THE PROCEEDINGS OF
THE PHYSICAL SOCIETY
Section A

VOL. 68, PART 1 1 January 1955 No. 421A

A Radio-Frequency Probe for the Mass-Spectrometric Analysis of Ion Concentrations

BY R. L. F. BOYD AND D. MORRIS†
Department of Physics, University College London

Communicated by H. S. W. Massey; MS. received 4th March 1954

Abstract. It has become increasingly evident of recent years that a detailed study of the processes occurring in gas discharges often requires a means of analysing and studying separately the various ionic species. This is true even in the case of the inert gases.

This paper describes the development, and analyses the action, of a versatile probe which can readily be moved radially into and out of a discharge tube and which is able to distinguish between ions (positive or negative) of various masses. With this instrument it is therefore now possible to make probe studies on a particular species of ion in the presence of others.

Basically the instrument is a very small 12-stage linear accelerator which discriminates in favour of ions of a particular mass–charge ratio passing through its sampling orifice. It is of high sampling efficiency and this together with its mobility and the absence of a magnetic field gives it certain pronounced advantages over the magnetic method of analysis.

§ 1. INTRODUCTION

THE need to know the nature of the ions present in an electrical discharge when seeking to analyse the processes operative has been brought out by much of the recent work on decaying plasmas in the inert gases. Processes such as attachment to form molecular ions, charge exchange and ionization by metastable particles may readily exert an over-riding control upon the concentrations of the various ionic species. A preliminary account of the application of radio-frequency time of flight methods to the mass analysis of ions reaching a probe in a discharge plasma has already been given in a note to *Nature* (Boyd 1950). The purpose of this paper is to record the development and performance of the present form of the instrument. As originally developed the probe was intended principally for work with electronegative discharges at pressures of a few microns of mercury. Current interest in the inert gas plasmas at rather higher pressures, however, prompted the production of a probe suitable for use in discharges at pressures of 1 mm Hg and higher. In addition a robust, easily demountable construction has been aimed at.

---

† Now at the Physics Division, National Research Council, Ottawa, Canada.

§ 2. Choice of the Method of Mass Discrimination

Reference to the reasons for employing a time of flight instead of a magnetic means of mass analysis has been made in the note referred to above. The principal factors are: (i) the ease with which the radio-frequency mass spectrometer can be moved into and out of the discharge; (ii) the absence of magnetic disturbance of the plasma; (iii) the shortness of the total ion path (about 3 cm); (iv) the very moderate pumping requirements (quite a small oil or mercury diffusion pump giving a speed of about 10 litres sec^{-1} is adequate); (v) very simple collimation arrangements are possible thus eliminating the need for focusing and giving a high current efficiency (a large part of the current passing through the initial orifice reaches the collector).

Against these advantages must be set the need to provide a suitable radio-frequency source, problems associated with the screening of the radio frequency especially from the electrometer equipment, and, in the particular arrangement used here, the fact that the sampling efficiency and resolution depend somewhat upon the energy (distribution) of the ions entering the initial orifice.

In selecting the method to be used here there were four over-riding considerations: (i) simplicity was aimed at, both in the geometrical arrangement and in the signal generating equipment. (ii) The size of the analyser was required to be very small both as regards path length, so that only a moderate vacuum would be required, and also as regards diameter, so that the disturbance of the discharge by the probe should be a minimum. (iii) It is necessary to ensure (Boyd 1950) that ions travelling at submultiples of the resonant speed should be rejected. Several otherwise simple systems capable of high resolution suffer from the disadvantage that it is not possible without considerable elaboration to distinguish between ions for which 1, 2 or 3, etc. cycles of the applied frequency have elapsed during their time of flight. (iv) Adequate sensitivity for use in weak plasmas was required.

Considerations of size and sensitivity together make it necessary to employ a system which integrates the current collected over many cycles.

By arranging a system of fields like those in a linear accelerator the diameter of the probe is kept small and a system results in which mass selection is based on the dependence of ion energy gain upon the time of flight. An initial d.c. accelerating field converts the mass spectrum into a velocity spectrum. Since therefore the acceleration due to the radio-frequency fields affects the time of flight the radio frequency must not be permitted to supply energy to the ions comparable to that gained in their initial acceleration. Certain advantages in resolution and sensitivity can result from the use of shaped wave forms. With the small path length in the present instrument, however, this is not practicable, and a simple sine wave oscillator is used. This has the advantage that the form of the signal arriving at the radio-frequency electrodes may with confidence be taken to be the same as that generated.

It will be shown that ions travelling at submultiple speeds are rejected by arranging that the time an ion spends in the radio-frequency field is an appreciable part of a cycle. Such ions will then experience reversals of field which will greatly reduce their energy gain.

§ 3. The Arrangement of Electrodes

The arrangement of electrodes may be seen in figure 1. The orifice A is a plane platinum electrode about 3 mm diameter pierced with a small hole.

For the highest pressures in the discharge a hole 50 μ in diameter is used in order to obtain good differential pumping. In discharges at lower pressure a considerably larger hole may be employed so as to give greater sensitivity. Under such circumstances the orifice carries a fine wire grid (14 mm^{-1} pitch 0·013 mm diameter tungsten wire) to prevent penetration of the accelerating potential through the orifice into the discharge and to give a uniform accelerating field. The orifice electrode operates as a Langmuir probe, being covered by a space charge sheath. It may be at space potential or a few volts positive or negative to it.

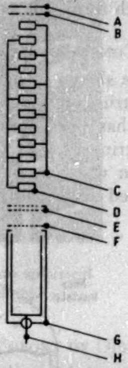

Figure 1. Schematic diagram of electrode system.

The accelerator electrode B is a grid (pitch and wire diameter as above) carrying an accelerating d.c. potential V of between 500 and 1000 volts, relative to the space potential in front of the orifice. This voltage is large compared with the energy of the ions entering the orifice and so gives rise to a velocity spectrum $v=(2V\boldsymbol{e}/\boldsymbol{m})^{1/2}$ dependent almost entirely on $\boldsymbol{e}/\boldsymbol{m}$ for the ions and not significantly on their initial velocity.

The radio-frequency electrodes C and D are the elements of a linear accelerator system which acts specifically to accelerate ions of particular velocity (i.e. $\boldsymbol{e}/\boldsymbol{m}$). These ions are said to be ‘ resonant ’. The radio-frequency electrodes are connected to a symmetrical radio-frequency oscillator and have the same d.c. potential as the accelerator. The amplitude of the applied radio frequency is usually about 5 volts so that although the gain in energy of the ions is sufficient to make discrimination possible the change in velocity of flight is so small that the spacing of the electrodes can be kept constant.

The retarder E is a pair of (crossed) grids carrying a retarding potential V_r relative to space potential such that only those ions which have been in resonance with the applied radio frequency have sufficient energy to pass them. The use of two grids effectively eliminates field penetration.

The suppressor F is an electrode normally maintained at an accelerating voltage slightly in excess of the initial accelerating potential. Its function is to reject ions of opposite sign to those in the beam, which may have been produced by collisions in the radio-frequency region. This is particularly important when working with negative ions, as electrons in the radio-frequency region may readily give rise to positive ions by ionization of the residual gas.

The collector shield G is a cylinder which shields the collector from electric fields and spurious charges.

The collector H (and its shield) is maintained at an attracting potential some 40 volts or so above space potential, so that particles moving obliquely after passing through the retarder are accelerated into the collector.

Electrodes B, C and D are surrounded by a screen (not shown) at the same potential as the initial accelerating electrode. This screen and all except the radio-frequency and collector electrodes are decoupled to earth by high permittivity silvered ceramic condensers which form part of the structure.

§ 4. The Constructional Details

The constructional details are shown in figures 2–6 (figure 6 is included to show an alternative form of construction, using discs instead of cylinders in the radio-frequency section, which has been found to be satisfactory when the pressure requirements are not stringent. In this instrument the retarder and suppressor grids were carried on discs about 16 mm diameter decoupled by sandwiching between other earthed discs insulated from them by thin sheets of mica).

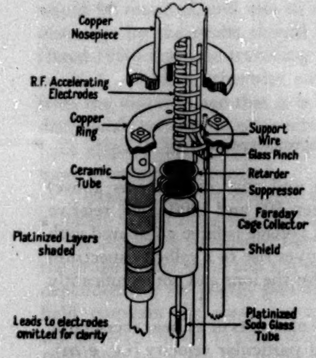
Copper Nosepiece
R.F. Accelerating Electrodes
Copper Ring
Ceramic Tube
Platinized Layers shaded
Leads to electrodes omitted for clarity
Support Wire
Glass Pinch
Retarder
Suppressor
Faraday Cage Collector
Shield
Platinized Soda Glass Tube

Figure 2. Drawing of radio-frequency and collector systems.

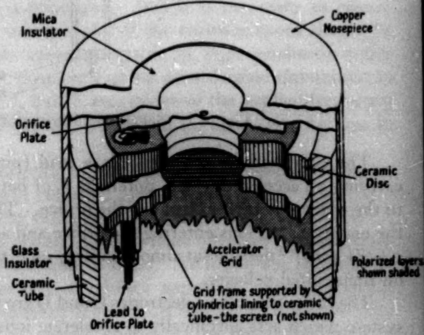
Mica Insulator
Copper Nosepiece
Orifice Plate
Ceramic Disc
Glass Insulator
Ceramic Tube
Lead to Orifice Plate
Accelerator Grid
Grid frame supported by cylindrical lining to ceramic tube - the screen (not shown)
Polarized layers shown shaded

Figure 3. Sectional drawing of nosepiece.

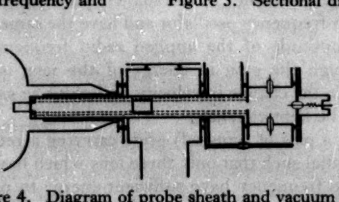

Figure 4. Diagram of probe sheath and vacuum head.

The analyser is built on a pair of 3 mm diameter stainless steel tubes (figure 2) which carry at their ends the nose piece, a self-contained unit (figure 3) made of thin copper tube and ceramic, which supports the orifice and accelerator grid. Silvered ceramic cylinders surrounding the 3 mm tubes carry the retarder and suppressor grids, the leads to these electrodes passing up the centre of the 3 mm tubes through glass sleeving. This whole system, except for the nose which protrudes from the end, is encased in a stainless steel tube of 2 cm diameter, vacuum seals being formed by compressed neoprene rings (figure 4). Figure 5 shows the assembly inserted into a radio-frequency discharge vessel.

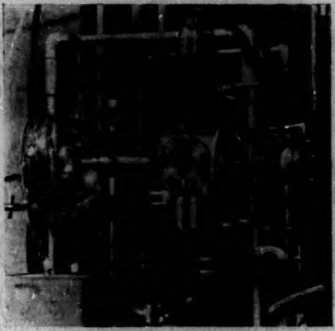

Figure 5. Probe inserted into spherical radio-frequency discharge.

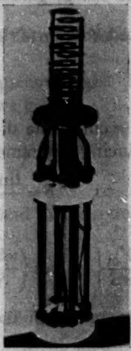

Figure 6. Early model of probe using disc electrodes.

§ 5. THEORY OF OPERATION

A generalized theory applicable to this instrument has been given by Redhead (Redhead 1952, Redhead and Crowell 1953) who has developed independently an almost identical system on a rather larger scale for use as a general purpose mass spectrometer. A very brief resumé of his theory as it concerns resolution and sensitivity will be given here, with appropriate modifications.

The following assumptions are made: (*a*) The energy of the ions at the orifice and the energy gained in the radio-frequency fields may both be neglected in comparison with that gained in the initial acceleration. (*b*) All the electrodes are assumed to act like equipotentials in their plane of symmetry. In the case of the cylinders there is actually a slight focusing action. In view of assumption (*a*), however, it is negligibly weak. No analytical solution is possible apart from these assumptions. However, an approximate solution for the effect of finite orifice energy will be given later.

The energy gain is worked out as a function of the phase angle ϕ, such that $V_m \sin\phi$ is the radio-frequency voltage at the instant an ion enters the first radio-frequency field where V_m is the maximum value of the radio-frequency voltage. From this the resolution and collector current are obtained.

Let f c/s be the radio frequency; $\omega = 2\pi f$. Let V_a volts be the accelerator potential, v cm sec^{-1} the velocity of an ion and m its mass in grammes. Only singly charged ions (charge $\mathbf{e}$ coulomb) will be considered. All potentials are referred to that of the orifice as zero.

The value of the field between each radio-frequency electrode is given by

$$X = \frac{2V_m}{S} \sin(\omega t + \phi)$$

where the time t is zero at the instant the ion enters the first radio-frequency field and S cm is the spacing between the idealized equipotential planes representing the electrodes. Between the accelerator and the first radio-frequency electrode and between the retarder and the last radio-frequency electrode the field has half this value.

The energy gain is therefore given by

$$\Delta E=\tfrac{1}{2}X\int_{0}^{S}\sin(\omega t+\phi)\,dx-X\int_{S}^{2S}\sin(\omega t+\phi)\,dx+X\int_{2S}^{3S}\sin(\omega t+\phi)\,dx-\dots$$
$$+X\int_{11S}^{12S}\sin(\omega t+\phi)\,dx-\tfrac{1}{2}X\int_{12S}^{13S}\sin(\omega t+\phi)\,dx \text{ electron volts}$$

where x cm is the displacement of the particle from the accelerator electrode. Introducing a parameter

$$\beta=\frac{\text{time taken for ion to travel distance }2S}{\text{period of radio frequency}}=\frac{2S}{vT}$$

we get

$$\Delta E=\frac{V_{\mathrm{m}}}{\pi\beta}\left\{-\left[\cos\left(\frac{\pi\beta x}{S}+\phi\right)\right]_{0}^{S}+2\left[\cos\left(\frac{\pi\beta x}{S}+\phi\right)\right]_{S}^{2S}-2\left[\cos\left(\frac{\pi\beta x}{S}+\phi\right)\right]_{2S}^{3S}\right.$$
$$\left.+\dots-2\left[\cos\left(\frac{\pi\beta x}{S}+\phi\right)\right]_{11S}^{12S}+\left[\cos\left(\frac{\pi\beta x}{S}+\phi\right)\right]_{12S}^{13S}\right\}$$

which for optimum ϕ gives for maximum $\Delta E=\Delta E_{\mathrm{m}}$

$$\Delta E_{\mathrm{m}}=\frac{4V_{\mathrm{m}}}{\pi\beta}\sin(\tfrac{1}{2}\pi\beta)\,[\cos 6\pi\beta-2\cos 5\pi\beta+2\cos 4\pi\beta-2\cos 3\pi\beta+2\cos 2\pi\beta$$
$$-2\cos\pi\beta+1].$$

Values of ΔE_{m} occur close to $\beta=1$, 3, 5, etc. Those at $\beta=3$, 5, 7, etc. however have values 1/3, 1/5, 1/7, etc. of the value at $\beta=1$. In addition there is a spectrum of much smaller subsidiary maxima on each side of those at $\beta=1$, 3, 5, etc. This effect is shown in figure 7 where the values of ΔE_{m} for values of β from 0 to 2 have been plotted. The highest value of ΔE_{m} occurs at $\beta=0{\cdot}992$ and is $12{\cdot}07\times 4V_{\mathrm{m}}/\pi$, i.e. $15{\cdot}4V_{\mathrm{m}}$.

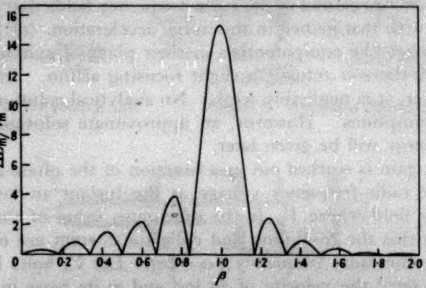

Figure 7. Variation of maximum ion energy gain with frequency.

By setting the retarder voltage at a sufficiently high value, i.e. greater than $15{\cdot}4V_{\mathrm{m}}/3$, all ions corresponding to maxima other than that at $\beta=1$ are rejected and a single characteristic frequency is found for each ionic mass–charge ratio.

§ 6. RESOLUTION

If we define the mass resolution R by $R=100(m_1-m_2)/2m_0\%$ where m_0 is the mass of the 'resonant' ion and m_1 and m_2 are the masses of the ions which are just rejected then (Redhead 1952)

$$R=\frac{2}{\pi}\left\{\frac{3\pi}{2N(N^2-1)}\frac{\delta E}{V_{\mathrm{m}}}\right\}^{1/2}\times 100\%$$

for N equal radio-frequency stages where δE is the excess of the maximum energy gained (in electron volts) over the retarder potential V_{r}.

In our case we have two half and eleven whole radio-frequency stages. Making the approximation $N=12$ and putting $\delta E=15\cdot 4V_{\mathrm{m}}-V_{\mathrm{r}}$ we get

$$R=3\cdot 34(15\cdot 4-V_{\mathrm{r}}/V_{\mathrm{m}})^{1/2}\%.$$

§ 7. ION CURRENT

If the ion current of 'resonant' ions at the orifice is i_0 and that arriving at the collector is i_{c} then

$$\frac{i_{\mathrm{c}}}{i_0}=T\,\frac{\phi(\Delta E>V_{\mathrm{r}})}{2\pi}$$

where T is a transparency factor for the grids (assumed independent of ion velocities and electrode potentials) and $\phi(\Delta E>V_{\mathrm{r}})$ is the angular range of phase for which the energy gain is greater than the retarder potential. Since the dependence of ΔE on ϕ is of the form $\Delta E_{\mathrm{m}}\cos(\phi+\theta)$ where θ is some constant, $\phi(\Delta E>V_{\mathrm{r}})=2\cos^{-1}(V_{\mathrm{r}}/\Delta E_{\mathrm{m}})$. Thus

$$\frac{i_{\mathrm{c}}}{i_0}=\frac{T}{\pi}\cos^{-1}\left(\frac{V_{\mathrm{r}}}{15\cdot 4V_{\mathrm{m}}}\right)$$

since $\Delta E_{\mathrm{m}}=15\cdot 4V_{\mathrm{m}}$ at $\beta=0\cdot 992$. For typical values of the parameters this gives an overall transmission efficiency of about 10%, a high value due to the acceptance of all ions entering the orifice into the initial beam, that is, there is no cutting down of the beam by collimation.

§ 8. EFFECT OF INITIAL ION ENERGIES

The possession of initial energies by the ions entering the probe orifice affects the collector current in two ways: (i) the energy gained by the ions in the radio-frequency fields depends on their velocity, (ii) the energy gain necessary to enable an ion to pass the retarder depends on its initial energy.

(i) *Energy Gain*

The energy gain in the radio-frequency fields depends both on the velocity of the ions and on the radio frequency. Hence, if the ions possess a range of energies then the curve of the energy gain plotted against β in the region of the maximum will consist of the superposition of a number of resonance curves, each peak occurring at a slightly different value of β. However, in practice the spectrometer will 'tune' to the frequency which satisfies the resonant condition ($\beta=0\cdot 992$) for ions of the most probable initial energy, eV. Consider a group of ions with energy $e\Delta V$ less than the latter. Then for the ions of energy eV at resonance $\beta=0\cdot 992$. For the second group of ions the value of β is given by $\beta=0\cdot 992\{(V_{\mathrm{a}}+V)/(V_{\mathrm{a}}+V-\Delta V)\}^{1/2}$.

Taking as a rather extreme example: $V=25$ volts, $\Delta V=25$ volts, and two values of V_a, viz. a very low value $V_a=200$ volts and the more normal value $V_a=800$ volts, we find $\beta=1{\cdot}052$ and $1{\cdot}003$ respectively. The corresponding energy gains are $12{\cdot}3V_m$ and $15{\cdot}25V_m$, i.e. differing by 20% and 1% respectively from the energy gained by ions of energy V (which is $15{\cdot}4V_m$). These values are obtained by a consideration of figure 7. From this example it can be seen that by keeping the accelerator voltage large in comparison with the ion entrance energies measured in electron volts the effect of the latter on the energy gain can be made small.

(ii) *Effect of Energy Spread on Retarder Action*

Since the range of phase of the radio frequency over which ions can arrive at the collector varies with the energy of the ions, the form and magnitude of the initial ion energy distribution will affect the collector current. In order to determine the magnitude of the effect, the form of the energy distribution must be known. An exponential distribution

$$dN=\frac{N}{V_p}\exp\left(-\frac{V_i}{V_p}\right)dV_i$$

is an approximation to the form of energy distribution likely to occur in practice. Here V_p electron volts is a characteristic ion mean energy, N is the total number of ions entering the orifice and dN is the number of ions with energies in the range V_i to V_i+dV_i electron volts. A situation in which such a distribution is approximately valid is that in which collisions made by the ions reaching the orifice are chiefly charge exchange collisions, with the electric field remaining sensibly constant over a path length. The collector current is given by

$$\frac{i_c}{i_0}=\frac{T}{2\pi}\frac{\int_0^\infty \phi_i\,dN}{N}$$

where ϕ_i is the angular range of phase for which ions can pass the retarder; for ions of energy V_i, $\phi_i=2\cos^{-1}a(V_r-V_i)$ where $1/a=15{\cdot}4V_m$. In obtaining this value of ϕ_i it is assumed that all ions entering at optimum phase receive the maximum energy gain, $15{\cdot}4V_m$. This is justified by the considerations in the preceding section.

The value of i_c/i_0 then becomes

$$\frac{i_c}{i_0}=\frac{T}{2\pi}\left\{2\int_0^{V_r+1/a}\exp\left(-\frac{V_i}{V_p}\right)\cos^{-1}a(V_r-V_i)\,dV_i+\int_{V_r+1/a}^{\infty}\exp\left(-\frac{V_i}{V_p}\right)dV_i\right\}$$

which can be reduced to

$$\frac{i_c}{i_0}=T\left[\frac{1}{2}\left\{1-\left(1-\frac{1}{\pi}\right)\exp\left(-\frac{V_r+1/a}{V_p}\right)\right\}-\frac{1}{\pi V_p}\right.$$
$$\left.\times\int_0^{V_r+1/a}\exp\left(-\frac{V_i}{V_p}\right)\sin^{-1}a(V_r-V_i)\,dV_i\right].$$

The integral cannot be evaluated analytically but some results can be obtained by taking the first few terms of the series expansion for $\sin^{-1}a(V_r-V_i)$. Even with only three terms the computation is long, and gives the shape of the retardation curve (collector current versus retarder voltage) only for low values of the retarder voltage. To obtain the shape of the curve under high resolution conditions a very lengthy and tedious computation would be necessary. However, in figure 8 curves obtained by using the above approximation are given (for small values of V_{r}) for the cases $V_{\mathrm{p}} = 1{\cdot}54V_{\mathrm{m}}$ and $6{\cdot}12V_{\mathrm{m}}$, these values being chosen for ease of computation. The curves shown are over the range of V_{r} for which the first three terms of the series expansion of $\sin^{-1} a(V_{\mathrm{r}} - V_{\mathrm{i}})$ differ from the exact value by less than 1%.

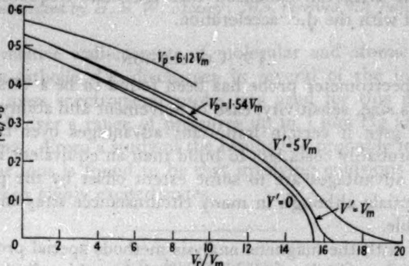

Figure 8. Influence of initial ion energy distribution on idealized theoretical collector current-retarder potential relationship.

In order more clearly to illustrate the effect of initial ion energies a simplified form of energy distribution will be chosen. It is such that the number of ions with energy in a given range decreases linearly with the energy, becoming zero at a 'cut-off' value V', i.e.

$$dN = \frac{2N}{V'}\left(1 - \frac{V_{\mathrm{i}}}{V'}\right) dV_{\mathrm{i}}.$$

This gives for the collector current

$$\frac{i_{\mathrm{c}}}{i_0} = \frac{2T}{\pi V'}\int_0^{V'}\left(1 - \frac{V_{\mathrm{i}}}{V'}\right)\cos^{-1} a\,(V_{\mathrm{r}} - V_{\mathrm{i}})\,dV_{\mathrm{i}}$$

and yields on integration

$$\frac{i_{\mathrm{c}}}{i_0} = \frac{T}{2\pi}\left(\frac{1}{aV'}\right)^2 [\{2a^2(V_{\mathrm{r}} - V')^2 + 1\}\cos^{-1} a(V_{\mathrm{r}} - V') - \{2a^2 V_{\mathrm{r}}(V_{\mathrm{r}} - 2V') + 1\}$$
$$\times \cos^{-1} aV_{\mathrm{r}} - 3a(V_{\mathrm{r}} - V')\{1 - a^2(V_{\mathrm{r}} - V')^2\}^{1/2} + a(3V_{\mathrm{r}} - 4V')\{1 - a^2 V_{\mathrm{r}}^2\}^{1/2}].$$

Retardation curves plotted from this expression are also shown in figure 8 for the cases $V' = 0$, V_{m} and $5V_{\mathrm{m}}$. The general shape of the curves is similar at low values of V_{r} but under high resolution conditions the effect of the initial energies becomes particularly apparent.

In experimental work it is usually required to determine the relative currents arriving at the probe orifice of two (or more) types of ions, from measurements of the corresponding collector currents. If both types of ions have zero energies on arriving at the orifice then the ratio of the orifice currents will be equal to the ratio of the collector currents. This also applies if the two types of ions have similar energy distributions of the same mean energy. However, in general, this may not be the case and the ratio of collector currents will not give an accurate value of the orifice current ratio. From the curves for $V' = V_{\mathrm{m}}$ and $V' = 5V_{\mathrm{m}}$ in figure 8, for example, it is obvious that a comparison of the collector currents under high resolution conditions will give results differing greatly from the orifice current ratio. A comparison at lower values of V_{r} will give more accuracy, however (to within 6% at $V_r=0$ in the case cited), but the greatest accuracy can be obtained by comparing the slopes of the curves at low V_r since the effect of initial energies tends to zero and the shapes of the curves therefore become very similar at low retarder voltages. The effect of the ion entrance energies can be reduced by using as high a value of the radio-frequency voltage V_m as is compatible with the condition that the radio-frequency energy gain is small compared with the d.c. acceleration.

§ 9. CONCLUSION

The mass-spectrometer probe has been found to be a versatile and reliable instrument. Its size, sensitivity, ease of movement and ability to work at fairly high pressures give it certain important advantages over magnetic analysis. In addition it probably costs less to build than an equivalent magnetic spectrometer. These advantages are to some extent offset by the presence of high-frequency potentials although in many circumstances stray magnetic fields are no more desirable.

In common with the magnetic analysis methods special problems connected with sampling and sensitivity are introduced when probing discharges at pressures above about 0·1 mm Hg. With care in interpretation useful data may be obtained with the present system at pressures up to about 1 mm Hg. Some typical results showing the ratio of wall currents of He_2^+ to He^+ in a d.c. discharge are shown in figure 9. A full discussion of this work on inert gases is given by Morris (1955).

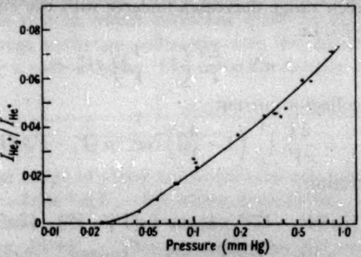

Figure 9. Variation of helium ion currents to tube wall with pressure.

An oscillator giving an automatically controlled output over a wide frequency range has been developed for use with the instrument (Boyd and Morris 1953). This oscillator may be used together with a recording camera to give complete spectrograms.

ACKNOWLEDGMENTS

In conclusion the authors wish to express their gratitude to Professor H. S. W. Massey for his unfailing interest and advice. Acknowledgments are also due to the I.C.I. Fellowship Committee of the University of London and to the Ministry of Education.

REFERENCES

BOYD, R. L. F., 1950, *Nature, Lond.*, **165,** 142.
BOYD, R. L. F., and MORRIS, D., 1953, *Electron. Engng*, **25,** 389.
MORRIS, D., 1955, *Proc. Phys. Soc.* A, **68,** 11.
REDHEAD, P. A., 1952, *Canad. J. Phys.*, **30,** 1.
REDHEAD, P. A., and CROWELL, C. R., 1953, *J. Appl. Phys.*, **24,** 331.

Molecular Ions in Discharges in the Inert Gases

By D. MORRIS†
Department of Physics, University College, London

Communicated by H. S. W. Massey; *MS. received 9th July* 1954

Abstract. The relative wall-currents of molecular and atomic ions have been measured in hot-cathode d.c. discharges in several of the inert gases. The radio-frequency mass spectrometer probe was used for this investigation and results were taken over a range of pressures up to 1 mm Hg and tube currents from 50 to 500 mA. From a study of the results the probable formation process for the molecular ions is found to be that involving collisions between normal atoms and atoms in highly excited states.

§ 1. INTRODUCTION

THE formation of molecular ions of the inert gases has been studied under various conditions. Mass spectrometric investigations of the ions formed by electron impact at gas pressures of the order of 10^{-3} mm Hg have been made by Arnot and M'Ewen (1939) for helium, and by Hornbeck and Molnar (1951) for all the inert gases except radon. The relative proportions of atomic and molecular ions in helium afterglows have been determined at pressures above 1 mm Hg by Phelps and Brown (1952). The only studies of the ions present in steady discharges in the inert gases have been those of Tüxen (1936) for helium, neon and argon at pressures greater than 5 mm Hg, and the preliminary results of Boyd (1950 a) for helium. The present work was undertaken at Boyd's suggestion to check the latter results, which were difficult to account for by theory, and to extend the measurements to higher pressures and to the other inert gases. It was intended to determine if possible the most important formation process for the molecular ions in these discharges.

§ 2. EXPERIMENTAL METHOD

The wall-currents of molecular and atomic ions in the discharge were measured by means of an improved version of the radio-frequency mass spectrometer probe (Boyd 1950 b). This instrument is fully described by Boyd and Morris (1955) and no details will be given here. The probe was mounted in a side-arm of a 3 in. diameter Pyrex glass discharge tube so that the probe orifice was flush with the tube wall. The discharge tube was 25 in. long and had a disc anode of molybdenum and a tungsten loop as filament. Differential pumping was used to keep the pressure inside the probe much lower than that in the discharge tube. The minimum attainable pressure in the apparatus after baking out the discharge tube was better than 10^{-5} mm Hg.

The gas used in the experiments was supplied by British Oxygen Company as 'spectrally' pure, and the gas passed through only a few inches of glass tubing and a liquid air trap before entering the discharge tube. A slow flow of gas was maintained while the readings were taken.

---

† Now at Physics Division, National Research Council, Ottawa, Canada.

The wall-currents were measured at gas pressures up to nearly 1 mm Hg in helium, neon and argon, and a few readings were taken at lower pressures in krypton and xenon. The latter were not studied in detail owing to the lower purity of the available gases. Above 1 mm Hg the pressure in the probe became high enough to cause serious attenuation of the ion beam inside it, and results at these pressures were not reliable. The probe had been constructed as an instrument capable of radial movement into the discharge, although such movement was not required in the present investigation. It was the provision of this radial motion that restricted the pressure range over which the probe could be used.

§ 3. RESULTS

Over the range of parameters used in this work, the current of molecular ions to the wall of the discharge did not exceed 8% of the atomic ion current for any of the inert gases studied. These results are at variance with Boyd's preliminary results, which appeared to show that the molecular ions were predominant in a helium discharge even at pressures as low as 0·01 mm Hg. In the present investigation it has been found that the results have been reasonably consistent even when the amounts of impurity ions present were varied. In view of this and the fact that no comparable results were obtained for argon in the earlier work it has been concluded, in discussion with Boyd, that the earlier results in helium must be attributed to some unknown error or effect in the earlier mass spectrometer probe.

The present results are displayed in the form of graphs showing the variation of the ratio of the wall-currents of the two ion species with pressure (figures 1–3) and tube current (figures 4, 5). The accuracy of these ion ratios is not better than within 10 to 15%, owing to the fact that they could not be obtained directly by comparison of the ion currents at a particular retarding potential, but had to be obtained by extrapolation of curves of ion current versus retarder voltage. This was necessitated both by the variation of the output voltage with frequency of the radio-frequency oscillator used in conjunction with the probe, and by the possession of initial energies by the ions on entering the probe orifice. This extrapolation procedure (Boyd and Morris 1955) was found to give the most consistent results in practice and was shown theoretically to be the most accurate method. However, since two retardation curves had to be plotted at each value of discharge pressure and tube current, there was sometimes a small drift in pressure during the observations. Such pressure variations are indicated on the graphs by horizontal lines.

The impurity ions present in the discharge were usually OH^+, H^+, N_2^+ and C^+, the first being the main impurity. The heights of these impurity peaks were noted when the other readings were taken, and the only points shown on the graphs are those obtained when the impurity ion peaks were less than the molecular ion peaks.

Besides the results shown for helium, neon and argon, a few results were also obtained in krypton and xenon. The only krypton available contained 1% xenon, so that the predominant ion in the discharge under most conditions was Xe^+. However, a trace of Kr_2^+ was found. The available xenon contained 1% krypton but the Xe_2^+ peak was easily found. The ion current ratio was 0·01 at a pressure of 0·07 mm Hg. Readings at higher pressures were rendered

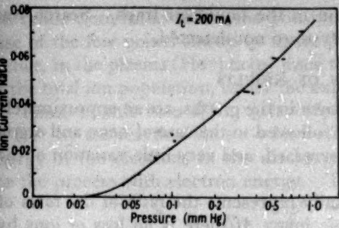

Figure 1.
Variation of helium ion ratio with pressure.

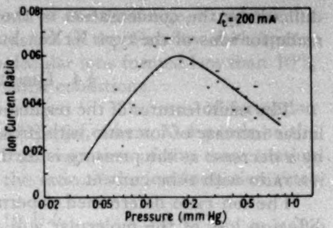

Figure 2.
Variation of neon ion ratio with pressure.

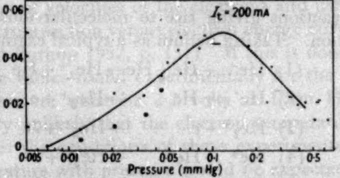

Figure 3. Variation of argon ion ratio with pressure. (Large points below curve represent results taken in the Faraday dark space.)

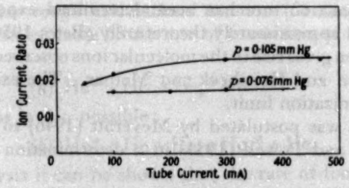

Figure 4. Variation of helium ion ratio with tube current.

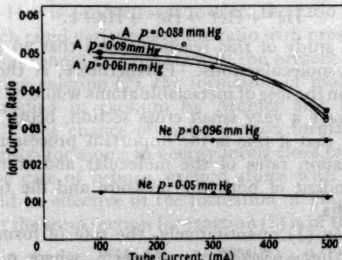

Figure 5. Variation of ion ratio with tube current for A and Ne.

difficult by the condensation of the xenon in the liquid air traps. Search was made for ions of the type $KrXe^+$ but they were not detected.

§ 4. DISCUSSION OF RESULTS

The main features of the results, as shown in the graphs, are an approximately linear increase of ion ratio with pressure, followed in the case of neon and argon by a decrease as the pressure is further increased, and very little variation of the ion ratio with tube current.

The ion ratio determined experimentally represents the ratio of the rates of diffusion loss of the molecular and atomic ions. If there is no loss of ions by other processes, then the measured ratio will also give the ratio of the formation rates of the ions, under the conditions of the discharge. It is possible to make some predictions concerning the relative formation rates, and so the most probable formation process for the molecular ions can be determined.

There are five reactions giving rise to molecular ions which appear to be worthy of consideration. Taking helium as a typical example, these are:

$$
\begin{array}{lll}
(1) & He^+ + He + He & \rightarrow He_2^+ + He \\
(2) & He' + He & \rightarrow He_2^+ + e \\
(3) & He_2^* + e & \rightarrow He_2^+ + 2e \\
(4) & He^* + He^* & \rightarrow He_2^+ + e \\
(5) & He^+ + He & \rightarrow He_2^+ + h\nu.
\end{array}
$$

Here the asterisks represent metastable states and the dashes represent excited states.

The first of these is known to account for the formation of He_2^+ in helium afterglows and the reaction rate has been determined experimentally (Phelps and Brown 1952) and approximately theoretically (Bates 1950).

The second reaction gives rise to the molecular ions observed in the experiments of Arnot and M'Ewen and Hornbeck and Molnar. The excited state must lie close to the atomic ionization limit.

The third process was postulated by Meyerott (1946) to explain the results obtained by Tyndall and Powell (1931) in a determination of the mobility of helium ions in helium.

The fourth and fifth processes appear energetically possible but have not been observed, and may be rejected as not important in the present experiments. The collision of two metastable helium atoms gives rise mostly to atomic ions:

$$He^* + He^* \rightarrow He^+ + He + e.$$

Biondi (1952) in a study of this reaction states that no evidence was found for the production of molecular ions. Furthermore, at the pressures used in the present investigation the loss of metastable atoms would be mainly by diffusion.

Reaction (5) will have a very small cross section, being a radiative process. Also, it can be shown that if this is the important process in the present work the ratio of the formation rates of the molecular and atomic ions should be approximately independent of both the pressure and the tube current, which is contrary to the results.

Considering reaction (1) quantitatively, the rate of formation of molecular helium ions is $d[He_2^+]/dt = 65p^2[He^+]$ cm^{-3} sec^{-1}, where p is the pressure in mm Hg and Phelps and Brown's experimental value has been used. All the ion ratios were measured in the positive column of the discharge, except in the case of the few points shown in figure 3 for results in the Faraday dark space. Hence, in the plasma $[\mathrm{He}^+] \simeq [\mathrm{e}]$ since the molecular ions formed less than 10% of the total ion population, under the experimental conditions.

Thus, in this case $d[\mathrm{He}_2{}^+]/dt = 65p^2[\mathrm{e}]\ \mathrm{cm}^{-3}\ \mathrm{sec}^{-1}$. The rate of formation of He^+ by the reaction $\mathrm{He} + \mathrm{e} \rightarrow \mathrm{He}^+ + 2\mathrm{e}$ is $K[\mathrm{He}][\mathrm{e}]$, where K depends on the energy of the electrons in the discharge and the variation of the cross section for the process with electron energy. Thus the ratio of the ion formation rates

$$R = \frac{65p^2}{K[\mathrm{He}]} \simeq 2 \times 10^{-15} \frac{p}{K}.$$

Assuming that K does not vary with pressure or electron density, it is seen that the ion ratio should increase linearly with pressure and be independent of the tube current. However, a rough calculation of K can be made assuming a Maxwellian distribution of velocities of the electrons and using the known form and magnitude of the cross section versus electron energy curve for the ionization of helium (Massey and Burhop 1952, p. 151). If this is done it is found that in order to reproduce the values found experimentally for the ion ratio, the value of the electron temperature must be 2·2 volts at 1 mm Hg and 2·0 volts at 0·1 mm Hg. It is very unlikely that the electron temperature could be as low as this in helium under the conditions of these experiments, and the variation of the electron temperature with pressure would be expected to be greater than 0·2 volt in the pressure range 0·1 to 1·0 mm Hg. Taking a more reasonable value of 5 volts for the electron temperature gives results at least an order of magnitude too low. It is not possible to make quantitative calculations for the other inert gases.

By making similar rough calculations reaction (3) can also be eliminated. Meyerott has given an estimate of the rate of formation of metastable molecules by the process

$$(a)\quad \mathrm{He}^* + \mathrm{He} \rightarrow \mathrm{He}_2{}^* + h\nu.$$

A three-body process is also possible:

$$(b)\quad \mathrm{He}^* + \mathrm{He} + \mathrm{He} \rightarrow \mathrm{He}_2{}^* + \mathrm{He}.$$

By a rough analysis it can be shown that the rate of formation of metastable molecules will be proportional to $p^2[\mathrm{e}]$ in case (*a*) and $p^3[\mathrm{e}]$ in case (*b*). Hence the rate of formation of $\mathrm{He}_2{}^+$ by (3) will be roughly proportional to $p^3[\mathrm{e}]^2$ or $p^4[\mathrm{e}]^2$, depending on the predominant mode of formation of $\mathrm{He}_2{}^*$. Since the rate of formation of He^+ is proportional to $p[\mathrm{e}]$, the ratio of the rates will vary as $p^2[\mathrm{e}]$ or $p^3[\mathrm{e}]$. Such rapid variations of the ratio with pressure and tube current show that this reaction cannot be important in the present instance.

Finally, considering reaction (2), the formation of molecular ions by such a process has been studied in caesium by Mohler and Boeckner (1930) and Freudenberg (1931). The chance of molecular ion formation was found to be nearly unity per collision for atoms in energy levels close to the atomic ionization limit. Hence, in the case of helium, excited atoms with energies greater than about 22 volts should be effective in the formation of $\mathrm{He}_2{}^+$.

If we assume that the cross section for reaction (2) is of the order of gas kinetic, then

$$\frac{d[\mathrm{He}_2^+]}{dt} \simeq P \frac{d[\mathrm{He}']}{dt}$$

where P is the probability of He′ colliding with a helium atom before decaying by radiation: $P=\tau/(\tau+T)$, where τ is the mean life of the excited state and T is the time between collisions. If λ is the mean free path of the gas atoms and v is their mean velocity, the expression becomes $P=(1+\lambda/v\tau)^{-1}$. Owing to the number of excited states which could contribute to the formation of molecular ions, the total rate of formation $d[\mathrm{He}']/dt$ cannot easily be estimated. A similar difficulty arises in the estimation of a mean value for τ. However, making the reasonable assumption that the rate of formation of the excited atoms is of the same order as that of the atomic ions, it is found that the ion ratio will be of the order of P.

In the case of helium, $\lambda=0{\cdot}014/P$ cm and $v\simeq 10^5$ cm sec^{-1}, and taking a lower limit of 10^{-8} sec for τ gives $P=p/(p+14)$. At low pressures P should vary almost linearly with pressure and be independent of tube current. If $p=1$ mm Hg then $P=0{\cdot}067$, which is of the right order to account for the experimental results. The results are also of the right order of magnitude in the case of neon and argon. Comparison of the theoretical ion ratio versus pressure curve obtained by these considerations with the experimental curve for helium is of little value, owing to the lack of knowledge of the exact reaction rates and the value of τ. Nevertheless the process (2) does give rise to ion ratios of the right order of magnitude and having approximately the correct variation with pressure and tube current.

One further point needs clarification however. In figures 2 and 3 it is seen that the curves for neon and argon rise to a maximum and then decrease. This effect must be attributed to loss of the molecular ions more rapidly than the atomic ions by some process other than diffusion. The most probable removal process is by dissociative recombination e.g.

$$\mathrm{Ne}_2^+ + e \rightarrow \mathrm{Ne}' + \mathrm{Ne}''.$$

The coefficients for dissociative recombination are large, the coefficient for argon being greater than for the lighter inert gases. Rough estimates show that the effect is large enough to explain the loss of A_2^+ at the pressures considered and also probably of Ne_2^+, but is not large enough to cause a decrease in the ion ratio in helium until higher pressures are reached.

Thus the experimental results show that the molecular ions in the discharge are formed most probably by collisions of normal atoms and those in high-lying excited states, although the possibility of three-body collisions between atomic ions and atoms being effective cannot be entirely ruled out. The principal loss of molecular ions in the 7 cm diameter discharge tube is by diffusion to the walls in helium at pressures up to 1 mm Hg. In neon and argon the effects of dissociative recombination become important at pressures above 0·1 mm Hg.

It would be of interest to extend the investigations to higher pressures in order to determine the formation process for the molecular ions under these conditions. By suitable modification it should be possible to use the mass spectrometer probe up to pressures of 5 mm Hg and perhaps above.

ACKNOWLEDGMENTS

The author wishes to express his thanks to Professor H. S. W. Massey for his interest and useful criticism, to Dr. R. L. F. Boyd for many helpful discussions of the work and to Dr. E. H. S. Burhop who read and criticized the manuscript. Thanks are also due to the Ministry of Education for financial assistance.

References

Arnot, F. L., and M'Ewen, M. B., 1939, *Proc. Roy. Soc.* A, **171**, 106.

Bates, D. R., 1950, *Phys. Rev.*, **77**, 718.

Biondi, M. A., 1952, *Phys. Rev.*, **88**, 660.

Boyd, R. L. F., 1950 a, *Proc. Phys. Soc.*, **63**, 543; 1950 b, *Nature, Lond.*, **165**, 142.

Boyd, R. L. F., and Morris, D., 1955, *Proc. Phys Soc.* A, **68**, 1.

Freudenberg, K., 1931, *Z. Phys.*, **67**, 417.

Hornbeck, J. A., and Molnar, J. P., 1951, *Phys. Rev.*, **84**, 621.

Massey, H. S. W., and Burhop, E. H. S., 1952, *Electronic and Ionic Impact Phenomena* (Oxford : University Press).

Meyerott, R., 1946, *Phys. Rev.*, **70**, 671.

Mohler, F. L., and Boeckner, C., 1930, *Bur. Stand. J. Res., Wash.*, **5**, 51.

Phelps, A. V., and Brown, S. C., 1952, *Phys. Rev.*, **86**, 102.

Tüxen, O., 1936, *Z. Phys.*, **103**, 463.

Tyndall, A. M., and Powell, C. F., 1931, *Proc. Roy. Soc.* A, **134**, 125.

Measurement of γ-Transition Lifetimes by Recoil Methods

By S. DEVONS, G. MANNING and D. St. P. BUNBURY
Department of Physics, Imperial College, South Kensington S.W.7

MS. received 22nd July 1954

Abstract. Methods of utilizing the recoil motion of excited nuclei produced in disintegrations, to obtain estimates of the half-lives of excited states, are described. They involve measurement either of the distance moved by the recoiling nucleus before radiation occurs, or of the small Doppler shift in frequency produced by the recoil motion. Details are given of the application of some of the methods to the measurement of the half-lives of the levels of ^{16}O at 6·13 MeV (E3 transition), 6·9 MeV (E2) and 7·1 MeV (E1), with the following results: 6·13 MeV, $5\times10^{-12}\lesssim\tau\lesssim10^{-11}$ sec; 6·9 MeV, $\tau\lesssim1{\cdot}2\times10^{-14}$ sec; 7·1 MeV, $\tau\lesssim8\times10^{-15}$ second.

---

§ 1. Introduction

Most of the γ-transitions between excited states of light nuclei take place too rapidly for their absolute lifetimes to be measured by conventional techniques, i.e. by clock or electronic timing. Most of the information that exists about such lifetimes is deduced from radiation width measurements in particle resonance reactions, but this method is not applicable to bound states, which form the large majority of the low-lying states. Measurement of the absolute cross section for excitation of bound states through a known form of electromagnetic interaction (e.g. the so-called 'Coulomb excitation') provides another method of estimating absolute radiation widths, but it is only conveniently applicable to low-lying states. In a few instances the recoil motion of the radiating nucleus excited in a nuclear reaction has been utilized to provide a suitable time scale with which to measure absolute radiation lifetimes. Such measurements are not, except in favourable circumstances, very accurate; often they provide no more than an order of magnitude or a limit, but they are useful for radiation lifetimes which are typical for γ-transitions in light nuclei, i.e. in the range 10^{-8}–10^{-14} sec, and where other methods are not readily available.

In view of the current interest in the properties of the low-lying states of light nuclei, and of the transitions between them, it has been considered worth while to explore in more detail the possibilities of the recoil techniques for studying these transitions. Typical recoil velocities of light nuclei produced in exothermic reactions, or in endothermic reactions with energies a few MeV above threshold, are of the order 10^8–10^9 cm sec^{-1}. With a typical radiation mean lifetime of, say, 10^{-13} sec, the mean distance traversed by an excited nucleus before radiating is 10^{-4}–10^{-5} cm. Measurement of the transition lifetime is thus reduced to measurement of this small distance (or larger distances for slow transitions). We have used such methods to obtain absolute values, or limits, for the lifetimes of the transitions in a number of light nuclei, the energies of the transitions ranging from 0·42 to 7·1 MEV and the multipolarities E1, M1, E2, E3. In this paper a brief account is given of the methods used, *some* of which are illustrated by the measurements of the first few levels of ^{16}O. It is intended to publish measurements of other nuclear levels in due course.

§ 2. EXPERIMENTAL METHODS

2.1. *Direct Method*

The distance traversed by the recoiling nucleus before de-excitation can, if sufficient, be measured directly by localizing the bombarded nuclei to a thin layer, and the region from which the radiation is observed by an arrangement of slits. On account of the limited absorption coefficient for γ-radiation of practical slit materials, ideally narrow slits cannot be constructed, and this factor determines the smallest distance and shortest lifetime that can be determined. This method was first used by Jacobsen (1924) to obtain an estimate (10^{-6} sec) of the half-life of RaC′. More quantitative application of the method in disintegration experiments has been made by Devons *et al.* (1949, 1954) to measure a half-life for electron pair emission of $(5 \pm 0{\cdot}5) \times 10^{-11}$ sec, and Thirion *et al.* (1953, 1954), who have measured several γ-transition half-lives ranging from $2{\cdot}5 \times 10^{-10}$ sec in ^{17}O to 8×10^{-8} sec in ^{19}F.

This method can be used, as the above measurements show, both with exo-momental† and endo-momental† reactions, although in the former case the interpretation of the measurements involves knowledge of the angular distributions in the reaction more sensitively than in the latter.

In the present series of experiments most of the transitions investigated were too fast for this method to be employed, but it has provided a useful method of placing an upper limit on the half-life. The limit attainable varies with the energy and intensity of the γ-radiation and the momentum of recoil nucleus, and is typically of the order 10^{-11} second.

2.2. *Measurement of Doppler Shift*

The motion of the recoil nucleus produces a Doppler shift, of the order 1% in a typical case, in the energy of the γ-transition. If the radiating nuclei are slowed down, either by passing through some material or by impinging on a solid surface, there is a relation between the average Doppler shift or line broadening, the mean range of the recoil nuclei in the material and the lifetime for the radiation transition which can be used to provide an estimate of this latter. The methods that we have used differ according as the nuclear reaction is exo- or endo-momental, so that it is convenient to consider these two types separately.

(*a*) *Endo-momental reactions.*

In this case the recoil motion of the radiating nucleus is primarily in the direction of the bombarding particles, so that the γ-ray energy is different according as one observes the γ-radiation in the same direction as the bombarding particles or oppositely, provided the radiation is not so slow that the recoil nuclei have been brought to rest in the target material or its support. If one assumes, for the moment, that *all* the recoil momentum derives from the bombarding particle, and that the residual range of the recoil nucleus in the stopping material, assumed uniform, is proportional to its velocity (Blackett and Lees 1932), then it can easily be shown that the average energy of the radiation, measured at an angle θ to the direction of the recoil is,

---

† For the sake of brevity we shall use these terms to denote reactions in which the recoil velocity of the radiating nucleus with respect to the centre of mass is larger than that of the centre of mass itself, and vice versa, i.e. reactions in which most of the momentum of the radiating nucleus is supplied by the outgoing or ingoing particles respectively.

$$E_0\left[1+\frac{v}{c}\cos\theta\,\frac{\lambda\alpha}{\lambda\alpha+1}\right],\quad \lambda=\tau^{-1}\ln 2 \qquad \ldots\ldots(1)$$

where E_0 is the radiation energy for nuclei at rest, v is the initial recoil velocity, τ the half-life for the radiation transition and $\alpha=R/v$, where R is the range of recoil nuclei of velocity v in the stopping material.†

Measurement of the difference in the mean energies of the radiation at, say, $\theta=0$ and π for a particular reaction provides a value of the ratio $\lambda\alpha$. Such Doppler shifts have been observed by Devons and Hine (1949) and Jones and Wilkinson (1952). The observations were consistent with no appreciable slowing down of the recoil nuclei before radiation, so that upper limits were obtained for the lifetime. Rasmussen, Lauritsen and Lauritsen (1949), using a magnetic lens spectrometer, measured the energy of the 480 kev transition in ^{7}Li in the reaction ^{7}Li(p, p′), and by comparison of this energy with that of the transition from stationary nuclei, $^7\mathrm{Be}(\beta)\rightarrow{}^7\mathrm{Li}$, concluded that the full recoil motion was present.

Measurements of Doppler shifts in this form suffer from several limitations. Firstly, the interpretation requires a knowledge of α, the range–velocity relationship in the medium, secondly, the bombarded material is the same as the stopping material, and thirdly, movement of the γ-measuring equipment is not always practical, or at best may involve small changes in the energy calibration of this equipment, which is a serious disturbance when small energy changes are being measured.

In order to overcome these limitations we have modified this method in several respects. We have used thin (in the range 10^{-5}–10^{-6} cm) evaporated layers for the target material, and these have been deposited on several backing materials of widely different densities to provide a range of stopping media for the recoil motion. In cases where there is a substantial difference in the recoil motion, and therefore in the Doppler shift, for two different backing materials a measurement which is much less dependent on the range–velocity relationships can be made by interposing a layer of known thickness of the less dense material between the target layer and a backing of the dense material. For example, suppose the retardation of the recoil nuclei is very small in the layer of light material (full Doppler shift) and very large in the backing material (no Doppler shift), then the mean Doppler shift ΔE using a 'sandwich' of light material with thickness x (in the direction of the bombarding beam) between target and backing will be approximately

$$\Delta E=E_0\frac{v}{c}\cos\theta\left[1-\exp\left(-\frac{\lambda x}{v}\right)\right] \qquad \ldots\ldots(2)$$

which is, of course, independent of range–velocity data.

---

† The recoil motion due to the momentum of the γ-radiation itself and scattering in the stopping material are here neglected.

In the more general, practical, case there will be some slowing down in the light material, and some residual recoil motion before radiation occurs in the dense material. Assuming again a linear relationship between v and R, we obtain for $x \leqslant R$ the following expression for the mean shift:

$$\Delta E = \frac{E_0 v \cos\theta}{c}\left\{\frac{\lambda\alpha'}{\lambda\alpha'+1}\left[1-\left(1-\frac{x}{R}\right)^{\lambda\alpha'+1}\right]+\left(\frac{R-x}{R}\right)^{\lambda\alpha'+1}\left(\frac{\lambda\alpha''}{\lambda\alpha''+1}\right)\right\}. \quad \ldots(3)$$

In this expression v refers to the velocity of recoil with which the nuclei enter the first, light, layer, and α', α'' refer to the light and dense materials respectively. The first term represents the contribution to the shift from nuclei radiating whilst passing through the light layer and the second term that from the residual motion of nuclei radiating in the dense backing. Expression (3) approximates to (2) when the second term in (3) is negligible ($\lambda\alpha'' \ll 1$) and the slowing in the light material is small, $x \ll R$, $\alpha'\lambda \gg 1$.

The Doppler shift can be measured either by making observations at two angles ($\theta = 0$ and π) for several values of x, or by measuring the shift in the mean γ-energy, at a fixed angle of observation, for different types and thicknesses of stopping material. This latter method avoids the complications associated with moving the γ-measuring equipment, but suffers from the limitation that unless one medium used has zero stopping (vacuum) it is not possible to distinguish between extremely fast transitions (full Doppler shift in all materials) and extremely slow ones (no Doppler shift in all cases). The shifts measured are also smaller in this latter method.

In the above discussion it has been assumed that all the recoil motion derives from the bombarding particle. In many cases there is a smaller contribution from the products of the reaction whose emission precedes the γ-transition.

In such cases the expression (3) has to be averaged over a range of values of v, x and θ, with due allowance for the fact that the probability of detection of the γ-ray will, in general, be different for different directions of the recoil motion due to possible angular correlation between particle and γ-emission. However, it is usually possible to choose experimental conditions so that the uncertainties in evaluating this average are not large, especially when it is remembered that the recoil shift itself cannot usually be measured with great accuracy.

(*b*) *Exo-momental reactions*.

When the major part of the recoil momentum is provided by the particle produced in a reaction, then there will be recoil motion in all directions, following the angular distribution of the process. The main consequence will be a broadening of the radiation from a sharp line to a band which is given by (1) together with a term dependent on the angular distribution of the recoil and the correlation between recoil direction and γ-emission, which is denoted by f, assuming the recoil takes place in a uniform medium. One of the few recoil measurements of lifetimes that have been made, that of the first state of ^{7}Li (480 kev) (Elliott and Bell 1949, Rasmussen, Lauritsen and Lauritsen 1949, see also Thomas and Lauritsen 1952), utilized this broadening in the reactions ^{10}B(n, α)^{7}Li and ^{9}Be(d, α) respectively to provide estimates of $\lambda\alpha$ and hence the lifetime.

In most reactions the broadening is of the order or less than 1%, so that, in addition to knowledge of f, the angular correlation function, very high spectral resolutions would be required in the γ-measurements. We have not therefore attempted to utilize this method.

If the broadening can be converted into a definite shift in mean energy of the same order of magnitude, then its measurement becomes rather easier and does not require the same degree of resolution. This we have done in two ways. Firstly we can examine those γ-transitions corresponding to particular directions of recoil motion by measuring only the γ-rays in coincidence with the preceding heavy particles moving in a fixed direction. For example, if the γ-spectrum is measured with the particle- and γ-detectors first in opposite directions with respect to the target, and then in the same direction, the mean γ-energy in the former case exceeds that in the latter by $2E_0(v/c)(\lambda\alpha)/(1+\lambda\alpha)$, where the assumptions are as in (1).† In practice we can either keep the particle detector fixed and move the γ-counter, or move both particle counter and, if necessary, the target (since it is not normally possible to detect the heavy particle through the target backing) and keep the γ-counter fixed. This latter alternative, although somewhat more elaborate, is the one we have adopted since it obviates the difficulties associated with change in calibration, on moving, of the γ-detector. One form of such an apparatus is shown schematically in figure 1. The second method is to introduce an anisotropy in the target arrangements. In the simplest form the target is a thin layer on a solid backing. Recoil motion in the direction of the backing will be slowed down and stopped, that in the direction away from the target (i.e. into vacuum) will be unimpeded. There will then, in general, be a *net* recoil motion away from the target surface. Consider an ideal arrangement in which the incident beam impinges on the target layer at zero grazing angle, and the γ-detector observes at 90° to the beam (figure 2(*a*)). Then if the target and backing are rotated by 180° (figure 2(*b*)) the mean energy of the γ-radiation will shift. To compensate for any change in intensity or scattering an absorber equal to the target backing is placed as shown in figure 2(*c*).

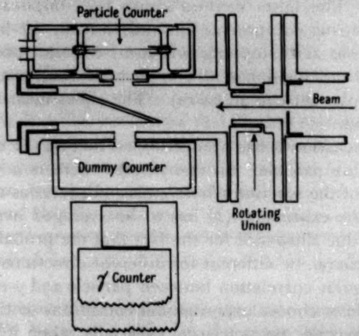

Figure 1. Coincidence apparatus. Approximately $\frac{1}{3}$ actual size.

Neglecting the small angle between target plane and beam, which is necessary in practice, the finite thickness of the target layer itself, and the finite sizes of target spot and γ-detector, the mean γ-energy in the two cases is

$$E_0\left\{1 \pm \frac{v}{2c}\left[1-\frac{\lambda\alpha}{\lambda\alpha+1}\right]g\right\}. \qquad \ldots\ldots(4)$$

---

† Also the centre-of-mass motion of the whole system is here neglected.

The observed shift will then be

$$E_0\frac{v}{c}\left[1-\frac{\lambda\alpha}{\lambda\alpha+1}\right]g \qquad \ldots\ldots(5)$$

where g is a factor (obtained by integrating f over half the sphere) of the order $\frac{1}{2}$ depending on the angular distribution and correlation (exactly $\frac{1}{2}$ if these are isotropic). Precise knowledge of g is not necessary to enable (5) to be used with as great an accuracy as the Doppler shift measurements warrant.

In practice small corrections are necessary to allow for the contribution to the recoil motion by the bombarding particles (or, more directly, the function f must refer to the laboratory and not the centre-of-mass frame), and also for the fact that the beam incidence is at a finite grazing angle. Figure 2(*c*) shows schematically a practical target arrangement employing this principle.

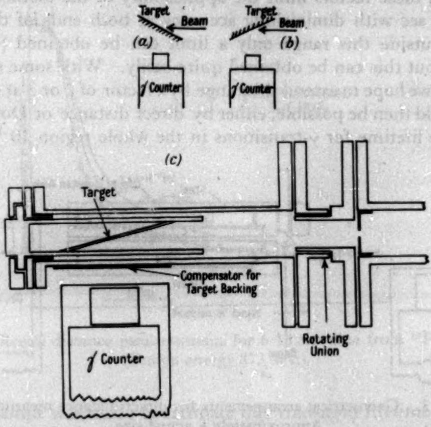

Figure 2. Target rotation apparatus. Approximately $\frac{1}{3}$ actual size.

We have sometimes found it convenient to compare the Doppler shift in two retarding media directly, and this can be done by using the target rotation method and covering one side of the target layer with one medium and the other with the second. In place of (5) we then get for the shift

$$\pm E_0\frac{v}{c}\left[\frac{\lambda\alpha'}{\lambda\alpha'+1}-\frac{\lambda\alpha''}{\lambda\alpha''+1}\right]g. \qquad \ldots\ldots(5\,a)$$

This method is useful when $\lambda\alpha \ll 1$ in all suitable media.

Both the above methods can be used in conjunction with the target 'sandwich' method described earlier, in which case the shifts will be given by straightforward modifications of (3), just as (4) is of (1). The coincidence method has two advantages as compared with the target rotation method, Firstly, the shifts are, on the average, about four times larger, and secondly no knowledge of the angular distribution is required. As against this, the more elaborate coincidence arrangement provides much slower counting rates in the measurement of the

γ-radiation, and we have found this in many cases more than offsets its 'theoretical' advantages over the simpler target rotation method.

2.3. *Scope of Methods*

All the expressions for the Doppler shift become insensitive to λ when $\lambda\alpha \gg 1$ or $\lambda\alpha \ll 1$, i.e. when the radiation lifetime τ is very much shorter or longer than the slowing down time α. The range over which one can obtain an estimate of λ depends then on the accuracy or sensitivity with which one can measure shifts and the range over which α can be varied by choice of material. Unfortunately the many practical limitations which govern the choice of target backing, and the absence of solid materials with density greater than about 20, limits the range of α to about a factor of 10 or less. With the present accuracy, in typical cases, we can measure shifts of down to 0·1% with moderate accuracy. For light nuclei ($A<30$) these factors limit the applicability of the method to the region 5×10^{-12}–10^{-14} sec with diminishing accuracy at both ends of the range. For γ-transitions outside this range only a limit can be obtained ($\tau>5\times10^{-12}$ or $\tau<10^{-14}$ sec), but this can be obtained quite easily. With some straightforward improvements we hope to extend this range by a factor of 2 or 3 at each end of the scale. It should then be possible, either by direct distance or Doppler methods, to estimate the lifetime for γ-transitions in the whole region 10^{-9}–10^{-14} second.

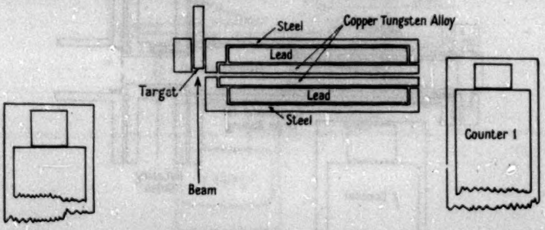

Figure 3. Geometrical arrangements for direct distance measurement. Approximately $\frac{1}{3}$ actual size.

§ 3. MEASUREMENTS OF LEVELS OF ^{16}O

3.1. *The* 6·13 MEV *Level* (3^-) *in* ^{16}O

The E3 transition of 6·13 MEV from the 3^- to the 0^+ state of ^{16}O (Ajzenberg and Lauritsen 1952, Seed and French 1952, Devons and Goldring 1954) was first studied using the direct, distance method. The apparatus used was a modified form of that used by Devons *et al.* (1954). The level in ^{16}O was excited by the reaction ^{19}F(p, α)^{16}O at a proton energy of 873 kev. The arrangements of the slits and detectors are shown diagrammatically in figure 3. The accuracy with which the target plane was flat, and to which its position could be determined, was 10^{-3} cm or better. With ideally opaque slit walls the only γ-radiation that would be detected in counter 1 would be from those nuclei where recoil motion had brought them opposite the slit opening. In the absence of recoil motion no γ-radiation should be observed when the target layer is moved to a position outside the slit aperture. The imperfection of the slit, due to finite opacity of its walls, was determined by measuring the variation in γ-intensity in counter 1 as a function of target position, using a CaF_2 target covered with a thin evaporated copper layer to suppress the recoil motion. The small residual recoil motion in this copper layer and the target backing have a negligible effect on this variation. Using this experimental result (figure 4, $\tau = 0$) and a knowledge of the angular distribution of the α-particles and the α–γ correlation function (Seed and French 1952), the expected variation of γ-intensity, in counter 1, with position of the target was calculated. Theoretical curves for $\tau = 3 \times 10^{-11}$ and 10^{-10} sec are shown in figure 4. The experimental variation, using as targets uncovered layers of CaF_2 of 10^{-5} cm or less, is also shown in figure 4. In making the measurement care was exercised to avoid or allow for backlash in the target-moving mechanism and errors due to thermal expansion of parts of the apparatus. From figure 4 we can conclude that the half-life for the transition is of the order or less than 10^{-11} second.

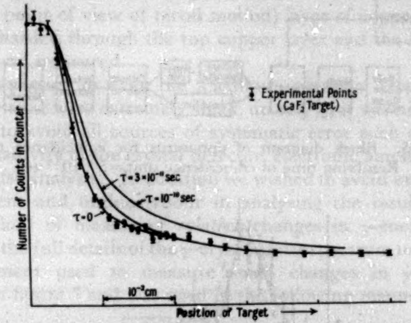

Figure 4. Recoil distance measurements for 6·13 MeV line from $^{19}F(p, \alpha)^{16}O$. (Proton energy 873 kev.)

A second attempt was made to estimate this transition lifetime by use of the coincidence technique described above and the apparatus used is shown in figure 1. The α-particles in the reaction $^{19}F(p, \alpha)^{16}O$, at 340 kev proton energy, were detected in the proportional counter, and coincident pulses in this counter and the γ-detectors were used to gate an amplifier which fed proportional pulses from the γ-detector into a 25-channel pulse analyser. This latter was arranged with two similar banks of 25 registers so that information could be stored in one bank whilst being collected in the other.

It was also arranged that a constant voltage could be subtracted from the pulse height from the γ-detector and the remainder subsequently amplified. In this way an expanded picture was obtained of the γ-spectrometer pulses. A block diagram of the electronic equipment is shown in figure 5.

Measurements of the coincidence-gated γ-spectrum were made with the α-detector in both parallel and antiparallel positions with respect to the γ-detector. The target and α-detectors were rotated through 180° every few minutes and the readings were stored in the two register banks during such a sequence of measurements. The purpose of this alternation was to minimize drifts or fluctuations in the energy sensitivity of the γ-detector. These were separately studied, as far as the electronic equipment was concerned, by feeding standard battery-produced pulses into the first γ-detector amplifier over long periods and observing the pulse-analyser records. With the alternate sequence of measurements used, the fluctuations in amplification introduced uncertainties rather smaller than the intrinsic accuracy with which the energy shifts could be measured. A typical set of observations obtained with this technique using a thin CaF$_2$ target on an aluminium backing is shown in figure 6. The energy shift between the two curves could be estimated visually, and using such an estimate the curves could be normalized to the same height. Comparison of the ordinates at the same analyser channel could then be used to provide a better estimate of the shift. This in turn could be used to provide better estimates of the normalization; and so after two or three successive approximations an *objective* estimate of the shift could be obtained. In three such experiments these were found to be $0{\cdot}15\% \pm 0{\cdot}3\%$, $0{\cdot}3\% \pm 0{\cdot}4\%$, $-0{\cdot}13\% \pm 0{\cdot}25\%$, with a

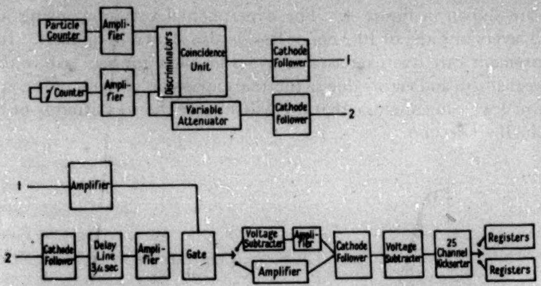
Particle Counter
Amplifier
Discriminators
Coincidence Unit
Cathode Follower
1
γ Counter
Amplifier
Variable Attenuator
Cathode Follower
2
1
Amplifier
2
Cathode Follower
Delay Line 3μ sec
Amplifier
Gate
Voltage Subtracter
Amplifier
Amplifier
Cathode Follower
Voltage Subtracter
25 Channel Kicksorter
Registers
Registers

Figure 5. Block diagram of apparatus for coincidence method. Resolving time of coincidence unit $= 5 \times 10^{-7}$ sec.

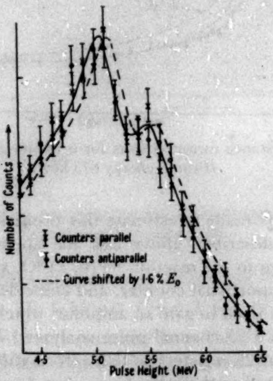

Figure 6. Coincidence method. Spectrum of 6·13 Mev line in ^{19}F(p,α)^{16}O. (Proton energy 340 kev.)

mean of 0·06% ± 0·15% (mean deviations). The full computed shift, assuming no retardation in the target backing, is 1·6%.

Using equation (1), we obtain $\lambda\alpha = 0{\cdot}04 \pm 0{\cdot}10$.

Additional estimates of this quantity were made using the target rotation method.

Firstly a thin CaF_2 target deposited on aluminium was used with protons of 340 kev, and the Doppler shift was found to be approximately equal to the full value to be expected if the recoil motion was completely destroyed by the time radiation occurred. To be certain that the shift was exactly equal to the full shift would mean very careful assessment of the theoretically expected shift, taking into account complicated geometrical corrections, in addition to precise experimental measurement. A more reliable procedure, using the differential Doppler shift for two materials, as described previously, was employed. A thin CaF_2 layer was deposited on a thick layer of calcium which was then covered with a thick (from the point of view of recoil motion) layer of copper. The composite target was bombarded through the top copper layer and the Doppler shift with target rotation was measured.

Since the expected, or even the maximum possible, Doppler shifts in this type of measurement were extremely small, up to ½%, it was necessary to exercise particular care to avoid all sources of systematic error such as fluctuations and drifts in the sensitivity of the crystal detector, electronic amplification and power supplies and pulse analysis. In addition we wished to avoid excessive elaboration of the equipment and undue labour in analysing the results. We therefore adopted a method of measuring *relative* changes in γ-energy without being concerned with the full details of the γ-crystal pulse spectrum to any high accuracy.

The equipment used to measure small changes in γ-energy is shown schematically in figure 7 and was used in the following manner.

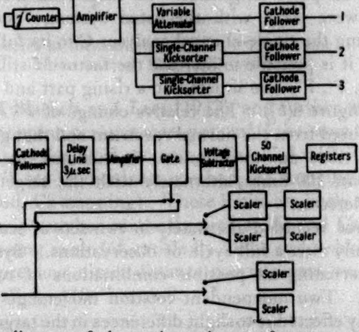
Counter
Amplifier
Variable Attenuator
Single-Channel Kicksorter
Single-Channel Kicksorter
Cathode Follower
Cathode Follower
Cathode Follower
1
2
3
1
Cathode Follower
Delay Line 3μ sec
Amplifier
Gate
Voltage Subtractor
50 Channel Kicksorter
Registers
Scaler
Scaler
Scaler
Scaler
Scaler
Scaler
2
3

Figure 7. Block diagram of electronic equipment for target rotation method.

The spectrum of the pulses from the photomultiplier was first recorded directly with moderate accuracy. The single channel pulse analyser F was then set so that it covered a small band in the spectrum where the number of pulses was a rapid function of pulse height, and the spectrum was again taken with a 50-channel pulse analyser gated by the output pulse of this single-channel analyser. A second single-channel analyser C was set so as to cover a much wider band of the spectrum, this band having limits at points in the spectrum where the intensity was changing only very slowly with pulse amplitude. A third spectrum was taken with the 50-channel analyser gated by this second single-channel analyser (figure 8(*a*)). From these three spectra it was a simple matter to compute, with adequate precision, the change in the relative number F/C, of counts in the two single-channel analysers F and C for a small change in energy in the γ-radiation. For the small energy changes with which we are concerned we can express the result of the measurements by stating that for a fractional change in γ-energy of ϵ the change in the ratio F/C will be $M\epsilon$, and we refer to M as the magnification of the measurement. M depends on the shape of the spectrum and the position and size of the selected band F. In these, and other measurements, we have used values of M ranging from 8 to 30.

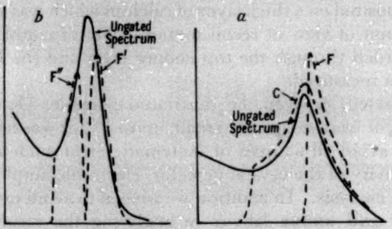

Figure 8. Gated spectra in measurements of Doppler shift.

It was found that the passage of pulses through the gate had a small, but detectable, effect on pulse amplitude. In later measurements, therefore, all relevant spectra were taken with the gated system, 'normal' spectra being obtained by opening the single-channel analyser C to its full width.

In some cases it is possible to increase the factor M still further by utilizing *two* narrow bands, F', F'', one situated on a rising part and one on a falling part of the spectrum (figure 8(*b*)). The relative change of F'/F'' with γ-energy can similarly be computed from the normal spectrum and that gated with F' and F''.

To minimize errors due to drifts and fluctuations the ratios F/C or F'/F'' were measured some 100 times, alternately with the target facing towards and away from the γ-detector.

Information was recorded alternately in two sets of scalers so that readings had to be taken only after a full cycle of observations. Systematic errors were minimized by alternating all possible combinations of rotations, scalers and starting positions. Two independent rotation movements for the target were possible, so that any effects due to slight differences in the target spot when towards and away from the γ-detector were eliminated.

A full set of observations, providing eight estimates of $M\epsilon$, took one to two hours and all eight values normally agreed within the statistical accuracy. If not, the results were not used. Spectra obtained with a bombarding voltage of 873 + 400 kev (energy loss in copper covering layer) are shown in figure 9. At this resonance the γ-spectrum contains about 35% of the 6·9 and 7·1 Mev lines in addition to the 6·13 Mev line (Hornyak *et al.* 1950). Allowance for this is easily made since, as we shall see below, these two components show no measurable shift even when conditions are favourable for detecting any that might occur.

The differential shift observed was, in four sets of measurements, $-0{\cdot}085\% \pm 0{\cdot}06\%$, $+0{\cdot}082\% \pm 0{\cdot}06\%$, $+0{\cdot}033\% \pm 0{\cdot}06\%$ and $0{\cdot}000\% \pm 0{\cdot}06\%$ giving a mean of $0{\cdot}008\% \pm 0{\cdot}03\%$. Using equation (5 *a*) and the computed value of $0{\cdot}48\%$ for gE_0v/c we get

$$\left[\frac{\lambda\alpha'}{\lambda\alpha'+1} - \frac{\lambda\alpha''}{\lambda\alpha''+1}\right] = 0{\cdot}017 \pm 0{\cdot}06$$

where α'' refers to copper and α' to calcium. Both $\lambda\alpha'$ and $\lambda\alpha''$ are much smaller than unity, and $\alpha'' \simeq 0{\cdot}2\alpha'$. We can then write this result as $\lambda\alpha' = 0{\cdot}02 \pm 0{\cdot}08$.

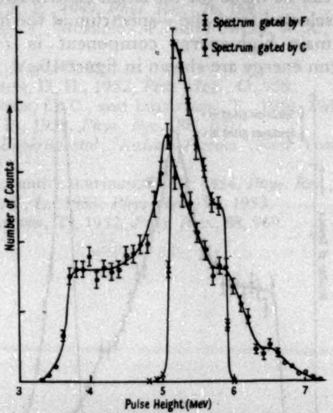

Figure 9. Spectra in measurement of the 6·13 MEV line in ^{19}F (p, α). Proton energy 1273 = 873 + 400 kev.

If we use the data of Blackett and Lees (1932), and further assume that for Al and Ca the effective stopping per unit mass per cm^2 is the same for these materials and air, we get $\alpha(\text{Al}) = 4{\cdot}3 \times 10^{-13}$ sec and $\alpha'(\text{Ca}) = 7{\cdot}3 \times 10^{-13}$ sec, giving for τ the limits $\tau > 2 \times 10^{-12}$ sec (coincidence method, Al stopping), $\tau > 5 \times 10^{-12}$ sec (target rotation method, Ca stopping). These limits are likely to be conservative since the higher atomic number materials such as Al and Ca are not likely to be as effective in stopping as air (cf. article by Bethe and Ashkin in Segrè 1953). Combined with the previous direct distance measurement we can state that for this transition $5 \times 10^{-12} \lesssim \tau \lesssim 10^{-11}$ second.

3.2. *The* 7·1 *and* 6·9 *Levels in* ^{16}O

Measurements of the Doppler shift in these two transitions were made using the same energy shift technique, the target rotation method and simple targets consisting of thin CaF$_2$ layers on copper backing.

The measurements are complicated in this case by the fact that it is not possible to produce these transitions without also exciting in somewhat greater degree the 6·13 MEV transition. However, by choosing appropriate settings of the single-channel pulse analyser F narrow bands of the composite γ-spectrum could be selected where the major contribution was from the higher energy transitions. The relative intensities of the three lines at the proton resonances used are (see Hornyak *et al.* 1950 for references):

	6·13	6·9	7·1 Mev
340 kev	0·96	(0·04)	
873·5 kev	0·65	0·24	0·11
935·3 kev	0·76	0·025	0·21

At 340 kev the spectrum is almost that of a pure 6·13 Mev line, and a correction for the 4% admixture can be made semi-theoretically. Using this corrected spectrum, allowance can be made for the small contribution from this transition to the narrow bands selected from the γ-spectrum at the higher resonances.

At 935 kev the main high-energy component is 7·1 Mev. The spectra measured at this proton energy are shown in figure 10.

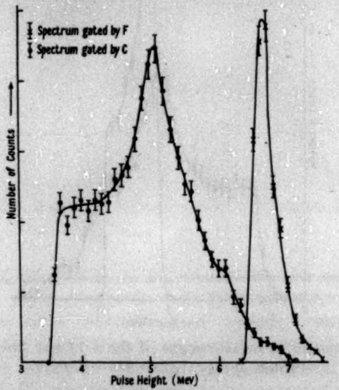

Figure 10. Spectra in measurement of 7·1 Mev line in $^{19}F(p, \alpha)^{16}O$. (Proton energy 935 kev.)

The observed value of $M\epsilon$ was $0{\cdot}63 \pm 0{\cdot}47\%$. Allowing for the contribution from the 6·1 Mev line, this gave a value of ϵ of $0 \pm 0{\cdot}03\%$. About half this error is due to uncertainty in the contribution from the 6·1 Mev line. The calculated maximum value of ϵ is 0·4%, corresponding to $\lambda\alpha \ll 1$.

Using (1) again we get $\lambda\alpha \gtrsim 11$. Assuming a value of $\alpha(\mathrm{Cu})$ of $1{\cdot}3 \times 10^{-13}$ sec, we get $\tau(7{\cdot}1) \lesssim 8 \times 10^{-15}$ second.

In view of the absence of any shift from the 7·1 Mev γ-line it was possible to examine also the 6·9 Mev line at the 873 Mev resonance, where both lines are present in comparable quantities. The observed values of $M\epsilon$ were $0{\cdot}56\% \pm 0{\cdot}6\%$. Allowing for the contributions of both 6·1 and 7·1 Mev lines, we get a value of ϵ of $0 \pm 0{\cdot}065\%$, as compared with a maximum of 0·5%. This gives an upper limit for the half-life of the transition $\tau(6{\cdot}9)$ of $1{\cdot}2 \times 10^{-14}$ second. The absence of an observable shift in this case justifies the neglect of the weak 6·9 Mev component in interpreting the measurements of the 7·1 Mev line at the 935 kev resonance.

ACKNOWLEDGMENTS

We should like to express our thanks to Dr. A. Folkierski and Mr. B. White for much technical assistance. One of us (G. Manning) is indebted to the Department of Scientific and Industrial Research for a maintenance grant.

REFERENCES

AZJENBERG, F., and LAURITSEN, T., 1952, *Rev. Mod. Phys.*, **24,** 321.

BLACKETT, P. M. S., and LEES, C. H., 1932, *Proc. Roy. Soc.* A, **134,** 658.

DEVONS, S., and GOLDRING, G., 1954, *Proc. Phys. Soc.* A, **67,** 413.

DEVONS, S., GOLDRING, G., and LINDSEY, G. R., 1954, *Proc. Phys. Soc.* A, **67,** 134.

DEVONS, S., HEREWARD, H. G., and LINDSEY, G. R., 1949, *Nature, Lond.*, **164,** 586.

DEVONS, S., and HINE, M. G. N., 1949, *Proc. Roy. Soc.* A, **199,** 56.

ELLIOTT, L. G., and BELL, R. E., 1949, *Phys. Rev.*, **76,** 168.

HORNYAK, W. F., LAURITSEN, T., MORRISON, P., and FOWLER, W. A., 1950, *Rev. Mod. Phys.*, **22,** 291.

JACOBSEN, J. C., 1924, *Phil. Mag.*, **47,** 23.

JONES, G. A., and WILKINSON, D. H., 1952, *Phil. Mag.*, **43,** 958.

RASMUSSEN, V. K., LAURITSEN, C. C., and LAURITSEN, T., 1949, *Phys. Rev.*, **75,** 199.

SEED, J., and FRENCH, A. P., 1952, *Phys. Rev.*, **88,** 1007.

SEGRÈ, E., 1953 (Ed.), *Experimental Nuclear Physics* (New York: Wiley; London: Chapman and Hall).

THIRION, J., BARNES, C. A., and LAURITSEN, C. C., 1954, *Phys. Rev.*, **94,** 1076.

THIRION, J., and TELEGDI, V. L., 1953, *Phys. Rev.*, **92,** 1953.

THOMAS, R. G., and LAURITSEN, T., 1952, *Phys. Rev.*, **88,** 969.

The Magnetic Susceptibility of Potassium Manganicyanide

By A. H. COOKE and H. J. DUFFUS†
Clarendon Laboratory, Oxford

MS. received 26th August 1954

Abstract. The magnetic susceptibility of potassium manganicyanide has been measured at temperatures from 4·2°K to 300°K. The susceptibility, which at room temperature approximately follows Curie's law, approaches a temperature-independent value at very low temperatures. This behaviour is compared with the theoretical prediction of Kotani.

It is well known that the paramagnetism of the covalently bonded compounds of the iron transition group of elements differs from that of the ionic compounds. This may be explained as the effect of the very strong covalent binding fields not only quenching the orbital magnetism but also breaking down the Russell–Saunders coupling. In the complex cyanides, for example, in which the metal is surounded by six CN groups of approximately octahedral symmetry, the orbital levels split into a doubly degenerate dγ group and a trebly degenerate dϵ group of lower energy. The 3d electrons must be housed in these dϵ states. If their number exceeds three, some of them must have their spins opposed. Hence the chromicyanides have a paramagnetic susceptibility corresponding to a spin $S=3/2$, the manganicyanides to $S=1$, the ferricyanides to $S=1/2$, and the cobalticyanides with $S=0$ are diamagnetic. Kotani (1949) has pointed out that while this 'spin-only' theory describes the general behaviour of the complex cyanides, the detailed predictions are considerably modified when account is taken of spin–orbit coupling. A particularly striking case arises when there are four 3d electrons, as in the manganicyanides, for spin–orbit coupling then splits the $(d\epsilon)^4$ level in such a way that the lowest energy level is a singlet. Such a state is diamagnetic (i.e. it has no first-order Zeeman displacement). The theory therefore predicts that as the temperature is lowered, and the upper states become depopulated, the magnetic susceptibility approaches a temperature-independent value, and the effective Bohr magneton number p (defined from $p^2=3\chi \boldsymbol{k}T/\boldsymbol{N}\beta^2$ where χ is the molar susceptibility at an absolute temperature T, $\boldsymbol{k}$ is Boltzmann's constant, $\boldsymbol{N}$ is Avogadro's number, and β is the Bohr magneton) approaches zero.

We have measured the magnetic susceptibility of a powdered specimen of potassium manganicyanide, $K_3Mn(CN)_6$, at temperatures from 4·2°K to 300°K. A Sucksmith ring balance was adapted to cover this temperature range (Cooke and Duffus 1954). Fixed temperatures were obtained from boiling liquid oxygen, hydrogen and helium. Intermediate temperatures were reached by the use of an electrical heater wound on a copper cryostat surrounding the specimen, the measurements being made when equilibrium had been established between the supply of heat and the loss by conduction to the cooling bath. The temperatures were measured by a resistance thermometer calibrated by a constant volume helium gas thermometer in contact with the cryostat. The absolute value of the susceptibility of the specimen was obtained by comparison with three specimens of manganous ammonium sulphate. The diamagnetic correction due to the Perspex specimen holder was measured, and that of the specimen was calculated. The total diamagnetic correction was only 2½% of the paramagnetic susceptibility at room temperature, and on cooling below 100°K was negligible compared with the experimental error.

---

† Now at the Pacific Naval Laboratory, British Columbia.

The results, corrected for diamagnetism, are shown in the diagram, in which the square of the effective magneton number is plotted against temperature. Kotani (1949) reports that various workers have obtained different values of p at room temperature, viz. Blitz (1928), 3·61; Ray and Bhar (1928), 2·95; Szego and Ostinelli (1930), 3·40; Goldenberg (1940), 3·25; our value was $3{\cdot}50 \pm 0{\cdot}05$.

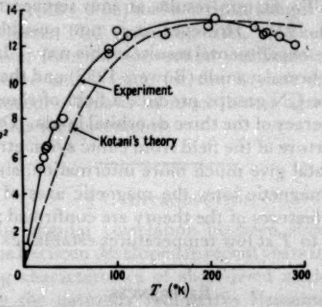

Variation with temperature of the effective Bohr magneton number of potassium manganicyanide. Experimental points are shown as circles. The broken curve shows the variation predicted theoretically by Kotani.

In comparing the experimental results with theory, we neglect any effect due to interactions between the magnetic ions. This is justified by the results of unpublished measurements by Cooke, Meyer and Wolf on the susceptibilities of powdered specimens of potassium chromicyanide and potassium ferricyanide in the liquid helium temperature range. Apart from temperature-independent effects, which were not determined, the susceptibility of each salt followed a Curie–Weiss law, $\chi = C/(T-\theta)$, with $\theta = -0{\cdot}09°$ for the chromicyanide and $\theta = -0{\cdot}28°$ for the ferricyanide. Crystalline field theory would predict a Curie law ($\theta = 0$) in each case. The discrepancy is small and may be neglected at temperatures above a few degrees absolute. The variation of p with temperature was calculated by Kotani (1949), assuming that the CN groups form a regular octahedron, producing an electric field of cubic symmetry at the Mn^{3+} ion. The $d\epsilon$ orbital levels are then completely degenerate. Under the action of spin–orbit interaction we then have a singlet ground state, a triplet state at an energy $A/2$, and a quintuplet state at an energy $3A/2$, where A is the spin–orbit coupling constant. This leads to the expression

$$p^2 = \frac{3\{24 + (x/2 - 9)\exp(-x/2) + (5x/2 - 15)\exp(-3x/2)\}}{x\{1 + 3\exp(-x/2) + 5\exp(-3x/2)\}}$$

where $x=A/\mathbf{k}T$. According to this formula, p^2 is proportional to T at low temperatures, rises to a broad maximum at $x=2{\cdot}2$, with a maximum value $p^2=13{\cdot}1$, and at high temperatures falls slowly to an asymptotic value $p^2=10$. The broken curve in the diagram shows the variation of p^2 calculated from this formula, taking $A/\mathbf{k}=492°$, the value for the free Mn^{3+} ion. It will be seen that the two curves are very similar, but that both the rise of p^2 at low temperatures and the fall at high temperatures are more rapid than the theory predicts. The discrepancy may be ascribed to the departure of the electric field at the Mn^{3+} ion from cubic symmetry and the departure of the electron orbits from pure d-orbits. Stevens (1953) has shown that the departure from pure d-orbits has the effect of lowering the orbital g-factor and reducing the spin–orbit coupling constant A below the free ion value. Such a reduction would bring Kotani's curve nearer to our experimental results. For example, at low temperatures Kotani's theory gives $p^2 \rightarrow 72\mathbf{k}T/A$. To fit our results at low temperatures requires a value $A/\mathbf{k}=270°$ instead of 492°. However, it is not possible to fit the complete theoretical curve to the experimental results in this way. It is to be expected that as in the case of the chromicyanide (Bowers 1952) and the ferricyanide (Bleaney and Ingram 1952), the CN groups produce a field of rhombic symmetry, which raises the initial degeneracy of the three $d\epsilon$ orbital levels. Our results do not suffice to determine the departure of the field from cubic symmetry (nor would measurements on a single crystal give much more information, since the unit cell of the crystal contains two magnetic ions, the magnetic axes of which are unknown). However, the general features of the theory are confirmed; in particular, the fact that p^2 is proportional to T at low temperatures establishes that the lowest energy level is diamagnetic.

REFERENCES

Bleaney, B., and Ingram, D. J. E., 1952, *Proc. Phys. Soc.* A, **65**, 953.
Blitz, W., 1928, *Z. Anorg. Chem.*, **170**, 161.
Bowers, K. D., 1952, *Proc. Phys. Soc.* A, **65**, 860.
Cooke, A. H., and Duffus, H. J., 1954, *Proc. Phys. Soc.* A, **67**, 525.
Goldenberg, N., 1940, *Trans. Faraday Soc.*, **36**, 847.
Kotani, M., 1949, *J. Phys. Soc. Japan*, **4**, 293.
Ray, P., and Bhar, H., 1928, *J. Indian Chem. Soc.*, **5**, 497.
Stevens, K. W. H., 1953, *Proc. Roy. Soc.* A, **219**, 542.
Szego, L., and Ostinelli, P., 1930, *Gazz. Chim. Ital.*, **60**, 946.

Alpha-Gamma Angular Correlations and Internal Conversion Measurements in ThCC″ and ThC′D

By J. W. WEALE
Department of Physics, Imperial College, London†

Communicated by S. Devons; MS. received 23rd June 1954

Abstract. The angular correlation between all γ-rays leading to ThC′ ground state and the ThC′D α-rays has been measured and found isotropic, in agreement with theory. The angular correlation between the 6·04 MeV α-ray and the 40 keV γ-ray in ThCC″ has been measured and found anisotropic, the best fitting curve being $W(\theta)=1-(0{\cdot}22\pm0{\cdot}05)\cos^2\theta$. Spin assignments of 1 or 2, 4 and 5 are deduced for the levels ThC (ground), ThC″ (40 kev) and ThC″ (ground) respectively. The total internal conversion coefficient of the 40 kev ThCC″ γ-ray has been measured and a value for the L shell conversion coefficient of $\alpha_L=15{\cdot}7\pm1{\cdot}6$ is deduced. This is in much better agreement with theoretical prediction than previous measurements.

§ 1. INTRODUCTION

The study of the angular correlation between successive radiations from the same nucleus has been developed in recent years into a powerful technique for determining characteristics of short-lived nuclear states. It is particularly useful among the naturally radioactive elements which provide many cascades suitable for the application of this method. An earlier application to the $\alpha\gamma$ cascade in ThCC″ was made by Kulchitski (1950), but the results were not easily interpreted and, in view of improvements in experimental techniques, a new measurement has been made. As the present work was nearing completion a brief report of another measurement of this correlation was published (Horton and Sherr 1953). The present result agrees with that obtained by Horton and Sherr and is completely at variance with that obtained by Kulchitski.

§ 2. APPARATUS

The complexity of the decay scheme (see figure 1), particularly the presence of a number of $\alpha\gamma$ cascades, makes accurate discrimination of great importance. The two main $\alpha\gamma$ cascades are the (6·04 MeV) α, (40 kev) γ cascade in ThCC″ and the (0·72 MeV to 2·2 MeV) γ, (8·8 MeV) α cascade in ThC′D, the γ-rays being emitted in transitions to the ThC′ ground state which has a half-life for α-decay of only 3×10^{-7} second. Either of these cascades can be eliminated by α-energy discrimination. For this purpose a scintillation counter was not considered to provide a sufficiently sharp discrimination and a proportional counter was therefore used. This has the additional advantage that the path lengths in the counter gas can be arranged so that the lower energy α-particle yields the larger pulse and the higher energy particle can be eliminated by simple discrimination, thus simplifying the electronics.

---

† Now at Atomic Weapons Research Establishment, Foulness, Essex.

The proportional counter was filled with a mixture of argon and carbon dioxide at a pressure of 24 cm Hg. It had a mica end window 0·48 cm in diameter and 2·0 cm air-equivalent thickness. The geometrical arrangement was such that no particles were allowed to strike the walls of the counter within the counting region. The γ-detector was a scintillation counter consisting of a single crystal of NaI(Tl) mounted on an EMI 5311 photomultiplier tube. The surfaces of the crystal were etched clean and covered with an aluminium reflector and the crystal was enclosed in an air-tight polythene cap. The end thickness of the cap was sufficient to prevent any β-rays from the source reaching the crystal.

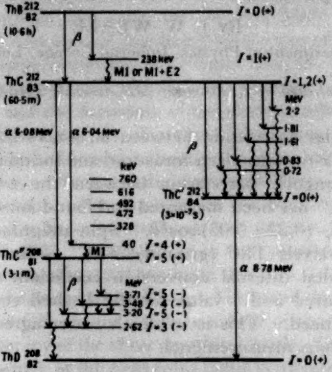

Figure 1. Simplified level scheme for ThBD. Some transitions irrelevant to the discussion have been omitted. Most of the data are from N.B.S. Circular 499. The remainder are contained in the references quoted.

The counters were followed by amplifiers and Harwell-type simple discriminator units. A variable delay circuit was used to balance the delays in the two channels and was followed by a Rossi-type coincidence unit with a resolving time variable from 3×10^{-7} to $1{\cdot}2 \times 10^{-6}$ second.

ThB in transient equilibrium with its decay products was used as a source of ThC. Sources were prepared by deposition from thorium active deposit on to polished aluminium foil 0·001 in. thick. Each source was cut to the form of a strip of foil with the deposit covering an area about 1 mm square on one side only. This was mounted in a small Perspex holder attached to the front of the proportional counter.

§ 3. INTERNAL CONVERSION OF THE 40 kev ThCC″ γ-RAY

The apparatus was used initially for the determination of the internal conversion coefficient of the 40 kev γ-ray in the ThCC″ transition. Earlier measurements of this have been based on the intensities of the L conversion electrons, as shown by a β-ray spectrograph. The best determination by this method is that derived by Kinsey (1948) from the measurements of Flammersfeld (1939). He found an L shell conversion coefficient $\alpha_L = 4{\cdot}7$. Kinsey (1947) reports a measurement by the method of $\alpha\gamma$ coincidence using a xenon-filled proportional counter for the γ-rays with the result $\alpha_L = 3{\cdot}6$.

The present determination was by the $\alpha\gamma$ coincidence method using a 0·5 cm NaI(Tl) crystal scintillation counter for the γ-ray. The ThC′D $\gamma\alpha$ coincidences were eliminated by a simple discriminator. The clear separation of the two groups of α-rays is shown by figure 2 (*a*). Coincidences between the 6·04 MeV α-rays and the L X-rays following internal conversion of the 40 kev γ-rays were eliminated by a careful adjustment of the discriminator in the γ-line. The response of the scintillation counter in this region is shown by figure 2 (*b*), which is a graph of the true $\alpha\gamma$ coincidence rate against the γ-line discriminator setting. The 40 kev γ-ray and 15 kev L X-ray peaks are clearly shown and it is evident that the X-ray peak can be eliminated by a discriminator setting of 30 volts. The contribution of the $\alpha\gamma$ cascades via higher excited states of ThC″ is negligible compared with that via the 40 kev level.

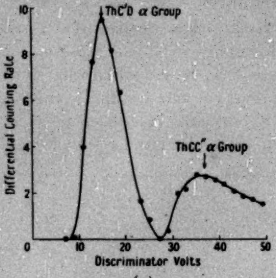

(*a*)

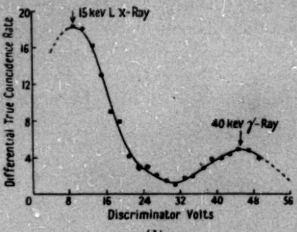

(*b*)

Figure 2 (*a*). ThB+C α-pulse height distribution. The ThCC″ and ThC′D α-groups are clearly separated by the proportional counter.

Figure 2 (*b*). Differential $\alpha\gamma$ coincidence rate as a function of γ discriminator setting. The coincidences between α-rays and internal conversion X-rays are eliminated by a discriminator setting of 30 volts.

A careful study of the variation of true coincidence rate with coincidence resolving time τ showed that variations in the delay time of pulse formation caused the coincidence rate to fall off slowly for $\tau<6\times10^{-7}$ second. The resolving time was therefore set at $\tau=8\times10^{-7}$ second. The counters were set opposite each other in line with the source and the solid angles were, for the α-counter, $1{\cdot}0\times10^{-2}$ of 4π and, for the γ-counter $1{\cdot}9\times10^{-2}$. The total coincidence rate and the α and γ rates, N_α and N_γ, were measured in a number of experiments and the random coincidence rate was calculated using the measured value of τ. The mean ratio of true coincidence rate to α counting rate was

$$N_{\mathrm{T}}/N_\alpha=(3{\cdot}86\pm0{\cdot}15)\times10^{-4}.$$

To allow for the angular correlation between the α- and γ-rays a small correction was applied using the result of § 5. The correction factor is the ratio of the mean coincidence rate ($\theta=90°$ to $\theta=270°$) to the coincidence rate at $\theta=180°$, using the experimental figures uncorrected for finite angular resolution. Its value is $\overline{N}_{\mathrm{T}}/N_{\mathrm{T}}(180)=1{\cdot}13$. A further correction was made to allow for scattering of γ-rays into the γ-counter at this setting. The 40 kev γ-counting rate is slightly increased at $\theta=180°$ by this effect and the correction factor was derived from the measurement of this variation described in § 5. Its value is $1/1{\cdot}09=0{\cdot}917$.

In calculating the overall efficiency of the γ-counter allowance was made for the 'escape peak' pulses and for absorption in the polythene cap. The escape peak represents pulses in which the iodine x-ray (33 kev) escapes from the face of the crystal which thus only absorbs 7 kev of the γ-ray energy. West *et al.* (1951) have measured the relative areas under the escape and normal photoelectric peaks for a 44 kev γ-ray and find that 22% of the iodine x-rays escape. Sterk and Wapstra (1953) have published calculated curves of the escape probability with a value of 20·6% at 40 kev. The figure of 21% was adopted in the present calculations. Absorption in the polythene cap was measured in the same geometrical conditions and found to be 21%. Since the absorption is entirely photoelectric and is virtually complete in a few millimetres of sodium iodide, the nominal efficiency of detection is 100% and the overall efficiency is therefore 62% with an estimated error of ±4%.

The above results together with the α-transition probability to the first excited state, which is 0·70 (Lewis and Bowden 1934), yield a total internal conversion coefficient of $\alpha = 19{\cdot}6 \pm 1{\cdot}7$. Using the Kinsey–Flammersfeld value of 0·80 for the ratio of L shell conversion to total conversion, the L shell internal conversion coefficient is $\alpha_L = 15{\cdot}7 \pm 1{\cdot}6$. Relativistic calculations of L shell conversion coefficients have been published by Gellmann *et al.* (1950, 1952). The results for $Z = 84$ and $E = 42{\cdot}6$ kev are

	L_I	L_{II}	L_{III}	L_{total}
E1	0·2910	0·2606	0·3544	0·9060
E2	5·300	195·4	195·9	396·6
M1	27·85	2·397	0·0298	30·28

The 40 kev γ-ray can therefore be confidently identified as M1 radiation in agreement with Graham and Bell (1953). Interpolation between the values calculated by Gellmann *et al.* (1950) yields a value of α (L total) $= 22{\cdot}8$ for $Z = 81$ and $E = 40$ kev. Comparing this with the experimental result, the discrepancy between the two is seen to be in a direction opposite to that which would be expected for an admixture of E2 radiation. The discrepancy may be accounted for by the displacement of the nucleus in the electronic configuration as a result of the α-emission and the recoil of the nucleus. (The lifetime of the excited state is less than 10^{-10} sec (Graham and Bell 1953).)

§ 4. THE ThC′D $\gamma\alpha$ ANGULAR CORRELATION

The half-life of ThC′ for α-emission is 3×10^{-7} sec and, for resolving times of this order, γ-rays leading to the ThC′ ground state are therefore in coincidence with the ThC′D α-rays (figure 1). Since ThC′ is an even–even nucleus, it is presumed to have zero ground state spin and all cascades having this as the intermediate level should therefore have isotropic angular correlations. This was checked experimentally by measuring the integrated $\gamma\alpha$ angular correlation for all the transitions $\text{ThC}'^{*} \rightarrow \text{ThD}$. The ThCC″ α-rays were eliminated by inserting a mica absorber of 3·5 cm air equivalent in the α-ray path. The γ-ray discriminator was set at 120 kev, thus admitting most of the γ-pulses (mainly Compton absorption) while rejecting the background of x-rays from Pb and Bi. The energy calibration was obtained from a measurement of the photoelectric spectrum from a source of ^{170}Tm. Solid angles were $1{\cdot}0 \times 10^{-2}$ of 4π for the α-counter and $1{\cdot}90 \times 10^{-2}$ of 4π for the γ-counter. The coincidence resolving time was set at 4×10^{-7} sec and was accurately measured at the start of each day's run. The total coincidence rate and the α- and γ-rates were recorded for periods of 30 minutes at 15° intervals from $\theta=90°$ to $\theta=270°$ with a 60-minute count at $\theta=180°$ so that all points had equal weight (θ is the angle between the two counters). The chance coincidence rate was calculated and a correction for variation of source strength was made by dividing the true coincidence rate by the α-rate for each reading. A correction was applied to allow for the measured variation of the γ-rate with θ due to geometrical anisotropy of the experimental arrangement. This amounted to 1·2% at $\theta=90°$ and 270°.

The results were found to be symmetrical about $\theta=180°$ and readings at θ and $2\pi-\theta$ were therefore combined. The final results represent the mean of five separate experimental runs and are shown in figure 3. Each point on the graph represents about 2000 true coincidence counts. The correlation is isotropic to within ±1% in agreement with theoretical prediction.

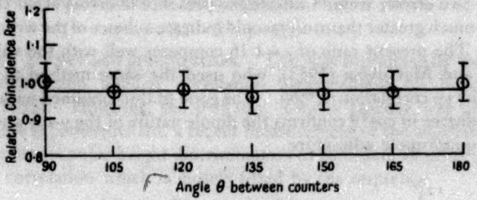

Figure 3. ThC′D $\gamma\alpha$ angular correlation.

§ 5. THE ThCC″ α (6·04 MEV) γ (40 kev) ANGULAR CORRELATION

For this measurement the experimental arrangement and the counter solid angles were the same as those in the internal conversion determination except that a resolving time of $\tau=4\times10^{-7}$ sec was used. Thirty-minute counts of the total coincidence rate, the α-rate N_α and the γ-rate N_γ were recorded at 15° intervals from $\theta=90°$ to 270°. The number of chance coincidences was calculated using an accurately measured value of τ. The variation of N_γ with θ was found to depend on the γ-energy, indicating that scattering was an important factor. To allow for this variation each experimental run included a measurement of the variation with θ of the γ-rate in the discriminator range 35 kev to 45 kev and the results were combined into a mean correction factor. Variation in source strength was allowed for by dividing the true coincidence rate at each setting by the α-rate. The correlation was found to be symmetrical about $\theta=180°$ and readings at θ and $2\pi-\theta$ were therefore combined. The mean results and correction factors are shown in the table and the angular correlation curve is shown in figure 4. Each experimental point corresponds to about 1000 true coincidence counts.

The 40 kev γ-ray is established as magnetic dipole from internal conversion and lifetime measurements, so the correlation function should not contain higher powers than $\cos^2\theta$. The function $W(\theta)=\alpha_0+\alpha_2P_2(\cos\theta)$ was therefore fitted by a least squares procedure to the experimental points with the result:

$$W(\theta)=0{\cdot}946-(0{\cdot}140\pm0{\cdot}039)P_2(\cos\theta).$$

Summarized Experimental Results: ThCC″ $\alpha\gamma$ Angular Correlation

θ (deg.)	90	105	120	135	150	165	180
Relative normalized coincidence rates	1·000	1·055	0·958	1·049	0·842	0·969	0·847
Correction factor for γ rate variation	1·09	1·07	1·05	1·02	1·01	0·99	1·00
Corrected coincidence rates	1·00	1·033	0·919	0·984	0·781	0·887	0·777

This is shown by the full line in figure 4. The error in α_0 is negligible compared with that in α_2, and the latter error was analysed by two methods as suggested by Rose (1953). A derivation solely in terms of the statistical errors of the individual readings yields a mean square error in α_2 of $\sigma^2(\alpha_2)=0{\cdot}039^2$. A derivation in terms of the residuals between the experimental points and the least squares line, which should therefore include all types of error, yields a mean square error $\sigma^2(\alpha_2)=0{\cdot}044^2$. A value considerably greater than unity for ϵ, the ratio of the two errors, would indicate the presence of errors other than statistical and a value much greater than unity would indicate a choice of the wrong polynomial for $W(\theta)$. The present ratio of $\epsilon=1{\cdot}16$ compares well with the values obtained by Klema and McGowan (1953), who used the same method to analyse their results on the $\gamma\gamma$ correlation in ^{60}Ni. The good fit thus obtained with a polynomial of the first degree in $\cos^2\theta$ confirms the dipole nature of the γ-ray and the absence of electric quadrupole admixture.

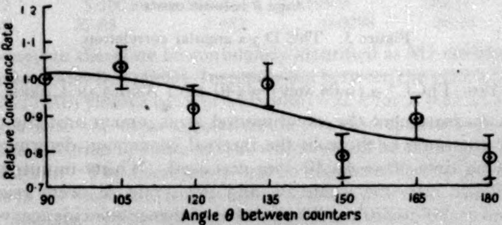

Figure 4. ThCC″ $\alpha\gamma$ angular correlation. The full line is the least squares curve $W(\theta)=\alpha_0+\alpha_2 P_2(\cos\theta)$ with $\alpha_0=0{\cdot}946\pm0{\cdot}024$ and $\alpha_2=-0{\cdot}140\pm0{\cdot}039$, i.e. $W(\theta)=1{\cdot}016-0{\cdot}209\cos^2\theta$.

A correction for the finite angular resolution of the counters was made by the method of Rose (1953). α_0 remains unchanged and α_2 is multiplied by an attenuation factor $Q_2(\alpha)Q_2(\gamma)$ where, in the present case, $Q_2(\gamma)=0{\cdot}946$, $Q_2(\alpha)=0{\cdot}972$. This gives an attenuation of the theoretical α_2 of $Q_2=0{\cdot}919$, but it is more convenient to apply the inverse of this factor to the experimental result giving a final angular correlation function:

$$W(\theta)=1-(0{\cdot}22\pm0{\cdot}05)\cos^2\theta.$$

The possible effect of electric or magnetic fields on the correlation can only be assessed in rather qualitative terms. The lifetime of the intermediate state is less than 10^{-10} sec (Graham and Bell 1953), so crystalline or molecular inhomogeneous electric fields, which do not produce precession periods smaller than about 10^{-9} sec, are expected to have a negligible effect. The atomic shell of thallium has a non-zero magnetic moment in its ground state but it is likely to be in a disturbed condition as a result of the α-emission and the recoil of the nucleus. Some attenuation of the correlation could be caused by magnetic interaction of nucleus and atomic shell since precession periods of the order of 10^{-11} sec are possible. However, the effect is small when the intermediate nucleus has a large spin and when one of the radiations is dipole, both of which conditions are fulfilled here, so the disturbance has been assumed to be negligible.

A simplified level scheme for the ThB, C, C″, D system is shown in figure 1. The even–even nuclei, ThB and ThD, are assumed to have zero spin and even parity in their ground states. Since an allowed β-transition leads to the first excited state of ThC, this state must have even parity and unit spin. Internal conversion measurements (Martin and Richardson 1950) show that the 238 kev γ-ray to the ThC ground state is M1 + E2 or pure M1, so ThC ground state has even parity and a spin of 0, 1 or 2. The angular correlation between the 2·6 Mev and 0·58 Mev γ-rays in the transition ThC″ → ThD was first measured by Petch and Johns (1950) and resulted in the assignment of spin values

$$4(+)-\mathrm{E2}-2(+)-\mathrm{E2}-0(+)$$

for the 3·2 Mev, 2·6 Mev and ground states. This was supported by the result of a directional-polarization angular correlation measurement by Kraushaar and Goldhaber (1953). However, the 0·58 Mev, 2·6 Mev cascade was not uniquely selected in these experiments and a recent measurement of the angular correlation using single channel pulse height discriminators to eliminate all other $\gamma\gamma$ cascades resulted in a correlation which is closely fitted by the sequence

$$5(-)-\mathrm{E2}-3(-)-\mathrm{E3}-0(+)$$

(Elliott *et al.* 1954). The internal conversion coefficient of the 2·6 Mev γ-ray was measured and found to be in good agreement with the E3 assignment. Further $\gamma\gamma$ angular correlation and internal conversion measurements by these authors determined the spins and parities of the 3·48 and 3·71 Mev states as 4(−) and 5(−) respectively. Recent $\beta\gamma$ coincidence measurements by Elliott and Wolfson† have detected a weak β-ray transition to the 2·6 Mev level, the ft value being in good agreement with the assignment $\Delta I = 2$, yes. This determines the ground state of ThC″ as $I = 5(+)$, all the β transitions then being first forbidden. It follows that the first excited state of ThC″ has $I = 4$, 5 or 6(+) and the 6·04 and 6·08 Mev α-rays must have even integer angular momenta since there is no parity change. On this basis and with the assumptions of single values for the orbital angular momenta of the α-transitions and negligible disturbance by magnetic interaction, the only spin assignments which agree with the present experimental result within the limits of error are

$W(\theta)$	ThC	ThC″ (40 kev)	ThC″	L_α (6·04 Mev)	L_α (6·08 Mev)
$1-0{\cdot}215\cos^2\theta$	1	4	5	4	4
$1-0{\cdot}200\cos^2\theta$	2	4	5	2	4

§ 6. Discussion

The lower levels of ThC″ are expected to be combinations of those of AcC″ (proton hole in the doubly closed shell), which has a ground state $d_{3/2}$ and first excited state $s_{1/2}$ (Gorodetzky *et al.* 1953) and ^{209}Pb (extra neutron) which has a ground state $i_{11/2}$ or $g_{9/2}$ (Pryce 1952). All of these give even parity combinations and the ground and first excited states of ThC″ could be interpreted for example as members of the $(i_{11/2})_N(d_{3/2})_P$ quartet. The higher excited states reveal a remarkable energy regularity which is suggestive of rotational states of the collective nuclear model. Their energies may be written as follows:

---

† Private communication by J. Walker.

Level	Energy (kev)	Level	Energy (kev)
ground	0	4	492
1	40	5	$616=40+4\times144$
2	$328=40+2\times144$	6	$760=40+5\times144$
3	$472=40+3\times144$		

ThC has three neutrons and one proton outside the doubly closed ^{208}Pb shell. In terms of the independent particle model two of the neutrons should form a pair with resultant spin zero and the nuclear spin would be the resultant of the remaining neutron and the odd proton. There is then only one $I=1(+)$ possibility, viz. $(i_{11/2})_N(i_{13/2})_P$ and this must be interpreted as the first excited state, so the ground state must be $I=2(+)$. In collective model terms, however, the coupling between core and particles may be sufficiently strong to reduce this to $I=1(+)$. Some evidence that ThC ground state is $I=1(+)$ is provided by the measurements of Martin and Richardson (1949) on the shape of the ThCC′ β-spectrum. The extension of the $\alpha\gamma$ angular correlation method to the study of another of the ThCC″ cascades would provide decisive evidence on this point.

ACKNOWLEDGMENTS

The author is indebted to Professor S. Devons for his interest and advice throughout this work and to the Department of Scientific and Industrial Research for a maintenance grant.

REFERENCES

Elliott, L. G., Graham, R. L., Walker, J., and Wolfson, J. L., 1954, *Phys. Rev.*, **93,** 356.

Flammersfeld, A., 1939, *Z. Phys.*, **114,** 227.

Gellmann, H., Griffith, B. A., and Stanley, J. P., 1950, *Phys. Rev.*, **80,** 866; 1952, *Ibid.*, **85,** 944.

Gorodetzky, S., Gallmann, A., Knipper, A., and Armbrustier, R., 1953, *C.R. Acad. Sci., Paris*, **237,** 245.

Graham, R. L., and Bell, R. E., 1953, *Canad. J. Phys.*, **31,** 377.

Horton, J., and Sherr, R., 1953, *Bull. Amer. Phys. Soc.*, **28,** No. 1.

Kinsey, B. B., 1947, *Phys. Rev.*, **72,** 526; 1948, *Canad. J. Res.* A, **26,** 426.

Klema, E. D., and McGowan, F. K., 1953, *Phys. Rev.*, **91,** 616.

Kraushaar, J. J., and Goldhaber, M., 1953, *Phys. Rev.*, **89,** 1081.

Kulchitski, L. A., 1950, *Doklady Akad. Nauk.*, **73,** No. 6.

Lewis, W. B., and Bowden, B. V., 1934, *Proc. Roy. Soc.* A, **145,** 235.

Martin, D. G. E., and Richardson, H. O. W., 1949, *Proc. Roy. Soc.* A, **195,** 287; 1950, *Proc. Phys. Soc.* A, **63,** 223.

Petch, H. E., and Johns, M. W., 1950, *Phys. Rev.*, **80,** 478.

Pryce, M. H. L., 1952, *Proc. Phys. Soc.* A, **65,** 773.

Rose, M. E., 1953, *Phys. Rev.*, **91,** 610.

Sterk, M. J., and Wapstra, A. H., 1953, *Physica*, **19,** 669.

West, H. I., Jr., Mayerhof, W. E., and Hofstadter, R., 1951, *Phys. Rev.*, **81,** 141.

RESEARCH NOTES

Scattering of 14·3 Mev Neutrons by ^{4}He Nuclei

By D. F. SHAW
The Clarendon Laboratory, Oxford

MS. received 30*th August* 1954

The angular distribution of 14–15 Mev neutrons scattered by ^{4}He nuclei has recently been investigated by Seagrave (1953) who measured the recoil pulse height distribution in an ionization chamber containing helium, and by Alston, Crewe *et al.* (1954) using a diffusion cloud chamber. Dodder and Gammel (1952) analysed the data on p–^{4}He scattering up to 9·5 Mev and by comparing the mirror nuclei ^{5}Li and ^{5}He predicted values for the phase-shifts in n–^{4}He scattering. Seagrave found good agreement with these predictions at 14·3 Mev in the backscattering region but obtained three divergent experimental curves from independent runs in the forward scattering hemisphere. He attributed the observed discrepancies to the effects of energy-degraded neutrons and stated in a footnote that a cloud chamber investigation over all angles by J. R. Smith (unpublished) gave good agreement with theory. Alston, Crewe *et al.* using 15·7 Mev neutrons were unable to make reliable measurements in the forward scattering region because of the small range of the recoils under their experimental conditions.

Before these results were published we had commenced a similar investigation at 14·3 Mev in this laboratory by the cloud chamber method. We used gas fillings of much less stopping power than Alston *et al.* and so have been able to make measurements of the small angle scattering. The cloud chamber method enables both the direction and energy of the recoils to be determined and thus can discriminate against the presence of lower energy neutrons in the incident flux. Our results are in good agreement with the theoretical curve over the range 20°–90° for the scattered neutrons. Our data on the backscattering are not sufficient to give any further useful information.

The experiment was carried out using a 9 in. diameter random expansion chamber and neutrons from the bombardment of a thick Zr–T target by a pulsed beam of 400 kev deuterons. The cloud chamber was arranged to receive neutrons from this target at 90° relative to the deuteron beam. Two independent runs were made, one with a chamber filling of 60 cm Hg pressure of helium and the other with 11·5 cm helium plus 53·5 cm argon. In each case the condensable vapour was a 40%–60% by volume mixture of water and ethyl alcohol. The range and direction of the recoil nuclei were measured by projecting stereoscopic photographs of the tracks through the cameras on to a movable screen on which each scattering event could be reconstructed. The energy of each helium recoil ion observed was deduced from a range–energy curve based on the data tabulated by Allison and Warshaw (1953). The lengths of the tracks measured were 0·7–5·4 cm in the helium run and 0·3–4·4 cm in the helium plus argon mixture and could be determined to ±0·1 cm. The directions could be measured quite accurately and the tracks included in the analysis were all within ± 2° of the direction calculated from their observed range. The majority of tracks rejected were well outside these limits and were probably due to neutrons of energy below 14 MEV. The chance of the observed background yielding recoils which would meet our criterion for acceptance is calculated to be negligible.

The results are given in the table. ϕ is the measured recoil direction relative to the incident neutron and θ the corresponding neutron scattering angle in the centre of mass system. N_1 and N_2 are the observed numbers of tracks in each angular interval in the helium and helium plus argon runs respectively. A track with ϕ an exact multiple of 5° was counted half in each adjacent interval. After correcting for the different effective volume of the chamber in the two runs the results were normalized and combined to give a weighted mean value for the differential cross section $d\sigma/d\Omega$ in millibarns per steradian. The errors quoted are the standard deviations.

ϕ (°)	θ (°)	N_1	N_2	$d\sigma/d\Omega$
80–75	20–30	49	48	280 ± 33
75–70	30–40	29½	43	184 ± 22
70–65	40–50	24½	42½	172 ± 22
65–60	50–60	11	31½	127 ± 21
60–55	60–70	—	33	140 ± 25
55–50	70–80	—	16½	81 ± 20
50–45	80–90	—	10	63 ± 19

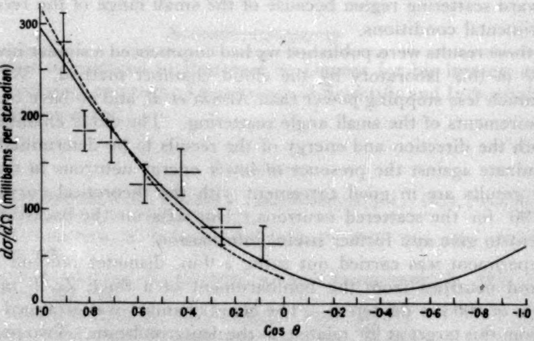

The figure depicts the results graphically. The vertical lines represent the standard deviations of the plotted points and the horizontal lines the included angular range. The full line is the theoretical curve of Dodder and Gammel. The broken curve is the lower of the three experimental curves given by Seagrave extrapolated and normalized to the same partial cross section as that covered by our measurements. The theoretical curve gives a better fit to our results. The root mean square deviation of the experimental points from the theoretical curve is 22% and from Seagrave's curve 37%. The deviation from the other two steeper curves obtained by the latter author would be considerably greater.

A curve of lesser slope would present a better fit to our measurements but it would then be necessary to choose much larger values for the D-wave phase-shifts to maintain the good fit to Seagrave's results for the backscattering hemisphere. Our statistical accuracy is not sufficient to support this.

ACKNOWLEDGMENTS

The author is grateful to Dr. G. Preston who operated the h.t. set during the experimental runs and to Mr. C. H. Collie for his helpful discussions. He also wishes to thank Professor Lord Cherwell for the interest he has shown in this work.

REFERENCES

ALLISON, S. K., and WARSHAW, S. D., 1953, *Rev. Mod. Phys.*, **25,** 779.

ALSTON, M. H., CREWE, A. V., EVANS, W. H., GREEN, L. L., and WILLMOTT, J. C., 1954, *Proc. Phys. Soc.* A, **67,** 657.

DODDER, D. C., and GAMMEL, J. L., 1952, *Phys. Rev.*, **88,** 520.

SEAGRAVE, J. D., 1953, *Phys. Rev.*, **92,** 1222.

Electron Scattering in Photographic Emulsions

BY A. HUSAIN
Department of Physics, University College London†

Communicated by E. H. S. Burhop; MS. received 21st September 1954

ILFORD G5 plates of dimensions 2 in. by 2 in. and emulsion thickness 200 microns were exposed to electrons accelerated to high energies by the 20 MeV synchrotron at University College, London. Electrons of energies 6·6, 11·5 and 18·0 MeV respectively were incident on the plates at a grazing angle of approximately 5° and the plates were processed using the temperature development method.

Measurements of the plates were made using a Beck binocular microscope. A 2 mm (80 ×) oil immersion objective was used in conjunction with 15 × compensating eyepieces fitted with a calibrated graticule and a protractor.

Two types of scattering measurement were carried out with these plates. The angle of ejection and range of electron recoils were measured in a study of electron–electron scattering. Multiple scattering measurements were also carried out on a number of the fast electron tracks.

§ 1. ELECTRON–ELECTRON SCATTERING

In these measurements about 90 cm of electron track were scanned for each of the three incident energies and the total number of scattering events observed in the three cases were 726, 775 and 634 respectively. Measurements were made when possible of (i) the projected angle of recoil, (ii) the projected length of recoil parallel to the surface of the emulsion, (iii) the projected length of recoil perpendicular to the emulsion surface. To estimate (iii) the contraction factor of the emulsion was assumed to be 2·3.

---

† Now at National Research Council Laboratories, Ottawa, Canada.

For very low energy knock-on electrons the angle of ejection was difficult to measure and only the range of the knock-on electron was available. Many of the recoils of energy greater than 0·2 MEV left the emulsion so that in these cases only the angle of ejection was available.

The knock-on electrons should be uniformly distributed in azimuth about the incident direction. The actual distribution in azimuth showed a marked deficiency of recoils corresponding to ejection at a large angle to the plane of the surface of the emulsion, as might have been expected owing to the difficulty of observation under these conditions, so that it was necessary to make a loss correction. From the departure of the distribution in azimuthal angle from uniformity it was estimated that this loss correction was 11%, 12% and 16·5% for incident electron energies of 6·6, 11·5 and 18·0 MEV respectively. The error in the estimate of the loss correction could have been as high as 25% however.

The corrected numbers of recoils in a range of energy intervals for the three incident energies investigated are shown in the table.

Table 1

E_I (MEV)	E_R (MEV)	N	Theoretical estimate of no. of events Rutherford (relativistic)	Mott	Möller
6·6	0·03–0·06	424±23	419	419	419
	0·06–0·10	158±13	164	164	164
	0·10–0·20	117±11	122	122	122
	0·20–0·50	71± 9	74	74	74
	0·50–1·0	22± 5·5	24·5	22	25
	1·00–2·00	10± 3·5	13	10	14
	2·00–3·25	6± 2·5	8	5	9
11·5	0·03–0·06	448±27	408	408	408
	0·06–0·10	187±14	162	162	162
	0·10–0·20	121±11	120	120	120
	0·20–0·50	64± 8	72	72	72
	0·50–1·00	27± 5·5	24	24	24
	1·00–2·00	13± 3·5	12·5	11	13
	2·00–5·75	9± 3	10	7	11
18·0	0·03–0·06	394±24	401	401	401
	0·06–0·10	145±13	160	160	160
	0·10–0·20	102±10·5	117	117	117
	0·20–0·50	63± 8	67	67	67
	0·50–1·00	22±45	24	24	24
	1·00–2·00	9± 3	12·5	11	13
	2·00–5·00	5± 2·5	6	4·8	6·5
	5·00–9·35	1± 1	1·9	1·5	2·2

E_I=incident energy; E_R=recoil energy;
N=number of observed events (including loss correction).

In the table the observed number of recoils is compared with the number to be expected on the basis of the relativistic Rutherford formula, the Mott formula (Mott 1930) which takes account of the identity of the two particles, and the Möller (Möller 1932) formula which takes account also of retardation and spin effects.

The observations are in general agreement with any of these three expressions since in the region of small energy transfer to the recoil there is no appreciable difference between the results of the three theories. Unfortunately in the region where the theories differ appreciably in their predictions there are insufficient recoils to make a significant comparison between them, and a prohibitively long scanning time would be needed to accumulate sufficient observations for such a comparison.

§ 2. MULTIPLE SCATTERING

Multiple scattering measurements were carried out on the tracks of the incident electrons employing the coordinate method of Fowler (1950). Observations were made on 120 tracks of length greater than 700 microns of an energy of 6·6 MEV and on 70 tracks of length greater than 1400 microns at an energy of 11·5 MEV. The electron energies were determined by range measurements in aluminium and should be accurate to within approximately 5%. These electron energies corresponded to maximum magnet currents in the synchrotron of 30 and 50 amp respectively. Further measurements were also carried out with electrons extracted under similar conditions from the synchrotron when the maximum magnet currents were 70 amp and 80 amp respectively.

If p and $\beta\mathbf{c}$ are respectively the momentum in units MEV C^{-1} and velocity of the electron, the mean projected angle of multiple scattering α degrees in a length t microns of the emulsion can be written as

$$\alpha = \frac{K}{p\beta}\left(\frac{t}{100}\right)^{1/2}$$

where K is conventionally defined as the scattering constant for the emulsion. If $\bar{D}$ microns is the mean magnitude of the second differences measured in the coordinate method

$$\bar{D}^2 = (\pi K/1800 p\beta)^2 t^3 + \langle \epsilon \rangle^2$$

where the quantity $\langle \epsilon \rangle$ represents the mean absolute second difference due to 'noise' which contributes to the observed second difference. The relation between D^2 and t^3 is not quite linear, however, since the scattering constant K increases slowly with cell length. Measurements of the second differences were carried out using cell lengths of 38, 76 and 114 microns respectively and the mean noise level determined by fitting a parabolic curve to the observed variation of D^2 with t^3.

To reduce the influence of single scattering on the observed second differences an experimental 'cut-off' criterion was adopted, all second differences greater in magnitude than four times the mean second difference for a given electron energy and cell length being ignored.

In table 2 the observed scattering constant is compared with the theoretical constant (allowing for cut-off) calculated using the theories of Williams (1940)

Table 2. Comparison of Observed and Theoretical Scattering Constants

Cell length	Experiment		Theory	
(μ)	6·6 MEV	11·5 MEV	Williams	Molière
38	$22{\cdot}3 \pm 1{\cdot}3$	$21{\cdot}9 \pm 1{\cdot}3$	21·8	21·6
76	$23{\cdot}3 \pm 1{\cdot}4$	$22{\cdot}8 \pm 1{\cdot}4$	23·0	22·7
114	$23{\cdot}7 \pm 1{\cdot}4$	$23{\cdot}6 \pm 1{\cdot}4$	23·6	23·2

and of Molière (1948) respectively. The results of the Williams theory were calculated using the expression given by Voyvodic and Pickup (1952) in which Molière's γ-factor was incorporated into the theory of Williams. The results are generally in agreement with those of Bosley and Muirhead (1952). More than 2500 second differences were used to derive the scattering constant for each energy and each cell length, and the uncertainty in the absolute value of the scattering constant arose mainly from the uncertainty in the energy value obtained from absorption measurements.

Using the theoretical scattering constant, the multiple scattering measurements with electrons extracted from the synchrotron when the maximum magnet current was 70 amp and 80 amp respectively were used to estimate the kinetic energy of the electrons under these conditions. Values of 15·6 Mev and 18·0 Mev were obtained for these two values of the magnet current.

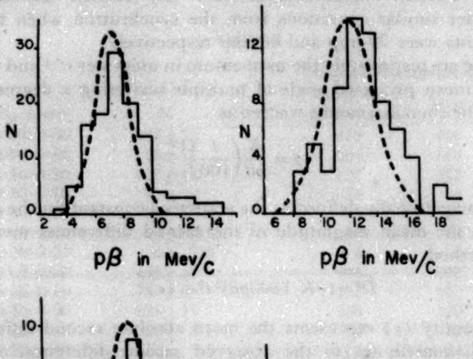

Energy distribution of the electrons. The ordinates N show the number of electrons per 1 Mev energy interval. The dotted lines are the expected gaussian distributions for the statistical errors in the measurements.

The distribution in energy estimated from multiple scattering for 120 tracks at 6·6 Mev, 70 at each of 11·5 Mev and 15·6 Mev and 39 at 18 Mev is shown in the histograms of the figure. In each case the dotted line shows the gaussian distribution to be expected, the width of the gaussian curve corresponding to the standard error of each determination.

Acknowledgments

I am much indebted to Professor H. S. W. Massey and to Dr. E. H. S. Burhop for their interest in this work and especially to Dr. C. Dodd and Mr. A. J. Egginton for exposing the plates to the extracted beam of the synchrotron. I also wish to express my deep gratitude to the Royal Commissioners of the Exhibition of 1851 for the award of an Overseas Scholarship.

References

Bosley, W., and Muirhead, H., 1952, *Phil. Mag.*, **43**, 63.
Fowler, P. H., 1950, *Phil. Mag.*, **41**, 169.
Molière, G., 1948, *Z. Naturforsch.*, **3** a, 78.
Möller, C., 1932, *Ann. Phys., Lpz.*, **14**, 531.
Mott, N. F., 1930, *Proc. Roy. Soc.* A, **126**, 259.
Voyvodic, L., and Pickup, E., 1952, *Phys. Rev.*, **85**, 91.
Williams, E. J., 1940, *Phys. Rev.*, **58**, 292.

LETTERS TO THE EDITOR

A Proposed Notation for Quantized Angular Momenta

Calculations concerned with states of quantized angular momentum are often cumbersome because of the large number of symbols which occur in the formulae. The following 'condensed' notation is accordingly proposed:

(i) Let the pair of quantum numbers (j, m) specifying states in which an angular momentum is quantized with respect to a given set of axes be denoted by a single bold-face symbol, thus $\mathbf{j} \equiv (j, m)$. Also $-\mathbf{j} \equiv (j, -m)$.

(ii) When the same bold-face symbol occurs two or more times in an expression, let summation over the z-component (only) be automatic.

(iii) Let states in which an angular momentum is quantized with respect to axes rotated from the original axes be distinguished by primes or numerical suffixes placed *before* the bold-face symbol, thus ${}'\mathbf{j}$, ${}''\mathbf{j}$, etc. Note that $j = {}'j = {}''j \ldots$, etc.

(iv) Phase factors[†]: Define $\varpi(\mathbf{j}) = (-1)^{j-m}$. Appearances as arguments of $\varpi(\mathbf{j})$ are not to count for the purpose of rule (ii) above.

In virtue of (i) and (iii) above, the notation of transformation theory (Dirac 1947) can be used without being unduly cumbersome for vector-addition coefficients (Condon and Shortley 1935) or insufficiently explicit for rotation coefficients. Thus for vector addition:

$$\psi(\mathbf{j}) = \psi(\mathbf{j}_1, \mathbf{j}_2)(\mathbf{j}_1, \mathbf{j}_2 | \mathbf{j}), \qquad \ldots\ldots(1)$$

$$\psi(\mathbf{j}_1, \mathbf{j}_2) = \textstyle\sum_j \psi(\mathbf{j})(\mathbf{j} | \mathbf{j}_1, \mathbf{j}_2), \qquad \ldots\ldots(2)$$

$$\begin{aligned}(\mathbf{j} | \mathbf{j}_1, \mathbf{j}_2) &= (\mathbf{j}_1, \mathbf{j}_2 | \mathbf{j}) \\ &= (-\mathbf{j}_2, -\mathbf{j}_1 | -\mathbf{j}) = (-1)^{j_1+j_2-j}(\mathbf{j}_2, \mathbf{j}_1 | \mathbf{j}) \\ &= [(2j+1)/(2j_1+1)]^{1/2}\varpi(-\mathbf{j}_2)(-\mathbf{j}, \mathbf{j}_2 | -\mathbf{j}_1). \qquad \ldots\ldots(3)\end{aligned}$$

For rotation of axes:

$$\psi({}'\mathbf{j}) = \psi(\mathbf{j})(\mathbf{j} | {}'\mathbf{j}), \qquad \ldots\ldots(4)$$

$$\psi(\mathbf{j}) = \psi({}'\mathbf{j})({}'\mathbf{j} | \mathbf{j}), \qquad \ldots\ldots(5)$$

$$(\mathbf{j} | {}'\mathbf{j}) = ({}'\mathbf{j} | \mathbf{j})^* = \varpi({}'\mathbf{j})(-{}'\mathbf{j} | -\mathbf{j})\varpi(\mathbf{j}), \qquad \ldots\ldots(6)$$

$$(\mathbf{j} | {}'\mathbf{j})({}'\mathbf{j} | {}''\mathbf{j}) = (\mathbf{j} | {}''\mathbf{j}). \qquad \ldots\ldots(7)$$

Relation between vector-addition coefficients and rotation coefficients:

$$(\mathbf{j} | \mathbf{j}_1, \mathbf{j}_2)(\mathbf{j}_1 | {}'\mathbf{j}_1)(\mathbf{j}_2 | {}'\mathbf{j}_2) = (\mathbf{j} | {}'\mathbf{j})({}'\mathbf{j} | {}'\mathbf{j}_1, {}'\mathbf{j}_2). \qquad \ldots\ldots(8)$$

In transformation theory notation these are alternative expressions for the transformation $(\mathbf{j} | {}'\mathbf{j}_1, {}'\mathbf{j}_2)$. Transposing a vector-addition coefficient (see equations (1) and (2) above):

$$(\mathbf{j}_1 | {}'\mathbf{j}_1)(\mathbf{j}_2 | {}'\mathbf{j}_2) = \textstyle\sum_j (\mathbf{j}_1, \mathbf{j}_2 | \mathbf{j})(\mathbf{j} | {}'\mathbf{j})({}'\mathbf{j} | {}'\mathbf{j}_1, {}'\mathbf{j}_2), \qquad \ldots\ldots(9)$$

i.e. an expression for the rotation $(\mathbf{j}_1, \mathbf{j}_2 | {}'\mathbf{j}_1, {}'\mathbf{j}_2)$ of states in which two uncoupled angular momenta are quantized.

[†] This convention was suggested to the author by U. Fano (private communication). It has certain advantages when the invariance of tensors under Hermitian conjugation is considered.

Racah recoupling coefficients (Racah 1942):

$$(\mathbf{j}_1, \mathbf{j}_2 | \mathbf{j})(\mathbf{j}, \mathbf{j}_3 | \mathbf{j}_4) = \textstyle\sum_s [(2s+1)(2j+1)]^{1/2} \quad W(j_1 j_2 j_4 j_3 ; js)(\mathbf{j}_2, \mathbf{j}_3 | \mathbf{s})(\mathbf{j}_1, \mathbf{s} | \mathbf{j}_4). \qquad \ldots\ldots(10)$$

Further relations follow by transposing one or both vector-addition coefficients (see equations (1) and (2) above), and by using (3).

Where it is necessary to specify a particular numerical value of a z-component the relevant symbol must of course be written out in full: $(j_1 m_1, j_2 m_2 | jm)$ or $(jm | j'm)$.

As an example of the condensed notation consider the angular correlation $W(A_1, A_2)$ of two successive nuclear radiations (Biedenharn and Rose 1953):

$$W(A_1, A_2) = \langle \mathbf{j}_1 | \mathbf{j}, A_1 \rangle^* \langle \mathbf{j}_1 | \mathbf{j}', A_1 \rangle \langle \mathbf{j} | \mathbf{j}_2, A_2 \rangle^* \langle \mathbf{j}' | \mathbf{j}_2, A_2 \rangle \qquad \ldots\ldots(11)$$

where $\langle \mathbf{j}_1 | \mathbf{j}, A_1 \rangle$, etc. are the probability amplitudes for the emission A_1, etc. (specified in direction and polarization), with nuclear spin change $\mathbf{j}_1 \rightarrow \mathbf{j}$, etc. Making the transformation $('\mathbf{L}, \pi | A)$ to states of the radiation with parity π and total angular momentum $'\mathbf{L}$ quantized with the direction of emission A as axis, and using 'reduced matrix elements',

$$\langle \mathbf{j}_1 | \mathbf{j}, A \rangle = \textstyle\sum_L \langle \mathbf{j}_1 | \mathbf{j}, \mathbf{L}\pi \rangle (\mathbf{L} | '\mathbf{L})('\mathbf{L}, \pi | A), \qquad \ldots\ldots(12)$$

$$\langle \mathbf{j}_1 | \mathbf{j}, \mathbf{L}\pi \rangle = (j_1 || L, \pi || j)(\mathbf{j}_1 | \mathbf{j}, \mathbf{L}). \qquad \ldots\ldots(13)$$

Using equations (6) and (9), then a variant of (10),

$$\langle \mathbf{j}_1 | \mathbf{j}, A \rangle^* \langle \mathbf{j}_1 | \mathbf{j}', A \rangle = \textstyle\sum T(LL')(\mathbf{j}_1 | \mathbf{j}, \mathbf{L})(\mathbf{j}_1 | \mathbf{j}', \mathbf{L}') \quad [\varpi(\mathbf{L})(-\mathbf{L}, \mathbf{L}' | \boldsymbol{\nu})(\boldsymbol{\nu} | '\boldsymbol{\nu})('\boldsymbol{\nu} | -'\mathbf{L}, '\mathbf{L}')\varpi('\mathbf{L})]('\mathbf{L}, \pi | A)^*('\mathbf{L}', \pi | A), \qquad (14)$$

$$= \textstyle\sum T(LL')(-1)^{j_1+L-j} \varpi(\mathbf{j})(\mathbf{j}, -\mathbf{j}' | -\boldsymbol{\nu}) W(jjLL' ; \nu j_1)(\boldsymbol{\nu} | '\boldsymbol{\nu}) C('\boldsymbol{\nu}, LL') \qquad (15)$$

where

$$T(LL') = (j_1 || L, \pi || j)^* (j_1 || L', \pi || j), \qquad \ldots\ldots(16)$$

$$C('\boldsymbol{\nu}, LL') = ('\boldsymbol{\nu} | -'\mathbf{L}, '\mathbf{L}')\varpi('\mathbf{L})('\mathbf{L}, \pi | A)^*('\mathbf{L}', \pi | A). \qquad \ldots\ldots(17)$$

The C coefficients depend only on the type of radiation emitted and can be summed over any unobserved properties, e.g. polarization. All other properties of the transition except spin values enter through the factor $T(LL')$ only. The summation Σ is over L, L' and ν.

Finally, using equation (7),

$$W(A_1, A_2) = \textstyle\sum_\nu D^{(2)}(''\boldsymbol{\nu})^* (''\boldsymbol{\nu} | '\boldsymbol{\nu}) D^{(1)}('\boldsymbol{\nu}), \qquad \ldots\ldots(18)$$

$$D^{(1)}('\boldsymbol{\nu}) = \textstyle\sum_{L_1 L_1'} T(L_1 L_1')(-1)^{L_1} W(jjL_1 L_1' ; \nu j_1) C('\boldsymbol{\nu}, L_1 L_1') \qquad \ldots\ldots(19)$$

with a corresponding expression for $D^{(2)}(''\boldsymbol{\nu})$. The z'' axis lies in the direction A_2. The only angular dependence occurs in the coefficients $(''\boldsymbol{\nu} | '\boldsymbol{\nu})$; there remains no reference to the original (unprimed) axes.

The Clarendon Laboratory,
Oxford.

J. A. Spiers.

24th March 1954; and in final form 18th October 1954.

Biedenharn, L. C., and Rose, M. E., 1953, *Rev. Mod. Phys.*, **25**, 729.

Condon, E. U., and Shortley, G. H., 1935, *Theory of Atomic Spectra* (Cambridge: University Press).

Dirac, P. A. M., 1947, *The Principles of Quantum Mechanics*, 3rd Edn (Oxford: University Press).

Racah, G., 1942, *Phys. Rev.*, **62**, 438.

Absolute Calibration of Neutron Counters with Po–α–Be

Po–α–Be sources are frequently used to calibrate neutron detectors, but because of the complex energy spectrum and the difficulty of standardizing the neutron source strength the method is of limited value. This letter describes a means of calibration without knowing the strength of the source, by detecting only those neutrons from Po–α–Be which are in coincidence with the well-known 4·43 Mev γ-rays. This has the further advantage that the spectrum of neutrons is considerably simplified.

The greater part of the neutrons from Po–Be arise from the reaction ^{9}Be(α, n)^{12}C, which is shown schematically in the figure (Ajzenberg and Lauritsen 1952, Hoyle, Dunbar, Wenzel and Whaling 1953). If a γ-ray counter which detects only γ-rays of 4·43 Mev and over (such as a suitably biased scintillation counter) is connected in a coincidence circuit with the neutron detector to be calibrated, only those neutrons which excite one of the two upper levels will be recorded as coincidences. The mean efficiency of the neutron counter for these neutrons will then be given by the ratio of the coincidence counting rate to the γ-ray counting rate, since the 4·43 Mev γ-ray is only emitted following neutron emission.

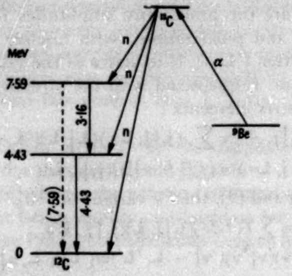

Energy levels in the reaction ^{9}Be(α, n)^{12}C.
(The ^{13}C level shown corresponds to the full α-particle energy of 5·3 Mev.)

This method would be invalidated if the 7·59 Mev level were de-excited by the emission of a single γ-ray quantum; however, it has been shown by Beghian, Halban, Husain and Sanders (1953) that such a γ-ray is not emitted with an intensity greater than 0·04% of that of the 4·43 Mev ray. There is some evidence that this level may be de-excited by internal pair production (Harries and Davies 1952); these pairs will not be recorded either as γ-ray counts or as coincidences, and the validity of the neutron counter calibration will not be affected: their effect will be to reduce slightly the low-energy component of the neutron spectrum.

It is not known for certain what the spectrum of neutrons detected is in practice; using monoenergetic α-particles and a thin beryllium target, three groups of neutrons corresponding to the three energy levels were found by Guier, Bertini and Roberts (1952), but in the usual type of polonium + powdered beryllium source the neutron energy depends on (*a*) the amount of energy lost by the α-particle before striking a beryllium nucleus, (*b*) the angle at which it is emitted relative to the α-particle, and (*c*) the moderating effect of the beryllium and container. The total spectrum from such a source has been measured by Elliott, McGarry and Faust (1954), and by analogy with their results the spectrum of neutrons detected in the present measurement will probably contain all energies from zero up to 6·4 MeV, with maximum intensity at 3–4 MeV.

In making this calibration care must be exercised that errors are not introduced by: (i) Angular correlation between γ-rays and neutrons: although there is at present no experimental evidence on this point, there is a strong possibility of correlation. (ii) Simultaneous detection of the 3·16 MeV and 4·43 MeV γ-rays, with higher efficiency than that for the 4·43 MeV quantum alone: since the relative intensity of the 3·16 MeV γ-ray is only 3% (Beghian *et al.* 1953), this effect will be small unless large solid angles are used. (iii) False coincidences due to neutrons scattered by the neutron detector and then captured, giving rise to γ-rays which are detected in the γ-ray counter.

An experimental test of this system was made by using it to calibrate a recoil chamber having a 10 mg cm^{-2} polythene radiator, the γ-rays being detected in a NaI(Tl) crystal and EMI type 6260 photomultiplier. Assuming that the neutron spectrum was as described above, reasonable agreement was obtained with the calculated value of the efficiency.

Atomic Energy Research Establishment,
Harwell, Berks.
9th September 1954.

G. N. HARDING.

AJZENBERG, F., and LAURITSEN, T., 1952, *Rev. Mod. Phys.*, **24**, 321.
BEGHIAN, L. E., HALBAN, H. H., HUSAIN, T., and SANDERS, L. G., 1953, *Phys. Rev.*, **90**, 1129.
ELLIOTT, J. O., MCGARRY, W. I., and FAUST, W. R., 1954, *Phys. Rev.*, **93**, 1348.
GUIER, W. H., BERTINI, H. W., and ROBERTS, J. H., 1952, *Phys. Rev.*, **85**, 426.
HARRIES, G., and DAVIES, W. T., 1952, *Proc. Phys. Soc.* A, **65**, 564.
HOYLE, F., DUNBAR, D. N. F., WENZEL, W. A., and WHALING, W., 1953, *Phys. Rev.*, **92**, 1095.

Dislocations and the Biot–Savart Law

The following notation, not particularly mentioned in the text, is given here for convenience:—$r \equiv |v - v'|$ distance between field point and source point, dL amount of the vector line element dL_α. Let a dislocation line of Burgers vector $\mathbf{b}_\alpha$ take its course in an infinite elastic medium along a space curve L. The displacement field connected with such a dislocation line (L, b_α) can be described by a surface integral over a surface F which is bounded by L, but which is otherwise arbitrary (Burgers 1939). This surface integral can be transformed by means of the Stokes theorem to a line integral as first indicated by Peach and Koehler (1950). From this line integral for the displacements one obtains in the usual manner the stress field of the dislocation line, also as a line integral. Peach and Koehler have pointed out the analogy with the Biot–Savart law.

It will be shown here that one can obtain the equations of Peach and Koehler for the stresses more directly by following the procedure generally used for deriving the Biot–Savart law.

The Burgers circuit $\oint du_\alpha$ round a dislocation line (L, b_α) gives, as is well known, a vector $\mathbf{b}_\alpha$ different from zero, because the compatibility equations for the strain components are not valid along L. From the analogous relations with the magnetic field of stationary currents it follows that one can characterize the stress field of the dislocation by the measure of divergence $\eta_{\alpha\beta}$ from the compatibility equations as well as by the displacement jump b_α on F. The quantities $\eta_{\alpha\beta}$ are appropriately to be defined by the equations

$$\epsilon_{\alpha\beta\gamma}\epsilon_{\delta\epsilon\zeta}\nabla_\alpha\nabla_\zeta e_{\gamma\delta}=\eta_{\beta\epsilon}=\eta_{\epsilon\beta} \qquad \ldots\ldots(1)$$

where $\epsilon_{\alpha\beta\gamma}\ldots$ is the Levi–Civita tensor and $e_{\gamma\delta}$ the strain tensor. For $\eta_{\alpha\beta}=0$ these are exactly the compatibility equations for the strain components. Substituting in equation (1) for the three-dimensional stress functions $\chi_{\alpha\beta}$ defined (Kroener 1954) by

$$\sigma_{\beta\epsilon}=2G\epsilon_{\alpha\beta\gamma}\epsilon_{\delta\epsilon\zeta}\nabla_\alpha\nabla_\zeta\left(\chi_{\gamma\delta}+\frac{\nu}{1-\nu}\chi_{\eta\eta}\delta_{\gamma\delta}\right),\quad \nabla_\alpha\chi_{\alpha\beta}=0 \qquad \ldots\ldots(2)$$

one gets

$$\Delta\Delta\chi_{\alpha\beta}=\eta_{\alpha\beta}. \qquad \ldots\ldots(3)$$

Here σ is the stress tensor, G the shear modulus, ν Poisson's ratio and δ the unit tensor. The equilibrium equations $\nabla_\alpha\sigma_{\alpha\beta}=0$ are as well satisfied by equation (2) as is the equation $\nabla_\alpha\mathbf{B}_\alpha=0$ in the analogous magnetic field theory by the equations $\mathbf{B}_\alpha=\epsilon_{\alpha\beta\gamma}\nabla_\beta\mathbf{A}_\gamma$, $\nabla_\alpha\mathbf{A}_\alpha=0$, introducing the vector potential $\mathbf{A}_\alpha$. In an infinite medium the equations

$$\chi_{\alpha\beta}(v)=\frac{1}{8\pi}\int_{L'}dL'\bar{\eta}_{\alpha\beta}(v')r,\quad \bar{\eta}_{\alpha\beta}\equiv\lim_{f\to 0}\int_f\eta_{\alpha\beta}\,df \qquad \ldots\ldots(4)$$

give as a particular solution of equation (3) the field of the stress functions resulting from a one-dimensional distribution of incompatibilities $\bar{\eta}_{\alpha\beta}$ ($f\equiv$cross section of the dislocation line). The analogous equation $\mathbf{A}_\alpha\sim\int_{L'}dL'j_\alpha(v')/r$ give the vector potential field produced by a linear current j.

Now one substitutes

$$\bar{\eta}_{\alpha\beta}dL'=\tfrac{1}{2}(dL'_\alpha b_\gamma\epsilon_{\beta\gamma\delta}\nabla_\delta-dL'_\beta b_\gamma\epsilon_{\alpha\gamma\delta}\nabla_\delta) \qquad \ldots\ldots(5)$$

in equation (4), differentiations being with respect to r. Introducing equation (4) into (2) and performing all differentiations, one obtains exactly the same stress field as from Burgers' surface integral by means of the Stokes theorem and the Hooke law. Equation (5) shows that a dislocation line is described not by means of an ordinary distribution of incompatibilities along L, but by a certain double distribution of incompatibilities. This is implied by the differentiations in equation (5). In the equation (4) substituted by (5) one can put most quantities before the integral. Then the stress function field of the dislocation (L, $\mathbf{b}_\alpha$) becomes

$$\chi_{\alpha\beta}(v)=\frac{1}{8\pi}\,\mathrm{SY}\{\epsilon_{\beta\gamma\delta}b_\gamma\nabla_\delta\mathscr{L}_\alpha(v)\},\quad \mathscr{L}_\alpha(v)\equiv\int_{L'}dL_\alpha'r$$

where SY$\equiv$symmetrical part of the tensor. This formula shows the superiority of the method of stress functions over the previous method. Only the integral $\mathscr{L}_\alpha(v)$, which is extremely simple relative to the Peach–Koehler one, has to be defined for this method. The stress field of the dislocation can then be obtained by ordinary differentiation.†

In the theory of magnetic fields of stationary currents the application of the vector potential is preferred in certain problems. It can be presumed that the application of the stress function tensor $\chi_{\alpha\beta}$ offers advantages in analogous problems in elastic theory.

The author would like to thank Professor U. Dehlinger for his interest and encouragement.

Institut für theoretische und
angewandte Physik der
Technischen Hochschule,
Stuttgart-N,
Germany.
11th October 1954.

E. KROENER.

BURGERS, J. M., 1939, *Proc. Kon. Ned. Acad. Wet.*, **42,** 378.
KROENER, E., 1954, *Z. Phys.*, **139,** 175 ; 1955, *Z. angew. Phys.*, in the press.
NABARRO, F. R. N., 1952, *Advances in Physics* (*Phil. Mag.* Suppl.), **1,** 269.
PEACH, M., and KOEHLER, J. S., 1950, *Phys. Rev.*, **80,** 436.

† The author has given a general statement of the theory of internal stresses in analogy to the theory of magnetic fields of stationary currents (Kroener 1955). There, also, the superiority of the method of stress functions will be shown by a numerical calculation (stress field of ' solenoidally ' arranged dislocations, important for the age hardening of Al–Cu alloys).

Nuclear Spins and Ratio of Magnetic Moments of Europium 151 and 153

Hyperfine structure has been observed in the paramagnetic resonance spectrum of the Eu^{2+} ion, and the known spins of 5/2 for the two stable isotopes have been confirmed. The anomalous ratio of the nuclear magnetic moments (151 : 153), previously given as 2·2 (Schuler and Schmidt 1935) is found to be $2{\cdot}23_5 \pm 0{\cdot}03$.

Measurements were made at room temperature and 3 cm wavelength on powdered samples of a phosphor of strontium sulphide containing a few parts in a thousand of europium and about one tenth this quantity of samarium. Two groups of six $(=2I+1)$ lines were clearly resolved, with nearly equal intensity corresponding to the relative abundances (47·8%, 52·2%, Hess 1948). The ratio of the nuclear moments is determined from the overall widths of the hyperfine structures. The half-width of the lines at half intensity was about two gauss, and the positions were measured with proton resonance. The narrowness of these lines in a powder shows that the g-value and hyperfine structure must be isotropic; the spectrum is described by the formula

$$h\nu = g\beta H + Am + \tfrac{1}{2}\left(\frac{A^2}{h\nu}\right)\{I(I+1)-m^2\}$$

with $g=1{\cdot}991_2 \pm 0{\cdot}001$, $A_{151}=30{\cdot}8_2 \pm 0{\cdot}2$, $A_{153}=13{\cdot}7_9 \pm 0{\cdot}2$ (A in units of 10^{-4} cm^{-1}).

The ground state of the Eu^{3+} ion is $^7F_0$, giving no resonance absorption, while that of the Eu^{2+} ion is $^8S_{7/2}$, the same as that of Gd^{3+}. The measured g-value is identical with that previously observed for salts of Gd^{3+}. Strontium sulphide has a simple cubic structure, and a small electronic splitting of the ^8S state is to be expected. Presumably only the electronic $+\frac{1}{2}\leftrightarrow-\frac{1}{2}$ transition is observed in the powder, other transitions being smeared out by the random orientation of the crystallites.

As in the case of the Mn^{2+} $3d^5$, ^6S ion, no hyperfine structure should be present except from unpaired s-electron states such as $4f^75s6s$ which are mixed to $4f^75s^2$ by configurational interaction. In terms of the non-dimensional constant κ introduced by Abragam and Pryce (1951), the hyperfine constant

$$A=2\gamma\,\beta\beta_N\,\overline{(1/r^3)}\kappa.$$

With $\overline{(1/r^3)}\sim 55A^{-3}$ (Elliott and Stevens 1953), and a nuclear moment of 3·6 n.m. for Eu 151 (Schmidt 1938, Klinkenberg 1952), this gives a value of the order of 0·08 for κ, which is appreciably smaller than in the other transition groups. No effect due to a term of this type has previously been detected in the 4f group, and its magnitude is too small to affect appreciably the theory of Elliott and Stevens (1953). The upper limit of 40 gauss for any hyperfine structure in gadolinium ethyl sulphate given by Bleaney and Scovil (1950) would indicate that the nuclear moments of the odd neutron isotopes Gd 155 and Gd 157 are not greater than about 1·0 n.m., if the degree of configurational interaction is the same as in Eu^{3+}.

There is some evidence (Stockmann 1952) that in this (infra-red stimulated) phosphor the dominant activator (Eu) exists in the divalent state and the auxiliary activator (Sm) in the trivalent state. On excitation with ultra-violet light the following reaction is postulated:

$$Eu^{2+}+h\nu\rightarrow Eu^{3+}+e^-,$$
$$Sm^{3+}+e^-\rightarrow Sm^{2+}.$$

On stimulation with infra-red light the reverse process occurs and visible light is emitted as the ions revert to their original valencies. Our experiment proves the presence of divalent europium, but no diminution in intensity of the spectrum could be observed after activation by ultra-violet light, presumably because insufficient numbers of Eu ions were changed in valency. At most a 10% effect would be expected, owing to the lower concentration of samarium; as anticipated, no spectrum due to the latter ion could be observed.

Our thanks are due to Dr. L. Weidenfeld for providing the samples of phosphors. This work was carried out while one of us (W.L.) was on leave from the Hebrew University, Jerusalem; he is indebted to the Humanitarian Trust and the Friends of the Hebrew University of Jerusalem for a grant.

Clarendon Laboratory,
Oxford.
20th September 1954.

B. Bleaney.
W. Low.

Abragam, A., and Pryce, M. H. L., 1951, *Proc. Roy. Soc.* A, **205**, 135.
Bleaney, B., and Scovil, H. E. D., 1950, *Proc. Phys. Soc.* A, **63**, 1369.
Elliott, R. J., and Stevens, K. W. H., 1935, *Proc. Roy. Soc.* A, **218**, 553.
Klinkenberg, P. F. A., 1952, *Rev. Mod. Phys.*, **24**, 63.
Hess, D. C., 1948, *Phys. Rev.*, **74**, 773.
Schmidt, T., 1938, *Z. Phys.*, **108**, 408.
Schuler, H., and Schmidt, T., 1935, *Z. Phys.*, **94**, 457.
Stockmann, F., 1952, *Naturwissenschaften*, **10**, 226.

Paramagnetism of Caesium Titanium Alum

Paramagnetic resonance in a powdered sample of caesium titanium alum was first observed by Bijl (1950). The shape of the absorption curve was interpreted as arising from a doublet ground state with anisotropic g-values. Resonance has now been observed in a single crystal at temperatures between 4·2 and 2·5°K. The spectrum indicates that the crystal has the usual alum structure, with four ions in unit cell, and yields the values $g_{\parallel}=1{\cdot}25$, $g_{\perp}=1{\cdot}14$ (accurate to $\pm 0{\cdot}02$). The line width is constant over the temperature range given above at 250 ± 50 gauss. This is considerably larger than that expected for pure magnetic dipole interaction between the ions, and indicates that there is considerable exchange interaction, in agreement with paramagnetic relaxation measurements of the specific heat (Benzie and Cooke 1951).

In a cubic crystalline electric field, the ^{2}D state of the Ti^{3+} ion is split into a lower orbital triplet and upper orbital doublet. The triplet with its twofold spin degeneracy is split by a trigonal field and by the spin–orbit coupling, and the g-values can be expressed in terms of one independent variable (Bleaney 1950) if matrix elements with the upper doublet are neglected. The closest fit with the observed values that can be obtained is $g_{\parallel}=1{\cdot}40$, $g_{\perp}=0{\cdot}95$, and the difference is well outside the experimental error. If matrix elements with the upper doublet are included, the g-values may be expressed in terms of two parameters, and these are both determined on fitting the observed g-values. Then the complete secular equation, with spin–orbit coupling and a trigonal field operating in a d-electron manifold, can be used to find the relative positions of the energy levels without any approximation. It is found that the state with the measured g-values is the ground state only if $\zeta \gg D$, where ζ is the spin–orbit coupling constant and D is the splitting produced by the cubic field. Since $\zeta=154$ cm^{-1} in the free ion, while the absorption spectrum of the Ti^{3+} ion both in the alum and in solution (Hartmann and Schläfer 1951) suggests that $D\simeq 20\,000$ cm^{-1}, this condition is very far from being fulfilled. The lowest state is then one with $g_{\parallel}=g_{\perp}=0$; it is thus evident that the simple crystalline field theory is inadequate in this case.

Van Vleck (1935) has shown that for a d^1 ion in an octahedral complex the magnetic electron does not take part in any σ-bonding. It may, however, take part in π-bonding, and though there is little evidence for such bonding in hydrated iron group compounds, it is most likely to occur with the Ti^{3+} ion, which has a very spreading 3d radial wave function. One effect of this will be to introduce a factor $k\leqslant 1$ in the matrix elements of the orbital angular momentum (Stevens 1953). (Actually, with trigonal symmetry two constants occur, k_1 and k_2, but these are unlikely to be very different and may be assumed equal.) The theory then shows that the observed g-values can be fitted with the right state lowest provided that $k<0{\cdot}95$, and the separation from the next level increases as k is reduced further.

The fact that the water molecules are not axially symmetric about the line joining them to the titanium ion suggests that the π-bonding may take place in a preferred plane. In this case the value of k given by a particular degree of bonding would be smaller than if the attached molecules were axially symmetric. The g-values of some complex halides of the 4d and 5d groups have been fitted using $k\sim 0{\cdot}85$ (Griffiths, Owen and Ward 1953), so that for titanium alum k might be as low as 0·7, when the separation of the two lowest energy levels would be about 30 cm^{-1}. In any case the theory leads to an excited state within a few tens of cm^{-1} of the ground state; this would explain the anomalous behaviour of the susceptibility found by Van den Handel (1940), and verified by preliminary measurements in this laboratory.

Clarendon Laboratory,
Oxford.
18th October 1954.

B. BLEANEY.
G. S. BOGLE.
A. H. COOKE.
R. J. DUFFUS.
M. C. M. O'BRIEN.
K. W. H. STEVENS.

BENZIE, R. J., and COOKE, A. H., 1951, *Proc. Roy. Soc.* A, **209**, 269.
BIJL, D., 1950, *Proc. Phys. Soc.* A, **63**, 405.
BLEANEY, B., 1950, *Proc. Phys. Soc.* A, **63**, 407.
GRIFFITHS, J. H. E., OWEN, J., and WARD, I. M., 1953, *Proc. Roy. Soc.* A, **219**, 526.
VAN DEN HANDEL, 1940, *Thesis*, Leiden University.
HARTMANN, H., and SCHLÄFER, H. L., 1951, *Z. Phys. Chem.*, **197**, 116.
STEVENS, K. W. H., 1953, *Proc. Roy. Soc.* A, **219**, 542.
VAN VLECK, J. H., 1935, *J. Chem. Phys.*, **3**, 807.

ADDENDUM

The Resolving Time of an Internal Counter Controlled Wilson Chamber, by P. J. CAMPION,† and W. T. DAVIES. (*Proc. Phys. Soc.* A, 1954, **67**, 944.)

In connection with our note of the above title (1954) our attention has been drawn to a recent paper by de Laboulaye, Tzara and Olkowsky (1954) in which substantially the same resolving time is reported using the same method, and to earlier work (de Laboulaye *et al.* 1952) which gave indications of the possibility of the method.

Clarendon Laboratory,
Oxford.
8th November 1954.

DE LABOULAYE, H., TZARA, C., and OLKOWSKY, J., 1954, *J. Phys. Radium*, **15**, 470.
DE LABOULAYE, H., TZARA, C., and STUDINOWSKI, J., 1952, *J. Phys. Radium*, **13**, 359.

† Now at Atomic Energy of Canada Ltd., Chalk River, Ontario.

REVIEWS OF BOOKS

Structure Reports—Vols. 11 *and* 12 (1947–48, 1949). International Union of Crystallography, edited by A. J. C. Wilson. Pp. x+779; viii+478 (Utrecht: Oosthoek, 1951, 1952).

It is often felt among x-ray crystallographers that their main concern is with the determination of structures by ever more ingenious and certain methods. Once the structure is determined they are apt to lose interest in it. If it were undertaken as an exercise in analytic methods this is understandable, if for the solution of some particular chemical problem once that problem is solved it is time to pass on to others. Nevertheless, it is particularly in structural crystallography that the full advantage of knowledge is lost if its units are isolated. It is only by bringing together the results of many analyses that we can hope to grasp the general principles underlying crystal structures. It was for this reason, as well as on account of the value of determined structures as an aid to the analyses of others, that the invaluable ' Strukturbericht ' of the *Zeitschrift für Kristallographie* was started by Professor Ewald in 1931. The war interrupted its publication but the rapidly resumed increase of structure determinations called ever more urgently for some form of record, especially as they were to be found in a bewildering variety of publications. It was for that reason that the newly formed International Union of Crystallography, in addition to its own journal *Acta Crystallographica*, decided at its first Congress in 1948 to take up the task where the Strukturbericht had laid it off, and by working backwards and forwards to fill the gap and bring the record up to date. So far three volumes have been published and another is about to appear.

The treatment follows that of the Strukturbericht somewhat simplified. Where new structures appear published, a summary but adequate description is given, usually with a diagram. In new cases of already known structures it is usually sufficient to refer back. These accounts are more than abstracts and except when detailed further work is contemplated they are usually sufficient for reference purposes. The standard of presentation is exceptionally high as assured by the experience of the three sectional editors, C. S. Barrett (metals), J. M. Bijvoet (inorganic and mineral), and J. M. Robertson (organic), and of the general editor, A. J. C. Wilson. The coverage is very thorough; there must be few determined structures, I know of none myself, that slip through the net.

Naturally the *Structure Reports* are indispensable to crystallographers; after them they are, or should be, of use to chemists. Their direct value to physicists until recently was likely to be small. Now, however, that the physics of solids has become, both theoretically and practically, one of the most important and live branches of physics, the *Structure Reports* will be found a most convenient reference work. The volumes covering specific years have in themselves only a limited interest, they must be taken as part of the larger whole of recorded information on structures. Nevertheless, one can note trends of interest in structure determination which reflect both external demands, for example of barium titanate for which there are seven references in Volume 10, 24 in Volume 11, and 17 in Volume 12, or on account of intrinsic interest in analysis, such as oxalic acid dihydrate or sucrose, or both, as in penicillin or protein structures.

Overall the picture is one of a well distributed effort; roughly two fifths of the space is given to inorganic, one third to organic, and one quarter to metallic structures. The value of the *Structure Reports* will much increase when the gap of the war years is filled, when it may be possible for a critical comparison and the putting together of all established results in a more ordered way; till then they remain the only convenient reference source to the architecture of the solid state.

J. D. BERNAL.

Structure Reports for 1950 (Volume 13), General editor A. J. C. Wilson. Pp. viii + 643. Published for the International Union of Crystallography by N. V. A. Oosthoek's Uitgevers Mij., Utrecht. 80 *Dutch florins*.

Structure Reports are an established institution. With the appearance of the fourth volume of the post-war series this institution now has a distinctive character, a uniform style and a tried format. The publication has not been going long enough to be showing signs of tiredness—although only the most dedicated editor could continue year after year—it has in fact not yet reached the steady state, as the accumulation of war-time papers has still to be reported. There are, therefore, very few criticisms to make of this addition to the series.

The field of crystallography, thanks to the admirable publications of the International Union of Crystallography, is one of the most united and self-conscious in science, but one may wonder whether metallurgists, mineralogists, physicists and even chemists use Structure Reports as much as they might. Pepinsky suggests that there are no crystallographers, but only users of crystallographic techniques. The latter, and those working on solid state physics, alloys and all branches of chemistry, even if not direct users of the techniques, should have access to this publication as the work reported affects them. To those preoccupied with crystals, the organized mass of data presented is an invitation to the generalization and theoretical synthesis which may lead to the easier and quicker digestion of future data on the structures of crystals.

The measured and temperate comments by the editors are most valuable to readers in guiding them on the relative importance of different papers. The comparative tables of interatomic distances ' from paper ' and ' as calculated by abstractor ', together with the astonishingly frequent corrected values of calculated densities should have a salutary effect on authors. One could imagine an author with a paper in the press breaking into a sweat and rechecking his calculations when he saw examples of the searching criticism to which it would be subjected. The assiduity of the editors in correcting errors and misprints is attested by the numerous references to ' private communication '. Their own misprints are remarkably few for a work of such complexity. To see a rising standard of published papers should be one of the editors' rewards. Editorial encouragement to the measurement of the optical constants of crystals of the new compounds examined might usefully be applied.

As there are many concessions to European usage, the systematic spelling ' Aluminum,' which seems so distinctively Transatlantic, and is, moreover, a departure from the practice of ending the names of metallic elements in ' -ium,' may be overlooked.

With every new volume of Structure Reports the user's task in extracting all the information on a particular topic from the separate indexes becomes more tedious. Perhaps when Volumes 8 and 9 (the war years) are published, a general index to the first thirteen volumes can be prepared.

This volume covers only the papers published in 1950 and comprises 643 pages. What is to be done when the annual quantity of new work becomes double this is a question which will soon have to be considered very seriously.

A. L. MACKAY.

Mathematics, Queen and Servant of Science, by E. T. BELL. Pp. 459. (London: Bell, 1952.) 21*s*.

The jaunty vigour of Professor Bell's writings is so well known that it is scarcely necessary to remark on the healthy good spirits that abound in the present expanded compound of two of his earlier books. He is one of the few writers capable of employing academic slang in a convincing way.

The first two chapters of the book under review might well have appeared as a separate essay on the object and nature of mathematics. Professor Bell takes the standpoint that the 'ethos' of mathematics is neither art for art's sake nor mere practical application, but both. A lot of mathematics was created by a spirit of curiosity without thought of practical applications, and equally a great deal of pure mathematics—the theory of Fourier series for example—arose out of working on a practical problem. To illustrate the futility of attempting to define what mathematics is, several such attempts are quoted. To describe the content of mathematics itself in its varied ramifications seems to be the only practical way of defining mathematics, and Professor Bell's book sets about this task in a workmanlike fashion, covering an astonishing number of fields of both pure and applied mathematics.

Chapters 3–6 deal with ordinary algebra, the continuum of numbers, mathematical logic, modern algebras, matrices and linear transformations. Not many applications are found in these chapters, although the application of Boolean algebra to electrical circuits could well have been cited.

There follows an account of the more modern approaches to geometry, of which the following definition due to Klein is quoted: " Given a manifold and a group of transformations of the same, to develop the theory of the invariants relating to that Group ". Of this, Professor Bell remarks: " It is a pity to spoil the beautiful simplicity of this by explanations . . . ". Apparently this is a serious comment, but it is difficult not to suspect a bit of leg-pulling.

The book continues to bound along, taking in its easy stride group theory—including Galois' theorem and the impossibility of algebraic solutions of the general equation of any degree greater than the fourth, Riemannian geometry, the theory of numbers, electromagnetism, the theory of planetary motion, continuity, the calculuses, waves and Fourier analysis, and the theory of probability. In this last some very sobering observations on the 'theory' of intelligence testing occur. The book ends with a discussion of convergence, and finally the nature of a mathematical proof—with an all too brief a comment on Gödel's work.

For those with more mathematics than the author assumes in his readers this is an exciting book. Few will want to miss the pleasure of reading it.

H. H. HOPKINS.

Molecular Structure and Related Problems, edited by Y. Asami and K. Higasi. Pp. 139 (Sapparo, Japan: The Research Institute of Applied Electricity, Hokkaido University. Monograph Series No. 4, 1954.)

It is a remarkable sign of the vitality of Japanese science that a university such as Hokkaido in northern Japan should be able to issue this collection of nine papers, more than half of which are the work of its own scientists. These articles are similar to the type of article found in *Discussions of the Faraday Society*. Some of them are of the nature of reviews, e.g. the structure of tropolone, the original derivative of which, hinokitiol, was discovered in Japan in 1936 and of which no less than 700 other derivatives have now been prepared in Japan. Others, such as the discussion of anomalous dispersion of ultrasonic waves in the gas–liquid critical region, represent original contributions. It will come as a surprise to most Europeans to discover how much and how varied is the work on molecular structure in just one of the many Japanese universities. A list of the topics covered includes (in addition to those previously mentioned) π-electron calculations in Japan (a review article), the structure of the activated complex in organic reactions, dipole moment calculation, H-bonding, electrical conductivity in solid alcohols, paramagnetic resonance in copper fluorosilicates, and intermolecular potentials derived from thermal diffusion.

Not all the articles are equally valuable. Some of them would appear to have been better placed in a normal scientific journal. But this is a useful little book, in impeccable English, which we welcome as showing the healthy condition of theoretical and experimental science in Japan. C. A. COULSON.

The Theory of Metals, by A. H. Wilson. Pp. viii + 346. 2nd Edn. (Cambridge: University Press, 1953.) 45*s*.

The first edition of this book was published in 1936, and it soon gained recognition as one of the standard works on the electron theory of metals. It was, however, difficult to read, since the treatments of many of the topics considered were presented in a very abbreviated form. The book has now been re-written and enlarged; there are many more diagrams, a fuller discussion of experimental results and numerous references to original papers, and the whole is published in a much more attractive format.

One of the most valuable features of the earlier edition was the detailed and critical account of the theory of electrical conduction and other transport effects which it contained. There is again a strong emphasis on these topics in the new edition, approximately one third of the book being devoted to them. A chapter on the historical development of the theory of conduction serves to introduce, *inter alia*, the concepts of the 'transport equation' and the 'time of relaxation'. Later, these themes are developed in a masterly account of the modern theory of transport effects, contained in three chapters on the formal theory of conduction, the mechanism of conductivity and the application of the variation principle to the solution of the transport equation. The topics treated include electrical and thermal conduction, thermoelectric, galvanomagnetic and thermomagnetic effects in metals; and conduction in semi-conductors and thin films. The theory is intrinsically complex and the mathematics correspondingly formidable, but no attempt is made to evade or gloss over the difficulties. A number of important points which are often not considered explicitly are discussed here, for example, the precise significance of a time of relaxation.

The other parts of the book cover a wider range of subjects, and, consequently, not all of these are treated at such great length, although again, in many places details of the theory which are sometimes merely hinted at are here given explicitly. There are chapters dealing with the motion of an electron in a perfect lattice, the crystal structures and electronic structures of metals and alloys, and the properties of semi-conductors. Chapters on thermal and magnetic properties include accounts of the theories of lattice and electronic specific heats, electron spin paramagnetism, diamagnetism and the collective electron theory of ferromagnetism.

All these chapters precede the three on transport effects, but it has seemed proper to mention the latter first, since it is they which are concerned with the dominant theme of the book. Indeed, in one sense, they may be said to cast a shadow before them on to the preceding chapters. The complexity of the theory of transport effects is such that, in order to make any progress, it is necessary to adopt the 'one-electron approximation', but this is not necessarily so in all the other branches of the theory of metals; and yet throughout the book the approximation is used with little more than passing references to the quantum mechanical treatment of many-electron systems. Although the problems raised by that subject are some of the most intractable in the theory of metals, it may, perhaps, be regretted that they are not discussed at some greater length.

As has already been implied, this second edition is in effect a new book by an author who has himself made important original contributions to the theory of metals, and as such it will need no additional recommendation to anyone who has any familiarity with the field; to others, it may be strongly recommended as a means of obtaining a thorough understanding of many aspects of a difficult and important branch of physics.

P. RHODES.

CONTENTS OF SECTION B

PAGE

Dr. R. Cade. An Electrostatic Problem Involving a Non-Linear Fluid Dielectric . . . 1

Mr. G. G. E. Low. Modulation of the Surface Conductance of Germanium and Silicon by External Electric Fields 10

Dr. P. C. Banbury and Mr. J. Houghton. Measurement of Injection Ratio of Point Contacts on Germanium 17

Dr. E. H. Putley. The Hall Coefficient, Electrical Conductivity and Magneto-Resistance Effect of Lead Sulphide, Selenide and Telluride 22

Dr. E. H. Putley. Thermoelectric and Galvanomagnetic effects in Lead Selenide and Telluride 35

Mr. J. B. Arthur, Dr. W. Bardsley, Mr. M. A. C. S. Brown and Dr. A. F. Gibson. Carrier Extraction in Germanium 43

Research Notes:

Dr. G. B. Greenough and Mrs. E. M. Smith. Deformation Faults in Cold-Worked Metals 51

Letters to the Editor:

Dr. M. J. Dumbleton. The Infra-Red Luminescence of Solid Halogens . 53

Dr. G. N. Lance and Mr. E. C. Deland. On the Differential Analyser Solution of the Water Bells Problem 54

Reviews of Books 56

Contents of Section A 64

The [110] Magnetostriction of some Single Crystals of Iron and Silicon-Iron

By E. W. LEE
Department of Physics, University of Nottingham

Communicated by L. F. Bates; MS. received 10th August 1954

Abstract. Using the results of a previous paper by the author on the shape of magnetization curves, the magnetostriction of single crystals of iron parallel to the [110] direction have been calculated as functions of intensity of magnetization and field strength, using the Néel model of domain structure. It is found that the magnetostriction is dependent on crystal width in a manner analogous to that found for the magnetization curves. Measurements on three crystals of Si–Fe show good agreement with their calculated behaviour. It is shown that in general the domain vectors in the demagnetized state are not uniformly distributed along all the easy axes and the distribution varies from one crystal to another. The actual distribution is evaluated in the two cases where it is found possible.

---

§1. INTRODUCTION

In a previous paper (Lee 1953, hereafter referred to as I), magnetization curves were calculated for single crystals of iron along the [110] direction taking into account the detailed domain structure of the crystal. The model used for the calculation was that proposed by Néel (1944) and subsequently verified in essentials by the powder pattern technique (Williams, Bozorth and Shockley 1949, Bates and Mee 1952 a, b). It was shown that in low fields the steepness of the (I, H) curve, i.e., the susceptibility, decreases with decreasing crystal width. In the present paper the magnetostrictive behaviour of such crystals is investigated both theoretically and experimentally.

§2. THEORETICAL TREATMENT

As in I, it is necessary to know the domain structure as a function of field strength, and therefore the present calculations are confined to the particular case in which this is fairly well known. This is a single crystal of iron of (strictly speaking) infinite length and of rectangular cross section cut with its long axis parallel to the [110] direction in a (100) plane. In a small applied field the primary domains are leaf-like sections with their planes perpendicular to the $[0\bar{1}1]$ axis and with their magnetization vectors alternately along [001] and $[0\bar{1}0]$ directions (see I, figure 1). In addition, there are two types of closure domains on the (011) planes whose purpose is to reduce the large magnetostatic energy that would otherwise exist due to the component of magnetization normal to the (011) plane. These are the q domains whose magnetization vectors are directed along the [100] and $[\bar{1}00]$ directions, perpendicular to the plane of the crystal, and the p domains with magnetization vectors along the long axis of the crystal parallel to the applied field.

The magnetostriction of any domain in the crystal is given by the general equation

$$dl/l = \tfrac{3}{2}\lambda_{100}\,(\alpha_1^2\beta_1^2+\alpha_2^2\beta_2^2+\alpha_3^2\beta_3^2-\tfrac{1}{3})+3\lambda_{111}\,(\alpha_1\alpha_2\beta_1\beta_2+\alpha_2\alpha_3\beta_2\beta_3+\alpha_3\alpha_1\beta_3\beta_1) \qquad \ldots\ldots(1)$$

where α_1, α_2, α_3 and β_1, β_2, β_3 are the direction cosines of the magnetization vector and the direction of observation respectively, with respect to the cubic crystal axes. The direction of observation here coincides with the long axis of the crystal and the direction of the applied field, and therefore $\beta_1=\beta_2=1/\sqrt{2}$, $\beta_3=0$. In the crystal under consideration there are three different sets of domains to which equation (1) must be applied separately, neglecting certain complications discussed by Bates and Mee.

For the primary domains $\alpha_1=\alpha_2=\cos\theta$, θ being the angle between I_s and the applied field, $\alpha_3=0$, whence from (1) $dl/l=\frac{1}{4}\lambda_{100}+\frac{3}{4}\lambda_{111}\cos 2\theta$. For the p domains $\alpha_1=\alpha_2=1/\sqrt{2}$, $\alpha_3=0$, and $dl/l=\frac{1}{4}\lambda_{100}+\frac{3}{4}\lambda_{111}$. For the q domains $\alpha_1=\alpha_2=0$, $\alpha_3=1$, and $dl/l=-\frac{1}{2}\lambda_{100}$.

In order to calculate the magnetostriction of the whole crystal the assumption is made that the magnetostrictive strains of the individual domains may be added algebraically after being multiplied by a suitable weighting factor. The assumption is rather different from that used in calculating the magnetostrictive energies of closure domains where it is usually assumed that these are held in place by the primary domains. The correct situation, no doubt lies somewhere between these two extremes, but it seems likely that the latter assumption will be nearer the truth when the closure domains are very much smaller than the primary domains, a state of affairs which exists in wide crystals. For narrow crystals the former assumption seems preferable and since the effects of closure domains are really only apparent with narrow crystals the former assumption is made here. The total magnetostriction of the crystal is thus

$$\frac{dl}{l}=(\tfrac{1}{4}\lambda_{100}+\tfrac{3}{4}\lambda_{111}\cos 2\theta)\frac{V_0}{V}+(\tfrac{1}{4}\lambda_{100}+\tfrac{3}{4}\lambda_{111})\frac{V_{\mathrm{p}}}{V}-\tfrac{1}{2}\lambda_{100}\frac{V_{\mathrm{q}}}{V} \qquad \ldots\ldots(2)$$

where V_0, V_{p} and V_{q} are the volumes of the primary and p and q domains and $V_0+V_{\mathrm{p}}+V_{\mathrm{q}}=V$: V_{p} and V_{q} are given by

$$V_{\mathrm{p}}=\frac{d^2}{4}\left(\frac{W_{\mathrm{q}}}{W_{\mathrm{p}}+W_{\mathrm{q}}}\right)^2\frac{\sin\theta}{1-\cos\theta}, \quad V_{\mathrm{q}}=\frac{d^2}{4}\left(\frac{W_{\mathrm{p}}}{W_{\mathrm{p}}+W_{\mathrm{q}}}\right)^2\tan\theta$$

where d is the distance between successive q domains and W_{p} and W_{q} are the energies of formation per cm^3 of the p and q domains as in I. These expressions differ from those given in I in which the exponent of the term in brackets was incorrectly omitted. The (V_{p}, H) and (V_{q}, H) curves given in I thus require correction, but the magnetization curves obtained remain sensibly unchanged since the only significant contribution of the closure domains to the mean magnetization comes from the q domains in very low fields and in the fields considered in I the quantity $W_{\mathrm{p}}/(W_{\mathrm{p}}+W_{\mathrm{q}})$ is not sensibly different from unity. V is equal to $\frac{1}{2}Ld$ where L is the width of the crystal and $d^2W_{\mathrm{p}}W_{\mathrm{q}}=\gamma L(W_{\mathrm{p}}+W_{\mathrm{q}})$, γ being the wall energy per cm^2 between adjacent primary domains.

Magnetostriction curves for iron crystals of various widths have been calculated from (2) taking $\lambda_{100}=20{\cdot}5\times10^{-6}$, $\lambda_{111}=-21\times10^{-6}$ (Carr and Smoluchowski 1952), and these are reproduced in figures 1 and 2. It is evident that the form of the curves depends on the crystal width in a manner analogous to the (I, H) curves. $dl/l=0$ corresponds to a hypothetical demagnetized state in which the domain magnetization vectors are distributed uniformly among the six easy directions. With the model used here this presumably means that the q domains occupy one third of the total volume and the primary domains two thirds. The latter is, however, separated into two equal volumes magnetized in opposite directions, separated by one or more 180° walls. There is some evidence for a break up of the primary domains in this manner from the powder pattern experiments of Williams, Bozorth and Shockley (1949).

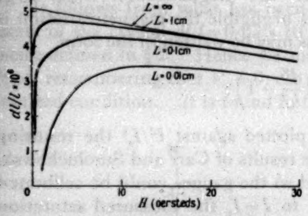

Figure 1. Calculated magnetostriction curves for single crystals of iron, of various widths in the [110] direction.

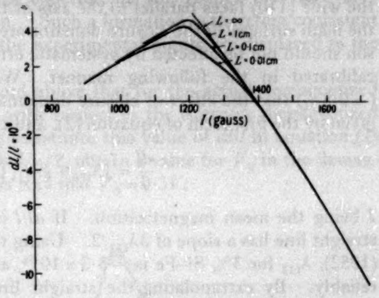

Figure 2. As in figure 1, as a function of the intensity of magnetization.

§ 3. EXPERIMENTAL MEASUREMENTS AND RESULTS

No magnetostriction data for crystals of the prescribed form appear to exist in the literature, all previous measurements having been made on rods or oblate spheroids for which the domain model used here is not applicable. Experiments were therefore made on three crystals of silicon–iron of the required shape. The relevant data for these crystals are given in the table.

	Composition	Dimensions (cm)			D
		length	breadth	thickness	
A	3·0% Si–Fe		0·135	0·615	—
B	2·8% Si–Fe	4·5	0·404	0·019	0·017
C	2·8% Si–Fe	2·8	1·28	0·254	0·067

Crystal A had been previously investigated by Bates and Mee (1952 a, b), and B and C by Bates and Neale (1949, 1950), using the powder pattern technique. The demagnetization factor D given in the table is approximate only and was obtained by assuming that the initial susceptibility of such a crystal with zero demagnetizing factor is infinite, i.e., that the observed initial susceptibility of the actual crystal is limited solely by the demagnetizing factor. The magnetostriction was measured using Tinsley Type 6 J strain gauges and a sensitive galvanometer, while the magnetization was measured ballistically in the usual way. As each of the crystals was required to serve a different purpose, each will be discussed separately.

Crystal A was the best of the available crystals, its sides having been cut to an accuracy of better than 0·5°, and this was used for a quantitative comparison of the observed and calculated behaviours. On account of its very large demagnetizing factor the magnetic field applied by the solenoid used was not great enough to ensure saturation, so that to overcome this and also to avoid magnetostriction due to the form effect, the crystal was lightly clamped in a yoke made of two soft iron rods tapered and flattened to be continuous with the crystal under investigation. The effective demagnetizing factor of this arrangement was 0·012, and the magnetostriction caused by the form effect was reduced to a negligible quantity. Owing to the very small width of the crystal the gauges were placed on the wide (110) faces parallel to the axis of the crystal, i.e., on the faces on which the main surfaces of the closure domains are formed. In order that the comparison should not be affected by systematic errors of measurement, the gauges were calibrated in the following manner. When the magnetization is so large ($>0{\cdot}8\,I_s$) that the effect of closure domains is negligible the magnetostriction is given by the first term of equation (2), and this may be written in the form

$$\frac{dl}{l}=\tfrac{1}{4}\lambda_{100}+\tfrac{3}{4}\lambda_{111}\left(2\frac{I^2}{I_s^2}-1\right)$$

I being the mean magnetization. If dl/l is plotted against I^2/I_s^2 the resulting straight line has a slope of $3\lambda_{111}/2$. Using the results of Carr and Smoluchowski (1952), λ_{111} for 3% Si–Fe is $-5{\cdot}3\times10^{-6}$, and so the gauges could be calibrated reliably. By extrapolating the straight line to $I=I_s$ the measured saturation magnetostriction was found to be $1{\cdot}73\times10^{-6}$. This is obtained with the actual demagnetized state as a reference state. From equation (2) the calculated saturation magnetostriction is $\tfrac{1}{4}(\lambda_{100}+3\lambda_{111})$. Using $\lambda_{100}=25{\cdot}6\times10^{-6}$ from Carr and Smoluchowski the last expression gives $2{\cdot}40\times10^{-6}$. But this value, however, is based on the hypothetical demagnetized state defined in § 2. The large difference between these two values can only mean that the distribution of domain vectors in the actual demagnetized state is not isotropic, there being a slight preponderance of domain vectors in the (100) plane. In comparing the experimental curves with the calculated ones the former were therefore normalized by adding $0{\cdot}63\times10^{-6}$ to each of the experimental points obtained. The comparison is shown in figures 3 and 4. The agreement between the calculated

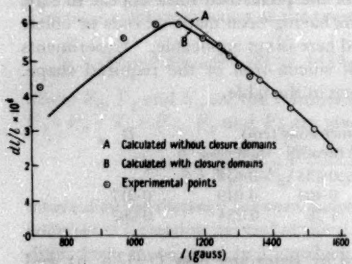

Figure 3. Calculated and observed magnetostriction of single crystal A along the [110] direction.

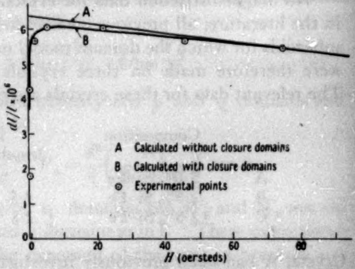

Figure 4. As in figure 3, as a function of the field strength (corrected for demagnetization).

curves and the experimental points is very good, in particular the calculated maximum magnetostriction of $6{\cdot}1\times10^{-6}$ (to be compared with $6{\cdot}4\times10^{-6}$ for an infinite crystal) coincides exactly with the experimental value and the values of the intensity of magnetization and field strength at which this occurs also agrees with the calculated values within the limits of experimental error. Below about 1100 gauss the agreement is not so good and this may be attributed to the fact that the domain structure is probably more complicated than the simple model used. In particular the formation of 180 walls within the primary domains as has been observed in powder pattern experiments will reduce the value of I without affecting the magnetostriction. Such a formation is therefore consistent with the fact that below 1000 gauss the experimental points are displaced to the left of the theoretical curve.

It follows from what has been said above that for the actual demagnetized state of the crystal $dl/l=0{\cdot}63\times10^{-6}$ with respect to the isotropic demagnetized state defined in § 2. Hence we may substitute this value of dl/l in equation (2) and, remembering that $V_p=0$, $\cos\theta=1/\sqrt{2}$, obtain a value for V_q in the demagnetized condition. It is found in this way that $V_q=0{\cdot}3V$.

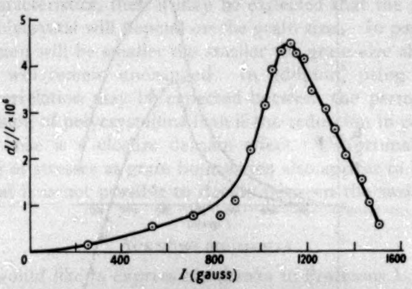

Figure 5. Magnetostriction of crystal B.

The q domains are magnetized perpendicular to the main plane of the crystal. One would expect a considerable magnetostatic energy to be associated with these and that for very thin strips they may be suppressed in order to reduce this energy. The magnetostriction of the very thin crystal B was measured to see to what extent this actually occurs. Owing to the very small thickness of this crystal these measurements, particularly of the magnetization, are not as reliable as the previous ones. The results obtained are shown in figure 5. In the previous discussion of magnetostriction in the [110] direction of iron (e.g. by Akulov 1931) it is shown that initial expansion is caused by 90° boundary movements between domains perpendicular to the field and those making an angle of 45° with it. It is natural to associate this expansion therefore with a reduction in the volume of q domains accompanied by an increase in the volume of the primary and p domains. Thus the magnitude of the initial expansion is a direct measure of the volume of q domains present in the demagnetized condition. The measured saturation magnetostriction is $-0{\cdot}4\times10^{-6}$. The calculated value using $\lambda_{100}=26{\cdot}0\times10^{-6}$ $\lambda_{111}=-6{\cdot}4\times10^{-6}$ for 2·8% Si–Fe (Carr and Smoluchowski) is $1{\cdot}70\times10^{-6}$. Interpreting this difference in the same way as for crystal A it is found that

$V_q = 0{\cdot}22V$ in the demagnetized state. It thus appears that even for this very thin crystal a considerable volume is magnetized perpendicular to its plane and that the suppression of easy axes due to shape anisotropy is much less than has hitherto been supposed.

Crystal C was 1·2 cm wide and it seems unlikely that the assumptions made in § 2 to calculate the magnetostriction curves are applicable here. In fact for a crystal of this size it seems unlikely that the strain is uniform but may vary in magnitude throughout the crystal. An attempt was made to investigate this by fixing two strain gauges on the same side of the crystal, one at the centre parallel to the axis of the crystal and the other off the axis but parallel to it along one of the crystal edges. The results obtained are shown in figure 6 where the magnetostriction observed at two different places is plotted against the mean magnetization. The two curves obtained may not be strictly comparable since the gauge placed at the edge of the crystal is not operating under quite the same conditions as that at the centre, but differences between the two are too great to be completely accounted for in this way.

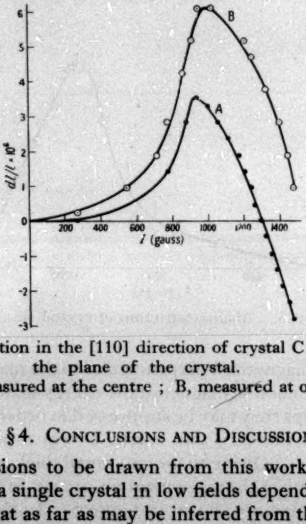

Figure 6. Magnetostriction in the [110] direction of crystal C measured at two places in the plane of the crystal.
A, measured at the centre ; B, measured at one edge.

§ 4. CONCLUSIONS AND DISCUSSION

The main conclusions to be drawn from this work are that the magnetostrictive behaviour of a single crystal in low fields depends to a large extent on its shape and size, and that as far as may be inferred from the three crystals studied here the domain magnetization vectors are not equally divided amongst the easy directions in the demagnetized state and, moreover, that the actual distribution varies from one crystal to another. The distribution does not seem to be as much affected by a large reduction in one dimension of the crystal as might be expected. It follows that no reliance can be placed on the values of the magnetostriction constants λ_{100} and λ_{111} obtained by measurements using the demagnetized state as a reference state. Kaya and Takaki (1936) sought to overcome this difficulty by using the remanent state as a reference state. In order to assess the reliability of this procedure it is necessary to know to what extent the magnetization is reversible. It is known that as the magnetization of a crystal of the form used here is increased to approach saturation the domain width *d* decreases and so new domain walls have to be formed. The formation of domain walls is however an irreversible process and it is not certain that, when the applied field is decreased to zero, the same domain processes will occur in the reverse order. Bates and Martin (1953) have observed the changes in domain structure when a magnetically saturated crystal is demagnetized and have observed the growth of closure domains at imperfections as the field acting is reduced to zero. The domains were always magnetized perpendicular to the original direction of saturation until a reverse field was applied. It seems likely that closure domains of the q type will appear on the (110) surfaces as well, although these may not be of the same size as before since this is determined by *d*. In any case it seems reasonable to suppose that the domain structure at remanence will depend on the number of imperfections in the surface and possibly on the width of the crystal. Thus the remanent state is not likely to be a unique one, and measurements using it as a reference state cannot really be preferred to those using the demagnetized state.

If the crystallites existing in a polycrystalline ferromagnetic retain any of their single crystal characteristics, then it may be expected that the magnetostrictive behaviour of a polycrystal will depend on the grain size. In particular for iron, the initial expansion will be smaller the smaller the grain size although the final saturation value will remain unchanged. In addition, using the conclusions reached in I a correlation may be expected between the permeability and the maximum expansion of polycrystalline iron if the reduction in permeability with decreasing grain size is a closure domain effect. Unfortunately the existing theories in terms of stresses at grain boundaries also appear to lead to the same conclusion so that it is not possible to decide between the two explanations by these means.

ACKNOWLEDGMENTS

The author would like to express his thanks to Professor L. F. Bates for his interest in this work. He is also indebted to Dr. S. Chikazumi for pointing out an error in I, which is corrected here in § 2. Both the author and this paper have benefited considerably from discussions with Dr. D. H. Martin.

REFERENCES

AKULOV, N., 1931, *Z. Phys.*, **69**, 253.
BATES, L. F., and MARTIN, D. H., 1953, *Proc. Phys. Soc.* A, **66**, 162.
BATES, L. F., and MEE, C. D., 1952 a, *Proc. Phys. Soc.* A, **65** 129; 1952 b, *Ibid.*, **65**, 140.
BATES, L. F., and NEALE, F. E., 1949, *Physica*, **15**, 220; 1950, *Proc. Phys. Soc.* A, **63**, 374.
CARR, W. J., and SMOLUCHOWSKI, R., 1952, *Phys. Rev.*, **83**, 1236.
KAYA, S., and TAKAKI, H., 1936, *Anniversary Vol. of Sci. Rep. Tohoku University, dedicated to Prof. K. Honda*, 314.
LEE, E. W., 1953, *Proc. Phys. Soc.* A, **66**, 623.
NÉEL, L., 1944, *J. Phys. Radium*, **5**, 241.
WILLIAMS, H. J., BOZORTH, R. M., and SHOCKLEY, W., 1949, *Phys. Rev.*, **75**, 155.

The Effect of 3pπ Electrons : Energy Levels of Ethylene

By J. JACOBS
Mathematical Institute, The University, Liverpool

MS. received 20th October 1954

Abstract. The usual LCAO MO method for obtaining wave functions of organic molecules with double bonds uses only 2pπ atomic orbitals. As a refinement we include 3pπ atomic functions in the basic molecular orbitals. Detailed calculations are made for ethylene, taking into account the interaction of configurations of like symmetry. The first excitation energy is calculated to be 8·7 ev, a much improved value compared with that obtained with only 2pπ orbitals. The implication for MO theory is that in any refined treatment the higher energy atomic orbitals can no longer be ignored. A list of newly computed atomic integrals is given.

§ 1. INTRODUCTION

In recent years several improvements have been proposed in both the principal methods available for the theoretical investigation of molecular properties, the MO and the VB methods. Both treatments were adequate for ground state phenomena but not for the interpretation of ultra-violet spectra. The aim has therefore been towards approximations which provide more reliable evaluations of excited levels, while retaining some of the simplicity of the initial theories. In both cases any logical extension or relaxation of approximations has, however, led to considerably more labour in computing; hence detailed applications have often been made only to simple molecules. It is for this reason that we also restrict our calculations to the simplest of organic molecules containing a double bond, ethylene.

One of the usual approximations made in applying the MO method to molecules with double bonds is to represent the wave functions of eigenstates by contributions from atomic orbitals of 2pπ type only. Now even within the framework of the MO theory there are several objections to this limitation.

Firstly, the 2pπ orbitals do not form a complete basis, so that for a better representation of the molecular wave function other atomic orbitals, such as 3pπ, 3dπ . . . with the same symmetry relative to the molecule, should be introduced.

Secondly, the overlap in ethylene between adjacent 2pπ and 3pπ atomic orbitals is 0·17, which is by no means negligible compared with 0·28 for the 2pπ–2pπ case.

Thirdly, the difference in energy in a free carbon atom between a 2p and a 3p orbital is of the same order of magnitude (8 ev) as are some molecular energy differences. Hence configurations which include 3pπ orbitals may well fall within some 8 ev of the corresponding ones constructed out of 2pπ orbitals only. And it has been shown that configurations separated by more than 10 ev interact significantly.

For these reasons it is considered necessary to include 3pπ configurations, our aim indeed being two-fold: to investigate whether the neglect of 3pπ atomic orbitals in the usual MO method is justified, and, by reference to ethylene, to examine the energy changes brought about by inclusion of 3pπ orbitals.

The two-electron problem (two electrons of 2pπ-type) of ethylene was first studied by Penney (1934) and Mulliken (1942). Recently a number of authors have diverged from the simple MO method in an effort to determine more accurately the excitation energy values of ethylene. Hitherto, however, these have differed widely from the experimental values, if Mulliken's interpretation of the 1630 Å absorption band as the first allowed transition is correct. The following corrections of the MO theory have been applied to the case of planar ethylene: Configuration interaction (Parr and Crawford 1948), variation of effective nuclear charge (Murai 1952, Craig 1950) and internuclear distance between ground and excited states (Craig 1950), semilocalized orbitals (Müller 1954); the use of different values for some atomic integrals (Moser 1953) and the semi-empirical approach (Pariser and Parr 1953) should also be mentioned. Some allowance for σ-electrons has been made (Altmann 1952) and in the most recent ethylene paper the 1s-electrons of the H and C atoms have been taken into some account; also SCF wave functions were used (Sponer and Löwdin 1954). The effect of 3p electronic orbitals has so far been ignored, although Dooling (1953) investigated their influence on bond energy. His conclusion that the contributions of 3pπ orbitals to the wave function is insignificant is perhaps too general, as he dealt with one-electron wave functions only.

Merely in order to ease computation we have abandoned again some of the refinements introduced by these authors, retaining only the interaction of configurations in our treatment. We follow the approach developed by Goeppert-Mayer and Sklar (1938) in which the π-electrons move in a field provided by all other electrons. In so far as ethylene is concerned our results are therefore most comparable with those of Parr and Crawford. But we believe that a more valuable result of this work is the general implication that the inclusion of atomic wave functions of higher order is essential in any refined MO treatment.

§2. METHOD AND APPLICATION TO ETHYLENE

The model chosen for ethylene is the planar molecule with the C–C link 1·353 Å long (Gallaway and Barker 1942). The presence of the H atoms is ignored.

There are two mobile electrons, and we make available to them the 2pπ and 3pπ atomic orbitals. Then, according to the MO theory, there exist four molecular orbitals, of which the first and third are bonding, as follows:

$$\phi_1 = N_1(\psi_a+\psi_b), \qquad \phi_3 = N_3(\chi_a+\chi_b),$$
$$\phi_2 = N_2(\psi_a-\psi_b), \qquad \phi_4 = N_4(\chi_a-\chi_b).$$

Here ψ_a, ψ_b are 2pπ atomic orbitals centred on a, b respectively, and χ_a, χ_b are 3pπ atomic orbitals centred on a, b respectively, and N_1, N_2, N_3, N_4 are normalizing factors involving the overlap integrals

$$S(2\text{pa}, 2\text{pb}) = \int \psi_a(\nu)\psi_b(\nu)\, d\tau_\nu = S_1, \qquad S(3\text{pa}, 3\text{pb}) = \int \chi_a(\nu)\chi_b(\nu)\, d\tau_\nu = S_2.$$

The non-orthogonality of these basic ϕ's is expressed in terms of two further integrals

$$S(2\text{pa}, 3\text{pa}) = \int \psi_a(\nu)\chi_a(\nu)\, d\tau_\nu = S_3, \qquad S(2\text{pa}, 3\text{pb}) = \int \psi_a(\nu)\chi_b(\nu)\, d\tau_\nu = S_4.$$

On the basis of the simplest MO picture these molecular orbitals are assumed to correspond to the ascending order of energy ϕ_1, ϕ_2, ϕ_3, ϕ_4. In what follows we restrict ourselves to some of the configurations which can be constructed from these wave functions, namely those which seem energetically the lowest.

We use ${}^rE_n^{pq}$ to denote an energy level of multiplicity r, for which n electrons have been raised and the molecular orbitals concerned with the excitation are p→q ; then ${}^r\Psi_n^{pq}$ denotes the corresponding configurational wave function. The five normalized configurational wave functions considered are:

$$ {}^1\Psi_0=\frac{1}{\sqrt{2!}}\begin{vmatrix}\phi_1(1)\alpha(1) & \phi_1(1)\beta(1)\\ \phi_1(2)\alpha(2) & \phi_1(2)\beta(2)\end{vmatrix}, $$

${}^1\Psi_2^{12}$ similarly, replacing ϕ_1 by ϕ_2,

$$ {}_{(3)}{}^1\Psi_1^{12}=\frac{1}{\sqrt{2!}}\,\frac{1}{\sqrt{2}}\left\{\begin{vmatrix}\phi_1(1)\alpha(1) & \phi_2(1)\beta(1)\\ \phi_1(2)\alpha(2) & \phi_2(2)\beta(2)\end{vmatrix}\begin{matrix}-\\(+)\end{matrix}\begin{vmatrix}\phi_1(1)\beta(1) & \phi_2(1)\alpha(1)\\ \phi_1(2)\beta(2) & \phi_2(2)\alpha(2)\end{vmatrix}\right\}, $$

${}_{(3)}{}^1\Psi_1^{13}$, ${}_{(3)}{}^1\Psi_1^{14}$ similarly, replacing ϕ_2 by ϕ_3, ϕ_4 respectively. If $\mathscr{H}$ is the Hamiltonian of the two-electron system, including an electron repulsion term (for details see Jacobs 1949) then the configuration energies become

$$ {}^1E_0=\int {}^1\Psi_0\mathscr{H}\,{}^1\Psi_0 d\tau=2\epsilon_{11}+\gamma_{11},\qquad {}^1E_2^{12}=2\epsilon_{22}+\gamma_{22}, $$

$$ {}_{(3)}{}^1E_1^{12}=\epsilon_{11}+\epsilon_{22}+\gamma_{12}\overset{+}{(-)}\delta_{12}, $$

$$ {}_{(3)}{}^1E_1^{13}=\epsilon_{11}+\epsilon_{33}+\gamma_{13}\overset{+}{(-)}\delta_{13}\overset{+}{(-)}2N_1N_3(S_3+S_4)(\epsilon_{13}+\epsilon_{31}), $$

$$ {}_{(3)}{}^1E_1^{14}=\epsilon_{11}+\epsilon_{44}+\gamma_{14}\overset{+}{(-)}\delta_{14}. $$

Here
$$ \zeta rp\,.\,st=\int \phi_r(\nu)\,\phi_p(\nu)\,\frac{1}{r_{\nu\mu}}\,\phi_s(\mu)\phi_t(\mu)\,d\tau_\nu\,d\tau_\mu $$

and $\zeta(r=p,s=t)=\gamma_{rt}$, $\zeta(r=s,p=t)=\delta_{rt}$, $\epsilon_{rs}=\int \phi_r(\nu)[H(\nu)+T(\nu)]\phi_s(\nu)\,d\tau_\nu$.

Let W_{2p}, W_{3p} be the energies of a 2pπ and a 3pπ electron in a neutral C atom. In the usual way the molecular integrals ϵ, ζ are reduced to integrals over atomic wave functions by expanding the ϕ in terms of ψ, χ.

$$ \begin{aligned}
\epsilon_{11}&=W_{2p}-2N_1^2(R+C+Q+B)\\
\epsilon_{22}&=W_{2p}+2N_2^2(R+C-Q-B)\\
\epsilon_{33}&=W_{3p}-2N_3^2(R_1+C_1+Q_1+B_1)\\
\epsilon_{44}&=W_{3p}+2N_4^2(R_1+C_1-Q_1-B_1)
\end{aligned} $$

$$ \begin{aligned}
\epsilon_{13}&=2N_1N_3(S_3+S_4)W_{3p}-(R_3+C_5+Q_2+B_3)\\
\epsilon_{31}&=2N_1N_3(S_3+S_4)W_{2p}-(R_2+C_2+Q_2+B_3)\\
\epsilon_{24}&=2N_2N_4(S_3-S_4)W_{3p}+(R_3+C_5-Q_2-B_3)\\
\epsilon_{42}&=2N_2N_4(S_3-S_4)W_{2p}+(R_2+C_2-Q_2-B_3)
\end{aligned} $$

$$ \begin{aligned}
\gamma_{11}&=2N_1^4(A+B+4C+2D)\\
\gamma_{22}&=2N_2^4(A+B-4C+2D)
\end{aligned} $$

$$ \begin{aligned}
\gamma_{12}&=2N_1^2N_2^2(A+B\quad-2D)\\
\gamma_{13}&=2N_1^2N_3^2(A_1+B_1+2C_1+2C_4+2D_1)\\
\gamma_{14}&=2\mathrm{N}_1^2N_4^2(A_1+B_1-2C_1+2C_4-2D_1)
\end{aligned} $$

$$ \begin{aligned}
\delta_{12}&=2N_1^2N_2^2(A-B)\\
\delta_{13}&=2N_1^2N_3^2(A_2+B_2+2C_3+2C_6+D_2+D_3)\\
\delta_{14}&=2N_1^2N_4^2(A_2-B_2+2C_3-2C_6+D_2-D_3)
\end{aligned} $$

$$ \begin{aligned}
\zeta_{11.13}&=2N_1^3N_3(A_3+B_3+C_5+C_2+2C_7+2D_4)\\
\zeta_{11.24}&=2N_1^2N_2N_4(A_3+B_3-C_5-C_2+2C_7-2D_4)\\
\zeta_{12.14}&=2N_1^2N_2N_4(A_3-B_3-C_5+C_2)\\
\zeta_{12.23}&=2N_1N_2^2N_3(A_3-B_3+C_5-C_2)
\end{aligned} $$

In defining below the integrands of integrals over atomic orbitals the following abbreviations are used: d denotes an atomic wave function ψ or χ; each integrand is then of the form

$$d_1(\nu)\,d_2(\nu)\,\frac{1}{r_{\nu\mu}}\,d_3(\mu)\,d_4(\mu)$$

and the d's are centred on nucleus a or b. This is shown by the sequence of a's and b's, thus ab.ba means d_1 on a, d_2 on b, d_3 on b, d_4 on a, and these sequences are constant within each type of integrand.

aa . aa	A: $\psi\psi.\psi\psi$	A_1: $\psi\psi.\chi\chi$	A_2: $\psi\chi.\psi\chi$	A_3: $\psi\psi.\psi\chi$
aa . bb	B: $\psi\psi.\psi\psi$	B_1: $\psi\psi.\chi\chi$	B_2: $\psi\chi.\psi\chi$	B_3: $\psi\psi.\psi\chi$
aa . ab	C: $\psi\psi.\psi\psi$	C_1: $\psi\psi.\chi\chi$	C_2: $\psi\psi.\chi\psi$	C_3: $\psi\chi.\chi\psi$
	C_4: $\chi\chi.\psi\psi$	C_5: $\psi\psi.\psi\chi$	C_6: $\psi\chi.\psi\chi$	C_7: $\psi\chi.\psi\psi$
ab . ab	D: $\psi\psi.\psi\psi$	D_1: $\psi\psi.\chi\chi$	D_2: $\psi\chi.\psi\chi$	D_3: $\psi\chi.\chi\psi$
	D_4: $\psi\psi.\psi\chi$			

With a similar notation the exchange-penetration integrals are

$-{}_{a}H_{a}^{C}{}_{b}$	R: $\psi.\psi$	R_1: $\chi.\chi$	R_2: $\chi.\psi$	R_3: $\psi.\chi$
$-{}_{b}H_{a}^{C}{}_{b}$	Q: $\psi.\psi$	Q_1: $\chi.\chi$	Q_2: $\chi.\psi$	

The following further approximations and assumptions are made: In the 2p*x*, 3p*x* Slater functions Z is taken as 3·18, 1·45 respectively throughout. The additional amount of labour required for the D type integrals is large, and as they are probably small like the purely 2p ones, these integrals are ignored with the exception of D itself. For numerical values of excitation energies the difference between W_{2p} and W_{3p} is required; we use the approximate relation for a free atom $W_{3p} = W_{2p} + 8$ ev.

It is necessary first of all to evaluate most of the atomic integrals listed above. These integrals are derived from existing formulae (Barnett 1951), after computation of the necessary Bessel functions. The numerical integrations are straightforward.

Table. Configuration (C) and State (S) Energies (ev) Zero at $E = 2W_{3p}$

^1A_gC	^1A_gS	^1B_uS	^1B_uC	^3A_gC	^3B_uC
		13·5—			
					12·4—$^3E_1^{14}$
			11·3—$^1E_1^{14}$		
	2·2—				
0·7—$^1E_2^{12}$					
			−1·6—$^1E_1^{12}$		
	−3·1—				
				−4—$^3E_1^{13}$	
		−4·9—			
−5·7—$^1E_1^{13}$					
					−10 —$^3E_1^{12}$
−11·8—E_0					
	−13·6—				

Once the atomic integrals are available the procedure is now quite standard: one derives configuration energies, configuration interaction, and finally state wave functions and energies (see table and appendix). We shall not describe the method here in detail (see Jacobs 1949).

§ 3. DISCUSSION—THE ETHYLENE SPECTRUM

The ultra-violet absorption spectrum of ethylene shows a strong band with a maximum at about 1630 Å and a less strong band near 2000 Å (Wilkinson and Johnston 1950). Various interpretations have been given; it is usually agreed that the 1630 Å band corresponds to the first allowed transition, probably ${}^1\mathrm{A}_g$–${}^1\mathrm{B}_u$. Theoretical calculations hitherto have, however, predicted the lowest allowed transition at a much higher energy, thus Parr and Crawford found 11·5 ev (but see Moser 1953). Our value of 8·7 ev falls very much nearer to the experimental value of 7·6 ev, so that the computed first excitation energy is quite satisfactory.

As regards the next band the situation is less well defined. It is not even agreed whether this represents the tail end of the 1630 Å band (Mulliken 1942) or whether it corresponds to a separate transition (Craig 1950), and, if the latter is correct, the symmetry is still uncertain. Craig has suggested that this is a forbidden ${}^1\mathrm{A}_g$–${}^1\mathrm{A}_g$ transition, made apparent by nuclear vibrations of the appropriate symmetry. The band might, however, belong to an excitation to a forbidden triplet level.

It is not possible, on the basis of the results reported here, to decide definitely between the various assignments that have been proposed. According to our work, where no configuration interaction in the triplet class is evaluated, the first ${}^1\mathrm{A}_g$–${}^3\mathrm{B}_u$ forbidden transition certainly lies nearer to 3400 Å than 2000 Å. A triplet band in this region was predicted by Lewis and Kasha (1944). On the other hand, our lowest ${}^1\mathrm{A}_g$–${}^1\mathrm{A}_g$ transition corresponds to 1200 Å, and this energy gap would probably be lessened by interaction of further ${}^1\mathrm{A}_g$ configurations, though this is difficult to assert without further calculation.

Our conclusion is that while no exact interpretation of the whole ultra-violet absorption spectrum of ethylene can yet be given, certainly the inclusion of $3p\pi$ wave functions has helped to determine the energy of the first allowed transition in a very satisfactory way. Indeed, the inclusion of $3p\pi$ orbitals makes a strong contribution to the stabilization of configurations into states. Thus in the ${}^1\mathrm{A}_g$ class, the $3p\pi$ orbitals effect a further lowering of the ground state by 0·5 ev (1·28 ev, Parr and Crawford; 1·78 ev, author), a considerable proportion of the whole stabilization. Again in the ${}^1\mathrm{B}_u$ class Parr and Crawford had only a single configuration to consider, and no configuration interaction; whereas the interaction with the ${}^1E_1{}^{14}$ level stabilizes the lowest ${}^1\mathrm{B}_u$ level by 3·3 ev.

It has long been realized that the MO method determines excited states less well than the ground state. This is reflected in our work where the refinement of considering $3p\pi$ orbitals has a more drastic effect on the first excited level than on the ground state, as is shown by the stabilization energies 3·3 and 1·8 ev respectively.

The weights with which the various configurations of suitable symmetry enter the lowest state wave functions are also reported, both for ${}^1\mathrm{A}_g$ and ${}^1\mathrm{B}_u$.

Now our basic ϕ are not orthogonal, owing to overlap and to non-orthogonality of the Slater 2p and 3p functions used. We therefore introduce the configuration wave functions ${}^1\Theta_1{}^{13}$ and ${}^1\Theta_1{}^{14}$ (linear combinations of Ψ functions), which are orthogonal to ${}^1\Psi'_0$ and ${}^1\Psi'^{12}_1$ respectively. In terms of these mutually orthogonal functions the state wave functions of the lowest state in each symmetry are

$$\begin{array}{llll} X({}^1\mathrm{A_g}) = & 0{\cdot}94\,{}^1\Psi'_0 & -\,0{\cdot}27\,{}^1\Psi'^{12}_2 & +\,0{\cdot}23\,{}^1\Theta^{13}_1 \\ c_r^2: & 0{\cdot}88 & 0{\cdot}07 & 0{\cdot}05 \\ X({}^1\mathrm{B_u}) = & 0{\cdot}91\,{}^1\Psi'^{12}_1 & +\,0{\cdot}42\,{}^1\Theta^{14}_1 & \\ c_r^2: & 0{\cdot}83 & 0{\cdot}17 & \end{array}$$

The weights (c_r^2) now indicate clearly the extent to which 3pπ admixture plays a part. And we have shown the 3pπ functions to be of considerable importance—at least within the present approach. It may be argued that the Slater 2p functions are not the most suitable ones to use anyway, so that the 3p addition is mainly a compensation for the bad initial 2p functions. This may well be the case. Calculations are now in progress to assess the extent to which we are merely improving the Slater 2p orbitals; results of this investigation will be published shortly.

However, we may at this stage comment on the state wave functions here determined: A comparison of the weights shows that in the ${}^1\mathrm{B_u}$ class the wave function containing 3pπ orbitals represents as much as 20% of the purely 2pπ one. In the ${}^1\mathrm{A_g}$ class the proportions are somewhat smaller: 8% ${}^1\Psi'^{12}_2$ and 6% ${}^1\Theta^{13}_1$. In both symmetry types therefore the 3pπ wave functions contribute a not insignificant proportion. Furthermore, it may be noticed that in the ground state wave function the functions ${}^1\Psi'^{12}_2$ and ${}^1\Theta^{13}_1$ are of comparable importance. This would suggest that higher energy orbitals are almost as decisive as is the mixing of 2pπ configurations. We ought to stress, however, that not too much meaning should be attached to the exact numerical coefficients of the wave functions, for two reasons. It is well known that wave functions are very sensitive to variations and so are, in any approximation, less good than energy values. Furthermore, previous experience has shown that it is not necessarily the least energetic configurations which contribute most to the lowest state, in any symmetry type. It should therefore be borne in mind that configurations which we have ignored will affect the state wave functions, perhaps as much as those which we have included.

ACKNOWLEDGMENTS

The writer is indebted to Professor C. A. Coulson for some discussions and to Mr. T. Murphy for computation of the Bessel functions.

REFERENCES

Altmann, S. L., 1952, *Proc. Roy. Soc.* A, **210,** 327.
Barnett, M. P., 1951, *Phil. Trans. Roy. Soc.* A, **243,** 221.
Craig, D. P., 1950, *Proc. Roy. Soc.* A, **200,** 272.
Dooling, J. S., 1953, *J. Chem. Phys.*, **21,** 859.
Gallaway, W. S., and **Barker**, E. F., 1942, *J. Chem. Phys.*, **10,** 88.
Goeppert-Mayer, M. G., and **Sklar**, A. L., 1938, *J. Chem. Phys.*, **6,** 645.
Jacobs, J., 1949, *Proc. Phys. Soc.*, **52,** 710.
Lewis, G. N., and **Kasha**, M., 1944, *J. Amer. Chem. Soc.*, **66,** 2100.
Moser, C. M., 1953, *J. Chem. Phys.*, **21,** 2098.
Müller, C. R., 1954, *J. Chem. Phys.*, **22,** 120.
Mulliken, R. S., 1942, *Rev. Mod. Phys.*, **14,** 265.
Murai, T., 1952, *Progr. Theor. Phys., Osaka*, **7,** 345.

PARISER, R., and PARR, R. G., 1953, *J. Chem. Phys.*, **21**, 466, 767.
PARR, R. G., and CRAWFORD, B. L., 1948, *J. Chem. Phys.*, **16**, 526.
PENNEY, W. G., 1934, *Proc. Roy. Soc.* A, **144**, 166.
SPONER, H., and LÖWDIN, P. O., 1954, *J. Phys. Radium*, **15**, 607.
WILKINSON, P. G., and JOHNSTON, H. L., 1950, *J. Chem. Phys.*, **18**, 190.

APPENDIX

All values except for S-type integrals are in ev

$A = 16{\cdot}93$
$A_1 = 4{\cdot}46$
$A_2 = 0{\cdot}31$
$A_3 = 2{\cdot}34$

$B = 9{\cdot}26$
$B_1 = 4{\cdot}02$
$B_2 = 0{\cdot}22$
$B_3 = 1{\cdot}38$

$C = 3{\cdot}58$
$C_1 = 4{\cdot}04$
$C_2 = 1{\cdot}14$
$C_3 = 0{\cdot}19$

$C_4 = 1{\cdot}20$
$C_5 = 1{\cdot}81$
$C_6 = 0{\cdot}28$
$C_7 = 0{\cdot}50$

$D = 1{\cdot}08$
$Q_1 = 0{\cdot}99$
$Q_2 = 0{\cdot}10$
$Q_3 = 0{\cdot}25$

$R = 2{\cdot}06$
$R_1 = 0{\cdot}10$
$R_2 = 0{\cdot}25$
$R_3 = 1{\cdot}82$

$S_1 = 0{\cdot}277$
$S_2 = 0{\cdot}932$
$S_3 = 0{\cdot}184$
$S_4 = 0{\cdot}166$

$\gamma_{11} = 13{\cdot}07$
$\gamma_{22} = 13{\cdot}44$
$\gamma_{12} = 13{\cdot}01$
$\gamma_{13} = 3{\cdot}84$

$\gamma_{14} = 16{\cdot}08$
$\delta_{12} = 4{\cdot}16$
$\delta_{13} = 0{\cdot}30$
$\delta_{14} = -0{\cdot}53$

$\zeta_{11.13} = 0{\cdot}20$
$\zeta_{11.24} = 3{\cdot}11$
$\zeta_{12.14} = 0{\cdot}51$
$\zeta_{12.23} = 0{\cdot}72$

$\epsilon_{11} = W_{2p} - 12{\cdot}44$
$\epsilon_{22} = W_{2p} - 6{\cdot}37$
$\epsilon_{33} = W_{2p} + 3{\cdot}72$
$\epsilon_{44} = W_{2p} + 8{\cdot}20$

$\epsilon_{13} = 0{\cdot}22W_{2p} - 1{\cdot}58$
$\epsilon_{31} = 0{\cdot}22W_{2p} - 1{\cdot}93$
$\epsilon_{24} = 0{\cdot}08W_{2p} + 9{\cdot}66$
$\epsilon_{42} = 0{\cdot}08W_{2p} - 1{\cdot}10$

An Extension of the Analysis of the Yttrium Spectrum

By L. F. H. BOVEY
Atomic Energy Research Establishment, Harwell, Didcot, Berks.

MS. received 30th September 1954

Abstract. Nineteen lines of the yttrium spectrum have been found in the region 9400–11500 Å and have been assigned to term combinations in the Yt I and Yt II spectra.

---

§ 1. Introduction

In order to try to extend the spectrum of lutetium to longer wavelengths, experiments have been carried out to assess the sensitivity of Kodak Z photographic plates in the region 10 000–12 000 Å. These plates have recently become available again in this country. During the course of the preliminary trial runs, yttrium was examined and eighteen lines additional to those reported by Meggers (1928) found. The wavelengths of these and their assigned positions in the term scheme are given here.

§ 2. Experimental Details

The Hilger compact 3-metre spectrograph (Model E.661) instrument was used in the first order with Z I plates previously sensitized by immersion in 4% ammonia solution for three minutes and a one-minute dip in methyl alcohol with subsequent rapid drying in a stream of dust free air. Conventional arcing from copper or silver electrodes proved unsatisfactory and graphite electrodes were used. The yttrium oxide was mixed with graphite powder and the mixture compressed into a small hole in the graphite anode. Exposure times of approximately 30 minutes were required to record the spectrum up to 11 500 Å although only a few seconds sufficed for the comparison iron arc (in the third order). A 6-amp d.c. arc operating off the 230-volt supply was used. The wavelengths of the lines were measured on a comparator against the superimposed iron arc and the vacuum conversion factor determined from Edlen's Tables. Wavelengths quoted in the table have been measured on at least two plates.

§ 3. Assignment of Terms

With the aid of the comprehensive analysis made by Meggers and Russell (1929), the determination of the combining levels was not very difficult. Considerable help was given by the use of tables of differences computed by the Mathematics Division of the National Physical Laboratory. The agreement between experimental and calculated values seems remarkably good particularly when it is realized that the lines are measured against a strong background of lines arising from the graphite electrodes themselves. This agreement, the intensity relationships and consideration of selection rules are taken as evidence for the correctness of the assignment.

Table of Classified Lines

λ_A (Å)		ν_{vac} (cm^{-1})	ν_{vac} (calc.)	Terms†	Spectrum
9405·8	VS	10628·9	10628·9	$a^3P_1-z^3P_2^0$	II
9476·9	VS	10549·1	10549·0	$a^3P_2-z^3P_2^0$	II
‡9494·9	VS	10529·1	10529·2	$a^2D_2-z^2P_1$	I
10105·5	S	9892·9	9892·8	$a^3P_0-z^3P_1^0$	II
10186·4	M	9814·3	9814·2	$b^1D_2-z^3P_2^0$	II
10245·2	M	9758·0	9758·1	$a^3P_1-z^3P_1^0$	II
10293·0	M	9712·7	9712·8	$y^2F_3^0-e^2D_2$	I
10329·8	VS	9678·1	9678·2	$a^3P_2-z^3P_1^0$	II
10373·7	VW	9637·2	9637·1	$y^2F_3^0-e^4P_2$	I
10390·4	VW	9621·6	9621·8	$y^2F_4^0-e^4P_3$	I
10511·5	W	9510·8	9510·8	$y^2D_3^0-e^2D_3$	I
10540·2	VW	9484·9	9485·0	$y^2D_3^0-e^2D_2$	I
10605·2	VS	9426·8	9426·9	$a^3P_1-z^3P_0^0$	II
10683·4	VS	9357·8	9357·9	$y^2F_4^0-e^2D_3$	I
10722·6	W	9323·5	9323·4	$y^2F_3^0-e^2P_2$	I
10784·5	VW	9270·0	9269·9	$a^4P_3-y^2D_3^0$	I
10876·0	VW	9192·0	9192·0	$a^2F_3-y^2F_3^0$	I
10921·3	M	9153·9	9153·8	$a^2F_3-y^2P_2^0$	I
11484·8	W	8704·8	8704·7	$b^2D_2-y^2P_1^0$	I

VS very strong; S strong; M medium; W weak; VW very weak.

† Nomenclature follows that of Moore (1952) except that whole numbers a half unit larger than the true *j* values for levels of even multiplicities are used.

‡ Previously observed (Meggers 1928).

§4. Discussion

The stronger lines in this region belong to the $a^3P-z^3P^0$ levels of the ionized atom and of the nine possible combinations, six have been observed. It is a little surprising that the $a^3P_0-z^3P_0^0$ combination at 10 457 Å is not seen on the plates.

The lines arising from the Yt I spectrum are nearly all accounted for by a series of combinations between doublet levels. Missing members which might have been expected in this region have been looked for but since they would probably be weak and possibly masked by the background lines, their absence is not significant.

The opportunity was also taken of examining whether the 69 lines unassigned by Meggers could be fitted into the term system. This did not prove possible and further work is being done on the assumption that fresh levels are concerned.

Acknowledgments

The author would like to thank Kodak Ltd. for their cooperation in supplying the Z plates and Mr. C. W. Nott of the Mathematics Division, National Physical Laboratory, for his patient help in producing the various lists of differences.

References

MEGGERS, W. F., 1928, *J. Res. Nat. Bur. Stand.*, **1**, 319 (RP 12).
MEGGERS, W. F., and RUSSELL, H. N., 1929, *J. Res. Nat. Bur. Stand.*, **2**, 733 (RP 55).
MOORE, C. E., 1952, *Atomic Energy Levels*, Circ. Nat. Bur. Stand., 467.

The Electronic Spectra of Aromatic Molecules

II : A Theoretical Treatment of Excited States of Alternant Hydrocarbon Molecules based on Self-Consistent Molecular Orbitals

BY J. A. POPLE
Department of Theoretical Chemistry, University of Cambridge

MS. received 13*th August* 1954

Abstract. The theoretical treatment of the electronic spectrum of benzenoid hydrocarbons recently given by Dewar and Longuet-Higgins (Part I) is generalized so that full account is taken of electron interaction. The method is based on the use of a self-consistent molecular orbital function for the ground state and corresponding functions for excited states. It is found that all the general features of the method of Part I carry over, although certain accidental degeneracies are removed. Approximate numerical calculations based on the new method give support to the assignments made by Dewar and Longuet-Higgins.

---

§ 1. INTRODUCTION

IN a previous paper, Dewar and Longuet-Higgins (1954) have given a theoretical interpretation of the singlet electronic spectra associated with the mobile electrons of benzenoid hydrocarbons. Their procedure, in outline, is as follows:

(1) A set of orbital energies is obtained from the Hückel LCAO molecular orbital theory (based on an effective one-electron Hamiltonian and neglecting overlap). If the mobile electrons were really independent and non-interacting, the excitation levels would be the differences between these energies.

(2) It is well known that the Hückel theory by itself leads to an oversimplified picture of the spectra. The mutual repulsion of the electrons leads to interaction between the various excited configurations and modifies the energy levels. To allow for this in a simple way, interaction is permitted between configurations which the Hückel theory predicts to be degenerate. Such levels are then split by amounts which are related to the matrix elements of the complete many-electron Hamiltonian between the corresponding antisymmetrized configurational wave functions. By applying this method to the lowest levels, Dewar and Longuet-Higgins are able to interpret the general features of the p, α, β and β' bands classified by Clar.

Although this is undoubtedly an improvement over the Hückel theory by itself, the use of the incompletely defined one-electron Hamiltonian in step (1) is still rather unsatisfactory. It would be better if the *whole* treatment could be based on the many-electron Hamiltonian with electron interaction. That some such further development is needed is suggested by the fact that the Dewar–Longuet-Higgins method still oversimplifies the spectra in some respects. For example, it predicts that the B_{1u} and B_{2u} levels of benzene should be degenerate, whereas in fact they are distinct. A second reason for improving the theory is that a treatment including electron interaction at all stages should show the relation between singlet and triplet levels.

Recently the work of Pariser and Parr (1953) on the spectra of ethylene and benzene has suggested that useful conclusions about the effect of electron interaction can be drawn without detailed calculation of complicated integrals characteristic of earlier work. Using a similar series of approximations, the present author (Pople 1953) has discussed the determination of self-consistent orbitals for the ground states of alternant hydrocarbons and has shown how many of the features of the Hückel theory (uniform charge-density, pairing of orbitals, etc.) hold also when electron interaction is taken into account explicitly. The present paper introduces a generalization of the work of Dewar and Longuet-Higgins which is based on the self-consistent molecular orbital function and which allows for electron interaction at all stages. The principal features of their work carry over almost without change to this more rigorous method, although certain accidental degeneracies are removed. It is possible to get explicit expressions for the lowest energy levels in terms of the self-consistent orbital coefficients, so that the integrals of Pariser and Parr can be used to make a more quantitative test of the assignments.

§ 2. EXCITED STATES OF ALTERNANT HYDROCARBONS

The wave function χ_0 for the π-electrons in the ground state of an alternant hydrocarbon will be taken as a Slater determinant built up from orthogonal molecular orbitals $\psi_1, \ldots . \psi_m$ which are themselves linear combinations of carbon $2p\pi$ atomic orbitals $\phi_1 \ldots . \phi_{2m}$

$$\psi_i = \sum_\mu c_{i\mu}\phi_\mu. \qquad \ldots\ldots(2.1)$$

In the self-consistent treatment, the coefficients $c_{i\mu}$ are chosen to minimize the electronic energy

$$\mathscr{E} = \int \ldots . \int \bar{\chi}_0 \mathscr{H} \chi_0 d\tau \qquad \ldots\ldots(2.2)$$

where $\mathscr{H}$ is the complete electronic Hamiltonian

$$\mathscr{H} = \sum_i H_i^{\text{core}} + \sum_{i<j}^{2m} (1/r_{ij}). \qquad \ldots\ldots(2.3)$$

H^{core} represents the kinetic energy and the potential energy of the σ-core.

A general set of equations for $c_{i\mu}$ has been given by Roothaan (1951). Making certain simplifying approximations about the integrals that arise (Pople 1953), these can be reduced to the eigenvalue equations

$$\sum_\nu F_{\mu\nu} c_{i\nu} = E_i c_{i\mu}. \qquad \ldots\ldots(2.4)$$

where

$$F_{\mu\mu} = U_{\mu\mu} + \tfrac{1}{2} p_{\mu\mu}\gamma_{\mu\mu} + \sum_{\sigma(\neq\mu)} (p_{\sigma\sigma} - 1)\gamma_{\mu\sigma} \qquad \ldots\ldots(2.5)$$

$$F_{\mu\nu} = H_{\mu\nu} - \tfrac{1}{2} p_{\mu\nu}\gamma_{\mu\nu} \qquad \ldots\ldots(2.6)$$

$$P_{\mu\nu} = 2\sum_{i=1}^{m} \bar{c}_{i\mu} c_{i\nu}. \qquad \ldots\ldots(2.7)$$

In these expressions $\gamma_{\mu\nu}$ has been written for the coulomb electrostatic repulsion integral

$$\gamma_{\mu\nu}=\int\int\phi_\mu^2(1)(1/r_{12})\phi_\nu^2(2)\,dv_1\,dv_2. \qquad \ldots\ldots(2.8)$$

$U_{\mu\mu}$ is a core matrix element which may reasonably be taken as the same for all carbon centres and $H_{\mu\nu}$ is the off-diagonal matrix element of the core Hamiltonian

$$H_{\mu\nu}=\int\phi_\mu(1)H_1^{\text{core}}\phi_\nu(1)\,dv_1. \qquad \ldots\ldots(2.9)$$

This is taken to be equal to a constant β for all pairs of neighbours and zero otherwise. E_i are the eigenvalues of the matrix $F_{\mu\nu}$.

Since there are $2m$ atomic orbitals, equations (2.2) determine $2m$ molecular orbitals. Of these only m corresponding to the lower E_i are occupied in the ground state. The other unoccupied orbitals will be used in formulating wave functions for excited states.

From the form of the self-consistent equations (2.4) certain general results can be derived which are applicable to all alternant hydrocarbons (Pople 1953). In particular,

(i) $p_{\mu\mu}=1$ for all μ.

(ii) The eigenvalues E_i are symmetrically arranged about the value $U+\frac{1}{2}\gamma_{11}$. That is, if $U+\frac{1}{2}\gamma_{11}-\epsilon$ is an eigenvalue, so is $U+\frac{1}{2}\gamma_{11}+\epsilon$.

(iii) The coefficients of the orbitals are paired. This means that, if the atoms are divided into starred and unstarred sets in the usual way, then the pair of molecular orbitals with energies $U+\frac{1}{2}\gamma_{11}\pm\epsilon$ can be written

$$\left.\begin{aligned}\psi_i&=\sum_\mu{}^{*}c_{i\mu}\phi_\mu+\sum_\mu{}^{0}c_{i\mu}\phi_\mu\\ \psi_{2m+1-i}&=\sum_\mu{}^{*}c_{i\mu}\phi_\mu-\sum_\mu{}^{0}c_{i\mu}\phi_\mu\end{aligned}\right\} \qquad \ldots\ldots(2.10)$$

where the molecular orbitals are numbered 1, 2.... $2m$ with increasing eigenvalues E_i; Σ^* and Σ^0 are written for sums over starred and unstarred atoms respectively.

Once the self-consistent problem for the ground state has been solved, the unoccupied molecular orbitals $\psi_{m+1}\ldots.\psi_{2m}$ can be used to construct configurational wave functions for excited states. We shall write ${}^1\chi_{i\to k}$ for the singlet configurational wave function in which one electron is excited from an occupied orbital ψ_i to an unoccupied one ψ_k. ${}^1\chi_{i\to k}$ will be a sum of two Slater determinants (Roothaan 1951). The corresponding triplet wave function will be written ${}^3\chi_{i\to k}$. (There are in fact three triplet functions with three different spin component eigenvalues. It is immaterial which component is selected as long as the same one is used for all configurations.) Other functions for two-electron excitations could be developed, but for a discussion of the lower absorption levels they will not be taken into account.

The matrix elements of the total Hamiltonian $\mathscr{H}$ between the $\chi_{i\to k}$ and χ_0 can be reduced to integrals over one or two electrons utilizing the orthogonality property of molecular orbitals. The results are (see Appendix)

$$({}^1\chi_{i\to k}|\mathscr{H}|{}^1\chi_{i\to k})-(\chi_0|\mathscr{H}|\chi_0)=E_k-E_i-(ik|G|ik)+2(ik|G|ki) \qquad \ldots\ldots(2.11)$$

$$({}^3\chi_{i\to k}|\mathscr{H}|{}^3\chi_{i\to k})-(\chi_0|\mathscr{H}|\chi_0)=E_k-E_i-(ik|G|ik) \qquad \ldots\ldots(2.12)$$

$$({}^1\chi_{i\to k}|\mathscr{H}|\chi_0)=0 \qquad \ldots\ldots(2.13)$$

$$({}^1\chi_{i\to k}|\mathscr{H}|{}^1\chi_{j\to l})=2(jk|G|li)-(jk|G|il)\ \text{(unless } i=j \text{ and } k=l) \qquad \ldots\ldots(2.14)$$

$$({}^3\chi_{i\to k}|\mathscr{H}|{}^3\chi_{j\to l})=-(jk|G|il)\ \text{(unless } i=j \text{ and } k=l) \qquad \ldots\ldots(2.15)$$

the two-electron matrix elements being defined by

$$(pq|G|rs)=\int\int\bar{\psi}_p(1)\bar{\psi}_q(2)(1/r_{12})\psi_r(1)\psi_s(2)\,dv_1\,dv_2. \qquad \ldots\ldots(2.16)$$

All matrix elements between singlet and triplet functions are zero by integration over spin.

Equations (2.11) and (2.12) show that $({}^1\chi_{i\to k}|\mathscr{H}|{}^1\chi_{i\to k})-(\chi_0|\mathscr{H}|\chi_0)$ and $({}^3\chi_{i\to k}|\mathscr{H}|{}^3\chi_{i\to k})-(\chi_0|\mathscr{H}|\chi_0)$, which may be described as configurational excitation energies, are not equal to the difference between the two eigenvalues if electron interaction is included. In fact E_k-E_i is generally larger.

In spite of this, it is still possible to generalize the method of Dewar and Longuet-Higgins, using the pairing properties described above. As explained in the introduction, their procedure is to include interaction only between configurations which are degenerate according to the one-electron Hamiltonian theory. The obvious generalization of this is to include interaction between configurations whose excitation energies are equal according to (2.11) and (2.12).

The most important degeneracy predicted by the Hückel theory for the general alternant hydrocarbon is that between the configurational excitations $m-1\to m+1$ and $m\to m+2$. An interaction element of the type (2.14) splits the singlets into two levels which Dewar and Longuet-Higgins identify with Clar's α and β bands. We shall now show that the same degeneracy occurs for both singlets and triplets in the self-consistent theory, that is

$$({}^1\chi_{m-1\to m+1}|\mathscr{H}|{}^1\chi_{m-1\to m+1})=({}^1\chi_{m\to m+2}|\mathscr{H}|{}^1\chi_{m\to m+2}) \qquad \ldots\ldots(2.17)$$

$$({}^3\chi_{m-1\to m+1}|\mathscr{H}|{}^3\chi_{m-1\to m+1})=({}^3\chi_{m\to m+2}|\mathscr{H}|{}^3\chi_{m\to m+2}). \qquad \ldots\ldots(2.18)$$

$E_{m+1}-E_{m-1}$ is clearly equal to $E_{m+2}-E_m$ on account of the pairing property noted above, so it only remains to demonstrate equality of the two-electron integrals. This is easily done by expanding the molecular orbitals in terms of atomic orbitals and neglecting all integrals except those of the Coulomb type (2.8). If, following Dewar and Longuet-Higgins, we write the highest occupied and lowest unoccupied orbitals in the form

$$\left.\begin{aligned}\psi_{m-1}&=\textstyle\sum^* b_\mu\phi_\mu+\sum^0 b_\mu\phi_\mu\\ \psi_m&=\textstyle\sum^* a_\mu\phi_\mu+\sum^0 a_\mu\phi_\mu\\ \psi_{m+1}&=\textstyle\sum^* a_\mu\phi_\mu-\sum^0 a_\mu\phi_\mu\\ \psi_{m+2}&=\textstyle\sum^* b_\mu\phi_\mu-\sum^0 b_\mu\phi_\mu\end{aligned}\right\} \qquad \ldots\ldots(2.19)$$

then

$$(m-1,m+1|G|m-1,m+1)=(m,m+2|G|m,m+2)=\sum_{\mu\nu}a_\mu{}^2b_\nu{}^2\gamma_{\mu\nu} \qquad \ldots\ldots(2.20)$$

$$(m-1,m+1|G|m+1,m-1)=(m,m+2|G|m+2,m)=\Big[\sum_\mu{}^*\sum_\nu{}^*+\sum_\mu{}^0\sum_\nu{}^0-2\sum_\mu{}^*\sum_\nu{}^0\Big]\,a_\mu b_\mu a_\nu b_\nu\gamma_{\mu\nu}. \qquad \ldots\ldots(2.21)$$

For the interaction elements

$$({}^1\chi_{m-1\to m+1}|\mathscr{H}|{}^1\chi_{m\to m+2})=\Big[\sum_\mu{}^*\sum_\nu{}^*+\sum_\mu{}^0\sum_\nu{}^0-6\sum_\mu{}^*\sum_\nu{}^0\Big]a_\mu b_\mu a_\nu b_\nu\gamma_{\mu\nu} \qquad \ldots\ldots(2.22)$$

$$({}^3\chi_{m-1\to m+1}|\mathscr{H}|{}^3\chi_{m\to m+2})=-\Big[\sum_\mu{}^*\sum_\nu{}^*+\sum_\mu{}^0\sum_\nu{}^0+2\sum_\mu{}^*\sum_\nu{}^0\Big]a_\mu b_\mu a_\nu b_\nu\gamma_{\mu\nu}. \qquad \ldots(2.23)$$

Equation (2.22) has already been given by Dewar and Longuet-Higgins. Other integrals are easily evaluated by the same method.

In the absence of further degeneracy, Dewar and Longuet-Higgins assign wave-functions to the excited states as follows

$$\begin{aligned} &\mathrm{p}:\ {}^1\chi_{m\to m+1} && \alpha:\ ({}^1\chi_{m-1\to m+2}-{}^1\chi_{m\to m+2})/\sqrt{2} \\ &\beta':\ {}^1\chi_{m-1\to m+2} && \beta:\ ({}^1\chi_{m-1\to m+1}+{}^1\chi_{m\to m+2})/\sqrt{2}. \end{aligned} \qquad \ldots\ldots(2.24)$$

By analogy, we may classify a corresponding set of triplet states

$$\begin{aligned} &{}^3\mathrm{p}:\ {}^3\chi_{m\to m+1} && {}^3\alpha:\ ({}^3\chi_{m-1\to m+1}-{}^3\chi_{m\to m+2})/\sqrt{2} \\ &{}^3\beta':\ {}^3\chi_{m-1\to m+2} && {}^3\beta:\ ({}^3\chi_{m-1\to m+1}+{}^3\chi_{m\to m+2})/\sqrt{2}. \end{aligned} \qquad \ldots\ldots(2.25)$$

The excitation energies can be found from the matrix elements. For the singlet bands they are

$$\mathscr{E}(\mathrm{p})-\mathscr{E}_0=E_{m+1}-E_m+\Big[\sum_\mu{}^*\sum_\nu{}^*+\sum_\mu{}^0\sum_\nu{}^0-6\sum_\mu{}^*\sum_\nu{}^0\Big]a_\mu{}^2a_\nu{}^2\gamma_{\mu\nu} \qquad \ldots\ldots(2.26)$$

$$\mathscr{E}(\alpha)-\mathscr{E}_0=E_{m+1}-E_{m-1}-\sum_{\mu\nu}a_\mu{}^2b_\nu{}^2\gamma_{\mu\nu}+\Big[\sum_\mu{}^*\sum_\nu{}^*+\sum_\mu{}^0\sum_\nu{}^0+2\sum_\mu{}^*\sum_\nu{}^0\Big]a_\mu b_\mu a_\nu b_\nu\gamma_{\mu\nu} \qquad \ldots\ldots(2.27)$$

$$\mathscr{E}(\beta)-\mathscr{E}_0=E_{m+1}-E_{m-1}-\sum_{\mu\nu}a_\mu{}^2b_\nu{}^2\gamma_{\mu\nu}+\Big[3\sum_\mu{}^*\sum_\nu{}^*+3\sum_\mu{}^0\sum_\nu{}^0-10\sum_\mu{}^*\sum_\nu{}^0\Big]a_\mu b_\mu a_\nu b_\nu\gamma_{\mu\nu} \qquad \ldots\ldots(2.28)$$

$$\mathscr{E}(\beta')-\mathscr{E}_0=E_{m+2}-E_{m-1}+\Big[\sum_\mu{}^*\sum_\nu{}^*+\sum_\mu{}^0\sum_\nu{}^0-6\sum_\mu{}^*\sum_\nu{}^0\Big]b_\mu{}^2b_\nu{}^2\gamma_{\mu\nu} \qquad \ldots\ldots(2.29)$$

and for the triplets

$$\mathscr{E}({}^3\mathrm{p})-\mathscr{E}_0=E_{m+1}-E_m-\sum_{\mu\nu}a_\mu{}^2a_\nu{}^2\gamma_{\mu\nu} \qquad \ldots\ldots(2.30)$$

$$\mathscr{E}({}^3\alpha)-\mathscr{E}_0=E_{m+1}-E_{m-1}-\sum_{\mu\nu}a_\mu{}^2b_\nu{}^2\gamma_{\mu\nu}+\Big[\sum_\mu{}^*\sum_\nu{}^*+\sum_\mu{}^0\sum_\nu{}^0+2\sum_\mu{}^*\sum_\nu{}^0\Big]a_\mu b_\mu a_\nu b_\nu\gamma_{\mu\nu} \qquad \ldots\ldots(2.31)$$

$$\mathscr{E}({}^3\beta)-\mathscr{E}_0=E_{m+1}-E_{m-1}-\sum_{\mu\nu}a_\mu{}^2b_\nu{}^2\gamma_{\mu\nu}-\Big[\sum_\mu{}^*\sum_\nu{}^*+\sum_\mu{}^0\sum_\nu{}^0+2\sum_\mu{}^*\sum_\nu\Big]^0a_\mu b_\mu a_\nu b_\nu\gamma_{\mu\nu} \qquad \ldots\ldots(2.32)$$

$$\mathscr{E}({}^3\beta')-\mathscr{E}_0=E_{m+2}-E_{m-1}-\sum_{\mu\nu}b_\mu{}^2b_\nu{}^2\gamma_{\mu\nu}. \qquad \ldots\ldots(2.33)$$

Even without detailed calculations, certain general features of the spectra can be deduced from these formulae. Dewar and Longuet-Higgins have indicated that the interaction element (2.22) leading to the separation of the α and β levels will be positive so that $\mathscr{E}(\beta)>\mathscr{E}(\alpha)$. They also showed that the transition moment between the ground state and the α-state is theoretically zero. This depends only on the pairing of orbitals and is still valid in the present theory. In a similar way we now predict the existence of a pair of associated triplet states ${}^3\alpha$ and ${}^3\beta$. The matrix element (2.23) is negative, so that $\mathscr{E}({}^3\alpha)>\mathscr{E}({}^3\beta)$. One interesting point is that the theory leads to degeneracy between the α and ${}^3\alpha$ states. This, no doubt, is partly a fortuitous result of the approximations made and would not hold accurately in a more refined calculation. There are not yet sufficient experimental data to test predictions about triplet states other than the lowest. The general effect of configuration interaction on the singlet and triplet levels is illustrated diagrammatically in the figure.

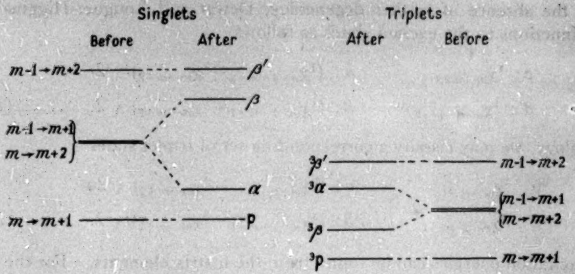

Effect of configuration interaction between degenerate configurational excitations.

§ 3. APPLICATION TO PARTICULAR HYDROCARBONS

When applied to benzene, the present treatment is equivalent to that of Pariser and Parr (1953). The molecular orbitals $\psi_{m-1} \ldots \psi_{m+2}$ are determined by symmetry and, in their real form, are

$$\left.\begin{aligned}
\psi_2 &= \tfrac{1}{2}(\phi_2+\phi_3-\phi_5-\phi_6)\\
\psi_3 &= \tfrac{1}{\sqrt{3}}(\phi_1+\tfrac{1}{2}\phi_2-\tfrac{1}{2}\phi_3-\phi_4-\tfrac{1}{2}\phi_5+\tfrac{1}{2}\phi_6)\\
\psi_4 &= \tfrac{1}{\sqrt{3}}(\phi_1-\tfrac{1}{2}\phi_2-\tfrac{1}{2}\phi_3+\phi_4-\tfrac{1}{2}\phi_5-\tfrac{1}{2}\phi_6)\\
\psi_5 &= \tfrac{1}{2}(-\phi_2+\phi_3-\phi_5+\phi_6)
\end{aligned}\right\} \quad \ldots\ldots (3.1)$$

Since ψ_2, ψ_3 and ψ_4, ψ_5 are degenerate pairs of orbitals, there will be degeneracy between the configurational excitations 3→4 and 2→5 as well as that between 3→5 and 2→4. But since the configurational excitation energies are no longer differences between one-electron energies, all four need not be degenerate. In fact they are not. The method of the previous section gives

$$({}^1\chi_{3\to4}|\mathscr{H}|{}^1\chi_{3\to4})-(\chi_0|\mathscr{H}|\chi_0) = -2\beta+\tfrac{1}{4}\gamma_{11}-\tfrac{1}{12}\gamma_{12}+\tfrac{1}{4}\gamma_{13}-\tfrac{5}{12}\gamma_{14} \quad \ldots\ldots (3.2)$$

$$({}^1\chi_{2\to4}|\mathscr{H}|{}^1\chi_{2\to4})-(\chi_0|\mathscr{H}|\chi_0) = -2\beta+\tfrac{1}{12}\gamma_{11}+\tfrac{5}{12}\gamma_{12}-\tfrac{7}{12}\gamma_{13}+\tfrac{1}{12}\gamma_{14}. \quad \ldots\ldots (3.3)$$

For this molecule, additional configuration interaction must be taken into account between $\chi_{3\to4}$ and $\chi_{2\to5}$.

The appropriate values for the β and γ integrals have been thoroughly discussed by Pariser and Parr (1953) (they use the symbol $(\mu\mu|\nu\nu)$ for $\gamma_{\mu\nu}$). On a partly empirical basis they select $\beta=-2{\cdot}39$ ev, $\gamma_{11}=10{\cdot}53$ev, $\gamma_{12}=7{\cdot}30$ev, $\gamma_{13}=5{\cdot}46$ev and $\gamma_{14}=4{\cdot}90$ev. Using these values and including configuration interaction, they calculate the energy levels of excited states as shown in table 1. It is clear that the difference between (3.2) and (3.3) removes the degeneracy between the ${}^1\beta_{1u}$ and ${}^1\beta_{2u}$ levels predicted by the method of Dewar and Longuet-Higgins.

The numerical parameters quoted above can be used to apply the method of this paper to other less symmetrical hydrocarbons. Since the application to benzene is comparatively successful, this should provide a quantitative test of the general assignments made by Dewar and Longuet-Higgins. It should also lead to energy-level predictions for as yet unobserved triplets.

Detailed calculations have been carried out for napthalene and anthracene. It has been assumed that all bond lengths can be taken as equal to that in benzene, each ring forming a perfect hexagon. The inverse distance approximation (Pople 1953) has been used for $\gamma_{\mu\nu}$ for atoms further apart than the opposite pair in benzene. The self-consistent equations (2.4) were solved by a cyclic process and the coefficients then used in the energy level expressions (2.26)–(2.33). The results are given in tables 2 and 3.

Table 1. Spectrum of Benzene

Band	Wave function	Symmetry	Frequency (cm^{-1})	
			calc	expt
α	$\chi_{2\to4}-\chi_{3\to5}$	$^1B_{2u}$	39500	38000 (*a*)
p	$\chi_{3\to4}+\chi_{2\to5}$	$^1B_{1u}$	43000	48000 (*a*)
β, β'	$\left\{\begin{matrix}\chi_{2\to4}+\chi_{3\to5}\\ \chi_{3\to4}-\chi_{2\to5}\end{matrix}\right\}$	$^1E_{1u}$	56500	54500 (*a*)
^{3}p	$^3\chi_{3\to4}+{}^3\chi_{2\to5}$	$^3B_{1u}$	32000	29500 (*b*)
$^3\beta$, $^3\beta'$	$\left\{\begin{matrix}{}^3\chi_{2\to4}+{}^3\chi_{3\to5}\\ {}^3\chi_{3\to4}-{}^3\chi_{2\to5}\end{matrix}\right\}$	$^3E_{1u}$	36000	—
$^3\alpha$	$^3\chi_{2\to4}-{}^3\chi_{3\to5}$	$^3B_{2u}$	39500	—

(*a*) Klevens and Platt (1949). (*b*) McClure (1949).

Table 2. Spectrum of Naphthalene

Band	Wave function	Symmetry	Frequency (cm^{-1})	
			calc	expt
α	$\chi_{4\to6}-\chi_{5\to7}$	$^1B_{1u}$	35500	32000 (*a*)
p	$\chi_{5\to6}$	$^1B_{2u}$	37500	34500 (*a*)
β	$\chi_{4\to6}+\chi_{5\to7}$	$^1B_{1u}$	49500	45500 (*a*)
β'	$\chi_{4\to7}$	$^1B_{2u}$	50000	60000 (*a*)
^{3}p	$^3\chi_{5\to6}$	$^3B_{2u}$	25000	21300 (*b*)
$^3\beta$	$^3\chi_{4\to6}+{}^3\chi_{5\to7}$	$^3B_{1u}$	33000	—
$^3\alpha$	$^3\chi_{4\to6}-{}^3\chi_{5\to7}$	$^3B_{1u}$	35500	—
$^3\beta'$	$^3\chi_{4\to7}$	$^3B_{2u}$	39000	—

(*a*) Klevens and Platt (1949). (*b*) McClure (1949).

Table 3. Spectrum of Anthracene

Band	Wave function	Symmetry	Frequency (cm^{-1})	
			calc	expt
p	$\chi_{7\to8}$	$^1B_{2u}$	30000	26500 (*a*)
α	$\chi_{6\to8}-\chi_{7\to9}$	$^1B_{1u}$	33500	[28000]
β	$\chi_{6\to8}+\chi_{7\to9}$	$^1B_{1u}$	45500	39000 (*a*)
β'	$\chi_{6\to9}$	$^1B_{2u}$	52000	45500 (*a*)
^{3}p	$^3\chi_{7\to8}$	$^3B_{2u}$	18000	14700 (*b*)
$^3\beta$	$^3\chi_{6\to8}+{}^3\chi_{7\to9}$	$^3B_{1u}$	32000	—
$^3\alpha$	$^3\chi_{6\to8}-{}^3\chi_{7\to9}$	$^3B_{1u}$	33500	—
$^3\beta'$	$^3\chi_{6\to9}$	$^3B_{2u}$	43500	—

(*a*) Klevens and Platt (1949). (*b*) Lewis and Kasha (1944).

There is satisfactory general agreement between the calculated and observed frequencies listed in these tables. The calculated values are mostly too high, but the relative arrangement tallies very well with the experimental assignments.

It is probable that further configuration interaction with other singly excited configurations would improve the detailed agreement, but these calculations do show that the general features of the low-frequency electronic spectra can be understood in terms of the simple relations derived in this paper.†

The assignment in anthracene differs slightly from that of Dewar and Longuet-Higgins and deserves comment. They note that according to the Hückel theory the transitions 6→9 and 5→10 are degenerate, so they assign wave functions $\chi_{6\to9}+\chi_{5\to10}$ and $\chi_{6\to9}-\chi_{5\to10}$ to two bands at 45 500 cm^{-1} and 53 500 cm^{-1}. This accidental degeneracy disappears when electron interaction is included, however, the energy of $\chi_{6\to9}$ being lower. As a result, the β' state is assigned a wave function $\chi_{6\to9}$. In a complete calculation there will probably be partial mixing between these two.

ACKNOWLEDGMENT

The author is indebted to Professor H. C. Longuet-Higgins for some valuable discussions on this topic.

APPENDIX

REDUCTION OF MATRIX ELEMENTS FOR SELF-CONSISTENT DETERMINANTAL FUNCTIONS

Equations (2.11) and (2.12) for the diagonal matrix elements of the many-electron Hamiltonian between determinantal functions are well known (Roothaan 1951). The off-diagonal elements (2.13)–(2.15) are also of considerable interest, so a brief outline of their derivation is given here.

The molecular orbital wave function for the ground state χ_0 can be written as an antisymmetrized product

$$\chi_0=[(2m)!]^{-1/2}\sum_P(-1)^P P\{(\psi_1\alpha)(\psi_1\beta)(\psi_2\alpha)\ldots.(\psi_m\beta)\}. \qquad \ldots\ldots(\mathrm{A1})$$

Here $\Sigma_P(-1)^P P$ is the usual antisymmetrizing summation over all permutations of the electrons. The corresponding expressions for ${}^1\chi_{i\to k}$ and one component of ${}^3\chi_{i\to k}$ are

$$\chi_{i\to k}=[2(2_m)!]^{-1/2}\sum_P(-1)^P P\{(\psi_1\alpha)\ldots.(\psi_{i-1}\beta)(\psi_i\alpha)(\psi_k\beta)\ldots.(\psi_m\beta)$$

$$\pm(\psi_1\alpha)\ldots.(\psi_{i-1}\beta)(\psi_k\alpha)(\psi_i\beta)\ldots.(\psi_m\beta)\} \qquad \ldots\ldots(\mathrm{A2})$$

the positive and negative signs being taken for singlet and triplet respectively.

The reduction of the many-electrons integrals between the determinantal functions can be performed by the usual method (Condon and Shortley 1935).

---

† Dr. R. G. Parr informs the author that Dr. Pariser has recently completed a more extensive treatment of the polyacene spectra using an electronic calculating machine and does, in fact, get better results.

This leads to

$$\left.\begin{array}{l}
({}^1\chi_{i\to k}|\mathscr{H}|\chi_0)=\sqrt{2}F_{ki}\\
\left.\begin{array}{l}
({}^1\chi_{i\to k}|\mathscr{H}|{}^1\chi_{i\to l})=F_{kl}+2(ik|li)-|G(ik|G|il)\\
({}^3\chi_{i\to k}|\mathscr{H}|{}^3\chi_{i\to l})=F_{kl}-(ik|G|il)
\end{array}\right\}(k\neq l)\\
\left.\begin{array}{l}
({}^1\chi_{i\to k}|\mathscr{H}|{}^1\chi_{j\to k})=-F_{ji}+2(kj|G|ik)-(kj|G|ki)\\
({}^3\chi_{i\to k}|\mathscr{H}|{}^3\chi_{j\to k})=-F_{ji}-(kj|G|ki)
\end{array}\right\}(i\neq j)\\
\left.\begin{array}{l}
({}^1\chi_{i\to k}|\mathscr{H}|{}^1\chi_{j\to l})=2(jk|G|li)-(jk|G|il)\\
({}^3\chi_{i\to k}|\mathscr{H}|{}^3\chi_{j\to l})=-(jk|G|il)
\end{array}\right\}(i\neq k, k\neq l)
\end{array}\right\}\quad\ldots\ldots(\mathrm{A3})$$

where

$$F_{ki}=(H^{\mathrm{core}})_{ki}+\sum_{j=1}^{m}\{2(jk|G|ji)-(jk|G|ij)\}.\qquad\ldots\ldots(\mathrm{A4})$$

But if we are using self-consistent orbitals, the matrix F_{kl} is diagonal. Nesbet (1955) has emphasised the importance of this property in the reduction of similar matrix elements. Equations (A3) can then be written in the compact form (2.13)–(2.15).

REFERENCES

CONDON, E. U., and SHORTLEY, G. H., 1935, *The Theory of Atomic Spectra* (Cambridge : University Press).

DEWAR, M. J. S., and LONGUET-HIGGINS, H. C., 1954, *Proc. Phys. Soc.* A, **67**, 795.

KLEVENS, H. B., and PLATT, J. R., 1949, *J. Chem. Phys.*, **17**, 470.

LEWIS, G. N., and KASHA, M., 1944, *J. Amer. Chem. Soc.*, **66**, 2100.

MCCLURE, D. S., 1949, *J. Chem. Phys.*, **17**, 905.

NESBET, R. K., 1955, *Proc. Roy. Soc.*, in preparation.

PARISER, R., and PARR, R. G., 1953, *J. Chem. Phys.*, **21**, 767.

POPLE, J. A., 1953, *Trans. Faraday Soc.*, **49**, 1375.

ROOTHAAN, C. C. J., 1951, *Rev. Mod. Phys.*, **23**, 61.

Inelastic Collisions between Heavy Particles

IV : Contribution of Double Transitions to certain Cross Sections including that associated with the Ionization of Hydrogen Atoms in Fast Encounters with other Hydrogen Atoms

By D. R. BATES and G. W. GRIFFING†
Department of Applied Mathematics, The Queen's University of Belfast

MS. received 5*th August* 1954

Abstract. Born's approximation is used to calculate the cross sections associated with the processes $H(1s)+H(1s)\rightarrow H(3s, p \text{ or } d)+H(3s, p \text{ or } d)$ and $H(1s)+H(1s)\rightarrow H^{+}+e+H(3s, p \text{ or } d;\ \text{or } C)$ where C represents the continuum. These cross sections and others calculated in papers I and II are combined to yield the cross section for excitation to the third quantum level, the cross sections for ionization and the total cross section for all inelastic collisions. Both single and double transitions are taken in account. The ratio of the electron loss cross section to the electron capture cross section is computed.

---

§ 1. Introduction

Amongst the processes investigated in paper I of this series (Bates and Griffing 1953) were the single-transition collisions

$$H(1s\,|\,A)+H(1s\,|\,B)\rightarrow H(nl\,|\,A)+H(1s\,|\,B) \qquad \ldots\ldots(1)$$

and

$$H(1s\,|\,A)+H(1s\,|\,B)\rightarrow H^{+}(\,|\,A)+e(\kappa)+H(1s\,|\,B): \qquad \ldots\ldots(2)$$

in the first of these the hydrogen atom A is excited to the state nl; in the second it is ionized, the magnitude of the propagation vector of the ejected electron relative to the parent nucleus being between κ and $\kappa+d\kappa$; in neither does the other hydrogen atom B suffer any change of configuration. Attention was, however, drawn to the possibility that the double-transition collisions

$$\left.\begin{array}{lr} H(1s\,|\,A)+H(1s\,|\,B)\rightarrow H(nl\,|\,A)+H(n'l'\,|\,B) & (a)\\ \qquad\qquad (\text{or } H^{+}(\,|\,B)+e(\kappa')) & (b)\end{array}\right\} \ldots\ldots(3)$$

and

$$\left.\begin{array}{lr} H(1s\,|\,A)+H(1s\,|\,B)\rightarrow H^{+}(\,|\,A)+e(\kappa)+H(n'l'\,|\,B) & (a)\\ \qquad\qquad (\text{or } H^{+}(\,|\,B)+e(\kappa')) & (b)\end{array}\right\} \ldots\ldots(4)$$

might be important. In papers II and III (Bates and Griffing 1954, Moiseiwitsch and Stewart 1954) it was shown that at high impact energies such double-transition collisions give a far greater contribution to certain excitations than do the single-transition collisions. This makes it of interest to undertake the much more laborious task of making a corresponding study of ionization.

The present paper is mainly devoted to the calculation of $Q(1s\text{–}C;\ 1s\text{–}\Sigma)$, the cross section describing the ionization of a *specified* one of a pair of colliding hydrogen atoms, the other being left in *any* state. Denoting the cross sections for processes (4*a*) and (4*b*) by $Q(1\text{s–}\kappa;\ 1\text{s–}n'l')\,d\kappa$ and $Q(1\text{s–}\kappa;\ 1\text{s–}\kappa')\,d\kappa\,d\kappa'$ respectively and introducing

---

† Affiliated to the Cambridge Geophysics Research Directorate of the United States Air Force.

$$Q(1\text{s–C};\ 1\text{s–}n'l') = \int_\kappa Q(1\text{s–}\kappa;\ 1\text{s–}n'l')\,d\kappa \qquad \ldots\ldots(5)$$

$$Q(1\text{s–C};\ 1\text{s–C}) = \int_\kappa \int_\kappa Q(1\text{s–}\kappa;\ 1\text{s–}\kappa')\,d\kappa\,d\kappa' \qquad \ldots\ldots(6)$$

it is apparent that

$$Q(1\text{s–C};\ 1\text{s–}\Sigma) = \sum_{n'l'} Q(1\text{s–C};\ 1\text{s–}n'l'). \qquad \ldots\ldots(7)\dagger$$

Computations need only be carried out on $Q(1\text{s–C};\ 1\text{s–C})$ and on

$$Q(1\text{s–C};\ 1\text{s–}\overline{3\text{spd}}) \equiv Q(1\text{s–C};\ 1\text{s–3s}) + Q(1\text{s–C};\ 1\text{s–3p}) + Q(1\text{s–C};\ 1\text{s–3d}) \qquad \ldots\ldots(8)$$

since $Q(1\text{s–C};\ 1\text{s–1s})$ and $Q(1\text{s–C};\ 1\text{s–}\overline{2\text{sp}})$ have already been evaluated (cf. papers I and II) and since the states with principal quantum number 4 or higher may be neglected without causing a significant error.

In addition to their main use the partial cross sections are combined together to yield $Q(1\text{s–}\overline{3\text{spd}};\ 1\text{s–}\Sigma)$, the cross section for the excitation of a specified atom to the third quantum level. A further combination is taken to obtain the cross section associated with collisions in which *either or both* of the atoms are excited or ionized, that is the total inelastic cross section

$$\mathcal{Q}((1\text{s})^2 - (\Sigma, \Sigma')) = Q(1\text{s–1s};\ 1\text{s–}\Sigma') + \sum_{nl\neq 1\text{s}}{}' Q(1\text{s–}nl;\ 1\text{s–}\Sigma). \qquad \ldots\ldots(9)\ddagger$$

The inelastic cross section due to single transitions only

$$\mathcal{Q}((1\text{s})^2 - (1\text{s}, \Sigma')) = 2\sum_{nl\neq 1\text{s}}{}' Q(1\text{s–}nl;\ 1\text{s–1s}) \qquad \ldots\ldots(10)$$

is also computed.

§ 2. THEORY

It was shown in paper II that according to the simple Born approximation the cross sections for double-transition collisions between hydrogen atoms are given by

$$Q(1\text{s–}nl;\ 1\text{s–}n'l') = \left[\frac{8}{s^2}\int_{t_{\min}}^{t_{\max}} |\mathcal{I}(1\text{s–}nl)|^2 |\mathcal{I}(1\text{s–}n'l')|^2 t^{-3}\,dt\right] \pi a_0^2 \qquad \ldots(11)$$

$$Q(1\text{s–}\kappa;\ 1\text{s–}n'l')\,d\kappa = \left[\frac{8\,d\kappa}{s^2}\int_{t_{\min}}^{t_{\max}} |\mathcal{I}(1\text{s–}\kappa)|^2 |\mathcal{I}(1\text{s–}n'l')|^2 t^{-3}\,dt\right] \pi a_0^2 \qquad \ldots(12)$$

$$Q(1\text{s–}\kappa;\ 1\text{s–}\kappa')\,d\kappa\,d\kappa' = \left[\frac{8\,d\kappa\,d\kappa'}{s^2}\int_{t_{\min}}^{t_{\max}} |\mathcal{I}(1\text{s–}\kappa)|^2 |\mathcal{I}(1\text{s–}\kappa')|^2 t^{-3}\,dt\right] \pi a_0^2 \qquad ..(13)$$

where $s^2 = \tfrac{1}{2} m v_\text{i}^2 / I_\text{H}, \quad \mathbf{t} = 2\pi M(\mathbf{v}_\text{f} - \mathbf{v}_\text{i}) a_0 / h; \qquad \ldots\ldots(14)$

the $\mathcal{I}$'s are certain functions of t (which are displayed in paper I for the transitions with which we are concerned); $\mathbf{v}_\text{i}$ and $\mathbf{v}_\text{f}$ are the initial and final velocities of relative motion of the nuclei; m is the mass of the electron and M the reduced mass of the system; a_0 is the radius of the first Bohr orbit; and I_H is the binding energy of a normal atom (that is one rydberg). Formulae (11) and (12) require no comment.

---

† Here and throughout the paper the continuum is included in the summation.

‡ As in the earlier papers $1\text{s–}\Sigma'$ signifies $1\text{s–}\sum_{nl\neq 1\text{s}}{}' nl$.

It should be mentioned, however, that formula (13) depends on the assumption that each of the ejected electrons may be regarded as moving solely under the influence of the field of its parent nucleus. This assumption is justified by the fact that the velocity of ejection is usually very much smaller than the velocity of one nucleus relative to the other (cf. § 3.1). The situation is thus essentially the same as that which arises in ionization by electron impact (cf. Bates, Fundaminsky and Massey 1950).

An account of the procedure followed in evaluating the cross sections for double excitation and excitation–ionization collisions has been given in the earlier papers of the series and need not be repeated. Little, too, need be said on double ionization for the computational problem presented, though formidable in practice, is trivial in principle. From formulae (6) and (13) of the present paper and formula (27) of paper I it may be seen that

$$Q(\text{1s–C};\ \text{1s–C}) = \frac{64\pi a_0^2}{9s^2}$$

$$\times \int_{\kappa=0}^{\infty}\int_{\kappa'=0}^{\infty}\int_{x=w}^{\infty} \frac{f(x,\kappa)f(x,\kappa')}{(\kappa\kappa')^5\{1-\exp(-2\pi/\kappa)\}\{1-\exp(-2\pi/\kappa')\}}\,d\kappa\,d\kappa'\,dx \quad \ldots .(15)$$

where
$$f(x,y) = \frac{(1+3x+y^2)\exp[-(2/y)\tan^{-1}\{2y/1+x-y^2\}]}{[\{(1+x+y^2)/2y\}^2-x]^3} \quad \ldots\ldots(16)$$

and w is determined by the equation

$$s^2 = \frac{(2+\kappa^2+\kappa'^2)^2}{4w}\left\{1+\frac{mw}{M(2+\kappa^2+\kappa'^2)}\right\}^2. \quad \ldots\ldots(17)$$

A rather troublesome triple numerical integration must thus be carried out for each chosen value of the impact energy.

Several useful asymptotic formulae may readily be derived. It has previously been established that in the high energy limit

$$\mathcal{Q}((\text{1s})^2-(\Sigma,\Sigma')) \sim (209{\cdot}5/\mathcal{E})\pi a_0^2 \quad \ldots\ldots(18)$$

$$\mathcal{Q}((\text{1s})^2-(\text{1s},\Sigma')) \sim (82{\cdot}8/\mathcal{E})\pi a_0^2 \quad \ldots\ldots(19)$$

$\mathcal{E}$ being the impact energy† measured in kev (paper II). By the same method it follows that

$$Q(\text{1s–C};\ \text{1s–}\Sigma) \sim \frac{16\pi a_0^2}{3s^2}\int_{\kappa=0}^{\infty}\int_{x=0}^{\infty}\frac{f(x,\kappa)\{1-256/(4+x)^4\}}{x\kappa^5\{1-\exp(-2\pi/\kappa)\}}\,d\kappa\,dx$$

$$+\,Q(\text{1s–C};\ \text{1s–1s}) \sim (92{\cdot}0/\mathcal{E})\pi a_0^2 + Q(\text{1s–C};\ \text{1s–1s}). \quad \ldots\ldots(20)$$

§ 3. RESULTS

3.1. Figure 1 shows the derived cross sections $Q(\text{1s–C};\ \text{1s–2}\overline{\text{sp}})$, $Q(\text{1s–C};\ \text{1s–3}\overline{\text{spd}})$ and $Q(\text{1s–C};\ \text{1s–C})$ as functions of the impact energy $\mathcal{E}$, a log–log scale being used. In harmony with the trend found earlier, collisions in which only one atom is ionized have the larger cross section at low impact energies and collisions in which both atoms are ionized have the larger cross sections at high impact energies.

---

† The impact energy is the kinetic energy of one of the colliding atoms, the other being taken to be at rest.

Since $Q(1s{-}3\overline{spd};\,1s{-}1s)$ and $Q(1s{-}3\overline{spd};\,1s{-}2\overline{sp})$ are known from papers I and II the calculations on $Q(1s{-}3\overline{spd};\,1s{-}C)$ just reported together with similar calculations on $Q(1s{-}3\overline{spd};\,1s{-}3\overline{spd})$ enable $Q(1s{-}3\overline{spd};\,1s{-}\Sigma)$ to be determined, the contribution to the sum of transitions to the discrete states with $n \geqslant 4$ being insignificant. The [log (cross section), log (impact energy)] curves for the collision processes $(1s{-}3\overline{spd};\,1s{-}\Sigma)$ and $(1s{-}3\overline{spd};\,1s{-}1s)$ are displayed in figure 2 in which are included for comparison the corresponding curves for the collision processes $(1s{-}2\overline{sp};\,1s{-}\Sigma)$ and $(1s{-}2\overline{sp};\,1s{-}1s)$ these last being obtained from results presented in paper II. Double-transition collisions are relatively slightly less important for the excitation of the third quantum level than they are for the excitation of the second quantum level.

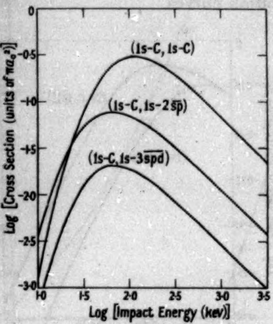

Figure 1.

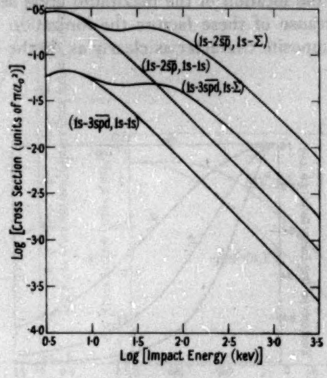

Figure 2.

Figure 1. Cross sections $Q(1s{-}C;\,1s{-}2\overline{sp})$, $Q(1s{-}C;\,1s{-}3\overline{spd})$ and $Q(1s{-}C;\,1s{-}C)$.

Figure 2. Cross sections $Q(1s{-}2\overline{sp};\,1s{-}\Sigma)$, $Q(1s{-}2\overline{sp};\,1s{-}1s)$, $Q(1s{-}3\overline{spd};\,1s{-}\Sigma)$ and $Q(1s{-}3\overline{spd};\,1s{-}1s)$.

During the course of the basic computation work $Q(1s{-}\kappa;\,1s{-}2\overline{sp})$, $Q(1s{-}\kappa;\,1s{-}3\overline{spd})$ and $Q(1s{-}\kappa;\,1s{-}C)$ were naturally obtained. Their sum is a close approximation to

$$Q(1s{-}\kappa;\,1s{-}\Sigma') = 2\kappa Q(1s{-}\kappa^2;\,1s{-}\Sigma'). \qquad \ldots\ldots(21)$$

For fixed $\mathcal{E}$ the function $Q(1s{-}\kappa^2;\,1s{-}\Sigma')$ gives the energy distribution of the electrons ejected from the stationary hydrogen atom in double-transition collisions. In figure 3 the distribution when $\mathcal{E}$ is 1000 kev† is compared with the corresponding distributions for the electrons ejected in single-transition collisions and for those ejected in collisions with protons (cf. paper I). As would be expected the distribution associated with double-transition collisions lies between the other two distributions.

---

† Provided it is high the impact energy has little influence on the distribution.

Figure 4 depicts the variations of $Q(1s\text{–}C\,;\ 1s\text{–}\Sigma)$ and $Q(1s\text{–}C\,;\ 1s\text{–}1s)$ with $\mathcal{E}$ on a log–log scale. In carrying out the summation required for the first of these cross sections, transitions to the higher discrete states were once again ignored. To demonstrate that this causes little error the asymptote to the true curve, given by formula (20), is also represented. As was predicted in paper II the influence of double-transition collisions in the case of ionization is much less than in the case of excitation. Moreover the location of the maximum cross section due to such collisions lies much closer, on the log (impact energy) scale, to the location of the maximum cross section due to single-transition collisions. Because of these factors the ionization curve does not by its form exhibit its composite character as clearly as do the excitation curves.

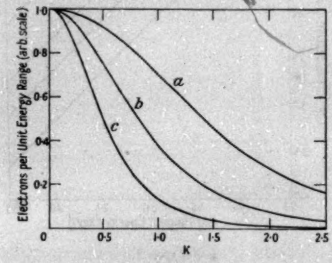

Figure 3.

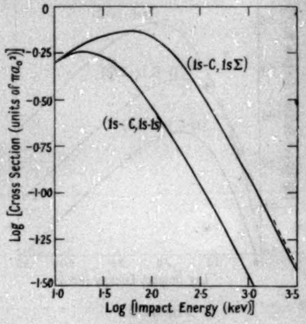

Figure 4.

Figure 3. Energy distribution of electrons ejected from a stationary hydrogen atom. Curves *a* and *b* respectively refer to single- and double-transition collisions with other hydrogen atoms; curve *c* refers to collisions with protons. In all cases the impact energy is 1000 kev. The units of κ are such that κ^2 is the kinetic energy of the ejected electron in rydbergs.

Figure 4. Cross sections $Q(1s\text{–}C\,;\ 1s\text{–}\Sigma)$ and $Q(1s\text{–}C\,;\ 1s\text{–}1s)$. The broken line represents the asymptotic behaviour of the former as given by formula (20) of the text.

Since the process

$$\mathrm{H}(1s\,|\,\mathrm{A}) + \mathrm{H}(1s\,|\,\mathrm{B}) \rightarrow \mathrm{H}^{+}(\,|\,\mathrm{A}) + \mathrm{H}^{-}((1s)^{2}\,|\,\mathrm{B}) \qquad \ldots\ldots(22)$$

is certainly very inefficient it is permissible to regard $Q(1s\text{–}C\,;\ 1s\text{–}\Sigma)$ as equivalent to σ_1, the *electron loss* cross section. Now σ_c, the *electron capture* cross section, that is the cross section associated with

$$\mathrm{H}^{+}(\,|\,\mathrm{A}) + \mathrm{H}(1s\,|\,\mathrm{B}) \rightarrow \mathrm{H}(\text{all } nl\,|\,\mathrm{A}) + \mathrm{H}^{+}(\,|\,\mathrm{B}), \qquad \ldots\ldots(23)$$

has been calculated, the Born approximation† being used as in the present paper (Bates and Dalgarno, 1952, 1953, Jackson and Schiff 1953). It is therefore possible to evaluate the Born approximation to σ_1/σ_c which is a ratio of considerable interest (figure 5).

---

† It has recently been asserted that the Born approximation grossly overestimates the capture cross section. This is incorrect. Such an overestimation is however caused by the erroneous Brinkman–Kramers approximation.

Finally the inelastic cross sections $\mathcal{Q}((1s)^2\text{–}(\Sigma,\Sigma'))$ and $\mathcal{Q}((1s)^2\text{–}(1s,\Sigma'))$, defined in equations (9) and (10) respectively, were computed. Transitions to the higher discrete states were as usual neglected.† The results are presented in the customary way in figure 6, formulae (18) and (19) being used to obtain the asymptotes. Clearly the relative importance of double-transition collisions is here not as great as it is for either excitation or ionization (cf. figures 2 and 4). The reason for this is that the contribution from certain of these (including (1s–C; 1s–C) which is the most effective double-transition collision at high impact energies) has a weighting of only *unity* in the summation involved whereas the contribution from all single-transition collisions has a weighting of *two*.

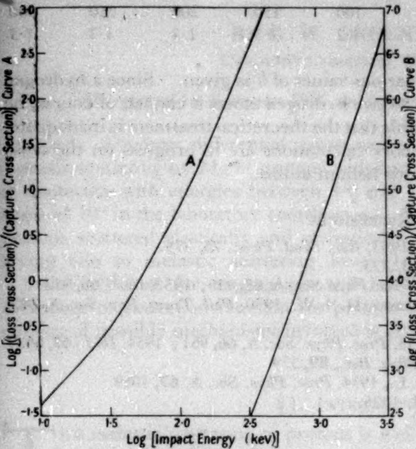

Figure 5.

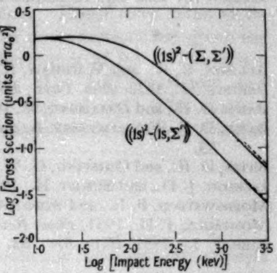

Figure 6.

Figure 5. Ratio of σ_l the electron loss cross section (for H(1s)+H(1s) collisions) to σ_c the electron capture cross section (for H^++H(1s) collisions).

Figure 6. Cross sections $\mathcal{Q}((1s)^2\text{–}(\Sigma,\Sigma'))$ and $\mathcal{Q}((1s)^2\text{–}(1s,\Sigma'))$. The broken lines represent the asymptotic behaviour as given by formulae (18) and (19) of the text.

3.2. Unfortunately laboratory studies have not yet been carried out on any of the processes we have studed. However, it is reasonable to suppose that a hydrogen molecule is approximately equivalent to two hydrogen atoms. Consequently at least some comparision data are available from the experiments of Bartels (1932), Montague (1951) and Ribe (1951) who have investigated the passage of H atoms and H^+ ions through ordinary gaseous hydrogen and have measured σ_l', the electron loss cross section, σ_c' the electron capture cross section and σ_l'/σ_c' the ratio of these cross sections (cf. the review by Allison and Warshaw 1953).

---

† The fractional error caused by this neglect, though still small, is naturally larger for $\mathcal{Q}((1s)^2\text{–}(\Sigma\Sigma'))$ than for the other cross sections.

Jackson and Schiff (1953) have shown that the calculated σ_c and measured σ_c' are almost equal for $\mathcal{E}$ between 50 kev and 150 kev (the upper limit of the impact energy range covered in the work on capture). The position regarding loss is rather different as can be seen from the table, in which the ratio of the calculated σ_l to the measured σ_l' at various values of $\mathcal{E}$ is given. Since a hydrogen molecule is not exactly equivalent to two hydrogen atoms it cannot, of course, be concluded from the entries in this table that the theoretical treatment is inadequate. To provide a better test of the theory calculations are in progress on the cross section for loss due to collisions with helium atoms.

Electron loss

Impact energy (kev)	50	100	150	200	250	300
Calculated σ_l/Measured σ_l'	1·0	1·2	1·3	1·3	1·3	1·3

REFERENCES

ALLISON, S. K., and WARSHAW, S. D., 1953, *Rev. Mod. Phys.*, **25,** 779.

BARTELS, H., 1932, *Ann. Phys., Lpz.*, **13,** 373.

BATES, D. R., and DALGARNO, A., 1952, *Proc. Phys. Soc.* A, **65,** 919; 1953, *Ibid.*, **66,** 972.

BATES, D. R., FUNDAMINSKY, A., and MASSEY, H. S. W., 1950, *Phil. Trans. Roy. Soc.* A, **243,** 93.

BATES, D. R., and GRIFFING, G. W., 1953, *Proc. Phys. Soc.* A, **66,** 961; 1954, *Ibid.*, **67,** 663.

JACKSON, J. D., and SCHIFF, H., 1953, *Phys. Rev.*, **89,** 359.

MOISEIWITSCH, B. L., and STEWART, A. L., 1954, *Proc. Phys. Soc.* A, **67,** 1069.

MONTAGUE, J. H., 1951, *Phys. Rev.*, **81,** 1026.

RIBE, F. L., 1951, *Phys. Rev.*, **83,** 1217.

Excitation Functions for the Scattering of Protons and Deuterons by Be and Mg

By G. W. GREENLEES†
Cavendish Laboratory, Cambridge

MS. received 1*st September* 1954 *and in amended form* 11*th October* 1954

Abstract. Absolute differential cross sections are given for the elastic and inelastic scattering by Mg of protons with energies between 3·0 and 6·5 Mev and of deuterons with energies between 4·0 and 7·8 Mev. These were taken at an angle of 70° in the laboratory coordinates. Similar cross sections are given for protons scattered elastically and inelastically by beryllium at 90°. The levels giving rise to inelastic scattering have Q values of $-1{\cdot}37 \pm 0{\cdot}04$ Mev and $-2{\cdot}43 \pm 0{\cdot}05$ Mev for magnesium and beryllium respectively. The marked difference of excitation function for protons and deuterons is noted and a discussion of possible mechanisms involved is given.

§1. Introduction

The inelastic scattering of protons is well known and has been investigated by several workers. It is generally assumed that the process involves the formation of a compound nucleus between the incident proton and the target nucleus with the subsequent emission of a proton of reduced energy from this compound state.

The inelastic scattering of deuterons is also well established (Greenlees, Kempton and Rhoderick 1949, Greenlees 1951, Holt and Young 1949, and others). Such a reaction is difficult to explain if the only mechanism involved in the inelastic scattering process requires the formation of a compound nucleus.

This paper describes experiments performed to measure the excitation functions for the inelastic and elastic scattering of both protons and deuterons. A comparison of the excitation functions for the (p, p′) and (d, d′) reaction is made in an effort to throw light on the mechanisms involved.

§2. Apparatus

The source of particles used was the Cavendish cyclotron giving a maximum energy of 8 Mev deuterons and 6·5 Mev protons.

The extracted beam from the cyclotron passes through a focusing magnet and then into a scattering chamber (figure 1). Curved plates, carrying windows at intervals of 10°, can be fixed into two recessed slots running from 20° to 90°. One such plate is shown in position in figure 1. The chamber is also fitted with an absorber wheel to vary the energy of the incident beam. Using this, different thicknesses of aluminium foil can be introduced into the path of the incident beam at a position between two sets of collimating stops. In the worst case (using the thickest absorbing foils) the angular spread of the incident beam on the target is ±5°. Proportional counters, of the end window type, together with aluminium absorbing foils, are used to detect the scattered particles.

---

† Now at Department of Physics, The University of Birmingham.

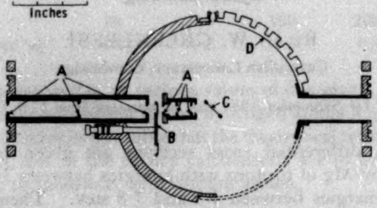

Figure 1. Scattering chamber. A, defining stops; B, foil wheel for incident energy variation; C, scattering foil; D, curved plate carrying observation windows.

§3. PROCEDURE

To determine the energy spectra of the scattered particles the counter was biased to give a differential curve so that only those particles having passed through the counter near the end of their range were recorded. The counting rate was observed as a function of thickness of aluminium foil placed in front of the counter. The beam was monitored using a second counter operated at low bias. The arrangement was such that the monitor could be calibrated to give absolute cross sections and it was found possible to do this quite consistently. However, for a large majority of the measurements, a more satisfactory method was used. The scattering foil of Mg or Be was backed with a piece of gold foil. Owing to the large difference in the atomic mass of gold and Mg, the recoil energy taken by the scattering nuclei is different and hence the energy and range of the elastically scattered particle varies. The two groups could be resolved with the present arrangement except for the experiments with low energy protons (less than 5 MeV). With low energy protons the calibrated monitor mentioned above was used. At the energies used in these experiments gold is assumed to give only elastic coulomb scattering. Since the variation of this scattering with energy and angle is accurately known, comparison of the two elastic groups and of other scattered groups gives an accurate estimate of relative intensities at different energies and angles. It also gives a reasonably accurate estimate of the absolute cross sections based on the assumption of coulomb scattering for gold. In the present experiments the ratio of peak heights of groups was taken as a measure of the ratio of the numbers of particles in each group. This procedure assumes the resolution to be independent of energy. Corrections to allow for this can be shown to be small in the present experiments.

Owing to the variation of gold scattering cross section with angle, precautions were taken to avoid movement of the beam on the target which involves a change of scattering angle. To avoid errors due to this effect, the beam was swung to and fro across the defining telescope giving uniform illumination of the target for all components of the beam. Oscillation of the beam was effected using two parallel plates fed with 50 c/s a.c. at 4 kv.

Final tests on the consistency of the whole arrangement showed it to be satisfactory to within the statistical errors of counting (1% in these tests).

§4. EXPERIMENTAL RESULTS

4.1. *Deuterons on Mg*

The target used in these experiments was a piece of pure Mg foil weighing 1·94 mg cm^{-2}, together with a piece of gold leaf weighing 0·18 mg cm^{-2}. This combination was found to give elastic peaks from Mg and gold of approximately the same size in the range of energies used. All results were taken at an angle of 70° for a range of incident energies between 3·8 and 7·5 MEV. A typical range curve obtained in these experiments is given in figure 2. The group marked C is due to elastic scattering from gold, the group marked B is due to elastic scattering from Mg and the group marked A is due to inelastic scattering from a level in Mg. The Q value for this (d, d′) reaction was found to be $-1·37 \pm 0·04$ MEV. Group A was only observable down to incident energies of 4·65 MEV due to its shorter range.

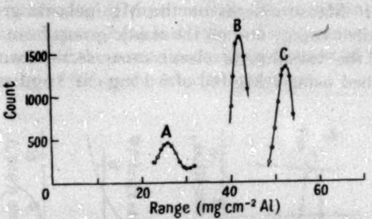

Figure 2. Range curve for the scattering of 7·5 MEV deuterons by Mg and gold. Foil: 1·94 mg cm^{-2} Mg and 0·18 mg cm^{-2} gold. Group A, inelastic scattering from Mg by a level of $1·37 \pm 0·04$ MEV excitation; Group B, elastic scattering from Mg; Group C, elastic scattering from gold.

The incident energy with no absorber in the path of the incident beam was determined by a magnetic deflection method. The incident energy for other cases was computed from the shift in position of the elastic peaks.

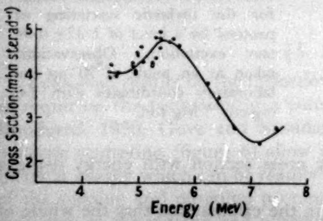

Figure 3. Variation of Mg differential cross section with incident energy for the inelastic scattering of deuterons by a level of 1·37 MEV excitation. Observations taken at an angle of 70° in the laboratory coordinates.

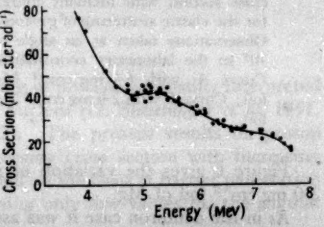

Figure 4. Variation of Mg differential cross section with incident energy for the elastic scattering of deuterons. Observations taken at an angle of 70° in the laboratory coordinates.

The ratios of the Mg to gold peak heights of the curves gives the ratio of Mg to gold scattering. These ratios can be used to obtain the absolute differential cross sections for inelastic and elastic scattering from Mg by using the Rutherford formula and the known weights of the targets. These cross sections are given in figures 3 and 4. In these calculations it was assumed that the whole of the Mg target gave rise to the observed scattering. For the inelastic scattering only one isotope will be responsible and this is almost certainly ^{24}Mg. This has an abundance of 78·6%, so that the inelastic cross sections should be increased accordingly.

These results are for an angle of 70° in the laboratory system. The angle in the centre-of-mass system varies slightly with the incident energy but this variation is small compared with the angular definition of the apparatus (approximately ± 3°) and can be neglected.

4.2. *Protons on Mg*

A set of range curves similar to those described above was taken using protons as the incident particles. Observations were made at an angle of 70° to the incident beam. Measurements on the Mg inelastic group extended from 4·0 to 6·5 MeV incident energy and on the elastic group from 3·0 to 6·5 MeV.

Figure 5 gives the variation of elastic cross section with incident energy. Curve A was obtained using a Mg foil of 6·1 mg cm^{-2} and curve B using one of 2·0 mg cm^{-2}.

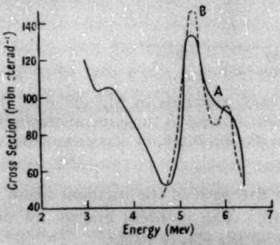

Figure 5. Variation of Mg differential cross section with incident energy for the elastic scattering of protons. Observations taken at an angle of 70° in the laboratory coordinates. Curve A, with 6·1 mg cm^{-2} Mg foil; Curve B with 2·0 mg cm^{-2} Mg foil.

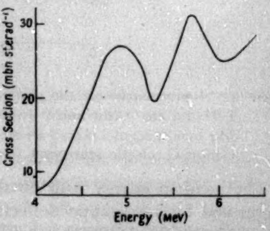

Figure 6. Variation of Mg differential cross section with incident energy for the inelastic scattering of protons by a level of 1·37 ± 0·04 MeV excitation. Observations taken at an angle of 70° in the laboratory coordinates with 2·0 mg cm^{-2} Mg foil.

Figure 6 gives the variation of inelastic cross section with energy using a 2·0 mg cm^{-2} foil of Mg.

As in the deuteron case it was assumed in the calculations that the whole of the Mg target gave rise to the elastic and inelastic scattering, no correction being made for isotopic abundance.

The observations were made at 70° in the laboratory system. The variation with energy of the centre-of-mass angle is small compared with the angular definition and sufficiently close to the value for deuterons to allow of a comparison.

4.3. *Protons on Be*

A Be and gold target was prepared by evaporating Be on to gold leaf *in vacuo* and the emitted range spectrum examined under proton bombardment. The exact weight of Be on the target was uncertain because of oxidation occurring in air. Neglecting this the foil used contained 1·85 mg cm^{-2} of Be and 0·54 mg cm^{-2} of gold.

The range curves obtained in these experiments were similar to those of figure 2 but exhibited five groups of particles. Three of these were due to elastic scattering from gold, oxygen and Be. The fourth group was due to deuterons from the Be (p, d) reaction and the fifth group was attributed to protons inelastically scattered from Be.

For group 4 the mean Q value of ten determinations was $0{\cdot}54 \pm 0{\cdot}05$ Mev; for group 5 the mean Q value of fifteen determinations was $-2{\cdot}43 \pm 0{\cdot}05$ Mev. These values are in good agreement with those of other workers (cf. Ajzenberg and Lauritsen 1952).

As before, these results were used to give the differential cross sections for the elastic and inelastic scattering of protons from Be at various incident energies. The results are given in figures 7 (*a*) and 7 (*b*). These curves will be subject to a systematic error because of the uncertain oxygen content of the foil. All these results are for scattering at 90° in the laboratory system.

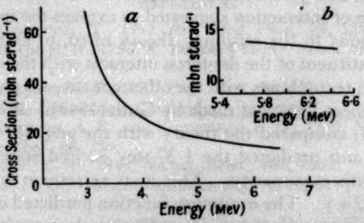

Figure 7. Variation of Be differential cross section with incident energy. Observations taken at an angle of 90° in the laboratory coordinates. (*a*) Elastic scattering of protons. (*b*) Inelastic scattering of protons by a level of $2{\cdot}43 \pm 0{\cdot}05$ Mev excitation.

§ 5. Discussion

Published results on the inelastic scattering of protons are readily interpreted as requiring the formation of a compound nucleus (cf. Shoemaker *et al.* 1951, Rhoderick 1950, Gove and Stoddard 1952). The present results on proton inelastic scattering (figure 6) show an increasing cross section with increasing incident energy which can be readily explained on the basis of barrier penetration of the ingoing and outgoing protons assuming only low values for the angular momenta of the ingoing and outgoing wave.

In contrast to this the evidence concerning the inelastic scattering of deuterons is difficult to fit into a compound nucleus theory. The angular distribution for the inelastic scattering of 8 Mev deuterons by the 1·37 Mev (2+) level of ^{24}Mg was measured by Holt and Young (1949). These results showed a marked forward peaking normally associated with high incident deuteron angular momenta.

These would not be expected to play any part in the compound nucleus formation The present results on the excitation function from the same level (figure 3) shows a decreasing cross section with increasing incident energy in contrast to the proton case (figure 6). These results are difficult to explain in terms of compound nucleus formation.

Two possible alternative mechanisms have been suggested to explain the inelastic scattering of deuterons. In the first the excitation is supposed due to the electric (coulomb) interaction of the two charged particles. The second type of interaction is analogous to the stripping theory for (d, p) and (d, n) reactions with only one of the constituents of the deuteron interacting with the nucleus.

Excitation by coulomb forces has been investigated by several authors (Weisskopf 1938, Mullin and Guth 1951, Huby and Newns 1951 a, Ter-Martirosyan 1952, and others). The treatment given by Ter-Martirosyan only applies when the incident energy is well below the barrier height and the energy transfer is small. These conditions are not fulfilled in the present experiments.

The transition from the ground state to the 1·37 MEV excited state of ^{24}Mg is known to be electric quadrupole. The treatment of Mullin and Guth for electric quadrupole transitions is known to be in error (Bohr and Mottelson 1953). As published, it predicts cross sections too small by a factor of 10^6 to explain the present results. Modification of the theory seems unlikely to increase the cross section sufficiently to predict the measured cross sections. The treatment given by Huby and Newns also predicts much smaller cross sections than are observed.

The second type of interaction suggested to explain the inelastic scattering of deuterons is analogous to the stripping theory of (d, p) and (d, n) reactions in which only one constituent of the deuteron interacts with the nucleus, raising it to an excited state, and recombines with the other constituent on re-emission. The first attempt along these lines was made by Guth (1945). A later paper by Huby and Newns (1951 b) compared the theory with the angular distribution of Holt and Young (1949) and predicted the 1·37 MEV excited state of ^{24}Mg to have a spin of 1, 2 or 3 with even parity. This is in agreement with the known properties of the state (2+). The excitation function predicted on this model gives a reasonable fit with the present results. The expression for the cross section contains a Bessel function giving rise to a set of maxima and minima in the excitation curve. These maxima and minima can be fitted to the corresponding variations in the experimental curve (figure 3). Whilst the theory gives a precise value for the cross section difficulty is encountered in assigning values to the physical quantities involved in the expression. If reasonable values are given to these quantities an estimate of the cross section can be made. Such estimates are of the correct order of magnitude to explain the observed cross sections. The evidence at present is in favour of a stripping type theory to explain the inelastic scattering of deuterons.

The results on elastic scattering here presented only apply to one angle of observation (70° laboratory coordinates). It is nevertheless interesting to compare the proton and deuteron results (figures 5 and 4). At high energies (above 5 MEV) the deuteron cross section falls steadily with increasing energy, approximately according to a coulomb law, whereas the proton cross section increases appreciably. In the proton case this is interpreted as scattering via a compound nucleus for incident proton energies above the barrier. The corresponding nuclear scattering does not occur appreciably with deuterons.

The excitation function for the elastic scattering of protons from ^{24}Mg has been measured by Mooring *et al.* (1951) using proton energies between 0·5 and 4·0 MEV. These results were taken at an angle of 164° (laboratory coordinates). This excitation function overlaps the present one (figure 5) in the region 3–4 MEV. Both sets of results show a broad peak in the cross section in this region and the magnitude of cross section observed is the same (110 mbn sterad^{-1}). The sharp discontinuities observed by Mooring *et al.* would not be noticed in the present results because of poorer resolution.

The beryllium elastic scattering results show appreciably greater cross sections than expected on a coulomb law (figure 7) over the whole observed energy range. Resonances observed in other work (cf. Ajzenberg and Lauritsen 1952) would not be resolved in the present experiment.

ACKNOWLEDGMENTS

The author wishes to acknowledge the help given by members of the Cambridge cyclotron team without which these experiments would not have been possible. In particular, thanks are due to Dr. A. E. Kempton for his interest in the work and assistance in recording the results. Thanks are also due to the Department of Scientific and Industrial Research for financial support covering the period of this work.

REFERENCES

AJZENBERG, F., and LAURITSEN, T., 1952, *Rev. Mod. Phys.*, **24,** 321.
BOHR, A., and MOTTELSON, B. R., 1953, *K. Danske Vidensk. Selsk. Mat. Fys. Medd.*, **27,** no. 16.
GOVE, H. E., and STODDARD, H. F., 1952, *Phys. Rev.*, **86,** 572.
GREENLEES, G. W., 1951, *Dissertation*, Cambridge University.
GREENLEES, G. W., KEMPTON, A. E., and RHODERICK, E. H., 1949, *Nature, Lond.*, **164,** 663.
GUTH, E., 1945, *Phys. Rev.*, **68,** 280.
HOLT, F. R., and YOUNG, C. T., 1949, *Nature, Lond.*, **164,** 1000.
HUBY, R., and NEWNS, H. C., 1951 a, *Proc. Phys. Soc.* A, **64,** 619; 1951 b, *Phil. Mag.* [7], **42,** 1442.
MOORING, F. P., KOESTER, L. J., GOLDBERG, E., SAXON, D., and KAUFMANN, S. G., 1951, *Phys. Rev.*, **84,** 703.
MULLIN, C. J., and GUTH, E., 1951, *Phys. Rev.*, **82,** 141.
RHODERICK, E. H., 1950, *Proc. Roy. Soc.* A, **201,** 348.
SHOEMAKER, F. C., FAULNER, J. E., BOURICIUS, G. M. B., KAUFMANN, S. G., and MOORING, F. P., 1951, *Phys. Rev.*, **83,** 1011.
TER-MARTIROSYAN, K. A., 1952, *J. Exp. Theor. Phys.*, **22,** 284.
WEISSKOPF, V. F., 1938, *Phys. Rev.*, **53,** 1018.

The Slow Neutron Cross Section of Scandium

By N. J. PATTENDEN
Atomic Energy Research Establishment, Harwell, Didcot, Berks.

MS. received 20th September 1954

Abstract. The neutron total cross section of scandium oxide has been measured from 0·0015 ev to 5000 ev. A resonance in scandium was observed at (3600 ± 200) ev, with $\Gamma \sim 180$ ev, and at lower energies the cross section varied in a way which could be explained by the existence of a level with parameters $E_r = -(130 \pm 30)$ ev, $\Gamma_n{}^0 = (0{\cdot}84 \pm 0{\cdot}25)$ ev and $\Gamma_a = (0{\cdot}25 \pm 0{\cdot}1)$ ev.

§ 1. INTRODUCTION

No measurements of the variation of the total cross section of scandium with slow neutron energy have yet been reported. However, several partial cross section measurements have been made. Seren, Friedlander and Turkel (1947) measured the activation cross section, and found it to be 22 barns ± 20%. Goldhaber and Muehlhause (1948) observed two activities in ^{46}Sc, of 20 second and 85 day half lives, and measured the activation cross section of the 20 second activity to be about 10 barns. They also measured cadmium ratios for both activities, and found them to be greater than the cadmium ratio of a $1/v$ absorber. They considered that this strong thermal absorption indicated the existence of a negative energy level in scandium. Harris, Muehlhause and Thomas (1950) measured the scandium cadmium ratio, and found that it corresponded to that of a $1/v$ absorber. Pile neutron cross section measurements using pile oscillators have been made by Harris, Muehlhause, Rasmussen, Schroeder, and Thomas (1950), Pomerance (1951), and Lockett and Bowell (1953). The latter also made a rough measurement of cadmium ratio, which showed scandium to be approximately a $1/v$ absorber. Hibdon (1952) measured the scattering cross section for thermal and cadmium filtered neutrons, and also the total cross section at certain energies corresponding to scattering resonances in his detector. From his results he concluded that there was a negative energy level in scandium, and also other levels in the thousand electron volts region. Milligan, Vernon, Levy and Peterson (1953) have measured the total and coherent scattering cross section at a neutron wavelength of 1·15 Å.

When the experiments reported in this paper were started, there were two discrepancies in the published data. One was the value of the pile neutron absorption cross section; this has now been resolved (Lockett and Bowell 1953). The other was whether scandium is a $1/v$ absorber. This question is resolved in this work, where the existence of a negative energy level is confirmed. Using the level parameters obtained here, it can be shown that a plot of the absorption cross section against energy drops slightly below the $1/v$ curve, but at 1 ev, it is only about 2% less. Hence Harris, Muehlhause and Thomas (1950) were not so likely to observe this departure as Goldhaber and Muehlhause (1948), who used a neutron beam containing more fast neutrons.

§ 2. EXPERIMENTAL METHODS

2.1. *Spectrometers*

The measurements were made with three spectrometers, using neutron beams from the Harwell pile, BEPO. Over the energy range 0·0015 ev to 0·10 ev, the measurements were taken with the slow chopper, previously described by Egelstaff (1954). Over the energy range 0·08 ev to 40 ev, the measurements were taken with the crystal spectrometer, previously described by Taylor (1952). Over the energy range 10 ev to 5000 ev, the measurements were taken with the fast chopper, previously described by Egelstaff (1953 a).

2.2. *Samples*

The samples for these measurements were prepared from ' specpure ' brand scandium oxide powder, supplied by Messrs. Johnson, Matthey and Co. Ltd. This powder was the same as that used for the Harwell pile oscillator experiment (Lockett and Bowell 1953), on which a chemical analysis had already been made. A further analysis for certain rare earth elements by an activation method showed that the contribution of impurities to the thermal absorption cross section was less than 0·5 barn. Before each sample for the transmission measurements was made, the powder to be used was heated in a vacuum furnace for about 10 hours at 400°c, to ensure that all water vapour was removed.

The containers for the samples used on the slow chopper and crystal spectrometer were hollow brass cylinders with a thin-walled Dural end, into which the powder was spread uniformly, and then compressed by a close fitting brass piston with a thin-walled Dural head. Thus the powder was formed into a disc whose dimensions were known accurately. The container used for the fast chopper sample was a rectangular aluminium tube, filled with powder and plugged at both ends. Before the samples were used, they were radiographed, to ensure that the powder was uniformly distributed. The three samples had thicknesses of oxide of 1·07 g cm^{-2}, 2·23 g cm^{-2}, and 4·90 g cm^{-2}.

2.3. *Counting Schedule*

For each spectrometer setting, whether time of flight or Bragg angle, the sample transmission was taken by counting the neutron beam intensity, first with the sample inserted in it, and then with the sample replaced by an identical empty container. In the cases of the slow and fast choppers, the beam intensity was monitored continuously with the same counter that was feeding into the timed channels. From the monitor counts, a correction for the difference in the mean beam intensity between the sample-in and the sample-out counts was obtained, and applied to the transmission. In the case of the slow chopper, background readings were taken at approximately every hour during counting; with the fast chopper, the background was taken continuously from a timed channel arranged to operate before the neutron pulse emerged from the rotor, but after all the neutrons from the previous pulse had passed the detector. In the case of the crystal spectrometer, the beam intensity was not monitored, but the total counts at each setting were split up into a series of short in and out runs, and background readings were taken between each run. From the transmission T the total cross section σ_t was obtained from the relation $T=\exp(-n\sigma_t)$ where n is the number of molecules per square centimetre of the sample in the direction of the neutron beam.

§ 3. RESULTS

The total cross section of scandium oxide has been measured from 0·0015 ev to 5000 ev. For the slow chopper points, a sufficient number of counts was taken for the statistical errors on the oxide cross sections to be less than 2% in all cases. The same limit applies to the crystal spectrometer points up to 5 ev. Above 5 ev, due to the counts to background ratio becoming less, the statistical errors steadily increase to 12% on the 39 ev point. For the fast chopper points, the statistical errors are about 7% for the points below 700 ev, and about 10% for the points above. The experimental points for scandium above 1 ev are plotted in figure 1, taking the oxygen cross section to be 3·73 barns (Melkonian 1949).

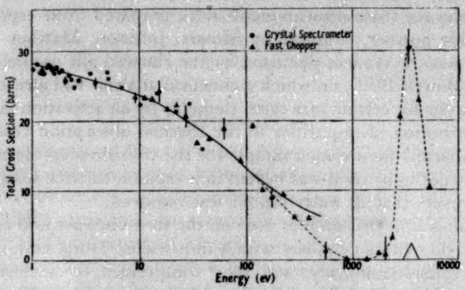

Figure 1. Total cross section of scandium.

It was thought that, at the low energy end, small-angle scattering (Krueger, Meneghetti, Ringo and Winsberg 1950, Weiss 1951) might be affecting the observed cross section. This was confirmed by repeating some of the slow chopper points with a different distance between sample and counter. When this distance was changed from 69 cm to 230 cm the observed cross section increased by 19% at 1500 μsec m^{-1}, 10% at 1200 μsec m^{-1} and was unchanged at 770 μsec m^{-1}. As it was inconvenient to reduce the sample-to-counter distance to less than 69 cm with the experimental arrangement used, there may be a systematic error in the results at times of flight greater than 1000 μsec m^{-1}, which makes the observed cross section greater than the true cross section. It is unlikely that this error is greater than 10% in the worst case, evaluated from the angle subtended by the counter at the sample, and the previous data on small angle scattering.

§ 4. ANALYSIS OF RESULTS

A complete analysis of the total cross section of the sample over the thermal range into its component absorption and scattering cross sections, in the manner described by Egelstaff (1953 b) is not possible, because the crystal diffraction breaks are not at all well marked. This is presumably due to the resolution of the spectrometer, and to the relatively large absorption and incoherent scattering components of the total cross section. Hence the coherent scattering cross section cannot be calculated. However, to show the magnitude of the diffraction breaks, the cross section is plotted on a time of flight scale in figure 2, and the cut-off positions of some of the more important planes put in.

The Harwell pile oscillator value for the pile neutron absorption cross section is (23 + 1 or − 3) barns (Lockett and Bowell 1953) related to a boron cross section of 710 barns. Although scandium is not a perfect $1/v$ absorber, at low energies it approaches this very closely, and at higher energies its absorption becomes small, so that it is a good approximation to assume that it obeys a $1/v$ law. A more recent value for the boron cross section at 2200 m sec^{-1} is 783 barns (Green, Littler, Lockett, Small, Spurway and Bowell 1954). Using this, and the improved chemical analysis of the material, we find for the absorption cross section $\sigma_a = 4{\cdot}05/\sqrt{E}$ barns ± 4% where E is the neutron energy in electron volts. Figure 3 shows the total scattering cross section, obtained by subtracting the absorption cross section from the measured total cross section, plotted on a time of flight scale. It is substantially constant down to about 30 μsec m^{-1}, at 23·6 barns ± 5%, which represents the free atom total scattering cross section. Multiplication by $\{(A+1)/A\}^2$ to obtain the bound atom cross section gives (24·7 ± 1·2) barns. The coherent scattering cross section of scandium has been measured by Milligan, Vernon, Levy and Peterson (1953), to be (17·5 ± 1·5) barns (positive amplitude), hence the incoherent scattering cross section is (7·2 ± 1·9) barns.

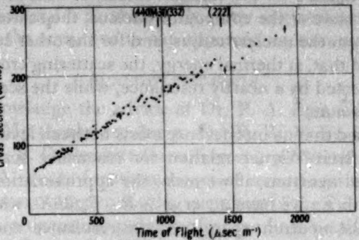

Figure 2. Total cross section of scandium oxide. At times of flight of more than 1000 μsec m^{-1}, there may be a negative systematic error of up to 10%, due to small angle scattering.

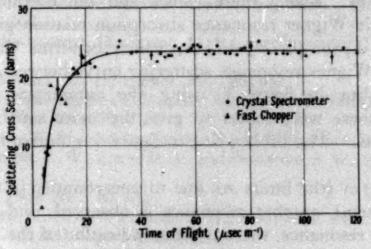

Figure 3. Scattering cross section of scandium.

Scandium is a mono-isotopic element whose nuclear spin is 7/2 (Mattauch 1949), hence the scattering lengths of each compound nuclear spin state can be calculated from the total and coherent scattering cross sections σ_s and σ_{coh}, using the usual relations (Hughes 1953). We find for the two scattering lengths, a_+ and a_-, the values $a_+ = +(0{\cdot}52 \pm 0{\cdot}18) \times 10^{-12}$ cm and $a_- = +(2{\cdot}04 \pm 0{\cdot}05) \times 10^{-12}$ cm or $a_+ = +(1{\cdot}85 \pm 0{\cdot}06) \times 10^{-12}$ cm and $a_- = +(0{\cdot}32 \pm 0{\cdot}28) \times 10^{-12}$ cm. These may be compared to the nuclear radius of scandium, $0{\cdot}53 \times 10^{-12}$ cm. Thus, for one spin state of the compound nucleus, the scattering length is significantly different from the nuclear radius, and for the other state it is not. From this it can be argued that, at thermal energy, the scattering cross section due to one state is strongly affected by a nearby resonance, while the scattering cross section for the other state is not.

It will be assumed that no interference exists between levels, and hence we may use the one-level Breit–Wigner relation for resonance scattering. From this relation, for thermal neutrons, if we make the approximations that E and Γ are small compared with E_r, we have a_+ or $a_- = R - \Gamma_n/2kE_r$, where k is the neutron wave number, E the neutron energy, E_r the resonance energy, R the nuclear radius and Γ_n and Γ the scattering and total widths respectively. Let us use for a_- the value $+2{\cdot}04 \times 10^{-12}$ cm. Then $\Gamma_n/2kE_r = -1{\cdot}50 \times 10^{-12}$ cm and hence E_r is negative. Assuming that the resonance is entirely scattering (i.e., $\Gamma_n \simeq \Gamma$), let us put this value into the Breit–Wigner relation, together with the measured scattering cross section at some energy other than thermal (say 100 ev). Then we obtain for E_r a value of $-(141 \pm 20)$ ev, which in turn gives a value for $\Gamma_n{}^0$ of $(0{\cdot}94 \pm 0{\cdot}17)$ ev, where $\Gamma_n{}^0$ is the scattering width at 1 ev. Alternatively, if we use for a_+ the value $+1{\cdot}85 \times 10^{-12}$ cm in the same way, we obtain values for the resonance parameters of $-(127 \pm 25)$ ev for E_r, and $(0{\cdot}74 \pm 0{\cdot}18)$ ev for $\Gamma_n{}^0$. As there is no way of knowing from this information which spin state is producing the level, all we can say is that the parameters are $E_r = -(130 \pm 30)$ ev, and $\Gamma_n{}^0 = (0{\cdot}84 \pm 0{\cdot}25)$ ev. Using these values and the thermal absorption cross section in the Breit–Wigner resonance absorption relation gives a value for the absorption width Γ_a of $(0{\cdot}25 \pm 0{\cdot}1)$ ev, which confirms the assumption that $\Gamma_n \simeq \Gamma$. A Breit–Wigner resonance scattering curve between 1 ev and 500 ev is drawn as a full line in figure 1, using the parameters $E_r = -137$ ev, and $\Gamma_n{}^0 = 0{\cdot}83$ ev, as these were found to give the most satisfactory fit with the experimental points. The broken line in figure 1 is drawn through the experimental points.

At (3600 ± 200) ev (the limits are due to uncertainties in the inherent delays in the timing system), another resonance is observed, and from the apparent asymmetry of this resonance, there is some indication of the existence of a third resonance at a few thousand electron volts higher energy. For the conditions under which the spectrometer was operating at the time of this measurement, the full width at half height of the resolution function at 3600 ev was about 600 ev, and therefore a resonance at this energy is poorly resolved. From a measurement of the area in the dip in the transmission curve at this energy, a value for $\sigma_0\Gamma^2$ of $(3{\cdot}4 \pm 1{\cdot}6) \times 10^7$ barn (ev)^2 is obtained in the manner described by Melkonian, Havens and Rainwater (1953), where σ_0 is the true peak cross section of the resonance. If this resonance is assumed to be entirely scattering, its peak cross section is given by the Breit–Wigner relation to be 370 barns, and this is the maximum possible value for σ_0. With the above value of $\sigma_0\Gamma^2$, this implies a minimum value for Γ of (300 ± 140) ev. It is very unlikely that the absorption width could contribute significantly to a total width of this magnitude, since absorption widths of that size are not known. Hence the assumption that the resonance is entirely scattering is reasonable. However, the peak cross section and width which this implies does not correspond with the known resolution width of the instrument and the observed peak cross section, which is only 31 barns. These favour the lower limit of Γ. Hence we may say that Γ is about 180 ev. The value of $\sigma_0\Gamma^2$ is necessarily very approximate, because of the difficulty in judging the area, due to the apparent asymmetry of the resonance.

ACKNOWLEDGMENTS

I gratefully acknowledge the advice of Dr. P. A. Egelstaff, obtained during many discussions. My thanks are due to Dr. R. W. Cornish, for the chemical analysis, to Mr. R. T. P. Derbyshire for radiographing the samples, to Mr. A. H. Baston and Mr. B. A. Booty for many hours of recording readings on the slow chopper and crystal spectrometer, to other members of the Pile Neutron Research Group for assistance in operating and recording readings on the fast chopper, and to the Pile Operating Group for their general cooperation and assistance.

REFERENCES

Egelstaff, P. A., 1953 a, *Proceedings of the Kjeller Conference on Heavy Water Reactors* (Kjeller per Lillestrøn : Jener Publications, No. 7); 1953 b, *A.E.R.E. Report N/R* 1147; 1954, *J. NuclearEnergy*, **1**, 57.

Goldhaber, M., and Muehlhause, C. O., 1948, *Phys. Rev.*, **74**, 1877.

Green, A., Littler, D. J., Lockett, E. E., Small, V. G., Spurway, A. H., and Bowell, E., 1954, *J. Nuclear Energy*, in the press.

Harris, S. P., Muehlhause, C. O., Rasmussen, S., Schroeder, M. P., and Thomas, G. E., 1950, *Phys. Rev.*, **80**, 342.

Harris, S. P., Muehlhause, C. O., and Thomas, G. E., 1950, *Phys. Rev.*, **79**, 11.

Hibdon, C. T., 1952, *Argonne National Laboratory, Progress Report* ANL–4982.

Hughes, D. J., 1953, *Pile Neutron Research* (Cambridge, Mass. : Addison-Wesley Publishing Co.), p. 262.

Krueger, H. H. A., Meneghetti, D., Ringo, G. R., and Winsberg, L., 1950, *Phys. Rev.*, **80**, 507.

Lockett, E. E., and Bowell, E., 1953, *Phys. Rev.*, **89**, 657.

Mattauch, J., 1949, *Isotopic Report* (Tübingen : Verlag der Z. Naturforsch.).

Melkonian, E., 1949, *Phys. Rev.*, **76**, 1750.

Melkonian, E., Havens, W. W., and Rainwater, L. J., 1953, *Phys. Rev.*, **92**, 702.

Milligan, W. O., Vernon, L. W., Levy, H. A., and Peterson, S. W., 1953, *J. Phys. Chem.*, **57**, 535.

Pomerance, H., 1951, *Phys. Rev.*, **83**, 641.

Seren, L., Friedlander, H. N., and Turkel, S. H., 1947, *Phys. Rev.*, **72**, 888.

Taylor, B. T., 1952, *A.E.R.E. Report N/R* 1005.

Weiss, R. J., 1951, *Phys. Rev.*, **83**, 379.

A Nuclear Emulsion Study of the Radioactive Decay of Actinium X(^{223}Ra)

By B. F. BAYMAN and M. A. S. ROSS
Department of Natural Philosophy, University of Edinburgh

Communicated by N. Feather ; *MS. received* 13*th August* 1954
and in final form 16*th September* 1954

Abstract. A nuclear emulsion method has been used to obtain the absolute intensity of the conversion electron spectrum following the radioactive decay of AcX. The results have been used in conjunction with the other available knowledge about the decay to show that in the level scheme of An there are three strong transitions having energies of 144, 154 and 268 kev and probably a fourth of 122 kev, all of which are either pure M1 or M1 with only a small admixture of E2. All four of these transitions probably go directly to the ground state of An. Estimates of the absolute intensities of these transitions and of several other less strong transitions have been made, and it is shown that the absolute intensity of K x-ray fluorescence is at least 0·3 and probably 0·5 quanta per disintegration.

---

§ 1. Introduction

The investigation of the radiations emitted in the disintegration of the X-body of the actinium series,

$$ {}^{227}_{90}\mathrm{RdAc} \xrightarrow[18\mathrm{d}]{\alpha} {}^{223}_{88}\mathrm{AcX} \xrightarrow[11\mathrm{d}]{\alpha} {}^{219}_{86}\mathrm{An} \xrightarrow[3{\cdot}9\mathrm{s}]{\alpha} {}^{215}_{84}\mathrm{AcA} $$

$$ \xrightarrow[1{\cdot}8\times10^{-3}\mathrm{s}]{99\%\ \alpha} {}^{211}_{82}\mathrm{AcB} \xrightarrow[36\mathrm{m}]{\beta} {}^{211}_{83}\mathrm{AcC} \xrightarrow[2{\cdot}16\mathrm{m}]{99{\cdot}68\%\ \alpha} {}^{207}_{81}\mathrm{AcC}'' \xrightarrow[4{\cdot}8\mathrm{m}]{\beta} {}^{207}_{82}\mathrm{Pb} $$

is rendered difficult by the short half-lives characteristic of the whole series. A further complication is the extreme richness of the internal conversion spectra of RdAc, AcX and An. These have been studied in magnetic deflection spectrometers by Hahn and Meitner (1925), Surugue (1937) and Ouang and Surugue (1944), and the first results of a new examination of the conversion spectrum of RdAc have been given by Frilley, Rosenblum, Valadares and Bouissières (1954). The conversion electrons of the An decay were examined in a cloud chamber by Bennett (1938). The result of this work is that with a few significant exceptions the attribution of the conversion lines to their element of origin is fairly certain. The relative intensities of the conversion lines have been obtained by visual estimation (Hahn and Meitner 1925) and by microphotometry (Surugue 1937). Using a rotating crystal spectrograph, Frilley (1940) has studied the γ-rays emitted by RdAc and by AcX derivatives. The α-spectrum of AcX has been obtained from RdAc and AcX sources by Curie, Rosenblum and co-workers (1932, 1933, 1936, 1937, 1952) and from an AcX source by Asaro and Perlman (1952). The latter authors found this spectrum difficult to measure because of the presence of a random background of tracks arising from the liberation of An by their source.

Consideration of this body of data reveals a number of anomalies concerning the decay of AcX. It appears that some transitions attributed to this decay and found to be strong both in emission and conversion cannot be fitted into the level scheme for An deduced from the fine structure of the α-particles of AcX. Moreover, the intensity of the accompanying K-fluorescence, which is ten times as great as that of any other element in the chain (Frilley 1940), is anomalously high. These observations suggest that, in the decay of AcX, α-emission leading directly to the ground state of An is feeble or non-existent and that γ- or electron-conversion transitions to the ground state occur in about 100% of all disintegrations. The object of the present work has been to elucidate this situation which is suitable for study by nuclear emulsion methods.

§ 2. EXPERIMENTAL METHOD

Advantage is taken of a diffusion effect occurring in nuclear emulsions (Demers 1947, Eichholz and Flack 1951) which makes it possible to separate the track produced by the α-particle of AcX from the tracks produced by the α- and β-particles of subsequent products. The emulsion is impregnated with a neutralized solution of the citrate of AcX + barium carrier, and is then dried and stored under controlled relative humidity for four days before processing. The immediate product of the AcX decay, An, is a rare gas which does not make a chemical bond with the gelatine and so diffuses away from the seat of the AcX decay. The products of subsequent disintegrations are normally chemically active and remain fixed in the gelatine, giving rise to the familiar 'radioactive star'. The higher the relative humidity during storage, the greater the diffusion, but high relative humidity introduces uncertainties regarding the stopping power and shrinkage factor of the emulsion. In order to ensure reliability of range measurements, the relative humidity normally used for nuclear emulsion work in this laboratory, namely 44%, was employed. The diffusion was then small.

A photograph of a typical good separation in Ilford G5 emulsion, 200 μ in thickness, is shown in figure 1 (Plate). The single α-track formed by the decay of AcX is here accompanied by two conversion electron tracks. The star includes two long electron tracks produced by the β-disintegration of AcB and AcC″. The smallness of the separations obtained at 44% relative humidity made the events rather difficult to study, and it was therefore necessary to adopt a rigid criterion for the acceptance of an event, namely that the An nucleus had diffused outside a cylinder of unlimited length, having a radius of 1 micron and the AcX α-track as axis. By ensuring that the track of the AcX α-particle did not lie in line with the star centre, this criterion eliminated spurious separations arising from the occurrence of a gap in the track near its origin. It also prevented bias in favour of events with larger An recoil energies. The remaining difficulties of interpretation were greatest when the track of a conversion electron associated with the α-particle of AcX became entangled with tracks belonging to the star.

Approximately 10 000 events were inspected. Of these, 809 satisfied the criterion of acceptance. If an electron track was certainly associated with the AcX α-track, it was recorded as a 'certain' electron. The number of grains forming its track was noted and the three-dimensional range of the track was measured. In a few cases the electron track passed out of the emulsion or was otherwise not sufficiently well defined to give a definite grain count or range measurement. If an electron track had a possible but not certain association with the AcX α-track, it was recorded as a 'doubtful' electron. The number of grains in such tracks was noted but range measurements were not made. The three-dimensional range of the separated α-track was measured to check its attribution to the AcX decay. Out of the 809 events, 367 show 'certain' electrons, 172 may or may not have electrons and 270 are certainly unaccompanied by electrons.

According to Zajac and Ross (1949), the standard deviation of either the grain counts or the ranges of the tracks of electrons of a monoenergetic group in nuclear emulsion is of the order of 20% of the mean grain count or mean range. When dealing with an extensive spectrum it is therefore convenient to display the spectrum as a function of the logarithm of grain count or range. This procedure gives all lines an approximately equal width; its effect on the line shape is unimportant.

A histogram of the 343 measured values of the range R of 'certain' electrons is shown in figure 2 as a function of log R, the interval of log R being 3 log (25/24).

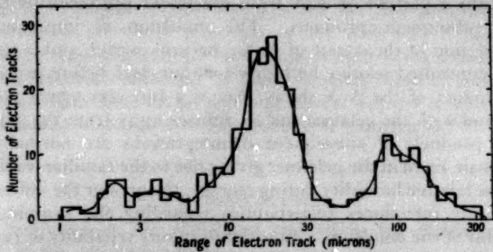

Figure 2. Range histogram of 'certain' electrons.

The accompanying smooth curve was calculated by Spencer's 21-term formula, the data being grouped in intervals of log (25/24). A logarithmic treatment of grain counts is less elegant since the grain count is not continuously variable. For comparison, however, the grain count histogram for the 354 'certain' electrons having definite grain counts is shown in figure 3. The logarithmic intervals are the same as those in figure 2. It is evident that the spectra shown in figures 2 and 3 are substantially the same, and that the grain counts give slightly higher resolution than the range measurements.

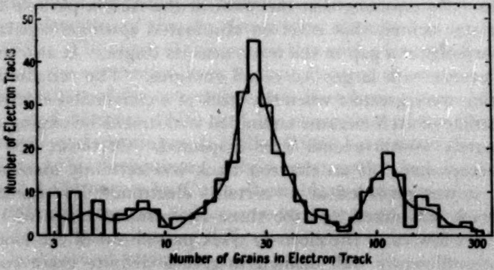

Figure 3. Grain number histogram of 'certain' electrons.

The group of 'certain' electrons, for each of which both grain count and range were available, was used to plot a dot diagram with log R as abscissa and log of grain count as ordinate. From this diagram the regression of log of grain count on log R was obtained. The relationship between mean range and energy was taken from Zajac and Ross (1949).

Of the electrons recorded as 'doubtful', 195 had a definite grain count. The histogram for this group, shown in figure 4, is clearly consistent with the assumption that these electrons have the same energy spectrum as the 'certain' electrons, although in figure 4 there is a relatively much lower intensity of tracks having grain counts between 12 and 58 than in the spectrum of 'certain' electrons. This is, however, to be expected, since electrons with such grain counts are less subject to difficulties of interpretation than those having either larger or smaller grain count. It is considered that while some 'doubtful' electrons may not be genuine, most of them do, in fact, belong to the spectrum of AcX.

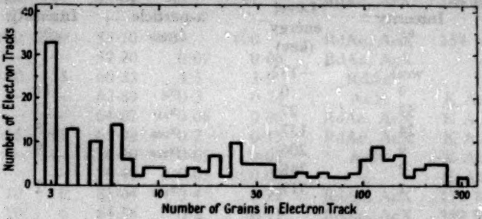

Figure 4. Grain number histogram of 'doubtful' electrons.

The spectrum shown in figures 2–4 resolves itself into four main regions. Definite limits for these regions were obtained from the dot diagram, and the total number of electrons in each region was counted for both 'certain' and 'doubtful' electrons. Results are shown in table 1. Electrons having neither definite range nor definite grain count are entered as 'unallocated'.

Table 1. The Number of Electrons in 809 Events

Group No.	I	II	III	IV	Unallocated
Approx. energy limits (kev)	<20	20–27	27–92	>92	
Range limits (μ)	<3	3–6	6–42	>42	
Grain count limits	<5	5–11	12–58	>58	
No. of 'certain' electrons	21	38	212	109	10
No. of 'doubtful' electrons	56	47	66	79	12

The electrons which fall in group I include the L-Auger electrons, a small proportion of which can normally be seen in such nuclear emulsion events. In seeking evidence of cascade de-excitation from electron–electron coincidences we therefore exclude all cases in which one of the electrons belongs to group I. We are then left with 12 events having two 'certain' electrons, 18 events having one certain and one 'doubtful' electron, and some 30 events having two 'doubtful' electrons. A discussion of the details of cascade events will be given in the next section.

§ 3. Discussion of the Decay Scheme of AcX

The evidence available for the discussion of the decay scheme of AcX includes

(i) The energies and intensities of the lines in the α-particle spectrum of AcX shown in table 2.

Table 2. Energy Levels of An from the α-particle fine Structure of AcX assuming for the 53% Group an Absolute Energy of 5·704 mev

Rosenblum *et al.* (1952)			Asaro and Perlman (1952)		
α-particle lines	Intensity %	Level energy (kev)	α-particle lines	Intensity %	Level energy (kev)
α_{-130}	weak	−132			
α_0	9	0	α_0	11	0
α_{26}	53	27	α_{31}	53	32
α_{134}	24	137	α_{143}	25	147
α_{202}	9	206	α_{210}	9	214
α_{243}	2	248			
α_{311}	3	317	α_{317}	2	323

(ii) The energies of the γ-rays from AcX and derivatives obtained by Frilley (1940) with attributions due to Surugue (1937), namely 144, 155, 180, 270 and 340 kev attributed to AcX, 123 kev attributed to An and 44, 52, 62 and 90·5 kev, unattributed. The relative intensities of some of these γ-rays are listed in table 4.

(iii) The energies and relative intensities of the lines in the magnetic spectrum of conversion electrons. The data are shown in table 3. Columns (2) and (3) of this table give the results of Hahn and Meitner (1925), columns (5) and (6) are taken from Surugue (1937). All lines attributed in whole or in part to AcX by Surugue are entered and in addition some to which he gave a different attribution. Column (8) gives Surugue's attribution and column (9) the interpretation of those lines which are attributed to AcX in the present paper. Some of these interpretations are discussed below. The factor given by Arnoult (1939) for converting photographic blackening to electron intensity is used to give the corrected intensities in columns (4) and (7).

(iv) The absolute intensities of conversion electrons in the four regions shown in table 1. The 'certain' and the 'certain' + 'doubtful' intensities give the minimum and approximate maximum values for each band. These limits, expressed as a percentage of the total number of acceptable events, are entered in column (10) of table 3. The counted number of electrons in each group is of course subject to statistical fluctuation. Reference to table 1 will show that statistical errors of 16%, 7% and 10% are applicable to groups II, III and IV respectively. These errors are small compared with the variation introduced by the 'doubtful' electrons.

By distributing each absolute band intensity in proportion to the relative intensities of the lines in the band as observed by Hahn and Meitner and by Surugue, two different estimates are obtained of minimum and approximate maximum absolute intensities of all the conversion lines. These calculations provide the data shown in columns (3) and (4) of table 4.

The 144 keV transition. Hahn and Meitner (1925) and Surugue (1937) agree that the conversion line at 45·6 kev arises partly from RdAc decay and partly from AcX decay. The work of Frilley *et al.* (1954) shows in agreement with

Table 3. Magnetic Spectrum of Conversion Electrons of AcX Decay

(1)	(2)	(3)	(4)	(5)	(6)	(7)	(8)	(9)	(10)
1	—	—	—	8·02	0·3	3·5	RdAc, AcX	L Auger	2·6 to 9·5%
2	—	—	—	9·10	0·07	0·76	AcX	L Auger	
3	—	—	—	17·75	12	76	AcX	—	
4	—	—	—	21·70	<0·05	<0·25	AcX	—	
5	23·7	20	92	23·71	1·5	6·9	RdAc	122 K	4·7 to 10·5%
6	45·4	80	121	45·64	60	91	RdAc, AcX	144 K	26·2 to 34·4%
7	48·3	10	13	—	—	—	—	?	
8	55·9	100	100	55·70	100	100	RdAc, AcX	154 K	
9	—	—	—	59·20	0·07	0·06	RdAc, AcX	—	
10	59·5	40	35	60·33	4·5	3·9	RdAc	?	
11	—	—	—	62·89	0·3	0·24	AcX	K Auger	
12	—	—	—	64·07	0·08	0·06	RdAc, AcX	K Auger	
13	66·0	15	11	65·92	0·2	0·15	RdAc, AcX	K Auger	
14	—	—	—	76·30	0·05	0·03	AcX	K Auger	
15	—	—	—	78·49	<0·05	<0·03	—	K Auger	
16	79·2	10	6	81·04	0·4	0·22	RdAc, AcX	179 K	
17	82·3	10	6	84·54	0·2	0·11	RdAc, AcX	182 K	
18	—	—	—	98·32	1·5	0·78	AcX	?	
19	104·2	10	5	103·8	2	1·05	An	122 L_{I}	13·5 to 23·2%
20	—	—	—	104·3	<0·05	<0·03	An	122 L_{II}	
21	113	10	6	—	—	—	—	211 K	
22	125·9	50	31	129·9	6	3·8	RdAc	144 L_{I}	
23	—	—	—	130·9	0·7	0·45	RdAc	144 L_{II}	
24	—	—	—	133·7	0·1	0·06	AcX	144 L_{III}	
25	135·5	50	33	134·3	8	5·4	AcX	154 L_{I}	
26	—	—	—	136·0	1	0·7	AcX	154 L_{II}	
27	138·5	25	17	139·1	0·07	0·05	AcX	—	
28	—	—	—	146·5	0·05	0·04	AcX	?	
29	148·2	15	11	149·2	0·7	0·5	RdAc, AcX	154 M	
30	151·2	15	11	151·3	0·6	0·44	—	154 N	
31	—	—	—	161·8	0·05	0·036	AcX	179 L	
32	170·8	100	77	169·8	20	15·5	RdAc, AcX	268 K	
33	175·8	25	20	—	—	—	—	?	
34	179·8	15	12	181·5	0·8	0·6	AcX, An	An	
35	—	—	—	213·4	<0·05	<0·05	AcX	?	
36	222·8	30	25	223·6	2	1·7	AcX	322 K	
37	236·7	30	26	238·2	0·05	0·05	—	335 K	
38	250·5	30	26	249·0	2·5	2·2	RdAc, AcX, An	268 L	
39	—	—	—	261·4	0·4	0·36	RdAc, AcX	?	
40	—	—	—	304·1	0·1	0·1	AcX	322 L	
41	—	—	—	329·6	<0·05	<0·05	AcX	?	
42	—	—	—	346	0·05	0·05	AcX active dep.	444 K	
43	—	—	—	426	<0·05	<0·05	AcX	444 L	

(1) Line number, (2), (3), (4) energy (kev), relative blackening and corrected relative intensity in the AcX spectrum of Hahn and Meitner, (5), (6), (7) energy (kev), relative blackening and corrected relative intensity in Surugue's spectrum, (8) Surugue's attribution, (9) present interpretation (AcX lines), (10) total intensity per 100 disintegrations in the group of lines.

Lines 3, 5, 6, 8, 19, 20, 22, 23, 24. See discussion below.

Line 10. From Frilley *et al.* (1954) we deduce that 4·0 of the intensity 4·5 (Surugue) comes from AcX: corrected rel. intensity is 3·5.

Line 38. From Hahn and Meitner we deduce that 2·0 of the intensity 2·5 (Surugue) comes from AcX: corrected rel. intensity is 1·8.

Table 4. Intensities of Transitions in the An Nucleus Following AcX Decay

(1)	(2)	(3)	(4)	(5)	(6)	(7)†	(8)
5	122 K	4·7 –10·5	4·7 –10·5				
19	122 L_I	0·2 – 0·4	0·43– 0·74	25	13	4	5·5–12·5
20	122 L_{II}		0·02				
6	144 K	10·9 –14·2	10·9 –14·3				
22	144 L_I	1·4 – 2·4	1·5 – 2·7	7	5	6	14·3–19·9
23	144 L_{II}		0·18– 0·32				
24	144 L_{III}		0·02– 0·04				
8	154 K	9·0 –11·8	14·7 –19·3				
25	154 L_I	1·5 – 2·6	2·2 – 3·8	5	5	12	13·8–28·6
26	154 L_{II}		0·29– 0·49				
27	154 L_{III}		0·02– 0·03				
29	154 M	0·5 – 0·9	0·20– 0·35				
30	154 N		0·18– 0·31				
16	179 K	0·5 – 0·7	0·03– 0·04				
31	179 L		0·01– 0·03			1	
17	182 K	0·5 – 0·7					
21	211 K	0·3 – 0·5					
32	268 K	3·5 – 6·0	6·3 –10·9	3	9	20	8·3–23·7
38	268 L	1·2 – 2·0	0·73– 1·27				
36	322 K	1·1 – 1·9	0·7 – 1·2				
40	322 L		0·04– 0·07				
37	335 K	1·2 – 2·0	0·02– 0·03			15	
42	444 K		0·02– 0·03				
43	444 L		0·03				

(1) line number, (2) transition energy (kev) and shell of conversion, (3) and (4) intensity per 100 disintegrations according to Hahn and Meitner, and Surugue, respectively, (5) K/L ratio from column (3), (6) K/L ratio from column (4), (7) approximate relative intensity of γ-radiation, (8) calculated total intensity of the transition per 100 disintegrations.

† Approximate values kindly provided by M. Frilley.

Hahn and Meitner that in the electron spectrum of pure RdAc the lines at 43 and 46 kev have an intensity ratio of 9 : 10. Surugue's spectrum of RdAc in equilibrium with its products shows an intensity ratio for these lines of 10 : 60. We conclude that for the line at 46 kev, 49 out of the 60 parts on Surugue's intensity scale come from AcX or a derivative. Meitner's (1925) assignment of the stronger part of this line to K-conversion of a γ-ray of 144 kev in the AcX decay is supported by the observation of a γ-ray of this energy (Frilley 1940) and by Hahn and Meitner's observation of relatively strong lines at energies appropriate for L_I and M_I conversion (Meitner's assignments). The energy tabulated by Surugue for the L_I line appears to be about 4 kev too high.

The 122, 154 *and* 268 *keV transitions.* Both Hahn and Meitner and Surugue find a moderately strong line at 23·7 kev. Hahn and Meitner attribute it to AcX decay, Surugue attributes it to RdAc. Frilley *et al.* (1954) say it is not a RdAc line. Our spectrum shows an appreciable intensity in the band 20–27 kev and supports the attribution of the 23·7 kev line to AcX. In figure 1 the shorter electron track associated with the separated α-particle track belongs to the line. We propose to assign this line to K-conversion of a transition of 122 kev. In support of this assignment Frilley (1940) finds a γ-ray of 123 kev from AcX and derivatives. Further, there is a line in Hahn and Meitner's AcX spectrum at 104·2 kev and two lines in Surugue's spectrum at 103·8 and 104·3 kev. Surugue's attribution of these lines to An is not confirmed by Bennett (1938). We assign the lines at 104 kev to L-conversion of the transition of 122 kev. However, we must emphasize that further work is required to substantiate the existence of this proposed transition. There is a further difficulty in the low-energy region, the occurrence of a very strong line in the spectrum of Surugue at 17·75 kev attributed to AcX. There is no visible counterpart in the apparently amply sensitive recordings of Hahn and Meitner and we therefore disregard this line. Inconsistencies do not arise in connection with the transitions of 154 and 268 kev. These are found to be strong both in emission and conversion and their attribution to AcX appears to be quite certain.

Level scheme of Asaro and Perlman. Turning now to the level scheme of An given by the α-particle spectrum of AcX (table 2, data of Asaro and Perlman 1952) it appears that none of the transitions 122, 154 and 268 kev corresponds to an energy difference between levels excited by α-emission. It is also clear that the 268 kev transition, having a conversion intensity of at least 4·7%, cannot on intensity grounds be fitted into this scheme unless a level is introduced below the lowest level found by Asaro and Perlman. If, however, it is assumed that the ground state of An lies 122 kev below the lowest level found by Asaro and Perlman, it becomes possible to accommodate not only the 154 and 268 kev transitions, but also the much weaker transitions of 335 and 444 kev for which there is evidence in table 3, all these transitions then going to the assumed ground state (see figure 5(*a*)). It may be noted that Rosenblum *et al.* (1952) found evidence of a weak α-line which he attributed to AcX and which lies within 10 kev of the energy proposed here for the ground state.

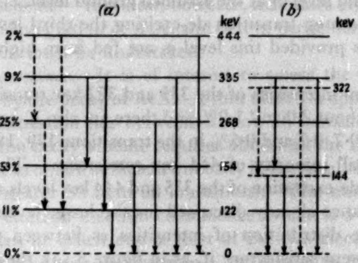

Figure 5. Proposed level scheme of An based on the data of Asaro and Perlman (1952).

It will now be shown that, assuming this decay scheme and using the intensities in table 4, the transitions of 122, 144, 154 and 268 kev are either pure M1 or predominantly M1 with a small admixture of E2. The K/L ratios shown in table 4 are too large for predominant E2 or higher electric polarities. From the approximate constancy (within a factor of 5) of the ratio of K-conversion intensity to γ-ray relative intensity, it follows that if one of these transitions is E1 all must be E1. The resulting total intensities of the 144, 154 and 268 kev transitions would in this case be too large to be accommodated otherwise than in series in a cascade descending from a level not higher than the 154 kev level. Such a cascade would imply a total disintegration energy not less than 6·38 Mev or at least 0·3 Mev greater than that required by Feather (1953). E1 transitions are therefore excluded. The K/L ratios are too large for high magnetic polarities and suggest M1 but do not in all cases exclude M2. M2 can be ruled out however by the ratios of conversion in the $(L_I + L_{II})$ and L_{III} shells using Surugue's data.

In column (8) of table 4 the total intensity is entered for the four strong transitions, assuming these to be pure M1. The intensity is found by calculating the γ-radiation intensity from the observed K-conversion intensity using the internal conversion coefficients of Rose *et al.* (1951 and private communication) and adding to the total observed conversion intensity. The values should be slightly raised above those shown in the table to take account of weak conversion lines. Still higher intensities would result if a small admixture of E2 were assumed. The following argument is however independent of such minor intensity changes.

The main problem presented by the modified Asaro and Perlman scheme concerns the total intensity of transitions exciting and de-exciting the first (122 kev) level. This is directly fed (11%) by α-emission and appears to be fed also by the strong 144 kev transition. It is clear, however, that the maximum intensity allowed by our measurements is only sufficient to de-excite a small feed to the level in addition to its primary excitation. There is as yet no definite evidence of electron or γ-ray lines which could form a cascade in parallel with the 122 kev transition. But even if such a cascade exists a difficulty remains, for the 154 kev transition to ground does not seem strong enough to carry all de-excitation of the second level even if some admixture of E2 polarity is taken into account. If, however, the 144 and 154 kev transitions both pass to ground, both difficulties are overcome. It is of course necessary to postulate a level splitting of 10 kev either at the second level or at the assumed ground level. The 268 kev transition is now the only strong transition de-exciting the third level and its intensity is sufficient for this provided this level is not fed from higher levels to any great extent.

The maximum intensities of the 335 and 322 kev transitions in K-conversion are respectively about 2·0 and 1·9% and there are also K-conversion intensities of not greater than 0·7, 0·7 and 0·5% in the transitions 179, 182 and 211 kev respectively, and a small intensity of 444 kev conversion. These intensities appear adequate for the de-excitation of the 335 and 444 kev levels and should not disturb the intensity balance already discussed for the lower levels.

However, the distribution of intensities as between the 335 and 444 kev levels does not seem satisfactory if, as in figure 5 (*a*), the 444, 322 and 182 kev transitions all de-excite the highest level. It may be necessary to postulate a splitting of the 335 kev level and the de-excitation of the resulting doublet by all four of the transitions 335, 322, 182 and 179 kev with $322 = 144 + 179$ and $335 = 154 + 182$ (figure 5 (*b*)).

Level scheme of Rosenblum et al. The level scheme of Rosenblum is in its principal features consistent with the level scheme of Asaro and Perlman, the main difference between the two schemes being the finding by Rosenblum of a level of 2% excitation at about 380 kev above the ground level. This introduces the possibility of transitions between neighbouring levels into which γ-rays of 44 and 62 kev energy might be fitted. The existence of a 322 kev level as shown in figure 5 (*b*) permits of a transition between this level and the 268 kev level of about the same energy as the 52 kev γ-ray. However, the absolute intensity of such transitions would be low and they should tend to occur in cascades.

Cascade evidence. The discussion of the cascade evidence is confined to the 30 cases of electron–electron coincidence in which at least one of the electrons is 'certain'. There are seven or eight examples in the cascades of the occurrence of conversion electrons having 14–18 grains, or an energy of about 35 kev. This electron line is also suggested by small bulges in the smooth curves of figures 2 and 3. Some confirmation of the existence of such a line is also found in Surugue's spectrum, for there is a line in his spectrum (not shown in table 3) at 33·92 kev which appears too strong to be entirely accounted for as L_{III} conversion of the 50 kev transition following the decay of RdAc (Frilley *et al.* 1954). The line may be assigned either to L-conversion of a transition of 52 kev, for which there is γ-ray evidence (Frilley 1940), or to K-conversion of a transition of 132 kev, in which case the γ-ray would coincide with the second-order spectrum of 268 kev.

The detailed information provided by the electron–electron coincidences includes the following events :

(*a*) Conversion of 268 kev with an electron of ~35 kev: 2 cases.
(*b*) Conversion of ~144 (or ~62) kev with an electron of ~35 kev: 4 cases.
(*c*) Conversion of ~144 (or ~62) kev with conversion of 122 kev: 5 cases.
(*d*) Conversion of 154 or 144 (or 62) kev with conversion of 179 or 182 kev: 5 to 7 cases.
(*e*) There are 5 or 6 events which could be K-conversions followed by K-Auger electrons

The events (*a*) indicate that the ~35 kev conversion electron arises in a level higher than the 268 kev level. (*c*) suggests the existence of a weak transition of 148 kev between the 268 and 122 kev levels. (*b*) is most easily interpreted as a cascade of ~62 + 44 kev between the 444 and 335 kev levels. The occurrence of (*d*) is implied by the decay scheme. It is clear, however, that more evidence is required on the details of the disintegration of AcX, and that in particular a high resolution coincidence experiment must be undertaken.

Intensity of K-fluorescence. It is of interest to assess the total intensity of K x-radiation excited by the decay of AcX. From table 3 it appears that the total intensity of K-shell ionization lies between 30 and 56 ionizations per 100 disintegrations. Since the decay scheme requires almost all the doubtful electrons to be included in order to obtain sufficient intensity in the transitions, the probable intensity is certainly nearer 56 than 30 ionizations. The number of K-Auger electrons seen in the electron–electron coincidence events is 5 to 6, considering only those coincidences in which one at least of the two electrons is 'certain'. The total number of K-Auger electrons may be nearer to 10 out of the 809 acceptable events. This indicates a fluorescence yield of about 98 ± 1% and a K-fluorescence intensity of between 30 and 55 quanta per 100 disintegrations. This is certainly an abnormally high intensity and is entirely consistent with Frilley's (1940) statement that the K-fluorescence of element 86 is ten times that of any other element in the chain. If our intensities are accurate it follows that the other elements of the chain show intensities of K-fluorescence of the order of 5 quanta per 100 disintegrations.

ACKNOWLEDGMENTS

The authors wish to thank Dr. N. Miller for his advice on the radiochemical separations. The participation in this work by one of us (B.F.B.) was made possible by a Fulbright Award.

References

Arnoult, R., 1939, *Ann. Phys., Paris*, **12**, 282.

Asaro, F., 1953, *Thesis*, University of California, Berkeley, *UCRL*–2180, 127.

Asaro, F., and **Perlman**, I., 1952, results quoted in *Tables of Isotopes, UCRL*–1928; 1953, *Rev. Mod. Phys.*, **25**, 469.

Bennett, W. E., 1938, *Proc. Camb. Phil. Soc.*, **34**, 282.

Curie, Mme. P., and **Rosenblum**, S., 1932, *C.R. Acad. Sci., Paris*, **194**, 1232; 1933, *Ibid.*, **196**, 1598.

Demers, P., 1947, *Phys. Rev.*, **72**, 536.

Eichholz, G. G., and **Flack**, F. C., 1951, *J. Chem. Phys.*, **19**, 363.

Feather, N., 1953, *Advances in Physics* (*Phil. Mag.* suppl.), **2**, 141.

Frilley, M., 1940, *J. Phys. Radium*, **1**, 34.

Frilley, M., **Rosenblum**, S., **Valadares**, M., and **Bouissières**, G., 1954, *J. Phys. Radium*, **15**, 45.

Hahn, O., and **Meitner**, L., 1925, *Z. Phys.*, **34**, 795.

Meitner, L., 1925, *Z. Phys.*, **34**, 807.

Ouang, T. T., and **Surugue**, J., 1944, *C.R. Acad. Sci., Paris*, **218**, 591.

Rose, M. E., *et al.*, 1951, *Phys. Pev.*, **83**, 79.

Rosenblum, S., **Guillot**, M., **Perey**, M., 1936, *C.R. Acad. Sci., Paris*, 202, 1274; 1937, *Ibid.*, **204**, 175.

Rosenblum, S., **Perey**, M., **Valadares**, M., **Guillot**, M., 1952, private communication to G. T. Seaborg, quoted in 1953, *Rev. Mod. Phys.*, **25**, 469.

Surugue, J., 1937, *Ann. Phys., Paris*, **8**, 484.

Zajac, B., and **Ross**, M. A. S., 1949, *Nature, Lond.*, **164**, 311.

The Theory of the Reflectivity of Metals

By R. WOLFE†
H. H. Wills Physical Laboratory, University of Bristol

Communicated by N. F. Mott; MS. received 8th September 1954

Abstract. The reflectivity of an ideal metal is calculated for infra-red light by a quantum-mechanical method. It is assumed that the conduction electrons in the metal absorb light by a photoelectric process which takes place near the surface, that these electrons behave as if they are free and that the light within the metal decays according to the formula given by the classical skin effect. Two types of wave functions are assumed for the electrons, corresponding to the assumptions of specular and diffuse reflection of the electrons at the surface of the metal. The absorptivity ($1-R$, where R is the reflectivity) in the case of specular electron reflection is found to be $A_S=(Ne^2/2\pi m\nu^2)v_0^3/c^3$; for diffuse reflection, $A_D=\frac{3}{4}v_0/c$. These results are the same as those obtained by Holstein and by Dingle using different methods which are essentially classical. Since A_D gives the better agreement with experiment, it is concluded that the 'diffuse reflection' wave functions are a better approximation to the exact electronic wave functions than the 'specular reflection' wave functions which have been used in previous work on the photoelectric effect and reflectivity.

§ 1. INTRODUCTION

In the theories which do not consider explicitly the reflection of electrons at the surface, the reflectivity of a metal is found to tend to unity as the conductivity increases (cf. Mott and Jones 1936). Recent experiments have shown that the reflectivity of metallic surfaces, however prepared, is lower than that predicted by these theories and that it tends to a limit which is less than unity as the temperature is lowered (Ramanathan 1952, Schultz 1954). The theory derived by Dingle (1953 a) which is an extension of the theory of the anomalous skin effect (Reuter and Sondheimer 1948, Sondheimer 1952) gives results which are in much better agreement with experiment. For the limiting case of infinite electron free paths and infra-red light, Holstein (1952) found the same results by a much simpler physical argument. Both authors found that the reflectivity depends very markedly on the behaviour of the electrons at the surface of the metal. The close agreement with experiment was found using the assumption of diffuse electron reflection at the surface rather than specular reflection.

In the calculations based on the theory of the anomalous skin effect, the change in the electronic distribution function due to the light is found, and the surface impedance which is determined by this electron distribution is used to calculate the absorptivity. In Holstein's treatment, the energy absorbed by the electrons as they oscillate in the alternating electric field of the light, which decays exponentially within the metal as in the normal skin effect, gives the absorptivity directly. In both methods the interaction between the electrons and the light is assumed to be given by the classical electromagnetic equations.

---

† Now at the Research Laboratories of the General Electric Co. Ltd., Wembley, Middlesex.

In this paper the problem is treated quantum-mechanically. The conduction electrons are assumed to absorb energy from the light by a photoelectric process. The approximations are the same as those used by Holstein. By considering an ideal metal at 0°K the effects of thermal vibrations and impurities in restricting the free path of the electrons are eliminated. The variation of the light in the metal is assumed to be given by the normal skin effect calculations. To obtain simple expressions for the absorptivity, only the infra-red region of the spectrum is considered. The transition probabilities due to the light are calculated for two different types of electronic wave functions corresponding to the two types of electron reflection in the previous theories. From these the total energy absorbed is calculated and then the absorptivities are found.

§ 2. ASSUMPTIONS

We assume that the electrons in the conduction band of the metal behave like free electrons of effective mass m except that they are confined to a rectangular box which extends distances L_1, L_2 and L_3 from the origin in the positive x, y and z directions respectively. There are no imperfections or thermal oscillations to scatter the electrons, so that their free path is infinite. We make two different assumptions about the behaviour of the electrons at the surface of the metal, the plane $x=0$:

Assumption S (S for specular). If the surface is perfectly smooth the electron density is uniform throughout the metal and vanishes at the surface and outside the metal. The electronic wave functions in the metal are of the form:

$$\psi=(2V)^{-1/2}\{\exp(ik_1x)-\exp(-ik_1x)\}\exp(ik_2y)\exp(ik_3z). \quad \ldots\ldots(1)$$

$V=L_1\,L_2\,L_3$ is the volume of the metal, $k^2=k_1^2+k_2^2+k_3^3=2mE/\hbar^2$ where E is the energy of the electron measured from the bottom of the conduction band, and $k_1\leqslant 0$. This assumption corresponds to specular reflection of the electrons at the surface in the classical calculations.

Assumption D (D for diffuse). If the surface of the metal is rough on an electronic scale though the departures from a plane are small compared with the wavelength of the light, or if impurities in the surface layer scatter the electrons, the wave functions are of the more general form

$$\psi=(2V)^{-1/2}\{\exp(i\mathbf{k}\,.\,\mathbf{r})-a_{k'}\exp(-i\mathbf{k}'\,.\,\mathbf{r})\} \quad \ldots\ldots(2)$$

where $a_{k'}$ is a phase factor such that $|a_{k'}|=1$ and $k'^2=k^2=2mE/\hbar^2\,(k_1\leqslant 0, k_1'\leqslant 0)$. This form corresponds to the classical picture of an electron wave approaching the surface with the wave vector $\mathbf{k}$ and being reflected back from the surface in a direction given by the vector $\mathbf{k}'$ and with an arbitrary phase $a_{k'}$. The energy is conserved in the reflection process. Corresponding to any specific model which might be chosen for the form of the surface or for the arrangement of scattering centres at the surface, a particular linear combination of these wave functions would be found which would satisfy the boundary conditions. In the absence of such a model we assume that, for any $\mathbf{k}$, all wave vectors $\mathbf{k}'$ which obey the above conditions occur with equal probability and with arbitrary phases. These wave functions do not satisfy any boundary conditions but we assume that they are valid throughout the metal and that outside the metal the wave functions are zero.

We assume that the light is incident normally on the plane $x=0$ and is plane-polarized in the y-direction. The vector potential therefore has only a y-component and its amplitude outside the metal is A_0. If δ is the skin depth characteristic of a free-electron gas, the vector potential just inside the metal is found by classical electromagnetic theory to be

$$A(0)=(2i\omega/\alpha c)A_0 \qquad \ldots\ldots(3)$$

where $\alpha=1/\delta$ and ω is the angular frequency of the light.

At a distance x inside the metal the vector potential is

$$A(x)=\exp(-\alpha x)(2i\omega/\alpha c)A_0. \qquad \ldots\ldots(4)$$

For high frequencies it is found that

$$\alpha=(4\pi Ne^2/mc^2)^{1/2} \qquad \ldots\ldots(5)$$

where N is the number of electrons per unit volume.

The mechanism of absorption of light is assumed to be as follows: A metallic electron in an occupied energy level (below the Fermi level) absorbs a photon of energy $h\nu$ from the light in the metal and jumps to a vacant level (above the Fermi energy). With our free electron model this upper level is of course in the same band. No inter-band transitions are considered. The total energy absorbed is given by the total probability P of all such allowed transitions multiplied by the energy per photon $h\nu$. The absorptivity (1 − reflectivity) is then obtained by dividing the energy absorbed by the incident flux. We shall now carry out the calculations of P and hence of the absorptivity for the two cases S and D corresponding to the two types of wave functions.

§ 3. CALCULATION OF ABSORPTIVITY: ASSUMPTION S

The probability per unit time of transitions due to the incident light from a state ψ_1 with energy E_1 to a state ψ_2 with energy near E_2 is (Heitler 1944)

$$w_{12}=(2\pi/\hbar)n(E_2)|H_{12}|^2 \qquad \ldots\ldots(6)$$

where H_{12} is the matrix element

$$H_{12}=\frac{ie\hbar}{2mc}\int\psi_2^*\mathbf{A}\,.\,\mathrm{grad}\,\psi_1\,d\tau$$

which, with the expression for $\mathbf{A}$ given by equation (4), reduces to

$$H_{12}=-\frac{e\hbar\omega}{\alpha mc^2}A_0 I \qquad \ldots\ldots(7)$$

where $$I=\int\psi_2^*e^{-\alpha x}\frac{\partial}{\partial y}\psi_1\,d\tau.$$

$n(E_2)$ is the density of states with energy E_2 per unit solid angle in the hemisphere of k-space (since $k_1\leqslant 0$). For a free-electron gas this density of states is (Seitz 1940)

$$n(E)=2V(2m)^{3/2}E^{1/2}/h^3=4mV\hbar k/h^3. \qquad \ldots\ldots(8)$$

In the derivation of equation (7), the wave vector of the light is neglected since it is very small compared with the wave vectors of the electrons.

Using wave functions given by equation (1), the integral I is

$$I=(2V)^{-1}\int_0^{L_1}\int_0^{L_2}\int_0^{L_3}[\{\exp(-iK_1x)-\exp(iK_1x)\}\exp(-iK_2y)\exp(-iK_3z)]\,e^{-\alpha x}$$
$$\times\frac{\partial}{\partial y}[\{\exp(ik_1x)-\exp(-ik_1x)\}\exp(ik_2y)\exp(ik_3z)]\,dx\,dy\,dz. \qquad \ldots\ldots(9)$$

Since the depth L_1 of the box is large, $\exp(-\alpha L_1)$ may be neglected. The result of this integration is then

$$I=\frac{ik_2\alpha}{V}\left[\frac{4k_1K_1}{(\alpha^2+k_1^2+K_1^2)^2-4k_1^2K_1^2}\right]\left[\frac{\exp\{-i(K_2-k_2)L_2\}-1}{K_2-k_2}\right]$$
$$\times\left[\frac{\exp\{-i(K_3-k_3)L_3\}-1}{K_3-k_3}\right]. \qquad \ldots\ldots(10)$$

W_{12}, the probability per unit time of transitions between all states of energy near $E_1=\hbar^2k^2/2m$ and all states of energy near $E_2=\hbar^2K^2/2m=E_1+h\nu$, is obtained by multiplying w_{12} by $n(E_1)$, the appropriate density of states with energy E_1, and then integrating over all directions of the electron wave vectors $\mathbf{k}$ and $\mathbf{K}$. To take into account the conservation of electronic spin in these transitions this results must be divided by 2. Thus

$$W_{12}=\tfrac{1}{2}\iiiint n(E_1)w_{12}\sin\theta\,d\theta\,d\phi\sin\Theta\,d\Theta\,d\Phi \qquad \ldots\ldots(11)$$

where θ and ϕ are the polar angles in the k-hemisphere and Θ and Φ are the polar angles in the K-hemisphere. Changing the variables of integration in K-space to K_2 and K_3 instead of Θ and Φ, and substituting for w_{12} we find

$$W_{12}=\tfrac{1}{2}\iiiint\frac{2\pi}{\hbar}n(E_1)n(E_2)|H_{12}|^2\frac{1}{K_1K}dK_2\,dK_3\sin\theta\,d\theta\,d\phi$$
$$=\frac{\pi}{\hbar}\left(\frac{4mV\hbar}{h^3}\right)^2kK\left(\frac{e\hbar\omega A_0}{\alpha mc^2}\right)^2\frac{\alpha^2}{V^2}J \qquad \ldots\ldots(12)$$

where
$$J=\iiiint\frac{k_2^2}{K_1K}\frac{16k_1^2K_1^2}{[(\alpha^2+k_1^2+K_1^2)^2-4k_1^2K_1^2]^2}\left[\frac{2\{1-\cos(K_2-k_2)L_2\}}{(K_2-k_2)^2}\right]$$
$$\times\left[\frac{2\{1-\cos(K_3-k_3)L_3\}}{(K_3-k_3)^2}\right]dK_2\,dK_3\sin\theta\,d\theta\,d\phi. \qquad \ldots\ldots(13)$$

The function of K_2 in the integrand has a sharp peak at $K_2-k_2=0$ and is close to zero elsewhere. Similarly the function of K_3 has a peak at $K_3-k_3=0$. Since the remaining function of K_1 varies slowly in the region of this double peak, it can be taken outside the integration with K_1 replaced by the value corresponding to $K_2=k_2$ and $K_3=k_3$, i.e. $K_1^2=k_1^2+2mh\nu/\hbar^2$. The range of integration over K_2 and K_3 can be taken to be from $-\infty$ to ∞, since only the peaks contribute to the integrals (see Heitler 1944, p. 90). Since

$$\int f(K_1)\left[\frac{2\{1-\cos(K_2-k_2)L_2\}}{(K_2-k_2)^2}\right]dK_2=2\pi L_2\,\mathrm{f}(K_1:K_2=k_2) \qquad \ldots\ldots(14)$$

the result is

$$J=\iint\frac{4\pi^2L_2L_3}{K}\left[\frac{16k_2^2k_1^2(k_1^2+n^2)^{1/2}}{\{(\alpha^2+2k_1^2+n^2)^2-4k_1^2(k_1^2+n^2)\}^2}\right]\sin\theta\,d\theta\,d\phi \qquad \ldots\ldots(15)$$

where K_1^2 has been replaced by $k_1^2+n^2$ and n^2 has been written for $2mh\nu/\hbar^2$.

In the infra-red region, the skin depth is large compared with the distance travelled by even the fastest electrons in one oscillation of the electromagnetic field, i.e. $1/\alpha \gg v_0/\omega$ where v_0 is the velocity of an electron with energy equal to the Fermi energy $F(\frac{1}{2}mv_0^2 = F)$. Therefore, expressing ω in terms of n and v_0 in terms of $k_{\max}$, $2\alpha k_{\max} \ll n^2$. Therefore, *a fortiori*, $2\alpha k_1 \ll n^2$. Also for infra-red light $h\nu < F$, i.e. $n^2 < k^2$ and therefore $\alpha^2 \ll n^2$. Making use of these inequalities we find that the denominator in equation (15) is approximately equal to n^8. In the numerator, $(k_1^2 + n^2)^{1/2}$ is approximately equal to k_1 over most of the range of the integrations over θ and ϕ except where k_1 is very small. Therefore only a small error is introduced by replacing $(k_1^2 + n^2)^{1/2}$ by k_1. Therefore

$$J \simeq \frac{4\pi^2 L_2 L_3}{K} \int\int \frac{16 k_2^2 k_1^3}{n^8} \sin\theta \, d\theta \, d\phi$$

$$= \frac{64\pi^2 L_2 L_3}{K n^8} k^5 \int\int \sin^6\theta \sin^2\phi \cos^3\phi \, d\theta \, d\phi. \qquad \text{......(16)}$$

The limits of integration are, for θ, 0 to π, and for ϕ, $\frac{1}{2}\pi$ to $3\pi/2$ (since $k_1 \leqslant 0$). The result of the integration is

$$J = \frac{64\pi^2 L_2 L_3 k^5}{K n^8} \frac{\pi}{12}. \qquad \text{......(17)}$$

This may now be substituted in equation (12) to give W_{12}.

The total probability per unit time of all transitions in which energy $h\nu$ is absorbed is obtained by integrating over all possible values of the initial energy:

$$P = \int_{F-h\nu}^{F} W_{12} \, dE_1 = \int W_{12} \frac{\hbar^2}{m} k \, dk. \qquad \text{......(18)}$$

With the value of W_{12} given by equations (12) and (17), this final integration is elementary. If we neglect terms of the order of $h\nu/F$ and smaller, we find

$$P = \frac{\pi}{\hbar} \left(\frac{4mV\hbar}{h^3}\right)^2 \left(\frac{e\hbar\omega A_0}{\alpha mc^2}\right)^2 \frac{\alpha^2}{V^2} \frac{16\pi^3}{3} \frac{L_2 L_3}{n^8} \frac{\hbar^2}{m} \frac{1}{2} \left(\frac{2m}{\hbar^2}\right)^4 F^3 h\nu. \qquad \text{......(19)}$$

Since the energy incident on the surface of the metal per unit time is $(\pi\nu^2 A_0^2/2c) L_2 L_3$, the absorptivity is

$$A_S = \frac{Ph\nu}{(\pi\nu^2 A_0^2/2c) L_2 L_3}. \qquad \text{......(20)}$$

Substituting $2mh\nu/\hbar^2$ for n^2, and making use of the relations $F = \frac{1}{2}mv_0^2 = (h^2/2m)(3N/8\pi)^{2/3}$ we find the absorptivity in the simplest form:

$$A_S = \frac{1}{2\pi} \frac{Ne^2}{m\nu^2} \frac{v_0^3}{c^3}. \qquad \text{......(21)}$$

In deriving this result we have made use of the fact that the light decays exponentially within the metal but we have not used the particular expression for the skin depth given by equation (5).

§4. CALCULATION OF ABSORPTIVITY: ASSUMPTION D

The steps in this calculation are identical with those of the previous section. We use equations (6) and (7) exactly as before but with the new wave functions given by equation (2); equation (9) must now be replaced by

$$I^* = \frac{1}{2V} \int_0^{L_1} \int_0^{L_2} \int_0^{L_3} \{\exp(-i\mathbf{K} . \mathbf{r}) - a_{K'} \exp(i\mathbf{K}' . \mathbf{r})\} \, e^{-\alpha x}$$

$$\times \frac{\partial}{\partial y} \{\exp(i\mathbf{k} . \mathbf{r}) - a_{k'} \exp(-i\mathbf{k}' . \mathbf{r})\} \, dx \, dy \, dz. \qquad \text{......(9*)}$$

Since $\exp(-\alpha L_1) \to 0$, this gives

$$\begin{aligned} I^* = \frac{1}{2V}\Bigg[& \frac{ik_2}{i(K_1-k_1)+\alpha}\left(\frac{\exp\{-i(K_2-k_2)L_2\}-1}{i(K_2-k_2)}\right)\left(\frac{\exp\{-i(K_3-k_3)L_3\}-1}{i(K_3-k_3)}\right) \\ & + \frac{ia_{K'}k_2}{i(K_1'+k_1)-\alpha}\left(\frac{\exp\{i(K_2'+k_2)L_2\}-1}{i(K_2'+k_2)}\right)\left(\frac{\exp\{i(K_3'+k_3)L_3\}-1}{i(K_3'+k_3)}\right) \\ & + \frac{ia_{k'}k_2'}{i(K_1+k_1')+\alpha}\left(\frac{\exp\{-i(K_2+k_2')L_2\}-1}{i(K_2+k_2')}\right)\left(\frac{\exp\{-i(K_3+k_3')L_3\}-1}{i(K_3+k_3')}\right) \\ & + \frac{ia_{k'}a_{K'}k_2'}{i(K_1'-k_1')-\alpha}\left(\frac{\exp\{i(K_2'-k_2')L_2\}-1}{i(K_2'-k_2')}\right)\left(\frac{\exp\{i(K_3'-k_3')L_3\}-1}{i(K_3'-k_3')}\right)\Bigg] \end{aligned} \qquad \ldots\ldots(10^*)$$

To obtain W_{12}^* we multiply w_{12}^* by one half of the density of states with energy E_1 as before, but now we must integrate not only over all possible directions of the wave vectors $\mathbf{k}$ and $\mathbf{K}$ but also over all directions of the wave vectors $\mathbf{k}'$ and $\mathbf{K}'$. In this way we make use of the assumption that for any $\mathbf{k}$, all directions of $\mathbf{k}'$ occur with equal probability. I^*, which is the sum of four terms, occurs squared in the integrand. By an argument similar to that used in deriving equation (15) from equation (13), we find that the crossed terms in the squared expression contribute nothing to the integral. In the squared terms each phase factor, $a_{k'}$ etc., is multiplied by its own complex conjugate and thus gives unity. The integral of a typical squared term is

$$\begin{aligned} & \int \cdots \int \frac{k_2^2}{|i(K_1-k_1)+\alpha|^2}\left|\frac{\exp\{-i(K_2-k_2)L_2\}-1}{i(K_2-k_2)}\right|^2 \left|\frac{\exp\{-i(K_3-k_3)L_3\}-1}{i(K_3-k_3)}\right|^2 \\ & \quad \times \frac{1}{KK_1}\, dK_2\, dK_3 \sin\theta\, d\theta\, d\phi \sin\theta'\, d\theta'\, d\phi' \sin\Theta'\, d\Theta'\, d\Phi' \\ & \quad = 4\pi^2 L_2 L_3 \int \cdots \int \frac{k_2^2}{|i(K_1-k_1)+\alpha|^2} \sin\theta\, d\theta\, d\phi \sin\theta'\, d\theta'\, d\phi' \sin\Theta'\, d\Theta'\, d\Phi' \end{aligned} \qquad \ldots\ldots(14^*)$$

with $K_1^2 = k_1^2 + n^2$ as above.

Each of these four terms is a function of two of the four wave vectors $\mathbf{k}$, $\mathbf{k}'$, $\mathbf{K}$ and $\mathbf{K}'$. Each of the two double integrations over the directions of the two wave vectors which do not occur in a term multiplies the result by 2π, the solid angle in a hemisphere. The remaining double integration is simplified if we make the same approximations which we used above to simplify equation (16). When the four terms are added together we find

$$\begin{aligned} J^* & \simeq \frac{4\pi^2 L_2 L_3}{K} 4\pi^2 \iint \frac{8k_2^2 k_1}{n^4} \sin\theta\, d\theta\, d\phi \\ & = \frac{128\pi^4 L_2 L_3 k^3}{Kn^4} \iint \sin^4\theta \sin^2\phi \cos\phi\, d\theta\, d\phi. \end{aligned} \qquad \ldots\ldots(16^*)$$

The result of this integration is:

$$J^* = 32\pi^5 L_2 L_3 k^3 / Kn^4. \qquad \ldots\ldots(17^*)$$

$n^*(E)$ in this case is the density of states of energy E per unit solid angle in the k-hemisphere per unit solid angle in the k'-hemisphere, i.e. $1/2\pi$ times the value used above in equation (8).

$$n^*(E)=2mV\hbar k/\pi h^3. \qquad \ldots\ldots(8^*)$$

Using equation (18) as above, we find the total transition probability

$$P^*=\frac{\pi}{\hbar}\left(\frac{2mV\hbar}{\pi h^3}\right)^2\left(\frac{e\hbar\omega A_0}{\alpha mc^2}\right)\frac{1}{4V^2}\frac{32\pi^5L_2L_3}{n^4}\frac{\hbar^2}{m}\frac{1}{2}\left(\frac{2m}{\hbar^2}\right)^3F^2h\nu. \qquad \ldots\ldots(19^*)$$

Since α does not cancel out in this equation as it did in equation (19) we must substitute the expression in equation (5) to find the absorptivity. We use equation (20) and the other substitutions given above and find:

$$A_{\mathrm{D}}=\tfrac{3}{4}v_0/c. \qquad \ldots\ldots(21^*)$$

In this case we find that the absorptivity depends only on the Fermi energy of the metallic electrons and not on their effective mass or on the wavelength of the light.

§5. CONCLUSION

The two absorptivities given by equations (21) and (21*) are identical with those obtained by Holstein and by Dingle for this limiting case of infinite conductivity and infra-red light. Since A_{D} is the result which agrees well with experiments (Dingle 1953 b) we may conclude that the wave functions of equation (2) are a better approximation to the accurate electronic wave functions than the more usual form of equation (1) which has been used before in most work on the photoelectric effect (Makinson 1937, Mitchell 1934, 1936) and in a previous quantum-mechanical theory of reflectivity (Schiff and Thomas 1935). More accurate wave functions might be found if some specific model were chosen for the surface roughness (cf. Müser 1954) or for the distribution of scattering centres in the surface layer of the metal.

ACKNOWLEDGMENTS

I am pleased to express my gratitude to Professor N. F. Mott for suggesting this problem and for his valuable guidance, to Dr. H. Müser and Mr. K. M. Howell for helpful discussions and to the Research Council of Ontario for a scholarship which made this work possible.

REFERENCES

DINGLE, R. B., 1953 a, *Physica*, **19**, 311 ; 1953 b, *Ibid.*, **19**, 348.

HEITLER, W., 1944, *The Quantum Theory of Radiation*, 2nd Edn (Oxford : University Press).

HOLSTEIN, T., 1952, *Phys. Rev.*, **88**, 1427; *Westinghouse Research Report* R-94411-9-J.

MAKINSON, R. E. B., 1937, *Proc. Roy. Soc.* A, **162**, 367.

MITCHELL, K., 1934, *Proc. Roy. Soc.* A, **146**, 442; 1936, *Ibid.*, **153**, 513.

MOTT, N. F., and JONES, H., 1936, *The Theory of the Properties of Metals and Alloys* (Oxford : University Press).

MÜSER, H., 1954, *Phil. Mag.*, **45**, 1237.

RAMANATHAN, K. G., 1952, *Proc. Phys. Soc.* A, **65**, 532.

REUTER, G. E. H., and SONDHEIMER, E. H., 1948, *Proc. Roy. Soc.*, **195**, 336.

SCHIFF, L. I., and THOMAS, L. H., 1935, *Phys. Rev.*, **47**, 860.

SCHULTZ, L. G., 1954, *J. Opt. Soc. Amer.*, **44**, 357, 362.

SEITZ, F., 1940, *The Modern Theory of Solids* (New York : McGraw-Hill).

SONDHEIMER, E. H., 1952, *Advances in Physics*, **1**, 1.

REVIEWS OF BOOKS

The Quantum Theory of Radiation, 3rd Ed., by W. Heitler. Pp. xiii + 430. (Oxford: University Press, 1954.) 45*s*.

The appearance of a new edition of this standard work is an exciting event for all theoretical physicists working in the field of high energy radiation physics and for many experimentalists as well. It sometimes happens that owing to the rapidity of development of a subject and the necessity to enlarge the contents later editions of a well known classic lose the distinctive approach that contributed to its original success. It can be said at once that while the length of this edition has been increased considerably the style and discrimination in choice of material has been more than maintained.

As previously this work is indispensable both for those workers whose main interest lies in the formal development of the theory as well as for those interested chiefly in the application of the theory to concrete problems of the interaction of high energy radiation with matter. Although the most substantial modifications in the new edition concern the former, sections on the comparison between the predictions of the theory and the results of experiment have been brought right up to date.

In chapter I the main change consists in the addition of a section on the Fourier expansion of the field quantities defined using the Coulomb gauge, while in chapter II, in preparation for later requirements, a new section is added on the quantization of the electromagnetic field using Lorentz gauge. In addition, in chapter II there is a new section dealing with the properties of delta and related functions.

In chapter III, in line with more recent treatments, a canonical formalism of the field variables is developed without an actual Fourier expansion of the field, while in addition a much needed section on second quantization has been added.

The former chapter III has in fact now been split into three chapters, enlarged sections on general perturbation theory and radiation damping being placed in a new chapter IV, while the application of the theory to the study of radiation processes in the first approximation now forms the basis of a new chapter V. The treatment of electron–electron scattering has been considerably enlarged and sections on pair production, bremsstrahlung, and positron annihilation have been brought up to date, as have also the sections on electron energy loss, and cascade shower development in chapter VII.

But the most important addition to the book is the new chapter VI which under the title ‘ Radiative corrections, ambiguous features ’, deals with questions such as mass and charge renormalization, the Feynmann–Dyson method for the evaluation of matrix elements occurring in the application of radiation theory, vacuum polarization effects and the application of the new techniques to the calculation of the anomalous magnetic moment of the electron, the Lamb–Retherford shift, and radiative reaction corrections to elastic electron scattering and to the Compton effect.

More use could perhaps have been made throughout the book of Feynmann graphs for illustrating the interaction with the radiation field, because these diagrams are helpful in making clear the processes being discussed even to those unable to follow the details of a calculation. But this is a minor point. The new edition is in every way worthy of its predecessors. E. H. S. BURHOP.

Theoretical Physics—Mechanics of Particles, Rigid and Elastic Bodies, Fluids and Heat Flow, by F. W. CONSTANT. Pp. xiv+281. (Cambridge, Mass.: Addison-Wesley, *Principles of Physics* Series.) $6.50.

It is in many ways a point in favour of a textbook of mechanics that the subject matter and mode of presentation should be fairly conventional. The student meets with courses on mechanics at various levels of sophistication in his studies, and the courses and textbooks used should dovetail together readily. This new book by Professor F. W. Constant does in fact meet this requirement. It begins at a level suitable for the average student in an Honours course in Physics and follows the logical and well-tried line of development till it forms an introduction to post-graduate work.

The book is divided into three parts. Part I is a very clear and well-written set of three chapters on vector algebra, vector calculus and on dyadics, the latter being introduced for use in connection with principal axes of a rigid body, stresses and strains in elasticity, and rates of strain in viscous media. Part II, the main part of the book, contains the usual particle and rigid body dynamics including such topics as the linear oscillator, forced oscillation, coupled oscillations and normal coordinates, planetary motion and its inverse in α-particle scattering, Euler's equations for a rotating rigid body, and a brief introduction to Lagrange's and Hamilton's equations. In addition to particle and rigid body dynamics are chapters on elasticity and elastic waves, viscous media and fluid dynamics. Part III consists of a chapter on the mathematical formulation of heat flow, following logically after fluid dynamics with which of course it has much in common.

As mentioned before the general standard is about that which a student of good ability will attain during his undergraduate courses and the book will undoubtedly be used as a standard textbook by the more able student. The author states that the book is intended to bridge the gap between undergraduate and post-graduate courses and if by this is meant a thorough resumé and consolidation of undergraduate work, with a mathematical background suitable for the next step, then it is very successfully done. There is still, however, a considerable gap between this and, for example, *Classical Mechanics* by Goldstein which is a representative textbook on advanced mechanics.

The printing, illustrations, binding, etc., are all of high quality and there are plenty of problems to assist the process of consolidation. R. LATHAM.

Textbook of Physics, edited by R. KRONIG (translated from 3rd Dutch edition, 1951). Pp. xiv+855. (London: Pergamon Press, 1954.) 70*s*.

This textbook is an English translation of a work by several eminent Dutch physicists. According to the publishers the original work has been well received in Holland but the reception which, in all probability, will be accorded here to the new version may not be more than a very mixed one. Even a casual perusal of the work makes one doubt the advisability of any authors or publishers making an attempt to give in one volume for degree students a really workable summary of physics. To the reviewer this book appears to fail in that it tries to combine things which are very elementary with others which are most advanced. Moreover, in order to find space, it seems as if the mathematical proofs have been shortened to such an extent that no typical student will be able to follow them.

The book also suffers from the fact that the notation used will be difficult for English students ; in particular the use of the letter O for surface area is very questionable here, although in the original no objection to it could be raised.

In a book of this nature it is surprising to find that there is no reference to any modern determination of the velocity of light or to Michelson's and later work on the metre. Since the measurement of spectral wavelengths has reached a degree of precision unequalled in any other branch of physics, and this is primarily due to the fact that Michelson did measure with great accuracy the wavelength of the red cadmium line with reference to the standard metre, such omissions are much to be deprecated.

Attention must also be called to some errors which should not have escaped the eyes of a team of experts. Only some can be mentioned. On p.100 we find a reference to a force–strain diagram when stress–strain is intended. On p.132 it is not pointed out that Poiseuille's equation is valid only for flow through a horizontal tube. The subject of non-Newtonian flow is not mentioned. On p. 309 Fig. 84 lines of force are shown cutting a metal surface at angles other than $\pi/2$. On p. 514 there appears a diagram showing the rise of a liquid in a capillary tube and the liquid therein is *flat*. In deriving a formula on p. 511 concerning falling drops, the writers appear to have ignored the work of Rayleigh and of Harkins and Brown.

On p. 405 there is an account of Michelson's stellar interferometer and here the errors are somewhat blatant. Rays fom a star must be parallel ; those shown do not satisfy this condition and the authors have not realized that Michelson only used a large telescope on account of the mechanical strength it possessed. The two mirrors which reflected light into the telescope actually covered only a small portion of the telescope objective. In the diagram they are shown covering nearly all the objective. This is an error common to many books. Michelson only covered a small portion of the aperture in order that the central ' blob ' of the diffraction image should be large ; this was absolutely necessary since it was across this portion of the field that interference fringes were obtained, and then caused to disappear.

Finally, on p. 605 it is not made clear that the expression pv^{γ} only applies to a reversible adiabatic or isentropic change.

At the end of the book there is a somewhat comprehensive biographical note. This makes very interesting reading. The book is well illustrated and the production is good but the price of 70*s*. will put the book beyond the reach of nearly all students. C. J. SMITH.

Einführung in die Physik, Band 3, *Optik und Atomphysik*, by R. W. POHL. Pp. viii + 356. (Berlin, Göttingen, Heidelberg : Springer.) DM 29.70.

The author describes a large number of experiments, many of them lecture demonstrations, and then gives a very brief account of the associated theories. In this way, starting from rudimentary beginnings, he is able to introduce a large number of topics very rapidly. Near the beginning of chapter 2, the reader is introduced to the laws of reflection and of refraction. On page 12, a lens is considered as an assembly of prisms and on page 17 there is an elementary treatment of resolving power. On page 19 the idea of dispersion is first introduced and on page 21 the properties of infra-red and ultra-violet radiation are described. The chapter ends with a discussion of mirror systems (pentagonal prisms, corner cubes, etc.). Chapter 4 begins on page 32 with nodal points and principal planes and includes the third-order aberrations, the Schmidt camera, achromatization, telescopic systems, magnification, field of view, stops, and the theory of perspective. The lectures on which this book is based are probably useful to the students for whom they are intended especially when illustrated by many good lecture demonstrations (some of which are described) and illuminated by the personality of the distinguished author. As the above summaries suggest they are so different from a course of lectures in a British University that a translation could not be recommended to British students.

One is shocked by the ease with which topics appear and then are allowed to fade out so that one chapter includes work which we should regard as school work and also material suitable for a Special Honours course. Yet, for the teacher of Physics, it is not sufficient to review this book as the Victorian lady reviewed *Antony and Cleopatra* with the phrase " How unlike the home life of our own dear Queen ". We need not imitate, but can it be that the somewhat pedestrian systematic, logical exposition (" starting at the beginning and going on to the end "), which constitutes our typical lecture course, would be improved by an occasional ' preview ' of something interesting which logically should come much later, and that students should occasionally be taken out of their depths, even though most of them prefer to paddle ! Any British University lecturer in optics who has given the same lectures for five years might profitably read this book and reconsider his course before saying " Same again ".

Part II on ' Atomic Physics ' includes sections on atomic and molecular spectra, temperature radiation, fundamental particles and on the author's own special subject ' Quantum Optics of Solids '. The treatment of spectra is in terms of the Bohr orbits. Here, and in a number of other places, a more modern viewpoint could, with advantage, be adopted. The 565 illustrations include many perspective drawings of lecture bench apparatus where line diagrams would be more useful. There are also a large number of excellent photographic illustrations.

R. W. DITCHBURN.

CONTENTS OF SECTION B

PAGE

Dr. V. I. Little and Mrs. V. Smith. The Ionic Conductivity of Dilute Potassium Chloride Solutions at Centimetric Wavelengths 65

Mr. M. A. Lonappan. Thermal Expansion of Potassium Chlorate 75

Mr. J. de Klerk and Mr. M. J. P. Musgrave. Internal Conical Refraction of Transverse Elastic Waves in a Cubic Crystal 81

Dr. F. C. Roesler. Some Applications of Fourier Series in the Numerical Treatment of Linear Behaviour 89

Dr. F. C. Roesler and Mr. W. A. Twyman. An Iteration Method for the Determination of Relaxation Spectra 97

Mr. G. Hughes and Dr. R. T. Spurr. An Experimental Investigation of Non-Metallic Wear 106

Dr. J. Franks, Dr. G. A. Geach, and Dr. A. T. Churchman. Lamellar Defects in Single Crystals of Silicon 111

Research Notes:

Mr. F. F. Roberts and Dr. J. R. Tillman. The Barrier Height of Point-Contact Germanium Diodes inferred from Measurements of the Voltage Dependence of Capacitance 113

Reviews of Books 116

Contents of Section A 120

Figure 1. Typical good separation between the α-particle track of AcX and the tracks of subsequent products. Two electrons are here associated with the AcX α-particle.

The Temperature Dependence of Magnetostriction in a Nickel Crystal

By W. D. CORNER and G. H. HUNT †
Department of Physics, Durham Colleges in the University of Durham

MS. received 16*th August* 1954, *and in amended form* 21*st October* 1954

Abstract. From a single crystal of nickel two specimens have been prepared in the form of prolate spheroids whose major axes lie along the [100] and [111] crystallographic directions. By the use of a special capacitance bridge arrangement described elsewhere, the longitudinal magnetostriction of each specimen has been measured over the temperature range −180°c to 360°c.

The results obtained indicate that at low temperatures the magnetostriction below saturation varies with magnetization approximately in the manner given by the domain treatment suggested by Heisenberg, and that with increasing temperature there is a steady departure from the calculated values. The saturation magnetostriction was found to depend on temperature in a way which did not correspond to any known theory.

§ 1. Introduction

The theory of ferromagnetic phenomena in its present form provides a satisfactory qualitative, and to some extent quantitative, account of the fundamental processes of ferromagnetism. For example, the dependence of intensity of magnetization on temperature may be closely represented by a theoretical expression. There is, however, no satisfactory explanation in more fundamental terms of the phenomenon of magnetostriction, which is the spontaneous distortion of the lattice of a ferromagnetic crystal. Spin–spin interaction is incapable of producing values of strain of the correct order, and the case of spin–orbit interaction has not yet been theoretically treated. Knowledge of the magnetostriction of ferromagnetic substances is required in any evaluation of the strain-dependent energies involved in the magnetization process.

Although there have been many investigations of the magnetostriction of polycrystalline specimens, measurements on single crystals have been very few. A knowledge of the single crystal magnetostriction over the whole range of temperatures up to the Curie temperature is desirable for many purposes, e.g. the calculation of magnetic effects of stresses. Such measurements have been carried out by Takaki (1937) using single crystals of iron, but the authors are not aware of any measurements on nickel or cobalt over a corresponding temperature range. They have therefore undertaken the measurement of the changes in length which accompany magnetization in the [100] and [111] directions in a single crystal of nickel over a range of temperatures from −180°c to 360°c, the latter being slightly greater than the Curie temperature.

§ 2. Apparatus

The apparatus was designed to measure the longitudinal magnetostriction of single crystals some 2 cm in length over the above temperature range. The apparatus used by Takaki (1937) for measurements of the dependence on temperature of the magnetostriction of single crystals of iron is not really comparable with that used here since he was able to use specimens some 20 cm long. All previous measurements over large temperature ranges have used mechanical methods of amplification, but with the small specimens used for these experiments it was felt that the greater sensitivity obtainable from electronic devices was desirable. Although modern practice tends towards the use of resistive strain gauges, this is difficult at high temperatures where the normal adhesives are prohibited, and a capacitance method was chosen. A differential condenser is used as the strain measuring instrument, and movement of the central plate produces a proportional out-of-balance voltage in a capacitance bridge network. The apparatus has already been described (Corner and Hunt 1955).

---

† Now at the Royal Aircraft Establishment, Farnborough, Hants.

The general arrangement of the apparatus when set up for high temperature measurements is shown in figure 1. The specimen A is placed in a quartz tube B, the top of which is fused to the large diameter quartz tube C. This tube is mounted on the frame D by means of the quartz rods E, one rod only being shown in the diagram. The differential condenser is also mounted on this frame. Thus there is a continuous length of quartz between the specimen and the condenser.

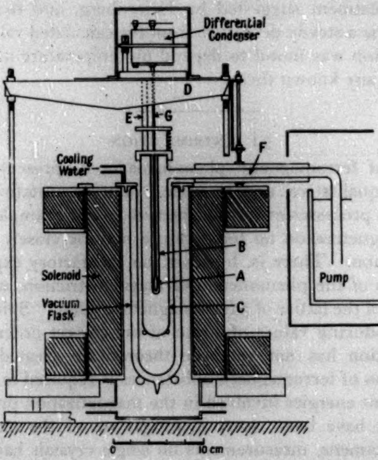

Figure 1. General arrangement of apparatus for magnetostriction measurements above room temperature.

The tube C is surrounded by a vacuum flask, and this is in turn surrounded by the solenoid which is designed to produce uniform fields of up to 1000 oersteds over a length of 2 cm at its centre. Due to the supplementary coils mounted at the ends of the solenoid, the uniformity of field is greater than that produced by a normal solenoid of the same length. Lewis (1950) suggested a solenoid with supplementary coils and Heddle (1952) described a similar arrangement in which two pairs of such coils were used. It was found by the authors that one pair was sufficient, since an extra adjustable parameter could be obtained by making both the diameter and the length of the supplementary coils variable. The solenoid is wound with silicone-bonded glass covered wire, and the heat dissipation, which for maximum field is 1000 watts, may be conducted away by a flow of water passing between the outside of the vacuum flask and the solenoid wall.

The earth's magnetic field was compensated by means of additional coils mounted on the solenoid, not shown in the figure.

The specimen is heated by a stream of silicone liquid MS 550 which is driven through the quartz tube C by means of a pump into which dip the two side tubes F. This pump contains a heater which allows the liquid to be maintained at any desired temperature between room temperature and the boiling point of the silicone liquid, 405°c. The pump itself has no mechanical contact with the feed-tubes F, since vibrations from the motor driving it cannot be allowed to reach the specimen and the condenser. It merely maintains a difference in levels between two cups into which dip the two feed-tubes, and it is attached to the laboratory wall while the rest of the apparatus is mounted on a rigid brick pillar having separate foundations.

The pump has a large thermal capacity, and the temperature of the silicone liquid may be kept constant to better than 1°c over long periods without the use of an automatic temperature controller. There is a fall of about 20°c between the pump and the specimen, but the temperature of the latter may be maintained with the same constancy as that of the liquid in the pump.

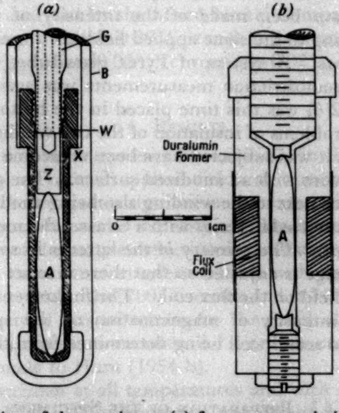

Figure 2. Mounting of the specimen, (*a*) for magnetostriction measurements, (*b*) for magnetization measurements.

The mounting of the specimen is shown in more detail in figure 2(*a*). To minimize the effect of changes in length of the specimen due to thermal expansion while under test, it is mounted in a metal tube with which it is in good thermal contact, and which compensates for length changes by expanding in the reverse direction to the specimen. Although it would have been possible to obtain temperature compensation in this way over a small range of temperatures, due to the large range over which tests were carried out, it was necessary to use a combination of two compensating metals since no single non-ferromagnetic metal could be found with similar expansion characteristics to those of nickel. The specimen A together with an aluminium cylinder Z are allowed to expand in opposition to a copper tube W which rests on the shoulder X of the quartz tube B shown in figure 1.

The movement of the free end of the specimen is transmitted to the differential condenser by means of a twin-bore quartz tube G. This also carries the leads from the thermocouple used to measure the temperature of the specimen. The thermojunction rests in the top of the cylinder Z, and because of the good thermal contact between this and the specimen, the temperature indicated by the e.m.f. of the thermocouple must be very nearly that of the specimen. The e.m.f. is applied to a potentiometer which will measure temperatures to an accuracy better than 1°c.

For low temperature measurements the pumping system is not used and cooling of the specimen is effected by the simple method of raising a vacuum flask containing liquid nitrogen round the outside of the quartz tube C of figure 1. This tube is then filled with iso-pentane, which has a freezing point of -159°c. With only the bottom of the tube immersed in liquid nitrogen there is a temperature gradient along the iso-pentane, and by adjusting the height of the vacuum flask the temperature of the specimen can be made any desired value. Using this arrangement the temperature could be maintained constant to better than $\frac{1}{2}$°c at temperatures down to -180°c, the lowest value obtained.

Measurements have been made of the intensity of magnetization of the specimen corresponding to the same applied fields as those used in the magnetostriction measurements. A system of Pyrex glass tubes similar to the quartz tube C used for magnetostriction measurements was again used, but the flux coil shown in figure 2(*b*) was this time placed in the bottom of a slightly larger central tube. The problems of insulation of the coil winding caused by the high temperature to which it was subjected have been overcome by making the coil of 36 s.w.g. aluminium wire with an anodized surface. The coil former is made of Duralumin, the surface next to the winding also being anodized.

The flux coil is connected in series with a Grassot fluxmeter and the secondary of a mutual inductance. The primary of the latter is in series with the solenoid winding, and the linkage is adjusted so that there is exact compensation for the effect of the solenoid field on the flux coil. The fluxmeter throw is then directly proportional to the intensity of magnetization of the specimen, the linkage between specimen and search coil being determined from the equations given by Hunt (1954 a).

§ 3. PREPARATION OF THE SPECIMENS

The single crystal from which the specimens were prepared was grown by Mr. R. F. Pearson of the University of Leeds using the method described in his paper (see Pearson 1953). It was examined by the x-ray reflection method, and this showed that two specimens each 1·8 cm long and 0·3 cm diameter could be cut from the crystal, one with its axis in the [111] crystallographic direction and the other in the [100] direction.

The crystal was mounted in Marco SB 26 C resin, the two specimens cut out, and faces milled on them perpendicular to the required crystallographic axis.

Each crystal was again set in resin, mounted in the lathe, and then gradually turned down to $\frac{1}{8}$ inch diameter. The final shaping to the form of a prolate spheroid was made in the lathe using a very fine file, the profile of the specimen being projected on to an outline of the correct shape. Previous tests had shown that lattice distortion caused by working a crystal in this way extended to a depth of 0·015 cm, and a layer of this thickness was therefore removed from the specimens by electrolytic polishing. The agreement between the calculated ellipsoidal shapes and the actual shapes of the specimens was good; each specimen had a length of 1·770 cm and a maximum diameter of 0·275 cm. The actual profile of each specimen was carefully measured with a travelling microscope and the dimensions of the ellipsoid which best fit these measurements were used in each case in the calculation of the demagnetizing factor. For the [100] specimen the value $N=0{\cdot}491$ was obtained and for the [111] specimen $N=0{\cdot}495$. These values compare well with those calculated from the initial slope of the magnetization curves, $0{\cdot}495 \pm 0{\cdot}01$ and $0{\cdot}4935 \pm 0{\cdot}002$ respectively.

Both specimens were annealed by heating them in a stream of hydrogen to a temperature of 910°c, maintaining them at that temperature for two hours, and cooling them at a rate not exceeding 100°c per hour. This is substantially the treatment used by Bates and Wilson (1951) for specimens whose domain structures were later studied by the Bitter pattern technique. After annealing further x-ray reflection photographs were taken which showed that the specimens remained single crystals. They also showed that the chosen crystallographic axis was in each case parallel to the ellipsoid axis to within 1°.

The crystals were analysed by the Mond Nickel Company who found 0·72% of impurities, consisting of cobalt 0·29%, iron 0·17%, manganese 0·10%, silicon 0·04%, copper 0·04%, carbon 0·02%, chromium 0·02%, titanium 0·02% and magnesium 0·02%.

§4. Results

The magnetostriction measurements were initially in the form of changes in length corresponding to various applied fields at certain fixed temperatures. By interpolation of the magnetization measurements, which were in general made at different temperatures, the intensity of magnetization and the true field corresponding to each of the magnetostriction measurements could be calculated. Measurements of the variation of magnetostriction with applied field were made at 27 different temperatures for the [100] direction and at 24 for the [111] direction. In table 1 are shown nine sets of results for the [100] direction and a similar number for the [111] direction in table 2. For the complete set of results reference should be made to Hunt (1954 b).

With the [111] specimen at all temperatures and with the [100] specimen at temperatures above about −50°c saturation was obtained before the maximum field available (1680 oersteds) was reached. After the application of a certain field the values of $\Delta L/L$ and I remained constant within the discrimination of the measuring devices. These values were taken as λ and I_s respectively. Between about 250°c and the Curie temperature these quantities alone were measured by this method. The measurements were made at arbitrary temperatures, often different for the two specimens, and for the sake of conciseness interpolated values for fixed temperatures are given in table 3, the values of I_s in this table being the average for the two specimens.

Table 1. Dependence of Magnetostriction in the [100] Direction on Field and Intensity of Magnetization at Various Temperatures

	−161°c			−100°c			−43°c		
H_{app}	$\Delta L/L$	I	H	$\Delta L/L$	I	H	$\Delta L/L$	I	H
100	0·6	196	4	0·6	196	4	1·5	196	4
200	3·7	314	46	5·2	319	43	8·5	331	38
300	7·6	332	137	11·0	348	129	20·8	374	117
400	11·6	350	228	17·2	374	216	31·1	411	198
500	15·8	368	319	23·8	397	305	39·6	442	283
600	17·7	388	409	29·9	418	395	46·5	467	371
700	22·0	404	502	34·8	440	484	50·7	490	459
800	25·0	420	594	40·8	462	573	52·5	502	554
900	28·7	434	687	47·0	475	667	53·1	506	652
1000	31·1	446	781	50·0	487	761	53·7	508	758
1310	39·1	482	1074	53·7	512	1059	53·7	508	1061
1680	45·7	499	1435	54·8	518	1415	53·7	508	1430

	0°c			43°c			105°c		
H_{app}	$\Delta L/L$	I	H	$\Delta L/L$	I	H	$\Delta L/L$	I	H
50	0·6	100	1						
100	1·2	197	3	2·4	198	3	2·4	199	4
150	5·5	284	11						
200	13·4	344	31	18·7	359	24	20·9	369	19
300	30·5	402	103	40·0	444	82	38·4	452	78
400	40·8	448	180	46·8	472	168	40·3	455	176
500	47·8	476	266	48·2	480	264	40·8	457	276
600	51·0	488	361	48·4	484	362	41·0	459	375
700	51·8	494	457						
800	52·2	499	555	48·6	485	562	41·0	459	575
900	52·5	499	655	48·9	485	662			
1000	52·5	499	755	48·9	485	762			

	155°c			196°c			265°c		
H_{app}	$\Delta L/L$	I	H	$\Delta L/L$	I	H	$\Delta L/L$	I	H
50	0·9	100	1	0·9	100	1	1·0	100	1
100	4·6	199	4	4·7	199	4	4·2	199	4
150	9·7	292	7	10·8	291	7	12·2	280	13
200	23·1	369	19	21·6	364	21	16·9	330	38
300	33·7	431	88	28·2	402	103	16·9	336	135
400	34·2	431	188	28·2	402	203	16·9	336	235
600	34·7	431	388						

Values of field in oersteds, intensity in c.g.s. units and temperature in degrees c.

Effective field H calculated from applied field H_{app} and the demagnetizing factor for the ellipsoidal specimen.

All values of $\Delta L/L$ multiplied by 10^6.

Table 2. Dependence of Magnetostriction in the [111] Direction on Field and Intensity of Magnetization at Various Temperatures

	−154°c			−108°c			−47°c		
H_{app}	$\Delta L/L$	I	H	$\Delta L/L$	I	H	$\Delta L/L$	I	H
50	0·8	102	0	0·6	102	0	0·8	102	0
100	2·8	203	0	2·8	203	0	2·9	202	0
150	6·8	300	2	6·8	300	2	7·0	299	2
200	12·6	398	3	12·8	398	3	12·8	397	4
250	18·0	495	5	18·0	494	6	17·9	489	8
300	20·3	514	46	20·2	513	46	19·4	505	50
400	20·9	517	144	20·8	515	145	20·2	507	149
500	21·7	521	242						
600				21·4	517	344	20·4	509	348
800	22·3	523	541	21·6	518	544			
1000	22·3	523	741	21·6	518	743	20·4	511	747

	0°c			77°c			127°c		
H_{app}	$\Delta L/L$	I	H	$\Delta L/L$	I	H	$\Delta L/L$	I	H
25				0	51	0	0·1	51	0
50	0·5	102	0	0·6	101	0	0·9	102	0
75				1·5	152	0	1·7	152	0
100	2·6	202	0	2·6	202	0	2·8	202	0
125				3·9	250	1	4·1	248	2
150	6·6	298	3	6·2	297	3	5·8	294	4
175				8·4	346	4	8·4	342	6
200	11·8	395	5	11·4	390	7	11·0	382	11
250	17·2	482	12	16·4	454	25	15·1	432	30
300	18·8	493	56	17·7	464	70	16·2	440	82
400	19·3	495	155	18·1	468	168	16·6	444	180
1000	19·4	499	753	18·1	470	767	16·6	444	780

	171°c			197°c			260°c		
H_{app}	$\Delta L/L$	I	H	$\Delta L/L$	I	H	$\Delta L/L$	I	H
50	0·9	102	0	0·2	102	0	0·6	101	0
75	1·5	152	0	1·5	151	0			
100	2·4	201	0	2·4	200	1	2·2	200	1
125	3·7	246	3	4·1	245	4			
150	5·0	290	7	5·6	288	8	5·4	279	12
175	7·9	338	8	7·9	330	12			
200	10·8	372	16	10·6	364	20	7·9	328	37
225	12·0	392	31	11·2	377	38			
250	13·1	408	48	11·8	389	57			
300	14·2	415	95	12·9	396	104	8·6	336	134
400	14·4	417	194	12·9	398	203	8·6	336	234
1000	14·4	417	794						

Values of field in oersteds, intensity in c.g.s. units and temperature in degrees c.

Effective field H calculated from applied field H_{app} and the demagnetizing factor for the ellipsoidal specimen.

All values of $\Delta L/L$ multiplied by 10^6.

Table 3. Variation of Saturation Magnetostriction and Magnetization with Temperature between 250°c and the Curie Temperature (interpolated results)

Temp. (°c)	200	220	240	260	280	300	320	340	350	352	354	356	358
$\lambda_{100} \times 10^6$	28·1	25·0	22·0	18·9	15·6	12·3	8·8	4·6	1·9	1·4	0·7	0·1	0
$\lambda_{111} \times 10^6$	12·9	11·6	10·3	8·9	7·2	5·6	3·7	1·6	0·5	0·2	0	0	0
I_s (c.g.s.)	398	382	363	342	314	279	235	172	120	104	84	54	8

The values of λ and I_s may be obtained directly from the three tables with the exception of those for the [100] specimen at temperatures below −50°c. The method of extrapolation employed to estimate these is described in § 5.

It is important that an estimate should be made of the probable accuracy of the results quoted in this section. A distinction must be drawn between the absolute accuracy of the complete set of measurements, and the accuracy of one measurement relative to another. The latter was checked by repeating measurements after the apparatus had been stripped and re-assembled, and measurements of saturation magnetostriction were shown to be reproducible to within 1% of the value at room temperature. The magnetostriction values corresponding to intermediate values of the magnetization were reproducible to 5% of the saturation value at room temperature.

The absolute accuracy is more difficult to estimate, but is thought to be closer than 5%. Agreement at room temperature with the results of Masiyama (1928) and Bozorth and Hamming (1953) is good.

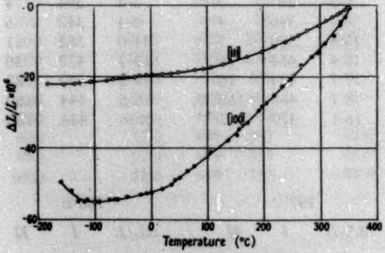

Figure 3. Variation of saturation magnetostriction with temperature in the [111] and [100] directions.

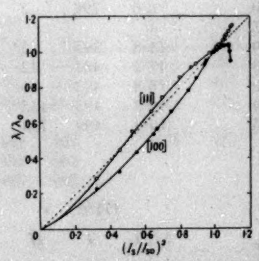

Figure 4. Saturation magnetostriction as a function of saturation magnetization. Both parameters reduced taking values at 0°c as standard.

§ 5. Discussion

5.1. *Saturation Magnetostriction*

In figure 3 is shown the saturation magnetostriction plotted against the temperature for both specimens. The saturation values at low temperatures in the [100] direction could not be obtained directly since the applied field was then too small to obtain saturation. The method adopted was to use values of saturation intensity of magnetization obtained with the [111] specimen as valid for the [100], and then extrapolate the curve of $\Delta L/L$ against I for the low temperature [100] measurements; values of $\Delta L/L$ corresponding to saturation were then obtained. The accuracy of such values is estimated to be better than 5%, and no reasonable extrapolation of the ($\Delta L/L, I$) curves can prevent the saturation magnetostriction in the [100] direction from falling at the lowest temperatures.

The temperature dependence of magnetostriction of polycrystalline nickel has been measured by a number of workers. Döring (1936) found proportionality between the saturation value of the magnetostriction λ and the square of the magnetization I_s in agreement with a dipole theory developed by Becker (1934). Vlasov (1952) found that λ varied linearly with temperature in agreement with the theory of Akulov (1939); Kirkham (1937) and Sucksmith (1950) have also investigated the dependence. Neither of the two laws mentioned above can be fitted to the curves shown in figure 3, in which the relationship between λ and temperature is seen to be of different form for the two crystallographic directions.

In figure 4 is shown a graph of λ/λ_0 plotted against $(I_s/I_{s0})^2$, λ_0 and I_{s0} being the values of λ and I_s at 0°c. The results for both directions are significantly different from the dotted line corresponding to $\lambda/\lambda_0=(I_s/I_{s0})^2$ which corresponds to the result found by Döring. An interesting point to note is that if the polycrystalline magnetostriction is calculated from the formula

$$\lambda_{\text{poly}}=\tfrac{2}{5}\lambda_{100}+\tfrac{3}{5}\lambda_{111}$$

derived by Becker, then over the range of $(I_s/I_{s0})^2$ from 0·7 to 1·0, the poly crystalline magnetostriction is found to be closely proportional to I_s^2. An examination of Döring's results shows that strict proportionality is only found over a similar range of values of $(I_s/I_{s0})^2$, but below 0·7 there is a significant departure. The values agree best with those found by Kirkham (1937).

No values corresponding to temperatures greater than 300°c are plotted in figure 4, since small errors in temperature measurements cause large errors in the corresponding values of λ and I_s deduced from the (λ, T) and (I_s, T) curves. The Curie temperatures indicated by the four different series of experiments are [111] magnetostriction 353°c, magnetization 358°c; [100] magnetostriction 356°c, magnetization 359°c.

The difference between the temperatures at which magnetization and magnetostriction become zero is probably due to the different temperature distributions round the specimen, since in neither case did the thermocouple junction touch the specimen. The temperatures recorded in magnetostriction measurements are considered to be the most reliable.

It may be mentioned that in neither the magnetization nor the magnetostriction measurements was there any indication of the curve tailing away as it approached the Curie temperature; on the contrary in both cases it cut the temperature axis very sharply, and at higher temperatures neither magnetostriction nor magnetization could be detected.

It has not been possible to find a law governing the relationship between λ and I_s, neither has a satisfactory theory been advanced to explain the fundamental mechanism of magnetostriction, and it is therefore difficult to draw any definite conclusions from the (λ, T) curves of figure 3. Corresponding to a change in temperature there are changes in magnetization, lattice constant, anisotropy, elastic moduli, and almost every other physical property associated with a solid, and it appears to be impossible to separate the effects of each of these on the magnetostriction. A simple relationship between saturation magnetostriction and either saturation magnetization or temperature is therefore not to be expected.

5.2. *Magnetostriction below Saturation*

The relationships between magnetization and magnetostriction below saturation have been calculated theoretically for iron single crystals by Heisenberg (1931) on the assumption that the anisotropy energy is sufficiently large to cause all the domain boundary movement to occur before any rotation of the direction of magnetization. The theory has been extended by Fowler (1936) to cover the case of nickel. It would be expected that experimental measurements would best agree with this theory at temperatures at which the anisotropy is greatest; for nickel, anisotropy increases sharply below room temperature.

Graphs of $\Delta L/L$ against I are shown in figures 5 and 6 for the [100] and [111] directions respectively; these are typical of the whole series of measurements and show the very good agreement at low temperatures with the curves derived from the theoretical equations given by Fowler.

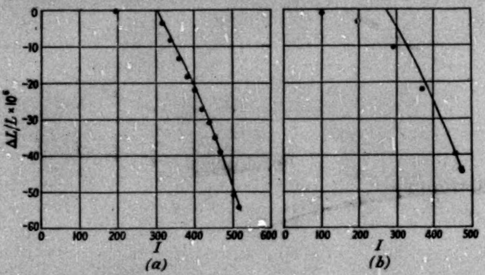

Figure 5. Variation of magnetostriction with intensity of magnetization in the [100] direction, (*a*) at −130°c, (*b*) at 76°c. Lines indicate theoretical values from Heisenberg's equations.

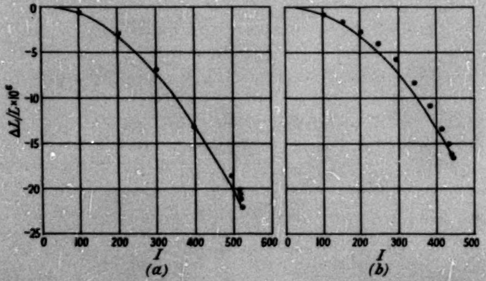

Figure 6. Variation of magnetostriction with intensity of magnetization in the [111] direction, (*a*) at −135°c, (*b*) at 127°c. Lines indicate theoretical values from Heisenberg's equations.

In order to show the transition with temperature of the shape of the $(\Delta L/L, I)$ curves, the graphs shown in figures 7 and 8 were drawn. These show values of reduced magnetostriction $(\Delta L/L)/\lambda$ corresponding to fixed values of reduced intensity of magnetization I/I_s plotted against temperature. The dotted lines on the left of these graphs indicate the calculated values of $(\Delta L/L)/\lambda$.

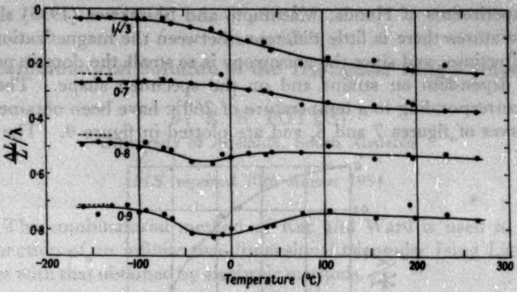

Figure 7. Variation of reduced magnetostriction with temperature for fixed values of reduced magnetization (shown on left). [100] direction.

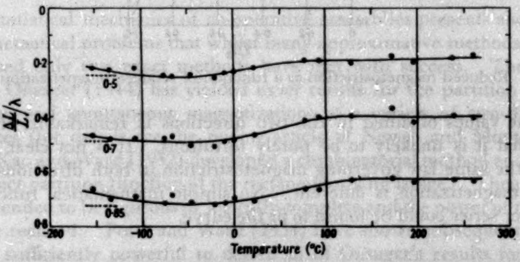

Figure 8. Variation of reduced magnetostriction with temperature for fixed values of reduced magnetization (shown on left). [111] direction.

In the [100] direction the theory predicts zero length change when the magnetization increases from 0 to $I_s/\sqrt{3}$ as shown in figure 5. The gradual transition from the sharp kink at $I_s/\sqrt{3}$ to a smooth curve as the temperature is raised is shown in figure 7, and may be accounted for by the decrease of anisotropy energy which makes the domain configuration less dependent on the anisotropy energy and more on the energy due to random strains and inclusions, boundary walls, and the demagnetizing field of the whole specimen. The depressions in the $I/I_s=0{\cdot}8$ and $I/I_s=0{\cdot}9$ curves at about −30°c are a reflection of the tendency found in the range −70°c to 50°c for the $(\Delta L/L, I)$ curves to tail off near saturation.

In the [111] direction the curves seem to agree with their calculated values at about −75°c, but to fall away again at lower temperatures. It will be seen from figures 7 and 8 that in the [111] direction the experimental results are never greater than the theoretical, while in the [100] direction they are never less. In the [100] case this is readily accounted for by the assumption that rotations are taking place before all the boundary movements are completed. In the [111] direction it is likely that the initial domain distribution does not agree with that assumed in the calculation of the theoretical curve to the same degree of accuracy that it does in the [100] direction. Evidence for this is provided by room temperature hysteresis measurements which have been discussed elsewhere (Hunt 1954 b).

The experiments of Honda, Masumoto and Shirakawa (1935) show that at high temperatures there is little difference between the magnetization curves in different directions, and since the anisotropy is so small, the domain pattern must be highly dependent on strains and on the specimen shape. The values of $(\Delta L/L)/\lambda$ corresponding to a temperature of 260°c have been obtained from the smooth curves of figures 7 and 8, and are plotted in figure 9. The agreement between the values obtained in the two directions is remarkable, and of such accuracy that it is unlikely to be purely fortuitous. It is not clear why there should be the same law governing magnetostriction in both directions when the saturation magnetization is different. No simple mathematical function other than a power series could be found to fit the curve.

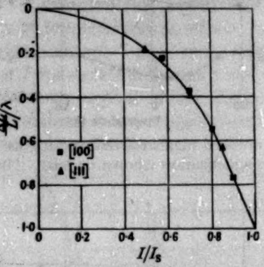

Figure 9. Reduced magnetostriction as a function of reduced magnetization at 260°c.

ACKNOWLEDGMENTS

The authors wish to thank Professor J. E. P. Wagstaff for the facilities placed at their disposal, and the Council of the Durham Colleges for a grant for the purchase of equipment. One of them (G.H.H.) is indebted to the Council of the Durham Colleges, to the British Association and to the Ministry of Education for maintenance grants.

REFERENCES

AKULOV, N. S., 1939, *Ferromagnetism*, ONTE, M–L.
BATES, L. F., and WILSON, G. W., 1951, *Proc. Phys. Soc.* A, **64,** 691.
BECKER, R., 1934, *Z. Phys.*, **87,** 547.
BOZORTH, R. M., and HAMMING, R. W., 1953, *Phys. Rev.*, **89,** 865.
CORNER, W. D., and HUNT, G. H., 1955, *J. Sci. Instrum.*, **34,** 445.
DÖRING, W., 1936, *Z. Phys.*, **103,** 560.
FOWLER, R. H., 1936, *Statistical Mechanics* (Cambridge : University Press), p. 520.
HEDDLE, T. A., 1952, *Brit. J. Appl. Phys.*, **3,** 95.
HEISENBERG, W., 1931, *Z. Phys.*, **69,** 287.
HONDA, K., MASUMOTO, H., and SHIRAKAWA, Y., 1935, *Sci. Rep. Tôhoku Univ.*, **24,** 291.
HUNT, G. H., 1954 a, *Brit. J. Appl. Phys.*, **5,** 260; 1954 b, *Thesis*, University of Durham.
KIRKHAM, D., 1937, *Phys. Rev.*, **52,** 1162.
LEWIS, B., 1950, *Brit. J. Appl. Phys.*, **1,** 238.
MASIYAMA, Y., 1928, *Sci. Rep. Tôhoku Univ.*, **17,** 945.
PEARSON, R. F., 1953, *Brit. J. Appl. Phys.*, **4,** 342.
SUCKSMITH, W., 1950, *E.R.A. Technical Report*, N/T 51.
TAKAKI, H., 1937, *Z. Phys.*, **105,** 92.
VLASOV, A. Y., 1952, *Izv. Akad. Nauk., S.S.S.R. Ser. Fiz.*, **16,** 718.

Combinatorial Solution of the Triangular Ising Lattice

By R. B. POTTS†
University of Adelaide, South Australia

MS. received 30th August 1954

Abstract. The combinatorial method of Kac and Ward is used to derive the partition function of an infinite two-dimensional triangular Ising Lattice. The result agrees with that obtained by algebraic methods.

§ 1. Introduction

The statistical mechanics of co-operative assemblies presents such difficult mathematical problems that whilst many approximative methods have been devised only two exact methods have met with success. The algebraic method of Onsager (1944) has yielded exact results for the partition functions, correlations, and spontaneous magnetizations of a variety of two-dimensional Ising lattices (for details see the review article of Newell and Montroll 1953). Recently, Kac and Ward (1952) developed a combinatorial method and used it to find the exact partition function of the rectangular Ising lattice. Their treatment was not intended to be rigorous or logically complete and the power of the method was hardly realized. Potts and Ward (1954) have shown subsequently that the method is sufficiently powerful to derive all of Onsager's results for the finite rectangular lattice and the correlations.

In the present paper the combinatorial method is applied to the problem of evaluating the partition function of the triangular Ising lattice. The purpose of the paper is not so much to give an alternative derivation of a well-known result but rather to develop and indicate the power and scope of an elementary exact method, which is of some importance in a field of research largely confounded by mathematical difficulties.

§ 2. Combinatorial Method

The starting point of the combinatorial method of evaluating the partition function $Z_{m,n}$ of a m row n column triangular Ising lattice wrapped on a torus is the relation

$$Z_{m,n}^{2}=(2\cosh H_1\cosh H_2\cosh H_3)^{2mn}\sum g(r,s,t)\tanh^{r}H_1\tanh^{s}H_2\tanh^{t}H_3 \qquad \ldots\ldots(1)$$

where $g(r, s, t)$ is the number of oriented graphs with r vertical, s horizontal, and t diagonal bonds, H_1, H_2, H_3 being the variables associated with the interactions in the vertical, horizontal, and diagonal directions respectively (figure 1 illustrates a 4-row 5-column triangular lattice, unwrapped from the torus and distorted to form a rectangular lattice with interactions along one diagonal).

---

† Now at Institute for Applied Mathematics, University of Maryland.

The combinatorial method consists, essentially, in the construction of a $6mn$ by $6mn$ matrix $\mathbf{E}-\mathbf{A}$ ($\mathbf{E}$ is the unit matrix) whose determinant performs with negligible error, the counting of the oriented graphs; thus

$$|\mathbf{E}-\mathbf{A}| \simeq \sum g(r,s,t)\tanh^r H_1 \tanh^s H_2 \tanh^t H_3. \qquad \ldots\ldots(2)$$

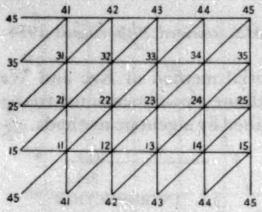

Figure 1. A 4-row 5-column triangular lattice unwrapped from a torus.

§ 3. THE COUNTING MATRIX

The matrix $\mathbf{A}$ is constructed by analysing the graphs into links, overlapping bonds cancelling out to leave separated polygons. This corresponds to the analysis of a permutation as a product of cycles, and to achieve the correct sign the links ending in the vertical, horizontal and diagonal directions are associated with the values $-\tanh H_1$, $-\tanh H_2$, $-\tanh H_3$. Changes in direction are allowed for by the factors α (one change counter-clockwise), α^2 (two changes counter-clockwise) and $\bar{\alpha}$ and $\bar{\alpha}^2$ for clockwise changes. By choosing $\alpha=\exp(i\pi/6)$ it is ensured that a polygon with r vertical, s horizontal and t diagonal bonds is counted as the term $\tanh^r H_1 \tanh^s H_2 \tanh^t H_3$.

If the six possible directions of a link are denoted by ± 1, ± 2, ± 3 then the terms corresponding to links ending in the $+1$ direction are, apart from the factor $\tanh H_1$,

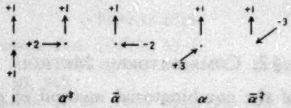

and can be represented by the matrix $\mathbf{A}(1)$. Similar considerations give the matrices $\mathbf{A}(-1)$, $\mathbf{A}(\pm 2)$, $\mathbf{A}(\pm 3)$.

$$\mathbf{A}(1)=\begin{array}{c}\\ +1\\ -1\\ +2\\ -2\\ +3\\ -3\end{array}\!\!\begin{array}{c}\begin{array}{cccccc}+1 & -1 & +2 & -2 & +3 & -3\end{array}\\ \left[\begin{array}{cccccc}1 & 0 & 0 & 0 & 0 & 0\\ 0 & 0 & 0 & 0 & 0 & 0\\ \alpha^2 & 0 & 0 & 0 & 0 & 0\\ \bar{\alpha} & 0 & 0 & 0 & 0 & 0\\ \alpha & 0 & 0 & 0 & 0 & 0\\ \bar{\alpha}^2 & 0 & 0 & 0 & 0 & 0\end{array}\right]\end{array} \qquad \mathbf{A}(-1)=\begin{bmatrix}0 & 0 & 0 & 0 & 0 & 0\\ 0 & 1 & 0 & 0 & 0 & 0\\ 0 & \bar{\alpha} & 0 & 0 & 0 & 0\\ 0 & \alpha^2 & 0 & 0 & 0 & 0\\ 0 & \bar{\alpha}^2 & 0 & 0 & 0 & 0\\ 0 & \alpha & 0 & 0 & 0 & 0\end{bmatrix}$$

$$\mathbf{A}(2)=\begin{bmatrix} 0 & 0 & \bar{\alpha}^2 & 0 & 0 & 0 \\ 0 & 0 & \alpha & 0 & 0 & 0 \\ 0 & 0 & 1 & 0 & 0 & 0 \\ 0 & 0 & 0 & 0 & 0 & 0 \\ 0 & 0 & \bar{\alpha} & 0 & 0 & 0 \\ 0 & 0 & \alpha^2 & 0 & 0 & 0 \end{bmatrix} \qquad \mathbf{A}(-2)=\begin{bmatrix} 0 & 0 & 0 & \alpha & 0 & 0 \\ 0 & 0 & 0 & \bar{\alpha}^2 & 0 & 0 \\ 0 & 0 & 0 & 0 & 0 & 0 \\ 0 & 0 & 0 & 1 & 0 & 0 \\ 0 & 0 & 0 & \alpha^2 & 0 & 0 \\ 0 & 0 & 0 & \bar{\alpha} & 0 & 0 \end{bmatrix}$$

$$\mathbf{A}(3)=\begin{bmatrix} 0 & 0 & 0 & 0 & \bar{\alpha} & 0 \\ 0 & 0 & 0 & 0 & \alpha^2 & 0 \\ 0 & 0 & 0 & 0 & \alpha & 0 \\ 0 & 0 & 0 & 0 & \bar{\alpha}^2 & 0 \\ 0 & 0 & 0 & 0 & 1 & 0 \\ 0 & 0 & 0 & 0 & 0 & 0 \end{bmatrix} \qquad \mathbf{A}(-3)=\begin{bmatrix} 0 & 0 & 0 & 0 & 0 & \alpha^2 \\ 0 & 0 & 0 & 0 & 0 & \bar{\alpha} \\ 0 & 0 & 0 & 0 & 0 & \bar{\alpha}^2 \\ 0 & 0 & 0 & 0 & 0 & \alpha \\ 0 & 0 & 0 & 0 & 0 & 0 \\ 0 & 0 & 0 & 0 & 0 & 1 \end{bmatrix} \qquad \ldots\ldots(3)$$

From the cyclic properties of the lattice it follows that, by numbering the rows and columns of $\mathbf{A}$ by 11, 12, . . $1n$, 21, . . , mn, this matrix can be expressed as the sum of direct products:

$$\begin{aligned}\mathbf{A}=\tanh H_1\{&\mathbf{R}_m\times\mathbf{E}_n\times\mathbf{A}(1)+\mathbf{R}_m{}'\times\mathbf{E}_n\times\mathbf{A}(-1)\}\\ +\tanh H_2\{&\mathbf{E}_m\times\mathbf{R}_n\times\mathbf{A}(2)+\mathbf{E}_m\times\mathbf{R}_n{}'\times\mathbf{A}(-2)\}\\ +\tanh H_3\{&\mathbf{R}_m\times\mathbf{R}_n\times\mathbf{A}(3)+\mathbf{R}_m{}'\times\mathbf{R}_n{}'\times\mathbf{A}(-3)\} \qquad \ldots\ldots(4)\end{aligned}$$

where $\mathbf{R}$ is permutation matrix

$$\mathbf{R}=\begin{bmatrix} 0 & 1 & 0 & . & . & 0 \\ 0 & 0 & 1 & . & . & 0 \\ . & . & . & . & . & . \\ 0 & 0 & 0 & . & . & 1 \\ 1 & 0 & 0 & . & . & 0 \end{bmatrix} \qquad \ldots\ldots(5)$$

and $\mathbf{R}'$ is the transpose of $\mathbf{R}$.

§4. EVALUATION OF DETERMINANT

The determinant $|\mathbf{E}-\mathbf{A}|$ is evaluated by first reducing $\mathbf{A}$ by a unitary transformation to the direct sum of matrices of order 6. If $\mathbf{U}(\delta)$ is the unitary matrix of order m with its i, jth element given by $m^{-1/2}\delta^{ij}$, $\delta=\exp(2\pi i/m)$, and similarly if $\mathbf{U}(\epsilon)$ is the unitary matrix of order n, $\epsilon=\exp(2\pi i/n)$, then the unitary matrix $\mathbf{R}=\mathbf{U}(\delta)\times\mathbf{U}(\epsilon)\times\mathbf{E}_4$ transforms $\mathbf{E}-\mathbf{A}$ to the direct sum of mn matrices $\mathbf{B}_{kl}$, $k=1,\ldots,m$; $l=1,\ldots,n$ where
$|\mathbf{B}_{kl}|\coth{}^2H_1\coth{}^2H_2\coth{}^2H_3$

$$=\begin{vmatrix} 1-\delta^k\coth H_1 & 0 & \bar{\alpha}^2 & \alpha & \bar{\alpha} & \alpha^2 \\ 0 & 1-\delta^{-k}\coth H_1 & \alpha & \bar{\alpha}^2 & \alpha^2 & \bar{\alpha} \\ \alpha^2 & \bar{\alpha} & 1-\epsilon^l\coth H_2 & 0 & \alpha & \bar{\alpha}^2 \\ \bar{\alpha} & \alpha^2 & 0 & 1-\epsilon^{-l}\coth H_2 & \bar{\alpha}^2 & \alpha \\ \alpha & \bar{\alpha}^2 & \bar{\alpha} & \alpha^2 & 1-\delta^k\epsilon^l\coth H_3 & 0 \\ \bar{\alpha}^2 & \alpha & \alpha^2 & \bar{\alpha} & 0 & 1-\delta^{-k}\epsilon^{-l}\coth H_3 \end{vmatrix} \qquad \ldots\ldots(6)$$

A rather laborious calculation gives the result

$$\begin{aligned}|\mathbf{B}_{kl}| = {} & (1+\tanh^2 H_1)(1+\tanh^2 H_2)(1+\tanh^2 H_3)+8\tanh H_1 \tanh H_2 \tanh H_3 \\ & -\tanh^2 H_1(1-\tanh^2 H_2)(1-\tanh^2 H_3)(\delta^k+\delta^{-k}) \\ & -\tanh^2 H_2(1-\tanh^2 H_3)(1-\tanh^2 H_1)(\epsilon^l+\epsilon^{-l}) \\ & -\tanh^2 H_3(1-\tanh^2 H_1)(1-\tanh^2 H_2)(\delta^k\epsilon^l+\delta^{-k}\epsilon^{-l}) \qquad \ldots\ldots(7)\end{aligned}$$

from which follows:

$$|\mathbf{E}-\mathbf{A}| = \prod_{k=1}^{m}\prod_{l=1}^{n}|\mathbf{B}_{kl}|. \qquad \ldots\ldots(8)$$

§5. PARTITION FUNCTION

The determinant evaluated above performs the required counting correctly except that graphs looping the torus are counted with the wrong sign. The error thereby introduced is negligible for large lattices so that from (1) and (2) it follows that if

$$\lim_{m,n\to\infty}(Z_{m,n})^{1/mn}=Z$$

then

$$\begin{aligned}\ln(\tfrac{1}{2}Z) = {} & \lim_{m,n\to\infty}\frac{1}{2mn}\sum_{k=1}^{m}\sum_{l=1}^{n}\ln\Big\{\cosh 2H_1\cosh 2H_2\cosh 2H_3 \\ & +\sinh 2H_1\sinh 2H_2\sinh 2H_3-\sinh 2H_1\cos\left(\frac{2k\pi}{m}\right) \\ & -\sinh 2H_2\cos\left(\frac{2l\pi}{n}\right)-\sinh 2H_3\cos\left(\frac{2k\pi}{m}+\frac{2l\pi}{n}\right)\Big\} \\ = {} & \frac{1}{8\pi^2}\int_0^{2\pi}\!\!\int \ln\{\cosh 2H_1\cosh 2H_2\cosh 2H_3+\sinh 2H_1\sinh 2H_2\sinh 2H_3 \\ & -\sinh 2H_1\cos w_1-\sinh 2H_2\cos w_2-\sinh 2H_3\cos(w_1+w_2)\}\,dw_1\,dw_2. \\ & \qquad\ldots\ldots(9)\end{aligned}$$

This is precisely the result given by the algebraic method.

§6. CONCLUSION

It has been shown that the exact partition function of the triangular Ising lattice can be derived by the elementary combinatorial method. As is well known, the partition function for the honeycomb lattice can be derived from that for the triangular lattice; it can also be derived directly along the lines of this paper. Perhaps the most interesting feature of the method is the fact that the graphs on a variety of two-dimensional lattices can be counted by a suitably constructed determinant.

REFERENCES

KAC, M., and WARD, J. C., 1952, *Phys. Rev.*, **88,** 1332.
NEWELL, G. F., and MONTROLL, E. W., 1935, *Rev. Mod. Phys.*, **25,** 353.
ONSAGER, L., 1944, *Phys. Rev.*, **65,** 117.
POTTS, R. B., and WARD, J. C., 1955, *Progr. Theor. Phys., Osaka*, **13,** No. 1.

On the Method of Atoms in Molecules

By A. C. HURLEY

Chemical Physics Section, Division of Industrial Chemistry, Commonwealth Scientific and Industrial Research Organisation, Melbourne, Australia

Communicated by A. L. G. Rees ; MS. received 3rd August 1954 *and in amended form 20th October* 1954

Abstract. The method of atoms in molecules is investigated in detail for the case of covalent-ionic resonance in the ground state of the hydrogen molecule. It is shown that the method is reliable if, and only if, different orbitals are used to approximate atomic and ionic states of the same molecule.

---

§ 1. INTRODUCTION

A NEW technique for calculating the electronic structure of molecules, the method of atoms in molecules, has recently been developed by Moffitt (1951 b). It is based on an expansion of the molecular wave function in terms of accurate atomic wave functions. The total energy of the molecule is then derived in terms of various integrals involving these accurate atomic functions. Although it is not possible to evaluate these integrals directly, Moffitt has shown how to obtain useful approximations to them. For this purpose the energy expression is divided into atomic terms and perturbation terms. The atomic terms are evaluated either from atomic spectral data or from accurate wave mechanical calculations, while the perturbation terms are evaluated using simple orbital approximations to the accurate atomic functions.

It is clear that there are two distinct sources of error in any calculation by the method of atoms in molecules. Firstly there are the errors introduced by expressing the molecular wave function in terms of a finite number of accurate atomic wave functions and secondly there are the errors arising from the approximate evaluation of the integrals involving these accurate atomic functions. Previous applications of the method have been to the relatively complex systems O_2 (Moffitt 1951 a), C_2H_4 (Moffitt and Scanlan 1953 a) and C_6H_6 (Moffitt and Scanlan 1953 b), for which it is not possible to distinguish between these two sources of error. For these systems the situation is further complicated by various additional approximations (e.g. the Hückel approximation) which are not inherent in the method itself.

In this note the method of atoms in molecules is investigated fully for the simplest possible case, that of covalent-ionic resonance in the ground state of the hydrogen molecule. This system is unique in that the exact wave function for the ground state of the hydrogen atom is known. Furthermore a very accurate approximation to the ground state wave function of the ion H^- is available

(Chandrasekhar 1944). It is also possible to carry through the complete programme of the method of atoms in molecules without any extraneous approximations.

Throughout the paper all equations and numerical values are expressed in atomic units.

§ 2. THE METHOD OF ATOMS IN MOLECULES FOR THE HYDROGEN MOLECULE

For the case of covalent-ionic resonance in the ground state of the hydrogen molecule, the method of atoms in molecules is based on the wave function

$$\Psi = \Psi_C + \lambda\Psi_I, \qquad \ldots\ldots(2.1)$$

with

$$\Psi_C = 2^{-1/2}[a(1)\,b(2) + b(1)\,a(2)], \qquad \ldots\ldots(2.2)$$

and

$$\Psi_I = 2^{-1/2}[\phi_a(1, 2) + \phi_b(1, 2)]. \qquad \ldots\ldots(2.3)$$

Here *a*, *b* are exact wave functions for the ground state of the hydrogen atom, and ϕ_a, ϕ_b are exact wave functions for the ion H^-.

In terms of the functions (2.2) and (2.3) we define the 2 × 2 matrices *H* and *M* by the equations

$$H_{ij} = \int \Psi_i^* \mathscr{H} \Psi_j \, d\tau, \ \ (i, j = \mathrm{I, C}) \qquad \ldots\ldots(2.4)$$

and

$$M_{ij} = \int \Psi_i^* \Psi_j \, d\tau, \ \ (i, j = \mathrm{I, C}) \qquad \ldots\ldots(2.5)$$

where

$$\mathscr{H} = \frac{1}{2}\nabla_1^2 - \frac{1}{2}\nabla_2^2 - \frac{1}{r_{a1}} - \frac{1}{r_{a2}} - \frac{1}{r_{b1}} - \frac{1}{r_{b2}} + \frac{1}{r_{12}} + \frac{1}{R} \qquad \ldots\ldots(2.6)$$

in the usual notation.

The energy of the hydrogen molecule ground state is now given by the lowest root λ_0 of the equation

$$\det(H - \lambda M) = 0, \qquad \ldots\ldots(2.7)$$

and the wave function for this state is obtained by substituting $\lambda = \lambda_0$ in equation (2.1).

Following Moffitt (1951 b) we express the matrix *H* in the form

$$H = MW + V = \tfrac{1}{2}(MW + WM) + \tfrac{1}{2}(V + V^\dagger), \qquad \ldots\ldots(2.8)$$

where

$$W = \lim_{R \to \infty} H, \qquad \ldots\ldots(2.9)$$

and $V^\dagger$ is the Hermitian conjugate of *V*. Moffitt (1951 b) has shown that equation (2.8) represents a satisfactory separation of the matrix *H* into atomic terms and perturbation terms, and has given explicit formulae for the perturbation terms *V* and $V^\dagger$ in terms of integrals involving the accurate atomic functions, in our case the functions (2.2) and (2.3).

In our case these formulae reduce to the following expressions:

$$\left.\begin{aligned}
V_{\mathrm{CC}} = V_{\mathrm{CC}}{}^{\dagger} &= 2\left[-\int\frac{a^2\,dv}{r_b} - \left(\int ab\,dv\right)\left(\int\frac{ab\,dv}{r_a}\right)\right] \\
&\quad + \int\frac{a^2(1)b^2(2)\,dv_1\,dv_2}{r_{12}} + \int\frac{a(1)b(2)b(1)a(2)\,dv_1\,dv_2}{r_{12}} \\
&\qquad + \frac{1}{R}\left\{1 + \left(\int ab\,dv\right)^2\right\}, \\
V_{\mathrm{CI}} = V_{\mathrm{IC}}{}^{\dagger} &= 2\left[-\int\frac{a(1)b(2)\phi_a(1,2)\,dv_1\,dv_2}{r_{b1}}\right. \\
&\quad \left. - \int\frac{a(1)b(2)\phi_a(1,2)\,dv_1\,dv_2}{r_{b2}} + \frac{1}{R}\int a(1)\,b(2)\,\phi_a(1,2)\,dv_1\,dv_2\right], \\
V_{\mathrm{IC}} = V_{\mathrm{CI}}{}^{\dagger} &= 2\left[-\int\frac{\phi_a(1,2)a(1)b(2)\,dv_1\,dv_2}{r_{a2}}\right. \\
&\quad - \int\frac{\phi_a(1,2)a(1)b(2)\,dv_1\,dv_2}{r_{b1}} + \int\frac{\phi_a(1,2)a(1)b(2)\,dv_1\,dv_2}{r_{12}} \\
&\qquad \left. + \frac{1}{R}\int\phi_a(1,2)\,a(1)\,b(2)\,dv_1\,dv_2\right], \\
V_{\mathrm{II}} = V_{\mathrm{II}}{}^{\dagger} &= 2\left[-\int\frac{\phi_a{}^2(1,2)\,dv_1\,dv_2}{r_{b1}}\right. \\
&\quad \left. - \int\frac{\phi_a(1,2)\phi_b(1,2)\,dv_1\,dv_2}{r_{a1}}\right] + \frac{1}{R}\left(1 + \int\phi_a(1,2)\,\phi_b(1,2)\,dv_1\,dv_2\right).
\end{aligned}\right\} \quad \ldots\ldots(2.9')$$

To carry the analysis further we must introduce orbital approximation to the exact atomic functions (2.2) and (2.3). These functions $\widetilde{\Psi}_{\mathrm{C}}$ and $\widetilde{\Psi}_{\mathrm{I}}$ are defined by

$$\widetilde{\Psi}_{\mathrm{C}} = \Psi_{\mathrm{C}} = 2^{-1/2}[a(1)\,b(2) + b(1)\,a(2)], \qquad \ldots\ldots(2.10)$$

and

$$\widetilde{\Psi}_{\mathrm{I}} = 2^{-1/2}[a'(1)\,a'(2) + b'(1)\,b'(2)], \qquad \ldots\ldots(2.11)$$

where a', b' are the normalized hydrogen-like functions

$$a' = \left(\frac{c^3}{\pi}\right)^{1/2}\exp(-cr_a), \quad b' = \left(\frac{c^3}{\pi}\right)^{1/2}\exp(-cr_b). \qquad \ldots\ldots(2.12)$$

In terms of these functions we define the 2×2 matrices $\tilde{\tilde{H}}$, $\widetilde{M}$, and $\widetilde{W}$ by the equations

$$\tilde{\tilde{H}}_{ij} = \int\widetilde{\Psi}_i{}^*\,\mathscr{H}\,\widetilde{\Psi}_j\,d\tau, (i, j = \mathrm{I}, \mathrm{C}), \qquad \ldots\ldots(2.13)$$

$$\widetilde{M}_{ij} = \int\widetilde{\Psi}_i{}^*\,\widetilde{\Psi}_j\,d\tau, (i, j = \mathrm{I}, \mathrm{C}) \qquad \ldots\ldots(2.14)$$

and

$$\widetilde{W} = \lim_{R\to\infty}\tilde{\tilde{H}}. \qquad \ldots\ldots(2.15)$$

We now consider three distinct approximations to the energy matrix H and the overlap matrix M of equation (2.7):

Approximation 1.

$$H \simeq \tilde{\tilde{H}}, \quad M \simeq \widetilde{M}.$$

This is the approximation employed in the usual orbital theories.

Approximation 2.

$$M \simeq \widetilde{M}$$

$$H \simeq \widetilde{H}_1 = \widetilde{\widetilde{H}} + \tfrac{1}{2}[\widetilde{M}(W-\widetilde{W}) + (W-\widetilde{W})\widetilde{M}].$$

This is the approximation used by Moffitt and Scanlan (1953 a, b) in their calculations on ethylene and benzene.

Approximation 3.

$$M \simeq \widetilde{M}$$

$$H \simeq \widetilde{H}_2 = \tfrac{1}{2}(\widetilde{M}W + W\widetilde{M}) + \tfrac{1}{2}(\widetilde{V} + \widetilde{V}^{\dagger}),$$

where the matrices $\widetilde{V}$ and $\widetilde{V}^{\dagger}$ are obtained by replacing Ψ_C and Ψ_I by $\widetilde{\Psi}_C$ and $\widetilde{\Psi}_I$ respectively in the definitions of V and $V^{\dagger}$ (Moffitt 1951 b). Thus in the expressions (2.9′) the functions a and b remain unaltered, whereas $\phi_a(1,2)$ and $\phi_b(1,2)$ are replaced by $a'(1)\,a'(2)$ and $b'(1)\,b'(2)$ respectively. This approximation is also considered by Moffitt, but for reasons of convenience he rejects it in favour of approximation (2). However, for the present system both approximations may be carried through without difficulty.

We note that

$$\lim_{R\to\infty} \widetilde{H}_1 = \lim_{R\to\infty} \widetilde{H}_2 = W. \qquad \ldots\ldots(2.16)$$

§3. NUMERICAL CALCULATIONS AND DISCUSSION

In place of the exact wave function for the ion H⁻ we use Chandrasekhar's eleven term function. Thus we take

$$\phi_a(1,2) = N\mathrm{e}^{-\alpha s}(1 + \beta u + \gamma t^2 + \delta s + \epsilon s^2 + \zeta u^2 + \chi_6 t^4 + \chi_7 t^6 + \chi_8 t^4 u^2 + \chi_9 t^2 u^2 + \chi_{10} t^2 u^4),$$

where $s = r_{a1} + r_{a2}$, $t = -r_{a1} + r_{a2}$, $u = r_{12}$, N is a normalization constant, and the parameters $\alpha, \beta, \ldots \chi_{10}$ are determined by the variational method. This function leads to a total energy of $-0{\cdot}52756$ (Chandrasekhar 1944). The errors involved in assuming this to be the exact total energy of the system H⁻ are quite negligible in the present context. It would, of course, be extremely difficult to carry out an exact molecular calculation in terms of such a complex wave function. This would involve the evaluation of all the integrals in the equations (2.9′). However, the method of atoms in molecules enables us to approximate to such a calculation without undue labour.

Two different approximations to the orbital functions (2.10) and (2.11) are considered. In the first of these, which corresponds to the approximation employed by Moffitt and Scanlan in their calculations (Moffitt 1951 a, 1953, Moffitt and Scanlan 1953 a, b), the screening constants of the ionic orbitals a' and b' are assumed to be the same as those of the atomic orbitals a and b. That is, we take

$$a' \equiv a = \pi^{-1/2}\exp(-r_a),\quad b' \equiv b = \pi^{-1/2}\exp(-r_b). \qquad \ldots\ldots(3.1)$$

The integrals required in this calculation were taken from the tables given by Hirschfelder and Linnett (1950). The results of this first calculation are shown in figures 1 and 2, which give the behaviour of the total energy E and the parameter λ for the three approximations considered in the previous section. In figure 1 the experimental energy curve (Hirschfelder and Linnett 1950) is also shown.

At first sight the results shown in figure 1 appear quite satisfactory. Approximations 2 and 3 both lead to energy curves which are much closer to the experimental curve than is the curve given by approximation 1. However, two features of the curves suggest that these good results are not due to the accuracy of the original wave function (2.1). Firstly, both curves are below the experimental curve for some values of the nuclear separation, and secondly there are considerable discrepancies between the results of approximations 2 and 3. These features of the curves suggest that the good results shown in figure 1 arise from a cancellation of the errors due to the inaccuracies of the original wave function (2.1) by the errors introduced by using the orbital approximations (2.2), (2.3) and (3.1).

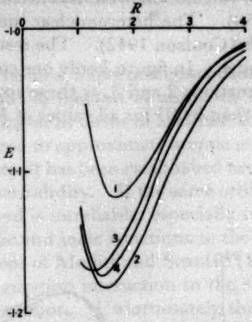

Figure 1. Energy of hydrogen molecule ground state: equal screening constants.

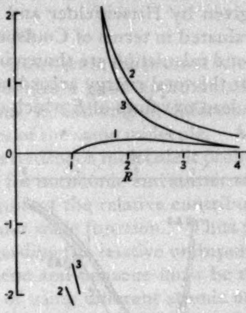

Figure 2. Behaviour of parameter λ: equal screening constants.

Curves 1, uncorrected orbital approximation; 2, first form of method of atoms in molecules; 3, second form of method of atoms in molecules; 4, experimental.

These suspicions are immediately confirmed by a glance at figure 2. Here we see that for both versions of the method of atoms in molecules (approximations 2 and 3) the parameter λ is extremely large near the equilibrium nuclear separation and indeed tends to infinity for $R \simeq 1{\cdot}4$. This corresponds to the absurd result that the wave function for the ground state of the hydrogen molecule is purely ionic at this nuclear separation, with no contribution from the covalent function (2.2).

It is not hard to locate the source of this error. It arises from the use of the same screening constant for the atomic and ionic orbital functions. The use of a large screening constant for the ionic function leads to a gross overestimate of the interaction energy of the two ions H^+ and H^-. In effect the interaction between these two ions is given by the simple Coulomb attraction $1/R$ down to quite small nuclear separations (1·5–2·0). When this large interaction energy, together with a resonance energy between H^+–H^- and H^-–H^+, is added to the low energy at infinite nuclear separation ($-0{\cdot}52756$) given by Chandrasekhar's wave function, it is found that the energy of the structure $H^{\pm}$–$H^{\mp}$ (wave function (2.3)) is considerably less than that of the covalent structure H–H (wave function (2.2)). Hence the ionic function (2.3) dominates the wave function (2.1) for small nuclear separations.

In the second calculation different values are used for the screening constants of the ionic and atomic orbital functions. The screening constant of the ionic orbitals a' and b' is given the value 0·6875. This is the value which results from a treatment of the ion H^- by the variational method using a wave function which is the product of equivalent hydrogenic functions. Thus in this calculation we have

$$\left.\begin{aligned} a&=(1/\pi)^{1/2}\exp(-r_a), & a'&=(c^3/\pi)^{1/2}\exp(-cr_a),\\ b&=(1/\pi)^{1/2}\exp(-r_b), & b'&=(c^3/\pi)^{1/2}\exp(-cr_b),\end{aligned}\right\}\qquad\ldots\ldots(3.2)$$

where $$c=0{\cdot}6875.$$

The homonuclear integrals required in this calculation were taken from the tables given by Hirschfelder and Linnett (1950). The heteronuclear integrals were evaluated in terms of Coulson's J-integrals (Coulson 1942). The results of this second calculation are shown in figures 3 and 4. In figure 3 only one curve is given for the total energy according to approximations 2 and 3, as these approximations lead to values of E which differ by less than 0·003 for all values of R considered.

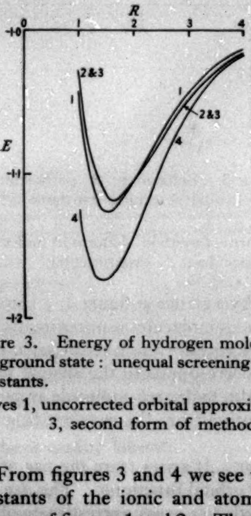

Figure 3. Energy of hydrogen molecule ground state: unequal screening constants.

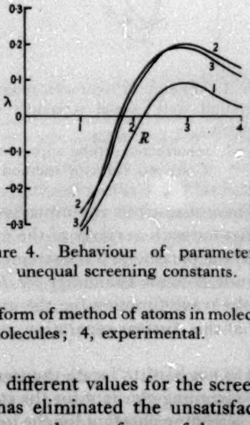

Figure 4. Behaviour of parameter λ unequal screening constants.

Curves 1, uncorrected orbital approximation; 2, first form of method of atoms in molecules; 3, second form of method of atoms in molecules; 4, experimental.

From figures 3 and 4 we see that the use of different values for the screening constants of the ionic and atomic functions has eliminated the unsatisfactory features of figures 1 and 2. The agreement between the two forms of the method of atoms in molecules is very striking. This good agreement strongly suggests that both forms of the theory provide an accurate approximation to an exact calculation in terms of the wave function (2.1). The differences between the results of the method of atoms in molecules and of the simple orbital method, although not large, are those to be expected from an accurate calculation in terms of the wave function (2.1). Thus for large values of the nuclear separation ($R>2{\cdot}5$) the use of the accurate function (2.2) stabilizes the ionic structure relative to the covalent structure. This stabilization is reflected in a larger value of λ for these nuclear separations and a lowering of the total energy of the system. For small nuclear separations ($R < 2$), however, it appears that the highly specialized Chandrasekhar function is less suitable than a simple orbital type function. For all these approximations the negative values of λ for small nuclear separations probably correspond to a form of in–out correlation similar to that which has been discussed for the helium atom ground state by Lennard-Jones and Pople (1952).

The failure of the more accurate form of the method of atoms in molecules to produce a significant lowering of the total energy for the present system, should not be regarded as a defect of the method. It arises solely from the fact that, for the hydrogen molecule, Ψ_C and $\tilde{\Psi}_C$ are identical. For more complex systems it is clear that a calculation in terms of accurate atomic functions instead of orbital functions would lead to a very substantial lowering of the total energy.

§ 4. Conclusions

The most important conclusion that can be drawn from the present calculations is that the method of atoms in molecules provides a good approximation to a calculation in terms of accurate atomic functions, if, and only if, different orbitals are used to approximate atomic and ionic states of the same molecule. Although this result has been established here only for the hydrogen molecule it probably has a wider validity. If the same orbitals are used for both ionic and atomic states the method is unreliable, especially in the estimation of the relative contributions of atomic and ionic functions to the total molecular wave function. Thus the conclusions of Moffitt and Scanlan (1953 a, b) regarding the relative unimportance of configuration interaction in the systems ethylene and benzene must be regarded with caution. Unfortunately the refinement of using different atomic and ionic orbitals greatly complicates the application of the method of atoms in molecules to complex molecules. In particular the close formal relationship between this method and the method of molecular orbitals is destroyed. Furthermore the evaluation of the necessary integrals for homonuclear molecules is rendered much more difficult. Nevertheless, this refinement seems essential if reliable results are to be obtained.

References

Chandrasekhar, S., 1944, *Rev. Mod. Phys.*, **16**, 301.

Coulson, C. A., 1942, *Proc. Camb. Phil. Soc.*, **38**, 210.

Hirschfelder, J. O., and Linnett, J. W., 1950, *J. Chem. Phys.*, **18**, 130.

Lennard-Jones, Sir John, and Pople, J. A., 1952, *Phil. Mag.*, **43**, 581.

Moffitt, W., 1951 a, *Proc. Roy. Soc.* A, **210**, 224; 1951 b, *Ibid.*, A, **210**, 245; 1953, *Ibid.*, A, **218**, 486.

Moffitt, W., and Scanlan, J., 1953 a, *Proc. Roy. Soc.* A, **218**, 464; 1953 b, *Ibid.*, A, **220**, 530.

The Coulomb Scattering of High-Energy Electrons and Positrons by Nuclei

BY R. M. CURR

Department of Physics, University College, London

Abstract. The Mott cross section for the Coulomb scattering of high-energy electrons and positrons by atomic nuclei has been expressed by McKinley and Feshbach in terms of series in powers of $Z/137$, up to terms in Z^4, where Z is the atomic number of the scattering nucleus. The coefficients of these series, which were evaluated numerically, have been re-calculated and some minor errors corrected. Further coefficients have been calculated to enable application of the method to heavy elements and the resulting cross section, expressed as a ratio to the Rutherford cross section, is given in the form of a single power series.

---

§ 1. INTRODUCTION

THE cross section for the single scattering of electrons and positrons by a Coulomb field has been expressed by Mott in terms of two conditionally convergent infinite series. These series have been expanded by McKinley and Feshbach (1948) in power series in α and α/β, where

$$\alpha = -ZZ'\mathbf{e}^2/\hbar\mathbf{c} = \pm Z/137(-\text{for positrons}), \quad \beta = v/\mathbf{c}. \qquad \ldots\ldots(1)$$

These expansions, which give results accurate to 1% for nuclei up to about $Z=40$, have been extended so that they are applicable for higher Z. The results have been further simplified by putting the cross section in the form of a single power series. The series gives results accurate to 1% for α/β less than 0·6.

§ 2. THEORY

The Mott cross section for scattering of electrons of velocity $\beta(=v/\mathbf{c})$ through an angle θ is given by

$$\sigma = 1/\kappa^2[q^2(1-\beta^2)|F|^2 \operatorname{cosec}^2 \theta/2 + |G|^2 \sec^2 \theta/2] \qquad \ldots\ldots(2)$$

where $q=\alpha/\beta$, $\kappa^2 = m_0{}^2v^2/\hbar^2(1-\beta^2)$. The functions F and G are given by:

$$\left.\begin{aligned} &F = F_0 + F_1, \quad G = G_0 + G_1 \\ &F_0 = \tfrac{1}{2}i \exp(iq \ln \sin^2 \theta/2)\Gamma(1-iq)/\Gamma(1+iq) \\ &G_0 = -iqF_0 \cot^2 \theta/2 \\ &F_1 = \tfrac{1}{2}i \sum_{k=0}^{\infty} [kD_k + (k+1)D_{k+1}](-)^k P_k(\cos\theta) \\ &G_1 = \tfrac{1}{2}i \sum_{k=0}^{\infty} [k^2D_k - (k+1)^2D_{k+1}](-)^k P_k(\cos\theta) \end{aligned}\right\} \qquad \ldots\ldots(3)$$

where

$$\left.\begin{aligned} &D_k = \exp(-\pi ik)\frac{\Gamma(k-iq)}{\Gamma(k+1+iq)} - \exp(-\pi i\rho_k)\frac{\Gamma(\rho_k-iq)}{\Gamma(\rho_k+1+iq)} \\ &\rho_k = (k^2-\alpha^2)^{1/2}. \end{aligned}\right\} \qquad \ldots\ldots(4)$$

The notation used is that of McKinley and Feshbach.

We wish to expand F and G in powers of α and α/β. The expansion of F_0 yields

$$F_0 = \tfrac{1}{2}i - qL_1 - iq^2L_1^2 + aq^3 + ibq^4 + cq^5 + \dots \qquad \dots\dots(5)$$

where

$$\left.\begin{aligned} L_1 &= \ln \sin\theta/2 - \psi_1(1) \\ a &= \tfrac{2}{3}L_1^3 - \tfrac{1}{6}\psi_3(1) \\ b &= -\tfrac{1}{3}L_1(L_1^3 - \psi_3(1)) \\ c &= -\tfrac{1}{3}(\tfrac{2}{5}L_1^5 - L_1^2\psi_3(1) - \tfrac{1}{40}\psi_5(1)). \end{aligned}\right\} \qquad \dots\dots(6)$$

Here $\psi_n(k)$ are the polygamma functions, defined by

$$\psi_n(k) = \frac{d^n}{dk^n}\ln\Gamma(k).$$

The expansion of D_k yields

$$\begin{aligned} D_k = (-)^{k+1}\frac{1}{k}\Bigg[&\frac{\pi i\alpha^2}{2k} + \frac{\alpha^2}{2k^2} + \frac{i\alpha^3}{2\beta}\left(\frac{\psi_2^*}{k} - \frac{\psi_1^*}{k^2}\right) \\ &+ \frac{\pi\alpha^3}{2k\beta}\psi_1^* - \frac{\pi i\alpha^4}{2k\beta^2}(\psi_1^2)^* + \frac{3\pi i\alpha^4}{8k^3} \\ &+ \frac{\alpha^4}{\beta^2}\left\{\frac{1}{k}(\psi_1\psi_2)^* - \frac{1}{2k^2}(\psi_1^2)^*\right\} - \frac{\pi^2\alpha^4}{8k^2} \\ &+ \frac{i\alpha^5}{\beta^2}\left\{\frac{(\psi_1^3)^*}{3k^2} - \frac{(\psi_1^2\psi_2)^*}{k} + \frac{\psi_3^*}{2k^2} - \frac{\psi_4^*}{12k}\right\} \\ &+ \frac{i\alpha^5}{\beta}\left\{\frac{\pi^2\psi_1^*}{8k^2} - \frac{3\psi_1^*}{8k^4} + \frac{3\psi_2^*}{8k^3} - \frac{\psi_3^*}{8k^2}\right\} \\ &- \frac{\pi\alpha^5}{2k\beta^3}\left(\frac{2}{3}\psi_1^3 + \frac{\psi_3}{6}\right)^* + \frac{\pi\alpha^5}{\beta}\left(\frac{3\psi_1^*}{8k^3} - \frac{\psi_2^*}{4k^2}\right) \\ &+ \frac{\pi i\alpha^6}{6k^2\beta^4}(\psi_1^4 + \psi_1\psi_3)^* + \frac{\pi i\alpha^6}{\beta^2}\left\{\frac{(\psi_1\psi_2)^*}{2k^3} - \frac{3(\psi_1^2)^*}{48k^4}\right\} \\ &+ \pi i\alpha^6\left(\frac{5}{16k^6} - \frac{\pi^2}{48k^4}\right) + \dots\Bigg] \end{aligned} \qquad \dots\dots(7)$$

where

$$F^*(k) = F(k) + F(k+1).$$

This series was given, up to the terms in α^4, by McKinley and Feshbach. Substituting (5) in (3) gives expansions for F and G of the form

$$\left.\begin{aligned} F = F_0 &+ A(\theta)\alpha^2 + B(\theta)\alpha^3/\beta + C(\theta)\alpha^4/\beta^2 + D(\theta)\alpha^4 \\ &+ Q(\theta)\alpha^5/\beta^3 + S(\theta)\alpha^5/\beta + \dots \\ G = G_0 &+ E(\theta)\alpha^2 + H(\theta)\alpha^3/\beta + I(\theta)\alpha^4/\beta^2 + J(\theta)\alpha^4 \\ &+ K(\theta)\alpha^5/\beta^3 + M(\theta)\alpha^5/\beta + N(\theta)\alpha^6/\beta^4 + O(\theta)\alpha^6/\beta^2 \\ &+ P(\theta)\alpha^6 + \dots \end{aligned}\right\} \qquad \dots\dots(8)$$

The terms in F_1 involve summations which converge as $1/k^2$ or better and were computed directly, but a method of analysis suggested by Bartlett and

Watson (1940) was used for G_1, which would otherwise have involved series of the type

$$\sum_{k=1}^{\infty} \{\psi_1(k)\}^n P_k.$$

These conditionally convergent series are difficult to sum accurately since they converge only very slowly.

The analysis of G_1 given by Bartlett and Watson is as follows:

$$G_1 = G_1^{F_0} + G_1^{\Phi} + G_1^{E}$$

where

$$\left.\begin{aligned} G_1^{F_0} &= [\pi^2\alpha^4 - 4\alpha^2(1+2iq)]iF_0/8q \\ G_1^{\Phi} &= \tfrac{1}{4}\pi\alpha^2(1+\cos\theta)\Phi/\Gamma(1+2iq) \\ G_1^{E} &= \tfrac{1}{2}i\sum_{0}^{\infty}(E_k - E_{k+1})(-)^k P_k(\cos\theta) \\ \Phi &= (2\sin\theta/2)^{2iq-2}\sin(\theta/2)|\Gamma(1+iq)|^2 F(\tfrac{1}{2}, 1+iq, 2;\ \cos^2\theta/2) \\ E_k &= k^2 D_k + \tfrac{1}{2}\pi i\alpha^2 k S_k - [\pi^2\alpha^4 - 4\alpha^2(1+2iq)]S_k/8. \end{aligned}\right\} \quad \ldots\ldots(9)$$

Here F is the hypergeometric function defined by

$$F(\alpha, \beta, \gamma;\ x) = \sum_{r=0}^{\infty} \frac{\Gamma(\alpha+r)\Gamma(\beta+r)}{r!\ \Gamma(\gamma+r)} x^r. \quad \ldots\ldots(10)$$

and S_k is given by

$$S_k = (-)^k \Gamma(k-iq)/\Gamma(k+1+iq). \quad \ldots\ldots(11)$$

The term $G_1^{F_0}$ can be expressed as a power series by use of (5). The function G_1^{Φ} can also be expanded in series, with coefficients involving summations of the type

$$\sum_{r=0}^{\infty} \frac{(2r)!}{2^{2r}(r!)^2(r+1)!}(\cos\theta/2)^{2r}\frac{d^n}{dr^n}\Gamma(r+1). \quad \ldots\ldots(12)$$

These summations converge rapidly for $\theta \geqslant 60°$; for $\theta < 60°$ Bartlett and Watson suggest the use of a connection formula between $F(\alpha, \beta, \gamma;\ x)$ and $F(\alpha', \beta', \gamma';\ 1-x)$. However, it was found that even at 30° expression (12) could be summed fairly readily; at this angle the first forty terms of the series were summed and the remainder estimated by noting that the terms converge slightly faster than $(\cos\theta/2)^{2r}$ for large r.

Using (7), (9) and (11) the expansion for E_k is found to be

$$\begin{aligned} E_k = (-)^{k+1}\Big[& \frac{i\alpha^3}{2\beta}\left(\psi_2^* - \frac{2}{k}\right) + \frac{\alpha^4}{2\beta^2}\left\{\psi_1^*\left(\psi_2^* - \frac{2}{k}\right) - \frac{1}{k^4}\right\} + \frac{3\pi i\alpha^4}{8k^2} \\ & + \frac{\pi\alpha^5}{8k\beta}\left(\frac{3}{k}\psi_1^* - 2\psi_2^*\right) - \frac{i\alpha^5}{2\beta^3}\left\{\psi_1^{2*}\left(\psi_2^* - \frac{2}{k}\right) + \frac{\psi_4^*}{3!} - \frac{\psi_1^*}{k^3}\right\} \\ & + \frac{i\alpha^5}{8k\beta}\left(-\frac{3\psi_1^*}{k^2} + \frac{3\psi_2^*}{k} - \psi_3^*\right) + \frac{\pi i\alpha^6}{8k\beta^2}\left\{2\psi_1^*\psi_2^* - \frac{3}{k}(\psi_1^2)^* - \frac{2}{k^3}\right\} \\ & + \frac{\pi i\alpha^6}{48k^2}\left(\frac{15}{k^2} - \pi^2\right) + \ldots\Big]. \end{aligned} \quad \ldots\ldots(13)$$

This is of order $1/k^2$, so that the coefficients in the expansion of G_1^E can be computed numerically.

The Rutherford cross section is given by

$$\sigma_R=\left(\frac{Ze^2}{2m_0v^2}\right)^2(1-\beta^2)\operatorname{cosec}^4\theta/2=\frac{q^2}{4\kappa^2}\operatorname{cosec}^4\theta/2. \qquad \ldots\ldots(14)$$

Substituting (5) and (8) in (2) we obtain the following series for the ratio of the Mott to the Rutherford cross section:

$$\begin{aligned}R=1-\beta^2\sin^2\theta/2+\alpha\beta R_1+\alpha^2R_2+\alpha^2\beta^2R_2'+(\alpha^3/\beta)R_3+\alpha^3\beta R_3'+(\alpha^4/\beta^2)R_4\\+\alpha^4R_4'+\alpha^4\beta^2R_4''+(\alpha^5/\beta^3)R_5+(\alpha^5/\beta)R_5'+\alpha^5\beta R_5''+\ldots\end{aligned} \qquad \ldots\ldots(15)$$

where

$$\left.\begin{aligned}
R_1&=4E_\mathrm{r}\sin^2\tfrac{1}{2}\theta\\
R_2&=4\sin^2\tfrac{1}{2}\theta(A_\mathrm{i}+H_\mathrm{r}+2E_\mathrm{i}L_1)\\
R_2'&=4\sin^2\tfrac{1}{2}\theta(|E|^2\tan^2\theta/2-A_\mathrm{i})\\
R_3&=4\sin^2\tfrac{1}{2}\theta(I_\mathrm{r}+B_\mathrm{i}+2H_\mathrm{i}L_1-2E_\mathrm{r}L_1{}^2-2A_\mathrm{r}L_1)\\
R_3'&=4\sin^2\tfrac{1}{2}\theta[2(H_\mathrm{r}E_\mathrm{r}+H_\mathrm{i}E_\mathrm{i})\tan^2\tfrac{1}{2}\theta-B_\mathrm{i}+2A_\mathrm{r}L_1+J_\mathrm{r}]\\
R_4&=4\sin^2\tfrac{1}{2}\theta[C_\mathrm{i}-2L_1B_\mathrm{r}-2A_\mathrm{i}L_1{}^2+K_\mathrm{r}+2I_\mathrm{i}L_1-2H_\mathrm{r}L_1{}^2-2E_\mathrm{i}a]\\
R_4'&=4\sin^2\tfrac{1}{2}\theta[|A|^2+D_\mathrm{i}-C_\mathrm{i}+2L_1B_\mathrm{r}+2A_\mathrm{i}L_1{}^2+M_\mathrm{r}+2J_\mathrm{i}L_1\\
&\qquad+\tan^2\tfrac{1}{2}\theta\{|H|^2+2(E_\mathrm{r}I_\mathrm{r}+E_\mathrm{i}I_\mathrm{i})\}]\\
R_4''&=4\sin^2\tfrac{1}{2}\theta[2(E_\mathrm{r}J_\mathrm{r}+E_\mathrm{i}J_\mathrm{i})\tan^2\tfrac{1}{2}\theta-|A|^2-D_\mathrm{i}]\\
R_5&=4\sin^2\tfrac{1}{2}\theta[Q_\mathrm{i}-2C_\mathrm{r}L_1-2B_\mathrm{i}L_1{}^2+2aA_\mathrm{r}+N_\mathrm{r}+2K_\mathrm{i}L_1-2aH_\mathrm{i}+2bE_\mathrm{r}]\\
R_5'&=4\sin^2\tfrac{1}{2}\theta[-Q_\mathrm{i}+S_\mathrm{i}+2C_\mathrm{r}L_1-2D_\mathrm{r}L_1+2B_\mathrm{i}L_1{}^2-2aA_\mathrm{r}\\
&\qquad+2(A_\mathrm{r}B_\mathrm{r}+A_\mathrm{i}B_\mathrm{i})+O_\mathrm{r}+2M_\mathrm{i}L_1-2I_\mathrm{r}L_1{}^2\\
&\qquad+2\tan^2\tfrac{1}{2}\theta(H_\mathrm{r}I_\mathrm{r}+H_\mathrm{i}I_\mathrm{i}+E_\mathrm{r}K_\mathrm{r}+E_\mathrm{i}K_\mathrm{i})]\\
R_5''&=4\sin^2\tfrac{1}{2}\theta[-S_\mathrm{i}+2D_\mathrm{r}L_1-2(A_\mathrm{r}B_\mathrm{r}+A_\mathrm{i}B_\mathrm{i})+P_\mathrm{r}\\
&\qquad\qquad-2J_\mathrm{r}L_1{}^2+2\tan^2\tfrac{1}{2}\theta(H_\mathrm{r}J_\mathrm{r}+H_\mathrm{i}J_\mathrm{i}+E_\mathrm{r}M_\mathrm{r}+E_\mathrm{i}M_\mathrm{i})].
\end{aligned}\right\} \ldots(16)$$

The coefficient R_1 is equal to $\pi\sin\frac{1}{2}\theta[1-\sin\frac{1}{2}\theta]$ as given by McKinley and Feshbach, Dalitz (1951) and Schwinger (unpublished).

§ 3. RESULTS

The coefficients A to M, N_r, O_r, P_r, Q_i and S_i have been calculated† as is indicated above; they are given in table 1. The suffix r refers to the real part and i to the imaginary part. The values of A to J are in good agreement with those given by McKinley and Feshbach, except in the case of H_r, I_r, J_r and J_i. These coefficients were calculated by McKinley and Feshbach by direct use of the expansion (7) for D_k. This gives

$$\left.\begin{aligned}
H_\mathrm{r}&=\tfrac{1}{2}\sum_1^\infty\left(\psi_2-\frac{\psi_1}{k}-\frac{1}{k^2}\right)(P_k+P_{k-1})\\
I_\mathrm{r}&=-\frac{\pi}{2}\sum_1^\infty\left(\psi_1{}^2+\frac{\psi_1}{k}+\frac{1}{2k^2}\right)(P_k+P_{k-1})\\
J_\mathrm{r}&=\frac{3\pi}{16}\sum_1^\infty\frac{1}{k^2}(P_k+P_{k-1})\\
J_\mathrm{i}&=\frac{\pi^2}{16}\sum_1^\infty\frac{1}{k}(P_k+P_{k-1})-\frac{3}{16}\sum_1^\infty\frac{1}{k^3}(P_k+P_{k-1}).
\end{aligned}\right\} \ldots\ldots(17)$$

---

† The polygamma functions are tabulated by H. T. Davis (1935) and the Legendre polynomials are tabulated up to P_{32} by Tallqvist (1938).

In the case of J_r the 'Bartlett and Watson' analysis also yields the above expression; McKinley and Feshbach give $J_r = 0$ at all angles, which is obviously incorrect.

In order to verify the values for H_r, I_r and J_i given in table 1 these sums were also obtained directly from (17) and good agreement was obtained. The agreement was within the accuracy of these check calculations viz. $\pm 0{\cdot}002$ in the case of H_r and J_i and $\pm 0{\cdot}01$ in the case of I_r.

The coefficients $R_1 \ldots$ in the series expansion (15) of R have been calculated using the above values of A to S and are given in table 2.

§4. CALCULATION OF THE CROSS SECTION FOR $\beta \sim 1$

For energies greater than about 0·5 MEV ($\beta > 0{\cdot}87$) R varies nearly linearly with $1-\beta^2$. Thus we may write

$$R(\beta) = R(1) + (1-\beta^2)\Delta R \qquad \ldots\ldots(18)$$

where $R(1)$ is the value of R for $\beta = 1$ and ΔR is independent of energy. The series for R is obtained in this form by substitution of the constant and $1-\beta^2$ terms in the expansion

$$\beta^n = [1-(1-\beta^2)]^{n/2} = 1 - \frac{n}{2}(1-\beta^2) + \frac{1}{2!}\frac{n}{2}(\tfrac{1}{2}n-1)(1-\beta^2)^2 \ldots$$

into (15). We obtain

$$R(1) = 1 - \sin^2\theta/2 + \sum_1 \alpha^n \mathscr{R}_n \qquad \ldots\ldots(19)$$

where $\mathscr{R}_1 = R_1$, $\mathscr{R}_2 = R_2 + R_2'$, etc. ΔR is given by

$$\Delta R = \sum_0 \alpha^n \Delta R_n$$

where

$$\Delta R_0 = \sin^2\theta/2$$
$$\Delta R_1 = -\tfrac{1}{2}R_1$$
$$\Delta R_2 = -R_2'$$
$$\Delta R_3 = \tfrac{1}{2}(R_3 - R_3')$$
$$\Delta R_4 = R_4 - R_4''$$
$$\Delta R_5 = \tfrac{1}{2}(3R_5 + R_5' - R_5'').$$

The coefficients R_n, ΔR_n are given in tables 3 and 4. These tables include additional terms R_6, R_7, R_8, ΔR_6 and ΔR_7 which were estimated by comparison of the series with the exact calculations of Bartlett and Watson (1940), Massey (1942) and Feshbach (1952) for energies of 0·66 mc^2 and higher. In the case of the calculations at 0·66 mc^2 comparison was made with the series (15) modified by addition of the terms

$$\alpha^6\mathscr{R}_6 + \alpha^7\mathscr{R}_7 + \alpha^8\mathscr{R}_8 + (1-\beta^2)(\alpha^6\Delta R_6 + \alpha^7\Delta R_7)$$

rather than with (18). At the higher energies (1·28 mc^2, 3·35 mc^2 and $\beta = 1$) the modified series (15) and (18) give results differing from one another by less than the probable error of the 'exact' calculations (about ½%), so that it is sufficient to use the simpler form (18). The use of (18) rather than (15) involves an error which is roughly proportional to $(1-\beta^2)^2$ and would be about 2% of αR_1 at 0·66 mc^2.

Table 1. Coefficients in the Series Expansions (8) of F_1 and G_1

θ (deg.)	30	45	60	80	90	100	120	135	150	180
A_r	−0·3616	−0·5090	−0·6369	−0·7797	−0·8400	−0·8934	−0·9799	−1·0277	−1·0618	−1·0888
A_i	0·0640	0·1141	0·1666	0·2343	0·2657	0·2947	0·3443	0·3732	0·3943	0·4112
B_r	−0·0866	−0·2005	−0·3386	−0·5373	−0·6357	−0·7298	−0·8965	−0·9974	−1·0720	−1·1330
B_i	0·4913	0·3743	0·2091	−0·0330	−0·1503	−0·2611	−0·4544	−0·5683	−0·6514	−0·7199
C_r	0·5746	0·4053	0·3132	0·2886	0·3049	0·3327	0·4083	0·4639	0·5107	0·5515
C_i	−0·0112	−0·0674	−0·1670	−0·3481	−0·4490	−0·5528	−0·7494	−0·8750	−0·9713	−1·0510
D_r	−0·1072	−0·2165	−0·3441	−0·5248	−0·6134	−0·6984	−0·8491	−0·9395	−1·0068	−1·0621
D_i	−0·1289	−0·2201	−0·3096	−0·4167	−0·4636	−0·5053	−0·5735	−0·6115	−0·6385	−0·6596
E_r	2·2492	1·2669	0·7854	0·4364	0·3253	0·2399	0·1215	0·0646	0·0277	0
E_i	−0·6758	−0·4802	−0·3466	−0·2210	−0·1732	−0·1332	−0·0719	−0·0397	−0·0173	0
H_r	1·3711	1·1859	0·9628	0·6799	0·5531	0·4384	0·2475	0·1394	0·0619	0
H_i	1·0486	1·3709	1·1735	0·8187	0·6571	0·5134	0·2824	0·1566	0·0688	0
I_r	2·976	1·200	0·371	−0·060	−0·134	−0·157	−0·1289	−0·0835	−0·0401	0
I_i	0·4697	0·7322	0·7809	0·6782	0·5909	0·4948	0·3028	0·1773	0·0811	0
J_r	1·3635	1·1107	0·8813	0·6150	0·4993	0·3953	0·2231	0·1258	0·0559	0
J_i	1·2767	0·8450	0·5709	0·3358	0·2538	0·1887	0·0960	0·0511	0·0218	0
K_r	−1·6077	−1·1855	−0·9787	−0·7575	−0·6488	−0·5390	−0·3295	−0·1944	−0·0893	0
K_i	−5·858	−2·246	−1·097	−0·553	−0·419	−0·3208	−0·1807	−0·1033	−0·0466	0
M_r	1·5680	0·8861	0·5668	0·3425	0·2691	0·2093	0·1172	0·0663	0·0298	0
M_i	1·8568	1·7543	1·5405	1·1793	0·9911	0·8078	0·4756	0·2747	0·1240	0
N_r	−3·119	0·045	0·553	0·525	0·450	0·369	0·218	0·126	0·057	0
O_r	−1·330	−1·314	−1·237	−1·032	−0·898	−0·755	−0·467	−0·276	−0·127	0
P_r	0·220	0·257	0·260	0·226	0·199	0·169	0·106	0·063	0·029	0
Q_i	−0·255	0·062	0·262	0·449	0·526	0·596	0·716	0·792	0·846	0·893
S_i	−0·122	−0·284	−0·497	−0·829	−1·002	−1·173	−1·487	−1·682	−1·831	−1·954

Table 2. Coefficients in the Series Expansion (15) for R

θ (deg.)	30	45	60	80	90	100	120	135	150	180	$R=1+$
$-\sin^2\frac{1}{2}\theta$	−0·0670	−0·1465	−0·2500	−0·4132	−0·5000	−0·5868	−0·7500	−0·8535	−0·9330	−1·0000	$\times\beta^2$
R_1	0·6027	0·7420	0·7854	0·7213	0·6506	0·5631	0·3645	0·2209	0·1034	0	$\times\alpha\beta$
R_2	0·6650	0·9772	1·2097	1·4121	1·4778	1·5265	1·5885	1·6155	1·6324	1·6449	$\times\alpha^2$
R_2'	0·0890	0·1176	0·0791	−0·1089	−0·2596	−0·4408	−0·8536	−1·1596	−1·4157	−1·6449	$\times\alpha^2\beta^2$
R_3	−0·379	−0·140	0·139	0·535	0·744	0·962	1·395	1·692	1·937	2·148	$\times\alpha^3/\beta$
R_3'	0·475	0·829	1·053	0·992	0·789	0·483	−0·339	−1·014	−1·604	−2·148	$\times\alpha^3\beta$
R_4	−1·093	−1·174	−1·158	−1·045	−0·955	−0·845	−0·589	−0·394	−0·225	−0·068	$\times\alpha^4/\beta^2$
R_4'	0·254	0·884	1·590	2·381	2·658	2·851	3·016	3·003	2·937	2·848	$\times\alpha^4$
R_4''	0·083	0·171	0·206	0·044	−0·151	−0·424	−1·151	−1·751	−2·282	−2·780	$\times\alpha^4\beta^2$
R_5	0·935	−0·056	−0·456	−0·734	−0·891	−1·065	−1·400	−1·554	−1·641	−1·664	$\times\alpha^5/\beta^3$
R_5'	−1·932	−1·394	−0·910	0·184	0·958	1·823	3·589	4·740	5·583	6·567	$\times\alpha^5/\beta$
R_5''	−0·125	0·607	1·265	1·467	1·190	0·673	−0·865	−2·245	−3·457	−4·903	$\times\alpha^5\beta$

Table 3. Expansion of R as a Power Series for $\beta=1$

$$R(1)=1-\sin^2\theta/2+\sum_{1}^{8}\alpha^n\mathscr{R}_n$$

θ (deg.)	30	45	60	80	90	100	120	135	150	180
$1-\sin^2\frac{1}{2}\theta$	0·9330	0·8535	0·7500	0·5868	0·5000	0·4132	0·2500	0·1465	0·0670	0
$\mathscr{R}_1$	0·6027	0·7422	0·7854	0·7213	0·6506	0·5631	0·3645	0·2209	0·1034	0
$\mathscr{R}_2$	0·7540	1·0948	1·2888	1·3032	1·2180	1·0858	0·7349	0·4559	0·2168	0
$\mathscr{R}_3$	0·096	0·689	1·192	1·526	1·533	1·445	1·056	0·679	0·333	0
$\mathscr{R}_4$	−0·756	−0·119	0·638	1·381	1·551	1·582	1·276	0·858	0·430	0
$\mathscr{R}_5$	−1·122	−0·842	−0·101	0·916	1·258	1·431	1·324	0·941	0·486	0
$\mathscr{R}_6$	−1·2	−1·4	−1·0	0·3	0·6	1·3	1·7	1·1	0·5	0
$\mathscr{R}_7$	−0·2	−1·2	−1·4	−0·6	0	0·5	1·1	0·9	0·5	0
$\mathscr{R}_8$	1	0	−0·5	−1	0	−0·5	−1	0	0·5	0

Table 4. Expansion of ΔR as a Power Series for Energies greater than 0·5 Mev

$$\Delta R=\sum_{0}^{7}\alpha^n\Delta R_n$$

θ (deg.)	30	45	60	80	90	100	120	135	150	180
ΔR_0	0·067	0·146	0·250	0·413	0·500	0·587	0·750	0·854	0·933	1·000
ΔR_1	−0·301	−0·371	−0·393	−0·361	−0·325	−0·282	−0·182	−0·110	−0·052	0
ΔR_2	−0·089	−0·118	−0·079	0·109	0·260	0·441	0·854	1·160	1·416	1·645
ΔR_3	−0·43	−0·48	−0·46	−0·23	−0·02	0·24	0·97	1·35	1·77	2·15
ΔR_4	−1·17	−1·35	−1·36	−1·08	−0·90	−0·42	0·56	1·36	2·06	2·71
ΔR_5	0·50	−1·08	−1·77	−1·78	−1·45	−1·02	0·13	1·17	2·05	3·24
ΔR_6	1	−1	−2	−3	−3	−3	−2	0	2	3·5
ΔR_7	−1	1	0	−1	−2	−2	−2	−1	1	3·5

For energies greater than about 0·66 mc^2 the error in (15) should be of the order of q^9. Exact cross sections for electron scattering by uranium ($\alpha^9=0{\cdot}028$) have been calculated by Yadav (1955). A comparison of Yadav's results at 20 mc^2 with the α^8 approximation of this paper is shown in the figure, together with the results obtained by use of the McKinley and Feshbach approximation and the α^5 approximation of this paper. It can be seen that the error is of the expected order of magnitude. For energies greater than 0·5 MeV and for heavy elements up to $Z\sim 82$ ($\alpha=0{\cdot}6$) the error is probably less than $\frac{1}{2}q^9$ (1% for $q=0{\cdot}65$) since the series has been fitted to the exact calculations in this energy region. Equation (18), which is valid in this energy region, is particularly convenient when the cross section for $\beta=1$ is known, for example from the exact calculations of Feshbach.

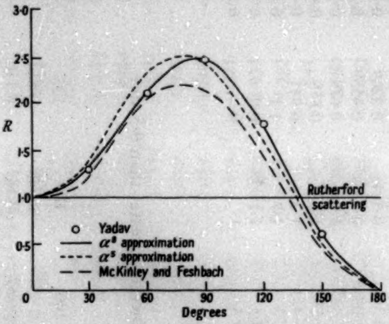

Comparison of the α^8 approximation with the exact calculation of Yadav for uranium. The McKinley and Feshbach and α^5 approximations are also shown for comparison. The electron energy is $20mc^2$. R is the ratio of the scattering cross section to Rutherford scattering.

ACKNOWLEDGMENTS

The author wishes to thank Dr. E. H. S. Burhop for his keen interest and encouragement, Dr. C. Henderson for checking the expansions obtained, and Dr. H. N. Yadav for letting him have the results of his calculations prior to publication. He would also like to thank the Department of Scientific and Industrial Research for the award of a maintenance allowance.

REFERENCES

Bartlett, J. H., and Watson, R. E., 1940, *Proc. Amer. Acad. Arts. Sci.*, **74,** 53.
Dalitz, R. H., 1951, *Proc. Roy. Soc.* A, **206,** 509.
Davis, H. T., 1935, *Tables of Higher Functions*, Vol. II (Bloomington : University of Indiana Press).
Feshbach, H., 1952, *Phys. Rev.*, **88,** 295.
Massey, H. S. W., 1942, *Proc. Roy. Soc.* A, **181,** 14.
McKinley, W. A., Jr., and Feshbach, H., 1948, *Phys. Rev.*, **74,** 1759.
Tallqvist, H., 1938, *Acta Soc. Scient. Fennica*, Vol. II.
Yadav, H. N., 1955, *Proc. Phys. Soc.* A, **68,** in the press.

The Effect of Finite Nuclear Size on Bremsstrahlung Production

By S. J. BIEL and E. H. S. BURHOP

Physics Department, University College, London

MS. received 8th October 1954

Abstract. Calculations have been made of the bremsstrahlung spectrum emitted in different directions following electron–nuclear collisions, allowing for the finite distribution of the nuclear charge.

Calculations were carried out for charge distributions of the uniform sphere, spherical shell, gaussian and exponential forms, as well as for a uniform spherical core with a distribution falling off exponentially at the surface. In each case the parameters of the distribution were chosen to agree with the elastic electron scattering data at 16 MeV.

The modification of the angular distribution obtained from the Bethe–Heitler formula for a point nucleus is large for electron energies above 20 MeV.

§1. INTRODUCTION

In their well-known calculation of the differential cross section for bremsstrahlung production in the collision of electrons with nuclei, Bethe and Heitler (1934) assumed that the nucleus could be considered as a point charge. As a result of the development of machines producing intense beams of high-energy electrons experimental studies of electron scattering can now be made under conditions where the effect of the finite size of the nuclear charge distribution is important and in recent years several investigations, both experimental and theoretical, have been made of the effect of the nuclear charge distribution on elastic scattering of fast electrons by nuclei (Lyman, Hanson and Scott 1951, Hofstadter *et al.* 1954, Rose 1948, Elton 1950, Yennie, Ravenhall and Wilson 1954).

It is of interest therefore to investigate the modifications introduced into the cross section for bremsstrahlung production when allowance is made for the effect of the nuclear charge distribution. Hough (1948) made a rough estimate of the magnitude of the effect to be expected and showed that under some conditions it could be large. In the present paper calculations have been made of the bremsstrahlung spectrum emitted at various angles to the incident electron beam as a result of collisions with Hg, Ag, Cu and Al nuclei, assuming forms of nuclear charge distribution suggested by the interpretation of the elastic electron scattering data.

§2. THE EXTENDED BETHE–HEITLER FORMULA

Following the notation used by Bethe and Heitler, E_0, p_0 denote respectively the total energy and momentum of the incident electron in units mc^2, mc respectively, while E, p are the corresponding quantities for the electron after scattering. A quantum of energy k (in units mc^2) is emitted in a direction making an angle θ_0 with that of the incident electron. The direction of the scattered electron is specified by the angle θ it makes with the direction of the quantum and the dihedral angle ϕ between the planes $(\mathbf{p}_0\mathbf{k})$ and $(\mathbf{pk})$.

The differential cross section $d\Phi$ for emission of a quantum of energy in the range between k and $k+dk$ in a direction making an angle between θ_0, $\theta_0+d\theta$ with the direction of the incident electron, while the electron is scattered into the solid angle $\sin\theta\,d\theta\,d\phi$, is given by

$$\begin{aligned} d\Phi = {} & \frac{Z^2e^4}{2\pi 137}\frac{dk}{k}\frac{\sin\theta_0\,d\theta_0\sin\theta\,d\theta\,d\phi}{q^4}\cdot\frac{p}{p_0}|\mathrm{F}(q)|^2 \\ & \times\left\{\frac{p^2\sin^2\theta(4E_0{}^2-q^2)}{(E-p\cos\theta)^2}+\frac{p_0{}^2\sin^2\theta_0(4E^2-q^2)}{(E_0-p_0\cos\theta_0)^2}\right. \\ & \left.-\frac{2pp_0\sin\theta\sin\theta_0\cos\phi(4E_0E-q^2+2k^2)}{(E-p\cos\theta)(E_0-p_0\cos\theta_0)}+\frac{2k^2(p^2\sin^2\theta+p_0{}^2\sin^2\theta_0)}{(E-p\cos\theta)(E_0-p_0\cos\theta_0)}\right\} \end{aligned} \qquad \ldots\ldots(1)$$

where q is the magnitude of the recoil momentum transferred to the nucleus and is given by

$$q^2=p_0{}^2+p^2+k^2-2p_0k\cos\theta_0+2pk\cos\theta-2p_0p(\cos\theta\cos\theta_0+\sin\theta\sin\theta_0\cos\phi)$$

and

$$\mathrm{F}(q)=\frac{4\pi}{Ze}\int_0^\infty\rho(r)\,\frac{\sin\kappa r}{\kappa r}\,r^2\,dr \qquad \ldots\ldots(2)$$

is the nuclear form factor determined by the distribution of the nuclear charge density $\rho(r)$, where $\kappa\hbar=q$ (Bethe 1934, Hough 1948).

The Bethe–Heitler formula is obtained by writing $\mathrm{F}(q)=1$, as is the case for a point nucleus.

To obtain the cross section per unit solid angle per unit energy range for the emission of a bremsstrahlung quantum in a direction θ_0 to the incident electron beam (1) has to be integrated over the angles θ, ϕ. These integrations have been carried out by Hough (1948) for the point nucleus case.

§3. THE FORM OF THE NUCLEAR CHARGE DISTRIBUTION

The following forms of the nuclear charge distribution have been used in these calculations. The corresponding expression for the nuclear form factor $\mathrm{F}(\kappa R)$ is given in each case.

(1) *Uniform spherical nucleus.*

$$\left.\begin{aligned} \rho&=\rho_0\ , r<R \\ \rho&=0,\ \ r>R \\ \mathrm{F}(\kappa R)&=3(\sin\kappa R-\kappa R\cos\kappa R)/\kappa^3R^3. \end{aligned}\right\} \qquad \ldots\ldots(3)$$

(2) *Uniform spherical shell of radius R.*

$$\mathrm{F}(\kappa R)=\sin\kappa R/\kappa R. \qquad \ldots\ldots(4)$$

(3) *Gaussian charge distribution.*

$$\left.\begin{aligned} \rho&=\rho_0\exp\{-(r/R)^2\} \\ \mathrm{F}(\kappa R)&=\exp\{-\kappa^2R^2/4\}. \end{aligned}\right\} \qquad \ldots\ldots(5)$$

(4) *Exponential charge distribution.*

$$\left.\begin{aligned} \rho&=\rho_0\exp\{-(r/R)\} \\ \mathrm{F}(\kappa R)&=(1+\kappa^2R^2)^{-2}. \end{aligned}\right\} \qquad \ldots\ldots(6)$$

(5) *Uniform spherical case with exponential fall-off near boundary.*

$$\rho=\rho_0, \qquad r<R$$

$$\rho=\rho_0 \exp\{-(r-R)/R_0\}, \qquad r>R$$

$$\begin{aligned}\kappa^3\{\tfrac{1}{3}R^3+R^2R_0+2RR_0^2+2R_0^3\}\mathrm{F}(\kappa R,\kappa R_0)\\ =\sin\kappa R[1+\kappa^2R_0^2+\kappa^2R_0R-\kappa^4R_0^3(1+\kappa^2R_0^2)^{-2}\{R+3R_0+\kappa^2R_0^2(R+R_0)\}]\\ -\cos\kappa R[\kappa R-\kappa^2R_0^2(R+2R_0)+\kappa^5R_0^4(1+\kappa^2R_0^2)^{-1}(R+2R_0)\\ +2\kappa^5R_0^5(1+\kappa^2R_0^2)^{-2}].\end{aligned} \qquad \ldots\ldots(7)$$

The elastic electron scattering data and other evidence suggests that the best radius to be used for the uniform spherical nucleus is $R=1{\cdot}20\times10^{-13}A^{1/3}$ cm for a nucleus of atomic mass A.

The radii in the other cases were adjusted so as to be consistent with the scattering data for 16 MeV electrons where only a single phase is important in determining the departure from point nucleus scattering. The values of R used were $R=0{\cdot}924\times10^{-13}A^{1/3}$ cm for the spherical shell,

$R=0{\cdot}756\times10^{-13}A^{1/3}$ cm for the gaussian distribution,

$R=0{\cdot}264\times10^{-13}A^{1/3}$ cm for the exponential distribution.

For the two-parameter distribution (5) the following three cases were taken:

$5(a)$, $R_0/R=\frac{1}{4}$, $R=0{\cdot}795\times10^{-13}A^{1/3}$ cm.
$5(b)$, $R_0/R=\frac{1}{2}$, $R=0{\cdot}50\times10^{-13}A^{1/3}$ cm.
$5(c)$, $R_0/R=\frac{1}{7}$, $R=0{\cdot}995\times10^{-13}A^{1/3}$ cm.

The constants of $5(c)$ satisfy the criteria given by Ravenhall and Yennie (1955) for a two-parameter charge distribution that will explain the experimental results on high-energy elastic electron scattering in gold†.

The quantity $\{\mathrm{F}(\kappa R)\}^2$ was expanded as a power series in $(\kappa R)^2$, viz.

$$\{\mathrm{F}(\kappa R)\}^2=1+\alpha_1(\kappa R)^2+\alpha_2(\kappa R)^4+\alpha_3(\kappa R)^6+\alpha_4(\kappa R)^8+\ldots.$$

By taking terms up to $(\kappa R)^8$ it was possible to obtain the ratio of extended nucleus to point nucleus cross section to within a few per cent for angles of emission up to 120° for an incident electron energy of 50 MeV and up to 60° for 100 MeV incident energy.

Table 1 shows the coefficients α for the different charge distributions considered.

Table 1

		α_1	α_2	α_3	α_4
Uniform sphere	(1)	$-0{\cdot}2$	$+1{\cdot}7143\times10^{-2}$	$-8{\cdot}47\times10^{-4}$	$+2{\cdot}628\times10^{-5}$
Shell	(2)	$-0{\cdot}3333$	$4{\cdot}444\times10^{-2}$	$-3{\cdot}175\times10^{-3}$	$1{\cdot}411\times10^{-4}$
Gaussian	(3)	$-0{\cdot}5$	$0{\cdot}125$	$-2{\cdot}083\times10^{-2}$	$2{\cdot}604\times10^{-3}$
Exponential	(4)	-4	10	-20	$+35$
Sphere and exponential fall-off	(5*a*)	$-0{\cdot}4528$	$0{\cdot}10256$	$-1{\cdot}608\times10^{-2}$	$2{\cdot}022\times10^{-3}$
	(5*b*)	$-1{\cdot}1474$	$0{\cdot}7661$	$-0{\cdot}3965$	$0{\cdot}1770$
	(5*c*)	$-0{\cdot}3003$	$4{\cdot}312\times10^{-2}$	$-3{\cdot}780\times10^{-3}$	$2{\cdot}299\times10^{-4}$

§4. THE BREMSSTRAHLUNG DISTRIBUTION

The angular integrations that have to be carried out are of the form

$$\int_{-1}^{1}\frac{(1-\mu^2)^m\mu^n\,d\mu}{(d-\mu)^p(a+b\mu+c\mu^2)^q}$$

---

† We are indebted to Dr. L. R. B. Elton for drawing our attention to this work.

where a, b, c, d are constants and the index m takes the values 0, 1 or 2, n takes the values 0 or 1, p takes the values 0, 1 or 2, and q the values 0, $\frac{1}{2}$ or $\frac{3}{2}$. These integrations can be carried out explicitly. After integration the approximation E_0, $E \gg 1$ is made so that one can write $E_0 = p_0$, $E = p$ (in units mc^2, mc for E and p respectively).

It is to be expected that finite size effects will only be appreciable for incident electron energies for which this approximation is satisfactory. We also write $E_0 = E + k$, thus neglecting the kinetic energy of recoil communicated to the nucleus. This is certainly justified for energies up to a few hundred MEV with which the present calculation is concerned.

To facilitate comparison with the calculations of Hough (1948) who used similar approximations for the point nucleus case we use a similar notation to his and write $\gamma = E/E_0$ and $\sigma^2 = \gamma^2 + 4(1-\gamma)\sin^2\theta_0/2$.†

After a good deal of algebraic manipulation the differential cross section $d\Phi_k$ for emission of a quantum of energy in the range $k, k+dk$ in a solid angle $d\omega_k$ in a direction θ_0 to the incident direction can be written in the form

$$d\Phi_k = \frac{Z^2 r_0^2}{137 E_0^2} \frac{d\omega_k}{4\pi} \frac{dk}{k} \times \left\{ H_0 + \alpha_1 \left(\frac{RE_0}{r_C}\right)^2 H_1 + \alpha_2 \left(\frac{RE_0}{r_C}\right)^4 H_2 + \alpha_3 \left(\frac{RE_0}{r_C}\right)^6 H_3 + \alpha_4 \left(\frac{RE_0}{r_C}\right)^8 H_4 \right\} \qquad \ldots\ldots(8)$$

where $r_0 = e^2/mc^2$, the classical electron radius, and $r_C = \hbar/mc$, the Compton wavelength.

$$H_n = 2^{2n}(1+\gamma^2) C^2 S^{2(n-2)} \ln(2\gamma E_0) + h_n(\theta_0, \gamma) \qquad n = 0, 1, 2, 3, 4 \quad \ldots\ldots(9)$$

where $C = \cos\frac{1}{2}\theta_0$, $S = \sin\frac{1}{2}\theta_0$;

$$h_0 = -\frac{(1+\gamma^2)C^2}{S^4}\ln(1-\gamma) - \frac{\gamma(5+2\gamma)}{4S^4} + \frac{\gamma^2 - 2\ln(1-\gamma)}{S^2} - \frac{\gamma^2}{8S^6}\left\{\frac{\gamma}{\sigma^2}(2S^2-\gamma)+1\right\} - \frac{\{3\sigma^2+\gamma(2-\gamma)\}(1-\gamma)}{2\sigma^3 S^2}\ln\left\{\frac{\sigma+\gamma}{\sigma-\gamma}\right\} \qquad \ldots\ldots(10)$$

$$h_1 = 4(1-\gamma)^2\ln(1-\gamma) - 8\gamma C^2/S^2 - \frac{2\gamma(1-\gamma)^2(\gamma-2S^2)}{\sigma^2 S^2} - \frac{4(1-\gamma)^2\{\gamma+2(1-\gamma)S^2\}}{\sigma^3}\ln\left\{\frac{\sigma+\gamma}{\sigma-\gamma}\right\} \qquad \ldots\ldots(11)$$

$$h_2 = 4\gamma^2(1+\gamma^2)/S^2 + 16\gamma(2+\gamma)S^2 - 16\gamma(2+\gamma^2) \qquad \ldots\ldots(12)$$

$$h_3 = \frac{16}{3}\frac{\gamma^4(1+\gamma^2)}{S^2} + 16\gamma^2\left(5 - \frac{14}{3}\gamma + 5\gamma^2 - \frac{10}{3}\gamma^3\right) - \frac{64}{3}\gamma(14+4\gamma+\gamma^2-4\gamma^3)S^2 + 128\gamma\left(3-\frac{2\gamma^2}{3}\right)S^4 \qquad \ldots\ldots(13)$$

$$h_4 = \frac{32}{3}\frac{\gamma^6(1+\gamma^2)}{S^2} + \frac{128}{3}\gamma^4(5-7\gamma+5\gamma^2-2\gamma^3) + \frac{64}{3}\gamma^2(33-64\gamma+57\gamma^2-24\gamma^3+4\gamma^4)S^2 - \frac{256}{3}\gamma(15-2\gamma^2+6\gamma^3-2\gamma^4)S^4 + \frac{128}{3}\gamma(30-9\gamma-12\gamma^2+22\gamma^3)S^6. \qquad \ldots(14)$$

---

† We use σ instead of Hough's ρ to avoid confusion with the symbol for charge density.

Equation (10) is the same as that obtained by Hough for the point nucleus.†

At very high energies when the quantities h_0, h_1, h_2, h_3, h_4 can be neglected in comparison with the terms involving $\ln 2\gamma E_0$

$$d\Phi_k \sim \frac{Z^2 r_0^2}{137 E_0^2}\frac{d\omega_k}{4\pi}\frac{dk}{k}\frac{(1+\gamma^2)C^2}{S^4}\ln 2\gamma E_0\left\{\mathrm{F}\left(\frac{2RE_0S}{r_C}\right)\right\}^2 \quad \ldots\ldots(15)$$

so that the effect of the finite size correction is simply to multiply the cross section by $\{\mathrm{F}(2RE_0S/r_C)\}^2$ where F is the nuclear form factor (equations (3)–(7)). An analysis of the size of the various terms in H_1, H_2, H_3, H_4 indicates that this should give a fair approximation to the effect of finite nuclear size for incident electron energies above 500 mc^2.

Table 2

θ_0 (°)	γ	h_0	h_1	h_2	h_3	h_4
5	0·1	−122970	−732·4	18·043	0·7030	0·03477
	0·3	−133330	−1346·4	196·41	30·26	5·602
	0·5	−74150	−2123	639·6	232·7	116·27
	0·7	+95380	−2946	1508·4	1026·2	1002·0
	0·9	649800	−3781	3045	3359	5429
30	0·1	−27·92	−13·453	−2·388	−1·3056	−0·1303
	0·3	−93·02	−43·59	−3·434	−0·0648	+2·005
	0·5	−83·37	−65·33	+2·002	+9·040	11·330
	0·7	+62·95	−82·27	17·741	36·47	49·26
	0·9	535·2	−100·81	49·89	106·30	191·78
60	0·1	−1·277	−3·289	−2·214	−4·557	−4·593
	0·3	−3·648	−8·876	−5·702	−11·347	−8·617
	0·5	−3·139	−14·214	−8·000	−14·960	−8·416
	0·7	+6·002	−18·235	−8·646	−13·048	+3·309
	0·9	40·32	−21·88	−6·566	+0·1296	44·16
90	0·1	−0·1850	−1·1784	−1·455	−5·052	−13·587
	0·3	−0·3599	−3·363	−3·727	−14·566	−34·14
	0·5	+0·1559	−5·182	−5·500	−23·84	−55·07
	0·7	2·532	−6·477	−6·927	−31·35	−69·08
	0·9	11·870	−7·403	−7·855	−33·96	−65·66
120	0·1	−0·0286	−0·6248	−0·6421	−0·7594	−15·366
	0·3	−0·0474	−1·6199	−1·2288	−3·586	−43·19
	0·5	+0·4507	−2·266	−1·3333	−9·408	−80·80
	0·7	2·118	−2·579	−1·3140	−17·248	−113·43
	0·9	5·370	−2·5709	−1·3248	−23·90	−114·48
150	0·1	0·0063	−0·4096	−0·0379	+5·409	−5·395
	0·3	0·1236	−0·9504	+0·6887	+3·318	−19·834
	0·5	0·4651	−1·1411	1·9994	15·503	−57·66
	0·7	1·2831	−1·0134	3·455	12·522	−88·26
	0·9	3·705	−0·6731	4·783	7·186	−63·99
180	0·1	0·0139	−0·3508	0·1844	8·323	+1·709
	0·3	0·1369	−0·7680	1·4004	21·48	−4·416
	0·5	0·4594	−0·8345	3·250	27·77	−35·79
	0·7	1·1923	−0·5931	5·272	27·59	−58·24
	0·9	3·3014	−0·15201	7·160	23·47	−16·42

---

† Our h_0 is not quite the same as Hough's g because we have taken the argument of the logarithm of the first term in H_0 as $2\gamma E_0$ while Hough took $2E_0$ as this argument and absorbed the γ in his expression for g.

§5. NUMERICAL CALCULATIONS

The quantities h_0, h_1, h_2, h_3, h_4 are tabulated in table 2 for a series of values of γ and θ_0. From these quantities the bremsstrahlung distribution for different energies and different assumed nuclear charge distributions can be obtained readily by calculating $\ln 2\gamma E_0$ and using equation (8) with the appropriate values of $\alpha_1, \alpha_2, \alpha_3, \alpha_4$ from table 1.

§6. THE EFFECT OF THE NUCLEAR CHARGE DISTRIBUTION

Figures 1–3 show the effect of finite nuclear size on the bremsstrahlung spectrum for different incident electron energies and different assumed charge distributions. These curves indicate that at large angles of emission the effect is appreciable even for electron energies of 20 MEV and may become very large at higher energies. The effect is most marked for the production of high energy quanta (γ small).

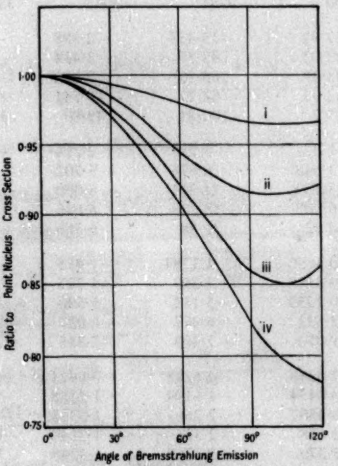

Figure 1. Ratio of differential cross section for bremsstrahlung emission to that for a point nucleus. These curves refer to a uniform spherical distribution of charge for the case $A=200$, radius $=1{\cdot}2\times10^{-13}A^{1/3}$.

(i) $E_0=10$ MEV, $\gamma=0{\cdot}5$; (ii) $E_0=20$ MEV, $\gamma=0{\cdot}9$;
(iii) $E_0=20$ MEV, $\gamma=0{\cdot}5$; (iv) $E_0=20$ MEV, $\gamma=0{\cdot}1$

where E_0 is the incident electron energy, γE_0 the electron energy after scattering. At these energies almost identical curves are obtained for any reasonable assumed charge distribution.

At energies of 50 MEV and higher, different assumed nuclear charge distributions influence the bremsstrahlung spectrum but the difference between the distributions tried is small compared with the difference of any of them from that

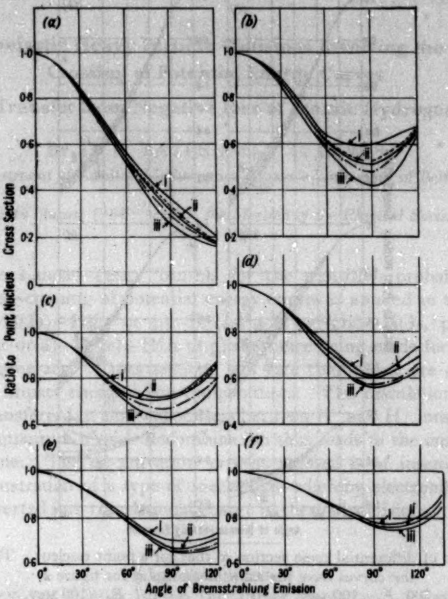

Figure 2. Ratio of differential cross section for bremsstrahlung emission to that for a point nucleus. Full curve (i) exponential distribution of charge; full curve (ii), gaussian distribution; full curve (iii), spherical shell; dashed curve, uniform spherical core with exponential fall-off on boundary with $R_0/R=\frac{1}{4}$; chain curve, uniform sphere. Two other cases with a uniform spherical core and exponential fall-off on boundary were calculated. The case $R_0/R=\frac{1}{2}$ gave results indistinguishable from full curve (i) for the exponential distribution. The case $R_0/R=\frac{1}{7}$ gave results very close to full curve (ii) for a gaussian distribution.

(*a*) $A=200$, $E_0=50$ MeV, $\gamma=0{\cdot}1$; (*d*) $A=107$, $E_0=50$ MeV, $\gamma=0{\cdot}5$;
(*b*) $A=200$, $E_0=50$ MeV, $\gamma=0{\cdot}5$; (*e*) $A=63$, $E_0=50$ MeV, $\gamma=0{\cdot}5$;
(*c*) $A=200$, $E_0=50$ MeV, $\gamma=0{\cdot}9$; (*f*) $A=27$, $E_0=50$ MeV, $\gamma=0{\cdot}5$.

to be expected for a point nucleus. In view of these comparatively small differences and the difficulties of measurement of bremsstrahlung at large angles of emission it does not appear likely that bremsstrahlung will be as useful as elastic electron scattering in determining nuclear charge distributions. Of the composite two parameter distributions tried type 5(*b*) gives a distribution nearly indistinguishable from the exponential distribution (4) while 5(*a*) and 5(*c*) give results close to that of the gaussian distribution (3). As pointed out above distribution 5(*c*) is closest to that required to explain the high energy elastic electron scattering data.

One interesting result is the apparent tendency of the ratio to point nuclear scattering to pass through a minimum and to increase at large angles of emission.

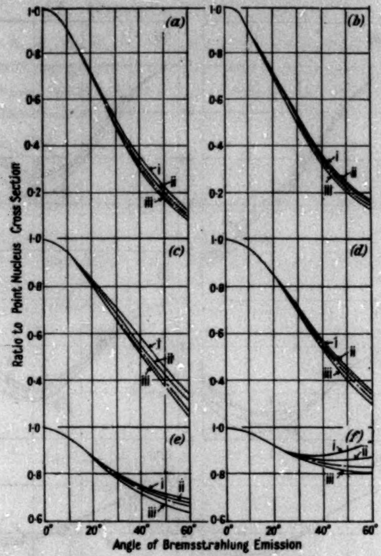

Figure 3. Ratio of differential cross section to that for a point nucleus. The markings on the curves have the same meanings as for figure 2.
(*a*) $A=200$, $E_0=100$ MeV, $\gamma=0{\cdot}1$; (*d*) $A=107$, $E_0=100$ MeV, $\gamma=0{\cdot}5$;
(*b*) $A=200$, $E_0=100$ MeV, $\gamma=0{\cdot}5$; (*e*) $A=63$, $E_0=100$ MeV, $\gamma=0{\cdot}5$;
(*c*) $A=200$, $E_0=100$ MeV, $\gamma=0{\cdot}9$; (*f*) $A=27$, $E_0=100$ MeV, $\gamma=0{\cdot}5$.

REFERENCES

BETHE, H. A., 1934, *Proc. Camb. Phil. Soc.*, **30,** 524.
BETHE, H. A., and HEITLER, W., 1934, *Proc. Roy. Soc.* A, **146,** 83.
ELTON, L. R. B., 1950, *Proc. Phys. Soc.* A, **64,** 1115.
HOFSTADTER, R., HAHN, B., KNUDSEN, A. W., and MCINTYRE, J. A., 1954, *Phys. Rev.*, **95,** 512.
HOUGH, P. V. C., 1948, *Phys. Rev.*, **74,** 80.
LYMAN, F. M., HANSON, A. O., and SCOTT, M. B., 1951, *Phys. Rev.*, **84,** 626.
RAVENHALL, D. G., and YENNIE, D. R., 1955, *Phys. Rev.* in the press.
ROSE, M. E., 1948, *Phys. Rev.*, **73,** 279.
YENNIE, D. R., RAVENHALL, D. G., and WILSON, R. N., 1954, *Phys. Rev.*, **95,** 500.

Inelastic Heavy Particle Collisions Involving the Crossing of Potential Energy Curves

III : Charge Transfer from Negative Ions of Atomic Hydrogen to Protons

By D. R. BATES and J. T. LEWIS
Department of Applied Mathematics, Queen's University of Belfast

MS. received 24th August 1954 ; *read at the Meeting of the Physical Society at Dublin, March* 1954

Abstract. The Landau–Zener formula for the transition probability arising from the pseudo-crossing of potential energy curves is applied to the processes $H^-(1s)^2+H^+\rightarrow H(1s)+H(2s \text{ or } p)$, $H^-(1s)^2+H^+\rightarrow H(1s)+H(3s, p \text{ or } d)$ and $H(1s)+H(3s, p \text{ or } d)\rightarrow H(1s)+H(2s \text{ or } p)$ allowance being made for the effect of the orbital degeneracy. Cross sections and rate coefficients are given over a wide range of impact energies and temperatures. The calculations show that the electron transferred in slow encounters between H^- and H^+ ions falls mainly into the third quantum level. Recombination thus leads to the emission of the first Balmer line. The de-activation process studied is of interest in that it provides an illustration of a type of mechanism whereby electronic energy can readily be converted into translational energy in thermal collisions.

§ 1. Introduction

This series is concerned with those inelastic collisions which are controlled essentially by the pseudo-crossing of the initial and final potential energy curves of the systems concerned. In the first two papers (I Bates and Moiseiwitsch 1954, II Dalgarno 1954) consideration was given to a few exothermic processes of the type

$$A+B^{2+}\rightarrow A^{+}+B^{+}. \qquad \ldots\ldots(1)$$

The calculations were facilitated by the Coulombic character of one of the potentials (which renders easier, for example, the determination of the location of the crossing point). A potential of this character is also a feature of

$$A^{-}+B^{+}\rightarrow A+B. \qquad \ldots\ldots(2)$$

Some exploratory work on such processes has already been done (Bates and Massey 1943, Magee 1952) but unfortunately the majority cannot be treated quantitatively owing to lack of precise enough information on the energy required to detach the electron (cf. Massey 1950). Amongst the exceptions are processes involving the negative ion of atomic hydrogen. This ion has been investigated in great detail by Chandrasekhar and his associates; and the value which Henrich (1943) finally obtained for the detachment energy, $0{\cdot}74_7$ ev, may be accepted with some confidence.

The present paper is mainly devoted to the calculation of the cross sections and rate coefficients of

$$H^-(1s)^2+H^+\rightarrow H(1s)+H(2s \text{ or } p)+2{\cdot}65_2\,\text{ev} \qquad \ldots\ldots(3)$$

$$\rightarrow H(1s)+H(3s, p \text{ or } d)+0{\cdot}76_3\,\text{ev}. \qquad \ldots\ldots(4)$$

These are the only members of the

$$H^-(1s)^2 + H^+ \rightarrow H(1s) + H(nl) \qquad \ldots\ldots(5)$$

family which can proceed rapidly; for when n either is 1 or is 5 or greater the potential energy curves do not intersect; and when it is 4 the internuclear distance at the crossing point is much too extreme.

Though of rather less importance the de-activation process

$$H(1s) + H(3s, p \text{ or } d) \rightarrow H(1s) + H(2s \text{ or } p) + 1{\cdot}88_9\,\text{ev} \qquad \ldots\ldots(6)$$

which takes place as a result of a *double* transition, is also studied. The basic parameters needed are the same as those which arise in connection with the charge-transfer processes so that little extra effort is incurred.

§2. THEORY

Let $U_i^0(R)$ and $U_f^0(R)$ be the zero-order initial and final potential energy curves, that is those obtained by neglecting the interaction between the states concerned; and assuming that this interaction is not zero let $U_i(R)$ and $U_f(R)$ the corresponding true potential energy curves. Though $U_i^0(R)$ and $U_f^0(R)$ may intersect at some point R_x, $U_i(R)$ and $U_f(R)$ cannot do so owing to what may be regarded as a mutual repulsion (cf. Coulson 1952). Since even and odd states do not interact with each other degeneracy arising from the symmetry properties of the wave functions does not cause any complication. The position regarding orbital degeneracy is rather different.

For a given symmetry processes (3) and (4) have a single initial state and a degenerate set of final states which we shall denote by i and $f_1 - f_n$ respectively. Noting that the interaction between i and the f's is very much greater than that between pairs of the f's it is immediately apparent from the appropriate secular equation that the potential energy curves are as sketched in figure 1, the essential feature being that they consist of two isolated branches, α and β, each of weight unity (corresponding to the similar branches arising in the standard non-degenerate case) together with an intermediate branch γ of weight $n-1$ which, unlike the others, is almost unaffected by the interaction. As R increases towards R_x the branches α and γ gradually converge and then diverge, and as it increases beyond the branches β and γ approach asymptotically†.

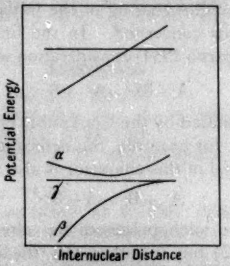

Figure 1. Pseudo-crossing point in the case of orbital degeneracy. The upper sketch shows the zero-order potential energy curves; the lower shows the true potential curves, allowance being made for the interaction between them.

---

† The potential energy curves are discussed more fully elsewhere (Lewis 1955).

The wave functions associated with the isolated branches change *rapidly* with internuclear distance in the region of the crossing point: thus according as R is much smaller or greater than R_x that of the upper of these branches, α, is predominantly homopolar or predominantly ionic while that of the lower, β, has the opposite characteristics. Furthermore the homopolar components of the two wave functions are of closely the same form; and of course the ionic components are necessarily identical in form since ($H^+, H^-(1s)^2$) has no orbital degeneracy. In complete contrast the wave functions associated with the intermediate branch, γ, change very *slowly* in the region of the crossing point and contain no appreciable part of *either* the homopolar *or* the ionic components of the other wave functions. It follows at once that transitions occur mainly between α and β, and that as far as they are concerned the existence of γ may be ignored. Now at the crossing point the energy separation of the isolated branches may readily be shown to be

$$\Delta U_{\alpha\beta}(R_x) = \left[\sum_{p=1}^{n} \{\Delta U_{\mathrm{if}_p}(R_x)\}^2\right]^{1/2} \quad \ldots\ldots(7)$$

where $\Delta U_{\mathrm{if}_p}(R_x)$ is what the separation would be if i and f_p were the only interacting states. From the Landau–Zener formula (cf. Mott and Massey 1949) we therefore have that the probability of a transition from one of these branches to the other in passing through the crossing point is

$$P = \exp(-w) \quad \ldots\ldots(8)$$

with

$$w = \pi^2\left[\sum_{p=1}^{n} \{\Delta U_{\mathrm{if}_p}(R_x)\}^2\right] \Big/ hv(R_x)\left|\frac{d}{dR}(U_\mathrm{i}^0 - U_\mathrm{f}^0)\right|_{R=R_x} \quad \ldots\ldots(9)$$

$v(R)$ being the radial component of the velocity of relative motion.

The fact that the ($H^+, H^-(1s)^2$) potential has important crossings *both* with the (H(1s), H(2s or *p*)), potential *and* with the (H(1s), H(3s, p or d)) potential has now to be taken into account. We shall use the numbers 1, 2 and 3 respectively to designate the asymptotic parts of these potentials and the letters b and c to designate the inner and outer crossing points (cf. figure 2); and we shall use the same numbers and letters as distinguishing subscripts on the symbols for associated quantities. To avoid making the notation unnecessarily cumbersome we

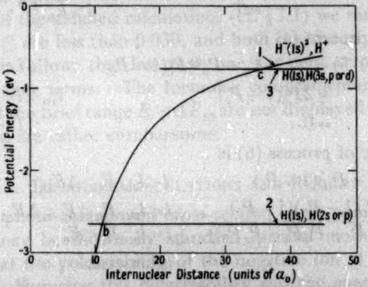

Figure 2. Potential energy diagram for the systems [$H^-(1s)^2, H^+$], [H(1s), H(2s or p)], [H(1s), H(3s, p or d)]. The zero is chosen to be the potential energy of the first-named system when the internuclear distance is infinite.

shall not in general include any specific reminder of the dependence on the angular momentum of the colliding systems about their centre of mass. This angular momentum, which we shall describe by the quantum number l, naturally controls how close the systems can come together. The homopolar curves are effectively horizontal since in the R-range of interest the inverse cube terms due to the dipole–dipole resonance forces (cf. King and Van Vleck 1939) are very small. Consequently if the approach is made along asymptote 1 crossing point b cannot be reached unless l is smaller than l_{1b}, and crossing point c cannot be reached unless l is smaller than l_{1c} where

$$l_{1b} = k_{12} R_{xb},\ l_{1c} = k_{13} R_{xc} \qquad \ldots\ldots(10)$$

$$k_{12}{}^2 = k_i{}^2 + \frac{8\pi^2 M}{h^2} \Delta E_{12},\ k_{13}{}^2 = k_i{}^2 + \frac{8\pi^2 M}{h^2} \Delta E_{13} \qquad \ldots\ldots(11)$$

$$k_i{}^2 = \frac{8\pi^2 M}{h^2} E_i \qquad \ldots\ldots(12)$$

M being the reduced mass, ΔE_{12} and ΔE_{13} being the amounts by which processes (3) and (4) are exothermic, and E_i being the initial kinetic energy of relative motion. The corresponding limits for approach along asymptote 3 are

$$l_{3b} = k_{32} R_{xb},\ l_{3c} = k_i R_{xc} \qquad \ldots\ldots(13)$$

with

$$k_{32}{}^2 = k_i{}^2 + \frac{8\pi^2 M}{h^2} \Delta E_{32} \qquad \ldots\ldots(14)$$

and with ΔE_{32} the amount by which process (6) is exothermic. It may be noted that

$$l_{1c} > l_{1b} \qquad \ldots\ldots(15)$$

and

$$(l_{3c} - l_{3b})/(E_i - E_0) > 0 \qquad \ldots\ldots(16)$$

where

$$E_0 = \{R_{xb}{}^2/(R_{xc}{}^2 - R_{xb}{}^2)\}\Delta E_{32}. \qquad \ldots\ldots(17)$$

Taking cognizance of the various paths that may be traversed during an encounter we find that if an approach along the requisite asymptote is made the probability of process (3) is

$$\left.\begin{aligned} \mathscr{P}(1,2) &= 2P_b(1-P_b)P_c & l &< l_{1b} \\ &= 0 & l &> l_{1b} \end{aligned}\right\} \qquad \ldots\ldots(18)$$

the probability of process (4) is

$$\left.\begin{aligned} \mathscr{P}(1,3) &= 2(1-P_b+P_b{}^2)P_c(1-P_c) & l &< l_{1b} \\ &= 2P_c(1-P_c) & l_{1b} < l &< l_{1c} \\ &= 0 & l &> l_{1c} \end{aligned}\right\} \qquad \ldots\ldots(19)$$

and the probability of process (6) is

$$\left.\begin{aligned} \mathscr{P}(3,2) &= \tfrac{2}{3} P_b(1-P_b)(1-P_c) && l < l_{3b}, E_i > \Delta E_{13} \\ &= \frac{2P_b(1-P_b)(1-P_c)}{3(1-P_c+P_bP_c-P_cP_b{}^2)} && \begin{cases} l < l_{3b}, E_0 < E_i < \Delta E_{13} \\ l < l_{3c}, E_i < E_0 \end{cases} \\ &= 0 && \text{otherwise.} \end{aligned}\right\} \qquad \ldots\ldots(20)\dagger$$

The probabilities of the reverse processes are of course related; we have

$$\mathscr{P}(2,1) = \tfrac{1}{2}\mathscr{P}(1,2),\ \mathscr{P}(3,1) = \tfrac{1}{3}\mathscr{P}(1,3),\ \mathscr{P}(2,3) = \tfrac{3}{2}\mathscr{P}(3,2). \qquad \ldots\ldots(21)$$

---

† If E_i is greater than ΔE_{13} particles reaching asymptote 1 continue to move apart indefinitely; but if it is smaller they fall back into the potential well and oscillate to and fro until ultimately they separate along either of the other asymptotes. A single formula is thus not applicable for all energies.

The associated cross sections are given by the standard formula

$$Q=\frac{\pi p}{k_{\mathrm{i}}^{2}}\sum_{l}(2l+1)\mathscr{P}_{l} \qquad \ldots\ldots(22)$$

in which p is the probability that the specified systems are initially on one of the interacting potentials (cf. Mott and Massey 1949). Since such potentials are associated only with singlet σ-states of the quasi-molecule we have that

$$p[\mathrm{H}^{+},\mathrm{H}^{-}(1\mathrm{s})^{2}]=1,\, p[\mathrm{H}(1\mathrm{s}),\mathrm{H}(2\mathrm{s}\ \text{or}\ \mathrm{p})]=\tfrac{1}{8},\, p[\mathrm{H}(1\mathrm{s}),\mathrm{H}(3\mathrm{s},\mathrm{p}\ \text{or}\ \mathrm{d})]=\tfrac{1}{12}. \quad \ldots(23)$$

The integrals equivalent to the required summations may be expressed in terms of the combination

$$F_{n}(x)=E_{n}(x)-E_{n}(2x) \qquad \ldots\ldots(24)$$

of the functions

$$E_{n}(x)=\int_{1}^{\infty} t^{-n}\exp(-xt)\,dt \qquad \ldots\ldots(25)$$

which are now well tabulated (Placzek 1946). Introducing

$$\left.\begin{aligned}\kappa&=\{2\pi Mv(R_{x})/h\}w\\ \zeta_{\mathrm{b}}&=\kappa_{1\mathrm{b}}/k_{12},\, \zeta_{\mathrm{c}}=\kappa_{1\mathrm{c}}/k_{13},\, \theta=\sin^{-1}(R_{x\mathrm{b}}k_{12}/R_{x\mathrm{c}}k_{13})\\ \xi_{\mathrm{b}}&=\kappa_{3\mathrm{b}}/k_{32},\, \xi_{\mathrm{c}}=\kappa_{3\mathrm{c}}/k_{\mathrm{i}},\, \phi=\sin^{-1}(R_{x\mathrm{b}}k_{32}/R_{x\mathrm{c}}k_{\mathrm{i}})\end{aligned}\right\} \qquad \ldots\ldots(26)\dagger$$

and substituting in (22) from (18), (19), (20) and (23) we obtain the following approximations for the cross sections:

$$Q[\mathrm{H}^{-}(1\mathrm{s})^{2},\mathrm{H}^{+};\ \mathrm{H}(1\mathrm{s}),\mathrm{H}(2\mathrm{s}\ \text{or}\ \mathrm{p})]=4\pi R_{x\mathrm{b}}^{2}(k_{12}^{2}/k_{\mathrm{i}}^{2})\exp(-\zeta_{\mathrm{c}}\sec\theta)\,F_{3}(\zeta)_{\mathrm{b}}\,.\ (27)$$

$$Q[\mathrm{H}^{-}(1\mathrm{s})^{2},\mathrm{H}^{+};\ \mathrm{H}(1\mathrm{s}),\mathrm{H}(3\mathrm{s},\mathrm{p}\ \text{or}\ \mathrm{d})]=4\pi R_{x\mathrm{c}}^{2}(k_{13}^{2}/k_{\mathrm{i}}^{2})\,F_{3}(\zeta_{\mathrm{c}}) \qquad \ldots\ldots(28)$$

$$\begin{aligned}Q[\mathrm{H}(1\mathrm{s}),H(3\mathrm{s},\mathrm{p}\ \text{or}\ \mathrm{d});\ \mathrm{H}(1\mathrm{s}),\mathrm{H}(2\mathrm{s}\ \text{or}\ \mathrm{p})]&=\frac{\pi}{9}R_{x\mathrm{b}}^{2}(k_{32}^{2}/k_{\mathrm{i}}^{2})\xi_{\mathrm{c}}\sec\phi\\ &\times[(1-\tfrac{1}{2}\xi_{\mathrm{c}}\sec\phi)F_{3}(\xi_{\mathrm{b}})-\tfrac{1}{2}\tan^{2}\phi(1-\xi_{\mathrm{c}}\sec\phi)F_{5}(\xi_{\mathrm{b}})\\ &+\tfrac{3}{8}\tan^{4}\phi(1-\tfrac{4}{3}\xi_{\mathrm{c}}\sec\phi)F_{7}(\xi_{\mathrm{b}})\\ &-\tfrac{5}{16}\tan^{6}\phi(1-\tfrac{8}{5}\xi_{\mathrm{c}}\sec\phi)\,F_{9}(\xi_{\mathrm{b}})],\ E_{\mathrm{i}}>\Delta E_{13}.\end{aligned} \qquad \ldots\ldots(29)$$

In the derivation of these formulae we have assumed that ζ_{c}, ξ_{c}, $\tan^{2}\theta$, and $\tan^{2}\phi$ are small enough to permit their use in short power series expansions. Anticipating the results of the detailed calculations (cf. § 3.1) we may note here that in them, both ζ_{c} and ξ_{c} are less than 0·030, and both $\tan^{2}\theta$ and $\tan^{2}\phi$ are less than 0·51, from which it follows that less than one per cent error is caused by the omission of the higher terms. The formulae complementary to (29) covering the various parts of the brief range $E_{\mathrm{i}}<\Delta E_{13}$ are not displayed as they are of more limited interest and are rather cumbersome.

§ 3. DETAILED CALCULATIONS AND RESULTS

3.1. From the photo-detachment cross-section curve computed by Chandrasekhar (1945) it may be shown by standard quantal methods (cf. Mott and Sneddon 1948) that the polarizability of the negative ion of hydrogen is about 230 atomic units. Knowing this polarizability and the energies of the isolated systems it is a simple task to determine the internuclear distances at which the pseudo-intersections of the potentials occur. We find that

$$R_{x\mathrm{b}}=11{\cdot}1a_{0},\, R_{x\mathrm{c}}=35{\cdot}6a_{0} \qquad \ldots\ldots(30)$$

---

† The first subscript on the κ's refers to the asymptote along which the approach is made and the second refers to the crossing point.

a_0 being the radius of the first Bohr orbit. Hence E_0 (defined by equation (17)) is $0{\cdot}20_3$ ev.

An account of the procedure for obtaining the energy separations, $\Delta U(R_x)$, has already been published (papers I and II) and need not be repeated. For $H^-(1s)^2$ we adopted the wave function given by Löwdin (1953) which is of the form

$$\psi(\mathbf{r}', \mathbf{r}'') = \{C_1 \exp(-\gamma_1 r') + C_2 \exp(-\gamma_2 r')\}\{C_1 \exp(-\gamma_1 r'') + C_2 \exp(-\gamma_2 r'')\} \quad \ldots\ldots(31)$$

where $\mathbf{r}'$ and $\mathbf{r}''$ are the position vectors of the two electrons relative to the parent nucleus and the C's and γ's are constants; and for H(1s, 2s or p and 3s, p or d) we used the exact wave functions. Describing the quasi-molecules (H^+, $H^-(1s)^2$), (H(1s),H(2s or p)) and (H(1s), H(3s, p or d)) by properly symmetrized combinations of these the required matrix elements may be computed without difficulty since they are expressible as the sums of products of the J-functions of Coulson (1942)[†]. As would be expected certain of the contributing integrals yield terms which contain factors of the type $\exp[(-\gamma_1 \text{ or } \gamma_2)R_x]$, and are therefore very sensitive to the γ's which are not accurately determined. Fortunately there is exact algebraic cancellation between the more important of such terms; and the dominant remaining terms are not very dependent on the constants of the $H^-(1s)^2$ wave function. Were it not for this the energy separation could scarcely be calculated with sufficient accuracy.

Table 1. Data Relating to Potential Energy Curves

Interacting states	Energy separation at crossing point (ev)	Root of sum of squares of energy separations (ev)
($H^-(1s)^2$, H^+) (H(1s), H(2s))	$3{\cdot}33 \times 10^{-1}$	$5{\cdot}26 \times 10^{-1}$
($H^-(1s)^2$, H^+) (H(1s), H(2p))	$4{\cdot}07 \times 10^{-1}$	
($H^-(1s)^2$, H^+) (H(1s), H(3s))	$4{\cdot}91 \times 10^{-3}$	$9{\cdot}27 \times 10^{-3}$
($H^-(1s)^2$, H^+) (H(1s), H(3p))	$6{\cdot}40 \times 10^{-3}$	
($H^-(1s)^2$, H^+) (H(1s), H(3d))	$4{\cdot}58 \times 10^{-3}$	

Table 1 gives the values finally obtained for the $\Delta U(R_x)$'s at the two crossing points together with the roots of the sum of the squares of each set (which are the quantities actually needed). It may be remarked that an increment of δR_x in R_x would cause the $\Delta U(R_x)$'s to diminish by the factor $\exp(-g\delta R_x)$ where g is about $0{\cdot}4_1/a_0$ for the b-crossing and is about $0{\cdot}2_8/a_0$ for the c-crossing. There is still some slight uncertainty about the true electron affinity of hydrogen. If the adopted value should be in error by, say, 0·01 ev then the derived values of R_{xb} and R_{xc} would be in error by $0{\cdot}0_4 a_0$ and $0{\cdot}4_7 a_0$ respectively.

Substitution from table 1 in definition (26) with use of the appropriate modification of equation (15) of paper I yields that

$$\zeta_b = 8{\cdot}5_5/(\mathscr{E} + 5{\cdot}30)^{1/2}, \zeta_c = 3{\cdot}6_5 \times 10^{-2}/(\mathscr{E} + 1{\cdot}53)^{1/2} \quad \ldots\ldots(32)$$

$$\xi_b = 8{\cdot}5_5/(\mathscr{E} + 3{\cdot}78)^{1/2}, \xi_c = 3{\cdot}6_5 \times 10^{-2}/\mathscr{E}^{1/2} \quad \ldots\ldots(33)$$

[†] It should perhaps be mentioned that having chosen the wave functions further approximations were not made in the evaluation of the matrix elements (as was done in paper II for the sake of reducing the computational labour).

where $\mathscr{E}$ is the impact energy of one of the particles (measured in ev), the other particle being taken to be at rest. For head-on collisions these quantities are identical with the corresponding w's appearing in formula (8) and their values give a useful indication of the general situation. In the case of such collisions it is apparent that P_b is much less than unity if $\mathscr{E}$ is below about 30 ev and that $(1-P_c)$ is much less than unity except when $\mathscr{E}$ is minute.

3.2. Using the formulae presented in § 2 the cross sections Q for processes (3), (4) and (6) were calculated over a range of impact energies $\mathscr{E}$ the results being shown in figures 3 and 4 in the form of $\log Q - \log \mathscr{E}$ curves. It should be noted that the approximations of Landau and Zener are not valid for very fast collisions. The region where they first begin to lead to serious error as yet cannot be specified definitely. However, failure undoubtedly occurs unless the velocity of relative motion is small compared with the relative velocity of the bound electrons (cf. paper I). The cross sections are therefore given only for impact energies up to 10^4 ev; and it is not certain that the approximations made are justified near this limit. According to the Landau–Zener formula the cross-sections for processes (3) and (4) ultimately fall off as $\mathscr{E}^{-1/2}$ and that for process (6) ultimately falls off as $\mathscr{E}^{-1}$ (being different because of the double transition involved). The true rates of fall off must be far more rapid since momentum transfer occurs. As the impact energy tends to zero the cross sections for processes (3) and (4) naturally tend to infinity as $\mathscr{E}^{-1}$ owing to the collecting action of the attractive Coulomb field. For process (6) the limit may for practical purposes be regarded as finite as is apparent from equation (33) and the succeeding remarks.

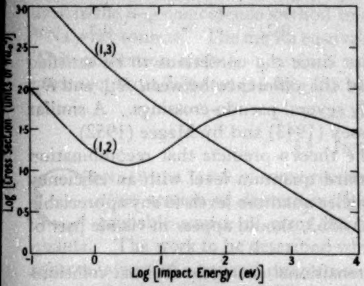

Figure 3. Cross sections for charge transfer from $H^-(1s)^2$ to H^+.

Curve (1, 2) refers to
$H^-(1s)^2 + H^+ \rightarrow H(1s) + H(2s \text{ or } p)$
and curve (1, 3) refers to
$H^-(1s)^2 + H^+ \rightarrow H(1s) + H(3s, p \text{ or } d)$.

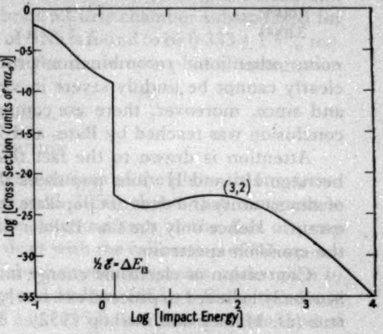

Figure 4. Cross section for the de-activation process
$H(3s, p \text{ or } d) + H(1s) \rightarrow H(2s \text{ or } p) + H(1s)$.

The rate coefficients associated with the processes were computed for a number of temperatures by averaging the products of the cross sections and the velocities of relative motion over the appropriate Maxwellian distribution. Table 2 gives the values obtained.

It will be observed that the rate coefficients for processes (3) and (4) are *both* large. This would suggest that large rate coefficients are likely to occur with

Table 2

Temperature (°K)	Rate coefficients Process (3) $\alpha(1, 2)$ (10^{-9} cm^3 sec^{-1})	Process (4) $\alpha(1, 3)$ (10^{-7} cm^3 sec^{-1})	Process (6) $\alpha(3, 2)$ (10^{-11} cm^3 sec^{-1})
250	$6\cdot_7$	1·3	1·9
500	$4\cdot_9$	$0\cdot9_3$	2·2
1000	$3\cdot_8$	$0\cdot6_8$	2·3
2000	$2\cdot_9$	$0\cdot5_0$	2·1
4000	$2\cdot_5$	$0\cdot3_9$	1·6
8000	$2\cdot_6$	$0\cdot3_2$	$0\cdot9_0$
16000	$3\cdot_4$	$0\cdot2_7$	$0\cdot5_2$
32000	$5\cdot_7$	$0\cdot2_5$	$0\cdot3_2$

many other ionic recombination processes since the conditions to be satisfied clearly cannot be unduly severe in view of the difference between R_{xb} and R_{xc} and since, moreover, there are commonly several pseudo-crossings. A similar conclusion was reached by Bates and Massey (1943) and by Magee (1952).

Attention is drawn to the fact that the theory predicts that recombination between H^+ and H^- ions populates the third quantum level with an efficiency of almost unity and does not populate the higher quantum levels to any appreciable extent. Hence only the first Balmer line, λ 6563, should appear in visible part of the emission spectrum.

Conversion of electronic energy into transitional energy in thermal collisions is usually believed to proceed extremely slowly and undoubtedly this is frequently true (cf. Massey and Burhop 1952). It is therefore of considerable interest that the calculated rate coefficient for process (6) is far from being small. The double transition mechanism responsible must also be operative in certain other cases. Further work is in progress.

ACKNOWLEDGMENT

One of us (J. T. L.) wishes to thank the Ministry of Education of Northern Ireland for the award of a maintenance allowance.

REFERENCES

BATES, D. R., and MASSEY, H. S. W., 1943, *Phil. Trans. Roy. Soc.* A, **239,** 269.

BATES, D. R., and MOISEIWITSCH, B. L., 1954, *Proc. Phys. Soc.* A, **67,** 805.

CHANDRASEKHAR, S., 1945, *Astrophys. J.*, **102,** 395.

COULSON, C. A., 1942, *Proc. Camb. Phil. Soc.*, **38,** 210 ; 1952, *Valence* (Oxford : Clarendon Press).

DALGARNO, A., 1954, *Proc. Phys. Soc.* A, **67,** 1010.

HENRICH, L. R., 1943, *Astrophys. J.*, **99,** 59.

KING, G. W., and VAN VLECK, J. H., 1939, *Phys. Rev.*, **55,** 1165.

LEWIS, J. T., 1955 *Proc. Phys. Soc.* A, **68,** in the press.

LÖWDIN, PER-OLOV, 1953, *Phys. Rev.*, **90,** 120.

MAGEE, J. L., 1952, *Discussions of the Faraday Society*, **12,** 33.

MASSEY, H. S. W., 1950, *Negative Ions* (Cambridge : University Press).

MASSEY, H. S. W., and BURHOP, E. H. S., 1952, *Electronic and Ionic Impact Phenomena* (Oxford: Clarendon Press).

MOTT, N. F., and MASSEY, H. S. W., 1949, *Theory of Atomic Collisions*, 2nd Edn (Oxford : Clarendon Press).

MOTT, N. F., and SNEDDON, I. N., 1948, *Wave Mechanics and Its Applications* (Oxford : Clarendon Press).

PLACZEK, G., 1946, *The Functions E_n (x)*. (National Research Council of Canada; Chalk River.)

The Radium Equivalent of ^{24}Na Sources and the Photodisintegration Cross Section of Deuterium

BY W. R. McMURRAY AND C. H. COLLIE
The Clarendon Laboratory, Parks Road, Oxford

MS. received 17*th August* 1954, *and in amended form* 5*th October* 1954

Abstract. A stable β-detecting proportional counter has been constructed and used in the β–γ coincidence method to calibrate a Curie chamber substandard for ^{24}Na γ-ray sources. The mg Ra equivalent of ^{24}Na is found to be 0·333 ± 1·5% mc. This calibration leads to a revised value of the deuterium photodisintegration cross section at 2·76 MEV (15·05 ± 0·5 barns).

---

§ 1. INTRODUCTION

CONSIDERATION of some recent determinations of the photodisintegration cross section of deuterium (Bishop *et al.* 1950) shows that the greatest probable source of error lies in the determination of the flux of γ-ray quanta. The work to be described which deals with the calibration of ^{24}Na γ-ray sources is part of a general programme of absolute measurements undertaken to remedy this uncertainty (cf. Marin, Bishop and Halban 1953). Since the decay scheme of ^{24}Na is well known (Hedgran and Lind 1952) the coincidence method of calibration can be used (Putman 1950, Barnothy and Forro 1951). As the original measurements made in this laboratory were made by this method and it is usually considered the most accurate for absolute measurements when the β–γ decay scheme is known, we have confined ourselves to it. The alternative method (Seliger and Schwebel 1954) of counting all the β-particles emitted from a thin source ('4π counting') is in use at the Atomic Energy Research Establishment, Harwell, and as a result of a parallel measurement we are able to report agreement within the experimental error between the two methods. A report on other British intercomparisons is given by Perry (1953).

In elementary theory, the absolute disintegration rate, N particles per second, of a source emitting β- and γ-rays in coincidence is given by $N = N_\beta N_\gamma / N_c$ in which N_β is the number of β-particles recorded, N_γ the number of γ-rays recorded, and N_c the number of β–γ coincidences between the two counters. The geometrical conditions under which this simple result obtains (Putman 1950) are not difficult to satisfy experimentally for β-counters subtending a few tenths of a steradian at the source. If 1% overall accuracy is aimed at, a high β counting rate must be used in order to obtain a sufficiently high coincidence rate. Small Geiger–Müller counters are not very reliable at high counting rates even when externally quenched. Furthermore, when counting at 20 000 per minute, the dead time correction enters largely into the final answer. The obvious way to overcome this difficulty is to use a proportional counter for the β-particles or a scintillation counter for the γ-rays. The equally obvious objection to this solution of the problem is that both these counters are very sensitive to small changes in their working conditions and are therefore unsuited to absolute measurements.

However, by careful attention to detail these difficulties can now be overcome.

§ 2. THE PROPORTIONAL β-COUNTER

The characteristic and desirable independence of counting rate upon applied voltage, the plateau, shown by a Geiger–Müller counter will also be shown by a proportional counter provided all the particles entering the counter are counted. For our purpose it is thus necessary to design a proportional counter in which the output pulses, due to the fastest weakly ionizing β-particles, reach the stable bias setting of the counter at an applied voltage considerably below that at which the counter ceases to behave as a proportional counter and becomes unstable or enters the Geiger region. The relative pulse height distribution for an idealized counter can be calculated from established data and is shown in figure 1 together with the distribution actually observed using our counter. In the calculation no allowance has been made for scattering in the window and from the inside walls of the counter, or for statistical spread in the number of ion pairs formed in the active volume of the counter. The peak in the distribution is due to β-particles of energy $E_\beta > 0{\cdot}2$ MEV. The high amplitude tail is due to particles for which $0{\cdot}2 > E_\beta > 0{\cdot}0006$ MEV; 99·8% of all the pulses are included between the finite limits set in figure 1. It should therefore be possible to detect at least 99·8% of the particles entering the counter with a finite gas amplification factor. A simple calculation shows that all the particles will not be counted until a gas gain of 300 is reached and that to obtain a satisfactory working plateau the counter must remain stable up to gas gains of 1000–2000.

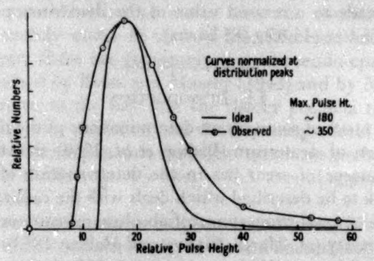

Figure 1. Pulse height distribution in the β-proportional counter.

A satisfactory design was worked out experimentally, taking as a basis the flow type loop counter developed at Atomic Energy Research Establishment, Harwell (Taylor 1953). Some preliminary experiments showed that the action of this counter depended on the purity of the argon and the conditions of flow. Systematic work was undertaken to explain many puzzling features about its action which were found experimentally.

The final design is shown in figure 2. Its performance is satisfactory as can be seen from the counting rate voltage curve (figure 3). The slope of the plateau is less than 0·4% per 100 volts. The amplifier was modified (Magee, Bell and Jordan 1952) so as to improve its overload characteristics in order to work several hundred volts along the plateau.

The counter is baked and filled with a methane, argon (~25%) mixture to about atmospheric pressure. The use of pure gases is not very important, provided they are dry and that the value of X/p (vcm^{-1} per mm Hg) does not fall below 0·5. This is ensured if the loop-window distance is kept below 1·0 cm. Under these conditions even 5% of air in the filling mixture can be tolerated without spoiling the plateau; however, the formation of negative ions in the regions of small X/p is shown by the appearance, at high gain, of a large number of small spurious pulses well below the discriminator bias. A detailed investigation showed the action of these counters could be explained in terms of the measured properties of the filling gas (Colli and Facchini 1952, English and Hanna 1953). The potential applied to the counter was obtained from a simple stabilized power pack, which was shown, by direct measurement, to be sufficiently stable for use with the β proportional counter.

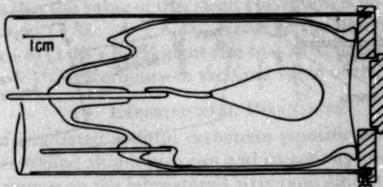

Figure 2. The proportional counter used to count the β-particles. The cathode is a silver deposit on walls and window. The 1/1000 in. window is made from a glass bubble or aluminium foil.

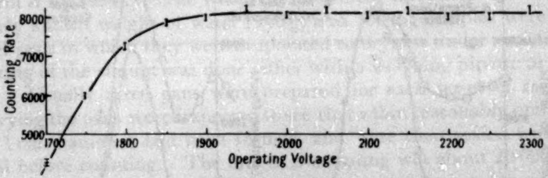

Figure 3. A ‘ plateau ’ obtained with a β-proportional counter using a ^{24}Na source.

§ 3. THE CORRECTION FOR THE γ-BACKGROUNDS IN THE β–γ COINCIDENCE

The simple formula $N = N_\beta N_\gamma / N_c$ assumes that the β-counter only registers β-rays and that all coincidences are between β-rays registered in the β-counter and γ-rays detected by the γ-counter. This is not so. Some of the particles detected by the β-counter are secondary electrons produced by the γ-rays. Since the ^{24}Na source emits two γ-rays (2·76 and 1·38 MEV) in cascade some of the coincidences are due to the detection of both members of a cascade, one in each counter.

The $\gamma\gamma$ coincidence rate and the true β rate can be approximately measured by slipping an aluminium disc, sufficiently thick to stop all the β-rays, over the counter window. This method over-estimates the correction because the efficiency of the β-counter for γ-rays is increased by the presence of the aluminium screen which stops the β-rays.

In our experiments this increase in efficiency was directly determined in a separate measurement in which the β-rays were deflected by a magnetic field. The apparatus is shown in figure 4.

The counter and head amplifier are mounted so that they can be rotated about a vertical axis and so vary the part of the counter window irradiated by a small, well collimated γ-ray beam. The axis of rotation is arranged to be 4 cm from the window of the counter. Since this is the usual source to window distance when a measurement is being made, a graphical integration of the counting rate curves with and without the absorber (figure 5) enables one to determine the desired ratio

$$\frac{\text{Total } \gamma \text{ counts with } \beta \text{ absorber over the window}}{\text{Total } \gamma \text{ counts with window uncovered}}.$$

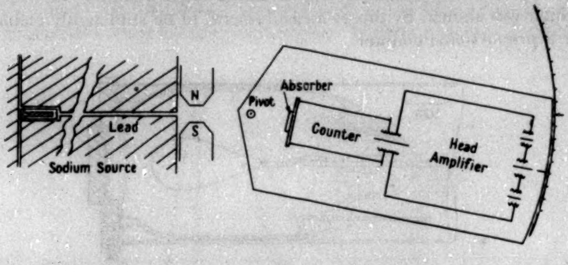

Figure 4. Apparatus used to determine the change in γ-counting efficiency of the β-counter when the β-screen (absorber) is placed over the window of the β-counter.

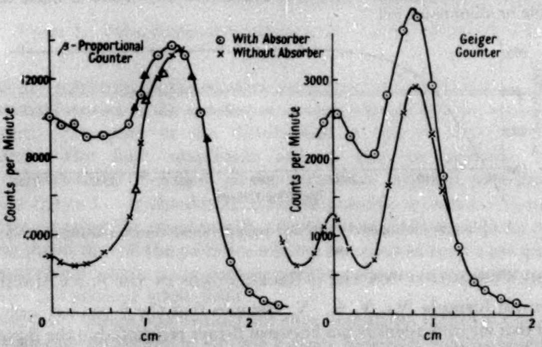

Figure 5. The variation of counting rate with point of entry of a collimated γ-ray beam into a proportional and Geiger counter with and without window absorbers.

For the proportional counter this ratio was 1·18. For a GM4 Geiger counter it was 1·39. The correction is applied in the following way.

If a and b are the efficiencies of the β-counter for the two γ-rays, γ_1 and γ_2, of the cascade, c its efficiency for β-rays, all measured in the absence of the absorber, $a+\delta a$, $b+\delta b$, and zero the corresponding efficiencies with the β-absorber in position, and ϵ_1, ϵ_2 the efficiencies of the γ-counter for the two γ-rays, then it is easily shown that

$$\frac{N_\beta N_\gamma}{N_c} = N\frac{(\epsilon_1+\epsilon_2)(c-\delta a-\delta b)}{c(\epsilon_1+\epsilon_2)-\delta a\epsilon_2-\delta b\epsilon_1}.$$

In this expression N_β and N_c are the differences between the pairs of values N_β, N_β'; N_γ, N_γ', measured with (N_β', N_γ') and without (N_β, N_γ) the absorber in position.

The correcting factor cannot be evaluated as it stands. However, as the ratio of the efficiency of a counter for γ-rays of energies 2·76 and 1·38 MEV is not very different from 1·8 (Segrè 1953), we can put $a=1{\cdot}80\,b$, $\epsilon_1=1{\cdot}8\epsilon_2$ and $\delta a=1{\cdot}8\delta b$, to obtain

$$\frac{N_\beta N_\gamma}{N_c}=N(1-1{\cdot}5\,\delta b/c).$$

The small quantity $\delta b/c$ may be calculated from the counting rate of the β-counter with and without the absorber, and is about 0·0028, making the correction about 0·42%.

It is easily seen that the value of this small correction is not very sensitive to the assumed value of ϵ_1/ϵ_2 (1·8). A ±4·25% error in the determination of the ratio $(a+b+\delta a+\delta b)/(a+b)$ (1·18 ± 0·05) gives rise to a 25% uncertainty in the value of the correction, i.e. 0·1% uncertainty in the final value of the disintegration rate.

§4. EXPERIMENTAL PROCEDURE

About 0·1 g of irradiated sodium carbonate (specific activity 10 mc g^{-1}) was weighed into a thin walled aluminium pan and its activity compared with that of a standard radium source on the laboratory Curie type ionization chamber (Wilson and Bishop 1949). The ionization current due to sodium was never more than six times that of the standard radium source. (N.P.L. Certificate C.2521; 1·01 mg radium content, and effective strength on our Curie chamber 0·96 mg (cf. Marin *et al.* 1954).) The whole of the sodium carbonate was dissolved in an accurately known weight of water (100 g) and 100 mg samples were transferred to nickel pans in which they were evaporated to dryness under an infra-red lamp. The taking of the aliquot was done either with a weighing pipette or a calibrated syringe. Usually three pans were prepared for each series of measurements. After drying the pans were inspected to see that a thin reasonably uniform deposit (about 1 cm diameter) had been formed, and were then sealed with 1/1000 in. styrofoil before counting. The rate of β-counting was about 20 000 per minute and with a γ-counting rate of 40 000 per minute a measurement to ±1% could be made in 30 minutes. Each pan was usually measured twice so that six separate sets of measurements were generally made for each comparison with the Curie chamber.

The runs in which the β-counter was screened provided a valuable check on the performance of the γ-counter, which should of course be unaffected by the screening.

The γ-counter was either a GM4 or B6 counter shielded with ¼ in. aluminium, or a sodium iodide scintillator (one inch cube) and EMI 6260 photomultiplier. It was found that sufficient stability in the working potential of the photomultiplier could be obtained using a standard 1007 stabilized power pack, but that care had to be taken to select a photomultiplier tube which had not developed a time drift in its sensitivity.

The Geiger counter was used without external quenching owing to the long delay (6 μsec) introduced by the conventional quenching circuit. The coincidence unit used was a type 1036A whose variable resolving time was used to check that no coincidences were lost. A typical set of experimental results is given below.

Date: 6th October 1953.
Time.
08.45 h Weight of $Na_2CO_3 = 0{\cdot}1065$ g.
10.00 h Comparison with Ra standard $I(\mathrm{Ra})/I(\mathrm{Na}) = 0{\cdot}1670 \pm 0{\cdot}0002$.
12.15 h Made up to 136·61 g of solution.
12.30 h Transferred aliquot parts to pans with a calibrated syringe.
  Pan 2 Weight of solution deposited = 59·5 mg.
  Pan 3 Weight of solution deposited = 100·2 mg.
  Pan 4 Weight of solution deposited = 59·5 mg.
16–24 h Six complete β–γ coincidence measurements.

A set of results and calculations is tabulated below.

Pan 2, Run 2

(1)	(2)	(3)	(4)	(5)	(6)	(7)	(8)
	Main coincidence run 1840 h–1905 h						
γ	1019683	40787		41093	39991		39991
Coinc.	23370	934·8	−36·7	909	908·4		872·8
β	663494	26540		26668	26613		25294
	γ-Background coincidence run 19.08 h–19.28 h						
γ	802594	40130		40445	39343	39999	
Coinc.	741	37·03	−1·83	35·5	34·9	35·6	
β	26916	1346		1349	1294	1319	

(1) Channel; (2) total count; (3) mean counting rate; (4) random coincidence correction; (5) dead time corrected counting rates; (6) background corrected counting rates; (7) decay corrected rates; (8) counting rates (corrected for γ–γ coincidences).

All counting rates are in counts per minute.

$$\text{Source strength at } 1852\tfrac{1}{2}\text{ h} : = \frac{N_\beta N_\gamma}{N_c} \times \frac{1}{60 \times 3{\cdot}7 \times 10^4} \times 1{\cdot}0042 = 0{\cdot}524\,\mu\text{c.}\dagger$$

The factor 1·0042, evaluated in §3, corrects for the error in the observed γ-background counting rates.

The dead time (about 10 μsec) was measured using a double pulse generator with a variable pulse separation. When a Geiger counter was used to detect the γ-rays, the dead time (about 100 μsec) was obtained by displaying the pulses on a triggered cathode-ray oscilloscope with a calibrated time-base.

§5. THE MILLIGRAMME EQUIVALENT OF ^{24}Na AND THE CROSS SECTION FOR THE PHOTODISINTEGRATION OF DEUTERIUM

The milligramme radium equivalent of ^{24}Na is the number of millicuries of ^{24}Na required to give the same ionization current in a Curie chamber as 1 milligramme of radium. The result of our measurements spread over a year, using a variety of equipment, is that the Curie chamber radium equivalent of ^{24}Na, is $0{\cdot}333 \pm 1{\cdot}5\%$ mc per mg.

							6							
						7	5							
				7		7	3			4				
				7		5	2			4				
				6	7	5	2	6		4	4			
	7			6	6	3	2	3	4	2	4			
	7	7		3	3	1	1	2	1	2	1		3	
0·319	0·321	0·323	0·325	0·327	0·329	0·331	0·333	0·335	0·337	0·339	0·341	0·343	0·345	0·347

---

† At its meeting in 1950, the International Commission on Radiological Units (ICRU) recommended that the unit of radioactivity, the curie, be defined as $3{\cdot}7 \times 10^{10}$ disintegrations per second as first suggested in 1947 (*Nature, Lond.*, **160**, 778).

The results of the 38 determinations of the milligramme equivalent are shown in the table. Each determination is represented by a number in the appropriate column. As already described 3–6 coincidence measurements were made for each Curie chamber comparison of a sample of irradiated sodium carbonate. In all, seven separate samples of ^{24}Na were compared on the Curie chamber and the numbers in the columns refer to these samples. Thus, column six indicates that three determinations gave a result between 0·328 and 0·330 mc mg^{-1} Ra of which one measurement was made with Na_2CO_3, sample 3, one with sample 6 and one with sample 7.

If these results are treated as if they formed part of a gaussian distribution the standard deviation of the mean would be $\pm 0{\cdot}3\%$. However, it is clear from inspection that they do not form a gaussian distribution, and deviations within a sample are less than the deviations from sample to sample. We interpret this to mean that the, at first sight, simple processes of weighing out the sodium carbonate samples, comparison on the Curie chamber, and dilution, introduce greater errors than would be expected. The quoted error of 1·5% is our estimate of the total uncertainty in our result. Of this uncertainty, 0·5% is due to the uncertainty of the absolute value of the radium source, and therefore does not apply to other measurements using the same radium standard.

The measurements previously made (Bishop *et al.* 1950) on the deuteron photodisintegration cross section for 2·76 Mev γ-rays, used ^{24}Na sources whose strengths were determined with the original value of the mg Ra equivalent of ^{24}Na on the Curie chamber. The new value of the mg Ra equivalent enables a recalculation of the cross section at this energy. In the original measurements the main ^{24}Na source was compared on the Curie chamber with a large (assumed effective strength = 229·5 mg) radium source, RaI, and the absolute disintegration rate determined in an aliquot. In the present measurements the comparison on the Curie chamber was made with a small radium source RaII (assumed effective strength = 0·960 mg). To allow a comparison of the old with the new mg Ra equivalent, the two-substandard Ra sources must be compared on the Curie chamber. Their disparity in strength makes a direct measurement impracticable; the comparison was made in three ways: (*a*) through an intermediate constant source (8·7 mg Ra) giving RaI/RaII = 235 ± 1; (*b*) through an intermediate decaying source (^{24}Na) giving RaI/RaII = 236 ± 1; 233 ± 1; (*c*) through an intermediate decaying source (Rn) giving RaI/RaII = 235·8 ± 0·3. Measurements (*a*) and (*c*) were made by Marin *et al.* (1954). The weighted mean of this ratio = 235·6.

To obtain the modified value of the deuteron photodisintegration cross section, the original value (15·9 ± 0·6 barns) is multiplied by the factor

$$\frac{229{\cdot}5}{0{\cdot}960} \times \frac{1}{235{\cdot}6} \times \frac{\text{old mg Ra equivalent}}{\text{new mg Ra equivalent}} = 0{\cdot}947$$

making the cross section equal to 15·05 ± 0·5 barns. This is in better agreement with the theoretical value (Squires 1952).

ACKNOWLEDGMENTS

We have to thank the Atomic Energy Research Establishment, Harwell, for their interest and cooperation. One of us (W. R. M.) held a Union Scholarship (South Africa) while the work was done. We also have to thank Dr. Halban and his colleagues for much helpful discussion, P. Marin for help with the Curie chamber and for making his measurements available to us, and Lord Cherwell for extending to us the facilities of the Clarendon Laboratory.

REFERENCES

BARNOTHY, J., and FORRO, M., 1951, *Rev. Sci. Instrum.*, **22,** 415.

BISHOP, G. R., COLLIE, C. H., HALBAN, H., HEDGRAN, A., SIEGBAHN, K., DE TOIT, S., and WILSON, R., 1950, *Phys. Rev.*, **80,** 15.

COLLI, L., and FACCHINI, U., 1952, *Phys. Rev.*, **88,** 987.

ENGLISH, W. N., and HANNA, G. C., 1953, *Canad. J. Res.*, **31,** 768.

HEDGRAN, A., and LIND, D., 1952, *Ark. Fys.*, **5,** 178.

MAGEE, F. I., BELL, P. R., and JORDAN, W. H., 1952, *Rev. Sci. Instrum.*, **23,** 30.

MARIN, P., BISHOP. G. R., and HALBAN, H., 1953, *Proc. Phys. Soc.* A, **66,** 608; *Ibid.*, **67,** 1113.

PERRY, W. E., 1953, *Standardisation of Radioactive Isotopes*, N.P.L. report.

PUTMAN, J. L., 1950, *Brit. J. Radiol.*, **23,** 46.

SEGRÈ, E., 1953, *Experimental Nuclear Physics*, Vol. 1 (London: Chapman and Hall), p. 47.

SELIGER, H. H., and SCHWEBEL, A., 1954, *Nucleonics*, **12,** No. 7, 54.

SQUIRES, G. L., 1952, *Progress in Nuclear Physics*, Vol. 2 (London: Pergamon Press), p. 111.

TAYLOR, D., 1953, *Nucleonics*, **11,** 40.

WILSON, R., and BISHOP, G. R., 1949, *Proc. Phys. Soc.* A, **62,** 457.

Studies in Intermediate Coupling : III
The Lithium Isotopes

By A. M. Lane†

Atomic Energy Research Establishment, Harwell, Berks.

MS. received 24th August 1954

Abstract. The methods of a previous paper are applied to the analysis of the reaction data on the lithium isotopes in terms of an intermediate coupling shell model of the nucleus. It is found that, to within the expected uncertainties, all of twelve data are consistent with the predictions of the model. The mean value of the intermediate coupling parameter a/K is about 3. As an incidental result, it is found that the β-decay data cannot be fitted with the old interaction mixture based on mirror transitions, but requires a new mixture based on the ^{14}O Fermi transition.

§ 1. Introduction

In the first paper of this series (Lane 1953, referred to as I‡) it was shown how the nuclear reaction data on light nuclei can be used to investigate the detailed structure of these nuclei. Assuming a shell model of the nucleus, general formulae were given for the values of reduced nucleon widths and M1 matrix elements. As an example, these formulae were applied to the data on the nuclei ^{13}C and ^{13}N. As a general rule, it was found that the values of the theoretical predictions were sensitive to the assumed mode of nucleon coupling (L–S or j–j or intermediate). Comparison with the experimental data then enabled the nature of the coupling in the mass-13 nuclei to be deduced. The result of this was gratifying in that all the data examined could be fitted with about the same mode of coupling, viz. intermediate coupling characterized (in terms of the usual constants a and K) by $a/K \sim 5$.

In the present paper, the available data on the states of the lithium isotopes of the configurations $(1p)^n$ with $n=1, 2, 3, 4$ are exposed to the same kind of analysis. In the next three sections, the data on reduced widths, β-decay and electromagnetic properties are discussed. The methods for calculating the wave functions of intermediate coupling are the same as those described in I, and details of the calculations will be omitted. Several of the spin–orbit matrices used in the present work have been given by Elliott (1953). (These are correct apart from the first non-diagonal elements in the $J=\frac{1}{2}$, $T=\frac{1}{2}$ and $J=\frac{3}{2}$, $T=\frac{1}{2}$ matrices for ^{7}Li, which should be multiplied by 3. Elliott uses a spin–orbit parameter D', which is related to a, the usual one, by $a=6D'$.) In computing the central force matrices, a Rosenfeld force has been assumed as in I, with the usual relation $L=6K$ between the direct and exchange integrals. Much of the experimental data used in this paper is to be found in the compilation of Ajzenberg and Lauritsen (1952) along with detailed energy level diagrams of the nuclei involved.

---

† Now at Massachusetts Institute of Technology, Cambridge, Boston, Massachusetts, U.S.A.

‡ The second paper, Lane and Radicati (1954), is referred to as II.

The paper is concluded with a discussion of the theoretical significance of the results obtained. Finally, in an Appendix, general formulae are given for allowed β-decay matrix elements and E2 moments in *L–S* coupling.

§ 2. THE REDUCED NUCLEON WIDTHS

In table 1, four data on nucleon widths are given together with the predicted values of these quantities in *L–S* and *j–j* coupling. These predicted values, computed from formulae given in I, are given in terms of the quantity x_1. This is the single-particle reduced width of a 1p nucleon in units of $\hbar^2/MR^2$ (M= nucleon mass, R=interaction radius). This quantity is always of order unity and, in I, it was actually assumed to be unity. In fact, however, x_1 has a certain dependence on the average binding energy of the nucleons in the compound state under consideration. At the beginning of the 1p shell, the single-particle nuclei ^{5}He and ^{5}Li are not bound (by about 1 MEV). The average binding energies of a 1p nucleon in the states quoted in table 1 in ^{7}Li and ^{8}Li are about 1 and 2 MEV. The average binding in ^{13}C is about 7 MEV. The effect of binding energy on the value of x_1 can be obtained from the curves labelled ' 1p ' in figures 1 and 2 of I.

Table 1. The Reduced Nucleon Widths of the Lithium Isotopes

(1)	(2)	(3)	(4)	(5)	(6)	(7)	(8)	(9)
^{6}Li(1p)	0	$\frac{3}{2}-, \frac{1}{2}$	^{4}He+p	~1	3·5	~1	x_1	x_1
^{7}Li(1p)^3	7·46	$\frac{5}{2}-, \frac{1}{2}$	^{6}Li+n ^{4}He+^{3}H	0·050	4·0	0·24	0	0·70x_1
^{8}Li(1p)^4	2·28	3+, 1	^{7}Li+n	0·031	4·0	0·135	0·40x_1	0·26x_1
	~3·3	1+(?), 1	^{7}Li+n ^{7}Li*+n	~1·0	4·0	~1	0·67x_1 0·67x_1	0·26x_1 1·0 x_1

(1) Compound nucleus; (2) excitation energy; (3) spin and isotopic spin; (4) modes of decay; (5) nucleon width (MEV); (6) radius assumed (10^{-13} cm); (7) observed reduced width (units of $\hbar^2/MR^2$); (8) *L–S* prediction; (9) *j–j* prediction.

The value of x_1 is discussed in the text. The last entry is derived from recent work (Freeman, Lane and Rose 1954).

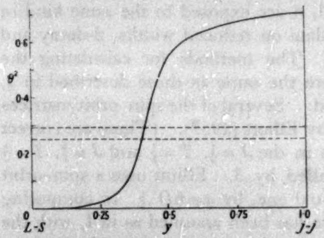

Figure 1. The reduced width of the transition ^{7}Li($\frac{5}{2}-$) → ^{6}Li(1+) in units of $\hbar^2/MR^2$.

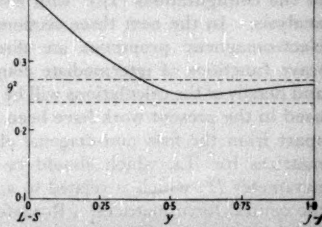

Figure 2. The reduced width of the transition ^{8}Li(3+) → ^{7}Li($\frac{3}{2}-$) in units of $\hbar^2/MR^2$.

These curves plot f_1, the logarithmic derivative of the radial 1p wave function evaluated at the nuclear surface, and x_1. Now, as the binding energy of a 1p nucleon increases from zero to 7 MEV, the value of f_1 (which fits on to the external wave function) increases negatively from about zero to about -3. From the graphs quoted, x_1 can be seen to decrease correspondingly from about unity to 0·4. We adopt the following values for x_1: ^{5}Li, 1·0; ^{7}Li, 0·8; ^{8}Li, 0·67; (^{13}C, 0·40). The last quoted value does not upset the agreement obtained in I where x_1 was taken as unity. This can be seen on examining figure 6 of I.

Since ^{5}Li is a one-particle state, its features are independent of the mode of coupling. The first line in table 1 merely confirms the well-known result that the reduced width is a one-particle one (Sack *et al.* 1954).

The second and third reduced widths in table 1 have predicted values dependent on the mode of coupling. The actual dependences of the predicted values on a/K are given in figures 1 and 2. The method of plotting is that used in I, with $y=(a/K)/(5+a/K)$, and L–S coupling on the left, j–j coupling on the right. The horizontal lines are the experimental values assuming the above values of x_1. It can be seen that the theoretical curves cut the experimental values, and that agreement is obtained with $y \sim 0{\cdot}4$ in both cases. It must be borne in mind that the positions of the experimental lines depend on (1) the values of the reduced widths extracted from the observed widths of table 1. These values depend somewhat on the choice of interaction radius, (2) the values taken for x_1. These two uncertainties can be estimated as giving a combined uncertainty of $\pm 15\%$ in the positions of the experimental lines.

The last entry in table 1 is discussed in Freeman, Lane and Rose (1954). The experimental results are not precise enough to conclude anything about the mode of coupling.

§ 3. THE β-DECAY *ft*-VALUES

There are four known *ft*-values involving the lithium isotopes and these are listed in table 2 together with the predicted values of L–S and j–j coupling.

Table 2. The *ft*-values of β-decay in the Lithium Isotopes

Initial nucleus	Final nucleus	ft_{exp}	ft_{L-S}	ft_{j-j}
^{6}He(0+)	^{6}Li(1+)	825 ± 75	825	1480
^{7}Be($\frac{3}{2}-$)	^{7}Li($\frac{3}{2}-$)	2240 ± 40	2040	3000
^{7}Be($\frac{3}{2}-$)	^{7}Li*($\frac{1}{2}-$)	3600 ± 600	3700	7400
^{8}Li(2+)	^{8}Be*(2+)	4.10^5	∞	3900

The last two columns give the predictions of L–S and j–j coupling.

These predicted values are obtained with the formula for allowed Gamow–Teller and Fermi matrix elements given in the Appendix, and with certain assumptions about the β-interaction constants. These latter have been defined by Winther and Kofoed-Hansen (1953) so that any allowed *ft*-value is given by:

$$ft = B/[(1-X)D_{\mathrm{F}} + XD_{\mathrm{GT}}]$$

where D_{F} and D_{GT} are the squares of the Fermi and Gamow–Teller matrix elements. The above authors analyse the *ft*-values of one-particle levels to derive values of B and X and quote $B = 2650 \pm 85$ sec; $X = 0{\cdot}50 \pm 0{\cdot}05$. In the light of recent results on the pure Fermi 0–0 transition in ^{14}O (Gerhart 1954) which gives a relation between X and B, we prefer the mean values suggested by Gerhart: $B = 2820$ sec; $X = 0{\cdot}57$. These are the values assumed in table 2 and in figures 3, 4, 5 and 6, which show the variation of the *ft*-values with the mode of coupling. It should be mentioned that the mean constants of Winther and

Kofoed-Hansen do not give reasonable results in the present investigation[†]; either no agreement with experiment is obtained at all, or else it is only obtained with most unlikely values of a/K.

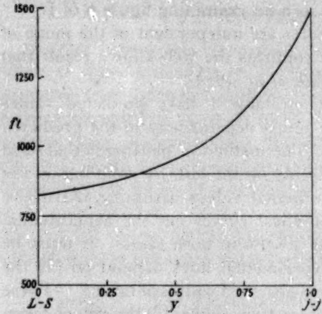

Figure 3. The ft-value of the ^{6}He → ^{6}Li β-decay.

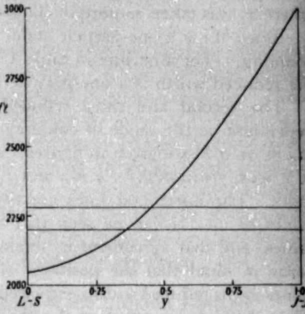

Figure 4. The ft-value of the ^{7}Be → ^{7}Li β-decay.

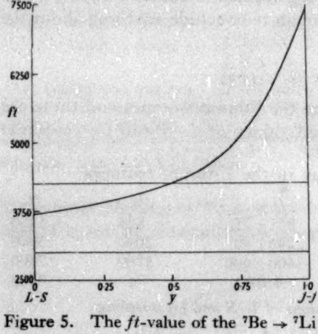

Figure 5. The ft-value of the ^{7}Be → ^{7}Li* β-decay.

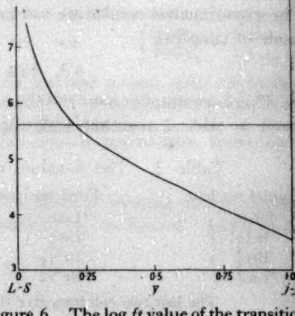

Figure 6. The log ft value of the transition ^{8}Li → ^{8}Be(2+).

One can see from figures 3–6 that experiment and theory always agree within the experimental error for some value of y. In the first three figures, the ft-values are all small and agreement is obtained for $y \sim 0{\cdot}4$ for the mass 7 nuclei, and for $0 < y \lesssim 0{\cdot}4$ for the mass 6 nuclei. In the last figure, the observed ft-value is very large and this means that small impurities in the assumed shell-model states could considerably change the theoretical predictions. In consequence, one should not attach much significance to the fact that agreement is obtained at about $y = 0{\cdot}2$.

[†] It should also be mentioned that Winther and Kofoed-Hansen made use of an old ft-value for the ^{39}Ca–^{39}K decay. This has recently been re-measured (Hunt *et al.* 1954) and the result is in complete disagreement with any of the interaction constants mentioned here. This would seem to imply that, if the experiment is correct, then ^{39}Ca and ^{39}K are not one-particle $d_{3/2}$ nuclei.

§ 4. THE ELECTROMAGNETIC DATA

In tables 3(*a*), 3(*b*) and 3(*c*), we list the available electromagnetic data on the lithium isotopes. We only include this data rather tentatively in the present investigation because of a certain correction to the theoretical predictions, which does not apply to the nucleon and β-decay data, and which is hard to take into account. This correction arises from the centre-of-mass motion of the α-particle core of the lithium nuclei. Considered as a single composite particle, this core has mass 4 and charge 2. If ^{5}Li were a bound nucleus, the centre-of-mass motion in this case would consist simply of the recoil motion of the core as the 1p nucleon moved in its orbit, and one could easily compute the appropriate corrections to the magnetic moment and E2 moment. (These quantities are not known experimentally because ^{5}Li is unstable.) The corrections would be: M1 moment, $\frac{1}{8}$ nuclear magneton; E2 moment, $\sqrt{\frac{1}{10}}Q_{\mathrm{SP}} \sim 3 \times 10^{-26} e\,\mathrm{cm}^2$. Compared with the magnitudes of the theoretical predictions in tables 3, these corrections are serious. In the absence of any reported study of the corrections in the general case, we can guess that those applying to the present work are rather less than those for ^{5}Li. Presumably the correction for core motion decreases as more 1p nucleons are added (merely because the more nucleons there are outside the core, the less the need, on the average, for recoil core motion to keep the centre of mass fixed).

Table 3(*a*). Magnetic Moments, μ, of the Lithium Isotopes

Nucleus	μ_{obs} (n.m.)	$\mu_{L\text{-}S}$	$\mu_{j\text{-}j}$	Reference
^{6}Li	+0·822	0·88	0·62	Mack 1950
^{7}Li	+3·256	3·07	3·04	

Table 3(*b*). Electric Quadrupole Moments, Q, of the Lithium Isotopes

Expl. quantity	Observed value	L–S	j–j	Reference
$Q(^{6}\mathrm{Li})/Q(^{7}\mathrm{Li})$	$(1{\cdot}9 \pm 0{\cdot}1) \times 10^{-2}$	0	0·50	Cranna 1953
$Q(^{7}\mathrm{Li})$	$-0{\cdot}02 \pm 0{\cdot}02 \times 10^{-24}\, e\,\mathrm{cm}^2$	$0{\cdot}190 Q_{\mathrm{SP}}$	$0{\cdot}232 Q_{\mathrm{SP}}$	Mack 1950

The L–S and j–j predicted values are given in units of Q_{SP}, the single particle value, defined in II as $\langle l \| H^{(2)} \| l \rangle$, and estimated as $\sim 10^{-25}\, e\,\mathrm{cm}^2$.

Table 3(*c*). The Λ-values of M1 Transitions in ^{7}Li and ^{7}Be

Transition	Λ_{obs}	$\Lambda_{L\text{-}S}$	$\Lambda_{j\text{-}j}$	Reference
$0{\cdot}479(\frac{1}{2}-) \rightarrow 0(\frac{3}{2}-)$ in ^{7}Li	22 ± 7	18·36	7·22	Bell and Elliott 1949
$0{\cdot}430(\frac{1}{2}-) \rightarrow 0(\frac{3}{2}-)$ in ^{7}Be	15 ± 3	13·42	7·22	S. Devons (private commn)

The Λ are defined in II as convenient dimensionless measures of the squared M1 matrix elements.

Figures 7, 8, 9, 10 and 11 show the variation of the magnetic moments and other electromagnetic properties with the mode of coupling. It can be seen that agreement or near agreement with the observed values can be obtained in all cases for some value of y. In the case of the magnetic moment of ^{7}Li (figure 8), the theoretical curve, without corrections, does not actually cut the experimental line. However, the ordinate scale is greatly expanded in this figure and the discrepancy is well within the error expected from core motion and the usual relativistic and exchange current effects. Allowing 0·1 nuclear magneton for these errors means that, for ^{6}Li and ^{7}Li, the experimental values of the magnetic moments are consistent with most values of y. From figure 9, the ratio of the E2 moments, allowing errors† of $0{\cdot}05\,Q_{SP}$ for core motion means that one can

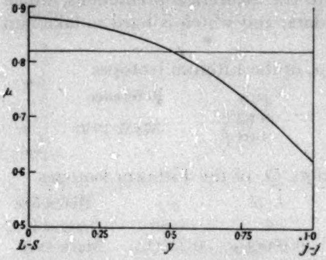

Figure 7. The magnetic moment of ^{6}Li in nuclear magnetons.

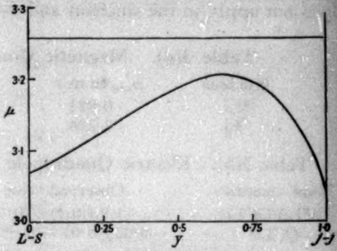

Figure 8. The magnetic moment of ^{7}Li in nuclear magnetons.

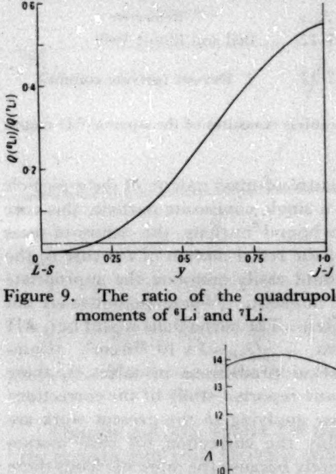

Figure 9. The ratio of the quadrupole moments of ^{6}Li and ^{7}Li.

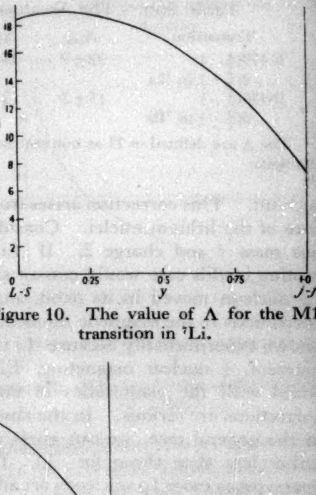

Figure 10. The value of Λ for the M1 transition in ^{7}Li.

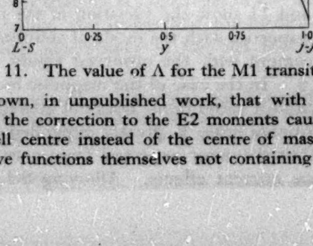

Figure 11. The value of Λ for the M1 transition in ^{7}Be.

---

† J. P. Elliott has shown, in unpublished work, that with harmonic oscillator wave functions in the 1p shell, the correction to the E2 moments caused by the operator being taken with respect to well centre instead of the centre of mass, is zero. However, the correction due to the wave functions themselves not containing centre-of-mass motion is not zero.

only conclude that $y < 0{\cdot}5$. The experimental error on the absolute value of the ^{7}Li E2 moment is so great that little can be gained from comparison with theory.

Figures 10 and 11 show the dependence on y of the two M1 transition strengths in table 3(*c*). The exact definition of ' transition strength ', denoted by Λ is given in II. Although the dependence on y is quite strong in both cases, the experimental uncertainties are such that any value of y less than $0{\cdot}5$ can be said to give agreement with experiment.

§ 5. DISCUSSION

Previous intermediate coupling studies on the lithium isotopes (e.g. Elliott 1953, Inglis 1953, Tauber and Wu 1954) have considered only the energy level schemes and the static moments. Inglis, in particular, concludes that an intermediate coupling model can give quite good agreement with the known data if a/K is taken to increase from about $1{\cdot}5$ in ^{5}Li to about $5{\cdot}0$ in ^{8}Li (i.e. y increases from about $0{\cdot}25$ to $0{\cdot}5$). There is an anomaly in ^{7}Li (the relative splittings of the ^{22}P and ^{22}F doublets are not correctly given) but, apart from this, the general picture is satisfactory. Recently, Allen (1954) has shown that the first six predicted levels of the ^{6}Li spectrum fit in beautifully with the experimental results obtained by himself and others.

In the investigation of ^{13}C and ^{13}N in I, it was shown that the analysis of the reaction data offered very strong support for an intermediate coupling model of these nuclei. Mainly because of larger experimental errors, the conclusion of the present paper cannot be quite as positive. However, it is certainly possible to say that, within these errors and certain theoretical uncertainties mentioned in the text, all twelve data in the present investigation are consistent with an intermediate coupling model of the nucleus characterized by $2 \lesssim a/K \lesssim 4$.

Finally, we would like to make the following more specific remarks :

(i) As in the ^{13}C investigation, the experimental quantity which is most sensitive to the mode of coupling (and which is therefore the most useful datum) is a reduced width (see figure 1).

(ii) Reasonable results are obtained for the β-decay only if the interaction constants of Winther and Kofoed-Hansen are replaced by those given in the text.

(iii) The present work in conjunction with I corroborates the conclusion of Inglis (1953) that the value of a/K increases through the 1p shell from ~ 2 to ~ 6. It is very desirable to try to account for this increase theoretically. Calculations by J. P. Elliott and the author (1954) suggest that a neutral two-body spin–orbit force may account for all the manifestations of spin–orbit forces in light nuclei, including this increase in a/K.

APPENDIX

In the course of obtaining results on the E2 moments and *ft*-values, the following general formulae for E2 moments and Gamow–Teller matrix elements of allowed transitions are obtained:

$$Q = n\left(\frac{J(2J-1)}{(J+1)(2J+3)}\right)^{1/2} U(2LJS,\, LJ)\sqrt{\left(\frac{16\pi}{5}\right)}\langle l\| H^{(2)} \| l\rangle \sum_{\mathrm{p}} \langle \alpha \,|\}\sigma_{\mathrm{p}}\rangle^2$$
$$\times\; U(2lLL_{\mathrm{p}},\, lL)(\tfrac{1}{2}\delta_{\Gamma 1'} - \mathscr{T}_{\mathrm{p}}). \qquad \ldots\ldots\text{(A1)}$$

This is the E2 moment of the state $\langle l^n, \alpha TSL, J|$. The various symbols are all defined in II.

$$D_{\mathrm{GT}}{}^{1/2} = \frac{3n}{\sqrt{2}}(-)^{S+S'}\delta_{LL'}C^{1T'T}_{1M_{T'}M_T}U(1S'JL, SJ')\sum_{\mathrm{p}}\langle\alpha|\}\alpha_{\mathrm{p}}\rangle\langle\alpha'|\}\alpha_{\mathrm{p}}\rangle$$
$$\times U(1\tfrac{1}{2}\,TT_p, \tfrac{1}{2}T')\,U(1\tfrac{1}{2}\,SS_p, \tfrac{1}{2}S'). \qquad \ldots\ldots\text{(A2)}$$

This is the Gamow–Teller matrix element for the allowed β-decay

$$\langle l^n, \alpha TSL, J| \rightarrow \langle l^n, \alpha' T'S'L'J'|.$$

The Fermi matrix element is simply:

$$D_{\mathrm{F}}{}^{1/2} = [(T+M_T)(T-M_T+1)]^{1/2}\,\delta_{\alpha TSLJ,\ \alpha'T'S'L'J'}\,. \qquad \ldots\ldots\text{(A3)}$$

ACKNOWLEDGMENT

The author wishes to thank the Director, Atomic Energy Research Establishment for permission to publish this paper.

REFERENCES

AJZENBERG, F., and LAURITSEN, T., 1952, *Rev. Mod. Phys.*, **24,** 321.
ALLEN, K., 1954, *Glasgow Conference on Nuclear Physics* (forthcoming report).
BELL, R. E., and ELLIOTT, L. G., 1949, *Phys. Rev.*, **76,** 168.
CRANNA, N. G., 1953, *Canad. J. Phys.*, **31,** 1185.
ELLIOTT, J. P., 1953, *Proc. Roy. Soc.* A, **218,** 345.
ELLIOTT, J. P., and LANE, A. M., 1954, *Phys. Rev.*, **96,** 160.
FREEMAN, J., LANE, A. M., and ROSE, B., 1955, *Phil. Mag.*, **46,** 17.
GERHART, J. B., 1954, *Phys. Rev.*, **95,** 288.
HUNT, W. A., KLINE, R. M., and ZAFFARANO, D. J., 1954, *Bull. Amer. Phys. Soc.*, **29,** No. 4, 23.
INGLIS, D. R., 1953, *Rev. Mod. Phys.*, **25,** 390.
LANE, A. M., 1953, *Proc. Phys. Soc.* A, **66,** 977.
LANE, A. M., and RADICATI, L. A., 1954, *Proc. Phys. Soc.* A, **67,** 167.
MACK, J. E., 1950, *Rev. Mod. Phys.*, **22,** 64.
SACK, S., BIEDENHAM, L. C., and BREIT, G., 1954, *Phys. Rev.*, **93,** 321.
TAUBER, G., and WU, T.-Y., 1954, *Phys. Rev.*, **93,** 295.
WINTHER, A., and KOFOED-HANSEN, O., 1953, *K. Danske Vidensk. Selsk. Mat. Fys. Medd.*, **27,** No. 14.

Studies in Intermediate Coupling
IV: Further Remarks on the Nuclei ^{13}C and ^{13}N

By A. M. Lane†

Atomic Energy Research Establishment, Harwell, Berks.

MS. received 15*th September* 1954

Abstract. The results reported in a previous paper on the nuclei ^{13}C and ^{13}N are extended in three ways: (i) The β-decay *ft*-value for the allowed mirror transition has been examined in intermediate coupling and is shown to be in excellent agreement with the previous results. (ii) Some properties of the nuclei have been recalculated with different assumptions about the central force between nucleons. It is found that the previous results are not very much changed, even when the central force mixture is quite severely modified. (iii) Some discussion is given about the even parity states of ^{13}C and ^{13}N. In particular the application of the 'unique parent' concept to these states, and its justification, is considered.

§ 1. Introduction

In the first and second papers of the present series (Lane 1953 a, Lane and Radicati 1954, to be referred to as I and II‡), the available experimental data on the nuclei ^{13}C and ^{13}N were interpreted theoretically with the aid of the nuclear shell model. In the present paper, this work is extended to additional data, and the dependence of the previous results on certain assumptions is investigated.

The data used in I included two reduced nucleon widths, a magnetic moment and an M1 radiation width. Section 2 discusses the *ft*-value of the mirror β-transition between ^{13}N and ^{13}C. As with the previous data, the states involved are assumed to belong to the shell-model configuration $(1p)^9$, and theoretical predictions are made allowing an arbitrary degree of spin–orbit coupling with the object of establishing the strength of this coupling by comparison with the experimental result. It will be recalled that all the data previously considered were consistent with a value of the spin–orbit parameter a of about $5K$, where K is the usual central force exchange integral.

Section 3 presents results answering some queries raised in the conclusions of I, viz. to what extent are the results given there sensitive to changes in the assumed exchange nature of the force between nucleons and the ratio L/K of the direct to the exchange integrals? In calculations, assumptions have to be made about both of these and it is important to know how rather different assumptions can affect the results. If, in fact, the results were very sensitive to alterations in the force mixture and the value of L/K, then the success of the results in I would be strong evidence in favour of the Rosenfeld force mixture and the value $L/K=6$ that were used in all the calculations.

---

† Now at Massachusetts Institute of Technology, Cambridge, Massachusetts.

‡ The third paper (Lane 1955) is referred to as III.

The last section discusses the states of even parity in ^{13}C and ^{13}N belonging to the mixed configurations $(1p)^8 2s$ and $(1p)^8 1d$. It is pointed out that all the experimental data of these states are consistent with a single particle model, i.e. it appears that the states can be constructed by simply coupling on the unlike nucleon (2s or 1d) to definite ' parent ' states of $(1p)^8$, and then anti-symmetrizing. Physically this implies that the presence of an added 2s or 1d nucleon does not appreciably perturb the $(1p)^8$ core, so that the coupling of a 2s or 1d nucleon to the 1p nucleons is *effectively* much weaker than the coupling of the core nucleons amongst themselves. There is no reason for this situation at first sight because the interaction integrals for the 2s–1p and 1d–1p interactions are certainly as large as those of the 1p–1p interactions. However, more detailed considerations show why the ' unique parent ' description of the states is indeed a good one in spite of this fact.

Finally, in the concluding remarks, some general observations are made on the results of shell-model calculations on nuclei in the 1p shell.

§ 2. THE β-TRANSITION ^{13}N $\rightarrow$ ^{13}C

The theoretical calculation of the *ft*-value of the ' mirror β-transition ' $^{13}\mathrm{N} \rightarrow {}^{13}\mathrm{C}$ for any degree of intermediate coupling is precisely the same in principle as the intermediate coupling calculations described in the previous papers I and III. Consequently details of the methods used will be omitted here and only the results will be given.

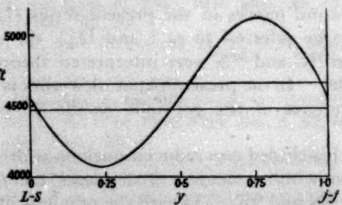

Figure 1. The *ft*-value of the β-decay ^{13}N → ^{13}C.

Figure 1 shows the theoretical variation of the *ft*-value of the transition as the quantity y is varied from 0 to 1. It will be recalled that y is defined in terms of the usual intermediate coupling parameter a/K by $y=(a/K)/(5+a/K)$. As y runs from 0 to 1, a/K varies from 0 to ∞, and the coupling situation is changed from extreme L–S to extreme j–j. The horizontal line in the diagram represents the experimental value along with the estimated error $ft=4560 \pm 100$ (Winther and Kofoed-Hansen 1953).

In calculating figure 1, a Rosenfeld exchange force mixture has been assumed as in the previous papers and the ratio of the direct and exchange integrals L/K has been taken as 6. The values used for the β-decay constants, X and B, are those given in III, where it is pointed out that some previously suggested values (Winther and Kofoed-Hansen 1953) do not give reasonable results.

The form of the curve in figure 1 is an excellent illustration of the rule that one must not guess anything about the behaviour of an intermediate coupling curve from knowledge of the extreme L–S and j–j values. It might have been supposed in the case of the present β-transition that the curve would be roughly horizontal since the extreme L–S and j–j values are the same ($ft=4570$). In fact, the curve is not at all so, and it is remarkable that it only crosses the range of experimental values at $y \sim 0{\cdot}5$ in excellent agreement with the values of y giving agreement with other data in I.

If we had chosen the β-interaction constants of Winther and Kofoed-Hansen, the theoretical curve would cross the experimental line at $y \sim 0{\cdot}7$ which is not in agreement with the results of I.

§ 3. THE EXCHANGE FORCE MIXTURE AND THE RATIO OF THE RADIAL INTEGRALS

There is considerable uncertainty as to the precise form of the central interaction force between nucleons. In setting up the central force matrices for intermediate coupling calculations, it is necessary to assume an exchange force mixture, and to specify the depth and range of the interaction potential. The latter two quantities determine L and K, the direct and exchange 1p shell integrals. The depth of the interaction potential enters as a multiplying factor into L and K, so that the ratio of these quantities does not depend on this. Consequently varying the interaction well-depth in the calculations of the present series of papers will not affect the results at all because only the ratio of L to K is involved. The values of L and K separately are only needed when calculations are made about level spacings and nuclear spectra generally.

(*a*) *Varying the Force Mixture*

In all the calculations of I, a Rosenfeld exchange force was assumed with the ratio $L/K=6$. The exchange force (Rosenfeld 1948) is chosen to fit the deuteron data and to give saturation, and it has the form:

$$(\tau_1 \cdot \tau_2)(0{\cdot}10 + 0{\cdot}23(\sigma_1 \cdot \sigma_2))V(r_{12})$$

or

$$-0{\cdot}13V_{\mathrm{W}} + 0{\cdot}93V_{\mathrm{M}} + 0{\cdot}46V_{\mathrm{B}} - 0{\cdot}26V_{\mathrm{H}}$$

where the subscripts W, M, B and H distinguish the usual Wigner, Majorana, Bartlett and Heisenberg contributions. In order to check the dependence of the results of I on the form assumed for the exchange mixture, one must repeat the calculations with a different mixture. Since four parameters are available to be varied, there is considerable arbitrariness in selecting a new mixture. However, we are restrained somewhat in our choice by the desire to adhere to a mixture that reproduces at least the gross features of previous predictions of nuclear spectra, i.e. in L–S coupling, the ordering of states by their spatial symmetry character.

This means retaining a large positive Majorana component. A force mixture which seems to be a reasonable change in this sense from the Rosenfeld mixture is the Serber mixture (Serber 1947) which fits the high energy n–p scattering data:

$$[0{\cdot}75 - 0{\cdot}25(\sigma_1 \cdot \sigma_2) - 0{\cdot}25(\tau_1 \cdot \tau_2) - 0{\cdot}25(\sigma_1 \cdot \sigma_2)(\tau_1 \cdot \tau_2)]\,\frac{V(r_{12})}{2}$$

or

$$0{\cdot}5V_{\mathrm{W}} + 0{\cdot}5V_{\mathrm{M}}.$$

Both the magnetic moment of ^{13}C (given in I) and the Λ-value of the $\frac{3}{2}^- \rightarrow \frac{1}{2}^-$ $M1$ transition in ^{13}N (given in I, corrected in II) have been re-calculated with the Serber mixture in intermediate coupling. The results are shown in figures 2 and 3.

The new curve for the magnetic moment (figure 2) is seen to follow the old curve so closely that the curve can be said to be substantially independent of the force mixture. The end-points (the *L–S* and *j–j* values) of the two curves closely coincide because the *j–j* state, $p_{1/2}$, is exactly, and the *L–S* state, ^{22}P, is nearly, independent of the force mixture. Since this in itself helps to ensure that the curve cannot be very sensitive to changes in the mixture, the result is not too surprising.

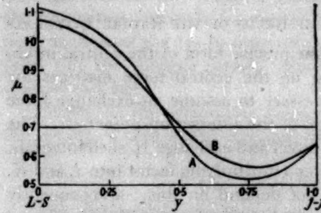

Figure 2. The magnetic moment of ^{13}C in nuclear magnetons. Curves A and B are calculated for Rosenfeld and Serber force mixtures respectively (assuming $L=6K$ in both cases).

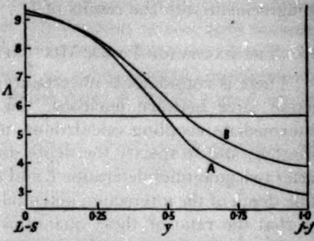

Figure 3. The Λ-value of the M1 transition in ^{13}N. Curves A and B are calculated for Rosenfeld and Serber force mixtures respectively (assuming $L=6K$ in both cases).

In the case of the Λ-value of the M1 transition (figure 3), the two curves do not coincide in the *j–j* coupling limit. The reason is that the upper state, which has quantum numbers $J=\frac{3}{2}^-$, $T=\frac{1}{2}$, belongs to the configuration $(1p_{3/2})^7\,(1p_{1/2})^2$, which possesses two states of these numbers. The separation of these states, which are degenerate in the *j–j* limit, is determined by the central force mixture, and, in particular, the Serber and Rosenfeld forces give different states and separations. However, in spite of this, the two curves in figure 3 are not very different.

(*b*) *Varying L/K*

The 1p-shell interaction, integrals *L* and *K* are defined explicitly by Feenberg and Phillips (1937). Assuming definite wave functions (usually those of a harmonic oscillator), the ratio *L/K* depends only on the form of the interaction force. If we assume a Yukawa type force, then *L/K* depends only on the ratio of the range of the force *a* to the harmonic oscillator well parameter a_0 (Swiatecki 1951). Feenberg and Phillips chose $L/K=6$ and this is the value used in our calculations. This ratio corresponds to $a/a_0 \sim 0{\cdot}9$. It can be said with some confidence that the value of a/a_0 lies between 0·5 and 1·0. (J. P. Elliott in a private communication informs the author that Coulomb energies in the 1p shell are fitted by $a_0 \sim 1{\cdot}65\times10^{-13}$ cm; the value of *a* has been variously taken at several values between 1·10 and $1{\cdot}50\times10^{-13}$ cm.) In this range, *L/K* varies from 5·0 to 6·3. Thus, a reasonable change in the value 6 taken for *L/K* seems to be $L/K=5$, and the magnetic moment of ^{13}C and the Λ-value of the M1 transition in ^{13}N have been re-calculated with this new value. The results are shown in figures 4 and 5. It can be seen that both of the curves are very insensitive to the value chosen for *L/K*.

§ 4. The Even Parity States of ^{13}C and ^{13}N

There are two well-established even parity states below 5 Mev in ^{13}C and ^{13}N. These are the first excited state (spin $\frac{1}{2}^+$, configuration $(1p)^8 2s$) and the third excited state (spin $\frac{5}{2}^+$, configuration $(1p)^8 1d$). In ^{13}N, these states are unbound against proton emission and they can be formed by bombarding ^{12}C with protons of the appropriate energies. The extensive experimental data on these states is summarized in the compilation of Ajzenberg and Lauritsen (1952). As the starting point of our discussion, we use the fact pointed out in a previous publication (Lane 1953 b) and based on unpublished calculations, that all of six data on the states are consistent with a purely single-particle picture. By this, we mean that all the data can be predicted correctly with a simple model in which a 2s or a 1d nucleon moves in a potential well of some radius and depth to be chosen from fitting two of the data.

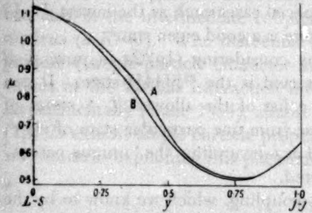

Figure 4. The magnetic moment of ^{13}C in nuclear magnetons. Curves A and B are calculated with the assumptions $L=6K$ and $L=5K$ respectively (with a Rosenfeld force mixture in both cases).

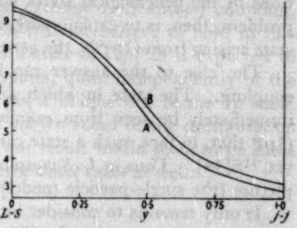

Figure 5. The Λ-value of the M1 transition in ^{13}N. Curves A and B are calculated with the assumptions $L=6K$ and $L=5K$ respectively (with a Rosenfeld force mixture in both cases).

The interesting implication of this fact is that the interaction of the 2s or 1d nucleon with the core particles in the configuration $(1p)^8$ is *effectively* very small. For instance when the two states in ^{13}N are formed in a reaction by bombarding ^{12}C with protons, the fact that the reaction data are all fitted by a single-particle picture implies that the ^{12}C core, initially in its ground state is essentially undisturbed by the addition of a 2s or 1d nucleon. More quantitatively, this means that the wave function for the total system can be written simply as an (anti-symmetrized) product of the wave functions of the single particle ϕ and the core of ^{12}C in its ground state:

$$\frac{1}{\sqrt{9}}\sum_P (-)^P \Psi_{-P}((1p)^8\,;\ J=0^+,\ T=0)\phi_P.$$

In extreme *j-j* coupling where the two states belong to the configurations $(1p_{3/2})^8 2s_{1/2}$ and $(1p_{3/2})^8 1d_{5/2}$ the single-particle picture is expected since eight $1p_{3/2}$ particle form a closed shell. In *L–S* coupling and intermediate coupling, however, this explanation no longer holds and we must look for new reasons for the validity of the single-particle picture. For definiteness, we shall consider the $J=\frac{1}{2}^-$ state, belonging to the configuration $(1p)^8 2s$.

In general, when we are dealing with mixed configurations of the type $l^{n-1}l'$, we can construct complete sets of independent states by simply vector-coupling the unlike nucleon l' on to 'core' states of the equivalent nucleons l^{n-1}, and then anti-symmetrizing.

The above wave function is an example of such states which are said to be defined 'genealogically'. By their definition each of such states can be said, in the language of fractional parentage (Racah 1943), to possess a 'unique parent state' (the state of the core) as far as the unlike orbit is concerned. The corresponding coefficient of fractional parentage is just $n^{-1/2}$.

There is no reason, in general, why these simply constructed states are good eigen states, i.e. why they should be diagonal in the total interaction. For instance, in pure L–S coupling, we know that the eigen states are those which, besides possessing quantum numbers T, S and L, also possess definite spatial symmetry. In general, for mixed configurations, such states are linear combinations of the genealogical states not possessing definite spatial symmetry. Our problem, then, is to explain why, in some special cases such as the lowest $J=\frac{1}{2}^{+}$ state arising from $(1p)^8 2s$, the genealogical state is a good eigen state.

The clue to the answer can be seen by considering $(1p)^8 2s$ in pure L–S coupling. The state in which we are interested is the ${}^{22}S[441]$ state. It can immediately be seen from examination of a list of the allowed L–S states of $(1p)^8$ that, in fact, such a state can only arise from one particular state of $(1p)^8$, viz. ${}^{11}S[44]$. Thus in L–S coupling, as well as j–j coupling, the 'unique parent' picture (the single-particle model) is predicted.

It only remains to consider intermediate coupling, which we know to be the correct coupling situation for ${}^{13}C$ and ${}^{13}N$. It is very laborious to examine this situation in detail because the complete set of states of $(1p)^8 2s$ with which we must work contains 18 component states, beginning with ${}^{22}S[441]$. This effort is not necessary for our purposes, however, because, for the intermediate coupling situation $a/K \sim 5$, we can make reasonable estimates of the position. Since the ground state ${}^{11}S[44]$ of $(1p)^8$ is so widely separated in energy from the next higher state (viz. ${}^{13}P[431]$) that can give $J=\frac{1}{2}^{+}$, $T=\frac{1}{2}$ when coupled to a 2s particle, a considerable amount of spin–orbit force must be introduced to affect the L–S coupling nature of the ${}^{11}S[44]$ state of $(1p)^8$ and the ${}^{22}S[441]$ state of $(1p)^8 2s$. The separation between the states of $(1p)^8$ is about $16K$, whereas the values of the components of the spin–orbit matrices lie in the range from 0 to a. Consequently, even for $a=5K$, there should be no serious departure from the L–S character of the lowest states of $(1p)^8$ and $(1p)^8 2s$. In the former case, the amplitude of the impurities has been calculated to be 0·10. It follows that we expect the observed state in ${}^{13}C$ and ${}^{13}N$ to exhibit single particle properties essentially because it retains its L–S character.

Finally, it is important to note that these results are substantially independent of the magnitude of the 1p–2s interaction integrals relative to L and K, although, at first sight, the experimental results seem to demand that these integrals be much smaller than L and K.

§ 5. CONCLUSIONS

The conclusions are summarized under three headings corresponding to the results presented in the three preceding sections.

(i) The β-decay ft value of the transition ${}^{13}N \rightarrow {}^{13}C$ has been predicted with the intermediate coupling model used in previous work. This makes a total of six data on the two states of $(1p)^9$ to be fitted by the same model. It is significant that, as in the work on the lithium isotopes in III, the β-decay constants of Winther and Kofoed-Hansen (1953) did not give reasonable results, but had to be replaced by values based on more recent data (Gerhart 1954).

(ii) The results on intermediate coupling problems in the present series of papers have been shown to be almost independent of reasonable changes in the character of the central interaction force. This is an important result because it means that nuclear reaction data can be used to establish the mode of coupling in the nucleus without any uncertainties arising from lack of knowledge of the nucleon–nucleon potential. Consequently, in a given nucleus, one can find a/K from the reaction data, and then predict the spectrum of levels (which depends on the interaction potential) in the hope of determining some features of the potential from comparison with experiment.

(iii) It has been shown that the even-parity levels in ^{13}C and ^{13}N are expected to exhibit a one-particle character, not only in extreme L–S and j–j coupling, but also in the intermediate coupling situation that we believe to hold in this nucleus ($a/K\sim5$). The incidental result that a state of $(1p)^n2s$ is expected to possess a single-particle character in L–S coupling, quite independently of the values of the various interaction integrals, is not a unique one in the 1p shell. Experimentally (Lane 1954), almost all of the known states of the configuration $(1p)^n2s$ exhibit single particle properties, and our result would seem to go some way towards explaining this phenomenon in these other cases as well.

REFERENCES

AJZENBERG, F., and LAURITSEN, T., 1952, *Rev. Mod. Phys.*, **24**, 321.

FEENBERG, E., and PHILLIPS, M., 1937, *Phys. Rev.*, **51**, 95.

GERHART, J. B., 1954, *Phys. Rev.*, **95**, 288.

LANE, A. M., 1953 a, *Proc. Phys. Soc.* A, **66**, 977; 1953 b, *Phys. Rev.*, **92**, 839; 1954, *Harwell Report T/R* 1289 (also Lane, A. M., and Thomas, R. G., to be published); 1955, *Proc. Phys. Soc.* A, **68** (preceding paper).

LANE, A. M., and RADICATI, L. A., 1954, *Proc. Phys. Soc.* A, **67**, 167.

RACAH, G., 1943, *Phys. Rev.*, **63**, 367.

ROSENFELD, L., 1948, *Nuclear Forces* (Amsterdam : North Holland Publishing Co.), p. 234.

SERBER, R., 1947, *Phys. Rev.*, **72**, 1114.

SWIATECKI, W. J., 1951, *Proc. Roy. Soc.* A, **205**, 238.

WINTHER, A., and KOFOED-HANSEN, O., 1953, *Dan. Mat. Fys. Medd.*, **27**, No. 14.

The Spin, Energy and Lifetime of ^{8}Be

By P. B. TREACY
Research School of Physical Sciences, Australian National University, Canberra

Communicated by Prof. E. W. Titterton; MS. received 3rd July 1954 *and in amended form 27th October* 1954

Abstract. Coincidences are used in studying the $^{11}B(p,\alpha)^8Be(\alpha)^4He$ reaction to infer directional correlations between successively emitted α-particles. From this the spin of the ground state of ^{8}Be is found to be zero and its break-up energy 90 ± 5 kev. The absence of any measurable loss of kinetic energy in the ^{8}Be nucleus when recoiling into a dense material enables us to place an upper limit on its half-life of 4×10^{-15} sec, which confirms the assignment of zero spin.

---

§ 1. INTRODUCTION

THE nucleus ^{8}Be, which is unstable by approximately 0·1 MeV with respect to disintegration into two α-particles, is known to exist as a short-lived intermediate product in many nuclear reactions (Ajzenberg and Lauritsen 1952: data on light nuclei quoted below are mostly taken from this review). This is often the case when an excited compound nucleus of ^{12}C has been formed, e.g., in $^{11}B + p$, $^{10}B + d$ and $^{12}C + \gamma$. The reaction $^7Li(p,\gamma)$ at a resonant proton energy of 441 kev also produces ^{8}Be in its ground state and an excited state at 2·94 MeV, and from a study of this process it has been inferred that the spins of these two states are different. No direct determination has been reported of these spins, although from other experiments it seems likely they are 0 and 2 respectively (Thomson *et al.* 1952, Treacy 1953 and references of Ajzenberg and Lauritsen). The breakup energy of ^{8}Be has been studied extensively, the most accurate determination being due to Jones *et al.* (1953), who find a value $94{\cdot}5 \pm 1{\cdot}4$ kev. All published values are consistent with this, except one which has been withdrawn (Allison 1953). An upper limit to the lifetime of ^{8}Be has been placed by Hodgson (1951) at 2×10^{-14} second. The value of the lifetime, taken in conjunction with the break-up energy, has a bearing on possible assignments for the spin of ^{8}Be.

The experiments described below are concerned with measurements on the spin and lifetime of ^{8}Be in the $^{11}B(p,\alpha)$ reaction. In the course of these experiments a value was also found for the break-up energy and it is consistent with the more accurate determination mentioned above.

§ 2. PRINCIPLE OF EXPERIMENTS

In the process

$$^{11}B + p \rightarrow \alpha_1 + {}^8Be + Q_1$$
$$^8Be \rightarrow \alpha_2 + \alpha_2 + Q_2,$$

the large reaction energy Q_1 of 8·58 MeV ensures that the ^{8}Be recoils from the primary α-particle α_1 with kinetic energy sufficiently great that the α-particles

α_2 from its disintegration are confined to a cone centred along its recoil axis, of semi-angle about $10\frac{1}{2}°$. This geometrical arrangement is similar to that studied in a previous experiment (French and Treacy 1951). Using a time coincidence one may observe the energy spectrum of α_2's corresponding to an α_1 being detected in a fixed direction. To each angle of emission of α_2 there corresponds a definite α_2-energy, and the energy spectrum is simply proportional to the angular correlation function $f(\theta)$, where $f(\theta)\,d\Omega$ is the number of α_2's emitted into a solid angle $d\Omega$ in the centre-of-mass system of ^{8}Be, at an angle θ to the ^{8}Be recoil axis.

The energy spectrum of coincident α_2's thus is a measure of the directional correlation between α_1 and α_2. This in turn depends on the spins of nuclei involved, and in particular if the spin of ^{8}Be is zero one must expect the energy spectrum to be uniform. The first experiment consists in the measurement of this spectrum and is described in § 4.

The directional correlation between α_1 and α_2 in the laboratory frame of reference depends on the break-up energy of ^{8}Be. In fact, the cone semi-angle or ' spray angle ' is $\sin^{-1}(v/V)$, where $v\,(\propto \sqrt{Q_2})$ is the α_2-velocity relative to ^{8}Be, and V the recoil velocity of the latter. Once the angular mode of disintegration of ^{8}Be is known, the form of directional correlation between α_1 and α_2 can be predicted. By comparison with experiment (making allowance for finite aperture of α_1-detector and target) one can deduce the value of Q_2. This was done, and the experiment is described in § 5.

Both the above experiments depend on the assumption that ^{8}Be is sufficiently short-lived that the spray angle is unaffected by recoil motion before decay. This assumption is certainly justified since the recoiling nucleus, which has a kinetic energy about 3 MEV, moves only some 10^{-5} cm in 10^{-14} sec and the lifetime of ^{8}Be, at most is of this order. Furthermore if (as was done) one arranges that the ^{8}Be moves *in vacuo* before disintegration, it cannot lose energy in flight. The third experiment was simply to allow the ^{8}Be to travel in a dense (platinum) foil, of thickness several times 10^{-5} cm, and observe once more the spatial correlation between α_1 and α_2, these latter having sufficient energy to penetrate the foil. A simple calculation shows that the effect of a ^{8}Be lifetime of order 10^{-14} sec under such conditions is to *increase* the spray angle by several degrees. The details of the experiment are given in § 6.

§ 3. DETAILS OF APPARATUS

The experimental arrangement used was similar to one previously described (French and Treacy 1951). The detector for α_1 was in this case a shallow proportional counter, whose axis could be tilted slightly forward of 90° to the proton beam, by means of syphon bellows. The α_1-particles constitute a group of well-defined energy 5·8 MEV at the upper end of the spectrum, so sufficient mica absorbers were mounted between this counter and the target for the detection of all alphas of energy greater than 5·6 MEV. The counter subtended an angle of 2·4° at the target.

The detector for α_2 was also a proportional counter, arranged so that pulses from α_2's entering it were a measure of their energy. This counter (to be described elsewhere) had a rather unconventional arrangement of electrodes: its active region was a cube of side 8 in., within which there were 16 anode wires perpendicular to the counter axis, with each anode wire surrounded by eight thicker wires constituting the cathode. This design was chosen for two reasons: first, that very fast electron collection times ($\sim 10^{-7}$ sec) are obtained, thus reducing fluctuations in pulse rise times; secondly by this design one eliminates any axial symmetry, which could obviously lead to spurious effects in this experiment. This counter had an aperture of semi-angle 17·75°, so that it was possible to detect all α_2's with a fixed position of counter. With the α_2-counter axis set at 90° to the beam, the α_1-counter should be at an angle of 84·9° and, of course, in a plane containing the α_2-counter and beam.

As the α_2's have ranges in air distributed from 0·5 to 1·5 cm, a very thin vacuum-tight window was necessary for the α_2-counter. This was made in the usual way from a 2 : 1 mixture of collodion and glyptal, and mounted on a fine brass grid, whose back was countersunk to allow wide-angle penetration. A window thickness of 0·3 cm air equivalent was chosen as suitable for exclusion of most scattered protons. The geometry of the experiment required that, in order to detect the continuous α_2-energy spectrum, it was necessary for this window to have a transmission factor much less than unity, thus preferentially detecting single α_2's rather than pairs. This window had a transmission factor of $\frac{1}{4}$. The α_2-counter was filled to only 2·5 cm Hg pressure of argon, thus putting no undue strain on the window.

For the purpose of measuring the spatial α_1–α_2 correlation an externally controlled iris diaphragm was incorporated between target and α_2-counter. Thus all coincident α_2's at less than any pre-assigned cone angle could be recorded.

Thin targets were made by evaporating a layer of B_2O_3 on a thin platinum backing, which was originally made by evaporation on aluminium foil. Under bombardment the aluminium evaporated, as also did the B_2O_3 at the target centre. The target therefore consisted in effect of a ring of B_2O_3 on platinum. It was mounted between two water-cooled brass plates, and set at 45° to the beam. The latter was defined by stops to a diameter of 5/16 inch.

The electronic arrangements were conventional: α_1-counts were set to trigger a blocking oscillator which gated a coincidence unit for the more numerous α_2-counts to pass through. The gated pulses were lengthened, displayed and photographed in an oscilloscope and their total number recorded on a scaling unit. A simultaneous record was made of true and random coincidences by the usual delayed coincidence method.

§4. THE SPIN

The B_2O_3 side of the target was set towards the wide-angle α_2-counter, with its iris diaphragm wide open. The proton beam of the Canberra high tension machine was set at the 5 kev wide resonance in $^{11}B + p$ at 163 kev. The target was of approximately 1 mm air equivalent, but by using only the low-energy edge of this narrow resonance one could ensure that any recoiling ^8Be nuclei did not lose more than a few kev of kinetic energy. A beam current of about 30 μA was used and, with the apertures as described, the true-to-random coincidence ratio was not less than ten to one.

The energy spectrum of about 8000 coincident pulses is plotted in figure 1; probable errors of ordinates are shown where significant. In this, allowance has been made for the spectrum of random coincidences. The large probable errors for small pulse heights are due to large numbers of small random coincident pulses, from scattered protons not stopped by the α_2-counter window. In figure 1 a calibration run using Th C + C′ alphas is also shown: the smallness of the pulse size is due to the fact that these particles did not lose all their energies in the counter. Using a calculated range–energy relation for alphas in argon† this calibration pulse should correspond to a mean energy loss for the two alpha groups of 0·42 MeV, and this gives an approximate calibration for the energy scale. The dispersion of this curve, assumed gaussian, is ± 21% of the mean, and is due partly to amplifier noise.

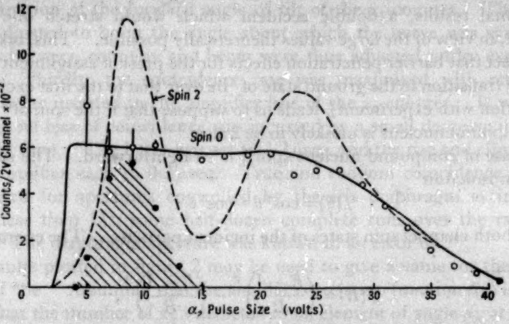

Figure 1. Open circles: spectrum of α–α coincidences. Full circles: ThC+C′ calibration peak (shaded). Curves are calculated from ‘ideal’ spectra with end-points corresponding to 4 v and 28 v, for different ^{8}Be spin assignments.

In figure 1 two curves are shown, which are the predicted forms of energy spectrum for the case of ^{8}Be spin 0 and 2. These curves were obtained as follows: *Spin* 0. This must lead to an isotropic angular correlation function $f(\theta)$ and consequently a uniform energy spectrum of α_2-particles. As mentioned in § 3, in the experimental arrangement used one must take account of the finite possibility that both α_2's enter the counter simultaneously, giving rise always to a pulse of constant size. Since the transmission factor of the gridded collodion window was $\frac{1}{4}$, the proportion of ‘double’ to ‘single’ pulses contained by the points in figure 1 must be $\frac{1}{4}/[2(1-\frac{1}{4})]$ or $\frac{1}{6}$. The full curve, labelled ‘spin 0’, was calculated using a (‘single’) uniform energy spectrum of pulse sizes extending from 4 v to 28 v; these are the end-points of the continuous α_2-spectrum predicted from the thorium calibration after making allowance for window thickness, and assuming the break-up energy of ^{8}Be to be 96 kev. It was assumed that the detector gave rise to a gaussian energy spread of dispersion ± 15%, and the answer was calculated by numerical integration. The area of the theoretical curve was suitably normalized. *Spin* 2. In this case the angular correlation will not, in general, be isotropic. Thomson *et al.* (1952) give evidence that the 163 kev resonance is due to p-wave protons, and have shown that their results are consistent with the assumption that the ^{12}C compound nucleus has spin 2 (with some interference between this state and a higher broad one). It is possible that both low states of ^{8}Be have non-zero spins, and in this case one must allow also the possibility of spin 0, 1, or 3 for the compound nucleus. The case of ^{12}C spin 0 may be rejected as it could not, by itself, give rise to any anisotropy of the α_1-distribution on resonance, and likewise spin 3 can be shown to yield insufficient anisotropy. For ^{12}C spin 2 there results ambiguity, not only in the ^{11}B + p channel-spin ratio but also in the relative contributions of s- and d-wave α_1's. The best one could do here would be to try to calculate the relative phases of the latter from Coulomb wave functions and fit the former from the results of Thomson *et al.* In the angular correlation function $f(\theta)$, there would then be one undetermined parameter entering into the coefficients of $\cos^2\theta$ and $\cos^4\theta$, both of which must be small ($\lesssim 0{\cdot}1$) to account for the present experimental results, a double accident which would stretch one's credulity somewhat, in view of the large values theoretically possible. This, taken together with the fact that barrier penetration effects for the present assignment would help favour the transition to the ground state of ^{8}Be over that to the first excited state (in contradiction with experiment), leads us to suppose that if the spin of ^{8}Be is 2, that of the compound nucleus is unlikely to be 2 also.

---

† I am indebted to Mr. A. C. Riviere for these figures.

The case of compound nucleus spin 1 is straightforward. The same angular correlation function

$$f(\theta)=\cos^2\theta-\cos^4\theta \qquad \ldots\ldots(1)$$

holds for both channel spin states of the incident particles. The energy spectrum is

$$g(E)=\left(\frac{E-A}{B}\right)^2-\left(\frac{E-A}{B}\right)^4, \qquad \ldots\ldots(2)$$

where A and B are equated to 16 v and 12 v respectively, being given by the end points $A-B=4$ and $A+B=28$ of the continuous spectrum. Using (2), the energy spread $\pm 15\%$ and transmission factor $\frac{1}{4}$, the dotted curve in figure 1 labelled 'spin 2' is obtained. Comparing the curves and points, and bearing in mind the above discussion regarding states of the compound nucleus, the evidence for ^{8}Be spin zero is strong. Further evidence to confirm this assignment will be given in §6.

§5. THE ENERGY

It was a consequence of the experimental arrangement that the α_2-particles were confined to a narrow cone whose axis lay along the direction of ^{8}Be recoil. A confirmation of this is shown in figure 2, in which the coincidence rate per α_1-count is plotted against α_2-counter aperture. It is seen that the counting

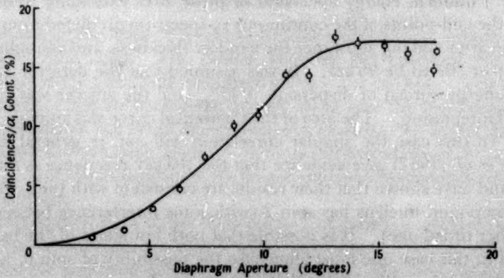

Figure 2. Points : directional correlation in energy measurement. Curve is that predicted theoretically for ^{8}Be energy 90 kev.

rate rises rapidly to a plateau for apertures beyond approximately 13°. The points are corrected for random coincidences, and plotted with probable errors. The total number of true coincidences recorded in this plot is approximately 8000.

In order to obtain the readings of figure 2, the following procedure was adopted. First, the target was set with its B_2O_3 side towards the α_2-counter, and a plot was made of the yield, over the resonance, of α_1-counts as a function of bombarding energy. Next the beam was set on the low-energy side of the resonance, and a curve was plotted of coincidence rate, for α_2-counter aperture 10°, as a function of the forward angle of tilt of the α_1-counter. This counter was then adjusted to be at the angle about which the curve was symmetrical. The angles between counters and beam were thus adjusted under experimental conditions. Thirdly, the coincidence rate was maximized with respect to a small time delay inserted in the amplifier line of the α_2-counter. It was further verified that no loss of coincidence was incurred by a small decrease in the coincidence gate time. The latter was set to $1{\cdot}2\,\mu$sec, and the rise and clipping times of the α_2-amplifier each to $0{\cdot}3\,\mu$sec. True and random coincidence rates were now recorded for apertures controlled by the iris diaphragm at intervals of somewhat less than $1\frac{1}{2}$°, some half-dozen complete runs over the range being recorded. The diaphragm aperture was known to an error of 3%.

The results plotted in figure 2 may be used to give a value for the energy of break-up of ^{8}Be. Assuming that the angular correlation function $f(\theta)$ is constant, it follows that the number of α_2's detected in an element of angle $d\chi$ at an angle χ to the ^{8}Be recoil axis is $n(\chi)\,d\chi$ where

$$n(\chi) \propto \frac{1-(V^2/v^2)(1-2\cos^2\chi)}{\{1-(V^2/v^2)\sin^2\chi\}^{1/2}}, \qquad \ldots\ldots(3)$$

in which V and v are as defined in §2 and $\chi \leqslant \sin^{-1} v/V$. For infinitely small apertures of α_1-counter and target (3) may be integrated analytically up to any desired value of diaphragm aperture, and attains a constant value beyond the angle $\sin^{-1}(v/V)$. A numerical calculation has been made of the expected modification to this function for finite apertures. The method used is described in the Appendix. The result was calculated for a ^{8}Be break-up energy of $Q_2 = 96$ kev. This curve showed a somewhat greater cut-off angle than that required by experiment, and a better fit, drawn in figure 2, was obtained by choosing $Q_2 = 90$ kev. From the statistical uncertainty in experimental points and error in diaphragm calibration, a probable error ± 5 kev must be associated with this answer.

The possibility must be considered of the necessary modifications of the theoretical form (3) for the case of 'double' α_2-coincidences mentioned in §5. A simple geometrical calculation gives a correction of order $v/V \sim 20\%$. Since the number of 'double' is only 17% of the number of 'single' coincidences, the overall correction of 3% may be ignored.

§6. THE LIFETIME

Figure 3 shows the ratio of coincident to α_1-counts plotted against diaphragm aperture when the ^{8}Be recoil nucleus was released from the compound nucleus into a platinum foil. This was achieved by leaving the counters fixed and simply turning the target over in its holder, so that the B_2O_3 faced the α_1-counter. It was now necessary for the proton beam to traverse the platinum target 'backing' in order to encounter boron nuclei, and for this an increase of 110 kev in proton energy was needed for the 163 kev resonance to appear. (This figure gives directly the platinum foil thicknes.) All α_2's thus recorded had penetrated through the platinum either as alphas or as parts of ^{8}Be nuclei. A calculation has been made, and is described in the Appendix, of the modification expected to the plot of points in figure 2, when the lifetime of ^{8}Be is sufficiently long that it loses appreciable energy in the foil. The best fit to the points of figure 2 is given by the full curve in figure 3, labelled $\tau=0$. Modifications expected, ignoring finite apertures, for half-lives τ of 5×10^{-15} sec and 10^{-14} sec are given as broken curves in the same figure. These are normalized to the same ordinate as in the full curve at the largest aperture ($17\frac{3}{4}°$) and the experimental points are themselves similarly normalized: reasons for this procedure are given below. It is not possible to distinguish between the experimental points and the full curve. A study of figure 3 shows that the half-life of ^{8}Be must be less than 4×10^{-15} second.

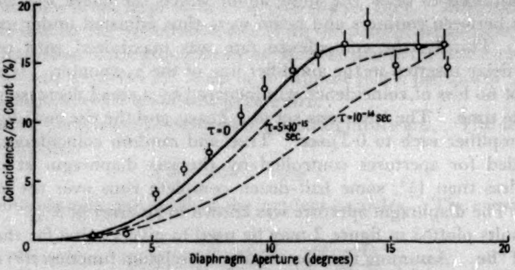

Figure 3. Points: directional correlation in lifetime measurement. Full curve: best fit to points of figure 2. Broken curves: theoretical prediction for finite ^{8}Be half-life τ.

It was not possible to compare absolutely the ordinates of points plotted in figures 2 and 3. In fact, the ratio of true coincidences to α_1-counts throughout the experiment was less than would be expected were 'α_1-counts' all genuinely due to primary alphas in the reaction under study. The continuous background of α-particles due to the ^{11}B(p, α) process occurring via the broad excited state of ^{8}Be unfortunately overlaps the α_1-energy selected. According to the reaction dynamics this continuous spectrum would give rise to a negligible number of coincidences, so that the numbers of particles recorded in the α_1-counter due to the ground-state primaries and excited-state secondaries were here apparently about equal. Their ratio must depend critically on the α_1-energy selected, as well as, in the plot of figure 3, on the degree of uniformity of the platinum foil, for the relative yields of the two processes differ markedly beyond the 163 kev resonance (Beckman *et al.* 1953). For these reasons, it was only possible in the present experiment to compare relative shapes of curves in figure 3, and under these conditions the lifetime of ^{8}Be is too small to be measured.

Should a small residual effect be evident in any future experiment of this nature, one would need to investigate the degree to which theoretical curves of the type described above will be modified by small-angle alpha scattering. An application of the usual criterion for plural scattering (Rutherford *et al.* 1930) for the target backing used in this experiment shows that scattering through greater than 1·6° is single, the probability of single scattering through angles greater than this value being 0·7%. Values of this order are certainly small enough not to affect the considerations of § 5.

The upper limit we are able to place on the ^{8}Be lifetime is consistent with the lower limit calculated from the sum rule (Teichmann and Wigner 1952), according to which for ^{8}Be spin zero the lifetime is greater than 4×10^{-17} sec; the corresponding limit of 2×10^{-14} sec for spin 2 is clearly excluded by the present result.

ACKNOWLEDGMENTS

I wish to acknowledge invaluable help from Dr. F. C. Barker in analysing the experimental data. This work was part of the research programme of this laboratory in nuclear physics under Professor E. W. Titterton.

APPENDIX

Correction for Finite Apertures

Referring to figure 4 (not to scale), which is supposed drawn in the frame of reference in which the compound nucleus (^{12}C) is at rest† the subscripts 1, 2 and 3 refer to α_1-counter, target and α_2-counter respectively. The α_1-counter aperture is of radius R_1 (maximum of r_1) = 19/64 inch, and its distance d_{12} from the target $7\frac{3}{16}$ inch. The equivalent distance d_{23} for the α_2-counter is $2\frac{1}{32}$ inch. Apertures of the latter up to $12\frac{1}{2}$° were considered, corresponding to R_3 (maximum of r_3) = 0·4503 inch. The target is considered as a ring of radius $R_2 = \frac{5}{32}$ inch. With the azimuths ϕ_1 and ϕ_3 as shown, the distances x_{12}, x_{23} and x_{13} are given by

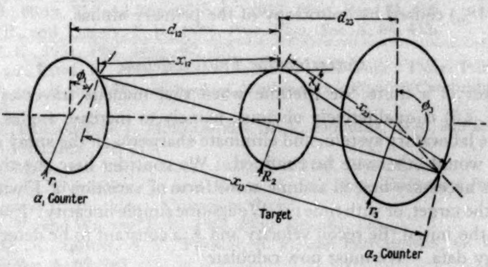

Figure 4. Isometric view of counters and target (not to scale).

$$x_{12}^2 = (r_1 \cos\phi_1 - R_2)^2 + (r_1 \sin\phi_1)^2 + d_{12}^2,$$
$$x_{23}^2 = (r_3 \cos\phi_3 - R_2)^2 + (r_3 \sin\phi_3)^2 + d_{23}^2,$$
$$x_{13}^2 = (r_3 \cos\phi_3 - R_1 \cos\phi_1)^2 + (r_3 \sin\phi_3 - r_1 \sin\phi_1)^2 + (d_{12} + d_{23})^2.$$

---

† The effect of motion of the centre of mass due to finite proton energy is negligible.

For any aperture $R_3 = d_{23} \tan \alpha$, the complete expression to be calculated is, apart from constant factors,

$$\int_0^{2\pi} d\phi_1 \int_0^{\pi} d\phi_3 \int_0^{R_1} r_1 \, dr_1 \int_0^{R_3} r_3 \, dr_3 \, \frac{n(\chi)}{x_{12}{}^3 x_{23}{}^3}, \qquad \ldots\ldots(4)$$

in which $n(\chi)$ is given by (3), § 5, and

$$\cos \chi = \frac{x_{13}{}^2 - x_{12}{}^2 - x_{23}{}^2}{2x_{12}x_{23}}.$$

Each integrand of the quadruple integral (4) was calculated for six equally spaced values of the independent variables ϕ_1, ϕ_3, r_1 and α. For large values of χ the integrand is very large, and actually becomes infinite at the critical value $\sin^{-1}(v/V)(=10{\cdot}66°$ for $Q_2 = 96$ kev). Under such conditions the calculation of an integral by conventional numerical methods is unsatisfactory (Jeffreys 1946). For χ above the arbitrarily chosen value 9·22° the integrand was replaced by its value averaged over the range of two increments of ϕ_3—an approximation which assumes $d\phi_3/d\chi$ constant over this range. Ignoring the slowly varying numerator of $n(\chi)$ such an average reduces to the difference of two incomplete elliptic integrals

$$\int \frac{d\chi}{\{1 - (V^2/v^2)\sin^2\chi\}^{1/2}},$$

tabulated by Jahnke and Emde (1945); this difference is closely proportional to the increment of χ over the range of integration, so that the averaging process is simple.

The numerical integration was carried out using Gregory's formula (Jeffreys 1946) to second differences. No attempt was made to apply small corrections (of order 0·1%) caused by anisotropy of the primary alphas.

Correction for Finite Lifetime

The effect of a finite ^{8}Be lifetime when that nucleus traverses a stopping material (cf. § 6) is qualitatively obvious, namely to increase angles of emission of α_2's in the laboratory system, and eliminate sharpness in the spray angle within which they would otherwise be confined. We consider here the theory of this effect. It is necessary first to assume some form of variation of V with distance x travelled in the target, or with time t. We assume simple linearity: $V = V_0(1 - Kt)$, where V_0 is the initial ^{8}Be recoil velocity and K a constant to be determined from range–energy data. We must now calculate

$$\int_0^{\infty} \lambda f(t) \exp(-\lambda t) \, dt,$$

where λ is the ^{8}Be decay constant and

$$f(t) = \int_0^{\alpha} n(\chi) \, d\chi = 1 - \cos\alpha\{1 - (V^2/v^2)\sin^2\alpha\}^{1/2}$$

is the integrated form of (3) for negligible α_1-counter and target apertures. It is convenient to neglect $K^2x^2/2V_0{}^2$ as compared with unity, and the answer becomes

$$1 - \left(\frac{2K}{\lambda}\right)^{1/2} \frac{V_0}{v} \sin\alpha \cos\alpha [\tfrac{1}{2}\sqrt{\pi} \exp(-\lambda t_0)$$
$$\{\Phi[\lambda(t_2 - t_0)]^{1/2} - \Phi[\lambda(t_1 - t_0)]^{1/2}\} + \exp(-\lambda t_1)\{\lambda(t_1 - t_0)\}^{1/2}], \qquad \ldots\ldots(5)$$

in which Φ is the error integral tabulated by Jahnke and Emde, and

$$t_0=\frac{(V_0^2/v^2)\sin^2\alpha-1}{2K(V_0^2/v^2)\sin^2\alpha};\quad \begin{array}{ll} t_1=t_0 & [(V_0/v)\sin\alpha>1] \\ t_1=0 & [(V_0/v)\sin\alpha\leqslant 1] \end{array};\quad t_2=\frac{X}{V_0-\frac{1}{2}KX}.$$

Here X is the effective target thickness for a 45° tilt to the α_2-counter. In calculating the above formula from the tables the approximation was made that for $[\lambda(t_1-t_0)]^{1/2}>3$,

$$\tfrac{1}{2}\sqrt{\pi}\exp(-\lambda t_0)\{\Phi[\lambda(t_2-t_0)]^{1/2}-\Phi[\lambda(t_1-t_0)]^{1/2}\}=\tfrac{1}{2}[\lambda(t_1-t_0)]^{-1/2}.$$

The target thickness X corresponds to a proton energy loss from 273 kev to 163 kev. Assuming that 3·85 mg cm^{-2} of platinum equals 1 cm of air (Livingston and Bethe 1937) one finds X is $2{\cdot}90\times10^{-5}$ cm. The other constant K may be estimated by remembering that ^{8}Be loses four times as much energy as an alpha of the same velocity, and using a standard range–energy relation for α-particles. The result is that ^{8}Be loses velocity from 0·85 to $0{\cdot}60\times10^9$ cm sec^{-1} in traversing a distance equal to $\frac{1}{2}X$, and hence $K=0{\cdot}24\times10^{14}$ sec^{-1}. Using these values the approximation made in our calculation ($K^2x^2/2V_0^2\leqslant1$) incurs an error of only 4%. The assumption of a linear loss in V is accurate to an error of less than 1%. The neglect of finite apertures in this calculation will, however, lead to an error of order 15% for the larger lifetime, but this approximation could not be eliminated simply.

REFERENCES

ALLISON, S. K., 1953, *Phys. Rev.*, **91**, 882.

AJZENBERG, F., and LAURITSEN, T., 1952, *Rev. Mod. Phys.*, **24**, 321.

BECKMAN, O., HUUS, T., and ZUPANČIČ, Č., 1953, *Phys. Rev.*, **91**, 606.

FRENCH, A. P., and TREACY, P. B., 1951, *Proc. Phys. Soc.* A, **64**, 452.

HODGSON, P. E., 1951, *Phil. Mag.*, **42**, 207.

JAHNKE, E., and EMDE, F., 1945, *Tables of Functions* (New York : Dover Publications).

JEFFREYS, H. and B. S., 1946, *Methods of Mathematical Physics* (Cambridge : University Press).

JONES, K. W., DONAHUE, D. J., MCELLISTREN, M. T., DOUGLAS, R. A., and RICHARDS, H. T., 1953, *Phys. Rev.*, **91**, 879.

LIVINGSTON, M. S., and BETHE, H. A., 1937, *Rev. Mod. Phys.*, **9**, 245.

RUTHERFORD, E., CHADWICK, J., and ELLIS, C. D., 1930, *Radiations from Radioactive Substances* (Cambridge : University Press).

TEICHMANN, T., and WIGNER, E. P., 1952, *Phys. Rev.*, **87**, 123.

THOMSON, D. M., COHEN, A. V., FRENCH, A. P., and HUTCHINSON, G. W., 1952, *Proc. Phys. Soc.* A, **65**, 745.

TREACY, P. B., 1953, *Phil. Mag.*, **44**, 325.

On the State of Solid Hydrogen

By KAZUHISA TOMITA†
Mathematical Institute, Oxford

Communicated by C. A. Coulson ; MS. received 12th August 1954

Abstract. Co-operative appearance of the rotation of hydrogen molecules in the solid phase is described using a semi-classical theory. The order of magnitude of the restriction to the rotation which is experienced by a molecule at the lowest temperature is estimated to be about 4°K using several different types of experiments, and the results are in reasonable agreement with each other. For the case of pure ortho-hydrogen a calculation of the potential energy and the anisotropy based on intermolecular forces is carried out in the Appendix.

§1. Introduction

More than twenty years ago it was found by Giauque and Johnston (1928) that the molar entropy of crystalline normal hydrogen at temperatures somewhat below the melting point exceeds the entropy expected from Debye's theory by 4·3 ± 0·1 e.u. Pauling (1930) suggested that the excess entropy is due to the presence of molecular rotation at this low temperature. At about the same time Mendelssohn, Ruhemann and Simon (1930) observed an anomaly in the specific heat of normal hydrogen in the expected temperature range. This anomalous heat is apparently connected with the ortho-component, because it increases with increasing concentration of the ortho-component. Also the saturated vapour pressure was found higher for a sample containing some ortho-component than for pure para-hydrogen (Keesom, Bijl and van der Horst 1932). The x-ray analysis of solid para-hydrogen (Keesom, de Smedt and Mooy 1930) suggests a hexagonal close-packed structure with $a_0 = 3{\cdot}75$ Å (i.e. 7·087 atomic units). It will be assumed that the structure of an ortho–para mixture in the solid phase is not very far from that of pure para-hydrogen. This assumption is made reasonable by the fact that normal and para-hydrogen have nearly the same density in liquid phase (Scott and Brickwedde 1937).

To explain the anomalous specific heat and the vapour pressure difference Schaefer (1939) proposed the following model. He assumed that the energy of an ortho-molecule under the influence of the crystalline field due to neighbouring molecules can be described by

$$-AP_2^0(\cos\theta) \qquad \ldots\ldots(1)$$

as far as the anisotropic part is concerned. Here θ is the angle between the axis of the central molecule and the axis inherent in the crystalline field, the 'z axis' (figure 1), P_2^0 is a second order spherical harmonic, and A is a constant characterizing the magnitude of anisotropy which is experienced by the central molecule.

---

† On leave from Department of Physics, Faculty of Science, University of Kyoto, Kyoto, Japan.

As far as the lowest state of the ortho-molecule ($J=1$) is concerned, (1) is the only relevant type of axially symmetric field. Under this type of crystalline field the three-fold degenerate state $J=1$ is split into a doublet (state μ which corresponds to $M_J=\pm 1$) above a singlet (state λ which corresponds to $M_J=0$) (figure 2). The alternative level scheme with the singlet above the doublet is not possible because the recently measured value for the anomalous part of the entropy is approximately $k \ln 3$ and not $k \ln 3/2$ (Hill and Ricketson 1954). Adjusting a Schottky-type curve to fit the specific heat data known in 1939, Schaefer estimated the value of the parameter A to be 14·1°K in temperature units. This is equivalent to saying that the separation between the two groups of levels is 5·6°K ($=2A/5$). However, this theory is not satisfactory because compared with the experimentally determined specific heat curve the theoretical curve has far too great a curvature, at least above 4°K. Little more has been done either experimentally or theoretically on this problem until fairly recently.

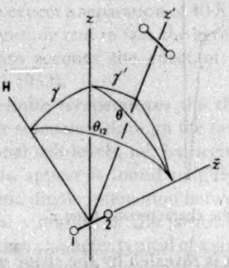

Figure 1. Relation between angles.

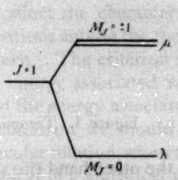

Figure 2. Level structure under an axially symmetric crystalline field.

§ 2. NUCLEAR MAGNETIC RESONANCE

As soon as the new technique of the nuclear magnetic resonance was developed Hatton and Rollin (1949) carried out a resonance experiment on protons in solid hydrogen. They measured the line shape as well as the lattice relaxation time T_1 down to 1·1°K, and found that in the lowest temperature region the separation of the two resonance peaks for the proton–proton system in the molecule is less than one expects for stationary molecules. In addition, they found a further sudden reduction of the separation at about 1·5°K. Essentially the same result was obtained recently by Reif and Purcell (1953) with higher accuracy as far as the line shape is concerned.

The spin–lattice relaxation time T_1, which corresponds to the rate at which energy is transferred from the spin system to other degrees of freedom (so-called ‘ lattice ’ degrees of freedom) can be related to a life time τ_c of the orientational configuration of a molecule by the following formula (Bloembergen, Purcell and Pound 1948)

$$\frac{1}{T_1}=K_1\left\{\frac{\tau_c}{1+(2\pi\nu_0\tau_c)^2}+\frac{2\tau_c}{1+(4\pi\nu_0\tau_c)^2}\right\} \qquad \ldots\ldots(2)$$

where $K_1=0{\cdot}3\gamma^4\hbar^2\times r_{ij}^{-6}$.

Using the experimental values of T_1 in this formula, we obtained (Tomita and Mannari 1953) the variation of τ_c with temperature as shown in figure 3. The fairly linear character of this plot indicates that τ_c is expressible in a form such as

$$\tau_c \propto \exp(-V/kT) \qquad \ldots\ldots(3)$$

with a constant value of the activation energy V. This gives us an idea about the magnitude of the inner field which hinders the molecular reorientation. It is estimated that V is of the order of 3 to 4 degrees absolute. The fact that V is fairly independent of temperature suggests that the local field constraining the molecular reorientation may be considered as axially symmetric at least in the first approximation, otherwise the effective value of V would continuously change with temperature.

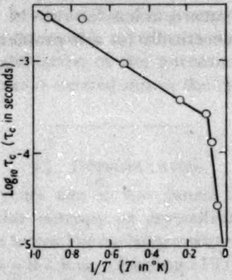

Figure 3. Temperature dependence of the characteristic time τ_c.

On the other hand the spin–spin interaction is revealed by the shape and the width of the resonance absorption, which accordingly tells us about the relative spatial configuration of the relevent spins and the time change of it. The fact that the separation between two peaks is less than half of the 102 gauss which is expected for a stationary configuration suggests that each molecule is in a state of motion. We can neglect the migration of molecules at this low temperature, and furthermore the vibration of the molecular centre of gravity will not affect the line shape very much. Therefore, to get the observable character of the resonance spectrum we need only take into account the rotational motion of the molecule, and this we do by averaging the interaction operator between two nuclei over the orientational wave function of the molecule. When the Zeeman energy of the nuclei under a constant magnetic field is much bigger, as it usually is, than the magnetic dipole–dipole interaction between the nuclei, the dominant part of the local field due to the latter interaction is given by the so-called semi-diagonal elements with respect to the magnetic quantum number arising from the external field:

$$D_0 = \gamma^2\hbar^2 r_{12}^{-3} \mathrm{P}_2^0(\cos\theta_{12})\{(\mathbf{I}_1 . \mathbf{I}_2) - 3I_{1z}I_{2z}\}. \qquad \ldots\ldots(4)$$

Here θ_{12} is the angle between the molecular axis (the $\bar{z}$-axis) and the direction of the constant magnetic field. Taking account only of the spin operators in (4), the secular equation arising from it has been solved and the separation of the two peaks turns out to be proportional to the factors in (4) outside the curly bracket. Remembering the addition theorem of spherical harmonics, P_2^0 ($\cos\theta_{12}$) can be replaced by a sum of products of spherical harmonics of θ, already introduced, and of γ, the angle between the crystalline axis and the constant magnetic field.

If we assume axial symmetry of the crystalline field, this sum reduces to one term after taking an average over the orientational wave function of the molecule. Hence the separation between two resonance peaks is proportional to

$$\gamma^2\hbar^2 r_{ij}^{-3} \mathrm{P}_2^0(\cos\gamma)\langle \mathrm{P}_2^0(\cos\theta)\rangle \qquad \ldots\ldots(5)$$

of which the only difference from the factor in (4) is the additional term $\langle \mathrm{P}_2^0(\cos\theta)\rangle$ and the replacement of θ_{12} by γ. If we take the polycrystalline nature of the sample into account, we must take an average over possible values of either θ_{12} or γ after we have calculated the absorption line position, and the result turns out to be the same in either case. Therefore, the term $\langle \mathrm{P}_2^0(\cos\theta)\rangle$ gives a scale factor as compared with the case where the configuration of the molecule is stationary.

At absolute zero temperature we assume that each molecule is confined in its lowest state $M_J = 0$ and take a wave-mechanical average of P_2^0 (cos θ) over this state. Then we get

$$\langle \mathrm{P}_2^0(\cos\theta)\rangle_{M_J=0} = -2/5$$

and we expect a separation of 40·8 gauss (102 × 2/5) which gives the observed order of magnitude and in fact the agreement in line shape is also satisfactory when we take into account the effect of protons in neighbouring molecules (Reif and Purcell 1953).

At finite temperatures the thermal motion may affect the character of the nuclear resonance through the fact that it causes transitions among the molecular rotational sub-levels, i.e. by urging the molecule to turn. The criterion for this effect to appear is found roughly by comparing the energy associated with the magnetic dipole interaction between nuclear spins and the energy associated with thermal vibration of the lattice. If the former is dominant we should have a resonance character typical of a single substate of molecular rotation, whereas if the latter is dominant we ought to expect a character typical of a statistical mixture of several substates. According to the estimate of Reif and Purcell (1953) the situation in solid hydrogen corresponds to the latter case at least above 1°K, and so the scale factor of the resonance must be

$$\begin{aligned}\langle \mathrm{P}_2^0(\cos\theta)\rangle_T &= \mathrm{Tr}\,[\exp(-H/kT)\mathrm{P}_2^0(\cos\theta)]/\mathrm{Tr}\,[\exp(-H/kT)]\\ &= -\tfrac{2}{5}\{1-\exp(-3A/5kT)\}/\{1+2\exp(-3A/5kT)\}. \qquad \ldots\ldots(7)\end{aligned}$$

Accordingly, if the magnitude of the anisotropy parameter A is independent of temperature, the scale factor of resonance is expected to decrease gradually with increasing temperature as shown in figure 4. However, the abrupt change in

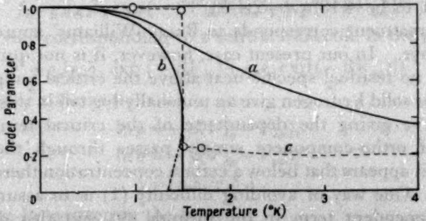

Figure 4. Order parameter or scale factor of the nuclear resonance. *a*, temperature independent crystalline field model; *b*, Bragg–Williams type model; *c*, observed scale factor of the nuclear resonance. (The separations between the two peaks are plotted below the transition point, and the width is plotted above the transition point.)

the observed width of resonance at about 1·5°K is obviously difficult to fit to this type of curve (cf. figure 4). This fact suggests strongly that there is a co-operative character in the appearance of molecular rotation. In this connection it is to be remembered that the simple Schottky-type curve was also unsatisfactory in describing the specific heat. And recently, in fact, the co-operative character was clearly observed by Hill and Ricketson (1954) as a λ-type transition in the specific heat in the very temperature range corresponding to the abrupt change of nuclear resonance.

§ 3. THEORETICAL TREATMENT AS A CO-OPERATIVE PHENOMENON

It is not very difficult to understand the essential nature of the transitions in the specific heat and the resonance character. Let us interpret tentatively the anisotropy constant A as an effective quadrupole moment Q_0 of the molecule multiplied by the magnitude of the gradient q of an axially symmetric crystalline field. Then we can calculate the average quadrupolarization $\langle Q\rangle_T$ per molecule at temperature T by the formula

$$\langle Q\rangle_T = Q_0\{1-\exp(-3Q_0 q/5kT)\}/\{1+2\exp(-3Q_0 q/5kT)\}. \quad \ldots\ldots(8)$$

The quantity $\langle Q\rangle_T/Q_0 = s$ has a meaning of an order parameter and is essentially proportional to $\langle P_2{}^0(\cos\theta)\rangle_T$ which is given by (7). In our present case, however, the quantity q is not to be considered as a temperature independent constant. It is the magnitude of an inner field due to the configuration of the neighbouring molecules, which in turn essentially depends upon the temperature motion. Let us assume for the moment that q is proportional to the average quadrupolarization $\langle Q\rangle_T$ and also to the fractional concentration ζ of the ortho-component.

$$q = c\zeta\langle Q\rangle_T = c\zeta Q_0 s. \quad \ldots\ldots(9)$$

Then we get from (8)

$$s = \{1-\exp(-3T_c s/T)\}/\{1+2\exp(-3T_c s/T). \quad \ldots\ldots(10)$$

The temperature dependence of s turns out to be co-operative in type, and the critical temperature is given by

$$T_c = c\zeta Q_0{}^2/5k \quad \ldots\ldots(11)$$

(cf. figure 4). As the scale factor of the resonance is simply proportional to the order parameter s, we now expect quite an abrupt narrowing of the resonance when we reach the critical temperature, as shown in figure 4. This corresponds satisfactorily to the experimental result. From the value of the transition temperature in resonance we can estimate the level separation at absolute zero, which turns out to be 4·10°K ($=2A/5$).

The above treatment corresponds to Bragg–Williams' approximation in the treatment of alloys. In our present case, however, it is not quite satisfactory in that (1) it gives no residual specific heat above the critical temperature (experimental results for solid hydrogen give an unusually big tail in this particular case), and (2) the curve giving the dependence of the critical temperature on the concentration of ortho-component simply passes through the origin of plot (experimentally it appears that below a certain concentration there is no indication of a transition). One way of avoiding difficulty (1) is to assume an additional temperature-independent term in the formula (9), but this does not remove difficulty (2) if the additional term vanishes with vanishing concentration of the ortho-component.

Both difficulties are removed, at least qualitatively, when we proceed to the next approximation corresponding to the Bethe–Peierls treatment of alloys. As the precise form of the interaction between hydrogen molecules is still unknown and as there is a possibility of lattice deformation in a solidified ortho–para hydrogen mixture, we take for the moment a phenomenological approach. Let us assume again a rotational level structure of the type described already (cf. figure 2), and introduce three parameters of interaction $V_{\lambda\lambda}$, $V_{\lambda\mu}$, $V_{\mu\mu}$ between a neighbouring pair of molecules. We assume that these interactions depend only on the rotational state of each molecule in the pair, a process corresponding to the Ising approximation in the case of ferromagnetism. In addition, several assumptions are made in order to apply a simple model to the actual case: (i) A theoretical estimate based on intermolecular force (Carlson 1950) suggests that the interaction between a pair of ortho-molecules is by far more important in producing the anisotropy than that between an ortho–para pair or a para–para pair. Therefore, for the moment we consider only the interaction between ortho–ortho pairs. (ii) We assume a more or less uniform distribution of ortho-molecules over the whole crystal and consider only the average number z of ortho-molecules on the nearest neighbouring sites (the first shell) of an ortho-molecule, that is to say we introduce the concentration of the ortho-component only through the value of parameter z. This can not be true in a rigorous sense, because there should be a local fluctuation in the value of z. However, if the migration of ortho-molecules through the crystal is sufficiently small during the time of the thermal observation, we need an average over the above fluctuation only in the final stage of the calculation.

Suppose that the central ortho-molecule is in a λ-state and that out of z neighbouring ortho-molecules L are in the λ-state, and let us write down the interaction between the central and first shell molecules explicitly by using $V_{\lambda\lambda}$, $V_{\lambda\mu}$ and $V_{\mu\mu}$. For the first-shell molecule, however, we are not going to write the remaining part of the interaction in the same way, but replace it by a kind of average potential which does not depend on its surroundings. In this approximation the partition function can be written in the following form

$$f_\lambda(L) = g_\lambda \frac{z}{L(z-L)} g_\lambda{}^L g_\mu{}^{z-L} \exp\left[-\beta\{LV_{\lambda\lambda} + (z-L)V_{\lambda\mu}\}\right] \delta_\lambda{}^L \delta_\mu{}^{z-L}. \qquad (12)$$

Here g_λ and g_μ are statistical weights, δ_λ and δ_μ are parameters due to the effective average potential for the first shell molecule, and $\beta = 1/kT$. Summing (12) over all possible values of L, we get

$$f_\lambda = g_\lambda[g_\lambda\delta_\lambda \exp(-\beta V_{\lambda\lambda}) + g_\mu\delta_\mu \exp(-\beta V_{\lambda\mu})]^z \qquad \ldots\ldots(13)$$

and in a similar way corresponding to a central molecule in the μ-state we find

$$f_\mu = g_\mu[g_\lambda\delta_\lambda \exp(-\beta V_{\lambda\mu}) + g_\mu\delta_\mu \exp(-\beta V_{\mu\mu})]^z. \qquad \ldots\ldots(14)$$

If we introduce the substitutions

$$\ln\rho = -\beta(V_{\lambda\lambda} - V_{\lambda\mu}), \qquad \ldots\ldots(15.1)$$

$$\ln\sigma = -\beta(V_{\lambda\mu} - V_{\mu\mu}), \qquad \ldots\ldots(15.2)$$

and

$$\gamma = (g_\mu\delta_\mu / g_\lambda\delta_\lambda), \qquad \ldots\ldots(15.3)$$

(13) and (14) can be written in the form

$$f_\lambda = [g_\mu\delta_\mu \exp(-\beta V_{\lambda\mu})]^z g_\lambda (\rho\gamma + 1)^z \qquad \ldots\ldots(13')$$

$$f_\mu = [g_\mu\delta_\mu \exp(-\beta V_{\lambda\mu})]^z g_\mu (\sigma\gamma + 1)^z. \qquad \ldots\ldots(14')$$

Using these partition functions, we find the average fractional population θ_0 of the λ-state at the central site to be

$$\theta_0 = f_\lambda/(f_\lambda + f_\mu). \qquad \ldots\ldots(15)$$

On the other hand, the average fractional population of the λ-state θ_1 at any site on the first shell is given by

$$\theta_1 = \frac{\delta_\lambda}{z}\frac{\partial}{\partial\delta_\lambda}\ln(f_\lambda + f_\mu). \qquad \ldots\ldots(16)$$

As there is no reason to discriminate the central site from first shell sites, we should put $\theta_0 = \theta_1$, and we have

$$\frac{\theta}{1-\theta} = \sigma\gamma\frac{(\rho\gamma+1)}{(\sigma\gamma+1)}. \qquad \ldots\ldots(17)$$

If we eliminate θ from (15) and (17) we get

$$\sigma\gamma = \frac{g_\lambda}{g_\mu}\left(\frac{\rho\gamma+1}{\sigma\gamma+1}\right)^z. \qquad \ldots\ldots(18)$$

Then, in order to obtain the condition appropriate to the critical temperature we require $\partial T/\partial\gamma = 0$, which, when applied to (18), gives an additional condition

$$\frac{1}{\sigma\gamma+1} - \frac{1}{\rho\gamma+1} = \frac{1}{z-1}. \qquad \ldots\ldots(19)$$

Eliminating γ from (17) and (19), we have

$$\rho/\sigma = \left(\theta + \frac{1}{z-2}\right)\left(1-\theta+\frac{1}{z-2}\right)\Big/\theta(1-\theta). \qquad \ldots\ldots(20)$$

As the long-range order should vanish at the critical temperature, we put $\theta_{\text{crit}} = g_\lambda/(g_\lambda + g_\mu)$ in (20).

Then we get

$$(\rho/\sigma)_c = (z^2 + Gz - G)/(z-2)^2 \qquad \ldots\ldots(21)$$

where

$$G = (g_\lambda - g_\mu)^2/g_\lambda g_\mu. \qquad \ldots\ldots(22)$$

Coming back to the original notation, we have

$$kT_c = \frac{-V}{\frac{1}{2}\ln(z^2+Gz-G) - \ln(z-2)} \qquad \ldots\ldots(21')$$

where

$$V = -\tfrac{1}{2}(V_{\lambda\lambda} + V_{\mu\mu}) + V_{\lambda\mu} \qquad \ldots\ldots(23)$$

which may be compared with an excitation energy per molecule and per pair.

If z_0 is the maximum possible number of the ortho-molecules on the first-shell sites, the concentration ζ of the ortho-component can be regarded in our approximation as z/z_0 and we have

$$\frac{(T_c)_{\zeta=\zeta}}{(T_c)_{\zeta=1}} = \frac{\frac{1}{2}\ln(z_0^2 + Gz_0 - G) - \ln(z_0 - 2)}{\frac{1}{2}\ln(z^2 + Gz - G) - \ln(z-2)}. \qquad \ldots\ldots(24)$$

At higher concentrations of the ortho-component the critical temperature is again shown to be proportional to the concentration, but this is not true at lower concentrations. In fact, there is a finite lower limit in the concentration for which a critical temperature can exist. In the case of hydrogen we get

$$\zeta_{\min} = 1/6 \qquad \ldots\ldots(25)$$

using the values $g_\lambda = 1$, $g_\mu = 2$, and $z_0 = 12$. The concentration dependence of the critical temperature in this particular case is shown in figure 5 (calculated by (24)). In a real crystal the value of z cannot be the same everywhere, and according to our assumption (ii) we are led to take a kind of average over the real values of z. However, if this distribution is symmetric around the maximum, the effect of averaging causes little deviation from the original formula (24), at least for a high concentration, because of the proportionality between T_c and ζ. For lower concentrations the result of averaging is expected to be a reduction of the value of T_c as compared with the value given by (24). Taking the above situation into account, we fixed the value of V in (21) by fitting the theory to the data at $\zeta = 0{\cdot}74$, which is the highest concentration observed by Hill and Ricketson. We found

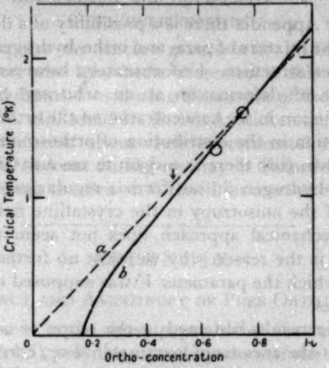

Figure 5. Dependence of the critical temperature T_c upon the fractional concentration of the ortho-component. (*a*) Bragg–Williams type theory. (*b*) Bethe–Peierls type theory. The arrow indicates the fact that there is no transition above that temperature.

$$V = 0{\cdot}447^\circ\text{K} \qquad \ldots\ldots(27)$$

per molecule and per pair interaction, which suggests an excitation energy per ortho-molecule in normal hydrogen

$$V_{\text{normal}} = 4{\cdot}023^\circ\text{K}(= Vz_0 \times 0{\cdot}75). \qquad \ldots\ldots(28)$$

Although there is only a small number of observed data (cf. table 1 and figure 5), the tendency of the concentration dependence of T_c is consonant with the theory. The theoretical (T_c, ζ) curve based upon equation (24) lies above the experimental curve in the non-linear region (see figure 5). This is not unreasonable because in a real situation the concentration factor z does not have a constant value throughout the solid but is subject to small variation from place to place. Taking into account the ' spread ' of z about each value, the theoretical curve can be brought into better agreement with the experimental one.

Table 1. Concentration Dependence of the Critical Temperature

ζ (ortho-concentration)	0·74	0·66	0·55
T_c(°K), calc.	1·60	1·40	1·14
T_c(°K), obs. in specific heat	$1{\cdot}6 \pm 0{\cdot}1$	$1{\cdot}35 \pm 0{\cdot}1$	$<1{\cdot}2$
T_c(°K), obs. in nuclear resonance†	1·55	1·33	$<1{\cdot}19$

§4. DISCUSSION AND CONCLUSION

As we show in the Appendix there is a possibility of a distortion or a deformation of the lattice in the mixture of para- and ortho-hydrogen as compared with the hexagonal close-packed structure. Unfortunately, however, it is not very easy to estimate the amount of deformation at an arbitrary concentration, because (i) there is a local variation in the concentration of the ortho-component, (ii) there is an additional variation in the distribution of ortho-molecules even if the local concentration is known, (iii) there is a definite amount of evidence for the fact that ortho- and para-hydrogen do not form a regular mixture. Therefore, the microscopic origin of the anisotropy in the crystalline field is not simple and a detailed quantum-mechanical approach does not seem to be justified at the present stage. This is the reason why we went no further than a phenomenological treatment in which the parameter V was supposed to cover various effects due to different causes.

To summarize the results obtained in the scope of our treatment, we may compare the values of the anisotropy parameter A or, corresponding to the level separation at absolute zero, the values of parameter $V(=2A/5)$, which are derived from entirely independent observations (cf. table 2). Although we are not quite sure that different types of observations lead to precisely the same quantity, the figures found in table 2 are all the same in order of magnitude and together they give some idea of the magnitude of hindrance restricting the motion of a molecule in the crystal.

Table 2. The Magnitude of Anisotropy

	Phenomenon observed	Theory employed	Anisotropy $V=2A/5$
1.	Specific heat above 4°K	Temperature-independent crystalline field (Schaefer's theory)	5·6°K
2.	Nuclear magnetic resonance (spin–lattice relaxation time T_1)	Bloembergen–Purcell–Pound theory	3·0 ∼ 4·0°K
3.	Nuclear magnetic resonance (temperature of abrupt change in resonance)	Co-operative phenomenon (Bragg–Williams' type theory)	4·10°K
4.	Critical temperature in specific heat in normal hydrogen	Co-operative phenomenon (Bethe–Peierls' type theory)	4·02°K

---

† Y. Masuda 1954, private communication.

In our particular case the anomalous specific heat above the critical point has a fairly big tail and the shape of the hump is symmetrical around its maximum rather than lambda-type. Both of these facts deviate from the simple theory, but can be explained qualitatively by taking the local variation in the value of z into account. For, when we average the specific heat over a more or less symmetrical distribution in the value of z, we may reasonably expect that the tail will tend to become bigger and the hump will become more symmetrical.

ACKNOWLEDGMENTS

I should like to express my sincere gratitude to Professor M. Kotani and Professor C. A. Coulson who have been interested in this work and have given valuable comments and discussions during the course of the investigation. I also wish to thank Dr. R. W. Hill and Mr. B. W. A. Ricketson, and Mr. Y. Masuda for their kind communication about their experimental results. The greater part of this work was carried out during my stay in Oxford for the academic year 1953/4, and I wish to thank the British Council for a research scholarship.

APPENDIX

CRYSTAL ENERGY AND ANISOTROPY OF PURE ORTHO-HYDROGEN

One of our conclusions in the above paper is that the value 4°K for the anisotropy parameter $V(=2A/5)$ provides a good measure of the restriction to rotation experienced by molecules in solid hydrogen. We shall now try to examine the conclusion in detail on the basis of intermolecular forces. The force between two hydrogen molecules is anisotropic and particularly for ortho-molecules it remains so even after an average over the rotational state of each molecule in the crystal. Hence there is no reason to exclude the possibility of lattice deformation in the mixture of ortho- and para-components as compared with pure para-hydrogen, which is hexagonal close-packed. This deformation might play an important part in producing the anisotropy (Nagamiya and Urano 1952). Therefore, we calculated the potential energy and anisotropy for a uniform deformation of the lattice.

We used various types of force which were calculated quantum-mechanically by de Boer (1942), Margenau (1943), Evett and Margenau (1953) and Carlson (1950). For the sake of computational convenience we studied the case of pure ortho-hydrogen which, although absent in nature, may be expected to give some idea about the mixture. Hence we always assumed a hexagonal structure.

The various different types of force between two hydrogen molecules can be expressed in a common form

$$\begin{aligned} E = K[a + b(z_1'^2 + z_2'^2) + c(z_1'^2 z_2'^2) \\ + d\{x_1'^2 x_2'^2 + y_1'^2 y_2'^2 + e(z_1'^2 z_2'^2)\} + f(z_1'^4 + z_2'^4)]. \qquad \ldots\ldots (\mathrm{A1}) \end{aligned}$$

Here a, b, c, d, e and f are numerical constants, and (x_1', y_1', z_1') are the direction cosines of the axis of the ith molecule with respect to a coordinate system in which the intermolecular direction is taken as the z' axis. The values of the numerical constants chosen for the various types of force in our calculation are given in table A1.

Table A1. Numerical Constants of the Intermolecular Force

Type of force	K	a	b	c	d	e	f
Exchange repulsion	$4A/R^{11}=48000/R^{11}$	1	0	0	0	0	0
	$4AnQ_2/4R^{n+2}=129360/R^{13}$	-2	$n+2$	0	0	0	0
	$4An(n+2)Q_2^2/16R^{n+4}=412011/R^{15}$	1	$-(n+4)$	$-(n+2)(n+4)$	2	$-(n+3)$	0
	$4An(n+2)Q_4/48R^{n+4}=68640/R^{15}$	6	$-6(n+4)$	0	0	0	$(n+4)(n+6)$
Quadrupole–quadrupole	$3\theta^2/4R^5=0{\cdot}146261/R^5$	1	-5	-15	2	-4	0
Induced dipole–dipole	$-3E\alpha^2/4R^6=-10{\cdot}9/R^6$	$1-\gamma$	$3\gamma(1-\gamma)/2$	0	$3\gamma^2/2$	-2	0
	oscillator model$=-118{\cdot}87/R^8$	$1-(2\gamma/5)$ $-(4\omega/7)$	$(3\gamma/5)+(6\omega/7)$	0	0	0	0
Induced dipole–quadrupole	oscillator model$=-620/R^{10}$	1	0	0	0	0	0

$A=12000$, $n=11$, $Q_2=0{\cdot}980$, $Q_4=0{\cdot}480$ (cf. de Boer 1942). $\theta=0{\cdot}4416$ (cf. James and Coolidge 1938).
$\alpha=5{\cdot}3280$, $\gamma=0{\cdot}1173$ (cf. Ishiguro *et al.* 1952). $E=0{\cdot}5168$ (14·095 ev). $\omega=0{\cdot}124837$ (cf. Carlson 1950).

We then transformed the coordinate system from z' to z, which is the direction of the crystalline axis. If we concentrate our attention on the total energy of the crystal, we should take an average over the rotational state of each molecule. We assumed that each of them is confined in the state $M_J=0$, and took an average over this state. On the other hand, when we consider the anisotropy we apply the same condition except for the central molecule, which was assumed to be fixed in its direction θ as measured from the crystalline axis, and we calculated the coefficient A of $P_2^0(\cos\theta)$.

In both cases the result can be expressed in the form

$$\sum_i K_i(c_{0i}+c_{2i}\gamma'^2+c_{4i}\gamma'^4) \qquad \ldots\ldots(\text{A2})$$

where γ' is the cosine of the angle between axes z and z', and the summation is over all different types of interaction. γ' depends only upon the relative orientation of the pair of molecules with respect to the crystalline axis. The values of c_{0i}, c_{2i} and c_{4i} for the different types of interaction are given in table A2. The K_i's were calculated by using a form like $K_i=K_{0i}(R_0/R)^{n_i}$. The results of the calculation are shown in figures 6 and 7, where constant energy contours are plotted against possible deformations described by $\alpha=a/a_0$ for the lateral deformation and $\beta=c/c_0$ for the longitudinal deformation. a_0 and c_0 are the constants characterizing the pure para-hydrogen lattice.

Several points follow from these results. (i) In order to obtain a consistent picture for the anisotropy we must have a negative value for the quantity $(-A)$, because it assures the fact that the central molecule is, like the other molecules, in the $M_J=0$ state in the crystalline field. In the close-packed case (i.e. $\alpha=\beta=1$), however, $-A$ is positive and our picture is not consistent. (ii) On the other hand, the close-packed structure does not correspond to the minimum in potential energy, which lies in a deformed structure where $\alpha=0{\cdot}85$ and $\beta=0{\cdot}94$.

In this deformed structure $-A$ is negative and $A=1{\cdot}5\times10^{-6}$ A.U. per mole and per two pairs, i.e. one lateral and one longitudinal. This corresponds to the value

$$V_{\text{normal}}=(2A/5)6(3/4)=2{\cdot}7\times10^{-6}\ \text{A.U. mole}^{-1}=0{\cdot}845^\circ\text{K}.$$

This result seems to be consistent with the original assumption but numerically it is much smaller than other estimates (cf. table 1).

However, we have not taken into account the effect of the kinetic energy, which is not negligible in solid hydrogen. For, if we calculate the crystal energy of pure para-hydrogen using a similar method, we find that the actual lattice constant is 13·6% bigger than that expected from the position of the minimum in potential energy. For this particular case the energy of zero-point vibration is estimated to be $0{\cdot}166\times10^{-3}$ A.U. mole^{-1}, and the sublimation energy is $0{\cdot}395\times10^{-3}$ A.U. mole^{-1} which is to be compared with the observed value $0{\cdot}287\times10^{-3}$A.U. mole^{-1} (Simon 1923, Johnston *et al.* 1950).

Unfortunately there are several serious difficulties in an exact treatment of the whole problem.

(i) Even if we have an exact potential function plotted against possible deformations, we must solve a Schrödinger equation for more than one dimension, which is not always easy. If we could solve this dynamical problem, we then should calculate the average value of several different powers of the intermolecular distance by using the wave function to obtain the lattice constant and the anisotropy.

Table A2

	n_i	K_0 (10^{-6}A.U.)	Crystal energy c_{0i}	Crystal energy c_{2i}	Crystal energy c_{4i}	Anisotropy c_{0i}	Anisotropy c_{2i}	Anisotropy c_{4i}
Quadrupole–quadrupole	5	8·18314	0·48	−0·48	5·6	1·2	−12	14
Induced dipole–dipole	6	−86·0544	0·956370	0·11436	0·02973	−0·050403	0·109917	0·074325
	8	−18·6868	0·924164	0·227508	0	−0·094795	0·284385	0
Induced dipole–quadrupole	10	−1·94076	1	0	0	0	0	0
Exchange repulsion	11	21·2020	1	0	0	0	0	0
	13	1·13776	3·2	10·4	0	−4·3	13·0	0
	15	0·072157	3·68	9·6	40·8	−7·46	−26	102
	17	0·0120211	13·7143	102·8571	0	−42·8571	128·5713	0

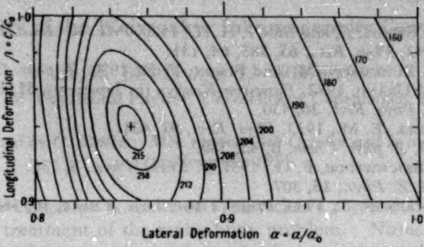

Figure 6. The crystal energy of pure ortho-hydrogen. (The number attached to the contour indicates the energy associated with two pairs of interaction, i.e. one lateral and one longitudinal, in 10^{-6} atomic units.)

(ii) To calculate the potential energy, we assumed a uniform deformation, i.e. the deformation with the longest wavelength. But the ground state of the crystal seems to be essentially dependent on the modes with shorter wavelength, for which the potential energy calculation is prohibitively complicated. Although there is a possibility that the greater part of the shorter waves has rather low frequency and is not so important as it seems to be (because shearing modes accompany little change in the volume), we cannot be sure about the long wave approximation in a quantitative sense.

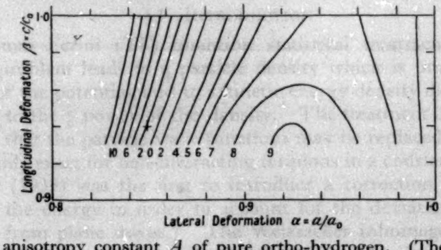

Figure 7. The anisotropy constant *A* of pure ortho-hydrogen. (The number attached to the contour indicates the value of anisotropy constant *A* which is associated with two pairs of interaction, i.e. one lateral and one longitudinal, in 10^{-6} atomic units.)

References

Bloembergen, N., Purcell, E. M., and Pound, R. V., 1948, *Phys. Rev.*, **73**, 679.

de Boer, J., 1942, *Physica*, **9**, 363.

Carlson, B. C., 1950, *Thesis*, University of Oxford.

Evett, A. A., and Margenau, H., 1953, *Phys. Rev.*, **90**, 1021, *J. Chem. Phys.*, **21**, 958.

Giauque, W. F., and Johnston, H. L., 1928, *J. Amer. Chem. Soc.*, **50**, 3221.

Hatton, J., and Rollin, B. V., 1949, *Proc. Roy. Soc.* A, **199**, 222.

Hill, R. W., and Ricketson, B. W. A., 1954, *Phil. Mag.*, **45**, 277.

Ishiguro, E., Arai, T., Kotani, M., and Mizushima, M., 1952, *Proc. Phys. Soc.* A, **65**, 178.

James, H. M., and Coolidge, A. S., 1938, *Astrophys. J.*, **87**, 438.

Johnston, H. L., Clarke, J. T., Rifkin, E. B., and Kerr, E. C., 1950, *J. Amer. Chem. Soc.*, **72**, 3933.

Keesom, W. H., Bijl, A., and van der Horst, H., 1932, *Commun. phys. Lab. Univ. Leiden*, 217a.
Keesom, W. H., de Smedt, J., and Mooy, H. H., 1930, *Proc. K. Akad. Wet. Amst.*, **33**, 814.
Margenau, H., 1943, *Phys. Rev.*, **63**, 385, **64**, 131.
Mendelssohn, K., Ruhemann, M., and Simon, F. E., 1930, *Z. phys. Chem.* B, **15**, 121.
Nagamiya, T., and Urano, 1952, *Busseiron-Kenkyu* (in Japanese), **51**, 64.
Pauling, L., 1930, *Phys. Rev.*, **36**, 430.
Reif, R., and Purcell, E. M., 1953, *Phys. Rev.*, **91**, 631.
Schaefer, K., 1939, *Z. phys. Chem.* B, **42**, 380.
Scott, R. B., and Brickwedde, F. G., 1937, *J. Chem. Phys.*, **5**, 736.
Simon, F. E., 1923, *Z. Phys.*, **15**, 307.
Tomita, K., and Mannari, I., 1953, *Progr. Theor. Phys., Osaka*, **10**, 367.

On the Validity of the Weizsäcker Inhomogeneity Correction Term

By R. BERG and L. WILETS†
Institute for Theoretical Physics, University of Copenhagen, Denmark

Communicated by C. Møller; MS. received 4th October and in amended form 12th November 1954

Abstract. An investigation is made of Weizsäcker's correction to the Thomas–Fermi statistical treatment of the many-body problem. Numerical solutions of Weizsäcker's equation were obtained for the isotropic harmonic oscillator and the step potential in plane symmetry. These particular potentials were chosen as approximations to nuclear potentials. In the case of the harmonic oscillator, the error in the energy is an order of magnitude greater than for the Thomas–Fermi equation, but a reduction in the magnitude of the Weizsäcker correction term by a factor of $\frac{1}{5}$ gives substantial improvement over the Thomas–Fermi solution. The step potential also shows that the Weizsäcker term is too great, but the reduction factor necessary to give substantial improvement is between $\frac{1}{2}$ and 1. It is concluded that the Weizsäcker correction term is not reliable as such, but that a reduction in the magnitude of the term may give plausible solutions for the density. The reduction factor depends, however, upon the form of the potential.

§ 1. INTRODUCTION

THE Thomas–Fermi (TF) quantum statistical treatment of the many-particle problem leads to a particle density which is proportional to the $\frac{3}{2}$ power of the potential, and to a kinetic energy density distribution which is proportional to the $\frac{5}{3}$ power of the density. The treatment is based upon the approximation that the particle wave functions may be replaced locally by plane waves, and is only exact for non-interacting fermions in a constant potential.

Weizsäcker (1935) was the first to introduce a correction term to the TF expression for the energy in order to account for the deviation of the particle wave function from plane waves.‡ The Weizsäcker inhomogeneity correction term varies as the square of the gradient of the particle density, and thus leads to solutions with qualitatively correct behaviour in that it prevents rapid density variation in regions of rapidly varying potential.

Weizsäcker's derivation of the correction term, however, is not very plausible and, in fact, breaks down just for the type of potentials which were assumed. The Weizsäcker term has been used by various researchers with varying (and frequently unknown) degrees of success in atomic and nuclear problems. An investigation of the validity of the correction term would seem to be desirable for analysis of the results of calculations based upon it.

---

† U.S. National Science Foundation Postdoctoral Fellow.

‡ Plaskett (1953) has derived a modification for the TF equation, and Ballinger and March (1954) have made numerical calculations with Plaskett's equation in the case of the one-dimensional harmonic oscillator. The latter authors point out that the equation does not have a unique solution. No member of the family of solutions obtained appears to be an improvement over the Weizsäcker solution.

Weizsäcker's equation is not amenable in general to analytical methods, but a measure of its validity can be obtained by comparing numerical solutions of the equation with exact quantum mechanical solutions in the case of simple fixed potentials. We have carried out such calculations with potentials designed to approximate nuclear potentials. The result of our investigations indicate that Weizsäcker's equation as such is not completely reliable and in many cases is not an improvement over the TF equation. A reduction in the magnitude of the Weizsäcker correction term, however, appears to lead to more satisfactory solutions, although the amount of the reduction depends upon the form of the potential in question.

§ 2. SKETCH OF THE DERIVATION OF WEIZSÄCKER'S INHOMOGENEITY CORRECTION TERM

Derivations of Weizsäcker's inhomogeneity correction term are given by Weizsäcker (1935) and by Gombás (1949); we outline briefly the former derivation here.

In the neighbourhood of a point taken as $\mathbf{r}=0$, the wave functions of the particles are assumed to be given approximately by

$$\psi_{\mathbf{p}}=\frac{1}{\sqrt{V}}(1+\mathbf{a}\,.\,\mathbf{r})\exp(i\mathbf{p}\,.\,\mathbf{r}/\hbar) \qquad \ldots\ldots(1)$$

where V is a normalizing volume. The vector $\mathbf{a}$ is assumed to be small, but may depend upon $\mathbf{p}$. The density at $\mathbf{r}=0$ is then approximately given by the Fermi value

$$\rho=\frac{8\pi}{3h^3}P^3, \qquad \ldots\ldots(2)$$

where P is the maximum magnitude of $\mathbf{p}$. The gradient of the density is given by

$$\nabla\rho=\frac{4}{h^3}\int^P \mathbf{a}(\mathbf{p})\,d\mathbf{p}, \qquad \ldots\ldots(3)$$

and the kinetic energy per unit volume may be written

$$E_{\mathrm{kin}}=E_{\mathrm{k}}+E_{\mathrm{W}}, \qquad \ldots\ldots(4)$$

where

$$E_{\mathrm{k}}=\frac{3}{40}\left(\frac{3}{\pi}\right)^{2/3}\frac{h^2}{m}\rho^{5/3}\equiv\kappa_{\mathrm{k}}\rho^{5/3} \qquad \ldots\ldots(5)$$

is the usual Fermi energy and

$$E_{\mathrm{W}}=\frac{1}{4\pi^2hm}\int^P[\mathbf{a}(\mathbf{p})]^2\,d\mathbf{p} \qquad \ldots\ldots(6)$$

is Weizsäcker's correction. Weizsäcker then shows that the expression in (6) is a minimum for a given gradient of the density (3) if $\mathbf{a}$ is independent of $\mathbf{p}$. In this case, E_{W} can be expressed as

$$E_{\mathrm{W}}=\frac{\hbar^2}{8m}\frac{(\nabla\rho)^2}{\rho}\equiv\kappa_{\mathrm{W}}\frac{(\nabla\rho)^2}{\rho}. \qquad \ldots\ldots(7)$$

The total energy of the system is given by

$$E=\int (E_{\mathrm{k}}+E_{\mathrm{W}}+V\rho)\,dv, \qquad \ldots\ldots(8)$$

where V is the energy potential. When this expression is minimized for a fixed number of particles, the corresponding differential equation for the density is given by

$$\kappa_{\mathrm{k}}\rho^{2/3}+\kappa_{\mathrm{W}}\left[\frac{(\nabla\rho)^2}{\rho^2}-2\frac{\nabla^2\rho}{\rho}\right]+V=E', \qquad \ldots\ldots(9)$$

where E' is a Lagrange multiplier related to the total number of particles. The potential is here assumed to be independent of ρ. It can be directly verified that the equation (9) satisfies the virial theorem,

$$E_{\mathrm{k}}+E_{\mathrm{W}}=E_{\mathrm{kin}}=\tfrac{1}{2}\int \rho\nabla V\,.\,\mathbf{r}\,dv \qquad \ldots\ldots(10)$$

as does the TF equation.†

There are several points which may bear criticism in the derivation, but probably the most serious is the use of oscillating wave functions (positive kinetic energy) for all particles in regions of varying potential. When the potential increases, the density associated with the particles of positive kinetic energy increases, while the density associated with particles of negative kinetic energy decreases due to the decay of the non-oscillating wave functions. The total density decreases and this decrease is due to the decay of the wave functions of the particles of negative energy. Thus, the approximation (1) is not valid for the particles which contribute most to the change in density.‡

Although the derivation given by Weizsäcker does not appear to be valid, the correction term does have the proper form in that it leads to a smoothing of the density in regions of rapid potential variation. A term of similar form, but with some (different) coefficient might be expected to give plausible results. The approach of the present work is to test the validity of the Weizsäcker, or similar, term in explicit cases. Since it is not immediately clear whether the expression should be better for slowly or for rapidly varying potentials, the potentials for which the method was tested were especially chosen to approximate nuclear potentials, as there is considerable current interest in the application of statistical methods to nuclear problems.

---

† This is not the case for Plaskett's equation. An expression for the total energy can be obtained by adding the potential energy to the kinetic energy which is obtained by substituting Plaskett's equation into the right-hand side of (10), but the minimization of this expression for a fixed number of particles does not lead back to Plaskett's differential equation. As Ballinger and March (1954) point out, the non-uniqueness of the Plaskett equation may be connected with the (apparent) absence of any expression for the energy which, by minimization, would lead to the differential equation.

‡ A similar objection may be raised in the case of Plaskett's derivation. Plaskett identifies a smoothly varying function P_E with the average density of a single particle. The justification that the identification is reasonable is based upon the equality of the integral of the function P_E with the integral of the actual single particle density between two nodes of the wave function. This is indeed reasonable in regions where the wave function oscillates rapidly, but since the only nodes outside the classical turning points are at ±∞, it is not clear that the function should represent the actual single particle density accurately in the forbidden region, or that the resulting total density should be represented accurately in regions of varying potential. In fact, all members of the family of solutions which Ballinger and March (1954) give for Plaskett's equation in the case of a one-dimensional harmonic oscillator considerably overestimate the density in the forbidden region, and none is even as good as the Weizsäcker solution which errs in the same direction.

§3. NUMERICAL EXAMPLES

Two specific fixed potential problems were considered: a three-dimensional isotropic harmonic oscillator, and a step potential in plane symmetry.

Equation (9) was expressed in the form of finite difference equations subject to the proper boundary conditions. The resulting set of n simultaneous algebraic equations in n unknowns (the value of ρ at each of the mesh points) was solved numerically by a modification of Newton's method of successive approximations (see Appendix).

The numerical calculations were performed on the BESK in Stockholm. A problem employing fifty mesh points would require about twenty iterations for convergence of the trial function to the correct solution when the criterion for convergence was chosen to be such that at each mesh point the value of ρ differs from the value obtained from the previous iteration by less than one part in 10^{-3}. The actual calculating time (exclusive of preparation and printing) to obtain the solution for one problem was less than one minute.

The examples and results are discussed below.

A. *Three-dimensional Isotropic Harmonic Oscillator*

The potential is given by

$$V=\tfrac{1}{2}m\omega^2r^2, \qquad \ldots\ldots(11)$$

where ω is the characteristic angular frequency of the oscillator. The quantum energy levels are given by

$$E_{n_1n_2n_3}=(n_1+n_2+n_3+\tfrac{3}{2})\hbar\omega, \qquad \ldots\ldots(12)$$

and the corresponding quantum wave functions by (cf. Schiff 1949)

$$\psi_{n_1n_2n_3}(x,y,z)=\left(\frac{\alpha}{\pi^{1/2}2^{n_1+n_2+n_3}n_1!\,n_2!\,n_3!}\right)^{1/2}H_{n_1}(\alpha x)H_{n_2}(\alpha y)H_{n_3}(\alpha z)\exp\left(-\tfrac{1}{2}\alpha^2r^2\right) \qquad \ldots\ldots(13)$$

where $\alpha=(m\omega/\hbar)^{1/2}$ and the H_n are the Hermitian polynomials of order n. The number of particles which fill all the energy levels (two particles per state) up to and including the levels characterized by the major quantum number $N=n_1+n_2+n_3$ is given by

$$\mathcal{N}=\tfrac{1}{3}(N+1)(N+2)(N+3), \qquad \ldots\ldots(14)$$

and the total energy of these particles is given by

$$E_{\mathcal{N}}=\tfrac{1}{8}(N+1)(N+2)^2(N+3)\hbar\omega=\tfrac{3}{4}\mathcal{N}\left[(3\mathcal{N})^{1/3}+\frac{1}{3(3\mathcal{N})^{1/3}}+\ldots\right]\hbar\omega. \qquad \ldots(15)$$

The energy given by the TF solutions is

$$E_{\mathcal{N}}^{(\mathrm{TF})}=\tfrac{3}{4}\mathcal{N}(3\mathcal{N})^{1/3}\hbar\omega. \qquad \ldots\ldots(16)$$

It can be shown from equation (9) that, for an harmonic oscillator, a solution of a given problem characterized by the Weizsäcker coefficient κ_W is equivalent (by a change in scale) to the solution of another problem characterized by $\kappa_W' = \xi\kappa_W$, and in which $\mathcal{N}' = \xi^{3/2}\mathcal{N}$ and $E' = \xi^2 E$. Thus, any numerical solution gives rise to a family of solutions of varying ξ.

Since the Weizsäcker equation (9) satisfies the virial theorem (10), we have the relationship

$$E_{\text{pot}} = \tfrac{1}{2}m\omega^2 \int r^2 \rho \, dv = E_k + E_W = \tfrac{1}{2}E. \qquad \ldots\ldots(17)$$

Thus, the energy alone gives directly the second moment (i.e. the integral weighted by r^2) of the density distribution. In figure 1 is plotted a comparison of the energies obtained from three sources: the exact quantum eigenvalues (equation (15)), the classical TF solutions (equation (16)), and the numerical solutions of the Weizsäcker equation (for various ξ). Whereas the classical TF solutions give too small energies because the particles are confined within the classical turning points, the Weizsäcker term causes the particles to extend too far into the forbidden region and thus results in energies which are too large. These results appear to be in agreement with those of Ballinger and March (1954) for the one-dimensional harmonic oscillator with the first ten states filled. The errors in the energy obtained, using the Weizsäcker term ($\xi = 1$), is an order of magnitude greater than for the classical TF case. An improvement in the former can be obtained by reducing the coefficient κ_W of the Weizsäcker term. A reduction of ξ to one quarter leads to energies which are about as good as the TF energies, but still erring on the side of overestimation. It appears that a ξ of $\frac{1}{8}$ or less would be necessary to give a substantial improvement over the TF solutions.

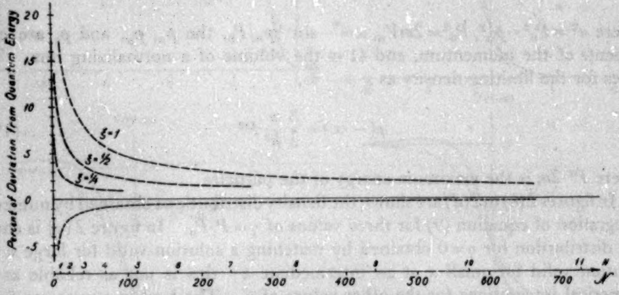

Figure 1. Harmonic oscillator.

The percentage deviation of the TF (lowest curve) and Weizsäcker ($\xi = 1$) energies from the quantum mechanical energies is plotted as a function of the number of particles (filling two per state). Curves are also given for solutions where the Weizsäcker coefficient κ_W is replaced by $\kappa_W' = \xi\kappa_W$. Another scale along the abscissa gives the major quantum number N.

B. *Step Potential in Plane Symmetry*

Neither the wave-mechanical nor the Weizsäcker solutions depend sensitively upon the precise form of the potential. Thus, a step potential was employed to approximate a smooth potential which varies rapidly over a distance of one wavelength, such as is to be expected in a nucleus. The use of plane symmetry and a semi-infinite distribution simplifies the interpretation of the problem.

The potential is assumed to be zero for $x<0$ and V_0 for $x>0$. The quantum wave functions are given by

$$\left.\begin{aligned} \psi_{\mathbf{p}}^{-} &= \left(\frac{2}{\Omega}\right)^{1/2} \exp\{i(p_y y + p_z z)/\hbar\} \sin(p_x x/\hbar + \alpha), \quad x<0, \\ \psi_{\mathbf{p}}^{+} &= \left(\frac{2}{\Omega}\right)^{1/2} \exp\{i(p_y y + p_z z)/\hbar\} \exp(-\kappa x/\hbar) \frac{p_x}{P_0}, \quad x>0, \end{aligned}\right\} \qquad \ldots\ldots(18)$$

where $\kappa^2 = P_0^2 - p_x^2$, $P_0^2 = 2mV_0$, $\alpha = -\sin^{-1} p_x/P_0$, the p_x, p_y, and p_z are components of the momentum, and Ω is the volume of a normalizing box. This gives for the limiting density as $x \to -\infty$,

$$\rho(-\infty) = \frac{8}{3}\frac{\pi}{h^3} P^3, \qquad \ldots\ldots(19)$$

where $P^2/2m$ is the maximum energy of the particles.

In figures 2(*b*) to 2(*d*) are shown the density distributions obtained by numerical integration of equation (9) for three values of $\eta = P/P_0$. In figure 2(*a*) is shown the distribution for $\eta = 0$ obtained by matching a solution valid for large x to a solution valid for small x at an intermediate x; this is not as reliable as the numerical integrations for the other values of x. The broken curves are fits to the quantum mechanical densities (see caption). The effect of oversmoothing the density is evident in all cases. Figure 3 shows a comparison of the barrier penetration given by the Weizsäcker equation with that given by the quantum solutions, which also indicates the over-compensation of the Weizsäcker term. The density at the step, however, is well reproduced, as is shown in figure 4.

Another measure of the accuracy of the Weizsäcker solutions can be obtained from the energy, or rather what we define as the surface energy. We define the surface energy as the difference between the energy of (say) N particles (per unit area) and the energy which the same number of particles would have in a Fermi gas filled to the asymptotic density. If N is a large number, the surface energy is independent of N and is given in units of energy per unit area. Thus, if we take $\mathrm{K}(L)$ and $\mathrm{N}(L)$ to be kinetic energy and number of particles per unit area within the region $-L<x<\infty$ we may define the surface kinetic energy by

$$\mathrm{K}_{\mathrm{S}} = \lim_{L\to\infty} \left\{ \mathrm{K}(L) - \frac{3P^2}{10m} \mathrm{N}(L) \right\}. \qquad \ldots\ldots(20)$$

The total surface energy is obtained by adding to the potential energy

$$N^+ V_0 = N^+ P^2/(2m\eta^2).$$

The kinetic and total surface energies are given in figure 5. It can be seen that the Weizsäcker solutions give too small kinetic energies and too great total energies.

In the case of the plane step, as in the case of the harmonic oscillator, a change in the coefficient of the Weizsäcker correction term results in a change of scale of the solutions only. Thus, for the step potential, if we replace κ_W by $\kappa_W' = \xi\kappa_W$, we change the units of length and energy so that $L' = \sqrt{\xi}L$ and $\epsilon_0' = \sqrt{\xi}\epsilon_0$. Thus, by a suitable choice of ξ, the various Weizsäcker density distributions can be

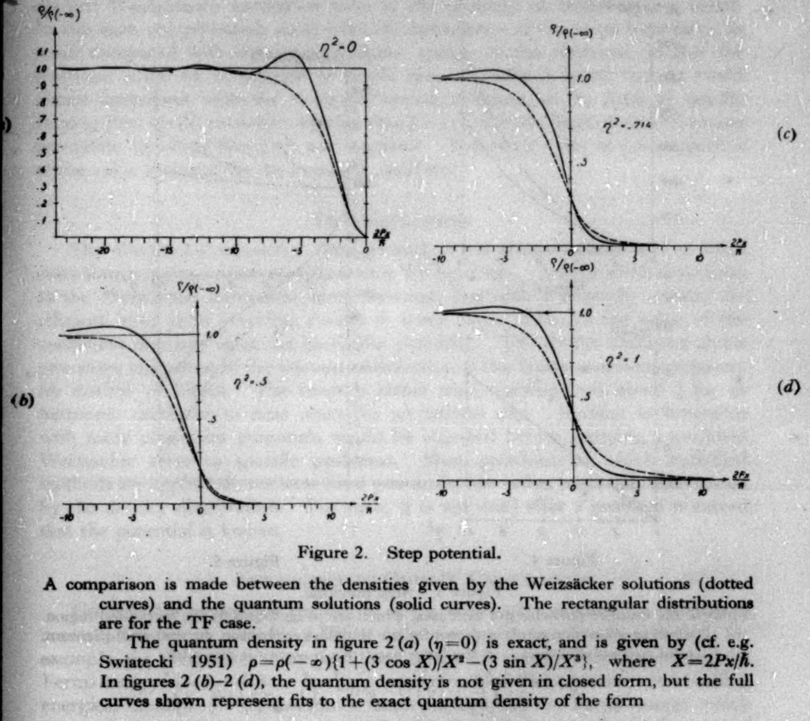

Figure 2. Step potential.

A comparison is made between the densities given by the Weizsäcker solutions (dotted curves) and the quantum solutions (solid curves). The rectangular distributions are for the TF case.

The quantum density in figure 2 (*a*) ($\eta=0$) is exact, and is given by (cf. e.g. Swiatecki 1951) $\rho=\rho(-\infty)\{1+(3\cos X)/X^2-(3\sin X)/X^3\}$, where $X=2Px/\hbar$. In figures 2 (*b*)–2 (*d*), the quantum density is not given in closed form, but the full curves shown represent fits to the exact quantum density of the form

$$\rho=\rho(-\infty)\{1-(a+bx+cx^2)\exp(dx)\}, \qquad x<0$$

$$\rho=\rho(-\infty)(a'+b'x+c'x^2)\exp(-d'x), \qquad x>0$$

where the coefficients were adjusted to give the proper values of ρ, ρ' and ρ'' at $x=0$, and the proper integral of ρ for $-\infty<x<0$, and $0<x<\infty$. These quantities can be obtained easily from the wave functions given in equation (18). The actual quantum densities are sharper near the maximum, and show oscillations behind the maximum, as is the case in figure 2 (*a*) ($\eta=0$).

The Weizsäcker solution in figure 2 (*a*) ($\eta=0$) was obtained by matching a power series solution valid for small x to an exponential solution,

$$\rho \simeq \rho(-\infty)(1-A\exp\{2\pi^{2/3}x/3^{1/6}\}),$$

valid for large x at an intermediate value of $x=x_0$. This solution is not as reliable as those solutions (figures 2 (*b*)–2 (*d*)) which were obtained by numerical integration.

brought into better agreement with the quantum solutions. Similarly, better agreement can be obtained for the surface energies. It is to be noted, however, that the value of ξ depends upon η (i.e. the height of the step) and is thus not uniquely given. Furthermore, the value of ξ which rectifies the kinetic energy is not generally the value which also rectifies the potential or total energies.

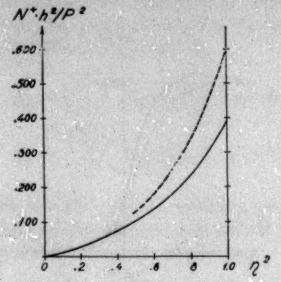

Figure 3.

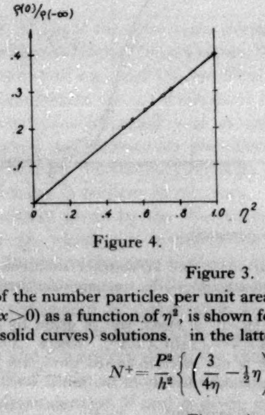

Figure 4.

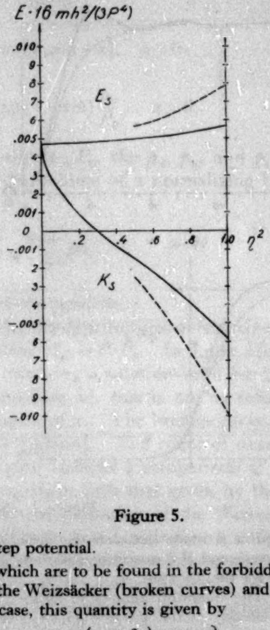

Figure 5.

Figure 3. Step potential.

A plot of the number particles per unit area, which are to be found in the forbidden region ($x>0$) as a function of η^2, is shown for the Weizsäcker (broken curves) and quantum (solid curves) solutions. in the latter case, this quantity is given by

$$N^+=\frac{P^2}{h^2}\left\{\left(\frac{3}{4\eta}-\tfrac{1}{2}\eta\right)(1-\eta^2)^{1/2}+\left(1-\frac{3}{4\eta^2}\right)\sin^{-1}\eta\right\}.$$

Figure 4. Step potential.

A plot of the density at the step, $\rho(0)$ as a function of η^2 is shown for the Weizsäcker (circles) and quantum (solid curve) solutions. In the latter case, this quantity is given by $\rho(0)=\rho(-\infty)\frac{2}{5}\eta^2$.

Figure 5. Step potential.

A plot of the kinetic and total surface energies as a function of η^2 is shown for the Weizsäcker (broken curve) and quantum (solid curve) solutions. The quantum kinetic surface energy is given by

$$K_S=\frac{3}{16}\,\frac{P^4}{mh^2\eta^4}\left\{\eta(1-\eta^2)^{1/2}\left(\frac{2}{5}\eta^2-1\right)+\left(-\frac{8}{15}\eta^4-\frac{16}{15}\eta^2+1\right)\sin^{-1}\eta+\frac{2}{15}\pi\eta^4\right\}.$$

The total surface energy is obtained by adding the potential energy,

$$N^+V_0=N^+P^2/(2m\eta^2),$$

to the kinetic surface energy.

A value of ξ of roughly 0·5 would, however, give significant improvement in most quantities for large η, while for small η it would appear that a ξ near unity would do quite well.

C. *Other Information*: *Calculations by Lindhard*

We have learned from J. Lindhard (private communication) that he has applied Weizsäcker's correction term to the problem of electrons in a metal. In this case, the potentials away from the boundaries of the metal were taken as small compared with the average kinetic energy of the electrons, so that the electrons could be considered as nearly free. Lindhard found that he could obtain agreement with the wave-mechanical solutions in the limit of rapidly varying (but small) potentials by choosing $\xi = 1$, but in the limit of slowly varying potentials, he found that $\xi = \frac{1}{9}$ was required. This latter value of ξ is suggestive of the value required for the harmonic oscillator.

§4. CONCLUSIONS

The Weizsäcker correction term as such is not always reliable and in some cases does not give improvement over the TF equation. A term of the same form as the Weizsäcker correction term, however, but with a generally smaller coefficient, may yield plausible results in many cases, although the value of the coefficient depends upon the particular potential. The results discussed above give some indication of the amount of reduction of the Weizsäcker term necessary for nuclear problems. The range is rather wide, varying from about $\frac{1}{8}$ for an harmonic oscillator to near unity for an infinite step. Further investigation with more consistent potentials would be required before applying a modified Weizsäcker term to specific problems. Most problems to which statistical methods are applied do not have fixed potentials, but rather potentials determined by the density distribution. For such, it is not until after a problem is solved that the potential is known.

§5. APPLICATION TO GOMBÁS' CALCULATIONS

Gombás has recognized the failure of the Weizsäcker equation in the case of a small number of particles. When only one quantum state is occupied, for example, the Weizsäcker term gives the total kinetic energy of the system and the Fermi energy is redundant. In the investigation of nuclear densities and binding energies, Gombás (1952) inserted a factor multiplying the Fermi energy which approaches unity for large A and vanishes for $A = 4$ (helium). Later, for general problems with spherical symmetry, Gombás (1953 a) introduced a modification to the kinetic energy expression which depends upon the radius vector in order to correct this particular defect; for large values of the radius vector, Gombás' equation reduces to Weizsäcker's equation. The objections which we have raised above are not accounted for by Gombás' modification since, for example, in the case of plane symmetry or for heavy nuclei, the modification either vanishes or is negligible.

Although Gombás' (1952) investigation of nuclei included necessarily crude assumptions about nuclear forces, he was able to fit nuclear binding energies over nearly the entire range of nuclear masses quite well, using only a single adjustable parameter (the strength of the forces). The resulting nuclear densities, however, appear to be greater at the centre and smoother in shape (nearly gaussian) than current experiments indicate. It is to be noted that the Weizsäcker energy for heavy nuclei is comparable to the net binding energy. A reduction of the Weizsäcker coefficient would reduce this contribution to the energy, and also increase the (negative) nuclear potential energy due to the sharpening of the nuclear surface which would also result. Since Gombás uses the binding energy as the criterion of his fit, a reduction of the Weizsäcker term would lead to a smaller value of his adjustable parameter and larger nuclei. Actually, the total binding energy is too sensitive a criterion to use in such a crude model if the shape of the density distribution is sought.

Gombás (1953 b) used the Weizsäcker term with his modifications to solve atomic problems. The correction term is then only of importance near the centre of the atom, where the TF solution for the density has a singularity. The major discrepancy between TF and (for example) Hartree atomic binding energies appears to arise from this singularity. Thus, the removal of the singularity by Gombás' modification of Weizsäcker's correction term gives an impressive improvement in the binding energies. It may be, however, that any of several devices which could remove this singularity would also lead to good binding energies. The validity of Gombás' approach could be tested by solving his equations for a fixed Coulomb field and comparing the results with the exact quantum solutions.

ACKNOWLEDGMENTS

We wish to thank Professor Niels Bohr for extending to us the hospitality of the Institute for Theoretical Physics. Suggestions and comments by several members of the Institute have proved invaluable, and for these we should particularly like to thank Professor L. L. Foldy, Dr. Aage Bohr and Mr. J. Lindhard. We are grateful to the Swedish Board of Computing Machinery and the staff associated with the BESK for their very kind cooperation in the solution of the numerical problems.

One of us (L.W.) gratefully acknowledges the kind support of the U.S. National Science Foundation.

APPENDIX

Numerical Method†

Equation (9) presents a boundary value problem which possesses certain characteristic solutions. We restrict ourselves to one dimension and let the independent variable range $0 < x < \infty$, and subject the dependent variable to the boundary conditions

$$\left.\begin{aligned}\omega'(0)&=0\\ \omega(\infty)&=0\end{aligned}\right\}. \qquad \ldots\ldots(\mathrm{A1})$$

---

† The iterative method for solving non-linear differential equations discussed here has been used by Henyey and Wilets (University of California, unpublished) for solving equations of stellar structure. The method is particularly useful when several coupled differential equations are involved or when acccurate solutions at both boundaries are required. In the case of n-coupled differential equations, we think of ω_i and $H_i(\omega_1 \ldots \omega_N)$ as n-dimensional vectors for each mesh point i. The following development is then quite general.

This does not fix $\omega(0)$ or the behaviour as $x \to \infty$. There are only certain characteristic values of $\omega(0)$ (perhaps only one) which are consistent with the conditions (A1), and in this sense $\omega(0)$ is an eigenvalue. The usual method of guessing $\omega(0)$ and integrating outward until the behaviour of the solution can be ascertained, and then repeating the procedure with a better value of $\omega(0)$, is not always an efficient method for electronic computing machines. Rather, we choose a trial function which satisfies the boundary conditions (A1) and, by a series of iterations, improve the function; at each step, the boundary conditions are satisfied, but the differential equations are not. The method is outlined as follows:

Let us replace equation (9) by a set of difference equations. We think of $\omega(x_i) \equiv \omega_i$ as being an N-dimensional vector defined at the N mesh points of x. Our boundary conditions require $\omega_{-1} = \omega_1$ and $\omega_N = 0$, where N is sufficiently large to assure us that the latter condition does not differ significantly from $\omega(\infty) = 0$. The difference equations may be written formally as

$$\mathbf{H}(\boldsymbol{\omega}) = 0, \qquad \ldots\ldots(\text{A2})$$

where $\mathbf{H}$ is a non-linear operator acting on the vector $\boldsymbol{\omega} = (\omega_i)$; $\mathbf{H}(\boldsymbol{\omega})$ is a vector, and thus (A2) represents N coupled equations. If $\tilde{\boldsymbol{\omega}} = \boldsymbol{\omega} - \delta\boldsymbol{\omega}$ is an approximate solution of (A2), then we may formally expand $\mathbf{H}(\boldsymbol{\omega})$ in a Taylor series,

$$\mathbf{H}(\tilde{\boldsymbol{\omega}} + \delta\boldsymbol{\omega}) = \mathbf{H}(\tilde{\boldsymbol{\omega}}) + \sum_i \left(\frac{\partial \mathbf{H}(\tilde{\boldsymbol{\omega}})}{\partial \omega_i}\right) \delta\omega_i + \ldots. = 0. \qquad \ldots\ldots(\text{A3})$$

We rewrite this in the form

$$\mathbf{H}(\tilde{\boldsymbol{\omega}}) + \left(\frac{\partial \mathbf{H}(\tilde{\boldsymbol{\omega}})}{\partial \boldsymbol{\omega}}\right) \delta\boldsymbol{\omega} + \ldots. = 0, \qquad \ldots\ldots(\text{A3}a)$$

where $\partial\mathbf{H}/\partial\boldsymbol{\omega}$ is to be considered a linear operator, or matrix. The approximate solution of (A3 *a*), neglecting the higher derivatives of $\mathbf{H}$, gives an improved value for $\boldsymbol{\omega}$. The process is iterated until $\mathbf{H}(\tilde{\boldsymbol{\omega}})$ (hence $\delta\boldsymbol{\omega}$) is sufficiently small. The method is formally equivalent to Newton's method for solving algebraic equations.

Because we are here dealing with a second-order difference equation, the matrix $\partial\mathbf{H}/\partial\boldsymbol{\omega}$ possesses elements along the main diagonal and the diagonals one above and one below the main diagonal. A third-order difference equation would lead to matrices with four diagonals grouped about the main diagonal, etc. The number of operations necessary to solve for $\delta\boldsymbol{\omega}$ is, in general, only proportional to the order of the matrix.

We shall not discuss here the problems of convergence of the iterative method. It would appear, however, that if the matrix $\partial\mathbf{H}/\partial\boldsymbol{\omega}$ is finite in the neighbourhood of the true solution, the method gives convergence provided the trial solution is sufficiently close to the true solution. If the successive iterations do converge to a limit ($\delta\boldsymbol{\omega} \to 0$), one can be assured that the function thus obtained is a proper solution of equation (A2).

REFERENCES

Ballinger, R. A., and March, N. H., 1954, *Proc. Phys. Soc.* A, **67**, 378.

Gombás, P., 1949, *Die statistische Theorie des Atoms* (Vienna: Springer); 1952, *Acta Physi a Hung.*, **1**, 329; **2**, 224; 1953 a, *Ibid.*, **3**, 105; 1953 b, *Ibid.*, **3**, 127.

Plaskett, J. S., 1953, *Proc. Phys. Soc.* A, **66**, 178.

Schiff, L. I., 1949, *Quantum Mechanics* (New York: McGraw-Hill).

Swiatecki, W. J., 1951, *Proc. Phys. Soc.* A, **64**, 226.

Von Weizsäcker, C. F., 1935, *Z. Phys.*, **96**, 431.

The Detachment of Electrons from Negative Hydrogen Ions by impact with Neutral Atoms

By D. W. SIDA
Physics Department, University College, London

Communicated by H. S. W. Massey; MS. received 18*th August* 1954

Abstract. Born's approximation is applied to calculate the cross section for detachment of an electron from a negative ion of hydrogen in collision with a helium atom as a function of the energy of the ion. The results are compared with observed data and show agreement to within a factor of two or so over an energy range from 100 to 20 000 ev.

---

§ 1. INTRODUCTION

IN the last few years the first measurements of the cross section for detachment of electrons from negative ions by impact with neutral atoms have been made (Hasted 1952, Hasted and Stedeford 1955). These measurements are rather easier to carry out than the corresponding ones for ionization of neutral atoms by atom impact and may be used as a basis for further examination of the theoretical problem of calculating accurately the cross sections for inelastic collisions between systems both of which are of atomic, as distinct from electronic, mass. The status of Born's approximation in this connection is still far from clear. Although first thought to be quite inapplicable when the relative velocity of the colliding atoms is less than the velocities of the electrons concerned in the internal motions involved it was pointed out by Bethe (1930) that in certain circumstances it could be expected to continue to give quite good results even under these conditions. Thus inner shell ionization of a heavy atom by a proton can be treated adequately even for energies very close to the threshold. Recently Bates, Massey and Stewart (1953) have examined the matter further and consider that there may be many circumstances in which Born's approximation is not likely to be incorrect by a large factor. It is therefore of interest to apply the approximation to as many cases as possible which have been investigated experimentally, in order to obtain a reliable idea of its range of validity. In carrying out a programme of this kind it is necessary to restrict consideration to relatively simple systems for otherwise the approximations which have to be made in dealing with the wave functions for the internal motions may lead to greater errors than Born's approximation itself. The observations which have been made by Hasted and by Stedeford of the cross sections for detachment of electrons from negative hydrogen ions by impact with helium atoms have therefore been selected as the simplest to consider. In this paper an account is given of the calculation and the result obtained in comparison with observation.

§ 2. METHOD OF CALCULATION

The Born approximation, without exchange, gives the cross section for detachment (Mott and Massey 1949, Ch. XI) as

$$Q=\frac{M^2}{4\pi^2}\iiint\frac{k'}{k}\,|\mathscr{M}|^2\,d\Omega\,d\omega\,d\kappa, \qquad \ldots\ldots(1)$$

where M is the reduced mass, $d\Omega$, $d\omega$ are the elements of the solid angles of scattering and ejection, $\mathbf{k}$, $\mathbf{k}'$ are the relative momentum vectors of the incident ion and scattered atom and $\boldsymbol{\kappa}$ is the relative momentum of the ejected electron. The equations are expressed in Hartree units.

$$\mathscr{M}=\int V(\mathbf{r}_1\mathbf{r}_2\boldsymbol{\rho}_3\boldsymbol{\rho}_4\mathbf{R})\,|\phi(\rho_3\rho_4)|^2\psi_i(r_1r_2)\psi_f^*(r_1r_2)\exp\{-i(\mathbf{k}-\mathbf{k}').\mathbf{R}\} \\ \times d\mathbf{r}_1\,d\mathbf{r}_2\,d\boldsymbol{\rho}_3\,d\boldsymbol{\rho}_4\,d\mathbf{R} \qquad \ldots\ldots(2)$$

where $\phi(\rho_3\rho_4)$ is the wave function for the scattering helium atoms, $\psi_i(r_1r_2)$ for the incident ion and $\psi_f(r_1r_2)$ for the scattered atom and free electron. $\mathbf{R}$ is the nuclear separation and V the interaction,

$$V=\frac{2}{|\mathbf{R}|}-\frac{1}{|\boldsymbol{\rho}_3+\mathbf{R}|}-\frac{1}{|\boldsymbol{\rho}_4+\mathbf{R}|}-\frac{2}{|\mathbf{r}_1-\mathbf{R}|}-\frac{2}{|\mathbf{r}_2-\mathbf{R}|}+\frac{1}{|\mathbf{r}_1-\boldsymbol{\rho}_3-\mathbf{R}|} \\ +\frac{1}{|\mathbf{r}_1-\boldsymbol{\rho}_4-\mathbf{R}|}+\frac{1}{|\mathbf{r}_2-\boldsymbol{\rho}_3-\mathbf{R}|}+\frac{1}{|\mathbf{r}_2-\boldsymbol{\rho}_4-\mathbf{R}|}. \qquad \ldots\ldots(3)$$

We express the scattering and ejection in momentum coordinates by

$$\mathbf{K}=\mathbf{k}-\mathbf{k}' \qquad \mathbf{H}=\mathbf{K}-\boldsymbol{\kappa}$$

thus $$\int d\Omega=\frac{2\pi}{kk'}\int K\,dK \qquad \text{and} \qquad \int d\omega=\frac{2\pi}{K\kappa}\int H\,dH.$$

On using the theorem,

$$\int\frac{\exp(ik\mathbf{n}.\mathbf{r}')}{|\mathbf{r}-\mathbf{r}'|}\,d\mathbf{r}'=\frac{4\pi}{k^2}\exp(ik\mathbf{n}.\mathbf{r})$$

(Bethe 1930) and the property that $\psi_i(r_1r_2)$ and $\psi_f(r_1r_2)$ are orthogonal,

$$Q=\frac{256\pi^2M^2}{k^2}\iiint\left(1-\int\exp(-i\mathbf{K}.\boldsymbol{\rho}_3)\,|\phi(\rho_3\rho_4)|^2\,d\rho_3\,d\rho_4\right)^2 \\ \times\left|\int\exp(-i\mathbf{K}.\mathbf{r}_2)\psi_i\psi_f^*\,d\mathbf{r}_1\,d\mathbf{r}_2\right|^2\frac{dK\,H\,dH\,d\kappa}{K^4\kappa}. \qquad \ldots\ldots(4)$$

For the wave function for the helium atom we used a Hylleraas (1929) wave function suitably normalized,

$$\phi(\rho_3\rho_4)=\frac{\mu^3}{\pi}\exp\{-\mu(\rho_3+\rho_4)\}$$

where $\mu=1{\cdot}69$, so that

$$Q=\frac{256\pi^2M^2}{k^2}\iiint\left(1-\frac{16\mu^4}{(4\mu^2+K^2)^2}\right)^2|\mathscr{N}|^2\frac{dK\,H\,dH\,d\kappa}{K^4\kappa} \qquad \ldots\ldots(5)$$

where $$\mathscr{N}=\iint\exp(-i\mathbf{K}.\mathbf{r}_2)\psi_i\psi_f^*\,d\mathbf{r}_1\,d\mathbf{r}_2. \qquad \ldots\ldots(6)$$

The wave function for the incident hydrogen negative ion ψ_i is represented by a one parameter Hylleraas (1929) function

$$\psi_i(r_1,r_2)=\frac{\alpha^3}{\pi}\exp\{-\alpha(r_1+r_2)\}$$

where $\alpha=0{\cdot}688$.

A first approximation for the ejected electron would be to express it as a plane wave, but it was found that lack of orthogonality of ψ_i and ψ_f led to serious difficulties below about 2 kev. A more refined wave function calculated by variational methods by Massey and Moiseiwitsch (1951) was therefore used with an additional term, of the form given in (7) below, inserted to make ψ_i and ψ_f orthogonal. Even this leads to a sudden increase in cross section below 150 ev probably introduced by this extra term.

If we assume only zero order phase shift, the solution to the wave equation for this detached electron is

$$\Psi = \exp(i\eta_0)L_0(r) + \sum_{n=0}^{\infty}(2n+1)i^n L_n(r)P_n(\cos\theta)$$

which is satisfied asymptotically by

$$\Psi = \exp(i\eta_0)L_0(r) + \exp(i\boldsymbol{\kappa}\cdot\mathbf{r}) - \frac{\sin\kappa r}{\kappa r}.$$

We introduce for $L_0(r)$ a trial form which is also asymptotically correct

$$\cos\eta_0\left\{\frac{\sin\kappa r}{\kappa r} + (a+b\,\mathrm{e}^{-r})(1-\mathrm{e}^{-r})\frac{\cos\kappa r}{\kappa r} - c\,\mathrm{e}^{-\alpha r}\right\}, \qquad \ldots\ldots(7)$$

where $a=\tan\eta_0$ and b were calculated by variational methods by Massey and Moiseiwitsch (1951) and c is defined by $\int\psi_i\psi_f^*\,d\tau=0$. The complete wave function for the scattered atom and ejected electron normalized and symmetrized to allow for exchange relations, becomes

$$\psi_f(r_1, r_2) = \frac{\kappa}{2\sqrt{2\pi^2}}\{\exp(-r_1)\Psi(r_2) + \exp(-r_2)\Psi(r_1)\}.$$

Substituting into equation (6) and integrating analytically over r_1 and r_2

$$\mathcal{N} = \frac{8\sqrt{2}}{\pi}\frac{\alpha^3\kappa}{(1+\alpha)^3}\left\{\frac{2\alpha}{[H^2+\alpha^2]^2} - \frac{2\alpha}{[\alpha^2+(K-\kappa)^2][\alpha^2+(K+\kappa)^2]} + B\exp(i\eta_0)\right\}.$$

Putting $|\mathcal{N}|^2$ into the equation (5) and integrating over dH from $K-\kappa$ to $K+\kappa$

$$Q = \frac{16M^2}{k^2}\left(\frac{4\alpha}{1+\alpha}\right)^6 \iint \frac{(8\mu^2+K^2)^2}{(4\mu^2+K^2)^4}\left\{\frac{\alpha^2}{3K\kappa}\left[\frac{1}{[\alpha^2+(K-\kappa)^2]^3} - \frac{1}{[\alpha^2+(K+\kappa)^2]^3}\right]\right.$$
$$\left. - \frac{4\alpha^2}{[\alpha^2+(K-\kappa)^2][\alpha^2+(K+\kappa)^2]} + B^2\right\} \times K\,dK\,\kappa^2\,d\kappa, \qquad \ldots\ldots(8)$$

where

$$B = \cos\eta_0\left\{\frac{2\alpha}{[\alpha^2+(K-\kappa)^2][\alpha^2+(K+\kappa)^2]} + \frac{a(1+2\alpha)}{2K\kappa}\right.$$
$$\times\left[\frac{K-\kappa}{[\alpha^2+(K-\kappa)^2][(1+\alpha)^2+(K-\kappa)^2]} + \frac{K+\kappa}{[\alpha^2+(K+\kappa)^2][(1+\alpha)^2+(K+\kappa)^2]}\right]$$
$$+ \frac{b(2\alpha+3)}{2K\kappa}\left[\frac{K-\kappa}{[(1+\alpha)^2+(K-\kappa)^2][(2+\alpha)^2+(K-\kappa)^2]}\right.$$
$$\left.\left. + \frac{K+\kappa}{[(1+\alpha)^2+(K+\kappa)^2][(2+\alpha)^2+(K+\kappa)^2]}\right] - \frac{4\alpha c}{[4\alpha^2+K^2]^2}\right\}.$$

The final integrations over dK and $d\kappa$ must be evaluated numerically.

From conservation of energy, $k^2 - k'^2 = M(\kappa^2 + 2\Delta)$ where Δ is the electron affinity of hydrogen 0·026 in Hartree units (Williamson 1942). Thus the minimum value of K is

$$K_{\text{min}} \simeq \frac{1}{2v}(\kappa^2 + 2\Delta)$$

where v is the incident relative velocity. The upper limits of both K and κ may be each taken infinitely large.

§ 3. CONCLUSION

The total cross section for detachment by neutral helium atoms was calculated for energies of the incident ion up to about 20 kev and is shown in comparison with the experiments of Hasted (1952) and of Hasted and Stedeford (1955).

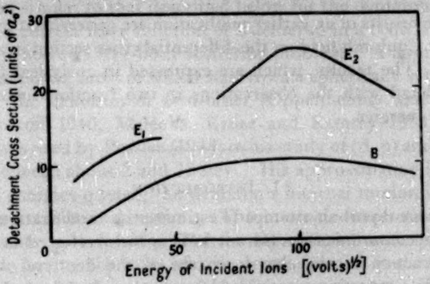

Comparison of observed and calculated cross sections for detachment of electrons from H^- in impact with He atoms: B, calculated using Born's approximation; E_1, observed (Hasted 1952); E_2, observed (Hasted and Stedeford 1955).

In the low energy regions the two curves have the same shape but do not agree in absolute values of the cross section. In the higher energy region, the maxima occur at comparable energies 10 kev but that given by this calculation is very much less pronounced than the experimental result. Despite these discrepancies, part of which may well be ascribed to the approximate nature of the wave functions used for the initial and final (continuum) states of H^-, Born's approximation gives results which are not too far wrong and certainly of the correct order of magnitude.

ACKNOWLEDGMENTS

I wish to thank Professor H. S. W. Massey for his guidance and interest in this problem, the Essex Education Committee for the award of a County Exhibition, and the Department of Scientific and Industrial Research for a maintenance grant.

REFERENCES

BATES, D. R., MASSEY, H. S. W., and STEWART, A. L., 1953, *Proc. Roy. Soc.* A, **2116,** 437.
BETHE, H., 1930, *Ann. Phys., Lpz.*, **5,** 325.
HASTED, J. B., 1952, *Proc. Roy. Soc.* A, **212,** 235.
HASTED, J. B., and STEDEFORD, J. B. H., 1955, *Proc. Roy. Soc.* A, in the press.
HYLLERAAS, E., 1929, *Z. Phys.*, **54,** 347.
MASSEY, H. S. W., and MOISEIWITSCH, B. L., 1951, *Proc. Roy. Soc.* A, **205,** 483.
MOTT, N. F., and MASSEY, H. S. W., 1949, *Theory of Atomic Collisions* (Oxford: Clarendon Press), Ch. VIII.
WILLIAMSON, E., 1942, *Astrophys. J.*, **96,** 438.

Theory of (d, p) and (d, n) Reactions
II : Coulomb Corrections and Numerical Results

By I. P. GRANT
Clarendon Laboratory, Oxford

MS. received 27*th August* 1954, *and in amended form* 27*th September* 1954

Abstract. The results of an earlier publication are generalized to take account of the effect of the Coulomb field on the differential cross section in a deuteron stripping reaction. The results, which are expressed in analytical form, have been compared in detail with the observations in two reactions using ^{9}Be as target nucleus at low energies.

---

§ 1. INTRODUCTION

In this paper we report an attempt to estimate the modifications to the results of an earlier communication (Grant 1954 a, to be referred to as I) produced by the interaction of the electric charge of the deuteron with that of the target nucleus in a stripping reaction at low energy. In § 2 we shall consider the effect of the Coulomb field on the scattering wave functions, which are used in § 3 for the evaluation of the amplitude $g^{c}{}_{l_{\mathrm{n}}}{}^{m_{\mathrm{n}}}$ analogous to the $g_{l_{\mathrm{n}}}{}^{m_{\mathrm{n}}}$ of I, equation (19). Finally we have compared the differential cross section given by our calculations with two of the experimentally observed angular distributions using ^{9}Be as target—the (d, n) reaction leading to the fourth excited state of ^{10}Be (Green, Scanlon and Willmott 1953), and the (d, p) reaction leading to the ground state of ^{10}Be (Canavan 1952), the former at a bombarding energy of 860 kev, and the latter at an energy of 1 MeV.

The angular distributions calculated with inclusion of Coulomb effects, but without nuclear scattering effects, are entirely similar to those in other recent investigations (Austern and Butler 1954, Yoccoz 1954). The principal difference between these calculations and the present one is the part played in them by numerical integration. This has no place here, as all our results are given in an analytical form.

The notation used is basically the same as that of I, and as before we shall refer to the (d, p) reaction unless the contrary is stated explicitly.

§ 2. THE WAVE FUNCTIONS

The heart of our problem is the integration of the analogue $g^{c}{}_{l_{\mathrm{n}}}{}^{m_{\mathrm{n}}}$ of

$$g_{l_{\mathrm{n}}}{}^{m_{\mathrm{n}}} = \left\{ \int Y_{l_{\mathrm{n}}}{}^{m_{\mathrm{n}}*}(\theta_{\mathrm{n}}\phi_{\mathrm{n}}) \exp(-i\mathbf{k}_{\mathrm{p}}\cdot\mathbf{r}_{\mathrm{p}}')\psi(s)\exp\{\tfrac{1}{2}i\mathbf{k}_{\mathrm{d}}\cdot(\mathbf{r}_{\mathrm{n}}+\mathbf{r}_{\mathrm{p}})\}\,d\omega_{\mathrm{n}}\,d\mathbf{r}_{\mathrm{p}} \right\}_{r_{\mathrm{n}}=R} \quad \ldots (1)$$

when the Coulomb field is no longer ignored ($\mathbf{s}=\mathbf{r}_{\mathrm{n}}-\mathbf{r}_{\mathrm{p}}$). In order to do this we have to obtain the appropriate generalizations of the factor $\exp(-i\mathbf{k}_{\mathrm{p}}\cdot\mathbf{r}_{\mathrm{p}}')$

(i.e. of the proton Green's function in unbounded space (cf. I, equation (12)), and of the deuteron plane wave.

We deal first with the simpler case of the proton. The Green's function for the Coulomb scattering of a particle is well known (compare, for example, Sommerfeld 1949, p. 206) and we obtain in place of $\exp(-i\mathbf{k}_p . \mathbf{r}_p')$

$$\exp\{-\tfrac{1}{2}\pi\eta_p\}\Gamma(1+i\eta_p)\exp[-i\mathbf{k}_p . \mathbf{r}_p']\,F[-i\eta_p, 1\,;\, i(k_p' r_p + \mathbf{k}_p' . \mathbf{r}_p)]. \qquad \ldots.(2)$$

Here $\eta_p = Ze^2/\hbar v_p$ and $\mathbf{k}_p = \{M_p M_A/(M_p + M_A)\}\,\mathbf{v}_p/\hbar$ where $\mathbf{v}_p$ is the proton velocity, and Ze the nuclear charge. F is the usual confluent hypergeometric function. The expression (2) was derived assuming that for the duration of the scattering process the deuteron ' sees ' a point charge at the origin. The result includes effects due to the fact that the centre of mass of B is not at the origin in an approximation similar to that described below for the deuteron.

To obtain the correct wave function of a deuteron in a central Coulomb field we should have to solve a three-body scattering problem. A number of approximations have been used, most of which start from a spherically symmetric charge distribution for the deuteron in zero-order (Oppenheimer and Phillips 1935, Bethe 1938, Volkoff 1940, Malenka, Kruse and Ramsey 1953). A different approximation was used by Peaslee (1948) in his study of (d, p) and (d, n) reaction cross sections between about 2 and 15 MeV. His approximation is based on the idea that at the energies quoted, the deuteron's internal motion is slow in comparison with its translational motion. The internal distribution is still given by the ground state wave function, but the translational motion is described as that of a particle having the mass of a deuteron situated at the position of the proton. Peaslee does not give a proof of this approximation. The approximation which we shall now derive is in a sense intermediate to these two. The deuteron's internal distribution is given by the ground state wave function, but its translational motion is described as that of the deuteron plane wave

$$\exp\{\tfrac{1}{2}i\mathbf{k}_d . (\mathbf{r}_n + \mathbf{r}_p)\}$$

modified by the Coulomb distortion for a free proton at $\mathbf{r}_p$ moving with the deuteron velocity $\mathbf{v}_d$.

The Schrödinger equation for a deuteron in a central Coulomb field may be transformed to the relative coordinates $\mathbf{s} = \mathbf{r}_n - \mathbf{r}_p, \mathbf{r}_p$ (cf. Margenau and Murphy 1943, p. 395) in the form

$$\left\{-\frac{\hbar^2}{2m_p}\nabla_p{}^2 + \frac{\hbar^2}{M_p}\nabla_p . \nabla_s - \frac{\hbar^2}{2m_d}\nabla_s{}^2 + V_{np}(\mathbf{s}, \sigma_n, \sigma_p) + \frac{Ze^2}{r_p} - E\right\}\psi = 0. \qquad \ldots\ldots(3)$$

m_p and m_d are the reduced masses

$$m_p = M_p M_A/(M_p + M_A),\ m_d = M_p M_n/(M_p + M_n).$$

The plane wave involved in (1) is a solution of (3) when $Z = 0$

$$\psi_0 = \psi(s)\exp\{\tfrac{1}{2}i\mathbf{k}_d . (\mathbf{r}_n + \mathbf{r}_p)\}. \qquad \ldots\ldots(4)$$

The Coulomb field has no matrix elements involving different spin states, and it follows that the correct scattering wave function may contain triplet states only. With this understanding we may ignore the spin part of the wave function as being irrelevant to the present discussion.

The correct wave function may be written in the form

$$\psi = \psi_0 f_0(\mathbf{r}_p) + \Phi(\mathbf{s}, \mathbf{r}_p) \qquad \ldots\ldots(5)$$

when $Z \neq 0$. Φ may involve only neutron–proton states orthogonal to $\psi(s)$ (i.e. states of the neutron–proton system belonging to the continuous spectrum) and $f_0 \to 1$, $\Phi \to 0$ as $Z \to 0$. Substituting (5) in (3) we obtain the equation

$$\left(\nabla_{\mathrm{p}}{}^2 + i\frac{M}{M_{\mathrm{B}}}\mathbf{k}_{\mathrm{d}}\,.\,\nabla_{\mathrm{p}} - \frac{M}{M_{\mathrm{B}}}\frac{k_{\mathrm{d}}\eta_{\mathrm{d}}}{r_{\mathrm{p}}}\right)f_0(\mathbf{r}_{\mathrm{p}}) = 2\frac{M_{\mathrm{A}}}{M_{\mathrm{B}}}\int \psi_0{}^*(\nabla_{\mathrm{p}}\,.\,\nabla_{\mathrm{s}})\Phi\, d\mathbf{s} \qquad \ldots\ldots(6)$$

for $f_0(\mathbf{r}_{\mathrm{p}})$, M being the total mass of the system. A similar equation may be obtained for each term of $\Phi(\mathbf{s}, \mathbf{r}_{\mathrm{p}})$.

We may obtain a first approximation to (6) by ignoring the right-hand side. Since $\psi(s)$ is an S-state, the only terms contributing from Φ will be P-states, so that our approximation ignores the effect of the dissociation by the electric field. The approximate solution of (6) satisfying the correct boundary conditions is

$$f_0(\mathbf{r}_{\mathrm{p}}) = \text{constant} \times F[-i\eta_{\mathrm{d}}, 1\,; i(k_{\mathrm{d}}'r_{\mathrm{p}} - \mathbf{k}_{\mathrm{d}}'\,.\,\mathbf{r}_{\mathrm{p}})] \qquad \ldots\ldots(7)$$

where $\mathbf{k}_{\mathrm{d}}' = \{M_{\mathrm{p}}M_{\mathrm{A}}/(M_{\mathrm{p}} + M_{\mathrm{A}})\}\,\mathbf{v}_{\mathrm{d}}/\hbar$, and in the same approximation

$$\psi = \exp(-\tfrac{1}{2}\pi\eta_{\mathrm{d}})\Gamma(1 + i\eta_{\mathrm{d}})\exp\{\tfrac{1}{2}i\mathbf{k}_{\mathrm{d}}\,.\,(\mathbf{r}_{\mathrm{n}} + \mathbf{r}_{\mathrm{p}})\}\psi(s)F[-i\eta_{\mathrm{d}}, 1\,; i(k_{\mathrm{d}}'r_{\mathrm{p}} - \mathbf{k}_{\mathrm{d}}'\,.\,\mathbf{r}_{\mathrm{p}})], \qquad \ldots\ldots(8)$$

the normalization being chosen so that the incident plane wave has unit amplitude.

This approximation should be adequate for all but the heaviest nuclei at the deuteron energies which have usually been employed in stripping reactions (up to about 15 MEV). Calculations of the anomalous electric scattering cross section by perturbation methods (for example Malenka, Kruse and Ramsey 1953) have shown that its ratio to the Rutherford scattering cross section varies from unity at small angles of scattering to something a little less at large angles —values of about 4·2% for 10 MEV deuterons on U ($Z = 92$) and 2·7% for 8 MEV deuterons on Bi ($Z = 83$) at an angle of 180° have been quoted for the deficit. The validity of our approximation depends on the magnitude of the electric disintegration terms in (6). The electric disintegration cross section is approximately proportional to Z^2 (Mullin and Guth 1951, Huby and Newns 1951) so that these terms will be proportional to Z. Therefore we may expect that the error incurred by our approximation is unimportant for all practical purposes in comparison with the drastic approximations made in the formal calculations of I.

§ 3. THE COULOMB CORRECTIONS

Using the wave functions defined in the preceding paragraph we may write

$$g^{c}{}_{l_{\mathrm{n}}}{}^{m_{\mathrm{n}}} = \exp\{-\tfrac{1}{2}\pi(\eta_{\mathrm{d}} + \eta_{\mathrm{p}})\}\Gamma(1 + i\eta_{\mathrm{d}})\Gamma(1 + i\eta_{\mathrm{p}})g'{}_{l_{\mathrm{n}}}{}^{m_{\mathrm{n}}}$$

for the (d, p) reaction, and

$$g^{c}{}_{l_{\mathrm{p}}}{}^{m_{\mathrm{p}}} = \exp(-\tfrac{1}{2}\pi\eta_{\mathrm{d}})\Gamma(1 + i\eta_{\mathrm{d}})g'{}_{l_{\mathrm{p}}}{}^{m_{\mathrm{p}}}$$

for the (d, n) reaction, where

$$g'{}_{l_{\mathrm{n}}}{}^{m_{\mathrm{n}}} = \left\{\int \mathrm{Y}_{l_{\mathrm{n}}}{}^{m_{\mathrm{n}}*}(\theta_{\mathrm{n}}\phi_{\mathrm{n}})\exp(-i\mathbf{k}_{\mathrm{p}}\,.\,\mathbf{r}_{\mathrm{p}}')F[-i\eta_{\mathrm{p}}, 1\,; i(k_{\mathrm{p}}'r_{\mathrm{p}} + \mathbf{k}_{\mathrm{p}}'\,.\,\mathbf{r}_{\mathrm{p}})]\right.$$
$$\left. \times\, \psi(s)\exp\{\tfrac{1}{2}i\mathbf{k}_{\mathrm{d}}\,.\,(\mathbf{r}_{\mathrm{n}} + \mathbf{r}_{\mathrm{p}})\}F[-i\eta_{\mathrm{d}}, 1\,; i(k_{\mathrm{d}}'r_{\mathrm{p}} - \mathbf{k}_{\mathrm{d}}'\,.\,\mathbf{r}_{\mathrm{p}})]\,d\omega_{\mathrm{n}}\,d\mathbf{r}_{\mathrm{p}}\right\}_{r_{\mathrm{n}}=R} \qquad \ldots\ldots(9\,a)$$

$$g'{}_{l_{\mathrm{p}}}{}^{m_{\mathrm{p}}} = \left\{\int \mathrm{Y}_{l_{\mathrm{p}}}{}^{m_{\mathrm{p}}*}(\theta_{\mathrm{p}}\phi_{\mathrm{p}})\exp\{-i\mathbf{k}_{\mathrm{n}}\,.\,\mathbf{r}_{\mathrm{n}}'\}\psi(s)\exp\{\tfrac{1}{2}i\mathbf{k}_{\mathrm{d}}\,.\,(\mathbf{r}_{\mathrm{n}} + \mathbf{r}_{\mathrm{p}})\}\right.$$
$$\left. \times\, F[-i\eta_{\mathrm{d}}, 1\,; i(k_{\mathrm{d}}'r_{\mathrm{p}} - \mathbf{k}_{\mathrm{d}}'\,.\,\mathbf{r}_{\mathrm{r}})]\,d\omega_{\mathrm{p}}\,d\mathbf{r}_{\mathrm{n}}\right\}_{r_{\mathrm{p}}=R}. \qquad \ldots\ldots(9\,b)$$

Clearly both integrals are convergent. To evaluate them we make use of the well-known contour integral representation (Erdelyi 1953, p. 272)

$$F[-i\eta, 1; i\xi] = \left(\frac{i}{2\pi}\right)\int_1^{(0+)} (-u)^{-i\eta-1}(1-u)^{i\eta}\, e^{iu\xi}du. \qquad \ldots\ldots(10)$$

The path of integration is a single loop starting and finishing at $u=1$ and encircling $u=0$ in the positive sense. All powers have their principal values. Inverting the order of spatial and contour integration

$$g'_{l_{\mathrm{n}}}{}^{m_{\mathrm{n}}} = \left(\frac{i}{2\pi}\right)\int_1^{(0+)} du(-u)^{-i\eta_{\mathrm{p}}-1}(1-u)^{i\eta_{\mathrm{p}}}$$

$$\times\left(\frac{i}{2\pi}\right)\int_1^{(0+)} dv(-v)^{-i\eta_{\mathrm{d}}-1}(1-v)^{i\eta_{\mathrm{d}}}\gamma_{l_{\mathrm{n}}}{}^{m_{\mathrm{n}}}(u, v). \qquad \ldots\ldots(11\,a)$$

$$g'_{l_{\mathrm{p}}}{}^{m_{\mathrm{p}}} = \left(\frac{i}{2\pi}\right)\int_1^{(0+)} du(-u)^{-i\eta_{\mathrm{d}}-1}(1-u)^{i\eta_{\mathrm{d}}}\gamma_{l_{\mathrm{p}}}{}^{m_{\mathrm{p}}}(u) \qquad \ldots\ldots(11\,b)$$

where

$$\gamma_{l_{\mathrm{n}}}{}^{m_{\mathrm{n}}}(u, v) = \left\{\int \mathrm{Y}_{l_{\mathrm{n}}}{}^{m_{\mathrm{n}}*}(\theta_{\mathrm{n}}\phi_{\mathrm{n}})\psi(s)\exp i[(\mathbf{K}+\mathbf{k}).\mathbf{r}_{\mathrm{n}} - (\mathbf{K}+\mathbf{q}).\mathbf{s} + K'r_{\mathrm{p}}]d\omega_{\mathrm{n}}d\mathbf{r}_{\mathrm{p}}\right\}_{r_{\mathrm{n}}=R}$$

$$\ldots\ldots(12\,a)$$

$$\gamma_{l_{\mathrm{p}}}{}^{m_{\mathrm{p}}}(u) = \left\{\int \mathrm{Y}_{l_{\mathrm{p}}}{}^{m_{\mathrm{p}}*}(\theta_{\mathrm{p}}\phi_{\mathrm{p}})\psi(s)\exp i[(-\mathbf{k}_{\mathrm{d}}'u+\mathbf{k}).\mathbf{r}_{\mathrm{p}} + \mathbf{q}.\mathbf{s} + k_{\mathrm{d}}'ur_{\mathrm{p}}]d\omega_{\mathrm{p}}d\mathbf{r}_{\mathrm{n}}\right\}_{r_{\mathrm{p}}=R}.$$

$$\ldots\ldots(12\,b)$$

Here $\mathbf{K} = \mathbf{k}_{\mathrm{p}}'u - \mathbf{k}_{\mathrm{d}}'v$, $K' = k_{\mathrm{p}}'u + k_{\mathrm{d}}'v$ and the vectors $\mathbf{k}$ and $\mathbf{q}$ have their usual meanings $\mathbf{k} = \mathbf{k}_{\mathrm{d}} - M_{\mathrm{A}}\mathbf{k}_{\mathrm{p}}/M_{\mathrm{B}}$, $\mathbf{q} = \frac{1}{2}\mathbf{k}_{\mathrm{d}} - \mathbf{k}_{\mathrm{p}}$ for a (d, p) reaction, and

$$\mathbf{k} = \mathbf{k}_{\mathrm{d}} - M_{\mathrm{A}}\,\mathbf{k}_{\mathrm{n}}/M_{\mathrm{B}},\ \ \mathbf{q} = \tfrac{1}{2}\mathbf{k}_{\mathrm{d}} - \mathbf{k}_{\mathrm{n}}$$

for a (d, n) reaction.

We may start with the evaluation of (12 *b*), which is performed most conveniently with ω_{p} and $\mathbf{s}$ as integration variables instead of ω_{p} and $\mathbf{r}_{\mathrm{n}}$ and by expanding the exponentials $\exp(-iu\mathbf{k}_{\mathrm{d}}'.\mathbf{r}_{\mathrm{p}})$ and $\exp(i\mathbf{k}.\mathbf{r}_{\mathrm{p}})$ in terms of partial waves with $\mathbf{k}$ as axis of quantization. Making use of the formula

$$\mathrm{Y}_l{}^m(\theta\phi)\mathrm{Y}_{l'}{}^{m'}(\theta\phi) = \sum_L\left[\frac{(2l+1)(2l'+1)}{4\pi(2L+1)}\right]^{1/2} C(ll'L; 00)C(ll'L; mm')\mathrm{Y}_L{}^{m+m'}(\theta\phi)$$

$$\ldots\ldots(13)$$

we obtain

$$\gamma_{l_{\mathrm{p}}}{}^{m_{\mathrm{p}}}(u) = 4\pi(2l_{\mathrm{p}}+1)^{-1/2}K_0(0)\sum_l (2l+1)i^l j_l(\rho_k)$$

$$\times\sum_\nu (-i)^\nu \exp(iu\rho'_{\mathrm{d}})j_\nu(u\rho'_{\mathrm{d}})\Psi_l{}^{m_{\mathrm{p}}*}(\nu). \qquad \ldots\ldots(14)$$

The $j_\nu(x)$ are spherical Bessel functions of the first kind (Schiff 1949, p. 77) and the other functions are defined in Appendix I. In (14) the notation ρ has been used to denote a wave number multiplied by the length R, e.g. $\rho_{\mathrm{q}} = qR$ etc.

The evaluation of (12 *a*) follows a similar, though more complex pattern. The only difficulty is due to the presence of the term $\exp(iK'r_{\mathrm{p}})$ and we have to resort to approximation to deal with this. The behaviour of $\psi(s)$ will encourage the contribution from small values of s, that is to say from values of r_{p} near to r_{n}. Therefore we replace $\exp(iK'r_{\mathrm{p}})$ by $\exp(iK'r_{\mathrm{n}})$ in the integral. This procedure is unlikely to lead to serious error.

It is now possible to evaluate the contour integrals (11) with the aid of the results of Appendix III. In both cases we may write

$$g'_{l_c}{}^{m_c} = [4\pi(2l_c+1)]^{1/2}\, i^{l_c} \sum_l \left(\frac{2l+1}{2l_c+1}\right) i^{l-l_c} A_l^{m_c} j_l(\rho_k) \qquad \ldots\ldots(15)$$

where the subscript c is an n or p according to whether we are discussing a (d, p) or a (d, n) reaction. A similar result holds for the generalization of the scattering terms of I, which can be written in the form of (15) with coefficients $B_l^{m_c}$ replacing the $A_l^{m_c}$. The detailed formulae for the $A_l^{m_c}$ are given in Appendix I, and those for the $B_l^{m_c}$ will be found in Appendix II. The complete stripping cross section is

$$\frac{d\sigma}{d\omega} = \frac{M_p^* M_d^*}{2\pi\hbar^4} \frac{k_p}{k_d} \left(\frac{2j_B+1}{2j_A+1}\right) \left(\frac{2\pi\eta_p}{\exp(2\pi\eta_p)-1}\right) \left(\frac{2\pi\eta_d}{\exp(2\pi\eta_d)-1}\right) \times \sum_{j_n l_n m_n} |B_\beta(j_n l_n)|^2 |\mathscr{I}_{l_n}{}^{m_n}(j_n)|^2 \qquad \ldots\ldots(16\,a)$$

in the (d, p) case, and

$$\frac{d\sigma}{d\omega} = \frac{M_n^* M_d^*}{2\pi\hbar^4} \frac{k_n}{k_d} \left(\frac{2j_B+1}{2j_A+1}\right) \left(\frac{2\pi\eta_d}{\exp(2\pi\eta_d)-1}\right) \sum_{j_p l_p m_p} |B_\beta(j_p l_p)|^2 |\mathscr{I}_{l_p}{}^{m_p}(j_p)|^2 \ldots.(16\,b)$$

in the (d, n) case (cf. I, equation (37)). The amplitude

$$\mathscr{I}_{l_c}{}^{m_c}(j_c) = \sum_l \left(\frac{2l+1}{2l_c+1}\right) i^{l-l_c} N_l^{m_c}(j_c) j_l(\rho_k) \qquad \ldots\ldots(17)$$

where

$$N_l^{m_c}(j_c) = A_l^{m_c} + \lambda(j_c l_c) B_l^{m_c}. \qquad \ldots\ldots(18)$$

In a (d, p) reaction $B_\beta(j_n l_n)$ is the reduced nuclear matrix element of V_n occurring in the Born approximation calculation of I, where V_n is the interaction potential of neutron and nucleus,

$$B_\beta(j_n l_n) = \langle \beta j_B || V_n || \alpha j_A j_n(l_n\tfrac{1}{2}) \rangle;$$

and

$$\lambda(j_n l_n) = U \langle \beta j_B || \alpha j_A j_n(l_n\tfrac{1}{2}) \rangle / \langle \beta j_B || V_n || \alpha j_A j_n(l_n\tfrac{1}{2}) \rangle$$

where the numerator is U times the reduced matrix element of the unit operator. U is the depth of the potential well with which the proton is assumed to interact. $|B_\beta(j_n l_n)|^2$ is thus the usual intrinsic neutron capture probability, and $\lambda(j_n l_n)$ is a measure of the relative importance of nuclear scattering and ' pure ' stripping (cf. I, equation (30)). Similar definitions can be given for the (d, n) reaction.

If the x-axis be taken in the plane of the reaction all the spherical harmonics implicit in (18) have azimuths 0 or π and it follows that $N_l^m = (-1)^m N_l^{-m}$.

It is easy to verify that (17) reduces to the result of I, equation (38) in the limit of high energy or of vanishing nuclear charge by making use of the properties of the function $\phi_\nu{}^r(\rho, \eta)$ defined in Appendix III.

§ 4. DISCUSSION AND NUMERICAL RESULTS

(*a*) *General Remarks*

We recapitulate briefly the data which a measurement of the defferential cross section can yield in a (d, p) or (d, n) reaction. The parameters defining the angular distribution (16) are (*a*) the bombarding energy E_d, (*b*) the energy release Q, (*c*) the nuclear radius R, (*d*) the orbital angular momentum $\hbar l_c$ transferred to the target nucleus, and (*e*) the corresponding total (spin + orbit) angular momentum $\hbar j_c$. The last parameter occurs only in the definition of $B(j_c l_c)$ and $\lambda(j_c l_c)$. Whilst a particular particle group will usually be connected with a single l_c, there will be in general two values of $j_c(=l_c \pm \frac{1}{2})$. The summation in (16) will be written

$$\sum_{j_c=l_c\pm\frac{1}{2}} \sum_{m_c} |B(j_c l_c)|^2 |\mathscr{I}_{l_c}{}^{m_c}(j_c)|^2 = \sum_{r=0}^{2} a_r I_r \qquad \ldots\ldots(19)$$

for a single l_c, where $a_0 = |B(+)|^2 + |B(-)|^2$, $a_1 = \lambda(+)|B(+)|^2 + \lambda(-)|B(-)|^2$, and $a_2 = |\lambda(+)B(+)|^2 + |\lambda(-)B(-)|^2$. The ± signs refer to $j_c = l_c \pm \frac{1}{2}$, and I_0, I_1 and I_2 are the contributions to the sum arising from pure stripping, interference and nuclear scattering terms respectively. In the following numerical calculations we have assumed that only a single value of j_c is effective.

The analysis of the angular distribution will only give estimates of l_c, R and the ratios a_r/a_0. An absolute measurement of the differential cross section will give the value of a_0 also. The reduced widths for nucleon emission from the final state of the residual nucleus are proportional to the $|B(j_c l_c)|^2$ but the values obtained by fitting the Butler formula to the experimental data are usually too small (Huby 1953, p. 207). The effects that we have discussed can be expected to modify these values considerably, but it is difficult to make any general prediction because of the complexity of our results.

In fitting angular distribution curves we have to assume a value of R. In the Butler or Born approximation theories this has to be taken considerably larger than the conventional radius used in discussing nuclear reactions -7×10^{-13} cm for the ^{9}Be reactions discussed below as compared with the Gamow radius of (about) $4{\cdot}25 \times 10^{-13}$ cm. Physically this implies that the interaction between deuteron and target nucleus appears to become appreciable rather a long way out. It follows that we can expect the Coulomb field in particular, and, to a lesser degree, the nuclear interaction with the emitted particle, to reduce the effective radius to a more conventional value.

(*b*) *Angular Distributions*

Because of the tedious nature of the numerical calculation we have not attempted to give typical curves for the angular distributions, but have considered two cases only at low energies. These are the angular distributions of Green, Scanlon and Willmott (1953) for the ^{9}Be(d, n)^{10}B reaction at an energy $E_d = 860$ kev, and the results of Canavan (1952) for ^{9}Be(d, p)^{10}Be at $E_d = 1$ Mev. The Q-value in the (d, n) case, which involves a transition to the fourth excited state of ^{10}B$(l_p = 1)$ is 800 kev, and that of the (d, p) reaction, which goes to the ground state of ^{10}Be$(l_n = 1)$ is 4·585 Mev.

In both computations a value $R = 4{\cdot}25 \times 10^{-13}$ cm was assumed. For calculations of the nuclear scattering term we have taken the harmonic oscillator potential well cut off at a radius $r_p = R$ as proposed in I. The main difficulty is that the field of integration over s is bounded, and the radial integral has an upper limit depending on ω_n and ω_s. The integration can only be performed by cutting off the radial integration at some mean radius αR where $0 \leqslant \alpha \leqslant 2$. For numerical work we have used $\alpha = 1$ and 2. In figure 1 we have compared the best fit to the experimental angular distribution obtained from the Born approximation

($R=7\times10^{-13}$ cm) and from our calculation for the (d, n) case. All curves are normalized to the same arbitrary maximum. In this reaction the dominating distortion of the Born approximation curve is due to the Coulomb interaction, and the nuclear scattering is of relatively minor importance. The amplitudes I_0, I_1 and I_2 are compared in figure 2 and it is clear that only a small amount of overlap between the initial and final nuclear states (as measured by $\lambda(j_p l_p)$) is necessary to produce an appreciable effect from nuclear scattering.

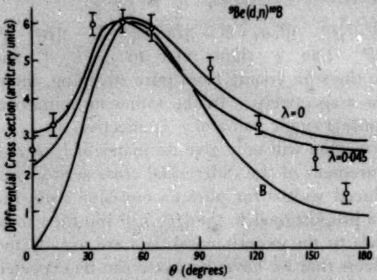

Figure 1. ^{9}Be(d, n)^{10}B. Measured angular distribution of neutrons leaving ^{10}B in fourth excited state. E_d(lab.) $=0{\cdot}860$ MeV, $Q=0{\cdot}800$ MeV (Green *et al.* 1953). Curve B: Born approximation $l_p=1$, $R=7\times10^{-13}$ cm. Other curves: present calculation, $l_p=1$, $R=4{\cdot}25\times10^{-13}$ cm, $\alpha=2$, $\lambda=0$ and $0{\cdot}045$.

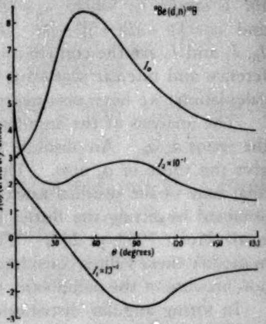

Figure 2. ^{9}Be(d, n)^{10}B. Calculated values of I_0, I_1 and I_2 for $\alpha=2$.

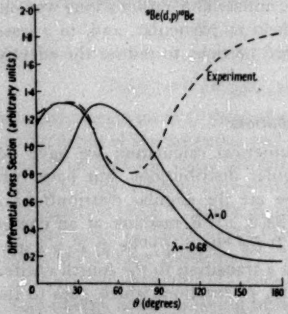

Figure 3. ^{9}Be(d, p)^{10}Be. Measured angular distribution of protons leaving ^{10}Be in ground state. E_d(lab.) $=1$ MeV, $Q=4{\cdot}585$ MeV. Broken curve: best fitting curve given by least squares analysis using a series of Legendre polynomials (Canavan 1952). Solid curves: present calculation, $l_n=1$, $R=4{\cdot}25\times10^{-13}$ cm, $\alpha=1$, $\lambda=0$ and $-0{\cdot}68$.

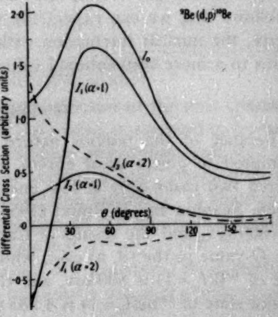

Figure 4. ^{9}Be(d, p)^{10}Be. Calculated values of I_0, I_1 and I_2 for $\alpha=1$ and 2. The scales for I_1 ($\alpha=2$) and for both the I_2 have been divided by 10.

The corresponding curves for the (d, p) case are shown in figures 3 and 4. The agreement with Canavan's experimental best fit curve is poor, showing that stripping, although important, is not the only process in this particular reaction. The calculated angular distribution is essentially similar in shape to that of the (d, n) case. A rough calculation of the relative magnitudes of the reduced width for the ^{10}Be ground state indicated that our calculation would yield a value between 5 and 20 times larger than that given by the Born approximation. No direct comparison was possible since Canavan's results are not absolute in magnitude.

(*c*) *Polarization*

A general formula for the components of the polarization vector of the outgoing particles in a stripping reaction was given in I, equation (39). Since with our choice of axes

$$N_l^m = (-1)^m N_l^{-m} \qquad \ldots\ldots(20)$$

the polarization vector lies along the *y*-axis (perpendicular to the plane of the reaction) and has a magnitude *P* given by

$$P = \pm \frac{4}{3} \frac{\sum_{j_c s_c} |B(j_c l_c)|^2/(2j_c+1) \,.\, \sum_{\mu>0} [(l_c+\tfrac{1}{2})^2 - \mu^2]^{1/2} \operatorname{Im}(\mathscr{I}^{\mu+1/2*} \mathscr{I}^{\mu-1/2})}{\sum_{j_c s_c} |B(j_c l_c)|^2 \sum_{m_c} |\mathscr{I}^{m_c}|^2} \qquad \ldots\ldots(21)$$

Assuming that only a single j_c is present, we have computed (21) as a function of angle θ for the two reactions discussed above. The results for the (d, n) case are given in figure 5. The polarization in the (d, p) reaction, ignoring the effect of nuclear interaction of the proton, has a similar angular dependence but only about half the intensity. In the general case the polarization will be a weighted mean of the two curves depending on the magnitudes of the $B(j_c l_c)$. The polarization appears to be too small to be of much use in deciding the relative magnitudes of these matrix elements.

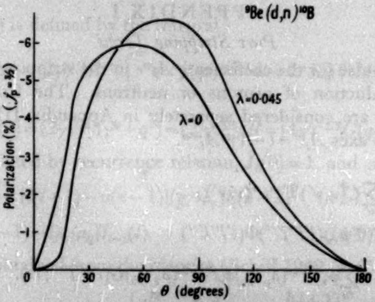

Figure 5. ^{9}Be(d, n)^{10}B. Curves give calculated polarization *P* (equation (21)) for $j_p=3/2$, $\alpha=2$, $\lambda=0$ and 0·045. Note that $P(j_p=1/2) = -2P(j_p=3/2)$.

(*d*) *Discussion*

The main conclusion emerging from the calculations is that the combination of Coulomb and nuclear interactions we have chosen is unable to account for the experimental results. It is unlikely that the angular distribution will depend strongly on the shape of the potential well assumed; but the present description of the nuclear scattering is unsatisfactory from a mathematical point of view since it is clear from figure 4 that the angular distribution depends rather strongly on the arbitrary parameter α which had to be introduced to avoid the difficulties of integration due to the finite range of our harmonic oscillator potential. A potential such as a gaussian, which is perhaps more simple to handle mathematically, would avoid this difficulty. An alternative choice, the hard-sphere scattering model of Horowitz and Messiah (1953), is not easily adapted to the present mode of calculation of Coulomb corrections. In spite of the ambiguity of our results it is clear that a small amount of overlap of the initial and final nuclear wave functions is capable of producing strong modifications to the angular distribution from nuclear scattering.

The principal advantage of our method of calculation of Coulomb corrections is its analytical expression, which shows at a glance the way in which the Coulomb interaction produces deviations from the simple Born approximation. In order of importance, the terms of the summation (17) are those with $l=l_e, l_e-1, l_e+1, \ldots$. In the cases we have discussed the convergence appeared to be a little slower for the (d, n) than the (d, p). An accuracy to about 5% was obtained by taking terms up to $l=l_p+1$ in the former case, and up to $l=l_n-1$ in the latter.

In conclusion, it seems that further work on the interaction of the emitted particle and the target nucleus is necessary. The present calculations will permit us to derive reasonably accurate estimates for R, l_e and a_0 provided that the angular distributions do not differ too much from Butler's, but are powerless if this is not the case. In addition it is not possible to determine the relative magnitudes of the $B(+)$ and $B(-)$ without performing some other experiment, such as a (d, p, γ) angular correlation, which involves different combinations of the parameters $\lambda(j_n l_n)$ and $B(j_n l_n)$. An expression for this correlation has been derived by Satchler (private communication) using our results.

APPENDIX I

Pure Stripping Terms

We quote formulae for the coefficients $A_l^{m_e}$ in the stripping part of the amplitude for the production of protons or neutrons. The Coulomb correction functions $\phi_\nu^r(\rho,\eta)$ are considered separately in Appendix III. We note that with our choice of axes $A_l^m=(-1)^m A_l^{-m}$.

(*a*) (d, p) *reactions*.

$$\left.\begin{aligned} A_l^{m_n} &= (4\pi)^3 \sum_{\nu\nu'} C(\nu,\nu')\Psi^{\nu}{}_l^{m_n *}(\nu,\nu') \\ C(\nu,\nu') &= \sum_{l'l''l'''} i^{\nu-\nu'}\psi_{\nu\nu'}(l'l''l''')\Phi(l'l''l''') \\ \psi_{\nu\nu'}(l'l''l''') &= i^{l'''-l''-l'}\sum_{rs}\phi_\nu^{l''+2r}(\rho_p'\eta_p)\phi_{\nu'}^{l'''+2s}(\rho_d'\eta_d)G(l'l''l''';rs). \end{aligned}\right\} \quad \ldots\ldots(\mathrm{A1})$$

(*b*) (d, n) *reactions*.

$$A_l^{m_p} = 4\pi K_0(0)\sum_\nu(-i)^\nu\phi_\nu^0(\rho_d'\eta_d)\Psi^{\nu}{}_l^{m_p *}(\nu). \quad \ldots\ldots(\mathrm{A2})$$

(*c*) *Angular Functions.*

The vectors whose polar angles are involved are $\mathbf{k}_d, \mathbf{k}_p, \mathbf{q}=\frac{1}{2}\mathbf{k}_d-\mathbf{k}_p$ and $\mathbf{k}=\mathbf{k}_d-M_A\mathbf{k}_p/M_B$. The last is taken as the z-axis. The vectors are all coplanar, and we take the x-axis in their common plane. Thus all spherical harmonics are real quantities. The polar angles are denoted by θ_{d}, θ_{p} and θ_{q} respectively and the corresponding azimuths ϕ_{d}, ϕ_{p} and ϕ_{q} are all 0 or π respectively.

The functions Ψ and Φ of (A1, 2) are defined by

$$\left.\begin{aligned}
\Psi_l^m(\nu,\nu') &= [(2\nu+1)(2\nu'+1)]^{1/2}\sum_n C(lal_{\mathrm{n}};00)C(lal_{\mathrm{n}};0m)C(\nu\nu'a;00)\\
&\quad\times\sum_\sigma C(\nu\nu'a;\sigma m-\sigma)\mathrm{Y}_\nu^\sigma(\theta_{\mathrm{p}}\phi_{\mathrm{p}})\mathrm{Y}_{\nu'}^{m-\sigma}(\theta_{\mathrm{d}}\phi_{\mathrm{d}})\\
\Phi(l'l''l''') &= [(2l'+1)(2l''+1)(2l'''+1)]^{1/2}C(l''l'''l';00)C(l'l'0;00)\\
&\quad\times C(l''l'''l';m'',-m'-m'')C(l'l'0;m',-m')\\
&\quad\times \mathrm{Y}_{l'}^{m'}(\theta_{\mathrm{q}}\phi_{\mathrm{q}})\mathrm{Y}_{l''}^{m''}(\theta_{\mathrm{p}}\phi_{\mathrm{p}})\mathrm{Y}_{l'''}^{-m'-m''}(\theta_{\mathrm{d}}\phi_{\mathrm{d}})
\end{aligned}\right\}\quad\ldots.(\mathrm{A3})$$

for the (d, p) case, and

$$\Psi_l^m(\nu)=(2\nu+1)^{1/2}C(l\nu l_{\mathrm{p}};00)C(l\nu l_{\mathrm{p}};\,0m)\mathrm{Y}_\nu^m(\theta_{\mathrm{d}}\phi_{\mathrm{d}})\quad\ldots\ldots(\mathrm{A4})$$

for the (d, n) case. $C(j_1j_2j;m_1m_2)$ is a vector addition coefficient, whose parameters are limited by the usual triangular inequalities (for example $|j_1-j_2|\leqslant j\leqslant j_1+j_2$), and, in our case, by the fact that j_1+j_2+j must be an even integer.

(*d*) *Radial Integrals.*

$G(l'l''l''';rs)$ is defined as the coefficient of $u^{l''+2r}v^{l'''+2s}$ in the power series expansion of the integral

$$(2\gamma)^{1/2}\int_0^\infty j_{l'}(qs)j_{l''}(uk_{\mathrm{p}}'s)j_{l'''}(vk_{\mathrm{d}}'s)\,\mathrm{e}^{-\gamma s}s\,ds.$$

We have

$$\begin{aligned}
G(l'l''l''';rs) &= (2\rho_{\mathrm{p}}')^{l''}(2\rho_{\mathrm{d}}')^{l'''}\frac{(l''+r)!}{(2l''+2r+1)!}\;\frac{(l'''+s)!}{(2l'''+2s+1)!}\;\frac{(-\rho_{\mathrm{p}}'^2)^r}{r!}\\
&\quad\times\frac{(-\rho_{\mathrm{d}}'^2)^s}{s!}K_{l'}(l''+l'''+2r+2s).
\end{aligned}\quad\ldots\ldots(\mathrm{A5})$$

The function $K_l(n)$ is defined by the integral

$$K_l(n)=(2\gamma)^{1/2}R^{-n}\int_0^\infty \mathrm{e}^{-\gamma s}j_l(qs)s^{n+1}ds=2^nK_0(0)I_l(n)\quad\ldots\ldots(\mathrm{A6})$$

with

$$K_0(0)=(2\gamma)^{1/2}/(\gamma^2+q^2)=(2/\gamma)^{1/2}gR=(4\pi)^{-1/2}G(q).\quad\ldots\ldots(\mathrm{A7})$$

The $I_l(n)$ are calculated by recurrence relation, $I_0(0)=1$, and

$$\left.\begin{aligned}
I_l(n)&=ngI_l(n-1)+[l(l+1)-n(n-1)](g/4\rho_\gamma)I_l(n-2)\qquad(n>l)\\
I_l(l)&=(l/\rho_{\mathrm{q}})I_{l-1}(l-1)-(\rho_\gamma/\rho_{\mathrm{q}})I_{l-1}(l)\qquad(l>0).
\end{aligned}\right\}\ldots\ldots.(\mathrm{A8})$$

The first result is obtained from the identity (Schiff 1949, p. 77)

$$\int_0^\infty \exp\{-(\rho_\gamma/\rho_{\mathrm{q}})u\}u^{n+1}\left\{\frac{d^2}{du^2}+\frac{2}{u}\frac{d}{du}+1-\frac{l(l+1)}{u^2}\right\}j_l(u)du=0$$

on integration by parts, and the second is based on the relation (Schiff 1949, p. 78)

$$-u^{-(l-1)}j_l(u)=\frac{d}{du}[u^{-(l-1)}j_{l-1}(u)].$$

The function g is defined by $g=\rho_\gamma/(\rho_\gamma{}^2+\rho_{\mathrm{q}}{}^2)$.

APPENDIX II

Scattering Terms

The general formulae are given first, and the specialization to the case of the bounded harmonic oscillator scattering potential discussed in I is given in (*d*). We note that $B_l^m = (-1)^m B_l^{-m}$.

(*a*) (d, p) *reactions.*

$$\left.\begin{aligned} B_l^{m_\mathrm{n}} &= (4\pi)^3 \sum_{\lambda\mu} \sum_{\nu\nu'} D_\lambda^\mu(\nu,\nu') \Psi_l^{m_\mathrm{n}+\mu^*}(\lambda;\nu,\nu') \\ D_\lambda^\mu(\nu,\nu') &= i^{\nu-\nu'} \sum_{l'l''l'''} \Psi_{\nu\nu'}^{\lambda}(l'l''l''') \Phi_\lambda^\mu(l'l''l''') \\ \Psi_{\nu\nu'}^{\lambda}(l'l''l''') &= i^{l'''-l''-l'} \sum_{rs} \phi_\nu^{l''+2r}(\rho_\mathrm{p}',\eta_\mathrm{p}) \phi_{\nu'}^{l'''+2s}(\rho_\mathrm{d}',\eta_\mathrm{d}) G_\lambda(l'l''l''';rs). \end{aligned}\right\} \quad ..\text{(A9)}$$

(*b*) (d, n) *reactions.*

$$\left.\begin{aligned} B_l^{m_\mathrm{p}} &= 4\pi \sum_{\lambda\mu} \sum_{\nu} D_\lambda^\mu(\nu) \Psi_l^{m_\mathrm{p}+\mu^*}(\lambda;\nu) \\ D_\lambda^\mu(\nu) &= (-i)^{\nu+\lambda} \phi_\nu^0(\rho_\mathrm{d}',\eta_\mathrm{d}) G_\lambda(\lambda 00;00) \mathrm{Y}_\lambda^\mu(\theta_\mathrm{q}\phi_\mathrm{q}). \end{aligned}\right\} \quad ......\text{(A10)}$$

The function $G_\lambda(\lambda 00;00) = (4\pi)^{-1/2} G(q) M_\lambda(q)$ (cf. I, equation (27)).

(*c*) *Angular Functions.*

$$\left.\begin{aligned} \Psi_l^m(\lambda;\nu,\nu') &= [(2\nu+1)(2\nu'+1)]^{1/2}(-1)^{m-m_\mathrm{n}} \\ &\quad \times \sum_{ab} C(lab;00) C(\lambda b l_\mathrm{n};00) C(lab;0m) C(\lambda b l_\mathrm{n}; m_\mathrm{n}-m, m) \\ &\quad \times C(\nu\nu' a;00) \sum_\mu C(\nu\nu' a;\mu m-\mu) \mathrm{Y}_\nu^\mu(\theta_\mathrm{p}\phi_\mathrm{p}) \mathrm{Y}_{\nu'}^{m-\mu}(\theta_\mathrm{d}\phi_\mathrm{d}) \\ \Phi_\lambda^\mu(l'l''l''') &= [(2l'+1)(2l''+1)(2l'''+1)]^{1/2} \sum_a C(l''l'''a;00) C(l'a\lambda;00) \\ &\quad \times \sum_{m'm''} C(l''l'''a;m'',\mu-m'-m'') C(l'a\lambda;m'\mu-m') \\ &\quad \times \mathrm{Y}_{l'}^{m'}(\theta_\mathrm{q}\phi_\mathrm{q}) \mathrm{Y}_{l''}^{m''}(\theta_\mathrm{p}\phi_\mathrm{p}) \mathrm{Y}_{l'''}^{\mu-m'-m''}(\theta_\mathrm{d}\phi_\mathrm{d}) \end{aligned}\right\} \quad ..\text{(A11)}$$

in the (d, p) case, and

$$\begin{aligned} \Psi_l^m(\lambda;\nu) &= [(2\nu+1)(2\lambda+1)]^{1/2}(-1)^{m-m_\mathrm{p}} \\ &\quad \times \sum_a C(l\nu a;00) C(\lambda a l_\mathrm{p};00) C(l\nu a;0m) C(\lambda a l_\mathrm{p}; m_\mathrm{p}-m, m) \mathrm{Y}_\nu^m(\theta_\mathrm{d}\phi_\mathrm{d}) \quad .\text{(A12)} \end{aligned}$$

for the (d, n) reaction.

(*d*) *Radial Integrals.*

We have used the harmonic oscillator potential well cut off at a radius $r_\mathrm{p} = R$ as proposed in I. The integration procedure has been described in the text. Otherwise the definition of $G_\lambda(l'l''l''';rs)$ is exactly parallel to the corresponding definition in Appendix I.

$$\begin{aligned} G_\lambda(l'l''l''';rs) &= (2\rho_\mathrm{p}')^{l''} (2\rho_\mathrm{d}')^{l'''} \frac{(l''+r)!}{(2l''+2r+1)!} \frac{(l'''+s)!}{(2l'''+2s+1)!} \frac{(-\rho_\mathrm{p}'^2)^r}{r!} \frac{(-\rho_\mathrm{d}'^2)^s}{s!} \\ &\quad \times \{\delta_{\lambda,0} K_{l'}(l''+l'''+2r+2s+2)_{\alpha R} - \tfrac{2}{3}\delta_{\lambda,1} K_{l'}(l''+l'''+2r+2s+1)_{\alpha R}\} \end{aligned}$$

$$......\text{(A13)}$$

where

$$K_l(n)_{\alpha R} = (2\gamma)^{1/2} R^{-n} \int_0^{\alpha R} \mathrm{e}^{-\gamma s} j_l(qs) s^{n+1} ds = 2^n K_0(0) \mathrm{J}_l(n)_{\alpha R}. \quad ......\text{(A14)}$$

$J_l(n)_{\alpha R}$ is given by the relations

$$\left.\begin{aligned}
J_0(0)_{\alpha R} &= 1+\exp(-\alpha\rho_\gamma)\{\alpha\rho_q j_1(\alpha\rho_q)-(1+\alpha\rho_\gamma)j_0(\alpha\rho_q)\}\\
J_l(n)_{\alpha R} &= \frac{2n}{\alpha}gJ_l(n-1)_{\alpha R}\\
&\quad +[l(l+1)-n(n-1)](g/\alpha^2\rho_\gamma)J_l(n-2)_{\alpha R}\\
&\quad +n\exp(-\alpha\rho_\gamma)j_l(\alpha\rho_q)-\exp(-\alpha\rho_\gamma)\{(1+\alpha\rho_\gamma)j_l(\alpha\rho_q)\\
&\quad +\frac{\alpha\rho_q}{2l+1}[lj_{l-1}(\alpha\rho_q)-(l+1)j_{l+1}(\alpha\rho_q)]\}\qquad (n>l)\\
J_l(l)_{\alpha R} &= \frac{2l}{\alpha}\frac{1}{\rho_q}J_{l-1}(l-1)_{\alpha R}-\frac{\rho_\gamma}{\rho_q}J_{l-1}(l)_{\alpha R}\\
&\quad -\alpha\exp(-\alpha\rho_\gamma)\left(\frac{\rho_\gamma{}^2+\rho_q{}^2}{\rho_q}\right)j_{l-1}(\alpha\rho_q)\qquad (l>0).
\end{aligned}\right\}\quad \ldots\text{(A15)}$$

Care has to be exercized in the use of these relations for computation since they share the disadvantages of the corresponding relations for Bessel functions.

APPENDIX III

Coulomb Distortion Functions

The Coulomb distortion function $\phi_\nu{}^r(\rho,\eta)$ is defined by the contour integral

$$\phi_\nu{}^r(\rho,\eta)=(-1)^r\left(\frac{i}{2\pi}\right)\int_1^{(0+)}du(-u)^{r-i\eta-1}(1-u)^{i\eta}\,e^{iu\rho}j_\nu(u\rho).\quad\ldots\ldots\text{(A16)}$$

A power series representation of the function may be obtained by using the relation

$$e^{iu\rho}j_\nu(u\rho)=\frac{\nu!}{(2\nu+1)!}(2u\rho)^\nu{}_1F_1(\nu+1,2\nu+2;2iu\rho)$$

(Erdelyi 1953, p. 265, equation (9)). The confluent hypergeometric function has a power series expansion uniformly convergent in any finite region of the *u*-plane, and on substituting this in (A16) and making use of the contour integral representation of the beta function (Erdelyi 1953, p. 15) we obtain

$$\begin{aligned}
\phi_\nu{}^r(\rho,\eta) &= (2\rho)^\nu\sum_{n=0}^{\infty}\frac{(\nu+n)!}{(2\nu+1+n)!}\;\frac{\Gamma(\nu+r-i\eta+n)}{\Gamma(-i\eta)(\nu+r+n)!}\;\frac{(2i\rho)^n}{n!}\\
&= (2\rho)^\nu\frac{\nu!}{(2\nu+1)!}\;\frac{\Gamma(\nu+r-i\eta)}{\Gamma(-i\eta)(\nu+r)!}\,{}_2F_2[\nu+1,\nu+r-i\eta;2\nu+2,\nu+r+1;2i\rho]
\end{aligned}\quad\ldots\ldots\text{(A17)}$$

after a little reduction. It follows that

$$\lim_{Z\to 0}\phi_\nu{}^r(\rho,\eta)=\delta_{\nu,0}\,\delta_{r,0}$$

so that in this limit our theory reduces to that of the Born approximation of I.

The function has been computed from the series for both the cases discussed in the text, and values of $|\phi_\nu{}^r(\rho,\eta)|$ for the (d, p) case are plotted against r in figure 6. Since the computation from (A17) becomes tedious for large values of ρ it is convenient to have an asymptotic expansion. The asymptotic expansion of the generalized hypergeometric function has been given by Wright (1940) and has been applied to our special case. For large ρ we obtain

$$\phi_\nu{}^r(\rho,\eta)=\delta_{\nu,0}\,\delta_{r,0}+O(\eta)\quad\ldots\ldots\text{(A18)}$$

($\rho\eta = m_p ZR/2{\cdot}905 \times 10^{-12}$ cm, $m_p = M_p M_A/(M_p + M_A)$ (Bloch *et al.* 1951). The full expression is too complicated to give here, but the details will be found in the author's thesis (Grant 1954 b). It follows from (A18) that our theory reduces to the Born approximation in the high energy limit also, but it must be emphasized that the deviation from this limit may be by no means negligible until the bombarding energy is several MEV above the Coulomb barrier height.

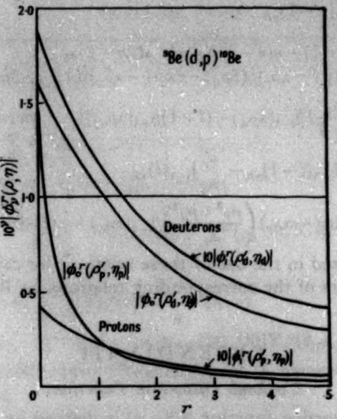

Figure 6. ⁹Be(d, p)¹⁰Be. Coulomb correction functions $10^\nu \times |\phi_\nu{}^r(\rho,\eta)|$, $\rho_d{}' = 0{\cdot}591$, $\eta_d = 0{\cdot}890$; $\rho_p{}' = 2{\cdot}039$, $\eta_p = 0{\cdot}258$.

REFERENCES

AUSTERN, N., and BUTLER, S. T., 1954, *Phys. Rev.*, **93**, 355.
BETHE, H. A., 1938, *Phys. Rev.*, **53**, 39.
BLOCH, I., HULL, M. H., BROYLES, A. A., BOURICIUS, W. G., FREEMAN, B. E., and BREIT, G., 1951, *Rev. Mod. Phys.*, **23**, 147.
CANAVAN, F. L., 1952, *Phys. Rev.*, **87**, 136.
ERDELYI, A. (Editor), 1953, *Higher Transcendental Functions*, Vol. 1 (New York: McGraw-Hill).
GRANT, I. P., 1954 a, *Proc. Phys. Soc.* A, **67**, 981 ; 1954 b, *Thesis*, University of Oxford.
GREEN, L. L., SCANLON, J. P., and WILLMOTT, J. C., 1953, *Phil. Mag.*, **44**, 919.
HOROWITZ, J., and MESSIAH, A. M. L., 1953, *J. phys. Radium*, **14**, 695.
HUBY, R., 1953, *Progr. Nucl. Phys.*, **3**, 177 (London : Pergamon Press).
HUBY, R., and NEWNS, H. C., 1951, *Phil. Mag.*, **42**, 1442.
MALENKA, B. J., KRUSE, U. E., and RAMSEY, N. F., 1953, *Phys. Rev.*, **91**, 1165.
MARGENAU, H., and MURPHY, G. M., 1943, *The Mathematics of Physics and Chemistry* (New York : Van Nostrand).
MULLIN, C. J., and GUTH, E., 1951, *Phys. Rev.*, **82**, 141.
OPPENHEIMER, J. R., and PHILLIPS, M., 1935, *Phys. Rev.*, **48**, 500.
PEASLEE, D. C., 1948, *Phys. Rev.*, **74**, 1001.
SCHIFF, L. I., 1949, *Quantum Mechanics* (New York : McGraw-Hill).
SOMMERFELD, A., 1949, *Partial Differential Equations in Physics* (New York: Academic Press).
VOLKOFF, G. M., 1940, *Phys. Rev.*, **57**, 866.
WRIGHT, E. M., 1940, *Proc. Lond. Math. Soc.* (2), **46**, 389.
YOCCOZ, J., 1954, *Proc. Phys. Soc.* A, **67**, 813.

LETTERS TO THE EDITOR

The Nuclear Spin and Magnetic Moment of Terbium 159

The paramagnetic resonance spectrum of the Tb^{3+} ion has been observed in a crystal of yttrium ethyl sulphate containing about 0·1% terbium ethyl sulphate. The spectrum consists of a single electronic transition split into four hyperfine lines; this confirms the nuclear spin of terbium 159 as 3/2. The spectrum can be described by the following Hamiltonian:

$$\mathscr{H} = g_{\parallel}\beta H_z S_z + A S_z I_z + \Delta S_x$$

where the effective spin $S=\frac{1}{2}$, $I=3/2$, $g_{\parallel}=17{\cdot}72 \pm 0{\cdot}02$, $A=0{\cdot}209 \pm 0{\cdot}002$ cm^{-1} and $\Delta = 0{\cdot}387 \pm 0{\cdot}001$ cm^{-1}.

The ground state of the free Tb^{3+} ion is $4f^8$, $^7F_6$. In a crystalline electric field of complete axial symmetry the ground state would be split into six doublets characterized by $J_z = \pm 6 \pm 5, \ldots, \pm 1$ and a singlet $J_z=0$. The values of $g_{\parallel}=g_z$ for the doublets would be $2\Lambda J_z$, where Λ is the Landé factor and equals 3/2 for Tb^{3+}. The measured value of $g_{\parallel}$ is so large that the observed doublet can only correspond to $J_z = \pm 6$ ($g_{\parallel}=18$ in this approximation). In the ethyl sulphates the crystal field has C_{3h} symmetry, which has matrix elements between states whose values of J_z differ by 6. Thus the states $J_z = \pm 6$ have matrix elements with $J_z=0$, and this splits the doublet and admixes the states in a way which can be represented by the term ΔS_x in the spin Hamiltonian. Transitions within the split doublet are allowed when a radio-frequency magnetic field is applied along the crystal axis, as observed in praseodymium ethyl sulphate (Bleaney and Scovil 1952) and plutonyl rubidium nitrate (Bleaney, Llewellyn, Pryce and Hall 1954). There is a significant difference in the present case, however, in that no departure from the C_{3h} symmetry is required to admix the doublet states.

An approximate value of the nuclear magnetic moment of ^{159}Tb can be obtained using the theory of Elliott and Stevens (1953). Matrix elements of the crystal field between the ground configuration $J=6$ and excited states such as $J=5$ prove to be negligible in the present case, and we have then

$$A/g_{\parallel} = \frac{2\beta\beta_N \mu_N}{I}\,\overline{r^{-3}}\,\frac{\langle J\|N\|J\rangle}{\langle J\|\Lambda\|J\rangle}$$

where $\langle J\|N\|J\rangle = 49/90$ and $\langle J\|\Lambda\|J\rangle = \Lambda = 3/2$. Elliott and Stevens give also $\overline{r^{-3}} = (12 \pm 3)(Z-55)^{3/4}$, which for Tb yields $\overline{r^{-3}} = 68 \pm 17 A^{-3}$. From this we find $\mu_N = 1{\cdot}5 \pm 0{\cdot}4$ nuclear magnetons. The approximation used neglects any contribution to the hyperfine structure from configurations with unpaired s electrons, but an effect of the order of magnitude observed by Bleaney and Low (1954) in Eu^{2+} would change the result only by about 5%. The error due to this is small compared with that assumed for $\overline{r^{-3}}$.

Clarendon Laboratory,
Oxford.
J. M. Baker.
B. Bleaney.

11th November 1954.

Bleaney, B., Llewellyn, P. M., Pryce, M. H. L., and Hall, G. R., 1954, *Phil. Mag.*, **45**, 991.

Bleaney, B., and Low, W., 1955, *Proc. Phys. Soc.* A, **68**, 55.

Bleaney, B., and Scovil, H. E. D., 1952, *Phil. Mag.*, **43**, 999.

Elliott, R. J., and Stevens, K. W. H., 1953, *Proc. Roy. Soc.* A, **219**, 387.

Paramagnetic Resonance Absorption by the Ferrous Ion

Paramagnetic resonance absorption has been observed with Fe^{2+} ions present as substitutional impurities in single crystals of ZnF_2 grown from the melt. According to spectroscopic analysis, the concentration of iron was less than 0·03%. This crystal has the rutile structure with two cations per unit cell. Since the axes for the two ions are orthogonal, the macroscopic symmetry is tetragonal although each cation has surroundings of only rhombic symmetry.

The splitting of the ground term $3d^6\,{}^5D$ in a crystal field of this symmetry has been calculated by standard methods (Bleaney and Stevens 1953). With values of the parameters suggested by a simple model, this calculation yields the following general scheme. The five-fold orbital degeneracy is reduced by the cubic field to an upper doublet and a lower triplet separated by approximately $10^4\,\mathrm{cm}^{-1}$. Addition of the terms of only rhombic symmetry lifts all the remaining orbital degeneracy. In particular, it leaves the lower triplet levels split with intervals of the order $10^3\,\mathrm{cm}^{-1}$. If now the spin–orbit coupling is considered, the five-fold spin degeneracy of each orbital level is lifted. The ground orbital level is split into a low-lying close doublet and three levels spaced several cm^{-1} apart and located roughly $30\,\mathrm{cm}^{-1}$ above the ground doublet. The separation Δ of the ground doublet is a fraction of a wave number.

Since the interaction with the upper levels in the presence of an external magnetic field is negligible for the field strengths used, it is convenient to treat the doublet in an $S=1/2$ formalism, neglecting the other levels. An appropriate spin Hamiltonian is then

$$\mathscr{H}=g_{\parallel}\beta S_z H_z+\Delta S_x \qquad \ldots\ldots(1)$$

where the z-axis is the c-axis of the crystal, which is common to both ions in the unit cell. This simple form is possible since $g_{\perp}=0$. The two eigenvalues of (1) differ by

$$h\nu=(\Delta^2+g_{\parallel}{}^2\beta^2H_z{}^2)^{1/2}.$$

Experimental data at several wavelengths between 1·25 and 3·85 cm and at several angles confirm this dependence. At 20°K the values of the parameters are $g_{\parallel}=8{\cdot}97\pm0{\cdot}02$ and $\Delta=0{\cdot}203\pm0{\cdot}004\,\mathrm{cm}^{-1}$. Similar precision could not be obtained at 90°K because of the lower signal/noise ratio. The data at 90° are consistent with the $g_{\parallel}$ given above, but require that Δ have the different value $0{\cdot}224\pm0{\cdot}010\,\mathrm{cm}^{-1}$.

The high g-value is readily understood by noting that in the high field limit the two levels concerned are really characterized by $S_z=\pm2$ in the original $S=2$ picture, which includes the full spin multiplicity of the ground term. Thus the spin-only $g_{\parallel}$ would be 8 in the $S=1/2$ formalism. The deviation from this value is the result of orbital angular momentum which is mixed in by the spin–orbit coupling. Since $g_{\perp}=0$, transitions are only induced by the component of the microwave magnetic field along the z-axis, in which case S_z does not change. Therefore transitions are only possible to the extent that the ΔS_x term in (1) mixes the eigenfunctions of S_z. This gives a transition probability proportional to $(\Delta/h\nu)^2$. A very similar situation was recently found in terbium ethyl sulphate (Baker and Bleaney 1955).

At 90°K the relaxation time is roughly 4×10^{-9} second giving a line so broad that with 3 cm wavelengths there is appreciable absorption at zero field. At 20°K the line has narrowed considerably, and at approximately 12°K hyperfine structure begins to be resolved. This structure is tentatively ascribed to the interaction of the magnetic electrons with the nuclei of the fluorine ions which surround the ferrous ion. This interpretation indicates that charge transfer, a characteristic of covalent bonding (Stevens 1953, Griffiths, Owen, and Ward 1953), is important even in a crystal as ionic as this one. It is hoped that further experiments at lower temperatures will clarify the situation.

The author is grateful to Dr. B. Bleaney for most helpful discussions and to Mr. J. M. Baker for assistance with the K-band measurements. He also wishes to acknowledge the help of the Crystal Growing Section, Natural Philosophy Department, Aberdeen University, who grew the ZnF_2 crystals. Finally, it is a pleasure to acknowledge the Fellowship from the U.S. National Science Foundation which has enabled the author to carry out this research.

Clarendon Laboratory,
Oxford.
23rd November 1954.

M. TINKHAM.

BAKER, J. M., and BLEANEY, B., 1955, *Proc. Phys. Soc.* A, **68**, 257.
BLEANEY, B., and STEVENS, K. W. H., 1953, *Rep. Progr. Phys.*, **16**, 108 (London: Physical Society).
GRIFFITHS, J. H. E., OWEN, J., and WARD, I. M., 1953, *Proc. Roy. Soc.* A, **219**, 526.
STEVENS, K. W. H., 1953, *Proc. Roy. Soc.* A, **219**, 542.

The Total Cross Sections for the Nuclear Scattering of High Energy Nucleons

In a recent publication (Gatha, Shah and Patel 1954) we have analysed the nuclear differential scattering of 340 MEV nucleons on the basis of the Born approximation. As a result, we have derived a characteristic nuclear density distribution for light elements described by

$$\rho(r') = N \sum_{q=1}^{3} \alpha_q \exp(-\beta_q r'^2) \qquad \ldots\ldots(1)$$

where $r' = rA^{-1/3}$ and the constants N, α_q and β_q have been determined numerically. In this analysis, the nuclear complex refractive index has been written as

$$n = 1 + (k'_1 + iK'/2)\rho/k \qquad \ldots\ldots(2)$$

where we have taken $k'_1 = 8$ mbn and $K' = 26$ mbn at this energy. In the present investigation, we have calculated σ_t, the total cross section for this scattering process.

Since the spin effects can be shown to be negligible, we can write the potential as

$$U = -k(2k'_1 + iK')\rho \qquad \ldots\ldots(3)$$

neglecting the quadratic term which has been found to give a negligible contribution to σ_t. We have used the expression (Lax 1950) for the total cross section

$$\sigma_t = -\frac{1}{k}\,\mathrm{Im}\left\{\int e^{-ikz}\, U\psi\, d\mathbf{r}\right\} \qquad \ldots\ldots(4)$$

where ψ is the exact wave function. It can be shown that to evaluate σ_t up to the first Born approximation it is necessary (Morse and Feshbach 1953) to evaluate the above integral at least up to the second Born approximation. Neglecting powers of U higher than the second power, we obtain, by a straightforward procedure,

$$\sigma_t = K'A + \lambda(k_1'^2 - K'^2/4)A^{4/3} \qquad \ldots\ldots(5)$$

where

$$\lambda = \pi^2 N^2 \sum_{q,q'} \alpha_q \alpha_{q'} / (\beta_q \beta_{q'})^{1/2} (\beta_q + \beta_{q'})$$

$$= 0{\cdot}016 \times 10^{27}\ \mathrm{cm}^{-2},$$

and wherein we have dropped an exponential term which gives a negligible contribution. In the above expression, the second term gives a contribution which lies between 10% and 20% of the first term. This indicates that the Born series should converge rapidly enough.

We have used Hildebrand's curves (private communication) for σ_t against energy for the nuclear scattering of nucleons from a few MEV to 280 MEV. Since these curves for various elements almost level off at high energies it has been possible for us to extrapolate them without introducing any significant errors and thus obtain σ_t at 340 MEV for several light elements. These experimental values of σ_t have been compared with the theoretical values calculated from equation (5) as shown below.

The Total Cross Sections in millibarns at 340 MEV

Element	Be	C	O	Al	S
σ_t (theoretical)	203	267	349	566	662
σ_t (experimental)	200	270	355	550	670

The above comparison shows that the characteristic nuclear density distribution for light elements and the parameters of the complex refractive index given above provide reasonable values for the total cross sections for the scattering process.

M. G. Science Institute,
Navarangpura,
Ahmedabad, 9, India.

K. M. GATHA.
G. Z. SHAH.

11th April 1954 and in amended form 30th August 1954.

GATHA, K. M., SHAH, G. Z., and PATEL, N. J., 1954, *Proc. Phys. Soc.* A, **67**, 773.
LAX, M., 1950, *Phys. Rev.*, **78**, 306.
MORSE, P. M., and FESHBACH, H., 1953, *Methods of Theoretical Physics* (New York: McGraw Hill), p. 1073.

A New Static Spherically Symmetric Solution of Einstein's Unified Field Theory

In the current formulation of the field equations of the unified field theory (Einstein 1953) the determinant g of the fundamental non-symmetric tensor g_{ik} is assumed to be non-zero. However, it can be easily verified that the method of Lagrangian variation, which is used to derive the field equations, does not require this assumption. Beginning with a fundamental non-symmetric tensor density $\mathfrak{g}^{ik}$ and a non-symmetric affinity Γ_{ik}^{l} one can apply all the analysis used by Einstein or Schrödinger without ever using the assumption $\det|\mathfrak{g}^{ik}|=g\neq 0$ and get the field equations of the unified theory in the form

$$\mathfrak{g}^{ik}{}_{,l}+\mathfrak{g}^{is}\Gamma_{ls}{}^{k}+\mathfrak{g}^{sk}\Gamma_{sl}{}^{i}-\mathfrak{g}^{ik}\Gamma_{\underline{ls}}{}^{s}=0, \qquad \ldots\ldots(1)$$

$$\Gamma_{\underset{\smile}{sl}}{}^{l}=0 \text{ or } \mathfrak{g}^{\underset{\smile}{is}}{}_{,s}=0,$$

$$\mathbf{R}_{\underline{ik}}=0, \qquad \ldots\ldots(2)$$

$$\mathbf{R}_{\underset{\smile}{ik},l}+\mathbf{R}_{\underset{\smile}{kl},i}+\mathbf{R}_{\underset{\smile}{li},k}=0. \qquad \ldots\ldots(3)$$

It will be seen that this assumption ($g\neq 0$) is only used in getting tensors out of the fundamental tensor density in the usual straightforward manner.

We have worked out a simple mathematical solution of equations (1), (2) and (3) which is static and spherically symmetric and for which $\det|\mathfrak{g}^{ik}|$ is zero. The general form of static spherically symmetric tensor density fields can be derived in the manner of Papapetrou (1948) or Vaidya (1953). We have taken the following form:

$$\mathfrak{g}^{ik}=\begin{pmatrix} -\alpha\sin\theta & 0 & 0 & 0 \\ 0 & -\beta\sin\theta & i\beta & 0 \\ 0 & -i\beta & -\beta\operatorname{cosec}\theta & 0 \\ 0 & 0 & 0 & \gamma\sin\theta \end{pmatrix}. \qquad \ldots\ldots(4)$$

α, β, γ are functions of r only and

$$\det|\mathfrak{g}^{ik}|=0, \qquad \ldots\ldots(5)$$

r, θ, ϕ being the usual spherical polar coordinates. For the form (4) of $\mathfrak{g}^{ik}$, the 64 algebraic equations (1) for the affinities $\Gamma_{ik}{}^{l}$ are very much simplified. They split up into independent sets of six or seven equations each. The procedure adopted for solving these equations is essentially similar to that adopted by Papapetrou (1948) or Bonnor (1952) in deriving their spherically symmetric solutions. However, there is a fundamental difference in the solutions so obtained. The 64 equations (1) do not determine all the 64 affinities $\Gamma_{ik}{}^{l}$. They determine 63 affinities and one component of the density $\mathfrak{g}^{ik}$. The affinity that is left undetermined at this stage is $\Gamma_{22}{}^{1}$ and the density component that is determined at this stage is $\mathfrak{g}^{44}$ or γ. The equation (1) leads to

$$\alpha\gamma=1 \qquad \ldots\ldots(6)$$

and the following values of the non-vanishing $\Gamma_{ik}{}^{l}$:

$$\Gamma_{11}{}^{1}=\frac{\beta'}{2\beta}-\frac{\alpha'}{2\alpha}\,; \quad \Gamma_{14}{}^{4}=\Gamma_{41}{}^{4}=\frac{\beta'}{2\beta}+\frac{\alpha'}{2\alpha}\,; \quad \Gamma_{22}{}^{1}=B=B(r);$$

$$\Gamma_{32}{}^{1}=-\Gamma_{23}{}^{1}=iB\sin\theta; \qquad \Gamma_{23}{}^{3}=\Gamma_{32}{}^{3}=\cot\theta; \qquad \Gamma_{33}{}^{1}=B\sin^{2}\theta;$$

$$\Gamma_{33}{}^{2}=-\sin\theta\cos\theta; \quad \Gamma_{44}{}^{1}=\alpha^{2}\left(\frac{\beta'}{2\beta}+\frac{\alpha'}{2\alpha}\right).$$

Here a prime indicates differentiation with regard to r. $\Gamma_{22}{}^{1}=B=B(r)$ is left undetermined. The Einstein tensor $\mathbf{R}_{ik}$ can now be formed and the field equations (2) and (3) are satisfied if

$$B=\frac{1}{\beta}(K-\textstyle\int\beta\,dr) \qquad \ldots\ldots(7)$$

and

$$\alpha=\frac{M}{\beta}(N+\textstyle\int\beta\,dr). \qquad \ldots\ldots(8)$$

K, M, N are undetermined constants. Equations (6) and (8) give the components of the fundamental density $\mathfrak{g}^{ik}$, $\beta=\beta(r)$ being left arbitrary.

Now that the $\det|\mathfrak{g}^{ik}|=0$, we cannot get tensors out of this density in the usual straightforward manner. Taking the skew part first, a covariant tensor $\mathbf{F}_{\underset{\smile}{ik}}$ can be obtained from it by the relation

$$\tfrac{1}{2}\epsilon^{ikmn}\mathbf{F}_{\underset{\smile}{ik}}=\mathfrak{g}^{\underset{\smile}{mn}},$$

where ϵ^{ikmn} is the Levi–Civita density. In the present solution we find that

$$\mathbf{F}_{\underset{\smile}{14}}=i\beta \qquad \ldots\ldots(9)$$

is the only surviving component of $\mathbf{F}_{\underset{\smile}{ik}}$.

For obtaining a symmetric tensor we form the determinant of the tensor density $\mathfrak{g}^{\underline{ik}}$

$$\bar{g}=\det|\mathfrak{g}^{\underline{ik}}|=-\alpha\gamma\beta^2\sin^2\theta.$$

Now putting $g^{\underline{ik}}=\mathfrak{g}^{\underline{ik}}/\sqrt{(-\bar{g})}$ one gets

$$g^{11}=-\frac{\alpha}{\beta},\ g^{22}=-1,\ g^{33}=-\operatorname{cosec}^2\theta,\ g^{44}=\frac{1}{\alpha\beta}.$$

Lowering the indices in the usual manner one gets

$$g_{11}=-\frac{\beta}{\alpha},\ g_{22}=-1,\ g_{33}=-\sin^2\theta,\ g_{44}=\alpha\beta.$$

If we take this g_{ik} as giving the metric of space-time, the line-element corresponding to this metric takes the form

$$ds^2=-\frac{\beta}{\alpha}\,dr^2-\frac{1}{r^2}(r^2\,d\theta^2+r^2\sin^2\theta\,d\phi^2)+\alpha\beta dt^2. \qquad \ldots\ldots(10)$$

This metric of our solution belongs to a class of metrics which is quite distinct from the class of spherically symmetric metrics used in general relativity in that a line-element of the form (10) cannot be transformed to a line-element of the type

$$ds^2=-e^{\lambda}\,dr^2-r^2\,d\theta^2-r^2\sin^2\theta\,d\phi^2+e^{\nu}\,dt^2. \qquad \ldots\ldots(11)$$

It is obvious that the class of line-elements of which (10) is a type, cannot represent an isolated distribution because these line-elements do not yield flat space-time at large distances. However, they may represent some cosmological situations. They can also be used to represent certain electromagnetic fields which are surrounded by Schwarzschild's empty field over a sphere of definite radius. The detailed treatment of this singular class of line-elements in the scheme of general relativity will be published elsewhere.

Vallabh Vidyanagar,
India.

P. C. Vaidya.

12th November 1954.

Einstein, A., 1953, *The Meaning of Relativity* (Princeton : University Press). Appendix II.
Bonnor, W. B., 1952, *Proc. Roy. Soc.* A, **210**, 427.
Papapetrou, A., 1948, *Proc. R. Irish Acad.* A, **52**, 69.
Vaidya, P. C., 1953, *Phys. Rev.*, **90**, 695.

REVIEWS OF BOOKS

X-ray Diffraction Procedures, by H. P. KLUG and L. E. ALEXANDER. Pp. xiii + 716. (London : Chapman and Hall, 1954.) 120*s*.

The book under review is directed primarily to physicists who use x-rays as a tool in either industrial or in academic research laboratories. Only about a third of the book is devoted to a review of the properties of x-rays, the geometrical character of crystals and the theoretical background of x-ray diffraction. This naturally leads to a great deal of compression and a certain amount of background information is necessary if the reader is to appreciate fully all the points made. The subjects covered are, however, set out clearly and full use is made of diagrams and of tables.

The main part of the book is devoted to experimental techniques and to the interpretation of experimental data. The description of the Geiger counter spectrometer and of its operation forms the main feature of this part. This relatively new technique is described in very useful detail. The analysis and interpretation of diffraction patterns from powders, especially those composed of non-cubic crystals, are discussed very fully.

The applications which are considered are many and varied. The quantitative analysis of crystalline powders and the determination of the size of crystallites from line broadening form two examples. The analysis of the information which can be derived from x-ray data on non-crystalline solids forms an interesting chapter. Of particular interest to physicists will be the section on x-ray scattering at very small angles, both the measurement of large crystal spacings and the determination of particle sizes by this method being relatively new.

The book is written in a very clear style, is well illustrated and well documented. It will certainly be indispensable to the specialist but it can be read and studied with profit by physicists who are not primarily concerned with x-ray techniques.

M. BLACKMAN.

CONTENTS OF SECTION B

PAGE

Mr. J. B. Arthur, Dr. W. Bardsley, Dr. A. F. Gibson and Dr. C. A. Hogarth. On the Measurement of Minority Carrier Lifetime in n-Type Silicon . . 121

Dr. R. G. Fowler. Constriction of the Positive Column of a Glow Discharge at High Pressure 130

Dr. G. Francis. The Growth of Electrodeless Discharges in Hydrogen . . 137

Mr. J. R. Cook. Photoconductivity in Calcium Tungstate 148

Dr. G. D. Archard. Two New Simplified Systems for the Correction of Spherical Aberration in Electron Lenses 156

Dr. D. A. Jones. Growth of Lead Fluoride Crystals from the Melt 165

Mr. M. H. N. Potok. The Diffraction of a Non-Monochromatic Electromagnetic Wave by a Slit and a Grating 171

Research Notes :

- Dr. S. R. Mohanty and Mr. P. Srinivasa Rao. Inversion Potential of the Joshi Effect and Light Intensity 177
- Dr. J. S. Halliday and Dr. W. Hirst. The Examination of Oxide Films by Reflection Electron Microscopy 178
- Prof. L. F. Bates, Mr. S. J. Leach, Mr. R. G. Loasby and Dr. K. W. H. Stevens. The Magnetic Susceptibility of Metallic Neodymium . . . 181
- Mr. R. D. Knott, Mr. I. D. Colson and Mr. M. R. P. Young. Breakdown Effect in p–n Alloy Germanium Junctions 182

Letters to the Editor :

- Prof. E. A. Guggenheim. The Computation of Electric Dipole Moments . 186

Reviews of Books 188

Contents of Section A 192

The Binding Energies of ^{3}H and ^{4}He

By G. ABRAHAM†, L. COHEN‡, and A. S. ROBERTS*
Physical Laboratories, University of Manchester

Communicated by L. Rosenfeld; MS. received 24th August 1954
and in final form 19th October 1954

Abstract. The binding energies of ^{3}H and ^{4}He are calculated as part of an attempt to solve the 'consistency' problem of light nuclei. A phenomenological two-body interaction, with central and tensor forces of different range, is assumed, the parameters being taken from a recent paper by Feshbach and Schwinger. The inclusion of additional sets of D-states in the wave functions is found to have a very appreciable effect on the binding energies. A rough calculation shows that the contribution of spin–orbit forces may not be negligible. Without a more extensive investigation into the effects of the additional D-states and the effect of spin–orbit forces, it is impossible to conclude that the interaction used leads to a satisfactory solution of the 'consistency' problem.

§ 1. Introduction

Briefly stated, the 'consistency' problem of light nuclei is to find an interaction, with suitable parameters, which will yield the correct binding energies for ^{2}H, ^{3}H, ^{3}He and ^{4}He, and the experimental value of the deuteron quadrupole moment, and which will be consistent with the low-energy two-body scattering data. The position at the commencement of the present calculation may be summarized as follows:

(i) Central forces can account for the binding energies of ^{2}H, ^{3}H and ^{3}He, but the same interaction with the same parameters leads to too high a binding energy for ^{4}He. Irving (1951), for example, obtained a binding energy of about 40 Mev for ^{4}He with an interaction that gave reasonable results for the lighter nuclei. Central forces fail, also, to explain the deuteron quadrupole moment.

(ii) A mixture of central and tensor forces of the same range adjusted to fit the ^{2}H data leads to binding energies for ^{3}H and ^{4}He which are much too small. Using an interaction of this kind, with a square well radial dependence, Gerjuoy and Schwinger (1942) obtained only 32% and 50% of the observed binding energies of ^{3}H and ^{4}He respectively.

(iii) A mixture of central and tensor forces of different range (first suggested by Gerjuoy and Schwinger 1942) has not yet been fully treated. However, calculations of the triton binding energy with a mixture of this form have been fairly successful (Pease and Feshbach 1951).

(iv) The effect of spin–orbit forces on the binding energies of light nuclei is usually assumed to be negligible. However, the situation is by no means clear. Measurements of the magnetic moments of light nuclei indicate the existence of a spin–orbit coupling; the large splitting between the virtual $P_{1/2}$ and $P_{3/2}$ levels in ^{5}He and ^{5}Li suggests that this coupling may be considerable. However, in the absence of a satisfactory explanation of the ^{5}He and ^{5}Li splitting in terms of a spin–orbit interaction no reliable conclusion regarding the strength of such an interaction can be drawn from the data; this is discussed further in § 5.

---

† Now at the Tata Institute, Bombay.
‡ Now at the Durham Colleges in the University of Durham.
* Now at the British Rayon Research Association, Manchester.

(v) Many-body forces will also contribute to binding energies, but since no manageable formalism exists it is impossible, at the present time, to estimate their effects.

In this paper we investigate whether a mixture of the form (iii), i.e. an interaction consisting of a sum of central and tensor forces of different range, leads to a satisfactory solution of the 'consistency' problem. Spin–orbit forces are neglected but a rough estimate of their effect is given in § 5. The forces are taken to be charge independent and the singlet and triplet central interactions are assumed to be of the same range; both of these assumptions are consistent with the low-energy scattering data (Blatt and Jackson 1949, Bethe 1949), at least when the radial dependence of the interaction is assumed to have the Yukawa form. On this basis, the form of interaction best suited to our purpose is that used by Feshbach and Schwinger in their paper on the triplet neutron–proton interaction (1951). This paper is, in fact, indispensable to the present calculation in that it lists sets of parameters, corresponding to various pairs of central and tensor force ranges, all of which give the correct deuteron binding energy and quadrupole moment; some sets of parameters also fit the low energy scattering data (see table VI of Feshbach and Schwinger's paper).

It was originally intended to extend the present programme to include heavier nuclei (^{6}Li, ^{7}Li, etc.) and it was therefore necessary to keep numerical work to a minimum. For this reason we chose radial wave functions of the form introduced by Irving (1951); all integrals can then be evaluated explicitly. The accuracy of these wave functions is discussed briefly in § 7.

We have calculated, by a simple variational method, the ^{3}H and ^{4}He binding energies for each set of the Feshbach and Schwinger parameters, using a mixture of S- and D-states. The integrals occurring in the helium calculation are more manageable than those in the triton calculation; it has therefore been possible to carry the investigation of the helium binding energy somewhat further than that of the triton binding energy. The ^{3}H calculation is given in § 3 and the ^{4}He calculation in § 4. A dicussion of spin–orbit coupling is given in § 5. The final results are discussed in § 6.

§ 2. THE INTERACTION

Since saturation conditions appear to favour a charge-symmetric interaction between nucleons it was considered desirable to use an interaction of this type. However, in the calculation involving the additional D-states of helium it was found that the use of the neutral interaction made computation appreciably simpler. For the work involving only the principal S- and D-states of triton and helium, both forms of interaction were used; the results (for all likely values of the parameters) were found to be much the same for both forms. This, to a certain extent, justifies the use of only the neutral interaction for the calculation on the additional D-states of helium.

For the triplet neutron–proton interaction Feshbach and Schwinger (1951) use the form

$$V(1,2) = -[V_c f_c(r_{12}/r_c) + V_t S_{12} f_t(r_{12}/r_t)], \qquad \ldots\ldots(1)$$

where $f_c(x)=f_t(x)=e^{-x}/x$; $r_{12}=|\mathbf{r}_{12}|=|\mathbf{r}_1-\mathbf{r}_2|$; V_c and V_t $(=\gamma V_c)$ are the central and tensor force strengths; r_c and r_t are the central and tensor force ranges, and

$$S_{12}=3(\boldsymbol{\sigma}_1 . \mathbf{r}_{12})(\boldsymbol{\sigma}_2 . \mathbf{r}_{12})/r_{12}^2-\boldsymbol{\sigma}_1 . \boldsymbol{\sigma}_2.$$

For the three- and four-body problems it is necessary, of course, to include a singlet potential and to specify the exchange character of the interaction. The two potentials considered in this paper (one corresponding to charge-symmetric, the other to neutral meson theory) may be expressed in one form as follows (assuming the same range for the singlet and triplet potentials)

$$\mathscr{V}(1,2)=\mathscr{V}_c(1,2)+\mathscr{V}_t(1,2),$$

where

$$\mathscr{V}_c(1,2)=-PV_c[1+\tfrac{1}{2}g(\boldsymbol{\sigma}_1 . \boldsymbol{\sigma}_2-1)]f_c(r_{12}/r_c) \qquad \ldots\ldots(2)$$

$$\mathscr{V}_t(1,2)=-PV_t S_{12} f_t(r_{12}/r_t)$$

$$P=\begin{cases} 1 & \text{(neutral theory)} \\ -\tfrac{1}{3}(\boldsymbol{\sigma}_1 . \boldsymbol{\sigma}_2)(\boldsymbol{\tau}_1 . \boldsymbol{\tau}_2) & \text{(charge-symmetric theory)}\,; \end{cases}$$

the parameter g is obtained from the singlet and triplet force strengths by means of the formula $V_s=(1-2g)V_c$. The singlet strength V_s is obtained from the central force range through the expansion (Rosenfeld 1948, page 131),

$$V_s=4{\cdot}67\times10^{-4}(M_m/m)^2-0{\cdot}965\times10^{-2}(M_m/m),$$

where M_m/m is the ratio of the meson mass M_m to the electron mass m. In terms of the central force range $M_m/m=\hbar c/mr_c$.

Various parameters used in the paper of Feshbach and Schwinger (1951) and which occur in the present paper are defined below:

$$\lambda=MV_c r_c^2/\hbar^2;\quad \tau=r_c/r_t;\quad \eta=(M\epsilon^{(2)}/\hbar^2)^{1/2}r_c;\quad \eta/\tau=(M\epsilon^{(2)}/\hbar^2)^{1/2}r_t;$$

M is the nucleon mass (proton and neutron are assumed to have the same mass) and $\epsilon^{(2)}$ is the binding energy of the deuteron.

The numerical values assumed for the constants were as follows:

$$\epsilon^{(2)}=2{\cdot}23\,\text{Mev};\quad M/\hbar^2=2{\cdot}4162\times10^{18}\,\text{ev}^{-1}\,\text{cm}^{-2};\quad e^2=1{\cdot}437\times10^{-7}\,\text{ev cm}.$$

Hence $(M\epsilon^{(2)}/\hbar^2)^{1/2}=2{\cdot}3212\times10^{12}\,\text{cm}^{-1}$, $r_c=4{\cdot}3081\times10^{-13}\,\eta\,\text{cm}$,
and $r_t=4{\cdot}3801\times10^{-13}\,\eta/\tau\,\text{cm}$.

The values of λ, γ and g corresponding to the various values of η and η/τ used in the paper are given in table 1.

Table 1

η	η/τ	λ	γ	g	η	η/τ	λ	γ	g
0·313	0·640	2·10	0·129	0·130	0·256	0·640	1·99	0·096	0·102
	0·492	1·94	0·275	0·099		0·492	1·82	0·207	0·064
	0·355	1·44	0·974	−0·040		0·355	1·33	0·734	−0·097
	0·320	1·12	1·786	−0·195		0·320	1·02	1·352	−0·278
0·275	0·640	2·02	0·107	0·110	0·224	0·640	1·92	0·078	0·085
	0·492	1·85	0·231	0·074		0·492	1·75	0·170	0·044
	0·355	1·34	0·836	−0·088		0·355	1·27	0·599	−0·129
	0·320	1·04	1·507	−0·256		0·320	0·95	1·124	−0·336

The parameters V_c, γ, r_c and r_t were taken directly from Feshbach and Schwinger's paper.

§ 3. THE BINDING ENERGY OF ^{3}H

3.1. *The Wave Functions*

The total orbital angular momentum L is not conserved, owing to the presence of the tensor force; neither, in a three-particle system, is the total intrinsic spin S. Since, for the ^{3}H ground state, $J=1/2$ and the maximum value of S is $3/2$, L can take only the values 0, 1 and 2. The ground state, therefore, is a mixture of S- P- and D-states. The component T_3 of isotopic spin, defined in an analogous manner to S_z and representing the net charge, is a constant having the value $\frac{1}{2}$. Corresponding to this value of T_3 the total isotopic spin T can have either of the values 1/2 and 3/2. In order to restrict the number of possible states we consider only the case $T=1/2$; it can be shown that states with this value of T lie lower than those with $T=3/2$. Assuming that the central forces predominate over the tensor force the ground state is, in a first approximation, an S-state. In the next approximation D-states but no P-states must be included since the tensor force couples S- and D- but not S- and P-states.

For the radial parts of the wave functions we use functions of the form used by Irving (1951). If $\mathbf{r}_1$, $\mathbf{r}_2$ and $\mathbf{r}_3$ are the position vectors of the three nucleons measured from an arbitrary origin then the radial wave function is

$$f(\mu)=\exp\left[-\tfrac{1}{2}\mu(\mathbf{r}_{12}{}^2+\mathbf{r}_{13}{}^2+\mathbf{r}_{23}{}^2)^{1/2}\right], \qquad \ldots\ldots(3)$$

where $\mathbf{r}_{12}=\mathbf{r}_1-\mathbf{r}_2$, etc.

We define new coordinates by the orthogonal transformation

$$\left.\begin{aligned}\mathbf{R}&=\sqrt{\tfrac{1}{3}}(\mathbf{r}_1+\mathbf{r}_2+\mathbf{r}_3),\\ \mathbf{r}&=\sqrt{\tfrac{2}{3}}\{\mathbf{r}_3-\tfrac{1}{2}(\mathbf{r}_1+\mathbf{r}_2)\},\\ \boldsymbol{\rho}&=\sqrt{\tfrac{1}{2}}(\mathbf{r}_2-\mathbf{r}_1).\end{aligned}\right\}, \qquad \ldots\ldots(4)$$

In terms of these the radial function becomes

$$f(\mu)=\exp\left[-\tfrac{1}{2}\sqrt{3}\mu(\mathbf{r}^2+\boldsymbol{\rho}^2)^{1/2}\right]. \qquad \ldots\ldots(5)$$

The motion of the centre of mass does not enter into the calculation.

The non-radial parts of the wave functions are most readily obtained by the operator method introduced by Gerjuoy and Schwinger (1942). The principal S and D wave functions (with radial parameters μ and ν respectively), anti-symmetric or symmetric in particles 1 and 2 and normalized for spin alone are

$$\left.\begin{array}{llll}{}^2\mathrm{S}_{1/2} & : \ \chi f(\mu) \quad ; & {}^4\mathrm{D}_{1/2}(\mathbf{r},\mathbf{r}): & \mathrm{D}(\mathbf{r},\mathbf{r})\chi f(\nu)\\ {}^4\mathrm{D}_{1/2}(\mathbf{r},\boldsymbol{\rho}): & \mathrm{D}(\mathbf{r},\boldsymbol{\rho})\chi f(\nu); & {}^4\mathrm{D}_{1/2}(\boldsymbol{\rho},\boldsymbol{\rho}): & \mathrm{D}(\boldsymbol{\rho},\boldsymbol{\rho})\chi f(\nu)\end{array}\right\} \quad \ldots(6)$$

where
$$\chi=\sqrt{\tfrac{1}{2}}(\chi_1{}^+\chi_2{}^- - \chi_1{}^-\chi_2{}^+)\chi_3{}^+,$$
$$\mathrm{D}(\mathbf{a},\mathbf{b})=\tfrac{3}{2}(\boldsymbol{\sigma}_1\,.\,\mathbf{a})(\boldsymbol{\sigma}_2\,.\,\mathbf{b})+\tfrac{3}{2}(\boldsymbol{\sigma}_1\,.\,\mathbf{b})(\boldsymbol{\sigma}_2\,.\,\mathbf{a})-(\mathbf{a}\,.\,\mathbf{b})(\boldsymbol{\sigma}_1\,.\,\boldsymbol{\sigma}_3),$$

and $\chi_i{}^+$ and $\chi_i{}^-$ are the two spin states of nucleon i; the subscripts 1 and 2 stand for the neutrons.

Using these and the isotopic spin wave functions and restricting ourselves to the case $T=\frac{1}{2}$, $T_3=\frac{1}{2}$ we construct states anti-symmetric in all three particles

$$\left.\begin{array}{ll}{}^{22}\mathrm{S}_{1/2}: & \Psi_{\mathrm{S}}'=[(\boldsymbol{\tau}_1\,.\,\boldsymbol{\tau}_3)-(\boldsymbol{\sigma}_1\,.\,\boldsymbol{\sigma}_3)]\,\chi\phi f(\mu)\\ {}^{24}\mathrm{D}_{1/2}: & \Psi_{\mathrm{D}}{}^{0\prime}=[\mathrm{D}(\boldsymbol{\rho},\boldsymbol{\rho})-\mathrm{D}(\mathbf{r},\mathbf{r})-(2/\sqrt{3})(\boldsymbol{\tau}_1\,.\,\boldsymbol{\tau}_3)\mathrm{D}(\mathbf{r},\boldsymbol{\rho})]\,\chi\phi f(\nu)\end{array}\right\} \quad \ldots(7)$$

where ϕ is the same function of isotopic spin as χ is of ordinary spin.

With normalization factors the wave functions are

$$\left.\begin{aligned}\Psi_S &= \tfrac{3}{4}(15\pi^3)^{-1/2}\mu^3\Psi_S{}';\\ \Psi_D{}^0 &= \tfrac{3}{2}(5.7\,!\,\pi^3)^{-1/2}\nu^5\Psi_D{}^{0\prime}.\end{aligned}\right\} \qquad \ldots\ldots(8)$$

These principal states are the lowest, and are unique in the sense that in order to form other wave functions with the same quantum numbers and the same radial factors it is necessary to introduce further scalar functions of the relative position vectors $\mathbf{r}$ and $\boldsymbol{\rho}$ corresponding to higher orbital angular momenta of the individual nucleons. Of these scalar functions the ones corresponding to the lowest individual angular momenta are

$$(\mathbf{r}\,.\,\boldsymbol{\rho});\quad (\mathbf{r}\,.\,\mathbf{r})=r^2;\quad (\boldsymbol{\rho}\,.\,\boldsymbol{\rho})=\rho^2.$$

The lowest additional D-states, anti-symmetric in particles 1 and 2 are

$$\left.\begin{aligned}& r^2\mathrm{D}(\mathbf{r},\boldsymbol{\rho})\chi f(\nu); && \rho^2\mathrm{D}(\mathbf{r},\boldsymbol{\rho})\chi f(\nu);\\ & (\mathbf{r}\,.\,\boldsymbol{\rho})\mathrm{D}(\mathbf{r},\mathbf{r})\chi f(\nu); && (\mathbf{r},\boldsymbol{\rho})\mathrm{D}(\boldsymbol{\rho},\boldsymbol{\rho})\chi f(\nu)\end{aligned}\right\} \qquad \ldots\ldots(9)$$

where, in order to restrict the number of parameters, we have assumed the radial parameters to be the same as that for the principal D-state.

The corresponding totally anti-symmetric states (again with $T=\frac{1}{2}$, $T_3=\frac{1}{2}$) are

$$\left.\begin{aligned}&(1)\ \Psi_D{}^{1\prime}=\{[(2r^2-\rho^2)\mathrm{D}(\boldsymbol{\rho},\boldsymbol{\rho})-\rho^2\mathrm{D}(\mathbf{r},\mathbf{r})+2(\mathbf{r}\,.\,\boldsymbol{\rho})\mathrm{D}(\mathbf{r},\boldsymbol{\rho})]\\ &\qquad +(1/\sqrt{3})(\boldsymbol{\tau}_1\,.\,\boldsymbol{\tau}_3)[(\mathbf{r}\,.\,\boldsymbol{\rho})\mathrm{D}(\boldsymbol{\rho},\boldsymbol{\rho})+3(\mathbf{r}\,.\,\boldsymbol{\rho})\mathrm{D}(\mathbf{r}\,.\,\mathbf{r})-2\rho^2\mathrm{D}(\mathbf{r},\boldsymbol{\rho})]\}\chi\phi f(\nu),\\ &(2)\ \Psi_D{}^{2\prime}=\{[r^2\mathrm{D}(\boldsymbol{\rho},\boldsymbol{\rho})+(r^2-2\rho^2)\mathrm{D}(\mathbf{r},\mathbf{r})-2(\mathbf{r}\,.\,\boldsymbol{\rho})\mathrm{D}(\mathbf{r},\boldsymbol{\rho})]\\ &\qquad +(1/\sqrt{3})(\boldsymbol{\tau}_1\,.\,\boldsymbol{\tau}_3)[3(\mathbf{r}\,.\,\boldsymbol{\rho})\mathrm{D}(\boldsymbol{\rho},\boldsymbol{\rho})+(\mathbf{r}\,.\,\boldsymbol{\rho})\mathrm{D}(\mathbf{r},\mathbf{r})-2r^2\mathrm{D}(\mathbf{r},\boldsymbol{\rho})]\}\chi\phi f(\nu),\\ &(3)\ \Psi_D{}^{3\prime}=(r^2+\rho^2)\Psi_D{}^{0\prime}.\end{aligned}\right\}$$

$$\ldots\ldots(10)$$

These additional D-states are directly coupled by the tensor interaction to the principal S-state. Clapp (1949), Hu and Hsu (1950) and Pease and Feshbach (1951) have emphasized the importance of the contribution made by such states to the triton binding energy.

The triton binding energy was calculated first with a wave function containing only the principal S- and D-states (8). The contribution of the additional D-states (10) was then estimated by adding these states separately and one at a time to the original wave function. A more satisfactory method would have been to use a wave function consisting of a sum of the principal S- and D-states and all the additional D-states (10). However this would have entailed a much more laborious calculation. The approximate method showed that only $\Psi_D{}^{1\prime}$ contributes appreciably to the binding energy. The D part of the final wave function was therefore taken to be a sum of the principal D-state and $\Psi_D{}^{1\prime}$.

The normalized function had the form

$$\Psi_D=\tfrac{3}{2}(5\,.\,7\,!\,\pi^3)^{-1/2}\nu^5(1+0{\cdot}22a'+0{\cdot}46a'^2)^{-1/2}(\Psi_D{}^{0\prime}+a\Psi_D{}^{1\prime}), \qquad \ldots\ldots(11)$$

where a is a variational parameter and $a'=100a/3\nu^2$.

3.2. *The Matrix Elements*

The matrix elements of the kinetic and potential energy operators are written separately. The kinetic energy operator

$$\mathscr{K} = -\sum_{i=1}^{3} (\hbar^2/2M)\nabla_{r_i}^2$$

becomes, in the new coordinates,

$$\mathscr{K} = -(\hbar^2/2M)(\nabla_R^2 + \nabla_r^2 + \nabla_\rho^2). \qquad \ldots\ldots(12)$$

The matrix elements in the two cases, neutral and charge-symmetric, are the same for the principal D-states, except for the D–D interaction elements which, however, are very small. With the additional D-states there is no precise correspondence between the two cases, but their contributions to the binding energy were found to be of the same order. The matrix elements given below are for the charge-symmetric case.

$$\left.\begin{aligned}
\langle\Psi_S|\mathscr{K}|\Psi_S\rangle &= \tfrac{1}{4}Cx^2\\
\langle\Psi_D|\mathscr{K}|\Psi_D\rangle &= \tfrac{1}{4}Cy^2\frac{1+0{\cdot}14a'+0{\cdot}45a'^2}{1+0{\cdot}22a'+0{\cdot}46a'^2}\\
\langle\Psi_S|\mathscr{V}(1,2)+\mathscr{V}(1,3)+\mathscr{V}(2,3)|\Psi_S\rangle &= \langle\Psi_S|3\mathscr{V}(1,2)|\Psi_S\rangle\\
&= -C\lambda(1-g)\frac{48}{5\pi}I(x;\,1,5)\\
\langle\Psi_S|3\mathscr{V}(1,2)|\Psi_D\rangle &= -C\lambda\gamma\frac{2^5}{\pi}\left(\frac{3}{35}\right)^{1/2}\frac{x^3y^5}{z^8}\frac{1+0{\cdot}62a'}{1+0{\cdot}22a'+0{\cdot}46a'^2}I(z;\,3,7)\\
\langle\Psi_D|3\mathscr{V}(1,2)|\Psi_D\rangle &= -C\lambda\frac{64}{135\pi}\left\{\frac{1+0{\cdot}35a'+0{\cdot}55a'^2}{1+0{\cdot}22a'+0{\cdot}46a'^2}[9I(y;\,1,9)\right.\\
&\qquad -28I(y;\,3,9)+28I(y;\,5,9)]\\
&\qquad \left.-2\gamma\frac{1+2{\cdot}5a'+2a'^2}{1+0{\cdot}22a'+0{\cdot}46a'^2}[7I(y/\tau;\,3,9)-16I(y/\tau;\,5,9)]\right\}
\end{aligned}\right\} \qquad \ldots\ldots(13)$$

where $C=\hbar^2/Mr_c^2$; $x=\sqrt{\tfrac{3}{2}}\mu r_c$; $y=\sqrt{\tfrac{3}{2}}\nu r_c$; $z=\tfrac{1}{2}(x+y)$;

$$I(x;\,l,n) = x^{n+1}\int_0^{\pi/2}\frac{\sin^2\theta\cos^l\theta}{(x+\cos\theta)^n}\,d\theta;$$

λ and τ are auxiliary parameters used by Feshbach and Schwinger and are defined in §2. Explicit expressions for the integrals are given in Appendix I.

The matrix elements for the principal states are easily obtained from those above by putting $a'=0$; then Ψ_D becomes identical with Ψ_D^0.

3.3. *The Variation Calculation*

The calculation consisted in the minimizing of the binding energy with respect to the parameters μ, ν and a, for each set of the Feshbach and Schwinger parameters. The usual variational procedure was followed and details of the calculation will not be given. The procedure, for each set of the Feshbach and Schwinger parameters, was carried out in three stages as follows: (*a*) An approximate value of μ was obtained by using the S wave function only. (*b*) The value of μ so obtained was used to obtain an approximate value of ν, the trial function now being a sum of the S wave function and the principal D wave function, $\Psi_D{}^0$. Both μ and ν were then varied slightly until the maximum binding energy was obtained. (*c*) The additional D wave function $\Psi_D{}^1$ was now added to the trial function of (*b*) and the above procedure repeated to obtain a. The absolute values of the binding energies obtained in the three stages are denoted by ϵ_0, ϵ_1 and ϵ_2 respectively.

3.4. *Results*

In order to avoid confusion our results are expressed in terms of the same auxiliary parameters as are used in Feshbach and Schwinger's paper; the definitions are given in §2.

The main results are set out in table 2. The successive columns give the values of ϵ_0, ϵ_1, ϵ_2 (in MEV) and the percentage D-state obtained from the calculation of ϵ_2.

Table 2. Binding Energies for Various Values of η and η/τ

η	η/τ	ϵ_0 (MEV)	ϵ_1 (MEV)	ϵ_2 (MEV)	D-state (%)
0·313	0·640	4·65	5·9	6·6	1·6
	0·492	2·85	4·6	5·65	2·3
	0·355	0·95	2·15	3·2	4·3
	0·320	−0·4	1·15	2·4	5·5
0·275	0·640	5·1	6·6	7·45	1·5
	0·492	2·6	5·15	6·5	2·4
	0·355	0·75	2·5	3·95	4·5
	0·320	−0·85	1·4	3·1	5·6
0·256	0·640	5·35	7·1	8·15	1·5
	0·492	2·6	5·45	7·1	2·3
	0·355	0·8	2·9	4·55	4·5
	0·320	−1·1	1·55	3·55	5·6
0·224	0·640	5·8	7·8	9·25	1·4
	0·492	2·15	5·85	8·3	2·5
	0·355	0·7	3·55	5·55	4·4
	0·320	−1·9	1·65	4·2	5·4

The increase $\epsilon_2-\epsilon_1$ in the binding energy due to the additional D-state (for a particular value of η and η/τ) is seen to be quite large and is about 60% of the increase $\epsilon_1-\epsilon_0$ due to the principal D-state (for the same value of η and η/τ). It is probable that still higher order D-states will continue to add to the binding energy. Pease and Feshbach (1952) obtained an increase of 30% of the experimental binding energy with two additional D-states and a further increase of 15% of the experimental binding energy with five more D-states. This indicates that the series ϵ_0, ϵ_1, $\epsilon_2, \ldots$ will increase steadily up to some limiting value $\epsilon^{(3)}$ as more and more D-states are included in the wave function.

§4. THE BINDING ENERGY OF ^{4}He

The helium calculation follows a pattern similar to that of the triton calculation, except that it is carried out, in the main, for the neutral interaction. It was not therefore found necessary to express all the wave functions in a completely anti-symmetric form.

4.1. *The Wave Functions*

For the He ground state $J=0$, so that the possible values of L are 0, 1 and 2. The ground state is therefore a mixture of S-, P-, and D-states. Only the D-state is directly coupled to the S-state by the tensor force. The component

T_3 of isotopic spin is zero. Neglecting the Coulomb interaction the ground state will correspond to $T=0$. The Coulomb interaction will cause a slight admixture of charge triplet and quintet terms; this is neglected.

If $\mathbf{r}_1, \mathbf{r}_2, \mathbf{r}_3, \mathbf{r}_4$, are the position vectors measured from an arbitrary origin, then the radial parts of the wave functions are taken to contain exponential functions of the form

$$f(\mu)=\exp\left[-\tfrac{1}{2}\mu\Big(\sum_{i<j}\mathbf{r}_{ij}^2\Big)^{1/2}\right], \qquad \ldots\ldots(14)$$

where $\mathbf{r}_{ij}=\mathbf{r}_j-\mathbf{r}_i$.

We define new coordinates by the transformation

$$\left.\begin{aligned} \mathbf{R}&=\tfrac{1}{2}(\mathbf{r}_1+\mathbf{r}_2+\mathbf{r}_3+\mathbf{r}_4), & \mathbf{r}&=\tfrac{1}{2}(\mathbf{r}_4+\mathbf{r}_3-\mathbf{r}_2-\mathbf{r}_1),\\ \boldsymbol{\rho}_1&=\sqrt{\tfrac{1}{2}}(\mathbf{r}_2-\mathbf{r}_1), & \boldsymbol{\rho}_2&=\sqrt{\tfrac{1}{2}}(\mathbf{r}_4-\mathbf{r}_3). \end{aligned}\right\} \qquad \ldots\ldots(15)$$

In terms of these coordinates the exponential function becomes

$$f(\mu)=\exp\left[-\mu(\mathbf{r}^2+\boldsymbol{\rho}_1^2+\boldsymbol{\rho}_2^2)^{1/2}\right]. \qquad \ldots\ldots(16)$$

The wave functions must be anti-symmetric with respect to interchange of the protons (particles 1 and 2), and with respect to interchange of the neutrons (particles 3 and 4). Since we shall treat the Coulomb energy as a perturbation the wave functions must also be invariant with respect to interchange of both neutrons with both protons.

Accordingly the principal S- and D-states can be written

$$\left.\begin{aligned} {}^{11}\mathrm{S}_0: &\qquad \phi_1=\chi f(\mu)\\ {}^{15}\mathrm{D}_0: &\qquad \phi_2=\mathrm{D}(\boldsymbol{\rho}_1,\boldsymbol{\rho}_2)\chi f(\nu) \end{aligned}\right\} \qquad \ldots\ldots\ldots(17)$$

where $\chi=(\tfrac{1}{4}\pi)^{3/2}\cdot\tfrac{1}{2}(\chi_1^+\chi_2^- - \chi_1^-\chi_2^+)(\chi_3^+\chi_4^- - \chi_3^-\chi_4^+)$,

$$\mathrm{D}(\boldsymbol{\rho}_1,\boldsymbol{\rho}_2)=\tfrac{3}{2}(\boldsymbol{\sigma}_1\cdot\boldsymbol{\rho}_1)(\boldsymbol{\sigma}_3\cdot\boldsymbol{\rho}_2)+\tfrac{3}{2}(\boldsymbol{\sigma}_1\cdot\boldsymbol{\rho}_2)(\boldsymbol{\sigma}_3\cdot\boldsymbol{\rho}_1)-(\boldsymbol{\rho}_1\cdot\boldsymbol{\rho}_2)(\boldsymbol{\sigma}_1\cdot\boldsymbol{\sigma}_3),$$

and χ_i^+, χ_i^- are the two spin states of the ith nucleon.

In order to obtain further D-states it is necessary to introduce appropriate scalar functions formed from the vectors $\mathbf{r}$, $\boldsymbol{\rho}_1$, $\boldsymbol{\rho}_2$. To simplify the calculation all the D-states are assumed to contain the exponential factor $f(\nu)$ with the same parameter ν. In accordance with the required symmetry properties the next most important D-states will be

$$\left.\begin{aligned} \phi_3&=(\boldsymbol{\rho}_1\cdot\boldsymbol{\rho}_2)\mathrm{D}(\mathbf{r},\mathbf{r})\chi f(\nu);\\ \phi_4&=(\boldsymbol{\rho}_1\cdot\boldsymbol{\rho}_2)[\mathrm{D}(\boldsymbol{\rho}_1,\boldsymbol{\rho}_1)+\mathrm{D}(\boldsymbol{\rho}_2,\boldsymbol{\rho}_2)]\chi f(\nu);\\ \phi_5&=[(\mathbf{r}\cdot\boldsymbol{\rho}_2)\mathrm{D}(\mathbf{r},\boldsymbol{\rho}_1)+(\mathbf{r}\cdot\boldsymbol{\rho}_1)\mathrm{D}(\mathbf{r},\boldsymbol{\rho}_2)]\chi f(\nu);\\ \phi_6&=r^2\mathrm{D}(\boldsymbol{\rho}_1,\boldsymbol{\rho}_2)\chi f(\nu);\\ \phi_7&=(\rho_1^2+\rho_2^2)\mathrm{D}(\boldsymbol{\rho}_1,\boldsymbol{\rho}_2)\chi f(\nu). \end{aligned}\right\} \qquad \ldots\ldots(18)$$

The ground state wave function is then taken to be a linear combination of $\phi_1,\ldots,\phi_7$. Although these latter are not orthogonal it is simpler to leave them in this form than to attempt to construct orthogonal wave functions.

The normalized wave functions are

$$\left.\begin{aligned} \Phi_1&=(8\mu^9/3\pi)^{1/2}\phi_1\;; & \Phi_5&=(2\nu^{17}/99225\pi)^{1/2}\phi_5\;;\\ \Phi_2&=(16\nu^{13}/2025\pi)^{1/2}\phi_2\;; & \Phi_6&=(4\nu^{17}/212625\pi)^{1/2}\phi_6\;;\\ \Phi_3&=(2\nu^{17}/42525\pi)^{1/2}\phi_3\;; & \Phi_7&=(\nu^{17}/425250\pi)^{1/2}\phi_7.\\ \Phi_4&=(\nu^{17}/127575\pi)^{1/2}\phi_4\;; \end{aligned}\right\} \qquad \ldots(19)$$

Since the Φ's are not orthogonal, the 'normalization' matrix N where $N_{kl} = \langle \Phi_k | \Phi_l \rangle$ is required in the calculation.

Normalization matrix elements N_{kl}

$$\left.\begin{matrix}
1 & 0 & 0 & 0 & 0 & 0 & 0 \\
0 & 1 & 0 & \frac{1}{3}\sqrt{\frac{7}{2}} & \frac{1}{2} & \frac{1}{2}\sqrt{\frac{21}{10}} & \frac{1}{4}\sqrt{\frac{35}{3}} \\
0 & 0 & 1 & 0 & \frac{2}{\sqrt{21}} & 0 & 0 \\
0 & \frac{1}{3}\sqrt{\frac{7}{2}} & 0 & 1 & \frac{2}{3}\sqrt{\frac{2}{7}} & \frac{2}{3}\sqrt{\frac{3}{5}} & 2\sqrt{\frac{2}{15}} \\
0 & \frac{1}{2} & \frac{2}{\sqrt{21}} & \frac{2}{3}\sqrt{\frac{2}{7}} & 1 & \sqrt{\frac{10}{21}} & \sqrt{\frac{5}{21}} \\
0 & \frac{1}{2}\sqrt{\frac{21}{10}} & 0 & \frac{2}{3}\sqrt{\frac{3}{5}} & \sqrt{\frac{10}{21}} & 1 & \frac{1}{\sqrt{2}} \\
0 & \frac{1}{4}\sqrt{\frac{35}{3}} & 0 & 2\sqrt{\frac{2}{15}} & \sqrt{\frac{5}{21}} & \frac{1}{\sqrt{2}} & 1
\end{matrix}\right\} \quad \ldots\ldots(20)$$

4.2. *The Matrix Elements*

The matrix elements of the kinetic and potential energy operators are written separately as in the triton case. In terms of the coordinates defined in §4.1 the kinetic energy operator becomes

$$\mathscr{K} = -(\hbar^2/2M)(\nabla_R{}^2 + \nabla_r{}^2 + \nabla_{\rho 1}{}^2 + \nabla_{\rho 2}{}^2). \qquad \ldots\ldots(21)$$

In particular the kinetic energy matrix elements for the principal S- and D-states are

$$\langle \Phi_1 | \mathscr{K} | \Phi_1 \rangle = (\hbar^2/2M)\mu^2,$$
$$\langle \Phi_2 | \mathscr{K} | \Phi_2 \rangle = (\hbar^2/2M)\nu^2.$$

The matrix $\mathscr{K}$ where the (kl)th element $\mathscr{K}_{kl} = \langle \Phi_k | \mathscr{K} | \Phi_l \rangle$ has the form:

Matrix elements of the kinetic energy operator $\mathscr{K}$ (divided by $(\hbar^2/2M)\nu^2$)

$$\left.\begin{matrix}
\mu^2/\nu^2 & 0 & 0 & 0 & 0 & 0 & 0 \\
0 & 1 & 0 & \frac{5}{3}\sqrt{\frac{1}{14}} & \frac{5}{14} & \frac{1}{2}\sqrt{\frac{15}{14}} & \frac{5}{4}\sqrt{\frac{5}{21}} \\
0 & 0 & 1 & 0 & \frac{2}{\sqrt{35}} & 0 & 0 \\
0 & \frac{5}{3}\sqrt{\frac{1}{14}} & 0 & \frac{7}{9} & \frac{2}{3}\sqrt{\frac{1}{14}} & \frac{1}{3}\sqrt{\frac{3}{5}} & \frac{7}{3}\sqrt{\frac{1}{30}} \\
0 & \frac{5}{14} & \frac{2}{\sqrt{35}} & \frac{2}{3}\sqrt{\frac{1}{14}} & \frac{6}{7} & \frac{1}{2}\sqrt{\frac{14}{15}} & \frac{1}{2}\sqrt{\frac{5}{21}} \\
0 & \frac{1}{2}\sqrt{\frac{15}{14}} & 0 & \frac{1}{3}\sqrt{\frac{3}{5}} & \frac{1}{2}\sqrt{\frac{14}{15}} & \frac{7}{10} & \frac{1}{2\sqrt{2}} \\
0 & \frac{5}{4}\sqrt{\frac{5}{21}} & 0 & \frac{7}{3}\sqrt{\frac{1}{30}} & \frac{1}{2}\sqrt{\frac{5}{21}} & \frac{1}{2\sqrt{2}} & \frac{7}{12}
\end{matrix}\right\} \quad \ldots\ldots(22)$$

The potential energy matrix elements are rather complicated and are listed in Appendix III. It is convenient to adopt the following abbreviations:

$$J=\sum_{i<j} f_{\mathrm{c}}(r_{ij}/r_{\mathrm{c}}); \qquad K=\sum_{i<j} (\boldsymbol{\sigma}_i\,.\,\boldsymbol{\sigma}_j) f_{\mathrm{c}}(r_{ij}/r_{\mathrm{c}}); \qquad S=\sum_{i<j} S_{ij} f_{\mathrm{t}}(r_{ij}/r_{\mathrm{t}}); \quad \ldots(23)$$

the total potential energy operator may then be written

$$V=\sum_{i<j}\mathscr{V}(i,j)=-(\hbar^2\lambda/Mr_{\mathrm{c}}^2)[(1-\tfrac{1}{2}g)J+\tfrac{1}{2}gK+\gamma S].$$

The matrix elements are expressed in terms of $x=\sqrt{2\mu}r_{\mathrm{c}}$, $y=\sqrt{2\nu}r_{\mathrm{c}}$ and $z=\frac{1}{2}(x+y)$, where x and y are variable parameters.

4.3. *The Variation Calculation*

The normalized wave function for the ground state is written

$$\Psi=a_k\Phi_k \quad (k=1,\ldots,7), \qquad \ldots\ldots(24)$$

where the a_k are real and the summation convention is used. Since Ψ is normalized, the relation

$$N_{kl}a_k a_l=1 \quad (k,l=1,\ldots,7) \qquad \ldots\ldots(25)$$

must be satisfied, where $N_{kl}=\langle\Phi_k|\Phi_l\rangle$. The variational method now consists in finding values of x, y and the a_k which make the total energy of the system a minimum subject to the condition (25).

The calculation was carried out in three stages (the Coulomb energy is neglected for the purpose of the variation calculation, and is introduced later as a perturbation): (*a*) The ground state of helium is predominantly an S-state, so that a first approximation $x^{(0)}$ to the value of x was obtained by minimizing the energy Φ_1 arising from the S-state only. (*b*) The next stage consisted in including the contributions to the energy from the principal D-state Φ_2 and minimizing the total energy with respect to variation of x and y by an iteration method using $x^{(0)}$ as a first approximation. (*c*) All the wave functions were now included, and using the values of x and y obtained in stage (*b*) minimization was carried out in respect to variation of the a_k.

The Coulomb energy operator is given by $\mathscr{C}=e^2/r_{12}$, where we assume that particles 1 and 2 are protons. The contribution to the Coulomb energy from the D-states is so small that it can be neglected. This is shown by considering the calculation for the case when only the principal S- and D-states are used. The required matrix elements are

$$\langle\Phi_1|\mathscr{C}|\Phi_1\rangle=(35\sqrt{2}/128)e^2\mu=0{\cdot}09125\ x/\eta \quad \text{Mev},$$

$$\langle\Phi_2|\mathscr{C}|\Phi_2\rangle=(77\sqrt{2}/2048)e^2\nu=0{\cdot}1255\ y/\eta \quad \text{Mev},$$

since $$e^2\mu=0{\cdot}236\ x/\eta \ \text{Mev}, \qquad e^2\nu=0{\cdot}236\ y/\eta \ \text{Mev}.$$

The percentage D-state is very small (less than 4%), so that we can certainly neglect the contribution of the principal D-state to the Coulomb energy. The other D-states are present in even smaller amounts, so that the same will hold true for them as well. We need therefore only consider the contribution of the S-state to the Coulomb energy, i.e.

$$\text{Coulomb energy} = 0{\cdot}09125\ x/\eta \quad \text{Mev.} \qquad \ldots\ldots(26)$$

The calculated values are shown in table 3.

The binding energies obtained in the three stages (*a*), (*b*), (*c*) above and including the Coulomb energy are denoted by ϵ_0, ϵ_1^{neut} and ϵ_2 respectively.

Table 3. Helium Binding Energy

η	η/τ	Coulomb energy (Mev)	ϵ_0 (Mev)	ϵ_1^{sym} (Mev)	(Mev)	ϵ_2 (Mev)
0·313	0·640	1·4	34·6	36·9	37·3	39·0
	0·492	1·3	27·3	30·6	31·2	34·2
	0·3555	1·2	9·6	15·6	14·6	19·8
	0·320	0·9	2·4	7·5	6·3	11·8
0·275	0·640	1·6	41·5	44·1	44·6	46·6
	0·492	1·5	31·9	36·4	36·6	40·3
	0·3555	1·3	10·0	18·0	16·6	23·5
	0·320	1·0	2·0	8·4	6·7	14·1
0·256	0·640	1·7	45·8	48·6	49·2	51·3
	0·492	1·6	35·0	39·9	40·1	44·2
	0·3555	1·4	11·2	19·4	17·8	24·4
	0·320	1·1	1·9	9·2	7·2	15·4
0·224	0·640	1·9	55·4	58·8	59·4	62·0
	0·492	1·8	42·2	48·0	48·2	52·5
	0·3555	1·5	12·8	23·0	21·0	29·4
	0·320	1·2	1·1	10·6	7·8	18·3

4.4. *Symmetric Interaction*

The exchange character of the interaction used above for the helium calculations is that which would arise from a neutral meson theory. It is of interest to examine the effect of the corresponding symmetric interaction.

It was found convenient for this purpose to introduce the isotopic spin coordinates and to obtain totally anti-symmetric wave functions. Since we are here only concerned with comparing the binding energies for the two interactions we shall only consider the principal S- and D-states. The corresponding totally anti-symmetric wave functions are

$$\left.\begin{aligned} {}^{11}\mathrm{S}_0 &: \psi_{\mathrm{S}} = [(\boldsymbol{\tau}_1 \cdot \boldsymbol{\tau}_3) - (\boldsymbol{\sigma}_1 \cdot \boldsymbol{\sigma}_3)]\,\chi\phi f(\mu); \\ {}^{15}\mathrm{D}_0 &: \psi_{\mathrm{D}} = [-\mathrm{D}(\mathbf{r},\mathbf{r}) + \tfrac{1}{2}\mathrm{D}(\boldsymbol{\rho}_1,\boldsymbol{\rho}_1) + \tfrac{1}{2}\mathrm{D}(\boldsymbol{\rho}_2,\boldsymbol{\rho}_2) - \mathrm{D}(\boldsymbol{\rho}_1,\boldsymbol{\rho}_2)(\boldsymbol{\tau}_1 \cdot \boldsymbol{\tau}_3)]\,\chi\phi f(\nu); \end{aligned}\right\} \quad ..(27)$$

where $\phi = \tfrac{1}{2}(\zeta_1^+\zeta_2^- - \zeta_1^-\zeta_2^+)(\zeta_3^+\zeta_4^- - \zeta_3^-\zeta_4^+)$,

ζ_i^+, ζ_i^- being the two isotopic spin wave functions of the *i*th nucleon.

With normalization factors the states are

$${}^{11}\mathrm{S}_0: \quad \Psi_{\mathrm{S}} = (4\mu^9/9\pi)^{1/2}\psi_{\mathrm{S}}; \qquad {}^{15}\mathrm{D}_0: \quad \Psi_{\mathrm{D}} = (8\nu^{13}/6075\pi)^{1/2}\psi_{\mathrm{D}}. \quad \ldots\ldots(28)$$

The matrix elements for the charge-symmetric interaction are given below:

$$\left.\begin{aligned}
\langle\Psi_S|\mathscr{H}|\Psi_S\rangle &= \tfrac{1}{4}Cx^2\\
\langle\Psi_D|\mathscr{H}|\Psi_D\rangle &= \tfrac{1}{4}Cy^2\\
\langle\Psi_S|\sum_{i>j}\mathscr{V}(i,j)|\Psi_S\rangle &= \langle\Psi_S|6\mathscr{V}(1,2)|\Psi_S\rangle\\
&= -C\lambda(1-g)\frac{315}{32}I(x;\ 1,2,8)\\
\langle\Psi_S|6\mathscr{V}(1,2)|\Psi_D\rangle &= C\lambda\gamma\frac{63\sqrt{6}}{16}\frac{x^{9/2}y^{13/2}}{z^{11}}I(z/\tau;\ 3,2,10)\\
\langle\Psi_D|6\mathscr{V}(1,2)|\Psi_D\rangle &= -C\lambda\frac{231}{64}\Big\{\frac{25}{16}I(y;\ 1,4,12)\\
&\quad +I(y;\ 5,2,12)-\frac{5}{3}I(y;\ 3,3,12)\\
&\quad -2\gamma[I(y/\tau;\ 5,2,12)-\frac{7}{6}I(y/\tau;\ 3,3,12)]\Big\}
\end{aligned}\right\}\quad\ldots(29)$$

where $C=\hbar^2/Mr_c^2$; $x=\sqrt{2}\mu r_c$; $y=\sqrt{2}\nu r_c$; $z=\tfrac{1}{2}(x+y)$;

$$I(x;\ l,m,n)=x^{n+1}\int_0^1\frac{t^l(1-t^2)^m}{(x+t)^n}\,dt.$$

An explicit expression for the above integral is given in Appendix II.

The matrix elements for the corresponding neutral interaction differ only in the D–D potential energy term. The net result is to replace $-(5/3)I(y;\ 3,3,12)$ and $-(7/6)I(y/\tau;\ 3,3,12)$ occurring in this term by $5I(y;\ 3,3,12)$ and $(7/2)I(y/\tau;\ 3,3,12)$ respectively.

The corresponding binding energy, including the Coulomb energy, for the symmetric interaction is denoted by $\epsilon_1^{\mathrm{sym}}$ and is tabulated in table 3.

4.5. *Results*

The main results are tabulated in tables 3, 4 and 5. Table 3 gives the Coulomb energy, and the values of ϵ_0, $\epsilon_1^{\mathrm{sym}}$, $\epsilon_1^{\mathrm{neut}}$ and ϵ_2. (Note that we take the binding energy as the absolute value of the energy.)

Table 4 gives the detailed results for the calculation using only the principal S- and D-states with a neutral interaction. B_S is the contribution to the binding energy from the S–S terms; B_{SD} is the contribution from the S–D terms; and B_D is the contribution from the D–D terms (all binding energy values are in MeV).

The values of the variation coefficients $a_1, \ldots, a_7$ are given in table 5. The contributions to the binding energy from the various wave functions have been calculated but are not tabulated. Of the additional D-states only Φ_5 and Φ_7 make any important contribution to the binding energy, and Φ_3, Φ_4, and Φ_6 could be omitted completely without altering the binding energy by more than about 0·3 MeV. However, the effect of the additional D-states is appreciable and is of the same order as the increase in binding energy due to the principal D-state above. One can expect that further D-states would again increase the binding energy and that the increase would be considerable for the smaller values of η/τ. Fortunately, as we shall see in § 6, these values can be rejected from the point of view of the consistency problem.

Table 4. Helium Binding Energy using Principal S and D States

η	η/τ	x	y	B_S (Mev)	B_{SD} (Mev)	B_D (Mev)	Total K.E. (Mev)	D-state (%)	ϵ_1^{neut} (Mev)
0·313	0·640	4·92	6·5	35·4	5·3	−2·0	139·4	1·7	37·3
	0·492	4·61	6·5	27·9	7·8	−3·3	123·5	2·2	31·2
	0·3555	4·05	5·5	9·9	10·7	−4·8	95·9	3·3	14·6
	0·320	3·1	5·0	3·1	7·8	−3·7	57·0	2·6	6·3
0·275	0·640	4·82	6·5	42·4	6·4	−2·6	173·5	1·6	44·6
	0·492	4·48	6·5	32·8	9·2	−3·8	151·2	2·0	36·6
	0·3555	3·8	5·2	10·4	13·8	−6·3	109·7	3·4	16·6
	0·320	3·0	5·2	2·7	9·7	−4·7	69·4	2·3	6·7
0·256	0·640	4·75	6·5	46·8	6·7	−2·6	194·2	1·4	49·2
	0·492	4·42	6·4	35·9	10·0	−4·2	169·7	1·9	40·1
	0·3555	3·8	5·1	11·5	14·1	−6·4	126·1	3·3	17·8
	0·320	3·0	5·0	2·4	11·4	−5·5	79·9	2·5	7·2
0·224	0·640	4·64	6·5	56·6	7·9	−3·2	242·0	1·2	59·4
	0·492	4·31	6·0	43·1	11·8	−4·9	210·1	1·9	48·2
	0·3555	3·7	5·2	13·1	17·5	−8·1	156·5	3·0	21·0
	0·320	3·0	5·0	1·3	15·0	−7·3	104·4	2·5	7·8

Table 5. Helium Binding Energy when Further D-States are included

η	η/τ	a_1	a_2	a_3	a_4	a_5	a_6	a_7	ϵ_2 Mev
0·313	0·640	0·9886	−0·1457	−0·0006	0·0152	0·0982	0·0065	−0·0474	39·0
	0·492	0·9834	−0·1576	0·0060	0·0227	0·1244	0·0043	−0·0742	34·2
	0·3555	0·9727	−0·2268	0·0132	0·0335	0·1728	0·0214	−0·0693	19·8
	0·320	0·9719	−0·1746	0·0296	0·0342	0·1846	0·0020	−0·1098	11·8
0·275	0·640	0·9891	−0·1245	−0·0048	0·0164	0·1086	−0·0225	−0·0513	46·6
	0·492	0·9843	−0·1399	0·0086	0·0213	0·1198	−0·0012	−0·0821	40·3
	0·3555	0·9710	−0·2325	0·0159	0·0387	0·1787	0·0201	−0·0731	23·5
	0·320	0·9731	−0·1395	0·0311	0·0289	0·1797	−0·0142	−0·1289	14·1
0·256	0·640	0·9901	−0·1208	0·0032	0·0164	0·0892	0·0014	−0·0582	51·3
	0·492	0·9848	−0·1373	0·0087	0·0210	0·1176	−0·0019	−0·0814	44·2
	0·3555	0·9735	−0·2266	0·0152	0·0378	0·1677	0·0204	−0·0673	24·4
	0·320	0·9722	−0·1534	0·0302	0·0311	0·1823	−0·0106	−0·1234	15·4
0·224	0·640	0·9908	−0·1074	0·0046	0·0154	0·0859	−0·0035	−0·0624	62·0
	0·492	0·9854	−0·1461	0·0071	0·0220	0·1146	0·0018	−0·0703	52·5
	0·3555	0·9747	−0·1990	0·0170	0·0342	0·1647	0·0079	−0·0835	29·4
	0·320	0·9723	−0·1468	0·0299	0·0302	0·1802	−0·0156	−0·1275	18·3

§ 5. SPIN–ORBIT COUPLING

We have assumed in the previous sections that the effect of a spin–orbit force on the binding energies of ^{3}H and ^{4}He is negligible. In the following we investigate whether it is possible to justify this assumption.

We shall consider the following spin–orbit interactions

$$M_1^{(ij)} = -\frac{V_{\mathrm{m}}}{\hbar}\frac{\exp(-r_{ij}/r_{\mathrm{m}})}{r_{ij}/r_{\mathrm{m}}}(\boldsymbol{\sigma}_i+\boldsymbol{\sigma}_j)\,.\,(\mathbf{r}_i-\mathbf{r}_j)\times(\mathbf{p}_i-\mathbf{p}_j), \qquad \ldots\ldots(30)$$

$$M_2^{(ij)} = \frac{1}{3}(\boldsymbol{\sigma}_i\,.\,\boldsymbol{\sigma}_j)(\boldsymbol{\tau}_i\,.\,\boldsymbol{\tau}_j)\frac{V_{\mathrm{m}}'}{\hbar}\frac{\exp(-r_{ij}/r_{\mathrm{m}})}{r_{ij}/r_{\mathrm{m}}}(\boldsymbol{\sigma}_i+\boldsymbol{\sigma}_j)\,.\,(\mathbf{r}_i-\mathbf{r}_j)\times(\mathbf{p}_i-\mathbf{p}_j) \qquad \ldots.(31)$$

between nucleons i and j, $\mathbf{p}_i$ and $\mathbf{p}_j$ being the linear momentum operators of the nucleons. The exchange factors in equations (30) and (31) correspond with those in the neutral and charge-symmetric interactions in § 2. We adopt a value $r_m = 1{\cdot}5 \times 10^{-13}$ cm for the range of the interactions, but, for the moment, leave the strengths V_m and V_m' unspecified. In order to relate V_m and V_m' we shall require that the two forms of interaction lead to the same splitting of the P level in ^{5}He. Since, for this particular case, the exchange factor has no effect, we have the results: $V_m' = -3V_m$. Then (31) may be rewritten

$$M_2^{(ij)} = (\boldsymbol{\sigma}_i \cdot \boldsymbol{\sigma}_j)(\boldsymbol{\tau}_i \cdot \boldsymbol{\tau}_j) M_1^{(ij)}. \qquad \ldots\ldots(31')$$

In order to estimate its effect the spin–orbit interaction is treated as a perturbation and, for simplicity, only the principal D-state (in the isotopic spin representation) for each nucleus is considered (the S–S and S–D matrix elements are, of course, zero; P-states are neglected throughout).

For the interaction (30) the relevant matrix elements are

$$\left.\begin{aligned} {}^3\text{H}:\ \langle \Psi_D^0 | \sum_{i<j} M_1^{(ij)} | \Psi_D^0 \rangle &= (256/15\pi) V_m [5I(y_m;\, 3, 9) - 2I(y_m;\, 5, 9)] \\ &\qquad \text{with } y_m = \sqrt{\tfrac{3}{2}}\, \nu r_m, \\ {}^4\text{He}:\ \langle \Psi_2 | \sum_{i<j} M_1^{(ij)} | \Psi_2 \rangle &= (693/32) V_m [5I(y_m;\, 3, 3, 12) + 2I(y_m;\, 5, 2, 12)] \\ &\qquad \text{with } y_m = \sqrt{2}\nu r_m. \end{aligned}\right\} \qquad \ldots\ldots(32)$$

For the interaction (31′) the corresponding expressions are

$$\left.\begin{aligned} {}^3\text{H}:\ \langle \Psi_D^0 | \sum_{i<j} M_2^{(ij)} | \Psi_D^0 \rangle &= (256/15\pi) V_m [5I(y_m;\, 3, 9) - 14I(y_m;\, 5, 9)] \\ &\qquad \text{with } y_m = \sqrt{\tfrac{3}{2}}\, \nu r_m, \\ {}^4\text{He}:\ \langle \Psi_2 | \sum_{i<j} M_2^{(ij)} | \Psi_2 \rangle &= (693/32) V_m [5I(y_m;\, 3, 3, 12) - 6I(y_m;\, 5, 2, 12)] \\ &\qquad \text{with } y_m = \sqrt{2}\nu r_m. \end{aligned}\right\} \qquad \ldots\ldots(33)$$

The explicit forms of $I(y_m;\, 3, 9)$, etc. are given in the Appendices. The above expressions have to be multiplied by the percentage D-state (divided by 100) in order to obtain the contributions to the binding energies.

We have evaluated these expressions for the potential parameters $\eta = 0{\cdot}275$, $\eta/\tau = 0{\cdot}492$; these are not the 'best' values of the parameters (see § 6) but the set nearest to the 'best' for which we have explicit values of the wave function parameters; the results do not depend critically on the values of η and η/τ. The percentage D-state for the above values of the parameters is approximately 2 for both triton and helium. For comparison we have calculated the contributions made by $M_1^{(ij)}$ and $M_2^{(ij)}$ to the deuteron binding energy using wave functions constructed in the manner of § 3. Table 6 gives the results together with the approximate values of the binding energies obtained with the parameters $\eta = 0{\cdot}275$, $\eta/\tau = 0{\cdot}492$. The small differences in binding energies given by the neutral and charge-symmetric interactions are neglected.

Table 6. The Effect of Spin–Orbit Coupling on the Binding Energies of ^{2}H, ^{3}H and ^{4}He

		^{2}H	^{3}H	^{4}He
Increase in binding energies due to	$M_1^{(ij)}$	$-0{\cdot}08V_m$	$-0{\cdot}10V_m$	$-0{\cdot}25V_m$
	$M_2^{(ij)}$	$0{\cdot}24V_m$	$0{\cdot}05V_m$	$-0{\cdot}07V_m$
Approximate binding energies (without spin–orbit force) (Mev)		1·7	5·1	36·5

The most significant fact which emerges is that the contribution to the deuteron binding energy is of the same order or, in the case of $M_2^{(ii)}$, considerably greater than the contribution to the triton binding energy.† There are no reliable estimates of V_m. The rather crude calculation of Hughes and Le Couteur's on ^{5}He (1950), when corrected to fit the present data (Ajzenberg and Lauritsen 1952), gives a value of about 8 MEV. It is clear from table 6 that a spin–orbit force with a strength of this magnitude would make a very large contribution to the deuteron binding energy. The effects on the ^{3}H and ^{4}He binding energies would be relatively less important but by no means negligible. The results indicate that the binding energy of the deuteron should be re-calculated, taking into account spin–orbit forces. Until this is done it is not possible to say anything regarding the contribution of these forces to the binding energies of ^{3}H and ^{4}He.

§ 6. DISCUSSION AND CONCLUSION

The potential parameters used yield accurately the experimental values for the deuteron binding energy and quadrupole moment. The range of η/τ chosen is probably consistent with the deuteron magnetic moment, although there is some doubt as to the correct percentage D-state in the deuteron ground state.

Only some of the sets of parameters are consistent with the neutron–proton scattering and deuteron photodisintegration data. Feshbach and Schwinger give the triplet effective range corresponding to these data as

$$r_{0t} = (1{\cdot}73 \pm 0{\cdot}04) \times 10^{-13}\,\text{cm}.$$

Consideration of the binding energies of ^{3}H and ^{4}He enables us to reduce the choice of parameters still further. Table 7 gives the sets of potential parameters corresponding to the limits for r_{0t} (obtained by graphical interpolation from Feshbach and Schwinger's values). The corresponding binding energies of ^{3}H and ^{4}He are also given in the table, and were obtained by graphical interpolation. For $\eta = 0{\cdot}224$, the best value of r_{0t} which can be obtained is

$$1{\cdot}68 \times 10^{-13}\,\text{cm},$$

and η/τ can be anywhere between 0·492 and 0·640.

Table 7

	η	r_{0t} (10^{-13} cm)	η/τ	Binding energies ^{3}H (MEV)	^{4}He (MEV)
(1)	0·313	1·69	0·313	2·3	10·0
		1·77	0·345	3·0	17·8
(2)	0·275	1·69	0·335	3·5	18·2
		1·77	0·430	5·5	35·2
(3)	0·256	1·69	0·360	4·7	25·7
		1·77	0·492	7·1	44·2
(4)	0·224	1·68	0·492	8·3	52·5
		1·68	0·640	9·2	62·0

---

† The results in table 6 for ^{3}H and ^{4}He are not strictly correct since we have neglected the contribution of the additional D-states. Nevertheless, an error of even 100% would not materially affect the conclusions.

Set (4) can definitely be excluded since the calculated binding energies are too large. Set (1) must also be exluded since it is very unlikely that increasing the number of D-states will increase the calculated binding energies sufficiently to reach the experimental values. Set (3) can also be excluded since it can be expected that on increasing the number of D-states the calculated ^{4}He binding energies will be too large for all the allowed values of η/τ. The second set therefore seems the most likely to give calculated binding energies close to the experimental values of 8·4 MeV (triton) and 28·2 MeV (helium).

Since the above work was completed a paper by Pease and Feshbach (1952) has appeared on the binding energy of ^{3}H. Their treatment differs from the present one in two respects. First, the radial wave functions used consist of exponentials in the sum of the inter-particle distances, that is they are of the form $\exp\{-\mu(r_{12}+r_{13}+r_{31})\}$. Second, a larger number of D-states is considered. As pointed out by Irving (1953) radial wave functions of the above form appear to give much better results than those of the form (2) in the case of ^{3}H. The resulting increase in binding energy may be as large as 2 MeV for the S-state alone. The additional D-states are responsible for about 2 MeV of the binding energy. The calculation of Pease and Feshbach was carried through in five stages, a more elaborate wave function being introduced at each stage. The correct ^{3}H binding energy was obtained for the parameters $\eta=0{\cdot}275$, $\eta/\tau=0{\cdot}3946$. For these parameters we obtain, by interpolation, a helium binding energy of 30·2 MeV.

That the Irving wave functions, with the same parameter for all the D-states, are also inadequate for the ^{4}He calculations is indicated by the work of Clark (1954). Although Clark uses a rather different approach, his method, apart from a modification due to the presence of D-states, amounts effectively to using a wave function containing six variable parameters. With only one D-state the energy obtained is little better than that obtained with Irving wave functions. However, with a further D-state (ϕ_5 in our notation) a binding energy of 30 MeV is obtained for the parameter values $\eta=0{\cdot}275$, $\eta/\tau=0{\cdot}367$. This is already larger than our (interpolated) value of 26 MeV for the same parameters using five additional D-states (of which only two are, however, of any importance). Apart from the possibility of numerical error, the difference must be attributed to the difference in wave functions.

At the same time one must remember that the variation calculation gives only an upper limit to the energy, and we have no means of estimating the accuracy of the result. The calculation might be improved by a different choice of radial function or by introducing further D-states. Indeed the main weakness of all the calculations hitherto is that they have been stopped at an arbitrary stage. It would seem logical to continue the process until the addition of more stages made little difference to the result. However, the labour involved in the calculations so far is already considerable; to extend them much further may well be prohibitive.

Moreover, another source of uncertainty lies in the assumed interaction itself. We cannot expect it to be more than a rough approximation to the truth. Apart from many-body forces we have seen that the exchange character of the interaction and spin–orbit coupling may make not insignificant differences to the calculated binding energies. It would therefore be unrealistic to require too close an agreement with experiment.

The calculations that have been carried out so far do not therefore permit one to reach a decision on the 'consistency' problem, i.e. on whether or not it is possible to find a phenomenological two-body interaction capable of accounting for the binding energies of the deuteron, triton and helium, of the deuteron quadrupole moment, and of the low-energy two-body data. The most that can be said is that if such an interaction, of meson well type, can be found, the value of the central force range will probably be $r_c = 1{\cdot}184 \times 10^{-13}$ cm (i.e. $\eta = 0{\cdot}275$).

ACKNOWLEDGMENTS

We are indebted to Professor L. Rosenfeld for suggesting the problem and for many helpful discussions. We are obliged to Dr. J. Irving and Dr. Robert L. Pease for sending us details of their work prior to publication. One of us (A. S. R.) wishes to thank the British Rayon Research Association for the award of a scholarship during the tenure of which this work was carried out.

APPENDIX I

The integrals occurring in the triton calculation are of the form

$$I(x\,;\,l,n) = x^{n+1}\int_0^{\pi/2}\frac{\sin^2\theta\cos^l\theta}{(x+\cos\theta)^n}\,d\theta.$$

The explicit forms of those required are given below.

$$I(x\,;\,l,n) = \frac{x^{l+2}}{(n-1)!\,(x^2-1)^{n-2}}\left[f_1(x\,;\,l,n) - \frac{x^{n-l}\sec^{-1}x}{(x^2-1)^{1/2}}f_2(x\,;\,l,n)\right], \quad x>1\,;$$

$$f_1(x\,;\,1,5) = 8x^4+9x^2-2,$$
$$f_1(x\,;\,1,9) = 13440x^{12}+102480x^{10}+3600x^8+26817x^6-15594x^4+5112x^2-720,$$
$$f_1(x\,;\,3,7) = 96x^6+741x^4+120x^2-12,$$
$$f_1(x\,;\,3,9) = 5376x^{10}+77928x^8+54081x^6-3234x^4+1128x^2-144,$$
$$f_1(x\,;\,5,9) = 3072x^8+56481x^6+71622x^4+4200x^2-240,$$
$$f_2(x\,;\,1,5) = 15,$$
$$f_2(x\,;\,1,9) = 315(144x^4+240x^2+45),$$
$$f_2(x\,;\,3,7) = 315(x^2+2),$$
$$f_2(x\,;\,3,9) = 315(72x^4+285x^2+72),$$
$$f_2(x\,;\,5,9) = 315(45x^4+240x^2+144).$$

APPENDIX II

The explicit form of the integrals occurring in the helium calculation is as follows:

$$I(x\,;\,l,m,n) = x^{n+1}\int_0^1\frac{t^l(1-t^2)^m}{(x+t)^n}\,dt$$
$$= \frac{x^{l+2}}{(x+1)^{l+m+2}}\sum_{s=0}^{m+1}a_s\left(\frac{x-1}{2}\right)^s,$$

$$a_s = n\frac{(-1)^m 2^m m!}{s!\,(m+2-s)!}\sum_{r=0}^{s}\frac{\binom{s}{r}}{\binom{l+m+2-s+2r}{m+2-s}}.$$

APPENDIX III

The potential energy matrix elements for helium are as follows (the coefficients A, $c_1 \ldots d_1 \ldots$ are given on the following page):

(*a*) *Matrix elements* $J_{kl} = \langle \Phi_k | J | \Phi_l \rangle$

$k, l = 1, 2$:

$$J_{11} = \frac{315}{32} I(x;\, 1, 2, 8),$$

$$J_{22} = \frac{231}{64}\left[I(y;\, 5, 2, 12) + 5I(y;\, 3, 3, 12) + \frac{25}{16} I(y;\, 1, 4, 12)\right],$$

$$J_{12} = 0.$$

$k = 1, 2;\quad l = 3, \ldots, 7$:

$$J_{1l} = 0,$$

$$J_{2l} = A[I(y;\, 7, 2, 14) + c_1 I(y;\, 5, 3, 14) + c_2 I(y;\, 3, 4, 14) + c_3 I(y;\, 1, 5, 14)].$$

$k, l = 3, \ldots, 7$:

$$J_{kl} = A[I(y;\, 9, 2, 16) + c_1 I(y;\, 7, 3, 16) + c_2 I(y;\, 5, 4, 16) + c_3 I(y;\, 3, 5, 16) + c_4 I(y;\, 1, 6, 16)].$$

(*b*) *Matrix elements* $S_{kl} = \langle \Phi_k | S | \Phi_l \rangle$

$k, l = 1, 2$:

$$S_{11} = 0,$$

$$S_{22} = -\frac{231}{32}\left[I\left(\frac{y}{\tau};\, 5, 2, 12\right) + \frac{7}{2}\left(\frac{y}{\tau};\, 3, 3, 12\right)\right],$$

$$S_{12} = -\frac{63}{16}\sqrt{6}\,.\,\frac{x^{9/2}y^{13/2}}{z^{11}} I\left(\frac{z}{\tau};\, 3, 2, 10\right).$$

$k = 1, 2;\quad l = 3, \ldots, 7$:

$$S_{1l} = -A\frac{x^{9/2}y^{17/2}}{z^{13}}\left[I\left(\frac{z}{\tau};\, 5, 2, 12\right) + d_1 I\left(\frac{z}{\tau};\, 3, 3, 12\right)\right],$$

$$S_{2l} = -2A\left[I\left(\frac{y}{\tau};\, 7, 2, 14\right) + d_1 I\left(\frac{y}{\tau};\, 5, 3, 14\right) + d_2 I\left(\frac{y}{\tau};\, 3, 4, 14\right)\right].$$

$k, l = 3, \ldots, 7$:

$$S_{kl} = -2A\left[I\left(\frac{y}{\tau};\, 9, 2, 16\right) + d_1 I\left(\frac{y}{\tau};\, 7, 3, 16\right) + d_2 I\left(\frac{y}{\tau};\, 5, 4, 16\right) + d_3 I\left(\frac{y}{\tau};\, 3, 5, 16\right)\right].$$

(*c*) *Matrix elements* $K_{kl} = \langle \Phi_k | K | \Phi_l \rangle$

$k, l = 1, 2$:

$$K_{11} = -J_{11};\quad K_{22} = J_{22};\quad K_{12} = 0.$$

$k, l = 2, \ldots, 7$:

$$K_{kl} = J_{kl}.$$

k	l	A	c_1	c_2	c_3	c_4	d_1	d_2	d_3
1	3	$\frac{495}{64}\sqrt{\frac{7}{2}}$	—	—	—	—	$-\frac{7}{6}$	—	—
1	4	$\frac{165}{128}\sqrt{21}$	—	—	—	—	$\frac{1}{6}$	—	—
1	5	$\frac{495}{64}\sqrt{6}$	—	—	—	—	$-\frac{5}{6}$	—	—
1	6	$\frac{495}{64}\sqrt{\frac{7}{5}}$	—	—	—	—	$-\frac{1}{6}$	—	—
1	7	$\frac{495}{128}\sqrt{\frac{7}{10}}$	—	—	—	—	$\frac{13}{6}$	—	—
2	3	$\frac{429}{256}\sqrt{21}$	$-\frac{13}{6}$	$\frac{25}{48}$	$\frac{1}{4}$	—	$-\frac{5}{3}$	$-\frac{1}{24}$	—
2	4	$\frac{429}{256}\sqrt{\frac{7}{2}}$	$\frac{31}{6}$	$\frac{65}{48}$	$\frac{45}{32}$	—	5	$\frac{77}{48}$	—
2	5	$\frac{1287}{128}$	$-\frac{5}{6}$	$\frac{65}{48}$	$\frac{9}{32}$	—	$-\frac{5}{6}$	$\frac{7}{6}$	—
2	6	$\frac{429}{256}\sqrt{\frac{42}{5}}$	$\frac{5}{6}$	$\frac{205}{48}$	$\frac{19}{32}$	—	$\frac{1}{3}$	$\frac{131}{48}$	—
2	7	$\frac{429}{512}\sqrt{\frac{21}{5}}$	$\frac{67}{6}$	$\frac{425}{48}$	$\frac{81}{32}$	—	$\frac{23}{3}$	$\frac{427}{96}$	—
3	3	$\frac{45045}{2048}$	$-\frac{4}{3}$	$\frac{29}{24}$	$\frac{23}{12}$	$\frac{13}{128}$	$-\frac{11}{6}$	$\frac{61}{48}$	$\frac{49}{96}$
3	4	$\frac{15015}{2048}\sqrt{\frac{3}{2}}$	-2	$\frac{3}{8}$	$-\frac{3}{8}$	$\frac{13}{128}$	$-\frac{3}{2}$	$\frac{13}{16}$	$-\frac{73}{160}$
3	5	$\frac{6435}{1024}\sqrt{21}$	-2	$\frac{19}{24}$	$\frac{13}{24}$	$\frac{9}{128}$	-2	$\frac{53}{48}$	$\frac{7}{24}$
3	6	$\frac{45045}{2048}\sqrt{\frac{2}{5}}$	$-\frac{7}{3}$	$\frac{7}{12}$	$-\frac{7}{48}$	$\frac{7}{128}$	$-\frac{11}{6}$	$\frac{13}{48}$	$\frac{17}{480}$
3	7	$\frac{45045}{4096}\sqrt{\frac{1}{5}}$	0	$-\frac{31}{8}$	$\frac{5}{4}$	$\frac{1}{128}$	$\frac{1}{2}$	$-\frac{53}{16}$	$\frac{13}{40}$
4	4	$\frac{15015}{4096}$	$\frac{28}{3}$	$\frac{187}{24}$	$\frac{4}{3}$	$\frac{257}{128}$	$\frac{325}{36}$	$\frac{211}{32}$	$\frac{133}{48}$
4	5	$\frac{6435}{2048}\sqrt{14}$	$-\frac{2}{5}$	$-\frac{1}{8}$	$\frac{25}{24}$	$\frac{1}{8}$	$-\frac{1}{2}$	$\frac{5}{16}$	$\frac{191}{240}$
4	6	$\frac{15015}{2048}\sqrt{\frac{3}{5}}$	1	1	$\frac{49}{16}$	$\frac{43}{128}$	$\frac{1}{2}$	$\frac{31}{16}$	$\frac{73}{80}$
4	7	$\frac{15015}{4096}\sqrt{\frac{3}{10}}$	$\frac{34}{3}$	$\frac{289}{24}$	$\frac{59}{24}$	$\frac{317}{128}$	$\frac{65}{6}$	$\frac{605}{48}$	$\frac{1093}{480}$
5	5	$\frac{19305}{512}$	$-\frac{5}{3}$	$\frac{5}{4}$	$\frac{31}{48}$	$\frac{53}{384}$	$-\frac{5}{3}$	$\frac{7}{8}$	$\frac{259}{480}$
5	6	$\frac{6435}{512}\sqrt{\frac{21}{10}}$	-1	$\frac{11}{12}$	$\frac{53}{48}$	$\frac{23}{128}$	-1	$\frac{41}{48}$	$\frac{35}{48}$
5	7	$\frac{6435}{2048}\sqrt{\frac{21}{5}}$	$\frac{4}{3}$	$\frac{1}{8}$	$\frac{263}{192}$	$\frac{49}{128}$	$\frac{4}{3}$	$-\frac{1}{8}$	$\frac{463}{384}$
6	6	$\frac{9009}{1024}$	$\frac{2}{3}$	$\frac{59}{24}$	$\frac{97}{24}$	$\frac{41}{128}$	$\frac{1}{6}$	$\frac{25}{48}$	$\frac{803}{480}$
6	7	$\frac{9009}{2048}\sqrt{\frac{1}{2}}$	3	$\frac{35}{4}$	$\frac{69}{16}$	$\frac{111}{128}$	$\frac{5}{2}$	$\frac{71}{16}$	$\frac{367}{160}$
7	7	$\frac{9009}{8192}$	$\frac{64}{3}$	$\frac{823}{24}$	$\frac{52}{3}$	$\frac{4337}{768}$	$\frac{101}{6}$	$\frac{1199}{48}$	$\frac{3961}{480}$

REFERENCES

AJZENBERG, F., and LAURITSEN, T., 1952, *Rev. Mod. Phys.*, **24,** 326.
BETHE, H., 1949, *Phys. Rev.*, **76,** 38.
BLATT, J., and JACKSON, J., 1949, *Phys. Rev.*, **76,** 18.
CLAPP, R. E., 1949, *Phys. Rev.*, **76,** 873.
CLARK, A. C., 1954, *Proc. Phys. Soc.* A, **67,** 323.
FESHBACH, H., and SCHWINGER, J., 1951, *Phys. Rev.*, **84,** 194.
GERJUOY, E., and SCHWINGER, J., 1942, *Phys. Rev.*, **61,** 138.
HU, T.-M., and HSU, K-N., 1950, *Phys. Rev.*, **78,** 633.
HUGHES, J., and LE COUTEUR, K. J., 1950, *Proc. Phys. Soc.* A, **63,** 1219.
IRVING, J., 1951, *Phil. Mag.*, **42,** 338 ; 1953, *Proc. Phys. Soc.* A, **66,** 17.
PEASE, R. L., and FESHBACH, H., 1951, *Phys. Rev.*, **81,** 142; 1952, *Ibid.*, **88,** 945.
ROSENFELD, L., 1948, *Nuclear Forces* (Amsterdam : North Holland Publishing Co.).

The Effect of a Potential Gradient on the Density of a Degenerate Fermi Gas

BY W. J. SWIATECKI
Institute for Mechanics and Mathematical Physics and The Gustaf Werner Institute for Nuclear Chemistry, Upsala, Sweden

Communicated by R. E. Peierls; MS. received 8th September 1954

Abstract. By studying the properties of a degenerate gas in a linearly varying potential a modified relation is derived between density and potential which replaces the usual $\rho=\text{const.}\ V^{3/2}$, takes into account explicitly the presence of potential gradients and can be used in regions of negative kinetic energy. When combined with Poisson's equation this gives a modified Thomas–Fermi differential equation. The resulting change in the density distribution of electrons in an atom is most marked in the outer regions, where the new equation leads to an $r^{-2}\exp(-r/a)$ decrease of density for a neutral atom. Applications to nuclear surface problems are mentioned.

§1. INTRODUCTION

THE simple statistical relation stating the proportionality between the density and the 3/2 power of the maximum kinetic energy T† for a completely degenerate gas of particles obeying the Pauli principle has been of great value in atomic and nuclear problems. When combined with Poisson's equation for particles interacting by electrostatic forces it gives the Thomas–Fermi equation which can be applied to the calculation of average density distributions of electrons in atoms and molecules. In nuclear problems the applications of the above relation have been of a more qualitative nature, but it is an important factor in discussions of nuclear structure (especially of nuclear stability and binding energies).

The relation

$$\rho=\frac{8\pi(2m)^{3/2}}{3h^3}T^{3/2} \qquad \ldots\ldots(1)$$

for spin $\frac{1}{2}$ particles of mass m, represents only a limiting case valid when $T(=-V)$ is sufficiently large and/or sufficiently slowly varying in space. In fact (1) is the equation for the density of particles in a *constant* potential well of infinite size when the density itself is also constant in space. In any actual application, where one has to deal with a variable potential, equation (1) will be only an approximation to the actual density.‡

Attempts have been made in the past to derive correction terms associated with the presence of density gradients, the best known being the so-called Weizsäcker term used to modify the inverse relation $T\propto\rho^{2/3}$ between kinetic energy and density (Gombas 1949). Apart from the modifications of the electron density distributions for atoms and molecules which such corrections introduce, the question is of interest in any discussion of surface problems (e.g. of the nuclear surface). For such problems it may be essential to take into account explicitly effects associated with the deviation of the density from a constant, and consequently the deviations from equation (1).

---

† Or the 3/2 power of the absolute magnitude of the potential, if this is reckoned from the maximum kinetic energy as zero, i.e. $T=-V$.

‡ In certain cases equation (1) fails altogether, e.g. in a region of space where T is negative.

The purpose of the present paper is to derive a relation analogous to (1), but generalized so as to contain features arising specifically from the presence of gradients in the potential.

§2. OUTLINE OF METHOD

The idea behind the present generalization can be stated very simply. When we use equation (1) in a problem where the potential is given, we approximate to the true density by the value it would have if the potential were everywhere constant and equal to the actual potential at the point in question.† Let us generalize this by *approximating to the true density by the value it would have if the potential were everywhere linear with a slope equal to the slope of the actual potential at the point in question.* (A levelling off and rise at infinity is again necessary—see below.)

The problem is now stated and the rest is a more or less straightforward calculation involving the solution of Schrödinger's equation in a linear potential and the squaring and adding of the properly normalized wave functions to obtain the total density. The result will be a density ρ depending on two parameters: the value of V and the absolute magnitude of the gradient $|V'|$. What will be the nature of this dependence?

We note that, together with $\hbar$ and m, we can construct the quantity

$$(4/9)2m|V'|/\hbar^2 \equiv l^{-3}$$

of dimensions (length)$^{-3}$ so that l is a length and $(-V)/l|V'| \equiv \xi$, say, is dimensionless. (The reason for the 4/9 in the definition of l appears later.) The density in a linear potential must therefore be of the form (see below)

$$\rho = l^{-3} f(\xi). \qquad \ldots\ldots(1\,a)$$

The problem is thus reduced to the calculation (once and for all) of a certain function $f(\xi)$. This will be done in § 3.

Once f has been tabulated the application to an actual problem consists in using equation (1 *a*) in place of (1). For instance if we are given a potential well, filled with particles up to a certain energy and we want to know the density at some point, we take V and $|V'|$ at that point, construct ξ and look up the value of $f(\xi)$.

Further discussion is reserved for a later section; first let us derive the modified relation between ρ and V.

§3. THE MODIFIFD RELATION BETWEEN ρ AND V

The treatment in this section follows closely that of Swiatecki (1951). We are interested in the solution of the Schrödinger equation in a linearly varying potential

$$V(x) = V'x, \qquad \ldots\ldots(2)$$

---

† Except for a final rise at infinity necessary to keep the particles from dispersing, but whose details are immaterial.

where V' is a constant (say negative). Since V would tend to $-\infty$ for large x we suppose the potential to level off at $x=x_0$, $V=V_0$ and then to be constant for a distance $L \gg x_0$. As usual, we imagine the potential to rise to positive values at still larger values of x, in order to ensure the existence of a steady distribution for which one can speak of a density of particles at a point. The resulting potential well is sketched in figure 1. The potential is assumed to be independent of the y and z coordinates except that, also in these directions, it rises to positive values outside a region of dimensions L. The origin of x and of the energy (counted positive upwards) is at O. We shall confine our attention to values of x much less than x_0, with a view to making the results independent of the levelling off at x_0, and the final rise at large x.

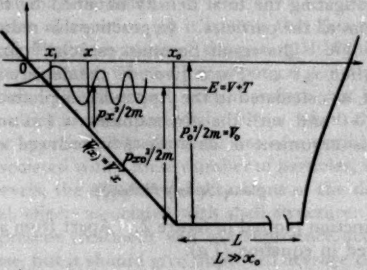

Figure 1. The potential well described in § 3. The well is filled with particles from the bottom up to a maximum kinetic energy $P_0^2/2m$ which is taken as the zero of the energy scale. The wave function of a particle with total energy $E\,(=V+T)$ is sketched in. The limiting case discussed in the text corresponds to making x_0 tend to ∞, while keeping V' constant. Consequently the depth of the well also tends to infinity. All the time L is kept much greater than x_0.

Note the following relations :

$$-x_0V'=P_0^2/2m, \qquad -(x-x_1)V'=p_x^2/2m, \qquad -(x_0-x_1)V'=p_{x0}^2/2m$$

and

$$p_x^2/2m+V(x)=p_{x0}^2/2m+V_0.$$

Consider the Schrödinger equation in the above potential well for a particle with total energy E

$$[-(\hbar^2/2m)\Delta+V(x)]\Psi=E\Psi. \qquad \ldots\ldots(3)$$

The solution can be written as a product $\psi(x)\psi_y\psi_z$ and, if the boundary conditions in the y and z directions are, as usual, replaced by conditions of periodicity† we have

$$\Psi=L^{-1/2}\exp(ip_y y/\hbar)L^{-1/2}\exp(ip_z z/\hbar)\psi(x). \qquad \ldots\ldots(4)$$

The quantities p_y, p_z are the y and z components of the total momentum.

Substituting (4) in (3) we find the following equation for $\psi(x)$:

$$-\frac{\hbar^2}{2m}\frac{d^2\psi}{dx^2}=\left[E-V(x)-\frac{p_y^2+p_z^2}{2m}\right]\psi. \qquad \ldots\ldots(5)$$

The quantity in square brackets is the component of the kinetic energy associated with the x direction and vanishes at a point x_1, the classical turning point (see figure 1). In fact, using (2), we can write it as $(x-x_1)(-V')$ for $x<x_0$, so that (5) becomes

---

† This must not be done in the x direction.

$$\frac{d^2\psi}{d(x-x_1)^2}+\left[-V'\frac{2m}{\hbar^2}\right](x-x_1)\psi=0, \text{ for } x<x_0. \qquad .....(5\,a)$$

The solutions of this equation are well known and are expressible in terms of Bessel functions of order 1/3 (for details see Appendix). The solution which is finite everywhere will be called $F(\epsilon)$. A free-hand drawing of F is included in figure 1. The argument ϵ is not $x-x_1$ itself but the dimensionless quantity $(x-x_1)/l$.

So far we have considered a single particle in the potential well. In fact we are interested in filling the well with particles (paying due regard to the exclusion principle) and investigating the total density obtained by squaring and adding up contributions from all the particles. In practice this reduces to the evaluation of an integral over F^2. The result becomes especially simple in the limiting case here studied when $x_0 \gg x$. For a given V' the density is then a function of x only. The result, as calculated in the Appendix, is plotted in figure 2 in units of the density at $x=0$ and with the dimensionless x/l as argument. In virtue of equation (2) this argument is also the ξ introduced earlier. The actual expression for ρ is

$$\rho=\sqrt{3}(4\pi)^{-2}l^{-3}\phi(\xi) \qquad ......(6)$$

where $\phi(\xi)$ is the function plotted in figure 2. Apart from a constant this is the function f anticipated in equation (1 *a*).

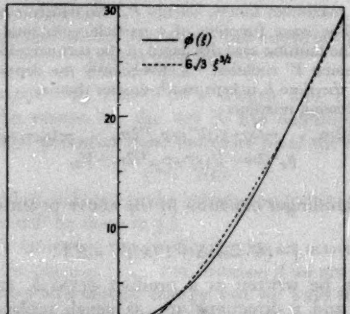

Figure 2. The particle density in a linearly varying potential. The potential, not shown in this diagram, is zero at $\xi=0$ and decreases linearly with increasing ξ. The function $\phi(\xi)$ is the total particle density in units of the density at $\xi=0$. The dotted line shows the result corresponding to the usual approximation which neglects the effect of the potential gradient.

We note that the density extends now to regions of negative kinetic energy $(x<0)$. For large ξ, i.e. for large densities, $\phi(\xi)$ is shown in the Appendix to tend to $6\sqrt{3}\xi^{3/2}$ and this, substituted in (6), gives at once the original relation (1).

A short table of the function $\phi(\xi)$ is given below:

ξ	$\phi(\xi)$	ξ	$\phi(\xi)$	ξ	$\phi(\xi)$
−2·0	0·00	0·0	1·000	1·2	13·12
−1·0	0·033	0·2	1·733	1·4	17·03
−0·8	0·071	0·4	2·866	1·6	21·1
−0·6	0·147	0·6	4·514	1·8	25·4
−0·4	0·290	0·8	6·768	2·0	29·5
−0·2	0·551	1·0	9·657	large ξ	10·392 $\xi^{3/2}$

§4. DISCUSSION OF THE MODIFIED RELATION

A systematic discussion of the possible applications and an assessment of the usefulness of the above modifications will not be attempted in the present paper. The following points may be noted.

From the derivation of equation (6) it is clear that this relation will only be accurate when the effect of derivatives of the potential higher than the first are negligible,† or, more generally, when a linear potential is a good approximation to the actual potential. The treatment will, therefore, not be valid near singularities or discontinuities in the potential. Even when these conditions are satisfied, the present approach, based on the use of a semi-infinite distribution, disregards effects associated with a finite number of particles, such as the existence of discrete energy levels, the associated fluctuations of the density from atom to atom and, in general, effects associated with shell structure. When such effects are important the present treatment will not reproduce accurately the density in any individual case, but it should give improved *average* density distributions. With these limitations the relation is valid for any value of the first derivative (and therefore not only for slowly varying potentials) and it is also applicable to the region of negative kinetic energy. In this sense it is more general than modifications of the type of the Weizsäcker term, whose derivation (Gombas 1949) appears to rest on a discussion of the density in a slowly varying potential in the region of positive kinetic energy.

The first application of the present calculations is to afford a criterion for the validity of the relation (1) and consequently of the usual Thomas–Fermi equation. From figure 2 it appears that for $\xi > 0{\cdot}4$ formula (1) does not differ from (6) by more than about 10%, and for $\xi > 1{\cdot}4$ by not more than about 1%. (Of course, if derivatives higher than V' are important, both (1) and (6) may be out by more than these figures.)

To see what the conditions are like in an atom as regards the magnitude of ξ let us take the usual Thomas–Fermi solution for $V(r)$ and calculate the quantity

$$[(4/9)2m|V'|/\hbar^2]^{1/3}(-V)/|V'|. \qquad \ldots\ldots(7)$$

The ξ found in this way is zero at the origin, increases to a maximum (proportional to $Z^{2/9}$ and equal to 1·4 for the heaviest atom) and then decreases again to zero for large r. Despite the smallness of ξ near the origin neither (1) nor (6) are expected to be valid there. (The approximation by a linearly varying potential is clearly inadequate near the singularity in V at $r=0$.) For heavy atoms and intermediate radii the effect of taking account of the gradient would not modify seriously the simple Thomas–Fermi solution. At large r the Thomas–Fermi treatment will break down. The actual radius at which this occurs according to the criterion discussed here could be estimated by determining the point at which ξ falls below about 0·4.

---

† The generalization of the present approach to include higher derivatives is imaginable. For example to include second derivatives one might try to approximate to ρ by the value it would have if the potential were everywhere parabolic with the first and second derivatives equal to those of the actual potential at the point in question.

§ 5. A MODIFIED THOMAS–FERMI EQUATION

A modified differential equation for the density distribution of electrons can be obtained by combining (6) with Poisson's equation $\Delta V = -4\pi \mathbf{e}^2 \rho$. We find

$$\Delta(-V) = \mathbf{e}^2 \sqrt{3}(4\pi)^{-1} l^{-3} \phi(\xi). \qquad \ldots\ldots.(8)$$

When $\xi \to \infty$ this reduces to the usual Thomas–Fermi equation

$$\Delta(-V) = 4\mathbf{e}^2 (3\pi)^{-1} (2m/\hbar^2)^{3/2} (-V)^{3/2}. \qquad \ldots\ldots(9)$$

In general (8) would have to be solved numerically, as is the case with the ordinary Thomas–Fermi equation. We have seen, however, that for a heavy atom ξ would be near 1 for intermediate distances from the origin, so that the solution of (8) would not be expected to differ from that of (9) by more than a few % in that region.† The region of greatest interest from this point of view is the periphery of the atom where $\xi \to 0$, and there equation (8) reduces to the very simple form‡

$$\Delta(-V) = \mathbf{e}^2 (3\sqrt{3\pi})^{-1} (2m/\hbar^2) V'. \qquad \ldots\ldots(10)$$

This equation can be integrated immediately. The equation for the density is, however, even simpler. Thus, using (6) with $\xi \to 0$ we have

$$\Delta V \equiv r^{-2} \frac{d}{dr}(r^2 V') = 12\sqrt{3}\pi^2 \frac{\hbar^2}{2m} r^{-2} \frac{d}{dr}(r^2 \rho),$$

so that (10) becomes

$$\frac{d}{dr}(r^2 \rho) = -\frac{2m\mathbf{e}^2}{\hbar^2} (3\sqrt{3\pi})^{-1} (r^2 \rho).$$

Hence $\rho = \text{constant}.\ r^{-2} \exp(-r/a)$, where the decay constant a is $3\sqrt{3\pi}/2$ times the Bohr radius of hydrogen and is independent of Z. This behaviour at large r would appear to be an improvement over the inverse power law resulting from the usual Thomas–Fermi equation.

Since the modified equation (8) can be used in regions of negative kinetic energy, it should be possible to apply it to the study of the average electron densities for *ionized* atoms, even for large r. It will be recalled that the usual Thomas–Fermi equation leads to density distributions for ions which become zero at a finite radius.

§ 6. APPLICATION TO THE STUDY OF THE NUCLEAR SURFACE

The system of particles confined to move in the potential well discussed in § 3 provides a simple model of a surface region, i.e. a region where the density decreases gradually to zero under the action of a one-sided resultant force. An attempt to apply such a model to the study of conditions in the nuclear surface was made earlier (Swiatecki 1951). The case studied there was in fact the more general one in which x_0 was kept finite. It might be interesting to examine what progress could be made along the lines of the above reference but in the case when the simplifications resulting from putting $x_0 \to \infty$ are exploited. The validity of this assumption in the case of a nucleus can be tested by estimating ξ at the point x_0 when the magnitudes of V_0 and V' are chosen to represent conditions in the nuclear surface. No entirely reliable estimates of these quantities are available, but if we take $V_0 \sim -22$ MeV, and the thickness of the nuclear surface region as about 2×10^{-13} cm (i.e. $|V'| \sim 11$ MeV per 10^{-13} cm) as suggested by recent electron scattering experiments, we find $\xi(x_0) = 1 \cdot 2$. Figure 2 then suggests that the results should not be drastically sensitive to the assumption $x_0 \to \infty$ and, in view of the many other uncertainties involved in treating the nuclear surface, it might be reasonable to begin by studying this much more tractable case.†

---

† The author is indebted to Dr. Radcliffe for valuable correspondence in this connection. Dr. Radcliffe (then at Birmingham University), examined the solution of equation (8) for an atom with $Z = 60$. The results appear to be consistent with the remarks made above in showing that the corrections to the usual Thomas–Fermi densities are not more than a few per cent out to quite large radii.

‡ Since for an atom V is an increasing function of r we have put $|V'| = V'$.

ACKNOWLEDGMENT

Most of the work described in this paper was carried out in 1950 at the Department of Mathematical Physics, Birmingham University. The author wishes to acknowledge the great help and inspiration which, during his stay there, he received from Professor R. E. Peierls. The author is also indebted to Professor Peierls and Dr. L. Wilets (Copenhagen) for valuable suggestions concerning the manuscript.

APPENDIX

In order to write down the solution of equation (5 *a*) we use the definition of ϵ and re-write (5 *a*) in the following form:

$$\frac{d^2\psi}{d\epsilon^2} + \frac{9}{4}\epsilon\psi = 0.$$

The solution which is finite everywhere is $\psi \propto F(\epsilon)$, where (Watson 1922)

$$F(\epsilon) = \begin{cases} (\epsilon/3)^{1/2}\,[\mathrm{J}_{1/3}(\epsilon^{3/2}) + \mathrm{J}_{-1/3}(\epsilon^{3/2})] & \text{for } \epsilon > 0 \\ \pi^{-1}(-\epsilon)^{1/2}\mathrm{K}_{1/3}\,[(-\epsilon)^{3/2}] & \text{for } \epsilon < 0 \end{cases} \quad \ldots\ldots(11)$$

For $\epsilon > 0$, $F(\epsilon)$ can also be written in terms of $\mathrm{H}_{1/3}^{(1)}$, the Hankel function of the first kind:

$$F(\epsilon) = \epsilon^{1/2}|\mathrm{H}_{1/3}^{(1)}(\epsilon^{3/2})| \cos[\arg \mathrm{H}_{1/3}^{(1)}(\epsilon^{3/2}) + 30^\circ].$$

The functions $\mathrm{H}_{1/3}^{(1)}$, $\arg \mathrm{H}_{1/3}^{(1)}$ and $\mathrm{K}_{1/3}$ are tabulated by Watson (1922).

For $x > x_0$, ψ will have the form of a plane wave

$$\psi \propto \sin[(p_{x0}/\hbar)(x - x_0) + \Delta],$$

where p_{x0} is the x component of the momentum for $x > x_0$ and is given by $p_{x0}^2/2m = E - V_0$, and Δ is a phase independent of x.

If, in the normalization integral, we disregard contributions from outside the region $x_0 < x < x_0 + L$, we can write the normalized solution as

$$\psi(x) = (2/L)^{1/2} \begin{cases} [\sin\Delta / F(\epsilon_0)]\,F(\epsilon) & \text{for } x < x_0 \\ \sin[(p_{x0}/\hbar)(x - x_0) + \Delta] & \text{for } x > x_0 \end{cases} \quad \ldots\ldots(12)$$

---

† Arguments have recently been discussed which suggest that the average gradient of the nuclear potential may, in fact, be considerably smaller than the estimate made above, so that, as in the atomic case, the simplest Thomas–Fermi average densities may be adequate for certain purposes (Swiatecki 1955 b). A simpler approach to the question of nuclear surface energy has also been discussed by Swiatecki (1955 a).

where $\epsilon_0 = (x_0 - x_1)/l$. The factor $\sin\Delta/F(\epsilon_0)$ ensures continuity of ψ at $x - x_0$. Smoothness is ensured by taking

$$\tan\Delta = \frac{p_{x0}}{\hbar}\,\frac{F(\epsilon_0)}{F'(\epsilon_0)}\,\frac{x_0 - x_1}{\epsilon_0} \qquad \text{......(13)}$$

which serves to define Δ.

To find the density at any point x when the well is filled with particles we have to evaluate

$$\rho = \sum |\Psi|^2, \qquad \Psi = \psi(x)\psi_y\psi_z,$$

where the sum is taken over all the particles in the well. If each wave function is labelled by the three components of momentum p_{x0}, p_y, p_z appropriate to the region $x_0 < x < x_0 + L$ the summation extends over a Fermi hemisphere of radius $P_0(P_0^2/2m = -V_0)$. (Because in the x direction we consider standing waves, p_{x0} is taken positive. On the other hand p_y and p_z may be positive or negative) The density of states in the p_{x0}, p_y, p_z space is $4L^3/h^3$.† As $L \to \infty$ we may replace the sum by an integral. The integrations over p_y and p_z can be carried out at once giving a factor $\pi(P_0^2 - p_{x0}^2)$ and we obtain

$$\rho = \frac{4L\pi}{h^3}\int_{p_{x0}=0}^{P_0} (P_0^2 - p_{x0}^2)|\psi|^2 dp_{x0}. \qquad \text{......(14)}$$

So far we have not assumed x_0 to be large. To proceed with the integration we assume that $x_0 \to \infty$. The factor $\sin\Delta/F(\epsilon_0)$ in ψ can then be written down explicitly. Since $\epsilon_0 \to \infty$ as $x_0 \to \infty$ we can use the asymptotic formulae for $J_{\pm 1/3}(\epsilon_0^{3/2})$ in evaluating $F(\epsilon_0)$. This gives

$$F(\epsilon_0) \to (2/\pi)^{1/2}\epsilon_0^{-1/4}\sin(\epsilon_0^{3/2} + \tfrac{1}{4}\pi). \qquad \text{......(14 a)}$$

Using this in (13) we find $\Delta \to \epsilon_0^{3/2} + \frac{1}{4}\pi$ and $\sin\Delta/F(\epsilon_0) \to (\frac{1}{2}\pi)^{1/2}\epsilon_0^{1/4}$. Hence, the normalized solution to be inserted in (14) is (for $x \ll x_0$):

$$\psi(x) = (\pi/L)^{1/2}\epsilon_0^{1/4}F(\epsilon).$$

The integrand in (14) contains by now a mixture of variables p_{x0}, ϵ, ϵ_0. We tidy up by making use of the relations between them which follow from the definitions of ϵ and ϵ_0, and the relations

$$-(x_0 - x_1)V' = p_{x0}^2/2m$$

$$-(x - x_1)V' = p_x^2/2m \qquad \text{(see figure 1).}$$

Adopting ϵ as the variable of integration one finds readily

$$\rho = (2\pi^2/h^3)(-2mV)^{3/2}\left[\xi^{-1/2}\int_{-\infty}^{\xi} F^2(\epsilon)d\epsilon - \xi^{-3/2}\int_{-\infty}^{\xi} \epsilon F^2(\epsilon)d\epsilon\right]. \qquad \text{......(15)}$$

The lower limit of integration contained $-x_0$ and has therefore been taken as $-\infty$.

It may be of interest to write down explicitly the expression for the number of particles in an interval dx, whose x – component of kinetic energy lies between T_x and $T_x + dT_x$. This number (say $W(x, T_x)dxdT_x$) is given by the differential form of (14) and, in the limit x_0, $L \to \infty$, we find

$$W(x, T_x)dxdT_x = 2\pi^2 h^{-3}(2m)^{3/2}\sqrt{\epsilon}F^2(\epsilon)(T - T_x)T_x^{-1/2}dT_x dx,$$

$$\text{where } \epsilon = T_x/l|V'|, \quad T = -V.$$

---

† One factor 2 comes from the spin degeneracy and the second from the fact that we are using a hemisphere in momentum space.

This relation is analogous to the expression for the density of states in phase space for an ordinary Fermi gas, with which it becomes identical when $V' \to 0$ and the average of the rapidly oscillating $\sqrt{\epsilon} F^2(\epsilon)$ (equal to π^{-1}) is inserted. The distribution function $W(x, T_x)$ is independent of x_0 and L, and can be used as the starting point in calculations of the properties of a Fermi gas in a linear potential when one is content to omit the more elementary procedure of introducing a finite well and carrying out the limiting process $x_0, L \to \infty$.

The two integrals in equation (15) are evaluated as follows:

$$\int_{-\infty}^{\xi} F^2 d\epsilon = \int_{-\infty}^{0} F^2 d\epsilon + \int_{\xi}^{0} F^2 d\epsilon.$$

Now $$\int_{-\infty}^{0} F^2 d\epsilon = (2/3\pi^2) \int_{0}^{\infty} y^{1/3} \mathrm{K}_{1/3}^2(y) dy = \Gamma^2(\tfrac{2}{3})/2^{2/3}\pi^2 \text{ (Watson 1922, p. 440).}$$

Similarly $$\int_{-\infty}^{0} \epsilon F^2 d\epsilon = -2/(9\sqrt{3}\pi).$$

The indefinite integrals are evaluated by using power series representations of the products of the Bessel functions occurring in F^2 and integrating term by term (Watson 1922, p. 147). The result is a power series in ξ and (15) can then be written in the final form

$$\rho = \sqrt{3}(4\pi)^{-2} l^{-3} \phi(\xi)$$

where $$\phi(\xi) = 1 + c_1\xi + c_2\xi^2 + \ldots\ldots$$

The coefficients up to c_{19} are given below:

$c_1 = 2{\cdot}86582$
$c_2 = 3{\cdot}53302$
$c_3 = 2{\cdot}25000$
$c_4 = 0{\cdot}53734$
$c_5 = -0{\cdot}26498$
$c_6 = -0{\cdot}25313$
$c_7 = -0{\cdot}057572$
$c_8 = 0{\cdot}024842$
$c_9 = 0{\cdot}020340$
$c_{10} = 0{\cdot}0039581$
$c_{11} = -0{\cdot}0014679$
$c_{12} = -0{\cdot}0010401$
$c_{13} = -0{\cdot}00017645$
$c_{14} = 0{\cdot}000057466$
$c_{15} = 0{\cdot}000036005$
$c_{16} = 0{\cdot}0000054354$
$c_{17} = -0{\cdot}0000015845$
$c_{18} = -0{\cdot}00000089349$
$c_{19} = -0{\cdot}00000012200$

The convergence of the above series is reasonably rapid up to $|\xi| \sim 2$. For instance at $\xi = 2$ the term $c_{20}\xi^{20}$ would contribute approximately 0·03 or 0·1%.

For large ξ we may use the asymptotic formula for F employed earlier in the evaluation of the phase Δ (equation (14 *a*)). Replacing the rapidly oscillating factor $\sin^2(\epsilon^{3/2} + \frac{1}{4}\pi)$ by $\frac{1}{2}$, and neglecting the contributions to the integrals in (15) coming from $\epsilon < 0$ (this, incidentally, illustrates the nature of the neglections underlying formula (1)), we find that the value of the square bracket in (15) reduces to $4/3\pi$ and we obtain for ρ the usual relation (1). This way of approximating to the integrals in (15) gives for $\phi(\xi)$ the limiting form $\phi(\xi) \sim 6\sqrt{3}\xi^{3/2}$. This is plotted for comparison in figure 2.

REFERENCES

Gombas, P., 1949, *Die Statistische Theorie des Atoms und ihre Anwendungen* (Wien: Springer-Verlag).

Swiatecki, W. J., 1951, *Proc. Phys. Soc.* A, **64**, 226; 1955 a, *Phys. Rev.*, in the press; 1955 b, *Ibid.*, in the press.

Watson, G. N., 1922, *Theory of Bessel Functions* (Cambridge: University Press).

Performance of Hot Wire Thermal Diffusion Columns

By R. C. SRIVASTAVA
Department of Physics, University of Lucknow, India

Communicated by B. N. Srivastava ; MS. received 3rd August 1954

Abstract. Furry and Jones' theory of the thermal diffusion column for the extreme cylindrical case has been extended to take into account the temperature variation of the thermal diffusion constant α with temperature in the usual form $\alpha = A - B'/T$. The expressions so obtained for the column constant H are shown to agree closely with the experimental data of Simon on argon.

---

§ 1. Introduction

The thermal diffusion column has been extensively used during the last decade for the separation of isotopes and the components of fluid mixtures. It consists essentially of two vertical concentric cylinders or a wire and a concentric cylinder having a radial temperature gradient. Furry, Jones and Onsager (1939) gave the first rigorous theory of the column for the plane case assuming molecules to be either of Maxwellian or of rigid sphere type.

The mathematical theory of the cylindrical case, which is rather complicated, was first given by Furry and Jones (1946) who obtained approximate solutions for the nearly plane and the extreme cylindrical cases only for the Maxwellian type of molecules. Their investigations show that in the cylindrical case the separation obtained is quite sensitive to the temperature dependence of α, the thermal diffusion constant. Unfortunately, however, they have not taken into account the temperature variation of α. Our present knowledge shows that α is strongly dependent upon the temperature, and the variation of α with temperature can be written in the form $\alpha = A - B'/T$ where A and B' are constants for any gas and T is the temperature in degrees absolute.

For the nearly plane case, this temperature variation of α has already been taken into account by B. N. Srivastava and R. C. Srivastava (1954). The purpose of the present paper is to take into account this experimentally observed variation of α with T for the extreme cylindrical case. This case, according to Furry and Jones (1946) corresponds to columns for which t_2 is greater than 2·5 and will occur in columns having a thin wire as the hot surface.

§ 2. Theory of the Cylindrical Case

Using Furry and Jones' terminology, the column constants H, K_c and K_d for the extreme cylindrical case are given by the expressions

$$H = \frac{2\pi}{6\,!}\left(\frac{\alpha\rho^2 g}{\eta}\right)_1 r_1^4 h \qquad \ldots\ldots(1)$$

$$K_c = \frac{2\pi}{9\,!}\left\{\frac{\rho^3 g^2}{\eta^2 D}\right\}_1 r_1^8 k_c \qquad \ldots\ldots(2)$$

$$K_d = 2\pi(\rho D)_1 r_1^2 k_d \qquad \ldots\ldots(3)$$

where
$$h \simeq 6!\,t_1^3 \exp(2t_1^2)\,\frac{h_\infty - (h''/t_2)}{1-(\delta''/t_2)} \qquad \ldots\ldots(4)$$

$$k_c \simeq 9!\,t_1^7 \exp(4t_1^2)\,\frac{k_\infty - (2k_1''/t_2) + (k_2''/t_2^2)}{\{1-(\delta''/t_2)\}^2} \qquad \ldots\ldots(5)$$

$$k_d = \tfrac{1}{2} - (t_2/2t_1)\exp(t_1^2 - t_2^2) + \tfrac{1}{2}f_{12} \qquad \ldots\ldots(6)$$

with
$$h_\infty = \int_{t_1}^{\infty}\left(\frac{\alpha}{\alpha_1}\right)\left(\frac{\gamma_\infty}{t_1}\right)dt\,; \quad h'' = \int_{t_1}^{\infty}\left(\frac{\alpha}{\alpha_1}\right)\left(\frac{\gamma''}{t}\right)dt\,; \qquad \ldots\ldots(7)$$

$$k_\infty = \int_{t_1}^{\infty}\gamma_\infty^2\,dt\,; \quad k_1'' = \int_{t_1}^{\infty}\gamma_\infty\gamma''\,dt\,; \quad k_2'' = \int_{t_1}^{\infty}\gamma''^2\,dt\,; \qquad \ldots\ldots(7')$$

where ρ, D, λ, α are respectively the density, diffusion constant, thermal conductivity and the thermal diffusion constant; $t=(\lambda/QT)^{1/2}T$, $2\pi Q$ is the heat flow by conduction per unit length of the cylinder and γ_∞, γ'' and δ'' are given by equations (67)–(69) of Furry and Jones (1946).

Since the expressions for K_c and K_d do not contain α they remain unchanged. From (1), (4) and (7) we have

$$H \simeq (2\pi)\left(\frac{\rho^2 g}{\eta}\right)_1 r_1^4 t_1^3 \exp(2t_1^2)\,\frac{h_1 - (h_1''/t_2)}{1-(\delta''/t_2)}, \qquad \ldots\ldots(8)$$

where
$$\begin{aligned} h_1 &= \int_{t_1}^{\infty}(A - B'/T)(\gamma_\infty/t)\,dt \\ &= A\int_{t_1}^{\infty}\frac{\gamma_\infty}{t}\,dt - \frac{B't_1}{T_1}\int_{t_1}^{\infty}\frac{\gamma_\infty}{t^2}\,dt \\ &= Ah_\infty - (B'/T_1)h_{\infty B} \qquad \ldots\ldots(9) \end{aligned}$$

and similarly
$$\begin{aligned} h_1'' &= A\int_{t_1}^{\infty}\frac{\gamma''}{t}\,dt - \frac{B't_1}{T_1}\int_{t_1}^{\infty}\frac{\gamma''}{t^2}\,dt \\ &= Ah'' - (B'/T_1)h_B''. \qquad \ldots\ldots(10) \end{aligned}$$

As shown by Furry and Jones (1946), the integrals

$$\int_{t_1}^{\infty}(\gamma/t^2)\,dt \quad \text{and} \quad \int_{t_1}^{\infty}(\gamma''/t^2)\,dt$$

can only be evaluated in terms of exponentials, error functions and a small number of new functions defined by integrals. The formulae so obtained would, however, be so complicated that the only way to give them any practical meaning would be to carry out a laborious process of numerical evaluation for each chosen pair of values of t_1, t_2. For this purpose the functions γ_∞/t^2 and γ''/t^2 were plotted for specific values of t_1 and numerical integrations performed. In this way the values of $h_{\infty B}$ and h_B'' were found. These are given in table 1, together with the values of h_∞ and h'' given by Furry and Jones.

Table 1. Values of $h_{\infty B}$, h_B'', h_∞ and h'' (Furry and Jones)

t_1	0·5	0·8	1·0	1·2
h_∞(F.J.)	838×10^{-6}	1113×10^{-7}	$256{\cdot}5\times10^{-7}$	$531{\cdot}4\times10^{-8}$
h'' (F.J.)	1409×10^{-6}	2076×10^{-7}	$511{\cdot}3\times10^{-7}$	1132×10^{-8}
$h_{\infty B}$	430×10^{-6}	704×10^{-7}	$178{\cdot}3\times10^{-7}$	$394{\cdot}8\times10^{-8}$
h_B''	720×10^{-6}	1358×10^{-7}	$348{\cdot}2\times10^{-7}$	$825{\cdot}6\times10^{-8}$

§ 3. COMPARISON WITH EXPERIMENTAL RESULTS

For testing our equations we have to select the experimental data on such gases for which the temperature variation of α is accurately known. The best and the most extensive experimental data regarding the variation of α with T

are those of Stier (1942) for argon. Fortunately, very reliable data on the thermal diffusion column by Simon (1946) for the same gas are also available. These are, therefore, utilized for testing the theoretical conclusions arrived at in this paper. Simon has tried to interpret his experimental data in terms of the theory for the plane case, as the theory for the cylindrical case was not known at that time. His comparisons with the theory were unsatisfactory as the theory employed was clearly inapplicable.

From Simon's data t_2 is found to be 2·80 and 2·85 corresponding to the hot surface temperatures of 1500°K and 1100°K. Hence our equations are applicable to this case.

Simon's experimental data are in the form

$$\ln f = \frac{a'/p^2}{1+(b'/p^4)}, \qquad \ldots\ldots(11)$$

where p is the pressure in centimetres of mercury and

(i) $a'=3{\cdot}42\times10^3$, $b'=8{\cdot}95\times10^5$ for $T_2=1500$°K,

(ii) $a'=1{\cdot}10\times10^3$, $b'=1{\cdot}95\times10^5$ for $T_2=1100$°K.

In view of the uncertainty about K_p, the asymmetry term, the experimental values of H were calculated from the relation $H=(a/b)p^2(K_d/L)$ by substituting the theoretically calculated values of K_d. Here L is the total length of the column.

The values of K_p were calculated from the following two relations:

$$(p^2/a)=(K_c+K_p)/HL; \quad b/p^4=K_d/(K_c+K_p) \quad \ldots\ldots(12\,a,b)$$

after substituting the theoretically calculated values of K_c and K_d, which are

(i) $K_c=1{\cdot}50\times10^{-9}p^4$, $K_d=2{\cdot}48\times10^{-3}$ for $T_2=1500$°K,

(ii) $K_c=5{\cdot}19\times10^{-9}p^4$, $K_d=2{\cdot}00\times10^{-3}$ for $T_2=1100$°K.

The results are given in table 2.

Table 2. Values of H and K_p

Temp. (°K)	$(H/p^2)\times10^8$ Theoretical	Experimental	$(K_p/p^4)\times10^9$ (theor.) From equation (12*a*)	(12*b*)
1500	4·61	4·76	1·28	1·27
1100	7·28	6·93	7·41	7·40

Thus the agreement between the calculated and the experimental values of H is quite satisfactory for both the temperatures and fully justifies the basis of our calculations. The agreement between the two values of K_p calculated from the two formulae further confirm the correctness of the deductions.

ACKNOWLEDGMENT

Thanks are due to Professor B. N. Srivastava for suggesting the problem and for useful advice and encouragement.

REFERENCES

FURRY, W. H., and JONES, R. C., 1946, *Phys. Rev.*, **69**, 459.
FURRY, W. H., JONES, R. C., and ONSAGER, L., 1939, *Phys. Rev.*, **55**, 1083.
SIMON, R., 1946, *Phys. Rev.*, **69**, 596.
SRIVASTAVA, B. N., and SRIVASTAVA, R. C., 1954, *Physica, Eindhoven*, **20**, 237.
STIER, L. G., 1942 *Phys. Rev.*, **62**, 548.

Note on a Search for Simple Analytic Wave Functions for Configurations $(1s)^2(2s)$ and $(1s)^2(2s)^2$ in Atoms and Ions from He to C

By E. HOLÖIEN
Blindern Universitet, Oslo, Norway

MS. received 2nd July 1954

§ 1. INTRODUCTION

It is well known that many atomic and molecular properties can be predicted if we know the relevant accurate wave functions. For this reason the construction of simple analytic expressions as approximations to the true wave functions has often been attempted. Such functions should ideally be obtained with the least expenditure of labour for any given accuracy.

The present paper deals with simple analytic expressions for the configurations $(1s)^2(2s)$ and $(1s)^2(2s)^2$ of atoms and ions from He to C, one-electron functions (orbitals) being used in the construction of the complete wave function.

The interest in these functions arises chiefly from their simplicity; for even in the four-electron problems there are only two parameters to be determined variationally. But they are also of interest on account of their excellent approximation to the Hartree–Fock 1s- and 2s-wave functions.

§ 2. PROCEDURE AND WAVE FUNCTIONS

The procedure is to set up the usual Slater determinants, with certain parameters to be determined by variation methods. These Slater determinants are built up from one-electron wave functions, whose forms, apart from the conventional spin factor, are:

$$1s: \quad R(1,0:kr)=(a^3k^3/\pi N_{1s})^{1/2}(e^{-akr}+\alpha e^{-bkr}) \qquad \ldots\ldots(1)$$

$$2s: \quad R(2,0:kr)=(k^5/3\pi N_{2s})^{1/2}(re^{-kr}+\beta k^{-1}e^{-ckr})+(N_{1s}/3N_{2s}a^3)^{1/2}KR(1,0:kr) \qquad \ldots\ldots(2)$$

where N_{1s} and N_{2s} are two different normalization factors, K is a factor which orthogonalizes the functions (1) and (2), and a, b, c, α, β and k are potentially variable parameters. The latter parameter k is a scale factor whose best value, as is well known, can be determined analytically. The other parameters enter the energy integrals in such a complicated way that their best values must be found numerically. This process, which has usually to be done graphically, is a very tedious one, particularly when many such parameters have to be determined. But the numerical work can sometimes be lightened by choosing definite fixed values for the less sensitive parameters.

Several calculations have already been made along these lines. All but two of them are special cases of the more general functions (1) and (2). Thus we get Wilson's four-parameter function (1933) when $\alpha=0$, Zener's three-parameter function (1930) when $\alpha=0$ and $c=1$, Eckart's two-parameter function (1930) when $\alpha=0$, $\beta=-1$, $c=1$, and Slater's two-parameter function (1930) when $\alpha=0$, $\beta=0$. Furthermore, we have the three-parameter function of Morse, Young and Haurwitz (1935, referred to hereafter as MYH) which was later improved by Duncanson and Coulson (1944) and the two-parameter function by Fock and Petrashen (1935). These two latter functions, both of which have an additional type of orthogonality, cannot be derived directly from (1) and (2).

Obviously the flexibility of our trial wave function is seriously limited by arbitrarily fixing any of the parameters. Fortunately, however, by adjusting the more insensitive parameters (see later) in conjunction with the more sensitive ones, as in this present paper, it is possible to reduce the number of parameters whose optimum values have to be found numerically, without at the same time limiting the flexibility of the wave function too severely. In this way we shall be able to reduce the number of effective parameters in (1) and (2) from five to one.

The following very convenient forms for the 1s- and 2s-functions appear to be excellent representations of the true radial parts of these functions, when the atoms and ions are in their ground states, with configurations $(1s)^2(2s)$ and $(1s)^2(2s)^2$,

$$R(1,0:kr)=(a^3k^3/\pi N_{1s})^{1/2}\times(e^{-akr}+21\times10^{-5}\,e^{-2a(kr-1)}) \qquad \ldots\ldots(3)$$

$$R(2,0:kr)=(k^5/3\pi N_{2s})^{1/2}\times\{re^{-kr}-(2/apk)\,e^{-akr/2}\}+(N_{1s}/3N_{2s}a^3)^{1/2}\,KR(1,0:kr) \qquad \ldots\ldots(4)$$

where $p=1$ for the configuration $(1s)^2(2s)$, and $p=2$ for $(1s)^2(2s)^2$. It will be seen that (3) and (4) are derived from (1) and (2) by putting

$$\alpha=21\times10^{-5}\,e^{2a},\ \beta=-2/ap,\ b=2a,\ c=a/2. \qquad \ldots\ldots(5)$$

The only remaining parameter whose value must be found numerically is a. We write this as a ratio $a=2Z_{1s}/Z_{2s}$ where Z_{1s} and Z_{2s} are effective nuclear charges for the 1s- and 2s-electrons in the outer parts of their orbitals. The other parameter—the scale factor k—may be written $k=\frac{1}{2}Z_{2s}$.

Some justification is needed for the conditions (5). First of all, we calculate the optimum values of all the parameters in the full function (1) to give an energy minimum for the ground states of the series from He to Ne^{8+} which have the simple configuration $(1s)^2$. The results, shown in table 1, indicate that $b/a\simeq2$ for the whole series.

Table 1. Values of Parameters in equation (1) which give Energy Minima

Atom or ion	ak	α	b/a	Atom or ion	ak	α	b/a
He	1·46	0·60	2·0	N^{5+}	6·44	0·15	1·7
Li^{+}	2·45	0·36	1·9	O^{6+}	7·43	0·14	1·7
Be^{2+}	3·44	0·26	1·8	F^{7+}	8·43	1·13	1·7
B^{3+}	4·44	0·20	1·8	Ne^{8+}	9·43	0·13	1·7
C^{4+}	5·44	0·17	1·8				

In order to estimate the relation $\alpha=f(a)$ connecting α and a, it would be desirable to find corresponding values of α and a for all the atoms of table 1. At this stage, however, we are only able to estimate a rather roughly. Our values of a and α are shown in table 2, in which the values of k are taken from Slater's rules (1930) because these values agree closely with those found by the self-consistent-field method. Once again these k-values are appropriate to the atoms in their ground states only. The values of ak and α, taken from table 1, may differ slightly from the best values obtained variationally from the less flexible functions (3) and (4).

Table 2. Estimated Values of the Quantities α and a for the Atoms from Li to Ne in the first row

Atoms	ak	k	a	α	α/e^{2a}
Li	2·45	0·650	3·77	0·36	19.10^{-5}
Be	3·44	0·975	3·53	0·26	23.10^{-5}
B	4·44	1·300	3·42	0·20	21.10^{-5}
C	5·44	1·625	3·35	0·17	21.10^{-5}
N	6·44	1·950	3·30	0·15	20.10^{-5}
O	7·43	2·275	3·27	0·14	20.10^{-5}
F	8·43	2·600	3·24	$0{\cdot}13_5$	21.10^{-5}
Ne	9·43	2·925	3·22	0·13	21.10^{-5}

From the last column of this table it follows that the ratio $\alpha/e^{2a} \simeq 21 \times 10^{-5}$ throughout the whole series of atoms.

Similarly, when justifying the other two equations in (5), we first put $\alpha = 0$ in (1) and determine the best values of the parameters β and c for the ground states $(1s)^2(2s)\ {}^2S(p=1)$ of the series Li to C^{3+}, and the ground states $(1s)^2(2s)^2\ {}^1S(p=2)$ of the series Be to C^{2+}. In this way we find the approximate relations $a\beta \simeq 2/p$ and $c/a \simeq \frac{1}{2}$ for the whole series of atom and ions.

It has therefore seemed worth while to carry out the energy calculations using the simplified functions (3) and (4) for the component atomic orbitals, and to study the ground states of two-, three- and four-electron systems from He to C. We shall compare the resulting energies with those associated with other related types of wave function. Even with the appreciable simplifications of (1) and (2) which are implied in (3) and (4) the amount of numerical work is still considerable. The full expressions for the energy integrals are complicated functions of the parameter a, and are too long and tedious to be given here. We therefore confine ourselves to the final numerical results. Energy tables for various values of a have been constructed so that both the energy minimum and the adjustment of the parameters for any atomic state which is the lowest of its particular spin symmetry, involving only 1s- and 2s-orbitals, can be determined approximately by quadratic interpolation. The computations have been carefully checked, and it is believed that no errors, other than those due to the accumulation of rounding-off errors, are present in the final values. It should be mentioned here that all the energies in the tables of this paper are expressed in rydberg units (1 rydberg unit = $\frac{1}{2}$ atomic unit). The experimental values of the total energies and the ionization energies are taken from the tables compiled for the National Bureau of Standards (1949).

§ 3. Results and Discussion

3.1. *Two-Electron Configurations*

Table 3 shows the values of the total energies and parameters calculated for the isoelectronic series from He to C^{4+} in the ground state $(1s)^2\ {}^1S$ using both the wave functions (1) and (3). The same table also lists the Hartree–Fock energies, the total energies of the function (1) when $\alpha = 0$, and also the experimental values. Some comments may be given on the figures in the table. Comparison of the second and the sixth columns shows that the 1s-function (3) is almost equally

Table 3. Comparison of Total Energies for Atoms and Ions in the $(1s)^2$ Configuration obtained by various Wave Functions

Atom or ion	The 1s-function (3)				The 1s-function (1)	Hartree–Fock	Function (1) when $\alpha=0$	Exptl.
	E_{calc}	a	k	ak				
He	− 5·723	3·99	0·366	1·46	− 5·723	− 5·723	− 5·695	− 5·807$_5$
Li^+	−14·472$_5$	3·62	0·688	2·49	−14·473	−14·420	−14·445	−14·561
Be^{2+}	−27·222	3·36	1·046	3·51	−27·223	−27·235	−27·195	−27·314
B^{3+}	−43·972	3·23	1·397	4·51	−43·973	—	−43·945	−44·071
C^{4+}	−64·720$_5$	3·15	1·748	5·51	−64·722	—	−64·695	−64·834

as good as the three-parameter function (1). For helium both functions give the same energy value, up to the third decimal place, as that reported for the Hartree–Fock function. This Hartree–Fock energy which is essentially different from that reported by Bethe (1929), is taken from Wilson (1935). According to the theory, however, the self-consistent-field approximation including exchange should give the lowest energy which is obtainable by separated one-electron functions. Hence, there may be an error in the Hartree–Fock energy quoted by Wilson. This energy should be appreciably nearer to the experimental value, and there is reason to believe that the value −5·734 Ryd earlier reported by Bethe (1929) is more correct than the later value −5·723 Ryd. Obviously the Hartree–Fock energy for the lithium ion reported by Fock and Petrashen (1935) is too high and incorrect. The same energy for Be^{2+} is taken from data by Hartree (1935). It seems probable, however, that we could obtain a lower Hartree–Fock energy for Be^{2+} by using the 1s-function given by Hartree in a later paper (1936): but the energy integrals would then all have to be recalculated.

It is interesting to consider the energy values in the second column of table 3 obtained with our two-parameter function (3). By comparing these values with those in column six, we see at once that there is a very slight difference of energies of the function (1), more noticeable when the atomic number increases. We conclude therefore that, although this defect in (3) is mainly due to the somewhat poor approximation $b/a=2$ in (5), our 1s-function (3) is still remarkably good.

The functions (3) and (4) also give a good approximation to the Hartree–Fock energy for the lowest triplet state of helium, namely −4·349 Ryd.

3.2. *Three-Electron Configurations*

The values of the parameters are summarized in table 4 together with total energies and ionization energies obtained by the functions (3) and (4) for the series isoelectronic with Li in the ground state $(1s)^2(2s)\ {}^2S$. The tables 5 and 6 give a comparison of the quantities given in the second and third columns of table 4 with experimental values and energy values associated with other related functions.

Some comments may be given on the figures in tables 4 to 7. It will easily be seen from the tables that our two-parameter function (3, 4) shows lower calculated energies than any other separated one-electron function previously reported for the ground state of this series. Thus according to the generally accepted energy criterion, this function is the best approximation to the Hartree–Fock 1s- and 2s-function. From table 5 it follows that the improvement in total energy is appreciable, decreasing from 0·19% for Li to 0·03% for C^{3+}. This is mostly due to the more flexible 1s-function (3) used in our calculations. Obviously the Wilson three-parameter 2s-function gives the best ionization energy, but as can be seen from tables 6 and 7, our two-parameter 2s-function is almost equally good, the energy difference (correct to three decimals) increasing only from zero to 0·04% for C^{3+}. To facilitate a comparison with the Hartree–Fock energy, the figures in the first row of table 6 and in the fourth column of

Table 4. The Energies and the Corresponding Parameters calculated for the Series from He$^-$ to C^{3+} in the Ground State

Atom or ion	Total energies	Ionization energies	Parameters a	k	ak
He$^-$	− 5·694		4·62	0·250	1·16
Li	−14·865$_5$	0·393	3·67	0·672	2·47
Be$^+$	−28·553	1·331	3·04	1·151	3·50
B^{2+}	−46·749	2·777	2·75	1·636	4·50
C^{3+}	−69·449	4·728	2·60	2·119	5·51

Table 5. Comparison of the Total Energies with those obtained by other Functions

Atom or ion	2-parameter fn. (3, 4) E_{calc}	Diff (%)	Wilson's function E_{calc}	Diff(%)	Slater's function E_{calc}	Diff(%)	Exptl.
He$^-$	− 5·694						
Li	−14·865$_5$	0·61	−14·838	0·80	−14·836	0·81	−14·957
Be$^+$	−28·553	0·35	−28·528	0·44	−28·517	0·48	−28·653
B^{2+}	−46·749	0·24	−46·726	0·28	−46·700	0·34	−46·860
C^{3+}	−69·449	0·18	−69·426	0·21	−69·380	0·28	−69·574

Table 6. Comparison of the Ionization Energies with those obtained by Wilson's Function

Atom or ion	2-parameter fn. (3, 4) E_{calc}	Diff (Ryd)	Wilson's function E_{calc}	Diff (Ryd)	Exptl.
Li	0·3930	0·0033	0·3931	0·0032	0·3963
Be$^+$	1·331	0·008	1·333	0·006	1·339
B^{2+}	2·777	0·011	2·780	0·008	2·788
C^{3+}	4·728	0·012	4·730	0·010	4·740

Table 7. Comparison of Total Energies and Ionization Energies for Li with those obtained by various Analytic Functions

Functions	Total energies	Diff (%)	Ionization energies	Diff (Ryd)
Exptl.	−14·957		0·3963	
Hartree–Fock			0·3934	0·0029
Author	−14·865$_5$	0·61	0·3930	0·0033
Wilson	−14·838	0·80	0·3931	0·0032
MYH	−14·838	0·80	0·3926	0·0037
Zener	−14·837	0·80	0·3913	0·0050
Slater	−14·836	0·81	0·3905	0·0058
Eckart	−14·784	1·16	0·3392	0·0571

table 7 are given to four decimals; to the best of the author's knowledge, no Hartree–Fock energy for the other members of this series is yet available. It must be noted that the energies calculated by Wilson's, Zener's and Slater's functions are taken from the original paper by Wilson (1933), and the MYH energy value has been accurately recalculated up to the fourth decimal place by using the best parameters reported by Duncanson and Coulson (1944).

3.3. *Four-Electron Configuration*

The wave functions (3, 4) of the component orbitals have also been applied to the members of the series isoelectronic with beryllium. In table 8 are listed the values of the total binding energies and the appropriate parameters calculated for this series. It may be noted once more that we are solely concerned with the atom and the ions in their ground states $(1s)^2(2s)^2\ {}^1S$.

Table 8. Calculated Energies and Parameters for the Series from Li^- to C^{2+} compared with the Experimental Values

Atom or ion	Total energies E_{calc}	Exptl.	Diff (%)	Parameters a	k	ak	$E(A^{2+})-E(A)$ Calc.	Exptl.
Li^-	−14·832			4·10	0·520	2·13		
Be	−29·145	−29·338	0·66	3·48	0·995	3·46	1·932	2·024
B^+	−48·450	−48·708	0·53	3·13	1·431	4·48	4·478	4·637
C^{2+}	−72·766	−73·093	0·44	2·93	1·874	5·49	8·045	8·259

Table 9. Comparison of Total and Ionization Energies for Be with those obtained by various analytic Wave Functions

Functions	Total energies E_{calc}	Diff (%)	$E(A^{2+})-E(A)$ Calc.	Diff (Ryd)	$E(A^+)-E(A)$ Calc.	Diff (Ryd)
Exptl.	−29·338		2·024		0·685	
Boys	−29·274 (1)	0·22				
Hartree–Fock	−29·159 (2)	0·61	1·924 (2)	0·100		
Author	−29·145	0·66	1·923	0·101	0·590	0·095
Wilson	−29·119 (4)	0·75	1·924	0·100	0·591	0·094
MYH	−29·119 (3)	0·75	1·924	0·100		
Zener	−29·115 (4)	0·76	1·921	0·103		
Slater	−29·113 (4)	0·77	1·918	0·106	0·596	0·089
Fock–Petrashen	−29·060	0·95	1·865	0·159		

(1) This value obtained by the poly-detor variational method comprises also some contributions from the angular correlation energy of the electrons, and it is only included here for the completeness of the table.

(2) The Hartree–Fock value for the ionization energy, namely 1·924 Ryd, is taken from Hartree (1936); by adding the energy value of 27·235 Ryd for Be^{2+} as reported by Hartree (1935) we get the total energy of 29·159 Ryd.

(3) This total MYH energy has been accurately recalculated by the author using the best values of the parameters reported by Duncanson and Coulson (1944).

(4) These energy values which were not available for Be, have been variationally determined by the author.

The results presented in table 9 are very interesting and show clearly that the two-parameter function (3, 4) also gives a better approximation to the total Hartree–Fock energy than any other separated one-electron function previously reported for the ground state of Be. It follows from table 8 that the goodness of the function is nearly the same for the whole series. It must be remembered that Boys's poly-detor function does not use separated orbitals, but that it does take into account the mutual polarization of the electrons.

When considering the results given in the fourth column of table 9, it will be seen immediately that both Wilson's and MYH's functions give the same energy value to three decimals as the Hartree–Fock function. However, since the Hartree–Fock function must give the lowest energy, this is a very strange situation, which leads us to believe either that the Hartree–Fock energy for Be is still incorrect, or that there is some error in our own energy calculations. For that reason we have checked our own numerical work with great care, for in the MYH case when the parameters already determined by Duncanson and Coulson were used no error was detected. Although Wilson's and MYH's 2s-functions are apparently very good approximations to the Hartree–Fock function, our two-parameter 2s-function gives almost an equally good approximation as can be seen from the same column in the table. When the goodness of a function is determined by the well-known criterion, namely the lowness of the calculated energy, it is obvious that the very simple Slater's function is also a fairly good approximation to the 2s-orbital in a $(2s)^2$ group. The results which are given for the ionization energy $E(A^+)-E(A)$ in the last two columns of the table, are a little confusing. It will be seen that Slater's function gives the best energy difference, even much better than Wilson's function, but this is doubtless due to an erroneous energy value for Be^+ calculated by Wilson (1933) when the Slater function was used. Finally, it must be noted that, to the author's knowledge, so far no Hartree–Fock value for the ionization energy $E(A^+)-E(A)$ is available.

ACKNOWLEDGMENTS

The author would like to express his gratitude to Professor E. A. Hylleraas for suggesting the problem discussed in this note and for the Institute's kind hospitality during the time he was working there. It is also a pleasure to thank the referees for several helpful suggestions.

REFERENCES

BETHE, H., 1929, *Z. Phys.*, **55,** 431; 1933, *Handb. Phys.*, **24,** 370.
BOYS, S. F., 1953, *Proc. Roy. Soc.* A, **217,** 136.
DUNCANSON, W. E., and COULSON, C. A., 1944, *Proc. Roy. Soc. Edinb.*, **62,** 37.
ECKART, C., 1930, *Phys. Rev.*, **36,** 878.
FOCK, V., and PETRASHEN, M. J., 1935, *Phys. Z. Sowjet.*, **8,** 547.
HARTREE, D. R., and HARTREE, W., 1935, *Proc. Roy. Soc.* A, **149,** 210; 1936, *Ibid.*, **156,** 45.
MOORE, C. E., 1949, *Atomic Energy Levels*, National Bureau of Standards.
MORSE, P. M., YOUNG, L. A., and HAURWITZ, E. S., 1935, *Phys. Rev.*, **48,** 948.
SLATER, J. C., 1930, *Phys. Rev.*, **36,** 57.
WILSON, E. B., 1933, *J. Chem. Phys.*, **1,** 210.
WILSON, W. S., 1935, *Phys. Rev.*, **48,** 536.
ZENER, C., 1930, *Phys. Rev.*, **36,** 51.

The Angular Correlation of Annihilation Radiation

By K. L. ERDMAN
The University of British Columbia, Vancouver 8, Canada

Communicated by J. B. Warren ; MS. received 4*th May* 1953
and in final form 3*rd September* 1954

Abstract. The departure from exact 180° angular correlation of quanta resulting from positrons annihilating in various materials has been measured. This provides data as to the momenta of the centres of mass of the annihilating electron–positron pairs. It does not appear possible to account for the data on the assumption that the positron achieves thermal energy by lattice collisions before annihilating, so that such measurements may not be simply related to the momentum distribution of the more loosely bound electrons in the absorbing substance.

---

§ 1. Introduction

THE departure from exact 180° angular correlation between annihilation quanta in the two-quantum annihilation process has been measured with some precision by various workers (de Benedetti *et al.* 1950, Argyle and Warren 1951, Griffiths and Warren 1951, Maier-Leibnitz 1951). It may be shown from conservation of momentum and energy that the residual momentum p of the mass centre of the annihilating positron and electron is given by the expression $p=\mathbf{m}\mathbf{c}\theta_0$ where θ_0 is the departure from exact 180° angular correlation of the two quanta emitted, $\mathbf{m}$ is the rest mass of the electron, and $\mathbf{c}$ is the velocity of light. The expression is valid in the region where θ is a small angle.

In his book Heitler (1944) shows that positrons of initial kinetic energy approximately 1 Mev lose energy in passing through a solid by ionization and excitation processes, until they reach an energy so low that such processes do not occur. Only 2 or 3% of the positrons are annihilated 'in motion' and the subsequent rate of annihilation is determined by the number of effective electrons per unit volume. This slowing down process to energies of a few tens of electron volts would take only 10^{-11} to 10^{-12} second.

In order to analyse the final stages of the annihilation process more exactly, de Benedetti *et al.* (1950) postulate that subsequent energy loss may occur by inelastic collisions with the lattice and that, in a metallic solid, the positrons are thermalized in a time of the order of 10^{-10} second. Such thermalized positrons may then diffuse through the lattice, preferentially occupying interstitial positions due to the Coulomb repulsion by the positive ions, and hence annihilate with the outermost electrons. In this way de Benedetti *et al.* show that the average residual momentum p_{av} depends partly on the momenta of the thermalized positron and more particularly on that of the annihilating electron. Consequently it was possible that measurements of p_{av} might give information as to the momentum distribution of the outer electrons in solids, in contrast to the average momentum of the complete electron configuration obtained from measurements of the profile of the Compton line in x-ray scattering.

The experimental work referred to above showed that the relation between $N(c)$, the coincident counting rate in the plane of the measurements determined by the two annihilation quanta detectors, and θ was a very simple one viz.: $N(c) \propto \exp(-\theta/\theta_0)$, the relation being a very good fit in some cases and poorer in others. The values of the average centre of mass momentum may be deduced from such data using $p_{av} = 2mc\theta_0$ (de Benedetti *et al.* 1950). The values so determined, although of the right order of magnitude, did not vary in any systematic way among the substances investigated. It seemed of interest to repeat the measurements with rather greater precision and with a wider variety of positron absorbers in the hope that the final details of the annihilation process might be elucidated thereby.

§ 2. EXPERIMENTAL

(i) *Source of Positrons*

All the measurements were made at the Laboratories of Atomic Energy of Canada Ltd., Chalk River, where, owing to the high neutron flux available from the heavy water nuclear reactor, extremely thin yet powerful sources of ^{64}Cu positrons could be made. Activated copper foils, less than 0·0005 in. thick, gave a high flux of positrons with very little internal annihilation (less than 10%).

(ii) *Counting System*

A coincidence circuit of the Bell and Petch type was employed (Bell *et al.* 1952). The detectors were two 1 in. × 1 in. × $\frac{1}{4}$ in. crystals of trans-stilbene mounted on the ends of two 11 stage E.M.I. photomultipliers (type 5311). The coaxial lines from pulse shapers in the head amplifiers were shorted by a stub giving a resolving time of 4×10^{-9} second. This resolving time was measured in two ways: firstly by using true coincidences from a positron source and varying the length of line between a pulse shaper and the shorted stub and plotting coincidence rate against pulse delay time, and secondly by taking random coincidence rates using the counters at large angles from the 180° position.

(iii) *Geometrical Arrangement*

The counters and source were mounted at a height of three feet from the floor in the middle of a large room to reduce scattering effects. One counter was rigidly fastened to the end of a table; the other was attached to the carriage of a travelling microscope to allow a precise determination of θ. The source consisted of a sandwich of activated copper foil placed between two sheets of absorber of sufficient mass to stop all the emerging positrons within them. This sandwich was placed in a slot cut into the end of a round rod, 1 in. in diameter, of air filled polystrene (styrofoam) of density 0·02 g cm^{-3}, which was in turn fastened to the top of a block, 6 in. × 4 in., for rigidity as shown in figure 1. For absorbers in the form of powders, holes of the correct depth were carved into styrofoam blocks which were then filled, clamped together on the copper foil, and positioned on the main styrofoam pillar.

The apparatus was arranged as in figure 2. The source (1 cm × 3 cm) was turned through a small angle to decrease the gamma-ray path through the source itself and also to present a source of constant width for different thickness of absorbers. The angle in the horizontal plane subtended by the source at the detector was 0·08°; that of the detector at the source was 0·25°. The 180° counter–source–counter position was established roughly with a tightly stretched thread, and was more precisely determined in each material by counting over a small angle at the 180° position.

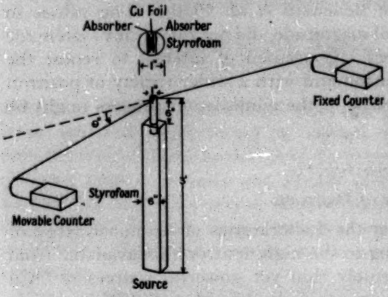

Figure 1. Positron source.

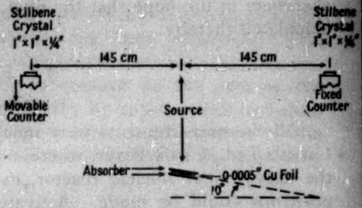

Figure 2. Experimental arrangement.

(iv) *Counting Rates*

The activity of a source at the beginning of a run was of the order of 200 millicuries. This gave a single channel counting rate of about 80 000 counts per minute and a coincidence rate at $\theta=0°$ of about 1000 counts per minute. The chance coincidence rate was about 0·5 count per minute. This allowed the true coincidence rate to be measured out to $\theta=1·8°$ at which point the true rate became equal to the chance rate.

§ 3. Corrections to the Observed Data

(*a*) *Counting corrections.* The values obtained for the observed coincidence rate were corrected for the source decay, the accidental coincidence rate and for the dead times of the circuits.

(*b*) *Geometrical corrections.* The finite width of both the source and the counters contributes little to the shape of the $(N(\mathrm{c}), \theta)$ curve, the effect being a slight decrease in the slope and hence of θ_0 (Griffiths and Warren 1951). This has been neglected here since the prime purpose of the experiment was to make a comparison between curves obtained with different absobers rather than to determine accurately the absolute magnitude of the quantity θ_0, and to this end the source and counter widths were kept as constant as possible for all the materials investigated.

(*c*) *Scattering corrections.* Compton scattering is negligibly small for the thickness of absorbers used in the experiment. Likewise scattering from the surroundings has no significant effect on the measured coincidence rates.

Rayleigh scattering has been demonstrated by Moon (1950) to be up to 100 times as great as Compton scattering at small angles. Measurements made by Storruste (1950) were in agreement with the cross-section values as calculated by Franz (1935) for this process. The cross section for scattering in the case of high Z absorbers is large enough to be significant, as shown in the calculated corrections to the experimental data in figure 3, where the broken curve represents the plot of the uncorrected values of the coincidence rate against angle in each case. In the case of low Z elements, such as lithium, the Rayleigh scattering cross section is also of negligible magnitude.

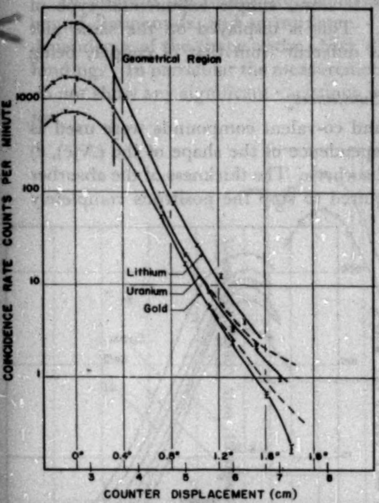

Figure 3. Effect of correction for Rayleigh scattering.

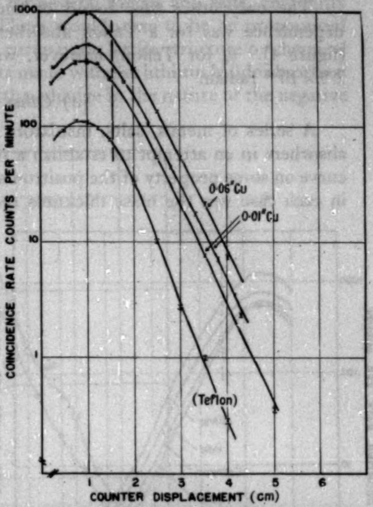

Figure 4. Angular correlation for annihilation in copper and Teflon.

The cross sections were calculated for single Rayleigh scattering of quanta from inside the region of geometrical overlap into angles outside of this region. Since the number of coincident quanta outside of this region was much smaller, their effect on the scattering correction was not significant. A numerical integration was therefore carried out over the experimental (N(c), θ) curve. As an example, with a gold absorber the cross section for scattering into 10^{-4} steradian (the angle subtended by the detector at the source) varied from 4×10^{-26} cm^2 at 0·4° to 1×10^{-26} cm^2 at 2·0°. The large Z dependence reduced these values by a factor of 1000 in the case of lithium. In no case did the integrated effect account to more than 0·8 count per minute at an angle of 1·2°, which was the value observed for uranium when the coincidence peak height was 1600 counts per minute.

§ 4. Results

(i) *Annihilation in Copper*

A comparison of these results (figure 4) with those of previous workers shows that the results obtained are very similar. The value obtained for θ_0 ($3{\cdot}80 \times 10^{-3}$ radian) uncorrected for finite source and counter width, agrees with the value given by Griffiths and Warren (1951), $3{\cdot}81 \times 10^{-3}$ radian. The thickness of absorber was increased by a factor of 6 to determine the effect of scattering.

The similarity of results obtained from the thin and thick source verifies the assumption concerning the small influence of scattering. An exponential type of dependence between $N(\mathrm{c})$ and θ of the form $N(\mathrm{c}) = N_0 \exp(-\theta/\theta_0)$ appears to hold quite accurately over the angular range studied.

The only other case found of such a close, simple exponential type of dependence was for a Teflon absorber. This is displayed on the same plot (figure 4). θ_0 for Teflon, however, was different from that of copper, being $2{\cdot}9 \times 10^{-3}$ radian.

(ii) *Other Substances*

A series of metals, salts, insulators and co-valent compounds were used as absorbers in an attempt to establish a dependence of the shape of the $(N(\mathrm{c}), \theta)$ curve on some property of the positron absorber. The thickness of the absorber in each case was the mass thickness required to stop the positrons completely within it. Since the source assembly was turned through a small angle (figure 2) substantially constant source widths were used, except in the case of materials of very low density such as lithium. The geometrical regions of overlap, determined by a straight line between the extremes of the counters and the source, are marked on all curves. The results are displayed in figures 5, 6, 7.

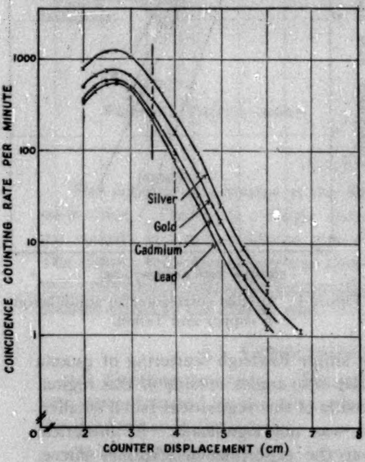

Figure 5. Angular correlation for annihilation in Ag, Au, Cd, Pb.

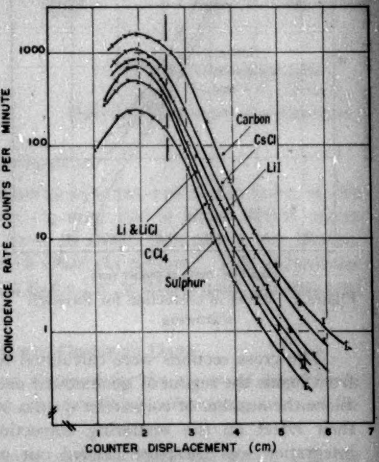

Figure 6. Angular correlation for annihilation in C, CCl_4, S, CsCl, Li, LiCl, LiI.

The statistical fluctuations varied from 2% on the peaks of the curves to 6% at the tails. The counting rates were not normalized to a fixed source strength as the display of the measurements would then become very confused. Normalization of the curves with respect to source strength, and a further correction due to the variation in photoelectric absorption among the various substances, does, in fact, give a set of curves which are closely superimposed.

It is immediately obvious that a 'good' exponential dependence of the coincidence rate with angle is not a general rule. Groups of materials have the same general shape.

The results for a group of metals, figure 5, exhibiting similar dependence of $N(c)$ on θ but varying in electronic shell structure and therefore having momentum distributions for outer electrons which would not be expected to be the same, seem to rule out dependence on this property.

In figure 6 the results are displayed for several metals and salts, covalently bound compounds, and an insulator. There would seem to be no pronounced dependence of the shape of the $(N(c), \theta)$ curve upon lattice structure or chemical binding. In particular the measurements made with the lithium halide absorbers do not show any significant variations with a change in the nature of the negative ion.

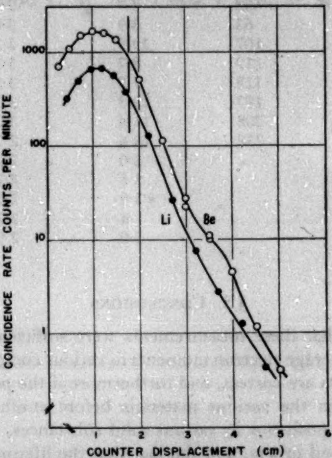

Figure 7. Angular correlation for annihilation in Be and Li.

One anomalous curve was obtained, figure 7. There appears to be an inflection in the $(N(c), \theta)$ curve for a beryllium positron absorber at about 1·1°. In view of the magnitude of statistical fluctuations existence of this inflection can be questioned. The momentum of the annihilating pairs giving this inflection would be $2{\cdot}65\ \boldsymbol{mc}/137$.

Thus to summarize:

(1) No curves, with the exception of those for copper and Teflon, appear to be simple exponentials.

(2) The table shows that the values of p_{av} are independent of density, atomic number and valency. Likewise there appeared to be no dependence on lattice spacing, lattice structure or chemical binding. These values for p_{av} were obtained from the average slopes of the $(\log N(c), \theta)$ lines over the range from the end of the geometrical overlap region to a point at which the counting rate had diminished by a factor of eight. Such values serve only for comparison purposes so that they are given with an accuracy to ±5%.

(3) Most of the curves for $N(c)$ as a function of θ show a marked similarity in shape, particularly in the tails.

Table. Average Momenta of Mass Centre of Annihilating Pair (using mean slope of logarithmic plots)

Absorber	Z	A	ρ (g cm^{-3})	θ_0 (deg$\times 10^{-3}$)	p_{av} ($mc \times 10^{-3}$)
Li	3	7	0·53	2·6	5·2
Be	4	8	1·8	2·3	4·6
C	6	12	2·3	2·5	5·0
Mg	12	24	1·7	3·0	6·0
Al	13	27	2·7	2·4	4·8
S	16	32	2·0	2·4	4·8
Fe	26	56	7·9	3·4	6·8
Ni	28	58	8·9	3·4	6·8
Cu	29	63	8·9	3·8	7·6
Ag	47	107	10·5	3·3	6·6
Cd	48	112	8·7	3·3	6·6
Sn	50	118	7·3	3·3	6·6
Au	79	197	19·3	3·3	6·6
Pb	82	208	11·4	3·2	6·4
U	92	238	18·6	2·7	5·4
LiCl			2·0	2·7	5·4
LiI			3·5	2·7	5·4
CsCl			3·9	2·7	5·4
CCl_4			1·6	2·7	5·4
Teflon			2·0	2·9	5·8

§ 5. CONCLUSIONS

It is considered that these measurements were sufficiently accurate to have shown variations in average electron momenta in various compounds, if the current ideas of such momenta are correct, and furthermore if the positrons had reached 'thermal' velocities in the various materials before annihilation. In view of the short lifetimes of positrons in various solid substances, as measured by Bell and Graham (1952) and others, and the fact that the lifetimes calculated on the basis of range–energy relationships for electrons are in fair agreement with these values, it would appear the the energy losses due to lattice excitations as postulated by de Benedetti *et al.* may not occur.

An attempt to explain these results might, perhaps, be aided by a measurement of the (N(c), θ) dependence through a change in state, liquid to solid, in order to check possible diffraction effects, and also by a measurement of the dependence as a function of temperature. It would also be of interest to see if there is a variation in the dependence of N(c) on θ in materials such as amorphous and crystalline quartz that exhibit different positron lifetimes (Bell and Graham 1952).

ACKNOWLEDGMENTS

I wish to express my thanks to Dr. J. B. Warren for suggesting the experiment and for his continuing interest in it. The experimental work was carried out while the author was a summer student at the Chalk River Laboratories of Atomic Energy of Canada Limited, in the summer of 1951.

I am also obliged to Dr. W. Opechowski for much valuable discussion of the interpretation of the data.

REFERENCES

ARGYLE, P. E., and WARREN, J. B., 1951, *Canad. J. Phys.*, **29,** 32.
BELL, R. E., and GRAHAM, R. L., 1952, *Proc. Roy. Soc. Can.* and *Atomic Energy of Canada, Ltd.*; 1953, *Phys. Rev.*, **90,** 644.
BELL, R. E., GRAHAM, R. L., and PETCH, H. E., 1952, *Canad. J. Phys.*, **30,** 35.
DE BENEDETTI, S., COWAN, G. E., KONNEKER, W. R., and PRIMAKOFF, H., 1950, *Phys. Rev.*, **77,** 205.
FRANZ, W., 1935, *Z. Phys.*, **98,** 314.
HEITLER, W., 1944, *The Quantum Theory of Radiation* (Oxford: University Press).
MAIER-LEIBNITZ, H., 1951, *Z. Naturf.*, **11,** 665.
MOON, P. B., 1950, *Proc. Phys. Soc.* A, **63,** 1189.
STORRUSTE, A., 1950, *Proc. Phys. Soc.* A, **63,** 1197.
WARREN, J. B., and GRIFFITHS, G. M., 1951, *Canad. J. Phys.*, **29,** 325.

The Electrical Conductivity of Cadmium Oxide at Low Temperatures

By J. A. BASTIN and R. W. WRIGHT
Department of Physics, University College, Ibadan, Nigeria

MS. received 27th May 1954, *and in amended form* 15*th November* 1954

Abstract. Measurements of the variation of conductivity with temperature in the range 1°K–250°K together with similar measurements by Wright (1951) in the range 100°K–700°K are compared with the theoretical expression for the conductivity in an ionic crystal derived by Howarth and Sondheimer (1953). The comparison gives the number of free electrons and the characteristic temperature for each specimen. The resistance at zero temperature is discussed in relation to impurity scattering and crystalline boundary resistances.

---

§ 1. INTRODUCTION

CADMIUM oxide has a cubic ionic lattice structure. In general it exists with a non-stoichiometric excess of cadmium atoms which take interstitial positions in the lattice. The concentration of these 'impurity centres' in compressed powder specimens depends largely on the previous treatment, both thermal and mechanical (Wright 1951). In the case of heavily compressed and very heavily sintered specimens, which concern us here, it is considered that the impurity centres are ionized at all temperatures so that the concentration of free electrons is constant (Wright 1951). Howarth and Sondheimer (1953) have derived an expression for the resistivity due to the thermal vibrations of the lattice ions on a wave-mechanical basis, assuming a single vibrational frequency for the lattice. The experimental results extended down to 1°K will be compared with the theoretical expression for the resistivity for the special case of a constant concentration of free electrons and high degeneracy.

§ 2. MEASUREMENTS

Specimens of sintered cadmium oxide were prepared by heating the compressed powder at 1000°K for 24 hours. The specimens were ground to small rectangular slabs about 20 mm × 4 mm × 1 mm. Each specimen was clamped at either end by two pairs of copper terminals; one of each pair acting as potential probes and the other two as current leads. Continuous readings of temperature and resistance were made in the range 20°K–250°K whilst the specimen was heating up, the temperature being measured with a platinum resistance thermometer. This thermometer and the specimen holder were wrapped together in metallic foil, and the rate of heating was kept to less than 1°K per minute, so that the temperature of the thermometer and the specimen should be appreciably the same. Measurements were also made in the range 1°K–4°K using the cryostat attached to a Simon liquifier, and in this case the temperature was measured from the helium vapour pressure. In both cases the specimens were surrounded by an atmosphere of helium. The graphs show the results of two separate runs of measurements on two different specimens.

§ 3. DISCUSSION

Howarth and Sondheimer give the following expression for the conductivity in an ionic crystal:

$$\sigma = \frac{16a^3 M\nu_0 \boldsymbol{k}^2 T^2 (\mathrm{e}^z - 1) G(\zeta z T)}{3\boldsymbol{e}^2 h^2} \qquad \ldots\ldots(1)$$

in which a is the interatomic lattice distance, $1/M$ the sum of the reciprocals of the ionic masses, $z = h\nu_0/\boldsymbol{k}T = \Theta/T$ (where Θ is the characteristic temperature of the substance), and ζ is the Fermi energy of the conduction electrons. $G(\zeta, z, T)$ is a complicated function of ζ, z, and T which, for high degeneracy, takes the form

$$G(\zeta, z, T) = \frac{\zeta^2}{\boldsymbol{k}^2 T^2} \frac{(1 - \mathrm{e}^{-z})}{2z}. \qquad \ldots\ldots(2)$$

This gives with equation (1)

$$\sigma = \frac{32a^3 M\boldsymbol{k}\zeta^2}{3\boldsymbol{e}^2 h^3} T \sinh^2\left(\frac{\Theta}{2T}\right) \qquad \ldots\ldots(3)$$

$$= AT \sinh^2\left(\frac{\Theta}{2T}\right) \qquad \ldots\ldots(4)$$

where A is a constant for any given specimen and depends on the number n of free electrons per unit volume and hence on the impurity concentration of the specimen. In the degenerate case considered here

$$\zeta = \frac{h^2}{2\boldsymbol{m}} \left(\frac{3n}{8\pi}\right)^{2/3}, \qquad \ldots\ldots(5)$$

so that from equations (3), (4) and (5)

$$A = \frac{3^{1/3}}{2} \frac{a^3 M\boldsymbol{k}h}{\boldsymbol{e}^2 \boldsymbol{m}^2} \left(\frac{n}{\pi}\right)^{4/3}. \qquad \ldots\ldots(6)$$

Thus

$$n \simeq 5 \times 10^{20} A^{3/4} \qquad \ldots\ldots(7)$$

where A is measured in ohm^{-1} cm^{-1} deg^{-1} and n in cm^{-3}. Equation (7) assumes a crystalline density of 8·0 g cm^{-3} and that the effective electron mass is equal to that of a free electron.

The actual resistance is assumed to be the sum of a temperature-independent residual resistance (due mainly to the scattering by the impurity centres but also to the scattering at intercrystalline boundaries) and to the resistance due to the thermal vibrations of the lattice. Thus the resistivity takes the form

$$\rho = \rho_0 + \frac{1}{AT \sinh^2(\Theta/2T)}. \qquad \ldots\ldots(8)$$

Jones (1951) has pointed out that this is not always true even using a particle treatment since the fact that two sources of scattering give rise to a free path formed by a reciprocal law from the independent free paths does not necessarily imply the additivity of the resistivities. In the case of the specimens considered with a highly degenerate electronic band this would not affect the problem provided that a mean free path could in fact be defined (Howarth and Sondheimer 1953).

Suitable values of ρ_0, A and Θ are chosen to give the best possible graphical agreement. The functions (8) with those values inserted are shown on the graph as full lines. The expressions for neighbouring values of Θ are shown as broken lines. The values of ρ_0, A, n and Θ are given in table 1 together with those for measurements made by Wright (1951) on more highly compressed specimens in the range 100°K–700°K.

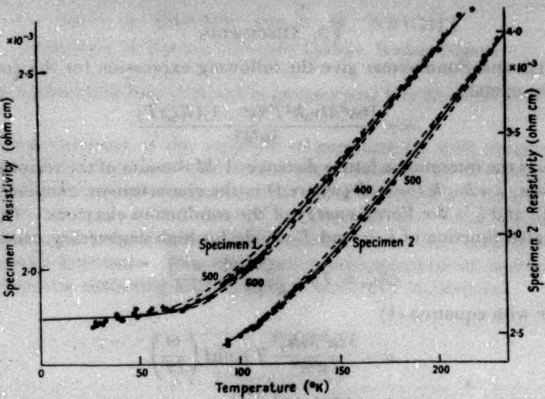

Table 1

Specimen	Temp. range (°K)	A (ohm^{-1} cm^{-1} deg^{-1})	n (cm^{-3})	Θ (°K)	ρ_0 (ohm cm)
B1	20–250	2·5	10×10^{20}	560	$1{\cdot}8\times10^{-3}$
B2	1–250	2·0	8×10^{20}	450	$2{\cdot}3\times10^{-3}$
W1	100–700	1·8	7×10^{20}	800–1000	$1{\cdot}3\times10^{-3}$
W2	100–250	8·0	23×10^{20}	680	$2{\cdot}9\times10^{-4}$

The values of Θ vary considerably from specimen to specimen. They do not bear any obvious relation to n or A. Measurements are at present being made on the variation of specific heat with temperature for various specimens. Comparison of values of Θ obtained from resistance measurements with those from the measurements of the specific heat would be uncertain since the assumption of a single characteristic frequency is far from exact.

The values of n obtained do not justify the assumption that ζ can be treated as a constant except at temperatures below about 250°K. It will be seen from table 1 that in the case of the specimen W1 the characteristic temperature rose from 800°K to 1000°K in the range of temperatures above 250°K. This is equivalent to a larger conductivity at higher temperatures than that calculated from equation (8) and may be due to the spreading of the upper energy levels as the non-degenerate state is approached. In view of the necessary simplifying assumptions no great reliance can be placed on values of n deduced from resistivity measurements. Indeed, using similar specimens Wright has deduced values of n of the order of 2×10^{19} from Hall effect measurements. The high apparent values of n obtained from the conductivity may merely imply a low effective electronic mass.

It is important to note that in addition to the assumptions given above the value of $G(\zeta, z, T)$ is only given exactly by equation (2) at high temperatures. Considering the assumptions made (e.g. n and ζ constant, ρ_0 independent of temperature), the fit of the theoretical curve to the points is very satisfactory. Small inconsistencies do not show up in the figure. For example for all specimens and all runs there were small irregularities near the oxygen point. These may be due to the effect of changes of oxygen pressure or they may be a true anomaly. Since the conductivity is dependent upon oxygen pressure (Blakemore 1950, Hogarth 1951) measurements below the oxygen point will always be difficult to interpret.

Using a classical model an extension of the Conwell-Weisskopf (1950) equation for the residual resistance due to impurity scattering gives

$$\rho_0 = 6{\cdot}0 \times 10^3 \times n^{-1/3} \text{ ohm cm.} \qquad \ldots\ldots(9)$$

Table 2 gives the values of ρ_0 obtained from this equation for two specimens with extreme values of n. The deviations of the observed from the calculated values of ρ_0 may be accounted for by : (i) The value of m used in equation (6) is that for the free electron. If a lower effective mass, as is used frequently in semiconductor work, is applicable this would lead to lower values for ρ_0 calculated than those given in table 2. (ii) Equation (9) assumes each scattering process by impurity atoms to be independent. This is not the case for a concentration of impurity of the order of 10^{21} cm^3. Consideration of this effect would again reduce the values of ρ_0 calculated in table 2. (iii) The effects of intercrystalline boundary resistances have been ignored. Consideration of this would clearly make the values of ρ_0 calculated in table 2 larger. Other experiments would be necessary to eliminate these boundary resistances but the fact that specimens with the same value of n have approximately the same value of ρ_0 suggests that they may in fact be small.

Table 2

Specimen	ρ_0 (calc)	ρ_0 (obs)	n
B2	$6{\cdot}5\times10^{-4}$	24×10^{-4}	8×10^{20}
W2	$4{\cdot}5\times10^{-4}$	3×10^{-4}	23×10^{20}

Measurements were made in the range 1°–4°K and it was found that the change in resistance over this range was less than 1 part in 10^4 of the change of resistance from 1°K to 300°K. This is in agreement with equation (8) using the values of the constants obtained above. These measurements were also of interest in showing the absence of superconductivity in a substance whose temperature variation of resistance resembles that of metals to some extent.

ACKNOWLEDGMENTS

We would like to thank Dr. H. Rosenberg, Dr. A. von Engel, and in particular Dr. K. Mendelssohn, of the Clarendon Laboratory, Oxford, without whom this work would not have been possible.

REFERENCES

BLAKEMORE, J., 1950, *Thesis* (University of London).
CONWELL, E., and WEISSKOPF, V. F., 1950, *Phys. Rev.*, **77**, 388.
HOGARTH, C. A., 1951, *Proc. Phys. Soc.* B, **64**, 691.
HOWARTH, D. J., and SONDHEIMER, E. H., 1953, *Proc. Roy. Soc.* A, **219**, 53.
JONES, H., 1951, *Phys. Rev.*, **81**, 149.
WRIGHT, R. W., 1951, *Proc. Phys. Soc.* A, **64**, 350.

The Effect of Radiative Corrections on a Charged Spin 1/2 Particle in a Constant Magnetic Field

By A. H. de BORDE

Natural Philosophy Department, Glasgow University

MS. received 23rd August 1954, *and in amended form 5th November* 1954

Abstract. As an alternative approach to the problem of determining magnetic moments the *S*-matrix formalism for a Dirac particle in an electromagnetic field is re-expressed as an integral equation of the Feynman type for a one-electron wave function. For a constant magnetic field, the equation reduces to a differential equation which may be solved for the energy eigenvalues in a non-relativistic approximation with arbitrary radiative correction terms. Provided conditions resulting from gauge invariance are satisfied, application of charge renormalization shows that the cyclotron frequency is unaltered in all orders. The magnetic moment derived is the same as that derived direct from the *S*-matrix.

---

§ 1. Introduction

As is well known, the *S*-matrix formalism has been applied with conspicuous success to the calculation of the anomalous magnetic moment of the electron. Similar calculations have also been carried out for nucleons though with less success because of the large value for the meson coupling constant.

The basis of most of these methods (see for instance Case 1949, Karplus and Kroll 1950) has been to consider the matrix element between two free particle states for scattering by a weak periodic potential. This matrix element is then compared with the corresponding matrix element produced by the addition of a magnetic moment term to the free Hamiltonian.

In other work, radiative corrections to the Hamiltonian for a free particle (Schwinger 1949, 1951) or a particle in a magnetic field (Gehenniau and Villars 1950) have been computed, giving directly the spin dependent energy of the particle in a constant magnetic field, the experimentally measurable quantity, as is also given by the work of Luttinger (1948). Both types of method give the same result for the lowest order anomalous magnetic moments, but it is not obvious that they would continue to do so in fourth and higher orders.

The latter methods show directly to the order calculated that all radiative energy corrections directly proportional to the magnetic field can be ascribed to the anomalous magnetic moment. In particular, radiative corrections to the non-relativistic cyclotron frequency are absent.

The purpose of the present paper is to show how a Dirac equation for a particle in a constant magnetic field, modified by arbitrary radiative terms (mesic or electrodynamic) can be solved in non-relativistic approximation to the first order in the magnetic field strength, thus providing a more direct basis for the computation of the anomalous magnetic moment.

In addition, the energy eigenvalues give the cyclotron frequency. If the correction terms satisfy the Dyson condition for charge renormalization, and certain conditions resulting from gauge invariance, this frequency is unaltered to all orders in e, g. Applying the same conditions to the spin dependent part of the energy, the equivalence of the method with the conventional S-matrix method is shown.

§ 2. Derivation of Equations

We may start from the integral equation formulation of Feynman (1949). The single particle wave function $\psi(x)$ of a Dirac particle with charge e, mass m, satisfies the equation

$$\psi(x) = i \int d\sigma_\mu' K(x, x')\gamma_\mu \psi(x') \qquad \ldots\ldots(1)$$

where the integration is over a closed three-dimensional surface of space time enclosing the point x, $d\sigma_\mu'$ has the direction of an inward drawn normal, the γ_μ are the Pauli matrices and the usual summation convention is implied. Natural units are used throughout.

The kernel $K(x, x')$ satisfies

$$K(x, x') = K_+(x, x') + \int dx''\, dx'''\, K_+(x, x'')\bar{G}(x'', x''')K(x''', x'). \qquad \ldots\ldots(2)$$

$\bar{G}(x'', x''')$ is defined as the sum over all possible irreducible† graphs which may be inserted into a single Dirac particle line, and which have no external lines other than those involving interactions with the external electromagnetic field. Both mesic and electrodynamic corrections are included. It is assumed that all renormalizations have been explicitly performed. Thus only renormalized masses and coupling constants appear in the equations. $K_+(x, x')$ is the propagation factor for a Dirac particle satisfying the equation

$$-i\left(\gamma_\mu \frac{\partial}{\partial x_\mu} + m\right) K_+(x, x') = \delta(x - x'). \qquad \ldots\ldots(3)$$

Substituting (2) into (1) operating with the free Dirac operator and using (3) we obtain the equation

$$-i\left(\gamma_\mu \frac{\partial}{\partial x_\mu} + m\right)\psi(x) = \int dx'''\, \bar{G}(x, x''')\psi(x'''). \qquad \ldots\ldots(4)$$

It is convenient to split $\bar{G}$ into parts involving different numbers of interactions with the electromagnetic field. We write

$$\bar{G}(x, x') = \sum_{n=0}^{\infty} \int dx_1 \ldots dx_n \{\Lambda^n_{\mu_1 \ldots \mu_n}(x, x'; x_1 \ldots x_n) A_{\mu_1}(x_1) \ldots A_{\mu_n}(x_n)$$
$$- e\gamma_\mu A_\mu(x)\delta(x - x')\}. \qquad \ldots\ldots(5)$$

The tensor indices will be left understood except where confusion may arise. Λ^n is independent of the potentials and can therefore be expressed as a function of the $n+1$ coordinate differences $x - x'$, $x_1 - x'$, $\ldots$ $x_n - x'$. Transforming (4) to momentum space, we obtain

$$(\gamma p - im)\psi(p) = \sum_n \int dl_1 \ldots dl_n \Lambda^n(p; l_1, \ldots, l_n) A(l_1) \ldots A(l_n) \psi\left(p - \sum_{r=1}^{n} l_r\right)$$
$$- e \int dl \gamma A(l) \psi(p - l) \qquad \ldots\ldots(6)$$

---

† Irreducible here means that the graph cannot be divided into two parts by a line cutting the open golygon of Dirac lines.

where

$$\left.\begin{aligned} \psi(x)=\int dp\psi(p)\mathrm{e}^{ipx}; \quad A(x)=\int dlA(l)\mathrm{e}^{ilx} \\ \Lambda^n(x,x';x_1\ldots x_n)=(2\pi)^{-4(n+1)}\int dp\,dl_1\ldots dl_n\Lambda^n(p;l_1,\ldots l_n) \\ \times\exp i\left\{p(x-x')-\sum_{r=1}^{n}l_r(x_r-x')\right\}. \end{aligned}\right\} \quad \ldots\ldots(7)$$

For a constant electromagnetic field $F_{\mu\nu}$ we may choose

$$A_\mu(l)=\tfrac{1}{2}iF_{\mu\nu}\frac{\partial}{\partial l_\nu}[\delta(l_\nu)].$$

Equation (6) then becomes

$$\left[\gamma_\mu\left(p_\mu+\tfrac{1}{2}ieF_{\mu\nu}\frac{\partial}{\partial p_\nu}\right)-im\right]\psi(p)=\sum_n(-\tfrac{1}{2}i)^nF_{\mu_1\nu_1}\ldots F_{\mu_n\nu_n}$$
$$\times\left[\frac{\partial}{\partial l_{\nu_1}}\cdots\frac{\partial}{\partial l_{\nu_n}}\Lambda^n_{\mu_1\ldots\mu_n}\psi(p-\sum_r l_r)\right]_{l_1=l_2\ldots=l_n=0}. \quad \ldots\ldots(8)$$

§ 3. SOLUTION OF EQUATIONS

We wish to solve (8) where $F_{\mu\nu}$ is a weak magnetic field $\mathscr{H}$ in the z-direction ($F_{12}=F_{21}=\mathscr{H}$ other components zero). Neglecting the terms on the right-hand side, the resulting equation is simply solved. A full discussion of many solutions is given by Johnson and Lippman (1949). If we suppose the z component of the momentum is diagonal, and for convenience zero, the energy eigenvalues are given by

$$E^2=m^2+e\mathscr{H}(2n+s+1) \quad \ldots\ldots(9)$$

where n is any positive integer or zero.

The corresponding normalized eigenfunctions for $s=\pm 1$ are

$$\psi_n{}^+=N\left\{\begin{matrix}\phi_n(m+E)\\0\\0\\{[2e\mathscr{H}(n+1)]^{1/2}\phi_{n+1}}\end{matrix}\right\}, \quad \psi_n{}^-=N\left\{\begin{matrix}0\\\phi_n(m+E)\\(2e\mathscr{H}n)^{1/2}\phi_{n-1}\\0\end{matrix}\right\} \quad \ldots\ldots(10)$$

where ϕ_n is a normalized solution of

$$\left[p_1{}^2+p_2{}^2+ie\mathscr{H}\left(p_1\frac{\partial}{\partial p_2}-p_2\frac{\partial}{\partial p_1}\right)-\frac{e^2\mathscr{H}^2}{4}\left(\frac{\partial^2}{\partial p_1{}^2}+\frac{\partial^2}{\partial p_2{}^2}\right)-E_t\right]\phi_n=0 \quad \ldots\ldots(11)$$

corresponding to an eigenvalue

$$E_t=e\mathscr{H}(2n+1) \quad \ldots\ldots(12)$$

and

$$N=[2E(E+m)]^{-1/2}. \quad \ldots\ldots(13)$$

The wave functions are infinitely degenerate as they must be to ensure invariance of the energy under translations in coordinate space. This condition is automatically satisfied by a gauge invariant theory.

Taking these functions as unperturbed solutions, we can now assess which of the perturbing terms can contribute only amounts to the energy of $O(\mathscr{H}^{3/2})$ and neglect these. Since this will involve neglect of the small components of relation (10) in which $\mathscr{H}$ is involved in the combination $\mathscr{H}n$ the approximation will necessarily be non-relativistic. From equation (11), it is immediately seen that p_1, p_2 are measured in terms of a characteristic momentum of $O(\mathscr{H}^{1/2})$. Thus p^2+m^2 is $O(\mathscr{H})$. The lowest order contribution arising from a given Λ^n arises when it occurs in a scalar product of the form

$$\Lambda^n{}_{\mu_1\ldots\mu_n} F_{\mu_1\nu_1}\ldots F_{\mu_n\nu_n}\frac{\partial}{\partial p_{\nu_1}}\cdots\frac{\partial}{\partial p_{\nu_n}}$$

and this is clearly $O(\mathscr{H}^{n/2})$. Thus only terms with $n \leqslant 2$ need be considered. Expanding the right-hand side of (8) in powers of p^2+m^2 and neglecting terms which are clearly $O(\mathscr{H}^{3/2})$ the remaining terms allowed by relativistic invariance may be reduced to the form

$$\begin{aligned}\Lambda^0 &= b_0(\gamma p - im)(p^2+m^2)\\ i\Lambda^1{}_\mu &= l_\mu\{b_1+ib_2\gamma p\}+\gamma_\mu\{ib_3+b_4\gamma p+b_5\gamma l+b_6(lp)\}\\ &\qquad +p_\mu\{b_7+ib_8\gamma p+ib_9\gamma l+b_{10}(lp)\}+ib_{11}\gamma_\mu(\gamma l)(\gamma p)\\ \Lambda^2{}_{\mu\nu} &= ib_{12}\gamma_\mu\gamma_\nu+b_{13}\gamma_\mu\gamma_\nu\gamma p+ib_{14}\delta_{\mu\nu}+b_{15}\delta_{\mu\nu}\gamma p. \qquad \ldots\ldots(14)\end{aligned}$$

Here the b_i are numerical coefficients. The Dyson renormalization procedure fixes the form of Λ^0 and also asserts the relation

$$b_3+m(b_4+b_7-mb_8)=0. \qquad \ldots\ldots(15)$$

Equation (10) shows that the expectation value of non-diagonal combinations of the γ matrices for any state is $O(\mathscr{H}^{1/2})$. All matrix elements between states with different s values vanish. Thus with the neglect of terms of $O(\mathscr{H}^2)$ (8) becomes

$$\begin{aligned}\Big[\gamma p - im + \mathscr{H}\Big\{ic_1\Big(\gamma_1\frac{\partial}{\partial p_2}-\gamma_2\frac{\partial}{\partial p_1}\Big)+\frac{ic_0}{2m}\sigma_3-\frac{b_4}{2}\sigma_3\Big(p_1\frac{\partial}{\partial p_1}+p_2\frac{\partial}{\partial p_2}\Big)\\ +\frac{c_2}{2m}\Big(p_1\frac{\partial}{\partial p_2}-p_2\frac{\partial}{\partial p_1}\Big)+\frac{ic_3\mathscr{H}^2}{2m}\Big(\frac{\partial^2}{\partial p_1{}^2}+\frac{\partial^2}{\partial p_2{}^2}\Big)\Big]\psi(p)=0 \qquad \ldots\ldots(16)\end{aligned}$$

where

$$\left.\begin{aligned}c_0&=2m(mb_{11}-b_5), & c_1&=\tfrac{1}{2}(e-b_3-mb_4),\\ c_2&=m(mb_8-b_7-b_4), & c_3&=\tfrac{1}{2}m(b_{12}+b_{14}+mb_{13}+mb_{15}).\end{aligned}\right\}\ldots\ldots(17)$$

If we now write

$$\psi=\Big[\gamma p+im+ic_1\mathscr{H}\Big(\gamma_1\frac{\partial}{\partial p_2}-\gamma_2\frac{\partial}{\partial p_1}\Big)\Big]\chi \qquad \ldots\ldots(18)$$

it is readily verified that all non-diagonal terms in the resulting equation give only energy contributions $O(\mathscr{H}^2)$. Thus we obtain

$$\begin{aligned}\Big[p^2+m^2+\mathscr{H}\Big\{(2c_1-c_0)\sigma_3+i(2c_1+c_2)\Big(p_1\frac{\partial}{\partial p_2}-p_2\frac{\partial}{\partial p_1}\Big)-\tfrac{1}{2}mb_4\sigma_3\Big(p_1\frac{\partial}{\partial p_1}+p_2\frac{\partial}{\partial p_2}\Big)\Big\}\\ -\mathscr{H}^2(c_3+c_1{}^2)\Big(\frac{\partial^2}{\partial p_1{}^2}+\frac{\partial^2}{\partial p_2{}^2}\Big)\Big]\chi=0. \qquad \ldots\ldots(19)\end{aligned}$$

If

$$p_1=\{\tfrac{1}{2}(2c_1+c_2)\mathscr{H}q\}^{1/2}\cos\theta,\quad p_2=\{\tfrac{1}{2}(2c_1+c_2)\mathscr{H}q\}^{1/2}\sin\theta \qquad \ldots\ldots(20)$$

and X is a constant eigenvector of σ_3 with eigenvalue s then equation (19) is satisfied by

$$\chi=e^{-\alpha q}q^{|M|/2}{}_1F_1(-N;\,C;\,kq)e^{-iM\theta}X. \qquad \ldots\ldots(21)$$

Here ${}_1F_1(-N;C;kq)$ is a hypergeometric function. M is any integer and the remaining quantities are defined by

$$\left.\begin{aligned}&\beta=\frac{(2c_1+c_2)^2}{4(c_3+c_1{}^2)},\gamma=-\frac{mb_4s(2c_1+c_2)}{8(c_3+c_1{}^2)},\quad \alpha^2+\alpha\gamma-(\beta/4)=0,\ k=2\alpha+\gamma,\\&C=(|M|+1)/k,\quad N=\frac{|M|}{2k}+\frac{\alpha}{k^2}-\beta\left(\frac{\lambda-2M}{4k^2}\right)\\&\lambda=m^2-E^2+\mathscr{H}s(2c_1-c_0).\end{aligned}\right\}\quad\ldots\ldots(22)$$

For the solutions χ to be integrable, the hypergeometric function must be a polynomial. N must therefore be a positive integer or zero. In addition, to satisfy the condition of invariance of the solutions under translations in coordinate space, each energy eigenvalue must be infinitely degenerate. This requirement can only be satisfied in view of (22) if $\beta=k=1$ thus fixing the values of $\alpha=\frac{1}{2}$, $\gamma=0$ and therefore $b_4=0$. We thus obtain the energy values from (22) and (17) on applying the renormalization condition (15)

$$E^2=m^2+e\mathscr{H}\{2N+M+|M|+1\}+s\mathscr{H}\{e-b_3-2m(mb_{11}-b_5)\}.\ldots.(23)$$

It will be observed that the non-spin-dependent part of the energy is exactly the same as (9) for a particle without radiative corrections, as a direct result of gauge invariance and the renormalization condition, and thus the cyclotron frequency is unchanged. The only effect is the extra contribution to the energy of the anomalous magnetic moment. This is directly deduced to be

$$-\frac{b_3+2m(mb_{11}-b_5)}{2me}\text{ Bohr magnetons.}\qquad\ldots\ldots(24)$$

§ 4. EQUIVALENCE WITH SCATTERING MATRIX CALCULATIONS

The method of abstracting the magnetic moment from the scattering matrix has frequently been described. The matrix element for a single scattering of a free particle by a single Fourier component of the electromagnetic field may be written

$$\begin{aligned}\psi^+(p)H'\psi(p-l)&=-i\bar{\psi}(p)\Lambda^1{}_\mu\psi(p-l)A_\mu(l)\\&=\bar{\psi}(p)[l_\mu\{m(b_2+\tfrac{1}{2}b_8+b_{11})-b_1-b_5-\tfrac{1}{2}b_7\}+i\gamma_\mu(m^2b_8-mb_7-b_3)\\&\qquad+i\sigma_{\mu\nu}l_\nu\{b_5+\tfrac{1}{2}(b_7-mb_8-2m^2b_{11})\}+O(l^2)]\psi(p-l)A_\mu(l).\end{aligned}$$

The free particle properties of $\bar{\psi}(p)$, $\psi(p-l)$ and $b_4=0$ are used in deriving the latter form. The term l_μ gives zero contribution because of the gauge condition and the γ_μ term is zero because of relation (15). The term $\sigma_{\mu\nu}l_\nu$ may be directly interpreted as the interaction with the electromagnetic field of an additional magnetic moment of magnitude $e^{-1}\{b_5+\frac{1}{2}(b_7-mb_8-2m^2b_{11})\}$ Bohr magnetons. Use of the renormalization condition (15) shows that this is exactly equal to (24).

§ 5. CONCLUSIONS

The equivalence of the scattering matrix and energy eigenvalue methods for the determination of the anomalous magnetic moment has thus been demonstrated. In addition the complete absence of radiative corrections (mesic or electrodynamic) to the non-relativistic cyclotron frequency has been shown.

ACKNOWLEDGMENTS

I should like to thank Dr. W. K. Burton, Dr. J. S. R. Chisholm and Professor J. C. Gunn for discussions and comments on the manuscript. The work was carried out during the tenure of a Nuffield Research Fellowship.

REFERENCES

CASE, K. M., 1949, *Phys. Rev.*, **76,** 1.

DYSON, F. J., 1949, *Phys. Rev.*, **75,** 1736.

FEYNMAN, R. P., 1949, *Phys. Rev.*, **76,** 749, 769.

GEHENNIAU, J., and VILLARS, F., 1950, *Helv. Phys. Acta*, **23,** 178.

GREEN, H. S., 1953, *Proc. Phys. Soc.* A, **66,** 873.

JOHNSON, M. H., and LIPPMAN, B. A., 1949, *Phys. Rev.*, **76,** 828.

KARPLUS, R., and KROLL, N. M., 1950, *Phys. Rev.*, **77,** 536.

LUTTINGER, J. M., 1948, *Phys. Rev.*, **74,** 893.

SCHWINGER, J., 1949, *Phys. Rev.*, **76,** 790; 1951, *Ibid.*, **82,** 664.

On the Identification of X-Ray Satellites

By D. J. CANDLIN

Department of Mathematical Physics, The University, Birmingham

Communicated by R. E. Peierls; MS. received 8th November 1954

Abstract. The wave numbers of Kα satellites from $Z=19$ to $Z=42$ are calculated with analytical wave functions, and the spectroscopic terms from which the observed lines are derived are identified.

---

§ 1. Introduction

The classic experimental papers on Kα satellite wavelengths, intensities and widths are those of Parratt (1936c) for $Z=16$ to 32, and of Shaw and Parratt (1936) for $Z=30$ to 46. Of the earlier results the most extensive are those of Ford (1932), including elements down to $Z=12$, but naturally the resolution is not so good as that of the later work. Other measurements have been made in France by Hulubei (1935, 1937), Groven (1949) and Morlet (1950), confirming Parratt's results and filling in some gaps in the table of elements.

In all this work the lines observed are α', α_3, α_3', α_4 and α_3'' (the $\alpha_{3,4}$ group) and another line, α'', nearer the principal $\alpha_{1,2}$ doublet. Wentzel suggested that satellites were due to atoms doubly ionized in the inner shells. Parratt (1936 a) showed that the excitation potential of the $\alpha_{3,4}$ group in titanium was approximately the sum of the K and L ionization potentials, so that this group could arise by the knocking out of a K and an L electron from the atom by a cathode electron, followed by the jumping of an L electron into the K hole with emission of the $\alpha_{3,4}$ quantum. The α'' line has an excitation potential approximately equal to the sum of the K and M ionization potentials, according to Parratt (1936 b: $Z=20$); this line would be explained on the Wentzel theory as $K^{-1}M^{-1} \rightarrow L^{-1}M^{-1}$.

The most recent experimental work is that of Edamoto (1950), who has used a high resolution spectrometer for the elements $Z=25$ to 30. He gives wavelengths for α_3', α_4, α_3, α_3'', α', α'', and a number of other lines of longer wavelength (nearer the principal doublet), which in most cases do not seem to lie on smooth curves against Z. These may be due to impurities in the target or to coupling of the K hole with holes in outer shells. For some of the elements Edamoto observes two lines, which he calls α_0', α_0'', of shorter wavelength than α_3'.

Theoretical work on Kα satellites using Wentzel's hypothesis has been done by Wolfe (1933) and by Kennard and Ramberg (1934), but their conclusions did not agree, owing to the scarcity of experimental data. For a review and further references see Hirsh (1942).

In the present work the expected structure of satellite lines due to $K^{-1}L^{-1} \rightarrow L^{-2}$ transitions for eleven elements between $Z=19$ and $Z=42$ is calculated using first order perturbation theory and hydrogen-like wave functions. The detailed agreement with experiment is fair, but the general trends with Z allow unambiguous identification of the observed lines. In §3 the structure for four elements is calculated using improved wave functions, and the interpretation is confirmed.

§ 2. PREDICTED SATELLITE WAVE NUMBERS, USING HYDROGENIC WAVE FUNCTIONS

In this section the calculation of the displacement of the mean satellite lines from the mean principal line is given. By mean line is meant the energy difference between the mean of the initial and final configurations. This displacement is obtained by calculating the diagonal matrix elements of the total Hamiltonian

$$\sum_i \left(\frac{p_i^2}{2m} - Z\frac{\mathbf{e}^2}{r_i}\right) + \sum_{i>j} \frac{\mathbf{e}^2}{r_{ij}}$$

together with relativistic corrections to order α_0^2, using antisymmetric combinations of hydrogen-like wave functions, with effective charge $Z-\sigma$.

Consider first the mean line $1s^{-1}\,2p^{-1} \rightarrow 2p^{-2}$. Let α, β, γ, δ be the configurations $1s^{-1}\,2p^{-1}$, $2p^{-2}$, $1s^{-1}$ and $2p^{-1}$ respectively. Then the energy displacement required is $E_\alpha - E_\beta - E_\gamma + E_\delta$. Following Condon and Shortley (1951, chap. VI) we find that terms derived from $\mathbf{e}^2/r_{ij}$ involve two single-particle wave functions in each of the initial and final states, and the other terms only one. The terms involving only electrons with principal quantum number $n \geqslant 3$ are almost equal for α and β, and again for γ and δ. The discrepancies which remain nearly cancel, giving a negligible contribution. Similar considerations hold for terms from $\mathbf{e}^2/r_{ij}$ involving one electron with $n \geqslant 3$ and one electron with $n = 1$ or 2. Here the cancellation will not be quite so complete; in terms of an asymptotic expansion in Z, the remainder is $O(1/Z)$ instead of $O(1/Z^2)$ but we still neglect it. From terms involving only 1s electrons the energy† contribution is

$$-(Z^2-\sigma^2) - \tfrac{1}{4}\alpha_0^2 (Z-\sigma')^4 \qquad \text{for a single 1s electron,}$$

and $$-2(Z^2-\sigma^2) - \frac{\alpha_0^2}{2}(Z-\sigma')^4 + \frac{5}{4}(Z-\sigma) \qquad \text{for two 1s electons.}$$

Similarly, for 2s or 2p electrons,

$$-\tfrac{1}{4}(Z^2-\sigma^2) - \frac{5\alpha_0^2}{64}(Z-\sigma')^4 \qquad \text{for a single 2s electron,}$$

$$-\tfrac{1}{2}(Z^2-\sigma^2) - \frac{5\alpha_0^2}{32}(Z-\sigma')^4 + \frac{77}{256}(Z-\sigma) \qquad \text{for two 2s electrons,}$$

$$-(Z^2-\sigma^2) - \frac{7\alpha_0^2}{48}(Z-\sigma')^4 + \frac{1341}{640}(Z-\sigma) \qquad \text{for four 2p electrons,}$$

$$-\tfrac{5}{4}(Z^2-\sigma^2) - \frac{35\alpha_0^2}{192}(Z-\sigma')^4 + \frac{447}{128}(Z-\sigma) \qquad \text{for five 2p electrons,}$$

and $$-\tfrac{3}{2}(Z^2-\sigma^2) - \frac{7\alpha_0^2}{32}(Z-\sigma')^4 + \frac{1341}{256}(Z-\sigma) \qquad \text{for six 2p electrons.}$$

From terms derived from $\mathbf{e}^2/r_{ij}$ involving one 1s and one 2s electron the contribution is

$$F_0 - \tfrac{1}{2}G_0 = \frac{290}{729}(Z-\sigma) \qquad \text{per pair}$$

(for example, $1s\,2s^2$ involves two such pairs, and $1s^2\,2s^2$ four). Similarly, for 1s and 2p electrons it is

$$F_0 - \tfrac{1}{2}G_1 = \frac{3074}{6561}(Z-\sigma) \qquad \text{per pair,}$$

---

† In this paper the Rydberg unit is used, and where conversion is necessary it is taken to be 13·52 electron volts. The fine structure constant α_0 is taken as 1/137·2.

and for 2s and 2p electrons

$$F_0 - \tfrac{1}{2} G_1 = \frac{151}{512}(Z-\sigma) \qquad \text{per pair.}$$

These formulae are derived from chapters V and VI of Condon and Shortley (1951) and use the same notation. The screening constant σ will of course be different in the different terms. It is found (e.g. Pauling and Goudsmit 1930) that agreement with experiment is better for ordinary x-ray spectra if the screening constants for the electrostatic and spin–orbit energies are allowed to be different, and for this reason σ and σ' have been written above. Different screening constants should also be taken for the F's and G's in the 'mixed electrostatic' terms.

$$F_0 = \int_0^\infty R_1^2(\text{inner}) \left[\frac{1}{r_1} \int_0^{r_1} R_2^2(\text{outer})\, dr_2 + \int_{r_1}^\infty \frac{1}{r_2} R_2^2(\text{outer})\, dr_2 \right] dr_1$$

for two shells (e.g. 1s and 2s), one of which is classically outside the other. Here the second of the two integrals within the square bracket makes a much larger contribution than the other, so that F_0 is approximately $Z-\sigma$ times the hydrogen value, where σ is a screening constant for the outer shell. With the G's, however, the main contribution comes from the overlap region, and σ will be intermediate between the values appropriate to the two shells involved; but since the G/2 is less than one twentieth of the F in the two cases (1s 2s and 1s 2p) in which the difference in σ is large, the σ appropriate to the outer shell is taken for all terms.

With these assumptions the displacement of the mean line, $E_\alpha - E_\beta - E_\gamma + E_\delta$, is $0{\cdot}118Z + A\alpha_0^2 Z^3$ + a constant term of order 1, where A is a linear combination of the σ',

$$\begin{aligned} A = {} & (\sigma_{1s}'^{(\alpha)} - 2\sigma_{1s}'^{(\beta)} - \sigma_{1s}'^{(\gamma)} + 2\sigma_{1s}'^{(\delta)}) \\ & + \tfrac{5}{8}(\sigma_{2s}'^{(\alpha)} - \sigma_{2s}'^{(\beta)} - \sigma_{2s}'^{(\gamma)} + \sigma_{2s}'^{(\delta)}) \\ & + \tfrac{7}{48}(5\sigma_{2p}'^{(\alpha)} - 4\sigma_{2p}'^{(\beta)} - 6\sigma_{2p}'^{(\gamma)} + 5\sigma_{2p}'^{(\delta)}). \end{aligned}$$

It will be noted that only the differences of the σ' within any one shell are involved, and these were estimated from charge distributions in published Hartree fields to give $A = 0{\cdot}08 \pm 0{\cdot}11$. Thus the displacement of the mean satellite due to an extra 2p hole is

$$0{\cdot}118 + (0{\cdot}08 \pm 0{\cdot}11)\,\alpha_0^2 Z^3 + \text{constant}.$$

Similarly that due to an extra 2s hole is

$$0{\cdot}103 + (0{\cdot}10 \pm 0{\cdot}25)\,\alpha_0^2 Z^3 + \text{constant}.$$

For the structure of the set of satellite lines, the F's, G's and ζ's required were obtained as follows. For the $2p^{-2}$ level $F_2(2p, 2p)$ was taken as $Z-\sigma_0$ times the hydrogen value and ζ_{2p} as $Z-\sigma_2$ times the hydrogen value. Garstang (1951) has analysed the levels of the $1s^2 2s^2 2p^4$ configuration (oxygen I sequence) as given in Miss Moore's compilation (1949). $E(^1D) - E(^3P)$ in Garstang's work is $6F_2$; $E(^1S)$ cannot be used since the $1s^2 2s^2 2p^4\,{}^1S_0$ and $1s^2 2p^6\,{}^1S_0$ levels perturb each other. Reduction of these results gives screening constants which tend with increasing Z to the limits $\sigma_0 = 4{\cdot}4$, $\sigma_2 = 2{\cdot}8$. For the present application an addition varying from 0·29 for $Z=19$ to 0·45 for $Z=42$ was made to allow for the screening by electrons with $n \geqslant 3$, estimated from self-consistent charge distributions. For the set of ions considered by Garstang, the levels of the $1s^2 2s 2p^5$ configuration are also available, and values of $G_1(2s, 2p)$ and ζ_{2p} for the $2s^{-1} 2p^{-1}$ configuration were derived and fitted to similar formulas, giving $\sigma_0 = 3{\cdot}10$ and $\sigma_2 = 2{\cdot}92$. The allowance made for outer shells varied from 0·31 for $Z = 19$ to 0·70 for $Z = 42$. For the $1s^{-1}\,2p^{-1}$ and $1s^{-1}\,2s^{-1}$ configurations only crude estimates for the screening constants could be made, based once again on the self-consistent distributions. The values $\sigma_0 = 2{\cdot}5$ and $\sigma_2 = 3{\cdot}0$ were used in both cases.

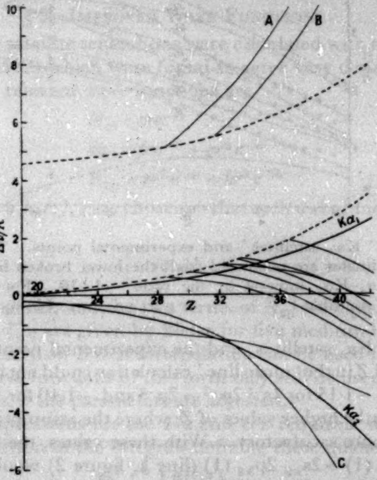

Figure 1. Predicted ' $K\alpha_2$ ' and ' forbidden ' satellites. The ordinates are measured from the weighted mean of the main doublet. The region within broken lines, which contains the ' $K\alpha_1$ satellites ' and all the experimental points, is shown on an enlarged scale in figure 2.

With these values the separations of the expected lines from the weighted mean of the main doublet were calculated. Out of twenty possible dipole lines, nine have approximately the right slope to account for the observed satellites at Z between 30 and 40; these can best be described in terms of *jj* coupling, as being due to the hole transition $1s_{1/2} \rightarrow 2p_{3/2}$ coupled with an extra $2s_{1/2}$, $2p_{1/2}$ or $2p_{3/2}$ hole, each of these possibilities giving three lines, according to the J values involved. These lines may be called ' $K\alpha_1$ satellites ', and lie within the broken lines in figure 1. The two due to the hole transition $1s_{1/2}\,2p_{1/2} \rightarrow 2p_{3/2}{}^2$ (lines A, B in figure 1) have much shorter wavelength, and that due to $1s_{1/2}\,2p_{3/2} \rightarrow 2p_{1/2}{}^2$ (line C in figure 1) has much longer wavelength, but all three are forbidden in both LS and *jj* coupling, and may therefore be expected to be weak in the intermediate region. The remaining eight lines are due to the hole transition $1s \rightarrow 2p_{1/2}$ coupled with an additional 2s or 2p hole, and may be called ' $K\alpha_2$ satellites '. They are also shown in figure 1 (between $K\alpha_1$ and $K\alpha_2$ at the higher Z values). It appears from the experiments of Parratt, that a satellite whose intensity is of the order of 1% of that of the main doublet would be unobservable if it lay within four or five half-widths of one of the doublet components. This would prevent the observation of any of the '$K\alpha_2$ satellites', for their intensity may be expected to fall with increasing Z (like that of the observed satellites) in such a way as to compensate for the increasing separation of the predicted lines from the main doublet.

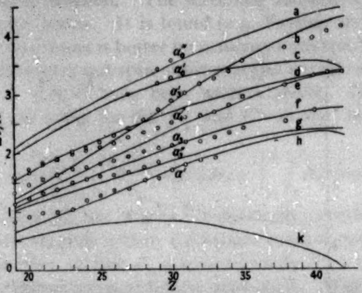

Figure 2. Predicted '$K\alpha_1$ satellites' and experimental points. To display the results clearly, the ordinates are measured from the lower broken line of figure 1, which divides the $K\alpha_1$–$K\alpha_2$ interval in the ratio $-1:10$. For the labelling of the predicted lines see table 1.

In figure 2 the '$K\alpha_1$ satellites' and the experimental points are shown. The term independent of Z in the 'mean line' calculation could not be reliably estimated and was taken to be $-1{\cdot}15$ for $1s^{-1}\,2p^{-1} \to 2p^{-2}$ and $-1{\cdot}40$ for $1s^{-1}\,2s^{-1} \to 2s^{-1}\,2p^{-1}$ to give the best fit at the higher values of Z, where the assumption of hydrogen-like wave functions is more satisfactory. With these values, the line due to the hole transition $1s_{1/2}\,2s_{1/2}\,(1) \to 2s_{1/2}\,2p_{3/2}\,(1)$ (line k, figure 2) would be masked by α_1 and it will be seen from figure 2 that the remaining eight predicted lines for $Z = 27$ to 42 agree well enough with the experimental points to allow the origin of the satellites to be unambiguously identified, as in table 1. It is assumed there that the experimental line α_4 is an unresolved doublet. At lower Z the '$K\alpha_2$ satellites' also lie in the interesting region, but in any case our assumptions are not good enough here. In particular, we can no longer neglect terms of order $1/Z$.

Table 1

	Predicted line	Correlated observed line
Label in fig. 2	Hole transition involved	
a	$1s_{1/2}2p_{1/2}(1) \to 2p_{1/2}2p_{3/2}(1)$	α_0''
b	$1s_{1/2}2p_{3/2}(1) \to 2p_{3/2}{}^2(2)$	α_3'
c	$1s_{1/2}2s_{1/2}\,(0) \to 2s_{1/2}2p_{3/2}\,(1)$	α_0'
d	$1s_{1/2}2p_{1/2}(1) \to 2p_{1/2}2p_{3/2}(2)$	α_4
e	$1s_{1/2}2p_{1/2}(0) \to 2p_{1/2}2p_{3/2}(1)$	
f	$1s_{1/2}2p_{3/2}(2) \to 2p_{3/2}{}^2(2)$	α_3
g	$1s_{1/2}2p_{3/2}(1) \to 2p_{3/2}{}^2(0)$	α_3''
h	$1s_{1/2}2s_{1/2}\,(1) \to 2s_{1/2}2p_{3/2}\,(2)$	α'
k	$1s_{1/2}2s_{1/2}\,(1) \to 2s_{1/2}2p_{3/2}\,(1)$	None

No calculations of expected intensities have been made, but it is interesting to note that the variation of line width against Z (Parratt 1936 c, Shaw and Parratt

1936) of α_3', α_4 and α_3 is very different from that of α'. In table 1 α_3', α_4 and α_3 are assumed to arise from the $1s^{-1}2p^{-1}$ configuration and α' from the $1s^{-1}2s^{-1}$. Also the relative intensities for α_3', α_4 and α_3 at $Z=40$ are roughly those to be expected, if one uses the *jj* coupling values of Condon and Shortley (1951) and assumes that all the $1s^{-1}\,2p^{-1}$ states are equally excited. However, the curious fall in total intensity at $Z=38$ is due to lack of excitation, as is shown by the continuity of the line widths against Z, and the last assumption may not be justified.

§ 3. IMPROVED WAVE FUNCTIONS

In this section the satellite separations were calculated with the analytical wave functions of Slater (1932) which were found to agree very closely with published Hartree fields. The relevant wave functions are

$$R_{1s}=cre^{-\gamma r}$$

$$R_{2s}=fre^{-\epsilon r}+gr^2\,e^{-\zeta r}$$

$$R_{2p}=ar^2\,e^{-\alpha r}+br^2\,e^{-\beta r}$$

where the coefficients a, b, c, f, g are chosen so that each wave function is normalized in the sense

$$\int_0^\infty R^2\,dr=1,$$

R_{1s} and R_{2s} are orthogonal, and the two terms of R_{2p} are equal for $\eta r=2$. The parameters α, β, γ, ϵ, ζ, η are given by Slater for five medium light elements, and depend so nearly linearly on Z that interpolation can be used for other elements. It is assumed that wave functions of this form may still be used when the atom is ionized in x-ray shells, if the parameters are adjusted.

The analytical expressions for the F's and G's required may be obtained by straightforward reduction of the integrals defining these quantities. To obtain

$$\zeta_{2p}=\frac{\alpha_0{}^2}{2}\int_0^\infty\frac{1}{r}\frac{dU(r)}{dr}\,R_{2p}{}^2(r)\,dr,$$

where U is the effective potential for 2p electrons,† U is expressed in terms of R_{2p} by means of the Schrödinger equation

$$-\tfrac{1}{2}\frac{d^2R_{2p}}{dr^2}+\left(U+\frac{1}{r^2}\right)R_{2p}=ER_{2p},$$

where E is a constant. This gives

$$\zeta_{2p}=\frac{\alpha_0{}^2}{4}\int_0^\infty r^{-4}\left[7R_{2p}{}^2-2r^2\left(\frac{dR_{2p}}{dr}\right)^2\right]dr,$$

and provided that errors in R_{2p} are $O(r^2)$ at the origin, as R_{2p} itself is, the errors in ζ_{2p} from this formula are much less than one might have feared.

The structure of the lines arising from the configuration change $1s^{-1}\,2p^{-1}\rightarrow 2p^{-2}$ was calculated for $Z=19$, 29, 35, 40. According to Slater, $\gamma=Z-0{\cdot}30$ for a neutral atom in this range. If it is assumed that this screening is due to the 1s electrons themselves only, a reasonable conjecture is to put $\gamma=Z-0{\cdot}15$ for an atom with one 1s electron missing. In the 2p wave function the first term is predominant inside the maximum and the second outside. In the $2p^{-2}$ configuration it is reasonable to assume that the effective nuclear charge is increased by 1/2 inside the maximum and 3/2 outside, so that α and β, which vary roughly as $Z/2$

---

† In this paragraph atomic units are used.

plus a constant, are increased by 1/4 and 3/4 respectively, compared with the neutral atom. Similarly η is increased by 1/2. For the $1s^{-1}2p^{-1}$ configuration α, η and β are increased by 5/8, 3/4 and 7/8 respectively. The results are shown in table 2, with the results of the calculations of § 2 and the experimental lines, adopting the assignments of table 1. It will be seen that the agreement for $Z = 19$ is still poor, but for the other elements it is improved. Particularly gratifying is the close coincidence of the two lines correlated with α_4. It should be mentioned that the adjustable constant in the 'mean line' was reduced from $-1{\cdot}15$ to $-1{\cdot}19$ for the calculations of this section.

Table 2

Element		Line				
		α_0''	α_3'	α_4		α_3	α_3''
K (19)	a	1·98	1·34	1·40	1·28	1·19	1·14
	b	2·18	1·30	1·63	1·23	1·16	1·10
	c	—	1·59	1·69		1·42	1·22
Cu (29)	a	3·90	3·38	3·08	3·06	2·72	2·42
	b	4·06	3·37	3·26	2·95	2·69	2·44
	c	4·09†	3·40	3·08		2·74	2·50
Br (35)	a	5·53	5·11	4·57	4·56	4·01	3·68
	b	5·53	5·12	4·59	4·44	4·00	3·77
	c	—	5·11	4·49		3·95	—
Zr (40)	a	7·14	6·74	6·07	6·22	5·46	4·96
	b	7·19	6·95	6·13	6·08	5·50	5·17
	c	—	6·74	6·09		5·49	—

Row a contains values calculated from Slater wave functions, b those from hydrogen-like wave functions, and c the experimental values.

† It may be that α_0' at 3·85 should be correlated with the calculated values, instead of α_0'' as shown here. These two lines are only observed in three elements, and there is naturally some ambiguity.

ACKNOWLEDGMENTS

The author is greatly indebted to Mr. J. M. C. Scott for suggesting this problem and for helpful discussions, and to Trinity College, Cambridge (where most of this work was carried out), and to the Department of Scientific and Industrial Research for financial support.

REFERENCES

CONDON, E. U., and SHORTLEY, G. H., 1951, *The Theory of Atomic Spectra* (Cambridge: University Press).

EDAMOTO, I., 1950, *Sci. Rep. Tohoku Univ.*, **A2**, 561.

FORD, O. R., 1932, *Phys. Rev.*, **41**, 577.

GARSTANG, R. H., 1951, *Mon. Not. R. Astr. Soc.*, **111**, 115.

GROVEN, L., 1949, *Ann. Phys. Paris*, **4**, 62.

HIRSH, F. R., JR., 1942, *Rev. Mod. Phys.*, **14**, 45.

HULUBEI, H., 1935, *C.R. Acad. Sci., Paris*, **201**, 544; 1937, *Ibid.*, **205**, 444.

KENNARD, E. H., and RAMBERG, E. G., 1934, *Phys. Rev.*, **46**, 1040.

MOORE, C. E., 1949, *Nat. Bur. Stand. Circular No.* 467 (*Atomic Energy Levels*).

MORLET, J., 1950, *C.R. Acad. Sci., Paris*, **230**, 942.

PARRATT, L. G., 1936 a, *Phys. Rev.*, **49**, 132; 1936 b, *Ibid.*, **49**, 502; 1936 c, *Ibid.*, **50**, 1.

PAULING, L., and GOUDSMIT, S., 1930, *The Structure of Line Spectra* (New York: McGraw-Hill).

SHAW, C. H., and PARRATT, L. G., 1936, *Phys. Rev.*, **50**, 1006.

SLATER, J. C., 1932, *Phys. Rev.*, **42**, 33.

WOLFE, H. C., 1933, *Phys. Rev.*, **43**, 221.

The Electronic Spectra of Aromatic Molecules
III : The Effect of Inductive Substituents

By J. N. MURRELL and H. C. LONGUET-HIGGINS†
Wheatstone Physics Laboratory, King's College, University of London

MS. received 13*th August* 1954 *and in amended form* 25*th October* 1954

Abstract. The theoretical interpretation of aromatic hydrocarbon spectra in Paper I of this series is used as a basis for interpreting the effects of inductive substituents on the spectra of these molecules. It is shown that of the four main bands in the hydrocarbon spectrum, the α band of Clar is the most sensitive to substitution, and relations are derived between the intensity increase and the wavelength shift in the observed bands for various positions of substitution in benzene. The theoretical results are shown to be in reasonable agreement with available data on the fluorobenzenes.

---

§ 1. Introduction

In the first paper of this series (Dewar and Longuet-Higgins 1954), to be referred to as I, a general interpretation was given of the near ultra-violet and visible spectra of aromatic hydrocarbons. The essential feature of this interpretation was that the wave functions of the lower electronic states were simply and definitely specified in terms of molecular orbital configurations. Though such wave functions cannot claim any great accuracy, their compact form makes them particularly useful for discussing the effects of perturbations on the observed spectra.

There are two main ways in which a substituent may affect the electronic structure of an aromatic hydrocarbon. In the first place, if the substituent possesses π-electrons it may enter into conjugation with the aromatic system. This is normally described as the mesomeric effect. Secondly, the substituent will as a rule modify the potential acting on the π-electrons of the hydrocarbon. This effect may be described as an inductive perturbation, and will predominate when the electrons of the substituent are most firmly bound. Of these two effects the latter is easier to treat theoretically, because a purely inductive substituent will not change the effective number of π-electrons, so that the wave functions of the perturbed π-electron system may be expanded in terms of those for the unperturbed hydrocarbon. It should be emphasized that this procedure is only possible when the mesomeric effect is small, or can be allowed for. Only the inductive effect will be discussed in this paper; the theoretical results obtained will therefore be of rather limited application.

§ 2. Theoretical Assumptions

In the LCAO MO theory (Coulson and Longuet-Higgins 1947), the one-electron Hamiltonian is completely specified by its matrix elements between the various pairs of atomic orbitals in the system. The same therefore applies to any one-electron perturbation, in particular to the inductive effect of a substituent. If this perturbation is denoted by h', it is reasonable to suppose that its most important matrix elements are those of the type

---

† Now at Department of Theoretical Chemistry, University of Cambridge.

$$\delta_r = \int \phi_r^{(i)} h'_i \phi_r^{(i)} \, d\tau_i, \qquad \ldots\ldots(2.1)$$

where ϕ_r is the 2p orbital of one of the substituted carbon atoms. Furthermore, δ_r may be presumed to depend only on the nature of the substituent, and not on the position of attachment. If the non-diagonal matrix elements $\int \phi_r^{(i)} h'_i \phi_s^{(i)} d\tau_i$ can be neglected compared with δ_r, then the matrix elements of $H' = \Sigma_i h'_i$ between the various electronic states of the hydrocarbon are linear in the δ_r, and may be evaluated once the wave functions of these states are known. It is then a simple matter, in principle, to determine the perturbed wave functions and their energies in terms of those of the unperturbed system. This programme would strictly require a knowledge of all the unperturbed wave functions and the matrix elements of H' between them. However, it is a familiar result of perturbation theory that the largest terms in the expansion of a perturbed wave function arise from those unperturbed states whose energies differ least from that of the unperturbed wave function. It will therefore be a reasonable approximation to ignore completely the Rydberg and other high-energy states of the hydrocarbon, and to expand the lower electronic states of the substituted molecule in terms of the corresponding lower states of the hydrocarbon. To be specific, we suppose that under inductive substitution the ground state and the upper states of the α, p, β and β' bands mix only with one another. To generalize this assumption we should need to know the energies and wave functions of other electronic states, and no such other states have yet been identified with any certainty.

§ 3. APPLICATION TO ALTERNANT HYDROCARBONS IN GENERAL

To demonstrate the application of the theory we shall first consider inductive substitution in a general alternant hydrocarbon, possessing no centre of symmetry and no orbital degeneracy. A typical example would be phenanthrene.

In I it was shown that if the highest bonding and lowest antibonding orbitals are written ψ_{m-1}, ψ_m and ψ_{m+1}, ψ_{m+2} respectively, then the lowest excited electronic states can be represented as follows :

$$\begin{aligned}
\Psi_{\beta'} &= \psi_{m-1}{}^{-1}\psi_{m+2}\\
\Psi_{\beta} &= \sqrt{\tfrac{1}{2}}(\psi_m{}^{-1}\psi_{m+2} + \psi_{m-1}{}^{-1}\psi_{m+1})\\
\Psi_{\mathrm{p}} &= \psi_m{}^{-1}\psi_{m+1}\\
\Psi_{\alpha} &= \sqrt{\tfrac{1}{2}}(\psi_m{}^{-1}\psi_{m+2} - \psi_{m-1}{}^{-1}\psi_{m+1})\,.
\end{aligned}$$

The symbol Ψ_0 will be used to represent the ground state.

The matrix elements of H' between these five electronic states are determined by its matrix elements between the component configurations. These may be evaluated from the following formulae:

$$\begin{aligned}
\int(\psi_l{}^{-1}\psi_m)H'(\psi_p{}^{-1}\psi_q)\,d\tau &= 0 \text{ unless } p=l \text{ or } q=m,\\
&= \int\psi_m h'\psi_q\,d\tau \text{ if } p=l,\, q\neq m,\\
&= -\int\psi_l h'\psi_p\,d\tau \text{ if } q=m,\, p\neq l;\\
\int(\psi_l{}^{-1}\psi_m)H'\Psi_0\,d\tau &= \sqrt{2}\int \psi_l h'\psi_m\,d\tau;\\
\int(\psi_l{}^{-1}\psi_m)H'(\psi_l{}^{-1}\psi_m)\,d\tau &= W' + \int\psi_m h'\psi_m\,d\tau - \int\psi_l h'\psi_l\,d\tau,
\end{aligned} \qquad \ldots\ldots(3.1)$$

where

$$W' = \int\Psi_0 H'\Psi_0\,d\tau.$$

The matrix elements of h' between the molecular orbitals are in turn determined by the perturbations δ_r and the atomic orbital coefficients in the expansion

$$\psi_l = \sum_r C_{lr}\phi_r.$$

The matrix elements of H' between the five states are set out in table 1. The relative simplicity of these elements is due to the fact that for an alternant hydrocarbon, the atomic orbital coefficients of a pair of 'conjugate' molecular orbitals are equal in magnitude and either equal or opposite in sign (Longuet-Higgins 1950). It will be observed that inductive substitution causes Ψ_0 and Ψ_α to interact with Ψ_{p}, Ψ_β and $\Psi_{\beta'}$, but that the latter three states do not interact among themselves, nor does Ψ_α interact with the ground state.

One other point of interest in table 1 is that the elements $H'_{\alpha\mathrm{p}}$ and $H'_{\alpha\beta'}$ are equal in magnitude but opposite in sign. We shall return to this point later.

To calculate the energy shifts in the observed bands on substitution we make use of the second-order energy equations

$$\left.\begin{aligned}\Delta E_0 &= H_{00}' + \left\{\frac{(H_{0\mathrm{p}}')^2}{E_0 - E_{\mathrm{p}}} + \frac{(H_{0\beta}')^2}{E_0 - E_\beta} + \frac{(H_{0\beta'}')^2}{E_0 - E_{\beta'}}\right\} = \Delta E_0' + \Delta E_0'' \\ \Delta E_\alpha &= H_{\alpha\alpha}' + \left\{\frac{(H_{\alpha\mathrm{p}}')^2}{E_\alpha - E_{\mathrm{p}}} + \frac{(H_{\alpha\beta}')^2}{E_\alpha - E_\beta} + \frac{(H_{\alpha\beta'}')^2}{E_\alpha - E_{\beta'}}\right\} = \Delta E_\alpha' + \Delta E_\alpha''\end{aligned}\right\} \quad \ldots\ldots(3.2)$$

etc. In these equations the energy denominators are obtained from the electronic spectrum of the hydrocarbon. When the equations (3.2) are subtracted to give the change in energy of a band, the first order terms H_{00}' and $H_{\lambda\lambda}'$ cancel, so that the observed spectral shifts should be purely second-order. For a molecule in which all the substituents are identical, the displacement of each band should be proportional to δ^2 where δ is characteristic of the substituent.

To complete the theoretical discussion it is necessary to consider how the intensities of the bands are affected by inductive substitution, and for this purpose one must evaluate the transition moments between the various electronic states. Since the dipole moment $\mathbf{M}$ is a sum of one-electron operators, the rules for evaluating the transition moments $\mathbf{M}_{\rho\sigma}$ are precisely analogous to those for determining the matrix elements $H_{\rho\sigma}'$. The transition moments between the states will form a matrix of the same type as that shown in table 1. Table 2 gives this matrix, where $\mathbf{M}_r = \int\phi_r e r \phi_r d\tau$. The diagonal elements vanish because the electron distribution is uniform in each of the five states (see I).

From table 2 one can draw some general conclusions about the intensities of the various bands. The change in transition moment for $\Psi_0 \to \Psi_\sigma$ is given by the equation

$$\mathbf{M}_{0\sigma}' = \sum_\rho{}' \frac{H_{0\rho}'\mathbf{M}_{\rho\sigma}}{E_0 - E_\rho} + \sum_\rho{}' \frac{H_{\rho\sigma}'\mathbf{M}_{0\rho}}{E_\sigma - E_\rho}. \qquad \ldots\ldots(3.3)$$

For $\sigma = \mathrm{p}$, β or β', $\mathbf{M}_{\rho\sigma}$ is zero unless $\rho = \alpha$, in which case $H_{0\alpha}' = 0$; and $H_{\rho\sigma}'$ $(\rho \neq \sigma)$ is zero unless $\rho = 0$ or $\rho = \alpha$, in which case $\mathbf{M}_{0\rho} = 0$. Hence both sums on the right-hand side vanish, and there should be no first order change in the intensities of the p, β and β' bands.

This general result, based on the assignments

$$\Psi_{\mathrm{p}} = \psi_m{}^{-1}\psi_{m+1}, \text{ and } \Psi_{\beta'} = \psi_{m-1}{}^{-1}\psi_{m+2}$$

remains valid, as we shall see, when owing to orbital degeneracy the states Ψ_{p} and $\Psi_{\beta'}$ are more correctly represented as linear combinations of these two configurations. In general then the α band is the only one whose intensity will be appreciably changed by inductive substitution.

Table 1. Interactions between the Electronic States of an Alternant Hydrocarbon

	$\Psi_{\beta'}$	Ψ_{β}	Ψ_{p}	Ψ_{α}	Ψ_{0}
$\Psi_{\beta'}$	W'	0	0	$\sqrt{2}\sum_r C_{(m-1)r}C_{mr}\delta_r$	$\sqrt{2}\sum_r C_{(m-1)r}C_{(m+2)r}\delta_r$
Ψ_{β}	0	W'	0	$\sum_r (C_{mr}^2 - C_{(m-1)r}^2)\delta_r$	$2\sum_r C_{(m-1)r}C_{(m+1)r}\delta_r$
Ψ_{p}	0	0	W'	$-\sqrt{2}\sum_r C_{(m-1)r}C_{mr}\delta_r$	$\sqrt{2}\sum_r C_{mr}C_{(m+1)r}\delta_r$
Ψ_{α}	$\sqrt{2}\sum_r C_{(m-1)r}C_{mr}\delta_r$	$\sum_r (C_{mr}^2 - C_{(m-1)r}^2)\delta_r$	$-\sqrt{2}\sum_r C_{(m-1)r}C_{mr}\delta_r$	W'	0
Ψ_{0}	$\sqrt{2}\sum_r C_{(m-1)r}C_{(m+2)r}\delta_r$	$2\sum_r C_{(m-1)r}C_{(m+1)r}\delta_r$	$\sqrt{2}\sum_r C_{mr}C_{(m+1)r}\delta_r$	0	W'

Table 2. The Matrix Elements of the Transition Moment Operator between the Five States

	$\Psi_{\beta'}$	Ψ_{β}	Ψ_{p}	Ψ_{α}	Ψ_{0}
$\Psi_{\beta'}$	0	0	0	$\sqrt{2}\sum_r C_{(m-1)r}C_{mr}\mathbf{M}_r$	$\sqrt{2}\sum_r C_{(m-1)r}C_{(m+2)r}\mathbf{M}_r$
Ψ_{β}	0	0	0	$\sum_r (C_{mr}^2 - C_{(m-1)r}^2)\mathbf{M}_r$	$2\sum_r C_{(m-1)r}C_{(m+1)r}\mathbf{M}_r$
Ψ_{p}	0	0	0	$-\sqrt{2}\sum_r C_{(m-1)r}C_{mr}\mathbf{M}_r$	$\sqrt{2}\sum_r C_{mr}C_{(m+1)r}\mathbf{M}_r$
Ψ_{α}	$\sqrt{2}\sum_r C_{(m-1)r}C_{mr}\mathbf{M}_r$	$\sum_r (C_{mr}^2 - C_{(m-1)r}^2\mathbf{M}_r$	$-\sqrt{2}\sum_r C_{(m-1)r}C_{mr}\mathbf{M}_r$	0	0
Ψ_{0}	$\sqrt{2}\sum_r C_{(m-1)r}C_{(m+2)r}\mathbf{M}_r$	$2\sum_r C_{(m-1)r}C_{(m+1)r}\mathbf{M}_r$	$\sqrt{2}\sum_r C_{mr}C_{(m+1)r}\mathbf{M}_r$	0	0

To find the change in intensity of the α band we put $\sigma=\alpha$ in equation (3.3), and obtain

$$\mathbf{M}_{0\alpha}'=\frac{H_{0\mathrm{p}}'\mathbf{M}_{\alpha\mathrm{p}}}{E_0-E_\mathrm{p}}+\frac{H_{0\beta}'\mathbf{M}_{\alpha\beta}}{E_0-E_\beta}+\frac{H_{0\beta'}'\mathbf{M}_{\alpha\beta'}}{E_0-E_{\beta'}}+\frac{H_{\alpha\mathrm{p}}'\mathbf{M}_{0\mathrm{p}}}{E_\alpha-E_\mathrm{p}}+\frac{H_{\alpha\beta}'\mathbf{M}_{0\beta}}{E_\alpha-E_\beta}+\frac{H_{\alpha\beta'}'\mathbf{M}_{0\beta'}}{E_\alpha-E_{\beta'}}. \qquad \ldots\ldots(3.4)$$

We have calculated the relative magnitudes of the moments $\mathbf{M}_{0\mathrm{p}}$, $\mathbf{M}_{0\beta}$ and $\mathbf{M}_{0\beta'}$ for several molecules neglecting overlap between adjacent atomic orbitals. Comparison with the observed intensities of the bands indicates that although our wave functions give the correct order of magnitude for the intensities, they are not sufficiently accurate to give exact values. The magnitudes of $\mathbf{M}_{\alpha\mathrm{p}}$, $\mathbf{M}_{\alpha\beta}$ and $\mathbf{M}_{\alpha\beta'}$ cannot therefore be reliably obtained from theoretical calculations.

If however the contribution from the first three terms in equation (3.4) can be neglected, or is identically zero as in the special case of a molecule with a centre of symmetry, then the increase in intensity of the α band on substitution is determined by $\mathbf{M}_{0\mathrm{p}}$, $\mathbf{M}_{0\beta}$ and $\mathbf{M}_{0\beta'}$, which may all be estimated from the observed spectrum of the hydrocarbon.

§ 4. APPLICATION TO BENZENE

Benzene belongs to the symmetry group D_{6h}, which gives rise to degeneracy in the molecular orbitals, and causes the β and β' bands to coincide. There seems to be general agreement about the assignment of the lowest three electronic bands (Göppert-Mayer and Sklar 1938). Table 3 summarizes the relevant information.

In the second column of this table χ_1, χ_2, χ_3, χ_4, represent the singlet configurations $(\psi_3^{-1}\psi_4)$, $(\psi_3^{-1}\psi_5)$, $(\psi_2^{-1}\psi_4)$, $(\psi_2^{-1}\psi_5)$ respectively; the molecular orbitals are to be taken in their real forms, with atomic orbital coefficients as in figure 1.

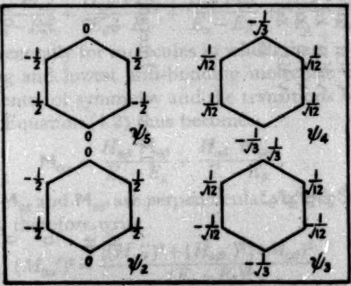

Figure 1. Molecular orbitals of benzene (real forms).

It was noted that in table 1 the elements $H_{\alpha\mathrm{p}}'$ and $H_{\alpha\beta'}'$ were equal in magnitude but opposite in sign. Therefore when through orbital degeneracy the states Ψ_p and $\Psi_{\beta'}$ must be represented by the sum and difference of the configurations χ_1 and χ_4, the matrix element $H_{\alpha\mathrm{p}}'$ becomes zero. Table 4 gives the matrix elements of H' between the five electronic states under consideration.

Table 3. The Electronic States of Benzene

Symbol	Assignment	Symmetry	Excitation energy (ev)	Oscillator strength (*f*)
$\Psi_{\beta'}$	$\sqrt{\tfrac{1}{2}}(\chi_1-\chi_4)$	E_1	$6{\cdot}69_3$	0·69
Ψ_{β}	$\sqrt{\tfrac{1}{2}}(\chi_2+\chi_3)$			
Ψ_{p}	$\sqrt{\tfrac{1}{2}}(\chi_1+\chi_4)$	B_1	$5{\cdot}95_0$	0·10
Ψ_{α}	$\sqrt{\tfrac{1}{2}}(\chi_2-\chi_3)$	B_2	$4{\cdot}73_5$	0·002
Ψ_{0}	χ_0	A_1	—	—

Table 4. Interactions between the Electronic States in Benzene

	$\Psi_{\beta'}$	Ψ_{β}	Ψ_{p}	Ψ_{α}	Ψ_{0}
$\Psi_{\beta'}$	W'	0	0	$2\sum_r C_{2r}C_{3r}\delta_r$	$\sum_r(C_{3r}C_{4r}-C_{2r}C_{5r})\delta_r$
Ψ_{β}	0	W'	0	$\sum_r(C_{2r}^2-C_{3r}^2)\delta_r$	$2\sum_r C_{3r}C_{5r}\delta_r$
Ψ_{p}	0	0	W'	0	$\sum_r(C_{3r}C_{4r}+C_{2r}C_{5r})\delta_r$
Ψ_{α}	$2\sum_r C_{2r}C_{3r}\delta_r$	$\sum_r(C_{2r}^2-C_{3r}^2)\delta_r$	0	W'	0
Ψ_{0}	$\sum_r(C_{3r}C_{4r}-C_{2r}C_{5r})\delta_r$	$2\sum_r C_{3r}C_{5r}\delta_r$	$\sum_r(C_{3r}C_{4r}+C_{2r}C_{5r})\delta_r$	0	W'

The energy shifts in the observed bands on substitution are consequently given by the equations

$$\left.\begin{aligned}\Delta E_0 &= H_{00}' + \left\{\frac{(H_{0\mathrm{p}}')^2}{E_0 - E_\mathrm{p}} + \frac{(H_{0\beta}')^2}{E_0 - E_\beta} + \frac{(H_{0\beta'}')^2}{E_0 - E_{\beta'}}\right\} = \Delta E_0' + \Delta E_0'', \\ \Delta E_\alpha &= H_{\alpha\alpha}' + \left\{\frac{(H_{\alpha\beta}')^2}{E_\alpha - E_\beta} + \frac{(H_{\alpha\beta'}')^2}{E_\alpha - E_{\beta'}}\right\} = \Delta E_\alpha' + \Delta E_\alpha'', \text{ etc.}\end{aligned}\right\} \quad \ldots\ldots(4.1)$$

Table 5 gives the calculated second-order energy displacements in terms of δ^2. The values of $\Delta E_\alpha''$ are seen to be proportional to the numbers given by Sklar (1942) and Forster (1947).

Table 5. The Calculated Second-Order Energy Changes of the Lowest Electronic States of Substituted Benzenes

Substitution	$\frac{-\Delta E_0''}{\delta^2}$	$\frac{-\Delta E_\alpha''}{\delta^2}$	$\frac{\Delta E_\mathrm{p}''}{\delta^2}$	$\frac{\Delta E_\beta''}{\delta^2}$	$\frac{\Delta E_{\beta'}''}{\delta^2}$
1	0·0352	0·0567	0·0187	0·0567	0·0166
1, 2	0·0498	0·0567	0	0·0267	0·0799
1, 3	0·0913	0·0567	0·0747	0·0267	0·0467
1, 4	0	0·2269	0	0·2269	0
1, 2, 3	0·0851	0	0·0187	0·0498	0·0166
1, 2, 4	0·0352	0·1702	0·0187	0·1401	0·0467
1, 3, 5	0·1681	0	0·1681	0	0
1, 2, 3, 4	0·0498	0·0567	0	0·1702	0
1, 2, 3, 5	0·0913	0·0567	0·0712	0·0267	0·0467
1, 2, 4, 5	0	0·2269	0	0·0567	0·1702
1, 2, 3, 4, 5	0·0352	0·0567	0·0187	0·0267	0·0467
1, 2, 3, 4, 5, 6	0	0	0	0	0

The matrix elements for the dipole moment operator $\mathbf{M}$ are similar to those of H' in table 4 ; in particular $\mathbf{M}_{\alpha\mathrm{p}}$ and $\mathbf{M}_{0\mathrm{p}}$ are zero. Just as in the general case the p, β and β' bands are unaffected in intensity by substitution, and equation (3.4), which gives the transition moment of the transition $\Psi_0' \rightarrow \Psi_\alpha'$, becomes

$$\mathbf{M}_{0\alpha}' = \frac{H_{0\beta}'\mathbf{M}_{\alpha\beta}}{E_0 - E_\beta} + \frac{H_{0\beta'}'\mathbf{M}_{\alpha\beta'}}{E_0 - E_{\beta'}} + \frac{H_{\alpha\beta}'\mathbf{M}_{0\beta}}{E_\alpha - E_\beta} + \frac{H_{\alpha\beta'}'\mathbf{M}_{0\beta'}}{E_\alpha - E_{\beta'}}. \quad \ldots\ldots(4.2)$$

(This equation holds generally for molecules in which there is orbital degeneracy in the highest bonding and lowest anti-bonding molecular orbitals.) Furthermore, benzene has a centre of symmetry and the transitions between the excited states are forbidden. Equation (4.2) thus becomes

$$\mathbf{M}_{0\alpha}' = \frac{H_{\alpha\beta}'\mathbf{M}_{0\beta}}{E_\alpha - E_\beta} + \frac{H_{\alpha\beta'}'\mathbf{M}_{0\beta'}}{E_\alpha - E_{\beta'}}. \quad \ldots\ldots(4.3)$$

Now in benzene itself $\mathbf{M}_{0\beta}$ and $\mathbf{M}_{0\beta'}$ are perpendicular vectors of equal magnitude; and $E_\beta = E_{\beta'}$. We may therefore write

$$\begin{aligned}(M_{0\alpha}')^2 &= \frac{\{(H_{\alpha\beta}')^2 + (H_{\alpha\beta'}')^2\}(M_{0\beta})^2}{(E_\alpha - E_\beta)^2} \\ &= \frac{\Delta E_\alpha''(M_{0\beta})^2}{E_\alpha - E_\beta}, \quad \text{by (4.1).}\end{aligned} \quad \ldots\ldots(4.4)$$

Furthermore, the intensities of the β, β' band in benzene and the α band in the substituted molecule depend on $(M_{0\beta})^2$ and $(M_{0\alpha}')^2$ according to the equations

$$I_{0\beta} = k(E_\beta - E_0)\{(M_{0\beta})^2 + (M_{0\beta'})^2\} = 2k(E_\beta - E_0)(M_{0\beta})^2$$

and $$I_{0\alpha}' = k(E_\alpha' - E_0')(M_{0\alpha}')^2 \simeq k(E_\alpha - E_0)(M_{0\alpha}')^2, \quad \ldots\ldots(4.5)$$

where k is a constant. Therefore the intensity increase and second-order part of ΔE_α are connected by the simple relation

$$\frac{I_{0\alpha}'}{\Delta E_\alpha''} = \frac{I_{0\beta}(E_\alpha - E_0)}{2(E_\alpha - E_\beta)(E_\beta - E_0)}. \qquad \ldots\ldots(4.6)$$

§ 5. COMPARISON WITH EXPERIMENT

It was emphasized in § 1 that the theory developed in this paper would apply only to those substituents which could be considered as exerting a purely inductive effect on the π-electrons of the aromatic system. The monatomic substituent which most closely conforms to this requirement is probably fluorine, since its valence electrons are very tightly bound.

Sponer (1954) has recently carried out an extensive investigation of the electronic spectra of some fluorinated benzenes, and has measured the change in frequency and intensity of the α-band relative to benzene. These data are collected in table 6, together with our calculated values of $\Delta E_\alpha''$ and $\Delta E_\alpha'' - \Delta E_0''$.

Table 6. Comparison of the Observed and Calculated Data for the α band of some Fluorinated Benzenes

Substitution	$\Delta E_\alpha''$ (ev)	$\Delta E_\alpha'' - \Delta E_0''$ (ev)	$(E_\alpha' - E_0')_{\text{obs}}$ (ev)	$(\Delta E_\alpha - \Delta E_0)_{\text{obs}}$ (ev)	$I_{0\alpha}(\text{obs})$ (f)
1	$-0{\cdot}0567\delta^2$	$-0{\cdot}0215\delta^2$	4·6875	−0·0335	0·0073
1, 3	$-0{\cdot}0567\delta^2$	$+0{\cdot}0345\delta^2$	4·6987	−0·0223	0·0080
1, 4	$-0{\cdot}2269\delta^2$	$-0{\cdot}2269\delta^2$	4·5666	−0·1544	0·0208
1, 2, 4	$-0{\cdot}1702\delta^2$	$-0{\cdot}1350\delta^2$	4·6012	−0·1198	0·0176
1, 3, 5	0	$+0{\cdot}1681\delta^2$	4·7753	+0·0543	0·0004
1, 2, 4, 5	$-0{\cdot}2269\delta^2$	$-0{\cdot}2269\delta^2$	4·5370	−0·1840	—

In figure 2, the calculated second-order change in energy of the α band for these fluorobenzenes is plotted against the observed change in energy.

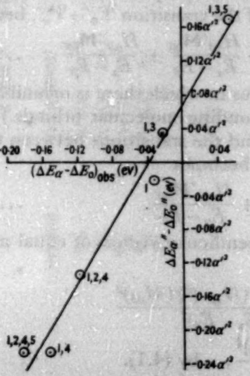

Figure 2. Comparison of the observed change in energy of the α-band on fluoro-substitution with the calculated second-order energy change.

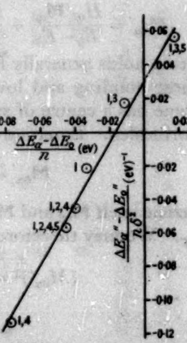

Figure 3. A graph of $(\Delta E_\alpha - \Delta E_0)_{\text{obs}}/n$ against $(\Delta E_\alpha'' - \Delta E_0'')/n\delta^2$ for the fluorobenzenes.

According to our simple theory the line drawn in figure 2 should go through the origin, since the first-order terms H_{00}' and $H_{\alpha\alpha}'$ are equal; actually the line passes below the origin. Two possible explanations suggest themselves. If interactions involving electronic states of higher energy had been included, there would probably have been a larger decrease in the energy of Ψ_α than in the energy of Ψ_0, leading to a larger expected decrease in the energy of the α band. An alternative explanation is that there is a difference between the first-order terms H_{00}' and $H_{\alpha\alpha}'$ proportional to the number of substituents. The change in energy of the α band is then related to the first and second-order terms by the following equation

$$(\Delta E_\alpha - \Delta E_0)_{\text{obs}} = nA + (\Delta E_\alpha'' - \Delta E_0'')$$

where n is the number of substituents and A the first-order energy difference $H_{\alpha\alpha}' - H_{00}'$. A plot of $(\Delta E_\alpha - \Delta E_0)_{\text{obs}}/n$ against $(\Delta E_\alpha'' - \Delta E_0'')/n\delta^2$ is shown in figure 3, which is seen to be a noticeable improvement on figure 2.

Some theoretical justification for this second explanation can be obtained from the fact that the atomic orbitals in the ground state will be slightly smaller than in the excited states; there would be little difference between the size of the atomic orbitals in the four excited states. This would mean that δ would have a smaller absolute value for the ground state than for the upper states. This difference would produce no noticeable change in the second-order term $\Delta E_0''$, but would lead to significant (negative) first-order terms $H_{\alpha\alpha}' - H_{00}'$ etc. If we attribute the first-order term entirely to a difference in the element H_{00}', then the first-order term A should be the same for each of the four main bands.

From figure 3 the values of δ and A for fluoro-substitution are found to be

$$\delta = -0{\cdot}751 \text{ ev}, \quad A = -0{\cdot}017 \text{ ev}.$$

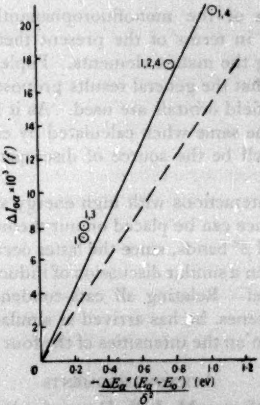

Figure 4. A graph of the observed increase of the α-band $\Delta I_{0\alpha}$ against $-\{\Delta E_\alpha''(E_\alpha' - E_0')\}/\delta^2$ for the fluorobenzenes.

The increase in intensity of the α band is related to the intensities of the p, β and β' bands by the formulae given in § 3. A graph of $\Delta I_{0\alpha}$ against

$$-(\Delta E_{\alpha}'')(E_{\alpha}'-E_{0}')/\delta^{2}$$

is shown in figure 4 for the fluorobenzenes. The points should in fact lie on the broken line whose slope is $-\{I_{0\beta}\delta^{2}\}/\{2(E_{\alpha}-E_{\beta})(E_{\beta}-E_{0})\}$. It is seen from figure 4 that although the relationship is linear to a good approximation, the points fail to be along the line which has the theoretical slope.

It is interesting also to compare the data for chlorinated benzenes with our theoretical results. Here it appears that the linear relationships which were observed for fluorine substitution are not so well satisfied. If we attempt to interpret those data by our equations, the change in energy is seen to be nearly all due to the first order term A, which increases seven-fold on going from fluorine to chlorine whilst the value of δ decreases. However, this behaviour is almost certainly connected with the increase in importance of the mesomeric effect together with the decrease of the inductive effect as the halogen series is descended from fluorine to chlorine.

§ 6. DISCUSSION

It has been shown how the simple wave functions used in I for describing the lower electronic states of aromatic hydrocarbons provide a convenient basis for a perturbation theory of the spectral changes produced by inductive substituents. This treatment explains the most striking change in the spectrum of an aromatic hydrocarbon on substitution, namely that the intensity of the α band is greatly enhanced, whilst the p, β and β' bands are little altered in intensity.

The data which are available on the spectra of fluorinated hydrocarbons are rather limited, but there is good agreement between our calculated energy shifts and the observed data of Sponer. This agreement is not so good when the mesomeric effect becomes appreciable, as is the case in the chlorobenzenes.

Dewar and Bavin (private communication) have recently measured the ultraviolet absorption spectra of the monofluorophenanthrenes. We have failed to interpret their results in terms of the present theory, using Hückel orbital coefficients for evaluating the matrix elements. Pople in paper II of this series (Pople 1955) has shown that the general results proposed in I only apply strictly when the self-consistent field orbitals are used. As it happens, the forms of the orbitals in benzene are the same when calculated by either method, but the use of Hückel orbitals may well be the source of discrepancy in our calculations on phenanthrene.

Lastly, the fact that interactions with high energy states have been neglected will mean that more reliance can be placed on our theoretical results for the α and p bands than for the β and β' bands, since the latter occur at shorter wavelengths.

Moffitt (1954) has given a similar discussion of inductive substitution using the so-called perimeter model. Relating all cata-condensed hydrocarbons to the corresponding cyclic polyenes, he has arrived at similar conclusions with regard to the effect of substitution on the intensities of the four principal bands.

ACKNOWLEDGMENTS

We wish to thank Professor M. J. S. Dewar for helpful discussion. One of us (J. N. M.) also wishes to thank King's College London for the award of a Layton Research Studentship during the tenure of which this work was carried out.

References

Coulson, C. A., and Longuet-Higgins, H. C., 1947, *Proc. Roy. Soc.* A, **192,** 16.
Dewar, M. J. S., and Longuet-Higgins, H. C., 1954, *Proc. Phys. Soc.* A, **67,** 795.
Forster, T., 1947, *Z. Naturforsch.* A, **2,** 149.
Göppert-Mayer, M., and Sklar, A. L., 1938, *J. Chem. Phys.*, **6,** 645.
Longuet-Higgins, H. C., 1950, *J. Chem. Phys.*, **18,** 265.
Moffitt, W., 1954, *J. Chem. Phys.*, **22,** 320.
Pople, J. A., 1955, *Proc. Phys. Soc.* A, **68,** 81.
Sklar, A. L., 1942, *J. Chem. Phys.*, **10,** 135.
Sponer, H., 1954, *J. Chem. Phys.*, **22,** 234.

RESEARCH NOTES

The Mean Free Path of Slow Neutrons in Nuclear Matter

BY C. B. O. MOHR
Physics Department, The University of Melbourne, Australia

Communicated by L. H. Martin; MS. received 22nd November 1954

THE variation of the low energy neutron-nucleus cross section with mass number A indicates a size-resonance effect which is particularly marked near $A=150$ (Adair 1954, Scott 1954 a). Such resonances are predicted by the optical model of the nucleus, which also accounts for the diffraction effects observed in the scattering of fast neutrons (Feshbach *et al.* 1953) and protons (Woods and Saxon 1954) by nuclei. But quantitative agreement is obtained only if account is taken of the absorption of the nucleons in the target nucleus, by the adoption of a complex interaction energy of the form $V=-V_0(1+i\zeta)$. The effect of absorption in reducing the size-resonance effect in the low energy neutron cross section has not previously been allowed for, and the observed variation in cross section will set an upper limit to the nuclear absorption coefficient.

Taking the accepted value of the nuclear well depth of about 40 MEV with the usual linear relation between the nuclear radius R and $A^{1/3}$ leads to a resonance near $A=150$ for $KR=3\frac{1}{2}\pi$, where $2\pi/K$ is the wavelength of the neutron when inside the nucleus. The scattering length a divided by R may be expressed simply in terms of the logarithmic derivative of the wave function at the nuclear boundary. For a rectangular potential well the result may be written down in terms of quantities which are complex when account is taken of absorption, and one must take the modulus of the expression for a. The values obtained for a/R are graphed in part (a) of the diagram, and it is seen that the variation in a near resonance is strongly reduced by comparatively small values of the quantity ζ determining the magnitude of the nuclear absorption.

A potential well with rounded edges must, however, be used in order to obtain close agreement with the observed angular distribution of the scattering of fast protons (Woods and Saxon 1954). One such form of well was therefore tried, illustrated in the inset figure to diagram (b), which permits relatively quick computation. The slope of the potential near the rim of the nucleus was taken to be the maximum slope of the potential used in the proton calculations mentioned, but the potential was taken to be constant well inside and well outside the nucleus instead of weakly exponential, with rounding-off at the inner and outer edges of the well. Then the wave function, which is complex when absorption is introduced, has a simple analytic form over the interior region of constant potential. The wave function was then extended to the nuclear boundary by numerical integration of the pair of coupled differential equations (Milne 1953) into which the wave equation splits, when the real and imaginary parts are separated. From the logarithmic derivative of the wave function follows at once the value of a/R.

The results are shown in diagram (b). The effect of taking a rounded potential well is to increase the variation in a near resonance, as might be expected (Scott 1954 b). Using a potential well with a slightly longer tail like that of Woods and

Saxon or Scott will not increase the variation much more. The points denote values obtained by Adair (1954) by averaging experimental values of the low energy cross section over narrow resonances. Comparison of the experimental and theoretical variations in a/R indicates that the value of ζ is less than 0·1.

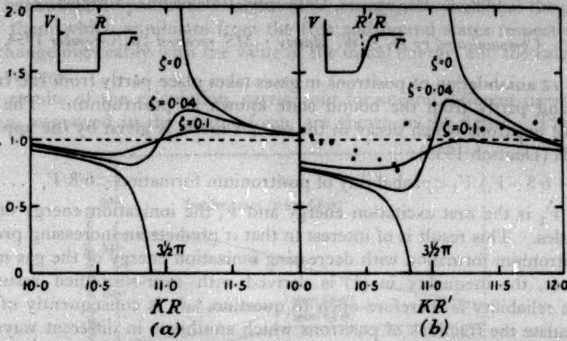

Illustrating the variation of scattering length a for slow neutrons as a function of the nuclear radius R for mass numbers near 150, for different values of ζ which specifies the nuclear absorption, and for two forms of potential well (shown inset). The experimental points are taken from Adair (1954).

The results of Scott are based on the assumption of a random variation in the phase of the wave function inside the nuclear boundary, and on experimental values of a which were not averaged over resonances and which exhibit a larger scatter than those obtained by Adair from the published data. Scott obtains a fit with these values with neglect of absorption, and with a rounded potential well similar in form to that used here but for the length of the tail. Any but very small values of ζ would appear to reduce the variation in a sufficiently to upset the agreement.

The small value of ζ suggested here for thermal neutrons is of the same order as the value of 0·05 obtained by Feshbach *et al.* (1953) for neutrons of energies 0·1–3 Mev. But it is notably smaller than the value of 0·24 obtained by Woods and Saxon for 20 Mev protons. One would not expect the mean free path of neutrons in nuclear matter to be so much greater than for protons, so that the results would indicate an increase in the mean free path at low energies. After all, a large mean free path for bound nucleons, which have negative energy, is indicated by the success of the independent particle model of the nucleus.

Finally, we may remark that the maximum variation in a/R is greater at the lower resonances corresponding to $KR = 2\frac{1}{2}\pi$ and $1\frac{1}{2}\pi$, being 30% and 85% respectively for $\zeta = 0{\cdot}1$ and for a rectangular well, as against 20% for the resonance at $KR = 3\frac{1}{2}\pi$. Greater variations are also apparent in the experimental results for elements in the region of the lower resonances (Adair 1954).

References

Adair, R. K., 1954, *Phys. Rev.*, **94**, 737.
Feshbach, H., Porter, C. E., and Weisskopf, V. F., 1953, *Phys. Rev.*, **90**, 166.
Milne, W. E., 1953, *Numerical Solution of Differential Equations* (New York : Wiley), p. 89.
Scott, J. M. C., 1954 a, *Phil. Mag.*, **45**, 751; 1954 b, *Ibid.*, **45**, 441.
Woods, R. D., and Saxon, D. S., 1954, *Phys. Rev.*, **95**, 577.

Positronium Formation in Gases and its Pressure Dependence

By C. B. O. MOHR
Physics Department, University of Melbourne, Australia

Communicated by H. S. W. Massey ; MS. received 1st *November* 1954

The annihilation of positrons in gases takes place partly from the free state, and partly from the bound state known as positronium. The fraction of positrons which decay in the second mode is given by the approximate formula (Deutsch 1953):

$$(V_1+6\cdot8-V_i)/V_1 < \text{probability of positronium formation} < 6\cdot8/V_i \quad \ldots\ldots(1)$$

where V_1 is the first excitation energy and V_i the ionization energy of the gas molecules. This result is of interest in that it predicts an increasing probability of positronium formation with decreasing ionization energy of the gas molecule. However, the inequality in (1) is derived with over-simplified assumptions, and its reliability is therefore open to question. It is consequently of interest to calculate the fractions of positrons which annihilate in different ways for the case of atomic hydrogen, for which the cross sections for the various processes involved have been calculated.

Firstly a positron may either lose energy in various amounts in excitation or ionization collisions with the hydrogen atoms (Mott and Massey 1949), or it may capture an electron from a hydrogen atom to form ortho- or para-positronium in either the ground or the excited states. Then, if the positronium is formed in the ground state, it may be excited or ionized by collision with a hydrogen atom (Massey and Mohr 1954), or it may decay with the production of two or three quanta (Deutsch 1953). If the positronium is formed in the excited state, it may drop to the ground with the emission of a quantum (Condon and Shortley 1935), it may suffer ionization by collision with a hydrogen atom, or it may decay. The chain of processes is terminated by the annihilation of the positron. We suppose that electron exchange—which quenches the ortho-positronium—does not take place, in order to typify the case of gas molecules without an unpaired electron spin.

With so many processes involved, a Monte Carlo type of calculation is indicated. Sets of curves are drawn for the positron, for the normal positronium and for the excited positronium, the relative spacings between the curves in each set being proportional to the relative probabilities of the possible processes the body could undergo (e.g. Wilson 1952). It is found much quicker in the present instance, however, to follow the life history of the positrons as a whole rather than singly, and backwards in time rather than forwards. We note that if a positron manages to reach an energy below 6·8 ev through collision losses, it will have insufficient energy to capture an electron to form positronium, so that it can only annihilate as a free positron. If a positron lands in the energy range 6·8 to 10·2 ev, it will be unable to lose further energy in excitation or ionization collisions, and—since free positron annihilation is very improbable in comparison—will form positronium with insufficient energy to do else but decay. Positrons in successive energy groups of width 1 ev above 10·2 ev are considered in turn, the fraction of them which finally annihilates from either the free or the bound state being readily calculable for the first few groups. Soon one works back to energy groups of positrons which will, if they do not first annihilate, lose amounts of energy in collision processes which will bring them into one of the energy groups already considered, and their ultimate fate will immediately be known. When one has worked backwards to positrons of about 50 ev energy, one finds that the proportions of them which annihilate from the free and bound states respectively no longer change noticeably with the value of the initial energy, and the calculation may be stopped.

The results of the calculation, carried out for several different pressures of hydrogen, supposed in the atomic form, are shown in the figure. The broad features of the curves may be accounted for in general terms as follows. The time of slowing down of positrons is much less than the mean life for free annihilation; hence practically only those positrons which are 'trapped' in the energy region below 6·8 ev annihilate from the free state. Positronium formed with kinetic energy below 6·8 ev is unable to dissociate in a collision and can only decay, three-quarters of it from the ortho form, one-quarter from the para form. Ortho-positronium formed with kinetic energy above 6·8 ev is extremely unlikely to decay before being dissociated by collision with a hydrogen atom, owing to its relatively long life. The shorter-lived para-positronium will, if formed with kinetic energy above 6·8 ev, contribute appreciably to the sum total of para-positronium decays; but this contribution will arise mainly from positrons with energies not too far above 13·6 ev, since the cross section for positron capture is largest at 12 ev and falls off rapidly with increasing energy, whereas the cross section for ionization of positronium by impact with hydrogen atoms is much larger except just near the threshold for ionization. The decay time of para-positronium is comparable with the mean time between positronium collisions at the lower pressures, so that the amount of para-positronium formed with energy above 6·8 ev will increase noticeably as the pressure is diminished.

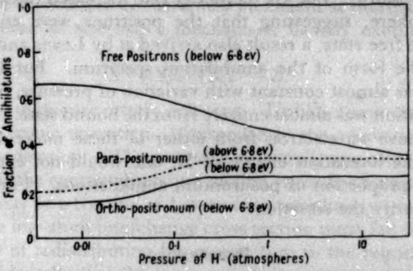

The vertical separation of the curves gives the fraction of positrons which annihilate from the free state or from the bound state when they pass through atomic hydrogen at various pressures.

According to relation (1) the fraction of positrons which annihilate as positronium lies between the limits $\frac{1}{3}$ and $\frac{1}{2}$ for atomic hydrogen, whereas the values calculated here are seen to lie between these limits only for pressures above $\frac{1}{2}$ atmosphere. In other gases, even above $\frac{1}{2}$ atmosphere, the fraction of positronium annihilation may not satisfy (1), since the calculated result depends not only on the ionization and excitation energies of the molecules, but to some degree also on the relative magnitudes of the cross sections for the various capture and loss processes.

The fraction of positrons which form ortho-positronium has been measured for H_2, He, N_2 and A at 1 atmosphere by Pond (1952). If one assumes that the ratio of para to ortho formation in these gases is about the same as for H at 1 atmosphere, the total fraction of positronium formation lies between the limits in (1).

Experiments on positron annihilation at different pressures have been carried out in O_2 and CCl_2F_2 by Deutsch (1953), the decay time being measured as a function of pressure. For O_2 the decay rate increased linearly with pressure above ½ atmosphere, suggesting that the positrons were annihilating almost entirely from the free state, a result also arrived at by Lewis and Ferguson (1953) in a study of the form of the annihilation spectrum. For CCl_2F_2, however, the decay rate was almost constant with variation of pressure, indicating that the positron annihilation was almost entirely from the bound state. Since the energy required to remove an electron from either of these molecules is not greatly different from the ionization energy of H, one would not expect this extreme variation in the proportion of positronium annihilations. Further experiments are needed to clarify the situation.

REFERENCES

CONDON, E. U., and SHORTLEY, G. H., 1935, *The Theory of Atomic Spectra* (Cambridge : University Press), p. 136.

DEUTSCH, M., 1953, *Progr. Nucl. Phys.*, **3,** 131.

LEWIS, G. M., and FERGUSON, A. T. G., 1953, *Phil. Mag.*, **44,** 1011.

MASSEY, H. S. W., and MOHR, C. B. O., 1954, *Proc. Phys. Soc.* A, **67,** 695.

MOTT, N. F., and MASSEY, H. S. W., 1949, *The Theory of Atomic Collisions*, 2nd Edn (Oxford : University Press), Chap. XI.

POND, T. A., 1952, *Phys. Rev.*, **85,** 489.

WILSON, R. R., 1952, *Phys. Rev.*, **86,** 261.

Charge Transfer and Ion–Atom Interchange Collisions

BY D. R. BATES

Department of Applied Mathematics, The Queen's University of Belfast

MS. received 25*th November* 1954

IN theoretical studies on recombination in the F layers of the upper atmosphere and similar problems it is important to know whether atomic ions can readily be converted into molecular ions in collisions with neutral molecules (Bates and Massey 1947).

The most obvious mechanism to consider is exothermic charge transfer which in the general case† may be written

$$X^+ + YZ \rightarrow X + YZ^+. \qquad \ldots\ldots(1)$$

---

† For the sake of definiteness the discussion is restricted to positive ions but it is equally applicable to negative ions.

Provided the impact energy E satisfies the condition

$$E \ll \{36l^2(\Delta E)^2 M\} \text{ ev} \qquad \ldots\ldots(2)$$

where l is a number of order unity, M is the mass of the incident ion on the ^{16}O scale and ΔE is the reaction energy in ev, the internal motion is normally able to adjust itself almost completely to the perturbation and the encounter is nearly adiabatic (Massey 1949). In such encounters the charge transfer cross section is small and diminishes rapidly towards zero as the impact energy is decreased. This general and well-known picture is in harmony with the measurements of Hasted (1951, 1952), Potter (1954) and Dillon, Sheridan, Edwards and Ghosh (1955). Except in special circumstances (cf. Bates and Massey 1954) process (1) would therefore be expected to be extremely inefficient at thermal energies.

There is however an alternative mechanism, namely exothermic ion–atom interchange

$$X^+ + YZ \rightarrow XY^+ + Z. \qquad \ldots\ldots(3)\dagger$$

The characteristics of this are utterly different. Unlike charge transfer it does not necessitate an electronic transition. Consequently the adiabatic condition does not enter into consideration. The process is essentially an ordinary chemical one. It can take place if the energy of relative motion exceeds an activation energy A, which threshold may be a fraction of 1 ev or even vanishingly small. At energies much above A the ion–atom interchange cross section must fall off because of the growing difficulty of redistributing the momentum in the required manner. It may be noted incidentally that the mean translational, rotational and vibrational energies of the molecular ions formed would be expected to be greater than the corresponding energies of those resulting from charge transfer.

In applications the rate coefficient associated with process (3) is what is of most direct interest. It can be expressed in the standard Arrhenius form and in many instances is probably quite large (perhaps as much as 10^{-10} cm^3 sec^{-1}) since steric hindrance can scarcely be unduly severe for such a simple rearrangement.

Experiments on the passage of beams of atomic ions through molecular gases have up to the present been confined to the moderate and high energy regions where charge transfer is most favoured. In view of the possibility of ion–atom interchange becoming dominant caution clearly must be exercised in any attempt at extrapolating the results of such experiments to obtain an estimate of the cross section describing the conversion of atomic ions into molecular ions at thermal energies.

REFERENCES

BATES, D. R., and MASSEY, H. S. W., 1947, *Proc. Roy. Soc.* A, **192,** 1; 1954, *Phil. Mag.*, **45,** 111.

DILLON, J. A., SHERIDAN, W. F., EDWARDS, H. D., and GHOSH, S. N., 1955, *J. Geophys. Res.*, in the press.

HASTED, J. B., 1951, *Proc. Roy. Soc.* A, **205,** 421; 1952, *Ibid.*, **212,** 235.

MASSEY, H. S. W., 1949, *Rep. Progr. Phys.*, **12,** 248 (London: Physical Society).

POTTER, R. F., 1954, *J. Chem. Phys.*, **22,** 974.

---

† In some cases as, for example,

$$O^+ + O_2 \rightarrow O_2^+ + O$$

the two mechanisms give the same products.

The Branching Ratios of ^{86}Rb and ^{42}K

By E. W. EMERY† and N. VEALL‡
† Department of Medicine, University of Manchester
‡ Physics Department, Guy's Hospital, London S.E.1

MS. received 25*th November* 1954

THE assessment of the relative intensities of the individual components by analysis of a complex β-ray spectrum is usually an inaccurate procedure. In the special case, however, when there are two β-ray branches, only one of which leads to the emission of γ-rays, a fairly accurate estimate of the branching ratio can be made from a comparison of the rate of emission of γ-ray energy, as determined by the ionization chamber method (Gray 1949), with the total disintegration rate as determined by 4π β-ray counting (Perry 1953).

^{42}K and ^{86}Rb have decay schemes of this type. ^{42}K goes to the ground state of ^{42}Ca by emission of a 3·6 Mev β-ray or by a 2·1 Mev β-ray followed by a 1·51 Mev γ-ray; ^{86}Rb decays by emission of a 1·80 Mev β-ray or alternatively by a 0·72 Mev β-ray followed by a 1·08 Mev γ-ray. With γ-rays of such energy internal conversion is expected to be negligible, and, further, energy is lost in light elements almost entirely by the Compton process. In these circumstances the energy transferred from γ-rays per electron in the medium at unit distance is $h\nu_{e}\sigma_{a}\phi/4\pi$ per disintegration where ${}_{e}\sigma_{a}$ is the Compton absorption cross section per electron, and ϕ is the fraction of disintegrations yielding a γ-ray. At 1·51 and 1·08 Mev the values of ${}_{e}\sigma_{a}$ are respectively 0·847 and $0{\cdot}916\times10^{-25}$ cm^2, giving a transfer of energy to secondary electrons in 1 g of air at 1 cm of 3·05 kev with ^{42}K and 0·99 kev with ^{86}Rb for each disintegration yielding a γ-quantum.

In the measurements reported here the γ-ray measurement was made by comparison of the ionization current produced in a graphite chamber with that produced by a standard radium source at the same distance. Assuming that the energy required for the formation of an ion pair in air is 32·5 ev, and that γ-ray output from 1 mg of radium screened by 0·5 mm of platinum is 8·3 röntgens per hour at 1 cm, the rate of energy absorption in 1 g of air at 1 cm from 1 mg of radium is $1{\cdot}207\times10^{11}$ ev sec^{-1}. With both the isotopes considered here the emission of β-ray energy is so much greater than the emission of γ-ray energy that a significant part of the observed ionization current was due to bremsstrahlung. With ^{86}Rb a good estimate of this contribution can be made from the effect produced under similar experimental conditions by a sample of ^{32}P, a pure β-emitter of very similar energy. Assuming that the bremsstrahlung intensity varies roughly as the square of the maximum energy, and allowing for the presence of the low energy branch, the bremsstrahlung from ^{86}Rb would be 4% greater than from a ^{32}P sample of the same disintegration rate, and would have contributed 5% of the observed ionization current. With ^{42}K there was no pure β-emitter of comparable energy available, and the effect was estimated by calculation, using the total energy emission given by Heitler (1944) and the approximation to the spectral distribution suggested by Wyard (1952). At low energies the calculation is unreliable owing to uncertainty in the spectral distribution and in the allowances to be made for absorption and for the wall effect in the chamber.

Radiation of low quantum energy, up to about 0·07 MeV, was therefore estimated experimentally by differential absorption in copper, and found to contribute 2·0% of the total ionization. The effect of radiation above 0·07 MeV was calculated giving a result of 6% of the total ionization, and the slight uncertainty as to the effective lower limit, corresponding to the cut-off in copper, has little effect on the result. With ^{42}K, therefore, the total bremsstrahlung effect was 8% of the total ionization, under the particular experimental conditions.

Aliquots of the solutions used for the λ-ray measurements were assayed by 4π β-ray counting, and the disintegration rate was so determined. In view of the high energy of the β-rays, self-absorption and source mounting corrections are small, so there should be no serious error in these measurements.

Combining the results of the two sets of measurements, it was concluded that a γ-ray is emitted in $8{\cdot}5 \pm 0{\cdot}5\%$ of disintegrations of ^{86}Rb, and in $10{\cdot}8 \pm 0{\cdot}6\%$ of disintegrations of ^{42}K. The limits of accuracy have been estimated from experience of determining the disintegration rates of β–γ emitters of known decay scheme by 4π counter and by the γ-ray ionization chamber (Perry 1953), where it has been found that the two methods usually agree to within 5%. The values may be compared with the following, taken from the *Table of Isotopes* (Hollander *et al.* 1953) ^{86}Rb: 20%, 33%, 12%; ^{42}K: 25%, 30%, 17%. It is possible that these variations are due, in part at least, to varying degrees of contamination with ^{134}Cs and ^{24}Na respectively. In the present experiments, the ^{42}K was prepared by irradiation of spectroscopically pure K_2CO_3, and the ^{86}Rb was purified by repeatedly recrystallizing the acid tartrate until the β–γ count ratio remained constant.

ACKNOWLEDGMENTS

We wish to thank the Medical Research Council for the loan of the equipment used for the ionization measurements, and Dr. J. E. S. Bradley of the Post-Graduate Medical School, London, for preparing a sample of radiochemically pure ^{86}Rb.

REFERENCES

GRAY, L. H., 1949, *Brit. J. Radiol.*, **22,** 677.

HEITLER, W., 1944, *The Quantum Theory of Radiation*, 2nd Edn (Oxford : University Press).

HOLLANDER, J. M., PERLMAN, I., and SEABORG, T. G., 1953, *Rev. Mod. Phys.*, **25,** 469.

PERRY, W. E., 1953, *Standardisation of Radioactive Isotopes* (London : National Physical Laboratory).

WYARD, S. J., 1952, *Proc. Phys. Soc.* A, **65,** 339.

LETTERS TO THE EDITOR

The Nuclear Scattering of Electrons by Uranium

The differential cross sections for the elastic scattering of electrons by the coulomb field of the uranium nucleus have been calculated exactly for the energy range $0{\cdot}145\boldsymbol{mc}^2$–$20\boldsymbol{mc}^2$, $\boldsymbol{m}$ being the mass of the electron. The differential cross section, $\sigma(\theta)$ is given by Mott's formula (Mott and Massey 1949)

$$k^2\sigma(\theta) = q^2(1-\beta^2)FF^* \operatorname{cosec}^2(\theta/2) + GG^* \sec^2(\theta/2) \qquad \ldots\ldots(1)$$

where $q=\alpha/\beta$, $\alpha = Ze^2/\hbar\boldsymbol{c}$, $\beta = v/\boldsymbol{c}$ and $k\hbar$ is the momentum of the incident electron. F and G are calculated following the procedure of Bartlett and Watson (1940). The ratios R of the differential cross sections obtained from (1) to those obtained by using the Rutherford formula

$$\sigma(\theta) = (Ze^2/2\boldsymbol{mc}^2)^2\{(1-\beta^2)/\beta^4\} \operatorname{cosec}^4(\theta/2) \qquad \ldots\ldots(2)$$

have also been obtained.

The values of the differential cross sections obtained from (1) and the ratios R are given in the table.

Values of $\sigma(\theta)$ and R

θ = angle of scattering in degrees, E = energy in $\boldsymbol{mc}^2$ of the incident electron

E/θ	30	60	90	120	150	180	
			(i) Values of $\sigma(\theta)$				
0·145	50·165	4·118	1·391	0·744	0·527	0·473	$\times 10^{-20}$ cm^2
0·314	12·752	1·269	0·419	0·193	0·113	0·091	$\times 10^{-20}$ cm^2
0·666	3·783	0·412	0·130	0·052	0·023	0·016	$\times 10^{-20}$ cm^2
3·350	2·863	0·328	0·097	0·032	0·0080	0·0016	$\times 10^{-21}$ cm^2
20·000	11·269	1·297	0·380	0·122	0·026	0·00026	$\times 10^{-23}$ cm^2
			(ii) Values of R				
0·145	0·988	1·130	1·527	1·836	2·013	2·075	
0·314	1·041	1·443	1·905	1·979	1·782	1·661	
0·666	1·147	1·742	2·192	1·975	1·367	1·058	
3·350	1·298	2·072	2·448	1·826	0·708	0·158	
20·000	1·321	2·118	2·481	1·793	0·593	0·0068	

I am greatly indebted to Dr. E. H. S. Burhop for his keen interest in the work. I express my sincere thanks to Dr. B. N. Singh for providing every facility to complete the work. I also thank Mr. L. S. Singh for checking some of the calculations.

Physics Department,
Patna University,
Patna, India.
20th December 1954.

H. N. Yadav.

Bartlett, J. H., and Watson, R. E., 1940, *Proc. Amer. Acad. Arts and Sci.*, **74,** 53.

Mott, N. F., and Massey, H. S. W., 1949, *Theory of Atomic Collisions* (Oxford : University Press), p. 80.

Angular Correlation Parameters for Oriented Nuclei

The population $W(M)$ of the magnetic substates of nuclei oriented by various mechanisms has been exhaustively studied by Steenberg (1953, 1954). It has been customary to give the angular distribution of radiation from these nuclei as a sum of intensities $I_M(\theta)$ from the M substates weighted by their population $W(M)$,

$$I(\theta)=\sum_M W(M)I_M(\theta). \qquad \ldots\ldots(1)$$

However, in view of the extensive tabulation of various radiation parameters (Biedenharn and Rose 1953) for angular correlation studies, it is useful to consider orientation from the same point of view. We can then write (1) in the form (Steenberg 1952, Tolhoek and Cox 1952)

$$I(\theta)=\sum A_\nu P_\nu(\cos\theta) \qquad \ldots\ldots(2)$$

where the coefficient A_ν splits into factors: $B_\nu(T)$, temperature dependent, for orientation, C_ν for the observed radiation, and U_ν for each intervening unobserved radiation, so $A_\nu=B_\nu C_\nu U_\nu(1)U_\nu(2)\ldots$ (see Satchler 1953, Appendix III, and 1954). Each factor then depends only on the orientation process, or on the two nuclear spins and radiation multipolarity of the relevant transition, and may be tabulated independently. Two advantages ensue; the degree of anisotropy of radiation may be estimated simply from A_ν, and the irreducible spin moments of the nuclear orientation at temperature T are given immediately by $B_\nu(T)$ (a measure of $\langle M^\nu\rangle_{\text{av.}}$). $B_1(T)/B_1(T=0)$ gives the degree of polarization, and $B_2(T)/B_2(T=0)$ the degree of alignment.

We find in terms of the tabulated coefficients $(AB\alpha\beta|ABC\gamma)$ (Simon 1954)

$$B_\nu(J\,;\,T)=\sum_M(2J+1)^{1/2}W(M)(-)^{J-M}(JJM-M|JJ\nu0).$$

$B_0=1$ if $\Sigma_M W(M)=1$, and B_ν vanish for odd ν if $W(-M)=W(M)$ ('alignment'). Explicit formulae for $W(M)$ are given by Steenberg (1953).

A cascade of particular interest is 2^L-pole γ-radiation following β-decay, with a spin sequence $J_0(j)J_1(L)J_2$. j is the *total* angular momentum carried off in the β process. The angular distribution of γ-rays is given by (2), with

$$A_\nu=B_\nu(J_0\,;\,T)F_\nu(LJ_2J_1)U_\nu(jJ_0J_1)$$

where $A_0=1$ and $U_\nu=[(2J_0+1)(2J_1+1)]^{1/2}(-)^{J_0+J_1-j}\,W(J_0J_0J_1J_1\,;\,\nu j)$. Tables of γ-parameters F_ν (Biedenharn and Rose 1953), and Racah functions W (Simon *et al.* 1954) have been published. If the linear polarization of the γ-ray is observed, we replace $P_\nu(\cos\theta)$ in (2) by

$$[P_\nu(\cos\theta)\pm\kappa_\nu(L)\cos 2\phi\,P_\nu^2(\cos\theta)].$$

Numerical values of $\kappa_\nu(L)$ were given by Satchler (1953).

Curves for $J=7/2$ and $\nu=1, 2, 4$ are given in figure 1 for $W(M)=a\exp(-\beta M)$. The curves for $\nu=2$, 4 also apply when $W(M)=a\cosh\beta M$. Normalization is such that $B_0\equiv1$. Only the B_ν for ν odd depend on the *sign* of β:

$$B_\nu(-\beta)=(-)^\nu B_\nu(\beta).$$

Curves for other J values have the same form, with a change in vertical scale; the larger J, the larger B, as indicated by the asymptotic values ($\beta=\infty$, $T=0$) at the side of figure 1. These are given by

$$B_1(\beta=\pm\infty)=\mp[3J/(J+1)]^{1/2}$$
$$B_2(\beta=\pm\infty)=[5J(2J-1)/(J+1)(2J+3)]^{1/2}.$$

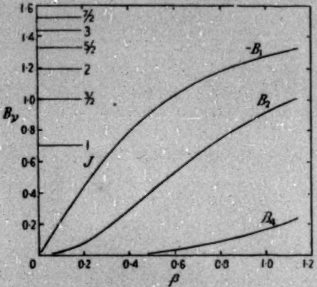

Figure 1. Variation of $B_{1,2,4}$ with β when $W(M)=a\exp(-\beta M)$, for $J=7/2$. Saturation values ($\beta=\infty$, $T=0$) of B_2 for other J values indicated at the left.

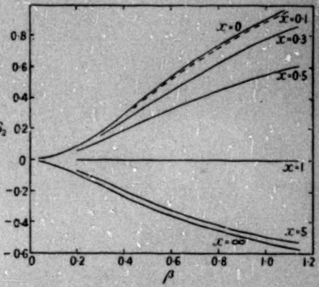

Figure 2. Variation of B_2 with $x=B/A$ in the Bleaney method, for $J=7/2$. $\beta=A/2\boldsymbol{k}T$ when $x<1$, $\beta=B/2\boldsymbol{k}T$ when $x>1$.

Tables of $B_{1,2,4}$ are available at this laboratory for $\beta=0(0{\cdot}1)1{\cdot}0$, 1·5, 2·0, ∞, with $J=1(\frac{1}{2})\,5$.

In the Bleaney method, $W(M)$ depends also on $x=B/A$, the hyperfine structure constants. The variation of B_2 with x is indicated in figure 2 for $J=7/2$; other values of J show similar behaviour. When x is small, $B_2(x)=(1-x^2)B_2(x=0)$, where the $x=0$ values are as for $\cosh\beta M$ (figure 1) with $\beta=A/2\boldsymbol{k}T$. Then B_4 departs negligibly from the $x=0$ value. This approximation is also true for all x when the temperature is high. In fact, to this approximation,

$$B_1=\alpha[J(J+1)/3]^{1/2}$$
$$B_2=\tfrac{1}{6}\beta^2[J(J+1)(2J-1)(2J+3)/5]^{1/2}$$

where α and β are given by Steenberg (1953) for various orientation methods.

Clarendon Laboratory,
Oxford.
23rd December 1954.

T. P. Gray.
G. R. Satchler.

Biedenharn, L. C., and Rose, M. E., 1953, *Rev. Mod. Phys.*, **25,** 729.

Satchler, G. R., 1953, *Proc. Phys. Soc.* A, **66,** 1081; 1954, *Phys. Rev.*, **94,** 1304.

Simon, A., 1954, *Table of Clebsch–Gordan Coefficients* (Oak Ridge National Laboratory Report 1718).

Simon, A., Vander Sluis, J. H., and Biedenharn, L. C., 1954, *Table of Racah Coefficients* (Oak Ridge National Laboratory Report 1679).

Steenberg, N. R., 1952, *Proc. Phys. Soc.* A, **65,** 791; 1953, *Ibid.*, **66,** 391, 399; 1954, *Phys. Rev.*, **93,** 678.

Tolhoek, H. A., and Cox, J. A. M., 1952, *Physica*, **18,** 357.

The Magnetic Ground State of UF_3

Paramagnetic resonance has recently been observed by Ghosh, Gordy and Hill (1954) in a powdered specimen of UF_3. The resonance was interpreted as being due to ions with $g_{\parallel}=2{\cdot}8$ and $g_{\perp}=2{\cdot}1$. Since, apart from complexes such as the uranyl ion, so little is known of the configuration and types of coupling in the heaviest elements, it is of interest to see what can be deduced about them from these g values.

UF_3 grows with the Tysonite structure, which was described by Oftedal (1931). Each uranium has five fluorines as nearest neighbours and six as next-nearest neighbours. In the idealized structure the symmetry is trigonal, and the five nearest neighbours form a trigonal bi-pyramid. The distortion from the idealized structure will be ignored in what follows.

The crystal field at the uranium was calculated by replacing these eleven fluorines and the six nearest U^{3+} ions by point charges and ignoring the rest of the crystal. Such a procedure is known to give the arrangement of energy levels quite well if certain plausible assumptions are made about the magnitude of the matrix elements concerned. This calculation gives values for the crystal field parameters A_2^0, A_4^0, A_6^0 and A_6^6, and it shows that $A_6^6 \simeq 10A_6^0$. This notation and the method used to calculate the parameters are from Bleaney and Stevens (1953). The field is expanded in spherical harmonics, and A_n^m is proportional to the coefficient of $r^n Y_n^m(\theta, \phi)$ in this expansion.

The U^{3+} ion has three magnetic electrons. Dawson (1952) has shown that in this part of the periodic table the energies of the configurations $5f^3$ and $6d^3$ are nearly equal, so that the ground state of this ion is not easy to predict, and may even be different in different compounds. A $5f^26d^1$ configuration has also been proposed to account for the magnetic properties of UCl_3, UBr_3 and UI_3 (Dawson 1951).

The configuration $5f^3$ has the ground state $^4I_{9/2}$. It is assumed that, as for the rare earth ions which have $4f^n$ magnetic electrons, the crystal field is not strong enough to break down the coupling by which J is a good quantum number. On the calculated crystal field the ground state should be the Kramers doublet

$$\cos\alpha|\pm 7/2\rangle + \sin\alpha|\mp 5/2\rangle,$$

in which the states $|J_z \pm 6\rangle$ are admixed to the state $|J_z\rangle$ by the Y_6^6 term in the crystal field. J_z is the component of J along the principal axis of the crystal. The g values of such a doublet depend only on α, and are

$$g_{\parallel} = \frac{8}{11}(1+6\cos 2\alpha) \quad g_{\perp} = \frac{32}{11}\sin 2\alpha.$$

The best fit with the experimental results is obtained with $\alpha = 71°$, when $g_{\parallel}=2{\cdot}6$ and $g_{\perp}=1{\cdot}8$. The prediction from the crystal field method is that $\alpha=68°$. These g values are reasonably close to the experimental ones, and a more detailed theory would modify them in two ways : the field would admix states with the same values of J_z but different values of J, as in the rare earths, and deviations from the ideal symmetry would admix states with other values of J_z (Elliott and Stevens 1953).

The configuration $6d^3$ could behave either like the majority of ions in the $3d^n$ group, in which L remains a good quantum number but the spin–orbit coupling is broken down, or like the $4d^n$ and $5d^n$ groups, in which the crystal field is stronger than both the spin–orbit coupling and the coulomb interaction. In either of these cases the ground state would have $g_\perp = 0$ in the idealized symmetry. Another possibility is that the spin–orbit coupling is the most important interaction, as its magnitude goes up very rapidly with increasing atomic number. In this case there is *jj* coupling, and the *g* values of the ground state are $g_{\parallel} = 0{\cdot}8$, $g_\perp = 1{\cdot}4$.

The configuration $5f^2 6d^1$ allows a great many possible types of coupling. If, as seems likely, the interaction of the d electron with the crystal field and its spin–orbit coupling are both much larger than the coulomb interaction with the other electrons, then $g_\perp$ is less than about 0·5 in a field of the ideal symmetry. The ground state suggested by Dawson, $^4K_{11/2}$, would have $g_\perp = 0$ with J remaining a good quantum number.

It should be pointed out that, although the language of the method of crystal fields has been used throughout, the matrix elements calculated in this way have only been used for the f electrons. The results quoted for the other configurations depend only on the symmetry and the order of the energy levels, which would not be altered by a small amount of covalent bonding.

The configurations considered above are those most likely to occur in the U^{3+} ion. It appears that, of the predicted *g* values for the ground-states, only those of the $5f^3$ configuration are near the experimental ones, and the agreement is then as good as could be expected in the first approximation.

Clarendon Laboratory,
Oxford.
22nd January 1955.

M. C. M. O'Brien.

Bleaney, B., and Stevens, K. W. H., 1953, *Rep. Progr. Phys.*, **16,** 108 (London: Physical Society).
Dawson, J. K., 1951, *J. Chem. Soc.*, 429; 1952, *Nucleonics*, **10,** 39.
Elliott, R. J., and Stevens, K. W. H., 1953, *Proc. Roy. Soc.* A, **219,** 387.
Ghosh, S. N., Gorly, W., and Hill, D. G., 1954, *Phys. Rev.*, **96,** 36.
Oftedal, I., 1931, *Z. Phys. Chem.*, **13,** 190.

The Second Maxima in the Transition Curve of Cosmic Ray Showers

If the coincidence counting rate between two or more Geiger counters is obtained as a function of the thickness of material placed above them several investigators (see Thurn and Bothe 1951) have found that the resultant curve shows two or more maxima. The first is readily explained in terms of cascade showers; the second sharp maxima is found by some authors under 15–20 cm of lead, but not by others (George, Jánossy and McCaig 1942). For this reason it was decided to carry out an experiment on lines similar to that of Bothe *et al.*

The apparatus is shown in figure 1, and is fully described, together with all results and conclusions, elsewhere (Harding 1954). Briefly, we have recorded the frequency of events in which one counter is discharged in tray A coincidently with one in tray B and at least two in tray D as a function of the lead absorber thickness. Results have been corrected for changes in atmospheric pressure and are shown in graphical form in figure 2, curve A. The apparatus was raised bodily so that tray D was three feet above the ground, and the experiment repeated. The results of this second experiment are shown in figure 2, curve B. The apparatus was surrounded by side-trays E and only events which did not discharge these are shown in the graph.

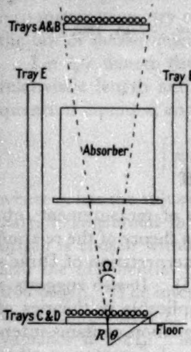

Figure 1.

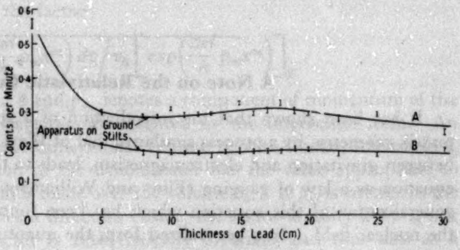

Figure 2.

The results of figure 2, curve A indicate a secondary maximum between 15 and 20 cm of lead. Unlike the results of other experiments (Thurn and Bothe 1951), this is an extended, not a sharply peaked, maximum. The barometric coefficient of -3% per cm Hg, suggests that the majority of these small showers must be produced by the μ-meson component of the cosmic radiation. With the apparatus above the ground a secondary maximum was not observed.

With the apparatus on the ground, it seems likely (Harding 1954) that a number of events, sufficient to cause the secondary maximum, could be produced by the following mechanism. A single μ-meson may pass through the four counter trays A B C and D, decay in the ground immediately below the apparatus, and give rise to a decay electron which travels upwards and passes through the tray D within the resolving time of the apparatus. If the differential μ-meson spectrum is slightly peaked in the region 15–20 cm Pb, then this process should produce events which would show up a secondary maximum under the conditions of the first experiment. With the apparatus placed well above the ground, the small solid angle Θ subtended by tray D would considerably reduce the number of such events. This accounts for the disappearance of the secondary maximum in the second experiment.

We conclude that if sufficient care is taken to eliminate events caused by μ-mesons and their associated decay electrons and if the lead absorber is separated from the shower detecting trays by about 40 cm, then there is no evidence for a secondary maximum in the transition curve even when the apparatus is capable of detecting narrow angled (3°) showers. In the experiments of Thurn and Bothe, when sharp secondary maxima were detected, the absorber and shower detectors were separated by at least 100 cm, but if this instrumental difference be the reason for the difference in results, the particles produced in these showers must possess unusual properties.

Atomic Energy Research Establishment,[†]
Harwell, Berks.
1st November 1954.

J. B. Harding.

George, E. P., Jánossy, and McCaig, M., 1942, *Proc. Roy. Soc.* A, **180,** 219.
Harding, J. B., 1954, *A.E.R.E. Report N/R.* 1550.[‡]
Thurn, H., and Bothe, W., 1951, *Z. Naturf.*, **6 a,** 576.
Thurn, H., 1953, *Z. Naturf.*, **8 a,** 134.

A Note on the Relativistic Cut-Off

It has been shown that the introduction of a system of measurement into matrix geometry, by a process similar to that of Weyl in his theory of the relation between gravitation and electromagnetism, leads to the interpretation of Dirac's equation as a law of gauging (Flint and Williamson 1953). It also suggests a generalization of this equation which has been found applicable in theories of the nuclear field. In a generalized form the quantum equation contains interaction terms which may be interpreted as arising from scalar, vector or other types of field. These terms fall into four groups corresponding to the four possible types of field and each is multiplied by a different constant, often denoted by the symbol g_n ($n=1$, 2, 3 or 4). The difficulties concerning divergences occur in these terms and suggest that some further condition must be included in the gauging equation.

It is well known in the theory of relativity that space–time can be divided into three domains, the future, to which signals may be sent, the past, from which they may be received and an intermediate region within which no such communications are possible. An observer cannot get into causal communication with this region. If the coordinates of a point in it are (x, y, z), if t is the time of an event at the point and if the observer be regarded as being at the origin both in space and time, the region is characterized by the relation

$$x^2+y^2+z^2-c^2t^2>0.$$

This region could be excluded from consideration by imposing the condition that points of importance in physics must satisfy the condition

$$x^2+y^2+z^2-c^2t^2\ngtr 0.$$

The notation of projective geometry and of five-dimensional Riemannian geometry, which has proved especially applicable to quantum phenomena, suggests that in the region of matrix geometry the limitation :

$$x^2+y^2+z^2-c^2t^2+x_5{}^2\ngtr 0$$

[†] Present address, Air Ministry, London S.W.1.

[‡] This report is obtainable from H.M. Stationery Office, London. Copies may also be seen in the Physical Society's Library.

might apply. The coordinate x_5 turns out to be a scalar quantity from the point of view of four dimensions and in applications to particular problems it has the character of a fundamental length, l_0.
Thus the condition

$$c^2t^2 - x^2 - y^2 - z^2 \nless l_0^2$$

may be adopted. This is a condition reminiscent of one introduced by Yukawa in his theory of non-local fields. The appropriate place to introduce this idea into matrix geometry or matrix mechanics is in the law of gauging, in other words the law of measurement.

Let l_0/c denote the minimum interval of proper time and l_0 the minimum relativistic length and let the constants of the various additional terms in the quantum equation contain the factor

$$\int \exp\left(\frac{2\pi i}{h} p_m x^m\right) dv \Big/ v_0 \left[\exp\left(\frac{2\pi i}{h} p_m x^m\right)\right]_0$$

where m has the values 1 . . . . 4 and p_m denotes a component of momentum of the particle concerned in the transition represented by the interaction term. An origin is chosen within a four-dimensional volume v_0 with linear dimensions l_0 and the exponential function in the denominator has the value appropriate to this origin. The integration is made over the volume v_0. If p_m is written in the form hl_m/λ, where l_m denotes a direction cosine, the factor is unity if $\lambda \gg l_0$ but vanishes if $\lambda \ll l_0$. The factor is relativistically invariant and thus acts as a relativistic cut-off. The introduction of the factor in this way into the quantum equations makes them at the same time the expression of a law of measurement and of a law of limitation of measurement. Professor A. March suggested some years ago the introduction of a new law limiting the possibility of measurement (March 1951). According to this it is not possible to give significance in physics to intervals of length less than l_0 ($\sim 10^{-13}$ cm). This has led him to the introduction of a factor similar to that given above to act as a cut-off in the interaction terms of nuclear field theories.

Bedford College,
University of London.
22nd November 1954.

H. T. Flint.
E. M. Williamson.

Flint, H. T., and Williamson, E. M., 1953, *Z. Phys.*, **135**, 260.
March, A., 1951, *Quantum Mechanics of Particles and Wave Fields* (New York: Wiley), p. 271.

REVIEWS OF BOOKS

Statistical Mechanics, by D. TER HAAR. Pp. xix + 468. (New York: Rinehart, 1954.) $8.50 (64*s*.). Also produced in England by Constable & Co. 45*s*.

The writer of a textbook on a branch of theoretical physics usually has to decide whether to follow the historical evolution of the subject, or to develop the subject formally and logically from certain basic assumptions. In most cases the former method provides the better elementary approach, and having grasped the problems and ideas as they arose historically, the student is in a favourable position to appreciate the more rigorous developments.

In statistical mechanics the opposite is true, and a formal development based on a quantum theoretical statement of axioms leads rapidly to an understanding of the range and power of the subject, and does not initially require the more sophisticated classical concept of phase space. However this can only suffice as a first introduction to the subject, and Dr. ter Haar's book, which tends to follow the historical development, is intended for the student who wishes to acquire a deeper understanding of the background to the basic assumptions, and a wider knowledge of the applications.

The book is divided into four sections. Section A deals with assemblies consisting of independent particles starting from the ideas of Maxwell and Boltzmann on the kinetic theory of gases. Section B, which is devoted to ensemble theory, follows along the lines of the fundamental papers of Gibbs, and thence proceeds to deal with the modifications necessitated by the quantum theory. Section C contains applications of the methods of statistical mechanics to a wide variety of problems; and section D consists of a number of important appendices which could not easily be fitted into the text of the other sections. The bibliographical notes at the end of each chapter are a useful feature of the whole book. They give detailed references to the classical original papers, as well as to the more recent developments, and Dr. ter Haar is particularly to be commended on the brief summaries of the important papers given in these notes.

A substantial portion of the book is devoted to fundamental questions such as ergodic properties and Boltzmann's H-theorem, and the author has here been strongly influenced by the work of the famous Dutch physicists H. A. Kramers and P. and T. Ehrenfest. Appendix 1 entitled "The H-theorem and the Ergodic Theorem" provides a valuable summary of the various attempts which have been made to justify the use of statistical mechanics in describing physical systems. Appendix 3 on the Third Law of Thermodynamics is a welcome corrective to the many misleading accounts in the literature. It states clearly that the Law has complete thermodynamic validity and the so-called 'exceptions' to the law arise from systems not in thermodynamic equilibrium. There are several other useful short appendices; perhaps we may specifically mention those on Irreversible Processes, Intermolecular Forces, and Relativistic Statistics.

Most of the new material in the book is contained in Section C. Some of the chapters (e.g. those on rubber elasticity and statistical methods in nuclear physics) give only a brief introduction to a whole field, but are useful to the general student since they give an idea of the range of problems to which the techniques of statistical mechanics can be applied. By contrast the chapter on the Equation of State provides a compact summary of this subject, and will surely now become a central reference. The chapter on Co-operative Phenomena contains an account (albeit rather brief) of Onsager's outstanding contributions to this field, which have previously been available only in original papers. The author points out in the preface that no attempt is made to cover all standard topics ; many subjects such as liquids, solutions, and lattice dynamics have not been considered.

The present reviewer has only two very minor criticisms to offer. The list of references at the end of the chapter on Rubber Elasticity does not contain the important book of L. R. G. Treloar. The footnote on p. 256 in the chapter on Co-operative Phenomena regarding the relation between the binary alloy and the ferromagnetic is unjustified for the wider problem when the ratio of constituents differs from unity ; the relation established by Rushbrooke is then essential to a clear understanding of the problem.

Dr. ter Haar has provided us with a valuable addition to the literature on statistical mechanics, and his book should be warmly recommended to all serious students of the subject. C. DOMB.

An Atlas of Typical Expansion Chamber Photographs, by W. GENTNER, H. MAIER-LEIBNITZ and W. BOTHE. Pp. x + 199. (London : Pergamon Press, 1954.) 105*s*.

The cloud chamber provides us with a very direct visual approach to the study of the properties of atomic nuclei and high energy particles bringing in consequence a high degree of realism to the many and varied phenomena which can be investigated by this means. In an age when atomic nuclei have acquired an all too special significance for mankind it is not unusual to hear the complaint that the basic concepts of nuclear physics are too abstract to be understood by any but the experts. It should not be difficult, however, for anyone with a little knowledge of physics to appreciate and understand some of the fundamentals merely by studying this collection of cloud chamber photographs together with their explanatory captions.

Whilst this volume deals mainly with the application of the cloud chamber to the study of nuclear physics and radioactivity it also includes a representative selection of cosmic ray photographs. There are sections dealing with α, β, γ and X-rays, nuclear transmutations, nuclear fission and artificial radioactivity. A description and interpretation in English, French and German accompanies each picture and many useful tables, graphs and diagrams have been included. This atlas will be of value to all who are engaged either in research or in the teaching of nuclear physics and the quality of many of the photographs will provide a standard of perfection for those who use the cloud chamber as an implement of research. The publishers are to be congratulated on the high quality of the reproductions which has helped to make this volume a remarkable tribute to the elegance and power of the tool devised by C. T. R. Wilson.

H. ELLIOT.

Nuclear Species, by H. E. HUNTLEY. Pp. xix + 193. (London: MacMillan, 1954.) 21*s*.

The expressed aim of this book is to present the systematics of nuclei for the honours undergraduate, and for others who are not already familiar with this field of study. The author also expresses the hope that it may serve as a general introduction to the subject of nuclear physics and, no doubt with this in mind, has leavened his text with a good deal of descriptive and historical material. This permits him in this first chapter to sketch the development of the subject from the time of Becquerel onwards, and enables him to round off the work with a final chapter on the origin of the elements.

The main emphasis is, of course, on the ground states of stable nuclei and of nuclei with a relatively long life. The reader is introduced first to certain basic concepts, such as nuclear size and density, and there follows a description of methods of nuclear mass determination. From this point the book is devoted almost entirely to a presentation, in charts and tables and descriptive text, of what is at present known about the nuclides and their relationships. A theme is furnished by the set of empirical rules covering this field, and the author uses simple physical arguments wherever possible to show what lies behind them. Considerable attention is given to the study of mass defects, binding energies, and the stability relations of isobars. This main part of the book comes to an end with a discussion of the Weizsäcker mass formula; it is followed by a brief presentation of ideas concerning nuclear energy levels, with special reference to the shell model and nuclear isomerism.

The book is not entirely up to date. Thus, for example, the author says that he is not aware of any other orderly presentation of nuclear systematics; one feels that he should have been able to mention Glasstone's *Source Book on Atomic Energy* (1950) and Feather's *Nuclear Stability Rules* (1952), both of which contain much relevant material. Again, in the discussion of measurements of nuclear size, no mention is made of the recent studies of mesic x-rays and of high-energy electron scattering, which in yielding different results from the earlier methods have aroused much interest. And in a later chapter, on isobars, it is categorically stated that the existence of both osmium and rhenium at mass 187 is due to a long-lived instability in the osmium, which is just the reverse of the present view. These are not, perhaps, matters of great moment in a work that is meant as a textbook. There are, however, some more serious criticisms that make it impossible to recommend this book as suitable for students in its present form.

These major criticisms concern errors of fact, on the one hand, and looseness of expression on the other. It is implied that nuclear forces are entirely of an exchange nature, and that mu-mesons are associated with the nuclear force field. It would be hard to sustain either of these views against the weight of present knowledge. There is a gross misstatement (p. 15) of what quantum mechanics has to say about spins and magnetic moments. The theory of alpha-radioactivity (pp. 26–7) emerges in a mangled form that is likely to induce schizophrenia in the uninitiated reader. The sketch of the nuclear shell model (pp. 161–4) appears to confuse the spin–orbit splitting with the separation of levels of different *l*. But what seems to this reviewer even more alarming, in a work that is largely concerned with nuclear masses and mass differences, is a lack of care in distinguishing between nuclei and atoms. Thus in tables on p. 17, and again on

p. 52, the proton is plainly credited with the mass of the hydrogen atom, whereas on p. 107 it is given its correct value. It is a pity that one is driven to make such criticisms, for the author has achieved his intention of making out of this rather awkward subject a very readable book, and if it were not marred by these faults it would have been a pleasing addition to the literature of nuclear physics.

A. P. FRENCH.

Table of Sine and Cosine Integrals for Arguments from 10 *to* 100. U.S. Department of Commerce, N.B.S. Applied Mathematics Series 32 (Reissue of Mathematical Table 13). Pp. xv + 187. (Washington : U.S. Government Printing Office, 1954.) $ 2.25.

This is a re-issue with minor modifications and additions of a table issued in 1942 by the Mathematical Tables Project. The interval is 0·01 in the argument, and entries are given to 10 places of decimals. Second differences are printed in the table, and an ancillary table of coefficients is provided to facilitate the use of Everett's interpolation formula. H. H. HOPKINS.

A Concise History of Mathematics, by D. J. STRUIK. Pp. xix + 299. (London : Bell, 1954.) 14*s*.

Professor Struik has attempted to summarize the development of the main ideas in mathematics prior to 1900. The result is a very readable account of the subject for those who know rather more about mathematics than he presupposes. A particularly useful feature of the book is the inclusion of a good bibliography at the end of each chapter. H. H. HOPKINS.

CONTENTS OF SECTION B

PAGE

Dr. S. C. Mossop. The Freezing of Supercooled Water 193

Miss N. E. Hill. Mutual Viscosity and Diffusion in Liquid Mixtures . . 209

Dr. W. D. Cussins. Effects Produced by the Ionic Bombardment of Germanium 213

Dr. M. Levy and Dr. J. H. O. Varley. Radiation Induced Colour Centres in Fused Quartz 223

Mr. R. H. Gough. Entrainment and Turbulence in Open Gas Streams . . 234

Dr. G. T. Wright. Absolute Quantum Efficiency of Photofluorescence of Anthracene Crystals : 241

Prof. H. N. Bose. Thermoluminescence of Alkali Halide Phosphors . . 249

Letters to the Editor:

Mr. J. Kirkbride. Borazole and Boron Nitride Scintillators 253

Corrigendum (Guggenheim) 253

Reviews of Books 254

Contents of Section A 256

Elastic Scattering of Polarized Protons from Complex Nuclei

By J. M. DICKSON, B. ROSE and D. C. SALTER
Atomic Energy Research Establishment, Harwell, Berks.

Communicated by D. W. Fry; *MS. received* 21*st October* 1954

Abstract. The degree of polarization obtained when approximately 130 Mev protons are scattered from Be, C, Al, Fe, Ag, Cd, Bi and U has been studied as a function of the laboratory scattering angle from 10° to 45°. Irregularities in the patterns so obtained may be associated with the diffraction patterns of the elements concerned. The degree of polarization from Be and C has been found to fall rapidly as the proton energy is reduced below 130 Mev.

§ 1. Introduction

Previous experiments have shown that a high degree of polarization is produced in the elastic scattering of protons from nuclei, and that in certain cases the magnitude of this polarization is several times the free p–p polarization (for example Chamberlain *et al.* 1954 a, Dickson and Salter 1954, Marshall *et al.* 1954). We have studied the elastic scattering of polarized protons from complex nuclei as a function of (i) the angle of scattering, (ii) the atomic number of the target nucleus and (iii) the energy of the bombarding protons.

§ 2. Experimental Method

The polarization was examined by the now familiar double scattering experiment, first successfully performed by Oxley, Cartwright and Rouvina (1954). In this method, the asymmetry e after the second scattering process is measured, where $e=(L-R)/(L+R)$, L and R are the normalized counting rates for left and right scattering from the second target, and the scattering at the first target is to the left. It may be shown (Oxley *et al.* 1954) that $e=P_1P_2$ where P_1 and P_2 are the degrees of polarization produced by the first and second scattering respectively. The general experimental arrangement is shown in figure 1.

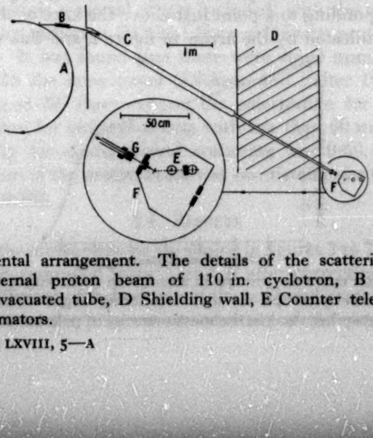

Figure 1. Experimental arrangement. The details of the scattering geometry are to scale. A Internal proton beam of 110 in. cyclotron, B Magnetic deflector channel, C Evacuated tube, D Shielding wall, E Counter telescope, F Scattering table, G Collimators.

2.1. *First Scattering Process*

The internal, presumably unpolarized, beam of the Harwell cyclotron was scattered by a 10 Mev thick carbon target through an angle of 20° into a magnetically shielded channel and brought out of the cyclotron tank through an evacuated pipe. The extracted polarized beam had a mean energy of 135 Mev and an energy spread of approximately 6 Mev as determined by absorption methods. The energy spectrum of those incident protons which could, by scattering in the first target, result in a proton passing out along the shielded channel extended from 135 Mev to 166 Mev.

2.2. *Second Scattering Process*

The polarized beam was led through a concrete shielding wall six feet thick to the second scattering target, which was set up at a distance of 25 ft from the first target.

The beam at this point had an intensity of 10^5 protons $\mathrm{cm}^{-2}\,\mathrm{sec}^{-1}$.

After the second scattering, the protons were detected in a double-coincidence scintillation counter telescope which had an angular resolution of $\pm 1\frac{1}{2}^\circ$. The telescope could be moved in the plane of the scattering to vary the scattering angle, and the framework on which it was mounted could be rotated about the axis of the proton beam to vary the angle between the first and second scattering planes. The axis of rotation of the framework was aligned with the axis of the beam with the aid of photographic films placed at the front and rear of the framework. The alignment could be adjusted to be true within $\pm 2'$ by a double exposure technique, whereby the films were exposed with and without ancillary collimators, which were located accurately on the axis of rotation and were placed immediately in front of the films. The residual magnetic field in the region of the counters was about 7 gauss directed axially along the EMI 6260 photomultipliers of the counter telescope, but did not adversely affect the counters when they were set on a counting rate plateau. The deflection of the high energy protons due to this field was negligible.

2.3. *Selection of Scattered Protons*

The elastically scattered protons were selected by inserting an aluminium absorber in the counter telescope. In order to determine a suitable value of the absorber thickness, an absorption curve was taken with the second target in place and the counter telescope set to 0° scattering angle. A thickness of aluminium corresponding to a point just above the knee of the absorption curve was selected, as indicated by the arrow in figure 2 and this was not changed as

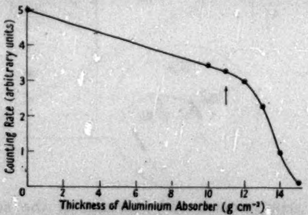

Figure 2. Absorption curve for protons in aluminium taken with a second target in place, and the counter telescope set to 0° scattering angle. The arrow indicates the thickness of absorber used in the measurements of polarization.

the angle of scattering was varied. The energy selection achieved by this method was sufficient to reveal the characteristic diffraction patterns for the elements from Al to In ; the minima were somewhat smeared out by effects such as the angular resolution of the telescope, multiple scattering in the targets, and the counting of some inelastically scattered protons.

2.4. *Measurements at Reduced Proton Energies*

The elastic scattering at energies less than 130 MEV was investigated by placing appropriate aluminium absorbers in the polarized proton beam and reducing the absorber in the counter telescope by the same amount.

The energy resolution became relatively worse as the energy was reduced, since energy straggling was introduced before the scattering. At 66 MEV bombarding energy the telescope absorber had become zero and the threshold for proton counting 37·5 MEV. Observations were repeated at this bombarding energy with an extra absorber in the telescope sufficient to raise the threshold to 59 MEV in order to check on any systematic errors due to the wide band of scattered protons which were being detected.

2.5. *Beam Monitoring*

The polarized beam intensity was monitored both by a proton counter telescope placed directly in the path of the beam about eight feet behind the second target, and by a boron trifluoride neutron counter embedded in paraffin wax which detected the general background of low energy neutrons in the cyclotron pit. The ratio of these counting rates was constant throughout the experiment for each of the second targets, though the value of the ratio depended on the target material.

§ 3. BEAM POLARIZATION

The polarization of the beam could ideally be determined by two identical scattering events, in which the polarizations P_1 and P_2 are equal. In practice, however, ideal conditions can never be realized due mainly to the wide energy spectrum of the internal cyclotron beam. The polarized beam always contains a fraction of protons which have been inelastically scattered by the first target, but this fraction is not easily determinable. An estimate of the relative numbers of elastic and inelastic scattering events in the first target which contributed to the 135 MEV beam was made by combining the measured internal proton energy spectrum (with multiple traversal effects included) with the energy spectrum of protons scattered by carbon at 20° (lab) from a 135 MEV proton beam (Dickson and Salter 1954). It was found that there were equal numbers of elastic and inelastic events. In the same paper (Dickson and Salter 1954) it was shown that, for scattering at 20° from carbon, the polarization for elastic events was twice the polarization for inelastic events with less than 60 MEV energy loss, and that the asymmetry for elastic second scattering was 0·60. From the above data, the polarization of the proton beam was calculated to be 0·68 (with absolute limits of 0·60 and 0·78).

§ 4. RESULTS

The results of the measurements are shown in figures 3 to 7. The differential cross sections were computed from L and R after correcting for the variation with angle of the efficiency for detection of the scattered protons. The variation of efficiency is due to the progressive reduction of the proton energy as the

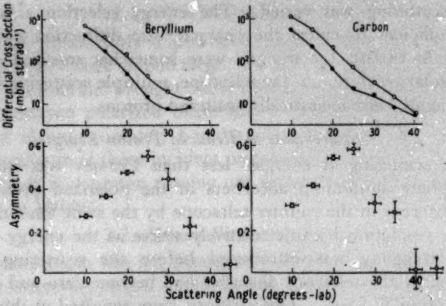

Figure 3. Differential cross section and asymmetry curves for beryllium and carbon.

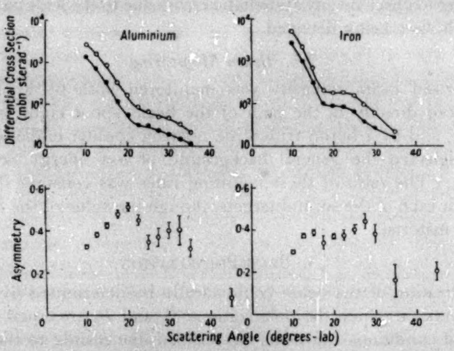

Figure 4. Differential cross section and asymmetry curves for aluminium and iron.

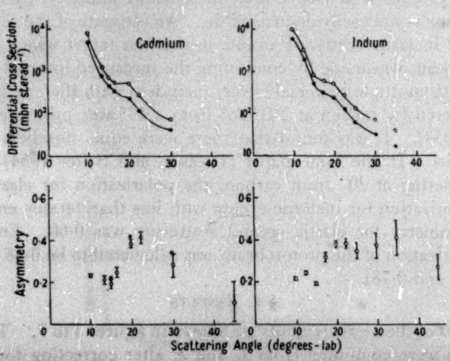

Figure 5. Differential cross section and asymmetry curves for cadmium and indium. The filled in circles on the cadmium curve were taken for silver and had similar errors. When plotted on the same graph, the points for cadmium, indium and silver can be followed by the same curve within the accuracy set by the errors.

scattering angle is increased. No correction was made for the counting of inelastic events. The accuracy of the absolute values of the differential cross sections is believed to be not worse than ±40%.

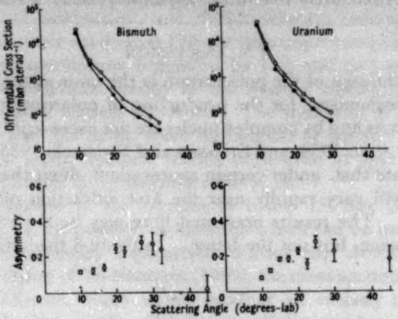

Figure 6. Differential cross section and asymmetry curves for bismuth and uranium.

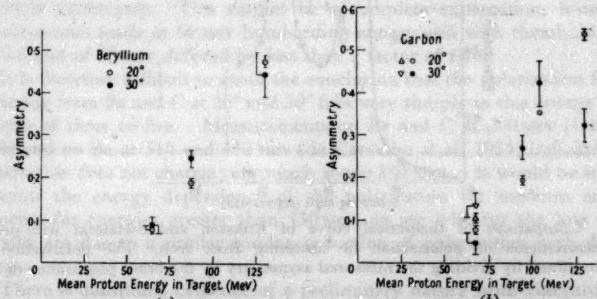

(*a*) (*b*)

Figure 7. Variation of asymmetry with energy in scattering from beryllium and carbon targets at 20° and 30°. The points marked by triangles on the carbon curve were taken with extra proton absorber (see text).

The main features of the asymmetry curves can be summarized as follows :

(i) There are no changes in the sign of the asymmetry, which is the same as that found in polarized p–p scattering.

(ii) The angular variations are not smooth functions of θ except for the lightest elements.

(iii) Neighbouring elements, Cd and In, produce very similar results (a few points obtained for Ag, the other neighbour of Cd were indistinguishable from the Cd and In points).

(iv) The angle of the first maximum and of the first minimum decrease regularly with increasing atomic weight.

(v) The maxima and minima of the asymmetry curves lie close to the maxima and minima of the differential cross section curves. However, these are not well defined in our experiment.

(vi) The asymmetry in general decreases with increasing atomic weight of the target material.

(vii) As the energy is reduced from 130 Mev to 66 Mev, there is a reduction by a factor of approximately five in the asymmetry after scattering from Be and C at 20° and 30°.

§ 5. Discussion

The fact that the sign of the polarization is the same as that in p–p scattering means that the mechanisms for the production of polarization in the scattering of protons by protons and by complex nuclei are not necessarily different. Various papers (e.g. Snow *et al.* 1954, and Eriksson and Swiatecki 1955) on the theory of polarization indicate that, under certain assumptions about the nuclear potential, the polarization will vary rapidly near the first diffraction minimum, and may even change sign. The results presented here may be regarded as support for the former conclusion, but not the latter. In figure 8 theoretical results for the scattering of 150 Mev neutrons by copper are compared with the present values for 130 Mev protons scattered by iron. There is qualitative agreement between them as to the position of the maxima and the mean degree of polarization, though not as regards the magnitude of the variation of polarization.

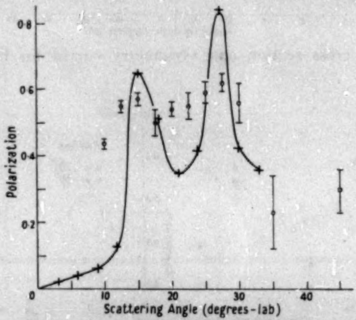

Figure 8. Comparison of theoretical curve of Eriksson and Swiatecki with present measurements of polarization in scattering from iron. The polarization was determined by dividing the measured asymmetry by the beam polarization of 0·68.

However, there is an alternative explanation for the fluctuation of the polarization near a diffraction minimum. As stated earlier, with the present energy resolution a certain fraction of slightly inelastically scattered protons must have been detected at all angles, and this fraction would be expected to have a maximum value near a diffraction minimum. Since inelastically scattered protons are less polarized than those due to elastic events, a minimum in polarization would be expected near a diffraction minimum. It is extremely difficult to distinguish between elastic and ‘ slightly inelastic ’ events at the bombarding energies used in these experiments, and considerable development in technique will be necessary in order to decide between these two explanations.

A pronounced dip in the variation of polarization with angle was found close to the first diffraction minimum in the scattering of protons from aluminium at

280 Mev by Chamberlain *et al.* (1954 b). On the other hand, de Carvalho *et al.* (1954) using a Be target, did not find any such dip either at 310 or at 430 Mev. It may be significant that the scattering from aluminium shows a well defined diffraction minimum at energies of 95 Mev (Strauch and Titus, private communication) and 280 Mev (Chamberlain *et al.* 1954 b) whereas carbon, and presumably any smaller nucleus, does not do so at 130 Mev (this paper) and 320 Mev (Richardson *et al.* 1952). The conclusions suggested by (iii) and (iv) are that the effects observed here are functions mainly of the nuclear radius, and are not much affected by the detailed nuclear structure. The similarity of the curves for Ag, Cd, and In illustrates this point, since Ag consists of equally abundant isotopes of spin 1/2, Cd of many isotopes, mainly even–even of spin 0, and In of two isotopes of spin 9/2 with an abundance ratio of 20 : 1.

The sharp reduction in the asymmetry below 130 Mev for Be and C is of particular interest. One possible explanation which can be immediately rejected is that the beam becomes depolarized during the slowing down process. According to the theory of Wolfenstein (1949), the cross section for depolarization is $6\times10^{-30}(Z^2+2Z)\,\mathrm{cm}^2$, which would produce an entirely negligible effect in the aluminium absorber used. Another possibility is that due to the energy straggling in the absorber a much greater fraction of inelastically scattered protons would be counted at the lower energies, and this would be expected to reduce the observed asymmetry. This cannot be a complete explanation, however, for measurements made at 66 Mev bombarding energy and with threshold energies of 37·5 and of 59 Mev differed by less than a factor of two.

It is therefore difficult to avoid the conclusion that the polarization for elastic scattering from Be and C at 20° and 30° falls very sharply in this energy range by a factor of three to five. Measurements on Be and C at 200 Mev (Oxley *et al.* 1954) and on Be at 310 and 430 Mev (de Carvalho *et al.* 1954) indicate that the polarization does not change very much above 130 Mev. It would be interesting to know the energy dependence of the polarization for medium and heavy elements for energies greater than 130 Mev, to see whether the low values at 130 Mev are due to a similar sudden reduction of polarization with decreasing energy.

There is additional evidence of a preliminary nature from Harvard that the polarization effect below 100 Mev is much smaller than at 130 Mev (Strauch, private communication). In a double scattering experiment from carbon in which both scatterings were made at 20° scattering angles and the mean first and second scattering energies were 87 Mev and 66 Mev respectively, the measured asymmetry was less than 0·05. From the results presented in this paper, an asymmetry of approximately 0·03 would be expected under these conditions.

ACKNOWLEDGMENTS

We wish to thank Dr. Swiatecki for pre-publication information on his calculations of polarization effects, Dr. Strauch for permission to refer to his work in advance of publication, Professor Ramsey whose communication of the preliminary results obtained by Strauch led us to look for the energy variation of polarization, and our colleagues for many stimulating discussions. Our thanks are due to Mr. L. Bird for his assistance throughout the experiment, and to the members of the cyclotron operating crew for their ready co-operation.

REFERENCES

DE CARVALHO, H. G., MARSHALL, J., and MARSHALL, L., 1954, *Phys. Rev.*, **96**, 1081.

CHAMBERLAIN, O., SEGRÈ, E., TRIPP, R., WIEGAND, C., and YPSILANTIS, T., 1954 a, *Phys. Rev.*, **93**, 1430; 1954 b, *Ibid.*, **95**, 1105.

DICKSON, J. M., and SALTER, D. C., 1954, *Nature, Lond.*, **173**, 946.

ERIKSSON, T., and SWIATECKI, W. J., 1955, *Ark. Fys.*, **9**, 28.

MARSHALL, J., MARSHALL, L., and DE CARVALHO, H. G., 1954, *Phys. Rev.*, **93**, 1431.

OXLEY, C. L., CARTWRIGHT, W. F., and ROUVINA, J., 1954, *Phys. Rev.*, **93**, 806.

RICHARDSON, R. E., BALL, W. P., LEITH, C. E., and MOYER, B. J., 1952, *Phys. Rev.*, **86**, 29.

SNOW, G. A., STERNHEIMER, R. M., and YANG, C. N., 1954, *Phys. Rev.*, **94**, 1073.

WOLFENSTEIN, L., 1949, *Phys. Rev.*, **75**, 1664.

Angular Distributions and Angular Correlations in the Reaction ^{23}Na(p, γ)^{24}Mg

By P. J. GRANT, J. G. RUTHERGLEN, F. C. FLACK†
and G. W. HUTCHINSON
Natural Philosophy Department, University of Glasgow

MS. received 29th July 1954

Abstract. The angular distributions and angular correlations of the more intense γ-ray components in the reaction ^{23}Na (p, γ) ^{24}Mg have been determined at four resonances. Those at proton energies of 310 kev, 515 kev and 679 kev are assigned $J=2^-$, $J=1^+$ and $J=3^+$ formed by p-, s- and d-wave protons respectively. The resonance at 593 kev has $J=2^-$ formed by p-wave protons and is therefore distinct from that in the (p, α) reaction at this energy. The level in ^{24}Mg at 4·24 Mev is assigned $J=2^+$ and that at 5·26 Mev $J=3$, probably with odd parity.

§ 1. Introduction

In a previous paper (Flack *et al.* 1954, to be referred to as FI) we have reported the results of investigations of the γ-ray spectra from the reaction ^{23}Na (p, γ)^{24}Mg at four resonances between proton energies of 250 kev and 700 kev. The present paper describes the determination of the angular distributions of the more prominent components at each resonance, together with the angular correlations between γ-rays in certain cascades. The results of these measurements enable spin and parity assignments to be made to each resonance and to two lower states in ^{24}Mg. The latter deductions are in accord with those of Newton (1955) who has investigated this reaction at proton energies above 700 kev.

§ 2. Angular Distributions

The experimental arrangement, which has been previously described, embodies as γ-ray detector a cylindrical sodium iodide crystal 1$\frac{3}{4}$ in. diam. × 2 in. long with photomultiplier. Pulses from the photomultiplier, after amplification, are fed into a 100-channel pulse-height analyser (Hutchinson and Scarrott 1951). Measurement of the complete pulse-height spectrum at each angular position of the detector and analysis into its components (FI) make possible the determination of the angular distributions of all the more intense γ-rays at each resonance.

The decay scheme of the γ-radiation is the same at all resonances, apart from variations in the relative intensities of the components. This scheme is shown in figure 1, the spin and parity values deduced in this paper being given in italics (top six figures).

Table 1 lists the results of angular distribution experiments made at the resonances at proton energies of 310, 515, 593 and 679 kev.

§ 3. Angular Correlations

The angular correlation of γ_1 and γ_8 was determined at each resonance and the correlation of γ_2 and γ_5 at the resonances at $E_p=593$ and 679 kev. In these experiments the first γ-ray of the cascade was detected at right angles to the

---

† Now at Department of Physics, University College of the South-West, Exeter.

direction of the proton beam and the angular correlation of the second γ-ray with the first was measured in the same plane (correlation $\pi/2$, θ, 0), the second γ-ray being detected in a scintillation spectrometer similar to the first. Pulses from the first spectrometer in the selected energy-band were used to gate the input of the pulse-height analyser which received pulses from the second spectrometer, thus recording the coincident spectrum at each angular position. The results are shown in figures 2 (*a*)–(*f*) together with certain theoretical correlation functions corrected for the finite solid angles of acceptance of the spectrometers.

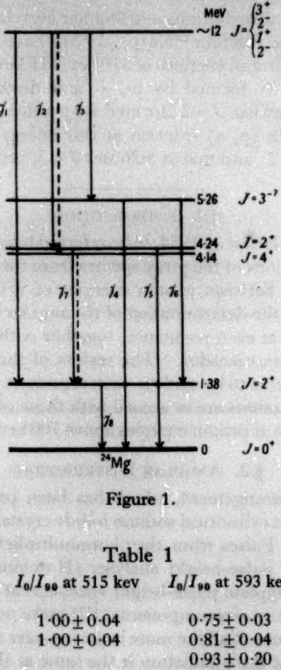

Figure 1.

Table 1

	I_0/I_{90} at 310 kev	I_0/I_{90} at 515 kev	I_0/I_{90} at 593 kev	W_θ at 679 kev
γ_1	$0\cdot82\pm0\cdot02$	$1\cdot00\pm0\cdot04$	$0\cdot75\pm0\cdot03$	$1+(0\cdot14\pm0\cdot03)\cos^2\theta$
γ_2	$0\cdot82\pm0\cdot04$	$1\cdot00\pm0\cdot04$	$0\cdot81\pm0\cdot04$	$1-(0\cdot38\pm0\cdot04)\cos^2$
γ_3	$1\cdot1\ \pm0\cdot3$		$0\cdot93\pm0\cdot20$	$1+(0\cdot9\pm0\cdot2)\cos^2\theta$
γ_5	$0\cdot94\pm0\cdot15$		$0\cdot75\pm0\cdot10$	$1+2\cdot4\cos^2\theta$ $-1\cdot6\cos^4\theta$
γ_6	$0\cdot67\pm0\cdot5$		$0\cdot72\pm0\cdot5$	
γ_7	$0\cdot89\pm0\cdot2$		$1\cdot05\pm0\cdot10$	
γ_8	$0\cdot91\pm0\cdot03$	$1\cdot00\pm0\cdot10$	$1\cdot03\pm0\cdot03$	$1+0\cdot6\cos^2\theta$ $-0\cdot37\cos^4\theta$

§ 4. INTERPRETATION

515 *keV resonance.* This resonance does not emit α-particles to the ground state of ^{20}Ne (FI); it is therefore most probable that it has odd spin with even parity or even spin with odd parity. All γ-ray components measured had isotropic angular distributions. This resonance level must therefore have either $J=1^+$, formed

by S-wave protons, or $J=0^-$, formed by p-wave protons, since ^{23}Na has spin 3/2 (assuming the shell-model prediction to be correct, that ^{23}Na has even parity). The angular correlation between γ_1 and γ_8 (figure 2(*b*)) makes possible a clear choice in favour of $J=1^+$. It is interesting to note that there is no measurable ground-state γ-ray transition even though transitions to the ground state and first

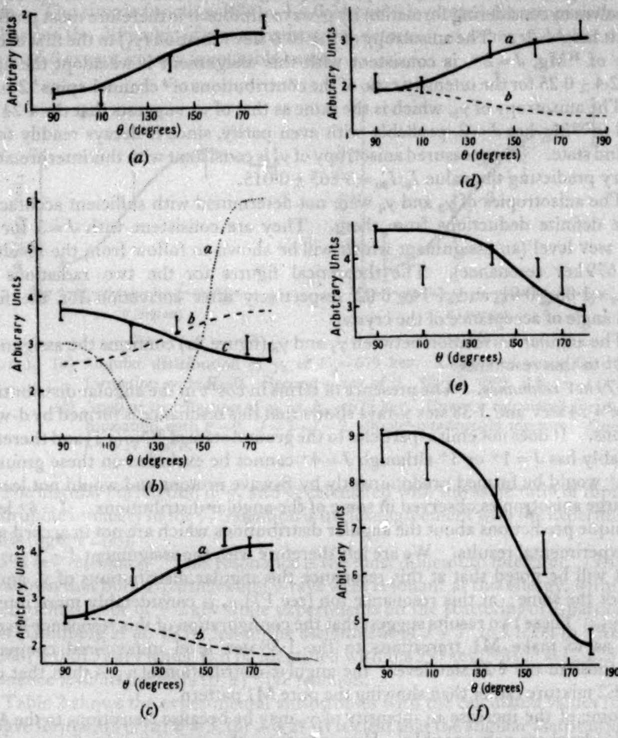

(*a*) (*d*) (*b*) (*e*) (*c*) (*f*)

Figure 2. (*a*) γ_1–γ_8 correlation at $E_p=310$ kev. Calculated curve for p-wave formation with $F=2{\cdot}4$, $2\rightarrow2\rightarrow0$.

(*b*) γ_1–γ_8 correlation at $E_p=515$ kev. Curve *a* calculated for p-wave formation $0\rightarrow2\rightarrow0$; curve *b*, s-wave formation $2\rightarrow2\rightarrow0$; curve *c*, s-wave formation $1\rightarrow2\rightarrow0$.

(*c*) γ_1–γ_8 correlation at $E_p=593$ kev. Curve *a* calculated for p-wave formation with $F=3{\cdot}0$, $2\rightarrow2\rightarrow0$; curve *b*, p-wave formation $3\rightarrow2\rightarrow0$.

(*d*) γ_2–γ_5 correlation at $E_p=593$ kev. Curve *a*, p-wave formation with $F=3{\cdot}0$, $2\rightarrow2\rightarrow0$; curve *b*, p-wave formation $3\rightarrow2\rightarrow0$.

(*e*) γ_1–γ_8 correlation at $E_p=679$ kev. Calculated curve for d-wave formation with $F=0$, $3\rightarrow2\rightarrow0$. Interference in first transition between dipole and quadrupole radiations.

(*f*) γ_2–γ_5 correlation at $E_p=679$ kev. Calculated for d-wave formation with $F=0$, $3\rightarrow2\rightarrow0$. First γ-ray pure dipole.

excited state of ^{24}Mg should be of the same type, namely M1. A similar result has been noted before in the case of the 669 kev resonance in the reaction ^{19}F (p, γ) ^{20}Ne where the cascade transition predominates (Rae *et al.* 1950) although both radiations are of the M1 type (Seed 1953).

310 *keV resonance.* This resonance does not emit α-particles to the ground state of ^{20}Ne (FI) and shows anisotropic γ-ray angular distributions. If we restrict ourselves to considering formation by p-wave protons it is therefore most probable that it has $J=2^-$. The anisotropy of the 10·6 MeV radiation (γ_1) to the first excited state of ^{24}Mg, $J=2^+$, is consistent with this assignment if we adopt the figure $F=2\cdot4\pm0\cdot25$ for the intensity ratio of the contributions of 'channel-spins' 2 and 1.

The anisotropy of γ_2, which is the same as that of γ_1, suggests that the 4·24 MeV level in ^{24}Mg has $J=2$, probably with even parity, since it decays readily to the ground state. The measured anisotropy of γ_5 is consistent with this interpretation, theory predicting the value $I_0/I_{90}=0\cdot865\pm0\cdot015$.

The anisotropies of γ_3 and γ_6 were not determined with sufficient accuracy to make definite deductions from them. They are consistent with $J=3$ for the 5·26 MeV level (an assignment which will be shown to follow from the results at the 679 kev resonance). The theoretical figures for the two radiations are $I_0/I_{90}=1\cdot06\pm0\cdot01$ and $1\cdot14\pm0\cdot02$ respectively after correction for the finite solid angle of acceptance of the crystal.

The angular correlation between γ_1 and γ_8 (figure 2*a*) confirms the assignment $J=2^-$ to this resonance.

679 *keV resonance.* The presence of terms in $\cos^4\theta$ in the angular distributions of the 4·24 MeV and 1·38 MeV γ-rays shows that this resonance is formed by d-wave protons. It does not emit α-particles to the ground state of ^{20}Ne (FI) and therefore probably has $J=1^+$ or 3^+ although $J=4^+$ cannot be excluded on these grounds. $J=1^+$ would be formed predominantly by S-wave protons and would not lead to the large anisotropies observed in some of the angular distributions. $J=4^+$ leads to unique predictions about the angular distributions which are not in accord with the experimental results. We are left therefore with the assignment $J=3^+$.

It will be noted that at this resonance the angular distributions of γ_1 and γ_2 are not the same; at this resonance too (see FI) γ_2 is considerably more intense than γ_1. These two results suggest that the configuration of this resonance level is such as to make M1 transitions to the 1·38 MeV level unfavoured compared with those to the 4·24 MeV level; the angular distribution of γ_1 is then that of a M1–E2 mixture rather than showing the pure M1 pattern.

Some of the increase in intensity of γ_2 may be because transitions to the 4·14 ($J=4^+$) level are now possible. However, from the γ-ray intensity figures given in F1 one may deduce that only 10–20% of the transitions γ_2 proceed in this way.

The angular distributions of γ_2, γ_3 and γ_5 and the angular correlation between γ_2 and γ_5 can best be fitted by assuming that the resonance is formed almost entirely via 'channel-spin' 1. We shall therefore put $F=0$. The calculated distribution for a transition $J=3\rightarrow J=2$ (dipole), corrected for solid angle, is $W(\theta)\sim1-0\cdot40\cos^2\theta$, in excellent agreement with the result for γ_2. (An admixture of 10% of transitions to the $J=4^+$ state leads to a distribution $W(\theta)\sim1-0\cdot38\cos^2\theta$.) $J=3\rightarrow J=3$ (dipole) leads to $W(\theta)\sim1+0\cdot66\cos^2\theta$, in agreement with the experimental result for γ_3. The calculated distribution for γ_5, corrected for solid angle, is shown in figure 3 (*a*) with the experimental points. The correlation between γ_2 and γ_5 (figure 2(*f*)) is well fitted by a dipole–quadrupole correlation.

In order to fit the experimental distribution of γ_1 we must assume a mixture of M1 and E2 radiations, in phase, with an intensity ratio I_1/I_2 of about 16. The calculated result, corrected for solid angle, is then

$$W(\theta) \sim 1 + 0{\cdot}26 \cos^2\theta - 0{\cdot}11 \cos^4\theta.$$

It will be seen from figure 3 (*b*) that this provides a good fit to the experimental points. The simple function $W(\theta) \sim 1 + 0{\cdot}14 \cos^2\theta$ is plotted for comparison and emphasizes the difficulty of the experimental detection of terms of higher order than $\cos^2\theta$ except in very favourable cases.

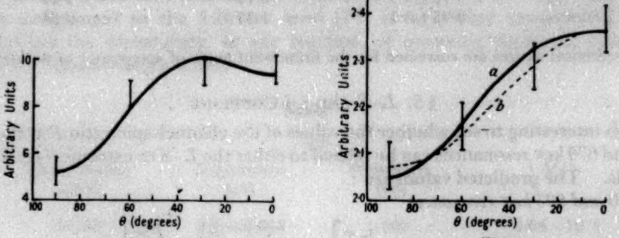

(*a*) (*b*)

Figure 3. (*a*) Angular distribution of γ_5 at $E_p = 679$ kev. Calculated curve for d-wave formation with $F = 0$. Second γ-ray of $3 \xrightarrow{\text{dip.}} 2 \xrightarrow{\text{quad.}} 0$.
(*b*) Angular distribution of γ_1 at $E_p = 679$ kev. Curve *a* calculated for d-wave formation with $F = 0$, $J = 3 \rightarrow J = 2$, dipole–quadrupole mixture. Curve *b*, $1 + 0{\cdot}14 \cos^2\theta$.

The angular correlation of γ_1 and γ_8 calculated with the same ratio of dipole to quadrupole intensity in the γ_1 transition is in close agreement with the experimental points (figure 2 (*e*)).

593 *kev resonance.* This resonance is the most difficult to interpret. In FI it was shown that both α-particles and γ-rays were resonant at this energy, within the experimental error of 1–2 kev while experiments on the scattering of α-particles in neon (Goldberg *et al.* 1954) led to the assignment of $J = 3^-$ to a level in ^{24}Mg* at 12·288 (±0·015) Mev which can be identified with the 593 kev (^{24}Mg* = 12·275 Mev) resonance level in the ^{23}Na (p, α) ^{20}Ne reaction.

Table 2 shows the experimental anisotropies with the calculated values for the p-wave formation of (*a*) $J = 3$, (*b*) $J = 2$. It is clear that the angular distributions of γ_3, γ_5 and γ_7 are not in accord with the assignment $J = 3^-$ but can all be fitted with $J = 2^-$ and a 'channel-spin ratio' $F = 3$. It will also be seen from figures 2 (*c*) and 2 (*d*) that this assignment gives good agreement with the angular correlations γ_1–γ_8 and γ_2–γ_5 whereas $J = 3^-$ does not.

Preliminary measurements of the polarization of γ_1 at this resonance (Hughes and Grant, to be published) show that the transition involves a change of parity. Since a level with $J = 2^-$ could not emit α-particles to the ground state of ^{20}Ne we are forced to conclude that there are two levels in ^{24}Mg with a separation of less than 2 kev, one having $J = 3^-$ and the other $J = 2^-$. This result may be compared with the reactions ^{27}Al(p, α)^{24}Mg and ^{27}Al(p, γ)^{28}Si in which two levels separated by 5 kev are known, at $E_p = 728$ and 733 kev, only one of which emits α-particles (Rutherglen and Smith 1953). It explains also the great similarity in the γ-ray spectra from the 310 and 593 kev resonances.

Table 2. 593 kev Resonance

γ-ray energy (MeV)	Anisotropy I_0/I_{90} Experimental	Theory for $J=3$	Theory for $J=2$ (and $F=3$)
10·9 (γ_1)	$0{\cdot}75 \pm 0{\cdot}03$	0·705	0·78
8·0 (γ_2)	$0{\cdot}81 \pm 0{\cdot}04$	0·705	0·78
7·0 (γ_3)	$0{\cdot}93 \pm 0{\cdot}20$	1·48	1·07
4·24 (γ_5)	$0{\cdot}75 \pm 0{\cdot}10$	1·56	0·84
3·9 (γ_6)	$0{\cdot}72 \pm 0{\cdot}5$	0·77	1·17
2·86 (γ_7)	$0{\cdot}95 \pm 0{\cdot}1$	1·37	0·85

The theoretical figures are corrected for the finite solid angle of acceptance of the detector.

§ 5. *L–S* AND *j–j* COUPLING

It is interesting to see whether the values of the channel-spin ratio F at the 310, 593 and 679 kev resonances can be related to either the L–S or extreme j–j coupling models. The predicted values are :

310 and 593 keV resonances

j–j		$j_p = \frac{1}{2}^-$	$F=1$
		$j_p = (3/2)^-$	$F=1$
L–S			
	$^{23}\mathrm{Na} \equiv {}^2\mathrm{D}_{3/2}$	$^{24}\mathrm{Mg}^* \equiv {}^3\mathrm{D}_2^-$	$F=2{\cdot}8$

679 keV resonance

j–j		$j_p = (3/2)^+$	$F=2/3$
		$j_p = (5/2)^+$	$F=3/2$
L–S	$^{23}\mathrm{Na} \equiv {}^2\mathrm{D}_{3/2}$	$^{24}\mathrm{Mg}^* \equiv {}^3\mathrm{G}_3^+$	$F=1/6$

Within the experimental errors the values of the channel-spin ratio F at the 310 and 593 kev resonances can be closely fitted by the L–S coupling value of $F=2{\cdot}8$ for formation of a $^3\mathrm{D}_2$ state of odd parity. The extreme j–j coupling does not fit the experimental results. At the 679 kev resonance again the j–j model is not in accord with experiment whereas the L–S model ($^{24}\mathrm{Mg}^* \equiv {}^3\mathrm{G}_3^+$) predicts a value of F of $\frac{1}{6}$ which provides as good a fit with our experimental results as does the value $F=0$ assumed in the preceding section. Other possible states in the L–S coupling scheme are not in agreement with experiment.

It must be emphasized that these calculations represent a considerable oversimplification of the problem, since a detailed calculation should take account of the fact that three particles are contributing to the resultant spin of ^{23}Na ; nevertheless the results may be taken as evidence that the L–S model provides a better approximation to the true state of affairs than does the extreme j–j model.

§ 6. γ-RAY WIDTHS

Since the absolute yields of the γ-rays are known at each resonance, by assuming $\Gamma_p \gg \Gamma_\gamma$, we may derive the absolute γ-ray widths. From consideration of the barrier penetrability we would expect proton widths considerably larger than the experimental values and hence the yields must be determined by the γ-ray widths. The assumption may be further justified by considering the other extreme, $\Gamma_\gamma \gg \Gamma_p$.

Under this condition the measured yields would be proportional to Γ_p and one would expect much larger variations from one resonance to another than are, in fact, observed. The widths are shown in table 3 and are compared with the predictions of the simplified single-particle model (Weisskopf 1951). Two conclusions may be drawn from these results : (*a*) The single-particle model is not valid here. This is hardly suprising since at least two particles must be involved in the transitions. Also, it is to be expected that at this level of excitation there will be considerable mixing of the single-particle states. (*b*) Experimentally there is no consistent difference between electric and magnetic dipole radiations. [It should be noted here that there is some doubt about the nature of γ_3 since the parity assignment to the 5·26 MeV level (FI) is somewhat speculative.] This emphasizes the uncertainty, in any reaction, of assigning multipole orders by intensity considerations alone.

Table 3

E1

Proton energy (MeV)	Experiment (ev)	Weisskopf (ev)	$\lvert M \rvert^2$
0·310	$\Gamma\gamma_1 = 0\cdot044$	1090	$4\cdot05 \times 10^{-5}$
	$\Gamma\gamma_2 = 0\cdot066$	425	$15\cdot5 \times 10^{-5}$
0·515	$\Gamma\gamma_3 = 0\cdot011$	302	$3\cdot65 \times 10^{-5}$
0·593	$\Gamma\gamma_1 = 0\cdot027$	1180	$2\cdot3 \times 10^{-5}$
	$\Gamma\gamma_2 = 0\cdot051$	470	$10\cdot9 \times 10^{-5}$
0·679	$\Gamma\gamma_3 = 0\cdot063$	325	$19\cdot5 \times 10^{-5}$

M1

Proton energy (MeV)	Experiment (ev)	Weisskopf (ev)	$\lvert M \rvert^2$
0·310	$\Gamma\gamma_3 = 0\cdot015$	6·4	$2\cdot35 \times 10^{-3}$
0·515	$\Gamma\gamma_1 = 0\cdot089$	26·4	$3\cdot4 \times 10^{-3}$
	$\Gamma\gamma_2 = 0\cdot022$	10·5	$2\cdot1 \times 10^{-3}$
0·593	$\Gamma\gamma_3 = 0\cdot016$	7·2	$2\cdot2 \times 10^{-3}$
0·679	$\Gamma\gamma_1 = 0\cdot033$	27·6	$1\cdot2 \times 10^{-3}$
	$\Gamma\gamma_2 = 0\cdot13$	11·1	12×10^{-3}

Transitions from the 5·26 *MeV level in* ^{24}*Mg*.

Direct transitions from this level to the ground state of ^{24}Mg were believed to occur at all resonances (FI). At the 679 kev resonance where the 5·36 MeV level is fed to a sufficient degree to make intensity measurements feasible it is found that the ratio of the intensity of the direct ground-state transition E3 to that of the E1 transition to the 1·38 MeV level is about 0·3. Using the single-particle model as a guide, the expected ratio is about 7×10^{-9}.

This result clearly throws doubt on the interpretation of this γ-ray as being the direct ground-state radiation. Invoking the isotopic spin selection rules (Radicati 1953) will only reduce the intensity of the E1 transition by a factor of approximately 10^{-4}, leaving a further factor 10^{-4} unexplained. Even after allowance has been made for the uncertainty of the single-particle model, it seems probable that the γ-ray (γ_4) of about 5·4 MeV energy must belong to a separate cascade which is only weakly excited.

Transitions from the 4·24 MeV level.

The two competing radiations are here 4·24→0 MeV (E2) and 4·24→1·38 MeV (M1). Using the single-particle model we would expect an intensity ratio $I_2/I_1 \sim 1/40$. Experimentally the ratio is about 2, showing a slowing down of dipole relative to quadrupole transitions by a factor of about 100. This may represent only the inapplicability of the single-particle model, nevertheless reductions of up to 1000 in dipole transition rates have been observed in some heavy elements (e.g. Steffen 1955) and the present example may be related to these.

ACKNOWLEDGMENTS

We would like to acknowledge the receipt of a set of tables (Sharp *et al.* 1953) which has immeasurably lightened the burden of the calculations. One of us (F.C.F.) wishes to acknowledge the award of an Imperial Chemical Industries Research Fellowship during the course of this work.

REFERENCES

FLACK, F. C., RUTHERGLEN, J. G., and GRANT, P. J., 1954, *Proc. Phys. Soc.* A, **67**, 973.

GOLDBERG, E., HAEBERLI, W., GALONSKY, A. I., and DOUGLAS, R. A., 1954, *Phys. Rev.*, **93**, 799.

HUTCHINSON, G. W., and SCARROTT, G. G., 1951, *Phil. Mag.*, **42**, 792.

NEWTON, J. O., 1955, *Proceedings of the* 1954 *Glasgow Conference on Nuclear and Meson Physics* (London : Pergamon Press); also 1954, *Phys. Rev.*, **96**, 241.

RADICATI, L. A., 1953, *Proc. Phys. Soc.* A, **66**, 139.

RAE, E. R., RUTHERGLEN, J. G., and SMITH, R. D., 1950, *Proc. Phys. Soc.* A, **63**, 775.

RUTHERGLEN, J. G., and SMITH, R. D., 1953, *Proc. Phys. Soc.* A, **66**, 800.

SEED, J., 1953, *Phil. Mag.*, **44**, 921.

SHARP, W. T., KENNEDY, J. M., SEARS, B. J., and HOYLE, M. G., 1953, *Tables of Coefficients for Angular Distribution Analysis*, Atomic Energy of Canada, A.E.C.L. No. 97.

STEFFEN, R. M., 1955, *Proceedings of the* 1954 *Glasgow Conference on Nuclear and Meson Physics* (London : Pergamon Press).

WEISSKOPF, V. F., 1951, *Phys. Rev.*, **83**, 1073.

The Layzer Approximation for the Treatment of Collisions of Electrons with Atoms

By U. ÖPIK†
Department of Applied Mathematics, The Queen's University of Belfast

Communicated by D. R. Bates; MS. received 24th March 1954, and in final form 21st October 1954; read at the meeting of the Physical Society in Dublin, March 1954

Abstract. A new approximation, proposed by Layzer, is investigated theoretically and applied to the excitation by electron impact of the 2^2S and 2^2P levels of hydrogen (the latter level only in the case of a reversal of the spin of the atomic electron) and of the $1s2s\,^1S$, $1s2s\,^3S$ and $1s2p\,^3P$ levels of helium. The cross sections are evaluated for a number of incident electron energies. The theoretical basis of the approximation is shown to be unsatisfactory.

In the case of the final states being S states, a comparison of the cross sections calculated by the new method with those obtained by other methods suggests that, for slow incident electrons, most of them may be expected not to differ by more than a factor of about two from the true cross sections. However, the 1^2S–2^2S cross section of hydrogen associated with an antisymmetrical spatial wave function for the electrons seems to be too large by a greater factor. No reliable comparison data are at present available for the S–P transitions, but the results do not seem unreasonable. The approximation is shown to give correctly the asymptotic variation of the non-exchange cross sections for large incident electron energies, but not the numerical coefficients. The pure exchange S–P cross sections fall off too slowly with increasing incident energy. In spite of the theoretical defects, there is some hope that the new approximation may prove useful, at least as an empirical method.

§ 1. Introduction

INFORMATION on cross sections for the excitation of atoms by slow electrons is needed in many connections. The earliest approximation used for calculating these cross sections, that due to Born (1926), treats the colliding electron as if it were distinguishable from the atomic electrons. In spite of this it is often found to give results in a fairly satisfactory agreement with experiment except, of course, in the case of collisions involving a change of multiplicity of the atomic state. An attempt at an improvement was made by Oppenheimer (1928), who introduced wave functions which were antisymmetrical in the electrons, but it has actually been found that for slow incident electrons the apparently better treatment often gives far less accurate results than Born's approximation (Bates, Fundaminsky, Leech and Massey 1950).

Layzer (1951) has advanced a possible reason for this failure and proposed an interesting new approximation, based, like the earlier ones, on the first-order perturbation theory, and employing antisymmetrical wave functions. Whatever the reason for the failure of Oppenheimer's approximation for slow electrons, it is certainly worth while to investigate Layzer's approximation, both theoretically and by applying it to some simple cases and comparing the results with those obtained by other methods, theoretical and experimental; for, being an approximation *different* from that of Oppenheimer, it may happen to be a *better* approximation, even if it is so for some reason other than suggested. The purpose of the present paper is to report on such an investigation.

---

† Now at the Department of Physics, University of Bristol.

To be sure, refined methods, giving improved results, have recently been applied to collision problems by Massey and Moiseiwitsch (1953, 1954), Seaton (1953) and others, but nevertheless Layzer's approximation would be of value should it yield cross sections that do not differ from the true cross sections by more than, say, a factor of 2, since it has the great advantage of being comparatively simple.

The theoretical investigation shows the basis of the new approximation to be unsatisfactory, but in spite of this the numerical results obtained by it are in fairly good agreement with other results.

§ 2. THEORY

We shall employ Layzer's notation as far as possible. References to equations in Layzer's original paper (1951) will be distinguished by a letter L before the equation number, to avoid confusion with references to equations in the present paper. We shall have occasion to use a function $\zeta(x)$, defined by

$$\left.\begin{array}{l}\zeta(x)=0 \text{ for } x<0,\\ \zeta(x)=1 \text{ for } x>0,\\ \zeta(0) \text{ is finite.}\end{array}\right\} \qquad \ldots\ldots(1)$$

By means of this function the unperturbed wave functions, as well as the various energy operators, can be written in a form suitable for substituting into equations, without having to state conditions such as $r_i>r_j$ (all $j\neq i$). Thus, for example, equation (L27) may be written as

$$\langle \mathbf{X}\,|\beta(\alpha\mathbf{k})\rangle=\sum_{i=1}^{N+1}\delta_i\hbar^{-3/2}\Big\{\prod_{j(\neq i)}\zeta(r_i-r_j)\Big\}\psi(\mathbf{x}_i,\,\mathbf{k})\,\langle\mathbf{X}^i\,|\alpha\rangle,$$

which makes both the theoretical discussion and the actual application much easier.

2.1. Certain criticisms may be made of the theory of the new approximation.

(*a*) The derivation of (L21) is based on Dirac's (1947) treatment with the momentum representation. But if the wave functions $\langle \mathbf{X}\,|\beta(\alpha\mathbf{k})\rangle$ are not orthogonal—and Layzer himself admits that they are not—then this treatment requires that if we take one of the terms into which the antisymmetrical function $\langle \mathbf{X}\,|\beta(\alpha\mathbf{k})\rangle$ may be split—say the term

$$\delta_1\hbar^{-3/2}\Big\{\prod_{j(\neq 1)}\zeta(r_1-r_j)\Big\}\psi(\mathbf{x}_1,\mathbf{k})\langle\mathbf{X}^1\,|\alpha\rangle$$

which represents the first electron as the colliding electron—then it should be orthogonal to the *corresponding* term (i.e. first electron free) taken out of a wave function with a different value of $\mathbf{k}$; and this condition is not satisfied.

(*b*) Expression (L36) for $V_{\delta ij}$ seems to have been derived by applying (L33) with $f(x)$ replaced by the first derivatives of $\langle \mathbf{X}\,|\beta\rangle$, in order to evaluate the second derivatives at the discontinuity of this function. This procedure is objectionable, because the first derivative of $\langle \mathbf{X}\,|\beta\rangle$ is not merely discontinuous but has a singularity in the form of a δ-function. Should it be answered that equation (L33) must be unconditionally valid as we get agreement if we integrate both sides of it with respect to x, we may point out that if $b\delta'(x-a)$ is added to the right-hand side, where b is independent of x and δ' is the derivative of δ with respect to its argument, we still get agreement on integration with respect to x; yet, if we multiply the right-hand side by another function $g(x)$ and integrate, the result is *not* independent of b, and we have no right to assume that b vanishes. A correct method of obtaining the second derivative is by direct differentiations. Taking $\langle \mathbf{X} | \beta \rangle$ to be of the form

$$\langle \mathbf{X} | \beta \rangle = \zeta(r_i - r_j)\beta_i + \zeta(r_j - r_i)\beta_j, \quad (r_i = r_j > r_k, \text{ all } k \neq i,j) \quad \ldots\ldots(2)$$

and assuming that

$$d\zeta(x)/dx = \delta(x), \quad \ldots\ldots(3)$$

we obtain

$$V_{\delta ij} \langle \mathbf{X} | \beta \rangle = -\frac{\hbar^2}{m}\{\delta'(r_i - r_j)\beta_i + \delta'(r_j - r_i)\beta_j\} - \frac{\hbar^2}{m}\delta(r_i - r_j)\Delta_{r_i r_j}\left(\frac{\partial}{\partial r_i} - \frac{\partial}{\partial r_j}\right)\langle \mathbf{X} | \beta \rangle. \quad \ldots\ldots(4)$$

If we attempted to take the terms involving δ' into account in (L21) by means of the relationship

$$\int g(x)\delta'(x-a)dx = -g'(a), \quad \ldots\ldots(5)$$

these terms would give an infinite contribution (which in certain special cases, but not in general, vanishes on further integrations). The reason is that the function here represented by $g(x)$ would involve the discontinuous function $\langle \beta^*(\alpha'\mathbf{k}') | \mathbf{X} \rangle$ as a factor and would have an infinite derivative for $r_i = r_j > r_k$ (all $k \neq i,j$). Moreover, the last term in equation (4) is *twice* the right-hand side of (L36), suggesting that the factor $\frac{1}{2}$ should be omitted in the latter.†

It may be possible to meet the criticism concerning the infinite contribution by assuming the functions $\langle \mathbf{X} | \beta \rangle$ to be not discontinuous but merely rapidly varying for $r_i \simeq r_j > r_k$ (all $k \neq i,j$). This region of variation would have to be on the one hand so large that those additional contributions which would tend to infinity if we let the extension of this region tend to zero are not unduly great; on the other hand, the region of variation must not be so large that the neglect of any finite terms in $V_{\delta ij}$, as well as the inaccuracy of the terms given by (L36), would affect the results too seriously. If we expect cross sections which are correct within a factor of 2, this may prove to be quite satisfactory, but whether or not this is so, only a detailed investigation can show.

(*c*) The choice of the value $2^{-1/2}$ for $\zeta\,(r_i - r_j)$ when $r_i = r_j$ in (L28) seems rather arbitrary; $\frac{1}{2}$ would seem to be a more natural choice.† When giving the form (L28) of the unperturbed wave function for $r_i = r_j > r_k$ (all $k \neq i,j$), Layzer states he assumes that for such values of the coordinates " the electrons i and j share equally the status of colliding electron ". The argument seems to be that the system must be equally likely to be found in the state

$$\delta_i h^{-3/2}\psi(\mathbf{x}_i, \mathbf{k}) \,.\, |s_i\rangle \langle \mathbf{X}^i | \alpha \rangle$$

as in the state $\delta_j h^{-3/2}\psi(\mathbf{x}_j, \mathbf{k}) \,.\, |s_j\rangle \langle \mathbf{X}^j | \alpha \rangle$ and hence these wave functions must be multiplied by the *same* coefficient and added together; and in order that the total wave function should have the same normalization when $r_i = r_j > r_k$ (all

---

† See, however, § 3.

$k \neq i, j$) as when $r_i > r_k$ (all $k \neq i$), the coefficient is taken to be $2^{-1/2}$. However, such an argument would imply an incorrect physical interpretation of the wave functions. The true meaning of the value which we use for $\zeta(0)$ is that it is an effective value which takes into account the rapid variation of the *electron density* in the $3(N+1)$ dimensional configuration space when $r_i \simeq r_j > r_k$. Considering for simplicity the hydrogen atom and a colliding electron, so that

$$\langle \mathbf{X} | \beta \rangle = -\zeta(r_1 - r_2)\Psi(2)F(1) + \zeta(r_2 - r_1)\Psi(1)F(2),$$

Ψ being the hydrogen wave function and F a free wave function, it would be incorrect to say that for $r_1 > r_2$, the system is in such a *state* that 1 is the colliding electron, and it is in a different *state* when $r_2 > r_1$; we must rather say that the system is *always* partly in the state $\zeta(r_1 - r_2)\Psi(2)F(1)$, in which 1 is the colliding electron, and partly in the state $\zeta(r_2 - r_1)\Psi(1)F(2)$, in which 2 is the colliding electron, and *both* states are such that the density of the colliding electron falls rapidly to zero when the distance from the nucleus decreases beyond that of the atomic electron. We see the physical meaning of the wave functions particularly clearly if we consider the case of the colliding and atomic electrons having different spin quantum numbers.

2.2. The criticisms listed above show that Layzer's derivation of his formula is not satisfactory, but nevertheless we shall now test the formula, regardless of the derivation, by applying it to some simple particular cases. The formula applied is that originally given by Layzer, without any modification (except, of course, that with the normalization that seems to be implied, the matrix element in (L21) must be multiplied by $(N+1)^{-1}$ to give the scattering coefficient correctly, and this factor has been included). As in the case of the Oppenheimer approximation, the work essentially reduces to the calculation of a direct integral f and an exchange integral g. For the hydrogen atom

$$f = -\frac{1}{2\pi}\iint \zeta(r_1 - r_2)\Psi_{\alpha'}^*(\mathbf{r}_2)\exp(-i\mathbf{k}'.\mathbf{r}_1)V\zeta(r_1 - r_2)\Psi_{\alpha^0}(\mathbf{r}_2)\exp(i\mathbf{k}^0.\mathbf{r}_1)d\tau_1 d\tau_2, \qquad \ldots\ldots(6)$$

$$g = -\frac{1}{2\pi}\iint \zeta(r_1 - r_2)\Psi_{\alpha'}^*(\mathbf{r}_2)\exp(-i\mathbf{k}'.\mathbf{r}_1)V\zeta(r_2 - r_1)\Psi_{\alpha^0}(\mathbf{r}_1)\exp(i\mathbf{k}^0.\mathbf{r}_2)d\tau_1 d\tau_2, \qquad \ldots\ldots(7)$$

and for the helium atom

$$f = -\frac{1}{2\pi}\iiint \zeta(r_1 - r_2)\zeta(r_1 - r_3)\Psi_{\alpha'}^*(\mathbf{r}_2,\mathbf{r}_3)\exp(-i\mathbf{k}'.\mathbf{r}_1)V\zeta(r_1 - r_2)\zeta(r_1 - r_3) \times \Psi_{\alpha^0}(\mathbf{r}_2,\mathbf{r}_3)\exp(i\mathbf{k}^0.\mathbf{r}_1)d\tau_1 d\tau_2 d\tau_3, \qquad \ldots\ldots(8)$$

$$g = -\frac{1}{2\pi}\iiint \zeta(r_1 - r_2)\zeta(r_1 - r_3)\Psi_{\alpha'}^*(\mathbf{r}_2,\mathbf{r}_3)\exp(-i\mathbf{k}'.\mathbf{r}_1)V\zeta(r_2 - r_1)\zeta(r_2 - r_3) \times \Psi_{\alpha^0}(\mathbf{r}_1,\mathbf{r}_3)\exp(i\mathbf{k}^0.\mathbf{r}_2)d\tau_1 d\tau_2 d\tau_3, \qquad \ldots\ldots(9)$$

where Ψ is the spatial part of an atomic wave function and atomic units are used. f and g are used in the same way as in Oppenheimer's approximation (cf. Bates, Fundaminsky and Massey 1950, eq. (58), (59), (88)–(91)). It will be noticed that the only contribution to a g-integral comes from that part of V which is denoted by $V_{\delta ij}$, as the ζ-factors always make the other contribution vanish.

The wave functions used for hydrogen were, of course, exact. For helium the variational wave functions given by Morse, Young and Haurwitz (1935) were adopted.

The integrations in (6)–(9) can be carried out in spherical polar coordinates. The S wave functions used in the present work are independent of the angular coordinates, which brings about two simplifications : (i) The exchange integrals g for S–S transitions are independent of the angle of scattering (i.e. the angle between $\mathbf{k}^0$ and $\mathbf{k}'$). (ii) The only contribution even to the direct integrals f for S–S transitions comes from V_{bij}.

The integrations are quite straightforward. The direct integrals f can be analytically expressed in terms of K^2 and the various constants characterizing the atomic wave functions, where

$$K = |\mathbf{k}^0 - \mathbf{k}'|. \qquad \ldots\ldots(10)$$

In the case of hydrogen the expression for f was found to be sufficiently simple for the scattering coefficient to be analytically integrated over the scattering angles; for this purpose the substitution

$$K^2 + (9/4) = x \qquad \ldots\ldots(11)$$

was found very helpful. In the case of helium analytical integration of the scattering coefficient, although possible, would have been too complicated, and therefore the integration over the scattering angles was done numerically.

The exchange integrals g could be analytically expressed as functions of $k^0 + k'$ and $k^0 - k'$. The exchange integral gave rise to no difficulties of integration over the scattering angles, because even in the case of the S–P transitions the pure exchange scattering coefficient, summed over the three degenerate P states, was found to be independent of the angle of scattering.

§ 3. RESULTS

The cross sections for exciting the 2^2S level of atomic hydrogen are presented in table 1. That for a collision which reverses the spin of the atomic electron is (for an unpolarized beam of incident electrons, as usual)

$$Q^g/2 = (k'/2k^0)\int |g|^2 d\omega, \qquad \ldots\ldots(12)$$

where $d\omega$ is the solid angle differential in the $\mathbf{k}'$-space. In the case of an S–S transition this reduces to $2\pi k' g^2/k^0$ in Layzer's approximation.

Table 2 gives the 1^1S–2^1S and 1^1S–2^3S excitation cross sections of helium. In the calculation of the D.W.B.O. cross sections only the s and p waves of the free electron were taken into account, the p-wave cross section being calculated by the simple Oppenheimer approximation. k^0 is calculated from the energy of the scattered electron by using the *theoretical* term values corresponding to the wave functions of Morse, Young and Haurwitz (1935), rather than the true spectroscopic energies.

The cross sections obtained by the Layzer approximation for the 1^1S–2^1S and 1^1S–2^3S transitions in helium appear to be very satisfactory, except for energies just above the threshold, where of course this simple method could not be expected to reproduce the sharp peak. The close agreement of Massey and Moiseiwitsch's results (D.W.B.O.) for 1^1S–2^3S with those of Maier-Leibnitz (E.) at low energies makes it very likely that at 6·76 and 20·87 ev the former are even closer to the true cross sections, and if this is so, then the Layzer cross sections, which are close to those of Massey and Moiseiwitsch, are quite good.

The results presented in table 1 appear less conclusive, except that there is little doubt that the values of Q^-, as calculated by Layzer's method, are too large for energies not quite near the threshold. If the distorted wave (D.W.B.O.) cross sections should be as near to the true ones as they appear to be in the case of helium, then that would imply that the Layzer values of Q^+ are quite satisfactory. The Layzer cross sections neglecting exchange (not included in the table) disagree

Table 1. The 1^2S–2^2S Excitation Cross Sections of Atomic Hydrogen

Incident electron energy (ev)	Spin of atomic electron reversed, $\frac{1}{2}Q^{g}$			Symmetrical, Q^+			Antisymmetrical, Q^-		
	L.	D.W.B.O.	V.	L.	D.W.B.O.	V.	L.	D.W.B.O.	V.
10·2	0	0	0	0	0	0	0	0	0
13·5	0·0598	0·067	0·004$_2$	0·529	0·714	0·167	0·050	0·0316	0·002
19·4	0·0133	0·029$_5$	0·011$_5$	0·204	0·344	0·124	0·098	0·010	0·004†
26·5	0·00237			0·111			0·092		
30·4	0·00095	0·011$_5$	0·006	0·0922	0·127	0·057	0·0845	0·010	0·007
34·6	0·00037			0·0794			0·0765		
43·8	0·00004			0·0627			0·0623		
54	0·00000	0·000$_8$	0·001$_2$	0·0514	0·0255	0·016	0·0514	0·006	0·005

L. = Layzer's approximation; D.W.B.O. = the distorted-wave Born–Oppenheimer approximation (Erskine and Massey 1952); V. = the variational method (Massey and Moiseiwitsch 1953). All cross sections are in units πa_0^2.

† Dr. Moiseiwitsch has informed the author that $Q^- = 0{\cdot}004\pi a_0^2$ is the correct value for 19·4 ev incident electrons, the figure given in the paper cited being a misprint.

Table 2. The 1^1S–2^1S and 1^1S–2^3S Excitation Cross Sections of Atomic Helium

Scattered electron energy (ev)	1^1S–2^1S				1^1S–2^3S			
	k°_{theor}	L.	D.W.B.O.	E.	k°_{theor}	L.	D.W.B.O.	E.
0	1·183	0		0	1·161	0	0	0
0·135†	1·187			0·017	1·165	0·0051	0·058$_6$	0·046
0·443†	1·197			0·027	1·174			0·039
1·26	1·222	0·0158	0·010$_5$	(0·014‡)	1·200	0·0145	0·0260	0·017
6·76	1·378	0·0323	0·039$_0$		1·359	0·0188	0·0216	
12·22					1·500	0·0127		
20·87	1·715	0·0508	0·042$_5$		1·700	0·0056	0·0052	
31·76	1·936	0·0524	0·036$_5$					

L. = Layzer's approximation; D.W.B.O. = the distorted-wave Born–Oppenheimer approximation (Massey and Moiseiwitsch 1954); E. = experimental (Maier-Leibnitz 1935). All cross sections are in units πa_0^2.

† The value 0·443 ev was so chosen as to coincide with the peak of Maier-Leibnitz's experimental curve for 1^1S–2^1S. The value 0·135 ev, which is one of the energies used by Massey and Moiseiwitsch, very nearly coincides with the peak of the experimental curve for 1^1S–2^3S.

‡ Uncertain.

Table 3. The Asymptotic Excitation Cross Sections of Hydrogen and Helium, for High-Speed Incident Electrons

	L.	Born's approx.
H, 1^2S–2^2S	$0{\cdot}223(k^0)^{-2}$	$0{\cdot}444(k^0)^{-2}$
He, 1^1S–2^1S	$0{\cdot}304(k^0)^{-2}$	$0{\cdot}074(k^0)^{-2}$

Unit of cross section : πa_0^2

Table 4. The Layzer Cross Sections $\frac{1}{2}Q^g$ for the 1^2S–2^2P Transition in Hydrogen for Collisions which reverse the Spin of the Atomic Electron

Incident electron energy (ev)	$\frac{1}{2}Q^g$	Incident electron energy (ev)	$\frac{1}{2}Q^g$	Incident electron energy (ev)	$\frac{1}{2}Q^g$	Incident electron energy (ev)	$\frac{1}{2}Q^g$
10·15	0	11·78	0·170	16·37	0·0976	39·10	0·0395
10·46	0·126	12·12	0·166	19·48	0·0737	43·84	0·0368
10·79	0·156	12·46	0·160	22·87	0·0603	48·84	0·0343
10·96	0·164	12·81	0·153	26·52	0·0522	54·12	0·0320
11·11	0·168	13·17	0·146	30·44	0·0468	59·67	0·0300
11·44	0·172	13·53	0·140	34·64	0·0428		

The cross sections are in units πa_0^2.

Table 5. The Layzer Cross Sections, Q, for the 1^1S–2^3P Excitation of Helium

Scattered electron energy (ev)	k^0_{theor}	Q	Scattered electron energy (ev)	k^0_{theor}	Q
0	1·197	0	5·59	1·359	0·130
1·40	1·24	0·150	11·04	1·5	0·079
2·77	1·28	0·157	19·70	1·7	0·043
3·82	1·31	0·150	30·58	1·922	0·028

The cross sections are in units πa_0^2.

with those calculated by other methods as seriously (and in the same direction) as do the values of Q^-. The cross sections $Q^g/2$, however, depending upon the exchange integral only, would seem to agree somewhat better, although the Layzer values seem to fall off too rapidly as the energy increases. But there is the possibility that the Layzer approximation is more successful in the treatment of exchange effects than it is in the treatment of non-exchange scattering.

Although Layzer apparently intended his approximation to be used for the treatment of the scattering of *slow* electrons, it is interesting to compare the asymptotic cross sections, for incident electron energy tending to infinity, with those given by the Born approximation. This comparison is made in table 3, the asymptotic Born cross section of helium being calculated from the value $0{\cdot}0025\ \pi a_0^2$ which Massey and Mohr (1933) give for the cross section at 400 ev incident energy.†

---

† The helium 1^1S and 2^1S wave functions used in the present work are not orthogonal and are therefore unsuitable for the application of Born's approximation. Massey and Mohr used a different wave function for 2^1S, as did also Fundaminsky (see Bates, Fundaminsky, Leech and Massey 1950), whose result does not differ much from that of Massey and Mohr.

In Layzer's approximation, as in Oppenheimer's approximation, the S–S exchange cross sections tend to zero much more rapidly than $(k^0)^{-2}$, and are not considered in table 3. The Layzer non-exchange cross sections behave like $(k^0)^{-2}$ for k^0 large, being in this respect in agreement with the Born cross sections which latter are quite reliable at high energies. The numerical coefficients, however, disagree quite seriously.

It was suggested in § 2·1 that the expression for $V_{\delta ij}$ to be used ought to be twice that given by Layzer, and that $\zeta(0)$ should be taken to be $\frac{1}{2}$ instead of $2^{-1/2}$. The effect of making both these corrections would be to increase all the Layzer cross sections given in this paper by a factor of 2. In most cases this would increase the discrepancies, and so it must be admitted that these theoretical suggestions receive no support from the numerical results so far obtained.

Lastly, tables 4 and 5 give the 1S–2P pure exchange excitation cross sections of hydrogen and helium, respectively, given by the Layzer formula, without comparison data. The cross sections given in table 4 are for such collisions that reverse the spin of the atomic electron, assuming the beam of incident electrons to be unpolarized.

The peak of the 1^1S–2^3P excitation function seems to be at least three times larger than it could possibly be according to the measurements by Maier-Leibnitz (1935) ‡ of the total inelastic cross section, but on the other hand it is six times smaller than an estimate based on a combination of the measurements of Thieme (1932) and of Woudenberg and Milatz (1941).

It must be remarked that the asymptotic fall-off of the S–P exchange cross sections with increasing k^0 is too slow; namely, these cross sections behave like $(k^0)^{-2}$ for k^0 large. On the other hand, the S–P non-exchange cross sections vary correctly for large k^0 in the case of hydrogen (and most probably also in the case of helium)—namely, like $(k^0)^{-2} \log (k^0 - k')$, as in Born's approximation (see, for example, Bates, Fundaminsky and Massey 1950). Since there is hardly any hope of improving upon the accuracy of Born's approximation, no numerical calculations were done on these cross sections, and consequently we can say nothing about the numerical factor in the asymptotic case.

In conclusion, it may be said that the present approximation gives results which are surprisingly good in view of the serious defects in the theory by which it is suggested (see § 2.1). In fact, the Layzer cross sections presented in this paper agree about as closely with those obtained by other methods as those other cross sections agree among themselves. This certainly justifies further work on this approximation, which may lead to more definite conclusions as regards its usefulness.

ACKNOWLEDGMENTS

The author wishes to thank Professor D. R. Bates for suggesting this problem, and for helpful advice and discussion during the progress of the work.

Thanks are also due to Professor H. S. W. Massey, and Dr. B. L. Moiseiwitsch, for allowing their distorted-wave cross sections of helium to be quoted in advance of publication.

‡ See Bates, Fundaminsky, Leech and Massey (1950), both for this and for a discussion of the other measurements mentioned below.

REFERENCES

BATES, D. R., FUNDAMINSKY, A., LEECH, J. W., and MASSEY, H. S. W., 1950, *Phil. Trans. Roy. Soc.* A, **243,** 93.
BORN, M., 1926, *Z. Phys.*, **38,** 803.
DIRAC, P. A. M., 1947, *The Principles of Quantum Mechanics*, 3rd Edn (Oxford : Clarendon Press).
ERSKINE, G. A., and MASSEY, H. S. W., 1952, *Proc. Roy. Soc.* A, **212,** 521.
LAYZER, D., 1951, *Phys. Rev.*, **84,** 1221.
MAIER-LEIBNITZ, H., 1935, *Z. Phys.*, **95,** 499.
MASSEY, H. S. W., and MOHR, C. B. O., 1933, *Proc. Roy. Soc.* A, **140,** 613.
MASSEY, H. S. W., and MOISEIWITSCH, B. L., 1953, *Proc. Phys. Soc.* A, **66,** 406; 1954, *Proc. Roy. Soc.* A, **227,** 38.
MOISEIWITSCH, B. L., 1951, *Phys. Rev.*, **82,** 753.
MORSE, P. M., YOUNG, L. A., and HAURWITZ, E. S., 1935, *Phys. Rev.*, **48,** 948.
OPPENHEIMER, J. R., 1928, *Phys. Rev.*, **32,** 361.
SEATON, M. J., 1953, *Phil. Trans. Roy. Soc.* A, **245,** 469.
THIEME, O., 1932, *Z. Phys.*, **78,** 412.
WOUDENBERG, J. P. M., and MILATZ, J. M. W., 1941, *Physica*, **8,** 871.

Angular Distributions from (d, n) Reactions at 0·86 Mev Deuteron Energy

By L. L. GREEN, J. P. SCANLON† and J. C. WILLMOTT
Nuclear Physics Research Laboratory, University of Liverpool

Communicated by H. W. B. Skinner; MS. received 12*th November* 1954

Abstract. The angular distributions of neutron groups from the reactions ^{9}Be(d, n)^{10}B and ^{13}C(d, n)^{14}N have been measured for a deuteron energy of 0·86 Mev. The excitation energies of the first few excited states of ^{10}B and ^{14}N have been measured, and are in good agreement with previous measurements. The angular distributions have been analysed in terms of both compound nucleus and stripping interactions. Only the fourth excited state of ^{10}B and the third excited state of ^{14}N were found to be formed to a large extent by deuteron stripping.

---

§ 1. Introduction

PREVIOUS authors (Pruitt, Hanna and Swartz 1952, 1953, Burke and Risser 1952, Burke, Risser and Phillips 1954) have reported work on the angular distributions of neutron groups produced by the bombardment of light elements by deuterons of approximately 1 Mev energy. In all these results there have been cases where the angular distributions show peaks in the forward directions characteristic of stripping, though superimposed on a background presumably due to a contribution from compound nucleus formation.

The present investigation was made to examine in greater detail the reaction ^{9}Be(d, n)^{10}B, which had previously been studied by Pruitt *et al.* (1952) at low bombarding energy, and the reaction ^{13}C(d, n)^{14}N, on which no previous angular distribution measurements have been reported at low bombarding energy. The present measurements were made using the nuclear emulsion method, and a search was made for the weak groups from the ^{9}Be(d, n)^{10}B and ^{13}C(d, n)^{14}N reactions corresponding to levels in ^{10}B at 2·85 Mev and in ^{14}N at 3·47 Mev as reported by Dyer and Bird (1953) and Mandeville and Swann (1950) respectively.

§ 2. Experimental Procedure

A beam of 865 ± 1 kev deuterons was accelerated by a 1·2 Mv Philips H.T. Set, electronically stabilized to within 1 kilovolt. The voltage was known to the same degree of accuracy from a previous calibration.

The beam was bent through 90° by a permanent magnet and defined by two $\frac{1}{4}$ in. water cooled collimators. Thus a deuteron current of 100 μA was focused on to a target $\frac{1}{4}$ in. in diameter.

The target chamber and detector are shown diagrammatically in figure 1. The targets were clamped to a water-cooled brass holder at the centre of a $\frac{1}{32}$ in. walled cylindrical chamber. The target holder could be rotated about the axis of the chamber and was electrically insulated from the rest of the chamber by an ebonite mounting.

---

† Now at the Atomic Energy Research Establishment, Harwell.

A light tight brass plate holder containing 2 in. × 2 in. × 400 micron Ilford C2 emulsions was positioned accurately with respect to the centre of the target chamber by means of locating studs. The plates were mounted in milled grooves cut radially from the target at 5° intervals between $-5°$ and $+170°$ to the incident beam; the front edge of each plate was located against the front wall of the holder at a distance of 20 cm from the target.

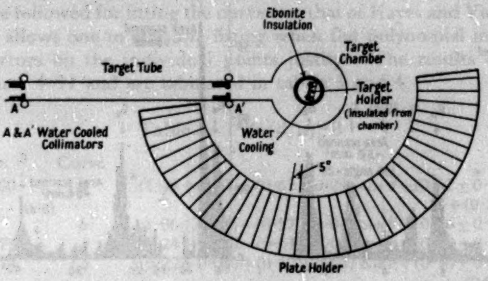

Figure 1.

A ^{9}Be target about 30 kev thick was made by evaporating metallic beryllium on to 0·005 in. thick copper backing. The ^{13}C target was prepared by Dr. R. Dawton at the Atomic Energy Research Establishment and was 20 kev thick on 0·005 in. aluminium backing.

A stilbene scintillation counter was used to monitor the neutron and γ-ray yield at 90° to the incident beam.

All the plates used in one particular exposure were taken from the same batch in the hope that the composition and moisture content would be similar and that the whole set would have the same range–energy relation. The plates used in one exposure were developed together so that the shrinkage factor would be similar for the whole batch.

The plates were scanned for neutron recoils using the normal method. The criteria for track acceptance were fixed so that only those recoils occurring with a projected angle in the emulsion less than or equal to 10° from the incident neutron direction, and with a dip angle into the emulsion plane less than, or equal to 10° in the processed emulsion were accepted.

§ 3. NEUTRON SPECTRA

Examples of the neutron spectra obtained from the two reactions are shown in figures 2 and 3. These are not corrected for the variations of (n, p) scattering cross section with energy or for escape losses from the emulsion, but represent the numbers of counted proton recoils plotted against the corresponding incident neutron energies. It will be seen that a certain amount of neutron background from the ^{2}H(d, n)^{3}He reaction was observed. The energy of this group varies much more rapidly with angle than that of the groups being measured, and it was possible to subtract it at all angles, knowing the form of its angular distribution at a similar deuteron energy (Allen *et al.* 1950).

The Q-values of the reactions, and the corresponding excitation energies of the levels of the residual nuclei have been calculated from all the angles measured, and are shown in tables 1 and 2, compared with previous measurements. The errors shown in the present measurement are based on the spread of the measurements at individual angles, and an allowance has been made for the possible errors in the range–energy relation.

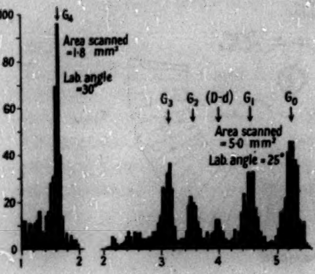

Figure 2.

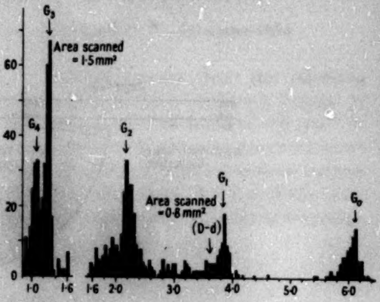

Figure 3.

Table 1. $^{9}Be(d, n)^{10}B$

Present authors.	$E_d=0{\cdot}860$ MeV	Pruitt *et al.*	$E_d=0{\cdot}945$ MeV
Q-Values (MeV)	Excitn Energy (MeV)	Q-Values (MeV)	Excitn Energy (MeV)
4·54±0·06	0·00	4·43±0·08	0·00
3·79±0·05	0·75±0·08	3·69±0·07	0·74±0·11
2·75±0·04	1·79±0·07	2·66±0·06	1·77±0·10
2·31±0·03	2·23±0·07	2·23±0·05	2·20±0·10
0·77±0·04	3·77±0·07	0·76±0·05	3·67±0·09

Table 2. $^{13}C(d, n)^{14}N$

Present authors.	$E_d=0{\cdot}86$ MeV	Benenson (1952).	$E_d=3{\cdot}87$ MeV
Q-Value (MeV)	Excitn Energy (MeV)	Q-Value (MeV)	Excitn Energy (MeV)
5·41±0·06	0·00	5·40±0·10	0·00
3·07±0·04	2·34±0·07	3·09±0·10	2·23±0·10
1·39±0·02	4·02±0·07	1·47±0·09	3·85±0·08
0·39±0·01	5·02±0·07	0·52±0·08	4·80±0·07
0·21±0·02	5·20±0·07	0·35±0·08	4·97±0·07

Q-value plots were made for both reactions, combining the data from all angles, in an endeavour to locate the weak groups mentioned above, but no trace of either was found.

§ 4. ANGULAR DISTRIBUTIONS

The angular distributions were computed by counting the numbers of proton recoils in the individual peaks in the spectra. The D–D background was subtracted where necessary. Allowances were also made for any other neutron background present. The number of recoils was corrected for conversion from the laboratory to the centre-of-mass system of coordinates, for variation of the (n, p) scattering cross section, and the estimated number of proton tracks which escaped from the emulsion and were in consequence not counted.

For each level the results at the various angles were fitted by the method of least squares, firstly to a polynominal in $\cos\theta$, secondly to a polynomial in $\cos\theta$ plus a Butler stripping function $B_l(\theta)$ (Butler 1951), the maximum value of the Butler curve being normalized to unity. The value of orbital angular momentum transferred by the ingoing proton was selected on the basis of the result obtained at higher bombarding energies by Ajzenberg (1952) in the case of ^{9}Be and Bromley and Goldman (1952) and Benenson (1952) in the case of ^{13}C. The procedure followed for fitting the curve was that of Hayes and Vickers (1951). This method allows one to stop the fitting when the polynomial in $\cos\theta$ fits as well as the errors on the individual points justify. The results obtained are shown in figures 4–11 and are tabulated in tables 3 and 4.

Table 3. $^{9}\mathrm{Be}(\mathrm{d,n})^{10}\mathrm{B}$

Group	*E*×	Curve	
g_0	0·00	*a*	$(1{\cdot}00\pm0{\cdot}12)-(0{\cdot}63\pm0{\cdot}24)\cos\theta+(0{\cdot}32\pm0{\cdot}13)\cos^2\theta$ $+(0{\cdot}18\pm0{\cdot}43)B_1(\theta)$
		b	$(1{\cdot}06\pm0{\cdot}05)-(0{\cdot}57\pm0{\cdot}04)\cos\theta+(0{\cdot}36\pm0{\cdot}08)\cos^2\theta$
g_1	0·75	*a*	$(1{\cdot}24\pm0{\cdot}05)-(0{\cdot}61\pm0{\cdot}04)\cos\theta-(0{\cdot}09\pm0{\cdot}07)\cos^2\theta$
g_2	1·79	*a*	$(0{\cdot}22\pm0{\cdot}04)+(0{\cdot}17\pm0{\cdot}03)\cos\theta+(0{\cdot}10\pm0{\cdot}03)\cos^2\theta$ $-(0{\cdot}04\pm0{\cdot}07)B_1(\theta)$
		b	$(0{\cdot}19\pm0{\cdot}02)+(0{\cdot}00\pm0{\cdot}02)\cos\theta+(0{\cdot}11\pm0{\cdot}02)\cos^2\theta$
g_3	2·23	*a*	$(0{\cdot}31\pm0{\cdot}08)-(0{\cdot}14\pm0{\cdot}06)\cos\theta+(0{\cdot}15\pm0{\cdot}05)\cos^2\theta$ $+(0{\cdot}28\pm0{\cdot}11)B_1(\theta)$
		b	$(0{\cdot}46\pm0{\cdot}09)+(0{\cdot}18\pm0{\cdot}07)\cos\theta+(0{\cdot}10\pm0{\cdot}04)\cos^2\theta$ $-(0{\cdot}24\pm0{\cdot}12)\cos^3\theta$
		c	$(0{\cdot}49\pm0{\cdot}04)-(0{\cdot}09\pm0{\cdot}03)\cos\theta+(0{\cdot}07\pm0{\cdot}06)\cos^2\theta$
g_4	3·77	*a*	$(0{\cdot}37\pm0{\cdot}07)+(0{\cdot}10\pm0{\cdot}03)\cos\theta-(0{\cdot}13\pm0{\cdot}08)\cos^2\theta$ $+(0{\cdot}36\pm0{\cdot}07)B_1(\theta)$
		b	$(0{\cdot}66\pm0{\cdot}09)+(0{\cdot}07\pm0{\cdot}08)\cos\theta-(0{\cdot}34\pm0{\cdot}15)\cos^2\theta$
		c	$(0{\cdot}54\pm0{\cdot}05)+(0{\cdot}40\pm0{\cdot}09)\cos\theta+(0{\cdot}35\pm0{\cdot}23)\cos^2\theta$ $-(0{\cdot}31\pm0{\cdot}10)\cos^3\theta-(0{\cdot}65\pm0{\cdot}22)\cos^4\theta$

Table 4. $^{13}\mathrm{C}(\mathrm{d,n})^{14}\mathrm{N}$

Group	*E*×	Curve	
g_0	0·00	*a*	$(1{\cdot}00\pm0{\cdot}04)+(0{\cdot}29\pm0{\cdot}05)\cos\theta$
g_1	2·34	*a*	$(0{\cdot}09\pm0{\cdot}01)+(0{\cdot}10\pm0{\cdot}02)\cos\theta+(0{\cdot}48\pm0{\cdot}03)\cos^2\theta$
g_2	4·02	*a*	$(0{\cdot}63\pm0{\cdot}02)-(0{\cdot}049\pm0{\cdot}03)\cos\theta+(0{\cdot}27\pm0{\cdot}04)\cos^2\theta$
g_3	5·02	*a*	$(0{\cdot}06\pm0{\cdot}02)-(0{\cdot}24\pm0{\cdot}05)\cos\theta+(1{\cdot}07\pm0{\cdot}10)B_0(\theta)$

§ 5. DISCUSSION

At the bombarding energy used in these experiments the results show that both the stripping and compound nuclear modes of action occur, contrasting with the results on these reactions at higher bombarding energies where all the groups show very much more pronounced stripping.

The stripping theories of Butler and of Bhatia *et al.* do not take into account the Coulomb potential, but according to Yoccoz (1954), the effect of this is largely to broaden the peaks.

At these bombarding energies there are still signs of structure in the excitation functions and so presumably at this excitation energy there are still discrete, if broad, levels in the compound nucleus. Because of this, and the fact that the lower deuteron velocity means that the particle which is unaffected in the stripping

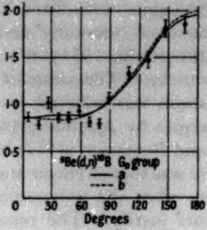

Figure 4.

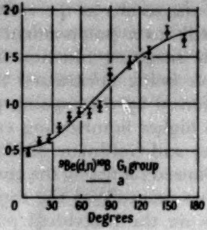

Figure 5.

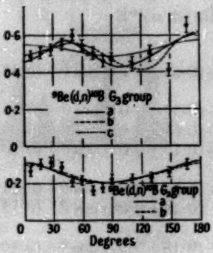

Figure 6.

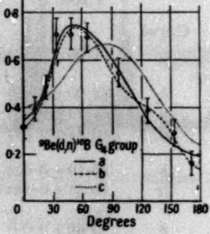

Figure 7.

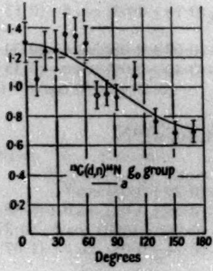

Figure 8.

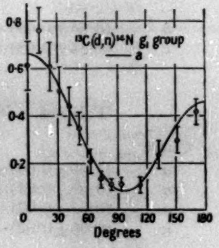

Figure 9.

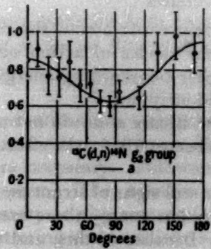

Figure 10.

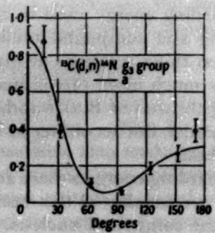

Figure 11.

mechanism spends more time close to the nucleus, compound nucleus formation should be relatively more probable at low bombarding energies.

In discussing whether or not a particular angular distribution requires a stripping term, or is adequately described by compound nuclear terms alone, we must have some idea as to what angular distributions we may expect from compound nucleus formation. In both these reactions we are in a region of broad overlapping levels but not yet in the continuum. Consequently we expect interference terms due to the excitation of levels of different parities. These terms, the odd powers of $\cos\theta$, vanish in the two extremes of sharp resonances, and a statistical density of levels. Due to the falling penetrability of higher l-waves, terms above $\cos^2\theta$ in the polynomial may be expected to be small. For 860 kev deuterons approaching ^{9}Be the penetrabilities are shown in table 5.

For ^{13}C the relative penetrabilities are almost the same, though the absolute values are somewhat lower.

Table 5

l	0	1	2
Absolute Penetrability	0·33	0·12	0·014
Relative Penetrability	1	0·35	0·04

Thus terms in $\cos^4\theta$ should be small unless for some reason a matrix element involving an $l=2$ wave is unusually large, and in any case terms in $\cos^3\theta$, being due to interference between $l=1$ and $l=2$ should not be large unless accompanied by a significant term in $\cos^4\theta$.

The compound nucleus and Butler contributions may be incoherent, or there may be interference between the two modes. In the former case the Butler term and the compound nucleus contribution are additive and the analysis described above will give the correct magnitude for the Butler contribution. If there is interference the coefficient of all the terms derived above may be incorrect, but the presence of a Butler term nevertheless indicates that there is a definite stripping contribution.

The ground state of ^{10}B and the first two excited states are adequately described by compound nucleus terms to $\cos^2\theta$ without any anomalies in the coefficients. The third excited state needs higher terms and can either be fitted by the addition of an $l=1$ Butler curve or a term in $\cos^3\theta$ which is twice the size of the term in $\cos^2\theta$ and half the size of the leading term ; no $\cos^4\theta$ term is required. This would be an unusual form for an angular distribution for a compound nucleus reaction and for this reason the function involving the Butler term may be preferable. The fourth excited state shows the characteristic peak of a stripping pattern with $l=1$. This curve could be fitted with a polynomial in $\cos\theta$ with terms up to $\cos^4\theta$, this term having the largest coefficient. This would be a very unusual function for a compound nucleus reaction. At higher bombarding energies all these levels are fitted with an $l=1$ stripping pattern.

All the levels of ^{14}N examined are fitted by polynomials up to $\cos^2\theta$ except for the third excited state which shows a very strong $l=0$ stripping pattern plus a term in $\cos\theta$. This requires terms to at least $\cos^6\theta$ to fit with a polynomial in $\cos\theta$. This is the only state which requires $l=0$ in results of Benenson (1952) at a higher bombarding energy, all the other levels requiring an $l=1$

curve. The results on the fourth excited state are not included in the tables. This is a very weak group and the separation in range between the tracks produced by this group and those produced by neutrons leaving ^{14}N in the third excited state is small, particularly in the backward direction. This latter group of neutrons is a strong group and consequently the results in the fourth excited state were not very reliable, but the neutron intensity from this group was approximately isotropic.

§ 6. CONCLUSIONS

Thus at 0·86 MEV deuteron bombarding energy there is evidence that a stripping term is needed in two cases; for one neutron group in each reaction studied. There is a further angular distribution for which the best fit is obtained with the addition of a Butler term and for which the alternative polynomial in $\cos\theta$ would be unusual. The remaining angular distributions are all fitted adequately by polynomials in $\cos\theta$ which are quite plausible angular distribution functions for compound nucleus formation.

ACKNOWLEDGMENTS

We are grateful to Professor H. W. B. Skinner for helpful discussions, to Miss E. Burrows and Miss Robinson for help with the track measurements, and one of us (J. P. S.) is indebted to the Department of Scientific and Industrial Research for the award of a maintenance grant.

REFERENCES

AJZENBERG, F., 1952, *Phys. Rev.*, **88**, 298.

ALLEN, K. W., LIVESEY, D. L., and WILKINSON, D. H., 1950, *Proc. Camb. Phil. Soc.*, **46**, 339.

BENENSON, R. E., 1952, *Phys. Rev.*, **90**, 420.

BROMLEY, D. A., and GOLDMAN, L. M., 1952, *Phys. Rev.*, **86**, 790.

BURKE, W. H., and RISSER, J. R., 1952, *Phys. Rev.*, **85**, 742.

BURKE, W. H., and RISSER, J. R., and PHILLIPS, G. C., 1954, *Phys. Rev.*, **93**, 188.

BUTLER, S. T., 1951, *Proc. Roy. Soc.* A, **208**, 559.

DYER, A. J., and BIRD, J. R., 1953, *Aust. J. Phys.*, **6**, 45.

HAYES, J. C., and VICKERS, T., 1951, *Phil. Mag.*, **42**, 1387.

MANDEVILLE, C. E., and SWANN, C. P., 1950, *Phys. Rev.*, **79**, 787.

PRUITT, J. S., HANNA, S. S., and SWARTZ, C. D., 1952, *Phys. Rev.*, **87**, 534; 1953, *Phys. Rev.*, **92**, 1456.

YOCCOZ, J., 1954, *Proc. Phys. Soc.* A, **67**, 813.

An Investigation of ^{7}Li(d, n)^{8}Be and ^{11}B(d, n)^{12}C Nuclear Reactions

By M. A. IHSAN
Nuclear Physics Research Laboratory, University of Liverpool

Communicated by H. W. B. Skinner ; MS. received 10*th August* 1954
and in amended form 19*th November* 1954

Abstract. The energy levels of ^{8}Be and ^{12}C have been studied by means of the (d, n) reaction using deuterons of energy 686 kev. Evidence of levels in ^{8}Be was found at 2·98 and 7·53 Mev. Investigation of energy levels of ^{12}C has shown energy peaks at 4·40, 7·63 and 9·72 Mev respectively. The angular distribution of neutrons from the ^{11}B(d, n)^{12}C reaction also has been investigated.

§ 1. INTRODUCTION

THE photographic plate technique has been used for the study of the spectrum of low lying states of ^{8}Be from the reaction

$$^7_3\text{Li} + ^2_1\text{D} \rightarrow ^8\text{Be} + ^1_0\text{n} + Q \qquad \ldots\ldots(1)$$

which has a Q value of 15·03 Mev. The reaction (1) has been studied by Richards (1941) and also by Green and Gibson (1949). Richards measured the energy distribution of the emitted neutrons at right angles to the direction of the incident deuteron beam, while Green and Gibson measured the neutron spectrum at 0° and 120° with respect to the initial direction of the deuterons. They found evidence of the neutron groups corresponding to the ground state of ^{8}Be, followed by a broad group for the first excited state, and accompanied by two more levels superimposed on a continuous background. Recently Trumpy *et al.* (1952) have studied the same reaction. They found evidence of energy levels in ^{8}Be at 2·9, 4·1 and 5·1 Mev. Their analysis suggests two energy levels at 4·1 and 2·92 Mev in place of the broad level corresponding to the first excited state of ^{8}Be. Erdös *et al.* (1953) have resolved the first excited state of ^{8}Be into three energy levels at 2·2, 2·9 and 3·4 Mev.

Lately Malm and Inglis (1953) have investigated the ^{8}Be energy levels using the following reaction:

$$^{10}_5\text{B} + ^2_1\text{D} \rightarrow ^8_4\text{Be} + \alpha + Q. \qquad \ldots\ldots(2)$$

They measured the energy of α-particles with a proportional counter extending their investigations from 0 to 7 Mev excitation energy of ^{8}Be. They found a sharp peak corresponding to the formation of ^{8}Be in its ground state having a width of 0·06 Mev which is by far the best resolution so far reported. Their experimental evidence suggests that there is only one broad energy level at 2·9 Mev which corresponds to the first excited state of ^{8}Be. We have studied the reaction (1) in order to investigate the energy levels of ^{8}Be in general and its first excited state in particular. Neutron spectra were measured at three different angles, 90°, 115° and 145° respectively. Finally a combined result is plotted in terms of excitation energy of ^{8}Be, which will be discussed below.

§ 2. EXPERIMENTAL ARRANGEMENT

A thin lithium target was used and kept cool during the time of bombardment. It was bombarded by a homogenous beam of deuterons of mean energy 686 kev from the Nuclear Physics Research Laboratory's 1-Mev h.t. generator. Ilford C2 400-micron nuclear research plates were used for the detection of neutrons. The plates were held lengthwise so as to receive the incoming neutrons tangentially. After an exposure of two hours they were developed by the temperature control method. The proton tracks in the emulsion formed by the collision of incoming neutrons were scanned with a Cooke, Troughton and Simms nuclear research microscope with an oil-immersed objective of × 45 and a Kellner eyepiece of × 10. The following criteria were used for the acceptance of a track for measurement: angle θ of proton in the forward direction $\leqslant 10°$, dip of proton track $\leqslant 4°$. Only those tracks were measured whose range was greater than or equal to 199 microns or 4·99 Mev.

§ 3. ENERGY LEVELS OF ${}^8_4\text{Be}$

In addition to reaction (1) with which we are mainly concerned, there is a possibility of the reaction

$$ {}^7_3\text{Li} + {}^2_1\text{D} \rightarrow 2\,{}^4_2\text{He} + {}^1_0\text{n} + Q. \qquad \ldots\ldots(3) $$

The reaction (3), being a three-body disintegration of low Q, produces a continuous distribution of neutrons of low energy in the spectrum of figure 1, which was obtained by plotting the excitation energy as abscissa against the neutron number as ordinate at an energy interval of 0·22 Mev. The spectrum of ${}^8\text{Be}$ shows a sharp peak corresponding to the ground state, having a half-width of 0·5 Mev, followed by a broad peak for the first excited state and a level at 7·53 Mev which is in agreement with the other reported experimental results (Green and Gibson 1949, Richards 1941, Steigert and Sampson 1953).

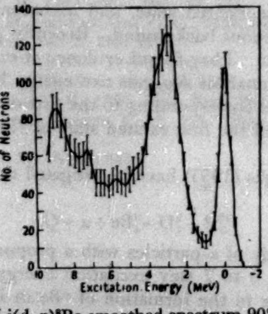

Figure 1. ${}^7\text{Li(d, n)}{}^8\text{Be}$ smoothed spectrum 90°, 115°, 145°.

The peak of the first excited state appears to be slightly asymmetric in shape and perhaps suggests a second level at about 4·1 Mev besides the level at 3 Mev. The existence of a level at 4·01 Mev has also been discussed by Titterton (1954). A number of authors (Trumpy *et al.* 1952, Calcraft and Titterton 1951, Brinkworth and Titterton 1951, Inall and Boyle 1953), have reported this level, but in some cases (Calcraft and Titterton 1951, Brinkworth and Titterton 1951) the statistics are too poor for definiteness. A number of other authors (Malm and Inglis 1953, Richards 1941, Trail and Johnson 1954, Treacy 1953, Kunz *et al.* 1953) have failed to find this level. Our evidence is not sufficient to establish this level, and it may be in any case that the 4·1 MEV level appears in some reactions but not in others. Titterton (1954) also discusses a level at 5·3 MEV but our evidence for this level is inconclusive.

§ 4. ENERGY LEVELS OF $^{12}_{6}C$

We have studied the reaction $^{11}B(d, n)^{12}C$ using a separated isotopic target of ^{11}B at a mean deuteron bombarding energy of 0·8 MEV with Ilford C2 photographic plates. Figure 2 shows the neutron spectrum from the above reaction at 95° to the initial direction of the deuteron beam. This spectrum is measured over a plate area of 1·8 × 5 mm for eighteen scans. The total number of tracks in this histogram is about 646. Evidence is found for neutron groups at 13·39, 9·33, 6·34 and 4·42 MEV. Their Q values and the corresponding excitation energy levels and their peak intensities are given in the table.

State	Q (MEV)	Energy level (MEV)	Peak intensity
Ground	13·81	0·0	11
1st excited	9·41	4·40	28
2nd excited	6·18	7·63	7
3rd excited	4·10	9·71	36

The groups corresponding to the ground, first, second and third excited states are marked G_0, G_1, G_2 and G_3 respectively. At the low energy end of the spectrum of figure 2, there is another apparent peak at 2·59 MEV which has also high intensity. This is probably due to the method of selection of tracks for measurement.

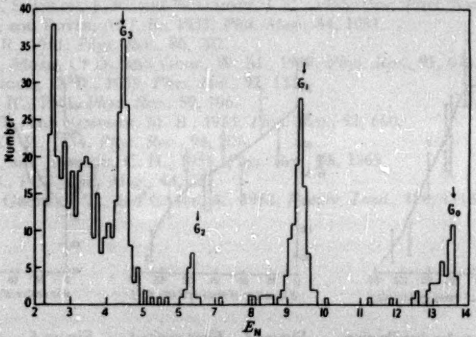

Figure 2. $^{11}B(d, n)^{12}C$; 95°. $E_d = 0·87$ MEV.

The neutron groups observed in the bombardment of ^{11}B by deuterons arise through the reaction

$$^{11}_{5}B + ^{2}_{1}D \rightarrow ^{12}_{6}C + ^{1}_{0}n + Q \qquad \ldots\ldots (4)$$

which has a Q value of 13·78 MeV agreeing reasonably well with the experimental value given in the table. The continuous distribution at low energies probably arises from a four-body type of break-up and is also due to the contamination of the target by deuterons producing D–D neutrons.

The energy levels of ^{12}C have been the subject of previous investigations by Gibson (1949), who studied the reaction $^{11}_{5}B(d, n)^{12}C$. He found levels in ^{12}C at 4·47, 7·7 and 9·72 MeV. Johnson (1951) also studied the levels of ^{12}C using an unseparated target of boron and found levels at 4·4, 9·6, 10·8 MeV etc., with no sign of any group at 7 MeV. Energy levels of ^{12}C have also been investigated by Bonner and Brubaker (1936). Dunbar *et al.* (1953) investigated the $^{14}N(d, \alpha)^{12}C$ reaction using 0·62 MeV deuterons and found a level at 7·68 MeV with a half-width of 0·31 MeV. Our result also shows a second excited state in ^{12}C at 7·63 MeV, which is one-fourth of the intensity of the first excited state of ^{12}C, and its half-width is 0·30 MeV.

§ 5. ANGULAR DISTRIBUTION OF NEUTRONS FROM $^{11}B(d, n)^{12}C$

For the measurement of angular distribution, plates were placed in a circular brass plate holder. They were mounted radially about the target in such a way that neutrons entered the emulsion surface at grazing incidence. Ten plates in all, placed at the angular positions 0°, 20°, 40°, 60°, 80°, 95°, 100°, 120°, 140, and 160° were scanned. The plates were 2 in. × 2 in. and an area of 2·5 mm × 0·8 mm of each plate was scanned, measuring in all 4627 tracks.

The angular distribution of neutrons for any energy level was calculated from the total number of tracks in the corresponding peak of each plate. The laboratory angle of emission of neutrons for each energy level was converted into the centre-of-mass system of angles and the following corrections were applied to every group in order to find the relative number of neutrons responsible for each energy level: solid angle correction, plate thickness, escape correction, neutron–proton scattering cross section.

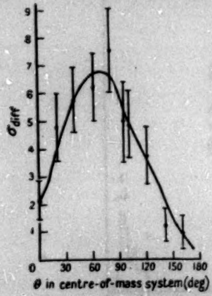

Figure 3. Angular distribution of neutron group leaving ^{12}C in the ground state.

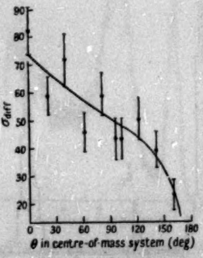

Figure 4. First excited state of ^{12}C. $E_d = 0·870$ MeV.

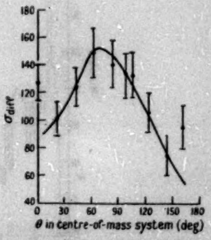

Figure 5. Third excited state of ^{12}C.

The three angular distributions for three energy levels of ^{12}C computed in this way, taking differential cross section as ordinate and the neutron angle of emission in the centre-of-mass system as abscissa, are plotted in figures 3, 4 and 5, corresponding to the ground, first and third excited state respectively. The errors indicated are due to the statistics. The angular distribution of the second excited state is omitted as it is far too weak a level to give reliable results.

Superficially the distribution of the ground and the third excited states look something like stripping patterns, but they could also be explained in terms of compound nucleus formation since they would not involve terms higher than $\cos^2 \theta$. The same applies to the very similar angular distribution published by Burke *et al.* (1954) which resembles the angular distribution of the first excited state shown in figure 4. Although the authors themselves suggest a stripping mechanism, we have no definite evidence for stripping at 800 kev for the reactions studied in this paper. The low energy stripping reactions to be published by Green *et al.* (1955) therefore seem rather exceptional.

ACKNOWLEDGMENTS

The author is profoundly indebted to Professor H. W. B. Skinner for the encouragement and experimental facilities made available to him for the performance of this experiment. He also acknowledges with gratitude the stimulating discussions with Dr. J. C. Willmott and the helpful guidance and useful criticism of Dr. L. L. Green.

REFERENCES

BONNER, T. W., and BRUBAKER, W. M., 1936, *Phys. Rev.*, **49,** 778.
BRINKWORTH, M. J., and TITTERTON, E. W., 1951, *Phil. Mag.*, **42,** 952.
BURKE, W. H., RISSER, J. R., and PHILLIPS, G. C., 1954, *Phys. Rev.*, **93,** 188.
CALCRAFT, M. E., and TITTERTON, E. W., 1951, *Phil. Mag.*, **42,** 666.
DUNBAR, D. N. F., PIXLEY, R. E., WENZEL, W. A., and WHALING, W., 1953, *Phys. Rev.*, **92,** 649.
ERDÖS, P., STOOLL, P., and SCHERRER, P., 1953, *Helv. Phys. Acta*, **26,** 207.
GIBSON, W. M., 1949, *Proc. Phys. Soc.* A, **62,** 587.
GREEN, L. L., GIBSON, W. M., 1949, *Proc. Phys. Soc.* A, **62,** 407.
GREEN, L. L., SCANLON, J. P., and WILLMOTT, J. C., 1955, *Proc. Phys. Soc.* A, **68,** 386.
INALL, E. K., and BOYLE, A. J. F., 1953, *Phil. Mag.*, **44,** 1081.
JOHNSON, V. R., 1951, *Phys. Rev.*, **86,** 302.
KUNZ, W. E., MOAK, C. D., and GOOD, W. M., 1953, *Phys. Rev.*, **91,** 676.
MALM, R., INGLIS, D. R., 1953, *Phys. Rev.*, **92,** 1326.
RICHARDS, H. T., 1941, *Phys. Rev.*, **59,** 796.
STEIGERT, F. E., and SAMPSON, M. B., 1953, *Phys. Rev.*, **92,** 660.
TITTERTON, E. W., 1954, *Phys. Rev.*, **94,** 206.
TRAIL, C. C., and JOHNSON, C. H., 1954, *Phys. Rev.*, **95,** 1363.
TREACY, P. B., 1953, *Phil. Mag.*, **44,** 325.
TRUMPY, B., GROTDAL, T., and GRAUE, A., 1952, *Nature, Lond.*, **170,** 1118.

The Break-up of Negative Ions in the Cyclotron

By J. H. FREMLIN and V. M. SPIERS
Physics Department, University of Birmingham

MS. received 30*th September* 1954

Abstract. A pinhole camera at the periphery of the cyclotron was used to record neutral products of dissociation of molecular ions accelerated to various radii. From the numbers of particles reaching different parts of a C2 nuclear plate in the camera, the attenuation of the accelerated ions due to collisions with residual air molecules could be deduced. This was compared with the attenuation for H_2^+ ions observed in a similar way. The cross section for dissociation of these by air is known, so the cross sections for other ions could be determined. At a velocity corresponding to 1 Mev per nucleon, the cross sections for D^- and HeH^+ were found to be respectively $7{\cdot}6 \times 10^{-16}\,cm^2$ and $1{\cdot}0 \times 10^{-14}\,cm^2$ with an accuracy to about 30%.

---

§ 1. Introduction

The cyclotron is usually used to accelerate simple bare nuclei, such as deuterons or alpha particles. It is, however, sometimes used to accelerate molecular ions such as H_2^+ or ions such as $^{14}N^{3+}$, which still carry with them several atomic electrons. In such cases there is a risk of loss of ions by collisions with residual gas atoms in which the ion is broken up or changes its e/m and can no longer be accelerated. This effect was investigated quantitatively for the H_2^+ ion by Effat (1952), who showed that the cross section for such breakup agreed with theory (Salpeter 1950) to within the accuracy of the experiments (20%). It was thought interesting to find the corresponding cross section for other ions. This was particularly the case for negative ions such as D^-, since, if such ions could be successfully accelerated, the problem of extraction of the beam from the magnetic field would be eliminated. Passage of such an ion through the thinnest foil would reverse its charge, enabling sensibly 100% extraction to be achieved.

§ 2. Method

Since the currents of D^- ions in the Birmingham cyclotron were known to be small, the calorimetric method of measuring the change of ion current with pressure, used by Effat, was not attempted. Instead, it was decided to use Effat's results for H_2^+ and to obtain a direct comparison of the attenuation with radius of D^- ions with that of H_2^+ at a single pressure.

To do this, the D^- and H_2^+ ions were not observed directly, but advantage was taken of the fact that, in each case, some proportion of collisions gives rise to a neutral atom; in the D^- case by the removal of one electron and in the H_2^+ case by the removal of one proton. The energies involved in the collisions are only a few ev, while the ions have an energy of some Mev in the range investigated. Hence the directions of motion of the neutral atoms are not significantly different from those of the original ions. If, therefore, we place a ' pinhole ' camera near the outside of the cyclotron, those neutral atoms passing through the ' pinhole ' will strike the plate at a point from which their original line of motion can be derived. If the axis of the camera lies along the radius of the cyclotron, particles coming directly from the source will strike the centre of the plate, while particles originally revolving in orbits will strike the plate at a distance from its centre dependent on the radius of the orbit. Neutral atoms derived from positive ions will strike the plate on one side of the centre and those derived from negative ions on the other, owing to their opposite direction of revolution in the cyclotron magnet field.

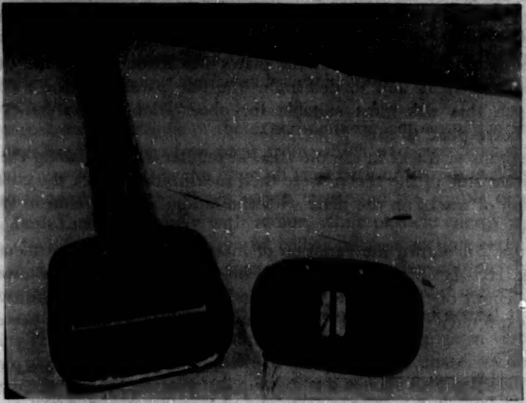

Figure 1. The ' camera ' used to receive neutral particles with the front, carrying a slit $1\frac{1}{2}$ mm wide, removed and one plate in position.

The details of the method were as follows: A camera, the form of which is shown in figure 1, carried two Ilford C2 nuclear plates at a suitable angle to give conveniently measurable tracks, and had in place of the ' pinhole ' a long vertical slit so as to avoid any errors due to variation of the mean vertical position of the beam.

The camera was placed in the cyclotron with the slit at a radius of 69 cm. The source was fed with nitrogen rather than with deuterium or hydrogen, the arc contamination with these gases being ample to give an adequate ion beam. The cyclotron was otherwise run in the normal conditions for acceleration of D^+ or H_2^+. An exposure of 2 seconds gave a convenient density of tracks on the plates. These received simultaneously neutral deuterium atoms on one side of the centre and neutral hydrogen atoms on the other side, pressure and other conditions certainly being identical for both.

After development, by counting tracks across the plate it was possible to find the variation with radius of the numbers of ions breaking up. The numbers breaking up depend both on numbers surviving to the radius concerned and on the collision cross section, and we need some further information to define these separately. This information is given by the known law of variation of cross section, which is shown by Salpeter (1950) to be inversely proportional to particle energy in the energy range concerned. Using this fact the plate results enable us to compare the cross sections for the H_2^+ and D^- at various energies. It was also possible, by measuring the track lengths, to determine accurately the mean energies and the energy spread of ions at any given radius.

§ 3. Experimental Results and Analysis

Several plates were exposed to the break-up products of H_2^+ and D^- ions, and two to the products of HeH^+ ions which can also be accelerated, at five-sixths of the D^+ magnetic field and one-third of the normal angular velocity. In each case the gas in the cyclotron was simply residual air, due to leakages, at a pressure of about 3×10^{-5} mm, the effect of the gas from the source being negligible.

A preliminary examination of the plates was made to find the density and distribution of tracks and to determine the line parallel to the median plane along which this was most suitable for observation. A reference line was drawn to correspond to this.

The lengths of tracks in sample areas at regular intervals along the reference line on either side of the centre were then measured to check the correlation of the position of tracks on the plate with the radius of the cyclotron from which they came.

In figure 2 is shown the variation of mean track length with distance along one of the H_2^+–D^- plates. The tracks on the negative side are clearly about twice the length of those at the corresponding position on the positive side, as would be expected if the D^- and H_2^+ ions have the same velocities at corresponding radii.

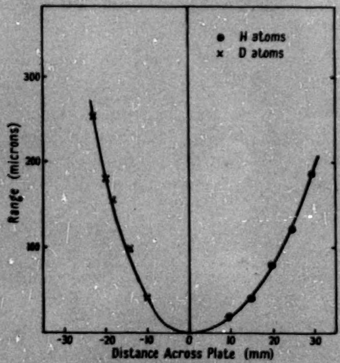

Figure 2. Variation of lengths of tracks with position on the plate.

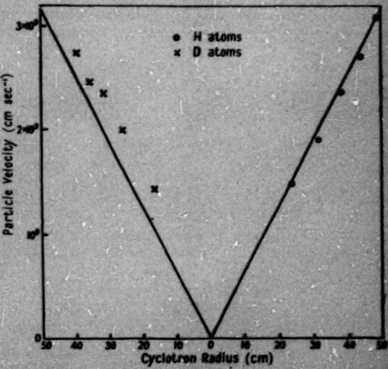

Figure 3. Variation of measured particle velocity with the distance from the centre of the cyclotron at which they originated. The straight lines show the theoretical values.

For each of the experimental points in figure 2 the cyclotron radius from which the particle came was calculated from the position on the plate and the velocity of the particles was found using the range–energy relation given by Rotblat (1950). The relation between these quantities is shown in figure 3.

The two straight lines show the theoretical relation given by simple cyclotron theory, and it will be seen that the experimental points lie very close to these. The small systematic deviation is believed to be due to the fact that the orbit centres did not coincide with the geometrical centre of the cyclotron. In the later figures below, this is allowed for by giving the radii of orbits determined from the particle energies and the known magnetic field rather than the distance of the points of origin of the neutral particle from the centre of the machine.

The qualitative agreement with theory thus being satisfactory, the main task of counting the tracks was undertaken. The number of deuteron tracks per unit area was counted over a strip 1 mm wide and 20 mm long along the reference line already mentioned. These readings were divided up into suitable areas to give reasonable statistical accuracy. It was not necessary to count over such a large total area for the proton tracks owing to their much greater density, 1 mm² being sufficient for each point. A total of about 3000 tracks of each kind was counted.

The geometrical conditions of the experiment are not simple, as the density of orbits, the length of arc of an orbit from which particles can reach the slit and the obliquity of arrival at the plate all vary with orbit radius. Fortunately the density of tracks and the above length of arc, on the simple theory of the cyclotron, both increase linearly with radius, while particle energy increases as (radius)². In this region of energy the collision cross section certainly varies inversely as energy, so that these effects cancel each other completely as far as the number of particles entering the slit is concerned, and it is needful only to make the small correction (up to 30%) for the obliquity of arrival at the plate. Two effects remain which cannot be allowed for: the change in vertical depth of the beam and the loss of particles which have got out of phase. Consideration of the mechanism of acceleration in the known magnetic field distribution and at the radio frequency voltage concerned suggested that these effects will work in opposite directions and that neither will exceed 30% over the range concerned. As will be seen later, the results themselves show that the error resulting does not have a serious effect.

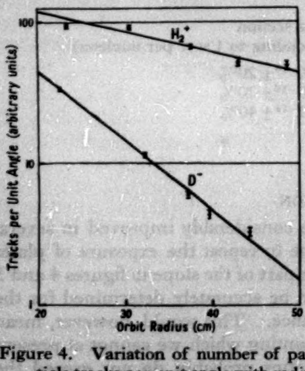

Figure 4. Variation of number of particle tracks per unit angle with radius of orbit of original D^- and H_2^+ ions.

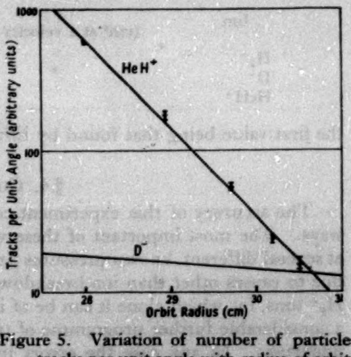

Figure 5. Variation of number of particle tracks per unit angle with radius of orbit of original HeH^+ ions. The D^- line from figure 4 is shown for comparison.

In figure 4 the number of tracks for unit solid angle is plotted against orbit radius for each kind of particle. It is seen that with the exception of extreme points, the graphs represent an exponential fall-off of number with radius as was expected, the rate of fall-off being much larger for the D^- ions.

Now, we can calculate from Effat's results the loss of H_2^+ ions to be expected over the range from say 25 cm to 50 cm radius, for the pressure and radio frequency voltage used ($3{\cdot}2 \times 10^{-5}$ mm and 120 kv dee-to-dee). This gives a calculated loss by a factor of $1{\cdot}95 \pm 0{\cdot}15$, while the factor given by figure 4 is $2{\cdot}25 \pm 0{\cdot}2$. This leaves a loss of particles from other causes by a factor of $1{\cdot}15 \pm 0{\cdot}15$, which confirms the statement above concerning the factors mentioned.

Over the same range the D^- beam falls by a factor of 17. Hence the ratio of the cross section for break-up of D^- to that for H_2^+ is $(\log(17/1{\cdot}15))/(\log 1{\cdot}95)$ or 4·0 with an uncertainty of perhaps 20%. This uncertainty is not more than the probable absolute error of Effat's results which was also estimated as 20%.

In figure 5 is shown, on a different scale, the rather limited results obtained from a similar investigation of the break-up of HeH^+, accelerated as described above, at the same tank pressure, and with an effective radio frequency voltage of 128 kv dee-to-dee.

The main difficulties involved were due to the very short lengths of the large numbers of tracks near the centres of the plates and the very rapid fall in numbers to near zero further out. The tracks were far too short to measure the change in length properly so that no independent check could be made of the divergence of the centre of revolution from the geometrical centre of the machine.

Nevertheless, a ratio for the destruction cross section to that for D^- can be found and, though the random errors are greater, uncertainty resulting from other causes of particle loss is much less. At a given radius the energy is nine times lower, but the interval between successive orbits is nine times larger than that for a similar particle moving with the normal angular velocity and no correction is required if a cross section varying as $1/E$ is assumed as before. The ratio of cross sections is then $13{\cdot}5 \pm 3$.

The final results may then be put in the form:

Ion	Cross section (cm² at a velocity corresponding to 1 MEV per nucleon)
H_2^+	$1{\cdot}9 \times 10^{-16} \pm 20\%$
D^-	$7{\cdot}6 \times 10^{-16} \pm 30\%$
HeH^+	$1{\cdot}0 \times 10^{-14} \pm 40\%$

the first value being that found by Effat.

§ 4. CONCLUSION

The accuracy of this experiment could be considerably improved in several ways. The most important of these would be to repeat the exposure of plates at several different, known pressures; then the part of the slope in figures 4 and 5 due to causes other than ion breakdown could be accurately determined for the H_2^+ ions, for which alone it can be of importance. This would, however, mean a considerable further programme of track-counting which we cannot at present undertake. In any case the errors in our ratios probably do not exceed the errors in the best absolute values available and an improvement of accuracy may not be important until further theoretical estimates are available for comparison.

The accuracy obtained is already quite adequate to show that the loss of negative ions would be very high in any practical particle accelerator in which they could be valuable. For a fixed-frequency cyclotron of moderate size, a pressure of 4×10^{-6} mm would not be too high, but in such cyclotrons there is less difficulty in extracting the beam than there would be in obtaining such a working pressure. Negative particles have been observed near the centre of a synchro-cyclotron (Lofgren 1951), but with a dee voltage of 50 kv a pressure of 10^{-7} mm would be needed to avoid serious loss of particles before reaching the outside and for a synchrotron in the kMev range it would have to be more like 10^{-10} mm.

ACKNOWLEDGMENTS

We are grateful to Mr. P. J. Bateman for his careful counting of a test plate which showed that the experiment was feasible.

REFERENCES

EFFAT, K. E. A., 1952, *Proc. Phys. Soc.* A, **65**, 433.
LOFGREN, E. J., 1951, *Rev. Sci. Instr.*, **22**, 321.
ROTBLAT, J., 1950, *Nature, Lond.*, **165**, 387.
SALPETER, E. E., 1950, *Proc. Phys. Soc.* A, **63**, 1295.

Electron Excitation Functions of Infra-Red Nitrogen Spectra

By D. T. STEWART
Physics Department, Queen's University, Belfast

Communicated by K. G. Emeléus ; MS. received 28th October 1954

Abstract. The relative excitation functions of lines and bands in the near infra-red spectrum of nitrogen have been determined using photographic photometry. The maximum of intensity of the (2, 0) and (3, 1) Meinel bands of N_2^+ occurs at 60 v while that of the N I lines at 8200 Å resulting from the $3s^4P-3p^4P^0$ transition occurs at 90 v.

§ 1. Introduction

A knowledge of the excitation functions of nitrogen band spectra, besides being of interest in itself, is of some importance in auroral and gas discharge phenomena. Experiments are in progress in this laboratory to determine these, using both photographic and photoelectric photometry with electron beam sources. Whilst photoelectric photometry has proved to be the more satisfactory method in the visible region, a sufficiently sensitive photoelectric detector has not been available for the infra-red. The present paper gives some preliminary results obtained photographically for the near infra-red. Kodak I.R.E.R. plates hypersensitized in a weak solution of ammonia were chosen for this investigation, as their maximum sensitivity occurs at about 8000 Å, enabling measurements to be made on the (3, 1) and (2, 0) Meinel bands of $N_2^+(A^2\Pi-X^2\Sigma_g^+)$ near 8105 Å and 7878 Å respectively. Some results were also obtained for the strong group of N lines near 8200 Å resulting from the $3s^4P-3p^4P^0$ transition and for the (2, 0) first positive band of N_2 near 7750 Å. As the usual calibrating source for the determination of light intensity in absolute units in the visible, a tungsten filament lamp, is at present unreliable in the near infra-red, only relative excitation functions have been obtained.

§ 2. Experimental Procedure

2.1. *Apparatus*

The radiation to be studied was produced in the tube shown diagrammatically in figure 1. A was a circular oxide-coated cathode, slightly more than 0·5 cm in diameter, mounted on a ground glass joint for convenience of renewal and alignment. In front of the cathode lay the first accelerating electrode B, controlling the beam current. D was a second accelerating electrode, controlling the final electron energy in the beam. C was a focusing cylinder, held in most cases at cathode potential. E was the collision box, maintained at the same potential as D. W was the viewing window, about 1 cm square. Directly behind W a further slightly larger window was cut in E, and a light trap, in the form of a bent glass cone blackened on the outside, was attached to the tube opposite these windows. J and J′ were gauze screens to assist in the capture of scattered electrons. H was the electron collector, lined with gauze to counteract secondary emission. At accelerating voltages above 50 v, H was made 2–4 v positive to the collision box in order to collect slow secondary electrons. M and M′ were two coils coaxial with the tube, which give a longitudinal magnetic field of the order of 10 gauss in the collision region, which further collimates the electron beam into H. All the electrodes were constructed of nickel which had been previously outgassed in a vacuum by induction heating.

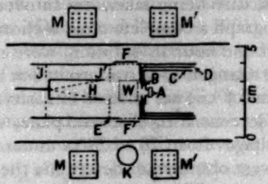

Figure 1. Electrode system for electron collision apparatus. The envelope was Pyrex.

The tube was operated in a continuously flowing stream of gas from a cylinder of commercial nitrogen. The pressure could be controlled by a needle valve, and in general was of order of 3×10^{-3} mm Hg. Mercury was excluded from the tube by traps cooled with liquid oxygen, and no bands or lines other than those from nitrogen were observed.

Contact potentials were checked by setting the plates F F′ mounted above grids in the collision box 40 v negative to E, and measuring the positive ion current to them for electron accelerating voltages from 12 to 30 v, at constant pressure and current. The resultant curve of positive ion current plotted against accelerating voltage had an appearance potential of 16 v, corresponding to the formation of N_2^+ ions in the $x^2\Sigma_g^+$ state, whilst a further break occurred at 24·5 v, usually taken to correspond to the formation of N^+ ions by dissociative ionization ; these are so close to the standard values (15·7 ± 0·2 v and 24·3 ± 0·2 v) (Hagstrum 1951) that contact potential differences can therefore be disregarded.

The use of currents from 1×10^{-5} amp to 2×10^{-4} amp did not affect the observed values of accelerating voltage at which the formation of N_2^+ and N^+ began, indicating that the space charge effects of the electron beam are small. A further test for the absence of space-charge effects can be made, as, if present they would lead to a non-proportionality of light intensity to beam current, which was not found.

The electron energy distribution in the beam was determined by applying retarding potentials between H and E. Due to disturbing effects, such as secondary emission and changes in the positive ion space charge around the collector, these retarding runs only give an upper limit to the inhomogeneity of electron energies in the beam. However, they did show that, after passing through the collision region, at least 90% of the electrons lay within a 5 v range of the applied accelerating voltage, for the range of the latter used in the present experiments.

2.2. *Measurement of Intensities*

The (density, log intensity) curve of each plate was determined in the following manner. A small disc of glass (K, figure 1) ground on both sides, was placed directly beneath the viewing window and illuminated by a 6 v 18 w tungsten filament lamp, run at a constant current. This lamp was mounted on an optical bench placed at about 20° to the collimator of a f/9 Hilger constant deviation spectrograph. Varying the distance of the lamp from K and using the inverse square law, different known relative intensities of continuous spectra could thus be obtained from the disc.

The beam and illuminated disc were focused on the slit of the spectrograph with a large aperture lens, care being taken not to overfill the collimator of the spectrograph and to photograph a complete cross section of the beam.

Seven exposures, each one hour in duration, were made on each plate, each exposure consisting of the nitrogen spectrum excited at a certain electron energy, and a continuous spectrum of known relative intensity. Two principal sets of plates were obtained, each set consisting of several plates with exposures taken over a range of accelerating voltages from 20 to 200 v at constant pressure and beam current. Further plates were obtained to determine the dependence of intensity on beam current and pressure. The plates were hypersensitized and developed under standardized conditions.

At wavelengths corresponding to the N I lines at 8200 Å, the (3, 1) and (2, 0) Meinel bands of N_2^+, and the (2, 0) first positive band, inverse calibration curves (Sawyer 1944) were plotted from the microphotometer traces of the continuous spectra of each plate. Over a range of intensity of factor 8 the majority of the points lay on straight lines.

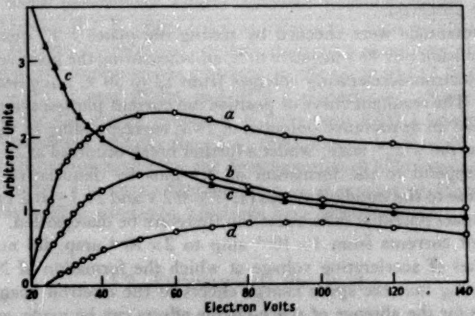

Figure 2. Electron excitation functions (ordinates) in arbitrary units for: *a*, the (2, 0) Meinel band; *b*, the (3, 1) Meinel band; *c*, the (2, 0) first positive band; and *d*, the blended N I lines at 8216–8200 Å. Abscissae are electron energies in electron volts.

A number of microphotometer traces were obtained of the cross sections of the bands and lines. It was found that the width of the electron beam remained at a constant value of about 5 mm to within 5% or better over the complete range of accelerating voltages. It was therefore decided that peak heights of the microphotometer traces gave a true measure of relative intensities.

Graphs of intensity of the bands and lines in arbitrary units plotted against accelerating voltage are shown in figure 2, for the case where the pressure was $3{\cdot}1 \times 10^{-3}$ mm Hg and the beam current 4×10^{-4} amp. Results indistinguishable from those shown in figure 2 were obtained from the second principal set of plates, for which the pressure was $2{\cdot}1 \times 10^{-3}$ mm Hg and the beam current $4{\cdot}4 \times 10^{-4}$ ampere.

§ 3. Discussion of Results

3.1. *Meinel Bands of* N_2^+

At electron energies below 24 v the N_2^+ bands were masked by the (6, 5) and (7, 6) first positive bands, but by extrapolation their appearance potentials were found to be 18 v, in reasonable agreement with values calculated from wavelength measurements (Dalby and Douglas 1951). These N_2^+ bands show direct proportionality of intensity to both current and pressure, indicating that secondary mechanisms of excitation are of little importance in their production. The ratio of intensity of the (3, 1) band to the (2, 0) band was definitely less than unity. This would be expected from Bates's tables (1952) of Franck–Condon factors, if the process of excitation of the $\mathrm{A}^2\Pi$ state was, as has been assumed,

$$N_2(\mathrm{X}^1\Sigma_g^+) + e \rightarrow N_2^+(\mathrm{A}^2\Pi) + 2e,$$

but not if it had been

$$N_2^+(\mathrm{X}^2\Sigma_g^+) + e \rightarrow N_2^+(\mathrm{A}^2\Pi) + e,$$

for which the ratio calculated from these tables is 1·5.

The broad peak of the excitation function at approximately four times the excitation potential is in accord with the changes in electron configuration in the first process.

3.2. N I *Lines*

Because of their relatively small intensity most of the points obtained for these lines did not lie on the straight line portions of the calibration curves, which makes the results for their excitation function less certain than for the Meinel bands. At pressures less than 10^{-2} mm Hg the intensity of the lines was directly proportional to both current and pressure, indicating that they were mainly produced by single electron impact with N_2 molecules in the $\mathrm{X}^1\Sigma_g^+$ ground state. At pressures above 10^{-2} mm Hg there was, however, some evidence that cumulative effects were occurring.

In the lower pressure range the N I lines were observed for electron energies as small as 24 v and possibly 1 v lower. This is not incompatible with an energy of dissociation of 9·76 ev for $\mathrm{X}^1\Sigma_g^+$ N_2 and an excitation potential of 11·8 v for the $3p^4P^0$ state from the ground state of N, from which the appearance potential of the N I lines could, on purely energetic grounds, be as low as 21·6 v.

3.3. *First Positive Bands*

The maximum of the curve (intensity, accelerating voltage) for the (2, 0) band is believed from previous work (Langstroth 1934) to be at about 15 v. The present results support this, showing a smooth fall off in intensity as the voltage is increased. The intensity of the band was found to be directly proportional to current, but not, at the higher pressures used, to the pressure. This is probably related to the fact that the light of the first positive bands is partly emitted from well outside the electron beam (Thompson and Williams 1934, Stewart, Gribbon and Emeléus 1954).

ACKNOWLEDGMENTS

The author wishes to thank Professor K. G. Emeléus for suggesting and supervising this work, Dr. R. H. Sloane for advice on many points, and Professor D. R. Bates for many stimulating discussions.

REFERENCES

BATES, D. R., 1952, *Mon. Not. R. Astr. Soc.*, **112**, 614.
DALBY, F. W., and DOUGLAS, A. E., 1951, *Phys. Rev.*, **84**, 843.
HAGSTRUM, H., 1951, *Rev. Mod. Phys.*, **23**, 185.
LANGSTROTH, O., 1934, *Proc. Roy. Soc.* A, **146**, 167.
SAWYER, R. A., 1944, *Experimental Spectroscopy* (New York : Prentice-Hall, Inc.).
STEWART, D. T., GRIBBON, P. W. F., and EMELÉUS, K. G., 1954, *Proc. Phys. Soc.* A, **67**, 188.
THOMPSON, N., and WILLIAMS, S. E., 1934, *Proc. Roy. Soc.* A, **147**, 583.

Measurements of the Momentum Spectrum of μ-Mesons at Sea Level

I: The Momentum Range 5×10^8 ev/c–2×10^{10} ev/c

By B. G. OWEN† and J. G. WILSON‡

† The Physical Laboratories, University of Manchester
‡ University of Leeds

MS. received 9th November 1954

Abstract. The μ-meson momentum spectrum near sea level in 57° N geomagnetic latitude has been measured for strictly defined angles of collection near the vertical direction. Results are given, covering the momentum range $5\times10^8\,\text{ev/c}<p<2\times10^{10}\,\text{ev/c}$, which are based on the measurement of about 60 000 trajectories.

---

§ 1. Introduction

The development of direct instrumental methods for measuring the magnetic deflection of particle trajectories, the so-called magnetic spectrographs, has made possible significant improvements in our knowledge of the sea-level cosmic-ray flux. A measurement of the vertical proton flux, made with the Manchester spectrograph, has already been described (Mylroi and Wilson 1951), while the Melbourne team has published a hard particle spectrum which differs considerably from that adopted by Rossi in 1948.

Measurements of the hard particle spectrum using the Manchester spectrograph have been undertaken in two stages: the first, dealing with the spectrum at moderate momenta ($5\times10^8\,\text{ev/c}<p<2\times10^{10}\,\text{ev/c}$) where the relevant particles are abundant, and the second dealing with the spectrum at higher momenta ($p>2\times10^{10}\,\text{ev/c}$) for which the available supply of particles is much scantier and the difficulties of measurement are greater. The results of the first part of the work are given in this paper while those of the second are given in a succeeding paper.

The main advantages shown by the magnetic spectrographs over the earlier methods involving curvature measurements in a cloud chamber lie in the higher rate of collection which is possible, and in the fact that both the directional description of the accepted particle beam as a whole and the relative efficiency with which particles of different momenta are registered are strictly defined in terms of the geometry of the apparatus. Moreover, difficulties of selection of material do not arise in the way in which they affect a cloud chamber spectrum determination. In a cloud chamber it is necessary to reject certain tracks either on account of technical poorness of the photograph or because of the presence of non-circular track distortions comparable in magnitude to the curvature of the track as a whole. Unless exceptional measures are taken, the criteria of rejection will be momentum-sensitive, and it is not clear that in any of the cloud chamber work these criteria have been completely independent of momentum.

In the present work, the spectrum refers to particles with trajectories the great majority of which lie within 10° from the vertical: the spectrum is accordingly described as that of the vertical flux at Manchester (50 m altitude, geomagnetic latitude 57° N).

§ 2. Principle of the Spectrum Determination

The spectrum determination with the counter spectrograph (with which this paper is concerned) uses the apparatus in the form described by Hyams *et al.* (1950), and the application will be discussed in terms of the treatment given there.

The instrument does not assign a particular momentum to each measured particle, but rather assigns each particle to a certain 'momentum category' which covers a finite range of momenta and within which the accepted spectrum of particles is a function of the incident particle spectrum and of a geometrical factor which is discussed in § 2.1 of the paper by Hyams and his colleagues. The data from which our spectrum is now derived consist of relative numbers of particles observed in the various momentum categories. These must be related to the respective accepted spectra of the momentum categories but they must also be related to the relative efficiency of collection as between momentum categories.

The relative efficiency of collection in given momentum categories is a further factor which is defined by the geometry of the apparatus. The counts in a single momentum category are made up of counts from a number of channels each of which is defined by three particular counters, one in each of the three measuring levels of the spectrograph. The essential unit of counting is such a channel, and the differing relative efficiencies of collection from one momentum category to another arise because different numbers of unit channels are available for the various momentum categories. We therefore count the number of particles recorded in a given momentum category and reduce this to the number of counts per unit channel in this category. It is this quantity which is characteristic of the integral over the accepted spectrum of particles falling into the particular momentum category.

To derive the incident spectrum, it is convenient to adopt an analytical trial, or comparison, spectrum which does not differ greatly from the actual incident spectrum, and to compare the actual counts per unit channel in a given momentum category with that to be expected had the incident spectrum been of the form of the comparison spectrum. In this way a series of small and slowly varying differences between the actual incident spectrum and the comparison spectrum are established from category to category.

We have adopted, for the comparison spectrum, a form based on the first-order approximation to the process of formation of the sea-level μ-meson component. At the energies under investigation, it is improbable that the intermediate phase between the initiating nuclear encounter and the eventual creation of a μ-meson is important, and the uncertain factors in setting down a suitable comparison spectrum are the actual μ-meson spectrum at formation, the effective height of formation and, to a lesser extent, the mass distribution of the atmosphere between the height of formation and sea level. For the present purpose reasonable values of the latter factors have been adopted; the assumed spectrum at formation at a single altitude has then been adjusted to bring the comparison spectrum into approximate agreement with the measured spectrum.

The comparison spectrum is, accordingly,

$$S(p) = P(t,p)\, S_t(p+p_t)$$

where $S(p)$, the sea-level spectrum, is given in terms of the effective spectrum of formation S_t at atmospheric depth t, and of the survival probability, $P(t,p)$, of a meson existing at depth t to reach sea level with momentum p. The survival probability $P(t,p)$ is

$$P(t,p)=\left\{\frac{t_0}{t}\left(1+\frac{p_0}{p}\right)-\frac{p_0}{p}\right\}^{-(h/c\tau)[\mu c/(p+p_0)]}$$

where t_0 is the total mass thickness of the atmosphere, p_0 is the ionization loss through the atmosphere, h the scale height of the atmosphere, and τ, μ the lifetime and mass of the μ-meson. We have used the following values of the constants: $t/t_0=10$, $p_0=2{\cdot}28\times10^9$ ev/c, $h=7{\cdot}02$ km, $\tau=2{\cdot}15\times10^{-6}$ sec, $\mu=215\,m_e$, together with the spectrum at formation

$$S_t(p+p_t)\sim(p+p_t)^{-\gamma}$$

where $p_t=(1-t/t_0)p_0=2{\cdot}05\times10^9$ ev/c, $\gamma=2{\cdot}85$. Since effective production of mesons has been assumed to take place at the 100 mb level, the scale height is based on the height to this level over the time of the experiment as given in published meteorological data.

The deviations of the actual incident spectrum from the comparison spectrum defined in this way will be shown to be small. They are never greater than ±7% through the whole accessible spectrum and vary slowly with momentum. The deviations may accordingly, to the accuracy of the experiment as a whole, be regarded as constant over the momentum spread of a single momentum category.

§ 3. THE GEOMETRICAL CHARACTERISTICS OF THE APPARATUS

3.1. *The Angular Distribution of the Measured Particles*

The particles of a given momentum category (and of given sign) enter the apparatus in a cone of semi-angle about 1° in the E–W plane and of semi-angle varying up to about 8° in the N–S plane. The mean zenith angle of the cone varies from 2° for category 0 particles to 5° for category 7 particles and 9° for category 12 particles. Thus, while 50% of category 0 particles are within 2°, and all are within 8°, of the zenith, category 7 particles fall on average 5° from the zenith, and may come from an inclination of as much as 10° to the vertical.

The correction to the measured spectrum arising because the particles in the low-momentum categories are collected from a direction inclined to the vertical is small but significant to the accuracy of the present work. The numerical data given below have throughout been corrected on the assumption of a $\cos^2\theta$ angular distribution for the particles concerned; if, as some recent work suggests (Kraushaar 1949, Zar 1951, Voisin 1951, Quercia and Rispoli 1953), the angular distribution for mesons of low momentum near the zenith is more nearly $\cos^3\theta$ the intensities in table 4 at the lowest momenta will be increased by about 1·5%.

The mean angles of collection for the various categories are shown in table 1 and the zenith angle correction is incorporated in the last column of that table.

3.2. *The Effective Number of Unit Counter Channels in a Momentum Category*

The actual number of counters comprising each of the three 'measuring levels' (Hyams *et al.* 1950) gives a certain maximum number of combinations of counters corresponding to a given trajectory deflection, and so to a maximum number of unit channels within the momentum category defined by this deflection. The effective number of unit channels is reduced below this maximum by the additional condition, imposed by 'defining counters', that the trajectory shall pass through a sufficiently uniform part of the deflecting magnetic field. The uncertainty of the effective number of channels arises because of the uncertainty in length of the active volume of the defining counters.

The active length of the defining counters is derived from the internal evidence of selected categories and is obtained in this way to ± 0·2 cm. Since a change of length of defining counters either increases or decreases the number of effective channels for *all* momentum categories, the *relative efficiencies* of different categories only undergo a second-order change. The indefiniteness of length of the defining counters given above leads to uncertainty of the relative efficiency of different momentum categories of the order of ± 1%. For the purpose of the present work this accuracy is entirely adequate; for a more precise spectrum determination it would be necessary to establish the 'gate', which is now placed for the particle trajectories in the region of the deflecting magnetic field by means of defining counters, to a correspondingly increased precision.

3.3. *The Equivalence of Counter Channels*

The description of the relative efficiency of the different momentum categories in terms of the number of effective unit channels implicitly assumes that the actual counter channels may be regarded as identical. However, these channels are certainly not identical; there are slight differences in the dimensions of the counters forming the three measuring levels; it is also likely that from time to time one or more counters may have deteriorated or may have been operated inefficiently.

The justification for treating all channels as of equal collecting properties can be demonstrated if it is noted that the counting rate of a single channel involves the product of three factors, one connected with each of the counters comprising the channel, and that each counter participates in many channels spread over all momentum categories. Hence the effect of the presence of an abnormal counter appears in all momentum categories, and it is only to the extent of the difference of frequency in which it enters into various categories that it will affect their relative efficiency.

The estimated variation of effective area of the counters used in the measuring layer is ± 3%. Assuming a normal distribution of variation of area of this magnitude, detailed computation of the actual frequency in which particular counters contribute shows that the relative efficiency of categories 0 to 8 will be uncertain to less than 0·3% while the uncertainty up to category 12 will be a little greater, but still small compared with the statistical errors of the data given below.

3.4. *Numerical Values of the Geometrical Characteristics*

The geometrical factors which define the relative efficiencies of collection in the various momentum categories are summarized in table 1.

§ 4. EXPERIMENTAL DATA

Measurements were made at three values of the deflecting magnetic field. This procedure allows a particular part of the momentum scale to be investigated using different momentum categories and in this way affords some check of the efficiencies assigned to these categories in the previous section. The data are summarized in table 2.

Table 1

(1)	(2)	(3)	(4)	(1)	(2)	(3)	(4)
0	2	73·2	2·00	8	6	45·3	1·63
1	—	72·8	1·01	9	—	39·5	1·87
2	—	70·3	1·04	10	7	34·6	2·14
3	3	67·3	1·09	11	—	29·5	2·51
4	—	63·8	1·15	12	9	25·5	2·93
5	4	59·8	1·23	13	—	21·2	3·54
6	—	55·5	1·32	14	10	18·0	4·22
7	—	50·6	1·45	15	—	14·0	5·40

(1) Momentum category; (2) mean zenith angle of collection (deg); (3) effective number of unit channels; (4) reciprocal of relative efficiency.

In table 3, the last column of table 2, which represents the number of counts in a vertical unit channel for the appropriate momentum category over an arbitrary time interval, is related to the calculated number of counts to be expected if the incident spectrum had the form adopted in the comparison spectrum. (The comparison spectrum is computed at arbitrary intensity, but the relative intensities for the three values of deflecting field have been adjusted to correspond to the total numbers of particles of momentum greater than 10^9 ev/c which have actually been observed in each.)

The values of the last column (table 3) are plotted as a function of momentum in figure 1 together with a smooth curve which will be used in the discussion of the spectrum.

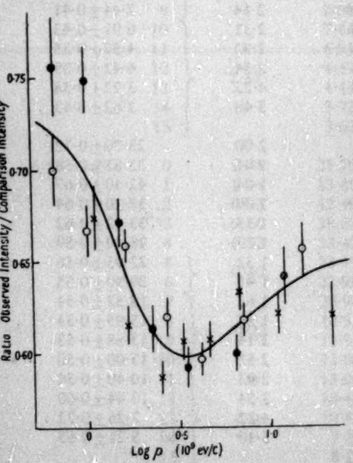

Figure 1. Deflecting field: ● 2·9 $\times 10^5$ gauss cm,
○ 3·35 $\times 10^5$ gauss cm,
× 6·15 $\times 10^5$ gauss cm.

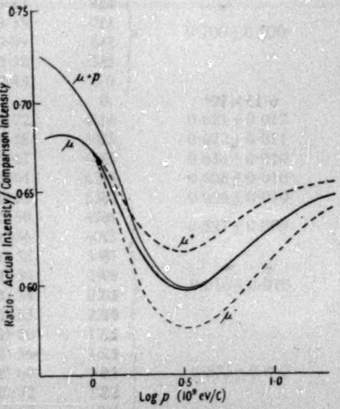

Figure 2. Spectra, as a function of the comparison spectrum, for the total hard component $\mu+p$, for the total meson component μ, and for negative and positive mesons separately.

Table 2. Experimental Material for Spectrum Determination

(1)	(2)	(3)	(4)	(5)
$2{\cdot}9 \times 10^5$	0	1644	2·00	32·88±0·82
	1	3543	1·01	35·61±0·60
	2	3075	1·04	32·00±0·57
	3	2217	1·09	24·10±0·51
	4	1490	1·15	17·10±0·45
	5	1173	1·23	14·40±0·42
	6	809	1·32	10·70±0·37
	7	598	1·45	8·70±0·35
	8	407	1·63	6·62±0·33
	9	275	1·87	5·13±0·32
	10	238	2·14	5·09±0·32
	11	154	2·51	3·87±0·30
	12	97	2·93	2·84±0·29
$3{\cdot}35 \times 10^5$	0	1958	2·00	39·20±0·88
	1	4235	1·01	42·56±0·65
	2	3915	1·04	40·80±0·66
	3	3102	1·09	33·70±0·61
	4	2333	1·15	26·80±0·55
	5	1702	1·23	20·90±0·50
	6	1136	1·32	15·03±0·45
	7	933	1·45	13·58±0·45
	8	624	1·63	10·13±0·41
	9	423	1·87	8·08±0·39
	10	348	2·14	7·44±0·41
	11	275	2·51	6·91±0·43
	12	156	2·93	4·57±0·35
	13	125	3·54	4·43±0·39
	14	88	4·22	3·72±0·38
	15	67	5·40	3·62±0·43
$6{\cdot}15 \times 10^5$	0	1285	2·00	25·70±0·72
	1	3368	1·01	33·85±0·58
	2	4063	1·04	42·40±0·67
	3	3509	1·09	38·20±0·64
	4	2911	1·15	33·42±0·62
	5	2321	1·23	28·49±0·59
	6	1735	1·32	22·95±0·56
	7	1444	1·45	20·90±0·55
	8	1139	1·63	18·52±0·54
	9	855	1·87	15·95±0·54
	10	640	2·14	13·68±0·53
	11	517	2·51	13·00±0·50
	12	355	2·93	10·40±0·56
	13	295	3·54	10·44±0·60
	14	172	4·22	7·26±0·72
	15	152	5·40	8·21±0·65

(1) Deflecting field (gauss cm); (2) momentum category; (3) number of particles recorded; (4) reciprocal efficiency function; (5) intensity per channel in arbitrary time interval.

Table 3. Relation of Experimental Counting Rates to a Comparison Spectrum of Index −2·85

(1)	(2)	(3)	(4)	(5)	(6)
2·9 $\times 10^5$	0	1·08	32·88 ± 0·82	51·2	0·642 ± 0·016
	1	0·81	35·61 ± 0·60	59·4	0·600 ± 0·010
	2	0·54	32·00 ± 0·57	54·0	0·593 ± 0·011
	3	0·35	24·10 ± 0·51	39·3	0·614 ± 0·013
	4	0·18	17·10 ± 0·45	27·1	0·672 ± 0·013
	5		14·40 ± 0·42	19·4	
	6	0·00	10·70 ± 0·37	15·1	0·749 ± 0·018
	7		8·70 ± 0·35	11·4	
	8		6·62 ± 0·33	8·5	
	9	$\bar{1}$·82	5·13 ± 0·32	7·2	0·756 ± 0·027
	10		5·09 ± 0·32	6·0	
	11		3·87 ± 0·30	4·9	
	12		2·84 ± 0·29	4·2	
3·55 $\times 10^5$	0	1·18	39·20 ± 0·88	59·9	0·657 ± 0·014
	1	0·85	42·56 ± 0·65	68·9	0·618 ± 0·009
	2	0·62	40·80 ± 0·66	68·6	0·596 ± 0·009
	3	0·43	33·70 ± 0·61	54·5	0·620 ± 0·011
	4	0·21	26·80 ± 0·55	40·6	0·658 ± 0·009
	5		20·90 ± 0·50	30·8	
	6		15·03 ± 0·45	24·2	
	7	0·00	13·58 ± 0·45	19·7	0·667 ± 0·014
	8		10·13 ± 0·41	15·5	
	9		8·08 ± 0·39	12·6	
	10	$\bar{1}$·82	7·44 ± 0·41	10·3	0·700 ± 0·020
	11		6·91 ± 0·43	9·2	
	12		4·57 ± 0·35	7·3	
	13		4·43 ± 0·39	6·5	
	14		3·72 ± 0·38	5·6	
	15		3·62 ± 0·43	5·0	
6·15 $\times 10^5$	0	1·34	25·70 ± 0·72	41·4	0·621 ± 0·017
	1	1·04	33·85 ± 0·58	54·5	0·622 ± 0·011
	2	0·83	42·40 ± 0·67	66·9	0·634 ± 0·010
	3	0·66	38·20 ± 0·64	62·9	0·608 ± 0·010
	4	0·52	33·42 ± 0·62	55·2	0·606 ± 0·010
	5	0·40	28·49 ± 0·59	47·4	0·587 ± 0·009
	6		22·95 ± 0·56	40·5	
	7	0·22	20·90 ± 0·55	34·7	0·616 ± 0·010
	8		18·52 ± 0·54	29·8	
	9		15·95 ± 0·54	27·5	
	10		13·68 ± 0·53	22·0	
	11	0·04	13·00 ± 0·50	19·1	0·673 ± 0·017
	12		10·40 ± 0·56	16·9	
	13		10·44 ± 0·60	14·8	
	14		7·26 ± 0·72	12·8	
	15		8·21 ± 0·65	9·4	

(1) Deflecting field (gauss cm); (2) momentum category; (3) log *p* (10^9 ev/c); (4) measured rate; (5) calculated rate; (6) ratio of rates: measured/calculated.

§ 5. DERIVATION OF SPECTRUM AND DISCUSSION OF RESULTS

The spectrum described by the data of figure 1 is that of vertical particles with the exclusion of electrons. Electrons are eliminated by placing a ½ in. lead layer over the spectrograph; the number of electrons, which is already small at the momenta covered in the present work, is then still further reduced by degradation of energy in this layer and electrons may also be rejected on account of multiple discharges in the top layer of the spectrograph.

In figure 2 following Mylroi and Wilson (1951), the smoothed curve of figure 1 is corrected for the presence of protons, while in this diagram also the difference of spectrum for the positive and negative meson components is estimated using values of the ratio of positive and negative particles given by the full line in the diagram of Owen and Wilson (1951).

The curve including particles of both signs but excluding protons has been used to derive the adopted form of the spectrum given in table 4. Our measurements do not lead to a reliable value of the absolute intensity of the spectrum, and so in table 4 it has been normalized at momentum 10^9 ev/c to the value adopted by Rossi (1948) : $2{\cdot}45 \times 10^{-6}$ particles cm^{-2} sec^{-1} sterad^{-1} (Mev/c)$^{-1}$.

Table 4. Derivation of the Vertical Intensity of μ-Mesons as a Function of Momentum

(1)	(2)	(3)	(4)	(5)
0·5	1·577	0·676	1·065	2·72
0·6	1·570	0·680	1·068	2·72
0·8	1·518	0·682	1·035	2·64
1·0	1·417	0·677	0·959	2·45†
1·2	1·313	0·663	0·869	2·22
1·4	1·201	0·645	0·775	1·98
1·6	1·096	0·631	0·692	1·77
2·0	0·908	0·611	0·555	1·42
2·5	0·722	0·599	0·432	1·10
3	0·577	0·596	0·344	0·878
4	0·384	0·598	0·230	0·587
5	0·266	0·605	0·161	0·410
7	0·143	0·618	0·0883	0·225
10	0·0677	0·630	0·0426	0·109
15	0·0267	0·642	0·0171	0·0436
20	0·0131	0·647	0·0085	0·0220

† Normalization point.

(1) $p(10^9$ ev/c); (2) $S(p)_{\text{comp.}}$; (3) relative correction factor (figure 2); (4), (5) $S(p)_{\text{incid.}}$ (cm^{-2} sec^{-1} sterad^{-1} (Mev/c)$^{-1}$); (4) unnormalized, (5) normalized ($\times 10^6$).

It will be useful to compare the spectrum now derived with forms which have been adopted by other workers and which have been widely referred to.

The earlier work is summarized in a form given by Rossi (1948, p. 543), who took into consideration both direct measurements of momentum spectrum and the information to be deduced from range measurements to great depths in the earth. Rossi gives his estimate of the probable form of the spectrum in a curve which has been very widely used. We compare our spectrum with values read from the published curve; since our results do not include an absolute intensity of the particle flux we have fitted them for purposes of comparison with Rossi's curve at

$p = 10^9$ ev/c, ($S(p) = 2{\cdot}45 \times 10^{-6}$ particles cm^{-2} sec^{-1} sterad^{-1} (Mev/c)$^{-1}$), and the existing uncertainty concerning this absolute intensity (York 1952) will apply to the values quoted for the present work.

The spectrum given by Caro, Parry and Rathgeber (1951) was obtained at Melbourne using an instrument similar in principle to the Manchester spectrograph, and of resolution greater than that used in this first part of the Manchester work. Caro's spectrum is based, as is the present work, on near-vertical particle trajectories, and measurements upon upwards of 6000 are included. In addition to the published curve we have had at our disposal numerical values of the various measured points on the spectrum which were kindly supplied to one of us (J. G. W.) by Dr. Rathgeber.

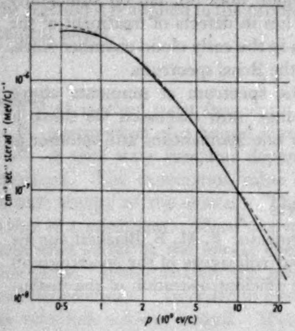

Figure 3. The adopted spectrum of this work (full line) and the Rossi spectrum (broken line). Curves fitted at $p = 10^9$ ev/c.

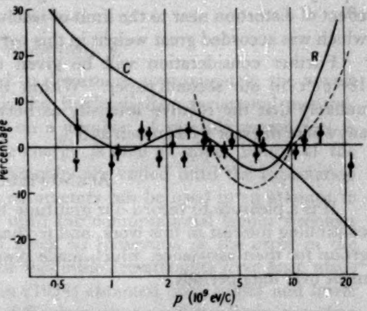

Figure 4. Deviations of other measurements from the spectrum of table 4. C : Caro *et al.*, R : Rossi, broken line : Glaser *et al.*

Spectrum measurements in which the total deflection of particles in the magnetic field is observed in cloud chambers placed above and below the pole gap have been reported by Glaser, Hamermesh and Safonov (1950). While the statistical accuracy of their work is not high (only about 1500 trajectories were measured), a useful analytical approximation is given : $S(p) \sim p^{-x}$, where $x = 1{\cdot}8 \pm 0{\cdot}2$, $2{\cdot}5 \times 10^9$ ev/c $< p < 10^{10}$ ev/c ; $x = 2{\cdot}1 \pm 0{\cdot}6$, 10^{10} ev/c $< p$, and we compare this approximation with our measurements.

In so far as the work incorporated in these publications is based upon direct observations of magnetic deflection, it is not of great statistical weight as compared with the present measurements which are based on about 60,000 trajectories.

Our spectrum is compared with the Rossi spectrum in figure 3 and in figure 4 the deviations of the Rossi, Caro and Glaser spectra from that now determined are given as percentages. The measured points upon which our spectrum is based are included in figure 4 to illustrate the statistical uncertainty of the adopted line. The discontinuity in the deviation of the Glaser spectrum from our adopted value arises from the analytical form of his approximation.

Over the range 7×10^8 ev/c $< p < 11 \times 10^9$ ev/c the agreement between the Rossi spectrum and our own is striking, no difference greater than ±6% being found, but at lower momenta our spectrum is markedly flatter than that adopted by Rossi, with a maximum between 5×10^8 and 6×10^8 ev/c rather than between 4×10^8 and 5×10^8 ev/c. Even here, however, the difference does not exceed about 10%. At the lower momenta, the approximation of Glaser is not relevant, while the Caro spectrum shows a strong excess of low energy particles.

Between $p = 10^{10}$ ev/c and $p = 2 \times 10^{10}$ ev/c, there is a very considerable difference between the spectra of Rossi and of Caro. The Glaser approximation is in general accord with Rossi's spectrum but the statistical precision of the actual measurements of Glaser and his colleagues is low, and these are quite consistent with our spectrum. In this range our spectrum falls between those of Rossi and of Caro and rather closer to the latter. It seems likely that the actual measurements of Caro *et al.* are, like those of Glaser, consistent with our spectrum. There can be little doubt that the Rossi spectrum in this region does not fall off sufficiently rapidly with momentum; the reason probably lies in defects of treatment of the effect of distortion near to the limit of resolution in the early cloud chamber work, which was accorded great weight in this part of the Rossi spectrum.

Further consideration will be given to the spectrum at momenta above 10^{10} ev/c in our second paper. Within the range now discussed we think it unlikely that the relative intensity as between one momentum and another is anywhere in error by as much as 5%.

ACKNOWLEDGMENTS

It is a pleasure to record our gratitude to Professor P. M. S. Blackett for his continuing interest in this work, and to thank our colleagues of the spectrograph group for their assistance, which made possible efficient operation of the instrument over long periods.

REFERENCES

CARO, D. E., PARRY, J. K., and RATHGEBER, H., 1951, *Aust. J. Sci. Res.* A, **4,** 16.
GLASER, D. A., HAMERMESH, B., and SAFONOV, G., 1950, *Phys. Rev.*, **80,** 625.
HYAMS, B. D., MYLROI, M. G., OWEN, B. G., and WILSON, J. G., 1950, *Proc. Phys. Soc.* A, **63,** 1053.
KRAUSHAAR, W. L., 1949, *Phys. Rev.*, **76,** 1045.
MYLROI, M. G., and WILSON, J. G., 1951, *Proc. Phys. Soc.* A, **64,** 404.
OWEN, B. G., and WILSON, J. G., 1951, *Proc. Phys. Soc.* A, **64,** 417.
QUERCIA, I. F., and RISPOLI, B., 1953, *Nuovo Cim.*, **10,** 357.
ROSSI, B., 1948, *Rev. Mod. Phys.*, **20,** 537.
VOISIN, A. G., 1951, *Phys. Rev.*, **84,** 850.
YORK, C. M., 1952, *Phys. Rev.*, **85,** 998.
ZAR, J. L., 1951, *Phys. Rev.*, **83,** 761.

A Variation-Perturbation Method : I

By L. COHEN
Mathematics Department, Durham Colleges, University of Durham

Communicated by L. Rosenfeld ; MS. received 19*th August* 1954

Abstract. A perturbation procedure is used to improve to any order the approximate value obtained by the Rayleigh–Ritz variational method for the lowest eigenvalue of the one-dimensional Schrödinger equation. As an illustration of the method it is applied to the problem of the binding energy of the deuteron using central forces.

---

§ 1. INTRODUCTION

THE method most frequently used to determine approximately the lowest energy level of a bound system is the Rayleigh–Ritz variational method. A trial wave function depending on a number of variable parameters is assumed. The expectation value of the energy is then an upper bound of the lowest energy of the system. The parameters are varied until the expectation value is a minimum. More and more parameters can be used in an attempt to approach closer to the lowest energy, until the computational labour becomes too great. Unfortunately the method gives no indication of the error in the calculated value. In order to overcome this difficulty attempts have been made to establish a lower bound. Weinstein (1934) obtained both upper and lower bounds, but in practice the method is difficult to apply and the limits are often too wide to be of any value. Kato (1949) and Temple (1952) developed an elegant method for obtaining a close lower bound, but unfortunately its application depends on knowing a lower bound of the next eigenvalue. In practice this would be difficult to obtain. It is not sufficient, as is done in one example by Temple, simply to evaluate the expectation value in a state orthogonal to that assumed for the ground state. An upper bound of the next eigenvalue may result, as it in fact does in the particular example discussed by Temple.

An important development in perturbation theory has been made by Price (1954) in expressing a perturbed eigenvalue of the one-dimensional Schrödinger equation in terms of an unperturbed wave function. In the present paper Price's results are used to show how the approximation to the lowest energy obtained by the variational method may be improved to any order. Makinson and Turner (1953) indicated a similar, but much more complicated, formulation up to the second order only. The question of the conditions for convergence of the method is not discussed in the present paper.

§ 2. PERTURBATION EXPANSION

We first establish Price's results in a slightly different form which we shall find convenient for later applications. We consider real solutions of the one-dimensional Schrödinger equation in the interval (a, b). The wave function is assumed to vanish at $x=a$ and $x=b$, and at nowhere else in the interval ; that is, for a given one-dimensional equation we consider only the ground state of this equation, although the equation itself could correspond to a state of a system other than its ground state. If ψ_0 is the normalized wave function of the ground state, and E_0 the corresponding energy

$$-\frac{d^2\psi_0}{dx^2}+V(x)\psi_0=E_0\psi_0. \qquad \ldots\ldots(1)$$

Introduce a perturbation $v(x)$ and let the perturbed wave function be ψ, and the perturbed eigenvalue $E_0+\epsilon$, so that

$$-\frac{d^2\psi}{dx^2}+V(x)\psi+v(x)\psi=(E_0+\epsilon)\psi. \qquad \ldots\ldots(2)$$

Now write $$\psi=A(x)\psi_0 \qquad \ldots\ldots(3)$$

where $A(x)$ may have a singularity at $x=a,\ b$, provided that $A\psi_0$ is zero at these points.

Multiply equation (1) by $A(x)$ and subtract from (2). Then on multiplying by ψ_0 we obtain

$$-\frac{d}{dx}\left(\psi_0{}^2\frac{dA}{dx}\right)+vA\psi_0{}^2=\epsilon A\psi_0{}^2. \qquad \ldots\ldots(4)$$

Replace v by λv, and expand ϵ and A formally

$$\epsilon=\sum_1^\infty\lambda^n\epsilon_n,\ A=1+\sum_1^\infty\lambda^nA_n. \qquad \ldots\ldots(5)$$

$$\left.\begin{aligned}\text{Then}\,\psi_0{}^2\frac{dA_n}{dx}&=-\int_a^x[\epsilon_n+\epsilon_{n-1}A_1+\ldots+\epsilon_2A_{n-2}+(\epsilon_1-v)A_{n-1}]\psi_0{}^2dx,\\ \epsilon_n&=-\int_a^b[\epsilon_{n-1}A_1+\ldots+(\epsilon_1-v)A_{n-1}]\psi_0{}^2dx.\end{aligned}\right\}\ldots\ldots(6)$$

Hence

$$\left.\begin{aligned}&\epsilon_1=\int_a^b v\psi_0{}^2dx\ ;\quad \psi_0{}^2\frac{dA_1}{dx}=-\int_a^x[\epsilon_1-v]\psi_0{}^2dx;\\ &\epsilon_2=-\int_a^b\left(\frac{dA_1}{dx}\right)^2\psi_0{}^2dx;\\ &\quad\psi_0{}^2\frac{dA_2}{dx}=-\int_a^x\left[\epsilon_2+\left(\frac{dA_1}{dx}\right)^2\right]\times\psi_0{}^2dx+A_1\frac{dA_1}{dx}\psi_0{}^2;\\ &\epsilon_3=-2\int_a^b\frac{dA_1}{dx}\frac{dA_2{}^*}{dx}\psi_0{}^2dx,\\ &\quad\psi_0{}^2\frac{dA_2{}^*}{dx}=-\int_a^x\left[\epsilon_2+\left(\frac{dA_1}{dx}\right)^2\right]\psi_0{}^2dx=\psi_0{}^2\frac{dA_2}{dx}-\psi_0{}^2A_1\frac{dA_1}{dx}\ ;\end{aligned}\right\}\ldots\ldots(7)$$

and so on.

The relationship between A and Price's Ω is given by

$$A(x)=\exp\int_a^x\Omega(x')dx'. \qquad \ldots\ldots(8)$$

The higher order expressions can be expressed more conveniently in terms of Ω than in terms of A. One can go from one to the other by equating the coefficients of the powers of λ in (8).

§ 3. VARIATION-PERTURBATION METHOD

Suppose now that we wish to obtain the lowest eigenvalue and corresponding wave function of the Schrödinger equation

$$-\frac{d^2\psi}{dx^2}+V(x)\psi=E\psi \qquad \ldots\ldots(9)$$

with the condition that ψ vanishes at the ends of the interval.

We first adopt the variational procedure and take as our trial wave function ϕ_0 depending on some variable parameters. We suppose ϕ_0 is normalized. Then the corresponding expectation value of the energy is

$$E_0 = \int_a^b \left(-\phi_0 \frac{d^2\phi_0}{dx^2} + V\phi_0^2 \right) dx. \qquad \ldots\ldots(10)$$

E_0 will be a function of the variable parameters which can be chosen to minimize E_0.

Now E_0 and ϕ_0 are the *exact* solutions of the Schrödinger equation

$$-\frac{d^2\psi}{dx^2} + \left(\frac{1}{\phi_0}\frac{d^2\phi_0}{dx^2} + E_0 \right)\psi = E\psi. \qquad \ldots\ldots(11)$$

We can start with equation (11) as our unperturbed equation, and add the perturbation

$$v(x) = -\frac{1}{\phi_0}\frac{d^2\phi_0}{dx^2} + V(x) - E_0. \qquad \ldots\ldots(12)$$

The perturbed equation is then the original equation (9) which we wish to solve. Starting with the wave function ϕ_0 and the perturbation $v(x)$, the perturbation expansion of the previous paragraph can now be used to improve the energy value to any degree of approximation, provided that expansion is convergent.

It should be noted that

$$\epsilon_1 = \int_a^b v\phi_0^2 dx = 0. \qquad \ldots\ldots(13)$$

The idea that an approximate wave function and the corresponding expectation value of the energy are the exact solutions of another Schrödinger equation has also been used by Laforgue (1954). (The author is indebted to the referee for drawing his attention to this paper.) Laforgue's perturbation expansion is the usual one requiring a set of orthonormal solutions of the new equation. The present method however, expresses everything in terms of the one initial trial function only. This method is of course directly applicable only to a one-dimensional equation, but other problems can often be reduced to this form in the manner indicated in § 6.

§ 4. EXAMPLE

As an example we consider the simple equation

$$-\frac{d^2\psi}{dx^2} = E\psi \qquad \ldots\ldots(14)$$

with ψ vanishing at $x=0$ and $x=1$. The lowest eigenvalue is then known to be $\pi^2 = 9{\cdot}86961$, and the corresponding eigenfunction is $\sin \pi x$. For the initial normalized trial wave function we take

$$\phi_0 = \sqrt{30}\, x(1-x). \qquad \ldots\ldots(15)$$

The expectation value E_0 is then

$$E_0 = 60\int_0^1 x(1-x)dx = 10, \qquad \ldots\ldots(16)$$

a value already correct to within about 1·3%; and

$$v(x) = -10 + \frac{2}{x(1-x)}. \qquad \ldots\ldots(17)$$

Substituting the numerical values for μ, E_0 we find $\epsilon_2 = -0{\cdot}0154$. Hence to second order the eigenvalue is $E_0 + \epsilon_2 = -0{\cdot}0949$. The third-order terms are much more complicated and involve numerical integration, and so are not considered here. However it is clear that the second-order terms alone bring about a considerable improvement in the calculated value of the energy. Although the initial approximation was in error by about 20%, the value to the second order is in error only by about 5%.

§ 6. DISCUSSION

The method developed in this paper could be applied to a wide variety of problems by using the device adopted by Morpurgo (1952) in the triton and helium binding energy problems with central forces. In a general system it is assumed that the wave function contains as unknown only a single unknown function $\phi(r)$ of a suitably chosen variable r. Calculation of the expectation value of the energy then leads to an integral over r alone, since the dependence of the wave function on the other variables is assumed known. The integrand is a function of ϕ, and so the integral can be considered as providing a variational principle for the determination of ϕ. This leads to a Schrödinger equation for ϕ, and the variation-perturbation method of the present paper can be applied. In nuclear problems with Yukawa forces, trial wave functions of the form $r^n \exp(-\mu r)$ with n integral and $r^2 = \Sigma r_{ij}^2$ (i.e. of the type used by Irving (1951)), will enable the second-order approximation to be evaluated analytically.

REFERENCES

BROMWICH, T. L. I'a., 1942, *Theory of Infinite Series*, 2nd Edn (London : Macmillan).
IRVING, J., 1951, *Phil. Mag.*, **42,** 338.
KATO, T., 1949, *J. Phys. Soc., Japan*, **4,** 334.
LAFORGUE, A., 1954, *C.R. Acad. Sci., Paris*, **238,** 1033.
MAKINSON, R. E. B., and TURNER, J. S., 1953, *Proc. Phys. Soc.* A, **66,** 857.
MORPURGO, G., 1952, *Nuovo Cim.*, **9,** 461.
PRICE, P. J., 1954, *Proc. Phys. Soc.* A, **67,** 383.
ROSENFELD, L., 1948, *Nuclear Forces* (Amsterdam : North Holland).
TEMPLE, G., 1952, *Proc. Roy. Soc.* A, **211,** 204.
WEINSTEIN, D. H., 1934, *Proc. Nat. Acad. Sci., Wash.*, **20,** 529.

A Variation-Perturbation Method : II

By L. COHEN
Mathematics Department, Durham Colleges, University of Durham

Communicated by L. Rosenfeld ; *MS. received* 19*th August* 1954

Abstract. The method developed in a previous paper is extended to simultaneous Schrödinger equations, and is applied to the problem of the binding energy of the deuteron with non-central forces.

---

§ 1. Introduction

In a previous paper (Cohen 1955, hereafter called I) a method is developed applicable to problems in which the wave function can be assumed to contain as unknown only a single function of a suitably chosen variable. In many cases however it is more reasonable to assume that the wave function contains linearly a number of different unknown functions of the same suitably chosen variable r (say); this is particularly so for nuclei with non-central forces. Calculation of the expectation value of the energy will then lead to an integral over r alone, since the dependence of the wave function on the other variables is assumed known, the integrand being a function of the unknown functions. An example of this extension of Morpurgo's (1952) device to the case of helium with non-central forces is given by Clark (1954). Using this integral in a variational principle will yield a number of simultaneous differential equations. In the present paper it is shown how the method of I may be extended to deal with simultaneous Schrödinger equations in one variable. As an illustration the method is applied to the deuteron with non-central forces. In a later paper the problems of triton and helium with non-central forces will be considered.

§ 2. Perturbation Expansion

We first extend the perturbation expansion of I to the case of simultaneous Schrödinger equations. For simplicity only two equations are considered, but the method can readily be extended to more. Let the unperturbed equations be two simultaneous uncoupled Schrödinger equations having the same eigenvalue. They can be represented in the matrix form

$$(\mathbf{H}+\mathbf{V})\mathbf{u}_0=E_0\mathbf{u}_0 \qquad \ldots\ldots(1)$$

where

$$\mathbf{H}=\begin{bmatrix} -\dfrac{d^2}{dx^2} & 0 \\ 0 & -\dfrac{d^2}{dx^2} \end{bmatrix}, \qquad \mathbf{V}=\begin{bmatrix} V_{11}(x) & 0 \\ 0 & V_{22}(x) \end{bmatrix},$$

and

$$\mathbf{u}_0=\begin{bmatrix} a_0\alpha_0(x) \\ b_0\beta_0(x) \end{bmatrix}.$$

We require $\alpha_0(x)$, $\beta_0(x)$ to vanish at the ends of the interval and at nowhere else in the interval. We suppose $\alpha_0(x)$ and $\beta_0(x)$ are normalized. The coefficients a_0 and b_0 are arbitrary since the equations are uncoupled.

Now add the symmetric perturbation $\mathbf{v}(x)$ where

$$\mathbf{v}(x)=\begin{bmatrix} v_{11}(x) & v_{12}(x) \\ v_{21}(x) & v_{22}(x) \end{bmatrix} \qquad \ldots\ldots(2)$$

with $v_{12}=v_{21}$.

Let $E_0+\epsilon$ be the new perturbed eigenvalue, and $\mathbf{u}$ the corresponding eigenfunction. We can write $\mathbf{u}$ in the form

$$\mathbf{u}=\mathbf{A}(x)\mathbf{u}_0 \qquad \ldots\ldots(3)$$

with

$$\mathbf{A}(x)=\begin{bmatrix} A(x) & 0 \\ 0 & B(x) \end{bmatrix}. \qquad \ldots\ldots(4)$$

Here $\mathbf{u}$ is assumed to vanish at $x=a$, $x=b$ but at nowhere else in the interval. $\mathbf{A}(x)$ may have a singularity at the ends of the interval provided $\mathbf{Au}_0$ vanishes there. The perturbed equations are then

$$(\mathbf{H}+\mathbf{V}+\mathbf{v})\mathbf{Au}_0=(E_0+\epsilon)\mathbf{Au}_0. \qquad \ldots\ldots(5)$$

Premultiply equation (1) by $\mathbf{A}$ and subtract from (5). Since

$$(-\mathbf{AH}+\mathbf{HA})\mathbf{u}_0=\begin{bmatrix} -\dfrac{a_0}{\alpha_0}\dfrac{d}{dx}\left(\alpha_0{}^2\dfrac{dA}{dx}\right) \\ -\dfrac{b_0}{\beta_0}\dfrac{d}{dx}\left(\beta_0{}^2\dfrac{dB}{dx}\right) \end{bmatrix}$$

and $(-\mathbf{AV}+\mathbf{VA})\mathbf{u}_0=0$, we obtain, on putting $a_0/b_0=\kappa$, the differential equations

$$\left.\begin{aligned} -\frac{d}{dx}\left(\alpha_0{}^2\frac{dA}{dx}\right)+v_{11}A\alpha_0{}^2+\frac{v_{12}B\alpha_0\beta_0}{\kappa}&=\epsilon A\alpha_0{}^2 \\ -\frac{d}{dx}\left(\beta_0{}^2\frac{dB}{dx}\right)+\kappa v_{21}A\alpha_0\beta_0+v_{22}B\beta_0{}^2&=\epsilon B\beta_0{}^2. \end{aligned}\right\} \qquad \ldots\ldots(6)$$

We can replace $\mathbf{v}$ by $\lambda\mathbf{v}$ and expand formally

$$A=1+\sum_1^\infty \lambda^n A_n, \qquad B=1+\sum_1^\infty \lambda^n B_n, \qquad \epsilon=\sum_1^\infty \lambda^n \epsilon_n. \qquad \ldots\ldots(7)$$

The first-order equations are therefore

$$\left.\begin{aligned} -\frac{d}{dx}\left(\alpha_0{}^2\frac{dA_1}{dx}\right)+v_{11}\alpha_0{}^2+\frac{v_{12}\alpha_0\beta_0}{\kappa}&=\epsilon_1\alpha_0{}^2 \\ -\frac{d}{dx}\left(\beta_0{}^2\frac{dB_1}{dx}\right)+\kappa v_{21}\alpha_0\beta_0+v_{22}\beta_0{}^2&=\epsilon_1\beta_0{}^2. \end{aligned}\right\} \qquad \ldots\ldots(8)$$

For the consistency of these two equations we must have, on integrating from a to b,

$$\epsilon_1=\int_a^b (v_{11}\alpha_0{}^2+v_{12}\alpha_0\beta_0/\kappa)\,dx=\int_a^b (\kappa v_{21}\alpha_0\beta_0+v_{22}\beta_0{}^2)\,dx. \qquad \ldots\ldots(9)$$

This gives a quadratic for κ, and so two values for ϵ_1. Since we will be interested in the lowest eigenvalue we choose the value of κ which gives the smaller value of ϵ_1. Both ϵ_1 and κ are now determined, and so integrating from a to x we have

$$\left.\begin{aligned} \alpha_0{}^2\frac{dA_1}{dx}&=-\int_a^x\left[(\epsilon_1-v_{11})\alpha_0{}^2-\frac{v_{12}\alpha_0\beta_0}{\kappa}\right]dx \\ \beta_0{}^2\frac{dB_1}{dx}&=-\int_a^x[-\kappa v_{21}\alpha_0\beta_0+(\epsilon_1-v_{22})\beta_0{}^2]\,dx. \end{aligned}\right\} \qquad \ldots\ldots(10)$$

The second-order equations are

$$\left.\begin{aligned}-\frac{d}{dx}\left(\alpha_0^2\frac{dA_2}{dx}\right)+v_{11}A_1\alpha_0^2+\frac{v_{12}B_1\alpha_0\beta_0}{\kappa}&=\epsilon_1A_1\alpha_0^2+\epsilon_2\alpha_0^2\\-\frac{d}{dx}\left(\beta_0^2\frac{dB_2}{dx}\right)+\kappa v_{21}A_1\alpha_0\beta_0+v_{22}B_1\beta_0^2&=\epsilon_1B_1\beta_0^2+\epsilon_2\beta_0^2.\end{aligned}\right\}\quad\ldots\ldots(11)$$

Integration from a to b apparently gives two values for ϵ_2. However A_1 and B_1 are only determined up to arbitrary constants of integration. We can therefore determine, at least partially, the constants of integration by requiring that the equations are consistent, i.e. give the same value of ϵ_2. Integrating from a to b, multiplying the first equation of (11) by κ^2 and adding to the second, we have

$$\begin{aligned}(\kappa^2+1)\epsilon_2&=\int_a^b[\kappa^2v_{11}A_1\alpha_0^2+\kappa v_{12}B_1\alpha_0\beta_0+\kappa v_{21}A_1\alpha_0\beta_0+v_{22}B_1\beta_0^2\\&\qquad-\kappa^2\epsilon_1A_1\alpha_0^2-\epsilon_1B_1\beta_0^2]\,dx\\&=\int_a^b\left[\kappa^2A_1\frac{d}{dx}\left(\alpha_0^2\frac{dA_1}{dx}\right)+B_1\frac{d}{dx}\left(\beta_0^2\frac{dB_1}{dx}\right)\right]dx\end{aligned}$$

(from equations (8) provided $v_{12}=v_{21}$)

$$=-\int_a^b\left[\kappa^2\alpha_0^2\left(\frac{dA_1}{dx}\right)^2+\beta_0^2\left(\frac{dB_1}{dx}\right)^2\right]dx,$$

i.e.

$$\epsilon_2=-\frac{1}{a_0^2+b_0^2}\int_a^b\left[a_0^2\alpha_0^2\left(\frac{dA_1}{dx}\right)^2+b_0^2\beta_0^2\left(\frac{dB_1}{dx}\right)^2\right]dx.\quad\ldots\ldots(12)$$

The expressions for the higher order approximations are rather more involved than in the case of the single differential equation. The quantities A_1, B_1 and so on will enter into these expressions but now of course the constants of integration will be sufficiently determined by the requirement of consistency of the equations. For example the difference between the two integration constants occurring in A_1, B_1 is given by

$$\int_a^b\left[v_{12}(B_1-A_1)\frac{\alpha_0\beta_0}{\kappa}\right]dx=\epsilon_2+\int_a^b\left(\frac{dA_1}{dx}\right)^2\alpha_0^2\,dx,$$

and it is this difference which also occurs in the expressions for dA_2/dx, dB_2/dx and ϵ_3.

§ 3. VARIATION-PERTURBATION METHOD

We now consider the coupled Schrödinger equations

$$\left.\begin{aligned}-\frac{d^2\alpha}{dx^2}+V_{11}\alpha+V_{12}\beta&=E\alpha\\-\frac{d^2\beta}{dx^2}+V_{21}\alpha+V_{22}\beta&=E\beta\end{aligned}\right\}\quad\ldots\ldots(13)$$

where $V_{12}=V_{21}$, and α,β vanish at the ends of the interval and nowhere else. In order to find the lowest eigenvalue we first adopt the variational procedure and take as trial wave function

$$\mathbf{u}_0=\begin{bmatrix}a_0\alpha_0\\b_0\beta_0\end{bmatrix}$$

where α_0, β_0 are normalized, vanish only at the ends of the interval, and usually contain variable parameters. The expectation value of the energy is then

$$E_0=\frac{1}{a_0^2+b_0^2}\int_a^b\left[-a_0^2\alpha_0^2\frac{d^2\alpha_0}{dx^2}+a_0^2V_{11}\alpha_0^2-b_0^2\beta_0\frac{d^2\beta_0}{dx^2}+b_0^2V_{22}\beta_0^2\right.$$
$$\left.+2a_0b_0V_{12}\alpha_0\beta_0\right]dx. \qquad \text{......(14)}$$

We wish to minimize E_0 with respect to the coefficients a_0 and b_0, and to the variable parameters occurring in α_0, β_0. Minimization with respect to a_0, b_0 requires

$$\left.\begin{aligned}a_0\int_a^b\left(-\alpha_0\frac{d^2\alpha_0}{dx^2}+V_{11}\alpha_0^2\right)dx+b_0\int_a^b V_{12}\alpha_0\beta_0\,dx&=a_0E_0\\ a_0\int_a^b V_{21}\alpha_0\beta_0\,dx+b_0\int_a^b\left(-\beta_0\frac{d^2\beta_0}{dx^2}+V_{22}\beta_0^2\right)dx&=b_0E_0.\end{aligned}\right\} \qquad \text{......(15)}$$

In other words E_0 is the minimum characteristic root of the matrix

$$\begin{bmatrix}\int_a^b\left(-\alpha_0\frac{d^2\alpha_0}{dx^2}+V_{11}\alpha_0^2\right)dx & \int_a^b V_{21}\alpha_0\beta_0\,dx\\ \int_a^b V_{12}\alpha_0\beta_0\,dx & \int_a^b\left(-\beta_0\frac{d^2\beta_0}{dx^2}+V_{22}\beta_0^2\right)dx\end{bmatrix}. \qquad \text{......(16)}$$

E_0 will also be a function of the other parameters which may be chosen to make E_0 least. This choice of E_0 will determine the ratio $\kappa=a_0/b_0$.

Now E_0 and $\mathbf{u}_0$ are the exact solutions of the uncoupled Schrödinger equations

$$\left.\begin{aligned}-\frac{d^2\alpha}{dx^2}+\left(\frac{1}{\alpha_0}\frac{d^2\alpha_0}{dx^2}+E_0\right)\alpha&=E\alpha\\ -\frac{d^2\beta}{dx^2}+\left(\frac{1}{\beta_0}\frac{d^2\beta_0}{dx^2}+E_0\right)\beta&=E\beta.\end{aligned}\right\} \qquad \text{......(17)}$$

We take equations (17) as the unperturbed equations with eigenvalue and eigenfunction E_0 and $\mathbf{u}_0$, and in order to obtain the initial coupled equations (13) we must add as perturbation

$$\mathbf{v}(x)=\begin{bmatrix}v_{11} & v_{12}\\ v_{21} & v_{22}\end{bmatrix}$$

where

$$\left.\begin{aligned}v_{11}(x)&=-\frac{1}{\alpha_0}\frac{d^2\alpha_0}{dx^2}-E_0+V_{11}(x)\\ v_{22}(x)&=-\frac{1}{\beta_0}\frac{d^2\beta_0}{dx^2}-E_0+V_{22}(x)\\ v_{12}(x)&=V_{12}(x),\quad v_{21}(x)=V_{21}(x)=v_{12}(x).\end{aligned}\right\} \qquad \text{......(18)}$$

Starting with the wave function $\mathbf{u}_0$ and the perturbation $\mathbf{v}(x)$, the perturbation procedure of the previous paragraph can now be applied.

The first order term ϵ_1 will now automatically vanish as a result of our choice of E_0. For consistency we require the coefficients a_0, b_0 to satisfy equation (9), i.e.

$$\begin{aligned}a_0\int_a^b\left(-\alpha_0\frac{d^2\alpha_0}{dx^2}+V_{11}\alpha_0^2\right)dx+b_0\int_a^b V_{12}\alpha_0\beta_0\,dx&=a_0E_0\\ a_0\int_a^b V_{21}\alpha_0\beta_0\,dx+b_0\int_a^b\left(-\beta_0\frac{d^2\beta_0}{dx^2}+V_{22}\beta_0^2\right)dx&=b_0E_0.\end{aligned}$$

But these are precisely the equations (15) which a_0, b_0 satisfy when they are chosen to minimize E_0. Having found κ, E_0 we have

$$\left.\begin{aligned} \alpha_0{}^2\frac{dA_1}{dx} &= \int_a^x \left[-\alpha_0\frac{d^2\alpha_0}{dx^2}+V_{11}\alpha_0{}^2-E_0\alpha_0{}^2+\frac{V_{12}\alpha_0\beta_0}{\kappa}\right]dx \\ \beta_0{}^2\frac{dB_1}{dx} &= \int_a^x \left[-\beta_0\frac{d^2\beta_0}{dx^2}+V_{22}\beta_0{}^2-E_0\beta_0{}^2+\kappa V_{21}\alpha_0\beta_0\right]dx, \end{aligned}\right\} \quad \ldots\ldots(19)$$

and the higher order terms are then obtained as before.

§ 4. DEUTERON WITH NON-CENTRAL FORCES

As an example we deal with the binding energy of the deuteron with tensor forces. This problem has been solved accurately by Feshbach and Schwinger (1951) using the variation–iteration method, but it is instructive to apply the present method to the problem in order to obtain some idea of its accuracy.

The two-body interaction is taken to be of the form

$$V(\mathbf{r}) = -[V_c f(r/r_c)+V_t f(r/r_t)S_{12}], \quad \ldots\ldots(20)$$

with $\mathbf{r}$ the distance between the nucleons,

$$S_{12}=\frac{3(\boldsymbol{\sigma}_1\,.\,\mathbf{r})(\boldsymbol{\sigma}_2\,.\,\mathbf{r})}{r^2}-(\boldsymbol{\sigma}_1\,.\,\boldsymbol{\sigma}_2)$$

and $\qquad f(x)=\mathrm{e}^{-x}/x.$

The wave function will have the general form

$$\psi=\frac{1}{r}\left[\alpha(r)+\frac{1}{2\sqrt{2}}S_{12}\beta(r)\right]\chi_{\mathrm{m}}, \quad \ldots\ldots(21)$$

where χ_{m} is the (triplet) spin state of the system. The differential equations for $\alpha(r)$, $\beta(r)$ can in this case be obtained directly by equating coefficients of spin wave functions. They are (Feshbach and Schwinger 1951)

$$\left.\begin{aligned} -\frac{d^2\alpha}{dx^2}-\lambda f(x)\alpha-2\sqrt{2}\gamma\lambda f(\tau x)\beta &= -\eta^2\alpha \\ -\frac{d^2\beta}{dx^2}-2\sqrt{2}\gamma\lambda f(\tau x)\alpha+\left[\frac{6}{x^2}-\lambda f(x)+2\lambda\gamma f(\tau x)\right]\beta &= -\eta^2\beta \end{aligned}\right\} \quad \ldots\ldots(22)$$

where $x=r/r_c$, $\tau=r_c/r_t$, $\gamma=V_t/V_c$, $\lambda=MV_c r_c{}^2/\hbar^2$, $\eta=(M\epsilon/\hbar^2)^{1/2}r_c$, ϵ is the binding energy of the deuteron, and α, β are zero at $x=0$, ∞.

Feshbach and Schwinger were concerned with the more realistic problem of finding the force parameters corresponding to the experimental values of the energy and quadrupole moment. For illustrative purposes we here suppose the force parameters known and apply the variation-perturbation method to find the eigenvalue. We use the following numerical values from Feshbach and Schwinger: $\eta=0{\cdot}275$, $\eta/\tau=0{\cdot}492$, $\tau=0{\cdot}559$, $\lambda=1{\cdot}8512$, $\gamma=0{\cdot}2305$, so that the accurate eigenvalue in this numerical case is $E=-\eta^2=-0{\cdot}0756$.

It will be convenient to write $\xi=2\lambda\gamma/\tau=1{\cdot}5267$ for the particular numerical values above.

Convenient normalized trial wave functions are

$$\alpha_0=2\mu^{3/2}x\mathrm{e}^{-\mu x}, \qquad \beta_0=(2/\sqrt{3})\nu^{5/2}x^2\mathrm{e}^{-\nu x}. \quad \ldots\ldots(23)$$

With these functions the integrals involved in the second-order approximation may be evaluated without recourse to numerical integration. The following expressions are required:

$$\int_0^x x^n \mathrm{e}^{-mx}\,dx = \left[-\frac{x^n}{m} - \frac{nx^{n-1}}{m^2} - \ldots - \frac{n!}{m^{n+1}}\right]\mathrm{e}^{-mx} + \frac{n!}{m^{n+1}}$$

and $$\int_0^\infty x^n \mathrm{e}^{-mx}\,dx = \frac{n!}{m^{n+1}},$$

in both of which $m>0$, and n is a positive integer.

The expectation value of E is

$$E_0 = \frac{1}{a_0{}^2 + b_0{}^2}\left[a_0{}^2\mu^2 - \frac{4a_0{}^2\lambda\mu^3}{(2\mu+1)^2} + \frac{7}{3}b_0{}^2\nu^2 - \frac{8b_0{}^2\lambda\nu^5}{(2\nu+1)^4} + \frac{8b_0{}^2\xi\nu^5}{(2\nu+\tau)^4}\right.$$
$$\left. - 16\sqrt{(2/3)}\frac{a_0 b_0 \xi \mu^{3/2}\nu^{5/2}}{(\nu+\mu+\tau)^3}\right]. \qquad \ldots\ldots(24)$$

In order that E_0 be minimized with respect to variation of a_0, b_0 we must have

$$\left.\begin{aligned} a_0\mu^2 - \frac{4a_0\lambda\mu^3}{(2\mu+1)^2} - \frac{8\sqrt{(2/3)}\,b_0\xi\mu^{3/2}\nu^{5/2}}{(\nu+\mu+\tau)^3} &= a_0 E_0 \\ -\frac{8\sqrt{(2/3)}a_0\xi\mu^{3/2}\nu^{5/2}}{(\nu+\mu+\tau)^3} + \frac{7}{3}b_0\nu^2 - \frac{8b_0\lambda\nu^5}{(2\nu+1)^4} + \frac{8b_0\xi\nu^5}{(2\nu+\tau)^4} &= b_0 E_0. \end{aligned}\right\} \qquad \ldots\ldots(25)$$

These equations give a quadratic for E_0, and the least root is chosen. It will be a function of μ, ν which can be chosen (by trial and error) so that E_0 is minimized with respect to these parameters also. The values finally adopted were $\mu = 0{\cdot}65$, $\nu = 1{\cdot}2$, with the corresponding values $E_0 = -0{\cdot}0601$, and $\kappa = a_0/b_0 = 6{\cdot}0047$. (This is to be compared with the actual eigenvalue $-0{\cdot}0756$.)

Applying the general expressions we have

$$\alpha_0{}^2\frac{dA_1}{dx} = \int_0^x [-4\mu^3(-2\mu x + \mu^2 x^2)\,\mathrm{e}^{-2\mu x} - 4\lambda\mu^3 x\,\mathrm{e}^{-(2\mu+1)x}$$
$$-4E_0\mu^3 x^2\,\mathrm{e}^{-2\mu x} - 4\sqrt{(2/3)}(\xi/\kappa)\,\mu^{3/2}\,\nu^{5/2}\,x^2\,\mathrm{e}^{-(\nu+\mu+\tau)x}]\,dx. \qquad \ldots\ldots(26)$$

After integrating and dividing by α_0 we find

$$\alpha_0\frac{dA_1}{dx} = (\mu^2 + E_0)\mu^{1/2}x\mathrm{e}^{-\mu x} - 2\mu p\mathrm{e}^{-\mu x} - \frac{p\mathrm{e}^{-\mu x}}{x} + (2\mu+1)\,q\mathrm{e}^{-(\mu+1)x}$$
$$+\frac{q\mathrm{e}^{-(\mu+1)x}}{x} + \tfrac{1}{2}(\nu+\mu+\tau)^2 rx\,\mathrm{e}^{-(\nu+\tau)x} + (\nu+\mu+\tau)\,r\,\mathrm{e}^{-(\nu+\tau)x}$$
$$+\frac{r\mathrm{e}^{-(\nu+\tau)x}}{x}, \qquad \ldots\ldots(27)$$

where $$p = \frac{\mu^2 - E_0}{2\mu^{3/2}}, \quad q = \frac{2\lambda\mu^{3/2}}{(2\mu+1)^2}, \quad r = 4\sqrt{\frac{2}{3}}\,\frac{\xi}{\kappa}\,\frac{\nu^{5/2}}{(\nu+\mu+\tau)^3}, \qquad \ldots\ldots(28)$$

and $p - q - r = 0$ in virtue of equations (25).

Similarly we obtain

$$\begin{aligned}\beta_0\frac{dB_1}{dx} = {} & \frac{1}{\sqrt{3}}(\nu^2+E_0)\,\nu^{3/2}x^2\,\mathrm{e}^{-\nu x}-\frac{2}{\sqrt{3}}(\nu^2-E_0)\,\nu^{1/2}x\,\mathrm{e}^{-\nu x}\\ & -2\nu^2 l\,\mathrm{e}^{-\nu x}-\frac{2\nu l\mathrm{e}^{-\nu x}}{x}-\frac{l\mathrm{e}^{-\nu x}}{x^2}+\frac{1}{6}(2\nu+1)^3\,m\,x\,\mathrm{e}^{-(\nu+1)x}\\ & +\tfrac{1}{2}(2\nu+1)^2m\mathrm{e}^{-(\nu+1)x}+\frac{(2\nu+1)m\mathrm{e}^{-(\nu+1)x}}{x}+\frac{m\mathrm{e}^{-(\nu+1)x}}{x^2}\\ & -\tfrac{1}{6}(2\nu+\tau)^3nx\mathrm{e}^{-(\nu+\tau)x}-\tfrac{1}{2}(2\nu+\tau)^2\,n\,\mathrm{e}^{-(\nu+\tau)x}\\ & -\frac{(2\nu+\tau)n\mathrm{e}^{-(\nu+\tau)x}}{x}-\frac{n\mathrm{e}^{-(\nu+\tau)x}}{x^2}\\ & +\tfrac{1}{2}(\nu+\mu+\tau)^2\,k\mathrm{e}^{-(\mu+\tau)x}+\frac{(\nu+\mu+\tau)k\mathrm{e}^{-(\mu+\tau)x}}{x}\\ & +\frac{k\mathrm{e}^{-(\mu+\tau)x}}{x^2},\end{aligned} \qquad \text{......(29)}$$

where

$$\left.\begin{aligned} l &= \frac{\sqrt{3}}{2}\left[\frac{7}{3}\nu^2-E_0\right]\nu^{-5/2}, & n &= \frac{4\sqrt{3}\xi\nu^{5/2}}{(2\nu+\tau)^4},\\ m &= \frac{4\sqrt{3}\lambda\nu^{5/2}}{(2\nu+1)^4}, & k &= \frac{4\sqrt{2}\xi\kappa\mu^{3/2}}{(\nu+\mu+\tau)^3},\end{aligned}\right\} \qquad \text{......(30)}$$

and $l-m+n-k=0$ in virtue of equations (25).

These expressions may be squared and integrated by using the formula in the Appendix. On substituting numerical values we find

$$\int_0^\infty \alpha_0{}^2\left(\frac{dA_1}{dx}\right)^2dx=0{\cdot}00955, \qquad \int_0^\infty \beta_0{}^2\left(\frac{dB_1}{dx}\right)^2dx=0{\cdot}05900,$$

and so $\epsilon_2=-0{\cdot}01089$. Hence $E_0+\epsilon_2=-0{\cdot}0710$. Thus although our initial approximation was nearly 20% in error, the value to the second order is in error only by about 6%. To carry the calculation to higher order in this example would require numerical integration, and so is not attempted here. (It should be noted that since v_{22} behaves like x^{-2} at the origin, B_1 will actually behave like $\log x$ at the origin.)

APPENDIX

The second-order contribution to the eigenvalue is obtained by making use of the following result (cf. Bromwich 1942, p. 473).

Let

$$\begin{aligned} I = {} & \frac{1}{x^n}\sum_i a_{-n}{}^{(i)}\exp(-\alpha^{(i)}x)+\frac{1}{x^{n-1}}\sum_i a_{-(n-1)}{}^{(i)}\exp(\quad\alpha^{(i)}x)\\ & +\ldots+\frac{1}{x}\sum_i a_{-1}{}^{(i)}\exp(-\alpha^{(i)}x)\end{aligned}$$

where

$$\begin{aligned} & \sum_i a_{-n}{}^{(i)}=0,\\ & \sum_i\left[a_{-(n-1)}{}^{(i)}-\alpha^{(i)}a_{-n}{}^{(i)}\right]=0,\\ & \ldots\ldots\ldots\ldots\ldots\ldots\ldots\ldots\\ & \sum_i\Big[a_{-1}{}^{(i)}-\alpha^{(i)}a_{-2}{}^{(i)}+\tfrac{1}{2}(\alpha^{(i)})^2a_{-3}{}^{(i)}+\ldots\\ & \qquad +(-1)^{n-1}\frac{1}{(n-1)!}(\alpha^{(i)})^{n-1}a_{-n}{}^{(i)}\Big]=0.\end{aligned}$$

Then
$$\int_0^\infty I dx = -\sum_i \Big[a_{-1}{}^{(i)} - \alpha^{(i)} a_{-2}{}^{(i)} + \dots + (-1)^{n-1} \frac{1}{(n-1)!} (\alpha^{(i)})^{n-1} a_{-n}{}^{(i)} \Big] \log \alpha^{(i)} - \sum_i [a_{-2}{}^{(i)} - c_3 \alpha^{(i)} a_{-3}{}^{(i)} + \dots + (-1)^n c_n (\alpha^{(i)})^{n-2} a_{-n}{}^{(i)}] \alpha^{(i)},$$

where
$$c_n = \frac{1}{(n-1)!} \left(1 + \tfrac{1}{2} + \dots + \frac{1}{n-1} \right) \text{ for } n > 1.$$

REFERENCES

BROMWICH, T. L. I'a., 1942, *Infinite Series*, 2nd Edn (London: Macmillan).

CLARK, A. C., 1954, *Proc. Phys. Soc.* A, **67**, 323.

COHEN, L., 1955, *Proc. Phys. Soc.* A, **68**, 419.

FESHBACH, H., and SCHWINGER, J., 1951, *Phys. Rev.*, **84**, 194.

MORPURGO, G., 1952, *Nuovo Cim.*, **9**, 461.

Isotope Shifts and Hyperfine Structure in the Atomic Spectrum of Tin

By W. R. HINDMARSH† and H. KUHN
Clarendon Laboratory, Oxford

MS. received 30*th November* 1954

Abstract. The spectrum of tin was excited in a liquid oxygen cooled hollow cathode tube, and examined by means of a Fabry–Perot interferometer. With the use of highly enriched samples of tin isotopes, isotope shifts of all the even isotopes were measured in the spark line $5s^2 6s\ {}^2S_{1/2} - 5s^2 6p\ {}^2P_{3/2}$, $\lambda 6454$. The shifts between successive even isotopes vary from 0·0015 cm^{-1} for ^{122}Sn and ^{124}Sn to 0·0067 cm^{-1} for ^{112}Sn and ^{114}Sn, and this change occurs in two 'jumps'. The probable error is about 0·0002 cm^{-1}. The corresponding isotope shift constants (C values), calculated without allowance for the specific mass shift, vary from 15×10^{-3} cm^{-1} to 40×10^{-3} cm^{-1}. The hyperfine structures of the line $\lambda 6454$ of the odd isotopes ^{117}Sn and ^{119}Sn were measured. The ratio of the splittings is 1·042, in good agreement with the value 1·046 calculated from the nuclear resonance values of the nuclear magnetic moments.

§ 1. Introduction

The elements of even atomic number near the middle of the periodic table possess large numbers of stable isotopes. By measurements of shifts for the different isotopes of one element, the effect of the addition of successive pairs of neutrons on the nuclear charge distribution can be studied. It is sometimes possible to examine the relative shifts in iso-neutronic sets of isotopes in different elements. There are often, however, great experimental difficulties in the measurements of shifts in these elements. The shifts are sometimes extremely small, and the Doppler widths of the lines increase as one proceeds to lighter elements. Further, the specific mass shift, which cannot be calculated, may not be negligible, though its presence does not affect the detection of irregularities in the volume shift.

Isotope shifts have not previously been measured in the tin spectrum, though Tolansky (1934) noticed broadening in two lines which he attributed to isotope shift.

Tin possesses ten stable isotopes, three odd and seven even. The atomic number is 50, and the mass numbers and natural abundances of the isotopes are as follows :

Mass numbers	112	114	115	116	117	118	119	120	122	124
% abundances	1·0	0·68	0·34	14·4	7·54	24·1	8·62	32·5	4·7	5·9

With the use of highly enriched isotopes supplied by the Atomic Energy Research Establishment, Harwell, measurements have been made of the isotope shift in one of the lines of the atomic spectrum of tin. Some of the results of this work have already been published (Hindmarsh, Kuhn and Ramsden 1954) but partly in an uncorrected form owing to the lack, at that time, of mass analysis data.

The hyperfine structures of the same line of the odd isotopes ^{117}Sn and ^{119}Sn have also been observed and measured.

---

† Now at the Atomic Energy Research Establishment, Harwell, Didcot, Berkshire.

§ 2. EXPERIMENTAL METHOD

2.1. *The Choice of Lines*

Preliminary experiments with natural tin revealed that some of the lines in the visible and ultra-violet regions of the tin spectrum were broader than expected. No splitting of the lines attributable to isotope shift was observed. The choice of lines for work with separated isotopes was limited to the brightest lines of the tin spectrum, as only these could be excited with appreciable intensity with the limited quantities of separated isotope available. The line $5s^2 6s\ ^2S_{1/2}$–$5s^2 6p\ ^2P_{3/2}$, λ 6454, of the spark spectrum seemed likely to show a comparatively large isotope shift, and was also well suited for comparison with the theory, owing to the relatively simple electron configurations.

2.2. *The Light Source*

The light source used in this investigation was a hollow cathode discharge tube similar in design to that described by Kelly, Kuhn and Pery (1954), with an interchangeable cathode block made of high purity aluminium. It was, however, made larger, having a cavity of depth 2 cm and diameter 1 cm in order to allow the discharge to be run at low pressures. This was necessary in order to reduce the relative intensity of the molecular lines of helium, which carried the discharge.

Considerable research was devoted to discovering how best to excite the tin spectrum with the milligramme quantities of enriched tin isotope available. This proved to be very difficult. The following method was finally adopted. The tin was introduced into the cathode cavity in the form of stannous sulphide, a suspension of which in water was spread round the roughened walls of the cavity. When the water evaporated the cavity was left coated with a uniform deposit of stannous sulphide. With about 1 mg of tin introduced in this manner, the spark line λ 6454 was bright enough at first to be photographed in half an hour, but gradually faded with continued running of the discharge. Currents of about 50 mA and exposure times of up to four hours were used. Helium was found to be the best carrier gas. Liquid oxygen cooled charcoal traps were used, but it was not necessary to circulate the gas.

2.3. *The Spectrograph and the Fabry–Perot Interferometer*

Two identical discharge tubes, one for each of a pair of isotopes under examination, were connected to a vacuum line. They were tilted so that their axes met in the spectrograph axis, and were contained in a plane normal to the spectrograph axis. A mirror was fitted to a mount so that light from either one or the other discharge tube could, in turn, be reflected into the spectrograph. Lenses formed an image, 1·5 times enlarged, of the hollow cathode discharge on the spectrograph slit. Great care was taken to align the optical system accurately for reasons which are discussed later.

A Hilger spectrograph of focal length 50 cm was used, with a 65° prism of refractive index 1·75, in order to separate λ 6454 from neighbouring lines.

The etalon plates were made of fused silica and were 6 cm in diameter. In use the aperture was stopped down to 5 cm. The plates were coated with very thin silver films of reflectivity 75% and transmission 20%. Under these conditions, the instrumental width with a 2 cm spacer was about 0·02 cm^{-1} while the Doppler width at 150°K was about 0·013 cm^{-1}. The resulting loss of resolution was an advantage for the measurements of some fringes which were blends due to the isotopic impurity of some samples. By making the line width considerably larger than the splittings (the largest splittings were about 0·006 cm^{-1}) it was ensured that the measured position of the fringe represented the centre of gravity of the components forming the blend. Also the loss of intensity when the instrumental width is much smaller than the Doppler width would have been a serious drawback to the use of dense films.

The etalon was mounted between the collimator and prism of the spectrograph, and it was enclosed in an air-tight box. The etalon and spectrograph were in a room thermostatically controlled to about ± 0·1°c.

Separate photographs of the centre portion of the ring systems of the two isotopes of a pair were taken, with photographs of the cadmium red line, λ 6438, before the first and after the second tin exposure, and between the two tin exposures.

All the isotopes were examined using at least two and sometimes three, different etalon spacers. Spacers of 1·5 cm, 2 cm, and 2·5 cm were employed.

Figure 1 shows photometer tracings of the isotopes ^{112}Sn and ^{120}Sn. The two tracings have been superposed so that the centres of the ring systems coincide. The magnitude of the isotope shift and its relation to the line width are thus displayed.

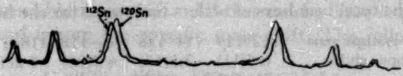

Figure 1.

For the investigation of the hyperfine structure of the line λ 6454 of the odd isotopes ^{117}Sn and ^{119}Sn, only one discharge tube was used. The etalon films were somewhat denser to provide adequate resolution.

2.4. *Sources of Error*

There is a number of possible sources of error to be considered in the isotope shift measurement. Spurious shifts may be recorded if the optical path between the etalon plates varies during an exposure. Any such shift was revealed by comparison of the ring diameters of the three photographs of the cadmium red line λ 6438, mentioned above. Only plates with a total shift of less than 0·01 of an order between the first and third cadmium exposures were used, but a correction to the apparent isotope shift was made, when necessary, to allow for the etalon shift. Such a correction could be made roughly by subtracting from the apparent shift one half the total shift between the first and the third cadmium photographs. However, there always appeared on the plates, near the tin line, a number of unidentified sharp single lines. Invariably at least one of these was suitably exposed. The ring diameters of the suitably exposed line were compared on each of the two photographs, and the order difference between them applied as a correction to the apparent isotope shift.

Very serious systematic errors may arise in any measurement of the relative positions of two lines from two different discharge tubes. If the distribution of intensity over the surface of the etalon is not precisely the same for the two discharge tubes, the two tubes are effectively using different parts of the etalon, and plate imperfections could cause a serious error. This was the reason for the care taken in the aligning of the optical system. The illumination condition was checked by filling the two discharge tubes with krypton (to provide narrow lines) and photographing light from a krypton discharge in each of the two tubes. The diameters of interference rings from the two tubes agreed to better than 1/300 of an order. A further check was obtained in the case of one pair of isotopes by exchanging the two cathodes. An error in illumination would be detected when the etalon was dismantled and reassembled with the same or a different spacer. The new adjustment would be slightly different from the old, so that any error caused by illumination differences would differ by a quantity of the same order as the error itself, and so a systematic difference in the results would be recorded.

Another source of error is the presence of unwanted spectral lines overlapping the tin line. Their presence would be revealed by a change of spacer, when a systematic difference would be apparent between the results from different spacers.

No systematic difference of any kind was ever observed, and it was therefore concluded that the effects described in the last two paragraphs were smaller than the random errors of measurement.

§ 3. Results

The following were the results obtained from measurements of the plates with a travelling microscope. The limits quoted are probable errors, and the figures in brackets are the total numbers of orders measured for the isotope concerned.

Mass numbers of isotope pair	112–114	114–116	116–118	118–120	120–122	122–124
Uncorrected isotope shifts (10^{-3} cm^{-1})	6·5(11)	2·5(17)	4·5(26)	4·2(17)	1·2(8)	1·7(13)
	±0·2	±0·15	±0·1	±0·2	±0·25	±0·2

These results were subsequently corrected for isotopic impurities in the samples. The assumption was made that the measured position of a fringe was the centre of gravity of the blend formed by the principal component and the impurities. This must be very closely true as long as the fringe appears symmetrical. In fact, no asymmetry was ever observed, either on photometer tracings or by direct inspection of the plates. In some of the isotopes the correction was large, but knowledge of the mass analyses of the specimens allowed it to be made with sufficient accuracy. The final results obtained after correction in this way are quoted in the following table. The errors given here are outside limits of error, being four times the probable error. Though the results are, of course, too few to make a proper statistical treatment possible, it is believed to be very improbable that the true values lie outside the quoted error limits. The sign of the shift is such that the lighter the isotope, the higher the frequency of the component.

Isotope pair	112–114	114–116	116–118	118–120	120–122	122–124
Shift (10^{-3} cm^{-1})	6·7	6·2	4·7	4·4	1·5	1·5
	±0·7	±0·6	±0·5	±0·7	±0·9	±0·8

The analogy of one of the observed 'jumps' in the values of the shifts with that found in the iso-neutronic isotopes of cadmium has been pointed out previously (Hindmarsh, Kuhn and Ramsden 1954); the significance of these results regarding nuclear structure will be discussed in another publication.

Results of measurements of the isotope shift due to the nuclear volume effect are commonly expressed in terms of the isotope shift constant C, introduced by Kopfermann (see for example Brix and Kopfermann 1949). The isotope shift of a term, ΔT, may be written as $\Delta T = C\beta$, where C depends on nuclear properties and β on the atomic wave function. If the shift is entirely due to an s electron β is given by the expression

$$\beta = (\pi a_0^3/Z)\psi^2(0)$$

where a_0 is the radius of the first Bohr orbit, Z the atomic number and $\psi^2(0)$ the square of the Schrödinger wave function at the centre of the nucleus. The magnetic hyperfine structure splitting of the same term, if due to the same s electron, is given by

$$\Delta W = \frac{8}{3}\,\frac{\pi a_0{}^3 \boldsymbol{R}\alpha^2 g_I}{1838}\,\psi^2(0)\ \mathrm{cm}^{-1}$$

where α is the fine structure constant, $\boldsymbol{R}$ the Rydberg constant and g_I the nuclear g factor.† Thus

$$\beta = \frac{3\times 1838}{8\boldsymbol{R}\alpha^2 Z g_I}\,\Delta W.$$

ΔW was measured for the odd isotopes ^{117}Sn and ^{119}Sn (see below) and g_I has been determined for these by nuclear resonance (Proctor 1949). In this way β was determined. It was assumed that the shift due to the $6p_{3/2}$ electron was negligible compared with that due to the 6s electron. This method of evaluating β, which avoids the calculation of $\psi^2(0)$, has been described by Brix and Kopfermann (1951). The C values can now be evaluated if allowance can be made for the mass shift. It was impossible to allow for the specific mass shift, and since only one line has been examined there is no experimental evidence for the presence or absence of an appreciable mass shift. All that can be done is to allow for the normal mass shift and ignore the specific mass shift. The following C values are thus obtained.

$$C_1\,(^{112}\mathrm{Sn}-{}^{114}\mathrm{Sn}-{}^{116}\mathrm{Sn}) = 40\times 10^{-3}\ \mathrm{cm}^{-1}$$
$$C_2\,(^{116}\mathrm{Sn}-{}^{118}\mathrm{Sn}-{}^{120}\mathrm{Sn}) = 30\times 10^{-3}\ \mathrm{cm}^{-1}$$
$$C_3\,(^{120}\mathrm{Sn}-{}^{122}\mathrm{Sn}-{}^{124}\mathrm{Sn}) = 15\times 10^{-3}\ \mathrm{cm}^{-1}$$

The specific mass shift is unlikely to cause an error of more than $\pm 10\times 10^{-3}\ \mathrm{cm}^{-1}$ in the C values. The fact that C_1 agrees with the C value for the cadmium isotopes with the same neutron numbers (due allowance being made for the difference in nuclear charge) is an indication that the specific mass effect is small in both elements.

The expected form of the hyperfine structure of the line λ 6454 for the odd isotopes of tin both of which have nuclear spin ½, is shown in figure 2. The nuclear magnetic moment is assumed negative in these diagrams. The dotted component M is that due to the even isotopes, which exist as impurities in the samples of enriched odd isotopes. The hyperfine structure of this line was observed using natural tin by Tolansky (1934) and using an enriched sample of ^{115}Sn by Gurevitch (1949). In all the investigations, including the present one, the components S′ and S″ were completely unresolved, appearing as one component S. The results of the present measurements were as follows ; outside errors are quoted.

	^{117}Sn		^{119}Sn	
	LS	LM	LS	LM
Splitting (10^{-3} cm^{-1})	200·6 ± 1	153·4 ± 3	209·0 ± 1	160·2 ± 3

The reason for the greater uncertainty of the measurements of the distances LM was that the component M was subject to considerable distortion by the nearby strong component S.

The magnetic moments determined from nuclear resonance measurements are (^{117}Sn) = −0·995 n.m. and (^{119}Sn) = −1·041 n.m. Thus the ratio of the

---

† The relativistic factor $\chi(j, Z)$ has been omitted; it is insignificant for the present calculation.

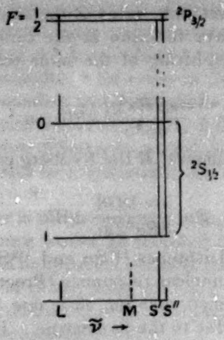

Figure 2.

moments of the two isotopes is 1·046, while the ratio of the measured hyperfine structure splittings LS is 1·042. The agreement is within the experimental error of the spectroscopic measurements. The present measurements also agree with Tolansky's values obtained with natural tin, though our accuracy is higher. Allowing for the calculated splitting of the upper term $^2P_{3/2}$, the measured splitting of the lower term $^2S_{1/2}$ is 0·221 cm^{-1} for ^{119}Sn. This compares with 0·248 cm^{-1} calculated using the nuclear resonance value of the magnetic moment and the Goudsmit–Fermi–Segrè formula. In this case, as in alkali like spectra (Kelly, Kuhn and Pery 1954) the formula gives too high a value for the hyperfine structure splitting.

It should be possible to obtain the isotope shift of the odd isotopes from such measurements as those described above, but the number of plates taken was not sufficient to give the required accuracy.

ACKNOWLEDGMENTS

The authors wish to thank the Electromagnetic Group and the Mass Spectrometry Group of the Atomic Energy Research Establishment, Harwell, for the provision of the samples of separated tin isotopes and some of the mass analyses, and the Research Department of Messrs. Metropolitan-Vickers Ltd. for carrying out the remaining mass analyses.

The authors are indebted to Mr. S. A. Ramsden, who carried out some of the measurements on ^{119}Sn.

One of us (W. R. H.) wishes to express his gratitude to the Department of Scientific and Industrial Research for the award of a maintenance grant during the tenure of which the above work was carried out.

REFERENCES

BRIX, P., and KOPFERMANN, H., 1949, *Z. Phys.*, **126**, 344; 1951, *Akad. Wiss. Gött.*, p. 17.
GUREVITCH, M., 1949, *Phys. Rev.*, **75**, 767.
HINDMARSH, W. R., KUHN, H., and RAMSDEN, S. A., 1954, *Proc. Phys. Soc.* A, **67**, 478.
KELLY, F. M., KUHN, H., and PERY, ANNE, 1954, *Proc. Phys. Soc.* A, **67**, 450.
PROCTOR, W. G., 1949, *Phys. Rev.*, **76**, 684.
TOLANSKY, S., 1934, *Proc. Roy. Soc.* A, **144**, 574.

RESEARCH NOTES

Note on the Network Approximation in Metals

By AMALKUMAR RAYCHAUDHURI

Theoretical Physics Department, Indian Association for the Cultivation of Science,
Jadavpur, Calcutta, India

MS. received 14*th December* 1954

FOLLOWING the impressive and rather surprising success of the so-called 'free electron model' in dealing with conjugated and aromatic molecules (Ruedenberg and Scherr 1953, Scherr 1953), Coulson (1954) has investigated the applicability of the 'free-electron network approximation' in the case of metals—the electrons being supposed to move freely in a constant potential along different crystallographic axes—and has obtained results strikingly similar to those obtained in the tightly bound approximation.

It seems interesting to investigate as to how far this agreement is sensitive to the form of potential function chosen, i.e. whether it will survive if one changes over to a non-constant potential; this is of particular importance because (as Coulson himself has remarked) for impure metals, in the presence of atoms of different kinds, it would be absurd to suppose that the potential function is even approximately constant and thus the free electron hypothesis would be inapplicable. On the other hand, as results obtained from such manifestly different starting points as the tight binding approximation and the free electron network approximation are strikingly similar, one may expect that many of these results essentially depend on their common features (e.g. periodicity of potential leading to Bloch type wave functions and lattice structure) and would persist even if one changes over to a non-constant potential in the network approximation.

In the present note we shall consider the case of a simple cubic lattice and shall assume that our wave functions satisfy precisely the same conditions as in Coulson's paper (1954) except that now the Schrödinger equation† is

$$\frac{d^2A}{dx^2} + q^2A = 0 \qquad \ldots\ldots(1)$$

with similar equations for B and C, where

$$q^2 = \frac{8\pi^2 m}{h^2}(E - V). \qquad \ldots\ldots(2)$$

About V, we shall only assume that it is periodic with the periodicity of the lattice. Further, owing to the cubic symmetry, it would be a symmetric function of x, y and z.

The general solution of (1) will be of the form

$$\left.\begin{aligned} A_{ijk} &= f_1(x) + af_2(x) \\ B_{ijk} &= f_1(y) + bf_2(y) \\ C_{ijk} &= f_1(z) + cf_2(z) \end{aligned}\right\} \qquad \ldots\ldots(3)$$

---

† The symbols and the notation used have the same significance as in Coulson (1954) except where specifically indicated.

where f_1 and f_2 are two independent solutions of (1) and we take them to be normalized according to the following conditions

$$\left.\begin{array}{ll} f_1(0)=1, & f_2(0)=0 \\ f'_1(0)=0, & f_2'(0)=q_0 \end{array}\right\} \qquad \ldots\ldots(4)$$

where primes denote differentiation and $q_0=q(x=y=z=0)$. The Bloch condition requires

$$A_{i-1,j,k}=\exp(-iK_xl)[f_1(x')+af_2(x')] \text{ etc.} \qquad \ldots\ldots(5)$$

and the condition of continuity gives

$$\left.\begin{array}{l} af_2(l)+[f_1(l)-\exp(iK_xl)]=0 \\ bf_2(l)+[f_1(l)-\exp(iK_yl)]=0 \\ cf_2(l)+[f_1(l)-\exp(iK_zl)]=0. \end{array}\right\} \qquad \ldots\ldots(6)$$

The vanishing of Σ grad ψ leads to the equation

$$\begin{aligned} &a[q_0-\exp(-iK_xl)f_2'(l)]+b[q_0-\exp(-iK_yl)f_2'(l)]+c[q_0-\exp(-iK_zl)f_2'(l)] \\ &\quad -f_1'(l)[\exp(-iK_xl)+\exp(-iK_yl)+\exp(-iK_zl)]=0. \qquad \ldots\ldots(7) \end{aligned}$$

The equations (6) and (7) are consistent only if the determinant of the coefficients vanishes and this condition gives

$$\begin{aligned} &[f_1(l)f_2'(l)-f_2(l)f_1'(l)][\exp(-iK_xl)+\exp(-iK_yl)+\exp(-iK_zl] \\ &\quad +q_0[\exp(iK_xl)+\exp(iK_yl)+\exp(iK_zl)]-3f_2'(l)-3q_0f_1(l)=0. \quad \ldots\ldots(8) \end{aligned}$$

As f_1, f_2 are solutions of equation (1), we have $f_1f_2'-f_2f_1'=$ constant. And in view of our normalization (4), the constant is equal to q_0. So that equation (8) becomes

$$2q_0(\cos K_xl+\cos K_yl+\cos K_zl)-3f_2'(l)-3q_0f_1(l)=0. \qquad \ldots\ldots(9)$$

Now expanding $f_2'(l)$ and $f_1(l)$ in Taylor's series and using (1), (2) and (4), we get

$$\begin{aligned} f_2'(l)&=f_2'(0)+f_2''(0)l+\ldots\ldots \\ &=q_0\left(1-\frac{q_0{}^2l^2}{2!}+\text{higher powers of } q_0l\right) \\ &\quad -q_0(\text{terms involving derivatives of } V \text{ at } x=y=z=0 \text{ but not } E \text{ and } K) \\ &\quad -q_0(\text{terms involving derivatives of } V \text{ at } x=y=z=0 \text{ and powers of } E-V) \end{aligned}$$

and a similar expression for $f_1(l)$. Finally we obtain for (9)

$$\begin{aligned} \cos K_xl+\cos K_yl+\cos K_zl&=3(1-\tfrac{1}{2}q^2{}_0l^2+\ldots) \\ &\quad -[\text{terms involving derivatives of } V \text{ at } x=y=z=0 \text{ but not } E] \\ &\quad -[\text{terms involving derivatives of } V \text{ and powers of } E-V]. \end{aligned}$$

The first group of terms on the right is essentially the same as Coulson obtains on the free electron approximation, the second group merely shifts all the energy states by a constant amount, while regarding the third group of terms we note the following. The first term is, apart from a numerical coefficient,

$$q_0{}^2\,\frac{8\pi^2m}{h^2}\left(\frac{\partial V}{\partial x}\right)_0 l^5$$

and if we take $(\partial V/\partial x)_0\sim V_0/l\sim(E-V_0)/l$, this term is of the order $q_0{}^4l^4$ and hence can be neglected in the region where the free electron approximation gives results in agreement with the tightly bound approximation. A similar consideration holds good for the succeeding terms and thus one sees that even a change over to a much more general non-constant potential does not materially affect the (E, K) relation. One is thus led to expect that the free electron model may be applicable to the case of impure metals as well provided the periodicity of the potential is not seriously affected.

REFERENCES

COULSON, C. A., 1954, *Proc. Phys. Soc.* A, **67**, 608.
RUEDENBERG, K., and SCHERR, C. W., 1953, *J. Chem. Phys.*, **21**, 1565.
SCHERR, C. W., 1953, *J. Chem. Phys.*, **21**, 1582.

On the Interaction of Electrons in Metals

BY J. HUBBARD
Department of Mathematics, Imperial College, London, S.W.7

Communicated by S. Raimes ; MS. received 8*th December* 1954 *and in final form* 7*th January* 1955

THE chief difficulty in the treatment of the electronic interactions in metals by the Rayleigh–Schrödinger perturbation theory is the long-range nature of the Coulomb interaction; this interaction gives rise to long-range correlation effects which cannot easily be handled by the perturbation theory. To obtain an adequate treatment of the interactions it is therefore necessary to find some other method of dealing with the long-range correlations. One such method is the plasma oscillation theory of Bohm and Pines (1953); Bohm and Pines show that in a free electron gas the principal effect of the long-range interaction is to bring about the plasma oscillations; these are fairly easily discussed, leading to a treatment of the interactions in a free electron gas. It is the purpose of this note to indicate a rather more general treatment of the problem; this treatment will in the case of a free electron gas lead to essentially the same results as the plasma oscillation theory, but will also be capable of taking into account the effects due to the core electrons, to the conduction electron binding and the 'damping' effects which occur in real metals.

The essential feature of this treatment is the recognition that, so far as long-range phenomena are concerned, the behaviour of the system is *medium-like*; as long as we consider interaction phenomena over distances rather greater than the period of the lattice (or the inter-particle distance in a free electron gas), the microscopic structure of the system is unimportant, only its average properties contributing to the phenomena.

To treat the long-range interactions we have therefore to give a treatment of the electromagnetic field in a medium. It can be shown by a straightforward generalization of Wilson's results (Wilson 1935) that an electric field

$$\mathbf{E}(\mathbf{r},t)=\mathbf{E}_0\exp(i\omega t+i\mathbf{k}.\mathbf{r})+\mathbf{E}_0{}^*\exp(-i\omega t-i\mathbf{k}.\mathbf{r}) \qquad \ldots\ldots(1)$$

will induce a current

$$\mathbf{J}(\mathbf{r},t)=\boldsymbol{\alpha}_{\omega\mathbf{k}}.(d\mathbf{E}/dt)+\boldsymbol{\sigma}_{\omega\mathbf{k}}.\mathbf{E} \qquad \ldots\ldots(2)$$

in a metal, where $\boldsymbol{\alpha}_{\omega\mathbf{k}}$ and $\boldsymbol{\sigma}_{\omega\mathbf{k}}$ are tensors independent of $\mathbf{r}$, t provided that k is not too large. Thus the current $\mathbf{J}(\mathbf{r},t)$ depends linearly upon $\mathbf{E}(\mathbf{r},t)$ and

$(d/dt)[\mathbf{E}(\mathbf{r},t)]$ and we can regard $\boldsymbol{\alpha}_{\omega\mathbf{k}}$ and $\boldsymbol{\sigma}_{\omega\mathbf{k}}$ as (ω and $\mathbf{k}$ dependent) polarizability and conductivity tensors, and can define a complex dielectric constant (see Seitz 1940, p. 631)

$$\boldsymbol{\epsilon}_{\omega\mathbf{k}} = 1 + 4\pi\boldsymbol{\alpha}_{\omega\mathbf{k}} + \frac{4\pi}{i\omega}\boldsymbol{\sigma}_{\omega\mathbf{k}}. \qquad \ldots\ldots(3)$$

Having shown that the induced current depends linearly upon the electric field and its rate of change, we can proceed in the same way as in the theory of the electromagnetic field in ponderable media, but must use the Fourier transforms with respect to $\mathbf{r}$ and t everywhere on account of the ω and $\mathbf{k}$ dependence of $\boldsymbol{\epsilon}_{\omega\mathbf{k}}$. In particular, we find that the Fourier transform $\phi_{\omega\mathbf{k}}$ of the scalar potential $\phi(\mathbf{r},t)$ is given, in a gauge in which the longitudinal part of the vector potential vanishes (we concern ourselves here with the Coulomb interactions only, neglecting the radiation field), by

$$\phi_{\omega\mathbf{k}} = \frac{4\pi}{k^2\epsilon_{\omega\mathbf{k}}}\rho_{\omega\mathbf{k}}, \qquad \epsilon_{\omega\mathbf{k}} \equiv \hat{\mathbf{k}}\,.\,\boldsymbol{\epsilon}_{\omega\mathbf{k}}\,.\,\hat{\mathbf{k}} \qquad \ldots\ldots(4)$$

where $\rho_{\omega\mathbf{k}}$ is the Fourier transform of the charge density $\rho(\mathbf{r},t)$ generating the field (as opposed to the charge density induced by the field through the induced current).

The quantities $\alpha_{\omega\mathbf{k}} \equiv \hat{\mathbf{k}}\,.\,\boldsymbol{\alpha}_{\omega\mathbf{k}}\,.\,\hat{\mathbf{k}}$, $\sigma_{\omega\mathbf{k}} \equiv \hat{\mathbf{k}}\,.\,\boldsymbol{\sigma}_{\omega\mathbf{k}}\,.\,\hat{\mathbf{k}}$, which are obtained by the generalization of Wilson's results (Wilson dealt only with the case of very small $\mathbf{k}$'s which occur in optical theory), are given by

$$\alpha_{\omega\mathbf{k}} = -\frac{ne^2}{m\omega^2} + \frac{2e^2}{m^2\omega^2}\sum_{\mathbf{k}',m,m'} N_{\mathbf{k}',m}(1-N_{\mathbf{k}'+\mathbf{k},m'})\,|\hat{\mathbf{k}}\,.\,\mathbf{M}_{m'm}(\mathbf{k}',\mathbf{k})|^2 \times \frac{E_{\mathbf{k}'+\mathbf{k},m'} - E_{\mathbf{k}'m}}{(E_{\mathbf{k}'+\mathbf{k},m'} - E_{\mathbf{k}'m})^2 - (\hbar\omega)^2}, \qquad \ldots\ldots(5)$$

$$\sigma_{\omega\mathbf{k}} = \frac{\pi e^2}{m^2\omega}\sum_{\mathbf{k}',m,m'} N_{\mathbf{k}'m}(1-N_{\mathbf{k}'+\mathbf{k},m'})\,|\hat{\mathbf{k}}\,.\,\mathbf{M}_{m'm}(\mathbf{k}',\mathbf{k})|^2 \times \{\delta(E_{\mathbf{k}'+\mathbf{k},m'} - E_{\mathbf{k}',m} - \hbar\omega) - \delta(E_{\mathbf{k}'+\mathbf{k},m'} - E_{\mathbf{k}'m} + \hbar\omega)\} \qquad \ldots\ldots(6)$$

where n is the particle density of the electrons,

$$\mathbf{M}_{m'm}(\mathbf{k}',\mathbf{k}) \equiv \int \psi^*_{\mathbf{k}'+\mathbf{k},m'}\,e^{i\mathbf{k}\cdot\mathbf{r}}(\mathbf{p} + \tfrac{1}{2}\hbar\mathbf{k})\psi_{\mathbf{k}'m}\,d\mathbf{r} \qquad \ldots\ldots(7)$$

the $\psi_{\mathbf{k}m}$ are Bloch wave functions, $N_{\mathbf{k}m}$ is the occupation number and $E_{\mathbf{k}m}$ the energy of the state $(\mathbf{k}, m)$; the factors $(1-N_{\mathbf{k}'+\mathbf{k},m'})$ etc. take care of the exclusion principle.

In the case of a free electron gas $\epsilon_{\omega\mathbf{k}}$ is very small at some frequency $\omega = \omega_{\mathbf{k}}$ near to ω_{P} ($\omega_{\mathbf{k}} = \omega_{\mathrm{P}}$ for $\mathbf{k} = 0$, and $\omega_{\mathrm{P}}{}^2 = 4\pi ne^2/m$) if the damping is small. Thus any fluctuation of the charge density leading to a non-zero component $\rho_{\omega\mathbf{k}}$, $\omega = \omega_{\mathbf{k}}$, will by (4) lead to a very large $\phi_{\omega\mathbf{k}}$, corresponding to strong oscillations at this frequency, which we identify with the plasma oscillations. In the case of a real metal such strong oscillations will occur only if $\epsilon_{\omega\mathbf{k}}$ obtained from (3), (5) and (6) becomes very small for some frequency (or frequencies).

Two applications of (4) are of especial interest. The first of these is the case in which $\rho(\mathbf{r},t)$ is the charge distribution corresponding to a fast electron passing through a metal. This will give rise to a field described by (4). This field, treated as a perturbation, will lead to transitions of the electrons of the metal from occupied levels to unoccupied levels, the electron making the transition taking up momentum $\hbar\mathbf{k}$ and energy $\hbar\omega$ from the fast electron. The cross section for this process can be calculated and is given by

$$\frac{32\pi^2e^2}{\hbar\omega k^2}\frac{\sigma_{\omega\mathbf{k}}}{|\epsilon_{\omega\mathbf{k}}|^2}\delta(\omega+\mathbf{k}\,.\,\mathbf{v}) \qquad \ldots\ldots(8)$$

where $\mathbf{v}$ is the velocity of the fast electron. This treatment closely resembles the Weizsäcker–Williams method (see Heitler 1936, p. 263).

In the case of a free electron gas in the limit of no damping

$$\sigma_{\omega\mathbf{k}}/|\epsilon_{\omega\mathbf{k}}|^2=\tfrac{1}{8}\omega_{\mathbf{k}}{}^2\delta(\omega-\omega_{\mathbf{k}})$$

apart from certain small terms, and the fast electron loses all its energy in amounts of about $\hbar\omega_{\mathrm{P}}$. In the general case, substitution of (5), (6) into (8) will lead to a rather complicated energy loss spectrum. It should be noticed that (5) and (6) already contain the contribution to the polarizability and conductivity of the core electrons and inter-zone transitions. Thus (8) will then give the energy loss spectrum taking into account the core electron polarizability and damping and also the effects of inter-zone transitions. Several treatments of electron penetration in metals have been carried out along similar lines by various authors (Fermi 1940, Kramers 1947, A. Bohr 1948, Halpern and Hall 1948); all the previous non-relativistic results can be obtained as special cases of (8).

The second case of especial interest is that in which $\rho(\mathbf{r},t)$ is the ordinary charge density of the metal in the independent electron approximation. This will not be constant and uniform, but will show fluctuations. In the classical case these fluctuations will be purely thermal, but in the quantum mechanical case will be partly of quantum mechanical origin and will not disappear even at the absolute zero. These fluctuations will by (4) give rise to a fluctuating electric field in the metal. For a free electron gas these fluctuations of the electric field will be very strong at $\omega\sim\omega_{\mathrm{P}}$, and will represent the plasma oscillations in the metal. Calculation of the energy of this field and the modification of the kinetic and potential energy of the electrons by the fluctuating field should lead to a value for the correlation energy of the metal. Such calculations are at present in progress. It is hoped to give further details of this theory in a paper at some later date.

ACKNOWLEDGMENTS

I should like to thank Dr. S. Raimes for his advice and encouragement with this work. I am indebted also to the University of London for the award of a Postgraduate Studentship.

REFERENCES

BOHM, D., and PINES, D., 1953, *Phys. Rev.*, **92,** 609.
BOHR, A., 1948, *K. Danske Vidensk. Selsk. Mat. Fys. Medd.*, **24,** No. 19.
FERMI, E., 1940, *Phys. Rev.*, **57,** 485.
HALPERN, O., and HALL, H., 1948, *Phys. Rev.*, **73,** 477.
HEITLER, W., 1936, *The Quantum Theory of Radiation*, 2nd Edn (Oxford : University Press).
KRAMERS, H. A., 1947, *Physica*, **13,** 401.
PINES, D., 1953, *Phys. Rev.*, **92,** 626.
SEITZ, F., 1940, *Modern Theory of Solids* (New York : McGraw-Hill).
WILSON, A. H., 1935, *Proc. Roy. Soc.*, **151,** 274.

The Interaction of Two Excited Hydrogen Atoms

BY M. A. JASWON AND H. AGHAJANIAN
Department of Mathematics, Imperial College, London S.W.7

MS. received 26th October 1954 *and in final form* 17*th December* 1954

THE theory of the cohesion of covalent molecules and crystals is based almost entirely on an approximation known in the literature as 'perfect pairing', i.e. the pairing of the spins of overlapping directed orbitals from neighbouring atoms so as to enable us to build up a wave function for the system. As a means towards making some assessment of the significance of this approximation, we have considered it worth while undertaking an investigation of a simple system in which essentially the same issues are involved, viz. the interaction of two hydrogen atoms each in its first excited state. The relevance of this interaction stems from the fact that the first excited state of the hydrogen atom is doubly degenerate, thus enabling us to construct hybridized s–p orbitals similar to those envisaged in the theory of directed valence. In the present note we set up a wave function for this system using the approximation of 'perfect pairing', and then compare it with the more accurate wave function in which no possible pairing scheme is neglected.

The interaction of two hydrogen atoms, each in the first excited state, defines a state of the molecule in which both electrons occupy excited molecular orbitals (m.o's), and these (using the separated-atom symbolism) will be of the type $\sigma 2s$, $\sigma 2p$ or $\pi 2p$, i.e. deriving adiabatically from the 2s or 2p wave functions of the free atoms as the nuclei are brought together. We are particularly interested in the lowest stable state of the system in these circumstances and therefore ignore the π-orbitals, i.e. those deriving from atomic p-functions perpendicular to the molecular axis, since they involve negligible interactions compared with the σ-orbitals. Of the latter, $\sigma_g 2s$ and $\sigma_g 2p$ are bonding and, for H_2, have comparable energies in the molecular field owing to the 2s, 2p degeneracy, thus suggesting the electronic configuration $(z\sigma_g)^2\, {}^1\Sigma_g$ (where $z\sigma_g$ is a hybrid of $\sigma_g 2s$ and $\sigma_g 2p$) as that which defines the lowest stable state of the molecule arising from the prescribed interaction. The energy of this hypothetical state lies at a level of about 24 ev $(4{\cdot}48 + 2 \times 10{\cdot}4 = 25{\cdot}28)$ above the ground level of the molecule, and is therefore quite beyond the range of the spectroscopically observed (doubly excited) levels listed in the standard work of Herzberg (1950). It is indeed open to doubt whether the state can lead an independent physical existence, for it must certainly compete with various alternative excited states of comparable energy, e.g. one electron occupying the ground m.o. $\sigma_g 1s$ and the other promoted into the ionized spectrum. However, the issues of interest in the present context refer solely to the formal properties of the particular interaction under consideration, and from this point of view the question of physical status may be dismissed as irrelevant.

At infinite separation R_∞ of the nuclei the two axially symmetric m.o's $\sigma_g 2s \equiv S$, $\sigma_g 2p \equiv P$ are orthogonal and degenerate, and therefore (omitting for the moment the inter-electronic interaction term e^2/r_{12} in the Hamiltonian) define the three independent zero order singlet wave functions

$$\mathrm{S}(1)\mathrm{S}(2),\quad \mathrm{S}(1)\mathrm{P}(2)+\mathrm{P}(1)\mathrm{S}(2),\quad \mathrm{P}(1)\mathrm{P}(2) \qquad \ldots\ldots(1)$$

of which some proper linear combination

$$\mathrm{S}(1)\mathrm{S}(2)+\alpha\{\mathrm{S}(1)\mathrm{P}(2)+\mathrm{P}(1)\mathrm{S}(2)\}+\beta\mathrm{P}(1)\mathrm{P}(2) \qquad \ldots\ldots(2)$$

constitutes an allowable representation of the state $(z\sigma_g)^2\ {}^1\Sigma_g$ of the system at any finite internuclear distance R. An alternative, more powerful, approach is to work with the hybridized m.o's $\mathrm{S}+\mu\mathrm{P}\equiv\mathrm{A}$, $\mathrm{S}+\lambda\mathrm{P}\equiv\mathrm{B}$ which constitute allowable representations of stationary states of the system $\mathrm{H}_2{}^+$ at all R; A and B are necessarily orthogonal at all R, degenerate at R_∞ (where they can be replaced by S and P), and are such that B is strongly bonding if λ is suitably chosen. In place of the three singlets (1) we then have

$$\psi_{\mathrm{I}}=\mathrm{B}(1)\mathrm{B}(2),\quad \psi_{\mathrm{II}}=\mathrm{B}(1)\mathrm{A}(2)+\mathrm{A}(1)\mathrm{B}(2),\quad \psi_{\mathrm{III}}=\mathrm{A}(1)\mathrm{A}(2) \qquad \ldots\ldots(3)$$

but now ψ_{I} alone is evidently the allowed representation of $(z\sigma_g)^2\ {}^1\Sigma_g$ at all R. On expanding ψ_{I}, we have

$$\psi_{\mathrm{I}}=\mathrm{B}(1)\mathrm{B}(2)=\mathrm{S}(1)\mathrm{S}(2)+\lambda\{\mathrm{S}(1)\mathrm{P}(2)+\mathrm{P}(1)\mathrm{S}(2)\}+\lambda^2\mathrm{P}(1)\mathrm{P}(2), \qquad \ldots\ldots(4)$$

which is seen to be a linear combination of the three original singlets (1); since (4) may be identified with (2), we must necessarily have $1:\alpha:\beta=1:\lambda:\lambda^2$.

The introduction of the interaction term e^2/r_{12} requires careful consideration in relation to the m.o. approximation. We may regard it in the first place as a straightforward perturbing potential, relevant at about R_0 but not at R_∞, and the zero order function (4) may then be used as it stands for calculating a first order energy correction. In a more refined treatment we should allow for configurational interaction between ψ_{I}, ψ_{II} and ψ_{III}—a procedure which amounts to using a linear variation treatment on the original combination (2). With the integrals available it would be quite feasible to determine α and β so that (2) constitutes a stationary state, and hence test the accuracy of the less rigorous hybridization treatment based on (4), but the work is sufficiently involved to warrant description in a separate paper. In view of the marked energy difference between the m.o's A and B, there is a marked (zero order) energy difference between the states (3), and we may therefore anticipate, on general grounds, that configurational interaction between these states will not turn out to be an effect of very great importance. A compromise procedure, which has been adopted here, is to regard λ as a parameter to be determined so that (4) constitutes a stationary state with respect to the total Hamiltonian of the system; this is an improvement on the straightforward use of (4) as a zero-order function in a perturbation process, but it is less accurate than the use of (2), for in (2) we have two independent parameters α and β at our disposal in a linear variation process whereas in (4) they are constrained to be of the form $1:\lambda:\lambda^2$.

To appreciate the significance of ψ_{I}, we note that

$$\mathrm{B}=\mathrm{S}+\lambda\mathrm{P}=(\mathrm{s_a}+\mathrm{s_b})+\lambda(\mathrm{p_a}+\mathrm{p_b})=(\mathrm{s_a}+\lambda\mathrm{p_a})+(\mathrm{s_b}+\lambda\mathrm{p_b}) \qquad \ldots\ldots(5)$$

where $\mathrm{s_a}$ stands for a 2s-function centred about nucleus a, etc., i.e. B may be regarded as a bonding m.o. made up from the overlapping hybridized a.o's $\mathrm{s_a}+\lambda\mathrm{p_a}$, $\mathrm{s_b}+\lambda\mathrm{p_b}$ centred respectively about the two nuclei. This means, in effect, that ψ_{I} represents a state of the system in which $\mathrm{s_a}+\lambda\mathrm{p_a}$ is paired with $\mathrm{s_b}+\lambda\mathrm{p_b}$ to form the dominant pairing scheme, the other pairing schemes being

$s_a+\lambda p_a$ with $s_b+\mu p_b$ (represented by ψ_{II}) and $s_a+\mu p_a$ with $s_b+\mu p_b$ (represented by ψ_{III}). Accordingly, the use of ψ_I alone is analogous to the approximation of 'perfect pairing' used with covalent structures, the only difference being that ψ_I includes an admixture of ionic states due to its being a m.o. representation of the pairing rather than a valence bond representation. In the present problem we have the advantage of being able to compare ψ_I with the more correct function (2) which is a linear combination of ψ_I, ψ_{II} and ψ_{III}.

Fairly straightforward energy calculations (Aghajanian 1954) yield a binding energy, relative to two excited atoms at infinite separation, of approximately 4·4 ev, at an equilibrium separation $R_0 \sim 1{\cdot}6$ Å, with a vibrational frequency approximately 2263 cm^{-1}. At first sight the estimate obtained for the binding energy seems anomalously high, but it should be remembered that H_2 differs from other diatomic molecules in several important respects:

(i) The existence of the 2s, 2p degeneracy, which effect must considerably reinforce the cohesion. In the case of carbon, where the self-consistent 2p level lies at about 3 ev above the self-consistent 2s level, even the approximate degeneracy is effective in producing the strong σ-bonding characteristic of carbon.

(ii) The absence of ion-core electrons, which in other diatomic molecules are known to have a marked effect in reducing the stability (Coulson 1952).

(iii) The extremely high binding energy of the ground state. It is not surprising to find the binding energy at least as great as this for a doubly occupied m.o. which is excited, since the overlap of the relevant atomic wave functions is much more marked than in the ground state.

On writing B in the form (5), and then forming the mean value of the Hamiltonian of the system with respect to B(1)B(2), it may be verified without difficulty that we are led to energy integrals of the types (using the cyclic notation of Slater 1931)

$$C_{\alpha\beta}=\alpha_a\left|-\frac{\hbar^2}{2\mu}\nabla^2-\frac{e^2}{r_a}\right|\beta_a,\quad C'_{a\beta}=\alpha_a\left|-\frac{\hbar^2}{2\mu}\nabla^2-\frac{e^2}{r_b}\right|\beta_b$$

$$Q_{\alpha\beta}=\alpha_a\left|\frac{e^2}{r_b}\right|\beta_a,\quad Q'_{\alpha\beta}=\alpha_a\left|\frac{e^2}{r_b}\right|\beta_b,\quad \Delta_{\alpha\beta}=\alpha_a\left|1\right|\beta_b$$

$$J_{\alpha\beta\gamma\delta}=\alpha_a\beta_b\left|\frac{e^2}{r_{12}}\right|\gamma_a\delta_b,\quad J'_{\alpha\beta\gamma\delta}=\alpha_a\beta_b\left|\frac{e^2}{r_{12}}\right|\gamma_b\delta_a$$

$$M_{\alpha\beta\gamma\delta}=\alpha_a\beta_b\left|\frac{e^2}{r_{12}}\right|\gamma_a\delta_a,\quad H_{\alpha\beta\gamma\delta}=\alpha_a\beta_a\left|\frac{e^2}{r_{12}}\right|\gamma_a\delta_b$$

where α_a stands for an α-function centred about nucleus a, etc. The $C_{\alpha\beta}$ present no difficulty, analytic expressions for $C'_{\alpha\beta}$ may be found from Roothaan (1951); $Q_{\alpha\beta}$, $Q'_{\alpha\beta}$, $\Delta_{\alpha\beta}$, $J_{\alpha\beta\gamma\delta}$ and $J'_{\alpha\beta\gamma\delta}$ are given by Kopineck (1950); $M_{\alpha\beta\gamma\delta}$ may be obtained from Barnett and Coulson (1951), and also independently from the relation $M_{\alpha\beta\gamma\delta}\rightarrow\mathrm{Lim}_{R\rightarrow 0}J_{\alpha\beta\gamma\delta}$: after these had been evaluated by us, the were found to be tabulated by Araki and Watari (1951); $H_{\alpha\beta\gamma\delta}$ were integrated on IBM computing machines on the basis of the ζ-function technique of Barnett and Coulson: they were afterwards found to be tabulated by Araki and Watari.

The function ψ_I, whether defined by (2) or (4), is not rigorously orthogonal to the ground m.o. wave function of the system, for neither $\sigma_g 2s \equiv 2s_a+2s_b$ nor $\sigma_g 2p \equiv 2p_a+2p_b$ are rigorously orthogonal to the ground m.o. $\sigma_g 1s \equiv 1s_a+1s_b$; certainly $2s_a$, $2p_a$ are orthogonal to $1s_a$, but unfortunately they are not quite orthogonal to $1s_b$ even though $R_0 \sim 1{\cdot}6$ Å. This lack of orthogonality implies that $\psi_{\rm I}$ includes a small admixture of the ground wave function, thus leading to a spurious lowering of the energy—and hence to a spurious overestimation of the binding energy—by an amount estimated to be of the order of 1 ev. Unfortunately it has been found necessary to adopt Slater function representations of $2s_a$ and $2s_b$, for most of the tabulated integrals refer to such functions and not to hydrogenic functions. This introduces certain obscurities into the analysis and, moreover, has the obvious effect of aggravating the non-orthogonality difficulty; nevertheless, since the self energy of each excited atom is calculated with respect to Slater functions, they should lead to no marked overestimation of the binding energy, and in any case by 1 ev at most. The two sources of overestimation have been allowed for in the figure 4·5 ev mentioned earlier. If this figure is accepted, our results imply that hybridization is effective in producing strong σ-bonds between excited hydrogen atoms, and it can therefore be anticipated that the hybridized orbitals of Slater and Pauling similarly provide an explanation of the extremely high cohesion and elastic constants of diamond.

ACKNOWLEDGMENT

The authors acknowledge helpful remarks from the referee as regards the presentation.

REFERENCES

AGHAJANIAN, H., 1954, *Thesis*, University of London.
ARAKI, G., and WATARI, W., 1951, *Progr. Theor. Phys., Osaka*, **6**, 961.
BARNETT, M. P., and COULSON, C A., 1951, *Phil. Trans. Roy. Soc.* A, **243**, 221.
COULSON, C. A., 1952, *Valence* (Oxford : University Press), p. 177.
HERZBERG, G., 1950, *Spectra of Diatomic Molecules*, 2nd Edn (New York : Van Nostrand), p. 340.
KOPINECK, H. J., 1950, *Z. Naturf.*, **5a**, 420.
ROOTHAAN, C. C. J., 1951, *J. Chem. Phys.*, **19**, 1445.
SLATER, J. C., 1931, *Phys. Rev.*, **38**, 1109.

The Use of Overlapping Intervals in Multiple Scattering Measurements

BY D. S. SCHONLAND
University of Southampton

Communicated by E. H. S. Burhop ; *MS. received 20th December* 1954

FOLLOWING the usual method of measuring multiple scattering (Fowler 1950), the y coordinates y_k of points on the track of a fast ionizing particle are measured at equal intervals τ along the x axis, which is aligned along the general direction of the track. From these measurements the quantities

$$\beta_k^{(l)} = [y_{k+l} - 2y_k + y_{k-l}]/l\tau \qquad \ldots\ldots(1)$$

can be formed and, in small angle approximation, represent the angles between successive overlapping chords of the track of length $l\tau$. Then if $a_0^{(l)}$ and $e_0^{(l)}$ are the mean square values of the true multiple scattering chord angle and the 'noise' respectively for chords of length $l\tau$, one can estimate $a_0^{(l)}$ from the equation

$$[a_0^{(l)}]_{\rm est} = \langle b_0^{(l)} \rangle - e_0^{(l)} \qquad \ldots\ldots(2)$$

where $\langle b_0^{(l)} \rangle$ represents the measured mean square value of the $\beta_k^{(l)}$ and $e_0^{(l)}$ is assumed to have been independently determined.

The probable (r.m.s.) error in the estimation of $a_0^{(l)}$ by equation (2) has been calculated for $l=1$, 2 and 3, using the method described in a previous paper (Schonland 1952, referred to below as I), on the assumption that the multiple scattering and the noise both have gaussian distributions, with correlations between the $\beta_k^{(1)}$ as given in I equation (3*a*).

In the notation of I, the probable error in an estimate of a_0 is denoted by $a_0\mathsf{F}(a_0)$; this is a function of the ratio τ/τ_0, where τ_0 is the interval length for which $a_0^{(1)}=e_0^{(1)}$. One may compare the efficacy of various methods of estimating a_0 for a track of given total length $T=N_0\tau_0$ by plotting $\sqrt{N_0}\mathsf{F}(a_0)$ as a function of τ/τ_0.

The results are shown in figure 1, where $\sqrt{N_0}\mathsf{F}(a_0)$ is plotted as a function of τ/τ_0 (i) for $l=1$ (singly overlapping intervals), (ii) for $l=2$ (doubly overlapping intervals), (iii) for $l=3$ (triply overlapping intervals). The broken curve in the figure shows the 'minimum possible error' obtained when the information contained in a set of values of the y_k is used to best advantage (I, § 2 (ii)). It is clear that equation (2) for the various values of l considered will yield good results provided that the basic interval length τ is properly chosen in relation to τ_0. The best value of l to use for a given set of measurements will be determined by the value of τ/τ_0: it may be noted that for $\tau>1{\cdot}4\tau_0$ the use of singly overlapping intervals will be preferable to that of double or triple intervals.

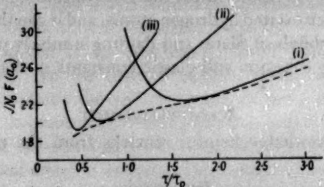

Figure 1. The relative error in the use of equation (2): (i) with $l=1$, (ii) with $l=2$, (iii) with $l=3$. The broken curve represents the minimum possible error.

Another way of exhibiting these results is shown in figure 2 where (i) shows $\sqrt{N_0}\mathsf{F}(a_0)$ for singly overlapping intervals of length τ plotted as a function of τ/τ_0, (ii) shows the result that would be obtained if the interval were halved and doubly overlapping intervals were used, and (iii) shows the effect of trisecting the interval and using triply overlapping intervals, both (ii) and (iii) being plotted as functions of the basic interval ratio τ/τ_0. Thus the difference between (i) and (ii) shows,

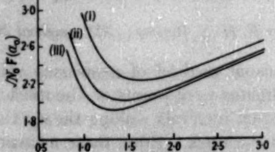

Figure 2. Relative errors in the use of equation (2), (i) with $l=1$, and interval τ, (ii) with $l=2$ and interval $\tau/2$, (iii) with $l=3$ and interval $\tau/3$.

for a particular value of τ/τ_0, what improvement would be gained by halving the interval length (and consequently doubling the number of measurements) and using doubly overlapping intervals. Similarly, the difference between (i) and (iii) shows the effect of trebling the number of measurements and using triple intervals.

Translated into terms of N, the total number of measurements made on a particular track, and taking $\tau = 1{\cdot}5\tau_0$ which is close to the minima of the curves of figure 2, these results give for single intervals with $N = N_1$, $\mathsf{F}(a_0) = 1{\cdot}85/\sqrt{N_1}$; for double intervals with $N = 2N_1$, $\mathsf{F}(a_0) = 2{\cdot}32/\sqrt{N} = 1{\cdot}64/\sqrt{N_1}$; for triple intervals with $N = 3N_1$, $\mathsf{F}(a_0) = 2{\cdot}73/\sqrt{N} = 1{\cdot}58/\sqrt{N_1}$. (In order to obtain a value for $\mathsf{F}(a_0)$ from the figures one uses the relation $N = N_0\tau_0/\tau$.)

From these figures one may conclude that the extra work required to use doubly or triply overlapping intervals is not commensurate with the resultant improvement in the accuracy of the estimation. This conclusion is supported by the work of O'Ceallaigh and Rochat (1951), and is due to the rather slow decrease of the minimum possible error with interval length.

In the limit of no noise, i.e. as $\tau/\tau_0 \to \infty$, one finds $\mathsf{F}(a_0)$ equal to $(6{\cdot}47/N)^{1/2}$ for triply overlapping intervals; $(4{\cdot}32/N)^{1/2}$ for doubly overlapping intervals; and $(2{\cdot}25/N)^{1/2}$ for singly overlapping intervals, whereas the minimum possible error in this limit is $(2/N)^{1/2}$.

The author would like to thank Dr. E. H. S. Burhop for suggesting this problem to him.

REFERENCES

FOWLER, P. H., 1950, *Phil. Mag.*, **41**, 169.
O'CEALLAIGH, C., and ROCHAT, O., 1951, *Phil. Mag.*, **42**, 1050.
SCHONLAND, D. S., 1952, *Proc. Phys. Soc.* A, **65**, 640.

LETTERS TO THE EDITOR

Nuclear Electric Quadrupole Moment of Potassium 39

We have applied the 'double resonance' method (Brossel and Kastler 1949, Brossel and Bitter 1952, Sagalyn 1954, Althoff and Kruger 1954) to an investigation of the state $5^2P_{3/2}$ of potassium, and have obtained resonances in magnetic fields which produce splittings of the sub-levels both small and great compared with the hyperfine structure. Although the experiments are still in progress, it is possible at this stage to quote the preliminary values $a = 1{\cdot}9 \pm 0{\cdot}2$ Mc/s for the magnetic dipole interaction constant, and $b/a = +1{\cdot}0 \pm 0{\cdot}25$, where b is the electric quadrupole interaction constant defined by the Hamiltonian

$$\mathscr{H} = a\mathbf{I}\,.\,\mathbf{J} + \frac{b}{2I(2I-1)J(2J-1)}\,[3(\mathbf{I}\,.\,\mathbf{J})^2 + \tfrac{3}{2}(\mathbf{I}\,.\,\mathbf{J}) - I(I+1)J(J+1)] + \beta g_J\mathbf{J}\,.\,\mathbf{H} + \beta_N g_I\mathbf{I}\,.\,\mathbf{H}. \qquad \ldots\ldots(1)$$

This value of a is in good agreement with the value 1·93 Mc/s which is obtained from the Goudsmit formula (see Kopfermann 1940) by taking $\mu = 0{\cdot}391$, $I = 3/2$ (Mack 1950) and $Z_I = 14{\cdot}8$ (Casimir 1936). Using the relation

$$b/a = Q\,\frac{3}{8}\,\frac{\mathbf{e}^2}{\beta^2}\,\frac{M}{m}\,\frac{I}{\mu}$$

(Davis *et al.* 1949) and without applying any corrections (Sternheimer 1950) we find the preliminary value for the electric quadrupole moment of ^{39}K,

$$Q = +0{\cdot}14 \times 10^{-24}\,\text{cm}^2 \pm 25\%.$$

Potassium in the form of an atomic beam traversing a glass bulb is illuminated by plane polarized radiation from a water-cooled hollow-cathode discharge in which potassium is used in the cathode and neon as the carrier gas. The scattered resonance radiation of the second doublet of the Principal Series (λ 4044 and 4047 Å) is isolated by filters and received by a photomultiplier in a direction at right angles to the incident beam. The resonance bulb is surrounded by Helmholz coils which produce a steady magnetic field in the direction of observation, and by smaller coils which produce a radio-frequency magnetic field at right angles both to the incident light beam and to the steady field. The signal (i.e. the change produced by the radio-frequency resonance in the intensity of the resonance radiation in the direction of observation) is modulated, amplified, detected by a phase-sensitive detector and recorded.

In the experiments in 'strong' fields (about 24 gauss) the incident light is plane polarized with the electric vector in the direction of observation of the scattered light, i.e. in the direction of the steady field. Since the ground state $4S_{1/2}$ has the same value of J as the $5P_{1/2}$ state, the magnetic sub-levels of this excited state are equally populated by the optical excitation, and no radio-frequency resonances are observed. Thus the signal is entirely due to transitions in the $5P_{3/2}$ state in which the sub-levels are not equally populated. The radio frequency is held constant while the magnetic field is continuously varied. A small oscillating magnetic field at 60 c/s is superimposed upon the steady field and a reference voltage from the same oscillator is used for the phase-sensitive detector.

The deflection of the recorder is then proportional to the differential of a plot of light signal against magnetic field at constant radio frequency. These differentiated resonance curves are particularly valuable in detecting and locating incompletely resolved lines.

The resonance curves obtained in these experiments are interpreted as a partly resolved pattern of eight lines of equal intensity arising from the transitions $m_J = \pm 1/2 \pm 3/2, \Delta m_I = 0$. The lines fall into two overlapping groups of four (m_I may take the values $\pm 1/2$, $\pm 3/2$), and by means of a quarter-wave plate and Nicol prism it has been shown that one group corresponds to right, the other to left circularly polarized light. The Hamiltonian (1) predicts patterns of the type observed if the ratio b/a is suitably chosen. The intervals in gauss may be converted into Mc/s either by the use of the theoretical value of g_J, 1·33, or the ratio of frequency to field at the centre of the pattern which yields $g_J = 1{\cdot}35 \pm 0{\cdot}02$. From a comparison of observed with calculated patterns we arrive at the values of a and b given above.

Slight asymmetries observed in the patterns can be accounted for by correction terms which arise because the decoupling of I and J is not quite complete. That the sign of b is the same as that of a is deduced from the orientation of the patterns separated by the $\lambda/4$ plate, from the influence of the correction terms, and also from an examination of the resonance curves obtained at frequencies in the region of 19 Mc/s where we were able to observe resonances with the radio-frequency field parallel to the steady field ($\Delta(m_I + m_J) = 0$).

The values of a and b deduced above are supported by exploratory experiments made in the earth's magnetic field alone. In these experiments the relative orientation of component parts of the apparatus was as above, but the radio-frequency current was modulated at 60 c/s, and the resonance curves plotted point by point as a function of frequency. Resonances about 2 Mc/s wide were observed in the regions of 7·0 and 1·4 Mc/s. We interpret these as due to the transitions F = 3–2 and 2–1 respectively. Setting these resonance frequencies equal to $3a+b$, $2a-b$, as predicted by (1), yields $a = 1{\cdot}7$ Mc/s, $b = 2{\cdot}0$ Mc/s. While it is reassuring that these figures are in good agreement with those obtained from the 'strong' field experiments, they are regarded as very provisional because of the large amplitude of the radio-frequency magnetic field (about 1 gauss) necessary to obtain the signals. Both this and the earth's field will produce a perturbation comparable with the interval between F = 2 and 1, and the theoretical interpretation of these experiments is not straightforward.

We hope to make a fuller publication at a later stage. In the meantime we wish to express our thanks for helpful discussions with many of our colleagues in the Clarendon Laboratory, and especially with Dr. B. Bleaney and Dr. H. Kuhn. One of us (G. J. R.) is indebted to the Rhodes Trust for a Scholarship.

Clarendon Laboratory,
Oxford.
18th January 1955.

G. J. Ritter.
G. W. Series.

Althoff, K. H., and Kruger, H., 1954, *Naturwissenschaften*, **41,** 368.
Brossel, J., and Bitter, F., 1952, *Phys. Rev.*, **86,** 308.
Brossel, J., and Kastler, A., 1949, *C.R. Acad. Sci., Paris*, **229,** 1213.
Casimir, H. B. G., 1936, *On the Interaction Between Atomic Nuclei and Electrons* (Haarlem : Teylers Tweede Genootschap).

Davis, L., Feld, B. T., Zabel, C. W., and Zacharias, J. R., 1949, *Phys. Rev.*, **76**, 1080 (equation 20; see also footnote).
Kopfermann, H., 1940, *Kernmomente* (Michigan : Edwards).
Mack, J. E., 1950, *Rev. Mod. Phys.*, **22**, 64.
Sagalyn, P. L., 1954, *Phys. Rev.*, **94**, 885.
Sternheimer, R., 1950, *Phys. Rev.*, **80**, 102.

The Yield of ^{7}Li(p,n)^{7}Be* Neutrons for Proton Energies between 2·5 and 2·9 MeV

It is now well established that when lithium 7 is bombarded with protons of energies greater than 2·378 MeV, two groups of neutrons are emitted, corresponding to the formation of beryllium 7 in the ground and in a 430 kev excited state. Previous results on the ratio of the intensities of the low and high energy groups have been reviewed by Ajzenberg and Lauritsen (1952). More recently Cranberg (1954) has measured this ratio and found it to be approximately 10% for proton energies between 3·9 and 5·4 MeV using a time-of-flight technique. The present letter gives results for proton energies between 2·5 and 2·9 MeV, and for neutrons emitted in the forward direction, obtained with a helium 3 fast neutron spectrometer (Batchelor 1952).

The instrument used for these measurements was more highly developed than that described in the previous communication and further details will be published in due course. A typical pulse height distribution obtained when it was placed 17 inches from a 40-kev thick lithium fluoride target is shown in figure 1. The relative intensities of the two groups, shown in figure 2, were calculated from the total number of counts in each peak. Corrections were made for the variation with neutron energy of the ^{3}He(n,p)^{3}H cross section and the wall effect of the counter.

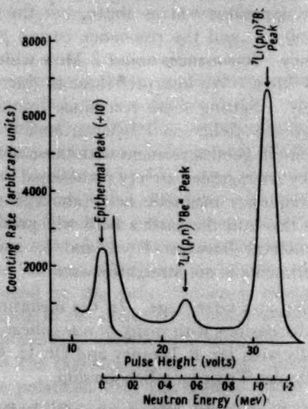

Figure 1. Pulse height distribution. Proton energy = 2·77 MeV.

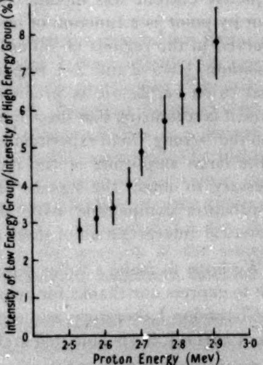

Figure 2. Relative intensities of the low and high energy neutron groups.

I wish to thank Mr. M. J. Elliott for his help in taking the measurements, and Dr. W. D. Allen for the use of the Van de Graaff machine.

Atomic Energy Research Establishment,
Harwell, Didcot, Berks.
9th February 1955. R. Batchelor.

Ajzenberg, F., and Lauritsen, T., 1952, *Rev. Mod. Phys.*, **24**, 334.
Batchelor, R., 1952, *Proc. Phys. Soc.* A, **65**, 674.
Cranberg, L., 1954, *United States Atomic Energy Report*, L.A. 1654.

REVIEWS OF BOOKS

Quantum Mechanics, by F. Mandl. Pp. viii + 232. (London: Butterworths Scientific Publications, 1954.) 35*s*.

Only some eighteen months elapsed between the giving of a course of lectures by Dr. Mandl and the printing of this book which he has based on them. Such haste is the probable cause of its failings. It is, indeed, little more than a somewhat expanded set of lecture notes, and it is difficult to see that it adds much to what has already been written on the subject.

It is intended to " bring out the unifying mathematical scheme underlying quantum mechanics " and, accordingly, there are few experimental examples of the formal theory. It is therefore, presumably, meant primarily for those who wish to appreciate and study this scheme. Such a short book cannot and does not set out to present original work or to be a treatise on the subject. Nevertheless, it can still be useful as a guide for the theoretician and, even more, for the experimentalist, provided it is concise, orderly and accurate. Unfortunately, this book is lacking in all three qualities.

It is repetitive and has no clear scheme of presentation. Thus, although many quantum mechanical terms have already been introduced and defined, it is not until we have read over a third of the book that we come to " *Definition* 1." " *Definition* 2. Two operators *A* and *B commute*, if . . . " occurs five pages after the terms *commutator* and *non-commutability* have been used. Most of the operator and eigenfunction theory presented in Chap. 2 is unnecessary for Chap. 3 and is repeated, more generally, in Chap. 4.

Although we do not expect mathematically rigorous proofs of all the rules and theorems given, they should be true, with mention of the qualifications and exceptions, if any, and, preferably, some reference to more thorough discussion elsewhere. The more general the statement, the more important this becomes. It is surprising, therefore, to find a rule given for the construction of quantum mechanical operators for generalized coordinate systems supported only by the comment that it is a ' natural generalization ', when Dirac has pointed out that it has only rather limited applicability and Kemble has given explicit examples of its failure.

The scope of the book is good and the problems given at the end of each chapter cover useful ground. The atomic or nuclear physicist who works through them with the aid of the hints provided at the end of the book would acquire a good background of quantum theory. N. C. B.

Advanced Level Examples in Physics, by R. V. Johns and W. F. Ware. Pp. viii + 346. (London: Macmillan, 1954). 16*s*.

The authors largely succeed in their aim of supplementing the theoretical and laboratory work of students preparing for examinations in Physics at the Advanced Level of the G.C.E. and for Intermediate examinations, particularly in the case of the weaker candidates.

The book contains about one thousand examples of graded difficulty, arranged by topics, with answers at the end. Each section is preceded by a useful summary of relevant principles and formulae, together with worked examples. These examples are very lucidly set out. In the main, arithmetical methods are employed in preference to those involving juggling with formulae, and ample verbal explanation of the steps is given. In a few cases only, unnecessarily long methods of solution are given.

One or two omissions have been noticed. There are not many examples involving the wave theory of light, and there is no mention of this subject in the text, nor are there any worked examples upon it. The sections on electromagnetism seem rather curtailed : for example, self induction is not mentioned, and there is but a bare minimum on alternating current, inadequate for the Advanced Level syllabus of at least one examining body.

There is a useful set of over one hundred revision examples at the end of the book, and many of these are suitable for the brighter students.

The ' real is positive ' optical sign convention is used.

R. SHEWELL.

CONTENTS OF SECTION B

PAGE

Dr. A. J. KENNEDY. Recovery and Recrystallization in Metals examined in terms of the Restoration of the Transient Creep Properties 257

Prof. F. KREITH and Mr. F. E. ROMIE. A Study of the Thermal Diffusion Equation with Boundary Conditions corresponding to Solidification or Melting of Materials Initially at the Fusion Temperature. 277

Dr. THONG SAW PAK. Noise from Hot-cathode Discharges 292

Dr. D. J. WRIGHT. Hysteresis of the Angle of Contact of Mercury against Steel . 297

Prof. L. F. BATES and Dr. N. P. R. SHERRY. The Heat Changes Accompanying Magnetization Processes in Ferrites 304

Mr. G. G. E. LOW. Carrier Concentration Disturbances in Semiconductors. . 310

Research Notes :

Mr. P. T. NARASIMHAN. Temperature Dependence of the Dielectric Constant of Diamond 315

Letters to the Editor :

Dr. L. PINCHERLE. Auger Effect in Semiconductors 319

Prof. G. O. JONES. An Improved Miniature Liquefier-Cryostat 320

Reviews of Books. 322

Contents of Section A 324

Cross Sections for 2s–2p Transitions in H and 3s–3p Transitions in Na Produced by Electron and by Proton Impact

By M. J. SEATON
Department of Physics, University College London

MS. received 13*th October* 1954

Abstract. Reliable cross sections for 2s–2p transitions in H produced by electron and by proton impact are required in certain astrophysical problems. In calculating these cross sections it is necessary to allow for strong coupling effects. Such effects are also important for 3s–3p transitions in Na produced by electron impact, for which experimental results are available.

The total cross section Q is the sum of components Q^l arising from the components of the incident wave with angular momenta $\hbar[l(l+1)]^{1/2}$. For these a limiting value $Q^l{}_{\text{max}}$ is set by the requirement of charge conservation. The approximation adopted is to calculate the Q^l using the Bethe approximation, to accept the values obtained if $Q^l{}_{\text{Bethe}} < \frac{1}{2}Q^l{}_{\text{max}}$ and to put $Q^l = \frac{1}{2}Q^l{}_{\text{max}}$ if $Q^l{}_{\text{Bethe}} \geqslant \frac{1}{2}Q^l{}_{\text{max}}$. The conditions for the validity of this approximation are examined, some use being made of an exactly soluble schematic model. It is considered that the final results for the H transitions should be correct to within ±20%. The results obtained for electron collisions with Na are found to be in good agreement with experiment, the approximation used being considerably superior to the Born approximation at low energies.

§ 1. Introduction

Information on the relative population of the 2s metastable state of hydrogen is required in at least two astrophysical problems. The first concerns the continuum intensities of gaseous nebulae, to which 2s → 1s transitions with the emission of two quanta may give an important contribution (Spitzer and Greenstein 1951, Kipper 1952). The second concerns the microwave radiation from the solar chromosphere, in which radiative 2s–2p transitions might be detected if the population of H(2s) is sufficiently great (Wild 1952, Purcell 1952). In order to calculate the relative population of H(2s) accurate cross sections for collisionally induced 2s–2p transitions are required.

Cross sections for electron impact have been calculated by Breit and Teller (1940) using the approximation of Bethe (1930) and cross sections for both electron and proton impact have been calculated by Purcell (1952) using a semi-classical method similar to the method of Weizsäcker (1934) and of Williams (1934). The method consists in calculating the probabilities of radiative transitions induced by the field of the impinging particle, the motion of which is treated classically. The results obtained show that, for equal proton and electron densities, collisions with protons will be more important than collisions with electrons.

From a classical standpoint it is obvious that the total transition probability per encounter should not exceed unity. The method used by Purcell ensured that the individual $2s \rightarrow 2p_{1/2}$ and $2s \rightarrow 2p_{3/2}$ transition probabilities should not exceed unity but does not appear to satisfy the somewhat more stringent condition that the sum of the transition probabilities should not exceed unity.

The quantum mechanical analogue of this classical condition is provided by the conservation theorem of Mott (1931) and of Bohr, Peierls and Placzek (unpublished, see Massey and Burhop 1952, and Mott and Massey 1949, p. 133). This gives an upper limit $Q^l_{\max}$ for the sum of all partial inelastic cross sections, Q^l_{in}, arising from the component of the incident wave with angular momentum $\hbar[l(l+1)]^{1/2}$. A necessary condition for the validity of the usual weak coupling approximations, such as Born's approximation, is that the calculated values of Q^l_{in} should be less than $Q^l_{\max}$ for all values of l. The results of Purcell for H 2s–2p transitions suggest that weak coupling approximations will violate this condition for the smaller values of l (close encounters), and that it is therefore necessary to take strong coupling effects into account. It has previously been remarked by Bates, Fundaminsky, Leech and Massey (1950) that the Born approximation tends to be unreliable at low energies for strong optically allowed transitions, such as 3s–3p transitions in Na, and it appears to be very probable that this is also due to the neglect of strong coupling effects.

The present paper describes calculations made for 2s–2p transitions in H and 3s–3p transitions in Na produced by proton and by electron impact, using proper quantum mechanical methods and allowing for strong coupling effects. The conditions for the validity of the particular approximation used are discussed and it is concluded that the H results should be correct to within ±20%. The results for electron collisions with Na are found to be in good agreement with experiment.

Application of the results obtained for H to the calculation of continuum intensities in gaseous nebulae has been described elsewhere (Seaton 1954).

§ 2. Notation and General Formulation

2.1. *Notation*

Consider particles of mass M_i and charge Ze incident on atoms of mass M_a. For electrons $Z=-1$ and for protons $Z=+1$. The reduced mass is

$$M=M_iM_a/(M_i+M_a).$$

The relative velocity at large separation, the atom being in energy level n, is denoted by v_n and k_n is defined as $Mv_n/\hbar$. For transitions from energy level n to energy level n' the cross section is denoted by $Q(n\rightarrow n')$ and the corresponding *collision strength* is defined as

$$\Omega(n',n)=\frac{k_n{}^2\omega_n}{\pi}Q(n\rightarrow n'), \qquad \ldots\ldots(1)$$

ω_n being the statistical weight of level n.

The term collision strength is suggested by analogy with the *line strength* as used by Condon and Shortley (1951). For radiative transitions between states ν and ν' with wave functions $\psi(\nu|\mathbf{r}_1,\mathbf{r}_2\ldots\mathbf{r}_N)$ and $\psi(\nu'|\mathbf{r}_1,\mathbf{r}_2\ldots\mathbf{r}_N)$ the dipole line strength is defined as

$$\mathbf{S}(\nu',\nu)=e^2\left|\int\psi^*(\nu'|\mathbf{r}_1,\mathbf{r}_2\ldots\mathbf{r}_N)\left[\sum_{j=1}^{N}\mathbf{r}_j\right]\psi(\nu|\mathbf{r}_1,\mathbf{r}_2\ldots\mathbf{r}_N)\,d\mathbf{r}_1\,d\mathbf{r}_2\ldots d\mathbf{r}_N\right|^2. \quad .(2)$$

The line strength $\mathbf{S}(n', n)$ connecting two degenerate levels is obtained on summing (2) over all initial and final states. Both the collision strengths and the line strengths are symmetrical in n and n' but unlike the line strength the collision strength is a dimensionless pure number.†

If the density of impinging particles per unit volume is N_i and the density of atoms in state n is N_n the total number of $n \to n'$ transitions per unit volume per unit time is $N_i N_n W(n \to n')$ where

$$W(n \to n') = \int v_n Q(n \to n') f(v_n)\, dv_n$$

and where $f(v_n)$ is the normalized distribution function for the relative velocity. For a Maxwell distribution with a kinetic temperature T (°K) this becomes

$$W(n \to n') = \frac{8{\cdot}63 \times 10^{-6}}{\omega_n T^{1/2}} \Upsilon(T;\, n, n')\, \mathrm{cm}^3\, \mathrm{sec}^{-1} \qquad \ldots\ldots(3)$$

with

$$\Upsilon(T;\, n, n') = \left(\frac{m}{M}\right)^{3/2} \int_0^\infty \Omega(n', n) \exp(-M v_n{}^2/2\kappa T)\, d(M v_n{}^2/2\kappa T) \qquad \ldots\ldots(4)$$

it being noted that the reduced mass occurs in the Maxwell distribution function for the relative velocity. The electron mass is denoted by m.

The total collision strength may be expanded in the form

$$\Omega(n', n) = \sum_{l=0}^{\infty} \Omega^l(n', n) \qquad \ldots\ldots(5)$$

where the partial collision strength $\Omega^l(n', n)$ is the contribution from the initial state in which the relative angular momentum is $\hbar[l(l+1)]^{1/2}$ and the atom is in level n. Charge conservation requires that

$$\sum_{n' \neq n} \Omega^l(n', n) \leqslant (2l+1)\omega_n \qquad \ldots\ldots(6)$$

(Mott and Massey 1949, p 133).

For practical calculations it is convenient to use atomic units ($m=1$, $e=1$ and $\hbar=1$). Unless the contrary is stated these will be adopted in the present paper. Cross sections in units of $\pi a_0{}^2$ ($8{\cdot}806 \times 10^{-17}$ cm^2), where a_0 is the atomic unit of length, are given by

$$Q(n \to n') = \frac{13{\cdot}60\,\Omega(n', n)}{M \omega_n E_n(\mathrm{ev})} \qquad \ldots\ldots(7)$$

where E_n(ev) is the initial energy of relative motion in ev and M is the reduced mass in atomic units, i.e. $M = M_i M_a / m(M_i + M_a)$.

2.2. *Formulation of the Collision Problem*

For reasons of simplicity the general theory will be discussed with particular reference to transitions in hydrogen; however the main results obtained are applicable for any optically allowed transition. For collisions with H atoms the complete wave function may be expanded in the form

$$\Psi(\mathbf{r}', \mathbf{r}) = \sum_{\nu} \psi(\nu \,|\, \mathbf{r}')\, u(\nu \,|\, \mathbf{r}) \qquad \ldots\ldots(8)$$

---

† The term ' target area ' which is sometimes used in referring to the quantity defined by (1) does not seem to be particularly appropriate for a dimensionless quantity.

where the $\psi(\nu|\mathbf{r}')$ are H atom wave functions. This will be a solution of the Schroedinger equation if the functions $u(\nu|\mathbf{r})$ satisfy

$$(\nabla^2+k_\nu^2)u(\nu|\mathbf{r})=2M\sum_{\nu'}V(\nu;\,\nu'|\mathbf{r})u(\nu'|\mathbf{r}) \qquad \ldots\ldots(9)$$

where
$$V(\nu;\,\nu'|\mathbf{r})=Z\int\psi^*(\nu|\mathbf{r}')\,\frac{1}{|\mathbf{r}-\mathbf{r}'|}\,\psi(\nu|\mathbf{r}')\,d\mathbf{r}'-\frac{Z}{r}\,\delta_{\nu,\nu'}. \qquad \ldots(10)$$

For transitions with initial state ν solutions of the equations (9) are required with asymptotic form

$$\left.\begin{aligned} u(\nu|\mathbf{r}) &\sim \exp(ik_\nu z)+\frac{1}{r}\,f_{\nu\nu}(\theta,\phi)\exp(ik_\nu r)\\ u(\nu'|\mathbf{r}) &\sim \frac{1}{r}\,f_{\nu'\nu}(\theta,\phi)\exp(ik_{\nu'}r) \quad (\nu'\neq\nu). \end{aligned}\right\} \qquad \ldots\ldots(11)$$

The collision strength connecting states ν and ν' is then given by

$$\Omega(\nu',\nu)=\frac{k_\nu k_{\nu'}}{\pi}\iint\left|f_{\nu'\nu}(\theta,\phi)\right|^2\sin\theta\,d\theta\,d\phi. \qquad \ldots\ldots(12)$$

The collision strength $\Omega(n',n)$ connecting two degenerate levels is obtained on summing equation (12) over all states of the two levels.

2.3. *The Born and Bethe Approximations*

The Born approximation may be used if the following conditions are satisfied: (i) the potentials $V(\nu;\nu)$ and $V(\nu';\nu')$ are sufficiently small to be neglected and (ii) the coupling terms $V(\nu;\nu')$ are sufficiently small to ensure that the transition probability per encounter is always much less than unity (cf. the condition (6)). When these are satisfied the equations (9) may be replaced by

$$\left.\begin{aligned} (\nabla^2+k_\nu^2)u(\nu|\mathbf{r}) &=0\\ (\nabla^2+k_{\nu'}^2)u(\nu'|\mathbf{r}) &=2MV(\nu';\,\nu|\mathbf{r})u(\nu|\mathbf{r}) \end{aligned}\right\} \qquad \ldots\ldots(13)$$

where ν is the initial state and $\nu'\neq\nu$. The Born approximation collision strengths are then given by equation (12) with

$$f_{\nu'\nu}(\theta_{k_{\nu'}},\phi_{k_{\nu'}})=-\frac{2M}{4\pi}\int\exp\{i(k_\nu z-\mathbf{k}_{\nu'}.\mathbf{r})\}V(\nu';\,\nu|\mathbf{r})\,d\mathbf{r} \qquad \ldots\ldots(14)$$

where $\mathbf{k}_{\nu'}$ is a vector of length $k_{\nu'}$ in the $\theta_{k_{\nu'}}$, $\phi_{k_{\nu'}}$ direction.

It is convenient to consider first the total 2s–2p collision strength for H assuming an effective 2s–2p level separation of $\Delta E=|E(2s)-E(2p)|$; this will be denoted by $\Omega(\Delta E)$. It may be shown (Mott and Massey 1949, p. 225) that (12) and (14) give

$$\Omega_{\rm Born}(\Delta E)=\frac{M^2}{2\pi^2}\int_{|k-k'|}^{k+k'}\left|\int\exp(-iKz)V(2\mathrm{p},m_l=0;\,2\mathrm{s}|\mathbf{r})\,d\mathbf{r}\right|^2K\,dK \quad ..(15)$$

(with $Z^2=1$). In this expression K measures the scalar magnitude of the change of relative momentum and $\Delta E=|k^2-k'^2|/2M$, atomic units being used. It should be noted that the convention is adopted of neglecting spin statistical weight factors, so that equation (14) should be substituted in (1) or (4) with a statistical weight of unity for the 2s state.

The integration over $\mathbf{r}$ in (15) may be carried out (Mott and Massey 1949, p. 226) to give

$$\Omega_{\rm Born}(\Delta E)=8M^2\int_{|k-k'|}^{k+k'}\left|\int\exp(-iKz')\psi^*(2\mathrm{p},m_l=0|\mathbf{r}')\psi(2\mathrm{s}|\mathbf{r}')\,d\mathbf{r}'\right|^2\frac{dK}{K^3}. \quad (16)$$

The Bethe approximation is obtained on replacing† $\exp(-iKz')$ in (16) by $1-iKz'$, giving

$$\Omega_{\text{Bethe}}(\Delta E)=\tfrac{8}{3}M^2\mathbf{S}\ln[(k+k')/|k-k'|], \qquad \ldots\ldots(17)$$

where **S** is the line strength defined by (2). For 2s–2p transitions in H, $\mathbf{S}=27$ atomic units.

In practice it is necessary to consider separately the $2s\rightarrow 2p_{1/2}$ and $2s\rightarrow 2p_{3/2}$ transitions, for which the collision strengths will be denoted by Ω' and Ω'' respectively. The corresponding energy differences are $\Delta E'=0{\cdot}0354\,\text{cm}^{-1}$ and $\Delta E''=0{\cdot}327\,\text{cm}^{-1}$ (Lamb 1951). In both the Born and the Bethe approximations these are given by

$$\Omega'=\tfrac{1}{3}\Omega(\Delta E') \quad\text{and}\quad \Omega''=\tfrac{2}{3}\Omega(\Delta E''). \qquad \ldots\ldots(18)$$

2.4. *The Born and Bethe Approximations for the Partial Collision Strengths*

On expanding $1/|\mathbf{r}-\mathbf{r}'|$ in spherical harmonics the following expression for the interaction potential may be obtained:

$$V(2p, m_l=0;\, 2s|\mathbf{r})=Z\sqrt{\tfrac{2}{3}}\,\Theta_{1,m_l}(\theta)\exp(-im_l\phi)y_1(2p;\, 2s|r) \qquad \ldots\ldots(19)$$

where

$$y_1(2p;\, 2s|r)=\frac{1}{r^2}\int_0^r P(2p|r')P(2s|r')r'\,dr'+r\int_r^\infty P(2p|r')P(2s|r')\frac{1}{r'^2}\,dr'. \quad .(20)$$

The functions $P(2s|r')/r'$ and $P(2p|r')/r'$ are radial functions for hydrogen and the $\Theta_{1,m_l}(\theta)$ are normalized spherical harmonics

$$\Theta_{1,0}=\sqrt{(3/2)}\cos\theta, \quad \Theta_{1,\pm1}=\mp\sqrt{(3/4)}\sin\theta.$$

Using the usual collision theory expansion for $\exp(ikz)$ (Mott and Massey 1949, p. 20), and carrying out the angular integrations it may be shown that the Born approximation partial collision strengths are given by

$$\Omega^l{}_{\text{Born}}(\Delta E)=\frac{16M^2}{3k^2}\left\{l\left|\int_0^\infty F_l(kr)y_1(2p;\, 2s|r)F_{l-1}(k'r)\,dr\right|^2 + (l+1)\left|\int_0^\infty F_l(kr)y_1(2p;\, 2s|r)F_{l+1}(k'r)\,dr\right|^2\right\} \qquad \ldots\ldots(21)$$

where

$$F_\lambda(kr)=(\tfrac{1}{2}\pi kr)^{1/2}J_{\lambda+1/2}(kr). \qquad \ldots\ldots(22)$$

Evaluation of the angular integrals will be discussed in detail elsewhere (Seaton 1955).

The asymptotic form of $y_1(2p;\, 2s|r)$ for large r is $y_1\sim s(2p;\, 2s)/r^2$ where

$$s(2p;\, 2s)=\int_0^\infty P(2p|r')P(2s|r')r'\,dr' \qquad \ldots\ldots(23)$$

and $s^2=\mathbf{S}$. An alternative derivation of the Bethe approximation is to replace y_1 by its asymptotic form; thus it is readily shown that substitution of

$$V(2p, m_l=0;\, 2s|\mathbf{r})=Z\frac{\sqrt{2}}{3}\,\Theta_{1,0}(\theta)\,\frac{s}{r^2}$$

---

† This may be expected to give too large a contribution from large values of K (close encounters). The expedient is therefore frequently adopted of replacing the upper limit of the integral over K by $\alpha(k+k')$ with $\alpha\leqslant 1$. The choice of α is, however, largely arbitrary. This expedient is not adopted in the present paper since an alternative method of correcting the Bethe approximation is employed.

in (15) gives (18). The Bethe approximation for the partial collision strengths is therefore

$$\Omega^l{}_{\mathrm{Bethe}}(\Delta E)=\tfrac{4}{3}\pi^2M^2\mathrm{S}\left\{l\left|\int_0^\infty \mathrm{J}_{l+1/2}(kr)\,\frac{1}{r}\,\mathrm{J}_{l-1/2}(kr)\,dr\right|^2\right.$$
$$\left.+(l+1)\left|\int_0^\infty \mathrm{J}_{l+1/2}(kr)\,\frac{1}{r}\,\mathrm{J}_{l+3/2}(k'r)\,dr\right|^2\right\}. \qquad \ldots\ldots\ldots(24)$$

The partial collision strengths prove to be very useful in assessing the validity of the various approximations made. The functions $F_\lambda(kr)$ defined by equation (22) are solutions of the equation

$$\left[\frac{d^2}{dr^2}-\frac{\lambda(\lambda+1)}{r^2}+k^2\right]F_\lambda(kr)=0. \qquad \ldots\ldots(25)$$

For small values of r they behave as $r^{\lambda+1}$ and for large values of r they have asymptotic form

$$F_\lambda(kr)\sim\sin(kr-\tfrac{1}{2}\lambda\pi). \qquad \ldots\ldots(26)$$

The first point of inflexion of $F_\lambda(kr)$ occurs at the value r_λ of r given by

$$k^2=\lambda(\lambda+1)/r_\lambda{}^2. \qquad \ldots\ldots(27)$$

For $r\ll r_\lambda$, $F_\lambda(kr)$ will be very small. It follows that $\Omega^l{}_{\mathrm{Bethe}}$ will be a good approximation to $\Omega^l{}_{\mathrm{Born}}$ if

$$r_l\gg\text{atomic dimensions}. \qquad \ldots\ldots(28)$$

If l is such that this condition is satisfied it is also to be expected that the neglected exchange terms will be small, since there will be very little overlap between the bound wave functions and the wave functions of relative motion.

The condition for the effect of distortion to be small (Mott and Massey 1949, p. 205) is that $2MV(\nu;\,\nu|\mathbf{r})$ and $2M(\nu';\,\nu'|\mathbf{r})$ should be small compared with $k_\nu{}^2$ and $k_{\nu'}{}^2$ respectively when $r\geqslant r_l$.

Finally the condition that the transition probability per encounter should be small is that $\Omega^l(n',n)$ should be much less than $(2l+1)\omega_n$.

2.5. *Evaluation of the Radial Integrals in the Bethe Approximation Partial Collision Strengths*

To evaluate the integrals occurring in equation (24) the following relation may be used:

$$\int_0^\infty \mathrm{J}_{l+1/2}(kr)r^{-1}\mathrm{J}_{l'+1/2}(k'r)\,dr=$$
$$\frac{\Gamma\left[\frac{1}{2}(l+l'+1)\right]z^{(l'+1/2)/2}}{2\Gamma\left[\frac{1}{2}(2-l'+l)\right]\Gamma(l'+3/2)}\,F[\tfrac{1}{2}(l+l'+1),\ \tfrac{1}{2}(l'-l);\ l'+3/2;\ z] \qquad \ldots\ldots(29)$$

(Watson 1948), where $k'\leqslant k$ and $z=(k'/k)^2$. The functions F are hypergeometric functions defined by

$$F(a,b;c;z)=\frac{\Gamma(c)}{\Gamma(a)\,\Gamma(b)}\sum_{n=0}^{\infty}\frac{\Gamma(a+n)\,\Gamma(b+n)}{n\,!\,\Gamma(c+n)}\,z^n \qquad \ldots\ldots(30)$$

the functions occurring here being of the form $F(a,b;a+b+1;z)$. It is convenient to introduce the functions $E_1(a,b;z)$ defined by

$$E_1(a,b;z)=\frac{\Gamma(b+1)\,\Gamma(a+1)}{\Gamma(a+b+1)}\,F(a,b;a+b+1;z) \qquad \ldots\ldots(31)$$

for which $E_1(a, b; 1) = 1$. Using these functions the Bethe approximation collision strengths may be written quite generally for any optically allowed transition as

$$\left.\begin{aligned} \Omega^0{}_{\text{Bethe}} &= \tfrac{4}{3} M^2 Z^2 \mathbf{S} \zeta(\epsilon, 0) \\ \Omega^l{}_{\text{Bethe}} &= \tfrac{4}{3} M^2 Z^2 \mathbf{S} \frac{(2l+1)}{l(l+1)} \zeta(\epsilon, l), (l>0), \end{aligned}\right\} \qquad \ldots\ldots(32)$$

where $\epsilon = 1 - z$,

$$\left.\begin{aligned} &\zeta(\epsilon, 0) = z^{3/2}[E_1(1, \tfrac{1}{2}; z)]^2 \\ &\text{and} \\ &\zeta(\epsilon, l) = \frac{z^{l-1/2}}{2l+1} \{(l+1)[E_1(l, -\tfrac{1}{2}; z)]^2 + l z^2 [E_1(l+1, \tfrac{1}{2}; z)]^2\} \end{aligned}\right\} \qquad \ldots\ldots(33)$$

for $l > 0$.

Evaluation of the functions $\zeta(\epsilon, l)$ is discussed in an appendix to the present paper.

The Bethe approximation for the total collision strength is

$$\Omega_{\text{Bethe}} = \tfrac{8}{3} M^2 Z^2 \mathbf{S} \ln \{(1 + z^{1/2})/(1 - z^{1/2})\}. \qquad \ldots\ldots(34)$$

In terms of the energies of relative motion, $z = (E'/E)$ and $\epsilon = \Delta E/E$ where $E \geqslant E'$ and $\Delta E = E - E'$.

§ 3. EVALUATION OF THE PROBABILITIES OF COLLISIONALLY INDUCED 2s–2p TRANSITIONS IN HYDROGEN

3.1. *The Born and Bethe Approximations*

The coefficients $W(2\text{s} \to 2\text{p}_{1/2})$ and $W(2\text{s} \to 2\text{p}_{3/2})$ will be denoted by W' and W'' with subscripts e and p for electron and proton impact. For astrophysical applications these coefficients are required for kinetic temperatures of order 10^4 °K corresponding to mean kinetic energies of order 1 ev $= 8{\cdot}07 \times 10^3$ cm^{-1}. Since these kinetic energies are much larger than $\Delta E'$ or $\Delta E''$ the following approximations may be used:

$$k + k' = 2Mv, \qquad |k - k'| = \Delta E/v. \qquad \ldots\ldots(35)$$

The Bethe approximation then becomes

$$\Omega_{\text{Bethe}}(\Delta E) = 72 M^2 \ln (2Mv^2/\Delta E). \qquad \ldots\ldots(36)$$

For the Born approximation the following integral is required:

$$\int \exp(-iKz') \psi^*(2\text{p}, m_l = 0 | \mathbf{r}') \psi(2\text{s} | \mathbf{r}')\, d\mathbf{r}' = \frac{3iK(1-K^2)}{(1+K^2)^4}. \qquad \ldots\ldots(37)$$

Substitution in (17) gives

$$\Omega_{\text{Born}}(\Delta E) = 72 M^2 [\ln (2Mv^2/\Delta E) - \mu_{\text{B}}] \qquad \ldots\ldots(38)$$

with

$$\mu_{\text{B}} = \frac{1}{2} \left\{ \frac{4}{7} \left(1 - \frac{1}{\eta^7}\right) + \sum_{\nu=1}^{5} \frac{1}{\nu} \left(1 - \frac{1}{\eta^\nu}\right) + \ln \eta \right\} \qquad \ldots\ldots(39)$$

where $\eta = 1 + 4k^2$.

The coefficients W_{e}', W_{e}'', W_{p}' and W_{p}'' are given in table 1 for temperatures of 1×10^4 and 2×10^4 deg K. Approximation I is the Bethe approximation, approximation II the Born approximation and approximation III the semi-classical approximation† of Purcell (1952).

---

† For proton impact the results of Purcell have been recalculated allowing for the reduced mass (Purcell put M equal to the proton mass).

In the semi-classical calculations allowance has been made for strong coupling. The quantum mechanical treatment of strong coupling is clarified by considering first a particularly simple schematic model.

3.2. *A Schematic Model*

In the schematic model the interaction potentials are taken to vary as $1/r^2$, as in the Bethe approximation, but in addition the approximation is made of neglecting their angular dependence. This gives collision equations of the form

$$\left.\begin{aligned}(\nabla^2+k^2)u&=\frac{A}{r^2}\,u'\\ (\nabla^2+k'^2)u'&=\frac{A}{r^2}\,u.\end{aligned}\right\}\qquad\ldots\ldots(40)$$

The Born approximation for these equations is readily evaluated as

$$\Omega_{\text{S.M., Born}}(\Delta E)=\tfrac{1}{2}(\pi A)^2\ln(2Mv^2/\Delta E).\qquad\ldots\ldots(41)$$

This is seen to be identical with the Bethe approximation (36) if

$$\pi A=12M\qquad\ldots\ldots(42)$$

corresponding to $\pi A=12$ for electrons and to $\pi A=1{\cdot}10\times10^4$ for protons.

The Born partial collision strengths for the schematic model are given by

$$\Omega^l_{\text{S.M., Born}}(\Delta E)=(\pi A)^2(2l+1)\left|\int_0^\infty \mathrm{J}_{l+1/2}(kr)\,r^{-1}\,\mathrm{J}_{l+1/2}(k'r)\,dr\right|^2.\qquad\ldots\ldots(43)$$

The integrals are readily evaluated (Watson 1948) to give

$$\Omega^l_{\text{S.M., Born}}(\Delta E)=\frac{(\pi A)^2}{2l+1}\,z^{l+1/2}$$

where $k'\leqslant k$ and $z=(k'/k)^2$. Since $\epsilon=1-z$ is much less than unity‡ we may put $z=\mathrm{e}^{-\epsilon}$ giving finally

$$\Omega^l_{\text{S.M., Born}}(\Delta E)=\frac{(\pi A)^2}{2l+1}\,\mathrm{e}^{-\epsilon l}.\qquad\ldots\ldots(44)$$

This will give $\Omega^l\leqslant 2l+1$, consistent with the conservation limit (6), for values of l such that $2l+1\geqslant\pi A$ but since $\mathrm{e}^{-\epsilon l}$ will be close to unity‡ when $2l+1\leqslant\pi A$, the expression (44) will violate the condition (6) when $2l+1$ is appreciably less than πA.

If the additional approximation is made of putting $k=k'$ an exact solution of the schematic equations is readily obtained, although in this case the total collision strength diverges. Expanding the functions u and u' into spherical harmonics multiplied by radial functions $G_l(r)/r$ and $G_l'(r)/r$, the equations satisfied by the latter are

$$\left[\frac{d^2}{dr^2}-\frac{l(l+1)}{r^2}+k^2\right]G_l=\frac{A}{r^2}\,G_l'\qquad\ldots\ldots(45\,a)$$

$$\left[\frac{d^2}{dr^2}-\frac{l(l+1)}{r^2}+k^2\right]G_l'=\frac{A}{r^2}\,G_l.\qquad\ldots\ldots(45\,b)$$

---

‡ We are interested in values of ϵ of order 10^{-5} and values of $\pi A\leqslant 1{\cdot}1\times10^4$.

On adding and subtracting equations (45 *a*) and (45 *b*) uncoupled equations may be obtained which have as solutions bounded at the origin† $F_{\lambda\pm}=G_l\pm G_l'$ where F_λ is defined by (22) and

$$\lambda^{\pm}=-\tfrac{1}{2}+\tfrac{1}{2}\{(2l+1)^2\pm 4A\}^{1/2}. \qquad \ldots\ldots(46)$$

Using the asymptotic form (26) for F_λ and the usual theory of exact resonance collisions (Mott and Massey 1949, p. 146) the following expression for the partial collision strengths may be obtained:

$$\Omega^l_{\text{S.M.}}(\Delta E=0)=(2l+1)\sin^2\{\tfrac{1}{4}\pi[(2l+1)^2+4A]^{1/2}-\tfrac{1}{4}\pi[(2l+1)^2-4A]^{1/2}\}. \quad .(47)$$

For $2l+1\gg\pi A$ this gives $\Omega^l_{\text{S.M.}}(\Delta E=0)=(\pi A)^2/(2l+1)$ in agreement with the Born approximation (44) for $\Delta E=0$.

Some results obtained from the schematic equations are shown in figure 1 for $\pi A=10^4$ (close to the value appropriate for protons). The following are plotted as functions of l: the exact solution for Ω^l with $\epsilon=0$; the Born approximation for Ω^l with $\epsilon=0$; the Born approximation for Ω^l with $\epsilon=2\times10^{-5}$; the limiting value $2l+1$.

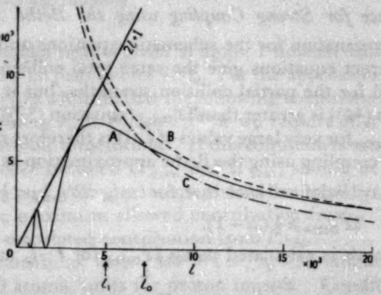

Figure 1. Partial collision strengths Ω^l obtained from the schematic equations with $\pi A=10^4$. A, exact solution for $\epsilon=0$. B, Born approximation for $\epsilon=0$. C, Born approximation for $\epsilon=2\times10^{-5}$. The values l_1 and l_0 of l are shown for $\epsilon=0$; these are defined in the text.

It is seen that the Born approximation gives Ω^l to be much too large for the smaller values of l and therefore leads to an over-estimate of the total collision strength. An improved estimate may be obtained on defining l_1 as the nearest integer less than l_1' where

$$2l_1'+1=\pi A. \qquad \ldots\ldots(48)$$

The values of Ω^l may be considered for $l>l_1$ and for $l\leqslant l_1$. (i) For $l>l_1$ the solutions shown in figure 1 indicate that the Born approximation (44) should be reliable. Replacing the sum over l by an integral we obtain

$$\sum_{l=l_1+1}^{\infty}\Omega^l_{\text{S.M.}}=\tfrac{1}{2}(\pi A)^2\,\text{Ei}\,[\tfrac{1}{2}\pi A\epsilon] \qquad \ldots\ldots(49)$$

where

$$\text{Ei}\,(x)=\int_x^\infty\frac{e^{-t}}{t}\,dt.$$

---

† Provided that $(2l+1)^2>4\,|\,A\,|$, which is all that is required in the present context. For a discussion of the difficulty which arises when this condition is not satisfied see Mott and Massey 1949, p. 40.

(ii) The maximum allowed contribution from $l \leqslant l_1$ is found to be small compared with the contribution from $l > l_1$; thus with $\pi A = 10^4$ and $\epsilon = 2 \times 10^{-5}$ (49) gives

$$\sum_{l=l_1+1}^{\infty} \Omega^l = 9 \cdot 1 \times 10^7 \text{ compared with } \sum_{l=0}^{l_1} (2l+1) = 2 \cdot 5 \times 10^7.$$

In consequence Ω is insensitive to the contribution assumed for $l \leqslant l_1$. We may take the latter to be one half of the limiting value, giving

$$\sum_{l=0}^{l_1} \Omega^l = \tfrac{1}{2}(l_1+1)^2 \simeq \tfrac{1}{8}(\pi A)^2. \qquad \ldots\ldots(50)$$

Combining (49) and (50) we obtain

$$\Omega_{\text{S.M.}}(\Delta E) = 72M^2\{\tfrac{1}{4} + \text{Ei}(6M\epsilon)\} \qquad \ldots\ldots(51)$$

for $\pi A = 12M$. Rate coefficients W calculated using this result are given in table 1 as approximation IV. In calculating the individual Ω' and Ω'' the relations (18) have been used; this should not cause significant error.

3.3. *Allowance for Strong Coupling using the Bethe Approximation*

The Born approximation for the schematic equations and the Bethe approximation for the correct equations give the same total collision strengths and the same general trend for the partial collision strengths, but it may be shown that $\Omega^l_{\text{S.M., Born}}$ (equation (44)) is greater than Ω^l_{Bethe} (equation (32)) for small values of l and is less than Ω^l_{Bethe} for very large values of l. It is therefore necessary to consider the effect of strong coupling using the Bethe approximation as a guide.

A value l_0 of l may be defined such that, for $l > l_0$, $\Omega^l_{\text{Bethe}} < \tfrac{1}{2}(2l+1)$ ...(52 a)

and that, for $l \leqslant l_0$, $\Omega^l_{\text{Bethe}} \geqslant \tfrac{1}{2}(2l+1)$. ......(52 b)

The collision strength is calculated using Ω^l_{Bethe} for $l > l_0$ and $\Omega^l = \tfrac{1}{2}(2l+1)$ for $l \leqslant l_0$. This gives

$$\Omega = \tfrac{1}{2}(l_0+1)^2 + \sum_{l=l_0+1}^{\infty} \Omega^l_{\text{Bethe}}. \qquad \ldots\ldots(53)$$

For kinetic energies of order 1 ev it is found that $l_0 = 7 \cdot 8 \times 10^3$ for protons and $l_0 = 8$ for electrons. When $l \leqslant l_0$ the factor $\zeta(\epsilon, l)$ occurring in equation (32) and evaluated in the appendix does not differ from unity by more than 4%. Putting this factor equal to unity for $l \leqslant l_0$ we have

$$\sum_{l=l_0+1}^{\infty} \Omega^l_{\text{Bethe}} = \Omega_{\text{Bethe}} - 36M^2\left\{1 + \sum_{l=1}^{l_0} \frac{2l+1}{l(l+1)}\right\}. \qquad \ldots\ldots(54)$$

This gives finally

$$\Omega(\Delta E) = 72M^2\{\ln(2Mv^2/\Delta E) - \mu\}, \qquad \ldots\ldots(55)$$

where $\mu = 8 \cdot 99$ for protons and $\mu = 2 \cdot 21$ for electrons, μ being effectively independent of energy within the energy range of interest. Rate coefficients calculated using (55) together with (18) are given as approximation V in table 1.

3.4. *Summary of Results for* 2s–2p *Transitions in Hydrogen and Discussion of their Accuracy*

Final results for the rate coefficients are summarized in table 1. The total rate coefficient W is calculated for equal densities of electrons and protons. Of the approximations considered approximation V should be the most accurate.

Table 1. Rate Coefficients W in cm^3 sec^{-1} for Collisionally Induced 2s$\rightarrow$2p Transitions in H

Approximation	$T=1\times10^4$ deg K					$T=2\times10^4$ deg K				
	I	II	III	IV	V	I	II	III	IV	V
$10^4\times W_p'$	8·15	5·67	2·72	1·77	2·51	6·07	4·16	2·21	1·50	2·08
$10^4\times W_p''$	13·52	8·58	2·80	1·34	2·23	10·18	6·37	2·56	1·36	2·19
$10^4\times W_e'$	0·27	0·25	0·24	0·19	0·22	0·20	0·18	0·17	0·15	0·17
$10^4\times W_e''$	0·45	0·42	0·38	0·30	0·35	0·34	0·31	0·29	0·23	0·27
Total $10^4\times W$	22·4	14·9	6·1	3·6	5·3	16·8	11·0	5·2	3·2	4·7

W' for 2s $\rightarrow$ 2p$_{1/2}$ and W'' for 2s $\rightarrow$ 2p$_{3/2}$ with subscripts p and e for proton and electron impact.

Approximations: I Bethe; II Born; III semi-classical (Purcell 1952); IV schematic model, with allowance for strong coupling; V Bethe, with allowance for strong coupling.

The schematic model results given in figure 1 indicate that the assumption of weak coupling should be justified for $l>l_0$. For the approximation V results to be reliable it is necessary in addition that the following conditions should be satisfied:
Condition (1). Defining r_0 as $[l_0(l_0+1)]^{1/2}/k$ we require that r_0 should be large compared with the atomic dimensions. If this condition is satisfied it follows that, for $l>l_0$, the difference between $\Omega^l{}_{\text{Born}}$ and $\Omega^l{}_{\text{Bethe}}$ should be small and that the neglected distortion and exchange terms should be small (cf. § 2.4).
Condition (2). The maximum allowed contribution from $l\leqslant l_0$ should be small compared with the calculated contribution from $l>l_0$.

For H 2s–2p transitions with $\frac{1}{2}Mv^2=1$ ev, $r_0=31$ atomic units for electron impact and $r_0=950$ atomic units for proton impact. Condition (1) is therefore satisfied. The estimated contribution to W from $l\leqslant l_0$ is 18% of the total for $T=1\times10^4\,^\circ$K and is 15% for $T=2\times10^4\,^\circ$K; therefore condition (2) is also satisfied. The maximum possible error in the estimated contribution from $l\leqslant l_0$ is $\pm100\%$ but in practice the error is likely to be much less since the Ω^l for $l\leqslant l_0$ will be oscillatory functions of l, as in figure 1, and we may expect the mean value for Ω^l to be not far different from one half of the maximum allowed value, giving

$$\sum_{l=0}^{l_0}\Omega^l=0{\cdot}5\,(l_0+1)^2.$$

It may be noted that the exact solution of the schematic equations for $\epsilon=0$ and $\pi A=10^4$ gives

$$\sum_{l=0}^{l_0}\Omega^l=0{\cdot}66\,(l_0+1)^2.$$

It would seem reasonable to conclude that the error in the approximation V results for W should not exceed† $\pm20\%$.

---

† Coupling terms other than those connecting the 2s, 2p states will be much smaller than the 2s–2p coupling terms, and their neglect should not cause significant error. It is also necessary to consider the possibility of radiative 2p $\rightarrow$ 1s transitions occurring during the collision process. An order of magnitude calculation shows that the time duration of the collisions will be too small for such effects to be important.

§ 4. CROSS SECTIONS FOR 3s–3p TRANSITIONS IN Na PRODUCED BY ELECTRON AND BY PROTON IMPACT

4.1. *Electron Impact*

The cross section has been calculated using the method of § 3.3 above (equation (53)). The energy difference between the 3s and 3p levels is $\Delta E = 2{\cdot}104$ ev and the line strength is $\mathbf{S} = 19{\cdot}0$ atomic units, corresponding to an f-value‡ of 0·98 (Seaton 1951). The values of $\Omega^l{}_{\text{Bethe}}$ for $l \leqslant l_0$ are obtained using table 2A of the appendix and the total collision strength is then obtained from

$$\Omega = \Omega_{\text{Bethe}} - \sum_{l=0}^{l_0} \Omega^l{}_{\text{Bethe}} + \tfrac{1}{2}(l_0+1)^2. \qquad \ldots\ldots(56)$$

Figure 2 gives the cross sections $Q(3\text{s} \rightarrow 3\text{p})$ as functions of the energy E, in ev, of electrons incident on Na atoms in the 3s state. The experimental curve obtained by Haft (1933) in arbitrary units has been fitted to the absolute measurements of Christoph (1935) as quoted by Bates *et al.* (1950). We also include the Born approximation calculated by Fundaminsky (see Bates *et al.* 1950). It is seen that for energies greater than about 2 ev above the threshold the approximation of equation (53) gives good agreement with experiment.

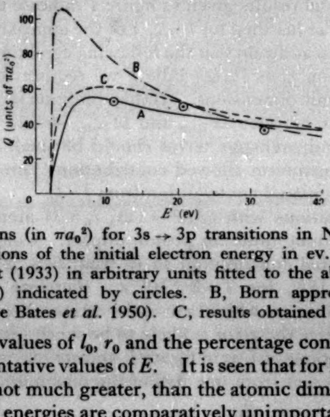

Figure 2. Cross sections (in $\pi a_0{}^2$) for $3\text{s} \rightarrow 3\text{p}$ transitions in Na produced by electron impact, as functions of the initial electron energy in ev. A, experimental curve obtained by Haft (1933) in arbitrary units fitted to the absolute measurements of Christoph (1935) indicated by circles. B, Born approximation calculated by Fundaminsky (see Bates *et al.* 1950). C, results obtained using equation (53).

Table 2 gives the values of l_0, r_0 and the percentage contribution coming from $l \leqslant l_0$ for a few representative values of E. It is seen that for low energies the values of r_0 are greater, but not much greater, than the atomic dimensions. The smaller values of r_0 for higher energies are comparatively unimportant since a large contribution to Ω then comes from values of l much greater than l_0. It should be noted that the method used gives fair agreement with experiment even when the condition (2) of § 3.4 is not satisfied, which confirms that

$$\sum_{l=0}^{l_0} \Omega^l \simeq 0{\cdot}5\,(l_0+1)^2.$$

Table 2. $3\text{s} \rightarrow 3\text{p}$ Transitions in Na produced by Electron Impact

$\dfrac{E-\Delta E}{\Delta E}$	E (ev)	l_0	r_0(A.U.)	% from $l \leqslant l_0$
0·5	3·16	3	7	81
1	4·21	3	6	49
4	10·52	5	6	38
15	33·66	6	4	23

---

‡ Spin statistical weight factors are consistently omitted.

4.2. *Proton Impact*

Results of some similar calculations† for proton impact are given in table 3. For the lower energies the results obtained will not be of a high accuracy due to the small value of r_0 and the large contribution from $l \leqslant l_0$.

Table 3. 3s → 3p Transitions in Na produced by Proton Impact

$\log_{10}$ (E (ev))	r_0 (A.U.)	Q(3s → 3p) (πa_0^2)	% from $l \leqslant l_0$
2·0	3·8	9	82
2·5	5·4	19	78
3·0	7·0	34	72
3·5	8·1	54	60
4·0	8·2	82	43
4·5	6·0	60	30

§ 5. CONCLUSIONS

Strong coupling effects may be expected for the following types of inelastic collisions: (i) certain collisions between atoms and electrons involving a change of atom spin, (ii) strong optically allowed transitions produced by electron impact and (iii) slow inelastic collisions between heavy particles.

Processes of type (i) have been discussed in two previous papers (Seaton 1953 a, b). The method of the present paper (equation (53)) is applicable for impact of charged particles producing optically allowed transitions for which the line strength is very large. As an example of the failure of the present method when the line strength is not sufficiently large we may consider 1s → 2p transitions in H, for which $S = 1{\cdot}66$. For 51 ev electrons the present method gives $Q\,(1s \to 2p) = 2{\cdot}6\,\pi a_0^2$ and $r_0 = 0{\cdot}73$ atomic units. This may be compared with $Q_{\mathrm{Born}}(1s \to 2p) = 1{\cdot}1\,\pi a_0^2$ at the same energy, which is itself probably rather too large (Bates *et al.* 1950). The failure of the present method is to be expected from the small value found for r_0.

It would seem that a suitable modification of the present method, using the Born or distorted wave approximation in place of the Bethe approximation and if necessary calculating matrix elements other than those directly connecting the initial and final states, might be usefully employed for a number of other collision processes, especially slow inelastic collisions between atoms and heavy charged particles.

APPENDIX

EVALUATION OF THE HYPERGEOMETRIC FUNCTIONS

It is required to evaluate the quantities defined by

$$\zeta(\epsilon, l) = \frac{z^{l-1/2}}{2l+1}\,\{(l+1)[E_1(l, -\tfrac{1}{2}\,;\,z)]^2 + lz^2[E_1(l+1, \tfrac{1}{2}\,;\,z)]^2\} \qquad \ldots\ldots(\mathrm{A1})$$

for $l > 0$ and by

$$\zeta(\epsilon, l) = z^{3/2}[E_1(1, \tfrac{1}{2}\,;\,z)]^2 \qquad \ldots\ldots(\mathrm{A2})$$

---

† The simplest procedure is to choose various values of ϵl_0 and to solve for l_0 and hence for E. The results quoted in table 3 have been interpolated from calculations made in this manner.

for $l=0$, where $z=1-\epsilon$ and

$$E_1(a,b\;;\;z)=ab\sum_{n=0}^{\infty}\frac{\Gamma(a+n)\,\Gamma(b+n)}{\Gamma(1+n)\,\Gamma(a+b+1+n)}\,z^n. \qquad \ldots\ldots\text{(A3)}$$

The expansion (A3) is found to be very slowly convergent for the values of l and ϵ of interest and alternative expressions for the functions E_1 must therefore be obtained. It is convenient to consider separately the following cases: (*a*) $l \leqslant 7$, $0 \leqslant \epsilon \leqslant 1$, which is important for collisions of electrons with atoms and (*b*) $l \gg 1$, $\epsilon \ll 1$, which is important for collisions of heavy charged particles with atoms. For case (*b*) it will be shown that, to a good approximation, $\zeta(\epsilon, l)$ may be regarded as a function of the single variable ϵl. Case (*b*) is conveniently subdivided into (i) $\epsilon l<1$, (ii) ϵl of order 1 and (iii) $\epsilon l \gg 1$.

Case (*a*): $l \leqslant 7$, $0 \leqslant \epsilon \leqslant 1$. The functions E_1 may be expressed in closed form on expanding the coefficients of z^n into partial fractions and using the series expansion for $z^{1/2}\ln\{(1+z^{1/2})/(1-z^{1/2})\}$. The following expressions are obtained, valid for $0<z\leqslant 1$:

$$\begin{aligned}E_1(\lambda,-\tfrac{1}{2}\,;\,z)=\frac{\lambda}{2^{\lambda-1}}\Bigg\{&\tfrac{1}{2}z^{1/2}\sum_{p=0}^{\lambda}\alpha(\lambda-p,\lambda)\,z^{-p}\ln\left[\frac{1+z^{1/2}}{1-z^{1/2}}\right]\\&-\alpha(\lambda,\lambda)-z\sum_{p=2}^{\lambda}\alpha(\lambda-p,\lambda)\,z^{-p}\sum_{\nu=0}^{p-2}\frac{z^{\nu}}{2\nu+1}\Bigg\}\end{aligned} \qquad \ldots\ldots\text{(A4)}$$

and

$$\begin{aligned}E_1(\lambda,\tfrac{1}{2}\,;\,z)=\frac{\lambda}{2^{\lambda-1}}\Bigg\{&\tfrac{1}{2}z^{-1/2}\sum_{p=0}^{\lambda}\alpha(p,\lambda)\,z^{-p}\ln\left[\frac{1+z^{1/2}}{1-z^{1/2}}\right]\\&-\sum_{p=1}^{\lambda}\alpha(p,\lambda)\,z^{-p}\sum_{\nu=0}^{p-1}\frac{z^{\nu}}{2\nu+1}\Bigg\}\end{aligned} \qquad \ldots\ldots\text{(A5)}$$

with

$$\left.\begin{aligned}&\alpha(p,\lambda)=\frac{(2p-1)!!\,(2\lambda-2p-3)!!}{p!\,(\lambda-p)!}\quad\text{for } p<\lambda\\ &\text{and}\\ &\alpha(\lambda,\lambda)=-\frac{(2\lambda-1)!!}{\lambda!}.\end{aligned}\right\} \qquad \ldots\ldots\text{(A6)}$$

For integral n, $(2n+1)!!$ is defined as

$$(2n+1)!!=1\,.\,3\,.\,5\,\ldots\ldots(2n+1) \qquad \ldots\ldots\text{(A7)}$$

and the convention is adopted that $(-1)!!=1$ and $(0)!=1$. Summations such as $\sum_{p=p_1}^{p_2}$ are to be taken to be zero if $p_2<p_1$.

The functions $E_1(l,-\frac{1}{2}\,;\,z)$ and $E_1(l+1,\frac{1}{2}\,;\,z)$, calculated† from equations (A4) and (A5), are given in table 1A for various values of $y=(1-\epsilon)/\epsilon$. Table 2A gives the functions

$$\frac{\Omega^0{}_{\text{Bethe}}}{M^2Z^2\mathrm{S}}\equiv\frac{4}{3}\,\zeta(\epsilon,0),\quad \frac{\Omega^l{}_{\text{Bethe}}}{M^2Z^2\mathrm{S}}\equiv\frac{4}{3}\,\frac{(2l+1)}{l(l+1)}\,\zeta(\epsilon,l) \qquad \ldots\ldots(8)$$

for $0\leqslant l\leqslant 7$. Values for $l=6$ and 7 are extrapolated; they should not be in error by more than two or three units in the last decimal place.

---

† The author is indebted to Miss J. Nicholson for assistance in computing these functions.

Case (*b*): $l \gg 1$ and $\epsilon \ll 1$. We may put

$$z^l = \{\exp[\ln(1-\epsilon)]\}^l \simeq \exp(-\epsilon l) \qquad \ldots\ldots(\mathrm{A9})$$

and

$$\zeta(\epsilon, l) \simeq \tfrac{1}{2} e^{-\epsilon l}\{[E_1(l, -\tfrac{1}{2};\ z)]^2 + [E_1(l, \tfrac{1}{2};\ z)]^2\}. \qquad \ldots\ldots(\mathrm{A10})$$

Case (*b*), (i): $l \gg 1$, $\epsilon \ll 1$, $\epsilon l < 1$. The expansion

$$E_1(a, b;\ 1-\epsilon) = 1 + \frac{1}{\Gamma(a)\,\Gamma(b)} \sum_{n=1}^{\infty} \frac{\Gamma(a+n)\,\Gamma(b+n)}{\Gamma(n)\,\Gamma(n+1)}$$

$$\times \left\{\ln\epsilon - \frac{1}{n} - 2\psi(n) + \psi(a+n) + \psi(b+n)\right\}\epsilon^n \qquad \ldots\ldots(\mathrm{A11})$$

where $\psi(x) = d\ln[\Gamma(x)]/dx$ (Bateman Manuscript Project, 1953, p. 74) is found to converge very rapidly if ϵ is sufficiently small and may then be terminated at a value

Table 1A

$E_1[l, -\tfrac{1}{2}; y/(1+y)]$

$l=$ \ $y=$	0·0	0·5	1·0	2·5	4	7	10	15	20
1	2·0000	1·7603	1·6232	1·4188	1·3228	1·2272	1·1782	1·1332	1·1075
2	2·6667	2·2810	2·0581	1·7214	1·5610	1·3992	1·3152	1·2375	1·1927
3	3·2000	2·7026	2·4132	1·9730	1·7611	1·5457	1·4332	1·3281	1·2673
4	3·6571	3·0664	2·7213	2·1935	1·9379	1·6764	1·5390	1·4100	1·3350
5	4·0635	3·3912	2·9973	2·3927	2·0983	1·7959	1·6361	1·4857	1·3977

$E_1[l+1, \tfrac{1}{2}; y/(1+y)]$

$l=$ \ $y=$	0·0	0·5	1·0	2·5	4	7	10	15	20
0	0·6667	0·7190	0·7536	0·8136	0·8465	0·8832	0·9041	0·9246	0·9371
1	0·5333	0·5948	0·6375	0·7154	0·7604	0·8129	0·8436	0·8750	0·8945
2	0·4571	0·5198	0·5646	0·6495	0·7003	0·7615	0·7983	0·8366	0·8610
3	0·4063	0·4679	0·5130	0·6005	0·6818	0·7209	0·7616	0·8050	0·8329
4	0·3694	0·4291	0·4687	0·5619	0·6175	0·6873	0·7311	0·7780	0·8087
5	0·3410	0·3987	0·4432	0·5303	0·5868	0·6588	0·7046	0·7544	0·7872

Note that $E_1(l, -\tfrac{1}{2}; 1) = E_1(l+1, \tfrac{1}{2}; 1) = 1$

Table 2A. $\Omega^l{}_{\mathrm{Bethe}}/M^2Z^2\mathrm{S}$

$l=$ \ $y=$	0	0·5	1·0	2·5	4	7	10	15	20	$\to\infty$
0	0·000	0·133	0·268	0·533	0·684	0·851	0·945	1·035	1·088	1·333
1	0·000	2·400	2·531	2·416	2·307	2·194	2·139	2·092	2·068	2·000
2	0·000	0·670	1·010	1·250	1·262	1·230	1·202	1·175	1·159	1·111
3	0·000	0·209	0·461	0·773	0·846	0·856	0·845	0·829	0·818	0·778
4	0·000	0·067	0·219	0·507	0·603	0·648	0·650	0·642	0·634	0·600
5	0·000	0·022	0·106	0·343	0·448	0·512	0·524	0·523	0·519	0·489
6	0·000	—	—	—	—	0·426	0·435	0·441	0·441	0·413
7	0·000	—	—	—	—	0·357	0·369	0·381	0·384	0·357

Note that $y = E'/\Delta E$ where E' is the smaller of the initial or final energies of relative motion and ΔE is the change of energy involved in the atomic transition.

n_0 of n such that $n_0 \ll l$. Using Stirling's formula we may put, for $n \leqslant n_0$, $\psi(n+l) \simeq \ln(l)$. For $n \leqslant n_0$ we may also put $\Gamma(n+l)/\Gamma(l) \simeq l^n$. Substituting these approximations in (A11) gives

$$E_1(l, -\tfrac{1}{2}; 1-\epsilon) = 1 - 2\{\ln(\tfrac{1}{4}\epsilon l) - 1 - \psi(1)\}(\tfrac{1}{4}\epsilon l) - 4\sum_{n=2}^{n_0} \frac{(2n-3)!}{n!(n-1)!(n-2)!}\{\ln(\tfrac{1}{4}\epsilon l) - \frac{1}{n} - 3\psi(n) + 2\psi(2n-1)\}(\tfrac{1}{4}\epsilon l)^n \qquad \text{......(A12)}$$

$$E_1(l, +\tfrac{1}{2}; 1-\epsilon) = 1 + 2\sum_{n=1}^{n_0} \frac{(2n-1)!}{n!(n-1)!^2}\{\ln(\tfrac{1}{4}\epsilon l) - \frac{1}{n} - 3\psi(n) + 2\psi(2n)\}(\tfrac{1}{4}\epsilon l)^n. \qquad \text{......(A13)}$$

For $\epsilon l \leqslant 0{\cdot}8$ and $n_0 \leqslant 5$ it is found that the convergence is sufficiently rapid to give the function E_1 correct to at least three decimal places. These expressions have been used to compute the values of $\zeta(\epsilon, l)$ given in table 3A for $0 \leqslant \epsilon l \leqslant 0{\cdot}8$.

Case (*b*), (ii): $l \gg 1$, $\epsilon \ll 1$, ϵl of order 1. The following integrals may be obtained (cf. Bateman Manuscript Project, 1953, pp. 114, 115):

$$E_1(l, -\tfrac{1}{2}; 1-\epsilon) = 2\epsilon l \int_0^\infty (1+t^2)^{1/2}(1+\epsilon t^2)^{-l-1}\,dt \qquad \text{......(A14)}$$

$$E_1(l, \tfrac{1}{2}; 1-\epsilon) = \int_0^\infty (1+t^2)^{-3/2}(1+\epsilon t^2)^{-l}\,dt. \qquad \text{......(A15)}$$

For $l \gg 1$, $\epsilon \ll 1$ we may put $(1+\epsilon t^2)^{-l} \simeq \exp(-\epsilon l t^2)$. Changing the integration variable to $\theta = \arctan t$ we obtain

$$E_1(l, -\tfrac{1}{2}; 1-\epsilon) = 1 + 2\epsilon l \int_0^{\pi/2} \left(\frac{1-\sin\theta}{\cos^3\theta}\right) \exp(-\epsilon l \tan^2\theta)\,d\theta \qquad \text{...(A16)}$$

and

$$E_1(l, \tfrac{1}{2}; 1-\epsilon) = \int_0^{\pi/2} \cos\theta \exp(-\epsilon l \tan^2\theta)\,d\theta. \qquad \text{.....(A17)}$$

These forms are convenient for numerical integration. They have been used to calculate the values of $\zeta(\epsilon, l)$ given in table 3A for $0{\cdot}8 \leqslant \epsilon l \leqslant 2{\cdot}0$.

Case (*b*), (iii): $l \gg 1$, $\epsilon \ll 1$, $\epsilon l \gg 1$. Since $\exp(-\epsilon l t^2)$ will decrease very rapidly for large t an asymptotic expansion may be obtained on expanding the functions $(1+t^2)^{1/2}$ and $(1+t^2)^{-3/2}$ in powers of t and substituting in (A14) and (A15). This gives

$$\zeta(\epsilon, l) = \tfrac{1}{2}\pi\epsilon l\, e^{-\epsilon l}\left\{1 + \tfrac{1}{4}(\epsilon l)^{-1} + \frac{7}{32}(\epsilon l)^{-2} + \dots\right\}. \qquad \text{......(A18)}$$

For $\epsilon l = 2$ the terms included in (A18) give $\zeta = 0{\cdot}502$ compared with the value $0{\cdot}540$ given in table 3A; for larger values of ϵl the accuracy of (A18) should be much improved.

Table 3A. $\zeta(\epsilon, l)$ for $l \gg 1$, $\epsilon \ll 1$

ϵl	$\zeta(\epsilon, l)$	ϵl	$\zeta(\epsilon, l)$
0·00	1·000	0·4	1·039
0·04	1·004	0·6	1·009
0·08	1·011	0·8	0·962
0·12	1·019	1·0	0·900
0·16	1·025	1·2	0·829
0·20	1·030	1·4	0·754
		1·6	0·680
		1·8	0·608
		2·0	0·540

This completes the calculation of $\zeta(\epsilon, l)$ for case (*b*); it is of interest to compare the results obtained with those calculated for $l=5$. This comparison is given in table 4A. It is seen that, for $\epsilon \leqslant 0{\cdot}2$, the values of $\zeta(\epsilon, l)$ for case (*b*) give agreement with the values for $l=5$ to within a few per cent.

Table 4A

ϵl	$l=5$		$l\gg1,\ \epsilon\ll1$
	ϵ	$\zeta(\epsilon, l)$	$\zeta(\epsilon, l)$
3·3333	0·6667	0·045	0·205†
2·5000	0·5000	0·218	0·366†
1·4286	0·2857	0·701	0·743
1·0000	0·2000	0·917	0·900
0·6250	0·1250	1·047	1·003
0·4545	0·0909	1·072	1·031
0·3125	0·0625	1·070	1·035
0·2381	0·0476	1·062	1·032
0·0000	0·0000	1·000	1·000

† Values computed from the asymptotic expansion (A18).

REFERENCES

Bates, D. R., Fundaminsky, A., Leech, J. W., and Massey, H. S. W., 1950, *Phil. Trans. Roy. Soc.* A, **243**, 93.

Bateman Manuscript Project, 1953, Vol. 1, prepared by Erdélyi, A., Magnus, W., Oberhettinger, F., and Tricomi, F. G. (New York: McGraw-Hill).

Bethe, H., 1930, *Ann. Phys., Lpz.*, **5**, 325.

Breit, G., and Teller, E., 1940, *Astrophys. J.*, **91**, 215.

Christoph, W., 1935, *Ann. Phys., Lpz.*, **23**, 51.

Condon, E. U., and Shortley, G. H., 1951, *The Theory of Atomic Spectra* (reprint of 1st Edn with corrections) (Cambridge: University Press), p. 98.

Haft, G., 1933, *Z. Phys.*, **82**, 73.

Kipper, A. Y., 1952, *Tartu Astr. Obs. Publ.*, **32**, 63.

Lamb, W. E., 1951, *Rep. Progr. Phys.* (London: Physical Society), **14**, 19.

Massey, H. S. W., and Burhop, E. H. S., 1952, *Electronic and Ionic Impact Phenomena* (Oxford: Clarendon Press), p. 143.

Mott, N. F., 1931, *Proc. Roy. Soc.* A, **133**, 228.

Mott, N. F., and Massey, H. S. W., 1949, *The Theory of Atomic Collisions*, 2nd Edn (Oxford: University Press).

Purcell, E. M., 1952, *Astrophys. J.*, **116**, 457.

Seaton, M. J., 1951, *Proc. Roy. Soc.* A, **208**, 418; 1953 a, *Phil. Trans. Roy. Soc.* A, **245**, 469; 1953 b, *Proc. Roy. Soc.* A, **218**, 400; 1954, *Ann. Astrophys.*, **17**, 296; 1955, *Proc. Roy. Soc.*, in the press.

Spitzer, L., and Greenstein, J. L., 1951, *Astrophys. J.*, **114**, 407.

Watson, G. N., 1948, *Bessel Functions*, 2nd Edn (Cambridge: University Press), p. 403.

von Weizsäcker, C. F., 1934, *Z. Phys.*, **88**, 612.

Wild, J. P., 1952, *Astrophys. J.*, **115**, 206.

Williams, E. J., 1934, *Phys. Rev.*, **45**, 729.

General Perturbation Theory in Neutronics

By E. D. PENDLEBURY
Atomic Weapons Research Establishment, Aldermaston, Berks.

MS. received 21*st January* 1955

Abstract. A general approach to perturbation theory in neutronics is given, and particular cases of one and two energy groups are considered. A method is also suggested for the treatment of large perturbations.

---

§ 1. Introduction

PREVIOUS accounts of perturbation theory in neutronics have been given by Fuchs (1949), by Glasstone and Edlund (1952), and by Tait (1954). Fuchs' account deals with only one energy group and he approaches the problem by way of the one-group integral equation and assumes that scattering is isotropic. Glasstone and Edlund's account (1952) deals with multigroup perturbation theory but their approach is from the diffusion equations and consequently their treatment is really only applicable to systems which are large compared with the mean free path of the neutrons. Tait considers two-group perturbation theory and he approaches the problem from the two-group integral equations and also assumes that scattering is isotropic, his analysis following closely that of Fuchs for the one-group theory. The approach given below is different from any of the above, the basis of the analysis being the Boltzmann transport equation, and in the first general treatment, anisotropic scattering and continuous energy dependence are taken into account. The particular cases of isotropic scattering with one and two energy groups are then considered. (As an alternative approach these particular cases could be dealt with separately from first principles using matrix notation.) In § 5 a method is suggested for dealing with large perturbations; the method consists essentially of the simultaneous perturbation of two or more known solutions and by suitable choice of these solutions corresponds to an interpolation, and if sufficient known solutions are perturbed simultaneously then results of any desired accuracy ought to be obtainable.

§ 2. General Perturbation Theory

Let $N(\mathbf{r}, v, \mathbf{\Omega}, t)\,dv$ be the number of neutrons whose speeds lie between v and $v+dv$ at the point $\mathbf{r}$ per unit volume, and per unit solid angle around $\mathbf{\Omega}$ at time t. Let $\alpha(\mathbf{r}, v)$ be the inverse mean free path for neutrons of speed v at the point $\mathbf{r}$. Let $\beta\{\mathbf{r}, (v', \mathbf{\Omega}' \rightarrow v, \mathbf{\Omega})\}\,ds\,dv\,d\Omega/4\pi$ be the probability that a neutron of speed v' moving a distance ds at $\mathbf{r}$ in the direction $\mathbf{\Omega}'$ gives rise, by fission or scattering, to a neutron with speed between v and $v+dv$ and whose direction of motion lies within the solid angle $d\Omega$ about $\mathbf{\Omega}$. The Boltzmann transport equation for stationary media in the absence of sources is then

$$\partial N(\mathbf{r}, v, \mathbf{\Omega}, t)/\partial t + v\mathbf{\Omega} \,.\, \operatorname{grad} N(\mathbf{r}, v, \mathbf{\Omega}, t) + v\alpha(\mathbf{r}, v) N(\mathbf{r}, v, \mathbf{\Omega}, t)$$

$$= \frac{1}{4\pi}\iint v'\beta\{\mathbf{r}, (v', \mathbf{\Omega}' \rightarrow v, \mathbf{\Omega})\} N(\mathbf{r}, v', \mathbf{\Omega}', t)\, dv'\, d\Omega'. \qquad \ldots\ldots(2.1)$$

Consider solutions of this equation of the form

$$\partial N(\mathbf{r}, v, \mathbf{\Omega}, t)/\partial t = \lambda N(\mathbf{r}, v, \mathbf{\Omega}, t) \qquad \ldots\ldots(2.2)$$

where λ is a constant, whence

$$N(\mathbf{r}, v, \mathbf{\Omega}, t) = N(\mathbf{r}, v, \mathbf{\Omega}) \exp(\lambda t).$$

Substitution of this in equation (2.2) gives

$$\begin{aligned} &-v\mathbf{\Omega} \,.\, \mathrm{grad}\, N(\mathbf{r}, v, \mathbf{\Omega}) - v\alpha(\mathbf{r}, v) N(\mathbf{r}, v, \mathbf{\Omega}) \\ &+ \frac{1}{4\pi} \int\!\!\int v' \beta\{\mathbf{r}, (v', \mathbf{\Omega}' \to v, \mathbf{\Omega})\} N(\mathbf{r}, v', \mathbf{\Omega}')\, dv'\, d\Omega' = \lambda N(\mathbf{r}, v, \mathbf{\Omega}). \qquad \ldots\ldots(2.3) \end{aligned}$$

In particular, the solution of this equation corresponding with the maximum value of λ permitted by the boundary conditions will be considered. $N(\mathbf{r}, v, \mathbf{\Omega})$ will be referred to as the neutron current density in the direction $\mathbf{\Omega}$ at the point $\mathbf{r}$, and, corresponding to the maximum value of λ, $N(\mathbf{r}, v, \mathbf{\Omega})$ is everywhere positive. This follows from physical considerations. Consider now the adjoint equation† of (2.3).

Suppose L is an operator and is a function of variables which we denote by ξ. If functions P and Q are functions of ξ then the adjoint operator of L, which we denote by L^+, is defined by

$$\int PLQ\, d\xi = \int QL^+P\, d\xi$$

where the integrations are taken over all ξ space. Thus if either N or the adjoint function N^+ are zero at infinity for a fixed value of $\mathbf{\Omega}$ (cf. after equation (2.7)) then the adjoint operator of 'grad' is '$-$grad'. Also the adjoint operator of

$$\int\!\!\int \beta\{\mathbf{r}, (v', \mathbf{\Omega}' \to v, \mathbf{\Omega})\} \ldots dv'\, d\Omega'$$

is

$$\int\!\!\int \beta\{\mathbf{r}, (v, \mathbf{\Omega} \to v', \mathbf{\Omega}')\} \ldots dv'\, d\Omega'.$$

The adjoint equation of (2.3) is then‡

$$\begin{aligned} &v\mathbf{\Omega} \,.\, \mathrm{grad}\, N^+(\mathbf{r}, v, -\mathbf{\Omega}) - v\alpha(\mathbf{r}, v) N^+(\mathbf{r}, v, -\mathbf{\Omega}) \\ &+ \frac{1}{4\pi} \int\!\!\int v' \beta\{\mathbf{r}, (v, \mathbf{\Omega} \to v', \mathbf{\Omega}')\} N^+(\mathbf{r}, v', -\mathbf{\Omega}')\, dv'\, d\Omega' = \lambda^+ N^+(\mathbf{r}, v, -\mathbf{\Omega}). \quad (2.5) \end{aligned}$$

N^+ is written thus: $N^+ \equiv N^+(\mathbf{r}, v, -\mathbf{\Omega})$ so that if $\mathbf{\Omega}$ is replaced by $-\mathbf{\Omega}$ in equation (2.5) and $\beta\{\mathbf{r}, (v, -\mathbf{\Omega} \to v', -\mathbf{\Omega}')\}$ is written in the form§ $\gamma\{\mathbf{r}, (v', \mathbf{\Omega}' \to v, \mathbf{\Omega})\}$ then the resulting equation is exactly similar in form to equation (2.3) and so, in the physical interpretation of equation (2.5), $N^+(\mathbf{r}, v, \mathbf{\Omega})$ represents a neutron current density in the direction $\mathbf{\Omega}$. Thus for a given problem, $N^+(\mathbf{r}, v, \mathbf{\Omega})$ corresponding to the maximum value of λ^+ will be everywhere positive.

---

† The adjoint equation is considered by Wilson (1950) to derive certain general properties of the transport equation, and in his report he obtains an equation similar to equations (2.8) and (2.9) of the present paper.

‡ This equation can still be considered even if there is no restriction on the behaviours of N and N^+ at infinity.

§ This is quite in order, since, from a mathematical point of view, β is merely a function of $\mathbf{r}, v', v, \mathbf{\Omega}'$ and $\mathbf{\Omega}$.

It will be shown later (after equation (2.8)) that $\lambda^+=\lambda$ for the maximum values of λ^+ and λ.

Consider now the adjoint equation of a system for which the corresponding α's and β's are α^* and β^*. (This can be considered as a perturbed system of the original one.) Let the (maximum) value of λ^+ for this adjoint system be λ^* and denote the corresponding neutron current density by $\Psi^+(\mathbf{r}, v, \mathbf{\Omega})$. The adjoint equation for this system is then

$$v\mathbf{\Omega}\,.\,\mathrm{grad}\,\Psi^+(\mathbf{r}, v, -\mathbf{\Omega})-v\alpha^*(\mathbf{r}, v)\Psi^+(\mathbf{r}, v, -\mathbf{\Omega})$$
$$+\frac{1}{4\pi}\iint v'\beta^*\{\mathbf{r}, (v, \mathbf{\Omega}\rightarrow v', \mathbf{\Omega}')\}\Psi^+(\mathbf{r}, v', -\mathbf{\Omega}')\,dv'\,d\Omega=\lambda^*\Psi^+(\mathbf{r}, v, -\mathbf{\Omega}). \qquad \ldots\ldots(2.6)$$

Multiply equation (2.3) by $v\Psi^+(\mathbf{r}, v, -\mathbf{\Omega})$ and equation (2.6) by $vN(\mathbf{r}, v, \mathbf{\Omega})$ and subtract. Integrate the resulting equation over v, $\mathbf{\Omega}$, and $\mathbf{r}$ denoting the element of volume by $d\tau$ to obtain

$$-\iiint[\Psi^+(\mathbf{r}, v, -\mathbf{\Omega})\mathbf{\Omega}\,.\,\mathrm{grad}\,N(\mathbf{r}, v, \mathbf{\Omega})+N(\mathbf{r}, v, \mathbf{\Omega})\mathbf{\Omega}\,.\,\mathrm{grad}\,\Psi^+(\mathbf{r}, v, -\mathbf{\Omega})]$$
$$\times v^2\,dv\,d\Omega\,d\tau-\iiint[\alpha(\mathbf{r}, v)-\alpha^*(\mathbf{r}, v)]v^2N(\mathbf{r}, v, \mathbf{\Omega})\Psi^+(\mathbf{r}, v, -\mathbf{\Omega})\,dv\,d\Omega\,d\tau$$
$$+\frac{1}{4\pi}\int\!\!\int\!\!\int\!\!\int\!\!\int v\Psi^+(\mathbf{r}, v, -\mathbf{\Omega})\beta\{\mathbf{r}, (v', \mathbf{\Omega}'\rightarrow v, \mathbf{\Omega})\}v'N(\mathbf{r}, v', \mathbf{\Omega}')\,dv'\,dv\,d\Omega'\,d\Omega\,d\tau$$
$$-\frac{1}{4\pi}\int\!\!\int\!\!\int\!\!\int\!\!\int vN(\mathbf{r}, v, \mathbf{\Omega})\beta^*\{\mathbf{r}, (v, \mathbf{\Omega}\rightarrow v', \mathbf{\Omega}')\}v'\Psi^+(\mathbf{r}, v', -\mathbf{\Omega}')\,dv'\,dv\,d\Omega'\,d\Omega\,d\tau$$
$$=(\lambda-\lambda^*)\iiint vN(\mathbf{r}, v, \mathbf{\Omega})\Psi^+(\mathbf{r}, v, -\mathbf{\Omega})\,dv\,d\Omega\,d\tau. \qquad \ldots\ldots(2.7)$$

Another similar equation is obtained by considering the adjoint of the unperturbed system together with the ordinary equation of the perturbed system. The integrals over $\mathbf{r}$ in equation (2.7) are taken over all space to infinity; free space is considered as a medium for which $\alpha\equiv\beta\equiv0$, and there is no restriction that the boundaries of the perturbed and unperturbed systems should be the same but the particular (hypothetical) case of a non-absorbing scattering medium extending to infinity is excluded, and so, with no neutron source at infinity, $\Psi^+(\mathbf{r}, v, \mathbf{\Omega})$ and $N(\mathbf{r}, v, \mathbf{\Omega})$ are zero for all directions entering the sphere at infinity.

Consider the first integral on the left-hand side of equation (2.7). It can be written as

$$-\iint v^2\,dv\,d\Omega\int\mathbf{\Omega}\,.\,\mathrm{grad}\,\{\Psi^+(\mathbf{r}, v, -\mathbf{\Omega})N(\mathbf{r}, v, \mathbf{\Omega})\}\,d\tau$$

which equals

$$-\iint v^2\,dv\,d\Omega\int_S\mathbf{\Omega}\,.\,\mathbf{1}\Psi^+(\mathbf{r}, v, -\mathbf{\Omega})N(\mathbf{r}, v, \mathbf{\Omega})\,dS$$

where the integral over S is the surface integral over the sphere at infinity, $\mathbf{1}$ is the unit vector normal to the surface, and dS is an element of surface. Since the particular (hypothetical) case of a non-absorbing scattering medium extending to infinity is excluded and $\Psi^+(\mathbf{r}, v, -\mathbf{\Omega})$ and $N(\mathbf{r}, v, \mathbf{\Omega})$ are zero for all directions entering the sphere at infinity, then for each value of $\mathbf{\Omega}$, either $\Psi^+(\mathbf{r}, v, -\mathbf{\Omega})$ or $N(\mathbf{r}, v, \mathbf{\Omega})$ is zero on the sphere at infinity and thus the above integral is zero. In view of this, and re-writing v' for v and $\boldsymbol{\Omega}'$ for $\boldsymbol{\Omega}$ in the fourth integral, equation (2.7) then becomes

$$\begin{aligned}
&-\int\!\!\int\!\!\int[\alpha(\mathbf{r},v)-\alpha^*(\mathbf{r},v)]v^2N(\mathbf{r},v,\boldsymbol{\Omega})\Psi^+(\mathbf{r},v,-\boldsymbol{\Omega})\,dv\,d\Omega\,d\tau\\
&+\frac{1}{4\pi}\int\!\!\int\!\!\int\!\!\int\!\!\int[\beta\{\mathbf{r},(v',\boldsymbol{\Omega}'\to v,\boldsymbol{\Omega})\}-\beta^*\{\mathbf{r},(v',\boldsymbol{\Omega}'\to v,\boldsymbol{\Omega})\}]\\
&\times v'N(\mathbf{r},v',\boldsymbol{\Omega}')v\Psi^+(\mathbf{r},v,-\boldsymbol{\Omega})\,dv'\,dv\,d\Omega'\,d\Omega\,d\tau\\
&=(\lambda-\lambda^*)\int\!\!\int\!\!\int vN(\mathbf{r},v,\boldsymbol{\Omega})\Psi^+(\mathbf{r},v,-\boldsymbol{\Omega})\,dv\,d\Omega\,d\tau. \qquad \ldots\ldots(2.8)
\end{aligned}$$

Consider the case of zero perturbation so that

$$\begin{gathered}
\alpha^*(\mathbf{r},v)=\alpha(\mathbf{r},v)\\
\beta^*\{\mathbf{r},(v',\boldsymbol{\Omega}'\to v,\boldsymbol{\Omega})\}=\beta\{\mathbf{r},(v',\boldsymbol{\Omega}'\to v,\boldsymbol{\Omega})\}\\
\Psi^+(\mathbf{r},v,\boldsymbol{\Omega})=N^+(\mathbf{r},v,\boldsymbol{\Omega})\\
\lambda^*=\lambda^+
\end{gathered}$$

then equation (2.8) gives

$$(\lambda-\lambda^+)\int\!\!\int\!\!\int vN(\mathbf{r},v,\boldsymbol{\Omega})N^+(\mathbf{r},v,-\boldsymbol{\Omega})\,dv\,d\Omega\,d\tau=0$$

and since for the maximum values of λ and λ^+, N and N^+ are both positive everywhere it then follows that $\lambda=\lambda^+$. Hence the equation obtained by considering the adjoint equation of the unperturbed system together with the ordinary equation of the perturbed system is

$$\begin{aligned}
&-\int\!\!\int\!\!\int[\alpha(\mathbf{r},v)-\alpha^*(\mathbf{r},v)]v^2N^+(\mathbf{r},v,-\boldsymbol{\Omega})\Psi(\mathbf{r},v,\boldsymbol{\Omega})\,dv\,d\Omega\,d\tau\\
&+\frac{1}{4\pi}\int\!\!\int\!\!\int\!\!\int\!\!\int[\beta\{\mathbf{r},(v',\boldsymbol{\Omega}'\to v,\boldsymbol{\Omega})\}-\beta^*\{\mathbf{r},(v',\boldsymbol{\Omega}'\to v,\boldsymbol{\Omega})\}]\\
&\times v'\Psi(\mathbf{r},v',\boldsymbol{\Omega}')vN^+(\mathbf{r},v,-\boldsymbol{\Omega})\,dv'\,dv\,d\Omega'\,d\Omega\,d\tau\\
&=(\lambda-\lambda^*)\int\!\!\int\!\!\int vN^+(\mathbf{r},v,-\boldsymbol{\Omega})\Psi(\mathbf{r},v,\boldsymbol{\Omega})\,dv\,d\Omega\,d\tau. \qquad \ldots\ldots(2.9)
\end{aligned}$$

Equations (2.8) and (2.9) are exact equations and they are the fundamental equations of the present treatment and all the subsequent results are derived from them. It is interesting at this stage to consider the general case of a small perturbation. The problem of large perturbations will be dealt with in § 5.

Write

$$\left.\begin{aligned}
\alpha^*(\mathbf{r},v)-\alpha(\mathbf{r},v)&=\Delta\alpha(\mathbf{r},v)\\
\beta^*\{\mathbf{r},(v',\boldsymbol{\Omega}'\to v,\boldsymbol{\Omega})\}-\beta\{\mathbf{r},(v',\boldsymbol{\Omega}'\to v,\boldsymbol{\Omega})\}&=\Delta\beta\{\mathbf{r},(v',\boldsymbol{\Omega}'\to v,\boldsymbol{\Omega})\}\\
\lambda^*-\lambda&=\Delta\lambda
\end{aligned}\right\}\ldots\ldots(2.10)$$

and also put $\Psi=N+\Delta N,\quad \Psi^+=N^++\Delta N^+$ ......(2.11)

but it will be seen on substitution in equations (2.8) and (2.9) that ΔN and ΔN^+ give only second order contributions and can therefore be neglected. In this case equations (2.8) and (2.9) reduce to one and the same equation which is

$$\begin{aligned}
&-\int\!\!\int\!\!\int\Delta\alpha(\mathbf{r},v)v^2N(\mathbf{r},v,\boldsymbol{\Omega})N^+(\mathbf{r},v,-\boldsymbol{\Omega})\,dv\,d\Omega\,d\tau\\
&+\frac{1}{4\pi}\int\!\!\int\!\!\int\!\!\int\!\!\int\Delta\beta\{\mathbf{r},(v',\boldsymbol{\Omega}'\to v,\boldsymbol{\Omega})\}v'N(\mathbf{r},v',\boldsymbol{\Omega}')vN^+(\mathbf{r},v,-\boldsymbol{\Omega})\,dv'\,dv\,d\Omega'\,d\Omega\,d\tau\\
&=\Delta\lambda\int\!\!\int\!\!\int vN(\mathbf{r},v,\boldsymbol{\Omega})N^+(\mathbf{r},v,-\boldsymbol{\Omega})\,dv\,d\Omega\,d\tau. \qquad \ldots.(2.12)
\end{aligned}$$

This is the general perturbation equation for small perturbations and in the next sections the particular cases of isotropic scatter with one and two energy groups are considered. From the above equation, knowing N and N^+ for a given system, one can calculate the change $\Delta\lambda$ in λ as a result of small changes $\Delta\alpha$ and $\Delta\beta$ in α and β.

§ 3. ONE-GROUP PERTURBATION THEORY

In the case of the one-energy-group approximation all the neutrons are considered to have the same mean energy, and the adjoint equation is the same as the ordinary equation and so

$$N(\mathbf{r}, v, \mathbf{\Omega}) = N(\mathbf{r}, \mathbf{\Omega})\delta(v - v_0) = N^+(\mathbf{r}, \mathbf{\Omega})\delta(v - v_0) \qquad \ldots\ldots(3.1)$$

where v_0 is the speed of the neutrons in the group and $\delta(v - v_0)$ is the Kronecker delta symbol and has the following properties

$$\begin{aligned} \delta(v - v_0) &= 0 \text{ if } v \neq v_0 \\ &= 1 \text{ if } v = v_0 \end{aligned}$$

$$\int_{v}^{v_0+} f(v)\delta(v - v_0)\, dv = f(v_0).$$

Write $\alpha(\mathbf{r}, v) = \alpha(\mathbf{r})$ when $v = v_0$, and for the particular case of isotropic scatter

$$\beta\{\mathbf{r}, (v_0, \mathbf{\Omega}' \to v, \mathbf{\Omega})\} = \beta\{\mathbf{r}, (v_0 \to v)\}\delta(v - v_0) \equiv \beta(\mathbf{r}) \text{ when } v = v_0. \qquad \ldots\ldots(3.2)$$

Substitution of (3.1) and (3.2) in equation (2.12) gives

$$-\iint \Delta\alpha(\mathbf{r}) N(\mathbf{r}, \mathbf{\Omega})\, N(\mathbf{r}, -\mathbf{\Omega})\, d\Omega\, d\tau + \frac{1}{4\pi}\int \Delta\beta(\mathbf{r}) n^2(\mathbf{r})\, d\tau$$

$$= \frac{\Delta\lambda}{v_0}\int N(\mathbf{r}, \mathbf{\Omega}) N(\mathbf{r}, -\mathbf{\Omega})\, d\Omega\, d\tau \qquad \ldots\ldots(3.3)$$

where $n(\mathbf{r}) = \int N(\mathbf{r}, \mathbf{\Omega})\, d\Omega$. Defining the function $g(\mathbf{r})$ by

$$g(\mathbf{r}) = 4\pi \int N(\mathbf{r}, \mathbf{\Omega}) N(\mathbf{r}, -\mathbf{\Omega})\, d\Omega / n^2(\mathbf{r})$$

equation (3.3) can then be written in the form

$$\int [\Delta\beta(\mathbf{r}) - g(\mathbf{r})\Delta\alpha(\mathbf{r})] n^2(\mathbf{r})\, d\tau = \frac{\Delta\lambda}{v_0}\int g(\mathbf{r}) n^2(\mathbf{r})\, d\tau \qquad \ldots\ldots(3.4)$$

which is the one-group perturbation equation (for small perturbations) and the same equation can be deduced from Fuchs' analysis. If equation (3.4) is derived directly from the transport equation omitting the general approach of the previous section, the derivation is extremely simple. Even obtaining it as has been done here by way of the general equations the derivation is simpler than by way of Fuchs' analysis.

§ 4. TWO-GROUP PERTURBATION THEORY

In the two-energy-group approximation all neutrons are considered to have one of two mean energies. Let the mean speed of the neutrons in the two groups be v_i $(i = 1, 2)$ then

$$\left.\begin{aligned} N(\mathbf{r}, v, \mathbf{\Omega}) &= N_1(\mathbf{r}, \mathbf{\Omega})\delta(v - v_1) + N_2(\mathbf{r}, \mathbf{\Omega})\delta(v - v_2) \\ N^+(\mathbf{r}, v, \mathbf{\Omega}) &= N_1^+(\mathbf{r}, \mathbf{\Omega})\delta(v - v_1) + N_2^+(\mathbf{r}, \mathbf{\Omega})\delta(v - v_2). \end{aligned}\right\} \qquad \ldots\ldots(4.1)$$

$$\left.\begin{aligned}&\text{Write}\qquad \alpha(\mathbf{r}, v_i) \equiv \alpha_i(\mathbf{r}) \qquad\qquad (i=1, 2)\\ &\text{and, for the particular case of isotropic scatter,}\\ &\qquad \beta\{\mathbf{r}, (v_i, \boldsymbol{\Omega}' \to v, \boldsymbol{\Omega})\} = \beta\{\mathbf{r}, (v_i \to v)\}\delta(v - v_j) \qquad (i, j = 1, 2)\\ &\qquad\qquad\qquad\qquad\qquad \equiv \beta_{ij}(\mathbf{r}) \quad \text{when} \quad v = v_j.\end{aligned}\right\} \qquad \ldots\ldots(4.2)$$

Thus† $\beta_{ij}(\mathbf{r})$ is the probability that a neutron in group i gives rise to a neutron in group j per unit length of its path. Substitution of equations (4.1) and (4.2) in equation (2.12) gives

$$-\iint \sum_i \Delta\alpha_i(\mathbf{r}) v_i^2 N_i(\mathbf{r}, \boldsymbol{\Omega}) N_i^+(\mathbf{r}, -\boldsymbol{\Omega})\, d\Omega\, d\tau + \frac{1}{4\pi}\int \sum_i \sum_j \Delta\beta_{ij}(\mathbf{r}) v_i v_j n_i(\mathbf{r}) n_j^+(\mathbf{r})\, d\tau$$
$$= \Delta\lambda \iint \sum_i v_i N_i(\mathbf{r}, \boldsymbol{\Omega}) N_i^+(\mathbf{r}, -\boldsymbol{\Omega})\, d\Omega\, d\tau \qquad \ldots\ldots(4.3)$$

where

$$n_i(\mathbf{r}) = \int N_i(\mathbf{r}, \boldsymbol{\Omega})\, d\Omega$$

and

$$n_i^+(\mathbf{r}) = \int N_i^+(\mathbf{r}, \boldsymbol{\Omega})\, d\Omega.$$

Defining

$$g_{ii}(\mathbf{r}) = 4\pi \int N_i(\mathbf{r}, \boldsymbol{\Omega}) N_i^+(\mathbf{r}, -\boldsymbol{\Omega})\, d\Omega / n_i(\mathbf{r}) n_i^+(\mathbf{r}), \qquad \ldots\ldots(4.4)$$

equation (4.3) can then be written in the form

$$-\int \sum_i \Delta\alpha_i(\mathbf{r}) v_i^2 g_{ii}(\mathbf{r}) n_i(\mathbf{r}) n_i^+(\mathbf{r})\, d\tau + \int \sum_i \sum_j \Delta\beta_{ij}(\mathbf{r}) v_i v_j n_i(\mathbf{r}) n_j^+(\mathbf{r})\, d\tau$$
$$= \Delta\lambda \int \sum_i v_i g_{ii}(\mathbf{r}) n_i(\mathbf{r}) n_i^+(\mathbf{r})\, d\tau. \qquad \ldots\ldots(4.5)$$

This is the two-group perturbation equation (for small perturbations) and it will be observed that it appears to be somewhat simpler than the corresponding equation obtained by Tait, but Tait's equation can, by a suitable transformation, be transformed into a similar equation.

§ 5. SUGGESTED METHOD FOR DEALING WITH LARGE PERTURBATIONS

The perturbation equations (2.12), (3.4) and (4.5) derived in the above sections are, strictly speaking, only suitable for use when the perturbations are small, but they may be used to give approximate results for the case of large perturbations. However, this is not always a satisfactory procedure. Suppose instead of extrapolating from a known system by means of perturbation theory to obtain the solution of the perturbed system, one were to interpolate between two known systems, then in general a better result should be obtained. It is with this idea in mind that the following method is obtained.

Consider the one-group approximation and suppose the solutions to two systems are known. Let the solutions to the known systems be ${}_1N(\mathbf{r}, \boldsymbol{\Omega})$ and ${}_2N(\mathbf{r}, \boldsymbol{\Omega})$ respectively and define

$${}_in(\mathbf{r}) = \int {}_iN(\mathbf{r}, \boldsymbol{\Omega})\, d\Omega. \qquad \ldots\ldots(5.1)$$

Let the α's and β's of the known systems be

$${}_i\alpha(\mathbf{r}) \text{ and } {}_i\beta(\mathbf{r}) \qquad (i = 1, 2)$$

and let $\alpha^*(\mathbf{r})$, $\beta^*(\mathbf{r})$ and $\Psi(\mathbf{r}, \boldsymbol{\Omega})$ refer to the perturbed system. Write

$$\begin{aligned}\alpha^*(\mathbf{r}) - {}_i\alpha(\mathbf{r}) &= \Delta_i\alpha(\mathbf{r})\\ \beta^*(\mathbf{r}) - {}_i\beta(\mathbf{r}) &= \Delta_i\beta(\mathbf{r})\\ \lambda^* - {}_i\lambda &= \Delta_i\lambda.\end{aligned}$$

---

† These functions differ from those used in some neutronics reports in that they do not include a velocity factor v_i/v_j.

In one-energy-group theory, equations (2.8) and (2.9) reduce to the same, since for one energy group $N^{+}(\mathbf{r}, \mathbf{\Omega}) = N(\mathbf{r}, \mathbf{\Omega})$ and $\Psi^{+}(\mathbf{r}, \mathbf{\Omega}) = \Psi(\mathbf{r}, \mathbf{\Omega})$. A perturbation equation corresponding to the one-energy-group form of equations (2.8) and (2.9) is obtained for each of the known systems, thus, writing $v_0 = v$ (cf. § 3)

$$\left.\begin{aligned}
&\frac{1}{4\pi}\int \Delta_1\beta(\mathbf{r})\,{}_1n(\mathbf{r})\psi(\mathbf{r})\,d\tau - \int \Delta_1\alpha(\mathbf{r})\,d\tau \int {}_1N(\mathbf{r}, \mathbf{\Omega})\Psi(\mathbf{r}, -\mathbf{\Omega})\,d\Omega \\
&\qquad = \frac{\Delta_1\lambda}{v}\iint {}_1N(\mathbf{r}, \mathbf{\Omega})\Psi(\mathbf{r}, -\mathbf{\Omega})\,d\Omega\,d\tau \\
&\frac{1}{4\pi}\int \Delta_2\beta(\mathbf{r})\,{}_2n(\mathbf{r})\psi(\mathbf{r})\,d\tau - \int \Delta_2\alpha(\mathbf{r})\,d\tau \int {}_2N(\mathbf{r}, \mathbf{\Omega})\Psi(\mathbf{r}, -\mathbf{\Omega})\,d\Omega \\
&\qquad = \frac{\Delta_2\lambda}{v}\iint {}_2N(\mathbf{r}, \mathbf{\Omega})\Psi(\mathbf{r}, -\mathbf{\Omega})\,d\Omega\,d\tau
\end{aligned}\right\} \quad \ldots\ldots(5.2)$$

where

$$\psi(\mathbf{r}) = \int \Psi(\mathbf{r}, \mathbf{\Omega})\,d\Omega.$$

These equations are exact—subject of course to the one-group approximation—and it seems most natural to expand Ψ in terms of ${}_1N$ and ${}_2N$ so that

$$\Psi(\mathbf{r}, \mathbf{\Omega}) = A_1\,{}_1N(\mathbf{r}, \mathbf{\Omega}) + A_2\,{}_2N(\mathbf{r}, \mathbf{\Omega})$$

where A_1 and A_2 are taken to be constants. Substitution in (5.2) and elimination of A_1 and A_2 gives

$$\begin{vmatrix}
\begin{gathered}\int\left[\Delta_1\beta(\mathbf{r}) - G_{11}(\mathbf{r})\left\{\Delta_1\alpha(\mathbf{r}) + \frac{\Delta_1\lambda}{v}\right\}\right] \\ \times\,{}_1n^2(\mathbf{r})\,d\tau\end{gathered} & \begin{gathered}\int\left[\Delta_1\beta(\mathbf{r}) - G_{12}(\mathbf{r})\left\{\Delta_1\alpha(\mathbf{r}) + \frac{\Delta_1\lambda}{v}\right\}\right] \\ \times\,{}_1n(\mathbf{r})\,{}_2n(\mathbf{r})\,d\tau\end{gathered} \\
\begin{gathered}\int\left[\Delta_2\beta(\mathbf{r}) - G_{12}(\mathbf{r})\left\{\Delta_2\alpha(\mathbf{r}) + \frac{\Delta_2\lambda}{v}\right\}\right] \\ \times\,{}_1n(\mathbf{r})\,{}_2n(\mathbf{r})\,d\tau\end{gathered} & \begin{gathered}\int\left[\Delta_2\beta(\mathbf{r}) - G_{22}(\mathbf{r})\left\{\Delta_2\alpha(\mathbf{r}) + \frac{\Delta_2\lambda}{v}\right\}\right] \\ \times\,{}_2n^2(\mathbf{r})\,d\tau\end{gathered}
\end{vmatrix} = 0 \quad \ldots\ldots(5.3)$$

where

$$G_{ij}(\mathbf{r}) = 4\pi\int {}_iN(\mathbf{r}, \mathbf{\Omega})\,{}_jN(\mathbf{r}, -\mathbf{\Omega})\,d\Omega / {}_in(\mathbf{r})\,{}_jn(\mathbf{r})$$

from which an approximation to the value of λ for the perturbed system can be calculated. Now with equation (5.3) there is not the same need as with equation (3.4) for the perturbation to be small, since it is effectively an interpolation between known results. In general, higher accuracy should be obtained by making use of more known solutions and thus effectively interpolating between 3, 4 or even more systems. In this way it seems likely that results of any desired accuracy can be obtained.

In the general case of continuous velocity dependence the procedure suggested is similar to that for one-group theory. Let prefix i refer to system i, and for simplicity consider only two systems. Let the solutions to the known systems be ${}_iN(\mathbf{r}, v, \mathbf{\Omega})$ and the adjoint solutions ${}_iN^{+}(\mathbf{r}, v, \mathbf{\Omega})$, then, if $\Psi(\mathbf{r}, v, \mathbf{\Omega})$ and $\Psi^{+}(\mathbf{r}, v, \mathbf{\Omega})$ are the ordinary and adjoint solutions of the perturbed system, put

$$\left.\begin{aligned}
\Psi(\mathbf{r}, v, \mathbf{\Omega}) &= A_1\,{}_1N(\mathbf{r}, v, \mathbf{\Omega}) + A_2\,{}_2N(\mathbf{r}, v, \mathbf{\Omega}) \\
\Psi^{+}(\mathbf{r}, v, \mathbf{\Omega}) &= B_1\,{}_1N^{+}(\mathbf{r}, v, \mathbf{\Omega}) + B_2\,{}_2N^{+}(\mathbf{r}, v, \mathbf{\Omega})
\end{aligned}\right\} \quad \ldots\ldots(5.4)$$

where A_i and B_i are taken to be constants. Substitution of these quantities in equations (2.8) and (2.9), for the perturbations from systems 1 and 2 in turn gives four simultaneous equations and the subsequent elimination of the A_i and

B_i gives a 4×4 determinantal equation from which an approximation to the value of λ for the perturbed system can be calculated. This determinantal equation is the analogue of equation (5.3) of the one-group treatment but contains twice as many rows and columns, because in the general case, the ordinary and adjoint solutions are distinct whereas in the one-group approximation they are the same. As in the one-group case higher accuracy should be obtained by simultaneously perturbing three or more known solutions but in practice a limit will be set by the computational effort available.

ACKNOWLEDGMENTS

I wish to express my thanks to the Director of the Atomic Weapons Research Establishment, Aldermaston, Berks., for permission to publish this paper and also to Dr. J. H. Tait of the Atomic Energy Research Establishment, Harwell, for his comments during preparation of the manuscript.

REFERENCES

FUCHS, K., 1949, *Proc. Phys. Soc.* A, **62**, 791.

GLASSTONE, S., and EDLUND, M. C., 1952, *The Elements of Nuclear Reactor Theory* (New York: Van Nostrand).

TAIT, J. H., 1954, *Proc. Phys. Soc.* A, **67**, 615.

WILSON, A. H., 1950, *Atomic Energy Research Establishment Report MS.* 105A.

On Star Production by μ-Mesons Underground

By G. N. FOWLER
The Physical Laboratories, The University, Manchester

Communicated by L. Rosenfeld; MS. received 13th December 1954

Abstract. The application of Williams' method to underground star production by μ-mesons is discussed. It is shown that the virtual photon spectrum derived by Williams is not applicable to this process and the appropriate virtual photon spectrum is deduced. The results on star production are then re-examined and it is shown that photo-nuclear effects are unable to explain the observed cross sections. The relationship of this result to the observations on the anomalous scattering of μ-mesons is also discussed.

---

§ 1. INTRODUCTION

RECENT experimental results on the scattering of high energy μ-mesons by nuclei (Whittemore and Shutt 1952, McDiarmid 1954, Rochester and Wolfendale 1954, Leontic and Wolfendale 1953) have shown a larger number of scattering events of large angle ($p\theta \gtrsim 3$ kMev θ/c, where p is the momentum of the μ-meson) than can be accounted for by electromagnetic processes. On the other hand, processes involving greater energy and momentum transfers—underground star production by μ-mesons—have been explained as photo-nuclear reactions produced by virtual photons from the incident meson. It is the purpose of the present note to examine the latter type of process in more detail and to relate it to the large angle scattering. It will be shown that electromagnetic interactions are not able to account for the production of stars with the observed frequency, and that the two processes are consistent with the same anomalous μ-meson–nucleon interaction.

§ 2. DISCUSSION OF THE WILLIAMS METHOD

The method of virtual quanta (Williams 1935) for the treatment of radiation and collision phenomena has come into extensive use in problems in which specifically photo-nuclear effects may be important. The method enables these effects to be included without the necessity for a detailed theory by making use of the experimental results.

The transition probability in an electromagnetic collision process may be written

$$P = K|\langle f|\,\mathbf{E}_W\,.\,e\mathbf{r}\,|i\rangle|^2 \qquad \ldots\ldots(1)$$

where $e\mathbf{r}$ is the electric displacement of the perturbed system and $\mathbf{E}_W$ is given by

$$\mathbf{E}_W = \int_{-\infty}^{\infty} \mathbf{E}(\mathbf{r}, t) \exp\{i(W/\hbar)t\}. \qquad \ldots\ldots(2)$$

Here $\mathbf{E}(\mathbf{r},t)$ is the electric field due to the incident particle at the position of the target.

One may show, using the Møller (1931) potentials, that this field is given by

$$\mathbf{E}=\mathbf{E}'\exp\{i(\mathbf{q}.\mathbf{r}-Wt)/\hbar\}. \qquad \ldots\ldots(3)$$

Here

$$\mathbf{E}'=\frac{\hbar ie(a_0\mathbf{q}-(W/c)\mathbf{a})}{q^2-W^2/c^2} \qquad \ldots\ldots(4)$$

$$\mathbf{q}=\mathbf{p}-\mathbf{p}', \quad W=E-E'$$

with p, p', E, E', the momentum and energy of the μ-meson before and after the collision. The wave function of the incident particle is given by

$$\psi=\phi(p)\exp\{i(\mathbf{p}.\mathbf{r}-Et)/\hbar\} \qquad \ldots\ldots(5)$$

and the symbols a_0 and $\mathbf{a}$ are defined by

$$a_0=-\phi^*(p')\phi(p), \quad \mathbf{a}=-\phi^*(p')\alpha\phi(p). \qquad \ldots\ldots(6)$$

In the first Born approximation the transition probability is now

$$P=K|\langle f|\mathbf{E}'.e\mathbf{r}\exp(i\mathbf{q}.\mathbf{r}/\hbar)|i\rangle|^2. \qquad \ldots\ldots(7)$$

Williams assumed the electric field to be uniform over the perturbed system so that the transition probability could be written

$$P=K|\mathbf{E}'|^2|\langle f|e\mathbf{r}|i\rangle|^2.$$

A factor $(c/2\pi)|\mathbf{E}'|^2$ may be interpreted as a virtual photon flux and $|\langle f|e\mathbf{r}|i\rangle|^2$ may be expressed in terms of the photo-absorption cross section.

It will be seen that a necessary condition for the application of the Williams method is

$qR\ll\hbar$, where R is the dimension of the perturbed system. ......(8)

In the case of star production underground we have

$$\langle f|\mathbf{E}'.e\mathbf{r}\exp(i\mathbf{q}.\mathbf{r}/\hbar)|i\rangle=\sum_{n=1}^{Z}e\int\psi_f^*\mathbf{E}'.\mathbf{r}_n\exp(i\mathbf{q}.\mathbf{r}_n/\hbar)\psi_i\,d\tau \quad \ldots(9)$$

where ψ_f is the final nuclear state wave function containing a free proton wave and ψ_i is the initial nuclear state wave function. The quantity R in (8) is then the nuclear radius. In star production processes the energy transfers, being not greater than 150 MeV, are such that they take place to individual nucleons with momentum conservation. In fact, the experimental data have been interpreted making this assumption (George and Evans 1950) together with the use of the Williams method. However, in such cases we have $qR\gg\hbar$ and so the Williams method, at least in its usual form, is not applicable. Thus the conclusions of George that the production of stars underground is due to photonuclear reactions initiated by the electromagnetic field of the incident meson, based as they are on the use of the Williams method, should be revised.

In the following paragraphs we will derive a more accurate expression for the virtual photon flux carried by the incident particle appropriate to the case of star production by μ-mesons.

§ 3. DERIVATION OF THE VIRTUAL PHOTON SPECTRUM

(i) $qR\sim p\theta R\ll\hbar$ (Williams' approximation valid)

It is useful to consider this case here, although the result will be the same as that found by Williams, in order to see how the argument should be modified for the case $qR\gg\hbar$.

With **E** given by (3) and (4) one finds, using (7), the following expression for the cross section for scattering into the element of solid angle $d\omega$

$$d\sigma = \frac{4e^4 p' E E' |\mathbf{q} - W\mathbf{p}/E|^2}{c^4 p (q^2 - W^2/c^2)^2} \left| \sum_{n=1}^{Z} \int \psi_f^* \mathbf{r}_n \psi_i \, d\tau \right|^2 d\omega. \qquad \ldots\ldots(10)$$

The photo-absorption cross section may be introduced by using the relation

$$\left| \sum_{n=1}^{Z} \int \psi_f^* r_n \psi_i \, d\tau \right|^2 = \frac{\hbar^2 f_{if}}{2M_p(E_f - E_i)} = \frac{\hbar c \sigma_{\text{ph}} \, dW}{4\pi^2 e^2 W}. \qquad \ldots\ldots(11)$$

In order to derive Williams' result for the total cross section, we must integrate over θ and ϕ bearing in mind condition (8). The integral over θ is therefore cut off at $\theta = \theta_{\max}$ which may be defined by $\theta_{\max} = \hbar/pR$. This excludes close collisions which do not contribute very much to the total cross section provided the energy transfer is not too large compared with the nucleon binding energies.

On substituting in (10) from (11) and carrying out the integrations the result is

$$\sigma \, dW = \frac{2e^2 c^2 \sigma_{\text{ph}} \, dW}{\pi \hbar c v^2 W} \left\{ \log \frac{E\hbar}{\mu c W R} - \frac{V^2}{c^2} \right\}. \qquad \ldots\ldots(12)$$

This result agrees with that given by Williams when the lower limit of impact parameters, in his derivation, is taken to be equal to the nuclear radius. Thus, as has been said above, the use of Williams' expression for the number of virtual photons accompanying the incident particle assumes the limitation $qR \ll \hbar$.

(ii) $qR \sim p\theta R \gg \hbar$

In this case we will be interested in the case of nuclear collisions in which the energy transfer is large compared with the binding energy of a nucleon. The nuclear forces will play only a secondary part and we assume that ψ_f contains the free proton wave of the struck particle of momentum **P**.

The angular distribution corresponding to (7) will then have a maximum for an angle such that

$$\frac{q^2}{2M_p} = \frac{|p - p'|^2}{2M_p} = W \qquad \ldots\ldots(13)$$

since the matrix element will only be appreciable when $\mathbf{P} = \mathbf{q}$ which implies (13) when $\mathbf{q}$ is large.

The same procedure as that used in § 3(i) may now be followed except that in this case only a small range of values of θ will contribute to the result.

Now $2q\,dq \sim (2E^2/c^2) \sin\theta \, d\theta$, so that the integration over θ may be replaced by an integration over q; this may be carried out approximately by taking the value of the integrand at $q = (2M_p W)^{1/2}$ and multiplying by $\Delta = 2\hbar/R$. Here Δ is the allowable variation in q; for values outside this the matrix element falls rapidly to zero. The integration over θ and ϕ therefore yields

$$\sigma = \frac{16\pi e^4}{c^2} \frac{\left| \sum_{n=1}^{Z} \int \psi_f^* r_n \exp(i\mathbf{q}\,.\,\mathbf{r}_n/\hbar) \psi_i \, d\tau \right|^2}{R\hbar q} \qquad \ldots\ldots(14)$$

with $q = (2M_p W)^{1/2}$, and assuming $q > W$. Substituting for the sum in (14) from (11), generalized in an obvious way, we have

$$\sigma(W)\,dW = \frac{4e^2 \hbar \sigma_{\text{ph}} \, dW}{\pi \hbar c R (2M_p)^{1/2} W^{3/2}}. \qquad \ldots\ldots(15)$$

The virtual photon spectrum is thus given by

$$N(h\nu)\,d(h\nu)=\frac{4\alpha\hbar\,d(h\nu)}{\pi R(2M_p)^{1/2}(h\nu)^{3/2}}. \qquad \ldots\ldots(16)$$

In order to compare the theory with the experimental observations on star production underground we must integrate (15) over the energy spectrum of the incident meson. This is given by

$$N(E)\,dE=2E_0^{\,2}\,dE/(E+E_0)^3 \qquad \ldots\ldots(17)$$

where E_0 is the ionization loss at the depth at which the observations are made. The averaged cross section is

$$\bar{\sigma}(W)\,dW=\int_W^\infty N(E)\sigma(W)\,dE\,dW$$

$$\simeq\frac{4\alpha\hbar E_0^{\,2}\sigma_{\rm ph}\,dW}{\pi R(2M_p)^{1/2}(W+E_0)^2\,W^{3/2}}. \qquad \ldots\ldots(18)$$

The cross section for the production of stars of energy larger than ϵ is then

$$\sigma_\epsilon=\int_\epsilon^\infty \bar{\sigma}(W)\,dW\simeq\frac{8\alpha\hbar\sigma_{\rm ph}}{\pi R(2M_p)^{1/2}\epsilon^{1/2}}. \qquad \ldots\ldots(19)$$

This result is to be compared with that found by George (1952), namely

$$\sigma_\epsilon\sim 0\cdot 9\alpha\sigma_{\rm ph}\{\log(E_0/\epsilon)\}^2/\pi. \qquad \ldots\ldots(20)$$

With ϵ taken to be 150 Mev, $\sigma_{\rm ph}=10^{-28}\,{\rm cm}^2$/nucleon, and[†] $R=3\cdot 6\times 10^{-13}$ cm, one finds a theoretical cross section of $1\cdot 6\times 10^{-31}\,{\rm cm}^2$/nucleon compared with the experimental result (George and Evans 1950, George 1952) of $\sim 5\times 10^{-30}\,{\rm cm}^2$/nucleon. In addition the cross section (19) is independent of depth although the experimental results seem to indicate some increase with depth. The absence of such an increase from the theoretical results is due to the approximations made but more accurate calculation should not show as marked an increase as that given by (20).

One may obtain a rough check on (21) in the following way. When the interaction is assumed to be an elastic collision between the μ-meson and a single nucleon, the cross section for energy transfer W to the nucleus is given approximately by

$$\sigma'\,dW=2\pi e^4 Z'\,dW/c^2 M_p W^2. \qquad \ldots\ldots(21)$$

Here Z' is the effective nuclear charge taking into account all photo-nuclear absorption processes. We may define Z' by

$$Z'=\sum_f f'_{if}=\frac{M_p c}{2\pi^2 e^2\hbar}\int\sigma_{\rm ph}\,dW \qquad \ldots\ldots(22)$$

where $\sigma_{\rm ph}$ is the photo-nuclear absorption cross section and the integration extends over the energy spectrum of the incident radiation. According to Levinger and Bethe (1952) the experimental value of $\int\sigma_{\rm ph}\,dW$ is

$$\int\sigma_{\rm ph}\,dW=0\cdot 14NZ/A \ \ \text{Mev barns} \qquad \ldots\ldots(23)$$

where Z is the nuclear charge. This is consistent with the value $\sigma=10^{-28}\,{\rm cm}^2$/nucleon used above.

From (22) and (23) we have

$$Z'=3\cdot 2NZ/A. \qquad \ldots\ldots(24)$$

[†] The value of R has been calculated assuming that for the photographic plate $A=27$.

Substituting this value for Z' in (21) we have

$$\sigma' dW = 6{\cdot}4\pi e^4 NZ\, dW/c^2 M_p A W^2. \qquad \ldots\ldots(25)$$

If we take $N = Z = 13$ and carry out the same averaging procedure as before we find for the total cross section per nucleon

$$\sigma_\epsilon' \simeq 1{\cdot}6\pi e^4/M_p c^2 \epsilon. \qquad \ldots\ldots(26)$$

The ratio of this to the previous result (19) is

$$\sigma_\epsilon'/\sigma_\epsilon \sim 5 \text{ (when } \epsilon = 150\,\text{Mev}). \qquad \ldots\ldots(27)$$

This confirms the result already obtained in equation (19) as to order of magnitude. It may be added here that the result (27) is not unreasonable since the expression (21) is an upper limit to the inelastic collision cross section (Gatto 1953). This fact, together with the difference in dependence on ϵ of the two results, implies that (19) still over-estimates the effect of the high energy stars.

§ 4. Conclusions

It is interesting to discuss the results obtained above in the light of the observations on large-angle scattering of μ-mesons referred to in § 1.

The anomalous scattering cross section is found to differ from that predicted theoretically, on the basis of an electromagnetic interaction, by a factor of the same order of magnitude as that found here in the case of the production. It seems therefore that the anomalous scattering and star production are due to the same anomalous μ-meson nucleon interaction.

However, it should be noted that the star production involves momentum transfers which are larger by a factor of at least three compared with the largest transfers observed in cloud chambers. It seems reasonable therefore to suggest that the interaction between the meson and the nucleons is anomalous over a much wider range of momentum transfers than has been so far observed in cloud chambers.

An interesting difference between the two types of phenomena concerns their A (or Z) dependence. The cloud chamber observations appear to be proportional to A^2 (or Z^2) whereas in the case of star production, in which it is certainly reasonable to suppose that the interaction takes place with single nucleons, the cross section should be proportional to A or Z. A reasonable interpretation of these observations is that the cloud chamber results correspond to elastic, and the star production to inelastic, anomalous interactions.

It might be added that there is some slight experimental evidence for an increase with depth in the cross section for star production which, if real, might indicate an increase of the interaction with energy.

At this stage it is useful to examine some of the possible consequences of the assumption that the anomalous interactions of μ-mesons are due to a new force between μ-mesons and nucleons. We will assume that it may be represented by a square well of width of the order of the nuclear radius.

The clearest test of the existence of such a force lies in measurements of the μ-mesic atom. The K and L orbits should be affected to a different extent and so the photon spectrum should be different from that to be expected with no nuclear interaction.

With regard to the scattering cross section, an ordinary force would give rise to interference effects with the Coulomb field which would be markedly different for μ-mesons of opposite charge. So far the experimental results do not indicate any such interference effects. This may be due to peculiarities of the interaction itself (for example a sharp boundary) which restrict the range of angles over which interference effects are possible, or to the fact that the experimentally observed quantity is usually the projected angle and this would tend to smooth out irregularities in the differential cross section.

The cross section for capture of μ-mesons with subsequent reaction $\mu + \mathrm{P} \rightarrow \mathrm{N} + \nu$ could be affected in two ways: the initial state wave function of the meson could be changed and the interaction could affect the second and higher orders of a perturbation calculation. (When it is assumed that the interaction is independent of isotopic spin there is no first order contribution.) Bearing in mind the experimental results discussed above, it is safe to say that these effects would not be such as to disturb significantly the agreement between the coupling constant for the above reaction and that for the reaction

$$\mathrm{N} \rightarrow \mathrm{P} + \mathrm{e} + \nu$$

so that the possibility of a universal Fermi interaction would remain. There remain the possible effects on the number of nucleons emitted after μ-meson capture by the nucleus. At present the usual statistical theory is not able to account for the experimental results without rather drastic modifications (Sard and Crouch 1954, Lang 1952). However, the existence of a μ-meson–nucleon force could lead to greater nuclear excitations which would help to explain the observed multiplicity. One might also expect a capture probability proportional to Z^3 rather than Z^4. This follows when the well depth is taken to be the same for all nuclei and the probability that the meson is inside the nucleus taken to be that of a meson in a K shell. This Z-dependence is not excluded by the experimental evidence.

In additional the experimental results for the ratio of a μ-meson capture probability in heavy and light nuclei is larger than that predicted by the theory of Wheeler (1949) (cf. Sard and Crouch 1954). An additional ordinary force would be expected to produce such an effect since it would tend to concentrate the μ-meson cloud inside the nucleus to a greater extent for the light than for the heavy nucleus.

Further experiments on the lower energy stars in which the incident and out-going μ-meson might be identifiable would be of interest in that they would give information on the angular dependence of the inelastic scattering. Also further observations on the depth dependence of the result should help to determine the dependence on the energy of the incident meson of the anomalous interaction.

Finally, more accurate cloud chamber measurements of the scattering cross section in which positive and negative μ-mesons are distinguished would be useful in deciding whether the interference effects, referred to above, exist.

Acknowledgments

I am indebted to Drs. G. D. Rochester and A. Wolfendale for many interesting discussions.

References

Gatto, R., 1953, *Nuovo Cim.*, **10**, 1559.

George, E. P., 1952, *Progress in Cosmic Ray Physics* (Amsterdam : North Holland Publishing Co.).

George, E. P., and Evans, J., 1950, *Proc. Phys. Soc.* A, **63**, 1248.

Lang, J. M. B., 1952, *Proc. Phys. Soc.*, A, **65**, 995.

Leontic, B., and Wolfendale, A. W., 1953, *Phil. Mag.*, **44**, 1101.

Levinger, J. S., and Bethe, H. A., 1952, *Phys. Rev.*, **85**, 577.

McDiarmid, I. B., 1954, *Phil. Mag.*, **45**, 933.

Møller, C., 1931, *Z. Phys.*, **70**, 786.

Rochester, G. D., and Wolfendale, A. W., 1954, *Phil. Mag.*, **45**, 980.

Sard, R. D., and Crouch, M. F., 1954, *Progress in Cosmic Ray Physics*, Vol. II (Amsterdam: North Holland Publishing Co.).

Whittemore, W. L., and Shutt, R. P., 1952, *Phys. Rev.*, **88**, 1312.

Williams, E. J., 1935, *K. Danske Vidensk. Selsk. Mat. Fys. Medd.*, **13**, 4.

Wheeler, J. A., 1949, *Rev. Mod. Phys.*, **21**, 133.

Some Proton Synchrotron Beam Studies with the Induction Electrode

By L. RIDDIFORD, H. B. van der RAAY and R. F. COE
Department of Physics, The University of Birmingham

Communicated by P. B. Moon; *MS. received* 10*th November* 1954

Abstract. The principle of the induction electrode and its application to the detection of the circulating proton beam in the Birmingham synchrotron are discussed. Investigations have been made of the phase width of the bunch of protons being accelerated, and of the period of the phase oscillations. These provide a confirmation of the theory of Bohm and Foldy concerning the acceleration process in a synchrotron. A study of the effects of pressure and aperture on the circulating beam shows that the requirements are more stringent than anticipated from the Blachman–Courant theory of gas scattering in such an accelerator. The difference is explainable in terms of characteristics particular to the Birmingham accelerator.

---

§ 1. Introduction

In the Birmingham synchrotron (University of Birmingham 1953) protons are injected with an energy of 460 kev into a vacuum tube in the form of a hollow ring of mean radius 450 cm. They are then accelerated by a radio-frequency potential applied to a drift tube called a cee, until at a time about one second after injection they attain an energy of 1000 Mev. During this time the magnetic field increases from 200 to 12 600 gauss, and the radio frequency has to be increased accurately from 0·3 to 9·7 Mc/s so that the particles remain close to the mean orbit. The nature of the accelerating mechanism is such that only those particles which lie within a certain range of phase with respect to the radio-frequency potential may be accelerated. As a result there exists inside the doughnut a circulating bunch of protons as drawn schematically in figure 1.

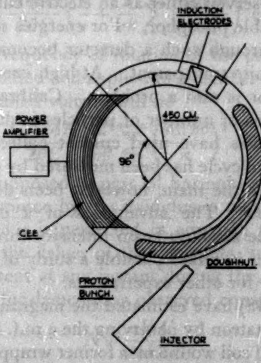

Figure 1. Schematic diagram of the Birmingham synchrotron.

The protons oscillate on complicated orbits about the mean orbit, deviations from this orbit being limited by the aperture available within the vacuum tube. The effective horizontal aperture is 26 cm and the vertical aperture 9 cm. The tube is located in a magnetic field which varies with radius as $r^{-2/3}$. The accelerating electrode extends for 96° and in-phase potentials of 300 volts r.m.s. appear on each end, so that the maximum energy gain per revolution is 630 electron volts. The phase of a particle adjusts itself with respect to that of the accelerating potential so that the average energy increment per revolution is about 200 electron volts. This is the amount required to keep it on the mean orbit as the magnetic field increases. The average pressure in the doughnut is normally $1{\cdot}3 \times 10^{-6}$ mm measured with air calibrated ionization gauges. Most of the results presented in this paper describe the beam properties during the first 100 milliseconds of the acceleration cycle. The pertinent machine parameters during this interval are plotted in figure 2.

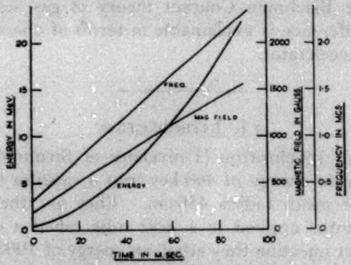

Figure 2. Parameters of the Birmingham synchrotron.

The possible methods of detecting the circulating beam divide broadly into two classes: those which destroy it, and those which leave it undisturbed. In the former case the beam is made to move to either the inner or outer wall of the doughnut, and is then observed either as an electric current or by means of the light emitted from a suitable phosphor. For energies above a few Mev multiple traversals of the beam through such a detector become possible, and at about 100 Mev the detector is quite transparent. At high energies secondary emission from the current collector is also a problem. Calibration of the light output from a scintillator in terms of number of particles is difficult. However, those engaged in injection studies have used current collectors and the beam size throughout the acceleration cycle has been measured by use of a potassium iodide crystal. The beam has in the main, however, been detected by the induction electrode described below. The advantages of a detector which provides a continuous record of the absolute beam intensity throughout the acceleration cycle are obvious; further it makes possible a study of beam fine structure and serves as a useful monitor for other experiments.

Bess and Hanson (1948) have estimated the magnitude of the electron beam circulating in a 20 Mev betatron by observing the e.m.f. induced by its associated magnetic field in a toroidal coil wound on a former wrapped around the doughnut. The beam in a betatron is not bunched and an e.m.f. results only if it is destroyed.

We have attempted to observe the proton synchrotron beam by means of the radio frequency e.m.f. induced in a simple one thousand turn coil of area 500 cm^2 placed outside the doughnut and to one side of the mean orbit. In principle this should be possible; the induced e.m.f. is proportional to the square of the radio frequency. At low frequencies the signal is too small in comparison with the interference due to radiation from the synchrotron power amplifier, while at high frequencies the signal is substantially reduced as a result of the self-capacitance of the coil. For these reasons, magnetic induction is difficult to use.

As an alternative, the electrostatic field associated with the proton beam may be converted into an electrical impulse by means of the so-called induction electrode. This method was studied by Le Caine (1951) and has also been used with success in the Brookhaven cosmotron (Swatz 1953). If an insulated electrode is placed inside the vacuum tube, the circulating bunch of protons induces charges on the condenser formed by the electrode and ground. This results in a train of voltage pulses whose fundamental frequency is the rotational frequency of the particles in the machine.

§ 2. THE INDUCTION ELECTRODE

The induction electrode consists of an insulated plate over which the circulating beam passes. If the azimuthal length ϕ of the electrode is small compared with the length of the bunch, the charge induced on the electrode will be a constant fraction K of the charge of those protons that are over the electrode at the instant in question; K takes account of the fact that all the lines of induction from the protons do not end on the electrode. If the bunch has a total azimuthal length 4θ and contains N protons, and if the number of protons decreases linearly from the centre of the bunch to each end, the pulses of voltage induced on the electrode will be of triangular form with a peak value

$$V = \frac{Ne\phi K}{2\theta C} \qquad \text{......(1)}$$

where e is the charge of each proton and C the capacity of the electrode. These pulses may be represented by the Fourier series

$$V(t) = \frac{Ne\phi K}{2\theta C}\left(\frac{\theta}{\pi} + \frac{2}{\pi\theta}\sum_{n=1}^{\infty}\left(\frac{\sin n\theta}{n}\right)^2 \mathrm{ccs}\, n\omega t\right) \qquad \text{......(2)}$$

where ω is the angular frequency of rotation of the particles.

If this voltage is amplified and applied to a rectifier which records its peak-to-peak amplitude, the rectified voltage will be

$$V' = \frac{GNe\phi K}{2\theta C}\left|\frac{2}{\pi\theta}\sum_{n=1}^{n=m}\left(\frac{\sin n\theta}{n}\right)^2 \cos n\omega t\right| \qquad \text{......(3)}$$

where the amplifier is supposed to pass all harmonics from the first to the mth with constant gain G. Since by the modulus is meant the peak-to-peak value of the series, the term θ/π is neglected in equation (3). Thus by measuring V' and θ, and knowing the values of the constants, an accurate estimate of the number of particles present at any instant during the acceleration cycle may be made. When only the fundamental is observed equation (2) may be written

$$N = \frac{\pi V' C}{\phi e K G}, \qquad \text{......(4)}$$

θ having been assumed small.

33-2

At times close to injection where all important harmonics are amplified, the number of particles can be estimated from equation (1). At full energy use is made of equation (4). According to equation (1) N is proportional to θ, whilst in equation (4) it is independent of θ. For a bunch 180° long ($\theta = 45°$), equation (4) is in error by 23%, and for a bunch 120° long by 9%. In the present case equation (4) shows that a beam of $4{\cdot}4 \times 10^8$ particles produces an output potential to the amplifier of one millivolt r.m.s.

In practice the limit to sensitivity is set at about 10^7 protons by the interference signals mentioned above. In the absence of these, the limit would be about 10^5 protons because of amplifier tube noise.

To determine the effect of beam position on the signal induced on the electrode, an electrostatic analogue was used. Two representations of the beam were used, one a wire of small diameter, the other metal sheets shaped to simulate the beam contour determined by experiments described later. The potential on the electrode was measured by a Lindemann electrometer. With the sheets it is necessary to take care that the charges remain approximately uniformly distributed as its position is varied. Figure 3(a) shows the results obtained with an 18 gauge wire and the normal induction electrode drawn in figure 4(a). Similar results are obtained for the metal sheets. It is evident that there is quite a strong dependence on the vertical position of the beam, but only a weak dependence on the horizontal position, over the region of interest.

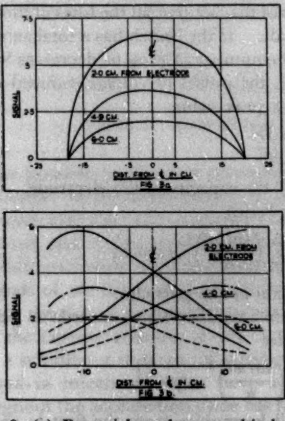

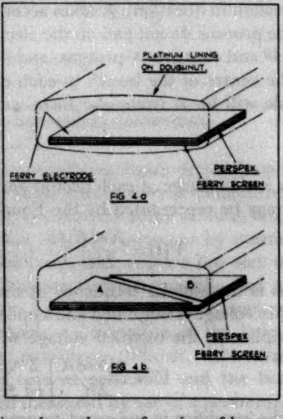

Figure 3. (a) Potential on the normal induction electrode as a function of beam position. (b) Potential on a tapered induction electrode as a function of beam position.

Figure 4. (a) Normal induction electrode. (b) Difference induction electrodes.

A strong radial dependence is obtained if the induction electrode is tapered as in figure 4(b). The results with an 18 gauge wire are drawn in figure 3(b). If a difference signal is taken from two adjacent plates with the tapers in opposite directions, and compared with the equivalent sum signal from the normal electrode, an estimate can be made of any radial displacement of the beam from the mean orbit. Similarly any vertical displacement could be estimated from the difference signal between identical normal electrodes placed one at the top and one at the bottom of the vacuum tube. In the Birmingham synchrotron the beam is below the middle of the vacuum tube; for this reason the value of K for a single electrode is larger than it would be were the beam centrally placed.

The induction electrodes at present in use are drawn in figure 4. They are constructed from sheets of Ferry 0·010 in. thick attached to light Perspex frames. Similar Ferry sheets on the undersides of the frames, and the platinum lining on the inside of the doughnut, form a common screen. The capacity of the normal electrode and the input cable to the amplifier is 203 pF. The signal from the induction electrode is amplified and then rectified so that a voltage equal to the peak-to-peak value of the amplified signal is obtained. This signal is displayed on a long persistence oscilloscope. The gain of the system is constant to 3 dB in the range 0·1–10 Mc/s and effectively zero outside this range. The system is linear over the range of beam intensities normally encountered. The amplifiers are placed inside thick steel tubes to shield them from the magnetic fringing field of the synchrotron. The cathode-ray tube of the recording oscilloscope is screened from the magnetic field by two concentric mumetal cylinders 0·094 in. thick.

For the study of bunch shapes the output from the radio frequency amplifier is connected directly to the deflector plates of a post-deflection acceleration cathode-ray tube with a fast time base. The timing pulses for triggering the various time bases were obtained from the synchrotron radio frequency control room. Figure 5 is a block diagram of the detection system.

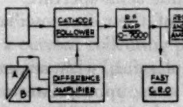

Figure 5.

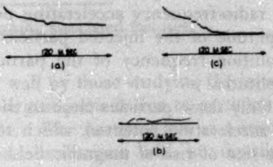

Figure 6.

Figure 5. Block diagram of the detection system.

Figure 6. (*a*) Trace of a rectified signal from the normal induction electrode. (*b*) Trace of a rectified signal from the difference induction electrodes. (*c*) Trace from normal electrode showing losses of beam.

Under good conditions the loss of particles is small from shortly after the instant at which the radio-frequency accelerating potential is applied, until the beam has attained full energy. This is shown by the photograph of a rectified induction electrode pattern reproduced in figure 6(*a*). The structure on the trace is due to spurious interference.

Normally the beam intensity is about 3×10^9 particles, but on occasions high energy pulses of $5\text{-}6 \times 10^9$ particles have been obtained. A pattern from the difference induction electrodes is reproduced in figure 6(*b*). From this it may be shown that the centre of the beam is never more than a few centimetres from the ideal orbit, verifying that the acceleration radio frequency is always close to the desired value. Figure 6(*c*) is a photograph of a trace from the normal electrode showing several sudden losses of beam. It demonstrates the value of a detector which does not require destruction of the beam for its operation. In figures 6(*a*), (*b*) and (*c*) the signal is of 120 msec duration.

§ 3. Free Oscillations and Phase Oscillations

A particle trapped in the magnetic field of a synchrotron will execute free oscillations, of the type first described by Kerst and Serber (1941) about the equilibrium orbit to which its energy is appropriate. The frequencies of such horizontal and vertical oscillations are respectively $(1-n)^{1/2}$ and $n^{1/2}$ times the particle revolution frequency, and in the absence of fresh disturbances, the initial oscillations are damped as $\{Hr(1-n)^{1/2}\}^{1/2}$ and $(Hrn^{1/2})^{1/2}$ respectively, n being the magnetic field index which in the present instance is about 2/3. The ratio of horizontal to vertical amplitudes for equal angular displacements from the equilibrium orbit is $\{n/(1-n)\}^{1/2}$. The free oscillations arise from two causes. One is the deviations from the ideal orbit due to scattering by the nuclei of the residual gas atoms in the doughnut, and is discussed later. The other is a result of the method of fixed energy injection at the outer edge of the doughnut into an increasing magnetic field.

The first particle to revolve inside the doughnut will have a small oscillation amplitude, and will spiral smoothly inwards as the magnetic field increases. But by the time it has reached the centre of the doughnut the incoming particles, although having a small angular spread, will have an oscillation amplitude equal to the doughnut semi-aperture, for their energy is inappropriate to the increased field. No more particles can be successfully injected and it is at this instant that the radio-frequency accelerating potential is applied. The average oscillation amplitude of the injected particles is half the doughnut semi-aperture. The revolution frequency of the particles is independent of their free oscillation amplitude.

Only those particles close to the point of constant phase ϕ_s, with respect to the accelerating potential, which receive an energy $eV \sin \phi_s$ appropriate to the time-rate of rise of magnetic field, continue to move as before. Many of the others commence to execute phase oscillations of the type described by Bohm and Foldy (1946) in their general theory of the synchrotron. The oscillations in phase ϕ are accompanied by associated variations in energy E and consequently radius r. Only those particles which lie within a certain region on the $(\phi, \Delta E)$, or $(\phi, \Delta r)$, diagram are accelerated. In our accelerator ϕ_s is equal to about 20° early in the acceleration cycle, and the region of stable phase is 220° long. It may be shown from equations (14) and (19) of Bohm and Foldy's paper that the maximum radial excursion is 15 cm. Consequently the appropriate $(\phi, \Delta r)$ diagram showing the stable region is as drawn in figure 7. Particles inside this region will rotate in an anticlockwise direction with the phase oscillation frequency along contours of the type dotted in the figure. Those outside it will not be accelerated and will quickly be lost to the inner wall of the doughnut.

As injection occurs at constant energy, the injected particles lie in a strip along the ϕ axis of the $(\phi, \Delta r)$ diagram as indicated in figure 7. The difference in energy between the first and last successfully injected particles is of the order of 1 kev only, and is due to the decelerating betatron action of the changing magnetic field.

For two reasons, as indicated in figure 7, the effective semi-aperture is less than the maximum radial excursion due to stable phase oscillations. Firstly, the maximum excursion is greater than the true semi-aperture. Secondly, the cumulative effect of factors such as any error in the relationship between the initial radio frequency and magnetic field, which cause the equilibrium orbit to be displaced from the ideal orbit, will also reduce the effective aperture. Further the free injection oscillations discussed above have frequencies corresponding to periods of a few microseconds, compared to the phase oscillation frequency of period about 200 microseconds, and so may be considered independent of and superimposed upon the phase oscillations as drawn schematically in the figure. Thus, after a quarter of a phase oscillation period, the particles will lie in a strip along the Δr axis, and at this time there will be a substantial loss of beam to the inner and outer walls of the doughnut. The particles lost to the wall of the doughnut for this reason have been observed on a current collecting probe near the inner wall by those studying the injection phenomena. In figure 8(*a*) the initial and largest pulse is due to particles with the maximum injection oscillation amplitude. The particles lost as a result of free oscillations superimposed upon phase oscillations will be distributed uniformly between the instant of the large pulse and a time one-quarter of a phase oscillation period later. Those lost due to the stable region extending beyond the walls of the doughnut will appear after a quarter of a phase oscillation period, and those lying outside the phase stable region will be lost to the inner wall some time before this. The result is a complex one, but there is clear evidence for a small pulse about 50 microseconds after the main pulse. Further a small discrete pulse appears about 150 microseconds after the main pulse, and is considered due to particles lost after three-quarters of a phase oscillation period as a result of gas scattering or instability (see later) between 50 and 150 microseconds. The phase oscillation period is therefore estimated to be about 200 microseconds.

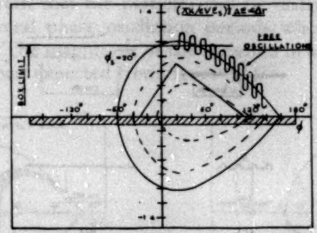

Figure 7. **Phase-stable diagram showing associated features.**

This early loss of beam is also evident in figure 8(*b*), which shows an induction electrode trace using a relatively fast time-base sweep. The initial pulse due to the injected beam is followed almost immediately by a substantial drop before the beam intensity settles down to a constant level. It will be shown below that the fine structure on the trace is due to phase oscillations. It is not possible from our measurements to estimate the fraction of the injected particles lost when the accelerating potential is applied, for the induction electrode signal has no significance before the beam is bunched.

Following the loss of particles one quarter of a phase oscillation period after acceleration is commenced, as a result of the aperture restrictions mentioned above, the bunch length immediately afterwards will be less than the maximum possible value of 220°. The observed value is about 140°. Figure 8(*c*) is a photograph of a train of pulses from the induction electrode due to the bunch of protons circulating in the machine with a revolution frequency equal to the frequency of the accelerating potential. It is apparent that the pulses are approximately triangular in shape, and this may be accounted for as follows. Initially particles are distributed uniformly in the strip of useful length 220° along the ϕ axis. All particles near the extremities of useful phase will be lost about 50 microseconds after the onset of acceleration for there is no aperture available to accommodate the free oscillations superimposed on the phase oscillations. No particles near the phase ϕ_s will be lost for the maximum free oscillation amplitude is just equal to the effective semi-aperture. At intermediate phases an assessable fraction of the particles initially present will be lost, and after a quarter of a phase oscillation period the bunch of particles, instead of being rectangular, will be triangular in form as drawn in figure 7. At later times the shape could change, for as we shall see, the particles distribute themselves throughout the stable region on the $(\phi, \Delta r)$ diagram. At most the shape could become similar to that of a contour in figure 7, but there will always tend to be a concentration of particles close to ϕ_s. The triangles in figure 8(*c*) are asymmetrical as expected. The triangular shape is maintained to the furthest instant at which we have photographed bunches, i.e. 120 milliseconds after the radio-frequency potential is applied.

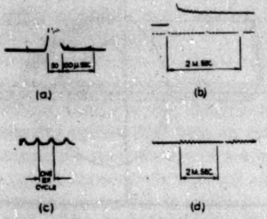

Figure 8 (*a*) Trace of a signal from a current collector showing early loss of particles due to phase oscillations. (*b*) Normal induction electrode trace showing phase oscillations. (*c*) Train of pulses from the induction electrode. (*d*) Difference induction electrode trace showing phase oscillations.

Theoretically then, assuming no other losses, 140/360 or 40% of the particles successfully injected will be accelerated, and of these a further 50% will be lost during the first quarter of the phase oscillation period.

Equation (2) shows that at low frequencies the signal from the induction electrode is inversely proportional to the bunch width. For a strip of particles as in figure 8, the bunch width will be seen to oscillate at twice the phase oscillation frequency. Thus the signal from the induction electrode will vary in amplitude with a frequency twice the phase oscillation frequency. The effect is evident in figure 8(*b*), from which it is estimated that the initial phase oscillation period is 200 micro-seconds. The variation in amplitude is smaller than would be expected from figure 7, and vanishes in a time of the order of twenty phase oscillation periods. This can be explained as follows: Equation (21) of Bohm and Foldy (1946) shows that for large phase amplitudes the phase oscillation period depends on the amplitude, increasing with amplitude. Further, since the oscillations are not symmetrical about ϕ_s, the time spent in each quadrant of the stable region on the $(\phi, \Delta r)$ diagram is not the same. Consequently the true distribution of the particles in this region after the first quarter of a phase oscillation period is as shown in figure 9(*a*) and not as in the idealized diagram in figure 7. The width of the band is due to the injection energy spread previously mentioned. In figure 9(*b*) the spreading out of the particles in the $(\phi, \Delta r)$ diagram during the first six quarter phase oscillation periods is illustrated. To avoid confusion the spread in injection energy is neglected. It is apparent that the particles will be distributed throughout the stable region after several phase oscillation periods whence the effect will no longer be detectable. The magnitude of the variation in amplitude in figure 8(*b*) is still rather smaller than expected from figure 9(*b*).

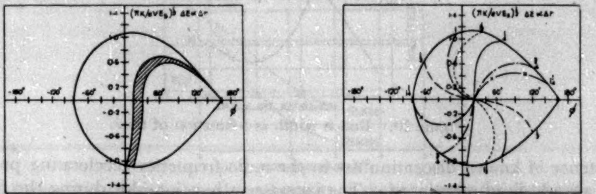

Figure 9. (*a*) Distribution of particles on the $(\phi, \Delta r)$ diagram after the first quarter phase oscillation period. (*b*) $(\phi, \Delta r)$ diagram showing the dependence of phase oscillation frequency on amplitude during the first one and a half periods.

The phase oscillations have also been observed shortly after injection with the difference electrodes, a typical trace being shown in figure 8(*d*). In this case the frequency of the signal is equal to the phase oscillation frequency; it is observable with the difference electrodes as the strip of phase stable particles is divided asymmetrically by the point ϕ_s. After a quarter phase oscillation period there are therefore more particles adjacent to say the electrode A than to the electrode B (see figure 4(*b*)). After three quarters of a phase oscillation period the majority of particles are adjacent to the electrode B. A symmetrically divided strip would yield no signal from the difference electrodes if the beam were centred on the mean orbit. The measured period is again 200 microseconds. There exist several small discontinuities in the voltage applied to the cee during the first sixty milliseconds of the acceleration cycle, which result from the method used to tune the cee. Phase jumps presumed to occur at these instants cause small losses of beam, and make it possible once more to observe phase oscillations. The effect of a phase jump is to cause the loss of all particles outside the region of overlap between the old and the new phase stable diagrams.

Those remaining will continue to rotate, now in an asymmetrical manner, on the $(\phi, \Delta r)$ diagram, and produce effects on the induction electrodes similar to those described above which occur shortly after injection. It is found that the frequency of the oscillations is constant during the first sixty milliseconds, in agreement with theory. The theoretical phase oscillation period is 250 microseconds, and the observed value 200 microseconds.

According to the theory of Bohm and Foldy the phase oscillation amplitude will be damped as $(E\cos\phi_s/\omega^2K)^{1/4}$, where $K=1+n/(1-n)\beta^2\}$ which in the present case means a reduction of only 30% throughout the acceleration cycle, and negligible damping, whilst the energy of the protons is non-relativistic. In the non-relativistic case the radial oscillations associated with the phase oscillations are however damped in proportion to H.

Unpublished calculations by the late Dr. J. S. Gooden suggested that strong phase damping would be obtained if the accelerating gaps were tapered at about 45° to the radius (see figure 1). The bunch width during the first 120 milliseconds of the acceleration cycle has been measured, and the results plotted in figure 10. The width shortly after injection has already been explained. The existence of known discontinuities in the radio-frequency accelerating potential has already been mentioned. The increase in bunch width during the first 50 milliseconds is probably due to these. Such an increase is possible only if the radial excursions associated with the phase oscillations are damped as expected. The rate of increase would probably be greater were it not for the fact that gas scattering will cause particles with large phase amplitudes to be lost during this time. The decrease in bunch width between 50 and 90 milliseconds is clear evidence for strong damping. The apparent further increase after 90 milliseconds must be considered a result of amplifier response, for at the last experimental point only three harmonics of the signal are recorded.

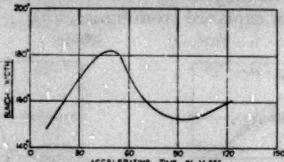

Figure 10. Bunch width as a function of time.

Two further interesting observations have been made. The region of stable phase extends in one direction to $\pi-\phi_s$. Particles at this phase receive the correct energy increment per revolution to maintain them on the equilibrium orbit, and the point is one of metastable phase. The slightest perturbation, however, will cause these particles either to be lost or to oscillate in phase about the stable phase position ϕ_s. At times very close to injection small bunches spaced between the main bunches of particles of the type shown in figure 8(c) have been observed. The group of metastable particles is observable as a discrete bunch because the width of the main bunch is reduced below the maximum possible by the injection oscillations, as described above. It has been found at all times that the bunched beam becomes completely incoherent within about 200 microseconds of the radio-frequency accelerating potential being removed.

§ 4. The Effects of Gas Scattering and Aperture

Shortly after being injected, the protons will experience small angle deflections as a result of Coulomb scattering by the nuclei of the residual atoms within the doughnut. These occur at random and soon the particles possess free oscillations, the phases of which are uniformly distributed in azimuth. Their properties are identical with those of the free injection oscillations. At any instant a particle will have a particular amplitude of oscillation, but this amplitude will either decrease or increase depending upon whether the $H^{1/2}$ damping or the scattering due to new collisions is predominant. The scattering will on the average decrease with increasing energy. The theory of gas scattering in betatrons and synchrotrons has been worked out by Blachman and Courant (1948, 1949) and by Courant (1953), and some results from the theory have been presented by one of us (Riddiford 1951). Theoretically the r.m.s. gas scattering amplitude reaches a maximum at four times the injection energy, and thereafter diminishes slowly. The oscillations can be resolved into horizontal and vertical components, and in the theory only the loss due to vertical scattering is considered. After a finite acceleration time almost all particles have experienced oscillations of amplitude greater than a certain minimal value in both horizontal and vertical directions.

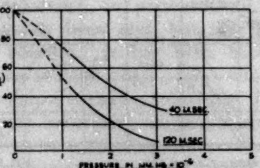

Figure 11. Dependence of beam intensity on the pressure in the doughnut.

The dependence of beam intensity on pressure has been investigated by increasing the amount of air in the doughnut by means of five artificial leaks. These are placed one on each of the five pumping manifolds (Riddiford 1951) to ensure a uniform pressure in a vacuum system in which substantial pressure gradients would otherwise exist. The results are shown in figure 11, the pressure being recorded with air calibrated ionization gauges. For our accelerator the main loss from scattering will occur for energies up to say 5 Mev and times up to say 40 milliseconds (figure 2). A steady loss of particles should, and does, continue for some time thereafter, for the distribution of the particles in oscillation amplitude is a Rayleigh one, and further the direct loss of particles from single scattering is not unimportant (Courant 1953). The effects of varying the horizontal and vertical apertures have been investigated, the effective horizontal aperture being varied by moving a $\frac{3}{16}$ in. diameter brass post transversely across the doughnut and the vertical aperture by rotating a centrally supported cranked rod which extends across the doughnut. Some of the results are shown in figure 12(*a*) and (*b*). During these measurements the horizontal aperture was 30 cm. The existence of minimal useful apertures is evident. In the vertical case it is seen that the axis of symmetry of the experimental curves is about one centimetre below the geometrical median plane of the magnet. It was considered, as was subsequently proved, that this is a result of the magnetic median plane being lower than the geometrical median plane. The ratio of horizontal to vertical minimal apertures is 4·5. Similar results were obtained at a different azimuth.

The pressure and effective aperture are several times more important than anticipated from the Blachman–Courant theory. There are good reasons for the discrepancy. As stated above the theory assumes that particles are lost only as a result of insufficient vertical aperture. The effective vertical aperture is substantially less than the available doughnut aperture because of the error in the median plane. As the mean square gas scattering amplitude is directly proportional to the pressure, this means that in the present case the pressure needs to be about 1·6 times lower for a given loss of particles. Further, there is no doubt that in the Birmingham synchrotron the horizontal aperture is just as important as the vertical aperture. Theory suggests that by the time gas scattering has become most important the injection oscillations and more particularly the radial excursions due to phase oscillations would be sufficiently damped for vertical gas scattering to matter most. But the results presented in figure 10 have shown that there is apparent anti-damping of the phase oscillations immediately following injection. For this reason the superposition of gas-scattering-free oscillations upon the phase oscillations will result in a substantially greater loss of particles than would otherwise occur. The phase jumps in the radio-frequency accelerating potential responsible for the early instability, combined with the effect of what frequency errors do exist, are responsible for the ratio of the minimal apertures being substantially greater than the theoretical value $\{n/(1-n)\}^{1/2} = \sqrt{2}$. The radial excursions due to phase oscillations and horizontal injection oscillations result in a greater loss of beam for a given aperture but would not affect the minimal aperture. Low harmonic magnetic field inhomogeneities are known to be small, and in any event would cause a radial displacement of the beam as well as an increase in its size. For both azimuths at which measurements were taken the beam was symmetrically spread about the mean doughnut radius.

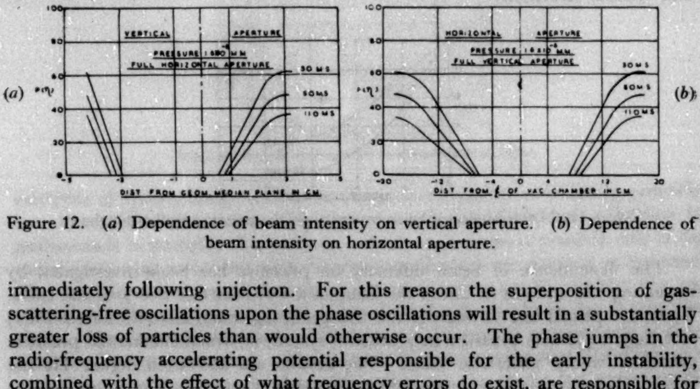

Figure 12. (*a*) Dependence of beam intensity on vertical aperture. (*b*) Dependence of beam intensity on horizontal aperture.

Several precautions were taken in the above measurements. The accelerated beam may vary by about 50% from pulse to pulse, largely as a result of variations in the number of particles injected. The experimental points are averages from a number of induction electrode traces each normalized to take account of variations in the number of particles remaining after the first quarter phase oscillation period. Experiments made using a faster time base and traces similar to that in figure 8(*c*) have shown that the number of injected particles is not significantly affected by the wires used to restrict the aperture, and that the spread in injection angles is small. As the horizontal aperture is reduced the loss after a quarter of a phase oscillation period increases rapidly, however, and the point at which the plateau such as is shown in figure 8(*c*) joins the injection pulse falls rapidly. This effect is automatically corrected for by the normalization mentioned above. Elder *et al.* (1947) have published results of aperture studies with a 70 MEV electron synchrotron, but without an induction electrode were unable to separate injection, pressure and phase phenomena.

The phase width of the circulating bunch of protons depends strongly on pressure and both horizontal and vertical apertures, but the shape is always triangular. The dependence of the induction electrode signal on bunch width has already been discussed. If corrections were not made for this, the beam intensity would not vary as rapidly with pressure and aperture as indicated in figures 11 and 12. Some typical results are as follows. The average pressure in the doughnut was $1{\cdot}2 \times 10^{-6}$ mm.

	Horizontal		Vertical	
Aperture (cm)	13	26	5·5	7·9
Bunch width 8 msec after injection (deg.)	55	140	45	142

The reason for the dependence on pressure and horizontal aperture is apparent from what has already been said, but that for the dependence on vertical aperture is more obscure. It has been shown that early in the acceleration cycle the particles at large phase angles will mostly have small free oscillation amplitudes. Further it is shown below that there is some preferential coupling between large (small) horizontal oscillations and small (large) vertical free oscillations. A reduction in vertical aperture causes the loss of particles with large vertical and consequently small horizontal oscillation amplitudes, thereby reducing the bunch width.

The beam contour has been determined experimentally by the use of two stops as drawn in figure 13. These consist simply of short $\frac{3}{16}$ in. diameter brass posts which may be inserted given distances into the beam at various radii from top and bottom, by longitudinal displacement and rotation of the supporting rods. These pass into the doughnut through O-ring vacuum seals. It has been shown that after sufficient time each particle has experienced both horizontal and vertical free oscillations with certain minimal amplitudes. If the radial

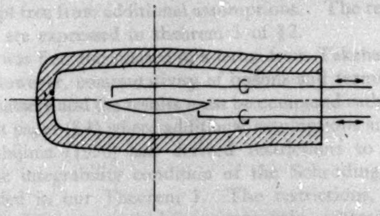

Figure 13. Contour of the minimal aperture, showing the device used for plotting it.

position of a post is inside the minimal horizontal aperture, and its vertical position is varied, the beam would be completely destroyed when the post is at or inside the minimal vertical aperture. The experimental contour of the minimal aperture determined in this way is shown in figure 13. It is displaced downwards from the median plane as expected, but is not rectangular. This means that particles with a large oscillation in one direction do not at the same time have a large oscillation in the other direction. Otherwise the contour plotted in figure 13 would be inconsistent with the minimal aperture studies discussed earlier. The result suggests that a doughnut of rectangular cross section has no real advantage over one of elliptical cross section.

The effect of reducing the average pressure in the doughnut by the assistance of liquid air traps, and the use of the results to throw some light on the nature of the residual molecules in an oil diffusion pump, are discussed by Coe and Riddiford (to be published).

ACKNOWLEDGMENTS

We wish to thank Professor P. B. Moon for his interest and encouragement in this work. It would not have been possible without the collaboration of several other members of the synchrotron group.

REFERENCES

BESS, L., and HANSON, A. O., 1948, *Rev. Sci. Instrum.*, **19**, 108.
BLACHMAN, N., and COURANT, E. D., 1948, *Phys. Rev.*, **74**, 140; 1949, *Ibid.*, **75**, 315.
BOHM, D., and FOLDY, L. L., 1946, *Phys. Rev.*, **70**, 249.
COURANT, E. D., 1953, *Rev. Sci. Instrum.*, **24**, 836.
ELDER, F. R., *et al.*, 1947, *J. Appl. Phys.*, **18**, 810.
KERST, D. W., and SERBER, R. B., 1941, *Phys. Rev.*, **60**, 53.
LE CAINE, H., 1951, *Thesis*, University of Birmingham.
RIDDIFORD, L., 1951, *J. Sci. Instrum.*, Supp. No. 1, p. 47.
SWATZ, C. E., 1953, *Rev. Sci. Instrum.*, **24**, 851.
UNIVERSITY OF BIRMINGHAM, 1953, *Nature, Lond.*, **172**, 704.

Commutation Relations between Different Fields

By H. UMEZAWA†, THE LATE J. PODOLANSKI† AND S. ONEDA‡

† The Physical Laboratories, University of Manchester
‡ Kanazawa University, Japan.

Communicated by L. Rosenfeld; MS. received 27th September 1954
and in final form 1st December 1954

Abstract. The commutation relations between fields representing different particles are not, as has been suggested, arbitrary. In general, only certain types of commutation relations are compatible with a specified Hamiltonian. The restrictions on the commutation relations—arising from the requirement of canonical invariance of field theory—are derived.

Further restrictions can be imposed by the assumption that the fermions form 'families'. A family comprises a set of mutually anticommuting particle fields. Members of different families commute. As a consequence of the family postulate bosons commute with fermions.

It is shown that the family postulate is consistent with the restrictions imposed by canonical invariance and that the two requirements together fix uniquely the commutation relations of the baryon-π system.

§ 1. INTRODUCTION

(*a*) In the first part of this paper (§§ 1, 2, 3) we show how the commutation relations between different fields are restricted by the form of the interaction Hamiltonian, and so by the possible transmutations. These restrictions follow from the canonical invariance of quantum field theory only, and this part of the paper has been kept free from additional assumptions. The results are therefore strictly valid and are expressed in theorem 1 of § 2.

This theorem was first formulated in a letter from Takahashi and Umezawa (1953). There, however, commutativity of bosons and fermions was assumed, implicitly, at the outset† and the results must be compared rather with the second part of the present paper (§ 4) where additional assumptions are introduced.

Previously Nishijima (1950) had derived restrictions to the commutation relations from the integrability condition of the Schrödinger equation. His results are included in our Theorem 1. The restrictions, contained in this theorem and derived from canonical invariance only, contradict Klein's (1938) conclusion that the commutation relations between different fields are arbitrary. We have therefore devoted the last section of this part (§ 3) to an analysis of Klein's method.

---

† This assumption is taken over by Kinoshita (1954) in a recent paper. He is therefore in a position, to derive as did Takahashi and Umezawa in their letter, the existence of 'families'. In the present paper we prefer to keep the treatment of the family hypothesis separate.

(*b*) Canonical invariance alone can never fix commutation relations completely. In order to arrive at more specific results we introduce in §4 a new postulate which separates bosons and fermions, grouping the latter into families.

The existence of families of fermions has already been derived in the above mentioned letter. There, families appear as a consequence of the assumption made about the commutativity of bosons and fermions. This assumption is thus (more or less) equivalent to the postulates of §4 of the present paper (cf. end of §4).

(*c*) Before we enter on the general proof of Theorem 1 we shall sketch, for the (nucleon, π) system, the physical meaning of our way of selecting commutation relations between different fields and shall show that the process $P \to N + \pi$ excludes, e.g. the commutation relations†

$$[P, N]_- = [P, \pi]_- = [N, \pi]_- = 0,$$

where P, N, π stand for the wave functions of the particles.

In quantum field theory canonical invariance guarantees the conservation of the probability of finding a set of transmuting particles. For the (nucleon, π) system canonical invariance obtains only in the Hilbert space made up of the state vectors of proton states, $N + \pi$ states and so on—not in any of these subspaces separately. A canonical transformation will affect the whole of the Hilbert space, and, because the commutation relations must be invariant under any canonical transformation, we expect canonical theory to give rise to some restrictions on the types of commutation relations between different particles. For the (nucleon, π) system such a restriction arises in the following way.

Canonical invariance is expressed by the existence of a unitary transformation $U[t]$ connecting the proton field operator to the incoming proton operator, so that

$$P(\mathbf{x}, t) = U^{-1}[t] P^{\text{in}}(\mathbf{x}, t) U[t] \qquad \ldots\ldots(1)$$

for any time t. The proton operator may be expanded as

$$P(\mathbf{x}, t) = P^{\text{in}}(\mathbf{x}, t) + \int a(\mathbf{x}, \mathbf{x}', t) N^{\text{in}}(\mathbf{x}', t) \pi^{\text{in}}(\mathbf{x}', t)\, d^3x' + \ldots, \qquad \ldots\ldots(2)$$

where a is a c-number function. Since

$$[P, P]_+ = [P^{\text{in}}, P^{\text{in}}]_+ = 0,$$

we have

$$[P^{\text{in}}, N^{\text{in}}\pi^{\text{in}}]_+ = 0. \qquad \ldots\ldots(3)$$

This relation, and the one obtained by exchanging proton and neutron, can be satisfied in two alternative ways,

(*a*) $[P, N]_+ = 0\,;\quad [P, \pi]_- = [N, \pi]_- = 0$ ......(4)

(*b*) $[P, N]_- = 0\,;\quad [P, \pi]_+ = [N, \pi]_+ = 0,$ ......(4)

and excludes therefore the above quoted combination of commutation relations.

To summarize: Canonical invariance requires the bare and the dressed proton to have the same statistics since they are connected by a unitary transformation. This, in turn, leads to restrictions on the commutation relations between the operators of the particles belonging to the proper fields.

These restrictions do not fix the commutation relations uniquely, but leave us, for the (nucleon, π) system, with the two possibilities (*a*), (*b*). The second possibility is excluded when one considers proton and neutron as different states of one Fermi particle, i.e. as members of the nucleon ‘ family ’. We shall later (§4) generalize the concept of families of Fermi particles and show that this construction leads to further restrictions of the commutation relations.

---

† Commutation relations refer, with a few obvious exceptions, to field operators at different points at the same time.

This, at any rate, will be our starting point. One could as well exclude (4*b*) by postulating that bosons commute with fermions as Kinoshita (1954) does. The relationship between these two assumptions will be discussed in §4.

§2. COMMUTATION RELATIONS BETWEEN DIFFERENT PARTICLES

The restrictions on the commutation relations will be derived from the equation (11) below. Here we shall give the proof of (11) only for the simple case in which the field operator is a canonical variable. Let $\mathbf{X}(x)$ and $X(x)$ be the field operator in Heisenberg and interaction representation and $\mathrm{U}(\sigma)$ the unitary transformation connecting them. We introduce the operator

$$\mathbf{X}(x,\sigma)\equiv \mathrm{U}^{-1}[\sigma]X(x)\mathrm{U}[\sigma], \qquad \ldots\ldots(5)$$

which goes over in $\mathbf{X}(x)$ if σ passes through x, and form the variation of $\mathbf{X}(x,\sigma)$ in the point x' on σ:

$$i\,\frac{\delta}{\delta\sigma(x')}\,\mathbf{X}(x,\sigma)=\mathrm{U}^{-1}[\sigma][X(x),H'(x')]_{-}\mathrm{U}[\sigma], \qquad \ldots\ldots(6)$$

where H' is the interaction Hamiltonian.

On the other hand, if L' is the interaction Lagrangian, $\mathbf{X}(x,\sigma)$ and $X(x)$ are connected by

$$\mathbf{X}(x,\sigma)=X(x)+\int_{-\infty}^{\sigma}\frac{\bar{\delta}\mathbf{L}'(x')}{\bar{\delta}\mathbf{X}^{*}(x')}\,\Delta_{X}(x-x')\,d^{4}x'. \qquad \ldots\ldots(7)$$

Here Δ_X, defined by

$$[X(x),X^{*}(x')]_{\pm}=i\Delta_{X}(x-x'), \qquad \ldots\ldots(8)$$

is related to the Green function (Takahashi and Umezawa 1953), and

$$\frac{\bar{\delta}\mathbf{L}'}{\bar{\delta}\mathbf{X}^{*}}=\frac{\partial\mathbf{L}'}{\partial\mathbf{X}^{*}}-\frac{\partial\mathbf{L}'}{\partial(\partial_{\mu}\mathbf{X}^{*})}\,\partial_{\mu}+\ldots \qquad \ldots\ldots(9)$$

differs from the (negative) source strength

$$-\mathbf{j}=\frac{\delta\mathbf{L}'}{\delta\mathbf{X}^{*}}=\frac{\partial\mathbf{L}'}{\partial\mathbf{X}^{*}}-\partial_{\mu}\,\frac{\partial\mathbf{L}'}{\partial(\partial_{\mu}\mathbf{X}^{*})}+\ldots$$

only by a divergence.

Equations (6) and (7) yield

$$[X(x),H'(x')]_{-}=-i\mathrm{U}[\sigma]\left\{\frac{\bar{\delta}\mathbf{L}'(x')}{\bar{\delta}\mathbf{X}^{*}(x')}\,\Delta_{X}(x-x')\right\}\mathrm{U}^{-1}[\sigma]. \qquad \ldots\ldots(10)$$

If H' satisfies (10), it will also satisfy

$$[X(x),H'(x')]_{-}=i\,\frac{\bar{\delta}H'(x')}{\bar{\delta}X^{*}(x')}\,\Delta_{X}(x-x'). \qquad \ldots\ldots(11)$$

Equations (10) and (11) remain valid, as can be shown, for a general field operator X (Takahashi and Umezawa 1953). Either of these equations expresses a necessary condition H' has to obey, and leads to restrictions on the commutation relations. To demonstrate this we prove the following theorem.†

---

† Two different A_k may stand for the same particle or may represent particle and anti-particle. For the meaning of ‘ commuting ’ and ‘ anticommuting ’ see footnote on previous page.

Theorem 1. Each interaction Hamiltonian must contain an even number of field operators $A_1, \ldots, A_{2n}$ which anticommute with a field X; thus each transmutation process must involve an even number of such particles.

For the proof, we suppose that H' contains an odd number of fields $A_1, \ldots, A_{2n+1}$ which anticommute with a field X. Denoting the remainder, which commutes with X, by B and substituting $H' = gA_1 \ldots A_{2n+1}B$ (with g a c-number) in the left-hand side of (11), we have

$$\begin{aligned}
&[X, A_1 \ldots A_{2n+1}B]_- \\
&\quad = [X, A_1]_+ A_2 \ldots - A_1[X, A_2]_+ A_3 \ldots \\
&\qquad + A_1 A_2 [X, A_3]_+ A_4 \ldots \mp \ldots \\
&\qquad + A_1 \ldots A_{2n}[X, A_{2n+1}]_- B \\
&\qquad + A_1 \ldots A_{2n+1}[X, B]_-.
\end{aligned}$$

The term containing the commutator $[X, A_{2n+1}]_-$ can neither vanish nor give rise to a Δ function, since X and A_{2n+1} anticommute. Thus the above expression cannot equal the right-hand side of (11).

Furthermore, we can prove the following theorem.

Theorem 2. If a field operator A commutes (anticommutes) with a field X, then the hermitian conjugate A^* also commutes (anticommutes) with X.

Indeed, the representation can always be chosen so that a part of the free field Hamiltonian containing A^*A is treated as an interaction. Applying Theorem 1 to this mass-type interaction we obtain Theorem 2.

We summarize the results which are obtained by applying Theorems 1 and 2 to the (baryon, π) system, the (π, θ, τ) system, the (lepton, μ) system and to photons.

Baryon, π. The processes concerned are

[1*a*]	$P \to P + \pi^0$;	[2*a*]	$\Lambda^+ \to P + \pi^0$
[1*b*]	$P \to N + \pi^+$;	[2*b*]	$\Lambda^0 \to P + \pi^-$
[1*c*]	$N \to P + \pi^-$;	[2*c*]	$\Lambda^- \to N + \pi^-$

Theorems 1 and 2 yield the following results:

(i) π^0 commutes with any field, and must therefore† be a boson (from [1*a*]).

(ii) The members of each of the following sets have the same commutation relations with any field:

π^+, π^- (theorem 2)
P, Λ^+, Λ^- (from [2*a*] or [2*c*], [1*c*])
N, Λ^0 (from [2*b*], [1*b*]).

That shows that all baryons have the statistics of the nucleons and leads to the commutation relations

$$[P, \Lambda^\pm]_+ = [N, \Lambda^0]_+ = 0.$$

(iii) All baryons (P, N, $\Lambda^\pm$, Λ^0) have the same commutation relations with the charged π-field. Depending on whether we assume the proton to commute or anticommute with $\pi^{\pm}$, the processes [1] and [2] yield two alternative sets of commutation relations :

---

† Our method gives Bose statistics for π^0, θ^0, γ no matter what the statistics of nucleons, electrons and charged pions is assumed to be.

$$\left.\begin{array}{ll}(a) & [\mathrm{P},\pi^{\pm}]_{-}=[\mathrm{N},\pi^{\pm}]_{-}=[\Lambda^{\pm,0},\pi^{\pm}]_{-}=0\\ & [\mathrm{P},\mathrm{N}]_{+}=[\mathrm{N},\Lambda^{\pm,0}]_{+}=[\mathrm{P},\Lambda^{\pm,0}]_{+}=[\Lambda^{0},\Lambda^{\pm}]_{+}=0\,;\\ (b) & [\mathrm{P},\pi^{\pm}]_{+}=[\mathrm{N},\pi^{\pm}]_{+}=[\Lambda^{\pm,0},\pi^{\pm}]_{+}=0\\ & [\mathrm{P},\mathrm{N}]_{-}=[\mathrm{P},\Lambda^{0}]_{-}=[\mathrm{N},\Lambda^{\pm}]_{-}=[\Lambda^{0},\Lambda^{\pm}]_{-}=0\\ & [\mathrm{P},\Lambda^{\pm}]_{+}=[\mathrm{N},\Lambda^{0}]_{+}=0.\end{array}\right\}\quad\ldots\ldots(12)$$

A decision between these two possibilities can be reached by an additional assumption, the family requirement, which we shall formulate in §4.

π, θ, τ. The decay schemes assumed are

$$[3a]\quad \theta^{0}\rightarrow\pi^{+}+\pi^{-}\,;\qquad [4a]\quad \tau^{\pm}\rightarrow\pi^{\pm}+\pi^{+}+\pi^{-}$$

$$[3b]\quad \theta^{\pm}\rightarrow\pi^{\pm}+\pi^{0}\,;\qquad [4b]\quad \tau^{0}\rightarrow\pi^{0}+\pi^{+}+\pi^{-}.$$

Application of Theorems 1 and 2 shows that

(iv) θ^{0} and τ^{0} commute with any field, and must therefore be bosons ;

(v) θ^{+}, θ^{-}, τ^{+}, τ^{-}, π^{+}, π^{-} have the same commutation relations with any field and commute with each other. The charged θ and τ fields have thus the same statistics as the charged π's.

μ, e, ν. If we assume the μ-meson to decay according to

$$[5]\quad \mu^{\pm}\rightarrow e^{\pm}+\nu+\nu$$

we find that

(vi) μ^{+}, μ^{-}, e^{+}, e^{-} obey the same commutation relations with any field and anticommute with each other. From this follows that the $\mu^{\pm}$ field has the same statistics as the electrons.

Photon. The process of bremsstrahlung, e.g.

$$[6]\quad e+\mathrm{P}\rightarrow e+\mathrm{P}+\gamma$$

shows that

(vii) γ commutes with any field and is thus a boson.

§ 3. KLEIN'S METHOD

Klein (1938) has shown that, under certain conditions, the commutation relations between different components of a Fermi field, and between different Fermi fields (Rosenfeld 1948), are arbitrary. For example, in the case of the nucleon system, according to Klein, the neutron can be described by either of two wave functions ψ_{N}, χ_{N}, of which one anticommutes and the other commutes with ψ_{P}. The two neutron operators are connected by

$$\chi_{\mathrm{N}}=(-1)^{n_{\mathrm{P}}}\psi_{\mathrm{N}}\qquad\ldots\ldots(13)$$

with n_{P} as the proton number operator. Indeed if $[\psi_{\mathrm{N}},\psi_{\mathrm{P}}]_{+}=0$, then

$$\begin{aligned}[\chi_{\mathrm{N}},\psi_{\mathrm{P}}]_{-}&=[(-1)^{n_{\mathrm{P}}}\psi_{\mathrm{N}},\psi_{\mathrm{P}}]_{-}\\&=(-1)^{n_{\mathrm{P}}}[\psi_{\mathrm{N}},\psi_{\mathrm{P}}]_{+}-[(-1)^{n_{\mathrm{P}}},\psi_{\mathrm{P}}]_{+}\psi_{\mathrm{N}}\\&=0.\end{aligned}$$

Our point is that, in general, one of the two neutron operators turns out to be a non-local function and therefore must be rejected.

Only for special types of interaction, to which the one considered by Klein belongs, are both ψ and χ point functions and only then does Klein's method apply. These are, indeed, just the instances in which our Theorem 1 does not lead to restrictions on the commutation relations. An example is the direct interaction between two protons and two neutrons,

$$H' = g\bar{\psi}_{\mathrm{P}}\psi_{\mathrm{P}}\bar{\psi}_{\mathrm{N}}\psi_{\mathrm{N}}.$$

There are, however, interactions which do not admit the transition (13) from ψ_{N} to χ_{N} and for which the method of Klein fails. For the interaction

$$H' = g\bar{\psi}_{\mathrm{N}}\Omega\psi_{\mathrm{P}}\phi_{\pi} + \text{h.c.}, \qquad \ldots\ldots(14)$$

e.g., with Ω made up of γ matrices, Theorem 1 leads to the alternative (cf. (4))

$$(a) \quad [\phi_{\pi}, \psi_{\mathrm{P}}]_{-} = [\phi_{\pi}, \psi_{\mathrm{N}}]_{-} = 0\ ; \quad [\psi_{\mathrm{P}}, \psi_{\mathrm{N}}]_{+} = 0$$
$$(b) \quad [\phi_{\pi}, \psi_{\mathrm{P}}]_{+} = [\phi_{\pi}, \psi_{\mathrm{N}}]_{+} = 0\ ; \quad [\psi_{\mathrm{P}}, \psi_{\mathrm{N}}]_{-} = 0.$$

Starting from the assumption that ϕ_{π} commutes with the nucleon operators (case (*a*)), we can now show that the neutron operator *anticommutes* with ψ_{P}. Klein's transformation to commuting nucleon operators is thus not allowed since it leads to a non-local neutron operator. The same is true in the case (*b*), i.e. if we make ϕ_{π} anticommute with ψ_{P} and ψ_{N} : the nucleon operators are both point functions only if they commute with one another. We shall give the proof for the first case.

A field operator ψ is local only if

$$[H'(x'), \psi(x)]_{-} = 0, \qquad \ldots\ldots\ldots(15)$$

where x' and x are any two points on a space-like surface. This is evident from

$$\frac{\delta\Psi(x)}{\delta\sigma(x')} = i\mathrm{U}^{-1}[\sigma][H'(x'), \psi(x)]_{-}\mathrm{U}[\sigma], \qquad \ldots\ldots(16)$$

where Ψ is the operator in the Heisenberg representation connected to ψ by

$$\Psi(x) = \mathrm{U}^{-1}[\sigma]\psi(x)\mathrm{U}[\sigma].$$

If the right-hand side of (16) were not zero, the implication would be that $\psi(x)$ is disturbed by π-production at a point x', separated from x by a space-like distance.

The condition (15) implies, just as equation (11) did, that the form of the interaction Hamiltonian is restricted by the commutation properties of the field operators. In our example the field operators $\psi_{\mathrm{N}}(x)$, $\psi_{\mathrm{P}}(x)$ both commute with $H'(x')$ of (14) only if they anticommute with each other. To make a commutable set χ_{N}, χ_{P} local we have to supplement the Hamiltonian by non-local operators :

$$\left.\begin{array}{lll} (a) & [\psi_{\mathrm{N}}, \psi_{\mathrm{P}}]_{+} = 0 & \rightarrow \quad H_a' = g\bar{\psi}_{\mathrm{N}}\Omega\psi_{\mathrm{P}}\phi_{\pi} + \text{h.c.} \\ (b) & [\chi_{\mathrm{N}}, \chi_{\mathrm{P}}]_{-} = 0 & \rightarrow \quad H_b' = g(-1)^{n_{\mathrm{P}}}(-1)^{n_{\mathrm{N}}}\bar{\chi}_{\mathrm{N}}\Omega\chi_{\mathrm{P}}\phi_{\pi} + \text{h.c.} \end{array}\right\} \quad \ldots.(17)$$

This discussion shows, indeed, that for a given Hamiltonian† only one of the two sets of field operators can be local. However, the second one which is commutable can only be made local by taking the Hamiltonian to be non-local. We feel justified in excluding such interactions—as we have done in deriving Theorem 1—and, consequently, in excluding the commutation relations

$$[\phi_{\pi}, \psi_{\mathrm{N}}]_{-} = [\phi_{\pi}, \psi_{\mathrm{P}}]_{-} = 0\ ; \quad [\psi_{\mathrm{P}}, \psi_{\mathrm{N}}]_{-} = 0.$$

In the same way it can be shown that the combination

$$[\phi_{\pi}, \psi_{\mathrm{N}}]_{+} = [\phi_{\pi}, \psi_{\mathrm{P}}]_{+} = 0\ ; \quad [\psi_{\mathrm{P}}, \psi_{\mathrm{N}}]_{+} = 0$$

is excluded if we insist on the field operators being local. We are left with the two possibilities (4*a*, *b*) which are compatible with Theorem 1.

---

† Klein's transformation $\chi_{\mathrm{P}} = \psi_{\mathrm{P}}$; $\chi_{\mathrm{N}} = (-1)^{n_{\mathrm{P}}}\psi_{\mathrm{N}}$ does not transform H_a' into H_b'.

§ 4. FAMILIES OF FERMI PARTICLES

Further restrictions can be imposed on the commutation relations between different fields by the requirement that all Fermi particles form *families*. A family will be defined as a set of mutually anticommuting fields which commute with any field not belonging to the family. Thus we assume that the commutation relations

$$[A_1, A_2]_+ = 0 \quad \text{and} \quad [A_1, A_3]_+ = 0 \quad \text{imply} \quad [A_2, A_3]_+ = 0, \qquad \ldots\ldots(18a)$$

and that

$$[A_1, A_2]_+ = 0 \quad \text{and} \quad [A_1, B]_- = 0 \quad \text{imply} \quad [A_2, B]_- = 0. \qquad \ldots\ldots(18b)$$

A consequence of (18) is that bosons commute with all fields.

The family postulate is consistent with Theorem 1 of § 2. Corresponding to any set of transmutations, commutation relations can be constructed satisfying both family postulate and Theorem 1. We prove this by induction, noting that Theorem 1 can now be formulated as:

Theorem 1′. A family of fermions always contributes an even number of particles to a transmutation process.

This is in accordance with the fact that each transmutation process must involve an even number of Fermi particles.

Suppose† that, corresponding to a set of transmutations, the fermions have been classified, by means of Theorem 1 and the family postulate, into groups, $A_1', A_2', \ldots ; A_1'', A_2'', \ldots$, of mutually anticommuting fields. *Any* additional transmutation process can be dealt with by amalgamating even numbers of these groups into anticommuting sets. The groups concerned are, according to Theorem 1′, those which contribute odd numbers of fermions to the process.

The family postulate applied to the process

$$[7] \qquad \mathrm{N} \rightarrow \mathrm{P} + \pi,$$

leads to

$$[\mathrm{P}, \pi^\pm]_- = [\mathrm{N}, \pi^\pm]_- = 0$$

and consequently excludes the commutation relations (12*b*) of § 2. The commutation relations of the (*baryon*, π) *system* are therefore fixed *uniquely* by Theorem 1 and the family postulate (see (12*a*)), the baryons constitute an anticommuting set. From

$$[8] \qquad \mathrm{N} \rightarrow \mathrm{P} + \mathrm{e} + \nu$$

it then follows that the leptons also form an anticommuting set. However, we cannot decide whether they, as a whole, commute or anticommute with the nucleons; i.e. whether they constitute a separate family or are part of the baryon family. (Since even numbers of both nucleons and leptons are involved in the transmutation, Theorem 1 does not lead to restrictions and Klein's method is applicable.)

Thus the Fermi particles separate themselves into three groups of anticommuting fields: baryons, muons and leptons. The processes considered hitherto do not enable us to tell whether these groups commute with each other, i.e. form separate families, whether they have to be amalgamated into two families, or whether all fermions form one family.

---

† From the proof it is evident that we may always start from such a situation. As a first step we can assume each group to contain only one fermion.

The assumption that the μ-meson decays according to

$$[9] \quad \mu^{\pm} \to e^{\pm} + \mu^{0} + \nu$$

leaves open the possibility that muons and leptons form separate families. On the other hand the decay into three leptons

$$[10] \quad \mu^{\pm} \to e^{\pm} + \nu + \nu$$

entails that muons and leptons belong to the same family, as does the assumption

$$[11] \quad \pi^{\pm} \to \mu^{\pm} + \nu.$$

The existence of a separate baryon family is not contradicted by any known process. It could be disproved only by a transmutation violating the conservation of number of baryons. On the other hand, the assumption that all fermions constitute one family is compatible with any transmutation process.

If we accept one of the decay schemes [10], [11] we are left with two possibilities :

(i) The fermions form two families, the baryon family and the muon-lepton family.

(ii) All fermions belong to the same family.

From Theorem 1′ it is evident that in any transmutation process the number of particles belonging to the same family can only change by an even number. If we wish to ensure conservation of the number† of particles in a family we have to make the additional assumption that the phases of particles belonging to different families are independent. In other words, we require the Lagrangian to be invariant with respect to the transformation‡

$$\left.\begin{array}{lcl} \psi_{A_k} & \to & \psi_{A_k} e^{i\alpha} \\ \psi_{B_k} & \to & \psi_{B_k} e^{i\beta} \end{array}\right\} \qquad \ldots\ldots(19)$$

where $A_k, B_k, \ldots$ belong to different families and $\alpha, \beta, \ldots$ are arbitrary constants.

One can, as Kinoshita does, take as the starting point not the family postulate (18), but the weaker requirement that bosons commute with any field. The results are the same with one exception : the commutation relations between members of different families now remain undetermined, whilst (18) requires commutativity. It seems difficult to say whether or not experiment can decide these commutation relations. If not our commutativity postulate becomes a mere convention. However, it seems to us that the family concept is incomplete unless the commutation relations between different families are fixed.

A treatment based solely on the commutation relations can hardly be expected to lead to a complete theory of families. The commutation properties cannot be considered to be the ultimate basis of the family concept which probably needs a group theoretical foundation. We expect a more fundamental theory to fix all the commutation relations and so to justify our assumption regarding the commutativity of different families.

---

† The number of anti-particles taken with the negative sign.

‡ Anti-particles transform, of course, as the complex conjugate.

Acknowledgments

We wish to thank Professor Rosenfeld and Dr. A. Visconti for inspiring discussions. To Mr. J. R. Maddox we are indebted for his helpful collaboration and to the referee for much good advice.

References

Kinoshita, T., 1954, *Phys. Rev.*, **96**, 199.

Kleiñ, O., 1938, *J. Physique*, **9**, 1.

Nishijima, K., 1950, *Progr. Theor. Phys.*, **5**, 405.

Rosenfeld, L., 1948, *Nuclear Forces* (Amsterdam: North Holland Publishing Co.), p. 49.

Takahashi, Y., and Umezawa, H., 1953, *Progr. Theor. Phys.*, **9**, 14.

Calculation of Reduced Widths from Stripping Curves

By J. E. BOWCOCK
Mathematical Physics Department, University of Birmingham

Communicated by R. E. Peierls; *MS. received 9th December* 1954

Abstract. A method of calculating the reduced widths of bound states of light nuclei from stripping curves is described. It is essentially a comparison between the experimental curve and the theoretical curve due to Butler. The comparison is done in such a way as to allow for some of the factors neglected in the Butler theory, in particular the type of proton–nucleus interaction included in Horowitz and Messiah's theory.

---

§ 1. Introduction

There exist several theories which predict differential cross sections for (d, p), (d, n) reactions (Butler 1951, Bhatia *et al.* 1952, Horowitz and Messiah 1953). In each of these the reduced width γ^2 of the nucleon energy level into which the nucleon is captured, appears as a constant multiplying factor, i.e. $\sigma(\theta_p)=\gamma^2 F(\theta_p)$. For any given reaction $F(\theta_p)$ is determined uniquely by assigning values to the radius of the target nucleus, the spins of the initial and final nuclei and the orbital angular momentum of the captured nucleon. The theories usually predict reasonably well the angles at which the maxima and minima occur in the cross section, but the relative magnitudes at these points are not in good agreement with experiment (figure 1). Hence the value of γ^2 determined from a comparison of experimental and theoretical curves depends somewhat upon the manner of fitting, the uncertainty in some cases amounting to a factor of three or four. It is the purpose of this paper to describe a method for lessening this uncertainty in the calculation of reduced widths from stripping curves.

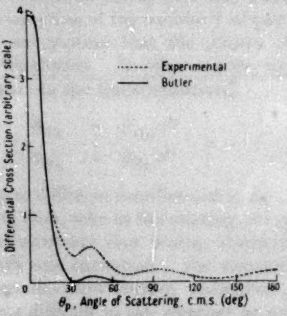

Figure 1. The lack of agreement between theoretical and experimental cross sections over the whole range of angles is shown for the typical case $^{16}O(d, p)^{17}O^*$. The experimental curve is due to Burge *et al.*

§ 2. THE BUTLER THEORY

We consider the approximations in the theory which lead to this lack of agreement between experiment and theory over the whole range of angles. For ease of notation we take the case of (d, p) reactions in which the neutron is captured into a bound state with orbital angular momentum, l_n equal to zero, i.e.

$$d+\mathcal{N}_1 \rightarrow p+\mathcal{N}_2.$$

Let Ψ be the stationary state for the collision $(d+\mathcal{N}_1)$, $V_{\alpha\beta}$ the interaction potential between particles α and β, r_N, r_P the coordinates of the neutron and proton from the deuteron, T_N and T_P their kinetic energies.

Then Butler makes the following assumptions:

(i) $V_{PN_1}=V_{PN_2}=0$

(ii) $V_{NP}=0$ for $r_N \leqslant R$ the nuclear radius

(iii) $V_{NN_1}=0$ for $r_N > R$

(iv) for $r_N > R$, $\Psi=\psi_D+\Phi$

where ψ_D is an incoming plane wave of deuterons satisfying

$$(T_N+T_P+V_{NP}-E)\psi_D=0$$

and Φ satisfies $(T_N+T_P-E)\Phi=0$ being everywhere outgoing in protons.

The angular distribution of protons is then obtained by smoothly fitting the wave function Ψ across the nuclear boundary.

Interpreting these assumptions physically we see that: (i), (*a*) all Coulomb forces are neglected, (*b*) the nucleus is transparent to protons and (*c*) that compound nucleus foundation is not taken into account; (ii), the neutron is stripped off without reaction on the proton; (iv), the effects of elastic and inelastic scattering of deuterons and other energetically possible processes are neglected. The assumption (iii) that V_{NN_1} for $r_N > R$ is a definition of nuclear radius. These are drastic approximations and the good agreement between theory and experiment is a little surprising.

However, using formal collision theory we may write Butler's theoretical cross section in the form

$$\sigma_B(\cos\theta_p)=\gamma^2\,\Big|\sum_{\lambda p} b_{\lambda p}P_{\lambda p}(\cos\theta_p)\Big|^2$$

where $P_{\lambda p}$ is the Legendre polynomial of order λ_p; then $b_{\lambda p}P_{\lambda p}$ represents the contribution to the cross section from protons with angular momentum $\hbar\{\lambda_p(\lambda_p+1)\}^{1/2}$. The approximations (i) (*b*) and (*c*) will be important only for $\lambda_p \leqslant \lambda_p^{\min}$ (say) when the proton is 'near' the nucleus. Therefore if we could write the experimental cross section $\sigma_E=|\Sigma_{\lambda p}e_{\lambda p}P_{\lambda p}|^2$ and find the ratio $\gamma b_{\lambda p}/e_{\lambda p}$ for $\lambda_p > \lambda_p^{\min}$, it is hoped that this ratio would be nearly constant. Choosing γ to make this constant unity a more accurate value of γ^2 would be arrived at.

$b_{\lambda p}$ may be found directly by drawing the curve $\Sigma_{\lambda p}b_{\lambda p}P_{\lambda p}(\cos\theta_p)$ from the Butler theory and analysing it numerically into Legendre polynomials. The analytic form for $b_{\lambda p}$ using Horowitz and Messiah's notation is

$$\text{constant}\times\int_{r>R} j_{\lambda p}(k_p r)\,j_{\lambda p}(K_d r)\,h_0^{(1)}(itr)\,r^2\,dr$$

but some numerical integration must be done to evaluate this and therefore it was found easier to use the former method. For bound states of the neutron it is found from the general Butler formula that $b_{\lambda p}$ is always *real*.

How may we find e_{λ_p} when we know only $|\Sigma_{\lambda_p} e_{\lambda_p} P_{\lambda_p}|^2$? If e_{λ_p} were real we could take the square root of the experimental cross section, making the resultant curve smooth by choosing correctly the ± sign, and analyse this into Legendre polynomials. In general, however, e_{λ_p} is complex and hence cannot be calculated from the experimental curve. In order to see more easily how we may find e_{λ_p} for $\lambda_p > \lambda_p^{\min}$ with some accuracy we consider first a theory in which the interaction of the proton with the nucleus is taken into account approximately.

§ 3. HOROWITZ AND MESSIAH'S THEORY

In this theory of (d, p) reactions an allowance is made for the interaction of the proton with the target nucleus by assuming this interaction to be that between a proton and an impenetrable sphere. This displaces only slightly the characteristic maxima and minima of Butler's angular distribution but reduces the absolute magnitude of the cross section at the main peak by a factor of from two to three. If Butler's cross section is written as

$$\sigma_B = \gamma^2 \Big|\sum_{\lambda_p} b_{\lambda_p} P_{\lambda_p}\Big|^2$$

then Horowitz and Messiah's may be written

$$\sigma_{HM} = \gamma^2 \Big|\sum_{\lambda_p} (b_{\lambda_p} + c_{\lambda_p}) P_{\lambda_p}\Big|^2$$

where c_{λ_p} is complex. It must be shown that $|c_{\lambda_p}| \ll |b_{\lambda_p}|$ for $\lambda_p > \lambda_p^{\min}$ if we are to maintain that Butler's theory for high λ_p is good against correction factors arising from proton–nucleus interaction.

A calculation was done for the reaction $^{16}O(d, p)^{17}O^*$ (0·88 MEV excitation) with a deuteron energy of 8 MEV. The results are shown in table 1.

Table 1. Relative values of the Butler coefficient b_{λ_p} of the Legendre polynomial of order λ_p and the correction factor c_{λ_p} of the same order from the theory of Horowitz and Messiah.

λ_p	Rel. value b_{λ_p}	c_{λ_p}		λ_p	Rel. value b_{λ_p}	c_{λ_p}	
0	0·0018	−0·0021	−i·0006	4	0·1271	−0·0486	−i·0078
1	−0·0263	0·0415	+i·0293	5	0·0892	−0·0123	−i·0013
2	0·0262	−0·0443	+i·0322	6	0·0531	−0·0014	−i·00007
3	0·1216	−0·1588	−i·0235	7	0·0327	−0·0002	−i·000004

It is seen that the magnitude of c_{λ_p} falls off more rapidly than does b_{λ_p} and that for $\lambda_p \geqslant 5$ the two theories give almost identical contributions. By a consideration of the forms of b_{λ_p} and c_{λ_p} it can be shown in general that $c_{\lambda_p} \ll b_{\lambda_p}$ for some λ_p. This is due to the magnitude of the wave function of the outgoing proton (a spherical Bessel function) at the nuclear boundary being diminished as λ_p is increased.

§ 4. COMPARISON OF $\sigma_B(\theta)$ AND $\sigma_{HM}(\theta)$

Suppose now that the Horowitz and Messiah differential cross section were the experimental result, then only

$$\sigma_{HM} = \gamma^2 \Big|\sum_{\lambda_p} (b_{\lambda_p} + c_{\lambda_p}) P_{\lambda_p}\Big|^2 = \Big|\sum_{\lambda_p} d_{\lambda_p} P_{\lambda_p}\Big|^2$$

would be known. How, with only this information, could γb_{λ_p} and d_{λ_p} be compared for high λ_p in order to yield the reduced width? An answer to this question would given an idea how to attempt the comparison between Butler's theory and the real experimental curve.

(i) One possibility is to analyse the differential cross sections directly into Legendre polynomials i.e.

$$\sigma_{\mathrm{B}}=\gamma^2\sum_L B_L P_L; \qquad \sigma_{\mathrm{HM}}=\sum_L D_L P_L.$$

Then

$$B_L=\sum_{\lambda_{\mathrm{p}}}\sum_{\lambda_{\mathrm{p}}'}(C_{0\ 0\ 0}^{L\ \lambda_{\mathrm{p}}\ \lambda_{\mathrm{p}}'})^2 b_{\lambda_{\mathrm{p}}} b_{\lambda_{\mathrm{p}}'}$$

where $C_{0\ 0\ 0}^{L\ \lambda_{\mathrm{p}}\ \lambda_{\mathrm{p}}'}$ is a Clebsch–Gordan coefficient. For a given L, $\lambda_{\mathrm{p}}+\lambda_{\mathrm{p}}'$ must have the same parity as L and also $|L-\lambda_{\mathrm{p}}|\leqslant\lambda_{\mathrm{p}}'\leqslant L+\lambda_{\mathrm{p}}$. In particular for high L, low λ_{p}'s are associated with high values of λ_{p}' where $b_{\lambda_{\mathrm{p}}'}$ is small. Therefore the terms $b_{\lambda_{\mathrm{p}}}$ which are ' incorrect ' for small $\lambda_{\lambda\mathrm{p}}$, are associated with $b_{\lambda_{\mathrm{p}}'}$'s which are very small in magnitude. In the example chosen it was found that the major contribution to B_L came from terms where $\lambda_{\mathrm{p}}\simeq\lambda_{\mathrm{p}}'\simeq L/2$. Thus for sufficiently high L we expect B_L not to be affected by correction factors due to proton-nucleus interaction.

Using the above example B_L was calculated and compared with D_L. The relative values are shown in table 2.

Table 2

L	10	11	12	13
$D_L/\gamma^2 B_L$	0·532	0·752	0·874	0·961

To reach a stage where the Horowitz and Messiah correction factor to the Butler theory is negligible, it is necessary to go to $L>12$.

These ratios were calculated directly from $b_{\lambda_{\mathrm{p}}}$ and $b_{\lambda_{\mathrm{p}}}+c_{\lambda_{\mathrm{p}}}$. If we really knew only σ_{HM} it would be impracticable to perform

$$\int_1^{-1} P_L(x)\sigma_{\mathrm{HM}}(x)dx$$

for $L>12$ to any degree of accuracy and hence we must consider other ways in which the comparison may be made.

(ii) If we write the two cross sections

$$\sigma_{\mathrm{B}}(\theta)=\gamma^2[b(\theta)]^2; \qquad \sigma_{\mathrm{HM}}(\theta)=\gamma^2|h_{\mathrm{R}}(\theta)+ih_{\mathrm{I}}(\theta)|^2=\gamma^2(h_{\mathrm{R}}^2+h_{\mathrm{I}}^2)$$

where h_{R}, h_{I} are real, and plot the contributions from the real and imaginary parts h_{R}^2 and h_{I}^2 separately, it may be seen that at the peaks of $\sigma_{\mathrm{HM}}(\theta)$, $h_{\mathrm{I}}^2\ll h_{\mathrm{R}}^2$ for the reaction considered above (figure 2).

This fact may be used to draw approximately the real part of Horowitz and Messiah's amplitude factor h_{R}. At each peak of σ_{HM}, $[\gamma^2(h_{\mathrm{R}}^2+h_{\mathrm{I}}^2)]^{1/2}$ may be taken approximately as γh_{R}. There is no reason for $h_{\mathrm{R}}(\theta)$ to be discontinuous for any particular θ and therefore by smoothly joining the peaks, with alternate signs, an approximate $h_{\mathrm{R}}(\theta)$, say $h_{\mathrm{R}}'(\theta)$ is found. This is shown in figure 3 (with the true $h_{\mathrm{R}}(\theta)$ for comparison) and it is this curve which will be used for comparison with the Butler curve $b(\theta)$.

There is no necessity to know the imaginary part of the amplitude $h_{\mathrm{I}}(\theta)$ since this is small and if $h_{\mathrm{I}}(\theta)=\Sigma_{\lambda_{\mathrm{p}}}h_{\mathrm{I}\lambda_{\mathrm{p}}}P_{\lambda_{\mathrm{p}}}$ then $h_{\mathrm{I}\lambda_{\mathrm{p}}}$ falls off rapidly for $\lambda_{\mathrm{p}}>3$. Hence $h_{\mathrm{I}\lambda_{\mathrm{p}}}$ would be negligible in the comparison between $h_{\mathrm{R}}'+ih_{\mathrm{I}\lambda_{\mathrm{p}}}$ and $b_{\lambda_{\mathrm{p}}}$. There are in practice two ways of comparing this approximate amplitude curve h_{R}' with the Butler amplitude curve $b(\theta)$. The two curves are analysed into the form $\gamma\Sigma_{\lambda_{\mathrm{p}}}h'_{\mathrm{R}\lambda_{\mathrm{p}}}P_{\lambda_{\mathrm{p}}}$ and $\gamma\Sigma_{\lambda_{\mathrm{p}}}b_{\lambda_{\mathrm{p}}}P_{\lambda_{\mathrm{p}}}$. Then for $\lambda_{\mathrm{p}}\geqslant\lambda_{\mathrm{p}}^{\min}$, $h_{\mathrm{R}\lambda_{\mathrm{p}}}$ is expected to be equal to $b_{\lambda_{\mathrm{p}}}$. Hence we may either (*a*) compare directly the coefficients $h'_{\mathrm{R}\lambda_{\mathrm{p}}}$

and $b_{\lambda p}$ for $\lambda_p \geqslant \lambda_p^{\min}$ or (*b*) find the coefficients $h'_{R\lambda p}$ and $b_{\lambda p}$ for $\lambda_p < \lambda_p^{\min}$ and subtract their contributions from the total curve, i.e. compare

$$h'_R(\theta) - \sum_{\lambda p=0}^{\lambda_p^{\min}} h'_{R\lambda p} P_{\lambda p}(\theta) \qquad \text{and} \qquad b(\theta) - \sum_{\lambda p=0}^{\lambda_p^{\min}} b_{\lambda p} P_{\lambda p}(\theta),$$

until a good fit between the remaining curves is obtained.

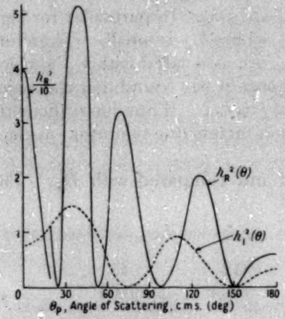

Figure 2.

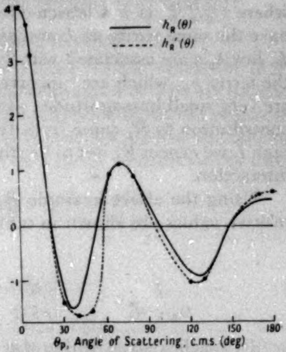

Figure 3.

Figure 2. Horowitz and Messiah's cross section may be written $\sigma_{HM}(\theta) = \gamma^2 |h_R(\theta) + ih_I(\theta)|^2 = \gamma^2\{h_R^2(\theta) + h_I^2(\theta)\}$. h_R^2 and h_I^2 are plotted for the case $^{16}O(d, p)^{17}O^*$ to show that at the peaks of $\sigma(\theta)$, $h_I^2 \ll h_R^2$.

Figure 3. By taking $(h_R^2 + h_I^2)^{1/2}$ at its peaks (circled points) and interpolating a smooth curve (dotted line) an approximate h_R is obtained, h_R'. h_R and h_R' are plotted for the case $^{16}O(d, p)^{17}O^*$.

Method (*a*) was used on the curves for $^{16}O(d, p)^{17}O^*$ drawn in figure 3. The relative values of $b_{\lambda p}$, $h_{R\lambda p}$, $h'_{R\lambda p}$ are shown in table 3. There is agreement to 10% between all three coefficients for $\lambda_p \geqslant 5$.

Table 3. The relative values of the coefficients from the expansions $b(\theta) = \sum_{\lambda p} b_{\lambda p} P_{\lambda p}$; $h_R(\theta) = \sum_{\lambda p} h_{R\lambda p} P_{\lambda p}$; $h_R'(\theta) = \sum_{\lambda p} h'_{R\lambda p} P_{\lambda p}$.

λ_p	$b_{\lambda p}$	$h_{R\lambda p}$	$h'_{R\lambda p}$
0	0·0018	−0·0003	−0·0085
1	−0·0263	0·0152	0·0181
2	0·0262	−0·0181	−0·0168
3	0·1216	−0·0371	0·0387
4	0·1271	0·0179	0·1058
5	0·0892	0·0767	0·0728
6	0·0531	0·0517	0·0479
7	0·0327	0·0327	0·0296

§ 5. COMPARISON OF $\sigma_B(\theta)$ AND $\sigma_E(\theta)$

The use of the above methods (ii) (*a*) and (*b*), depends primarily upon the fact that $h_I^2(\theta) \ll h_R^2(\theta)$ at the peaks of $\sigma_{HM}(\theta)$. If the experimental curve is written

$$\sigma_E(\theta) = |\sum_{\lambda p} (e_{R\lambda p} + ie_{I\lambda p}) P_{\lambda p}|^2 = e_R^2(\theta) + e_I^2(\theta)$$

and there were reasons to consider that $e_I^2(\theta) \ll e_R^2(\theta)$ at the peaks of $\sigma_R(\theta)$ then, by using either of the methods described, the reduced width might be calculated with a considerably greater accuracy than previously.

In order to investigate the magnitude of $e_I(\theta)$ write $e_{R\lambda p} = \gamma b_{\lambda p} + \delta_{\lambda p}$, i.e. $\delta_{\lambda p}$ is the real part of the correction factor to Butler's theory. Then

$$\begin{aligned} \sigma_E &= |\gamma(\sum_{\lambda p} b_{\lambda p} P_{\lambda p}) + (\sum_{\lambda p} \delta_{\lambda p} P_{\lambda p}) + i(\sum_{\lambda p} e_{I\lambda p} P_{\lambda p})|^2 \\ &= |\gamma b(\theta) + \delta(\theta) + i e_I(\theta)|^2 \\ &= (\gamma b(\theta) + \delta(\theta))^2 + e_I^2(\theta). \end{aligned}$$

At the zeros of the Butler theory, at points θ_m say,

$$\sigma_E(\theta_m) = \delta^2(\theta_m) + e_I^2(\theta_m)$$

and therefore $e_I^2(\theta_m) \leqslant \sigma_E(\theta_m)$. $\sigma_E(\theta_m)$ is an upper limit of $e_I^2(\theta_m)$, but $e_I^2(\theta_m)$ may be much smaller than this value. Figure 1 is a typical stripping curve for $l_n = 0$ and here it is seen that $\sigma_E(\theta_m)$ is small compared with the main peak at least. Also $e_I^2(\theta)$ is unlikely to show any large fluctuations in magnitude (such as the large forward peak) since it must be due to effects other than the pure stripping described by the Butler theory. With these considerations it seems probable that $e_I^2(\theta) \ll e_R^2(\theta)$ at the peaks of the experimental curve. One test of this assumption will be to see if, by using the methods described, good agreement between $e'_{R\lambda p}$ (derived from the approximate $e_{R\lambda p}$) and $b_{\lambda p}$ can be found. If the assumption is false neither of the methods should produce any agreement.

Since $e_R'(\theta)$ may be analysed into Legendre polynomials only if it is known over all angles, the experimental cross section must be known in absolute magnitude over the whole range of angles 0° to 180° in the centre of mass system. Many previous experimental workers have been interested only in deducing l_n from their curves and hence performed the experiments only over a limited range of angles as it is only necessary to have the positions of the first one or two maxima. There are also experimental difficulties in determining the cross section to low angles especially when the reaction has a negative or low positive Q value.

It is of interest to consider here what effect variations of the approximate amplitude curve for large angles have upon the coefficients $e'_{R\lambda p}$. There are two reasons for this. One is that at large angles the peaks are not very high compared with the minima and so it is not really sure that $e'^2_R(\theta) \gg e_I^2(\theta)$. Hence the $e_R'(\theta_m)$ found are not so accurate as at small angles. In some cases the curve is not known for $\theta > 90°$ and to use the method we may have to guess the remaining part of the curve.

The effect is found to vary with the height of $\sigma_E(\theta)$ at larger angles relative to the height at the main peaks. The main contribution to $e'_{R\lambda p}$ i.e. to

$$\frac{2\lambda_p + 1}{2} \int_1^{-1} e_R'(x) P_{\lambda p}(x)\, dx$$

comes from the first large peak. It was found in the examples taken that the percentage of the total $e'_{R\lambda p}$ contributed by the curve at angles greater than 90° is larger for higher λ_p.

If the curve is very small at large angles this contribution is small and $e'_{R\lambda p}$ is not sensitive to any 'reasonable' variation in the curve at these angles. Therefore either of methods (ii) (*a*) and (*b*) would be applicable in such a case.

However, if the curve at large angles is of greater magnitude (compared with the main peak) any variation in it is found to alter the $e'_{R\lambda_p}$ appreciably for high λ_p but *not* for low λ_p. For such a case the first method of comparing $e'_{R\lambda_p}/b_{\lambda_p}$ would not give good results, but if the second method were used the coefficients of the polynomials to be subtracted are not sensitive to high angle curve variations. Hence a good fit may be obtained between

$$\sum_{\lambda_p=\lambda_p^{\min}}^{\infty} e'_{R\lambda_p}P_{\lambda_p} \quad \text{and} \quad \sum_{\lambda_p} b_{\lambda_p}P_{\lambda_p}$$

over the lower angles where the stripping contribution is predominant.

Therefore the first method should be used only for the case where $e_{\lambda_p}'(\theta)$ is small at large angles compared to the main peak of the curve. This is usually the case for $l_n=0$. For all other cases the second method should be used.

§ 6. REDUCED WIDTHS FROM THE REACTIONS $^{16}O(d, p)^{17}O^*$, $^{12}C(d, p)^{13}C$, $^{24}Mg(d, p)^{25}Mg^*$

(*a*) $^{16}O(d, p)^{17}O^*$

This is the reaction to the state of 0·88 MEV excitation with $l_n=0$. The results of Burge *et al.* (1952) were used. From the approximate e_R' the coefficients $e'_{R\lambda_p}$ were extracted and these are plotted in figure 4 as $e'_{R\lambda_p}/b_{\lambda_p}$. Good agreement between $e'_{R\lambda_p}$ and b_{λ_p} is found for $\lambda_p \geqslant 3$ giving $\gamma^2=0{\cdot}36\times10^{-18}$ erg cm

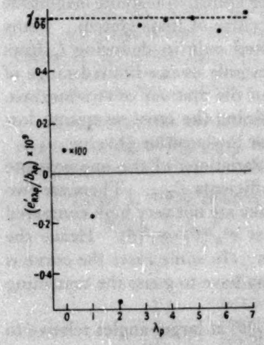

Figure 4.

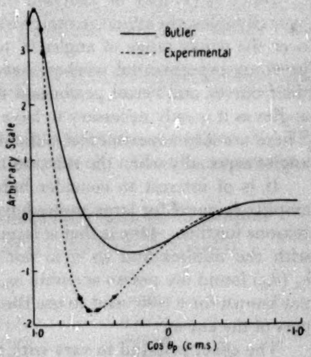

Figure 5 (*a*).

Figure 4. $e'_{R\lambda_p}/b_{\lambda_p}$ is plotted for the case $^{16}O(d, p)^{17}O^*$. For $\lambda_p \geqslant 3$ the ratio is approximately constant, giving $\gamma^2=0{\cdot}36\times10^{-18}$ erg cm.

Figure 5 (*a*). For the reaction $^{24}Mg(d, p)^{25}Mg^*$ the Butler amplitude curve is plotted with the approximate real part of the experimental amplitude curve.

(*b*) $^{12}C(d, p)^{13}C(l_n=1)$

The experimental results were from Rotblat (1951) and Holt and Marsham (private communication). Using method (ii) (*b*) good agreement was found between the experimental curve and the Butler curve for $\gamma^2=0{\cdot}25\times10^{-18}$ erg cm.

(*c*) ^{24}Mg(d, p)^{25}Mg*($Q = 1{\cdot}69$ MeV)

This reaction was chosen for a special reason. The energy level into which the neutron is captured has a corresponding level in the mirror nucleus ^{25}Al which is virtual. The reduced width of this virtual energy level has been investigated by Koester (1952) using the inelastic scattering of protons from ^{24}Mg. On the assumption of charge independence of nuclear forces these reduced widths should be equal. Hence there is a check on the reduced width calculated from the stripping curve.

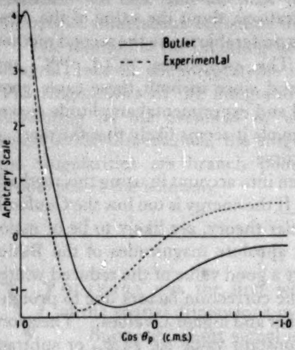

(*b*)

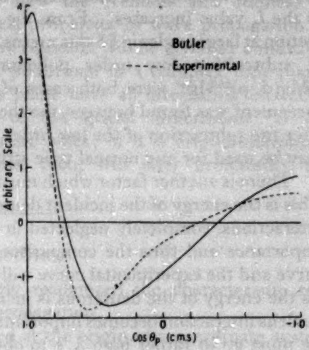

(*c*)

Figure 5 (*b*). Curves of figure 5 (*a*) after subtraction from each of the contribution from the zero order Legendre polynomial in their respective expansions into Legendre polynomials.

Figure 5 (*c*). Curves of figure 5 (*a*) after subtraction of the respective contributions from the Legendre polynomials of zero and first order.

The experimental results were taken from Holt and Marsham (1953). Figures 5 (*a*), (*b*), (*c*) illustrate the method of subtracting low order polynomials. Unfortunately the experimental curve was known only to 90° (c.m.s.) and the remaining portion of the curve was guessed. However it was found that a variation of this curve figure 5 (*a*) produced a change of only 10% in the final reduced width. γ^2 calculated from these curves $= 0{\cdot}41 \times 10^{-18}$ erg cm whereas Koester gives the value $\gamma^2 = 0{\cdot}37 \times 10^{-18}$ erg cm. Since Holt and Marsham give their experimental cross section to only 15% accuracy and the value of γ^2 calculated from the inelastic scattering depends upon parameters which are not known exactly, this is good agreement and seems to indicate that the method really does give reduced widths of bound states to quite good accuracy.

§ 7. MISCELLANEOUS CONDISERATIONS

In the early discussion the problem was limited to a (d, p) reaction in which the neutron was captured into a bound state with $l_n = 0$. We now consider the effect of raising these restrictions.

(*a*) The method should also work for (d, n) reactions but few experiments have been done in which the absolute magnitude of such cross sections has been measured.

(*b*) If the neutron is captured into a virtual level, the Butler coefficients $b_{\lambda p}$ are no longer entirely real and hence the method of this paper is not applicable to these cases.

(*c*) For $l_n > 0$, $|\lambda_p - l_n| \leqslant l_d \leqslant \lambda_p + l_n$.

A proton of given λ_p may come from a deuteron of angular momentum $\hbar(\lambda_p - l_n)$ which ' moves close to the nucleus '. Hence the method is expected not to work so well for $l_n > 0$.

Another point to be taken into account in this case is that usually in stripping curves the height of the main peak with respect to the background becomes lower as the l_n value increases. From the considerations about the value of the cross section at large angles in § 5 this means that it is preferable to use the second method of subtracting low order polynomials. The two cases $^{12}C(d, p)^{13}C$ and $^{24}Mg(d, p)^{25}Mg^*$ were both cases of $l_n = 1$ and since in both these cases good agreement was found between the theoretical and experimental amplitude curves after the subtraction of the low order polynomials it seems likely that the method may be used for any normal type stripping curve.

There is another factor which must be taken into account in using this method. This is the energy of the incident deuterons. If the energy is too low the Coulomb interactions, completely neglected in the Butler theory, are likely to be of major importance and thus the comparison of the absolute magnitudes of the Butler curve and the experimental curve will not give a good value of the reduced width. As the energy of the deuterons is increased the correction factors due to proton–nucleus interaction becomes important for higher and higher λ_p values. Therefore we must go to rather high λ_p's to obtain a constant value for $e_{\lambda p}/b_{\lambda p}$ or subtract more and more low order polynomials if method (ii) (*b*) is to be used. In the former case it is difficult to find the coefficients of the Legendre polynomials of high order to any accuracy by numerical analysis.

Theoretically the reduced widths of the energy level should be independent of the incident deuteron energy. However, Fairbairn (1954), using an ' uncorrected ' method of curve fitting, found variations of a factor of two in the calculated reduced widths of two particular energy levels when the deuteron energy is increased from 8 to 19 MEV. It will therefore be of interest, when sufficient experimental data are to hand, to see if, using the method described in this paper the reduced widths calculated from stripping curves are found to be independent of the deuteron energy.

ACKNOWLEDGMENTS

The author wishes to thank Professor R. E. Peierls for suggesting this problem and for many valuable discussions and Professor W. E. Burcham for help in the selection of experimental curves. He is also indebted to the Department of Scientific and Industrial Research for a grant.

REFERENCES

BHATIA, A. B., KUN HUANG, HUBY, R., and NEWNS, H. C., 1952, *Phil. Mag.*, **43**, 485.
BURGE, E. J., BURROWS, A. B., GIBSON, W. M., and ROTBLAT, J., 1952, *Proc. Roy. Soc.* A, **210**, 534.
BUTLER, S. T., 1951, *Proc. Roy. Soc.* A, **208**, 559.
FAIRBAIRN, W. M., 1954, *Proc. Phys. Soc.* A, **67**, 564.
HOLT, J. R., and MARSHAM, T. N., 1953, *Proc. Phys. Soc.* A, **66**, 258.
HOROWITZ, J., and MESSIAH, A. M. L., 1953, *J. Phys. Radium*, **14**, 12, 695.
KOESTER, L. J., 1952, *Phys. Rev.*, **85**, 643.
ROTBLAT, J., 1951, *Nature, Lond.*, **167**, 1027.

Wave Propagation in Even and Odd Dimensional Spaces

By N. L. BALAZS
Department of Physics, University of Alabama

MS. received 26th October 1954 *and in amended form* 11*th January* 1955

Abstract. In this note we plan to show how the evenness and oddness of the spatial dimensions influence the general properties of wave propagation.

The solution of the inhomogeneous wave equation will be given by a multiple integral; one of the integrations is to be performed in a complex time-plane. The singularities of the integrand in this plane have an alternating character depending on the evenness or oddness of the spatial dimensions. If the space is odd-dimensional, the singularities are poles; if it is even-dimensional, the singularities are branch points. This, then, will alter profoundly the properties of the solution.

---

§ 1. Introduction

VOLTERRA was the first who clearly recognized the characteristic role of the spatial dimensions in wave propagation.

Suppose a short signal is emitted at the origin of a coordinate system in a space. This signal will be observed at a point having the distance r only after r/c seconds (c being the velocity of propagation of the disturbance). This is true, irrespectively of the number of spatial dimensions. However, if the space is odd-dimensional, the effect will disappear after a correspondingly short time. If the space is even-dimensional the effect will not, in general, disappear. In odd-dimensional spaces short signals, as observed at a point, have a sharp front and sharp rear; in even dimensional spaces they still have a sharp front, but a tail, or diffuse rear.

The mathematical theory of Volterra was generalized by Hadamard (1952) and Riesz (1936). Their methods are very beautiful, and rather sophisticated. It is, however, not easy to see why this characteristic difference arises. (For an excellent review of Volterra's and Hadamard's methods see Courant and Hilbert 1937).

Our aim here is to show, by a very elementary method, how the evenness and oddness of the spatial dimensions can give rise to such a profound difference.

§ 2. Outline of Approach

The method we will use is an extension of an idea conceived by Herglotz (1904) and Sommerfeld (1910).

Imagine a differential equation $F(x,y,\ldots;\, u,\ldots)=0$. F is an analytic function of all of its arguments, and $u(x,y,\ldots)$ is analytic in $x,y,\ldots$ Then one can continue F and u in the complex domain conceiving $x=x_1+ix_2$, $y=y_1+iy_2$ etc. as complex variables. As soon as this is done the difference between hyperbolic and elliptic differential equations disappears, and the solution of one type can be used in the construction of the solution of the other type. For our purpose a simplification can be introduced: keeping the spatial variables in the wave equation real and letting only the time variable be complex. Then we are still able to pass at will from the wave equation to the potential equation and vice versa; (the potential equation refers to the same number of dimensions as the space–time dimensions appearing in the wave equation). For, if the time variable is a pure imaginary we obtain the wave equation; if it is real, the potential equation.

Our plan will then be as follows: (i) We construct the solution of the n-dimensional inhomogeneous potential equation by the standard methods. The solution will be given in form of integrals. (ii) We continue it in the complex domain introducing a complex x_n (which then corresponds to the time variable), and obtain in this way the complete solution of the inhomogeneous wave equation, also in the form of integrals. When performing the indicated integration in the complex x_n plane we must pay due regard to the singularities of the integrand in this plane. (iii) Next we show that the alternating character of the solutions for even and odd dimensions arises in the following manner. If n is even (space–time even, space odd) the integrands in the solution, as constructed according to (ii), have a pole in the complex time plane; if n is odd they have a branch point. If the integrand has a pole the path of integration in the complex time plane can be deformed into a small circle around the pole, which is then contracted. Hence after performing this integration the result will refer to one time value only, to that of the pole.

If the integrand has a branch point, we cannot let the path of integration encircle the singularity; it will have to run along both edges of the branch cut and consequently the solution will contain contributions from all times along the branch cut.

As an example we will work out the most important case, when $n=4$ (the spatial dimensions are 3). The solution so obtained contains, indeed, both the solution of the homogeneous and inhomogeneous wave equation, i.e. the well-known Kirchhoff solutions, and the advanced or retarded potentials.

§ 3. THE SOLUTION

The solution of the n-dimensional, inhomogeneous potential equation can be obtained by the standard methods. We use the fundamental solution of the homogeneous equation and Green's theorem. The solution of the equation $\Delta_n v = -f$ is then given immediately by (Δ_n is the n-dimensional Laplacian, $n > 2$)

$$v(x_1, \ldots, x_n) = \frac{1}{2\omega_n}\left[-\int_{S_{n-1}}\left\{v\frac{\partial}{\partial\nu}\left(\frac{1}{R^{n-2}}\right) - \frac{1}{R^{n-2}}\frac{\partial v}{\partial \nu}\right\} d\sigma + \int_{V_n}\frac{f}{R^{n-2}}\, d^n\xi\right] \qquad \ldots\ldots(1)$$

Here $R^2 = (x_1-\xi_1)^2 + \ldots + (x_n-\xi_n)^2$; ω_n is the area of a unit sphere in n dimensions. S_{n-1} is a $n-1$ dimensional hypersurface with the surface element $d\sigma$, positive outward normal ν; it encloses the n dimensional volume V_n with the volume element $d^n\xi = d\xi, \ldots d\xi_n$. V must not have singularities in V_n, or on S_{n-1}.

We shall obtain from (1) the solution of the wave equation in a space of $n-1$ dimensions by putting $x_n = ict$ where t is the time variable, c the velocity of propagation. Since each integrand is supposed to be an analytic function of ξ_n regarded as a complex variable, we can alter the path of integration with respect to ξ_n from the real axis into some other path in the complex plane if attention is paid to the singularities of the integrand in this plane.

The integrals are of the form $\int g/R^{n-2}\,d\xi_n$. This applies for the integrands involving the normal derivatives as well, if the observer is at rest with respect to S_{n-1}. The integrand has singularities where $R=0$, i.e. where $r^2+(ict-\xi_n)^2=0$; $r^2=(x_1-\xi_1)^2+\ldots+(x_{n-1}-\xi_{n-1})^2$. Hence the singularities are located on the imaginary axis at the points $\xi_n=ict\pm ir$. *If n is even these singularities are poles; if n is odd, they are branch points.*

If we put, for the moment $\xi_n=ic\tau$, then τ is a time variable; only values of τ less than t are relevant for physical reasons. (In this way only those values of f which refer to the past can influence the solution at time t.) Hence, if n is even we can deform the path from $-\infty$ to $+\infty$ along the real ξ_n axis into a small circle running clockwise round the point $\xi_n=i(ct-r)$. The value of the integral will then be the residue evaluated at $\xi_n=i(ct-r)$, multiplied by $-2\pi i$. Consequently the value of $v(x_1,x_2,\ldots,x_{n-1},ict)$ will be related to events at $(\xi_1,\xi_2,\ldots,\xi_{n-1},ict-ir)$.

If n is *odd*, the point $\xi_n=i(ct-r)$ is a branch point. We introduce a branch cut along the imaginary axis, extending from $i(ct-r)$ to $-i\infty$ (and of course from $i(ct+r)$ to $i\infty$). The path of integration will now run along the cut going from $-i\infty$ to $i(ct-r)$ in the third quadrant, and going back on the other side of the cut.

Then the value of $v(x_1,x_2,\ldots,x_{n-1},ict)$ will be related to events taking place at points $(\xi_1,\xi_2,\ldots,\xi_{n-1},ic\tau)$ where τ takes on all values up to the time $t-r/c$.

This shows that the entirely different propagation process in even and odd dimensional spaces depends upon the alternating character of the singularities of the fundamental solution of the potential equation.

As an example let us give the solution for the important case $n=4$. In the neighbourhood of $\xi_4=i(ct-r)$

$$\oint\frac{f}{R^2}\,d\xi_4=\oint\frac{f}{r^2+(ict-\xi_4)^2}\,d\xi_4=\oint\frac{f\,d\xi_4}{(\xi_4-ict-ir)(\xi_4-ict+ir)}\quad\ldots\ldots(2)$$

$$=-2\pi i\{\text{residue of integrand at } i(ct-r)\}=\pi f(\xi_1,\xi_2,\xi_3,t-r/c)/r.$$

Hence the volume integral in (1) gives

$$\pi\int\frac{f(\xi_1,\xi_2,\xi_3,t-r/c)}{r}\,d^3\xi=\pi\int\frac{[f]}{r}\,d^3\xi,$$

if we indicate the retarded value of f by $[f]$. This is the well-known retarded potential. (The other pole would give the advanced potential.)

To solve the surface integral we proceed as follows. Take S_3 to be a right hypercylinder whose base is that closed portion Γ of the physical space in which the wave process occurs.

The axis of the hypercylinder is parallel to the time axis. The surface integral will consist of three parts; the two arising by the integration over the bases of the cylinder, and one due to the integration over the mantle. It can be easily shown that if the cylinder is of infinite length the contributions from the bases vanish. Hence, we have to compute only the integral over the mantle. On this hypersurface the surface element $d\sigma$ can be written as $do\,d\xi_4$ where do

is the two dimensional surface element of the surface Ω enclosing the three-space Γ. Moreover, ν is the outward normal to *do*. Physically speaking, this cylinder contains all those space–time points which will describe the history of a process taking place in Γ. It is supposed that Γ is the same portion of our physical space (hence the cylindrical shape), and that the observer is at rest with respect to Γ (hence the stipulation that our cylinder should be a right cylinder).

The surface integral can be written now as

$$\int_{\xi_4}\int_{\Omega}\left\{v\frac{\partial}{\partial\nu}\left(\frac{1}{R^2}\right)-\frac{1}{R^2}\frac{\partial v}{\partial\nu}\right\}do\,d\xi_4=\int_{\Omega}\frac{\partial}{\partial\nu}\left\{\int_{\xi_4}\frac{v}{R^2}\,d\xi_4\right\}do$$
$$-2\int_{\Omega}\left\{\int_{\xi_4}\frac{1}{R^2}\frac{\partial v}{\partial\nu}\,d\xi_4\right\}do.$$

Using (2) with an appropriate change in the meaning of f, we immediately obtain

$$\pi\int_{\Omega}\frac{\partial}{\partial\nu}\left\{\frac{[v]}{r}\right\}do-2\pi\int_{\Omega}\frac{1}{r}\left[\frac{\partial v}{\partial\nu}\right]do, \qquad \ldots\ldots(3)$$

with $[v]=v(\xi_1,\xi_2,\xi_3;\ t-r/c)$. Now

$$\frac{\partial[v]}{\partial\nu}=\left[\frac{\partial v}{\partial\nu}\right]-\frac{1}{c}\frac{\partial r}{\partial\nu}\left[\frac{\partial v}{\partial t}\right];$$

hence we obtain

$$\pi\int_{\Omega}\left\{[v]\frac{\partial}{\partial\nu}\left(\frac{1}{r}\right)-\frac{1}{r}\left[\frac{\partial v}{\partial\nu}\right]-\frac{1}{cr}\frac{\partial r}{\partial\nu}\left[\frac{\partial v}{\partial t}\right]\right\}do. \qquad \ldots\ldots(4)$$

Substitute now (2) and (4) into (1) and observe that $\omega_4=2\pi^2$. The result is

$$v(x_1,x_2,x_3,t)=-\frac{1}{4\pi}\int_{\Omega}\left\{[v]\frac{\partial}{\partial\nu}\left(\frac{1}{r}\right)-\frac{1}{r}\left[\frac{\partial v}{\partial\nu}\right]-\frac{1}{cr}\frac{\partial r}{\partial\nu}\left[\frac{\partial v}{\partial t}\right]\right\}do$$
$$+\frac{1}{4\pi}\int_{\Gamma}\frac{[f]}{r}\,d^3\xi. \qquad \ldots\ldots(5)$$

This is indeed the well-known solution of the wave equation, provided the observer is at rest with respect to Γ.

It is equally easy to show that proceeding in a completely analogous manner we obtain from (1) the usual expressions for wave propagation in a two dimensional space, if we take n to be three.

ACKNOWLEDGMENTS

I should like to express my thanks to Professor Carl Eckart for reading the manuscript and giving valuable suggestions. My thanks are also due to the Scripps Institution of Oceanography for their hospitality and to the Research Committee of the University of Alabama for their grant to pursue this research.

REFERENCES

COURANT, H., and HILBERT, D., 1937, *Methoden der Mathematischen Physik*, Vol. II (Berlin: Springer).
HADAMARD, J., 1952, *Lectures on Cauchy's Problem* (New York: Dover Publications).
HERGLOTZ, G., 1904, *Nachr. Ges. Wiss. Göttingen*, Kl., 549.
RIESZ, M., 1936, *Comptes rendus du congrès int. des math.* (Oslo), **2**, 44.
SOMMERFELD, A., 1910, *Ann. Phys., Lpz.*, **33**, 649.

Plasma Oscillations and Energy Loss of Charged Particles in Solids

By H. FRÖHLICH and H. PELZER†

Department of Theoretical Physics, The University of Liverpool

MS. received 22nd November 1954

Abstract. It is shown that the frequencies of logitudinal electric oscillations in solids satisfy the condition $\epsilon(\omega)=0$, where $\epsilon(\omega)$ is the dielectric constant for the frequency $\omega/2\pi$ which can be obtained from the optical constants n, κ. Such longitudinal waves include so-called plasma oscillations. It is shown that energy losses of fast charged particles in discrete steps $\hbar\omega_{\mathrm{p}}$ (the plasma quantum) can be expected only if the quantity $n\kappa/(n^2+\kappa^2)^2$ has a sharp maximum at a frequency ω_{p}. This holds for the alkali metals and for silver.

§ 1. INTRODUCTION

RECENTLY Bohm and Pines (1951, 1952, 1953) and Pines (1953) have demonstrated that the long range Coulomb interaction of the conduction electrons in metals can be treated successfully by introducing the collective modes of motion known as plasma oscillations. These are longitudinal oscillations of frequency $\omega_{\mathrm{p}}/2\pi$ where

$$\omega_{\mathrm{p}}^2=4\pi e^2N/m \qquad \ldots\ldots(1)$$

if N is the number of free electrons per unit volume. Already some time ago Kronig and Korringa (1943) (cf. also Kronig 1949) have made use of collective electronic motion in order to treat the energy loss of fast charged particles in metals.

The frequency ω_{p} plays an important role in the optical properties of a gas of charged particles; electromagnetic waves of frequency $\omega<\omega_{\mathrm{p}}$ are totally reflected by such a system whereas they are transmitted if $\omega>\omega_{\mathrm{p}}$. In metals this property has been found with the alkalis; in many other cases absorption and diffraction connected with electronic transitions veil the effect.

It is the purpose of the present paper to point out that there exists a phenomenological connection between the possible frequencies of longitudinal electric waves and the optical constants. The theory of plasma oscillations is, therefore, a special case of the theory of absorption and dispersion. Furthermore, the energy loss of fast particles can be predicted from a knowledge of the optical constants, and if the latter are known then it is possible to decide whether or not to expect energy loss in discrete steps.

Phenomenological considerations do not, of course, permit the determination of the lower limit for plasma wavelengths or a possible dependence of frequency on wavelength.

---

† British Electrical and Allied Industries Research Association.

§ 2. CONDITION FOR LONGITUDINAL ELECTRIC WAVES

If the wavelength of a longitudinal wave is small compared with the dimensions of the substance, then

$$\operatorname{curl} \mathbf{H} = \operatorname{curl} \mathbf{E} = 0 \qquad \ldots\ldots(2)$$

where **H** and **E** are the magnetic and the electric field vectors, respectively. It then follows from the Maxwell equations that

$$\frac{\partial \mathbf{D}}{\partial t} + 4\pi \mathbf{j} = 0 \qquad \ldots\ldots(3)$$

where

$$\mathbf{D} = \mathbf{E} + 4\pi \mathbf{P} \qquad \ldots\ldots(4)$$

is the electric displacement, **P** the polarization and **j** the density of the conduction current. **D** and **j** are correlated to **E** by the dielectric constant ϵ and the conductivity σ. Both depend on the frequency $\omega/2\pi$. It is useful to eliminate the conductivity in favour of a complex dielectric constant (cf. for example Fröhlich 1949, A1, ii), i.e. to replace (3) by

$$\partial \mathbf{D}/\partial t = 0 \qquad \ldots\ldots(5)$$

and introduce

$$\epsilon_2(\omega) = 4\pi\sigma(\omega)/\omega \qquad \ldots\ldots(6)$$

such that

$$\epsilon(\omega) = \epsilon_1(\omega) + i\epsilon_2(\omega) \qquad \ldots\ldots(7)$$

and

$$\mathbf{D}(\omega) = \epsilon(\omega)\,\mathbf{E}(\omega). \qquad \ldots\ldots(8)$$

Here the partial waves of frequency ω of **D** and **E** are represented by the real parts of $\mathbf{D}(\omega)$ and $\mathbf{E}(\omega)$. The time dependence of the latter is given by $\exp(-i\omega t)$.

In the absence of free charges (including surface charges) the condition (5) for the existence of longitudinal waves reduces to $\mathbf{D}(\omega) = 0$ or with the use of (8) to

$$\epsilon(\omega) = 0. \qquad \ldots\ldots(9)$$

This represents an equation for the frequency ω which in general is solved by complex quantities ω_l,

$$\omega_l = \omega_0 - i\omega_1 \qquad \ldots\ldots(10)$$

with positive ω_0 and ω_1. Hence

$$\mathbf{E}(\omega_l) = \mathbf{E}_0(\omega_l)\exp(-i\omega_0 t)\exp(-\omega_1 t). \qquad \ldots\ldots(11)$$

Here $\mathbf{E}_0(\omega_l)$ is independent of time but may depend on the spatial coordinates in an arbitrary way provided that the spatial Fourier development of $\mathbf{E}_0(\omega_l)$ does not contain wavelengths of macroscopic dimensions. If equation (9) has only a single solution ω_l then any longitudinal electric field created say at a time $t = 0$, carries out damped oscillations with frequency ω_0 and relaxation time $1/\omega_1$. In special cases, of course, ω_0 or ω_1 may vanish. In quantum mechanical interpretation, the energy of the longitudinal vibrations is quantized in integer multiples of $\hbar\omega_0$ (including a zero point energy $\frac{1}{2}\hbar\omega_0$). The transition probabilities between quantum states are connected with the frequency ω_1. It must be realized, however, that ω_1 represents a statistical average on the assumption that all other degrees of freedom of the substance are in thermal equilibrium.

§ 3. Special Cases

(i) *Debye Dielectric*

In the simplest case of this type assume (ϵ_s = static dielectric constant)

$$\epsilon(\omega) = 1 + \frac{\epsilon_s - 1}{1 - i\omega\tau}. \qquad \ldots\ldots(12)$$

From condition (9) it follows that

$$\omega_l = -i\epsilon_s/\tau. \qquad \ldots\ldots(13)$$

In this case, therefore, a longitudinal field decays exponentially proportional to $\exp(-\epsilon_s t/\tau)$.

(ii) *Conduction Electrons*

Assume N free electrons per unit volume in interaction with a frictional medium leading to a relaxation time τ. This is, for instance, the case of a metal where the electrons interact with the lattice vibrations provided that the possibility of optical transitions into other energy levels is ignored. In this case

$$\epsilon_1(\omega) = 1 - \frac{\omega_p^2}{\omega^2 + 1/\tau^2}, \quad \sigma(\omega) = \frac{1}{4\pi}\frac{\omega_p^2\tau}{1+\omega^2\tau^2}. \qquad \ldots\ldots(14)$$

Hence with (6) and (7),

$$\epsilon(\omega) = 1 - \frac{\omega_p^2\tau^2}{\omega\tau(\omega\tau + i)}. \qquad \ldots\ldots(15)$$

Equation (9) is solved by

$$\omega_l = {}_{(}{}^{+}_{-}{}_{)}(\omega_p^2 - 1/4\tau^2)^{1/2} - i/2\tau. \qquad \ldots\ldots(16)$$

Usually $\omega_p\tau \gg 1$, so that

$$\omega_l \simeq \omega_p - i/2\tau, \quad \omega_p\tau \gg 1. \qquad \ldots\ldots(17)$$

Clearly this is the case of the plasma oscillations mentioned in the introduction.

(iii) *Ionic Crystals*

For ionic crystals of the alkali halide type,

$$\epsilon(\omega) = \epsilon_\infty + \frac{(\epsilon_s - \epsilon_\infty)\omega_t^2}{\omega_t^2 - \omega^2 - i\omega/\tau}. \qquad \ldots\ldots(18)$$

where ϵ_s is the static dielectric constant, $\sqrt{\epsilon_\infty}$ is the optical refractive index, considered here as independent of ω, and ω_t is the frequency of residual waves. The above expression is correct only in the limiting case $\omega_t\tau \to \infty$ in which ϵ_2 is a delta function. This case has already been treated by Pelzer (1954). Solution of condition (9) yields

$$\omega_l \simeq {}_{(}{}^{+}_{-}{}_{)}(\epsilon_s/\epsilon_\infty)^{1/2}\omega_t - i/2\tau, \quad \omega_t\tau \gg 1. \qquad \ldots\ldots(19)$$

The real part represents a well-known relation (cf. Fröhlich 1949 (18·23)). If Szigeti's (1949) formula for ϵ_s (e.g. Fröhlich 1949 (18·31)),

$$\epsilon_s - \epsilon_\infty = 4\pi\left(\frac{\epsilon_\infty + 2}{3}\right)^2 \frac{e^{*2}N_0}{M\omega_t^2} \qquad \ldots\ldots(20)$$

is introduced into (19), then

$$\omega_l^2 \simeq \omega_t^2 + \frac{1}{\epsilon_\infty}\left(\frac{\epsilon_\infty + 2}{3}\right)^2 \frac{4\pi e^{*2}N_0}{M}. \qquad \ldots\ldots(21)$$

Here M is the reduced ionic mass, N_0 is the number of ion pairs per unit volume and e^* is an effective ionic charge. In the limiting case $e^* = e$ and $\epsilon_\infty = 1$, the second term is equal to ω_p^2 provided m is substituted for M.

§ 4. ENERGY LOSS OF FAST CHARGED PARTICLES

If the energy per collision of a particle with charge e and velocity v is small compared with its kinetic energy then the rate of energy loss, $-dW/dt$ can be expressed in terms of the complex dielectric constant $\epsilon(\omega)$ by a method first developed by Fermi (1924). This method has recently been applied by Fröhlich and Platzmann (1953) to dielectrics of the Debye type (our case (i)). In general (cf. their equation (10)),

$$-\frac{dW}{dt}=\frac{2e^2}{\pi v}\int_0^\infty \frac{\omega\epsilon_2(\omega)}{\epsilon_1^2(\omega)+\epsilon_2^2(\omega)}\,x\mathrm{K}_0(x)\mathrm{K}_1(x)\,d\omega \qquad \ldots\ldots(22)$$

where K_0 and K_1 are the modified Bessel functions and

$$x=\omega p_{\min}/v. \qquad \ldots\ldots(23)$$

Here $p_{\min}$ is the minimum value of the collision parameter. It may vary, of course, for different mechanisms of absorption in which case equation (22) has to be modified appropriately.

In quantum mechanical interpretation, the quantity

$$P(\omega)=\frac{2e^2}{\pi v\hbar\omega}\frac{\omega\epsilon_2(\omega)}{\epsilon_1^2(\omega)+\epsilon_2^2(\omega)}\,x\mathrm{K}_0(x)\mathrm{K}_1(x)\,d\omega \qquad \ldots\ldots(24)$$

represents the probability that the particle loses in a single collision energy in the range between $\hbar\omega$ and $\hbar(\omega+d\omega)$. Clearly the energy loss occurs in discrete steps when the quantity $\epsilon_2(\omega)/\{\epsilon_1^2(\omega)+\epsilon_2^2(\omega)\}$ is very large near one or several values of ω. This is fulfilled, of course, in the case of discrete optical absorption lines. It also holds for our case (ii) i.e. for conduction electrons. For in this case, using (15),

$$\frac{\epsilon_2}{\epsilon_1^2+\epsilon_2^2}=\frac{\omega_p^2\tau^2\omega\tau}{(\omega^2-\omega_p^2)^2\tau^4+\omega^2\tau^2}\,. \qquad \ldots\ldots(25)$$

If $\omega_p\tau$ is very large, this becomes a delta function,

$$\lim_{\omega_p\tau\to\infty}\frac{\epsilon_2(\omega)}{\epsilon_1^2(\omega)+\epsilon_2^2(\omega)}=\frac{\pi}{2}\delta\left(1-\frac{\omega}{\omega_p}\right),\quad \omega>0. \qquad \ldots\ldots(26)$$

Hence with (22),

$$-dW/dt=(e^2/v)\omega_p^2x_p\mathrm{K}_0(x_p)\mathrm{K}_1(x_p) \qquad \ldots\ldots(27)$$

where

$$x_p=\omega_p p_{\min}/v. \qquad \ldots\ldots(28)$$

Also $x_p \ll 1$ for sufficiently large velocity v so that

$$\mathrm{K}_0(x_p)\simeq\log\frac{2}{\gamma x_p},\quad x_p\mathrm{K}_1(x_p)\simeq 1,\quad \gamma=1{\cdot}78 \qquad \ldots\ldots(29)$$

and hence

$$\frac{1}{v}\frac{dW}{dt}=-\frac{e^2\omega_p^2}{v^2}\log\frac{2v}{\gamma\omega_p p_{\min}} \qquad \ldots\ldots(30)$$

a formula which has been previously derived by Kramers (1947) (cf. also Kronig 1949). It must be mentioned that the above phenomenological treatment leading to energy loss in discrete steps $\hbar\omega_p$ breaks down in the case of very close collisions. These latter should lead to different energy loss which might better be calculated on the basis of a strongly screened Coulomb interaction.

It should now be strongly emphasized that the above results have been derived on the assumption that the optical properties of a metal near the frequency ω_p are essentially determined by the free electron contributions. Only then can one expect an energy loss in steps $\hbar\omega_p$ of the plasma quantum with the probability $(1/\hbar\omega)\, dW/dt$ per second using (30). The assumption requires that the quantity

$$\frac{\epsilon_2(\omega)}{\epsilon_1^2(\omega)+\epsilon_2^2(\omega)}=\frac{2n\kappa}{(n^2+\kappa^2)^2} \qquad \ldots\ldots(31)$$

should have a sharp maximum near $\omega=\omega_p$. Empirically this can be checked if the optical constants n, κ are known. For alkali metals the work of Wood (1933) shows that the condition is well fulfilled. These metals should, therefore, exhibit the discrete energy loss in steps of $\hbar\omega_p$. Of the other monovalent metals (Cu, Ag, Au) only silver shows a fairly sharp maximum (see figure) which should be noticeable in terms of the energy loss of charged particles. No other metal to our knowledge shows a sharp maximum of the quantity (31). It might be, however, that for some metals such maxima occur in the far ultra-violet where the optical constants have not yet been measured.

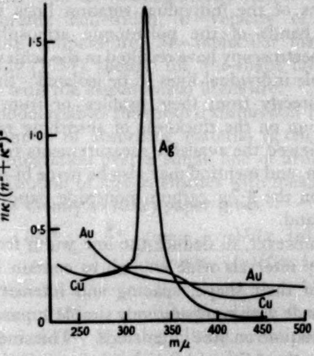

ACKNOWLEDGMENT

We should like to express our thanks to Dr. S. Whitehead, Director of the British Electrical and Allied Industries Research Association, for permission to publish this paper.

REFERENCES

Bohm, D., and Pines, D., 1951, *Phys. Rev.*, **82,** 625; 1952, *Ibid.*, **85,** 338; 1953, *Ibid.*, **92,** 609.
Fermi, E., 1924, *Z. Phys.*, **29,** 315.
Fröhlich, H., 1949, *Theory of Dielectrics* (Oxford : Clarendon Press).
Fröhlich, H., and Platzmann, R. L., 1953, *Phys. Rev.*, **92,** 1152.
Kramers, H. A., 1947, *Physica*, **13,** 401.
Kronig, R., 1949, *Physica*, **15,** 667.
Kronig, R., and Korringa, J., 1943, *Physica*, **10,** 406, 800.
Pelzer, H., 1954, *E.R.A. Report* L/T 316.
Pines, D., 1953, *Phys. Rev.*, **92,** 626.
Szigeti, B., 1949, *Trans. Faraday Soc.*, **45,** 155.
Wood, R. H. 1933, *Phys. Rev.*, **44,** 353.

Line Widths in the 9·6 μ Band of Ozone

By C. D. WALSHAW
Cavendish Laboratory, Cambridge

MS. received 7th December 1954

Abstract. Intensity measurements at low resolution and low pressures in the 9·6 μ fundamental rotation–vibration band of ozone are shown to be consistent with a mixed Doppler and Lorentz shape for the rotation lines. For collisions with air molecules the average Lorentz width for this band is shown to be 0·078 cm^{-1} at 760 mm Hg and 20°c.

---

§ 1. INTRODUCTION

In the study of radiative energy transfer in the earth's atmosphere it is necessary to know the widths of the individual rotation lines which constitute the rotation–vibration bands of the polyatomic atmospheric gases. Recent advances in infra-red spectroscopy have resulted in the achievement of sufficiently high resolution to enable individual lines to be isolated; their widths may then be estimated either directly from their profiles or from the dependence of integrated line absorption on the thickness of absorbing material. Curtis and Goody (1954) have reviewed the available measurements from the point of view of atmospheric radiation, and mention may also be made of recent work by Locke and Herzberg (1953) on the 4·7 μ carbon monoxide band and by Adel (1953) on the 17 μ ammonia band.

It is also possible, however, to deduce the line width from measurements of absorption in frequency intervals wide enough to contain many rotation lines, provided that details of their shape, spacing and intensity are known. The measurements can be made with comparatively simple apparatus, and at the same time give useful information on line intensities. This method was employed by Matheson (1932) for the 4·7 μ and 2·4 μ carbon monoxide bands, and more recently by Goody and Wormell (1951) in an investigation of the 7·8 μ and 8·6 μ bands of nitrous oxide. These simple molecules have regular rotation–vibration bands of equally spaced lines, and the spacing can be readily calculated from the molecular dimensions.

But the rotation–vibration bands of non-linear molecules are of far greater complexity, demanding new methods for inferring line widths from low-resolution absorption measurements. The problem is especially acute in the case of the ozone molecule, whose fundamental band at 9·6 μ is very active in radiative processes in the stratosphere (see for instance Goody 1954) but whose infra-red spectrum still presents a number of puzzling features. Consequently particular interest attaches to a method by which estimates of line widths, spacings, and intensities can be derived from purely experimental sources of information.

Measurements of mean transmission in this band for ozone amounts up to 1·5 cm at s.t.p. with the total pressure (ozone plus dry air) ranging from 10 to 760 mm Hg have been discussed in a previous paper (Walshaw and Goody 1954).

Fairly good agreement was found with a statistical model of the band having lines of Lorentz shape randomly distributed in position and intensity (Goody 1952); in this way it was possible to estimate the ratios of mean line width and intensity to mean line spacing. Additional information is required, however, to yield absolute values of these quantities. The purpose of this paper is to demonstrate that this can be obtained by extending the measurements to lower pressures, when Doppler broadening has a considerable influence on the mean transmission.

§ 2. THEORETICAL

The shape of an absorption line with mixed Doppler and Lorentz broadening is given by (Unsöld 1938)

$$k_\nu = \frac{k}{\alpha_D\sqrt{\pi}}\,\frac{a}{2\pi}\int_{-\infty}^{+\infty}\frac{\exp(-t^2)dt}{(x-t)^2+(\tfrac{1}{2}a)^2} = \frac{k}{\alpha_D\sqrt{\pi}}H(x,\tfrac{1}{2}a) \quad \ldots\ldots(1)$$

in which $x=(\nu-\nu_0)/\alpha_D$, $a=2\alpha_L/\alpha_D$ and $\alpha_D=(\nu_0/\mathbf{c})(2\boldsymbol{k}\theta/M)^{1/2}$ ......(2)

where k_ν = monochromatic absorption coefficient at frequency ν, k = line intensity = $\int k_\nu d\nu$ from $-\infty$ to $+\infty$, ν_0 = frequency of line centre, α_D = Doppler half-width, α_L = Lorentz half-width, $\mathbf{c}$ = velocity of light, $\boldsymbol{k}$ = Boltzmann's constant, θ = absolute temperature, M = molecular mass. The notation used here is that of Goody (1954), though the line-shape function $H(x, \tfrac{1}{2}a)$ has been defined to conform with the astronomical literature.

The statistical model enables the mean transmission T^* for a beam of radiation traversing an amount m of absorbing material (g cm^{-2} or cm at S.T.P.) to be determined by an integration over a single line of arbitrary shape. Assuming an exponential distribution of line intensities with mean intensity σ, insertion of (1) in equation (3) of Goody's (1952) paper gives

$$\frac{\delta D^*}{\alpha_D} = \int_{-\infty}^{+\infty}\frac{(\sigma m/\alpha_D\sqrt{\pi})H(x,\tfrac{1}{2}a)}{1+(\sigma m/\alpha_D\sqrt{\pi})H(x,\tfrac{1}{2}a)}\,dx \quad \ldots\ldots(3)$$

where $D^* = -\ln T^*$.

From this equation $\delta D^*/\alpha_D$ was calculated as a function of $\sigma m/\alpha_D\sqrt{\pi}$ using the values of H tabulated by Hjerting (1938). Simpson's rule was used out to $x=20$; the remaining contribution from the far wings was estimated analytically from the approximation $H \simeq a/2\sqrt{\pi}x^2$. For pure Doppler broadening ($a=0$), the line shape becomes $H = \exp(-x^2)$ and insertion of this in (3) gave an expression which was also integrated by Simpson's rule.

Transmission of Statistical Model with Doppler–Lorentz Line Shape and Exponential Distribution of Line Intensities: Values of $\delta D^*/\alpha_D$

$\sigma m/\alpha_D\sqrt{\pi}$	$a=0$	0·06	0·20	1·00
0·1	0·166	—	—	—
0·316	0·461	—	—	0·504
1	1·07	—	1·14	1·33
3·16	1·95	2·02	2·20	2·94
10	2·82	3·06	3·54	5·48
31·6	3·56	4·16	5·35	9·77
100	4·18	5·70	8·26	17·0
316	4·73	8·30	13·8	—
1000	5·16	11·9	—	—

The results of these computations are shown in the table. They are sufficient to allow interpolation and extrapolation to a sufficient degree of accuracy for all values of the parameters owing to the known asymptotic forms for pure Lorentz broadening (Goody 1952) and for small amounts of absorbing matter (the linear law of absorption, see for example Goody 1954).

The behaviour of the mean transmission under the influence of Doppler broadening is conveniently represented on a diagram developed for treating the previous results for higher pressures (Walshaw and Goody 1954), where $\log_{10}(D^*/m)$ is plotted as a function of $\log_{10}(m/p)$. If the lines have the Lorentz shape, a single curve should be obtained with zero slope at high pressures (to the left in figure 1) and a slope of $-1/2$ at low pressures (broken lines in figure 1). The effect of Doppler broadening is to prevent this continual fall-off as the pressure is lowered, and, if the pressure is low enough, to make the transmission independent of pressure, giving the S-shaped curves shown by the full lines in figure 1.

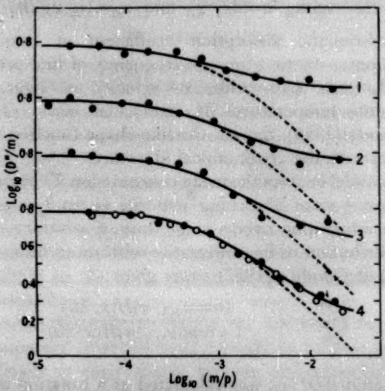

Figure 1. Transmission in the 9·6 μ band at 1017 cm^{-1}. m is in cm at s.t.p. and p in mm Hg, and the optical density $D^* = -\ln I^*$. The lines are calculated from the statistical model with $\alpha_L/\delta = 1{\cdot}59$ at 760 mm Hg and $\sigma/\delta = 6{\cdot}10$ (cm s.t.p.)$^{-1}$; full lines : $\alpha_D/\delta = 0{\cdot}0204$, broken lines : $\alpha_D/\delta = 0$. The values of m are : curve 1, 0·0074 ; 2, 0·0126 ; 3, 0·0200 ; 4, 0·0327. The different symbols on curve 4 denote two experimental runs of nearly equal m.

The four curves in figure 1 are for different amounts of ozone but the same value of the Doppler half-width. The Lorentz curves should be superimposed to give a single curve for all amounts and pressures, but they have been separated by vertical displacements in order to show the effects of Doppler broadening more clearly. It will be seen that deviations from the Lorentz curve are more obvious for the lower ozone amounts.

§ 3. Experimental

The 9·6 μ band was recorded photographically by a conventional rocksalt prism spectrometer using a Hilger d.c. thermocouple with galvanometer amplification and a Nernst filament source. The slit width was kept constant and equivalent to 6·5 cm^{-1} at the band centre. Experimental runs were made by evaporating into the evacuated absorption tube a suitable quantity of pure ozone from the fractionally distilled liquid, and taking spectra after the admission of successive amounts of dry air until atmospheric pressure was reached. Control spectra of the Nernst filament with the tube evacuated were also taken at the beginning and end of each run to enable the ozone absorption to be calculated and to give a check on the stability of the apparatus.

Pressures were measured on a barometer and McLeod gauge using a sensitive glass spoon gauge as an intermediate null indicator to avoid contact between the mercury and ozone. The amount of ozone traversed by the beam was determined from simultaneous measurements of absorption in the ultra-violet bands made by a Hilger E.1 spectrometer fitted with a 27M3 photomultiplier and arranged for double-beam working through a cross arm of the absorption tube; a mercury arc source was used and the results converted to ozone amounts with the aid of the absorption coefficients of Ny and Choong (1933).

The optical path length was 35 centimetres. The measured pressures were adjusted to apply to conditions of infinite dilution in air by using the fact that ozone molecules are 1·61 times as effective as air molecules in collision broadening; this result was obtained from subsidiary measurements made with a much shorter (6·5 cm) absorption tube (Walshaw 1954).

§ 4. RESULTS

Transmissions were measured at eight points in the band, and results were plotted in the manner described above; figure 1 shows the results for a frequency of 1017 cm^{-1} for four different ozone amounts with arbitrary shifts on the vertical scale. The results show the characteristic shape which is to be expected if Doppler broadening is important, and a very good fit to the experimental points can be made by choosing appropriate values for the parameters σ/δ, α_D/δ, and α_L/δ at one atmosphere pressure.

Similar fits were obtained for the results at the other seven frequencies, and the values of α_D/δ obtained are shown in figure 2, together with a vertically displaced curve showing the run of α_L/δ through the band as obtained from the previously reported work at higher pressures. Since values of α_L/δ and σ/δ were available from this earlier work, it was only strictly permissible to vary the one parameter α_L/α_D to obtain the best fit to these results. In fact it was also found necessary to vary the value of σ/δ in order to produce a good fit. The reason for this is not quite clear, but is thought to be due to errors in the measurements of the very

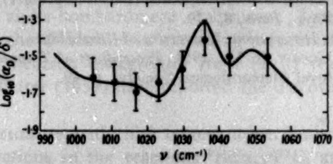

Figure 2. Variation of α_D/δ in the 9·6 μ band. The points are values derived from the comparison of the observations with the transmission function for the mixed Doppler–Lorentz line shape. The line is the curve of α_L/δ at 760 mm Hg obtained from measurements in the Lorentz region with a vertical displacement corresponding to $\log_{10} \alpha_L/\alpha_D = 1{\cdot}85$ at 760 mm Hg.

small ozone amounts used in these experiments. These errors could be partly caused by inaccuracies in the ultra-violet absorption coefficients, and partly by adsorption effects on the windows such as those reported by Vassy (1937) and confirmed by other experiments in this laboratory. Whatever the cause of these errors they only lead to displacements of the curves in figure 1 and not to changes in shape, and so do not influence the values of α_L/α_D deduced from them.

Figure 2 suggests that this ratio does not vary sensibly over the band and that a mean value of 71 ± 4 (standard error) can be adopted at 20°c and 760 mm Hg pressure.

An estimate may now be made of the value of the Lorentz line half-width, since the Doppler half-width can be found from (2) to be $1{\cdot}10 \times 10^{-3}$ cm^{-1} at the band centre. The resulting value at 20°c and 760 mm Hg under conditions of infinite dilution in air is $0{\cdot}078$ cm^{-1}, which is very close to values found by recent workers on other infra-red bands using high-resolution techniques.

ACKNOWLEDGMENTS

It is a pleasure to thank Dr. T. W. Wormell and Dr. R. M. Goody for their constant advice and encouragement, and Mr. A. R. Curtis for some preliminary calculations and helpful discussions. I am also indebted to the Gassiot Committee of the Royal Society and to the Department of Scientific and Industrial Research for the financial support which enabled the work to be undertaken.

REFERENCES

ADEL, A., 1953, *J. Opt. Soc. Amer.*, **43,** 1053.

CURTIS, A. R., and GOODY, R. M., 1954, *Quart. J. R. Met. Soc.*, **80,** 58.

GOODY, R. M., 1952, *Quart. J. R. Met. Soc.*, **78,** 165; 1954, *The Physics of the Stratosphere* (Cambridge: University Press), p. 142.

GOODY, R. M., and WORMELL, T. W., 1951, *Proc. Roy. Soc.* A, **209,** 178.

HJERTING, F., 1938, *Astrophys. J.*, **88,** 508.

LOCKE, J. L., and HERZBERG, L., 1953, *Canad. J. Phys.*, **31,** 504.

MATHESON, L. A., 1932, *Phys. Rev.*, **40,** 813.

NY TSI-ZÉ and CHOONG SHIN PIAW, 1933, *Chin. J. Phys.*, **1,** 38.

UNSÖLD, A., 1938, *Physik der Sternatmosphären* (Berlin: Springer), p. 148.

VASSY, E., 1937, *Ann. Phys., Paris*, **8,** 679.

WALSHAW, C. D., 1954, *Dissertation*, University of Cambridge.

WALSHAW, C. D., and GOODY, R. M., 1954, *Proceedings of Toronto Meteorological Conference* (London: Royal Meteorological Society), p. 49.

RESEARCH NOTES

A Search for Capture Processes in Alpha-Particle and Deuteron Bombardments

By H. R. ALLAN and N. SARMA
Physics Department, Imperial College, London

MS. received 8th January 1955

An attempt has been made to detect the process of radiative capture in the alpha-particle and deuteron bombardment of various target elements, using beams of accelerated particles from the Imperial College Van de Graaff generator. No definite evidence has been obtained for any of these processes, but new upper limits have been placed upon the cross sections.

Three methods of detection were employed : a scintillator counter spectrometer, threshold detection, and detection of induced radioactivity.

(i) *Scintillation Counter Spectrometer*

A 2 in. thick NaI (thallium activated) crystal was used as a scintillation counter in conjunction with a fifty-channel pulse height analyser to detect the high-energy quanta that would be emitted during any radiative capture. The sensitivity of this method was limited by the pile-up of small pulses due to the background of neutrons and low energy gamma-quanta. This method has been used previously by Sinclair (1954) who set limits of 5×10^{-29}, 10^{-28}, and 5×10^{-28} cm^2 on the cross sections for the reaction (d, γ) in deuterium, helium, and oxygen respectively at bombarding energies near 1·1 Mev. Using coincidence counting of secondary electrons, Fowler, Lauritsen and Tollestrup (1949) set a limit of $\sigma < 10^{-31}$ cm^2 for the $D(d, \gamma)^4He$ reaction at near 1 Mev. Bennett, Roys and Toppel (1951) and Jones and Wilkinson (1952, 1954) have successfully detected the capture of gamma rays in the alpha-bombardment of lithium; Jones and Wilkinson (1953) have also noted the difficulties in extending measurements to other elements because of the neutron background from (α, n) reactions. Recently Blair, Hintz and Van Patter (1954) have reported the discovery of the reaction $^3He\,(d, \gamma)^5Li$.

In the present experiments, with thick targets, upper limits were obtained for the integrated cross sections in the reactions $^9Be(\alpha, \gamma)^{13}C$, and $^{12}C(\alpha, \gamma)^{16}O$ by comparing the counting rates in the high-energy channels of the analyser with the counting rate due to the 4·43 Mev quanta from the reaction $^9Be(\alpha, n\gamma)^{12}C$ for which the gamma-ray yield is known (Halpern 1949, Bradford and Bennett 1950). The results are as follows :

Reaction	E_α	Integrated cross section
$^9Be(\alpha, \gamma)^{13}C$	1600 kev	$< 2 \times 10^{-29}$ cm^2 Mev
$^{12}C(\alpha, \gamma)^{16}O$	1600 kev	$< 3 \times 10^{-29}$ cm^2 Mev

On the assumption that the excitation functions of $^9Be(\alpha, \gamma)^{13}C$ and $^9Be(\alpha, n\gamma)^{12}C$ are similar in shape, the result for $^9Be(\alpha, \gamma)^{13}C$ corresponds to a cross section at 1·6 MeV less than 3×10^{-29} cm^2. For ^{12}C, on the other hand, the excitation function is expected to show marked resonances, since the (α, n) and (α, p) reactions are energetically impossible.

(ii) *Threshold Detector*

In this method, praseodymium was used as a detector of high-energy gamma-quanta. These produce in praseodymium a 3·5 minute β^+ activity by the reaction ^{141}Pr(γ, n)^{140}Pr (Hollander, Perlman and Seaborg 1953). This reaction has a threshold at about 9·5 MeV and a maximum cross section of about 300 millibarns near 15 MeV (Montalbetti, Katz and Goldemberg 1953). A compressed tablet of PrO$_2$, 1 in. in diameter and $\frac{1}{8}$ in. thick was therefore held close to the target for five minutes and its subsequent activity examined. In these circumstances, low energy quanta could produce no activity, while low energy neutrons produced the 19·2-hour β^- activity of ^{142}Pr by neutron capture. Considerable discrimination against the neutron-induced activity was provided by the difference in half-lives; further discrimination was achieved by using two NaI(Tl) scintillation counters in coincidence to detect the annihilation quanta from the positrons, the PrO$_2$ tablet being mounted between the crystals.

The limitations of this method of detecting capture radiation arise from the production of high-energy neutrons in the target which cause the same positron activity by the reaction ^{141}Pr(n, 2n)^{140}Pr. Such neutrons are formed by the (d, n) reactions in ^{7}Li, ^{11}B, ^{15}N, and ^{19}F (Ajzenberg and Lauritsen 1952), and minute traces of any of these elements on a target are sufficient to mask the capture radiation. The cross section for (d, n) reactions may be 10^4 to 10^6 times that for a (d, γ) reaction; the (n, 2n) reaction in praseodymium has a cross section some ten times greater than the (γ, n) cross section (Paul and Clark 1953). Consequently, contamination of the target to the extent of one part in 10^5 or 10^7 will mask the capture process. On some of the targets used, the presence of lithium contamination was established by detecting the alpha particles from the ^{7}Li(p, α)^{4}He reaction, and the amounts were sufficient to explain the radioactivity induced in the praseodymium tablet.

The detection efficiency (determined using the known gamma ray yield from the reaction ^{7}Li(p, γ)^{8}Be (Fowler and Lauritsen 1949)) was found to be 1 in 10^5 quanta, and the smallest detectable yield, with beam currents of 50 microamperes, was about 10^{-10} quanta per deuteron. Limits were thereby obtained for the (d, γ) yield with thick targets of beryllium and carbon :

Reaction	E_d	Gamma yield per deuteron	Estimated σ at incident energy
^{9}Be(d, γ)^{11}B	900 kev	$<4 \times 10^{-10}$	$<1{\cdot}8 \times 10^{-30}$ cm^2
	1500 kev	$<10^{-9}$	$<2 \times 10^{-29}$ cm^2
^{12}C(d, γ)^{14}N	1500 kev	$<10^{-10}$	$<10^{-30}$ cm^2

(iii) *Induced Radioactivity*

In some cases, the residual nucleus formed by the capture of a deuteron or alpha particle is radioactive and the activity can therefore be used to establish the occurrence of the reaction. Such a case has been reported by Weimer, Pool and Kurbatov (1943) who bombarded barium with 6 MeV deuterons and found ^{140}La among the products. The yield was remarkably high, 1/1300 of the yield of the (d, n) reaction. Another instance is given by Sharma (1951) who obtained ^{30}P by deuteron bombardment of ^{28}Si at 6 MeV.

In the present experiments, a search was made for the residual activity formed by the reaction $^{22}Ne(d, \gamma)\,^{24}Na$. For deuteron capture in neon, a gas target was used, 5 microamperes of 1·6 MEV deuterons being admitted to the target chamber through a quartz window. Any activity produced in the gas was allowed to settle on an aluminium collecting cylinder and then measured with a Geiger counter. The background counting rate was reduced by taking measurements 100 ft below ground level.

After bombardment of the neon for some 12 hours, the aluminium collector was examined ; the 15-hour period due to ^{24}Na was found to be present, together with a 2-hour period due to ^{18}F formed by the reaction $^{20}Ne(d, \alpha)^{18}F$. However, ^{24}Na was also produced when a control experiment was carried out with nitrogen in the chamber instead of neon. The cause appears to have been the presence of sodium in the quartz window; the ^{24}Na formed by the reaction $^{23}Na(d, p)^{24}Na$ could be transferred to the collecting cylinder by recoil. Because of this, the occurrence of deuteron capture in ^{22}Ne could not be definitely established. Comparison of the ^{18}F and ^{24}Na yields gave an upper limit of 4×10^{-31} cm² for the cross section of $^{22}Ne(d, \gamma)^{24}Na$ at 1·5 MEV.

The upper limits to the cross sections for the various (d, γ) and (α, γ) reactions found above may be compared with the predictions of the usual statistical theory of the compound nucleus, according to which (with standard notation)

$$\frac{\sigma(\alpha, \gamma)}{\sigma(\alpha, n)} = \frac{\Gamma_\gamma}{\Gamma_n}.$$

Γ_γ normally lies between 0·1 ev and 10 ev, while Γ_n may be some tens or hundreds of kev. Apart from barrier effects, $\sigma(\alpha, n)$ is typically between 10^{-25} and 10^{-26} cm². Thus $\sigma(\alpha, \gamma)$ would be expected to lie between 10^{-28} and 10^{-32} cm², apart from any reduction due to the Coulomb barrier. For deuterons, the occurrence of stripping complicates the situation, but the relative magnitudes of the (d, α) and (d, p) cross sections in light elements, and angular distribution studies, suggest that compound nucleus formation predominates in the energy region below 2 MEV. The expected cross section for (d, γ) reactions is therefore of the same order as for (α, γ) reactions.

The experimental results are seen to be consistent with the theoretical expectations. There are indications in the literature that at higher bombarding energies, abnormally high yields may occur. One instance is the $^{138}Ba(d, \gamma)^{140}La$ reaction referred to above. Katz and Penfold (1951 a, b) find evidence for a giant resonance in the reaction $^{32}S(\gamma, d)^{30}P$ at a deuteron energy of 6 MEV; a detailed balancing argument shows that this must imply a correspondingly large (d, γ) cross section at this energy. Thus it may be that the detection techniques here described would prove adequate at bombarding energies greater than were available in the present experiment.

REFERENCES

AJZENBERG, F., and LAURITSEN, T., 1952, *Rev. Mod. Phys.*, **24**, 321.
BENNETT, W. E., ROYS, P. A., and TOPPEL, B. J., 1951, *Phys. Rev.*, **82**, 20.
BLAIR, J. M., HINTZ, N. M., and VAN PATTER, D. M., 1954, *Phys. Rev.*, **96**, 1023.
BRADFORD, C. E., and BENNETT, W. E., 1950, *Phys. Rev.*, **78**, 302.
FOWLER, W. A., and LAURITSEN, C. C., 1949, *Phys. Rev.*, **76**, 314.
FOWLER, W. A., LAURITSEN, C. C., and TOLLESTRUP, A. V., 1949, *Phys. Rev.*, **76**, 1767.

Halpern, I., 1949, *Phys. Rev.*, **76**, 248.
Hollander, J. M., Perlman, I., and Seaborg, G. T., 1953, *Rev. Mod. Phys.*, **25**, 469.
Jones, G. A., and Wilkinson, D. H., 1952, *Phys. Rev.*, **88**, 423; 1953, *Proc. Phys. Soc.* A, **66**, 1176; 1954, *Phil. Mag.*, **45**, 703.
Katz, L., and Penfold, A. S., 1951 a, *Phys. Rev.*, **81**, 815; 1951 b, *Ibid.*, **83**, 169.
Montalbetti, R., Katz, L., and Goldemberg, J., 1953, *Phys. Rev.*, **91**, 659.
Paul, E. B., and Clarke, E. T., 1953, *Canad. J. Phys.*, **31**, 267.
Sharma, H. D., 1951, *UCRL*-1265.
Sinclair, R. M., 1954, *Phys. Rev.*, **93**, 1082.
Weimer, K. E., Pool, M. L., and Kurbatov, J. D., 1943, *Phys. Rev.*, **63**, 67.

The Radiative Capture of Protons of 669 kev in Fluorine

By A. B. CLEGG, G. A. JONES and D. H. WILKINSON
Cavendish Laboratory, Cambridge

MS received 7th February 1955

S wave protons of 669 kev are captured by ^{19}F into a 1^+ level of ^{20}Ne at 13·50 Mev which de-excites by gamma-ray emission to the 2^+ state of ^{20}Ne at 1·63 Mev with a radiative width of 2·2 ev ($\pm 15\%$) (All References A). That the 13·50 Mev level whose assignment is established from the reaction ^{19}F(p, $\alpha\gamma$)^{16}O and the level concerned in the radiative capture are the same is made virtually certain by the carefully measured excitation functions of Sanders (1952) and Sinclair (1954) in which the level positions as observed in the two reactions are found to be the same and the widths the same (to within 1 kev). Since this level shows by far the strongest radiative transition known in ^{20}Ne the character of the radiation becomes of some interest; in particular we must enquire whether it is M1 (with a strength of 0·064 Weisskopf (1951) units) or perhaps a strong E2 (strength 1·8 Weisskopf units). To settle this point we have measured the angular correlation between the two cascade gamma rays in the plane at right angles to the proton beam. We used NaI(T1) crystals; one was biased to correspond to a gamma-ray energy of 8 Mev so as to be sensitive only to the gamma rays of radiative capture and not to those of 6 and 7 Mev from ^{16}O that follow the (p, α) reaction; the output from the other crystal was recorded by a kicksorter if it corresponded to a gamma ray of greater than 0·7 Mev in coincidence (resolving time 0·5 μsec) with a high-energy gamma ray. The background of chance coincidences is seen chiefly as gamma rays of 6 and 7 Mev and may be accurately subtracted to leave the 1·63 Mev spectrum of genuine coincidences. The results are displayed in the figure where θ is the angle between the directions of emission of the two cascade gamma rays.

A least squares analysis yields the distribution $1-(0{\cdot}342\pm0{\cdot}054)\cos^2\theta$ which, when corrected for the finite angular resolution of the detectors, becomes $1-(0{\cdot}389\pm0{\cdot}078)\cos^2\theta$. Any term in $\cos^4\theta$ is rather small. The theoretical angular correlation for the sequence $1+(\mathrm{Ml\ and\ E2})\ 2+(\mathrm{E2})0^+$ is:

$$\tfrac{3}{8}(3-\cos^2\theta)+\delta^2\frac{(15+75\cos^2\theta-80\cos^4\theta)}{24}+\delta\,\frac{\sqrt{5}}{4}(3\cos^2\theta-1)$$

where δ is the amplitude of the E2 component relative to the M1 in the first gamma ray. It is clear that the E2 component is small and that the transition is predominantly M1 (we find that δ is less than about 0·1 although it would be dangerous to base any quantitative conclusion on this figure owing to the influence on the $\gamma-\gamma$ correlation of possible small d-wave proton components in the formation of the ^{20}Ne compound nucleus).

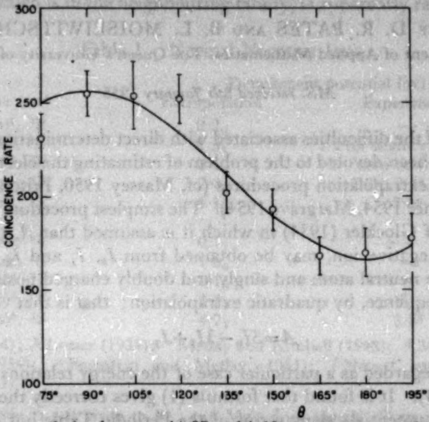

Angular correlation between 11·87 and 1·63 MEV gamma rays from the 13·50 MEV level of ^{20}Ne.

We have also sought the M1 direct ground state transition from this level and find its radiative width to be less than 0·02 ev. Since we now know both possible transitions from the 13·50 MEV level to be M1 the striking difference in their radiative widths demands that a significant re-arrangement take place in ^{20}Ne between the ground and first excited states. On the shell model this could well correspond to the ground state's being rather pure $2s_{1/2}{}^4$ with the first excited state of $2s_{1/2}{}^3\,1d_{5/2}+2s_{1/2}{}^2\,1d_{5/2}{}^2+\ldots\ldots$ on the basis of which assignment we should expect all M1 transitions to the ground state to be forbidden to first order.

At all events the present observations make it unlikely that the ground state and first excited states of ^{20}Ne may both be written $1d_{5/2}{}^4$ and it seems well possible that the considerable pairing energy of the $2s_{1/2}$ shell, presumably seen reflected in the notorious change of parity at 110 kev in ^{19}F, has effected the purification of the ground state of ^{20}Ne to something close to $2s_{1/2}{}^4$. The great strength of the observed M1 transition to the first excited state remains noteworthy and in turn implies that the state at 13·50 MEV cannot have too complicated a shell-model description.

REFERENCES A

CARVER, J. H., and WILKINSON, D. H., 1951, *Proc. Phys. Soc.* A, **64,** 199.
DEVONS, S., and HEREWARD, H. G., 1948, *Nature, Lond.*, **162,** 331.
JONES, G. A., and WILKINSON, D. H., 1952, *Proc. Phys. Soc.* A, **65,** 1055.
RAE, E. R., RUTHERGLEN, J. G., and SMITH, R. D., 1950, *Proc. Phys. Soc.* A, **63,** 775.
SEED, J., 1953, *Phil. Mag.*, **44,** 921.
SEED, J., and FRENCH, A. P., 1952, *Phys. Rev.*, **88,** 1007.

OTHER REFERENCES

SANDERS, J. E., 1952, *Thesis*, University of Cambridge.
SINCLAIR, R. M., 1954, *Phys. Rev.*, **93,** 1082.
WEISSKOPF, V. F., 1951, *Phys. Rev.*, **83,** 1073.

Energies of Normal and Excited Negative Ions

By D. R. BATES and B. L. MOISEIWITSCH
Department of Applied Mathematics, The Queen's University of Belfast

MS. received 8th January 1955

BECAUSE of the difficulties associated with direct determinations considerable effort has been devoted to the problem of estimating the electron affinities of atoms by extrapolation procedures (cf. Massey 1950, Pritchard 1953, Pritchard and Skinner 1954, Margrave 1954). The simplest procedure yielding useful results is that of Glockler (1934) in which it is assumed that A, the detachment potential of a negative ion, may be obtained from I_0, I_1 and I_2, the ionization potentials of the neutral atom and singly and doubly charged positive ions of the iso-electronic sequence, by quadratic extrapolation; that is that

$$A=3I_0-3I_1+I_2 \qquad \ldots\ldots(1)$$

which may be regarded as a particular case of the energy relations of Bacher and Goudsmit (1934). It is found that formula (1) gives correctly the main trend of the detachment potentials along a row of the Periodic Table but that the values it predicts tend to be too low (Bates 1947). In a modification proposed by Wu (1936) the variation principle is invoked to calculate approximations $\mathscr{A}$, $\mathscr{I}_0$, $\mathscr{I}_1$ and $\mathscr{I}_2$, to A, I_0, I_1 and I_2 respectively, and the correction $A-\mathscr{A}$ is then estimated by carrying out a quadratic extrapolation of the corrections $I_0-\mathscr{I}_0$, $I_1-\mathscr{I}_1$ and $I_2-\mathscr{I}_2$ which are comparatively small. This modification has been applied in the cases of H^-, Li^-, O^- and F^- (Wu 1936, Moiseiwitsch 1954). The improvement brought about is disappointingly slight. Once again the negative ion appears to be an anomalous member of the isoelectronic sequence.

It was tentatively suggested some years ago (Bates 1947) that in certain cases the error arising from the unknown effect characteristic of negative ions might partially cancel out in the formula analogous to (1) concerned with excitation potentials, these being the *difference* between the energies of two bound terms; and it was further suggested that the lowest term of the first excited configuration of a negative ion would in general lie only slightly below or slightly above the limit of the continuum so that its excitation potential (computed in the manner indicated) might be taken as giving an estimation of the detachment potential. An incidental practical advantage is that the excitation potentials of neutral atoms and positive ions are much better determined than are the ionization potentials (which in some vital cases are still not known with the high precision that is required so that corrections, assessed by differencing, must be introduced before they can be used). The method is of course essentially empirical. When it was first put forward there were very few measurements on detachment potentials which could be regarded as reliable. The position in this respect is now somewhat better and it was therefore thought worth repeating the original computations using carefully selected modern spectroscopic data. Table 1 gives the results thus obtained in the case of p-shell negative ions which are of the type for which the method is best suited. The agreement with the laboratory results is not unsatisfactory and is certainly better than that achieved by the other extrapolation methods mentioned. It is peculiar that whereas the calculated values for F^- and Cl^- are apparently rather too large (and by about the same amount) the calculated value for O^- (which is in the neighbouring family) is apparently rather too small.

Table 1. Normal Negative Ions

Negative ion†	Detachment potential (ev) Extrapolation	Detachment potential (ev) Experiment
$\mathrm{B}^-(2p)^2$, ^3P	$0{\cdot}2_0$	—
$\mathrm{C}^-(2p)^3$, ^4S	$1{\cdot}3_5$	1·2 (or slightly greater)[a]
$\mathrm{N}^-(2p)^4$, ^3P	$0{\cdot}1_5$	zero or small
$\mathrm{O}^-(2p)^5$, ^2P	$2{\cdot}0_0$	2·2[b], 2·3[c], 2·0[d]
$\mathrm{F}^-(2p)^6$, ^1S	$4{\cdot}1_0$	3·6[e]
$\mathrm{Al}^-(3p)^2$, ^3P	$0{\cdot}7_5$	—
$\mathrm{Si}^-(3p)^3$, ^4S	$1{\cdot}6_0$	—
$\mathrm{P}^-(3p)^4$, ^3P	$1{\cdot}1_0$	—
$\mathrm{S}^-(3p)^5$, ^2P	$2{\cdot}5_5$	>1[f]
$\mathrm{Cl}^-(3p)^6$, ^1S	$4{\cdot}2_5$	3·8[g]

[a] Honig (1954); [b] Lozier (1934); [c] Metlay and Kimball (1948); [d] Marriott, Thorburn and Craggs (1954); [e] Bernstein and Metlay (1951); [f] Neuert and Clasen (1952); [g] Pritchard (1953).

† Consideration is not given to Be^- and Mg^- since special effects arise with negative ions possessing only a single outer electron. In the case of the former the 3s orbital may lie below the 2p; and in the case of the latter the 4s orbital may lie below the 3p (Bates 1947).

For the reasons stated above it would be expected that quadratic extrapolation would yield the energy differences between the terms of the ground configuration of a negative ion quite accurately. The values derived, which may be of interest in connection with the interpretation of electron collision experiments, are presented in table 2. In a few instances the predicted excitation potentials are less than, or about the same as, the predicted detachment potentials so that *metastable negative ions* (probably $\mathrm{Si}^-(^2D)$, $\mathrm{Al}^-(^1D)$, $\mathrm{P}^-(^1D)$ and possibly $\mathrm{Si}^-(^2P)$, $\mathrm{C}^-(^2D)$) may exist. If the excitation potential is greater than the detachment potential there is generally an almost instantaneous disintegration through a radiationless transition into the adjacent continuum. The case of $\mathrm{N}^-(^1D)$ merits

Table 2. Excited Negative Ions

Configuration and term	$n=2$ (1)	$n=2$ (2)	$n=2$ (3)	$n=3$ (1)	$n=3$ (2)	$n=3$ (3)
$(np)^2$ ^1S	B^-	1·25		Al^-	1·07	
^1D		0·61			0·44	
^3P		0	$0{\cdot}2_0$		0	$0{\cdot}7_5$
$(np)^3$ ^2P	C^-	2·07		Si^-	1·54	
^2D		1·40			0·94	
^4S		0	$1{\cdot}3_5$		0	$1{\cdot}6_0$
$(np)^4$ ^1S	N^-	2·77		P^-	2·00	
^1D		1·34			0·84	
^3P		0	$0{\cdot}1_5$		0	$1{\cdot}1_0$

(1) Negative ion; (2) excitation potential (ev); (3) detachment potential (ev).

special mention. If the estimates given in tables 1 and 2 are correct the total energy of this system lies well below that of N(^{2}D) the excitation potential of which is 2·38 ev. Consequently the only energetically allowed disintegration is

$$N^-(^1D)\rightarrow N(^4S)+e \qquad \ldots\ldots(2)$$

which involves a *forbidden* radiationless transition. The life of N$^-$(^{1}D) towards auto-detachment, though still brief, should therefore be less transitory than is usual for unstable negative ions.

Note added in proof. Drs. L. M. Branscomb and S. J. Smith have kindly informed us, prior to publication, that they have recently carried out experiments which give the detachment energy of O$^-$ to be 1·45 ± 0·15 ev. This is lower than the usually accepted value but is in harmony with the work of Moiseiwitsch (1954) which suggested a value of less than 1·7 ev. If the new determination is correct the peculiarity regarding O$^-$ mentioned in the text disappears (and for S$^-$ a value of about 2·1 ev would appear to be indicated); indeed it would seem that the errors in the values obtained by the extrapolation procedure of Glockler and that described here both vary smoothly with atomic number, as suspected originally, and are opposite in sign.

REFERENCES

BACHER, R. F., and GOUDSMIT, S., 1934, *Phys. Rev.*, **46**, 948.
BATES, D. R., 1947, *Proc. R. Irish Acad.* A, **51**, 151.
BERNSTEIN, R. B., and METLAY, M., 1951, *J. Chem. Phys.*, **19**, 1612.
GLOCKLER, G., 1934, *Phys. Rev.*, **46**, 111.
HONIG, R. E., 1954, *J. Chem. Phys.*, **22**, 126.
LOZIER, W. W., 1934, *Phys. Rev.*, **46**, 268.
MARGRAVE, J. L., 1954, *J. Chem. Phys.*, **22**, 636, 1937.
MARRIOTT, J., THORBURN, R., and CRAGGS, J. D., 1954, *Proc. Phys. Soc.* B, **67**, 437.
MASSEY, H. S. W., 1950, *Negative Ions*, 2nd Edn (Cambridge : University Press).
METLAY, M., and KIMBALL, G. E., 1948, *J. Chem. Phys.*, **16**, 779.
MOISEIWITSCH, B. L., 1954, *Proc. Phys. Soc.* A, **67**, 25.
NEUERT, H., and CLASEN, H., 1952, *Z. Naturf.*, **7a**, 410.
PRITCHARD, H. O., 1953, *Chem. Rev.*, **52**, 529.
PRITCHARD, H. O., and SKINNER, H. A., 1954, *J. Chem. Phys.*, **22**, 1936.
WU, TA-YOU, 1936, *Phil. Mag.*, **22**, 837.

Spectroscopic Identification of Diatomic PS and New Band Systems of PO and P_2

BY K. DRESSLER AND E. MIESCHER
Physical Institute, University of Basel

Communicated by R. F. Barrow ; MS. received 3rd December 1954

THE band spectra of the molecules NO and NS have been reinvestigated recently. Baer and Miescher (1953) have identified in the near Schumann region a new system of emission of NO (β' bands), which represents a transition $^2\Delta - x^2\Pi$ (Miescher 1955). For NS, Barrow, Drummond and Zeeman (1954) have shown that the well-known bands designated as β system also represent a transition $^2\Delta - x^2\Pi$. It is of interest to compare the spectra of the analogous molecules PO and PS with these results. Whereas no experimental work has been done before on PS, two systems belonging to PO are known in the ultra-violet. The γ bands ($^2\Sigma - {}^2\Pi$) have been examined well, but the analysis of the β bands is still uncertain.

Therefore emission spectra were photographed with a discharge tube containing circulating He at a pressure of about 1 mm Hg, with a small additional amount of P_2O_3 vapour or P_4S_3 vapour respectively. Prism spectrographs of medium dispersion, a 3m grating (2·8 Å mm^{-1}) for the long wavelength region, and a 1m vacuum grating (8·4 Å mm^{-1}) served as spectrographs.

Table 1. Constants for the New Band Systems (cm^{-1})

		Present Investigation						PO $x^2\Pi$		
	$\lambda\lambda$	$\nu_{0,0}$ (head)	$\Delta\nu$	ω_e''	$\omega_e''x_e''$	ω_e'	$\omega_e'x_e'$	ω_e''	$\omega_e''x_e''$	$\Delta\nu$
PO	1825–1930	53 096·0 53 320·8	224·8	1233	7	$\Delta G_{1/2}' = 1454·5$		1230·6	6·5	223·8
								Ghosh and Ball (1931)		
PS	2700–3100	34 265·6 34 587·0	321·4	740	3	534	3			
PS^+	2300–2750	40 499·0	—	845	3·5	610	5			
								$P_2\, x^1\Sigma$		
								ω_e''	$\omega_e''x_e''$	
P_2	1680–1750	59 407	—	$\omega'' = 772$		—	—	780·4	2·8	
								Herzberg (1932)		
	1510–1530	66 275	—	$\omega'' = 770$		$\omega' = 680$				

Table 1 contains provisional data of some previously unknown band spectra appearing on the plates. The new bands partly overlap with the wide spread band systems of P_2 and S_2; but by maintaining suitable conditions of discharge, we were able to get clearly measurable plates.

PO. Five pairs of bands, degraded to shorter wavelengths, have been measured. Each sub-band consists of one strong head, accompanied by a close pair of weaker heads at a distance of 30–40 cm^{-1} towards longer wavelengths. Vibrational analysis shows the new $c - x^2\Pi$ system to involve the ground state of PO in common with the known β and γ bands.

PS. Two new band systems appear in the region 2300–3100 Å. One of them shows a doublet splitting (321·4 cm^{-1}), the other one seems to represent a singlet system. The bands of both systems are shaded to the red. 12 single-headed bands belonging to the singlet system have been measured, whereas some 20 double-headed bands (separation 4 cm^{-1}) were found to fit into the doublet system. Apart from the bands of P_2 and S_2, the plates contain only the atomic lines of P, S and He, lines of other atoms being completely absent. Therefore it is suggested that the spectra mentioned above should be attributed to a molecule consisting of P and S.

Table 2 shows a comparison of the results with known data concerning analogous molecules. This supports the assignment of the doublet spectrum to PS, and of the singlet spectrum to PS^+. Additional support for this assignment is provided by a comparison of the following relations between the ground state frequencies of molecules formed by elements of the first and second period of the periodic system :

$$\frac{\omega(P_2)}{\omega(N_2)} = \frac{780}{2360} = 0·33, \qquad \frac{\omega(PS^+)}{\omega(NO^+)} = \frac{845}{2372} = 0·36,$$

$$\frac{\omega(PS)}{\omega(NO)} = \frac{740}{1904} = 0·39, \qquad \frac{\omega(S_2)}{\omega(O_2)} = \frac{726}{1580} = 0·46.$$

In PS as well as in PS$^+$ the level of excitation corresponds to the value known for the electronic transitions $w\pi \rightarrow v\pi$ or $x\sigma \rightarrow v\pi$ of the neighbouring molecules ; and the expected loosening of binding force is found in the decrease of vibrational frequency. Ionization of PS, i.e. removal of the antibonding $v\pi$ electron, results as expected in a considerable increase of this frequency.

Table 2. Doublet Separations and Vibrational Frequencies (cm^{-1}) for Pairs of Isoelectronic Molecules

		$\text{x}^2\Pi$					$\text{x}^1\Sigma$	$^1\Pi$	
		$\Delta\nu$		ω_e			ω_e	ω_e	T_e
NO		121		1904		N$_2$	2360	1692	69290
	CF		77		1308	NO$^+$	2372	1560	73080
NS		223		1220					
	CCl		138		846			$^1\Sigma$	
PO		224		1230		P$_2$	780	475	46940
	SiF		161		857	PS$^+$	845	610	40500
PS		321		740					
	SiCl		208		535				

P$_2$. Those plates on which the $\text{A}^1\Sigma - \text{X}^1\Sigma$ bands of P$_2$ were strongly developed showed some new bands which seem to be part of transitions from two highly excited states to the ground state of P$_2$. Four red degraded bands with λλ 1683·3, 1705·5, 1728·2, 1751·4 Å probably form a v'-constant progression of a $\text{B} - \text{X}^1\Sigma$ transition, and two groups of red degraded bands at λλ 1510 and 1530 Å probably represent two sequences of a $\text{C} - \text{X}^1\Sigma$ transition. No correlation could be found between these bands and those in the visible reported by Herzberg (1932).

Further details will soon be reported in *Helv. Phys. Acta*.

References

Baer, P., and Miescher, E., 1953, *Helv. Phys. Acta*, **26,** 91.

Barrow, R. F., Drummond, G., and Zeeman, P. B., 1954, *Proc. Phys. Soc.* A, **67,** 365.

Ghosh, P. N., and Ball, G. N., 1931, *Z. Phys.*, **71,** 362.

Herzberg, G., 1932, *Ann. Phys., Lpz.*, **15,** 677.

Miescher, E., 1955, *Canad. J. Phys.*, in the press.

The Continuous Atomic Absorption Cross Sections for Neutral Atomic Systems

By G. V. MARR †

Physics Research Laboratory, University of Reading

Communicated by R. W. Ditchburn; MS. received 17*th December* 1954

§ 1. Introduction

The calculation of the absorption cross sections σ for the photoionization of atoms involves considerable difficulties (Bates 1946). Experimental measurements are possible for certain elements but difficult for those which have high boiling points. Measurements have been obtained for the alkali metals and a comparison between theory and experiment has been made for these elements by Ditchburn, Jutsum and Marr (1953, to be referred to as I). More recently measurements have been made on elements with more complicated atomic systems. It therefore seems desirable to assemble the available data so as to produce curves which show whether there is a reasonable continuity between similar elements and which may be used to give estimates for other elements.

---

† Now at the University of Western Ontario, London, Canada.

§ 2. THE VALUE OF σ AT THE SPECTRAL HEAD

The atomic systems may be divided into types of electron configurations denoted by the electrons in the outer shell. Since the experimental observations on metallic vapours indicate a maximum value for σ at the spectral head, it is proposed to use this value (σ_{LT}) as a comparison of the cross sections from element to element.

2.1. *Configurations with a Single s Electron in the Outer Shell*

Hydrogen and the alkali metals constitute this type of atomic configuration. While no conclusive experimental measurements appear to have been made on hydrogen, the indication is that the calculations are not subject to the uncertainties of those for more complicated systems, and the theoretical prediction of $6{\cdot}3 \times 10^{-18}$ cm^2 (Trumpy 1931) is probably correct. The experimental work on the alkali metals has been summarized in I. Using these values, a plot of log σ_{LT} against the atomic number *A* is shown in curve *a* of the figure.

The effect of the completed inner shells on this type of configuration is indicated by the variation of the absorption cross section from element to element. The points are joined by straight lines and the graph shows a minimum in the region of atomic number 19 (potassium), after which it rises again towards higher atomic numbers.

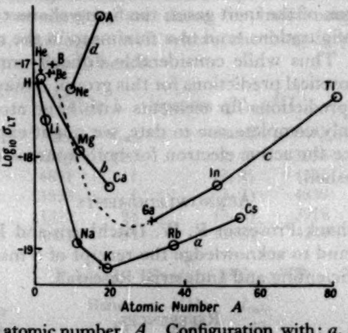

Plots of log σ_{LT} against atomic number, *A*. Configuration with: *a*, a single s electron in the outer shell; *b*, s^2 electrons in the outer shell; *c*, s^{2}p electrons in the outer shell; *d*, s^{2}p^6 electrons in the outer shell. Circles indicate experimental results, crosses theoretical predictions.

2.2. *Elements with s^2 Electrons in the Outer Shell*

The elements with this type of configuration are the alkali earths and helium. A plot of log σ_{LT} against *A* is shown in curve *b*, for the available elements of this group. The value for helium was obtained from some experimental results by

Professor Weissler (private communication) while those for magnesium and calcium were taken from the experimental reports of Ditchburn and Marr (1953) and Jutsum (1954) respectively. The general trend of the graph is similar to that for curve *a*. As yet little theoretical evidence is available; the calculation for calcium by Bates and Massey (1941) neglected polarization effects and predicted a value of σ_{LT} considerably in excess of that observed by Jutsum. The approximate calculation for beryllium (Bates 1946) predicted a value of $8{\cdot}2 \times 10^{-18}$ cm^2 at the spectral head, which is about twice the value indicated by curve *b* for this element.

2.3. *Elements Containing s^2p Electrons in the Outer Shell*

With the exception of boron, no theoretical predictions have been made for this group of elements. The absorption for thallium has been observed experimentally by Marr (1954 a). An approximate value of 5×10^{-19} cm^2 is indicated for indium (Marr 1954 b) from some observations by Garton (1950). It is possible to extend this kind of prediction to gallium and an examination of Garton's work (1952) suggests that σ_{LT} is probably less than 4×10^{-19} cm^2 for this element. The curve *c* plotted in the figure for this configuration is therefore less accurately defined than the others. However by including a value of 2×10^{-19} cm^2 for gallium it shows the same general trend as the corresponding portion of curve *a*.

2.4. *The Inert Gases with s^2p^6 Configurations*

Values of σ have been obtained for neon (Weissler and Lee 1953) and for argon (Weissler, private communication). These elements have been included in curve *d* of the figure for the sake of completeness. Very little can be said about the results until information becomes available for the other elements in this configuration.

§ 3. DISCUSSION

With the exception of the inert gases, the figure shows that the curves joining atoms of similar configurations tend to a minimum in the region of Group II of the periodic table. Thus while considerable difficulty must be anticipated in making accurate theoretical predictions for this group, it may be possible to obtain reasonably reliable predictions for elements with large atomic numbers. While the curve *a* is the only complete one to date, we might expect the curve *c* to be similar in shape since the active electron for both systems is the first electron of an uncompleted subshell.

ACKNOWLEDGMENTS

I would like to thank Professor R. W. Ditchburn and Professor D. R. Bates for their comments and to acknowledge the receipt of a maintenance grant from the Department of Scientific and Industrial Research.

REFERENCES

BATES, D. R., 1946, *Mon. Not. R. Astro. Soc.*, **106**, 423.
BATES, D. R., and MASSEY, H. S. W., 1941, *Proc. Roy. Soc.* A, **177**, 329.
DITCHBURN, R. W., and MARR, G. V., 1953, *Proc. Phys. Soc.* A, **66**, 655.
DITCHBURN, R. W., JUTSUM, P. J., and MARR, G. V., 1953, *Proc. Roy. Soc.* A, **219**, 89.
GARTON, W. R. S., 1950, *Nature, Lond.*, **166**, 150; 1952, *Proc. Phys. Soc.* A, **65**, 268.
JUTSUM, P. J., 1954, *Proc. Phys. Soc.* A, **67**, 190.
MARR, G. V., 1954 a, *Proc. Roy. Soc.* A, **224**, 83; 1954 b, *Proc. Phys. Soc.* A, **67**, 196.
TRUMPY, B., 1931, *Z. Phys.*, **71**, 720.
WEISSLER, G. L., and LEE, P., 1953, *Proc. Roy. Soc.* A, **220**, 71.

Intensities in Band Systems of CH

By M. E. PILLOW
Northern Polytechnic, London

MS. received 24th January 1955, *and in revised form* 16*th February* 1955

THREE band systems attributed to the 'molecule' CH are known, being observed in many flames, as well as in suitable arcs and discharges. Durie (1952) noted some unusual features in the relative intensities of some of the bands in the spectra of hydrocarbon flames, and Broida (1953) has made a detailed study of a few bands and attempted to relate the degrees of excitation of the vibrational and rotational levels in terms of 'temperatures'. For this to be done, the vibrational transition probabilities are required. These were not at the time available, and Broida used a very rough approximation. It has therefore appeared useful to calculate these transition probabilities, using the distortion method with wave functions approximately normalized (Pillow 1951, 1952), which is satisfactory at low levels provided that the molecular constants used are reliable. The values for these constants used here are those given by Herzberg (1950), and are taken mainly from measurements by Gerö (1941).

The values given in tables 1–3 are for the quantity

$$I_{\text{calc}} = [\int \psi'\psi''\,dr]^2\nu^4$$

where ψ', ψ'', are the two vibrational wave functions connected with a band, and ν (cm^{-1}) is the wave number of the band origin. This quantity should be proportional to the intensity of the band if distribution among the vibrational levels were uniform, that is, at infinite 'vibrational temperature'. The scale of intensity is arbitrary, being so chosen for each system that the value for the (0, 0) band is 100. The wavelengths are those for band origins calculated from Herzberg's constants, and agree well where checking is possible with Gerö's measurements (1941) on the Q heads.

Table 1. System $A^2\Delta$–$X^2\Pi$

Band	λ(Å)	I_{calc}	Band	λ(Å)	I_{calc}
(0, 0)	4314	100	(2, 1)	3884	2
(0, 1)	4891	<1	(2, 2)	4321	97
(1, 0)	3858	1	(2, 3)	4839	<1
(1, 1)	4313	98	(3, 2)	3918	1
(1, 2)	4858	<1	(3, 3)	4339	96

Table 2. System $B^2\Sigma^-$–$X^2\Pi$

Band	λ(Å)	I_{calc}	Band	λ(Å)	I_{calc}	Band	λ(Å)	I_{calc}
(0, 0)	3888	100	(1, 0)	3634	43	(2, 0)	3501	36
(0, 1)	4350	20	(1, 1)	4035	35	(2, 1)	3872	39
(0, 2)	4909	3	(1, 2)	4509	30	(2, 2)	4306	2
			(1, 3)	5076	12	(2, 3)	4820	19

Table 3. System $C^2\Sigma^+$–$X^2\Pi$

Band	λ(Å)	I_{calc}	Band	λ(Å)	I_{calc}
(0, 0)	3145	100	(1, 1)	3156	98
(0, 1)	3440	<1	(2, 2)	3177	90

Broida's intensity measurements were made on the first system, $A^2\Delta - X^2\Pi$, and he derived a 'temperature' from two bands only, (0, 0) and (1, 1), by assuming transition probabilities, represented by $[\int \psi' \psi'' \, dr]^2 \nu^3$, to be in the ratio 1 : 1. The corresponding ratio now calculated is very nearly 1 : 1, so that Broida's 'temperature' probably needs no modification on this score.

It is obvious that extremely long exposures would be needed if any sequence of this system other than $\Delta v = 0$ were to appear, even faintly, in a photograph of the spectrum, and this is the case in practice.

It is interesting to compare the calculated values for the second system, $B^2\Sigma^- - X^2\Pi$, with Durie's observations. An estimate of the intensity ratio of the (1, 1) and (0, 0) bands was made by him as 1 : 4, or 25 : 100. It can be seen from the table that this would indicate populations of the $v' = 1, 0$, levels in the ratio of 25 : 35, i.e. 0·7 : 1, which represents a high, but not impossible, degree of excitation. On this basis, the intensities of the (1, 0), (1, 2) bands would be reduced from those shown in the table to 31 and 21 respectively. One would therefore expect the (1, 2) band to be visible, though somewhat faint, and in fact it was observed by Durie, under the conditions considered here, for the first time, and identified. The (0, 1) band, which should then appear also, would be completely masked by the P-branch of the (0, 0) band of the $A^2\Delta - X^2\Pi$ system, and no comparison with this can therefore be made. If the population of successive levels fell off in a constant ratio (which is not necessarily to be expected in a flame), the bands (2, 0), (2, 1), would have intensities of about 18 and 20 on the scale used. The second would in any case be masked by the (0, 0) band, thus upsetting slightly the ratios considered above, and the first might perhaps appear, but very faintly, in a region where faint HCO bands are also present, according to Durie. No other bands of this system are to be expected unless the excitation of the upper levels is still further increased.

In the $C^2\Sigma^+ - X^2\Pi$ system, the $\Delta v = 0$ sequence is the only one at all likely to be observed, and this is borne out by experiment.

REFERENCES

BROIDA, H. P., 1953, *J. Chem. Phys.*, **21,** 340.

DURIE, R. A., 1952, *Proc. Phys. Soc.* A, **65,** 125.

GERÖ, L., 1941, *Z. Phys.*, **118,** 27.

HERZBERG, G., 1950, *Spectra of Diatomic Molecules*, 2nd Edn (New York : Van Nostrand).

PILLOW, M. E., 1951, *Proc. Phys. Soc.* A, **64,** 772; 1952, *Thesis*, University of London.

LETTERS TO THE EDITOR

Effect of Finite Nucleus on the Radiative Correction

The radiative correction to the essentially elastic scattering of electrons by nuclei has been evaluated by Schwinger (1949) on the assumption that nuclei can be treated as point charges. The scattering cross section can be written (Elton and Robertson 1952)

$$I(\theta, \Delta E) = I_{B1}(1 + \delta_{B2} - \delta_R),$$

where I_{B1} is the cross section in first Born approximation, $I_{B1}\delta_{B2}$ is the second Born correction (Dalitz 1951) and $I_{B1}\delta_R$ is the radiative correction. ΔE, which is small, is the energy lost in bremsstrahlung. Now the matrix elements leading to I_{B1} and to $I_{B1}\delta_R$ are proportional to the momentum transform of the scattering potential. Hence it follows that δ_R is completely independent of the scattering potential and, in particular, will be the same for a nucleus of finite size and for a point nucleus. This is not the case with δ_{B2}. As the second Born correction involves an integration over intermediate states of the potential, δ_{B2} will depend on the particular form of the potential.

It should be stressed that the above argument applies only to light nuclei, for which higher order corrections are negligible. For heavy nuclei, the radiative correction will certainly not be independent of the scattering potential.

Wheatstone Department of Physics,
King's College,
London.
L. R. B. Elton.

21st March 1955.

Dalitz, R. H., 1951, *Proc. Roy. Soc.* A, **206**, 509.
Elton, L. R. B., and Robertson, H. H., 1952, *Proc. Phys. Soc.* A, **65**, 145.
Schwinger, J., 1949, *Phys. Rev.*, **76**, 790.

Energy Loss Distribution for Minimum Ionizing Electrons in a Pressure Proportional Counter

The experiments described are an extension of work carried out by Rothwell (1951) and West (1953), who found that the energy loss distribution for relativistic electrons was broader than that predicted by Landau (1944) in a theoretical paper, and by Moyal (1955) in an extension of Landau's work. West found, also, that the distribution showed a tendency to become narrower as the pressure of the gas filling in his counter was increased, and it seemed probable that at still higher pressures Landau's value might be reached. Recent theoretical work by Hines, however, suggests that Landau's formula is incorrect, and that higher values of width are to be expected.

The proportional counter used was 7·2 cm effective diameter, fitted with windows of aluminium foil, 1·0 cm in diameter, and 0·004 in. thick. They were at opposite ends of a counter diameter, halfway along its length. The filling throughout the experiment was of argon plus a little methane, and energy calibrations were made with 59·8 kev γ-rays from ^{241}Am, and with 20 kev fluorescence x-rays from Pd excited with x-rays from ^{153}Gd.

Minimum ionizing electrons selected by a β-spectrometer were passed through the thin windows of the proportional counter, and then into an end-window Geiger counter. The pulse from the Geiger counter operated a gating unit which allowed the proportional counter pulse to pass to a pulse amplitude analyser.

Measurements were made of the most probable energy loss Δ_0, and of the width of the energy loss distributions for pressures of gas filling up to ten atmospheres total pressure. These results are given in the table. The distributions obtained were found to be broader than those obtained by West, in the region where they overlapped, but they showed the same tendency to become narrower with increasing pressure.

Filling					
Argon (atm)	CH$_4$ (cm)	Δ_0 Exp. (kev)	Δ_0 Exp./Δ_0 Landau	$\xi/\overline{I_0Z}$	% Width
9·98	6·0	144	1·14	37·2	35·5
7·94	6·0	108	1·09	30·1	36·7
5·93	6·0	77	1·06	22·8	40·1
3·86	2·4	45·1	1·00	14·5	44·1
2·83	1·8	30·6	0·94	10·7	48·7
1·83	1·2	17·4	0·86	6·9	55·3

In order to compare the results with those of other experimenters, the widths were plotted against $\xi/\overline{I_0Z}$. The mean ionization potential of electrons in an atom of atomic number Z is $\overline{I_0Z}$, and ξ is an energy chosen so that, on the average, only one collision transferring more energy than ξ occurs in the path length considered. Collisions transferring energy in the neighbourhood of ξ are mainly responsible for the spread in the distribution (Cranshaw 1952).

This resulted in the curve shown in the figure. The broken curve gives Landau's theoretical widths for argon, and it can be seen that, even at high pressures, the experimental curve gives considerably greater values of width.

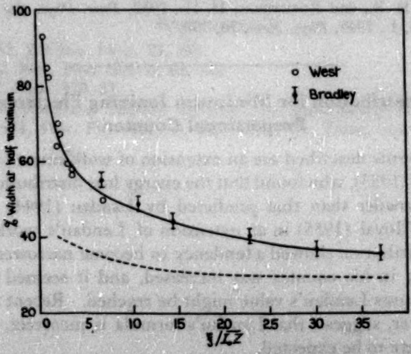

Since this work was completed, Palmatier *et al.* (1955) have published results on the Landau distribution for mesons using pressure proportional counters. The shape of their curve of distribution width against pressure is similar to that for electrons, but indicates broader widths. Hines' (1955 and private communication) theory, however, treats mesons and electrons independently, and he sees no reason to suppose that they lie on a common width–pressure curve.

The experimental values of most probable energy loss are given in the table. For values of ξ/I_0Z greater than 10, the experimental values of Δ_0 are substantially the same as Landau's values, but too much weight should not be put on the two highest points given, as the value of Δ_0 in these cases is considerably greater than the highest calibration energy available.

Thanks are due to Dr. P. E. Cavanagh, and Mr. J. F. Turner for the use of their β-spectrometer, and to Mr. D. West for his guidance during the experiment.

Atomic Energy Research Establishment,
Harwell, Berks.
28th March 1955.

E. F. BRADLEY.

CRANSHAW, T. E., 1952, *Progress in Nuclear Physics*, Vol. II (London : Pergamon Press).
HINES, K. C., 1955, *Phys. Rev.*, **97**, 1725.
LANDAU, L., 1944, *J. Phys., Moscow*, **8**, 201.
MOYAL, J. E., 1955, *Phil. Mag.*, **46**, 263.
PALMATIER, E. D., MEERS, J. T., and ASKEY, C. M., 1955, *Phys. Rev.*, **97**, 486.
ROTHWELL, P., 1951, *Proc. Phys. Soc.* B, **64**, 911.
WEST, D., 1953, *Proc. Phys. Soc.* A, **66**, 306.

CONTENTS OF SECTION B

PAGE

Dr. S. P. F. Humphreys-Owen. The Scattering of Light in Sodium Chloride Monocrystals 325

Miss B. I. H. Hall. Experimental Investigation of the Motions of Electrons in a Gas in the Presence of a Magnetic Field 334

Mr. J. H. Phillips, Dr. J. C. Woolley and Dr. R. Street. The Influence of Temperature on Magnetic Viscosity 345

Dr. H. K. Henisch and Dr. W. N. Reynolds. Surface Recombination in Germanium in the Presence of Strong Electric Fields 353

Dr. V. I. Little. The Dielectric Constant of Aqueous Ionic Solutions . . 357

Dr. P. T. Landsberg. The Effect of Field-Dependent Mobilities on the Diffusion Theory of Rectification 366

Dr. G. Francis. The Growth of an Electron Avalanche Retarded by its Own Space Charge 369

Research Notes :

Prof. L. G. H. Huxley and Mr. R. W. Crompton. A Note on the Diffusion in a Gas of Electrons from a Small Source 381

Dr. V. D. Farris. Diffusion in Moving Striations 383

Dr. D. H. Parkinson and Mrs. L. M. Roberts. A Resistance Thermometer for Use at Helium Temperatures 386

Dr. F. E. Hoare, Dr. J. C. Matthews and Mr. B. Yates. Carbon Resistor Thermometers 388

Letters to the Editor :

Dr. M. Smollett and Mr. R. G. Pratt. The Effect of Adsorbed Air on Photoconductive Layers of Lead Sulphide 390

Contents of Section A 392

The Radiative Capture of Alpha Particles in ^{14}N

By P. C. PRICE
Cavendish Laboratory, Cambridge

Communicated by E. S. Shire; MS. received 15*th December* 1954, *and in amended form* 1*st February* 1955

Abstract. The $^{14}N(\alpha, \gamma)^{18}F$ reaction has been examined from 1·2 to 2·2 MeV bombarding energy. Two narrow resonances have been found; their positions have been measured, and upper limits obtained for their total widths. The cascade schemes at each resonance have been partly elucidated, and the position of another level involved in these cascades has been measured. The partial radiation widths of these resonances have been determined, except for a statistical factor. Some of the angular distributions have been studied, and conclusions have been drawn about the possible values of the spins and parities of the levels concerned.

---

§ 1. INTRODUCTION

A KNOWLEDGE of the position and nature of the energy levels in ^{18}F has some theoretical value, because in the shell model some states of this nucleus are represented by a proton and a neutron in orbits outside a symmetrical ^{16}O ‘core’, and it would be useful to learn something about the interaction of these outer nucleons. Very little is known about the levels of this nucleus; nine excited states have been detected by Middleton and Tai (1951) by using the $^{20}Ne(d, \alpha)^{18}F$ reaction, but no spins or parities have been obtained. Even the spin of the ground state is not known, although the allowed nature of the beta-decay of ^{18}F indicates that it must be 0^+ or 1^+.

We can confidently predict that a further undiscovered level exists, the analogue of the ground states of ^{18}O and ^{18}Ne. By applying a correction to the difference in the mass defects of ^{18}O and ^{18}F, we deduce that this level should be found at $1{\cdot}1 \pm 0{\cdot}3$ MeV; this value is consistent with the recent measurement of the positron energy in the decay of ^{18}Ne (Gow and Alvarez 1954). This level is unlikely to be identical with any of those found by Middleton and Tai, because the appearance of such a level in their reaction is forbidden by the conservation of isotopic spin; this theoretical reason is supported by the fact that, in the similar reaction $^{16}O(d, \alpha)^{14}N$, no alpha-particle group is found corresponding to the level of isotopic spin unity at 2·31 MeV in ^{14}N (Van de Graaff *et al.* 1952).

The investigation of the $^{14}N(\alpha, \gamma)^{18}F$ reaction is one way of studying the lower levels of ^{18}F, which has not previously been undertaken. Section 2 contains a description of the apparatus and methods used, and §3 is an account of the experimental results. In §4 their interpretation is discussed.

§ 2. EXPERIMENTAL METHODS

The experiments were all performed with the Cavendish Electrostatic Generator, which produces a beam of singly charged helium ions. The gamma-rays were detected in a 1 in. cube NaI(Tl) crystal, suitably mounted on an

EMI 6262 photomultiplier tube. The output of this system was amplified in a commercial wide-band pulse amplifier, and fed into a Hutchinson–Scarrott pulse height analyser (Hutchinson and Scarrott 1951). The energy of the radiation was determined by comparison using five standard sources: annihilation radiation (0·511 MEV), ^{137}Cs (0·661 MEV), ^{65}Zn (1·12 MEV), ThC″ (2·61 MEV), and the ^{15}N (p, α, γ)^{12}C reaction (4·43 MEV).

The coincidence experiment described in the next section was performed by sending the output from another similar crystal and photomultiplier tube system into a single-channel pulse height analyser, which was designed to operate the permissive 'gate' incorporated in the Hutchinson–Scarrott instrument.

Three different kinds of nitrogen target were employed. Thick tantalum nitride targets were made by heating tantalum foil to 1300°C in an atmosphere of dry ammonia; this was made from ammonium nitrate in a way similar to that of Malm and Buechner (1950). Moderately thick magnesium nitride targets were made by heating to dull redness in dry ammonia a thin layer of magnesium that had been evaporated to the required thickness on a molybdenum backing. Very thin targets were made by using a tantalum foil as the cathode of a nitrogen discharge tube. All these targets gave satisfactory yields in the ^{15}N(p, α, γ)^{12}C reaction, but only the thick tantalum nitride targets were resistant to prolonged bombardment by intense beams.

§ 3. RESULTS

A thick target yield curve for quanta above 1 MEV obtained from the bombardment of tantalum nitride with alpha-particles was obtained from 1·2 to 2·2 MEV. Two steps in this yield curve were observed.

The identification of the reaction was effected by studying the residual radioactivity of the target. After the target had been bombarded for a few hours, the beam was shut off and a search for radiation made. A single line at 0·5 MEV was observed, and its intensity was found to decay with a half-life of 105 ± 5 minutes. The only light element that emits positrons with such a half-life is ^{18}F.

The yield curve was examined in detail near the two resonances, and their widths were found to be too small to be measurable. Upper limits were placed on these quantities. The absolute resonance energies were obtained by comparison with some narrow resonances in the reaction ^{27}Al(p, γ)^{28}Si (Brostrom *et al.* 1947).

Table 1 shows the energies and total widths of the ^{14}N(α, γ)^{18}F resonances.

Table 1

Bombarding energy (MEV)	1·530 ± 0·003	1·617 ± 0·003
Excitation energy (MEV)	5·600 ± 0·020	5·668 ± 0·020
Total width (kev)	<1·5	<1·0

The spectrum of the radiation at each resonance was determined by using the multi-channel pulse height analyser on three ranges of quantum energy, covering altogether the range from 0·5 to 6·0 MEV. The overlapping lines were separated by comparison with the spectra of the calibration lines given in the last section; the complex nature of the pulse-height spectrum produced by a single line near 2·5 MEV made the identification of all the lines in the spectrum very difficult, and the low intensity of the reaction did not permit the use of a crystal pair spectrometer. The spectrum analysis given in table 2 is consistent with all the results obtained, and these cannot be explained on any simpler system.

Table 2

5·60 MEV resonance		5·67 MEV resonance	
Line	Energy (MEV)	Line	Energy (MEV)
A	$5\cdot6\pm0\cdot1$		
B	$4\cdot52\pm0\cdot02$	B′	$4\cdot59\pm0\cdot03$
C	$3\cdot00\pm0\cdot05$	C′	$2\cdot9\pm0\cdot2$
D	$2\cdot55\pm0\cdot05$	D′	$2\cdot55\pm0\cdot05$
E	$2\cdot10\pm0\cdot10$	E′	$2\cdot05\pm0\cdot10$
F	$1\cdot075\pm0\cdot010$	F′	$1\cdot075\pm0\cdot010$
G	$0\cdot945\pm0\cdot010$		

The obvious interpretation of table 2 involves a level at 1·075 MEV excitation. A study was made of the pulse-height distribution of pulses from one crystal occurring in coincidence with pulses greater than various bias values received in the other. This experiment indicated that the line B is in coincidence with the line F, with a delay of less than 5 μsec. The number of coincidences received showed that an analysis of the whole cascade scheme by this method was impracticable because of the poor statistics that could be obtained in any reasonable observing time; the further study of the cascades was therefore abandoned.

The angular distributions of the lines A, B and B′ were studied and at the same time the intensities of all the lines, integrated over all directions, were obtained relative to the 90° yield of 4·43 MEV quanta from the ^{15}N(p, α, γ)^{12}C reaction. This yield has been determined with an accuracy to within about 20% by Schardt *et al.* (1952) and this gives the absolute values of the yields in the ^{14}N(α, γ)^{18}F reaction to the same degree of accuracy.

It can easily be shown that the total yield of a reaction of this kind at an isolated resonance is proportional to an effective radiation width Γ_R, given by $\Gamma_R=(2J+1)\Gamma_\alpha\Gamma_\gamma/\Gamma$ where J is the spin of the level, and Γ_α, Γ_γ, and Γ are the partial widths for alpha-particle emission and for the radiative transition considered, and the total width, respectively. Table 3 shows all the angular distributions and partial widths for the quanta identified as the first members of cascades; estimates are also given of the values of Γ_R for all the unanalysed transitions at each resonance.

Table 3

Line	Γ_R (ev)	Angular distribution
A	$0\cdot7\pm0\cdot2$	$1+(0\cdot20\pm0\cdot26)P_2(\cos\theta)+(0\cdot48\pm0\cdot28)P_4(\cos\theta)$
B	$2\cdot2\pm0\cdot4$	$1+(0\cdot38\pm0\cdot08)P_2(\cos\theta)-(0\cdot08\pm0\cdot08)P_4(\cos\theta)$
others	3 ± 1	
B′	$2\cdot2\pm0\cdot4$	$1+(0\cdot44\pm0\cdot04)P_2(\cos\theta)-(0\cdot03\pm0\cdot08)P_4(\cos\theta)$
others	2 ± 1	

No terms in $P_6(\cos\theta)$ were found to be statistically significant.

§ 4. INTERPRETATION

The cascade scheme is illustrated in the figure, which also displays the levels below 6 MEV excitation previously discovered. The 5·60 and 5·67 MEV levels can be identified with the level at $5\cdot61\pm0\cdot10$ MEV, and the 1·075 MEV level is probably identical with the $1\cdot05\pm0\cdot02$ MEV level of Middleton and Tai (1951).

It is not possible to compare the partial widths with theory unless the spins and parities of the levels are known. It is not possible to derive unique values of these from the present results, but a good deal of information about them can be obtained. Apart from the angular distributions, there are three considerations limiting the possible values of some of the spins and parities:

(i) It may be assumed that no transitions can occur with a partial width greater than one hundred times the value predicted by the formulae of Blatt and Weisskopf (1952). This assumption is supported by the survey of available experimental evidence given by those authors. The lines A, B and B′ cannot then be of higher multipolarity than dipole or electric quadrupole, and so the spin of the 5·60 Mev level cannot be greater than 2^- or 3^+.

(ii) On the same assumption, the line F cannot be of higher multipolarity than octupole, because its lifetime is less than 5 μsec. Hence the spin of the 1·075 Mev level cannot exceed 4.

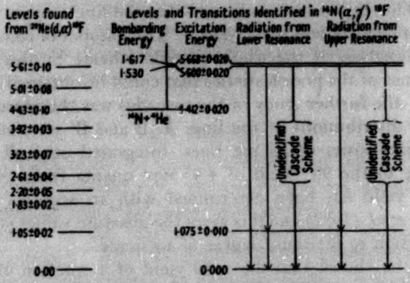
Levels found from ^{20}Ne(d,α)^{18}F
Levels and Transitions Identified in ^{14}N(α,γ) ^{18}F
Bombarding Energy
Excitation Energy
Radiation from Lower Resonance
Radiation from Upper Resonance
5·61±0·10
5·01±0·08
4·43±0·10
3·92±0·03
3·23±0·07
2·61±0·04
2·20±0·05
1·83±0·02
1·05±0·02
0·00
1·617
1·530
5·668±0·020
5·600±0·020
4·412±0·020
^{14}N+^{4}He
Unidentified Cascade Scheme
Unidentified Cascade Scheme
1·075±0·010
0·000

Energy levels below 6 Mev in ^{18}F. (All energies are in Mev.)

(iii) If it is assumed that the reduced alpha-particle width cannot exceed five times the ‘Wigner limit’, it is possible to show by calculating the penetrabilities from the tables of Bloch *et al.* (1951) that the angular momentum of the incoming alpha-particles cannot be greater than 4 at either resonance. Therefore the spin of the 5·67 Mev level does not exceed 4^- or 5^+.

In order to obtain as much information as possible about the spins and parities of the levels from the angular distributions, theoretical distributions were computed for all the possible values of the spins, using the methods and tables of Biedenharn and Rose (1953); as a check, they were also calculated from the tables of Sharp *et al.* (1953). In many cases the theoretical angular distributions were rendered ambiguous by one of two factors: the mixing of two possible incoming alpha-particle momenta and the mixing of different multipole transitions. It was assumed that the latter would not be present except in the case of dipole and quadrupole transitions.

It is possible to predict rough values for the intensity ratios, both of the competing alpha-particle waves and of the multipole orders. In the first case the estimate is derived from the computed penetrabilities, and in the second from the formulae of Blatt and Weisskopf. In many cases the experimental and theoretical distributions could be reconciled only by adopting improbable values of these mixing ratios. In compiling table 4 improbable mixing ratios were taken to be: a ratio of the intensities of two alpha-particle partial waves differing from the penetrability ratio by more than a factor of 5, and a quadrupole : dipole intensity ratio exceeding that given by the formulae of Blatt and Weisskopf by more than a factor of 10.

It was found by comparing all these theoretical and experimental distributions at the 1% level of significance, that isotropic distributions could definitely be excluded. Therefore neither of the upper two levels could have zero spin. The remaining possible assignments of spins and parities are represented by the intersections of rows and columns in table 4; at each intersection a letter is placed indicating the degree of agreement between the observed and the theoretical angular distributions. The letter A denotes agreement, B indicates agreement if improbable values (in the sense explained above) are adopted for the mixing ratios, and C indicates definite disagreement. An asterisk added to a letter denotes that that assignment involves pure electric quadrupole radiation, which on the assumption of the Blatt and Weisskopf formulae would be about thirty times too weak. This factor is too small to justify the exclusion of these assignments from possible consideration; transitions greater than quadrupole can definitely be so excluded, and are 'boxed off' in table 4. The table contains no reference to line A, as the accuracy of this angular distribution was insufficient to exclude any of the assignments consistent with the previous considerations.

Table 4

Properties of upper levels	Level	5·60 mev					5·67 mev								
Spin of 1·075 mev level	Spin	1	1	2	2	3	1	1	2	2	3	3	4	4	5
	Parity	+	−	+	−	+	+	−	+	−	+	−	+	−	+
0		A	A	C*	A*		C	A	C*	A*					
1		A	B	B	B	A*	A	B	B	B	A*	A*			
2		B	A	A	A	B	C	B	A	A	B	B	A*	A*	
3		C*	C*	B	B	A	C*	C*	C	B	A	A	B	B	A*
4				C*	C*	B			C*	C*	B	B	A	A	B

There is one further consideration. It is improbable that either of the upper levels is 1^-, because we know that a low-lying 0^+ level exists with unit isotopic spin. It is likely that any 1^- level would decay radiatively exclusively to this level, and with a partial width near the value predicted by Blatt and Weisskopf (1952) for electric dipole radiation; this does not occur, which suggests that neither of the upper levels can be 1^-.

The object of table 4 is to enable exact assignments of spins and parities to be made when further information becomes available.

ACKNOWLEDGMENTS

The writer is obliged to Mr. E. S. Shire for suggesting the study of the radiative capture of alpha particles, and for his constant advice and encouragement. He is also grateful to Mr. H. R. McK. Hyder for his work on the maintenance and improvement of the Electrostatic Generator. He wishes to express his thanks to Trinity College, Cambridge, for a Senior Scholarship and to the Department of Scientific and Industrial Research for a maintenance grant.

REFERENCES

BIEDENHARN, L. C., and ROSE, M. E., 1953, *Rev. Mod. Phys.*, **25,** 729.

BLATT, J. M., and WEISSKOPF, V. F., 1952, *Theoretical Nuclear Physics* (New York: Wiley).

BLOCH, I., HULL, M. M., Jr., BROYLES, A. A., BOURICIUS, W. G., FREEMAN, B. E., and BREIT, G., 1951, *Rev. Mod. Phys.*, **23,** 147.

BROSTROM, K. J., HUUS, T., and TANGEN, R., 1947, *Phys. Rev.*, **75,** 1953.

GOW, J. D., and ALVAREZ, L. W., 1954, *Phys. Rev.*, **94,** 365.

HUTCHINSON, G. W., and SCARROTT, G. G., 1951, *Phil. Mag.*, **42,** 792.

MALM, R., and BUECHNER, W. W., 1950, *Phys. Rev.*, **80,** 771.

MIDDLETON, R., and TAI, C. T., 1951, *Proc. Phys. Soc.* A, **64,** 801.

SCHARDT, A., FOWLER, W. A., and LAURITSEN, C. C., 1952, *Phys. Rev.*, **86,** 527.

SHARP, W. T., KENNEDY, J. M., SEARS, B. J., and HOYLE, M. G., 1953, *Atomic Energy of Canada Ltd.*, Report CRT-556.

VAN DE GRAAFF, R. J., SPERDUTO, A., BUECHNER, W. W., and ENGE, H. A., 1952, *Phys. Rev.*, **86,** 966.

On the Scattering of High Energy Electrons

By G. N. FOWLER
University of Manchester

Communicated by L. Rosenfeld; *MS. received 20th December* 1954

Abstract. The effect of the finite nuclear size on the scattering of high energy electrons depends upon the ratio of the small to the large radial Dirac function inside the nuclear charge distribution. An approximate expression for this ratio is given, valid for energies of the order of 150 Mev. The result is used to discuss the model independence of the scattering for the case of uniform and shell charge distributions.

---

§ 1. Introduction

The scattering of electrons of energies larger than about 5 Mev deviates from that to be expected when the nucleus is considered as a point charge. In fact, provided that the energy of the incident particle is not so large that its de Broglie wavelength becomes comparable with the internucleon separation, the nuclear protons may be treated as a smoothed out charge distribution giving rise to a potential in which the electron moves. Furthermore, it has been shown by several authors, for example, Feshbach (1951) and Bodmer (1953), that for energies equal to or less than 20 Mev the corrections to the pure Coulomb phase shifts are related to the fourth and higher even moments over this nuclear charge distribution. In particular the corrections to the s and p phase shifts determine the fourth and sixth moments for these engeries.

In the present paper we consider the information to be obtained from the corrections to the s and p phase shifts at higher energies. The results are most easily expressible in terms of the potential distribution within the nucleus and an approximate expression is obtained, valid for energies less than about 150 Mev, for the integral over the potential distribution, which replaces the appropriate moment of the low energy case. The value of this average can then be used to determine another parameter of the charge distribution.

In addition, the model independence of the scattering at high energies is discussed.

§ 2. Calculation of the Phase Shift Corrections

The corrections to the Coulomb phase shifts produced by the finite nuclear size are given by

$$\tan \delta_k = \frac{X_k \sin(\eta^{c}_{k,\mathrm{I}} - \eta^{c}_{k,\mathrm{R}})}{X_k \cos(\eta^{c}_{k,\mathrm{I}} - \eta^{c}_{k,\mathrm{R}}) - 1}$$

where

$$X_k = \frac{K_k(r_1) g^{c}_{k,\mathrm{R}}(r_1) - f^{c}_{k,\mathrm{R}}(r_1)}{f^{c}_{k,\mathrm{I}}(r_1) - K_k(r_1) g^{c}_{k,\mathrm{I}}(r_1)}$$

and

$$K_k = f_k(r_1)/g_k(r_1)$$

with

$$k = \mp(j + \tfrac{1}{2}) \text{ for } j = l \pm \tfrac{1}{2}.$$

In these formulae the index c refers to quantities calculated for the case of the nucleus considered as a point and the functions f_k and g_k are the small and large components of the radial Dirac functions corresponding to the interior of the nucleus. The suffixes R, I refer to regular and irregular solutions of the radial Dirac equation in the case of the point nucleus. The point r_1 at which the various functions are evaluated is chosen to be sufficiently far out for the potential to be Coulomb, i.e. for ρ, the charge density of the nucleus, to be zero. It will be seen that the corrections to the phase shifts produced by the finite nuclear size depend on the nuclear charge distribution only through the K_k.

§ 3. CALCULATION OF K_k

In units such that $\hbar = m_e = c = 1$, the equation satisfied by K_k is

$$\frac{dK_k}{dr} = \frac{2kK_k}{r} - \{E+1-U(r)\}K_k^2 - \{E-1-U(r)\}. \qquad \ldots\ldots(1)$$

In the extreme relativistic case, $E \gg 1$, this becomes

$$\frac{dK_k}{dr} = \frac{2kK_k}{r} - \{E-U(r)\}(1+K_k^2). \qquad \ldots\ldots(2)$$

Bodmer's method of treating (1) is to use r^{-2k} as an integrating factor and thus to convert (1) into the following integral equation for $K_k(r)$:

$$K_k(r) = r^{2k}\int_0^r [U(r')-E+1+\{U(r')-E-1\}K_k^2]r'^{-2k}dr'. \qquad \ldots\ldots(3)$$

This is solved by successive iteration starting with $K_k = 0$. However, the function K_k has simple poles (Rose and Newton 1951) at the zeros of the large component g_k so that this method is only satisfactory when the range of integration in (3) does not approach a pole of K_k. At high energies, however, we must expect that the range of r comprised by $0 \leqslant r \leqslant r_1$ does include such a singularity, so that for high energies we must look for a different method of solving (2).

To do this we introduce the phase ϕ of the Dirac functions by the substitution (cf. Brait and Brown 1949, Rose and Newton 1951) $K_k = \tan\phi_k$. One finds the following equation for ϕ at high energies, with $k \to -k$,

$$\frac{d\phi_k}{dr} = -\frac{k}{r}\sin 2\phi_k - (E-U) \qquad \ldots\ldots(4)$$

with the boundary condition

$$\phi_k = \frac{\{U(0)-E\}}{2k+1}\,r \text{ for } |r| \ll 1. \qquad \ldots\ldots(4')$$

It should be noted that ϕ_k will have no singular points in a finite range of r since this would lead to an essential singularity in the solution of the Dirac equation at a finite point.

One recovers Bodmer's first iteration on putting $|\phi_k| \ll 1$. In this case it will be seen that, to be accurate, the energy should be restricted by the condition $Er_{\max}/(2k+1) \ll 1$ which is not very well satisfied for $E \gtrsim 50$ MEV, unless k be large.

A more accurate approximate result may be found in the following way. With

$$\phi_k = \phi_k^0 + \phi_k^1,$$

where ϕ_k^0 satisfies (4) and (4′) with $U=0$ and ϕ_k^1 is assumed to be small, we find for the equation satisfied by ϕ_k^1

$$\frac{d\phi_k^1}{dr} = -\frac{2k\phi_k^1\cos 2\phi_k^0}{r} + U(r) \qquad \ldots\ldots(5)$$

with ϕ_k^1 satisfying the boundary condition

$$\phi_k^1 = \frac{U(0)r}{2k+1} \text{ for } |r| \ll 1. \qquad \ldots\ldots(5')$$

ϕ_k^0 is given by

$$\phi_k^0 = -\tan^{-1}\{J_{k+1/2}(Er)/J_{k-1/2}(Er)\}. \qquad \ldots\ldots(6)$$

Equation (5) then becomes

$$\frac{d\phi_k^1}{dr} = -\frac{2k\phi_k^1}{r}\left[1-\frac{2}{1+\{J_{k-1/2}(Er)/J_{k+1/2}(Er)\}^2}\right]. \qquad \ldots\ldots(7)$$

The ratio of Bessel functions occurring in (7) is given in terms of a continued fraction (Courant and Hilbert 1931, p. 423):

$$\frac{J_{k-1/2}(Er)}{J_{k+1/2}(Er)} = \frac{2k+1}{Er} - \cfrac{1}{\cfrac{2k+3}{Er} - \cfrac{1}{(2k+5)/Er}}. \qquad \ldots\ldots(7')$$

This form permits the values of the function to be bracketed rather closely, but for reasons of simplicity we will use only the first approximation.

The integrating factor of (5) then becomes

$$\exp\left[\int\frac{2k}{r}\left\{1-\frac{2E^2r^2}{E^2r^2+(2k+1)^2}\right\}dr\right] = \left\{\frac{r}{(Er)^2+(2k+1)^2}\right\}^{2k}. \qquad \ldots\ldots(8)$$

The solution of (4) which satisfies the boundary condition (4′) is then

$$\phi_k^0(r)+\phi_k^1(r) = \left\{\frac{(Er)^2+(2k+1)^2}{r}\right\}^{2k}\int_0^r U(r')\left\{\frac{r'}{(Er)^2+(2k+1)^2}\right\}^{2k}dr'$$
$$-\tan^{-1}\{J_{k+1/2}(Er)/J_{k-1/2}(Er)\}. \qquad \ldots\ldots(9)$$

When $Er \ll 2k+1$ we recover the first iteration solution of equation (2).

In deriving this result we have made two approximations: (i) The result (9) is essentially an approximation to the Taylor expansion of ϕ_k with respect to $U(r)$. Thus it will be most accurate when the term depending on U is small compared with the term independent of U. (ii) We have taken the first term only in (7′).

The approximation (ii) is obviously very poor for r such that $Er \gg 2k+1$. For such values of r we will use the asymptotic expressions for the Bessel functions so that

$$\phi_k^0(Er) \sim \pm\tan^{-1}(\cot Er) = \mp Er - \pi/2, \qquad k \text{ odd},$$

or

$$\phi_k^0(Er) \sim \pm\tan^{-1}(\tan Er) = \pm Er, \qquad k \text{ even}. \qquad \ldots\ldots(10)$$

Substituting this in (5) gives

$$\left.\begin{aligned}\frac{d\phi_k^1}{dr} &= \frac{2k\phi_k^1\cos 2Er}{r}+U, \qquad k \text{ odd},\\ &= -\frac{2k\phi_k^1\cos 2Er}{r}+U, \qquad k \text{ even}.\end{aligned}\right\} \qquad \ldots\ldots(5'')$$

The integrating factor then becomes

$$\exp\left\{\pm 2k\int^{r}\cos(2Er')/r'\,dr'\right\} \qquad \ldots\ldots(8')$$

in the two cases.

With r greater than zero and at high energies the integral in (8′) is small, as a result of the oscillation of the integrand, so that we find, under these conditions

$$\phi_k^{1}\sim\int_a^r U(r')\,dr' \qquad \ldots\ldots(11)$$

where a is chosen so that (10) is valid for $r\geqslant a$.

The solution of (4) satisfying the boundary condition (4′) is then found by smoothly joining the solution (9) to the solution (11) at the point a. In the following we put $a=2k/E$. Then the approximate solution of (4) is given by (9) for $Er\leqslant 2k$ and by

$$\phi_k(r)=-\tan^{-1}\{J_{k+1/2}(Er)/J_{k-1/2}(Er)\}$$

$$+\left\{\frac{4k^2+(2k+1)^2}{2k/E}\right\}^{2k}\int_0^{2k/E}U(r')\left\{\frac{r'}{(Er')^2+(2k+1)^2}\right\}^{2k}dr'+\int_{2k/E}^{r}U(r')\,dr' \qquad \ldots\ldots(12)$$

for $Er>2k$.

Thus the potential dependence of the result may be written

$$\phi_k^{1}(r_1)\sim\int_0^{r_1}U(r')\left\{\frac{r'}{(Er')^2+(2k+1)^2}\right\}^{2k}dr'$$

for $Er_1\leqslant 2k$

or $$\phi_k^{1}(r_1)\sim\int_0^{2k/E}U(r')\left\{\frac{r'}{(Er')^2+(2k+1)^2}\right\}^{2k}dr'+\int_{2k/E}^{r_1}U(r')\,dr'$$

for $Er_1>2k$.

These are to be compared with the result

$$\phi_k^{1}(r_1)\sim\int_0^{r_1}U(r')r'^{2k}\,dr'$$

valid for $Er_1\ll 2k+1$.

One may say, therefore, that at the highest energies for which the present treatment is applicable, say 150 MEV, one gains relatively little new information from the phase shifts with $k\ll 2$.

§ 4. COMPARISON WITH THE EXACT SOLUTION

The accuracy of this solution may be tested by comparing it with the exact solution for the case $U=\text{const}=-a/R$. In this case we have, for $k=1$,

$$K_1(R)=\tan\phi_1(R)=-\frac{1}{a+ER}+\cot(a+ER). \qquad \ldots\ldots(13)$$

The comparison is shown in figure 1 for the case of lead with the radius given by $r_1=R=1{\cdot}0\times 10^{-13}A^{1/3}$ cm. Also shown is the result found from Bodmer's second iteration.

It will be seen that the agreement between (12) and the exact solution is reasonable up to 150 MEV, except near a singularity of K.

It may be shown (Bodmer 1953) that the second iteration is good enough to compare different charge distributions up to 50 Mev; we may therefore conclude that the present approximate solution (9) or (12) enables a comparison to be made up to energies of the order of 150 Mev. In addition the accuracy is such that the approximate solution is probably accurate enough for use in the calculation of the phase shift corrections themselves for lighter nuclei and higher angular momenta up to energies of the order of 100 Mev.

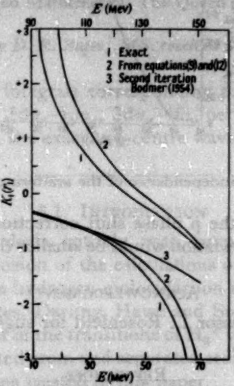

Figure 1. Exact value of $K_1(r_1)$ compared with various approximations.

§ 5. Model Independence of the Scattering

At a given energy the δ_k may be made model independent by a suitable choice of the radii of the different models. This choice will, in general, depend on the energy and to obtain model independence over an energy range we must require δ_k and $\partial\delta_k/\partial E$ to be model independent separately. It has been shown by Feshbach (1951) that, when only the s phase shift correction is important, i.e. for $E \leqslant 20$ Mev, the uniform and the shell nuclear charge distributions give the same scattering when the radii of the distributions are in the ratio $r_s/r_u = 0{\cdot}77$.

For energies in the range 20 to 40 Mev, Elton (1953) has shown that the scattering is not quite model independent, since, for such energies, the s and p phase shift corrections are model independent separately at $r_s/r_u = 0{\cdot}75$ and $r_s/r_u = 0{\cdot}81$ respectively.

For energies larger than 40 Mev we may investigate the model independence of the scattering for the shell and uniform models using equation (12).

The difference in phase shift corrections will depend on the difference in the ϕ_k' for the different models. We have assumed an energy such that the s, p and d phase shift corrections are important and we have fixed the ratio r_s/r_u by the requirement that the d phase shift correction should be model independent.

Now for large k it will be seen that the solution (12) reduces to the first iteration (or low energy) solution obtained by Bodmer, even for energies as high as 100 Mev. Thus we may take $r_s/r_u = 0{\cdot}83$ which gives model independence of the d phase shift correction at low energies.

With this choice of r_s/r_u we have calculated $(\phi_1^{1u}-\phi_1^{1s})/\phi_1^{1s}$. The result is shown in figure 2. It will be seen that the deviation from model independence is pronounced for energies greater than 50 MeV and that beyond 100 MeV the tendency is towards model independence, as one would expect from the result of § 3.

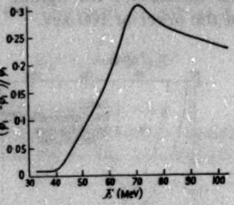

Figure 2. Model independence of the scattering, $40 \leqslant E \leqslant 100$ MeV.

On would expect that the p phase shift correction would also not be model independent but that the deviation would be smaller than that for the s correction.

ACKNOWLEDGMENT

I am indebted to Professor L. Rosenfeld for suggesting this problem to me and for helpful discussions.

REFERENCES

BODMER, A. R., 1953, *Proc. Phys. Soc.* A, **66**, 1041.
BRAIT, G., and BROWN, G. E., 1949, *Phys. Rev.*, **76**, 1307.
COURANT, R., and HILBERT, D., 1931, *Methoden der mathematikalischen Physik* (Berlin: Springer).
ELTON, L. R. B., 1953, *Proc. Phys. Soc.* A, **66**, 806.
FESHBACH, H., 1951, *Phys. Rev.*, **84**, 1206.
HOFSTADTER, R., FECHTER, H. R., and MCINTYRE, J. A., 1953, *Phys. Rev.*, **92**, 978.
ROSE, M. E., and NEWTON, K. R., 1951, *Phys. Rev.*, **82**, 470.
YENNIE, D. R., WILSON, R. N., and RAVENHALL, D. G., 1953, *Phys. Rev.*, **92**, 1325.

Properties of the Hydrogen Molecular Ion
V: Transitions Connecting the Lowest Even and Lowest Odd π-States with Higher σ-States

By J. T. LEWIS, M. R. C. McDOWELL and B. L. MOISEIWITSCH
Department of Applied Mathematics, The Queen's University of Belfast

Communicated by D. R. Bates; MS. received 13*th January* 1955

Abstract. The transition integrals corresponding to the $2p\pi_u-2s\sigma_g$, $2p\pi_u-3s\sigma_g$, $2p\pi_u-3d\sigma_g$ and $3d\pi_g-3p\sigma_u$, $3d\pi_g-4p\sigma_u$, $3d\pi_g-4f\sigma_u$ perpendicular type transitions of H_2^+ are computed from the exact two-centre wave functions.

---

§ 1. INTRODUCTION

THIS paper, which deals entirely with perpendicular type transitions, represents the conclusion of the calculations on the oscillator strengths of the transitions of the hydrogen molecular ion using exact two-centre wave functions (Bates 1951, Bates, Darling, Hawe and Stewart 1953, 1954).

In table 1 is shown a list of the transitions of H_2^+ which have been investigated previously both in the united atom and separated atoms notation, while in table 2 are displayed the transitions treated in this paper.

Table 1. Transitions of H_2^+ investigated earlier

	United atom notation	Separated atoms notation
S	$1s\sigma_g-2p\sigma_u$	$\sigma(1s)-\sigma^*(1s)$
X	$1s\sigma_g-3p\sigma_u$	$\sigma(1s)-\sigma^*(2s, 2p_z)$
X	$1s\sigma_g-4p\sigma_u$	$\sigma(1s)-\sigma^*(3s, 3p_z, 3d_z)$
	$1s\sigma_g-4f\sigma_u$	$\sigma(1s)-\sigma^*(2s, 2p_z)$
S	$1s\sigma_g-2p\pi_u$	$\sigma(1s)-\pi(2p_x)$
	$2p\sigma_u-2s\sigma_g$	$\sigma^*(1s)-\sigma(2s, 2p_z)$
X	$2p\sigma_u-3s\sigma_g$	$\sigma^*(1s)-\sigma(3s, 3p_z, 3d_z)$
	$2p\sigma_u-3d\sigma_g$	$\sigma^*(1s)-\sigma(2s, 2p_z)$
S	$2p\sigma_u-3d\pi_g$	$\sigma^*(1s)-\pi^*(2p_x)$
S	$2p\pi_u-3d\pi_g$	$\pi(2p_x)-\pi^*(2p_x)$

Table 2. Transitions of H_2^+ investigated in this paper

	United atom notation	Separated atoms notation
	$2p\pi_u-2s\sigma_g$	$\pi(2p_x)-\sigma(2s, 2p_z)$
X	$2p\pi_u-3s\sigma_g$	$\pi(2p_x)-\sigma(3s, 3p_z, 3d_z)$
	$2p\pi_u-3d\sigma_g$	$\pi(2p_x)-\sigma(2s, 2p_z)$
	$3d\pi_g-3p\sigma_u$	$\pi^*(2p_x)-\sigma^*(2s, 2p_z)$
	$3d\pi_g-4p\sigma_u$	$\pi^*(2p_x)-\sigma^*(3s, 3p_z, 3d_z)$
	$3d\pi_g-4f\sigma_u$	$\pi^*(2p_x)-\sigma^*(2s, 2p_z)$

The symbols within the brackets represent the atomic orbitals. Odd (u) σ-states are marked with an asterisk while even (g) σ-states are unmarked. The reverse is done for the π-states.

The transitions designated with an X have transition integrals which pass through zero. Of the others those designated with an S have transition integrals which cannot change sign for, as symmetry considerations show, cancellation effects are completely absent.

§ 2. CALCULATIONS

If the nuclei are regarded as stationary at a distance R apart, the oscillator strength corresponding to the transition between a lower state A and an upper state B is given by

$$f(\mathrm{A}-\mathrm{B}\,|\,R)=\tfrac{1}{3}E(\mathrm{A}-\mathrm{B}\,|\,R)G(\mathrm{A}-\mathrm{B})\,|\,Q(\mathrm{A}-\mathrm{B}\,|\,R)\,|^2 \qquad \ldots\ldots(1)$$

where $E(\mathrm{A}-\mathrm{B}\,|\,R)$ is the vertical energy difference in rydbergs, $G(\mathrm{A}-\mathrm{B})$ is the orbital degeneracy factor and $Q(\mathrm{A}-\mathrm{B}\,|\,R)$ is the dipole length transition integral expressed in atomic units (Mulliken 1939). This transition integral is given by

$$Q(\mathrm{A}-\mathrm{B}\,|\,R)\mathbf{t}=\int \mathrm{X}_\mathrm{B}^*(\mathbf{r}\,|\,R)\mathbf{r}\mathrm{X}_\mathrm{A}(\mathbf{r}\,|\,R)\,d\mathbf{r} \qquad \ldots\ldots(2)$$

in which $\mathbf{t}$ is some unit vector, $\mathbf{r}$ is the position vector of the electron and X_A and X_B are the electronic wave functions of the states concerned.

In the case of the hydrogen molecular ion the wave functions can be written in the form

$$\mathrm{X}(\mathbf{r}\,|\,R)=\Lambda(\lambda\,|\,R)\mathrm{M}(\mu\,|\,R)\Phi(\phi) \qquad \ldots\ldots(3)$$

where λ and μ are the usual confocal elliptic coordinates and ϕ is the azimuthal angle. Λ and M can be obtained from the tables given by Bates, Ledsham and Stewart (1953) while Φ is merely unity for σ-states, and $\cos\phi$ or $\sin\phi$ for π-states.

For π–σ transitions equation (2) reduces to

$$Q(\mathrm{A}-\mathrm{B}\,|\,R)=\pi(R/2)^4\left[\int_1^\infty \lambda^2(\lambda^2-1)^{1/2}\Lambda_\mathrm{A}\Lambda_\mathrm{B}\,d\lambda\int_{-1}^1(1-\mu^2)^{1/2}\mathrm{M}_\mathrm{A}\mathrm{M}_\mathrm{B}\,d\mu - \int_1^\infty(\lambda^2-1)^{1/2}\Lambda_\mathrm{A}\Lambda_\mathrm{B}\,d\lambda\int_{-1}^1\mu^2(1-\mu^2)^{1/2}\mathrm{M}_\mathrm{A}\mathrm{M}_\mathrm{B}\,d\mu\right] \qquad \ldots\ldots(4)$$

the normalization being such that

$$(R/2)^3\int_1^\infty\int_{-1}^1\int_0^{2\pi}\Lambda^2\mathrm{M}^2\Phi^2(\lambda^2-\mu^2)\,d\lambda\,d\mu\,d\phi=1. \qquad \ldots\ldots(5)$$

The μ integrations can be done analytically but the λ integrations must be done numerically.

§ 3. DISCUSSION OF THE RESULTS

In figures 1 and 2 are illustrated the transition integrals Q as functions of the internuclear distance R for the six π–σ transitions treated in the present paper. The corresponding oscillator strengths are of less interest than the transition integrals and have not been displayed since they can be immediately obtained from them by using equation (1) and the exact total energies given by Bates, Ledsham and Stewart (1953).

Treated exactly in this paper are the four transitions

$$2\mathrm{p}\pi_\mathrm{u}\text{–}2\mathrm{s}\sigma_\mathrm{g},\qquad 2\mathrm{p}\pi_\mathrm{u}\text{–}3\mathrm{d}\sigma_\mathrm{g},\qquad 3\mathrm{d}\pi_\mathrm{g}\text{–}3\mathrm{p}\sigma_\mathrm{u},\qquad 3\mathrm{d}\pi_\mathrm{g}\text{–}4\mathrm{f}\sigma_\mathrm{u}$$

which are characterized by the fact that on dissociation the upper state in each case has the same principal quantum number as the lower state. In the limit of large internuclear separation all the above transitions are allowed due to the mixing of the 2s and $2\mathrm{p}_z$ states of hydrogen (cf. table 2) and so none of these transitions belongs to the *sub-Rydberg* type (Herzberg 1950) as one might have supposed at first sight. It can be seen by reference to figures 1 and 2 that the four transitions mentioned above have absolute intensities which are rather large in contrast to sub-Rydberg transitions (not of the charge-transfer type) whose intensities are generally quite small.

The calculation of the relative intensities in band systems depends essentially on a knowledge of the behaviour of the transition integrals. It is often assumed in such calculations that Q is a slowly varying function of the internuclear distance R. However, as was noted in a preceding paper (Bates *et al.* 1954), for certain cases the fractional change in Q can be very large. Thus, for the $2p\pi_u$–$3s\sigma_g$ transition, Q changes sign at an intermediate value of R. All the transitions which have been investigated so far for which Q passes through zero are marked with an X in tables 1 and 2. From an inspection of these tables it is evident that the wave function of the upper state in each of these cases has at least one radial node (none of the wave functions of the lower states involved in any of the transitions have radial nodes). Of the remaining transitions those marked with an S have transition integrals which cannot pass through zero due to the symmetrical arrangement of the nodes. If we exclude these, as large a fraction as one third of the transitions so far considered have transition integrals which change sign at some intermediate value of the internuclear separation. For more complex systems than the hydrogen molecular ion this fraction may be even greater as the states of interest will tend to have wave functions with several nodes.

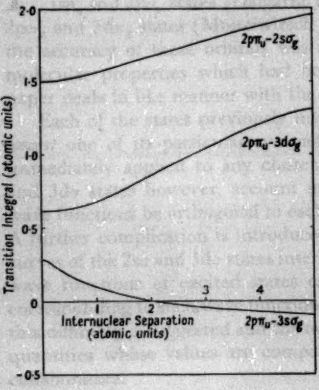

Figure 1. $2p\pi_u$–$2s\sigma_g$, $2p\pi_u$–$3s\sigma_g$, $2p\pi_u$–$3d\sigma_g$ transition integrals calculated from the exact wave functions.

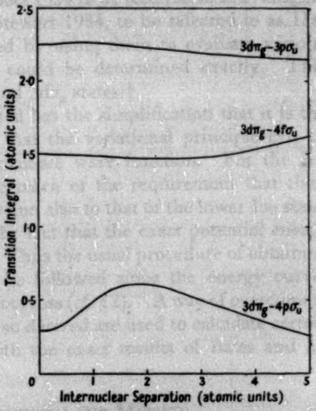

Figure 2. $3d\pi_g$–$3p\sigma_u$, $3d\pi_g$–$4p\sigma_u$, $3d\pi_g$–$4f\sigma_u$ transition integrals calculated from the exact wave functions.

The LCAO approximation has not been used in this paper as a study of the results obtained with it in the previous papers of this series indicates that it is not reliable. In general, it not only does not give the correct absolute values for the transition integrals but it also fails to give the correct slope as has been assumed by some authors. Furthermore, there seems to be no justification for the supposition that as one progresses to heavier molecules the position with regard to the LCAO approximation improves.

ACKNOWLEDGMENTS

We are greatly indebted to Professor D. R. Bates for suggesting this problem and for useful discussions.

One of us (J. T. L.) wishes to thank the Ministry of Education of Northern Ireland for the award of a maintenance grant.

REFERENCES

BATES, D. R., 1951, *J. Chem. Phys.*, **19**, 1122.

BATES, D. R., DARLING, R. T. S., HAWE, S. C., and STEWART, A. L., 1953, *Proc. Phys. Soc.* A, **66**, 1124; 1954, *Ibid.*, **67**, 533.

BATES, D. R., LEDSHAM, K., and STEWART, A. L., 1953, *Phil. Trans. Roy. Soc.* A, **246**, 215.

HERZBERG, G., 1950, *Spectra of Diatomic Molecules*, 2nd Edn (London : Macmillan).

MULLIKAN, R. S., 1939, *J. Chem. Phys.*, **7**, 14, 20.

Approximate Molecular Orbitals—III: The $2s\sigma_g$ and $3d\sigma_g$ states of H_2^+

By T. R. CARSON and A. DALGARNO
Department of Applied Mathematics, Queen's University of Belfast

Communicated by D. R. Bates; MS. received 7th December 1954, *and in final form* 31*st January* 1955

Abstract. A modified variational method is used to obtain approximate wave functions for the $2s\sigma_g$ and $3d\sigma_g$ states of H_2^+. Their accuracy is assessed by comparing various quantities computed using them with the exact values of these quantities. The dependence of the kinetic and potential energies on the nuclear separation is briefly discussed.

§ 1. Introduction

Previous papers of this series have used the Rayleigh–Ritz variational principle to determine approximate molecular orbitals of H_2^+ for the $1s\sigma_g$ and $2p\sigma_u$ states (Dalgarno and Poots 1954 to be referred to as I) and the $2p\pi_u$ and $3d\pi_g$ states (Moiseiwitsch and Stewart 1954, to be referred to as II); the accuracy of these orbitals was assessed by using them to evaluate various molecular properties which had been or could be determined exactly. This paper deals in like manner with the $2s\sigma_g$ and $3d\sigma_g$ states.†

Each of the states previously investigated has the simplification that it is the *lowest* one of its particular symmetry so that the variational principle can be immediately applied to any chosen approximate wave function. For the $2s\sigma$ and $3d\sigma$ states however, account must be taken of the requirement that their wave functions be orthogonal to each other and also to that of the lower $1s\sigma$ state. A further complication is introduced by the fact that the exact potential energy curves of the $2s\sigma$ and $3d\sigma$ states intersect. Thus the usual procedure of obtaining wave functions of excited states cannot be followed since the energy curves corresponding to such wave functions cannot cross (cf. § 2). A way of overcoming this difficulty is suggested and the orbitals so derived are used to calculate certain quantities whose values are compared with the exact results of Bates and his collaborators.

§ 2. Choice of Wave Functions and Method

Apart from some essentially qualitative considerations of Morse and Stueckelberg (1929), Lennard-Jones (1929) and Gilbert (1933), little attention has been paid to the problem of obtaining approximate wave functions for the excited states of H_2^+. In the case of the $2s\sigma$ and $3d\sigma$ states, the only quantitative calculations appear to be those of Pritchard and Skinner (1951) who used a wave function

$$\Psi\begin{Bmatrix}2s\sigma\\3d\sigma\end{Bmatrix}=a_1\{(1-\tfrac{1}{2}r_a)\exp(-\tfrac{1}{2}r_a)+(1-\tfrac{1}{2}r_b)\exp(-\tfrac{1}{2}r_b)\}$$
$$+a_2\{r_a\cos\theta_a\exp(-\tfrac{1}{2}r_a)+r_b\cos\theta_b\exp(-\tfrac{1}{2}r_b)\}\quad\ldots\ldots(1)$$

---

† In the separated atoms notation these are *both* designated $\sigma(2s, 2p_z)$.

where $\mathbf{r}_a$ and $\mathbf{r}_b$ are the position vectors of the electron relative to the nuclei A and B respectively and the ratios $a_1 : a_2$ are determined by minimizing the energy E where

$$E = -\int \Psi^* \left(\nabla^2 + \frac{2}{r_a} + \frac{2}{r_b}\right) \Psi \, d\tau \bigg/ \int \Psi^* \Psi \, d\tau. \qquad \ldots\ldots(2)$$

The function (1) is the familiar LCAO approximation and has the correct form when the nuclear separation R is infinite.

The minimization procedure leads to a secular equation of degree two in the energy whose roots are the required values. However although the wave functions so obtained are orthogonal to each other, they are not orthogonal to that of the lower 1sσ state.† This defect may be unimportant if the wave functions have closely the correct form at any given internuclear distance but even if this is not so, the defect may be partially removed by adding to function (1) a third component such as

$$a_3\{\exp(-r_a) + \exp(-r_b)\} \qquad \ldots\ldots(3)$$

from which one obtains a set of three mutually orthogonal wave functions. But it is well known that the energy curves associated with such a set of wave functions cannot cross (Wigner and Witmer 1928, MacDonald 1933),‡ whereas the exact 2sσ, 3dσ curves do in fact cross at a value of $R = R_X$ between $4a_0$ and $5a_0$ ($a_0 = 5{\cdot}29 \times 10^{-9}$ cm) (Bates, Ledsham and Stewart 1953). Thus the LCAO approximation and indeed any approximation obtained by varying the coefficients of a linear combination of functions cannot be valid both for R greater than, and for R less than R_X.

In order to obtain curves which cross it is necessary therefore to derive the orbitals of the 2sσ and 3dσ states by separate treatments with the consequence that mutual orthogonality is no longer automatic. However by careful choice of trial wave functions, the effect of the departure from orthogonality can be rendered unimportant.

In paper I, Dalgarno and Poots introduced a type of united-atom approximation, which is capable of straightforward generalization to excited states. It was shown to possess high accuracy in spite of its extreme simplicity.§ Moiseiwitsch and Stewart (paper II) found, as was to be expected, that it was still better for excited states. If we define elliptical coordinates $\lambda = (r_a + r_b)/R$, $\mu = (r_a - r_b)/R$ and $\phi(r, \theta)$ is the atomic wave function corresponding to $R = 0$, the united atom approximation at any R is obtained according to

$$\phi(r, \theta) \longrightarrow \phi(\lambda R/2, \cos^{-1}\mu). \qquad \ldots\ldots(4)¶$$

Thus

$$\psi(2s\sigma) = (1 - \tfrac{1}{2}\lambda R)\exp(-\tfrac{1}{2}\lambda R) \qquad \ldots\ldots(5)$$

$$\psi(3d\sigma) = \lambda^2 R^2 \exp(-\tfrac{1}{3}\lambda R)(3\mu^2 - 1). \qquad \ldots\ldots(6)$$

---

† Due to this lack of orthogonality, the wave function corresponding to the lower root is properly regarded as a (rather poor) approximation to the 1sσ orbital so that the magnitude of the lower root will tend to be an overestimate.

‡ For a simple discussion, cf. Coulson (1952).

§ Almost all molecular properties calculated using this united-atom approximation are simple rational functions of R.

¶ An important property of wave functions obtained by the relation (4) which they share with the exact wave functions is that the matrix elements of the Hamiltonian between states corresponding to different values of the azimuthal quantum number of the united atom vanish at *all* values of R.

An obvious improvement to (5) and (6) is to introduce screening parameters and it then seems imperative to ensure orthogonality to the lower orbital. We choose finally

$$\Psi(2\mathrm{s}\sigma)=(1-\alpha\lambda R)\exp(-\alpha\lambda R)+q\Psi(1\mathrm{s}\sigma) \qquad \ldots\ldots(7)$$

$$\Psi(3\mathrm{d}\sigma)=\lambda^2R^2\exp(-\alpha'\lambda R)(3\mu^2-1)-q'\Psi(1\mathrm{s}\sigma) \qquad \ldots\ldots(8)$$

where q, q' are determined by the condition

$$\int \Psi^*(2\mathrm{s}\sigma)\Psi(1\mathrm{s}\sigma)d\mathbf{r}=\int \Psi^*(3\mathrm{d}\sigma)\Psi(1\mathrm{s}\sigma)d\mathbf{r}=0 \qquad \ldots\ldots(9)$$

and α, α' are varied to obtain minimum energies.

§ 3. DESCRIPTION OF CALCULATIONS

The functions studied were of the type (7), (8) with

(i) $\alpha=\frac{1}{2}$, $q=0$; $\alpha'=\frac{1}{3}$, $q'=0$;

(ii) $\alpha=\frac{1}{2}$, q determined by (9); $\alpha'=\frac{1}{3}$, q' determined by (9);

(iii) α variable, q determined by (9); α' variable, q determined by (9).

The orbital $\Psi(1\mathrm{s}\sigma)$ was taken to be the best of those obtained in paper I; it is extremely accurate at all values of R.

Using the three functions (i), (ii) and (iii), the 2sσ–2pπ, 3dσ–2pπ, 2sσ–2pσ and 3dσ–2pσ transition integrals Q were computed, the wave functions for the 2pσ and 2pπ states being taken from papers I and II. Both the dipole length and dipole velocity forms of Q were used:

$$Q_{\mathrm{L}}\mathbf{t}=\int \chi_{\mathrm{i}}\mathbf{r}\chi_{\mathrm{f}}d\mathbf{r} \qquad \text{(dipole length)} \qquad \ldots\ldots(10)$$

$$Q_{\mathrm{V}}\mathbf{t}=-\frac{2}{\Delta E}\int \chi_{\mathrm{i}}\nabla\chi_{\mathrm{f}}d\mathbf{r} \qquad \text{(dipole velocity)} \qquad \ldots\ldots(11)$$

where χ_{i} and χ_{f} are the initial and final wave functions, ΔE is the photon energy of the radiation in rydbergs and **t** is some unit vector. The exact values have been computed by Bates, Darling, Hawe and Stewart (1954) and Lewis, McDowell and Moiseiwitsch (1955).†

In addition the potential energy of the electron in the field of the nuclei has been computed:

$$V=-\int \Psi^*\left(\frac{2}{r_{\mathrm{a}}}+\frac{2}{r_{\mathrm{b}}}\right)\Psi\, d\mathbf{r} \Big/ \int \Psi^*\Psi d\mathbf{r}.$$

Exact values of V can be derived from the exact values of E (Bates, Ledsham and Stewart 1953) by the use of the quantal virial theorem (Slater 1933) and, besides providing comparison data, give some insight into the difference between bonding and non-bonding orbitals.

§ 4. RESULTS

The values of α, α', q and q' obtained for (ii) and (iii) are given in table 1 for the 2sσ state and in table 2 for the 3dσ state. The total and the potential energies corresponding to (i), (ii) and (iii) are compared with the exact values in tables 3, 4 and 5, 6 respectively, whilst tables 7, 8 and 9, 10 compare the 2sσ–2pσ, 3dσ–2pσ and 2sσ–2pπ, 3dσ–3dπ transition integrals Q_{L} and Q_{V} computed using functions (i), (ii) and (iii) in expressions (10) and (11) with the exact values.

---

† We are indebted to the latter three authors for allowing us to use their results prior to publication.

Table 1. Parameters of the $2s\sigma$ Wave Functions

Internuclear distance R		0·0	0·4	0·8	1·2	1·6	2·0	3·0	4·0	5·0
Function (ii)	q	0·0000	0·1322	0·3179	0·4899	0·6251	0·7339	0·8543	0·8098	0·6748
Function (iii)	α	0·500	0·470	0·433	0·404	0·380	0·360	0·321	0·296	0·291
	q	0·0000	0·0725	0·1938	0·3310	0·4680	0·6014	0·8972	1·1268	1·2551

Table 2. Parameters of the $3d\sigma$ Wave Functions

Internuclear distance R		0·0	0·4	0·8	1·2	1·6	2·0	3·0	4·0	5·0
Function (ii)	q'	0·0000	0·0146	0·0734	0·2088	0·4640	0·8967	2·9066	6·4666	10·6378
Function (iii)	α'	0·333	0·334	0·337	0·343	0·351	0·364	0·413	0·472	0·508
	q'	0·0000	0·0146	0·0698	0·1865	0·3864	0·6651	1·4900	2·0792	2·4277

Table 3. Total Electronic Energies $-E$ of the $2s\sigma$ State

R	0·0	0·4	0·8	1·2	1·6	2·0	3·0	4·0	5·0
Function									
(1)		0·6877	0·6737	0·6568	0·6384	0·6205	0·5762	0·5367	0·5030
(i)	1·0000	0·9551	0·9443	1·0062	1·1049	1·2000	1·3134	1·2783	1·1848
(ii)	1·0000	0·9407	0·8435	0·7529	0·6711	0·6005	0·4893	0·4459	0·4508
(iii)	1·0000	0·9478	0·8763	0·8142	0·7622	0·7178	0·6312	0·5715	0·5360
Exact	1·0000	0·9482	0·8778	0·8166	0·7652	0·7217	0·6378	0·5770	0·5310

Table 4. Total Electronic Energies $-E$ of the $3d\sigma$ State

R	0·0	0·4	0·8	1·2	1·6	2·0	3·0	4·0	5·0
Function									
(1)		1·5426	1·4557	1·3563	1·2597	1·1700	0·9906	0·8638	0·7728
(i)	0·4444	0·4453	0·4481	0·4528	0·4594	0·4680	0·4961	0·5281	0·5575
(ii)	0·4444	0·4453	0·4481	0·4528	0·4594	0·4679	0·4944	0·5205	0·5361
(iii)	0·4444	0·4454	0·4482	0·4531	0·4606	0·4711	0·5115	0·5630	0·5968
Exact	0·4444	0·4454	0·4482	0·4532	0·4608	0·4716	0·5150	0·5715	0·6120

Table 5. Electronic Potential Energies $-V$ of the $2s\sigma$ State

R	0·0	0·4	0·8	1·2	1·6	2·0	3·0	4·0	5·0
Function									
(i)	2·000	1·834	1·620	1·504	1·479	1·500	1·552	1·513	1·419
(ii)	2·000	2·055	2·047	1·992	1·876	1·643	1·849	1·906	1·854
(iii)	2·000	1·842	1·636	1·478	1·345	1·246	1·080	0·987	0·997
Exact	2·000	—	1·622	1·465	1·342	1·243	1·064	0·945	0·860

Table 6. Electronic Potential Energies $-V$ of the $3d\sigma$ State

R	0·0	0·4	0·8	1·2	1·6	2·0	3·0	4·0	5·0
Function									
(i)	0·889	0·889	0·892	0·898	0·905	0·914	0·940	0·962	0·975
(ii)	0·889	0·889	0·892	0·898	0·904	0·911	0·915	0·877	0·791
(iii)	0·889	0·892	0·903	0·925	0·957	1·003	1·172	1·321	1·306
Exact	0·889	0·893	0·904	0·925	0·956	1·004	1·187	1·386	1·461

Table 7. The $2s\sigma$–$2p\sigma$ Transition Integrals

k		0·0	0·4	0·8	1·2	1·6	2·0	3·0	4·0	5·0
Function										
(i)	Q_L	1·50	1·48	1·41	1·32	1·27	1·26	1·37	1·55	2·04
	Q_V	−0·00	−0·09	−0·07	0·04	0·17	0·31	0·64	0·86	0·90
(ii)	Q_L	1·50	1·45	1·31	1·13	0·95	0·78	0·08	−0·15	−0·20
	Q_V	1·89	1·67	1·46	1·25	1·05	0·86	0·41	−0·07	−0·59
(iii)	Q_L	1·50	1·47	1·33	1·12	0·92	0·76	0·50	0·28	0·10
	Q_V	−0·00	−0·04	0·00	0·07	0·15	0·23	0·27	0·26	0·23
Exact $Q_L = Q_V$		1·50	1·47	1·34	1·14	0·95	0·82	0·63	0·55	0·51

Table 8. The 3dσ–2pσ Transition Integrals

R		0·0	0·4	0·8	1·2	1·6	2·0	3·0	4·0	5·0
Function										
(i)	Q_L	1·23	1·20	1·09	0·96	0·88	0·84	0·92	1·10	1·22
	Q_V	1·23	1·18	1·06	0·92	0·82	0·77	0·75	0·81	0·90
(ii)	Q_L	1·23	1·20	1·09	0·96	0·88	0·82	0·87	0·94	1·03
	Q_V	1·23	1·18	1·06	0·92	0·83	0·78	0·78	0·88	1·04
(iii)	Q_L	1·23	1·20	1·10	0·98	0·91	0·90	1·03	1·18	1·17
	Q_V	1·23	1·18	1·07	0·96	0·89	0·88	1·00	1·16	1·16
Exact	$Q_L=Q_V$	1·23	1·18	1·08	0·96	0·89	0·87	0·99	1·15	1·15

Table 9. The 2sσ–2pπ Transition Integrals

R		0·0	0·4	0·8	1·2	1·6	2·0	3·0	4·0	5·0
Function										
(i)	Q_L	1·50	1·52	1·58	1·63	1·68	1·70	1·71	1·67	1·63
	Q_V	−0·30	−0·83	−1·37	−1·92	−2·46	−2·92	−3·79	−4·39	−4·92
(ii)	Q_L	1·50	1·49	1·50	1·52	1·56	1·59	1·74	1·80	1·69
	Q_V	2·72	2·74	2·78	2·88	3·05	3·25	3·72	3·39	2·05
(iii)	Q_L	1·50	1·52	1·55	1·60	1·64	1·70	1·87	2·05	2·25
	Q_V	2·67	2·44	2·35	2·34	2·36	2·38	2·45	2·45	2·33
Exact	$Q_L=Q_V$	1·50	1·52	1·54	1·59	1·63	1·67	1·77	1·88	1·96

Table 10. The 3dσ–2pπ Transition Integrals

R		0·0	0·4	0·8	1·2	1·6	2·0	3·0	4·0	5·0
Function										
(i)	Q_L	0·61	0·62	0·66	0·70	0·74	0·79	0·90	0·99	1·06
	Q_V	0·61	0·62	0·66	0·69	0·74	0·81	1·07	1·81	6·48
(ii)	Q_L	0·61	0·62	0·66	0·70	0·75	0·80	0·93	1·08	1·21
	Q_V	0·61	0·62	0·66	0·70	0·76	0·83	1·19	2·35	10·28
(iii)	Q_L	0·61	0·63	0·66	0·71	0·76	0·82	0·95	1·02	1·08
	Q_V	0·61	0·63	0·66	0·72	0·79	0·88	1·23	2·13	8·44
Exact	$Q_L=Q_V$	0·61	0·63	0·66	0·72	0·78	0·85	1·03	1·20	1·31

A comparison of the LCAO energies with the exact energies has previously been made by Bates *et al.* (1953). Their results and some additional values are included in tables 3, 4.†

§ 5. DISCUSSION

The most encouraging feature of the results is the continued success of the united-atom approximation introduced in paper I. The derived electronic energy curves cross as they should and even at internuclear distances as large as $5a_0$ they are much superior to those obtained using the LCAO approximation. The inaccuracy of the LCAO approximation should perhaps be emphasized; at $R=5$, the total energy $E'=E+2/R$ (which is usually the quantity of interest to chemists) derived using the LCAO approximation is in error by 21% and 76% for the 2sσ and 3dσ states respectively whereas the corresponding errors with the united atom approximation (iii) are 4% and 7%.

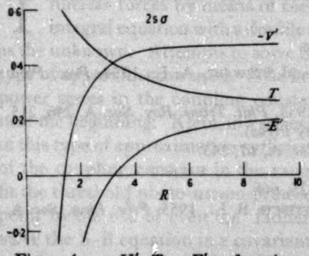

Figure 1. $-V'$, T, $-E'$ as functions of R for the 2sσ state.

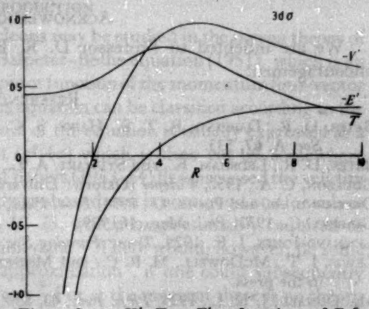

Figure 2. $-V'$, T, $-E'$ as functions of R for the 3dσ state.

When the screening parameters are unvaried, the requirement of orthogonality leads to little or no improvement in the computed quantities other than the 2sσ energy whose values are much too large in magnitude unless orthogonality is imposed. Variation of the screening parameters without ensuring orthogonality leads to completely erroneous results in the 2sσ case but not in the 3dσ case, whose values are frequently slightly improved by neglect of orthogonality. The apparent unimportance of orthogonality in the 3dσ case is due presumably to the near orthogonality already ensured by the united-atom approximation.‡

When the screening parameters are varied and orthogonality is imposed, there is in general a marked improvement in all quantities. The accuracy is high except for the transition integrals involving the 2sσ function computed using the dipole velocity formula. That it is unwise to use the dipole velocity form of Q in cases when the photon energy is very small is, of course, obvious; in addition the integral is very sensitive to the position of the node (in λ, μ space) of the wave function.† The dipole length formula however is not so sensitive and yields quite good results. In the 3dσ case, the dipole velocity formula is to be preferred for small R and the dipole length for large R, the correct value usually lying between them.

---

† The values obtained disagree with those calculated by Pritchard and Skinner (1951). Their work on the 1sσ state has also been repeated and again we are in disagreement with them; contrary to the remarks of Pritchard and Skinner the conclusion cannot be drawn from the calculations that hybridization is significant for the 1sσ state.

‡ The essential difference between the 2sσ and 3dσ wave functions is that at $R=0$ the azimuthal quantum number of one is the same as that of the 1sσ state whilst that of the other is different.

The variation with R of the potential energy, $V' = V + 2/R$ and the kinetic energy T of the 2sσ and 3dσ states is illustrated in figures 1 and 2. It had been shown previously that for the 1sσ and 2pπ states (which are bonding), T passes through a minimum as the atoms approach. However, it is not possible to say whether this occurs for the bonding 3dσ state or not. Apart from the minima in T, figure 1 is similar to the curves for the 1sσ and 2pπ states and figure 2 is similar to the curves for the 2pσ and 3dπ states; it may be noted that the 2sσ, 1sσ and 2pπ are unpromoted orbitals and 3dσ, 2pσ, 3dπ promoted orbitals.

ACKNOWLEDGMENT

We are indebted to Professor D. R. Bates for his continued interest and encouragement.

REFERENCES

BATES, D. R., DARLING, R. T. S., HAWE, S. C., and STEWART, A. L., 1954, *Proc. Phys. Soc.* A, **67**, 533.

BATES, D. R., LEDSHAM, K., and STEWART, A. L., 1953, *Phil. Trans. Roy. Soc.* A, **246**, 215.

COULSON, C. A., 1952, *Valence* (Oxford: University Press).

DALGARNO, A., and POOTS, G., 1954, *Proc. Phys. Soc.* A, **67**, 343.

GILBERT, C., 1933, *Phil. Mag.*, **16**, 929.

LENNARD-JONES, J. E., 1929, *Trans. Faraday Soc.*, **25**, 668.

LEWIS, J. T., MCDOWELL, M. R. C., and MOISEIWITSCH, B. L., 1955, *Proc. Phys. Soc.* A, in the press.

MACDONALD, J. K. L., 1933, *Phys. Rev.*, **43**, 830.

MOISEIWITSCH, B. L., and STEWART, A. L., 1954, *Proc. Phys. Soc.* A, **67**, 457.

MORSE, P. M., and STUECKELBERG, E. C. G., 1929, *Phys. Rev.*, **33**, 932.

PRITCHARD, H. O., and SKINNER, H. A., 1951, *J. Chem. Soc.*, **2**, 945.

SLATER, J. C., 1933, *J. Chem. Phys.*, **1**, 687.

WIGNER, E., and WITMER, E. E., 1928, *Z. Physik*, **51**, 859.

---

† That for the 2sσ transition Q_V is incorrect even at $R=0$ (where the wave functions are exact) is due to Q_V being of the form 0/0.

Covariant Treatment of the Nucleon–Nucleon Interaction

By H. S. GREEN
University of Adelaide, South Australia

MS. received 4th January 1955

Abstract. An approximate covariant solution of the Salpeter–Bethe equation is obtained by a modification of the Fredholm theory. This solution is developed to the point where only numerical substitutions are required to obtain the scattering amplitudes and differential cross sections for elastic nucleon–nucleon collisions, for any energy and any spins of the incident and scattered particles.

§ 1. Introduction

The interaction between two nucleons may be studied in the meson theory of nuclear forces by means of the Salpeter–Bethe equation (1951), which is an integral equation with a double spinor function of the momentum four-vector as the unknown. Attempts to solve this equation can be classified according to the type of approximation used. The kernel of the equation is usually expressed as a power series in the coupling constant ($g^2/4\pi$) which is then cut off somewhere near the beginning. Klein, in a series of papers (1953–54) has discussed the validity of this type of approximation sufficiently to show that it is not a good one for values of the coupling constant in the range 10–25, which are presumably required to fit the threshold photo-meson production data. There would, however, be some point to the use of even the 'ladder approximation', if one could subsequently solve the S–B equation in a covariant way. For at the moment there is no theory which makes any kind of detailed prediction concerning nuclear interactions at high energies, apart from the crude and frankly tentative theory of Fermi (1950).

Yet nearly all of the attempts to solve the S–B equation (e.g. Brueckner and Watson 1953, Henley and Ruderman 1953) have been based on additional non-covariant approximations which frustrate from the outset any application to the relativistic region. In particular the validity of a common approximation which makes the speed of the virtual mesons infinite is not apparent even in the non-relativistic region. Any attempt to solve the S–B equation covariantly is therefore of special interest. Unfortunately existing attempts due to Edwards (1953) and Goldstein (1953) would apply to a system of two nucleons only if their binding energy were equal to their combined rest energies. Under this unrealistic condition, Goldstein obtained a particular solution of the homogeneous equation for arbitrary values of the coupling constant. This, however, failed to reveal the existence of a bound state ; and the only way in which he could obtain a discrete solution was by the addition of a convergence factor to the kernel of the equation. The author (Green 1955) has since shown that even this solution was the result of a mathematical error, and that the S–B equation with zero total energy has a pathological character.

Goldstein's essential idea, however, that bound-state solutions can be separated from the homogeneous S–B equation by introducing a convergence factor, seems likely to be correct in general. McCarthy and Green (1954), using the Fredholm method to solve the integral equation, have shown how to eliminate the cut-off mass and obtain a discrete spectrum from the homogeneous equation as well as a general formal solution of the inhomogeneous equation.

The solution of the inhomogeneous S–B equation, which represents the amplitude for nucleon–nucleon scattering, can be expressed as the ratio of two convergent power series in the coupling constant. The first few terms in these series are definite integrals not essentially different from terms in the perturbation expansion, they therefore appear in the perturbation calculations of Watson and Lepore (1949) and Beard and Bethe (1951). Unfortunately these authors succeeded in evaluating the fourth-order integrals only in non-relativistic approximation, and it has been necessary to undertake a new and exact computation for the purpose of the present paper.

To those unfamiliar with the rapidity of convergence of the Fredholm method, it might appear doubtful that a trustworthy solution of the S–B equation could be constructed from perturbation material, with a coupling constant as large as nuclear theory requires. The efficacy of the method has, however, been amply demonstrated in non-covariant calculations by Jost and Pais (1951) and Gammel (1954). The purpose of the present paper is to facilitate a test of the method, applied directly to the S–B equation. The calculations are carried to the point where nothing more than numerical substitutions are required to obtain the differential cross sections for nucleon–nucleon scattering, for any energy, and for polarized or unpolarized nucleons. The author hopes to confront the predictions of the theory with experiment in a subsequent paper. It is expected that the results will not suffer by comparison with those of the non-covariant theories. But radiative effects and crossed meson lines will probably have to be considered before a final judgment on pseudoscalar meson theory can be made. Apart from the ladder approximation, the only approximations which will be made consist in the neglect of the meson mass μ, compared with the nucleon mass m, in terms of order $\mu^2/2m^2$, and the neglect of terms of order $(g^2/4\pi)^3$ and higher in the Fredholm numerator and denominator.

§ 2. NEUTRON–PROTON INTERACTION

For the neutron–proton system, one has to take account of ordinary and exchange forces, and the charge independence of the meson interaction will be taken for granted. Denote by p one half of the resultant momentum four-vector of the system, so that if p_1 and p_2 are the initial and final momenta of the proton, and p_3 and p_4 are those of the neutron,

$$\begin{gathered} 2p = p_1 + p_3 = p_2 + p_4 \\ p_1 = p + k \qquad p_3 = p - k \\ p_2 = p + l \qquad p_4 = p - l. \end{gathered} \qquad \ldots\ldots(1)$$

Since p_1, p_2, p_3 and p_4 are free-particle momenta, $p_1{}^2 = m^2$ etc., and

$$\begin{gathered} k^2 = l^2 = -\kappa^2 \; ; \\ p \, . \, k = p \, . \, l = 0 \; ; \qquad p^2 = m^2 + \kappa^2 = E^2, \end{gathered} \qquad \ldots\ldots(2)$$

where E and κ represent the energy and scalar momentum of each particle relative to the mass centre. If s_1, s_2, s_3 and s_4 represent *twice* the spin of each particle, resolved in its direction of motion, and u_1, u_2, u_3 and u_4 are the corresponding spinors, one will have

$$u_1\bar{u}_1 = \frac{\mathbf{p}+\mathbf{k}+m}{2E}\cdot\frac{E\kappa+i\mathbf{k}\mathbf{p}\gamma_5 s_1}{2E\kappa},$$

$$u_3\bar{u}_3 = \frac{\mathbf{p}-\mathbf{k}+m}{2E}\cdot\frac{E\kappa-i\mathbf{k}\mathbf{p}\gamma_5 s_3}{2E\kappa}, \qquad \ldots\ldots(3)$$

etc., where $\mathbf{p}=\gamma\,.\,p$, $\mathbf{k}=\gamma\,.\,k$ and $\gamma_5=\gamma_1\gamma_2\gamma_3\gamma_4$.

If θ_1, θ_2, θ_3 and θ_4 are the angles made by the directions of the tracks of the particles with some fixed direction in the plane of the relative motion one finds easily from (3) that

$$|\bar{u}_1 u_2|^2 = \mathrm{spur}\,(u_1\bar{u}_1 u_2\bar{u}_2)$$

$$= \tfrac{1}{4}(1-s_1s_2)(1-\cos\theta_{12}) + \tfrac{1}{4}(m/E)^2(1+s_1s_2)(1+\cos\theta_{12}), \qquad \ldots\ldots(4)$$

where $\theta_{12}=\theta_1-\theta_2$; so that, with the simplest choice of the arbitrary phase factor,

$$\bar{u}_1 u_2 = \tfrac{1}{2}(s_1-s_2)\sin(\tfrac{1}{2}\theta_{12}) + \tfrac{1}{2}(m/E)(1+s_1s_2)\cos(\tfrac{1}{2}\theta_{12}). \qquad \ldots\ldots(5)$$

Similarly

$$\bar{u}_3 u_4 = \tfrac{1}{2}(s_3-s_4)\sin(\tfrac{1}{2}\theta_{34}) + \tfrac{1}{2}(m/E)(1+s_3s_4)\cos(\tfrac{1}{2}\theta_{34}),$$

$$\bar{u}_1 u_4 = \tfrac{1}{2}(s_1-s_4)\sin(\tfrac{1}{2}\theta_{14}) + \tfrac{1}{2}(m/E)(1+s_1s_4)\cos(\tfrac{1}{2}\theta_{14}),$$

$$\bar{u}_3 u_2 = \tfrac{1}{2}(s_3-s_2)\sin(\tfrac{1}{2}\theta_{32}) + \tfrac{1}{2}(m/E)(1+s_3s_2)\cos(\tfrac{1}{2}\theta_{32}), \qquad \ldots\ldots(6)$$

where $\theta_{34}=\theta_3-\theta_4$, etc. If θ is the scattering angle, one has

$$\theta_{12}=\theta_{34}=\theta, \text{ but } \theta_{14}=\theta+\pi \text{ and } \theta_{32}=\theta-\pi.$$

These formulae will enable one to calculate the scattering amplitude explicitly and derive the cross section simply by squaring the modulus of the amplitude, instead of evaluating spurs of complicated expressions as commonly done.

The scattering amplitude is

$$\mathrm{S.A.} = \bar{u}_{1\alpha}\bar{u}_{3\beta}\{S_{\alpha\beta,\gamma\delta}(k,l) + S_{\beta\alpha,\gamma\delta}(-k,l)\}u_{2\gamma}u_{4\delta} \qquad \ldots\ldots(7)$$

where α, β, γ, δ denote spinor components, and $S_{\alpha\beta,\gamma\delta}(k,l)$ satisfies the integral equation

$$S_{\alpha\beta,\gamma\delta}(k,l) = F_{\alpha\beta,\gamma\delta}(k,l) + 2\int K_{\alpha\beta,\lambda\mu}(k,j)S_{\lambda\mu,\gamma\delta}(j,l)d^4j \qquad \ldots\ldots(8)$$

in which

$$F_{\alpha\beta,\gamma\delta}(k,l) = g^2\{(k-l)^2-\mu^2\}^{-1}(\gamma_5)_{\alpha\gamma}(\gamma_5)_{\beta\delta} \qquad \ldots\ldots(9)$$

and

$$(2\pi)^4 K_{\alpha\beta,\gamma\delta}(k,l) = ig^2\{(k-l)^2-\mu^2\}^{-1}$$

$$\times\{\gamma_5(\mathbf{p}+\mathbf{l}-m)^{-1}\}_{\alpha\gamma}\{\gamma_5(\mathbf{p}-\mathbf{l}-m)^{-1}\}_{\beta\delta}. \qquad \ldots\ldots(10)$$

The second term on the right-hand side of (7) takes account of the possibility of charge exchange between the nucleons ; the factor 2 on the right-hand side of (8) is necessary because both charged and uncharged mesons can be exchanged in intermediate virtual processes.

Writing (8) in the matrix form $S=F+2KS$, the Fredholm solution is

$$S = \frac{F+2(K-\mathrm{tr}\,K)F+\ \ldots}{1-2\,\mathrm{tr}\,K+2\{(\mathrm{tr}\,K)^2-\mathrm{tr}\,K^{(2)}\}-\ \ldots} \qquad \ldots\ldots(11)$$

where

$$K^{(2)}{}_{\alpha\beta,\gamma\delta}(k,l) = \int K_{\alpha\beta,\lambda\mu}(k,j)K_{\lambda\mu,\gamma\delta}(j,l)d^4j \qquad \ldots\ldots(12)$$

and $\mathrm{tr}\, K$, for example, means $\int K_{\alpha\beta,\alpha\beta}(j,j)d^4j$. Actually $\mathrm{tr}\, K$ vanishes, and $\mathrm{tr}\, K^{(2)}$ only converges when a cut-off factor is added to the kernel K. But, as explained by McCarthy and Green (1954), the cut-off mass can be eliminated from the solution (11) without spoiling its convergence ; and the final result is to replace $\mathrm{tr}\, K^{(2)}$, $\mathrm{tr}\, K^{(3)}$, . . . by $\mathrm{tr}'K^{(2)}$, $\mathrm{tr}'K^{(3)}$, . . . , where $\mathrm{tr}'K^{(2)}$, for example, is obtained by subtracting from $\mathrm{tr}\, K^{(2)}$ the value it assumes when $p=0$.

The Fredholm solution (11), even after the replacement of $\mathrm{tr}\, K^{(2)}$ by $\mathrm{tr}'K^{(2)}$, etc., is not the most rapidly convergent one which can be devised. The reason for this is that, for every solution corresponding to spins $\frac{1}{2}s_1$, $\frac{1}{2}s_2$, $\frac{1}{2}s_3$ and $\frac{1}{2}s_4$ of the incident and scattered particles, there is another corresponding to the spins $-\frac{1}{2}s_1$, $-\frac{1}{2}s_2$, $-\frac{1}{2}s_3$ and $-\frac{1}{2}s_4$. These solutions contribute equal factors to the Fredholm denominator, which is therefore the square of a convergent series beginning $1-\mathrm{tr}\, K^{(2)}+\ldots$, which is a simple factor of the numerator also. Cancelling the redundant factor, one obtains

$$S=\frac{F+2KF+\ldots}{1-\mathrm{tr}'K^{(2)}+\ldots}. \qquad \ldots\ldots(13)$$

The author has made tests with somewhat simplified equations which show that this procedure greatly improves the rate of convergence of the solution, and in most cases allows a very good approximation to S to be computed from the terms actually shown above.

§ 3. PROTON–PROTON INTERACTION

The analysis for the two-proton system is very similar, and even somewhat simpler since one does not have to consider charge exchange. It is necessary, however, to anti-symmetrize the initial wave function of the system with respect to the proton spin coordinates and momenta (the final wave function will then be automatically anti-symmetrical). The scattering amplitude is therefore

$$\mathrm{S.A.}=\bar{u}_{1\alpha}\bar{u}_{3\beta}\{S'_{\alpha\beta,\gamma\delta}(k,l)-S'_{\beta\alpha,\gamma\delta}(-k,l)\}u_{2\gamma}u_{4\delta} \qquad \ldots\ldots(14)$$

where S' satisfies the equation $S'=F+KF$ and is therefore given by

$$S'=\frac{F+KF+\ldots}{1-\frac{1}{4}\mathrm{tr}'K^{(2)}+\ldots}. \qquad \ldots\ldots(15)$$

Here F and K have the same significance as in the previous section.

§ 4. COMPUTATIONAL PROCEDURES

Write

$$\begin{aligned} J_+&=(p+j)^2-m^2, & J_-&=(p-j)^2-m^2,\\ K_+&=(p+k)^2-m^2, & K_-&=(p-k)^2-m^2,\\ A&=(k-j)^2-\mu^2, & B&=(l-j)^2-\mu^2. \end{aligned} \qquad \ldots\ldots(16)$$

Then, neglecting some terms of order $\mu^2/2m^2$,

$$\mathrm{tr}\, K^{(2)}=-\frac{g^4}{64\pi^8}\iint\frac{(J_++K_+-A)(J_-+K_--A)d^4j\, d^4k}{J_+K_+J_-K_-A^2} \qquad \ldots\ldots(17)$$

and

$$(KF)_{\alpha\beta,\gamma\delta}=\frac{ig^4}{16\pi^4}\int\frac{(\mathbf{p}+\mathbf{j}-m)_{\alpha\gamma}(\mathbf{p}-\mathbf{j}-m)_{\beta\delta}d^4j}{J_+J_-AB}. \qquad \ldots\ldots(18)$$

In evaluating the right-hand side of (17), it is not possible to split up the integral without introducing bad divergences. To circumvent this difficulty one uses the identity

$$\frac{(J_+ + K_+ - A)(J - + K_- - A)}{J_+ K_+ J_- K_- A^2} = \tfrac{3}{2}\iiiint \gamma\left(\frac{\partial}{\partial\alpha_1}+\frac{\partial}{\partial\beta_1}\right)\left(\frac{\partial}{\partial\alpha_2}+\frac{\partial}{\partial\beta_2}\right)$$
$$\times(\alpha_1 J_+ + \alpha_2 J_- + \beta_1 K_+ + \beta_2 K_- + \tfrac{1}{2}\gamma A)^{-4} d\alpha_1\, d\alpha_2\, d\beta_1 d\beta_2 \qquad \ldots\ldots(19)$$

where $\gamma = 1 - \alpha_1 - \alpha_2 - \beta_1 - \beta_2$ and the domain of integration is such that α_1, α_2, β_1, β_2 and γ are all positive. The integrations with respect to j and k are then carried out using Feynman's technique (1949), and new variables $x_1 = \alpha_1 + \beta_1$, $x_2 = \alpha_2 + \beta_2$, $y_1 = \beta_1 - \alpha_1$ and $y_2 = \beta_2 - \alpha_2$ are introduced. One finds

$$\mathrm{tr}'K^{(2)} = \left(\frac{g}{4\pi}\right)^4 \int_0^1 dx_1 \int_0^{1-x_1} dx_2 \int_{-x_1}^{x_1} dy_1 \int_{-x_2}^{x_2} dy_2 \frac{\gamma\partial^2}{\partial x_1 \partial x_2} f(x_1, x_2, y_1, y_2)$$
$$\ldots\ldots(20)$$

with

$$f(x_1, x_2, y_1, y_2) = \frac{1}{M^2}\ln\left\{1 + \frac{(N - xM)\phi}{M(x + \gamma\theta)}\right\},$$
$$M = \tfrac{1}{4}(2x - x^2 - y^2), \quad N = \tfrac{1}{2}\xi(\xi - \eta y) + \tfrac{1}{4}x(\eta^2 - \xi^2),$$
$$x = x_1 + x_2 = 1 - \gamma, \quad y = y_1 + y_2,$$
$$\xi = x_2 - x_1, \quad \eta = y_2 - y_1, \quad \phi = p^2/m^2, \quad \theta = \tfrac{1}{2}\mu^2/m^2. \qquad \ldots\ldots(21)$$

The integration is very long, and details are omitted here, but will be supplied privately by the author to interested persons. If $\phi = p^2/m^2 = \cos^2\epsilon$, the result is

$$\mathrm{tr}'K^{(2)} = \left(\frac{g}{2\pi}\right)^4 [2\ln 2 - \tfrac{3}{2} + (3 + 2\ln\theta)\{1 - (\tfrac{1}{2}\pi - \epsilon)\tan\epsilon\}$$
$$+ \tfrac{1}{2}(1 - \tan^2\epsilon)(\tfrac{1}{2}\pi - \epsilon)^2 + 2\tan\epsilon\{(\tfrac{1}{2}\pi - \epsilon)(2\ln\sin\epsilon + \ln\cos\epsilon)$$
$$+ \int_0^\epsilon (2\ln\sin\beta + \ln\cos\beta)d\beta + (\tfrac{1}{2}\pi + \epsilon)\ln 2\}]. \qquad \ldots\ldots(22)$$

If $p^2 > m^2$, as is the case for scattering, $\epsilon = -i\lambda$, where λ is real and positive ; furthermore such imaginary values are reached by analytic continuation in the lower right-hand quadrant of the complex plane. The definite integrals in (22) can be expressed in terms of the function

$$\mathrm{Rl}(x) = \int_1^x \frac{\ln x\, dx}{x - 1}$$

tabulated by Powell (1943); if $\tau = \tanh\lambda$,

$$\int_0^\lambda \ln\cosh\mu d\mu = \tfrac{1}{2}[\mathrm{Rl}\{\tfrac{1}{2}(1+\tau)\} + \tfrac{1}{12}\pi^2 - \tfrac{1}{2}(\ln 2)^2$$
$$+ \ln 2\ln(1-\tau) - \tfrac{1}{2}\ln(1-\tau)\ln(1+\tau) + \tfrac{1}{4}\{\ln(1-\tau)\}^2$$
$$- \tfrac{1}{4}\{\ln(1+\tau)\}^2] \;; \qquad \ldots\ldots(23)$$

and if $\sigma = \coth\lambda$,

$$\int_0^\lambda \ln\sinh\mu d\mu = \tfrac{1}{2}[\mathrm{Rl}\{\tfrac{1}{2}(1+\sigma)\} - \tfrac{1}{6}\pi^2 - \tfrac{1}{2}(\ln 2)^2$$
$$+ \ln 2\ln(\sigma - 1) - \tfrac{1}{2}\ln(\sigma - 1)\ln(1+\sigma) + \tfrac{1}{4}\{\ln(\sigma - 1)\}^2$$
$$- \tfrac{1}{4}\{\ln(1+\sigma)\}^2]. \qquad \ldots\ldots(24)$$

Equation (18) is readily reduced by Feynmans' technique to the form

$$(KF)_{\alpha\beta,\gamma\delta}=\frac{g^4}{16\pi^2}\left\{\tfrac{1}{2}(\gamma^\lambda)_{\alpha\gamma}(\gamma_\lambda)_{\beta\delta}+(\mathbf{p})_{\alpha\gamma}(\mathbf{p})_{\beta\delta}\frac{\partial}{\partial b}+(\mathbf{k})_{\alpha\gamma}(\mathbf{k})_{\beta\delta}\frac{\partial}{\partial c}\right\}R(a,b,c) \qquad \ldots\ldots(25)$$

where

$$R(a,b,c)=\int_0^1 dx\int_0^1 dy\int_0^1 dz\left\{\frac{z(1-z)}{\alpha z^2(1-x^2)+(1-z)^2(by^2+c)}\right\},$$
$$a=-\tfrac{1}{2}(1-\cos\theta)k^2,\; b=p^2,\; c=k^2. \qquad \ldots\ldots(26)$$

This result is, in fact, equivalent to that obtained by Watson and Lepore, who, however, used non-covariant approximations to evaluate the integral. It is, however, possible to obtain an exact result, after terms of order $\frac{1}{2}\,\mu^2/m^2$ have been neglected. The z-integration is performed first to give

$$R=\int_0^1 dx\int_0^1 dy\left\{\frac{(A-B)}{2(A+B)^2}\ln\left(\frac{A}{B}\right)-\frac{1}{(A+B)}+\frac{\pi(AB)^{1/2}}{(A+B)^2}\right\},$$
$$A=a(1-x^2),\; B=by^2+c. \qquad \ldots\ldots(27)$$

When B is negative, $B^{1/2}$ means $-i(-B)^{1/2}$, and $\ln(A/B)$ means $\ln(-A/B)+i\pi$. The only term on the right-hand side of (27) which presents difficulty is the first, and this is handled by using

$$\frac{A-B}{(A+B)^2}=\frac{a}{(a+c)}\frac{\partial}{\partial y}\left(\frac{y}{A+B}\right)-\frac{c}{(a+c)}\frac{\partial}{\partial x}\left(\frac{x}{A+B}\right)$$

and integrating by parts to eliminate the logarithm from the double integral. In this way one obtains after some calculation

$$R=R_1+R_2,$$
$$R_1=\frac{\tanh v}{a+c}\left\{\int_0^v \ln\,(2\sinh u)du+\tfrac{1}{4}\pi^2\right\},$$
$$R_2=\frac{\tan\epsilon}{a+c}\left\{\int_0^\epsilon \ln(2\sin\beta)\,d\beta+\tfrac{1}{2}(\tfrac{1}{2}\pi-\epsilon)\ln(c/a)\right\}, \qquad \ldots\ldots(28)$$

where $\sinh v=a^{1/2}(b+c)^{-1/2}$ and ϵ has the same meaning as in (22) above. Again the definite integrals can be expressed in terms of the Rl function by means of (24). Further,

$$\frac{\partial R_1}{\partial b}=-\frac{R_1}{2(a+b+c)}-\frac{\sinh^2 v\ln(2\sinh v)}{2(a+c)(a+b+c)}$$
$$\frac{\partial R_1}{\partial c}=\frac{\partial R_1}{\partial b}-\frac{R_1}{(a+c)}$$
$$\frac{\partial R_2}{\partial b}=-\frac{R_2}{2b}-\frac{\sin^2\epsilon}{2b(a+c)}\{\ln(2\sin\epsilon)-\tfrac{1}{2}\ln(c/a)\}$$
$$\frac{\partial R_2}{\partial c}=-\frac{R_2}{(a+c)}+\frac{b}{c}\frac{\partial R_2}{\partial b}+\frac{\tan\epsilon}{2c(a+c)}(\tfrac{1}{2}\pi-\epsilon). \qquad \ldots\ldots(29)$$

Although c is negative, imaginary quantities arise only through the occurrence of $\epsilon=-i\lambda$ in the above formulae.

§ 5. THE DIFFERENTIAL CROSS SECTIONS

It is now possible to derive explicit expressions for the scattering amplitudes. For n–p scattering, it follows from (7) and (13) that

$$\text{S.A.} = \frac{F_o + F_e + 2(KF)_o + 2(KF)_e}{1 - \text{tr}' K^{(2)}} \qquad \ldots\ldots(30)$$

where, according to (9),

$$F_o = \bar{u}_{1\alpha}\bar{u}_{3\beta} F_{\alpha\beta,\gamma\delta}(k, l)\, u_{2\gamma} u_{4\delta} = \frac{g^2 \gamma_5{}^{(12)} \gamma_5{}^{(34)}}{(k-l)^2 - \mu^2},$$

$$F_e = \bar{u}_{1\alpha}\bar{u}_{3\beta}\, F_{\beta\alpha,\gamma\delta}(-k, l)\, u_{2\gamma} u_{4\delta} = \frac{g^2 \gamma_5{}^{(14)} \gamma_5{}^{(32)}}{(k+l)^2 - \mu^2},$$

$$\gamma_5{}^{(12)} = \bar{u}_1 \gamma_5 u_2, \text{ etc.} \qquad \ldots\ldots(31)$$

and, according to (25),

$$(KF)_o = \frac{g^4}{16\pi^2}\left\{ \tfrac{1}{2}\gamma^{\lambda(12)}\gamma_\lambda{}^{(34)} R_o + \mathbf{p}^{(12)}\mathbf{p}^{(34)} \frac{\partial R_o}{\partial b} + \mathbf{k}^{(12)}\mathbf{k}^{(34)} \frac{\partial R_o}{\partial c} \right\},$$

$$(KF)_e = \frac{g^4}{16\pi^2}\left\{ \tfrac{1}{2}\gamma^{\lambda(14)}\gamma_\lambda{}^{(32)} R_e + \mathbf{p}^{(14)}\mathbf{p}^{(32)} \frac{\partial R_e}{\partial b} + \mathbf{k}^{(14)}\mathbf{k}^{(32)} \frac{\partial R_e}{\partial c} \right\}. \qquad \ldots\ldots(32)$$

Here R_o is the value of R, obtained in the last section, with $a = \frac{1}{2}(1 - \cos\theta)\kappa^2$, $b = E^2$ and $c = -\kappa^2$, while R_e is obtained from R_o by reversing the sign of $\cos\theta$. The values of $\gamma_5{}^{(12)}$, etc. can be obtained as follows:

Using (3), one computes in succession

$$\bar{u}_1 \mathbf{k}\mathbf{l} u_2 = -E^{-2}\bar{u}_1(i\mathbf{k}p\gamma_5)(i\mathbf{l}\mathbf{p}\gamma_5)u_2 = -s_1 s_2 \kappa^2 \bar{u}_1 u_2,$$

$$m\bar{u}_1 \mathbf{k} u_2 = \tfrac{1}{2}\bar{u}_1\{(\mathbf{p}+\mathbf{k})\mathbf{k} + \mathbf{k}(\mathbf{p}+\mathbf{l})\}\, u_2 = -\tfrac{1}{2}(1 + s_1 s_2)\kappa^2 \bar{u}_1 u_2,$$

$$\bar{u}_1 \mathbf{k}\mathbf{p} u_2 = \bar{u}_1 k(m - \mathbf{l})u_2 = -\tfrac{1}{2}(1 - s_1 s_2)\kappa^2 \bar{u}_1 u_2,$$

$$\bar{u}_1 \gamma_5 u_2 = -(E\kappa)^{-1} s_1 \bar{u}_1(i\mathbf{k}\mathbf{p})u_2 = \tfrac{1}{2}i(s_1 - s_2)(\kappa/E)\bar{u}_1 u_2$$

and, in the centre-of-mass frame, since

$$\kappa^2 \sin^2\theta\, \boldsymbol{\gamma} = \boldsymbol{\gamma}\,.\,\mathbf{k}\mathbf{k} + \boldsymbol{\gamma}\,.\,\mathbf{l}\mathbf{l} - \cos\theta(\boldsymbol{\gamma}\,.\,\mathbf{k}\mathbf{l} + \boldsymbol{\gamma}\,.\,\mathbf{l}\mathbf{k}) + (\mathbf{k}\mathbf{l} + \mathbf{k}\,.\,\mathbf{l})\gamma_4\gamma_5\kappa^{-2}\mathbf{k}\times\mathbf{l}$$

$$\ldots\ldots(33)$$

one has

$$\bar{u}_1 \boldsymbol{\gamma} u_2 = \frac{(1 + s_1 s_2)(\mathbf{k} + \mathbf{l} + i s_1 \kappa^{-1}\mathbf{k}\times\mathbf{l})}{2m(1 + \cos\theta)}$$

$$\bar{u}_1 \gamma_4 u_2 = \frac{m}{E}\left\{ 1 + \tfrac{1}{2}(1 + s_1 s_2)\frac{\kappa^2}{m^2} \right\} \bar{u}_1 u_2.$$

From these relations one has

$$\gamma_5{}^{(12)} = \tfrac{1}{2}i(s_1 - s_2)(\kappa/E)\bar{u}_1 u_2,$$

$$\mathbf{p}^{(12)} = m\{1 + \tfrac{1}{2}(1 + s_1 s_2)(\kappa/m)^2\}\bar{u}_1 u_2,$$

$$\mathbf{k}^{(12)} = -\tfrac{1}{2}(1 + s_1 s_2)(\kappa^2/m)\bar{u}_1 u_2, \qquad \ldots\ldots(34)$$

etc., and

$$\begin{aligned}\gamma^{\lambda(12)}\gamma_\lambda{}^{(34)} = {} & [(m/E)^2\{1 + \tfrac{1}{2}(1 + s_1 s_2)(\kappa/m)^2\}\{1 + \tfrac{1}{2}(1 + s_3 s_4)(\kappa/m)^2\} \\ & + \tfrac{1}{2}(\kappa/m)^2(1 + \cos\theta)^{-1}(1 + s_1 s_2)(1 + s_3 s_4) \\ & + \tfrac{1}{4}(\kappa/m)^2(1 - \cos\theta)(1 + \cos\theta)^{-1}(s_1 + s_2)(s_3 + s_4)]\bar{u}_1 u_2 \bar{u}_3 u_4.\end{aligned}$$

$$\ldots\ldots(35)$$

One can now substitute from (5) and (6), and use the relations $(s_1+s_2)(s_1-s_2)=0$, $\frac{1}{2}(1+s_1s_2)(s_1+s_2)=s_1+s_2$, etc. to obtain simple explicit expressions for all quantities appearing in (31) and (32).

For p–p scattering, one has, instead of (30)

$$\text{S.A.}=\frac{F_o-F_e+(KF)_o-(KF)_e}{1-\frac{1}{4}\,\mathrm{tr}'K^{(2)}}. \qquad \ldots\ldots(36)$$

In either case, the differential cross section in the centre-of-mass frame is given by

$$\text{D.C.S.}=(4\pi)^{-2}E^2\,|\text{S.A.}|^2d\Omega. \qquad \ldots\ldots(37)$$

Zeros of the denominators of (30) and (36) can occur for $p^2<m^2$, i.e. for real values of the angle ϵ defined so that $p^2/m^2=\cos^2\epsilon$. Such zeros would correspond to the existence of stable bound states of the pair of nucleons concerned, and one would be inclined to fix the value of the coupling constant g to fit the observed binding energy of the deuteron. There is, however, an unfortunate ambiguity in the value of g obtained in this way, arising from the presence of the term proportional to $\ln\theta$, where $\theta=\frac{1}{2}\mu^2/m^2$, in (22). It is easily verified that the integrals of higher order $\mathrm{tr}'K^{(3)}$, $\mathrm{tr}'K^{(4)}$ which appear in the Fredholm denominator do not depend sensitively on $\frac{1}{2}\mu^2/m^2$ so the zero of the denominator ought not to depend sensitively on $\frac{1}{2}\mu^2/m^2$ either. One can show that the term proportional to $\ln(\frac{1}{2}\mu^2/m^2)$ in $\mathrm{tr}'K^{(2)}$ must arise from a factor of the type

$$\exp\left\{-\left(\frac{g}{2\pi}\right)^4(2-\pi\tan\epsilon+\epsilon\tan\epsilon)\ln(c\mu^2/m^2)\right\}$$

in the denominator of (30), but the value one assumes for c affects—not very sensitively, it is true—the estimate one makes of the value of g required to fit the energy of the bound state. Without undertaking the prohibitive labour of calculating $\mathrm{tr}'K^{(3)}$ or $\mathrm{tr}'K^{(4)}$, the best thing which can be done is to regard the θ in (22) as an adjustable parameter, and see how well the scattering data and binding energy of the deuteron can be fitted with both g and θ at one's disposal.

REFERENCES

Beard, D. B., and Bethe, H. A., 1951, *Phys. Rev.*, **83**, 1106.
Brueckner, K. A., and Watson, K. M., 1953, *Phys. Rev.*, **92**, 1023.
Edwards, S. F., 1953, *Phys. Rev.*, **90**, 284.
Fermi, E., 1950, *Progr. Theor. Phys., Osaka*, **5**, 570.
Feynman, R. P., 1949, *Phys. Rev.*, **76**, 769.
Gammel, J. L., 1954, *Phys. Rev.*, **95**, 209.
Goldstein, J. S., 1953, *Phys. Rev.*, **91**, 1516.
Green, H. S., 1955, *Phys. Rev.*, **97**, 540.
Henley, E. M., and Ruderman, M. A., 1953, *Phys. Rev.*, **92**, 1037.
Jost, R., and Pais, A., 1951, *Phys. Rev.*, **82**, 840.
Klein, A., 1953, *Phys. Rev.*, **90**, 1101; **91**, 740; **92**, 1017; 1954, *Ibid.*, **94**, 1052.
McCarthy, I. E., and Green, H. S., 1954, *Proc. Phys. Soc.* A, **67**, 719.
Powell, E. O., 1943, *Phil. Mag.* (7), **34**, 600.
Salpeter, E. E., and Bethe, H. A., 1951, *Phys. Rev.*, **84**, 1232.
Watson, K. M., and Lepore, J. V., 1949, *Phys. Rev.*, **76**, 1157.

The Rates of Penetrating Showers at Sea Level

By C. B. A. McCUSKER, J. G. DARDIS and B. G. WILSON
Dublin Institute for Advanced Studies

MS. received 8th December 1954, *and in amended form* 15*th February* 1955

Abstract. The times of arrival of 17 665 local and 2526 extensive penetrating showers have been recorded. The showers penetrated various thicknesses of lead from 17·5 cm to 97·5 cm. A variation of the rate of local showers with solar time which is correlated with the small diurnal pressure variations appears to be statistically established. This variation seems to have a much larger barometric coefficient than that derived from the large pressure changes associated with the weather. No significant variation of the rate of local showers with sidereal time was found.

Possible variations of the rates of penetrating extensive showers with solar and with sidereal time are discussed.

§ 1. Introduction

Many experiments on the rates of the various components of cosmic radiation have been carried out. There are several admirable summaries of the work (e.g. Duperier 1945, Elliott 1952, *Proceedings of the Bagnères Conference* 1953). The effects have been classified either as variations of the primary intensity or as variations produced in the atmosphere. The first class may throw light on conditions in interplanetary or interstellar space and possibly on the origin of cosmic radiation. The second may give information concerning the very high energy nuclear interactions which take place in the upper atmosphere. In either case primary particles of very high energy are of particular interest. Previously these have been studied by observing the electron component of extensive air showers (Elliott 1952, *Proceedings of the Bagnères Conference* 1953, Farley and Storey 1954, Cranshaw and Galbraith 1954) or by observing μ-mesons deep underground (Barrett *et al.* 1954, Sherman 1954). The present experiment was begun as an attempt to study the development of the nucleon cascade in lead. It was necessary to select high energy† primaries (on the apparatus) to do this and, in addition, dense penetrating extensive showers were recorded as a contamination. Since both of these classes are probably due to very high energy primary interactions at the top of the atmosphere it was thought that it might be worth while to study the variations (if any) of the rates with time.

§ 2. Apparatus

The apparatus used was a penetrating shower detector (figure 1). It consisted of five trays A B C D and E, each of 12 Geiger–Müller counters. The Geiger counters were each 50 cm long and 3·8 cm in diameter. Trays A and B were in contact; the axes of the counters in the two trays were at right angles. Tray C was separated from B by 60 cm air and 10 cm Pb. The two lowest trays were shielded at both sides and ends by 15 cm Pb and each individual counter in them was wrapped in lead sheet $\frac{1}{10}$ in. thick. Tray E was unshielded and placed at a horizontal distance of 2 m from the centre line of the penetrating shower set. Each counter in trays A and B could operate a neon lamp.

---

† The average energy of these primaries for 10 cm of lead over the apparatus was probably approximately 20 kmev. For greater thicknesses it would, of course, be greater.

A master pulse required the discharge of at least two counters in each of trays B, C and D. If tray E was also discharged the event was classed as an extensive penetrating shower; if not, it was classed as a local penetrating shower.

At first, there was no lead above tray A, then lead 5 cm thick and 4 feet × 4 feet in area was place immediately above this tray. Subsequently it was increased in thickness in steps up to 82·5 cm and then gradually decreased to zero thickness again. From 25th August 1953 up to the present the times of arrival of all showers have been recorded.

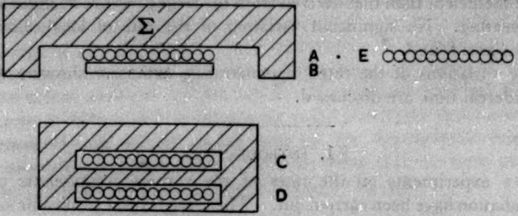

Figure 1. Diagram of the apparatus.

§ 3. RESULTS

The rates of local and of extensive penetrating showers were determined for nine different thicknesses of the lead from 5 to 82·5 cm. Thus about 2000 local showers were recorded for each thickness. The extensive showers were about seven times less frequent. Ideally one should have a well determined rate per hour for each of the twenty-four hours of the solar or sidereal day and for each thickness of lead. This, however, is not possible with the number of events recorded. To increase the statistical accuracy, therefore, the rates have been either averaged over all thicknesses of lead, or averaged over four-hour periods, or both. The results for solar time are given in figures 2 and 3 with mean values in table 1 and the results for sidereal time in figure 4, with mean values in table 2.

Table 1. Mean (Solar Time) Rates of Local and Extensive Penetrating Showers

Hours G.M.T.	01–05	05–09	09–13	13–17	17–21	21–01
Rate of local showers (counts per hour)	1·980 ±0·033	1·970 ±0·034	1·858 ±0·037	2·000 ±0·032	2·052 ±0·032	1·888 ±0·036
Rate of extensive showers (counts per hour)	0·315 ±0·014	0·251 ±0·013	0·259 ±0·013	0·288 ±0·014	0·279 ±0·013	0·285 ±0·014

Table 2. Mean (Sidereal Time) Rates of Local and Extensive Penetrating Showers

The showers were recorded from 25th August 1953 to 4th November 1954

Hours (G.S.T.)	23–03	03–07	07–11	11–15	15–19	19–23
Rate of local showers (counts per hour)	1·932 ±0·033	1·932 ±0·033	1·949 ±0·035	2·028 ±0·036	1·956 ±0·035	1·961 ±0·035
Rate of extensive showers (counts per hour)	0·292 ±0·014	0·273 ±0·014	0·266 ±0·013	0·245 ±0·013	0·293 ±0·014	0·305 ±0·014

§ 4. The Solar Variation of Local Showers

The most obvious feature of the results is an apparent variation of the rate of local showers with solar time (figure 2, upper curve). By taking the difference of the maximum and minimum hours the effect has been shown to be statistically significant (Dardis and McCusker 1954). An alternative treatment is to apply the χ^2 test on the null hypothesis to the results given in table 1. A value of $P=0{\cdot}001$ is obtained. A straight line is therefore a poor fit for these points.

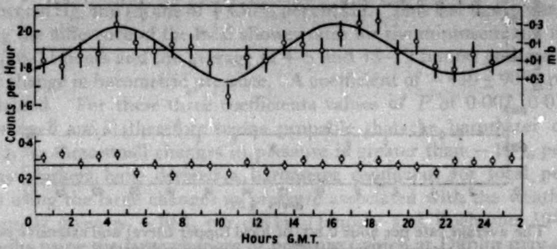

Figure 2. The average rate per hour G.M.T. of local (upper curve) and extensive penetrating showers. The straight lines give the average values. The curve on the upper graph is for the average hourly value of the pressure at Dublin Airport plotted as a departure from mean for the period September 1953 to August 1954 inclusive.

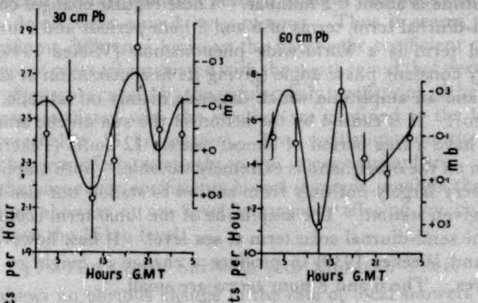

Figure 3. The average of local showers per four-hour period beginning 01–05 h. G.M.T. under four different thicknesses of lead are plotted as points with their statistical errors. The curve gives the average value, over the period of the run, pressure at Dublin Airport plotted as a departure from the mean.

The apparent minima of the curve lie at 1030 and 2230 G.M.T. These times coincide with the maxima of the semi-diurnal pressure wave and thus a possible connection with pressure is suggested.

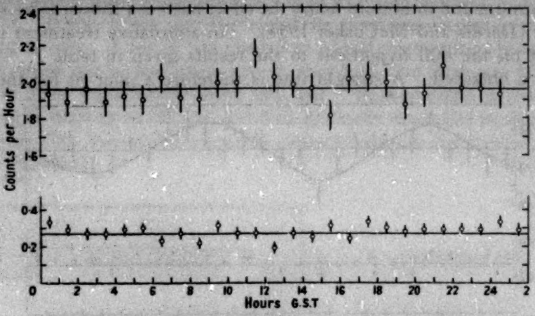

Figure 4. The average rate per hour G.S.T. of local (upper curve) and extensive penetrating showers. The straight lines give average values.

§ 5. The Daily Pressure Variations

The regular daily variations of pressure at sea level in Dublin are small. Their amplitude is about 0·2 millibar. These regular changes contain a diurnal term, a semi-diurnal term, terms of 6 and 8 hour periods and a lunar term. The semi-diurnal term is a world-wide phenomenon (Wilkes 1949, Mitra 1947). It has a very constant phase angle (giving its first maximum at about 1000 local solar time) and an amplitude which depends mainly on latitude, being greatest at the equator. It is caused by the action of the sun on the atmosphere which happens to have a free period of almost exactly 12 hours (Pekeris 1937). The diurnal term on the other hand is extremely variable. Both amplitude and phase angle vary very largely not only from station to station but also from month to month at a given station. The amplitude of the lunar term is only one fifteenth of that of the semi-diurnal solar term at sea level. It has, however, been shown (Appleton and Weekes 1939) to produce a change in height of the E layer of 1·7 kilometres. The 6 and 8 hour terms are small.

In order to compare the pressure variations with the cosmic ray rates the average daily variations of pressure (at Dublin Airport) for both the periods of the individual runs and for the year September 1953 to August 1954 inclusive have been computed. The necessary data were taken from the monthly weather report for Dublin of the Meteorological Service of the Department of Industry and Commerce. The results (which of course include the terms of all periods) are shown as continuous curves in figures 2 and 3. The pressure in millibars difference from average is given on the right-hand ordinate. Positive values are plotted downwards. The average pressure and the average local shower rate have been made to coincide. The different shapes of these pressure curves are largely due to the variations in the amplitude and phase of the diurnal term. Over the whole period September 1953 to August 1954 this term had an amplitude of only 0·03 mb and a phase angle of 15·1°. (For the same period the semi-diurnal term had amplitude 0·28 mb and phase angle 133°.) However, the average amplitude of the diurnal term for the month of January from 1950 to 1954 was

0·09 mb and its phase angle 164°. For July for the same period the values were 0·20 mb and 36·2°. For short periods the variation was even greater; e.g. for the period of the 20 cm run the values were 0·36 mb and 173°.

§ 6. THE BAROMETER COEFFICIENTS

The appearance of figures 2 and 3 suggests a connection between the local shower rate and these pressure changes. To see if this is indeed so, χ^2 tests were applied assuming (*a*) a barometer coefficient of -10% per cm Hg, (*b*) one of -50% per cm Hg, and (*c*) one of -430% per cm Hg. This last figure was obtained by taking the difference of the local shower rates for the minimum and maximum periods (10–11 hours and the average of 4–5 and 18–19 hours) and comparing it with the change in barometric pressure. A coefficient of $-430 \pm 90\%$ per cm Hg was obtained. For these three coefficients values of P of 0·002, 0·02 and 0·6 were obtained and it therefore seems probable that the barometer coefficient derived from these small changes in pressure is greater than -10% per cm Hg.

Many workers have derived a barometer coefficient for local penetrating showers using the large changes in pressure associated with the weather. The value usually given is -10% per cm Hg (Jánossy and Rochester 1944). Our own results using the large changes of pressure (which at Dublin may amount to as much as 80 mb) confirm this result. At all thicknesses of lead a value of this order was obtained with the exception of the run at 82·5 cm. Here the barometer coefficient seemed to be significantly less (about -5% per cm Hg). This, however, was not unexpected as other evidence seemed to show that about half the 'local' events at this depth were caused by μ-mesons. Thus it seems possible that there is a significant difference between the barometer coefficient derived from the large changes of pressure associated with the weather and that derived from the small changes of pressure caused by the regular daily oscillations of the atmosphere.

The changes associated with the weather are confined to the lower part of the atmosphere (below 15 kilometres). The oscillations on the other hand produce their biggest effects relatively in the upper atmosphere. Hence if the difference in the barometer coefficients is real it seems possible that the rate of local penetrating showers at sea level is strongly affected by changes in the atmosphere above the 15 km level.

§ 7. THE LOCAL SHOWERS AND SIDEREAL TIME

Figure 4 shows no obvious change in the rate of local showers with sidereal time. This conclusion was confirmed by a χ^2 test on the null hypothesis which gave a value $P = 0{\cdot}45$. Thus a straight line is a good fit for these results. This, of course, does not prove that there is no sidereal variation.

§ 8. THE EXTENSIVE SHOWERS

The results for the extensive showers are interesting but not conclusive. A straight line is a poor fit for the points for both solar and sidereal time. The respective values of P from χ^2 tests are 0·02 and 0·05. For solar time, a curve derived from the known pressure curve and a -430% per cm Hg barometer coefficient, $P = 0{\cdot}25$. On the other hand against sidereal time, the extensive showers show a maximum for the period 19–23 hours G.S.T. This in itself is not a conclusive result but this is the period at which the Galaxy crosses our meridian and maxima in the rates of soft extensive showers have been found at about 21 hours local sidereal time by Hodson (1951), Daudin (*Proceedings of the Bagnères Conference* 1953), Farley and Storey (1954) and Formaca and Martelli

(*Proceedings of the Bagnères Conference* 1953). A diurnal sine wave of 10% amplitude with its maximum at 21 hours G.S.T. gives a value of $P=0{\cdot}6$ on a χ^2 test when compared with the results in table 2. An amplitude of 10% is considerably larger than found by other observers. The showers selected in this experiment were, however, both penetrating and of high electron density (~ 200 particles per m^2).

Thus the position with regard to the extensive showers is rather confused. From the work on local showers presented here, and from work on extensive showers there seems to be some reason to believe that both variations may occur. But since we have averaged over many thicknesses of lead a real solar variation may have produced an apparent sidereal variation or vice versa. Thus while both variations may occur neither can yet be taken to be established.

§ 9. CONCLUSION

A variation of the rate of local penetrating showers with solar time appears to be established. It shows a strong negative correlation with the daily variations of barometric pressure. It seems likely that the associated barometric coefficient is greater than -10% per cm Hg. A value of $-430 \pm 90\%$ per cm Hg follows from the results. If this difference is significant it would appear that the rate of local penetrating showers at sea level is strongly affected by changes in the upper atmosphere.

Possible variations of the rate of high density extensive penetrating showers with both solar and sidereal time have been found.

ACKNOWLEDGMENTS

We are greatly indebted to Professor L. W. Pollak particularly for his help with the meteorological and statistical sections of this work, to Dr. N. A. Porter and Mr. P. D. McCormack for their help in running the apparatus, to Dr. E. Corinaldesi for many discussions and to Professor C. O'Ceallaigh, Dr. G. D. Rochester, Dr. F. C. Roesler and the Members of the Independent Research Group, Atomic Energy Research Establishment, for their criticisms of the original manuscript. We wish to thank the Director of the Meteorological Service of the Department of Industry and Commerce for his help.

REFERENCES

APPLETON, E. V., and WEEKES K., 1939, *Proc. Roy. Soc.* A, **171,** 171.

BARRETT, P., COCCONI, G., EISENBERG, Y., and GREISEN, K., 1954, *Phys. Rev.*, **95,** 1571, 1573.

CRANSHAW, T. E., and GALBRAITH, W., 1954, *Phil. Mag.*, **45,** 1109.

DARDIS, J. G., and MCCUSKER, C. B. A., 1954, *Proc. Phys. Soc.* A, **67,** 1026.

DUPERIER, A., 1945, *Proc. Phys. Soc.*, **57,** 464.

ELLIOT, H., 1952, *Progress in Cosmic Ray Physics*, Vol. I (Amsterdam : North Holland Publishing Co.).

FARLEY, F. J. M., and STOREY, J. R., 1954, *Proc. Phys. Soc.* A, **67,** 996.

HODSON, A. L., 1951, *Proc. Phys. Soc.* A, **64,** 1061.

JÁNOSSY, L., and ROCHESTER, G. D., 1944, *Proc. Roy. Soc.* A, **183,** 186.

MITRA, S. K., 1947, *The Upper Atmosphere* (Calcutta : The Royal Asiatic Society of Bengal).

PEKERIS, C. L., 1937, *Proc. Roy. Soc.* A, **158,** 650.

Proceedings of the Bagnères Conference, 1953, Imprimerie Universitaire Toulouse.

SHERMAN, N., 1954, *Phys. Rev.*, **93,** 208.

WILKES, M. V., 1949, *The Oscillations of the Earth's Atmosphere* (Cambridge : University Press).

The Electronic Spectra of Aromatic Molecules
IV : Excited States of Odd Alternant Hydrocarbon Radicals and Ions

By H. C. LONGUET-HIGGINS and J. A. POPLE
University Chemical Laboratory, Cambridge

MS. received 9th December 1954

Abstract. The lower excited electronic states of some unsaturated hydrocarbon radicals and ions are discussed in terms of molecular orbital theory, taking account of electron interaction. The following results emerge:

(i) In the absorption spectrum of an alternant radical there should appear two long wavelength bands. These arise jointly from excitations of electrons into and out of the singly occupied orbital. The lower frequency band should be weak, and the higher frequency band relatively strong. The existence of a low-lying quartet level is also predicted.

(ii) The absorption spectra of the corresponding anion and cation should be closely related, the lowest two excited states being for both types of ion a triplet and a singlet.

(iii) The singlet–triplet separation in the ions should be roughly equal to the separation of the two low-lying doublets of the radical.

These generalizations are supported by the experimental data for certain triaryl-methyl systems.

§ 1. INTRODUCTION

Odd alternant hydrocarbons are conjugated systems with an odd number of carbon atoms connected together in such a way that they can be divided into two classes, each member of one being bonded only to members of the other. According to the number of electrons present, they may be charged ions or free radicals. They form an important class of compounds whose spectra should be understandable in terms of molecular orbital theory.

The simplest molecular orbital theory of conjugated hydrocarbons is that due to Hückel (1931) according to which the orbitals are supposed to be approximate eigenfunctions of an effective one-electron Hamiltonian. The Hückel theory has been applied to odd alternants by Longuet-Higgins (1950) who showed that there are certain non-bonding orbitals restricted to one of the two classes of carbon atoms. We shall only consider systems of $2m-1$ centres with one non-bonding orbital restricted to starred atoms. This orbital will be empty in the cation, singly occupied in the radical and doubly occupied in the anion. The eigenvalues of the remaining orbitals are symmetrically placed in pairs above and below the energy of the non-bonding orbital.

If the excitation energies are taken to be the difference of Hückel orbital eigenvalues, then the lowest excited configurations of the cation, radical and anion will all be equally raised above their ground states (figure 1). These configurations will lead to a singlet and a triplet level for each of the two ions and two doublets for the radical. In addition, the radical will have an excited quartet state and two further doublets due to the configuration in which an electron is moved from the lowest to the highest of the three orbitals. However, these predictions of the Hückel theory are over-simplified because of the neglect of electron interaction. A similar situation arises in the corresponding theory of even alternants. In part I of this series, Dewar and Longuet-Higgins (1954) suggested an interpretation of the long-wave spectra of alternant hydrocarbons in which they allowed for the particular effect of electron interaction in splitting levels which were degenerate according to the Hückel theory. When applied to odd alternant radicals, they showed that this led to a splitting of the two lower doublet levels. In part II (Pople 1955), it was shown how the conclusions of Dewar and Longuet-Higgins on even alternants could be justified in terms of a more rigorous theory, based on self-consistent orbitals, in which electron interaction was taken into account at all stages. The first aim of the present paper is to develop a similar background for the application to odd radicals. This is followed by a treatment of the excited states of corresponding singly charged ions, also based on the use of self-consistent orbitals. It is important that electron interaction should be adequately allowed for in a discussion of the structure of ions, for one of the principal weaknesses of the Hückel theory is its assumption that the energy of an electron in one orbital is independent of whether the others are occupied or not. In the final section, the general relation between the spectra of corresponding radicals and ions is reconsidered.

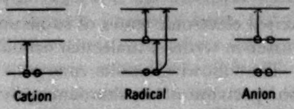

Figure 1. Configurational excitations in odd alternant hydrocarbons.

§ 2. Self-Consistent Orbital Functions for Alternant Radicals

The determination of LCAO self-consistent orbitals for radicals has been discussed generally by Pople and Nesbet (1954), who derived equations for the coefficients, and these equations were applied to odd alternant hydrocarbons by Brickstock and Pople (1954).

Pople and Nesbet suggested that the ground state of a radical containing $2m-1$ mobile electrons should be described by a wave function of the form

$$\chi_0 = |\psi_1{}^{\alpha} \dots \psi_m{}^{\alpha} \bar{\psi}_1{}^{\beta} \dots \bar{\psi}_{m-1}{}^{\beta}| \qquad \dots\dots(2.1)$$

in which m electrons are assigned to space orbitals $\psi_1{}^{\alpha} \dots \psi_m{}^{\alpha}$, with spin $\frac{1}{2}$, and the other $m-1$ electrons are assigned to orbitals $\psi_1{}^{\beta} \dots \psi_{m-1}{}^{\beta}$, with spin $-\frac{1}{2}$. They removed the restriction that the spatial orbitals $\psi_i{}^{\alpha}$ and $\psi_i{}^{\beta}$ be identical, so that one could no longer speak of doubly occupied molecular orbitals.

This description is convenient for a discussion of the unexcited radical, but is not altogether suitable for discussing electronic excitations, for the following reason. It is known that any eigenstate of a many-electron system must be not only an eigenfunction of the Hamiltonian $\mathscr{H}$ (assumed spin-free) but also of the spin component $\mathbf{S}_z$ and the total spin operator $\mathbf{S}^2$. The eigenvalue of $\mathbf{S}^2$, namely $S(S+1)\hbar^2$, determines the multiplicity $2S+1$ of the eigenstate; and the classification of electronic states according to their multiplicity is of fundamental importance in spectroscopy, since transitions are forbidden between states of different multiplicity. Now the function of Pople and Nesbet (1954), though an eigenfunction of $\mathbf{S}_z$ with eigenvalue $\frac{1}{2}\hbar$, is not an eigenfunction of $\mathbf{S}^2$, whereas the simpler function

$${}^2\chi_0 = |\psi_1 \bar{\psi}_1 \dots \psi_{m-1} \bar{\psi}_{m-1} \psi_m| \qquad \dots\dots(2.2)$$

in which the space parts of ψ_i and $\bar{\psi}_i$ are identical, may be shown to be an eigenfunction of $\mathbf{S}^2$ with eigenvalue $\frac{1}{2}(\frac{1}{2}+1)\hbar^2$, and is therefore one component ($S_z = \frac{1}{2}\hbar$) of a doublet. In this respect, therefore, the latter function is to be preferred to the former as a description of the ground state, which is normally a doublet.

One must now enquire how the orbitals $\psi_1 \ldots \psi_m$ are to be determined. The best orbitals are those which minimize the energy of the ground state ${}^2\chi_0$, subject to the orbitals themselves being orthonormal—a condition which involves no loss of generality. Assume for the moment that $\psi_1 \ldots \psi_m$ have been found, and that $\psi_k (k = m+1, m+2 \ldots)$ is some set of other functions which together with $\psi_1 \ldots \psi_m$ constitute a complete orthonormal set. Then any infinitesimal variation in the orbitals $\psi_1 \ldots \psi_m$, subject to the condition of orthonormality, has the effect of adding to ${}^2\chi_0$ small amounts of singly excited configurations, as follows:

$$\begin{aligned}
{}^2\chi_0 \rightarrow & \,|\psi_1\bar{\psi}_1 \ldots \psi_i\bar{\psi}_i \ldots \psi_{m-1}\bar{\psi}_{m-1}\psi_m| \\
& + \sum_{i=1}^{m-1} \lambda_{im} |\psi_1\bar{\psi}_1 \ldots \psi_i\bar{\psi}_m \ldots \psi_{m-1}\bar{\psi}_{m-1}\psi_m| \\
& + \sum_{k=m+1}^{\infty} \lambda_{mk} |\psi_1\bar{\psi}_1 \ldots \psi_i\bar{\psi}_i \ldots \psi_{m-1}\bar{\psi}_{m-1}\psi_k| \\
& + \sum_{i=1}^{m-1} \sum_{k=m+1}^{\infty} \lambda_{ik} \{ |\psi_1\bar{\psi}_1 \ldots \psi_i\bar{\psi}_k \ldots \psi_{m-1}\bar{\psi}_{m-1}\psi_m| \\
& + |\psi_1\bar{\psi}_1 \ldots \psi_k\bar{\psi}_i \ldots \psi_{m-1}\bar{\psi}_{m-1}\psi_m| \}. \qquad \ldots\ldots(2.3)
\end{aligned}$$

The associated change in energy is given by the expression

$$\begin{aligned}
& \sum_{i=1}^{m-1} \lambda_{im} \langle {}^2\chi_0 | \mathscr{H} | \psi_i^{-1}\psi_m \rangle + \sum_{k=m+1}^{\infty} \lambda_{mk} \langle {}^2\chi_0 | \mathscr{H} | \psi_m^{-1}\psi_k \rangle \\
& \qquad + \sum_{i=1}^{m-1} \sum_{k=m+1}^{\infty} \lambda_{ik} \langle {}^2\chi_0 | \mathscr{H} | \psi_i^{-1}\psi_k \rangle, \qquad \ldots\ldots(2.4)
\end{aligned}$$

where $\langle {}^2\chi_0 | \mathscr{H} | \psi_i^{-1}\psi_m \rangle$ represents the matrix element of the Hamiltonian $\mathscr{H}$ between ${}^2\chi_0$ and the wave function multiplying λ_{im} in (2.3), the other terms in (2.4) being similarly defined.

In passing we may note that the wave functions represented by $\psi_i^{-1}\psi_m$, $\psi_m^{-1}\psi_k$ and $\psi_i^{-1}\psi_k$ are eigenfunctions not only of $\mathbf{S}_z$ but of $\mathbf{S}^2$ also, with eigenvalue $\frac{1}{2}(\frac{1}{2}+1)\hbar^2$. They are therefore doublets, like ${}^2\chi_0$. For the energy of ${}^2\chi_0$ to be stationary, then, the matrix elements in (2.4) must all vanish, and this implies that the ground state ${}^2\chi_0$ cannot interact with any of the singly excited configurations appearing in (2.3).

We now express the Hamiltonian $\mathscr{H}$ in the form $H+G$, where H is a sum of one-electron operators (the 'core field' Hamiltonian) and G includes all the two-electron repulsion terms. This leads to the equations

$$\left.\begin{aligned}
& 0 = \langle {}^2\chi_0 | \mathscr{H} | \psi_i^{-1}\psi_m \rangle = H_{im} + \sum_{j=1}^{m-1} \{ 2(ji|G|jm) - (ji|G|mj) \} \\
& \qquad\qquad + (mi|G|mm) \\
& \qquad\qquad (i = 1, 2, \ldots, m-1) \\
& 0 = \langle {}^2\chi_0 | \mathscr{H} | \psi_m^{-1}\psi_k \rangle = H_{mk} + \sum_{j=1}^{m-1} \{ 2(jm|G|jk) - (jm|G|kj) \} \\
& \qquad\qquad (k = m+1, m+2, \ldots) \\
& 0 = \langle {}^2\chi_0 | \mathscr{H} | \psi_i^{-1}\psi_k \rangle = H_{ik} + \sum_{j=1}^{m-1} \{ 2(ji|G|jk) - (ji|G|kj) \} \\
& \qquad\qquad + \tfrac{1}{2} \{ 2(mi|G|mk) - (mi|G|km) \} \\
& \qquad (i = 1, 2, \ldots, m-1 ; k = m+1, m+2, \ldots).
\end{aligned}\right\} \quad \ldots(2.5)$$

In these equations H_{pq} represents the matrix element of the one-electron core Hamiltonian between ψ_p and ψ_q, and $(pq|G|rs)$ denotes the two-electron integral

$$\iint \psi_p{}^*(1)\psi_q{}^*(2)\,\frac{e^2}{r_{12}}\,\psi_r(1)\psi_s(2)\,d\tau_1 d\tau_2.$$

Proceeding by analogy with the closed-shell case we now introduce a one-electron operator F defined by the equation

$$\int \psi_p F \psi_q = F_{pq} = H_{pq} + \sum_{j=1}^{m-1}\{2(jp|G|jq)-(jp|G|qj)\} + \tfrac{1}{2}\{2(mp|G|mq)-(mp|G|qm)\}.$$

This makes it possible to rewrite equations (2.5) in the more compact form:

$$\begin{aligned} &F_{im}+\tfrac{1}{2}(mi|G|mm)=0\\ &F_{mk}-\tfrac{1}{2}(mm|G|mk)=0\\ &F_{ik}=0 \end{aligned}$$

where $i=1, 2, \ldots, m-1;\, k=m+1, m+2, \ldots$ ......(2.7)

These equations are not quite so simple as the corresponding equations for a closed shell; but if the terms $(mi|G|mm)$ and $(mm|G|mk)$ are small, as they will appear to be, the molecular orbitals may be taken to satisfy the simpler equations

$$F_{pq}=0. \qquad \text{......(2.8)}$$

Now F, being a linear Hermitian operator, generates a complete set of orthonormal eigenfunctions with real eigenvalues. Furthermore, the matrix element of F between any two of these eigenfunctions is necessarily zero. It follows then that the molecular orbitals we require are just eigenfunctions of the operator F, satisfying the eigenvalue equation

$$F\psi_i = E_i\psi_i. \qquad \text{......(2.9)}$$

The eigenvalues E_1 to E_{m-1} are then the 'energies' of the doubly occupied orbitals and E_m the energy of the singly occupied orbital. E_{m+1}, E_{m+2}, and so on, are the energies of the orbitals which are unoccupied in the ground state. It is not possible to identify the energies $E_1 \ldots E_m$ with the various ionization potentials, as in the closed shell case, but E_m can be identified with the mean of the ionization potential and electron affinity of the radical.

These orbitals can now be used to construct wave functions for excited states. The configurations most likely to contribute to the lowest excited states are those in which an electron is raised (i) from ψ_{m-1} to ψ_m, (ii) from ψ_m to ψ_{m+1} and (iii) from ψ_{m-1} to ψ_{m+1}. The first of these gives rise to a doublet configuration whose wave function is

$${}^2\chi_1 = |\psi_1\bar{\psi}_1 \ldots \psi_{m-1}\bar{\psi}_m\psi_m|. \qquad \text{......(2.10)}$$

The second also gives rise to a doublet configuration, namely

$${}^2\chi_2 = |\psi_1\bar{\psi}_1 \ldots \psi_{m-1}\bar{\psi}_{m-1}\psi_{m+1}|. \qquad \text{......(2.11)}$$

The third, however, gives rise to two doublets and a quartet. The doublet configurations may be taken in the forms

$${}^2\chi_3 = \sqrt{\tfrac{1}{2}}\,|\psi_1\bar{\psi}_1 \ldots \psi_{m-1}\bar{\psi}_{m+1}\psi_m| + \sqrt{\tfrac{1}{2}}\,|\psi_1\bar{\psi}_1 \ldots \psi_{m+1}\bar{\psi}_{m-1}\psi_m|, \qquad \text{......(2.12)}$$

$$\begin{aligned} {}^2\chi_3{}' = \sqrt{\tfrac{2}{3}}\,|\psi_1\bar{\psi}_1 \ldots \psi_{m-1}\psi_{m+1}\bar{\psi}_m| &- \sqrt{\tfrac{1}{6}}\,|\psi_1\bar{\psi}_1 \ldots \psi_{m-1}\bar{\psi}_{m+1}\psi_m| \\ &- \sqrt{\tfrac{1}{6}}\,|\psi_1\bar{\psi}_1 \ldots \bar{\psi}_{m-1}\psi_{m+1}\psi_m|, \end{aligned} \qquad \text{......(2.13)}$$

while the quartet configuration is

$$
\begin{aligned}
{}^4\chi_3 = \sqrt{\tfrac{1}{3}}\,|\psi_1\bar{\psi}_1\ldots\psi_{m-1}\psi_{m+1}\bar{\psi}_m| + \sqrt{\tfrac{1}{3}}\,|\psi_1\bar{\psi}_1\ldots\psi_{m-1}\bar{\psi}_{m+1}\psi_m| \\
+ \sqrt{\tfrac{1}{3}}\,|\psi_1\bar{\psi}_1\ldots\bar{\psi}_{m-1}\psi_{m+1}\psi_m|.
\end{aligned}
\qquad \ldots\ldots(2.14)
$$

It has already been established that ${}^2\chi_1$, ${}^2\chi_2$ and ${}^2\chi_3$ do not interact with ${}^2\chi_0$; and ${}^4\chi_3$ cannot do so either, as configurations of different multiplicity do not interact. ${}^2\chi_3'$, on the other hand, does interact with the ground state. However, it may be verified without difficulty that the transition moment between ${}^2\chi_0$ and ${}^2\chi_3'$ is zero, so that optical transitions between these two configurations are strictly forbidden. ${}^2\chi_3'$ is therefore analogous to a doubly excited configuration of a closed shell system, and we shall not consider it further.

The excitation energies of the configurations ${}^2\chi_1$, ${}^2\chi_2$, ${}^2\chi_3$ and ${}^4\chi_3$ may be evaluated in a straightforward manner, using the relationship

$$
\begin{aligned}
E_i = F_{ii} = H_{ii} + \sum_{j=1}^{m-1}\{2(ji\,|\,G\,|\,ji) - (ji\,|\,G\,|\,ij)\} \\
+ \tfrac{1}{2}\{2(mi\,|\,G\,|\,mi) - (mi\,|\,G\,|\,im)\}.
\end{aligned}
\qquad \ldots\ldots(2.15)
$$

The results are:

Configuration	Excitation energy
${}^2\chi_1$	$E_m - E_{m-1} - (m-1, m\,|\,G\,|\,m-1, m) + \tfrac{1}{2}(m-1, m\,|\,G\,|\,m, m-1) + \tfrac{1}{2}(mm\,|\,G\,|\,mm)$
${}^2\chi_2$	$E_{m+1} - E_m - (m, m+1\,|\,G\,|\,m, m+1) + \tfrac{1}{2}(m, m+1\,|\,G\,|\,m+1, m) + \tfrac{1}{2}(mm\,|\,G\,|\,mm)$
${}^2\chi_3$	$E_{m+1} - E_{m-1} - (m-1, m+1\,|\,G\,|\,m-1, m+1) + 2(m-1, m+1\,|\,G\,|\,m+1, m-1)$
${}^4\chi_3$	$E_{m+1} - E_{m-1} - (m-1, m+1\,|\,G\,|\,m-1, m+1) - \tfrac{1}{2}(m+1, m\,|\,G\,|\,m, m+1) - \tfrac{1}{2}(m-1, m\,|\,G\,|\,m, m-1)$.

(2.16)

In dealing with a conjugated radical such as benzyl it is most convenient to express these results in LCAO form. We set

$$\psi_i = \sum_{\nu} c_{i\nu}\phi_{\nu} \qquad \ldots\ldots(2.17)$$

where ϕ_ν are the various atomic orbitals of the conjugated system. Equation (2.9) then becomes

$$\sum_{\nu} c_{i\nu}F\phi_{\nu} = E_i \sum_{\nu} c_{i\nu}\phi_{\nu}. \qquad \ldots\ldots(2.18)$$

Multiplying both sides by ϕ_μ^*, integrating, and setting $\int\phi_\mu^*\phi_\nu d\tau = \delta_{\mu\nu}$, we obtain the secular equations

$$\sum_{\nu} F_{\mu\nu}c_{i\nu} = E_i c_{i\mu} \qquad \ldots\ldots(2.19)$$

where $F_{\mu\nu}$ is the matrix element of F between ϕ_μ and ϕ_ν. With the simplifying assumptions of Brickstock and Pople (1954), these elements take the form

$$
\left.
\begin{aligned}
F_{\mu\mu} &= U_{\mu\mu} + \tfrac{1}{2}p_{\mu\mu}\gamma_{\mu\mu} + \sum_{\sigma}^{\neq\mu}(p_{\sigma\sigma} - 1)\gamma_{\mu\sigma} \\
F_{\mu\nu} &= H_{\mu\nu} - \tfrac{1}{2}p_{\mu\nu}\gamma_{\mu\nu} \\
\text{where}\qquad p_{\mu\nu} &= \sum_{i=1}^{m-1} 2c_{i\mu}c_{i\nu} + c_{m\mu}c_{m\nu}
\end{aligned}
\right\}
\qquad \ldots\ldots(2.20)
$$

and $\gamma_{\mu\mu}$, $U_{\mu\mu}$ and $H_{\mu\nu}$ are coulomb repulsion integrals and core integrals as in part II. Let us now apply these equations to an alternant hydrocarbon radical, containing $2m-1$ conjugated atoms of which m are 'starred' and $m-1$ 'unstarred', each starred atom being linked only to unstarred atoms and vice versa.

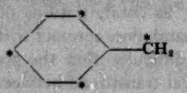

Let us assume that at some stage in the iterative calculation of the $c_{i\nu}$ (*a*) the diagonal elements $F_{\mu\mu}$ are all equal and (*b*) the off-diagonal elements $F_{\mu\nu}$ vanish if μ, ν are both starred or both unstarred. Then if equations (2.9) are solved to obtain the $p_{\mu\nu}$ it will be found that (α) the $p_{\mu\mu}$ are all unity and (β) the $p_{\mu\nu}$ vanish if μ, ν are both starred or both unstarred. This means that in the next iteration we must take

(*a*) $F_{\mu\mu} = U_{\mu\mu} + \frac{1}{2}\gamma_{\mu\mu}$,

(*b*) $F_{\mu\nu} = H_{\mu\nu} = 0$ if μ, ν are both starred or both unstarred,

(*c*) $F_{\mu\nu} = H_{\mu\nu} - \frac{1}{2}p_{\mu\nu}\gamma_{\mu\nu}$ if one of μ, ν is starred and the other unstarred (2.21).

Therefore if at one stage in the iterative calculation conditions (*a*) and (*b*) are satisfied, they will be satisfied at the next stage too; so we conclude that they will be satisfied by the elements $F_{\mu\nu}$ of the self-consistent Hamiltonian itself.

In consequence, the familiar pairing properties of the Hückel orbitals in a radical are exhibited by the self-consistent orbitals also. These properties are:

(i) If $\psi_i (i=1, \ldots, m-1)$ is a doubly occupied orbital, then there is a 'conjugate' unoccupied orbital ψ_{2m-i} such that

$$\left.\begin{aligned} c_{2m-i,\mu} &= c_{i\mu} && (\mu \text{ starred}) \\ c_{2m-i,\mu} &= -c_{i\mu} && (\mu \text{ unstarred}). \end{aligned}\right\} \qquad \ldots\ldots(2.22)$$

(ii) The energy parameters of a pair of conjugate orbitals are related by the equation

$$E_i + E_{2m-i} = 2U_{\mu\mu} + \gamma_{\mu\mu}. \qquad \ldots\ldots(2.23)$$

(iii) The singly occupied orbital ψ_m has the form

$$\psi_m = \sum{}^{*} c_{m\mu}\phi_\mu \qquad \ldots\ldots(2.24)$$

where the summation is confined to starred atoms only, and is non-bonding in the sense that

$$E_m = U_{\mu\mu} + \tfrac{1}{2}\gamma_{\mu\mu}. \qquad \ldots\ldots(2.25)$$

In view of these pairing properties the molecular orbitals ψ_{m+1}, ψ_m can be written

$$\left.\begin{aligned} \psi_{m-1} &= \sum{}^{*} b_\mu\phi_\mu + \sum{}^{0} b_\mu\phi_\mu \\ \psi_m &= \sum{}^{*} a_\mu\phi_\mu \\ \psi_{m+1} &= \sum{}^{*} b_\mu\phi_\mu - \sum{}^{0} b_\mu\phi_\mu, \end{aligned}\right\} \qquad \ldots\ldots(2.26)$$

where Σ^*, Σ^0 are sums over starred and unstarred atoms respectively. Their orbital energies satisfy the equality:

$$E_{m+1} - E_m = E_m - E_{m-1} = \Delta E, \text{ say.} \qquad \ldots\ldots(2.27)$$

Using (2.26) and (2.27), and the approximations introduced in II, we may express the excitation energies in (2.16) in terms of ΔE and the repulsion integrals $\gamma_{\mu\nu}$. It turns out that the excitation energies of ${}^2\chi_1$ and ${}^2\chi_2$ are identical, as predicted by the Hückel theory and illustrated schematically in figure 1. This means that there will be first-order configuration interaction between ${}^2\chi_1$ and ${}^2\chi_2$, the magnitude of the splitting (see I) being determined by the integral

$$\begin{aligned}\langle {}^2\chi_1 | \mathscr{H} | {}^2\chi_2 \rangle &= -(m+1, m-1 | G | m, m) \\ &= -\sum_{\mu\nu} a_\mu b_\mu a_\nu b_\nu \gamma_{\mu\nu}. \qquad \ldots\ldots(2.28)\end{aligned}$$

When this configurational interaction is taken into account, the excited states and their excitation energies become:

State	Excitation energy
$\sqrt{\tfrac{1}{2}}({}^2\chi_1 + {}^2\chi_2)$	$\Delta E - \sum_{\mu\nu} a_\mu{}^2 b_\nu{}^2 \gamma_{\mu\nu} + \tfrac{1}{2}\sum_{\mu\nu} a_\mu{}^2 a_\nu{}^2 \gamma_{\mu\nu} - \tfrac{1}{2}\sum_{\mu\nu} a_\mu b_\mu a_\nu b_\nu \gamma_{\mu\nu}$
$\sqrt{\tfrac{1}{2}}({}^2\chi_1 - {}^2\chi_2)$	$\Delta E - \sum_{\mu\nu} a_\mu{}^2 b_\nu{}^2 \gamma_{\mu\nu} + \tfrac{3}{2}\sum_{\mu\nu} a_\mu b_\mu a_\nu b_\nu \gamma_{\mu\nu} + \tfrac{1}{2}\sum_{\mu\nu} a_\mu{}^2 a_\nu{}^2 \gamma_{\mu\nu}$
${}^2\chi_3$	$2\Delta E - \sum_{\mu\nu} b_\mu{}^2 b_\nu{}^2 \gamma_{\mu\nu} + 2(\sum_\mu{}^* - \sum_\mu{}^0)(\sum_\nu{}^* - \sum_\nu{}^0) b_\mu{}^2 b_\nu{}^2 \gamma_{\mu\nu}$
${}^4\chi_3$	$2\Delta E - \sum_{\mu\nu} b_\mu{}^2 b_\nu{}^2 \gamma_{\mu\nu} - \sum_{\mu\nu} a_\mu b_\mu a_\nu b_\nu \gamma_{\mu\nu}.$

Dewar and Longuet-Higgins showed in I that the lowest of these states, namely $\sqrt{\tfrac{1}{2}}({}^2\chi_1 + {}^2\chi_2)$, should give only a weak band in the spectrum, but that the transition ${}^2\chi_0 \rightarrow \sqrt{\tfrac{1}{2}}({}^2\chi_1 - {}^2\chi_2)$ should give rise to a relatively intense band. This result still holds with self-consistent orbitals, since the pairing properties of the Hückel orbitals are preserved. The interpretation of alternant radical spectra suggested by Dewar and Longuet-Higgins is therefore confirmed by the self-consistent orbital theory.

Before discussing the alternant ions we should recall that the passage from equations (2.7) to (2.8) depends on the integrals $(im | G | mm)$ and $(mm | G | mk)$ being negligible. It is difficult to assess the accuracy of this assumption in general, but in the particular case of allyl the integrals $(12 | G | 22)$ and $(22 | G | 23)$ vanish by symmetry. Though this will not happen in general, we doubt whether the errors so introduced will be large, and feel that the assumption is justified in large measure by the great simplification which it makes possible.

§ 3. SELF-CONSISTENT ORBITAL FUNCTIONS FOR ODD ALTERNANT IONS

Singly charged odd alternant ions generally have closed shell ground states. The theory of excited states based on self-consistent orbitals is therefore similar to the treatment of even alternants given in II. In this section we shall show how certain pairing properties can be used to predict similarities between corresponding positive and negative ions.

The solution of the self-consistent equations has been discussed by Brickstock and Pople (1954). The LCAO coefficients for positive and negative ions must satisfy

$$\left.\begin{aligned}\sum_\nu F_{\mu\nu}{}^+ c_{i\nu}{}^+ &= E_i{}^+ c_{i\mu}{}^+ \\ \sum_\nu F_{\mu\nu}{}^- c_{i\nu}{}^- &= E_i{}^- c_{i\mu}{}^-\end{aligned}\right\} \qquad \ldots\ldots(3.1)$$

where F_μ^+, F_μ^- are defined as in (2.20) except that

$$\left.\begin{aligned} p_{\mu\nu}^+ &= 2\sum_{i=1}^{m-1} c_{i\mu}^+ c_{i\nu}^+ \\ p_{\mu\nu}^- &= 2\sum_{i=1}^{m} c_{i\mu}^- c_{i\nu}^- . \end{aligned}\right\} \quad \ldots\ldots (3.2)$$

With the same set of approximations, the following pairing properties can be deduced:

$$\text{(i)} \qquad p_{\mu\mu}^+ + p_{\mu\mu}^- = 2 \quad \ldots\ldots (3.3)$$

$$\text{(ii)} \qquad E_i^+ + E_{2m-i}^- = 2U_{\mu\mu} + \gamma_{\mu\mu} \quad \ldots\ldots (3.4)$$

$$\text{(iii)} \qquad \left.\begin{aligned} c_{i\mu}^+ &= c_{2m-i,\mu}^- \quad (\mu \text{ starred}) \\ c_{i\mu}^+ &= -c_{2m-i,\mu}^- \quad (\mu \text{ unstarred}). \end{aligned}\right\} \quad \ldots\ldots (3.5)$$

The simplest configurational excitations are $\psi_{m-1}^+ \to \psi_m^+$ for the cation and $\psi_m^- \to \psi_{m+1}^-$ for the anion. The corresponding determinantal wave functions for the ground states will be denoted by χ_0^+, χ_0^- and for the excited states by ${}^1\chi_1^+$, ${}^3\chi_1^+$ and ${}^1\chi_1^-$, ${}^3\chi_1^-$. By the pairing property (3.5) the orbitals involved can be written

$$\left.\begin{aligned} \psi_{m-1}^+ &= \sum_\mu{}^{*} b_\mu^+ \phi_\mu + \sum_\mu{}^{0} b_\mu^+ \phi_\mu \\ \psi_m^+ &= \sum_\mu{}^{*} a_\mu^+ \phi_\mu + \sum_\mu{}^{0} a_\mu^+ \phi_\mu \\ \psi_m^- &= \sum_\mu{}^{*} a_\mu^+ \phi_\mu - \sum_\mu{}^{0} a_\mu^+ \phi_\mu \\ \psi_{m+1}^- &= \sum_\mu{}^{*} b_\mu^+ \phi_\mu - \sum_\mu{}^{0} b_\mu^+ \phi_\mu . \end{aligned}\right\} \quad \ldots\ldots (3.6)$$

The excitation energies of these states can be evaluated by standard methods and are:

States	Excitation energies
${}^1\chi_1^+, {}^1\chi_1^-$	$E_m^+ - E_{m-1}^+ - \sum_{\mu\nu} a_\mu^{+2} b_\nu^{+2} \gamma_{\mu\nu} + 2\sum_{\mu\nu} a_\mu^+ b_\mu^+ a_\nu^+ b_\nu^+ \gamma_{\mu\nu}$
${}^3\chi_1^+, {}^3\chi_1^-$	$E_m^+ - E_{m-1}^+ - \sum_{\mu\nu} a_\mu^{+2} b_\nu^{+2} \gamma_{\mu\nu}$

The theory in this form therefore predicts that the energy levels of the lowest singlet and triplet states should be the same for corresponding positive and negative ions. In the next section we shall attempt to compare these with the excitation energies for the radicals derived previously.

§ 4. COMPARISON BETWEEN CORRESPONDING RADICALS AND IONS

It is not possible to make a direct comparison between radicals and ions on the basis of the formulae of the previous sections as the self-consistent coefficients are not simply related. We may get some idea of the relationship, however, by using the radical orbitals (2.26) as approximations in all cases. It then follows, if μ and ν are both starred or both unstarred, that

$$\left.\begin{aligned} p_{\mu\mu}^\pm &= 1 \mp a_\mu^2 \\ p_{\mu\nu}^\pm &= \ \mp a_\mu a_\nu . \end{aligned}\right\} \quad \ldots\ldots (4.1)$$

Further, if μ and ν belong to different classes, $p_{\mu\nu}$ is the same for the radical and both ions.

Although the orbitals are now taken to be identical, the eigenvalues E_i^+, E_i and E_i^- will not coincide. They are easily evaluated as diagonal elements of the corresponding operators, however, and it is found that

$$E_{m+1}-E_m=E_m-E_{m-1}=-2\sum_{\mu}{}^{*}\sum_{\nu}{}^{0}b_\mu b_\nu(H_{\mu\nu}-\tfrac{1}{2}p_{\mu\nu}\gamma_{\mu\nu}) \qquad \ldots\ldots(4.2)$$

$$\begin{aligned}E_{m+1}{}^{-}-E_m{}^{-}=E_m{}^{+}-E_{m-1}{}^{+}=&-2\sum_{\mu}{}^{*}\sum_{\nu}{}^{0}b_\mu b_\nu(H_{\mu\nu}-\tfrac{1}{2}p_{\mu\nu}\gamma_{\mu\nu})\\&+\sum_{\mu\nu}a_\mu{}^2b_\nu{}^2\gamma_{\mu\nu}-\tfrac{1}{2}\sum_{\mu\nu}a_\mu{}^2a_\nu{}^2\gamma_{\mu\nu}-\tfrac{1}{2}\sum_{\mu\nu}a_\mu b_\mu a_\nu b_\nu\gamma_{\mu\nu}.\end{aligned} \qquad \ldots\ldots(4.3)$$

Using these results the excitation energies of radicals and ions, (2.29) and (3.7) respectively, can be directly compared. The following general features of the results are of interest.

(i) The separation of the two doublet levels $\sqrt{\tfrac{1}{2}}(^2\chi_1\pm{}^2\chi_2)$ is equal to the singlet–triplet splitting of the ionic states $^1\chi_1{}^{\pm}$ and $^3\chi_1{}^{\pm}$.

(ii) The excitation energies of these two excited doublet levels are greater than those of the corresponding ionic singlet–triplet pair by an amount

$$\sum_{\mu\nu}a_\mu{}^2(a_\nu{}^2-b_\nu{}^2)\gamma_{\mu\nu}.$$

This is the difference between the averaged coulomb interaction between two electrons in ψ_m and that between one in ψ_m and one in ψ_{m-1}. It is not possible to prove that this is strictly positive, but it seems likely that it will usually be so.

(iii) The lowest quartet level of the radical will be considerably lower than would be expected on the basis of the Hückel theory, which would predict the excitation energy to be twice that of the doublets. Using the notation $\mathscr{E}(\chi)$ for the excitation energy of state χ, we have

$$\mathscr{E}(^4\chi)-2\mathscr{E}(\sqrt{\tfrac{1}{2}}(^2\chi_1+{}^2\chi_2))=-\sum_{\mu\nu}(a_\mu{}^2-b_\mu{}^2)(a_\nu{}^2-b_\nu{}^2)\gamma_{\mu\nu} \qquad \ldots\ldots(4.4)$$

which should be negative. This means that the excitation energy of the quartet is less than twice that of the *lower* doublet. But it is not possible to say whether it will be above or below the doublet $\sqrt{\tfrac{1}{2}}(^2\chi_1-{}^2\chi_2)$ without detailed calculations.

(iv) The doublet $^2\chi_3$ will lie above the quartet $^4\chi$ and will probably be the highest of the excited states considered.

These conclusions are illustrated schematically in the energy level diagram of figure 2.

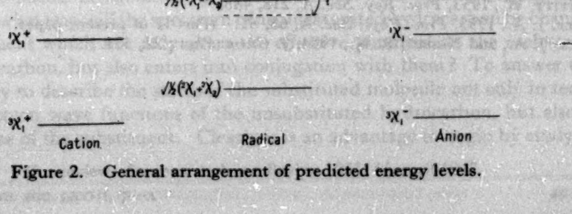

Figure 2. General arrangement of predicted energy levels.

The quantitative application of the theory can be illustrated by calculations on allyl and benzyl, two simple odd alternants (table 1). These are based on the formulae (4.4) using the same integrals β and $\gamma_{\mu\nu}$ as in part II.

Table 1. Calculated Excitation Energies of Odd Alternants (ev)

	Ion		Radical			
State	$^3\chi_1{}^+$	$^1\chi_1{}^+$	$\sqrt{\frac{1}{2}}(^2\chi_1+{}^2\chi_2)$ (weak)	$\sqrt{\frac{1}{2}}(^2\chi_1-{}^2\chi_2)$ (strong)	$^2\chi_3$	$^4\chi$
Allyl	2·39	4·94	2·74	5·29	7·74	4·51
Benzyl	1·96	2·68	3·46	4·18	6·23	3·97

The calculations of the allyl radical may be compared with those of Moffitt (1953). The results are similar, although Moffitt predicts the quartet level to be above both doublets $\sqrt{\frac{1}{2}}(^2\chi_1 \pm {}^2\chi_2)$.

Experimental data on the spectra of odd alternants is rather limited, but what there is fits in with the qualitative description. Recently, Chu and Weissman (1954) have observed the spectra of some triaryl-methyl radicals and their cations. They found that each free radical shows a weak absorption in the visible region and a much stronger one in the near ultra-violet. The corresponding cations have a region of intense absorption at an intermediate wavelength. The approximate energy levels (peak absorption) are given in table 2.

Table 2. Energy Levels in Triaryl-Methyl Radicals and Cations (cm^{-1})

Substance	Radical		Cation
	Weak	Strong	Strong
Triphenyl-methyl	19,000	29,000	23,500
Diphenyl-p-xenylmethyl	17,500	26,000	19,500
Phenyl-di-p-xenylmethyl	16,000	24,500	18,500
Tri-p-xenylmethyl	15,000	24,000	18,000

Although these systems are probably not planar, the theory of this paper ought to give a qualitative explanation of these results. It is suggested, therefore, that the two principal bands of the radicals arise from the doublet states with wave functions $\sqrt{\frac{1}{2}}(^2\chi_1 \pm {}^2\chi_2)$, while the excited state of the cation is $^1\chi_1{}^+$. For triphenyl-methyl and tri-p-xenylmethyl, Chu and Weissmann assign the weak radical band to a symmetry-forbidden transition. But if the present interpretation is correct, it will be of the same symmetry as the strong ultra-violet band.

REFERENCES

BRICKSTOCK, A., and POPLE, J. A., 1954, *Trans. Faraday Soc.*, **50**, 901.

CHU, T. L., and WEISSMAN, S. I., 1954, *J. Chem. Phys.*, **22**, 21.

DEWAR, M. J. S., and LONGUET-HIGGINS, H. C., 1954, *Proc. Phys. Soc.* A, **67**, 795. (Part I of present paper.)

HÜCKEL, W., 1931, *Z. Phys.*, **70**, 204, 279.

LONGUET-HIGGINS, H. C., 1950, *J. Chem. Phys.*, **18**, 265.

MOFFITT, W., 1953, *Proc. Roy. Soc.* A, **218**, 486.

POPLE, J. A., 1955, *Proc. Phys. Soc.* A, **68**, 81. (Part II of present paper.)

POPLE, J. A., and NESBET, R. K., 1954, *J. Chem. Phys.*, **22**, 571.

The Electronic Spectra of Aromatic Molecules
V : The Interaction of Two Conjugated Systems

By H. C. LONGUET-HIGGINS and J. N. MURRELL
Department of Theoretical Chemistry, University of Cambridge

MS. received 15*th December* 1954

Abstract. The electronic spectrum of a composite alternant hydrocarbon R–S is discussed theoretically in relation to the excited electronic states of the separate fragments RH and SH. The lowest excited states of RS are interpreted as arising from two types of excited configuration. In the first type an electron is raised from an occupied orbital of one fragment to an unoccupied orbital of the same fragment, and in the second, an electron is transferred from one fragment to the other. The self-consistent molecular orbital theory is used to evaluate the interactions between the various configurations, and the molecules butadiene, biphenyl and styrene are examined quantitatively. The following results are worthy of mention: (i) In butadiene the near ultra-violet transition arises primarily from an in-phase combination of local excitations in the two double bonds. (ii) In biphenyl a similar situation arises, there being strong configurational interaction in the perpendicular as well as in the planar conformation.

In all three molecules there is quite good agreement between the observed and calculated spectra.

§ 1. INTRODUCTION

A PROBLEM of great importance in spectroscopic theory is to find how the wave functions and energy levels of a composite system are related to those of its constituent parts. That such relationships exist has been established experimentally by extensive studies of the absorption spectra of organic molecules ; in a rough way one can frequently associate a particular band with a certain grouping in the molecule, and numerous attempts, more and less successful, have been made to find the relationship of bands of similar type in molecules of allied structure.†

In papers I and II of this series (Dewar and Longuet-Higgins 1954, Pople 1955) an interpretation was given of the principal bands in the electronic spectra of benzenoid hydrocarbons, and in paper III (Murrell and Longuet-Higgins 1955) the inductive effects of substituents were examined. An outstanding question remains: in what way will the spectrum of an unsaturated hydrocarbon be changed by a substituent which not only alters the effective potential on the π-electrons of the hydrocarbon, but also enters into conjugation with them? To answer this it is necessary to describe the states of the substituted molecule not only in terms of the π-electron wave functions of the unsubstituted hydrocarbon, but also in terms of those of the substituent. Clearly it is an advantage to begin by studying substituents whose electronic states can be identified with certainty, and for this reason we have turned our attention first to the case in which the substituent itself is an unsaturated hydrocarbon.

---

† For review of recent work see Bayliss 1952, Maccoll 1947.

Our first problem then is to find how the spectrum of a composite system R–S, where R and S are unsaturated hydrocarbon residues, is related to the electronic spectra of the fragments RH and SH.

§ 2. THEORY

Let R–S be an alternant hydrocarbon made up of two unsaturated hydrocarbon residues R and S joined by one bond. Examples of such hydrocarbons would be butadiene, styrene and biphenyl.

If R and S are initially regarded as separate, the self-consistent molecular orbitals for the molecule R–S are just those for the separate subsystems R and S. Our notation for these orbitals is as follows:

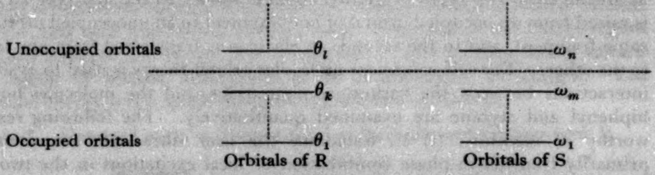

The question now arises: how are these orbitals modified when R and S are joined together? Suppose the bond is formed between atom μ in R and atom ν in S. Then Pople has shown that if ϕ_μ and ϕ_ν are the 2pπ atomic orbital functions of these atoms, the changes in the molecular orbitals are entirely determined by the value of the resonance integral

$$\beta_{\mu\nu}=\int \phi_\mu(i)H_i^{\text{core}}\phi_\nu(i)d\tau_i,$$

where H^{core} is the one electron core Hamiltonian. It is convenient to begin by ignoring the change in H^{core} as the systems are brought together, and to introduce it later as a perturbation which leads to a finite value for the resonance integral $\beta_{\mu\nu}$.

If $\beta_{\mu\nu}=0$, the excited electronic states of R–S will be of two kinds. There will be states associated with local excitations of electrons in R and S, and states which arise from the transfer of an electron from a bonding orbital of one subsystem to an antibonding orbital of the other. All such states can be described in terms of singly excited configurations of the type $\theta_k^{-1}\theta_l$, $\omega_m^{-1}\omega_n$, $\theta_k^{-1}\omega_n$, $\omega_m^{-1}\theta_l$. However, the excited states cannot in general be identified with individual configurations, since these will interact under the influence of electron repulsion. We will now investigate this interaction.

§ 3. THE EFFECTS OF ELECTRON REPULSION

The general expression for the interaction between two different singly excited configurations $\psi_a^{-1}\psi_b$ and $\psi_c^{-1}\psi_d$ is (Pople 1955)

$$\begin{aligned}\iint \psi_a^{-1}\psi_b H \psi_c^{-1}\psi_d\, d\tau &= 2\iint \psi_a(i)\psi_b(i)(1/r_{ij})\psi_c(j)\psi_d(j)\, d\tau_{ij}\\ &\quad - \iint \psi_a(i)\psi_c(i)(1/r_{ij})\psi_b(j)\psi_d(j)\, d\tau_{ij}, \qquad \ldots\ldots(3.1)\end{aligned}$$

where H is the total Hamiltonian of the system for which $\beta_{\mu\nu}=0$.

The following cases need to be considered separately:

(i) If $\psi_a^{-1}\psi_b$ and $\psi_c^{-1}\psi_d$ are locally excited configurations in the same fragment, the interaction between them will be independent of whether the subsystems R and S are juxtaposed or not. In setting up a scheme of interactions it is therefore best to begin by allowing the locally excited configurations of each fragment to interact among themselves; the resulting locally excited states will not then interact further when the subsystems are brought together.

(ii) If $\psi_a^{-1}\psi_b$ and $\psi_c^{-1}\psi_d$ are locally excited configurations in different fragments, they will interact by virtue of the first term in (3.1), but the second term will be zero if the orbitals of the different fragments do not overlap. In general therefore there will be interactions between the locally excited states of the two fragments, although in certain cases this interaction will vanish for other reasons.

(iii) If $\psi_a^{-1}\psi_b$ and $\psi_c^{-1}\psi_d$ represent configurations in which electrons are transferred in the same direction, these configurations will interact by virtue of the second term in equation (3.1), the first term being zero.

It is important to note, however, that there will be no interactions between locally excited and electron transfer configurations, nor between configurations in which electrons are transferred in opposite directions. Such interactions will only become allowed under the influence of the resonance integral $\beta_{\mu\nu}$. We conclude that if $\beta_{\mu\nu}$ is zero, the electron transfer configurations may be ignored in interpreting the electronic spectrum, since transitions to them from the ground state will be forbidden.

Application to Biphenyl

The effect of steric hindrance in biphenyl will be to give some preference to the configurations in which the two benzene rings are not coplanar. The value of the resonance integral $\beta_{\mu\nu}$ for these configurations will be small, and in the case of the rings being perpendicular will be zero.

The singly excited states of the two aromatic rings can be written (see paper I) as follows:

$$\Theta_{\beta'}=\sqrt{\tfrac{1}{2}}(\theta_3^{-1}\theta_4-\theta_2^{-1}\theta_5), \qquad \Omega_{\beta'}=\sqrt{\tfrac{1}{2}}(\omega_3^{-1}\omega_4-\omega_2^{-1}\omega_5)$$
$$\Theta_{\beta}=\sqrt{\tfrac{1}{2}}(\theta_3^{-1}\theta_5+\theta_2^{-1}\theta_4), \qquad \Omega_{\beta}=\sqrt{\tfrac{1}{2}}(\omega_3^{-1}\omega_5+\omega_2^{-1}\omega_4)$$
$$\Theta_{p}=\sqrt{\tfrac{1}{2}}(\theta_3^{-1}\theta_4+\theta_2^{-1}\theta_5), \qquad \Omega_{p}=\sqrt{\tfrac{1}{2}}(\omega_3^{-1}\omega_4+\omega_2^{-1}\omega_5)$$
$$\Theta_{\alpha}=\sqrt{\tfrac{1}{2}}(\theta_3^{-1}\theta_5-\theta_2^{-1}\theta_4), \qquad \Omega_{\alpha}=\sqrt{\tfrac{1}{2}}(\omega_3^{-1}\omega_5-\omega_2^{-1}\omega_4)$$

where the self-consistent orbitals are those shown in figure 1.

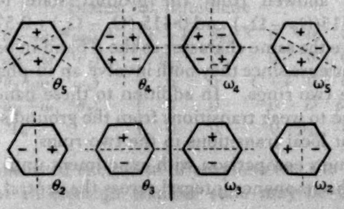

Figure 1. The self-consistent orbitals of the benzene fragments in biphenyl.

Since the orbitals θ and ω are self-consistent for the whole molecule as well as for the separate fragments, the ground state will not interact with any of the singly excited configurations. There will however be interaction between the locally excited states of the two benzene rings.

If the rings are perpendicular considerations of symmetry impose severe restrictions on the interactions which occur, and the resulting states have the form

$$\begin{gathered}\Theta_\alpha,\ \Omega_\alpha,\ \Theta_\beta,\ \Omega_\beta,\\ \lambda(\Theta_\mathrm{p}+\Omega_\mathrm{p})+\mu(\Theta_{\beta'}+\Omega_{\beta'}),\\ \mu(\Theta_\mathrm{p}+\Omega_\mathrm{p})-\lambda(\Theta_{\beta'}+\Omega_{\beta'}),\\ \rho(\Theta_\mathrm{p}-\Omega_\mathrm{p})+\sigma(\Theta_{\beta'}-\Omega_{\beta'}),\\ \sigma(\Theta_\mathrm{p}-\Omega_\mathrm{p})-\rho(\Theta_{\beta'}-\Omega_{\beta'}).\end{gathered}$$

The values of λ, μ, ρ and σ are determined by the matrix elements between the four states Θ_p, Ω_p, $\Theta_{\beta'}$ and $\Omega_{\beta'}$ and these in turn can be expressed in terms of molecular orbitals by (3.1). To evaluate them numerically we expand the molecular orbitals in terms of atomic orbital functions, and neglect all electron repulsion integrals except those of the form

$$\gamma_{rs}=\iint\phi_r(i)\phi_r(i)(1/r_{ij})\phi_s(j)\,\phi_s(j)\,d\tau_{ij}.$$

Using the inverse distance approximation suggested by Pople (1953), that is setting $\gamma_{rs}=R_{rs}^{-1}$, we obtain the following matrix elements of H between the four states.

Table 1. The Matrix Elements of H between the Locally Excited p and β' States of Biphenyl (ev)

$$\begin{array}{c}\Omega_{\beta'}\\ \Theta_{\beta'}\\ \Omega_\mathrm{p}\\ \Theta_\mathrm{p}\end{array}\begin{bmatrix}6{\cdot}62 & 0{\cdot}92 & 0 & -0{\cdot}31\\ 0{\cdot}92 & 6{\cdot}62 & -0{\cdot}31 & 0\\ 0 & -0{\cdot}31 & 6{\cdot}07 & 0{\cdot}18\\ -0{\cdot}31 & 0 & 0{\cdot}18 & 6{\cdot}07\end{bmatrix}$$

In this matrix the diagonal elements are just the observed energies for the onset of the p and β^1 bands in benzene (Klevens and Platt 1954). Table 2 gives the calculated energies and wave functions of the resulting states.

Table 2. The Wave Functions and Energies of the p and β' States of Perpendicular Biphenyl

$0{\cdot}156(\Theta_\mathrm{p}+\Omega_\mathrm{p})-0{\cdot}689(\Theta_{\beta'}+\Omega_{\beta'})$	7·61 ev
$0{\cdot}689(\Theta_\mathrm{p}+\Omega_\mathrm{p})+0{\cdot}156(\Theta_{\beta'}+\Omega_{\beta'})$	6·18 ev
$0{\cdot}573(\Theta_\mathrm{p}-\Omega_\mathrm{p})-0{\cdot}415(\Theta_{\beta'}-\Omega_{\beta'})$	6·12 ev
$0{\cdot}415(\Theta_\mathrm{p}-\Omega_\mathrm{p})+0{\cdot}573(\Theta_{\beta'}-\Omega_{\beta'})$	5·47 ev

Transitions are allowed from the ground state to the states Θ_β, Ω_β, $0{\cdot}573(\Theta_\mathrm{p}-\Omega_\mathrm{p})-0{\cdot}415(\Theta_{\beta'}-\Omega_{\beta'})$ and $0{\cdot}415\ (\Theta_\mathrm{p}-\Omega_\mathrm{p})+0{\cdot}573(\Theta_{\beta'}-\Omega_{\beta'})$. Of these the first two will have the same character as the β band in benzene. The third and fourth will also be intense since they both involve an in-phase combination of the β' transitions of the two rings. In addition to these bands we may also expect Θ_α and Ω_α to give rise to weak transitions from the ground state just as in benzene, since these represent local transitions in the two rings.

We shall postpone a comparison with experiment until we have discussed the situation in which the resonance integral across the central bond is not negligible.

§ 4. THE EFFECT OF CONJUGATION

Having dealt with the interactions which arise from electron repulsion alone, it is now necessary to consider the effect of introducing a resonance integral $\beta_{\mu\nu}$ between the two subsystems. As $\beta_{\mu\nu}$ is a one-electron element it will have the effect of mixing together configurations which differ by the position of just one electron. The relevant formulae are:

$$\begin{aligned}\int\Psi_0 H^{\text{core}}\psi_a^{-1}\psi_b\,d\tau &= \sqrt{2}\int\psi_a(i)H_i^{\text{core}}\psi_b(i)\,d\tau_i,\\ \int\psi_c^{-1}\psi_a H^{\text{core}}\psi_c^{-1}\psi_b\,d\tau &= \int\psi_a(i)H_i^{\text{core}}\psi_b(i)\,d\tau_i,\\ \int\psi_a^{-1}\psi_c H^{\text{core}}\psi_b^{-1}\psi_c\,d\tau &= -\int\psi_a(i)H_i^{\text{core}}\psi_b(i)\,d\tau_i. \qquad \ldots\ldots(4.1)\end{aligned}$$

These three expressions will be zero unless ψ_a belongs to one subsystem and ψ_b to the other, since the change in H_i^{core} as the subsystems are brought together affects only the resonance integral $\beta_{\mu\nu}$.

Application to Butadiene

Butadiene can exist in two forms *cis* and *trans*. In both of these the molecule is planar so that there will be a non-zero resonance integral β_{23} between the $2p\pi$ atomic orbital functions of the central carbon atoms.

Let us denote the molecular orbitals of the two ethylene fragments, regarded initially as independent, by

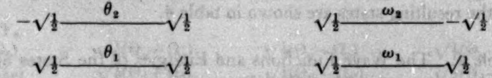

In terms of these orbitals the locally excited configurations are $\theta_1^{-1}\theta_2$ and $\omega_1^{-1}\omega_2$. By symmetry these must be taken in the combinations $\sqrt{\frac{1}{2}}(\theta_1^{-1}\theta_2+\omega_1^{-1}\omega_2)$ and $\sqrt{\frac{1}{2}}(\theta_1^{-1}\theta_2-\omega_1^{-1}\omega_2)$ with energies $C+\Gamma$ and $C-\Gamma$ where C is the energy of the first N→V transition of ethylene, and Γ is the electron repulsion integral

$$\Gamma = 2\iint\theta_1(i)\theta_2(i)(1/r_{ij})\omega_1(j)\omega_2(j)\,d\tau_{ij}. \qquad \ldots\ldots(4.2)$$

The electron transfer configurations $\theta_1^{-1}\omega_2$ and $\omega_1^{-1}\theta_2$ must be combined in a similar manner, but the resulting states will have the same energy D since the configurations arise from the transfer of electrons in opposite directions. The resonance integral β_{23} will cause these states to mix together, the matrix of the interaction elements taking the form shown in table 3.

Table 3. The Matrix of the Interactions between the 'Ethylenic States' of Butadiene

$$\begin{array}{c} \sqrt{\frac{1}{2}}(\theta_1^{-1}\theta_2-\omega_1^{-1}\omega_2)\\ \sqrt{\frac{1}{2}}(\theta_1^{-1}\omega_2-\omega_1^{-1}\theta_2)\\ \sqrt{\frac{1}{2}}(\theta_1^{-1}\theta_2+\omega_1^{-1}\omega_2)\\ \sqrt{\frac{1}{2}}(\theta_1^{-1}\omega_2+\omega_1^{-1}\theta_2)\\ \Psi_0 \end{array} \begin{bmatrix} C-\Gamma & \beta_{23} & 0 & 0 & 0\\ \beta_{23} & D & 0 & 0 & 0\\ 0 & 0 & C+\Gamma & 0 & 0\\ 0 & 0 & 0 & D & \beta_{23}\\ 0 & 0 & 0 & \beta_{23} & 0 \end{bmatrix}$$

The energy C of the observed excitation of ethylene has the value 7·06 ev (Platt 1950). The energy of an electron transfer state may be computed from the equation

$$\iint\theta_1^{-1}\omega_2 H\theta_1^{-1}\omega_2\,d\tau = E_2-E_1-\iint\theta_1(i)\theta_1(i)(1/r_{ij})\omega_2(j)\omega_2(j)\,d\tau_{ij}. \qquad \ldots(4.3)$$

E_2-E_1 which is the difference of the Hartree–Fock parameters of the two orbitals is evaluated by Pople's method (1953), and in the case of ethylene has the value

$-2\beta_{12}+\gamma_{12}$. As β_{12} and γ_{12} refer to two atoms of the same ethylene fragment, it seems best to use the values for these quantities which give a correct energy for the first N→V transition in ethylene. Pariser and Parr (1953) recommend the values $\gamma_{12}=7{\cdot}38$ ev $\beta_{12}=-2{\cdot}92$ ev. The electron repulsion integral in equation (3.3) has the value $\frac{1}{4}(\gamma_{23}+2\gamma_{13}+\gamma_{14})$; and Γ has the value $\frac{1}{2}(\gamma_{23}-2\gamma_{13}+\gamma_{14})$. In evaluating these quantities we have used the inverse distance approximation, the *cis* and *trans* forms being assumed to have the geometry indicated in figure 2.

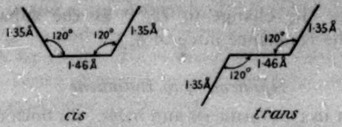

Figure 2. The geometry of the butadiene isomers.

The use of this approximation will be discussed later. The value of β_{23} has been taken as -1.68 ev as suggested by Pariser and Parr. The energies and wave functions of the resulting states are shown in table 4.

Table 4. The Wave Functions and Energies of the States of Butadiene

	Wave Function	Symmetry	Energy (ev)
trans	$0{\cdot}553(\theta_1{}^{-1}\theta_2-\omega_1{}^{-1}\omega_2)+0{\cdot}441(\theta_1{}^{-1}\omega_2-\omega_1{}^{-1}\theta_2)$	(A)	4·73
	$0{\cdot}441(\theta_1{}^{-1}\theta_2-\omega_1{}^{-1}\omega_2)-0{\cdot}553(\theta_1{}^{-1}\omega_2-\omega_1{}^{-1}\theta_2)$	(A)	8·18
	$\sqrt{\tfrac{1}{2}}(\theta_1{}^{-1}\theta_2+\omega_1{}^{-1}\omega_2)$	(S)	8·05
	$0{\cdot}225\Psi_0-0{\cdot}689(\theta_1{}^{-1}\omega_2+\omega_1{}^{-1}\theta_2)$	(S)	7·23
	$0{\cdot}974\Psi_0+0{\cdot}159(\theta_1{}^{-1}\omega_2+\omega_1{}^{-1}\theta_2)$	(S)	−0·39
cis	$0{\cdot}571(\theta_1{}^{-1}\theta_2-\omega_1{}^{-1}\omega_2)+0{\cdot}416(\theta_1{}^{-1}\omega_2-\omega_1{}^{-1}\theta_2)$	(A)	4·25
	$0{\cdot}416(\theta_1{}^{-1}\theta_2-\omega_1{}^{-1}\omega_2)-0{\cdot}571(\theta_1{}^{-1}\omega_2-\omega_1{}^{-1}\theta_2)$	(A)	7·78
	$\sqrt{\tfrac{1}{2}}(\theta_1{}^{-1}\theta_2+\omega_1{}^{-1}\omega_2)$	(S)	8·65
	$0{\cdot}235\Psi_0-0{\cdot}686(\theta_1{}^{-1}\omega_2+\omega_1{}^{-1}\theta_2)$	(S)	6·96
	$0{\cdot}971\Psi_0+0{\cdot}166(\theta_1{}^{-1}\omega_2+\omega_1{}^{-1}\theta_2)$	(S)	−0·41

Of these states those with the symbol S are symmetrcial about the central bond and those with A are antisymmetrical. In *trans* butadiene there are therefore two allowed transitions from the ground state with energies 5·12 ev and 8·57 ev. In *cis* butadiene on the other hand transitions are allowed by symmetry to any of the four upper states. However, in the absence of overlap between the atomic orbitals, transitions are forbidden between the last two states in table 4. The only additional allowed transition in *cis* butadiene is from the ground state to the state $\sqrt{\frac{1}{2}}(\theta_1{}^{-1}\theta_2+\omega_1{}^{-1}\omega_2)$. This transition has a moment perpendicular to the central bond and corresponds to a symmetric combination of local excitations in the two double bonds.

As far as the near ultra-violet spectrum is concerned the most important transition is to the lowest excited state. Although the wave function of this state involves electron transfer configurations, it may roughly be thought of as an antisymmetric combination of the locally excited states of the two ethylene fragments, and transitions to it from the ground state will therefore be strongly allowed. Our calculations give 4·66 ev and 5·12 ev for the energy of this transition in the *cis* and *trans* configurations. These values are to be compared with the observed intense band in butadiene with an origin at 5·33 ev (Platt 1950).

It is perhaps worth noting that the longest wavelength transition in *s-cis* dienes such as cyclohexadiene is normally found at a slightly longer wavelength than the corresponding transitions in *s-trans* dienes.

Application to Planar Biphenyl

In the planar configuration of biphenyl there will be a substantial resonance integral across the bond connecting the two benzene rings. As a result the electron-transfer configurations will interact with the locally excited configurations. However, only states of the same symmetry class can interact, and analysis shows that the various wave functions fall into symmetry classes as follows:

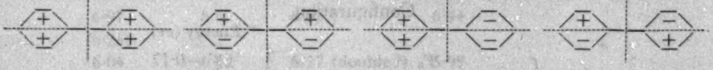

A_{1g}	B_{2u}	B_{3u}	B_{1g}
Ψ_0			
$\sqrt{\tfrac{1}{2}}(\Theta_p+\Omega_p)$	$\sqrt{\tfrac{1}{2}}(\Theta_\alpha+\Omega_\alpha)$	$\sqrt{\tfrac{1}{2}}(\Theta_p-\Omega_p)$	$\sqrt{\tfrac{1}{2}}(\Theta_\alpha-\Omega_\alpha)$
$\sqrt{\tfrac{1}{2}}(\Theta_{\beta'}+\Omega_{\beta'})$	$\sqrt{\tfrac{1}{2}}(\Theta_\beta+\Omega_\beta)$	$\sqrt{\tfrac{1}{2}}(\Theta_{\beta'}-\Omega_{\beta'})$	$\sqrt{\tfrac{1}{2}}(\Theta_\beta-\Omega_\beta)$
$\sqrt{\tfrac{1}{2}}(\theta_2{}^{-1}\omega_5+\omega_2{}^{-1}\theta_5)$	$\sqrt{\tfrac{1}{2}}(\theta_3{}^{-1}\omega_5+\omega_3{}^{-1}\theta_5)$	$\sqrt{\tfrac{1}{2}}(\theta_2{}^{-1}\omega_5-\omega_2{}^{-1}\theta_5)$	$\sqrt{\tfrac{1}{2}}(\theta_3{}^{-1}\omega_5-\omega_3{}^{-1}\theta_5)$
$\sqrt{\tfrac{1}{2}}(\theta_3{}^{-1}\omega_4+\omega_3{}^{-1}\theta_4)$	$\sqrt{\tfrac{1}{2}}(\theta_2{}^{-1}\omega_4+\omega_2{}^{-1}\theta_4)$	$\sqrt{\tfrac{1}{2}}(\theta_3{}^{-1}\omega_4-\omega_3{}^{-1}\theta_4)$	$\sqrt{\tfrac{1}{2}}(\theta_2{}^{-1}\omega_4-\omega_2{}^{-1}\theta_4)$

The interaction matrices for these symmetry classes are then

$$\begin{array}{c} \Psi_0 \\ \sqrt{\tfrac{1}{2}}(\theta_2{}^{-1}\omega_5+\omega_2{}^{-1}\theta_5) \\ \sqrt{\tfrac{1}{2}}(\theta_3{}^{-1}\omega_4+\omega_3{}^{-1}\theta_4) \\ \sqrt{\tfrac{1}{2}}(\Theta_p+\Omega_p) \\ \sqrt{\tfrac{1}{2}}(\Theta_{\beta'}+\Omega_{\beta'}) \end{array} \begin{bmatrix} 0 & 1{\cdot}12 & 0 & 0 & 0 \\ 1{\cdot}12 & 7{\cdot}21 & -0{\cdot}14 & 0 & 0 \\ 0 & -0{\cdot}14 & 7{\cdot}98 & 0 & 0 \\ 0 & 0 & 0 & 6{\cdot}29 & -0{\cdot}29 \\ 0 & 0 & 0 & -0{\cdot}29 & 7{\cdot}55 \end{bmatrix}$$

$$\begin{array}{c} \sqrt{\tfrac{1}{2}}(\Theta_\alpha+\Omega_\alpha) \\ \tfrac{1}{2}(\theta_3{}^{-1}\omega_5+\omega_3{}^{-1}\theta_5+\theta_2{}^{-1}\omega_4+\omega_2{}^{-1}\theta_4) \\ \sqrt{\tfrac{1}{2}}(\Theta_\beta+\Omega_\beta) \\ \tfrac{1}{2}(\theta_3{}^{-1}\omega_5+\omega_3{}^{-1}\theta_5-\theta_2{}^{-1}\omega_4-\omega_2{}^{-1}\theta_4) \end{array} \begin{bmatrix} 4{\cdot}61 & -0{\cdot}56 & 0 & 0 \\ -0{\cdot}56 & 8{\cdot}05 & 0 & 0 \\ 0 & 0 & 7{\cdot}00 & -0{\cdot}56 \\ 0 & 0 & -0{\cdot}56 & 8{\cdot}34 \end{bmatrix}$$

$$\begin{array}{c} \sqrt{\tfrac{1}{2}}(\Theta_p-\Omega_p) \\ \sqrt{\tfrac{1}{2}}(\Theta_{\beta'}-\Omega_{\beta'}) \\ \sqrt{\tfrac{1}{2}}(\theta_2{}^{-1}\omega_5-\omega_2{}^{-1}\theta_5) \\ \sqrt{\tfrac{1}{2}}(\theta_3{}^{-1}\omega_4-\omega_3{}^{-1}\theta_4) \end{array} \begin{bmatrix} 5{\cdot}86 & -0{\cdot}29 & -0{\cdot}79 & 0 \\ -0{\cdot}29 & 5{\cdot}68 & 0{\cdot}79 & 0 \\ -0{\cdot}79 & 0{\cdot}79 & 7{\cdot}21 & -0{\cdot}14 \\ 0 & 0 & -0{\cdot}14 & 7{\cdot}98 \end{bmatrix}$$

$$\begin{array}{c} \sqrt{\tfrac{1}{2}}(\theta_\alpha-\Omega_\alpha) \\ \tfrac{1}{2}(\theta_3{}^{-1}\omega_5-\omega_3{}^{-1}\theta_5-\theta_2{}^{-1}\omega_4+\omega_2{}^{-1}\theta_4) \\ \sqrt{\tfrac{1}{2}}(\Theta_\beta-\Omega_\beta) \\ \tfrac{1}{2}(\theta_3{}^{-1}\omega_5-\omega_3{}^{-1}\theta_5+\theta_2{}^{-1}\omega_4-\omega_2{}^{-1}\theta_4) \end{array} \begin{bmatrix} 4{\cdot}61 & -0{\cdot}56 & 0 & 0 \\ -0{\cdot}56 & 8{\cdot}34 & 0 & 0 \\ 0 & 0 & 6{\cdot}24 & -0{\cdot}56 \\ 0 & 0 & -0{\cdot}56 & 8{\cdot}05 \end{bmatrix}$$

The diagonal elements of the electron-transfer states have been calculated in the same way as in butadiene, that is using the Pariser and Parr integrals for atomic orbitals within a benzene ring and the inverse distance approximation for the repulsion integrals between atomic orbital functions belonging to different rings. The length of the central bond has been taken to be the same as that of the central bond in butadiene. The following points are worthy of comment: (i) As in the perpendicular configuration the p and β' states interact both in the representations A_{1g} and B_{3u}. (ii) The only states with which Θ_α and Ω_α interact are electron transfer states; they do not interact with one another. This is a quite general result in that the α state of any alternant system R cannot interact with any of the locally excited configurations of S, because if the wave function of the α state is written $\sqrt{\tfrac{1}{2}}(\psi_m{}^{-1}\psi_{m+2}-\psi_{m-1}{}^{-1}\psi_{m+1})$ (see paper I), the interaction element takes the form

$$\sqrt{2}\iint(\psi_m(i)\psi_{m+2}(i)-\psi_{m-1}(i)\psi_{m+1}(i))(1/r_{ij})\theta_a(j)\theta_b(j)\,d\tau_{ij},$$

which is zero because of the pairing of the orbitals (ψ_m, ψ_{m+1}) and (ψ_{m-1}, ψ_{m+2}).

The roots of the secular equations, relative to the energy of Ψ_0, together with the states from which they arise, are shown in table 6.

Table 6. The Energies of the States of Biphenyl in the Planar Configuration

		Energy (ev)
A_{1g}	Ψ_0	$-0{\cdot}17$
	$\sqrt{\tfrac{1}{2}}(\theta_2{}^{-1}\omega_5+\omega_2{}^{-1}\theta_5)$	$7{\cdot}32$
	$\sqrt{\tfrac{1}{2}}(\theta_3{}^{-1}\omega_4+\omega_3{}^{-1}\theta_4)$	$8{\cdot}04$
	$\sqrt{\tfrac{1}{2}}\Theta_p+\Omega_p)$	$6{\cdot}22$
	$\sqrt{\tfrac{1}{2}}\Theta_{\beta'}+\Omega_{\beta'})$	$7{\cdot}62$
B_{2u}	$\sqrt{\tfrac{1}{2}}(\Theta_\alpha+\Omega_\alpha)$	$4{\cdot}52$
	$\tfrac{1}{2}(\theta_3{}^{-1}\omega_5+\omega_3{}^{-1}\theta_5+\theta_2{}^{-1}\omega_4+\omega_2{}^{-1}\theta_4)$	$8{\cdot}14$
	$\sqrt{\tfrac{1}{2}}(\Theta_\beta+\Omega_\beta)$	$6{\cdot}80$
	$\tfrac{1}{2}(\theta_3{}^{-1}\omega_5+\omega_3{}^{-1}\theta_5-\theta_2{}^{-1}\omega_4-\omega_2{}^{-1}\theta_4)$	$8{\cdot}54$
B_{3u}	$\sqrt{\tfrac{1}{2}}(\Theta_p-\Omega_p)$	$5{\cdot}87$
	$\sqrt{\tfrac{1}{2}}(\Theta_{\beta'}-\Omega_{\beta'})$	$5{\cdot}05$
	$\sqrt{\tfrac{1}{2}}(\theta_2{}^{-1}\omega_5-\omega_2{}^{-1}\theta_5)$	$7{\cdot}73$
	$\sqrt{\tfrac{1}{2}}(\theta_3{}^{-1}\omega_4-\omega_3{}^{-1}\theta_4)$	$8{\cdot}08$
B_{1g}	$\sqrt{\tfrac{1}{2}}(\Theta_\alpha-\Omega_\alpha)$	$4{\cdot}53$
	$\tfrac{1}{2}(\theta_3{}^{-1}\omega_5-\omega_3{}^{-1}\theta_5-\theta_2{}^{-1}\omega_4+\omega_2{}^{-1}\theta_4)$	$8{\cdot}42$
	$\sqrt{\tfrac{1}{2}}(\Theta_\beta-\Omega_\beta)$	$6{\cdot}08$
	$\tfrac{1}{2}(\theta_3{}^{-1}\omega_5-\omega_3{}^{-1}\theta_5+\theta_2{}^{-1}\omega_4-\omega_2{}^{-1}\theta_4)$	$8{\cdot}21$

The level at $-0{\cdot}17$ ev is of course the ground state and transitions from this level to any of the states in classes A_{1g} and B_{1g} are forbidden by symmetry. Of the states in the other two classes there are four which lie in the near ultra-violet region. The level at 6·80 ev will have the characteristics of the β state in benzene, and transitions to it will have about the same intensity as the β band in benzene. The level at 4·52 ev for similar reasons will resemble the α state in benzene. As for the states at 5·05 ev and 5·87 ev it would be an over-simplification to describe these as combinations of β' states and p states respectively; transitions to both should be strongly allowed as both involve an in-phase excitation to the β' states of the two rings. The four remaining bands in these two classes lie at higher energies, and should be weaker as they arise mainly from exchange of electrons between the two rings. In any case the whole theory becomes less reliable at these higher energies. In short, we expect four bands in the spectrum at 4·69 ev, 5·22 ev, 6·04 ev and 6·97 ev.

It is interesting to note that if the two rings are twisted slightly out of the plane the states of class B_{1g} become optically accessible from the ground state, with a transition moment perpendicular to the central bond. We may therefore expect to observe in addition to the four bands described a fifth at 6·25 ev, and this should be quite intense being of the β type.

In table 7 are shown the results of our calculations for biphenyl in the planar and perpendicular configurations together with the observed spectra of biphenyl, fluorene, and 9:10–dihydrophenanthrene.

Table 7. †Comparison of the Calculated Energies of the Bands in the Spectrum of Biphenyl with the Observed Data

Calculated		Observed		
Planar Biphenyl	Perpendicular Biphenyl	Biphenyl‡	Fluorene‡	9:10 dihydro-phenanthrene§
ν_{onset}	ν_{onset}	ν_{max}	ν_{max}	ν_{max}
6·97	6·62	6·57 ?	6·44	
(6·25)				
6·04	6·12	6·17 (double ?)	5·98	
5·22	5·47	5·02	4·73	4·57
4·69	4·61	4·52	4·19	4·15

† It has been implicitly assumed throughout this paper that the nuclei do not move when the electrons are excited. Our calculations therefore yield vertical excitation energies, which by the Franck–Condon principle are correlated with ν_{max}, the frequency of most intense absorption. However, the energies of the locally excited states have been estimated from values of ν_{onset}, and so our calculated absorption frequencies for R–S will therefore correspond more closely to the observed values of ν_{onset} than to those of ν_{max}.

‡ Klevens and Platt 1954. § Jones 1941.

The observed spectra conform in general pattern with the predictions of the theory. It is not altogether surprising to find the absorption bands of fluorene and 9:10–dihydrophenanthrene lying at somewhat longer wavelengths than those in biphenyl, as it is well known that alkyl substitution produces red shifts in the principal ultra-violet bands.

Application to Styrene

The styrene molecule is presumably planar, with an angle of 120° between the double and single bonds of the side chain. Let us denote the degenerate orbitals of the benzene ring by θ_2, θ_3, θ_4 and θ_5 as in biphenyl, and the bonding and antibonding orbitals of the side chain by ω_1 and ω_2 respectively. We shall consider the excited states as arising from interactions between the following wave functions:

Locally excited states	Electron transfer states
$\Theta_{\beta'}=\sqrt{\tfrac{1}{2}}(\theta_3{}^{-1}\theta_4-\theta_2{}^{-1}\theta_5)$	$\sqrt{\tfrac{1}{2}}(\theta_2{}^{-1}\omega_2+\omega_1{}^{-1}\theta_5)$
$\Theta_{\beta}=\sqrt{\tfrac{1}{2}}(\theta_3{}^{-1}\theta_5+\theta_2{}^{-1}\theta_4)$	$\sqrt{\tfrac{1}{2}}(\theta_2{}^{-1}\omega_2-\omega_1{}^{-1}\theta_5)$
$\Theta_{\mathrm{p}}=\sqrt{\tfrac{1}{2}}(\theta_3{}^{-1}\theta_4+\theta_2{}^{-1}\theta_5)$	$\sqrt{\tfrac{1}{2}}(\theta_3{}^{-1}\omega_2+\omega_1{}^{-1}\theta_4)$
$\Theta_{\alpha}=\sqrt{\tfrac{1}{2}}(\theta_3{}^{-1}\theta_5-\theta_2{}^{-1}\theta_4)$	$\sqrt{\tfrac{1}{2}}(\theta_3{}^{-1}\omega_2-\omega_1{}^{-1}\theta_4)$
$\omega_1{}^{-1}\omega_2$	

It is found that these wave functions fall into two classes between which no interactions occur; and the interaction matrices for these two classes are:

$$\begin{array}{c} \Theta_\alpha \\ \sqrt{\tfrac{1}{2}}(\theta_3{}^{-1}\omega_2-\omega_1{}^{-1}\theta_4) \\ \Psi_0 \\ \sqrt{\tfrac{1}{2}}(\theta_2{}^{-1}\omega_2-\omega_1{}^{-1}\theta_5) \end{array} \begin{bmatrix} 4\cdot 61 & 0\cdot 69 & 0 & 0 \\ 0\cdot 69 & 7\cdot 94 & 0 & -0\cdot 10 \\ 0 & 0 & 0 & -1\cdot 37 \\ 0 & -0\cdot 10 & -1\cdot 37 & 7\cdot 17 \end{bmatrix}$$

$$\begin{array}{c} \sqrt{\tfrac{1}{2}}(\theta_3{}^{-1}\omega_2+\omega_1{}^{-1}\theta_4) \\ \sqrt{\tfrac{1}{2}}(\theta_2{}^{-1}\omega_2+\omega_1{}^{-1}\theta_5) \\ \omega_1{}^{-1}\omega_2 \\ \Theta_\beta \\ \Theta_{\beta'} \\ \Theta_p \end{array} \begin{bmatrix} 7\cdot 94 & -0\cdot 10 & 0 & 0\cdot 69 & 0 & 0 \\ -0\cdot 10 & 7\cdot 17 & 0\cdot 97 & 0 & 0\cdot 69 & -0\cdot 69 \\ 0 & 0\cdot 97 & 7\cdot 06 & -0\cdot 31 & 0\cdot 97 & -0\cdot 47 \\ 0\cdot 69 & 0 & -0\cdot 31 & 6\cdot 62 & 0 & 0 \\ 0 & 0\cdot 69 & 0\cdot 97 & 0 & 6\cdot 62 & 0 \\ 0 & -0\cdot 69 & -0\cdot 47 & 0 & 0 & 6\cdot 07 \end{bmatrix}$$

The roots of the secular equations are shown in table 8.

Table 8. The Energies of the States of Styrene

Wave function	Energy (ev)	Wave function	Energy (ev)
Θ_α	4·47	$\sqrt{\tfrac{1}{2}}(\theta_3{}^{-1}\omega_2+\omega_1{}^{-1}\theta_4)$	8·24
$\sqrt{\tfrac{1}{2}}(\theta_3{}^{-1}\omega_2-\omega_1{}^{-1}\theta_4)$	8·08	$\sqrt{\tfrac{1}{2}}(\theta_2{}^{-1}\omega_2+\omega_1{}^{-1}\theta_5)$	8·93
Ψ_0	−0·25	$\omega_1{}^{-1}\omega_2$	6·36
$\sqrt{\tfrac{1}{2}}(\theta_2{}^{-1}\omega_2-\omega_1{}^{-1}\theta_5)$	7·42	Θ_β	6·52
		$\Theta_\beta{}'$	5·90
		Θ_p	5·52

In computing the resonance integral and electron repulsion integrals we have assumed the six-membered ring to have the same geometry as benzene, and the external single and double bonds to have lengths 1·46 and 1·34Å respectively. Transitions to the states of energy 5·52, 5·90, 6·36 and 6·52 ev should be strongly allowed since these states have components, transitions to which give rise to the strong bands of benzene and ethylene. The state of energy 4·47 ev, however, will give rise to a weak band having the characteristics of the α band of benzene.

Table 9 summarizes the observed and calculated frequencies of the principal bands of the spectrum.

Table 9. Comparison of the Energies of the Observed and Calculated Bands in the Spectrum of Styrene

Calculated bands (ev) : ν_{onset}	6·77	6·61	6·15	5·77	4·73
Observed bands (ev) : ν_{max}	7·19		6·10	5·03	4·42

§ 5. DISCUSSION

In this paper we have attempted to relate the spectrum of a composite alternant hydrocarbon to the spectra of its component parts. In this interpretation we have supposed that the excited states of the joint system can be expressed as linear combinations of wave functions representing on the one hand local excitations in the two fragments, and on the other, states in which an electron has been transferred from one fragment to the other. In describing these states we have made use of the self-consistent molecular orbital theory, and have supposed that the only wave functions which need to be considered are those arising from singly excited configurations, in which one electron has been raised from an occupied molecular orbital to an unoccupied orbital in either fragment. This approximation makes it possible to relate the transitions occurring in the composite system to those observed in the separate fragments, without the necessity of making absolute calculations on the fragments themselves.

In butadiene and biphenyl we picture the strong bands as arising from in-phase transitions occurring in the two halves of the molecule. The principal interactions which occur are those between degenerate states, which give rise to a first order change in the energy. Electron transfer configurations play a relatively small role in these molecules, since the extent to which they contribute to the energy of the excited states is second order in the resonance integral $\beta_{\mu\nu}$. On the quantitative side we have obtained a very satisfactory interpretation of the principal bands in the spectrum of butadiene and biphenyl in relation to the known spectra of benzene and ethylene. The quantitative results for styrene are perhaps less satisfactory, but we feel confident as to the nature of the excited states responsible for the transitions.

With regard to our theoretical approximations, we have ignored completely the configurations in which more than one electron has been excited. To abandon this approximation would complicate the theory very considerably, but since these configurations lie at high energies, they are unlikely to make important contributions to the wave functions of the lower energy states. We have used throughout the approximations suggested by Pariser and Parr and by Pople of neglecting atomic orbital overlap and all electron repulsion integrals which depend on the overlapping of different atomic orbitals. The remaining electron repulsion integrals have been regarded by Pariser and Parr as parameters to be determined empirically, and we have adopted their values for pairs of atoms within the same fragment. However, for pairs in different fragments we have found that the inverse distance approximation $\gamma_{rs}=R_{rs}^{-1}$ gives better results, but we think our main conclusions are unlikely to be modified by slightly different values for these integrals.

We intend to extend the method we have described to systems consisting of more than two fragments joined by single bonds, and to systems in which the fragments are joined by more than one bond.

ACKNOWLEDGMENTS

We wish to thank Dr. J. A. Pople for helpful discussion, and Dr. G. G. Hall for assistance with the calculations on styrene. One of us (J. N. M.) wishes to thank the Department of Scientific and Industrial Research for the award of a maintenance grant.

REFERENCES

BAYLISS, N. S., 1952, *Annual Review of Physical Chemistry*, **3,** 229.
DEWAR, M. J. S., and LONGUET-HIGGINS, H. C., 1954, *Proc. Phys. Soc.* A, **67,** 795.
JONES, R. N., 1941, *J. Amer. Chem. Soc.*, **63,** 1658.
KLEVENS, H. B., and PLATT, J. R., 1954, *Technical report of the Laboratory of molecular structure and spectra*, Department of Physics, University of Chicago.
MACCOLL, A., 1947, *Quart. Rev. Chem. Soc., Lond.*, **1,** 16.
MURRELL, J. N., and LONGUET-HIGGINS, H. C., 1955, *Proc. Phys. Soc.* A, **68,** 329.
PARISER, R., and PARR, R. G., 1953, *J. Chem. Phys.*, **21,** 767.
PLATT, J. R., 1950, *J. Chem. Phys.*, **18,** 1168.
POPLE, J. A., 1953, *Trans. Faraday Soc.*, **49,** 1375; 1955, *Proc. Phys. Soc.* A, **68,** 81.

The Fluorescence Yields of the L Levels of Bismuth

BY M. A. S. ROSS, A. J. COCHRAN, J. HUGHES AND N. FEATHER
Department of Natural Philosophy, University of Edinburgh

MS. received 28th December 1954

Abstract. This paper is a supplement to the discussion by Kinsey of the fluorescence yields of the L sub-shells in the heavy elements; it suggests the use of experimental measurements other than those which he discussed for the calculation of these quantities. New observations are reported and collated with existing information. The fluorescence, Auger and Coster–Kronig yields of Bi are re-calculated. Suggestions are made about further experimental work.

The numerical results are, for the fluorescence yields of Bi, $\omega_1 = 0{\cdot}12 \pm 0{\cdot}01$, $\omega_2 = 0{\cdot}32 \pm 0{\cdot}04$, $\omega_3 = 0{\cdot}40 \pm 0{\cdot}05$, for the Auger yields $a_1 = 0{\cdot}11 \pm 0{\cdot}03$, $a_2 = 0{\cdot}62 \pm 0{\cdot}14$, $a_3 = 0{\cdot}60 \pm 0{\cdot}05$, and for the Coster–Kronig yields $f_{12} = 0{\cdot}19 \pm 0{\cdot}05$, $f_{13} = 0{\cdot}58 \pm 0{\cdot}05$, $f_{23} = 0{\cdot}06 \pm 0{\cdot}14$.

A discussion is added on some aspects of the radioactive disintegration of RaD.

---

§ 1. INTRODUCTION

DIRECT measurements of the total fluorescence yield of the L shell were made for twenty-one elements in the range of Z from 40 to 92 by Lay (1934) using x-rays to excite the fluorescence and photographic film to record the intensities. Measurements of the fluorescence yields ω_1, ω_2, and ω_3, for the levels L_I, L_{II} and L_{III} respectively, were made with ionization chambers by Küstner and Arends (1935) for seven elements in the range of Z from 73 to 83, but in their evaluation no account was taken of the possibility of the transfer of ionization from a low lying L level to a higher L level (Coster and Kronig 1935). Values of ω_3 are, however, unaffected by this omission, and, if ionization transfers of the type $L_{II} \rightarrow L_{III}$(N, O, etc.) are of negligible intensity, values of ω_2 should also be unaffected. Measurements of ω_3 were also made by Stephenson (1937) for Pb, Th and U. His results are consistent with the corresponding measurements of Küstner and Arends (see Kinsey 1948 a, figure 2) and this suggests that both sets of measurements for ω_3 are reliable.

Kinsey (1948 a) calculated values of ω_1, ω_2 and ω_3 for eight elements in the range of Z from 73 to 92 by estimating the radiation width Γ_r of each sub-shell and dividing this by the total width Γ of the sub-shell. Estimates of Γ_r were based on (i) the calculations by Massey and Burhop (1936) of the absolute transition probabilities of selected strong radiative transitions, and (ii) the measured relative intensities of all important lines in the L x-ray spectrum arising in the particular L sub-shell. For the total widths of the respective levels, Kinsey selected a 'best value' from the direct measurements of level widths made for Ta and W by Bearden and Snyder (1941) and for Au by Richtmyer, Barnes and Ramberg (1934). Values of Γ for neighbouring elements were estimated by using the equation $\Gamma = \Gamma_r + \Gamma_A + \Gamma_C$, where Γ_A is the Auger width and Γ_C the Coster–Kronig width of the level. Γ_A was assumed to be constant over the range of Z concerned and Γ_C was assumed to arise only from ionization transfers of the type $L_I \rightarrow L_{III}M_{IV,V}$ and to be given in magnitude by the measurements of Cooper (1942).

In a subsequent paper, Kinsey (1948 b) published measurements of the absolute intensities of the L x-rays excited by internal conversion of γ-radiation following the β-disintegration of ThB, the α-disintegration of ThC and the β-disintegration of RaD. He thereby established that the total L fluorescence yield was higher than his calculated value and also that the fraction of this yield due to $L_I + L_{II}$ fluorescence was larger in the cases of ThC and RaD than the calculations predicted. He concluded (i) that the calculated values of Massey and Burhop were too small by about 10% (these calculations used hydrogenic relativistic wave functions and took account of screening in accordance with Slater's rules), and (ii) that Coster–Kronig transitions of the type $L_I \rightarrow L_{II}N$ occur for about 12% of the L_I ionization. These modifications raise the predicted total fluorescence yields in bismuth following the conversion of nuclear magnetic dipole radiation of 40 to 50 kev energy from 32 to 41%. However, this increase was not considered by Kinsey to be sufficient to produce good agreement between calculated and observed values of the L x-ray intensity following the α-disintegration of ThC, and he finally employed a total fluorescence yield of 47% in his calculations for RaD, a figure which has been adhered to in subsequent discussions of this disintegration. Further evidence on the fluorescence yields would clearly be of value.

§ 2. THE EQUATIONS GOVERNING THE FLUORESCENCE YIELD

The equations are formulated for the case in which the primary ionization is produced by internal conversion of a single γ-ray, but the treatment is readily adapted to other methods of ionization by substituting in a suitable manner for the phrase 'per disintegration'.

The symbols employed are as follows.

n_1, n_2, n_3: the numbers of primary ionizing events per disintegration in the L_I, L_{II} and L_{III} levels respectively.

$\omega_1, \omega_2, \omega_3$: the fluorescence yields of the three L levels.

a_1, a_2, a_3: the Auger yields of the three L levels.

f_{12}, f_{13}, f_{23}: the Coster–Kronig transition yields for transfer of ionization from the level represented by the first suffix to the level represented by the second suffix.

I, F, and A: the total number per disintegration of L ionizations, L fluorescent quanta and L Auger electrons respectively.

R: the total number of γ-quanta radiated per disintegration.

$1:C_2:C_3$: the relative numbers of primary ionizations in the three levels.

$1:F_2:F_3$: the relative numbers of L x-ray quanta produced from the three levels.

$1:A_2:A_3$: the relative numbers of Auger electrons produced from the three levels.

Assuming only that, as proved by Kinsey (1948 a), the L fluorescence yield of an atom singly ionized in a given L level is to a good approximation the same as the L fluorescence yield for the atom ionized both in the given L level and in an M or higher shell, the following relations hold:

$$n_1 + n_2 + n_3 = I = A + F \qquad \ldots\ldots(1)$$

$$\omega_1 n_1 + \omega_2(n_2 + f_{12}n_1) + \omega_3[n_3 + f_{13}n_1 + f_{23}(n_2 + f_{12}n_1)] = F \qquad \ldots\ldots(2)$$

$$a_1 n_1 + a_2(n_2 + f_{12}n_1) + a_3[n_3 + f_{13}n_1 + f_{23}(n_2 + f_{12}n_1)] = A \qquad \ldots\ldots(3)$$

$$n_1 = n_2/C_2 = n_3/C_3 \qquad \ldots\ldots(4)$$

$$\omega_1 n_1 = \frac{\omega_2(n_2 + f_{12}n_1)}{F_2} = \frac{\omega_3[n_3 + f_{13}n_1 + f_{23}(n_2 + f_{12}n_1)]}{F_3} \qquad \ldots\ldots(5)$$

$$a_1 n_1 = \frac{a_2(n_2 + f_{12}n_1)}{A_2} = \frac{a_3[n_3 + f_{13}n_1 + f_{23}(n_2 + f_{12}n_1)]}{A_3} \qquad \ldots\ldots(6)$$

$$1 = f_{12} + f_{13} + \omega_1 + a_1 \qquad \ldots\ldots(7a)$$

$$1 = f_{23} + \omega_2 + a_2 \qquad \ldots\ldots(7b)$$

$$1 = \omega_3 + a_3. \qquad \ldots\ldots(7c)$$

The problem in its present form is to determine the quantities represented by small letters when the quantities represented by capital letters are determined by experiment. The equations are however neither independent nor sufficient. There are twelve 'unknowns', the *n*'s, the ω's, the *a*'s and the *f*'s, and of these, three (the *n*'s) refer to the process of primary ionization and nine are independent of that process. There are eight independent quantities experimentally determined (I, C_2, C_3, F, F_2, F_3, A_2 and A_3), and three of these (I, C_2, C_3) allow the *n*'s to be calculated. This leaves five experimentally determined quantities and three identities (equations (7)) for the calculation of the nine coefficients of de-excitation. Explicit expressions for four of the coefficients may be written down at once. They are

$$\omega_1 = \frac{F}{I}\,\frac{1 + C_2 + C_3}{1 + F_2 + F_3} \qquad \ldots\ldots(8a)$$

$$a_1 = \frac{I - F}{I}\,\frac{1 + C_2 + C_3}{1 + A_2 + A_3} \qquad \ldots\ldots(8b)$$

$$\frac{1}{\omega_3} = 1 + \frac{I - F}{F}\,\frac{A_3}{F_3}\,\frac{1 + F_2 + F_3}{1 + A_2 + A_3} \qquad \ldots\ldots(9a)$$

$$\frac{1}{a_3} = 1 + \frac{F}{I - F}\,\frac{F_3}{A_3}\,\frac{1 + A_2 + A_3}{1 + F_2 + F_3}. \qquad \ldots\ldots(9b)$$

Equations (9) involve a redundancy in view of (7*c*).

To proceed further it is necessary either to acquire an additional source of experimental information, or to introduce a simplifying assumption. The assumption $f_{23} = 0$ is mathematically convenient and is probably not greatly in error. If we adopt this assumption we have (again with a redundancy on account of equation (7*b*)),

$$\frac{1}{\omega_2} = 1 + \frac{I - F}{F}\,\frac{A_2}{F_2}\,\frac{1 + F_2 + F_3}{1 + A_2 + A_3} \qquad \ldots\ldots(10a)\dagger$$

$$\frac{1}{a_2} = 1 + \frac{F}{I - F}\,\frac{F_2}{A_2}\,\frac{1 + A_2 + A_3}{1 + F_2 + F_3} \qquad \ldots\ldots(10b)\dagger$$

and, from equations (4) and (5), in terms of (8*a*), (9*a*) and (10*a*) and with redundancy on account of (7*a*),

$$f_{12} = (\omega_1 F_2/\omega_2) - C_2 \qquad \ldots\ldots(11)$$

$$f_{13} = (\omega_1 F_3/\omega_3) - C_3. \qquad \ldots\ldots(12)\dagger$$

If no assumption is made regarding f_{23}, a second set of experiments is required

---

† Valid only if $f_{23} = 0$.

involving an alternative mode of primary ionization such that vacancies are created in the three L levels in ratios other than $n_1 : n_2 : n_3$. Such an experiment is possible if a stable isotope is available for experiments in which x-rays are the primary ionizing agent, or if a second unstable isotope exists the radioactive disintegration of which involves the emission and internal conversion of a single γ-ray producing L ionization ratios $n_1' : n_2' : n'_3$ different from those of the γ-ray already considered. As a good approximation, in most cases, species of neighbouring *Z* values may be used if pairs of isotopes are not available—thus Kinsey compared the disintegrations of ThB and ThC (internal conversion in $_{83}$Bi and $_{81}$Tl, respectively) though he had not available two complete sets of data for use as indicated here. In the present treatment, primed letters will be used to represent the second set of experimentally determined quantities, and also to distinguish duplicated values of the coefficients of de-excitation obtained through the use of these quantities.

By combining the first and second sets of experimental quantities (using (5) and (4)) we then have

$$\omega_2 = (\omega_1 F_2 - \omega_1' F_2')/(C_2 - C_2') \qquad \ldots\ldots(13a)$$

$$f_{12} = (C_2 \omega_1' F_2' - C_2' \omega_1 F_2)/(\omega_1 F_2 - \omega_1' F_2'). \qquad \ldots\ldots(14a)$$

Similarly (using (6) and (4))

$$a_2 = (a_1 A_2 - a_1' A_2')/(C_2 - C_2') \qquad \ldots\ldots(13b)$$

$$f_{12} = (C_2 a_1' A_2' - C_2' a_1 A_2)/(a_1 A_2 - a_1' A_2'). \qquad \ldots\ldots(14b)$$

These results enable f_{13} to be obtained from (7*a*) and f_{23} from (7*b*) thereby completing the solution of the problem. Here it may be noted that full duplication of the experimentally determined information would provide duplicated values of six of the coefficients of de-excitation (ω_1, a_1, ω_3, a_3, f_{12}, f_{13}) and single values of the other three coefficients.

Up to this point the solution of the equations has been regarded purely formally, without reference to the relative accuracy of the experimental information involved. It should be recognized, however, that all this information is not of the same accuracy, and that, in particular, individual values of the Auger yields from the three L sub-shells are difficult to determine with precision. Values of A_2 and A_3 are not involved in the calculation of the coefficients ω_1, ω_2 and f_{12} from equations (8*a*), (13*a*) and (14*a*) respectively, but they are involved in the calculation of a_1 and ω_3 by equations (8*b*) and (9*a*) and hence in the determination of a_3 and f_{13} using equations (7*c*) and (7*a*). The equations (13*b*) and (14*b*) for a_2 and f_{12} are particularly unreliable in that they require two sets of the Auger intensities; the errors in a_2 also affect f_{23} when the latter is found by difference using equation (7*b*). It is possible, however, in a favourable case to obtain f_{23} with useful accuracy from the relation

$$f_{23} = [(\omega_1 F_3/\omega_3) - C_3 - f_{13}]/(C_2 + f_{12}) \qquad \ldots\ldots(15)$$

and a_2 may then be found from (7*b*). It may be noted that if the ratio $A_3/(1 + A_2)$ is known more accurately than either A_2 or A_3, ω_3 is likely to be more accurate than a_1; in the subsequent discussion this condition will be encountered.

§ 3. THE EXPERIMENTAL VALUES RELATING TO BISMUTH

The disintegration of RaD followed by internal conversion in RaE of a single γ-ray of 46·5 kev energy provides a very suitable case for the study of L-shell fluorescence. This disintegration has been so often investigated that a considerable body of experimental results already exists for it, and there is available also some evidence regarding the ordinary fluorescent radiation of Bi. We therefore devote the rest of this paper to the discussion of the data concerning Bi and to the calculation of the fluorescence and other yields of the L levels of this element.

(i) C_2 *and* C_3

The results of recent work on the relative intensities of conversion of the 46·5 kev γ-ray in Bi following β-disintegration of RaD are shown in table 1 together with theoretical values taken from the tables of internal conversion coefficients for M1 radiation given by Rose *et al.* (private communication) for the L_I and L_{II} levels, and by Gellman *et al.* (1952) for the L_{III} level. The measured relative intensities are consistent with the assumption of pure M1 radiation and are close to the theoretical values. The rather difficult measurement of the relative intensity of conversion in the L_{III} level appears to give a value somewhat higher than theory predicts (although final theoretical values have not yet been obtained).

Table 1. The Relative Intensities of Conversion of the RaD γ-ray in the L Levels of Bi

Level of conversion	Cranberg (1950)	Wu *et al.* (1953)	Bashilov *et al.* (1953)	Theoretical M1	
				Relative	Absolute
L_I	100	100	100	100	16·3
L_{II}	$9\pm1{\cdot}5$	$7{\cdot}5\pm0{\cdot}5$	15 ± 3	8·9	1·45
L_{III}	$1{\cdot}9\pm0{\cdot}4$	$0{\cdot}7\pm0{\cdot}3$	$0{\cdot}86\pm0{\cdot}05$	0·13	0·022

This may be explained by the presence of an almost negligible E2 component, or alternatively by the occurrence under the conditions of experiment of a small amount of external conversion of the γ-ray in Pb, an explanation for which there is support in the finding by Bashilov *et al.* of a peak (labelled X by these authors) which may arise from external conversion in the L_{II} level of Pb. However, the quantity C_3 is so small by comparison with f_{13} and with $1+C_2$ that variations in it are unimportant and we therefore adopt the theoretical values $C_2=0{\cdot}089\pm0{\cdot}002$, $C_3=0{\cdot}0013$.

For the case of L ionization by soft x-rays, experimental values of the relative intensities of ionization are given by Robinson and Young (1930) but complete data are found in their work only for Au. They find ionization (produced by $K\alpha_1+K\alpha_2$ radiations of Ag) proportional to $3{\cdot}5\pm0{\cdot}25$, $5{\cdot}3\pm0{\cdot}5$ and $8{\cdot}5\pm0{\cdot}5$ in the L_I, L_{II} and L_{III} levels respectively, giving $C_2'=1{\cdot}5\pm0{\cdot}2$, $C_3'=2{\cdot}4\pm0{\cdot}3$ (errors estimated by present authors). However the intensities of ionization found by Robinson and Young are subject to two corrections: (i) for the conversion from photographic blackening to electron intensity, which will raise the intensity of L_I ionization and to a less extent that of L_{II} ionization relative to the L_{III} ionization intensity, and (ii) for the directionality of ejection of photoelectrons from the three L levels which probably enhances the reception of L_I photoelectrons under the geometrical conditions of the experiment. Considerable difficulties are also encountered in estimating the relative intensities of ionization from the 'absorption jump' ratios. Relative intensities obtained by this method for Bi are: 1 : 1·7 : 2·6 (Patten 1934), 1 : 2·1 : 2·26 (Carr 1934), and 1 : 1·77 : 2·74 (Küstner and Arends 1935). Because of the uncertainties associated with these measurements we take the mean of those measurements which give a reasonably good fit with the crude theoretical ionization ratio 2:3 for the L_{II} and L_{III} levels respectively, namely, those of Robinson and Young, Patten, and Küstner and Arends. This gives $C_2' = 1{\cdot}66 \pm 0{\cdot}15$ and $C_3' = 2{\cdot}6 \pm 0{\cdot}2$. A precision measurement of the relative ionizations using counters and a high resolution spectrograph and making allowance for the directionality of photoelectron ejection would obviously be of interest.

(ii) F_2 *and* F_3

Precision measurements of the relative intensities of the L x-rays of Bi following the disintegration of RaD have been made recently by Frilley *et al.* (1951), by Ewan† (1952) and for the present paper by Cochran.† In each case a curved crystal spectrometer with photographic recording on electron-sensitive emulsion was used, the resolution obtained by Frilley *et al.* being somewhat higher than that obtained by Ewan or Cochran. The calibration of the sensitivity of the spectrometers as a function of the energy of the radiation was calculated by Frilley *et al.* and Ewan and was experimentally determined by Cochran (thereby including in the calibration, corrections for absorption in the crystal, in the air path and in the paper cover of the electron-sensitive plate). The results obtained are shown in table 2. The total relative intensities in the Lα, Lβ and Lγ bands inclusive of the weaker lines are shown in table 3 and compared with the band intensities measured by Wu *et al.* (1953) and by Hughes† for the present paper. Wu *et al.* made their observations by proportional counter with krypton and methane filling and Hughes used a proportional counter with pure argon filling. Some allowance must be made for the presence of x-rays from Pb in the spectra of Wu *et al.* and of Hughes, which tends to lower the Lγ intensity relative to that of Lα and Lβ perhaps by 2 or 3%. The agreement between the five sets of results in the table is considered to be satisfactory. The total intensities

Table 2. Relative Intensities of the L x-ray Lines of Bi

	RaD disintegration			Excitation by soft x-rays		
	Frilley *et al.*	Ewan	Cochran	Frilley *et al.* ‡	Ewan	Cochran
α_2 + satellites of α_2	15	18	161	17·5	17	15·6
α_1 + satellites of α_1	150	145		137·5	135	137
β_4	25	35	31·5	6·3	6	7
β_2	20	100	100	30	100	100
β_1 + satellites of β_2	80			70		
β_3	40	46	38	7·5	7	7·5
β_5	—	3	—	3·7	—	4·3
γ_1		15	9·4		14	10·9
	$\frac{\gamma_2}{\gamma_1} \simeq 3$			$\frac{\gamma_2}{\gamma_1} \simeq 0{\cdot}1$		
γ_2		11	7·1		1·8	3·8
	$\frac{\gamma_3}{\gamma_2} \simeq 1$			$\frac{\gamma_3}{\gamma_2} \simeq 1$		
γ_3		14	8·8		1·8	
λ_4		4	2·7		—	0·3

---

† Fuller publication elsewhere.

‡ Normalized to bring the total intensity of the lines β_1 and β_2 to 100 units.

Table 3. Relative Intensities of Groups of L x-ray Lines of Bi

	Disintegration of RaD					Excitation by soft x-rays			
Group of lines	Frilley *et al.*	Ewan	Cochran	Wu *et al.*	Hughes	Frilley *et al.*	Ewan	Cochran	Hughes
Lα	170	168	166	1	1·00 ±0·10	159	157	157	1·00 ±0·15
Lβ	175	191	181	1	1·13 ±0·10	121	120	122	0·98 ±0·15
Lγ	38	45	29	0·2	0·23 ±0·02	15·2	18·9	15·8	0·19 ±0·04
L_I	94	115	91			19·2	17·1	18·0	
L_{II}	78	82	75			85	81	78	
L_{III}	211	207	210			191	197	199	

of radiation from the L_I, L_{II} and L_{III} shells are also entered in table 3. In the calculation of these intensities, auxiliary data were required to resolve the $\beta_1\beta_2$ line and to include weak lines. The required relative intensities were taken from the spectra of Ta (Hicks 1931, Bötzkes 1934), W (Jönsson 1926), U (Allison 1928) after correction for absorption in the source. The intensities of the Lγ lines in the spectrum of Frilley *et al.* were likewise calculated from these auxiliary spectra. Values of F_2 and F_3 were then calculated for each Bi spectrum and means taken to obtain $F_2 = 0{\cdot}79 \pm 0{\cdot}06$, $F_3 = 2{\cdot}12 \pm 0{\cdot}3$. Proceeding in a similar manner with the spectrum of Bi excited by soft x-rays (largely Ag K radiation), values of $F_2' = 4{\cdot}5 \pm 0{\cdot}2$, $F_3' = 10{\cdot}7 \pm 1{\cdot}0$ were derived. Hence $F_2'/F_2 = 5{\cdot}7 \pm 0{\cdot}5$, $F_3'/F_3 = 5{\cdot}1 \pm 0{\cdot}9$ and $F_3/F_2 = 2{\cdot}7 \pm 0{\cdot}4$, $F_3'/F_2' = 2{\cdot}4 \pm 0{\cdot}25$.

(iii) *The Value of F/I for the RaD Disintegration and for Excitation of Bi by Soft X-Rays*

For the case of excitation by soft x-rays we have $F/I = 0{\cdot}402$, as determined by Lay (1934).

For the RaD disintegration there is considerably more doubt about the best value. For this case an absolute determination of F by Stahel (1935) gave 0·252 per disintegration. Other (and probably less reliable) measurements are 0·30 (Gray 1932), 0·27 (Tsien 1944) and 0·19 ± 0·03 (Damon and Edwards 1954). Many workers have made measurements of I, either by comparing the total L-conversion intensity with the total intensity of the RaE continuum, or by determining the absolute intensity of L conversion and the absolute intensity of the source—the latter by various methods. Recent results are summarized in table 4. The value of I given by Butt and Brodie is considered to err on the low side on account of over-correction for back-scattering in the source.

Table 4. Values of I and F/I

	Method	I per disintegration	F/I	
Cranberg (1950)	Absolute source strength	0·54	0·465	F from Stahel
Butt and Brodie (1951)	RaE	0·467	0·54	
Wu *et al.* (1953)	RaE	0·64	0·393	
Bashilov *et al.* (1953)	RaE	0·45 ± 0·02	0·56	
Kinsey (1948)	Calculation		0·41	
,,	Final estimate		0·47	
Lay (1934)	X-ray excitation		0·402	

An alternative method of determining F/I for the RaD disintegration is through the ratios F/R and R/I separately determined. Values of F/R have been found by direct comparison (using proportional counter and pulse analyser) to be $4{\cdot}4 \pm 0{\cdot}7$ (Wu *et al.* 1953) and $6{\cdot}74 \pm 0{\cdot}5$ (Hughes for the present paper: uncorrected for source absorption). Absolute determinations by scintillation spectrometer give $F = 0{\cdot}19 \pm 0{\cdot}03$, $R = 0{\cdot}044 \pm 0{\cdot}003$ and hence $F/R = 4{\cdot}3 \pm 0{\cdot}9$ (Damon and Edwards 1954). R/I is the reciprocal of the total L internal conversion coefficient, the data for which are given in table 1, column 6. Here an error of the order of 2% is involved in the interpolation for Z and γ-ray energy in the tables of Rose *et al.* The maximum fractional error due to neglect of a possible E2 component of the γ-ray is 0·3% and is therefore negligible. Even allowing for approximations in the calculations of Rose *et al.* and of Gellman *et al.*, the theoretical value for R/I is considered to be better than any experimental value at present available. Using it with the data of Wu *et al.* and of Damon and Edwards, F/I by this method is about $0{\cdot}25 \pm 0{\cdot}04$ and with the more recent determination of Hughes, $F/I = 0{\cdot}38 \pm 0{\cdot}03$. By comparison with the results in table 4 it appears that the value of F/I obtained in this way from the published data is considerably too low to be acceptable. The value derived from the observations of Hughes would be slightly raised by correction for source absorption; in this way it would be brought nearer to the results in the table. From the experimental evidence discussed above we conclude that the value of F/I probably lies between 0·38 and 0·49.

(iv) *Evidence Concerning A_2 and A_3*

High resolution electron spectrometer studies of the L Auger electrons of RaD have been made by Kobayashi (1953) and by Bashilov *et al.* (1953). Allowing for the somewhat higher resolution achieved by Bashilov *et al.* at energies below about 6 kev, the published spectra are essentially the same. Kobayashi gives an analysis of the line intensities after applying a correction for absorption in the source and estimating the level of the background. The figure shows the

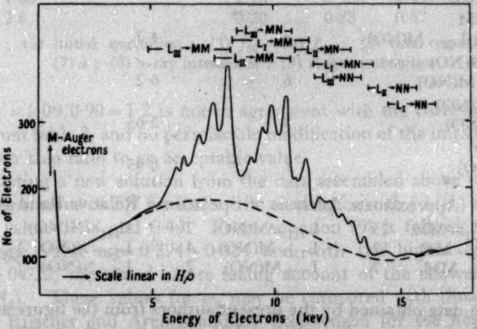

Spectrum of L-Auger electrons of Bi (after Bashilov *et al.*) uncorrected for absorption in the source. Background level as estimated by the present authors is indicated by the broken line.

spectrum after Bashilov *et al.* to which we have added a curve showing the approximate level of the background but no correction for source absorption. The energy ranges of the various Auger electron bands are shown in table 5 and it will be seen that the main features of the spectrum shown in the figure may be interpreted in terms of these bands. From 5·2 to 8·1 kev the $L_{III}\rightarrow$MM lines appear and the high-energy end of this band includes the low-energy tail of $L_{II}\rightarrow$MM. From 8·4 to 10·4 kev the main part of the $L_{II}\rightarrow$MM band occurs superposed on the $L_{III}\rightarrow$M(NO) band and a considerable portion of the $L_{I}\rightarrow$MM band. From 10·8 to 11·1 kev no L_{III} lines appear and the contributing bands are the high-energy portion of $L_{I}\rightarrow$MM and the low energy tail of $L_{II}\rightarrow$M(NO). From 11·4 to 13·6 kev the high-energy portion of $L_{II}\rightarrow$M(NO) is superposed on $L_{I}\rightarrow$M(NO) and $L_{III}\rightarrow$N(NO) and finally from 13·7 to 16·4 kev the $L_{I,\,II}\rightarrow$N(NO) lines occur. In table 6 the intensity analysis given by Kobayashi is reproduced together with data obtained by the present authors from the figure and corrected approximately for source absorption. For comparison the results of Robinson and Young (1930) for excitation by soft x-rays are included in the table, the figures in this case representing the relative photographic blackening. The rough analysis suggested in table 7 is based on the intensity measurements of Kobayashi and the intensity readings made from the graph of Bashilov *et al.* From this analysis we conclude that the ratio $A_3/(1+A_2)$ is $1{\cdot}3\pm0{\cdot}2$ and less confidently

Table 5. Energy Limits of L Auger Bands in kev based on the data of Cauchois (1952)

Shells of final ionization	Shell of initial ionization		
	L_I	L_{II}	L_{III}
MM	8·22–11·11	7·54–10·42	5·25– 8·15
M(NO etc.)	11·38–13·62	10·71–12·95	8·41–10·65
N(NO etc.)	14·4 –16·4	13·7 –15·7	11·4 –13·4

Table 6. Relative Intensities of the Auger Electron Bands

	Disintegration of RaD		x-ray excitation
	Kobayashi	after Bashilov *et al.*	Robinson and Young (blackening)
$L_{III}\rightarrow$ MM +small part $L_{II}\rightarrow$ MM	26·5	25·4	13·5
part $L_{II}\rightarrow$ MM +part $L_{I}\rightarrow$ MM $+L_{III}\rightarrow$ M(NO)	21	21	7·5+
part $L_{I}\rightarrow$ MM +small part $L_{II}\rightarrow$ M(NO)	4	4·7	3·5
part $L_{II}\rightarrow$ M(NO) +part $L_{I}\rightarrow$ M(NO)	6	6·2	5+
part $L_{I}\rightarrow$ M(NO) $+L_{III}\rightarrow$ N(NO)	3	2·65	2
$L_{II}\rightarrow$ N(NO) $+L_{I}\rightarrow$ N(NO)	?	0·95	0·1

Table 7. Approximate Analysis of Spectrum: Relative Band Intensities

$L_{III}\rightarrow$ MM	25	$L_{III}\rightarrow$ M(NO)	7	$L_{III}\rightarrow$ N(NO)	2
$L_{II}\rightarrow$ MM	12	$L_{II}\rightarrow$ M(NO)	4−	$L_{II}\rightarrow$ N(NO)	0·95
$L_{I}\rightarrow$ MM	7	$L_{I}\rightarrow$ M(NO)	2+	$L_{I}\rightarrow$ N(NO)	

that $1<A_2<2{\cdot}5$. For the analysis of the Auger spectrum of RaD it would be valuable to obtain, at equally high resolution, the Auger spectrum of the L_{III} shell alone.

For the case of x-ray excitation, the only observations of Auger intensities are those of Robinson and Young (1930) entered in table 6. It does not seem possible to make use of these because the correction factor for the conversion of photographic blackening units to electron intensity is too uncertain. We therefore rely on the theoretical relations $A_2/F_2=A_2'/F_2'(=a_2\omega_1/a_1\omega_2)$ and $A_3/F_3=A_3'/F_3'(=a_3\omega_1/a_1\omega_3)$ which follow from equations (5) and (6).

§ 4. CALCULATION OF THE YIELDS

It will first be shown that the values proposed by Kinsey do not give a satisfactory fit with the 'best values' of the experimental data adopted here. We take from § 3 (i) above the relative intensities of initial ionization entered in column 2 of table 8 and calculate from them and from Kinsey's values of f_{12} and f_{13} (entered in columns 3 and 4) the total excitations shown in column 5. Then using Kinsey's values of ω and a, the entries are obtained for columns 8 and 9. From column 8, we find the calculated ratio $F_3/F_2=0{\cdot}231/0{\cdot}106=2{\cdot}2$ in fairly satisfactory agreement with the value $2{\cdot}7\pm0{\cdot}4$ deduced from table 3, but the ratio $F_3'/F_2'=1{\cdot}09/0{\cdot}90=1{\cdot}2$ is not in agreement with the corresponding value $2{\cdot}4\pm0{\cdot}25$ from table 3, and no permissible modification of the initial x-ray excitations can alter this ratio to an acceptable value.

Table 8. Substitution of the Yields deduced by Kinsey

(1)	(2)	(3)	(4)	(5)	(6)	(7)	(8)	(9)
	RaD disintegration							
L_I	1·0	0·12	0·70	1·0	0·11	0·07	0·11	0·07
L_{II}	0·089			0·209	0·506	0·494	0·106	0·103
L_{III}	0·0013			0·7013	0·33	0·67	0·231	0·470
	X-ray excitation							
L_I	1·0	0·12	0·70	1·0	0·11	0·07	0·11	0·07
L_{II}	1·66			1·78	0·506	0·494	0·90	0·88
L_{III}	2·6			3·30	0·33	0·67	1·09	2·21

(1) Level ; (2) initial excitation ; (3) f_{12} ; (4) f_{13} ; (5) total excitation ; (6) ω ; (7) a ; (8) x-ray intensities ; (9) Auger intensities

In attempting a new solution from the data assembled above it is necessary first to choose a value of F/I for RaD. In accordance with § 3 (iii) above we take as extreme values 0·38 and 0·49. From equation (9) it follows that with the lower extreme value $\omega_3=0{\cdot}374\pm0{\cdot}024$ and with the higher extreme value $\omega_3=0{\cdot}476\pm0{\cdot}022$, the stated errors taking account of the allowable variations in $A_3/(1+A_2)$. These values for ω_3 may be compared with those determined directly by Küstner and Arends and by Stephenson for the heavy elements, namely

	Küstner and Arends		Stephenson
Pb	$Z=82$	$\omega_3=0{\cdot}337$	$\omega_3=0{\cdot}32$
Bi	$Z=83$	$\omega_3=0{\cdot}367$	
Th	$Z=90$		$\omega_3=0{\cdot}42$

The evidence of these experiments clearly supports the choice of a value of F/I much nearer 0·38 than 0·49. We therefore select a value of 0·40 ± 0·02 for F/I in order to continue the discussion of the yields.

The acceptance of the very rough data for A_2 and A_3 requires some justification. Adopting the assumption $f_{23}=0$ it is possible to obtain a value of ω_2 if a value can be obtained for A_2 (equation (10)). With A_2 equal to 1·0, 1·5 and 2·5 (see §3 (iv) above), ω_2 takes the values 0·375 ± 0·021, 0·345 ± 0·021 and 0·292 ± 0·020 respectively, where the error covers the allowed variation in $A_3/(1+A_2)$. This range for ω_2 is less than might have been expected considering the uncertainties in the analysis of the Auger spectrum; the three values all lie between 0·506 and 0·255 which are, respectively, the values of ω_2 calculated by Kinsey and determined experimentally by Küstner and Arends. Having in this way shown that the values deduced in §3 (iv) for A_2 and A_3 do not appear to be grossly in error nor to be unduly critical, we adopt finally $A_2=1\cdot7\pm0\cdot7$ and $A_3=3\cdot5\pm1\cdot2$, the latter value resulting from the substitution of the former in the equation $A_3/(1+A_2)=1\cdot3\pm0\cdot2$.

We now compute the yields in two ways. In the first we assume $f_{23}=0$ and use the data from the RaD experiments and equations (7) to (12) excluding (9*b*), (10*b*) and (11). The resulting yields, shown in the upper part of table 9 are then applied to the case of ionization by x-rays following the procedure employed in forming table 8, i.e. values of C_2' and C_3' are taken from §3 (i). This gives calculated values of x-ray intensities as shown in table 9 from which

Table 9. Calculation of Yields assuming $f_{23}=0$

RaD disintegration

Level	Initial excitation	f_{12}	f_{13}	ω	a
L_I	1·00	0·18 ± 0·04	0·605 ± 0·03	0·11 ± 0·01	0·105 ± 0·025
L_{II}	0·089			0·33 ± 0·15	0·67 ± 0·15
L_{III}	0·0013			0·39 ± 0·05	0·61 ± 0·05

X-ray excitation

Level	Initial excitation	Total excitation	X-ray intensities	Auger intensities
L_I	1·00	1·00	0·11 ± 0·01	0·105 ± 0·025
L_{II}	1·66 ± 0·15	1·84 ± 0·155	0·61 ± 0·3	1·23 ± 0·3
L_{III}	2·6 ± 0·2	3·205 ± 0·2	1·25 ± 0·17	1·955 ± 0·17

$F_3'/F_2'=1\cdot25/0\cdot61=2\cdot05\pm1\cdot0$. This is in better agreement with the experimental value 2·4 ± 0·25 than the corresponding result from table 8, but the significance of this agreement is low on account of the large error involved. The value of $F_3'=1\cdot25/0\cdot11=11\cdot4\pm1\cdot9$ is however more significantly in agreement with the value 10·7 ± 1·0 deduced in §3 (ii).

The second computation of the yields is made on the assumption that f_{23} may have a non-zero value. Equations (7*c*), (8) and (9*a*) are each used once with the RaD data (giving the values already entered in table 9 for ω_1, ω_3, a_1 and a_3) and once with the x-ray excitation data (giving ω_1', ω_3', a_1' and a_3'). The equations (13*a*) and (14*a*) are used once, and (15), (7*a*) and (7*b*) twice. The results are shown in table 10.

The agreement between ω_1 and ω_1' shows the consistency of the results obtained from the two independent sets of experimental data; ω_3', a_1' and a_3' are not completely independent of the RaD data since independent values of A_2' and A_3' are not available. The values of ω_3 and ω_3' agree within the limits

Table 10. Yields calculated on the assumption that f_{23} may be non-zero

$\omega_1=0{\cdot}11\pm0{\cdot}01$		$\omega_1'=0{\cdot}13\pm0{\cdot}012$
$\omega_3=0{\cdot}39\pm0{\cdot}05$		$\omega_3'=0{\cdot}41\pm0{\cdot}05$
$a_1=0{\cdot}105\pm0{\cdot}025$		$a_1'=0{\cdot}111\pm0{\cdot}03$
$a_3=0{\cdot}61\pm0{\cdot}05$		$a_3'=0{\cdot}59\pm0{\cdot}05$
	$\omega_2=0{\cdot}32\pm0{\cdot}04$	
	$f_{12}=0{\cdot}19\pm0{\cdot}05$	
$f_{13}=0{\cdot}59\pm0{\cdot}05$		$f_{13}'=0{\cdot}57\pm0{\cdot}06$
$f_{23}=0{\cdot}04\pm0{\cdot}14$		$f_{23}'=0{\cdot}08\ \pm0{\cdot}14$
$a_2=0{\cdot}64\pm0{\cdot}14$		$a_2'=0{\cdot}60\ \pm0{\cdot}14$

of error with the measurements of Küstner and Arends, but this agreement has been obtained by the choice of the value of F/I. The values of ω_2 and f_{12} are not appreciably altered by giving up the assumption $f_{23}=0$. It will be noted, however, that the accuracy of the ω_2 value is better in the second calculation than in the first. For ω_2, Küstner and Arends found a value 0·255, somewhat lower than our calculated value. The use by us of a lower value of F/I would have improved the agreement with Küstner and Arends, but the errors involved in their determination are too uncertain to justify any conclusions on this point. The quantity f_{23} is particularly sensitive to variation in the values of A_2 and A_3. The errors quoted for f_{23} and a_2 ignore the variations allowed in A_2 and A_3: if these had been included no significant result would have emerged. We take this to indicate that the values adopted here for A_2 and A_3 are better than our error estimates suggest. All other quoted errors include the full allowance for errors in A_2 and A_3. On account of the large error in f_{23} it is not possible to conclude that this quantity has a non-zero value.

§ 5. Implications of the Data Relating to the Disintegration of RaD

If F/I is approximately 0·40 and if Stahel's (1935) value $F=0{\cdot}252$ per disintegration is accurate, then I is approximately 0·63 per disintegration, a value in good agreement with the measurements of Wu *et al.* (1953), but somewhat higher than other recent determinations shown in table 4. For the γ-ray of RaD, the ratio of conversion in the L shell to conversion in M and higher shells is given by Wu *et al.* as 3·05 and by Cranberg (1950) as 2·84. Taking the mean of these values, we find the total conversion of the γ-ray to be 0·84 per disintegration. Adopting also the theoretical value for the internal conversion coefficient of this γ-ray, $I/R=17{\cdot}77\pm0{\cdot}35$ from table 1 column (6), then R is 0·035 per disintegration. This value for R is in good agreement with the measured values $0{\cdot}031\pm0{\cdot}012$ (Bramson 1930), 'somewhat less than 4%' (Gray 1932), 0·036 (von Droste 1933), 0·035 (Stahel 1935) and $0{\cdot}044\pm0{\cdot}007$ (Damon and Edwards 1954), but it is not in agreement with the value 0·07 calculated by Wu *et al.* (1953) from their measurement of F/R which we have had to discard for another reason in § 3 (iii) above. In accordance with the above assumptions, we thus find the total excitation of the 46.5 kev state of RaE to be of the order of 0·875 per disintegration and there remains 12·5% of the disintegrations to be otherwise explained.

This estimate, however, depends critically on the values chosen for F/I and F. If F/I is lowered to 0·38, the lower limit considered in our calculations, and if F is raised to 0·27, its value according to the measurements of Tsien (1944) calculations carried out as described in the previous paragraph would show 100%

excitation of the 46·5 kev state. It is therefore clear that F/I and F must be determined with high precision if an argument relying on their values is to establish with certainty the existence of an alternative mode of disintegration for RaD.

ACKNOWLEDGMENTS

We acknowledge with thanks the award by the Department of Scientific and Industrial Research of a maintenance grant to one of the authors (A. J. C.) which made it possible to carry out the crystal spectrograph experiments.

REFERENCES

ALLISON, S. K., 1928, *Phys. Rev.*, **32,** 1.
BASHILOV, A. A., DZHELEPOV, B. S., and CHERVINSKAYA, L. S., 1953, *Izv. Akad. Nauk. S.S.S.R., Ser. Fiz.*, **17,** 428.
BEARDEN, J. A., and SNYDER, T. M., 1941, *Phys. Rev.*, **59,** 162.
BÖTZKES, M., 1934, *Z. Phys.*, **89,** 667.
BRAMSON, S., 1930, *Z. Phys.*, **66,** 721.
BUTT, D. K., and BRODIE, W. D., 1951, *Proc. Phys. Soc.* A, **64,** 791.
CARR, L. H., 1934, *Phys. Rev.*, **46,** 92.
CAUCHOIS, Y., 1952, *J. Phys. Radium*, **13,** 113.
COOPER, J. N., 1942, *Phys. Rev.*, **61,** 234.
COSTER, D., and KRONIG, L., 1935, *Physica*, **2,** 13.
CRANBERG, L., 1950, *Phys. Rev.*, **77,** 155.
DAMON, P. E., and EDWARDS, R. R., 1954, *Phys. Rev.*, **95,** 1698.
VON DROSTE, G., 1933, *Z. Phys.*, **84,** 17.
EWAN, G. T., 1952, *Thesis*, University of Edinburgh (account to be published).
FRILLEY, M., GOKHALE, B. G., and VALADARES, M., 1951, *C. R. Acad. Sci., Paris*, **232,** 157.
GELLMAN, H., GRIFFITH, B. A., and STANLEY, J. P., 1952, *Phys. Rev.*, **85,** 944.
GRAY, J. A., 1932, *Nature, Lond.*, **130,** 738.
HICKS, V., 1931, *Phys. Rev.*, **38,** 572.
JÖNSSON, A., 1926, *Z. Phys.*, **36,** 426.
KINSEY, B. B., 1948a, *Canad. J. Res.*, **26,** 404 ; 1948b, *Ibid.*, **26,** 421.
KOBAYASHI, Y., 1953, *J. Phys. Soc., Japan*, **8,** 440.
KÜSTNER, H., and ARENDS, E., 1935, *Ann. Phys., Lpz.*, **22,** 443.
LAY, H., 1934, *Z. Phys.*, **91,** 533.
MASSEY, H. S. W., and BURHOP, E. H. S., 1936, *Proc. Camb. Phil. Soc.*, **32,** 461.
PATTEN, C. G., 1934, *Phys. Rev.*, **45,** 662.
RICHTMYER, F. K., BARNES, S. W., and RAMBERG, E. G., 1934, *Phys. Rev.*, **46,** 843.
ROBINSON, H. R., and YOUNG, C. L., 1930, *Proc. Roy. Soc.* A, **128,** 92.
STAHEL, E., 1935, *Helv. Phys. Acta*, **8,** 511.
STEPHENSON, R. J., 1937, *Phys. Rev.*, **51,** 637.
TSIEN, S.-T., 1944, *C. R. Acad. Sci., Paris*, **218,** 503.
WU, C. S., BOEHM, F., and NAGEL, E., 1953, *Phys. Rev.*, **91,** 319.

On the Positive Temperature Effect in the Cosmic Radiation

By H. TREFALL†
Imperial College of Science and Technology, London

Communicated by P. M. S. Blackett; MS received 14*th February* 1955

Abstract. The results of several underground measurements of the positive temperature effect are examined in order to obtain some information about the attenuation length of high-energy π-mesons in air. It is shown that this quantity can hardly be smaller than the attenuation length of the primary component. If this is so, competition between disintegration and nuclear capture of the π–mesons can account for but a very small part of the positive temperature effect which has been observed at sea level.

§ 1. INTRODUCTION

A POSITIVE partial correlation is known to exist between the meson intensity at sea level or underground and the stratospheric temperature, the other independent variables being the sea-level pressure and the height of the 100 mb level. This positive temperature effect was discovered by Duperier (1949), and was interpreted by him as being due to competition between decay and nuclear capture of the π-mesons. However, it has later been pointed out (Trefall 1953) that certain second-order effects of the μ–e decay must also give rise to a positive temperature effect which, in the case of measurements made at sea level, will be of the same order of magnitude as the effect which was expected to arise from the π–μ decay.

For a given energy, the positive temperature effect due to the π–μ decay depends essentially on the attenuation length λ_π of the π-mesons. Because of the possibility of reproduction of π-mesons in collisions with nuclei, λ_π need not be identical with the collision mean free path of π-mesons, and it therefore cannot be measured directly. It only seems possible to obtain any information about λ_π from the positive temperature effect itself, and then only if theoretical and experimental values are compared at such high energies that the second-order effects of the μ–e decay are small. This means that only underground measurements can be expected to give any significant information about λ_π. Such measurements have been performed by MacAnuff (1951) at a depth of 60 m water equivalent, by Sherman (1954) at 846 m water equivalent, by Barrett, Bollinger, Cocconi, Eisenberg and Greisen (1952) at 1574 m water equivalent and by Barrett, Cocconi, Eisenberg and Greisen (1954), also at 1574 m water equivalent. The information which these measurements can give about λ_π may then help us to estimate the positive temperature effect arising from the π–μ decay at lower energies.

§ 2. THEORY

We shall assume that the number of π-mesons produced in the layer dx with energies in the interval dE_π is proportional to $E_\pi^{-s} \exp(-x/\lambda_p)\, dx\, dE_\pi$, where E_π is the total energy of the mesons and x is the atmospheric depth in g cm^{-2}.

---

† On leave from Universitetet i Bergen, Norway.

Energies will always be measured in units of the rest energy of the particle under consideration. For mesons travelling vertically in an isothermal atmosphere, the survival probability from x' to x is $(x'/x)^{E'/E_\pi}\exp[-(x-x')/\lambda_\pi]$, where $E'\equiv H/ct_\pi$. H is the ' scale height ' of the atmosphere, t_π is the proper mean life of π-mesons, and energy losses are neglected.

For the sake of simplicity we shall now assume that $\lambda_\pi=\lambda_p=\lambda$. The intensity of π-mesons at the depth x is then found by a straightforward integration to be

$$I_\pi(x, E_\pi)=\frac{xE_\pi}{E_\pi+E'}E_\pi^{-s}e^{-x/\lambda}. \qquad \ldots\ldots(1)$$

As the atmospheric density is x/H, the number of π-mesons that decay per unit depth is

$$D_\pi(x, E_\pi)=\frac{H}{xct_\pi E_\pi}I_\pi(x, E_\pi)=\frac{E'}{E_\pi+E'}E_\pi^{-s}e^{-x/\lambda}. \qquad \ldots\ldots(2)$$

In order to obtain agreement with the observed sea-level energy spectrum of μ-mesons, one must take $s\simeq 2{\cdot}8$. Using the known properties of the π–μ decay, it can then be shown that μ-mesons of a given energy E are produced by π-mesons whose average energy is $0{\cdot}93E$. The production function for μ-mesons is therefore

$$S_\mu(x, E)=\frac{E'}{0{\cdot}93E+E'}E^{-s}e^{-x/\lambda}. \qquad \ldots\ldots(3)$$

Let $w(x, x_s, E)$ be the probability that a μ-meson which has been produced with the energy E at the atmospheric depth x shall reach the sea level depth x_s before it disintegrates. If we introduce a reference level at the depth x_r, we can write $w(x, x_s, E,)=w(x, x_r, E).\,w(x_r, x_s, E)$, where the second factor denotes the survival probability from the reference level to sea level. If $x<x_r$ the first factor will be the survival probability from the place of production to the reference level, but if $x>x_r$ this factor will be the inverse of the survival probability for a meson travelling from the reference level to the depth x. As nearly all high-energy μ-mesons are produced in the upper, practically isothermal, part of the atmosphere where also the reference level is situated, we find that

$$w(x, x_r, E)=(x/x_r)^{E''/E}$$

if energy losses in the atmosphere are neglected. Here $E''\equiv H/ct_\mu$, t_μ being the proper mean life of μ-mesons.

The differential energy spectrum of μ-mesons at sea level will therefore be of the form

$$\begin{aligned} n(E)&=\frac{E'}{0{\cdot}93E+E'}E^{-s}w(x_r, x_s, E)\int_0^{x_s}(x/x_r)^{E''/E}e^{-x/\lambda}\,d(x/\lambda) \\ &\simeq\frac{E'}{0{\cdot}93E+E'}E^{-s}w(x_r, x_s, E)(\lambda/x_r)^{E''/E}(E''/E)! \qquad \ldots\ldots(4)\end{aligned}$$

where we let ! denote the factorial function. The approximation is obtained by extending the upper limit of integration to infinity, which is permissible because $x_s\gg\lambda$. We have also assumed that μ-mesons which arrive with equal energies at sea level have been produced with equal energies, again neglecting the effect of ionization losses. These approximations do not, however, affect the estimate of the positive temperature effect due to the π–μ decay.

The effect of temperature changes in an isothermal atmosphere is then given by the formula

$$\frac{1}{n(E)}\frac{\partial n}{\partial T}=\frac{1}{w}\frac{\partial w}{\partial T}+\left\{\ln\frac{\lambda}{x_r}+\frac{d[\ln(E''/E)!]}{d(E''/E)}\right\}\frac{E''}{ET}+\frac{0{\cdot}93E}{0{\cdot}93E+E'}\frac{1}{T}. \qquad \ldots(5)$$

When deriving this formula, use was made of the fact that E' and E'' are both proportional to the scale height H and are therefore also proportional to the atmospheric temperature T.

The first term on the right-hand side of (5) contains the main effect of the μ–e decay. It represents the change in survival probability due to the change in height of the reference level.

The second term is due to the displacement of the mean level of meson production relative to the reference level. Its magnitude and its sign depend on the energy and on the choice of reference level. Because it is a second-order effect of the μ–e decay, it is usually very small and decreases rapidly with increasing energy.

The third term of (5) is the one which represents the effect of competition between disintegration and absorption of the π-mesons. At small energies, this effect is approximately proportional to the energy. At energies much greater than E' it will approach $1/T$ as an upper limit.

The integral temperature effect can now be calculated on the basis of (5) and the observed momentum spectrum of μ-mesons at sea level. For this purpose, we have used the empirical formula $n(p_s) \propto (p_s+38)^{-3\cdot0}$ to represent the sea-level spectrum, with the momentum p_s measured in units of $m_\mu c$. This formula very accurately reproduces the spectrum of Owen and Wilson (1955) in the interval $8<p_s<100$. For $p_s<8$, our formula is in better agreement with the spectrum of Caro, Parry and Rathgeber (1951) than with that of Owen and Wilson. For $p_s>100$, the formula strikes a compromise between the two spectra. The numerical results also depend on several parameters, for which we have used the following values : $t_\pi = 2\cdot65\times10^{-8}$ sec, $t_\mu = 2\cdot10\times10^{-6}$ sec, $m_\pi c^2 = 139\cdot5$ MeV, $m_\mu c^2 = 105\cdot7$ MeV, $T = 216\cdot5$°K, and consequently $H = 6330$ m, $E' = 800$ and $E'' = 10$. The results are presented in the table, where $p_s/m_\mu c$ is the cut-off momentum of the recording apparatus in units of $m_\mu c$ and C_T is the temperature effect in units of 10^{-5} per centigrade degree. We have taken the average momentum loss of μ-mesons in the atmosphere to be 18 $m_\mu c$.

$p_s/m_\mu c$	2	5	10	20	50	100	200	500	1000
$C_T(10^{-5}\ \text{deg}^{-1})$	28	30	34	42	64	95	143	231	302

§ 3. UNDERGROUND MEASUREMENTS

We shall first consider MacAnuff's measurements, which were performed at the equivalent depth of 60m of water. The positive temperature effect was first calculated on the basis of the observed day-to-day variations of the cosmic-ray intensity. Because of the relatively low counting rate and the high energies of the recorded mesons, no statistically significant correlation between the meson intensity and the height of the 100 mb level was found. MacAnuff therefore used only the sea-level pressure and the temperature of the 100–300 mb layer as independent variables in this analysis. The temperature coefficient obtained was $(0\cdot055 \pm 0\cdot005)\%\ \text{deg}^{-1}$, this being the mean of three independent determinations which all agreed well with each other. MacAnuff also analysed the seasonal variations and found positive temperature coefficients of $0\cdot054$ and $0\cdot070\%\ \text{deg}^{-1}$ for his two different recorders. The agreement with the ' day-to-day ' coefficient is satisfactory. In order to compare these results with the theory, we shall assume that the temperature variations are independent of the atmospheric depth. For mesons recorded under 60 m water equivalent, we shall take the minimum energy at production to be 155 $m_\mu c^2$, and this leads to a theoretical estimate of the positive temperature effect of the π–μ decay of 0·114% deg^{-1}. With $\lambda = 125$ g cm^{-2} and $x_r = 102$ g cm^{-2} the first-order effect of the μ–e decay, represented by the first term of (5), amounts to $-0{\cdot}048$% deg^{-1}. The second-order effect, represented by the second term of (5), is $-0{\cdot}006$% deg^{-1}. The net estimated positive temperature effect is therefore 0·060% deg^{-1}, which agrees very well with MacAnuff's results.

In addition to the analysis described above, MacAnuff corrected the observed seasonal variations for changes in the height of the 100 mb level, using a theoretically estimated decay coefficient of 0·07% km^{-1}, and obtained in this case coefficients of 0·112 and 0·096% deg^{-1} for his two separate recorders. Our theoretical estimate is in this case 0·108% deg^{-1}, as we now neglect the first term of (5).

As previously mentioned, underground measurements have also been made by Sherman and by Barrett *et al.* These measurements were all performed at such great depths that the effects of absorption and decay of the μ-mesons in the atmosphere were negligible. In both cases an effective temperature

$$T_{\text{eff}} = \int_0^{x_s} T(x) e^{-x/\lambda}\, dx \Big/ \int_0^{x_s} e^{-x/\lambda}\, dx \qquad \ldots\ldots(6)$$

was used as the only independent variable. Sherman found a positive temperature effect of (0·22 ± 0·06)% deg^{-1} at a depth of 846 m water equivalent, whereas our theoretical estimate turns out to be 0·36%. Barrett *et al.* (1952, 1954) have reported the results of two independent series of measurements at a depth of 1574 m water equivalent. Their first series gave (0·79 ± 0·20)% deg^{-1}, whereas the second one gave (0·33 ± 0·13)%, the weighted mean of these two values being (0·46 ± 0·11)% compared with the theoretical estimate of 0·41% deg^{-1}. At these very high energies, our theoretical estimates and the theoretical estimates of Barrett *et al.* (1952) agree very well, but at 60 m water equivalent they seem to be a little different.

Barrett *et al.* performed their measurements in order to obtain some information about the origin of extremely high-energy μ-mesons. As they could find no evidence for any significant production of μ-mesons by the decay of mesons different from the π-mesons, we shall assume that practically all μ-mesons are decay products of π-mesons. The further discussion concerning the attenuation length λ_π of the π-mesons is based on this assumption.

The interpretation and comparison of these underground measurements is rendered difficult because the same definition of the temperature was not used in all cases. It has already been pointed out by Barton (1954) that if MacAnuff also had used T_{eff} as his temperature variable, his positive temperature coefficient would have been reduced by a factor of approximately 2 because of the very great temperature variations at levels above the 100 mb level. For this reason, the very good agreement between MacAnuff's results and our theoretical estimates does not necessarily mean that the assumption of $\lambda_\pi = \lambda_p$ is correct.

If we accept a reduction of MacAnuff's coefficient by a factor of 2, as suggested by Barton, we must have $\lambda_\pi \simeq 2\lambda_p$, because the effect of the π–μ decay is approximately proportional to $1/\lambda_\pi$ at this energy. This value of λ_π is immediately seen to be in good agreement with Sherman's coefficient if we remember that the temperature effect must decrease more slowly than $1/\lambda_\pi$ at energies where the coefficient approaches the theoretical upper limit, which is $1/T = 0{\cdot}46$% deg^{-1}.

Such a value of λ_π is not incompatible with the results of Barrett *et al.*, even though their weighted mean is somewhat higher than the theoretical estimate with $\lambda_\pi = \lambda_p$. However, their original coefficient of 0·79% deg^{-1} may perhaps be regarded as insignificant because it so greatly exceeds the theoretical upper limit. Their later result, (0·33 ± 0·13)% deg^{-1}, obviously agrees very well with the theoretical estimate for $\lambda_\pi = 2\lambda_p$.

From the above comparison between the theoretical estimates of the positive temperature effect and the results of the underground measurements we may conclude that the attenuation length of the π-meson component is not less than that of the primary component, but probably not greater than twice that value.

§ 4. SEA-LEVEL MEASUREMENTS

A number of investigators have measured the positive temperature effect at sea-level. The following results have been published : Duperier (1949) (0·123 ± 0·024)% deg^{-1} under 25 cm of lead; Duperier (1951) (0·075 ± 0·010)% under 40 cm of lead; Dawton and Elliot (1953) (0·056 ± 0·018)% under 10 cm of lead; Trumpy and Trefall (1953) (0·036 ± 0·021)% under 10 cm of lead and (0·038 ± 0·019)% under 22 cm of lead; Chasson (1954) (0·068 ± 0·018)% under 20 cm of lead. In all these cases, the 100 mb level was used as the reference level. In most of the cases, the mean temperature of the 100–200 mb layer was used as the temperature variable, but in some cases the temperature at the 100 mb level was used. Only Cotton and Curtis (1951) have found no positive temperature effect at all.

The only measurements which have been made with the reference level at 50 mb are those of Duperier (1951) who obtained positive temperature coefficients of (0·228 ± 0·045)% deg^{-1} under 25 cm of lead and (0·143 ± 0·015)% under 40 cm of lead.

According to the data given in the table, and subject to the assumptions upon which those results are based, the positive temperature effect should in all the above-mentioned cases be close to 0·030% deg^{-1}, which is smaller than every quoted experimental value. In particular, the temperature coefficients which have been obtained with the reference level at 50 mb are incompatible with the theoretical estimates given in the table. We shall therefore re-examine the assumptions upon which those estimates rest to see whether this discrepancy between the experimental results and our theoretical estimates is real.

The theoretical estimates given in the table were based on the assumptions that $\lambda_\pi = \lambda_p$ and that the atmospheric temperature variations are independent of the atmospheric depth. However, all sea-level data have been analysed by correlating the cosmic-ray intensity with the temperature measured at the reference level or in a limited atmospheric layer immediately below it. Therefore, if the temperature variations in this layer are different from those of the other parts of the atmosphere, one would expect a discrepancy between these estimates and the experimental results even if the assumption of $\lambda_\pi = \lambda_p$ is correct. Now it is well known that at least the seasonal temperature variations are more pronounced above the 100 mb level than below, and the same may be true for the day-to-day variations. If this is so, it might seem possible to reduce the discrepancy between our theoretical estimates and the experimental results. However, during the discussion in the preceding section of MacAnuff's measurements, it was pointed out that if the greater seasonal variations of temperature above the 100 mb level had been taken into account, the positive temperature coefficient so obtained would have been reduced by a factor of about 2. This would then imply that $\lambda_\pi \simeq 2\lambda_p$, which would in turn reduce our estimates by a factor of 2. We conclude therefore that it is not possible to reduce the discrepancy between our theoretical estimates and the experimental values of the positive temperature effect at sea level by assuming that the temperature variations are much greater above the reference level than they are below.

When estimating the positive temperature effect, we have assumed for simplicity that the temperature variations of the different atmospheric layers can be considered independent. However, the experimental data have been analysed by the method of multiple correlation in an attempt to separate the positive temperature effect from the other atmospheric effects. A theoretical estimate made for comparison with the results of sea-level measurements should, strictly speaking, therefore have been based on a model of the atmosphere in which the two other variables, the sea-level pressure and the height of the reference level, are kept constant. In such a model, any increase of temperature in an atmospheric layer extending downwards from the reference level must be accompanied by a compensating decrease of temperature in the lower atmosphere. Consequently, a negative effect must arise from the π–μ decays which occur in the lower part of the atmosphere. At low energies, a considerable fraction of the μ-mesons reaching sea level have been produced below the 200 mb level. Thus, a considerable number of π–μ decays will be affected in a negative way, while the number of positively affected decays must decrease by the same amount. The net result must be a very considerable reduction of the expected positive temperature effect. Just how great the reduction will be cannot be said without a much more thorough investigation of the subject.

It must be emphasized that the remarks of the last paragraph do not apply to any of the underground measurements which were discussed in § 3. In neither of those cases was the positive temperature coefficient obtained from a correlation analysis in which the height of the reference level was used as an independent variable.

It has been assumed throughout that the attenuation length of the π-meson component is independent of the energy of the π-mesons. There is good reason to believe that at least it does not decrease with decreasing energy. Such a behaviour is improbable for the following reason : If λ_π is greater than the collision mean free path, nuclear collisions cannot be regarded as catastrophic in the sense that no new π-mesons are produced; on the contrary, there must be a transfer of energy from mesons of high energy to mesons of lower energy. The efficiency of this process will depend on the shape of the energy spectrum. The flatter the spectrum, the more efficient must this transfer process be. As the energy spectrum of π-mesons at any given depth becomes gradually steeper with increasing energy, it is to be expected that the attenuation length will decrease rather than increase with increasing energy. This conclusion can be upset only if the cross section for production of new mesons changes with energy in such a way as to cancel the effect of the changing energy spectrum. It is therefore very improbable that λ_π will change with energy in such a way as to increase our theoretical estimates.

In summing up, therefore, it seems that there is a real discrepancy in that the competing processes of decay and nuclear capture of the π-mesons can only account for a small part of the positive temperature effect observed at sea level. Such a discrepancy has already been noticed by Duperier (1951). It seems, therefore, that the greater part of the effect must have another origin, probably due to second-order effects of the μ–e decay (Trefall 1953, Olbert 1953).

§ 5. CONCLUSION

The underground measurements, in particular those of MacAnuff, have shown that if the attentuation length of the π-meson component is assumed to be independent of energy, it cannot be smaller than the attenuation length of the primary component. The particular importance of MacAnuff's measurements is due to the fact that the energy was sufficiently low to make the effect of the π–μ decay small compared with the theoretical upper limit of $1/T$, so that the results were rather sensitive to the value of λ_π. At the same time, the energy was high enough to make the second-order effects of the μ–e decay very small. On the other hand, the significance of MacAnuff's work is reduced by the fact that the cosmic-ray intensity could only be correlated with the temperature of a layer below the 100 mb level, and this layer may not have been a sufficiently representative sample of the atmosphere. For this reason, we can only say that λ_π probably lies somewhere in the interval $\lambda_p < \lambda_\pi < 2\lambda_p$.

Theoretical estimates of the positive temperature effect in an isothermal atmosphere have been presented for the case of $\lambda_\pi = \lambda_p$. However, if the positive temperature coefficient is determined by the method of multiple correlation usually employed, in which the height of the reference level is treated as an independent variable, the expected effect of the π–μ decay at low energies will be much less than these estimates. As these estimates were already small compared with the experimental values, we may conclude that the theory of competition between disintegration and nuclear capture of π-mesons is unable to explain the positive temperature effect which has been observed at sea level. The same theory does, however, successfully explain the positive temperature effect which has been observed at higher energies in underground measurements.

ACKNOWLEDGMENTS

The author is very much indebted to the British Council for a scholarship which made possible his stay in the United Kingdom. It is also a pleasure to acknowledge the hospitality given by Professor P. M. S. Blackett at the Imperial College of Science and Technology. Dr. H. Elliot has made several helpful suggestions, for which the author is very grateful.

REFERENCES

BARRETT, P. H., BOLLINGER, L. M., COCCONI, G., EISENBERG, Y., and GREISEN, K., 1952, *Rev. Mod. Phys.*, **24,** 133.
BARRETT, P. H., COCCONI, G., EISENBERG, Y., and GREISEN, K., 1954, *Phys. Rev.*, **95,** 1573.
BARTON, J. C., 1954, *Proc. Phys. Soc.* A, **67,** 637.
CARO, D. E., PARRY, J. K., and RATHGEBER, H. D., 1951, *Aust. J. Sci. Res.* A, **4,** 16.
CHASSON, R. L., 1954, *Phys. Rev.*, **96,** 1116.
COTTON, E. S., and CURTIS, H. O., 1951, *Phys. Rev.*, **84,** 840.
DAWTON, D. I., and ELLIOT, H., 1953, *J. Atmos. Terr. Phys.*, **3,** 295.
DUPERIER, A., 1949, *Proc. Phys. Soc.* A, **62,** 684; 1951, *J. Atmos. Terr. Phys.*, **1,** 296.
MACANUFF, J. W., 1951, *Thesis*, University of London.
OLBERT, S., 1953, *Phys. Rev.*, **92,** 454.
OWEN, B. G., and WILSON, J. G., 1955, *Proc. Phys. Soc.* A, **68,** 409.
SHERMAN, N., 1954, *Phys. Rev.*, **93,** 208.
TREFALL, H., 1953, *Nature, Lond.*, **171,** 888.
TRUMPY, B., and TREFALL, H., 1953, *Physica*, **19,** 636.

Ionic Configuration Interaction in Some Excited States of the Hydrogen Molecule

By J. T. LEWIS
Department of Applied Mathematics, The Queen's University of Belfast, N. Ireland

Communicated by D. R. Bates; *MS. received 22nd November* 1954

Abstract. Using the Rayleigh–Ritz variational method, the $^1\Sigma$ states of the hydrogen molecule arising from the [H(1s), H(2s or p)], [H^+, $H^-(1s)^2$] and [H(1s), H(3s, p or d)] configurations are investigated in the region of transition from ionic to homopolar character. Potential energy curves are given for these regions. It is shown that the admixture of configurations has a very considerable effect on the potential energy curves even at large nuclear separations. The ionic content is defined and calculated for [H(1s), H(3s, p or d)] states and is found to vary rapidly in the transition region. The bearing of this result on collision theory is discussed briefly.

§ 1. Introduction

Little is known quantitatively of the contribution of ionic configurations to the electronic states of molecules. In the case of H_2, the ground state has been investigated by Weinbaum (1933) and Coulson and Fischer (1949) who showed that at all values of the nuclear separation R the ionic contribution is unimportant; however, it is to be expected that in the excited states it is, for some values of R, significant or even dominant. For example, in the excited state ($B^1\Sigma^+_u$) the minimum in the potential energy curve is of an ionic character but the dissociation products are neutral atoms (Pauling 1928, Kemble and Zener 1929, Zener and Guillemin 1929). This arises since the force between two neutral atoms at large values of R is small and slowly varying and its energy curve may intersect a Coulombic curve arising from a positive and negative ion (represented by the broken lines in figure 1). In such an event the true potential energy curves (full lines) for the states arising from these atoms will not intersect if the ionic and homopolar configurations interact (since then the molecular states will be

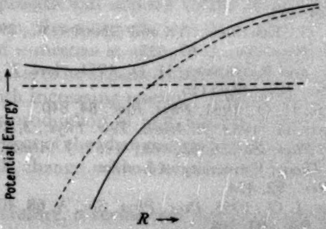

Figure 1. Avoidance of crossing. The broken lines show the approximate potential energy curves and the full lines the true potential energy curves.

mixtures of both). Instead they appear to be repelled, as shown in the figure, and change their character as they traverse the crossing region (for a fuller discussion see Coulson (1952)).

The $H(1s)+H(nl)$ homopolar curves cut the $H^{+}+H^{-}(1s)^2$ ionic curve if $n=2$, 3 or 4. In this paper the cases $n=2$ and $n=3$ are investigated† by the Rayleigh–Ritz variational method for the regions in which the change from ionic to homopolar character occurs. For the former the calculations cover an R range of from $8a_0$ to $12a_0$ and for the latter an R range of from $26\,a_0$ to $38\,a_0$ where a_0 is the radius of the first Bohr orbit.

It is shown that for the $^1\Sigma_u$ or $^1\Sigma_g$ states (which are the only ones affected) the magnitude of the ionic contribution, even at large separations, is such as to invalidate any calculation of long range forces which ignores it.

§ 2. THEORY

Let $\psi(A)$ and $\psi(B)$ be the wave functions of the negative ion of hydrogen when centred on nuclei A and B respectively and let $\phi(nl|A)$ and $\phi(nl|B)$ be the corresponding wave functions of the neutral atom. The ionic wave function describing H^{+}, $H^{-}(1s)^2$ and the homopolar wave function describing $H(1s)$, $H(nl)$ may be written (omitting all spin factors for brevity)

$$\Phi_1^{g,u}=\{2\pm 2S_1\}^{-1/2}\{\psi(A)\pm\psi(B)\}$$

$$\begin{aligned}\Phi_{l+2}^{g,u}=\{4\pm 4S_{l+2}^{g,u}\}^{-1/2}\{&\phi(1s\,|\,A1)\phi(nl\,|\,B2)\pm\phi(nl\,|\,A1)\phi(1s\,|\,B2)\\&+\phi(1s\,|\,A2)\phi(nl\,|\,B1)\pm\phi(nl\,|\,A2)\phi(1s\,|\,B1)\}\end{aligned}$$

with

$$S_i=\int\!\!\int\psi(A)\psi(B)\,d\tau_1 d\tau_2$$

$$S_{l+2}^{g,u}=\left\{\int\phi(1s\,|\,A)\phi(nl\,|\,B)\,d\tau\right\}^2\pm\int\phi(1s\,|\,A)\phi(1s\,|\,B)\,d\tau\int\phi(nl\,|\,A)\phi(nl\,|\,B)\,d\tau$$

the numbers 1 and 2 being used to distinguish the cordinates of the electrons, and the positive sign corresponding to the g state, the negative to the u state.

Because the ns, np, nd, ... states of hydrogen all have the same energy we must include all of them in our trial wave function which we take to be

$$\Psi=c_1\Phi_1+\sum_{l=0}^{n-1}c_{l+2}\Phi_{l+2}$$

determining the c's by minimizing the energy integral with respect to them. This yields the secular equation

$$|H_{ij}-S_{ij}E|=0$$

where

$$H_{ij}=\int\Phi_i\mathscr{H}\Phi_j\,d\tau,\quad S_{ij}=\int\Phi_i\Phi_j\,d\tau$$

and $\mathscr{H}$ is the total Hamiltonian of the system.

The term H_{11} is the energy corresponding to the ionic approximation to the state, and (neglecting overlap forces) is closely given (in atomic units) by

$$H_{11}(R)=H_{11}(\infty)-\left(\frac{1}{R}+\frac{1}{2}\frac{\alpha}{R^4}\right)$$

---

† The $n=4$ case is of less interest because the crossing occurs at an extremely large nuclear separation. The crossing points in the cases $n=2$, 3, 4 occur at approximately $11a_0$, $36a_0$ and $270a_0$ respectively.

where α is the polarizability of H⁻. The $H_{ii}(i \neq 1)$ are approximately constant and equal (being the energies corresponding to the homopolar approximations) and so may be conveniently chosen as the zero of the energy scale. Those off-diagonal matrix elements which do not contain the ionic wave function Φ_1 are found by calculation to be small compared with those which do, and are neglected.†

Thus the secular equation reduces in the case $n=2$ to

$$\begin{vmatrix} H_{11}-E \ , & H_{12}-S_{12}E, & H_{13}-S_{13}E \\ H_{12}-S_{12}E, & -E \ , & 0 \\ H_{13}-S_{13}E, & 0 \ , & -E \end{vmatrix} = 0$$

which may be diagonalized simply to

$$\begin{vmatrix} A_{11}-E, & A_{12}, & A_{13} \\ A_{12} \ , & -E, & 0 \\ A_{13} \ , & 0 \ , & -E \end{vmatrix} = 0$$

where $A_{11} = \{H_{11} - 2(H_{12}S_{12} + H_{13}S_{13})\}/\{1-(S_{12}{}^2 + S_{13}{}^2)\}$

$A_{12} = H_{12}/\{1-(S_{12}{}^2 + S_{13}{}^2)\}^{1/2}$, $A_{13} = H_{13}/\{1-(S_{12}{}^2 + S_{13}{}^2\}^{1/2}$.

This has roots $E=0$ or $E = \tfrac{1}{2}[A_{11} \pm \{A_{11}{}^2 + 4(A_{12}{}^2 + A_{13}{}^2)\}^{1/2}]$.

When $n=3$ the Φ's are approximately orthonormal in the crossing region (because of the large nuclear separation), which further simplifies the equation to

$$\begin{vmatrix} H_{11}-E, & H_{12}, & H_{13} \ , & H_{14} \\ H_{12} \ , & -E, & 0 \ , & 0 \\ H_{13} \ , & 0 \ , & -E, & 0 \\ H_{14} \ , & 0 \ , & 0 \ , & -E \end{vmatrix} = 0$$

with roots $E^2=0$ or $E = \tfrac{1}{2}[H_{11} \pm \{H_{11}{}^2 + 4(H_{12}{}^2 + H_{13}{}^2 + H_{14}{}^2)\}^{1/2}]$.

The approximate orthonormality makes a definition of the ionic content particularly simple and we take it to be $c_1{}^2/\{c_1{}^2 + c_2{}^2 + c_3{}^2 + c_4{}^2\}$.

It now remains to evaluate the non-vanishing off-diagonal elements. To do this we use for $\psi(\mathrm{A})$ an expression due to Löwdin (1953)

$$\psi(\mathrm{A}) = \{A_1 \exp(-a_1 r_{a1}) + A_2 \exp(-a_2 r_{a1})\}\{(A_1 \exp(-a_1 r_{a2}) + A_2 \exp(-a_2 r_{a2})\}$$

where $A_1 = 0{\cdot}30025$, $a_1 = 0{\cdot}4228$, $A_2 = 1{\cdot}0001$, $a_2 = 0{\cdot}9794$. The necessary integrals may be expressed in terms of the J, K-functions of Coulson (1942).

The polarizability α of H⁻ was calculated to be 230 atomic units using the very accurate oscillator strength values of Chandrasekhar (1945) in the standard expression (cf. Mott and Sneddon 1948). The value of the electron affinity of H used in calculating $H_{11}(\infty)$ is that obtained by Henrick (1943), $0{\cdot}74_7$ ev.

§ 3. Results and Discussion

The results for $n=2$ are displayed in figure 2, with the results of King and Van Vleck's (1939) calculation of the inverse cube term for comparison. (This term arises from the so-called excitation exchange which occurs when two like atoms are in states which combine in the optical sense. This is not included in the present calculation.)

---

† If we suppose these small neglected quantities to be all equal to ϵ, then it can be shown that the effect of their inclusion would be to increase the largest root and decrease the lowest root by $c\epsilon$ where c is close to unity.

The results for $n = 3$ are displayed in figure 3 together with a graph of the ionic content (as defined above) in the crossing region. This is of particular interest in collision theory since the rapid change of character in the crossing region (from 10% ionic to 80% ionic in less than 1 atomic unit) supports Zener's (1932) basic assumption in his treatment of non-adiabatic collisions. The change in character only occurs in branches E_1 and E_4, E_2 and E_3 having a constant, zero, ionic content. Thus in a calculation of the rate of recombination of H^+ and H^- the branches E_2 and E_3 must be ignored because the only important transitions will be between E_1 and E_4 (Bates and Lewis 1955).

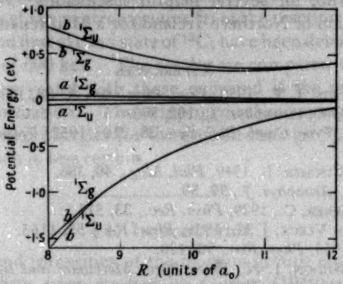

Figure 2. Potential energy curves of H_2. The curves *a* are those due to King and Van Vleck for the $^1\Sigma_{g,\,u}$ states of hydrogen tending at infinite separation to [H(1s), H(2p)]. The curves *b*, together with the line $E_{g,\,u} = 0$ represent the six $^1\Sigma_{g,\,u}$ states arising from the [H^+, H^-], [H(1s), H(2s)], [H(1s), H(2p)] configurations as calculated in this paper.

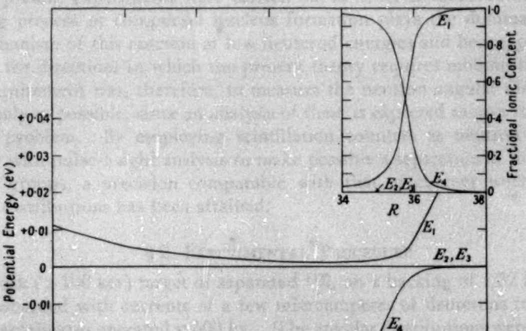

Figure 3. The curves E_1, E_2, E_3 and E_4 represent the potential energy of the eight $^1\Sigma_{g,u}$ states arising from the [H^+, H^-], [H(1s), H(3s, p or d)] configurations as calculated in this paper. (At these large values of R the g and u states are indistinguishable.) The inset shows the fractional ionic content (as defined in the text) of the four states in the transition region.

The effect upon the computed energies of including ionic terms in the system wave function is very considerable even at large nuclear separations (see figures 2 and 3). Thus in cases where a molecule is in a state which has a neighbouring ionic state of the same symmetry, calculations of long range forces which ignore ionic configuration interaction are likely to be grossly in error. It may be noted finally that this conclusion is equally valid for both heteronuclear and homonuclear molecules.

ACKNOWLEDGMENTS

The author wishes to thank Professor D. R. Bates, who suggested the problem, and Dr. A. Dalgarno, for several helpful discussions. He is indebted to the Ministry of Education of Northern Ireland for a Maintenance Allowance.

REFERENCES

BATES, D. R., and LEWIS, J. T., 1955, *Proc. Phys. Soc.* A, **68**, 173.
CHANDRASEKHAR, S., 1945, *Astrophys. J.*, **102**, 395.
COULSON, C. A., 1942, *Proc. Camb. Phil. Soc.*, **38**, 210; 1952, *Valence* (Oxford: Clarendon Press).
COULSON, C. A., and FISCHER, I., 1949, *Phil. Mag.*, **40**, 386.
HENRICK, L. R., 1943, *Astrophys. J.*, **99**, 59.
KEMBLE, E. C., and ZENER, C., 1929, *Phys. Rev.*, **33**, 512.
KING, G. W., and VAN VLECK, J. H., 1939, *Phys. Rev.*, **55**, 1165.
LÖWDIN, PER-OLOV, 1953, *Phys. Rev.*, **90**, 120.
MOTT, N. F., and SNEDDON, I. N., 1948, *Wave Mechanics and Its Applications* (Oxford: Clarendon Press).
PAULING, L., 1928, *Chem. Rev.*, **5**, 173.
WEINBAUM, S., 1933, *J. Chem. Phys.*, **1**, 593.
ZENER, C., 1932, *Proc. Roy. Soc.* A, **137**, 696.
ZENER, C., and GUILLEMIN, V., 1929, *Phys. Rev.*, **34**, 999.

The Reaction $^{11}B(d, n)^{12}C$

By A. WARD and P. J. GRANT
Department of Natural Philosophy, The University, Glasgow

MS. received 8*th January* 1955 *and in amended form* 15*th February* 1955

Abstract. Using scintillation-counter detection and pulse-height analysis, the angular distributions of the neutron groups from the reaction $^{11}B(d, n)^{12}C$ leading to the ground state and first excited state of ^{12}C, have been determined at a deuteron bombarding energy of 600 kev. The results are compared with those predicted by the stripping theory and with those expected if the reaction proceeds by compound nucleus formation. The stripping mechanism appears to be important even at low bombarding energies for the ground-state group, but for the excited state the interpretation is less certain.

---

§ 1. Introduction

The energies and intensities of the neutron groups emitted in the reaction $^{11}B(d, n)^{12}C$ have been studied by Gibson (1949) and Johnson (1952). The angular distributions of the emitted neutrons have not so far been very thoroughly examined, owing to the experimental difficulties involved, in particular the lack of a reliable neutron spectrometer (see, however, Burke *et al.* 1954, and Graue 1954).

The present experiments were carried out in order to discover whether the stripping process or compound nucleus formation plays the dominant role in the mechanism of this reaction at low deuteron energies and hence, possibly, to indicate the directions in which the present theory requires modification. The main requirement was, therefore, to measure the neutron angular distributions as precisely as possible, since an analysis of these is expected to give information on this problem. By employing scintillation counters as neutron detectors, together with pulse-height analysis to make possible a separation of the different neutron groups, a precision comparable with that of current work on γ-ray angular distributions has been attained.

§ 2. Experimental Procedure

A thick ($>$100 kev) target of separated ^{11}B, on a backing of 1/32 in. copper, was bombarded with currents of a few microamperes of deuterons from a high tension accelerator operated at 600 kv. The angular distributions were measured using the apparatus described by Rutherglen *et al.* (1954), a neutron detector being substituted for a γ-ray detector.

2.1. *The Neutron Detector*

The neutron detector consisted of a piece of plastic scintillator, effectively $(CH)_n$, approximately 4 cm in diameter by 0·7 cm thick, together with a DuMont photomultiplier type 6292 for detection of the light emission from recoil protons in the plastic. Optical contact between the scintillator and the photo-tube was made by a thin film of silicone grease while the scintillator was surrounded with tightly packed magnesium oxide to improve the efficiency of light collection.

Pulses from the photomultiplier, after amplification, were fed into a 100-channel pulse-height analyser (Hutchinson and Scarrott 1951). The shape of the pulse-height spectrum from a mono-kinetic neutron group (^{3}H(d, n)^{4}He) is shown in figure 1 and may be compared with the results of Poole (1952) who used a small anthracene crystal to detect neutrons from the D–D reaction.

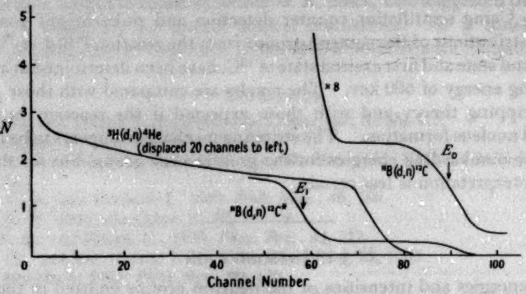

Figure 1.

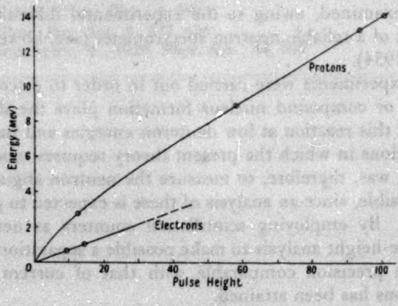

Figure 2.

Figure 2 is a plot of the channel number on the pulse-height analyser at which the counting rate has fallen to one half of the value on the plateau, observed for different neutron energies. The points on the curve for protons of energy 14·3 Mev and 2·8 Mev were obtained using neutrons from the reactions ^{3}H(d, n)^{4}He and ^{2}H(d, n)^{3}He respectively. The other two points were obtained from curves similar to those shown in figure 1 for the reaction ^{11}B(d, n)^{12}C. It can be seen that the points fall on a smooth curve which exhibits the characteristic non-linear response at low proton energies common to all organic scintillators. Two points are included for the pulse height observed at the peak in the Compton spectrum of electron recoils in the plastic from γ-rays of energies 0·51 and 1·28 Mev. These two points lie on a straight line passing through the origin. The range–energy relationship for electrons and protons in the plastic scintillator can be deduced from the tables of Aron *et al.* (1949). It is clear from the response curves, shown in figure 2, and the range–energy relationships of the plastic scintillator for protons and electrons that by a suitable choice of thickness, a plastic scintillator gives very large light pulses for protons recoiling from neutrons and small pulses for electrons due to γ-rays. Therefore, even though the cross sections for γ-ray absorption and n–p scattering in the plastic scintillator are comparable at medium energies it is possible to discriminate against pulses due to the absorption of γ-rays. Since the n–p scattering up to 15 MEV is due entirely to partial waves of angular momentum $l=0$, the angular distribution of recoil protons from a monokinetic neutron group in the centre-of-mass system is isotropic and the energy spectrum in the laboratory system is flat. The recoil carbon nuclei have, of course, much smaller energies but, in addition, the response curve for such heavy particles in organic scintillators which is expected from the reduced efficiencies observed by Wright (1953) of alpha particles as compared with protons of the same low energy shows that very small pulses result from the elastic scattering of neutrons by the carbon present in the plastic scintillator.

2.2. *Angular Distributions*

The pulse-height distribution at each angular position was recorded, measurements being taken for a definite number of counts in a fixed monitor counter. This procedure removes possible errors due to inhomogeneity or deterioration of the target. Measurements at the different positions were taken in a random order, and afterwards repeated in the reverse order, thus minimizing the effects of any slow changes in the electronic part of the apparatus.

A block of lead, ½ in. thick, was inserted between the target and the detector to absorb the β-particles from the decay of ^{12}B formed in the reaction ^{11}B(d, p)^{12}B. If not absorbed these electrons, which could pass right through the scintillator, produced a strong peak in the region corresponding to a neutron energy of about 4 MEV.

2.3. *Detector Efficiency*

The overall detection efficiency of the phosphor for a given energy group is very closely independent of the direction of observation relative to the incident deuteron beam. The effective solid angle of detection varies with direction (due to centre-of-mass motion) in the same way as the measured neutron energy E_n while the intrinsic detection efficiency of the phosphor (which is proportional to the n–p scattering cross section) varies as E_n^{-1} over the small energy range involved.

2.4. *Monitor*

The monitor consisted of another plastic scintillator similar to the first. For monitoring purposes no lead was inserted between the target and the detector, since the electron-produced peak from the mirror reaction can be used to help the monitor stability. If a discriminator is set below the pulse height corresponding to the electron pulses (but above that corresponding to the background of neutrons from the D–D reaction) then the counting rate is almost independent of small variations in either the gain of the monitor amplifier system or the discriminator threshold.

§ 3. RESULTS

3.1. *The Shape of the Pulse-Height Spectrum*

The shape of the pulse-height spectrum from a mono-kinetic neutron group (^{3}H(d, n)^{4}He) is shown in figure 1. Little saturation occurs in the plastic (figure 2) and, as expected, the pulse-height spectrum is seen to be substantially flat for most of its length, most of the slope being due to 'end effects' owing to the thinness of the plastic. Most of the sharp rise at low pulse heights is attributed to a background of neutrons from the D–D reaction. For the calculation of the relative intensities of different neutron groups we have assumed that the shape of the pulse-height spectrum from a mono-energetic neutron group is independent of its energy.

The resolution obtained would correspond, on a 'peaked' spectrum, to a full width at half-height of about 10%.

3.2. $^{11}B(d, n)^{12}C$ *Spectrum*

A typical spectrum from this reaction is shown in figure 1. It will be seen that the groups corresponding to the ground state and first excited state of ^{12}C at 4·43 MEV are well resolved.

No attempt was made to investigate in detail the low-energy region of the spectrum since it is hoped that this will be done more effectively by coincidence methods.

3.3. *Intensities*

The relative intensities of the groups to the ground and first excited states of ^{12}C were determined from the areas under the separated spectra. After correction for the detection efficiency of the phosphor, using the values for the n–p scattering cross section given by Blatt and Jackson (1949) we obtain at a bombarding energy of 600 kev: $I_{4\cdot 43}/I_0 = 2\cdot 3 \pm 0\cdot 5 (\theta = 90°)$. This figure is close to that obtained by Gibson (1949) at a bombarding energy of 0·9 MEV.

The absolute intensity (thick target yield) was determined at 600, 500 and 400 kev. After correction for the effect of the lead absorber the integrated yields for the ground state and first excited state groups are:

Deuteron energy (kev)		400	500	600
Yield per 10^{10}	ground state	9·4	41·5	190
deuterons (±20%)	1st excited state	24	108	530

3.4. *Angular Distributions*

(*a*) *Ground-state group.*

Figure 3 shows the angular distribution of the neutron group leading to the ground state of ^{12}C. The average error of any point on the curve is 1·5–2%.

The most important of the possible systematic errors was an instrumental anistropy due to misalignment of the target spot. This was determined by means of the reaction ^{19}F(p, α, γ)^{16}O at 340 kev, where the γ-radiation is known to be isotropic, and found to be less than 1%.

The curve represents the best fit that can be obtained to the experimental points (in the centre-of-mass system) by superposing a stripping curve for

$l_p = 1$ (calculated by the theory of Bhatia *et al.* (1952) using a nuclear radius $R = 5{\cdot}4 \times 10^{-13}$ cm) on an incoherent isotropic background. Assuming that this procedure is legitimate, we obtain a figure of about 30% for the ratio of the intensities of stripping and compound nucleus formation.

It will be noted that the experimental points show the anomalous dip at low forward angles which has been previously observed in some other stripping reactions (Evans *et al.* 1953, Holt *et al.* 1953).

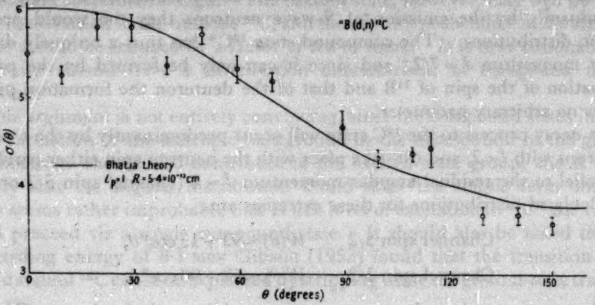

Figure 3.

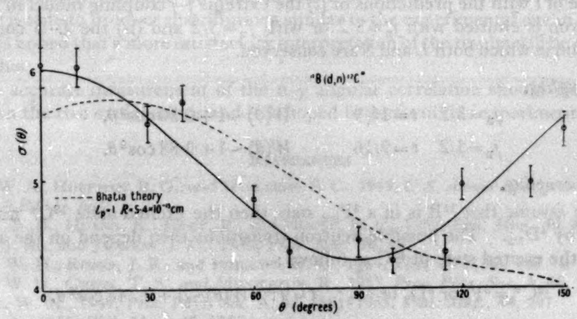

Figure 4.

(*b*) ***Excited-state group.***

Figure 4 shows the angular distribution of the neutron group leading to the first excited state of ^{12}C. It is seen to be very closely symmetrical about the 90° position, a result which is normally characteristic of compound nucleus formation and not of the stripping mechanism. The experimental distribution (in the centre-of-mass system) is best fitted by the expression $W(\theta) = 1 + (0{\cdot}41 \pm 0{\cdot}03)\cos^2\theta$ (full curve). After correction for the finite angle of acceptance of the detector we obtain the result $W_0(\theta) = 1 + (0{\cdot}45 \pm 0{\cdot}04)\cos^2\theta$.

We will first discuss this distribution on the assumption that the reaction is proceeding via the formation of a single compound state in ^{13}C.

Since the distribution is markedly anistropic the compound state cannot be formed entirely by S-wave deuterons, and in view of the low bombarding energy it seems unlikely that deuterons with $l \geqslant 2$ are involved. We shall therefore assume that p-wave formation is taking place.

^{11}B has spin 3/2 with odd parity; the capture of a p-wave deuteron can therefore lead to states with $J=7/2$, 5/2, 3/2 or 1/2, all with even parity. Of these states, $J=1/2^+$ would lead to an isotropic neutron angular distribution, and since the states $J=5/2^+$ and $J=3/2^+$ should decay to the $J=2^+$ state in ^{12}C predominantly by the emission of S-wave neutrons they too would produce isotropic distributions. The compound state ^{13}C* has thus a uniquely defined angular momentum $J=7/2^+$ and since it can only be formed by the parallel combination of the spin of ^{11}B and that of the deuteron the formation process involves no arbitrary parameter.

The decay process to the ^{12}C state will occur predominantly by the emission of neutrons with $l=2$, and can take place with the neutron spin either parallel or antiparallel to the residual angular momentum $J=2$ (channel spin 5/2 or 3/2). The calculated distributions for these extremes are:

$$\text{Channel spin } 5/2 \qquad W(\theta) \sim 93 + 15\cos^2\theta,$$

$$\text{Channel spin } 3/2 \qquad W(\theta) \sim 68 + 90\cos^2\theta.$$

To fit the experimental result we must assume a mixing ratio for the contributions of parallel and antiparallel spins given by $t = 2{\cdot}2 \pm 0{\cdot}4$. It is interesting to compare this value of t with the predictions of (i) the extreme j–j coupling model in which the neutron is emitted with $j_n = 5/2$ or with $j_n = 3/2$ and (ii) the L–S coupling description in which both L and S are conserved.

(i) *j–j coupling.*

$$j_n = 5/2 \quad t = 16/9 \qquad W(\theta) \sim 1 + 0{\cdot}50\cos^2\theta,$$

$$j_n = 3/2 \quad t = 9/16 \qquad W(\theta) \sim 1 + 0{\cdot}88\cos^2\theta.$$

(ii) *L–S coupling.*

If we assume that ^{11}B is in a $^2P_{3/2}$ state then the excited state ^{13}C* must be denoted by $^4D_{7/2}$. The possible neutron transitions then depend on the assignment of the excited state of ^{12}C as follows:

$$^{12}\text{C}^* = {}^3P_2 \text{ or } {}^3D_2 \text{ or } {}^3F_2; \quad t=9; \quad W(\theta) \sim 1 + 0{\cdot}248\cos^2\theta.$$

The experimental result is thus well fitted by the j–j coupling description with $j_n = 5/2$ but not by the L–S if the spin of ^{11}B is considered to be due simply to the odd particle. If this condition is relaxed to allow the formation of other compound states besides $^4D_{7/2}$ then, for example, the transition $^4F_{7/2} \rightarrow {}^3D_2$ also leads to an angular distribution $W(\theta) \sim 1 + 0{\cdot}50\cos^2\theta$.

3.5. *Stripping Mechanism*

If the reaction is proceeding via the stripping process then the captured proton must have either $l_p = 1$ or $l_p = 3$. It is to be expected that the contribution from $l_p = 3$ will be very small. The broken curve in figure 4 shows the best fit that can be obtained by superposing a normal stripping curve for $l_p = 1$ and an incoherent isotropic background. The agreement is very poor.

§ 4. DISCUSSION

From the preceding arguments it would seem that the ground-state group is due both to the stripping mechanism and to compound nucleus formation, while the excited-state group is produced almost entirely by the latter process. This might perhaps be justified by the following argument: in the case of the ground-state group the proton in the stripping process is being captured into a state which must approximate to a single-particle level, and the capture probability should therefore be high. The excited state, however, may well be due to multiple excitation in the nucleus ^{12}C, and the capture probability in the stripping process should be reduced by a factor of ten or more. It is thus reasonable that this group should have a distribution characteristic of compound nucleus formation.

This argument is not entirely convincing, since the compound states involved in the formation of the isotropic background in the distribution of the ground-state neutrons should also contribute to the excited-state group, and it is thus unlikely that the angular distribution would show the simple form observed. It also seems rather improbable that at this level of excitation in ^{13}C* the reaction would proceed via a single compound state. It should also be noted that at a bombarding energy of 8·1 MEV Gibson (1953) found that the transition to the excited state of ^{12}C could be explained by stripping while the ground-state transition could not.

However, a modification of the stripping theory (de Borde, private communication) designed to take account of the low deuteron bombarding energy is able to produce distributions similar to the experimental one in figure 4, and it is hoped that a more satisfactory interpretation of the results will be obtained from this.

An accurate measurement of the n–γ angular correlation should distinguish between the two explanations and it is hoped to perform this experiment shortly.

REFERENCES

ARON, W. A., HOFFMAN, B. G., and WILLIAMS, F. C., 1949, *U.S. Atomic Energy Commission, A.E.C.U.* 663.

BHATIA, A. B., HUANG, K., HUBY, R., and NEWNS, H. C., 1952, *Phil. Mag.*, **43,** 485.

BLATT, J. M., and JACKSON, J. D., 1949, *Phys. Rev.*, **76,** 18.

BURKE, W. H., RISSER, J. R., and PHILLIPS, G. C., 1954, *Phys. Rev.*, **93,** 188.

EVANS, W. H., GREEN, T. S., and MIDDLETON, R., 1953, *Proc. Phys. Soc.* A, **66,** 108.

GIBSON, W. M., 1949, *Proc. Phys. Soc.* A, **62,** 586; 1953, *Phil. Mag.*, **44,** 297.

GRAUE, A., 1954, *Phil. Mag.*, **45,** 1205.

HOLT, J. R., and MARSHAM, T. N., 1953, *Proc. Phys. Soc.* A, **66,** 249, 258, 467, 565, 1032.

HUTCHINSON, G. W., and SCARROTT, G. G., 1951, *Phil. Mag.*, **42,** 792.

JOHNSON, V. R., 1952, *Phys. Rev.*, **86,** 302.

POOLE, M. J., 1952, *Proc. Phys. Soc.* A, **65,** 453.

RUTHERGLEN, J. G., GRANT, P. J., FLACK, F. C., and DEUCHARS, W. M., 1954, *Proc. Phys. Soc.* A, **67,** 101.

WRIGHT, G. T., 1953, *Phys. Rev.*, **91,** 1283.

RESEARCH NOTES

On the Spin Paramagnetism of a Free Electron Gas: II

By B. DONOVAN†, A. B. LIDIARD‡ and N. H. MARCH§
† Department of Physics, Northern Polytechnic, London
‡ Atomic Energy Research Establishment, Harwell, Berks.
§ Department of Physics, The University, Sheffield

MS. received 11*th October* 1954 *and in final form* 27*th January* 1955

Recently two of the authors (March and Donovan 1953, subsequently referred to as I) have given a discussion of the effect of exchange interactions on the spin paramagnetism of a free electron gas. The temperature dependence of the susceptibility was investigated numerically for the particular case where the electron density was the same as that of the valence electrons in metallic sodium. The calculations employed a variation method based on an approximate distribution function (a fundamental analysis of this procedure has been given by Lidiard 1953). In general the aim is to choose a variation function which is sufficiently simple to leave the calculations tractable, but which does not introduce spurious features by departing too severely from the *best possible* distribution function. The distribution function used in I was specified by two analytic forms (1) roughly resembling a Fermi–Dirac function, for temperatures less than or equal to a certain critical value and (2) roughly resembling a Boltzmann function for temperatures greater than or equal to the critical value. It was pointed out that the calculated susceptibility might be expected to be least reliable at intermediate temperatures around the point where the two forms become identical.

In fact when the numerical calculations were performed with a suitably small interval an anomalous temperature variation was found in this region as shown in figure 3. Whilst the anomaly was relatively small for the case treated in I, more detailed investigation showed that the magnitude of the 'hump' on the curve of $(1/\chi, T)$ increased rapidly with the strength of the exchange interactions. Although it seemed to us that this behaviour was probably not inherent in the model but due instead to an inadequacy of the distribution function, it is clearly of interest to verify this and to be certain that the anomaly is not partly due to the exchange forces and therefore physically significant. This point is relevant to the theory of the magnetic susceptibilities of the transition metals (cf. Kriessman 1953, Kriessman and Callen 1954).

On the other hand there are other calculations which are facilitated by the use of approximate distribution functions, e.g. the discussions of exchange potential (March 1953) and distance correlations (Lidiard 1954). Information on the reliability of the distribution functions employed is useful here too.‖

The present note describes the application of a more accurate distribution function to the problem of calculating the paramagnetic susceptibility as a function of temperature. Numerical results are again presented for the case where the electron density is equal to that of the valence electrons in metallic sodium. It is found that the calculated susceptibility is in good agreement with the earlier work except in the region of intermediate temperatures, where the exchange interactions in this model do not give rise to maxima and minima in the susceptibility.

‖ A further application which might be made of approximate distribution functions is in extending calculations of the thermodynamic functions for a relativistic electron gas (cf. Kothari and Singh 1942).

The function used in I was due to Lidiard (1951, subsequently referred to as L); a similar form valid at low temperatures was originally suggested by Koppe (1947) and first applied correctly by Wohlfarth (1950). The defect of this function which is important here may be seen from the following considerations. Using Lidiard's notation and referring to L, figure 1, we see that $f(0)$, the value of the distribution function at the origin of the wave vector **k** space, is fixed at the value unity for all temperatures lying between absolute zero and the temperature corresponding to $x=1/\alpha=1$. Now we know that for a free electron gas *without* exchange interactions $f(0)$ is appreciably less than unity at the temperature corresponding to $x=1$. Thus from the simple Fermi–Dirac statistics

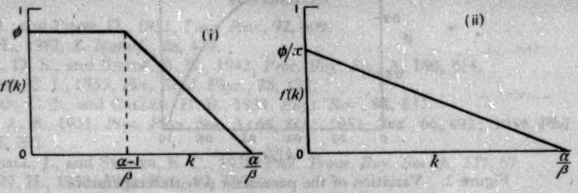

Figure 1. Approximate forms for the function $f(k)$: (i) $\alpha \geqslant 1$; (ii) $\alpha \leqslant 1$.

$$f(0)=[\exp(-\eta)+1]^{-1}.$$

By L, eqn (A2), $x=1$ leads to $kT/\epsilon_0 \sim 0{\cdot}50$. From the tables prepared by McDougall and Stoner (1938) we find that $kT/\epsilon_0 \sim 0{\cdot}50$ requires $\eta \sim 1{\cdot}5$ and hence $f(0)=0{\cdot}8$, which is appreciably less than unity. This suggests that in our problem also we need a distribution function which allows $f(0)$ to be less than unity even at the lower temperatures. In fact we proceed by introducing a new adjustable parameter ϕ equal to $f(0)$; both ϕ and the second unkown, x, are determined as before by minimizing the total free energy function for the system, i.e. by setting

$$\frac{\partial F}{\partial x}=\frac{\partial F}{\partial \phi}=0.$$

The new distribution function is specified in terms of the new parameter ϕ, as shown in figure 1. In place of L, eqns (2.9) and (2.10), we have the following forms for $f(k)$:

(i) $\alpha \geqslant 1$

$$\left.\begin{array}{ll} f=\phi, & 0 \leqslant k \leqslant (\alpha-1)/\beta, \\ f=\phi(\alpha-\beta k), & (\alpha-1)/\beta \leqslant k \leqslant \alpha/\beta, \\ f=0, & k \geqslant \alpha/\beta. \end{array}\right\} \quad \ldots\ldots(1a)$$

(ii) $\alpha \leqslant 1$

$$\left.\begin{array}{ll} f=\phi(\alpha-\beta k), & 0 \leqslant k \leqslant \alpha/\beta, \\ f=0, & k \geqslant \alpha/\beta. \end{array}\right\} \quad \ldots\ldots(1b)$$

The procedure for handling this function follows the same general lines as in L, and after much lengthy but relatively straightforward calculation the free energy can be obtained as a function of the relative magnetization ζ. By finding the second derivative of the free energy with respect to ζ and evaluating it at $\zeta = 0$ a system of complicated equations, which we omit here, can be obtained for the inverse susceptibility.

The numerical calculations have been carried through for the case when $\epsilon_s/\epsilon_0 = 1{\cdot}32$ (the value for sodium), and figure 2 shows the way in which the new parameter ϕ, which we have introduced here, varies with kT/ϵ_0. This curve has, of course, been obtained by minimizing the free energy and it can be seen that the value soon departs significantly from unity, the value which it had at all temperatures according to the old distribution function. The final curve showing the temperature dependence of the susceptibility obtained by the present method is given in figure 3. (The details of these calculations will be supplied on request.)

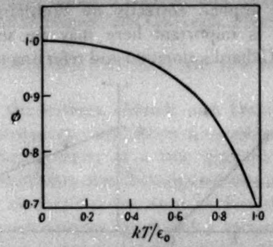

Figure 2. Variation of the parameter ϕ with temperature.

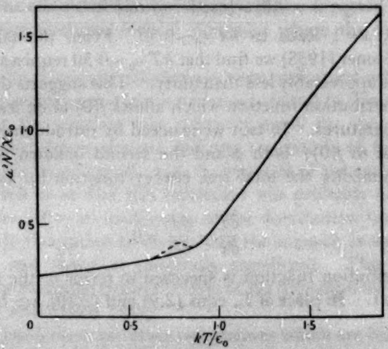

Figure 3. Variation of the inverse susceptibility with temperature. The dotted curve shows the corresponding result according to the previous method (I).

As can be seen from figure 3 the susceptibility calculated here is in good agreement with that obtained using the simpler distribution function at both high and low temperatures. In the intermediate region, however, the anomaly found previously is clearly removed by the introduction of the variational parameter ϕ. Since the susceptibility depends on a second derivative of the free energy it appears therefore that equations (1) represent a much better approximation to the true distribution function than do L (2.9) and (2.10).

More realistic calculations of metallic susceptibilities must include a consideration of correlation energy as well as exchange energy. At present most calculations of this nature reduce to semi-empirical discussions of the sort given by Stoner (1954). A notable exception is the free electron gas treated by the methods of Bohm and Pines (1953) (see also Pines 1953). This model can be examined at low temperatures with the aid of a variational distribution function which is even better than (1). Preliminary results indicate a substantial agreement with the semi-empirical studies of susceptibility and specific heat.

REFERENCES

BOHM, D., and PINES, D., 1953, *Phys. Rev.*, **92,** 609.
KOPPE, H., 1947, *Z. Naturf.*, **2a,** 429.
KOTHARI, D. S., and SINGH, B. N., 1942, *Proc. Roy. Soc.* A, **180,** 414.
KRIESSMAN, C. J., 1953, *Rev. Mod. Phys.*, **25,** 122.
KRIESSMAN, C. J., and CALLEN, H. B., 1954, *Phys. Rev.*, **94,** 837.
LIDIARD, A. B., 1951, *Proc. Phys. Soc.* A, **64,** 814; 1953, *Ibid.*, **66,** 492; 1954, *Phil. Mag.*, **45,** 202.
McDOUGALL, J., and STONER, E. C., 1938, *Phil. Trans. Roy. Soc.* A, **237,** 67.
MARCH, N. H., 1953, *Phys. Rev.*, **92,** 510.
MARCH, N. H., and DONOVAN, B., 1953, *Proc. Phys. Soc.* A, **66,** 1104.
PINES, D., 1953, *Phys. Rev.*, **92,** 626.
STONER, E. C., 1954, *Acta Metallurgica*, **2,** 259.
WOHLFARTH, E. P., 1950, *Phil. Mag.*, **41,** 534.

Absorption and Emission Spectra of Bismuth-Activated Phosphors

BY W. A. RUNCIMAN
Atomic Energy Research Establishment, Harwell, Didcot, Berks.

MS. received 14*th February* 1955

SOME phosphors show fine structure in their low-temperature absorption and emission spectra, and an investigation of this is likely to help our understanding of the nature of luminescent centres. Bismuth-activated oxide phosphors have a particularly well-defined vibrational fine structure and in consequence have been the subject of several investigations (Ewles 1938, Ewles and Curry 1950, Ewles and Lee 1953).

The frequencies of the maxima of the low-temperature emission bands have been represented (Ewles 1938) by the equation

$$\nu = \nu_e + (v' + \tfrac{1}{2})w' - (v'' + \tfrac{1}{2})w'', \qquad \ldots\ldots(1)$$

where v' and v'' are small integers or zero, w' and w'' are vibrational frequencies and ν_e is the frequency of the electronic transition. The plus sign indicates that the frequency w' refers to the excited state, and the minus sign that the frequency w'' belongs to the ground state.

Exactly the same bands can equally well be described by the equation

$$\nu = \nu_0 - v_1 w_1 - v_2 w_2 \qquad \ldots\ldots(2)$$

which has previously been applied to other fluorescent systems (e.g. Hausser, Kuhn and Kuhn 1935). The relations between the constants in equation (1) and (2) are:

$$v_1 = v'' \qquad w_1 = w''$$
$$v_2 = v' \qquad w_2 = w'' - w'$$
$$\nu_0 = \nu_e - \tfrac{1}{2}(w'' - w').$$

It is convenient to describe the bands by the number of vibrational quanta present (v_1, v_2) and the (0, 0) band will be called the fundamental band. For bismuth-activated phosphors v_1 ranges from 0 to 7 or 8, whereas v_2 is usually 0 or 1. The number of vibrational quanta excited by the electronic transition can only be integral, so the halves of equation (1) have been omitted. Any term due to the zero-point energy is effectively included in ν_0.

In equation (2) both frequencies w_1 and w_2 now belong to the ground state and hence at least two modes of vibration must be involved, whereas in (1) it was only necessary to postulate one normal mode whose frequencies were different in the ground and excited states.

The equation corresponding to (2) for absorption is

$$\nu_0 = \nu_0^* + v_1 w_1^* + v_2 w_2^* \qquad \ldots\ldots(3)$$

where w_1^* and w_2^* are vibrational frequencies of the excited state corresponding to w_1 and w_2 in the ground state.

The difference $\nu_0^* - \nu_0$ represents the energy difference between the electronic transitions for absorption and emission. If $\nu_0^* - \nu_0 = 0$ then the fundamental line is a resonance line. It has been maintained (Pringsheim 1949) that if $\nu_0^* - \nu_0 \neq 0$ then the first observed absorption and emission lines cannot be (0, 0) lines. Selection rules in solids are not very rigid and this explanation seems unlikely. An alternative explanation is that the surroundings of the activator ion are different in the ground and excited states. The neighbouring atoms do not readjust their positions during the electronic transitions by the Franck–Condon principle and hence the frequencies ν_0 and ν_0^* may be unequal.

For CaO(Bi) the frequencies, measured as wave numbers in cm^{-1}, of the emission bands have been represented (Ewles and Lee 1953) by

$$\nu = 25815 + 298(v' + \tfrac{1}{2}) - 493(v'' + \tfrac{1}{2}).$$

When this is rewritten in form (2) it becomes

$$\nu = 25717 - 493 v_1 - 195\, v_2, \qquad \ldots\ldots(4)$$

and this is in agreement within the limits of experimental error, ~10 cm^{-1}, with recent observations.

Furthermore, the absorption bands in CaO(Bi) have been obtained (figure, (*a*), Plate) by a reflection technique in which a 36w 6v tungsten lamp was focused through two pieces of Chance OX7 filter, each 2 mm thick, on to the phosphor in a Dewar flask.

In form (3) these bands are expressed by

$$\nu = 27230 + 430\, v_1 + 215\, v_2. \qquad \ldots\ldots(5)$$

Since different vibrational frequencies occur in (4) and (5), there are at least two modes of vibration active in both electronic states and equation (1) is not applicable. With a Boltzmann distribution of energy these vibrations will not be appreciably thermally excited at 77°K or lower temperatures. Hence the absorption bands only show vibrational levels of the upper state and the emission bands levels of the ground state. It might be argued that the centre retains some vibrational energy after excitation, but this is most improbable as the vibrational frequency is of the order of 10^{13} sec^{-1} and the excited state has usually a half-life of the order of 10^{-8} second.

There is no theoretical reason for there to be only two vibrational terms in (2) and (3), and weak bands due to a third term with a frequency of the order of 360 cm^{-1} have been observed in both the absorption and emission spectra of CaO(Bi). In the case of uranium activated phosphors many more vibrational terms are necessary in (2) and (3), although (1) has been used (Ewles and Lee 1953).

The electronic transmission ($^1S_0 \rightarrow {}^3P_1{}^0$) responsible for the absorption spectrum is that of Bi^{3+} ion going from a $6s^2$ to a 6s 6p state. In contrast with the earlier view (Ewles and Curry 1950) that the vibrations were those of the host lattice, it has been suggested (Williams 1955) that the main vibrational frequency w_1 is that of a radially symmetric oscillation of the six oxygen ions surrounding the bismuth ion. Extending this idea it appears (Runciman 1955) that the change in charge distribution during the electronic transition from a spherical 6s to a dumb-bell 6p state oriented along the [110] axis will cause the equilibrium position of the six oxygen ions to be changed in a way determined by three independent parameters, e.g. two to fix the radial and deformation motions of the four oxygen ions in the xy plane and one to fix the radial motion of the two oxygen ions on the z axis. Hence in addition to the radially symmetric mode two more modes of vibration are especially likely to occur. The three active normal modes may correspond roughly to the three Raman active modes of an octahedral molecule, e.g. UF_6.

Emission bands for SrO(Bi) have been expressed (Ewles and Curry 1950) by

$$\nu = 24180 + 190(v' + \tfrac{1}{2}) - 390(v'' + \tfrac{1}{2}),$$

and in form (2) this becomes

$$\nu = 24080 - 390\, v_1 - 200\, v_2. \qquad \ldots\ldots(6)$$

The present results for SrO(Bi), figure 1 (*b*) lead to the equation

$$\nu = 24320 - 400\, v_1 - 200\, v_2. \qquad \ldots\ldots(7)$$

The vibrational frequencies in (6) and (7) are in good agreement though it was with difficulty that the lines due to the second vibrational term were observed and measured. On the other hand the difference in the fundamental band is well outside the limits of experimental error and is probably due to the detection of a weak band at 4107Å not previously reported.

The reason for some discrepancies with earlier results may be partly due to the higher firing temperature, 1300°c, which has been used in the preparation of phosphors, as compared with temperatures as low as 650°c previously used (Ewles and Lee 1953).

REFERENCES

Ewles, J., 1938, *Proc. Roy. Soc.* A, **167,** 34.

Ewles, J., and Curry, C., 1950, *Proc. Phys. Soc.* A, **63,** 708.

Ewles, J., and Lee, N., 1953, *J. Electrochem. Soc.*, **100,** 392, 399, 402.

Hausser, K. W., Kuhn, R., and Kuhn, E., 1935, *Z. Phys. Chem.* B, **29,** 417.

Pringsheim, P., 1949, *Fluorescence and Phosphorescence* (New York: Interscience), pp. 304, 431.

Runciman, W. A., 1955, Cambridge Conference on Luminescence, *Brit. J. Appl. Phys.*, Suppl. No. 4, pp. 78, 84.

Williams, F. E., 1955, Cambridge Conference on Luminescence, *Brit. J. Appl. Phys.*, Suppl. No. 4, pp. 84, 97.

Neutron–Deuteron Scattering in the Range 80–200 kev

By W. D. ALLEN, A. T. G. FERGUSON and J. ROBERTS†
Atomic Energy Research Establishment, Harwell, Berks.

MS. received 17*th January* 1955, *and in amended form* 16*th February* 1955

§ 1. Introduction

The scattering of neutrons by deuterons in the range 0·1–2 Mev, has already been studied by Tunnicliffe (1953) in this laboratory and by Adair, Okazaki and Walt (1953). Above 300 kev, there was general agreement that the scattering was markedly anisotropic, although the distributions of Tunnicliffe, after approximate estimates have been made for end and wall corrections, show considerably greater anisotropy than those of Adair *et al.* At 220 kev, Adair *et al.* found the distribution almost isotropic, although the technique was not checked by comparison with n–p scattering. Tunnicliffe, on the other hand, observed appreciable anisotropy as low as 135 kev. He found, however, that the total cross section at this energy was 4·8 barns, a figure considerably higher than either the cross section at 1 Mev (3 barns) or the cross section for free deuterons at thermal energies (3·5 barns).

In view of these discrepancies, the work was repeated some 18 months ago by observing recoils in proportional counters filled with hydrogen and deuterium. It was found, as described below, that the distribution was anisotropic down to neutron energies of 100 kev, and that the total cross section was in the region of 3·3 barns. The results in the low energy region of the pulse distribution were obscured by gamma rays. In a recent repetition of the work, therefore, an experimental method was developed which minimized the effect of gamma rays. The results of the previous investigation were confirmed and improved.

§ 2. Apparatus and Method

The distribution of pulses from protons and deuterons recoiling from neutron impact were observed in a proportional counter of the type described by Skyrme, Tunnicliffe and Ward (1952). Protons from the Harwell electrostatic generator impinged on a ZrT target of thickness 20 kev; in the first experiment, the backing of the ZrT was copper. By observing the neutrons at a backward angle of 135°, the neutron energy spread due to target thickness was reduced to 5 kev; adding the contribution of the finite angle subtended by the counter at the target gives a total effective spread at 100 kev, for example, of 12 kev. The neutron flux was monitored by a BF_3 'long counter' at 0°. From the counts observed in the proportional counter was subtracted the background obtained by interposing a polythene scatterer between target and counter. The background due to neutrons scattered from the walls is effectively removed in this way. The polythene scatterer, however, also scatters out low energy gamma rays from the target, arising for example from Coulomb excitation; the net distribution in the counter therefore includes the pulses from these low-energy gamma rays, which predominate in the low-energy end of the recoil distribution. The effect of the gamma rays can be reduced by a reduction of pressure in the gas of the counter, but below one atmosphere, the counting rate becomes prohibitively low.

---

† Now at Imperial College, London, S.W.7.

In the latter experiment, therefore, the gamma rays were dealt with differently. In the first place, the ZrT was backed by silver, which was found to have a lower yield of gamma rays than the copper backing. In the second place, the target gamma rays were screened by $\frac{3}{4}$ in. of lead; this reduced the neutron intensity by some 30–40%, but eliminated low-energy gamma radiation. The polythene which scattered the neutrons was then transparent to the residual high-energy gamma radiation. The loss of intensity was compensated by higher pressures (130 cm) in the counters; this also reduced end and wall corrections.

§ 3. VOLTS PER ION PAIR

The differential distribution of pulses recorded by the pulse analyser corresponds to the energy distribution of the recoils only if volts per ion pair remain constant for the ions considered; the energy distribution of the recoils corresponds to the differential angular distribution in the centre-of-mass system, as first shown by Barschall and Kanner (1940). We have studied the variation in volts per ion pair of protons recoiling in hydrogen by varying the neutron energy and observing the corresponding variation in maximum pulse height. The 'neutron energy' is taken as the mean neutron energy: the 'maximum pulse height' as the centre point of the knee of the curve, i.e. points A in figure 4. The technique was first developed by Tunnicliffe and Ward (1952) who showed, by observing pulses from hydrogen and deuterium in the same counter, that volts per ion pair for recoil protons were constant in the 250–500 kev range. We have extended these observations to the 10–100 kev region by observing the variation in pulse height in a hydrogen-filled counter at different energies; at 10 kev the neutron yield in the backward direction from a ZrT target is quite low, but the centre point of the 'knee' can still be determined to 3–4%. At higher energies this error is about $\frac{1}{2}$%. Errors from neutron energy determination are about $\frac{1}{2}$% (the machine potentiometer was checked by comparing the Li(pn) and T(pn) thresholds), and in the electronics, about 1% (chiefly in the amplifier attenuator). The results are exhibited in figure 1; they show that volts per ion pair are very nearly constant in the range considered. As Crenshaw (1942) and others have shown, the rate of energy loss is the same for protons and deuterons moving with the same velocity. It is noteworthy that at 25 kev a recoiling proton is moving with approximately the same velocity as a molecular electron, and the cross section for charge exchange reaches a maximum. In spite of this, the proportion of energy lost in ion production remains constant at energies considerably lower than 25 kev. We should also comment that in methane at various pressures the volts per ion pair are not nearly so constant. Thus, a plot of pulse height against neutron energy in the range 250–1000 kev will give a straight line which extrapolates to zero pulse height at 40 kev.

§4. RESULTS

An exact calculation of end and wall corrections for deuterium would be tedious to compute. The corrections for hydrogen are small and almost linear; in the extreme case considered, at 200 kev, the theoretical distribution is almost a straight line from an ordinate of 1·07 on the left-hand end to 0·92 on the right-hand end. To demonstrate the corrections involved, figure 4 shows the distributions for hydrogen at 100 and 200 kev, uncorrected for end and wall effects.

Approximate corrections were made for deuterium, therefore, by simply taking the observed curves and multiplying by the appropriate corrections for hydrogen; the remaining errors are not significant.

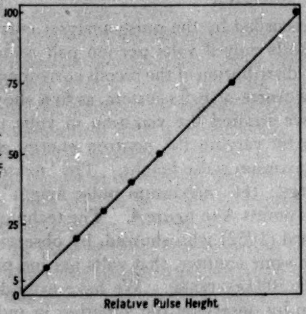

Figure 1. Relative pulse height plotted against E_n. Counter pressure 78 cm H_2; ZrT target at 135°.

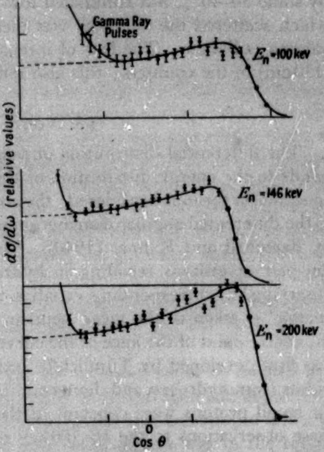

Figure 2. Angular distributions of neutrons recoiling from deuterium (counter pressure 78 cm D_2; corrected for end and wall effects).

The results for deuterium in the first experiment, at three energies between 100 and 200 kev, are shown in figure 2; it is seen that the gamma-ray contribution makes the anisotropy at 100 kev uncertain. When Tunnicliffe's result at 135 kev is corrected for end and wall effects, as in this paper, the agreement with our result at 146 kev is good. The results of the second experiment for deuterium are shown in figure 3 (both figures 2 and 3 include end and wall corrections); the anisotropy at 100 kev is clearly demonstrated, and is probably present even at 80 kev. The agreement in angular distribution between the first result at 200 kev (counter pressure 64 cm) and the second (counter pressure 130 cm) is reasonably good.

For the total cross section, the area under the distribution curve was integrated; for low-energy recoils this means the area under the dotted line. The ratio of the total counts for deuterium and hydrogen, suitably corrected for gas pressure and $1\frac{1}{2}\%$ H_2 contamination in the deuterium, then gives the ratio of $\sigma_{tot}(nD)$ to $\sigma_{tot}(nH)$. The latter was calculated using $a_s = -23{\cdot}7 \times 10^{-13}$, $a_t = 5{\cdot}38 \times 10^{-13}$, $r_s = 2{\cdot}5 \times 10^{-13}$, $r_t = 1{\cdot}703 \times 10^{-13}$, since all these quantities are accurately known except r_s, which does not materially affect the result. The (np) cross sections so obtained agree well with the curve for hydrogen in A.E.C.U. 2040, Supplement 1, which, however, differs at points by as much as 8% from the curve for hydrogen published in A.E.C.U. 2040.

The total statistical error is ± 3%. The results are shown in the table with figures of Adair *et al.* at 262 kev for comparison.

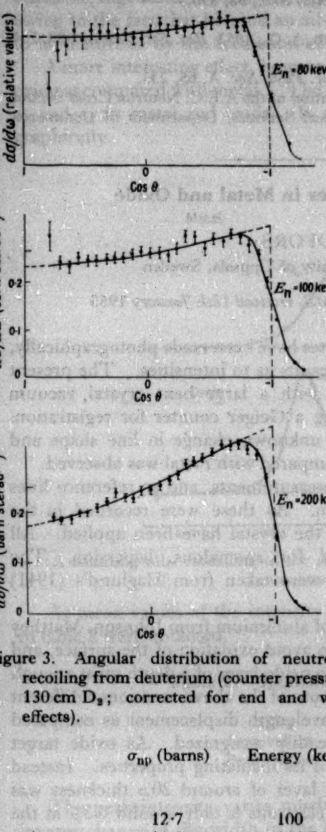

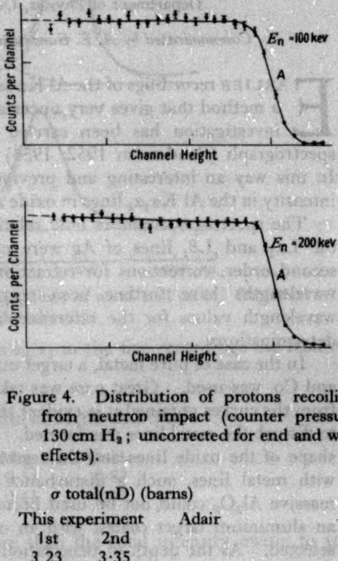

Figure 3. Angular distribution of neutrons recoiling from deuterium (counter pressure 130 cm D_2; corrected for end and wall effects).

Figure 4. Distribution of protons recoiling from neutron impact (counter pressure 130 cm H_2; uncorrected for end and wall effects).

σ_{np} (barns)	Energy (kev)	σ total(nD) (barns)		
		This experiment		Adair
		1st	2nd	
12·7	100	3 23	3·35	
11·0	146·5	3·07		
9·6	200	3·06	3·08	
	262			3·22

§ 5. Discussion

As observed by Adair, the back scattering observed in the n–D recoils at low energies arises primarily from the interference between the S waves and the quartet P waves. T. H. R. Skyrme of this Establishment has made a calculation of the ^4P scattering in the limit of zero energy; from this it would appear that the calculated amount of anisotropy is about two thirds of that required to account for the experimental data. We are indebted to Dr. Skyrme for carrying out the calculations.

References

Adair, R. K., Okazaki, A., and Walt, M., 1953, *Phys. Rev.*, **89**, 1165.
Barschall, H. H., and Kanner, M. H., 1940, *Phys. Rev.*, **58**, 590.
Crenshaw, C. M., 1942, *Phys. Rev.*, **62**, 54.
Skyrme, T. H. R., Tunnicliffe, P. R., and Ward, A. G., 1952, *Rev. Sci. Instrum.*, **23**, 204.
Tunnicliffe, P. R., 1953, *Phys. Rev.*, **89**, 1247.
Tunnicliffe, P. R., and Ward, A. G., 1952, *Proc. Phys. Soc.* A, **65**, 233.
A.E.C.U. 2040, *Neutron Cross Sections*, a compilation of the A.E.C. Neutron Cross Section Advisory Group, 1952 (Office of Technical Services, Department of Commerce, U.S.A.).

A Note on the Al $K\alpha_3\alpha_4$ Lines in Metal and Oxide

By B. NORDFORS
Department of Physics, University of Uppsala, Sweden

Communicated by A. E. Sandström ; MS. received 18*th January* 1955

Earlier recordings of the Al $K\alpha$ satellites have been made photographically, a method that gives very uncertain results as to intensities. The present investigation has been carried out with a large bent crystal vacuum spectrograph (Sandström 1952, 1954) using a Geiger counter for registration. In this way an interesting and previously unknown change in line shape and intensity in the Al $K\alpha_3\alpha_4$ lines in oxide as compared with metal was observed.

The spectrograph allows only relative measurements, and as reference lines the $L\alpha_1$ and $L\beta_1$ lines of Ag were chosen. As these were recorded in the second order, corrections for refraction in the crystal have been applied. All wavelengths have further been corrected for anomalous dispersion. The wavelength values for the reference lines were taken from Haglund's (1941) determinations.

In the case of pure metal, a target made of aluminium from Johnson, Matthey and Co. was used. Great care was taken to avoid oxidation of the surface, and from the curves obtained it is evident that no oxide layer of a depth great enough to disturb the metal lines was formed. Because of the above-mentioned different shape of the oxide lines and their great wavelength displacement as compared with metal lines, such a disturbance is readily recognized. As oxide target massive Al_2O_3 could not be used because of its insulating properties. Instead an aluminium target coated with an oxide layer of around $20\,\mu$ thickness was selected. As the depth of penetration for electrons is only around $0{\cdot}3\,\mu$ at the voltage used, this thickness is quite sufficient to ensure radiation from oxide only. The pressure in the spectrograph tank and the x-ray tube was usually less than 10^{-5} mm Hg during recordings. Occasionally it was as high as 2×10^{-5} mm Hg.

The wavelengths in the table below represent mean values of five determinations. The errors represent greatest fluctuations from the mean value. $\Delta\lambda$ has been measured separately, and thus the errors there are smaller than in λ.

Table 1. Wavelengths of the Al $K\alpha_3\alpha_4$ Lines in Metal and Oxide

	Metal λ (x.u.)	Oxide λ (x.u.)	$\Delta\lambda$ (x.u.)	ΔV (ev)
α_3	$8268{\cdot}7\pm0{\cdot}4$	$8265{\cdot}1\pm0{\cdot}5$	$3{\cdot}6\pm0{\cdot}2$	0·65
α_4	$8256{\cdot}8\pm0{\cdot}6$	$8253{\cdot}7\pm0{\cdot}5$	$3{\cdot}1\pm0{\cdot}2$	0·56

The wavelength displacement $\Delta\lambda$ is great as compared to that of Al K$\alpha_1\alpha_2$, which is only 1·7 X.U. The displacements of Al Kα satellites were measured by Carlsson (Ingelstam) in 1932. He got, however, somewhat lesser values, probably owing to the fact that he used an air-filled ion tube, thus causing the metal lines to be disturbed by the formation of oxide on the target.

A more interesting effect, however, is the change in line shape and intensity in oxide as compared with metal. The figure represents one of the five recordings of α_3 and α_4 in metal and oxide. It also shows an attempt to resolve the lines graphically.

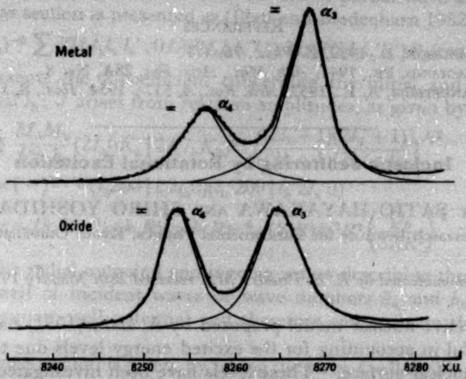

A counting tube recording of the Al K$\alpha_3\alpha_4$ lines in metal and oxide. Statistical uncertainty as indicated.

As mean values of the intensity ratio α_4/α_3 in the five recordings the results in table 2 were obtained.

Table 2. Intensity Ratio in Metal and Oxide

α_4/α_3	Metal	Oxide
Area values	0·54	0·82
Peak values	0·44	0·98

The peak intensity varies much more than the total intensity owing to an inverse change in the width of the lines according to table 3.

Table 3. Line Width in Metal and Oxide

	Metal		Oxide	
	α_3	α_4	α_3	α_4
Width at half maximum (X.U.)	5·3	6·9	6·2	4·9

The broadening effects are of the same order of magnitude as the uncertainty of the graphical resolution, and thus no corrections for broadening effects have been applied. It has further proved impossible to perform the graphical resolution in such a way that α_3 in metal becomes symmetrical. Whether α_3 itself is strongly asymmetrical or whether it is complex has not been possible to determine in spite of the high resolving power of the spectrograph.

The experimental results thus obtained in this investigation may possibly be of some significance in choosing between the different existing theories of the origin of satellite lines.

ACKNOWLEDGMENT

The work with the bent crystal vacuum spectrograph is being sponsored by the Swedish Natural Science Research Council. The author wishes to thank Dr. Arne Eld Sandström for his valuable advice and help.

REFERENCES

CARLSSON, E., 1932, *Z. Phys.*, **76**, 471.
HAGLUND, PH., 1941, *Ark. Mat., Astr. Fys.* **28A**, No. 8.
SANDSTRÖM, A. E., 1952, *Ark. Fys.*, **4**, 517; 1954, *Ibid.*, **8**, 129.

Inelastic Scattering by Rotational Excitation

BY SATIO HAYAKAWA AND SHIRO YOSHIDA†
Research Institute for Fundamental Physics, Kyoto University

Communicated by R. E. Peierls; *MS. received 28th January* 1955

THE collective nuclear model proposed by A. Bohr (1952) has been found successful in accounting for the excited energy levels due to the rotation of the nuclear surface. These levels have been investigated by means of electromagnetic radiation and by Coulomb excitation by charged particles. Through these experimental means one obtains the magnitude of the nuclear surface deformation which is intimately related to the nuclear quadrupole moment. This quantity can also be obtained by observing the inelastic scattering of nucleons, leaving a residual nucleus in a rotational level. Conversely, the influence of the rotational excitation on nuclear reactions should be noticed in interpreting experiments.

We consider a case where a nucleus is excited to the first rotational level through the inelastic scattering of a nucleon. According to the strong coupling approximation (Bohr and Mottelson 1953), the interaction of the nucleon takes place at the nuclear surface with a strength UR times a quantity proportional to the intrinsic quadrupole moment Q_0, where U is taken to be the depth of the nuclear potential for the nucleon and R the average nuclear radius. With this interaction alone the differential cross section under Born approximation can readily be obtained as

$$\frac{d\sigma}{d\Omega}=\frac{M_{\mathrm{a}}M_{\mathrm{b}}k_{\mathrm{b}}}{k_{\mathrm{a}}\hbar^4}(2I_{\mathrm{a}}0K_{\mathrm{a}}|2I_{\mathrm{a}}I_{\mathrm{b}}K_{\mathrm{b}})^2 5U^2R^6\left(\frac{Q_0}{3ZR^2}\right)^2|j_2(qR)|^2, \quad \ldots\ldots(1)$$

for the initial nucleus of atomic number Z and of spin I_{a} to make transition to the final nucleus of spin I_{b}. $K_{\mathrm{a}}=K_{\mathrm{b}}(=I_{\mathrm{a}})$ are the component sof the respective spins along the respective nuclear symmetry axes. M and k are the reduced mass and the wave number respectively in the initial and final states, designated by suffixes a and b ; $(2I_a0K_a|2I_aI_bK_b)$ are Clebsch–Gordan coefficients; $q = |\mathbf{k}_a - \mathbf{k}_b|$ is the absolute magnitude of the momentum transfer. The spherical Bessel function $j_2(qR)$ arises because the rotational angular momentum excited is $2\hbar$. The angular distribution appearing in (1) is characteristic for any scattering due to a surface interaction with absorption of two units of orbital angular momentum.

---

† Now at Department of Mathematical Physics, University of Birmingham.

As the Born approximation is not realistic in most cases, we take account of the distortion of nucleon waves by a potential well of depth U and radius R. This approximation is applicable to neutrons of low energies and the calculation of the cross section can be carried out with the aid of partial wave analysis. The differential cross section is presented as (Blatt and Biedenharn 1952)

$$d\sigma/d\Omega = (2k_a)^{-2} \sum Z(l_a l_a l_a' l_a'; 0L) Z(l_b l_a l_b' l_a'; 2L) J(l_a l_b l_a' l_b') P_L(\cos\theta), \quad \ldots(2)$$

where Z represents the Z-coefficient concerning the initial and final angular momenta, l_a and l_b; J arises from reaction amplitudes, as given by

$$\begin{aligned} J = \tfrac{1}{4} \frac{M_a M_b}{\hbar^4 k_a k_b} &(2I_a0K_a|2I_aI_bK_b)^2 5 \left(\frac{(2l_b+1)(2l_b'+1)}{(2l_a+1)(2l_a'+1)}\right)^{1/2} \\ &\times (-)^{l_b+l_b'} (l_b200|l_b2l_a0)(l_b'200|l_b'2l_a'0) \\ &\times u_{la}(k_aR) u^*_{la'}(k_aR) v_{lb}(k_bR) v^*_{lb'}(k_bR) U^2 R^2 \left(\frac{Q_0}{3ZR^2}\right)^2. \quad \ldots\ldots(3) \end{aligned}$$

u and v^* are the radial outgoing and ingoing waves describing the scattering by the potential well of incident waves of wave numbers k_a and k_b respectively. We assume a square-well potential and therefore can evaluate these functions exactly.

The total cross section is given, by taking the term $L=0$ in (2), as

$$\begin{aligned} \sigma = \frac{\pi}{k_a^2} \frac{M_a M_b}{\hbar^4 k_a k_b} &\tfrac{1}{4} (2I_a0K_a|2I_aI_bK_b)^2 5 U^2 R^2 \left(\frac{Q_0}{3ZR^2}\right)^2 \\ &\times \sum (2l_b+1)(l_b200|l_b2l_a0)^2 |u_{la}(k_aR)|^2 |v_{lb}(k_bR)|^2. \quad \ldots\ldots(4) \end{aligned}$$

By comparison with the Born approximation, the distortion caused by the potential has a considerable influence on the cross section. This is fairly sensitive to the magnitude of $(2MUR^2/\hbar^2)^{1/2}$. As this is approximately seven, a variation of ten per cent of U or R^2 gives rise to a change of this quantity of about $\pi/8$, which is not small in the argument of a trigonometric function.

For the comparison of our theory with experiments, we fix the magnitudes of the parameter as $R = 1{\cdot}4 \times 10^{-13} A^{1/3}$ cm, from reaction radii, and $U = 33$ MEV, to give reasonable binding energies. Experimental data with the best accuracy are available for the inelastic scattering by iron. The excitation of ^{56}Fe to its first excited level of 0·85 MEV is observed with neutrons of a few MEV (Eliot *et al.* 1954, Kiehn and Goodman 1954, and Scherrer *et al.* 1954) as well as protons of 17 MEV (Schrank *et al.* 1954). For such experiments $I_a = 0$ from observation, and $I_b = 2$, as inferred from the general characteristics of even–even nuclei. The intrinsic quadrupole moment Q_0 can be obtained by reference to the static quadrupole moments of neighbouring nuclei, ^{55}Mn and ^{59}Co, on account of the smooth variation of Q_0 with mass number. In the strong coupling limit, the Q_0's of these nuclei are evaluated as 1·1 ± 0·6 barns and 1·1 ± 0·4 barns respectively. It is more appropriate, however, to take account of the intermediate coupling nature for the magnitude of Q_0. Thus we fix $Q_0 = 0{\cdot}6$ barn.

Eliot *et al.* (1954) obtained $\sigma = 1{\cdot}0 \pm 0{\cdot}3$ barns with 2·5 MEV neutrons, while (4) gives us about 1 barn. Kiehn and Goodman (1954) observed the excitation curve for the process under consideration and noticed that the cascade gamma rays give a contribution above 2·1 MEV. In order to avoid this effect, comparison is made near the threshold where only $l'_a = 2$ and $l_b = 0$ are important. As our theory neglects compound nucleus formation, the resonances observed by them cannot be reproduced. However, the gross behaviour of the excitation curve is in rough agreement with the experiment and also with that predicted by Hauser and Feshbach (1952) under the assumption of the statistical theory. The agreement with the latter theory is to be expected for the energy dependence, but the absolute magnitude may be different because our theory contains physical constants. The rough agreement with experiments seems to show that our model of rotational excitation as well as the magnitudes of the parameters are not unreasonable. This success should not be taken too seriously, however, because we have over-simplified the derivation of the cross section, and consequently the result is too sensitive to the magnitudes of U and R.

This sensitivity does not come into the Born approximation formula (1), which may be compared with the proton experiment (Schrank *et al.* 1954). The angular distribution is approximately represented by $|j_2|^2$ and the differential cross section at the first peak (at about 40°) is observed as 11 mbn sterad^{-1}, while (1) yields about 50 mbn sterad^{-1}. The effect of the Coulomb repulsion is estimated to decrease this value approximately by a factor of 2. There still remains a discrepancy of a factor of 2, but the distortion by nuclear forces may alter this factor.

A detailed account will be published in the *Progress of Theoretical Physics*.

REFERENCES

BLATT, J. M., and BIEDENHARN, L. C., 1952, *Rev. Mod. Phys.*, **24**, 258.
BOHR, A., 1952, *K. Danske Vidensk. Selsk. Mat. Fys. Medd.*, **26**, 14.
BOHR, A., and MOTTELSON, B. R., 1953, *K. Danske Vidensk. Selsk. Mat. Fys. Medd.*, **27**, 16.
ELIOT, E. A., HICKS, D., BEGHIAN, L. E., and HALBAN, H., 1954, *Phys. Rev.*, **94**, 144.
HAUSER, W., and FESHBACH, 1952, *Phys. Rev.*, **87**, 366.
KIEHN, R. M., and GOODMAN, C., 1954, *Phys. Rev.*, **95**, 989.
SCHERRER, V. E., ALLISON, B. A., and FAUST, W. R., 1954, *Phys. Rev.*, **96**, 386.
SCHRANK, G., GUGELOT, P. C., and DAYTON, I. E., 1954, *Phys. Rev.*, **96**, 1156.

REVIEWS OF BOOKS

Table of the Gamma Function for Complex Arguments. National Bureau of Standards—Applied Mathematics Series 34. Pp. xvi + 105. (Washington: U.S. Government Printing Office, 1954.) $2.

Once again we are indebted to the Mathematical Tables Project of the National Bureau of Standards for a table of considerable importance to many engaged in computation in both pure and applied mathematics. In physical problems, the gamma function with complex argument often occurs as an external factor to complex hypergeometric series, and may need to be known with unusually high accuracy.

The table under review presents 12D values of the real and imaginary parts of $\log_e \Gamma(z)$ for $z=x+iy$, $x=0(0{\cdot}1)10$, $y=0(0{\cdot}1)10$. By means of the familiar $\sin \pi z$ formula, and the duplication formula, the values given can readily be extended to cover the ranges, $-18 \leqslant x \leqslant 20$, $-20 \leqslant y \leqslant 20$. Outside this region the asymptotic series of Stirling provides similar precision, so that in effect the quantitative behaviour of $\Gamma(z)$ in the whole complex plane is known. In a table of such wide range it is of course unreasonable to expect accurate interpolation to be everywhere straightforward. Linear interpolation is out of the question except for the crudest calculations, but one finds that a simple 4-point interpolation mostly provides 5D accuracy when $x, y>1$, improving to 8D accuracy for larger values of x and y. For uses needing greater precision details are given of interpolation formulae using up to 8 points in the table, and ensuring at least 9D accuracy when $x, y> 2$. Various formulae are also suggested for inverse interpolation.

There remains of course the awkward region near the singular point at $z=0$. Here the obvious procedure is to use this table to find $\Gamma(2+z)$ or $\Gamma(1+z)$, and hence $\Gamma(z)=\Gamma(1+z)/z$. There also exists the complementary table of Stanley and Wilkes (Toronto, 1950), giving 6D values of $1/\Gamma(z)$ for $x=-0{\cdot}5(0{\cdot}01)0{\cdot}5$, $y=0(0{\cdot}01)1$, which remains a valuable accessory. Otherwise the N.B.S. table has no rival, and is good value at the price.

R. A. B.

Variational Principles in Dynamics and Quantum Theory, by W. YOURGRAU and S. MANDELSTAM. Pp. ix + 155. (London: Pitman, 1955). 25*s*.

This is an excellent introduction to variational principles in theoretical physics. The intention of the study, in the authors' words, is the " co-ordination of the historical, mathematico-physical, and philosophic aspects of variational principles." In this they have succeeded admirably.

The book starts with an appraisal of the scientific thought in the age of Fermat and Maupertuis, who first enunciated the so-called ' least ' principles. This is followed by the precise mathematical development of these principles, due to Euler and Lagrange. The next sections discuss the full flowering of the theory in the hands of Hamilton and Jacobi. Even though the authors write about a very familiar part of the subject, the zest they bring to it gives the writing a new freshness.

Two shorter chapters deal with the discovery of the Schrödinger equation and the role which variational principles have played in quantum theory. The book closes with a discussion of the significance of these principles in natural philosophy.

This is one of the rare books which combine sound mathematics with a sound philosophic appraisal of its concepts and conclusions. The historical comments enhance the readability. Altogether the book provides most stimulating reading and is recommended to all students of natural philosophy. It will, in particular, be a suitable introduction to the subject for those in their final year's honours course in mathematical physics.

A. S.

Annual Review of Nuclear Science, Vol. 4, edited by J. G. Beckerley, M. D. Kamen and L. I. Schiff. Pp. ix + 483. (Stanford: Annual Reviews, Inc., 1954) $ 7.50.

The volume of original publications on nuclear physics is now so great that the frequent issue of review articles is a prime necessity. Publications such as *Progress in Nuclear Physics* (London: Pergamon Press) and *Annual Reviews of Nuclear Science* are becoming increasingly important to the nuclear physicist who wishes both to keep himself up to date in his own special interests and also to acquaint himself with advances in related fields. Most of the articles in the volume under review contain information as recent as April 1954 and some extend a few months further. The availability of the volume early in 1955 is a tribute both to the diligence of the contributors and to the enthusiasm of editors and publishers. The production maintains the standards set by previous volumes and the book is singularly free from typographical errors.

The articles in the volume under review cover a wide range of subjects and the treatment differs from article to article. Some are admittedly progress reports, covering only a brief period. In this category is ' Radiofrequency and Microwave Spectroscopy ' (G. E. Pake) which describes in detail a new ionization method for detecting atomic beams and also a method, due to Overhauser, for producing nuclear polarization by interaction with electronic spins. Similarly of current interest is J. P. Blewett's article on ' Recent Developments in Proton Synchrotrons '. This very clearly expounds the transition in design between operating machines and the new monster alternating gradient accelerators.

Several articles deal with subjects in which considerable progress has been made over a period of several years but which for one reason or another have now reached what appears to be a suitable reviewing point. The extremely well documented article by T. P. Kohman and N. Saito on ' Radioactivity in Geology and Cosmology ' gives a fascinating and particularly readable account of nuclear dating methods. Among the techniques used in these studies is that of isotopic dilution analysis, which is described by M. G. Inghram in a short technical review also in this volume. The remarkable progress in the discovery of new alpha emitting nuclei, made largely with the cyclotrons of the Radiation Laboratory at Berkeley, is well described by I. Perlman and F. Asaro, whose work has revealed many of the properties of these bodies. The collection of data on energies and life-times will be found useful by workers in this field. The short article on ' Fission Radiochemistry ' by L. E. Glendenin and E. P. Steinberg is perhaps of rather less general interest; despite its title it does not discuss chemical procedures but chiefly reports on fission yields as a function of mass number in a variety of experiments bearing on the fission mechanism. The behaviour of the positronium atom is a matter which on the grounds of elegance and importance to electromagnetic theory deserves frequent review. S. DeBenedetti and H. C. Corben have contributed a clear and well arranged article in which theory and experiment are displayed to mutual advantage. Recent work of interest in connection with the penetration of heavy charged particles through matter is discussed by E. A. Uehling. This article starts usefully with a review of the many previous reviews and data articles of the subject; he then deals particularly with the theory of energy loss including binding energy correction, the polarization effect, and the determination of mean excitation potentials. The article is primarily theoretical but the author briefly refers to experimental measurements of energy loss distributions and of the ratio of energy loss to ionization.

High energy physics is represented by three articles. M. Gell-Mann and K. M. Watson have written an expert monograph on ' The Interactions between π-Mesons and Nucleons '. This gives essentially a phenomenological discussion of the problem, based on the charge independence hypothesis and on the (empirical) fact of strong meson–nucleon interaction in the state of $J=3/2$, $T=3/2$. The concept of isotopic spin is well discussed and both scattering and meson production are examined. The article concludes with a short report on the present state of field theory. The following review, on ' Heavy Mesons ' by C. Dilworth, G. P. S. Occhialini and L. Scarsi deals only with particles with mass between that of the π-meson and the proton. This is one of the most interesting and least understood areas of high energy physics and it is helpful to have at this stage a collection of most of the available data. It would be ungracious to complain that the article reads too much like a conference report; this is inherent in the present state of the information and when well established conclusions are available they are given, as in the section on the τ-meson. The final table of ' possible particles ' summarizes a subject which " is if anything, growing in complexity ". In contrast with this, the theory of photonuclear reactions has to some extent been clarified recently by application of the ideas of the independent particle model. J. S. Levinger reports on this progress in an article which is concerned with the physical content of the theories and experiments rather than with the details of either.

The volume has four articles which may be broadly classed as technical. ' Standardisation of Radioactive Sources ' by G. G. Manov is a straightforward account of the primary standards of radioactivity such as ^{14}C, ^{60}Co, ^{131}I, ^{32}P and others. Nuclear particle detection is represented by reviews of progress in ' Fast Electronics ' (R. E. Bell), ' Characteristics of Scintillators ' (R. K. Swank), and Čerenkov Counters (J. Marshall). These subjects have been reviewed elsewhere recently but they are rapidly developing and deserve frequent attention. Each of this group of articles is well arranged and informative, and generously provided with references.

The policy of including biological articles in a review of nuclear science may perhaps be questioned. Of two such reviews in this volume, one, by J. F. Thomson on ' Lethal Actions and Associated Effects ' is readily intelligible and interesting to a physicist. The other, however, by K. P. DuBois and D. F. Peterson on ' Biochemical Effects of Radiation ' will probably be found difficult by many owing to unfamilarity with the technical language. Many of the purchasers of this volume might have been grateful for a simple introduction to to this very important field of investigation.

W. E. BURCHAM.

Superfluids, Vol. II. *Macroscopic Theory of Superfluid Helium*, by the late F. London. Pp. xvi+217. (New York: Wiley; London: Chapman and Hall, 1954.) 64*s*.

One tends automatically to expect that any book by the late Professor London shall be extremely readable. This volume abundantly fulfils expectations. It does so, moreover, without loss of precision and without glossing over any difficulties. In particular the limitations of the macroscopic theory are fully discussed.

The first section deals with the phase diagram of helium and with the observed behaviour of the superfluid modification of liquid helium. This is followed by considerations of the van der Waals forces, the radial distribution function and the zero-point energy for possible crystal structures. It is shown that the zero-point energy will prevent the liquid from solidifying except at high pressures; at ordinary pressures the interatomic spacing is large, and liquid helium is much more gas-like than other liquids.

The condensation of an ideal Bose–Einstein gas is discussed, and the macroscopic two-fluid theory is developed using concepts borrowed from the Bose–Einstein condensation. Landau's quantum hydrodynamics is also shown to lead to the two-fluid model. (The 'roton' concept is criticized, however: the author takes the view that the real elementary excitations should be phonons and single-atom translational motions.) Much of the volume is devoted to developing the consequences of two-fluid thermo- and hydrodynamics. The phenomenon of 'second sound' is fully discussed, including Ward and Wilks's interpretation of second sound at low temperatures as sound waves in a gas of phonons.

The recent rigorous quantization of the hydrodynamical equations by Kronig and Thellung is presented, but Ziman's work on the energy spectrum of rotons appears to have been completed too late for discussion. However, the very sensitive dependence of Ziman's hydrodynamical roton energy on a momentum cut-off strengthens the view that a microscopic theory is required to give Landau's excitation spectrum a sound foundation.

The inclusion of a chapter on the properties of ^{3}He and ^{3}He–^{4}He mixtures is very welcome. The behaviour of these systems supports the author's view that the superfluid properties of helium are intimately connected with its Bose–Einstein statistics. In conclusion, he draws attention to the many similarities between the macroscopic theories of superfluidity and of superconductivity. Both types of system are characterized by an inhomogeneity in momentum space rather than in configuration space.

The volume should be invaluable to all experimentalists and theoreticians working on liquid helium, despite the restriction of its scope to the macroscopic theory. The recent work of Feynman suggests that a full understanding of superfluidity may no longer be too remote. The untimely death of Professor London has, however, crushed the hope that he would complete this series with a third volume, on the microscopic theory of superfluids. C. G. KUPER.

Les Fonctions de Bessel (2nd Edn), by G. Goudet. Pp. 90. (Paris: Masson et Cie, 1954.) 600 *fr*.

This is an introductory text, which is addressed particularly to physicists. The first three chapters are devoted to the introduction of Bessel functions as solutions of Bessel's equation together with most of the better known recurrence formulae, integrals and expansions. The final chapter gives an account of some physical applications of the foregoing. These cover the oscillations of a cylindrical cavity, the skin effect, conduction of heat by a cylinder, and finally a group of problems in diffraction. The treatment is simple and a model of clarity. The inclusion of examples, however, would have been an advantage for the student. H. H. HOPKINS.

BOOK NOTICES

Science and its Background, by H. D. ANTHONY. 2nd Edn. Pp. ix + 337. (London: Macmillan, 1954.) 20*s*.

The Sources of Eddington's Philosophy, by H. DINGLE. Pp. vi + 64. (Cambridge: University Press, 1954.) 3*s*. 6*d*.

Equazioni alle derivate parziali di tipo ellittico, by C. MIRANDA. Pp. viii + 222. (Berlin, Göttingen, Heidelberg: Springer, 1955.) (Ergebnisse der Mathematik und ihrer Grenzgebiete, Neue Folge, Heft 2.) DM 28.80.

Transfinite Zahlen, by H. BACHMANN. Pp. vii + 204. (Berlin, Göttingen, Heidelberg: Springer, 1955.) (Ergebnisse der Mathematik und ihrer Grenzgebiete, Neue Folge, Heft 1.) DM 29.80.

Analytische Fortsetzung, by L. BIEBERBACH. Pp. 167. (Berlin, Göttingen, Heidelberg: Springer, 1955.) (Ergebnisse der Mathematik und ihrer Grenzgebiete, Neue Folge, Heft 3.) DM 24.80.

CONTENTS OF SECTION B

Mr. K. F. Hulme. On the Distribution of Impurity in Crystals Grown from Impure Unstirred Melts 393

Mr. M. Kerridge. Metal Transfer and the Wear Process 400

Dr. N. C. Gerson. Diurnal Variation in Auroral Activity 408

Dr. A. H. Cooke, Dr. S. Whitley, and Dr. W. P. Wolf. Demagnetization Experiments on Cerium Ethyl Sulphate 415

Dr. L. Hartshorn, Mr. J. V. L. Parry and Dr. L. Essen. The Measurement of the Dielectric Constant of Standard Liquids 422

Mr. G. G. E. Low. A Pulse Method for Measuring the Injection Ratio of Metal–Semiconductor Contacts 447

Dr. J. H. Gerrard. Measurements of the Sound from Circular Cylinders in an Air Stream 453

Dr. Mary D. Waller. A Study of Powder and Granular Ridges in a Sound Field 462

Research Notes:

Mr. Amar Nath Nigam. The Origin of Fine Structures in X-ray Absorption Spectra of Ionic Solutions 472

Letters to the Editor:

Dr. H. Wilman. The Temperatures attained at the Surfaces of Growing Deposits, and the Origin of Stress in Deposits 474

Reviews of Books 477

Contents of Section A 480

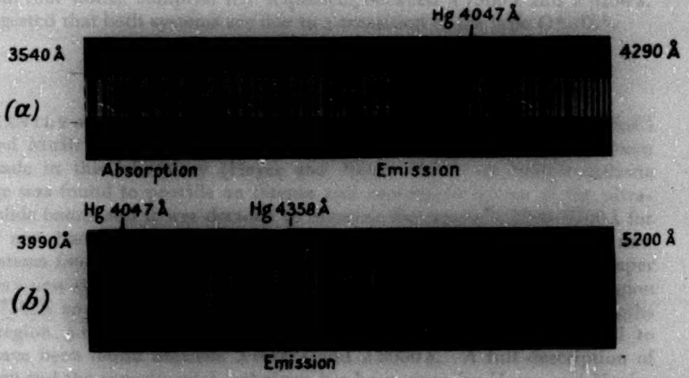
Hg 4047 Å
3540 Å
4290 Å
(a)
Absorption
Emission
Hg 4047 Å
Hg 4358 Å
3990 Å
5200 Å
(b)
Emission

(*a*) Absorption and emission spectra of CaO(Bi) at 77°K (2 min exposure Zenith plate).
(*b*) Emission spectrum of SrO(Bi) at 77°K with 3650 Å excitation (1 min exposure. Thin film half tone plate).

The spectra were obtained on a Hilger medium Quartz Spectrograph, and the wavelength limits are as shown.

New Band Systems of MnF and MnBr in the Red

By W. HAYES and T. E. NEVIN
Physics Department, University College, Dublin

MS. received 21*st February* 1955

Abstract. New band systems in the red attributed to MnF and MnBr have been observed in a hollow cathode discharge. The MnBr bands degraded to shorter wavelengths consist of two sequences of double headed bands in the region λ 6285–6246 Å. The MnF bands degraded to longer wavelengths, each band with four heads, comprise five sequences between λ 7300 Å and λ 6230 Å. It is suggested that both systems are due to a transition of the type $O^{\pm}$–$^5\Sigma^+$.

§ 1. Introduction

Recently a new study of the complex near ultra-violet bands of MnCl and MnBr which involve the transition $^7\Pi$–$^7\Sigma$ (Bacher 1948) has been made in this laboratory (Hayes and Nevin 1955). A hollow cathode discharge was found to provide an intense and convenient source of the ultra-violet halide bands and it was decided to examine the region λ 2200–9700 Å for possible new band systems of MnF, MnCl and MnBr. An account of new band systems found in the infra-red is being published elsewhere. This paper describes a new system of MnF degraded to long wavelengths lying in the region λ 6229–7302 Å and a new band system of MnBr degraded to short wavelengths in the region λ 6246–6285 Å. No strong bands which can be attributed to MnCl have been found between λ 6000 Å and λ 8000 Å. A full description of the source and the experimental technique has been given by Hayes and Nevin.

§ 2. Bands of MnF

Preliminary survey work using the glass prism of a Hilger E 478 spectrograph with Ilford Astra III and Kodak II N plates showed five sequences of double headed bands degraded to longer wavelengths the appearance of which can be seen from figure 1 (*a*) and (*b*) (Plate). The strongest sequence, the first pair of heads of which are at wavelengths λ 6890·7 Å and λ 6893·2 Å is interpreted as the $\Delta v = 0$ sequence of the system. In order of increasing wavelength the five sequences are therefore labelled $\Delta v = +3, +2, +1, 0, -1$ respectively. The sequences $\Delta v = -1, 0, +1$ were photographed and measured in the first and second orders of the 21 ft grating, dispersion 2·5 Å mm^{-1} and 1·2 Å mm^{-1} respectively. The resolution, however, was quite inadequate for a rotational analysis. The sequences $\Delta v = +3$ and $+2$ were poorly defined on the grating plates and have been measured only on the prism plates which in the region in question have a dispersion of about 21 Å mm^{-1}. On the high dispersion plates each band shows four heads three of which lie so close together that on the prism plates they are blended together and the bands appear to have double heads. The sequence $\Delta v = 0$ enlarged from a second order grating plate is reproduced in figure 1 (*c*).

Table 1. Band Heads of the Red System of MnF

Vacuum wave number (K)	*I*	Classification		Vacuum wave number (K)	*I*	Classification	
16049·6*	1	6, 3	T	14817·3*	1	6, 5	T
043·2*	2		Q, R, S	809·5*	3		Q, R, S
15980·5*	1	7, 4	T	759·7*	1	7, 6	T
973·9*	2		Q, R, S	752·8*	2		Q, R, S
912·6*	1	8, 5	T	702·7*	0	8, 7	T
904·5*	2		Q, R, S	695·3*	0		Q, R, S
844·5*	0	9, 6	T	14508·3	10	0, 0	T
835·0*	1		Q, R, S	503·6	10		S
771·5*	0	10, 7	T	500·8	20		R
764·2*	1		Q, R, S	500·1	15		Q
701·9*	0	11, 8	T	459·8	4	1, 1	T
696·2*	1		Q, R, S	454·9	4		S
617·6*	2	3, 1	T	452·0	8		R
612·3*	4		Q, R, S	451·0	8		Q
556·1*	2	4, 2	T	411·2	1	2, 2	T
549·8*	4		Q, R, S	407·2	1		S
493·8*	3	5, 3	T	404·2	2		R
487·5*	6		Q, R, S	402·8	2		Q
430·9*	3	6, 4	T	13871·9	4	0, 1	T
424·2*	6		Q, R, S	866·7	4		S
368·4*	3	7, 5	T	863·4	10		R
361·5*	6		Q, R, S	862·2	10		Q
297·3*	2	8, 6	T	829·8	5	1, 2	T
290·6*	4		Q, R, S	824·3	5		S
169·2*	1	10, 8	Q, R, S	820·9	10		R
113·5*	0	11, 9	T	819·8	10		Q
106·0*	1		Q, R, S	787·2	4	2, 3	T
097·3	4	1, 0	T	781·4	4		S
092·7	4		S	777·9	8		R
091·0	10		R	776·9	8		Q
089·9	10		Q	743·8	3	3, 4	T
042·2	5	2, 1	T	737·8	3		S
037·2	5		S	734·5	6		R
035·5	10		R	733·5	6		Q
034·5	10		Q	699·9	2	4, 5	T
14986·8	4	3, 2	T	693·9	2		S
981·5	4		S	691·0	4		R
978·9	8		R, Q	690·3†	4		Q
930·7	3	4, 3	T				
925·5	3		S				
922·5	6		R, Q				
875·0	2	5, 4	T				
869·0	2		S				
867·2	4		R, Q				

* Measured on prism plates only.

† The (5, 6) and (6, 7) bands are probably present but the heads are too confused for measurement.

A list of wave numbers and intensities of the observed heads with vibrational quantum number assignments is given in table 1. On the negatives and in the reproduction the two heads of longest wavelength in each band seem to have the same intensity. Since the two heads overlap somewhat because of their small wavelength separation, 0·6 Å, the longest wavelength head may in reality be weaker than the appearance would suggest. The mean of the wave numbers of the two longest wavelength heads measured on the grating is represented with a mean error of 0·5 K by the formula

$$v=14527{\cdot}7+595{\cdot}4(v'+\tfrac{1}{2})-3{\cdot}15(v'+\tfrac{1}{2})^2-645{\cdot}4(v''+\tfrac{1}{2})+3{\cdot}2(v''+\tfrac{1}{2})^2.$$

Rochester and Olsson (1939) have observed a system of single headed bands of MnF in the region λ 2380-2460 Å the vibrational constants of which are $\omega_e'=637{\cdot}2$ K, $x_e'\omega_e'=4{\cdot}46$ K, $\omega_e''=618{\cdot}8$ K, $x_e''\omega_e''=3{\cdot}01$ K. Though the values of the constants of the initial state of the ultra-violet bands are fairly close to the values of the constants of the final state of the red bands it seems certain that the two systems do not share one state in common.

§ 3. BANDS OF MnBr

The bands observed for MnBr lie between λ 6216 and λ 6285 Å. Under low dispersion there seem to be two double headed bands separated by 63 K degraded to shorter wavelengths. The higher dispersion of the grating shows that each 'band' is a close sequence of double headed bands, the appearance of which can be judged from the reproduction in figure 1 (*e*). In the long-wave sequence seven weak and eleven strong heads can be distinguished and the separation of corresponding pairs of heads is about 22 K. In the short-wave sequence six weak and eleven strong heads can be identified and the separation of pairs of heads is about 15 K. The intensity difference between weak and strong heads is more marked in the long-wave sequence. The wave numbers derived from measurements on first order grating plates and the intensities of the heads are given in table 2.

Table 2. Band Heads of the Red System of MnBr

Vacuum wave number (K)	*I*	Classification		Vacuum wave number (K)	*I*	Classification	
15905·5	2	0, 0	N	15975·5	6	0, 0	O
926·2	8		P	989·5	10		Q
907·6	2	1, 1	N	977·6	4	1, 1	O
928·5	6		P	991·9	7		Q
909·3	2	2, 2	N	979·6	4	2, 2	O
930·8	4		P	994·1	6		Q
911·1	2	3, 3	N	981·3	3	3, 3	O
932·9	3		P	996·1	5		Q
912·7	1	4, 4	N	983·1	2	4, 4	O
934·8	2		P	998·0	4		Q
914·2	1	5, 5	N	984·5	2	5, 5	O
936·6	2		P	999·7	3		Q
915·4	0	6, 6	N	985·7	0	6, 6	O
938·1	2		P	16001·2	2		Q
939·5	1	7, 7	P	002·6	1	7, 7	Q
940·8	1	8, 8	P	003·7	0	8, 8	Q
941·8	1	9, 9	P	004·8	0	9, 9	Q
942·8	0	10, 10	P				

The absence of an isotope effect suggests that each group of heads is an independent sequence of double-headed bands with $\Delta v=0$. On strongly exposed plates two very weak additional double maxima can be observed though no measurements are possible. The approximate wave numbers of the long-wave limits of these intensity maxima are

15655 K	16200 K
15716 K	16264 K

It seems that the first pair of maxima separated by 61 K are the (0,1) band and the second pair separated by 64 K the (1,0) band of the system. If these identifications are correct $\omega'=275$ K and $\omega''=272$ K, values which seem reasonable for MnBr.

Three additional weak heads have been observed in MnBr degraded to shorter wavelengths the wave numbers and intensities of which are

16375·0 (2) (276·8) 16098·2 (1) (268·0) 15830·2 (0).

These bands may be the (0,0), (0,1) and (0,2) bands of an MnBr system the final state of which is the same as the initial or final state of the main system. The heads seem to have a close complex structure but unfortunately the strongest head is overlapped by atomic lines and a more detailed description is not possible. A reproduction of the 16098 K band is shown in figure 1 (*d*).

§ 4. Discussion of MnBr Bands

If the two MnBr sequences are independent singlet systems with P and Q heads, the equality of the vibrational constants for the two systems in both the initial and final states implies near equality of the rotational constants and approximately equal separations of corresponding heads in the two sequences and approximately the same intensity ratio of P and Q heads. In fact there is a considerable difference in both the separation and intensity ratio of the heads in the two sequences.

It seems probable that the two sequences together constitute a transition of the type $0^{\pm}-{}^5\Sigma$. Since this appears to be the first example recorded of this type of transition a diagram showing the branches is given in figure 2. For a band degraded to short wavelengths $0^{+}-{}^5\Sigma^{+}$ gives an N form P branch forming a head and three P form P,Q and R branches which, when the fine structure of the ${}^5\Sigma$ state is unresolved, will give a single head approximately three times as strong as the N head. The transition $0^{-}-{}^5\Sigma^{+}$ gives O form R and Q branches

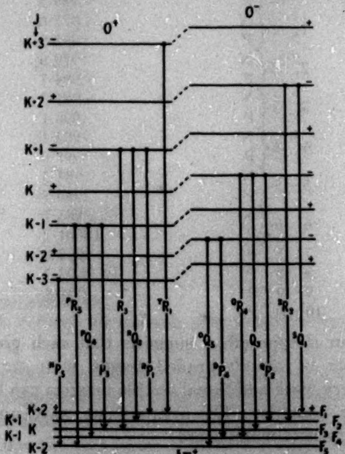

Figure 2.

forming one head and Q form P, Q and R branches forming a second head with an approximate intensity ratio of two to three. The separation of the N and P heads should be greater than that of the O and Q heads.

In conformity with these considerations the long wave sequence with the greater head separation and the greater intensity difference is assigned to the $O^+–{}^5\Sigma^-$ transition and the short wave sequence with the smaller head separation and small intensity difference to the $O^-–{}^5\Sigma^+$ transition. An inspection of the negatives suggests that the overall intensity of the $O^+–{}^5\Sigma^+$ transition may be somewhat greater than the intensity of the $O^-–{}^5\Sigma^+$ transition. The heads are identified in table 2 on the assumption that our interpretation is correct.

The ground state of MnBr is a $^7\Sigma$ state and the existence of a stable $^5\Sigma$ state is probable on general grounds. A Σ state with multiplicity other than five would not explain the observed appearance of the bands. A $^7\Sigma$ state would result in N and P heads in one component but M, O, Q heads in the other. A $^3\Sigma$ state would give a P head and O and Q heads.

§ 5. Discussion of MnF Bands

The spacing and intensities of the heads in the ten bands for which four heads have been measured are unusual and seem to preclude an interpretation of the system in terms of a transition like $^2\Pi–{}^2\Sigma$ or $^3\Pi–{}^3\Sigma$ with the Π state approximating to case *b*. The former interpretation moreover would require the emitter to be MnF$^+$ and it seems unlikely that this is the case as in preliminary experiments the bands were obtained in the heated positive column of a discharge tube with the same intensity relative to the ultra-violet bands as in the hollow cathode discharge.

If the heads, in order of increasing wavelength, are interpreted as T, S, R and Q heads the average separations are T–Q = 8·9 K, S–Q = 3·8 K, R–Q = 1·05 K, which are of the correct relative order of magnitude. Accordingly the system could arise from a transition like $^3\Pi_0–{}^3\Sigma$, $^5\Pi_{-1}–{}^5\Sigma$, $^5\Pi_0–{}^5\Sigma$. However, the T, S and R heads, particularly the T and S heads are anomalously intense relative to the Q head and a further difficulty is the absence of the bands arising from transitions from the other components of the Π state to the Σ state.

It seems reasonable to assume that the fluoride bands are the analogue of the bromide bands with a small separation between the O^+ and O^- states. As the bands are degraded to long wavelengths the T, S, R and Q branches form heads, the T and R heads belonging to $O^+–{}^5\Sigma^+$ and the S and Q heads to $O^-–{}^5\Sigma^+$.

The fact that the T and S heads are equally strong constitutes a difficulty. It is possible that the transition involving the O^+ state is more probable than that involving O^- causing the T and S heads to have approximately equal intensities. In this event the R head should be more intense than the Q head and as stated earlier this may indeed be the case. The identification of the heads is given in table 1.

References

Bacher, J., 1948, *Helv. Phys. Acta*, **21**, 379.
Hayes, W., and Nevin, T. E., 1955, *Proc. R. Irish Acad.*, **57**, 15.
Rochester, G. D., and Olsson, E., 1939, *Z. Phys.*, **114**, 495.

The Spectrum of MnBr in the Photographic Infra-red

By W. HAYES
Physics Department, University College, Dublin

Communicated by T. E. Nevin; MS. received 21*st February* 1955

Abstract. High dispersion spectrograms have shown the existence of two new band systems of MnBr in the region λ 8850–9700 Å. The bands in both systems are degraded to longer wavelengths. The shorter wavelength system is double headed and is considered to be the analogue of the Π–Σ system observed in MnCl. The longer wavelength system is single headed and is attributed to a Σ–Σ transition. Both systems show an isotope effect which confirms the vibrational analysis.

---

§ 1. Introduction

A recent investigation of the band spectra of the manganese halides has disclosed the existence of new systems in the photographic infra-red. The spectrum of MnF consists of a single strong sequence extending from λ 8180 Å to λ 8495 Å. The MnCl bands extend from λ 8180 Å to λ 9150 Å and form the two highest frequency components of a Π–Σ transition with a multiplicity at least five. In the $\Delta v = 0$ sequence of the first component the R and Q branches form heads and faint S and T branches are observed running back to shorter waves from the R head of the 0 , 0 band. Weak S and T heads occur in the $\Delta v = \pm 1$ sequences and also in the $\Delta v = 0$ sequence of the second component. A detailed account of the analysis of the spectrum has been given by Hayes and Nevin (1955 b). The present paper describes the extensive band spectrum of MnBr in the region λ 8850 Å to λ 9700 Å. The bands appear to form two separate systems.

§ 2. Description of the Bands

The spectrum was excited in a hollow cathode discharge in the manner described by Hayes and Nevin (1955 a) and photographed in the first order of a 21 ft concave grating at a dispersion of approximately 2·5 Å mm^{-1}. The region λ 8850 Å to λ 9400 Å was photographed on hypersensitized Kodak IIN plates with exposure times of about four hours but the bands between λ 9350 Å and λ 9400 Å were weak. Hypersensitized Kodak IQ plates were used for the region λ 9350 Å–9700 Å with an exposure time of ten hours. To obtain even a weak photograph of the bands between λ 9600 Å and λ 9700 Å it was necessary both to prefog and hypersensitize the plates and to increase the slit width from 0·05 to 0·1 mm. Second and third order iron comparison spectra were used.

The observed spectrum consists of four groups of heads degraded to longer wavelengths. The most intense group, reproduced in figure 1 (*a*), †consists of a close sequence of double-headed bands beginning at λ 9349 Å followed by a sequence of single headed bands beginning at λ 9383·5 Å. The presence of two sequences with different structure suggests the presence of two separate systems. This suggestion is confirmed by an examination of the three remaining groups, the heads in each of which seem also to contain two independent sequences.

---

† Plate.

The sequences of shorter wavelength in each of the groups form a system which can be assigned to a Π–Σ transition. The heads of the $\Delta v = 0$ sequence of the system begin at λ 9349 Å and the four sequences composing the system extend from λ 8878 Å to λ 9639 Å. The longer wavelength sequences form a system which arises from a Σ–Σ transition and extend from λ 8886 Å to λ 9680 Å. The $\Delta v = 0$ sequence of the system begins at λ 9383·5 Å. Very faint diffuse structure which cannot be assigned to either system has been observed in the region λ 9601 Å–9612 Å. The $\Delta v = +1$ sequences of both systems are reproduced in figure 1 (*c*). The heads of the Σ–Σ system are not clear due to lack of contrast.

§ 3. THE Π–Σ SYSTEM

The presence of R and Q heads in this system could be accounted for by a $^1\Pi$–$^1\Sigma$ transition. It was noticed however, on a strongly exposed plate, that what appears to be a weak continuum extends back from the R heads of the $\Delta v = 0$ sequence and fades out at approximately λ 9312 Å. This structure, reproduced in figure 1 (*b*), is probably caused by weak S and T branches of the $\Delta v = 0$ sequence, the lack of resolution being due to the large number of branches. The presence of S and T branches suggests that the bands are the analogue of the higher frequency component of the Π–Σ transition of MnCl. A tendency to case *c* in MnCl was indicated by the weakness of the S and T heads and the absence of these heads in the bromide bands might well be due to a more pronounced tendency to case *c* in MnBr. If this interpretation is correct a very weak second component is expected in the region λ 9700 Å to longer wavelengths. The exposure required to photograph this component would be prohibitively long.

The wave numbers of the observed heads and their classifications are given in table 1. The number of unclassified heads is small and these may be due in some cases to fortuitous line accumulations. The wave numbers of the Q heads of Mn ^{79}Br are given with a mean error 0·7K by the equation

$$\nu = 10682{\cdot}1 + 290{\cdot}4\ (v' + \tfrac{1}{2}) - 0{\cdot}13(v' + \tfrac{1}{2})^2 - 291{\cdot}3(v'' + \tfrac{1}{2}) + 0{\cdot}01(v'' + \tfrac{1}{2})^2.$$

The vibrational constants are nearly equal and this may be correlated with the large head–origin separations and the presence of an intense extensive $\Delta v = 0$ sequence.

The isotope effect arising from ^{79}Br and ^{81}Br has been observed and confirms the vibrational analysis. The isotope shift is calculated from the formula $\Delta\nu = (\rho - 1)\nu_v$ where ν_v is the distance of the Q head from the system origin. The effect of the rotational isotope shift on the positions of the R heads has been neglected. The observed and calculated shifts are given in table 2 and the agreement between them can be regarded as satisfactory.

Columns three and four of table 2 contain the observed isotope shifts for the Q and R heads.

§ 4. THE Σ–Σ SYSTEM

The interpretation of this sytem presents little difficulty. The structure of the bands is simple, each having a single head, and the system can therefore be assigned to a Σ–Σ transition of odd multiplicity. When the multiplicity is greater than one a single head only should occur in each band since the fine structure will not be resolved.

A list of the observed heads and their classification is given in table 3. Few measured heads remain unclassified. The identification of the heads in the $\Delta v = +2$ sequence is difficult due to the weakness of the heads and the presence of atomic lines. The intensity distribution corresponds to a narrow Condon parabola.

The wave numbers of the classified heads of $Mn^{79}Br$ are represented with a mean error 1.1K by the formula

$$\nu = 10667{\cdot}5 + 295{\cdot}6(v'+\tfrac{1}{2}) - 0{\cdot}62(v'+\tfrac{1}{2})^2 - 298{\cdot}8(v''+\tfrac{1}{2}) + 0{\cdot}61(v''+\tfrac{1}{2})^2.$$

The isotope effect is easily recognizable and the satisfactory agreement between the observed and calculated values can be seen from an inspection of table 4.

Table 1. Heads of the Infra-Red Bands of MnBr, II–Σ system

Vacuum wave number (K)	*I*	Classification	Vacuum wave number (K)	*I*	Classification
11261·0	3	3, 1 Q	10693·9	3	0, 0 R
59·0	2	4, 2 Q	93·3	3	1, 1 R
58·2	1	3, 1 Q*	92·5	2	2, 2 R
56·2	2	5, 3 Q. 4, 2 Q*	91·5	2	3, 3 R
55·1	2		90·3	2	4, 4 R
54·2	1	5, 3 Q*	89·0	1	5, 5 R
52·1	1	6, 4 Q	88·4	1	
10989·4	0	1, 0 R	87·9	1	
87·6	0	R*	87·4	A	6, 6 R
86·0	0	2, 1 R	85·6	1	7, 7 R
85·0	1	2, 1 R*. 3, 2 R	83·7	1	8, 8 R
83·4	1	3, 2 R*	82·6 ?	0	
82·8	1	4, 3 R	80·8	3	0, 0 Q
81·2	1	R*	79·9	7	1, 1 Q
80·4	1	5, 4 R	78·5	9	2, 2 Q
78·8	2	R*	76·7	9	3, 3 Q
78·0	2	6, 5 R	74·7	10	4, 4 Q
76·2	3	R*	10391·5	1	4, 5 R*
75·0	1	7, 6 R	93·8	2	R
73·5	2	R*	93·2	2	0, 1 Q*. 5, 6 R
71·9	2	1, 0 Q	91·3	4	0, 1 Q. 1, 2 Q*
71·1	2	8, 7 R	89·7	3	1, 2 Q. 2, 3 Q*
70·3	1	1, 0 Q*. 2, 1 Q	88·1	3	2, 3 Q. 3, 4 Q*
69·5	1	8, 7 R*	87·8 ?	2	
69·1	1	2, 1 Q*	86·6	3	3, 4 Q
68·5	3	3, 2 Q	85·9	5	4, 5 Q*
67·2	4	Q*	84·8	4	Q
66·3	5	4, 3 Q	84·4	4	
64·8	3	Q*	83·6	3	5, 6 Q*
63·5	6	5, 4 Q	82·4	2	Q
62·0	5	Q*	80·9	1	6, 7 Q*
61·2 ?	1		79·4	0	Q
60·6	4	6, 5 Q	77·4	0	7, 8 Q
56·6 ?	3	7, 6 Q	74·4	0	8, 9 Q
55·1	1	Q*			

The heads of the molecule $Mn^{81}Br$ are marked with a star. Doubtful heads are followed by a question mark. The wave number given for the 6, 6 R head is that of an argon line which coincides with the expected head position and it is followed by the letter A in the intensity column.

Table 2. Isotope Effect in the Π–Σ System

v', v''	$\Delta\nu_{\text{calc}}$	$\Delta\nu_{\text{obs}}$(Q)	$\Delta\nu_{\text{obs}}$(R)
3, 1	3·0	2·8	—
4, 2	2·9	2·8	—
5, 3	2·9	2·0 ?	—
1, 0	1·5	1·6	1·8
2, 1	1·5	1·2	1·8
3, 2	1·5	1·5	1·6
5, 4	1·4	1·5	1·6
6, 5	1·4	—	1·8
7, 6	1·4	1·5	1·5
8, 7	1·4	—	1·6
0, 1	1·5	1·9	—
1, 2	1·5	1·6	—
2, 3	1·5	1·6	—
4, 5	1·4	1·1	1·3
5, 6	1·4	1·2	—
6, 7	1·4	1·5	—

Table 3. Heads of the Infra-red Bands of MnBr, Σ–Σ System

Vacuum wave number (K)	I	v', v''	Vacuum wave number (K)	I	v', v''
11250·6	1	2, 0	10957·2 ?	3	1, 0
49·1	1		55·9* ?	3	
47·4*	0	2, 0	53·9	2	2, 1
47·0	Br	3, 1	52·5*	1	
43·7*	2		50·3	4	3, 2
42·9	1	4, 2	49·0*	4	
40·6*	2		47·8	2	
38·1	2	5, 3	46·5	1	4, 3
32·6	1	6, 4	43·7	1	
30·0*	1		42·6	3	5, 4
27·1	1	7, 5	41·3*	3	
23·9*	1		38·3	1	6, 5
22·2	1		37·0*	1	
20·5	1	8, 6	34·1	1	7, 6
18·1*	L		32·8*	1	
13·8	L	9, 7	29·5	1	8, 7
10·0*	1		28·1*	1	
07·7	1	10, 8	25·3	1	9, 8
04·9*	L		23·7*	1	
01·1	1	11, 9	20·6	1	10, 9
11198·9*	2		19·4*	1	
94·1	1	12, 10	16·0	1	11, 10
93·3 ?	2		14·8*	1	
92·1*	Br	12, 10	10665·5	4	0, 0
87·7	2	13, 11	62·0	5	1, 1
85·1*	2		58·2	3	2, 2
81·0	2	14, 12	10371·9*	L	0, 1
78·8*	2		70·1	1	
74·2	2	15, 13	68·3*	1	1, 2
71·7*	2		67·0	1	
67·7	1	16, 14	65·4*	1	2, 3
65·3*	1		63·8	1	

The letter L in the intensity column denotes the presence of an unidentified atomic line at the expected head position. Where this happens the wave number of the line is given. The 3, 1 head of Mn ^{79}Br and the 12, 10 head of Mn ^{81}Br coincide with atomic bromine lines and in these cases also the wave numbers of the lines are given and their presence indicated in the intensity column.

Table 4. Isotope Effect in the Σ–Σ System

v', v''	$\Delta\nu_{calc}$	$\Delta\nu_{obs}$	O–C	v', v''	$\Delta\nu_{calc}$	$\Delta\nu_{obs}$	O–C
2, 0	3·0	3·1	+0·1	16, 14	2·6	2·4	−0·2
3, 1	3·0	3·1	+0·1	1, 0	1·5	1·3	−0·2
4, 2	2·9	2·3	−0·6	2, 1	1·5	1·4	−0·1
6, 4	2·9	2·6	−0·3	3, 2	1·4	1·3	−0·1
7, 5	2·9	3·2	+0·3	5, 4	1·4	1·3	−0·1
8, 6	2·8	2·4	−0·4	6, 5	1·4	1·3	−0·1
9, 7	2·8	3·8	+1·0	7, 6	1·4	1·3	−0·1
10, 8	2·8	2·8	0·0	8, 7	1·3	1·4	+0·1
11, 9	2·7	2·2	−0·5	9, 8	1·3	1·6	+0·3
12, 10	2·7	2·1	−0·6	10, 9	1·3	1·2	−0·1
13, 11	2·7	2·6	−0·1	11, 10	1·3	1·2	−0·1
14, 12	2·6	2·2	−0·4	1, 2	1·5	1·3	−0·2
15, 13	2·6	2·5	−0·1	2, 3	1·5	1·6	+0·1

ACKNOWLEDGMENT

The author wishes to thank Professor T. E. Nevin for his encouragement and his interest in the work.

REFERENCE

HAYES, W., and NEVIN, T. E., 1955 a, *Proc. Roy. Irish Acad.*, **57** 15 1955 b, *Nuovo Cim.*, in the press.

On Lattice Scattering in Homopolar Semiconductors

By J. M. RADCLIFFE
Radar Research Establishment, Malvern, Worcs.

MS. received 2nd February 1955

Abstract. The conductivity of a homopolar semiconductor with an arbitrary band shape is considered. The corresponding Boltzmann equation is solved after making a simplifying assumption about the form of the matrix element of the lattice-scattering potential.

---

§1

OVER a considerable range of temperatures the mobility of electrons in single crystals of fairly pure semiconductors is determined by lattice scattering, rather than by the scattering from defects such as ionized impurities or from dislocations. In this note attention will be restricted to lattice scattering in homopolar crystals. An essentially different theory is required for ionic crystals, in which the scattering is due largely to the polarization associated with optical modes of lattice vibration.

The existing theories of lattice scattering in homopolar semiconductors (Wilson 1953, Seitz 1948, Bardeen and Shockley 1950) give essentially equivalent results. They predict in particular that the drift mobility μ_D should vary with temperature as $T^{-3/2}$, that if a Hall mobility μ_H is defined by $\mu_H = R\sigma$ then $\mu_H = (3\pi/8)\mu_D$, and that there should be an isotropic transverse magneto-resistance but no longitudinal magneto-resistance. Now the results of recent experiments are not always in accord with these theories. For instance, n-type germanium exhibits longitudinal magneto-resistance and an anisotropic transverse magneto-resistance (Pearson and Suhl 1951). Also Morin (1954) finds that the mobility of holes in germanium varies as $T^{-2.3}$ above 100°K.

It is clear that the behaviour of electrons in conduction phenomena must depend on the precise form of the scattering potential. It must also depend on the structure of the conduction band and in particular on the shape of its branches. The theories mentioned earlier employ the scattering potential given by the Bloch 'deformable atom' hypothesis and the simple parabolic band shape $E(\mathbf{k}) = \hbar^2k^2/2m$. This paper pursues some consequences of assuming a non-degenerate band of arbitrary shape whilst retaining the form of the scattering matrix element used by previous workers.

§2

The Boltzmann equation for the stationary states of a system subject to an electric field is

$$-(e\mathbf{F}/\hbar) . \nabla_{\mathbf{k}} f = [\partial f/\partial t]_{\text{collisions}} \qquad \ldots\ldots(1)$$

where f is the electron distribution function and $\mathbf{F}$ the applied electric field. If $W(\mathbf{k}\,;\mathbf{k}')$ is the probability per unit time that an electron make a transition from the state $\mathbf{k}$ to the state $\mathbf{k}'$, then

$$[\partial f/\partial t]_{\text{collisions}} = \int d^3\mathbf{k}'[W(\mathbf{k}'\,;\mathbf{k})f(\mathbf{k}')\{1-f(\mathbf{k})\} - W(\mathbf{k}\,;\mathbf{k}')f(\mathbf{k})\{1-f(\mathbf{k}')\}]. \qquad \ldots.(2)$$

At practical field strengths, the electron distribution f is never far from the equilibrium one f_0. It is thus justifiable to write

$$f(\mathbf{k}) = f_0(\mathbf{k}) + \Phi(\mathbf{k})(\partial f_0(\mathbf{k})/\partial E_{\mathbf{k}}), \qquad \ldots\ldots(3)$$

and neglect terms $O(\Phi^2)$ on the right-hand side of expression (2). As explained in the introduction, the usual form for the matrix element P of the interaction between electrons and the lattice vibrations will be used. The matrix element for a transition from a state of crystal momentum $h\mathbf{k}$ to one of momentum $h(\mathbf{k} \pm \mathbf{q})$, by absorption or emission respectively of a phonon of wavenumber $\mathbf{q}$ in a crystal of volume V is (Seitz 1948)

$$P(\mathbf{k} \pm \mathbf{q}\,;\mathbf{k}) = \mp \frac{i2C}{3(n_0 V)^{1/2}} \boldsymbol{\epsilon}\,.\,\mathbf{q} \left(\frac{\hbar}{2Mu\mathrm{q}}\right)^{1/2} \begin{cases} n_{\mathbf{q}}{}^{1/2} \\ (n_{\mathbf{q}}+1)^{1/2}. \end{cases} \qquad \ldots\ldots(4)$$

Here n_0 is the density of unit cells in the lattice, M is the mass in a unit cell, C is a parameter having the dimension of energy which measures the strength of the electron-lattice interaction, $\boldsymbol{\epsilon}$ is the polarization vector of the phonon, and u is the velocity of sound in the crystal. $n_{\mathbf{q}}$ is the number of phonons of wavenumber $\mathbf{q}$ in the field, and is taken to be that given by the equilibrium Bose–Einstein distribution. The physical content of equation (4) is that the electrons interact only with longitudinal waves, that is with waves which are associated with a density modulation in the crystal. After applying (4) to obtain $W(\mathbf{k}\,;\mathbf{k}')$ and using the definition (3), equation (2) becomes

$$\begin{aligned}{}[\partial f/\partial t]_{\text{collisions}} = (C^2/9\pi M n_0 \boldsymbol{k} T)\int & d^3q(q^2/uq) \\ & \times n_{\mathbf{q}}[f_0(\mathbf{k})\{1-f_0(\mathbf{k}+\mathbf{q})\}\delta(E_{\mathbf{k}}-E_{\mathbf{k}+\mathbf{q}}+h\nu_{\mathbf{q}}) \\ & +f_0(\mathbf{k}+\mathbf{q})(1-f_0(\mathbf{k})]\delta(E_{\mathbf{k}}-E_{\mathbf{k}+\mathbf{q}}-h\nu_{\mathbf{q}})\}[\Phi(\mathbf{k}+\mathbf{q})-\Phi(\mathbf{k})]. \end{aligned} \qquad \ldots\ldots(5)$$

At temperatures above about 1°K, that is at all temperatures for which lattice scattering is likely to be the dominant resistive mechanism, equation (5) can be reduced to

$$[\partial f/\partial t]_{\text{collisions}} = [C^2 f_0(\mathbf{k})/9\pi^2\hbar u^2 M n_0]\int d^3q\,\delta(E_{\mathbf{k}}-E_{\mathbf{k}+\mathbf{q}})[\Phi(\mathbf{k}+\mathbf{q})-\Phi(\mathbf{k})] \qquad \ldots\ldots(6)$$

for then the acoustic modes of long wavelength with which the electrons can interact have energies small compared with the mean thermal energy of the electron distribution, $3\boldsymbol{k}T/2$. Finally, neglecting terms $O(F^2)$ on the left-hand side, equation (1) becomes

$$-(e\mathbf{F}/\hbar)\,.\,\nabla_{\mathbf{k}} f_0 = [C^2 f_0(\mathbf{k})/9\pi^2\hbar u^2 M n_0]\int d^3q\,\delta(E_{\mathbf{k}}-E_{\mathbf{k}+\mathbf{q}})[\Phi(\mathbf{k}+\mathbf{q})-\Phi(\mathbf{k})]. \qquad \ldots.(7)$$

It will be shown now that this equation has a solution of the form

$$\Phi(\mathbf{k}) = \mathbf{g}(E_{\mathbf{k}})\,.\,\nabla_{\mathbf{k}} E_{\mathbf{k}}. \qquad \ldots\ldots(8)$$

Consider the integral I on the right-hand side of (7). By equation (8)

$$\begin{aligned} I &= \int d^3q\,\delta(E_{\mathbf{k}}-E_{\mathbf{k}+\mathbf{q}})[\Phi(\mathbf{k}+\mathbf{q})-\Phi(\mathbf{k})] \\ &= \int d^3q\,\delta(E_{\mathbf{k}}-E_{\mathbf{k}+\mathbf{q}}) \\ &\qquad \times [\mathbf{g}(E_{\mathbf{k}+\mathbf{q}})\,.\,\nabla_{\mathbf{k}+\mathbf{q}} E_{\mathbf{k}+\mathbf{q}} - \mathbf{g}(E_{\mathbf{k}})\,.\,\nabla_{\mathbf{k}} E_{\mathbf{k}}]. \end{aligned} \qquad \ldots\ldots(9)$$

Because of the δ-function in the integrand

$$\begin{aligned} I &= -\,\mathbf{g}(E_{\mathbf{k}})\,.\int d^3q\,\delta(E_{\mathbf{k}}-E_{\mathbf{k}+\mathbf{q}})\nabla_{\mathbf{k}}(E_{\mathbf{k}}-E_{\mathbf{k}+\mathbf{q}}) \\ &= -\,\mathbf{g}(E_{\mathbf{k}})\,.\int d^3q\,\nabla_{\mathbf{k}}\theta[E_{\mathbf{k}}-E_{\mathbf{k}+\mathbf{q}}]. \end{aligned} \qquad \ldots\ldots(10)$$

Here θ is a unit step function which is sufficiently defined by

$$\begin{aligned}\theta(x) &= (\alpha+1), \qquad x>0\\ &= \alpha, \qquad\quad\;\; x<0 \qquad\qquad \ldots\ldots(11)\end{aligned}$$

where α is arbitrary. The integral extends in principle over the whole spectrum of phonons in a volume Ω of $\mathbf{q}$-space which is bounded by some surface S_Ω. On the Debye model Ω is the sphere of radius $q_0 = \boldsymbol{k}\theta_D/hu$. In fact only a small part of the spectrum contributes to I. Now the integral

$$J = \int_\Omega d^3q\,\theta[E_\mathbf{k} - E_{\mathbf{k}+\mathbf{q}}] \qquad \ldots\ldots(12)$$

has an obvious geometrical interpretation if all points $\mathbf{k}'$ on $E(\mathbf{k}') = E'$ lie within the surface $E(\mathbf{k}) = E$ when $E' < E$, a condition which is always satisfied near a minimum in the energy surface. Then

$$\begin{aligned}J &= (\alpha+1)V[E_\mathbf{k}] + \alpha\{\Omega - V[E_\mathbf{k}]\}\\ &= V[E_\mathbf{k}] + \alpha\Omega \qquad\qquad \ldots\ldots(13)\end{aligned}$$

where $V[E_\mathbf{k}]$ denotes the volume of $\mathbf{k}$-space enclosed by the surface $E = E(\mathbf{k})$.

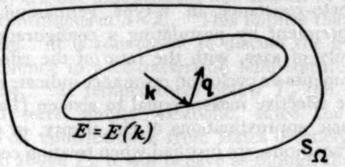

Thus,

$$\begin{aligned}I &= -\mathbf{g}(E_\mathbf{k})\,.\,\nabla_\mathbf{k} V[E_\mathbf{k}]\\ &= -\mathbf{g}(E_\mathbf{k})\,.\,\nabla_\mathbf{k} E_\mathbf{k}(\partial V[E_\mathbf{k}]/\partial E_\mathbf{k}). \qquad \ldots\ldots(14)\end{aligned}$$

This shows that equation (7) has a solution of the form (8), with

$$\mathbf{g} = \frac{e\mathbf{F}}{\hbar}\,\frac{9\pi^2\hbar u^2 M n_0}{C^2\boldsymbol{k}T}\bigg/\frac{\partial V[E]}{\partial E}. \qquad \ldots\ldots(15)$$

The right-hand side of (15) is a function of $\mathbf{k}$ only through $E(\mathbf{k})$, so that the theory is self-consistent and provides a solution to equation (1). If the relaxation time τ is defined in the usual way by

$$[\partial f/\partial t]_{\text{collisions}} = (f - f_0)/\tau$$

then

$$1/\tau(E) = (C^2\boldsymbol{k}T/9\pi^2\hbar u^2 M n_0)(\partial V[E]/\partial E). \qquad \ldots\ldots(16)$$

The use of this equation can be illustrated by applying it to the band $E(\mathbf{k}) = \hbar^2\mathbf{k}^2/2m^*$. The volume within the surface $E = E(\mathbf{k})$ is then $V[E_\mathbf{k}]$, where $V[E_\mathbf{k}] = 4\pi k^3/3 = 4\pi(2m^*E)^{3/2}/3\hbar^3$. Substitution in equation (16) yields the relaxation time obtained by Wilson and by Seitz, in the form

$$1/\tau = (4/9\pi)(C^2\boldsymbol{k}T/\hbar^3u^2n_0)(m^*/M)(2m^*E/\hbar^2)^{1/2}. \qquad \ldots\ldots(17)$$

It will be clear that the solution to the Boltzmann equation for a system subject to both electric and magnetic fields will not have the form implied by equation (8) in general. However, the solution does still have this simple form in some particular cases.

§3

In order to explain the anisotropic properties of n-type germanium, non-spherical energy surfaces must be introduced into the theory. The simplest non-spherical surface is an ellipsoid. If such surfaces are postulated, then overall cubic symmetry requires that there be at least six ellipsoids properly distributed about the Brillouin zone. The theory outlined above yields a solution to the Boltzmann equation for this model, if inter-ellipsoid transitions are neglected. It is one of the particular cases for which magnetic effects also can be treated. The relaxation time is determined by $\partial V[E_{\mathbf{k}}]/\partial E_{\mathbf{k}}$. But

$$V[E_{\mathbf{k}}]=(4\pi/3)(2\mu E_{\mathbf{k}}/\hbar^2)^{3/2},$$

where $\mu^3=m_1m_2m_3$, the m_i being the effective masses along the principal axes of the ellipsoid. Thus by (16)

$$1/\tau(E)=(4/9\pi)(C^2\boldsymbol{k}T/\hbar^3u^2Mn_0)(2\mu^3E_{\mathbf{k}}/\hbar^2)^{1/2}. \qquad \ldots\ldots(18)$$

This expression has also been obtained by Howarth (1953) and by Shibuya (1954), using methods specific to ellipsoidal energy surfaces. It is the form for the relaxation time which is assumed by Abeles and Meiboom (1954) in their treatment of magneto-resistance in n-type germanium. They obtain fair agreement with experiment by postulating a configuration of eight ellipsoids along the (111) family of axes, with the ratio of the effective masses equal to twenty. The experiments on cyclotron resonance indicate the same configuration with the ratio of the effective masses equal to sixteen (Lax *et al.* 1954). This suggests that the basic approximations of the theory, in particular the neglect of inter-ellipsoidal transitions, are justified when treating conduction phenomena. It is however likely that such inter-ellipsoidal transitions play an important part in the mechanism of infra-red absorption by free carriers.

§4

Another possible application of the theory is to bands which are spherically symmetrical but have an arbitrary profile. For these bands $\partial V[E_{\mathbf{k}}]/\partial E_{\mathbf{k}}=4\pi k^2/E'$, where $E'=dE(k)/dk$. Consequently the relaxation time is given by

$$1/\tau=(4/9\pi)(C^2\boldsymbol{k}T/\hbar u^2Mn_0)(\mathbf{k}^2/E'). \qquad \ldots\ldots(19)$$

On the basis of this formula for τ, formal expressions for such quantities as the drift mobility and the Hall constant can be derived. They cannot be evaluated analytically in general, and in order to understand the implications of equation (19) it is useful to consider the family of band shapes given by $E\sim k^n$. All the integrals involved may then be readily evaluated. It is found that the drift mobility would vary with temperature according to an equation of the form

$$\mu_{\mathrm{D}}(T)=\mu_{\mathrm{D}}(T_0)(T_0/T)^{(5/n)-1} \qquad \ldots\ldots(20)$$

and that the ratio of the Hall mobility μ_{H} to the drift mobility μ_{D} would be

$$\mu_{\mathrm{H}}/\mu_{\mathrm{D}}=3\Gamma(5-7/n)\Gamma(3/n)/n\{\Gamma(3-2/n)\}^2. \qquad \ldots\ldots(21)$$

Now the drift mobility of holes in germanium varies with temperature as $T^{-2\cdot3}$ above about 100°K (Morin 1954), rather than as $T^{-1\cdot5}$ as would be expected from Wilson's and Seitz' theories. The same is true in silicon above 150°K (Prince 1954). Enz (1954) has attempted to explain this behaviour by including multiple-phonon processes in the electron-lattice interaction. However, a detailed treatment of the two-phonon interaction gives a mobility dependence like $T^{-\alpha}$, with α not greater than 2. Adams and Dumke (1954) have proposed a phenomenological theory in which the mean free path is not constant, as in Wilson's and Seitz' theories, but of the form

$$l = l_0/(1+qE^p).$$

Calculations were done for $p=1, 2, 3$, the values of q being chosen to fit the observed ratio of Hall to drift mobility at room temperature. The mobility was found to vary as $T^{-1\cdot9}$ or $T^{-2\cdot0}$ in all cases.

According to equation (20) the observed variation of the mobility with temperature can be associated with a band of the simple type $E \sim k^n$ by taking $n=3/2$. This model can be refined slightly by taking account of the fact that near the origin the energy must be quadratic in the momentum k. Morin's data can be fitted quite well by a model in which

$$\begin{aligned} E(k) &= -\hbar^2(ka)^2/2m_1a^2, & k<k_0 \\ &= -\hbar^2(ka)^{3/2}/2m_2a^2+E_0, & k>k_0 \qquad \ldots\ldots(22) \end{aligned}$$

where a is some convenient length. This band can be given an exact treatment. The parameters in (22) are not independent but chosen so that the energy and its first derivative are continuous at $k=k_0$. This implies that the relaxation time is also continuous there. It is convenient to discuss the qualitative behaviour of this system by reference to a characteristic temperature T_c defined by the equation $\boldsymbol{k}T_c=\hbar^2k_0^2/2m_1$. At temperatures below T_c the system will behave as though the band were simply parabolic, since the Boltzmann factor $\exp(-E(\mathbf{k})/\boldsymbol{k}T)$ cuts off contributions from states of energy greater than $\boldsymbol{k}T$. At temperatures much above T_c, it will behave as though the band were entirely of the form $E\sim k^{3/2}$. The interesting transition region must be treated numerically. It is possible to obtain a good fit to Morin's data on the temperature dependence of the drift mobility in germanium by choosing the characteristic temperature T_c to be 250°K. It is also possible in fact to obtain a fit with Morin's values for the ratio of Hall to drift mobilities using the same parameters. However, this latter fit cannot be used to support the present model until it is clearly established that the magnetic fields used in the experiments were sufficiently small to justify Morin's employment of a weak-field theory to analyse the experimental data.

Since the mobility of holes in silicon is found to vary as $T^{-2\cdot3}$ down to 150°K, this theory requires that the valence band of both germanium and silicon should begin to deviate from a parabolic profile quite near the origin. Every band must eventually depart in this sense from a parabolic profile in order that the condition $\mathrm{grad}_{\mathbf{k}}E=0$ be satisfied on the zone boundary. A deviation so near the origin fits in well with the idea of a splitting of the valence band due to spin–orbit forces (Elliott 1954). An effect of the kind observed, namely hole mobility varying as T^{-p}, with $p>3/2$, would certainly be expected from band shape considerations in silicon, for which the spin–orbit splitting is estimated to be of the order of only 0·05 ev.

§ 5

It has been shown in § 4 that it is possible to understand the temperature variation of the mobility of holes in germanium and silicon by an application of the theory given in § 2 for a general band shape. The fitting was done by evaluating the formal general expression for the mobility for a particular family of band shapes and then comparing the experimental data with the results of this calculation. This approach was necessary because one of the general problems in this field has not been solved yet. Suppose that the relaxation time as a function of the crystal momentum **k** and the temperature T is known for an arbitrary band shape either theoretically or semi-empirically. Formal expressions for transport phenomena can then be written down. The problem is to carry out a general inversion so as to obtain the function $E(\mathbf{k})$ from a knowledge of the temperature dependence of these various transport properties of a crystal.

ACKNOWLEDGMENTS

I wish to thank my colleagues at the Radar Research Establishment for discussions and advice. Acknowledgment is made to the Chief Scientist, Ministry of Supply, and the Controller, H.M. Stationery Office, for permission to publish this paper.

REFERENCES

ABELES, B., and MEIBOOM, S., 1954, *Phys. Rev.*, **95**, 31.
ADAMS, E. N., II, and DUMKE, W., 1954, *Notes on the Energy Band Structure of Germanium and Silicon* (Chicago : Midway Laboratories Report).
BARDEEN, J., and SHOCKLEY, W., 1950, *Phys. Rev.*, **80**, 72.
ELLIOTT, R. J., 1954, *Phys. Rev.*, **96**, 256, 280.
ENZ, CH., 1954, *Proceedings of the Amsterdam Conference.*
HOWARTH, D. J., 1953, *Thesis*, University of London.
LAX, B., *et al.*, 1954, *Phys. Rev.*, **93**, 1418.
MORIN, F. J., 1954, *Phys. Rev.*, **93**, 62.
PEARSON, G., and SUHL, H., 1951, *Phys. Rev.*, **83**, 768.
PRINCE, M. B., 1954, *Phys. Rev.*, **93**, 1204.
SEITZ, F., 1948, *Phys. Rev.*, **73**, 547.
SHIBUYA, M., 1954, *Phys. Rev.*, **95**, 1385.
WILSON, A. H., 1953, *Theory of Metals* (Cambridge : University Press).

Electron Capture in the Decay of Sodium 22

By R. A. ALLEN[†], W. E. BURCHAM, K. F. CHACKETT,
G. L. MUNDAY and P. REASBECK
Department of Physics, University of Birmingham
† Atomic Energy Research Establishment, Harwell, Berks.

MS. received 3rd *March* 1955

Abstract. The fraction of electron capture transitions in the decay of ^{22}Na has been found by comparing the rate of evolution of ^{22}Ne from a source of ^{22}Na with the rate of emission of positrons. The ratio of electron capture to positron transitions is found to be $0{\cdot}122 \pm 0{\cdot}010$; a possible systematic error in the ^{22}Ne determination would increase this figure.

§ 1. INTRODUCTION

The decay scheme of ^{22}Na is shown in figure 1 (Endt and Kluyver 1954); there is, in addition to the well-known positron emission to the first excited state of ^{22}Ne, an alternative K-capture branch. The most recent measurements of the ratio P_K/P_+ of K capture to positron emission for the main transition are listed below.

Authors	Fraction of electron capture in ^{22}Na decay	Ratio P_K/P_+
Sherr and Miller 1954	$0{\cdot}099 \pm 0{\cdot}006$	$0{\cdot}110 \pm 0{\cdot}006$
Kreger 1954	$0{\cdot}110 \pm 0{\cdot}009$	$0{\cdot}123 \pm 0{\cdot}010$
Charpak 1955	$0{\cdot}061 \pm 0{\cdot}009$	$0{\cdot}065 \pm 0{\cdot}009$

In the first two determinations the number of positrons or of annihilation quanta emitted per disintegration was compared by counting methods with the number of 1·28 Mev quanta.

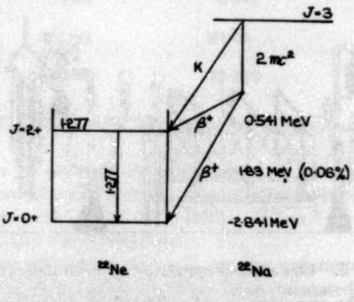

Figure 1. Decay scheme of ^{22}Na.

The K-capture process results in the formation of a ^{22}Ne atom with a K-shell vacancy, the filling of which leads to the emission of a K quantum or of Auger electrons. The K capture to positron ratio for the ^{22}Na disintegration may therefore also be found by comparing the number of positrons from a given source with the number of Auger electrons (correcting for fluorescence yield) or with the number of ^{22}Ne atoms formed (Alvarez 1936). The former method was used essentially by Charpak (1955); the latter method is described in the present paper.

The theoretical value for the ratio P_K/P_+ for ^{22}Na is 0·111 (Zweifel 1954) which is in agreement with the results of Sherr and Miller and of Kreger. The present result does not improve on the accuracy of this work but seems worth reporting since it incorporates at least in part an independent method of observation.

§ 2. EXPERIMENTAL METHOD

The production of ^{22}Ne by decay of ^{22}Na was first detected spectrographically by Weltin (1943). The present experiment used the gas analytical techniques developed by Paneth and his collaborators (Paneth, Chackett, Reasbeck and Wilson 1953) for measurement of the rate of evolution of neon from a ^{22}Na source. The rate of emission of positrons from an accurately known fraction of the same source was found by direct counting in a 4π Geiger counter.

A source of about 1·5 mc of ^{22}Na, made by bombarding magnesium metal for about 600 microampere hours with 19 MEV deuterons in the 60 in. Nuffield cyclotron, was used for the experiment.

§ 3. DETERMINATION OF RATE OF EVOLUTION OF NEON

The bombarded magnesium metal was dissolved in dilute sulphuric acid in a 500 ml. soda glass flask and 101·5 mg of sodium sulphate were added to the solution in order to prevent significant exchange of the radioactive sodium ions with positive ions in the glass. Soda glass was chosen as material for the flask since it is known to be almost impervious to helium and neon. The virtual absence of helium in the neon eventually measured was therefore a clear indication that no leakage of atmospheric air could have occurred during the experiment.

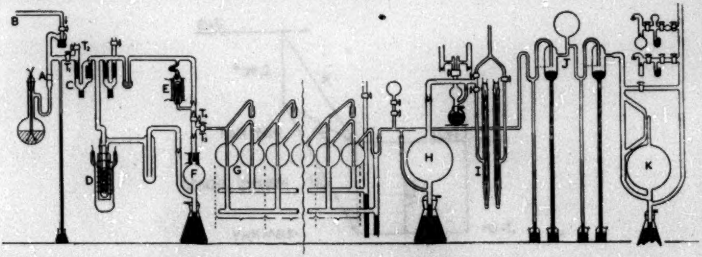

Figure 2. Gas analysis apparatus for neon determination.

Figure 2 shows the apparatus used. The flask containing the active solution was attached at A. It was fitted with a ground stopper carrying two platinum electrodes dipping into the liquid. The flask was evacuated via the stopcocks T_1 and T_2 with the non-return valve C closed, while electrolysing current was being passed, so that the solution was effectively freed from all initially dissolved gas.

After the lapse of a measured time (3 days, 6 days and 40 days in the three runs) T_1 was opened and the accumulated gas was swept through the non-return valve C by means of electrolytic gas together with pure oxygen from the reservoir B into the section of the apparatus between C and T_3. In this part of the system all hydrogen in the gas mixture was removed by combustion with excess oxygen in the heated palladium tube D, the gas being circulated by the reciprocating pump E. The remaining gas was then compressed using the Toepler pump F into the first stage of a fractionating system G via T_3, the cock T_4 being closed. The fractionating system comprised fifteen units arranged in tandem each consisting of a mercury displacement pump in contact with a charcoal tube cooled to -192°c. Careful preliminary work with pure helium and neon, and also mixtures of the two, proved that 99·3% of any helium and 0·7% of any neon put into the column were delivered into the receiving flask H after 36 strokes of the displacement pumps. Thereafter the remaining neon was delivered in a further 19 strokes under standard operating conditions.

The purified neon so obtained was compressed by raising the mercury in H and admitted to a Pirani gauge I. This formed one arm of a Wheatstone network, and the out-of-balance current caused by the admission of gas to the gauge was measured with a sensitive mirror galvanometer. On opening the gauge to vacuum, a deflection in the reverse sense was noted. The mean of the two deflections was taken as a measure of the volume of gas present. Calibrations were effected using pure helium and neon measured in a standard McLeod gauge K and accurately subdivided by the pipetting system J.

The results from the three runs are summarized below. The neon volumes are corrected for the very small amount collected in the helium fraction. The latter was in all cases so small that no appreciable correction has to be made for air leakage.

	Date	Collection time (hours)	Vol. of Ne ($\mathrm{cm}^3 \times 10^{-7}$)	Rate of evolution of neon ($\mathrm{cm}^3\ \mathrm{h}^{-1} \times 10^{-9}$)†
Run 1	27.4.54–30.4.54	73·66	6·971	8·443
Run 2	30.4.54–9.6.54	961·33	89·06	8·424
Run 3	9.6.54–15.6.54	142·48	13·230	8·559

† Corrected to 1.10.54, assuming ^{22}Na half-life = 948 days.

These results are in satisfactory agreement and when combined with equal weight, lead to the conclusion that the rate of evolution of ^{22}Ne from the ^{22}Na source on 1st October 1954 was $8{\cdot}475 \pm 0{\cdot}06 \times 10^{-9}\ \mathrm{cm}^3$ per hour, corresponding to a source strength of $1{\cdot}720 \pm 0{\cdot}012$ mc.

The error in this estimation depends on the volumetric calibration of the McLeod gauge and pipetting system and has been estimated at 0·6%. A systematic error may arise from the fact that the ^{22}Ne isotope only was measured whereas the natural mixture of neon isotopes was used for calibrating the gauges. The sensitivity of the Pirani gauge for the isotopes of neon might be expected to vary as $M^{-1/2}$ so that the sensitivity for ordinary neon would be 1·042 times that for ^{22}Ne. It was not possible to check this factor directly at the time of the experiment but comparison of the sensitivities for helium and neon gave a ratio of only 1·4 instead of the expected 2·25. This suggests that the sensitivity ratio for the neon isotopes is nearer to unity than to the predicted value. In the absence of direct information no correction for the mass difference 20–22 has been made and this is the major uncertainty in the experiment.

§ 4. Determination of Rate of Emission of Positrons

The active solution used in the neon determination was made up to about 100 ml. volume (actual mass = 109·90 g) and accurately weighed. Three weighed samples *A*, *B*, *C*, were then sealed in glass ampoules for comparison with a standard source *S* sealed in a similar ampoule. The comparison was made independently at Birmingham, using a Geiger counter and at Harwell, using a scintillation counter with a sodium iodide crystal; in each case sufficient absorber was placed round the source to stop the positrons. Enough counts (produced by the 1·28 Mev gamma radiation and 0·511 Mev annihilation quanta) were taken to establish the relative source strengths to 0·5%. The weight of solution in each source was also found in the two places independently. The Harwell weights were obtained after all the inter-comparison measurements had been carried out; the ampoules were weighed, broken open and emptied and weighed again. These weights served only to check those found earlier at Birmingham and were not used in the calculation. The results obtained are shown below.

Ratio of activities

Sample	Birmingham			Harwell			
A/S	0·299	0·290	0·309	0·298	0·295	0·298	0·296
B/S	0·285	0·281	0·303	0·292	0·286	0·294	0·291
C/S	0·313	0·316	0·335	0·323	0·314	0·324	0·328

Mass of solution *M* (g)

	Birmingham	Harwell
A	1·0284	1·0259
B	1·0237	1·0223
C	1·1288	1·1260

In each ratio listed in this table the error from the counting statistics is less than 0·001. The combined results give

$$A/S = 0{\cdot}2978 \pm 0{\cdot}0004, \qquad A/SM_{\rm A} = 0{\cdot}2896 \pm 0{\cdot}0004\,{\rm g}^{-1},$$
$$B/S = 0{\cdot}2903 \pm 0{\cdot}0004, \qquad B/SM_{\rm B} = 0{\cdot}2836 \pm 0{\cdot}0004\,{\rm g}^{-1},$$
$$C/S = 0{\cdot}3219 \pm 0{\cdot}0004, \qquad C/SM_{\rm C} = 0{\cdot}2851 \pm 0{\cdot}0004\,{\rm g}^{-1}.$$

The errors are those due to counting statistics. The mean value of the ratio of the activity per gram of solution to the activity of the standard is then 0·286 ± 0·001.

The standard source *S* had a positron strength of 48·75 ± 0·25 μc per gramme on 1st October 1954. This was found by counting the positrons emitted from a sample of the solution from which *S* had been prepared in a 4π Geiger counter at the Atomic Energy Research Establishment, Harwell. The source, of thickness 6 μg cm^{-2} was supported in the counter on a foil of thickness 260 μg cm^{-2} which stopped the emission of Auger electrons into the bottom half of the counter. By placing further similar foils above and below the source the correction (2·5%) to the counting rate due to Auger electrons was found. The positron absorption due to the aluminium foils was found in the same way. Although the 'sandwich foil' method is known to give a high result in the case of β^--spectra, the facts that the correction was small in the present case (0·8%) and that the low-energy end of a positron spectrum falls to zero more rapidly than for electron emission suggest that the observed correction is justified for ^{22}Na. The counting of K x-rays was neglected, as in the experiment of Sherr and Miller, because of the low value of the fluorescence yield of neon.

As a final check of the consistency of the measurements, the activity of sample A was measured in the 4π counter at the conclusion of the experiment. Using a half-life of 948 days for ^{22}Na and the value 0·2978 for the ratio A/S, the source strength of the standard on 1st October 1954 was deduced. The result was 1·5% lower than the value originally obtained directly for S. In view of the fact that the solution had been in a glass ampoule for several months and that some sodium ions might have adhered to the walls, this result was considered satisfactory.

From the strength of the standard source S and the mean value of the ratio of specific activity of the samples to the activity of S, the 'positron' strength of the main source was found to be 1·533 ± 0·010 mc on 1st October 1954.

§ 5. K CAPTURE FOR POSITRON RATIO FOR ^{22}NA

From the figures given in §§ 3 and 4

$$\frac{P_K}{P_+}=\frac{1{\cdot}720\pm0{\cdot}012-1{\cdot}533\pm0{\cdot}010}{1{\cdot}533\pm0{\cdot}010}=0{\cdot}122\pm0{\cdot}010.$$

The error in this value is based on standard deviations; its magnitude shows that the gas analysis method has an accuracy comparable with that of the counter experiments. There may be a systematic error due to neglect of the possible dependence of Pirani gauge sensitivity on isotopic mass. If the dependence found experimentally for the gases helium and neon is used to correct the ratio P_K/P_+ the figure 0·122 becomes 0·141. No correction for the small effect of the weak ground state β-transition on the ratio has been made.

ACKNOWLEDGMENT

We are grateful to Mr. M. Petravić for help in the measurement of the activities.

REFERENCES

ALVAREZ, L. W., 1936, *Phys. Rev.*, **54**, 486.
CHARPAK, G., 1955, *J. Phys. Radium*, **16**, 62.
ENDT, P. M., and KLUYVER, J. C., 1954, *Rev. Mod. Phys.*, **26**, 95.
KREGER, W. E., 1954, *Phys. Rev.*, **96**, 1554.
PANETH, F. A., CHACKETT, K. F., REASBECK, P., and WILSON, E. J., 1953, *Geochim. et Cosmoch. Acta*, **3**, 257.
SHERR, R., and MILLER, R. H., 1954, *Phys. Rev.*, **93**, 1076.
WELTIN, H., 1943, *Phys. Rev.*, **64**, 128.
ZWEIFEL, P. F., 1954, *Phys. Rev.*, **96**, 1572.

The Cellular Method for a Close-packed Hexagonal Lattice, with applications to Titanium

By B. SCHIFF

Department of Mathematics, Imperial College, London, S.W.7

Communicated by H. Jones; *MS. received* 1*st February* 1955

Abstract. The cellular method for obtaining electronic eigenvalues in crystals is formally extended to the close-packed hexagonal lattice, and the use of a double atomic cell is investigated, boundary conditions being obtained for a wave function with an arbitrary wave vector. The symmetry properties of wave functions at the zone centre are outlined. After calculating a potential function for the titanium ion-core, point boundary conditions are applied to determine eigenvalues for low-lying states at the centre of the zone in both modifications of the metal. The ground state is found to possess s-like symmetry in both cases.

---

§ 1. INTRODUCTION

CELLULAR-TYPE calculations for non-Bravais lattices have been confined to applications of the method of Slater (1934) to various substances possessing the diamond structure, the first of these being a calculation by Kimball (1935) for a diamond crystal. However, Slater's original method does not yield accurate results, even for Bravais lattices, because of the limited expansion used for the wave function, and the approximate way in which the boundary conditions are applied. More recently, von der Lage and Bethe (1947), and Howarth and Jones (1952) (hereinafter referred to as H. J.), have obtained accurate results for sodium by utilizing the symmetry properties of wave functions belonging to certain points in the zone. These enable many of the terms to be left out of the expansions for the functions, as well as simplifying the boundary conditions. In this paper, the cellular method will be extended to a close-packed hexagonal lattice, and will then be applied to determine eigenvalues for conduction electrons in metallic titanium.

The close-packed hexagonal lattice may be regarded as a simple hexagonal lattice, with a basis of two atoms in a unit cell. To apply the cellular method, therefore, we use a double cell, formed by joining two cells constructed in the usual manner about adjacent lattice points belonging to opposite sub-lattices. The double cell is shown in figure 1 (*b*). Through each lattice point there are three two-fold axes in the basal plane (one of which is shown in the figure), and a three-fold axis perpendicular to this plane. Herring (1942) has given a full account of the symmetry properties of the wave functions in a close-packed hexagonal lattice. Only the wave functions belonging to the centre point Γ, or to the centre of the top face, of the reduced zone possess a sufficiently high symmetry to permit the application of a method similar to that of H. J., and in this paper we shall only be concerned with functions at Γ.

Within a given half cell, we introduce spherical polar coordinates, with the origin at the lattice point. The polar axis is taken along the three-fold axis, and the plane $\phi=0$ is chosen so as to contain the three-fold axis and the particular two-fold axis shown in figure 1 (*b*). The function is expanded in the form

$$\psi=\sum_{l=0}^{\infty}\sum_{m=0}^{l}[A_{lm}\cos m\phi+B_{lm}\sin m\phi]\,P_l^m(\cos\theta)\,R_l(E,r)$$

where $R_l(E,r)$ is the solution of the radial wave equation of order l, inside the half cell. We now use the symmetry properties of the wave functions to set certain of the constants in this expansion equal to zero, and also to determine the behaviour of the functions on passing into the other half of the double cell. The group of the wave vector $\mathbf{k}=0$ is made up of a sub-group $\mathscr{A}$ and its cosets $Q\mathscr{A}$, $S\mathscr{A}$ and $QS\mathscr{A}$, and contains twenty-four operations. The subgroup $\mathscr{A}$ consists of the identity, rotations through $\pm 2\pi/3$ about the three-fold axis, and reflections in the planes $\phi=0$, $2\pi/3$ and $4\pi/3$. The operation S is a reflection in the basal plane, and Q denotes an inversion in the origin, followed by a translation equivalent to the vector joining the centres of the two halves of the cell. There are twelve wave functions with distinctive symmetries, referred to as symmetry types, which belong to the point Γ. They split into pairs, the members of a pair having the same type of expansion inside a given half cell, but being of opposite parity with respect to Q; Herring uses the symbols Γ^+ and Γ^- to denote even and odd parity respectively under this operation. The expansions of the functions in spherical harmonics may be obtained from the character table given by Herring, via the irreducible representations of the group, and are given in table 1. For example, the $\Gamma_1{}^+$ function may be expanded in the form

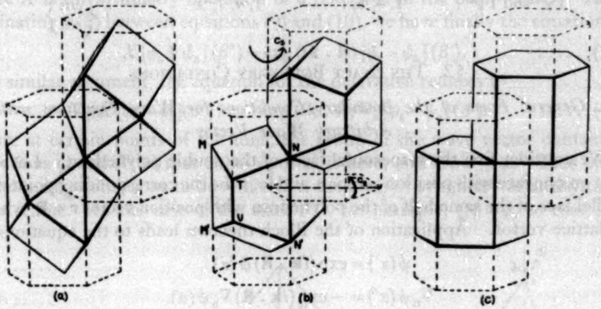

Figure 1.

$$\begin{aligned}\psi(\Gamma_1{}^+)=R_0&+AR_2P_2(\cos\theta)+BR_4P_4(\cos\theta)+\ldots\ldots\\&+\{FR_3P_3{}^3(\cos\theta)+GR_5P_5{}^3(\cos\theta)+HR_7P_7{}^3(\cos\theta)+\ldots\ldots\}\cos 3\phi\\&+\{KR_6P_6{}^6(\cos\theta)+LR_8P_8{}^6(\cos\theta)+MR_{10}P_{10}{}^6(\cos\theta)+\ldots\ldots\}\cos 6\phi\\&+\ldots\ldots\,.\end{aligned}$$

The two components of a degenerate function differ only in the exchange of cos $m\phi$ and sin $m\phi$. The table contains all of the information about the symmetries of the wave functions which may be obtained by theoretical considerations. The arbitrary constants in the expansion, and hence the eigenvalue, are obtained by applying the boundary conditions.

Table 1. Expansions of the Symmetry Types in Spherical Harmonics

Type	Values of l	Values of m	ϕ-dependence
Γ_1^+ and Γ_4^-	0, 2, 4, . . .	0, 3, 6, . . .	cos
Γ_4^+ and Γ_1^-	1, 3, 5, . . .	0, 3, 6, . . .	cos
Γ_2^+ and Γ_3^-	3, 5, 7, . . .	3, 6, 9, . . .	sin
Γ_3^+ and Γ_2^-	4, 6, 8, . . .	3, 6, 9, . . .	sin
Γ_6^+ and Γ_5^-	1, 3, 5, . . .	1, 4, 7, . . .	$\begin{Bmatrix}\cos\\ \sin\end{Bmatrix}$
Γ_5^+ and Γ_6^-	2, 4, 6, . . .	1, 4, 7, . . .	$\begin{Bmatrix}\cos\\ \sin\end{Bmatrix}$

§ 2. THE EXACT BOUNDARY CONDITIONS

2.1. *General Form of the Boundary Conditions for Wave Functions with an Arbitrary Wave Vector*

We consider first the trapezoidal faces of the double polyhedron. Let α be a point on one face with position vector $\mathbf{r}$, and let α' be the corresponding point on the parallel face of the same half of the polyhedron with position vector $\mathbf{r}+\mathbf{R}$, where $\mathbf{R}$ is a lattice vector. Application of the Bloch theorem leads to the equations

$$\psi(\alpha') = \exp(i\mathbf{k}\,.\,\mathbf{R})\,\psi(\alpha) \qquad \ldots\ldots(1)$$

$$\nabla_{\mathrm{n}}\psi(\alpha') = -\exp(i\mathbf{k}\,.\,\mathbf{R})\,\nabla_{\mathrm{n}}\psi(\alpha). \qquad \ldots\ldots(2)$$

Let X denote the symmetry operation which reflects in the plane through the origin normal to $\mathbf{R}$. Then $\psi(\alpha')$ may be replaced by $X\psi(\alpha)$, and similarly for the derivative, so that equations (1) and (2) may be written

$$X\psi(\alpha) = \exp(i\mathbf{k}\,.\,\mathbf{R})\,\psi(\alpha) \qquad \ldots\ldots(3)$$

$$\nabla_{\mathrm{n}}\{X\psi(\alpha)\} = -\exp(i\mathbf{k}\,.\,\mathbf{R})\,\nabla_{\mathrm{n}}\psi(\alpha). \qquad \ldots\ldots(4)$$

At certain points of high symmetry in the zone, amongst them the point Γ, the operation X is included in the group of the wave vector. In this case, we have that $X\psi = \pm\psi$, and the boundary conditions will thus necessitate the vanishing of the function or its derivative over the face. For example, in the case of the Γ_1^+ function, $\exp(i\mathbf{k}\,.\,\mathbf{R})$ is equal to unity and $X\psi=\psi$ for all $\mathbf{R}$, so that equation (3) is satisfied automatically, and equation (4) requires that $\nabla_n\psi$ should vanish over a trapezoidal face.

Each rhombic face will be parallel to a similar face on the opposite half of the double polyhedron. Two such parallel faces are shown in figure 2(*a*), on which O and O′ represent the two centres of the double cell. Let γ and β be corresponding points on the two faces, such that the lattice translation $\mathbf{R}$ takes γ into β. Application of the Bloch theorem leads to the equations

$$\psi(\beta) = \exp(i\mathbf{k}\,.\,\mathbf{R})\,\psi(\gamma) \qquad \ldots\ldots(5)$$

$$\nabla_{\mathrm{n}}\psi(\beta) = -\exp(i\mathbf{k}\,.\,\mathbf{R})\,\nabla_{\mathrm{n}}\psi(\gamma). \qquad \ldots\ldots(6)$$

The two parallel faces are also transformed into one another by the operation Q, which plays a somewhat similar role in a close-packed hexagonal lattice to that played by the inversion operator in a Bravais lattice. Using this idea, we write ψ in the form $\psi_{\mathrm{s}}+\psi_{\mathrm{a}}$, where ψ_{s} is symmetric and ψ_{a} antisymmetric with respect to Q.

(This step is also suggested by a comparison with the bonding and anti-bonding functions of molecular theory.) Referring to figure 2 (*a*), if β' is the reflection of β in B, the centre of the face, we have that

$$\psi(\gamma) = Q\psi(\beta') \qquad \ldots\ldots(7)$$

i.e.

$$[\psi_s + \psi_a](\gamma) = [\psi_s - \psi_a](\beta'). \qquad \ldots\ldots(8)$$

Eliminating $\psi(\gamma)$ between equations (5) and (8),

$$[\psi_s + \psi_a](\beta) = \exp(i\mathbf{k} \,.\, \mathbf{R})\,[\psi_s - \psi_a](\beta'). \qquad \ldots\ldots(9)$$

Again, if β'' is the reflection of β in the line BD,

$$[\psi_s + \psi_a](\beta) = X[\psi_s + \psi_a](\beta''), \qquad \ldots\ldots(10)$$

where X is the symmetry operation of a reflection in the plane O′BD. Hence, eliminating $\psi(\beta)$ between equations (9) and (10), we have finally the equation

$$X[\psi_s + \psi_a](\beta'') = \exp(i\mathbf{k} \,.\, \mathbf{R})\,[\psi_s - \psi_a](\beta'). \qquad \ldots\ldots(11)$$

By a similar argument, the equation for the derivative reduces to

$$\nabla_n\{X[\psi_s + \psi_a](\beta'')\} = -\exp(i\mathbf{k} \,.\, \mathbf{R})\,\nabla_n[\psi_s - \psi_a](\beta'). \qquad \ldots\ldots(12)$$

Again, at certain points of the zone, the group of the wave vector contains the operations Q and X, so that either ψ_s or ψ_a is zero, and $X\psi = \pm\psi$. This enables the boundary conditions to be reduced to the form of symmetry or antisymmetry about a line. In the case of the state $\Gamma_1{}^+$, for example, $Q\psi = \psi$, so that $\psi_a = 0$.

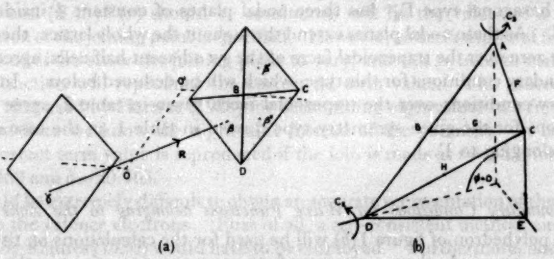

Figure 2.

Also $X\psi = \psi$. Thus equations (11) and (12) require that the function should be symmetric and its normal derivative antisymmetric about the line BC.

Although deduced for non-degenerate symmetry types, the above equations will also apply to the case of a degenerate type if the wave function is written as a vector, and the appropriate matrix representations are used for the operators. Before listing the boundary conditions for the types at Γ, it is useful to consider the shape of the double polyhedron over which they may be applied. For functions with any wave vector, the Bloch conditions (1), (2), (5) and (6) will determine the function inside a double cell, and hence will fix the eigenvalue uniquely. Equations (5) and (6), however, reduce to identities if applied to the interface between the two halves of the cell. Thus, in general, the boundary conditions must be applied over the whole of the double polyhedron. However, if the group of the wave vector contains the operation Q (thus indicating a definite connection between the symmetries of the function in the two halves of the cell), equation (8) and a similar equation for the derivative may be used. In this case the function need be fitted over, at most, one half of the double polyhedron.

2.2. *Choice of the Double Polyhedron*

Consider the double polyhedron shown in figure 1 (*b*). Let us rotate each rhombic face through an equal angle about the line (such as MN) through its centre parallel to the basal plane. During this process, lines such as TU will change in length, whilst lines such as MM′ will remain unaltered in length. The two limiting cases, in which the line TU either shrinks to a point, or becomes equal in length to the line MM′, are shown in figures 1 (*a*) and 1 (*c*) respectively. Throughout such a deformation of the double polyhedron, since the line MN is unaltered, the faces will still remain parallel to one another in pairs, the members of a pair still being separated by lattice vector displacements and transforming into each other under the operation Q. Furthermore, each face will remain symmetrical about the plane of constant ϕ passing through its centre, so that the operation X will take β^* into β as before. Thus the boundary condition equations (11) and (12) will apply equally well to any polyhedron between (and including) the two limiting cases shown in figures 1 (*a*) and 1 (*c*).

It might, at first sight, appear strange that we can vary the size of the trapezoidal faces of the cell, in the manner indicated, without affecting the boundary conditions for these faces. The reason lies in the build up of a non-Bravais lattice. Although, as in a Bravais structure, the nodal planes extend throughout the lattice, those nodal planes passing through the nuclei of one sub-lattice can form the edges of the half cells about atoms of the other sub-lattice. For example, the close-packed hexagonal type Γ_2^+ has three nodal planes of constant ϕ inside a given half cell. As these nodal planes extend throughout the whole lattice, the function must be zero over the trapezoidal faces of the six adjacent half cells, agreeing with the boundary conditions for this type, which will be deduced below. In fact, the boundary conditions over the trapezoidal faces, given in table 2, agree with the expansions for the given symmetry type quoted in table 1, in the case of all the types belonging to Γ.

2.3. *Boundary Conditions for Wave Functions belonging to the Zone Centre*

The polyhedron of figure 1 (*b*) will be used for the calculations on titanium in the next section. As there are twenty-four symmetry operations in the group of the wave vector $\mathbf{k}=0$, the boundary conditions for symmetry types at Γ need only be applied over the section shown in figure 2 (*b*), whose area is one twenty-fourth that of the double polyhedron. The conditions, deduced in the manner described above, are given in table 2, in which ψ' denotes the derivative of ψ normal to the face in question.

Table 2. Boundary Conditions for Symmetry Types at Γ

Type	Face CDE		Line BC		Type	Face CDE		Line BC	
	ψ	ψ'	ψ	ψ'		ψ	ψ'	ψ	ψ'
Γ_1^+		0	s	a	Γ_3^+	0		a	s
Γ_4^-		0	a	s	Γ_2^-	0		s	a
Γ_4^+		0	s	a	Γ_6^+		0	s	a
Γ_1^-		0	a	s	Γ_5^-		0	a	s
Γ_2^+	0		a	s	Γ_5^+		0	s	a
Γ_3^-	0		s	a	Γ_6^-		0	a	s

The two components of a degenerate function are required to satisfy the same boundary conditions as one another.

§3. EIGENVALUES FOR THE VALENCE ELECTRONS IN METALLIC TITANIUM

The theory will now be applied to determine eigenvalues for low-lying states belonging to the centre of the zone in close-packed hexagonal titanium, and eigenvalues will also be calculated for the body-centred cubic modification.

3.1. *The Potential Field in which a Valence Electron moves*

The existence of stable trivalent and tetravalent titanium compounds, and the small difference (0·23 Ryd) between the energies of the $3d^2 4s^1$ and the $3d^1 4s^2$ configurations for the Ti^+ ion, indicate that the 3d electrons in the free atom are fairly loosely bound. There is no reason why this should not also be the case in the metal, so that in calculating a potential function for the Ti^+ ion, is it essential to treat the 3d electrons as valence electrons. The procedure adopted is to calculate a function for the Ti^{4+} ion, and then to add the contribution from the valence electrons.

The potential function for the Ti^{4+} ion is obtained using the method of Prokofiew (1929) over as large a portion of the range of r as possible. The 6h, 5g and 4f and 4d term values give parabolae covering the range of r down to $r=0{\cdot}38$. No term values are available for the core electrons. As $V(r)$ tends to $-22/r$ as r tends to zero, the form $-r^2 V(r) = 22r + ar^2 + br^3$ is assumed for the region near the nucleus, the aim being to join this function smoothly to the innermost Prokofiew parabola at some point on the range of validity of the latter. The requirement that $V(r)$ and $(d/dr)V(r)$ should be continuous will fix the values of a and b, if the position of the joining point is specified. However, an extra degree of freedom is introduced if we allow the joining point to vary, and this is used to make sure that the function will reproduce the correct 3d term value. The procedure is similar to that used by Hartree (1928) for determining eigenvalues in a free atom, except that here we know the eigenvalue instead of the potential. It is found that the correct term value is reproduced if the join is made at $r=0{\cdot}82$, for which $a=-37{\cdot}469$ and $b=20{\cdot}963$.

It would be extremely difficult to obtain an accurate representation of the potential due to the valence electrons. First of all, a self-consistent method, similar to that used by Raimes (1950) would have to be employed. Furthermore, one would have to develop a procedure to calculate two functions simultaneously, as the 4s and 3d electrons move in different fields. Such a calculation would be very laborious, and would not be justified in view of the approximate nature of the function calculated for the Ti^{4+} ion. As the chief object of the calculation was to investigate the application of the cellular method to a close-packed hexagonal lattice and, in view of these difficulties, it was decided to approximate to the potential due to the valence electrons by adding the potential function of a uniform smeared charge, normalized so as to contain a charge of $-3e$ inside the equivalent sphere. The total potential function assumed for the Ti^+ ion is as follows:

$$-r^2V = 44r - 77{\cdot}876r^2 + 41{\cdot}925r^3 + 0{\cdot}1043r^4 \quad \ldots\ldots\ldots\ldots \quad r<0{\cdot}82$$

$$-r^2V = 4{\cdot}648 + 4{\cdot}473r - 2{\cdot}206r^2 + 0{\cdot}1043r^4 \quad \ldots\ldots\ldots\ldots \quad 0{\cdot}82<r<2$$

$$-r^2V = 2{\cdot}467 + 6{\cdot}655r - 2{\cdot}751r^2 + 0{\cdot}1043r^4 \quad \ldots\ldots\ldots\ldots \quad 2<r<3{\cdot}06$$

$$-r^2V = 2{\cdot}467 + 0{\cdot}655r + 0{\cdot}186r^2 \quad \ldots\ldots\ldots\ldots\ldots\ldots\ldots \quad 3{\cdot}06<r<3{\cdot}5$$

$$-r^2V = 0{\cdot}321 + 1{\cdot}881r + 0{\cdot}011r^2 \quad \ldots\ldots\ldots\ldots\ldots\ldots\ldots \quad 3{\cdot}5<r<5{\cdot}4$$

$$-r^2V = 2r \quad \ldots\ldots\ldots\ldots\ldots\ldots\ldots\ldots\ldots\ldots\ldots\ldots \quad 5{\cdot}4<r$$

The coefficients are only quoted to three places of decimals in order to make the function as smooth as possible for the integration. The method used to determine $V(r)$ does not, of course, yield results of such high accuracy.

3.2. *Integration of the Radial Wave Equation*

In order to fit the boundary conditions, the values of the radial wave functions are needed at various points on the surface of the cell, over a range of energies. We are only interested in the low-lying states, and the radial wave equation is therefore integrated at intervals of 0·1 Ryd for $l<6$ and 0·2 Ryd for $6 \leqslant l \leqslant 9$ over the range from +1 Ryd to −1 Ryd. The labour involved in computing by hand the necessary 170 integrations would be prohibitive, and they were therefore performed on the Manchester University Electronic Computer Mark II, to which reference is made later. The computer was also used to calculate the required values of the Legendre polynomials.

3.3. *The Point Boundary Conditions*

The eigenvalues are obtained by applying suitable point boundary conditions over the section of the atomic polyhedron shown in figure 2(*b*). In the case of the state $\Gamma_1{}^+$, for example, ten conditions referring to the points on the diagram may be deduced from the exact conditions of table 2, as follows:

Face CDE: (i) $\psi_C{}'=0$ (ii) $\psi_E{}'=0$ (iii) $\psi_H{}'=0$
Face ADC: (iv) $\psi_A-\psi_D=0$ (v) $\psi_F-\psi_H=0$ (vi) $\psi_A{}'+\psi_O{}'=0$
(vii) $\psi_B{}'=0$ (viii) $\psi_F{}'+\psi_H{}'=0$ (ix) $\psi_G{}'=0$
(x) $\psi_C{}'=0$.

ψ' denotes the derivative of ψ normal to the face in question. The expansion

$$\psi(\Gamma_1{}^+)=R_0+AR_2P_2(\cos\theta)+BR_4P_4(\cos\theta)+CR_6P_6(\cos\theta) \qquad \ldots\ldots(13)$$

is used for the wave function. On applying H.J.'s method for the determination of the eigenvalue from the point boundary conditions, it is not found possible to obtain reasonably consistent determinations, the latter being distributed fairly evenly between about −0·7 Ryd and −0·8 Ryd. The inclusion of the next term in the expansion (13) does not lead to any significant improvement in the results, and the work of Howarth (1953) and of Schiff (1954) indicates that only the terms with the lowest value of *m* play any significant part in the wave function. The inclusion of terms with still higher values of *l* would necessitate fitting the function at a much larger number of points, because of the rapid variation of the higher harmonics over the surface. Other states at Γ are found to yield equally unsatisfactory results.

3.4. *The 'Least Squares' Method*

In order to improve the results, it is desirable to use a method which allows the boundary conditions to be fitted at a fairly large number of points without increasing the number of terms in the expansion. This would remedy the chief defect of H.J.'s method, in which the number of conditions used for any given determination is restricted by the particular expansion used for the wave function. The procedure we adopt is to determine the constants in the expansion from the point boundary conditions by the method of 'least squares'. If *n* constants are used in the expansion, the *m* point boundary condition equations form a system of *m* linear equations in n unknowns ($m > n$). A measure of the inconsistency of such a set of equations is the residual left over on substituting back the least squares values of the constants.

Using the Choleski method of triangular resolution of the matrix of coefficients, the residual can be found without actually calculating the constants, although the latter may easily be determined if required. The method is simple to apply, as the inclusion of an extra term in the expansion just adds an extra row and column to the triangular matrices. To determine the eigenvalue, the residual is calculated at energies for which the radial wave functions are available, and a (residual, energy) curve is plotted. The energy at the minimum of this curve is taken as the eigenvalue for the particular expansion used. The proportionate decrease in the minimum residual as extra terms are added gives a good indication of the rate of convergence of the process, and hence of the probable error of the final eigenvalue. The accuracy of the eigenvalue is also affected by the shape of the residual curve. If the latter is flat, a small decrease in the residual, due to the inclusion of an extra term in the expansion, or to the use of unnormalized functions, will affect the position of the minimum considerably. On the other hand, if the curve is steep, the eigenvalue will be insensitive to such changes. The probable errors quoted in tables 3 and 4 are based on the above considerations.

The results for close-packed hexagonal titanium are given in table 3, which shows how these eigenvalues change as extra terms are added to the expansion. In general, it is found that only the terms with the lowest values of m play any significant part in the wave function, as in the previous work mentioned above. Because of the relatively small number of points at which the boundary conditions are fitted, no terms with values of l greater than 8 are included.

Table 3. Eigenvalues (Ryd) for Close-Packed Hexagonal Titanium

State	Eigenvalue for Expansion containing					Final
	1 Term	2 Terms	3 Terms	4 Terms	5 Terms	Eigenvalue
Γ_1^+	−0·718	−0·729	−0·735	−0·746	−0·747	−0·75 ± 0·01
Γ_4^-	+0·227	−0·008	−0·033	−0·034	−0·015	−0·02 ± 0·02
Γ_4^+	−0·157	−0·293	−0·291	−0·296		−0·3
Γ_6^+	+0·114	+0·097	+0·134	+0·141		+0·1
Γ_5^+	−0·475	−0·471	−0·471	−0·482		−0·48 ± 0·01
Γ_6^-	−0·351	−0·360	−0·359	−0·353		−0·355 ± 0·01

On performing a similar calculation for the body-centred cubic modification, using the expansions and boundary conditions given by H. J., it is also found necessary to use the least squares method in order to obtain consistent results. Eigenvalues for states belonging to the points Γ and H in the zone are given in table 4.

Table 4. Eigenvalues (Ryd) for Body-Centred Cubic Titanium

State	Eigenvalue for Expansion containing				Final
	1 Term	2 Terms	3 Terms	4 Terms	Eigenvalue
Γ_s	−0·755	−0·757	−0·775	−0·774	−0·774 ± 0·005
H_s	+0·488	+0·654	+0·666		+0·67 ± 0·05
H_p		+0·115	+0·154	+0·157	+0·16 ± 0·05
H_d^1	−0·477	−0·498	−0·478		−0·478 ± 0·005
Γ_d^1	−0·438	−0·426	−0·406		−0·406 ± 0·005

It will be noted that the eigenvalues for the body-centred cubic modification show a much more rapid convergence than those for the close-packed hexagonal metal. This is probably because the higher symmetry of the body-centred cubic lattice is more suited to a method based on a separation of the wave equation in spherical polar coordinates. The states whose expansions contain harmonics of odd order are found to have very flat residual curves. This is because the $l=1$ radial wave function, which dominates these functions, varies only slowly with energy. The eigenvalues for these states will thus be subject to quite a large error, and it is not possible to make any reasonably safe estimate of the error in the case of the close-packed hexagonal states Γ_4^+ and Γ_6^+.

3.5. *Discussion of the Results*

The results given above are subject to errors arising from two sources. Firstly there are the errors arising from the use of a terminated expansion for the wave function, and the consequent approximate fitting of the boundary conditions. Secondly, there is a considerable uncertainty in the results because of the nature of the potential function used. The estimates of the errors given in tables 3 and 4 make no allowance for this second factor. Recent work, particularly that of Howarth (1953), has shown that the eigenvalues are rather sensitive to fairly small changes in the potential function. It was therefore felt that there would be no justification for expending the considerable amount of labour which would be necessary in order to improve the boundary condition fitting (by the inclusion of more terms in the expansions, etc.). This uncertainty should also be borne in mind when attempting to draw any physical conclusions from the results.

It is not possible to make a rigid classification of the close-packed hexagonal states according to the number of nodal planes through the origin, as H. J. have made for the states in a body-centred cubic lattice. For instance, table 1 shows that only one component of the Γ_6^+ function possesses a nodal plane of constant ϕ, so that, strictly speaking, one component has p-like, and one component s-like symmetry. This is to be expected, as functions differing only in the rotation of a nodal plane through $\pi/2$ about a three-fold axis would not have the same eigenvalue. However, over the range of energies considered, only the terms with the lowest values of m play any significant part in the wave function. Thus it is reasonable to compare the state Γ_6^+ with states of p-like symmetry, as the terms $\cos 4\phi$, $\cos 10\phi$, etc., which have no nodal plane of constant ϕ, play only a very small part in this function. It must be pointed out, however, that this may no longer hold for much higher energies. This difficulty does not, of course, arise in the case of non-degenerate types, which can be classified exactly. Thus the types Γ_1^+ and Γ_4^-, Γ_4^+ and Γ_1^-, Γ_2^+ and Γ_3^-, and Γ_3^+ and Γ_2^- may be classified as pairs of s, p, f and g states respectively. Γ_6^+ and Γ_5^- may be considered as p-states, and Γ_5^+ and Γ_6^- as d-states.

In both modifications, the energy of the lowest d-state lies about 0·25 to 0·3 Ryd above that of the lowest s-state, whereas in the free atom, the $3d^2 4s^1$ Ti^+ ion has an energy 0·23 Ryd lower than the $3d^1 4s^2$ configuration. This would tend to support the assumption that the 3d electrons are fairly free to wander through the metal. The close-packed hexagonal ground state Γ_1^+ has an eigenvalue ($-0·75$ Ryd) considerably above the Wigner–Seitz energy of $-0·80$ Ryd, with the energy of the body-centred cubic ground state lying about midway between these two values.

The difference between these three figures probably arises because the (E_0, r_s) curve is much less flat than in the case of an alkali metal, so that the deviation from spherical symmetry will have more effect on the eigenvalue. This would account for the rather large deviation in the case of the close-packed hexagonal modification, which has a lower symmetry than the body-centred cubic. The body-centred cubic states $H_d{}^1$ and $\Gamma_d{}^1$ lie much closer together than in the case of lithium or sodium, the smallness of the difference between the energies of the two d-states (in either modification) being due mainly to the fact that, for a given value of r on the surface of the atomic cell, the $l=2$ radial wave function and its derivative have nodes at almost the same energies.

ACKNOWLEDGMENTS

It is a pleasure to express my gratitude to Professor H. Jones for the help and advice which he has given to me throughout the work. I am grateful to Mr. R. A. Brooker and the staff of the Manchester University Computing Machine Laboratory for allowing me to use the University Computer (Mark II), and particularly to Dr. N. E. Hoskin for his assistance in programming the problem for the machine. I would like to thank Dr. P. Rhodes for his help in the calculation of a potential function for the titanium ion-core.

My thanks are also due to the Senate of the University of London for the award of a Postgraduate Studentship.

REFERENCES

HARTREE, D. R., 1928, *Proc. Camb. Phil. Soc.*, **24**, 89.
HERRING, C., 1942, *J. Franklin Inst.*, **233**, 525.
HERRING, C., and HILL, A. G., 1940, *Phys. Rev.*, **58**, 132.
HOWARTH, D. J., 1953, *Proc. Roy. Soc.* A, **220**, 513.
HOWARTH, D. J., and JONES, H., 1952, *Proc. Phys. Soc.* A, **65**, 355.
KIMBALL, G. E., 1935, *J. Chem. Phys.*, **3**, 560.
VON DER LAGE, F. C., and BETHE, H. A., 1947, *Phys. Rev.*, **71**, 612.
PROKOFIEW, W., 1929, *Z. Phys.*, **58**, 255.
RAIMES, S., 1950, *Phil. Mag.*, **41**, 568.
SCHIFF, B., 1954, *Proc. Phys. Soc.* A, **67**, 2.
SLATER, J. C., 1934, *Phys. Rev.*, **45**, 794.

A Spectroscopic Study of Plasma–Electron Oscillations

By T. K. ALLEN

Physics Department, Queen's University, Belfast

Communicated by K. G. Emeléus; MS. received 6th January 1955

Abstract. A demountable discharge tube has been constructed for spectroscopic and probe exploration of low-voltage electron beam discharges through gas at low pressure. Using argon, the probe evidence for presence of electrons with excess energy when plasma–electron oscillations are occurring has been confirmed spectroscopically. The spectroscopic results also confirm the probe evidence for the distribution of oscillations in the discharge, and for the variation with discharge parameters of the position of the main oscillating region.

§ 1. Introduction

Most investigations of plasma–electron oscillations and associated phenomena in hot cathode, low pressure discharges have been made with exploring probes. Recent work (Bailey and Emeléus 1955) has shown definitely that the presence of a probe may influence the oscillations. It is therefore desirable to check where possible in other ways the results obtained with probes. This paper contains an account of some spectroscopic experiments which confirm the existence of the form of electron scattering first studied by Dittmer (1926) and later, in more detail, by Merrill and Webb (1939), and in this laboratory. In its simplest form the scattering consists of the superposition of a longitudinal spread of energy on the almost constant energy with which the electrons leave the thin space-charge sheath on the cathode and enter the plasma. It occurs rather abruptly at a distance of a few millimetres from the cathode. The longitudinal scattering is often accompanied by lateral deviation of the primary beam at the scattering region (Bailey and Emeléus 1955). The phenomena are due to self-maintained fields in the discharge, and not to collisions with gas molecules.

The main features of the appearance of an oscillating discharge of this type from a flat oxide-coated cathode are shown diagrammatically in figure 1. The scattering region usually takes the form of a bright meniscus M, convex to the cathode C. The primary electrons from the cathode, indicated by arrows, approach M from C in an almost parallel beam, and leave M in convergent and divergent beams. The space traversed by the primary electrons is distinguished from the rest of the plasma by difference in colour and intensity of the light emitted. Strong oscillations can be picked up by a probe only when this is exposed to primary electrons in or to the anode side of M. The position of the anode A is largely immaterial, so long as it is not close to M. The potential of the whole of the plasma is close to that of the anode.

The principle of the spectroscopic experiments is that if there are primary electrons present on the anode side of M with energy greater than on the cathode side, spectra requiring higher energy of excitation from the ground state of the gas should appear preferentially in the former region. As a convenient cathode fall in potential for this type of discharge is about 20 v, and since the energy changes which occur in scattering may be of the order of 20 v, the gas should have states requiring 35 to 40 ev for excitation from the ground state to show the effect. Argon, which has a large number of spark lines (AII) in the visible region with excitation potentials of this order from the ground state of neutral argon (Moore 1945), has been used. In view of the complexity of the phenomena, no attempt has been made to study in detail the complete energy distribution of the electrons from the excitation functions for the various spectroscopic levels.

§ 2. EXPERIMENTAL ARRANGEMENTS

A demountable discharge tube was constructed for this work, similar to the large cylindrical tube described by Bailey and Emeléus (1955), but 5 cm in diameter, and with the cathode mounted on a large ground joint. The cathode was a flat oxide-coated disc, 0·8 cm in diameter, and the anode a flat nickel sheet 3·5 cm in diameter, parallel to the cathode face and distant about 3·5 cm from it. The tube was mounted so that the primary electron beam which emerged perpendicular to the cathode was parallel to the slit of a spectrograph. The light from the primary beam, after passing through a plane window, was focused on the slit, so that with this arrangement each spectrum line was an image of a narrow slice along the beam. Intensity changes along a particular spectrum line therefore indicated corresponding changes in energy or flux of the primary electrons. The spectrographs used were, for visual observation, a Hilger f/9 constant deviation spectrograph, and for photography a Hilger f/5·6 two-prism glass spectrograph. The tube contained a movable cylindrical probe, 0·2 mm in diameter, shielded with glass to near its exposed end. Its position could be controlled accurately by differential screws. Unless otherwise stated, the probe was withdrawn from the primary beam. The main optical results were in no way dependent on its presence, and were also obtained from a tube from which the probe was absent.

§ 3. EXPERIMENTAL RESULTS

A typical spectrum is shown in the Plate, photograph (*a*), for the following discharge parameters : pressure, 9×10^{-3} mm Hg, tube voltage 25 v, tube current 60 mA. For this exposure, a magnetic field of 45 oersteds was applied parallel to the primary beam; beyond assisting in the collimation of the beam, it had no effect of present significance. The cathode image is at the top of the spectrum, the anode image at the bottom. The horizontal dark line is the shadow of a probe, which was out of the main discharge.

The long lines of fairly uniform intensity stretching from anode to cathode (the cathode sheath is too thin to appear separately) are AI. The short lines which appear more or less abruptly at a distance from the cathode which was 7 mm in the actual discharge, and near the meniscus M, are AII. A slight background of bands is present, due to a trace of impurity in the argon. The AII lines do not come from the region CM (figure 1), but only from MA, i.e. at and to the anode side of the meniscus, where probe measurements also indicate that scattering occurs. The decrease in intensity of the AII lines towards the anode was diminished by increasing the magnetic field, which prevented the lateral spread of the divergent cones of primary electrons in MA. The excitation potentials from the ground state of AI of the typical AII lines at 4806, 4609 and 4448 Å are 34·8, 36·7 and 39·9 v. As the space-potential of the plasma was about 2·5 v positive to the anode, this shows that some primary electrons had acquired extra energies of not less than 12·5 ev in the meniscus of this discharge.

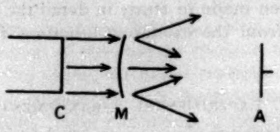

Figure 1. Diagram of oscillating discharge. C, cathode; M, meniscus-shaped oscillating and scattering region; A, anode. The primary beams are indicated by arrows.

The probe measurements of Dittmer and later workers have indicated that the maximum energy of the scattered primary electrons increases with increase in current density, other discharge parameters being held as far as possible constant. This has been verified visually in the present investigation by observing the appearance of AII lines with the constant deviation spectrograph. In addition, by photographing the spectrum, and taking probe characteristic curves, it has been found that AII lines were recorded only when the probe characteristics showed the presence of primary electrons with sufficient energy. The Plate (*b*) and (*c*) shows an example of this. The pressure was $1 \cdot 9 \times 10^{-2}$ mm Hg in each case. The other discharge parameters were, for (*b*), tube voltage 18·2 v, tube current 10 mA and for (*c*), tube voltage 19·2 v, tube current 52 mA. AII lines are absent from (*b*), and present feebly on (*c*), as on (*a*). The spectrum plate was exposed for 60 minutes for (*b*), and for only 15 minutes for (*c*). The corresponding relevant sections of the probe characteristics are shown in figure 2. The positions of the upward break mark the voltage at which the probe starts to

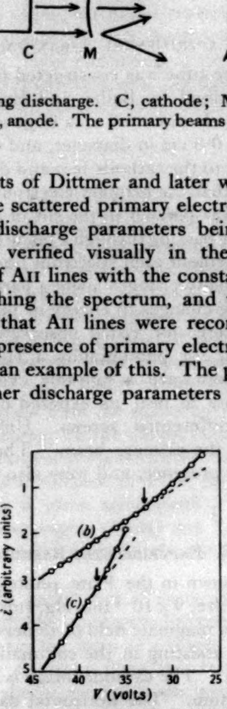

Figure 2. Net positive current to probe plotted against potential of probe negative to anode: see text for discharge parameters.

collect appreciable numbers of primary electrons. As the plasma space-potential was between 2 and 3 v positive to the anode, the maximum energy of the primary electrons in the discharge was about 35·5 ev in case (*b*), and 40·5 ev in case (*c*), in accord with the spectroscopic observations.

A further correlation of the probe and spectroscopic measurements has been made by examining the behaviour of AII lines with different excitation potentials in more detail. It has been shown in this way that the maximum energy of the primary electrons increases gradually by a few electron volts in the last few millimetres on the cathode side of M. This agrees with probe measurements of the maximum energy of the primary electrons. The confirmation of the probe measurements in this respect is of considerable importance in the theory of the production of the oscillations. Neglecting this relatively small dispersion, the distance from the cathode at which the main scattering occurs can be readily measured from the spectra for various series of discharge parameters. Figure 3 (curve *a*) shows, for example, the relation between this distance and gas pressure for a constant tube voltage (25 v) and current (58 mA). Figure 3 (curve *b*) shows the relation between distance and tube current for constant tube voltage (25 v) and gas pressure ($1{\cdot}2 \times 10^{-2}$ mm Hg). The changes in scattering distance agreed quite accurately with the variation of the position of the meniscus M, but only roughly with the changes in distance from the cathode beyond which oscillations were detected. Movement of a probe along the primary electron beam also shifted the position of appearance of the AII lines in the same manner as the position of the visible meniscus (Bailey and Emeléus 1955).

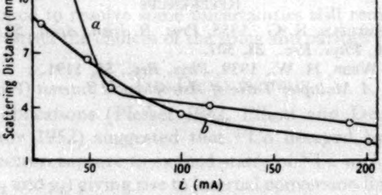

Figure 3. Scattering distance plotted against pressure *p* (curve *a*) and current *i* (curve *b*). For other discharge parameters see text.

A few observations have been made of the spectrum of the discharge in a line perpendicular to the unscattered primary beam, by essentially the same method as was used for observations along the beam. These have verified the absence of any considerable number of primary electrons outside the limits indicated in figure 1, and have given confirmatory evidence for the scattering at and to the anode side of M. Photographs (*d*), (*e*) and (*f*) (Plate) show spectra of three such transverse slices of a discharge with parameters, pressure $1{\cdot}3 \times 10^{-2}$ mm Hg, anode current 100 mA, anode voltage 21·2 v. Photographs (*d*), (*c*) and (*f*) were taken 2·5, 7·5 and 17·5 mm respectively from the cathode with equal exposures. The meniscus was about 6 mm from the cathode. In (*d*) only AI lines appear, but in (*e*) AII lines are present with length nearly equal to the diameter of the undisturbed primary beam. In (*f*) the AII lines are longer and less intense, on account of the divergence of the primary beam. Some band background appears in (*f*). It will be noticed that the AI lines do not all behave in the same way, presumably because of their different excitation functions.

§ 4. CONCLUSION

It has been assumed in § 3 that the excitation of AII lines has been due to single impact of electrons of appropriate energy on neutral argon atoms in the ground state. Rough calculations show that the probability of excitation of the AII lines by electron impact with A^+ ions in the ground state, or with metastable argon atoms, is at least one order of magnitude less likely than direct excitation. Apart from the scattering, the properties of the discharge are also so similar on opposite sides of the meniscus that it seems unlikely that cumulative processes should occur on one side only, with mean free paths of the order of 1 cm or greater. Indirect processes might however be responsible for the occasional appearance of AII lines of almost constant very low intensity between the cathode and scattering region, when the cathode fall was well below 35 v. With this possible minor reservation, the behaviour of the spectra can be taken to support the probe evidence for presence of high energy electrons in the primary beam in the neighbourhood of and to the anode side of the meniscus.

ACKNOWLEDGMENTS

The writer wishes to thank Professor K. G. Emeléus for suggesting this work, and for his assistance in preparation of the paper. The spectroscopes were purchased with the aid of a grant from the Guild of Queen's University.

REFERENCES

BAILEY, R. A., and EMELÉUS, K. G., 1955, *Proc. R. Irish. Acad.*, **57**A, 53.
DITTMER, A. E., 1926, *Phys. Rev.*, **28**, 507.
MERRILL, H. J., and WEBB, H. W., 1939, *Phys. Rev.*, **55**, 1191.
MOORE, C. E., 1945, *A Multiplet Table of Astrophysical Interest* (Princeton Observatory).

The Decay of Cobalt 57

H. R. LEMMER, O. J. A. SEGAERT† AND M. A. GRACE
Clarendon Laboratory, Oxford

MS. received 15*th March* 1955

Abstract. The X- and γ-radiations excited during the decay of ^{57}Co have been investigated with scintillation and proportional counters. These measurements showed that the $14\cdot4 \pm 0\cdot1$ kev γ-ray follows the 123 kev γ-ray with a half-life of $1\cdot0 \pm 0\cdot1 \times 10^{-7}$ sec and that its internal conversion coefficient (α_{total}) is 15 ± 1. No evidence for β^+ emission with an intensity greater than 1/1300 per disintegration was found and upper limits of about 14% were set on the number of disintegrations proceeding directly to the ground and first excited states of ^{57}Fe. Spin and parity assignments are suggested.

§ 1. Introduction

FOLLOWING the original identification of 270 day ^{57}Co by Livingood and Seaborg (1941) a considerable amount of work has been performed in attempts to establish the decay scheme of this isotope. Since ^{57}Co is suitable for investigation by the method of nuclear orientation it seemed valuable to extend our earlier measurements on the 137 and 123 kev γ-rays (Alburger and Grace 1954) to the investigation of the 14 kev γ-ray, the sequence of the transitions and the electron capture branching to the different excited states in ^{57}Fe. In this way it was hoped to resolve some uncertainties still remaining in the decay scheme and thus restrict the choices of the spins and parities for the levels.

§ 2. The Decay Scheme

The earlier publications (Plesset 1942, Elliott and Deutsch 1943, Cheng, Dick and Kurbatov 1952) suggested that ^{57}Co decayed by positron emission (0·26 Mev) and electron capture to excited states of ^{57}Fe with the excitation of at least two γ-rays (γ_1 and γ_2) giving rise to internal conversion lines of approximately equal intensity. A soft electron group attributed to a highly converted γ-ray of about 14 kev confirmed the opinion that the γ-ray γ_1 represented a cross-over transition. Deutsch and Wright (1950) found evidence for an isometric state of half-life $1\cdot1 \times 10^{-7}$ sec associated with the 14 kev transition. It was identified by Goldhaber and Sunyar (1951) as an M1 transition from this half-life. From proportional counter and β-spectrometer measurements Alburger and Grace (1954) determined the α_K/α_L ratios for the two γ-rays and approximate values for α_K. They determined the energies of these as $122\cdot8 \pm 0\cdot5$ kev (γ_2) and $137\cdot6 \pm 0\cdot5$ kev (γ_1) and concluded that they were dipole ($\alpha_K \simeq 0\cdot01$) and quadrupole ($\alpha_K \simeq 0\cdot14$) respectively although their electric or magnetic character remained undetermined. (From the present measurements on the energy of γ_3 it appears that the best values for the energies of these γ-rays would be $123\cdot0 \pm 0\cdot5$ kev and

---

† On leave from the University of Ghent.

137·4 ± 0·5 kev.) In comparison with the 123 kev γ-ray, the 137 kev γ-ray was very weak, the branching ratio for the unconverted γ-radiation being $1:15\pm7$ and the total branching $1:13\pm6$. These results could be understood most easily by the decay scheme due to Goldhaber and Hill (1952) shown in figure 1, although they are insufficient to determine the level sequence unambiguously. The conclusions of the present paper confirm the level sequence of figure 1; the multipole assignments and tentative values for the spins and parities also shown in this figure are discussed in the following sections.

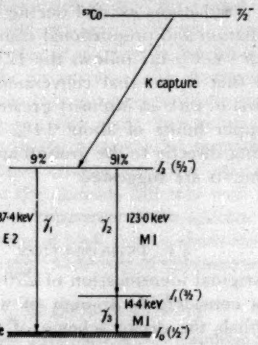

Figure 1. Decay scheme of ^{57}Co.

During the course of our experiments various other papers concerning these levels have appeared. Crasemann and Manley (1955) confirmed the approximately equal intensity of the 123 and 137 kev internal conversion lines and showed that positron decay is almost entirely absent ($<10^{-4}$ per disintegration). Temmer and Heydenburg (1954) succeeded in forming the 137 kev state by Coulomb excitation of ^{57}Fe and from the close agreement between their excitation curve and the predictions of theory (Alder and Winther 1953) concluded that the mode of excitation was electric quadrupole. By including ^{57}Co within a NaI(Tl) crystal in a scintillation spectrometer, Madansky and Rasetti (1955) have shown that the number of 14 kev γ-rays in coincidence with X-rays is negligible; they concluded that γ_2 and γ_3 are inverted in sequence, that the majority of the K capture transitions proceed directly to the 123 kev level and that γ_3 has a half-life long compared with the resolving time of their equipment ($1{\cdot}5\times10^{-6}$ sec). The long half-life for the 137 kev level required by this result appears to be quite incompatible with the value of approximately 5×10^{-9} sec which can be deduced from the transition probability ($B_2=0{\cdot}051\times10^{-48}$ cm^4) obtained by Temmer and Heydenburg from the cross section for Coulomb excitation.

§ 3. THE ^{57}Co SOURCE

A target containing ^{57}Co together with other activities was prepared by 18 Mev deuteron bombardment of 'Specpure' iron in the Nuffield cyclotron, Birmingham, in May 1952. Chemical separation of the cobalt activities from the bulk of the material was carried out and the extraction completed by complexing with α-nitroso-β-naphthol. Thin sources effectively free from other radioactive and carrier material were then obtained by electroplating on foils of aluminium. These sources originally contained approximately equal strengths of ^{56}Co and ^{57}Co but at the time of the present experiments (December 1954) the ratio of the strengths ^{56}Co/^{57}Co had decreased to about 1/150, a figure sufficiently small to enable useful results to be obtained on the disintegration of ^{57}Co.

§ 4. THE 14 kev TRANSITION

In this experiment and those described later both proportional counters and sodium iodide scintillation counters, employing E.M.I. type 6260 photomultiplier tubes have been used. The proportional counters were identical in construction with that described by Rothwell and West (1950) and were filled with krypton at 40 cm pressure, using methane at 4 cm pressure as the stabilizing organic vapour. The electronic equipment associated with these for the supply of the high voltages and for the pulse amplification and analysis was of conventional design.

In both types of counter it was found that the 14 kev γ-radiation, although weak, could be well resolved. The proportional counter was chosen for energy measurement of this radiation primarily because of its superior performance in the low-energy region. It also appeared from a preliminary examination that this γ-ray energy lies slightly above that of the K absorption edge of krypton (14·3 kev) and this was confirmed by the observation that an 'escape' peak (see figure 2) arising from escape of the krypton K radiation from the counter occurs at a low energy (1·8 ± 0·1 kev). This feature enables the γ-ray energy to be determined accurately as 14·4 ± 0·1 kev by adding the Kr K_α x-ray energy (12·6 kev) to that of the 'escape' peak. By comparing the intensity of this γ-ray

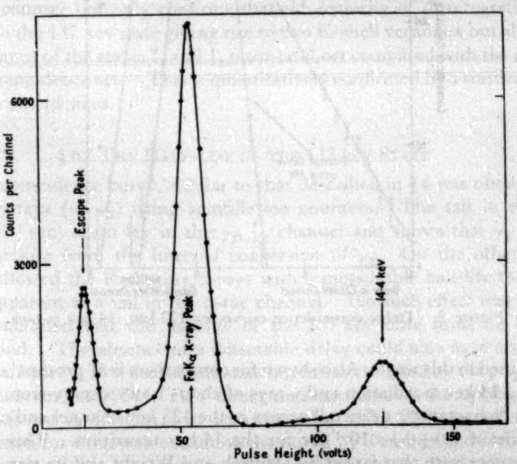

Figure 2. Pulse height distribution for the 14 kev γ-radiation and the iron K x-radiation using a krypton filled proportional counter.

using the proportional counter with the total γ-ray $(\gamma_1+\gamma_2)$ source strength, determined with a scintillation counter, a value for the internal conversion coefficient α_{total} of $14 \pm 1{\cdot}5$ was obtained; a small allowance was made for internal conversion of the 123 kev γ-ray and the presence of the 137 kev radiation. It was shown subsequently that no direct K capture to the 14 kev state occurred and that the transition followed rather than preceded the 123 kev transition and therefore this method of determining α_{total} is valid. The error in this value contributed by uncertainty in the branching ratio γ_1/γ_2 is negligible.

A pair of scintillation counters, operated in coincidence with a resolving time of 10^{-7} sec, was used to measure the lifetime of the 14 kev state by detecting the 123 and 14 kev γ-rays. One scintillation counter was fitted with a thin (1 mm) sodium iodide crystal for detecting the 14 kev γ-rays, the X-rays being eliminated by an aluminium absorber; the second counter whose pulse height discriminator was adjusted so as to make it insensitive to radiations below 100 kev in energy was fitted with a thick crystal. Figure 3 shows a typical delay-coincidence curve obtained in this way. Also shown for comparison is a 'prompt' coincidence curve using 14 kev X-radiation and γ-rays of about 1 MeV energy from a source of ^{88}Y. The characteristic delay tail occurs in the 123 kev channel and corresponds to a half-life of $1{\cdot}0 \pm 0{\cdot}1 \times 10^{-7}$ sec for the 14 kev transition. This value is in close agreement with that found by Deutsch and Wright and its sign establishes the fact that the 14 kev transition follows the 123 kev γ-ray. A comparison of the coincidence rate with the single channel counting rate shows that the 14 kev transition is associated with γ_2 rather than γ_1. The sequence of the transitions γ_2 and γ_3 agrees with that of figure 1 but is not in accord with the scheme proposed by Madansky and Rasetti.

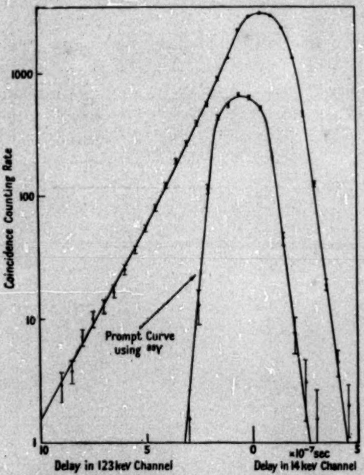

Figure 3. Delay coincidence curve for 123 kev, 14 kev γ-rays.

§ 5. X-Radiation from the Source

Using the proportional counter the yield of iron x-radiation from the source was determined from the area under the x-ray peak, combined with the calculated values of the counter efficiency, the solid angle subtended by the source and the transmission of the counter window. The total disintegration rate of the source was found from the γ-ray strength $(\gamma_1+\gamma_2)$ assuming that each disintegration involves the emission of one of these γ-rays. From these figures and the known fluorescence yield of iron (0·3) a value of $2{\cdot}1 \pm 0{\cdot}3$ K-shell vacancies per disintegration was obtained. It was concluded that about half of these originated in K capture while the remainder accompanied the internal conversion of the γ-radiation. Since γ_1 and γ_2 are only slightly internally converted the principal contribution must be due to γ_3.

This conclusion was confirmed by observing coincidences amongst the x-rays. To detect these a pair of krypton-filled proportional counters and a coincidence set with a resolving time of 10^{-6} sec were used. A large number of coincidences (approximately 10 per second) was observed. The contributions to this coincidence rate, after making allowance for the small background of fortuitous coincidences, were separated into the following categories by absorption in thin foils of aluminium and copper: coincidences amongst the x-rays 40%, between x-rays and γ_3 30%, x-rays and γ_2 15%, γ_2 and γ_3 10%, and cosmic-ray background 5%. The source strength determined from the x, x coincidence rate and the corresponding single channel counting rates was $2{\cdot}2 \pm 0{\cdot}4\,\mu$c. The agreement between this figure and that of $2{\cdot}2\,\mu$c determined by detecting $\gamma_1+\gamma_2$ with a scintillation counter not only confirms that the majority of disintegrations take place through the 137 kev state giving rise to two K-shell vacancies but also shows that the lifetimes of the states I_1 and I_2 must be short compared with the resolving time of the coincidence set. This is quantitatively confirmed by a similar analysis of the x, γ_3 coincidences.

§ 6. The Half-life of the 137 kev State

A delay–coincidence curve, similar to that described in § 4 was obtained with x-rays and γ-rays (γ_1, γ_2) using scintillation counters. The tail in the curve (half-life $\sim 10^{-7}$ sec) again lay in the γ_1, γ_2 channel and shows that γ_2 precedes the x-rays arising from the internal conversion of γ_3. On the other hand if γ_1, γ_2 had followed the K-capture x-rays with a measurable half-life this should have been apparent as a tail in the x-ray channel. No such effect was observed and it is concluded that the half-life of the 137 kev state must be less than 5×10^{-8} second. The absence of a detectable delay could also have arisen from a very long half-life ($>10^{-4}$ sec) of this state but this is excluded by the proportional counter measurements (§ 5). This direct measurement of the upper limit for this half-life is not in disagreement with the value of 5×10^{-9} sec deduced from the cross section for Coulomb excitation measured by Temmer and Heydenburg.

Confirmation of this cross section has been obtained by Coulomb excitation of this level with 850 kev protons using an enriched ^{57}Fe target. The thick target yield of γ-radiation $(\gamma_1+\gamma_2)$ was determined by direct comparison, with a standardized source of ^{57}Co in the same geometry. Using the treatment of Alder and Winther (1953) a value for the transition probability B_2 of $0{\cdot}015 \times 10^{-48}$ cm^4 was found. Although the accuracy of the measurement was vitiated by the high x-ray background it nevertheless confirms within an order of magnitude the value for B_2 of $0{\cdot}051 \times 10^{-48}$ cm^4 obtained by Temmer and Heydenburg and indicates that the half-life of this state must be in the neighbourhood of 10^{-8} second.

§ 7. THE β^+/K CAPTURE RATIO

A scintillation spectrometer was used to compare the intensity of the γ-radiation (γ_1, γ_2) with that of the positron annihilation radiation from a ^{57}Co source. The spectrometer was calibrated with γ-ray sources of known strength and hence a value of one positron per 400 disintegrations of ^{57}Co was obtained. After correcting for those positrons arising from the residual ^{56}Co activity, estimated from the intensity of the prominent 845 kev γ-ray and the proportion of disintegrations in ^{56}Co proceeding by β^+ emission (Sakai, Dick, Anderson and Kurbatov 1954), the number of positrons in the decay of ^{57}Co was found to be less than 1/1300 per disintegration. There was, in fact no evidence for the presence of positrons in the decay. This is in accord with the total energy available for the transition to the ground state of ^{57}Fe, $0{\cdot}45 \pm 0{\cdot}30$ MEV, as determined from the cycle of nuclear reactions, ^{57}Fe(n, γ)^{58}Fe, ^{58}Co(β^+, γ)^{58}Fe, ^{59}Co(γ, n)^{58}Co, ^{59}Co(p, n)^{59}Ni, ^{58}Ni(n, γ)^{59}Ni, ^{58}Ni(γ, n)^{57}Ni, ^{57}Ni(β^+, γ)^{57}Co (see Nussbaum 1955).

§ 8. K CAPTURE BRANCHING TO THE GROUND AND 14 kev STATES

Further single channel and coincidence measurements between x-rays and $\gamma_1 + \gamma_2$ and between γ_2 and γ_3 were made with scintillation counters using a coincidence resolving time of 3×10^{-7} second. This increased resolving time was chosen so that by suitably shaping the scintillation counter pulses only a small ($\sim$5%) loss of coincidences occurred; the exact value of this loss was determined in auxiliary experiments. From these measurements using the decay scheme of figure 1 it was possible to determine the number of K-capture transitions proceeding directly to the 14 kev level and to the ground state of ^{57}Fe; in each case this figure was less than 14% of the total number of disintegrations. A value of 15 ± 1 for α_{total} for the 14 kev transition was also deduced from these measurements, in agreement with that found using the proportional counter. Apart from the different technique used to obtain this figure it represents an improvement on that derived from the proportional counter measurements in that it requires no knowledge of the absence of K capture directly to the 14 kev state.

§ 9. DISCUSSION AND CONCLUSIONS

It is concluded from the present measurements that the basic features of the decay scheme are those displayed in figure 1. There was no evidence for β^+ decay ($< 8 \times 10^{-4}$) nor for K capture to the 14 kev or ground states of ^{57}Fe ($<$14%).

From the half-life of the 14 kev level Goldhaber and Sunyar (1951) suggest that this transition is predominantly M1 and consequently the level I_1 has the same parity as the ground state of ^{57}Fe. This half-life agrees well with other M1 half-lives which have been tabulated by Graham and Bell (1954), and is approximately 100 times longer than Weisskopf's single-particle estimate. Our value for α_{total} is in approximate agreement with Reitz's (1950) value for α_K of 13·3 evaluated for copper and with a value of about 8 extrapolated from the figures of Rose, Goertzel and Swift (unpublished) and thus supports this assignment; the value of α_K for an E2 transition of this energy is about 400 and this shows that if E2 radiation is also present its proportion must be small. The E2 character of the Coulomb excitation of the 137 kev level shows that this is also of the same parity as the ground state and thus all these levels of ^{57}Fe must have the same parity. Combining this information with the internal conversion data on γ_1 and γ_2 it is concluded that these are mainly E2 and M1 respectively. Such an assignment would be in accord with the known competition between M1 and E2 transitions of similar energy. The half-life of γ_2 ($\sim 5 \times 10^{-9}$ sec) is also in good agreement with Graham and Bell's figures and is again about 100 times longer than the single particle estimate.

The absence of K capture to the level I_1 suggests that this transition is at least one order more forbidden than that to the level I_2. From the calculated value for the disintegration energy it is found that the value of log *ft* for the K-capture transition cannot exceed 6·2. Comparing this with the data on β-transitions of Mayer, Moszkowski and Nordheim (1951), it is seen that this transition must be allowed or first forbidden with ΔI not greater than 1. Since all the ^{57}Fe levels have the same parity, I_1 must differ in spin from the ground state (7/2) of ^{57}Co (Baker *et al.* 1953) by at least 2 and therefore must be 1/2, 3/2, 11/2 or greater than 11/2. The nuclear shell model suggests that these low lying levels in ^{57}Fe are of low spin rather than high spin and therefore a spin of 11/2 or greater for I_1 is unlikely. The spin sequence I_2, I_1, I_0 which would fit this evidence most satisfactorily would be 5/2, 3/2, 1/2.

From the presence of a strong transition to a level close to the ground state in the neutron capture γ-ray spectrum of ^{56}Fe, Kinsey and Bartholomew (1954) concluded that one of the low lying levels in ^{57}Fe had a spin of 3/2 or 1/2 and odd parity. If this level can be identified with either the 14 kev or ground state it can be concluded that the parity of all these levels is odd. These proposed values for the spins and parities are incorporated in figure 1.

ACKNOWLEDGMENTS

We are indebted to the Nuffield Cyclotron Group at Birmingham for their cooperation in irradiating the iron target and to the Director of the Atomic Energy Research Establishment, Harwell, for the enriched ^{57}Fe target. Our thanks are due to Dr. P. F. D. Shaw for the chemical separation and preparation of the cobalt sources and to Dr. F. V. Price for his help in the experiments using the 1 MEV accelerator. We are most grateful to Professor H. Halban for much helpful advice and encouragement and to Lord Cherwell for his interest in this work. We wish to thank the Nuffield Foundation for a research fellowship (H.R.L.) and the Inter Universitair Instituut voor Kernwetenschappen (Belgium) for a scholarship (O.J.A.S.).

REFERENCES

ALBURGER, D. E., and GRACE, M.A., 1954, *Proc. Phys. Soc.* A, **67,** 280.
ALDER, K., and WINTHER, A., 1953, *Phys. Rev.*, **91,** 1578.
BAKER, J. M., BLEANEY, B., BOWERS, K. D., SHAW, P. F. D., and TRENAM, R. S., 1953, *Proc. Phys. Soc.* A, **66,** 305.
CHENG, L. S., DICK, J. L., and KURBATOV, J. D., 1952, *Phys. Rev.*, **88,** 887.
CRASEMANN, B., and MANLEY, D. L., 1955, *Phys. Rev.*, **98,** 66.
DEUTSCH, M., and WRIGHT, W. E., 1950, *Phys. Rev.*, **77,** 139.

Elliott, L. G., and Deutsch, M., 1943, *Phys. Rev.*, **64,** 321.
Goldhaber, M., and Hill, R. D., 1952, *Rev. Mod. Phys.*, **24,** 179.
Goldhaber, M., and Sunyar, A. W., 1951, *Phys. Rev.*, **83,** 906.
Graham, R. L., and Bell, R. E., 1954, *Canad. J. Phys.* **30,** 377.
Kinsey, B. B., and Bartholomew, G. A., 1954, *Phys. Rev.*, **93,** 1260.
Livingood, J. J., and Seaborg, G. T., 1941, *Phys. Rev.*, **60,** 913.
Madansky, L. and Rasetti, F., 1955, *Phys. Rev.*, **97,** 837.
Mayer, M. G., Moszkowski, S. A., and Nordheim, L. W., 1951, *Rev. Mod. Phys.* **23,** 315.
Nussbaum, R. H., 1955, *Nuclear Levels in the Neighbourhood of the* 1 $F_{7/2}$ *State.* (Assen : von Gorcum).
Plesset, E. H., 1942, *Phys. Rev.*, **62,** 181.
Reitz, J. R., 1950, *Phys. Rev.*, **77,** 10.
Rothwell, P., and West, D., 1950, *Proc. Phys. Soc.* A, **63,** 539.
Sakai, M., Dick, J. W., Anderson, W. S., and Kurbatov, J. D., 1954, *Phys. Rev.*, **95,** 101.
Temmer, G. M., and Heydenburg, N. P., 1954, *Phys. Rev.*, **96,** 426.

A New Phenomenon Associated with Active Nitrogen

By C. R. STANLEY
Department of Physics, Imperial College, London

MS. received 1st *February* 1955 *and in amended form* 28th *February* 1955

Abstract. An orange beam, obtained with the author's recent active nitrogen apparatus, is considered to constitute a nitrogen afterglow. Its spectrum is compared with the exciting arc spectrum over a range of pressure and current. The decay is exponential, with a mean life of the order of 10^{-4} second. Other physical and chemical properties are briefly discussed.

---

§ 1. Description

In the spring of 1952, the author was attempting to excite a fluorescence in nitrogen by means of a high-voltage arc with a hollow electrode. At a certain stage it was noticed that there was a slight red protrusion, somewhat similar in appearance to the positive column of the arc, from the hole in the hollow electrode; the pressure was then sufficiently high to confine the negative glow (which is normally more voluminous than the positive column) entirely within the hollow electrode and it was therefore very surprising to see part of the positive column apparently extending beyond it. The matter was investigated further and it was found that at somewhat higher pressures the red protrusion became unsymmetrical; the direction of asymmetry suggested that it was influenced by convection currents.

With a view to making the phenomenon more marked, another apparatus was constructed, in which the arc ran in a quartz capillary tube through which the nitrogen was allowed to stream. The hollow electrode was mounted outside the capillary, near one end of it, and the direction of flow was towards this electrode. With nitrogen at a pressure of a few mm Hg and a current of about 10 mA, an ordinary glow discharge was observed; a red positive column filled the capillary and the electrodes were immersed in the usual blue volume glow. At slightly higher pressure, a red core (similar to the protrusion seen with the first apparatus) appeared at the centre of the blue glow, and as the pressure was further increased the red core became larger, while the blue glow dwindled, until eventually the red core extended well beyond the boundary of the blue glow. At a pressure of several cm Hg, the blue volume glow had disappeared altogether. Filling the remainder of the vessel there appeared a yellow glow which was readily identified from its spectrum as the afterglow of active nitrogen, while the protruding red glow had taken on an orange hue and had become much narrower and longer, appearing as a pencil or beam of orange light on the yellow green background. The phenomenon is one of much visual beauty.

Details of the apparatus have already been published (Stanley 1954). With a fast pump, a current of around 100 mA, and a pressure of several cm Hg the 'beam' can be made at least as long as 10 cm and of considerable brilliance, suitable for demonstration to a large audience.†

In the remainder of this paper some of the properties of the beam will be examined in more detail.

§ 2. THE SPECTRUM OF THE BEAM

2.1. *Principal Features*

The spectrum of the beam has been photographed under various conditions, with Hilger medium quartz and medium glass spectrographs. The spectrograms show in general, the First Positive, Second Positive and First Negative band systems of nitrogen, all with an intensity distribution which (at least superficially) resembles that of an ordinary discharge spectrum. In particular there appears to be no selective enhancement of certain bands such as might be expected if the excitation were due to fluorescence or to collisions between ordinary nitrogen molecules and metastable atoms or molecules. The impurities OH, NH occur strongly and the NOγ system occurs moderately in all (or most) of the beam spectra. In arriving at these results, allowance has been made for the possibility of contamination by the yellow-green (Lewis–Rayleigh) afterglow which always accompanies the orange beam, and the blue-violet electrode glow which at the lower pressures extends as far from the electrode as does the beam.

2.2. *Comparison of Exciting Arc, Beam, and Chamber Glow*

Geometrically the beam appears to be a prolongation of the exciting discharge. The colour of the beam appears orange-red compared with the pink-red of the discharge; but as the latter is intrinsically a good deal brighter, the colour difference is not sufficiently great to be definite. Furthermore, the beam spectrum is very like an ordinary nitrogen discharge spectrum and for these reasons several observers have suggested that the beam is simply "part of the arc blown out of the capillary". It is consequently desirable to make a detailed comparison between the beam and its own exciting arc. To this end, several pairs of discharge and beam spectra, for diverse conditions, have been photographed. The Plate is a reproduction of one of these photographs, taken with a medium quartz spectrograph on an Ilford H.P. 3 plate. The pressure was about 1 cm Hg and the current about 90 mA. (*a*) shows the discharge spectrum. This was photographed through the side of the capillary tube to avoid contamination by the beam and the electrode glow. Because the arc is surrounded by a Pyrex jacket, the ultra-violet is cut off below about 3200 Å, and the comparison is therefore valid only at greater wavelengths than this. (*b*) shows the beam spectrum, photographed through the quartz window of the observation chamber (with the chamber glow (*c*) superimposed). The attenuation along the length of the beam is well illustrated here. (*c*) shows the spectrum of the yellow-green glow that fills the observation chamber, photographed with the same exposure time as (*b*).

In this, as in the other photographs obtained, it is clear that the beam and discharge spectra are different in detail. In the discharge, the First Positive and Second Positive systems of nitrogen occur with about the same relative intensity as in the beam and with no conspicuous difference in intensity distribution. However, the First Negative system which, in the beam, is rather stronger than the Second Positive, is only very faintly present in the discharge (only the (0, 0) sequence showing at all, on the plate which records the Second Positive about equally strongly in beam and discharge.) NH is present strongly in the beam but is absent from the discharge. The same appears to be true of OH but as this occurs near the Pyrex cut-off, the evidence for its absence in the discharge is a little uncertain.

---

† The apparatus was demonstrated by the author at the Royal College of Science Conversazione at Imperial College, in October 1953.

The chamber glow (*c*), exhibits simply the α, β and γ bands of Fowler and Strutt (1911) which at once identifies it with the afterglow of active nitrogen.

2.3. *Effect of Pressure Variation*

The beam spectrum has been photographed over a pressure range of a few mm Hg to about 10 cm Hg. The spectral changes are of special interest when compared with those of the exciting discharge. The latter exhibits the First Negative system strongly at very low pressures (of the order of 10^{-1} mm Hg). As the pressure is increased, the intensity of this sytem diminishes; over the entire range mentioned above, it is only faintly present. The First and Second Positive systems, both quite strong, undergo scarcely any alteration throughout this same pressure range. The beam behaves quite differently. At a few mm Hg it has very little First Negative while the Second Positive and also the First Positive are quite strong, but as the pressure rises the First Negative intensity rapidly increases while the Second Positive intensity falls, so that by 5 cm Hg the beam has strong First Negative and First Positive but practically no Second Positive radiation.

2.4. *Effect of Current Variation*

There is, as would be expected, an overall intensity increase that is at least (probably more than) in proportion to the current. But it is not the same for all systems: for a pressure of 1 cm Hg the First Negative system is not visible at lowest current (compared with medium intensity Second Positive) but at highest current it is much stronger than the Second Positive system; First and Second Positive systems show fairly similar variation, both increasing about proportionately with current (Second Positive rather more than proportionately). At lowest current, NH is much more prominent than the nitrogen Second Positive (0, 0) band but at higher currents NH has either vanished, or at least is obscured by the Second Positive (0, 0) band. Much the same is true of OH which is prominent at low current but absent, or obscured by N_2^+, at higher current. The third principal impurity, NO, has no chance of being obscured and is still very noticeable at high current, but is has definitely undergone an intensity increase, much less than proportionately to the current.

Thus it seems that the systems can be grouped as follows: for increasing current the nitrogen spectra N_2 and N_2^+ show a constant or an increasing intensity per unit current, while the impurities, NH, OH and NO, show a decreasing intensity per unit current.

§ 3. THE PHYSICAL NATURE OF THE BEAM

The possibility that the beam is part of the arc, carried forward by the stream of gas, is an obvious suggestion from the appearance of the phenomenon and from the similarity of the beam and arc spectra. However, it has been noted above that their spectra are different in detail; furthermore, this difference is not of the kind that would be expected to develop from a mere difference in decay times of the systems involved, for some features are stronger in the beam than in the arc, and in any case such a differential decay would be very apparent along the beam itself, but there is no evidence of it. An independent refutation of this possibility was obtained as follows: the arc was extinguished by reducing the voltage quickly to zero, whereupon the boundary between the Lewis–Rayleigh glow and the following unactivated gas could be seen moving along the observation tube. The speed of flow was obtained by observations with a stop watch, and with a knowledge of the apparatus dimensions and the ordinary principles of gas flow, the velocity of the gas stream leaving the capillary was calculated. The value obtained was of the order of 10^4 cm sec^{-1}, so that the time interval corresponding to the observed length of beam was about 5×10^{-4} second. This is the time for which the excited states responsible for the emission would have to persist, if the excitation took place in the arc and the radiation in the beam. In fact, the systems emitted correspond to permitted transitions for which the mean lifetime could scarcely be greater than about 10^{-7} second.†

A second possibility is the production in the capillary tube of very short wavelength ultra-violet radiation that could be absorbed by molecular nitrogen, with the production of fluorescence. This would account for the properties of the beam described above. In particular, the pencil of radiation would have the same geometrical form as is observed for the beam, and there would be an exponential attenuation along the beam as is illustrated in (*b*) of the Plate.

Thirdly there might be produced in the arc, some energy-carrying constituent which, by subsequent collision with nitrogen molecules, excites the states responsible for the observed emission from the beam. Such a constituent would be analogous to, though different from, active nitrogen, and the beam would constitute a nitrogen afterglow albeit of much shorter duration than the Lewis–Rayleigh afterglow.

A simple observation distinguishes between these last two possibilities: if the mechanism were fluorescence, the path of the beam would be defined by the path of the exciting radiation from the capillary and so could not be deflected in any way; on the other hand, if the phenomenon were an afterglow due to a material constituent of the gas stream, the beam path would be defined by the path of the stream and so would suffer deflection with the stream. Accordingly an auxiliary capillary tube was inserted through the wall of the observation vessel and used to direct a second stream of nitrogen at the beam. Thereupon the beam was seen to bend and waver.

Thus we are led to the conclusion that the phenomenon is due, not to persistence of the original discharge luminosity, nor to fluorescence of the gas stream through absorption of radiation from the discharge, but rather to some material constituent, carrying energy from the discharge and subsequently dissipating it as an afterglow.

§ 4. THE ACTIVE NATURE OF THE BEAM

It is natural to ask whether or not the energy-carrying constituent is 'active' in the same sense as is active nitrogen. No systematic study of this question has yet been made, but preliminary observations suggest that the answer may be in the affirmative. A piece of crystalline quartz, placed in the path of the beam, became covered with an immovable white film suggestive of chemical attack. Several metals similarly treated acquired a coating of their respective nitrides. In a darkened room, a strong green luminescence was seen to be excited in both Pyrex glass and quartz, placed in the path of the beam.

---

† The author is not aware of any experimental determination of the lifetimes of the actual states involved, but the states are not detected by the technique of Muschlitz and Goodman (1953) which implies that they have mean lifetimes certainly smaller than 10^{-6} second.

Closely related to the question of activity is that of the effect of heat. It was shown by Lord Rayleigh (1911) that the afterglow associated with active nitrogen was weakened if the observation vessel was heated; with sufficiently strong heating the afterglow disappeared completely but the glowless gas nevertheless retained its chemical activity. This fact has played an important part in the theories of active nitrogen for it suggests at once the presence of at least two constituents. In the present apparatus the phenomenon is very conspicuous; the chamber glow is visually very much brighter soon after switching on than it is when the tube has become hot. In contrast with this, there is no visually conspicuous change in the beam intensity; in fact it appears to become brighter rather than weaker, though a visual estimate is difficult on account of the changing background. To obtain a quantitative measure of the effect of heat on the beam several plates have been calibrated and exposed to both the 'hot' and the 'cold' beams. All the standard precautions for precise photographic photometry were taken. The First Positive band system was taken as representative of the whole beam and it was found that the intensity was *unchanged* within the experimental error (not greater than 5%), while the chamber glow intensity, under the same respective conditions, was diminished about four-fold.

It is concluded therefore, that heat quenching in the beam afterglow, if it exists at all, is of very much smaller magnitude than is the heat quenching of the Lewis–Rayleigh afterglow.

§ 5. DETERMINATION OF THE ATTENUATION CONSTANT OF THE BEAM

5.1. *Experimental*

A sharp image of the beam was formed in the plane of the spectrograph slit by a condensing lens; this lens was a quartz-fluorite achromat of long focal length so that the image was quite sharp for all parts of the visible spectrum simultaneously. The aperture was reduced to f/20 in order to minimize other aberrations.

The principal spectrograph employed was the medium glass Hilger instrument; for the near ultra-violet and for confirmatory results in the visible, the medium quartz instrument was used. Both have an aperture of about f/11 and consequently were much less than filled by the above condensing system, a desirable feature in photometric work since the scattered light is then quite small. A mask was made for the plate holder to intercept such scattered light as remained. A wide slit was used in order to give a flat topped peak to each band head, thus facilitating the subsequent measurement of photographic image density.

It had been found from previous experience that Ilford Astra III are among the best panchromatic plates for photographic photometry and Ilford Ordinary, although rather slow, are excellent for the shorter wavelengths. These plates had also been found to exhibit comparatively little reciprocity failure for the particular range of illumination employed in the present experiments.

Accordingly most of the calibration exposures were made with a fixed illumination for various times, the mean of which was about equal to the time of the principal exposure. A fine grain developer (Ilford D.11) was used, and the usual precautions for photometric work were taken.

The resulting spectrograms were examined with a Hilger non-recording microdensitometer and graphs were plotted showing the variation of intensity along the length of the beam, for each of several nitrogen bands, and for the (0, 0) and (1, 1) bands of NH.

The effect of the superimposed Lewis–Rayleigh glow was minimized by photographing from the side of the tube. It was then easy to make a correction for the slight effect that remained merely by taking a second photograph with twice the path length of Lewis–Rayleigh glow. (By itself the Lewis–Rayleigh glow produced an effect that was below the threshold of the photographic plate, so that direct measurement and subtraction were not possible.)

In the interpretation of the results, the assumption is made that the peak intensity of the band head can be regarded as proportional to the integrated band intensity. This is tantamount to supposing that there is no change of rotational energy distribution along the beam; a separate experiment has been performed to show that this is, in fact, the case.

5.2. *Results*

For the nitrogen First Positive system, the intensity I is found to diminish exponentially with distance along the beam. Graphs of log I against distance have been plotted for the (5, 1) (8 ,4) and (8, 5) bands and are found to be accurate straight lines, the slopes differing from one another by less than 3%. Thus the decay of the active particle evidently represents a monomolecular reaction. If the concentration of active particles at position x is denoted by $n(x)$, then

$$n(x) = n_0 e^{-\alpha x} = n_0 e^{-\alpha v t}$$

where v is the beam velocity and t denotes time. The intensity of the emitted radiation is presumably proportional to the concentration of the active particles, so that

$$\log I \propto \log n(x) = \log n_0 - \alpha x$$

and the constant α is therefore numerically equal to the slope of the graph of log I against x.

The value obtained for the attenuation constant αv is $0{\cdot}71 \times 10^4$. The mean life of the active particles, equal to $1/\alpha v$, is thus $1{\cdot}4 \times 10^{-4}$ second.

Since this value was obtained, Muschlitz and Goodman (1953) have published a paper describing a method for the measurement of the lifetime of the metastable $A^3\Sigma_u^+$ state of N_2 and giving the value $2{\cdot}3 \times 10^{-4}$ second. The proximity of this time to the value obtained above for the lifetime of the active particle, suggests that the latter may be identified with the $A^3\Sigma_u^+$ state N_2, a possibility which would otherwise have been merely conjectural.

In the experiments of Muschlitz and Goodman, the pressure of nitrogen was around 10^{-4} mm Hg which is sufficiently low to ensure that the life is not shortened by collisions. The effective diameter for collisions between metastable A-state molecules and ordinary molecules was also determined and found to be 3·8 Å which is very close to the kinetic theory value. It might therefore appear that at the much higher pressure of the present experiments, the combined effects of collisional de-excitation and radiative de-excitation would be a very much smaller lifetime than the value actually obtained. However it must be remembered that with the technique used by Muschlitz and Goodman any collision with a normal molecule would almost certainly remove the metastable molecule from the detected molecular ray, whereas in the present experiment it would merely result in the passing-on of the excitation energy to another nitrogen molecule, without any appreciable reduction in the metastable molecular density. There may, of course, be some loss in the form of superelastic collisions, but this process would be expected to have a much smaller probability than the exchange of the whole of the electronic energy with another nitrogen molecule (Oldenberg 1952, Franck and Jordan 1926). Such loss may account for the present value being lower than that of Muschlitz and Goodman, though it is doubtful if the accuracy is sufficient for the difference to be significant.

The mechanism of production of the First Positive bands would seem to be a consequence of the presence in the beam of a large concentration of N_2(A) molecules together with ordinary active nitrogen. If, as is now generally supposed, the latter consists of atomic nitrogen, then the recombination of two nitrogen atoms in a three-body collision with an N_2(A) molecule would release sufficient energy to raise the molecule to the B state from which radiation of the First Positive system occurs. Since resonance is not effective in such a recombination (Oldenberg 1952) there would not be any selectivity in the excitation of the various vibrational levels, in contradistinction to the situation obtaining in the Lewis–Rayleigh glow and in conformity with the observed spectrum of the beam afterglow.

The other parts of the beam afterglow spectrum have not been examined as carefully as was the nitrogen First Positive system. The graphs of log I plotted against x are, for all the bands examined, approximately straight lines, but the scatter of the points is not sufficiently small definitely to exclude the possibility of a bimolecular curve. The graphs of $1/\sqrt{I}$ plotted against x, which would be straight for a bimolecular reaction, do show a slight curvature but again not very definitely on account of the scatter. Thus it seems desirable to postpone discussion of these other bands until more precise data are available. It may perhaps be worth noting that the order of magnitude of the attenuation constants is the same for all the bands investigated, but there is a variation from one system to another by a factor of about two, which does not seem to be ascribable to experimental error and which therefore suggests that more than one mechanism is operative.

§ 6. OTHER AFTERGLOW PHENOMENA IN NITROGEN

A new afterglow in nitrogen, which bears some resemblance to the present beam afterglow, was detected in 1945 by Herman by the application to nitrogen of the newly developed phosphoroscope of Lejay (1944). The duration of this afterglow was about 10^{-3} second compared with several seconds for the visually observed auroral afterglow reported earlier by Kaplan (1932, 1934, 1935). The present beam afterglow has a duration similar to that of Herman's, but the method of production, the pressure range over which the phenomenon appears, and the spectrum are different. A more detailed consideration of the relations between the Kaplan, Herman and beam afterglows will be attempted in a later paper, after the presentation of further experimental results on the latter.

ACKNOWLEDGMENTS

My thanks are due to Mr. W. R. S. Garton and to Professors R. W. B. Pearse, P. M. S. Blackett and Sir George Thomson, for their interest in this work. I am indebted to Dr. J. F. Herringshaw of the Chemistry Department for the use of the Hilger microdensitometer.

REFERENCES

FOWLER, A., and STRUTT, R. J., 1911, *Proc. Roy. Soc.* A, **85**, 377.
FRANCK, J., and JORDAN, P., 1926, *Anregung von Quantensprungen durch Stosse* (Berlin : Springer).
HERMAN, R., 1945, *C. R. Acad. Sci., Paris*, **220**, 593, 878.
KAPLAN, J., 1932, *Phys. Rev.*, **42**, 807; 1934, *Ibid.*, **45**, 671; 1935, *Ibid.*, **48**, 800.
LEJAY, P., 1944, *C. R. Acad. Sci., Paris*, **216**, 536.
MUSCHLITZ, E. E., Jr., and GOODMAN, L., 1953, *J. Chem. Phys.*, **21**, 2213.
OLDENBERG, O., 1952, *Phys. Rev.*, **87**, 786.
RAYLEIGH, LORD (STRUTT), 1911, *Proc. Roy. Soc.* A, **85**, 219.
STANLEY, C. R., 1954, *Proc. Phys. Soc.* A, **67**, 821.

The K-Series Emission Spectrum of Neon

By H. R. MOORE[†] and the late F. C. CHALKLIN
Physics Department, Canterbury University College, Christchurch, New Zealand

MS. received 10*th December* 1954 *and in final form* 9*th March* 1955

Abstract. The K-spectrum of neon has been examined with a photographically recording bent crystal x-ray spectrometer. The radiation source was an electrodeless discharge tube. The intensity contour of the spectrum was derived leading to a study of the shape of the diagram line $K\alpha_{1,2}$ and an analysis of some satellite structure. Wavelength values are given for the diagram line $K\alpha_{1,2}$ (14·5847 kx units), the semi-optical diagram line $K\beta_1$ (14·430 kx units) and twenty satellite lines (14·278–14·539 kx units).

§ 1. Introduction

The precision with which x-ray spectroscopic data can be interpreted is determined firstly by the state of aggregation of the emitting element and secondly by the number of electrons involved. For these reasons the K-series emission spectrum of neon is of particular interest since it arises in a monatomic gas of low atomic number. Previous examinations of the neon K-spectrum have been made by Bačkovský (1936) and by Kunzl and Svobodová–Joanelli (1946). Using a low voltage ion tube as source and a plane grating Bačkovský obtained the diagram line $K\alpha_{1,2}$ at a wavelength of 14·61 Å. With a similar source but using a bent mica crystal spectrometer having limited focal properties, Kunzl and Svobodová-Joanelli showed that a number of satellite lines are also present in this spectrum. Their results are summarized in table 1. The present work was carried out with a photographically recording bent crystal vacuum spectrograph designed to operate at wavelengths up to about 20 kx units. An innovation for this wavelength region was the use of a high frequency electrodeless discharge tube as the radiation source.[‡]

Table 1

Neon K-series	Wavelength (kx units)	Remarks
$\alpha_{1,2}$	14·587	Most intense line of group
α' Long wavelength limit	14·550	A weak line broadened towards long wavelengths
α' Maximum of blackening	14·526	
$\alpha_{3,4}$	14·485 14·470	Only measurable as two lines on some plates
β_1	14·435	A very feeble line
α_8–α_9 β^{V}–β^{VI}	14·368– 14·271	Broad diffuse band

[†] Now with the Dominion Physical Laboratory, Department of Scientific and Industrial Research and seconded to the Physics Department, Canterbury University College.

[‡] This method of excitation has been used at shorter wavelengths by Groven (1949) and his associates at Brussels.

§ 2. Apparatus

The spectrometer, which is of the reflection type, is described elsewhere (Moore 1955). Using a muscovite mica crystal bent with a radius of 50 cm it has an inverse plate dispersion of about 37 x units mm^{-1} at a wavelength of 15 kx units in the first order. It is situated in a vacuum case to which the x-ray tube is directly attached.

The x-ray tube is a dual one, being effectively a hot filament high vacuum tube into whose glass envelope is sealed an external electrode ('electrodeless') discharge tube. A normal anti-cathode which emits radiation from a nickel target for wavelength calibration is mounted in a vacuum bellows and may be withdrawn into a side-arm. This permits radiation from the gas in the discharge tube to be emitted in precisely the same direction to fall on the spectrometer crystal. The pure silica discharge tube is about 20 cm long and has a rectangular (2 cm × 0·5 cm) cross section. Its normal operating power of 135 w r.m.s. is supplied from a valve oscillator (1·7 Mc/s) driving a Tesla coil whose unloaded terminal voltage is 40 kv. The discharge tube is cooled by immersion in an oil bath.

A circular window (1·6 cm diameter) placed between the x-ray tube and the spectrometer case retains the gas in the discharge tube at the operating pressure of about 0·1 mm Hg and also prevents the visible discharge from fogging the plates. It consists of a $1\cdot5 \times 10^{-5}$ cm thick film of Formvar which is rendered opaque to visible light by being vacuum coated with a 10^{-5} cm thick layer of aluminium. To avoid localized imperfections in the aluminium coatings two such films are placed in series, one of which makes the necessary vacuum seal. The window transmits about 10% of x-radiation with a wavelength of 15 kx units.

The spectrometer case is evacuated to its usual pressure of about 10^{-4} mm Hg by a baffled oil diffusion pump. A separate oil diffusion pump evacuates the x-ray tube through a cold trap to a pressure which is about 10^{-5} mm Hg when the calibration electrodes are being used. The pumping system is arranged to protect the tube window from excessive pressure differences. A simple monitoring system allows the gas under study to be introduced into the discharge tube at the required pressure.

§ 3. Experimental Procedure

The spectra were recorded with Ilford Q emulsions coated on plane glass plates. Two grades, Q1 and Q2, were used, the latter being the faster but having the larger grain size. A shutter on the plate holder allows several exposures (overlapping or separate) to be made on a plate. Some plates were exposed to the neon radiation alone (figure 1, Plate) while others were also exposed to nickel radiation to provide wavelength calibration lines (figure 2, Plate). Under favourable circumstances it has been possible to record the stronger lines in the neon spectrum on a Q1 plate in two hours while the complete spectrum is present on a Q2 plate in eight hours.

The useful plates were surveyed with the microdensitometer described by Tait and Chalklin (1953) and now adapted for use with a strip chart recorder.

The relationship between density of photographic blackening and intensity of incident radiation (the so-called blackening curve) was obtained for each plate by giving it two neon exposures for different times at constant source intensity. After determining the density values in equivalent regions of the two exposures the blackening curve was constructed in the usual manner (cf. Hill 1937). The curves obtained are smooth and reproducible, their good quality being attributed to the fact that unlike a solid emitter the discharge source is not liable to changes in its emission character due to contamination.

Apart from the second order of the silicon line $K\alpha_{1,2}$ (emitted by the silica discharge tube and recorded when the spectrometer is suitably focused, cf. figure 1) no characteristic radiation was detected when the discharge tube was operated with air under conditions identical with those for which the lines ascribed to the neon K-series were recorded. The neon spectrum is found to be complex. On the short wavelength side of the diagram line $K\alpha_{1,2}$ (readily identified from its strong intensity and wavelength position) there are at least twenty-one lines, none of which is completely resolved. They are conveniently labelled I–XXI in the microdensitometer record of the spectrum shown in figure 3.

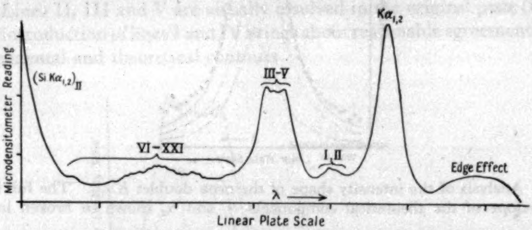

Figure 3. Tracing of average microdensitometer record of the K-series emission spectrum of neon showing the diagram line $K\alpha_{1,2}$ and satellite lines I-XXI. Also present is the second order of silicon $K\alpha_{1,2}$ and an effect due to the discharge tube wall.

The spectrum has a general background due to continuous radiation from both gas and tube. It is approximately constant over the region which corresponds to the central part of the discharge. The latter varies in a peculiar manner near the tube walls and may give rise to two diffuse line-like regions of blackening on the plate records. Such an 'edge-effect' is visible in figure 1.

§ 4. THE SHAPE OF THE NEON LINE $K\alpha_{1,2}$

Two plates were exposed to neon radiation under selected conditions. Microdensitometer records in the region of line $K\alpha_{1,2}$ from each plate were converted to an intensity scale and plotted as shown in figure 4 (the peaks have been scaled to the same value). Since the corresponding blackening curves were derived from extreme variations of the experimental conditions the excellent agreement between the two sets of experimental values (i and ii) justifies the method of establishing the intensity scale.

While the effect of the temperature and pressure of the source on the recorded line shapes may be assumed to be negligible, a detailed study has shown that they are also uninfluenced by the effect of the slit of the examining microdensitometer. The only other factor likely to influence the experimental line shape is the broadening due to diffraction in the mica crystal but it has not been possible to make a realistic estimate of its effect. In the first place, there is as yet no dynamical treatment available of the diffraction of x-rays by real bent crystals. The wave kinematical treatment of Borovskiĭ and Bezirganyan (1953) is only applicable to an ideal three-dimensional bent lattice. Secondly, as has been pointed out by Hendricks (1940) in a study of layer-silicate (mica) lattices, "while line width, line shape, and intensities are affected, the phenomenon (of the mosaic crystal) has not been very susceptible of study and the distribution of sizes of the mosaic volumes are unknown".

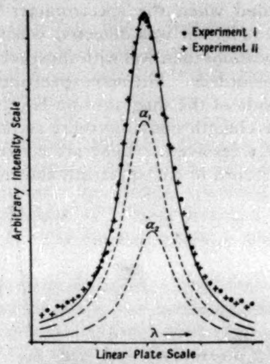

Figure 4. Analysis of the intensity shape of the neon doublet $K\alpha_{1,2}$. The full line is the envelope of the theoretical components α_1 and α_2 shown in broken line.

The theoretical distribution of intensity in an x-ray line, the natural line shape, may be expressed according to the quantum mechanical treatment of Weisskopf and Wigner (1930). In the present work the widths of the lines examined are small compared with the wavelength λ of their central maxima. Further, the inverse plate dispersion $\partial\lambda/\partial x$ is constant for plate distances x of the order of the widths of the recorded lines. It follows, that, if the Weisskopf–Wigner line shape is applicable to the experimental line, it may be written in the symmetrical form

$$I(x) = \frac{\gamma x}{2\pi} \frac{I_0}{(x-x_0)^2 + \frac{1}{4}\gamma x^2}$$

where I_0 is the total line intensity, x_0 is the position of the central maximum and γx is the full width of the line at half maximum intensity (half width).

The experimental shape of $K\alpha_{1,2}$ (figure 4) is asymmetrical about an axis through its peak, being broader on the long wavelength side. The most probable reason for this is a partial separation of the doublet components α_1 and α_2. Theory and experiment agree that for all elements line $\alpha_1(K \rightarrow L_{III})$ is about twice as intense as line $\alpha_2(K \rightarrow L_{II})$ while their half widths are nearly equal. Assuming this in the case of neon and giving the supposed doublet components a separation of about 0·05 mm (2 x units, which is in accord with the measured separations listed by Cauchois and Hulubei (1947) for elements down to $Z = 13$) the $K\alpha_{1,2}$ experimental shape was decomposed into two lines of Weisskopf–Wigner form. In fitting the envelope of the theoretical components to the experimental contour of this intense line it is reasonable to neglect the contribution of background and adjacent lines.

The analysis yields a half-width value for the $K\alpha_{1,2}$ components of $\gamma x = 0{\cdot}40$ mm on the plate scale which is equivalent to 14·7 x units or 0·85 ev. Since the experimental shape was not corrected for possible diffraction broadening, the agreement obtained indicates either that the diffraction pattern is of small breadth or that it has approximately the Weisskopf–Wigner form.

§ 5. ANALYSES OF SOME SATELLITE STRUCTURE

In figure 5 is shown an analysis of the satellite structure on the immediate short wavelength side of line $K\alpha_{1,2}$ the intensity contour having been derived from the microdensitometer record of figure 3. The non-satellite contribution to the contour consists of the base of line $K\alpha_{1,2}$ plus continuous radiation. Guided by the variation in background shown in the case of an exposure taken with air in the discharge tube the continuous radiation was given a constant value over the region concerned. The base of line $K\alpha_{1,2}$ was described by its previously discussed line shape fitted to the experimental line at the peak and half maximum points. Lines II, III and V are visually resolved in the original plate (figure 1), while the introduction of lines I and IV brings about reasonable agreement between the experimental and theoretical contours.

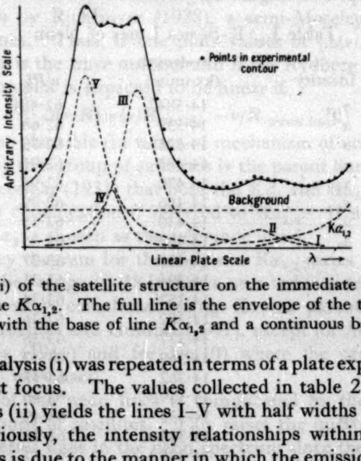

Figure 5. Analysis (i) of the satellite structure on the immediate short wavelength side of the neon line $K\alpha_{1,2}$. The full line is the envelope of the theoretical components I–V together with the base of line $K\alpha_{1,2}$ and a continuous background.

This satellite analysis (i) was repeated in terms of a plate exposed with a different wavelength in exact focus. The values collected in table 2 show that although this second analysis (ii) yields the lines I–V with half widths of the same order of magnitude as previously, the intensity relationships within the satellite group are different. This is due to the manner in which the emission intensity from the gas varies near the discharge tube walls and prevents a reliable estimate of the relative intensities. Those given by analysis (i) are more likely to be correct.

Table 2

Line	Analysis (i)			Analysis (ii)		
	Int. rel. to Line V	Half width		Int. rel. to Line V	Half width	
		x-units	ev		x-units	ev
I	0·15	12·6	0·73	0·06	12·3	0·72
II	0·3	16·2	0·95	0·1	17·6	1·03
III	1·6	13·2	0·78	0·9	15·0	0·88
IV	0·5	10·3	0·60	0·35	8·6	0·51
V	1·0	13·2	0·78	1·0	15·0	0·89

Towards shorter wavelengths there is a weak band consisting of many partially resolved lines. Figure 3 shows a tracing of the average of eight independent microdensitometer records of this region. At least five of these lines are discerned by the eye in the original plates, some of which have survived reproduction in figure 1. Although the low intensity of this complex band precludes any useful attempt to decompose it into its component lines, their minimum number can be decided from the maxima in the density contour. These will not be much displaced from the line peaks they represent and are accordingly labelled as lines VI–XXI.

§ 6. WAVELENGTH MEASUREMENTS

The wavelengths of the neon lines were measured relative to the wavelengths of the $L\beta_1$ and $L\alpha_{1,2}$ lines of nickel in the first order. The values obtained are collected in table 3. The relatively low intensity satellites occur too close to the nickel calibration lines to allow a direct comparison by overlapping the two spectra. This was possible, however, for the intense neon diagram line $K\alpha_{1,2}$ (figure 2). The satellites were then measured with reference to $K\alpha_{1,2}$ on plates not having the nickel spectrum present (figure 1).

Table 3. K-Series Lines of Neon

Line	Identity	Wavelength (kx units)	ν/R§	$\sqrt{(\nu/R)}$
	$\alpha_{1,2}$	14·5847	62·481	7·904$_5$
I	α''	14·539	62·68	7·917
II	α'	14·528	62·73	7·920
III	α_3	14·485	62·91	7·932
IV†	α_3', α_4'	14·476	62·95	7·934
V	α_4	14·466	62·99	7·937
VI	β_1	14·430	63·15	7·947
VII	β_0	14·407	63·25	7·953
VIII		14·402	63·27	7·954
IX	α_8	14·394	63·31	7·957
X		14·387	63·34	7·959
XI		14·382	63·36	7·960
XII		14·377	63·38	7·961
XIII	α_5	14·369	63·42	7·964
XIV		14·362	63·45	7·966
XV		14·539	63·46	7·966
XVI	α_7	14·352	63·49	7·968
XVII		14·343	63·53	7·971
XVIII		14·335	63·57	7·973
XIX	α_6	14·327	63·61	7·976
XX	β_x	14·315	63·66	7·979
XXI‡	α_9, β^V	14·278	63·82	7·989

† This ' line ' is probably more complex than the known data plotted in figure 6 indicates, and it has not therefore been specifically identified.

‡ Either identification is possibly correct.

§ To calculate the values of ν/R, ν was expressed in reciprocal x units and the generally accepted value of $R = 109{,}737$ cm^{-1} used.

The wavelength values due to Tyrén (1936) are considered to be the best available for the nickel L lines. They were measured in terms of hydrogen-like spark lines with a concave grating and are given on the grating scale as 14·279 Å ($L\beta_1$) and 14·566 Å ($L\alpha_{1,2}$). These values were converted to the crystal scale using a conversion factor of value 1·00202 (cf. Wood 1947).

The various line separations were determined between peaks on the microdensitometer (or analysed intensity) records and the wavelengths evaluated by a modification of the method described by Haglund (1942). It involves the Bragg equation and requires a knowledge of the {001} lattice constant of muscovite mica in the first order of reflection (d_1). The value $d_1 = 9927{\cdot}58$ x units due to Siegbahn (1943) was used.

Since the method of measurement is a relative one the wavelength values of the nickel lines and the value of the muscovite lattice constant are regarded as being free from error. The effect on the calculated neon wavelengths of the remaining sources of error (spectrometer construction, microdensitometer screw thread, etc.) has been considered. The wavelength value for neon K$\alpha_{1,2}$ given in table 3 is the mean of determinations from four plates, the error in any of which is not greater than $\pm 0{\cdot}001$ kx units. The error in the other wavelengths listed is not greater than $\pm 0{\cdot}0025$ kx units.

§7. IDENTIFICATION OF THE K-SERIES LINES OF NEON

An attempt has been made to identify the neon satellite lines, on a descriptive basis, by comparison with experimentally established data from adjacent elements.

As first shown by Richtmyer (1928), a semi-Moseley law exists between typical satellite lines. Thus, if one plots values of $\{\Delta(\nu/R)\}^{1/2}$ against atomic number Z (where ν is the wave number and R the Rydberg constant for an atom of infinite mass) the plot is expected to be linear if

$$\Delta(\nu/R) = (\nu/R_{\text{satellite}} - \nu/R_{\text{parent line}}).$$

Although it is most plausible (in terms of mechanism of origin) that the nearest strong diagram line to a group of satellites is the parent line of that group, it has been shown by Deodhar (1931) that both the Kβ_1 and K$\alpha_{1,2}$ satellite groups are more amenable to classification if referred to K$\alpha_{1,2}$. It makes little difference whether Kα_1 or Kα_2 is chosen as the reference line.†

A semi-Moseley diagram for the Kβ_1 and K$\alpha_{1,2}$ series lines of the elements in the atomic number range 10–18 is shown on a reduced scale in figure 6. The $\{\Delta(\nu/R)\}^{1/2}$ values were calculated (using Kα_1 as parent line) from the ν/R values listed by Cauchois and Hulubei (1947), except for A(18) which are due to Nilsson and Slätis (1944) and for Ne(10) where the present determinations collected in table 3 were used.

Identification of the neon lines is complicated by the overlapping of the Kβ_1 and K$\alpha_{1,2}$ groups of satellites. This raises the question of the possibility of obtaining Kβ series lines in the neon spectrum since the M level is normally unoccupied. In fact, however, the diagram line Kβ_1(K$\rightarrow$M$_{\text{III}}$) has been reported in both Na(11) and Mg(12) although here too the M level is normally vacant. The explanation is that for these elements the Kβ_1 line is 'semi-optical' (Bäcklin, Siegbahn and Thoraeus 1925). Such a line arises when an electron from an outer level is raised to an unoccupied optical level by the absorption of energy and then falls into a subsequently created inner vacancy (Maitra 1937). The neon line labelled VI was accordingly identified as the semi-optical diagram line Kβ_1 by extrapolation in a normal Moseley diagram. It follows that some of the satellite lines are possibly members of a semi-optical Kβ_1 series.‡

---

† For a critical discussion of Deodhar's method of classification see Hirsh (1932) and Ford (1932).

‡ A weaker component Kβ_3 (K$\rightarrow$M$_{\text{II}}$) may also exist but has not been recorded at these low atomic numbers.

In identifying the satellites (table 3) it is assumed that they occur only on the short wavelength sides of their parent lines so that no β-satellites are expected between the positions of $K\alpha_{1,2}$ and $K\beta_1$ in figure 6. Lines VIII, X, XI, XII, XIV, XV, XVII and XVIII have no obvious correlation with the known lines from the elements of higher atomic number. They could well be semi-optical β-satellites whose probability of occurrence has been favoured by the conditions in the discharge source where many atoms will be excited into optical states. The identity of line I is of some interest. It would appear to be the satellite $K\alpha''$ reported by Deodhar (1931) for Si(14) and P(15). However, Deodhar himself expressed some doubt as to the origin of his α'' lines (he regarded $K\alpha'$, α'' as being a doublet) particularly for silicon. The matter is referred to by Ford (1932) who did not find any trace of the doublet nature of a' between Mg(12) and Ge(32). Parratt (1936) reports an examination of a satellite line named $K\alpha''$ which occurs on the short wavelength side of the $K\alpha_1$ diagram line with elements S(16) to V(23). He refers to Deodhar's work on silicon and phosphorus. The present conclusion is that the line Parratt labels $K\alpha''$ for the elements in the atomic number range 16 to 23 is not to be classified with the line $K\alpha''$ reported by Deodhar for silicon and phosphorus. The positions of Parratt's for $K\alpha''$ S(16) and Cl(17) are noted in figure 6. Finally, the uncertainty which is present in regard to the reality of line I limits its use as an argument in favour of the doublet nature of $K\alpha'$. It seems in order, nevertheless, tentatively to designate it as $K\alpha''$.

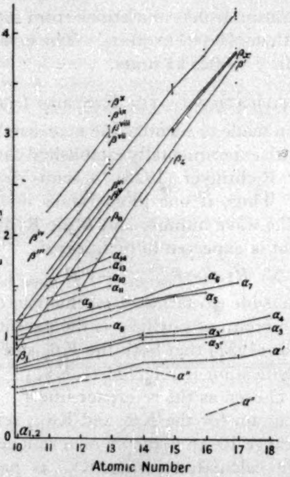

Figure 6. Semi-Moseley diagram for the $K\beta_1$ and $K\alpha_{1,2}$ series lines for elements $_{10}$Ne to $_{18}$A.

§ 8. Discussion of Results

The results obtained for neon may be compared with those of Kunzl and Svobodová-Joanelli summarized in table 1. Their wavelength values for lines $\alpha_{1,2}$, a', α_3, α_4 and β_1 are in reasonable agreement with the present ones. Kunzl and Svobodová-Joanelli were apparently unable to survey their plates with a microphotometer for they do not show an intensity (or density) contour of the spectrum. Presumably, their plates were examined with a microscope which lead them to regard the line α' as being broadened towards long wavelengths, a value being given for its long wavelength limit. The present analysis of the intensity contour is in favour of the presence of line α'' rather than an unexplained asymmetry in α'. Again, their (microscope ?) examination did not enable them to discern the line α_3', α_4' reported here, although they suspected its presence. The diffuse band found by Kunzl and Svobodová-Joanelli is now shown to consist of several lines, some of which have been identified and to all of which wavelength values have been ascribed.

Acknowledgments

The subject of this research was suggested by the late Professor F. C. Chalklin who supervised its progress up to the time of his death when the experimental work was practically complete. The writer (H. R. M.) wishes to thank Dr. G. T. P. Tarrant and Dr. N. K. Pope for their advice during the preparation of this paper. The work was made possible by the award of a National Research Scholarship (Department of Scientific and Industrial Research) and by the award of an apparatus grant and a Senior Research Fund Fellowship (Research Committee, University of New Zealand).

References

Bäcklin, E., Siegbahn, M., and Thoraeus, R., 1925, *Phil. Mag.*, **49,** 513.
Bačkovský, J. M., 1936, *C.R. Acad. Sci., Paris*, **202,** 1671.
Borovskiĭ, I. B., and Bezirganyan, P. A., 1953, *C.R. Acad. Sci. U.R.S.S.*, **88,** 639; 1953, *Ibid.*, **88,** 769.
Cauchois, Y., and Hulubei, H., 1947, *Constantes Sélectionnées Longueurs d'Onde des Émissions X et des Discontinuités d'Absorption X* (Paris : Hermann).
Deodhar, G. B., 1931, *Proc. Roy. Soc.* A, **131,** 633.
Ford, O. R., 1932, *Phys. Rev.*, **41,** 577.
Groven, L., 1949, *Ann. Phys., Paris*, **4,** 62.
Haglund, P., 1942, *Ark. Mat. Astr. Fys.* A, **28,** No. 8.
Hendricks, S. B., 1940, *Phys. Rev.*, **57,** 448.
Hill, R. D., 1937, *Proc. Roy. Soc.* A, **161,** 284.
Hirsh, F. R., 1932, *Phys. Rev.*, **40,** 151.
Kunzl, V., and Svobodová-Joanelli, M., 1946, *Acad. Int. Tchèque Sci.*, **47,** 91.
Maitra, A. T., 1937, *Indian J. Phys.*, **11,** 77.
Moore, H. R., 1955, *J. Sci. Instrum.*, **32,** 324.
Nilsson, Å., and Slätis, H., 1944, *Ark. Mat. Astr. Fys.* A, **31,** No. 8.
Parratt, L. G., 1936, *Phys. Rev.*, **49,** 502.
Richtmyer, F. K., 1928, *Phil. Mag.*, **6,** 64.
Siegbahn, M., 1943, *Nature, Lond.*, **151,** 502.
Tait, R. I., and Chalklin, F. C., 1953, *J. Sci. Instrum.*, **30,** 268.
Tyrén, F., 1936, *Z. Phys.*, **98,** 768.
Weisskopf, V., and Wigner, E., 1930, *Z. Phys.*, **63,** 54.
Wood, E. A., 1947, *Phys. Rev.*, **72,** 436.

Equations of State of Elements from the Thomas–Fermi Theory

By N. H. MARCH

Department of Physics, The University, Sheffield

MS. received 28th February 1955 and in final form 14th April 1955

Abstract. An investigation of the equations of state of elements as given by the Thomas–Fermi theory has been carried out in a region corresponding to higher pressures than have hitherto been discussed in detail. Both analytical and numerical methods have been used. The results thus obtained suggest modifications to be made in the recent formulae given by Gilvarry, who fitted the available numerical data with functions having the correct limiting forms. The introduction of exchange is also considered and the modifications thus caused are exhibited explicitly for very high pressures.

---

§ 1. Introduction

It is now well known that the Thomas–Fermi (TF) method is very valuable in yielding information about the equations of state of solids under extremely high pressures, as found for example in stars. The first suggestion of the usefulness of the theory in this field was made by Slater and Krutter (1935) in their original paper on the application of the TF method to metals and the detailed results have been worked out chiefly by Jensen (1938) and Feynman, Metropolis and Teller (1949; subsequently referred to as FMT). Whereas Jensen's work was restricted to the completely degenerate case, FMT also discussed the results given by the TF theory when generalized to take account of non-zero temperatures. Whilst under normal conditions the applicability of the TF method is rather restricted and the results are most appropriate to describe the alkali metals (March 1954), when the pressures of interest are sufficiently high for the detailed influence of the outer electronic structure to be obliterated, then the results become applicable to all elements and are of very considerable value in astrophysics (see, for example, Sommerfeld 1938, Scholte 1947, Brown 1950) and also to some extent in geophysics (Elsasser 1950, Bullen 1952).

Until recently, the work reported has been based entirely on numerical solutions of the basic TF equation, and results have therefore been available only over a limited range of pressures. Gilvarry (1954) in a recent paper, however, has gone some way towards making the results of the TF theory available over the entire range of pressures by fitting the numerical data with analytical expressions having the correct limiting forms. As he points out, the properties of his fitted functions ensure some kind of approximate validity outside the range of available data. Nevertheless, in view of the wide applicability of the results, it seemed very worth while to examine more carefully than has been attempted hitherto the results in the region of exceedingly high pressures, and this is our main concern in this paper. As we shall see, our results suggest some modifications which might be made in Gilvarry's formulae to put them on a more satisfactory theoretical basis. Gilvarry's investigations were solely confined to the unmodified TF case in which exchange is neglected, whereas we shall consider also the modifications introduced by exchange at very high pressures. Our considerations in this paper will be restricted to the completely degenerate case.

In § 2 we briefly summarize the basic method of obtaining equations of state from the TF theory, whilst in § 3 we consider the solution of the TF equation by means of a Taylor expansion around the boundary point. We are thus enabled to obtain the first two terms in a series giving the boundary value of the TF function for very high pressures. The first term agrees with the result obtained by Gilvarry, who used essentially intuitive arguments, but the second term is new and has interesting connections with Gilvarry's work which we discuss in § 4. In § 5 we deal in a similar manner with the Thomas–Fermi–Dirac (TFD) equation which includes the effect of exchange. We are hence able to demonstrate explicitly the modifications due to exchange at the highest pressures.

§ 2. CALCULATION OF EQUATIONS OF STATE FROM UNMODIFIED TF THEORY

The fundamental problem in obtaining equations of state of elements, as indeed in any application of the TF theory, is to solve the non-linear equation

$$\nabla^2(V-V_0)=\mu(V-V_0)^{3/2} \qquad \ldots\ldots(1)$$

for the electrostatic potential V, and hence the electron density n. Here $-eV_0$ is the maximum occupied electron energy level whilst

$$\mu=\frac{32\pi^2 e}{3h^3}(2me)^{3/2}.$$

Actually, for the particular crystal with which we are dealing, we should construct the appropriate polyhedron surrounding a given atom and then solve equation (1) within this polyhedron. So far, however, all the detailed work reported has been based on the sphere approximation introduced into the TF theory by Slater and Krutter following the original Wigner–Seitz work. This simply amounts to the replacement of the polyhedron by a sphere having equal volume. Some work has actually been carried out recently by the writer in which equation (1) has been solved approximately within the appropriate polyhedron for a diamond-type structure, and preliminary results were reported at a conference on the energy band structure of solids at the Radar Research Establishment, Malvern (see Coulson 1954). However, the procedure is very laborious and in order to achieve generality we shall have to be content with discussing equations of state with the sphere approximation. This should be quite good in many cases and then the TF equation (1) reduces to the usual dimensionless form

$$\frac{d^2\phi}{dx^2}=\frac{\phi^{3/2}}{x^{1/2}} \qquad \ldots\ldots(2)$$

when we make the substitutions

$$V-V_0=\frac{Ze}{r}\phi, \qquad r=bx \qquad \ldots\ldots(3)$$

where

$$b=\left(\frac{3}{32\pi^2}\right)^{2/3}\frac{h^2}{2me^2Z^{1/3}}.$$

The boundary conditions in terms of ϕ are

$$\left.\begin{aligned}\phi(0)&=1\\ \phi(x_0)/x_0&=(d\phi/dx)_{x_0}\end{aligned}\right\} \qquad \ldots\ldots(4)$$

the first arising from the fact that as we approach the origin the potential must tend to that due to the point charge Ze, whilst the second condition can be regarded either as expressing the requirement of electrical neutrality or the fact that the potential must be periodic, that is $(dV/dr)_R=0$, where R is the radius of the atomic sphere and $x_0=R/b$.

At this stage it is important to note that a knowledge of the boundary value $\phi(x_0)$ is sufficient to determine the equations of state and the complete solution need not necessarily be found. This was first shown by Slater and Krutter and stems from the fact that the pressure p in the TF model is simply the pressure which would be exerted by a free electron gas of density equal to the TF density at the surface of the sphere. This seems intuitively correct when we recall that the TF theory can be set up by applying free electron relations locally, and it can of course be justified rigorously (see, for example, March 1952 a). The pressure p is thus given by

$$p=\tfrac{2}{3}c_{\mathrm{k}}\{n(R)\}^{5/3} \qquad \ldots\ldots(5)$$

where

$$c_{\mathrm{k}}=\frac{3h^2}{10m}\left(\frac{3}{8\pi}\right)^{2/3}$$

and $n(R)$ is the TF density at the boundary of the atomic sphere. In terms of ϕ equation (5) becomes

$$pv=\frac{2}{15}\frac{Z^2e^2}{b}x_0^{1/2}\{\phi(x_0)\}^{5/2} \qquad \ldots\ldots(6)$$

where v is the atomic volume given in terms of x_0 by $v=4\pi(bx_0)^3/3$. It is also of interest to note here that the difference between the total energy for finite x_0 and for an isolated atom ($x_0=\infty$) is given by

$$E(x_0)-E(\infty)=\frac{Z^2e^2}{b}\left[\frac{3}{7}(a_2-a_{2\infty})+\frac{2}{35}x_0^{1/2}\{\phi(x_0)\}^{5/2}\right] \qquad \ldots\ldots(7)$$

and depends only on a_2 the slope of ϕ at the origin and on $\phi(x_0)$.

§ 3. SOLUTION OF TF EQUATION BY TAYLOR EXPANSION AROUND BOUNDARY POINT

Numerical solutions of the type required here have been given by a number of workers, the most recent tabulation being that of the present writer in the course of a discussion on the application of the TF method to molecules with high symmetry (March 1952 b), and values of $\phi(x_0)$ were given there for ten values of x_0 ranging from 2·8 to 8·0. Slater and Krutter had earlier obtained solutions down to a value of x_0 of 1·2, but no solutions corresponding to smaller values of x_0 have hitherto been given as far as the writer is aware. It is to bridge this gap that is our main concern here.

Gilvarry has already discussed the limiting form of $\phi(x_0)$ for $x_0\to 0$ by arguments that are essentially intuitive and based on the observation that the results of the TF method must go over into those appropriate for a Fermi–Dirac gas of completely free electrons when the pressure is sufficiently high. We shall now consider how this result follows from the properties of the dimensionless TF equation (2) and this will allow us to extend Gilvarry's result somewhat, with interesting consequences.

The method we shall use is to expand the solution $\phi(x)$ in a Taylor series around the boundary point x_0. Then we have

$$\phi(x)-\phi(x_0)=\sum_{n=1}^{\infty}\frac{(-1)^n}{n!}h^n\phi^n(x_0)=\sum_{n=1}^{\infty}t_nh^n \qquad \ldots\ldots(8)$$

where $h=x_0-x$, $\phi^n(x)$ is the nth derivative of $\phi(x)$ and

$$t_n=\frac{(-1)^n}{n!}\phi^n(x_0).$$

It is convenient at this stage to introduce a parameter a defined by

$$\frac{\phi(x_0)}{x_0}=\left(\frac{d\phi}{dx}\right)_{x_0}=a^2 \qquad \ldots\ldots(9)$$

and then to express the coefficients t_n in terms of a and x_0. The results are shown in table 1, where we give coefficients up to and including t_{12}.

Table 1. Coefficients t_n in Taylor Series Solution of TF Equation

$$\begin{array}{ll}
t_1=-a^2 & t_7=\dfrac{a^5}{3360} \\[2ex]
t_2=\dfrac{a^3x_0}{2} & t_8=\dfrac{a^5x_0^{-1}}{1344}+\dfrac{a^6x_0}{2240} \\[2ex]
t_3=-\dfrac{a^3}{6} & t_9=\dfrac{a^5x_0^{-2}}{1728}+\dfrac{a^6}{20160} \\[2ex]
t_4=\dfrac{a^4x_0}{16} & t_{10}=\dfrac{a^5x_0^{-3}}{2160}+\dfrac{43\,a^6x_0^{-1}}{1209600}+\dfrac{3\,a^7x_0}{89600} \\[2ex]
t_5=-\dfrac{a^4}{80} & t_{11}=\dfrac{a^5x_0^{-4}}{2640}+\dfrac{a^6x_0^{-2}}{172800}+\dfrac{47a^7}{2956800} \\[2ex]
t_6=\dfrac{a^5x_0}{160} & t_{12}=\dfrac{a^5x_0^{-5}}{3168}-\dfrac{a^6x_0^{-3}}{71280}+\dfrac{481\,a^7x_0^{-1}}{26611200}+\dfrac{13\,a^8x_0}{7884800}
\end{array}$$

The solution (8) satisfies of course the required boundary conditions at x_0, but in order to determine a as a function of x_0, and hence the boundary value $\phi(x_0)$, we must impose the condition that $\phi(0)=1$. It seems from investigation of the series (8) that this diverges when we are actually at the origin. Nevertheless, it is still useful from a practical point of view as a semi-convergent series and we apply it first of all to determine the limiting form of $\phi(x_0)$ as $x_0\to 0$. We proceed by writing down $\phi(0)$ as far as terms in a^3 (the terms in a^2 cancel one another). We then have

$$\phi(0)=1=a^3x_0^{\,3}/3 \qquad \ldots\ldots(10)$$

and hence

$$a=3^{1/3}/x_0. \qquad \ldots\ldots(11)$$

Thus $\phi(x_0)$ has the limiting form

$$\phi(x_0)=3^{2/3}/x_0 \qquad \ldots\ldots(12)$$

which is just Gilvarry's result. However, our method now allows us to go further. First we note the consistency of our approximation made in writing equation (10) as it can be seen that the first neglected term in $\phi(0)$ is of order x_0. Including the terms in a^4 we obtain

$$1=\frac{a^3x_0^{\,3}}{3}+\frac{a^4x_0^{\,5}}{20} \qquad \ldots\ldots(13)$$

and hence by substituting for a in the correction term from equation (11) we find

$$a=\frac{3^{1/3}}{x_0}\left[1-\frac{3^{1/3}}{20}x_0\right] \qquad \ldots\ldots(14)$$

and thus

$$\phi(x_0)=\frac{3^{2/3}}{x_0}\left[1-\frac{3^{1/3}}{10}x_0\right]. \qquad \ldots\ldots(15)$$

However, there is a difficulty when we try to go further. As can be seen from table 1, every coefficient t_n higher than t_5 contains a term in a^5. Even though the term in a^5 in the nth coefficient can be written down and the terms easily summed, we have not found any procedure which we can justify to calculate the next term. This is a pity, of course, but even equation (15) is very useful, as we shall see later.

Before going on, it is interesting to compare the approximation we have for $\phi(x)$ as far as terms in a^3 with that given by Gilvarry (1954, eqn (36)). Our expression may be written

$$\phi(x)=\tfrac{1}{3}a^3x_0^{\,3}+(a^2-\tfrac{1}{2}a^3x_0^{\,2})x+\tfrac{1}{6}a^3x^3. \qquad \ldots\ldots(16)$$

If we now substitute in this for a from equation (11) we obtain simply the equation given by Gilvarry, which was found from the potential due to a point charge Ze and a uniform distribution of Z electrons within the atomic volume, combined with a term calculated from the chemical potential of a Fermi–Dirac gas. It is clear from our treatment that this procedure will only give correctly the leading term (of order x_0^{-2}) in the coefficient of x.

In order to investigate numerically the usefulness of equation (15), as well as to check the results of our whole argument, we have solved the TF equation numerically in the usual way for two cases corresponding to x_0 approximately 0·1 and 0·5, using the semi-convergent expansion due to Baker to obtain starting values around the origin and then continuing by the usual step-by-step methods of numerical integration. In both cases we find excellent agreement with the boundary value calculated from equation (15). In order to illustrate the form of the solutions for small x_0 we have plotted the two solutions we have obtained in the figure (note, however, that the scales are different). Even for large values of x_0 the Taylor expansion we have given will be useful to obtain part of the solutions required, and then either numerical integration into the origin could be used to complete the solution (this should be done in terms of the variable $w=(2x)^{1/2}$, in order to avoid difficulties at the origin), or, when possible, the Taylor solution could be joined on numerically to a solution calculated from Baker's expansion. With the first alternative, no trial and error is called for, as the solution could be transformed to pass through the origin by using the property of the TF equation that if $\phi(x)$ is one solution, then another is given by $\chi(y)$ where

$$\phi=c\chi, \qquad x=dy \qquad \ldots\ldots(17)$$

provided that $cd^3=1$. The new boundary value is of course easily obtained.

The other parameter entering into the expression for the energy, namely a_2 the initial slope of ϕ (see equation (7)) can also be obtained from the Taylor expansion to the same approximation as $\phi(x_0)$ given by equation (15). The result is

$$a_2=\frac{3^{2/3}}{x_0^{\,2}}-\frac{9}{5x_0}. \qquad \ldots\ldots(18)$$

It is further confirmation of the correctness of our results that $\phi(x_0)$ and a_2, as given by equations (15) and (18), satisfy the relation

$$x_0^{1/2}\frac{da_2}{dx_0} = -\{\phi(x_0)\}^{5/2} - \tfrac{1}{3}x_0\{\phi(x_0)\}^{3/2}\frac{d\phi(x_0)}{dx_0} \qquad \ldots\ldots(19)$$

which any exact solution must obey (Gilvarry 1954, eqn (32)).

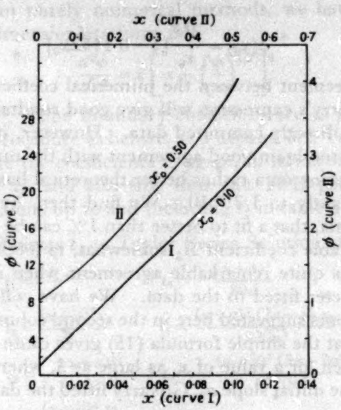

Solutions of TF equations for $x_0 = 0{\cdot}10$ and $0{\cdot}50$.

§ 4. DETAILED COMPARISON WITH PREVIOUS WORK AND IMPROVED EQUATIONS OF STATE

It is now of interest to compare our findings with the results given by Gilvarry. The form he used in fitting the available numerical data for the boundary value $\phi(x_0)$ was

$$\phi(x_0) = \left[\sum A_n x_0^{n/2}\right]^{-1} \qquad \ldots\ldots(20)$$

where n goes from 2 to 6, and the coefficients are given in the first column of table 2.

Table 2. Coefficients in Fitted Functions for $\phi(x_0)$ and a_2

	$\phi(x_0)$ Gilvarry	$\phi(x_0)$ March		$a_2 - a_{2\infty}$
A_2	$4{\cdot}8075\times10^{-1}$	$4{\cdot}8075\times10^{-1}$	B_2	$4{\cdot}8075\times10^{-1}$
A_3	$7{\cdot}009\times10^{-3}$	0	B_3	$4{\cdot}3462\times10^{-1}$
A_4	$7{\cdot}003\times10^{-2}$	$6{\cdot}934\times10^{-2}$	B_4	$6{\cdot}9203\times10^{-2}$
A_5	$8{\cdot}901\times10^{-3}$	$9{\cdot}700\times10^{-3}$	B_5	$5{\cdot}9472\times10^{-2}$
A_6	$3{\cdot}3704\times10^{-3}$	$3{\cdot}3704\times10^{-3}$	B_6	$-4{\cdot}9688\times10^{-3}$
			B_7	$4{\cdot}3386\times10^{-4}$
			B_{11}	$1{\cdot}5311\times10^{-6}$

A_2 and A_6 have been chosen so that $\phi(x_0)$ has the correct limiting forms for $x_0 \to 0$ and $x_0 \to \infty$. Equation (20) predicts that for small x_0

$$\phi(x_0) = \frac{3^{2/3}}{x_0}\left[1 - 3^{2/3}A_3 x_0^{1/2}\right] \qquad \ldots\ldots(21)$$

whereas the correct form is given by our equation (15). However, it is noteworthy that the coefficient A_3 found by Gilvarry is a factor of ten smaller than A_4. If we put $A_3=0$, in order to obtain agreement with our form (15), then Gilvarry's expression for small x_0 gives

$$\phi(x_0)=\frac{3^{2/3}}{x_0}[1-0\cdot 1457x_0] \qquad \ldots\ldots(22)$$

whereas we have

$$\phi(x_0)=\frac{3^{2/3}}{x_0}[1-0\cdot 1442x_0] \qquad \ldots\ldots(23)$$

with remarkable agreement between the numerical coefficients. All this points to the fact that Gilvarry's expression will give good results for small values of x_0, outside the range of directly computed data. However, it suggests further that we shall still be able to obtain good agreement with the numerical data when we put Gilvarry's expression on a rather better theoretical basis by choosing $A_3=0$, and changing A_4 slightly to $1/3^{1/3}.10$. We find then, by comparison with the existing numerical data, that a fit to better than 1% can be obtained by changing the remaining adjustable coefficient A_5 somewhat, to 0·0097. This, it seems to the present writer, is quite remarkable agreement when it is remembered that A_5 is the one parameter fitted to the data. We have collected for convenience the modified coefficients suggested here in the second column of table 2. Finally it is worth noting that the simple formula (15) gives quite a reasonable fit of the numerical values, even for a value of x_0 as large as 3, where it is in error by 9%.

With regard to the initial slope a_2, Gilvarry fitted the data in this case with the function

$$a_2-a_{2\infty}=\left[\sum B_n x_0{}^n\right]^{-1} \qquad \ldots\ldots(24)$$

where n ranges over the sequence $n=2, 3 \ldots 7, \lambda_1$, and $\lambda_1=\frac{1}{2}[73^{1/2}+7]=7\cdot 77200$. B_2 and $B_{\lambda 1}$ are again chosen to give the correct asymptotic forms, and the coefficients obtained by Gilvarry are given in the third column of table 2. Examining again the connection with our result for small x_0 we find that this time Gilvarry's form is in agreement with ours, and the numerical coefficient of the term proportional to $x_0{}^{-1}$ is $-1\cdot 88$, whereas our value from equation (18) is $-1\cdot 80$. Again, then, there is quite good agreement. Since Gilvarry's formula fits the numerical data well and has a form for small x_0 very near to the correct result, it seems unnecessary to modify it.

Finally, we can express the equations of state of elements in the form

$$p^{2/5}\left[\sum_{n=2}^{6} A_n\left(\frac{3v}{4\pi b^3}\right)^{(n+2)/6}\right]=\left(\frac{Z^2\epsilon^2}{10\pi b^4}\right)^{2/5} \qquad \ldots\ldots(25)$$

using equations (6) and (20). Taking the coefficients to be those suggested by the present work, this reduces for very high pressures to the correct result

$$pv=\frac{h^2}{5m}\left(\frac{3}{8\pi}\right)^{2/3}\frac{Z^{5/3}}{v^{2/3}}\left[1-\frac{2\pi me^2}{h^2}(4Zv)^{1/3}\right]. \qquad \ldots\ldots(26)$$

Omitting the second term in this equation, we have simply the well-known expression for the pressure exerted by Z free electrons enclosed in a volume v, and the term is of course independent of the electronic charge. On the other hand, the second term in equation (26) is new and shows the way in which the equations of state are modified at the highest pressures by including electron–nuclear and electron–electron interactions by means of the TF theory.

Similarly, we can write down immediately the difference in energy between the cases of finite and infinite x_0 using equations (7), (20) and (24).

§ 5. MODIFICATIONS DUE TO EXCHANGE

We shall now consider quite briefly the modifications brought about by exchange when the pressure is extremely high. In this case, not considered hitherto by other than purely numerical methods, we have to solve the TFD equation, which in dimensionless form is

$$\frac{d^2\phi}{dx^2} = x\left[\alpha + \left(\frac{\phi}{x}\right)^{1/2}\right]^3 \qquad \ldots\ldots(27)$$

where $\alpha = 6^{1/3}/4(\pi Z)^{2/3}$. The boundary conditions are as given in equation (4). We follow the same procedure as before, and expand in a Taylor series around x_0. Then we can calculate the coefficients t_n again, in terms of the parameter a, the dimensionless radius x_0, and also this time the TFD parameter α. We have recorded these coefficients up to and including t_7 in table 3. It will be seen that they reduce correctly to the corresponding coefficients in table 1 when we put $\alpha = 0$. Proceeding entirely as before we find

Table 3. Coefficients t_n in Taylor Series Solution of TFD Equation

$t_1 = -a^2$	$t_5 = -\dfrac{(\alpha+a)^5}{80a}$
$t_2 = \dfrac{(\alpha+a)^3 x_0}{2}$	$t_6 = \dfrac{(\alpha+a)^7\,(2a-\alpha)\,x_0}{320a^3}$
$t_3 = -\dfrac{(\alpha+a)^3}{6}$	$t_7 = -\dfrac{(\alpha+a)^7\,(5\alpha-2a)}{6720a^3}$
$t_4 = \dfrac{(\alpha+a)^5\,x_0}{16a}$	

$$\phi(x_0) = \frac{3^{2/3}}{x_0}\left[1 - \frac{3^{1/3}}{10}x_0 - \frac{2\alpha}{3^{1/3}}x_0\right]. \qquad \ldots\ldots(28)$$

In this case the pressure of the electrons is again that exerted by a free electron gas of density equal to the TFD density on the boundary. This time, however, we must treat the free electron gas by the Hartree–Fock approximation. The pressure is then (see, for example, March 1952 a)

$$p = \tfrac{2}{3}c_{\mathrm{k}}\{n(R)\}^{5/3} - \tfrac{1}{3}c_{\mathrm{e}}\{n(R)\}^{4/3} \qquad \ldots\ldots(29)$$

where

$$c_{\mathrm{e}} = \frac{3e^2}{4}\left(\frac{3}{\pi}\right)^{1/3}.$$

In terms of the boundary value of the TFD solutions this becomes

$$pv = \frac{2}{15}\frac{Z^2e^2}{b}x_0{}^3\left[\left(\frac{\phi(x_0)}{x_0}\right)^{1/2} + \alpha\right]^5\left[1 - \frac{\alpha/45}{\{\phi(x_0)/x_0\}^{1/2} + \alpha}\right]. \qquad \ldots\ldots(30)$$

Using equation (28) we obtain for small x_0

$$pv = \frac{h^2}{5m}\left(\frac{3}{8\pi}\right)^{2/3}\frac{Z^{5/3}}{v^{2/3}}\left[1 - \frac{2\pi me^2}{h^2}(4Zv)^{1/3} - \frac{10\pi me^2}{3^{2/3}h^2}(4Zv)^{1/3}\alpha\right] \ldots\ldots(31)$$

which reduces correctly the equation (26) when we put $\alpha = 0$. This equation demonstrates explicitly then the effect of exchange on the equations of state of elements at the highest pressures. By substituting for α it is easy to show that the exchange correction to the equations of state is simply the free electron exchange term for Z electrons in a volume v. Equations (28) and (31) will be useful in any attempt to set up functions which fit the numerical data for the TFD equations of state.

§ 6. CONCLUSIONS

We have shown here how solutions of the TF equation appropriate to describe solids under exceedingly high pressures can be obtained by means of a Taylor expansion, and in this way it is possible to calculate the first two terms in a series giving the boundary value $\phi(x_0)$. A similar approximate expression is obtained for the slope of the TF function at the origin, which enters the formula for the total energy. The results obtained indicate that the fitted functions given by Gilvarry will be good approximations outside the range of the data he considered. A modification of Gilvarry's equation for the boundary value is suggested which leaves the numerical fit quite unimpaired but puts the formula on a better theoretical basis, and leaves only one adjustable parameter. Even with this single constant to vary, the numerical data can be reproduced to better than 1% accuracy. The final formula given here for the equations of state predicted by the TF theory is thus proved to be completely reliable in all regions except possibly for very large values of x_0. In any case this is a relatively unimportant region, but there is no reason to believe that the formulae will not work well here too.

By examination of the TFD equation in a similar manner, the effect of exchange at the highest pressures has been investigated, and the way in which the corrections to be applied to the TF equations of state vary with atomic number is given explicitly. The exchange correction is shown to be just that for the case of completely free electrons.

We hope that it may prove possible to extend the results presented here to the case of elevated temperatures, and this problem is now receiving consideration.

REFERENCES

BROWN, H., 1950, *Astrophys. J.*, **111**, 641.
BULLEN, K. E., 1952, *Mon. Not. R. Astr. Soc., Geophys. Suppl.*, **6**, 383.
COULSON, C. A., 1954, *Nature, Lond.*, **174**, 949.
ELSASSER, W. M., 1950, *Rev. Mod. Phys.*, **22**, 1.
FEYNMAN, R. P., METROPOLIS, N., and TELLER, E., 1949, *Phys. Rev.*, **75**, 1561.
GILVARRY, J. J., 1954, *Phys. Rev.*, **96**, 934.
JENSEN, H., 1938, *Z. Phys.*, **111**, 373.
MARCH, N. H., 1952 a, *Phil. Mag.*, **43**, 1042 ; 1952 b, *Proc. Camb. Phil. Soc.*, **48**, 655 ; 1954, *Phil. Mag.*, **45**, 325.
SCHOLTE, J. G., 1947, *Mon. Not. R. Astr. Soc.*, **107**, 237.
SLATER, J. C., and KRUTTER, H. M., 1935, *Phys. Rev.*, **47**, 559.
SOMMERFELD, A., 1938, *Nuovo Cim.*, **15**, 14.

The Decay of RaD and the 46·5 keV Excited State of RaE

By G. M. LEWIS
Department of Natural Philosophy, University of Glasgow

MS. received 16*th February* 1955 *and in amended form* 22*nd March* 1955

Abstract. The lifetime of the 46·5 kev excited state following β-decay of RaD has been shown, by delayed coincidence methods, to be less than 3×10^{-9} sec; this specifies the 46·5 kev transition to be a dipole one. An investigation of the scintillations from an activated sodium iodide crystal containing RaD has determined the complete integrated spectrum of RaD, free from effects of source absorption. This spectrum consists in the main of a single peak, and indicates directly that at least 90% of the disintegrations involve soft β-decay to the 46·5 kev excited state followed by rapid de-excitation. Less than 5% of the disintegrations pass through metastable states. The β-decay is briefly discussed.

§1. Introduction

Various features of the decay of RaD are unspecified or uncertain because of the experimental difficulties associated with the study of the low energy radiations emitted by that element.

Detailed measurements of the soft β-spectrum have been of a coincidence type (Insch, Balfour and Curran 1952, Jaffe and Cohen 1953, Huster 1953), and a full interpretation of the measurements is dependent upon the lifetime of the 46·5 kev state following β-decay. It seemed desirable in the first instance to investigate this lifetime closely, using scintillation methods. Such a study also leads to a spin specification for the transition. Measurements latterly by Wu, Boehm and Nagel (1953) on the L-conversion coefficient ratios have suggested the transition to be a magnetic dipole one, on the basis of calculations by Gellman, Griffith and Stanley (1952).

The partially integrated spectrum from a gaseous source in a proportional counter was obtained by Jaffe and Cohen (1953), and Huster (1953), and involved essentially observation of β-rays, conversion electrons and Auger electrons. It seemed worth while to extend this type of experiment by carrying out a complete integration utilizing the scintillations of a crystal of activated sodium iodide grown from a melt contaminated with RaD. In this way a clear record can be obtained of the decay process as a whole. The γ-rays and all the various kinds of x-rays register in the solid, as well as all the various electrons, and the responses combine appropriately (cf. Bannerman, Lewis and Curran 1951, and Bannerman and Curran 1952). There is no source absorption and the particles are emitted inside the fluorescent material. Such measurements provide a direct assessment of the relative number of disintegrations involving the 46·5 kev state, and information concerning other possible modes of decay. Information on the soft β-spectrum, mostly of a confirmatory type is obtained incidentally here.

§ 2. LIFETIME MEASUREMENTS ON THE 46·5 kev EXCITED STATE OF RaE

Coincidences between the β-rays of RaD and subsequent electromagnetic emissions have been measured with a unit of short resolving time as a function of delay inserted on the β-counting side. Two EMI 14 stage photomultipliers type 6262 were used. One channel detecting the β-particles was activated only by pulses lying in a narrow energy band, so as to improve resolving time characteristics and to help eliminate unwanted radiations. The other channel detecting electromagnetic radiations was activated by pulses above a given height. The experimental arrangement is similar to that described by Ferguson and Lewis (1953), and involves kicksorting after mixing.

RaD from spent radon needles was dissolved in nitric acid and converted into a solution of chloride. RaE and RaF were removed as described by Cranberg (1950). Less than 5% of RaE was present in the sources used at the times of all the measurements, the amount of RaF was insignificant.

A thin source ($\sim 20 \mu$ g cm^{-2}), mounted on 2 mil aluminium foil, was placed in contact with a $\frac{1}{16}$ in. thick β-detecting stilbene crystal mounted on one multiplier. The narrow band of pulse energies accepted was centred at about 7 kev. (Rough calibration was effected by the RaD conversion electron response, and by using an external ^{71}Ge source emitting capture x-rays.)

The radiations emitted from the source in the other direction, traversed in succession a $\frac{1}{8}$ in. sheet of polythene, which removed the β-rays from the small amount of RaE, and a 2 mil sheet of copper, which absorbed L x-rays, then a 40 mil sheet of rubber and a 20 mil sheet of aluminium. The γ-rays remaining were then picked up in a $\frac{1}{4}$ in. thick sodium iodide crystal. This iodide crystal was mounted in paraffin on the other photomultiplier; the discriminator linked with this γ-ray counter eliminated energies below approximately 30 kev. The predominant radiation picked up is then the 46·5 kev γ-radiation, any possible weak lower energy γ-rays being attenuated or eliminated (Ewan and Ross 1952, and Wu, Boehm and Nagel 1953, and the review of past work on the γ-rays by Damon and Edwards 1953, 1954), and x-rays could not register. Furthermore, bremsstrahlung from RaE electrons in the polythene was small and fluorescence radiation from RaE unimportant (cf. Wu, Boehm and Nagel 1953); 46·5 kev radiation generating iodine x-escape radiation could not record.

Figure 1 shows one of several resolution curves taken under these conditions The downwards slope of such a curve, for positive delay on the β-side, sets an

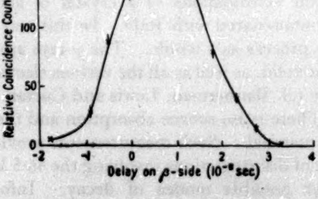

Figure 1. Coincidence rate, involving β-rays and 46·5 kev γ-rays, as a function of delay.

upper limit on the lifetime. From an examination of the slopes of this and the many similar curves which have been obtained, the lifetime concerned is less than 3×10^{-9} sec. This lifetime was shown to be that of the 46·5 kev excited state. For, from the β-channel counting rate the coincidence rate at the peak was found to be of the correct order of magnitude assuming the coincidences to involve 46·5 kev γ-rays; no other radiations could produce effects at all comparable. Moreover when the discriminator level was raised to eliminate 46·5 kev γ-rays, or when the narrow channel setting was positioned at an energy above that of the β-spectrum, the coincidences ceased.

Investigations were also made with a similar arrangement, but with 1 cm^3 of stilbene detecting L x-radiation, in the place of the iodide crystal, fronted by a polythene absorber only. Delayed coincidence curves were obtained both with, and without, a thin aluminium absorber on the electron side to stop RaD soft β-rays. A coincidence resolution curve involving prompt coincidences between a band of low energy scattered conversion electrons and L x-rays was in this way compared with one involving both β–L x coincidences and prompt coincidences. The findings supported, but did not extend the above results.

The lifetime results can be compared with predictions based on the possible character of the 46·5 kev transition. The probability of emission of a 46·5 kev γ-ray can be assessed from the theoretical formula of Blatt and Weisskopf (1952). Further, it is known from experiment that competing decay processes—mostly, if not entirely, those of internal conversion—are about 20 times as likely (Cranberg 1950; this is also discussed below). The predicted lifetime of the 46·5 kev state, on these grounds, would be of order 10^{-13} second for an electric dipole transition, or 2×10^{-11} second for a magnetic dipole transition. The state would be long lived for all other types of transition, being of order $2\,\mu$sec for the electric quadrupole case. The high speed of decay found experimentally here determines the transition to be a dipole one, but does not specify whether it is electric or magnetic in origin.

§ 3. DETERMINATION OF THE COMPLETE INTEGRATED SPECTRUM OF RaD

The rate of growth of RaE from RaD does not permit very slow processes to be used for the preparation of activated sodium iodide crystals containing RaD. However, small crystals of about 2 mm side are large enough for examining the RaD radiations. A drop taken from the surface of the source solution was placed in a small quartz tube, and the water removed. A small activated sodium iodide crystal cleaved from a block supplied by Harshaw Chemical Co. was inserted and the thin protecting layer of paraffin was removed by heating. The tube was sealed under vacuum, and the contents were melted and allowed to mix, and afterwards allowed to cool. Satisfactory crystals with radioactive contamination were obtained; the process took in all about 2 hours. One such crystal approximately 3 mm × 3 mm × 1½ mm was mounted in paraffin on a Du Mond 6292 photomultiplier, and provided with an aluminium reflector. After leaving the system for some while to minimize possible phosphorescence effects, measurements of the pulse height distribution were recorded with a single channel kicksorter. The pulses generated at the photomultiplier collector fell with a time constant of $3\,\mu$sec. Pulses arriving within a time short compared to $3\,\mu$sec would add completely.

A preliminary examination of the pulse height distribution was carried out. Figure 2 shows results obtained for a subsequent, more detailed, run of 2 hours duration, started about 7 hours after the commencement time of the whole experiment. The curve shows clearly a pronounced broad single peak, smooth in contour within the statistical errors, and only a relatively small number of pulses appear at the lower energies. The small peak on the right of the curve is due to amplifier saturation and is caused by pulses from RaE (see below); additional readings (not shown) were taken in the run determining the maximum height of this saturation peak. The photomultiplier noise and background were unimportant in the region above the lowest point shown (10v). No readings were taken below this point because of the increasing incidence of tube noise. Figure 3 shows the narrower calibration peak obtained during the run using an external source (RaD, E, F), of 46·5 kev γ-rays, covered by $\frac{1}{10}$ in. aluminium to remove β-rays and L x-rays. It lies below the peak of figure 2. The amount of RaE present in the crystal at the time of the measurements was expected, from previous sampling (§ 2), to be not far from 5%. By taking the pulse height

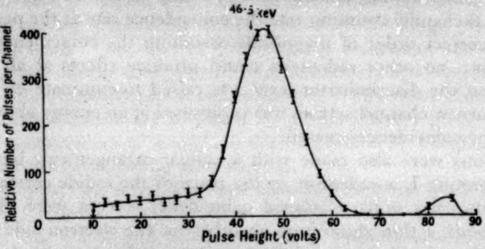

Figure 2. Integrated pulse height distribution observed with an activated sodium iodide crystal containing RaD, showing in the main a single peak representing the β-spectrum carried forward by 46·5 kev. (The small amplifier saturation peak lying near 85 v is due to RaE contamination.)

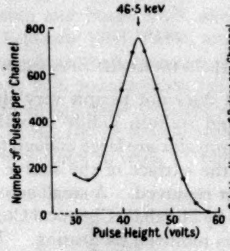

Figure 3.

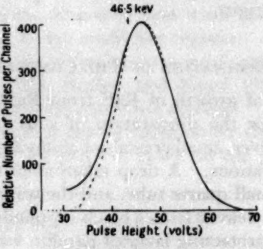

Figure 4.

Figure 3. Calibration peak obtained using an external source of RaD γ-rays with the crystal of figure 2.

Figure 4. Comparison of part of figure 2 (solid curve) with the predicted curve for a Fermi distribution allowing for finite crystal resolution (broken curve—this overlaps the solid curve above ~50 v and near the peak).

distribution with the crystal at a later date, the growth of RaE could be followed and the effect on the pulse height distribution could be determined. The percentage of pulses from RaE in figure 2 is just under 5% (mostly due to growth), of which about 3% occur in the saturation peak which is wholly due to RaE; the remainder are distributed broadly at lower energies. RaF contamination was insignificant.

Measurement work on a second contaminated crystal confirmed the forms of the pulse height distributions of figure 2 and 3 and their relative positioning.

§ 4. OBSERVED PULSE HEIGHT DISTRIBUTION AND THE DECAY OF RaD

Though some work reported in the past suggested the percentage of disintegrations involving emission of the 46·5 kev γ-ray and its conversion electrons was very low, later measurements gave a figure near 78% (cf. the review and work of Cranberg 1950,); more recently Wu, Boehm and Nagel (1953) obtained a value of about 92%. The comparative absence of pulses at lower energies in figure 2 indicates directly that the number of disintegrations involving the 46·5 kev state is very high, and that figure 2 consists essentially of the soft β-spectrum displaced forwards by 46·5 kev. To assess quantitatively the decay processes it is first necessary to discuss briefly this soft β-spectrum, taking into consideration the finite resolution of the crystal.

The front edge of the calibration curve of figure 3 is distorted, essentially by an iodine x-ray escape peak (West, Meyerhof and Hofstadter 1951). As this escape peak will not affect the form of the rear edge, the rear edge is taken as defining the resolution obtainable with electrons of energy 46·5 kev generated inside the crystal. The resolution of the crystal method is necessarily lower at these energies than that of the proportional counter; thus the half width at half height in figure 3 is 5·8 kev compared with the value of 1·7 kev employed by Jaffe and Cohen (1953). A close initial inspection of figure 2 indicates that the main bulk of the particles are emitted in the region 0–5 kev; moreover the maximum β-energy can be shown to be near 17 kev. These matters have been examined more stringently employing the finite resolution of the crystal as defined by the right-hand edge of figure 3. The actual response which can be expected in the crystal from β-rays of end point energy 17 kev obeying a Fermi distribution has been determined, allowing for Coulomb attraction (cf. Bleuler and Zünti 1946), but neglecting electron screening (figure 4). The calculated rear edge is seen to be in good agreement with the experimental rear edge, which it mostly overlaps. The calculated front edge can be expected to be low, the small drop between the full and dotted contours (involving 3% of the total number of particles) is of the order of effects associated with the liberation of a small number of electrons near the surface of the crystal. On the basis of these comparisons the end point energy of the β-rays can be assessed at 17 ± 2 kev. The total decay energy is given by figure 2 as $63{\cdot}5 \pm 2$ kev.

Jaffe and Cohen (1953) suggested their β-curve might deviate from a Fermi plot by peaking at about 2·4 kev. Though the curve of figure 2 runs close to Fermi predictions, the existence of a small number of extra β-particles over the Fermi distribution clustering around an energy below about $2\frac{1}{2}$ kev, would be possible. A broad maximum at about 5 kev as reported by Huster (1953) is however not compatible with the distribution found here.

It is now possible to consider quantitatively the lower energy region of figure 2. For a uniform source distribution about 2% of the total number of pulses from the crystal will be reduced in height because of electrons arising near the edge; further, 1% will be affected by the escape of L x-rays, and 2% by escape of 46·5 kev γ-rays or of the associated iodine x-rays. Thus including the effect of RaE, at the lower energies a tail in the pulse height distribution curve involving some 6% of the pulses might have been anticipated. Apart from the undetermined response between 0 and approximately 10 kev (which will be small taking into account the large resolution broadening at the lowest energies) the number of pulses at lower energies is approximately double that anticipated. The possibility that the small number of extra pulses are satellite or afterglow pulses, or that they arise from a greater concentration of source near the crystal surface, is very unlikely, but cannot be completely dismissed. Satellite and afterglow pulses, for instance, are very unlikely in view of a 15 μsec dead time elapsing in the kicksorter mechanism after the arrival of a real pulse; moreover the crystal had been several hours in the dark.

In considering the additional pulses it is of interest to note that an excess of pulses was reported by Jaffe and Cohen (1953), and that Cranberg (1950) observed a background continuum. These extra pulses here could be associated with the existence of a low intensity β-transition to the ground state, or with weak transitions involving metastable states with lifetimes in excess of about 3 μsec. From the distribution of figure 2, and making allowances for possible pulses below about 10 kev on the basis of the resolution broadening there, it is certain that at least 90% of the RaD disintegrations proceed by the soft β-transition to the 46·5 kev excited state followed by rapid de-excitation. Less than 5% of the RaD disintegrations can involve metastable states.

ACKNOWLEDGMENTS

The author wishes to thank Professor P. I. Dee for his interest in the work, and Mr. J. D. Prentice for some comments.

REFERENCES

BANNERMAN, R. C., and CURRAN, S. C., 1952, *Phys. Rev.*, **85**, 134.
BANNERMAN, R. C., LEWIS, G. M., and CURRAN, S. C., 1951, *Phil. Mag.*, **42**, 1097.
BLATT, J. M., and WEISSKOPF, V. F., 1952, *Theoretical Nuclear Physics* (New York: John Wiley), p. 627.
BLEULER, E., and ZÜNTI, W., 1946, *Helv. Phys. Acta*, **19**, 375.
CRANBERG, L., 1950, *Phys. Rev.*, **77**, 155.
DAMON, P. E., and EDWARDS, R. R., 1953, *Phys. Rev.*, **90**, 280; 1954, *Ibid.*, **95**, 1698.
EWAN, G. T., and ROSS, M. A., 1952, *Nature, Lond.*, **170**, 760.
FERGUSON, A. T. G., and LEWIS, G. M., 1953, *Phil. Mag.*, **44**, 1339.
GELLMAN, H., GRIFFITH, B. A., and STANLEY, J. P., 1952, *Phys. Rev.*, **85**, 944.
HUSTER, E., 1953, *Naturwissenschaften*, **40**, 197, *Phys. Rev.*, **92**, 1076.
INSCH, G. M., BALFOUR, J. G., and CURRAN, S. C., 1952, *Phys. Rev.*, **85**, 805.
JAFFE, A. A., and COHEN, S. G., 1953, *Phys. Rev.*, **89**, 454.
WEST, H. I., MEYERHOF, W. E., and HOFSTADTER, R., 1951, *Phys. Rev.*, **81**, 141.
WU, C. S., BOEHM, F., and NAGEL, E., 1953, *Phys. Rev.*, **91**, 319.

Effect of Electron Mass on High Energy Electron Scattering

By L. R. B. ELTON
Wheatstone Department of Physics, King's College, London

Communicated by H. S. W. Massey; MS. received 21*st March* 1955

Abstract. The effect of the electron mass on the differential cross section for the scattering of high energy electrons by atomic nuclei is investigated. It is shown that it is negligible for point nuclei above 5 MeV. The effect on the scattering by extended nuclei is more difficult to estimate, but is almost certainly negligible in the 100–200 MeV region.

---

§ 1. INTRODUCTION

BRENNER, BROWN AND ELTON (1954) have recently shown that the inclusion of a finite electron mass m changes the differential scattering cross section for electrons scattered by atomic nuclei only by terms of order m^2 and not m.† This effect will now be evaluated by calculating to order m^2 the phase differences between the kth partial scattered waves of a particle of zero mass and the corresponding waves of a particle of finite mass m, both scattered by the same potential. For it to be possible to define such a phase difference ζ_k it is necessary that the two waves have the same wavelength. Hence the momenta, but not the energies, of the two particles must be the same, and the energy of the particle of mass m is

$$E=(1+m^2)^{1/2}. \qquad \ldots\ldots(1)$$

This change in the energy, which is never greater than a fraction of a percent at the energies in which we are interested, is certainly quite negligible.

§ 2. THE PHASE DIFFERENCE ζ_k

The radial equations of the kth partial wave of the particle of mass m are

$$\left.\begin{aligned} S'+\frac{k}{r}S-(E-V+m)R=0,\\ R'-\frac{k}{r}R+(E-V-m)S=0,\end{aligned}\right\} \qquad \ldots\ldots(2)$$

where primes denote differentiation with respect to r. These are multiplied by m, and substitution is made for mR and mS in the resulting equations from (2). After a little simplification this yields

$$\left.\begin{aligned} R''+\left[(E-V)^2-\frac{k(k-1)}{r^2}\right]R-V'S=m^2R,\\ S''+V'R+\left[(E-V)^2-\frac{k(k+1)}{r^2}\right]S=m^2S.\end{aligned}\right\} \qquad \ldots\ldots(3)$$

This is exact. We now use m^2 as a perturbation parameter and denote the unperturbed solutions by R_0, S_0. It is then permissible to replace E by $1+\frac{1}{2}m^2$.

---

† Energies and masses are measured in units of the energy of the incident zero mass electron. Also $\hbar=c=1$.

This is done, equations (3) are multiplied by R_0, S_0 respectively, the corresponding equations for R_0, S_0 are multiplied by $-R$, $-S$ respectively, and the resulting four equations are added, to give

$$R''R_0 - RR_0'' + S''S_0 - SS_0'' + 2V'(RS_0 - SR_0) = m^2 V(R_0^2 + S_0^2). \qquad \ldots\ldots(4)$$

This can be integrated at once,

$$\Big[R'R_0 - RR_0' + S'S_0 - SS_0'\Big]_0^a = m^2 \int_0^a V(R_0^2 + S_0^2)dr - 2\int_0^a V'(RS_0 - SR_0)\,dr, \qquad \ldots\ldots(5)$$

where a will be taken to be an infinite constant. The last integral can be integrated by parts and simplified, using (2):

$$\int_0^a V'(RS_0 - SR_0)dr = \Big[V(RS_0 - SR_0)\Big]_0^a - m\int_0^a V(SS_0 - RR_0)\,dr$$
$$+ \tfrac{1}{2}m^2 \int_0^a V(S_0^2 + R_0^2)\,dr. \qquad \ldots\ldots(6)$$

Hence finally

$$\Big[R'R_0 - RR_0' + S'S_0 - SS_0' + 2V(RS_0 - SR_0)\Big]_0^a = 2m\int_0^a V(SS_0 - RR_0)\,dr. \qquad \ldots\ldots(7)$$

Now asymptotically the potential vanishes and the radial functions reduce to

$$\left.\begin{aligned} R &\sim (1-m)^{1/2}\cos(r + \alpha\beta\ln 2r - \tfrac{1}{2}k\pi + \chi_k + \zeta_k), \\ S &\sim (1+m)^{1/2}\sin(r + \alpha\beta\ln 2r - \tfrac{1}{2}k\pi + \chi_k + \zeta_k). \end{aligned}\right\} \qquad \ldots\ldots(8)$$

Here χ_k is the phase for zero mass particles, ζ_k the additional phase shift due to the finite mass, $\alpha = Ze^2$ and $\beta = (1-m^2)^{-1/2}$. Also the radial functions and their derivatives vanish for $r = 0$. Hence if we write

$$R = R_0 + mR_1 + O(m^2), \qquad S = S_0 + mS_1 + O(m^2), \qquad \ldots\ldots(9)$$

it follows from (7) that to $O(m^2)$

$$\zeta_k + \tfrac{1}{2}m^2 \ln 2a = -m\int_0^a V(S_0^2 - R_0^2)dr - m^2\int_0^a V(S_1S_0 - R_1R_0)\,dr. \qquad \ldots\ldots(10)$$

Here terms of order m^3 have been consistently neglected. It is easily shown that this result is independent of a, provided a is sufficiently large.

§ 3. THE DIFFERENTIAL CROSS SECTION

Although, as (10) shows, ζ_k contains a term of order m, the differential cross section does not. This will now be shown explicitly. It has been pointed out by Feshbach (1951) that

$$\chi_k = \chi_{-k}, \qquad R_{0,k} = S_{0,-k}, \qquad S_{0,k} = -R_{0,-k}, \qquad \ldots\ldots(11)$$

and hence it follows from (10) that to order m

$$\zeta_k = -\zeta_{-k}. \qquad \ldots\ldots(12)$$

The differential cross section to order m is

$$I(\theta) = I_0(\theta) + (f_0 f_1^* + g_0 g_1^* + \text{c.c.}) \qquad \ldots\ldots(13)$$

where $I_0(\theta), f_0, g_0$ refer to the cross section for zero mass and f_1, g_1 are the corrections to f_0, g_0 to order m. Here

$$2if_0 = \sum k\{\exp(2i\chi_k)\}(P_{k-1}+P_k), \qquad \ldots\ldots(14)$$

$$2ig_0 = \sum \{\exp(2i\chi_k)\}(P^1_{k-1}-P^1_k)\, e^{i\phi}, \qquad \ldots\ldots(15)$$

$$f_1 = -\sum k\zeta_k(P_{k-1}-P_k), \qquad \ldots\ldots(16)$$

$$g_1 = -\sum \zeta_k(P^1_{k-1}+P^1_k)\,\mathrm{e}^{i\phi}. \qquad \ldots\ldots(17)$$

These have been obtained from the standard formulae with the help of (11) and (12). It now follows from the recurrence formulae for the Legendre polynomials that

$$P^1_{k-1} \pm P^1_k = \pm k \begin{matrix}\cot\\ \tan\end{matrix} \tfrac{1}{2}\theta(P_{k-1} \pm P_k). \qquad \ldots\ldots(18)$$

When this is substituted into (15) and (17) we obtain

$$\begin{aligned} 2ig_0g_1^* &= \sum_k k\exp(2i\chi_k)(P_{k-1}+P_k)\sum l\zeta_l(P_{l-1}-P_l) \\ &= 2if_0f_1^*, \end{aligned} \qquad \ldots\ldots(19)$$

so that

$$f_0f_1^* + g_0g_1^* + \text{c.c.} = 0. \qquad \ldots\ldots(20)$$

We now write

$$\zeta_k = ma_k + m^2b_k \qquad \ldots\ldots(21)$$

and divide the mass effect on the cross section into two parts, that due to a_k^2 and that due to b_k. The latter is simply a phase shift correction and, provided that m^2b_k is less than the accuracy to which χ_k is known, it is negligible. The former is much more difficult to deal with, since it can only be investigated in the complete cross section.

On expanding f and g to the next order, we find that the contribution to $I(\theta)$ due to the a_k is

$$f_1f_1^* + g_1g_1^* + f_0f_2^* + f_0^*f_2 + g_0g_2^* + g_0^*g_2, \qquad \ldots\ldots(22)$$

where

$$f_1f_1^* + g_1g_1^* = m^2\operatorname{cosec}^2\tfrac{1}{2}\theta \sum_k ka_k(P_{k-1}-P_k)\sum_l la_l(P_{l-1}-P_l), \qquad \ldots\ldots(23)$$

$$f_0f_2^* + g_0g_2^* + \text{c.c.} = -m^2\sec^2\tfrac{1}{2}\theta \sum_k k\cos 2\chi_k(P_{k-1}+P_k)\sum la^2_l(P_{l-1}+P_l). \qquad \ldots\ldots(24)$$

Closed formulae for these sums can be obtained only in the special case of the Coulomb potential.

§ 4. THE COULOMB CASE

In the Coulomb case (superfix c) $a_k{}^{\mathrm{c}}$ and $b_k{}^{\mathrm{c}}$ can be found easily by expanding the explicit expression for $\chi_k{}^{\mathrm{c}} + \zeta_k{}^{\mathrm{c}}$ (Mott and Massey 1949) in powers of m. We obtain

$$a_k{}^{\mathrm{c}} = -\frac{\alpha}{2k}, \qquad \ldots\ldots(25)$$

$$b_k{}^{\mathrm{c}} = \frac{1}{4}\alpha\left\{\frac{\rho}{k^2} - \psi(\rho+1-i\alpha) - \psi(\rho+1+i\alpha)\right\}, \qquad \ldots\ldots(26)$$

where $\rho=(k^2-\alpha^2)^{1/2}$. The corrections (23) and (24) then reduce to

$$-\tfrac{1}{4}m^2\alpha^2\operatorname{cosec}^2\tfrac{1}{2}\theta, \qquad \ldots\ldots(27)$$

and

$$-\tfrac{1}{4}m^2\alpha^2\sec^2\tfrac{1}{2}\theta\ln\operatorname{cosec}^2\tfrac{1}{2}\theta\times i(f_0{}^c-f_0{}^{c*}). \qquad \ldots\ldots(28)$$

Here $\frac{1}{2}i(f_0{}^c-f_0{}^{c*})$ is the imaginary part of the $G(\theta)$ tabulated by Feshbach (1952).

Now (27) and (28) are corrections to the cross section and (26) gives a correction to the phases, of which never more than 10–15 are required (Yennie, Ravenhall and Wilson 1954). Numerical results for mercury are given in tables 1 and 2. Clearly the most important corrections are those to the phases, and these become negligible at energies above about 5 MeV. This confirms the result of McKinley and Feshbach (1948), who found that for a point nucleus the differential cross section was independent of energy above 4 MeV.

Table 1. Differential Cross Sections for Zero Mass Electrons and Corrections for Finite Mass for Scattering by a Point Nucleus, $Z=80$

θ(°)	$I_0{}^c$	$\lvert i(f_0{}^c-f_0{}^{c*})\rvert$	|Correction (27)|	|Correction (28)|
30	25·8	7·07	1·3 m^2	0·2 m^2
90	0·646	0·532	0·17 m^2	0·07 m^2
150	0·0377	0·074	0·009 m^2	0·007 m^2

Table 2. Phase Shifts for Zero Mass Electrons and Correction for Finite Mass for Scattering by a Point Nucleus, $Z=80$

k	$\chi_k{}^c$	|Correction (26)|
1	0·419	0·06 m^2
5	−0·881	1·26 m^2
10	−1·316	1·80 m^2
15	−1·563	2·13 m^2

§ 5. THE EXTENDED NUCLEUS

The situation is somewhat different for scattering by an extended nucleus. Closed formulae for (23) and (24) cannot now be obtained. Order of magnitude calculations can however be made on the assumption that the phase difference ζ_k is approximately the same for a point and for an extended nucleus. This is not unreasonable when it is remembered that calculations of χ_k in which the change from a point to an extended nucleus is treated as a perturbation (Elton 1953) give results which differ from the correct ones by less than 25%. Further, the only exact calculation available is one for the scattering of 20 MeV electrons by gold (Elton 1950), where the following results were obtained:

	$\chi_1+\zeta_1$	$\chi_1-\zeta_1$	$2\zeta_1$
Point nucleus	0·415	0·400	0·015
Homogeneous distribution	0·219	0·205	0·014
Surface distribution	0·144	0·132	0·012

The energy region of greatest interest for the scattering by an extended nucleus is 100–200 MeV. Because of the very large cancellations occurring in the calculations, it is necessary to know the χ_k to an accuracy of about 0·00005, but as the corrections to the χ_k will certainly be of the same order of magnitude as those in table 2 they are quite negligible. An estimate of the corrections to the cross sections has been obtained by using the point nucleus values of the a_k, but the extended nucleus values of $i(f_0-f_0{}^*)$, since the latter depends on the χ_k. The results are given in table 3. The corrections are negligible by several orders of magnitude, except at very large angles. At these the experimental accuracy of the most recent experiments (Hofstadter, Hahn, Knudsen and McIntyre 1954) is certainly insufficient to detect a discrepancy of even 50% in the cross section. The discrepancies between the experimental results and the theoretical curves of Ravenhall and Yennie (1954) and of Brown and Elton (1955) are most unlikely therefore to be due to the neglect of the electron mass.

Table 3. Differential Cross Sections for 125 MeV Electrons scattered by Extended Nuclei, $Z=80$. The corrections are approximate (see text)

$\theta(^\circ)$	I_0	$\lvert i(f_0-f_0^*)\rvert$	$\lvert$Correction (23)$\rvert$	$\lvert$Correction (24)$\rvert$
30	8	4·90	$2{\cdot}1\times10^{-5}$	$2{\cdot}2\times10^{-5}$
90	5×10^{-4}	$2{\cdot}5\times10^{-2}$	$2{\cdot}7\times10^{-6}$	$5{\cdot}3\times10^{-8}$
150	1×10^{-6}	$1{\cdot}6\times10^{-4}$	$1{\cdot}4\times10^{-7}$	$<10^{-10}$

REFERENCES

BRENNER, S., BROWN, G. E., and ELTON, L. R. B., 1954, *Phil. Mag.*, **45**, 524.

BROWN, G. E., and ELTON, L. R. B., 1955, *Phil. Mag.*, **46**, 164.

ELTON, L. R. B., 1950, *Proc. Phys. Soc.* A, **63**, 1115 ; 1953, *Ibid.*, **66**, 806.

FESHBACH, H., 1951, *Phys. Rev.*, **84**, 1206 ; 1952, *Ibid.*, **88**, 295.

HOFSTADTER, R., HAHN, B., KNUDSEN, A. W., and MCINTYRE, J. A., 1954, *Phys. Rev.*, **95**, 512.

MCKINLEY, W. A., and FESHBACH, H., 1948, *Phys. Rev.*, **74**, 1759.

MOTT, N. F., and MASSEY, H. S. W., 1949, *The Theory of Atomic Collisions*, 2nd Edn (Oxford : University Press), ch. IV, § 4.

RAVENHALL, D. G., and YENNIE, D. R., 1954, *Phys. Rev.*, **96**, 239.

YENNIE, D. R., RAVENHALL, D. G., and WILSON, R. N., 1954, *Phys. Rev.*, **95**, 500.

The Scattering of Nucleons by Alpha Particles—Determination of the Spin–Orbit Interaction

By S. HOCHBERG, H. S. W. MASSEY, H. ROBERTSON and L. H. UNDERHILL
Department of Physics, University College, London

MS. received 11*th February* 1955

Abstract. The p-phases for the scattering of neutrons by alpha-particles have been calculated by the resonating group structure method assuming an interaction between nucleons of the form

$$V_0\{mM_{ij}+hH_{ij}+bB_{ij}+w+S\hbar^{-2}(\mathbf{s}_i+\mathbf{s}_j)\,.\,\mathbf{r}_{ij}\times(\mathbf{p}_i-\mathbf{p}_j)\}\exp(-\beta r_{ij}{}^2)+(e^2/r_{ij})\epsilon_{ij},$$

where $\epsilon_{ij}=1$ if the nucleons are protons and zero otherwise. M_{ij}, H_{ij} and B_{ij} are the normal Majorana, Heisenberg and Bartlett exchange operators, $\mathbf{s}_i$, $\mathbf{s}_j$ and $\mathbf{p}_i$, $\mathbf{p}_j$ are the spin and orbital angular momentum of the two nucleons. m, h, w, b are constants which satisfy the conditions $m+h+w+b=1$, $m+w-(h+b)=x=0{\cdot}6$. V_0 and β are taken to be -45 MEV and $0{\cdot}2657\times10^{26}$ cm^{-2} respectively. The parameter S measures the relative strength of the spin–orbit interaction, and the aim of the work was to determine S to give the best fit with the observed scattering data. It is found that the mean p-phase shift is only given correctly when the exchange operator in the central interaction is close to the Serber form

$$m=w=\tfrac{1}{4}(1+x),\quad h=b=\tfrac{1}{4}(1-x).$$

A good fit is obtained with the following constants:

$$m=0{\cdot}258+0{\cdot}325x,\ h=0{\cdot}258-0{\cdot}325x,\ w=0{\cdot}242+0{\cdot}225x,\ b=0{\cdot}242-0{\cdot}225x,$$
$$S=0{\cdot}1.$$

The phase shifts were calculated from the integro-differential equations using the Pilot ACE electronic computer at the National Physical Laboratory, Teddington. Values of the d-phases have also been obtained for neutron energies up to 16 MEV.

---

§ 1. INTRODUCTION

In an earlier paper (Hochberg, Massey and Underhill 1954, to be referred to as I) we have developed the theory of the scattering of nucleons by alpha particles using the method of resonating group structure which is equivalent to the usual method of collision theory in which exchange of particles is included but polarization largely neglected. Using a central interaction between nucleons of gaussian form and approximate alpha-particle wave functions of the same form the s-phases for the scattering of both neutrons and protons by alpha particles were calculated. The method used did not assume that the approximate alpha-particle wave functions were exact solutions of the alpha-particle wave equation but merely satisfied an integral condition which ensured that they gave a good variational approximation to the binding energy of the alpha particle. The integro-differential equation which determined the s wave functions for the relative motion of nucleon and alpha particle was solved accurately by an iterative numerical procedure. Very good agreement was obtained with the s-phases derived from an analysis of experimental data provided the nuclear forces were assumed to have a symmetrical exchange character. The agreement was somewhat less satisfactory with Serber type forces but still reasonably good in view of the complexity of the problem and the uncertainty which still exists in some of the observed data.

The main aim of the work has, however, been directed towards the second stage. The observed data show that the p-phases are widely split, a result which appeared first from an analysis of single scattering data and which was directly confirmed by a double scattering experiment (Heusinkveld and Freier 1952). It was first thought that the non-central force responsible for this splitting is the tensor force known to form a substantial part of the main interaction between nucleons. However, estimates of the splitting which it can produce have all been very much too small and it has therefore been assumed that some other kind of non-central force must be introduced. The most obvious one to consider is of the spin–orbit type with which one is familiar in the theory of the fine structure of atomic spectra. There is no doubt that such an interaction, of sufficient strength, between nucleons can produce the observed splitting. So far no attempt has been made to determine the required strength from the scattering data though several authors have analysed the data on the assumption of a central nucleon–alpha-particle interaction with a spin–orbit term added. We have now extended the method of I to include the presence of a spin–orbit term in the fundamental internucleonic interactions. This does not affect the s-phases but leads to a splitting of the p-phases. To determine the strength of the spin–orbit interaction it has been necessary to calculate the $p_{3/2}$ and $p_{1/2}$ phases for several energies of the nucleons for a number of different assumed strengths in order to obtain the best fit. In addition to obtaining the correct ' centre of gravity ' of the p-phases it was found necessary to vary somewhat the assumed exchange character of the nuclear forces. Each such calculation involves the solution of an integro-differential equation. This very extensive programme has been rendered possible by the availability of an electronic computing machine. A good fit with the p-phases obtained by analysis of the neutron–alpha-particle scattering data has been obtained if an exchange character close to the Serber, but with slightly more pure exchange component, is assumed together with a spin–orbit interaction of a particular strength. The central interaction is the same as in I and the space variation of the spin–orbit term is taken to be the same as for the central component. The d-phase shifts have also been calculated assuming the same interaction.

§ 2. THE INTERNUCLEONIC INTERACTION AND NUCLEAR WAVE FUNCTION ASSUMED

The interaction between two nucleons distinguished by suffixes i, j was taken to be of the form

$$(mM_{ij}+hH_{ij}+bB_{ij}+w)\,V(r_{ij})+(e^2/r_{ij})\epsilon_{ij}+\hbar^{-2}\,U(r_{ij})\,(\mathbf{s}_i+\mathbf{s}_j)\,.\,\mathbf{r}_{ij}\times(\mathbf{p}_i-\mathbf{p}_j), \quad \ldots\ldots(1)$$

where M, H, B are respectively the Majorana, Heisenberg and Bartlett exchange operators, m, h, b and w are numerical constants such that $m+h+w+b=1$, $m+w-(h+b)=x$ and r_{ij} is the relative position vector of the particles, s_i, s_j and p_i, p_j the respective spin and linear momenta, in operator form, of the two nucleons. $\epsilon_{ij}=1$ if the nucleons are protons and zero otherwise.

The central potential function $V(r_{ij})$ was taken exactly as in I, i.e.

$$V(r_{ij}) = V_0 \exp\{-\beta r_{ij}^2\},$$

with

$$\beta = 0{\cdot}2657 \times 10^{26}\,\text{cm}^{-2}, \quad V_0 = -45\,\text{Mev}, \quad x = 0{\cdot}6. \qquad \ldots\ldots(2)$$

The non-central potential function $U(r_{ij})$ was taken to be a constant fraction S of $V(r_{ij})$ so that

$$U(r_{ij}) = SV_0 \exp\{-\beta r_{ij}^2\}. \qquad \ldots\ldots(3)$$

This is reasonable for a gaussian shape of interaction for, arguing by analogy, one might suppose that $U(r_{ij})$ should be proportional to $r_{ij}^{-1}\,\partial V(r_{ij})/\partial r_{ij}$ which is also of gaussian shape.

The problem is to determine S to give the best fit with the observed $p_{1/2}$ and $p_{3/2}$ phase shifts. m, h, b and w are, in principle, also available for adjustment, but reasonable consistency must be preserved with the observed s-phases which also depend quite strongly on these constants.

It will be noted that the spin–orbit interaction has been taken to be independent of isotopic spin. This was done in order to reduce the number of possible variants. In a later investigation the dependence of the spin–orbit strength parameter S on the isotopic spin dependence of the spin–orbit interaction will be determined.

As in I the wave function ϕ for the ground state of an alpha particle was taken to have the gaussian form

$$\phi(2345) = N \exp\{-\alpha \sum_{i>j=2}^{5} r_{ij}^2\}, \qquad \ldots\ldots(4)$$

with $\alpha = 0{\cdot}0789 \times 10^{26}\,\text{cm}^{-2}$. N is the normalizing factor.

§ 3. THE INTEGRO–DIFFERENTIAL EQUATION FOR THE SCATTERING

The inclusion of the spin–orbit interaction into the theory described in I, § 2, presents no difficulties. It is only necessary to replace the product $F(1)\alpha_1$ of the function F describing the relative motion of nucleon 1 and the alpha particle and the spin wave function α of the nucleon, by $G_M(\mathbf{r}_1, \mathbf{s}_1)$ where

$$G_M(\mathbf{r}_1, \mathbf{s}_1) = \sum_{J=1/2}^{\infty} \sum_{l=J-1/2}^{J+1/2} r_1^{-1} f_{JMl}(r_1)$$
$$\times [c_{JMl,M+1/2} Y_{l,M+1/2}(\theta_1,\phi_1)\beta_1 + c_{JMl,M-1/2} Y_{l,M-1/2}(\theta_1,\phi_1)\alpha_1], \quad \ldots\ldots(5)$$

$M\hbar$ being the z-component of total angular momentum, c_{JMlm} the appropriate Clebsch–Gordan coefficients and the $Y_{l,m}$ spherical harmonics. The coordinates (r_1, θ_1, ϕ_1) are spherical polar coordinates of the nucleon 1 relative to the centre of the alpha particle. The complete wave function describing the system is then written, in the notation of I, eqn. (4), in the form

$$\Psi_M = \sum_{\text{cyclic }1,2,3} G_M(\mathbf{r}_1, \mathbf{s}_1)\,\phi(-1)\,\chi(\widetilde{23}, \widetilde{45}). \qquad \ldots\ldots(6)$$

By following a procedure similar to that of I, uncoupled differential equations are obtained for the radial functions f_{JMl} but the direct and exchange interactions which appear in them depend now on both J and l, the quantum numbers of the total and of the relative orbital angular momentum respectively. We find that the equations which determine the phase shifts for a given value of l are

$$\frac{d^2 f_{l\pm1/2,l}(r)}{dr^2} + \left\{k^2 - W(r) - U_{l\pm1/2,l}(r) - \frac{l(l+1)}{r^2}\right\} f_{l\pm1/2,l}(r)$$
$$= \int_0^\infty \{k_l(r,r') + n_{l\pm1/2,l}(r,r')\} f_{l\pm1/2,l}(r')\,dr' \qquad \ldots\ldots(7)$$

where $W(r)$ and $k_l(r,r')$ are as in I eqn. (12).

$U_{l\pm 1/2,l}(r)$, $n_{l\pm 1/2,l}(r,r')$ arise from the spin–orbit interaction. In terms of the interaction (1) with (2) and (3) and with the form (4) for ϕ we have

$$W(r)=[2(2w+b)-(m+2h)]D, \qquad \ldots\ldots(8)$$

$$k_l(r,r')=[2(2m+h)-(w+2b]\,Q+P, \qquad \ldots\ldots(9)$$

$$U_{l\pm 1/2,l}=\frac{80\alpha}{32\alpha+3\beta}S\,\lambda_{l+1/2,l}\,D, \qquad \ldots\ldots(10)$$

$$n_{l\pm 1/2,l}=-\frac{40\alpha}{8\alpha-3\beta}S\,\lambda_{l+1/2,l}\,Q, \qquad \ldots\ldots(10)$$

where

$$D=\frac{MV_0}{\hbar^2}\left(\frac{2\alpha}{32\alpha+3\beta}\right)^{3/2}\frac{512}{5}\exp\left\{\frac{-32\alpha\beta}{32\alpha+3\beta}r^2\right\},$$

$$Q=\frac{MV_0}{\hbar^2}\left(\frac{6\alpha}{\pi}\right)^{3/2}\left(\frac{16}{15}\right)^3\frac{15\pi}{8\alpha-3\beta}\exp\left\{-\frac{16}{75}(17\alpha+3\beta)(r^2+r'^2)\right\}$$

$$\times I_{l+1/2}\left[\frac{32}{75}(8\alpha-3\beta)rr'\right],$$

$$P=\left(\frac{6\alpha}{\pi}\right)^{3/2}\left(\frac{16}{15}\right)^3R,$$

$$R=\frac{-MV_0}{\hbar^2}\left(\frac{3\alpha}{12\alpha+\beta}\right)^{1/2}\frac{45\pi}{4\alpha+\beta}\left[\exp\frac{-16}{25}\,\frac{\alpha}{12\alpha+\beta}\right.$$

$$\times\{(68\alpha+27\beta)r^2-(68\alpha+7\beta)r'^2\}+\exp\,\frac{-16}{25}\,\frac{\alpha}{12\alpha+\beta}$$

$$\left.\times\{(68\alpha+7\beta)r^2-(68\alpha+27\beta)r'^2\}\right]I_{l+1/2}\left\{\frac{256}{25}\,\frac{4\alpha+\beta}{12\alpha+\beta}\alpha rr'\right\}+\frac{M}{\hbar^2}\,\frac{15\pi}{8\alpha}$$

$$\times\left[E+E_\alpha-\frac{188}{5}\,\frac{\hbar^2\alpha}{M}-24(m+w)V_0\left(\frac{\alpha}{4\alpha+\beta}\right)^{3/2}-4e^2\left(\frac{\alpha}{\pi}\right)^{1/2}\right]\times$$

$$\exp\left\{-\frac{16\times 17}{75}\alpha(r^2+r'^2)\right\}I_{l+1/2}\left\{\frac{256}{75}\alpha rr'\right\}+\frac{2\alpha\pi}{75}\left[\left\{38(r^2+r'^2)+49\,\frac{75}{256\alpha}\right\}\right.$$

$$\left.\times I_{l+1/2}\left\{\frac{256}{75}\alpha rr'\right\}-49rr'I_{l+1/2}'\left\{\frac{256}{75}\alpha rr'\right\}\right]\exp\left\{-\frac{16\times 17}{75}\alpha(r^2+r'^2)\right\},$$

and $\qquad \lambda_{l+1/2,l}=l, \quad \lambda_{l-1/2,l}=-(l+1), \quad \lambda_{1/2,0}=0.$

$I_{l+1/2,l}(x)$ is the hyperbolic spherical Bessel function defined by

$$I_{l+1/2}(x)=(-1)^l(\pi x/2)^{1/2}\exp\{-(l+\tfrac{1}{2})i\pi/2\}J_{l+1/2}(ix),$$

the first two values being

$$I_{1/2}(x)=\sinh x,\; I_{3/2}(x)=\sinh x/x-\cosh x,$$

$I_{l+1/2}'(x)$ is written for $dI_{l+1/2}/dx$.

These expressions are obtained on the assumptions as for case (*a*) of I, § 2, which assumes merely that the function ϕ satisfies a variational condition in terms of the binding energy of the alpha particle (see I, § 3).

The asymptotic form of the solution of (7) which vanishes at the origin is given by

$$f_{l\pm 1/2,l}(r)\sim\sin(kr-\tfrac{1}{2}l\pi+\eta_{l\pm 1/2,l}). \qquad \ldots\ldots(12)$$

§ 4. METHOD OF CALCULATION

The phases $\eta_{l\pm 1/2,\, l}$ were calculated from the equation (7) by means of an electronic computing machine (Pilot ACE at the National Physical Laboratory, Teddington). Some time before, a programme for dealing with the determination of phases for nuclear scattering problems from the integro-differential equations which arise when gaussian interactions and gaussian wave functions are assumed had been set up by one of us (H.R.) following a suggestion of Dr. P. Swan. This programme, an account of which will be published separately (Robertson 1955) was immediately applicable to the present problem. With this technique it was possible to calculate a phase shift for given functions W, $U_{l\pm 1/2,\, l}$, k_l and $\eta_{l\pm 1/2,\, l}$ and a chosen value of the parameter S in a very short time. There was no difficulty therefore in scanning a wide range of possibilities and quickly deciding a first approximation to the correct value of S from which a more accurate value could be obtained.

§ 5. RESULTS AND DISCUSSION

In view of the fact that in I it was found that a central interaction of symmetrical exchange type gave the best fit with the ' observed ' s-phases, the first calculations of p-phases were carried out with this choice of values for m, h, b and w. It soon became clear that no fit with the ' observed ' p-phases could be obtained in this way. Roughly speaking the ' mean ' p-phase $(\frac{2}{3}p_{1/2}+\frac{1}{3}p_{3/2})$ is determined by the central interaction, the difference, $p_{1/2}-p_{3/2}$ by the spin–orbit term. Symmetrical exchange forces give a ' mean ' p-phase which is much too small. With this interaction the ordinary potential terms in equation (5) vanish. In general these terms are much more effective in producing p-phase shift than the exchange kernels, a result which also holds for n–d collisions (Buckingham and Massey 1941). It follows that complete consistency between the s and p phases cannot be obtained with the assumed interaction since it was shown in I that the best fit with the s-phases is obtained with a symmetrical interaction. However, reference to the figure in I shows that a Serber interaction does not give s-phases which are too seriously wrong and it was found that this does give a mean p-phase which is not far from correct. The following procedure was then adopted.

The exchange operator associated with the central interaction was taken as

$$(1-a)S_y + aS_e \qquad \ldots\ldots(13)$$

where S_y is the symmetrical and S_e the Serber exchange operator. a and the spin–orbit strength S were then adjusted to give the best fit with the observed p-phases. 58 p-phases in all were calculated and it was found that a good fit was obtained with

$$a=0{\cdot}90, \quad S=0{\cdot}10. \qquad \ldots\ldots(14)$$

Comparison of the p-phases calculated assuming these values with the ' observed ' p-phases is illustrated in figure 1. It will be seen that the agreement is probably as good as is justified from the accuracy of the experimental data available. To illustrate the sensitiveness of the calculated phases to the parameters assumed the phases obtained for different values of these parameters are also shown in figure 1.

In figure 2 the s-phases calculated with $a=0{\cdot}90$ are compared with those for $a=0$ and $a=1$ given in I, and the ' observed '. The disagreement with the 'observed ' phases is not very serious.

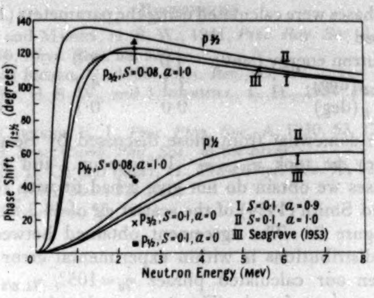

Figure 1. $p_{3/2}$ and $p_{1/2}$ phase shifts for scattering of neutrons by alpha particles.

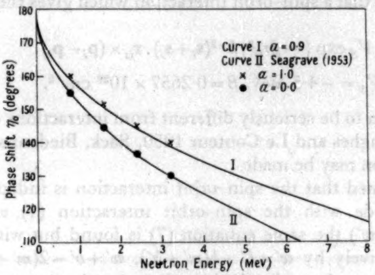

Figure 2. s-phase shifts for scattering of neutrons by alpha particles.

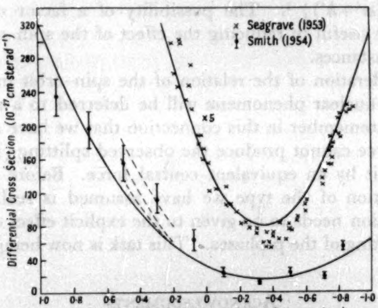

Figure 3. Comparison of observed and calculated differential cross sections for scattering of 14·3 MEV neutrons by alpha particles.

Full line curve calculated with $S=0\cdot10$, $p=0\cdot9$. Seagrave's observations are plotted on an absolute scale, the broken lines indicating the trend of three separate sets of measurements at smaller angles. Smith's observations are normalized so as to agree, on the average, with the calculated cross sections around the minimum.

Finally, the d-phases were calculated using the parameters (14). The following values were obtained:

Neutron energy (MeV)	4·0	8·0	16·0
$\eta_{5/2,\,2}$ (deg)	1·1	4·7	15·7
$\eta_{3/2,\,2}$ (deg)	0·0	0·1	0·8

These values differ somewhat from those discussed by Seagrave (1953). For example, at 16 MeV he took $\eta_{3/2,\,2} = -17°$ (approx.) and either $\eta_{5/2,\,2} = 0$ or $= \eta_{3/2,\,2}$. The phases we obtain do not give a bad fit with the observations of Seagrave (1953) and Smith (1954) of the scattering of 14·3 MeV neutrons. This is illustrated in figure 3. The agreement obtained between calculated and observed angular distributions is within experimental error over most of the angular range when our calculated phases $\eta_0 = 105°$, $\eta_{1,\,3/2} = 92°$, $\eta_{1,\,1/2} = 56°$, $\eta_{2,\,5/2} = 9°$, $\eta_{2,\,3/2} = 0$ are introduced. This suggests that the constants of (14) give as good a representation of the experimental data as is worth obtaining at this stage.

It appears then that a spin–orbit interaction which gives the observed splitting is given by

$$V_S \exp\{-\beta r_{ij}^2\}\,\hbar^{-2}(\mathbf{s}_i+\mathbf{s}_j)\,.\,\mathbf{r}_{ij}\times(\mathbf{p}_i-\mathbf{p}_j)$$

with

$$V_S = -4{\cdot}5 \text{ MeV}, \quad \beta = 0{\cdot}2657\times 10^{26}\text{ cm}^{-2}. \qquad \ldots\ldots(15)$$

This does not seem to be seriously different from interactions derived from other considerations (Hughes and Le Couteur 1950, Sack, Biedenharn and Breit 1954) as far as comparison may be made.

We have assumed that the spin–orbit interaction is independent of isotopic spin. If we include with the spin–orbit interaction (1) an operator factor $(m'M + h'H + b' + w')$ the same equation (7) is found but with $U_{l\pm 1/2,\,l}$; $n_{l\pm 1/2,\,l}$ multiplied respectively by $w' + b' - \frac{1}{2}(m' + h')$, $w' + b' - 2(m' + h')$. The contribution made to the p-phases by the kernels $n_{l\pm 1/2,\,l}$ is very small compared with that made by the potential term $U_{l\pm 1/2,\,l}$. It follows that if the operator factor is included the value of V_S given in (15) should be reduced approximately by the factor $\{w' + b' - \frac{1}{2}(m' + h')\}^{-1}$. The possibility of a factor of this kind being present may prove useful in reducing the effect of the spin–orbit interaction in in different circumstances.

A fuller consideration of the relation of the spin–orbit interaction we have obtained to other nuclear phenomena will be deferred to a subsequent paper. It is important to remember in this connection that we have assumed, as usual, that the tensor force cannot produce the observed splitting (Dancoff 1940) and have represented it by an equivalent central force. Before concluding that a spin–orbit interaction of the type we have assumed is really necessary more detailed consideration needs to be given to the explicit effect of the tensor force in producing splitting of the p-phases. This task is now being attempted.

ACKNOWLEDGMENTS

We are indebted to the Director of the National Physical Laboratory and to the Superintendent of the Mathematics Division for the use of the Pilot ACE electronic computer. One of us (L.H.U.) wishes to thank the University of Wales for the award of a Fellowship and another (S.H.) wishes to thank the University of London for the award of a Hoover Postgraduate Studentship during the period in which this work was carried out.

REFERENCES

Buckingham, R. A., and Massey, H. S. W., 1941, *Proc. Roy. Soc.* A, **179,** 123.

Dancoff, S. M., 1940, *Phys. Rev.*, **58,** 326.

Heusinkveld, M., and Freier, G., 1952, *Phys. Rev.*, **85,** 80.

Hochberg, S., Massey, H. S. W., and Underhill, L. H., 1954 *Proc. Phys., Soc.* A, **67,** 957.

Hughes, J., and Le Couteur, K. J., *Proc. Phys. Soc.*, A, 1950, **63,** 1220.

Robertson, H., 1955, *Proc. Camb. Phil. Soc.*, in the press.

Sack, S., Biedenharn, L. C., and Breit, G., 1954, *Phys. Rev.* **93,** 321.

Seagrave, J. D., 1953, *Phys. Rev.*, **92,** 1222.

Smith, J. R., 1954, *Phys. Rev.*, **95,** 730.

An Investigation of the Neutron Groups from the Disintegration of Phosphorus by 8 MeV Deuterons

By F. A. EL BEDEWI† and M. A. EL WAHAB‡

† Nuclear Physics Research Laboratory, University of Liverpool
‡ Faculty of Science, University of Alexandria, Egypt.

Communicated by H. W. B. Skinner : MS received 10*th February* 1955 *and in revised form* 11*th March* 1955

Abstract. The energy spectrum and angular distributions of some neutron groups emitted from the bombardment of a thin phosphorus target by 8 MeV deuterons have been investigated. The Q value of this reaction is found to be $6{\cdot}63 \pm 0{\cdot}08$ MeV. New excited states in ^{32}S at 6·29, 7·28 and 8·23 MeV, with errors of $\pm 0{\cdot}10$ MeV have been observed. Angular distributions of neutron groups corresponding to the transition to the ground state and two excited states at 2·25 MeV and 3·81 MeV in ^{32}S are compared with theoretical curves calculated on the basis of Butler and Born approximation stripping theories. The angular momentum of the captured proton to these states is found to be 0, 2 and 0 respectively. In an appendix, R. Huby and H. C. Newns discuss the interpretation of these results on the shell model.

§ 1. Introduction

Several investigators have reported measurements of the positions of the energy levels of ^{32}S but so far no assignments of spin and parity have been made. In this paper, we report the results of an investigation of the energy levels of this nucleus by the (d, n) stripping process using 8 MeV deuterons on a thin phosphorus target. The choice of the target nucleus is due to the fact that phosphorus naturally exists as a single isotope and the (d, n) reaction leads to a ^{32}S nucleus which contains an equal even number of protons and neutrons. It is of interest to find out whether they fill the subshell $2s_{1/2}$ of Mayer's model.

§ 2. Experimental Procedure

A thin (60 kev) phosphorus target deposited by sedimentation from a suspension in water on a thick gold backing was bombarded by deuterons of incident energy $8{\cdot}13 \pm 0{\cdot}05$ MeV. The neutrons were detected by eight 2 in. × 2 in. Ilford C2 600 μ nuclear plates mounted radially with their inner edges at 10 cm from the centre of the target. The plates were placed vertically at angles ranging from 0° to 35° with respect to the direction of the incident deuteron beam.

The exposure was made with the 37 in. cyclotron at the Nuclear Physics Research Laboratory, Liverpool, employing the experimental arrangement previously reported by Middleton, El Bedewi and Tai (1953). Investigation of the plates was carried out at Alexandria University, Egypt, using a Leitz binocular microscope with × 6 eyepieces and × 100 oil immersion objective. Measurement of recoil protons, in each plate, was confined to a strip of emulsion of width 4 mm and length 5 mm centred about the line joining the centres of the target and plate and commenced 8 mm from the inner edge of the plate. All tracks of ranges greater than 200 μ, and subtending a horizontal angle of less than or equal to 8° with the centre line and having a dip of less than 10 μ in a length of 100 μ at the beginning of the track were recorded. The corresponding neutron energy for each recoil proton was calculated from geometrical considerations and using the range–energy relation of El Bedewi (1951).

§ 3. ENERGY LEVELS

From the inelastic scattering of 2·5 MEV neutrons from sulphur, Day (1953) observed by means of a scintillation spectrometer γ-rays of energy 0·077 MEV and 2·23 MEV. The second level agrees with that previously reported by Grace, Beghian, Preston and Halban (1951) and corresponds to a known level in ^{32}S while the low-lying level could be better assumed to originate from the ^{32}S (n, p) ^{32}P reaction to the known 77 kev level in ^{32}P. An extensive study of the energy levels in ^{32}S was recently reported by Arthur *et al.* (1952) from the inelastic scattering of 8 MEV protons. They observed, by magnetic analysis, levels at 2·25, 3·81, 4·32, 4·50, 4·74, 5·04 and 5·83 MEV with errors of ± 0·02 MEV. Using the photographic plate technique Snowdon (1952) has investigated the neutrons emitted at 0° and 90° from a thick phosphorus target when bombarded by 1·6 MEV deuterons. An uncertain value of 6·2 MEV for the Q value of this reaction is given and the positions of the excited states do not agree well with those reported by Arthur *et al.* (1952). No higher levels than those previously mentioned have been reported except an indication of γ-rays of energy 6·2 MEV observed by Alburger (1949) by aluminium absorption from the bombardment of phosphorus by 3·7 MEV deuterons. It was not clear whether these γ-rays were due to a level in ^{32}S or in some other residual nucleus resulting from competing reactions such as (d, p) or (d, α). In the present work an energy level at 6·29 ± 0·10 MEV was observed.

To analyse the energy levels, histograms were plotted for the energy distribution of neutrons emitted at angles ranging from 0° to 35° with respect to the direction of the incident deuteron beam. The neutron energy scale, for each spectrum, was then transferred to the corresponding energy release Q and a superposition of all accepted tracks was made as shown in figure 1. Each point on this spectrum represents the number of tracks recorded in successive intervals of 100 kev in energy release Q. The positions of the arrows shown at N_1, N_2 . . . . N_7 are derived from the results of Arthur *et al.* (1952). The groups denoted by N_8, N_9 and N_{10} correspond to new excited states in ^{32}S at 6·29, 7·28 and 8·23 MEV, with errors of ± 0·10 MEV.

The Q-value of the present reaction is derived from the energy of the long range neutron group N_0 and it is found to be 6·63 ± 0·08 MEV. It is considered to be more accurate than that previously given (6·81 MEV) in the preliminary note by El Bedewi *et al.* (1952). Thus, using the mass of sulphur (31·982236 ± 0·00007 m.u.) as reported by Collins, Nier and Johnson (1952) and the mass of neutron and deuteron as given by Mattauch and Bieri (1954) the mass of ^{31}P is found to be 30·98360 ± 0·0009 m.u. This result is in excellent agreement with the value of 30·983609 ± 0·000012 m.u. calculated from the mass difference of the doublet O_2–PH which was reported by Ogata and Matsuda (1953).

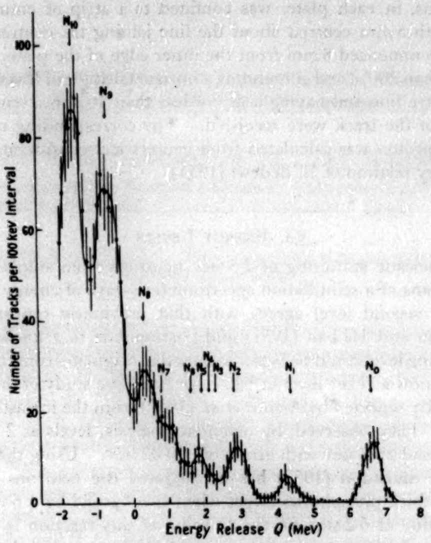

Figure 1. Neutron spectrum from the reaction ^{31}P (d, n) ^{32}S.

§4. ANGULAR DISTRIBUTIONS

Measurement of the angular distributions were carried out for the neutron groups denoted by N_0, N_1 and N_2 corresponding to the transition to the ground state and two excited states at 2·25 MEV and 3·81 MEV. The number of tracks belonging to each group was carefully estimated from the plotted histograms. To increase the statistical accuracy our criterion for selection of tracks was altered to allow for tracks subtending a horizontal angle of equal to or less than 12° and having a dip of less than 12μ in a length of 100μ at the beginning of the track. After calculating the relative intensities, correcting for the variation of the cross section of the (n, p) scattering with neutron energy (Adair 1950) the results were then transferred to the centre-of-mass system and represented, in the same units of intensity, as shown in figure (2). The experimental errors are the statistical standard deviation. The error due to escape is of the order of 6% and the observed escaping tracks were shared between the three groups in ratio corresponding to their intensities.

Figure 2 shows, with the experimental points, the theoretical curves calculated from the Butler (1951) and the Born approximation (Bhatia, Huang, Huby and Newns 1952) stripping theories. Good agreement was obtained with both theories by assuming the angular momentum transferred by the absorbed proton $l_p = 0$, 2 and 0 for the transition to the ground, first and second excited states respectively. It was found that while the radius of interaction used in Butler's formula was the Gamow radius $(1{\cdot}7 + 1{\cdot}22A^{1/3})10^{-13}$ cm satisfactory agreement could not be achieved in case of Born approximation theory unless the radius is somewhat higher, i.e. Gamow radius plus 1×10^{-13} cm in the case of the transition to the second excited state and Gamow radius plus 2×10^{-13} cm in the case of the transition to the other states.

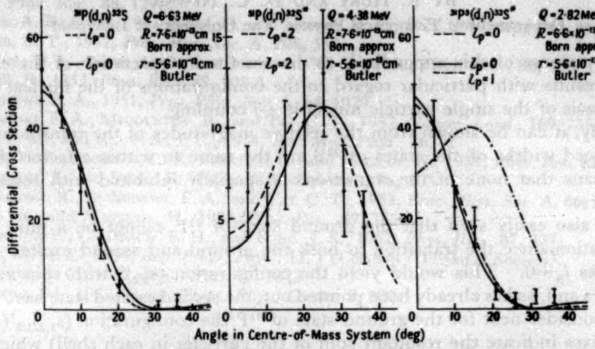

Figure 2. Angular distributions of the neutron groups corresponding to the ground-state and excited states of ^{32}S at 2·25 and 3·81 MEV.

Since the ground state of ^{31}P is known to have a spin $\frac{1}{2}^+$ (Endt and Kluyver 1954) the value of $l_p = 0$ for the transition to the ground state of ^{32}S indicates that it has even parity and spin 0 or 1. This is in agreement with the fact that the spin of all even–even nuclei is zero.

In the case of the transition to the first excited state, the value of $l_p = 2$ indicates that it has even parity and spin 1, 2 or 3. But there is a general tendency for light even–even nuclei to possess a first excited state with spin 2^+ (Pryce 1954), the only exception being ^{16}O the spin of which is found to be 0^+. No case has been found where the first excited state of an even–even nucleus has an even parity and odd value of its spin, so it is likely that this state in ^{32}S has spin 2 and even parity.

Finally, the value $l_p = 0$ for the transition to the second excited state indicates that this state has even parity and spin 0 or 1. Endt and Kluyver (1954) reported that Breckon, Martin, Henrikson and Foster (unpublished) observed a γ-ray transition from this state to the ground state. It follows that the assignment of spin 0 to the second excited state is excluded and it would have then spin 1 and even parity. Since it is rather surprising that an even–even nucleus should have a low-lying state of even parity and spin 1, great care was therefore taken to ensure that the assignment of $l_p = 0$ for this case is correct. The Butler theoretical curve for $l_p = 1$ with the Gamow radius is also shown in figure 2 and is seen not to agree with the experimental results. In order to get a reasonable fit for $l_p = 1$, a radius of about double the Gamow radius should be assumed and this would seem to be quite out of the question. There is thus no doubt that $l_p = 0$ is the correct assignment.

ACKNOWLEDGMENTS

We are grateful to Professor H. W. B. Skinner for his encouragement and advice. We would also like to express our sincere thanks to Professor M. A. El Shirbini, Dr. J. R. Holt and Dr. R. Middleton for helpful discussions.

APPENDIX

By R. Huby and H. C. Newns
Department of Theoretical Physics, The University of Liverpool

The purpose of this appendix is to discuss the interpretation of the experimental results with particular regard to the configurations of the nuclear states on the basis of the single particle model in *j–j* coupling.

Firstly, it can be shown from the relative magnitudes of the transitions that the reduced widths of the states of ^{32}S are the same to within a factor of two. This means that none of the transitions is specially inhibited with respect to the others.

It is also easily seen that the ground state of ^{31}P cannot be a pure $(s_{1/2})^3$ configuration since the transition to both the ground and second excited states of ^{32}S has $l_p = 0$. This would yield the configuration $(s_{1/2})^4$ with spin zero in both cases and, as has already been pointed out, the second excited state has $J = 1^+$.

We consider next for the ground state of ^{31}P the configuration $(s_{1/2})_{1/2}^{1}(d_{3/2})_0^{2}$ (the suffixes indicate the resultant spin of the particles in each shell) which has been shown by Umezawa (1952) to give reasonable agreement with the magnetic moment. The transition to the ground state of ^{32}S then yields the configuration $(s_{1/2})_0^{2}(d_{3/2})_0^{2}$, the state being $J = 0^+$. We obtain the configurations for the first and second excited states by adding a d and an s nucleon respectively to obtain $(s_{1/2})_{1/2}^{1}(d_{3/2})_{3/2}^{3}$ and $(s_{1/2})_1^{2}(d_{3/2})_0^{2}$. The configuration of the first excited state can couple to give $J = 1^+$ or 2^+ while the second excited state we know to be $J = 1^+$, which fixes the configuration.

However, this explanation of the experiments in terms of pure configurations is open to objection. A difficulty lies in the assignment of $(s_{1/2})_1^{2}(d_{3/2})_0^{2}$ as at least a component of the second excited state of ^{32}S since, if charge independence holds good, this configuration has $T = 1$. Thus this state, or the first excited state, should be the analogue of the ground state of ^{32}P. Comparison of the (d, p) (Parkinson *et al.* 1952) and (d, n) reactions on ^{31}P and the density of levels in ^{32}P shows that this is not so; and in any case, one would expect, from Coulomb energy considerations, the first $T = 1$ state in ^{32}S to lie at about 7 Mev. So the second excited state must be $T = 0$ and to ensure this we must assume a component of $(s_{1/2})_1^{2}(d_{3/2})_{3/2}^{1}$, $(d_{3/2})_{1/2}^{3}$ or $(s_{1/2})_{1/2}^{1}(d_{3/2})_1^{2}$ in ^{31}P.

A way out of this difficulty would be to assume that the second excited state is double, one component having $J = 0^+$ and the other some reasonable spin and parity, say $J = 2^+$ or 4^+. We note that if this level is double, the experiments of Arthur *et al.* (1952) indicate that the two components lie closer in energy than 20 kev. With these assumptions the stripping reaction could excite both these levels but the transition to the component having $J = 0^+$ masks the other. In addition the γ-ray transition to the ground state now no longer makes $J = 0^+$ impossible since it can arise from the component having non-zero spin. All these states are then reasonable according to the shell model, but one then would have to show that two such states exist, accidentally coinciding in energy to within 20 kev.

Although this discussion has been confined to the *j–j* coupling model, the main difficulties would remain for *L–S* coupling.

REFERENCES

ADAIR, R. K., 1950, *Rev. Mod. Phys.*, **22,** 249.

ALBURGER, D. E., 1949, *Phys. Rev.*, **75,** 51.

ARTHUR, J. C., ALLEN, A. J., BENDER, R. S., HAUSSMAN, H. J., and MCDOLE, C. J., 1952, *Phys. Rev.*, **88,** 1291.

BHATIA, A. B., HUANG, K., HUBY, R., and NEWNS, H. C., 1952, *Phil. Mag.*, **43,** 485.

BUTLER, S. T., 1951, *Proc. Roy. Soc.* A, **208,** 559.

COLLINS, T. L., NIER, A. O., and JOHNSON, W. H., 1952, *Phys. Rev.*, **86,** 408.

DAY, R. B., 1953, *Phys. Rev.*, **89,** 908 A.

EL BEDEWI, F. A., 1951, *Proc. Phys. Soc.* A, **64,** 1079.

EL BEDEWI, F. A., MIDDLETON, R., and TAI, C. T., 1952, *Nature, Lond.*, **169,** 235.

ENDT, P. M., and KLUYVER, J. C., 1954, *Rev. Mod. Phys.*, **26,** 95.

GRACE, M. A., BEGHIAN, L. E., PRESTON, G., and HALBAN, H., 1951, *Phys. Rev.* **82,** 969 (L).

MATTAUCH, J., and BIERI, R., 1954, *Z. Naturforsch.*, **9a,** 303.

MIDDLETON, R., EL BEDEWI, F. A., and TAI, C. T., 1953, *Proc. Phys. Soc.* A, **66,** 95.

OGATA, K., and MATSUDA, H., 1953, *Phys. Rev.*, **89,** 333.

PARKINSON, W. C., BEACH, E. H., and KING, J. S., 1952, *Phys. Rev.*, **87,** 387.

PRYCE, M. H. E., 1954, *Rep. Progr. Phys.*, **17,** 1 (London : Physical Society).

SNOWDON, S. C., 1952, *Phys. Rev.*, **87,** 1022.

UMEZAWA, M., 1952, *Progr. Theor. Phys., Osaka*, **8,** 509.

RESEARCH NOTES

Decay of ^{70}As Produced by ^{14}N Bombardment of Cu

By A. E. SOUCH
Physics Department, University of Birmingham

MS. received 15*th February* 1955

During an investigation of the products of the bombardment of various targets with ^{14}N ions in the 60-in. Nuffield cyclotron it appeared that arsenic activities, notably ^{70}As, were produced in large quantities in the thin copper foils used to screen the targets. Summarized data (Hollander, Perlman and Seaborg 1953) ascribe a 52-minute arsenic positron activity to mass number 70. Verkerk and Aten (1952) also formed ^{70}As by bombarding germanium with 26-Mev deuterons. They found a positron activity (K/β^+ ratio $\not> 0{\cdot}2$) of 52 ± 1 minutes half-life and of maximum energy 2·7 Mev by absorption in aluminium. Hard gamma radiation was observed in addition to the positron annihilation radiation.

In order to study the ^{70}As produced by heavy ion bombardment in more detail, copper foils of 25 microns thickness were placed in a shielded target probe and bombarded in the internal ^{14}N beam at 25 in. radius (maximum energy$\sim$125 Mev) with beam currents in the range 10^{-9}A–10^{-7}A. Two methods of chemical separation of arsenic were used; in the first $MgNH_4AsO_4$ was precipitated by magnesia mixture in alkaline solution and in the second (used as a check) As_2S_3 was distilled with HCl. Germanium and gallium were removed before the arsenic separations. Several arsenic activities up to mass 76 may be produced by ^{14}N bombardment of copper (Hollander *et al.* 1953), the reactions producing ^{70}As being ^{63}Cu(^{14}N, 3p4n)^{70}As and ^{65}Cu(^{14}N, 3p2n)^{70}As. Decay curves of separated As activities could not be analysed to identify all of the products with certainty but half-lives of 47 ± 2 minutes and 17 ± 1 days showed the presence of ^{70}As and ^{74}As respectively. Gamma spectra taken with a scintillation spectrometer identified ^{71}As, ^{72}As and ^{73}As and possibly ^{74}As.

The beta spectrum of ^{70}As was investigated with a simple semicircular focusing spectrometer which had a momentum resolution of 7%. It was calibrated for linearity of momentum with magnet current by means of a search coil and Grassot fluxmeter and an absolute calibration point was obtained with ^{137}Cs conversion electrons. The spectrometer was evacuated to a pressure of the order of 0·1 mm Hg with a rotary pump. Six positron spectra of the short-lived As activity were measured; each was taken immediately after separation using short counting periods and when the ^{70}As was judged to have decayed ($\sim$10 hours) a second spectrum was obtained using longer counting periods. From an examination of the decay curves the second spectrum was expected to be almost entirely due to ^{72}As and the observed shape was consistent with this assumption. The second spectrum was time-corrected forward to the first and the difference was taken as the ^{70}As spectrum; as can be seen from figure 1, this spectrum appears to be complex. The momentum distributions of the six spectra were analysed (Fano 1952) and the Fermi plots showed two components in each case; their relative abundances in the spectrum shown in figure 1 were obtained by dividing the number $N(B\rho)\, d(B\rho)$ by $B\rho$, and taking the ratio of the areas under these new curves. The relative intensities of the high energy and low energy components were 0·33 and 0·67 respectively.

The addition of corresponding points in the beta spectra, when analysed, gave the composite Fermi plot shown in figure 2. Assuming the transitions to be allowed, with linear plots, a 'least squares' analysis gave maximum energies of 1·35 ± 0·03 Mev and 2·45 ± 0·04 Mev. The comparative half-lives of the transitions are then:

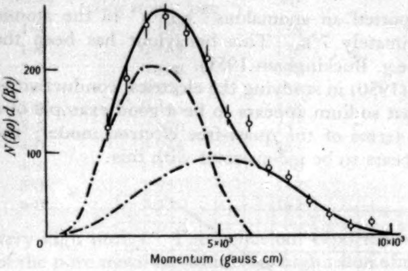

Figure 1.

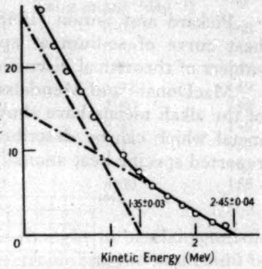

Figure 2.

Energy (Mev)	2·45	1·35
Relative intensities	0·33	0·67
log (*ft*)	5·6	4·05

Both of these values fall within the generally accepted range of 'allowed-unfavoured' transitions (4–6).

A $1\frac{1}{4}$ in. diameter × $\frac{1}{2}$ in. packed NaI(Tl) crystal was mounted on an E.M.I. type 6260 photomultiplier and used with a type 1049B linear amplifier and cathode-follower head unit. Several gamma spectra were measured using a single-channel differential discriminator. Since both of the beta transitions would appear to be allowed the gamma transition between the two levels excited by beta decay would be M1 or E2 on spin and parity considerations and should be observable. A peak (whose size obviated the possibility that it was an 'escape' peak from a pair-production process) was found and the mean of fourteen energy determinations gave 1·07 ± 0·04 Mev in excellent agreement with the beta energy difference of 1·10 ± 0·05 Mev. Other peaks of higher energy were also observed with mean energies of 3·25 ± 0·15 Mev, 2·75 ± 0·05 Mev, 2·15 ± 0·08 Mev and 1·5 ± 0·05 Mev. The small size of the crystal made quantitative analysis of these results impossible; there is little doubt, however, that some of the peaks correspond to the same gamma-ray energy with the escape of one or both of the positron-annihilation quanta.

ACKNOWLEDGMENTS

The author wishes to thank the cyclotron staff for their patient efforts to provide good bombardments; during the period in which this work was performed he was in receipt of a Department of Scientific and Industrial Research maintenance grant.

REFERENCES

FANO, U., 1952, *Appl. Math. Ser. U.S. Bur. Stand.*, 13.
HOLLANDER, J. M., PERLMAN, I., and SEABORG, G. T., 1953, *Rev. Mod. Phys.*, **25**, 469.
VERKERK, B., and ATEN, A. H. W., Jr., 1952, *Physica*, **18**, 974.

LETTERS TO THE EDITOR

The Atomic Heat of Sodium

Pickard and Simon (1948) reported an anomalous 'hump' in the atomic heat curve of sodium at approximately 7°K. This behaviour has been the subject of theoretical discussions (e.g. Buckingham 1951).

MacDonald and Mendelssohn (1950) in studying the electrical conductivities of the alkali metals have shown that sodium appears to be a good example of a metal which can be described in terms of the quasi-free electron model; the reported specific heat anomaly appears to be inconsistent with this.

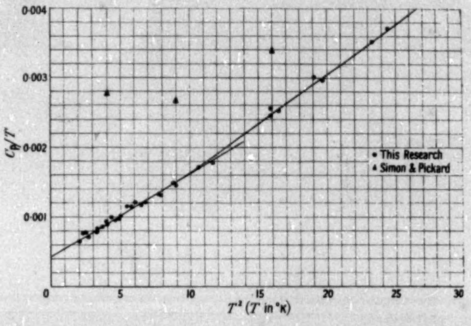

An experimental study of the atomic heats of the alkali metals has been in progress in this laboratory, and in particular sodium has been investigated between 1·4°K and 20°K. It has been found that the specific heat curve is quite smooth and no 'hump' appears; smoothed values are given in the table. The present results agree very well with those of Pickard and Simon between 10° and 20°K, but in the helium range the value of the specific heat is very much smaller. A conventional plot of C_p/T against T^2 is shown in the figure, whence a value of the electronic specific heat has been deduced, i.e. $0{\cdot}00043T$ cal (g atom)$^{-1}$ deg^{-1} which is about 1·6 times the theoretical value for free electrons. This value is believed to be correct to within 10% and is obviously dependent on the scatter of the points in the linear range of the figure. This is rather high and experiments are in progress to improve this.

In the table values of θ_D the Debye temperature have been deduced allowing for the free-electron contribution but ignoring the correction C_p to C_v. There is rather a sharp fall in θ_D above 3·0°K.

While this work was in progress, during the winter 1953–54, L. Smith (private communication) at the Clarendon Laboratory, Oxford, also showed that there was no 'hump' in the specific heat curve, but he was unable to deduce a satisfactory electronic specific heat term. More recently Rayne (1954) has produced evidence showing an anomalous behaviour in the atomic heat of sodium below 1°K.

The present specimen was given several days in which to ' self anneal ' at room temperature after sealing into the calorimeter and should therefore be comparatively strain free. It was provided by the Pure Metals Committee of the Department of Scientific and Industrial Research as redistilled sodium of very high purity. The behaviour reported here is thought to be characteristic of the pure metal for which the high value of the electronic specific heat could be explained in terms of the interactions proposed by Buckingham (1951).

T(°K)	$C_p \times 10^2$ (cal(g atom)$^{-1}$deg^{-1})	θ_D	T(°K)	$C_p \times 10$ (cal(g atom)$^{-1}$deg^{-1})	θ_D
1·5	0·105	158	7·0	0·52	148
1·8	0·145	158	8·0	0·78	148
2·0	0·180	158	9·0	1·06	149
2·5	0·290	158	10·0	1·42	149
3·0	0·445	158	12·0	2·50	148
3·5	0·670	157	14·0	3·85	149
4·0	0·985	154	16·0	5·35	152
4·5	1·45	150	18·0	7·10	153
5·0	1·95	149	20·0	9·00	155
6·0	3·45	147			

In the two instances where anomalies have been reported it is probable that the specimen was in a state of strain which may provide a mechanism for an electronic transition.

This work is continuing and being extended to the other alkali metals.

Acknowledgment is made to The Chief Scientist, Ministry of Supply and the Controller of H.M. Stationery Office, for permission to publish this letter.

Radar Research Establishment,
Great Malvern, Worcs.
9th May 1955.

D. H. PARKINSON.
J. E. QUARRINGTON.

BUCKINGHAM, M. J., 1951, *Nature, Lond.*, **168,** 281.
MACDONALD, D. K. C., and MENDELSSOHN, K., 1950, *Proc. Roy. Soc.* A, **202,** 523.
PICKARD, G. L., and SIMON, F. E., 1948, *Proc. Phys. Soc.*, **61,** 1.
RAYNE, J., 1954, *Phys. Rev.*, **95,** 1428.

REVIEWS OF BOOKS

Physicochemical Calculations, by E. A. GUGGENHEIM and J. E. PRUE. Pp. xii + 492. (Amsterdam: North Holland Publishing Company, 1955.) 53*s*.

This masterly collection of 171 worked problems based on published experimental data will be a boon to teachers and students of physical chemistry. The principle of the book is that textbooks are not enough, understanding only comes by applying, or, as here, studying the application of textbook knowledge to individual problems. A wide range of subjects in chemical physics and physical chemistry is covered with characteristic precision and clarity. Many of the problems are of direct interest to physicists; those on more specifically chemical subjects—chemical kinetics and thermodynamics, electrolyte solutions, surface chemistry, etc.—will be useful to physicists who require more than a textbook acquaintance with these subjects. The choice necessarily reflects the interests of the authors. A noteworthy omission is that despite the excellent and full collection illustrating the thermodynamic uses of reversible electrodes, none are included on electrode kinetics to provoke the student to consider how reversible potentials are established.

The discussion sections are illuminating but occasionally Olympian in shortness. Some might have been expanded into the blank spaces at the end of the problems (each problem starts elegantly—and very rightly—on a new page) with advantage to many readers and without loss of edge. For example, in problem 83 most readers would have welcomed a discussion of the advantages and snares of estimating the error in the slope of lines by numerical methods instead of by the method used here, judgment by eye. In problem 122 the impression will be left on the guileless that in estimating dy/dx (= constant) given y for three equally spaced values of x the middle value contributes nothing (it gives, of course, a rough measure of error). In problem 14 the effect on the estimate of Avogadro's number of taking the modern value of the disintegration rate of radium instead of Rutherford and Geiger's value should have been mentioned.

L. YOUNG.

Reihenentwicklungen in der mathematischen Physik, by J. LENSE. Pp. 216. (Berlin: de Gruyter, 1953.) DM. 26.

The use of expansions in terms of orthogonal functions is now such a commonplace in mathematical physics that an account of both these and related expansions and functions cannot fail to be of interest to a large number of physicists. Professor Lense's book, the first edition of which appeared more than twenty years ago, deals with the properties of Fourier series, and the polynomials associated with the names of Bernoulli, Laguerre, Hermite and Tschebyschef, together with extensive accounts of Bessel functions, spherical harmonics and Lamé functions. Complex theory is only used in connection with Bessel functions; for the rest a real variable is assumed. In addition to the treatment of specific functions, a number of techniques is also described, including, for example, the method of steepest descent and a discussion of 'completeness' as applied to orthogonal functions. Considered as a general view of this branch of mathematics, it is not easy to imagine more material being described so well in so short a space. H. H. HOPKINS.

Introduction to Mathematical Statistics, by P. G. HOEL. Pp. xi + 331. (2nd Edition.) (New York: John Wiley; London: Chapman and Hall, 1954.) 40*s*.

The satisfaction with which the first edition was received has encouraged Dr. Hoel to extend the contents of his book. The result is, for the student with an appreciation of lucid and moderated mathematics in a context of common-sense discussion and illustration, one of the best introductions to statistics now available.

The chapter on probability (which is now included!) provides the very necessary foundation for the whole subject and manages to be both compact and clear. It is immediately followed by a discussion of the main principles involved in the testing of hypotheses and the estimation of parameters, bringing the reader to the heart of the subject, so that he knows his purpose before studying the means of achieving it.

The computation of descriptive measures for empirical distributions of one variable leads into an analysis of the properties of the common model distributions by immediate use of the moment generating function, rounded off by illustrations of the application of the mathematical models to simple practical problems with ample warning that only rarely will the skeleton model appear as a perfect representation of reality.

After a concise explanation of the basis of sampling theory for one variable (large samples) and a descriptive and theoretical treatment of calculation and regression, the application of χ^2 for testing goodness of fit rounds off the first half of the book. Dr. Hoel now leads the reader to a more critical examination of the principles involved in testing simple and composite hypotheses: the Neyman–Pearson lemma of critical regions and the use of the likelihood ratio. This is followed by a more sophisticated account of the theory of estimation and a discussion of small sample theory to provide the necessary understanding of such significance tests as are normally met with in the analysis of experimental data.

It is now taken for granted that any book on statistics should not only stress the importance of good quality experimental data but also tell the reader something of the art of collecting it. Dr. Hoel sketches very briefly general principles for the design of experiments in which components of variation can be separated by the method of analysis of variance, stressing the link between a hypothetical model and the numerical analysis of the data. He regards industrial sampling inspection as essentially a branch of the design of experiments directed to obtaining desired quality production at nominal cost with specified risks.

The final chapter deals with the now very fashionable 'non-parametric' or 'distribution-free' methods, which our American friends more accurately and more realistically call 'quick and dirty'.

The whole book is attractively done and can be strongly recommended to those who are looking for a nice beginning that will carry them a very long way in practice. Dr. Hoel leaves no excuse for narrowness: every chapter has a list of references. Equally, he leaves no room for complacency: every chapter has an extensive set of exercises. But why no answers?

M. J. MORONEY.

Introduction to Atomic and Nuclear Physics, by H. SEMAT. Pp. xii+561. 3rd Edition. (London: Chapman and Hall, 1954.) 50*s*.

This is a new, revised and enlarged edition of Dr. Semat's now familiar textbook. The subject matter of the first two parts of the book, comprising roughly one half of the total, is atomic physics, and follows closely the lines of the earlier editions. The major changes and additions are in the second half of the book which deals with nuclear physics and high energy processes.

The treatment is broadly historical and everywhere elementary. ("The text is still intended for use at undergraduate level with students who have had a one-year course in physics and a course in the calculus".) As applied to the chapters on atomic physics this has not excluded some theoretical as well as the experimental and factual aspects of the subject; for example, elementary treatments are given of the theory of the hydrogen atom, Zeeman effect and the scattering of x-rays. The chapters on nuclear physics, however, are almost exclusively devoted to an account of the facts and experimental methods, and this is surely to be regretted.

Nuclear physics is no longer a collection of empirical information, and many of its aspects are capable of elementary theoretical discussion, in a manner not dissimilar from that habitually employed in teaching atomic physics. Certainly nuclear theory is generally more recondite and less settled than atomic theory, but many of its salient features are capable of some illumination by simple or semi-quantitative arguments. Even the use of classical–mechanical approximations is not always inappropriate.

The lack of a theoretical background is reflected in the present book in two respects. Firstly, particular important topics in nuclear physics are not always introduced in the most convenient or logical place, and some are omitted altogether. Secondly, a number of the brief theoretical statements that do occur are apt to be misleading. For example: the positron, artificial radioactivity and K-capture are all introduced in the chapter on Disintegration of Nuclei (XI), although β-decay, along with α-particle decay and the neutrino are dealt with partly in an earlier chapter, X, on natural radio activity and partly in a following chapter, XII, entitled Nuclear Processes. Similarly this latter chapter, although largely devoted to the question of nuclear stability concludes with an account of high energy nuclear collisions. There is practically no mention of scattering by nuclei (apart from the treatment of Rutherford scattering in the earlier part), little mention of the two-body problem in nuclear physics, and there is no mention of nuclear forces either in the index or text.

More surprising is the omission of any discussion of the processes occurring when ionizing particles or γ-radiation pass through matter, particularly some indication and explanation of the orders of magnitude of the distances and cross sections involved. Some of these omissions could be repaired without an overall increase in the bulk of the volume; for example by elimination of the first chapter which contains a brief résumé of electromagnetism. Surely no student should embark on a study of atomic and nuclear physics without a grasp of the principles of electromagnetism sufficiently thorough to make a treatment confined to some 30 pages superfluous?

One or two examples will suffice to show the sort of misleading theoretical remark that ought to be avoided. On p. 275, referring to the argument against the presence of electrons in the nucleus the author writes "the argument which follows is based on the assumption that the spin angular momentum of the nucleus is the vector sum of the spin angular momenta of the particles within the nucleus..."; and a brief account of the shell model includes the statement "A nuclear quantum state is usually specified by its total quantum number and by its parity" (p. 393). The occurrence of nuclear reaction resonances is adduced as evidence that "The transparency of the coulomb barrier is not always a smooth function of the energy of the projectile but exhibits the phenomenon of resonance". The likelihood of such loose statements being made or misunderstood would be greatly reduced if the 'theory' were presented as a simple logical framework, rather than as a number of disconnected remarks.

The book contains excellent descriptive accounts, beautifully illustrated, of many topics, ranging from the determination of the charge of the electron to V-particles, nuclear reactors and particle accelerators. A better ordered and more explanatory treatment of nuclear physics, similar to that adopted in the earlier parts of the book dealing with atomic physics, would greatly enhance its value as a current textbook.

S. DEVONS.

CONTENTS OF SECTION B

PAGE

Dr. G. J. Phillips and Dr. M. Spencer. The Effects of Anisometric Amplitude Patterns in the Measurement of Ionospheric Drifts 481

Dr. M. Spencer. The Shape of Irregularities in the Upper Ionosphere . . . 493

Dr. T. J. Lewis. The Mechanism of High-Field Electron Emission from Tarnished Metal Surfaces 504

Dr. M. J. Morant. Interpretation of Experiments on Electron Emission in Spark Gaps 513

Dr. C. Hurst. Phase Transitions of the First and Second Orders 521

Dr. J. C. E. Jennings and Mr. R. G. Pratt. Numerical Ray Tracing in Electron Lenses 526

Prof. L. F. Bates and Dr. D. H. Martin. A Study of Domain Structures in Alnico 537

Dr. E. G. Richardson. The Sounds of Impact of a Solid on a Liquid Surface . 541

Prof. S. Tolansky and Mrs. Anne P. Williams. Directional Hardness Studies on Single Crystals of Tin and Bismuth 548

Prof. S. Tolansky and Miss Sayeda H. Emara. An Occasional Mode of Growth in Diamond 559

Research Notes :

Mr. N. F. Durrant. Measurement of Minority Carrier Lifetimes in Semiconductors 562

Dr. P. F. Browne. The Transfer of Metal between Electrodes in a High Vacuum on Application of a High Electric Field 564

Dr. J. Woods and Dr. D. A. Wright. Field Enhanced Cathodo-Luminescence in Magnesium Oxide 566

Prof. R. E. Burgess. Low Frequency Noise in Illuminated Germanium Diodes 569

Reviews of Books 572

Contents of Section A 576

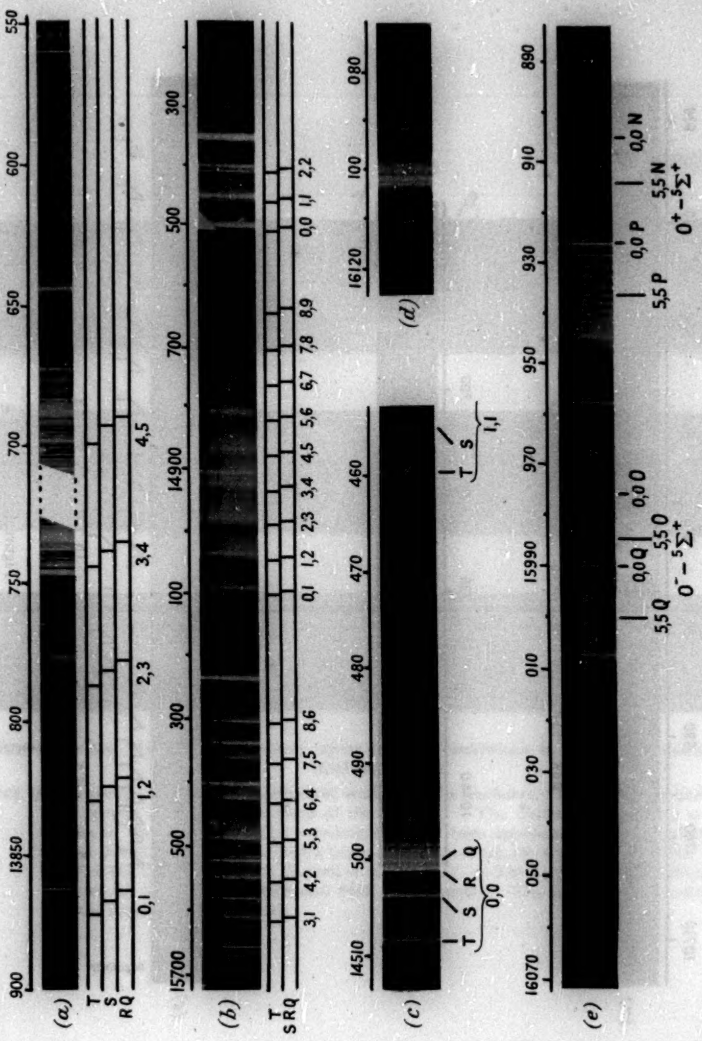
(a)
550
600
650
700
750
800
13850
900
T
S
R Q
4,5
3,4
2,3
1,2
0,1
(b)
300
500
700
14900
100
300
500
15700
T
S R Q
2,2
1,1
0,0
8,9
7,8
6,7
5,6
4,5
3,4
2,3
1,2
0,1
8,6
7,5
6,4
5,3
4,2
3,1
(d)
080
100
16120
(c)
460
470
480
490
500
14510
T S
1,1
T S R Q
0,0
(e)
890
910
930
950
970
15990
010
030
050
16070
0,0 N
5,5 N
0,0 P
5,5 P
$0^+ - {}^5\Sigma^+$
0,0 O
5,5 O
0,0 Q
5,5 Q
$0^- - {}^5\Sigma^+$

Figure 1

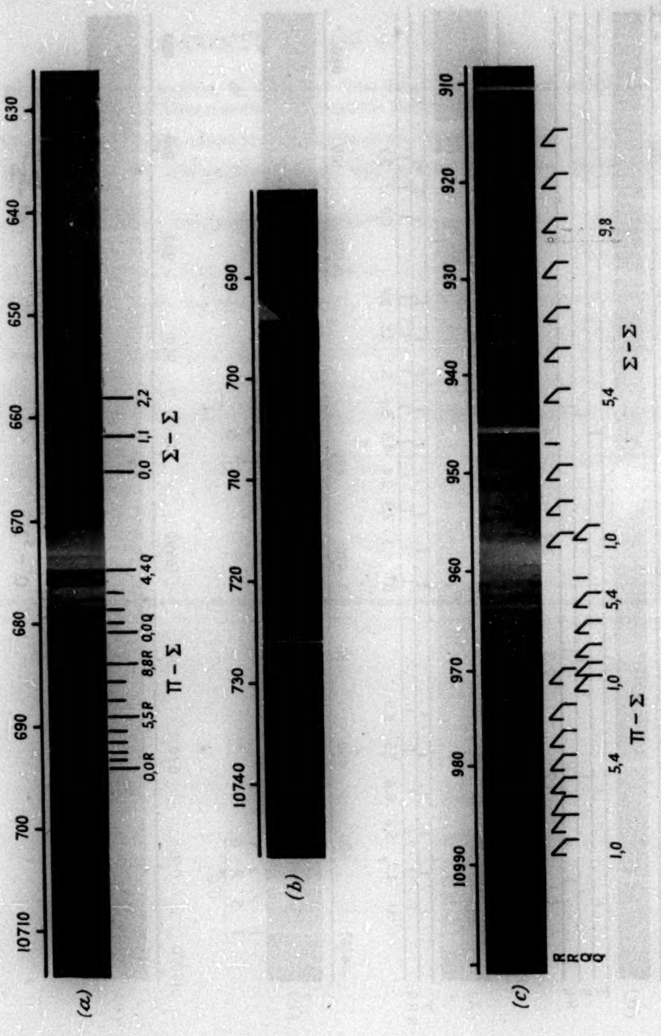
(a)
630
640
650
660
670
680
690
700
10710
2,2
1,1
0,0
Σ - Σ
4,4Q
0,0Q
8,8R
5,5P
0,0R
Π - Σ
(b)
690
700
710
720
730
10740
(c)
910
920
930
940
950
960
970
980
10990
9,8
Σ - Σ
5,4
1,0
5,4
1,0
5,4
1,0
Π - Σ
R
R
Q
Q

Figure 1

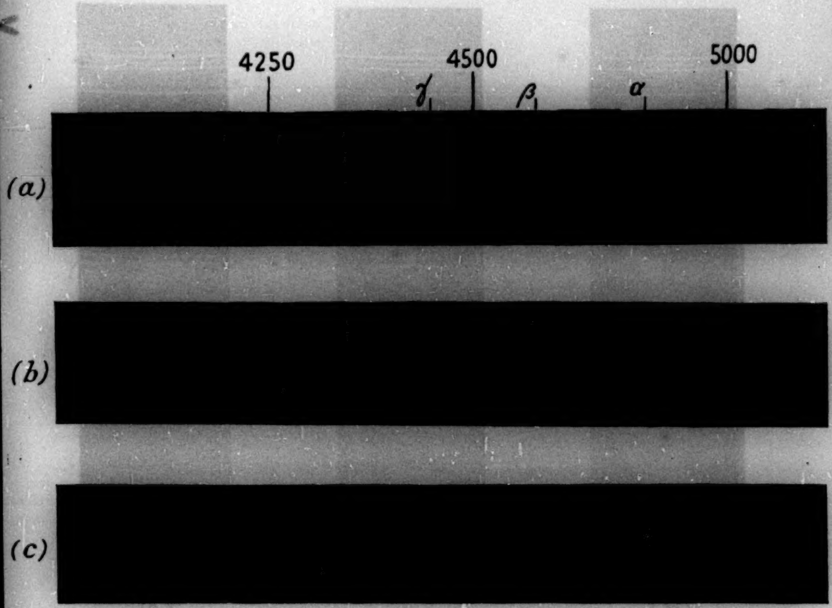

Argon spectra (A I and A II) excited under different conditions in beam and plasma discharges.

(*a*), (*b*), (*c*) are spectra of axial longitudinal sections of the discharge. (*d*), (*e*), (*f*), overleaf, are spectra of transverse sections of the discharge. The discharge parameters are given in the text (§ 3). The wavelengths range from approximately 4040 Å (left-hand side of (*a*), (*b*), (*c*)) to 5200 Å (right-hand side of (*a*), (*b*), (*c*)), and from 4200 Å (top of (*d*), (*e*), (*f*)) to 5150 Å (bottom of (*d*), (*e*), (*f*)). α, β and γ denote the positions of the A II lines at 4806, 4609 and 4448 Å respectively. The last is clearly visible on the originals of (*a*) and (*e*).

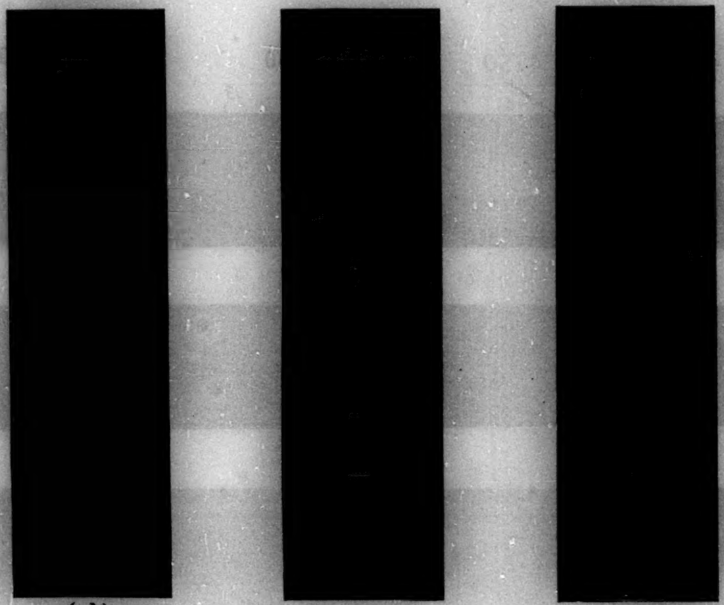

(d) (e) (f)

Argon spectra (AI and AII) excited under different conditions in beam and plasma discharges.

(*a*), (*b*), (*c*), overleaf, are spectra of axial longitudinal sections of the discharge. (*d*), (*e*), (*f*) are spectra of transverse sections of the discharge. The discharge parameters are given in the text (§ 3). The wavelengths range from approximately 4040 Å (left-hand side of (*a*), (*b*), (*c*)) to 5200 Å (right-hand side of (*a*), (*b*), (*c*)), and from 4200 Å (top of (*d*), (*e*), (*f*)) to 5150 Å (bottom of (*d*), (*e*), (*f*)). α, β and γ denote the positions of AII lines at 4806, 4609 and 4448 Å respectively. The last is clearly visible on the originals of (*a*) and (*e*).

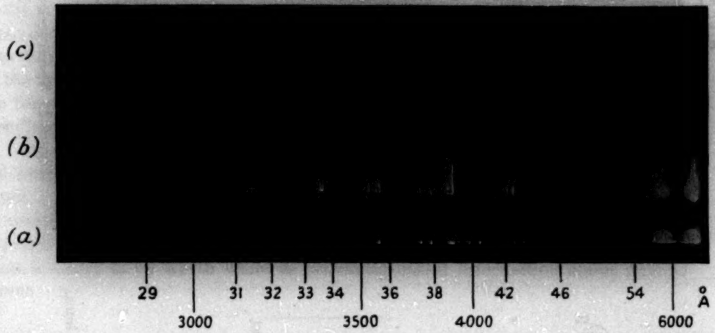
(c)
(b)
(a)
29
3000
31
32
33
34
3500
36
38
4000
42
46
54
6000
Å

Comparison of the spectra of (*a*) the exciting arc, (*b*) the beam, (*c*) the chamber glow.

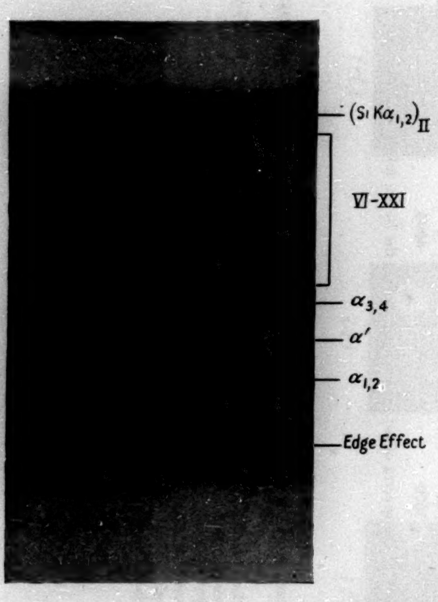
$(\mathrm{Si}\,K\alpha_{1,2})_{\mathrm{II}}$
VI-XXI
$\alpha_{3,4}$
α'
$\alpha_{1,2}$
Edge Effect

Figure 1. Spectrogram of the neon K-series emission lines.

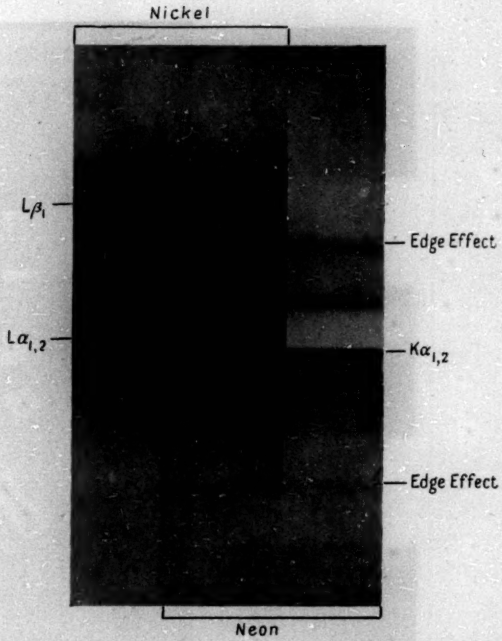
Nickel
$L\beta_1$
$L\alpha_{1,2}$
Edge Effect
$K\alpha_{1,2}$
Edge Effect
Neon

Figure 2. Spectrogram of the neon K-series and the nickel L-series lines.

The Collisions of Nucleons with Deuterons

By A. H. de BORDE† and H. S. W. MASSEY
Department of Physics, University College, Gower Street, London, W.C.1

MS. received 1st *March* 1955

Abstract. A considerable amount of theoretical data (assuming central nuclear forces) is now available concerning the elastic scattering of nucleons with energies up to 16 MeV by deuterons. Buckingham, Hubbard and Massey have taken the force to be of exponential shape with range consistent with the binding energy of the deuteron and triton while Christian and Gammel have used Yukawa and gaussian shape interactions with ranges consistent with all relevant two-body data but which are considerably too short to give the correct binding energy of the triton on the assumption of purely central forces. In the present paper the former calculations have been extended to allow fully for the contributions from high order phases.

The dependence of the theoretical predictions on the assumptions made about the range, shape and exchange character of the nuclear forces is discussed in detail. It is shown that the observed data are inconsistent with the assumption of mainly ordinary forces even for the least sensitive case of the short range gaussian interaction. Extension of the theory to include explicitly the tensor force is likely to be worth while as providing useful information about nuclear forces.

§ 1. Introduction

The theoretical analysis of phenomena involving more than two nucleons is very much more complicated than when only two nucleons are concerned. It remains true, however, that a satisfactory theoretical method for dealing at least with three-body problems would be of considerable value in the study of nuclear forces; it is obviously impossible to determine definitely whether many-body forces exist and if so what is their nature, without such a theory. Apart from this particular problem one could also hope to derive information about the two-body interactions: the neutron–neutron interaction for example can only be studied indirectly in terms of the binding energy of the triton or the scattering of neutrons by deuterons. Considerable progress has been made towards the calculation of the binding energy of the three-body nuclei even when tensor forces are included, but rather less attention has been paid to the theory of the scattering. Until recently the only detailed theoretical calculations for energies below 20 MeV were those of Buckingham and Massey (1941) and Buckingham, Hubbard and Massey (1952) in which the interaction was taken to be purely central and charge independent, of exponential form, with a range consistent with the binding energy of the deuteron and of the triton. The method used made accurate allowance for exchange of particles as well as in the character of the nucleonic interaction but did not take account of polarization of the deuteron by the incident nucleon. It was found that the results depended on the exchange character of the interaction, even at quite low energies, to such an extent that comparison with observation revealed much better agreement if either a symmetrical or Serber exchange interaction was assumed than with an ordinary force. Discrepancies at small and large angles of scattering were found which could be ascribed to the failure of the calculations to include the contributions from phase shifts of higher order than the second.

---

† Now at Department of Natural Philosophy, University of Glasgow.

Recently Christian and Gammel (1953) have carried out similar calculations using central interactions of Yukawa and gaussian shape with ranges consistent with all two-body data which do not depend essentially on the tensor force. This range is effectively shorter than that used by Buckingham and Massey and is inconsistent with the binding energy of the triton. They find considerably less sensitivity of the calculated cross sections to the exchange nature of the interaction.

On the other hand they do produce evidence which indicates that the neglect of polarization, which was regarded as likely to be serious, is not actually so. This suggests that the method of calculation probably gives good results if the interaction assumed is substantially correct.

It is debatable whether the best equivalent central interaction for the three-body scattering problem is the one which is consistent with the two-body data and yet gives erroneous results for the three-body binding energy. *A priori* it is at least arguable that for the three-body scattering problem it is best to use an interaction which is consistent with the three-body binding energy. The answer can only come by carrying out the scattering calculation with full explicit inclusion of the tensor force, a task which is now being undertaken. Meanwhile in this paper we examine in some detail the differences between the results of Christian and Gammel and those of the earlier authors to see whether any indication can be obtained about the degree of sensitivity to the exchange nature of the forces which might be expected from a thorough-going analysis employing the tensor force. The opportunity is also taken to remedy the defect of the earlier calculations (Buckingham and Massey 1941, Buckingham, Hubbard and Massey 1952) by including the contributions from all high order phases by a suitable device. When this is done quite good agreement with the observed data for nuclear energies up to 20 MEV is obtained over the whole angular range when a Serber interaction is employed. How far this can be taken as evidence that the nuclear forces are of this exchange type is discussed.

§ 2. EFFECT OF RANGE OF INTERACTION ON THE CALCULATED SCATTERING

If the internucleonic interaction is assumed to be purely central and of the form:

$$\mathcal{V}(r)=(mM+hH+w+bB)V(r) \qquad \ldots\ldots(1)$$

where M, H and B are the Majorana, Heisenberg and Bartlett exchange operators and m, h, w, b numerical constants which satisfy the relations $m+h+w+b=1$, $m-h+w-b=x$, the integro-differential equations which describe the scattering of neutrons by deuterons can be written in the form:

$$(\nabla^2+k^2)F(\mathbf{r})=\alpha U(r)F(\mathbf{r})+\beta\int Q(\mathbf{r},\mathbf{r}')F(\mathbf{r}')\,d\mathbf{r}'+\gamma\int S(\mathbf{r},\mathbf{r}')F(\mathbf{r}')\,d\mathbf{r}'. \qquad \ldots\ldots(2)$$

For the quartet scattering $\alpha = 2w + 2b - m - h$, $\beta = 2m + 2h - w - b$, $\gamma = 1$ and for the doublet $\alpha = 2w - b + \frac{1}{2}m - h$, $\beta = 2m - h + \frac{1}{2}w - b$, $\gamma = -\frac{1}{2}$. In terms of the normalized wave functions $\chi(R)$ for the ground state of the deuteron

$$U(r) = \frac{16\pi^2 M}{3h^2} \int |\chi(R)|^2 V(|\mathbf{r} + \tfrac{1}{2}\mathbf{R}|)\, d\mathbf{R},$$

$$Q(\mathbf{r}, \mathbf{r}') = \frac{16\pi^2 M}{3h^2} \left(\frac{4}{3}\right)^3 \chi(u) V(t) \chi(v),$$

$$S(\mathbf{r}, \mathbf{r}') = \frac{16\pi^2 M}{9h^2} \left(\frac{4}{3}\right)^3 [\chi(u)\{V(u) + V(v)\}\chi(v)$$

$$+ \frac{h^2}{\pi^2 M} \chi'(u) \frac{\mathbf{u}\,.\,\mathbf{v}}{uv} \chi'(v) + (3E_{\mathrm{n}} - 5E_{\mathrm{d}})\chi(u)\chi(v)],$$

$$u = \tfrac{2}{3}|2\mathbf{r}' + \mathbf{r}|, \qquad v = \tfrac{2}{3}|\mathbf{r}' + 2\mathbf{r}|, \qquad t = \tfrac{2}{3}|\mathbf{r} - \mathbf{r}'|. \qquad \ldots\ldots(3)$$

M is the mass and E_n is the relative kinetic energy of the incident neutron and E_d the energy of the ground state of the deuteron.

These equations were derived by Buckingham and Massey (1941) assuming that the function $\chi(R)$ is an exact solution of the deuteron wave equation. If approximate functions are used the procedure which leads to (2) with the forms (3) is inconsistent and it is better to work with equations in which the reduction has not been carried so far. In the earlier work (Buckingham and Massey 1941, Buckingham, Hubbard and Massey 1952) accurate deuteron wave functions were employed with expressions (3). In the recent work of Christian and Gammel (1953) only approximate deuteron wave functions were used but inconsistency was nevertheless avoided by working with a less reduced form for the kernels Q and S. A similar problem arises in dealing with the scattering of nucleons by alpha-particles (see Hochberg, Massey and Underhill 1954).

Essentially the only important difference between the calculations of Christian and Gammel and the earlier work is in the range and shape of the central interaction employed. Buckingham and Massey used

$$V(r) = -A \exp(-2r/a), \quad x = 0{\cdot}6, \qquad \ldots\ldots(4)$$

with $A = 242\, mc^2$ and $a = 1{\cdot}73 \times 10^{-13}$ cm. This was consistent with the nuclear data known at the time, including the binding energy of the triton which it gives quite accurately. The same interaction was used by Buckingham, Hubbard and Massey (1952). The best fit with the low energy two-body data now available is obtained with $a = 1{\cdot}35 \times 10^{-13}$ cm but this interaction gives too large a binding energy of the triton. Much of the work of Christian and Gammel (1953) was carried out with a Yukawa shape interaction

$$V(r) = -C(r/b)^{-1} \exp(-r/b), \qquad \ldots\ldots(5)$$

with $C = 68{\cdot}0$ MeV, $b = 1{\cdot}18 \times 10^{-13}$ cm, $x = 0{\cdot}69$. This gives the best fit with available two-body data but again leads to too large a binding energy for the triton; in fact to give this correctly b must be as large as $1{\cdot}83 \times 10^{-13}$ cm (Brown 1939). They also carried out calculations with the gauss interaction

$$V(r) = -D \exp(-r^2/c^2) \qquad \ldots\ldots(6)$$

$D = 86{\cdot}4$ MeV, $c = 1{\cdot}332 \times 10^{-13}$ cm. This again gives the best fit with the two-body data but too large a binding energy for the triton. For this to be given correctly c would have to be increased to $2{\cdot}25 \times 10^{-13}$ cm.

When allowance is made for a tensor force component the apparent discrepancy between the two-body and three-body data can be largely removed (Pease and Feshbach 1952) without any need to invoke three-body forces. It is to be expected that a satisfactory treatment of the three-body scattering must also make explicit allowance for the tensor force. Meanwhile it is difficult to say what is the best equivalent central force to employ: it seems clear that it will be appreciably different for use in three-body than in two-body problems and may well have a larger range than in the latter cases. Until a proper calculation has been carried out with explicit exclusion of tensor forces it is not possible to decide easily on purely theoretical grounds whether the earlier work or that of Christian and Gammel (1953) gives the better representation of the actual scattering. The correct results may lie in between and it is of interest to examine a little further the extent to which the two sets of calculations differ.

§ 3. THE ZERO-ORDER PHASES

The phases δ_0 do not depend appreciably on the exchange character of the forces. In figure 1 values of $k \cot \delta_0$ are given as a function of neutron energy for the quartet and doublet phases $\delta_0{}^q$ and $\delta_0{}^d$ respectively. The values calculated by Buckingham, Hubbard and Massey have been obtained using the interaction (4) and solving the corresponding integro-differential equation by an accurate numerical procedure for several values of k. The calculated values of Christian and Gammel have been obtained from the interaction (5) but it is only in the low-energy limit that they have been derived from accurate solutions of the integro-differential equations. At higher energies a less accurate procedure was adopted based on a 'zero range' approximation for the nuclear forces. The experimental values of $k \cot \delta$ have been derived from an analysis of the observed differential cross sections and the zero energy scattering lengths.

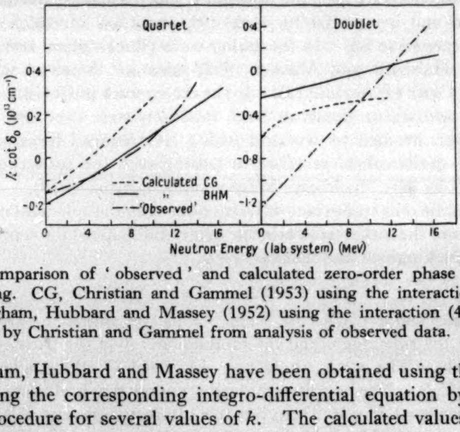

Figure 1. Comparison of 'observed' and calculated zero-order phase shifts for n–d scattering. CG, Christian and Gammel (1953) using the interaction (5); BHM, Buckingham, Hubbard and Massey (1952) using the interaction (4); 'observed' derived by Christian and Gammel from analysis of observed data.

It will be seen that the quartet phases are much less sensitive to the assumed interaction than the doublet phases. There is quite good agreement between the observed and both calculated curves for the variation of $k \cot \delta_0{}^q$ with energy. This agreement is absent for the doublet phases. The 'observed' shape of the variation of $k \cot \delta_0{}^d$ with energy is markedly different from that given either by the BHM or CG calculations. At energies below 10 MEV the latter gives results in less marked disagreement, while the reverse seems to be true above. It seems clear that there is room for much improvement in the theoretical determination of the zero-order doublet phase shifts. It is probable that polarization effects as well as the non-central nature of the interaction have a much more important effect than for the quartet phases: some theoretical justification for this has been given by Christian and Gammel (1953).

§ 4. THE FIRST-ORDER PHASES

The conspicuous feature of the earlier work was the marked dependence of the calculated scattering on the exchange character of the forces even at quite low energies. This was because the p-phases were found to be both sensitive to this character and quite important even at low neutron energies. In terms of the equation (2) this arose because the direct interaction $U(r)$ is, loosely speaking, much more effective in producing p-phase shift than the exchange kernels Q and S, the former being particularly ineffective. It follows that the larger the coefficient α relative to β and γ in (3), the larger the p-phase shift. The values of α, β, γ for ordinary (O), Serber (Ser) and symmetrical (Sym) exchange forces are as follows:

Table 1

	Quartet				Doublet		
	O	Ser	Sym		O	Ser	Sym
α	2	$\frac{1}{2}$	0	α	$\frac{1}{2}(1+3x)$	$\frac{1}{8}(1+9x)$	0
β	-1	$\frac{1}{2}$	1	β	$-\frac{1}{4}(1-3x)$	$\frac{1}{8}(1+9x)$	$\frac{1}{4}(1+9x)$
γ	1	1	1	γ	$-\frac{1}{2}$	$-\frac{1}{2}$	$-\frac{1}{2}$

For a qualitative examination of the possibilities we may concentrate on the quartet scattering. It will be seen from table 1 that since the interaction producing the scattering according to (2) is $\alpha U+\beta Q+\gamma S$ we would expect much larger p-phase shifts for an ordinary force between nucleons than for either a Serber or symmetrical exchange force. Serber forces would also be expected to give larger p-phases than symmetrical forces but the difference is likely to be much smaller. Since the p-phases for a given energy will decrease with decreased range of the effective interaction it is clear that sensitivity to the exchange character of the forces, at a given neutron energy, will decrease with the range of the effective central interaction between nucleons.

We now examine the numerical data given by the earlier investigation and by Christian and Gammel. In the earlier work the p-phases were calculated by accurate numerical solution of the appropriate integro-differential equations. It was found that, provided the coefficient α was considerably less than unity, Born's approximation gives quite satisfactory results for the phase shifts but for greater values of α it is quite unsatisfactory. The values of the p-phases used by Buckingham, Hubbard and Massey are given in table 2 for a number of neutron energies. For comparison the values found by Christian and Gammel, using Born's approximation in all cases, are given. These were read from figure 1 of their paper and so are not given accurately to the second decimal place.

It will be noticed first that the three sets of phases exhibit the same trend. For symmetrical exchange forces the results are not very different. The difference becomes appreciable for Serber forces at the lower energies and is quite marked for ordinary forces. It is probable, however, that, at least for the latter, the differences should be somewhat smaller than appears in the table. Born's

Table 2. Comparison of 'observed' p-phase shifts for n–d scattering with values calculated for various assumptions about the exchange values of the forces. Columns BHM are obtained from the calculations of Buckingham, Hubbard and Massey (1952) using interaction (4). The columns CG (5) and CG (6) are obtained from the calculations of Christian and Gammel (1953) using interactions (5) and (6) respectively.

Quartet

Neutron wave number (10^{13} cm^{-1})	Neutron energy (lab) (Mev)	Obs.	Ord. forces			Serber forces			Sym. exch. forces		
			BHM	CG (5)	CG (6)	BHM	CG (5)	CG (6)	BHM	CG (5)	CG (6)
0·2	1·85	0·35	0·57	0·31*	0·28*		0·26	0·25	0·25	0·25	0·24
0·3	4·2	0·52	1·18	0·57*	0·51*	0·59	0·365	0·45	0·50	0·365	0·40
0·4	7·4	0·57	1·35	0·73*	0·645*		0·48	0·51	0·55	0·39	0·41
0·5	11·5	0·575	1·22	0·88*	0·73*	0·59	0·51	0·51	0·45	0·38	0·39
	14·0	0·58	1·0	0·91	0·77	0·53	0·50	0·47	0·39	0·36	0·37
0·6	16·6			0·95*	0·79*		0·49	0·52	0·30	0·34	0·35

* These phase shifts having been obtained from Born's approximation are probably too small (see text). The corresponding BHM phases have been calculated accurately.

Doublet

Neutron wave number (10^{13} cm^{-1})	Neutron energy (lab) (Mev)	Obs.	Ord. forces			Serber forces			Sym. exch. forces		
			BHM	CG (5)	CG (6)	BHM	CG (5)	CG (6)	BHM	CG (5)	GC (6)
0·2	1·85	−0·10	−0·01	−0·08			--0·10		−0·08	−0·08	
0·3	4·2	−0·13	0·03	−0·07		0·0	−0·13		−0·22	−0·22	
0·4	7·4	−0·09	0·43	−0·01			−0·14		−0·25	−0·25	
0·5	11·5	−0·02	0·50	+0·08		0·08	−0·07		−0·22	−0·22	
	14·0	0·0	0·31	0·12	0·01	0·08	0·12	0·01	−0·20	−0·26	−0·26
0·6	16·6			0·11			−0·02		−0·19	−0·19	

approximation is *not* satisfactory for these cases even with the shorter range interaction used by Christian and Gammel. This was verified by calculating the p-phase shift to be expected for the case $\alpha = 2$, $k = 0{\cdot}4 \times 10^{13}$ cm^{-1} by numerical integration, using Christian and Gammel's interaction (5) and approximate deuteron wave function. The exact phase was found to be 0·56 radian whereas according to Born's approximation it would only be 0·28 radian. It is impossible to decide how much correction should be applied to Christian and Gammel's ordinary force results because of this marked failure of Born's approximation without carrying out a complicated numerical calculation of the contribution from the kernel S of (2) in these circumstances. From experience gained in the earlier calculations it is likely that the correct values for ordinary forces with the interaction (5) are appreciably greater than those given in table 2.

The dependence of the calculated phases on the exchange character of the forces is considerably less marked for the CG short range interactions than for the BHM interaction. This is particularly true for the gaussian shape but even with this the ordinary force phases become substantially larger than those obtained with the assumption of a Serber or symmetrical exchange operator, at the higher energies. There seems then to be a real hope at least of deciding whether or not the forces are effectively of ordinary type even if the extreme assumption of the short range gaussian interaction is made. We therefore proceed next to compare the various calculated phases and cross sections with experiment. The elimination of ordinary forces would be a distinct step forward in view of the lack of evidence from other sources on the exchange character of the forces:

the high energy data on the scattering and polarization in nucleon–nucleon collisions which were previously relied upon for conclusive evidence on this matter have so far defied any attempt at consistent interpretation.

§ 5. COMPARISON WITH OBSERVATION

Christian and Gammel have analysed the data on the scattering of protons by deuterons and obtain 'observed' p-phase shifts. These were obtained by first assuming that the p-phases calculated for the interaction (5) with Serber exchange operator, by Born's approximation, then adjusting the s-phases and finally readjusting the p-phases to give a least squares fit to the experimental data. Although we have been considering only neutron–deuteron scattering there is no difficulty in deriving the corresponding p-phase shifts from those for the proton collisions. Christian and Gammel show that the p-phases δ_1 for neutron collisions are related to those η_1, for proton collisions with the same relative velocity v, through the formula

$$\eta_1 = fC^2\delta_1$$

where $C^2 = 2\pi\zeta/\{\exp(2\pi\zeta)-1\}$, $\zeta = e^2/hv$ and f is a function of ζ which differs only slightly from unity in the energy range of interaction and is given graphically in figure 2 of Christian and Gammel's paper (1953). Using this relation δ_1 is obtained for both the quartet and doublet scattering from the curves of figure 3 of Christian and Gammel's paper. The values so obtained are given in table 2. They cannot be regarded as very accurate or indeed unambiguous but should not be far from the correct values. The doublet phases are probably considerably less accurate than the quartet.

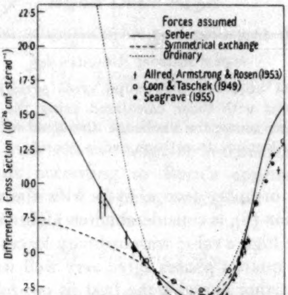

Figure 2. Comparison of observed differential cross section for elastic scattering of 14·1 MEV neutrons by deuterons with those calculated using the BHM interaction (4) with different assumptions about the exchange character of the forces and making full allowance for contributions from high order phases.

Christian and Gammel also present in table V of their paper a phase analysis of 14 MEV neutron–deuteron scattering and the p-phases for this case are also included in table 2.

Comparison of these observed p-phases with those calculated in various assumptions shows that, at neutron energies as high as 11·5 MEV, the quartet

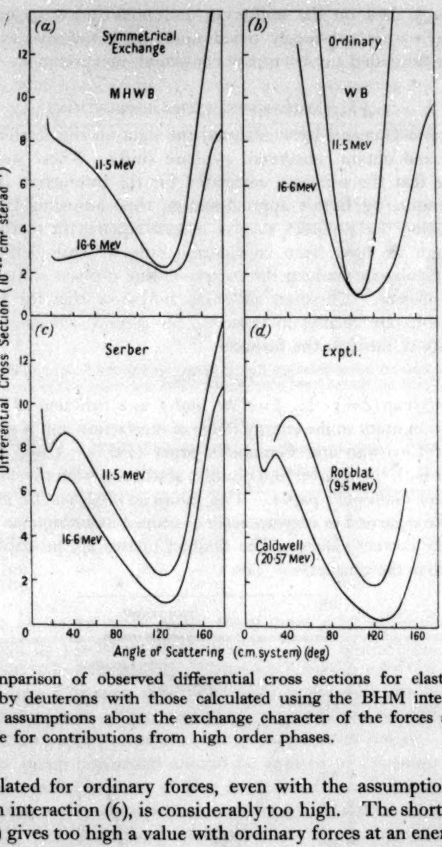

Figure 3. Comparison of observed differential cross sections for elastic scattering of protons by deuterons with those calculated using the BHM interaction (4) with different assumptions about the exchange character of the forces and making full allowance for contributions from high order phases.

p-phase calculated for ordinary forces, even with the assumption of the short range gaussian interaction (6), is considerably too high. The short range Yukawa interaction (5) gives too high a value with ordinary forces at an energy of 7·4 Mev. None of the calculated quartet phases agree very well with the 'observed' value at 1·85 Mev but at the other energies the best fit is probably obtained with the Serber forces, with the BHM interaction (4) or with the CG interaction (5).

Little can be derived from a study of the doublet phases. Most of the calculated values agree in giving small phase shifts in agreement with observation, the sole exceptions being ordinary forces with the BHM interaction (4) which rise much too rapidly at the higher energies.

The calculations of Buckingham, Hubbard and Massey (1952) did not include any allowance for phase shifts of order higher than the second in calculating the angular distributions for scattering of nucleons by deuterons at any energy. This is likely to be serious at angles of scattering in the centre-of-mass system over 0° and 180° at the higher energies and has given an impression of a greater disagreement between the predictions from the BHM interaction (4) and observation. In order to eliminate these effects the BHM calculations have been extended to allow fully for the contribution from higher order phases. This has been done by summing the series of partial cross sections in the scattered amplitude assuming Born's approximation and then allowing for the deviations from this sum due to failure of the approximation for the zero and first order phases. Details of the method are given in the appendix.

Figure 2 illustrates comparison of observed and calculated angular distributions for scattering of 14 MEV neutrons by deuterons. The calculations assume the BHM interaction and allow fully for higher order phases. It will be seen that if a Serber force is assumed the agreement of theory and experiment is quite good, but is much less satisfactory for symmetrical exchange and quite unsatisfactory with ordinary forces.

A similar situation is found for proton–deuteron scattering. Figure 3 illustrates comparison between observed and calculated angular distributions in the energy range from 10 to 20 MEV. The Serber interaction clearly gives the best agreement but even though this gives a very good representation of the shape of the observed curves there are considerable discrepancies in absolute magnitude at small angles. Similar discrepancies are found when the BHM interaction is replaced by the CG interaction (5).

APPENDIX

Calculation of Differential Cross Sections with Full Allowance for Higher Order Phases

We write the scattered amplitude for n–d collisions in the form

$$f(\theta)=f_{\mathrm{B}}(\theta)+\frac{1}{2ik}\sum_{l=0}^{\infty}(2l+1)(\exp 2i\delta_l-1-2i\epsilon_l)\mathrm{P}_l(\cos\theta) \qquad \ldots\ldots(7)$$

where $f_{\mathrm{B}}(\theta)$ is the amplitude given by Born's approximation. δ_l is the exact phase shift for motion with relative angular momentum $\{l(l+1)\}^{1/2}h$, ϵ_l the corresponding phase shift according to Born's approximation. The series converges rapidly, all terms with $l>2$ being negligible.

Referring to the equation (2) we have

$$f_{\mathrm{B}}(\theta)=\alpha I_1+\beta I_2+\gamma I_3, \qquad \ldots\ldots(8)$$

where

$$I_1(\theta)=-\frac{1}{4\pi}\int U(r)\exp\{i(\mathbf{k}_0-\mathbf{k}_1)\,.\,\mathbf{r}\}\,d\mathbf{r},$$

$$I_2(\theta)=-\frac{1}{4\pi}\iint Q(\mathbf{r},\mathbf{r}')\exp\{i(\mathbf{k}_0\,.\,\mathbf{r}'-\mathbf{k}_1\,.\,\mathbf{r})\}\,d\mathbf{r}\,d\mathbf{r}',$$

$$I_3(\theta)=-\frac{1}{4\pi}\iint S(\mathbf{r},\mathbf{r}')\exp\{i(\mathbf{k}_0\,.\,\mathbf{r}'-\mathbf{k}_1\,.\,\mathbf{r})\}\,d\mathbf{r}\,d\mathbf{r}',$$

$$\mathbf{k}_0\,.\,\mathbf{k}_1=k^2\cos\theta. \qquad \ldots\ldots(9)$$

To evaluate these integrals conveniently it is necessary to make one approximation not made in the earlier calculations; the deuteron wave function is represented by

$$\chi(R)\simeq R^{-1}B(\mathrm{e}^{-\alpha R}-\mathrm{e}^{-\beta R}), \qquad \ldots\ldots(10)$$

with $\alpha = 0{\cdot}2312$, $\beta = 2{\cdot}1444$ whereas in the earlier work an exact numerical form was used. Using (10) and the expressions (3) for U and S we obtain, without difficulty,

$$I_1 = -\frac{128\pi^2 N a^3}{K(K^2a^2+4)^2}\left\{\arctan\frac{K}{4\alpha} + \arctan\frac{K}{4\beta} - 2\arctan\frac{K}{2(\alpha+\beta)}\right\},$$

$$I_3 = 16\pi^2 N(\alpha^2\gamma^2 + \beta^2\delta^2 - \alpha^2\delta^2 - \beta^2\gamma^2)$$
$$\times \{(K'^2+\alpha^2)(K'^2+\beta^2)(K'^2+\gamma^2)(K'^2+\delta^2)\}^{-1}$$

where

$$\gamma = \alpha + 2/a, \quad \delta = \beta + 2/a, \quad K = |\mathbf{k}_0 - \mathbf{k}_1|, \quad K' = |\mathbf{k}_0 + \tfrac{1}{2}\mathbf{k}_1|, \quad N = 4\pi MAB^2/3h^2.$$

The evaluation of I_2 is more difficult. It may be evaluated explicitly using Feynman's technique of parametrization (Feynman 1949). This was carried through and yields an extremely cumbrous expression. As expected it was soon found that I_2 is very nearly independent of the angle between $\mathbf{k}_0$ and $\mathbf{k}_1$. This being so we have

$$I_2 \simeq I_2'(\alpha, \alpha) + I_2'(\beta, \beta) - 2I_2'(\alpha, \beta)$$

where

$$I_2'(\alpha, \beta) = -N \iint \exp\{\tfrac{3}{2}i\mathbf{k}_0 \cdot (\mathbf{u}-\mathbf{v}) - \alpha u - \beta v - 2|\mathbf{u}-\mathbf{v}|/a\}(uv)^{-1}\, d\mathbf{u}\, d\mathbf{v}.$$

The phase shifts ϵ_0, ϵ_1 and ϵ_2 may readily be calculated from the relation

$$\epsilon_l = \tfrac{1}{2}k\int_0^\pi f_{\mathrm{B}}(\theta)\mathrm{P}_l(\cos\theta)\sin\theta\, d\theta.$$

It was verified that, for $l = 2$ and for those conditions under which ϵ_1 should be nearly equal to the exact phase δ_1, the results agree quite closely with the earlier calculations, thereby confirming that the approximation (10) for χ is a good one.

There is no difficulty in extending this method to p–d collisions. The integro-differential equations (2) are replaced by

$$(\nabla^2 + k^2)F(\mathbf{r}) = \left\{\frac{Z}{r} + \alpha U(r)\right\} F(\mathbf{r}) + \int [\beta Q(\mathbf{r}, \mathbf{r}') + \gamma S(\mathbf{r}, \mathbf{r}')$$
$$-\gamma T(\mathbf{r}, \mathbf{r}')] F(\mathbf{r}')\, d\mathbf{r}',$$

where

$$\frac{Z}{r} = \frac{16\pi^2 Me^2}{3h^2}\int |\chi(R)|^2 (|\mathbf{r} + \tfrac{1}{2}\mathbf{R}|)^{-1}\, d\mathbf{R}$$

$$T(\mathbf{r}, \mathbf{r}') = \frac{16\pi^2 Me^2}{3h^2}\left(\frac{4}{3}\right)^3 \chi(u)\chi(v)t^{-1}.$$

The scattered amplitude is given by

$$f(\theta) = f_{\mathrm{B}}(\theta) + f_{\mathrm{C}}(\theta) - f_{\mathrm{BC}}(\theta) + \frac{1}{2ik}\sum_{l=0}^{\infty}(2l+1)[\exp(2i\xi_l)\{\exp(2i\eta_l) - 1\}$$
$$- 2i\epsilon_l']\mathrm{P}_l(\cos\theta),$$

where

$$\xi_l = \arg\Gamma(l + 1 + i\zeta), \qquad \zeta = 8\pi^2 Me^2/3kh^2,$$

$$f_{\mathrm{BC}}(\theta) = -\ 4\pi^2 Me^2/3h^2k^2 \sin^2\tfrac{1}{2}\theta,$$

$$\epsilon_l' = \tfrac{1}{2}\, k \int (f_{\mathrm{B}} - f_{\mathrm{BC}})\mathrm{P}_l(\cos\theta)\sin\theta\, d\theta.$$

The introduction of f_{BC} is required in order that the final integral be convergent. The ϵ_l' have the significance of the Born approximation to the phase shift produced by the deviation from a Coulomb potential.

$f_{\mathrm{B}}(\theta)$ is given by

$$\begin{aligned} f_{\mathrm{B}}(\theta) &= \alpha I_1 + \beta I_2 + \gamma I_3 + I_4 - \gamma I_5, \\ I_4 &= -\frac{1}{4\pi}\int \exp i(\mathbf{k}_0 - \mathbf{k}_1)\,.\,\mathbf{r}(Z/r)\,dr, \\ I_5 &= -\frac{1}{4\pi}\int T(\mathbf{r},\mathbf{r}')\exp i(\mathbf{k}_0\,.\,\mathbf{r} - \mathbf{k}_1\,.\,\mathbf{r}')\,dr\,dr'. \end{aligned}$$

Using the approximate form for χ, I_4 is simply evaluated giving

$$I_4 = -\frac{128\pi^3 Me^2B^2}{3h^2K^2}\left\{\arctan\frac{K}{4\alpha} + \arctan\frac{K}{4\beta} - 2\arctan\frac{K}{2(\alpha+\beta)}\right\}.$$

As with I_2 the evaluation of I_5 proves more difficult. Again employing the approximate form for χ

$$\begin{aligned} I_5 &= -\frac{4\pi Me^2}{h^2}B^2\{I_5'(\alpha,\alpha) + I_5'(\beta,\beta) - 2I_5'(\alpha,\beta)\}, \\ I_5'(\alpha,\beta) &= \iint (uv\,|\mathbf{v}-\mathbf{u}|)^{-1}\exp[i(\mathbf{K}'\,.\,\mathbf{u} - \mathbf{K}''\,.\,\mathbf{v}) - \alpha u - \beta v]\,d\mathbf{u}\,d\mathbf{v} \\ \mathbf{K}'' &= \tfrac{1}{2}\mathbf{k}_0 + \mathbf{k}_1. \end{aligned}$$

Transforming to momentum space

$$I_5'(\alpha,\beta) = 8\int \frac{d\mathbf{p}}{p^2\{\alpha^2 + (\mathbf{K}'+\mathbf{p})^2\}\{\beta^2 + (\mathbf{K}''+\mathbf{p})^2\}}.$$

This latter integral may again be evaluated using the parametrization techniques of Feynman, but the resulting expression is very complicated. It should be noted, however, that in the energy region of interest $\beta^2 \gg K'^2 = K''^2$, $\beta^2 \gg \alpha^2$ thus, it is to be anticipated that $I_5'(\alpha,\alpha) \gg I_5'(\alpha,\beta) \gg I_5'(\beta,\beta)$.

To evaluate $I_5'(\alpha,\alpha)$, we note the relation (Whittaker and Watson 1927)

$$(t-z)^{-1} = \sum_{n=0}^{\infty}(2n+1)\mathrm{P}_n(z)\mathrm{Q}_n(t), \qquad t > z,$$

where
$$\mathrm{Q}_n(t) = \frac{\pi^{1/2}}{2^{n+1}}\frac{\Gamma(n+1)}{\Gamma(n+\frac{3}{2})}\frac{1}{t^{n+1}}\,{}_2F_1(\tfrac{1}{2}n+\tfrac{1}{2}, \tfrac{1}{2}n+1, n+\tfrac{3}{2}, t^{-2}).$$

Applying this relation to both denominators, the angular integrations may then be performed to give

$$I_5'(\alpha,\alpha) = \frac{8\pi}{K'^2}\sum_n\int_0^\infty \frac{(2n+1)}{p^2}[\mathrm{Q}_n(\xi)]^2\mathrm{P}_n(\omega)\,dp,$$

where
$$\omega = \frac{\mathbf{K}'\,.\,\mathbf{K}''}{K'^2}, \qquad \xi = \frac{\alpha^2 + K'^2 + p^2}{2K'p}.$$

Noting the relation, (easily derived by expansion of the left-hand side in powers of z)

$$[{}_2F_1(a,b,c\,;z)]^2 = \sum_m \frac{\Gamma(c)\Gamma(a+m)\Gamma(b+m)}{\Gamma(a)\Gamma(b)\Gamma(c+m)\Gamma(1+m)}\,z^m\,{}_4F_3\left[\begin{matrix} a, b, 1-c-m, -m\,; & 1 \\ c, 1-a-m, 1-b-m\,; & \end{matrix}\right]$$

the integration over p may be performed term by term. After some reduction, it is found that

$$I_5'(\alpha, \alpha) = \sum_{n,m} \frac{8\pi^2}{(K'^2+\alpha^2)^{3/2}} \left(\frac{K'^2}{K'^2+\alpha^2}\right)^{n+m} \frac{2^{-2m}}{2n+2m+1} \frac{(n!)^2(n+2m)!}{(2n)!(n+m)!m!}$$

$$\mathrm{P}_n(\omega)\,{}_4F_3\left[\begin{matrix} \tfrac{1}{2}n+\tfrac{1}{2},\ \tfrac{1}{2}n+1,\ -n-\tfrac{1}{2}-m,\ -m;\ 1 \\ n+\tfrac{3}{2},\ \tfrac{1}{2}-\tfrac{1}{2}n-m,\ -\tfrac{1}{2}n-m; \end{matrix}\right].$$

$I_5(\alpha, \alpha)$ gives a sufficiently small contribution for the first term of the series to be an adequate approximation, thus rendering plausible the neglect of $I_5'(\alpha, \beta)$ and justifying the neglect of $I_5(\beta, \beta)$.

REFERENCES

ALLRED, J. C., ARMSTRONG, A. H., and ROSEN, L., 1953, *Phys. Rev.*, **91,** 91.

BROWN, F. W., 1939, *Phys. Rev.*, **56,** 1107.

BUCKINGHAM, R. A., and MASSEY, H. S. W., 1941, *Proc. Roy. Soc.* A, **179,** 123.

BUCKINGHAM, R. A., HUBBARD, S. J., and MASSEY, H. S. W., 1952, *Proc. Roy. Soc.* A, **211,** 183.

CALDWELL, S. J., 1955, *Phys. Rev.*, in the press.

CHRISTIAN, R. S., and GAMMEL, J. L., 1953, *Phys. Rev.*, **91,** 100.

COON, J. H., and TASCHEK, R. F., 1949, *Phys. Rev.*, **76,** 710.

FEYNMAN, R. P., 1949, *Phys. Rev.*, **76,** 769.

HOCHBERG, S., MASSEY, H. S. W., and UNDERHILL, L. H., 1954, *Proc. Phys. Soc.* A, **67,** 957.

PEASE, R. L., and FESHBACH, H., 1952, *Phys. Rev.*, **88,** 945.

ROTBLAT, J., 1955, *Proc.* 1954 *Glasgow Conference on Nuclear and Meson Physics* (London : Pergamon Press).

SEAGRAVE, J. D., 1955, *Phys. Rev.*, **97,** 757.

WHITTAKER, E. T., and WATSON, G. M., 1927, *Modern Analysis*, Fourth Edition (Cambridge : University Press), p. 322.

The Gamma Radiation from the Reaction $D(p, \gamma)^3He$

BY G. M. GRIFFITHS† AND J. B. WARREN
Physics Department, University of British Columbia

MS. received 11*th May* 1954 *and in revised form* 6*th January* 1955

Abstract. Using a scintillation counter for the measurement of the gamma radiation, the Q value of the reaction $D(p, \gamma)^3He$ was found to be $5{\cdot}50 \pm 0{\cdot}03$ MeV. The Doppler shift has been measured. The angular distribution was found to be nearly a pure $\sin^2 \theta$ pattern at all proton bombarding energies from 0·5 to 2 MeV but evidence has been obtained for a small isotropic component. Neutrons were detected, arising, via the $D(d, n)^3He$ reaction, from the knock-on deuterons. The relative yield curve has been measured with a thin target and is in accord with the formula given by Fowler and his co-workers.

An approximate measurement of the absolute cross section at $E_p = 1{\cdot}0$ MeV gave 4×10^{-30} cm² ± 50%.

§1. INTRODUCTION

THE existence of weak capture gamma radiation from the proton bombardment of deuterium was first reported by Curran and Strothers (1939). The reaction was studied by Fowler, Lauritsen and Tollestrup (1949), who found, by measuring the absorption coefficient in aluminium with three coincident Geiger counters, that the γ-ray energy was $6{\cdot}3 \pm 0{\cdot}3$ MeV for a proton bombarding energy of 1·4 MeV. These authors showed that the angular distribution could be represented by $I(\theta) = a + b \sin^2 \theta$, where a was very small or zero. They also measured the excitation function using a thick heavy ice target, and gave for the absolute cross section, at a proton energy E MeV, $\sigma = 0{\cdot}74\, E^{0{\cdot}72} \times 10^{-29}$ cm². The error quoted for the factor 0·74 was about 50% and for the exponent 15%.

From the angular distribution Fowler *et al.* suggested that the radiation was primarily electric dipole in character. Wilkinson (1952) has measured the polarization of the emitted radiation, using the angular dependence of the photodisintegration of deuterium on the polarization, and found that at 90° to the proton beam the radiation is predominantly polarized in the plane of the reaction, consistent with the character of electric dipole radiation. With the advent of the scintillation counter with its high gamma-ray detection efficiency it appeared that a more detailed study of this reaction was possible.

§2. APPARATUS AND GENERAL EXPERIMENTAL PROCEDURE

The layout of the target and detector is shown in figure 1. An analysed beam of protons from the University of British Columbia Van de Graaff generator, accurately stabilized in energy and position, was directed against a thin film of heavy ice. Quite smooth, uniform layers of heavy ice could be deposited up to a thickness of 250 kev to 1 MeV protons, using the dispenser shown in figure 1. Such layers did not deteriorate over several hours of running with beams as large as 10 μA.

---

† Now at Cavendish Laboratory, Cambridge.

In view of the low intensity of the radiation from this reaction, the background radiation coming from various metals when bombarded with 1½ MeV protons was measured. For example copper was found to give radiation with 7 and 8 MeV components presumably arising from ground state transitions in ^{64}Zn or ^{65}Zn. Gold was finally chosen for backing metal and was used on all surfaces in the vicinity of the target since it gave the least radiation above 2 MeV energy. Background from the magnet box, due in part to the D fraction in the mass 2 beam, was eliminated by lead shielding. Very great care was taken to avoid any flourine contamination in the target region, because of the prolific yield of 6 and 7 MeV radiation from the ^{19}F(p, $\alpha\gamma$)^{16}O reaction, and throughout the measurements background runs were taken before depositing the ice and at the end of a run after the ice had been evaporated to check for contamination.

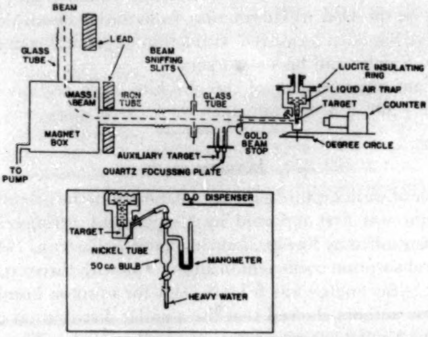
BEAM
GLASS TUBE
LEAD
BEAM SNIFFING SLITS
LUCITE INSULATING RING
LIQUID AIR TRAP
MASS I BEAM
IRON TUBE
GLASS TUBE
TARGET
COUNTER
MAGNET BOX
GOLD BEAM STOP
DEGREE CIRCLE
AUXILIARY TARGET
TO PUMP
QUARTZ FOCUSSING PLATE
D₂O DISPENSER
TARGET
NICKEL TUBE
50 c.c. BULB
MANOMETER
HEAVY WATER

Figure 1. The target and detection arrangement.

The main counter consisted of a cylinder of activated sodium iodide 2 in. long and 1¾ in. diameter mounted on an EMI VX6262 photomultiplier. Angles from − 150° through 0° to + 150° with respect to the incident beam direction were obtained by rotating the counter about an axis through the centre of the proton spot on the target. The output was fed to a 'kicksorter' and also to a scaler with discrimination set to exclude pulses corresponding to less than 4 MeV energy loss in the counter crystal. A monitor counter was fixed in the plane through the target perpendicular to the beam, and its output fed to a second scaler with a 4 MeV equivalent discrimination level. Care was taken to avoid counter fatigue, and soft iron shields eliminated magnetic effects.

§ 3. THE GAMMA-RAY ENERGY

In the reaction $D + P \rightarrow {}^3\text{He}^* \rightarrow {}^3\text{He} + h\nu$, the gamma ray energy is not only a function of the bombarding energy but also varies with the angle of observation at any particular proton energy due to the doppler shift resulting from the motion of the ^{3}He* nucleus. The gamma-ray energy is given by

$$h\nu' = Q + E_x - \frac{(Q+E_x)^2}{2M(^3\text{He}^*)c^2} \simeq Q + E_x - \frac{(Q+E_x)^2}{2M(^3\text{He})c^2} \qquad \ldots\ldots(1)$$

where $E_x = E_p M_d/(M_p + M_d)$ is the fraction of the proton energy which does not go into centre-of-mass motion and $Q = (M_p + M_d - M(^3\text{He}))\,c^2$. Owing to the motion of the $^3\text{He}^*$ with respect to the laboratory system, the gamma-ray energy, $h\nu$, as measured will depend on the angle of observation in accordance with the usual Doppler formulae:

$$h\nu = h\nu' \frac{1+\beta\cos\theta'}{(1-\beta^2)^{1/2}} \quad \ldots\ldots(2a) \qquad \cos\theta = \frac{\cos\theta' + \beta}{1+\beta\cos\theta'} \quad \ldots\ldots(2b)$$

where $\beta = \dfrac{v(^3\text{He}^*)}{c} = \dfrac{M_p}{M_p + M_d}\dfrac{v_p}{c} = \dfrac{M_p}{M_p + M_d}\left(\dfrac{2E_p}{M_p c^2}\right)^{1/2}$,

$v(^3\text{He}^*)$ and v_p are the velocities referred to the laboratory system, and θ is the angle of the observation in the laboratory system corresponding to an angle θ' between the $^3\text{He}^*$ nucleus and an observer in the centre of mass system.

The gamma-ray energy was measured at an angle of 90° to the proton beam by comparing the spectrum from the $D(p,\gamma)^3He$ reaction with that from a thin fluorine target bombarded with protons of 873 kev energy. Typical spectra are shown in figure 2. The two peaks used for calibration are pair peaks of energies 5·115 and 5·626 Mev arising from the 6·137 Mev component in the $^{19}F(p,\alpha,\gamma)^{16}O$ radiation (Chao *et al.* 1950). The proton energy was read from the generating voltmeter, calibrated in terms of the accurately known resonances in the $^{19}F(p,\alpha,\gamma)^{16}O$ reaction. Table 1 gives the gamma-ray energy so measured and the Q values deduced therefrom.

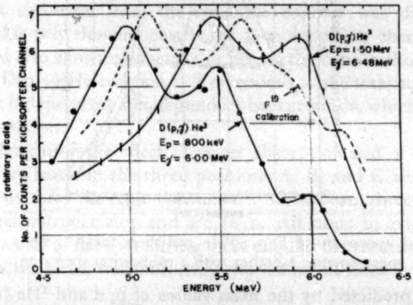

Figure 2. Typical Single Crystal Spectra of the gamma radiation from the $D(p,\gamma)^3He$ reaction at 90° to the incident beam, together with a calibration spectrum of radiation from the $^{19}F(p,\alpha,\gamma)^{16}O$ reaction. The ' photo peak ' is not shown on the spectrum taken at $E_p = 1{\cdot}50$ Mev.

Table 1. Experimental Q values for Reaction $D(p,\gamma)^3He$

E_p (Mev)	$h\nu$ (Mev)	Q (Mev)
0·80	6·00 ± 0·04	5·47 ± 0·04
1·00	6·16 ± 0·03	5·48 ± 0·03
1·50	6·48 ± 0·03	5·48 ± 0·03

The average Q value from this data is 5·48 ± 0·02 Mev. The thickness of the targets was estimated to be between 30 and 60 kev for these runs; applying a correction for this to the value of E_p gives an average $Q = 5{\cdot}50 \pm 0{\cdot}03$ Mev.

Further measurements were made using a three-crystal pair spectrometer at proton energies of 1·0 and 1·5 Mev, and, for calibration, spectra of the fluorine radiation at the 935 and 1355 kev resonances were used. A typical spectrum is shown in figure 3. The D(p, γ)^{3}He spectrum consists of a single peak with this pair spectrometer, which reduces the accuracy of estimating the gamma-ray energy, and, owing to the longer time needed to obtain such a spectrum of the weak radiation and consequent apparatus drifts, the width of the D(p, γ)^{3}He peak is wider than the calibration peaks from the fluorine γ-ray lines. After allowing for target thickness the three-crystal result was $Q = 5{\cdot}51 \pm 0{\cdot}05$ Mev.

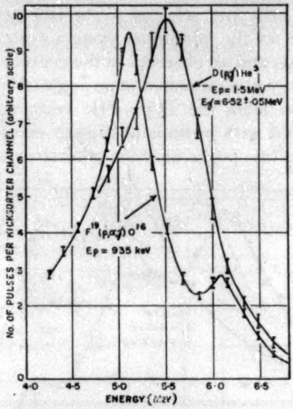

Figure 3. Typical spectrum of D(p, γ)^{3}He radiation taken with a three-crystal pair spectrometer, together with a calibration spectrum.

The Q value predicted by the mass values of p, d and ^{3}He (Li *et al.* 1951) is $5{\cdot}493 \pm 0{\cdot}012$ Mev which lies within the errors of this experimental determination. This result confirms the conclusion that the γ-ray transition goes to the ground state; no evidence was found for any other components.

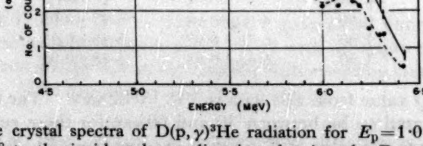

Figure 4. Single crystal spectra of D(p, γ)^{3}He radiation for $E_p = 1{\cdot}0$ Mev taken at 45° and 135° to the incident beam direction showing the Doppler shift.

The Doppler shift of the γ-ray energy was observed at angles of 45° and 135° for proton bombarding energies of 1·0 and 1·7 Mev. Figure 4 shows the spectra obtained with 1 Mev protons from which the shift was estimated as 130 ± 10 kev as compared with the calculated value of 135 kev. At 1·7 Mev the observed shift was 195 ± 15 kev compared with the calculated value of 190 kev. For these measurements the angular width of the counter as seen from the target was 16°. This agreement demonstrates that the ^{3}He* nucleus emits the γ-ray in a time short compared with its stopping time in the target, 10^{-12} second, as is expected. The transverse Doppler shift at $\theta = 90°$ is beyond our limit of resolution.

§ 4. THE ANGULAR DISTRIBUTION OF GAMMA RADIATION

4.1. *Experimental Procedure*

The angular distribution of the gamma radiation has been measured at several proton energies with targets of thicknesses from 50 to 100 kev. At each angle the counts in both the monitor and rotatable counter were recorded, with the discrimination levels set to correspond to at least a 4 Mev energy loss. At the same time the pulse height spectrum from the rotatable counter was displayed on the 'kicksorter', in this way showing clearly the Doppler effect, checking the overall gain stability, and also showing whether or not all the counts above the bias level were due to the D(p, γ)^{3}He reaction. Corrections to the total counts were made for both machine independent and dependent backgrounds, which were measured at each angular position.

In order to determine the effect of target absorption and of any asymmetry, measurements were made in the three positions A, B, and C shown in figure 5, position C being used for the region around 0°. The beam direction was defined by a ¼ in. diameter entrance stop and a 5/16 in. exit stop; to avoid errors due to small sideways wander of the spot during these angular distribution runs, the focus was spread out so the beam was uniformly clipped on all sides by the stops.

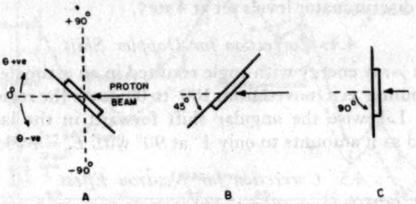

Figure 5. Target positions used for the angular distribution measurements.

A typical curve showing the variation of the number of counts in the movable counter as a function of angle, after background subtraction and normalization to the monitor counts is shown in figure 6 for a proton bombarding energy of 1·75 Mev. The angular distribution is clearly almost a pure $\sin^2\theta$ type; several corrections to these experimental curves have been made as outlined below. The main emphasis was placed on the $-45°$–0–$+45°$ region, in an attempt to determine the magnitude of the small, presumed isotropic, component.

4.2. *Correction for Target Absorption*

The absorption was measured experimentally by taking readings with the movable counter at +90° and −90° for the target in positions A and B. These readings also checked sideways asymmetry and agreed with the calculated value for 6·5 MeV radiation passing through the backing. For the radiation passing perpendicularly through the backing, the absorption was 4%.

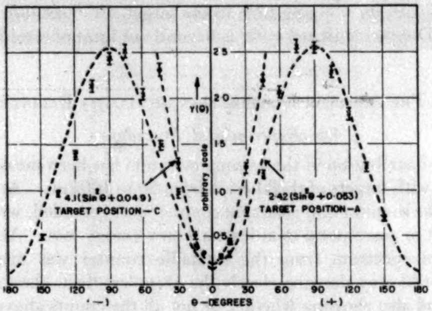

Figure 6. Angular distribution of the radiation from the D(p, γ)^{3}He reaction taken at $E_p = 1{\cdot}75$ MeV with background subtracted.

4.3. *Correction for Scattered Radiation*

The readings at 0° may be too high due to some of the much more intense radiation at 90° being scattered into the counter. Rayleigh scattering, without change of energy, is negligible. The scattered radiation would therefore have shown up as a change in the shape of the spectrum at 0° as compared with 45° or 90°, with more counts in the low energy region, an effect which was not distinguishable from the neutron effect (§ 4.5). Most of the scattered radiation was not counted with the discriminator levels set at 4 MeV.

4.4. *Correction for Doppler Shift*

The change in γ-ray energy with angle resulted in an estimated 3% increase in efficiency of the counter as it moved from 180° to 0°; over the region 45° to 0° it has been neglected. Likewise the angular shift forward in the laboratory system has been neglected as it amounts to only 1° at 90° with $E_p = 1{\cdot}75$ MeV.

4.5. *Correction for Neutron Effect*

Jennings *et al.* (1950) have reported that neutrons are produced by protons bombarding deuterium targets somewhat below the (p, n) threshold at 3·3 MeV. At proton bombarding energies of 2 MeV and below, a check with a neutron detector (a zinc sulphide–plastic scintillation counter, quite insensitive to gamma radiation) confirmed the presence of neutrons, presumably arising from the D on D reaction caused by deuterons knocked on by the protons, since photodisintegration does not account for the order of magnitude of the yield found. From estimates of the efficiency of this neutron counter using a radium beryllium source, it was concluded that there were rather more neutrons than gamma rays emitted at 0°. Such neutrons were not counted directly by the sodium iodide scintillation counter but were captured in the surrounding materials and in the iodine leading to gamma rays detected by this counter. Quite definite evidence for the latter effect was obtained by irradiating the counter with fast neutrons, following which an intense background below 3 MeV was found which decayed with a half-life of 25 minutes and the spectrum of which was characteristic of ^{128}I. While the ^{128}I activity would not have interfered with the measurement of the 6 MeV D(p, γ)^{3}He radiation, from the spectrum obtained during a D(D, n)^{3}He run there appeared to be prompt gamma rays with components around 4·5 and 6 MeV produced at the time of neutron capture.

The magnitude of this neutron effect was estimated in two ways. The first method involved a comparison of the counting rates in the neutron and gamma sensitive counters placed at 0°, when irradiated by neutrons from the D(d, n)^{3}He reaction, $N_n{}^D$ and N^D, and when irradiated by the products of the proton bombardment of heavy ice $N_n{}^P$ and N^P. The contribution of the knock-on process to N^P is given by

$$N^{P(D+D)} = (N^D/N_n{}^D) \, . \, N_n{}^P.$$

The deuteron bombarding energy was chosen to give neutrons of about the same mean energy as would arise from the knock-on process.

The second method was indirect and was based on a comparison of the shape of the gamma-ray spectra produced at 0° and 45° during the D(p, γ)^{3}He runs. Such spectra for $E_p = 1{\cdot}0$ MeV and $E_p \simeq 1{\cdot}75$ MeV are shown in figures 7 and 8, from which it is evident that in both cases the 0° spectrum is rather higher on the low-energy side than the 45° spectrum, the effect being more pronounced at 1·75 MeV as would be expected if the effect arises from knock-on deuterons giving D on D neutrons. Thus a background may be subtracted from the lower side of the 0° spectrum to reduce this spectrum to the same shape as the 45° spectra.

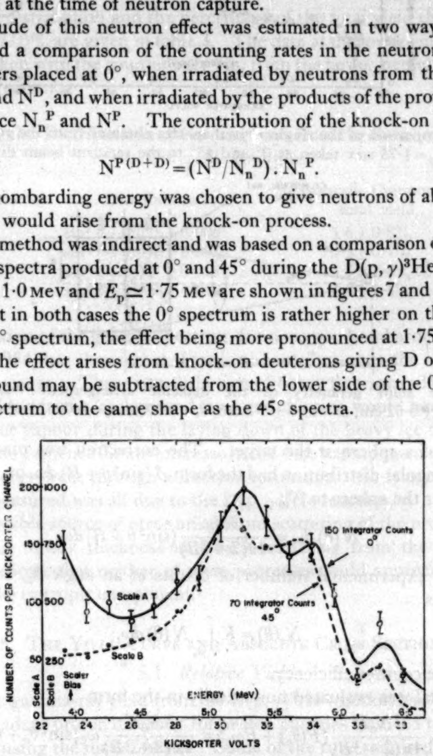

Figure 7. Comparison of the single crystal spectra obtained from the reaction D(p, γ)^{3}He at $E_p = 1{\cdot}0$ MeV taken at 0° and 45° to the incident beam direction.

Both methods gave similar corrections to the observed count at 0°, about 25% reduction at 1·75 MeV bombarding energy and 8% at 1 MeV.

4.6. *Correction for Solid Angle*

Figure 9 shows the geometry of crystal and target. For the solid angle corrections the crystal was approximated to by a spherical cap subtending a solid angle

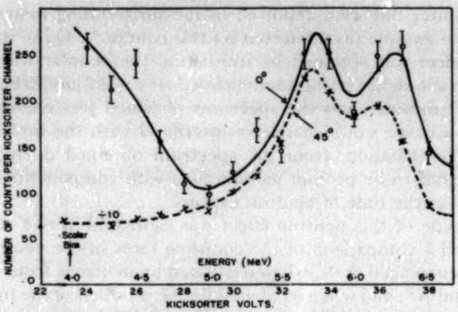

Figure 8. Comparison of the single crystal spectra obtained from the reaction D(p, γ)^{3}He at $E_p = 1{\cdot}75$ MeV taken at 0° and 45° to the incident beam direction.

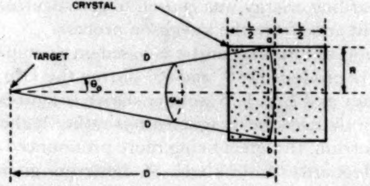

Figure 9. The solid geometry of the detector arrangement : $L=5{\cdot}10 \pm 0{\cdot}05$ cm, $R=2{\cdot}23 \pm 0{\cdot}02$ cm, $D=15{\cdot}5 \pm 0{\cdot}2$ cm, $\theta_0 = 8°\,15'$, $\omega_0 = 0{\cdot}00521$ of a sphere.

$\omega_0 = 0{\cdot}00521$ of a sphere at the target. The correction was made by assuming that the true angular distribution had the form $A(\sin^2\theta + B)\,d\omega$, or, normalizing the total yield over the sphere to N_0,

$$N(\theta)\,d\omega = \frac{3N_0}{4\pi(2+3B)}(\sin^2\theta + B)\,d\omega. \qquad \ldots\ldots(3)$$

The expected experimental number of counts at an angle θ_c, corresponding to equation (3), is

$$N_c(\theta) = K\int_{\omega_0} N(\theta)\,d\omega,$$

where K is the counter efficiency.

The integral was evaluated numerically in the form

$$N_c(\theta_c) = \frac{3N_0K}{4\pi(2+3B)}(F(\theta_c) + B\omega_0) = \frac{3N_0K}{4\pi(2+3B)}\,\omega_0\{\sin^2\theta_c + f(\theta_c) + B\}$$

in which $$F(\theta_c) = \int_{\theta_c - \sin^{-1}C}^{\theta_c + \sin^{-1}C} 2\sin^3\theta\,\sin^{-1}\frac{\{C^2 - \sin^2(\theta-\theta_c)\}^{1/2}}{\sin\theta\cos(\theta-\theta_c)}\,d\theta,$$

$C = R/D$ (see figure 9), and it has been assumed that the intersection of the cones of constant radiation intensity with the plane surface ab of figure 9 are straight lines. In table 2 are given the values of $F(\theta_c)$ and the values of $(\omega_0 \sin^2\theta)$ representing the $\sin^2\theta$ angular distribution without solid angle correction ; these values are accurate to about 3% and to this accuracy no correction was necessary for angles between 45° and 90°.

Table 2. Solid Angle Corrections

θ_c	$F(\theta_c)$	$\omega_0 \sin^2 \theta_c$	$F(\theta_c) - \omega_0 \sin^2 \theta_c$	$f(\theta_c)$
0°	0·00068	0·00000	0·00068	0·0103
15°	0·00495	0·00439	0·00056	0·0085
30°	0·0169	0·0164	0·0005	0·0076
45°	0·0334	0·0328		
90°	0·0657	0·0655		

4.7. *Angular Distribution Results and Possible Sources of Error*

The angular distribution and the percentage of the total yield that is isotropic $(3B \times 100)/(2+3B)\%$ are given in table 3. The data at the lower energies, 0·6 and 0·8 MeV, were taken with the counter only 4 in. from the target, necessitating a larger solid angle correction.

Table 3. Angular Distributions of Gamma Rays from the Reaction $D(p,\gamma)^3He$ at Different Energies

E_p (MeV)	Distribution	% Isotropic Component in total yield
1·75	$\sin^2 \theta + 0{\cdot}025 \pm 0{\cdot}006$	$3{\cdot}6 \pm 0{\cdot}8\%$
1·0	$\sin^2 \theta + 0{\cdot}046 \pm 0{\cdot}005$	$6{\cdot}5 \pm 0{\cdot}7\%$
0·8	$\sin^2 \theta + 0{\cdot}04 \pm 0{\cdot}015$	$5{\cdot}7 \pm 2{\cdot}0\%$
0·6	$\sin^2 \theta + 0{\cdot}026 \pm 0{\cdot}010$	$3{\cdot}8 \pm 1{\cdot}5\%$

An examination of the gamma spectrum from oxygen bombarded with protons (Warren *et al.* 1954) has shown that there is no contribution to the radiation above 4 MeV from this cause. There was little sign of 6 MeV fluorine radiation from the gold target backing in the background runs and fluorine would hardly be carried over in the water vapour during the laying down of the heavy ice targets; moreover, there was no evidence for any increase in the 6 MeV component of the radiation as the beam energy went through a fluorine resonance. So it is considered that the radiation measured was all due to the $D(p,\gamma)^3He$ reaction.

Another possible source of error arises from scattering of the protons in the ice targets of about 50 kev thickness and back-scattering from the gold backing. Calculations indicate that neither of these processes could appreciably affect the magnitude of the isotropic component.

§ 5. THE YIELD CURVE AND ABSOLUTE CROSS SECTION

5.1. *Relative Yield*

The relative gamma-ray yield from the $D(p,\gamma)^3He$ reaction has been measured at 90° to the incident proton direction for proton energies from 0·5 to 1·85 MeV and at 0·25 MeV by using the mass 2 beam. Some of the runs required a total time of 12 hours so that a careful check was kept of the gain stability of the electronic apparatus. The total count recorded above the discrimination level of 4 MeV, corrected for background, was taken as proportional to the gamma-ray yield. The total count so obtained was corrected for the variation in the efficiency of the counter, as the gamma-ray energy changed from 5·6 MeV at $E_p = 0{\cdot}25$ MeV to 6·6 MeV at $E_p = 1{\cdot}75$ MeV. The efficiency was calculated from the cross sections for the γ-ray interactions in the crystal, taking into account wall effects and the number of pulses below 4 MeV in the Compton distribution. As a check, the percentage of the pulses above the bias level was estimated from the kicksorter distribution, and this fraction times the total calculated theoretical efficiency gave another value for the actual efficiency. These two values were in fair agreement, i.e. 36% for $E = 6{\cdot}15$ MEV by the first method and 33% by the second.

During the long runs the integrated current could not be relied upon to give the relative normalization since the yield from the target did not remain quite constant. As an example at $E_p = 1{\cdot}25$ MEV the yield decreased by about 17% after 10 hours. Consequently, two check points were used, $E_p = 1{\cdot}0$ MEV for the lower proton energies and 1·25 MEV for the higher, corresponding to two different sets of focusing conditions for the beam. The background tended to rise quite sharply as E_p rose above 1·24 MEV and depended quite significantly on the exact focusing conditions. The proton energy was maintained to better than ± 10 kev during the runs. Correction was made for the target thickness which in these runs was about 70 kev for $E_p = 1{\cdot}0$ MEV.

Figure 10 shows the relative yield as a function of E_p together with a curve calculated from the formula $Y = KE^{0{\cdot}72}$ given by Fowler *et al.* (1949) and adjusted to fit the present data in the region of $E_p = 1{\cdot}0$ MEV. No errors have been shown since the statistical errors are less than other experimental errors, but the data agree within the errors of the two measurements.

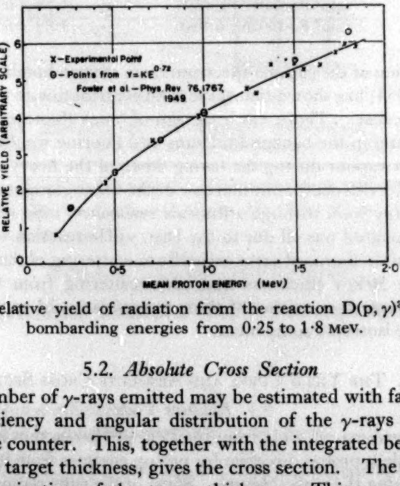

Figure 10. Relative yield of radiation from the reaction $D(p, \gamma)^3He$ for proton bombarding energies from 0·25 to 1·8 MEV.

5.2. *Absolute Cross Section*

The total number of γ-rays emitted may be estimated with fair precision from the counter efficiency and angular distribution of the γ-rays and solid angles subtended by the counter. This, together with the integrated beam current and a knowledge of the target thickness, gives the cross section. The main uncertainty lies in the determination of the target thickness. This was accomplished by standardizing the method of dispensing the water vapour by depositing a layer on to a thin calcium fluoride target and measuring the apparent shift in the $^{19}F(p, \alpha, \gamma)^{16}O$ resonances. From the energy loss so established and the data of Wenzel and Whaling (1952) the number of D atoms in the targets used was deduced.

The absolute cross section at $E_p = 1{\cdot}0$ MEV so obtained was $\sigma = 4 \times 10^{-30}\,cm^2 \pm 50\%$ in approximate accord with the previous measurement (Fowler *et al.* 1949). Since the angular distribution changes very little, the cross section at other energies may be deduced from the relative yield curve.

§ 6. DISCUSSION

The excitation function and the change in gamma-ray energy with incident proton energy indicate that the reaction takes place by direct radiative capture to the ground state of ^{3}He, without the formation of a compound nucleus in the Bohr sense. It would be of interest to extend the range of bombarding energy to perhaps 20 MEV to determine the position and the value of the maximum in the cross section.

The angular distribution of the radiation is of the form $\sin^2\theta+b$ where b is small but not zero. This, together with the polarization data, strongly suggests that the predominant transition is electric dipole. For this part of the radiation the angular momentum of the ingoing protons l_p cannot be zero and the simplest choice is p-wave protons. If it is assumed that the intermediate state, ^{3}He*, is one of well-defined angular momentum arising from the vector addition of l and the incident channel spin, then it is not possible to realize a distribution of the form $\sin^2\theta+b$, with b as small as experimentally observed, taking $l_p=1$ or even 2 or 3. Thus the simplest assumption for this reaction is that the spin of the proton remains unchanged throughout, so with p-wave protons the γ-ray transition is from ^{3}He* with orbital angular momentum $l=1$ and $l_z=0$ to the ground state of ^{3}He with $l=0$ and $l_z=0$. In this case $\Delta l=1$, $\Delta l_z=0$ leading directly to a pure $\sin^2\theta$ distribution with the required polarization.

The small 'isotropic' component, which seems to show a maximum around $E_p=1{\cdot}0$ MEV may be explained by including a little spin–orbit coupling. Thus for $l_p=1$ protons such coupling would introduce transitions for which $\Delta J=1$, $\Delta J_z=0$, giving a $\sin^2\theta$ distribution and also for which $\Delta J=1$, $\Delta J_z=\pm 1$ giving a $1+\cos^2\theta$ pattern, where J refers to the total angular momentum, spin plus orbital. However, part or all of this isotropic component may arise from magnetic dipole transitions following capture of S-wave protons. Such transitions may arise from non-central components in the nuclear force law (Verde 1950) and indeed the observation of the mirror reaction D(n, γ)T with thermal neutrons, for which l_n is presumably zero, is evidence for such an assignment. On the basis of Verde's theory the isotropic component should increase relative to the $\sin^2\theta$ component as the proton energy decreases in a similar manner to the D(γ, n)P reaction but our experimental results do not show this tendency. It would be of interest, though difficult, to study this mirror reaction, D(n,γ)T, with fast neutrons for comparison.

One possible way of distinguishing between these two alternative explanations of the isotropic component would seem to be to determine the polarization in the vicinity of 0°. However, it is not clear that this is possible, since the elliptic polarization of the small $1+\cos^2\theta$ component combined with a portion of the predominant plane polarized $\sin^2\theta$ component would look the same as the circular polarization of the magnetic dipole transitions of the second theory.

This reaction D(p, γ)^{3}He and its inverse would appear to be very suitable for testing the principle of reciprocity in nuclear physics. Unfortunately the cross section for the photodisintegration, deduced from the radiative capture cross section, is only about 10^{-28} cm^2 for 6 MEV quanta which is at the limit of detectability at the present time even taking into account the coincident appearance of the two charged particles in the photodisintegration.

Theoretical calculations for the direct radiative capture processes in very light nuclei usually proceed from a consideration of the inverse photodisintegration process to the radiative capture using the reciprocity theorem. It is first necessary to make some guess as to the wave function describing the nucleus in the ground state based on the binding energies, magnetic moments and a nuclear force law. This approach has been quite successful in the case of the deuteron, and calculations for the more difficult three-body case have been made by Burhop and Massey (1948), Verde (1950) and Gunn and Irving (1951). Except for Verde these authors have considered only the symmetric part of the ground-state wave function, so only the $\sin^2\theta$ part of the cross section is included. Since there seems to be some discrepancy between the three-body theory and results in the present case and in the scattering of neutrons by deuterons (Buckingham and Massey 1942, Adair *et al.* 1953), calculations which did include non-central force components required by two- and three-body binding energies and magnetic moments (Tsi-Ming Hu and Kung-Ngou Hsu 1951), and which covered a wider range of distance dependence of the wave functions than the gaussian used by Verde, would be of interest. At the present time it is not clear whether any greater precision in the measurement of the cross section for example, would be of value in choosing the form of the wave function owing to the approximations made in the theoretical calculations.

ACKNOWLEDGMENTS

We should like to acknowledge the help of Mr. E. Critoph with the preliminary measurements and of Mr. J. Sample who assisted with the neutron detection. One of us (G. M. G.) gratefully acknowledges the receipt of a National Research Council of Canada fellowship. This work was made possible by generous assistance from Atomic Energy of Canada Ltd.

REFERENCES

ADAIR, R. K., OKAZAKI, A., and WALT, M., 1953, *Phys. Rev.*, **89,** 1165.
BUCKINGHAM, R. A., and MASSEY, H. S. W., 1942, *Proc. Roy. Soc.* A, **179,** 123.
BURHOP, E., and MASSEY, H. S. W., 1948, *Proc. Roy. Soc.* A, **192,** 156.
CHAO, C., TOLLESTRUP, A. V., FOWLER, W. A., and LAURITSEN, C. C., 1950, *Phys. Rev.*, **79,** 108.
CURRAN, S. C., and STROTHERS, J., 1939, *Proc. Roy. Soc.*, **172,** 72.
FOWLER, W. A., LAURITSEN, C. C., and TOLLESTRUP, A. V., 1949, *Phys. Rev.*, **76,** 1767.
GUNN, J. C., and IRVING, J., 1951, *Phil. Mag.*, **42,** 1353.
JENNINGS, LEITER and SUN, 1950, *Westinghouse Technical Report*.
LI, C., WHALING, W., FOWLER, W. A., and LAURITSEN, C. C., 1951, *Phys. Rev.*, **83,** 512.
TSI-MING HU, and KUNG-NGOU HSU, 1951, *Proc. Roy. Soc.* A, **204,** 476.
VERDE, M., 1950, *Helv. Phys. Acta*, **23,** 453; 1951, *Ibid.*, **24,** 298.
WARREN, J. B., LAURIE, K. A., JAMES, D. B., and ERDMAN, K. L., 1954, *Canad. J. Phys.*, **32,** 563.
WENZEL, W., and WHALING, W., 1952, *Phys. Rev.*, **87,** 499.
WILKINSON, D. H., 1952, *Phil. Mag.*, **43,** 659.

The Ionization Loss of Relativistic μ-Mesons in Neon

By D. A. EYEIONS*, B. G. OWEN*, B. T. PRICE†, AND J. G. WILSON‡
(with an Appendix by J. M. Hammersley § and K. W. Morton†)

MS. received 4th March 1955

Abstract. Proportional counters filled with neon have been used in conjunction with the Manchester magnetic spectrograph to investigate the relationship between the momentum and the most probable ionization loss for μ-mesons at momenta greater than about 10^9 ev/*c*. The logarithmic increase of ionization loss with momentum is found to be in good agreement with that indicated by treatments which ignore interactions among the target molecules, and the onset of polarization effects is compared with that previously reported in oxygen.

§ 1. Introduction

Ghosh, Jones and Wilson (1952, 1954) have measured the ionization of μ-mesons traversing a gas by drop counting in a cloud chamber placed in the beam of the Manchester magnetic spectrograph (Hyams *et al.* 1950). They showed that for relativistic particles the ionization increased logarithmically with increasing momentum until polarization effects in the medium became important and the ionization appeared to approach a saturation maximum, the so-called 'Fermi plateau'.

Recently several workers (Becker *et al.* 1952, Price *et al.* 1953, Parry *et al.* 1953) have investigated the same phenomena by measuring the most probable ionization loss of particles traversing various gases contained in proportional counters. The results so far published establish the logarithmic increase, but there remains considerable uncertainty in the magnitude of the saturation value of the ionization corresponding to the Fermi plateau. This is mainly on account of the difficulty of measuring the momentum of mesons when this exceeds 10^{10} ev/*c*.

A modification of the Manchester spectrograph, in which a system of cloud chambers is used to define the particle trajectory (a detailed description will be published elsewhere), has greatly extended the resolution of the instrument; the momentum of single particles can now be measured with a maximum detectable momentum of the order 10^{12} ev/*c*. The modified spectrograph combines two instruments, the first of which, referred to as the 'counter spectrograph', has already been described (Hyams *et al.* 1950), while the second will be referred to as the 'cloud chamber spectrograph'. The determination of momentum using the cloud chamber spectrograph is relatively tedious and is normally used only if the momentum of the particle exceeds 10^{10} ev/*c*, but a small number of particles of lower momentum are also recorded by the cloud chamber spectrograph

* University of Manchester. † Atomic Energy Research Establishment, Harwell.
‡ University of Leeds. § University of Oxford.

to provide a reasonable overlap with the counter information. This instrument affords the opportunity to examine particles in the 'Fermi plateau' region of ionization loss uncontaminated by particles of lower momentum.

When ionizing particles all of the same momentum and mass traverse a given medium, the loss of energy is not unique but fluctuates over very wide limits. Landau (1944) calculated a distribution function applicable to thin absorbers, and the treatment has been extended by Symon (1948) to thicker absorbing layers. Landau calculated this distribution in terms of $(\Delta-\Delta_0)/\xi$ where Δ is the energy lost by the ionizing particle in travelling a distance x and Δ_0 is the most probable energy loss for a particle of velocity βc. For a singly charged particle:

$$\Delta_0=\xi\,(\ln \xi/\epsilon'+0{\cdot}37),$$

where

$$\xi=x\frac{2\pi Ne^4}{mc^2\beta^2}\rho\frac{\Sigma Z}{\Sigma A},$$

and

$$\epsilon'=\frac{I^2(Z)}{2mc^2\beta^2}(1-\beta^2)\exp\beta^2.$$

In these expressions N is Avogadro's number, e and m are the electronic charge and mass, while Z, A, ρ and $I\ (Z)$ are respectively the atomic number, atomic weight, density and average ionization potential of the medium traversed.

An essential condition for the validity of Landau's calculations is that

$$I(Z)\ll\xi\ll E_{\max}$$

where $E_{\max}$ is the maximum possible energy transferable to an electron in a single collision.

When ξ is not very large compared with $I(Z)$, which is the case for convenient sizes and fillings of proportional counters (including those used in this experiment), a broader distribution results; the exact shape of this distribution is best determined experimentally (West 1953). However, even when the condition is far from satisfied, all authors agree that the most probable ionization does not seem to be greatly different from Landau's value; so it is still convenient to compare the experimentally determined values of the most probable ionization with Landau's theoretical values, even though there is at present no rigorous justification for doing so.

§ 2. EXPERIMENTAL DETAILS

The magnetic spectrograph recorded the momentum of each particle and the ionization loss was simultaneously recorded in two rectangular proportional counters placed one above the other between the two magnets of the spectrograph. In this position the particle beam was collimated and did not extend beyond the sensitive volume of the proportional counters. The path lengths of all particles traversing the counters were the same to within ½%. The proportional counters and recording equipment have already been described by Price *et al.* (1953); no modifications were necessary for the present experiment, apart from the change of gas filling.

The dimensions of the counters were: useful length 25 cm, internal depth in the direction of the beam 7·0 cm, width 9 cm (effective width of the beam 6 cm). The counters were filled with neon and methane at partial pressures of 40·0 cm and 4·4 cm of mercury respectively at 15°c; the pulses from the counters were amplified and, after separation by delay lines, were displayed on an oscilloscope and photographed. The oscilloscope was triggered by master pulses generated by particles traversing the spectrograph and the ionization losses of the particles were determined from the height of the photographed pulses.

§ 3. THE TREATMENT OF RESULTS

The pulse records were assigned to twelve momentum ranges and the pulse amplitudes in each range plotted in the form of histograms. These momentum ranges were of two kinds: the first nine ranges, corresponding to groups of deflection categories of the counter spectrograph, contained mesons of momentum up to 10^{10} ev/c, the remaining three ranges contained the particles of high momentum directly measured in the cloud chamber spectrograph.

In experiments of this kind, the events lying in the 'high-energy tail' of the experimental ionization distribution cannot be observed with any accuracy, as they saturate the amplifier. Since it is therefore impossible to make a satisfactory measurement of the average ionization, it is preferable to determine the most probable ionization, i.e. the mode of the distribution. It has been pointed out by a number of earlier workers (Becker *et al.* 1952, Price *et al.* 1953, Parry *et al.* 1953 and Yeuseyev *et al.* 1953) that it is important when determining the mode to use some objective statistical method. The method adopted by all of these workers was to fit a suitable smooth curve to the ionization histograms, and to determine the mode of the fitted curve. In this way effectively the whole of the observations can be utilized in deriving the result, and not merely those lying in close proximity to the mode. In the work of Becker, Price and Parry and their respective co-workers an application of the method of 'maximum likelihood' was used to fit the 'ideal curves' (derived from auxiliary experiments with electrons) to the experimental distributions. A somewhat similar statistical treatment was used by Yeuseyev and his colleagues. However, neither of these methods of analysis is completely rigorous, although both yield results with only a moderate amount of computation.

In the present analysis, the curve fitting and determination of the mode was carried out using the method of 'linear unbiased estimators of minimum variance' in an application specially developed for the treatment of these results by Hammersley and Morton (1954). A very brief summary of the method, including a 'computing recipe' is given in the Appendix to this paper.

The 'ideal curve' fitted to the histograms was obtained by suitably combining the observations in the eight lower momentum groups, i.e. those *not* in the region of the polarization plateau. The median was first found for each distribution. This was possible because even though the magnitude of the saturation pulses corresponding to the large energy losses could not be determined, their number was known. The eight pulse-height distributions were then plotted, each with the median as origin, and all eight were then added together, giving a histogram containing a very large number of observations (~5000). The 'ideal curve' was obtained by smoothing this histogram, and it was then fitted to the individual histograms by adjusting both the mode and the width.

The method of preparing the ideal curve implicitly assumes that the width and shape of the ionization distributions for each of the eight histograms were the same, so that the only effect of the relativistic increase of ionization was to shift the whole distribution bodily. This assumption was subsequently justified by the computed results, which showed no significant variation in width over this range of momenta.

§ 4. ERRORS IN THE VALUE OF ENERGY LOSS

The amplifying system of the proportional counters was checked at the beginning of the experiment for linearity over the range used, and daily calibrations were made using the K x-rays from a ^{51}Cr source placed against the thin central windows of each counter (Rothwell and West 1950). This particular x-ray energy, 5·0 kev, was in the neighbourhood of the most probable energy losses measured in the experiment, and so extrapolation errors were minimized. The standard deviation of an individual calibration was $\pm 5\%$ and the mean of all the daily readings had a standard deviation of less than $\pm 1\%$.

Except for a short period when there was a partial failure in the recording equipment, the amplification of the proportional counter pulses varied by less than the observational uncertainties in the daily calibrations throughout the period of the experiment. The number of traversals per day was such that an additional check of the constancy of the amplification factor was possible by the examination of the distribution of energy losses of a group of particles within a well-defined momentum range over successive periods.

Because calibration was carried out throughout the experiment, systematic errors in the amplification factor are unlikely to be more than 1%; since the random errors were also reduced to less than 1%, the overall accuracy of the relationship between measured pulse height and energy lost in the counter is probably appreciably better than to 2%.

§ 5. TABULATED RESULTS

The tabulated results are based on the two different techniques of momentum determination:

(A) *Using the counter spectrograph.*

With this instrument the particles are grouped into 'momentum categories' (Hyams *et al.* 1950); the momentum spectrum in each category has been calculated from the incident spectrum and the geometry of the apparatus. To determine the 'effective momentum' the ionization distribution function (the 'ideal curve') was integrated numerically over the momentum spectrum of each category taking into account the existence of the relativistic increase of ionization. The 'effective' momentum was then assumed to be that value which would have a most probable ionization equal to the mode of the distribution obtained from this integration. The ninth group of this section of the table, corresponding to category '0' of the counter spectrograph data, contains particles of so wide a range of momenta that the 'effective' momentum of this group is probably less significant than that for other groups.

(B) *Using the cloud chamber spectrograph.*

The procedure adopted was the same as in (A) except that the directly observed incident spectrum between chosen deflection limits was used. The instrumental precision in the momentum determination will be discussed in detail elsewhere, but it may be stated that the accuracy to which deflections of the order 0·5 cm are measured is better than 0·1 cm.

Selection		No. of traversals	Effective momentum (10^9 ev/c)	Measured distribution of energy loss	
				Mode (kev)	Width at ½ height (kev)
	Category				
	>7	742	1·5	3·86 ± 0·06	3·14 ± 0·14
	7	255	2·0	3·91 ± 0·12	3·65 ± 0·23
	6	446	2·3	3·92 ± 0·08	3·17 ± 0·18
	5	559	2·8	4·02 ± 0·07	3·08 ± 0·16
A	4	745	3·7	4·05 ± 0·07	3·28 ± 0·14
	3	860	5·0	4·22 ± 0·06	3·20 ± 0·13
	2	999	6·9	4·51 ± 0·06	3·24 ± 0·12
	1	954	11·6	4·69 ± 0·06	3·63 ± 0·12
	(0)	(258)	(20)	(4·88 ± 0·12)	(3·46 ± 0·24)
	Deflection (cm)				
	2·0–1·0	262	17	4·96 ± 0·11	3·30 ± 0·23
B	1·0–0·5	157	33	4·97 ± 0·20	4·57 ± 0·33
	0·5–0·0	95	100	4·99 ± 0·23	4·12 ± 0·39

A : Counter spectrograph ; B : Cloud chamber spectrograph.

§ 6. Discussion of Results

The table shows, as does previous work, the difficulty of accumulating sufficient data at the higher momenta to follow closely the variation of ionization with momentum in this region of particular interest. It will be useful, however, to compare the results now given, and also those of Ghosh, Jones and Wilson (1954), with recent calculations by Sternheimer (1952, 1953).

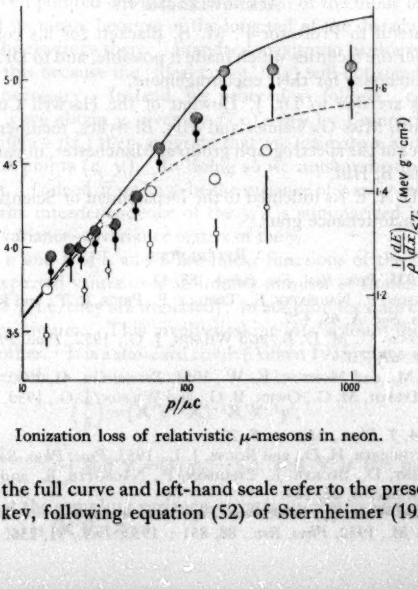

Ionization loss of relativistic μ-mesons in neon.

In the figure, the full curve and left-hand scale refer to the present experiment showing ϵ_{prob} in kev, following equation (52) of Sternheimer (1953), and using the values of constants given in tables I and II of Sternheimer (1952). The broken curve and the right-hand scale refer to oxygen at S.T.P. (Ghosh *et al.* 1954) and show $\rho^{-1}(dE/dx)_{<T_0}$ in units MEV g^{-1} cm^2, the average energy loss per gramme excluding collisions involving a transfer T_0 greater than 930 ev again following Sternheimer (1953, p. 261) and making the correction (model I) for the energy going into Cerenkov radiation. The two scales have been fitted at $p/\mu c = 10$.

Experimental results are shown as black circles (neon, present experiment) and open circles (oxygen, Ghosh *et al.*). The energy calibration of the former has been described above, for the latter the recorded number of ion pairs per centimetre have been transformed using Valentine's (1952) value for the energy required to produce each ion pair in oxygen. Although both calibrations essentially compare the ionization by very energetic particles with that of particles of low energy, there is at present no evidence to suggest that this procedure leads to an error of calibration.

In the region below the onset of polarization effects both experimental sets of points fall below the calculated curves, by about 8% for oxygen and by about 2% for neon. At the present time this discrepancy is probably not serious. For a comparison of the polarization effects in the two gases, the neon measurements raised by 2% (large shaded circles) and the oxygen measurements raised by 8% (large open circles without error limits) have been added to the figure. These show that, while both sets appear to fall off somewhat more rapidly than is predicted, the difference between them is of the kind and, as far as the precision of measurement permits any conclusion, of the magnitude which Sternheimer's calculations suggest. The difference is in part a simple density effect, the neon measurements being made at lower pressure than those in oxygen, but it is mainly an intrinsic property of the two gases.

ACKNOWLEDGMENTS

We are grateful to Professor P. M. S. Blackett for his constant interest in this work and for the facilities which made it possible, and to Dr. E. Bretscher and Mr. W. J. Whitehouse for their encouragement.

Our thanks are due to Dr. J. Howlett of the Harwell Computing Group, to Miss A. Beard, Miss G. Tanner and Mrs. B. Sykes, members of his staff, and to our colleagues of the spectrograph group at Manchester, in particular Mr. A. L. Rogers and Miss B. Hill.

One of us (D. A. E.) is indebted to the Department of Scientific and Industrial Research for a maintenance grant.

REFERENCES

AITKEN, A. C., 1935, *Proc. Roy. Soc. Edinb.*, **55,** 42.

BECKER, J., CHANSON, P., NAGEOTTE, E., TREILLE, P., PRICE, B. T., and ROTHWELL, P., 1952, *Proc. Phys. Soc.* A, **65,** 437.

GHOSH, S. K., JONES, G. M. D. B., and WILSON, J. G., 1952, *Proc. Phys. Soc.* A, **65,** 68; 1954, *Ibid.*, **67,** 331.

HAMMERSLEY, J. M., and MORTON, K. W., 1954, *Biometrika*, **41,** 296.

HYAMS, B. D., MYLROI, M. G., OWEN, B. G., and WILSON, J. G., 1950, *Proc. Phys. Soc.* A, **63,** 1053.

LANDAU, L., 1944, *J. Phys., Moscow*, **8,** 201.

PARRY, J. K., RATHGEBER, H. D., and ROUSE, J. L., 1953, *Proc. Phys. Soc.* A, **66,** 541.

PRICE, B. T., WEST, D., BECKER, J., CHANSON, P., NAGEOTTE, E., and TREILLE, P., 1953, *Proc. Phys. Soc.* A, **66,** 167.

ROTHWELL, P., and WEST, D., 1950, *Proc. Phys. Soc.* A, **63,** 541.

STERNHEIMER, R. M., 1952, *Phys. Rev.*, **88,** 851 ; 1953, *Ibid.*, **91,** 256.

Symon, K. R., 1948, quoted by Rossi, 1952, *High Energy Particles* (New York : Prentice-Hall), p. 32.
Valentine, J. M., 1952, *Proc. Roy. Soc.* A, **211**, 75.
West, D., 1953, *Proc. Phys. Soc.* A, **66**, 306.
Yeuseyev, G. P., Kosmachevsky, V. K., and Lyubimov, V. A., 1953, *C. R. Acad. Sci., U.R.S.S.*, **90**, 995.

APPENDIX

Analysis of the Histograms

By J. M. HAMMERSLEY and K. W. MORTON

For each momentum range we are given experimental values of $F(x)$, the proportion of counts with ionization loss less than x, for several fixed values x_i $(i=1, 2, \ldots n)$ of x. In addition we are given a cumulative distribution function $\Phi(x)$, the 'ideal curve', also obtained experimentally but with about ten times as many counts. It is assumed that $F(x)$ is of the same form as $\Phi(x)$ with a change of location and scale, i.e. $F(x) \equiv \Phi(\alpha+\beta x)$. We then wish to make estimates of α and β to enable us to estimate, for example, the mode of $f(x)$ given that of $\phi(x)$, where these are the frequency distributions corresponding to $F(x)$ and $\Phi(x)$ respectively. The validity of the above assumption can also be tested by evaluating

$$\chi^2 = \sum_{i=1}^{n} [f(x_i) - \phi(a+bx_i)]^2/\phi(a+bx_i).$$

The method adopted and the reasons for its adoption are set forth in more detail elsewhere (Hammersley and Morton 1954), but we shall give here a brief description followed by a computing recipe.

It has already been pointed out that an evaluation of the mode of $f(x)$ is more reliable than one of its mean, because of the long tail of the distribution and the lower accuracy of the readings there. Standard maximum likelihood techniques cannot be used for this because the 'ideal curve' $\Phi(x)$ will not stand the number of differentiations necessary. Instead, we proceed as follows: corresponding to each value x_i of x we obtain y_i given by $F(x_i)=\Phi(y_i)$. Comparison with the assumption $F(x_i)=\Phi(\alpha+\beta x_i)$ then suggests that we estimate α and β by fitting a straight line to the points (x_i, y_i). In doing so we must remember that the y_i are not independent. Indeed, if we let v_{ii} be the variance of y_i and v_{ij} the covariance of y_i and y_j, then the interdependence of the y_i's is summarized by the matrix $\mathbf{V}=(v_{ij})$, called the variance–covariance matrix of the y_i.

Our estimators a and b of α and β are linear functions of the y_i, and are so chosen that their expected values over an infinite number of similar experiments actually equal α and β (i.e. they are unbiased); in addition they are chosen so that their variance is a minimum. This involves taking into account the dependence of the y_i upon each other. It is a standard result (Aitken 1935) that such estimators are given by the formula

$$\begin{pmatrix} a \\ b \end{pmatrix} = (\mathbf{X}'\mathbf{V}^{-1}\mathbf{X})^{-1}\mathbf{X}'\mathbf{V}^{-1}\mathbf{y}', \qquad \ldots\ldots(1)$$

where $\mathbf{X}' = \begin{pmatrix} 1 & 1 \ldots 1 \\ x_1 & x_2 \ldots x_n \end{pmatrix}$ and $\mathbf{y}' = (y_1 y_2 \ldots y_n)$, and $\mathbf{V}$ is the matrix defined above; and also that the sampling variance–covariance matrix of these estimators (defined as for the y_i) is $(\mathbf{X}'\mathbf{V}^{-1}\mathbf{X})^{-1}$.

In the present case the elements v_{ij} of $\mathbf{V}$ are given by

$$v_{ij} = \operatorname{cov}(y_i, y_j) = \operatorname{cov}(F_i, F_j)/\phi_i\phi_j,$$

where $F_i = F(x_i)$ and $\phi_i = [\partial\Phi(x)/\partial x]_{x=y_i}$. Further, if N is the total number of counts for this momentum range, NF_j is the number of counts with energy loss not exceeding x_j. If p_j is the probability of such a loss, F_j is a binomial variate with mean p_j and variance $p_j(1-p_j)/N$; and when $i<j$ the covariance between F_i and F_j is given by $\operatorname{cov}(F_i, F_j) = p_i(1-p_j)/N$. Hence putting in the approximations F_i for p_i and combining with the case $i=j$ we have

$$v_{ji} = v_{ij} = F_i(1-F_j)/N\phi_i\phi_j \qquad \text{for} \qquad i \leqslant j. \qquad \ldots\ldots(2)$$

Further, by constructing the product $\mathbf{V}\mathbf{V}^{-1}$, it can be verified that the inverse matrix $\mathbf{V}^{-1}$ occurring in formula (1) is

$$\mathbf{V}^{-1} = N \begin{bmatrix} c_1 & \gamma_1 & 0 \ldots 0 & 0 & 0 \\ \gamma_1 & c_2 & \gamma_2 \ldots 0 & 0 & 0 \\ 0 & \gamma_2 & c_3 \ldots 0 & 0 & 0 \\ . & . & . \quad . & . & . \\ 0 & 0 & 0 & c_{n-1} & \gamma_{n-1} \\ 0 & 0 & 0 & \gamma_{n-1} & c_n \end{bmatrix}$$

where (with the convention $F_0 = 0$, $F_{n+1} = 1$)

$$c_i = \phi_i^2(F_{i+1} - F_{i-1})/(F_{i+1} - F_i)(F_i - F_{i-1}); \quad \gamma_i = -\phi_i\phi_{i+1}/(F_{i+1} - F_i). \ldots\ldots(3)$$

We are now in position to evaluate formula (1) in terms of the observations F_i.

After a little manipulation these results enable us to give a computing recipe as follows:

(i) From the given values x_i and F_i, compute y_i such that

$$\Phi(y_i) = F_i, \qquad \text{and} \qquad \phi_i = [\partial\Phi(x)/\partial x]_{x=y_i} \qquad \text{for} \qquad i = 1, 2 \ldots n.$$

(ii) Compute c_i $(i = 1, 2, \ldots n)$ and γ_i $(i = 1, 2, \ldots n-1)$ from (3).

(iii) Compute

$$S_{11} = \sum_{i=1}^{n} c_i + 2\sum_{i=1}^{n-1} \gamma_i; \qquad S_{1x} = \sum_{i=1}^{n} c_i x_i + \sum_{i=1}^{n-1} \gamma_i(x_i + x_{i+1})$$

$$S_{xx} = \sum_{i=1}^{n} c_i x_i^2 + 2\sum_{i=1}^{n-1} \gamma_i x_i x_{i+1}; \qquad S_{1y} = \sum_{i=1}^{n} c_i y_i + \sum_{i=1}^{n-1} \gamma_i(y_i + y_{i+1})$$

$$S_{xy} = \sum_{i=1}^{n} c_i x_i y_i + \sum_{i=1}^{n-1} \gamma_i(x_i y_{i+1} + y_i x_{i+1}); \qquad D = S_{11}S_{xx} - S_{1x}^2.$$

(iv) Then the estimates of α and β are

$$a = (S_{xx}S_{1y} - S_{1x}S_{xy})/D; \qquad b = (S_{11}S_{xy} - S_{1x}S_{1y})/D.$$

The sampling variances and covariances are

$$\operatorname{var} a = S_{xx}/ND; \qquad \operatorname{var} b = S_{11}/ND; \qquad \operatorname{cov}(a, b) = -S_{1x}/ND.$$

If the mode of $\phi(x)$ is μ, the estimate of that of $f(x)$ is $m = (\mu - a)/b$ and

$$\operatorname{var} m = [b^2 \operatorname{var} a + 2b(\mu - a)\operatorname{cov}(a, b) + (\mu - a)^2 \operatorname{var} b]/b^4.$$

Since m is the quantity we are interested in we should strictly have minimized $\operatorname{var} m$, but algebraic difficulties preclude this. As a result, m now has a small bias, but we can make a correction for this and in the present case this is nowhere greater than 0·2%.

The Detection of Mesic X-rays with Pressurized Proportional Counters using Cosmic Ray μ-Mesons stopped in Carbon

By D. WEST, R. BATCHELOR AND E. F. BRADLEY
Atomic Energy Research Establishment, Harwell, Didcot, Berks.

Communicated by W. J. Whitehouse ; MS. received 3rd March 1955

Abstract. The advantages of proportional counters over scintillation counters in the study of mesic x-rays from light elements are pointed out.

A preliminary investigation is described in which mesic x-rays from carbon are detected with proportional counters. Aluminium counters filled to a pressure of seven atmospheres of xenon were used.

§ 1. INTRODUCTION

WHEN a negatively charged μ-meson is brought to rest in matter, it is captured into a Bohr orbit round a nearby nucleus and cascades down to the lowest orbit, emitting mesic x-rays characteristic of the element in question (Wheeler 1947). Subsequently it decays or is captured into the nucleus. For a point nucleus the orbit size is μ times smaller than the corresponding size for an electron (where μ is the ratio of the mass of the meson to the mass of the electron) and the transition energies are μ times greater than in the corresponding electron case.

For elements of atomic number greater than ten an appreciable fraction of the lowest orbit lies within the nucleus and the transition energies are considerably modified. Fitch and Rainwater (1953) have been able to measure nuclear radii from the observed change of energy (factor of three reduction in the case of lead) in the 2p–1s transition.

For elements of low atomic number the nuclear size makes only a small difference to the energy of the 2p–1s transition ($-0{\cdot}5\%$ for carbon) and a correction due to vacuum polarization by the nucleus—a consequence of the Dirac theory of the electron—is equally important ($+0{\cdot}5\%$ for carbon (Foldy and Erikson 1954)). A determination of the energies of mesic x-rays from light elements is therefore capable of yielding a very accurate value for the mass of the μ-meson.

Measurements of mesic x-rays from light elements, using scintillation counters as detectors, have been carried out, in the case of μ-mesons, by Butement (1953), Stearns, De Benedetti, Stearns and Leipuner (1954) and Koslov, Fitch and Rainwater (1954). The last authors overcame the difficulties of the direct measurement of pulse size, due to the poor resolution of scintillation counters at low energies, by determining the energies with critical absorbers. They concluded that the mass of the μ-meson was between 206·89 and 208·95 electron masses.

An alternative approach is to use proportional counters as detectors. The energy resolution attainable is nearly six times better than that of a scintillation counter and opens up the possibility of a more detailed direct investigation of mesic x-ray spectra from light elements. A disadvantage of the proportional counter compared with the scintillation counter is its lower efficiency. For the present preliminary investigation, in which only cosmic ray μ-mesons were available, it was necessary to increase the efficiency of detection. This was achieved by using counters filled with xenon at a pressure of seven atmospheres.

§2. Experimental Method

The design of the experiment was largely conditioned by intensity considerations. Self-absorption and backscattering of mesic X-rays in the graphite source sets a limit to its thickness. The resulting distortion of a γ-ray spectrum was investigated using a one atmosphere xenon (+5% methane) filled counter and an artificial source of γ-rays (59·8 kev) whose energy is similar to that of mesic X-rays of carbon ($\sim$75 kev). Figure 1 shows the effects of absorption and backscattering when a block of graphite 1·5 cm in thickness is interposed between source and counter, and also when the source is placed in the centre of a graphite block 3 cm in thickness. A broad peak due to backscattered Compton radiation is very pronounced. Inset in figure 1 is the spectrum computed from this data for a block 1·4 cm in thickness as used for the main experiment. The restriction on the source thickness necessitates the use of a large area source to obtain adequate intensity. A block of graphite 20 cm × 32 cm was used with three proportional counters immediately below it. A conventional Geiger counter telescope as shown in figure 2 detected μ-mesons stopping in the graphite by means of the delayed coincidence technique. After reaching the K shell 90% of μ-mesons decay in graphite so that the decay electron can be used

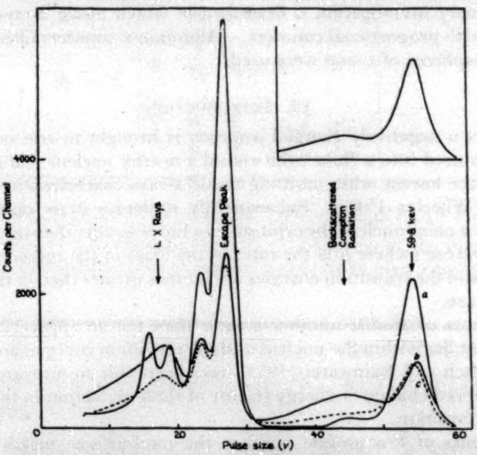

Figure 1. Effects of absorption and backscattering of graphite on the pulse height spectrum from 59·8 kev γ-rays of ^{241}Am in a proportional counter filled to 1 atmosphere pressure with xenon. *a*, no absorber, *b*, source in centre of graphite block (3·0 cm in thickness), *c*, 1·5 cm of graphite between source and counter.

Inset: Computed spectrum from a source in the centre of a graphite block 1·4 cm (2·2 g cm^{-2}) in thickness.

to identify a stopped μ-meson without an appreciable loss of efficiency. Only decay electrons emitted upwards can be used, since the remainder will pass through the proportional counters and although the decay electron is delayed with respect to the mesic x-ray it would mask the mesic x-ray pulse due to the slow collection time in the counters. The Geiger counters in A are connected in parallel. Those in B have their outputs mixed electronically since the tray is required to be sensitive to both the incident μ-meson and the decay electron.

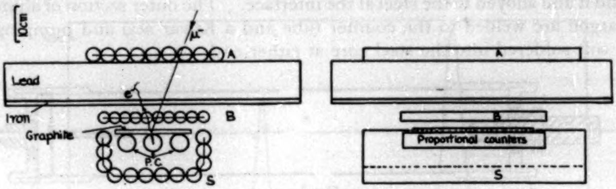

Figure 2. The counter telescope.

The circuit gives a standard size pulse when any counter is fired and these pulses are added (Hincks and Pontecorvo 1950). Consequently, a discriminator whose level is set above the height of the pulse from a single Geiger counter is only triggered when two or more counters in B have been fired and it is sensitive to a delayed pulse. The pulse at the input of the discriminator is put in coincidence with the output from the A tray. A coincidence between trays A and B (resolving time 0·5 μsec) caused by a penetrating particle, triggers a square wave of 5 μsec duration. This is differentiated and the trailing edge used to produce a sharp pulse delayed 5 μsec with respect to the passage of the particle. The threshold output B′ from the discriminator then triggers a square wave whose duration is set at 4 μsec. This square wave and the pulse from the AB coincidence (which is delayed by 5 μsec) are then fed into a gate. Consequently if the B′ (4 μsec) pulse occurs between 1 and 5 microseconds after the incident particle has triggered the telescope the AB pulse will get through the gate and give a trigger pulse 5 microseconds after the passage of the particle. It is necessary to use a minimum delay of 1 μsec otherwise delays in the Geiger counters give rise to a large background of spurious ABB'_{delayed} events. The tray S is in anticoincidence with the ABB'_{del} pulse and is used to reduce the number of background events as discussed in §4. An event $ABB'_{\text{del}} - S$ which always occurs 5 microseconds after the initiating particle has passed through the telescope then operates a triggered oscilloscope and camera (Type 1102A) for recording any pulses from the proportional counters.

The mesic x-ray is emitted at the same time as the initiating particle stops and the pulse from it, if suitably delayed, always appears at the same distance along the oscilloscope trace. The pulses from the three proportional counters were delayed artificially by 6·2, 10·7 and 16·7 microseconds respectively and the counter responsible could be identified from the position of a pulse on the time base (Becker *et al.* 1952). The counters could then be calibrated separately instead of being accurately adjusted to give the same output. In addition events in which more than one proportional counter participated could be identified and rejected.

§ 3. The Proportional Counters

The proportional counters were of conventional pattern but were made of aluminium to minimize absorption of x-rays in the walls. They were 4·4 cm in diameter, fitted with 0·005 in. diameter platinum wire and the counter walls were 1 mm in thickness. Their active length was 44 cm. The ends of the counter (figure 3) were made from short lengths of 'Al–fin' bar as suggested by Aves (1953). The bar consists of a solid steel core with aluminium moulded around it and alloyed to the steel at the interface. The outer section of aluminium was argon arc welded to the counter tube and a Kovar seal and pumping stem were soft soldered into the steel core at either end.

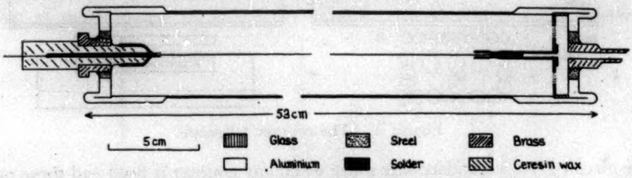

Figure 3. Aluminium pressure proportional counter.

Several problems were encountered in operating these counters at high pressures of xenon. In the first place the wire had to be chosen very carefully as it was found that the multiplication factor is very sensitive to the uniformity of the wire at high pressures. Some wires tested showed variations in multiplication factor of up to 10% along the length of the counter. This will be discussed more fully elsewhere (West, Morgan and Bradley, to be published later). A platinum wire was selected by trial and error. This wire showed variations in multiplication factor of up to 2% along its length when the counter was filled to seven atmospheres pressure. The behaviour of the counter becomes much more sensitive to impurities as the pressure is raised. Impurities which form negative ions reduce the number of ionization electrons available for initiating avalanches and the resolution of the counter is worsened. An effective way of purifying the gas (especially mixtures containing methane) was evolved. A glass flask 10 litres in capacity fitted with a condensing tube was coated on the inside with a mirror of sodium. This was produced by repeatedly melting sodium metal in the condensing stem and pumping the flask. A few days storage in this flask cleaned out any oxygen or water vapour. It is usual to add 5% of methane to counter fillings at one atmosphere pressure. At higher pressures a much smaller percentage was needed and the best conditions were obtained with the same absolute pressure ($\sim$4 cm Hg) as for one atmosphere fillings.

The counters operated at 8000 volts when filled to a pressure of seven atmospheres. Differentiation and integration time constants of five microseconds were used in the amplifier. Electrical breakdown was invariably encountered outside rather than inside the counters and was eliminated by moulding ceresin wax on to the Kovar end of the counter and around all soldered connections. The pulse size distribution in one of the counters from 59·8 kev γ-rays of ^{241}Am is shown in figure 4. The energy resolution, 4·3% half width at half maximum, is only slightly worse than that obtained at one atmosphere

(3·2%). After the counters had been filled for one month the resolution was found to have deteriorated to between 5% and 6%, presumably due to outgassing from the walls. The filling gas was therefore returned to the purifier flask for a few days at monthly intervals. On refilling, the original resolution was obtained. The overall efficiency of the counter was measured directly at 59·8 kev using a ^{241}Am source of known strength immediately outside the counter. The efficiency was found to be 16·5% which corresponds to 10·4% efficiency at 75 kev—the expected energy of μ-mesic x-rays of carbon.

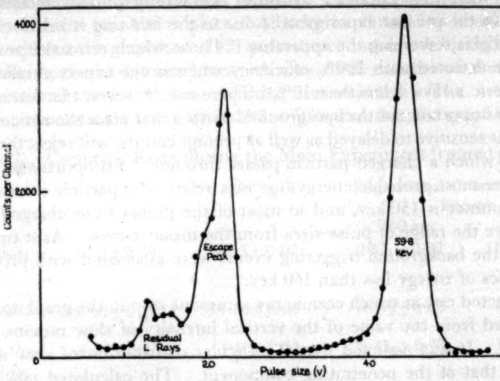

Figure 4. Pulse size distribution from γ-rays of ^{241}Am in one of the proportional counters filled to 7 atmospheres pressure with xenon.

§ 4. CHARACTERISTICS OF THE COUNTER TELESCOPE

The behaviour of the counter telescope was tested under various conditions prior to the main experiment. It was appreciated that the apparatus would respond to mesons stopping in any material below the B tray and so the telescope was erected on an open steel frame with a clear space of 1·6 m between the counters and the floor of the laboratory. The delayed coincidence and other counting rates are given in table 1. A disturbing feature is the high rate of delayed coincidences in the absence of the graphite, which greatly exceeds the casual rates It arises from μ-mesons stopping in the counter walls and boxes and from delay.

Table 1. Delayed Coincidence and other Counting Rates

	A	B	B′	S	AB	ABS	AB–S
Counts per minute	2750	1529	82	4013	480	370	120

(1)	(2)	(3)	(4)	(5)	(6)	(7)
ABB′$_{del}$ (ct/hr)	6·8±0·15	8·95±0·27	9·03±0·12	13·5±0·09	1·72	4·47±0·15
ABB′$_{del}$–S (ct/hr)		3·80±0·18	4·16±0·08	8·35±0·07	0·43	4·19±0·11

(1) Conditions; (2) nothing below B tray; (3) with anticoincidence tray only; (4) with anticoincidence tray and proportional counters; (5) with graphite, anticoincidence tray and proportional counters; (6) casuals; (7) difference due to graphite.

in the Geiger counters or associated circuits when two Geigers are fired simultaneously. The background rate is considerably reduced by the anticoincidence tray. The residual rate is due to μ-mesons stopping in the anticoincidence tray itself and to the inefficiency of the tray. Further reduction of the background rate could be achieved by using special thin walled Geiger counters and by increasing the efficiency of the tray. Even so it was estimated that a background of $\mathrm{ABB'_{del}}$–S events of about 3 counts per hour would remain and this improvement was not considered worth while. The background is comparable with that obtained by other workers with this technique. Its importance in the present experiment is due to the fact that it is associated with charged particles traversing the apparatus. Those which cross the proportional counters are detected with 100% efficiency whereas the expected efficiency for detecting mesic x-rays is less than 10%. There are, however, two features which diminish the importance of the background. In the first place the anticoincidence tray, which is sensitive to delayed as well as prompt counts, will reject the majority of events in which a charged particle passes through the proportional counters. Secondly, the most probable energy loss of a relativistic particle in crossing the gas of the counter is 150 kev, and so most of the pulses from charged particles will fall above the range of pulse sizes from the mesic x-rays. As it turned out, only 9% of the background triggering events were associated with proportional counter pulses of energy less than 160 kev.

The expected rate at which cosmic ray μ-mesons stop in the graphite (1·44 kg) was calculated from the value of the vertical intensity of slow mesons given by Rossi (1948). It was assumed that the angular distribution of slow mesons is the same as that of the penetrating component. The calculated rate at which mesons stop in the graphite after triggering the telescope is 20·2 per hour. An elementary calculation shows that a fraction equal to 0·19 is then detected by means of their decay electrons. The expected rate of delayed coincidences is therefore $0{\cdot}19 \times 20{\cdot}2 = 3{\cdot}8$ counts per hour, which agrees with the observed value of $4{\cdot}19 \pm 0{\cdot}11$ counts per hour.

§ 5. RESULTS

The pulses from the three proportional counters were fed into separate head amplifiers and were delayed and mixed before the main amplifier stage. The positions on the oscilloscope trace at which pulses from each counter occurred were determined by triggering the recording apparatus on particles which passed through the proportional counters. It was found that the pulses from any one counter appeared over a region corresponding to three microseconds on the trace. This is due to the long collection time of electrons in the counters at 7 atmospheres pressure. The separations between the pulses from the three counters were 4·5 and 6·0 microseconds so that no confusion between pulses from different counters should arise. The counters were calibrated with 59·8 kev γ-rays from ^{241}Am. Calibrations were carried out by allowing many pulses to record on the same frame of film (using a diminished brilliancy setting and lens aperture). The position of the calibration line could be clearly identified and measured. The three counters were operated at the same high tension (8000 volts) and separate gain controls in the mixing circuit were adjusted to give nearly equal outputs from each channel. Throughout the runs each counter was calibrated at intervals of about 40 hours. The position of the calibration line remained constant to within a few per cent. The oscilloscope and camera were triggered on each ABB'_{del}–S event. The individual counting rates of the trays and the AB, ABS, and AB–S rates were monitored daily and the number of ABB'_{del} and ABB'_{del}–S events were recorded. During the course of the measurements the gas filling in the counters was removed, purified and returned to the counters on three occasions at monthly intervals. The pulse heights were measured from the film using a microfilm reader. Pulses corresponding to an energy greater than 160 kev gave deflections beyond the limits of the oscilloscope screen and only the number of such pulses was recorded. The apparatus ran for a total of 1794 hours with the graphite in place. A background run, 368 hours in duration, was taken without the graphite. 1481 pulses were measured during the main run and 137 during the background run. A very small number of events in which two proportional counter pulses recorded was rejected. The mean counting rates in the two runs are given in table 2. It is seen that the graphite only gives rise to proportional counter pulses in the energy region below 160 kev. Above this energy the pulses are all due to background. The histogram of the energies of the proportional counter pulses is shown in figure 5 where the approximate background distribution is shown dotted. A well defined peak is seen at an

Table 2. Counting Rates during the Main Experiment (counts per hour)

	ABB'_{del}	ABB'_{del}–S	Proportional Counter Pulses of Energy <160 kev	Proportional Counter Pulses of Energy >160 kev
With graphite	13·5 ± 0·09	8·35 ± 0·07	$0{\cdot}82_5 \pm 0{\cdot}02$	0·92 ± 0·02
Without graphite	†9·03 ± 0·12	†4·16 ± 0·08	$0{\cdot}37_3 \pm 0{\cdot}03$	0·93 ± 0·05
Difference due to graphite	4·47 ± 0·15	4·19 ± 0·11	$0{\cdot}45_2 \pm 0{\cdot}03_6$	−0·01 ± 0·05

† Additional runs in which the proportional counter pulses were not recorded were also used in obtaining these values.

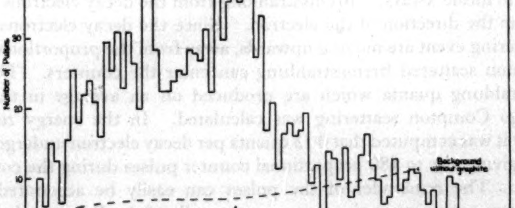

Figure 5. Energy histogram of proportional counter pulses. Total number of pulses 1481. Time 1794 hours.

energy close to 75 kev together with indications of an escape peak near $75-29{\cdot}6=45{\cdot}4$ kev. The energy of the 2p–1s transition in carbon is calculated to be 75·3 kev for a μ-meson mass of 207 m_e (Foldy and Erikson 1954).

The efficiency of the three proportional counters for detecting mesic x-rays from the graphite was computed from the measurements using ^{241}Am γ-rays already mentioned. The mean transmission of the graphite is 0·73 at 59·8 kev averaged over the three counters, which corresponds to a transmission of 0·76 at 75 kev. From the ratio of the photoelectric absorption coefficients of xenon at the two energies, one obtains an overall efficiency of $16{\cdot}5\times0{\cdot}76\times0{\cdot}63=7{\cdot}9\%$ at 75 kev. Of the number of stopped mesons of both signs which triggered the recording apparatus (7520 ± 200) it is calculated that 3410 ± 90 were negative mesons. From this one can calculate the expected number of mesic x-ray pulses, assuming there is one radiative 2p–1s transition for each stopped meson. Table 3 shows the numbers of pulses expected from mesic x-rays and background events. There is a residue of 373 ± 68 pulses which is not accounted for. A very inaccurate spectrum of these pulses was obtained by subtracting the expected distribution from mesic x-rays together with the known background without graphite from the histogram in figure 5. The residual pulses lay on a continuous distribution which rapidly went to zero above 90 kev.

Table 3. Analysis of the Number of Proportional Counter Pulses of energy <160 kev

Origin	No. of Pulses
Mesic x-rays (photo peaks)	269 ± 10
Mesic x-rays (backscattered Compton radiation)	148 ± 10
Background measured in absence of graphite	670 ± 54
Casuals due to background pulses in the proportional counters	21 ± 5
Total	1108
Number of pulses observed	1481
Excess	373 ± 68

The most likely source of these extra pulses is bremsstrahlung from the decay electrons and positrons. Owing to the slow collection of electrons in the counters, delayed pulses from bremsstrahlung cannot be distinguished from the prompt pulses due to mesic x-rays. Bremsstrahlung from the decay electrons is strongly collimated in the direction of the electron. Since the decay electrons associated with a triggering event are moving upwards, away from the proportional counters, only Compton scattered bremsstrahlung can enter the counters. The number of bremsstrahlung quanta which are produced on an average in the graphite and undergo Compton scattering was calculated. In the energy region from 5 to 100 kev it was computed that 0·13 quanta per decay electron undergo Compton scattering, giving rise to 180 proportional counter pulses during the course of the experiment. The remainder of the pulses can easily be accounted for by a similar process occurring in the glass counter walls of the B tray and the counter box. The total weight of the counters and the box is 3 kg to be compared with that of the graphite (1·44 kg). The contribution from the lead and iron between the trays A and B is negligible due to the high self-absorption of the radiation in these materials.

§6. CONCLUSIONS

It has been demonstrated that mesic x-rays from light elements can be detected with proportional counters.

The advantage of the proportional counter over the scintillation counter, as far as resolution is concerned, is to some extent counterbalanced in the present investigation by background events. The number of slow μ-mesons available in cosmic rays is approximately 10^{-4} of the flux of penetrating particles, and imperfections in the selection of events by Geiger counters constitutes a major background. An increased efficiency for detecting mesic x-rays is consequently required and can only be obtained at present with proportional counters by increasing the pressure. The collection time of electrons and hence the variation of time lags between an event and the appearance of a proportional counter pulse is also increased. Discrimination between prompt and delayed events is thereby lost and bremsstrahlung from the decay electrons constitutes an additional background. Both these sources of background will largely disappear if strong artificial sources of μ-mesons are used with lower pressure counters.

This investigation has also shown the desirability of using sources less than 2 g cm^{-2} thick to avoid an excessive amount of Compton scattered radiation.

ACKNOWLEDGMENTS

We wish to thank Dr. E. Bretscher and Mr. W. J. Whitehouse for their interest and advice during this experiment.

REFERENCES

AVES, R., 1953, *J. Sci. Instrum.*, **30**, 388.

BECKER, J., CHANSON, P., NAGEOTTE, E., TREILLE, P., PRICE, B. T., and ROTHWELL, P., 1952, *Proc. Phys. Soc.* A, **65**, 437.

BUTEMENT, F. D. S., 1953, *Phil. Mag.*, **44**, 208.

FITCH, V. L., and RAINWATER, J., 1953, *Phys. Rev.*, **92**, 789.

FOLDY, L. L., and ERIKSON, E., 1954, *Phys. Rev.*, **95**, 1048.

HINCKS, E. P., and PONTECORVO, B., 1950, *Phys. Rev.*, **77**, 102.

KOSLOV, S., FITCH, V., and RAINWATER, J., 1954, *Phys. Rev.*, **95**, 291.

ROSSI, B., 1948, *Rev. Mod. Phys.*, **20**, 537.

STEARNS, M. B., DE BENEDETTI, S., STEARNS, M., and LEIPUNER, L., 1954, *Phys. Rev.*, **93**, 1123.

WHEELER, J. A., 1947, *Phys. Rev.*, **71**, 462.

Properties of the Hydrogen Molecular Ion
VI: The Total Electronic Orbital Angular Momentum of the $1s\sigma_g$, $2s\sigma_g$ and $3s\sigma_g$ States

By R. W. McCARROLL and M. R. C. McDOWELL
Department of Applied Mathematics, The Queen's University of Belfast

Communicated by D. R. Bates; *MS. received* 25th *March* 1955

Abstract. The total electronic orbital angular momenta in the $1s\sigma_g$, $2s\sigma_g$ and $3s\sigma_g$ states of H_2^+ are calculated using the exact two-centre wave functions. For the lowest of these states, calculations are also carried out using apparently quite accurate approximate wave functions but the results obtained are seriously in error.

§ 1. INTRODUCTION

THE expectation value of the square of the total electronic angular momentum of a molecule (with nuclei held fixed) is of interest in that the variation with increasing internuclear distance is of assistance in visualizing the growing change in the character of the wave function: and, moreover, as its magnitude depends mainly on the angular distribution, calculations using exact and approximate wave functions provide a test of the accuracy of these latter different from those usually employed.

Exact two-centre wave functions are now available for a number of states of H_2^+ (Bates, Ledsham and Stewart 1953), as are also various approximate wave functions (Dalgarno and Poots 1954). The former are used to evaluate the expectation value of the square of the total electronic orbital angular momentum at various internuclear distances ($0 \leqslant R \leqslant 4$ atomic units) for the $1s\sigma_g$, $2s\sigma_g$ and $3s\sigma_g$ states; the latter are used for the $1s\sigma_g$ state only.

Throughout the paper all quantities are in atomic units.

§ 2. EXACT CALCULATIONS

Using the customary prolate spheroidal coordinates (λ, μ, ϕ), the exact two-centre wave functions for the σ states of H_2^+ may be expressed as

$$\Psi(r \mid R) = \Lambda(\lambda \mid R) M(\mu \mid R) \qquad \ldots\ldots(1)$$

where R, on which the wave functions depend parametrically, is the internuclear distance. The equations satisfied by M and Λ are

$$\frac{d}{d\mu}\left\{(1-\mu^2)\frac{dM}{d\mu}\right\} + \{-A + p^2\mu^2\}M = 0 \qquad \ldots\ldots(2)$$

and

$$\frac{d}{d\lambda}\left\{(\lambda^2-1)\frac{d\Lambda}{d\lambda}\right\} + \{A + 2R\lambda - p^2\lambda^2\}\Lambda = 0 \qquad \ldots\ldots(3)$$

in which A and p^2 are certain quantities tabulated by Bates, Ledsham and Stewart (1953). The solutions to these equations may be written in the form

$$M(\mu)=\sum_{s=0}^{\infty} f_{2s}P_{2s}(\mu) \qquad \ldots\ldots(4)$$

and

$$\Lambda(\lambda)=(\lambda+1)^{\sigma}\exp(-p\lambda)\sum_{n=0}^{\infty} g_n\left(\frac{\lambda-1}{\lambda+1}\right)^{n} \qquad \ldots\ldots(5)$$

σ, g_n and f_{2s} also being tabulated quantities and P_{2s} being the Legendre polynomial indicated.

For a given internuclear distance the expectation value of the square of the total electronic angular momentum about the mid-point of the line joining the nuclei is

$$\mathscr{M}^2=\int \Psi^*\mathfrak{M}^2\Psi\, d\tau \qquad \ldots\ldots(6)$$

the wave function being normalized as usual and $\mathfrak{M}^2$ being the relevant quantum mechanical operator, given by

$$\begin{aligned}\mathfrak{M}^2=-\Bigg[&\frac{(\lambda^2-1)(1-\mu^2)}{\lambda^2\mu^2}\left\{\mu^2\frac{\partial^2}{\partial\lambda^2}+\lambda^2\frac{\partial^2}{\partial\mu^2}-2\mu\lambda\frac{\partial^2}{\partial\lambda\partial\mu}-\mu\frac{\partial}{\partial\mu}-\lambda\frac{\partial}{\partial\lambda}\right\}\\ &+\frac{2\lambda\mu}{(\lambda^2-\mu^2)^3}\{\lambda^4+\mu^4-2\lambda^2-2\mu^2+2\}\left\{\mu\frac{\partial}{\partial\lambda}-\lambda\frac{\partial}{\partial\mu}\right\}\\ &+\frac{\lambda^2+\mu^2-1}{(\lambda^2-1)(1-\mu^2)}\frac{\partial^2}{\partial\phi^2}\Bigg]. \qquad \ldots\ldots(7)\end{aligned}$$

Making use of equations (2) and (3) and omitting the term involving differentiation with respect to the azimuthal angle ϕ, as it yields no contribution in the case of σ states, (7) becomes

$$\begin{aligned}\mathfrak{M}^2=-\Bigg\{&\frac{(1-\lambda^2)(1-\mu^2)}{(\lambda^2-\mu^2)^2}2\lambda\mu\frac{\partial^2}{\partial\lambda\partial\mu}\\ &+\frac{[3\lambda^5\mu^2-\lambda^5+\lambda^3-6\lambda^3\mu^2+\lambda^3\mu^4-\lambda\mu^4+3\lambda\mu^2]}{(\lambda^2-\mu^2)^3}\frac{\partial}{\partial\lambda}\\ &-\frac{[3\mu^5\lambda^2-\mu^5+\mu^3-6\mu^3\lambda^2+\mu^3\lambda^4-\mu\lambda^4+3\mu\lambda^2]}{(\lambda^2-\mu^2)^3}\frac{\partial}{\partial\mu}\\ &+\frac{\mu^2(1-\mu^2)}{(\lambda^2-\mu^2)^2}[p^2\lambda^2-2R\lambda-A]+\frac{\lambda^2(\lambda^2-1)}{(\lambda^2-\mu^2)^2}[A-p^2\mu^2]\Bigg\}. \qquad (8)\end{aligned}$$

The integrations over ϕ and μ in (6) may be carried out analytically. The resulting expression in λ must be integrated numerically; it is cumbersome and will not be presented in full. Briefly if we write

$$\mathscr{M}^2=\frac{\pi R^3}{4}\int_1^{\infty} F(\lambda)\,d\lambda \qquad \ldots\ldots(9)$$

then $F(\lambda)$ is of the form

$$\begin{aligned}F(\lambda)=\Lambda^2(\lambda)&\left\{AG_1(\lambda)-p^2G_2(\lambda)+G_3(\lambda)+[2\lambda(A-\lambda^2p^2)G_5(\lambda)-\lambda G_6(\lambda)]\ln\frac{\lambda+1}{\lambda-1}\right\}\\ &+2R\Lambda^2(\lambda)\left\{G_4(\lambda)-\lambda G_5(\lambda)\ln\frac{\lambda+1}{\lambda-1}\right\}\\ &+\Lambda(\lambda)\frac{d\Lambda(\lambda)}{d\lambda}\left\{G_7(\lambda)-\frac{1}{\lambda}G_8(\lambda)\ln\frac{\lambda+1}{\lambda-1}\right\} \qquad \ldots\ldots(10)\end{aligned}$$

where the G's are polynomials in even powers of λ, the degree of which depends on the number of terms included in the expansion of $M(\mu)$, e.g. if only two terms are included, G_2 and G_8 are of the eighth degree in λ and the other polynomials of the sixth degree, while if three terms are included the corresponding degrees are the twelfth and the tenth.

By expanding in inverse powers of λ, considerable simplification may be effected, giving

$$F(\lambda)=\lambda g(\lambda)\frac{d\Lambda(\lambda)}{d\lambda}\Lambda(\lambda)+h(\lambda)\Lambda^2(\lambda) \qquad \ldots\ldots(11)$$

where $g(\lambda)$ and $h(\lambda)$ have leading terms in λ^{-2} and λ^2 respectively. For λ greater than 3 approximately this series is much easier to evaluate than is expression (10), in which there is great cancellation.

§ 3. APPROXIMATE CALCULATIONS

We represent the wave functions by approximations II and IV of Dalgarno and Poots; that is, the separated atoms approximation

$$\Psi_s=N_s\{\exp(-\beta r_a)+\exp(-\beta r_b)\} \qquad \ldots\ldots(12)$$

and the united atom approximation

$$\Psi_u=N_u\exp\{-\alpha(r_a+r_b)\} \qquad \ldots\ldots(13)$$

in which $\mathbf{r}_a$ and $\mathbf{r}_b$ are the position vectors of the electron relative to the nuclei A and B, α and β are variable parameters chosen to minimize the electronic energy and

$$N_s^2=\frac{2\pi}{\beta^3}[1+(1+t+\tfrac{1}{3}t^2)\,e^{-t}] \qquad \ldots\ldots(14)$$

$$N_u^2=\frac{\pi}{24\alpha^3}(3+3p+p^2)\,e^{-p} \qquad \ldots\ldots(15)$$

$$t=\beta R \qquad p=2\alpha R. \qquad \ldots\ldots(16)$$

The distinguishing subscripts, s and u, affixed to the symbols Ψ and N will also be affixed to other symbols where necessary.

These approximations were adopted because of their simplicity and apparent accuracy. When R is 1, 2 and 4 the energies associated with Ψ_s are within 1%, 1·5% and 1% of the true energies; and those associated with Ψ_u are within 0·5%, 2% and 10% of the true energies.

Substituting (12) and (13) in (6) we obtain

$$\mathscr{M}_s^2=\frac{\pi R^2}{3\beta}\,\frac{(1+t)\,e^{-t}-1}{N_s^2} \qquad \ldots\ldots(17)$$

$$\mathscr{M}_u^2=\tfrac{1}{2}\alpha^2R^2-\frac{K_{49}(p)+\alpha K_{48}(p)}{N_u^2} \qquad \ldots\ldots(18)$$

$$\left.\begin{aligned} K_{48}(p)&=\int\cos^2\theta_a\exp[-2\alpha(r_a+r_b)]\,d\tau\\ K_{49}(p)&=\int\frac{1}{r_a}\cos^2\theta_a\exp[-2\alpha(r_a+r_b)]\,d\tau.\end{aligned}\right\} \qquad \ldots\ldots(19)$$

Expressions for K_{48} and K_{49} have been provided by Coulson (1941). The second of these is, however, given incorrectly.† It should read

$$\begin{aligned} K_{49}(\delta, R) = \frac{\pi R^2}{q^5}\,[& -4(15-15q+6q^2-q^3)\,e^{q}\,\mathrm{Ei}^*(2q) \\ & -4(15+15q+6q^2+q^3)\,e^{-q}(\gamma+\log 2q) \\ & +q(120+60q+15q^2+q^3)\,e^{-q}] \qquad \ldots\ldots(20) \end{aligned}$$

where γ is Euler's constant, $q=\delta R$ and

$$\mathrm{Ei}^*(x) = -\mathrm{Ei}(-x) = \int_x^\infty \frac{e^{-y}}{y}\,dy.$$

Approximation VII of Dalgarno and Poots

$$\Psi_{u,s} = \exp\{-\alpha(r_a+r_b)\} + d\{\exp(-\beta r_a)+\exp(-\beta r_b)\} \quad \ldots\ldots(21)$$

d being an additional variable parameter, is superior to approximations II and IV but its use was not thought to be justified since it leads to integrals which are linear combinations of the J(k, l, m)'s of Barnett and Coulson (1951) and are of great complexity.

§ 4. RESULTS AND DISCUSSION

Using the formulae based on the exact wave functions, $\mathscr{M}^2$ has been calculated as a function of R for the lowest three $ns\sigma_g$ states. The results are presented in figure 1. In the case of the $1s\sigma_g$ state computations were also carried out using the formulae based on the separated and united atom approximations. In figure 2 the values of $\mathscr{M}_s{}^2$ and $\mathscr{M}_u{}^2$ are compared with the true values.

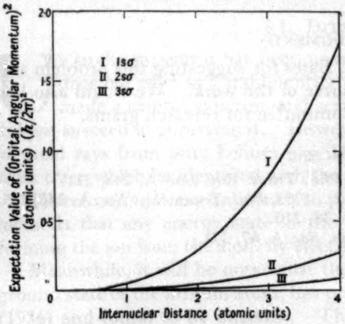

Figure 1. Electronic orbital angular momentum of the lowest three $ns\sigma_g$ states of $H_2{}^+$ using exact two-centre wave functions.

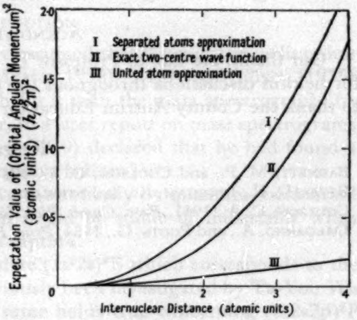

Figure 2. Electronic orbital angular momentum of the $1s\sigma_g$ state of $H_2{}^+$.

For a given state the square of the total electronic angular momentum is a rapidly increasing function of the internuclear distance; and for a given internuclear distance it is a rapidly decreasing function of the principal quantum number, as would be expected. The behaviour in the three cases is very similar; indeed over the range investigated all three $(\mathscr{M}^2, R)$ curves may be fitted closely to a single arbitrary function of the ratio f_2/f_0, where f_0 and f_2 are the first two coefficients in the Legendre polynomial expansion.

---

† Professor Coulson agrees that the original result is in error.

The small absolute value of $\mathcal{M}^2$ is due to the contribution from each element of space being small, rather than due to cancellation between the contributions from the different elements of space. Within the range of interest in molecular problems it is apparent that the azimuthal quantum number of the united atom is quite a good quantum number at least for the $2s\sigma_g$ and $3s\sigma_g$ states.

In view of their success in other applications (cf. Dalgarno and Poots 1954) the extent of the failure of the approximate wave functions as exhibited in figure 2 might at first seem rather surprising. This failure is a manifestation of the fact that Ψ_g and Ψ_u do not represent the angular distribution properly. Clearly $\mathcal{M}^2$ may be regarded as a measure of the departure from spherical symmetry. Another measure of this is given by

$$\epsilon = (\overline{Z^2} - \overline{X^2})/\overline{X^2} \qquad \ldots\ldots(22)$$

where

$$\overline{X^2} = \int \Psi^* x^2 \Psi \, d\tau, \qquad \overline{Z^2} = \int \Psi^* z^2 \Psi \, d\tau \qquad \ldots\ldots(23)$$

the z axis being taken along and the x axis perpendicular to the line joining the nuclei. From the tables of $\overline{Z^2}$ and $\overline{X^2}$ given by Dalgarno and Poots it is found, for example, that when R is 3 then ϵ is actually 1·54 but is 2·03 on the separated atoms approximation and is 0·43 on the united atom approximation. Since the corresponding values of $\mathcal{M}^2$ are 0·82, 1·17 and 0·14 respectively the fractional errors are comparable and in the same sense. It may be noted incidentally that approximation VII of Dalgarno and Poots (equation (21) of this paper) gives ϵ correct to within 1% so that this wave function must therefore be very accurate even as regards the angular distribution.

ACKNOWLEDGMENTS

Our thanks are due to Professor D. R. Bates for suggesting this problem and for helpful discussions throughout the course of the work. We would also like to thank the County Antrim Education Committee for research grants.

REFERENCES

BARNETT, M. P., and COULSON, C. A., 1951, *Phil. Trans. Roy. Soc.* A, **243,** 221.
BATES, D. R., LEDSHAM, K., and STEWART, A. L., 1953, *Phil. Trans. Roy. Soc.* A, **246,** 215.
COULSON, C. A., 1941, *Proc. Camb. Phil. Soc.*, **38,** 210.
DALGARNO, A., and POOTS, G., 1954, *Proc. Phys. Soc.* A, **67,** 343.

On a Metastable Energy State of the Negative Helium Ion

By E. HOLØIEN and J. MIDTDAL
University of Oslo, Oslo, Norway

MS. received 21*st March* 1955

Abstract. By applying the selection rules of auto-ionization to the (1s2s2p)^{4}P state of the negative helium ion, it is shown that only the $^4P_{5/2}$ energy level is not liable to auto-ionization. Provided the lowest triplet state of the atom has positive electron affinity, this ionic state is metastable in the same sense as the triplet state.

A thorough energy calculation of the quartet state of the ion has been carried through, and a positive electron affinity of at least 0·075 ev is found, enough to explain the experimental observation of it in the mass spectrograph as reported by Hiby. The unexplained line 310 061 cm^{-1} (322·5 Å) observed in the vacuum ultra-violet by Kruger may then probably correspond to the transition (2s2p^2) ^{4}P–(1s2s2p) ^{4}P in He$^-$, yielding an error of only 0·083 ev in the energy calculations.

§ 1. Introduction

Up to the present it has been usually assumed that the negative helium ion does not exist as a stable entity (Massey 1938). Although Tüxen (1936) made a careful experimental search for it with the mass spectrograph, he did not succeed in observing it. However, in a later report on mass spectrograms of canal rays from pure helium gas, Hiby (1939) declared that he had found a weak trace which he identified with the negative helium ion.

Therefore, it is very important to prove theoretically by quantum-mechanical methods that any energy state of the ion might be stable or metastable when forming the ion from the atom by electron capture.

Meanwhile, it will be noted that the state (1s^{2}2s)^{2}S which corresponds to the ground state of the lithium atom, has previously been investigated by Ta-You Wu (1936) and found to be unstable. The same holds true concerning (1s2s2p)^{2}P (Holøien 1951). Furthermore, the excited states (1s2s^2)^{2}S and (2s2p^2)^{4}P are both subject to auto-ionization, that is, spontaneous dissociation into a neutral helium atom and a free electron with positive energy in the continuum.

In the present paper we have focused our attention on the lowest quartet state (1s2s2p)$^4P_{5/2}$ because this is the only one which does not undergo auto-ionization.

§ 2. The State (1s2s2p)$^4P_{5/2}$ is Metastable

First of all, we note the selection rules of auto-ionization as follows (Condon and Shortley 1935):

If the matrix components of the Hamiltonian connecting a discrete level above the ionization energy with the states of the continuum at the same energy are not to vanish, these states must be of the same parity and the same J-value (the most important conditions), and, furthermore, in the case of Russell–Saunders coupling (LS coupling) they must have the same L and S values.

When applying these rules on the three levels $^4P_{1/2}$, $^4P_{3/2}$ and $^4P_{5/2}$ of the (1s2s2p)-configuration, it must be remembered that the auto-ionization arises by interaction with the ($1s^2kp$) states of the continuum only. Doing this, we see that no states of the continuum can be found which interact with the quartet state mentioned above if the selection rules in full are taken into account. Through partial breakdown of the LS coupling, however, $^4P_{1/2}$ and $^4P_{3/2}$ become respectively mixed with $^2P_{1/2}$ and $^2P_{3/2}$ of the same configuration, and hence they can show auto-ionization because the term ^2P itself is unstable (Holøien 1951). On the other hand, as the level $^4P_{5/2}$ is the only one with $J=5/2$ in the configuration concerned, it is not liable to breakdown of the LS coupling and in this way escapes auto-ionization.

Now we can explain the observation of the negative helium ion in an electrical discharge of helium atoms as reported by Hiby (1939) in the following way. We know that by a relatively small electrical discharge the helium atom becomes excited into the lowest triplet state $(1s2s)^3S$ and remains in this metastable state for a while (lifetime about 10^{-3} sec).

If now the total binding energy calculated for the negative ion in the $^4P_{5/2}$ state is lower than the actual (experimental) energy of the lowest triplet state of the neutral atom, one extra electron can be attached in a 2p orbital of the atom, all three electrons with their spins orientated parallel with the orbital angular momentum ($J=5/2$). Hence, it is evident that the negative ion can be formed, and it remains in this state (metastable) till collisions of the second kind, i.e. collisions with neighbouring particles or with the tube, cause the ion to give up its exciting energy without radiation.

§ 3. Procedure and Wave Functions

It is well known that the total energy of an electron system in the lowest state of a given multiplicity is defined by the absolute minimum of the variation integral concerned, and it should be kept in mind that by using approximate wave functions only an upper limit to the true total energy can be obtained.

The variation integral may be written

$$E=\frac{4\int \phi^* H\phi \, d\tau \, d\tau_s}{\int \phi^* \phi \, d\tau d\tau_s} \qquad \ldots\ldots(1)$$

where H is the Hamiltonian operator of the system moving in a Coulomb field, ϕ is the total spin-orbital wave function, and $d\tau_s$ is the volume element in the spin-space. Expressing the energy in rydberg units (1 Ryd $=\frac{1}{2}$ atomic unit) and the distance in units of $a_0/2$ the Hamiltonian is

$$H=-\sum_{i=1}^{3}\left\{\nabla_i^2+\frac{Z}{r_i}\right\}+\sum_{i>j}^{3}\frac{1}{r_{ij}}; \quad Z=2. \qquad \ldots\ldots(2)$$

As can be seen, we have neglected both the relativistic effects and the effect of spin–orbit interaction. Furthermore, assuming infinite mass of the nucleus, we can fix it in the space.

It is generally known that the total spin–orbital wave function must be antisymmetric for interchange of the electronic coordinates (Pauli principle).

$$\phi=\phi(\overparen{123})=\psi(\overparen{123})\,S(\overline{123}) \qquad \ldots\ldots(3)$$

bars $\frown$ and $—$ symbolizing antisymmetry and symmetry respectively.

In a quartet state the spin part $S(\overline{123})$ is symmetric for interchange of the electronic spin coordinates, and, hence the spatial part $\psi(\overparen{123})$ must be antisymmetric for interchange of the electronic space coordinates.

Introducing (3) into (1) and carrying out the spin integration we get, since the Hamiltonian is independent of the spin coordinates:

$$E=\frac{4\int\psi^*H\psi\,d\tau}{\int\psi^*\psi\,d\tau} \qquad \ldots\ldots(4)$$

or by substituting $\psi=\psi(\overparen{123})=\Sigma_P(-1)^P\,P\Psi(123)$ where $\Sigma_P(-1)^P\,P$ is an antisymmetrizing operator (here six permutations)

$$E=\frac{4\int\psi^*H\Psi\,d\tau}{\int\psi^*\Psi\,d\tau}. \qquad \ldots\ldots(5)$$

Furthermore, when introducing a scale constant k, we can write

$$\left.\begin{aligned}\Psi(123)&=g(kr_1,kr_2,kr_3,kr_{12},kr_{13},kr_{23})\\ \psi(123)&=\sum_P(-1)^P\,Pg=h(kr_1,kr_2,kr_3,kr_{12},kr_{13},kr_{23})\\ E&=\frac{k^2M+kV}{N}\end{aligned}\right\} \qquad \ldots\ldots(6)$$

where

$$M=-4\sum_{i=1}^{3}\int h\nabla_i^2g\,d\tau=4\sum_{i=1}^{3}\int \operatorname{grad}_i h\,\operatorname{grad}_i g\,d\tau$$

and

$$V=-4\int\left\{\sum_{i=1}^{3}\frac{Z}{r_i}-\sum_{i>j}^{3}\frac{1}{r_{ij}}\right\}hg\,d\tau.$$

We now look for an approximate wave function of the generalized form

$$g_p(123)=(1/4\pi^2)\,F_p(123)\,Y_{l|\nu|}(\theta_3,\phi_3)$$

where $Y_{l|\nu|}(\theta,\phi)$ are the normalized form of the spherical harmonics:

$$Y_{l|\nu|}(\theta,\phi)=\left[\frac{(2l+1)(l-|\nu|)!}{4\pi(l+|\nu|)!}\right]^{1/2}P_l^\nu(\cos\theta)\exp(i\nu\phi), \qquad \ldots\ldots(7)$$

and

$$F_p(123)=\sum_p c_pf_p(123)$$

$$\begin{aligned}f_p(123)&=f(mnq,stu)\\ &=\{N(mnq,stu)\}^{-1/2}\exp\{-\tfrac{1}{2}(\alpha r_1+\beta r_2+\gamma r_3)\}\,r_1{}^m r_2{}^n r_3{}^q r_{12}{}^s r_{13}{}^t r_{23}{}^u \qquad \ldots\ldots(8)\end{aligned}$$

the unit of length being $a_0/2$. $N(mnq,stu)$ is a normalizing factor and α, β and γ are potentially variable parameters. The letter p is used as an abbreviation for the numbers (mnq,stu).

Substituting from (7) and (8) into (6) and minimizing the energy with respect to the coefficients c_p, we get the following set of homogeneous equations

$$\sum_p c_p\{k^2M_{p'p}+k\,V_{p'p}-N_{p'p}E\}=0 \qquad \ldots\ldots(9)$$

and the corresponding energy minimum is the lowest root of the secular equation

$$|k^2 M_{p'p} + kV_{p'p} - EN_{p'p}| = 0, \qquad \ldots\ldots(10)$$

symbolizing $(m'n'q', s't'u')$ and (mnq, stu) with p' and p respectively.

Expressions of the matrix elements of energy $M_{p'p}$ and $V_{p'p}$ and of the unity $N_{p'p}$ together with some recurrence relations are given in the appendix.

§ 4. INCLUSION OF ANGULAR CORRELATION BETWEEN THE ELECTRONS

Ta-You Wu and Shen (1944) have calculated the total energy of He⁻ in the $(1s2s2p)^4P$ state by using approximate one-electron wave function products, obtaining the value $-4{\cdot}326$ Ryd. When using a more flexible 2s function, the energy value $-4{\cdot}340$ Ryd has been obtained (Holøien 1951).

Since the total charge distribution of the electrons in the ion is essentially effected by a closer interaction between the L-electrons, it was hoped that a more flexible wave function which, to a sufficient degree, takes into account the angular correlation of these electrons, might lead to a positive actual electron affinity of the atom in the lowest triplet state. It should be noted that in the present paper a preliminary calculation has been made with the aim of obtaining such a positive electron affinity of the atom by investigating the easiest cases $f(mnq, stu)\cos\theta_3$, when $stu = 000$, 200, 020 and 002.

§ 5. CHOICE OF TERMS. NUMERICAL RESULTS

In selecting terms we first started with the basic term $f(011, 000)$ of approximately the form which would be a solution of the problem with static screening charges. The optimum values of the screening parameters in this first approximation have been determined and found to be $\alpha = 4{\cdot}18$, $\beta = 1$ and $\gamma = 0{\cdot}72$. The corresponding total energy calculated is $E = -4{\cdot}335\,712$ Ryd.

When proceeding to higher approximations it would be desirable to permit independent variation of the parameters α, β and γ, that is, to find the optimum values of the screening constants for each term, but this degree of flexibility cannot be combined with that secured by the inclusion of many terms with adjustable coefficients without increasing the labour of computation too much.

Therefore, we have fixed (not quite arbitrarily) screening parameters both for the inner and the outer part of the electronic orbitals, denoted by α^*, β^* and γ^* in table 2.

Table 2 shows the fixed values together with the optimum values of the screening parameters, the latter values obtained by minimizing the energy when adding each term on the left to the basic term in the wave function. The deviating fixed values are chosen for convenience in computing numerical tables of the basic integrals.

Some comments may be given on the figures in table 1. The terms which have been investigated by inclusion in the wave function, are listed in the first column. In the next columns are given the total energy values (rydberg units) calculated with an approximate wave function containing terms written on the left (first column) and above.

As can be seen from table 1, the inclusion of terms $f(0nq, 002)$ in the wave function produces appreciable improvements in total energy. The terms $f(0nq, 020)$ are not so helpful, and $f(011, 200)$ is almost completely without value.

In table 1 the optimum values of the scale constants by different approximations are given in brackets, and table 3 shows the corresponding coefficients c_p.

Table 1. Total Energy by Different Approximations

Basic term : $f(1)=f(011, 000)$. $E=-4\cdot335712$ Ryd. $(k=0\cdot4778)$.

Terms	2nd approx. $f(1)$	3rd approx. $f(1)+f(2)$	4th approx. $f(1)+f(2)+f(3)$
$f(2)=f(011, 002)$	$-4\cdot346917$ $(0\cdot4843)$		
$f(3)=f(011^*, 002)$	$-4\cdot343123$ $(0\cdot4765)$	$-4\cdot354354$ $(0\cdot4830)$	
$f(4)=f(012, 002)$	$-4\cdot338737$ $(0\cdot4770)$	$-4\cdot350566$ $(0\cdot4837)$	$-4\cdot356035$ $(0\cdot4830)$
$f(5)=f(011^*, 000)$	$-4\cdot337936$ $(0\cdot4767)$	$-4\cdot350228$ $(0\cdot4835)$	$-4\cdot354451$ $(0\cdot4830)$
$f(6)=f(012, 000)$	$-4\cdot337450$ $(0\cdot4772)$	$-4\cdot349008$ $(0\cdot4838)$	
$f(7)=f(011^*, 020)$	$-4\cdot337137$ $(0\cdot4786)$		
$f(8)=f(01^*1, 000)$	$-4\cdot336321$ $(0\cdot4791)$	$-4\cdot347314$ $(0\cdot4851)$	
$f(9)=f(001, 000)$	$-4\cdot336009$ $(0\cdot4790)$		
$f(10)=f(011, 020)$	$-4\cdot335929$ $(0\cdot4785)$		
$f(11)=f(0^*11, 000)$	$-4\cdot335875$		
$f(12)=f(011, 200)$	$-4\cdot335813$ $(0\cdot4784)$		
$f(13)=f(111, 000)$	$-4\cdot335712$		

Table 2. Values of the Screening Parameters α, β and γ

Terms	α	β	γ	Optimum values
$f(011, 000)$	4·18	1	0·72	
$f(011^*, 000)$	4·18	1	2·3	2·27
$f(012, 000)$	4·18	1	4·18	3·66
$f(01^*1, 000)$	4·18	4·18	0·72	4·90
$f(001, 000)$	4·18	2·3	0·72	5–6
$f(0^*11, 000)$	0·65	1	0·72	0·65

Table 3. The Coefficients c_p by Different Approximations

2 terms	3 terms	4 terms
$c_2=$ 0·79138	$c_2=$ 0·90000	$c_2=$ 0·91401
$c_3=$ 0·17392	$c_3=$ 0·30116	$c_3=$ 0·64110
$c_4=$ 0·06785		$c_4=-0{\cdot}23517$
$c_5=$ 0·07727	$c_2=$ 0·85143	
$c_6=$ 0·04734	$c_4=$ 0·12722	$c_2=$ 0·92022
$c_7=$ 0·07245		$c_3=$ 0·27995
$c_8=-0{\cdot}01392$	$c_2=$ 0·92086	$c_5=$ 0·03659
$c_9=-0{\cdot}01784$	$c_5=$ 0·16670	
$c_{10}=$ 0·06931		
$c_{11}=$ 0·00962	$c_2=$ 0·82504	
$c_{12}=$ 0·02651	$c_6=$ 0·08760	
	$c_2=$ 0·76882	
	$c_8=-0{\cdot}01837$	

§ 6. THE TRANSITION $(2s2p^2)^4P$–$(1s2s2p)^4P$ IN He^- IS POSSIBLE

The energy level $(2s2p^2)^4P$ of He^- is found to be a closed one (Holøien 1951), that is, the negative ion can be formed from a helium atom excited either to the $(2s2p)^3P$ state or the $(2p^2)^3P$ state (the electron affinities are found to be at least 0·407 ev and 1·884 ev respectively), but the state is subject to auto-ionization. The auto-ionization probability of this three-electronic state is assumed to be of the same order of magnitude as in doubly excited states of He, namely of the order 10^{14} sec^{-1}.

Accordingly, the transition $(2s2p^2)^4P$–$(1s2s2p)^4P$ can take place and it is of interest to try to identify this with some of the unexplained helium lines in the vacuum ultra-violet.

According to our energy computations this transition gives as result an emission line with wave number 309 388 cm^{-1} (323·2 Å), in good agreement with the observed lines with wave numbers 310 061 cm^{-1} (322·5 Å) and 311 346 cm^{-1} (321·2 Å) as reported by Kruger (1930). The difference from the first line is only 673 cm^{-1} or 0·083 ev (0·2%).

Kruger does not specify the widths of the lines observed, but it seems not unlikely to assign to them a maximum width of 0·05 Å, which requires an auto-ionization probability of not more than 2×10^{12} sec^{-1} as reported by Bransden and Dalgarno (1953).

As mentioned above we here assume the probability of auto-ionization to be about 10^{14} sec^{-1}, similar to that of the two-electronic states, but it is possible that the probability might conceivably be so small that detectable broadening of the lines would not ensue.

At all events, the correspondence in wave numbers is very striking.

§ 7. CONCLUSION

An approximate wave function containing four terms and eight adjustable parameters (the scale constant and the coefficients included) may now be written

$$g = \{f(1) + c_2 f(2) + c_3 f(3) + c_4 f(4)\} \cos\theta_3 \qquad \ldots\ldots(11)$$

and the corresponding total energy

$$E = -4{\cdot}356\,035 \text{ Ryd.}$$

Accordingly, this approximation proves that the helium atom in the lowest triplet state actually has a positive electron affinity of at least

$$E^{\text{atom}}_{\text{exptl}} - E^{\text{ion}}_{\text{calc}} = (4{\cdot}356\,035 - 4{\cdot}350\,523)\text{ Ryd} = 0{\cdot}075 \text{ ev.}$$

Comparing the result of this approximation with the corresponding energy for the atom as calculated theoretically by using a wave function of the same form and flexibility, we obtain an electron affinity of

$$E^{\text{atom}}_{\text{calc}} - E^{\text{ion}}_{\text{calc}} = (4{\cdot}356\,035 - 4{\cdot}345\,000)\text{ Ryd} = 0{\cdot}150 \text{ ev.}$$

Even though we are not justified in relying upon such approximate considerations it appears reasonable to believe that some additional terms, especially angular correlation terms $f(mnq, 001)$, $f(mnq, 010)$ and $f(mnq, 100)$, which are postponed to later investigations, may yield an actual electron affinity that is a great deal better than 0·075 ev.

At all events, we have proved by the wave function given here, that the negative ion can exist as a stable structure in the lowest quartet state for a relatively long time (about 10^{-3} sec), enough to explain the observation of it in the mass spectrograph as reported by Hiby (1939).

ACKNOWLEDGMENT

One of the authors (E. H.) is indebted to the foundation Nansenfondet for financial grants.

APPENDIX

The calculation of the matrix elements of energy and unity in the secular equation (10) is based on the evaluation of integrals

$$I(mnq\,|\,\alpha\beta\gamma\,|\,stu)=\int \exp\{-(\alpha r_1+\beta r_2+\gamma r_3)\}\,r_1^{\,m}\,r_2^{\,n}\,r_3^{\,q}\,r_{12}^{\,s}\,r_{13}^{\,t}\,r_{23}^{\,u}\,d\tau. \quad \ldots\ldots(12)$$

By means of the relations

$$r_{ij}^{\,2}=r_i^{\,2}+r_j^{\,2}-2r_ir_j\cos\theta_{ij}$$

$$\cos\theta_{ij}=\cos\,\theta_i\cos\,\theta_j+\sin\,\theta_i\sin\,\theta_j\cos\,\phi_{ij}$$

and

$$\frac{1}{r_{ij}}=\sum_{n=0}^{\infty}\left\{\frac{r^n}{R^{n+1}}\right\}\mathrm{P}_n(\cos\theta_{ij}),$$

where r and R is the smaller and greater of r_i and r_j respectively, all the integrals occurring in the present paper can be evaluated without serious difficulties. It should, however, be noted that by the integration both interelectronic distances r_{ij} and angles θ_{ij} subtended at the nucleus between the electronic vectors $\mathbf{r}_i$ and $\mathbf{r}_j$ have been used as integration variables.

As already mentioned, we have used approximations containing terms $f(mnq,\ 000)$, $f(mnq,\ 002)$, $f(mnq,\ 020)$ and $f(mnq,\ 200)$ only, and in equation (7) we put

$$\mathrm{Y}_{l|\nu|}(\theta_3,\ \phi_3)=\mathrm{Y}_{10}(\theta_3,\phi_3)=\cos\theta_3.$$

The matrix elements of kinetic energy may therefore be written as follows:

$$\begin{aligned}
M_{p'p}&=4\sum_{i=1}^{3}\int \mathrm{grad}_i(h_{p'})\,\mathrm{grad}_i(g_p)\,d\tau\\
&=4\sum_{i=1}^{3}\int\left\{\frac{\partial h_{p'}}{\partial x_i}\frac{\partial g_p}{\partial x_i}+\frac{\partial h_{p'}}{\partial y_i}\frac{\partial g_p}{\partial y_i}+\frac{\partial h_{p'}}{\partial z_i}\frac{\partial g_p}{\partial z_i}\right\}d\tau\\
&=4\int\left\{\sum_{i=1}^{3}\left[\frac{\partial h_{p'}}{\partial r_i}\frac{\partial g_p}{\partial r_i}+\frac{1}{r_i^{\,2}}\frac{\partial h_{p'}}{\partial \theta_i}\frac{\partial g_p}{\partial \theta_i}\right]+2\sum_{i>j}^{3}\frac{\partial h_{p'}}{\partial r_{ij}}\frac{\partial g_p}{\partial r_{ij}}\right.\\
&\quad+\frac{1}{2}\sum_{i=1}^{3}\sum_{j\neq i}\frac{r_i^{\,2}+r_{ij}^{\,2}-r_j^{\,2}}{r_ir_{ij}}\left[\frac{\partial h_{p'}}{\partial r_i}\frac{\partial g_p}{\partial r_{ij}}+\frac{\partial g_p}{\partial r_i}\frac{\partial h_{p'}}{\partial r_{ij}}\right]\\
&\quad\left.+\frac{1}{4}\sum_{i=1}^{3}\sum_{k\neq j\neq i}\frac{r_{ij}^{\,2}+r_{ik}^{\,2}-r_{jk}^{\,2}}{r_{ij}r_{ik}}\left[\frac{\partial h_{p'}}{\partial r_{ij}}\frac{\partial g_p}{\partial r_{ik}}+\frac{\partial g_p}{\partial r_{ij}}\frac{\partial h_{p'}}{\partial r_{ik}}\right]\right\}d\tau.
\end{aligned}$$

As can be seen, the calculation of the components of this matrix element is reduced to evaluating of integrals of the form (12).

In the same way the matrix elements of potential energy and of unity

$$V_{p'p} = -4Z\sum_{i=1}^{3}\int\frac{h_{p'}g_p}{r_i}\,d\tau + 4\sum_{i>j}^{3}\int\frac{h_{p'}g_p}{r_{ij}}\,d\tau$$

and

$$N_{p'p} = \int h_{p'}g_p\,d\tau$$

can be directly evaluated.

The expressions of these components that have finally been obtained are too long and tedious to be given in the present paper. We may mention only that the first step of the computation is the construction of tables of some basic integrals as follows:

$$Q(n\,|\,a) = \int \mathrm{e}^{-ax}x^n\,dx = n!\,a^{-(n+1)} \quad \text{when } n \geqslant 0.$$

$$R(m,n\,|\,a,b) = \iint\limits_{x>y} \mathrm{e}^{-ax-by}x^m y^n\,dxdy = (-1)^{m+n}\frac{\partial^m}{\partial a^m}\frac{\partial^n}{\partial b^n}\frac{1}{(a+b)b}$$

$$= \sum_{s=0}^{n} b^{s-n-1}(a+b)^{-m-s-1}(m+s)!\,n!/s! \quad n \geqslant 0,\ m \geqslant 0$$

$$W(m,n,q\,|\,a,b,c) = \iiint\limits_{x>y>z} \mathrm{e}^{-ax-by-cz}x^m y^n z^q\,dxdydz$$

$$= a^{-1}\{m\,W(m-1,n,q\,|\,a,b,c) - R(m+n,q\,|\,a+b,c)\}$$

$$m \geqslant 1 \quad m+n \geqslant 0 \quad m+n+q \geqslant -1$$

$$R(0,-1\,|\,a,b) = a^{-1}\ln\{(a+b)/b\}.$$

Furthermore we have

$$W(0,n,q\,|\,a,b,c) = a^{-1}\{R(n,q\,|\,b,c) - R(n,q\,|\,a+b,c)\} \quad n \geqslant 0, \quad n+q \geqslant -1$$

and the recurrence relations when checking the computations:

$$R(m,n\,|\,a,b) = (a+b)^{-1}\{m\,R(m-1,n\,|\,a,b) + n\,R(m,n-1\,|\,a,b)\}$$

$$m \geqslant 1, \quad m+n \geqslant 0$$

$$W(m,n,q\,|\,a,b,c) = (a+b+c)^{-1}\{m\,W(m-1,n,q\,|\,a,b,c)$$

$$+\,n\,W(m,n-1,q\,|\,a,b,c) + q\,W(m,n,q-1\,|\,a,b,c)\}$$

$$m \geqslant 1,\ m+n \geqslant 0,\ m+n+q \geqslant -1.$$

When checking the numerical tables we have also the following useful relations:

$$R(0,n\,|\,a,b) = a^{-1}\{Q(n\,|\,b) - Q(n\,|\,a+b)\} \qquad n \geqslant 0$$

$$R(m,n\,|\,a,b) = a^{-1}\{m\,R(m-1,n\,|\,a,b) - Q(m+n\,|\,a+b)\} \qquad m \geqslant 1, \quad m+n \geqslant 0$$

$$= b^{-1}\{n\,R(m,n-1\,|\,a,b) + Q(m+n\,|\,a+b)\} \qquad m \geqslant 0. \quad m+n \geqslant 0$$

and

$$W(m,n,q\,|\,a,b,c) = b^{-1}\{n\,W(m,n-1,q\,|\,a,b,c) + R(m+n,q\,|\,a+b,c)$$

$$-\,R(m,n+q\,|\,a,b+c)\}$$

$$m \geqslant 0,\ m+n \geqslant 0,\ m+n+q \geqslant -1.$$

REFERENCES

BRANSDEN, B. H., and DALGARNO, A., 1953, *Proc. Phys. Soc.* A, **66**, 911.

CONDON, E. U., and SHORTLEY, G. H., 1935, *Theory of Atomic Spectra* (Cambridge: University Press), p. 371.

HIBY, J. W., 1939, *Ann. Phys., Lpz.*, **34**, 473.

HOLØIEN, E., 1951, *Arch. Math. Naturv.*, **51**, 81.

KRUGER, P. G., 1930, *Phys. Rev.*, **36**, 853.

MASSEY, H. S. W., 1938, *Negative Ions, Camb. Phys. Tracts*, **1**, 15.

TÜXEN, O., 1936, *Z. Phys.*, **103**, 463.

WU, TA-YOU, 1936, *Phil. Mag.*, **22**, 837.

WU, TA-YOU, and SHEN, S. T., 1944, *Chin. J. Phys.*, **5**.

The Triplet Band Systems of Aluminium Monofluoride

By P. G. DODSWORTH and R. F. BARROW
Physical Chemistry Laboratory, University of Oxford

MS. received 29th March 1955

Abstract. The vibrational analyses of three triplet band systems of aluminium monofluoride obtained in emission have been carried out. They arise from transitions from three $^3\Sigma$ states to a common lower $^3\Pi$ state. The order of the sub-levels of the $^3\Pi$ state and of the corresponding state for BF is considered. The relative position of the triplet and singlet levels for AlF is predicted.

---

§ 1. Introduction

Following the analysis of the singlet band systems of AlF observed in emission and absorption (Rowlinson and Barrow 1953 a, b, Naudé and Hugo 1953 a, b, 1954, Barrow and Rowlinson 1954), and the vibrational analysis of one triplet system $b^3\Sigma$–$a^3\Pi$ (Rowlinson and Barrow 1953 a), the vibrational analyses of two further triplet systems have been carried out. These systems lie in the ultra-violet at 2520–2650 Å and 2700–2912 Å and form system (2) of Naudé and Hugo (1953 a). A preliminary account of this work has already been given (Dodsworth and Barrow 1954).

§ 2. Experimental

The triplet systems of AlF were excited in emission as before in hollow cathode discharges using a 1000 v d.c. generator (Rowlinson and Barrow 1953 a). The bands in the region 2520–2912 Å were photographed on Ilford Process plates on the quartz optics of a Hilger E.478 prism instrument (focal length, NaD 1·7 m). Further heads were measured on spectrograms of the 3600 Å system previously obtained (Rowlinson and Barrow 1953 a) to enable a more complete analysis to be made. Wavelengths of the band-heads were determined by comparison with internal standards, mainly Fe and Mn lines from the hot cathode, and are given together with the frequencies and the allocation of the heads in tables 1–3. Internal evidence indicates that the measurements of the band-heads are correct to about ± 1 cm^{-1}.

§ 3. Analysis of the Triplet Systems

The bands observed fall into two systems closely resembling the $b^3\Sigma$–$a^3\Pi$ system at 3450–3720 Å which has been analysed previously (Rowlinson and Barrow 1953 a). Assuming then that these systems are also due to $^3\Sigma$–$^3\Pi$ transitions, there are expected in each band nine heads, three to each sub-band, and one of the three will be formed at the beginning of the branch, i.e. very close to the sub-band origin. This head is not always observed because of overlapping, more intense, structure, and the P_{13} head is formed at such high J values as to be unobserved in any band. A theoretical Fortrat diagram for the (0, 0) band of the system which we shall call c–a is shown in the figure. Assumed values of $B(B_0' = 0{\cdot}585\ \mathrm{cm}^{-1}, B_0'' = 0{\cdot}550\ \mathrm{cm}^{-1})$ have been used; these are chosen to give the correct head–origin separations for the branches and are not based on a full rotational analysis.

Table 1. Band Heads of the $b^3\Sigma$–$a^3\Pi$ System of AlF

λ (Å)	ν_{vac}(cm^{-1})	Head	v', v''
3717·90	26889·3	P_{23}, Q_{13}	
15·96	903·3	P_{33}, Q_{23}, R_{13}	
14·58	13·3	P_{12}	
10·94	39·7	P_{22}, Q_{12}	0, 1
09·41	50·8	P_{32}, Q_{22}, R_{12}	
06·85	69·4	P_{11}	
04·09	89·5	P_{21}, Q_{11}	
03·28	95·4	P_{31}, Q_{21}, R_{11}	
00·54	27015·4	P_{33}, Q_{23}, R_{13}	
3694·35	60·7	P_{32}, Q_{22}, R_{12}	1, 2
87·77	109·0	P_{31}, Q_{21}, R_{11}	
79·39	170·7	P_{32}, Q_{22}, R_{12}	2, 3
08·21	706·7	P_{23}, Q_{13}	
05·92	24·1	P_{12}; P_{33}, Q_{23}, R_{13}	
01·40	59·1	P_{22}, Q_{12}	0, 0
00·12	69·0	P_{32}, Q_{22}, R_{12}	
3597·74	27787·3	P_{11}	
94·85	809·7	P_{21}, Q_{11}	0, 0
94·22	14·5	P_{31}, Q_{21}, R_{11}	
94·85	809·7	P_{23}, Q_{13}	1, 1
80·31	922·6	P_{31}, Q_{21}, R_{11}	
3492·21	28627·0	P_{23}, Q_{13}	
89·82	46·7	P_{33}, Q_{23}, R_{13}	
89·60	48·4	P_{12}	
85·54	81·8	P_{22}, Q_{12}	1, 0
84·08	93·8	P_{32}, Q_{22}, R_{12}	
82·35	708·1	P_{11}	
79·32	33·1	P_{21}, Q_{11}	
78·40	40·7	P_{31}, Q_{21}, R_{11}	
67·15	833·9	P_{31}, Q_{21}, R_{11} P_{33}, Q_{23}, R_{13}	2, 1 3, 2
55·99	927·0	P_{31}, Q_{21}, R_{11} P_{33}, Q_{23}, R_{13}	3, 2 4, 3

Note. All heads are given for the (0, 1), (0, 0) and (1, 0) bands, but only additional heads (see § 2) for other bands.

Table 2. Band Heads of the $c^3\Sigma$–$a^3\Pi$ System of AlF

λ (Å)	ν_{vac}(cm^{-1})	Head	v', v''
2912·1	$34329\cdot_{2}$	P_{23}, Q_{13}	
11·3	$38\cdot_{9}$	P_{33}, Q_{23}, R_{13}	
09·8	$56\cdot_{6}$	P_{12}	
08·0	$77\cdot_{9}$	P_{22}, Q_{12}	0, 2
05·3	$409\cdot_{8}$	P_{11}	
03·9	$26\cdot_{6}$	P_{21}, Q_{11}	
03·2	$34\cdot_{2}$	P_{31}, Q_{21}, R_{11}	
01·6	$54\cdot_{2}$	P_{23}, Q_{13}	
00·6	$65\cdot_{8}$	P_{33}, Q_{23}, R_{13}	
2899·3	$80\cdot_{7}$	P_{12}	
97·4	$503\cdot_{1}$	P_{22}, Q_{12}	1, 3
96·8	$11\cdot_{0}$	P_{32}, Q_{22}, R_{12}	
94·7	$35\cdot_{3}$	P_{11}	
93·3	$52\cdot_{4}$	P_{21}, Q_{11}	
45·0	$35139\cdot_{0}$	P_{23}, Q_{13}	
44·0	$51\cdot_{7}$	P_{33}, Q_{23}, R_{13}	
42·9	$64\cdot_{5}$	P_{12}	
41·0	$88\cdot_{8}$	P_{22}, Q_{12}	0, 1
40·4	$96\cdot_{1}$	P_{32}, Q_{22}, R_{12}	
38·5	$219\cdot_{4}$	P_{11}	
37·0	$38\cdot_{5}$	P_{21}, Q_{11}	
36·7	$42\cdot_{4}$	P_{31}, Q_{21}, R_{11}	
35·6	$55\cdot_{8}$	P_{23}, Q_{13}	
34·6	$68\cdot_{1}$	P_{33}, Q_{23}, R_{13}	1, 2
34·3	$72\cdot_{9}$	P_{12}	
2831·6	$35304\cdot_{9}$	P_{22}, Q_{12}	
30·8	$15\cdot_{2}$	P_{32}, Q_{22}, R_{12}	
29·2	$34\cdot_{9}$	P_{11}	1, 2
27·7	$54\cdot_{7}$	P_{21}, Q_{11}	
27·0	$62\cdot_{6}$	P_{31}, Q_{21}, R_{11}	
2780·3	$957\cdot_{1}$	P_{23}, Q_{13}	
79·1	$72\cdot_{0}$	P_{33}, Q_{23}, R_{13}	
78·5	$80\cdot_{3}$	P_{12}	
76·3	$36008\cdot_{0}$	P_{22}, Q_{12}	0, 0
75·6	$17\cdot_{1}$	P_{32}, Q_{22}, R_{12}	
74·1	$36\cdot_{9}$	P_{11}	
72·4	$58\cdot_{7}$	P_{21}, Q_{11}	
72·0	$65\cdot_{1}$	P_{31}, Q_{21}, R_{11}	
68·2	$114\cdot_{2}$	P_{22}, Q_{12}	
66·9	$30\cdot_{4}$	P_{32}, Q_{22}, R_{12}	
65·9	$44\cdot_{6}$	P_{11}	1, 1
64·3	$64\cdot_{5}$	P_{21}, Q_{11}	
63·6	$74\cdot_{7}$	P_{31}, Q_{21}, R_{11}	
10·6	$881\cdot_{8}$	P_{23}, Q_{13}	
09·2	$900\cdot_{6}$	P_{33}, Q_{23}, R_{13}; P_{12}	
06·7	$35\cdot_{0}$	P_{22}, Q_{12}	
05·8	$46\cdot_{4}$	P_{32}, Q_{22}, R_{12}	1, 0
04·6	$63\cdot_{1}$	P_{11}	
02·9	$85\cdot_{8}$	P_{21}, Q_{11}	
02·4	$93\cdot_{2}$	P_{31}, Q_{21}, R_{11}	

Table 3. Band Heads of the $d^3\Sigma$–$a^3\Pi$ System of AlF

λ (Å)	ν_{vac}(cm^{-1})	Head	v', v''	λ (Å)	ν_{vac}(cm^{-1})	Head	v', v''
2648·6	$37744\cdot_3$	P_{23}, Q_{13}		2585·6	$38663\cdot_9$	P_{21}, Q_{11}	
46·8	$69\cdot_7$	P_{12}		85·2	$70\cdot_8$	P_{31}, Q_{21}, R_{11}	0, 0
44·6	$802\cdot_1$	P_{32}, Q_{22}, R_{12}	0, 1				
43·0	$25\cdot_0$	P_{11}		84·5	$81\cdot_2$	P_{23}, Q_{13}	
41·7	$43\cdot_9$	P_{21}, Q_{11}		81·0	$732\cdot_5$	P_{22}, Q_{12}	
				79·2	$60\cdot_9$	P_{11}	1, 1
39·6	$72\cdot_7$	P_{23}, Q_{13}		77·7	$83\cdot_0$	P_{21}, Q_{11}	
34·1	$952\cdot_0$	P_{11}	1, 2	77·3	$89\cdot_3$	P_{31}, Q_{21}, R_{11}	
32·8	$70\cdot_6$	P_{21}, Q_{11}					
2592·2	$38565\cdot_2$	P_{23}, Q_{13}		31·0	$39498\cdot_7$	P_{23}, Q_{13}	
91·4	$78\cdot_4$	P_{33}, Q_{23}, R_{13}		29·8	$516\cdot_8$	P_{33}, Q_{23}, R_{13}; P_{12}	
90·8	$86\cdot_3$	P_{12}		27·7	$50\cdot_1$	P_{22}, Q_{12}	1, 0
88·9	$614\cdot_5$	P_{22}, Q_{12}	0, 0	27·0	$61\cdot_2$	P_{32}, Q_{22}, R_{12}	
88·3	$23\cdot_9$	P_{32}, Q_{22}, R_{12}		25·9	$78\cdot_6$	P_{11}	
87·0	$42\cdot_8$	P_{11}		24·4	$601\cdot_3$	P_{21}, Q_{11}	

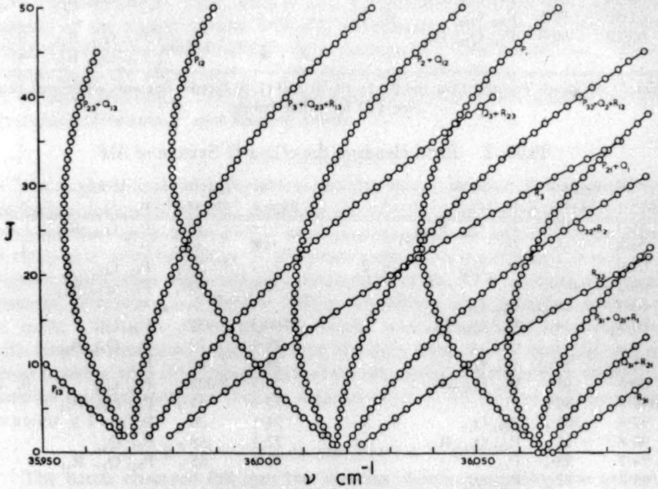

Fortrat diagram for the 0, 0 band of the c–a system.

From the branch formulae, the head–origin separations are given by

$$\nu_h = \nu_0^{(i)} - \frac{(B' + B^{(i)}{}_{\text{eff}})^2}{4(B' - B^{(i)}{}_{\text{eff}})}$$

where $i = 1$ for the $Q_{11} + P_{21}$ branch, $i = 2$ for the $Q_{12} + P_{22}$ branch, and $i = 3$ for the $Q_{13} + P_{23}$ branch, and

$$\nu_h = \nu_0^{(i)} + 2B' - \frac{(3B' + B^{(i)}{}_{\text{eff}})^2}{4(B' - B^{(i)}{}_{\text{eff}})}$$

where $i = 1$ for the P_{11} branch and $i = 2$ for the P_{12} branch.

Since for all three triplet systems $B' \simeq B''$, the head–origin separations are large, and in each sub-band the ratio of the two head–origin separations is very nearly four to one. This makes possible the estimation of the position of the sub-band origin when the head formed at the origin is obscured, except for the $^3\Sigma$–$^3\Pi_2$ sub-band where, as already explained, the P_{13} head is not observed.

The analyses of the three triplet systems were carried out simultaneously as follows. First of all, a table of sub-band origins was drawn up for each system, and from these an average value of A, the triplet splitting in $a^3\Pi$, was obtained. Then, from tables of the mean values of the band origins, the vibrational constants of the common lower state were calculated by a least squares treatment of all the $\Delta G''$ values. Finally, the vibrational constants of the upper states were found. The constants obtained are given in table 4.

Table 4. Constants of the Triplet States of AlF

State	T_0	ω_e	$x_e\omega_e$	$y_e\omega_e$	$\Delta G_{1/2}$
$d^3\Sigma$	a+38623·5	—	—	—	938·$_9$
$c^3\Sigma$	a+36017·6	—	—	—	930·$_2$
$b^3\Sigma$	a+27769·0	936·3	6·2$_6$	0·2$_1$	—
$a^3\Pi$	a	827·8	3·9$_3$	—	—

$A(a^3\Pi) = 46·6$

If we assume any one B value, it is possible to obtain a self-consistent set of rotational constants which will account for all the observed head–origin separations within the limits of experimental error. Owing to the large number of overlapping branches, however, it is not possible to carry out a full rotational analysis.

§ 4. THE $^3\Pi$ STATE OF BF

The rotational analysis by Paul and Knauss (1938) of the $b^3\Sigma$–$a^3\Pi$ system of BF presents several disturbing features. If one considers the upper state differences $R_i(K) - Q_i(K)$, the values for $i = 1$, 2 and 3 for the same K value in any one band do not agree within the limits of experimental error, although the differences for a given K and a given i but for different bands (the (0, 0), (0, 1) and (0, 2) bands) show much better agreement. As the triplet splitting of the $^3\Sigma$ state is too small to be observed, this points to the existence of appreciable Λ-type doubling in the lower state. The non-agreement of values of $R_i(K) - Q_i(K)$ and $Q_i(K+1) - P_i(K+1)$ confirms this view, although owing to the scarcity of unblended lines in the P branches of this analysis the reliable $Q_i(K+1) - P_i(K+1)$ differences are so few that it is not possible to calculate the magnitude or the variation of the Λ-type doubling in the three sub-bands, and thus to decide whether the $^3\Pi$ state is regular or inverted.

The second method of determining unambiguously the character of the $^3\Pi$ state is the observation of the first lines of the branches: the structure of these bands is so complex that this is not possible without the use of much greater resolution.

A third method, developed by Challacombe and Almy (1937), was applied by Paul and Knauss to this system of BF. The method involves the observation of lines of low K'' in corresponding branches and is difficult to apply in this case because of the overlapping of branches and blending of lines. If we plot $(R_i(K) - Q_i(K))/(K+1)$ against $(K+1)^2$ we should obtain straight lines of slope $-4D_v$ and intercept $2B_v$, neglecting Λ-type doubling, or at least a straight line at low K values with an intercept independent of i for the sub-bands where the doubling is a function of K. We find that at $K \simeq 10$ the values of the function plotted are abnormally low, much more so than can be accounted for by the lack of resolution in this region. Thus there may be some incorrect assignment of lines near the band origins.

Finally, we have calculated the positions of lines near the origin of the (0, 0) band of a $^3\Sigma$–$^3\Pi$ transition for a hypothetical molecule with rotational constants similar to those of BF. We have taken $B_0' = 1{\cdot}6235$ cm^{-1}, $D_0' = 6{\cdot}70 \times 10^{-6}$ cm^{-1}, $B_0'' = 1{\cdot}4030$ cm^{-1}, and $D_0'' = 6{\cdot}39 \times 10^{-6}$ cm^{-1}, and carried out the calculations for two values of the coupling constant Y, -12 and $+16$. Spin tripling in the upper state and Λ-type doubling in the lower state were ignored, and the formulae given by Herzberg (1950) for the levels of a $^3\Pi$ state intermediate between case (*a*) and case (*b*) were used. These calculations show that in the complex overlapping structure which is obtained it is most unlikely that one should be able to distinguish between the cases $Y = -x$ and $Y = x + 4$ without the use of greater resolution than was attained by Paul and Knauss. The positions of corresponding lines at $K'' = 3$, for example, differ by an average of only $0{\cdot}45$ cm^{-1}, while at $K'' = 9$ the average difference between corresponding lines for the two values of Y is only $0{\cdot}17$ cm^{-1}.

We conclude that there is no definite evidence for the inversion of the $^3\Pi$ state.

§ 5. THE $a^3\Pi$ STATE OF AlF

The observed $^3\Pi$ states of BF, AlF, GaF, and InF are very similar to each other, as we should expect for low-lying states arising from similar electron configurations. For example, the ratio $\omega_e(^3\Pi_1) : \omega_e(x^1\Sigma^+)$ for these molecules is 0·95, 1·03, 1·06 and 1·07 respectively. It seems probable that since the $^3\Pi$ states of GaF and InF are known to be regular, as is the corresponding case (*c*) triplet state for TlF, the $a^3\Pi$ states of BF and AlF are also $^3\Pi_r$.

We may furthermore expect that the dissociation products of these states are in similar states of excitation. The $B^3\Pi_1$ state of InF appears to dissociate into In($^2P_{1/2}$) + F(^2P) (Barrow, Jacquest and Thompson 1954) and we may assume that the corresponding $^3\Pi_1$ levels of all this group of molecules dissociate to give a metal atom in its ground state ($^2P_{1/2}$).

The dissociation energies D_0 of the $^3\Pi_1$ states of GaF and InF calculated on this basis are then 17167 ± 202 and 12988 ± 202 cm^{-1} respectively, or 34·2% and 29·6% of the dissociation energies of the corresponding ground states $^1\Sigma^+$. If the corresponding value for AlF is about 40%, then we should expect $\nu_{0,0}(a^3\Pi - x^1\Sigma^+)$ to be about 33000 cm^{-1}.

REFERENCES

Barrow, R. F., Jacquest, J. A. T., and Thompson, E. W., 1954, *Proc. Phys. Soc.* A, **67,** 528.

Barrow, R. F., and Rowlinson, H. C., 1954, *Proc. Roy. Soc.* A, **224,** 134.

Challacombe, C. N., and Almy, G. M., 1937, *Phys. Rev.*, **51,** 930.

Dodsworth, P. G., and Barrow, R. F., 1954, *Proc. Phys. Soc.* A, **67,** 94.

Herzberg, G., 1950, *Molecular Structure*: I: *Spectra of Diatomic Molecules* (New York: van Nostrand).

Naudé, S. M., and Hugo, T. J., 1953 a, *Phys. Rev.*, **90,** 318 ; 1953 b, *Canad. J. Phys.*, **31,** 1106 ; 1954, *Ibid.*, **32,** 246.

Paul, F. W., and Knauss, H. P., 1938, *Phys. Rev.*, **54,** 1072.

Rowlinson, H. C., and Barrow, R. F., 1953 a, *Proc. Phys. Soc.* A, **66,** 437 ; 1953 b, *Ibid.*, **66,** 771.

Further Observations of Cosmic-Ray Events in Nuclear Emulsions Exposed Below Ground

By E. P. GEORGE† and J. EVANS‡

† The F.B.S. Falkiner Nuclear Research and Adolph Basser Computing Laboratories, School of Physics,* The University of Sydney, Australia
‡ Messrs. Standard Telephones, London

Communicated by H. Messel; *MS. received* 1st *February* 1955

Abstract. Earlier work with underground emulsion has been extended by making observations at greater depths, and by obtaining more data at depths previously employed. The final result for the interaction cross section of fast μ-mesons with nucleons is $(4{\cdot}6 \pm 0{\cdot}5) \times 10^{-30}$ cm². The flux of fast π-mesons is certainly less than 0·17% of the flux of fast μ-mesons, and a more probable figure for this ratio is 0·04%.

§ 1. INTRODUCTOIN

In a previous paper (George and Evans 1950) we gave an account of cosmic-ray stars and mesons observed in nuclear emulsions prepared, stored and processed at various levels below ground. This work has been extended in two respects: more data have been accumulated at the depths previously employed and the maximum depth of observation has been extended to one equivalent to 600 metres of water. A brief account of these new observations is given in this paper.

§ 2. EXPERIMENTAL

In our earlier paper, we had exposed nuclear emulsions at various stations on the Underground Railway in London, estimating the depths to be equivalent to 20, 34 and 60 metres of water respectively from the given real depths. The equivalent depths have been checked by observing the counting rate of a three-fold vertical counter telescope containing a 10-cm lead absorber at these three places and at sea level, and then reading off the equivalent depths corresponding to the relative counting rates from figure 5 of the survey paper of Rossi (1948). The equivalent depths found in this way were 25, 45 and 57 m water respectively, and these we shall take as the most reliable estimates of the depths for these points of observation. In addition, emulsions were exposed on a new site on the City line at Waterloo, the depth being equivalent to 8 metres of water, and in a coal mine at Pensford, near Bristol. The depth of the coal mine was 300 metres below surface and the equivalent depth was taken at 600 metres of water. Ilford emulsions type G5, of thickness 200, 400 and 600 microns were used in these experiments.

§ 3. RESULTS

A total volume of 843 cubic centimetres of emulsion has been searched, and 265 stars of three or more prongs and 2816 mesons stopping in the emulsion have been observed.

---

* Also supported by the Nuclear Research Foundation within the University of Sydney.

Table 1

Location	Depth (m.w.e.)	μ-Mesons No. observed	μ-Mesons Frequency (cm^{-3} d^{-1})	σ-Mesons No. observed	σ-Mesons Frequency (cm^{-3} d^{-1})	π^+-Mesons No. observed	π^+-Mesons Frequency (cm^{-3} d^{-1})
Waterloo	8	589	$0{\cdot}91 \pm 0{\cdot}04$	12 (3)	$(1{\cdot}8 \pm 0{\cdot}5) \times 10^{-2}$	2	$(3{\cdot}1 \pm 2{\cdot}0) \times 10^{-3}$
Arsenal	25	1059	$0{\cdot}1 \pm 0{\cdot}003$	27 (7)	$(2{\cdot}6 \pm 0{\cdot}5) \times 10^{-3}$	1	1×10^{-4}
Holborn plat. 1	45	441	$0{\cdot}049 \pm 0{\cdot}002$	7 (0)	$(8{\cdot}0 \pm 3{\cdot}0) \times 10^{-4}$	4	$(4{\cdot}5 \pm 2{\cdot}0) \times 10^{-4}$
Holborn plat. 4	57	648	$0{\cdot}026 \pm 0{\cdot}001$	13 (2)	$(5{\cdot}2 \pm 1{\cdot}4) \times 10^{-4}$	11	$(4{\cdot}4 \pm 1{\cdot}3) \times 10^{-4}$
Pensford pit-bottom	600	1	2×10^{-5}	1 (1)	2×10^{-5}	0	—
Total		2738		60(13)		18	

Table 3. Frequencies of stars at various depths below ground

Location	Depth (m.w.e.)	No. of stars observed	Frequency of Stars (10^{-3} cm^{-3} d^{-1}) All types	 O_n	 I_p	 Showers	 O_p	 I_p + showers
Waterloo	8	64	33 ± 4 (64)	20 ± 3 (32)	$5 \pm 1{\cdot}6$ (10)	$3{\cdot}6 \pm 1{\cdot}4$ (7)	$2{\cdot}6 \pm 1{\cdot}1$ (5)	8·6 (17)
Arsenal	25	67	$6{\cdot}3 \pm 0{\cdot}7$ (67)	$2{\cdot}4 \pm 0{\cdot}5$ (25)	$2{\cdot}7 \pm 0{\cdot}5$ (29)	$0{\cdot}57 \pm 0{\cdot}2$ (6)	$0{\cdot}57 \pm 0{\cdot}2$ (6)	3·3 (35)
Holborn plat. 1	45	36	$4{\cdot}0 \pm 0{\cdot}6$ (36)	$1{\cdot}9 \pm 0{\cdot}5$ (17)	$0{\cdot}56 \pm 0{\cdot}2$ (5)	$0{\cdot}9 \pm 0{\cdot}3$ (8)	$0{\cdot}67 \pm 0{\cdot}25$ (6)	1·5 (13)
Holborn plat. 4	57	94	$3{\cdot}8 \pm 0{\cdot}4$ (94)	$1{\cdot}9 \pm 0{\cdot}3$ (48)	$0{\cdot}83 \pm 0{\cdot}2$ (20)	$0{\cdot}32 \pm 0{\cdot}1$ (8)	$0{\cdot}36 \pm 0{\cdot}12$ (9)	1·15 (28)
Pensford pit-bottom	600	3	$0{\cdot}06 \pm 0{\cdot}035$	$0{\cdot}06 \pm 0{\cdot}035$	—	—	—	—

(The figures in parentheses give the number of events observed.)

3.1. *Slow Mesons*

The results for the slow mesons are collected together in table 1. In this table, the errors given are the statistical standard deviations. The combined effects of the revision of the figures for the equivalent depths, and the use of thicker emulsions which give slightly higher rates result in good agreement between the observed frequencies of slow μ-mesons as a function of depth, down to 60 m water equivalent, and those given by Rossi (1948, fig. 6).

The exponent of the differential spectrum of the μ-mesons in the energy band 10^{10} to 10^{11} ev is close to 3, and hence the expected frequency of slow μ-mesons at 600 m depth is approximately one thousandth of the frequency at 57 m, viz. $2{\cdot}6 \times 10^{-5}$ cm^{-3} day^{-1}. The observed frequency at 600 cm depth (2×10^{-5}) is seen to be of the expected order of magnitude.

(*a*) σ-*Mesons*.

We have shown previously (George and Evans 1951) that the underground σ-mesons are mostly μ-mesons, the stars resulting from their capture being mostly one-prong disintegrations of rather low energy, corresponding to a mean nuclear excitation of about 15 Mev. The remaining σ-mesons are π-mesons. Using the method given in our previous paper, we have estimated the number of π^--mesons among the observed σ-mesons, and these are given in brackets in the fifth column of table 1. The remaining σ-mesons we assumed to be μ-mesons.

It is seen from table 1 that the 47 σ-mesons classified as μ-mesons were observed at the same time as 2738 stopping μ-mesons, a ratio of $(1{\cdot}7 \pm 0{\cdot}3)\%$. This corresponds to a figure of $(6 \pm 0{\cdot}9\%)$ for the ratio of the number of stopping μ-mesons producing visible disintegrations, to the total number of captured μ^--mesons.

(*b*) π-*Mesons*.

In table 2, we have divided the total number of π-mesons of either sign of charge (the bracketed figures in column 5, plus the figures in column 7 of table 1) by the frequency of stars at the same depth (cf. table 3).

Table 2

Depth (m.w.e.)	8	25	45	57	600
$\dfrac{\pi^\pm}{\text{Stars}}$	0·24 ± 0·11	0·13 ± 0·05	0·11 ± 0·5	0·14 ± 0·04	0·3

The weighted mean value of this ratio is $0{\cdot}15 \pm 0{\cdot}03$. The one σ-meson observed at 600 m water equivalent was of the π-meson type and it is seen that the observed number of π-mesons at this depth, 1, is close to the number expected (0.5), if the ratio of π-mesons to stars is a constant.

3.2. *Stars*

The final figures for the frequency of occurrence of nuclear-disintegration ' stars ' at various depths are given in table 3 ; column 4 gives the frequencies of stars of all types lumped together, and column 5 onwards, the frequencies of various star-types individually.

Some of our colleagues, believing that the frequency of stars may be substantially higher than that originally reported, have suggested that the plates used previously might have been searched inefficiently. We checked this point by arranging for a sample of our present plates, exposed at 57 m, to be searched at one tenth of the speed used in searching the remainder. The results of this test are given in table 4.

Table 4

Searching speed (cm^2 d^{-1})	2·5	25
No. of Events	14	94
Observed frequency of stars with 3 or more prongs	4·3 ± 1·1	3·8 ± 0·4

The results suggest that the number of events observed at the normal, faster, scanning speed could be as much as 30% low but the error is unlikely to be much more than this. Certainly the results cannot be out by an order of magnitude. In addition, to test the scanning efficiency, plates already searched by one observer were re-searched by a second one. No additional stars were found, again indicating a negligible loss of events by the scanners.

Previously (1950) we have given the following picture of the formation of underground stars. A certain fraction (viz. stars of type I_p and showers, all of which have fast charged primary particles) are produced directly by the electromagnetic excitation resulting from the passage of fast μ-mesons through nuclei. These primary stars emit strongly interacting particles, neutrons, protons and π-mesons, which often possess sufficient energy to cause secondary stars. These secondary events occur mainly as stars of type O_n and O_p.

(*a*) *Cross section for star production by fast μ-mesons.*

The cross section for star production by fast μ-mesons may therefore be evaluated from the sum of the frequencies of the I_p stars and showers, given in the last column of table 3. If S is the frequency of occurrence of stars per cm^3 of emulsion per day, and N the number of nucleons per cm^3, then the cross section for star production per nucleon by μ-mesons is given by

$$3S/2\pi NI \qquad \ldots\ldots(1)$$

where I is the μ-meson flux in the vertical direction per steradian per day.

Values for the cross section for star and for shower production at various depths obtained by inserting the relevant values of S in equation (1) are collected in table 5. Also given in table 5 are the values of I used, which were obtained from Rossi (1948).

Table 5

Depth (m.w.e.)	I (sterad d^{-1})	σ (I_p plus showers) 10^{-30} cm^2 nucleon^{-1}		σ (showers) 10^{-30} cm^2 nucleon^{-1}
8	378	4·5 ± 1·1		1·9 ± 0·7
25	138	4·7 ± 0·8		0·82 ± 0·4
45	67·5	4·4 ± 1·2		2·6 ± 0·8
57	47·2	4·8 ± 0·9		1·35 ± 0·4
	Mean	4·6 ± 0·5	Mean	1·7 ± 0·3

These figures are our final values for the cross section for the interactions of μ-mesons with nucleons.

(*b*) *Identification of shower particles.*

In our previous paper we reported the existence underground of stars accompanied by showers of thin tracks, and in line with the results of Fowler (1950) for high-altitude stars, we suggested that most of the shower particles in the underground stars also were π-mesons. With the larger amount of data we have since accumulated, it has been possible to confirm this guess. From among the shower tracks with grain density less than 1·4 times the plateau value, four were sufficiently long for the methods of the Bristol group to be applied. For these four tracks, the multiple scattering $\bar{\alpha}_{100}$ and ' blob '-density were measured. The ' plateau ' blob density was determined from the background of fast high-energy straight-through tracks. Defining in the usual way g^* as the ratio of blob density for a given track to the plateau value, it was found in all cases that the pairs of values of g^* and $\bar{\alpha}_{100}$ were consistent with those for π-mesons, although the experimental errors were such that the possibility that the particles forming the shower tracks were μ-mesons could not be excluded. The values of $p\beta$ for these four particles were found to be 70, 75, 600 and 630 MEV/C respectively.

§ 4. DISCUSSION

4.1. *Slow Mesons*

The probability of a scanner observing a slow meson depends on the length of track available, and this in turn depends on the thickness of the emulsion being used. In thin emulsions, therefore, the observed frequency of events is likely to be significantly lower than the true frequency. This is illustrated by the fact that the frequency of μ-mesons stopping in emulsions 200μ thick at 57 m water equivalent reported in our earlier paper was 0·017 cm^{-3} day^{-1}, whereas the figure we now obtain is 0·026. The difference is due to the fact that the new results were obtained using emulsions 400 and 600 microns thick. In fact, the result for the thick emulsions alone is 0·035 showing that our figure for 200μ plates is low by some 50%.

At a depth of 25 m water equivalent, emulsions 200μ thick only were used, and this means that the true frequency of slow μ-mesons is likely to be about twice the observed figure. Multiplying our observed figure by two, we get $0{\cdot}2 \pm 0{\cdot}06$ as the corresponding thick emulsion figure, at 25 m water equivalent which is in good agreement with the result of Kaneko *et al.* (1954), whose result for the frequency of slow μ-mesons in emulsion exposed at a depth equivalent to 23 m of water is $0{\cdot}22 \pm 0{\cdot}03$.

Our earlier work on the capture of negative μ-mesons (George and Evans 1951) was confirmed by workers using machine-produced negative μ-mesons (Fry 1952, Sherman *et al.* 1952), and it was obvious that the much greater statistical accuracy obtainable using machine-particle beams made the approach via the cosmic radiation unprofitable and we accordingly did not push our investigation any further. It remains to demonstrate that our results are consistent with those obtained using machine-produced particles.

The latest results are those of Morinaga and Fry (1953) who observed 591 cases of star production among 24 000 stopped negative μ-mesons, a ratio of 2·4%. From table 1, we obtain our figure for comparison as follows: 47 cases classified as the capture of μ-mesons in a total of 2738. Of the latter, 44% were negative (Owen and Wilson 1949) giving 1202 negative μ-mesons stopping. The ratio of 47 to 1202 is $3{\cdot}9 \pm 0{\cdot}6$%. The difference between this figure and that of Morinaga and Fry we do not regard as significant on account of the poor accuracy of our figures, and also because the efficiency of detecting μ-mesons ending in stars was likely to be somewhat higher than that of recording isolated μ-mesons.

4.2. *Stars*

Concerning the nuclear disintegrations, we have little to add to what we have said previously (George and Evans 1950; George 1952). The figures in table 4 are our best values for the cross section for the nuclear interactions of fast μ-mesons and are consistent with the underground cloud-chamber results of Braddick and Leontic (1954), Lovati *et al.* (1953) and McDiarmid (1954).

These interactions may be explained in terms of the coulomb interaction of the electric charge of the fast μ-mesons with nuclei. The details have been fully discussed in our earlier papers, and need not be repeated here. The numerical value of the cross section is consistent with that obtained from the known cross section for photo-nuclear disintegration obtained by Miller (1951).

Since we have shown that the shower particles are mostly π-mesons, it is clear that there must be a small flux of fast π-mesons underground, and it is of interest to enquire how big it is, and to what extent it may contribute to the frequency of stars, large-angle scatters etc. which have been observed.

The calculation will be performed for a depth of 60 m water equivalent. The mean free path in emulsion, λ_3 for the production of stars with three or more prongs by fast π-mesons will be required, and this will be taken from the work of Morrish (1954) who obtained $\lambda_3 = 115$ cm, for 200 MEV π-mesons.

For the sake of argument, we shall now assume that all the stars with charged primaries are produced by π-mesons: although we do not believe this assumption it will serve to give us an upper limit. From table 3, the frequency of such stars per cm^3 per day at 57 m is $(0{\cdot}83 + 0{\cdot}32 + 0{\cdot}36) \times 10^{-3} = 1{\cdot}5 \times 10^{-3}$. This, together with the value for λ_3 gives $1{\cdot}5 \times 10^{-3} \times 115 = (0{\cdot}17 \pm 0{\cdot}03)$ cm^{-2} day^{-1} as the upper limit to the flux of relativistic π-mesons at 60 m depth. Since the flux of fast μ's is of the order of 100 cm^{-2} d^{-1}, this means that the upper limit to the ratio

$$\frac{\text{Relativistic } \pi\text{-mesons}}{\text{Relativistic } \mu\text{-mesons}} = 0{\cdot}17\%. \qquad \ldots\ldots(2)$$

In actual fact, a more realistic figure would be obtained by assuming that the O_p stars are the ones due to the fast π's (Camerini *et al.* 1950), which reduces the ratio of π/μ to 0·04%.

This low figure for the flux of π-mesons renders unlikely any explanation of the anomalous scatter of fast particles below ground observed in emulsions by Kannangara and Shrikantia (1953) and in cloud chambers by George, Redding and Trent (1953) and McDiarmid (1954) in terms of a π-meson contamination of the underground cosmic radiation.

§ 5. CONCLUSIONS

From the work reported in this paper, we have drawn the following conclusions:

(i) The proportion of stopping negative μ-mesons in the cosmic radiation which causes stars with visible prongs is $(3{\cdot}9 \pm 0{\cdot}6)\%$. On account of possible systematic errors, the difference between this figure and that of Morinaga and Fry for machine-produced mesons, 2·4%, is not significant.

(ii) Over a wide range of depths, from 8 to 600 m water equivalent the ratio of $\pi^{\pm}$-mesons to stars is substantially constant, the ratio being $0{\cdot}15 \pm 0{\cdot}03$.

(iii) The flux of fast π-mesons is certainly less than 0·17% of the flux of fast μ-mesons, and a more probable figure for this ratio is 0·04%.

(iv) The 'shower'-particles produced in energetic nucleon disintegration observed below ground are mostly π-mesons.

(v) The frequency of large-angle scatters of fast particles observed below ground by various workers is greater by an order of magnitude than that calculated for the maximum possible flux of π-mesons. Hence the observed scatters are not, in the main, examples of π-meson interactions.

ACKNOWLEDGMENTS

This work was started in London and was finished after one of us moved to Sydney. The work was supported by a grant from the Department of Scientific and Industrial Research. We are also grateful to the Research Committees of London and Sydney Universities for financial support. We would like to thank Mrs. M. H. George, Miss Kurz and Mrs. Chartres for help in searching the emulsion. The co-operation of the London Transport Executive and of the National Coal Board is gratefully acknowledged. We are grateful to Professors J. D. Bernal and H. Messel for many stimulating discussions.

REFERENCES

BRADDICK, H. J. J., and LEONTIC, B., 1954, *Phil. Mag.*, **45**, 1287.
CAMERINI, U., FOWLER, P. H., LOCK, W. O., and MUIRHEAD, H., 1950, *Phil. Mag.*, **41**, 413.
FOWLER, P. H., 1950, *Phil. Mag.*, **41**, 169.
FRY, W. F., 1952, *Phys. Rev.*, **85**, 676.
GEORGE, E. P., 1952, *Progress in Cosmic Ray Physics* (Amsterdam: North Holland Publishing Co.), p. 434.
GEORGE, E. P., and EVANS, J., 1950, *Proc. Phys. Soc.* A, **63**, 1248; 1951, *Ibid.*, **64**, 193.
GEORGE, E. P., REDDING, J. L., and TRENT, P. T., 1953, *Proc. Phys. Soc.* A, **66**, 533.
KANEKO, S., KUBOZOE, T., and TAKAHATA, M., 1954, *J. Phys. Soc. Japan*, **9**, 147.
KANNANGARA, M. L. T., and SHRIKANTIA, G. S., 1953, *Phil. Mag.*, **44**, 1091.
LOVATI, A., MURA, A., SUCCI, C., and TAGLIAFERRI, G., 1953, *Nuovo Cim.*, **10**, 1201.
MCDIARMID, I. B., 1954, *Phil. Mag.*, **45**, 933.
MILLER, R. D., 1951, *Phys. Rev.*, **82**, 260.
MORINAGA, H. ,and FRY, W. F., 1953, *Nuovo Cim.*, **10**, 308.
MORRISH, A. H., 1954, *Phil. Mag.*, **45**, 47.
OWEN, B. G., and WILSON, J. G., 1949, *Proc. Phys. Soc.* A, **62**, 601.
ROSSI, B., 1948, *Rev. Mod. Phys.*, **20**, 537.
SHERMAN, D. F., HECKMAN, H. H., and BARKAS, W. H., 1952, *Phys. Rev.*, **85**, 771 (A).

RESEARCH NOTES

Determination of Proton Synchrotron Beam Size with a Crystal Scintillator

By B. LEDLEY and L. RIDDIFORD
Department of Physics, The University of Birmingham

Communicated by P. B. Moon; MS. received 23rd March 1955 and in amended form 21st April 1955

§ 1. Introduction and Apparatus

Crystal scintillators are now commonly used inside synchrotrons to detect accelerated particles. In the Birmingham proton synchrotron (*Nature* 1953) a $\frac{3}{16}$-inch square thallium activated potassium iodide crystal about $\frac{1}{16}$-inch thick has been employed. It is cemented with Canada Balsam to the end of a polished $\frac{1}{4}$-inch diameter Lucite rod which passes along and close to the bottom of the vacuum chamber. The rod is smoothly curved, as shown in figure 1, so that the crystal may be located near the back wall, where it does not interfere with injection or acceleration of the protons. The O-ring vacuum seals make rotational and translational motion possible. Light from the crystal passes along the $\frac{1}{4}$-inch rod and then down eight feet of one-inch rod to a type EMI 6262 photomultiplier tube. Both rods are enclosed in brass tubes which keep out spurious light. The photomultiplier tube is screened from the fringing field of the synchrotron by mumetal cylinders. A thin 0·0004-inch aluminium foil protects the crystal from spurious light, and the curved part of the Lucite rod is wrapped with copper foil. The aluminium foil serves also to prevent the intense flash of light associated with the pulse of 500 kev protons injected into the synchrotron if they are allowed to strike the crystal.

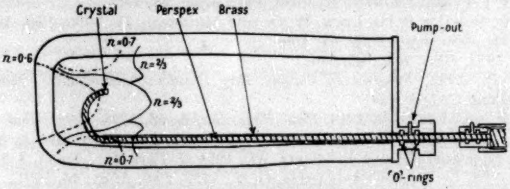

Figure 1. Cross section of vacuum chamber, with scintillator probe inserted. Contours of n are shown.

In a synchrotron the particles move on complex orbits about the mean orbit, which is determined by the magnetic field and the frequency of the potential used to accelerate them. The spatial distribution of protons in the bunch being accelerated is determined in the vertical direction solely by free oscillations and in the horizontal direction by both free and phase oscillations. If the radio-frequency accelerating potential is removed the particles spiral in towards the crystal as the magnetic field continues to increase, and finally strike it. The distribution in vertical oscillation amplitudes may be obtained by varying the position of the crystal in the vertical direction, and the distribution in horizontal amplitudes inferred from the time variation of the signal from the photomultiplier tube.

§ 2. Results

Figure 2 shows a typical photograph of an oscilloscope display of the scintillator signal (the upper trace) together with that from an induction electrode (Riddiford, Van der Raay and Coe 1955). The step in the induction electrode pattern is at the instant when the accelerating potential is removed. The area under the scintillation trace is a measure of the number of protons which have struck the crystal, and the height of the induction electrode trace is a measure of the number of protons which were circulating inside the synchrotron. It is necessary to normalize the scintillator's response to the number of circulating protons, since this may vary substantially from pulse to pulse in a proton synchrotron. Since the crystal is small compared with the vertical extent of the beam, it is assumed that when in a certain vertical position it will be struck by all particles with oscillation amplitudes equal to, or greater than, its distance from the centre of the beam, and by no others. This is reasonable, since the oscillation amplitude is unlikely to change in the time a particle takes to spiral radially inwards a distance equal to the crystal thickness, whereas the phase of one of the free oscillations which occur during this time is certain to be such as to make the particle strike the crystal. A plot of scintillator signal against vertical position obtained in this way is drawn in figure 3, curve *a*.

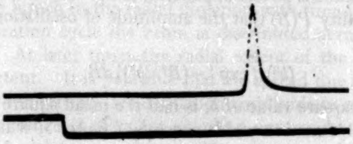

Figure 2. Oscilloscope traces of scintillation and induction electrode signals.

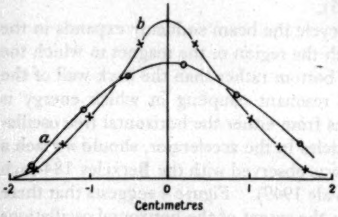

Figure 3.

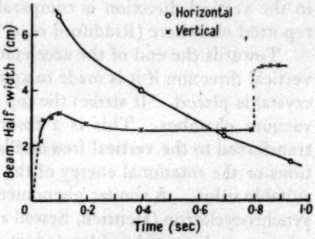

Figure 4.

Figure 3. A comparison between the measured vertical distribution of protons at 0·4 second and the theoretical value.

a, experimental ; *b*, integrated Rayleigh function.

Abscissae : *a*, vertical position of crystal (origin 1 cm below geometrical median plane); *b*, oscillation amplitude *B*.

Ordinates : *a*, integrated scintillator signal ; *b*, $\int_B^\infty P(B)\,dB$.

Figure 4. Variation of beam half-width during the acceleration cycle.

§ 3. DISCUSSION

3.1. *Vertical Distribution*

In general only free oscillations due to gas scattering will matter, for the divergence of the injected beam is known to be small, and the associated oscillations are rapidly damped. The distribution in oscillation amplitudes will then be a Rayleigh one if there is no loss of particles to the walls of the vacuum chamber. That is, the probability $P(B)$ that the amplitude of oscillation B lies between B and $B+dB$ is

$$(\overline{b^2})B\exp\{-(B^2/2\overline{b^2})\}\,dB$$

where $\overline{b^2}$, the mean square value of b, is half the mean square value of B. Integration of a Rayleigh function yields curve b of figure 3, which is seen to agree fairly well with experiment. The centre of the experimental curve is about one centimetre below the geometrical median plane of the synchrotron magnet, supporting other observations (Riddiford *et al.* 1955) that the magnetic median plane is low.

The variation in vertical size of the beam during acceleration is shown in figure 4. The points refer to the widths at half maximum of curves such as those in figure 3, which however correspond closely to the peak to peak widths of the Rayleigh distributions. That the beam width passes through a broad maximum during the acceleration cycle is in qualitative agreement with theory (Blachman and Courant 1948), but it should decrease steadily from the maximum until acceleration is complete. That it does not could be due to the steady decrease in n, the magnetic field index, in the region in which the crystal is located, associated with saturation of the steel in the magnet at greater field strengths. In any event, the crystal is near a field region where n varies in space, as is evident from the contours dotted in figure 1, which were obtained from electrolytic trough measurements (Bracher 1950). The vertical free oscillation amplitude is inversely proportional to $\sqrt{n}$, so that the beam size will be greater than that expected for the value of $n(\simeq\frac{2}{3})$ existent at low field strengths. The beam size in the vertical direction is comparable with that suggested by aperture studies reported elsewhere (Riddiford *et al.* 1955).

Towards the end of the acceleration cycle the beam suddenly expands in the vertical direction if it is made to approach the region of the magnet in which the crystal is placed. It strikes the top and bottom rather than the back wall of the vacuum chamber. This is a result of resonant coupling in which energy is transferred to the vertical free oscillations from either the horizontal free oscillations or the rotational energy of the particles in the accelerator, should n reach a suitable value. A similar phenomenon was observed with the Berkeley 184-inch synchrocyclotron (Henrich, Sewell and Vale 1949). Figure 4 suggests that there exists no substantial sudden reduction in the extent of the horizontal oscillations at the instant in question, which implies that the resonance arises from the rotational energy. Low order resonances may then occur for $n=\frac{1}{4}, \frac{4}{9}$, etc.

3.2. *Horizontal Distribution*

After the radio-frequency accelerating potential is removed the beam spirals at a rate given by

$$\frac{dr}{dt}=-\frac{r(dB/dt)}{B(1-n)}$$

where r is the radius, B the magnetic field and $B \propto r^{-n}$. Using this equation the distribution of radial oscillation amplitudes can be obtained from traces such as are shown in figure 2. Phase oscillations cease when the accelerating potential is removed, but the radial dispersion due to them will continue to exist, resulting in an apparent broadening of the Rayleigh distribution due to gas scattering. The trace will of course show only one half of the distribution. The variation in half-width of the bunch in the radial direction with time is shown in figure 4. Early in the acceleration cycle the beam is distributed across the whole of the vacuum chamber. At later times the radial extent of the beam becomes less than the vertical extent. It is probable that the spread due to phase oscillations is then small. For the vertical free oscillation amplitude to exceed the horizontal amplitude, in the absence of resonant coupling one would require n to be less than 0·5 in the field region in question. The resonance described above could then be one of low order.

REFERENCES

BLACHMAN, N. M., and COURANT, E. D., 1948, *Phys. Rev.*, **74,** 140.
BRACHER, D. F., 1950, *Thesis*, University of Birmingham.
HENRICH, L. R., SEWELL, D. C., and VALE, V., 1949, *Rev. Sci. Instrum.*, **20,** 887.
NATURE, *Lond.*, 1953, **172,** 704.
RIDDIFORD, L., VAN DER RAAY, H. B., and COE, R. F., 1955, *Proc. Phys. Soc.* A, **68,** 489.

CONTENTS OF SECTION B

PAGE

Dr. G. K. Williamson and Dr. R. E. Smallman. X-Ray Extinction and the Effect of Cold Work on Integrated Intensities 577

Mr. M. G. Harwood. The Crystal Structure of Lanthanum–Strontium Manganites 586

Dr. J. N. Hodgson. The Infra-red Properties of Some Metallic Films . . 593

Dr. E. Rabinowicz. The Relation between Friction and Wear for Boundary-Lubricated Surfaces 603

Mr. J. A. Greenwood and Dr. D. Tabor. Deformation Properties of Friction Junctions 609

Dr. J. C. Firmin and Mr. C. W. Oatley. Effects Produced by Metal Electrodes in Studies of Electron Bombardment Conductivity 620

Dr. R. W. Wilson. The Contact Resistance and Mechanical Properties of Surface Films on Metals 625

Prof. L. F. Bates and Dr. N. P. R. Sherry. The Direct Separation of the Reversible and Irreversible Components of the Magnetothermal Effect . 642

Mr. A. H. McIlraith. The Properties of Fine Virtual Slits formed by Oblique Reflection at Cylindrical Surfaces 649

Prof. H. Fröhlich. Theory of Secondary Electron Emission from Solids . . 657

Prof. R. E. Burgess. Fluctuations of the Numbers of Electrons and Holes in a Semiconductor 661

Dr. G. Burniston Brown. A Theory of Action-at-a-Distance 672

Research Notes :

Dr. G. Liebmann. The Field Distribution in Asymmetrical Magnetic Electron Lenses 679

Dr. G. Liebmann. The Magnetic Pinhole Electron Lens 682

Dr. C. Dodd. Radio-Carbon Content and Delayed Boiling of Liquids . 686

Letters to the Editor :

Dr. D. A. Bell. Distribution Function of Semiconductor Noise . . 690

Reviews of Books 692

Contents of Section A 696

The Scattering-in Correction

By B. A. CHARTRES and D. A. TIDMAN

The F. B. S. Falkiner Nuclear Research and Adolph Basser Computing Laboratories,
School of Physics, The University of Sydney, Sydney, Australia†

Communicated by H. Messel; *MS. received* 1*st February* 1955 *and in amended form* 23*rd March* 1955

Abstract. In experimental work with nuclear research emulsions, one sometimes makes scattering measurements to determine the energy distribution of a beam of particles incident on the emulsion. To do this, one selects particles which leave tracks longer than a certain minimum length. This sample is a biased sample, and a correction for this bias has been calculated, considering both single and multiple scattering.

§ 1. Introduction

In using the photographic plate to study charged particles, one sometimes requires to make a measurement of the number of particles of a particular energy which enter the emulsion or are produced by events inside the emulsion. For an accurate measurement of the energy of a particle to be made its track must be longer than a certain minimum length x_0, usually ranging from 0·1 cm to 1 cm. The elimination of all tracks shorter than this minimum length introduces a systematic bias into the estimate of the number of particles in a particular energy group, this bias arising through the scattering of the particles in the emulsion.

We have calculated a correction for this bias for the special case in which it is desired to measure the angular and energy distribution of cosmic radiation in the atmosphere using a photographic plate exposed in a vertical plane. A similar correction will be relevant in many other cases.

Ignoring scattering altogether, and considering the geometry of a photographic plate exposed in a vertical plane in the atmosphere, one expects a certain number of tracks of various lengths to be left by particles passing through the emulsion. We shall show that when scattering is considered one obtains more tracks longer than the minimum length than the geometrical number expected. The difference we call the scattering-in correction. In our calculation of this correction we have considered the effect of both multiple and single scattering.

§ 2. Statement of Problem

Define $I(\Psi, p\beta)$ to be the angular and energy distribution of cosmic radiation in the atmosphere, where Ψ is the angle a particle makes with the vertical, p is its momentum and $\beta = vc^{-1}$. Let $I_e(\gamma, p\beta, x_0)$ be the angular and energy distribution obtained by examination of tracks longer than a certain minimum length x_0 in the photographic emulsion; γ is the angle a track makes with the vertical projected on to the plane of the emulsion, the angle being measured where the particle first enters the emulsion (see figure 1 (*a*)). We require the relation between I and I_e when the scattering of particles in the emulsion is taken into account.

---

† Also supported by the Nuclear Research Foundation within the University of Sydney.

Consider a particle entering the emulsion of thickness d at an angle ϕ to the emulsion surface. If it entered at an angle $\phi < \tan^{-1}(d/x_0) = \phi_0$ and suffered no scattering it would be certain to have a track length greater than x_0. However, like particle 1 in figure 1 (*b*), it may be scattered out of the emulsion. Similarly, a particle entering at an angle $\phi > \phi_0$ may, like particle 2, be scattered into the emulsion in such a way as to leave a track length greater than x_0. We shall show that 'scattering-in' predominates over 'scattering-out'.

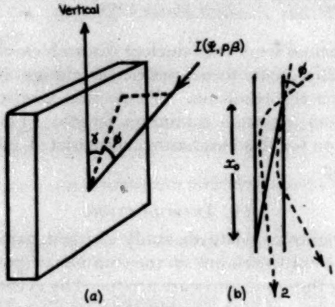

Figure 1.

Considering figure 1 (*a*), the incident particle makes an angle Ψ with the vertical given by the equation $\cos\Psi = \cos\phi\cos\gamma$. We shall need the probability $N(\phi, p\beta, x_0)$ that this particle makes a track in the emulsion of projected length greater than x_0.

To investigate the order of magnitude of the angles involved we consider as a typical example a minimum track length of 5 mm in a 200 micron plate which gives ϕ_0 equal to 2·3°. We shall show that even for the lowest energy particles we shall consider, the function $N(\phi, p\beta, x_0)$ tends to zero exponentially for angles ϕ greater than $2\phi_0$ and can be considered as zero for $\phi > 3\phi_0$. Consequently we see that the plate considered above accepts particles only within an angular range of seven degrees. Since $I(\Psi, p\beta)$ is known to be a slowly varying function of Ψ for small Ψ it follows that we can neglect the dependence of the incident spectrum on ϕ. Also for small ϕ we have $\cos\Psi = \cos\gamma$, and the distribution in γ will then be the same as in Ψ.

We define $I(\gamma, \phi, p\beta)d\phi d\gamma d(p\beta)$ as the number of particles in the intervals γ to $\gamma + d\gamma$, ϕ to $\phi + d\phi$ and $p\beta$ to $p\beta + d(p\beta)$ arriving on a unit area perpendicular to their direction of motion per unit time. Also $I_e(\gamma, p\beta, x_0)d\gamma d(p\beta)$ is defined as the number of tracks starting on a unit area of the emulsion surface in the ranges γ to $\gamma + d\gamma$ and $p\beta$ to $p\beta + d(p\beta)$ and of length greater than x_0, divided by the length of time for which the emulsion was exposed. We then have the relation

$$I_e(\gamma, p\beta, x_0) = \int_0^{\pi/2} d\phi \sin\phi I(\gamma, \phi, p\beta) N(\phi, p\beta, x_0).$$

Neglecting the dependence of I on ϕ, as justified in the preceding argument, we find

$$I_e(\gamma, p\beta, x_0) = K(p\beta, x_0) I(\gamma, p\beta) \qquad \ldots\ldots(2.1)$$

where

$$K(p\beta, x_0) = \int_0^{\pi/2} \sin\phi N(\phi, p\beta, x_0)\, d\phi. \qquad \ldots\ldots(2.2)$$

$K(p\beta, x_0)$ is the number of tracks longer than x_0 per unit angle as measured in the plane of the emulsion, when there is one particle per unit solid angle per unit area perpendicular to the direction of motion incident on unit surface area of the plate. It is this function that we shall calculate.

At very high energies when scattering can be ignored, the function $N(\phi, p\beta, x_0)$ is unity for ϕ less than ϕ_0 and zero for ϕ greater than ϕ_0. For this case of simple geometrical acceptance we have

$$\lim_{p\to\infty} K(p\beta, x_0)=K_g(x_0)=\tfrac{1}{2}\sin^2\phi_0\simeq\tfrac{1}{2}\phi_0{}^2. \qquad \ldots\ldots(2.3)$$

We now define the scattering-in correction C as

$$C=(K-K_g)/K_g. \qquad \ldots\ldots(2.4)$$

§ 3. SUMMARY OF METHOD

The scattering cross section σ of particles by emulsion nuclei has been divided into two parts, $\sigma_m+\sigma_s$ at an angle θ_c, such that σ_m takes account of the most probable deflections through small angles, and σ_s gives the probability of large deflections. We then work out the scattering-in correction for multiple scattering using σ_m, by defining an overestimate and an underestimate of the correction. Using σ_s an exact expression for the single-scattering correction is obtained on the assumption that a particle suffers at most one large-angle scatter in passing through the emulsion.

It is shown that it is possible to choose θ_c in such a way that the approximations made in the calculation are good ones, and that the single and multiple corrections can be combined additively.

§ 4. THE DISTRIBUTION FUNCTION

Let $\boldsymbol{\sigma}(p\beta, \boldsymbol{\theta})d\omega dx$ be the probability that a particle of momentum p suffers a deflection $\boldsymbol{\theta}$ into the solid angle $d\omega$ in travelling a distance dx. In the small angle approximation we can write $\boldsymbol{\theta}^2=\theta_y{}^2+\theta_z{}^2$ and $d\omega=d\theta_y d\theta_z$.

Let $\sigma(p\beta, \theta_y)d\theta_y dx$ be the probability that the particle suffers a deflection which has a component θ_y. Then the projected scattering probability σ is given by

$$\sigma(p\beta, \theta_y)=\int_{-\infty}^{+\infty}\boldsymbol{\sigma}(p\beta, [\theta_y{}^2+\theta_z{}^2]^{1/2})\,d\theta_z. \qquad \ldots\ldots(4.1)$$

We now consider a beam of particles incident along the x axis. The distribution function P is defined such that $P(\theta_y, y, x)d\theta_y dy$ is the number of particles at (y, x) passing through the line element dy in the angular interval θ_y to $\theta_y+d\theta_y$. Then this projected distribution function obeys the diffusion equation (Rossi 1952)

$$\frac{\partial P}{\partial x}+\theta_y\frac{\partial P}{\partial y}=\int d\theta'\sigma(\theta_y-\theta_y{}')[P(\theta_y{}', y, x)-P(\theta_y, y, x)]$$

with $$P(\theta_y, y, x=0)=\delta(\theta_y)\delta(y). \qquad \ldots\ldots(4.2)$$

This equation is soluble if certain assumptions are made. We will follow a procedure similar to that of Butler and split our cross section σ into two parts $\sigma_m+\sigma_s$ at an angle θ_c, so that σ_m takes account of the very frequent deflections through small angles and σ_s gives the probability of large deflections (Butler 1950).

Using σ_{m} as the scattering cross section in equation (4.2) we have a distribution function which is dependent on small-angle scattering. We can then expand P in the integrand of (4.2) into a Taylor series and take the first non-vanishing term which is proportional to the second moment of our cross section σ_{m}. Making this multiple-scattering approximation, and dropping the subscript y on θ as we shall not refer to the three-dimensional case again in this section, we have

$$\frac{\partial P}{\partial x}+\theta\frac{\partial P}{\partial y}=\mu\frac{\partial^2 P}{\partial\theta^2} \qquad \ldots\ldots(4.3)$$

where

$$\mu=\tfrac{1}{2}\int\theta^2\sigma_{\mathrm{m}}(\theta)\,d\theta \qquad \ldots\ldots(4.4)$$

the integral extending over all θ.

In an infinite medium equation (4.3) has the solution which was first derived by Fermi

$$P(\theta, y, x)=\frac{\sqrt{3}}{2\pi\mu x^2}\exp\left[-\frac{1}{\mu x^3}(3y^2-3xy\theta+x^2\theta^2)\right]. \qquad \ldots\ldots(4.5)$$

The lateral distribution $Y(y, x)$ irrespective of the angle θ is given by

$$Y(y, x)=\int P(\theta, y, x)\,d\theta=\left(\frac{3}{4\pi\mu x^3}\right)^{1/2}\exp\left[-\frac{3y^2}{4\mu x^3}\right]. \qquad \ldots\ldots(4.6)$$

Alternatively, using σ_{s} in (4.2) we can make use of the exact 'first-collision' integral equation corresponding to (4.2), namely

$$Y(y, x)=\int_0^x dx'\exp(-p_0x')\int_{-\infty}^{\infty}d\theta\sigma_{\mathrm{s}}(\theta)Y(y-\theta x-\theta x', x-x')+\delta(y)\exp(-p_0x) \qquad \ldots\ldots(4.7)$$

where

$$p_0=\int_{-\infty}^{+\infty}\sigma_{\mathrm{s}}(\theta)\,d\theta.$$

If θ_{c} is chosen so that the probability of scattering through angles greater than θ_{c} is small, that is if p_0x is small, we can use the convergent 'scatter-by-scatter' iterative solution of equation (4.7), viz.

$$Y=\sum_{n=0}^{\infty}Y_n \qquad \ldots\ldots(4.8)$$

$$Y_n(y, x)=\int_0^x dx'\exp(-p_0x')\int_{-\infty}^{\infty}d\theta\sigma_{\mathrm{s}}(\theta)Y_{n-1}(y-\theta x-\theta x', x-x') \qquad \ldots\ldots(4.9)$$

$$Y_0(y, x)=\delta(y)\exp(-p_0x).$$

Y_n is the contribution to the distribution function of particles which have suffered n scattering collisions.

We shall calculate the correction C using solutions (4.5) and (4.9). These two distribution functions cannot be added to yield the distribution for combined multiple and single scattering, but we shall show that, under certain conditions, the scattering-in corrections for these two extreme cases, which we shall write as C^{m} and C^{s}, are additive, and their sum is the required correction C.

§5. DEFINITION OF OVER AND UNDER ESTIMATES OF C^{m}

The functions P and Y give us the distribution in particle numbers in an infinite medium. In the emulsion a particle once having crossed out through either the emulsion–air or emulsion–glass surface is lost. (A particle passing out into the glass has a good chance of returning to the emulsion, but it is not recognized as the same particle). We therefore require to obtain from P and Y the 'first passage time distribution' for two imaginary parallel plane boundaries in an infinite medium, the boundaries representing the surface of the emulsion.

Consider a beam of particles of unit intensity incident at the surface of the emulsion at O, at an angle ϕ to the surface (see figure 2). Choosing the x axis along the direction of the beam and O as the origin of coordinates, the equations of the two surfaces are

$$y_1 = -x\phi, \qquad y_2 = d - x\phi \qquad \ldots\ldots(5.1)$$

if ϕ is a small angle.

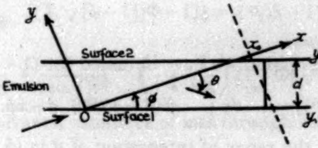

Figure 2.

If the emulsion were part of an infinite medium, then at $x = x_0$ the lateral distribution function Y would be

$$Y(y, x_0) = \left(\frac{3}{4\pi\mu x_0^3}\right)^{1/2} \exp\left[-\frac{3y^2}{4\mu x_0^3}\right]. \qquad \ldots\ldots(5.2)$$

Now consider the integral

$$N_1^{\mathrm{m}} = \int_{y_1(x)_0}^{y_2(x_0)} Y(y, x_0)\, dy. \qquad \ldots\ldots(5.3)$$

This counts all the particles between the boundaries at x_0 irrespective of how they got there. Hence a particle included in this integral may have crossed a boundary at some $x < x_0$ and returned again. This cannot happen in the actual emulsion, therefore N_1^{m} is an over-estimate of the number of particles still in the emulsion at $x = x_0$.

Now consider the integral

$$-\int_0^{x_0} dx \int_{-\pi/2}^{-\phi} d\theta \sin(\theta + \phi) P(\theta, -x\phi, x). \qquad \ldots\ldots(5.4)$$

This is the number of particles crossing out over surface 1. However, included in it are particles which have previously crossed out, returned, and are again crossing the boundary. Such a particle will be counted twice, in fact one particle lost will be counted as n particles lost if it crosses out and returns n times. The integral (5.4) is therefore an over-estimate of the number of particles lost through surface 1.

Since the function P decreases exponentially with increasing θ, we are able to extend the range of integration from $-\pi/2$ to $-\infty$ and replace $\sin(\theta + \phi)$ by $(\theta + \phi)$. In the same way, the loss through surface 2 is

$$\int_0^{x_0} dx \int_{-\phi}^{\infty} d\theta (\theta + \phi) P(\theta, d - x\phi, x). \qquad \ldots\ldots(5.5)$$

Therefore

$$1 - N_2^{\mathrm{m}} = \int_0^{x_0} dx \int_{-\phi}^{\infty} d\theta (\theta + \phi) P(\theta, d - x\phi, x) - \int_0^{x_0} dx \int_{-\infty}^{\phi} d\theta (\theta + \phi) P(\theta, -x\phi, x) \qquad \ldots\ldots(5.6)$$

which we write as

$$1-N_2{}^{\mathrm{m}}=(1-N_2{}^{\mathrm{m}})_2+(1-N_2{}^{\mathrm{m}})_1 \qquad \ldots\ldots(5.7)$$

where $N_2{}^{\mathrm{m}}$ is an under-estimate of the number of particles still in the emulsion at $x=x_0$.

We shall show that $N_1{}^{\mathrm{m}}$ and $N_2{}^{\mathrm{m}}$ are close limits bounding the correct value N^{m} of the number of particles of track length greater than x_0, and later will consider the best way of taking a weighted mean of the two limits.

We can also split $1-N_1{}^{\mathrm{m}}$ into a contribution from each surface, giving

$$(1-N_1{}^{\mathrm{m}})_1=\tfrac{1}{2}[1-\Phi(\psi\sqrt{X})] \qquad \ldots\ldots(5.8)$$

$$(1-N_1{}^{\mathrm{m}})_2=\tfrac{1}{2}[1-\Phi([1-\psi]\sqrt{X})] \qquad \ldots\ldots(5.9)$$

where $\psi=\phi/\phi_0$, $X=\frac{3}{4}\phi_0{}^2/\mu x$.

Now consider the expression we have obtained for $(1-N_2{}^{\mathrm{m}})_2$:

$$(1-N_2{}^{\mathrm{m}})_2=\int_0^{x_0}dx\int_{-\phi}^{\infty}d\theta(\theta+\phi)P(\theta,d-x\phi,x). \qquad \ldots\ldots(5.10)$$

If we were to extend the range of integration of θ in (5.10) to $-\infty$ it would count not only those particles passing out through surface 2 but also subtract those entering through the surface. But this would simply give us another expression for $(1-N_1{}^{\mathrm{m}})_2$. We therefore have

$$(1-N_2{}^{\mathrm{m}})_2-(1-N_1{}^{\mathrm{m}})_2=-\int_0^{x_0}dx\int_{-\infty}^{-\phi}d\theta(\theta+\phi)P(\theta,d-x\phi,x). \qquad \ldots\ldots(5.11)$$

We shall use this expression for numerical computation of $(1-N_2{}^{\mathrm{m}})_2$ as it is much smaller than (5.10). It can be simplified to

$$(1-N_2{}^{\mathrm{m}})_2-(1-N_1{}^{\mathrm{m}})_2=\frac{\sqrt{3}}{4\pi}\int_1^{\infty}\frac{d\eta}{\eta}\exp(-Y)\{\exp(-Z^2)-\sqrt{\pi}Z[1-\Phi(Z)]\} \qquad \ldots\ldots(5.15)$$

where $$Z=(\tfrac{1}{3}X\eta)^{1/2}(3\eta-\psi),\ Y=X\eta(\eta-\psi)^2.$$

§ 6. Isotropic Distribution of Incident Particles

So far we have obtained expressions which give us $N_1{}^{\mathrm{m}}$ and $N_2{}^{\mathrm{m}}$ for a parallel beam of particles incident on the surface of the emulsion at an angle ϕ. We now need the corresponding expressions for an isotropic distribution in ϕ. The quantities giving the over and under estimates of the number of tracks longer than x_0 are then

$$K_1{}^{\mathrm{m}}=\int_0^{\pi/2}N_1{}^{\mathrm{m}}(\phi)\sin\phi\,d\phi \qquad \ldots\ldots(6.1)$$

$$K_2{}^{\mathrm{m}}=\int_0^{\pi/2}N_2{}^{\mathrm{m}}(\phi)\sin\phi\,d\phi \qquad \ldots\ldots(6.2)$$

with $K_1{}^{\mathrm{m}}>K^{\mathrm{m}}>K_2{}^{\mathrm{m}}$.

From table 1, which has been calculated for the typical value $X=1{\cdot}4$, it can be seen that at $\psi=3$ the estimates of loss through surface 1 have become very nearly zero and through surface 2 nearly 100%. These limits are approached exponentially. Hence in integrating over ϕ, if we consider those quantities which tend to zero with increasing $\phi(=\phi_0\psi)$ it will be valid to replace $\sin\phi$ by ϕ and extend the range of integration to infinity. Table 1 also shows that the function $N(\phi, p\beta, x_0)$, as stated in § 3, tends rapidly to zero for $\psi>2$. This justifies the use of an isotropic angular distribution.

The quantities we used for computation are

(i) Over-estimate of loss through surface 1:

$$(1-K_2{}^{\mathrm{m}})_1=\int_0^\infty (1-N_2{}^{\mathrm{m}})_1\,\phi\,d\phi=0{\cdot}1523\phi_0{}^2/X. \qquad \ldots\ldots(6.3)$$

(ii) Under-estimate of loss through surface 1:

$$(1-K_1{}^{\mathrm{m}})_1=\int_0^\infty (1-N_1{}^{\mathrm{m}})_1\,\phi\,d\phi=0{\cdot}1250\phi_0{}^2/X. \qquad \ldots\ldots(6.4)$$

(iii) Over-estimate of number remaining in

$$K_1{}^{\mathrm{m}}=\int_0^\infty N_1{}^{\mathrm{m}}\,\phi\,d\phi$$

$$=\phi_0{}^2\left[\frac{1}{2}+\frac{1}{8X}+\frac{e^{-X}}{(4\pi X)^{1/2}}-\left(\frac{1}{4}+\frac{1}{8X}\right)\{1-\Phi(\sqrt{X})\}\right]. \qquad \ldots\ldots(6.5)$$

(iv) Difference between estimates of loss through surface 2:

$$(1-K_2{}^{\mathrm{m}})_2-(1-K_1{}^{\mathrm{m}})_2=\int_0^\infty [(1-N_2{}^{\mathrm{m}})_2-(1-N_1{}^{\mathrm{m}})_2]\,\phi\,d\phi. \qquad \ldots\ldots(6.6)$$

Table 1

ψ	$(1-N_1{}^{\mathrm{m}})_1$	$(1-N_1{}^{\mathrm{m}})_2$
0	0·5000	0·0463
0·4	0·2506	0·1565
1·0	0·0463	0·5000
2·0	0·0004	0·9537
3·0	0·0000	0·9996

The integrands in all these integrals tend exponentially to zero for $\phi>3\phi_0$. The above choice of quantities computed has been made so that the only one which requires a numerical integration, namely (iv) (which requires a double numerical integration), is an order of magnitude smaller than the others. In figure 3 are drawn curves of $K_1{}^{\mathrm{m}}$ and $K_2{}^{\mathrm{m}}$ as functions of X. It can be seen that the limits define the true value of K fairly closely down to quite small values of X.

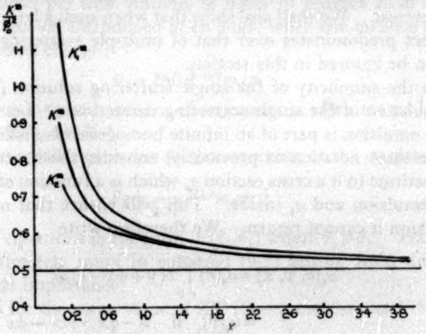

Figure 3.

§7. ESTIMATE OF THE CORRECTION FOR MULTIPLE SCATTERING

We have shown that the true value of K^{m} lies somewhere between K_1^{m} and K_2^{m}. We now investigate the possibility of obtaining from K_1^{m} and K_2^{m} an estimate for K^{m} which is more accurate than either of the former. This is done by comparing the relative magnitude of the errors in K_1^{m} and K_2^{m}.

The correct number of particles lost, viz. $1-K^{\mathrm{m}}$, is obtained by counting as one particle lost every particle which crosses either boundary any number of times between $x=0$ and $x=x_0$. The under-estimate $1-K_1^{\mathrm{m}}$ of the loss is obtained by counting as one particle lost any particle which crosses the boundaries an odd number of times, but not counting those which cross an even number of times. The over-estimate $1-K_2^{\mathrm{m}}$ counts 1 for a particle crossing once or twice, 2 for one crossing three or four times, and so on.

Now if a particle is much less likely to cross $n+1$ times than n times for fairly small n (and this is so when the scattering-in correction is a few per cent) we can take $K^{\mathrm{m}}-K_{\mathrm{g}}$ as an approximate expression for the number crossing once, $K_1^{\mathrm{m}}-K^{\mathrm{m}}$ for the number crossing twice and $K^{\mathrm{m}}-K_2^{\mathrm{m}}$ for those crossing three times. Assuming that the probability of a particle re-crossing a surface is independent of whether it has already crossed once or twice we obtain the following approximate relation

$$(K^{\mathrm{m}}-K_{\mathrm{g}})(K^{\mathrm{m}}-K_2^{\mathrm{m}})=(K_1^{\mathrm{m}}-K^{\mathrm{m}})^2 \qquad \ldots\ldots(7.1)$$

which reduces to

$$K^{\mathrm{m}}=[(K_1^{\mathrm{m}})^2-K_{\mathrm{g}}K_2^{\mathrm{m}}](2K_1^{\mathrm{m}}-K_2^{\mathrm{m}}-K_{\mathrm{g}})^{-1}. \qquad \ldots\ldots(7.2)$$

Although the above reasoning breaks down when the correction is large, that is for $X<0{\cdot}5$, we may still assume that equation (7.2) gives a better estimate of K^{m} than either K_1^{m} or K_2^{m}. K^{m}, as obtained from (7.2) is plotted, together with K_1^{m} and K_2^{m} in figure 3.

§8. SINGLE SCATTERING

In this section we calculate the correction which arises from one single large angle scatter. By a suitable definition of 'large angle', that is, by a suitable choice of θ_{c}, we can ensure that at most one such event will occur in the majority of tracks. We will show that this choice of θ_{c} is quite satisfactory over the range of physical interest. We shall also show that when such a large angle scatter does occur its effect predominates over that of multiple scattering, so that multiple scattering can be ignored in this section.

Owing to the simplicity of the single scattering solution (4.9) we can make an exact calculation of the single scattering correction C^{s}, i.e. we do not assume here that the emulsion is part of an infinite homogeneous medium.

Using the same notation as previously, consider the iterative solution (4.9). We must substitute in it a cross section σ_{s} which is a function of position, i.e. zero outside the emulsion and σ_{s} inside. This will ensure that once a particle has left the emulsion it cannot return. We therefore write

$$\begin{aligned}\sigma_{\mathrm{s}}(\theta, y, x)&=\sigma_{\mathrm{s}}(\theta)\int_0^d \delta(y+\phi x-\epsilon)\,d\epsilon\\ &=\sigma_{\mathrm{s}}(\theta) \quad \text{if} \quad d-\phi x>y>-\phi x\\ &=0 \quad \text{otherwise.}\end{aligned} \qquad \ldots\ldots(8.1)$$

If we make this substitution, (4.9) yields

$$Y_0(y,x)=\delta(y)\exp(-p_0x)$$

$$Y_1(y,x)=\exp(-p_0x)\int_0^x dx'\int_{-\infty}^{\infty}d\theta\int_0^d d\epsilon\sigma_s(\theta)\delta(\phi x'-\epsilon)\delta(y-\theta x+\theta x'). \qquad \ldots\ldots(8.2)$$

The number of particles which have suffered n collisions and are still in the emulsion at $x=x_0$ is given by

$$K_n^s=\int_0^{\infty}\phi d\phi\int_0^d dy Y_n(y-\phi x_0,x_0). \qquad \ldots\ldots(8.3)$$

Defining K_g exactly as before we have

$$K_g=\tfrac{1}{2}\phi_0^2\simeq\tfrac{1}{2}\phi_0^2\exp(-p_0x_0)(1+p_0x_0). \qquad \ldots\ldots(8.4)$$

The approximation is valid under the assumption that two or more large-angle scatters are highly improbable. The single scattering correction C^s then becomes

$$\begin{aligned}C&=\frac{K_0^s+K_1^s-K_g}{K_g}\\&=\frac{x_0\exp(-p_0x_0)}{K_g}\left[\frac{1}{12}p_2-\frac{1}{3}\int_{\phi_0}^{\infty}\sigma_s(\theta)(\theta-\phi_0)^3\frac{d\theta}{\theta}+\frac{1}{6}\int_{4\phi_0}^{\infty}\sigma_s(\theta)(\theta^2-4\theta\phi_0)^{3/2}\frac{d\theta}{\theta}\right]\end{aligned} \qquad \ldots\ldots(8.5)$$

where

$$p_2=\int_{-\infty}^{\infty}\sigma_s(\theta)\theta^2\,d\theta.$$

§9. COMBINATION OF THE SINGLE AND MULTIPLE SCATTERING CORRECTIONS

We take for the scattering cross section $\boldsymbol{\sigma}(\boldsymbol{\theta})$ the formula

$$\begin{aligned}\boldsymbol{\sigma}(\boldsymbol{\theta})&=R(\theta^2+\theta_1^2)^{-2} &&\text{if}\quad \boldsymbol{\theta}<\theta_2\\&=0 &&\text{if}\quad \boldsymbol{\theta}>\theta_2\end{aligned} \qquad \ldots\ldots(9.1)$$

where

$$R=4\sum_i \mathrm{N}_iZ_i^2r_e^2\left(\frac{m_ec}{p\beta}\right)^2,$$

r_e is the radius and m_e the mass of the electron. The summation is over the numbers N_i of nuclei per unit volume, of different charges Z_i in the emulsion. θ_2 is a large angle cut-off introduced at an angle when the nucleus can no longer be considered a point charge:

$$\theta_2=280A^{-1/3}m_ecp^{-1} \qquad \ldots\ldots(9.2)$$

where A is the atomic mass number. For a mixture of atoms we have taken the mean value $A^{1/3}=\Sigma_iN_iA_i^{1/3}N^{-1}$.

The angle θ_1 is small and is due to the screening of the nucleus by electrons

$$\theta_1=\frac{1}{137}Z^{1/3}m_ecp^{-1}. \qquad \ldots\ldots(9.3)$$

θ_1 enters into our equations in the form $\ln(\theta_2/\theta_1)$ where $\theta_0\gg\theta_1$. Hence numerical factors of approximately unity in equation (9.3) arising from different atomic models are of little importance.

We have used for the mean value of $Z^{1/3}$ (Scott and Snyder 1950)

$$Z^{1/3}=\left[\sum N_iZ_i^2\Big/\sum_i N_iZ_i^{4/3}\right]^{1/2}. \qquad \ldots\ldots(9.4)$$

Now consider the angle θ_c at which we have divided the scattering cross section σ into two parts. The condition $\theta_c \ll \phi_0$ is equivalent to making it only possible for a particle to get outside the emulsion at $x=x_0$ by suffering a large number of collisions, i.e. it is the condition that the multiple scattering distribution function should be gaussian as assumed.

The condition that we must impose in order to justify our assumption that more than one large angle scatter is very unlikely is $p_0 x_0 < \frac{1}{8}$ say. This imposes a lower limit on θ_c, which for a G5 emulsion is

$$\frac{4\cdot784}{(p\beta)^2}\left[\frac{1}{\theta_c^{\,2}} - \frac{4}{\pi\theta_2\theta_c}\right] x_0 < \tfrac{1}{8}\times 10^4 \qquad \ldots\ldots(9.5)$$

where $p\beta$ is in units MeV/c and x_0 in microns.

These two conditions on θ_c can be simultaneously satisfied only for a certain range of $p\beta$ and x_0. We shall give the scattering-in correction for this range which, fortunately, happens to be the range of most interest to experimenters.

As can be seen from figure 4, the single scattering correction C^s is consistently smaller than the correction C^m due to multiple scattering. But it should be noted that a single scatter occurs in only a small percentage of tracks, viz. one in every $(p_0x_0)^{-1}$ tracks. The magnitude of the correction in those tracks in which a large angle scatter does occur is therefore given by $C^s(p_0x_0)^{-1}$ which is plotted in figure 4. It can be seen that in those tracks which have a large angle scatter the multiple scattering correction is negligible in comparison with the single scatter correction. Consequently C^m and C^s are additive, and we get

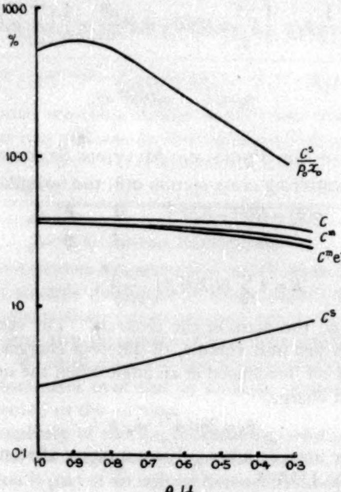

Figure 4.

$$C = \exp(-p_0x_0)C^m + C^s. \qquad \ldots\ldots(9.6)$$

Now, if θ_c is chosen correctly, the total correction should be insensitive to variation in it. For the particular emulsion, track length and energy considered in figure 4, the condition (9.5) reduces to $\theta_c > \frac{1}{6}\phi_0$. It can be seen from the graph that C is a slowly varying function over the range plotted, so for simplicity in calculation we take the value $\theta_c = \phi_0$.

The total correction C and the ratio K/K_g for G5 nuclear research emulsion are tabulated in table 2 as a function of $p\beta$ for four typical values of x_0 and d.

Table 2

$d=200\,\mu$, $x_0=5000\,\mu$

$p\beta$	C (%)	K/K_g
83	46·21	0·6838
100	37·01	0·7298
150	21·89	0·8204
200	14·25	0·8753
250	9·33	0·9146
300	6·93	0·9352
350	5·24	0·9502
400	4·01	0·9614
500	2·61	0·9745
600	1·81	0·9822
700	1·33	0·9869

$d=200\,\mu$, $x_0=10000\,\mu$

$p\beta$	C (%)	K/K_g
230	43·69	0·6959
250	39·77	0·7155
300	32·07	0·7572
350	26·59	0·7899
400	22·50	0·8163
450	19·07	0·8356
500	16·77	0·8564
600	12·78	0·8867
800	7·64	0·9290
1000	5·00	0·9524
1200	3·64	0·9649
1400	2·64	0·9743

$d=400\,\mu$, $x_0=5000\,\mu$

$p\beta$	C (%)	K/K_g
41	46·74	0·6815
100	14·25	0·8753
150	7·00	0·9346
200	4·02	0·9614
250	2·60	0·9747
300	1·71	0·9821

$d=400\,\mu$, $x_0=10000\,\mu$

$p\beta$	C (%)	K/K_g
115	43·61	0·6963
150	31·29	0·7617
200	23·00	0·8130
250	16·76	0·8565
300	12·60	0·8881
350	9·40	0·9141
400	7·63	0·9291
500	5·02	0·9522
600	3·52	0·9660
700	2·62	0·9745

From these tables we see that the scattering correction C is positive, i.e. the number of the tracks K longer than x_0 in the emulsion is greater than the geometric number K_g. This is true in all cases in which the intensity of radiation incident on the plate is slowly varying over an angular range of $\phi < 3\phi_0$. Using this correction the photographic plate can be used reliably to extend energy spectrum measurements down to the region $p\beta \sim 100$ MEV/c.

ACKNOWLEDGMENTS

We would like to thank Dr. E. P. George and Dr. A. J. Herz for useful discussions. One of us (B. A. C.) is indebted to the Commonwealth Scientific and Industrial Research Organisation, and one (D. A. T.) to the University of Sydney Research Committee for the provision of research grants. We would also like to thank Professor Messel for the excellent research facilities provided in the School of Physics.

REFERENCES

BUTLER, S. T., 1950, *Proc. Phys. Soc.* A, **63**, 599.
ROSSI, B., 1952, *High Energy Particles* (New York : Prentice-Hall).
SCOTT, W. T., and SNYDER, H. S., 1950, *Phys. Rev.*, **78**, 223.

The Variation of Track Length with Angle of Dip in Photographic Nuclear Research Emulsion

By R. B. J. PALMER and H. A. B. SIMONS
Physics Department, The Royal Free Hospital School of Medicine, London W.C.1

MS. received 25th February 1955 *and in final form* 10*th May* 1955

Abstract. Alpha particle and $\alpha + {}^3H$ tracks have been measured at angles of dip between 0 and 90° in Ilford C2 emulsions. No significant variation in track length with angle of dip has been found except in measurements made with one microscope. A fault in the depth measuring mechanism is shown to account for this effect.

---

§ 1. INTRODUCTION

MEASUREMENTS of an apparent variation in length of the track of a heavily ionizing particle with angle of dip in photographic emulsion for nuclear research have been reported with differing results.

Rotblat and Tai (1949, 1951) found that α and $\alpha + {}^3H$ particle track lengths observed in the processed emulsion increased with increasing angle of dip between the track direction and the surface of the emulsion for angles of dip greater than a certain critical value which they related to the grain spacing. They suggested that, when the emulsion shrinks during processing, tracks in which the silver grains are close together contract to some extent, but resist the full shrinkage of the gelatine. The track lengths obtained therefore for tracks at large angles of dip, which are calculated on the assumption that the track shrinkage in a vertical direction is the same as that of the gelatine, are too large. Horan (1953) using α-particles from ^{210}Po in Eastman N.T.A. and N.T.B. emulsions also found an increase in length of track with angle of dip. The track length is reported as increasing by 65% from measurements made in a plane parallel to the free surface of the emulsion to measurements made at 40° dip. Greenberg and Haslam (1953), using ^{210}Po particles calculated a shrinkage factor by measuring tracks incident at a known shallow angle (up to 5°) on the plate. Using this value, they obtained the lengths of tracks incident at greater angles to the emulsion surface, and concluded that the emulsion shrinkage was uniform and that track lengths do not vary with dip. The experiments reported here have been made to investigate further this effect.

§ 2. EXPERIMENTAL PROCEDURE

Measurements have been made on α-particle tracks from ThC′ in Ilford C2 emulsion and on ${}^3H + \alpha$ tracks in Li loaded C2 emulsion. The α-particle track measurements have included measurements on tracks formed by particles entering the surface of the emulsion and also on tracks distributed throughout the emulsion. The ${}^3H + \alpha$ tracks measured were all distributed throughout the emulsion.

The surface irradiation of C2 plates of 100μ thickness was made from an active deposit source of thorium. A brass plate carrying the source was fixed to the lid of a small vacuum chamber with a movable shutter beneath it. The plate, which had previously been stored at constant humidity, was attached to a small table beneath the shutter. This table was pivoted and weighted so that, as the vacuum chamber was tilted, the table always remained horizontal. The position of the radioactive source relative to the surface of the plate could thus be varied, and by tipping the evacuated chamber through angles up to 180° in a vertical plane whilst the shutter was drawn aside, particle tracks incident at widely varying angles were obtained over the whole surface.

Alpha particle tracks were obtained throughout the emulsion by preparing a solution of ThB and C in hydrochloric acid. This was diluted until the activity was such that the track density produced finally in the exposed plate was convenient for measurement. A 100μ plate which had been pre-soaked in water was immersed in the radioactive solution for 45 to 60 minutes. The plate was dried rapidly *in vacuo* and left for 2 or 3 days under conditions of constant humidity, by which time the activity had fallen to 3% or less, leaving tracks distributed throughout the plate. It was expected that these tracks would show a tendency to be shorter than the surface tracks since some were produced while the emulsion was swollen, but these should occur randomly at all orientations.

The $^3H + \alpha$ tracks were obtained by bombarding 200μ Li loaded C2 emulsions with low energy neutrons. Of these, the thermal neutrons reacted with the lithium nuclei releasing an α-particle and triton of fixed energy in each case. These particles produced straight tracks of constant length orientated randomly in the unprocessed emulsion.

Before development, the corners of each plate were cut off and a number of measurements of the emulsion thickness were made at each corner by scraping away part of the emulsion and focusing a microscope on the emulsion and glass surfaces in turn. The rest of the plate was soaked in water, cold-developed in amidol developer, soaked in a cold 2% acetic acid stop-bath and fixed in a 20% hypo solution with constant stirring. It was then washed thoroughly and allowed to dry in a horizontal position at room temperature and humidity.

After processing, each track length was determined by measuring the projected horizontal length x and the apparent depth z. By use of the apparent shrinkage factor S the total track length L is given by $L = (x^2 + S^2z^2)^{1/2}$, where S is the ratio of the apparent thickness of the processed emulsion, obtained by focusing a microscope on the surface and through the emulsion on to the glass backing, to the original thickness previously determined. The final processed thickness varied slightly over the whole plate, so that frequent measurements of this thickness were made as tracks in different parts of the plate were being observed and the appropriate value of S was used to compute the individual track lengths.

In addition the emulsions of some plates were swollen to more than their original thickness by soaking them in a 20% solution by volume of glycerine in water. They were then dried and coated with a thin film of Perspex in chloroform; this dried rapidly leaving a thin coating of Perspex on the surface which made the swollen plates easier to handle and prevented excessive absorption of moisture by the glycerine from the atmosphere. They were then re-examined, the shrinkage factor in this case being almost unity, and the total depth measurement of the processed emulsion therefore being rather less critical than in the previous examination.

§ 3. MEASUREMENT

The track measurements concerned were carried out on three different microscopes. Horizontal measurements of track lengths were made by means of an eyepiece graticule initially calibrated against a stage micrometer, and vertical measurements were made by means of a micrometer drum on the fine focus mechanism calibrated by the makers in micron divisions. The drum was re-calibrated on the same scale as the eyepiece graticule by fixing the stage micrometer in a vertical plane in the place of the microscope objective and viewing this horizontally through another microscope while the drum was rotated in 100 μ steps throughout its complete range.

A complete analysis of a number of plates, however, showed considerable discrepancies between plates examined by means of microscope 2 and those examined by means of microscopes 1 and 3. The microscopes were re-calibrated, particular care being taken with the vertical drum calibration, and microscope 2 was found to exhibit an error. Whilst the fine adjustment drum was being rotated consistently in one direction, 100 μ depths were consistently recorded on the drum as 100 μ. When, however, an attempt was made to repeat a particular 100 μ depth measurement and the drum was rotated back to a position just above the first setting and the depth measurement repeated, the depth measurement recorded on the drum was found on an average to be 102·5 μ. When the drum was rotated back to a position further from the first setting (e.g. 20 μ above that setting) the average value of the depth measurement on the drum tended to be smaller, and if the drum was rotated still further back (e.g. 100 μ above the original setting), the true 100 μ depth was recorded on the drum as 100 μ as before. In fact it was found that the reading obtained for any particular setting could vary by 2·5 μ depending on the conditions of approach. Thus any depth measurement of 20 μ or over was liable to a maximum error of 2·5 μ, seeing that the lower setting was always approached in approximately the same way. Smaller depth measurements were found to be liable to smaller maximum errors, as errors were obtained in both upper and lower settings and tended to cancel when the depth value was determined by subtraction. The fault was fully investigated and an estimate was made of its effect on measurements of a constant track length at different angles of dip, and it was found to account for the discrepancy in results. The fault may be inherent in the design of this type of fine focus adjustment, and its presence would not necessarily have been detected by normal calibration.

§ 4. ANALYSIS OF RESULTS

In figure 1 are shown the results obtained for ThC′ α-particles and $\alpha + {}^3\mathrm{H}$ tracks measured on microscopes 1 and 3. Track measurements have been divided into groups with angles of dip (0–10°, 10–20°, etc.) defined as dip relative to the surface of the emulsion. Line A is the result of measurements made with microscope 1 on 7 different plates, each point representing between 80 and 250 surface track measurements; line B is the result of measurements on two thorium loaded plates using microscope 3, each point representing approximately 50 track measurements. Line C is the result of measurements on one plate, both dry and swollen with glycerine, most points on it representing over 50 track measurements. The error shown at each point on the graphs is the standard deviation of the mean of the track lengths. It will be seen that there is no significant variation of track length with angle of dip in any case.

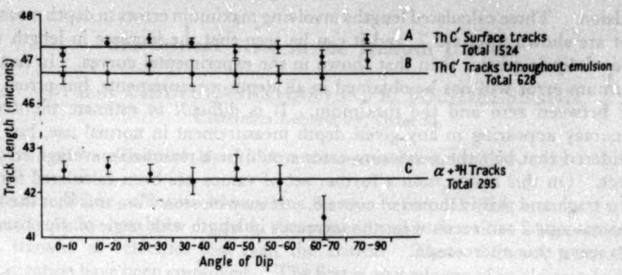

Figure 1.

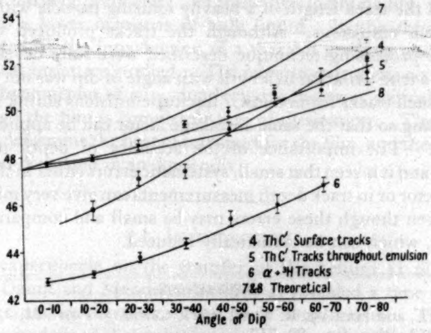

Figure 2.

In figure 2 are shown the results obtained from track measurements made using microscope 2. Curve 4 represents measurements made on about 240 surface α-particle tracks in one plate. Curve 5 represents measurements on two thorium loaded plates with a total of approximately 1000 tracks. Curve 6 represents measurements on 1100 $\alpha + {}^3\mathrm{H}$ tracks in three different plates. One of these plates had previously been analysed using microscope 3, with results included in line C. It can be seen that in all the above measurements track lengths apparently increase with angle of dip. Curves 7 and 8 show an attempt that has been made to investigate the effect of faulty depth measurements on the final calculated length of a track of true length 47·5 μ if it were measured at different angles of dip in the emulsion. It has been found by measurements made with the microscope that depths of 3 μ, 4·5 μ, 8 μ, 15 μ and 17 μ are recorded as 4 μ, 6 μ, 9·5 μ, 17 μ and 19·5 μ respectively when subject to a maximum consistent error. By assuming the 47·5 μ track to lie at such an angle that the necessary depth measurement coincides with each of the above values in turn, and that a maximum error is involved in each measurement, the final faulty value that would be obtained for the track length has been calculated, together with the corresponding angle of dip, a shrinkage factor of 2·7 being assumed for the emulsion. These calculated lengths involving maximum errors in depth measurement are shown in curve 7, and it can be seen that the increase in length with angle of dip is greater than that shown in the experimental curves. In fact the maximum error will not be obtained in all depth measurements, but errors will vary between zero and the maximum. It is difficult to estimate the overall inaccuracy appearing in any given depth measurement in normal use, but it is considered that half the maximum error would be a reasonable average error to expect. On this assumption a further set of values has been calculated for the $47{\cdot}5\,\mu$ track and this is shown in curve 8. It may be seen from this that the fault in microscope 2 can account for the increases in length with angle of dip observed when using this microscope.

§ 5. CONCLUSIONS

These results indicate that with the processing technique used by us there is no variation in the track length of a heavily ionizing particle with angle of dip in nuclear research emulsions. Although the tracks produced using Ilford C2 plates and the processing technique described were fully developed with close grain spacing, a true variation in length with angle of dip was not observed. This indicates that such tracks formed in C2 nuclear emulsions shrink with the gelatine during processing so that the same shrinkage factor can be applied to tracks at all angles of dip. The importance of the accuracy of depth measurements is demonstrated, and it is seen that small, systematic errors either in the determination of shrinkage factor or in track depth measurements can give very misleading results. This is true even though these errors may be small and comparable in size with random errors, which can be statistically reduced.

REFERENCES

GREENBERG, L. H., and HASLAM, R. N. H., 1953, *Canad. J. Phys.*, **31,** 7, 1115.
HORAN, J. R., 1953, *Phys. Rev.*, **90,** 717.
ROTBLAT, J., and TAI, C. T., 1949, *Nature, Lond.*, **164,** 835; 1951, *Photographic Sensitivity*, Ed. J. W. Mitchell (London : Butterworths Scientific Publications), p. 336.

Sub-Critical Flow in the Helium II Film

By B. S. CHANDRASEKHAR† and K. MENDELSSOHN
Clarendon Laboratory, Oxford

MS. received 10*th March* 1955 *and in amended form* 13*th May* 1955

Abstract. While in most observations on the helium II film, transport at the critical velocity has been studied, the present paper describes observations of film transfer at velocities less than the critical. Three different methods of investigation have been employed. The first is an analogue of an electrical circuit embodying a current–potential measurement on a superconductor. The second method uses as indicator the formation of bulk liquid out of a film which passes over a surface of varying perimeter. In these two methods film transfer occurs from a higher to a lower meniscus of bulk liquid. In the third method film transfer is initiated by the introduction of a thermal gradient and transfer rates under varying heat input are studied. The experiments show conclusively that, similar to the phenomenon of superconductivity, below a critical velocity, flow of helium through the film is completely free of dissipation. The third method has been used to determine the heat of transport for the film, and these experiments are described and discussed in an Appendix.

§ 1. Introduction

THE early experiments on the transfer of the helium II film along solid surfaces (Daunt and Mendelssohn 1939 a) revealed a type of flow which, though unusual in character, obeys fairly simple rules. The phenomena are in fact so clearly defined that subsequent investigations could add little to the original observations. Indeed those experiments which seemed to indicate a deviation from this simple pattern (Atkins 1948, de Haas and van den Berg 1949) could be traced to secondary effects, such as contamination of the solid surface (Bowers and Mendelssohn 1950), or surface irregularities (Chandrasekhar and Mendelssohn 1952, Chandrasekhar 1952, Daunt and Smith 1954).

In contradistinction to the flow properties of the helium II film, the transport phenomena in the bulk liquid are of very considerable complexity. Attempts have been made to interpret these phenomena as a mixture of two types of flow, classical viscous flow and 'superflow' with vanishing dissipation of energy. On the basis of this two-fluid model, it has been postulated that viscous flow is effectively suppressed in the thin transfer film, which therefore exhibits pure superflow. The most striking feature of liquid transfer by the film is that it takes place, for a given temperature, at a steady rate which is independent of the level difference, the height of the barrier and the length of the path. This has led to the concept of a critical rate of mass transfer in the film, for which recently indications have also been observed in the bulk liquid (Bowers and Mendelssohn 1952, Hung, Hunt and Winkel 1952, Chandrasekhar and Mendelssohn 1953). The invariance of the critical film rate with the nature of the experimental arrangement indicated that transfer up to this rate is free of friction.

---

† Now at Westinghouse Research Laboratories, East Pittsburgh, U.S.A.

The absence of dissipation below a critical transport rate in conjunction with other features creates an interesting parallelism between liquid helium II and superconductivity (Daunt and Mendelssohn 1942, F. London 1945, Mendelssohn 1945). In the early experiments the helium transfer always took place at the critical rate and thereby differed from the classical experiment on superconductivity demonstrating zero resistance. The latter is a current–potential measurement which, as shown in figure 1 (*a*), uses a battery B and a resistance R for limiting the current in the circuit so that its value in the superconductor S is sub-critical. The voltmeter V will then indicate zero potential difference across the superconductor. The question arose whether a similar experiment can be carried out in the case of liquid helium II, demonstrating mass flow under zero potential difference.

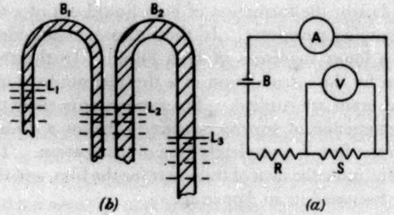

Figure 1. Analogue between a current–potential measurement on (*a*) a superconductor and (*b*) the helium film.

The fact that the rate of film transfer has been found to be accurately proportional to the available perimeter of solid surface offers such a possibility. Let us for instance consider transfer from a level L_1 to a level L_3 as shown in figure 1 (*b*) in which use is made of two solid bridges, B_1 leading from L_1 to an intermediate level L_2, and B_2 from L_2 to L_3. If the perimeter of the bridge from L_1 to L_2 is smaller than that between L_2 and L_3, the total transport of fluid will be determined by the width of the first bridge. The arrangement now is quite analogous to the circuit shown in figure 1 (*a*). The battery B providing the potential difference is represented by the level difference between L_1 and L_3. The bridge between L_1 and L_2 corresponds to the resistance R, since it limits the transfer to a value which is smaller than the critical rate across the wider bridge between L_2 and L_3. The latter therefore corresponds to the superconductor S and the potential drop across it is measured by the level difference between L_2 and L_3 corresponding to the voltmeter V. If the sub-critical flow of the helium film is free of friction, this difference will be zero.

An experiment based on the principle outlined in figure 1 (*b*) making use of two concentric beakers corresponding to B_1 and B_2 was carried out some years ago. The result mentioned in a brief communication (Daunt and Mendelssohn 1946) indeed showed that there existed a transfer of mass under zero potential difference.

The transport of helium by superflow is accompanied by a mechano-caloric effect (Daunt and Mendelssohn 1939 b). While it appeared unlikely that in the experiment with the double beaker mentioned above this effect influenced the phenomena, the importance of the result (cf. F. London 1954) made it desirable to check it more carefully. Moreover other questions connected with flow below and above the critical rate, as for instance the formation of bulk liquid from the film, required elucidation. Finally the thermo-mechanical effect (Allen and Jones 1938, Daunt and Mendelssohn 1939 b) seemed to offer another possibility of studying helium transfer at sub-critical rates. The work described in this paper deals with these three aspects of sub-critical transfer in the helium II film. For the sake of clarity, the results of each section are discussed together with the observations. The thermal measurements also offer a means for determining the heat of transport in the film, and these measurements are described in the Appendix.

§ 2. FILM TRANSFER UNDER ZERO POTENTIAL DIFFERENCE

2.1. *Method*

If helium is transferred from a higher level inside a beaker to a lower level outside, the observed quantity is the rate of change dh/dt of the level. For a cylindrical beaker $dh/dt = 2R_c/r$, where R_c is the critical rate of transfer of the helium film measured as volume per unit time per unit length of perimeter, and r is the radius of the beaker. Since dh/dt is inversely proportional to the radius, the outflow of helium from two concentric beakers is determined by the radius of the outer beaker. This means that when starting with the same height of level in the inner and the outer beakers, the transfer over the rim of the inner beaker takes place at a rate *smaller* than the critical rate R_c. Neglecting the wall thickness of the beakers, the flow rate from the inner to outer beaker at the start of the experiment is $(r_i/r_o)R_c$, where r_i and r_o are the radii of the inner and outer beakers respectively. Accordingly, in this experiment, the separation between the levels in the inner and outer beakers corresponds to the potential difference to be measured.

In order to make sure that the temperature in the three volumes of helium was the same, the lower part of the two beakers was made of thin-walled copper, as shown in figure 2. Thermal equilibrium was ensured between the inner and

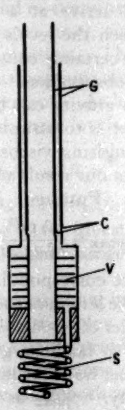

Figure 2. Diagram of improved double beaker.

outer beakers by the vanes V, and between the outer beaker and the bath by the copper spiral tube S. Cylindrical glass tubes G of inner diameters 0·84 and 1·26 cm respectively were sealed to the copper assembly at C. The wall thickness of these glass tubes was approximately 0·1 cm but this may be neglected in our subsequent discussion, as the results deduced are not affected.

2.2. *Results*

The equilibrium condition for the beaker partly immersed in the bath of liquid helium II was for the inner and outer levels to be at the same height as that of the bath. In fact the outer level was slightly raised above the other two levels owing to surface tension. The separation of the levels was not uniform throughout the annulus because it had been impossible to seal in the glass tubes in a perfectly concentric manner. The calculated rise due to surface tension was 0·04 cm, while the actually observed value varied between 0·02 and 0·05 cm.

For the experiment, the beaker was raised out of the equilibrium position, so that the levels in the beaker were about 2 cm above that of the bath. The menisci in the beaker were measured every 30 seconds and it was found that they stayed together, falling at a rate corresponding to the diameter of the outer beaker. This result therefore confirms our earlier observation and shows that the latter was not falsified by thermal effects. The slight separation of the two beaker levels due to surface tension did in fact facilitate the observation of equal fluid pressure.

It is immediately apparent that the film transfer cannot be due to acceleration by gravity. From the latest determinations of the film thickness (Ham and Jackson 1954) and of the transfer rate (Mendelssohn and White 1950), the average velocity of helium flowing from the inner into the outer beaker can be calculated for the temperature of the experiment (1·27°K). This is by assuming that all the helium in the film takes part in the motion. In this way we obtain the minimum velocity which the moving mass in the film can have, since if only a part of the film were engaged in the actual transport, the moving mass would be smaller and its velocity higher. In our case this minimum velocity was between 15 and 20 cm sec^{-1}. Thus in order to arrive at a final velocity of approximately 35 cm sec^{-1}, the separation between the levels would have to be about 0·6 cm. On the other hand, the levels were certainly coincident at all times within 0·02 cm, this being the uncertainty of the observation.

The only other way in which gravity can be made responsible for the flow from the inner to the outer beaker is to assume that the film forms a siphon in which helium can move with vanishing viscosity. Such a picture can in fact be used in order to determine from our result an upper limit for the coefficient of viscosity of helium II in the film. Putting

$$\eta_{\max} = \frac{\Delta p d^3}{6l\, dv/dt} \qquad \ldots\ldots(1)$$

where Δp is the pressure difference corresponding to the uncertainty of the level separation, d the film thickness, l the length of the film and dv/dt the rate of volume flow, we arrive at a value of the order of 10^{-14} poise. This is the lowest maximum value for the viscosity which has so far been given.

This limiting value of $\eta_{\max}$ must however not be considered to mean that the siphon model is a physical reality. $\eta_{\max}$ as determined in our experiments corresponds exactly to the maximum value of resistivity which can be ascribed to a superconductor. To interpret the transfer phenomenon as a siphon flow with vanishing viscosity would be equivalent to describing a superconductor as a normal metal with very small resistivity. The breakdown of the siphon model becomes apparent when instead of the flow from the inner to the outer beaker, we consider that from the outer beaker to the bath. With $\eta_{\max}$ in equation (1) becoming smaller, the rate of volume flow should nevertheless remain proportional to the pressure difference Δp and inversely proportional to the length of the film l. On the other hand, our present experiments, and indeed all earlier observations show that dv/dt is quite independent of either Δp or l. The only way out of this difficulty is to assume that in the helium film, similar to a superconductor, the resistance is actually zero, which would make equation (1) indeterminate. We further see that, again analogous to a superconductor, the condition of zero resistance by itself is insufficient to describe the phenomena. In order to prevent dv/dt from tending to infinity as η tends to zero, a limiting value has to be introduced, which in physical reality is represented by the critical transfer rate R_c. It has been suggested (Mendelssohn 1945) that the momentum of film transfer is derived from the zero-point energy. The critical rate of transfer is accordingly given as the speed under its zero-point momentum with which a mass of helium can be redistributed to a state of lower total energy. In the case of a beaker, the state of lower energy is clearly that with levels inside and outside the same, and the rate of redistribution should depend on the dimension of the connecting link, i.e. the film. The fact that the relation $\bar{v} \sim h/md$ (where m is the mass of the helium atom and d the film thickness) does indeed yield the correct order of magnitude for the average velocity of film flow $\bar{v}$ is encouraging although, owing to the dimensional nature of the relation, it can hardly be regarded as a proof for the model.

2.3. *Further Experiments with the Double Beaker*

Making use of the conclusions reached in the preceding paragraph, i.e. assuming frictionless transfer in the film which is limited by a critical rate R_c, one can predict any readjustment of the levels. There are six different mutual positions of the inner, outer and bath levels, two of which correspond to the initial conditions investigated in the earlier work and re-examined in the preceding section. These are the cases of the sequence: inner level, outer level, bath level, with the bath level in the highest or the lowest position. The four other cases present a slightly more complex aspect, but if our assumptions are correct, they should follow directly from the geometry of the arrangement. As long as the three levels are separate, the movements of the inner and outer levels dh_i/dt and dh_o/dt are given by the equations:

$$dh_i/dt = 2R_c/r_i \qquad \ldots\ldots(2)$$

$$dh_o/dt = 2R_c/(r_o \pm r_i). \qquad \ldots\ldots(2a)$$

The four remaining cases have been investigated and the results are shown schematically in figure 3. The slight change in the height of the bath level has been neglected.

The results of these observations show indeed that the prediction about the behaviour of the levels is fulfilled, and for practical purposes the assumptions made by us can be accepted for solving problems of film transfer. It should be emphasized again that these considerations can be applied only when the film transfer takes place isothermally on smooth and uncontaminated surfaces.

§ 3. FORMATION OF BULK LIQUID FROM THE FILM

It had already been observed in the early experiments that under certain conditions bulk liquid in the shape of drops can be formed out of the film. Under isothermal conditions no such formation can take place above the highest liquid level in the system. Otherwise an arrangement could be constructed which is equivalent to a perpetual motion machine. On the other hand one cannot predict under which conditions liquid will leave the film below the highest level or what will happen if in a non-equilibrium state there are a number of levels at different heights in the system. Evidently the size of the solid perimeter above the highest place where the film is in contact with the bulk liquid is of importance since it had been observed that film flow through a constriction in the perimeter has a different value according to whether or not this constriction was above the highest meniscus (Daunt and Mendelssohn 1939 a).

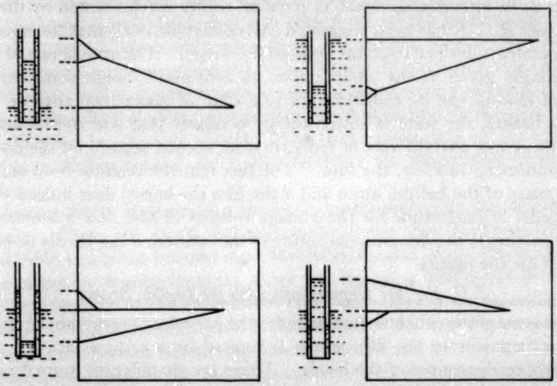

Figure 3. Movement of helium levels with time in the double beaker. The diagrams refer to the four relative positions not treated in the original experiment.

In order to investigate this problem a beaker was constructed in such a manner that the flow over a varying perimeter below the highest level could be made super-critical or sub-critical. The formation of drops could then be observed and the conditions under which this took place clearly defined.

The beaker was made of glass in the form shown in figure 4. Its diameter decreased in steps from the top downwards, the widest section A being at the top. The glass 'skirt' D was attached to the 'waist' of the beaker, and inside D was another 'skirt' E. The maximum diameter of D was greater than the inside diameter of A, and that of E was between the inside diameters of A and B. D and E each had a glass 'drop' (not shown) fused to the rim, to help collect any bulk liquid that might form. The actual dimensions of the apparatus, in centimetres, were as follows: inside diameters of: $A=1\cdot 8$, $B=0\cdot 8$, $C=0\cdot 35$; maximum diameters of: $D=2\cdot 2$, $E=1\cdot 4$, $F=0\cdot 5$. The beaker was enclosed in a thin-walled copper radiation shield, with two narrow vertical slits cut in it to permit observation. For the experiment the beaker was filled with liquid helium and raised out of the bath, which was at a temperature of 1·2°K. The following phenomena were observed: (i) With the inner level in A, drops were seen to form at all the three points D, E and F, detach themselves and fall into the bath. The rate of formation of these drops at each point remained constant as long as the inner level was in A. (ii) As the inner level passed through the narrowing part of the beaker from A to B, the intervals between successive drops from D increased and when the inner level entered B, these drops ceased altogether. The drops from E and F continued. (iii) When the inner level entered C, drops ceased to form at E also, and continued to appear at F only.

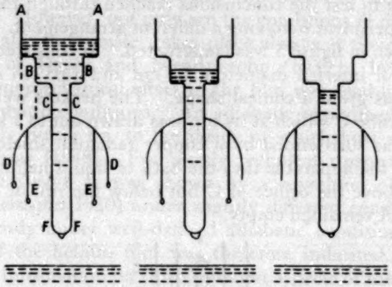

Figure 4. First experiment on the formation of bulk liquid from the film.

The observations listed under (i), (ii) and (iii) can be fully explained under the assumption that drops are formed because the film cannot exceed the critical rate. At the beginning of the experiment helium leaves the top reservoir in a film of perimeter A and at the rate AR_c. As it runs down over the outside of B and C pure film flow cannot be maintained, since the perimeter is smaller than A, and R_c would have to be exceeded. Bulk liquid will be formed, and from an observation of Jackson and Henshaw (1950) one might expect this to be in the form of droplets. This stream of liquid is subsequently distributed over a larger perimeter than A, when it reaches the rim of the outer skirt D. However in order to reach a lower level than the rim of D the helium will have to run up the inside of D and down the outside of the inner skirt E. Since E is smaller than A the flow in this section of the path cannot remain pure film transfer because the rate $R=(A/E)R_c$ would be super-critical. Free liquid will therefore form on the inside of D, collect at its rim and eventually fall down in drops. A similar process will take place at the next stage where helium has to run up the inside of E. Only that amount of helium, corresponding to FR_c, can reach the outside of the beaker. The rest must drop off at E in the form of free liquid.

As the level inside the beaker moves into B, the critical rate on the outside of E, ER_c would be larger than the rate BR_c at which the film is now formed. There is thus no necessity for surplus liquid to be separated out on the surface of D and consequently no drops are formed at the rim of D. The same argument can be used for the third case, when the helium level has dropped into C. Now the rates ER_c and FR_c are both larger than the generating rate CR_c. As a result, no drops are formed either at D or at E, and the helium transferred out of C moves in the form of the film over the whole surface of the beaker, until liquid is eventually formed into drops at the bottom of F.

The most remarkable of the three cases is (ii). It shows that even below the highest level in the system, the helium which has been in the form of droplets will be formed back into the film if the perimeter is larger than the generating one. The film issuing from B cannot move as such over the outside of C and droplets will be formed. The fact that these droplets of free liquid do not collect at the bottom of D shows that they have been re-formed into the film.

As mentioned earlier, the object of this experiment was to determine the conditions under which free liquid will be formed out of the film and it seemed therefore advisable to test the conclusions reached through the observations just described in an experiment involving a different arrangement. For this purpose, the apparatus shown in figure 5 was constructed. It consisted of two concentric beakers A and B of internal diameters 1·5 cm and 1·05 cm respectively. The lower part of A was given a conical shape. The beakers were held in position by a narrow glass tube C which at its top was drawn out to a small orifice. The whole assembly was surrounded by a copper radiation shield with observation slits. By dipping the apparatus into the bath of liquid helium so that the level of the latter was above the orifice of C but below the rim of A, liquid could be filled into B while A remained empty.

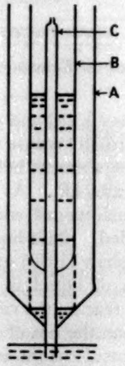

Figure 5. Second experiment on the formation of bulk liquid from the film.

For the experiment, B was partly filled in this manner. The time necessary to do this was very short, and no observable amount of free liquid collected in A due to transfer through the film from the bath. Then the apparatus was lifted out of the helium bath altogether. Film transfer now took place out of B into A and out of A in to the bath, and the rate of this transfer was determined by the inside perimeter of B. As the film reached the lower end of B on the outside, the solid connecting surface available to it decreased below the generating perimeter, and free liquid was formed. This liquid could be seen to collect in the bottom of A. As the experiment proceeded the level in A rose slowly until it finally came to rest still within the conical part. From now on helium kept on disappearing from B ultimately finding its way to the bath, but the level in A rose no further. The final position of this level was that at which the inside perimeter of the cone was just equal to the generating perimeter in B. This is precisely the result which had to be expected from our earlier conclusions. The total transport of liquid was determined by the inner perimeter of B multiplied by the critical transfer rate at this temperature (1·27°K). The final level in A simply marked that position above which the rate was always sub-critical.

§ 4. THERMOMECHANICAL FILM TRANSFER

Film transfer to a higher temperature will occur in any helium cryostat below the λ-point. However, not only are the conditions ill defined under these circumstances but also the transfer takes place always at the critical rate. The early experiments of Daunt and Mendelssohn (1939 b, 1950) in which the existence of a thermomechanical effect in the film was established were carried out under non-adiabatic conditions. An adiabatic experiment, using a Dewar vessel with a closely fitting lid, to the inside of which heat was supplied, was carried out by Atkins (1948). For purely technical reasons his results were unfortunately inconclusive as was shown by a repetition of his experiments (Brown and Mendelssohn 1950) under slightly different conditions.

A systematic study under well-defined adiabatic conditions of the thermomechanical flow of the helium film was therefore indicated. Experiments of this kind will yield information on three different aspects of the helium problem: (i) the relation between transfer rate R and heat input dQ/dt will give a measure of the dissipation, (ii) they will provide a measure of the critical rate, and (iii) they yield a determination of the 'heat of transport' which is required to convert unit mass of helium from film to bulk liquid. Only the first two aspects fall strictly under the scope of this paper, while the third, which is of more general significance, will be dealt with in an Appendix.

4.1. *Method*

The method used was identical with that of Brown and Mendelssohn (1950), i.e. helium was drawn into a Dewar vessel closed with a tight-fitting lid and the relation between heat input and mass flow determined. One of the objections to Atkins' experiments was that for purely geometrical reasons a critical rate which was apparently too high had been observed. In Brown and Mendelssohn's experiments this error had been eliminated by making the inside perimeter of the Dewar vessel larger than the outer one. This precaution was unnecessary in the present experiments, since the establishment of the numerical value of the critical transfer rate was of secondary importance.

The transfer beaker is shown in figure 6. A was a small unsilvered Dewar vessel of inside diameter 0·46 cm, depth 7 cm, and outside diameter 1·10 cm. The lip of the Dewar was blown flat and optically polished. A glass cap B, with its lower side also optically polished, fitted on the Dewar. This whole arrangement was surrounded by a cylindrical radiation shield made of thin copper. The shield was made in two parts C and D, which screwed together at H. By inserting the steel spring E between D and the glass cap, and then screwing down D, the cap was held firmly pressed against the Dewar. C had two narrow slits to permit observation of the helium level inside the beaker. Heat could be supplied to the inside of the beaker by passing a current through the resistance G.

The gap K between the optically polished surfaces was estimated by flow measurements, with air at room temperature and liquid helium at 4·2°K. The results by the two methods agreed, giving about 1 μ for the width of this gap. A small helium 'tank' F was attached to the top of the radiation shield by means of two stout copper supports. The tank had a small hole at the top, through which it could be kept filled with liquid helium right through the course of an experiment by dipping it into the bath from time to time. This tank prevented radiation from the warmer parts of the liquefier cryostat impinging on the top of the flow apparatus.

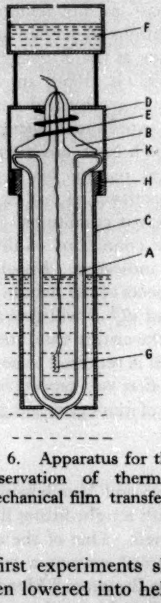

Figure 6. Apparatus for the observation of thermo-mechanical film transfer.

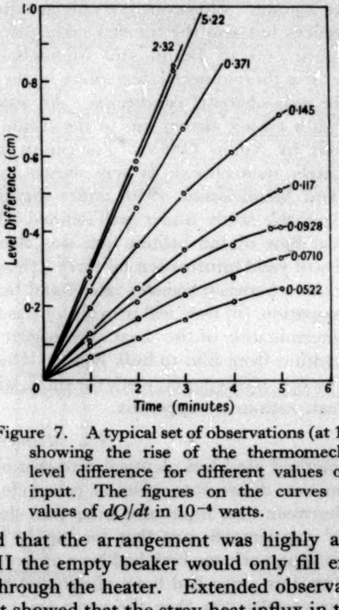

Figure 7. A typical set of observations (at 1·40°K) showing the rise of the thermomechanical level difference for different values of heat input. The figures on the curves denote values of dQ/dt in 10^{-4} watts.

The first experiments showed that the arrangement was highly adiabatic, since when lowered into helium II the empty beaker would only fill extremely slowly if no power were applied through the heater. Extended observations on the flow rate under zero heat input showed that the stray heat influx in the range of our experiments corresponded to 1% or less of the critical heating rate dQ_c/dt. This correction was at the limit of observation, and moreover will not affect our results since it would only produce a very small parallel shift of the $(R, dQ/dt)$ curves, but not alter their slope.

A feature of the experiments which was at first puzzling was that the inner level would occasionally become stable a few millimetres *below* the height of the outer level. This was explained when it was realized that the gap K was filled by surface tension with bulk liquid (cf. McCrum 1954). A temperature difference of 10^{-5}–10^{-4} degree between the gap K and the bath, as could easily be accounted for by stray heat influx, would be sufficient to stabilize the inner level at a millimetre or two below the bath level. This is because, owing to the adiabatic nature of the interior of the beaker, thermomechanical equilibrium between it and K exists, but not between K and the bath. It was further observed that when the temperature of the bath was suddenly reduced by pumping, drops of bulk liquid would form in the upper part of the beaker and run down on the lead wires. This again was due to the high adiabaticity of the arrangement which allowed the formation of bulk liquid at the inner rim of the gap K owing to the thermomechanical pressure difference between the warm inside and the cold outside of the beaker.

The experiments were carried out by applying, at constant bath temperature, different heat inputs dQ/dt to the inside of the beaker, and observing the rise of the liquid level in the beaker with time. A typical set of curves obtained at a temperature of 1·40°K is shown in figure 7. It can be seen that in the beginning the rise is linear, and only after some time does the rate of rise drop owing to loss of heat from the beaker. The linearity is a further proof of the adiabatic conditions of the experiment.

4.2. *Results*

The results of the flow rate R of helium into the beaker under varying heat input dQ/dt and at different temperatures, are given in figure 8. The experimental points all refer to the tangent at the origin of the curves typified in figure 7. Since, in the latter figure, the first observational points on all curves fall on straight lines, our values of R refer to conditions in which deviation from perfect adiabaticity could not be detected within the accuracy of our measurements.

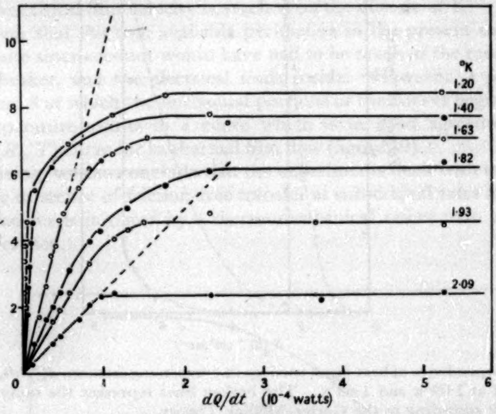

Figure 8. Variation of transfer rate R with heat input dQ/dt.

The curves for the different temperatures appear each to be made up of three sections. Starting at the origin, R rises first linearly with dQ/dt. Then follows a curved section in which the increase of R with dQ/dt becomes slower. Finally R remains independent of dQ/dt up to the highest values investigated. Only at the highest temperature is the curved section completely missing. This curved section seems, as will be discussed below, to be due to the geometry of the arrangement, and is not considered to be of general importance.

In general shape, the $(R, dQ/dt)$ curves for the film are similar to those obtained for the flow of bulk liquid through fine slits (Bowers and Mendelssohn 1952). In these observations, too, the first rise of R is linear, indicating that for small velocities the transport occurs without friction. Frictional forces only make their appearance beyond a certain critical flow rate R_c which in some of the experiments was very sharply defined. Originally a dependence of friction on the cube of the velocity had been postulated by Gorter and Mellink (1949) from measurements on wide slits filled with bulk helium II. However, the lack of friction for small velocities in narrow slits has recently been confirmed by Hung, Hunt and Winkel (1952). The distinguishing feature of the present results is the complete independence of R from dQ/dt for higher heat inputs. This gives the impression that in the film no thermomechanical flow at all can occur beyond a certain critical rate. How completely different the flow mechanism in the film is from that in wide capillaries is shown in figure 9, where our results at 1·63°K and 2·09°K have been compared with the Gorter–Mellink theory. This theory describes fairly well the occurrence of friction in all but the very narrow capillaries (Atkins 1951). Following the procedure of Bowers and Mendelssohn (1952) we have divided the $(R, dQ/dt)$ diagram into flow velocities with and without friction, the division being indicated by the broken lines for the two temperatures mentioned above in figure 8. For any given value of R the heat input dQ/dt is therefore divided into a presumably reversible part dQ_R/dt which is used to withdraw liquid from the film, and another part dQ_F/dt which is required to overcome friction in the liquid flow. In figure 9, R is plotted against dQ_F/dt. These experimental values are compared with the theroetical

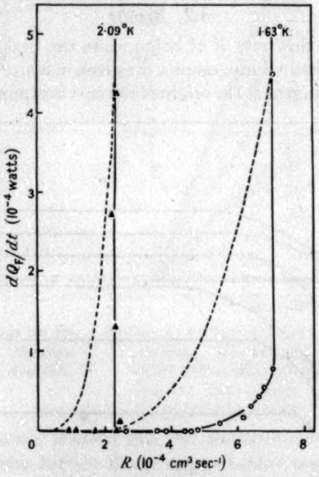

Figure 9. Dependence of heat input used up in overcoming friction, dQ_F/dt, on the transfer rate R at 2·09°K and 1·63°K. The broken lines represent the minimum values for dQ_F/dt according to the Gorter–Mellink Theory.

curves of the Gorter–Mellink theory, which have been fitted to our plots by normalizing the function at the highest value of dQ_F/dt covered by our experiments. It is obvious that the results on the film cannot be brought into accord with the flow phenomena in the bulk liquid. Besides the appearance of frictionless flow at low velocities, there is also no evidence for the existence of a cube law of friction at velocities higher than the critical. On the contrary, the friction seems to rise from the value zero, with only a short intermediate region (none at 2·09 °K), to infinity.

We are reluctant to draw conclusions concerning the small region in which the friction rises gradually. The object of the present experiments was to establish the linearity of the lower part of the (R, dQ/dt) curves and thereby to demonstrate the freedom from friction in the region of sub-critical flow rates. Since no attempt was to be made to establish the value of R_c, the latter being known from other experiments (Mendelssohn and White 1950), no special precautions had been taken in the geometrical design of the apparatus which was therefore open to the same objections as Atkins' original (1948) experiments. This means that as dQ/dt is rising, the limiting velocity will first be approached on the inner rim of the gap K and from then onwards helium can still enter the beaker by bulk liquid flow at super-critical velocities (cf. Bowers and Mendelssohn 1952) until the critical film velocity is reached on the outside of K. It should be noted moreover that the true available perimeters in the present case were not easy to compute since account would have had to be taken of the radiation shield outside the beaker, and the electrical leads inside. However, a plot of those points in figure 8 at which the horizontal portions of the curves begin against the absolute temperature results in a curve which is in good agreement with the well known (R_c, T) curve for isothermal film flow (figure 10).

Summarizing, we can conclude that the experiments dealt with in this section also show the existence of friction-free transfer at sub-critical rates in those cases where the transfer is initiated by a thermomechanical rather than a hydrostatic pressure difference.

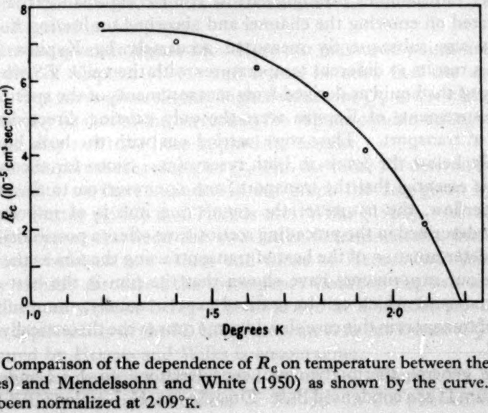

Figure 10. Comparison of the dependence of R_c on temperature between the present work (circles) and Mendelssohn and White (1950) as shown by the curve. The values have been normalized at 2·09°K.

§ 5. CONCLUSIONS

One of the main objects of the experiments described in this paper was to compare superfluidity in helium with the phenomena of electrical superconductivity. The striking features of the latter only become apparent below a certain critical current density which depends on temperature. While the two phenomena are similar, the analogy is of course not complete owing to the difference in the nature of the particles involved. However, a close resemblance to the superconducting phenomena could be expected in the case of the helium film where, owing to the small thickness, the hydrodynamical effect of the normal component can be disregarded. The conditions in helium under these circumstances are therefore similar to those in a superconductor at low frequencies. It was the aim of the present work to try and demonstrate in helium two basic phenomena observed in superconductivity: flow free of resistance, and the limitation of this flow by a critical current density. The first of these phenomena was demonstrated in §§ 2 and 4, and the second in §§ 2, 3 and 4.

The suggestion of a fundamental analogy between superconductivity and superfluidity (Daunt and Mendelssohn 1942, Mendelssohn 1945, 1954) was taken up in 1945 by F. London who has since elaborated the theoretical background of the analogy in many ways (F. London 1950, 1954). One of us (K. M.) likes to take this opportunity to record his gratitude to the late Professor F. London for many extensive and clarifying discussions on the subject.

APPENDIX

THE HEAT OF TRANSPORT

The mechano-caloric effect provides direct evidence that the liquid helium II passing in superfluid flow through a narrow channel has a lower entropy than the bulk liquid. The first direct observation (Daunt and Mendelssohn 1939 b) showed clearly that if under adiabatic conditions helium is forced from one container into another through narrow connecting channels, a quantity of heat is liberated on entering the channel and absorbed on leaving it. This heat of transport was subsequently measured accurately by Kapitza (1941) who compared his results at different temperatures with the value TS where S is the *total* entropy of the liquid as derived from measurements of the specific heat.

The measurements of Kapitza were the only existing direct determination of the heat of transport. They were carried out with the bulk liquid passing through a slit below the levels in both reservoirs. Since for theoretical interpretation it is essential that the transport from one reservoir to the other should be pure superflow, the nature of the connecting link is of importance. Our arrangement described in the preceding section now offers a possibility of carrying out a direct determination of the heat of transport using the *film* as the connecting link. Since our experiments have shown that the film is the best example of frictionless transport which can be realized experimentally, the results obtained for the heat of transport in this case should come near to the theoretically interesting quantity TS.

Applying general thermodynamic considerations to F. London's model (1938) of helium II as a condensed Bose–Einstein gas, H. London (1939) connected the heat of transport per gramme Q_T with the entropy per gramme S of the liquid at temperature T by the equation

$$Q_T/T=S. \qquad \ldots\ldots(3)$$

H. London assumes that the liquid flowing in the film will carry lattice vibrations, but that their entropy is only a negligible part of the total entropy S.

The data used for the determination of Q_T are those given in figure 8. If dV/dt is the rate at which helium enters the Dewar vessel under a rate of heat input dQ/dt, the heat of transport

$$Q_T=\frac{1}{\rho}\frac{d(dQ/dt)}{d(dV/dt)}. \qquad \ldots\ldots(4)$$

Since dV/dt was determined immediately after the heating current was switched on, the corresponding difference of temperature between the helium in the bath and that in the reservoir was vanishingly small. Because we use for our determination the tangents to the experimental curves drawn at the origin, the determination of Q_T corresponds to adiabatic conditions. The corrections which had to be applied are small but in view of the discrepancies to be discussed below, must be mentioned in some detail. One correction arises from the fact that the energy supplied by the heater will not only be used for drawing liquid into the Dewar but also for heating the liquid already inside the Dewar. The highest value of this correction was of the order of 0·5%. Secondly, as the helium in the container rises the vapour phase is compressed and some of it must condense, supplying its heat of condensation to the inside of the beaker. As is known from earlier experiments (Brown and Mendelssohn 1950) this process is instantaneous owing to the high heat conductivity of liquid helium II. This correction, which is very small at the lowest temperature, is, however, the most important one at the two highest points measured by us at 1·93°K and 2·09°K, where it amounts to 3 and 5% respectively. Other processes taking place, such as the evaporation of liquid due to the increase in vapour pressure and the specific heat of the vapour, did not provide detectable thermal effects. The effect of heat loss from the inside of the Dewar to the outside, and its elimination in the calculations, has already been discussed earlier in this paper.

Our results are given in figure 11. Here our measured points are compared with the results of Kapitza (1941) and it can be seen that the agreement is satisfactory. Our curve gives slightly higher values for Q_T at the higher temperatures, but this may be due to the correction for vapour condensation, which is not mentioned and may not have been applied in his case.

In order to compare these results for Q_T with the value TS derived from specific heat measurements, we have included in our graph the data given by Kramers, Wasscher and Gorter (1952) and Hercus and Wilks (1954). As can be seen, there is a discrepancy between the two latter determinations, but reasonably good agreement between our values and those of Hercus and Wilks. These authors have already discussed the discrepancy between the two sets of values of the specific heat without being able to arrive at a satisfactory explanation. However the applicability of the H. London formula to our values of Q_T and those of TS measured by Hercus and Wilks is encouraging.

In the temperature range investigated by us, any discrepancy between Q_T and calorimetrically determined values of TS due to the phonon contribution should, except at the lowest temperature, hardly be noticeable. Measurements of the specific heat of liquid helium below 1°K (Hull, Wilkinson and Wilks 1951, Kramers *et al.* 1952) indicate that in the neighbourhood of 0·7°K the T^6 law gives way to a T^3 law. This may indicate that the entropy of liquid helium is made up of a phonon contribution following a T^3 law to which is added a spectrum of anomalous excitations giving rise to the λ-phenomenon. The latter would then evidently follow a law of higher power of T and become noticeable at 0·7°K. If, as has been suggested (Tisza 1947, 1949), the anomalous thermal effects in helium II are due only to those extra excitations, H. London's formula should become invalid as the temperature of 0·7°K is approached. A preliminary measurement of the thermomechanical effect between 0·5°K and 1·1°K (Bots and Gorter 1953) has indeed indicated a lower value than that to be expected from the London equation. Measurements of this kind suffer from requiring the complex technique of adiabatic demagnetization, and the difficulty of maintaining temperature differences below 1°K. It would appear that the same information could be obtained more simply by isothermal measurements of Q_T such as are described in this paper. Using the published values of the specific heat and extrapolating the T^3 region with a Debye function of $\theta = 27{\cdot}5$, one should expect, if phonons are carried, that at 1°K and 0·8°K Q_T would be 50% and 25% respectively of the values of TS. Using a specially designed helium cryostat, it should be possible to make measurements of Q_T in the range between these two temperatures.

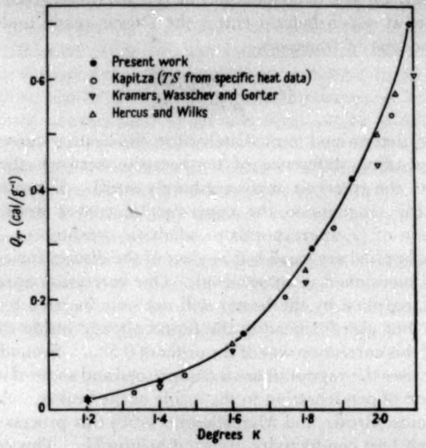

Figure 11. The heat of transport Q_T as a function of temperature.

At the lowest temperature at which measurements could be made with the apparatus described in this paper (1·2°K) the deviation of Q_T from TS would amount to only about 20%. It is worthy of note that our measured point at this temperature agrees well with the value TS derived from the specific heat measurements. Our results therefore seem to favour the suggestions made by Landau (1941) and by Ward and Wilks (1952) that the phonons also contribute to the heat of transport. A difference of 20% should certainly have been detected with the accuracy of our measurements. However, one is reluctant to base important conclusions on data obtained at one extreme end of our range of measurements and the final decision as to whether or not phonons are carried in the thermomechanical effect must be left to specially designed measurements of Q_T at somewhat lower temperatures.

REFERENCES

ALLEN, J. F., and JONES, H., 1938, *Nature, Lond.*, **141,** 243.
ATKINS, K. R., 1948, *Nature, Lond.*, **161,** 925; 1951, *Proc. Phys. Soc.* A, **64,** 833.
BOTS, G. J. C., and GORTER, C. J., 1953, *Phys. Rev.*, **90,** 1117.
BOWERS, R., and MENDELSSOHN, K., 1950, *Proc. Phys. Soc.* A, **63,** 178; 1952, *Proc. Roy. Soc.* A, **213,** 158.
BROWN, J. B., and MENDELSSOHN, K., 1950, *Proc. Phys. Soc.* A, **63,** 1312.
CHANDRASEKHAR, B. S., 1952, *Thesis* (University of Oxford).
CHANDRASEKHAR, B. S., and MENDELSSOHN, K., 1952, *Proc. Phys. Soc.* A, **65,** 226; 1953, *Proc. Roy. Soc.* A, **218,** 18.
DAUNT, J. G., and MENDELSSOHN, K., 1939 a, *Proc. Roy. Soc.* A, **170,** 423; 1939 b, *Nature, Lond.*, **143,** 719; 1942, *Ibid.*, **150,** 604; 1946, *Phys. Rev.*, **69,** 126; 1950, *Proc. Phys. Soc.* A, **63,** 1305.
DAUNT, J. G., and SMITH, R. S., 1954, *Rev. Mod. Phys.*, **26,** 172.
GORTER, C. J., and MELLINK, J. H., 1949, *Physica*, **15,** 285.
DE HAAS, W. J., and VAN DEN BERG, G. J., 1949, *Rev. Mod. Phys.*, **21,** 524.
HAM, A. C., and JACKSON, L. C., 1954, *Phil. Mag.*, **45,** 1084.
HERCUS, G. R., and WILKS, J., 1954, *Phil. Mag.*, **45,** 1163.
HULL, R. A., WILKINSON, K. R., and WILKS, J., 1951, *Proc. Phys. Soc.* A, **64,** 379.
HUNG, C. S., HUNT, B., and WINKEL, P., 1952, *Physica*, **18,** 629.
JACKSON, L. C., and HENSHAW, D. G., 1950, *Phil. Mag.*, **41,** 1081.
KAPITZA, P. L., 1941, *J. Phys., Moscow*, **5,** 59.
KRAMERS, H. C., WASSCHER, J. D., and GORTER, C. J., 1952, *Physica*, **18,** 329.
LANDAU, L. D., 1941, *J. Phys., Moscow*, **5,** 71.
LONDON, F., 1938, *Nature, Lond.*, **141,** 643; 1945, *Rev. Mod. Phys.*, **17,** 310; 1950, *Superfluids*, Vol. 1 (New York: Wiley); 1954, *Superfluids*, Vol. 2 (New York: Wiley).
LONDON, H., 1939, *Proc. Roy. Soc.* A, **171,** 484.
MCCRUM, N. G., 1954, *Phil. Mag.*, **45,** 1302.
MENDELSSOHN, K., 1945, *Proc. Phys. Soc.* A, **57,** 371; 1954, *Proc. Roy. Instn G.B.*, **35,** 619.
MENDELSSOHN, K., and WHITE, G. K., 1950, *Proc. Phys. Soc.* A, **63,** 1328.
TISZA, L., 1947, *Phys. Rev.*, **72,** 838; 1949, *Ibid.*, **75,** 885.
WARD, J. C., and WILKS, J., 1952, *Phil. Mag.*, **43,** 48.

Single Band Motion of Conduction Electrons in a Uniform Magnetic Field

By P. G. HARPER†
Department of Mathematical Physics, University of Birmingham

Communicated by R. E. Peierls ; MS. received 19th January and in amended form 27th April 1955

Abstract. The effect of a uniform magnetic field on the conduction band of a metal is investigated, using as model the tight-binding approximation for a simple cubic crystal. The normally discrete magnetic levels pertaining to free electrons are shown to be non-uniformly spaced and broadened as a result of the lattice forces.

§ 1. INTRODUCTION

THE effect of a uniform magnetic field on the conduction electrons in a metal is of general interest for a variety of magnetic phenomena. Little attempt, however, has been made to examine the problem rigorously. For some effects, e.g. diamagnetism, the approximation of an effective mass has been successfully used, thus reducing the problem to that of free electrons, which is then easily handled. This procedure has some support from a theorem first enunciated by Peierls (1933). This states that an approximate Hamiltonian describing the magnetic motion is obtained by replacing $E(\mathbf{k})$ by $E(\boldsymbol{\kappa})$ where $[\kappa_x, \kappa_y] = (ie/\hbar c)H_z$, etc., H being the magnetic field and $E(\mathbf{k})$ the energy relating to a particular band. This implies immediately that there is no mixing of bands and that they can be treated independently. If, therefore, the occupied levels lie at the top or bottom of a band, $E(\mathbf{k})$ may be represented by the use of effective-mass parameters (to describe anisotropy of the metal) and if one takes

$$\hbar\boldsymbol{\kappa} = \mathbf{p} - (e/c)\mathbf{A}(\mathbf{r}), \qquad \mathbf{p} = \hbar\nabla/i,$$

$E(\boldsymbol{\kappa})$ reduces to a quadratic differential operator whose eigenvalues are easily obtained.

The above theorem was initially obtained for the limiting case of tight binding. A more general derivation has been given by Luttinger (1951) using Wannier functions. There remain, however, several obscurities as regards the interpretation of $E(\boldsymbol{\kappa})$; more important, no useful estimate of the errors involved was provided. In this paper the theorem is assumed and used to investigate magnetic eigenvalues in the case of tight binding for a simple cubic lattice. This special case serves to illustrate features common to more complicated band structures. What is important to notice is that motion in a particular band is considered as independent of other bands, interband terms being omitted. This is usually described as the single-band approximation. A subsequent paper will complete the examination and indicate in what circumstances the approximation is justified (Harper 1955).

---

† Now at Division of Electrotechnology, Commonwealth Scientific and Industrial Research Organization, University Grounds, Sydney, Australia.

§ 2. SOLUTION OF THE EIGENEQUATION BY A W. K. B. METHOD

The eigenequation considered is

$$E(\boldsymbol{\kappa})u(\mathbf{r}) = Wu(\mathbf{r}) \qquad \ldots\ldots(1)$$

where

$$\hbar\boldsymbol{\kappa} = \frac{\hbar}{i}\nabla - \frac{e}{c}\mathbf{A}(\mathbf{r}). \qquad \ldots.(1.1)$$

A discussion of the exact meaning of $u(\mathbf{r})$ is reserved for a subsequent paper. It is sufficient at present to regard it as the actual wave function. Then a convenient gauge for $\mathbf{A}$ is $\mathbf{A} = (0, Hx, 0)$, i.e. $\mathbf{H}$ is directed along the z-axis. In the case of tight binding, $E = \delta(\cos k_x a + \cos k_y a + \cos k_z a)$ if the field $\mathbf{H}$ is assumed to coincide with a crystallographic axis. Then (1) and (1.1) give

$$\tfrac{1}{2}[u(x+a) + u(x-a) + \exp(i\epsilon Hxa)u(y+a) + \exp(-i\epsilon Hxa)u(y-a)$$
$$+ u(z+a) + u(z-a)] = Wu(\mathbf{r}).$$

$u(\mathbf{r}) \equiv \exp(ik_y y)\exp(ik_z z)u(x)$ separates the variables, giving

$$\tfrac{1}{2}[u(x+a) + u(x-a)] + \cos(\epsilon aHx - k_y a)u(x) = (W - \cos k_z a)u(x) \qquad \ldots\ldots(1.2)$$

where $\epsilon \equiv e/\hbar c$, and W is supposed measured in units of δ. The energy due to motion in the field direction is thus additive. Including it in the eigenvalue W, and changing the origin of x, (1.2) may be more simply presented as a difference equation,

$$\tfrac{1}{2}(u_{n+1} + u_{n-1}) + (\cos\alpha n - W)u_n = 0, \qquad \ldots\ldots(1.3)$$

where $\alpha = \epsilon a^2 H$. For fields $H \sim 10^4$ oersteds, and taking $a \sim 10^{-8}$ cm, $\alpha \sim 10^{-4}$. Consequently $\cos\alpha n$ may be regarded as slowly varying, and approximate eigenvalues may be found using an adaptation of the W.K.B. method. For convenience write $\cos\alpha n - W$ as k_n. Then for k_n less than 1, u_n is oscillatory; for k_n greater than 1, u_n behaves exponentially. $k_n = 1$ is therefore a classical turning point and in its vicinity u_n clearly behaves linearly.

It is now evident that $|W| < 2$, since for $|W|$ greater than 2, $|k_n|$ is always greater than 1 and therefore boundary conditions cannot be satisfied. Thus the eigenvalues W are confined to a band whose energy limits are identical with those occurring in the non-magnetic case. The levels are, of course, discrete (apart from the field-direction energy $\cos k_z a$) and may be obtained as follows:

For $|k_n| < 1$, put $u_n = \exp i\phi_n$. Then (1.3) becomes

$$\exp(i\Delta\phi_{n+1}) + \exp(-i\Delta\phi_n) + 2k_n = 0$$

where $\Delta\phi_n$ denotes the first difference $\phi_n - \phi_{n-1}$, i.e.

$$\exp\{i(\Delta\phi_n + \Delta^2\phi_{n+1})\} + \exp(-i\Delta\phi_n) + 2k_n = 0.$$

Assuming now that $\Delta\phi_n$ is slowly varying, then $\Delta^2\phi_{n+1} \sim \Delta^2\phi_n \ll 1$, and therefore,

$$\cos\Delta\phi_n + \tfrac{1}{2}i\exp(i\Delta\phi_n)\Delta^2\phi_n \simeq -k_n.$$

As a zero-order approximation, $\cos\Delta\phi_n{}^0 = -k_n$. Put $\Delta\phi_n = \Delta\phi_n{}^0 + \chi_n$, χ_n being of the same order of magnitude as $\Delta^2\phi_n$, then

$$\cos\Delta\phi_n{}^0 - \chi_n\sin\Delta\phi_n{}^0 + \tfrac{1}{2}i\Delta^2\phi_n{}^0\exp(i\Delta\phi_n{}^0) \simeq -k_n,$$

or

$$\chi_n = \tfrac{1}{2}i(\cot\Delta\phi_n{}^0 + i)\Delta^2\phi_n{}^0.$$

Consequently, $\phi_n = \sum^{n}(\Delta\phi_l^0 + \chi_l)$

$$= \sum^{n}\Delta\phi_l^0 + \tfrac{1}{2}i\log\sin\Delta\phi_n^0 - \tfrac{1}{2}\Delta\phi_n^0 + \text{const.}$$

(replacing $\sum\limits_{l}^{n}$ by $\int^{n} dl$).

Thus

$$u_n \simeq \text{const.}\,(\sin\Delta\phi_n^0)^{-1/2}\exp\left(\pm i\int^{n}\Delta\phi_l^0\,dl\right). \qquad \ldots\ldots(1.4)$$

This is in obvious analogy to the usual results for a continuous variable. For $k_n > 1$, the corresponding expression is

$$u_n \simeq \text{const.}(\sinh\Delta\phi_n^0)\exp \pm\int^{n}\Delta\phi_l^0\,dl, \qquad \ldots\ldots(1.5)$$

where $\cosh\Delta\phi_n^0 = -k_n$. These approximations fail near the turning point $k_n = 1$, since then $\Delta^2\phi_n^0$ is not small but of the order of unity.

In the usual way suitable combinations of these solutions have to be matched in order to provide eigenvalues. In the region $k_n \sim 1$, $\cos\alpha n - W$ may be expanded to $1 - \alpha(n - n_0)\sin\alpha n_0$ where $\cos\alpha n_0 - W = 1$. k_n is therefore linear in n and two independent solutions are

$$\mathrm{J}_{n-n_0-m}\left(\frac{2}{m}\right), \quad \mathrm{Y}_{n-n_0-m}\left(\frac{2}{m}\right) \qquad \ldots\ldots(1.6)$$

where $m = 1/\alpha\sin n_0\alpha$. For $|m| \gg 1$, and $n \sim n_0$, both these expressions behave linearly (see Nicholson's formulae, Watson 1944, p. 249) in accordance with an earlier remark. To effect matching, asymptotic expansions are available (Watson 1944, p. 244) and the arguments run parallel to those usually presented for the case of a continuous variable.

There is one important difference, namely that the turning points n_0 are infinite in number, and cyclic boundary conditions are necessary. It is clear that $u_{n+2\pi/\alpha}$ satisfies the same equation as u_n. It is permissible therefore to choose solutions u_n such that

$$u_{n+2\pi/\alpha} = u_n\exp(2\pi ik_x a/\alpha)$$

i.e.

$$u_n = v_n\exp(ik_x na), \qquad -\tfrac{1}{2}\alpha < k_x a < \tfrac{1}{2}a$$

where now v_n is periodic with period $2\pi/\alpha$. Equation (1.3) thus becomes

$$v_{n+1}\exp(ik_x a) + v_{n-1}\exp(-ik_x a) + v_n(\cos\alpha n - W) = 0. \qquad \ldots\ldots(1.7)$$

This simple procedure is, strictly speaking, correct only for special values of α, namely if $2\pi/\alpha$ is integral, or $N = 2\pi/\epsilon a^2 H$ an integer. This, however, is a mild restriction on the field since $N \sim 10^5$ for $H \sim 10^4$ oersteds. It is clear that only positive W (say) need be considered since putting $v_n = (-1)^n\omega_n$ and changing the origin of n by π/α reverses the sign of W. The eigenvalues are therefore symmetrical about $W = 0$.

The effect of phase factors $\exp(\pm ik_x a)$ in (1.7) is to add $k_x a$ to $\Delta\phi_n$ throughout the analysis. Thus $\Delta\phi_n^0$ is determined by

$$\cos(k_x a + \Delta\phi_n^0) + \cos\alpha n - W = 0. \qquad \ldots\ldots(1.8)$$

The matching of (1.4), (1.5) is carried out using the linear solutions (1.6) and their asymptotic expansions. The phase of (1.4) is determined and as usual is corrected by $\pi/4$. From familiar arguments quantization is then effected by requiring that

$$\int_{n_0}^{2\pi/\alpha - n_0} \Delta\phi_l^0 \, dl = (j+\tfrac{1}{2})\pi \qquad \ldots\ldots(1.9)$$

the upper and lower limits of the integral being two adjacent turning points which contain the oscillatory part of u_n.

§ 3. LEVEL BROADENING

Equations (1.8) and (1.9) are a particular instance of Onsager's results (1952). For completeness one should also take account of the phase $k_y a$ occurring in $\cos \alpha n$. There are then two parameters k_x, k_y, in addition to j, necessary to describe completely the level spectrum. It will presently appear that the former describe a broadening of a (nearly) discrete level j.

Omitting k_x, k_y for the present, the equation for eigenvalues is

$$\int_{-n_0}^{+n_0} \cos^{-1}(W - \cos \alpha n) \, dn = (j+\tfrac{1}{2})\pi \qquad \ldots\ldots(1.10)$$

where $\cos \alpha n_0 - W + 1 = 0$, $0 < \alpha n_0 \leqslant \pi$.

Plotting the integral in (1.10) as a function of W (see figure), one sees for example, that the unbroadened levels become more widely separated near $W=0$.

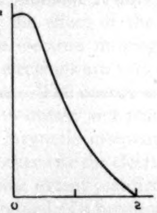

To examine broadening, consider k_x only. Then

$$\Delta\phi_n = -k_x\alpha + \cos^{-1}(W - \cos \alpha n),$$

and (1.9) becomes

$$\int_{-n_0}^{+n_0} \cos^{-1}(W - \cos \alpha n) \, dn - 2n_0 k_x a = (j+\tfrac{1}{2})\pi$$

or

$$\int_{-n_0}^{+n_0} \cos^{-1}(W - \cos \alpha n) \, dn = (j+\tfrac{1}{2})\pi + \frac{2k_x a}{\alpha} \cos^{-1}(W-1). \qquad \ldots\ldots(1.11)$$

Since $-\frac{1}{2}\alpha < k_x a < \frac{1}{2}\alpha$ the broadening term is always less than π so that the levels are always separated. Using equation (1.1) then the levels may be described as follows. For $W = 2 - \omega$, $\omega \ll 1$, an approximate solution is

$$\omega = (j+\tfrac{1}{2})\alpha + 2k_x a[(2j+1)a]^{1/2}.$$

Thus at the edge of the band the levels are uniformly spaced, the separation being given by the effective mass in the customary way. There is in addition a broadening, but so slight as to be negligible. Qualitatively the figure indicates how the levels vary throughout the band, the most important fact being that near the centre, $W=0$, the broadening is extremely large, the actual separation in fact being small compared with it. The situation here then is just the inverse of that occurring at the edge of the band.

It should be remarked that, strictly speaking, the above equations do not hold at the very centre $W=0$, since for this value the turning points n_0 are no longer linear and the preceding analysis does not apply. On grounds of continuity, however, the conclusions seem fairly assured.

Concerning Onsager's work it is perhaps worth emphasizing that the magnetic quantization of levels is a direct consequence of $[\kappa_x, \kappa_y] = i\epsilon H_z$ etc. and that the notion of wave packets is unnecessary.

REFERENCES

HARPER, P. G., 1955, *Proc. Phys. Soc.* A, **68,** 879.
LUTTINGER, J. M., 1951, *Phys. Rev.*, **84,** 814.
ONSAGER, L., 1952, *Phil. Mag.*, **43,** 1006.
PEIERLS, R. E., 1933, *Z. Phys.*, **80,** 763.
WATSON, G. N., 1944, *A Treatise on the Theory of Bessel Functions*, 2nd Edn (Cambridge : University Press).

The General Motion of Conduction Electrons in a Uniform Magnetic Field, with Application to the Diamagnetism of Metals

By P. G. HARPER†

Department of Mathematical Physics, University of Birmingham

Communicated by R. E. Peierls; MS. received 19th January 1955
and in amended form 27th April 1955

Abstract. Using translational properties of the Hamiltonian, a standard form is derived for the wave functions describing conduction electrons moving in a uniform magnetic field. This is used to obtain a solution of the Schrödinger equation in order to examine the magnetic energy levels. For non-overlapping bands the notion of effective mass is shown adequate (neglecting level broadening) but in an overlap region neighbouring bands interact strongly and distort the single band levels. A brief application to the diamagnetism of metals is considered.

INTRODUCTION

THE large diamagnetism of metals has long been understood to be due in some way to the 'free' conduction electrons. It is also well known that it is entirely quantum-mechanical in origin, since classically a mechanical system can possess no magnetic moment at all. To get a first understanding, therefore, one neglects entirely the effect of the crystal lattice and solves the Schrödinger equation for a free electron moving in a uniform magnetic field. For the alkali metals, where the electrons are very nearly free, the approximation is, in fact, likely to be a good one. The energy eigenvalues (including magnetic energy due to spin) are simple to obtain and may be used to calculate the free energy F from which the total magnetic moment is obtained as $M=-\partial F/\partial H$. Fermi–Dirac statistics are used, otherwise the electrons are treated as independent. That this is permissible is to some extent justified by the success of the model.

The susceptibility is thus obtained as a function of the field and temperature. Measurements of the constant susceptibility (weak fields, high temperature) of the alkali metals demand the variation of some parameter, however, and of the universal constants available the electronic mass is the only one permissible. The notion of 'effective mass' is, of course, also supported by the band theory of metals, and its use in the magnetic problem is already plausible. Further support comes from the (low temperature, strong field) susceptibility where it was pointed out by Peierls that if the electronic mass is sufficiently small and the electron density low, an oscillatory behaviour might be expected. Such an effect was indeed observed by de Haas and van Alphen in bismuth.

More direct support was provided by Peierls (1933) when he obtained an expression for the constant susceptibility for conduction electrons, of which the greatest contribution appeared essentially as an average of the effective Bohr magneton over the Fermi surface. For free electrons this reduced to the form obtained by Landau. There remained a contribution analogous to atomic diamagnetism (and thus small) and a third part having no simple interpretation but again apparently small.

---

† Now at Division of Electrotechnology, Commonwealth Scientific and Industrial Research Organization, University Grounds, Sydney, Australia.

These results were obtained, not by considering directly the energy eigenvalues, but by application of the interesting theorem that an equivalent energy operator is found (at least approximately) by replacing $E(\mathbf{k})$ by $E(\boldsymbol{\kappa})$, $[\boldsymbol{\kappa}_x, \boldsymbol{\kappa}_y] = i(e/\hbar c)H_z$, etc. All results were obtained for the limiting case of tight binding but have since been shown to be of more general application (Wilson 1936, Luttinger 1951).

For electrons lying near the top or bottom of a band, $E(\mathbf{k})$ may be taken as quadratic in $\mathbf{k}$ (not necessarily isotropic) and the replacement of $\mathbf{k}$ by $\boldsymbol{\kappa}$ then introduces the effective mass in a natural way. Blackman (1938) was thus able to extend the expression for the low-temperature susceptibility to allow for anisotropy of the metal. That is, by considering combinations of ellipsoids of suitable eccentricities to represent the Fermi surface (for holes and overflowing electrons), effective mass parameters are introduced and used to interpret the complicated modulations, phases, etc., of the susceptibility oscillations (Shoenberg 1952).

However, some doubt was thrown on the simple use of an effective mass when Adams (1953) showed that, at least in the case of the constant susceptibility, the previously neglected third contribution mentioned above could become very important in just those situations for which the effective mass approximation is most useful, that is, when the energy gap is small and consequently the effective mass small. Briefly, his argument was that in such a case there is a degeneracy of Bloch states, and that the magnetic field mixes them considerably.

The main purpose of the present paper is to examine this and other difficulties by means of a direct solution of the Schrödinger equation for a conduction electron moving in a uniform magnetic field. An exact solution in closed form is not, of course, to be expected since, even without the field, that does not exist. What is meant is a treatment analogous to the solution for nearly free electrons which establishes the existence of energy gaps, etc. A brief application of some of the results to the magnetic susceptibility is given though much more remains to be done.

§ 1. TRANSLATIONAL PROPERTIES OF THE STATE FUNCTION

If an electron moves in the periodic field of a crystal lattice, and an external uniform magnetic field $\mathbf{H}$ is imposed, the electron stationary states are determined by the Schrödinger equation

$$\left[-\frac{\hbar^2}{2m}\left(\nabla - \frac{ie}{\hbar c}\mathbf{A}\right)^2 + V(\mathbf{r}) - W\right]\psi = 0, \qquad \ldots\ldots(1.1)$$

where $\mathbf{H} = \operatorname{curl}\mathbf{A}$, and the vector potential $\mathbf{A}$ is linear in coordinates $\mathbf{r}$. $V(\mathbf{r})$ represents the lattice potential and therefore $V(\mathbf{r}+\boldsymbol{\tau}_i) = V(\mathbf{r})$, where $\boldsymbol{\tau}_i$, $i = 1, 2, 3$, are basic lattice vectors. Consider a displacement $\boldsymbol{\tau}_i$ of $\mathbf{r}$; then from the linearity of (1.1),

$$\psi_\lambda(\mathbf{r}+\boldsymbol{\tau}_i) = \exp\,[i\epsilon\mathbf{A}(\boldsymbol{\tau}_i)\,.\,\mathbf{r}]\sum_{\lambda'} C^i_{\lambda'\lambda}\psi_{\lambda'}, \qquad \ldots\ldots(1.2)$$

where $\epsilon = e/\hbar c$ and the index λ enumerates all states of energy W. The matrices $C^i_{\lambda'\lambda}$, together with the phase factors $\exp\,[i\epsilon\mathbf{A}(\boldsymbol{\tau}_i)\,.\,\mathbf{r}]$ (which simply effect a change of gauge) form representations of the elementary translations. Such operations commute and therefore

$$C^jC^i = C^iC^j \exp i\epsilon[\mathbf{A}(\boldsymbol{\tau}_j)\,.\,\boldsymbol{\tau}_i - \mathbf{A}(\boldsymbol{\tau}_i)\,.\,\boldsymbol{\tau}_j], \qquad \ldots\ldots(1.3)$$

matrix multiplication being understood. Thus C^i do not in general commute and cannot be simultaneously diagonalized. For example, taking a cubic lattice of lattice constant a, and $\mathbf{A}=(0, Hx, 0)$

$$C^y C^x = C^x C^y \exp(-i\epsilon H a^2)$$
$$C^z C^x = C^x C^z$$
$$C^z C^y = C^y C^z.$$

In this case C^z commutes with C^x, C^y and may be treated as diagonal. Since C^x, C^y do not commute, if C^x is diagonal, C^y is not, and vice versa.

It is interesting to note that symbolically C^i could be represented by $C^i=\exp(i\boldsymbol{\kappa}\,.\,\boldsymbol{\tau}_i)$, where $[\kappa_x, \kappa_y]=i\epsilon H_z$ etc. (for the case $\mathbf{A}=\frac{1}{2}\mathbf{H}\times\mathbf{r}$). A more useful representation is obtained by introducing a vector $\mathbf{k}$ and writing

$$(\mathbf{k}'\,|\,C^i\,|\,\mathbf{k}) = \exp(i\mathbf{k}\,.\,\boldsymbol{\tau}_i)\,\delta[\mathbf{k}'-\mathbf{k}+\epsilon\mathbf{A}(\boldsymbol{\tau}_i)]. \qquad \ldots\ldots(1.4)$$

(In the above example this makes C^x and C^z diagonal.) Thus, taking $\mathbf{A}=0$, (1.4) reduces to the diagonal Bloch representation. In the magnetic case however, the vector $\mathbf{k}$ is not to be identified as a momentum vector since the motion is not that of plane waves.

That (1.4) satisfies (1.3) is clear since

$$(\mathbf{k}'\,|\,C^j C^i\,|\,\mathbf{k}) = \exp[-i\epsilon\mathbf{A}(\boldsymbol{\tau}_i)\,.\,\boldsymbol{\tau}_j]\exp(i\mathbf{k}\,.\,\boldsymbol{\tau}_i+\boldsymbol{\tau}_j)\,\delta[\mathbf{k}'-\mathbf{k}+\epsilon\mathbf{A}(\boldsymbol{\tau}_i+\boldsymbol{\tau}_j)].$$

Interchanging i, j the result follows.

Choosing this representation then and using (1.2) and (1.4),

$$\psi_{\mathbf{k}}(\mathbf{r}+\boldsymbol{\tau}_i) = \exp(i\mathbf{k}\,.\,\boldsymbol{\tau}_i)\exp[i\epsilon\mathbf{A}(\boldsymbol{\tau}_i)\,.\,\mathbf{r}]\,\psi_{\mathbf{k}-\epsilon\mathbf{A}(\tau_i)}(\mathbf{r}). \qquad \ldots\ldots(1.5)$$

It should be noted that since the summation over $\mathbf{k}$ is restricted to the surface $W(\mathbf{k})=W$, if the only surviving term that the δ-function permits is to be included, it must follow that

$$W[\mathbf{k}-\epsilon\mathbf{A}(\boldsymbol{\tau}_i)] = W(\mathbf{k}),$$

i.e. that W be periodic in $\mathbf{k}$ with the (vector) period $\mathbf{A}(\boldsymbol{\tau}_i)$. For the case $\mathbf{A}=0$, (1.5) reduces to the familiar Bloch relation

$$\psi_{\mathbf{k}}(\mathbf{r}+\boldsymbol{\tau}_i) = \exp(i\mathbf{k}\,.\,\boldsymbol{\tau}_i)\,\psi_{\mathbf{k}}(\mathbf{r}).$$

A formal solution to the functional equation (1.5) is

$$\psi_{\mathbf{k}}(\mathbf{r}) = \exp(i\mathbf{k}\,.\,\mathbf{r})\,U[\mathbf{k}-\epsilon\mathbf{A}(\mathbf{r})\,;\,\mathbf{r}\,;\,\mathbf{k}], \qquad \ldots\ldots(1.6)$$

where U is understood to be formed from a unique function of three variables by replacing the first written by a linear combination of $\mathbf{r}$ and $\mathbf{k}$. Furthermore the dependence of U upon $\mathbf{r}$ is periodic, of lattice periodicity, the dependence of U upon $\mathbf{k}$ periodic with (vector) period $\mathbf{A}(\boldsymbol{\tau}_i)$. If such a function be constructed, it will be seen to be the most general function satisfying equation (1.5). That it is unique will presently appear when explicit representations are introduced.

By using the functional form (1.6) in the Schrödinger equation and taking the gradient with respect to $\mathbf{k}$, matrix relations analogous to those holding for Bloch functions may be obtained.

Thus,

$$\left.\begin{aligned}
&\int \psi^*_{\mathbf{k}\alpha}\Big(\mathbf{p}-\frac{e}{c}\mathbf{A}\Big)\psi_{\mathbf{k}\alpha}\,d^3\mathbf{r} = \frac{m}{\hbar}\nabla_{\mathbf{k}} W_\alpha(\mathbf{k}),\\
&\int \psi^*_{\mathbf{k}\alpha}\left(\mathbf{p}-\frac{e}{c}\mathbf{A}\right)\psi_{\mathbf{k}\alpha}\,d^3\mathbf{r} + \frac{m}{\hbar}(W_{\alpha'}-W_\alpha)\int U_{\mathbf{k}\alpha'}\nabla_{\mathbf{k}} U_{\mathbf{k}\alpha}\,d^3\mathbf{r} = 0,\\
&\qquad \frac{2}{m}\sum_{\alpha'}\frac{|(p_x-(e/c)A_x)_{\alpha\alpha'}|^2}{W_{\alpha'}-W_\alpha} = 1-\frac{m}{\hbar^2}\frac{\partial^2 W_\alpha}{\partial k_x{}^2}\ \text{etc.},
\end{aligned}\right\} \qquad \ldots\ldots(1.7)$$

where α denotes any other quantum variables necessary for a complete description.

For the particular case of free electrons, i.e. $V(\mathbf{r})=0$, and using $\mathbf{A}=(0, Hx, 0)$ say, all results obtained so far may be verified provided one is careful to choose the proper linear combinations of the degenerate states, W then being degenerate in k_x, k_y.

§ 2. REPRESENTATIONS FOR THE SCHRÖDINGER EQUATION

To avoid unnecessary complication, take $\mathbf{A}=\frac{1}{2}\mathbf{H}\times\mathbf{r}$. Then from (1.6)

$$\psi_{\mathbf{k}}=\exp(i\boldsymbol{\kappa}\,.\,\mathbf{r})U(\boldsymbol{\kappa}, \mathbf{r}), \qquad \text{where} \qquad \boldsymbol{\kappa}=\mathbf{k}-\epsilon\mathbf{A}(\mathbf{r}).$$

(The separate dependence of U upon $\mathbf{k}$ is now understood to be present and will not be written in explicitly.)

In this form it resembles a Bloch function though it must be remembered that $\boldsymbol{\kappa}$ is a linear combination of $\mathbf{k}$ and $\mathbf{r}$.

The Schrödinger equation (1.1) becomes therefore,

$$\left[\frac{1}{2m}\left(\mathbf{p}-\frac{e}{c}\mathbf{A}\right)^2+V(\mathbf{r})-W\right]\exp(i\boldsymbol{\kappa}\,.\,\mathbf{r})U(\boldsymbol{\kappa}, \mathbf{r})=0. \qquad \ldots\ldots(2.1)$$

$\mathbf{p}$, in the kinetic term, is a total differential operator; it acts on the explicit $\mathbf{r}$ (in which U, keeping $\boldsymbol{\kappa}$ constant, is periodic) and on the $\mathbf{r}$ contained implicitly in $\boldsymbol{\kappa}$. If $\partial/\partial x^\mu$ therefore be replaced by

$$\frac{\partial}{\partial x^\mu}+\frac{\partial \kappa^\nu}{\partial x^\mu}\frac{\partial}{\partial \kappa^\nu},$$

i.e. $\mathbf{p}\rightarrow\mathbf{p}-\frac{1}{2}\mathbf{H}\times i\nabla_{\boldsymbol{\kappa}}$ the two operations are separated and $\boldsymbol{\kappa}$ and $\mathbf{r}$ may be regarded as independent variables. This is nothing more than elementary implicit differentiation, but one should note that since the square of $\mathbf{p}$ occurs, it is important that $\boldsymbol{\kappa}$ be linear in $\mathbf{r}$.

Then (2.1) becomes a differential equation in the two independent vector variables, $\mathbf{r}$ and $\boldsymbol{\kappa}$, thus:

$$\left\{\frac{1}{2m}\left[\mathbf{p}-\frac{e}{c}\mathbf{A}(\mathbf{r})-\frac{e}{c}\mathbf{A}(i\nabla_{\boldsymbol{\kappa}})\right]^2+V(\mathbf{r})-W\right\}\exp(i\boldsymbol{\kappa}\,.\,\mathbf{r})U(\boldsymbol{\kappa}, \mathbf{r})=0 \qquad \ldots.(2.2)$$

($\nabla_{\boldsymbol{\kappa}}$ means gradient with respect to $\boldsymbol{\kappa}$).

There are now two different representations possible:

(i) $\exp(i\boldsymbol{\kappa}\,.\,\mathbf{r})U(\boldsymbol{\kappa}, \mathbf{r})$ having the translational symmetry of the lattice, may be expanded into the ordinary Bloch functions $\phi_{\boldsymbol{\kappa}, l}(\mathbf{r})$ where

$$\left[\frac{p^2}{2m}+V(\mathbf{r})-E_l(\boldsymbol{\kappa})\right]\phi_{\boldsymbol{\kappa}, l}(\mathbf{r})=0.$$

Thus,
$$\exp(i\boldsymbol{\kappa}\,.\,\mathbf{r})U(\boldsymbol{\kappa}, \mathbf{r})=\sum_l v_l(\boldsymbol{\kappa})\phi_{\boldsymbol{\kappa}, l}(\mathbf{r}),$$

the summation over l extending over all bands.

(ii) $U(\boldsymbol{\kappa}, \mathbf{r})$ being periodic in $\mathbf{r}$, may be expanded into Fourier plane waves, thus

$$\exp(i\boldsymbol{\kappa}\,.\,\mathbf{r})U(\boldsymbol{\kappa}, \mathbf{r})=\sum u_l(\boldsymbol{\kappa})\exp[i(\boldsymbol{\kappa}_l+\boldsymbol{\kappa})\,.\,\mathbf{r}],$$

where $\boldsymbol{\kappa}_l$ are the lattice vectors of the inverse lattice, i.e. $\exp(i\boldsymbol{\kappa}_l\,.\,\boldsymbol{\tau}_{l'})=1$ for all l, l'.

Considering (i), it is a matter of algebra to verify that it leads to a set of simultaneous differential equations in $\boldsymbol{\kappa}$ which may be written as follows:

$$\left.\begin{aligned} E_n v_n-\frac{e}{mc}\sum_{n'}[\mathbf{p}\,.\,\mathbf{A}+\mathbf{A}(i\nabla_{\boldsymbol{\kappa}})]_{nn'}v_{n'} \\ +\frac{e^2}{2mc^2}\sum_{n'}[\mathbf{A}^2+2\mathbf{A}\,.\,\mathbf{A}(i\nabla_{\boldsymbol{\kappa}})+\mathbf{A}^2(i\nabla_{\boldsymbol{\kappa}})]_{nn'}v_{n'} \\ -Wv_n=0 \end{aligned}\right\} \qquad \ldots\ldots(2.3)$$

where $(\mathbf{p}\,.\,\mathbf{A})_{nn'}$, $\mathbf{A}_{nn'}{}^2$ etc. are the matrix elements

$$\int \phi^*_{\boldsymbol{\kappa},n}(\mathbf{p}\,.\,\mathbf{A})\phi_{\boldsymbol{\kappa},n'}d^3\mathbf{r}, \qquad \int \phi^*_{\boldsymbol{\kappa},n}\mathbf{A}^2\phi_{\boldsymbol{\kappa},n'}d^3\mathbf{r} \text{ etc.,}$$

and $\mathbf{A}(i\nabla_{\boldsymbol{\kappa}})_{nn'}$ means $\mathbf{A}(i\nabla_{\boldsymbol{\kappa}})\delta_{nn'}$.

Equation (2.3) might be written more elegantly as

$$\sum_{n'}\left[E-\frac{e}{mc}\,\mathbf{p}\,.\,\mathfrak{A}+\frac{e^2}{2mc^2}\,\mathfrak{A}^2\right]_{nn'} v_{n'}=Wv_n, \qquad \ldots\ldots(2.4)$$

where $\mathfrak{A}_{nn'}\equiv\mathbf{A}(\mathbf{r}+i\nabla_{\boldsymbol{\kappa}})_{nn'}$ and $\mathfrak{A}^2$ is defined to mean the last term in (2.3) so that $\mathbf{A}i(\nabla_{\boldsymbol{\kappa}})\cdot\mathbf{A}$ does *not* occur.

An equation similar to (2.4) has been derived by Wilson (1936) though from quite different principles. It differed in being an equation for the density matrix rather than for eigenvalues.

Adams (1953) has also considered a somewhat similar equation though he used the formalism of Wannier functions to derive it. Both these authors were intent on calculating the constant magnetic susceptibility to which purpose the equation is well suited. For eigenvalues it is more convenient to use (ii).

With less trouble it is seen to produce

$$\frac{\hbar^2}{2m}\,[\boldsymbol{\kappa}+\boldsymbol{\kappa}_l-\epsilon\mathbf{A}(i\nabla_{\boldsymbol{\kappa}})]^2u_l(\boldsymbol{\kappa})+\sum_{l'l''} V_{l'}u_{l''}(\boldsymbol{\kappa})=Wu_l(\boldsymbol{\kappa}) \qquad \ldots\ldots(2.5)$$

where V_l are the Fourier components of $V(\mathbf{r})$ and $\Sigma_{l',l''}$ is restricted to l', l'' for which $\boldsymbol{\kappa}_{l'}+\boldsymbol{\kappa}_{l''}=\boldsymbol{\kappa}_l$.

Equation (2.5) is again a set of coupled second-order differential equations which are simpler than (2.4) in that the coupling occurs only through the numbers V_l and that no complicated matrix elements appear. The equations are an evident generalization of those holding in the absence of a magnetic field for the Fourier components of Bloch functions: $\mathbf{k}$ is replaced by $\boldsymbol{\pi}=\boldsymbol{\kappa}-\epsilon\mathbf{A}(\nabla_{\boldsymbol{\kappa}})$ so that $[\pi_x, \pi_y]=i\epsilon H_z$ etc.

It may be remarked that the unambiguous derivations of equations (2.4), (2.5) are further demonstrations, if such were needed, of the uniqueness of $U(\boldsymbol{\kappa}, \mathbf{r})$ as a function of the two independent variables, $\mathbf{r}$, $\boldsymbol{\kappa}$.

§ 3. DISCUSSION AND SOLUTION OF THE SCHRÖDINGER EQUATION

Since Adams has extensively discussed what is probably the only useful application of equation (2.4), nothing more will be said about it in this paper. In any case, (2.5), besides being simpler to treat, gives some useful insight into the origins of the non-diagonal contributions which Adams regarded as important.

In analogy with the non-magnetic case, $\mathbf{A}=0$, $V(\mathbf{r})$ is restricted for the sake of simplicity to be sinusoidal; it is not pretended that this is at all realistic but it may be expected to lead to results of qualitative importance and suggest extensions to more general potentials. An immediate consequence (which would not be generally true) is that motion in the field direction is separable and is simply the unperturbed Bloch motion. If this is removed there remains the motion in a plane normal to the field $\mathbf{H}$, which will be taken to be in the z direction.

A second simplification involving no loss of generality is to take $\mathbf{A}=(0,Hx,0)$. Since the equations were derived using $\mathbf{A}=\frac{1}{2}\mathbf{H}\times\mathbf{r}$, the necessary corrections are discussed in the Appendix and it is seen that $\mathbf{A}(i\nabla_{\boldsymbol{\kappa}})$ must be replaced by

$(-iH\partial/\partial\kappa_y, 0, 0)$. Supposing **H** to coincide with a crystallographic axis equation (2.5) may be simplified to

$$\left\{\frac{\hbar^2}{2m}\left[\left(\kappa_x+\frac{2\pi m}{a}+i\epsilon H\frac{\partial}{\partial\kappa_y}\right)^2+\left(\kappa_y+\frac{2\pi n}{a}\right)^2\right]-W\right\}u_{m,n}$$
$$+V(u_{m+1,n}+u_{m-1,n})+V'(u_{m,n+1}+u_{m,n-1})=0 \quad \ldots\ldots(3.1)$$

where the metal is supposed to have cubic symmetry of lattice constant a, and V, V' (taken as different for convenience) are the Fourier components of $V(x, y)$ in the x, y directions.

In (3.1), κ_x is a constant of the motion and, in fact, is equal to k_x since $A_x=0$. First suppose $V=0$, i.e. a periodic field in one dimension only (though the motion is, of course, two-dimensional). This is not physically interesting, but serves to illustrate simply how the calculation proceeds. Then the index m is redundant and (3.1) becomes

$$\left\{\frac{\hbar^2}{2m}\left[\left(k_x+i\epsilon H\frac{\partial}{\partial\kappa}\right)^2+\left(\kappa+\frac{2\pi n}{a}\right)^2\right]-W\right\}u_n+V'(u_{n+1}+u_{n-1})=0 \quad \ldots.(3.2)$$

where κ_y is abbreviated to κ.

Suppose the last term is small (the precise condition for this will appear shortly), then the effect of a lattice may be treated as a perturbation to the free magnetic motion, the zero-order wave function being

$$u_n(\kappa)=\exp\left[i\left(k_x+\frac{2\pi n}{a}\right)\Big/\epsilon H\right].\ \text{oscillator function of}\left(\kappa+\frac{2\pi n}{a}\right)$$

and $$W_j=(j+\tfrac{1}{2})\hbar\omega_{\mathrm{L}}, \qquad \omega_{\mathrm{L}}=\frac{eH}{mc}.$$

The perturbed energy then becomes

$$2V'\cos\frac{2\pi k_x}{\epsilon aH}\int u_j(\kappa)u_j\left(\kappa+\frac{2\pi}{a}\right)d\kappa.$$

Provided the overlap integral is sufficiently small, the level W_j is thus broadened since k_x can take a continuous range of values. That the lattice forces might produce such broadening was earlier suggested by Dingle and Shoenberg (1950), Dingle (1952 a) and Shoenberg (1952). Remembering the definition of u_n, it is seen that $\psi_{\mathbf{k}}$ extends throughout the lattice, this representing the proper linear combination of (localized) Landau solutions. These simple results are also obtainable more directly by treating $V(x, y)$ as a perturbation to such free-electron solutions and one then obtains the useful results $-\frac{1}{2}\epsilon aH<k_x<\frac{1}{2}\epsilon aH$, $k_x=2\pi t/L_x$, t an integer and L_x the x-dimension of the metal.

However, the requirement

$$V\int u_j(\kappa)u_j\left(\kappa+\frac{2\pi}{a}\right)d\kappa \ll \mu H,$$

necessary for the success of perturbation treatment, is satisfied only for $W\ll\epsilon_0=(\hbar^2/2m)(\pi/a)^2$, this being the energy at which $u(\kappa)$, $u(\kappa+2\pi/a)$ begin to overlap appreciably. An asymptotic expansion of the integral is given by

$$\int_{-\infty}^{\infty}u_j(\kappa)u_j\left(\kappa-\frac{2\pi}{a}\right)d\kappa\simeq\left(\frac{2\pi^4}{a^2\epsilon H}\right)^{-1/4}(j-j_0)^{-1/4}\cos\Theta, \quad W_j>\epsilon_0$$

Θ being a slowly varying function of j. The approximation is poor near $W\gtrsim\epsilon_0$, but improves with increasing W. Taking $H\sim10^4$ oersted, $V\sim1$ ev its order of magnitude is 0·02 ev, compared with $\mu H \sim 10^{-4}$ ev. Thus, perturbation methods fail for energies close to and beyond ϵ_0, that is, beyond the first energy gap region.

Returning to equation (3.2), an inspection of the non-magnetic solution (nearly-free electrons) suggests that a better method is to neglect all but two adjacent components, say u_0, u_1 and regard these as strongly coupled. Symmetry considerations will then show how to allow for a true solution.

Then (3.2) becomes,

$$\left.\begin{aligned} &\left\{\frac{\hbar^2}{2m}\left[\left(k_x + i\epsilon H \frac{d}{d\kappa}\right)^2 + \kappa^2\right] - W\right\} u_0 + V' u_1 = 0, \\ &\left\{\frac{\hbar^2}{2m}\left[\left(k_x + i\epsilon H \frac{d}{d\kappa}\right)^2 + \left(\kappa + \frac{2\pi}{a}\right)^2\right] - W\right\} u_1 + V' u_0 = 0. \end{aligned}\right\} \quad \ldots\ldots(3.3)$$

From the first,

$$u_1 = -\frac{1}{V'}\left\{\frac{\hbar^2}{2m}\left[\left(k_x + i\epsilon H \frac{d}{d\kappa}\right)^2 + \kappa^2\right] - W\right\} u_0. \quad \ldots\ldots(3.4)$$

Inserting (3.4) into the second of (3.3)

$$\left\{\left[\frac{\hbar^2}{2m}\left(D^2 + \left\{\kappa + \frac{2\pi}{a}\right\}^2\right) - W\right]\left[\frac{\hbar^2}{2m}(D^2 + \kappa^2) - W\right] - V'^2\right\} u_0 = 0, \quad \ldots(3.5)$$

abbreviating $k_x + i\epsilon H d/d\kappa$ to D. Define now $\vartheta_a'(\kappa)$, $\vartheta_b'(\kappa)$ to be the roots of

$$\left(\vartheta - \frac{\hbar^2\kappa^2}{2m}\right)\left[\vartheta - \frac{\hbar^2}{2m}\left(\kappa + \frac{2\pi}{a}\right)^2\right] - V'^2 = 0; \quad \ldots\ldots(3.6)$$

then (3.5) may be re-written as

$$\left\{\left[\frac{\hbar^2 D^2}{2m} + \vartheta_b'(\kappa) - W\right]\left[\frac{\hbar^2 D^2}{2m} + \vartheta_a'(\kappa) - W\right] + \left[\frac{\hbar^2 D^2}{2m}, \frac{\hbar^2\kappa^2}{2m} - \vartheta_a'(\kappa)\right]\right\} u_0 = 0, \quad \ldots\ldots(3.7)$$

the last (commutator) term arising from the necessary re-ordering of the operator D^2.

The potentials ϑ_a', ϑ_b' are illustrated below; the broken curve corresponds to the 'free electron' potentials.

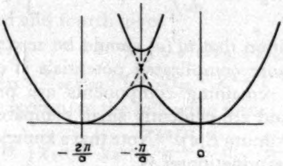

Consider first the region $\kappa > -\pi/a$. If $\vartheta_a'(\kappa)$ is chosen as the lower branch then $\hbar^2\kappa^2/2m - \vartheta_a'(\kappa)$ is slowly varying except near $\kappa = -\pi/a$. In zero order therefore, the commutator in (3.7) may be neglected, and $u_0(\kappa > -\pi/a)$ may be taken to satisfy

$$\left[\frac{\hbar^2 D^2}{2m} + \vartheta_a'(\kappa) - W\right] u_0 = 0,$$

and consequently from (3.4)

$$u_1 = -\frac{1}{V'}\left(\frac{\hbar^2\kappa^2}{2m} - \vartheta_a'\right) u_0. \quad \ldots\ldots(3.8)$$

Equation (3.8) is incomplete since boundary conditions are necessary to determine W. Considering now the region $\kappa < -\pi/a$, it is evident that (to a similar degree of approximation) a solution is

$$\left.\begin{aligned} &\left(\frac{\hbar^2 D^2}{2m} + \vartheta_a' - W\right) u_1 = 0, \\ &u_0 = -\frac{1}{V'}\left[\frac{\hbar^2}{2m}\left(\kappa + \frac{2\pi}{a}\right)^2 - \vartheta_a'\right] u_1. \end{aligned}\right\} \qquad \ldots\ldots(3.9)$$

The boundary condition adopted is that $u_0(\kappa > -\pi/a)$ (determined from equation (3·8)) join smoothly to $u_1(\kappa < -\pi/a)$ (determined from the first of (3.9)). Note that choosing ϑ_b' requires interchanging u_0, u_1.

One might at first object to such boundary conditions since from (3.8), for example, $u_1(\pi/a) = -u_0(-\pi/a)$ and therefore both u_0 and u_1 are discontinuous at $\kappa = -\pi/a$. There need be no discontinuity in $\psi_{\mathbf{k}}$ however; it is merely necessary to re-label the u_l such that the greatest is denoted by u_0 and simultaneously to change the origin of k_y by an inverse lattice vector, $2\pi/a$. This corresponds, in the non-magnetic problem, to adopting the convention of regarding all functions of **k** as periodic with the periodicity of the inverse lattice.

It should be remarked that, owing to the neglect of commutators, these solutions are only approximate, and choosing the largest component to be continuous (along with its derivative) means that in general the smaller one will not be. In fact there is a slight discontinuity in slope at $\kappa = -\pi/a$. It is of no special consequence however, and may be ignored.

It is now evident from symmetry how to include all components u_l: ϑ_a', ϑ_b' are to be replaced by $E_y^{(1)}(\kappa)$ and $E_y^{(2)}(\kappa)$, the latter being the first and second band energies (in κ) relating to a sinusoidal potential in the y direction. Equation (3.6) is the usual secular equation determining $E(\kappa)$ in the simple one-dimensional problem of nearly free electrons.

Thus u_0 satisfies the equation

$$\left[\frac{\hbar^2}{2m}\left(k_x + i\epsilon H \frac{d}{d\kappa}\right)^2 + E_y^{(1)}(\kappa) - W\right] u_0 = 0, \qquad \ldots\ldots(3.10)$$

with the boundary condition that $u_0'(\kappa)$ should be zero at a maximum of $E^{(1)}(\kappa)$. The generalization to more complicated potentials is obvious and will not be elaborated upon. The remaining components are provided (approximately) by equations like (3.8) and are evidently small compared with u_0 except in the immediate vicinity of maximum $E(\kappa)$. Note that a knowledge of such components is not necessary for a determination of W.

Since $E_y^{(1)}(\kappa)$ is periodic in κ, (3.10) is a Bloch-like equation whose eigenvalues are therefore bands. Considering dimensions however, one sees that far from an energy gap, the width of the potential barrier is so great that the bands must be very narrow; they are in fact, nothing but the broadened levels mentioned earlier.

The effect of a periodic potential in the x direction may also be considered, it now being necessary to factorize (approximately) the expression

$$\left\{\frac{\hbar^2}{2m}\left[\left(k_x + \frac{2\pi}{a} + i\epsilon H \frac{d}{d\kappa}\right)^2 + \kappa^2\right] - W\right\}\left\{\frac{\hbar^2}{2m}\left[\left(k_x + i\epsilon H \frac{d}{d\kappa}\right)^2 + \kappa^2\right] - W\right\} - V^2.$$

Using the Fourier transform of u_0

$$u_0(\kappa)=\int \bar{u}(q)\exp\left[-i(q-k_x)(\kappa-k_y)/\epsilon H\right]dq,$$

then $k_x+i\epsilon Hd/d\kappa\to q$, $\kappa\to k_y+i\epsilon Hd/dq$, and the equations reduce to the previous form, κ being replaced by q and k_x by k_y. The solutions for $\bar{u}_0(q)$, $\bar{u}_1(q)$ may be discussed as before and lead to similar conclusions, the broadening now being described by k_y.

The analogue of (3.10) is

$$\left[E_x^{(l)}\left(k_x+i\epsilon H\frac{d}{d\kappa}\right)+\frac{\hbar^2\kappa^2}{2m}-W\right]u_0=0, \qquad \ldots\ldots(3.11)$$

where the boundary conditions are now applied to $u_0(q)$, thus introducing the absent k_y. k_x in (3.11) is of course redundant, just as k_y is for (3.10); these degeneracies are removed when both V and V' are present.

One might guess that using a two-dimensional potential, i.e. including V, V', (3.10) and (3.11) would be combined in an obvious manner. In fact, a fresh difficulty arises which may be loosely described as a band coupling. To discuss this it is sufficient to consider the equations (3.1) retaining only u_{00}, u_{01}, u_{10}, u_{11}.

Then the equations run,

$$\left.\begin{aligned}H_{00}u_{00}+Vu_{10}+V'u_{01}=0,\\ H_{01}u_{01}+Vu_{11}+V'u_{00}=0,\\ H_{10}u_{10}+Vu_{00}+V'u_{11}=0,\\ H_{11}u_{11}+Vu_{01}+V'u_{10}=0,\end{aligned}\right\} \qquad \ldots\ldots(3.12)$$

where $H_{l,m}$ are abbreviations for the differential operators (including W) which appear in (3.1).

From the first and second equations of (3.12),

$$\left.\begin{aligned}u_{10}=-\frac{1}{V}(H_{00}u_{00}+V'u_{01}),\\ u_{11}=-\frac{1}{V}(H_{01}u_{01}+V'u_{00}).\end{aligned}\right\} \qquad \ldots\ldots(3.13)$$

Substitution in the third and fourth gives

$$\begin{aligned}(H_{10}H_{00}-V^2+V'^2)u_{00}+V'(H_{10}+H_{01})u_{01}=0,\\ V'(H_{11}+H_{00})u_{00}+(H_{11}H_{01}-V^2+V'^2)u_{01}=0.\end{aligned}$$

These are conveniently written in the following form:

$$\left(\vartheta_{\mathrm{b}}+\frac{\hbar^2\kappa^2}{2m}-W\right)\chi_1+V'\chi_2-\left[\frac{\hbar^2D^2}{2m}-\vartheta_{\mathrm{a}},\ \frac{\hbar^2\kappa^2}{2m}\right]u_{00}=0 \qquad \ldots\ldots(3.14)$$

$$V'\chi_1+\left[\vartheta_{\mathrm{b}}+\frac{\hbar^2}{2m}\left(\kappa+\frac{2\pi}{a}\right)^2-W\right]\chi_2-\left[\frac{\hbar^2D^2}{2m}-\vartheta_{\mathrm{a}},\ \frac{\hbar^2}{2m}\left(\kappa+\frac{2\pi}{a}\right)^2\right]u_{01}=0$$

where

$$\left.\begin{aligned}\chi_1=\left(\vartheta_{\mathrm{a}}+\frac{\hbar^2\kappa^2}{2m}-W\right)u_{00}+V'u_{01}\\ \chi_2=V'u_{00}+\left[\vartheta_{\mathrm{a}}+\frac{\hbar^2}{2m}\left(\kappa+\frac{2\pi}{a}\right)^2-W\right]u_{01}\end{aligned}\right\} \qquad \ldots\ldots(3.15)$$

(the argument of ϑ_{a}, ϑ_{b} being $D\equiv k_x+i\epsilon Hd/d\kappa$).

If the final commutators in (3.14) are omitted then a solution is $\chi_1=\chi_2=0$.

This, from (3.15), leads to

$$\left[(\vartheta_{\mathrm{a}}+\vartheta_{\mathrm{b}}'-W)(\vartheta_{\mathrm{a}}+\vartheta_{\mathrm{a}}'-W)+\vartheta_{\mathrm{a}},\left[\frac{\hbar^2\kappa^2}{2m}-\vartheta_{\mathrm{a}}'\right]\right]u_{00}=0.$$

Neglecting the final commutator, an approximate solution is

$$(\vartheta_{\mathrm{a}}+\vartheta_{\mathrm{a}}'-W)u_{00}=0. \qquad \ldots\ldots(3.16)$$

This is the form expected to appear from a combination of the two cases already discussed. From (3.15) the other components are given by

$$\left.\begin{aligned} u_{01}&=-\frac{1}{V'}\left(\frac{\hbar^2\kappa^2}{2m}-\vartheta_{\mathrm{a}}'\right)u_{00}\\ u_{10}&=-\frac{1}{V}\left(\frac{\hbar^2D^2}{2m}-\vartheta_{\mathrm{a}}\right)u_{00}\\ u_{11}&=\frac{1}{VV'}\left(\frac{\hbar^2D^2}{2m}-\vartheta_{\mathrm{a}}\right)\left(\frac{\hbar^2\kappa^2}{2m}-\vartheta_{\mathrm{a}}'\right)u_{00}.\end{aligned}\right\} \qquad \ldots\ldots(3.17)$$

Equation (3.16) may be discussed along similar lines as before except that now boundary conditions are to be applied to both $u_{00}(\kappa)$ and $\bar{u}_{00}(q)$. By choosing appropriate combinations of ϑ_{a}, ϑ_{b}, ϑ_{a}', ϑ_{b}', three other bands are obtainable, two of which, for $V'=V$, are degenerate.

Symmetry considerations again permit the immediate generalization of equations like (3.16) to

$$\left[E_x^{(n)}\left(k_x+i\epsilon H\frac{d}{d\kappa}\right)+E_y^{(m)}(\kappa)-W\right]u_{00}=0 \qquad \ldots\ldots(3.18)$$

with appropriate boundary conditions at the maxima of E_x, E_y.

Equation (3.18) is a particular instance of Peierls' theorem stated more exactly; namely, that replacing $E(\mathbf{k})$ by $E(\boldsymbol{\varkappa})$, $[\kappa_x,\kappa_y]=i\epsilon H_z$ etc., provides an approximate energy operator for the conduction electrons in a uniform magnetic field. $\boldsymbol{\varkappa}$, in this case, is $\mathbf{k}-\epsilon\mathbf{A}^0(i\nabla_{\mathbf{k}})$, $\mathbf{A}^0=\mathbf{H}\times\mathbf{r}-\mathbf{A}$ (see Appendix). Luttinger (1951) has also given a general demonstration of this theorem using the Wannier representation. An advantage of the present treatment is that the theorem is presented quite naturally as a zero-order approximation, the validity conditions of which are easy to obtain. To this end, consider again equations (3.14), (3.15). By eliminating χ_2, u_{01}, there results a pair of simultaneous equations u_{00}, χ_1 which may be written as:

$$\left.\begin{aligned} &\left[(\vartheta_{\mathrm{a}}+\vartheta_{\mathrm{b}}'-W)(\vartheta_{\mathrm{a}}+\vartheta_{\mathrm{a}}'-W)+\left[\frac{\hbar^2\kappa^2}{2m},\frac{\hbar^2D^2}{2m}-\vartheta_{\mathrm{a}}\right]\right.\\ &\qquad\left.+\left[\vartheta_{\mathrm{a}},\frac{\hbar^2\kappa^2}{2m}-\vartheta_{\mathrm{a}}'\right]\right]u_{00}\\ &\qquad=\left[\vartheta_{\mathrm{a}}-\vartheta_{\mathrm{b}}+\frac{\hbar^2}{2m}\left\{\left(\kappa+\frac{2\pi}{a}\right)^2-\kappa^2\right\}\right]\chi_1,\\ &\left[(\vartheta_{\mathrm{b}}+\vartheta_{\mathrm{b}}'-W)(\vartheta_{\mathrm{b}}+\vartheta_{\mathrm{a}}'-W)+\left[\vartheta_{\mathrm{b}},\frac{\hbar^2\kappa^2}{2m}-\vartheta_{\mathrm{a}}'\right]\right.\\ &\qquad\left.+\left[\frac{\hbar^2}{2m}\left(\kappa+\frac{2\pi}{a}\right)^2,\frac{\hbar^2D^2}{2m}-\vartheta_{\mathrm{a}}\right]\right]\chi_1\\ &\qquad=\left[\left\{\vartheta_{\mathrm{b}}+\frac{\hbar^2}{2m}\left(\kappa+\frac{2\pi}{a}\right)^2-W\right\}\left[\frac{\hbar^2D^2}{2m}-\vartheta_{\mathrm{a}},\frac{\hbar^2\kappa^2}{2m}\right]\right.\\ &\qquad\left.+\left[\frac{\hbar^2}{2m}\left(\kappa+\frac{2\pi}{a}\right)^2,\frac{\hbar^2D^2}{2m}-\vartheta_{\mathrm{a}}\right]\left(\vartheta_{\mathrm{a}}+\frac{\hbar^2\kappa^2}{2m}-W\right)\right]u_{00}.\end{aligned}\right\} \qquad \ldots\ldots(3.19)$$

Considering the left-hand sides of these equations, it is clear (from previous arguments) that in both the leading term is the first one written. For u_{00} the first operating factor represents (approximately) the first band; for χ_1, the second band. Their eigenvalues (or more properly, the eigenvalues of their generalizations to forms like equation (3.18)) themselves form bands of broadened levels lying between the same energy limits as those found in the non-magnetic problem (Harper 1955). Thus, in the present case of nearly free electrons, these bands will certainly overlap, though the equations might be regarded as including the less interesting situation that arises when they do not.

The commutator terms (still on the left-hand side) will modify these eigenvalues. Treating them as a perturbation, the first-order correction η to a level W will be given by

$$\eta \int \phi^*(\vartheta_a' - \vartheta_b')\phi \, d\kappa = \int \phi^* U \phi \, d\kappa$$

where U is the sum of the two commutators appropriately defined on both sides of κ, $q = -\pi/a$, and ϕ is an eigenfunction of $\vartheta_a + \vartheta_a'$. A typical term in U is

$$\left[\vartheta_a, \frac{\hbar^2\kappa^2}{2m} - \vartheta_a'\right] \sim \left[\frac{\hbar^2 D^2}{2m}, \frac{\hbar^2\kappa^2}{2m} - \vartheta_a'\right]$$
$$= \frac{\hbar^2}{2m}\left[2i\epsilon H \frac{d}{d\kappa}\left(\frac{\hbar^2\kappa^2}{2m} - \vartheta_a'\right)\left(k_x - i\epsilon H \frac{d}{d\kappa}\right) - (\epsilon H)^2 \left(\frac{d}{d\kappa}\right)^2 \left(\frac{\hbar^2\kappa^2}{2m} - \vartheta_a'\right)\right].$$

Now $\langle \vartheta_a' - \vartheta_b' \rangle$ is least when the electron is largely confined to the vicinity of $\kappa = -\pi/a$. This happens when $W \sim 2(\epsilon_0 - V)$, i.e. near the top of the first band. $\langle \vartheta_a' - \vartheta_b' \rangle$ is then of order $2V$ and the electron behaviour is described by the use of an effective mass m^*. The final term in the above expression is then approximately

$$-(\epsilon H)^2 \left(\frac{\hbar^2}{2m}\right)^2 \left(\frac{d}{d\kappa}\right)^2 \left(\kappa^2 - \frac{m}{m^*}\kappa^2\right) = -2(\mu H)^2 \left(1 - \frac{m}{m^*}\right)$$

where $\mu = e\hbar/2mc$.

Thus it contributes $(\mu H/V)(1 - m/m^*)\mu H$ to η which is a small correction even though $1 - m/m^*$ might be of the order of 10, since $\mu H/V \ll 1$. The first term is not constant and therefore more difficult to estimate, but on dimensional grounds it is probably of the same order of magnitude.

These commutator terms then are likely to be small and are conjectured to correspond, in the limiting case of tight binding, to perturbation of atomic levels, though this has not been verified directly.

The discussion so far applies, for example, to the case $\chi_1 = 0$ and neglects coupling between first and second band. Suppose now, as a better approximation χ_1 is determined from the second of (3.19) using u_{00} from the first (but with $\chi_1 = 0$). Then this contribution to η is given by

$$\eta \int \phi^*(\vartheta_a' - \vartheta_b')\phi \, d\kappa = \int \phi^* \left[\vartheta_a - \vartheta_b + \frac{\hbar^2}{2m}\left\{\left(\kappa + \frac{2\pi}{a}\right)^2 - \kappa^2\right\}\right] \chi_1 \, d\kappa.$$

But in the case when the eigenvalues $W^{a,a}$ of $\vartheta_a + \vartheta_a'$ overlap with $W^{b,a}$ of $\vartheta_b + \vartheta_a'$, it will frequently happen that a pair of them nearly coincide (periodically so, in fact, when the two effective masses in this region are constant) and consequently χ_1 becomes large since it contains components of the order $(W^{a,a} - W^{b,a})^{-1}$. The complexity of the coupled equations (3.19) makes any quantitative examination of their solution an unattractive programme. In any case they represent the situation only approximately since all but adjacent components were neglected. It is not difficult however to obtain the following dimensional estimate for η:

$$\eta \sim \frac{(\mu H)^2}{W^{a,a} - W^{b,a}} \qquad \text{provided} \qquad W^{a,a} \neq W^{b,a}, \qquad \ldots\ldots(3.20)$$

$W^{b,a}$ being the closest eigenvalue of $\vartheta_b + \vartheta_a'$ to $W^{a,a}$. (The resemblance of this result to perturbation theory seems fortuitous since, for example, there should be a factor $V(W^{a,a} - W^{b,a} + V)^{-1}$ which is supposed of order unity.)

If now the bands do overlap, $\eta \sim \mu H$ in the overlap region, i.e. of the order of the level spacing itself, which means that the coupling is strong and cannot be regarded as a weak perturbation to single band levels. However, an inspection of the matrix elements concerned shows that in the overlap region (where in general the use of effective masses for the separate bands is permissible) they are slowly varying and, since near coincidences of $W^{b,a}$ with $W^{a,a}$ will occur (almost) periodically, the actual level spectrum should still exhibit great regularity, even periodicity. Whether this situation can be represented by the use of effective mass parameters is not clear from such simple arguments. The success obtained in fitting experimental curves by such means suggests that it can, though the interpretation of such masses is then uncertain.

For non-overlapping bands, or far from an overlap region, (3.20) gives $\eta \sim (\mu H)^2/\Delta E$, ΔE being the energy gap, and thus, $\eta \ll \mu H$. The correction in this situation is thus comparable with the perturbation first considered, though its origin is different.

§ 4. SUMMARY AND CONCLUSIONS

Apart from some initial generalities concerning properties of the state functions, most results refer to a simplified model chosen in order to avoid purely mathematical difficulties. Firstly, the periodic potential describing the effect of the lattice was restricted to be sinusoidal. It is evident however, that results concerning single-band motion are immediately extendible to include all $V(\mathbf{r})$ of the form $V_1(x) + V_2(y) + V_2(z)$ using, of course, any convenient set of axes (x, y, z). Secondly, the magnetic field $\mathbf{H}$ was supposed to lie along such an axis (not necessarily a crystallographic axis). In consequence of this, and the fact that $E(\mathbf{k})$ is separable into $E_x(k_x) + E_y(k_y) + E_z(k_z)$, no ordering ambiguities arise in applying Peierls' theorem concerning $\mathbf{k} \to \boldsymbol{\kappa} - \epsilon \mathbf{A}(i\nabla\boldsymbol{\kappa})$.

The magnetic wave functions depend of course upon choice of gauge in $\mathbf{A}(\mathbf{r})$. Comparison with those for free electrons (in a magnetic field) show that in the particular case $\mathbf{A} = (0, Hx, 0)$ the wave functions are of the extended sort, being (for low energies at least) approximately linear combinations of the degenerate Landau functions. Application of the first of formulae (1.7) shows that there is a very slow linear motion of the electron in the x direction, this being a translation of the 'orbit' due to Bragg collisions with the lattice.

Of more interest are the magnetic energy levels. Neglecting field direction motion, the highly degenerate discrete levels of free electrons are broadened as a result of lattice forces. In the preceding paper (Harper 1955) the case of tight binding was discussed and some of the results are quite general. The level spacing is also affected, since it is no longer uniform. When there is no band overlap the variation in spacing is slow and the concept of effective mass certainly valid. For overlapping bands however, there appears to be a strong coupling which, while distorting the level structure in that vicinity, may still leave great regularity. It is not certain whether a description in terms of effective mass is applicable.

Knowing something of the magnetic level density what can one say of its effect on the magnetic susceptibility? Consider first the level broadening. Dingle has shown that the effect of collision broadening is to damp the low temperature susceptibility oscillation or what proves to be equivalent, raise the effective temperature by a degree or so. Lattice broadening has the same effect. Taking the spacing as uniform, simple perturbation theory indicates that the broadening might be well described by

$$\epsilon = b\left(\cos\frac{2\pi k_x}{\epsilon a H} + \cos\frac{2\pi k_y}{\epsilon a H}\right)$$

for each level, where $2b < \mu^* H$. If one now corrects the classical partition function by a factor

$$\sum_{k_x, k_y} \exp\{-\beta\epsilon(k_x, k_y)\}$$

and uses the analytical method of Sondheimer and Wilson (1951), the vth Fourier component of the level density is seen to be diminished by a factor $J[_0(bv\pi/\mu^* H)]^2$ J_0 being the zero-order Bessel function regular at the origin. Consequently the magnetic moment is damped by the same factor. Dingle (1951) also examined this question and arrived at a similar result to the one given above, namely, that a periodic perturbation in one direction (perpendicular to the field) reduces the susceptibility amplitude by the factor $J_0(bv\pi/\mu^* H)$, b being given by the overlap integral of two Landau wave functions. Taking $2b \lesssim \mu^* H$, i.e. extreme broadening, the first (and greatest component) is heavily damped. Since in the monovalent metals the Fermi surface may be supposed to lie in the centre of the band and since the broadening is greatest there (see Harper 1955), it suggests a possible explanation of the absence of any observed oscillations in these metals.

For $b \ll \mu^* H$, the broadening factor may be written approximately $\exp[-(bv\pi/\mu^* H)^2]$ and the broadening effect becomes additive to that due to collision as described by Dingle (1952 b).

The level structure in the vicinity of an energy gap near a zone boundary is all-important for the de Haas–van Alphen effect. Unfortunately, this seems very difficult to determine in detail, even for a sinusoidal potential. Apart from the regularity already mentioned there seems little one can say. It is likely, however, that if periodicity exists, the period will give rise to effective mass parameters much smaller than one would otherwise expect. This is because the level structure will consist of irregular groups, regularly repeated. Since the period is large, the oscillatory period will also be large and the effective mass correspondingly smaller.

ACKNOWLEDGMENTS

The author is grateful to Professor R. E. Peierls for suggesting this problem, and for his constant supervision and encouragement throughout the work. He would also like to thank the Ministry of Education for their financial support.

APPENDIX

With an arbitrary gauge $\mathbf{A}(\mathbf{r})$, the Schrödinger equation becomes

$$\left[-\frac{\hbar^2}{2m}\left(\nabla-\frac{ie}{\hbar c}A\right)^2+V(r)-W\right]\exp\left[i\epsilon\mathbf{A}(\mathbf{r})\,.\,\mathbf{r}\right]U(\boldsymbol{\varkappa},\mathbf{r})\exp\left(i\boldsymbol{\varkappa}\,.\,\mathbf{r}\right)=0$$

or

$$\left\{-\frac{\hbar^2}{2m}\left[\nabla-i\epsilon\mathbf{A}+i\epsilon\nabla(\mathbf{A}\{\mathbf{r}\}\,.\,\mathbf{r})\right]^2+V(\mathbf{r})+\frac{\hbar^2\nabla^2}{2m}(\mathbf{A}\,.\,\mathbf{r})i\epsilon\right\}\exp\left(i\boldsymbol{\varkappa}\,.\,\mathbf{r}\right)U(\boldsymbol{\varkappa},\mathbf{r})$$

Now $\nabla^2(\mathbf{A}\,.\,\mathbf{r})=0,\qquad \nabla(\mathbf{A}\,.\,\mathbf{r})=2\mathbf{A}-\mathbf{H}\times\mathbf{r},$

consequently, $+\mathbf{A}-\nabla(\mathbf{A}\,.\,\mathbf{r})=\mathbf{H}\times\mathbf{r}-\mathbf{A}$ replaces $\mathbf{A}(\mathbf{r})$ in the kinetic term. Considering now the implicit differentiation on $\boldsymbol{\varkappa}$,

$$\frac{\partial}{\partial x^\mu}\to\frac{\partial}{\partial x^\mu}-\epsilon\left(\frac{\partial A^\nu}{\partial x^\mu}\frac{\partial}{\partial\kappa^\nu}\right).$$

Writing curl $\mathbf{A}=\mathbf{H}$ and remembering that $\partial A^\nu/\partial x^\mu$ are constants,

$$\begin{aligned}\frac{\partial A^\nu}{\partial x^\mu}\frac{\partial}{\partial\kappa^\nu}&=-\mathbf{H}\times\nabla_\kappa+(\nabla_\kappa\,.\,\nabla)\mathbf{A}(\mathbf{r})\\&=-\mathbf{H}\times\nabla_\kappa+\mathbf{A}(\nabla_\kappa).\end{aligned}$$

Therefore in the kinetic term,

$$\nabla\to\nabla+\epsilon[\mathbf{H}\times\nabla_\kappa-\mathbf{A}(\nabla_\kappa)].$$

Then the whole term may be written

$$\left[\mathbf{p}-\frac{e}{c}\mathbf{A}^0(\mathbf{r}+i\nabla_\kappa)\right]^2$$

where $\mathbf{A}^0(\mathbf{r})=\mathbf{H}\times\mathbf{r}-\mathbf{A}(\mathbf{r}).$

For the case $\mathbf{A}=\frac{1}{2}\mathbf{H}\times\mathbf{r}$, $\mathbf{A}^0=\mathbf{A}$. For $\mathbf{A}=(0, Hx, 0)$, $\mathbf{A}^0=(-Hy, 0, 0)$ and vice versa. Note however, that the definition of $\boldsymbol{\varkappa}$ is unaltered, i.e. $\boldsymbol{\varkappa}=\mathbf{k}-\epsilon\mathbf{A}(\mathbf{r})$.

REFERENCES

ADAMS, E. N., 1953, *Phys. Rev.*, **89,** 633.

BLACKMAN, M., 1938, *Proc. Roy. Soc.* A, **166,** 1.

DINGLE, R. B., 1951, *Thesis*, University of Cambridge ; 1952 a, *Proc. Roy. Soc.* A, **211,** 500; 1952 b, *Ibid.*, **211,** 517.

DINGLE, R. B., and SHOENBERG, D., 1950, *Nature, Lond.*, **166,** 652.

HARPER, P. G., 1955, *Proc. Phys. Soc.* A, **68,** 874.

LUTTINGER, J. M., 1951, *Phys. Rev.*, **84,** 814.

ONSAGER, L., 1952, *Phil. Mag.*, **43,** 1006.

PEIERLS, R. E., 1933, *Z. Phys.*, **80,** 763.

SHOENBERG, D., 1952, *Phil. Trans. Roy. Soc.* A, **245,** 1.

SONDHEIMER, E. H., and WILSON, A. H., 1951, *Proc. Roy. Soc.* A, **210,** 173.

WILSON, A. H., 1936, *Theory of Metals*, ch. III (Cambridge : University Press).

On the Positive Temperature Effect in the Cosmic Radiation and the μ–e Decay

By H. TREFALL†
Imperial College of Science and Technology, London

Communicated by P. M. S. Blackett; MS. received 4th April 1955

Abstract. It is shown that the positive partial correlation which exists between the meson intensity at sea level and the stratospheric temperature can be interpreted as being due to the μ–e decay. Two 'second-order' effects of the μ–e decay contribute to the positive temperature effect which is observed at sea level. One is due to the fact that neither of the standard pressure levels (the 100 mb and 50 mb levels) which have been used as reference levels in the analysis of experimental data is a sufficiently good approximation to the mean level of meson production. The other is due to the fact that the survival probability of a μ-meson depends on the way in which its energy loss is distributed over the distance which the meson has to traverse. The theoretically predicted values of the positive temperature effect associated with the μ–e decay are in reasonable agreement with the available experimental results. The observed dependence of the effect on the choice of reference level is also explained.

§ 1. Introduction

The work of Duperier (1949, 1951) has proved the existence of a positive partial correlation between the sea-level flux of μ-mesons and the stratospheric temperature, the other independent variables being the barometric pressure at sea level and the height of the 100 mb level. This positive temperature effect was found to be of the order of 0·1% per degree, and it was interpreted as being due to competition between disintegration and nuclear capture of the π-mesons.

However, Duperier (1951) has pointed out that the observed effect appears to be considerably greater than it should be according to this interpretation. The experimental work on the positive temperature effect at sea level as well as that performed underground has recently been re-examined by the author (Trefall 1955) and compared with more accurate theoretical estimates of the effect due to the π–μ decay. It was then concluded that whilst Duperier's theory could adequately account for the results of the underground measurements, a real discrepancy existed between the theoretical estimates and the positive temperature effect observed at sea level.

A possible explanation of this discrepancy as an effect of the μ–e decay has already been put forward (Trefall 1953). A similar suggestion was made independently by Olbert (1953). Even though only second-order effects of the μ–e decay are involved, they may nevertheless be great compared with the effect of the π–μ decay if the mean energy of the recorded radiation is relatively low,

† On leave from Universitetet i Bergen, Bergen, Norway.

as is the case at sea level. It is the purpose of this paper to discuss the relevant effects of the μ–e decay to see whether they suffice to explain the discrepancy between the observed positive temperature effect and that which is expected to arise from the π–μ decay.

§ 2. THE ATMOSPHERIC EFFECTS IN THE COSMIC RADIATION

The observed correlation between the intensity of the hard component of the cosmic radiation at sea level and the atmospheric conditions is usually described by means of a linear regression equation with three independent variables, viz.

$$(I-\bar{I})/\bar{I}=\beta_1(B-\bar{B})+\beta_2(H-\bar{H})+\beta_3(T-\bar{T}). \qquad \ldots\ldots(1)$$

Here I denotes the intensity, B the barometric pressure at sea level, H the height of a suitably chosen reference level and T the temperature in the neighbourhood of this level. Bars denote mean values. The above representation of the atmospheric effects on the cosmic-ray intensity is due to Duperier (1949). The reference level is assumed to represent the mean level of meson production. Usually, the 100 mb level is chosen as the reference level, and Duperier (1949, 1951) has shown that this is a good choice. Occasionally, the 50 mb level has been used instead. The variable T is usually defined as the mean temperature of the layer between the reference level and the 200 mb level.

It is usually taken for granted that each term of this experimentally established formula can be given a unique physical interpretation. The first term on the right-hand side of (1) is regarded as representing the effect of absorption of μ-mesons in the atmosphere, whilst the second term is due to the instability of the μ-mesons and expresses the fact that their survival probability depends on the distance between their mean level of production and the place of observation. The third term was introduced by Duperier because it was found that a regression equation with B and H as the only independent variables was insufficient for the description of the observed atmospheric effects. Duperier found the coefficient β_3 to be positive and of the order of $0{\cdot}1\%$ per degree. This is the positive temperature effect which was interpreted as being due to competition between disintegration and nuclear capture of the π-mesons.

However, the assumption that it is possible to give each term of equation (1) a unique physical interpretation is not strictly true, for only in the first approximation can the survival probability of the μ-mesons be regarded as a function of H only, and the second term of (1) as the total effect of the μ–e decay. In a more accurate theory, the two other terms are both found to be 'contaminated' by second-order effects of the μ–e decay.

These second-order effects of the μ–e decay are particularly important in the theory of the positive temperature effect, for they seem to be responsible for the greater part of the effect observed at sea level. In this case two different second-order effects have to be considered. First, the chosen reference level may not coincide with the mean level of meson production. Such a coincidence is, in fact, highly improbable, for the reference level has, for reasons of convenience, always been chosen as one of the standard pressure levels for which meteorological data are available. Therefore, the distance between sea level and the mean level of meson production may not be uniquely determined by the height of the reference level, but may also depend on the temperature of the upper atmosphere.

If the mean level of production lies below the reference level, an increase in temperature in the upper atmosphere will reduce the distance between sea level and the production level, provided H and B remain constant. The survival probability of the μ-mesons will then increase, and a positive partial correlation between the meson intensity at sea level and the temperature of the upper atmosphere will be observed. As we shall see later on, this is exactly what happens, but the sign as well as the magnitude of this second-order effect of the μ–e decay must depend on the choice of reference level. The effect will also depend on the energy of the recorded radiation, not only because the mean life of a μ-meson depends on its energy, but also because the mean depth of meson production is a function of energy. With increasing energy, more of the mesons produced in the uppermost layers of the atmosphere will reach sea level and the mean depth of production will move towards smaller atmospheric depths. It is therefore quite possible that this second-order effect of the μ–e decay, which depends on the distance between the reference level and the mean level of meson production, can be positive at low energies and negative at high energies for certain choices of reference level. Such a change of sign actually occurs when the 100 mb level is used as reference level. With the reference level at 50 mb the effect is always positive whereas with the reference level at 200 mb it would always be negative, irrespective of the energy of the recorded mesons.

The other second-order effect of the μ–e decay which contributes to the observed positive temperature effect is a combined effect of the relativistic time-dilation and the slowing down of the μ-mesons in the atmosphere. If a μ-meson is to travel a given distance while losing a given amount of energy, the survival probability will depend upon how the energy loss is distributed along its path. Because the mean life of the μ-meson is an increasing function of its energy, the survival probability will increase if some of the energy loss can be transferred towards the end of the path. This is exactly what happens if the temperature of the stratosphere increases while B and H remain constant. Under these conditions, the temperature of the lower atmosphere must decrease. Consequently, some amount of air, and with it some energy loss, will be transferred towards the end of the path which the meson has to traverse, thereby increasing the survival probability and giving rise to a positive temperature effect. It will be shown that this effect of the μ–e decay also increases with decreasing atmospheric depth of the reference level.

During the above qualitative discussion we have used the concept of a mean level of meson production. In the following sections, the theory for the positive temperature effect associated with the μ–e decay will be developed for the general case in which mesons are produced throughout the atmosphere.

§ 3. ANALYSIS OF THE MESON COMPONENT

The hard component of the cosmic radiation at sea level is known to consist almost entirely of μ-mesons. According to our present knowledge, practically all μ-mesons are decay products of π-mesons. A comprehensive analysis of the meson component should therefore begin with a discussion of the π–μ decay. However, as the positive temperature effect due to the π–μ decay has already been investigated and found to be very small (Trefall 1955), the discussion may proceed without any explicit reference to the π–μ decay. The discussion in this section will be restricted to vertically travelling μ-mesons.

It will be assumed that the number of μ-mesons which are produced in an atmospheric layer dx with momenta in the interval dp is proportional to $p^{-s}\exp(-x/\lambda)\,dp\,dx$, where x is the atmospheric depth measured in g cm^{-2} and p is the momentum measured in units of $m_\mu c$, m_μ being the mass of the μ-meson. (Throughout the paper, momenta will be measured in units of $m_\mu c$.) The justification for the above assumption is the following: It is known that the intensity of that component of the cosmic radiation which produces penetrating showers decreases exponentially with increasing atmospheric depth, and Ticho (1952) has shown that the attenuation length of the shower-producing radiation is almost independent of its energy. Therefore, if we identify this component with that responsible for the production of π-mesons, it is reasonable to assume that the momentum spectrum of the produced π-mesons is independent of the atmospheric depth. The same will then apply to the production spectrum of the μ-mesons. A power law was assumed to hold for the production spectrum because it is then possible to obtain very good agreement with the observed sea-level momentum spectrum. For the attenuation length we will adopt the value $\lambda = 125$ g cm^{-2} found by Ticho (1952).

The momentum spectrum at sea level also depends on the survival probability of the μ-mesons and their momentum loss in the atmosphere. If it is assumed that the momentum loss per g cm^{-2} of air for relativistic particles is independent of their velocity, the differential momentum spectrum at sea level may be represented by the function

$$n_s(p_s)=\int_0^{x_s} w(x,x_s,p_0)(p_0-ax)^{-s}\exp(-x/\lambda)\,d(x/\lambda) \qquad \ldots\ldots(2)$$

where p_s is the sea-level momentum, $w(x,x_s,p_0)$ is the survival probability from the depth of production x to the sea-level depth x_s, a is the momentum loss per g cm^{-2} and p_0 is defined by

$$p_0 \equiv p+ax, \qquad \ldots\ldots(3)$$

p being the momentum with which the meson was produced. The connection between p_0 and p_s is

$$p_0=p_s+ax_s. \qquad \ldots\ldots(4)$$

The parameter p_0 will be called the "momentum of the μ-meson at the top of the atmosphere". It is a very useful quantity because mesons reaching sea level with equal momenta have equal values of p_0, even though they may have been produced with different momenta at different atmospheric depths.

The reference level can now be introduced by writing

$$w(x,x_s,p_0)=w(x,x_r,p_0)\,w(x_r,x_s,p_0), \qquad \ldots\ldots(5)$$

where x_r is the atmospheric depth of the reference level. The second factor on the right-hand side is the survival probability for a meson travelling from the reference level to sea level. If $x<x_r$ the first factor is the survival probability from the place of production to the reference level, but if $x>x_r$ this factor will be the inverse of the survival probability for a meson travelling from the reference level to the depth x.

According to (2) and (5) we can now write

$$n_s(p_s)=w(x_r,x_s,p_0)\,n_r(p_0) \qquad \ldots\ldots(6)$$

where

$$n_r(p_0)=\int_0^{x_s} w(x,x_r,p_0)(p_0-ax)^{-s}\exp(-x/\lambda)\,d(x/\lambda), \qquad \ldots\ldots(7)$$

the relation between p_0 and the sea-level momentum p_s being given by (4). The function $n_r(p_0)$ can be given the following physical interpretation: If μ-mesons were produced at the reference level only, $n_r(p_0)$ is the production spectrum which would give rise to a sea-level spectrum identical with that which is actually observed.

The general formula for the survival probability of a meson travelling from the depth x_1 to the depth x_2 is

$$w(x_1, x_2, p_0) = \exp\left[-\int_{x_1}^{x_2} \frac{(1-\beta^2)^{1/2}}{ct_\mu \beta} \frac{dx}{\rho}\right] \qquad \ldots\ldots(8)$$

where ρ is the density of air, t_μ is the proper mean life of the μ-mesons and the other symbols have their usual meaning. The factor $(1-\beta^2)^{1/2}$ accounts for the relativistic time-dilation. It is convenient to introduce the momentum $p = \beta/(1-\beta^2)^{1/2}$ and to write $\rho = x/H_0$, where H_0 is the scale height of the atmosphere. If an isothermal atmosphere is assumed, H_0 is independent of x, and one easily arrives at the formula

$$w(x_1, x_2, p_0) = \left[\frac{x_1(p_0 - ax_2)}{x_2(p_0 - ax_1)}\right]^v \qquad \ldots\ldots(9)$$

where

$$v \equiv H_0/ct_\mu p_0 \qquad \ldots\ldots(10)$$

and a denotes the momentum loss per g cm^{-2} of air.

Our next step is to derive an approximate formula for $n_r(p_0)$, defined by (7). For the survival probability $w(x, x_r, p_0)$ we will use the general formula (9). This is permissible because most μ-mesons are produced in the almost isothermal stratosphere, where also the reference level is situated. We then introduce the approximation

$$p_0 - ax \simeq p_0 \exp(-ax/p_0). \qquad \ldots\ldots(11)$$

This can be done because most μ-mesons are produced at such small depths that $x \ll x_s$, and the minimum value of p_0 for μ-mesons reaching sea level is, according to (4), ax_s. Usually, therefore, one has $ax \ll p_0$, and the above approximation is a good one. By means of (7), (9) and (11) one then finds that

$$n_r(p_0) \simeq p_0^{-s} x_r^{-v} \left[\frac{p_0 - ax_r}{p_0}\right]^v \int_0^{x_s} x^v \exp\left[-\frac{p_0 - (s+v)a\lambda}{p_0} . \frac{x}{\lambda}\right] d(x/\lambda). \qquad \ldots(12)$$

If the upper limit of integration could be extended to infinity, the integral could be transformed to the one defining the factorial function $v\,!$. This approximation is, in fact, permissible: Because $\lambda = 125$ g cm^{-2} and $x_s = 1033$ g cm^{-2}, we have $x_s/\lambda \gg 1$. Further, we have $s \simeq 3$, while $p_0 > ax_s$ and $v < 0{\cdot}5$ for all mesons reaching sea level. Therefore, at the upper limit of integration the argument of the exponential is numerically much greater than 1. This, combined with the fact that the exponent v is always small, shows that no significant error is introduced by extending the upper limit of integration to infinity, and we obtain

$$n_r(p_0) \simeq p_0^{-s}(v\,!)(\lambda/x_r)^v(1 - ax_r/p_0)^v[1 - (s+v)a\lambda/p_0]^{-(1+v)}. \qquad \ldots\ldots(13)$$

Finally, we need a formula for the survival probability of a μ-meson travelling from the reference level to sea level. We will use an approximation which corresponds to an atmosphere consisting of two isothermal layers, the stratosphere and the troposphere, and write, therefore,

$$w(x_r, x_s, p_0) \simeq \left[\frac{x_r(p_0 - ax_t)}{x_t(p_0 - ax_r)}\right]^v \left[\frac{x_t(p_0 - ax_s)}{x_s(p_0 - ax_t)}\right]^{v'} \qquad \ldots\ldots(14)$$

where x_t is the atmospheric depth of the tropopause, v is defined by (10) and $v' = H_0'/ct_\mu p_0$, H_0' being the mean scale height of the troposphere. H_0' will be defined by the equation

$$H_0' \ln(x_s/x_t) = H_t, \qquad \ldots\ldots(15)$$

where H_t is the height of the tropopause, for (15) is the formula for the vertical distance between the levels x_s and x_t in an isothermal atmosphere with scale height H_0'.

The actual values of x_t, H_0' and H_t used in this work have been chosen in accordance with the properties of the 'international standard atmosphere' (see, for example, Berry *et al.* 1945). Its definition is the following: The sea-level pressure is 1013·2 mb, corresponding to a sea-level depth $x_s = 1033\ \mathrm{g\,cm^{-2}}$. At any altitude $h < 11\,000$ m above mean sea level, the temperature is $(15 - 0{\cdot}0065h)^\circ$c, h being measured in metres. For $h > 11\,000$ m, the temperature is independent of h and equal to $-56{\cdot}5^\circ$c. One then finds that the tropopause height of 11 000 m corresponds to a pressure of 226 mb or a depth of 231 g cm^{-2}, which makes $H_0' = 7340$ m. The scale height of the stratosphere is $H_0 = 6330$ m.

The final step in the analysis of the meson component is to calculate the theoretical momentum spectrum at sea level for different values of the exponent s in the production spectrum and compare the results with the observed sea-level spectrum. Measurements of the sea-level spectrum have been performed by Caro, Parry and Rathgeber (1951) and by Owen and Wilson (1955). With $s = 3{\cdot}0$ one obtains very good agreement between the two experimental spectra and our theoretical spectrum. The momentum loss of μ-mesons in air was taken to be $0{\cdot}02m_\mu c$ per g cm^{-2}, which is a good average value for mesons in the atmosphere. For the mass of the μ-meson we have used a value of 207 electron masses (Smith, Birnbaum and Barkas 1953).

§ 4. THEORY OF THE POSITIVE TEMPERATURE EFFECT

In § 2 we discussed in a qualitative way the two second-order effects of the μ–e decay which would contribute to the positive temperature effect. In the preceding section we derived equations which will make it possible to deduce explicit formulae for those effects. It was found convenient to express the sea-level momentum spectrum as a product of the function $n_r(p_0)$, defined by (7) and approximated by (13), and the survival probability $w(x_r, x_s, p_0)$ for a μ-meson travelling from the reference level to sea level, approximated by (14). This representation is advantageous because it enables us to discuss separately each of the two second-order effects of the μ–e decay.

The function $n_r(p_0)$ depends on the stratospheric temperature T through the parameter v. According to (10), v is proportional to the atmospheric scale height H_0 and is, therefore, also proportional to T. Differentiation of $\ln[n_r(p_0)]$ with respect to T then yields the formula

$$\frac{1}{n_r(p_0)}\frac{dn_r}{dT} \simeq \left[\frac{d}{dv}\ln(v!) + \ln\left(\frac{\lambda}{x_r}\right) + \ln\left(\frac{p_0 - ax_r}{p_0 - (s+v)a\lambda}\right) + \frac{(1+v)a\lambda}{p_0 - (s+v)a\lambda}\right]\frac{v}{T} \qquad (16)$$

for the positive temperature effect relative to the reference level. However, the derivation of this formula may seem to rest on rather strange assumptions about the atmospheric temperature variations, for the basic formula (13) is valid only in an isothermal atmosphere. Therefore, during the derivation of (16) it has implicitly been assumed that the temperature variations are also independent of the atmospheric depth, but such an assumption is, strictly speaking, inconsistent with the atmospheric model which has been used in the analysis of experimental data.

According to equation (1), the positive temperature coefficient β_3 represents the change in cosmic-ray intensity which is observed if T changes while B and H remain constant, and H cannot remain constant if the temperature increases throughout the atmosphere. An exact theoretical estimate of the positive temperature effect should therefore have been based on an atmospheric model in which an increasing stratospheric temperature is compensated by a decrease of temperature in the troposphere, so that the height of the reference level can remain constant. However, as most of the μ-mesons reaching sea level have been produced in the stratosphere, the distance between the mean level of meson production and the reference level is not very sensitive to changes in the tropospheric temperature. Consequently, the positive temperature effect caused by movements of the mean production level relative to the reference level will be adequately represented by (16).

The positive temperature effect caused by the variation of the survival probability from the reference level to sea level will now be discussed. In this case the temperature variation in the lower atmosphere may not be neglected. According to (14), $w(x_r, x_s, p_0)$ depends on the stratospheric temperature T through v and on the mean tropospheric temperature T' through v', v and v' being proportional to H_0 and H_0' respectively. The stratospheric scale height H_0, the mean tropospheric scale height H_0' and the height H of the reference level are related to each other by the equation

$$H_0' \ln(x_s/x_t) + H_0 \ln(x_t/x_r) = H. \qquad \ldots\ldots(17)$$

If the atmospheric temperature distribution changes, H can remain unchanged only if the condition

$$\delta H_0' \ln(x_s/x_t) + \delta H_0 \ln(x_t/x_r) = 0 \qquad \ldots\ldots(18)$$

is fulfilled. By means of equations (14) and (18) and the fact that the parameters $v = H_0/ct_\mu p_0$ and $v' = H_0'/ct_\mu p_0$ are proportional to the atmospheric temperature, one obtains the expression

$$\frac{1}{w(x\,, x_s, p_0)}\frac{dw}{dT} = \left[\frac{\ln(x_t/x_r)}{\ln(x_s/x_t)}\ln\left(\frac{p_0 - ax_t}{p_0 - ax_s}\right) - \ln\left(\frac{p_0 - ax_r}{p_0 - ax_t}\right)\right]\frac{v}{T} \qquad \ldots\ldots(19)$$

for the second positive temperature effect due to the μ–e decay.

For comparison with the experimental results we need estimates of the temperature effect on the integral meson intensity, whereas the formulae (16) and (19) describe the effects on the differential momentum spectrum only. Integral positive temperature coefficients are easily calculated by integrating the differential coefficients (16) and (19) over that part of the momentum spectrum which is accepted by the recording apparatus. This has been done, and the integral coefficients have been plotted against the cut-off momentum of the recorder in figures 1 and 2, the reference levels being at 100 mb and 50 mb respectively. In order to show the relative importance of the two effects described by (16) and (19), they have also been plotted separately.

§ 5. ZENITH ANGLE DEPENDENCE

The formulae already developed in §§ 3 and 4 are valid for μ-mesons arriving from any zenith angle θ provided x is replaced by $x_\theta = x/\cos\theta$ and H_0 by $H_\theta = H_0/\cos\theta$. Instead of p_0 we will now use the symbol p_θ to denote the momentum of a meson at the top of the atmosphere. Inspection of the formulae (16) and (19) then shows that only the effect described by (16) will depend on θ provided p_0 and p_θ are related to each other by the equation

$$p_\theta = p_0/\cos\theta. \qquad \text{......(20)}$$

As the most significant change in (16) is the addition of a term $(v/T)\ln\cos\theta$, we see that the differential positive temperature effect associated with the μ–e decay decreases with increasing zenith angle if mesons with equal values of $p_\theta \cos\theta$ are compared.

Table 1. Experimental Values of the Positive Temperature Coefficient obtained with the Reference Level at 100 mb

Author and reference	Cut-off momentum (m_μ c)	Opening half-angle (°)	Temp. coeff. (% per deg.)
I. Duperier (1951)	4·1	23 × 59	0·124 ± 0·032
II. Duperier (1951)	5·9	36 × 71	0·075 ± 0·010
III. Chasson (1953)	3·6	38 × 60	0·068 ± 0·018
IV. Dawton and Elliot (1953)	2·3	58 × 58	0·056 ± 0·018
V. Trumpy and Trefall (1953)	3·8	45 × 57	0·038 ± 0·019
VI. Trumpy and Trefall (1953)	2·3	59 × 71	0·036 ± 0·021
VII. Cotton and Curtis (1951)	3·5	Max. 17	−0·023 ± 0·027
VIII. Wada and Kudo (1954)	3·1	52 × 52	0·271 ± 0·040 †‡
IX. Wada and Kudo (1954)	3·1	Chamber	0·135 ± 0·023 †

† Calculated on the basis of results obtained with the 200 mb level as reference level.
‡ Not plotted in figure 1.

Table 2. Experimental Values of the Positive Temperature Coefficient obtained with the Reference Level at 50 mb

Author and reference	Cut-off momentum ($m_\mu c$)	Opening half-angle (°)	Temp. coeff. (% per deg.)
X. Duperier (1951)	4·1	23 × 59	0·228 + 0·045
XI. Duperier (1951)	5·9	36 × 71	0·143 + 0·015
XII. Dolbear and Elliot (1953)	5·3	Inclined	0·14

It can further be shown that the integral positive temperature coefficient for mesons arriving from the direction θ is approximately given by the formula

$$\beta_3(\theta) = \beta_3(0) + k\ln\cos\theta \qquad \text{......(21)}$$

provided the cut-off momenta in the vertical and inclined directions are related to each other by equation (20). It has also been assumed that the attenuation length of the meson-producing radiation and the production spectrum of the μ-mesons are independent of the zenith angle. The factor k is a slowly varying function of the cut-off momentum of the meson recorder. When discussing the results of the various sea-level measurements one can always use the value $k \simeq 0{\cdot}12\%$ per degree.

Apart from measurements at specific zenith angles, the above considerations are of interest in connection with the interpretation of the measurements made with vertical cosmic-ray telescopes because the various workers have used recorders with quite different angular apertures. In any vertical telescope the cut-off momentum in the direction θ and the cut-off momentum in the vertical direction are related to each other by equation (20). On the basis of the results obtained above we therefore conclude that the positive temperature effect due to the μ–e decay will decrease with increasing aperture of the counter telescope.

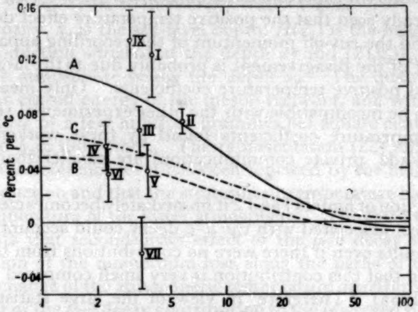

Figure 1. Positive temperature effect with the reference level at 100 millibar plotted against cut-off momentum

A. Total positive temperature effect due to the μ–e decay.
B. Effect due to movement of production level (formula (16)).
C. Effect due to redistribution of momentum loss (formula (19)).

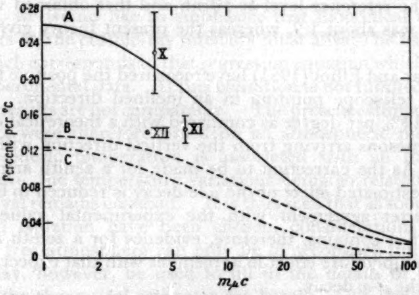

Figure 2. Positive temperature effect with the reference level at 50 millibar plotted against cut-off momentum.

A. Total positive temperature effect due to the μ–e decay.
B. Effect due to movement of production level (formula (16)).
C. Effect due to redistribution of momentum loss (formula (19)).

§ 6. COMPARISON WITH EXPERIMENTS

Several workers have now analysed the variations of the hard component of the cosmic radiation at sea level by fitting a regression equation of the form (1) to their data. The positive temperature coefficients thus obtained are given in tables 1 and 2. In order to facilitate the comparison between theory and experiment, the experimental results have been plotted together with the theoretical curves in figures 1 and 2. Each point representing an experimental value has been marked with a Roman numeral referring to the corresponding entry in tables 1 and 2.

There is clearly no good agreement between the results obtained by the many different workers. To some extent the apparent inconsistency may be accounted for by the very different experimental arrangements used by the different workers, for we have already seen that the positive temperature effect depends upon both the geometry and the cut-off momentum of the recording apparatus. However, the greater part of the disagreement is probably due to the large statistical errors of the measured positive temperature coefficients. Only measurement VIII of able 1 seems to be incompatible with the other experimental results. However, the positive temperature coefficients found by these workers in more recent experiments (Wada, private communication) are smaller than those quoted in table 1.

Upon inspection of figures 1 and 2 it immediately becomes clear that the positive temperature effect associated with the μ–e decay could account for almost all the experimental results even if there were no contributions from the π–μ decay. It is already known that this contribution is very small compared with the observed effect (Trefall 1955). Therefore, in view of the large statistical errors in the experimental results and the approximate nature of the theoretical estimates of the positive temperature effect associated with the μ–e decay, the agreement between theory and experiment must be considered satisfactory.

It is particularly satisfying that the present theory can explain the observed dependence of the positive temperature effect on the choice of reference level. Duperier (1951) found that the ratio between the positive temperature coefficient obtained with the reference level at 50 mb and that obtained with the reference level at 100 mb was about 1·9, whereas the present theory gives a ratio of about 2·5.

Only Dolbear and Elliot (1951) have measured the positive temperature effect with a counter telescope pointing in an inclined direction. They obtained a coefficient of 0·14% per degree as compared with a theoretical estimate of 0·21% per degree for mesons arriving from the vertical direction with a corresponding mean energy. As the correction to be made for a zenith angle of 45° is about 0·04%, the net estimated effect of the μ–e decay is reduced to 0·17% per degree, which gives better agreement with the experimental value. The result of Dolbear and Elliot contains, therefore, evidence for a zenith angle dependence of the positive temperature effect in agreement with that expected for the second-order effects of the μ–e decay.

§ 7. CONCLUSION

It has been shown that two second-order effects of the μ–e decay exist which contribute to the observed positive temperature effect. Of these effects, one is due to the fact that the mean level of meson production does not coincide with the usually employed reference level, while the other is caused by the redistribution of momentum loss along the paths of the μ-mesons which occurs when the atmospheric temperature distribution varies. Comparison with the experimental results has shown that the main features of the positive temperature effect observed at sea level can be explained by the properties of those second-order effects of the μ–e decay.

A comprehensive analysis of the atmospheric effects on the cosmic-ray intensity has been carried out by Olbert (1953), and it is interesting to compare his results with ours. Olbert analysed the atmospheric effects from a purely theoretical point of view, and suggested that the variation of the integral meson intensity at sea level ought to be represented by the formula

$$\delta I/I = A_P\delta x_s + A_H\delta H(\bar{x}_1) + A_K[\delta T(\bar{x}_2)]_{av} \qquad \ldots\ldots(22)$$

where I is the intensity, x_s is the sea-level depth, $H(\bar{x}_1)$ is the height of the mean level of meson production situated at the depth $\bar{x}_1$ and $[T(\bar{x}_2)]_{av}$ is the average temperature of the atmosphere below the depth $\bar{x}_2$. The quantities $\bar{x}_1$ and $\bar{x}_2$ are functions of the cut-off energy of the meson recorder, and with an amount of absorber of the order of a few hundred grammes per square centimetre they are $\bar{x}_1 \simeq 115\,\mathrm{g\,cm^{-2}}$ and $\bar{x}_2 \simeq 190\,\mathrm{g\,cm^{-2}}$. The representation (22) differs from (1) in that the height of the reference level has been replaced by the height of the mean level of meson production and that the stratopheric temperature has been replaced by the average temperature of the lower atmosphere. The third term of Olbert's equation represents that second-order effect of the μ–e decay which is caused by the redistribution of the momentum loss along the paths of the μ-mesons in connection with a change of the atmospheric temperature distribution. The other second-order effect of the μ–e decay contributing to the observed positive temperature effect is not explicitly represented in (22), for the reference level and the mean level of meson production are identical in Olbert's representation. However, because of this identity between reference level and mean level of meson production Olbert's decay coefficient A_H must differ from the coefficient β_2 of equation (1) by an amount equal to the magnitude of the corresponding second-order effect of the μ–e decay.

In conclusion, we would like to emphasize that theoretical estimates of the atmospheric effects on the cosmic-ray intensity must always be based on an atmospheric model which corresponds to that regression equation which was used in the analysis of the experimental data. If this condition is not fulfilled, the theoretical and experimental results are not comparable. The present estimates of the positive temperature effect were therefore based on an atmospheric model in which a decreasing tropospheric temperature is associated with an increasing stratospheric temperature, the temperature variations being so related that the height of the reference level remains constant. It is thus seen that as soon as the variables of the regression equation have been chosen, considerations of the general behaviour of the free atmosphere can only be of secondary importance. Such considerations may, however, be used to fill in the details of the atmospheric model on which the theoretical estimates are based. Our choice of tropopause depth is an example of this.

ACKNOWLEDGMENTS

The author is very much indebted to the British Council for a scholarship which made possible his stay in The United Kingdom. It is a pleasure to thank Professor P. M. S. Blackett for the hospitality given at the Imperial College of Science and Technology and for the interest he has taken in this work. The author also wishes to thank Dr. H. Elliot who read the first manuscript and made many valuable suggestions. This investigation was begun at the University of Bergen, and the author is very grateful for support given by L. Meltzer's Høyskolefond during the first phase of this work.

REFERENCES

BERRY, F. A., BOLLAY, E., and BEERS, R., 1945, *Handbook of Meteorology* (New York: McGraw-Hill).

CARO, D. E., PARRY, J. K., and RATHGEBER, H. D., 1951, *Aust. J. Sci. Res.* A, **4,** 16.

CHASSON, R. L., 1954, *Phys. Rev.*, **96,** 1116.

COTTON, E. S., and CURTIS, H. O., 1951, *Phys. Rev.*, **84,** 840.

DAWTON, D. I., and ELLIOT, H., 1953, *J. Atmos. Terr. Phys.*, **3,** 295.

DOLBEAR, D. W. N., and ELLIOT, H., 1951, *J. Atmos. Terr. Phys.*, **1,** 215.

DUPERIER, A., 1949, *Proc Phys. Soc.* A, **62,** 684; 1951, *J. Atmos. Terr. Phys.*, **1,** 296.

OLBERT, S., 1953, *Phys. Rev.*, **92,** 454.

OWEN, B. G., and WILSON, J. G., 1955, *Proc. Phys. Soc.* A, **68,** 409.

SMITH, F. M., BIRNBAUM, W., and BARKAS, W. H., 1953, *Phys. Rev.*, **91,** 765.

TICHO, H. K., 1952, *Phys. Rev.*, **88,** 236.

TREFALL, H., 1953, *Nature, Lond.*, **171,** 888; 1955, *Proc. Phys. Soc.* A, **68,** 625.

TRUMPY, B., and TREFALL, H., 1953, *Physica*, **19,** 636.

WADA, M., and KUDO, S., 1954, *J. Sci. Res. Inst., Tokyo*, **48,** 245.

Theoretical Studies of the Kerr Effect
I: Deviations from a Linear Polarization Law

By A. D. BUCKINGHAM and J. A. POPLE
Department of Theoretical Chemistry, University of Cambridge

MS. received 4*th April* 1955

Abstract. A theoretical expression is derived for the Kerr constant of a gas at low pressures using a general expression for the energy of a molecule in a strong electric field. It is shown that the temperature independent part is closely related to the change of molecular polarizability with field strength. For spherically symmetric systems, the measured Kerr constant can be used to find the magnitude of this hyperpolarizability.

---

§ 1. Introduction

When a substance is placed in a strong uniform electric field, it generally becomes birefringent, the optic axis corresponding to the direction of the lines of force. This effect, first discovered by Kerr (1875), indicates that the application of a static field leads to anisotropy in the molecular distribution. This can be either because the molecules are intrinsically anisotropic and consequently become orientated by the field, or because the applied field itself induces some anisotropy. For most substances the first of these two effects is dominant. The magnitude and temperature dependence of the effect for gases at low densities can be interpreted with the aid of the well-known formula for non-polar molecules due to Langevin (1910), extended to polar molecules by Born (1918). These theories have been widely used to estimate polarizability anisotropies.

The general theory of molecular polarizability at high field strengths throws light on the effect of the anisotropy produced by the field. If an atom is placed in a sufficiently strong electric field E, the induced dipole moment μ will no longer be directly proportional to E, but will be given by an expansion of the form

$$\mu=\alpha E+\tfrac{1}{6}\gamma E^3+\ldots, \qquad \ldots\ldots(1.1)$$

where α is the normal low field polarizability and γ is a coefficient representing the modification of the usual law at high field strengths. For molecules there may be terms with even powers of E and the coefficients may have to be replaced by tensors. The order of magnitude of this 'hyperpolarizability' has been discussed by Coulson, Maccoll and Sutton (1952). Sewell (1949) has calculated it for the hydrogen atom.

The aim of the present paper is to modify the Langevin–Born equations by including these distortion effects and to show their relation to polarizability coefficients such as γ in equation (1.1). Since the additional field due to the light wave is periodic, it is necessary to neglect any dispersion effects, but if the frequency is not close to any natural frequency of the molecule, this should be a reasonable approximation.

§ 2. The Polarization of a Molecule in a Strong Electric Field

In a full quantum-mechanical treatment of polarization, it is necessary to consider the alteration of each individual quantum state. For most molecules at normal temperatures, however, the rotational energy levels are close enough together for it to be sufficient to treat the corresponding degrees of freedom in a classical manner. We shall suppose, therefore, that we are dealing with a molecule whose position and orientation can be described by variables τ. When an electric field E_α (using a tensor suffix notation) is applied to a molecule in this configuration, the energy u can be developed in a power series

$$u(\tau, E) = u^{(0)} - \mu_\alpha{}^{(0)} E_\alpha - \tfrac{1}{2}\alpha_{\alpha\beta} E_\alpha E_\beta - \tfrac{1}{6}\beta_{\alpha\beta\gamma} E_\alpha E_\beta E_\gamma - \tfrac{1}{24}\gamma_{\alpha\beta\gamma\delta} E_\alpha E_\beta E_\gamma E_\delta - \dots \qquad \dots\dots(2.1)$$

where $\mu_\alpha{}^{(0)}$, $\alpha_{\alpha\beta}$, $\beta_{\alpha\beta\gamma}$, $\gamma_{\alpha\beta\gamma\delta}, \dots$, are tensors symmetric in all suffixes. Strictly these should be functions of the electronic and vibrational states of the molecule. However, dependence on electronic state is unimportant, as at normal temperatures most molecules will be found in their ground states. We shall also ignore any variation between vibrational states.

Using the general relation

$$du = -\mu_\alpha dE_\alpha, \qquad \dots\dots(2.2)$$

we find that the dipole moment μ_α in the presence of a field is

$$\mu_\alpha = \mu_\alpha{}^{(0)} + \alpha_{\alpha\beta} E_\beta + \tfrac{1}{2}\beta_{\alpha\beta\gamma\delta} E_\beta E_\gamma + \tfrac{1}{6}\gamma_{\alpha\beta\gamma\delta} E_\beta E_\gamma E_\delta + \dots\ . \qquad \dots\dots(2.3)$$

$\mu_\alpha{}^{(0)}$ represents the permanent dipole moment of the molecule, $\alpha_{\alpha\beta}$ the weak-field electric polarizability and $\beta_{\alpha\beta\gamma}$, $\gamma_{\alpha\beta\gamma\delta}, \dots$, describe the additional effects of strong fields. If the field is increased from E_α to $E_\alpha + \delta E_\alpha$, the corresponding increase in moment is

$$\delta\mu_\alpha = (\alpha_{\alpha\beta} + \beta_{\alpha\beta\gamma} E_\gamma + \tfrac{1}{2}\gamma_{\alpha\beta\gamma\delta} E_\gamma E_\delta + \dots)\,\delta E_\beta = \Pi_{\alpha\beta}\delta E_\beta. \qquad \dots\dots(2.4)$$

The tensor $\Pi_{\alpha\beta}$ will be referred to as the *differential polarizability*. It measures the increase in moment per unit increase in field and has to be distinguished from the ratio of the total moment to the total field. The two only coincide in the limit of weak field strengths.

For molecules possessing elements of symmetry, relations exist between the components of the tensors $\alpha, \beta, \gamma, \dots$. We shall not attempt any general analysis of these, but only consider the simple case of an axially symmetric molecule. Linear molecules satisfy such a condition exactly, and others do so approximately. If we take the direction O3 along the axis of symmetry, then the only non-vanishing elements are

$$\begin{array}{llll} \mu_3{}^{(0)} & \alpha_{11} = \alpha_{22} & \beta_{113} = \beta_{223} & \gamma_{1111} = \gamma_{2222} = 3\gamma_{1122} \\ & \alpha_{33} & \beta_{333} & \gamma_{1133} = \gamma_{2233} \\ & & & \gamma_{3333} \end{array} \qquad \dots\dots(2.5)$$

and elements obtained by interchanging suffixes. If the molecule has a centre of inversion (as in homonuclear diatomic molecules), only even powers of E can appear in equation (2.1), so that $\mu_\alpha{}^{(0)}$ and $\beta_{\alpha\beta\gamma}$ are identically zero. Finally, for spherical symmetry, we have

$$\begin{array}{l} \alpha_{11} = \alpha_{22} = \alpha_{33} = \alpha \\ \gamma_{1111} = \gamma_{2222} = \gamma_{3333} = 3\gamma_{1122} = 3\gamma_{2233} = 3\gamma_{3311} = \gamma. \end{array} \qquad \dots\dots(2.6)$$

and the dipole moment in a strong field is given by (1.1), and has the direction of the applied field.

§ 3. THEORETICAL EXPRESSION FOR THE MOLECULAR KERR CONSTANT

The experiment measuring the magnitude of the double refraction resulting from the application of the electric field compares the refractive indices of a substance in directions parallel and perpendicular to a strong electric field E_α. Let

$e_\alpha^{\parallel}$ and $e_\alpha^{\perp}$ be unit vectors in these two directions. If the period of oscillation of the light waves is small compared with the time of rotation of the molecule, we can obtain an expression for the difference between these refractive indices by evaluating the difference between the differential polarizabilities $\Pi_{\alpha\beta}e_\alpha^{\parallel}e_\beta^{\parallel}$ and $\Pi_{\alpha\beta}e_\alpha^{\perp}e_\beta^{\perp}$ for each configuration τ and then averaging over configurations with a Boltzmann-type weighting factor appropriate to the molecule in the static field E_α only. If we write

$$\Pi(\tau, E) = \Pi_{\alpha\beta}(e_\alpha^{\parallel}e_\beta^{\parallel} - e_\alpha^{\perp}e_\beta^{\perp}), \qquad \ldots\ldots(3.1)$$

then the difference between the refractive indices is given by

$$n_{\parallel} - n_{\perp} = \frac{2\pi N}{V}\overline{\Pi}, \qquad \ldots\ldots(3.2)$$

where N/V is the number of molecules in unit volume, and where

$$\overline{\Pi} = \frac{\int \Pi(\tau, E)\exp\{-u(\tau, E)/kT\}d\tau}{\int \exp\{-u(\tau, E)/kT\}\,d\tau}. \qquad \ldots\ldots(3.3)$$

Using (2.4) and writing $Ee_\alpha^{\parallel}$ for E_α, the full expression for $\Pi(\tau, E)$ is

$$\Pi(\tau, E) = (\alpha_{\alpha\beta} + \beta_{\alpha\beta\gamma}Ee_\gamma^{\parallel} + \tfrac{1}{2}\gamma_{\alpha\beta\gamma\delta}E^2e_\gamma^{\parallel}e_\delta^{\parallel} + \ldots)(e_\alpha^{\parallel}e_\beta^{\parallel} - e_\alpha^{\perp}e_\beta^{\perp}). \qquad \ldots\ldots(3.4)$$

We now proceed to expand $\overline{\Pi}$ as a power series in E, noting that it depends on E both through $\Pi(\tau, E)$ and through the energy u. It is convenient to use the notation $\langle X\rangle$ for the average value of a quantity $X(\tau, E)$ in the assembly with $E=0$, that is,

$$\langle X\rangle = \frac{\int X(\tau, 0)\exp\{-u^{(0)}/kT\}\,d\tau}{\int \exp\{-u^{(0)}/kT\}\,d\tau}. \qquad \ldots\ldots(3.5)$$

We first note that $\overline{\Pi}$ is zero when $E=0$, that is $\langle\Pi\rangle=0$. The coefficient of E in the power series expansion can be obtained by differentiating (3.3) with respect to E and then putting $E=0$. This gives

$$\left(\frac{\partial\overline{\Pi}}{\partial E}\right)_{E=0} = \left\langle\frac{\partial\Pi}{\partial E}\right\rangle - \frac{1}{kT}\left\langle \Pi\,\frac{\partial u}{\partial E}\right\rangle. \qquad \ldots\ldots(3.6)$$

The quantities $\partial u/\partial E$ and $\partial\Pi/\partial E$ at $E=0$ are easily obtained from (2.1) and (3.4):

$$\left(\frac{\partial u}{\partial E}\right)_{E=0} = -\mu_\alpha^{(0)}e_\alpha^{\parallel} \qquad \ldots\ldots(3.7)$$

$$\left(\frac{\partial\Pi}{\partial E}\right)_{E=0} = \beta_{\alpha\beta\gamma}e_\gamma^{\parallel}(e_\alpha^{\parallel}e_\beta^{\parallel} - e_\alpha^{\perp}e_\beta^{\perp}). \qquad \ldots\ldots(3.8)$$

It is clear that both terms in (3.6) vanish on averaging over all directions of $e_\alpha^{\parallel}$. The leading non-vanishing term in the expansion of $\overline{\Pi}$ is therefore in E^2, the coefficient being

$$\tfrac{1}{2}\left(\frac{\partial^2\overline{\Pi}}{\partial E^2}\right)_{E=0} = \tfrac{1}{2}\left\langle\frac{\partial^2\Pi}{\partial E^2}\right\rangle - \frac{1}{2kT}\left\langle 2\frac{\partial\Pi}{\partial E}\frac{\partial u}{\partial E} + \Pi\frac{\partial^2 u}{\partial E^2}\right\rangle + \frac{1}{2k^2T^2}\left\langle \Pi\left(\frac{\partial u}{\partial E}\right)^2\right\rangle. \qquad \ldots\ldots(3.9)$$

The second derivatives of (2.1) and (3.4) are

$$\left(\frac{\partial^2 u}{\partial E^2}\right)_{E=0} = -\alpha_{\alpha\beta}e_\alpha^{\parallel}e_\beta^{\parallel} \qquad \ldots\ldots(3.10)$$

$$\left(\frac{\partial^2\Pi}{\partial E^2}\right)_{E=0} = \gamma_{\alpha\beta\gamma\delta}(e_\alpha^{\parallel}e_\beta^{\parallel} - e_\alpha^{\perp}e_\beta^{\perp})e_\gamma^{\parallel}e_\delta^{\parallel}. \qquad \ldots\ldots(3.11)$$

The averaging in (3.9) can now be carried out by averaging over all directions $e_\alpha{}^\perp$ perpendicular to each $e_\alpha{}^{\parallel}$ and then over $e_\alpha{}^{\parallel}$, axes being fixed in the molecule (considering all possible directions of the fields is equivalent to averaging over all orientations of the molecule). Simple trigonometrical analysis leads to

$$\operatorname{av}(e_\alpha{}^{\parallel} e_\beta{}^{\parallel} e_\gamma{}^{\parallel} e_\delta{}^{\parallel}) = \tfrac{1}{15}(\delta_{\alpha\beta}\delta_{\gamma\delta} + \delta_{\alpha\gamma}\delta_{\beta\delta} + \delta_{\alpha\delta}\delta_{\beta\gamma}) \qquad \ldots\ldots(3.12)$$

$$\operatorname{av}(e_\alpha{}^{\parallel} e_\beta{}^{\parallel} e_\gamma{}^{\perp} e_\delta{}^{\perp}) = \tfrac{1}{30}(4\delta_{\alpha\beta}\delta_{\gamma\delta} - \delta_{\alpha\gamma}\delta_{\beta\delta} - \delta_{\alpha\delta}\delta_{\beta\gamma}), \qquad \ldots\ldots(3.13)$$

where $\delta_{\alpha\beta}$ is the substitution tensor (unity if $\alpha = \beta$ and zero otherwise). Substitution of (3.10) and (3.11) into (3.9) gives the dependence of $\overline{\Pi}$ on E^2.

We shall use the definition of the molecular Kerr constant ${}_{\mathrm{m}}K$ proposed by Otterbein (1934). In the limit of low densities this reduces to

$${}_{\mathrm{m}}K = \lim_{E\to 0} \frac{2(n_{\parallel} - n_{\perp})\, V_{\mathrm{m}}}{27E^2} = \frac{2\pi N}{27}\left(\frac{\partial^2\overline{\Pi}}{\partial E^2}\right)_{E=0}, \qquad \ldots\ldots(3.14)$$

where V_{m} is the molar volume and N Avogadro's number. From (3.2) and (3.9), we obtain

$${}_{\mathrm{m}}K = \frac{2\pi N}{405}\left\{2\gamma_{\alpha\alpha\beta\beta} + \frac{1}{kT}\left[4\mu_\alpha{}^{(0)}\beta_{\alpha\beta\beta} + 3(\alpha_{\alpha\beta}\alpha_{\alpha\beta} - 3\alpha^2)\right] + \frac{3}{k^2T^2}\left[\alpha_{\alpha\beta}\mu_\alpha{}^{(0)}\mu_\beta{}^{(0)} - \alpha(\mu^{(0)})^2\right]\right\}, \qquad \ldots\ldots(3.15)$$

where α is the mean low-field polarizability

$$\alpha = \tfrac{1}{3}(\alpha_{11} + \alpha_{22} + \alpha_{33}). \qquad \ldots\ldots(3.16)$$

Equation (3.15) has to be modified if it is necessary to distinguish between the polarizability coefficients in a static field and those in a high-frequency field. These may differ because of the so-called 'atomic polarization' of a molecule representing distortion of the nuclear framework. If the frequency of the light is higher than that of the vibrational modes, this polarization will not contribute to the additional oscillating dipole moments. If we use $a_{\alpha\beta}$ for the high-frequency polarizability, we then have

$$(\Pi)_{E=0} = a_{\alpha\beta}(e_\alpha{}^{\parallel} e_\beta{}^{\parallel} - e_\alpha{}^{\perp} e_\beta{}^{\perp}). \qquad \ldots\ldots(3.17)$$

There should be corresponding modifications of (3.8) and (3.11), but we shall ignore any variation of these with frequency. Equation (3.15) is then replaced by

$${}_{\mathrm{m}}K = \frac{2\pi N}{405}\left\{2\gamma_{\alpha\alpha\beta\beta} + \frac{1}{kT}[4\mu_\alpha{}^{(0)}\beta_{\alpha\beta\beta} + 3(\alpha_{\alpha\beta}a_{\alpha\beta} - 3\alpha a)] + \frac{3}{k^2T^2}[a_{\alpha\beta}\mu_\alpha{}^{(0)}\mu_\beta{}^{(0)} - a(\mu^{(0)})^2]\right\}. \qquad \ldots\ldots(3.18)$$

§ 4. DISCUSSION

Equation (3.18) is a generalization of the well-known Langevin–Born equation to include the effects of high field strengths on the polarizability. Since no account has been taken of molecular interaction (3.18) applies accurately only to gases at low pressures. A discussion of more dense media is presented in a following paper (Buckingham 1955).

The general result is of particular interest for spherically symmetric systems, when it reduces to

$${}_{\mathrm{m}}K = 4\pi N\gamma/81. \qquad \ldots\ldots(4.1)$$

This suggests that a measurement of the Kerr constant can be used to determine the hyperpolarizability constant γ, which would be very difficult to do by a direct measurement of dielectric saturation. The Kerr constants of argon and methane (which may be regarded as approximately spherically symmetrical) measured by Kuss (1940) have been used in this way to calculate the values of γ given in the table. The low-field polarizabilities are also given, and so are the theoretical values for atomic hydrogen as deduced from Sewell's (1949) calculation of the energy in an external field. The agreement in order of magnitude gives support to our interpretation of the non-vanishing Kerr constants of spherical systems.

Polarizability Constants of Spherical Systems

Substance	Argon	Methane	Atomic hydrogen
${}_{\mathrm{m}}K \times 10^{12}$ (e.s.u.)	0·07	0·25	—
$\alpha \times 10^{24}$ (cm^3)	1·63	2·60	0·667 (calc.)
$\gamma \times 10^{36}$ (e.s.u.)	0·7	2·6	0·672 (calc.)

For molecules with centres of inversion, equation (3.18) becomes

$$ {}_{\mathrm{m}}K = \frac{2\pi N}{405}\left\{2\gamma_{\alpha\alpha\beta\beta} + \frac{3}{kT}(\alpha_{\alpha\beta}a_{\alpha\beta} - 3\alpha a)\right\}. \qquad \ldots\ldots(4.2) $$

The temperature-dependent term is dominant for many molecules, but in some cases the direct distortion term may be appreciable. Molecular hydrogen, for example, according to detailed theoretical calculations made by Ishiguro, Arai, Kotani and Mizushima (1952) has $\alpha_{11} = \alpha_{22} = 0{\cdot}6968 \times 10^{-24}$ cm^3, $\alpha_{33} = 0{\cdot}9746 \times 10^{-24}$ cm^3; the most reliable observed values are those obtained by Volkmann (1935) from light scattering experiments, namely

$$ \alpha_{11} = \alpha_{22} = 0{\cdot}718 \times 10^{-24}\,\mathrm{cm}^3, \quad \alpha_{33} = 0{\cdot}934 \times 10^{-24}\,\mathrm{cm}^3. $$

The term $\gamma_{\alpha\alpha\beta\beta}$ will probably be rather larger for molecular hydrogen than for the single atom, so $\gamma = 1{\cdot}0 \times 10^{-36}$ e.s.u. should be a reasonable estimate. The calculated Kerr constant at 0°c is then $0{\cdot}131 \times 10^{-12}$ e.s.u., of which $0{\cdot}093 \times 10^{-12}$ e.s.u. arises from the temperature independent part. The two could only be separated by measurements of ${}_{\mathrm{m}}K$ as a function of temperature.

The position is more complex for molecules with permanent dipole moments. However, for strongly polar and anisotropically polarizable molecules at normal temperatures, the term in T^{-2} will be dominant, and in such cases measurements of ${}_{\mathrm{m}}K$ may be used to deduce principal polarizabilities. When this term is not dominant, interpretation of the measurements will be difficult, for although γ is probably small, there is no reason to suppose that the term in $\mu_\alpha^{(0)}\beta_{\alpha\beta\beta}$ is small compared with $\alpha_{\alpha\beta}a_{\alpha\beta} - 3\alpha a$.

ACKNOWLEDGMENT

One of the authors (A. D. B.) is indebted to the Royal Dutch/Shell Group for the award of a Postgraduate Scholarship.

REFERENCES

Buckingham, A. D., 1955, *Proc. Phys. Soc.* A, **68,** 910.
Born, M., 1918, *Ann. Phys., Lpz.*, **55,** 177.
Coulson, C. A., Maccoll, A., and Sutton, L. E., 1952, *Trans. Faraday Soc.*, **48,** 106.
Ishiguro, E., Arai, T., Kotani, M., and Mizushima, M., 1952, *Proc. Phys. Soc.* A, **65,** 178.
Kerr, J., 1875, *Phil. Mag.* [4], **50,** 337, 446.
Kuss, E., 1940, *Thesis* (University of Berlin).
Langevin, P., 1910, *Radium, Paris*, **7,** 249.
Otterbein, G., 1934, *Phys. Z.*, **35,** 249.
Sewell, G. L., 1949, *Proc. Camb. Phil. Soc.*, **45,** 678.
Volkmann, H., 1935, *Ann. Phys., Lpz.*, **24,** 457.

Theoretical Studies of the Kerr Effect
II : The Influence of Pressure

By A. D. BUCKINGHAM
Department of Theoretical Chemistry, The University of Cambridge

Communicated by J. A. Pople; MS. received 4th April 1955

Abstract. A statistical-mechanical theory of the Kerr constant is presented, and expressions are derived which are applicable at any density. For anisotropic molecules without permanent dipole moments, the Kerr constant is expanded in powers of the polarizability and the leading non-vanishing terms retained. To this order of accuracy, the molecular Kerr constant of molecules of this type is unaffected by pressure changes provided the forces acting between the molecules are independent of orientation. Experimental data for some compressed non-polar gases support this conclusion. For orientationally dependent intermolecular forces, the Kerr constant is expanded in powers of the density and the leading term representing a departure from ideal behaviour is discussed in some detail for both polar and non-polar molecules.

---

§ 1. INTRODUCTION

The Langevin–Born theory of the electro-optical Kerr effect is strictly applicable only to assemblies of independent molecules. No account is taken of the possible interaction of molecules, so that the equations deduced will only be accurate when applied to gases and vapours at low densities. However, differences between the refractive indices in the directions of the field and perpendicular to it are often small at low densities for readily obtainable field strengths, so experimental measurements are frequently made on liquids and compressed gases. There is a need, therefore, for a theory of the Kerr effect at densities at which molecular interactions are important.

Raman and Krishnan (1927) were the first to attempt a general theory applicable at any density, and subsequent treatments have been proposed by Oka (1937) and Piekara (1939). However, each of these theories rests on the assumptions inherent in the models employed, so that the limitations of the results are difficult to assess. A rigorous theory must invoke the methods of statistical mechanics. It is the aim of the present paper to give an account of such a theory.

§ 2. THE MOLECULAR KERR CONSTANT IN A DENSE MEDIUM

In this section we shall derive expressions for the molecular Kerr constant of an assembly of interacting molecules. Our discussion will be restricted to systems in which the static electric field is uniform. The molecular Kerr constant is defined by

$${}_{\mathrm{m}}K=\frac{6nV_{\mathrm{m}}}{(n^2+2)^2(\epsilon_0+2)^2}\lim_{E\to 0}\left(\frac{n_{\parallel}-n_{\perp}}{E^2}\right) \qquad \ldots\ldots(2.1)$$

where $n_{\parallel}$ and $n_{\perp}$ are the refractive indices of the specimen in the directions of the unit vectors $\mathbf{e}^{\parallel}$ parallel to $\mathbf{E}$ and $\mathbf{e}^{\perp}$ at right angles to it. V_{m} is the molar volume and n and ϵ_0 the refractive index and dielectric constant of the specimen.

In order to isolate the external electric field as the effective local field acting on a molecule, we shall consider a large spherical specimen of volume V_{m} containing N (Avogadro's number) similar molecules. If $\mathbf{E}_0$ is the strength of the uniform field in the absence of the specimen, $\mathbf{E}=3\mathbf{E}_0/(\epsilon_0+2)$, and equation (2.1) becomes

$$_{\mathrm{m}}K=\frac{2nV_{\mathrm{m}}}{3(n^2+2)^2}\lim_{E_0\to 0}\left(\frac{n_{\parallel}-n_{\perp}}{E_0{}^2}\right). \qquad \ldots\ldots(2.2)$$

In Part I of this series (Buckingham and Pople 1955 a, to be referred to as I) it was shown that terms representing departures from a linear polarization law can be important contributors to $_{\mathrm{m}}K$ in some special cases. The most interesting of these is that of spherical symmetry, when such a term is the only non-vanishing one for isolated molecules. We shall represent the configuration of the specimen by τ, and shall suppose that for this arrangement of molecules the moment is $\mathbf{M}(\tau,E_0)$. In the first instance we shall suppose that the molecules are spherically symmetric when isolated. For such an assembly, the mean local field acting on a molecule was shown by Kirkwood (1936) to be $E_0\{1+\mathrm{O}(\alpha^2)\}$, where α is the low field strength polarizability. Now α is usually small, and to a very good approximation (as is illustrated by the constancy of the Clausius–Mosotti function $V_{\mathrm{m}}(\epsilon_0-1)/(\epsilon_0+2)$ for assemblies of spherically symmetric molecules) the local field can be put equal to E_0. Thus, the molecular Kerr constant, as defined by equation (2.1), will be almost independent of pressure and therefore given by (4.1) of I, namely

$$_{\mathrm{m}}K=4\pi N\gamma/81. \qquad \ldots\ldots(2.3)$$

Thus the molecular Kerr constant of spherically symmetric molecules is independent of both temperature and pressure. The constancy over a considerable pressure range is illustrated in the table by the figures for methane, which is only approximately spherical.

For simplicity we shall from now on suppose that the polarizability of a molecule is independent of the field strength. Thus

$$\frac{n_{\parallel}{}^2-1}{n_{\parallel}{}^2+2}-\frac{n_{\perp}{}^2-1}{n_{\perp}{}^2+2}=\frac{4\pi N}{3V_{\mathrm{m}}}\overline{\Pi^{(1)}(\tau,E_0)} \qquad \ldots\ldots(2.4)$$

where $\Pi^{(1)}(\tau,E_0)$ is defined by

$$\Pi^{(1)}(\tau,E_0)=\alpha_{\alpha\beta}{}^{(1)}(e_\alpha{}^{\parallel}e_\beta{}^{\parallel}-e_\alpha{}^{\perp}e_\beta{}^{\perp}) \qquad \ldots\ldots(2.5)$$

$\alpha_{\alpha\beta}{}^{(1)}$ being the polarizability tensor of molecule 1. The averaging in equation (2.4) is over all possible configurations τ in the presence of the external field. Thus

$$\overline{\Pi^{(1)}(\tau,E_0)}=\frac{\int \pi^{(1)}(\tau,E_0)\exp\{-U(\tau,E_0)/kT\}\,d\tau}{\int \exp\{-U(\tau,E_0)/kT\}\,d\tau} \qquad \ldots\ldots(2.6)$$

where $U(\tau,E_0)$ is the potential energy of the system in the presence of E_0 and in the configuration τ. Thus

$$U(\tau,E_0)=U(\tau,0)-\int_0^{E_0}\mathbf{M}(\tau,E)\,.\,\mathbf{e}^{\parallel}\,dE. \qquad \ldots\ldots(2.7)$$

As in I, we shall employ the notation $\langle X\rangle$ for the average value of a quantity $X(\tau,E_0)$ in the assembly with $E_0=0$, that is

$$\langle X\rangle=\frac{\int X(\tau,0)\exp\{-U(\tau,0)/kT\}\,d\tau}{\int \exp\{-U(\tau,0)/kT\}\,d\tau}. \qquad \ldots\ldots(2.8)$$

We note that $\langle \Pi^{(1)} \rangle = 0$ if the specimen is isotropic in the absence of an external field, and we shall only deal with such assemblies. From (2.6), we find with our assumption that $\partial \Pi^{(1)}/\partial E_0 = 0$,

$$\left(\frac{\partial \overline{\Pi^{(1)}(\tau, E_0)}}{\partial E_0}\right)_{E_0=0} = -\frac{1}{kT}\left\langle \Pi^{(1)} \frac{\partial U}{\partial E_0} \right\rangle. \qquad \ldots\ldots(2.9)$$

On averaging over all directions of $\mathbf{e}^{\parallel}$, it is found, as in I, that $(\partial \overline{\Pi^{(1)}}/\partial E_0)_{E_0=0}$ is zero, so that the leading non-vanishing term in the expansion of $\overline{\Pi^{(1)}(\tau, E_0)}$ is in E_0^2. From (2.6) we find, on noting that $\langle \Pi^{(1)} \rangle = 0 = \langle \partial U/\partial E_0 \rangle$,

$$\left(\frac{\partial^2 \overline{\Pi^{(1)}(\tau, E_0)}}{\partial E_0^2}\right)_{E_0=0} = -\frac{1}{kT}\left\langle \Pi^{(1)} \frac{\partial^2 U}{\partial E_0^2} \right\rangle + \frac{1}{k^2T^2}\left\langle \Pi^{(1)} \left(\frac{\partial U}{\partial E_0}\right)^2 \right\rangle. \qquad \ldots(2.10)$$

From (2.7),

$$\left(\frac{\partial U}{\partial E_0}\right)_{E_0=0} = -M_\alpha(\tau, 0)\, e_\alpha^{\parallel} \qquad \ldots\ldots(2.11)$$

and

$$\left(\frac{\partial^2 U}{\partial E_0^2}\right)_{E_0=0} = -\left(\frac{\partial M_\alpha(\tau, E_0)}{\partial E_0}\right)_{E_0=0} e_\alpha^{\parallel}. \qquad \ldots\ldots(2.12)$$

Now the total moment $M_\alpha(\tau, E_0)$ can be written as the sum of moments of individual molecules

$$M_\alpha(\tau, E_0) = \sum_{i=1}^{N} \{\mu_{i\alpha}^{(0)} + \alpha_{\alpha\beta}^{(i)}(E_0 e_\beta^{\parallel} + F_\beta^{(i)})\} \qquad \ldots\ldots(2.13)$$

where $\mu_{i\alpha}^{(0)}$ is the permanent dipole moment of the ith molecule, and $F_\alpha^{(i)}$ is the field strength at the centre of molecule i due to the other $N-1$ molecules. From (2.12) and (2.13)

$$\left(\frac{\partial^2 U}{\partial E_0^2}\right)_{E_0=0} = -\sum_{i=1}^{N} \left\{\alpha_{\alpha\beta}^{(i)} \left(e_\alpha^{\parallel} e_\beta^{\parallel} + e_\alpha^{\parallel} \frac{\partial F_\beta^{(i)}}{\partial E_0}\right)\right\}. \qquad \ldots\ldots(2.14)$$

From (2.2) and (2.4) ,we therefore find

$$_{\mathrm{m}}K = \frac{2\pi N}{27}\left(\frac{\partial^2 \overline{\Pi^{(1)}(\tau, E_0)}}{\partial E_0^2}\right)_{E_0=0} \qquad \ldots\ldots(2.15)$$

which, with (2.10), (2.11) and (2.14), becomes

$$_{\mathrm{m}}K = \frac{2\pi N}{27kT}\left\langle \alpha_{\alpha\beta}^{(1)} \left\{\sum_{i=1}^{N} \alpha_{\gamma\delta}^{(i)} + \frac{1}{kT} M_\gamma M_\delta\right\} \{e_\gamma^{\parallel} e_\delta^{\parallel}(e_\alpha^{\parallel} e_\beta^{\parallel} - e_\alpha^{\perp} e_\beta^{\perp})\} \right\rangle. \qquad \ldots(2.16)$$

We have, in (2.16), neglected the term in $\partial F_\beta^{(i)}/\partial E_0$ in (2.14), but it is of the order of α^3 and hence normally unimportant.

Using (3.12) and (3.13) of I, (2.16) reduces to

$$_{\mathrm{m}}K = \frac{2\pi N}{405kT}\left\langle \left\{\sum_{i=1}^{N} 3\alpha_{\alpha\beta}^{(1)}\alpha_{\alpha\beta}^{(i)} - \alpha_{\alpha\alpha}^{(1)}\alpha_{\beta\beta}^{(i)}\right\} + \frac{1}{kT}\{3\alpha_{\alpha\beta}^{(1)} M_\alpha M_\beta - \alpha_{\alpha\alpha}^{(1)} M^2\} \right\rangle. \qquad \ldots\ldots(2.17)$$

Following the discussion in I, (2.17) will have to be modified if it becomes necessary to distinguish between the polarizability in static and high-frequency fields. These may differ because of the atomic polarization. If we use $a_{\alpha\beta}$ for the high frequency polarizability, then

$$\Pi^{(1)} = a_{\alpha\beta}^{(1)}(e_\alpha^{\parallel} e_\beta^{\parallel} - e_\alpha^{\perp} e_\beta^{\perp}). \qquad \ldots\ldots(2.18)$$

With this modification, (2.17) becomes

$$_{\mathrm{m}}K=\frac{2\pi N}{405kT}\left\langle\left\{\sum_{i=1}^{N}3a_{\alpha\beta}{}^{(1)}\alpha_{\alpha\beta}{}^{(i)}-a_{\alpha\alpha}{}^{(1)}\alpha_{\beta\beta}{}^{(i)}\right\}+\frac{1}{kT}\{3a_{\alpha\beta}{}^{(1)}M_{\alpha}M_{\beta}-a_{\alpha\alpha}{}^{(1)}M^{2}\}\right\rangle. \qquad \ldots\ldots(2.19)$$

If we express $a_{\alpha\beta}$ and $\alpha_{\alpha\beta}$ in terms of the principal components a_1, a_2, a_3 and α_1, α_2, α_3, then we obtain

$$_{\mathrm{m}}K=\frac{2\pi N}{135kT}\left[\left\{\sum_{s=1}^{3}a_s\alpha_s-3a\alpha+\sum_{s,t=1}^{3}a_s\alpha_t\iint(\cos^2\theta_{st}-\tfrac{1}{3})n_2(\mathbf{r},\omega)\,d\mathbf{r}\,d\omega\right\}\right.$$
$$\left.+\frac{1}{kT}\left\{\sum_{s}a_s\langle M_s{}^2\rangle-a\langle M^2\rangle\right\}\right] \qquad \ldots\ldots(2.20)$$

where θ_{st} is the angle between the s-principal axis of molecule 1 and the t-principal axis of another molecule whose position and orientation are represented by $(\mathbf{r},\omega)$ referred to molecule 1 fixed at the origin, and where $n_2(\mathbf{r},\omega)\,d\mathbf{r}\,d\omega$ is the probability of there being a molecule in the volume element $d\mathbf{r}$ and in the orientational element $d\omega$. Also, M_s is the component of $\mathbf{M}$ in the direction of the s-principal axis of molecule 1. For molecules which are symmetric about the 3-axis of polarizability, (2.20) becomes

$$_{\mathrm{m}}K=\frac{2\pi Na\kappa_a}{135kT}\left[3\kappa_{\alpha}\alpha\left\{2+3\iint(\cos^2\theta-\tfrac{1}{3})n_2(\mathbf{r},\omega)\,d\mathbf{r}\,d\omega\right\}+\frac{1}{kT}\langle 3M_3{}^2-M^2\rangle\right] \qquad \ldots\ldots(2.21)$$

where θ is the angle between the axes of molecule 1 and the molecule at $(\mathbf{r},\omega)$, and κ_a and κ_{α} are parameters describing the anisotropy of an axially symmetric molecule, thus

$$\kappa_a=(a_3-a_1)/3a, \qquad \kappa_{\alpha}=(\alpha_3-\alpha_1)/3\alpha. \qquad \ldots\ldots(2.22)$$

As a particular case of interest, we shall consider an assembly of molecules with centres of inversion. For such molecules $\langle M_s{}^2\rangle$ is proportional to α^2, whence the term in T^{-2} in (2.20) will usually be small in comparison with the term in T^{-1}. Thus, if we include the contribution of $\gamma_{\alpha\beta\gamma\delta}$, the molecular Kerr constant of a system of non-polar molecules can be represented by

$$_{\mathrm{m}}K=\frac{2\pi N}{405}\left[2\gamma_{\alpha\alpha\beta\beta}+\frac{3}{kT}\left\{\sum_{s=1}^{3}a_s\alpha_s-3a\alpha+\sum_{s,t=1}^{3}a_s\alpha_t\iint(\cos^2\theta_{st}-\tfrac{1}{3})n_2(\mathbf{r},\omega)\,d\mathbf{r}\,d\omega\right\}\right] \qquad \ldots\ldots(2.23)$$

which, for axial symmetry, reduces to

$$_{\mathrm{m}}K=\frac{4\pi N}{405}\left[\gamma_{\alpha\alpha\beta\beta}+\frac{9\kappa_a\kappa_{\alpha}a\alpha}{2kT}\left\{2+3\iint(\cos^2\theta-\tfrac{1}{3})n_2(\mathbf{r},\omega)\,d\mathbf{r}\,d\omega\right\}\right]. \qquad \ldots.(2.24)$$

An immediate consequence of (2.23) is that $_{\mathrm{m}}K$ for an assembly of non-polar molecules whose interaction potential energies do not depend on orientation is independent of pressure. This follows from the fact that for such a system $\langle\cos^2\theta_{st}\rangle=\frac{1}{3}$, and the remaining expression for $_{\mathrm{m}}K$ is simply that for the perfect gas, namely (4.2) of I.

A second case of interest is that of strongly polar optically anisotropic molecules. For these, the terms in T^{-2} in (2.20) and (2.21) are dominant, so that to a good approximation for such molecules, we can neglect the remaining terms. It is noteworthy that the resulting equations accurately represent the contribution to the Kerr constant of the so-called dipole term. They retain all powers of α, as can be seen by examining (2.10) and (2.11).

§ 3. DISCUSSION

Experimental data from which the molecular Kerr constants of nitrogen, carbon dioxide, ethylene and methane can be computed have been published by Kuss and Stuart (1941). Their measurements cover the range 0–400 atmospheres and include figures for carbon dioxide both above and below the critical temperature. The results of our calculations of ${}_{\mathrm{m}}K$ from these data are presented in the table. The measurements were all made using the green mercury line as light source, the wavelength of this being 5460 Å. The static field E was of the order of 50 000 volts per cm.

The molecular Kerr constants of nitrogen and methane are seen to be almost pressure independent over the range covered, whereas for carbon dioxide (both above and below the critical temperature) and ethylene some variation is found. This is not unexpected, for the forces between carbon dioxide or ethylene molecules will doubtless depend more on orientation than those between nitrogen or methane molecules.

For many molecules we would expect $\langle\cos^2\theta\rangle$ to differ from one third, and in the remainder of this paper we shall be concerned with such systems. We shall restrict the discussion to the imperfect gas, that is, we shall examine in detail the initial deviations from ideal behaviour. Both polar and non-polar molecules will be considered, and in the former case we might expect considerable variations in ${}_{\mathrm{m}}K$ with pressure changes.

§ 4. THE IMPERFECT GAS

If we write

$$ {}_{\mathrm{m}}K = A_{\mathrm{K}} + \frac{B_{\mathrm{K}}}{V_{\mathrm{m}}} + \frac{C_{\mathrm{K}}}{V_{\mathrm{m}}^2} + \dots \qquad \dots\dots(4.1) $$

then A_{K} is the molecular Kerr constant where there is no interaction between the molecules. The term in V_{m}^{-1} corresponds to the initial deviations from ideal gas behaviour and consequently depends on the interactions of molecules in pairs. We shall call A_{K}, B_{K}, $C_{\mathrm{K}}, \dots$, the first, second, third, ... , *Kerr constant virial coefficients*. A_{K}, equal to $\lim_{V_{\mathrm{m}}\to\infty}({}_{\mathrm{m}}K)$, is given by (3.18) of I.

As in the previous sections of this paper, we shall suppose that the molecular polarizability is independent of field strength, and we shall also only discuss in detail molecules with axial symmetry. Thus

$$ B_{\mathrm{K}} = \lim_{V_{\mathrm{m}}\to\infty}\{({}_{\mathrm{m}}K - A_{\mathrm{K}})V_{\mathrm{m}}\} $$
$$ = \frac{2\pi N a\kappa_a}{135kT}\lim_{V_{\mathrm{m}}\to\infty}\left[\{9N\kappa_\alpha\alpha\langle\cos^2\theta^{(12)} - \tfrac{1}{3}\rangle + \frac{1}{kT}\langle 3M_3{}^2 - M^2 - 2(\mu^{(0)})^2\rangle\}V_{\mathrm{m}}\right] \qquad \dots\dots(4.2) $$

where $\theta^{(12)}$ is the angle between the axes of molecules 1 and 2, and where the subscript 3 implies the component of a vector in the direction of the axis of molecule 1. For the calculation of B_{K} only a pair of molecules need be considered and we obtain

$$ B_{\mathrm{K}} = \frac{2\pi N^2\kappa_a a}{135kT\Omega}\int\Big[9\kappa_\alpha\alpha(\cos^2\theta^{(12)} - \tfrac{1}{3}) + \frac{1}{kT}\{3(\mu_3{}^{(1)} + \mu_3{}^{(2)})^2 - (\boldsymbol{\mu}^{(1)} + \boldsymbol{\mu}^{(2)})^2 $$
$$ - 2(\mu^{(0)})^2\}\Big]\exp\{-u_{12}/kT\}\,d\tau_2, \qquad \dots\dots(4.3) $$

Molecular Kerr Constants of Non-polar Substances as Functions of Pressure

N_2 at 25·1°c			CO_2 at 25·1°c			CO_2 at 40·0°c			C_2H_4 at 40·0°c			CH_4 at 25·0°c		
P (atm.)	d (g cm^{-3})	$_mK.10^{12}$ (e.s.u.)	P (atm.)	d (g cm^{-3})	$_mK.10^{12}$ (e.s.u.)	P (atm.)	d (g cm^{-3})	$_mK.10^{12}$ (e.s.u.)	P (atm.)	d (g cm^{-3})	$_mK.10^{12}$ (e.s.u.)	P (atm.)	d (g cm^{-3})	$_mK.10^{12}$ (e.s.u.)
111·6	0·127	0·248	36·7	0·085	2·26	37·5	0·078	2·10	54·1	0·089	1·81	103·6	0·080	0·22
147·7	0·165	0·248	49·3	0·13	2·34	51·3	0·120	2·22	76·2	0·171	1·80	129·5	0·102	0·24
166·0	0·184	0·248	63·4	0·24	2·30	74·3	0·234	2·16	97·8	0·26	1·74	178·6	0·144	0·27
224·0	0·238	0·252	69·5	0·74	2·08	84·8	0·38	2·33	195·3	0·37	1·44	216·8	0·173	0·27
245·0	0·256	0·249	88·2	0·80	1·99	94·0	0·58	2·07	301·5	0·42	1·27	399·1	0·249	0·24
312·9	0·306	0·254	176·0	0·90	1·83	109·9	0·69	1·96				419·7	0·257	0·24
387·3	0·356	0·246	238·3	0·94	1·77	142·2	0·77	1·93						
415·3	$0·371_5$	0·251	397·9	1·00	1·74	186·7	0·83	1·86						
						300·1	0·91	1·75						

where u_{12} is the intermolecular potential energy of molecules 1 and 2, and

$$\int d\tau_2 = \Omega V_{\mathrm{m}}$$

so that Ω is the integral over the angular coordinates. We shall now proceed to examine in detail a few special cases.

(*a*) *Non-polar Molecules with Anisotropic Dispersion Forces*

London (1942) discussed the dispersion forces between molecules with anisotropic polarizabilities in terms of a simple oscillator model. Combining his result with a Lennard-Jones 6–12 potential, we can use the force field (Pople 1954)

$$u_{12} = 4\epsilon\left\{\left(\frac{r_0}{r}\right)^{12} - \left(\frac{r_0}{r}\right)^{6}\right\} - \frac{6\kappa_\alpha \epsilon r_0^{\,6}}{r^6}\left[(1-\kappa_\alpha)\cos^2\theta_1 + (1-\kappa_\alpha)\cos^2\theta_2 - \tfrac{2}{3} + \kappa_\alpha(2\cos\theta_1\cos\theta_2 + \sin\theta_1\sin\theta_2\cos\phi)^2\right] \qquad \ldots\ldots(4.4)$$

where ϵ and r_0 are parameters having the dimensions of energy and length respectively, and where r is the molecular separation, θ_1 and θ_2 the angles between the line of centres and the axes of the molecules and ϕ the angle between the planes formed by the two axes with the line of centres.

Since the molecules do not have permanent moments, we can neglect the term in T^{-2} in (4.3), and we then have

$$B_{\mathrm{K}} = \frac{\pi N^2 \kappa_a \kappa_\alpha a\alpha}{15kT}\int_0^\infty r^2\,dr\int_0^\pi \sin\theta_1\,d\theta_1\int_0^\pi \sin\theta_2\,d\theta_2\int_0^{2\pi} d\phi\,\{\cos^2\theta_1\cos^2\theta_2 - 2\sin\theta_1\sin\theta_2\cos\theta_1\cos\theta_2\cos\phi + \sin^2\theta_1\sin^2\theta_2\cos^2\phi - \tfrac{1}{3}\}\exp(-u_{12}/kT) \qquad \ldots\ldots(4.5)$$

$$= \frac{4\pi^2 N^2 \kappa_a \kappa_\alpha^{\,3} a\alpha r_0^{\,3}}{3375y^2kT}\{H_6(y) + y^2 H_{12}(y)\} + \ldots \qquad \ldots\ldots(4.6)$$

where

$$y = 2\left(\frac{\epsilon}{kT}\right)^{1/2} \qquad \ldots\ldots(4.7)$$

$$H_n(y) = y^{(27-n)/6}\sum_{p=0}^{\infty}\Gamma\left(\frac{6p+n-3}{12}\right)\frac{y^p}{p!}. \qquad \ldots\ldots(4.8)$$

The functions $H_n(y)$ have been discussed and tabulated by Buckingham and Pople (1955 b).

(*b*) *Non-polar Non-spherical Molecules*

If the shapes of the interacting molecules are not spherical, then there will be steric hindrance to free rotation. We shall represent the interaction energy of two non-spherical molecules without permanent dipole moments by the equation

$$u_{12} = 4\epsilon\left\{\left(\frac{r_0}{r}\right)^{12} - \left(\frac{r_0}{r}\right)^{6}\right\} + \frac{4D\epsilon(r_0)^{12}}{r^{12}}\{3\cos^2\theta_1 + 3\cos^2\theta_2 - 2\} \qquad \ldots\ldots(4.9)$$

where D is a dimensionless parameter whose numerical value must lie between $-0{\cdot}25$ and $+0{\cdot}5$ in order that the molecules should repel one another in all orientations when r is small. For rod-shaped molecules orientations with $\theta_1 = \theta_2 = \pi/2$ will be favoured, so that D will be positive, whereas plate-like molecules will prefer positions with θ_1 and θ_2 equal to 0 or π, and for them D will be negative. On substituting (4.9) into (4.5), we find, to the second order in D,

$$B_{\mathrm{K}} = \frac{16\pi^2 N^2 \kappa_a \kappa_\alpha a\alpha r_0^{\,3} D^2 H_{24}(y)}{3375kT}. \qquad \ldots\ldots(4.10)$$

(*c*) *Non-dipolar Molecules with Quadrupole Moments*

Some molecules without permanent dipole moments may have a strong directional interaction on account of their possessing quadrupole moments. We shall represent the interaction energy of two axially symmetric molecules by

$$u_{12}=4\epsilon\left\{\left(\frac{r_0}{r}\right)^{12}-\left(\frac{r_0}{r}\right)^{6}\right\}+\frac{3\Theta^2}{4r^5}\{1-5\cos^2\theta_1-5\cos^2\theta_2+17\cos^2\theta_1\cos^2\theta_2$$
$$+16\sin\theta_1\sin\theta_2\cos\theta_1\cos\theta_2\cos\phi+2\sin^2\theta_1\sin^2\theta_2\cos^2\phi\} \qquad \ldots\ldots(4.11)$$

where the quadrupole moment Θ is defined as $\Sigma_i e_i(z_i^2-x_i^2)$, z_i being the distance along the axis of the charge e_i and x_i its distance from the axis. The effects of the quadrupole moment on B_K are two-fold. Firstly, the average value of $\cos^2\theta^{(12)}-\frac{1}{3}$ will not be zero since some configurations are weighted more than others, and secondly, even though the molecules have no permanent dipole moments, an interacting pair may possess a resultant dipole moment induced by the field of the quadrupoles. This effect has been discussed by Buckingham and Pople (1955 c) in connection with the dielectric constant of an imperfect gas. Its influence in this connection is considerable for strongly quadrupolar molecules such as carbon dioxide. In evaluating this second effect, represented by the term in T^{-2} in equation (4.3), we shall suppose that the molecules are isotropically polarizable and have central force interactions. We shall, then, only determine the leading term of this contribution to B_K. Thus, to this order,

$$B_K=\frac{2\pi^2N^2\kappa_a\kappa_\alpha a\alpha\Theta^4H_{10}(y)}{4725kT\epsilon^2r_0^{\,7}}+\frac{\pi N^2\kappa_a a\alpha^2}{135k^2T^2}\int_0^\infty r^2\,dr\int_0^\pi\sin\theta_1\,d\theta_1\int_0^\pi\sin\theta_2\,d\theta_2\int_0^{2\pi}d\phi$$
$$\times(3F_3^{\,2}-F^2)\exp\{-u^{(0)}/kT\} \qquad \ldots\ldots(4.12)$$

where F_3 is the component of the field at molecule 2 due to the moment of molecule 1 in the direction of the axis of molecule 1, and F is the total field at molecule 2, and where $u^{(0)}$ is the central force part of (4.11). Thus, with the above assumptions,

$$\left.\begin{aligned}F_3^{\,2}&=\frac{9\Theta^2}{4r^8}\{3\cos\theta_1-5\cos^3\theta_1\}^2\\ F^2&=\frac{9\Theta^2}{4r^8}\{1-2\cos^2\theta_1+5\cos^4\theta_1\}.\end{aligned}\right\} \qquad \ldots\ldots(4.13)$$

Thus

$$B_K=\frac{\pi^2N^2\kappa_a a\alpha\Theta^2}{4725kT\epsilon r_0^{\,2}}\left[\frac{2\kappa_\alpha\Theta^2}{\epsilon r_0^{\,5}}H_{10}(y)+\frac{5\alpha}{r_0^{\,3}y^2}H_8(y)\right]. \qquad \ldots\ldots(4.14)$$

(*d*) *Molecules with Permanent Dipole Moments*

As a first approximation to B_K for an assembly of polar molecules, we shall evaluate the integrals in (4.3) for molecules without polarizability—that is, we shall suppose that u_{12} is the Stockmayer potential (1941). We shall put

$$u_{12}=4\epsilon\left\{\left(\frac{r_0}{r}\right)^{12}-\left(\frac{r_0}{r}\right)^{6}\right\}+\frac{(\mu^{(0)})^2}{r^3}\{2\cos\theta_1\cos\theta_2+\sin\theta_1\sin\theta_2\cos\phi\}. \qquad \ldots(4.15)$$

We then have

$$B_K=\frac{\pi N^2\kappa_a a}{135kT}\int_0^\infty r^2\,dr\int_0^\pi\sin\theta_1\,d\theta_1\int_0^\pi\sin\theta_2\,d\theta_2\int_0^{2\pi}d\phi\left[\left(9\kappa_\alpha\alpha+\frac{3(\mu^{(0)})^2}{kT}\right)\right.$$
$$\left.\times(\cos^2\theta^{(12)}-\tfrac{1}{3})+\frac{4(\mu^{(0)})^2}{kT}\cos\theta^{(12)}\right]\exp(-u_{12}/kT). \qquad \ldots\ldots(4.16)$$

where $\cos\theta^{(12)} = -\cos\theta_1\cos\theta_2 + \sin\theta_1\sin\theta_2\cos\phi$. On performing the integrations in equation (4.16), we find

$$B_{\mathrm{K}} = \frac{8\pi^2N^2\kappa_a a r_0{}^3}{135kT}\left[\left(3\kappa_\alpha\alpha + \frac{y^2\tau r_0{}^3}{4}\right)\left\{\frac{\tau^2H_6(y)}{7200} + \frac{y^4\tau^4H_{12}(y)}{470\,400} + \dots\right\}\right.$$
$$\left. + \frac{y^2\tau r_0{}^3}{4}\left\{\frac{y^2\tau^3H_9(y)}{7200} + \frac{y^6\tau^5H_{15}(y)}{705\,600} + \dots\right\}\right] \quad \dots\dots(4.17)$$

where τ is a dimensionless parameter equal to $(\mu^{(0)})^2/\epsilon r_0{}^3$.

§ 5. DISCUSSION OF THE IMPERFECT GAS EQUATIONS

The equations of (*a*), (*b*), and (*c*) of § 4 all predict positive values of B_{K}. This is not surprising, since, for the configurations of figures 1, 2 and 3, $\kappa_\alpha\alpha$ for the dimer is twice that for an isolated molecule, whereas in figures 4 and 5 it has the same magnitude for both.

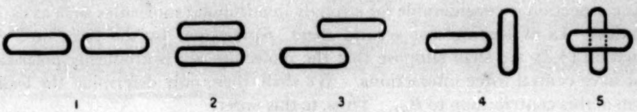

Figures 1–5.

Molecules with anisotropic dispersion forces prefer configurations as in figures 1 and 2, while plate-like molecules favour that in figure 1, and rod-like ones figures 2 and 5, and a quadrupole moment prefers the arrangements of figures 3 and 4.

To assess the orders of magnitude of B_{K} for the various fields for non-polar molecules discussed in the previous section, we shall substitute the following parameters into the several equations (the parameters correspond roughly to those of carbon dioxide at room temperature).

$y = 1{\cdot}6$, $r_0 = 3{\cdot}9$ Å, $\kappa_a = \kappa_\alpha = 0{\cdot}24$, $a = 2{\cdot}6 \times 10^{-24}\,\mathrm{cm}^3$,
$\alpha = 3 \times 10^{-24}\,\mathrm{cm}^3$, $\Theta = 5 \times 10^{-26}$ e.s.u., $D = 0{\cdot}1$, $T = 290°\mathrm{K}$.

(*a*) Anisotropic dispersion forces (4.6) $B_{\mathrm{K}} = 5{\cdot}5 \times 10^{-12}$ e.s.u. mole^{-2}.
(*b*) Non-spherical repulsive forces (4.10) $B_{\mathrm{K}} = 1{\cdot}3 \times 10^{-12}$ e.s.u. mole^{-2}.
(*c*) Non-dipolar molecules with quadrupoles (4.14)
$B_{\mathrm{K}} = (25 + 6) \times 10^{-12}$ e.s.u. mole^{-2}.

Thus the contribution of neither the anisotropic dispersion forces nor the non-spherical repulsive forces has an important influence on the molecular Kerr constant of an imperfect non-dipolar gas such as $\mathrm{CO_2}$. The major effect tending to increase ${}_{\mathrm{m}}K$ as the pressure increases is the directional field of the quadrupoles. The contribution of the induced dipoles, that is the second term in (4.14) and in (*c*) above, being proportional to $a\alpha^2$, is of secondary importance. In this respect B_{K} differs from the second dielectric virial coefficient (see Buckingham and Pople 1955 c). Unfortunately, the measurements of ${}_{\mathrm{m}}K$ shown in the table are not sufficiently precise for an accurate estimate of B_{K} to be made. The only conclusion that can be drawn from Kuss and Stuart's (1941) figures is that their results are not in disagreement with our calculations.

If the molecules possess permanent dipole moments then the configurations of figures 1, 2 and 3 will be preferred. Rod-like molecules will favour those of figures 2 and 3 and will have their dipoles in opposite directions, while plate-like ones will prefer to be in positions as in figure 1 with their dipoles adding algebraically. It might be anticipated therefore, that plate-like dipolar molecules will have large positive B_K values—considerably larger than those for corresponding rod-like ones owing to their larger net dipole moments.

To estimate the expected order of magnitude of B_K for a polar molecule, we shall apply equation (4.17) to figures corresponding roughly to those for methyl fluoride at room temperature. On putting $\mu^{(0)}=1{\cdot}8D$, $y=1{\cdot}6$, $r_0=3{\cdot}4$ Å, $\kappa_a=\kappa_\alpha=0{\cdot}09$, $\alpha=3{\cdot}5\times10^{-24}\,\mathrm{cm}^3$, $a=2{\cdot}8\times10^{-24}\,\mathrm{cm}^3$, $T=300°\mathrm{K}$, we find $B_K=1900\times10^{-12}$ e.s.u. mole^{-2}. Also, for these parameters, and with $\beta_{\alpha\beta\gamma}=\gamma_{\alpha\beta\gamma\delta}=0$, $A_K=27\times10^{-12}$ e.s.u. Thus measurements on dipolar gases should easily yield an experimental value for B_K, but at present there are no such data in the literature.

ACKNOWLEDGMENTS

The author is grateful to Dr. J. A. Pople for his advice on the foregoing topics, and to Professor W. H. Stockmayer for some helpful criticisms, and is indebted to the Royal Dutch/Shell Group for the award of a Postgraduate Scholarship.

REFERENCES

BUCKINGHAM, A. D., and POPLE, J. A., 1955 a, *Proc. Phys. Soc.* A, **68**, 905; 1955 b, *Trans. Faraday Soc.*, **51**, 1173, 1179; 1955 c, *Ibid.*, **51**, 1029.

KIRKWOOD, J. G., 1936, *J. Chem. Phys.*, **4**, 592.

KUSS, E., and STUART, H. A., 1941, *Phys. Z.*, **42**, 95.

LONDON, F., 1942, *J. Phys. Chem.*, **46**, 305.

OKA, S., 1937, *Proc. Phys.-Math. Soc. Japan* (3), **19**, 156.

PIEKARA, A., 1939, *Proc. Roy. Soc.* A, **172**, 360.

POPLE, J. A., 1954, *Proc. Roy. Soc.* A, **221**, 508.

RAMAN, C. V., and KRISHNAN, K. S., 1927, *Proc. Roy. Soc.* A, **117**, 1.

STOCKMAYER, W. H., 1941, *J. Chem. Phys.*, **9**, 398,

RESEARCH NOTES

Anharmonicity and Monomolecular Reactions

By R. H. TREDGOLD
Physics Department, University of Maryland

MS. received 28th February 1955

§ 1. Introduction

The subject of monomolecular reactions has been treated theoretically by Slater (1939, 1948, 1949, 1950, 1953). He considered reactions in a gas in which the mean time between a molecular collision and the subsequent disintegration of one of the molecules is long as compared with the mean time between collisions. Thus the reaction rate is proportional to the first power of the number of molecules not yet disintegrated.

In order to study the actual mechanism whereby the collisions lead to delayed disintegrations of the molecules he assumed that, up to a certain separation, the forces between the atoms constituting the molecules are linear but that, at a certain critical breaking separation, there is a sudden discontinuity. Thus if the internal motion of the molecule is represented by an appropriate number of normal mode coordinates, $q_1, q_2, q_3, \ldots$, then there will be certain regions in q-space corresponding to a disintegrated molecule and the problem of studying disintegration resolves itself into the problem of finding the mean period between excitation and the time when the point representing the configuration crosses into one of these regions. In the linear approximation this mean time is obviously a definite function of the distribution of energies amongst the various normal modes immediately after collision. If this distribution of energies is considered to be purely random, the problem of calculating the reaction rate is thus a statistical one.

It would be out of place to give a further discussion of this treatment here, but it should be noted that there will be many excited molecules having a sufficient energy to disintegrate which, until re-excited, will never be able to disintegrate as their energy will be distributed amongst the normal modes in such a manner that the point representing the configuration will never be able to cross one of the critical boundary regions.

Now as Slater has pointed out (1948), the linear approximation is not entirely satisfactory in this context as the force between atoms will really be a continuous function of separation and thus, if one is to consider separations large enough to lead to disintegration, the anharmonic forces will be quite important.

It is thus of interest to attempt to determine what the effect of anharmonicity is going to be. The problem of anharmonicity in the case of several bodies interacting according to a law which is treated as linear in the first approximation is also of interest in other contexts. Following Slater it will be assumed that the atoms are sufficiently massive and the degree of excitation sufficiently high so that it is legitimate to use classical mechanics.

§ 2. The Present Model

Since the effect of anharmonicity is assumed to be large it would obviously be out of place to use a perturbation method and one must therefore seek a model which embodies the essential physical problems under discussion, but which is nevertheless amenable to exact treatment.

We therefore consider three bodies whose masses are, for convenience, taken to be unity and which are constrained to move in a straight line.

We then take for the kinetic and potential energies respectively:

$$T=\frac{1}{2}\left[\left(\frac{dx_1}{dt}\right)^2+\left(\frac{dx_2}{dt}\right)^2+\left(\frac{dx_3}{dt}\right)^2\right]$$

$$U=\frac{1}{2}\left[\frac{b}{3}(x_{12}{}^2+x_{23}{}^2+x_{31}{}^2)-\frac{2c}{27}(x_{12}{}^4+x_{23}{}^4+x_{31}{}^4)\right]. \qquad \ldots\ldots(1)$$

Since one wishes to obtain solutions formally equivalent to the normal mode solutions of a linear problem, the following substitution is made:

$$\begin{aligned} x_1&=q_1-\tfrac{1}{2}q_2+\tfrac{1}{2}\sqrt{3}q_3\\ x_2&=q_1-\tfrac{1}{2}q_2-\tfrac{1}{2}\sqrt{3}q_3\\ x_3&=q_1+q_2 \end{aligned} \qquad \ldots\ldots(2)$$

giving

$$\left.\begin{aligned} &\frac{d^2q_1}{dt^2}=0\\ &\frac{d^2q_2}{dt^2}+bq_2-cq_2(q_2{}^2+q_3{}^2)=0\\ &\frac{d^2q_3}{dt^2}+bq_3-cq_3(q_2{}^2+q_3{}^2)=0. \end{aligned}\right\} \qquad \ldots\ldots(3)$$

Putting

$$q_2+iq_3=re^{i\phi} \qquad \ldots\ldots(4)$$

one obtains

$$\frac{d^2r}{dt^2}-r\left(\frac{d\phi}{dt}\right)^2+br-cr^3=0 \qquad \ldots\ldots(5)$$

$$\frac{d\phi}{dt}=\frac{\mu}{r^2} \qquad \ldots\ldots(6)$$

from which one may obtain

$$r=\left(\frac{\lambda}{bh}\right)^{1/2}\left\{(1+\gamma)+(\beta-\gamma)\,\mathrm{sn}^2\left[\left(\frac{\alpha-\gamma}{3}\right)^{1/2}b^{1/2}t\,\middle|\,m\right]\right\}^{1/2} \qquad \ldots\ldots(7)$$

where

$$m=(\beta-\gamma)/(\alpha-\gamma). \qquad \ldots\ldots(8)$$

The elliptic function notation as used, for example, by Milne Thomson (1950) is employed here and in equation (13). Here α, β, γ are defined as follows:

$$\alpha=A+B;\quad \beta=-\tfrac{1}{2}(A+B)-\tfrac{1}{2}(A-B)i\sqrt{3};\quad \gamma=-\tfrac{1}{2}(A+B)+\tfrac{1}{2}(A-B)i\sqrt{3} \qquad \ldots\ldots(9)$$

where

$$A=[\eta+(\eta^2-\sigma^3)^{1/2}]^{1/3},\qquad B=[\eta-(\eta^2-\sigma^3)^{1/2}]^{1/3} \qquad \ldots\ldots(10)$$

and

$$\sigma=1-2h\qquad \eta=1-3h+3h^2k^2/2 \qquad \ldots\ldots(11)$$

$$h=\frac{3\lambda c}{2b^2}\qquad k=\frac{\mu b^{1/2}}{\lambda}. \qquad \ldots\ldots(12)$$

Here λ is the internal energy of the system. It may be shown that $-1 \leqslant h \leqslant +1$ and that the solution (7), corresponding to a stable system is valid for $h<3/8$ irrespective of the value of k. For $h>3/8$ the system is unstable and another solution is applicable.

The expression for ϕ is somewhat cumbersome as it involves the incomplete elliptic integral of the third kind. However, one may obtain all the information that one requires to understand the behaviour of the system as follows.

It is easy to see that the point representing the configuration of the system in q-space will follow a somewhat distorted ellipse and that this ellipse will precess.

The precession is given by

$$\theta = \frac{4\sqrt{3}hkK}{(1+\gamma)(\alpha-\gamma)^{1/2}}\left\{1+\left[\frac{(\alpha-\gamma)(1+\gamma)}{(1+\alpha)(1+\beta)}\right]^{1/2}\right. \\ \left.\times\left[Z(\rho\,|\,m_1)+\frac{\pi\rho}{2KK'}-\operatorname{dn}(\rho\,|\,m_1)\operatorname{sc}(\rho\,|\,m_1)\right]\right\}-2\pi \quad \text{radians per cycle} \qquad \ldots\ldots(13)$$

where

$$\rho = \operatorname{sc}^{-1}\left[\frac{(\alpha-\gamma)^{1/2}}{(1+\gamma)^{1/2}}\,\middle|\,m_1\right] \qquad \ldots\ldots(14)$$

and $Z(\rho\,|\,m_1)$ is the Jacobian zeta function. θ is shown in the figure plotted as a function of k for $h=0{\cdot}1$ and $h=0{\cdot}2$.

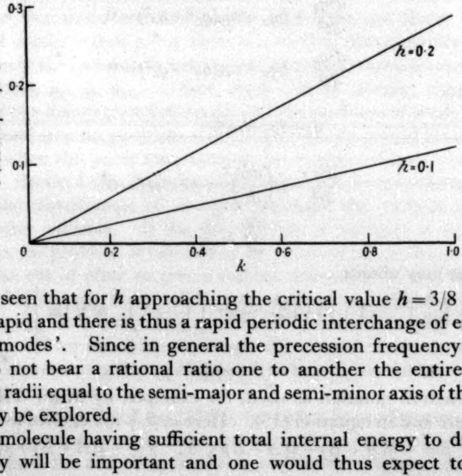

It will be seen that for h approaching the critical value $h=3/8$ the precession rate is quite rapid and there is thus a rapid periodic interchange of energy between the 'normal modes'. Since in general the precession frequency and the basic frequency do not bear a rational ratio one to another the entire area between circles having radii equal to the semi-major and semi-minor axis of the quasi-ellipse will ultimately be explored.

In a real molecule having sufficient total internal energy to disintegrate the anharmonicity will be important and one would thus expect to find a rapid interchange of energy between the normal modes as exemplified by the simple model discussed here.

Thus it appears that a treatment of monomolecular reactions based on a purely harmonic model is not entirely adequate as it will always yield a lower reaction rate than will actually be observed. It is of interest to note that the special case of degenerate normal modes occurring in highly symmetrical molecules and discussed in detail by Slater (1953) will, in the presence of anharmonicity, differ little from the non-degenerate case as the anharmonicity will remove the degeneracy. This effect, and indeed the entire effect of anharmonicity, will not be important at high pressures but could make a very substantial difference to the reaction rate at medium and low pressures.

ACKNOWLEDGMENT

This research was supported by the United States Air Force, through the Office of Scientific Research of the Air Research and Development Command.

REFERENCES

MILNE THOMSON, L. M., 1950, *Jacobian Elliptic Function Tables* (New York: Dover Publications).

SLATER, N. B., 1939, *Proc. Camb. Phil. Soc.*, **35,** 56; 1948, *Proc. Roy. Soc.* A, **194,** 112; 1949, *Proc. Leeds Phil. Lit. Soc.*, **5,** 75; 1950, *Proc. Camb. Phil. Soc.*, **46,** 525; 1953, *Phil. Trans. Roy. Soc.* A, **246,** 57, No. 906.

Radioactive Disintegration of ^{232}Th

BY S. W. PEAT AND M. A. S. ROSS
Department of Natural Philosophy, University of Edinburgh

MS. received 16*th May* 1955

THE nuclear emulsion method has been used to study the α-disintegration of ^{232}Th by Albouy (1952) and by Dunlavey and Seaborg (1952); Albouy concluded that the first excited state of ^{228}Ra lies about 75 kev above the ground state and is excited in 20% of the disintegrations; Dunlavey and Seaborg reported about 55 kev for the excitation energy and 24 ± 3% for the excitation intensity. In view of this discrepancy the present work was undertaken to obtain another determination of the excitation energy of the first excited state of ^{228}Ra. The thorium used was an analar grade supplied free from $MsTh_1$ and $MsTh_2$.

When the normal process of emulsion impregnation (Jarvis and Ross 1951) was employed, difficulties arose from the low solubility of thorium citrate in neutral solution and the high density of impregnation required for the study of an α-emitter having a half-life of the order of 10^{10} years. Strong solutions of the citrate with pH between 3·0 and 5·0 produced local desensitization of the emulsion but weak solutions containing about 1 μg of thorium per cm^3 did not show this effect. The cause of the desensitizing action may therefore be a chemical action of the thorium salt on the gelatin. Weak solutions were used in the main investigation. After impregnation the plates were stored for 28 days in an atmosphere with 44% relative humidity. They were then soaked for 30 minutes in a 2·5% solution of sodium bicarbonate to neutralize the acid in the plates and processed using the standard elon developer recommended by Messrs. Kodak.

Measurements were made at a magnification of 100 on the tracks of α-particles and conversion electrons in events having single α-particle tracks with range not greater than 25μ. The α-particles from the disintegration of ionium (mean range 18·6μ) and from the disintegration of radiothorium (mean range 23μ) were present, each with an intensity about 10% of the main peak due to the disintegration of ^{232}Th (mean range 15·3μ). The half-width at half maximum of the main peak was 0·6μ and the resolution of the ^{232}Th events from the ionium events was almost complete.

The figure shows a histogram and smoothed curve of the three-dimensional ranges of 142 conversion electrons associated with α-particles from ^{232}Th. The smoothed curve resolves the electrons into two groups with peak ranges of 11·4 and 17·5μ respectively. Resolution of the two groups in accordance with the broken line in the figure leads to mean ranges for the two groups of 11·25 ± 0·25 and 17·5 ± 0·4μ. From the mean-range versus energy relation of Zajac and Ross (1949) we infer mean energies for the two groups of 42·0 ± 0·5 and 54·5 ± 0·7 kev. Assuming the transition giving rise to these electrons to be of E2 type, and attributing the groups to L and M + N conversion, it follows that the L group arises almost entirely from conversion in the L_{II} and L_{III} shells having term values of 18·48 and 15·44 kev (Cauchois 1952) and relative conversion intensities 51 : 40 (Rose *et al.* private communication), and the M + N group arises mainly in the M_I, M_{II} and M_{III} shells having term values in the range 3·8 to 4·8 kev. The energy of the transition is therefore given by $42{\cdot}0 + 17{\cdot}0 = 59{\cdot}0$ kev from the L-conversion groups and $54{\cdot}5 + 4{\cdot}3 = 58{\cdot}8$ kev from the M-conversion group. Its value may therefore be taken as 59 ± 1 kev.

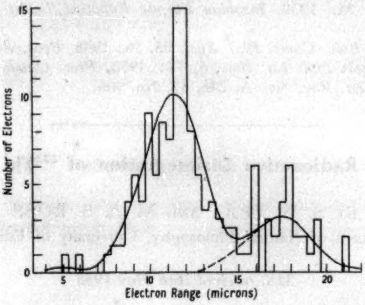

The absolute intensity of the conversion electrons is 24 ± 3% in agreement with Dunlavey and Seaborg (1952).

The mean range of the α-particle tracks having conversion electrons is 15·07 ± 0·04μ and the mean range of all α-particle tracks is 15·30 ± 0·04μ. Assuming that the α-spectrum of ^{232}Th contains only two lines of appreciable intensity, arising respectively in transitions to the ground and first excited states of ^{228}Ra, we infer that there is a difference of 0·30 ± 0·06μ in the mean ranges of the two groups of α-particles. This difference corresponds to a difference of 60 ± 12 kev in the kinetic energies of the α-particle groups. This energy difference is consistent with the conversion-electron results and their interpretation in terms of L and M + N conversion.

The resolution of the electron spectrum in the figure indicates that the ratio of L conversion intensity to M + N conversion intensity is about 3.

ACKNOWLEDGMENTS

This investigation was suggested by Professor N. Feather. Useful preliminary measurements were made by three undergraduate students, Miss Margaret D. Wilson, Mr. J. Carruthers and Mr. A. Rae. The radioactive solutions were prepared by Dr. N. Miller.

REFERENCES

ALBOUY, G., 1952, *J. Phys. Radium*, **13**, 309.
CAUCHOIS, Y., 1952, *J. Phys. Radium*, **13**, 113.
DUNLAVEY, D. C., and SEABORG, G. T., 1952, *Phys. Rev.*, **87**, 165.
JARVIS, C. J. D., and ROSS, M. A. S., 1951, *Proc. Phys. Soc.* A, **64**, 535.
ZAJAC, B., and ROSS, M. A. S., 1949, *Nature, Lond.*, **164**, 311.

The Energy Distribution of Protons from the Reaction Cu(n, p)Ni at 14 MeV

BY D. L. ALLAN
Atomic Energy Research Establishment, Harwell, Berks.

MS. received 9*th March* 1955 *and in final form* 23*rd May* 1955

IN recent years several workers have studied the energy distribution of neutrons and protons inelastically scattered by medium and heavy weight nuclei in the energy region 14–18 MEV. Some attention has also been given to (p, n) type reactions, but no results on the energy distribution of protons emitted by medium and heavy nuclei during (n, p) reactions have been reported. Paul and Clarke (1953) have shown that the cross sections for (n, p) reactions at 14 MEV are frequently significantly larger than predictions made on the basis of a compound nucleus theory and proposals that an additional reaction mechanism, involving mainly the surface of the nucleus, have been made to account for the observed cross sections (Austern, Butler and McManus 1953).

The energy distribution of neutrons and protons emitted during reactions involving the decay of a compound nucleus should be approximately given by the well known relations due to Weisskopf and Ewing (1940)

$$I(\epsilon)\,d\epsilon = \text{const.}\ S_{\text{b}}\epsilon\omega_{\text{R}}(E) \qquad \ldots\ldots(1)$$

$$\omega_{\text{R}}(E) = \exp(-\epsilon/T). \qquad \ldots\ldots(2)$$

A distinguishing feature of this distribution is the low probability for the emission of high-energy particles. In contrast to this, surface interactions should favour the emission of high-energy particles. Furthermore, the decay of a compound nucleus should lead to an isotropic angular distribution of the emitted particles, whereas the direct interaction mechanism is expected to have an angular distribution which is peaked in the forward direction. In order to determine the relative contributions of these two mechanisms we began the study of the energy distribution of protons emitted in the forward direction during 14 MEV (n, p) reactions with medium weight nuclei.

Metal targets 0·0005 in. and 0·001 in. thick in the form of narrow strips were placed at one end of an evacuated cylindrical chamber lined internally with 0·02 in. gold sheet. The chamber was placed with the targets 2 cm from a 14 MEV T–D neutron source, and the protons emitted were detected by a 300 μ Ilford type C2 photographic plate placed at the other end of the chamber 8 cm from the targets. A rapid survey was made to find which target materials gave good yields of protons. Pairs of target strips 1 cm wide and separated by 1 cm were placed side by side at the end of the chamber and at right angles to the plane of the emulsion. Since the points of origin of the particles leaving the target plane can be calculated from the positions and orientations of the tracks which they produce in the plates, plots such as illustrated in figure 1 (*b*) can be obtained. These give the relative number of protons originating in rectangular zones 1 mm wide lying in the target plane and parallel to the target strips. The figure shows clearly that the intensity of the protons which can be attributed to the targets is several times background for Cu and Ni. Good yields were also obtained from Al, Fe, Co, Zn, Mo, while Ag, Cd, In, Sn, Pt, gave yields which could not be resolved from the background. The yield from Pd was just measurable. The background was due mainly to proton recoils and other events originating near to the surface of the emulsion and indistinguishable from protons entering the emulsion from outside.

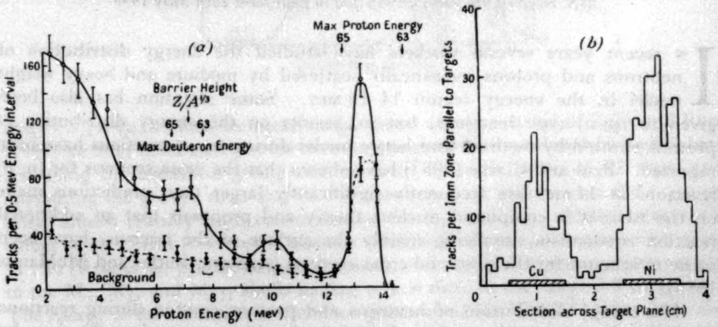

Figure 1. (*a*) Energy distribution of protons from reaction Cu(n, p)Ni. (*b*) Origin of tracks in target plane for Cu and Ni targets.

The energy distribution of protons from a 0·0005 in. Cu target is shown in figure 1 (*a*) (upper curve) with the background (lower curve) obtained from a run with the target strip removed. In this figure the data have not been corrected for target thickness, but the energy loss in the targets is indicated at two energies by square brackets. There is some indication that high energy particles are observed, but the most significant feature is the large number (about 85%) of low-energy protons below the barrier energy (7·2 MEV). The shape of the spectrum is more consistent with the Weisskopf model but with a greater coulomb barrier penetration than that usually assumed.

An attempt was made to check the identity of the tracks by grain counting. A sample of 50 tracks of all lengths appeared to be protons, but the spread in grain counts was such that the possibility that deuterons were also present cannot be ruled out. It may be significant that the break in the distribution at 7·5 MeV corresponds to the maximum possible deuteron energy (on a proton range–energy scale) for the two copper isotopes. A similar discontinuity occurs at the maximum deuteron energy in a spectrum for ^{27}Al(n, p)^{27}Mg. Byerly and Stephens (1951) have studied the photodisintegration of Cu with x-rays from a 24 MeV betatron using photographic plates, and by grain counting have shown that 25% of the singly charged particles emitted were due to deuterons. Using the same technique Toms and Stephens (1954) have shown that very few deuterons are emitted as a result of the photodisintegration of Co. The possibility therefore exists that the larger yields found for some elements in the present work may be due to deuterons. It may also be possible that some of the protons were produced by a (n, np) reaction.

In view of these doubts an examination of the data in terms of the Weisskopf model may have only limited validity. The present results were compared with those of Graves and Rosen (1953) for 14 MeV (n,n′) scattering by Cu, and of Gugelot (1954) for 18·3 MeV (p, p′) scattering by Cu. Using equation (1), relative values of log ω were plotted against the excitation energies of the residual nuclei. The rate of increase of log ω with excitation energy for the (n, p) data was very much higher than for the (n, n′) data when the theoretical values of S_b (protons) for a nucleus with $Z=30$ were used (Blatt and Weisskopf 1952). The (n, n′) and (n, p) results, which on a compound nucleus theory should differ only by a coulomb barrier penetrability factor, could only be reconciled if a barrier penetrability corresponding to a nucleus with $Z=10$ was used. The (n, p) results were even more at variance with the higher energy (p, p′) data of Gugelot, but good agreement was obtained when log ω was plotted against proton energy rather than excitation energy. A similar observation has been made by Gugelot (1954).

Approximate cross sections for the (n, p) reactions at 0° are given below. Relative values are probably accurate to 15%, the absolute magnitudes may have been underestimated by as much as 30%.

Element	Al	Fe	Co	Ni	Cu	Zn	Pd
mbn sterad^{-1}	16·0	8·4	3·8	17·3	15·5	14·1	10·0

REFERENCES

AUSTERN, N., BUTLER, S. T., and MCMANUS, H., 1953, *Phys. Rev.*, **92**, 350.
BLATT, J. M., and WEISSKOPF, V. F., 1952, *Theoretical Nuclear Physics* (New York : John Wiley), p. 352.
BYERLY, P. R., and STEPHENS, W. E., 1951, *Phys. Rev.*, **83**, 54.
GRAVES, E. R., and ROSEN, L., 1953, *Phys. Rev.*, **89**, 343.
GUGELOT, P. C., 1954, *Phys. Rev.*, **93**, 425.
PAUL, E. B., and CLARKE, R. L., 1953, *Canad. J. Phys.*, **31**, 267.
TOMS, M. E., and STEPHENS, W. E., 1954, *Phys. Rev.*, **95**, 1209.
WEISSKOPF, V. F., and EWING, D. H., 1940, *Phys. Rev.*, **57**, 472.

The Absolute Measurement of Differential Cross Sections for the Nuclear Scattering of Low Energy Relativistic Electrons

By K. R. CHAPMAN†, E. MATSUKAWA, P. H. ROSE†, and E. A. STEWARDSON
Physics Department, University College, Leicester

MS. received 4*th April* 1955

During recent years a number of studies of the nuclear scattering of electrons of energies in the range 0·1 to 3·0 Mev by metal foils has been made (Van de Graaff *et al.* 1946, 1947, Kinzinger and Bothe 1952, Kinzinger 1953, Reich 1950, Paul and Reich 1952, Bayard and Yntema 1954). Most of these experiments yield relative values only for the differential cross sections, and the only absolute determinations appear to be those of Van de Graaff *et al.* in the energy range 1·2–2·7 Mev, restricted to angles below 60° for Be, Al, Cu, Ag, Au and a single determination by Kinzinger and Bothe of the cross section in Al for 245 kev electrons scattered through 50°. No absolute measurements of the differential cross sections for scattering in the back direction appear to have been made. The difficulty lies in simultaneous measurement of the intensity of the incident and scattered electron beams when these differ by a factor of the order of 10^{-7} or 10^{-8} in the presence of a heavy x-ray background.

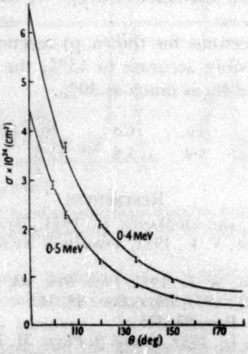

We have for some time been using a method which largely overcomes these difficulties and allows of the measurement of differential cross sections down to rather less than 10^{-25} cm². This consists in using an incident electron beam of some tens of μA produced in an electrostatic generator capable of giving energies up to 1 Mev, collecting the electrons in an aluminium Faraday cylinder and measuring them directly by means of an electrometer triode, the total incident beam being measured simultaneously by means of a galvanometer. This method of measurement is very insensitive to x-ray background and the slight effect arising from this cause is readily allowed for. Discrimination against secondary and inelastically scattered electrons is carried out by means of suitable absorbers placed before the collector. In agreement with Kinzinger we find it is necessary to discriminate against electron energies up to 70–75% of the incident beam energy. The accompanying curves show some typical results for the scattering cross sections of Al over the angular range 100°–150° at energies of 0·4 and 0·5 MEV. The curves have been drawn from theoretical cross sections calculated mostly by means of the α^4 expansion of McKinley and Feshbach (1948), a few values, however, having been obtained from the second Born approximation by the same authors with a correction derived from a comparison of the same approximation with α^4 values where these have been obtained. In this angular range scattering measurements made on the 'reflection' and 'transmission' sides of an inclined Al foil show that in the foil used (0·265 mg cm^{-2}) the plural scattering correction is less than our experimental error which probably amounts to two or three per cent. The conventional multiple scattering correction is also negligible at these angles. It will be seen that the experimental results agree very well with the theoretical curves. Other experiments have been carried out on scattering in the forward direction (from 25° to 90°) in Al and Au at 0·2 MEV. The results after correction for multiple scattering, electron–electron scattering, and electron screening, also show excellent agreement with theory, but as these merely extend the measurements of Van de Graaff *et al.* into the lower energy range we do not quote them here.

---

† Now at the University of Birmingham.

The experiments are being continued to cover nuclear scattering in heavier elements where discrepancies between theory and experiment have been reported by Kinzinger and Bothe and by Paul and Reich. Some preliminary results have already been obtained and we hope shortly to publish a full account of our results, together with details of apparatus and experimental methods.

REFERENCES

BAYARD, R. T., and YNTEMA, J. L., 1954, *Phys. Rev.*, **93**, 1412.
KINZINGER, E., 1953, *Z. Naturf.*, **89**, 312.
KINZINGER, E., and BOTHE, M., 1952, *Z. Naturf.*, **79**, 390.
MCKINLEY, W. A., JR, and FESHBACH, H., 1948, *Phys. Rev.*, **74**, 1759.
PAUL, W., and REICH, H., 1952, *Z. Phys.*, **131**, 326.
REICH, H., 1951, *Z. Phys.*, **130**, 144.
VAN DE GRAAFF, R. J., BUECHNER, W. W., BURRILL, E. A., JR, FESHBACH, H., and SPERDUTO, A., 1947, *Phys. Rev.*, **72**, 678.
VAN DE GRAAFF, R. J., BUECHNER, W. W., and FESHBACH, H., 1946, *Phys. Rev.*, **69**, 452.

Phase Shifts in p–p Scattering

By A. KELLER†
The Physical Laboratories, University of Manchester

Communicated by L. Rosenfeld; *MS. received* 18*th March* 1955

It is the purpose of this note to offer an interpretation of the P-wave phase shifts, recently observed in low energy p–p scattering.

A formula has been developed, valid for arbitrary angular momentum, relating the p–p phase shift to the corresponding n–p phase shift. For $l \geqslant 1$ it reduces to

$$-k^{-3}W_l(\eta, k^2) = \frac{\exp 2\pi\eta}{\exp(2\pi\eta)-1}\cot\delta_{l,\,\mathrm{p-p}} = \cot\delta_{l,\,\mathrm{n-p}} + f_{l,\,\mathrm{int}} \quad \ldots\ldots(1)$$

with $\eta = 1/2kR$. Here $R(=2{\cdot}88\times10^{-12}\ \mathrm{cm})$ is the Bohr radius of the system. The wave number k is related to the energy E of the incident proton (in the laboratory system) by $k^2 = 1{\cdot}206\,E$, when k is measured in $10^{12}\ \mathrm{cm}^{-1}$ and E in Mev. The term $f_{l,\,\mathrm{int}}$ represents a small interference effect of the Coulomb and the nuclear field and is of the order $1/R\mu$, with $1/\mu$ the range of the nuclear force.

Methods have been devised, based on an operational formulation, which allow accurate values of $\cot\delta_{l,\,\mathrm{n-p}}$ (including the case $l=0$), to be obtained with a minimum of labour. It is hoped to publish full details of this method later.

The interpretation of the experimental values of $\delta_{1,\,\mathrm{p-p}}$ were carried through on the basis of equation (1) with the small interference term neglected.

It can be shown (Blatt and Jackson 1950) that for scattering by a tensor force

$$V(r) = V_{\mathrm{C}}(r) + S_{12}V_{\mathrm{T}}(r), \quad \ldots\ldots(2)$$

at low energies the three phase shifts $\delta(^3\mathrm{P}_0)$, $\delta(^3\mathrm{P}_1)$ and $\delta(^3\mathrm{P}_2)$ will combine, provided they are small, as

$$\delta_1 = \tfrac{1}{9}\delta(^3\mathrm{P}_0) + \tfrac{3}{9}\delta(^3\mathrm{P}_1) + \tfrac{5}{9}\delta(^3\mathrm{P}_2) \quad \ldots\ldots(3)$$

to give the P-wave phase shift which is observed experimentally.

Using this result it can easily be shown that δ_1 can be derived from a Schrödinger equation, provided the Born approximation is valid, with a single central potential

$$V_{\mathrm{eff}}(r) = V_{\mathrm{C}}(r) - \frac{22}{45}\frac{M}{\hbar^2}r^2[V_{\mathrm{T}}(r)]^2 \quad \ldots\ldots(4)$$

(M is the mass of the proton).

We checked the assumption of the Born approximation being valid by comparing accurate values of δ_1, obtained for the Yukawa and the exponential well in the way indicated briefly above, with values calculated in Born approximation. The Born approximation was best at zero energy and gradually deteriorated with increasing energy. At 7 Mev the Born approximation still gave results correct to within 5%. These results are in agreement with the

† Now at the National Coal Board, Central Research Establishment, Cheltenham.

investigations of Kohn (1952) who showed that for $l \geqslant 1$, in the region of zero energy, the convergence of successive Born approximations will grow worse with increasing energy.

It should be noted that if $V_C(r)$ and $V_T(r)$ are both weak, then $V_C(r)$ will dominate (4).

The experimental values of the P-wave phase shifts are given in the table. It was not found possible, unfortunately, to utilize experimental data of an earlier date as these were not of sufficient accuracy.

Experimental Values of the P-wave Phase Shift for p–p Scattering

	Lab. energy E (MEV)	P-shift δ_1 (deg)	
Worthington *et al.* (1953)	1·855	−0·049	0·020
,,	1·858	−0·057	0·024
,,	2·425	−0·075	0·018
,,	3·037	−0·082	0·022
,,	3·527	−0·094	0·023
,,	3·899	−0·109	0·020
,,	4·203	−0·074	0·023
Kerman *et al.* (1953)	5·77	−0·08	0·05
Zimmerman & Kruger (1951)	5·86	−0·36	0·22
Cork & Hartsough (1954)	9·7	No P-wave scattering observed	
Yntema & White (private comm.)	18·2	1·0	

We attempted to obtain a fit to the above experimental data by taking in turn for $V_{\mathrm{eff}}(r)$ a pure Yukawa and an exponential potential. It was found that no satisfactory fit could be obtained above 4 MEV. Approximate calculations with the square and the gaussian well produced similar results.

A reasonable fit of the data was, however, obtained with the interaction

$$V_{\mathrm{eff}}(r) = V_1 \frac{\exp(-\mu_1 r)}{\mu_1 r} - V_2 \exp(-\mu_2 r) \qquad \ldots\ldots(5)$$

when we chose

$$V_1 = 136 \text{ MEV}, \qquad V_2 = 257 \text{ MEV},$$
$$1/\mu_1 = 1{\cdot}176 \times 10^{-13} \text{ cm}, \qquad 1/\mu_2 = 0{\cdot}7645 \times 10^{-13} \text{ cm}.$$

The values of $\delta_{1,\,\mathrm{n-p}}$ were calculated, using (5), in Born approximation; (1) then furnished the appropriate p–p shifts. In the figure, the results of the calculation are compared with the experimental values.

For 18 MEV, we obtained a value of $W(\eta, k^2)^{-1} = 0{\cdot}185 \times 10^{-39}$ cm^3. This is in good agreement with the value $0{\cdot}191 \times 10^{-39}$ cm^3 corresponding to the determination of Yntema and White, though of course at this energy the Born approximation is less reliable than at the lower energies.

A superficial comparison of (5) with (4) would appear to indicate a possible identification of the exponential and the Yukawa term of (5) with $V_C(r)$ and $V_T(r)$ respectively. This is not possible as the magnitudes of V_C and V_T would be so large that the condition that $\delta(^3P_0)$, $\delta(^3P_1)$ and $\delta(^3P_2)$ should all be small would be invalidated.

We are therefore led to the conclusion that the whole of (5) must be essentially identified with $V_C(r)$, the contribution of $V_T(r)$ being very small but indeterminate in the low energy region.

The main feature of (5) is such that near zero energy it will give a negative phase shift; somewhere in the region of 7 MeV δ_1 will pass through a zero; above 7 MeV the shorter ranged well will then predominate and produce positive phase shifts. At high energies (5) should give extremely strong scattering, in contrast to the very weak scattering at low energies.

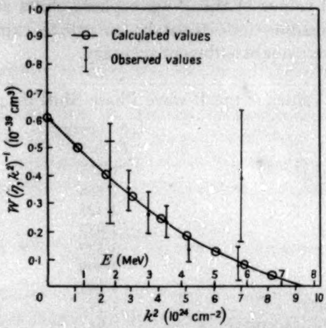

Belief in the change of sign is perhaps heightened by the recent determination of Rotblat and co-workers (private communication) at 9·5 MeV. They obtained $\delta_1 = +1{\cdot}1° \pm 0{\cdot}6°$.

More experiments in the 0–20 MeV region are particularly recommended as in this region the large experimental errors are to a considerable extent offset by the extreme sensitivity of δ_1 to the shape of the nuclear well. It is much more so for P states than it is for S states.

References

Blatt, J. M., and Jackson, J. D., 1950, *Rev. Mod. Phys.*, **22,** 77.
Cork, B., and Hartsough, W., 1954, *Phys. Rev.*, **94,** 1300.
Kerman, R. O., Kreger, W. E., and Kruger, P. G., 1953, *Phys. Rev.*, **89,** 908.
Kohn, W., 1952, *Phys. Rev.*, **87,** 539.
Worthington, H. R., McGruer, J. N., and Findley, D. E., 1953, *Phys. Rev.*, **90,** 899.
Zimmerman, E. J., and Kruger, P. G., 1951, *Phys. Rev.*, **83,** 218.

An Approximation for the High Order Phase Shifts in the Elastic Scattering of Slow Protons in the Inert Gases

By C. A. HAYWOOD
Physics Department, University College of Leicester

MS. received 4th *January* 1955 *and in amended form* 20th *May* 1955

To a first approximation the scattering of a charged particle by a neutral atom may be treated by replacing the field due to the electronic charge distribution by a static central field.

It has been shown (Faxen and Holtsmark 1927) by the method of partial cross sections that the total cross section Q for the scattering of a charged particle of de Broglie wavelength λ by a central field of force in which the potential energy of the particle at a distance r from the centre is $V(r)$ is given by

$$Q=\frac{4\pi}{k^2}\sum_{n=0}^{\infty}(2n+1)\sin^2\eta_n \qquad \ldots\ldots(1)$$

where $k=2\pi/\lambda$ and η_n is defined (Mott and Massey 1949) as the phase occurring in the asymptotic form of the bounded solution

$$G_n(r)\sim\sin\left(kr-\tfrac{1}{2}n\pi+\eta_n\right)$$

of

$$\frac{d^2G}{dr^2}+\left[k^2-U(r)-\frac{n(n+1)}{r^2}\right]G=0$$

where $U(r)=2mV(r)$, m being the mass of the particle. Atomic units are used throughout this paper.

Further it may be shown (Massey and Smith 1933) that

$$\eta_n=-\pi m\int_0^{\infty} rV(r)[\mathrm{J}_{n+1/2}(kr)]^2\,dr \qquad \ldots\ldots(2)$$

provided that η_n is small. $\mathrm{J}_{n+1/2}(kr)$ is the Bessel function of the first kind.

For low energy protons, the convergence of the series for Q is very slow and a large number of terms is required. Also for slow protons the expression (2) is only valid for large n.

The product $rV(r)$ is known as the 'effective nuclear charge for potential'. It is usually denoted by $Z_{\mathrm{p}}(r)$ and has been calculated by the 'self-consistent field' method of Hartree for helium (McDougall 1932, Wilson and Lindsay 1935), neon (Brown 1933), argon (Hartree 1938), and krypton (Holtsmark1930).

As tables of $\mathrm{J}_{n+1/2}$ do not exist for n greater than 18, Massey and Smith (1933) make use of an asymptotic expansion of the Bessel function and evaluate η_n numerically. The method of the present paper avoids the numerical integrations entirely. It involves finding a good fit to the $Z_{\mathrm{p}}(r)$ function of the form

$$Z_{\mathrm{p}}(r)\simeq a_1\exp(-b_1r)+a_2\exp(-b_2r)+a_3\exp(-b_3r)+\ldots \qquad \ldots\ldots(3)$$

It has been found that sufficient accuracy is obtainable with, at the most, three terms of the expansion and for neon only *one* term is necessary. The expansions are shown in the table and the agreement with the exact function $Z_{\mathrm{p}}(r)$ for helium is shown in the figure. Of the expansions shown in the table that for

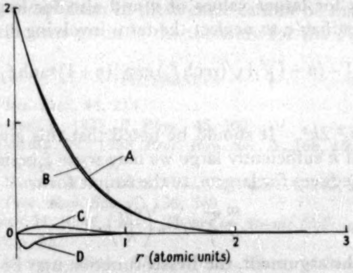

A: $\Sigma\, a_j \exp(-b_jr)$
B: $Z_{\mathrm{p}}(r)$
C: $\Sigma\, a_j \exp(-b_jr)-Z_{\mathrm{p}}(r)$
D: $\Sigma\, a_j \exp(-b_jr)-\alpha\, e^{-\beta r}-Z_{\mathrm{p}}(r)$

helium is the *least* accurate, and it will therefore be sufficient to consider that case in assessing the resultant error in η_n.

Making use of a generalization of a Lipschitz–Hankel integral (Watson 1944) we obtain for the phase shift

$$\eta_n = -\pi m \int_0^\infty \left\{ \sum_j a_j \exp(-b_j r) \right\} \mathrm{J}_{n+1/2}{}^2(kr)\, dr$$

$$= -\frac{m}{k} \sum_j a_j \mathrm{Q}_n \left(1 + \frac{b_j{}^2}{2k^2} \right) \qquad \ldots\ldots(4)$$

where Q_n is the Legendre function of the second kind. Tables of Q_n for large n do not exist but Watson (1918) gives an expression which exhibits the error involved in replacing a Legendre function by a Bessel function. The expression is:

$$\mathrm{Q}_n(\cosh\xi) = \exp\{-(n+\tfrac{1}{2})\xi\}\sqrt{(\operatorname{sech}\xi)}[\exp\{(n+\tfrac{1}{2})\tanh\xi\}\mathrm{K}_0\{(n+\tfrac{1}{2})\tanh\xi\} + 2\theta/3(n+\tfrac{1}{2})], \qquad (\xi \geqslant 0,\ n > 0) \qquad \ldots\ldots(5)$$

where K_0 is the modified Bessel function of the second kind and θ is a number which is less than unity. We then identify $\cosh\xi_j$ with $1 + b_j{}^2/2k^2$ and substitute from (5) into (4). The product $\mathrm{e}^x\mathrm{K}_0(x)$ is conveniently tabulated (Watson 1944) for x from 0 to 16.

Consider now the order of magnitude of the error involved in neglecting the term involving θ altogether. If $k \gg b_j$, $\tanh\xi_j \simeq b_j/k$ and the maximum error will be of order

$$\frac{\frac{2}{3}n^{-1}\Sigma_j a_j}{\Sigma_j a_j \exp(nb_j/k)\mathrm{K}_0(nb_j/k)} \times 100\%.$$

	a_1	b_1	a_2	b_2	a_3	b_3
Helium	+10	3·070	−8	3·486	—	—
Neon	+10	2·355	—	—	—	—
Argon	+31	2·138	−21	2·942	+8	8·831
Krypton (Hartree)	+60	1·766	−50	2·019	+26	4·887
Krypton (Fermi–Thomas)	+25·9	4·046	+9	1·197	+1·1	0·336
Xenon	+42·1	4·063	+10	1·377	+1·9	0·412
Radon	+55·8	6·566	+27	1·801	+3·2	0·483

Taking $n = 100$ and $k = 100$, for all the cases given in the table the maximum error is less than 1%. The value of k corresponds to a proton of energy about 70 ev. The error decreases for larger values of n and also for larger values of k. It therefore appears justifiable to neglect the term involving θ, and we have

$$\eta_n = -\frac{m}{k} \sum_j a_j \exp\{-(n+\tfrac{1}{2})\xi_j\}\sqrt{(\operatorname{sech}\xi_j)}\exp\{(n+\tfrac{1}{2})\tanh\xi_j\}\mathrm{K}_0\{(n+\tfrac{1}{2})\tanh\xi_j\} \qquad \ldots\ldots(6a)$$

where $\cosh\xi_j = 1 + b_j{}^2/2k^2$. It should be noted that this gives too *small* a value of η_n. For values of k sufficiently large we may write $\xi_j \simeq \sinh\xi_j \simeq \tanh\xi_j \simeq b_j/k$. Equation (6*a*) then reduces for large n, to the simple form

$$-\frac{m}{k} \sum_j a_j \mathrm{K}_0\left(\frac{nb_j}{k}\right). \qquad \ldots\ldots(6b)$$

For large values of the argument, the Bessel function may be calculated from the asymptotic expansion

$$\mathrm{e}^z\mathrm{K}_0(z) \sim \left(\frac{\pi}{2z}\right)^{1/2}\left(1 + \frac{1}{8z} + \frac{9}{128z^2} + \frac{75}{1024z^3} + \ldots\right). \qquad \ldots\ldots(7)$$

Consider now the error in η_n due to the lack of perfect 'fit' between $Z_p(r)$ and the series expansion. As already mentioned, the case of helium only will be considered. The figure shows that the error will be in excess because $J_{n+1/2}^2(kr)$ is positive. If then an extra term $\alpha e^{-\beta r}$ is subtracted from the expansion such that the error then becomes in deficit, it follows that the fractional error ϵ in the former case must be less than

$$\int_0^\infty \alpha e^{-\beta r} J_{n+1/2}^2(kr)\,dr \Big/ \int_0^\infty Z_p(r) J_{n+1/2}^2(kr)\,dr.$$

Without significant change this may be written as

$$\epsilon < \int_0^\infty \alpha e^{-\beta r} J_{n+1/2}^2(kr)\,dr \Big/ \sum_j \int_0^\infty a_j \exp(-b_j r) J_{n+1/2}^2(kr)\,dr \quad \ldots\ldots(8)$$

and may be calculated by application of equation (6) to both numerator and denominator. It is found in the case of helium that the function $\alpha e^{-\beta r} = 0{\cdot}24\, e^{-3{\cdot}34 r}$ converts the error from an excess to a deficit (see figure). The error, calculated from equation (8) for $n = 100$ and $k = 100$, is of the order of 3%. In view of the fact that the subtraction of the extra term $\alpha e^{-\beta r}$ makes the fit to the exact function $Z_p(r)$ considerably worse and also that the errors in equations (3) and (6) are of opposite sign, the error may be expected to be *substantially* less than 3%.

For fast collisions the series in equation (1) for Q converges rapidly, all the phases becoming small, and it is then unnecessary to use the above approximation. The range of applicability of the above method is thus between say 50 v and 20 kv energy.

The physical significance of the small error involved for slow proton impact presumably lies in the fact that the discrepancy between the exact and approximate forms of $Z_p(r)$ occurs mainly in the region of small r. On the classical theory the slow proton does not penetrate into this region and consequently the form of the atomic field there is unimportant. In this connection it is interesting to consider the effect on the high order phases due to using the Fermi–Thomas instead of the Hartree field for a relatively heavy atom such as krypton. The discrepancy here occurs in the region of large r. Using equation (6) in conjunction with the table, we find a difference of 27% between the values of η_{100} for $k = 100$. The Hartree fields for xenon and radon do not appear to have been calculated and so the comparison in these cases cannot be made. In these cases the values of the coefficients given in the table are for the Fermi–Thomas field.

REFERENCES

BROWN, F. W., 1933, *Phys. Rev.*, **44**, 214.

FAXEN, H., and HOLTSMARK, J., 1927, *Z. Phys.*, **45**, 307.

HARTREE, D. R., and HARTREE, W., 1938, *Proc. Roy. Soc.* A, **166**, 450.

HOLTSMARK, J., 1930, *Z. Phys.*, **66**, 49.

MASSEY, H. S. W., and SMITH, R. A., 1933, *Proc. Roy. Soc.* A, **142**, 142.

MCDOUGALL, J., 1932, *Proc. Roy. Soc.* A, **136**, 549.

MOTT, N. F., and MASSEY, H. S. W., 1949, ***Theory of Atomic Collisions***, 2nd Edn (Oxford: University Press), p. 25.

WATSON, G. N., 1918, *Messeng. Math.*, **47**, 151; 1944, ***Theory of Bessel Functions***, 2nd Edn (Cambridge: University Press), p. 389, *Ibid.*, Table II, p. 698.

WILSON, W. S., and LINDSAY, R. B., 1935, *Phys. Rev.*, **47**, 681.

LETTERS TO THE EDITOR

Hyperfine Structure of Praseodymium

Paramagnetic resonance in praseodymium ethyl-sulphate (diluted with the isomorphous lanthanum salt) was observed by Bleaney and Scovil (1952), who found rather broad lines. We have made measurements on the same salt with yttrium as the diluent and obtain rather narrower lines, with the asymmetrical shape characteristic of resonance from a doublet without Kramers degeneracy (see Bleaney, Llewellyn, Pryce and Hall 1954). The spectrum is fitted by the spin Hamiltonian

$$\mathscr{H}=g_z\beta H_zS_z+A_zS_zI_z+\Delta_xS_x+\Delta_yS_y$$

where $S=\frac{1}{2}$, $I=5/2$, $g_z=1{\cdot}52_5\pm0{\cdot}02$, $A_z=0{\cdot}075_5\pm0{\cdot}002\ \mathrm{cm}^{-1}$, and Δ_x, Δ_y each have a gaussian error distribution with average value zero. The values of g_z and A_z obtained in this way are rather smaller than the earlier values because of a change in the interpretation of the line shape. The separation between the hyperfine lines of 1059 ± 29 gauss (which is independent of this change) agrees with the previous value (1052 gauss) within the experimental error, and gives the ratio $A/g_z=0{\cdot}0495\pm0{\cdot}0015\ \mathrm{cm}^{-1}$.

The hyperfine structure of an ion with a $4\mathrm{f}^n$ configuration is given by the formula

$$2\beta\beta_ng_n\langle r^{-3}\rangle=a_{4\mathrm{f}}=\frac{A_1\langle J\|\Lambda\|J\rangle}{g_1\langle J\|N\|J\rangle}\qquad\ldots\ldots(1)$$

where $a_{4\mathrm{f}}$ is the "hyperfine structure parameter of a single 4f electron" as defined by Hin Lew (1953), and $\langle J\|N\|J\rangle$ is a numerical factor given by Elliott and Stevens (1953 a). For a free ion g_1 is isotropic and equal to the ordinary Landé g-factor ($\langle J\|\Lambda\|J\rangle$ in this nomenclature). In this formula matrix elements of the crystal field outside the ground state of the multiplet have been neglected, but in praseodymium ethyl-sulphate a correction must be applied for such elements between the ground state $^3\mathrm{H}_4$ and the first excited state $^3\mathrm{H}_5$. This correction can be found using the theory of Elliott and Stevens, if the size of the crystal field is known. A reasonable fit with the resonance g-value given above, and with measurements of the principal susceptibilities of a single crystal over the range 2° to 290°K (Fereday and Wiersma 1935, van den Handel 1941), is obtained using the crystal field parameters (for notation see Elliott and Stevens 1952) $V_2^0=50\ \mathrm{cm}^{-1}$, $V_4^0=-100\ \mathrm{cm}^{-1}$, $V_6^0=-48\ \mathrm{cm}^{-1}$, $V_6^6=660\ \mathrm{cm}^{-1}$, which are not greatly different from values obtained by interpolation between those given by Elliott and Stevens (1935 b) for the neighbouring ions cerium and neodymium.

With these crystal field parameters, the corrections to A_z and g_z have been calculated and it is found that $a_{4\mathrm{f}}$ is 10% smaller than given by equation (1), having the value $a_{4\mathrm{f}}=0{\cdot}0271\pm0{\cdot}0008\ \mathrm{cm}^{-1}$. Taking the value of $\langle r^{-3}\rangle$ as $37\pm2\ \text{Å}^{-3}$ (Bleaney 1955, following letter) the nuclear magnetic moment is estimated as

$$\mu_n=g_nI=3{\cdot}9_2\pm0{\cdot}2\ \mathrm{n.m.}$$

F the free Pr atom $4f^3 6s^2$, $^4I_{9/2}$ Hin Lew finds

$$a_{4f} = 0{\cdot}02354\ \mathrm{cm}^{-1}, \qquad \mu_n = 3{\cdot}8_5 \pm 0{\cdot}4\ \mathrm{n.m.}$$

assuming $\langle r^{-3}\rangle = 32 \pm 3$ Å^{-3}. This lower value of $\langle r^{-3}\rangle$ for the free atom corresponds to an increase of about 0·8 units in the screening constant, presumably owing to the effect of the 6s electrons. Although these are generally thought to be 'outside' the 4f electrons, they have a finite density at the nucleus and some screening action is to be expected in the region close to the nucleus from which the major contribution to $\langle r^{-3}\rangle$ arises.

These values of the nuclear magnetic moment are in good agreement with other measurements from optical spectroscopy, which give 3·9 ± 0·3 (Brix 1952) and 4·0 ± 0·1 (Murakawa and Suwa 1954). The effect of any unpaired s-electron character has been neglected in all cases; in our result its effect is estimated as only about 2% (Bleaney 1955).

Clarendon Laboratory,
Oxford.
11th July, 1955.

J. M. Baker.
B. Bleaney.

Bleaney, B., 1955, *Proc. Phys. Soc.*, A, **68,** 937.
Bleaney, B., Llewellyn, P. M., Pryce, M. H. L., and Hall, G. R., 1954, *Phil. Mag.*, **4,** 991.
Bleaney, B., and Scovil., H. E. D., 1952, *Phil. Mag.*, **43,** 999.
Brix, P., 1952, Z. *Phys.* **132,** 579.
Elliott, R. J., and Stevens, K. W. H., 1952, *Proc. Roy. Soc.* A, **215,** 437; 1953 a, *Ibid.*, **218,** 553; 1953 b, *Ibid.*, **219,** 387.
Fereday, R. A., and Wiersma, E. C., 1935, *Physica*, **2,** 575.
van den Handel, J., 1941, *Physica*, **8,** 513.
Hin Lew, 1953, *Phys. Rev.*, **91,** 619.
Murakawa, K., and Suwa, S., 1954. *J. Phys. Soc., Japan*, **9,** 93.

Nuclear Moments of the Lanthanons from Paramagnetic Resonance

The principal source of error in the calculation of nuclear moments from measurements of hyperfine structure in the paramagnetic resonance spectra of rare earth compounds is the uncertainty in the value of $\langle r^{-3}\rangle$. Elliott and Stevens (1953) have used the empirical formula

$$\langle r^{-3}\rangle = (12 \pm 3)(Z - 55)^{3/4}\ \text{Å}^{-3}$$

where the rather large error was assumed because of the considerable discrepancy between an estimate of 47 Å^{-3} for un-ionized europium based on the Fermi–Thomas model (Sternheimer 1950) and one of 64 Å^{-3} for triply ionized europium obtained from the spin–orbit coupling. The results for praseodymium (Baker and Bleaney 1955, preceding letter) indicate that the value of $\langle r^{-3}\rangle$ is appreciably smaller for the neutral atom, presumably because of the screening effect of the 6s electrons. Also, the Fermi–Thomas model is probably less reliable because it does not predict the start of the rare earth series at the right point. For these reasons it seems best to rely on values of $\langle r^{-3}\rangle$ obtained in the usual way from the spin–orbit coupling energy ζ of the trivalent ions. At first sight the multiplet splittings seem rather unpromising as a method of deducing ζ, because of the rather large deviations from the Landé interval rule; however, unpublished work of B. R. Judd has shown that these are due to intermediate coupling (spin–spin interaction is negligible) and fairly reliable values of ζ can be obtained from the overall multiplet splitting. Such values are given in table 1, and if these are fitted to the formula

$$\zeta = \frac{2(Z-\sigma)^4\beta^2}{n^3 l(l+\frac{1}{2})(l+1)a_0^{\,3}} \qquad \ldots\ldots(1)$$

the value of the screening constant σ is found to increase from approximately 34·6 at the start of the lanthanons to 35·9 at the end. A convenient empirical formula which fits the results within a few per cent over the whole range (see table) is

$$\zeta = 5{\cdot}4_6(Z-47)^2\ \mathrm{cm}^{-1}. \qquad \ldots\ldots(2)$$

Then the usual relation between ζ and $\langle r^{-3}\rangle$ gives

$$\langle r^{-3}\rangle = 0{\cdot}89(Z-47)^{3/2}\ \text{Å}^{-3}. \qquad \ldots\ldots(3)$$

Values of nuclear moments of the 4f series deduced from paramagnetic resonance measurements using this formula for $\langle r^{-3}\rangle$ are also given in the table.

Tri-valent ion	ζ (cm^{-1})		$\langle r^{-3}\rangle$(Å^{-3})	δ %	Iso-tope	Spin	Nuclear moments		
	(exp)	from (2)	from (3)				μ (n.m.)		Q (10^{-24} cm^2)
58 Ce	640	660	32·5	(1·5)	—		—		—
59 Pr	800	790	37	(1·9)	141	$\frac{5}{2}$	3·9		—
60 Nd	900	920	42	(2·4)	143	$\frac{7}{2}$	1·03	ratio =1·083	<1
					145	$\frac{7}{2}$	0·64		<1
61 Pm	—	1070	47	(2·9)	—		—		—
62 Sm	1200	1230	51	(4·1)	147	$\frac{7}{2}$	0·83	ratio =1·22	<0·7
					149	$\frac{7}{2}$	0·68		<0·7
63 Eu	1410	1390	57	—	151	$\frac{5}{2}$	—	ratio =2·23	—
					153	$\frac{5}{2}$	—		—
64 Gd	—	1580	62	—	—		—		—
65 Tb	1770	1770	68	(6·0)	169	$\frac{3}{2}$	1·52		—
66 Dy	1860	1970	74	(2·9)	—		—		—
67 Ho	2000	2180	80	(1·9)	165	$\frac{7}{2}$	3·31		—
68 Er	2350	2400	86	(1·4)	167	$\frac{7}{2}$	0·48		9·4
69 Tm	2660	2640	92	(1·1)	—		—		—
70 Yb	2940	2880	98	(0·9)	171	$\frac{1}{2}$	0·49	ratio =0·72	—
					173	$\frac{5}{2}$	0·68		—

Values of ζ from Gobrecht (1938) except for
Ce (Lang 1936), Pr (Spedding 1940) and Nd (Satten 1953).

They are generally close to those found from the spectra of the free atoms or ions where these are known, and the principal uncertainty arises from the same causes in both types of measurements. Apart from an error estimated as ±5% in the value of $\langle r^{-3}\rangle$ given by equation (3), there may be a contribution (cf. Abragam, Horowitz and Pryce 1955) to the hyperfine structure from unpaired s electrons. In the notation of Elliott and Stevens (1953), this would require the replacement of $\langle J\|N\|J\rangle$ by $\langle J\|N\|J\rangle+\kappa(\langle J\|\Lambda\|J\rangle-1)$. The value of κ is known only for Eu^{2+} (Bleaney and Low 1955), but if the same empirical rule holds as in the iron group, then the value of $\kappa\langle r^{-3}\rangle$, which is $(0{\cdot}080\times 57)$ Å^{-3} for Eu, would be the same for all 4f ions. The sign of κ is not known, and only the magnitude of the correction to the nuclear moments which this assumption gives is shown as δ in the table; it is small in all cases, the maximum being 6% for Tb, and can be neglected.

I am indebted to Dr. A. H. Cooke and Mr. J. G. Park for permission to quote unpublished results on ytterbium, and similarly to Dr. J. M. Baker on holmium.

Clarendon Laboratory,
Oxford.
11th July 1955.

B. Bleaney.

Abragam, A., Horowitz, J., and Pryce, M. H. L., 1955, *Proc. Roy. Soc.* A, **230,** 169.
Baker, J. M., and Bleaney, B., 1955, *Proc. Phys. Soc.* A, **68,** 936.
Bleaney, B., and Low, W., 1955, *Proc. Phys. Soc.* A, **68,** 55.
Elliott, R. J., and Stevens, K. W. H., 1953, *Proc. Roy. Soc.* A, **218,** 553.
Gobrecht, H., 1938, *Ann. Phys. Lpz.*, **31,** 755.
Lang, R. J., 1936, *Canad. J. Res.*, **14,** 127.
Satten, R. A., 1953, *J. Chem. Phys.*, **21,** 637.
Spedding, F. H., 1940, *Phys. Rev.*, **58,** 255.
Sternheimer, R., 1950, *Phys. Rev.*, **80,** 102.

The Entropy of Superfluid Helium

A recent paper (Chandrasekhar and Mendelssohn 1955) has emphasized the need for an accurate determination of the heat of transport of liquid helium II near 1°K. According to the simple two-fluid model, the heat of transport $Q_T = T\Delta S$ (H. London 1939), where T is the absolute temperature and ΔS the entropy difference between bulk fluid and superfluid. It appears from the specific heat data (Kramers, Wasscher and Gorter 1952) that the entropy of liquid helium II is made up of two contributions. At temperatures below about 0·6°K the only significant contribution is that due to phonon excitations (S_{ph}) which increases as T^3. Above this temperature, there is a further contribution due to anomalous excitations, which increases with a higher power of the absolute temperature, and becomes predominant at the higher temperatures near the lambda point.

The question arises whether the heat of transport contains contributions from the anomalous excitations only (Tisza 1947, 1949), or whether the phonon excitations also form part of it (Landau 1941, Ward and Wilks 1952). In the latter case, as superfluid is converted into bulk at the end of a flow channel, we should expect all modes to require excitation, whereas in the former case this would not be true for the phonon contribution. This question can therefore be decided by determining whether the measured heat of transport agrees with TS_{tot} or with $T(S_{\text{tot}}-S_{\text{ph}})$, where S_{tot} is the total entropy containing both kinds of excitations. Clearly the percentage difference between these two quantities is greatest at the lower temperatures, where below about 0·6°K the heat of transport would be zero if the phonons were carried in superflow. However, measurements at these temperatures suffer from difficulties in technique, and the question can in fact be decided at higher temperatures provided that the measurements are sufficiently accurate.

Such accurate measurements have now been carried out in this laboratory using an apparatus the details of which will be published later. It is similar in principle to that used by Chandrasekhar and Mendelssohn (1955) except that the flow channel consists of a tube containing tightly packed jewellers' rouge powder. Measurements were made in the usual way by observing the rate of flow of liquid produced by a given heat current, at temperatures from 1·14°K to 2·05°K. From the results, values of the entropy difference ΔS have been calculated with an estimated accuracy of better than 2%. These values agree fairly well with those of S_{tot} given by Kramers, Wasscher and Gorter (1952), being about 5% higher at 2·00°K, and showing a gradual trend to about 2% lower at 1·2°K. At this lower temperature $S_{tot}-S_{ph}$ is about 25% less than S_{tot}. In view of the accuracy of the experiments, it can therefore be concluded that both the anomalous excitations *and* the phonon excitations contribute to the heat of transport, and that phonons are not transported in superflow.

Details of these experiments will be given in a later publication.

Clarendon Laboratory,
Oxford.
21st July 1955.

D. F. Brewer.
D. O. Edwards.
K. Mendelssohn.

Chandrasekhar, B. S., and Mendelssohn, K., 1955, *Proc. Phys. Soc.* A, **68**, 857.
Kramers, H. C., Wasscher, J. D., and Gorter, C. J., 1952, *Physica*, **18**, 329.
Landau, L. D., 1941, *J. Phys. U.S.S.R.*, **5**, 71.
London, H., 1939, *Proc. Roy. Soc.* A, **171**, 484.
Tisza, L., 1947, *Phys. Rev.*, **72**, 838; 1949, *Ibid.*, **75**, 885.
Ward, J. C., and Wilks, J., 1952, *Phil. Mag.*, **43**, 48.

Elastic Scattering of 80 kev Neutrons

The considerable success of the 'complex potential' model of the nucleus (Feshbach, Porter and Weisskopf 1954) in accounting for the angular distributions of scattered neutrons of 1 Mev energy (Walt and Barschall 1954) led us to consider its experimental verification at lower energies. For neutrons of 80 kev energy there is a p-wave single particle resonance at about $A=92$ when considerable anisotropy in the angular distributions is expected. The theoretical ratios of intensities at 0°, 90° and 180° are 2·1 : 1 : 1·4 for $A=92$ decreasing almost to isotropy at $A=78$.

In the reaction ^{7}Li(p, n)^{7}Be, when 80 kev neutrons are produced in the direction of the incident beam, all the neutrons from the reaction lie within a cone of semi-angle about 40°. The proton energy is only 16 kev above threshold, and the neutron energy and intensity vary rapidly with proton energy in this region. The angle of the neutron cone also varies rapidly and the counting rate in a monitor at 40° changes by a factor of 2 for 2 kv change in proton energy. By adjusting the resolving magnet manually it is possible to hold the counting rate in this monitor constant so that the corresponding proton energy variation is less than 0·2 kv.

The experimental arrangement is shown in figure 1. The monitors at 0° and 40° are 'long-counters' (Hanson and McKibben 1947) and the scattered neutron detector is a proton recoil counter (Skyrme, Tunnicliffe and Ward 1952) filled with hydrogen at a pressure of about 1 atmosphere. The target is of Li metal some 5 kev thick. In the earlier stages of this work difficulties respecting the stability of these targets were encountered, but these have now been overcome by the use of a platinum backing. The scatterers were conical in form and had transmissions of about 60%. The correction for multiple scattering is less than ± 6% in the experimental range of angles. At each angle the recoil spectrum of the scattered neutrons was obtained by subtracting the pulse height distributions obtained with and without the scatterer, the neutron flux being monitored by a beam current integrator.

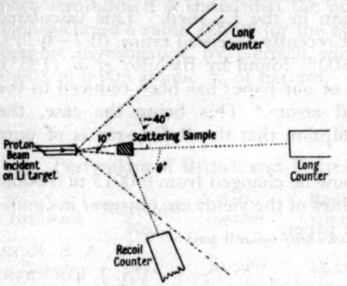

Figure 1. Experimental arrangement.

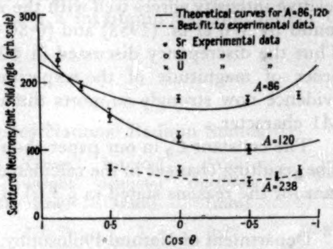

Figure 2. Angular distribution of scattered neutrons.

We can report the results obtained here using this method for tin and strontium. The observed angular distributions corrected for multiple scattering are shown in figure 2. These may be compared with the angular distributions calculated for the parameters $V_0 = 9$ MEV and $\xi = 0{\cdot}05$.

There is fair agreement between the experimental and theoretical results for tin while for strontium the experimental curve is rather flatter. Other results of the authors, not yet however sufficiently well established for publication, do not exhibit the degree of anisotropy expected in this region. Further experimental work on these elements is being continued and a more thorough comparison of theory and experiment will then be possible.

With the same arrangement, the angular distribution of neutrons elastically scattered from uranium, has been measured and found to be isotropic within the errors of the experiment.

ACKNOWLEDGMENT

The writers are indebted to Dr. A. M. Lane for valuable discussions of the theory, and for carrying out the calculations.

Atomic Energy Research Establishment,
Harwell, Berks.
25th May 1955.

W. D. ALLEN.
A. T. G. FERGUSON.

FESHBACH, H., PORTER, C. E., and WEISSKOPF, V. F., 1954, *Phys. Rev.*, **96**, 448.
HANSON, A. O., and MCKIBBEN, J. L., 1947, *Phys. Rev.*, **72**, 673.
SKYRME, T. H. R., TUNNICLIFFE, P. R., and WARD, A. G., 1952, *Rev. Sci. Instrum.*, **23**, **204**.
WALT, M., and BARSCHALL, H. H., 1954, *Phys. Rev.*, **93**, 1062.

Fluorescence Yields of the L Levels of Bi

In our paper on fluorescence yields (Ross, Cochran, Hughes and Feather 1955), calculated values of the internal conversion coefficient for M1 radiation in the L_{III} shell were taken from the paper by Gellman, Griffith and Stanley (1952). These calculations did not include an allowance for screening by atomic electrons. Calculated values which include screening have now been given for the L_{III} shell by Rose *et al.* (private communication). The new values give an internal conversion coefficient of 0·098 in place of 0·022 for the RaD γ-ray in the L_{III} shell of Bi, and make the intensity of conversion in the L_{III} shell 0·60% of the intensity of conversion in the L_I shell. This calculated relative intensity agrees well with the most recently observed ratios, $(0{\cdot}7 \pm 0{\cdot}3)\%$ found by Wu *et al.* (1953) and $(0{\cdot}86 \pm 0{\cdot}05)\%$ found by Bashilov *et al.* (1953). Thus the discrepancy discussed in § 3 (i) of our paper has been reduced to the order of magnitude of the experimental errors. This being the case, the evidence now strongly supports the assumption that the RaD γ-ray is of pure M1 character.

The constant C_3 in our paper should now be changed from 0·0013 to 0·0060. The resulting changes in the calculated values of the yields are however insignificant for the reasons stated in § 3 (i) of the paper.

M. A. S. Ross.
A. J. Cochran.
J. Hughes.
N. Feather.

Department of Natural Philosophy,
University of Edinburgh.
16th August 1955.

Bashilov, A. A., Dzhelepov, B. S., and Chervinskaya, L. S., 1953, *Izv. Akad. Nauk, S.S.S.R.*, Ser. Fiz., **17**, 428.

Gellman, H., Griffith, B. A., and Stanley, J. P., 1952, *Phys. Rev.*, **85**, 944.

Ross, M. A. S., Cochran, A. J., Hughes, J., and Feather, N., 1955, *Proc. Phys. Soc.* A, **68**, 612.

Wu, C. S., Boehm, F., and Nagel, E., 1953, *Phys. Rev.*, **91**, 319.

Comparison of British and United States National Radium Standards

The National Physical Laboratory has had the custody of the British national radium standard since 1913. The first standard (No. 3 issued by the International Radium Standard Commission) was a secondary standard, its radium content value being based on gamma-ray comparisons with the 1911 Paris and Vienna international standards (Meyer 1945). It was replaced in 1934 by one of twenty weighed standards prepared by Hönigschmid (1945); two of these standards were assigned as replacements of the 1911 Paris and Vienna standards (Chamié 1940, Karlik 1953) and two were acquired as national standards by the United States National Bureau of Standards. In 1952, one of the United States standards was compared at the N.P.L. with the British national standard, and the same two standards were subsequently compared at the N.B.S. (Davenport *et al.* 1954). The main purpose of this note is to place on record the results of the 1952 comparison.

Each standard consists of a sealed thin-walled tube containing a weighed quantity of RaCl$_2$. It is seen (table 1) that the standards differ slightly in length, gross weight and in the stated weights of their contents, but that they are equal in diameter and wall thickness. In each case the radioactive material, which is granular in form, occupies only a small fraction of the total volume of the glass tube. The British standard is certified by weight only, as it has not been compared with the international standards. Comparisons at the N.P.L. in 1934 showed that it was about 0·3% relatively more active than the first British national standard. The United States standard is certified by weight and by gamma-ray comparison with the 1911 Paris and Vienna standards. In the certificates for both standards it is stated that the purity of the radium chloride is testified by Hönigschmid's value 226·05 for the atomic weight of radium, and by a spectrographic investigation by Gerlach which gave a maximum barium content of 0·002 to 0·003 atomic % of barium.

Table 1

Particulars of British and United States National Radium Standards

Standard	Reference No.	Salt content (mg RaCl$_2$)	Radium content (mg element)	Gross weight (mg)	Internal diameter (mm)	Wall thickness (mm)	Length (mm)
British	5432	20·50(1)	15·60(1)	276·74	3	0·27	38·8
U.S.	5440, XV	26·86(1)	20·45(1) 20·38(2)	267·86	3	0·27	37

(1) The date of the weighing of both standards by Hönigschmid is given on the certificates as 2nd June 1934.

(2) By comparison with the 1911 Paris and Vienna standards as of June 1934. The certified value is 20·36 mg " towards the end of 1936 ".

Three different measuring equipments were used for the comparison, namely, the standard combined gamma-ray ionization chamber and projection gold leaf electroscope normally used for radium standardization at the N.P.L. (Perry 1936), an ionization chamber of almost the same construction and dimensions as the standard chamber but connected to a Lindemann electrometer which serves as a null instrument in a Townsend induction balance, and a gamma-ray Geiger–Müller counter. The gamma-rays were filtered by 0·5 cm of lead before entering the ionization chamber or counter. The normal procedure was followed to minimize instrumental and personal errors and the effects of asymmetry and absorption in the standards. The values of the ratio of the gamma-ray activity of the United States standard to that of the British standard by the three measuring devices are given in table 2 which also includes the results of the comparisons of the same two standards at the National Bureau of Standards (Davenport *et al.* 1954, Connor and Youden 1954, Mann 1954). The limits given are the standard deviations of the individual values from the mean.

It is necessary to note that as the glass tubes are very similar in dimensions and contain not very different quantities of radium salt, the absorption of the gamma rays in the glass wall and in the salt, estimated to be about 0·5%, is assumed to be the same for each standard.

Table 2

Results of comparisons of British and United States National Radium Standards given as ratio of activity of United States standard † to activity of British Standard

Institution	N.P.L.	N.B.S.
Ionization chamber and gold leaf electroscope	1·304 ± 0·002	1·3053
Ionization chamber and Lindemann electrometer (null) method	1·306 ± 0·001	—
Geiger–Müller counter	1·304 ± 0·001	1·3057
Scintillation counter	—	1·3116
Radiation balance	—	1·3077

The N.B.S. values are not the actual results of the direct comparisons of the two standards; the Hönigschmid standard No. 5437, which is in the possession of the N.B.S., was included in the measurements thus providing three pairs of standards. The directly measured activity ratios of the members of each pair were adjusted statistically to satisfy a consistency criterion (Connor and Youden 1954). The N.B.S. values given in table 2 are the adjusted values.

The comparisons indicate a difference of the order of a few parts per thousand between the gamma-ray activity ratio and the weight ratio. In discussing the standards, Hönigschmid (1945) stated that the error of a single weighing did not exceed 0·02 mg, and that as two weighings were involved for each standard, the maximum error could amount to 0·04 mg. The weight ratio is thus subject to an error of about 0·2%. The standard error of the mean (1·3047) of the N.P.L. activity ratios is about 0·1%. The observed difference (0·4%) between the mean activity ratio and the weight ratio is therefore not significant. Similar considerations applied to the N.B.S. values lead to the same conclusion.

The work described above was carried out as part of the research programme of the National Physical Laboratory and this letter is published by permission of the Director of the Laboratory. Acknowledgment is made to Dr. W. B. Mann of the National Bureau of Standards, for the loan and transport of the United States standard, and to Mr. W. Binks‡, Mr. E. E. Smith, Mr. W. J. Callow and Mr. J. W. G. Dale of the Physics Division, National Physical Laboratory, for advice and assistance with the measurements.

National Physical Laboratory,
Teddington,
Middlesex.
23rd June 1955.

W. E. Perry.

Chamié, C., 1940, *J. Phys. Radium* (8), **1**, 319.
Connor, W. S., and Youden, W. J., 1954, *J. Res. Nat. Bur. Stand.*, **53**, 273.
Davenport, T. I., Mann, W. B., McCraven, C. C., and Smith, C. C., 1954, *J. Res. Nat. Bur. Stand.*, **53**, 267.
Hönigschmid, O., 1945, *Anz. Akad. Wiss., Wien*, **8–9**, 30 (*Mitt. des Rad. Inst.* No. 453a).
Karlik, B., Report submitted to the Joint Commission on Radioactivity. Stockholm Meeting, 1953.
Mann, W. B., 1954, *J. Res. Nat. Bur. Stand.*, **53**, 277.
Meyer, S., 1945, *Anz. Akad. Wiss., Wien*, **8–9**, 25 (*Mitt. des Rad. Inst.* No. 542a).
Perry, W. E., 1936, *Brit. J. Radiol.*, **9**, 648.

---

† The ratio of the certified weights of $RaCl_2$ in the standards is 1·3102.

‡ Now Director, Radiological Protection Service, Sutton, Surrey.

Energy Levels of Mu-Mesic Atoms

It has been shown (Vachaspati 1954, Vachaspati and Shah 1954) that a nuclear charge distribution given by

$$Ze\rho = Ze\left[-(c-1)\delta^3(\mathbf{r}) + \frac{cB^2}{4\pi}\frac{e^{-Br}}{r}\right] \qquad \ldots\ldots(1)$$

consistently explains both the electron scattering and nuclear coulomb energy data when c is taken equal to 1·75 and B is related to the nuclear radius R of the uniform model by $(BR)^2 = 14{\cdot}8$.

The $2P_{3/2} \rightarrow 1S_{1/2}$ transition energy of a mu-mesic Pb atom provides an experimental result highly sensitive to the charge distribution. Hill and Ford (1954) have calculated this transition energy for a variety of nuclear models such that the charge density is everywhere positive. Their calculations exclude the case considered here, for our density given by equation (1) corresponds to negative charge at the centre and positive charge outside. We have calculated the above energy for this model. It has been stated (Cooper and Henley 1953) that, at least for light nuclei, two models would give the same result for electron scattering as well as mu-mesic transition energy, if the integral of the second moment of the charge density is the same in both cases. This criterion does not apply in our case as we are dealing with a heavy nucleus, and in addition, the integral in question has quite a different value for the given values of B and c from that for the uniform model.

The non-relativistic Schrödinger equation for the above model is

$$G'' + \left[k^2 + \lambda\left(\frac{1}{r} - \frac{ce^{-Br}}{r}\right) - \frac{l(l+1)}{r^2}\right]G = 0$$

where $G = R(r)/r$, $R(r)$ being the radial part of the wave function, $k^2 = 2\mu E/\hbar^2$, $\lambda = 2\mu Ze^2/\hbar^2$, E is the energy of the state and μ is the meson mass equal to 210 times the electron mass. From $Br = 0$ to $Br = \frac{1}{2}$ the equation is solved by expanding G into a series of increasing powers of Br, G starting as $(Br)^{l+1}$ for a given l. The value of G'/G is found at $Br = \frac{1}{2}$.

For a value of r sufficiently large for the exponential term in the potential to be neglected, the solution of the equation is given by

$$G = W_{\kappa\,[l(l+1)+1/4]^{1/2}}(\rho)$$

where W is the confluent hypergeometric function, $\kappa = \lambda/2(-k^2)^{1/2}$ and $\rho = 2(-k^2)^{1/2}r$ (Whittaker and Watson 1944). Values of G, G' and G'' are found with the help of this solution for $r \simeq 10^{-12}$ cm and the solution is carried back to $Br = \frac{1}{2}$ by point-by-point integration using the Runge–Kutta method. The value of G'/G at $Br = \frac{1}{2}$ obtained in this way is compared with the series expansion value, taking various values of E, until the solutions match, giving the correct value of the energy level.

In this manner, values for the 1S and 2P states are found for Pb, taking $R = 1{\cdot}2 \times 10^{-13}A^{1/3}$ cm. The spin–orbit interaction energy for the 2P state is calculated by the first-order perturbation theory using the above potential and point nucleus wave function, the fine structure splitting obtained being 0·19 MEV.

The $2P_{3/2} \rightarrow 1S_{1/2}$ transition energy found is 10·34 Mev − 4·53 Mev = 5·81 Mev. Relativistic corrections are expected to increase this value by about 2% bringing the transition energy to nearly 5·93 Mev. This compares favourably with the experimental value (Fitch and Rainwater 1953) of 6·0 Mev.

Thus the charge distribution (1) gives correct values for the electron scattering as well as for the transition energy of the mu-mesic Pb atom. It has the further advantage that it gives a smaller radius for these phenomena and a bigger one for coulomb energy (Vachaspati and Shah 1954).

I wish to thank Dr. Vachaspati for helpful discussions.

Physical Research Laboratory,
Ahmedabad 9,
India.
13th June 1955.

S. M. Shah.

Cooper, L. N., and Henley, E. M., 1953, *Phys. Rev.*, **92**, 801.
Fitch, V. L., and Rainwater, J., 1953, *Phys. Rev.*, **92**, 789.
Hill, D. L., and Ford, K. W., 1954, *Phys. Rev.*, **94**, 1617.
Vachaspati, 1954, *Phys. Rev.*, **93**, 502.
Vachaspati and Shah, S. M., 1954, *Proc. Phys. Soc.* A, **67**, 950.
Whittaker E. T., and Watson G. N., 1944, *Modern Analysis* (New York : Macmillan), Chap. 16.

REVIEWS OF BOOKS

Untersuchungen über die Elektronentheorie der Kristalle, by S. I. PEKAR. Pp. viii + 184. (Berlin: Akademie-Verlag, 1954.) DM 13.

This book represents in a systematic way the papers by the author on polarons (slow electrons in ionic crystals) as well as on F-centres. The theoretical methods underlying this treatment are described in a clear manner. The movement of the ions induced by the electronic motion is treated both classically and quantum mechanically. The main result in the theory of polarons leads to a very large effective mass. Unfortunately, the author did not know of recent developments in the theory of polarons which show that his method holds only for values of the interaction parameter α larger than 10. For smaller values of α another method which gives similar results to perturbation theory must be preferred (proof by variational technique). This makes the author's application of his method to alkali halides invalid; other substances may exist, however, for which the method may be applicable.

The section on F-centres is free from this objection. Here the author's values of the thermal ionization energy and of the width of the absorption bands are in good agreement with experiment. The book should be mainly of interest to theoretical physicists who wish to study Pekar's strong coupling approximation.

H. FRÖHLICH.

Molecular Theory of Gases and Liquids, by J. O. HIRSCHFELDER, C. F. CURTISS and R. B. BIRD. Pp. xxvi + 1219. (New York: John Wiley; London: Chapman and Hall, 1954.) 160*s*.

This book deals with the molecular theory of gases and liquids in a very comprehensive way. Little knowledge is assumed on the part of the reader, and the first two chapters consist of an account of simple kinetic theory, quantum mechanics and statistical mechanics. Apart from this introduction the book is divided into three parts, dealing with equilibrium properties of gases and liquids, non-equilibrium properties, and intermolecular forces. In each part the various theories are described in considerable detail and the results of a large number of numerical computations are given. For example the second virial coefficient of a gas is calculated for thirteen different types of potential function, corresponding partly to different degrees of elaboration of the theory, and partly to different types of molecule. In most cases a careful comparison with experimental results is made and the method of finding the force constants is described. Similar detailed treatment is given throughout the book, and this accounts for its considerable length. The treatment is not confined to classical gases and liquids, and there are chapters on the quantum theory of the equation of state and the quantum theory of transport phenomena. There is a useful section on the theory of flame propagation and also on the theory of detonation and the flow of propellant gases in rockets, subjects which were considerably developed during the war.

The authors state that they hope this book will be useful to several groups of people including students, and they have therefore incorporated problems at the end of some of the chapters. It is true that some sections could usefully be read by students, but the book's length and detail make it unsuitable for a text-book, since a student would normally read only a small fraction of the book. On the other hand this very detail will make it invaluable as a work of reference to many people; most sections, for example, provide information that could otherwise be acquired only by a great deal of time and labour in searching the literature.

There is one minor criticism to be made about the production of the book. Its sheer bulk and weight make it awkward to handle and carry about (it weighs over 2 kilos !) and it would have been more convenient to the reader if it could have been issued in three volumes, though this would presumably have made it more expensive. A. F. DEVONSHIRE.

Einführung in die Quantenelectrodynamik, by W. THIRRING. Pp. xii + 122. (Vienna : Franz Deuticke, 1955.) DM 17.50.

Apart from the Russian text of Akhieser and Berestetsky and the mimeographed notes of Dyson and others in private circulation, this is the first account of quantum electrodynamics developed entirely from the post-war point of view. The book is written for theoretical physicists who are beginning a study of modern quantum electrodynamics and pre-supposes a thorough knowledge of quantum mechanics including all of Chapter 5 of Dirac's book. After a brief chapter on the classical radiation theory, the author commences the quantum theory from the variational form of the action principle which has recently been formulated by Schwinger. The Heisenberg representation is used throughout and no mention is made of the interaction representation so that the development is from the Lagrangian rather than Hamiltonian point of view, a policy which with the reviewer concurs. After sections on non-interacting fields and on the uncertainty principle in field theory, the problem of interacting fields is tackled by the Feynman–Dyson expansion of the S-matrix which is then applied to the self-energy problems of electron and photon, and the anomalous moment of the electron and Lamb shift are briefly discussed. These problems of course require renormalization, and they are followed by a summary of the general renormalization question. Appendices discuss the properties of Dirac matrices and the various Green functions of the theory and there is also a set of examples which is unusual in a book at this level, but should prove very useful to the student. The author in his preface claims no completeness for the text on the references but one is nevertheless struck by some surprising omissions. The papers of Feynman which played so important a part in the development of the theory and contain the deepest discussion of it are not mentioned, nor is the fact that a paper of Schwinger quoted is the first of a comprehensive series or the subject. The two-body problem is given one paragraph from the graph summing point of view and though positronium is mentioned the papers solving its properties so well are not. The renormalization section does not refer to the general perturbation solution of this problem by Salam. There is also no index. In so brief a book it is unreasonable to expect all these matters to be discussed but it costs no space to mention their existence and to give proper references to papers which, after the book itself has been understood, should be the student's next task. These, however, are all faults of omission and the book can be recommended as a clear development of modern techniques, moreover the only consistently modern treatment which is easily available. S. F. EDWARDS.

Introduction to Experimental Physics, by W. B. Fretter. Pp. viii + 349. (London: Blackie and Son Ltd., 1955.) 35*s*.

According to the author's Preface this book has been compiled from notes taken at a course of lectures in experimental techniques given for some years to graduate students at the University of California. It is therefore not surprising to find that the techniques chosen for description are treated rather sketchily and in many cases inadequately from the point of view of the prospective user. The detailed instructions with which one had become familiar in books such as Strong's *Procedures in Experimental Physics* are given considerably less prominence in the present volume. On the other hand the condensed presentation and the shortness of the chapters makes for easy reading. On reaching the end of the book the reader may well be left with the feeling that he has accompanied Professor Fretter on a tour of the Physical Laboratories of the University of California. He will probably retain after a single reading the same sort of impressions that might be gathered from such a tour.

Most of the 32 chapters of the book are devoted to atomic and nuclear physics although many of the techniques described are useful in other fields. Thus the first chapters deal with selected topics in electrical and magnetic measurements, electronics, magnet design and vacuum techniques. The next group of chapters gives a condensed account of methods of particle and radiation detection. The material presented is obviously incomplete and is chosen mainly to acquaint the reader with the ' vocabulary ' of the subject and to suggest further reading. Chapters 16–20 are mainly descriptions of the large accelerating machines at Berkeley. Finally there are sections on cosmic-ray techniques, mass spectroscopy, β-ray, optical and microwave spectroscopy, molecular beams, magnetic resonance, pile techniques, x-ray diffraction and low temperature physics (with an average of about 12 pages each). The book concludes with a chapter on laboratory hazards (radiation exposure and toxicity of chemicals) and an interesting philosophical section on the design of experiments, which might well have prefaced the volume.

Professor Fretter has achieved his object of presenting a wide range of topics in readable form. The book is full of interesting pieces of information and is likely to remind most readers of some long-forgotten fact or trick as well as to suggest some new back-of-the-envelope calculation. Those who are giving or planning graduate courses on techniques will find the book useful both for its method of presentation and for the adequate but not overwhelming bibliographies at the end of each chapter. Altogether the author may be congratulated on having produced a volume which will both help and stimulate those who profess some interest in the arts of atomic and nuclear science.

W. E. BURCHAM.

Proceedings of the 1954 *Glasgow Conference on Nuclear and Meson Physics*, edited by E. H. Bellamy and R. G. Moorhouse. Pp. ix + 352. (London: Pergamon Press, 1955.) 63*s*.

The conference on nuclear physics held in Glasgow in July 1954 was sponsored by the International Union of Pure and Applied Physics. Partly for this reason the conference was attended by an unusually large number of distinguished visitors from overseas.

The formal business of the conference was divided into eight sections, each introduced by a survey paper; these were followed by specialized papers, totalling just over 100, and discussions. In the present volume of the Proceedings the editors have presented an extremely useful acount of the conference, an account which seems to have suffered little from the economies in text and diagrams which had inevitably to be made, although an index would have been helpful. The reports of the discussions, although brief, add considerably to the interest of the volume as a whole.

It is impossible in a short review to summarize the work of a large meeting but the scope of the papers may be gathered from the section headings. Part I (Nuclear Forces) opens with a survey article by H. S. W. Massey. Part II (Nuclear Data and Nuclear Models), which occupies nearly one third of the volume, is introduced by J. A. Wheeler and S. Devons and concludes usefully, after reports of many interesting experiments mainly on light nuclei, with a summary by V. F. Weisskopf. Part III is a brief account of Photodisintegration, with a review article by E. W. Titterton, and Part IV covers Beta and Gamma Ray Transitions, with an introductory lecture by Kai Siegbahn. The remainder of the volume deals with the sessions on high energy physics. The subject of π–Mesons (Part V) is surveyed by H. A. Bethe and is followed by reports of a session on Field Theory (Part VI) introduced by W. Heisenberg. This is mainly devoted to theoretical methods and is followedby a chapter (Part VII) on High Energy Experimental Techniques. The concluding section (Part VIII) is a survey of work up to June 1954 on Heavy Mesons and Hyperons; it is introduced by C. C. Butler.

Despite the wide range of topics covered certain unifying theories or hypotheses are obvious throughout the volume. The nuclear shell model and the nucleon isobar state are typical examples. Most of the contributions are distinguished by extreme clarity and concentration on essentials—a welcome result of the compression presumably exerted by the conference authorities. Among the large number of interesting articles will be found, for instance, news of a new theory of photodistintegration, some remarkable pictures of the operation of a bubble chamber, and an account of an attempt to co-ordinate theoretically the growing family of heavy mesons.

The ideal conference report would presumably appear in final form immediately after the conference. The present report has been delayed by some nine months, but much of the information contained in it, particularly the authoritative survey articles, is likely to be of value for several years to come. The editors and publishers have probably made the right decision in producing a volume of high quality which can be regarded as an addition to the literature of nuclear physics.

W. E. BURCHAM.

Neutron Diffraction, by G. E. BACON. Pp. ix + 299. (Oxford: University Press, 1955.) (Monographs on the Physics and Chemistry of Materials.) 35*s*.

It is only a decade since intense beams of neutrons from atomic piles have been available for the study of the structure of matter by neutron diffraction. Yet in that relatively short period a very large amount of work has been done and the technique has proven a most valuable one, both to the physicist and the chemist. All workers will be grateful to Dr. Bacon for this most timely discussion of the subject, especially so since the author treats the topic primarily from the practical viewpoint. Those workers who wish to find out what neutron diffraction is, the experimental techniques now employed and the kind of problems solved by its application will find that this book is ideal.

Following an introductory chapter on fundamental theory, the second and and third chapter deal with the scattering of neutrons by atoms in simple and more complex molecules and the diffraction of neutrons by crystals. In the next chapter the experimental techniques are surveyed. Then follows a discussion of the measurement of scattering amplitudes and in Chapter VI the principles of magnetic scattering are described. The author then deals with one of the most important applications of the technique, namely the determination of the positions of atoms of light elements in compounds, e.g. the position of hydrogen atoms in sodium hydride, the ammonium halides and potassium hydrogen fluoride. The remainder of the book is devoted mainly to the way in which neutron diffraction has been of value for the study of magnetic materials. Its importance in the study of ferro- and antiferromagnetic materials is very thoroughly surveyed. In the final chapter the results obtained by the application of neutron diffraction in gases, liquids and amorphous solids are discussed and an indication is given of present trends in this direction.

The book contains a large number of diagrams most of which are particularly clear and without unnecessary detail. The book is well up to the high standard of printing expected of the Oxford Press. The references, approaching 300, are well up to date ; there are many from journals published in 1953 and several from 1954. The author and publishers are to be complimented for ensuring that the book deals with so much very recent work, an important feature in a monograph dealing with a rapidly developing subject.

Practically no errors were observed but the reviewer does not claim to have checked more than a few of the values and equations which are quoted.

This is a book which should be on the bookshelves of both physicists and chemists, especially those interested in the structure of solid materials and magnetic substances, and it is highly recommended. R. S. NYHOLM.

CONTENTS OF SECTION B

PAGE

Dr. T. S. Moss. Measurements on p–n Junctions in Lead Sulphide 697

Dr. G. T. Wright. Fluorescence Excitation Spectra and Quantum Efficiencies of Organic Crystals 701

Dr. K. J. Standley and Dr. K. H. Reich. Ferromagnetic Resonance in Nickel and in some of its Alloys 713

Dr. D. J. Millard, Mr. P. C. Newman and Mr. J. W. Phillips. The Apparent Strength of Extensively Cracked Materials 723

Dr. G. Black. On the Automatic Design of Optical Systems 729

Dr. G. Liebmann. A Unified Representation of Magnetic Electron Lens Properties 737

Dr. R. Stratton. Field Emission from Semiconductors 746

Dr. A. Halperin and Dr. G. F. J. Garlick. The Absorption Spectrum of Excited Crystals of Cadmium Sulphide 758

Prof. R. E. Burgess. The A.C. Admittance of Temperature-Dependent Circuit Elements 766

Dr. G. F. Alfrey and Dr. J. B. Taylor. Electroluminescence in Single Crystals of Zinc Sulphide 775

Research Notes :

- Dr. Sampooran Singh. On the Jet Formation by Explosives with Lined Hemispherical Cavities 785
- Dr. B. K. P. Scaife. Isothermal Pressure Dependence of the Dielectric Properties of Eugenol, Glycerol and Water 790

Letters to the Editor :

- Prof. R. E. Burgess. Carrier Concentration Disturbances in Semiconductors 793

Reviews of Books 794

Contents of Section A 800

On the Barometer Effect on the Hard Component of the Cosmic Radiation

By H. TREFALL

Imperial College of Science and Technology, London†

Communicated by P. M. S. Blackett; MS. received 7th July 1955

Abstract. The interpretation of the observed partial correlation between the meson intensity at sea level and the barometric pressure, the other independent variables of the regression equation being the height of the 100 mb level and the stratospheric temperature, is discussed. It is shown that even though the decay effect due to changes in the height of the meson-producing layer is represented by a separate term in the regression equation, the barometer term does not represent a pure absorption effect but contains also a contribution from the μ–e decay. This decay contribution is due to the relativistic time dilation which makes the mean life of a μ-meson in the atmosphere depend on its energy loss and thereby causes its survival probability to change with changing sea-level pressure even if the height of the meson-producing layer remains constant. The decay effect is found to constitute about one third of the barometric effect observed in experiments performed at sea level. The simple total correlation between the meson intensity and the sea-level pressure is also discussed.

§ 1. INTRODUCTION

It is well known that a negative correlation exists between the cosmic-ray intensity at sea level and the barometric pressure, and the simple regression equation

$$(I-\bar{I})/\bar{I}=\beta(B-\bar{B}) \qquad \ldots\ldots(1)$$

can be used for a quantitative description of this effect. I denotes the cosmic-ray intensity and B the barometric pressure. The coefficient β will be referred to as the 'total barometer coefficient'.

This barometer effect was first observed by Myssowski and Tuwim (1928), and was interpreted as being due to the absorption of the radiation in the atmosphere. However, after it had been discovered that the greater part of the cosmic radiation at sea level consists of unstable particles (the μ-mesons), the observed barometer effect could no longer be regarded as a pure absorption effect. If the sea-level pressure increases, the height of the meson-producing layer will also increase, which has the effect of reducing the survival probability of the μ-mesons. Therefore, the observed barometer effect is partly due to absorption and partly due to the instability of the μ-mesons.

In order to separate the effects of absorption and decay, Duperier (1944) introduced the height of the meson-producing layer as a second independent variable in the regression equation, now writing

---

† On leave from Universitetet i Bergen, Bergen, Norway.

$$(I-\bar{I})/\bar{I}=\beta'(B-\bar{B})+\beta''(H-\bar{H}). \qquad \ldots\ldots(2)$$

The best correlation was obtained when the 100 mb level was taken to represent the mean level of meson production. The first term of equation (2) was then regarded as representing the pure absorption effect while the second term would represent the effect of the μ–e decay.

Later work by Duperier (1949, 1951) has shown that the representation of the atmospheric effects on the meson intensity at sea level is improved if the mean temperature between the 100 and 200 mb levels is introduced as a third independent variable in the regression equation, which then assumes the form

$$(I-\bar{I})/\bar{I}=\beta_1(B-\bar{B})+\beta_2(H-\bar{H})+\beta_3(T-\bar{T}). \qquad \ldots\ldots(3)$$

The interpretation of the third term of equation (3) has been discussed in detail in previous papers (Trefall 1955 a, b). The inclusion of this temperature term has no significant influence on the interpretation of the observed barometer effect. The coefficients β' and β_1 will be referred to as 'partial barometer coefficients'.

However, even if the experimental data are analysed according to equation (2) or (3), the barometer term still contains a contribution from the μ–e decay. The reason for this is the following: Because of the relativistic time dilation, the mean life of a μ-meson increases with its energy. The probability for decay between the place of production and sea level therefore depends not only on the height of production, but also on the energy with which the μ-meson was produced and on its energy loss in the atmosphere. As the energy loss increases with increasing sea-level pressure, the survival probability will decrease even if the height of production remains unchanged. Consequently, the partial barometer coefficients β' and β_1 will be greater than the true absorption coefficient. They will, however, be smaller than the total barometer coefficient β of equation (1) because this coefficient also includes the effect of the changes in height of the meson-producing layer which usually accompany changes in the sea-level pressure.

In the present paper an attempt is made to give a comprehensive analysis of the barometer effect on the meson component of the cosmic radiation at sea level. The absorption effect and the decay contributions to the total barometer coefficient β and to the partial barometer coefficient β_1 are calculated. The theoretical estimates are then compared with the available experimental results. Only vertically travelling μ-mesons are considered.

§ 2. THE ABSORPTION EFFECT

A shielded counter telescope or ionization chamber measures the integral meson intensity above a certain cut-off momentum which is determined by the amount of absorbing material in and above the recorder. The effect of a change in barometric pressure is equivalent to the combined effects of a change in cut-off momentum of the recorder and a change in the differential momentum spectrum of the μ-mesons arriving at the recorder. The change of cut-off momentum is due to the change in air mass above the recorder, whilst the change in the differential meson spectrum is caused by the above-mentioned decay effects.

Let $n(p)$ be the differential momentum spectrum of μ-mesons arriving from the vertical direction at sea level, and let $N(p)$ be the corresponding integral spectrum. The pure absorption effect caused by a change in the barometric pressure B is then given by

$$\frac{1}{N(p_c)}\frac{dN(p_c)}{dp_c}\frac{dp_c}{dB} = -\frac{n(p_c)}{N(p_c)}\frac{dp_c}{dB} \qquad \ldots\ldots(4)$$

where p_c is the cut-off momentum of the recording apparatus.

Formula (4) shows that reliable theoretical estimates of the pure absorption effect can be obtained only if the differential momentum spectrum of μ-mesons at sea level as well as the momentum loss of μ-mesons in air are accurately known. In these respects the absorption effect differs from all other atmospheric effects on the cosmic radiation. In the case of any other variation of atmospheric origin one measures what can be regarded as an effect integrated over the whole of the accepted momentum spectrum. Consequently, the magnitudes of those effects do not depend so critically on the exact form of the differential momentum spectrum of the meson component as does the absorption effect. For the same reason one can neglect the dependence of the momentum loss in air on the velocity of the μ-mesons when those other atmospheric effects are discussed. Only in the case of the absorption effect is it necessary to take into account the exact variation of the momentum loss with velocity.

Many measurements of the momentum spectrum of cosmic-ray mesons have been performed. Rossi (1948) has discussed the information which was available at that time, and we shall refer to his summary as the 'Rossi curve'. The later measurements agree very well with the Rossi curve except at very high momenta. The spectrum below $p = 0{\cdot}5$ kMev/c has recently been measured anew by Shamos (1954), who used an absorption method, and obtained results which are in good agreement with the Rossi curve. Measurements at higher momenta have been performed with magnetic counter spectrographs by Caro, Parry and Rathgeber (1951) and by Owen and Wilson (1955). In the region $0{\cdot}5$ kMev/$c < p < 10$ kMev/c the spectra of Caro *et al.* and of Owen and Wilson agree very well with the Rossi curve, but at higher momenta all three spectra differ. The spectrum of Caro *et al.* decreases most rapidly with increasing momentum, then comes the spectrum of Owen and Wilson and finally the Rossi curve.

For the purpose of the present investigation the following differential momentum spectrum has been adopted: The Rossi curve has been used as it stands for momenta less than $0{\cdot}5$ kMev/c whilst the empirical formula $n(p) = k(p+4)^{-3{\cdot}0}$, with p measured in kMev/c, has been used for momenta greater than $0{\cdot}5$ kMev/c. With a proper choice of the constant k the above formula very accurately reproduces the Rossi curve in the region $0{\cdot}5$ kMev/$c < p < 10$ kMev/c. For $p > 10$ kMev/c, where the Rossi curve and the spectra of Caro *et al.* and of Owen and Wilson begin to differ, our empirical formula strikes a good compromise between the last two of the above-mentioned spectra.

The factor dp_c/dB in equation (4) has been derived from that curve for the momentum loss of heavy charged particles per g cm^{-2} of air which has been published by Rossi (1952, p. 25). The absorption coefficient for the vertical meson component at sea level has been calculated and plotted against cut-off momentum as curve A of figures 1 and 2. The change in momentum loss with velocity has an appreciable effect on the shape of the curve.

§ 3. THE DECAY EFFECT WITH CONSTANT ATMOSPHERIC TEMPERATURE DISTRIBUTION

The effect of the μ–e decay is very simple if the atmospheric temperature distribution is independent of the sea-level pressure. An increase in the sea-level pressure then simply means that the whole atmosphere is lifted a certain distance upwards, which is $dh = dx_s/\rho_s$, where x_s is the atmospheric depth at sea level measured in g cm^{-2} and ρ_s is the density. Since all mesons must now travel this additional distance before they reach the recording apparatus, their new survival probability will be

$$w + dw = w \exp(-dh/L) \qquad \ldots\ldots(5)$$

where w denotes the original survival probability and L is the mean distance traversed by a meson before it decays. If the momentum p is measured in units of $m_\mu c$, where m_μ is the mass of the μ-meson, one finds that $L = pct_\mu$, where t_μ is the proper mean life of the μ-meson. After introducing in (5) the expressions for dh and L, one obtains the formula

$$\frac{1}{w}\frac{dw}{dx_s} = -\frac{1}{\rho_s pct_\mu} \qquad \ldots\ldots(6)$$

for the decay effect on mesons with sea-level momentum p. The corresponding integral effect is found by integration of (6) over the recorded part of the momentum spectrum with $n(p)$ as a weighting factor. The decay effect has been calculated as a function of the cut-off momentum and has been plotted as curve B in figure 1. The combined effect of absorption and decay is represented by curve C.

The total barometer effect has also been calculated by Olbert (1953) for this case, in which the atmospheric temperature distribution is independent of the sea-level pressure. Our results are found to be in good agreement with those of Olbert.

§ 4. THE DECAY EFFECT WITH CONSTANT HEIGHT OF THE REFERENCE LEVEL

When the height of a reference level, supposed to represent the mean level of meson production, is used as an independent variable in the regression equation, theoretical estimates of the decay contribution to the barometer effect must be computed for a model atmosphere in which the temperature distribution changes with sea-level pressure in such a way that the height of the reference level remains unchanged. Obviously, there is an infinite number of ways in which this condition can be fulfilled. For the purpose of the present investigation the following simple model has been used: The atmosphere consists of two independent layers, the troposphere and the stratosphere. In accordance with the properties of 'The International Standard Atmosphere' (see for example Berry, Bollay and Beers 1945) the stratosphere is assumed to be isothermal and the tropopause depth is taken to be 231 g cm^{-2}. The stratospheric temperature is assumed to be identical with the variable T of equation (3).

As all available experimental determinations of the partial barometer effect on the meson component have been made by means of the regression equation (3), the behaviour of our model atmosphere must be chosen so as to be in accordance with that equation. That implies that only the tropospheric temperature can be allowed to change with the sea-level pressure, for the stratospheric temperature has already been identified with the variable T of equation (3) and must therefore be regarded as being independent of B. Under such circumstances the height of the reference level can be independent of the sea-level pressure only if the height of the tropopause is also independent of B. The relation which must then exist between the tropospheric temperature and the sea-level pressure is determined by the equation

$$H_t = \int_{x_t}^{x_s} \frac{H_0(x)}{x}\,dx \qquad \ldots\ldots(7)$$

where $H_0(x)$ denotes the value of the atmospheric scale height at the depth x, and x_s and x_t denote the atmospheric depths at sea level and at the tropopause, respectively. Since the scale height is proportional to the atmospheric temperature, equation (7) can be regarded as determining the mean tropospheric temperature. The condition that the height of the tropopause (and thereby also the height of the reference level) shall be independent of x_s is then expressed mathematically by the equation

$$0 = \frac{H_0(x_s)}{x_s} + \int_{x_t}^{x_s} \frac{\partial H_0/\partial x_s}{x}\,dx \qquad \ldots\ldots(8)$$

found by differentiation of (7).

It will now be assumed that all μ-mesons reaching sea level have been produced above the tropopause. (It is not necessary to assume that they have all been produced at the same atmospheric depth.) The probability that a μ-meson shall not decay before it has reached sea level can then be written in the form

$$w = w(x, x_t, p)\,.\,w(x_t, x_s, p) \qquad \ldots\ldots(9)$$

where the factors on the right-hand side denote the survival probabilities from the place of production to the tropopause and from the tropopause to sea level, respectively. Since the stratospheric temperature is assumed to be independent of the sea-level pressure, the first factor on the right-hand side of (9) is independent of x_s.

If the momentum loss of a charged particle in air is assumed to be independent of its velocity, the general formula for the survival probability of a μ-meson travelling from the depth x_t to the depth x_s is

$$w(x_t, x_s, p) = \exp\left[-\int_{x_t}^{x_s} \frac{H_0(x)}{[p + a(x_s - x)]ct_\mu}\,\frac{dx}{x}\right] \qquad \ldots\ldots(10)$$

where a is the momentum loss per unit atmospheric depth, p is the sea-level momentum of the meson measured in units of $m_\mu c$ and $H_0(x)$ is the atmospheric scale height. Since only this second factor of (9) depends on the sea-level pressure the decay effect on mesons with sea-level momentum p is

$$\frac{1}{w(x_t, x_s, p)}\frac{\partial w}{\partial x_s} = -\frac{H_0(x_s)}{pct_\mu x_s} - \int_{x_t}^{x_s} \frac{\partial H_0/\partial x_s}{[p + a(x_s - x)]ct_\mu}\,\frac{dx}{x}\,. \qquad \ldots\ldots(11)$$

In this case no serious error is introduced by neglecting the variation of the momentum loss with velocity.

Some specific assumption must now be made about the tropospheric temperature variations, and the simplest one is that the temperature variations are independent of the atmospheric depth. Since $H_0(x)$ is proportional to the atmospheric temperature, this means that $\partial H_0/\partial x_s$ is independent of x. From equation (8) one then finds that

$$\frac{\partial H_0}{\partial x_s} = -\frac{H_0(x_s)}{x_s \ln (x_s/x_t)}\,. \qquad \ldots\ldots(12)$$

When (12) has been substituted in (11), the integration can be performed, and one obtains the formula

$$\frac{1}{w}\frac{\partial w}{\partial x_s}=\left[-\frac{ax_s}{p}+\frac{1}{\ln(x_s/x_t)}\ln\left(\frac{p+a(x_s-x_t)}{p}\right)\right]\frac{H_0(x_s)}{x_s(p+ax_s)ct_\mu} \qquad \ldots\ldots(13)$$

for the decay effect on mesons with sea-level momentum p.

The corresponding integral decay effect has been calculated as a function of the cut-off momentum of the meson recorder and has been plotted as curve B in figure 2. The combined effect of absorption and decay is represented by curve C. Comparison with curve A, which represents the pure absorption effect, shows that a significant decay contribution to the barometer effect remains even after the effects of changes in the height of meson production have been taken into account.

§ 5. COMPARISON WITH EXPERIMENTS

The available experimental values of the total and partial barometer coefficients are listed in the tables 1 and 2, respectively. In order to facilitate the comparison

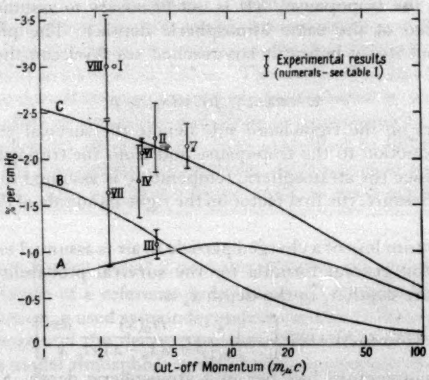

Figure 1. ' Total ' barometer effect. (No temperature variations.)
Curve A : Contribution from pure mass absorption.
Curve B : Contribution from μ–e decay.
Curve C : Combined effect of A and B.

Table 1. Experimental Values of the Total Barometer Coefficient β, determined by regression equation (1)

	Authors	Cut-off momentum ($m_\mu c$)	Barometer coefficient (% per cm Hg)
I.	Trumpy and Orlin (1941)	2·5	$-3{\cdot}0$
II.	Duperier (1949)	4·1	$-2{\cdot}22\pm0{\cdot}37$
III.	Duperier (1949)	4·1	$-1{\cdot}07\pm0{\cdot}16$
IV.	Rose (1951)	3·3	$-1{\cdot}75\pm0{\cdot}39$
V.	Rose (1951)	6·0	$-2{\cdot}13\pm0{\cdot}24$
VI.	Chasson (1954)	3·6	$-2{\cdot}07\pm0{\cdot}14$
VII.	Jacklyn (1954)	2·3	$-1{\cdot}63\pm0{\cdot}79$
VIII.	Jacklyn (1954)	2·3	$-2{\cdot}99\pm0{\cdot}56$

between theory and experiment, all the experimental results have been plotted together with the theoretical curves in figures 1 and 2. Each experimental point has been marked with a roman numeral which refers to the corresponding entry in the table.

5.1. *The Total Barometer Effect*

Inspection of figure 1 shows that there is a very great spread in the experimental values of the total barometer coefficient. This spread is too great to be completely accounted for by the statistical errors. Duperier (1949) has shown that it is due to changes in the general behaviour of the atmosphere from one period to another, for such changes will affect the decay contribution to the total barometer coefficient. The great difference between Duperier's two results (II and III of table 1) could thus be accounted for by the very different correlations which existed between the sea-level pressure and the height of the 100 mb level during the two periods of observation. The difference between Jacklyn's two results (VII and VIII of table 1) could also be explained in the same way.

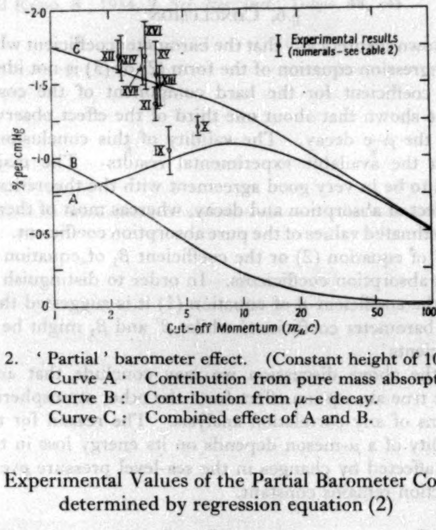

Figure 2. ' Partial ' barometer effect. (Constant height of 100 mb level).
Curve A · Contribution from pure mass absorption.
Curve B : Contribution from μ–e decay.
Curve C : Combined effect of A and B.

Table 2. Experimental Values of the Partial Barometer Coefficient β_1, determined by regression equation (2)

	Authors	Cut-off momentum ($m_\mu c$)	Barometer coefficient (% per cm Hg)
IX.	Duperier (1949)	4·1	$-1{\cdot}05 \pm 0{\cdot}16$
X.	Duperier (1951)	5·9	$-1{\cdot}21 \pm 0{\cdot}06$
XI.	Cotton and Curtis (1951)	3·5	$-1{\cdot}36 \pm 0{\cdot}11$
XII.	Trumpy and Trefall (1953)	2·3	$-1{\cdot}69 \pm 0{\cdot}11$
XIII.	Trumpy and Trefall (1953)	3·7	$-1{\cdot}49 \pm 0{\cdot}14$
XIV.	Dawton and Elliot (1953)	2·3	$-1{\cdot}67 \pm 0{\cdot}16$
XV.	Chasson (1954)	3·6	$-1{\cdot}56 \pm 0{\cdot}23$
XVI.	Wada and Kudo (1954)	3·1	$-1{\cdot}69 \pm 0{\cdot}23$
XVII.	Wada and Kudo (1954)	3·1	$-1{\cdot}62 \pm 0{\cdot}12$

However, even though the experimental points are so widely scattered, they are approximately evenly distributed about the theoretical curve C of figure 1. This indicates that the assumption that the atmospheric temperature distribution is independent of the sea-level pressure will lead to reasonable estimates of the total barometer coefficient if long periods of observation are considered.

5.2. *The Partial Barometer Effect*

Inspection of figure 2 shows that there are no statistically significant differences between the various experimental values of the partial barometer coefficient. The agreement between the experimental results and the theoretical curve C is also found to be very good. The experimental results do, however, differ significantly from the curve A for the pure absorption effect. It is thus quite clear that agreement between the theoretical estimates and the experimental values of the partial barometer coefficient can be obtained only if the contribution from the μ–e decay is taken into account.

§ 6. CONCLUSION

It has been shown theoretically that the barometer coefficient which is obtained by the use of a regression equation of the form (2) or (3) is not identical with the true absorption coefficient for the hard component of the cosmic radiation. Calculations have shown that about one third of the effect observed at sea level must be due to the μ–e decay. The validity of this conclusion is proved by comparison with the available experimental results. The majority of these results are found to be in very good agreement with the theoretical estimates for the combined effect of absorption and decay, whereas most of them differ significantly from the estimated values of the pure absorption coefficient. Consequently, the coefficient β' of equation (2) or the coefficient β_1 of equation (3) should not be referred to as absorption coefficients. In order to distinguish between these coefficients and the coefficient β of equation (1) it is suggested that β should be called 'the total barometer coefficient' whilst β' and β_1 might be called 'partial barometer coefficients'.

In view of the above discussion we may conclude that an experimental separation of the true absorption effect from the other atmospheric effects is not possible by means of any correlation analysis. The reason for this is that the survival probability of a μ-meson depends on its energy loss in the atmosphere and is therefore affected by changes in the sea-level pressure even if the height of meson production remains constant.

ACKNOWLEDGMENTS

The author wishes to thank Professor P. M. S. Blackett for the interest he has taken in this work and for the hospitality given at the Imperial College of Science and Technology. He is also very much indebted to the British Council for the scholarship which made possible his stay in the United Kingdom. The author is also grateful to Dr. H. Elliot for many valuable discussions. This work was begun at the University of Bergen, and the support given by L. Meltzer's Høyskolefond is gratefully acknowledged.

REFERENCES

BERRY, F. A., BOLLAY, E., and BEERS, R., 1945, *Handbook of Meteorology* (New York : McGraw-Hill).

CARO, D. E., PARRY, J. K., and RATHGEBER, H. D., 1951, *Aust. J. Sci. Res.* A, **4,** 16.

CHASSON, R. L., 1954, *Phys. Rev.*, **96,** 1116.

COTTON, E. S., and CURTIS, H. O., 1951, *Phys. Rev.*, **84,** 840.

DAWTON, D. I., and ELLIOT, H., 1953, *J. Atmos. Terr. Phys.*, **3,** 295.

DUPERIER, A., 1944, *Terr. Magn. Atmos. Elect.*, **49,** 1 ; 1949, *Proc. Phys. Soc.* A, **62,** 684 ; 1951, *J. Atmos. Terr. Phys.*, **1,** 296.

JACKLYN, R. M., 1954, *Aust. J. Phys.*, **7,** 315.

MYSSOWSKI, L., and TUWIM, L., 1928, *Z. Phys.*, **50,** 273.

OLBERT, S., 1953, *Phys. Rev.*, **92,** 454.

OWEN, B. G., and WILSON, J. G., 1955, *Proc. Phys. Soc.* A, **68,** 409.

ROSE, D. C., 1951, *Canad. J. Phys.*, **29,** 97.

ROSSI, B., 1948, *Rev. Mod. Phys.*, **20,** 543 ; 1952, *High-Energy Particles* (New York : Prentice-Hall Publishing Co.)

SHAMOS, 1954, *Phys. Rev.*, **96,** 1096.

TREFALL, H., 1955 a, *Proc. Phys. Soc.*, A, **68,** 625 ; 1955 b, *Ibid.*, **68,** 893.

TRUMPY, B., and ORLIN, J., 1941, *Arch. Math. Naturv.*, **44,** 99.

TRUMPY, B., and TREFALL, H., 1953, *Physica*, **19,** 636.

WADA, M., and KUDO, S., 1954, *J. Sci. Res. Inst., Tokyo*, **48,** 245.

Rotational Analysis of Bands of the $A^3\Pi_{0^+}$, $B^3\Pi_1$–$X^1\Sigma^+$ Systems of Indium Monofluoride

By R. F. BARROW†, D. V. GLASER† AND P. B. ZEEMAN‡

† Physical Chemistry Laboratory, University of Oxford
‡ Merensky Institute for Physics, University of Stellenbosch

MS. received 3*rd May* 1955

Abstract. A rotational analysis has been made of the 1,0, 0,0, 0,1 and 1,2 bands of the A–X system and of the 1,0, 0,0 and 0,1 bands of the B–X system of InF. Two branches are found in the A–X bands, and three in the B–X bands, confirming the identification of A as $^3\Pi_{0^+}$ and B as $^3\Pi_1$. The internuclear distance in the ground state, r_e'' is 1·985 Å.

§ 1. INTRODUCTION

THE object of recent spectroscopic and thermochemical studies of the halides of the Group IIIb elements has been to study as completely as possible the variations in bond properties throughout the group, from boron monofluoride to thallous iodide. This is a particularly attractive set of molecules for such a study, as not only the force constants and internuclear distances but also the bond energies may, in many cases at least, be determined with some precision. The present paper is primarily concerned with the determination of the internuclear distance in indium monofluoride.

§ 2. EXPERIMENTAL

The spectrum of indium monofluoride has been observed both in absorption (Welti and Barrow 1952) and in emission (Barrow, Jacquest and Thompson 1954). In the present work, the InF bands were excited in a hollow cathode discharge of the type described by Naudé and Hugo (1953). Helium gas at low pressure was used to carry the discharge; no auxiliary furnace was used as the hollow cathode was heated adequately by the discharge itself. Exposures were made on a 21-ft concave grating set up in a Paschen mounting at the University of Stellenbosch.

It was found in preliminary experiments that compressed pellets of aluminium trifluoride with finely divided indium metal in the cathode gave the InF bands with only rather low intensity. More intense spectra were obtained from compressed pellets of indium oxide, In_2O_3, with calcium fluoride and indium metal.

Bands of the C–X system (2300–2400 Å) were photographed in various orders up to the fifth order, and the triplet systems A, B–X (3100–3400 Å) up to the sixth order. Exposure times on Ilford Zenith plates were about two hours for the C–X system and 35 minutes for the triplet bands.

Exposures were also made in the visible and new infra-red regions of the spectrum in an attempt to observe systems similar to the visible and near infra-red

Table 1. System $\mathrm{A}^3\Pi_{0^+}-\mathrm{X}^1\Sigma^+$

	1,0 Band		0,0 Band		0,1 Band		1,2 Band	
J	R(*J*)	P(*J*)	R(*J*)	P(*J*)	R(*J*)	P(*J*)	R(*J*)	P(*J*)
0	31032·62		30465·99		29936·10			
1	33·18	31·56	66·53		36·69			
2	33·81	31·06	67·19		37·29			
3	34·39	30·58	67·79	63·95	37·92			
4	35·00	30·09	68·41	63·50	38·57			
5	35·63	29·67	69·08	63·09	39·23	33·31	29980·92	
6	36·31	29·21	69·76	62·64	39·95	32·85	81·70	
7	36·98	28·83	70·43	62·23	40·67	32·46	82·33	
8	37·65	28·45	71·21		41·40	32·13	83·08	
9	38·33	28·04	71·96		42·20	31·82	83·83	
10	39·08	27·65	72·71		43·02	31·52	84·64	
11	39·82	27·30	73·45	61·03	43·81	31·23	85·42	
12	40·57	26·96	74·32	60·78	44·65	31·00	86·31	
13	41·36	26·63	75·15	60·49	45·49	30·73	87·18	
14	42·12	26·33	75·99	60·28	46·39		88·07	
15	42·95		76·86	60·02	47·33		88·96	
16	43·81		77·76		48·28		89·95	
17	44·63		78·68		49·23		90·89	
18	45·50		79·62		50·23		91·89	
19	46·37		80·58		51·23	29·96$^{\mathrm{H}}$	92·93	71·82$^{\mathrm{H}}$
20	47·28		81·53		52·31	29·96$^{\mathrm{H}}$	93·93	71·82$^{\mathrm{H}}$
21	48·23		82·57		53·37	29·96$^{\mathrm{H}}$	95·02	71·82$^{\mathrm{H}}$
22	49·14		83·60		54·41	29·96$^{\mathrm{H}}$	96·10	71·82$^{\mathrm{H}}$
23	50·07		84·62	58·91$^{\mathrm{H}}$	55·58	29·96$^{\mathrm{H}}$	97·27	71·82$^{\mathrm{H}}$
24	51·26		85·69	58·91$^{\mathrm{H}}$	56·78		98·37	
25	52·02		86·78	58·91$^{\mathrm{H}}$	57·95		99·54	
26	53·05		87·90		59·12		30000·74	
27	54·04		89·03		60·35		01·96	
28	55·10		90·17		61·61		03·18	
29	56·15	24·21$^{\mathrm{H}}$	91·34		62·90	30·73	04·49	
30	57·25	24·21$^{\mathrm{H}}$	92·53		64·21	31·00	05·74	
31	58·32	24·21$^{\mathrm{H}}$	93·76		65·53	31·23	07·03	
32	59·40		95·01		66·91	31·52	08·38	
33	60·51		96·26	59·90	68·30	31·82	09·77	
34	61·64		97·55	60·02	69·70	32·13	11·16	
35	62·81		98·91	60·28	71·17	32·46		
36	63·98		500·28	60·49	72·72	32·85		
37	65·21		01·76	60·78	74·29	33·31		
38	66·45		02·65	61·11	75·39	33·81		
39	67·83		04·10		76·97	34·48		
40	68·59		05·50	61·38	78·48	34·48		
41	69·84		06·97	61·78	80·14	34·97		
42	71·23		08·39	62·23	81·70	35·54		
43	72·57		09·87	62·64	83·36	36·10		
44	73·82		11·33	63·09	85·03	36·69		
45	75·16		12·91	63·50	86·68	37·29		
46	76·53	26·33	14·39	63·95	88·42	37·92		
47	77·84	26·63	15·95	64·45	90·09	38·57		
48	79·27	26·96	17·55	64·94	91·89	39·23		80·92
49	80·61	27·30	19·17	65·39	93·70	39·95		81·70
50		27·65	20·77	65·99	95·46	40·67		82·33
51		28·04	22·37	66·53	97·27	41·40		83·08
52		28·45	24·11	67·19	99·18	42·20		83·83
53		28·83	25·76	67·79	30001·03	43·02		84·64
54		29·21	27·57	68·41	02·95	43·81		85·42
55		29·67	29·15	69·08	04·87	44·70		86·31
56		30·09	30·91	69·76	06·83	45·59		87·18
57		30·58		70·43	08·80	46·51		88·07
58		31·06		71·21	10·80	47·45		88·96
59		31·56		71·96		48·44		89·95
60		32·10		72·71		49·41		90·89
61		32·62		73·45		50·40		91·89
62		33·18		74·32		51·47		92·93
63		33·81		75·15		52·51		93·93
64		34·39		75·99		53·60		95·02
65		35·00		76·86		54·68		96·10
66		35·63		77·76		55·87		97·27
67		36·31		78·68		57·07		98·37
68		36·98		79·62		58·28		99·54
69		37·65		80·58		59·47		30000·74
70		38·33		81·53		60·70		01·96
71		39·08		82·57		62·04		03·18
72		39·82		83·60		63·26		04·49
73		40·57		84·62		64·63		05·74
74		41·36		85·69		65·94		07·03
75		42·12		86·78		67·35		08·38
76		42·95		87·90		68·74		09·77
77		43·81		89·03		70·21		11·16
78		44·63		90·17		71·61		

H indicates band head.

Table 2. System $B^3\Pi_1 - X^1\Sigma^+$

	1,0 Band			0,0 Band			0.1 Band		
	R(*J*)	Q(*J*)	P(*J*)	R(*J*)	Q(*J*)	P(*J*)	R(*J*)	Q(*J*)	P(*J*)
0									
1									
2									
3									
4									
5							30747·57		
6				31278·41		71·29	48·48		
7				79·03		70·91	49·04	44·69	40·83
8				79·83		70·55	49·86	44·95	40·50
9				80·55	75·18	70·21	50·64	45·17	40·20
10	31847·58	41·58		81·44	75·46	69·91	51·53	45·50	39·92
11	48·26	41·79		82·04	75·74	69·59	52·31	45·75	39·74
12	48·99	41·99	35·45	82·96	75·86	69·34	53·22	46·11	
13	49·74	42·23	35·16	83·78	76·22	69·14	53·92	46·39	
14	50·55	42·49	34·87	84·60	76·48	68·85	54·98	46·80	
15	51·38	42·76	34·62	85·52	76·93		55·95	47·17	
16	52·25	43·07	34·37	86·43	77·21		57·00	47·57	
17	53·13	43·38	34·14	87·36	77·62		57·86	48·07	
18	53·96	43·76	33·89	88·32	78·00		58·87	48·48	
19	54·88	44·07	33·76	89·32	78·41		59·92	49·04	
20	55·77	44·47	33·60	90·30	78·91		60·99	49·56	38·68$^{\mathrm{H}}$
21	56·68	44·82		91·33	79·38		62·08	50·09	38·68$^{\mathrm{H}}$
22	57·65	45·25		92·43	79·83		63·23	50·64	38·68$^{\mathrm{H}}$
23	58·67	45·64		93·46	80·36	67·85$^{\mathrm{H}}$	64·45	51·23	38·68$^{\mathrm{H}}$
24	59·61	46·07		94·53	80·92	67·85$^{\mathrm{H}}$	65·51	51·92	
25	60·57	46·53		95·65	81·44	67·85$^{\mathrm{H}}$	66·74	52·53	
26	61·64	46·99	32·94$^{\mathrm{H}}$	96·77	82·04	67·85$^{\mathrm{H}}$	67·96	53·22	
27	62·67	47·47	32·94$^{\mathrm{H}}$	97·93	82·61		69·24	53·92	
28	63·84	48·03	32·94$^{\mathrm{H}}$	99·12	83·27		70·52	54·67	
29	64·89	48·52	32·94$^{\mathrm{H}}$	300·29	83·91		71·80	55·40	39·74
30	65·88	49·09		01·60	84·60		73·17	56·22	39·92
31	66·97	49·68		02·76	85·30		74·54	57·00	40·20
32	68·15	50·28		03·95	86·00		75·92	57·86	40·50
33	69·21	50·84		05·26	86·74	68·85	77·39	58·70	40·83
34	70·38	51·48		06·58	87·45	69·14	78·77	59·58	41·19
35	71·74	52·16		07·99	88 32	69·34		60·54	41·55
36	73·01	52·83		09·33	89·10	69·59		61·48	41·96
37	74·14	53·48	33·60	10·67	89·91	69·91		62·46	42·39
38	75·26	54·15	33·76	12·03	90·79	70·21		63·44	42·84
39	76·49	54·88	33·89	13·43	91·64	70·55		64·45	43·33
40		55·66	34·14	14·87	92·53	70·91		65·51	43·85
41		56·38	34·37	16·33	93·46	71·29		66·57	44·37
42		57·15	34·62	17·85	94·46	71·69		67·69	44·95
43		57·95	34·87	19·36	95·37	72·11		68·83	45·50
44		58·75	35·16	20·84	96·39	72·59		69·94	46·11
45		59·61	35·45	22·36	97·38	73·07		71·14	46·80
46		60·42	35·75	23·96	98·41	73·52		72·33	47·57
47		61·32	36·10	25·61	99·46	74·05		73·58	48·07
48		62·15	36·41		300·53	74·62		74·82	48·92
49		63·05	36·79		01·60	75·18		76·12	49·56
50		64·04	37·20		02·76	75·74		77·39	50·37
51		64·89	37·54		03·95	76·22		78·77	51·23
52		65·88	38·04		05·08	76·93		80·15	51·92
53		66·86	38·44		06·29	77·62		81·51	52·91
54		67·78	38·93		07·49	78·41		82·89	53·80
55		68·77	39·41		08·70	79·03		84·39	54·67
56		69·81	39·92		09·96	79·83		85·86	55·61
57		70·88	40·42		11·25	80·55		87·27	56·60
58		72·00	40·91		12·57	81·44		88·90	57·56
59		73·01	41·47		13·90	82·04		90·40	58·70
60		74·14	42·14		15·23	82·96		91·95	59·58
61		75·26	42·69		16·61	83·78		93·55	60·54
62		76·49			17·85	84·30		95·19	61·81
63					19·36	85·52		96·77	62·90
64					20·84	86·43		98·55	64·09
65					22·29	87·36			65·23
66					23·74	88·32			66·57
67					25·25				67·69
68									68·83
69									70·23
70									71·55
71									72·91
72									74·27
73									75·62
74									77·03
75									78·47

systems of AlF (Naudé and Hugo 1953, 1954, Barrow and Rowlinson 1954). No such bands were found, even though in later experiments indium trifluoride was prepared separately, mixed with indium metal, and heated inside the hollow cathode as before.

The rotational lines were measured against Fe arc lines whose wavelengths were taken from the M.I.T. tables (1939). Wave numbers of the lines analysed are given in tables 1 and 2.

§ 3. ANALYSIS

The rotational structure of bands of the C–X system was not resolved, even on the fifth order plates, but many of the lines of the triplet bands are well resolved, and the fourth order plates proved the most useful. Microphotometer traces of parts of the 0, 1 bands of the A, B–X systems are illustrated in figures 1 and 2.

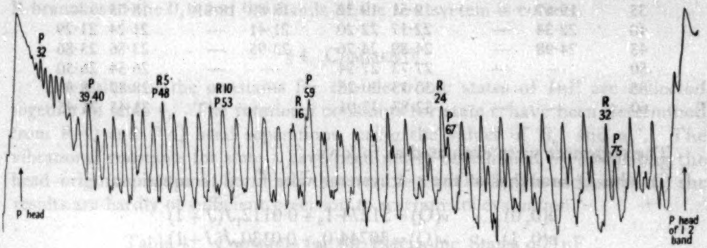

Figure 1. The 0, 1 band of system A–X.

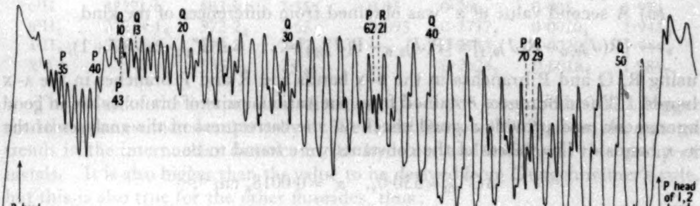

Figure 2. The 0, 1 band of system B–X.

The analysis started with the 0, 0 and 0, 1 bands of the B–X system. The Q branches were easily recognized, and their approximate J numberings were determined from the first differences. The R lines are well resolved only at low J values, and the P lines only at high J values, where they return from the head, so that the correct J numbering had to be found by trial and error from possible sets of $\Delta_1 F'(J)$. Only one arrangement gave sets identical within experimental error for the two bands. A selection of values of $\Delta_1 F'(J)$ is given in table 3; the analysis rests essentially upon these results, but is confirmed by the values of $\Delta_1 F''(J)$ obtained from the 0, 0 and 1, 0 bands of the B–X system, analysed later. Preliminary values of the ground-state rotational constants were then evaluated from the rather small selection of values of $\Delta_2F''(J)$ available, using $D=4B^3/\omega^2$: these were used to calculate values of $\Delta_2F''(J)$ for the analysis of the 1, 0 and 0, 1 bands of the A–X system.

Table 3. Combination Differences

	$\Delta_1F'(J)$				$\Delta_1F''(J)$			
	R(*J*)–Q(*J*)		Q(*J*+1)–P(*J*+1)		R(*J*)–Q(*J*+1)		Q(*J*)–P(*J*+1)	
J	0, 0	0, 1	0, 0	0, 1	0, 0	1, 0	0, 0	1, 0
10	5·98	6·03	6·15	6·01	5·70	5·79	5·87	—
15	8·59	8·78	—	—	8·31	8·31	—	8·39
20	11·39	11·43	—	11·41	10·92	10·95	—	—
25	14·21	14·21	14·19	—	13·61	13·58	13·59	13·59
30	17·00	16·95	—	16·80	16·30	16·20	—	—
35	19·67	—	19·51	19·52	18·89	18·91	18·73	—
40	22·34	—	22·17	22·20	21·41	—	21·24	21·29
45	24·98	—	24·89	24·76	23·95	—	23·86	23·86
50	—	—	27·73	27·54	—	—	26·54	26·50
55	—	—	30·13	30·25	—	—	28·87	28·85
60	—	—	32·83	33·01	—	—	31·45	31·45

The constants were evaluated as follows:

(i) The Q branches of the B–X systems were fitted to equations:

$$\mathrm{B}(0,0) \qquad \nu(\mathrm{Q}) = 31274\cdot1_8 + 0\cdot0112_1 J(J+1)$$
$$\mathrm{B}(0,1) \qquad \nu(\mathrm{Q}) = 30744\cdot0_3 + 0\cdot0130_9 J(J+1)$$
$$\mathrm{B}(1,0) \qquad \nu(\mathrm{Q}) = 31840\cdot5_7 + 0\cdot0091_8 J(J+1)$$

Thus $\Delta G'_{1/2}=566\cdot3_9$, $\Delta G''_{1/2}=530\cdot1_5$, $\alpha'=0\cdot0020_3$, $\alpha''=0\cdot0018_8\ \mathrm{cm}^{-1}$.

(ii) A second value of α'' was obtained from differences of the kind

$$[\mathrm{R}(J)_{0,0}-\mathrm{R}(J)_{0,1}]=[\mathrm{P}(J)_{0,0}-\mathrm{P}(J)_{0,1}]=\ldots=\Delta G''_{1/2}-\alpha''J(J+1),$$

using R, Q and P branches in the B–X bands and R and P branches in the A–X bands. The differences obtained from the various pairs of branches are in good agreement, and provide a good check on the correctness of the analyses of the A–X bands. The values of the constants were found to be:

$$\Delta G''_{1/2}=530\cdot0_8, \quad \alpha''=0\cdot0018_6\ \mathrm{cm}^{-1}.$$

(iii) The value of B_0'' was then evaluated for $v''=0$ and $v''=1$ from all reliable values of $\Delta_2F''(J)/(J+\frac{1}{2})$, using $\alpha''=0\cdot0018_6$ and $D''=2\cdot5\times10^{-7}\ \mathrm{cm}^{-1}$ (determined from Kratzer's relation). We obtain $B_0''=0\cdot2615_4\ \mathrm{cm}^{-1}$.

(iv) The remaining rotational constants were found as follows: B_e'', B'' were obtained from B_0'' and the value of α'' obtained in (ii). The constants for state B were derived from the results of (i). The constants for state A were obtained in two ways:

(*a*) From the sums R(*J*−1)+P(*J*) which gave

$$\mathrm{A}(0,1) \qquad \nu_0=29935\cdot5_8 \qquad \Delta B=0\cdot0126_4\ \mathrm{cm}^{-1}$$
$$\mathrm{A}(0,0) \qquad \nu_0=30465\cdot5_2 \qquad \Delta B=0\cdot0108_2$$
$$\mathrm{A}(1,0) \qquad \nu_0=31032\cdot1_7 \qquad \Delta B=0\cdot0088_1$$

thus $\Delta G'_{1/2}=566\cdot6_5$, $\alpha'=0\cdot0019_9\ \mathrm{cm}^{-1}$.

(*b*) From the differences $[R(J-1)_{1,0}-R(J-1)_{0,0}]$, $[P(J+1)_{1,0}-P(J+1)_{0,0}]$, which lead to $\Delta G'_{1/2}=566{\cdot}6_8$, $\alpha'=0{\cdot}0020_5\,\mathrm{cm}^{-1}$. The means of the estimates from (*a*) and (*b*) were accepted.

(v) The differences $[R(J)_{1,0}-R(J)_{1,2}]$, $[P(J)_{1,0}-P(J)_{1,2}]$ were used to analyse the 1, 2 band of the A–X system, and to derive

$$\Delta G''(0,2)=1054{\cdot}8_9,\quad \alpha''=0{\cdot}0018_6\,\mathrm{cm}^{-1}.$$

(vi) Values of the internuclear distances were obtained using

$$I=16{\cdot}8611/B\ \mathrm{a.m.u.\,\AA^2},\quad \text{and}\quad \mu=16{\cdot}3081\ \mathrm{a.m.u.}$$

A small perturbation in the R branch was detected at about $J=38$ in $v=0$ of $\mathrm{A}^3\Pi_{0^+}$. The effect in the P branch could not be observed with certainty, as the lines in this region returning from the head are not well resolved (see figure 1). However, it seems certain that the perturbation does in fact arise in the upper state. The observation provides a check that the relative numbering of the R branches of the 0, 0 and 0, 1 bands of the A–X system is correct.

§ 4. COMMENTS

The values of the constants for the electronic states of InF are collected together in table 4. The rotational constants for state C have been determined from R–Q and P–Q head separations, using the values of B_e'' and α_e''. The vibrational constants for state A have been newly determined by calculating the head–origin separations; it is likely that a cubic term in $G(v)$ is necessary, but the results are hardly of sufficient precision to warrant its evaluation.

Table 4. Constants for the Electronic States of InF

State	T_0	ω_e	$x_e\omega_e$	$y_e\omega_e$	B_e	α	r_e (Å)
D	(47536)	535	—	—	—	—	—
$\mathrm{C}^1\Pi$	42771·6	463·9	7·35	−0·05	$0{\cdot}266_4$	$0{\cdot}005_0$	$1{\cdot}97_0$
$\mathrm{B}^3\Pi_1$	$31274{\cdot}1_8$	$572{\cdot}2_5$	2·63	−0·095	$0{\cdot}2737_8$	$0{\cdot}0020_4$	$1{\cdot}943_3$
$\mathrm{A}^3\Pi_{0^+}$	$29935{\cdot}5_8$	575·2	$3{\cdot}67_6$	—	$0{\cdot}2733_6$	$0{\cdot}0020_2$	$1{\cdot}944_8$
$\mathrm{X}^1\Sigma^+$	0	$535{\cdot}3_5$	$2{\cdot}6_{35}$	—	$0{\cdot}2624_7$	$0{\cdot}0018_6$	$1{\cdot}984_7$

The value of the internuclear distance, $r_e''=1{\cdot}985$ Å is about 0·12 Å bigger than the value estimated empirically by Welti and Barrow (1952), from the general trends in the internuclear distance in the hydrides and halides of this group of metals. It is also bigger than the value to be derived from Guggenheimer's rule, but this is also true for the other fluorides, thus:

	r''_{obs}	r''_{calc}	$\Delta_{\mathrm{o-c}}$
BF	1·262	1·197	0·065
AlF	1·655	1·559	0·096
GaF		1·697	
InF	1·985	1·853	0·132

If GaF is regular, we should expect $r''=1{\cdot}81$ Å.

The second point concerns the difference between the internuclear distances in InF and InCl. Froslie and Winans (1947) derived $r_e''(\mathrm{InCl})=2{\cdot}315$ Å, so that $r_e''(\mathrm{InCl})-r_e''(\mathrm{InF})=0{\cdot}33$ Å. In the case of the boron and aluminium compounds, the differences are bigger, $0{\cdot}45_4$ and $0{\cdot}48_3$ Å, respectively. If the present value for InF is correct, it seems possible that the value for InCl is somewhat too low. This would suggest that the rotational analysis of the InCl bands may not be quite correct; a careful examination of the published measurements has led to no definite conclusions, but it is noteworthy that the plot of $\Delta_2F''(J)/(J+\frac{1}{2})$ for this molecule departs from linearity in an unusual way, and that the limiting slope gives a value of the centrifugal stretching constant D'' very different from that obtained from Kratzer's relation $D=4B^3/\omega^2$, which usually gives reliable results. The view that Froslie and Winan's value for r''(InCl) is a little too low is supported by the electron diffraction observations of Brode (1940), who obtained $r''(\text{InCl})=2{\cdot}42$ Å.† A similar difficulty arises in the rotational analysis of GaCl (Levin and Winans 1951); in this case a further problem arises in that a perturbation is apparently found in the ground state. Such a perturbation is not to be expected, and these anomalies in the published analysis, taken together with the difficulties arising from the isotope effect on this molecule, lead us to suspect that this analysis as well may need revision.

Some light will be thrown on these questions by a study of the rotational structure of the $^3\Pi-{}^1\Sigma^+$ bands of GaF now in progress.

REFERENCES

BARROW, R. F., JACQUEST, J. A. T., and THOMPSON, E. W., 1954, *Proc. Phys. Soc.* A, **67**, 528.
BARROW, R. F., and ROWLINSON, H. C., 1954, *Proc. Roy. Soc.* A, **224**, 134.
BRODE, H., 1940, *Ann. Phys. Lpz.*, **37**, 344.
FROSLIE, H. M., and WINANS, J. G., 1947, *Phys. Rev.*, **72**, 481.
LEVIN, F. K., and WINANS, J. G., 1951, *Phys. Rev.*, **84**, 431.
M.I.T. Wavelength Tables, 1939 (London : Chapman and Hall).
NAUDÉ, S. M., and HUGO, T. J., 1953, *Canad. J. Phys.*, **31**, 1106 ; 1954, *Ibid.*, **32**, 246.
WELTI, D., and BARROW, R. F., 1952, *Proc. Phys. Soc.* A, **65**, 629.

† *Note added in proof* (16. 9. 55). This is now confirmed by observations of the spectrum of InCl in the microwave region, which lead to $re''=2{\cdot}4012\pm0{\cdot}0001$ Å (Barrett, A. H., and Mandel, M., *Phys. Rev.*, 1955, **99**, 666).

The Electronic Spectrum of Aromatic Molecules
VI: The Mesomeric Effect

By J. N. MURRELL
Department of Theoretical Chemistry, University of Cambridge

MS. received 4*th May* 1955 *and in final form* 22*nd June* 1955

Abstract. The mesomeric effect is discussed in terms of a mixing of the 'locally excited' states of the hydrocarbon, and the 'electron transfer' states. If the substituent behaves as an electron donor, the energies of the lowest electron transfer states can be estimated from the ionization potential of the substituent.

A substituent which has a small ionization potential will be expected to exert a strong mesomeric effect, since the electron transfer states have low energies. These states may give rise to new bands in the spectrum. The spectrum of aniline is discussed in these terms, and the band at 2350 Å is attributed to an excitation to an electron transfer state.

If the ionization potential is large, then, in general, there will be only a weak mesomeric effect. In this case it is only possible to estimate the change in energy of the lowest electronic states. A method is described whereby the inductive effect can be allowed for, and this is applied to find the mesomeric effect of a methyl substituent from the various methylated benzenes.

---

§ 1. INTRODUCTION

THE mesomeric effect is exemplified by the tendency for the electrons of a substituent group to enter into conjugation with the π-electrons of an unsaturated molecule. One result of this conjugation is to bring about a change in the electronic spectrum of the molecule, the bands usually being shifted to longer wavelengths.

In paper III of this series (Murrell and Longuet-Higgins 1955, to be referred to as III) the effect of an inductive substituent on the spectrum of an aromatic hydrocarbon was considered. In this case, the substituent just alters the potential under which the π-electrons of the hydrocarbon move. In paper V (Longuet-Higgins and Murrell 1955) we dealt with the special case of the substituent itself being an unsaturated hydrocarbon. Both electron interaction and the mesomeric effect are important for this type of substituent, but on the molecular orbital model there is no inductive effect.

In this paper, substituent groups will be considered which contain no unsaturated bonds. With this restriction the excited states of the substituent will tend to have a rather high energy, and hence electron interaction will be of secondary importance. Furthermore, it will be assumed that the inductive effect is small, or that it can be allowed for by the method of paper III.

§ 2. METHOD

It was shown in V that in order to predict the change in the electronic spectrum of a hydrocarbon due to the mesomeric effect of a substituent, the following information is required: (i) The energies and wave functions of the electronic states of the hydrocarbon. These are called 'locally excited' states. (ii) The energies and wave functions of the states which arise from the transfer of an electron from the substituent to the hydrocarbon, or from the hydrocarbon to the substituent. These are the 'electron transfer' states. (iii) The resonance integral $\beta_{rs} = \int \phi_r(i) H_{(i)} \phi_s(i) d\tau_i$, where ϕ_r and ϕ_s are the atomic orbital functions associated with the atoms forming the bond between the hydrocarbon and the substituent.

If the self-consistent molecular orbitals of the hydrocarbon are written $\psi_1 \ldots \psi_p$, and those of the substituent $\theta_1 \ldots \theta_q$, then the locally excited states of the hydrocarbon will be linear combinations of singly excited configurations of the type $\psi_k^{-1}\psi_l$, and those of the substituent will be combinations of the configurations $\theta_m^{-1}\theta_n$ (see papers I and II in this series, Dewar and Longuet-Higgins 1954, Pople 1955.) The electron transfer states are of two kinds, according as the electron is transferred from the hydrocarbon R to the substituent S, or from the substituent to the hydrocarbon. The former will consist of configurations of the type $\psi_k^{-1}\theta_n$ and will be written R→S, and the latter of configurations $\theta_m^{-1}\psi_l$, written S→R.

Table 1 summarizes the interactions which occur between the states, when the hydrocarbon and the substituent come together to form a bond.

Table 1. A Summary of the Types of Interaction which occur between the Electronic States when R and S come together to form a Bond (see III and V)

	Locally excited states of R Ψ	Locally excited states of S Θ	Electron transfer states R → S	Electron transfer states S → R
Ψ	Inductive effect of substituent	Electron interaction	Mesomeric effect	Mesomeric effect
Θ	Electron interaction	Inductive effect of hydrocarbon	Mesomeric effect	Mesomeric effect
R → S	Mesomeric effect	Mesomeric effect	Inductive effect and electron interaction	No interaction
S → R	Mesomeric effect	Mesomeric effect	No interaction	Inductive effect and electron interaction

If the substituent can be classified either as an electron donor or an acceptor with reference to the hydrocarbon, then a further simplification arises, since one kind of electron transfer state will have a high energy and can be neglected. If the substituent is an electron acceptor we can neglect the states S→R, if it is an electron donor, we can neglect R→S.

With this approximation, and with a substituent for which electron interaction and the inductive effect can be either ignored or treated separately, the problem reduces to an evaluation of the interaction between the locally excited states of the hydrocarbon and one set of electron transfer states, which set being determined by the character of the substituent.

The energy of the electron transfer configuration $\theta_k^{-1}\psi_l$ is given by

$$E_{k,l}=E_l-E_k-\iint \theta_k^2(i)\frac{1}{r_{ij}}\psi_l^2(j)d\tau_{ij} \qquad \ldots\ldots(1)$$

where E_k and E_l are the energies of the self-consistent orbitals θ_k and ψ_l respectively. The energies and wave functions of the molecular orbitals of the substituent are often uncertain; however, if we restrict attention to the electron transfer state of lowest energy, then E_k will be given, to a good approximation, by the ionization potential of the molecule HS. The energy E_l can be obtained as the electron affinity of the hydrocarbon RH, or can usually be calculated with moderate accuracy. The integral in expression (1) can be evaluated using the approximations of Pople (1953). The molecular orbital of the hydrocarbon is expanded in terms of atomic orbital functions, and all integrals neglected except those of the form

$$\iint \theta_k^2(i)\frac{1}{r_{ij}}\phi_t^2(j)d\tau_{ij}.$$

These integrals are replaced by the interaction energy of point charges centred on the substituent and on the carbon atom ‘t’. This will be a good approximation if the substituent group is small and compact. The energies of the configurations $\psi_k^{-1}\theta_l$ are obtained in a similar way.

The matrix elements of the interaction between the electron transfer configurations and the locally excited configurations of the hydrocarbon are evaluated from the following formulae:

$$\int \psi_k^{-1}\theta_l H\psi_m^{-1}\psi_n d\tau=\delta_{k,m}\int \theta_l(i)H_{(i)}\psi_n(i)d\tau_i$$

$$\int \theta_k^{-1}\psi_l H\psi_m^{-1}\psi_n d\tau=-\delta_{l,n}\int \theta_k(i)H_{(i)}\psi_m(i)d\tau_i.$$

The interactions with the ground state χ_0 are given by

$$\int \psi_k^{-1}\theta_l H\chi_0 d\tau=\sqrt{2}\int \psi_k(i)H_{(i)}\theta_l(i)d\tau_i$$

$$\int \theta_k^{-1}\psi_l H\chi_0 d\tau=\sqrt{2}\int \theta_k(i)H_{(i)}\psi_l(i)d\tau_i.$$

The integral $\int\theta_p(i)H_{(i)}\psi_q(i)d\tau_i$ can be reduced to $C_{qr}\int\theta_p(i)H_{(i)}\phi_r(i)d\tau_i$, where C_{qr} is the coefficient of the *r*th atomic orbital in the expansion of the ψ_q, the substituent being attached to carbon atom ‘r’. If as we have suggested, we consider only the electron transfer states of lowest energy, then these will involve only one molecular orbital of the substituent—the highest filled orbital for the states S→R, and the lowest vacant orbital for the states R→S. All the interactions can then be expressed in terms of one parameter, namely

$$\beta_{\mathrm{RS}}=\int \theta(i)H_{(i)}\phi_r(i)d\tau_i.$$

Two examples will now be given, which will illustrate the scope and limitations of this theory. The amino group will be chosen as an example of a substituent which has a strong mesomeric effect, and the methyl group as one which has a weak effect.

§ 3. A STRONG MESOMERIC EFFECT

Let us first consider the interactions which occur between the locally excited states of a benzene molecule, and the electron transfer states which arise from taking an electron out of the highest filled orbital of the substituent, and placing it in either of the degenerate vacant orbitals of the benzene. These states will be favoured for an amino substituent, which has a tendency to donate electrons to the hydrocarbon. The locally excited states of benzene have wave functions and energies as follows:

Wave function	Energy (ev)
$\Psi_{\beta'} = \sqrt{\frac{1}{2}}(\psi_3^{-1}\psi_4 - \psi_2^{-1}\psi_5)$	6·74
$\Psi_{\beta} = \sqrt{\frac{1}{2}}(\psi_3^{-1}\psi_5 + \psi_2^{-1}\psi_4)$	6·74
$\Psi_{p} = \sqrt{\frac{1}{2}}(\psi_3^{-1}\psi_4 + \psi_2^{-1}\psi_5)$	6·14
$\Psi_{\alpha} = \sqrt{\frac{1}{2}}(\psi_3^{-1}\psi_5 - \psi_2^{-1}\psi_4)$	4·88

ψ_2 and ψ_3, ψ_4 and ψ_5 are the two pairs of degenerate molecular orbitals of benzene (see I).

The energies of the electron transfer states $\theta^{-1}\psi_4$ and $\theta^{-1}\psi_5$ have been calculated using the point charge approximation, taking the bond length of benzene to be 1·39 Å, and the bond joining the substituent to the hydrocarbon to be 1·46 Å. They have the following values:

$$E(\theta^{-1}\psi_4) = I - A - 4{\cdot}84 \text{ ev}, \qquad E(\theta^{-1}\psi_5) = I - A - 6{\cdot}03 \text{ ev}.$$

I is the ionization potential of the substituent, and A is the electron affinity of benzene.

The interactions which occur between the electronic states are shown in table 2.

Table 2. The Matrix Elements of the Interactions between the Electronic States due to the Mesomeric Effect

$$\begin{array}{c|ccc|}
 & \Psi_\alpha & \Psi_\beta & \theta^{-1}\psi_4 \\
\hline
\Psi_\alpha & E_\alpha & 0 & \sqrt{\frac{1}{6}}\beta_{RS} \\
\Psi_\beta & 0 & E_\beta & -\sqrt{\frac{1}{6}}\beta_{RS} \\
\theta^{-1}\psi_4 & \sqrt{\frac{1}{6}}\beta_{RS} & -\sqrt{\frac{1}{6}}\beta_{RS} & I-A-4{\cdot}84
\end{array}
\qquad
\begin{array}{c|cccc|}
 & \Psi_p & \Psi_{\beta'} & \chi_0 & \theta^{-1}\psi_5 \\
\hline
\Psi_p & E_p & 0 & 0 & -\sqrt{\frac{1}{6}}\beta_{RS} \\
\Psi_{\beta'} & 0 & E_{\beta'} & 0 & \sqrt{\frac{1}{6}}\beta_{RS} \\
\chi_0 & 0 & 0 & E_0 & \sqrt{\frac{2}{3}}\beta_{RS} \\
\theta^{-1}\psi_5 & -\sqrt{\frac{1}{6}}\beta_{RS} & \sqrt{\frac{1}{6}}\beta_{RS} & \sqrt{\frac{2}{3}}\beta_{RS} & I-A-6{\cdot}03
\end{array}$$

Taking the value of I as equal to the ionization potential of ammonia, 10·52 ev (Morrison and Nicholson 1952), and A as $-0{\cdot}54$ ev (Pople and Hush 1955), then the energies of $\theta^{-1}\psi_4$ and $\theta^{-1}\psi_5$ are 6·22 ev and 5·03 ev respectively. It is to be expected therefore that the spectrum of aniline will differ appreciably from that of benzene, and will possess an additional band at low energies. This is in fact what is observed.

If the secular equations are now solved, taking a reasonable value for β_{RS} of $-1{\cdot}6$ ev, we obtain the results shown in table 3.

Table 3. The Wave Functions and Energies of the Electronic States of Aniline

Wave function	Energy (ev)
$0{\cdot}167\Psi_\alpha - 0{\cdot}777\Psi_\beta - 0{\cdot}606\theta^{-1}\psi_4$	7·25
$0{\cdot}297\Psi_p - 0{\cdot}855\Psi_{\beta'} + 0{\cdot}419\theta^{-1}\psi_5 - 0{\cdot}032\chi_0$	7·06
$0{\cdot}861\Psi_p + 0{\cdot}431\Psi_{\beta'} + 0{\cdot}260\theta^{-1}\psi_5 - 0{\cdot}055\chi_0$	6·34
$0{\cdot}396\Psi_\alpha + 0{\cdot}612\Psi_\beta - 0{\cdot}684\theta^{-1}\psi_4$	6·01
$0{\cdot}416\Psi_p - 0{\cdot}285\Psi_{\beta'} - 0{\cdot}834\theta^{-1}\psi_5 + 0{\cdot}266\chi_0$	4·83
$0{\cdot}901\Psi_\alpha - 0{\cdot}125\Psi_\beta + 0{\cdot}414\theta^{-1}\psi_4$	4·58
$0{\cdot}025\Psi_p - 0{\cdot}023\Psi_{\beta'} - 0{\cdot}244\theta^{-1}\psi_5 - 0{\cdot}969\chi_0$	−0·33

The moment of a transition from the ground state to one of the electron transfer states is zero, if it is assumed that there is no overlap between the molecular orbitals of the hydrocarbon and those of the substituent. If this is not strictly true, then a transition to the state $\theta^{-1}\psi_5$ will have a larger moment than one to the state $\theta^{-1}\psi_4$, since ψ_4 has a node through the carbon atom to which the substituent is attached. The bands of aniline will derive most of their intensity from the contributions of Ψ_β and $\Psi_{\beta'}$ in their upper state, transitions to these states giving the very intense β band of benzene. Transitions to the states of energy 7·25 ev and 7·06 ev will be expected to give rise to intense bands similar to the β band of benzene; transitions to the states of energy 6·34 ev and 6·01 ev will give rise to less intense bands, but they should be more intense than the p band of benzene. Transitions to the states of energy 4·83 ev and 4·58 ev will have a small moment, but of these two the former will be at least five times more intense than the latter, due to the contribution from the β' state. In table 4 the observed and the calculated results are compared.

Table 4. A Comparison of the Observed and Calculated Spectrum of Aniline

Excitation energies (ev)	Calculated	7·58	7·39	6·67	6·34	5·16	4·91
	Observed	>7·06[1]		6·30[1]		5·27[1]	4·31[2]
Observed intensity ($\epsilon_{\max}$)		>10000		32000		8000	1300

[1] Klevens and Platt (1954–55).

[2] Grammaticakis (1951).

It is most probable that the electron transfer states for amino substituents arise from the excitation of an electron from the unshared pair of electrons on the nitrogen atom. In this case, if the plane of the substituent group is forced out of the plane of the benzene ring, the mesomeric effect will be considerably reduced. This is in fact observed when dimethylaniline is substituted in the ortho positions (see table 5).

Table 5. The Effect of Ortho Substituents on the Spectrum of Dimethylaniline (Klevens and Platt 1949)

Dimethylaniline				
ν(cm^{-1})	56800	50100	40000	33000
f	0·79	0·54	0·28	0·04
o–Methyldimethylaniline				
ν(cm^{-1})	54000	48000	40400	—
f	0·69	0·23	0·12	0·02
o–*o*–Dimethyldimethylaniline				
ν(cm^{-1})	54550	47400	38600	
f	0·66	0·15	0·05	
Benzene				
ν(cm^{-1})	54400	49500	39400	
f	0·69	0·10	0·0014	

There has been some controversy over the origin of the band at 5·27 ev in aniline. Klevens and Platt (1949) came to the conclusion that this band arose from the α band of benzene, basing their argument on the frequency of the band, and its relationship with the bands observed for methyl and hydroxyl substitution. From the intensity of the band however, we have reached the conclusion that this band does in fact arise from a transition to the electron transfer state. This state has a different symmetry from the α state. The α band appears, very much weaker, at longer wavelengths. The inductive effect has been ignored in this problem: it will be expected to increase the intensity and wavelength of the α band, but these changes will be small in comparison with the mesomeric effect.

§ 4. A WEAK MESOMERIC EFFECT

To consider mono-substitution, we chose our benzene orbitals to be so oriented that the electron transfer states could be represented simply by the configurations $\theta^{-1}\psi_4$ and $\theta^{-1}\psi_5$. Since all positions of substitution are identical it must be possible to set up orthogonal states of the type $a\theta^{-1}\psi_4+b\theta^{-1}\psi_5$ and $b\theta^{-1}\psi_4-a\theta^{-1}\psi_5$, for each position of substitution. One of these states will have an energy $I-A-4\cdot84$ ev and will interact with the α and β states; the other will have an energy $I-A-6\cdot03$ ev and will interact with p, β' and ground states of the molecule. Since there is no interaction between the electron transfer states associated with different positions of substitution, the mesomeric effect will just depend on the number of substituents, and not on the actual position of substitution. This is an important difference between the mesomeric effect and the inductive effect, the relative positions of substitution being very important in the latter case. Thus there is the same mesomeric effect on the α state for ortho, meta, and para substitution, yet, as was shown in III, the inductive effect varies in the ratio 1 : 1 : 4.

Since we have considered only the excited states of lowest energy, our method will probably be most reliable for determining the change in energy of the α band; the p, β and β' states may lie close to other high energy states. In addition the α band is unaffected by electron interaction, whereas the p, β and β' bands can be changed considerably. This is an important reason for restricting our attention to the α band when the mesomeric effect is weak.

It was suggested in III that the change in energy of the α band should be given by an expression of the form

$$(\Delta E_\alpha-\Delta E_0)_{\mathrm{obs}}=n\mathscr{A}+(\Delta E_\alpha''-\Delta E_0'')$$

where $\mathscr{A}$ is a constant for a given substituent, n is the number of substituents, and $\Delta E_\alpha''-\Delta E_0''$ is the calculated change in energy due to the inductive effect. Good agreement was found for an expression of this type for the fluoro-substitution of benzene, and a value for $\mathscr{A}$ of $-0\cdot017$ ev was obtained by comparison with experiment.

If the interaction between the electron transfer states and the ground state and α state is sufficiently weak to allow the second order perturbation theory to be used, then the constant $\mathscr{A}$ will be given by

$$-\mathscr{A}=\beta^2\left\{\frac{1}{6(E_\alpha-[I-A-4\cdot84])}-\frac{2}{3(E_0-[I-A-6\cdot03])}\right\}.$$

To obtain a value for $\mathscr{A}$ from experiment, it is necessary to be able to estimate the inductive effect. However, it is an exact result, within the limits of the LCAO molecular orbital approximation, that the inductive effect of substituents which are in the positions a, b, c, … is the same as that produced by substituents in all positions except a, b, c, …. This is true if the states of the molecule have a uniform charge distribution. The difference in energy of the α bands of a pair of substituted benzene molecules which are related in this way, is given by

$|6-2r|\mathscr{A}$, where one of the molecules has substituents in r of the six available positions.

Table 6 shows the result of applying this method to the methyl benzenes. The positions of the 0–0 band, and of the most intense band are shown for comparison. It is seen that $\mathscr{A}$ has a constant value to within about 0·01 ev for either the maximum absorption, or the position of the 0–0 band. This is extremely good when we consider that the frequency of a vibrational peak can only be estimated with an accuracy of about 0·005 ev.

Table 6. The Mesomeric Effect of Methyl Substituents in Benzene

Positions of substitution	0–0 band			Maximum adsorption		
	ν	$\Delta\nu$	$-\mathscr{A}$	ν	$\Delta\nu$	$-\mathscr{A}$
1	4·612	0·173	0·043	4·731	0·149	0·037
1, 2, 3, 4, 5	4·439			4·582		
1, 2	4·574	0·095	0·047	4·712	0·087	0·043
1, 2, 3, 4	4·479			4·625		
1, 3	4·548	0·074	0·037	4·673	0·051	0·025
1, 2, 3, 5	4·474			4·622		
1, 4	4·520	0·062	0·031	as 0–0 band		
1, 2, 4, 5	4·452					

These results are obtained from the American Petroleum Industry reports on ultraviolet spectroscopy.

From the observed ionization potential of methane, 13·04 ev (Honig 1948), the energies of the electron transfer configurations for a methyl substituent can be calculated. The states $\theta^{-1}\psi_4$ and $\theta^{-1}\psi_5$ are found to have the energies 8·74 ev and 7·55 ev respectively. With these energies the α band should increase rather than decrease in energy. However, the calculation of the energies of the electron transfer configurations is the most uncertain step in this theory, and I feel that not too much importance should be attached to the above discrepancy. The neglect of overlap between atomic orbitals, and the assumption that β_{RS} is a constant for all interactions, may also introduce significant errors when the mesomeric effect is weak.

ACKNOWLEDGMENT

I wish to thank Professor H. C. Longuet-Higgins for the interesting discussion we have had on this topic, and for reading the manuscript of this paper.

REFERENCES

Dewar, M. J. S., and **Longuet-Higgins**, H. C., 1954, *Proc. Phys. Soc.* A, **67,** 795 (Paper I).

Grammaticakis, P., 1951, *Bull. Soc. Chim. Fr.*, 534.

Honig, R. F., 1948, *J. Chem. Phys.*, **16,** 105.

Klevens, H. B., and **Platt**, J. R., 1949, *J. Amer. Chem. Soc.*, **71,** 1714; 1954–55, *Technical Report of the Laboratory of Molecular Structure and Spectra*, Department of Physics, University of Chicago.

Longuet-Higgins, H. C., and **Murrell**, J. N., 1955, *Proc. Phys. Soc.* A, **68,** 601 (Paper V).

Morrison, J. D., and **Nicholson**, A. J. C., 1952, *J. Chem. Phys.*, **20,** 1021.

Murrell, J. N., and **Longuet-Higgins**, H. C., 1955, *Proc. Phys. Soc.* A, **68,** 329 (Paper III).

Pople, J. A., 1953, *Trans. Faraday Soc.*, **49,** 1375; 1955, *Proc. Phys. Soc.* A, **68,** 81 (Paper II).

Pople, J. A., and **Hush**, N. S., 1955, *Trans. Faraday Soc.*, **51,** 600.

The Dielectric Theory of Electronic Interactions in Solids

By J. HUBBARD
Department of Mathematics, Imperial College, London S.W.7

Communicated by S. Raimes; MS. received 15*th March* 1955
and in amended form 17*th May* 1955

Abstract. It is suggested that the long-range part of the Coulomb interaction of the electrons in solids can be treated by regarding the solid as a homogeneous dielectric. The theory is developed in a semi-classical way. It is found that there is a possibility of sustained electric oscillations in metals, and these are identified in the case of a free electron gas with the plasma oscillations of Bohm and Pines. The theory is used to discuss the plasma frequencies of metals and the energy loss spectra of fast electrons in Ruthemann and Lang type experiments. The connection with the optical properties is indicated.

---

§ 1. INTRODUCTION

ONE of the most important problems in the theory of solids is that of obtaining an understanding of the effect on the behaviour of the conduction electrons of their mutual interactions and their interactions with the core electrons. This problem is, of course, a complex many-body problem, and we can only hope to treat it by some sort of approximational procedure. One obvious scheme would be to treat the interactions as though they were perturbations and apply the ordinary perturbation theory. But this method breaks down for two reasons. First, the interaction between the core and the conduction electrons is usually too strong to be treated by perturbation theory. This difficulty can probably be remedied by the use of Hartree self-consistent fields; the main part of the interaction is contained in the self-consistent field and the residual interaction can be treated by perturbation theory. It is hoped to give more details of this approach at a later date.

The second difficulty with the perturbation method arises from the long-range nature of the Coulomb interaction. Macke (1950) showed that even in a free electron gas, with the electrons so widely spaced that the interaction energy should be small, the perturbation method still diverged in the second order. This difficulty was found to arise not from the strength of the electronic interactions, but from the long-range nature of the interaction.

The same sort of difficulty frequently arises in attempts to treat the Coulomb interaction approximately. For example, the well-known peculiarity in the behaviour of the (E, $\mathbf{k}$) curve near the Fermi surface in the Hartree–Fock self-consistent field treatment (theoretically the best of the independent electron treatments) arises from the very long-range part of the interaction.

Thus we see that the principal difficulties in treating the interaction arise from the long-range part of it. If we could obtain a satisfactory treatment of this part, then we could treat the short-range part by means of self-consistent fields and perturbation theory in many cases. It is with obtaining such a treatment of the long-range interaction that the present theory is concerned.

Fortunately there is an important simplification which can be made in the treatment of the long-range interaction. So long as we are considering only interactions over distances rather greater than the dimensions of the atomic cell or the inter-electronic distance, whichever is the larger, we may reasonably treat the solid as though it were a continuous, homogeneous medium. Such a medium is described so far as we are concerned by its dielectric properties, which can be calculated theoretically or determined experimentally. We have then only to apply the classical theory of the electromagnetic field in dielectric media, or the corresponding quantum mechanical generalization, to the long-range interaction to obtain the required treatment. This is the treatment we shall develop in this paper; we shall call it the dielectric treatment of the long-range interaction.

The idea of treating the long-range interaction in this way is not new. It seems to have been first suggested by Fermi (1940), and was used by him to calculate that part of the stopping power of materials for fast charged particles due to 'long-range' collisions. Various authors (Halpern and Hall 1948, Kramers 1947, A. Bohr 1948) developed this theory and applied it to special cases.

In this paper we shall present a mainly classical version of the theory. In § 2 we shall develop the theory mathematically, and in § 3 we shall apply it to a free electron gas and find that it is equivalent to the plasma theory of Bohm and Pines (1953) in this case. In § 3 we shall also consider the dielectric behaviour of a general solid, and use it to discuss the plasma frequencies in solids. Finally, in § 4 we shall make an important application of the theory to obtain the formula quoted in an earlier note (Hubbard 1955) for the energy loss spectrum of fast electrons in Ruthemann and Lang type experiments.

We hope in a later paper to present a quantum mechanical version of the theory, which is required to treat such problems as the determination of the correlation energy in metals.

§ 2. THE CLASSICAL THEORY

In this section we shall develop the dielectric theory classically. Although a classical approach is not suitable for some problems, such as the calculation of the correlation energy, it is nevertheless simple to understand and apply, and can be used to obtain correct results in many cases.

The theory is quite straightforward. We shall separate the long- and short-range parts of the electric field and notice that we can treat the long-range part as though the solid were a homogeneous dielectric. This will enable us to obtain a simple connection between the long-range field and the charge distribution generating it, *taking into account the polarization* of the solid by the field. It is the inadequate treatment of this polarization that has led to difficulties with the long-range interaction in approximate treatments. This polarization is of course just equivalent to the long-range electronic correlation; it represents the movements of the electrons to screen out the field acting on them, and it is just these movements which we call electronic correlations.

To separate the long- and short-range parts of the electric field $\mathbf{E}$ we make a Fourier analysis of it:

$$\mathbf{E}(\mathbf{r},t)=\sum_{\mathbf{k}}\mathbf{E}_{\mathbf{k}}(t)\exp(i\mathbf{k}\,.\,\mathbf{r}) \qquad \ldots\ldots(1)$$

and split it into two parts, the first (the long-range part) containing terms with $k<k_c$, where k_c is some suitably chosen constant, and the second (the short-range part) the remaining terms. Thus

$$\mathbf{E}_{\mathrm{l.r}}=\sum_{k<k_c}\mathbf{E}_{\mathbf{k}}\exp(i\mathbf{k}\,.\,\mathbf{r}) \qquad \ldots\ldots(2)$$

$$\mathbf{E}_{\mathrm{s.r}}=\mathbf{E}-\mathbf{E}_{\mathrm{l.r}}\,.$$

We now work with $\mathbf{E}_{\mathrm{l.r}}$ only, treating the solid as a homogeneous dielectric. The details of such a treatment are well known in connection with the optical properties of solids (see, for example, Seitz 1940, ch. 17, Mott and Jones 1936, ch. 3). The dielectric properties of a solid can be described by a frequency dependent complex dielectric constant

$$\boldsymbol{\epsilon}_\omega=1+4\pi\boldsymbol{\alpha}_\omega+\frac{4\pi}{i\omega}\boldsymbol{\sigma}_\omega \qquad \ldots\ldots(3)$$

where $\boldsymbol{\alpha}_\omega$ and $\boldsymbol{\sigma}_\omega$ are the polarizability and conductivity tensors at frequency $\omega/2\pi$. The tensor $\boldsymbol{\epsilon}_\omega$ relates the Fourier components of the electric field $\mathbf{E}$ to those of the displacement $\mathbf{D}$ through the equation

$$\boldsymbol{\epsilon}_\omega\,.\,\mathbf{E}_{\omega\mathbf{k}}=\mathbf{D}_{\omega\mathbf{k}},\quad k<k_c \qquad \ldots\ldots(4)$$

where $\mathbf{E}_{\omega k}$ is the Fourier component of $\mathbf{E}$ with respect to $\mathbf{r}$ and t, i.e.

$$\mathbf{E}_{\mathrm{l.r}}(\mathbf{r},t)=\sum_{k<k_c}\sum_{\omega}\mathbf{E}_{\omega k}\exp(i\mathbf{k}\,.\,\mathbf{r}+i\omega t) \qquad \ldots\ldots(5)$$

and similarly for $\mathbf{D}$.

There are two differences between our treatment and the ordinary optical treatment. Firstly, we are concerned with longitudinal rather than transverse waves. Therefore we can write, neglecting the transverse part which only represents the very weak magnetic interactions, $\mathbf{E}_{\omega\mathbf{k}}\equiv\hat{\mathbf{k}}E_{\omega\mathbf{k}}$, $\mathbf{D}_{\omega\mathbf{k}}\equiv\hat{\mathbf{k}}D_{\omega\mathbf{k}}$, and then obtain instead of (4)

$$(\hat{\mathbf{k}}\,.\,\boldsymbol{\epsilon}_\omega\,.\,\hat{\mathbf{k}})E_{\omega\mathbf{k}}=D_{\omega\mathbf{k}},\quad k<k_c. \qquad \ldots\ldots(6)$$

The second difference from the optical case is that our $\mathbf{k}$'s may be very much longer than those occurring optically (the wavelength of optical radiation is very much greater than the lattice spacing). A simple generalization of Wilson's calculation (Wilson 1935) of $\boldsymbol{\alpha}_\omega$ and $\boldsymbol{\sigma}_\omega$ shows that in this case we should regard ϵ as $\mathbf{k}$ dependent as well as ω dependent and write (6)

$$\epsilon_{\omega\mathbf{k}}E_{\omega\mathbf{k}}=D_{\omega\mathbf{k}},\quad k>k_c, \qquad \ldots\ldots(7)$$

where

$$\epsilon_{\omega\mathbf{k}}\equiv\hat{\mathbf{k}}\,.\,\boldsymbol{\epsilon}_{\omega\mathbf{k}}\,.\,\hat{\mathbf{k}}. \qquad \ldots\ldots(8)$$

The $\mathbf{k}$ dependence of $\epsilon_{\omega\mathbf{k}}$ is generally not very strong, but will lead to a dispersion relation for the plasma frequency.

If we now write $\mathbf{E}=-\nabla\phi$, and use div $\mathbf{D}=4\pi\rho$, we obtain from (7) the equation

$$\epsilon_{\omega\mathbf{k}}\phi_{\omega\mathbf{k}}=\frac{4\pi}{k^2}\rho_{\omega\mathbf{k}} \qquad \ldots\ldots(9)$$

relating the Fourier components of the scalar potential ϕ to those of the charge distribution ρ generating the field, taking into account the polarization. This equation summarizes the theory in the classical case.

We shall now point out an important feature of equation (9). Let us first neglect $\sigma_{\omega\mathbf{k}}$, so that $\epsilon_{\omega\mathbf{k}}$ is real, and also ignore the $\rho_{\omega\mathbf{k}}$ on the right-hand side of (9). Now it may happen that the real part of $\epsilon_{\omega\mathbf{k}}$ vanishes for some frequency $\omega = \omega_{\mathbf{k}}$, say, (and always will for a metal, see § 3). Equation (9) shows that at $\omega = \omega_{\mathbf{k}}$, $\phi_{\omega\mathbf{k}}$ can have any magnitude whatsoever, independently of the charge distribution. This can only mean that it is possible for the solid to sustain electric oscillations at the frequency $\omega_{\mathbf{k}}/2\pi$. We shall see that in the case of a free electron gas we can identify these oscillations with the plasma oscillations of Bohm and Pines.

In the classical case, if we now take into account $\sigma_{\omega\mathbf{k}}$, the (complex) $\epsilon_{\omega\mathbf{k}}$ will not in general vanish at any frequency; this corresponds to the fact that the conductivity would damp out any oscillations. In the quantum mechanical case, however, we should expect to find zero-point oscillations at the classical oscillation frequency. For in the quantum mechanical case, although the damping (which damps out the oscillations completely in the classical case) can reduce any excitation of the oscillations down to the zero-point oscillations, it cannot damp out the oscillation completely.

Though the complex $\epsilon_{\omega\mathbf{k}}$ does not vanish, it may become very small at some frequencies. We see from (9) that any disturbance of the charge density which gives rise to a non-zero $\rho_{\omega\mathbf{k}}$ at one of these frequencies will lead to strong, slightly damped, oscillations. If the disturbance is due to the passage of a fast electron through the metal, then these oscillations will transfer energy from the fast electron to the metal electrons (see § 4).

§ 3. PLASMA OSCILLATIONS IN SOLIDS

In § 2 we found that the frequencies at which sustained oscillations could take place (at least in the quantum mechanical case) were those at which the real part of $\epsilon_{\omega\mathbf{k}}$ vanished. We shall now determine this frequency for a free electron gas, and verify that it is in fact the plasma oscillation frequency of Bohm and Pines.

We must first quote the results of the generalization of Wilson's calculation mentioned in § 2. These results are, neglecting the local field correction the effects of which we shall discuss later,

$$\boldsymbol{\alpha}_{\omega\mathbf{k}} = -\frac{\mathcal{N}e^2}{m\omega^2} + \frac{2e^2}{m^2\hbar}\sum_{\mathbf{k}',n,n'} N_{\mathbf{k}'n}\,\omega_{\mathbf{k}'+\mathbf{k},n';\mathbf{k}'n} \times \frac{\left|\int \psi^*_{\mathbf{k}'+\mathbf{k},n'} e^{i\mathbf{k}\cdot\mathbf{r}}\,\hat{\mathbf{k}}\cdot(\mathbf{p}+\tfrac{1}{2}\hbar\mathbf{k})\psi_{\mathbf{k}'n}\,d\mathbf{r}\right|^2}{\omega^2_{\mathbf{k}'+\mathbf{k},n';\mathbf{k}'n}-\omega^2} \qquad \ldots\ldots(10)$$

$$\boldsymbol{\sigma}_{\omega\mathbf{k}} = \frac{\pi e^2}{m^2\hbar\omega}\sum_{\mathbf{k}',n,n'} N_{\mathbf{k}'n}\left|\int \psi^*_{\mathbf{k}'+\mathbf{k},n'} e^{i\mathbf{k}\cdot\mathbf{r}}\,\hat{\mathbf{k}}\cdot(\mathbf{p}+\tfrac{1}{2}\hbar\mathbf{k})\psi_{\mathbf{k}'n}\,d\mathbf{r}\right|^2 \times\{\delta(\omega_{\mathbf{k}'+\mathbf{k},n';\mathbf{k}'n}-\omega)-\delta(\omega_{\mathbf{k}'+\mathbf{k},n';\mathbf{k}'n}+\omega)\} \qquad \ldots\ldots(11)$$

where $\alpha_{\omega\mathbf{k}} \equiv \hat{\mathbf{k}}\cdot\boldsymbol{\alpha}_{\omega\mathbf{k}}\cdot\hat{\mathbf{k}}, \quad \sigma_{\omega\mathbf{k}} = \hat{\mathbf{k}}\cdot\boldsymbol{\sigma}_{\omega\mathbf{k}}\cdot\hat{\mathbf{k}}$

$$\hbar\omega_{\mathbf{k}'+\mathbf{k},n';\mathbf{k}'n} = E_{\mathbf{k}'+\mathbf{k},n'} - E_{\mathbf{k}'n} \qquad \ldots\ldots(12)$$

and where $\mathcal{N}$ is the total electron density (core and conduction electrons), $\psi_{\mathbf{k}n}$ is the Bloch wave function belonging to the nth zone and to wave vector $\mathbf{k}$, $E_{\mathbf{k}n}$ the corresponding energy, and $N_{\mathbf{k}n}$ the occupation number (0 or 1) of the state $(\mathbf{k}, n)$. The sum over $\mathbf{k}$ runs over the first Brillouin zone, and the sums over n and n' run over all zones, including the core electron levels.

If we now treat a free electron gas as though it were a metal with a single zone, we obtain from (10)

$$\alpha_{\omega\mathbf{k}} = -\frac{\mathcal{N}e^2}{m\omega^2} + \frac{2e^2}{m^2\hbar\omega^2}\sum_{\mathbf{k}'} N_{\mathbf{k}'}\frac{[\hbar\mathfrak{k}\,.\,(\mathbf{k}'+\tfrac{1}{2}\mathbf{k})]^2[(\hbar/m)\mathbf{k}\,.\,(\mathbf{k}'+\tfrac{1}{2}\mathbf{k})]}{[(\hbar/m)\mathbf{k}\,.\,(\mathbf{k}'+\tfrac{1}{2}\mathbf{k})]^2-\omega^2} \quad \ldots\ldots(13)$$

which can be rearranged into the form

$$\alpha_{\omega\mathbf{k}} = -\frac{e^2}{m}\sum_{\mathbf{k}'}\frac{N_{\mathbf{k}'}}{[\omega-(\hbar/m)\mathbf{k}'\,.\,\mathbf{k}]^2-\hbar^2k^4/4m^2}. \quad \ldots\ldots(14)$$

The condition for the plasma frequency can be written $\alpha_{\omega\mathbf{k}} = -1/4\pi$. Using this together with (14), we obtain the equation

$$1 = \frac{4\pi e^2}{m}\sum_{\mathbf{k}'}\frac{N_{\mathbf{k}'}}{[\omega-(\hbar/m)\mathbf{k}'\,.\,\mathbf{k}]^2-\hbar^2k^4/4m^2} \quad \ldots\ldots(15)$$

for the oscillation frequency of a free electron gas. This is just equivalent to Bohm and Pines dispersion relation (Bohm and Pines 1953, eqn 57). From (11) we find that the conductivity, and hence the damping, vanishes at the plasma frequency given by (15), provided that the Fermi energy is less than about $\hbar\omega_{\mathrm{P}}$. Thus $\epsilon_{\omega\mathbf{k}}$ actually does vanish at the plasma frequency for a free electron gas. This only results of course from our neglecting other sources of damping, such as that due to collisions brought about by the short-range interaction; equation (11) only represents what might be called the 'long-range' damping.

We can now apply the equation $\alpha_{\omega\mathbf{k}} = -1/4\pi$ to obtain the oscillation frequencies in solids. It is first convenient to transform (10) using a slight generalization of the *f*-sum rule. We can obtain

$$\alpha_{\omega\mathbf{k}} = -\frac{e^2}{\hbar^2\omega^2}\sum_{\mathbf{k}',n}N_{\mathbf{k}'n}(\mathfrak{k}\,.\,\nabla)(\mathfrak{k}\,.\,\nabla)E_{\mathbf{k}'n}$$
$$+\frac{2e^2}{m^2\hbar}\sum_{\mathbf{k}',n,n'}N_{\mathbf{k}'n}\frac{\left|\int\psi^*{}_{\mathbf{k}'+\mathbf{k},n'}\,e^{i\mathbf{k}\cdot\mathbf{r}}\,\mathfrak{k}\,.\,(\mathbf{p}+\tfrac{1}{2}\hbar\mathbf{k})\psi_{\mathbf{k}'n}\,d\mathbf{r}\right|^2}{\omega_{\mathbf{k}'+\mathbf{k},n';\mathbf{k}'n}(\omega^2{}_{\mathbf{k}'+\mathbf{k},n';\mathbf{k}'n}-\omega^2)}. \quad \ldots\ldots(16)$$

In a cubic crystal the first term represents $\mathcal{N}$ times the average of $-e^2/m^*$ (m^* is the effective mass) over the occupied levels. In computing this term we can omit completely filled zones, since the average of $1/m^*$ over a whole zone vanishes; thus only partly filled zones contribute to this term, which might be called the plasma term, because it is the term analogous to this which leads to a plasma frequency in a free electron gas. In the case of an insulator this term will vanish altogether, corresponding to the absence of a Fermi surface, and showing that there are no oscillations in an insulator *analogous to the plasma oscillations* of a free electron gas.

In 'free electron' metals, such as the alkalis, we might expect the second term of (16) to be small at the plasma frequency. If we neglect it, we obtain the simple result for the plasma frequency

$$\omega_{\mathbf{k}}{}^2 = 4\pi ne^2/\langle m^*\rangle \quad \ldots\ldots 17$$

where n is the density of 'free' electrons and $\langle m^*\rangle$ the average of the effective mass over them. This result agrees with effective mass treatments (Wolff 1953, Hubbard 1954). To obtain the next approximation we put $\omega^2 = 4\pi ne^2/\langle m^*\rangle$ in the second term of (16) and thence obtain

$$\omega_{\mathbf{k}}{}^2 = \frac{4\pi ne^2}{\langle m^*\rangle} - \frac{8\pi e^2}{m^2\hbar}\left(\frac{4\pi ne^2}{\langle m^*\rangle}\right)\sum_{\mathbf{k}',n,n'}\frac{N_{\mathbf{k}'n}\left|\int\psi^*{}_{\mathbf{k}'+\mathbf{k},n'}\,e^{i\mathbf{k}\cdot\mathbf{r}}\,\mathfrak{k}\,.\,(\mathbf{p}+\tfrac{1}{2}\hbar\mathbf{k})\psi_{\mathbf{k}'n}\,d\mathbf{r}\right|^2}{\omega_{\mathbf{k}'+\mathbf{k},n';\mathbf{k}'n}(\omega^2{}_{\mathbf{k}'+\mathbf{k},n';\mathbf{k}'n}-4\pi ne^2/\langle m^*\rangle)}. \quad \ldots\ldots(18)$$

In computing the correction term, only those terms for which the level $\mathbf{k}'+\mathbf{k}, n'$ is unoccupied give any contribution, the other terms cancelling out. We can regard the correction term as made up of two parts: (i) the terms for which n is a conduction band and n' an unoccupied zone; these terms represent the effect on the plasma frequency of inter-zone transitions; (ii) the terms in which the 'band' n is a core electron level; these terms represent the effect on the plasma frequency of the polarization of the ion cores by the plasma field.

Obviously a similar interpretation can be given to the terms of (16) even when the approximation procedure of (17) and (18) cannot be used. In particular, we should notice that in a metal the first term of (16) always leads to the vanishing of $1+4\pi\alpha_{\omega\mathbf{k}}$ at some frequency (it ensures that $1+4\pi\alpha_{\omega\mathbf{k}}$ is negative for small values of ω, whilst this quantity must become positive for large ω), and hence there is always a plasma frequency in a metal. On the other hand in an insulator there is no plasma term and correspondingly no plasma frequency.

The above results, (10)–(18), have been obtained by neglecting the so-called local field correction. Nevertheless, the results (13)–(15) concerning a free electron gas are correct as they stand, since it is well known (Darwin 1934, 1943) that there is no need to apply a local field correction in the case of a free electron gas, and therefore the identification of the oscillation frequency of the gas with the plasma frequency of Bohm and Pines is unaffected.

In the case of a real metal, however, this correction will be of importance, because, although the conduction electrons can often be regarded as free, this correction will affect the core electron polarizability strongly. Although the appropriate correction is known in the case of a free electron gas, discussed above, and also in the case of a cubic lattice of compact ions (in which case it is just the ordinary Lorenz–Lorentz correction), so far as we are aware no general treatment covering the cases in which the conduction electrons cannot really be regarded as free or where the core electron wave functions are not compact enough for the Lorentz correction to be accurate, has ever been given. However, it seems possible to develop such a treatment, and it is hoped to publish details of it at some later date. For the moment we shall content ourselves with indicating the expected modifications to the above results by the local field correction.

In general we should expect the correction to alter the oscillation frequencies, since it will change the zeros of $1+4\pi\alpha_{\omega\mathbf{k}}$. Without an expression for the local field correction, it is not possible to give the corrected form of (16) or (18) in the general case. Nevertheless, it can be seen (by considering the case in which the Lorentz correction holds, for example) that it will no longer be possible to give the simple interpretations that were given to the terms of (16) or (18), since the polarization of one of the core electron shells may now depend upon that of the others through the local field correction.

There are, however, some cases in which the situation is rather simpler. In the case of the alkali metals the main contribution to the polarizability at the plasma frequency comes from the almost-free conduction electrons, and hence the oscillation frequency is very little changed in these metals. Again, many metals have almost-free conduction electrons together with compact ion cores. For the free electrons there is no correction and for the ion cores the Lorentz correction is accurate. In such cases, as Darwin has shown (1934), the correct polarizability is obtained by adding the uncorrected free electron polarizability to the Lorentz-corrected ion core polarizability.

We see that, apart from the uncertainties regarding the local field correction, the dielectric theory gives a straightforward account of the factors affecting the oscillation frequencies. Of course, not all factors affecting the oscillation frequencies have been taken into account in the above discussion, but it is not difficult to take into account other factors, since we have only to determine their effect on the polarizability. For example, to take into account the effect on the plasma frequency of the motion of the nuclei, one would include in the expression for the polarizability the (at the plasma frequency rather small) contribution due to the displacements of the nuclei.

Unfortunately the lack of accurate band structure calculations does not permit us to apply (16) or (18) together with the appropriate local field correction. There is, however, an alternative possibility of determining $\alpha_{\omega\mathbf{k}}$ and $\sigma_{\omega\mathbf{k}}$ for small **k**'s from the optical properties of the solid, since they are related to the refractive index n and the extinction coefficient κ by the equations

$$n^2-\kappa^2=1+4\pi\alpha_{\omega\mathbf{k}} \qquad \ldots\ldots(19)$$

$$n\kappa\omega=2\pi\sigma_{\omega\mathbf{k}}. \qquad \ldots\ldots(20)$$

Thus from the experimentally determined optical data we should be able to find the zeros of $1+4\pi\alpha_{\omega\mathbf{k}}$ and estimate the damping at these frequencies. Since it is not expected that $\alpha_{\omega\mathbf{k}}$ will vary very rapidly with **k**, these results for small **k**'s should give a good indication of the general behaviour of $\alpha_{\omega\mathbf{k}}$ with ω. At the present time, however, there are practically no measurements of the optical properties in the range 200 Å to 2500 Å, which is the interesting region for the present purpose because for most metals $\hbar\omega_{\mathbf{k}}\sim$5–20 ev. But we can apply this method in one or two cases. In particular, in the case of the alkali metals $\omega_{\mathbf{k}}$ is rather small and the corresponding optical wavelengths fall in the ultra-violet. In this region we have the results of Ives and Briggs (1936, 1937). These results confirm the free electron-like character of these metals (see Seitz 1940, p. 652), and show that the change in the plasma frequency due to inter-zone transitions, to the core electron polarizability and to the local field correction is very small in these metals. They further show that the damping (mainly due to transitions from the conduction band to the next zone, analogous to the photoelectric effect) is very small at the plasma frequency.

A further method of obtaining information about the behaviour of $\alpha_{\omega\mathbf{k}}$ and $\sigma_{\omega\mathbf{k}}$ should be the Ruthemann and Lang type experiments when results of sufficient certainty become available (see § 4).

Before leaving the question of oscillation frequencies, it should be pointed out that although we have shown above that there must be at least one oscillation frequency in a metal, we have not shown that there cannot be more than one, nor, indeed, that there cannot be oscillation frequencies in insulators. In fact, if the quantity $1+4\pi\alpha_{\omega\mathbf{k}}$ should vanish at more than one frequency in a metal, or should vanish at some frequency in an insulator, there seems to be no reason why oscillations should not take place at these frequencies also.

§ 4. THE SMALL ANGLE SCATTERING OF FAST ELECTRONS

One of the most interesting applications of the present theory is to obtain the energy loss spectrum of fast electrons in Ruthemann and Lang type experiments (Ruthemann 1948, Lang 1948).

In these experiments fast electrons (energy ~10 kev) are passed through metal films and the energy loss spectrum of those electrons suffering very small deflections determined. Since the deflection is very small, the momentum loss $\hbar\mathbf{k}$ of the fast electron is such that $k<k_c$, and it is the long-range part of the interaction which is responsible for the energy loss. Thus it is appropriate to treat the interaction by means of the dielectric theory.

In this section we shall derive the formula quoted earlier (Hubbard 1955). Essentially all we have to do is to study the earlier treatments of the stopping power, quoted in § 1, at a stage at which we can examine the spectral distribution of the energy loss. The treatment we shall give here will look slightly different from these earlier treatments because we shall work with the Fourier transforms of most quantities.

The treatment we shall give is rather similar to the Weizsäcker–Williams treatment of scattering (see, for example, Heitler 1954, p. 414). We shall represent the fast electron by the appropriate charge distribution $\rho(\mathbf{r}, t)$, and calculate the field it generates from (9). We shall then regard this field as a perturbation acting on the electrons of the metal. This perturbation will cause transitions from occupied to unoccupied levels. Any electron making such a transition will acquire energy $\hbar\omega$ and momentum $\hbar\mathbf{k}$ and the fast electron will suffer a corresponding loss. Since we can calculate the probability of a given transition by means of the dielectric theory, we can determine the energy loss spectrum and the angular distribution of the scattered electrons.

It might appear at first that this treatment is contrary to the picture of the energy losses as due to the excitation of plasma oscillations. This is not so, however, for we could look upon the treatment given here as follows: the fast electron excites oscillations, but in due course the excitation is damped out by a metal electron making an inter-zone transition, and it is the rate of these transitions that we calculate.

The charge distribution corresponding to a fast electron passing through a metal with velocity $\mathbf{v}$ can be written, with suitable choice of origin,

$$\rho(\mathbf{r}, t)=e\delta(\mathbf{r}-\mathbf{v}t) \qquad \ldots\ldots(21)$$

from which we obtain

$$\rho_{\omega\mathbf{k}}=e\delta(\omega+vk_{\parallel}) \qquad \ldots\ldots(22)$$

where $v=|\mathbf{v}|$ and $k_{\parallel}$ is the component of $\mathbf{k}$ parallel to $\mathbf{v}$. Then from (9) the scalar potential of the field due to the fast electron is given by

$$\phi_{\omega\mathbf{k}}=\frac{4\pi e}{k^2\epsilon_{\omega\mathbf{k}}}\delta(\omega+vk_{\parallel}). \qquad \ldots\ldots(23)$$

The interaction of the fast electron with a metal electron at $\mathbf{r}$ is just $e\phi(\mathbf{r}, t)$. If we regard this as a perturbation and apply the ordinary time dependent perturbation theory (see, for example, Schiff 1949, ch. 8), we find that the only component of ϕ which will induce a transition from the state $\psi_{\mathbf{k}'n}$ to the state $\psi_{\mathbf{k}'+\mathbf{k},n'}$ is $\phi_{\omega\mathbf{k}}\exp(i\mathbf{k}\,.\,\mathbf{r}+i\omega t)$ where

$$\hbar\omega=E_{\mathbf{k}'+\mathbf{k},n'}-E_{\mathbf{k}'n} \qquad \ldots\ldots(24)$$

and that the rate of such transitions is proportional to $|\phi_{\omega\mathbf{k}}|^2$. Thus we see that the rate of transitions $P(\mathbf{k}, \omega)$ in which the fast electron simultaneously loses energy $\hbar\omega$ and momentum $\hbar\mathbf{k}$ is proportional to $|\phi_{\omega\mathbf{k}}|^2$. To determine the constant of proportionality, we notice that (as is shown in the Appendix) the rate of energy loss associated with the component $\phi_{\omega\mathbf{k}}$ of the field is

$$2k^2\sigma_{\omega\mathbf{k}}|\phi_{\omega\mathbf{k}}|^2. \qquad \ldots\ldots(25)$$

Dividing this by $\hbar\omega$, we find

$$P(\mathbf{k},\omega)=\frac{2k^2\sigma_{\omega\mathbf{k}}}{\hbar\omega}|\phi_{\omega\mathbf{k}}|^2. \qquad \ldots\ldots(26)$$

Substituting for $\phi_{\omega\mathbf{k}}$ from (23), we obtain

$$P(\mathbf{k},\omega)=\frac{32\pi^2e^2}{\hbar\omega k^2}\frac{\sigma_{\omega\mathbf{k}}}{|\epsilon_{\omega\mathbf{k}}|^2}\delta(\omega+vk_{\parallel}) \qquad \ldots\ldots(27)$$

the result quoted earlier (Hubbard 1955).

This result gives a complete account of the energy loss spectrum and the angular distribution of the scattered electrons, since the angle θ through which the fast electron is scattered is given by

$$\theta=\hbar k_{\perp}/mv \qquad \ldots\ldots(28)$$

where $k_{\perp}$ is the component of $\mathbf{k}$ perpendicular to $\mathbf{v}$.

The probability per unit path length of the fast electron suffering a long-range collision in which it is scattered through an angle between θ and $\theta+d\theta$ and loses energy $\hbar\omega$ is given by

$$\frac{2\pi k_{\perp}dk_{\perp}}{v(2\pi)^3}\int_{-\infty}^{+\infty}P(k,\omega)\,dk_{\parallel}=\frac{8e^2}{\hbar\omega v^2}\frac{\sigma_{\omega\mathbf{k}}}{|\epsilon_{\omega\mathbf{k}}|^2}\frac{\theta\,d\theta}{\theta^2+(\hbar\omega/mv^2)^2}. \qquad \ldots\ldots(29)$$

Since $mv^2\gg\hbar\omega$, the scattering has a strong maximum near $\theta=0$. If we integrate with respect to θ between 0 and θ_0, we obtain the probability per unit path length of the fast electron suffering a long-range collision in which it is scattered through an angle $\theta<\theta_0$ and loses energy $\hbar\omega$. The result is

$$\frac{4e^2}{\hbar\omega v^2}\frac{\sigma_{\omega}}{|\epsilon_{\omega}|^2}\log\frac{\theta_0{}^2+(\hbar\omega/mv^2)^2}{(\hbar\omega/mv^2)^2} \qquad \ldots\ldots(30)$$

where we have neglected the $\mathbf{k}$ dependence of $\sigma_{\omega\mathbf{k}}$ and $\epsilon_{\omega\mathbf{k}}$ (most of the contribution to the integral comes from small $\mathbf{k}$'s).

Finally, putting $\theta_0=\hbar k_{\perp}/mv$, multiplying by $\hbar\omega$, and integrating over ω, we find the total rate of energy loss due to long-range collisions is

$$\frac{4e^2}{v^2}\int_0^{\infty}\frac{\sigma_{\omega}}{|\epsilon_{\omega}|^2}\log\frac{k_c{}^2+(\omega/v)^2}{(\omega/v)^2}\,d\omega \qquad \ldots\ldots(31)$$

per unit path length.

In applying these results to a free electron gas, we meet with the difficulty that both $\sigma_{\omega\mathbf{k}}$ and $\epsilon_{\omega\mathbf{k}}$ vanish at the plasma frequency. To avoid this difficulty we introduce a small damping at the plasma frequency proportional to γ (there is always some damping due to the collisions brought about by the short-range interaction in any case), and let $\gamma\to0$. Introducing this damping, we find that for ω near to ω_P

$$\sigma_{\omega\mathbf{k}}=\frac{\omega_{\mathbf{k}}{}^2}{4\pi}\frac{\gamma}{\omega^2+\gamma^2} \qquad \ldots\ldots(32)$$

$$|\epsilon_{\omega\mathbf{k}}|^2=\left[1-\frac{\omega_{\mathbf{k}}}{\omega^2+\gamma^2}\right]^2+\frac{\gamma^2}{\omega^2} \qquad \ldots\ldots(33)$$

where $\omega_{\mathbf{k}}$ is the plasma frequency corresponding to **k** given by (15). In the limit $\gamma \rightarrow 0$ we find from (32) and (33) that

$$\frac{\sigma_{\omega\mathbf{k}}}{|\epsilon_{\omega\mathbf{k}}|^2} = \tfrac{1}{8}\omega_{\mathbf{k}}^2\,\delta(\omega - \omega_{\mathbf{k}}), \quad \omega \text{ near to } \omega_{\mathrm{P}}. \qquad \ldots\ldots(34)$$

Putting this result into (27) or (29) we see that a free electron gas will absorb energy in quanta of $\hbar\omega_{\mathbf{k}} \sim \hbar\omega_{\mathrm{P}}$ from a fast electron. For a free electron gas we find from (11)

$$\sigma_{\omega\mathbf{k}} = \frac{\pi e^2 \hbar}{m^2\omega^2} \sum_{\mathbf{k}'} N_{\mathbf{k}'} [\hbar\hat{\mathbf{k}} \, . \, (\mathbf{k}' + \tfrac{1}{2}\mathbf{k})]^2 \,\delta\left\{\frac{\hbar}{m}\mathbf{k} \, . \, (\mathbf{k}' + \tfrac{1}{2}\mathbf{k}) - \omega\right\} \qquad \ldots\ldots(35)$$

and when this (together with the appropriate $\epsilon_{\omega\mathbf{k}}$) is put into (27) we obtain a further absorption at frequencies other than the plasma frequency. This absorption is, however, very small and can be neglected for fast electrons (it is represented by the second term of eqn (48) of Pines 1953). Neglecting this term we obtain from (31) the expression

$$\frac{2\pi n e^4}{m v^2} \log \frac{k_c^2 m^2 v^2}{\omega_{\mathrm{P}}^2} \qquad \ldots\ldots(36)$$

for the rate of energy loss per unit path length of a fast electron in a free electron gas, agreeing with the results of Kramers (1947) and Pines (1953).

In the case of a real metal, since we have no reliable theoretical estimates of $\alpha_{\omega\mathbf{k}}$ and $\sigma_{\omega\mathbf{k}}$, we cannot calculate the energy loss spectrum quantitatively from (27). We can, however, make some qualitative deductions as to the nature of the spectrum. We should first notice that $\alpha_{\omega\mathbf{k}}$ and $\sigma_{\omega\mathbf{k}}$ will not in general depend on ω in any very simple fashion, and consequently the energy loss spectrum obtained from (27) may be rather complex in character. In fact, (27) does not necessarily lead to the simple line spectrum that has been suggested. Nevertheless, it may very well happen that $|\epsilon_{\omega\mathbf{k}}|^2$ does become small at some frequency (for example at the plasma frequency of a metal if the damping is not too great at this frequency). Then (27) predicts strong absorption at such a frequency. This just corresponds to the situation discussed in the last paragraph of § 2.

It should be noticed that it is quite possible for $|\epsilon_{\omega\mathbf{k}}|^2$ to become small at more than one frequency. If it does, there will be a corresponding number of absorption peaks, rather than just one ‘ plasma ’ peak. Again it is quite possible for $|\epsilon_{\omega\mathbf{k}}|^2$ to become small at some frequency or frequencies in an insulator. It is then possible to obtain peaks in the energy loss spectrum of the insulator, although there can be no plasma oscillations in an insulator analogous to those in a free electron gas.

In the absence of theoretical calculations of $\alpha_{\omega\mathbf{k}}$ and $\sigma_{\omega\mathbf{k}}$, an alternative approach is to determine these quantities as functions of ω from the optical properties of the solid and substitute them into (27). We should thus obtain a direct connection between the optical properties and the Ruthemann and Lang type experiments. Unfortunately at the present time satisfactory experimental data of either kind covering a sufficiently wide range to make these comparisons are not available.

ACKNOWLEDGMENT

I should like to express my thanks to Dr. S. Raimes for his advice and encouragement in this work. I am indebted also to the University of London for the award of a Postgraduate Studentship.

APPENDIX

The total rate of energy loss of a field in a dielectric is given by

$$R=\int\overline{\mathbf{J}(\mathbf{r},t)\,.\,\mathbf{E}(\mathbf{r},t)}\,d\mathbf{r}$$

where $\mathbf{J}(\mathbf{r},t)$ is the current induced in the dielectric by the field, and the bar denotes the time average over a unit time. Taking the Fourier transforms of $\mathbf{E}$ and $\mathbf{J}$, we have

$$\begin{aligned}R&=\sum_{\mathbf{k},\mathbf{k}',\omega,\omega'}\mathbf{E}_{\mathbf{k}'\omega'}\,.\,\mathbf{J}_{\mathbf{k}\omega}\overline{\exp\{i(\omega+\omega')t\}}\int\exp\{i(\mathbf{k}+\mathbf{k}')\,.\,\mathbf{r}\}\,d\mathbf{r}\\&=\sum_{\mathbf{k},\omega}\mathbf{E}_{-\mathbf{k},-\omega}\,.\,\mathbf{J}_{\mathbf{k}\omega}\end{aligned}$$

using the result $\mathbf{E}_{-\mathbf{k},-\omega}=\mathbf{E}^*_{\mathbf{k},\omega}$ ......(A 1)

which follows from the reality of $\mathbf{E}$, and the equation

$$\mathbf{J}_{\mathbf{k}\omega}=(i\omega\boldsymbol{\alpha}_{\omega\mathbf{k}}+\boldsymbol{\sigma}_{\omega\mathbf{k}})\,.\,\mathbf{E}_{\mathbf{k}\omega}$$

which can easily be deduced from the ordinary theory of dielectrics, we obtain

$$\begin{aligned}R&=\sum_{\mathbf{k}}\sum_{\omega=-\infty}^{\infty}\mathbf{E}^*_{\mathbf{k},\omega}\,.\,(i\omega\boldsymbol{\alpha}_{\omega\mathbf{k}}+\boldsymbol{\sigma}_{\omega\mathbf{k}})\,.\,\mathbf{E}_{\mathbf{k}\omega}\\&=\sum_{\mathbf{k}}\sum_{\omega=-\infty}^{\infty}(i\omega\alpha_{\omega\mathbf{k}}+\sigma_{\omega\mathbf{k}})\,|E_{\mathbf{k}\omega}|^2\end{aligned}$$

using $\mathbf{E}_{\mathbf{k}\omega}=\hat{\mathbf{k}}E_{\mathbf{k}\omega}$. The term in $\alpha_{\omega\mathbf{k}}$ just vanishes, the contributions from positive and negative ω's cancelling one another out. We thus have

$$R=\sum_{\mathbf{k}}\sum_{\omega=-\infty}^{\infty}\sigma_{\omega\mathbf{k}}\,|E_{\omega\mathbf{k}}|^2=\sum_{\mathbf{k}}\sum_{\omega=0}^{\infty}2\sigma_{\omega\mathbf{k}}\,|E_{\mathbf{k}\omega}|^2=\sum_{\mathbf{k}}\sum_{\omega=0}^{\infty}2k^2\sigma_{\omega\mathbf{k}}\,|\phi_{\omega\mathbf{k}}|^2$$

using $\sigma_{\omega\mathbf{k}}=\sigma_{-\omega-\mathbf{k}}$ (A 1) and $E_{\mathbf{k}\omega}=-ik\phi_{\omega\mathbf{k}}$ (which follows from $\mathbf{E}=-\nabla\phi$). By inspection we see that the rate of energy loss associated with the component $\phi_{\omega\mathbf{k}}$ of the field is $2k^2\sigma_{\omega\mathbf{k}}\,|\phi_{\omega\mathbf{k}}|^2$.

REFERENCES

BOHM, D., and PINES, D., 1953, *Phys. Rev.*, **92,** 609.
BOHR, A., 1948, *K. Danske Vidensk. Selsk. Mat. Fys. Medd.*, **24,** No. 19.
DARWIN, C., 1934, *Proc. Roy. Soc.* A, **146,** 17; 1943, *Ibid.*, **182,** 152.
FERMI, E., 1940, *Phys. Rev.*, **57,** 485.
HALPERN, O., and HALL, H., 1948, *Phys. Rev.*, **73,** 477.
HEITLER, W., 1954, *Quantum Theory of Radiation*, 3rd Edn (Oxford : University Press).
HUBBARD, J., 1954, *Proc. Phys. Soc.* A, **67,** 1058; 1955, *Ibid.*, **68,** 441.
IVES, H. E., and BRIGGS, H. B., 1936, *J. Opt. Soc. Amer.*, **26,** 238; 1937, *Ibid.*, **27,** 181.
KRAMERS, H. A., 1947, *Physica*, **13,** 401.
LANG, W., 1948, *Optik*, **3,** 233.
MACKE, W., 1950, *Z. Naturf.*, **5a,** 192.
MOTT, N. F., and JONES, H., 1936, *The Theory of the Properties of Metals and Alloys* (Oxford : University Press).
PINES, D., 1953, *Phys. Rev.*, **92,** 625.
RUTHEMANN, G., 1948, *Ann. Phys., Lpz.*, **2,** 113.
SCHIFF, L. I., 1949, *Quantum Mechanics* (New York : McGraw-Hill).
SEITZ, F., 1940, *Modern Theory of Solids* (New York : McGraw-Hill).
WILSON, A. H., 1935, *Proc. Roy. Soc.* A, **151,** 274.
WOLFF, P. A., 1953, *Phys. Rev.*, **92,** 18.

The Self-Consistent Field for Zr^{4+}

By S. L. ALTMANN
Mathematical Institute, Oxford

MS. received 5*th April* 1955 *and in amended form* 8*th June* 1955

Abstract. A fairly general programme for the computation of atomic self-consistent fields without exchange has been prepared for the Manchester University electronic computer. Results obtained for the Zr^{4+} ion are given.

---

§ 1. Introduction

In the course of some work on the electronic structure of Zr metal it was found necessary to obtain a potential field for the ion core Zr^{4+}. This has been obtained by a self-consistent field computation without exchange which has been programmed for the Manchester University computer Mark II. This programme is expected to be useful in its present form for most ions of medium and high atomic number. For this reason we think it worth describing in a little detail.

The characteristics of the Manchester electronic computer are well known (Kilburn 1951). For our purposes it is enough to say that it possesses an electronic store where information is kept for its immediate use, and an auxiliary one, magnetic, with longer accessibility time. The electronic store consists of eight cathode-ray tubes, each of them storing 64 lines of 20 binary digits. This amount of information is called a page. The magnetic store consists of 256 tracks, each of them containing two pages. There is an additional line of twenty binary digits governed by hand switches by means of which miscellaneous information can be fed into the machine. The machine works with numbers of forty binary digits (about twelve decimal digits) with fixed binary points. This means that only fractional numbers in the range $-0{\cdot}5$ to $+0{\cdot}5$ can be used and that great care must be exercised to prevent the various quantities calculated by the machine going off-scale.

It was decided at the beginning to use a computational procedure based on the methods devised by Hartree (1928, 1932–33, 1933, 1946–47) for desk-machine computation. Although when an electronic computer is available it might be more economical to use an essentially different procedure, such as that given by Torrance (1934), we considered it advantageous to use the Hartree technique, which is very suitable for the Manchester computer, thanks to its large storage capacity. Later experience fully confirmed this expectation.

§ 2. The Programme

A form of the Hartree method was used in which $x=\log_{10} r$ is taken as the independent variable, rather than the radial distance r. Then a range in r from $\sim 0{\cdot}002$ to 10 atomic units was covered in steps of uniform length $(x=1/30)$ in the numerical integrations. The radial equation is certainly more complicated in the x variable than it is in r, as now the first derivative of the wave function is present (see equation (3) below), but this does not introduce any additional difficulty when the numerical integration is carried out on the electronic computer, whereas changing the interval of integration is quite an uneconomical operation on it.

The contributions to the effective nuclear charge Z, which we shall denote by the notation $\mathcal{Z}^{(0)}(nl, x)$,† for the eight groups $1s^2$, $2s^2$, $2p^6$, $3s^2$, $3p^6$, $3d^{10}$, $4s^2$, $4p^6$ were first estimated by a scaling procedure. Those for the groups $3p^6$ and $3d^{10}$ were very kindly provided for us by Professor Hartree. The remaining ones were obtained from the field of Rb^+ calculated by Hartree (1935). Details of the scaling procedure are given by Hartree (1946) and Arnot and McLauchlan (1934). The contributions to Z were first interpolated on the machine from the r to the x variable and then stored in two tracks per group, sixteen tracks in all, which we call the $\mathcal{Z}$ store.

The first step in the self-consistent field cycle for a group (nl) is then to form the effective nuclear charge

$$Z(x) = \mathcal{Z}_1(x) + [(4l+1)/(4l+2)]\mathcal{Z}^{(0)}(nl, x) \qquad \ldots\ldots(1)$$

where

$$\mathcal{Z}_1(x) = C + 1 + \sum_{n'l' \neq nl} \mathcal{Z}^{(0)}(n'l', x)$$

C being the net charge on the ion, four in our case.‡ The computation is started with a routine which forms $\mathcal{Z}_1(x)$ and $\mathcal{Z}^{(0)}(nl, x)$ by omitting the relevant group in the summation involved in $\mathcal{Z}_1(x)$, in accord with a code number assigned to the groups. It then stores each of the tables in two tracks. It will be noted that $\mathcal{Z}_1(x)$ is a constant during the time that a group is being made self-consistent, so that when entering the cycle in a second iteration it is only necessary to modify $\mathcal{Z}^{(0)}(nl, x)$. The $\mathcal{Z}$ store is then kept unaltered and is treated as a more permanent store, to be used only in making one group self-consistent with the others.

A second routine then forms $Z(x)$ in accord with (1). The equation for the effective nuclear charge for the potential Z_p,

$$dZ_p/dx = K(Z_p - Z) \qquad \ldots\ldots(2)$$

where $K = \log_e 10$, can now be solved. This is integrated inwards by means of a Gill–Runge–Kutta integration routine (Gill 1951). dZ_p/dr is obtained at the last point and Z_p extrapolated to $r = 0$, where it is compared with the atomic number N as a check.

The Runge–Kutta method was used as the only integrating procedure throughout this programme, and some comments about it will be useful. As is well known, this method requires values of the derivatives at half the interval used in the integration. It is not convenient to carry out the necessary interpolation jointly with the integration, as the Runge–Kutta routine works with terms belonging to one interval at a time, a very advantageous feature which should be preserved so that there is no need of any special operation when a new page is brought from the magnetic to the electronic store. We therefore interpolate the auxiliary functions beforehand, set them up in a special manner, so that each interval can be treated quite independently of any other, and store the tables in the magnetic store to be brought to the electronic store when the Runge–Kutta routine is used. This interpolation is done by a general routine which is called in before the integration starts, every time the Runge–Kutta routine is used.

---

† $2(2l+1)\,[1 - Z_0(nl, nl|r)]$ in Hartree's notation. Our upper index denotes the stage of the iteration.

‡ These equations and those below are obtained by simple transformation from those given by Hartree (1933, 1946–47).

The next step is to solve the radial equation

$$P'' - KP' + F(x)P = 0 \qquad \ldots\ldots(3)$$

where $P = r \times$ radial wave function, and $F(x)$ is defined as

$$F(x) = F_1(x) - \epsilon F_2(x). \qquad \ldots\ldots(4)$$

Here $F_1(x) = 2Z_p(x)K^2 \exp(Kx) - K^2 l(l+1)$ and $F_2(x) = K^2 \exp(2Kx)$. $F_1(x)$ and $F_2(x)$ are calculated only once, before (3) is solved, whereas (4) is recomputed every time the energy parameter ϵ (which is measured in rydberg units) is changed.

Equation (3) is transformed into a set of two first-order differential equations which can be solved by the Runge–Kutta method, but an iterative procedure for ϵ is necessary. This is done in two stages. The second stage is the standard one, namely to obtain the eigenvalue and the eigenfunction by integrating outwards and inwards and joining the two solutions at an adjustable point. This is done by computing for each value of ϵ the quantity $(P/P')_{\text{out}} - (P/P')_{\text{in}}$ at the point of join, and using it and the corresponding value of ϵ in an interpolation procedure carried out by a modified rule of false position of higher order than the first. To start this procedure we require two values of ϵ which bracket the eigenvalue. Moreover, this bracket should be quite narrow, lest the functions go off-scale, especially in the inwards integration. We have therefore introduced a preliminary stage, which is a routine that provides a bracket of the desired width by starting with any value of ϵ below the eigenvalue, so that a minimum amount of guesswork is necessary. This is essential as owing to the high speed of the machine one is passing from one group to another in a matter of a few minutes and a new ϵ must be guessed each time.

The initial routine for finding the eigenvalue is based on the following facts: (i) The eigenfunction of (3) and all the solutions of it corresponding to values of ϵ above the eigenvalue have $n-l$ nodes, the node at the origin being included. Those corresponding to values of ϵ below the eigenvalue have $n-l+1$ nodes. (ii) This extra node appears at a fraction of an atomic unit after the last maximum of P, even when ϵ differs from the eigenvalue by less than 1%. This means that the number of nodes ν of the solutions can be used to find the values of ϵ that bracket the eigenvalue, by integrating outwards only, for a fraction (adjustable) of the total range of x, so that the danger of the functions going off-scale in the machine is reduced. This is essential at the beginning, when values of ϵ differing widely from the eigenvalue might be used. The procedure used is the following: An initial guess for ϵ is set in the hand switches. A routine then operates which picks up this value automatically and integrates equation (3) outwards counting the number of nodes ν of P. An adjustable step Δ is then repeatedly added to ϵ until ν differs by one from the previous value. Then Δ is halved n times (n adjustable) and a check is made to ensure that the two final values of ϵ correspond to solutions with the right number of nodes over a second, wider range. These values of ϵ are used in starting the second stage.

In higher order iterations of the whole cycle a fairly good estimate of the bracketing values of ϵ is now possible, as the field must be almost correct and the variations in the eigenvalue are now small. Facilities are therefore provided for by-passing the nodes-counting routine and getting the machine to form a suitable pair of values of ϵ, from the last eigenvalue obtained.

Initial values of P and P' are necessary for both the outwards and inwards integration. The values of P are arbitrary and can be easily modified. This is necessary in going from one group to another, to ensure that in all cases the maximum value of P is as large as possible without going off-scale. The initial values of P' are then obtained from the values of P and ϵ by using two routines based on techniques described by Hartree (1928, 1932–33). In the integration inwards it is necessary to have a starting routine for a variable value of r smaller than $r=10$, because if the integration inwards is started too far from the last maximum of P, both P and P' increase so rapidly that they go off-scale before the point of join is reached. A starting routine for an easily variable value of x is therefore provided. Both starting routines are called in every time ϵ is changed.

Once a join is obtained to a specified accuracy a final outwards and inwards integration is run, a table of P now being built up. A new estimate for $\mathcal{Z}(nl,x)$, $\mathcal{Z}^{(1)}(nl,x)$, is then obtained by integration:

$$\mathcal{Z}^{(1)}(nl,x)=2(2l+1)\left[1-\int_{-\infty}^{x}P^2\exp(Kx)dx\Big/\int_{-\infty}^{+\infty}P^2\exp(Kx)dx\right]\ldots\ldots(5)$$

which finishes a complete cycle.

The differences $\mathcal{Z}^{(1)}(nl,x)-\mathcal{Z}^{(0)}(nl,x)$ are now obtained and printed. If they are of the desired order the iteration is interrupted by the operator by setting zero in the hand switches, whereupon $\mathcal{Z}^{(1)}(nl,x)$, P and the normalizing factor are printed, and $\mathcal{Z}^{(1)}(nl,x)$ transferred to its appropriate track in the $\mathcal{Z}$ store, to be used when working out another group. If it is judged that further iteration is necessary, the number one is set in the hand switches. A new estimate for $\mathcal{Z}(nl,x)$ is now necessary to start a new cycle. It is not always convenient to take $\mathcal{Z}^{(1)}(nl,x)$ as this new estimate, but rather to obtain one based in the values of $\mathcal{Z}^{(0)}(nl,x)$ and $\mathcal{Z}^{(1)}(nl,x)$. This would normally be taken to be near $\mathcal{Z}^{(1)}(nl,x)$ for small values of x and half way between $\mathcal{Z}^{(0)}(nl,x)$ and $\mathcal{Z}^{(1)}(nl,x)$ for large values of x, but if there is overstability (Hartree 1933) the new estimate should be nearer $\mathcal{Z}^{(0)}(nl,x)$. We have therefore prepared a very flexible weighting routine which can cover a variety of cases. This is based on building up a weighting function $w(x)$ (from a hyperbolic tangent) that goes from 0 to $1/h$ in the given range of x. Both h and the position of the inflection point of $w(x)$ can be easily altered by a decision on the hand switches. Then the weighted function

$$w(x)\mathcal{Z}^{(0)}(nl,x)+[1-w(x)]\mathcal{Z}^{(1)}(nl,x)$$

is formed. If h is taken to be 2 a new estimate is obtained which obeys the rule given before. On the other hand $\mathcal{Z}^{(0)}(nl,x)$ and $\mathcal{Z}^{(1)}(nl,x)$ can be interchanged when weighting by a decision on the hand switches, and this facility, in conjunction with an appropriate choice of h, permits cases of overstability to be treated. Another alternative provided is to by-pass the weighting operation and to substitute $\mathcal{Z}^{(1)}(nl,x)$ for $\mathcal{Z}^{(0)}(nl,x)$, which is convenient when dealing with inner shells. When the weighting operation is completed the weighted function is written over the table of $\mathcal{Z}^{(0)}(nl,x)$, and the whole cycle is automatically restarted.

The master routine that governs the various operations so that one routine follows the other automatically is provided with a flexible control number, so that a cycle can be started at any point, which is necessary when owing to a machine failure a routine must be restarted. To switch over from one group to another it is enough to run a short tape which contains the variable parameters that correspond to the given group. Each cycle takes from fifteen to twenty minutes.

§ 3. Results

The contributions to Z, which are given in table 1, have been made self-consistent within less than 0·0005 electron. This means that each group was iterated until the final estimate of $\mathcal{Z}(nl, x)$ differed in all points from the previous

Table 1. Contributions to Z, $2(2l+1)[1-Z_0(nl, nl\,|\,r)]$

	$r = A\times10^p$									
$3x$	A	p	$1s^2$	$2s^2$	$2p^6$	$3s^2$	$3p^6$	$3d^{10}$	$4s^2$	$4p^6$
$-\infty$	0·0000	(0)	2·000	2·000	6·000	2·000	6·000	10·000	2·000	6·000
−8·0	2·1544	(−3)	2·000	2·000	6·000	2·000	6·000	10·000	2·000	6·000
−7·5	3·1623	(−3)	1·997	2·000	6·000	2·000	6·000	10·000	2·000	6·000
−7·0	4·6416	(−3)	1·989	1·999	6·000	2·000	6·000	10·000	2·000	6·000
−6·5	6·8129	(−3)	1·966	1·997	6·000	1·999	6·000	10·000	2·000	6·000
−6·0	1·0000	(−2)	1·908	1·991	6·000	1·999	6·000	10·000	2·000	6·000
−5·5	1·4678	(−2)	1·776	1·979	5·999	1·996	6·000	10·000	1·999	6·000
−5·0	2·1544	(−2)	1·513	1·957	5·992	1·993	5·999	10·000	1·999	6·000
−4·8	2·5119	(−2)	1·361	1·946	5·985	1·991	5·997	10·000	1·999	6·000
−4·6	2·9286	(−2)	1·185	1·934	5·972	1·989	5·995	10·000	1·998	5·999
−4·4	3·4145	(−2)	0·989	1·924	5·948	1·988	5·991	10·000	1·998	5·999
−4·2	3·9811	(−2)	0·785	1·917	5·905	1·987	5·984	10·000	1·998	5·998
−4·0	4·6416	(−2)	0·584	1·914	5·833	1·986	5·972	10·000	1·998	5·996
−3·8	5·4117	(−2)	0·404	1·914	5·713	1·986	5·953	9·999	1·998	5·994
−3·6	6·3096	(−2)	0·255	1·911	5·526	1·986	5·924	9·998	1·998	5·990
−3·4	7·3564	(−2)	0·145	1·894	5·244	1·982	5·883	9·994	1·997	5·984
−3·2	8·5770	(−2)	0·072	1·845	4·844	1·973	5·829	9·987	1·996	5·977
−3·0	1·0000	(−1)	0·031	1·743	4·311	1·955	5·766	9·972	1·993	5·969
−2·9	1·0798	(−1)	0·019	1·667	3·996	1·943	5·733	9·958	1·991	5·964
−2·8	1·1659	(−1)	0·011	1·572	3·653	1·930	5·701	9·939	1·989	5·960
−2·7	1·2589	(−1)	0·006	1·458	3·287	1·915	5·673	9·912	1·986	5·957
−2·6	1·3594	(−1)	0·003	1·327	2·906	1·900	5·649	9·875	1·984	5·954
−2·5	1·4678	(−1)	0·002	1·183	2·518	1·886	5·632	9·823	1·982	5·952
−2·4	1·5849	(−1)	0·001	1·030	2·135	1·874	5·621	9·753	1·980	5·951
−2·3	1·7113	(−1)		0·873	1·766	1·866	5·617	9·659	1·979	5·951
−2·2	1·8478	(−1)		0·719	1·423	1·862	5·617	9·537	1·979	5·951
−2·1	1·9953	(−1)		0·573	1·112	1·860	5·615	9·378	1·979	5·950
−2·0	2·1544	(−1)		0·441	0·842	1·860	5·604	9·177	1·979	5·948
−1·9	2·3263	(−1)		0·327	0·616	1·858	5·574	8·926	1·978	5·942
−1·8	2·5119	(−1)		0·232	0·433	1·848	5·513	8·620	1·976	5·932
−1·7	2·7123	(−1)		0·158	0·293	1·826	5·407	8·254	1·971	5·916
−1·6	2·9286	(−1)		0·102	0·189	1·785	5·246	7·826	1·963	5·893
−1·5	3·1623	(−1)		0·063	0·116	1·720	5·018	7·337	1·952	5·862
−1·4	3·4145	(−1)		0·037	0·068	1·627	4·721	6·790	1·938	5·825
−1·3	3·6869	(−1)		0·020	0·037	1·506	4·354	6·194	1·921	5·784
−1·2	3·9811	(−1)		0·010	0·020	1·359	3·927	5·560	1·903	5·741
−1·1	4·2987	(−1)		0·005	0·010	1·191	3·453	4·902	1·886	5·702
−1·0	4·6416	(−1)		0·002	0·004	1·012	2·953	4·238	1·872	5·670
−0·9	5·0119	(−1)		0·001	0·002	0·829	2·450	3·586	1·863	5·648
−0·8	5·4117	(−1)			0·001	0·655	1·966	2·964	1·859	5·637
−0·7	5·8434	(−1)				0·496	1·521	2·388	1·858	5·634
−0·6	6·3096	(−1)				0·359	1·132	1·870	1·857	5·634
−0·5	6·8129	(−1)				0·249	0·808	1·421	1·850	5·623
−0·4	7·3564	(−1)				0·163	0·552	1·044	1·830	5·588
−0·3	7·9433	(−1)				0·102	0·358	0·740	1·788	5·511
−0·2	8·5770	(−1)				0·060	0·221	0·505	1·718	5·374
−0·1	9·2612	(−1)				0·033	0·129	0·330	1·616	5·162
0·0	1·0000	(0)				0·017	0·071	0·206	1·481	4·867
0·1	1·0798	(0)				0·008	0·036	0·123	1·318	4·488
0·2	1·1659	(0)				0·004	0·018	0·069	1·134	4·035
0·3	1·2589	(0)				0·001	0·008	0·037	0·941	3·525
0·4	1·3594	(0)					0·003	0·019	0·751	2·985
0·5	1·4678	(0)					0·001	0·009	0·573	2·442
0·6	1·5849	(0)						0·004	0·419	1·925
0·7	1·7113	(0)						0·002	0·291	1·457
0·8	1·8478	(0)						0·001	0·192	1·056
0·9	1·9953	(0)							0·120	0·730
1·0	2.1544	(0)							0·070	0·480
1·1	2·3263	(0)							0·039	0·298
1·2	2·5119	(0)							0·020	0·175
1·3	2·7123	(0)							0·009	0·096
1·4	2·9286	(0)							0·004	0·049
1·5	3·1623	(0)							0·002	0·023
1·6	3·4145	(0)							0·001	0·010
1·7	3·6869	(0)								0·004
1·8	3·9811	(0)								0·001

Table 2. Radial wave functions. Table of *P*

	$r=A\times 10^p$									
3*x*	*A*	*p*	1s	2s	2p	3s	3p	3d	4s	4p
−∞	0·0000	(0)	0·000	0·000	0·000	0·000	0·000	0·00000	0·000	0·000
−8·1	1·9953	(−3)	1·000	+1·000	0·010	+0·100	+0·010	0·00001	+0·100	+0·010
−8·0	2·1544	(−3)	1·073	+1·073	0·012	+0·107	+0·012	0·00001	+0·107	+0·012
−7·5	3·1623	(−3)	1·513	+1·511	0·025	+0·151	+0·025	0·00004	+0·151	+0·025
−7·0	4·6416	(−3)	2·093	+2·086	0·051	+0·209	+0·051	0·0001	+0·208	+0·051
−6·5	6·8129	(−3)	2·817	+2·793	0·106	+0·279	+0·106	0·0004	+0·279	+0·106
−6·0	1·0000	(−2)	3·641	+3·570	0·214	+0·356	+0·214	0·0011	+0·356	+0·214
−5·5	1·4678	(−2)	4·437	+4·232	0·421	+0·421	+0·420	0·0034	+0·420	+0·420
−5·0	2·1544	(−2)	4·957	+4·409	0·794	+0·434	+0·789	0·0098	+0·433	+0·789
−4·8	2·5119	(−2)	5·014	+4·221	1·008	+0·412	+0·999	0·0148	+0·411	+0·998
−4·6	2·9286	(−2)	4·956	+3·823	1·265	+0·369	+1·249	0·0223	+0·367	+1·247
−4·4	3·4145	(−2)	4·767	+3·175	1·567	+0·299	+1·540	0·0333	+0·296	+1·536
−4·2	3·9811	(−2)	4·443	+2·249	1·913	+0·200	+1·867	0·0492	+0·197	+1·861
−4·0	4·6416	(−2)	3·991	+1·034	2·296	+0·072	+2·218	0·0720	+0·068	+2·208
−3·8	5·4117	(−2)	3·435	−0·450	2·701	−0·082	+2·573	0·1041	−0·088	+2·556
−3·6	6·3096	(−2)	2·813	−2·146	3·107	−0·255	+2·898	0·1485	−0·261	+2·871
−3·4	7·3564	(−2)	2·175	−3·948	3·481	−0·432	+3·146	0·2085	−0·437	+3·104
−3·2	8·5770	(−2)	1·572	−5·707	3·785	−0·593	+3·261	0·2877	−0·596	+3·195
−3·0	1·0000	(−1)	1·051	−7·240	3·976	−0·711	+3·175	0·3891	−0·708	+3·077
−2·9	1·0798	(−1)	0·832	−7·861	4·016	−0·745	+3·036	0·4489	−0·738	+2·918
−2·8	1·1659	(−1)	0·642	−8·355	4·014	−0·758	+2·823	0·5149	−0·744	+2·682
−2·7	1·2589	(−1)	0·483	−8·702	3·967	−0·746	+2·532	0·5869	−0·725	+2·365
−2·6	1·3594	(−1)	0·358	−8·890	3·874	−0·706	+2·157	0·6646	−0·678	+1·963
−2·5	1·4678	(−1)	0·251	−8·908	3·734	−0·638	+1·699	0·7473	−0·600	+1·476
−2·4	1·5849	(−1)	0·172	−8·757	3·549	−0·540	+1·160	0·8343	−0·492	+0·908
−2·3	1·7113	(−1)	0·114	−8·440	3·324	−0·414	+0·545	0·9242	−0·354	+0·268
−2·2	1·8478	(−1)	0·073	−7·974	3·063	−0·260	−0·134	1·0154	−0·190	−0·432
−2·1	1·9953	(−1)	0·045	−7·378	2·776	−0·084	−0·863	1·1059	−0·004	−1·173
−2·0	2·1544	(−1)	0·026	−6·680	2·469	+0·110	−1·623	1·1985	+0·197	−1·932
−1·9	2·3263	(−1)	0·015	−5·913	2·154	+0·314	−2·392	1·2757	+0·404	−2·679
−1·8	2·5119	(−1)	0·008	−5·110	1·840	+0·522	−3·144	1·3497	+0·608	−3·383
−1·7	2·7123	(−1)	0·005	−4·307	1·537	+0·723	−3·852	1·4129	+0·796	−4·008
−1·6	2·9286	(−1)	0·002	−3·534	1·253	+0·910	−4·490	1·4627	+0·958	−4·519
−1·5	3·1623	(−1)	0·001	−2·820	0·996	+1·073	−5·032	1·4969	+1·082	−4·881
−1·4	3·4145	(−1)		−2·184	0·770	+1·206	−5·458	1·5137	+1·156	−5·064
−1·3	3·6869	(−1)		−1·639	0·578	+1·303	−5·750	1·5119	+1·174	−5·041
−1·2	3·9811	(−1)		−1·190	0·421	+1·359	−5·900	1·4911	+1·129	−4·796
−1·1	4·2987	(−1)		−0·834	0·296	+1·375	−5·905	1·4515	+1·018	−4·320
−1·0	4·6416	(−1)		−0·563	0·201	+1·351	−5·770	1·3940	+0·842	−3·615
−0·9	5·0119	(−1)		−0·365	0·132	+1·291	−5·508	1·3201	+0·607	−2·694
−0·8	5·4117	(−1)		−0·227	0·083	+1·200	−5·137	1·2320	+0·319	−1·579
−0·7	5·8434	(−1)		−0·135	0·050	+1·085	−4·679	1·1322	−0·008	−0·305
−0·6	6·3096	(−1)		−0·076	0·029	+0·955	−4·161	1·0239	−0·362	+1·084
−0·5	6·8129	(−1)		−0·041	0·016	+0·817	−3·609	0·9100	−0·724	+2·536
−0·4	7·3564	(−1)		−0·021	0·008	+0·678	−3·050	0·7941	−1·078	+3·991
−0·3	7·9433	(−1)		−0·010	0·004	+0·546	−2·509	0·6795	−1·404	+5·389
−0·2	8·5770	(−1)		−0·004	0·002	+0·426	−2·005	0·5692	−1·687	+6·667
−0·1	9·2612	(−1)		−0·002	0·001	+0·321	−1·555	0·4663	−1·911	+7·767
0·0	1·0000	(0)				+0·234	−1·168	0·3728	−2·067	+8·642
0·1	1·0798	(0)				+0·164	−0·848	0·2905	−2·149	+9·257
0·2	1·1659	(0)				+0·111	−0·594	0·2203	−2·157	+9·592
0·3	1·2589	(0)				+0·071	−0·401	0·1623	−2·095	+9·645
0·4	1·3594	(0)				+0·044	−0·260	0·1160	−1·972	+9·429
0·5	1·4678	(0)				+0·026	−0·161	0·0802	−1·802	+8·973
0·6	1·5849	(0)				+0·015	−0·096	0·0535	−1·597	+8·318
0·7	1·7113	(0)				+0·008	−0·054	0·0345	−1·374	+7·510
0·8	1·8478	(0)				+0·004	−0·029	0·0213	−1·146	+6·602
0·9	1·9953	(0)				+0·002	−0·015	0·0126	−0·926	+5·646
1·0	2·1544	(0)				+0·001	−0·007	0·0071	−0·724	+4·692
1·1	2·3263	(0)					−0·003	0·0038	−0·547	+3·782
1·2	2·5119	(0)					−0·001	0·0020	−0·398	+2·952
1·3	2·7123	(0)					−0·001	0·0009	−0·278	+2·227
1·4	2·9286	(0)						0·0004	−0·186	+1·618
1·5	3·1623	(0)						0·0002	−0·119	+1·130
1·6	3·4145	(0)						0·0001	−0·073	+0·756
1·7	3·6869	(0)							−0·042	+0·483
1·8	3·9811	(0)							−0·023	+0·294
1·9	4·2987	(0)							−0·012	+0·169
2·0	4·6416	(0)							−0·006	+0·092
2·1	5·0119	(0)							−0·003	+0·047
2·2	5·4117	(0)							−0·001	+0·023
2·3	5·8434	(0)								+0·010
2·4	6·3096	(0)								+0·004
2·5	6·8129	(0)								+0·002
2·6	7·3564	(0)								+0·001
2·7	7·9433	(0)								+0·000

one by less than 0·0005 electron, and that this situation was attained for the eight groups simultaneously, each one being integrated in the revised fields of the others. The values given in table 1 are therefore exact in all the figures printed. This accuracy, about ten times better than that of Hartree's standard computations (Hartree 1933) was obtained in about 30 hours of machine work. Values of P are given in table 2. Values of the r variable are also given in these tables so as to facilitate a comparison with other fields. The eigenvalues and normalizing factors are given in table 3.

Table 3. Values of ϵ (in rydberg units) and $I = \int_0^\infty P^2 dr$

	1s	2s	2p	3s	3p	3d	4s	4p
ϵ	1302·92	178·66	165·32	31·131	25·732	16·152	6·6947	5·1803
I	1·1780	11·9478	2·4330	0·7119	14·0735	1·0475	4·3754	101·83

We print in the tables values of the functions at varying intervals of x, which are considered suitable for most applications, but the values of $\mathcal{Z}(nl, x)$ and P for all the 112 points $x = -2{\cdot}7(1/30)1$ are available and are being deposited with the Royal Society, as well as an extra table (table 4) which gives the values of P for small values of r, with no less than four significant figures†.

ACKNOWLEDGMENTS

I should like to thank the following persons: Dr. N. E. Hoskin for introducing me to the techniques of electronic computing and for his unfailing help and advice during the development of the programme, Mr. R. A. Brooker and the staff of the Manchester University Computing Machine Laboratory, for the hospitality given to me and especially for the most generous provision of machine time, Professor D. R. Hartree for discussion and correspondence which was essential to this work and for providing me with the data for obtaining the initial estimates for the field, Dr. A. S. Douglas for discussion and Professor C. A. Coulson for his interest in this work and comments on the manuscript.

REFERENCES

ARNOT, F. L., and MCLAUCHLAN, J. C., 1934, *Proc. Roy. Soc.* A, **146**, 662.

GILL, S., 1951, *Proc. Camb. Phil. Soc.*, **47**, 96.

HARTREE, D. R., 1928, *Proc. Camb. Phil. Soc.*, **24**, 89, 111; 1932–33, *Mem. Manchr. Lit. Phil. Soc.*, **77**, 91; 1933, *Proc. Roy. Soc.* A, **141**, 282; 1935, *Ibid.*, **151**, 96; 1946–47, *Rep. Progr. Phys.*, **11**, 113 (London : Physical Society).

KILBURN, T., 1951, *Nature, Lond.*, **168**, 95.

TORRANCE, C. C., 1934, *Phys. Rev.*, **46**, 388.

---

† *Note added in proof.* Copies of these tables (The Self-Consistent Field for Zr^{4+}: supplementary tables, by S. L. Altmann, file no. 56) can be obtained from the Royal Society Depository of Unpublished Tables, The Royal Society, Burlington House, London W.1.

Inelastic Scattering of Neutrons by Deformed Nuclei

By D. M. BRINK
Clarendon Laboratory, Oxford

MS. received 16*th May* 1955 *and in final form* 17*th June* 1955

Abstract. The cross section for direct inelastic scattering from the nuclear surface deformation is calculated and compared with the compound nucleus inelastic cross section. It is found, using optical model wave functions, that the direct process can be important in the regions of atomic weight near $A = 150$ and $A = 240$.

---

§ 1. INTRODUCTION

MANY of the features of the process of inelastic scattering of neutrons by medium and heavy nuclei have been explained on the basis of Bohr's (1936) compound nucleus model. This model assumes that, when a neutron of moderate energy strikes a target nucleus it may be absorbed to form a compound system of some stability. Subsequently this compound system can decompose emitting a neutron and leaving the target nucleus in an excited state. The theory supposes that the formation and the decay of the compound nucleus may be treated as independent processes, so that the mode of decay of the compound system depends only on its energy, total angular momentum and parity, but not specifically on the way in which it was formed. Hauser and Feshbach (1952) have considered this theory in some detail and the results of their calculations account for most of the observed features of inelastic scattering for neutron energies up to about 5 MEV.

Recently the collective model of the nucleus proposed by Bohr (1952) has been very successful in describing the properties of low excited states in heavy nuclei. These states are assumed to be the various collective modes of motion of the nuclear surface and, in many nuclei, they arise from the rotation of a large ellipsoidal surface deformation. Consider the scattering of a neutron by such a nucleus. The incident neutron may be elastically scattered or it may be absorbed to form a compound system; but there is also the possibility that direct interaction with the nuclear surface will inelastically scatter the neutron and excite a surface mode. One can picture this process in the following way: The neutron enters the nucleus and is reflected within the walls of the nucleus. If the nucleus is non-spherical, there is a chance that by these reflections the nucleus is set in rotation or vibration. Evidently the cross section for this process will be highest for those nuclear radii for which a standing wave develops inside the nucleus, thus giving rise to many reflectors. In the present paper, we investigate this process and compare its cross section with the cross section for compound nucleus formation. We will be interested chiefly in the excitation of the rotational surface modes in strongly deformed nuclei.

§ 2. The Collective Model

The surface coordinates $\alpha_{\lambda\mu}$ of a nucleus are defined by the equation to the nuclear surface

$$R(\theta,\phi)=R_0\left[1+\sum_{\lambda\mu}\alpha_{\lambda\mu}Y_\lambda^\mu(\theta,\phi)\right] \qquad \ldots\ldots(1)$$

where R_0 is the radius of the undeformed nucleus and Y_λ^μ is a normalized spherical harmonic with Condon and Shortley (1935) phases. The rotational levels considered by Bohr (1952) are described by the coordinates $\alpha_{\lambda\mu}$ and the nuclear rotational Hamiltonian H_0 is a function of these coordinates. Deformations with $\lambda\neq 2$ do not contribute appreciably, thus need not be considered.

The Hamiltonian for the scattering of a neutron by a Bohr nucleus can be written H_0+T+V, where T is the neutron kinetic energy and V is the neutron nucleus interaction potential. Following Bohr we approximate the potential V by a square well,

$$\begin{aligned} V(\mathbf{r},\alpha_{2\mu}) &= -V_0 \quad \text{if} \quad r<R(\theta,\phi) \\ &= \quad 0 \quad \text{if} \quad r>R(\theta,\phi). \end{aligned} \qquad \ldots\ldots(2)$$

Because V depends on the neutron coordinate $\mathbf{r}$ and the nuclear surface coordinates $\alpha_{2\mu}$ it contains a direct interaction between the neutron and the surface deformations, and it is this coupling which gives rise to inelastic scattering with the excitation of surface modes. In order to calculate the cross section for the scattering, we split V into two parts by expanding as a power series in the surface deformations $\alpha_{2\mu}$. For small deformations, powers of $\alpha_{2\mu}$ higher than the first may be neglected, so that

$$\begin{aligned} V(\mathbf{r},\alpha_{2\mu}) &\simeq \bar{V}(r)+V_0R_0\delta(r-R_0)\sum_\mu \alpha_{2\mu}Y_2^\mu(\theta,\phi) \\ &= \bar{V}(r)+H', \end{aligned} \qquad \ldots\ldots(3)$$

with

$$\begin{aligned} \bar{V}(r) &= -V_0 \quad \text{if} \quad r<R_0 \\ &= \quad 0 \quad \text{if} \quad r>R_0 \end{aligned}$$

and $\delta(r-R_0)$ the Dirac delta function.

The averaged central potential $\bar{V}(r)$ represents the interaction of a neutron with an undeformed nucleus while the term H', containing both neutron and surface coordinates, is the coupling between the neutron and the surface deformations.

We want to compare the magnitude of the direct scattering with compound nucleus scattering so it is useful to include compound nucleus formation in our model. Feshbach, Porter and Weisskopf (1954) have proposed a simple description of neutron scattering in which they replace the neutron–nucleus interaction by a complex potential well. The imaginary part of the potential causes an absorption to be identified with compound nucleus formation. We use the results of their paper by taking V_0 the strength of the neutron–nucleus interaction (2) to be complex with a small imaginary part. The compound nucleus scattering can then be calculated from the theory of Hauser and Feshbach (1952). The decay of the compound nucleus is assumed to be independent of its mode of formation and, in particular, the phase of the inelastically scattered neutron wave is indeterminate. In contrast to this, the phase of the neutron waves inelastically scattered from the nuclear surface deformations, is completely determined by the phase of the incident wave. Thus the contributions to the scattering by direct interaction and due to compound nucleus formation (averaged over nuclear resonances) are incoherent.

§ 3. THE CALCULATION OF THE CROSS SECTION

The cross section for inelastic scattering has been calculated treating the potential $\overline{V}(r)$ exactly and the term H' as a perturbation on the scattering by this potential. As there is no spin interaction in the potential, we can write the unperturbed solution as a pure orbital wave function corresponding to scattering of plane waves by $\overline{V}(r)$. The solution with wave number k can be written

$$\psi(\mathbf{r})=\frac{i\pi^{1/2}}{k}\sum_{l}(-1)^{l}(2l+1)^{1/2}\psi_{l,0}(\mathbf{r}), \qquad \ldots\ldots(4)$$

where the functions $\psi_{l,m}$ are the bounded partial wave solutions for the potential $\overline{V}(r)$. We have

$$\psi_{l,m}=\frac{1}{r}\,u_l(kr)\mathrm{Y}_l^m(\theta,\phi) \qquad \ldots\ldots(5)$$

where $u_l(kr)\sim e^{-ikr}-\eta_l e^{ikr}$ for large r. η_l is the complex reflection factor of Feshbach, Porter and Weisskopf with $|\eta_l|<1$ because of the absorption term in the potential.

Suppose we are considering neutron scattering from an initial nuclear state $|I_0M_0\rangle$ to a final state $|IM\rangle$ with an incident neutron wave $\psi_0(\mathbf{r})$ with wave number k_0 and energy E_0 and a scattered neutron wave $\psi_s(\mathbf{r})$ of energy E and wave number k. To the first order of perturbation ψ_s is the solution of the inhomogeneous equation

$$\left(-\frac{\hbar^2}{2M}\nabla^2+\overline{V}(r)-E\right)\psi_s=-\langle IM|H'|I_0M_0\rangle\psi_0(\mathbf{r}) \qquad \ldots\ldots(6)$$

corresponding to outgoing waves. This equation can be solved by Green's function methods (Mott and Massey 1949) and for large r the wave function ψ_s has the asymptotic form

$$\psi_s\simeq\frac{e^{ikr}}{2ikr}\frac{2M}{\hbar^2}\sum_{l,m}\mathrm{Y}_l^m(\theta,\phi)[(-1)^m\psi_{l,m}(\mathbf{r}')\langle IM|H'|I_0M_0\rangle\psi_0(\mathbf{r}')\,d\mathbf{r}'. \qquad \ldots\ldots(7)$$

If we substitute for H' from (3) and evaluate the integrals, we get the explicit form

$$\psi_s\sim\frac{e^{ikr}}{r}\frac{V_0R_02M}{\hbar^2}\sum_{l,l_0,\mu}\left[\frac{[(2l_0+1)(2l+1)]^{1/2}}{4kk_0}u_{l_0}(k_0R_0)u_l(kR)\right.$$
$$\left.\times\,\mathrm{Y}_l^{\mu}(\theta,\phi)C(2ll_0,-\mu\mu)C(ll_02,00)\langle IM|\alpha_{2\mu}|I_0M_0\rangle\right] \qquad \ldots\ldots(8)$$

where the $C(2ll_0,-\mu\mu)$ are Clebsch–Gordan vector addition coefficients in the notation of Biedenharn, Blatt and Rose (1953).

In the following it is convenient to write $K^2=(2M/\hbar^2)|V_0|$, then K is approximately the wave number of the scattered neutron inside the nucleus for low incident neutron energies. Put $KR_0=X$, $k_0R_0=x_0$ and $kR_0=x$. The differential cross section for inelastic scattering is given in terms of ψ_s by

$$\sigma(\theta)=\frac{k}{k_0}\,[|\psi_s|^2r^2]_{r=\infty}$$

so, averaging over initial nuclear orientations and summing over final orientations we get for the differential cross section

$$\sigma(\theta)=\frac{X^4M(I_0I)}{k_0{}^2 16x_0x}\sum_{\mu}\Big|\sum_{l,l_0}[(2l_0+1)(2l+1)]^{1/2}u_{l_0}(x_0)u_l(x)$$

$$\times C(2ll_0,-\mu\mu)C(ll_02,00)Y_l^{\mu}(\theta,\phi)\Big|^2 \qquad \ldots\ldots(9)$$

and for the total cross section

$$\sigma=\frac{X^4M(I_0,I)}{k_0{}^2 16x_0x}\sum_{l,l_0}(2l_0+1)(2l+1)\,|\,u_{l_0}(x_0)\,|^2\,|\,u_l(x)\,|^2\,[C(ll_02,00)]^2. \qquad \ldots.(10)$$

The coefficient

$$M(I_0,I)=\frac{1}{2I_0+1}\sum_{M_0,M}|\,\langle IM\,|\,\alpha_{2\mu}\,|\,I_0M_0\rangle\,|^2$$

is the averaged square of the nuclear matrix element of the deformations $\alpha_{2\mu}$, and it is seen that the dependence of the cross section on the structure of the initial and final nuclear states enters only through this factor. In even–even nuclei we are interested in a $0^+\to2^+$ transition and for this transition

$$M(0,2)=\beta^2/5 \qquad \ldots\ldots(11)$$

if the two states have a rotational character. Here β is the nuclear deformation parameter defined by Bohr and Mottelson, $\beta^2=\Sigma_\mu|\alpha_{2\mu}|^2$. In odd A nuclei with a rotational sequence I_0, I_0+1, I_0+2 $(I_0\neq\frac{1}{2})$

$$M(I_0,I_0+1)=\frac{3}{5}\frac{\beta^2I_0}{(I_0+1)(I_0+2)}$$

and

$$M(I_0,I_0+2)=\frac{6}{5}\frac{\beta^2}{(I_0+1)(2I_0+1)}. \qquad \ldots\ldots(12)$$

Transitions with $\Delta I>2$ are forbidden on this model by angular momentum considerations if we neglect $\lambda\neq2$ in (1).

§ 4. RESULTS

In this section we give the results of some calculations of the inelastic cross section by the direct process and compare them with cross sections for the compound nucleus scattering calculated from the formulae of Hauser and Feshbach (1952). First, however, we express the direct cross section (10) explicitly in terms of optical model parameters introduced by Feshbach, Porter and Weisskopf (1954). We write for the logarithmic derivatives at the nuclear boundary

$$f_l+ig_l=R_0\left[\frac{du_l}{dr}\Big/u_l\right]_{r=R_0}$$

$$\Delta_l+iS_l=R_0\left[\frac{du_l{}^+}{dr}\Big/u_l{}^+\right]_{r=R_0}.$$

Here $u_l{}^+$ is the partial wave solution for a potential $\overline{V}(r)$ with only outgoing waves, If we put

$$M_l=S_l-g_l, \qquad N_l=f_l-\Delta_l$$

it can be shown that

$$|\,u_l(x)\,|^2=\frac{4xS_l}{M_l{}^2+N^2}$$

and substituting into (10) the total cross section for the direct inelastic process is

$$\sigma=\frac{M(I_0,I)}{k_0^{2}}\sum_{l,l_0}(2l_0+1)(2l+1)[C(ll_02,00)]^2\,\frac{X^2S_l}{M_l^2+N_l^2}\,\frac{X^2S_{l_0}}{M_{l_0}^{2}+N_{l_0}^{2}}.$$

Hauser and Feshbach (1952) give their results in terms of a 'barrier penetrability' $T_l(E)$ which is the probability that a neutron in a partial wave l and with energy E will be absorbed and form a compound nucleus. For the 'optical model' T_l has the form

$$T_l=1-|\eta_l|^2=\frac{-4S_lg_l}{M_l^2+N_l^2}.$$

In calculating both the direct scattering and the compound nucleus scattering we have chosen a potential well with $V_0=40(1+0{\cdot}05i)$ MeV and $R_0=1{\cdot}45\times10^{-13}A^{1/3}$ cm.

We have made calculations of the inelastic cross section for an even–even nucleus, i.e. for a $0^+\rightarrow2^+$ transition. The 2^+ state is assumed to have a pure rotational character and to lie 0·2 MeV above the 0^+ ground state. Incident neutron energies from zero to 1·5 MeV have been considered and the range of atomic weights $A=100$ to $A=240$ has been covered.

The nuclear distortion parameter β ranges from zero near closed shells to a maximum value of $\beta=0{\cdot}3$ in the regions $A=170$ and $A=240$. A value of $\beta^2=0{\cdot}05$ has been used throughout, but as the direct cross section is proportional to β^2 the results given here can easily be adapted to nuclei with different values of β. Values of β derived from quadrupole moments or γ-ray transition probabilities should be used rather than those derived from consideration of energy level spacings, since it is probable that the electromagnetic values give a truer picture of the nuclear shape (Ford 1954).

Figure 1 gives the direct inelastic cross section σ_{d} plotted against $X=KR_0$ and against A the atomic weight, for an incident neutron energy of 1 MeV. The same figure shows, for comparison, values of σ_{ci} the compound inelastic cross section for the same $0^+\rightarrow2^+$ transition. In figure 2 σ_{d} is plotted against the incident neutron energy E for values of E ranging from zero to 1·3 MeV and for $A=150$, 165, 230 and 240.

The Angular Distribution of Neutrons

Equation (9) for the differential cross section yields the following expression for the angular distribution of the inelastically scattered neutrons

$$\begin{aligned}W(\theta)\propto\sum_{\substack{l_0,l_0',l,l'\\J}}[&u_{l_0}(x_0)u_l(x)u^*_{l_0'}(x_0)u^*_{l'}(x)(2l_0+1)(2l_0'+1)(2l+1)(2l'+1)\\&\times C(l_0l2,00)C(l_0'l'2,00)C(l_0l_0'J,00)C(ll'J,00)\\&\times W(l_0l_0'll',J2)P_J(\cos\theta)].\end{aligned}$$

Here $W(l_0l_0'll',J2)$ is a Racah (1942) coefficient and $P_J(\cos\theta)$ is a Legendre polynomial. In the present theory we can estimate the forward–backward asymmetry by calculating the quantity $|\{W(0)-W(\pi)\}/\{W(0)+W(\pi)\}|$. In the region of atomic weights $A\sim150$ and $A\sim240$ the forward–backward asymmetry is of the order of 10% on the basis of optical model wave functions. The effect is small because the asymmetry arises from interference of P and S or D neutron partial waves and, according to the optical model, where S and D waves give an important contribution P waves are unimportant, and conversely. Compound nucleus scattering theory gives a differential cross section which is symmetrical about 90° to the direction of the incident neutrons.

Neglecting odd parity terms and assuming the neutron energy is large compared with the nuclear excitation under consideration, we get the following expressions for the angular distribution in the regions of atomic weight $A \sim 150$ and $A \sim 240$:

$$W(\theta) \simeq 1 + P_2(\cos\theta) \quad \text{for} \quad A \sim 150$$
$$\simeq 1 + 0{\cdot}2 P_2(\cos\theta) \quad \text{for} \quad A \sim 240.$$

The large anisotropy in the angular distribution for $A \sim 150$ arises from the interference of S and D partial waves. In the same region of atomic weight compound nucleus theory yields an almost isotropic distribution of scattered neutrons.

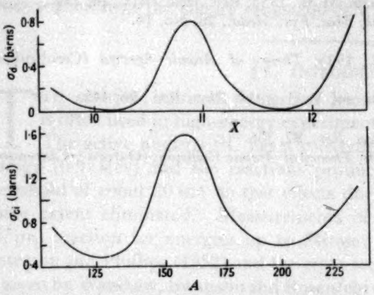

Figure 1. The direct inelastic cross section σ_d and the compound nucleus inelastic cross section σ_{cl} against X ($= KR_0$) and atomic weight A for a neutron energy of 1 Mev.

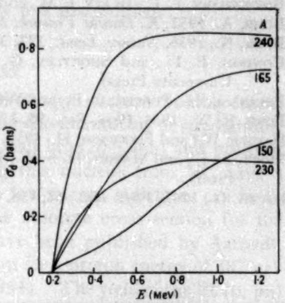

Figure 2. The direct cross section σ_d against energy for $A = 150$, 165, 230 and 240.

§ 5. Discussion

The curves of σ_d and σ_{cl} (figure 1) both show strong maxima in the regions $A \sim 150$ and $A \sim 240$. The maximum for $A \sim 150$ is due to the resonance for S and D neutron partial waves inside the nucleus while the maxima at $A \sim 240$ results from a P wave resonance. The cross sections σ_d and σ_{cl} are both of the same order of magnitude for $A \sim 150$ and $A \sim 240$ while between the maxima, at $A \sim 130$ and $A \sim 200$, σ_d falls almost to zero. Higher order effects will make the peaks less sharp, but the general features of the variation of cross section with atomic weight should remain. It is clear that for A between 190 and 216 the direct process should be quite unimportant.

In figure 2 the curves of σ_d against energy show a different behaviour in the regions $A \sim 150$ and $A \sim 240$. For $A = 150$ and 265 the increase in σ_d with E is almost linear while for $A = 230$ and 240, the initial rise just above threshold is much sharper. Only S and D partial waves contribute appreciably to σ_d for $A = 150$ and 165 and one expects a sharp rise in cross section just above threshold due to the emergence of S waves. The opposite behaviour shown in figure 2 for $A \sim 150$ is due to the fact that at 0·2 Mev the barrier penetrability for D waves is very small, so that almost the entire rise in σ_d from 0·2 to 1 MeV is due to the increase in D wave penetrabilities. The cross sections for $A = 230$ and 240 rise steeply above threshold because penetrabilities for P waves increase more rapidly with energy than for D waves. For $A = 240$ and for energies above 1 MeV, F partial waves give an appreciable contribution to the cross section.

ACKNOWLEDGMENTS

I am very grateful to Professor V. Weisskopf for valuable discussions during the course of the work and for reading the manuscript of this paper. Thanks are due to Dr. Satchler for discussion on angular distributions. I am indebted to the Royal Society for the award of a Rutherford Memorial Scholarship.

REFERENCES

BIEDENHARN, L. C., BLATT, J. M., and ROSE, M. E., 1953, *Rev. Mod. Phys.*, **24**, 251.
BOHR, A., 1952, *K. Danske Vidensk. Selsk. Mat. Fys. Medd.*, **26**, No. 14.
BOHR, N., 1936, *Nature, Lond.*, **137**, 344.
CONDON, E. U., and SHORTLEY, G. H., 1935, *Theory of Atomic Spectra* (Cambridge : University Press).
FESHBACH, H., PORTER, C. E., and WEISSKOPF, V. F., 1954, *Phys. Rev.*, **96**, 448.
FORD, K. W., 1954, *Phys. Rev.*, **95**, 1250.
HAUSER, W., and FESHBACH, H., 1952, *Phys. Rev.*, **87**, 366.
MOTT, N. F., and MASSEY, H. S. W., 1949, *Theory of Atomic Collisions* (Oxford : Clarendon Press).
RACAH, G., 1942, *Phys. Rev.*, **62**, 438.

The Production of ^{11}C from Carbon by Protons of Energy between 200 and 950 MeV

By W. E. BURCHAM, J. L. SYMONDS and J. D. YOUNG
Department of Physics, University of Birmingham

MS. received 27th May 1955 *and in amended form 24th June* 1955

Abstract. Polystyrene discs were irradiated in the scattered proton beam of the Birmingham synchrotron. The proton flux was found by counting tracks in a nuclear emulsion exposed near the polystyrene disc. From the observed activity of the discs the cross section for the production of 20·5 minute ^{11}C from carbon by 950 MeV protons was found to be $20{\cdot}5 \pm 1{\cdot}1$ mbn. The variation of cross section over the energy range 200–950 MeV was also studied.

§ 1. Introduction

The activity induced in carbon by high-energy nucleon bombardment is often used in high-energy experiments for the monitoring of irradiations. The active nucleus ^{11}C has a convenient half life (20·5 min) and positron energy (0·97 MeV) and the reactions producing this nucleus from ^{12}C have a threshold of about 20 MeV so that effects due to low-energy radiations can be to some extent eliminated. Measurements of the absolute cross section for the (p, pn) reaction for energies up to 340 MeV have been published by Aamodt, Peterson and Phillips (1952) and the cross section for a proton energy of 387 MeV is given by Warshaw, Swanson and Rosenfeld (1954). The yield of the $^{12}C(p, pn)$ reaction relative to the yield of ^{24}Na in the reaction $^{27}Al(p, 3pn)^{24}Na$ has been obtained by Wolfgang and Friedlander (1954), for proton energies between 500 and 2000 MeV. In this last work no specified account is taken of alternative modes of production of ^{11}C such as $^{12}C(n, 2n)$ or $^{12}C(p, pn\pi^0)$; moreover the absolute cross section is not directly determined but is derived from the cross section for the comparison reaction, which is itself not accurately established (Turkevich 1954). The present work was undertaken in order to provide an absolute measurement of the cross section for production of ^{11}C from carbon by protons of an energy near 1000 MeV, taking into account possible background effects from the (n, 2n) reaction. Some observations on the yield of the reaction at lower energies were also made.

§ 2. Experimental Method

2.1. *General*

Polystyrene discs were at first irradiated in the scattered external beam of the Birmingham proton synchrotron. The main features of this machine are described by Moon, Riddiford and Symonds (1955); the site 'A' chosen for the first irradiations is shown in the general plan view given by these authors in their figure 2 (region marked BC).

In this position the proton intensity is about 10^5 per cm^2 per pulse, and nuclear emulsion studies (mainly multiple coulomb scattering and p–p collision analysis by the nuclear emulsion group in this laboratory) show that the proton energy at the end of the acceleration period is 950 ± 50 MeV. The same value was calculated from the magnetic field at the time at which the beam strikes the target. The protons reaching this position are accompanied by neutrons produced by the impact of stray protons on the walls of the vacuum system. These neutrons produce ^{11}C activity in the polystyrene discs by the reaction ^{12}C(n, 2n)^{11}C and estimation of this effect involves some doubtful assumptions. Further irradiations were therefore made in a re-entrant tube mounted in the region E of the synchrotron vacuum system (Moon, Riddiford and Symonds 1955, fig. 2, site 'B'). In this position protons reaching the sample are scattered from a moving target placed upstream from the re-entrant tube. With this arrangement the proton to neutron ratio at the sample was expected to be more favourable than at site 'A'. Irradiations with protons of energy between 200 and 950 MeV were obtained in site B by switching the radio-frequency accelerating voltage of the synchrotron to a fixed frequency at the appropriate time during the acceleration cycle.

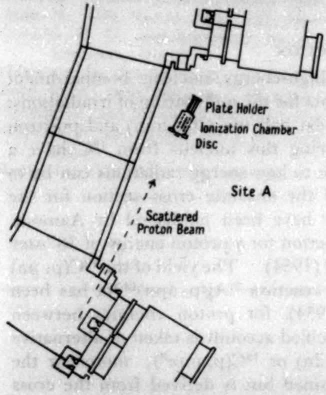

Figure 1. Ionization chamber and plate holder (site A).

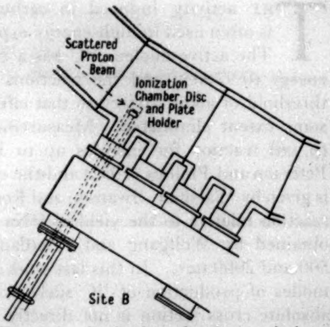

Figure 2. Ionization chamber and plate holder (site B).

The incident proton flux was found by exposing an Ilford G5 emulsion to one pulse under the machine conditions used in the irradiation. Since one pulse gives a satisfactory number of tracks in the emulsion, and at least 20 pulses are needed for a significant activation of the polystyrene samples, it was necessary to relate the strength of the 'calibration' pulse to that of the activation pulses. This was done by means of an argon filled ionization chamber placed in the scattered beam near the polystyrene sample as shown in figures 1 and 2. Pulses from this chamber were displayed directly on an oscilloscope trace, triggered from the synchrotron timing pulse and individually photographed.

The activity on the discs after irradiation was counted in a standard geometrical arrangement by a screened end-window Geiger counter.

2.2. *Measurement of Incident Proton Flux*

The tracks of 950 MeV protons in G5 emulsion have a grain density which is nearly equal to the plateau value. With such a low density it is difficult to make an accurate estimate of the number of tracks passing out through the top surface of the emulsion when the protons are allowed to travel obliquely through the plate. For this reason the plates were always set as nearly as possible parallel to the beam; the distribution in angle observed in plates set vertically and horizontally in site A was ± 1°. The number of tracks crossing an area of $100\mu \times 100\mu$ was counted, scanning through the emulsion depth. Many determinations of this number, over the whole plate, were made. The most suitable track density was 30 in an area $100\mu \times 100\mu$ of a G5 nuclear emulsion of thickness 200μ. Counting was done with an M4000 type microscope with a magnification of × 45 and a × 15 eyepiece.

The thickness of emulsion at the time of exposure was found by a method developed by Duke, Lock, March and Munir (1955). Correction for obliquity of the proton tracks with respect to the emulsion was found to be negligible.

2.3. *Measurement of Absolute Disintegration Rate of Activated Discs*

The maximum range of the positrons of ^{11}C is about 400 mg cm^{-2} and the surface density of the discs used was 130 mg cm^{-2}; thinner discs would have given rather low counting rates in a proton flux suitable for measurement by the nuclear emulsion method. The use of a thick disc reduces the fractional loss of ^{11}C by recoil; this was found experimentally to be less than 2% and has been neglected.

The activity of the discs was determined in a standard counter castle. Decay curves always gave a pure 20·5 minute period and the activity was followed until it merged with the background counting rate (about 7 per minute). The counting rate was extrapolated back to the mid-time of the bombardment, and the number N of active nuclei formed during the bombardment, whose decay positrons were emitted into the solid angle defined by the counter, was deduced using the formula $N = A_{\text{mid}}/\lambda$ where λ is the decay constant for ^{11}C. The conversion of this number to the total number of ^{11}C nuclei produced entails correction for the thickness of the discs, and a determination of the effective solid angle of the end-window counter for a thin source. The thickness correction was found by irradiating a stack of 130 mg cm^{-2} discs and 5 mg cm^{-2} discs together in a strong proton flux and finding the ratio of observed activities. The relative change in observed activity per gramme between the 130 mg cm^{-2} and the 5 mg cm^{-2} discs was $1{\cdot}75 \pm 0{\cdot}04$. Use of this factor permitted the activation in the main experiment to be referred to a source thickness of 5 mg cm^{-2}. Then the activity of a strongly irradiated 5 mg cm^{-2} disc was found using firstly the end-window counter and secondly a 4π Geiger counter. Comparison of the two activities, after small corrections for self-absorption in the 4π counter and difference in size of sources, gave an efficiency of $17{\cdot}1 \pm 0{\cdot}4\%$ for the end-window counter for a sample of thickness 5 mg cm^{-2}. An independent estimate of this efficiency was obtained using standardized ^{198}Au sources and good agreement with the result from the 4π counter was found, although rather large corrections for source thickness had to be made.

2.4. *Pulse-to-Pulse Monitoring*

The argon-filled ionization chambers used had a capacity of about 5 pF and were connected to the oscilloscope by a cable of capacity 1000 pF. The time constants of the oscilloscope amplifier were about 50 milliseconds. In relating the 'calibration' pulses to the activation pulses the maximum deflection during the pulse was used; in most of the runs the synchrotron operating conditions were stable and the pulses did not vary largely. Checks were made, using increased chamber voltages, to verify that the ionization chamber was not saturating; the oscilloscope deflections were also kept small in comparison with the output limit of the amplifier.

2.5. *Carbon Content of Foils*

The polystyrene was assumed to have the chemical composition $(CH)_n$ and the number of carbon atoms in the 130 mg cm^{-2} disc was calculated to be $3{\cdot}26 \times 10^{22}$.

2.6. *Relative Measurements*

Since the determination of absolute cross sections by the method so far described proved to be a rather lengthy process, the low-energy part of the excitation curve for the production of ^{11}C activity was studied by a different method. In this a shallow argon-filled ionization chamber was placed at the end of the re-entrant tube in site B and small polystyrene samples were put behind it. The assembly was then irradiated in a strong proton flux and a photographic record of the ionization chamber pulse size was taken as before. The activity of the polystyrene was also measured. The synchrotron beam energy was then varied by about 50 Mev and a similar exposure was made. In this way activations over the range 200–500 Mev at about 50 Mev intervals were obtained. Relative values of the cross section were calculated by assuming the ionization chamber signals to be proportional, for a given proton flux, to the theoretical value of the energy loss per centimetre in argon for protons of the appropriate energy. This was taken from the tables of Aron, Hoffman and Williams (1951).

§ 3. NEUTRON BACKGROUND

Several tests were made both to establish the existence of, and to estimate, the neutron intensity in the positions chosen for irradiation. It was found that for site A the activity induced in the discs, when 60 cm of lead were placed between the window and the disc, was only 5% of the activity obtained in a similar exposure without absorber. Since the mean free path for high energy nucleons in lead is about 5 cm this arrangement prevents both direct protons and neutrons from reaching the disc and shows only that background radiations, in particular low-energy neutrons, from surrounding materials do not contribute greatly to the activation.

Nuclear emulsions exposed in the irradiation position do, however, show a considerable number of neutron induced stars, as well as the more prolific stars with an incident proton. A general count† of all stars with more than two prongs (with or without primary) gave, for a given volume of emulsion, 'proton' stars 2098 ± 45, 'neutron' stars 861 ± 30.

It is not quite certain how best to use these figures to obtain the ratio of proton to neutron flux, since the star counts may be discriminatory (e.g. the two-prong star (n, 2p) would be counted while (p, np) would not) but as a first approximation the value $2098/861 = 2{\cdot}4 \pm 0{\cdot}1$ was used for the flux ratio. For site B the proton to neutron star ratio was found by counts on one of the calibration plates. These gave, for a given volume of emulsion, 'proton' stars 210, 'neutron' stars 77, giving a ratio of 2·7 ± 0·3. There is no evidence that the proton to neutron flux ratio is significantly different in sites A and B, and the more accurate value 2·4 ± 0·1 obtained for site A was used in the calculations. There was some indication that at energies of about 300 Mev the proton to neutron flux ratio was higher, but the value 2·4 has been used throughout.

---

† We are indebted to the nuclear emulsion group in this laboratory for this information.

§ 4. RESULTS

The results obtained in several independent measurements at an energy of 950 Mev are shown in table 1, and similar results for lower energies are given in table 2. Table 2 also includes the results of the relative cross section measurements.

Table 1. Production of ^{11}C from Carbon by 950 Mev Protons

(1)	(2)	(3)	(4)	(5)
31.8.54	A	198 ± 9	2·55 ± 0·14	7·80 ± 0·56
1.9.54	A	205 ± 12	3·14 ± 0·17	6·52 ± 0·53
2.9.54	A	363 ± 10	4·16 ± 0·19	8·99 ± 0·30
23.9.54	A	843 ± 13	9·66 ± 0·32	8·73 ± 0·30
7.10.54	A	326 ± 10	4·53 ± 0·22	7·19 ± 0·42
14.1.55	B	1630 ± 80	23·5 ± 1·0	6·94 ± 0·45
27.1.55	B	238 ± 9	2·72 ± 0·16	8·75 ± 0·62
27.1.55	B	3040 ± 30	37·3 ± 1·4	8·15 ± 0·33
10.12.54	C	253 ± 9	4·08 ± 0·17	6·20 ± 0·34

(1) Date ; (2) Irradiation site ; (3) N, number of ^{11}C atoms formed ; (4) ν, number of incident protons per cm^2, $\times 10^{-6}$; (5) $10^5 \times N/\nu$.

Table 2. Production of ^{11}C from Carbon by Protons of energy 200–950 Mev

(1)	(2)	(3)	(4)	(5)
238	9·8 ± 2·10	13·1 ± 0·92	39·4 ± 2·4	35·8 ± 2·4
310	11·3 ± 0·74		35·5 ± 2·3	31·9 ± 2·4
365		13·1 ± 0·99	41·0 ± 3·1	37·4 ± 3·1
420	11·1 ± 0·85	11·1 ± 0·41	34·8 ± 2·7	31·2 ± 2·8
465		10·5 ± 0·34	33·0 ± 1·1	29·4 ± 1·2
522		11·4 ± 0·51	35·8 ± 1·6	32·2 ± 1·6
648	8·75 ± 0·87		27·5 ± 2·7	23·9 ± 2·8
832	10·3 ± 0·50		32·3 ± 1·6	28·7 ± 1·6
950 (A & B)	8·06 ± 0·30		25·3 ± 0·95	21·7 ± 1·0
950 (C)	6·20 ± 0·34		19·4 ± 1·07	19·4 ± 1·07

(1) Energy (Mev) ; (2) N/ν (absolute measurement) $\times 10^5$; (3) N/ν (relative measurement) $\times 10^5$; (4) cross section without neutron correction (mbn); (5) cross section with neutron correction (mbn).

Column (4) of table 2 gives the absolute cross sections calculated with no correction for neutron induced effects. The relative cross sections have been normalized to agree with the absolute measurement at 420 Mev.

In order to make a correction for the beta activity produced in the discs by the (n, 2n) reaction, some assumption about the cross section for this reaction must be made. The average neutron energy for the 950 Mev proton exposures was estimated to be about 300 Mev from a prong-number distribution for the neutron induced stars in the nuclear emulsion. For an energy of about 400 Mev Warshaw, Swanson and Rosenfeld (1954) find that the ratio of the cross sections for the

^{12}C(p, pn) and ^{12}C(n, 2n) reactions is 2·4 ± 0·2. Since the cross section for the (n, 2n) reaction probably does not vary much with energy from 90 Mev to 300 Mev we have used the cross section ratio of 2·4 ± 0·2 and the flux ratio of 2·4 ± 0·1 to correct the absolute values given in column (4) of table 2; the final values of the cross section for the production of ^{11}C by protons as a function of energy are given in column (5) of this table.

The experiment labelled C in table 1 was carried out in site A but an attempt to estimate background was made by recording counts and proton tracks with 60 cm of lead in front of the sample and photographic plate. The values with absorber were subtracted from the values without absorber and the difference is given in columns (3) and (4) of the table. The cross section without neutron correction from this 'difference' experiment is 19·4 ± 1·8 mbn. The neutron correction in this case was based on the difference of star counts in the plates taken with and without absorber and was found to be negligible within the limits of accuracy of the experiment. This result agrees with the average value from the exposures marked A and B; taken together, the best value for the cross section for the reaction ^{12}C(p, pn) at 950 Mev is 20·5 ± 1·1 mbn. This figure is lower than the result presented at the 1955 Rochester Conference chiefly because of improved beta counting.

§ 5. Discussion

The cross sections listed in column (5) of table 2 are plotted against energy in figure 3, which also shows the results of Wolfgang and Friedlander (1954). The results of Aamodt, Peterson and Phillips (1952) are omitted since they appear to be in disagreement with later (1954) unpublished work in the same laboratory by Birnbaum, Crandall, Millburn and Pyle. The present results are lower in absolute value than those of the Brookhaven workers but like these, show a cross section which decreases with energy over the range 200–1000 Mev. The slow fall-off in cross section with energy shown in figure 3 is in agreement with the general picture of high energy nuclear reactions proposed by Serber (1947) in so far as energies below the meson production threshold are concerned. For energies above this threshold, where meson production forms an important part of the total proton cross section in carbon, the results indicate that meson re-absorption in the carbon nucleus is not an important effect.

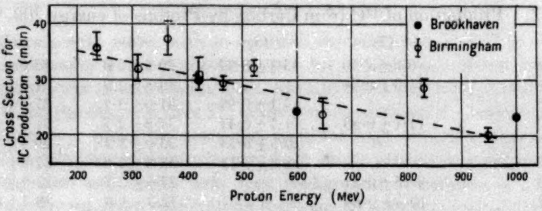

Figure 3. Cross section for ^{12}C (p, pn) reaction.

Acknowledgment

We are grateful to Miss D. Latham for processing the nuclear emulsions used in this work, for scanning the emulsions for proton tracks and stars, and for help in preparing the diagrams.

REFERENCES

AAMODT, R. L., **PETERSON**, V., and **PHILLIPS**, R., 1952, *Phys. Rev.*, **88**, 739.

ARON, W. A., **HOFFMAN**, B. G., and **WILLIAMS**, F. C., 1951, *United States Atomic Energy Commission Report* AECU 663.

DUKE, P. J., **LOCK**, W. O., **MARCH**, P. V., and **MUNIR**, B. A., 1955, *J. Sci. Instrum.*, **32**, 365.

MOON, P. B., **RIDDIFORD**, L., and **SYMONDS**, J. L., 1955, *Proc. Roy. Soc.* A, **230**, 204.

SERBER, R., 1947, *Phys. Rev.*, **72**, 1114.

TURKEVICH, A., 1954, *Phys. Rev.*, **94**, 775.

WARSHAW, S. D., **SWANSON**, R. A., and **ROSENFELD**, A. H., 1954, *Phys. Rev.*, **95**, 649.

WOLFGANG, R. L., and **FRIEDLANDER**, G., 1954, *Phys. Rev.*, **96**, 190.

Neutron Groups from Deuteron Stripping by ^{23}Na, ^{27}Al and ^{31}P

By J. M. CALVERT, A. A. JAFFÉ, A. E. LITHERLAND and
E. E. MASLIN
Nuclear Physics Research Laboratory, University of Liverpool

Communicated by H. W. B. Skinner; MS. received 27th April 1955 *and in final form* 4*th July* 1955

Abstract. Using a triple ionization chamber to collimate and record recoil protons from a hydrogenous radiator, angular distribution measurements have been carried out on a number of neutron groups emitted as a result of the bombardment by 9 MeV deuterons of targets of sodium carbonate, aluminium and phosphorus. Spins and parities of the resulting states of the 4n nuclei ^{24}Mg, ^{28}Si and ^{32}S have been assigned by applying the theory of the stripping process. In the case of ^{28}Si, the first $T=1$ level is identified and its characteristics compared with those of the ground state of ^{28}Al.

§ 1. Introduction

The analysis of the angular distributions of both protons and neutrons in deuteron stripping reactions in terms of partial waves of the angular momentum of the ingoing particle (Butler 1951, Bhatia *et al.* 1952) has proved a valuable method of establishing data of nuclear levels. Most investigations of stripping reactions, however, have been devoted to (d, p) reactions largely because of the ready detectability of protons and also because of the lack of a suitable fast-neutron spectrometer. Nuclear emulsions have proved a useful tool for studying neutron spectra but suffer from the disadvantage of being more sensitive to the lower energy groups. This means that exposures have to be kept to such a low level in order to avoid losing high energy neutron groups in the background of low energy neutrons and γ-ray fogging that the work of scanning is considerable.

The neutron spectrometer described in a previous paper (Holt and Litherland 1954) was developed and applied to meet these difficulties and although not a perfect solution of the problem, it enabled spectra to be obtained with an energy resolution sufficient to investigate many levels. The spectrometer consisted essentially of a high-pressure triple ionization chamber with which it was possible to identify and measure the range of collimated recoil protons from a hydrogenous radiator. Target nuclei investigated were ^{23}Na, ^{27}Al and ^{31}P all of which have high Q-values for the formation of the ground states of the 4n nuclei ^{24}Mg, ^{28}Si and ^{32}S.

§ 2. Details of Experimental Arrangement

The general experimental arrangement was very similar to that described by Middleton *et al.* (1953). The extracted deuteron beam from the Liverpool University 37 in. cyclotron was magnetically focused on to a water-cooled target some 10 feet away from the cyclotron tank. A concrete wall, 2 feet thick and replacing the earlier wall of whale-fat, was built between the focusing magnet and the target. Further shielding was introduced by using a thickness of 2 feet of whale-fat between the cyclotron tank and the focusing magnet. The target assembly described by Middleton *et al.* was used in a form modified to allow measurement of the beam energy and also monitoring of protons from the target as described below.

The triple ionization chamber was mounted on a horizontal table and could be rotated about a vertical axis passing through the target. The level of the table was adjustable so that the beam and the chamber axis were in the same horizontal plane. The distance between the ionization chamber and the target was adjusted to give an angular resolution of 3°.

The beam energy was determined using a modification of the target assembly described by Middleton *et al.* (1953). A thin gold scatterer was mounted so that it could be lowered into the path of the deuteron beam. The deuterons elastically scattered through 90° were collimated by a slit system which allowed a cone of half angle 0·75° to fall on a 100 μ C2 emulsion inclined at an angle of 8°. The beam energy was determined from the range of deuterons in the emulsion to be 9·02 ± 0·06 MEV. Measurements at an interval of one month were consistent with this value.

§ 3. MONITORS

In order to obtain reliable angular distributions of the neutron groups, effective monitoring of the deuteron beam was essential and was carried out in two ways: by integrating the beam current falling on the target and by counting protons from the (d, p) reactions in the target material.

The beam current integrator designed by Lewis and Collinge (1953) was used for the first. It was found necessary to insert a grid one inch in front of the target and to maintain it at a negative potential to suppress secondary electron emission. Consistent integrator readings were obtained with voltages greater than 50 applied to this grid. Since certain targets tend to evaporate under bombardment, it was considered necessary also to monitor either protons or neutrons from the target nuclei themselves. A constant ratio of integrator to monitor readings was taken as the criterion for satisfactory running conditions.

Initially a Hornyak button (1952) to monitor on neutrons was tried but was considered unsatisfactory because the slope of the integral bias curve was so steep that it was impossible to get consistent results. A further method which proved more reliable was to monitor protons coming from the target at 90° to the incident beam. For this purpose, a side-arm with a thin Be–Cu window was fitted to the target chamber. Behind the window was placed a photomultiplier with a thin flake of anthracene (about 10 mg cm^{-2}) as a scintillator. All protons of energy greater than a few MEV passing through the flake produce pulses of approximately the same size while protons just stopped by the flake produce somewhat larger pulses. It was found that if sufficient absorbers were placed between the target and monitor to cut out all except the two or three highest energy proton groups, an integral bias curve with a good plateau about 20 v long was obtained for proton pulses about 45 v in height.

When targets were mounted on a gold backing, it was sometimes found impossible to remove all protons from the ^{197}Au (d, p) reaction, which has the rather high *Q*-value of 4·1 MEV, and still maintain a good plateau. This was overcome by using target backings of bismuth which has the lower (d, p) ground state Q-value of 1·95 MeV (Harvey 1951). This method of monitoring was found to be very satisfactory as also the contribution to the counting rate from background γ-rays was negligible at the mid-point of the plateau.

§ 4. TARGET PREPARATION

In order to provide suitable backings, as discussed above, a layer of Bi about 50 mg cm^{-2} was evaporated on to gold foil and the target material was then deposited on the surface of the bismuth.

Sodium was used in the form of sodium carbonate which was painted on to the backing from a suspension and then dried. A sufficiently uniform layer was thus obtained to give satisfactory resolution of the neutron groups. The presence of carbon and oxygen only present difficulties for Q-values of less than zero, i.e. excitation energies of 9·76 MeV and above. As the levels are closely spaced at these excitations, this region was not examined in detail. A target thickness of 5·2 mg cm^{-2} was used.

Aluminium was used as metal foil fixed on to the backing. Targets of thickness 1·6 and 3·2 mg cm^{-2} were used.

Red phosphorus dried with alcohol and then ground to form a paste with alcohol was painted on to the backing as in the case of sodium. A target of thickness 4·4 mg cm^{-2} was used.

§ 5. ANALYSIS OF SPECTRA

An explanation of the principles and construction of the neutron spectrometer may be found in the literature (Holt and Litherland 1954). The spectra were found by projecting the films of oscillograph traces and plotting range histograms directly. Ranges were translated into energies by means of the range–energy data of Aron *et al.* (1949), the chamber pressure being known.

In order to determine the Q-value of an observed neutron group, it is necessary to allow for the energy spread arising from the following causes: (*a*) inhomogeneity of the deuteron beam, (*b*) target thickness, (*c*) radiator-target geometry, (*d*) radiator thickness, (*e*) geometry of collimation of recoil protons, (*f*) straggling. It can be shown that the resultant line shape should be roughly triangular but with a low-energy tail. Most of these effects tend to lower the energy of the group below the expected value and the correct value is found from the extrapolation of the high energy side of the triangular shape. A linear extrapolation gave energies consistently low by about 200 kev for all cases of known Q-values but this was not surprising as the spectral lines could not be expected to show an accurate linear fall-off.

For this reason, it was considered more convenient to use a reaction of known Q to calibrate each energy range where possible. The ^{12}C(d, n)^{13}N ground state and the ^{27}Al(d, n)^{28}Si first excited were used. Intermediate energies were covered by calibrating on a prominent Al group and, by overlapping energy ranges, this could be compared with the first excited state. The high energy side of the histogram for any particular group invariably showed a linear fall-off except towards the foot. The intersection of the extrapolation with the energy axis was taken as giving the energy of the group. In this way groups fitted in well with known level schemes. The method is not suitable for giving accurate Q-values as it depends on the precision of the extrapolation but it is generally possible to do this to 0·1 MeV.

§ 6. RESULTS

Angular distributions of the various neutron groups were plotted by measuring the area under individual peaks of the spectra obtained at several angles and normalizing with respect to the monitor. In those cases where groups were not resolved, the distribution of the composite groups has been plotted. Results have been fitted to theoretical stripping curves calculated on the Born approximation (Bhatia *et al.* 1952) and using a radius of $(2{\cdot}7 + 1{\cdot}22A^{1/3}) \times 10^{-13}$ cm. Previous work on stripping indicates that this is a reliable radius to use (Huby 1953). Individual points plotted on the curves show probable errors.

In calculating the cross sections, the data of Adair (1950) for the energy dependence of n–p scattering were used. Although it might appear that the stripping curves were each superimposed on a background probably arising from compound nucleus formation, no subtraction of this background was made in determining the proton capture probabilities from the measured cross sections because of the relatively large statistical errors on the experimental points. The relative cross sections have an estimated error of $\pm 20\%$ but the error in the absolute cross sections may be $\pm 50\%$.

^{23}Na(d, n)^{24}Mg. The energy levels of ^{24}Mg and previous work have been discussed by Endt and Kluyver (1954). In the present work, the energy range up to an excitation of 8·4 MeV was covered. Data obtained for the levels in this range are summarized in table 1. Differential cross sections are given at the angle quoted in each case which is the stripping maximum for levels showing a stripping angular distribution and 0° in other cases. Angular distributions of groups $n_2 + n_3$, n_7 and n_8 are given in figure 1.

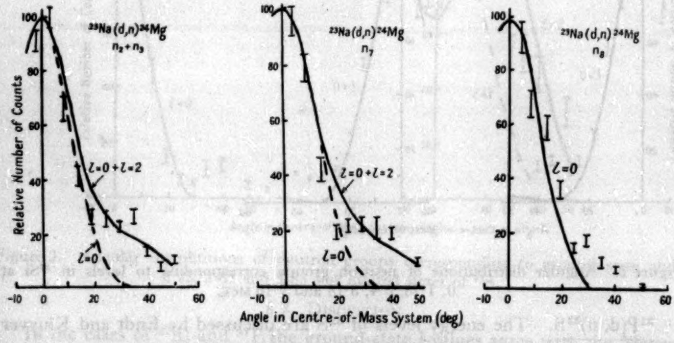

Figure 1. Angular distributions of neutron groups corresponding to excited states of ^{24}Mg at 4·2, 7·5 and 8·4 MeV.

^{27}Al(d, n)^{28}Si. The energy levels of ^{28}Si have been studied by Peck (1949) using ^{27}Al(d, n) and nuclear emulsions to study the neutron groups. We agree with his level scheme in that we find levels at similar energies without being able to measure these energies with any greater precision that he does, save that we cannot claim to find levels at 4·47 and 4·91 MeV. Our indication is of a level at 4·7 MeV but our work does not disprove the possible presence of a second weaker level in this region. The upper limit of the differential cross section for the sum of the groups $n_2 + n_3$ corresponding to these levels is given in table 2 together with a summary of the results for the other groups investigated. Angular distributions of groups n_0, n_1, $n_4 + n_5$, n_8 and n_9 fitted to theoretical curves are given in figure 2.

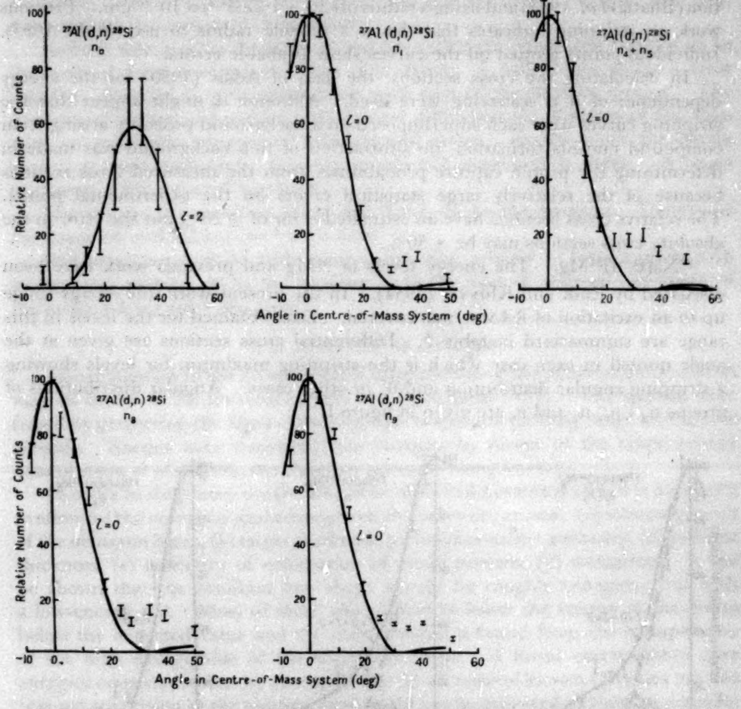

Figure 2. Angular distributions of neutron groups corresponding to levels in ^{28}Si at 0, 1·78, 6·4, 8·18 and 9·16 Mev.

^{31}P(d, n)^{32}S. The energy levels of ^{32}S are discussed by Endt and Kluyver (1954). A previous study of ^{31}P(d, n)^{32}S by Snowdon (1952) using the emulsion technique indicated more levels than have been found either by proton scattering on ^{32}S, by (p, γ) on ^{31}P or by the more recent work on ^{31}P(d, n) by El-Bedewi and El-Wahab (1955). In general, we agree with the latter work and do not for instance find the levels at 0·5 Mev and 1·5 Mev found by Snowdon. The levels between 3·81 Mev and 5·04 Mev were too close to resolve completely with our instrument but it was possible to plot the angular distribution for the compound of levels at 3·81, 4·32 and 4·50 Mev and similarly for those at 4·74 and 5·04 Mev. This division, while seeming arbitrary, occurs because of the difficulty of resolving a weak group in the foot of a strong group. The evidence of the present work indicates that the level at 3·81 MeV is the strong member of the compound (showing $l=0$ angular distribution) but as it is not possible to assess the contribution of the two adjacent levels, we prefer to present the results as indicated in table 3. Angular distributions of groups n_0, n_1, $n_2+n_3+n_4$ and n_7 are shown in figure 3.

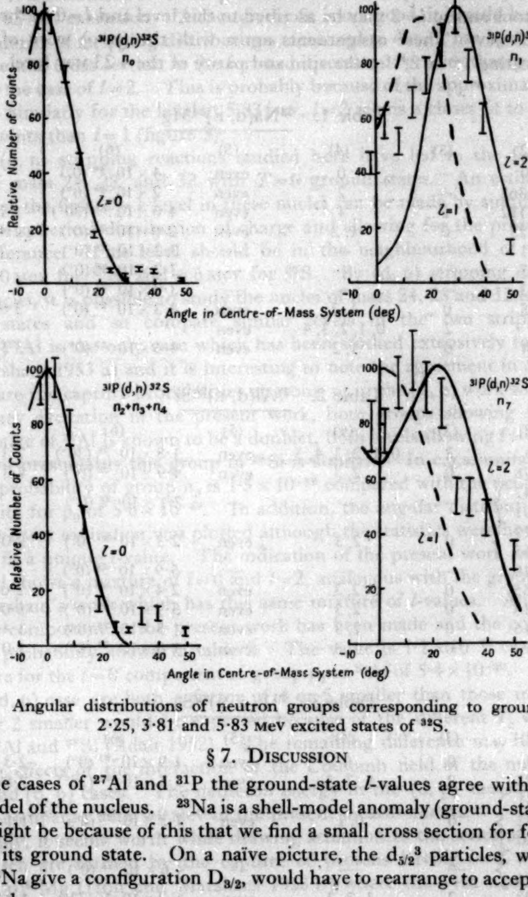

Figure 3. Angular distributions of neutron groups corresponding to ground state and 2·25, 3·81 and 5·83 MeV excited states of ^{32}S.

§ 7. DISCUSSION

In the cases of ^{27}Al and ^{31}P the ground-state l-values agree with the Mayer shell-model of the nucleus. ^{23}Na is a shell-model anomaly (ground-state spin 3/2) and it might be because of this that we find a small cross section for formation of ^{24}Mg in its ground state. On a naïve picture, the $d_{5/2}{}^3$ particles, which in the case of ^{23}Na give a configuration $D_{3/2}$, would have to rearrange to accept the fourth $d_{5/2}$ particle.

In the case of the other levels of ^{24}Mg, only a very small indication of the first and of the fourth to sixth excited states was found. The neutron yield was so low from all of these levels that is was impossible to obtain angular distributions with good statistics and it could only be concluded from our results that the distributions were fairly isotropic between 0° and 50°. Curves for the groups n_2+n_3, n_7 and n_8 (figure 1) are 'good' stripping distributions, the pattern being typical of $l=0$ in each case. In the first two cases a better fit could be obtained by adding together curves with $l=0$ and $l=2$ in suitable proportions. The group n_2+n_3 is known to correspond to unresolved levels at 4·122 MeV and 4·23 MeV. As the level at 4·122 MeV is known to have spin $J=4$, it cannot be formed by s-wave protons and so $l=2$ may be ascribed to this level and $l=0$ to the adjacent level at 4·23 MeV. These assignments agree with the (p, γ) work of Newton (1954) indicating 1^+ or 2^+ for the spin and parity of the 4·23 MeV level.

Table 1. ^{23}Na(d, n)^{24}Mg

(1)	(2)	(3)	(4)	(5)	(6)	(7)
n_0	0	—	0	even	4×10^{-29} (0°)	—
n_1	1·368	—	2	even	2×10^{-28} (0°)	—
n_2	4·122	2	4	even	$4{\cdot}0\times10^{-28}$ (30°)	$1{\cdot}1\times10^{-49}$
n_3	4·23	0	1, 2	even	$2{\cdot}0\times10^{-27}$ (0°)	$2{\cdot}4\times10^{-50}$
n_4	5·1	—	—	—	$3{\cdot}2\times10^{-28}$ (0°)	—
n_5	5·5	—	—	—	$3{\cdot}2\times10^{-28}$ (0°)	—
n_6	6·3	—	—	—	$3{\cdot}0\times10^{-27}$ (0°)	—
n_7	7·5	0	1, 2	even	$4{\cdot}3\times10^{-27}$ (0°)	$3{\cdot}6\times10^{-50}$
		2	0, 1, 2, 3, 4	even		
n_8	8·4	0	1, 2	even	$4{\cdot}4\times10^{-27}$ (0°)	$3{\cdot}5\times10^{-50}$

Table 2. ^{27}Al(d, n)^{28}Si

(1)	(2)	(3)	(4)	(5)	(6)	(7)
n_0	0	2	0, 1, 2, 3, 4, 5	even	$1{\cdot}8\times10^{-28}$ (30°)	$7{\cdot}3\times10^{-50}$
n_1	1·78	0	2, 3	even	$4{\cdot}9\times10^{-28}$ (0°)	$7{\cdot}3\times10^{-51}$
n_2	4·47	—	—	—	$2{\cdot}1\times10^{-28}$ (0°)	—
n_3	4·91					
n_4	6·11	0	2, 3	even	$2{\cdot}3\times10^{-27}$ (0°)	$2{\cdot}0\times10^{-50}$
n_5	6·65					
n_6	7·10	—	—	—	$5{\cdot}9\times10^{-28}$ (0°)	—
n_7	7·55	0	2, 3	even	$2{\cdot}4\times10^{-27}$ (0°)	$2{\cdot}0\times10^{-50}$
n_8	8·18	0	2, 3	even	$5{\cdot}9\times10^{-27}$ (0°)	$5{\cdot}0\times10^{-50}$
n_9	9·16	0	2, 3	even	$1{\cdot}5\times10^{-26}$ (0°)	$1{\cdot}4\times10^{-49}$
n_{10}	10·2	0	2, 3	even	$1{\cdot}0\times10^{-27}$ (0°)	$1{\cdot}0\times10^{-50}$

Table 3. ^{31}P(d, n)^{32}S

(1)	(2)	(3)	(4)	(5)	(6)	(7)
n_0	0	0	0	even	$1{\cdot}9\times10^{-27}$ (0°)	$2{\cdot}3\times10^{-50}$
n_1	2·25	2	1, 2, 3	even	$3{\cdot}5\times10^{-28}$ (28°)	$7{\cdot}8\times10^{-50}$
n_2	3·81	0	0, 1	even	$1{\cdot}3\times10^{-27}$ (0°)	$1{\cdot}1\times10^{-50}$
n_3	4·32					
n_4	4·50					
n_5	4·74	—	—	—	$4{\cdot}6\times10^{-28}$ (0°)	—
n_6	5·04					
n_7	5·83	2	1, 2, 3	even	$1{\cdot}2\times10^{-27}$ (22°)	$1{\cdot}3\times10^{-49}$

(1) Neutron group, (2) excitation energy of level in MeV as listed by Endt and Kluyver, (3) l-value, (4) possible spins of state, (5) parity, (6) differential cross section at centre of mass angle shown, (7) proton capture probability $\Lambda/(2j_i+1)$ in c.g.s. units.

The distribution of the neutron group leading to the 3·81 MeV level of ^{32}S is $l=0$ so that the spin of the state must be 0 or 1 with even parity. There is some evidence for the γ-ray transition from this level to the ground state (Breckon *et al.* 1954, Glass and Richardson 1954) which would indicate that the level spin is 1. However, these authors say that they cannot ascribe the observed γ-ray to this level with complete certainty, so the alternative spin values for this level must remain. A distribution $l=2$ has been fitted to the experimental points for the level at 2·25 MeV excitation. Although the fit is not good, it should be noted that in the majority of stripping distributions measured to date it has been found that the differential cross section in the forward direction is greater than predicted by theory in the case of $l=2$. This is probably because of the approximations of the theory. Similarly for the level at 5·83 MeV, $l=2$ seems a closer fit to the experimental points than $l=1$ (figure 3).

The (d, n) stripping reactions studied here have led to the formation of nuclei of mass 24, 28, and 32 with $T=0$ ground states. An estimate of the position of the first $T=1$ level in these nuclei can be made by simply assuming a uniform spherical distribution of charge and allowing for the proton–neutron mass difference. This level should be in the neighbourhood of 9·3 MeV for ^{24}Mg, 9·0 MeV for ^{28}Si and 6·6 MeV for ^{32}S. By (d, p) stripping on the same target nuclei, it is possible to study the nuclei of mass 24, 28 and 32 having $T=1$ ground states and so compare similar levels in the two stripping cases. ^{27}Al(d, p)^{28}Al is the only case which has been studied extensively to date (Holt and Marsham 1953 a) and it is interesting to note the agreement in l-values and to compare the capture probabilities of group p_0 in the (d, p) work with group n_9, at 9·16 MeV excitation in the present work, both groups showing $l=0$. (The ground state of ^{28}Al is known to be a doublet, both levels showing $l=0$ (Buechner 1954) and presumably this group in ^{28}Si is similar.) In c.g.s. units, the proton capture probability of group n_9 is $1{\cdot}5\times10^{-49}$ compared with the neutron capture probability for p_0 of $5{\cdot}6\times10^{-49}$. In addition, the angular distribution of group n_{10} at 10·2 MeV excitation was plotted although the statistics were not sufficiently good to fit a unique l-value. The indication of the present work would be that this level shows a mixture of $l=0$ and $l=2$, analogous with the group p_1 in Holt and Marsham's work which has this same mixture of l-values. An estimate of the $l=0$ component in the present work has been made and the corresponding capture probability shown in table 2. The value is $1{\cdot}1\times10^{-50}$ compared with the figure for the $l=0$ component of group p_1 in ^{28}Al of $5{\cdot}4\times10^{-50}$. The figures in the (d, n) case are both a factor of 4 or 5 smaller than those in the (d, p). A factor 2 smaller would be expected because of the different T_z values in the nuclei ^{28}Al and ^{28}Si (Adair 1952). The remaining difference may be due to the differing effects of the interaction of the Coulomb field of the nucleus in the (d, n) and (d, p) cases. The deuteron energy in the (d, p) measurements was 8·0 MeV compared with 9·0 MeV in the present measurements.

Finally, it seems worth while drawing attention to the series of six levels in ^{28}Si which are formed by the capture of protons having $l=0$. In the case ^{25}Mg(d, p)^{26}Mg (Holt and Marsham 1953 b) where the 14th neutron is being added (as distinct from the 14th proton in our work) a similar series having $l=0$ is found.

It is hoped to apply similar measurements to more elements in the near future.

ACKNOWLEDGMENTS

The authors would like to thank Professor H. W. B. Skinner and Dr. J. R. Holt for their continued interest in this work and for helpful discussions. One of us (E. E. M.) is grateful to the Department of Scientific and Industrial Research for the award of a maintenance grant.

REFERENCES

ADAIR, R. K., 1950, *Rev. Mod. Phys.*, **22,** 249; 1952, *Phys. Rev.*, **87,** 1041.
ARON, W. A., HOFFMAN, B. G., and WILLIAMS, F. C., 1949, University of California, UCRL–121.
BHATIA, A. B., HUANG, K., HUBY, R., and NEWNS, H. C., 1952, *Phil. Mag.*, **43,** 485.
BRECKON, S. W., HENRIKSON, A., MARTIN, W. M., and FOSTER, J. S., 1954, *Canad. J. Phys.*, **32,** 223.
BUECHNER, W. W., 1954, *Proceedings of the* 1954 *Glasgow Conference on Nuclear and Meson Physics* (London : Pergamon Press).
BUTLER, S. T., 1951, *Proc. Roy. Soc.* A, **208,** 559.
EL-BEDEWI, F. A., and EL-WAHAB, M. A., 1955, *Proc. Phys. Soc.* A, **68,** 754.
ENDT, P. M., and KLUYVER, J. C., 1954, *Rev. Mod. Phys.*, **26,** 95.
GLASS, N. W., and RICHARDSON, J. R., 1954, *Phys. Rev.*, **93,** 942.
HARVEY, J. A., 1951, *Phys. Rev.*, **81,** 353.
HOLT, J. R., and LITHERLAND, A. E., 1954, *Rev. Sci. Instrum.*, **25,** 298.
HOLT, J. R., and MARSHAM, T. N., 1953 a, *Proc. Phys. Soc.* A, **66,** 249; 1953 b, *Ibid.*, **66,** 258.
HORNYAK, W. F., 1952, *Rev. Sci. Instrum.*, **23,** 264.
HUBY, R., 1953, *Progress in Nuclear Physics*, Vol. 3 (London : Pergamon Press), p. 206.
LEWIS, I. A. D., and COLLINGE, B., 1953, *Rev. Sci. Instrum.*, **24,** 1113.
MIDDLETON, R., EL-BEDEWI, F. A., and TAI, C. T., 1953, *Proc. Phys. Soc.* A, **66,** 95.
NEWTON, J. C., 1954, *Phys. Rev.*, **96,** 241.
PECK, R. A., 1949, *Phys. Rev.*, **76,** 1279.
SNOWDON, S. C., 1952, *Phys. Rev.*, **87,** 1022.

An Investigation of the Reaction $^{19}F(d, n)^{20}Ne$ using a new Fast-Neutron Spectrometer

By J. M. CALVERT, A. A. JAFFE and E. E. MASLIN
Nuclear Physics Research Laboratory, University of Liverpool

Communicated by H. S. W. Skinner; *MS. received* 6th *June* 1955 *and in final form* 4th *August* 1955

Abstract. A description is given of a new fast-neutron spectrometer which utilizes scintillation counters and which has a relatively high efficiency of detection. The instrument is suitable for use at neutron energies of 4 MeV and above and has been used to investigate the stripping reaction $^{19}F(d, n)^{20}Ne$. The angular distribution of four neutron groups has been found and the theory of the deuteron stripping process has been applied to analyse the results and to obtain information about the corresponding levels in ^{20}Ne.

---

§ 1. Introduction

The angular distributions of the neutron groups from (d, n) stripping reactions have been investigated mainly by the use of photographic plates (Huby 1953) and also, recently, by means of a fast-neutron spectrometer utilizing ionization chambers (Holt and Litherland 1954, Calvert *et al.* 1955). The latter enabled neutron spectra to be obtained much more readily than by the scanning of nuclear emulsions. However, in order to maintain adequate energy resolution it was necessary to restrict the thickness of the hydrogenous radiator in which the recoil protons were produced, thus limiting the efficiency of neutron detection.

To investigate (d, n) stripping reactions in some of the many nuclei which have not yet been examined, or else have been studied only incompletely, a fast-neutron spectrometer has been developed having a relatively high efficiency of detection. This is of particular importance since, for the determination of neutron angular distributions, a large number of spectra must be obtained from each target nucleus.

A description of the apparatus and the results obtained from the reaction $^{19}F(d, n)^{20}Ne$ are given below.

§ 2. The Fast-Neutron Spectrometer

Two scintillators are mounted on the axis of the incident neutron beam so that recoil protons originating in the first scintillator, an anthracene crystal, complete their ranges in the second, which is of sodium iodide. The geometry is such that only those protons leaving the anthracene crystal within a small angle to the direction of the incident neutrons are accepted by the second crystal. Recoils having all, or almost all, the energy of the incident neutron produce simultaneous pulses from both crystals and the neutron energy may be determined by suitably analysing the heights of these pulses.

A neutron spectrometer based on similar principles has been described by Mozley and Shoemaker (1952). With their instrument, the neutron energy is determined by the addition of scintillation pulse heights from two anthracene crystals. When the pulses derived from the scintillations in the two crystals are to be added, however, their relative sizes must be adjusted so that their sum is as nearly as possible a constant for all neutrons of a given energy. For example, with two similar crystals and negligible absorption path between them, the overall photomultiplier and amplifier gains in the two channels would have to be equal. Actually the absorption path between the crystals would modify the above condition. In any case, the optimum amplifier gain settings would probably have to be determined by a time-consuming process of trial and error and would have to be maintained constant for long periods. Small drifts in photomultiplier or amplifier gain would cause serious loss in energy resolution.

In the arrangement to be described, provision has therefore been made for the separate analysis of the outputs of the scintillators, so that the exact setting of the amplifier gains, which is difficult to attain, is not necessary and gain stability need be maintained for much shorter periods. The system used for pulse analysis, coupled with the choice of a sodium iodide crystal as the second scintillator, also allows for a substantial improvement in resolution which, as will be seen, may be obtained by placing absorbing foils between the crystals.

Since the anthracene crystal may be as thick as the range of the recoil protons from the most energetic of the neutron groups being studied, much higher efficiency of neutron detection may be obtained than with neutron spectrometers restricted to thin radiators (Calvert *et al.* 1955, Trail and Johnson 1954). Any greater thickness of crystal would only increase the background counting rate, without increasing the efficiency.

§ 3. Experimental Details

The arrangement of the neutron spectrometer, target chamber and monitor is shown diagrammatically in figure 1. The anthracene crystal (usually about 1 cm square) is placed directly on the face of the photomultiplier nearest to the target.

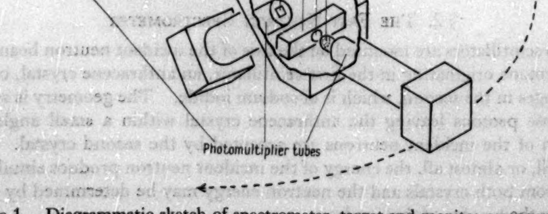

Figure 1. Diagrammatic sketch of spectrometer, target and monitor arrangement (spectrometer set in the 0° position).

This multiplier is inclined at an angle of 45° to the horizontal so that the distance between the anthracene crystal and the target may be reduced to as little as 8 cm if desired. The sodium iodide crystal is mounted on a short light pipe and is enclosed to prevent deterioration, the front surface being covered by thin aluminium foil over a circle of 1 cm diameter. Dumont type 6292 multipliers were chosen for their high cathode sensitivity. The crystals are normally 5 cm apart and between them, in the light-tight box which connects the multipliers, is a small proportional counter of rectangular section. Thin mica windows in the faces opposite the scintillators allow the recoil protons to pass through the counter. Access to the crystals and counter may be had through a lid in the top of the connecting box which also facilitates the insertion of absorbers. The spectrometer is mounted on a horizontal table and pivoted so that it may be rotated about the target.

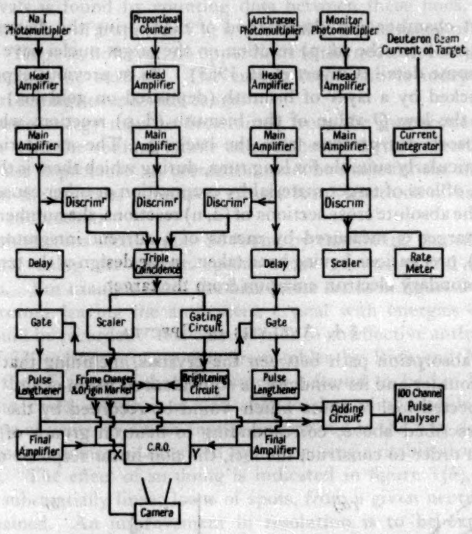
Na I Photomultiplier
Proportional Counter
Anthracene Photomultiplier
Monitor Photomultiplier
Deuteron Beam Current on Target
Head Amplifier
Head Amplifier
Head Amplifier
Head Amplifier
Main Amplifier
Main Amplifier
Main Amplifier
Main Amplifier
Current Integrator
Discrimr
Discrimr
Discrimr
Discrim
Delay
Triple Coincidence
Delay
Scaler
Rate Meter
Gate
Scaler
Gating Circuit
Gate
Pulse Lengthener
Frame Changer & Origin Marker
Brightening Circuit
Pulse Lengthener
Adding Circuit
100 Channel Pulse Analyser
Final Amplifier
X
C.R.O.
Y
Final Amplifier
Camera

Figure 2. Block diagram of electronic apparatus.

A block diagram (figure 2) illustrates the functions performed electronically. The proportional counter, used in triple coincidence with the scintillators, serves to help identify recoil protons, and virtually eliminates the otherwise unduly large number of random coincidences caused by the intense flux of γ-rays and neutrons from the target. When a triple coincidence occurs, the amplified pulses from the sodium iodide and anthracene crystals are lengthened to about 1 millisecond and are applied respectively to the X and Y deflecting plates of a cathode-ray oscillograph. The oscillograph beam is normally kept stationary, at the origin of deflections, at one corner of the tube screen and has very low intensity. On the arrival of the lengthened pulses, the beam is deflected to the appropriate position on the face of the tube and begins to return to the origin with a millisecond time constant. About 5 microseconds after the coincidence, a 10 microsecond brightening pulse is applied, and a single spot is recorded on stationary film in the oscillograph camera. After a predetermined number of such events (usually 100) the film is automatically moved on, and the position of the origin is marked on the new frame. While this is being done, the output of both the final amplifiers is momentarily short circuited to ensure the correct positioning of the origin. Since the coincidence rate never exceeds ten per second, and is usually much less, there is little danger of chance 'pile up' of the lengthened pulses.

While events are being recorded by the oscillograph, the lengthened pulses may also be fed into the adding circuit, in which the relative proportions of the pulses added from each of the two channels may be varied. The output from the adding circuit is then analysed on a Hutchinson–Scarrott 100-channel pulse analyser.

The target chamber and the method of monitoring the deuteron beam by counting protons from the (d, p) reaction on the target nuclei have already been described in some detail (Calvert *et al.* 1955). As in previous experiments, the targets are backed by a layer of bismuth (deposited on gold foil) so as to take advantage of the low *Q* value of the bismuth (d, p) reaction, which makes it possible to absorb out protons from the backing. The monitoring technique adopted is particularly suitable for long runs, during which there is the possibility, in some cases, of loss of target material by evaporation or other causes. In order to determine the absolute cross sections of (d, n) reactions, the number of deuterons reaching the target is measured by means of a current integrator (Lewis and Collinge 1953), precautions having been taken, in the design of the target chamber, to suppress secondary electron emission from the target.

§ 4. ANALYSIS OF SPECTRA

The total absorption path between the crystals, including that through the proportional counter and its windows, is equivalent to 14 cm of air. Figure 3 (*a*) shows the expected loci of spots which would be recorded by the oscillograph, in the way described above, corresponding to neutron groups of the energies indicated. In order to construct the loci, the non-linear response of anthracene

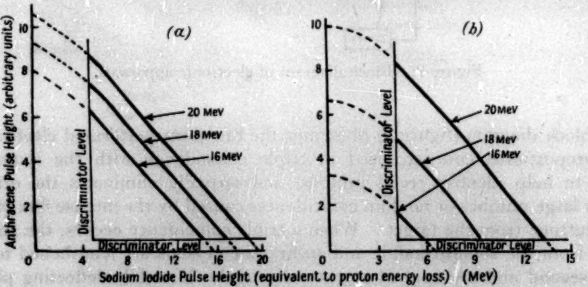

Figure 3. (*a*) Expected loci of recorded spots for neutrons of various energies. (*b*) Effect of interposing 300 mg cm^{-2} aluminium between the crystals.

to proton energy and the effect of the absorption of proton energy in the path between the crystals has been taken into account, using data from Taylor *et al.* (1951) and range–energy tables (Aron *et al.* 1949). As may be seen, points corresponding to all neutrons of a given energy lie approximately on straight lines, and the simplest method of analysis is to treat them as such. If better resolution is required, analyses may be made over the region of stricter linearity and, as in the figure, this may be selected by appropriate setting of the discriminator levels.

In practice the photographic records (on 35 mm film) are projected, with a linear enlargement of some 8 to 10 times, on to thin paper and the pattern of spots is copied by hand (this may be done extremely rapidly). The enlarged copy is then superimposed on a grid of parallel lines placed at the correct angle, which may be determined from prominent groups in the spectrum or from calibration targets, and a histogram showing the number of neutrons in given energy intervals is found by counting dots between these lines. In this way an energy resolution of from 5 to 7% is obtainable in the range of energies from 4 to 20 MeV. There is, however, no upper limit to the neutron energy range which may, in principle, be studied. The energy resolution is independent of the amplifier gain settings over a wide range.

The neutron energy may be determined from the intersection of the locus of the group with the sodium iodide axis, since the latter material has a linear energy response to protons. A correction must be made for the small absorption path between the crystals. Neutron groups from reactions of known Q values are used for calibration.

The absolute cross section may be found by calculating the effective radiator thickness, and using the known spectrometer geometry and n–p scattering cross section. For example, with the bias levels set as in figure 3 (*a*), for 20 MeV neutrons, protons leaving the anthracene crystal with energies of from 6·1 to 19·6 MeV would be recorded; this corresponds to an effective anthracene radiator thickness of 350 mg cm^{-2} (using data from tables by Rich and Madey (1954)). In this case the efficiency of the spectrometer is found to be 1 in $1{\cdot}72 \times 10^4$.

In certain cases, where it is desirable to determine angular distributions of two groups of neutrons which cannot be resolved in the way described above, enhanced resolution may be obtained by interposing suitable absorbers between the crystals. The effect of so doing is indicated in figure 3 (*b*), and it will be seen that a substantially linear locus of spots, from a given neutron group, may still be obtained. An improvement in resolution is to be expected for two reasons: (*a*) the form of the range–energy relation for protons is such that the lower the energy of the particle, the more energy will be lost in the absorber; (*b*) only part of the energy of each recoil proton is lost in the crystals, so that the statistical spread in the energy measured by the scintillation pulse heights is less in absolute value than it would be without absorbers. When such absorbers are used, only a restricted range of neutron energies may be studied at a time, and there is some loss in efficiency of neutron detection. The ultimate resolving power obtainable by this method should, however, be limited only by straggling in the energy loss of the protons in the absorber.

With the discriminator levels set to select the range of linearity between the pulses from the two channels, as in figure 3 (*a*), analysis of the neutron energies may also be performed by adding the pulses in proportions such that their sum is constant for neutrons of a given energy. As already stated, this condition is difficult to achieve and maintain, and consequently the resolution is inferior to that obtainable by the separate analysis of the pulses, as described above. Since both methods may, however, be used simultaneously, analysis of the added pulses by means of a 100-channel pulse analyser provides a means of checking the operation of the spectrometer during a run, since the spectra thus obtained may be continuously observed. If good resolution is not essential, it is possible to obtain spectra by means of the adding circuit alone, with some consequent saving of labour.

§ 5. THE ^{19}F(d, n)^{20}Ne REACTION

This reaction has been studied by Powell (1942) and by Bonner (1940) and neutron groups corresponding to several levels in ^{20}Ne have been reported. The angular distributions of these have not previously been measured, though the work of Bromley (1952) indicated that the group corresponding to the formation of the ground state of ^{20}Ne has a maximum in the forward direction.

In the present experiments, targets of CaF_2 and CF_2 were bombarded with a beam of deuterons of energy 9·06 MeV from the Liverpool 37 in. cyclotron, and the angular distributions of the neutron groups were investigated with the apparatus described above.

The neutron groups corresponding to the formation of the ground state, and of an excited state of 1·6 MeV, were found to show good stripping distributions. The Q values were, within the accuracy of our measurements, in agreement with those previously found by Powell (1942). Though these groups are fairly well resolved when of roughly equal intensity (e.g. at about 15°) it was necessary to use absorbers to separate them satisfactorily at other angles. Spectra obtained are shown in figure 4, and the angular distributions in figure 5. Theoretical curves calculated by the Born approximation theory (Bhatia *et al.* 1952) using a nuclear radius of $(2{\cdot}7+1{\cdot}22A^{1/3})\times 10^{-13}$ cm have been fitted. Neither of the levels previously reported at 4·3 MeV and 5·4 MeV could be identified with certainty in the range of angles of 0–50°. At a mean excitation of 7·3 MeV, an intense group, probably resulting from more than one level in ^{20}Ne, is observed. Because of the proximity of levels in this region the group has not been resolved into its components but the angular distribution indicates a mixture of two states corresponding to $l_p=0$ and $l_p=2$. Finally, a state at 9·3 MeV excitation was observed, formed with $l_p=1$. The results are summarized in the table.

(1)	(2)	(3)	(4)	(5)	(6)	(7)
n_0	0	0	0, 1	even	$2{\cdot}8\times10^{-27}$ (0°)	$7{\cdot}0\times10^{-50}$
n_1	1·63	2	1, 2, 3	even	$9{\cdot}0\times10^{-28}$ (33°)	$4{\cdot}4\times10^{-49}$
n_4	7·3	0	0, 1	even	$4{\cdot}7\times10^{-27}$ (0°)	$3{\cdot}9\times10^{-50}$
n_8		2	1, 2, 3	even	$4{\cdot}7\times10^{-28}$ (30°)	$1{\cdot}0\times10^{-48}$
n_9	9·2	1	0, 1, 2	odd	$1{\cdot}7\times10^{-28}$ (0°)	$5{\cdot}4\times10^{-50}$

(1) Neutron group ; (2) excitation energy of level in MeV as listed by Ajzenberg and Lauritsen (1952) ; (3) l_p value ; (4) possible spins of state ; (5) parity ; (6) differential cross section at centre of mass angle shown ; (7) Proton capture probability $\Lambda/(2j_i+1)$ in c.g.s. units.

§ 6. DISCUSSION

The ground state of ^{20}Ne is of interest when considering any nuclear model, because of the doubt about its configuration. As ^{19}F has spin ½ and even parity, the stripping distribution having $l_p=0$ for the formation of the ground state

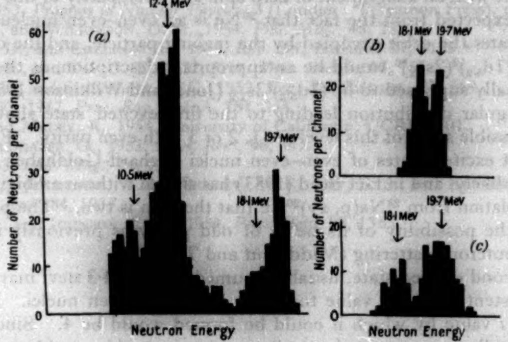

Figure 4. (*a*) Neutron energy spectrum obtained at 0° from ^{19}F(d, n)^{20}Ne. (*b*) 15° spectrum from ^{19}F(d, n)^{20}Ne showing neutrons corresponding to the ground and first excited states. (*c*) The same neutron spectrum as in (*b*) recorded with 260 mg cm^{-2} aluminium placed between the crystals.

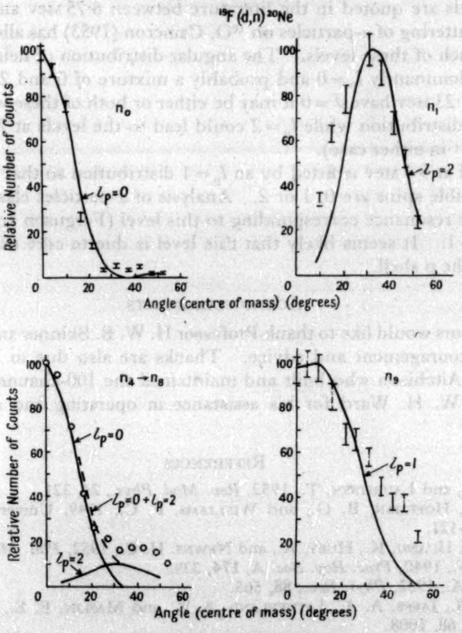

Figure 5. Angular distributions of neutrons corresponding to the formation of the ground state and excited states of 1·6, 7·3 and 9·2 mev.

is consistent with an assignment of zero spin and even parity to this state. This would be expected from the fact that ^{20}Ne is an even–even nucleus. If the l_p value indicates the orbit occupied by the ingoing particle, and the configuration is simple, $(1d_{5/2})^2(2s_{1/2})^2$ would be an appropriate description, as the ^{19}F ground state is usually supposed to be $(1d_{5/2})^2 2s_{1/2}$ (Jones and Wilkinson 1954).

The angular distribution leading to the first excited state shows $l_p = 2$, so that the possible spins of this level are 1, 2 or 3 with even parity. From the rule for the first excited states of even–even nuclei (Scharff-Goldhaber 1953) $J = 2^+$ is the most likely, and in fact Seed (1953) has shown without ambiguity from the (α, γ) correlation from ^{23}Na(p, $\alpha\gamma$)^{20}Ne that the spin is two. The present result discounts the possibility of its being of odd parity as previously indicated by inelastic deuteron scattering (Middleton and Tai 1952).

The second excited state, usually assumed to be at 4·3 MEV, may have a spin of 4, consistent with the value for other light even–even nuclei. If this is so, the lowest l value by which it could be formed would be 4. Since such high l values usually have extremely small cross sections, this would account for our failure to observe the formation of this state. Moreover, it seems quite likely that this level is an excited state of the configuration $(1d)^2(2s)^2$ and as stripping would require it to have an appreciable admixture of $(1d)^2 2s1g$ to give a spin of 4, it would make it still more difficult to observe stripping to this level.

Five levels are quoted in the literature between 6·75 MEV and 7·87 MEV and, by elastic scattering of α-particles on ^{16}O, Cameron (1953) has allocated spins and parities to each of these levels. The angular distribution of neutrons leading to these is predominantly $l_p = 0$ and probably a mixture of 0 and 2. As the levels at 6·75 and 7·23 MEV have $J = 0$ it may be either or both of these which contribute to the $l_p = 0$ distribution while $l_p = 2$ could lead to the levels at 7·46 or 7·87 MEV (giving $J = 2^+$ in either case).

The level at 9·3 MEV is fitted by an $l_p = 1$ distribution so that its parity is odd and the possible spins are 0, 1 or 2. Analysis of α-particles elastically scattered by ^{16}O at the resonance corresponding to this level (Ferguson and Walker 1940) indicates $J = 1$. It seems likely that this level is due to core excitation, that is, to a hole in the p shell.

ACKNOWLEDGMENTS

The authors would like to thank Professor H. W. B. Skinner and Dr. J. R. Holt for their encouragement and advice. Thanks are also due to Dr. B. Collinge and Mr. K. Aitchison who built and maintained the 100-channel pulse analyser and to Mr. W. H. Ward for his assistance in operating and maintaining the cyclotron.

REFERENCES

AJZENBERG, F., and LAURITSEN, T., 1952, *Rev. Mod. Phys.*, **24**, 321.

ARON, W. A., HOFFMAN, B. G., and WILLIAMS, F. C., 1949, University of California, UCRL-121.

BHATIA, A. B., HUANG, K., HUBY, R., and NEWNS, H. C., 1952, *Phil. Mag.*, **43**, 485.

BONNER, T. W., 1940, *Proc. Roy. Soc.* A, **174**, 339.

BROMLEY, D. A., 1952, *Phys. Rev.*, **88**, 565.

CALVERT, J. M., JAFFE, A. A., LITHERLAND, A. E., and MASLIN, E. E., 1955, *Proc. Phys. Soc.* A, **68**, 1008.

CAMERON, J. R., 1953, *Phys. Rev.*, **90**, 839.

FERGUSON, A. J., and WALKER, L. R., 1940, *Phys. Rev.*, **58**, 666.

Holt, J. R., and Litherland, A. E., 1953, *Rev. Sci. Instrum.*, **25**, 298.
Huby, R., 1953, *Progress in Nuclear Physics*, **3** (London : Pergamon Press), p. 177.
Jones, G. A., and Wilkinson, D. H., 1954, *Phil. Mag.*, **45**, 230.
Lewis, I. A. D., and Collinge, B., 1953, *Rev. Sci. Instrum.*, **24**, 1113.
Middleton, R., and Tai, C. T., 1952, *Proc. Phys. Soc.* A, **65**, 752.
Mozley, R. F., and Shoemaker, F. C., 1952, *Rev. Sci. Instrum.*, **23**, 569.
Powell, C. F., 1942, *Proc. Roy. Soc.* A, **181**, 344.
Rich, M., and Madey, R., 1954, University of California, UCRL-2301.
Scharff-Goldhaber, G., 1953, *Phys. Rev.*, **90**, 587.
Seed, J., 1953, *Phil. Mag.*, **44**, 921.
Taylor, C. J., Jentschke, W. K., Remley, M. E., Eby, F. S., and Kruger, P. G., 1951, *Phys. Rev.*, **84**, 1034.
Trail, C. C., and Johnson, C. H., 1954, *Phys. Rev.*, **95**, 1363.

The Hall Effect in Metals at High Frequencies

By B. DONOVAN
Department of Physics, Northern Polytechnic, London

MS. received 18*th May* 1955

Abstract. The theory of the Hall effect at high frequencies is developed in terms of the 'surface Hall coefficient' defined in a similar manner to the complex surface impedance for metals. Calculations of this coefficient have been carried through for a metal with two overlapping energy bands, and the variations with frequency and with field strength are shown graphically for certain special cases.

At very low frequencies the Hall coefficient is constant at the d.c. value; at higher frequencies it increases as the square root of the frequency and ultimately, in the infra-red region for normal metals, attains a limiting value independent of frequency. Furthermore a phase difference exists in general between the Hall field and the specimen current but this decreases to zero at very low and very high frequencies.

§ 1. Introduction

In a previous paper (Donovan 1954, subsequently referred to as I) an investigation was made of the magneto-resistance effect at high frequencies, on the basis of the two-band model well known in the theory of metals. The essential procedure in this treatment was the evaluation of the surface resistance as a function of frequency and applied magnetic field strength, and the importance of the relaxation time of the conduction electrons was demonstrated. In the present paper a similar analysis is applied to the problem of the corresponding Hall effect, i.e. the production of an alternating electric field when a specimen carrying a high frequency current is placed in a constant transverse magnetic field.

Very few experimental data on this problem have been obtained and for metals the only investigation at very high frequencies appears to be that briefly reported by Cooke (1948), who used a cavity technique at a wavelength of 3 cm. The Hall effect was detected in bismuth, iron, nickel and various ferromagnetic alloys but no numerical results were given. In the case of semiconductors, alternating currents of comparatively low frequency have been used occasionally for Hall measurements; thus Bottom (1948) carried out experiments on tellurium up to 10 kc/s. Recently the Hall effect in germanium has been used by Barlow (1955) as a means of measuring power in transmission lines at frequencies up to 300 Mc/s.

So far no theory has been given relevant to the situation at high frequencies. The purpose of the present paper is to develop such a theory and, starting from the same premises as in I, to establish the essential results for the case of a highly degenerate electron gas. For this purpose it is convenient to introduce the 'surface Hall coefficient', defined in an analogous manner to the complex surface impedance. Reference to this quantity has already been made in a preliminary note (Donovan and Sondheimer 1953) dealing with the free-electron model.

§ 2. THE SURFACE HALL COEFFICIENT

The present calculation is based upon the model with two overlapping bands of standard form, band 1 being normal and band 2 inverted. In each band the energy is taken to be proportional to the square of the wave number. The effective mass m and relaxation time τ of the electrons in the two bands will be distinguished by suffixes as usual.

We consider a semi-infinite metal whose surface corresponds to the plane $z=0$, the positive z-axis being directed into the metal. A constant magnetic field H is applied in the direction of the z-axis, and the alternating electric field is specified by $(\mathscr{E}_x(z), \mathscr{E}_y(z), 0)\,e^{i\omega t}$, where ω is the angular frequency. As in I, calculation of the current density is carried out by the usual method and leads to the expressions

$$J_x = \frac{e^2}{3\pi^2\hbar^4}(P\mathscr{E}_x - Q\mathscr{E}_y) \qquad \ldots\ldots(1)$$

$$J_y = \frac{e^2}{3\pi^2\hbar^4}(Q\mathscr{E}_x + P\mathscr{E}_y) \qquad \ldots\ldots(2)$$

where

$$P = \frac{(\hbar\tau_1/m_1)(1+i\omega\tau_1)(2m_1\zeta_1)^{3/2}}{\alpha_1{}^2\tau_1{}^2 + (1+i\omega\tau_1)^2} + \frac{(\hbar\tau_2/m_2)(1+i\omega\tau_2)(2m_2\zeta_2)^{3/2}}{\alpha_2{}^2\tau_2{}^2 + (1+i\omega\tau_2)^2} \qquad \ldots\ldots(3)$$

$$Q = \frac{(\hbar\alpha_1\tau_1{}^2/m_1)(2m_1\zeta_1)^{3/2}}{\alpha_1{}^2\tau_1{}^2 + (1+i\omega\tau_1)^2} - \frac{(\hbar\alpha_2\tau_2{}^2/m_2)(2m_2\zeta_2)^{3/2}}{\alpha_2{}^2\tau_2{}^2 + (1+i\omega\tau_2)^2} \qquad \ldots\ldots(4)$$

and $\alpha = eH/mc$. The parameters ζ_1 and ζ_2 give the position of the Fermi energy level relative to the bottom of band 1 and the top of band 2 respectively.

The surface Hall coefficient is defined by

$$Y = \frac{\mathscr{E}_y(0)}{H\int_0^\infty J_x dz} \qquad \ldots\ldots(5)$$

and depends in general upon the frequency and the applied magnetic field. It will be noted that Y differs dimensionally from the normal d.c. coefficient,

$$R_H = \mathscr{E}_y/J_xH.$$

The calculation of the surface Hall coefficient follows similar lines to the calculation of the surface impedance in I; equations (1) and (2) are combined with Maxwell's equations (neglecting the displacement current) and the total transverse current is set equal to zero. In this way one obtains†

$$Y(\omega, H) = -\frac{4\pi i\omega}{c^2H}\,\frac{\mathscr{E}_y(0)}{(d\mathscr{E}_x/dz)_0} = -(1+i)\frac{2\pi\omega}{c^2H}\left[\frac{(P^2+Q^2)^{1/2} - P}{\gamma(P^2+Q^2)}\right]^{1/2} \qquad \ldots\ldots(6)$$

where

$$\gamma = 4\omega e^2/3\pi\,\hbar^4c^2.$$

It is clear that the Hall coefficient given by equation (5), like the surface impedance, is in general a complex quantity, showing that a phase difference exists between the Hall field and the current. The usual experimental procedure, involving measurement of transverse e.m.f. and specimen current, would thus give $|Y|$.

---

† Gaussian units are used throughout this paper.

In discussing the behaviour of equation (6) for various cases it is convenient to introduce the carrier densities: if n_1 and n_2 represent respectively the numbers of electrons and positive holes per unit volume, then

$$n_1 = \frac{(2m_1\zeta_1)^{3/2}}{3\pi^2\hbar^3}, \qquad n_2 = \frac{(2m_2\zeta_2)^{3/2}}{3\pi^2\hbar^3}. \qquad \ldots\ldots(7)$$

In terms of these carrier densities the d.c. conductivity may be written

$$\sigma_0 = e^2\left(\frac{n_1\tau_1}{m_1} + \frac{n_2\tau_2}{m_2}\right). \qquad \ldots\ldots(8)$$

§ 3. The Free-Electron Model

As a preliminary special case we consider the application of equation (6) to a system of perfectly free electrons. Making use of (3), (4), (7) and (8), in which expressions the first term only appears, we find

$$Y(\omega, H) = -\frac{(1+i)}{H\sqrt{2}}\left[\frac{2\pi\omega}{c^2\sigma_0}\right]^{1/2}(1+i\omega\tau)^{1/2}\left[-1+\left\{1+\left(\frac{\alpha\tau}{1+i\omega\tau}\right)^2\right\}^{1/2}\right]^{1/2}. \quad \ldots(9)$$

This expression has a similar form to that of the corresponding surface impedance $Z(\omega, H)$, given in I, equation (17), and may be written as

$$Y(\omega, H) = -(1+i)R_n(a+ib)/H\sqrt{2} \qquad \ldots\ldots(10)$$

where $R_n = [2\pi\omega/c^2\sigma_0]^{1/2}$, the limiting value of the surface resistance in the non-relaxation region ($\omega\tau \ll 1$).

From (10) it follows that the modulus of the surface Hall coefficient is

$$|Y| = R_n(a^2+b^2)^{1/2}/H \qquad \ldots\ldots(11)$$

and the phase difference ϕ between the Hall field and the current is given by

$$\tan\phi = (a+b)/(a-b). \qquad \ldots\ldots(12)$$

The functions a and b must in general be determined by numerical methods but simple expressions may be found in various limiting cases. In the non-relaxation region $b=0$ and equation (9) becomes

$$Y(\omega, H) = -\frac{(1+i)}{H\sqrt{2}}R_n[-1+\{1+\alpha^2\tau^2\}^{1/2}]^{1/2}. \qquad \ldots\ldots(13)$$

If, further, we consider the case of weak fields ($\alpha\tau \ll 1$), we obtain

$$Y(\omega, H) = -(1+i)R_n(\sigma_0/2nec) \qquad \ldots\ldots(14)$$

showing that the surface Hall coefficient is here independent of the field strength and proportional to the square root of the frequency. Moreover, we see from (12) that $\phi = \pi/4$. The modulus of Y may be expressed as

$$|Y| = -\left(\frac{1}{nec}\right)\left(\frac{\pi\omega\sigma_0}{c^2}\right)^{1/2} \qquad \ldots\ldots(15)$$

where the first factor is the well-known d.c. coefficient.

As explained in I, the present treatment is not directly applicable to the case of very low frequencies, for which the penetration depth is very much greater than the dimensions of the specimen. Under such quasi-static conditions, however, so long as the variation of current density is negligible, the surface resistance is *constant* and hence, since $Y \propto R_n$, we should expect that the Hall coefficient would also be constant.

As the frequency increases Y rises to a limiting value and for $\omega\tau \gg 1$ it is independent of frequency and given by

$$|Y| = -\left(\frac{1}{nec}\right)\left(\frac{\pi\sigma_0}{c^2\tau}\right)^{1/2}. \qquad \ldots\ldots(16)$$

In this region Y is a *real* quantity and $\phi = 0$.

In order to illustrate the frequency variation of the Hall effect the quantities a and b have been evaluated from equation (9) taking $\alpha = 2 \times 10^{12}$ ($H = 1{\cdot}1 \times 10^5$ oersteds) and $\tau = 3 \times 10^{-14}$ sec, which is the room temperature value for sodium. In figure 1 curve (a) the function $\omega^{1/2}(a^2 + b^2)^{1/2}$ is plotted against the frequency $\omega/2\pi$ and against the product $\omega\tau$; it will be noticed that the curve bends over quite abruptly in the neighbourhood of $\omega\tau \sim 1$.

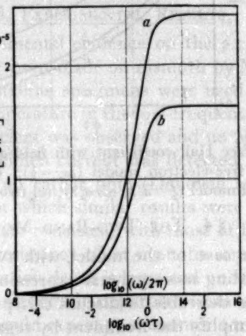

Figure 1. Variation of surface Hall coefficient with frequency for: (a) free-electron model ($\xi = 1$); (b) two-band model ($\xi = 2/3$). $\alpha\tau = 0{\cdot}06$ in both cases.

The behaviour of the phase angle ϕ, as given by (12), is shown in figure 2. The transition region in which ϕ decreases to zero is determined by the relaxation time, which assumes particular significance in the present theory, as it does in the high frequency magneto-resistance effect.

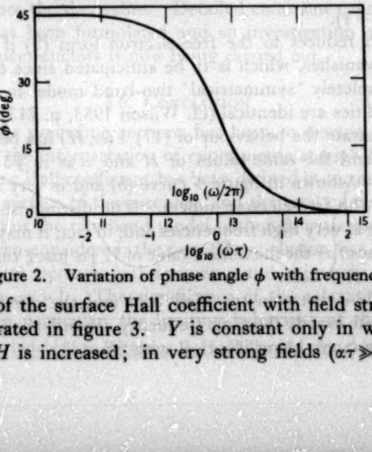

Figure 2. Variation of phase angle ϕ with frequency.

The variation of the surface Hall coefficient with field strength at constant frequency is illustrated in figure 3. Y is constant only in weak fields ($\alpha\tau \ll 1$) and decreases as H is increased; in very strong fields ($\alpha\tau \gg 1$), $Y \propto H^{-1/2}$ but, as noted in I, this case is strictly speaking outside the range of validity of the Boltzmann equation. In figure 3 the ratio $|Y(H)|/|Y(0)|$, where $Y(0)$ is the limiting value of Y for vanishingly small magnetic field, has been plotted against $\alpha\tau$ and it will be seen that very similar results are obtained in the non-relaxation region (curve (*a*)) and at $\omega\tau=\frac{1}{2}$ (curve (*b*)).

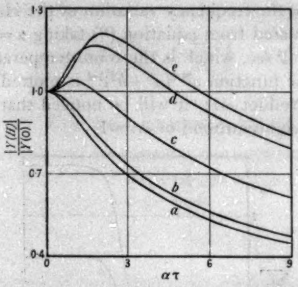

Figure 3. Variation of surface Hall coefficient with field strength for: (*a*) free-electron model ($\omega\tau\ll 1$); (*b*) free-electron model ($\omega\tau=\frac{1}{2}$); (*c*) two-band model ($\xi=4/5$, $\omega\tau\ll 1$); (*d*) two-band model ($\xi=2/3$, $\omega\tau\ll 1$); (*e*) two-band model ($\xi=2/3$, $\omega\tau=\frac{1}{2}$).

§ 4. The Two-Band Model

We now consider the case of the model with two overlapping bands, by returning to (6) and inserting more general expressions for P and Q. Clearly it is neither profitable nor desirable to discuss this problem in great generality at present and we shall simplify the treatment by regarding the effective masses and the relaxation times in the two bands as equal. Thus we write $m_1=m_2=m$ and $\tau_1=\tau_2=\tau$.

Taking the carrier density to be the distinguishing feature and writing $n_1=\kappa n_2$, we may derive the surface Hall coefficient in the form

$$Y(\omega,H)=-\frac{(1+i)}{H\sqrt{2}}R_n\left[\frac{(1+i\omega\tau)^2+\alpha^2\tau^2}{(1+i\omega\tau)^2+\alpha^2\tau^2\xi^2}\right]^{1/2}[\{(1+i\omega\tau)^2+\alpha^2\tau^2\xi^2\}^{1/2}-(1+i\omega\tau)]^{1/2} \qquad \ldots\ldots(17)$$

where $\xi=(\kappa-1)/(\kappa+1)$.

This expression reduces to the free-electron form (9) if $\xi=1$ (κ infinite). If $\xi=0$ ($\kappa=1$), Y vanishes, which is to be anticipated since the d.c. coefficient vanishes for a completely 'symmetrical' two-band model in which the carrier densities and mobilities are identical (cf. Wilson 1953, p. 213).

In order to illustrate the behaviour of (17) $Y(\omega,H)$ has been evaluated with $|\xi|=\frac{2}{3}$ ($\kappa=5$ or $\frac{1}{5}$) and the same values of H and τ as in § 3. The frequency dependence of $|Y|$ is shown in figure 1 curve (*b*) and is very similar in form to that obtained with the free-electron model. The distinguishing feature is the lower limiting value at very high frequencies and, in fact, it may readily be shown that, for a given value of $\alpha\tau$ the maximum value of $|Y|$ is just ξ times the expression (16) for the free-electron case.

The phase angle ϕ between the Hall field and the current has also been evaluated and exhibits exactly the same frequency dependence as the free-electron model, the resulting curve being identical with figure 2.

The variation of Y with field strength is shown in figure 3 and here the two-band model exhibits an essentially new feature. For sufficiently large values of $\alpha\tau$ $Y(H)$ tends to zero as found previously but as $\alpha\tau$ is increased from zero $Y(H)$ *increases* initially and passes through a maximum. This behaviour is a consequence of values of ξ less than unity and, for a given frequency, the maximum in $Y(H)$ increases and occurs at a higher value of $\alpha\tau$ if ξ is reduced.

Figure 3 shows the results obtained with $|\xi|=\frac{2}{3}$ and it will be seen that, as in the free-electron case, the non-relaxation curve lies slightly below that for $\omega\tau=\frac{1}{2}$. As an example of an intermediate case we have also plotted the curve for $|\xi|=\frac{4}{5}$ ($\kappa=9$ or $\frac{1}{9}$) in the low frequency region. The maximum in $Y(H)$ in this case (curve (*c*)) occurs at $\alpha\tau\sim 1$, which is about half the value obtained with $|\xi|=\frac{2}{3}$ (curve (*d*)).

§ 5. Experimental Results

In order to obtain experimental evidence on the a.c. Hall effect some preliminary measurements have been made on bismuth by Mr. G. Reichenbaum in this Department. Polycrystalline specimens were used and the measurements were carried out at room temperature in the low-frequency region. Up to 3 Mc/s no change in the Hall coefficient was observed and no phase difference between the Hall e.m.f. and the specimen current was detected. Further experimental details have been given in an earlier note (Donovan and Reichenbaum 1954) dealing with germanium, for which similar results were obtained.

The results for bismuth are consistent with those of Blunt (1948), who found no change in the magneto-resistance effect over the same frequency range. At these frequencies the penetration depth is large and under quasi-static conditions we should not expect any significant departure from d.c. behaviour. As the frequency is increased we should expect to encounter a transition region in which the phase angle increases from zero to the value $\pi/4$ characteristic of the low frequency limit of the present theory. Further, one would expect to observe the increasing Hall coefficient, as depicted in figure 1. In bismuth this effect should occur at much lower frequencies than in normal metals owing to the abnormally large relaxation time (cf. I, § 6).

In this connection it is of interest that recent experiments at the University of Pennsylvania† indicate that the Hall coefficient of germanium at 3000 Mc/s differs very little from the d.c. value. Detailed comment cannot be made until a suitable theory has been formulated and an investigation of high frequency conductivity in semiconductors is now being carried out.

§ 6. Conclusion

The object of the preceding sections has been to discuss the Hall effect in a form suitable for the interpretation of experiments at high frequencies. For this purpose a surface Hall coefficient has been defined in terms of the transverse electric field at the surface of the specimen and the total current per unit width in the specimen. For the two-band model, although variations in all the parameters have not been considered, the general conclusion has emerged that the surface Hall coefficient increases with frequency and ultimately reaches a constant value in the region $\omega\tau \gg 1$. The significance of the relaxation time has been emphasized, and, in particular, the limiting behaviour of the Hall coefficient takes place in a frequency range corresponding roughly to $1<\omega\tau<10$. For normal metals such frequencies are too high to be accessible with electrical techniques and necessarily come within the province of optics. In this connection it may be pointed out that the phenomenon of the high frequency Hall effect is relevant to the interpretation of the changes in polarization which are observed when electromagnetic waves are reflected from a metal surface in the presence of a magnetic field.

---

† The author is indebted to Professor P. H. Miller, Jr., for this information.

ACKNOWLEDGMENT

The author wishes to thank Dr. E. H. Sondheimer for helpful discussion on this work.

REFERENCES

BARLOW, H. E. M., 1955, *Proc Inst. Elect. Engrs*, **102** (Part B), 179

BLUNT, R. F., 1948, *Phys. Rev.*, **73**, 654.

BOTTOM, V. E., 1948, *Bull. Amer. Phys. Soc.*, **23**, 21.

COOKE, S. P., 1948, *Phys. Rev.*, **74**, 701.

DONOVAN, B., 1954, *Proc. Phys. Soc.* A, **67**, 305.

DONOVAN, B., and REICHENBAUM, G., 1954, *Physica*, **20**, 993.

DONOVAN, B., and SONDHEIMER, E. H., 1953, *Proc. Phys. Soc.* A, **66**, 849.

WILSON, A. H., 1953, *The Theory of Metals* (Cambridge : University Press).

The Beta Decay of the Ground State of ^{26}Al

By M. J. LAUBITZ
Cavendish Laboratory, Cambridge

Communicated by E. S. Shire ; MS. received 31st March 1955

Abstract. The beta-decay spectrum from the ground state of ^{26}Al has been observed by means of a scintillation spectrometer. It has an end point of 1·17 ± 0·05 Mev and corresponds to a second forbidden transition, $\Delta J = 3$, no. The beta decay is followed by a gamma ray of energy 1·76 ± 0·1 Mev.

---

§ 1. Introduction

Kluyver *et al.* (1954), Browne (1954), and Kavanagh *et al.* (1955) have established the levels in ^{26}Al produced by ^{25}Mg(p,γ) and ^{28}Si(d,α) reactions, and Kavanagh *et al.* also re-measured the previously known beta-ray spectrum. Their results point to the energy level scheme illustrated in figure 1 with the observed 6·68 sec beta ray transition coming from the first excited ($T = 1$) state (T is the total isotopic spin). The assumed ground state can thus decay by positron emission to the $J = 2^+$ level of ^{26}Mg by means of a second forbidden $\Delta J = 3$, no, transition. From *ft* value considerations, such a transition would have a half-life of 10^4–10^6 years. Recent work by Simanton *et al.* (1954) suggests that the half-life is closer to 10^6 years.

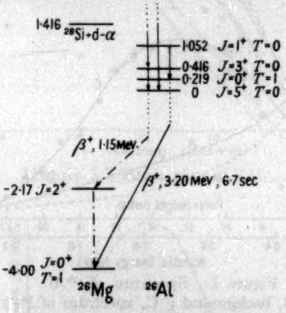

Figure 1. Decay scheme of ^{26}Al.
Solid lines : as given by Kavanagh *et al.*, broken lines : results of our experiments.

We now report experiments made with a scintillation spectrometer in which we have obtained the beta-ray spectrum of the ground-state disintegration and have observed the gamma-ray expected if the transition takes place to the first excited level of ^{26}Mg.

§ 2. Experimental Method

We irradiated a small piece (1 in. × 1 in. × $\frac{1}{8}$ in.) of silicon oxide in the Cavendish Laboratory cyclotron with 5 Mev deuterons for 126 hours at an average current of 5 μA in^{-2}. The reaction ^{28}Si(d, α)^{26}Al ensured the formation of states with $T = 0$. We began the measurements of the beta-ray spectrum 60 days after the irradiation, by which time the activity of the source had remained constant for a period of 20 days. The activity, however, was much too low for the use of a magnetic spectrometer and we used a scintillation spectrometer, consisting of a cylindrical anthracene crystal (1 in. diameter × 1 in.), an E.M.I. 6262 photomultiplier tube, and a multichannel pulse-height analyser. The spectrometer was calibrated by means of ^{35}S, ^{32}P and ^{106}Rh (a Kurie plot of ^{32}P is shown in figure 3), and its resolution, as given by the ^{137}Cs conversion line, was 18%.

For the gamma-ray measurements, we used a 1 in. cube NaI crystal in the spectrometer. The resolution was 20%. We calibrated the system by means of the gamma rays of ^{134}Cs, ^{137}Cs, ^{106}Rh and Th active deposit.

§ 3. EXPERIMENTAL RESULTS

The spectrum obtained with the ^{26}Al source is shown in figure 2. It is an average of several runs, totalling approximately 25 000 counts. The background counting rate was determined by interposing 4 mm of aluminium between the source and the crystal—enough to absorb 2 MeV beta rays. The high background caused considerable scatter of experimental points at lower energies, and the spectrum could not be extended lower than 0·3 MeV. Experiments performed with ^{137}Cs in the magnetic spectrometer showed that electrons backscattered from the silicon oxide source had no effect on the spectrum shape above 0·3 MeV. Figure 3 shows the spectrum analysed in terms of the allowed Kurie plot, and the Kurie plots for the second forbidden matrix elements R_{ij}, A_{ij}, T_{ij}, $\int(\boldsymbol{\alpha} \cdot \mathbf{r})$, and S_{ijk} (Konopinski and Uhlenbeck 1941). The best straight line is obtained using the S_{ijk} matrix ($\Delta J = \pm 2$, 3, no) and this is the only second forbidden matrix element in agreement with the proposed level assignments of ^{26}Al and ^{26}Mg. The higher energy points of the S_{ijk} matrix are off the Kurie plot by a considerable amount, but the deviation may be entirely ascribed to the 18% resolution of the spectrometer (figure 4). The end point obtained from the Kurie plot is $1{\cdot}17 \pm 0{\cdot}05$ MeV, in good agreement with the proposed energy level scheme.

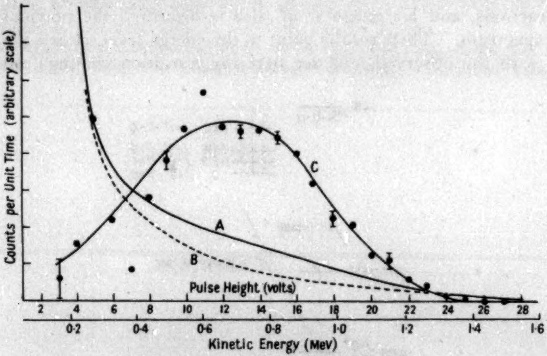

Figure 2. Spectrum of ^{26}Al.
A, total count ; B, background ; C, spectrum of ^{26}Al on enlarged scale.

The only other second forbidden matrix element which could qualify on the basis of linearity of the Kurie plot is the A_{ij}. However, its selection rules

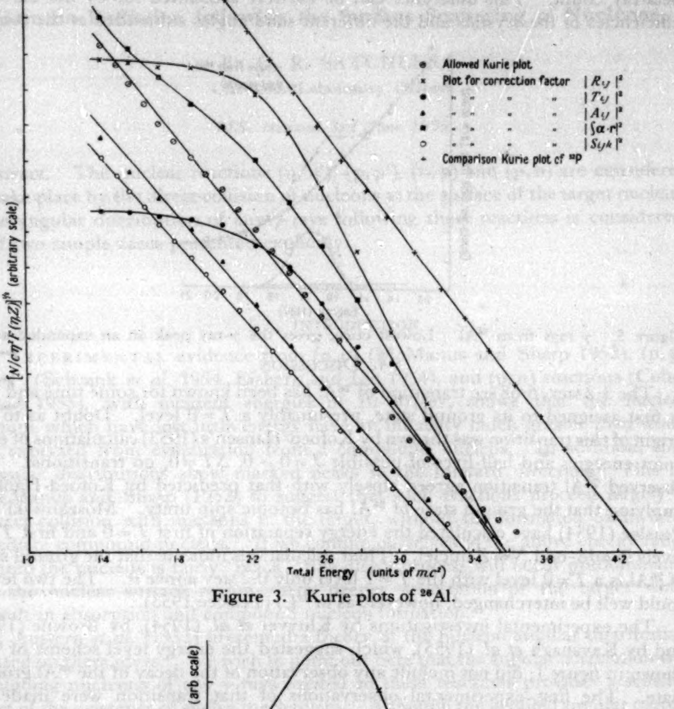

Figure 3. Kurie plots of ^{26}Al.

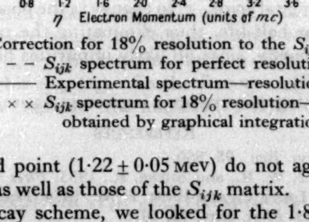

Figure 4. Correction for 18% resolution to the S_{ijk} spectrum.
– – – S_{ijk} spectrum for perfect resolution.
—— Experimental spectrum—resolution 18%.
× × × S_{ijk} spectrum for 18% resolution—
obtained by graphical integration.

($\Delta J = \pm 2$, no) and end point ($1{\cdot}22 \pm 0{\cdot}05$ MeV) do not agree with the proposed disintegration scheme as well as those of the S_{ijk} matrix.

To confirm the decay scheme, we looked for the 1·83 MeV gamma ray. A typical result is illustrated in figure 5. The energy found for the observed gamma ray from four runs of 1 hour each was $1{\cdot}76 \pm 0{\cdot}1$ MeV. The total recorded gamma ray count was about 10 per minute, compared with about 60 per minute for the beta-ray count. This difference can be entirely accounted for by the different efficiencies of the crystals and the different solid angles subtended at the source.

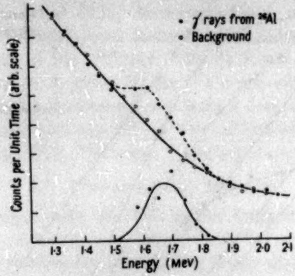

Figure 5. γ rays from ^{26}Al. Lowest curve gives the γ-ray peak on an expanded scale.

§ 4. Discussion

The 3·2 Mev, 6·68 sec transition of ^{26}Al has been known for some time and was at first assigned to its ground state, presumably a $T=0$ level. Doubt as to the origin of this transition was thrown by Kofoed-Hansen's (1953) calculations of end-point energies and half-lives of possible $J=0\rightarrow 0$, $\Delta T=0$, no transitions. The observed ^{26}Al transition agreed closely with that predicted by Kofoed-Hansen, implying that the ground state of ^{26}Al has isotopic spin unity. Moszkowski and Peaslee (1954) have calculated the energy separation of first $T=0$ and first $T=1$ levels in odd–odd $N=Z$ nuclei. Their calculations indicate that the ground state of ^{26}Al is a $T=0$ level with the $T=1$ level only 0·2 Mev above it. The two levels could well be interchanged, however, as in ^{34}Cl (Peaslee 1953).

The experimental investigations by Kluyver *et al.* (1954), by Browne (1954) and by Kavanagh *et al.* (1955), which suggested the energy level scheme of ^{26}Al shown in figure 1, did not include any observation of the decay of the ^{26}Al ground state. The first experimental observations of that transition were made by Simanton *et al.* (1954), who traced chemically to aluminium a long-lived gamma and beta activity obtained by bombarding commercial magnesium with deuterons.

The observed beta spectrum reported here has the correct end-point energy for, and is consistent as regards selection rules with, the decay scheme proposed by Kavanagh *et al.* The gamma ray observed also agrees with the proposed scheme within experimental error. No change in the observed rate of decay of the source indicates a long half-life, thus eliminating the possibility of the activity being due to some impurity, since all likely impurities have half-lives less than a few hours.

The complete disintegration scheme is given in figure 1.

References

Browne, C. P., 1954, *Phys. Rev.*, **95,** 860.
Kavanagh, R. W., Mills, W. R., and Sherr, R., 1955, *Phys. Rev.*, **97,** 248.
Kluyver, J. C., van der Leun, C., and Endt, P. M., 1954, *Phys. Rev.*, **94,** 1795.
Kofoed-Hansen, O., 1953, *Phys. Rev.*, **92,** 1075.
Konopinski, E. J., and Uhlenbeck, G. E., 1941, *Phys. Rev.*, **60,** 308.
Moszkowski, S. A., and Peaslee, D. C., 1954, *Phys. Rev.*, **93,** 455.
Peaslee, D. C., 1953, *Nuovo Cim.*, **10,** 1349.
Simanton, J. R., Rightmire, R. A., Long, A. L., and Kohman, T. P., 1954, *Phys. Rev.*, **96,** 1711.

Gamma Radiation following the Surface Scattering of Nucleons

By G. R. SATCHLER
Clarendon Laboratory, Oxford

MS. received 3rd June 1955

Abstract. The nuclear reactions (n, n′), (p, p′), (n, p) and (p, n) are considered to take place by the direct collision of nucleons at the surface of the target nucleus. The angular distribution of any γ-rays following these reactions is considered, and two simple cases presented explicitly.

---

§ 1. Introduction

Experimental evidence from (n, p) (McManus and Sharp 1952), (p, p′) (Schrank *et al.* 1954, Eisberg and Igo 1954), and (p, n) reactions (Cohen 1955), with incident energies of 10–30 Mev, shows that the nucleon groups which have lost little energy have an intensity much greater than would be expected from evaporation from a compound nucleus. In addition, their angular distributions show marked peaks in the forward direction. This led McManus and Sharp (1952) to suggest that such reactions proceed largely by direct collision with nucleons in the target, without the formation of an intermediate compound nucleus. If we confine ourselves to the above energy range, where the nucleus is fairly ‘black’, this direct process will occur predominantly in the nuclear surface region. Any deeper penetration of the target would result in absorption and compound nucleus formation.

Austern *et al.* (1953) presented a theory of the nucleon angular distributions based on these ideas. We wish to point out here that the angular correlation with outgoing nucleons of any γ-rays excited in these reactions provides a sensitive test of the existence of such a mechanism. Although the detailed angular correlation function in most cases depends upon the nature of the two-body forces, it exhibits certain symmetries which are very characteristic of the direct process.

§ 2. The Particle Angular Distribution

We reformulate briefly the theory of Austern *et al.* (1953) using the same simple model. A loosely bound nucleon is ejected with wave-vector $\mathbf{k}'$, from a definite orbit $\phi_{lm}(\mathbf{r}_1)$, by the incident nucleon with wave-vector $\mathbf{k}$, which is itself captured into orbit $\phi_{l'm'}(\mathbf{r}_2)$. In the free-wave (Born) approximation the collision in the region ‘outside’ the nucleus ($r \geqslant R$) is described by the matrix element

$$\langle l'm';\mathbf{k}'|V|lm;\mathbf{k}\rangle$$
$$=\int d\mathbf{r}_1\int d\mathbf{r}_2\phi_{l'm'}{}^*(\mathbf{r}_2)\exp(-i\mathbf{k}'.\mathbf{r}_1)V_{12}\phi_{lm}(\mathbf{r}_1)\exp(i\mathbf{k}.\mathbf{r}_2)\quad(r_1,r_2\geqslant R)\quad\ldots\ldots(1)$$

where V_{12} is the two-body interaction potential. As a first approximation we may assume the inter-nucleon force to have zero-range, that is

$$V_{12}=V_0\delta(\mathbf{r}_1-\mathbf{r}_2).\qquad\ldots\ldots(2)$$

Equation (1) then gives immediately the result of Austern *et al.*

$$V_0 \int d\mathbf{r} \exp(i\mathbf{Q}\,.\,\mathbf{r}) f_{l'}^*(r) f_l(r) \mathrm{Y}_{l'}^{m'*}(\theta\phi) \mathrm{Y}_l^m(\theta\phi) \quad (r \geqslant R) \qquad \ldots\ldots(3)$$

where $\mathbf{Q}=\mathbf{k}-\mathbf{k}'$ is the recoil momentum given to the nucleus. Expanding the exponential, and carrying out the angular integrations, we obtain

$$V_0 \sum_L i^L [(2l+1)(2l'+1)]^{1/2} C(ll'L; m-m) C(ll'L; 00)$$

$$\times (-)^m \delta(m, m') \int_R^\infty j_L(Qr) f_{l'}^*(r) f_l(r) r^2 dr \qquad \ldots\ldots(4)$$

where the C's are vector-addition coefficients. The approximation of taking the spherical Bessel function outside the integral and evaluating it at the nuclear boundary, $r=R$, gives the transition amplitude as a sum of terms whose angular dependence is contained in $j_L(QR)$,

$$Q^2 = k^2 + k'^2 - 2kk' \cos\theta$$

where θ is the angle between $\mathbf{k}'$ and $\mathbf{k}$. L is restricted by the vector-addition coefficients to be

$$|l-l'| \leqslant L \leqslant l+l'.$$

The parity change is given by $(-)^L$; i.e. $L+l+l'$ must be even. Hence only even or only odd values of L can contribute to any particular reaction. The lowest allowed value of L will give the most forward peak in the angular distribution of emitted particles, with a shape essentially that of $|j_L(QR)|^2$.

In the derivation of (4) we took $\mathbf{Q}$ as quantization axis when expanding the plane wave $\exp(i\mathbf{Q}\,.\,\mathbf{r})$ into partial waves. This recoil direction is an axis of symmetry for the process. We see that effectively the target nucleus receives a pulse of orbital angular momentum L with zero component along $\mathbf{Q}$, i.e. the reaction proceeds as though the target absorbed particles incident along $\mathbf{Q}$. We have, however, neglected the spins of the nucleons, which may interact in a singlet or a triplet state; the relative amount of each will depend upon the two-body force assumed (exchange character, etc.). This means that in addition to an orbital L, the hypothetical quanta absorbed carry an effective spin $S=0$ or 1; and in general the $S=1$ component behaves as though its spins were *aligned* (not polarized) along $\mathbf{Q}$. This allows the γ-ray angular distribution to be anisotropic even when $L=0$.

In addition, for identical particles, (n, n′) or (p, p′), the wave functions must be symmetrized. In the zero-range approximation (2), for example, this only allows interaction in the spin singlet state, that is, absorption with 'spin up' requires emission with 'spin down' if there is no spin exchange.

Thus, for a given L, the nucleus can absorb angular momentum $K=L$ or $L \pm 1$, so that for target and final nuclear spins J_0 and J_1,

$$|J_0 - J_1| \leqslant K \leqslant J_0 + J_1.$$

§ 3. Gamma Ray Angular Distribution

The above discussion shows that the γ-ray angular distribution about $\mathbf{Q}$ (in coincidence with outgoing nucleons along $\mathbf{k}'$) will be the same as though the target absorbed an incoherent mixture of alpha particles and aligned deuterons incident along $\mathbf{Q}$, the mixture being determined by inter-nucleon forces and the nuclear structure. We have calculated this with mixed l, l' and L values

(Satchler 1955), using standard techniques (Biedenharn and Rose 1953). In view of the complexity of the general formulae, we shall consider here explicitly only two simple cases. The general case, however, exhibits certain characteristic symmetries. The angle dependence consists of *even* powers of $\cos\gamma$, where γ is the angle between the γ-ray and the *recoil axis* $\mathbf{Q}$. That is, there is both azimuthal and backward–forward symmetry about $\mathbf{Q}$. *This is in sharp contrast to compound nucleus formation* where the axis $\mathbf{Q}$ has no special significance. Experimentally, one would sit the particle detector on an L peak (the most forward $L=|l-l'|$ will be best defined), thus defining $\mathbf{Q}=\mathbf{k}-\mathbf{k}'$ and count γ's in coincidence. Overlap from other peaks will be fairly small, hence interference from other L values reduced. Then the maximum power of $\cos\gamma$ appearing is restricted to equal to or less than $2L+2$.

This allows $\cos^2\gamma$ anisotropy even when $L=0$. In fact, with $L=0$, we find for excitation of spin J_1 from a target of J_0 that the distribution for de-excitation by 2^λ-pole γ to a level J_2 takes the simple form

$$W(\gamma)=1+f_2F_2(1J_0J_1)F_2(\lambda J_2J_1)P_2(\cos\gamma). \qquad \ldots\ldots(5)$$

The F's are the γ-correlation coefficients tabulated by Biedenharn and Rose (1953). The f_2 depends upon the two-body force; for (n, n′) or (p, p′) one expects it to be nearly unity.

In another important case we obtain a simple form, namely when the target nucleus is even–even with zero spin. If a level of spin J_1, with parity $(-)^{J_1}$, is excited, we have $L=J_1$ (e.g. the 2^+ states). Then if a nucleon is ejected from the same orbit, (j,l), as that capturing the incident one, which will often be the case, we find, in the notation of Biedenharn and Rose,

$$\begin{aligned}W(\gamma)&=\sum_\nu b_\nu(L;\alpha)F_\nu(L0L)F_\nu(\lambda J_2L)P_\nu(\cos\gamma)\\&=\sum C(LL\nu;00)F_\nu(\lambda J_2L)P_\nu(\cos\gamma) \qquad \ldots\ldots(6)\end{aligned}$$

i.e. the same form as an α–γ correlation. In particular, $C(220;00)=5^{-1/2}$, $C(222;00)=-(2/7)^{1/2}$ and $C(224;00)=(18/35)^{1/2}$. Then excitation by (p, p′) or (n, n′) of the 2^+ state in even–even nuclei would give the E2 γ-ray distribution about $\mathbf{Q}$:

$$\begin{aligned}W(\gamma)&=1+0{\cdot}714P_2(\cos\gamma)-1{\cdot}714P_4(\cos\gamma)\\&=\cos^2\gamma-\cos^4\gamma.\end{aligned}$$

These conclusions would be modified slightly in a more exact theory. For example, preliminary investigation indicates that a finite range for the interaction V, instead of (2), introduces some slight azimuthal asymmetry of the γ's about $\mathbf{Q}$. Again, use of correct functions to describe the free particles, instead of the plane waves in (1), will have a similar effect. We do not, however, expect the main features to be greatly changed, and more detailed theory will be deferred until experimental evidence shows it necessary. Mixtures of l, l' and L values (which are incurred by departures from the single-particle model) do not change the symmetries but merely increase the complexity of the theoretical formulae.

If γ-ray counts are not taken in coincidence with nucleons emitted in a definite direction $\mathbf{k}'$ we are no longer able to define the recoil axes $\mathbf{Q}$, and the above symmetries vanish. The γ-ray distribution is now azimuthally symmetrical about the incident axis $\mathbf{k}$, as it is in compound nucleus formation.

If the γ angular distribution *in* coincidence is $W(\gamma) = \Sigma_\nu A_\nu P_\nu(\cos\gamma)$, that *without* coincidence becomes $W(\beta) = \Sigma_\nu A_\nu G_\nu P_\nu(\cos\beta)$, where β is now measured from $\mathbf{k}$. The attenuation factor G_ν is the mean value over the particle distribution of $P_\nu(\cos q)$, where q is the angle between $\mathbf{k}$ and $\mathbf{Q}$. Unfortunately, when the particle distribution is peaked near the forward direction, for nucleons losing about 1–2 MEV in 15 MEV upon collision, both G_2 and G_4 are small. For example, under the conditions of the experiment of Schrank *et al.* (1954) with ^{56}Fe(p, p′), we find $G_2 \simeq -0{\cdot}2$, $G_4 \simeq 0$.

In addition to compound nucleus background, we lose the advantage that coincidence counting picks out the required γ-ray. On the whole, it would seem difficult to interpret unambiguously the results of such a non-coincidence measurement.

REFERENCES

AUSTERN, N., BUTLER, S. T., and MCMANUS, H., 1953, *Phys. Rev.*, **92**, 350.
BIEDENHARN, L. C., and ROSE, M. E., 1953, *Rev. Mod. Phys.*, **25**, 729.
COHEN, B., 1955, *Phys. Rev.*, **98**, 49.
EISBERG, R. M., and IGO, G., 1954, *Phys. Rev.*, **93**, 1039.
MCMANUS, H., and SHARP, W. T., 1952, *Phys. Rev.*, **87**, 188.
SATCHLER, G. R., 1955, *Thesis*, University of Oxford.
SCHRANK, G., GUGELOT, P. C., and DAYTON, I. E., 1954, *Phys. Rev.*, **96**, 1156.

Polarization in Nuclear Reactions

By G. R. SATCHLER
Clarendon Laboratory, Oxford

MS. received 28*th June* 1955

Abstract. Simple formulae are given for the polarization effects, in nuclear reactions, of spin $\frac{1}{2}$ particles and photons, and applied to elastic scattering by a potential well with spin–orbit coupling.

§ 1. INTRODUCTION

GENERAL formulae have been given (Blin-Stoyle 1951, 1952, Simon and Welton 1953, Simon 1953, Satchler 1955) for the angular distribution and polarization of products from nuclear reactions initiated by polarized particles and photons. These formulae are quite complicated, but we wish to point out here that they simplify greatly if only the polarization of photons or spin $\frac{1}{2}$ particles is considered. Suppose we know the angular distribution of intensity from a reaction with an unpolarized incident beam (Blatt and Biedenharn 1953, Biedenharn and Rose 1953, Satchler 1953). Then there is a simple prescription for obtaining the distribution when *either* the incident beam is polarized, *or* a polarization-sensitive detector is used for the outgoing radiation, provided this consists of photons or spin $\frac{1}{2}$ particles.

Let the 'unpolarized' distribution be given by

$$W(\theta)=\sum_{\nu jj'} a_\nu(jj')P_\nu(\cos\theta) \qquad \ldots\ldots(1)$$

where the j are *total* angular momenta of the spin $\frac{1}{2}$ particles (vector sum of orbital and spin, $\mathbf{j}=\mathbf{l}+\frac{1}{2}\boldsymbol{\sigma}$) or photons (multipolarity). θ is the angle between the incident $\mathbf{k}_1$ and outgoing $\mathbf{k}_2$ directions. The 'polarized' distribution is then obtained by replacing P_ν in (1) by

$$[P_\nu(\cos\theta)\pm p\kappa_\nu(jj')\cos 2\phi P_\nu^{\,2}(\cos\theta)]:\ \textit{photons} \qquad \ldots\ldots(2a)$$

or

$$[P_\nu(\cos\theta)+i\mathbf{n}\,.\,\mathbf{p}\phi_\nu(jj')(-)^{l'}P_\nu^{\,1}(\cos\theta)]:\ \textit{spin}\ \tfrac{1}{2}. \qquad \ldots\ldots(2b)$$

$\mathbf{p}$ is the polarization vector. For *incident* radiation its magnitude is the degree of polarization ($0\leqslant p\leqslant 1$), and its direction that of the electric vector (photons) or spin (particles). For the detection of *outgoing* radiation, $\mathbf{p}$ is directed along the axis of the polarimeter, and its magnitude may be taken as the polarimeter efficiency. In (2*a*) the azimuth angle ϕ, of $\mathbf{p}$, is measured from the reaction plane containing $\mathbf{k}_1$ and $\mathbf{k}_2$, and we take $\pm$ as the j' multipole is electric or magnetic. In (2*b*), $\mathbf{n}$ is a unit vector along $\mathbf{k}_1\times\mathbf{k}_2$, and l' is the orbital associated with j'. The $P_\nu^{\,m}(\cos\theta)$ are unnormalized associated Legendre functions (Jahnke and Emde 1945). The coefficients of the polarization terms are

$$\kappa_\nu(jj')=-\left[\frac{(\nu-2)!}{(\nu+2)!}\right]^{1/2}\frac{C(jj'\nu;11)}{C(jj'\nu;1-1)}$$

$$=\frac{(j-j')(j+j'+1)}{(\nu+2)(\nu+1)\nu(\nu-1)} \qquad \nu+j+j'\ \text{odd}$$

or

$$=\frac{2j(j+1)/(\nu+2)(\nu-1)}{\nu(\nu+1)-2j(j+1)} \qquad \nu\ \text{even and}\ j=j'$$

and $$\phi_\nu(jj') = (-)^{j'+1/2}[(2j'+1)+(-)^{\nu+j+j'}(2j+1)]/2\nu(\nu+1). \quad \ldots\ldots(3)$$

These prescriptions hold whether the intermediate state (for example, compound nucleus) has definite parity or not. Expression (2*a*) is the natural extension of the results of Biedenharn and Rose; the form of (2*b*) bears out the discussion of Wolfenstein (1949).

§ 2. DETAILED FORMULAE

We now rewrite the above results in a more useful explicit form. Previously, nuclear reactions have been discussed in terms of channel spins (vector sum of incident and target spins), but we choose to use the total angular momentum j of each radiation. This has some advantages (Satchler 1953), and the present simplifications would not be possible without it. The two representations are connected by a simple unitary transformation.

Suppose the target spin is J_0, the intermediate compound state J_1, final nucleus J_2, and the incident radiation (spin s_1, orbital l_1 or parity $(-)^{l_1}$) has total j_1, the emitted (s_2, l_2) has j_2. The angular distribution without polarization effects has the form (summed over $\nu, j_1, j_1', j_2, j_2', l_1, l_1', l_2, l_2', J_1, J_1'$)

$$\frac{d\sigma(\theta)}{d\omega} = \frac{\lambda\!\!\!^{-2}}{4(2J_0+1)(2s_1+1)}\sum A_\nu P_\nu(\cos\theta) \quad \ldots\ldots(4)$$

where A_ν contains a factor for each stage

$$A_\nu = B_\nu(j_1l_1j_1'l_1'J_0; J_1J_1')B_\nu(j_2l_2j_2'l_2'J_2; J_1J_1')$$
$$\times R(J_1; J_2j_2l_2; J_0j_1l_1)R^*(J_1'; J_2j_2'l_2'; J_0j_1'l_1'). \quad \ldots\ldots(5)$$

The form of (1) follows immediately. The R's are elements of the reaction matrix, $R \equiv S-1$, for the transitions indicated, so that

$$\sigma = \pi\lambda\!\!\!^{-2}\sum\frac{2J_1+1}{(2J_0+1)(2s_1+1)}|R|^2.$$

For particles of spin s,

$$B_\nu = (-)^{J_1-J_0+s}i^{\nu-l+l'}[(2J_1+1)(2J_1'+1)]^{1/2}Z(ljl'j'; s\nu)W(J_1J_1jj'; \nu J_0)$$

where the Z and W functions are tabulated (Biedenharn 1952, Simon *et al.* 1954). When $s=\frac{1}{2}$, the Z is independent of orbitals (except that $\nu+l+l'$ must be even), and becomes a Clebsch–Gordan coefficient (tabulated by Simon (1954))

$$i^{\nu-l+l'}Z(ljl'j'; \tfrac{1}{2}\nu) = [(2j+1)(2j'+1)]^{1/2}C(jj'\nu; \tfrac{1}{2}-\tfrac{1}{2}).$$

Then for $s=\frac{1}{2}$, when $J_1=J_1'$,

$$B_\nu = (2J_1+1)^{1/2}\eta_\nu(jj'J_0J_1).$$

Tables of η are given by Satchler (1953). For γ-rays,

$$B_\nu = (-)^{J_0-J_1+1}[(2j+1)(2j'+1)(2J_1+1)(2J_1'+1)]^{1/2}$$
$$\times C(jj'\nu; 1-1)W(J_1J_1'jj'; \nu J_0)$$

provided $\nu+j+j'$ is even when the j, j' multipoles are both electric or both magnetic, or odd when one is electric, the other magnetic. $B_\nu=0$ otherwise. For sharp spin, $J_1=J_1'$,

$$\begin{aligned} B_\nu &= (2J_1+1)^{1/2}F_\nu(jJ_0J_1) && \text{if} \quad j'=j \\ &= (-)^{J_0-J_1+1}[(2j+1)(2j'+1)]^{1/2}(2J_1+1)G_\nu(jJ_0J_1) && \text{if} \quad j'=j+1 \end{aligned}$$

in terms of the tabulated F, G of Biedenharn and Rose.

The same expressions for B_ν hold for the outgoing radiation, with obvious changes in suffixes. The B_ν are invariant under interchange of primed and unprimed arguments, while expressions (2), (3) show that the coefficient of the polarization term remains unchanged for photons, but changes sign for spin $\frac{1}{2}$. This has the immediate consequence that the linear polarization of γ-rays depends only on the real part of the matrix element product RR^* in equation (5), while spin $\frac{1}{2}$ polarization depends only on the imaginary part, as is well known. The intensity distribution, of course, depends only on the real part in both cases.

Thus (2*a*) may be applied to equation (4) as it stands. For spin $\frac{1}{2}$, (2*b*) becomes: replace $RR^*P_\nu(\cos\theta)$ in (4), (5) by

$$\mathscr{R}[RR^*]P_\nu(\cos\theta)-(-)^{l'}\mathscr{I}[RR^*]\phi_\nu(jj')\mathbf{n}\,.\,\mathbf{p}P_\nu^{\,1}(\cos\theta) \quad \ldots\ldots(6)$$

where $\mathscr{R}$ means real part, $\mathscr{I}$ imaginary part, and, of course,

$$RR^*\equiv R(J_1;J_2j_2l_2;J_0j_1l_1)R^*(J_1';J_2j_2'l_2'J_0j_1'l_1').$$

j, j' and l' refer to the radiation whose polarization is considered.

§ 3. AN APPLICATION

We may illustrate these remarks by considering the elastic scattering of low energy nucleons by a potential well $V(r)$ (Feshbach *et al.* 1954), with a spin–orbit term $\alpha(r)\mathbf{l}\,.\,\mathbf{s}$. This has eigenvalues $\frac{1}{2}\alpha l$ for $j=l+\frac{1}{2}$, and $-\frac{1}{2}\alpha(l+1)$ for $j=l-\frac{1}{2}$. That is, the nucleons in each partial wave l 'see' a different potential for each j,

$$\begin{aligned} V(+) &= V(r)+\tfrac{1}{2}\alpha(r)l && \text{if} \quad j=l+\tfrac{1}{2} \\ V(-) &= V(r)-\tfrac{1}{2}\alpha(r)(l+1) && \text{if} \quad j=l-\tfrac{1}{2}. \end{aligned}$$

For elastic scattering the S-matrix elements reduce to the partial wave reflection factor $\eta(jl)$ for these potentials (Feshbach *et al.* 1954)

$$R(J_1;J_2j_2l_2;J_0j_1l_1)\rightarrow 1-\eta(jl)\delta(j_2j_1)\delta(l_2l_1)\delta(J_2J_0).$$

We may now perform the sums over J_1 and J_1' in (4), and find immediately for the angular distribution

$$\frac{d\sigma}{d\omega}=\frac{1}{8}\lambda\!\!\!^{-2}\sum(2j+1)(2j'+1)C^2(jj'\nu;\tfrac{1}{2}-\tfrac{1}{2})R(jlj'l')P_\nu(\cos\theta)$$

summed over ν, j, j', l, l' with $\nu+l+l'$ even.

$$R(jlj'l')\equiv\mathscr{R}[1-\eta(jl)][1-\eta^*(j'l')].$$

The angular distribution from a polarized incident beam, or the polarization produced on scattering an unpolarized beam, is given immediately by using (6).

The results for s, p and d waves are

$$\begin{aligned} W(\theta\phi) = {} & A+BP_1(\cos\theta)+CP_2(\cos\theta)+DP_3(\cos\theta)+EP_4(\cos\theta) \\ & -\mathbf{n}\,.\,\mathbf{p}[FP_1^{\,1}(\cos\theta)+GP_2^{\,1}(\cos\theta)+HP_3^{\,1}(\cos\theta)+KP_4^{\,1}(\cos\theta)] \end{aligned}$$

where

$$\begin{aligned}
A &= 2R(\tfrac{1}{2}0\tfrac{1}{2}0) + 2R(\tfrac{1}{2}1\tfrac{1}{2}1) + 4R(\tfrac{3}{2}1\tfrac{3}{2}1) + 4R(\tfrac{3}{2}2\tfrac{3}{2}2) + 6R(\tfrac{5}{2}2\tfrac{5}{2}2)\\
B &= 4R(\tfrac{1}{2}0\tfrac{1}{2}1) + 8R(\tfrac{1}{2}0\tfrac{3}{2}1) + 8R(\tfrac{1}{2}1\tfrac{3}{2}2) + 1\cdot 6R(\tfrac{3}{2}1\tfrac{3}{2}2) + 14\cdot 4R(\tfrac{3}{2}1\tfrac{5}{2}2)\\
C &= 8R(\tfrac{1}{2}0\tfrac{3}{2}2) + 12R(\tfrac{1}{2}0\tfrac{5}{2}2) + 8R(\tfrac{1}{2}1\tfrac{3}{2}1) + 4R(\tfrac{3}{2}1\tfrac{3}{2}1) + 4R(\tfrac{3}{2}2\tfrac{3}{2}2)\\
&\qquad + 3\cdot 429R(\tfrac{3}{2}2\tfrac{5}{2}2) + 6\cdot 857R(\tfrac{5}{2}2\tfrac{5}{2}2)\\
D &= 12R(\tfrac{1}{2}1\tfrac{5}{2}2) + 14\cdot 4R(\tfrac{3}{2}1\tfrac{3}{2}2) + 9\cdot 6R(\tfrac{3}{2}1\tfrac{5}{2}2)\\
E &= 20\cdot 571R(\tfrac{3}{2}2\tfrac{5}{2}2) + 5\cdot 143R(\tfrac{5}{2}2\tfrac{5}{2}2)\\
F &= 4I(\tfrac{1}{2}0\tfrac{1}{2}1) - 4I(\tfrac{1}{2}0\tfrac{3}{2}1) + 4I(\tfrac{1}{2}1\tfrac{3}{2}2) + 3\cdot 2I(\tfrac{3}{2}1\tfrac{3}{2}2) - 7\cdot 2I(\tfrac{3}{2}1\tfrac{5}{2}2)\\
G &= 4I(\tfrac{1}{2}0\tfrac{3}{2}2) - 4I(\tfrac{1}{2}0\tfrac{5}{2}2) - 4I(\tfrac{1}{2}1\tfrac{3}{2}1) - 2\cdot 857I(\tfrac{3}{2}2\tfrac{5}{2}2)\\
H &= -4I(\tfrac{1}{2}1\tfrac{5}{2}2) + 4\cdot 8I(\tfrac{3}{2}1\tfrac{3}{2}2) - 0\cdot 8I(\tfrac{3}{2}1\tfrac{5}{2}2)\\
K &= -5\cdot 143I(\tfrac{3}{2}2\tfrac{5}{2}2).
\end{aligned}$$

$R(jlj'l')$ has been defined, and $I(jlj'l')$ is the imaginary part of the same product.

REFERENCES

BIEDENHARN, L. C., 1952, *Tables of Racah Coefficients* (Oak Ridge National Laboratory Report 1098).

BIEDENHARN, L. C., and ROSE, M. E., 1953, *Rev. Mod. Phys.*, **25**, 729.

BLATT, J. M., and BIEDENHARN, L. C., 1953, *Rev. Mod. Phys.*, **25**, 258.

BLIN-STOYLE, R. J., 1951, *Proc. Phys. Soc.* A, **64**, 700 ; 1952, *Ibid.*, **65**, 452.

FESHBACH, H., PORTER, C. E., and WEISSKOPF, V. F., 1954, *Phys. Rev.*, **96**, 448.

JAHNKE, E., and EMDE, F., 1945, *Tables of Functions* (New York : Dover).

SATCHLER, G. R., 1953, *Proc. Phys. Soc.* A, **66**, 1081 ; 1955, *Thesis*, University of Oxford.

SIMON, A., 1953, *Phys. Rev.*, **92**, 1050; 1954, *Tables of Clebsch–Gordan Coefficients* (Oak Ridge National Laboratory Report 1718).

SIMON, A., VANDER-SLUIS, J. H., and BIEDENHARN, L. C., 1954, *Tables of Racah Coefficients* (Oak Ridge National Laboratory Report 1679).

SIMON, A., and WELTON, T. A., 1953, *Phys. Rev.*, **90**, 1036.

WOLFENSTEIN, L., 1949, *Phys. Rev.*, **75**, 1664.

The Scattering of μ-Mesons in Lead and Iron

By J. L. LLOYD and A. W. WOLFENDALE
The Physical Laboratories, The University, Manchester

Communicated by G. D. Rochester; MS. received 12*th May* 1955

Abstract. A description is given of a cloud chamber experiment in which is investigated the dependence of the multiple and large-angle scattering of μ-mesons on momentum, sign and atomic number. The results are compared with Molière's theory for a point nucleus, Olbert's theory for an extended nucleus, and a more accurate modification of Olbert's theory. These theories give an adequate description of the multiple scattering for small momentum transfers. For large momentum transfers, where the size and structure of the nucleus should profoundly modify the scattering, Molière's theory is found to give a better description than Olbert's theory.

---

§ 1. INTRODUCTION

THE scattering distribution for charged particles traversing an absorber can be divided roughly into two regions: (*a*) the region of multiple scattering in which distant collisions yield small deflections, and (*b*) the region of large-angle scattering where the effects of single close collisions predominate. Region (*b*) should give information about the charge distribution in the nucleus and the presence of short-range interactions between the charged particle and the target nucleus. In this region the scattering is characterized by a spatial angle $\theta_{\mathrm{m}} = \lambda\!\!\!^{-}/R$ where $\lambda\!\!\!^{-}$ is the reduced de Broglie wavelength of the incident particle, and R is the nuclear radius. Thus if the moving particle is represented as a plane wave (Born approximation), and is scattered at a nucleus with a uniform charge distribution (uniform nuclear model—U.N.M.), the angle θ_{m} sets the scale of the scattering diffraction pattern. This pattern is expected to have pronounced maxima and minima but these are not observed in electron scattering at high energies (Hofstadter *et al.* 1953, 1954). Reasonable agreement with the scattering distribution which is actually observed for electrons can, however, be obtained by modifying the form of the U.N.M. and refining the calculation by a more exact computation of the phase shifts of the scattered waves.

In the present work the theoretical multiple scattering distributions are calculated on the following basic assumptions about the elementary single scattering: (i) the scattering is by Coulomb forces, (ii) the Born approximation is valid, (iii) the effects of nuclear size can be allowed for by using the results from electron scattering. Deviations from the expected distributions will then indicate a failure of one or more of the above assumptions.

The method used in the present experiment is similar to that employed by Whittemore and Shutt (1952), namely, momentum determination by magnetic deflection followed by scattering in cloud chamber plates. The range of momenta covered in the present experiment was approximately 0·5–20 kMev/c and the scattering elements were lead and iron. The thicknesses of the plates were chosen to contain roughly equal numbers of nucleons in order that any scattering effects dependent on short-range forces between μ-mesons and single nucleons should be the same, whilst Coulomb scattering, which varies as Z^2 per atom, should be very different for the two materials.

§ 2. EXPERIMENTAL ARRANGEMENT AND METHOD

2.1. *The Cloud Chamber*

The cloud chamber was of conventional type and contained two plates. A diagram of the arrangement is given in figure 1. The chamber was placed directly under the magnetic spectrograph (Hyams *et al.* 1950, referred to hereafter as I) and the expansions were triggered by particles traversing the spectrograph and a single tray of counters immediately above the chamber.

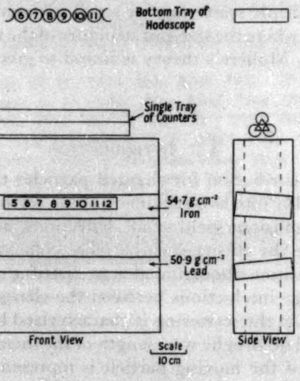

Figure 1. The experimental arrangement.

As explained in I, the spectrograph consists of three trays of Geiger counters and two regions of magnetic field each containing further counters. The counters in the three trays are connected to hodoscope circuits so that the approximate trajectories of single particles traversing the instrument can be determined from the hodoscope records. Each particle registered by the instrument is then allotted to a Momentum Category.

The chamber was photographed by a stereoscopic camera placed 102 cm from the central plane. The camera lenses were separated by 9·0 cm.

2.2. *Tracks Selected for Measurement*

(*a*) Consistency with hodoscope record. Tracks were accepted which, on inspection, could have traversed the correct counter in the bottom tray of the hodoscope. Events were rejected in which more than one counter in any tray was discharged. The question of spurious particles accepted for the analysis will be considered in § 5.1.

(*b*) Track distortion. The small number of tracks possessing curvatures such that the sagitta was greater than 3 track widths were measured but not considered in the analysis of the results. The scattering distributions for these obviously distorted tracks indicated that the effect of distortion on the accepted tracks was small.

2.3. *Measurement of Deflections*

The projected scattering angles ϕ were measured using an instrument described by McDiarmid (1954). Each deflection was measured twice and where the two angles differed by more than 0·4° the measurements were rejected and further readings taken. The mean of the two consistent angles was then taken. The distribution of differences between the two measurements of the same angle showed that the distribution of measuring errors was gaussian with a standard deviation 0·09° for the mean angle.

2.4. *Spectrograph Operation*

The spectrograph was operated successively with high and low magnetic fields in order to check the consistency of the analysis and for each value of the magnetic field half the photographs were taken with the direction of the field reversed. No evidence of misalignment of the counters was found. The numbers of photographs taken in each series are given in table 1.

Table 1. Measured Particles as a Function of Momentum

Category		0	1	2	3	4	5	6	7	8	9	10	≥11
CD Series	(*a*)	283	551	510	341	233	160	114	64	47	30	17	20
(Low field)	(*b*)	—	6·34	3·17	2·11	1·58	1·27	1·05	0·904	0·792	0·704	0·634	—
EF Series	(*a*)	188	446	516	400	320	285	199	148	111	73	52	69
(High field)	(*b*)	—	11·8	5·9	3·93	2·95	2·36	1·96	1·68	1·47	1·31	1·18	—

(*a*) No. in Category; (*b*) nominal momentum (kMeV/*c*).

§ 3. ANALYSIS OF THE RESULTS

3.1. *The Deflection Spectrum of Particles in each Category*

Since the trajectory of a particle is defined only to a counter width in each of the 'measuring trays' of the hodoscope, the particles in a given Category have a momentum spread or spectrum. The deflection spectrum is the product of the geometrical acceptance distribution $P(\Delta-\Delta_n)$ (see I) and the deflection spectrum $S(\Delta)$ of particles incident on the apparatus. The nominal deflection Δ_n is the distance from the centre of the counter discharged in the middle tray to the line joining the centres of the counters discharged in the two extreme trays. A further broadening of the spectrum is caused by scattering of particles in the apparatus. This scattering will now be considered.

3.2. *Correction to the Spectrum of Particles for Scattering in the Spectrograph*

The expected deflection of particles by scattering in the counter trays and air column of the instrument has been evaluated in I.† In the arrangement used by us further scattering was introduced by three shallow cloud chambers, introduced for another experiment (Holmes, Owen, Rodgers and Wilson, private communication, to be published later). The expected standard deviation of the displacement due to scattering is given by $\sigma = 0{\cdot}725/p\beta$ cm where p is the momentum of the particle in kMeV/c and βc its velocity. The deflection due to the magnetic field is $\Delta = k/p$ cm where k is a function of the linear dimensions of the instrument and the integrated field strengths. These relations give $\sigma_\Delta/\Delta = 0{\cdot}059$ for the low field Series CD and $\sigma_\Delta/\Delta = 0{\cdot}032$ for the high field Series EF.

---

† Although the relations for the expected scattering given in I are correct the numerical values quoted are incorrect.

In view of the importance of the scattering correction in this work the correction has been checked experimentally and good agreement found with the expected value (Holmes, Owen, Rodgers and Wilson, private communication).

Following the notation used in I if $S_n(\Delta)$ represents the deflection spectrum of particles in category n we have

$$S_n(\Delta) = P(\Delta - \Delta_n) \int S(\Delta')\, G(\Delta - \Delta')\, d\Delta'$$

where G is the gaussian error function having standard deviation σ_Δ. This integral has been evaluated numerically for each Category in each Series.

3.3. *The Momentum Spectrum of the Measured Particles*

The corrected deflection spectrum has been used to give the momentum spectrum of particles in each Category. In the evaluation of the multiple scattering parameter most of the Categories have been considered separately, but for a study of the form of the scattering distribution and the large-angle scattering the momentum spectrum is divided into 3 groups. Details of this division are given later. The nominal momenta p_n corresponding to the nominal deflections Δ_n are given for each Category in table 1.

3.4. *The Accuracy of the Angular Measurements*

In order to increase the accuracy of the scattering measurements an attempt was made to correct for systematic distortion. The chamber was divided into six regions, i.e. those traversed by particles crossing the individual counters used in the bottom tray of the hodoscope. The Series were divided in time so that each group contained about 30 tracks of fast particles in each region (categories 0, 1, 2 and 3) and the median angle for each region found. The accuracy of the median was to about 0·07° and the medians were evaluated to the nearest 0·1°. Small variations were found across the width of the chamber in a given group and between successive groups. All scattering measurements were then corrected using the appropriate median angle. The means of the moduli of the median angles ϵ are given in table 2.

The random errors due to random distortions and errors of measurement are also of importance and will now be considered.

The scattering distribution in the highest momentum category is profoundly modified by random errors whose magnitude can be calculated on certain assumptions. For small angles ($<0{\cdot}5°$) the theoretical scattering distribution is very insensitive to nuclear structure and if the scattering theory is assumed valid for high momenta a gaussian error distribution can be found which, after folding-in with the theoretical scattering, best fits the experimental results. Figure 2 shows these distributions for Category 0 (Series EF).

The standard deviations of the random errors σ for each Series and scattering element are given in table 2. If the standard deviations of the observed and expected scattering distributions are Σ_o and Σ_e respectively, then σ is also given by $\sigma^2 = \Sigma_o^2 - \Sigma_e^2$. The values of σ found in this way are also given.

The consistency in the values of σ found by the two methods indicates that the assumption of a gaussian distribution of random errors is reasonable. Since the values of σ and Σ_0 are comparable, an uncertainty in the validity of the scattering theory for these high momentum particles is not important.

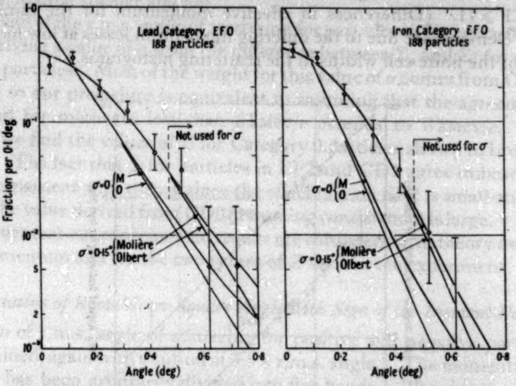

Figure 2. Comparison of the theoretical and experimental scattering for particles in the highest Momentum Category (σ is the standard deviation of the random errors).

Table 2. Systematic and Random Errors determined from observations on Particles of very high Momentum

Series		ϵ (0·1°)	Σ_r (0·1°)	Σ_0 (0·1°)	σ best fit (0·1°)	σ equation (0·1°)
CD	Fe	1·4	1·90	2·80 ± 0·18	2·3 ± 0·3	2·7 ± 0·3
CD	Pb	1·3	2·68	3·84 ± 0·24	2·3 ± 0·3	2·1 ± 0·2
EF	Fe	1·0	1·02	1·82 ± 0·14	1·5 ± 0·2	1·7 ± 0·2
EF	Pb	1·0	1·58	2·34 ± 0·18	1·5 ± 0·2	1·5 ± 0·2

§ 4. EXPERIMENTAL RESULTS ON MULTIPLE SCATTERING

The corrected deflection spectrum for each Momentum Category considered in § 3 has been used to calculate the scattering distributions expected on the theories of Molière (1947, 1948) and Olbert (1952). In the case of Olbert's theory we have used a value of $r_0 = 1{\cdot}1$ for the nuclear radius parameter.

4.1. *Variation of Root-Mean-Square Angle with Momentum and Z*

The root mean square angle of scattering has been found from the experimental results with a large-angle cut-off at 3·5 times the r.m.s. angle found from the smaller angles. The r.m.s. angle for each Category other than 0 has been corrected for the effects of random errors using the 'equation value' of σ given in table 2. The Molière distribution has been treated in a similar way after being plotted in histogram form with the same cell-width as the experimental distribution. The r.m.s. angles are plotted against momentum for each element in figure 3. Apart from the two points at the low momentum end of the lines, each point represents the r.m.s. angle Σ for a Category in each Series of the experiment. The effective momentum for each Category is such that the value of Σ for the theoretical distribution lies on the line. The two points at the low momentum end correspond to the appropriate mean scattering for the lowest momentum Categories in each Series: CD $\geqslant 7$, EF $\geqslant 11$. (Differences in effective momentum for the same Category in the two elements are due to the differing momentum losses at low momenta and the effect of the finite cell widths in the scattering histograms.)

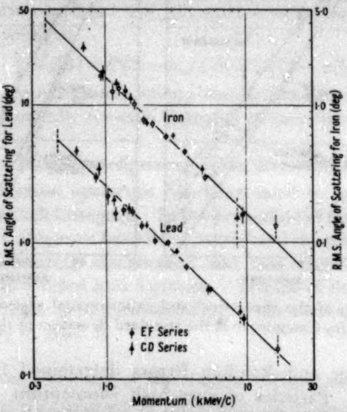

Figure 3. The variation of multiple scattering with momentum for iron and lead. The points have been corrected for the effects of random error.

For Category numbers greater than 2, i.e. momenta less than 6 kMev/c for the EF Series and 3·5 kMev/c for the CD Series, the effect of random errors on the values of Σ given in figure 3 is less than one standard deviation. For this region ($\sim$0·5–6 kMev/c) the weighted mean value of the scattering parameter γ has been compared with the value expected on Molière's theory. γ is given by the relation $\Sigma = \gamma / p$. The ratios of observed to expected r.m.s. angles with cut-off at 3·5 × r.m.s. are

$0{\cdot}995 \pm 0{\cdot}021$ for 50·9 g cm^{-2} Pb
and $0{\cdot}996 \pm 0{\cdot}022$ for 54·7 g cm^{-2} Fe.

Similar comparison with the theory of Olbert results in the ratios

$1{\cdot}066 \pm 0{\cdot}021$ for 50·9 g cm^{-2} Pb
and $1{\cdot}022 \pm 0{\cdot}022$ for 54·7 g cm^{-2} Fe.

The modified theory for iron gives

$1{\cdot}011 \pm 0{\cdot}022$ for 54·7 g cm^{-2} Fe.

The higher momentum points are modified by the effect of random errors and will now be considered in some detail. The points for Categories other than 0 are dependent on the multiple scattering theory holding for particles in Category 0 but this dependence is not great since the contributions from scattering and random errors are about equal in Category 0 (see table 2). For example, if the multiple scattering is reduced by a factor 2 in the region of 20 kMev/*c* (EF0) the effect is to raise the point for EF2 by less than one standard deviation, and the points for lower momenta by an even smaller amount.

An estimate of the r.m.s. angle of scattering for particles in Category 0 has been made by deriving a value of σ from the difference between Σ_0 and Σ_e for the lower momentum particles. Most of the weight for this value of σ comes from Categories 1 and 2 and so our procedure is equivalent to assuming that the agreement with theory found for momenta less than 6 kMev/*c* extends to 8 kMev/*c*. On this assumption we find the values of Σ for Category 0 particles shown in broken lines in figure 3. The fact that Σ for particles in EF2 and CD1 agree indicates that Σ for CD0 is consistent with theory since the effect of σ on EF2 is small and that on CD1 using the value derived from CD0 (assuming consistency) is large.

It is evident that our experimental results are consistent with theory over a wide range of momentum and for the two values of Z used in the experiment.

4.2. *Variation of Root-Mean-Square Angle with Sign of the Incident Particle*

The ratio of r.m.s. angle of scattering for positive and negative particles has been determined, again with a cut-off at 3·5 × r.m.s. angle. The momentum range investigated has been arbitrarily divided into five bands. The ratios and approximate mean momenta of the bands are given in table 3.

Table 3. The Ratios of the r.m.s. Angles of Scattering of Positive to Negative Particles as a function of Momentum

Lead	(*a*)	7·3	4·1	2·2	1·3	0·69
	(*b*)	1·065 ± 0·072	0·909 ± 0·051	1·062 ± 0·066	1·130 ± 0·081	1·000 ± 0·135
Iron	(*a*)	7·1	3·9	2·2	1·3	0·80
	(*b*)	1·050 ± 0·072	0·984 ± 0·054	0·962 ± 0·060	0·935 ± 0·066	1·060 ± 0·144

(*a*) Momentum (kMev/*c*); (*b*) ratio.

The ratios averaged over all momenta are 1·025 ± 0·015 for Pb and 0·987 ± 0·015 for Fe.

The ratios are independent of systematic instrumental errors and are consistent with unity for each element.

§ 5. THE FORM OF THE SCATTERING DISTRIBUTIONS AND THE LARGE-ANGLE SCATTERING

5.1. *Spurious Contributions to the Large-Angle Scattering*

Protons interacting in the plates will sometimes simulate μ-mesons scattered through large angles; their contribution must therefore be assessed.

Measurements on the flux of low-energy protons (below 1 kMev/*c*) at sea level are plentiful but only Mylroi and Wilson (1951) have extended the measurements beyond 3 kMev/*c*. Unfortunately their detection apparatus included at most only 1·5 interaction lengths, a value insufficient for the efficient detection of high-energy protons. If secondary π-meson production is taken into account, their results for 3 kMev/*c* should be increased by a factor of about 2·0, and for 6 kMev/*c* by about 2·6.

In the cloud chamber, slow protons will be recognized if they stop in one of the plates by ionization loss or lose energy in this way and emerge from the lower plate with ionization significantly above the plateau value. Fast protons will be recognized if they interact and (*a*) produce more than one secondary visible in the cloud chamber, (*b*) produce one or more heavily ionizing secondaries, (*c*) suffer catastrophic absorption in the plate, or (*d*) produce a lightly ionizing particle leaving the plate at an angle to the primary greater than a defined cut-off angle.

All protons entering the cloud chamber with momentum less than 980 MeV/*c* should be detected in this experiment; twenty-one such protons were observed in a total of about 260 (positive and negative) particles. This fraction of $8{\cdot}0 \pm 1{\cdot}8\%$ is not inconsistent with the expected value of about 5% (York 1952).

Twenty-eight other particles were classed as interacting protons; a further 19 should then have traversed the plates without interacting, making 47, compared with an expected number of 42. This agreement is however illusory. Above 2 kMeV/*c* 8·5 identifiable nuclear interactions are expected: seven were observed. On the same basis the number of interactions with a single track at minimum ionization throughout is expected to be only one or two, but ten abnormally large deflections (of positive particles only) were found. It is uncertain whether these are indeed protons; their identity is discussed later in § 5.3.

To avoid any uncertainty a cut-off in scattering deflection has been applied to the distributions; beyond this limit the number of μ-meson events should be small on any reasonable theory; within it the estimated effect of protons is small.

Whittemore and Shutt have studied the scattering of cosmic rays at 3·4 km altitude and at sea level, of much the same momentum as Groups L and M (see § 5·2 for the momentum spectra of these groups) and in approximately the same thickness of lead. By suitable subtraction of their two distributions, it is possible to determine the large-angle scattering of protons. Because the proton spectrum at sea level is similar in shape to that at 3·4 km, this distribution can be assumed to prevail at sea level, with reduced intensity.

The expected distributions so obtained are indicated on the graphs. It has been assumed that consecutive interactions in iron and lead would result in recognition of the event. Proton effects are evidently unimportant.

The effect of incident π-mesons is negligible (Mylroi and Wilson 1951).

Spurious hodoscope records are expected to be rarer than estimated in I. Showers could be recognized in the cloud chamber, and the presence of the chamber and the acceptance criteria reduced the fraction of casual coincidences to 0·05% of all events. Thus about three particles were accepted whose momenta are unknown; it is unlikely that they appear in the tails of the distributions.

5.2. *The Scattering Distributions*

Scattering distributions were computed for each Category. The acceptance function $P(\Delta - \Delta_n)$ was modified to take account of variations of the magnetic fields (amounting to about 2% of the mean values) and the scattering of particles into and out of the channel, using numerical methods. The chief effect was to add to the deflection spectrum of each Category a small and accurately known low-momentum tail. Loss of momentum in the scattering plates was also allowed for.

Thus determined, the deflection spectrum was used to give the scattering distribution for the category by numerical integration. Effects of random errors of measurement and track distortion were added as described in Appendix I, the values of σ used being found from the small-angle scattering of Category 0 for each Series, as illustrated in figure 2.

The distributions for each Category were set into histogram form because the experimental measurements were presented at 0·1 degree intervals. This was important when larger cell-widths for groups of Categories were used. In all our graphs the experimental point and the smooth curve should be compared at the same abscissa; adjustments to ordinate for finite cell-width have been made (see Appendix I).

Three groups of Categories have been formed: (*a*) Group H, where the effects of experimental errors are large and to some extent uncertain. This is made up of Categories 0 and 1, EF Series, and Category 0, CD Series. Because Category 0 has been used at small angles to find the values of σ, only the large-angle tail is made up from all three Categories; the small-angle region shows Category 1, EF alone. (*b*) Group M: here the momentum resolution is moderately good, especially at the low-momentum end. The correction for momentum loss is small and while the distortion of the distribution by experimental errors cannot be neglected, it can be accurately assessed. The angles of scatter are all small and geometrical corrections for loss of large-angle events are quite negligible. (*c*) Group L comprises Categories 6 (EF), and 3 (CD), and all slower particles. Here the momentum is quite well known and the experimental errors have little effect. The fractional momentum loss, however, can be large, the mean value for the group being 8·3% for particles scattered in the lead plate. No correction for the finite illuminated depth has been made, although angles approaching 20° occur. Thus the theoretical curves are slight over-estimates at large momentum transfer. The momentum spectrum for each group is shown in figure 4, and the distributions are given in figures 5, 6, and 7.

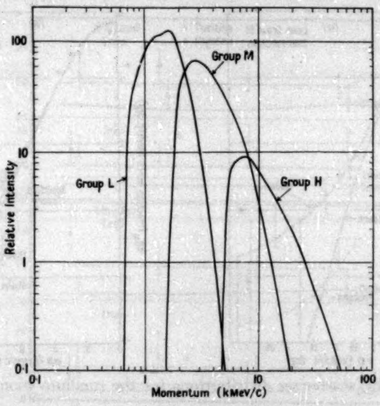

Figure 4. The momentum spectrum for the high, medium and low momentum groups.

It should be noted that in agreement with the results of Whittemore and Shutt (1952) there is no evidence of a variation of the anomalous large-angle

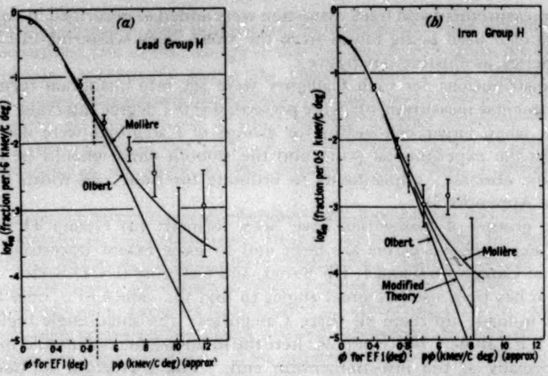

Figure 5. The scattering distributions for the high momentum group.

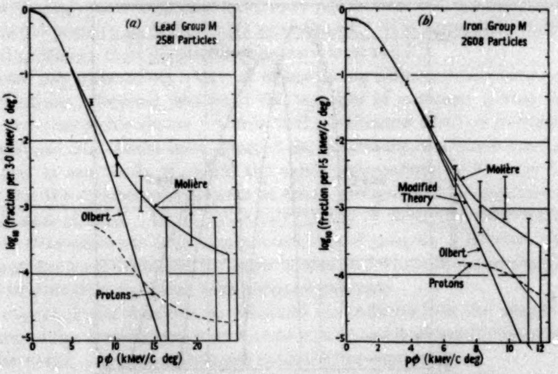

Figure 6. The scattering distributions for the medium momentum group.

scattering with momentum. This conclusion is made more positive by plotting the number of events exceeding a certain momentum transfer, as has been done in figure 8 for four momentum bands (not the same grouping as is described above) as a fraction of the number expected on Molière's theory. The cut-off in momentum transfer has been applied and protons allowed for. Two levels of momentum transfer have been considered, those where the integral numbers of events fall to 5% and 1% of the total.

It can further be seen that at the 5% level (which demonstrates the existence of the anomaly more significantly than the extreme 'tail') there is little difference between the scattering of positive and negative particles.

In figure 9 we plot the differential distributions for the composite group M + L, separating the events according to sign. The excess of positive over negative events in the extreme tails is discussed in § 5.3.

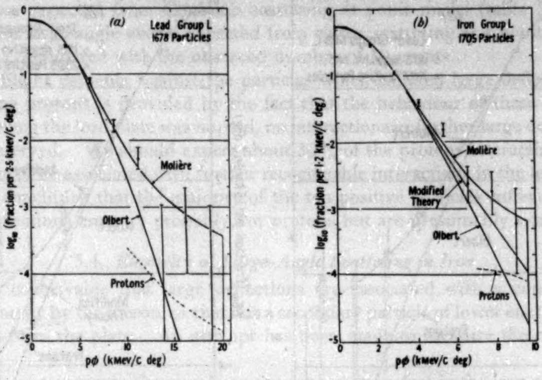

Figure 7. The scattering distributions for the low momentum group.

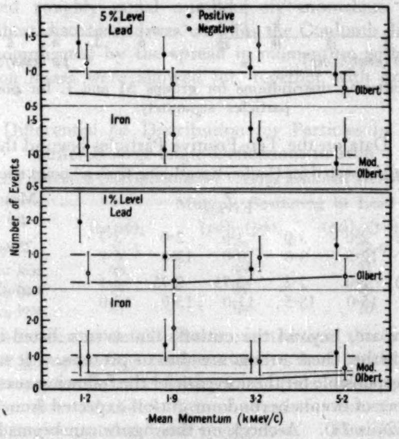

Figure 8. The variation with momentum of the number of events exceeding a certain momentum transfer expressed as a fraction of the number expected on Molière's theory. A comparison with Olbert's theory, and, in the case of iron, with the modified theory, is made.

5.3. *The Variation of the Large-Angle Scattering with Sign*

As pointed out previously, the anomalous scattering is present for both positive and negative particles. However there is evidence for a slight excess of positive over negative particles suffering large-angle deflections in the tails of the distributions within the cut-off. From considerations of the last three cells of the groups M and L for iron and lead, we find an excess of 6·9 ± 4·2 particles over the whole distribution, supposing they are not μ-mesons and are distributed uniformly.

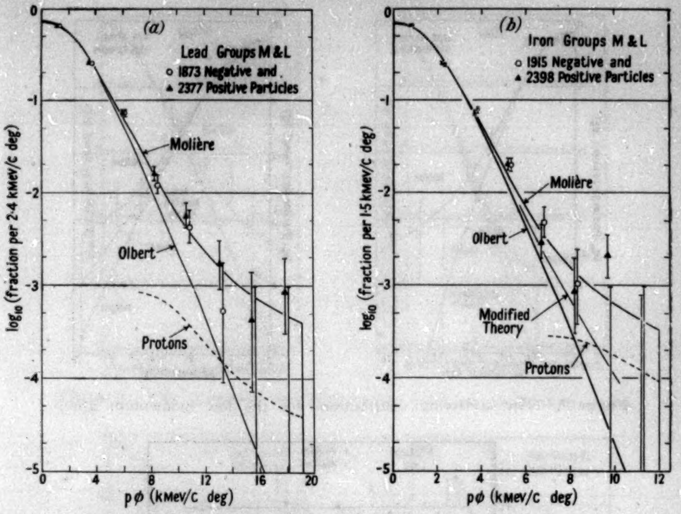

Figure 9. The scattering distributions for groups M and L for positive and negative particles separately.

Table 4. Data on the Ten Positive Particles beyond the Cut-Off

The mean value of $p\phi$ expected for Coulomb scattering from a 'point nucleus' is also given

Element		Events					Mean $p\phi$	Coulomb $p\phi$
Iron	p(kMev/c)	2·0	3·0	3·0	3·0	3·7	28·6	24
	ϕ (deg.)	12·5	8·0	10·0	13·0	6·7		
Lead	p(kMev/c)	2·0	2·2	2·75	2·75	5·1	40·6	38
	ϕ (deg.)	15·0	18·5	11·0	15·0	12·0		

In addition there are, beyond the cut-off, ten events listed in table 4. The question arises whether these events are due to protons. It seems improbable that protons are responsible for these events for the following reasons:

(i) The number of events beyond our cut-off expected from Whittemore and Shutt's data (1952) is 2·0. A check on this figure can be made by calculating the number of protons interacting and giving rise to one shower particle which escapes from the plates without interacting. The calculation is based on the modified proton spectrum of Mylroi and Wilson and work on star production in photographic emulsions by Camerini *et al.* (1952). In the calculation the presence of 'grey tracks', many of which would be seen in the cloud chamber, is ignored. This upper limit to the number of unrecognized protons interacting in the plates is 4·1, of which a fraction is expected beyond our cut-off. The two estimates are therefore not inconsistent.

(ii) Since there are no large-angle events between the cut-off values of $p\phi$ for iron and lead the means of $p\phi$ for iron and lead can be compared directly. We see from table 4 that the values are not equal, indicating that the interactions are probably not with individual nucleons. In fact, the mean values agree well with those expected from Coulomb scattering at point nuclei (table 5). The number of large-angle events expected from elastic scattering at a point nucleus is about 7, compared with the observed number of 10 events.

(iii) Slight evidence against the particles which suffered large deflections in iron being protons is provided by the fact that the behaviour of these particles on traversing the lead plate was normal, no interactions or further large deflections being observed. We should expect about 30% of the protons interacting in the iron plate to be associated with further recognizable interactions in the lead plate.

It is concluded that the majority of the ten positive particles suffering large-angle deflections are very probably not protons but are presumably μ-mesons.

5.4. *Elasticity of Large-Angle Scattering in Iron*

It is conceivable that large deflections are associated with a considerable loss of energy by the meson, or that it is a secondary particle of lower energy which emerges from the plate. An attempt has been made to measure the change in energy.

All μ-meson events showing large momentum transfers in the iron plate were selected and the multiple scattering in lead examined; the optimum angle in the iron provided roughly equal numbers of 'anomalous' and 'Coulomb' events. The Olbert distribution was used for the Coulomb distribution. The treatment was complicated by the spread in momentum within each category. Normal ionization losses were allowed for, together with experimental errors (the effect of σ).

Table 5. The Differential $p\phi$ Distribution for Particles in Lead which have suffered large-angle Deflections in Iron

The expected and observed distributions for various assumed inelasticities are given

		Multiple Scattering in Lead			
		0–$(p\phi)_1$	$(p\phi)_1$–$(p\phi)_2$	$(p\phi)_2$–$(p\phi)_3$	$>(p\phi)_3$
Expected Numbers		70·5	57·4	28·9	28·2
Observed Numbers	No loss	68	49	31	37
	17% loss	77	57	26	25
	23% loss	81	64	20	20

Table 5 gives numerical details of this examination, the events in lead being divided into four groups. One computation has been made and the expected distribution of events for zero inelasticity found (this is the expected distribution of table 5). The observed distribution of events for the same limits of $p\phi$ has been found and is given under 'zero energy loss'. The limits of $p\phi$ are then varied so that an assumed inelasticity is corrected for and the new observed distributions found. The inelasticity for which the observed and expected distributions agree can then, in principle, be found. The value of the energy change which best fits the results is a loss of $11 \pm 12\%$. The error quoted is statistical only and may be a little higher due to approximations in the calculations.

5.5. *The Variation of the Large-Angle Scattering with Atomic Number*

Some information on the dependence of the large-angle scattering on atomic number can be found from a study of the relative numbers of particles having large values of $p\phi$ in lead and iron. Considering firstly the particles within the cut-off in momentum transfer, 29 particles in lead have values of $p\phi$ greater than 9·6 kMev/c deg, much of which is presumably due to single scattering. Three particles only, in iron, have been observed for the same limit of $p\phi$. If the particles outside the cut-off (table 4) are also included, the respective numbers of events are 34 and 8. It is apparent that the results are inconsistent with a scattering cross section per atom proportional to Z since equal numbers of particles would be expected in the above comparison.

A Z^2-dependence for the scattering cross section, however, gives distributions in good agreement with experiment (Molière distributions).

§ 6. COMPARISON WITH OTHER EXPERIMENTS

6.1. *The Multiple Scattering*

Wilson (1940) and Code (1941) used magnet cloud chambers to obtain the scattering distribution for cosmic rays at sea level of momentum less than 2 kMev/*c*. With 185 and 359 particles respectively, each found good agreement with multiple scattering theory.

Whittemore and Shutt (1952) also investigated the scattering of cosmic rays at sea level in 5 cm Pb. Using a cloud chamber and associated magnetic field they accepted the range 0·3–3·1 kMev/*c*. Their results on multiple scattering agree well with the present experiment.

6.2. *The Large-Angle Scattering*

A summary of most of the work carried out prior to 1953 has been given by Leontic and Wolfendale (1953). None of the early work is inconsistent with the results reported here.

Whittemore and Shutt (1952) were able to demonstrate the anomalous scattering of μ-mesons; at the 5% (integral) level they found slightly more scatters than predicted by Molière's theory. However, they neglected the effect of experimental errors in broadening the distributions, and this is not inappreciable. The corrected distributions agree well with those given here up to $p\phi \sim 15$ kMev/*c* deg. In the extreme tail, however, Whittemore and Shutt found somewhat greater scattering of negative particles than positive. This is in disagreement with our results, which show a positive excess, but this excess is greatest above 2 kMev/c, where Whittemore and Shutt had fewer particles. A detailed comparison is given in table 6.

George, Redding and Trent (1953) working underground used a cloud chamber without magnetic field to measure the scattering of μ-mesons in two 2-cm lead plates. Counters were placed both above and below the chamber and in part of the experiment the particles were required to traverse a lead absorber below the cloud chamber. The angles so obtained were compared with those expected from a knowledge of the momentum spectrum of cosmic rays at that depth and appeared to show anomalous scattering, particularly below 250 Mev/*c*. The present authors, however, have recalculated the angular distributions expected from Molière's theory, and cannot find agreement with the distribution given by George, Redding and Trent. For example, in arrangement (*b*) (with 5 cm Pb below the cloud chamber) the theoretical scattering greater than 10° is underestimated by a factor of 3 and the new distribution eliminates the anomaly at large angles. For the intermediate angles and the other arrangements the experimental points fall below the theoretical distribution and the interpretation of the results is not clear. In view of the uncertainties in the knowledge of the spectrum of low momentum particles traversing the cloud chamber underground the results of this experiment cannot be accepted.

Table 6. Comparison between the Numbers of Events found by Whittemore and Shutt and the present Authors, for the extreme tail of the scattering distribution

Bracketed numbers are those expected on Molière's theory

$p\phi$ range (kMeV/c deg)	10–15	15–20	>20
(*a*) Negative			
Whittemore and Shutt	9(8·8)	1(2·4)	1(3·0)
Lloyd and Wolfendale	9(10·7)	0(2·4)	0(3·1)
(*b*) Positive			
Whittemore and Shutt	14(13·3)	0(3·3)	1(3·75+1·0 Proton)
Lloyd and Wolfendale	17(14·2)	3(3·3)	5(3·9+1·0 Proton)

Kannangara and Shrikantia (1953) studied photographic emulsions exposed underground. Their results have been re-analysed by Rochester and Wolfendale (1954) and are consistent with the point nucleus theory, but the statistics are poor.

Leontic and Wolfendale (1953) operated a multi-plate cloud chamber without a magnetic field at sea level beneath 100 cm of lead and confirmed the existence of anomalous scattering in lead. A defect in the statistical analysis has since been pointed out by Rainwater (private communication) and when this is allowed for the magnitude of the anomalous component is decreased by a factor of approximately 5, bringing the experimental results into better agreement with the point nucleus theory.

McDiarmid (1954, 1955) has operated a cloud chamber also without magnetic field underground, but containing six plates of lead or of iron. A detailed statistical analysis combined with a knowledge of the μ-meson spectrum (at high momentum only) indicates disagreement with theories which consider the extension of the nucleus and good agreement with the point nucleus theory.

§ 7. DISCUSSION AND CONCLUSIONS

7.1. *The Multiple Scattering*

We have verified the multiple scattering theory of Molière in the relatively small angle region (angles less than 3·5 × r.m.s. angle) in lead and iron for the momentum range 0·5 to 6 kMeV/c and our results are not inconsistent with the theory up to momenta of the order of 20 kMeV/c. In this region the effect of nuclear size is not very important and although agreement is better with Molière's theory for a point nucleus the disagreement with Olbert's theory is not very great, amounting to three times standard deviation for lead and to standard deviation for iron.

No significant difference in the multiple scattering of positive and negative μ-mesons has been found, again in agreement with theory for the momentum range investigated.

7.2. *The Large-Angle Scattering*

In agreement with all the μ-meson scattering experiments of any precision we find evidence for the existence of an anomalous large-angle scattering component.

For lead the observed distribution for negative μ-mesons is in good agreement with Molière's distribution up to a value of $p\phi$ of about 12 kMeV/c deg above which the number of events falls off rapidly. Positive μ-mesons definitely follow the Molière distribution to 20 kMeV/c deg and probably to much higher values of $p\phi$.

For iron a similar state of affairs exists, the values given above being replaced by 8 kMeV/c deg and 12 kMeV/c deg respectively. No evidence for an appreciable inelasticity for the large-angle scattering in iron has been found.

The validity of the initial assumptions (§ 1) can now be examined. For the relatively small scattering angles encountered in this experiment the Born approximation should be valid (Appendix II) and the form factor derived from electron scattering is expected to be a good approximation. Consequently the multiple scattering distribution for the extended nucleus should give a realistic estimate of the expected scattering of μ-mesons. It has been shown however that the observed large-angle scattering is in excess of the expected value and has a magnitude similar to the scattering from a point nucleus. The concept of the point nucleus has no physical significance; it represents only an extreme case of a nuclear model for which the multiple scattering by Coulomb forces has been evaluated. The agreement between the observed distributions and point nucleus scattering is presumably fortuitous but the variation of the large-angle scattering with momentum and atomic number, and the lack of appreciable inelasticity in the scattering in iron does suggest that the scattering may be due to some form of elastic Coulomb interaction.

The explanation of the inelastic scattering is likewise not clear. Stars and showers observed underground have been studied by George and Evans (1950) and George (1952) and attributed to the inelastic interactions of fast μ-mesons. The cross section for these events has been shown to be several orders of magnitude smaller than that for the anomalous scattering (Kannangara and Shrikantia 1953, Leontic and Wolfendale 1953). The inelastic events were explained by George and Evans in terms of the virtual quanta method of Williams (1935). Fowler (1955) has shown, however, that the virtual-photon spectrum derived by Williams is not applicable to this process and the accurate cross section for the process is too small to explain the results by a factor of about 30. The two processes, large-angle scattering and star production, may therefore correspond to elastic and inelastic anomalous interactions.

Davidson (1954) has attempted to show that the anomalous large-angle scattering can be explained by the excitation of the nucleus by virtual photons in the 'giant' photon resonance region. Fowler (private communication) has shown that the method is not valid.

In conclusion we can state that the anomaly in the large-angle scattering of μ-mesons has been confirmed but that experiments of higher statistical precision are needed to examine the fine structure of the scattering and give information on the mechanism of the scattering process.

ACKNOWLEDGMENTS

We are greatly indebted to Professor P. M. S. Blackett and Dr. G. D. Rochester for providing the facilities, and for their interest in the work. Dr. G. D. Rochester has given invaluable help in the preparation of the paper.

We wish to express our thanks to Mrs. M. Gorman for performing many of the computations, Miss B. Hill for carrying out the measurements of most of the

tracks, our colleagues in the Magnetic Spectrograph Group, Dr. B. G. Owen and Messrs Rodgers and Eyeions, for their assistance in the operation of the equipment, Professor S. Sciuti for his co-operation in the early part of the work, and Dr. G. N. Fowler, Dr. I. B. McDiarmid, Mr. J. L. Redding, and Dr. P. T. Trent for useful discussions.

Professor J. Rainwater kindly communicated his results on the theory of multiple scattering prior to publication.

APPENDIX I

(*a*) *The Effect of Random Errors on the Scattering Distributions*

Let the uncorrected (differential) scattering distribution be $f(\phi)\,d\phi$ and suppose that the experimental errors in ϕ are normally distributed with standard deviation σ.

The resultant distribution $g(\phi_0)\,d\phi$ at ϕ_0 is made up of contributions from $f(\phi)$ for all ϕ

$$g(\phi_0)\,d\phi = d\phi(2\pi\sigma^2)^{-1/2}\int_{-\infty}^{+\infty} f(\phi)\exp\{-(\phi_0-\phi)^2/2\sigma^2\}\,d\phi.$$

This integral may be evaluated numerically but often we may write

$$f(\phi)\,d\phi = A\exp(-m|\phi|)\,d\phi$$

(the scattering distributions for Olbert's theory are, in many categories, of this form over a wide range of ϕ).

A straightforward analytic integration gives

$$\frac{g(\phi_0)}{f(\phi_0)} = \tfrac{1}{2}\exp(m^2\sigma^2/2)\left\{1+\operatorname{erf}\left(\frac{\phi_0-m\sigma^2}{\sigma\sqrt{2}}\right)+\exp(2m\phi_0)\left[1-\operatorname{erf}\left(\frac{\phi_0+m\sigma^2}{\sigma\sqrt{2}}\right)\right]\right\}.$$

The term in brackets is almost 2 for values of ϕ_0 in the tail of the distribution for which $\phi_0 \gg m\sigma^2$; the ratio of the corrected and uncorrected distributions is then $g(\phi_0)/f(\phi_0)=\exp(m^2\sigma^2/2)$ where m may be a slowly varying function of ϕ.

(*b*) *Correction for Cell Width*

The experimental points have been plotted at the centres of the cells and the theoretical distributions must be modified so that an exact comparison is afforded.

A continuous distribution $g(\phi)$ must be transformed to a distribution

$$h(\phi_0) = \int_{\phi_0-\delta}^{\phi_0+\delta}\frac{g(\phi)d\phi}{2\delta} \quad \text{plotted at } \phi_0.$$

Often we may write $g(\phi)=A\exp(-m\phi+c\phi^2)$ where A, m, c are constants over the histogram cell and $|c\phi/m|\ll 1$.

An approximate solution gives

$$\frac{h(\phi_0)}{g(\phi_0)} = \exp(\tfrac{1}{3}\delta^2 c)\frac{\sinh(m\sigma)}{m\sigma}$$

and for small values of $\delta^2 c$

$$\frac{h(\phi_0)}{g(\phi_0)} \to \frac{\sinh(m\sigma)}{m\sigma}.$$

APPENDIX II

Calculation of the Multiple Scattering Distributions

The single scattering law for the scattering of charged particles through small angles by an atom is given by the relativistic Rutherford expression

$$f(\theta)\,d\theta = 2Q\,d\theta/\theta^3$$

where θ is the spatial angle of scattering and

$$Q = 4\pi\frac{Nt}{A}\left(\frac{Ze^2}{pc\beta}\right)^2$$

Here N = Avogadro's number, t = thickness in g cm^{-2}, Z and A are the atomic and mass numbers of the scattering atom, e is the electronic charge, p is the momentum and βc the velocity of the particle.

The Rutherford expression must be modified at very small angles due to the effects of screening of the nucleus by the electron cloud and at large angles because of the finite size of the nucleus. Molière has considered the first modification in detail and has derived the multiple scattering distribution for the case where the nucleus can be regarded as concentrated in a point.

Olbert has considered both modifications, that due to nuclear size being considered by cutting off sharply the *projected* angle distribution at $\phi_0 = \phi_{\mathrm{m}}\,(a/r_{\mathrm{n}})$ where a and r_{n} are the radii of atom and nucleus and ϕ_{m} is the screening angle. It has been shown however that the sharp cut-off does not give a good representation of the effect of the nucleus (Cooper and Rainwater 1954, McDiarmid 1955). These authors have simplified the problem by applying the nuclear form factor to the single scattering law for projected angles, instead of that for spatial angles.

Here we apply the form factor to the spatial single scattering distribution. The form factor has been evaluated for a U.N.M. of radius R by Rose (1948) and others in the Born approximation. This is given by the relation

$$K = \frac{9}{\eta^4}\left(\frac{\sin\eta}{\eta} - \cos\eta\right)^2$$

where

$$\eta = \frac{2p}{\hbar}R\sin\tfrac{1}{2}\theta \sim \frac{p\theta R}{\hbar}$$

for small angles. Figure 10 shows the variation for lead. Such pronounced diffraction minima are not observed in the electron scattering experiments of Hofstadter *et al.* (1953, 1954). Yennie *et al.* (1954) have made exact phase shift calculations for 125 and 150 MeV electrons in gold ($Z = 79$) and have shown that the maxima and minima are smoothed out considerably for the U.N.M. Yennie *et al.* find that better agreement with experiment results if a smoothed charge distribution is assumed of the following form (for example)

$$\rho(x) = \rho_0\{1 + \exp K(x-c)\}^{-1}.$$

Calculations have been made by Yennie *et al.* for two smoothed distributions with $K = 4{\cdot}40$, $c = 3{\cdot}86$, and $K = 1{\cdot}83$, $c = 3{\cdot}34$. The form factors taken over from the published distributions of Yennie *et al.* are presented approximately in figure 10 (the effect of the change in atomic number is small). The exact phase shift calculations have been made for large angles of scattering where the divergence from the Born approximation is great; for example, the ratio of exact to Born approximation for the point nucleus is of the order of 5 in the region of $\eta \sim 5$. For small angle deflections—the case in fast μ-meson scattering—the Born approximation is more accurate (e.g. Massey and Burhop 1952), and the phase shift form factors for extended nuclei will represent an upper limit. Consequently we have taken as a reasonable form factor for the coherent scattering the envelope of the Rose distribution $9/\eta^4$ fitted on to the Born approximation form factor at $\eta = 3{\cdot}15$.

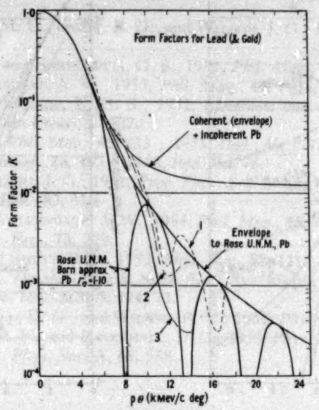

Figure 10. Form factors for lead and gold. The curves denoted by numbers are taken from the exact phase shift calculations of Yennie *et al.* for gold. (1) U.N.M. (2) Charge distribution smoothed over the outer 25% of the nuclear radius. (3) Charge distribution smoothed over the outer 50% of the nuclear radius.

In addition to the coherent scattering of particles by the nucleus, incoherent scattering by individual nucleons is expected for which the form factor is

$$K_I = Z^{-1}(1 - K_C) \text{ (Amaldi } et\ al. \text{ 1950).}$$

The resultant form factor for both coherent and incoherent scattering is thus $K_{C+I} = K_C + Z^{-1}(1 - K_C)$; K_{C+I} for lead is also shown in figure 10.

The single scattering distributions for the elements used must now be derived. Following Olbert we use a variable q, the projected angle of scattering ϕ expressed in units of $(GQ)^{1/2}$ where G is Molière's scattering parameter,

$$G = 5{\cdot}66 + 1{\cdot}24 \log_{10} [Z^{4/3} A^{-1} t / \{1{\cdot}13\beta^2 + 3{\cdot}76(Z/1{\cdot}37)^2\}] \quad \text{for} \quad G > 3.$$

The single scattering law for projected angles is then

$$f(q)\,dq = \frac{1}{2G}\frac{dq}{q^3}$$

for the point nucleus in the regions where atomic shielding is unimportant. The single scattering laws for coherent plus incoherent scattering from extended nuclei have been found by applying the approximate form factors to the single scattering law for spatial angles and then finding the distributions of projected angles $S(q)$ by numerical integration. The small angle approximation has been used throughout. The distributions are shown in figures 11 and 12. Olbert has derived the multiple scattering distribution from a projected single scattering distribution of the point nucleus form, cut off at a value $q_0=\phi_0/(GQ)^{1/2}$. Since our projected single-scattering law for the extended nucleus does not differ very greatly from the point nucleus law at q_0, we have used Olbert's distribution $f(q, q_0)$ to give the contribution to the multiple scattering from angles less than q_0,

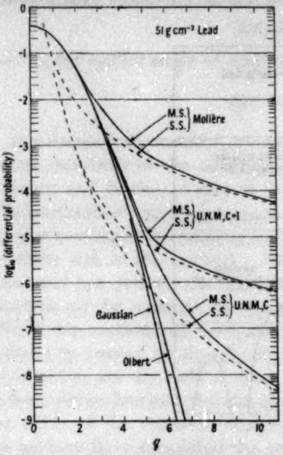

Figure 11. The differential scattering distributions for projected angles in lead (one sign only). M.S. = multiple scattering; S.S. = single scattering; C = coherent; I = incoherent.

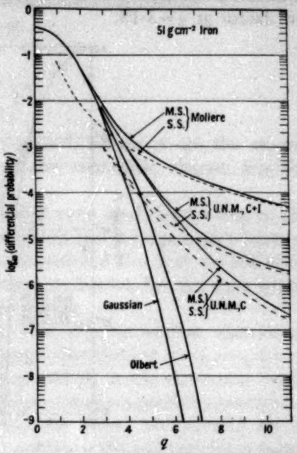

Figure 12. The differential scattering distributions for projected angles in iron (one sign only). M.S. = multiple scattering; S.S. = single scattering; C = coherent; I = incoherent.

and applied Butler's method (1950) for determining the complete distribution. The multiple scattering distributions for 51 g cm^{-2} Pb and Fe are given in figures 11 and 12, for one sign of deflection only, for coherent and coherent plus incoherent single-scattering distributions.

It will be noticed that for our thickness of iron the new distributions differ significantly from Olbert's over the range important for the present experiment. The modified distribution, i.e. the multiple distribution for coherent plus incoherent scattering from the smoothed U.N.M. model, has therefore been used for comparison with our scattering distributions in iron.

In the case of scattering in lead the difference between the modified and Olbert distributions is small over the important range and has therefore been neglected.

REFERENCES

AMALDI, E., FIDECARO, G., and MARIANA, F., 1950, *Nuovo Cim.*, **7,** 553.

ANNIS, M., BRIDGE, H. S., and OLBERT, S., 1953, *Phys. Rev.*, **89,** 1216.

BUTLER, S. T., 1950, *Proc. Phys. Soc.* A, **63,** 599.

CAMERINI, U., LOCK, W. O., and PERKINS, D. H., 1952, *Progress in Cosmic Ray Physics*, Vol. I, p. 1 (Amsterdam : North-Holland Publishing Co.).

CODE, F. L., 1941, *Phys. Rev.*, **59,** 229.

COOPER, L. N., and RAINWATER, J., 1954, *Phys. Rev.*, **95,** 1107.

DAVIDSON, J. P., 1954, *Nuovo Cim.*, **11**, 205.
FOWLER, G. N., 1955, *Proc. Phys. Soc.* A, **68**, 482.
GEORGE, E. P., 1952, *Progress in Cosmic Ray Physics*, Vol. I, p. 393 (Amsterdam : North-Holland Publishing Co.).
GEORGE, E. P., and EVANS, J., 1950, *Proc. Phys. Soc.* A, **63**, 1248.
GEORGE, E. P., REDDING, J. L., and TRENT, P. T., 1953, *Proc. Phys. Soc.* A, **66**, 553.
HOFSTADTER, R., FECHTER, H. R., and MCINTYRE, J. A., 1953, *Phys. Rev.*, **92**, 978.
HOFSTADTER, R., HAHN, B., KNUDSEN, A. W., and MCINTYRE, J. A., 1954, *Phys. Rev.*, **95**, 512.
HYAMS, B. D., MYLROI, M. G., OWEN, B. G., and WILSON, J. G., 1950, *Proc. Phys. Soc.* A, **63**, 1053.
KANNANGARA, M. L. T., and SHRIKANTIA, G. S., 1953, *Phil. Mag.*, **44**, 1091.
LEONTIC, B., and WOLFENDALE, A. W., 1953, *Phil. Mag.*, **44**, 1101.
MASSEY, H. S. W., and BURHOP, E. H. S., 1952, *Electronic and Ionic Impact Phenomena* (Oxford : Clarendon Press), p. 127.
MCDIARMID, I. B., 1954, *Phil. Mag.*, **45**, 933 ; 1955, *Ibid.*, **46**, 177.
MOLIÈRE, G., 1947, *Z. Naturf.*, **2a**, 133 ; 1948, *Ibid.*, **3a**, 78.
MYLROI, M. G., and WILSON, J. G., 1951, *Proc. Phys. Soc.* A, **64**, 404.
OLBERT, S., 1952, *Phys. Rev.*, **87**, 319.
ROCHESTER, G. D., and WOLFENDALE, A. W., 1954, *Phil. Mag.*, **45**, 980.
ROSE, M. E., 1948, *Phys. Rev.*, **73**, 279.
WHITTEMORE, W. L., and SHUTT, R. P., 1952, *Phys. Rev.*, **88**, 1312.
WILLIAMS, E. J., 1953, *K. Danske Vidensk. Selsk. Mat. Fys. Medd.*, **13**, 4.
WILSON, J. G., 1940, *Proc. Roy. Soc.* A, **174**, 73.
YENNIE, D. R., RAVENHALL, D. G., and WILSON, R. N., 1954, *Phys. Rev.*, **95**, 500.
YENNIE, D. R., WILSON, R. N., and RAVENHALL, D. G., 1953, *Phys. Rev.*, **92**, 1325.
YORK, C. M., 1952, *Proc. Phys. Soc.* A, **65**, 558.

Calculation of Magnetostriction Constants for Nickel

By G. C. FLETCHER
Department of Mathematics, University College of the South West, Exeter

MS. received 22nd March 1955 *and in revised form* 6th *May* 1955

Abstract. Calculations are made of the magnetostriction constants λ_{100} and λ_{111} for nickel at 0°K, based on the collective electron model and the calculations of the author of the $N(E)$ curve for the 3d electrons in that metal. The values of -187×10^{-6} and -44×10^{-6} obtained for λ_{100} and λ_{111} respectively are both rather larger than the latest experimental figures which, however, are available only for 120°K. The method of calculation is very similar to that used by the author in previous work on ferromagnetic anisotropy and the possible reasons for discrepancy between theory and experiment are also similar.

---

§ 1. Introduction

Kittel (1949) has pointed out that magnetostriction of ferromagnetics is closely related to their anisotropy energy in that no linear magnetostriction can arise unless this energy is taken into account and proves to be dependent on the state of strain of the crystal. Ferromagnetic anisotropy can be explained, at least qualitatively, on the collective electron model in terms of the effect of the crystalline field on the free atom wave functions together with spin–orbit interaction (Brooks 1940, Fletcher 1954) and Katayama (1951) has applied the same methods to the problem of magnetostriction. The author has developed a theory on similar lines to Katayama but for a face-centred cubic crystal subject to certain specific strains in order that a detailed calculation of λ_{100} and λ_{111} could be made in the case of nickel. These are obtained by comparison of the calculated energy of the strained crystal with a formula given by Kittel (1949, eqn 2.3.6) for the total energy density which depends on the strain and direction of magnetization.

§ 2. Physical Assumptions

Briefly the physical assumptions are that in a ferromagnetic crystal the magnetic effects are largely caused by d-type electrons which are subject to the electrical field of all atoms, exchange effects and spin–orbit interaction. The first is treated by normal tight-binding theory, which ignores the other two effects, resulting in a d energy band. The assumption is made that the effect of exchange is simply to alter the band energies already calculated by $\pm\delta$ according as the spin of the electron is antiparallel or parallel to the total spin of the crystal. It is further assumed that at 0°K all states of one spin are fully occupied while states of the other spin are occupied up to the level indicated by other magnetic measurements, e.g. leaving 0·54 hole per atom for nickel to explain the observed values of g and g'. Finally spin–orbit interaction is assumed to be negligible except between the spin of an electron and its own orbit; on the collective electron model this is introduced by the perturbing operator $\Sigma_{\mathbf{l}}\xi(|\mathbf{r}-a\mathbf{l}|)\mathbf{S}\,.\,\mathbf{L}(\mathbf{r}-a\mathbf{l})$ where $\mathbf{S}$, $\mathbf{L}$ are the spin and orbital angular momentum operators for the electron,

$\xi(r) \sim r^{-3}$ and summation is over all lattice points $a\mathbf{l}$ of the crystal. For simplicity it is further assumed that only states in the Γ_5 energy band need be considered and that it contains all the holes mentioned above. For a more detailed consideration of these assumptions and their possible effects see Fletcher (1954).

§ 3. CALCULATIONS

In order to calculate λ_{100} a face-centred cubic crystal strained in the (100) direction was considered while for λ_{111} one strained in the (111) direction was treated; in both cases it was assumed that the strain could be expressed in terms of a single parameter λ (no volume magnetostriction) and all calculations were restricted to the first order in λ. Starting from the three atomic 3d functions

$$\phi_1 = yzf(r)/r^2; \quad \phi_2 = zxf(r)/r^2; \quad \phi_3 = xyf(r)/r^2 \qquad \ldots\ldots(1)$$

employed by the author in his previous calculation for nickel (Fletcher and Wohlfarth 1951) a tight-binding calculation for the strained crystal was carried out by the normal methods and with the usual approximations. Using these results and allowing for the effect of exchange by the simple method mentioned above, a matrix was constructed for the given spin–orbit interaction operator with respect to the band wave functions. The methods used and approximations made were exactly the same as in the treatment of ferromagnetic anisotropy (Brooks 1940, Fletcher 1954). Assuming the introduction of spin–orbit interaction has not altered appreciably the occupation of states mentioned above, the energy of an average atom in the crystal was obtained by summing the energies of all occupied states. Each such energy was of the form

$$E_\tau'(\mathbf{k}) = E_\tau(\mathbf{k}) \pm \delta + A^2 f_\tau(\alpha_i^2, \alpha_i\alpha_j) + A^4 g_\tau(\alpha_i^4, \alpha_i^2\alpha_j^2) + \ldots \qquad \ldots\ldots(2)$$

where E_τ is the energy obtained from the tight-binding calculation, A the spin–orbit interaction parameter for a single electron (Fletcher 1954), $\boldsymbol{\alpha} = (\alpha_1, \alpha_2, \alpha_3)$ the direction of magnetization of the crystal and $f_\tau, g_\tau, \ldots$ are functions of $\mathbf{k}$ obtained by perturbation theory using the spin–orbit matrix. For the unstrained crystal this summation over occupied states yields no term involving $\boldsymbol{\alpha}$ below that of $O(A^4)$ but for the strained crystal $\boldsymbol{\alpha}$ is involved in the $O(A^2)$ term. The difference in energy density between the strained and unstrained crystals is obtained by multiplying the resulting expressions for both cases by n, the number of atoms per unit volume, and deducting the latter from the former. The first term obtained is of $O(A^2\lambda)$ and this is the only term of $O(\lambda)$ which confirms that there would be no linear magnetostriction if there were no anisotropy. This term corresponds to the second and third terms of Kittel's expression, i.e.

$$-\tfrac{3}{2}\lambda_{100}(c_{11} - c_{12})(\alpha_1^2 e_{xx} + \alpha_2^2 e_{yy} + \alpha_3^2 e_{zz}) - 3\lambda_{111}c_{44}(\alpha_1\alpha_2 e_{xy} + \alpha_2\alpha_3 e_{yz} + \alpha_3\alpha_1 e_{zx}) \qquad \ldots\ldots(3)$$

where $\mathbf{e}$ is the strain tensor and c_{ij} are elastic moduli. By suitable choice of $\mathbf{e}$ either term may be made zero, enabling λ_{100} or λ_{111} to be evaluated by comparison of (3) with the calculated difference in energy density.

In calculating the total energy densities it may be noted that for the third and subsequent terms in (2)

$$\Sigma\,(\text{occupied states}) = -\Sigma\,(\text{unoccupied states})$$

by the diagonal sum rule of perturbation theory. In calculating these terms degeneracy and near-degeneracy of the forms $E_\tau - E_\sigma = 0$, $E_\tau - E_\sigma < A$ and

$E_\tau - E_\sigma + 2\delta < A$ are found to occur for certain wave vectors **k** so that suitable modifications to the perturbation theory are necessary for such states (Fletcher 1954). It might be expected that the change of shape of the Brillouin zone and of the position of the Fermi surface on straining the crystal would cause added difficulties. It may be shown, however, that the density of states $N(E)$ and hence the energy at the Fermi surface is unaltered to $O(\lambda)$ and that these two factors may be ignored in calculating the change of energy density on straining the crystal.

§ 4. RESULTS AND COMPARISON WITH EXPERIMENT

In evaluating λ_{100} for nickel at 0°K it was assumed that $e_{xx} = 2\lambda$, $e_{yy} = e_{zz} = -\lambda$, $e_{rs} = 0\ (r \neq s)$ and that $\boldsymbol{\alpha} = (1, 0, 0)$ while for λ_{111} it was assumed that $e_{rr} = 0$, $e_{rs} = \lambda\ (r \neq s)$ and $\boldsymbol{\alpha} = 3^{-1/2}(1, 1, 1)$. It was found possible to express all formulae in terms of the energies $E_{\tau 0}$ and corresponding coefficients $a_{\tau n0}$ obtained from the tight-binding calculation for the unstrained crystal. These values were taken from the author's calculation for nickel (Fletcher and Wohlfarth 1951); using also the values $\delta = 0{\cdot}215$ ev, $A = 0{\cdot}0728$ ev, $n = 9{\cdot}25 \times 10^{22}$ atoms cm^{-3} (Fletcher 1954); $c_{11} = 2{\cdot}50 \times 10^{12}$; $c_{12} = 1{\cdot}60 \times 10^{12}$ and $c_{44} = 1{\cdot}185 \times 10^{12}$ erg cm^{-3} (Kittel 1949) the results obtained for nickel at 0°K were $\lambda_{100} = -187 \times 10^{-6}$; $\lambda_{111} = -44 \times 10^{-6}$.

These are respectively about 4 and 2 times as large as the most recent experimental values of -50×10^{-6} and -22×10^{-6} obtained by Corner and Hunt (1955). These measurements, however, were made at 120°K so that they are not strictly comparable with the values calculated here and unfortunately none have been made at lower temperatures. From the curves obtained by Corner and Hunt for the temperature variation down to 120°K it seems possible that at absolute zero λ_{100} may be about -30×10^{-6} and λ_{111} about -25×10^{-6} but these curves indicate that any such extrapolation must be regarded as very tentative. As in the case of the author's ferromagnetic anisotropy calculation it is considered that the main source of error lies in the oversimplified treatment of exchange effects, since the cases of degeneracy which then arise have a marked effect on the calculations. A second source is the neglect of two of the atomic 3d functions in the tight-binding calculations on which the evaluation of λ_{100} and λ_{111} is based.

APPENDIX

In the following the suffix zero is used to denote quantities referring to the unstrained crystal and the mathematics is restricted everywhere to the first order in e_{rs}. Consider a crystal strained so that the point $\mathbf{r}_0$ becomes the point $\mathbf{r} = (1 + \mathbf{e})\mathbf{r}_0$; with the usual notation and approximations of tight-binding theory assume one-electron wave functions of the form

$$\Psi_\tau(\mathbf{r}\,;\mathbf{k}) = N^{-1/2} \sum_m \sum_{\mathbf{l}} a_{\tau m}(\mathbf{k}) \exp(ia\mathbf{l}\,.\,\mathbf{k})\, \phi_m(\mathbf{r} - a\mathbf{l}).$$

It can then be shown that the roots of the usual secular equation are

$$E = E_\tau = E_{\tau 0} + h_{\tau\tau} \qquad \ldots\ldots(\mathrm{A}\,1)$$

where $\mathbf{h} = \mathbf{a}_0 \mathbf{h}' \mathbf{a}_0^{-1}$, $h_{nm}' = H_{nm} - H_{nm0}$ and $\mathbf{a}_0 = \{a_{\tau n0}\}$. The corresponding coefficients prove to be

$$a_{\tau m} = a_{\tau m0} + \sum_{\sigma \neq \tau} a_{\sigma m0}\, h_{\sigma\tau}\, \epsilon_{\tau\sigma 0}^{\ -1} \qquad \ldots\ldots(\mathrm{A}\,2)$$

where $\epsilon_{\tau\sigma 0} = E_{\tau 0} - E_{\sigma 0}$. For wave vectors **k** where degeneracy occurs between the $E_{\tau 0}$ more complicated expressions are obtained for E_τ and $a_{\tau m}$. Introducing spin–orbit interaction and applying perturbation theory in the manner detailed in the author's previous paper (Fletcher 1954) the energy of the state arising from the level $E_1(\mathbf{k})$ with spin antiparallel to that of the crystal is

$$E_1'^{+}(\mathbf{k}) = E_1(\mathbf{k}) + \delta + A^2[\alpha_3'^2\epsilon_{12}^{-1} + \alpha_2'^2\epsilon_{13}^{-1} + (1-\alpha_3'^2)\epsilon_{12\delta}^{-1} + (1-\alpha_2'^2)\epsilon_{13\delta}^{-1}] \\ + \mathrm{O}(A^3\epsilon_{\tau\sigma}^{-2}) \qquad \ldots\ldots(\mathrm{A}\,3)$$

where E_1 is given by (A 1), $\epsilon_{\tau\sigma} = E_\tau - E_\sigma$, $\epsilon_{\tau\sigma\delta} = E_\tau - E_\sigma + 2\delta$, $\boldsymbol{\alpha}$ is the direction of magnetization of the crystal and $\boldsymbol{\alpha}' = \mathbf{a}\boldsymbol{\alpha}$. To find the required difference in energy density from the unstrained crystal, (A 3) must be summed over all occupied states, multiplied by n and the corresponding quantity for the unstrained crystal deducted, i.e.

$$\Delta E = n[\sum_s E_1'^{+}(\mathbf{k}) - \sum_u E_{10}'^{+}(\mathbf{k})] \qquad \ldots\ldots(\mathrm{A}\,4)$$

where s, u denote occupied states for the strained and unstrained crystals respectively. It will be shown that Σ_s may be replaced in the first term by Σ_u and it is also found that $\Sigma_u h_{\tau\tau}(\mathbf{k}) = 0$ for all τ so that the first two terms in (A 3) may be ignored; this confirms that there would be no linear magnetostriction if there were no anisotropy. Thus (A 4) depends effectively on the difference between the coefficients of A^2 in (A 3) and the corresponding expression for $E_{10}'^{+}(\mathbf{k})$. For the particular case when $\boldsymbol{\alpha} = (1, 0, 0)$ this difference proves to be

$$\sum [2a_{m10}(a_{110}h_{m1}\epsilon_{m10}^{-1} + a_{n10}h_{mn}\epsilon_{mn0}^{-1})(\epsilon_{1n0}^{-1} - \epsilon_{1n\delta0}^{-1}) \\ + (h_{mm} - h_{11})\{a_{n10}^2\epsilon_{1m0}^{-2} + (1 - a_{n10}^2)\epsilon_{1m\delta0}^{-2}\}] \qquad \ldots\ldots(\mathrm{A}\,5)$$

where the summation is over $m=2$, $n=3$ and $m=3$, $n=2$. Similarly when $\boldsymbol{\alpha} = 3^{-1/2}(1, 1, 1)$ the difference proves to be

$$\tfrac{1}{3}\sum [2(J_{m1}h_{m1}\epsilon_{m10}^{-1} + J_{mn}h_{mn}\epsilon_{mn0}^{-1})(\epsilon_{1n0}^{-1} - \epsilon_{1n\delta0}^{-1}) \\ + (h_{mm} - h_{11})\{(1 + 2K_n)\epsilon_{1m0}^{-2} + (2 - 2K_n)\epsilon_{1m\delta0}^{-2}\}] \qquad \ldots\ldots(\mathrm{A}\,6)$$

where $J_{ij} = \Sigma_{\mu,\nu}\, a_{i\mu0}\, a_{j\nu0}$ and $K_i = \Sigma_{\mu<\nu}\, a_{i\mu0}\, a_{i\nu0}$. Expressions (A 5) and (A 6) are invalid for states $\mathbf{k}$ where degeneracy or near-degeneracy of the types mentioned above occur; similar expressions may be obtained in these cases by modifying the perturbation calculations and substituted in (A 4) instead of (A 5), (A 6) without affecting any other steps in the calculations.

Points concerning the Brillouin zone and Fermi surface for the strained crystal will now be considered. The first point of interest is that, if it is assumed that there is no change in volume to $\mathrm{O}(e_{rs})$ of the unit cell of the lattice on straining it, then it is easily shown that the volume of the Brillouin zone is also unaltered to this order. With regard to the distribution of energy in momentum space, if S, S_0 denote the constant energy surface of energy E in the strained and unstrained cases respectively and the element dS of the former is a distance δk_n from the corresponding element dS_0, measured in the direction of grad $E_{\tau0}$, then

$$\delta k_n = -h_{\tau\tau}/|\mathrm{grad}\, E_{\tau0}|. \qquad \ldots\ldots(\mathrm{A}\,7)$$

Hence the volume of momentum space enclosed by S is

$$K = K_0 - \int\!\!\int_{S_0} (h_{\tau\tau}/|\mathrm{grad}\, E_{\tau0}|)\, dS_0. \qquad \ldots\ldots(\mathrm{A}\,8)$$

Now S_0 has the symmetry of the unstrained lattice; similarly $|\mathrm{grad}\, E_{\tau0}|$ has the same value for all wave vectors which may be obtained from a given $\mathbf{k}$ by the symmetry operators of this lattice. For some of these, however, $h_{\tau\tau}$ will have different values owing to the loss of symmetry on straining the lattice; denoting this set of 'non-equivalent' vectors by g, the integration in (A 8) may be carried out by summing the integrand over g first and then integrating over part of S_0. But in the cases considered here it is found that $\Sigma_g h_{\tau\tau}=0$ and this appears likely to be true in general, in which case the integral vanishes and $K=K_0$. But the density of states $N(E)$ may be put in the form

$$N(E)=\sum_{\tau} N(E_\tau)=\frac{1}{4\pi^3}\sum_{\tau}\frac{dK}{dE_\tau} \qquad \ldots\ldots(\mathrm{A}\,9)$$

and therefore $N(E)=N_0(E)$, i.e. the density of states is unaltered on straining the lattice. In particular the upper and lower limits of the energy band are unchanged and, if one assumes that the number of occupied states is the same in both cases, the only possible assumption as long as this number is deduced from experiment, the Fermi surface must occur at the same energy as before. It will be of different shape, however, the change being given by (A 7). Now to $\mathrm{O}(A^2)$ $\Delta E/n$ in equation (A 4) may be put in the integral form

$$\begin{aligned}&\int_s (E_{10}+h_{11}+A^2f_1)\,d\mathbf{k}-\int_u (E_{10}+A^2f_{10})\,d\mathbf{k}\\ &\quad=\int_u [h_{11}+A^2(f_1-f_{10})]\,d\mathbf{k}+\int_{\mathrm{B}} (E_{10}+h_{11}+A^2f_1)d\mathbf{k}+\int_{\mathrm{F}} (E_{10}+h_{11}+A^2f_1)d\mathbf{k}\end{aligned} \qquad \ldots\ldots(\mathrm{A}\,10)$$

where the second term on the right-hand side is an integral over the volume between the boundaries of the Brillouin zones for the two cases and the third is a similar one for the Fermi surfaces. h_{11} in the first term may be ignored since $\Sigma_g h_{\tau\tau}=0$ and this term is then just the quantity calculated. h_{11} may also be dropped from the other two terms as it will only give a contribution of $\mathrm{O}\,(e_{rs}{}^2)$ and for the same reason f_1 may be replaced by f_{10}. Now to be accurate $E_{10}+A^2f_{10}$ should have the same symmetry as the Brillouin zone for the unstrained crystal, i.e. it should have the same value for the wave vectors g. But then

$$\sum_g (E_{10}+A^2f_{10})\delta\mathbf{k}=(E_{10}+A^2f_{10})\sum_g \delta\mathbf{k}=0$$

if

$$\sum_g \delta\mathbf{k}=\delta S_0\sum_g \delta k_n=0.$$

But by (A 7) $\Sigma_g\,\delta k_n=0$ for the third term in (A 10) and this is also found to be true for the second term. Thus both vanish and the method of calculation used here is justified.

For a face-centred cubic crystal strained in the (100) direction as defined above the faces of the Brillouin zone have the equations

$$ak_x=2\pi(1-2\lambda);\ ak_y=2\pi(1+\lambda);\ ak_z=2\pi(1+\lambda)$$
$$a\,(k_x+k_y+k_z)=3\pi\,(1+2\lambda)-3\lambda a\,(k_y+k_z)\ \text{etc.}$$

and in the tight-binding calculation one obtains

$$\begin{aligned}h_{11}'=4\lambda\{&-A_1(\eta\sin\eta\cos\zeta+\zeta\sin\zeta\cos\eta)+A_2[\cos\xi\,(\eta\sin\eta+\zeta\sin\zeta)\\ &-2\xi\sin\xi\,(\cos\eta+\cos\zeta)]-A_1'\cos\eta\cos\zeta+A_2'\cos\xi\,(\cos\eta+\cos\zeta)\}\\ h_{22}'=4\lambda\,\{&-A_1\,(\zeta\sin\zeta\cos\xi-2\xi\sin\xi\cos\zeta)+A_2\,[\cos\eta\,(\zeta\sin\zeta-2\xi\sin\xi)\\ &+\eta\sin\eta\,(\cos\zeta+\cos\xi)]+\tfrac{1}{2}\,A_1'\cos\zeta\cos\xi-A_2'\cos\eta\cos\zeta\\ &+A_2''\cos\eta\,(\cos\xi\ -\cos\zeta)\}\\ h_{12}'=4\lambda\,\{&A_3\,(\eta\cos\eta\sin\xi-2\xi\cos\xi\sin\eta)-A_3'\sin\xi\sin\eta\}\\ h_{23}'=4\lambda\,\{&A_3\,(\eta\cos\eta\sin\zeta+\zeta\cos\zeta\sin\eta)+2A_3'\sin\eta\sin\zeta\}\end{aligned}$$

where $\xi=\frac{1}{2}ak_x$, etc. h_{33}' and h_{31}' are obtained from h_{22}' and h_{12}' respectively by interchange of η and ζ; $h_{nm}'=h_{mn}'$. With the approximations, in particular to $f(r)$ and the crystal potential $V(\mathbf{r})$, used by the author previously for nickel (Fletcher and Wohlfarth 1951)

$$A_1=0{\cdot}1928;\quad A_2=0{\cdot}0572;\quad A_3=0{\cdot}0776;\quad A_1'=1{\cdot}0753;\quad A_2'=-0{\cdot}4216;$$
$$A_2''=0{\cdot}0441;\quad A_3'=-0{\cdot}2706$$

in units of $E_0=1{\cdot}349$ ev. For the same crystal strained along the (111) direction as defined above the faces of the Brillouin zone are

$$2ak_x=\pm 4\pi+\lambda a(k_y+k_z);\quad a(k_x+k_y+k_z)=\pm 3\pi(1-2\lambda)+\lambda a(k_x+k_y+k_z)\ \text{ etc.}$$

and one also obtains

$$\begin{aligned}h_{11}'=2\lambda\{&A_1[(\zeta+\xi)\sin\eta\cos\zeta+(\xi+\eta)\sin\zeta\cos\eta]-A_1'\sin\eta\sin\zeta\\&-A_2[(\xi+\eta)\sin\zeta\cos\xi+(\eta+\zeta)\sin\xi(\cos\eta+\cos\zeta)+(\zeta+\xi)\sin\eta\cos\xi]\\&-(A_2'+A_2'')\sin\xi(\sin\eta+\sin\zeta)\}\\h_{12}'=2\lambda\{&2(A_1-A_2)\sin\zeta(\sin\xi+\sin\eta)\\&-A_3[(\zeta+\xi)\sin\xi\cos\eta+(\eta+\zeta)\sin\eta\cos\xi]+2A_3'\cos\xi\cos\eta\}\end{aligned}$$

where h_{22}', h_{33}' are obtained from h_{11}' by cyclic permutation of ξ, η, ζ as are h_{23}' h_{31}' from h_{12}'; again $h_{nm}'=h_{mn}'$. The A_i and A_i' have the same values as before under the same approximations.

REFERENCES

BROOKS, H., 1940, *Phys. Rev.*, **58**, 909.

CORNER, W. D., and HUNT, G. H., 1955, *Proc. Phys. Soc.* A, **68**, 133.

FLETCHER, G. C., 1954, *Proc. Phys. Soc.* A, **67**, 505.

FLETCHER, G. C., and WOHLFARTH, E. P., 1951, *Phil. Mag.*, **42**, 106.

KATAYAMA, T., 1951, *Sci. Rep. Res. Insts Tôhoku Univ.* A, **3**, 341.

KITTEL, C., 1949, *Rev. Mod. Phys.*, **21**, 541.

RESEARCH NOTES

Transport of Energy by Knock-on Electrons

By J. W. GARDNER

The F.B.S. Falkiner Nuclear Research and Adolph Basser Computing Laboratories,
School of Physics,† The University of Sydney, Sydney, N.S.W.

MS. received 15*th March* 1955 *and in amended form* 26*th April* 1955

§ 1. Introduction

Theories of energy loss by ionizing particles (e.g. Bohr 1915, Landau 1944, Symon 1948) are concerned with calculating the probability that a particle loses certain energy in traversing a certain thickness of material. Experiments, on the other hand, usually record, directly or indirectly, the number of ion pairs deposited in a layer of material (e.g. the gas of an ionization chamber) by the passage through it of an ionizing primary, and the associated energy loss is then computed by assuming a certain proportionality between the number of ion pairs and the energy required to produce them. Without entering here into the vexed question of 'electron volts per ion pair',‡ we simply note that even if the assumption of proportionality were accurate and one knew the proportionality factor exactly, the energy loss computed in the above manner could not strictly be identified with the energy lost by the primary particle in traversing the layer. The reasons for this are twofold: first, the primary may be accompanied into the layer by knock-on electrons (generated, for example, in its passage through the chamber wall) which will give rise to ionization not correlated with energy lost by the primary in the layer itself; second, and conversely, there will be other knock-ons, generated by the primary inside the layer and accompanying it as it leaves, which remove from the layer some energy that the primary lost in traversing it. It is commonly assumed, explicitly or (more often) implicitly, in experimental work that the effects of these incoming and outgoing knock-ons mutually annul, so that one is justified in taking the number of ion pairs recorded in the layer as a measure of the energy lost by the primary during its traverse. The present note examines this assumption in general, and devotes particular attention to its effect on the interpretation of the cosmic-ray ionization burst statistics reported by Carmichael and Steljes (1954).

There are actually two questions to be examined: one is the effect of knock-on electrons on the average energy loss (as computed from the recorded ion pairs); the other is their effect on fluctuations from this average. The first of these questions is answered if we know the average number $N(E, x)$ of electrons with energy in dE at E, accompanying the primary at depth x. In §2, the diffusion equation for $N(E, x)$ is solved and the solution used to compute the knock-on correction to the average energy loss of a 1 kMev muon traversing the chamber of Carmichael and Steljes. In this case the correction amounts to about one or two per cent.

---

† Also supported by the Nuclear Research Foundation within the University of Sydney.

‡ Reviews, with bibliographies of this subject have been given by Taylor (1952) and by Rossi (1952). A recent theoretical paper by Moyal (1955) shows that energy loss and numbers of ion pairs can both be represented by the same 'universal' distribution, as one would expect if they were proportional.

The second question, that of the fluctuations, is important when one is measuring the distribution of energy loss rather than a mere average; a qualitative discussion in § 3 shows the knock-on correction in this case may well be significant, especially for the high energy tail of the distribution. No quantitative solution to the fluctuation problem is presented here. This problem is sufficiently akin to the fluctuation problem in cascade theory to be included in a programme of numerical computation on that subject.

§ 2. SOLUTION FOR AVERAGE NUMBERS

By considering the change in $N(E, x)$ across an infinitesimal thickness of material one readily obtains the diffusion equation:

$$\frac{\partial N(E, x)}{\partial x} = \phi(E) + \lambda(E)\frac{\partial N(E, x)}{\partial E} + \int_E^{E_m} N(E, x)\psi(E/E')\,dE'. \qquad \ldots\ldots(1)$$

The first term on the right side represents the knock-ons produced by the primary particle in traversing the layer: $\phi(E)dEdx$ is the probability for the primary to produce, in distance dx, an electron of energy in dE at E. Strictly ϕ should be a function of the primary energy E_p too, but we are assuming this to be constant, i.e. that E_p is so large, or the total thickness of our layer is so small, that only an insignificant fraction of E_p is lost in the traverse. In particular $E_p \gg E$.

The second term of the right side of (1) arises from the energy degradation of the knock-ons. We define $\lambda(E) \equiv dE/dx$ to be the *total* rate of energy loss for an electron of energy E: thus λ includes both collision and radiation losses, and in particular it includes energy losses from those occasional collisions which result in the production of secondary knock-ons. The second term, then, represents the change in $N(E, x)$ due to the fact that in traversing a layer δx some electrons with energy initially above E are degraded into the interval dE at E, whilst others with energy initially in this interval are degraded out of it.

The third term on the right of (1) represents the secondary knock-ons created with energy E at depth x: $\psi(E/E')$ is the probability for an electron of energy E' to create secondaries with energies E, $E'-E$. The upper limit E_m of the integral is the maximum energy a primary knock-on can acquire from the primary ionizing particle. This is usually severely limited by consideration of momentum conservation; e.g. a 1 kMev muon cannot communicate more than 10% of its energy to an electron with which it collides.†

To solve (1) an iteration procedure may be used, starting with the equation satisfied by $N_0(E, x)$, the number of *primary* knock-ons with energy in dE at E, at depth x:

$$\frac{\partial N_0(E, x)}{\partial x} = \phi(E) + \lambda(E)\frac{\partial N_0(E, x)}{\partial E}. \qquad \ldots\ldots(2)$$

---

† The fact that primary knock-ons may be removed from the energy interval dE at E in creating secondaries is taken care of by our definition of $\lambda(E)$ in the second term on the right of (1). Had $\lambda(E)$ been defined to exclude losses resulting from the production of secondaries, our third term would be

$$\int_E^{E_m} \{N(E', x) - N(E, x)\}\psi(E/E')\,dE'.$$

The iteration equation is then

$$\frac{\partial N_k(E, x)}{\partial x} = \phi(E) + \lambda(E)\frac{\partial N_k(E, x)}{\partial E} + \int_E^{E_m} N_{k-1}(E', x)\psi(E/E')\,dE'. \qquad \ldots\ldots(3)$$

Equations (2) and (3) may be formally solved using a Laplace transformation with respect to x, together with the boundary conditions: $N(E, 0) = N(0, x) = 0$. If we denote by μ_0 the transform of N_0, that is

$$\mu_0 = \int_0^\infty e^{-\alpha x} N_0\, dx,$$

then the transform of equation (2) is

$$\alpha\mu_0(\alpha, E) - \lambda(E)\frac{\partial \mu_0(\alpha, E)}{\partial E} = \frac{\phi(E)}{\alpha}. \qquad \ldots\ldots(2a)$$

Using the method of variation of parameters to solve for μ_0 and inverting the transform we obtain for N_0

$$N_0(E, x) = \int_E^{E_0} \frac{\phi(\sigma)}{\lambda(\sigma)}\, d\sigma. \qquad \ldots\ldots(4)$$

Here $E_0(x, E)$ is defined implicitly by

$$x = \int_E^{E_0} \frac{d\omega}{\lambda(\omega)}. \qquad \ldots\ldots(4a)$$

Physically E_0 represents the energy which a knock-on at zero depth must have if it is to arrive at depth x with energy E. Thus if we denote the range corresponding to energy ϵ by $R(\epsilon)$ then $R(E_0) - R(E) = x$, so that given E and x, E_0 may be determined from range–energy curves.

Values of $N_0(E, x)$ obtained from (4) by numerical integration may be substituted in (3) with $k = 1$ to start the iteration procedure which takes account of the secondaries. The production of secondaries affects the distribution in energy more than it affects the total energy being transported by knock-on electrons,† and it is of course the total energy $\int EN(E, x)\, dE$ rather than $N(E, x)$ itself which one ultimately needs in calculating the knock-on correction to the average energy deposited by the primary ionizing particle in a layer of material. In view of the probable smallness of the effect of secondaries on the total energy being transported by knock-ons it was not considered worth while to iterate for this in computing the knock-on correction for a 1 kMEV muon traversing the chamber of Carmichael and Steljes. The numerical work for even one iteration is quite heavy and, as we shall see below, the inclusion of secondaries could not affect the main result that the total knock-on correction is small (less than 2%) in the present case. Indeed, it is easy to see qualitatively by considering, say, a 10 MEV primary electron generating two 5 MEV secondaries, that the inclusion of such cases would reduce the total correction, since more energy is left behind as ionization.

Equation (4) was used to compute the knock-on correction to the mean energy deposited in the gas of the Carmichael–Steljes chamber by 1 kMEV muons during a diametric traverse. For $\phi(E)$ we used the standard expression, given, for example, by Rossi (1952). For $\lambda(E)$ we may write $\lambda_{\text{coll}} + \lambda_{\text{rad}}$; the formula of

---

† The effect of secondaries on the slowing-down spectra for mono-energetic sources ($4mc^2$ and $80mc^2$) in lead and aluminium has been computed by Spencer and Fano (1954); in every case secondaries become as numerous as the primaries at about 4% of the initial energy.

Bethe (1933) was used for λ_{coll}, and λ_{rad} was calculated from λ_{coll} using the familiar relation (cf. Fermi 1950)

$$\frac{\lambda_{\text{rad}}}{\lambda_{\text{coll}}} = \frac{Z(E+E_0)}{1600} \qquad \ldots\ldots(5)$$

where E and E_0 are in Mev. Although for the energies (<20 Mev) used in the calculation, λ_{rad} is small compared with λ_{coll}, it has much stronger Z-dependence, and it is this which essentially determines the knock-on correction, for the latter derives mainly from the difference in energy carried by knock-ons in the chamber wall ($Z=26$) and in the chamber gas ($Z=18$). Details of the calculation have been given elsewhere (Gardner 1954); the results are presented in the figure in the form of mean energy spectra of knock-on electrons accompanying a primary 1 kMev muon into and out of the chamber. It may be readily computed that

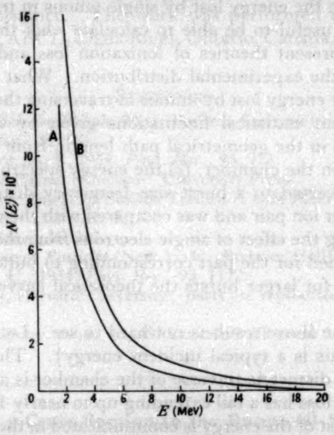

Energy spectrum of electrons accompanying a 1 kMev muon. (A) $N_{\text{IN}}(E)$: spectrum of electrons accompanying muon as it enters chamber gas, having penetrated 1·24 g cm⁻² Fe in wall. (B) $N_{\text{OUT}}(E)$: spectrum of electrons accompanying muon as it leaves chamber, having traversed 1·81 g cm⁻² A.

$$\int_{2\,\text{Mev}}^{20\,\text{Mev}} EN_{\text{IN}}(E)\,dE \simeq 0{\cdot}05 \text{ Mev}, \quad \text{and} \quad \int_{2\,\text{Mev}}^{20\,\text{Mev}} EN_{\text{OUT}}(E)\,dE \simeq 0{\cdot}09 \text{ Mev}.$$

Both these energies are small compared with the 3·6 Mev lost by the muon in traversing the chamber gas; their difference of 0·04 Mev represents a net transport out of the chamber of about 1% of the energy actually lost by the muon in the chamber gas. The remaining 99% stays behind (as ionization and excitation) and is recorded.

Our numerical computation of $N_{\text{IN}}(E)$ and $N_{\text{OUT}}(E)$ was restricted to values of E in the range 2–20 Mev for the following reasons. Below 2 Mev the neglect of multiple scattering is no longer justified; above 20 Mev radiation effects become larger and too complicated to be adequately represented by the simple formula (5). However, our approximations affect $N_{\text{IN}}(E)$ and $N_{\text{OUT}}(E)$ more or less equally so their effect on $\int E\{N_{\text{OUT}}(E)-N_{\text{IN}}(E)\}\,dE$ should be relatively small.

It seems reasonable to suppose therefore that the knock-on correction in the present case would not amount to more than 2% of the muon's energy loss even if we had done a more accurate calculation extending over a much wider range of energy values.

§ 3. FLUCTUATIONS FROM AVERAGE NUMBERS

The importance of fluctuations from $N(E, x)$ appears when one attempts to interpret experimental results like those of Carmichael and Steljes (1954) who measured the complete size–frequency distribution curve of ionization bursts due to cosmic-ray particles at sea level intersecting their chamber. One component of such a curve is the size–frequency distribution of ionization bursts due to fluctuations in the energy lost by single muons in traversing the chamber. It would have been useful to be able to calculate what this distribution should be on the basis of present theories of ionization loss and compare it with the appropriate part of the experimental distribution. What was in fact calculated was a distribution for energy lost by muons in traversing the chamber, taking into account: (*a*) inherent statistical fluctuations given by the theory of Symon (1948), (*b*) variations in the geometrical path length, from zero up to a chamber diameter, of muons in the chamber, (*c*) the energy spectrum of incident muons. This curve was converted to a burst size–frequency distribution by assuming 25·4 electron volts per ion pair and was compared with the experimental distribution (after subtracting the effect of single electrons from the latter). Reasonable agreement was obtained for the part corresponding to bursts up to several times the average size, but for larger bursts the theoretical curve predicted too high a frequency.

The reason for the above result is not hard to see. Let us consider a 1 kMev muon again, since this is a typical incident energy†. The average energy loss of such a muon for a diametric traverse of the chamber is about 3·6 Mev, but the *distribution* of energy loss has a tail extending up to nearly 100 Mev. When such high losses occur, most of the energy is communicated in the first instance to a few energetic primary knock-ons which will have a good chance of leaving the chamber without depositing much of their energy as ionization in the gas. By the same token, of course, when a muon suffers a large energy loss in the wall, much of this energy will be transferred to the chamber gas by knock-ons generated in the wall and accompanying the muon into the chamber. However, the frequency of such large energy losses is very small, so that the probability that the same muon will suffer such a loss both in the wall and in the chamber gas is for practical purposes zero. Most of the large muon energy losses in the gas are accompanied by near-average losses in the wall; in such cases the energy transferred to the gas by knock-ons entering from the wall—about 0·05 Mev in the example of § 2—is quite negligible compared with that removed by the energetic knock-ons resulting from a muon energy loss of say 20–100 Mev in the gas.

From the above paragraph it is clear that if one is interested in the distribution of energy loss, rather than an overall average, the unbalance between energy transported into and out of the medium by knock-ons can be very important, at any rate for the high-energy tail. To allow for this one would need to know the fluctuations from the average numbers $N(E, x)$ calculated in § 2, and how these fluctuations are correlated with fluctuations in the energy loss of the primary ionizing particle. Just as in cascade theory the fluctuation problem is at least an order of magnitude more difficult than the average number problem. Indeed, our present process is a special case of a cascade with a linear source of particles and a relatively small number of multiplications, and as such may be included in a programme of numerical work on all aspects of cascade theory already in hand at this laboratory.

---

† The energy-loss distribution for muons intersecting the chamber is in any case quite insensitive to their incident energy if this >0·1 kMev (see Gardner 1954).

ACKNOWLEDGMENTS

The author has enjoyed stimulating discussions on the above work with H. Carmichael, L. Elliott, G. Lee-Whiting and J. Moyal; he is also indebted to Professor H. Messel for a critical reading of the manuscript, and Miss P. Dyson for computational assistance. The work was performed during the tenure of research fellowships at AECL, Chalk River, Ontario, Canada, and at the University of Sydney, Australia.

REFERENCES

BETHE, H., 1933, *Handbuch der Physik*, **24**, 1 (Berlin : Springer).
BOHR, N., 1915, *Phil. Mag.*, **30**, 581.
CARMICHAEL, H., and STELJES, J., 1954, *Phys. Rev.*, **93**, 913.
FERMI, E., 1950, *Nuclear Physics* (Chicago : University Press).
GARDNER, J., 1954, *Atomic Energy of Canada Limited (Chalk River), Report No.* CRT-565.
LANDAU, L., 1944, *J. Phys. U.S.S.R.*, **8**, 201.
MOYAL, J., 1955, *Phil. Mag.*, **46**, 263.
ROSSI, B., 1952, *High Energy Particles* (New York : Prentice Hall), Ch. 2.
SPENCER, L., and FANO, U., 1954, *Phys. Rev.*, **93**, 1172.
SYMON, K., 1948, *Thesis*, Harvard University; parts are reproduced by Rossi in the above reference.
TAYLOR, A., 1952, *Rep. Progr. Phys.*, **15**, 49 (London : Physical Society).

The n–p Cross Section in the Range 60–550 kev

BY W. D. ALLEN and A. T. G. FERGUSON
Atomic Energy Research Establishment, Harwell, Berks.

MS. received 13*th May* 1955 *and in final form* 10*th June* 1955

§ 1. INTRODUCTION

THE n–p cross section is of considerable importance in flux measurements with recoil counters. The best available data on neutron cross sections are those compiled by the American A.E.C. neutron cross section advisory group under the title of 'Neutron Cross Sections' and reference number AECU–2040. For the n–p cross section, the first volume of AECU–2040 showed a large number of experimental points, with a smooth line drawn (approximately) through them. The first supplement showed, apparently, the same set of points, with a different line drawn through them : the difference (at 550 kev, for example) being as much as 8%. The second line was in much better agreement with the theoretical values and with an earlier curve of Adair (1950).

In view of these discrepancies, the figures were checked with polythene and graphite scatterers : because of apparent disagreement in the 120 kev region between long counter and proportional counter flux measurement, attention was concentrated on this region. The graphite was not heated to check constancy of weight; as it was pile graphite, it was assumed that the hydrogen content must have been much less than 1 atomic per cent. The neutron energy measurement at 120 kev was carefully checked by three different methods; the agreement of five different determinations within ±1%, at two angles (135° and 0°) to the incident proton beam, can be regarded as excellent. The results at lower energies can be regarded as fair, considering difficulties of background and intensity; the measurement at 550 kev was relatively easy.

§ 2. METHOD

Neutrons from an LiF target at 0° or 135° to the incoming proton beam were detected by a hydrogen-filled proportional counter, the counter being at a distance of 40 in. and the pressure determined by the neutron energy being investigated. A BF_3 counter monitored the neutron yield at an angle of 17°. The active diameter of the hydrogen-filled proportional counter was 2 in.; the scattering samples were also 2 in. in diameter and of lengths up to 3 cm of polythene and 9 in. of graphite. For this arrangement, the maximum in-scattering correction is less than 1%. The scatterers were held in a light (0·015 in. wall) brass cylinder, aligned by a simple optical arrangement.

At 120 kev in the forward direction, the proton energy is only 39 kev above threshold, and, with a neutron cross section varying rapidly with energy, it is necessary to check the neutron energy carefully. In addition to the usual method of neutron energy determination, which depends on the linearity of the potentiometer of the machine voltage control, the following methods were used to check the voltage :

(i) For neutron energies below 120 kev, the neutrons are in a forward cone; and the threshold of a long counter, set at an angle of say 60°, will give a figure for the neutron energy. The figure for neutron energy deduced from the threshold at a particular angle agreed well with the figure obtained from the potentiometer setting.

(ii) The volts per ion pair have been shown elsewhere (Allen, Ferguson and Roberts 1955) to be accurately constant for hydrogen. Hence the pulse height for 120 kev was compared with the pulse height for say 550 kev, for which the proportional error in neutron energy would be much smaller. Again, good agreement was obtained.

(iii) Finally, the attenuation at 0° in the forward direction was compared with that at 135°. The results for three runs at 0° and two at 135° agreed to within ±1 %.

The pulses from the recoil counter were recorded on a pulse analyser. The sequence of runs was without scatterer, with one scatterer, two, three. . . , very thick scatterer (for background), then a run without scatterer, so that drifts in the electronics were checked. The pulses were integrated above an arbitrary level, sufficiently high to avoid any gamma-ray effects. Attenuation curves plotted, for four different levels in a particular measurement, showed that the attenuation was insensitive to the level chosen, as it should be. A typical attenuation curve is shown in the figure.

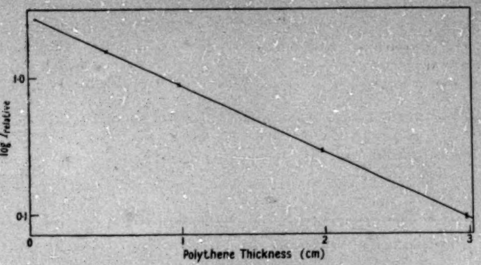

Attenuation of 120 kev neutrons in polythene.

§ 3. RESULTS

As noted above, the results give good agreement with previous work if the graphite is taken as $(CH_2)_n$ and the graphite as C. The values are exhibited in the table (for purposes of comparison, two values near 120 kev have been amended by a small correction to give the equivalent value at 120 kev). It is seen that the value at 120 kev is probably accurate to 1%, the others within 3%. Values marked A are those assuming that the polythene was $(CH_2)_n$; B, those assuming the polythene was $CH_{1\cdot 94}$, the figure given from chemical analysis. The figures for carbon contain the small correction for 0·2% hydrogen from the pile oscillator measurement. The theoretical figures for the n–p cross section were computed using $a_s = 23\cdot 7 \times 10^{-13}$; $a_t = 5\cdot 38 \times 10^{-13}$; $r_s = 2\cdot 5 \times 10^{-13}$ and $r_t = 1\cdot 704 \times 10^{-13}$ (Adair *et al.* 1953).

§ 4. CONCLUSION

It was decided that there were no grounds for suspecting discrepancies from the theoretical formula, but that more attention would be required to the choice of attenuating material if more accurate results were to be obtained.

Neutron Energy (kev)	σ_{np} (theor)	σ_{np} (exp)		σ carbon	σ_c (AECU–2040)
		A	B		
60	14·8	14·8 15·4	15·1 15·7	4·60	4·6
75	14·0	13·9	14·2	4·62	4·6
90	13·2	12·7	13·0	4·64	4·6
120	11·85	11·75 11·85 11·75 11·75 11·9	12·0 12·1 12·0 12·0 12·15	4·57	4·42
550	5·83	5·85	5·95	3·41	3·5

ACKNOWLEDGMENT

We are grateful to Mr. A. A. Smales for arranging the chemical analysis and to Mr. E. E. Lockett for the pile oscillator measurement.

References

Adair, R. K., 1950, ' Neutron Cross Sections ', *Rev. Mod. Phys.*, **22,** 3.

Adair, R. K., Okazaki, A., and Walt, M., 1953, *Phys. Rev.*, **89,** 6, 1165.

Allen, W. D., Ferguson, A. T. G., and Roberts, J., 1955, *Proc. Phys. Soc.* A, **68,** 650.

Note.—' Neutron Cross Sections ', a compilation by the U.S. Atomic Energy Commission neutron advisory group, A.E.C.U. 2040 (Office of Technical Services, Department of Commerce, Washington, D.C., U.S.A., 1952).

The Absolute Determination of Resonant Energies for Radiative Capture of Protons by Sodium in the Energy Range below 530 kev

By D. A. HANCOCK† and F. VERDAGUER‡

† Research Laboratory, Associated Electrical Industries Ltd., Aldermaston, Berks.
‡ Junta de Energia Nuclear, Madrid

Communicated by D. R. Chick ; *MS. received* 14*th April* 1955 *and in final form* 12*th July* 1955

Thin sodium targets were irradiated by the proton beam from an electrostatic generator. An absolute 63·6° electrostatic analyser described previously (Hunt 1952) was used to measure and stabilize the energy of the beam, mass analysis being obtained by a 26·4° magnetic analyser (Hunt and Jones 1953).

A thallium activated sodium iodide crystal and photomultiplier type EMI 5311 were used for the detection of the gamma rays. The target was continuously heated to a temperature of 150°c and preceded by a liquid nitrogen trap in order to prevent the deposition of carbon during irradiation.

Sodium chloride targets of thickness ΔE equal to 25, 4 and 0·8 kev were prepared by evaporating known quantities of the salt on to carefully polished copper backings in a vacuum system of known geometry. To check the stopping power of the 4 and 0·8 kev targets they were rotated through 60° to the beam, which effectively doubled their thickness, thereby displacing the resonance peak by $\frac{1}{2}\Delta E$. The 25 and 4 kev targets were used to investigate the energy range 220–530 kev and the resonance peaks were then selected on the 0·8 kev targets. Targets of sodium sulphate and potassium chloride were also irradiated in order to check that the observed resonances were due to sodium.

Using the 0·8 kev targets all the resonances except that at 373·5 kev gave half widths of approximately 1 kev. A more accurate determination of resonance half width was obtained by comparing the peak yields from the 0·8 and 4·0 kev targets using the formula (Fowler, Lauritsen and Lauritsen 1948) :

$$Y_{\max} = C\Gamma_0 \tan^{-1} (\Delta E/\Gamma_0)$$

where $Y_{\max}$ is the peak yield, C is a constant, Γ_0 the natural width at half maximum yield and ΔE the target thickness. The values obtained are shown in the table.

Present Work					
Resonant voltage (kev)	250·8 ± 0·2	307·8 ± 0·3	373·5 ± 0·4	443·8 ± 0·6	510·9 ± 0·6
Relative yield	1	110	2	4	65
Half width	0·3 ± 0·2	0·8 ± 0·3	2·0 ± 1·0	0·8 ± 0·3	0·8 ± 0·3
Tangen					
Resonant voltage (kev)	255 ± 3	310 ± 3	375 ± 4	445 ± 5	510 ± 5
Half width		0·5	1		

These resonances have been measured previously by Tangen (1946) with an accuracy to about 1% and his values are compared with those obtained in the present work in the table. The relative yields tabulated are those obtained with the 0·8 kev target.

Except for the measurement at 250·8 ± 0·2 kev, the resonance values obtained in the present work are within the limits of accuracy of Tangen's determinations and the 510·9 kev resonance is in agreement with the value of 512 ± 2 kev given by Nybö and Grotdal (1955). The errors quoted were obtained by taking the standard deviation of several determinations of each resonance and adding to this the estimated systematic error in beam energy measurement (Hunt 1952).

The limits of accuracy placed on the half widths include the extreme values obtained by using several values of the peak yields from different 0·8 and 4 kev targets.

The authors would like to acknowledge the guidance of Dr. S. E. Hunt in these measurements. Thanks are also due to Dr. T. E. Allibone for permission to publish this note.

Mr. F. Verdaguer wishes to thank the Junta de Energia Nuclear, Madrid, for financial support during the course of this work.

REFERENCES

FOWLER, W. A., LAURITSEN, T., and LAURITSEN, C. C., 1948, *Rev. Mod. Phys.*, **20**, 236.
HUNT, S. E., 1952, *Proc. Phys. Soc.* A, **65**, 982.
HUNT, S. E., and JONES, W. M., 1953, *Phys. Rev.*, **67**, 443.
NYBÖ, K., and GROTDAL, T., 1955, *Nature, Lond.*, **175**, 180.
TANGEN, R., 1946, *K. Norske vidensk. Selsk. Skr.* No. 1.

The Angular Distribution of ^{7}Li (p, n) ^{7}Be* Neutrons for Proton Energies between 2·5 and 2·9 MeV

BY R. BATCHELOR AND G. C. MORRISON
Atomic Energy Research Establishment, Harwell, Didcot, Berks.

Communicated by W. J. Whitehouse; MS. received 18*th May* 1955
and in final form 7*th July* 1955

IN a previous communication (Batchelor 1955) the relative forward intensities of the two neutron groups emitted in the proton bombardment of lithium 7 were reported. The two groups arise from the formation of the residual nucleus beryllium 7 in the ground and 430 kev excited states. Measurements have now been made at various angles of neutron emission for incident protons of mean energies 2·58, 2·68, 2·78 and 2·88 MeV.

As in the previous work a lithium fluoride target of 40 kev thickness was used, and the neutrons were detected with a helium 3 fast neutron spectrometer (Batchelor 1952). A current integrator monitored the proton current, and a previously calibrated long counter monitored the neutron yield at 30° to the incident proton beam direction. The detector subtended a solid angle of 0·026 steradian at the target, and the angular resolution was 6°. When the neutron component of lower energy was less than 150 kev it was not resolved from the large epithermal neutron peak, and measurements were then not possible.

An absolute yield scale was established by comparing the sum of the high and low energy neutron yields in the forward direction at 2·55 Mev proton bombarding energy with a previous value of 0·053 barn per steradian obtained by Taschek and Hemmendinger (1948).

(1)	(2)	(3)	(4)	(5)	(6)
2·58	0	48 ± 3	1·8 ± 0·3	0	0·8 ± 0·15
	30	39 ± 2	1·1 ± 0·2	44° 47′	0·55 ± 0·1
	60	25 ± 1·5	0·9 ± 0·15	86° 13′	0·6 ± 0·1
2·68	0	42 ± 2·5	1·9 ± 0·2	0	0·9 ± 0·1
	30	33 ± 2	1·7 ± 0·2	42° 18′	0·95 ± 0·1
	60	24 ± 1·5	1·3 ± 0·15	81° 39′	0·9 ± 0·1
	90	12 ± 0·7	0·8 ± 0·1	115° 12′	0·9 ± 0·1
2·78	0	38 ± 2	2·3 ± 0·3	0	1·2 ± 0·15
	30	30 ± 2	2·2 ± 0·3	40° 49′	1·25 ± 0·15
	60	22 ± 1·5	2·0 ± 0·25	78° 59′	1·5 ± 0·2
	90	12 ± 0·7	0·9 ± 0·1	112° 4′	1·0 ± 0·1
	120	7 ± 0·4	0·6 ± 0·1	138° 59′	1·05 ± 0·15
2·88	0	33 ± 2	3·2 ± 0·4	0	1·75 ± 0·2
	30	28 ± 1·5	2·6 ± 0·35	39° 51′	1·55 ± 0·2
	60	19 ± 1	2·8 ± 0·35	77° 14′	2·1 ± 0·25
	90	12 ± 0·7	1·6 ± 0·2	110°	1·65 ± 0·2
	120	7 ± 0·4	1·0 ± 0·15	137° 14′	1·6 ± 0·2

(1) Proton energy (Mev); (2) lab. angle of emitted neutron (°); (3) $d\sigma/d\theta$ for ^{7}Li(p, n)^{7}Be neutrons: lab. system (mbn sterad^{-1}); (4) $d\sigma/d\theta$ for ^{7}Li(p, n)^{7}Be* neutrons: lab. system (mbn sterad^{-1}); (5) centre of mass angle of emitted ^{7}Li(p, n)Be* neutron; (6) $d\sigma/d\theta$ for ^{7}Li(p, n)^{7}Be* neutrons: c.m. system (mbn sterad^{-1}).

The results are summarized in the table, where the errors quoted arise mainly from counting statistics, and estimation of the wall effect of the detector. In the centre of mass system, the angular distributions for the low energy component are roughly isotropic; for proton energies 2·78 and 2·88 Mev, however, the results indicate slight anisotropy. The figure shows the total low energy neutron yield calculated on the assumption that the distributions are isotropic. The earlier results obtained at 0° are included.

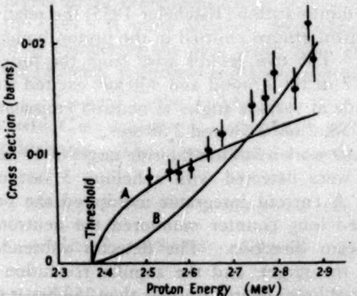

^{7}Li (p, n) ^{7}Be* reaction cross section plotted against proton energy.

If states of $\frac{3}{2}^-$ and $\frac{1}{2}^-$ are assumed for the ground state of lithium 7 and the 430 kev excited state of beryllium 7 respectively, then there can be no change in the parity of the partial waves of the ingoing proton and the outgoing neutron. In the figure, curves A and B show the shapes of the energy dependences predicted near the threshold, assuming s-waves in and out and p-waves in and out respectively (Wigner 1948). Curve A fits the observations at proton energies below 2·7 Mev. Moreover, the observed isotropic angular distribution is consistent with an s-wave interaction. It is tempting to associate the divergence of the observed points from curve A at proton energies greater than 2·7 Mev with a p-wave resonance involving a known 2^+ state of beryllium 8 at an excitation energy of 19·9 Mev (Ajzenberg and Lauritsen 1952), corresponding to 3 Mev proton energy. Interference between the large s-wave background and the p-wave resonance may then explain the slight anisotropy for proton energies of 2·78 and 2·88 Mev. More information, particularly at higher proton energies, is required before definite conclusions can be made.

ACKNOWLEDGMENTS

We wish to acknowledge in this paper the original suggestion of Dr. E. Bretscher which led to the development of the helium 3 spectrometer, and his continued interest in its application. We also thank Drs. J. Freeman, J. O. Newton and B. H. Flowers for helpful discussions, and members of the Van de Graaff Group for their cooperation.

REFERENCES

AJZENBERG, F., and LAURITSEN, T., 1952, *Rev. Mod. Phys.*, **24**, 334.
BATCHELOR, R., 1952, *Proc. Phys. Soc.* A, **65**, 674; 1955, *Ibid.*, **68**, 452.
TASCHEK, R., and HEMMENDINGER, N., 1948, *Phys. Rev.*, **74**, 373.
WIGNER, E. P., 1948, *Phys. Rev.*, **73**, 1001.

The Quadrupole Moments of Odd *A* Nuclei

BY M. A. PERKS[†]
Department of Mathematical Physics, University of Birmingham

Communicated by R. E. Peierls; MS. received 2nd June 1955 and in final form 11th July 1955

§ 1. INTRODUCTION

It has been shown in a previous paper (Blin-Stoyle and Perks 1954, to be referred to as I) that the deviations of the nuclear magnetic moments from the Schmidt lines can be accounted for in terms of simple interconfigurational mixing. In this Note the effect of this mixing on the electric quadrupole moments of odd *A* nuclei is considered.

The *j–j* coupling shell model gives fair agreement with the experimental values of the quadrupole moments of odd-proton nuclei with *A* less than 100 (see for example Sachs 1953). However, it fails in the region $100<A<200$ and cannot explain the moments of odd-neutron nuclei. The deformable core model (Bohr 1953) accounts for the large quadrupole moments in this region.

[†] Now at United Kingdom Atomic Energy Authority, Risley, Lancs.

§ 2. INTERCONFIGURATIONAL MIXING

As was the case for magnetic moments it is possible to obtain corrections to the quadrupole moment of a nucleus linear in the amplitude of the admixed state. Because of the form of the quadrupole moment operator

$$\widetilde{Q}=e\sum_{n=1}^{Z}(3z_n^2-r_n^2) \qquad \ldots\ldots(1)$$

which contains spherical harmonics of order 2, more types of admixed wave function can now lead to such corrections. They will arise when one proton in the shell model state l_j is transferred to a state $l'_{j'}$ where $l'=l$, $l\pm 2$. Thus in addition to the three cases listed in I there are now three more: viz. where a proton is excited (iv) from the state $(l\pm 2)_{j'}$ to l_j, (v) from the state l_j to $(l\pm 2)_{j'}$ and (vi) from the state $l'_{j'}$ to $(l'\pm 2)_{j''}$.

§ 3. CALCULATIONS

It is found that the amplitudes of admixture are small so that it is convenient to describe the mixing in terms of the wave function

$$\Psi_j=\chi_j+\sum_p \alpha_p\phi_{p,j} \qquad \ldots\ldots(2)$$

where χ_j represents the shell model state and $\phi_{p,j}$ the admixed state, exactly as in I. The amplitudes of admixture α_p are given by

$$\alpha_p=-\frac{\langle\chi_j|V|\phi_{p,j}\rangle}{\Delta E} \qquad \ldots\ldots(3)$$

where ΔE is the energy difference between the shell model and the admixed configurations. As in I we assume a delta function for the inter-nucleon potential $V(\mathbf{r})$.

The calculation of the corrections Q_c was performed exactly as in I for the magnetic moments. The results for odd-proton nuclei can all be written in form

$$Q_c=A(j,j',l,l')\zeta(l,l')e\langle r^2\rangle \qquad \ldots\ldots(4)$$

where A can be calculated explicitly, $\zeta=\epsilon_s/\Delta E$ (ϵ_s is the singlet interaction energy) and $\langle r^2\rangle=\langle nl|r^2|n'l'\rangle$ (r is the radial coordinate of the odd proton). This latter quantity is given approximately by

$$\langle r^2\rangle=2\times 10^{-26}A^{2/3}\,\mathrm{cm}^2. \qquad \ldots\ldots(5)$$

An inspection of the tables of nuclear shell structure drawn up by Klinkenberg (1952) shows that excitations of types (iv), (v) and (vi) are possible for many nuclei between adjacent levels. This means that for these cases ΔE is small compared with the spin–orbit splitting energy. Hence the corrections to the quadrupole moments are much greater for (iv), (v) and (vi) than for (i), (ii) and (iii).

The author has considered the magnitudes of these correction terms in detail (Perks 1954). It was found that in fact the corrections due to types (i), (ii) and (iii) of admixtures are negligible compared with those due to (iv), (v) and (vi). Types (iv) and (vi) lead to an increase in the magnitude of the quadrupole moment in agreement with experiment. Although type (v) gives a correction in the wrong direction, this is outweighed in every case by one of the right sign.

For odd-neutron nuclei equation (4) holds with $\zeta = (\epsilon_s + 3\epsilon_t)/\Delta E$ (ϵ_t is the triplet interaction energy) and the same A's as for the odd-proton cases (iii) and (vi).

Of the three cases of interest A only takes a simple form for (vi), when it is

$$A = \frac{1}{5}\frac{(2j+1)}{(j+1)}(2j''+1)\,|C^{2\,j''\,j'}_{\frac{1}{2}\,-\frac{1}{2}}|^2 . \qquad \ldots\ldots(6)$$

In this case $p = 2$ only but in the others a sum over p is involved.

§ 4. Comparison with Experiment

The sign of the corrections can be found by observing that the product $\zeta\langle r^2\rangle$ is always negative. The magnitude depends on ζ, which for types (i), (ii) and (iii) is given in I. For types (iv), (v) and (vi) we estimate that $|\zeta| \sim 0{\cdot}5 - 1{\cdot}5$ for the odd-proton nuclei of interest. For odd-neutron nuclei this should be multiplied by 11/4 (assuming $\epsilon_t = 1{\cdot}5\epsilon_s$).

The corrections are found to be only of the same order of magnitude as the single particle values of the quadrupole moments. Hence they cannot explain the large deviations found in the region $100 < A < 200$. They do however explain those of some odd-proton nuclei and how quadrupole moments can arise in odd-neutron nuclei.

§ 5. Conclusions

It has been shown that simple interconfigurational mixing does not meet with such success in attempting to account for the quadrupole moments of odd A nuclei as it did with the magnetic moments of such nuclei. The only explanation of the large quadrupole moments in the region $100 < A < 200$ appears to be that offered by the deformable core model.

Acknowledgments

The author wishes to thank Professor R. E. Peierls and Dr. R. J. Blin-Stoyle for helpful discussions during the course of this work. He is indebted to the Department of Scientific and Industrial Research for a grant.

References

Blin-Stoyle, R. J., and Perks, M. A., 1954, *Proc. Phys. Soc.* A, **67**, 885.
Bohr, A., 1953, *K. Danske-Vidensk. Selsk. Mat. Fys. Medd.*, **27**, No. 16.
Klinkenberg, P. F. A., 1952, *Rev. Mod. Phys.*, **24**, 63.
Perks, M. A., 1954, *Thesis*, University of Birmingham.
Sachs, R. G., 1953, *Nuclear Theory* (Cambridge, Mass.: Addison-Wesley).

LETTERS TO THE EDITOR

A Search for Secondary Maxima in Cosmic Ray Transition Curves: I

The existence of secondary maxima in the shower transition curve of the cosmic radiation has been reported by several workers (Thurn and Bothe 1951, and references therein to earlier work, Allegretti and El-Wahab Khalil 1951, Thurn 1952, 1953, Clay 1954, Bothe and Kraemer 1954). Others have either been unable to find the effect or have attributed it to trivial causes (George, Janossy and McCaig 1942, Harding and Robinson 1954). In particular three secondary maxima have recently been reported by Bothe and his co-workers (Thurn 1953). The large counting rates and sharpness of Bothe's secondary maxima are worth noting. However, Harding and Robinson (1954) using a very similar apparatus have found no effect similar to that of Bothe, and have attributed the small effect found when their apparatus was on the ground to the decay electrons of μ-mesons stopping immediately below the apparatus.

During the course of an investigation of the nucleon cascade in lead, our apparatus was tested by taking twofold coincidences from each of the three trays of Geiger counters in turn. This is rather similar to Bothe's experiment. The apparatus is shown in the figure. For the present purpose tray A is not considered. Tray B is placed 10 cm under the absorber. Trays C and D are located in a lead pile 60 cm below. 10 cm lead separate trays B and C, 5 cm trays C and D, with 2·5 cm between tray D and the floor. The counters in trays C and D are separately wrapped in 0·1 in. lead and are shielded at sides and ends by 15 cm lead.

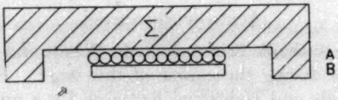

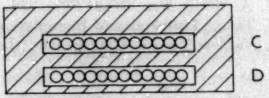

The test rates for each tray, corresponding to two or more counters discharged, are presented in the table. The rates are normalized to 1010 mb. All three transition effects show high attenuation lengths for the radiation responsible for the events. Taken with the high intensity and the experimentally determined -2% per cm Hg barometer coefficients, the events are clearly associated with μ-mesons.

The experimental points for tray B lie on a smooth curve, a typical absorption curve without any anomaly about 15 cm thickness. It is difficult, however, to fit a smooth curve through the data for tray C because the rate for $\Sigma = 2{\cdot}5$ cm (corresponding to a total lead thickness above C of 12·5 cm) is over three standard deviations below the expected rate. The probability that the points fit a smooth absorption curve is 0·008 on a χ^2-test. Tray D is shielded by 15 cm lead even with $\Sigma = 0$, and the best smooth curve through the data has a probability of the order of 0·15.

The most striking feature of these results is the absence of any large secondary maxima as found by Bothe. Our observations have been continued up to 98 cm Pb total, but no further anomalies in the transition curve were found. There does, however, seem to be some evidence in support of Harding's conclusions. The smooth curve from tray B confirms his results with his apparatus on stilts. The apparent small maxima at about 16 cm Pb total for trays C and D is not inconsistent with his curve for the apparatus on the floor. Compared with his experiment, where the chance of a μ-meson decaying within the resolving time of the set was about 63%, in our experiment, with lead as a ' floor ', only the μ^+-mesons will decay, so that the chance will be about 50%, since the resolving time (15 μsec) is long enough to include all the decays. In lead, however, the critical energy is only 7 MEV so that the total energy losses by the decay electrons emerging from the lead and passing through the lead wrappings of the counters will be greater than in Harding's experiment. The background events will be more frequent in our case because the wider acceptance angle will not always include Σ. The 1·5% effect obtained for the maximum is therefore in qualitative agreement with the $\sim$3% effect observed by Harding, and may be considered as evidence in favour of his explanation of the phenomenon.

Twofold Coincidence Rates, Normalized to 1010 mb

Σ (cm lead)	Tray B	Tray C (Counts per minute)	Tray D
0·0	209·50 ± 0·86	78·82 ± 0·43	78·52 ± 0·42
2·5	199·47 ± 1·51	76·12 ± 0·67	78·69 ± 0·65
5·0	175·81 ± 0·91	77·95 ± 0·45	78·14 ± 0·45
10·0	160·95 ± 0·79	76·88 ± 0·41	76·64 ± 0·42
15·0	153·90 ± 0·70	76·28 ± 0·36	76·93 ± 0·35
20·0	150·64 ± 0·65	75·63 ± 0·34	76·87 ± 0·36
30·0	148·11 ± 0·81	75·30 ± 0·42	75·98 ± 0·45
40·0	145·65 ± 0·51	75·75 ± 0·31	76·28 ± 0·33
82·5	135·26 ± 0·44	74·78 ± 0·28	74·41 ± 0·31

We wish to thank Mr. J. G. Dardis for his help in running the apparatus and Professor C. O'Ceallaigh for reading the manuscript.

Dublin Institute for Advanced Sciences.
11th August 1955.

C. B. A. McCUSKER.
B. G. WILSON.

ALLEGRETTI, L., and ABD EL-WAHAB KHALIL, M., 1951, *Nuovo Cim.*, **8**, 1011.
BOTHE, W., and KRAEMER, H., 1954, *Phys. Rev.*, **94**, 1402.
CLAY, J., 1954, *Proc. Acad. Sci. Amst.* B, **57**, 29.
GEORGE, E. P., JANOSSY, L., and McCAIG, M., 1942, *Proc. Roy. Soc.* A, **180**, 219.
HARDING, J. B., and ROBINSON, P. R., 1954, *A.E.R.E. N/R* 1550; (see also HARDING, J. B., 1955, *Proc. Phys. Soc.* A, **68**, 352).
THURN, H., 1952, *Z. Naturf.*, **7a**, 497; 1953, *Ibid.*, **8a**, 134.
THURN, H., and BOTHE, W., 1951, *Z. Naturf.*, **6a**, 576.

A Search for Secondary Maxima in Cosmic Ray Transition Curves: II

In recent papers, Bothe and his co-workers (Bothe and Thurn 1950, 1951, Thurn 1952, 1953, Bothe and Kraemer 1954) have reported a strong secondary maximum in the Rossi transition curve and suggested that it might be due to narrow angle showers (Thurn and Bothe 1951) or possibly to the decay of a neutral particle (Bothe and Kraemer 1954). We have used a cloud chamber to study the type of event which might contribute to such a maximum under lead.

Two distinct selection criteria have been used.

1. An analysis has been made using a penetrating shower set of conventional design, figure 1 (*a*). Tray A, immediately under the absorber, consisted of thirteen Geiger counters (10 cm × 2 cm). Tray B had fifteen 10 cm × 2 cm counters, separated by 0·1 in. lead and covered by 10 cm lead. The counter-pulses from tray B fed into an addition circuit followed by a discriminator. A master pulse operated a mechanical register and the cloud chamber when more than one counter in tray A and more than two counters in tray B were simultaneously discharged.

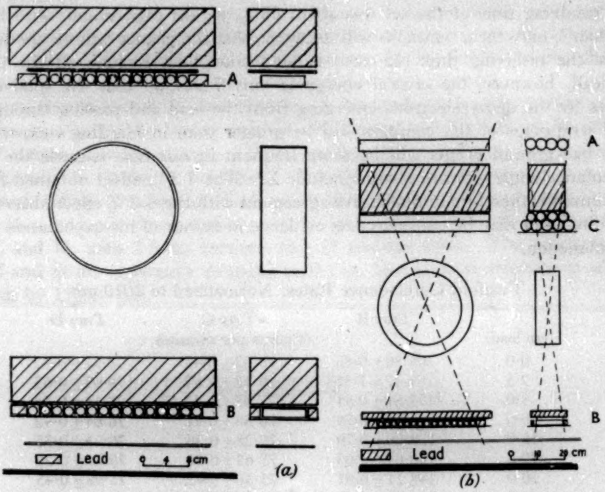

Figure 1.

The experiment was performed using three thicknesses of absorber, 12·5, 15 and 17·5 cm lead, above tray A for a total time of 2000 hours. About 5000 photographs were taken and the events subdivided into different categories. No increase in production of any type of event was observed at 15 cm. The rate of ' narrow angle ' events ($<5°$) was constant within statistical errors over the three thicknesses and formed only 6% of the total number of events. The ratio of narrow showers, detected using this selection system, to single meson traversals was 0·1%.

Using a similar apparatus, Pfotzer (1953) has found only 26 showers coming from the lead out of 500 events observed at 15 cm Pb. Only one narrow meson shower was observed. This is in good agreement with the results of Shutt (1946) who found the frequency of narrow meson showers to be 0·2% of single meson traversals. It seems clear that the frequency of production of narrow angle events is quite incompatible with their suggested role in the production of a second maximum. There is no evidence from these experiments that any type of event exists which offers a satisfactory explanation of the reported phenomenon.

2. The alternative explanation has been put forward by Bothe and Kraemer (1954), suggesting that the anomaly is produced by a neutral particle, produced in the lead by an ionizing primary. It is postulated that these are preferentially created without accompanying charged particles, so that a penetrating shower selector will discriminate against the events. An alteration in the selection system was accordingly made (figure 1 (*b*).)

A counter telescope was used to reduce the background due to the presence of a large magnet. Tray A consisted of four 50 cm × 4 cm counters, placed above the absorber; tray B consisted of fifteen 10 cm × 2 cm counters, separated by 0·1 in. lead and covered by 2·5 cm lead. An anti-coincidence tray, C, of nine 50 cm × 4 cm counters was introduced immediately below the lead. The rates were taken simultaneously when $A \geqslant 1$, $B \geqslant 2$, $C \geqslant 0$ and $A \geqslant 1$, $B \geqslant 2$, $C = 0$ master pulses were generated (A, B and C being the number of counters discharged in trays A, B and C respectively).

The experiment was run with $\Sigma = 0$, 10, 12·5, 15 and 17·5 cm lead for a total of 900 hours. A slight increase was observed in the number of anti-coincidence events with increasing absorber thickness, attributed to more effective shielding of the anti-coincidence tray from side and extensive showers. Neither rate showed any indication of a maximum at 15 cm lead. The cloud chamber was triggered on the anti-coincidence events for part of the time and an analysis made of these events. In 35% of the photographs no particles were observed in the chamber at all; 25% were due to showers produced in the material of the magnet, with origin outside the telescope; the remaining 40% showed evidence of low density extensive showers.

No examples of V-type decays were observed in the photographs examined and it is concluded that there is no evidence from this experiment either for a second maximum in the transition curve obtained using an anti-coincidence selection system or for any specific events which could be responsible for the reported effect under about 15 cm lead.

Dublin Institute for Advanced Studies.
11th August 1955.

P. D. McCormack.
C. B. A. McCusker.
B. G. Wilson.

Bothe, W., and Kraemer, H., 1954, *Phys. Rev.*, **94,** 1402.
Bothe, W., and Thurn, H., 1950, *Phys. Rev.*, **79,** 544.
Pfotzer, G., 1953, *Z. Naturf.*, **8a,** 353.
Shutt, R. P., 1946, *Phys. Rev.*, **69,** 261.
Thurn, H., 1952, *Z. Naturf.*, **7a,** 497; 1953, *Ibid.*, **8a,** 134.
Thurn, H., and Bothe, W., 1951, *Z. Naturf.*, **6a,** 576.

The Nuclear Magnetic Moment of Holmium 165

The paramagnetic resonance spectrum of the Ho^{3+} ion has been observed at 13°K in a crystal of yttrium ethyl sulphate containing about 1% of holmium ethyl sulphate. When the crystal is oriented so that the radio-frequency magnetic field is parallel to the crystal axis a spectrum of eight hyperfine lines is observed, verifying that the nuclear spin of ^{165}Ho is 7/2 (Schuler and Schmidt 1935). If this spectrum is described by the usual spin Hamiltonian for a non-Kramers doublet (Bleaney, Llewellyn, Pryce and Hall 1954)

$$\mathscr{H}=g_z\beta H_zS_z+A\,S_zI_z+\Delta_xS_x+\Delta_yS_y \qquad \ldots\ldots(1)$$

then the values of the parameters are $S=\frac{1}{2}$, $I=7/2$, $g_z=15{\cdot}36\pm0{\cdot}04$, $A=0{\cdot}334\pm0{\cdot}001\ \mathrm{cm}^{-1}$, while Δ_x, Δ_y (assumed to have a gaussian distribution) have the most probable value $\Delta=(\Delta_x{}^2+\Delta_y{}^2)^{1/2}=0{\cdot}065\pm0{\cdot}015\ \mathrm{cm}^{-1}$.

The ground state of the free Ho^{3+} ion is $4f^{10}$, $^5I_8$. The theory of Elliott and Stevens (1953) indicates that matrix elements of the crystal field between the states $J=8$ and 7 are negligible, so that the value of the nuclear magnetic moment can be calculated from the formula

$$A/g_z=\left(\frac{2\beta\beta_n\mu_n}{I}\right)\langle r^{-3}\rangle\frac{\langle J\,\|N\|\,J\rangle}{\langle J\,\|\Lambda\|\,J\rangle}$$

where $\langle J\,\|N\|\,J\rangle=23/30$, $\langle J\,\|\Lambda\|\,J\rangle=5/4$. Hence we obtain

$$\mu_n=3{\cdot}2_9\pm0{\cdot}17\ \text{n.m.},$$

on assuming $\langle r^{-3}\rangle=80\pm4\,A^{-3}$, and neglecting any possible contributions from s-electrons (estimated as ±2% (see Bleaney 1955)).

The large value of g_z means that the states involved in the resonance transition must consist principally either of $J_z=\pm8$ or ±7. Extrapolation of the crystal field theory indicates that the latter alternative must be chosen, with small admixtures of the states $J_z=\pm1$, ∓5. The theory also indicates that a singlet level (a mixture of $J_z=+6$, 0 and -6) lies nearby, and this is verified by the observation of lines in high external fields (12 to 16 kG) attributable to an electronic transition between one of the doublet levels and this singlet level. It may also be that the Jahn–Teller effect, which splits the doublet and gives allowed transitions within the doublet, admixes some of the singlet state to the doublet states. This is indicated in the low-field spectrum by a small deviation from equal spacing in the hyperfine structure, and the appearance of seven hyperfine lines corresponding to the transitions $S_z=+\frac{1}{2}$, $I_z=m \leftrightarrows S_z=-\frac{1}{2}$, $I_z=m+1$. These effects can be described by adding terms

$$B(S_xI_x+S_yI_y)+P\{I_z{}^2-\tfrac{1}{3}I(I+1)\}$$

to the Hamiltonian (1), with $B\simeq0{\cdot}02\ \mathrm{cm}^{-1}$ and $P\simeq10^{-3}\ \mathrm{cm}^{-1}$. The latter suggests a nuclear electric quadrupole moment $Q\simeq+2\times10^{-24}\ \mathrm{cm}^2$ (the positive sign is deduced on the assumption that μ_n is positive, since A, P have the same sign), but this result must be regarded as very provisional in the absence of a complete theory (some lines can also be observed when the external magnetic field is perpendicular to the z axis, suggesting that $g_\perp$ may not be zero). The effect of these small terms on the calculation of the nuclear magnetic moment is negligible.

Clarendon Laboratory,
Oxford.
26th August 1955.

J. M. Baker.
B. Bleaney.

Bleaney, B., 1955, *Proc. Phys. Soc.* A (in the press).
Bleaney, B., Llewellyn, P. M., Pryce, M. H. L., and Hall, G. R., 1954, *Phil. Mag.*, **45,** 991.
Elliott, R. J., and Stevens, K. W. H., 1953, *Proc. Roy. Soc.* A, **218,** 553; *Ibid.*, **219,** 387.
Schuler, H., and Schmidt, T., 1935, *Naturwissenschaften*, **23,** 69.

CORRIGENDA

Theoretical Studies of the Kerr Effect: I—Deviations from a Linear Polarization Law, by A. D. Buckingham and J. A. Pople (*Proc. Phys. Soc.* A, 1955, **68,** 905).

In equation (2.3) the third term on the right hand side should read

$$\tfrac{1}{2}\beta_{\alpha\beta\gamma}E_\beta E_\gamma \quad \text{and not} \quad \tfrac{1}{2}\beta_{\alpha\beta\gamma\delta}E_\beta E_\gamma.$$

Theoretical Studies of the Kerr Effect, II—The Influence of Pressure, by A. D. Buckingham (*Proc. Phys. Soc.* A, 1955, **68,** 910).

In equation (2.9) the left hand side should read

$$\left(\frac{\partial\overline{\Pi^{(1)}(\tau, E_0)}}{\partial E_0}\right)_{E_0=0} \quad \text{and not} \quad \left(\frac{\partial\overline{\Pi^{(1)}(\tau,}\, E_0)}{\partial E_0}\right)_{E_0=0}$$

REVIEWS OF BOOKS

Dynamical Theory of Crystal Lattices, by Max Born and Kun Huang. Pp. xii + 420. (Oxford: Clarendon Press, 1954.) 50*s*.

The dynamical theory of crystal lattices shares the distinction with the kinetic theory of gases of being a comprehensive attempt to deduce the macroscopic properties of a medium from a definite microscopic model. Following on some preliminary work of Voigt, Professor Born must rank as the chief inspirer of this discipline and his contributions to it range over a period of forty years. Since its conception, Born's programme has however been somewhat modified by the realization of the great part played by the exclusion principle in all situations where the metallic bond predominates and the theory of metals has developed its own special methods. The volume under review is a comprehensive account of the lattice theory of ideal, non-conducting crystals; it supersedes the review article of Born and Mrs. Mayer, which appeared in 1933 and is in German, and gives evidence on every page, if only in manner of presentation, of the progress made since that date.

The book is divided into two parts. The first part provides in 165 pages a very readable account of such topics as atomic forces, lattice energies, lattice vibrations and the theory of specific heat both from the Einstein–Debye and Born–Kármán point of view, elasticity and stability of lattices and the dispersion theory of polar lattices. This part of the book can be read by beginners without much reference to the philosophy of Born's general theory. The authors have bestowed much care on matters of exposition and a greatly improved notation to smooth their path. This will be particularly appreciated in the chapter dealing with the elasticity of the crystal lattice, where simplification is achieved through the simple expedient of regarding the potential energy of interaction as a function of the square of the inter-particle distance. The tone of these chapters is entirely physical and phenomenological model considerations are to the fore. Particular mention is due to the novel treatment of the dispersion theory of polar crystals which incorporates all the results which have been obtained in this field in recent years in a very satisfactory and yet elementary manner.

The second part of the book is quite different in style and makes much greater demands on the reader. It is very formal, runs to four chapters covering over 200 pages, and contains the deduction of the optical, thermodynamical and elastic properties of the infinite crystal lattice from the general potential function based on the Born–Oppenheimer adiabatic approximation. The authors achieve the complete identification of the medium-like, elastic description of the lattice and the lattice wave microscopic treatment in the limit of long wavelengths. Special care has again been bestowed on the polar crystal and the old ghosts which haunted the mathematics of the ionic lattice have been laid by a reformulation of the theory, and one finds here the justification of the continuum model used in the first part. The free energy of the crystal is expressed as a function of the lattice strain, electric field and temperature in such a way that the thermodynamics of finite lattice strain becomes accessible. The last chapter deals with optical effects. Apart from the Raman and Brillouin effects it contains a much simplified account of the Ewald–Born dispersion theory of optical wave transmission and a treatment of the effect of damping on the dispersion formula.

There are eight appendices, of which the most noteworthy is a treatment due to Peierls of the cyclic boundary condition and a new method for the elimination of the electronic coordinates in the quantum mechanical nucleon–electron Hamiltonian. The printing and layout are everywhere excellent.

It will be seen that this book contains within the same cover two essentially different approaches. In spite of the great measure of success, it is the general theory which appears open to some criticism. Since everything is based on the Born–Oppenheimer approximation, one misses a *criterion* for its applicability and the reader is never shown where the theory of the metallic bond diverges from that of the non-conducting solid.

The discussion of the Born–Ewald dispersion theory also leaves something to be desired. It was indeed high time that a version of this theory should be worked out using the convenient separation of the electromagnetic field into longitudinal and transverse components, instead of the unwieldy Hertz vector representation. For the extreme long wave limit there is little to quarrel with in the treatment, which in this approximation hardly gets beyond a more phenomenological discussion in the first part. But one misses a working out of the connection between the refractive index and the forward scattering amplitude: that is, the part played by radiation damping, and the effective field on the oscillators is not discussed; in vain does one look for the extinction theorem. The total lack of references to earlier or similar work is particularly annoying in this section (the name of Ewald does not occur once!) and the reader must turn to Rosenfeld's recent book or to a paper by Ewald in *Annales de l'Institut Poincaré*, 1938, to see what the real problem is.

It is in the nature of things that one finds no mention of the host of phenomena associated with crystal imperfections or surface properties. But one misses reference to the thermal conductivity of crystals. The only instance where the authors touch on irreversible effects is in their long discussion of the influence of the anharmonic potential on dispersion, and one would like to see this carried out with a more adequate mathematical apparatus—the quantum theory of damping is invoked—before judging its significance.

These are minor faults in a book which fills a real gap. In one respect they indicate no more than that Professor Born's ambitious programme will need to await further progress in the quantum mechanical many-body problem before it can be brought nearer to fulfilment. But it will be a long time before anyone writes a book to supersede Born–Huang. S. ZIENAU.

Numerical Methods, by A. D. BOOTH. Pp. vii + 195. (London: Butterworths Scientific Publications, 1955.) 35*s*.

The book is mainly based on a series of lectures given to honours mathematics students at Birkbeck College, London. Its aim is to give a general introduction to the basic techniques of Numerical Analysis with special reference to those methods which are most appropriate to automatic digital computers, with the development and use of which the author has been associated for the last ten years.

After a short introductory chapter of a general nature there are three chapters on the elementary theory of the difference calculus in which the main interpolation, integration and differentiation formulae are developed mainly by operational methods. It should be noticed that the formula giving the first derivative in terms of differences is incorrect and that the incorrect formula is used later in the book. There is a special section on the gaussian integration formulae which have proved of much greater use on automatic computers than on desk machines. A general method of estimating errors in approximate integration formulae in terms of derivatives is given, but it is not stressed that in general it is of much greater value to have errors in terms of differences.

The solution of ordinary differential equations starting from given initial values is treated in one short chapter. The main method described is the Adams–Bashforth, with the Picard process or the Taylor series method for the initial steps. Although the Taylor series method is fully described no mention is made of its value as a method in its own right for solving differential equations, rather than as a starting process, though in cases where it can be used it is often extremely powerful. The Runge–Kutta process is dismissed as inferior to the Picard or the Taylor series method for starting a solution and, rather surprisingly, no mention is made of Gill's excellent adaptation of the Runge–Kutta process though it is a good example of a method which is well suited to an automatic machine while having nothing to recommend it on desk machines.

The next chapter, dealing with matrix algebra, is the least satisfactory in the book, which is unfortunate in view of the great use of such methods which has been made on automatic computers. The method of pivotal condensation for solving linear equations is described and it is stated that the virtue of taking the largest element is that it keeps rounding errors to a minimum, but that it is not well suited to automatic machines. No mention is made of two far more important advantages, that of helping to keep the elements of the reduced matrices from growing too rapidly in magnitude and of avoiding the difficulty which otherwise arises when a principal minor, but not the whole matrix, is singular or nearly singular. Both of these are of fundamental importance on an automatic machine and if the largest element in the leading column, rather than in the whole matrix, is taken as pivot this is probably the most suitable of known methods. The final stages of the Choleski method for inverting a matrix are described in such a manner as to justify the author's comment that " the complexity of the process is self-evident ". An iterative process for finding the inverse of a matrix A by means of the formula $X_{n+1}=X_n(2I-AX_n)$ is illustrated by a most misleading example which obscures the great value of the formula for improving an approximate inverse found by some other method. In the section on latent roots of matrices, unsymmetric matrices receive little attention although they are of frequent occurrence, and complex roots of real matrices are dismissed with the erroneous statement that if A has a complex root AA' will have a real root equal to the square of the modulus of that of A.

By contrast the chapter on partial differential equations, which is mainly devoted to the quasi-linear equation of the second order, is well written and within the limits imposed by the space available is reasonably complete. The classification of second order equations into elliptic, hyperbolic and parabolic types by reduction to canonical form is described and there is an exposition of the main methods of treating the three types of equation, in which matrix methods, relaxation techniques and Monte-Carlo methods are fully described. The method of characteristics for solving hyperbolic equations receives less attention than it deserves however, and it is implied that it is only when the characteristics can be found analytically that the method is useful. This is rather surprising in view of the fact that the method has been extensively used on problems in compressible flow in which the characteristic systems are often very complex. Although the use of higher differences for estimating errors in results is described in several contexts there is no reference to the extensive work of L. Fox in this field.

The remaining chapters are devoted to short accounts of non-linear algebraic equations, the use of approximating functions, Fourier synthesis and integral equations. Each of these gives a concise account of the principal techniques involved, perhaps the only omission worthy of note being Bairstow's process for finding the complex zeros of real polynomials.

There is at present no other book which covers the whole range of topics treated in this volume, and workers in the field of numerical analysis will find a useful introduction to their subject together with fairly extensive references to the literature. Unfortunately, the work is marred by a surprising number of errors of a careless nature and this, together with the price, precludes an unconditional recommendation.

J. H. WILKINSON.

Physics—A Descriptive Interpretation, by C. H. BACHMAN. Pp. viii + 497. (London: Chapman and Hall; New York: John Wiley, 1955.) 44*s*.

This book is intended to give students who are not specialists in science a connected account of what physics is about and what ideas physicists use in their investigations. The scheme of the book depends on logical convenience rather than on conventional classification—the initial chapters on basic concepts, energy, momentum and the electromagnetic spectrum lead rapidly to atomic and nuclear physics. This ' microcosmic ' physics is followed by the ' macrocosmic ' physics of heat, classical electricity and magnetism, geometric and wave optics. The second half of the book is concerned with the application of physical ideas to the world we know—there are long sections on the ' cosmic physics ' of the weather, the earth, the stars and the galaxies and on the physics of biology, particularly of various processes in the human body. This is one of the most attractive sections of the book. There are final chapters on historic development, stressing the accelerating pace of scientific progress, and on the present structure of scientific research—the latter from a distinctly American point of view. The book is written without mathematics other than arithmetic and elementary algebraic formulae. There are a number of sets of discussion topics; many of them would probably prove unreasonably difficult to a person with no other guide than the text. The aims and arrangement of the book are original and commendable: it was obviously written with American college courses in mind, but in this country might find its greatest appreciation in the sixth forms of schools and in adult education classes, for both of which it is eminently suitable.

The reviewer detects no serious inaccuracies or misleading treatments though a few of the analogies seemed to him pointless and laboured. A few of the drawings seemed ill-chosen and some of them showed a comic-strip facetiousness which might repel the staider reader. H. J. J. BRADDICK.

CONTENTS OF SECTION B

PAGE

Dr. J. A. HULBERT and Prof. G. O. JONES. The Superconducting Bolometer as a Detector of Thermal Radiation from Low-Temperature Sources . . 801

Mr. W. W. H. CLARKE and Dr. L. JACOB. Some Anomalous Emission Effects in Low Energy Electron Beams 805

Dr. G. D. ARCHARD. A Possible Chromatic Correction System for Electron Lenses 817

Mr. G. L. BOOTH, Dr. F. E. HOARE and Mr. B. T. MURPHY. The Low Temperature (11°–20°K) Specific Heat of α and β Manganese 830

Dr. K. D. FROOME. The Refractive Indices of Water Vapour, Air, Oxygen, Nitrogen and Argon at 72 kMc/s 833

Dr. D. H. PRINGLE and Mr. W. E. J. FARVIS. Screened Probe Measurements in the Helium Negative Glow 836

Prof. L. F. BATES and Dr. A. W. SIMPSON. The Thermal Effects Associated with the Magnetization of High-Coercivity Materials 849

Prof. L. F. BATES, Mr. S. J. LEACH and Mr. R. G. LOASBY. The Magnetic Susceptibility of Metallic Cerium 859

Mr. G. S. BRINDLEY. A Photochemical Reaction in the Human Retina . . 862

Mr. L. R. BAKER. An Interferometer for measuring the Spatial Frequency Response of a Lens System 871

Dr. R. W. SILLARS. The Effect of Field Emission on the Behaviour of Semiconductor Contacts 881

Dr. F. W. G. ROSE and Mr. D. J. SANDIFORD. An Easy Derivation of the Hole Lifetime in an n-type Semiconductor with Acceptor Traps 894

Mr. D. BARBER. Measurements of Current Noise in Lead Sulphide at Audio Frequencies 898

Prof. R. E. BURGESS. The Turnover Phenomenon in Thermistors and in Point-Contact Germanium Rectifiers 908

Dr. D. G. AVERY and Mr. J. B. GUNN. The Use of a Modulated Light Spot in Semiconductor Measurements 918

Dr. J. LEES and Mr. S. WALTON. The Influence of Pressure on Metal–Germanium Contacts 922

Dr. G. T. WRIGHT. Absolute Scintillation Efficiency of Anthracene Crystals . 929

Dr. T. J. LEWIS. Some Factors Influencing Field Emission and the Fowler–Nordheim Law 938

Mr. C. B. RAYNER. Whitehead's Law of Gravitation in a Space–Time of Constant Curvature 944

Dr. L. CARTZ. Thermal Vibrations of Atoms in Cubic Crystals: I—The Temperature Variation of Thermal Diffuse Scattering of X-rays by Lead Single Crystals 951

Dr. L. CARTZ. Thermal Vibrations of Atoms in Cubic Crystals: II—The Amplitude of Atomic Vibrations 957

Research Notes:

- Dr. C. A. HOGARTH and Dr. W. BARDSLEY. The Effect of Illumination on the Excess Noise of Silicon Filaments 968
- Dr. A. MANY, Mr. D. GERLICH and Dr. E. HARNIK. Some Measurements connected with Carrier Deficit Phenomena in Germanium 970
- Dr. E. W. J. MITCHELL. The Infra-Red Faraday Effect due to Free Carriers in a Semiconductor 973
- Mr. D. C. NORTHROP and Dr. O. SIMPSON. Photoeffects in Condensed Aromatic Hydrocarbons 974

Corrigendum: N. A. LONAPPAN 977

Reviews of Books 978

Contents of Section A 984

The Spectra of the Manganese Halides in the Blue-Green

BY W. HAYES

Physics Department, University College, Dublin

Communicated by T. E. Nevin; MS. received 23rd May 1955 *and in amended form 7th July* 1955

Abstract. The bands of MnBr, MnCl and MnF in the region λ 4750–5200 Å have been photographed under high dispersion. The spectrum of each molecule consists of two separate systems one of which is assigned to a Π–Σ transition. The second system of MnCl may also be assigned to a Π–Σ transition. It is suggested that the second MnF system arises from a transition of the type $0^{\pm}$–Σ and the second MnBr system from a transition of the type $0^{\pm}$–1. The isotope effect observed in MnBr and MnCl is described in detail. A table of the constants of the band systems of the manganese halides is included.

---

§ 1. INTRODUCTION

EARLY investigations of the spectra of the manganese halides revealed the existence of strong complex systems in the region λ 4750–5200 Å. The spectra of MnCl and MnBr were first described by Mesnage (1939) and the spectrum of MnF by Bacher (1948). In an analysis made by Rao (1952, 1953) the bands are interpreted as a $^5\Pi$–$^7\Sigma$ transition. The analysis is based on prism plates taken at a dispersion of 25–30 Å mm^{-1}.

In the present paper it is shown that the spectrum of each of the halides consists of two separate systems one of which arises from a Π–Σ transition. Possible interpretations of the other systems are given. The presence of two systems was originally suggested by Mesnage.

§ 2. EXPERIMENTAL

The bands were excited using MnF_2 or $MnCl_2$ or $MnBr_2$ in the hollow cathode source described by Hayes and Nevin (1955 a). Low dispersion plates were taken using the glass prism of the Hilger E 478 spectrograph, but on these plates (dispersion ∼9 Å mm^{-1}) many groups of closely spaced heads were not resolved. The bands were also photographed in the first order of a 21ft concave grating at a dispersion of the order of 2·5 Å mm^{-1}. Astra 111 plates were used. Exposures of about 90 seconds were required with the prism spectrograph and from 30 minutes to three hours with the grating. The data given in this paper are taken from grating plates only.

§ 3. THE SPECTRUM OF MnBr

The spectrum consists of three groups of heads degraded to longer waves. The groups beginning at λ 4986 Å and λ 5068 Å are strong and equally intense while the third group which begins at λ 4915 Å is weak. The structures of the λ 4915 Å and λ 4986 Å groups are similar and bear no resemblance to the structure of the λ 5068 Å group.

The bands appear to form two separate systems one of which arises from a Π–Σ transition. The two intense groups are assigned to the $\Delta v=0$ sequences of the systems.

The Π–Σ *System*

The $\Delta v=0$ sequence of this system reproduced in figure 1 (*a*), (Plate I), consists of three groups of closely spaced heads beginning at λ 4986·4 Å, λ 4990·8 Å and λ 4993·7 Å, followed by intensity ridges, regularly spaced, which are caused by the fusion of diffuse heads. This structure can be interpreted as a $^5\Pi$–$^5\Sigma$ transition with the Π state near case *b*. In each band, when B' is less than B'', five Q and five R heads are expected and if the satellite structure is well developed, four weaker S heads. Head formation by T branches is unlikely.

The four heads in the group beginning at λ 4986·4 Å are the S heads of the (0, 0) band. The first five heads of the λ 4990·8 Å group are the R heads of the (0, 0) band. The two weaker diffuse heads present are the R_5 and R_4 heads of the (1, 1) band. The heads comprising the λ 4993·7 Å group are the Q_5 and Q_4 heads of the (0, 0) band. Faint unresolved T branches run back to shorter waves from the S heads of the (0, 0) band and fade out at ~λ 4983·6 Å. The heads of the $\Delta v=\pm 1$ sequences beginning at λ 4915 Å and λ 5063 Å are readily fitted into this scheme. Only three weak heads are observed in the $\Delta v=-1$ sequence, the rest being covered by the heads of the strong λ 5068 Å group. The multiplet splitting in the Π state is of the order of 1·8 K.

The wave numbers of the observed heads and their classification are given in table 1. Two measured heads remain unclassified. The Q_5 heads of $Mn^{79}Br$ are represented with a mean error 0·6 K by the equation

$$\nu=20024{\cdot}6+286{\cdot}6\,(v'+\tfrac{1}{2})-1{\cdot}4\,(v'+\tfrac{1}{2})^2-295{\cdot}9\,(v''+\tfrac{1}{2})+1{\cdot}6\,(v''+\tfrac{1}{2})^2.$$

The isotope effect associated with ^{79}Br and ^{81}Br is readily observed and is useful in identifying the heads of the weak $\Delta v=-1$ sequence.

The isotope shift is calculated using the formula

$$\Delta\nu=(\rho-1)\,\nu_v+(\rho^2-1)\nu_r.$$

The observed and calculated shifts are given in table 2 and the agreement between them may be regarded as satisfactory.

The Bands in the Region λ 5068–5100 Å

The group of heads beginning at λ 5068 Å (figure 2 (*a*), Plate II) appears to consist of two extensive sequences of double headed bands, the sequence of longer wavelength being the stronger. The heads in each band are equally intense suggesting they are R and Q heads. The R–Q head separation in the short wave sequence is of the order of 19K and in the long wave sequence of the order of 15K. The bands could be assigned to two $^1\Pi$–$^1\Sigma$ transitions or a transition of the type $0^{\pm}$–1. In the latter interpretation the difference in the R–Q head separation constitutes a difficulty.

The wave numbers of the observed heads and their classification are given in table 3. Column (6) contains five unclassified heads which lie between λ 5069·6 Å and λ 5072·1 Å. The direction of shading of these heads is indefinite. The heads of the weaker sequence in columns (2) and (3) are marked with a dash.

§ 4. THE SPECTRUM OF MnCl

In the chloride spectrum, besides weaker groups, two strong groups of heads degraded to longer wavelengths are observed extending from λ 4964 Å to λ 5009 Å and from λ 5011 Å to λ 5030 Å. As in the spectrum of MnBr the intense groups are assigned to the $\Delta v = 0$ sequences of two separate systems one of which arises from a Π–Σ transition. In Rao's analysis many of the heads present are not recorded due to inadequate dispersion. It is the author's experience with these systems that the high dispersion of the grating is essential for an investigation of the vibrational structure.

Table 1. Heads of MnBr in the Blue-Green. Π–Σ System

Vacuum Wave number	I	Classification		Vacuum Wave number	I	Classification	
20340·9	1	1, 0	S_5	20031·2	8	0, 0	R_5
339·0	2		S_5*	030·2	8		R_4
338·2	2		S_4	029·3	7		R_3
336·3	2		S_4*	027·9	5		R_2
335·4	2		S_3	025·4	3		R_1
333·7	2		S_3*	023·1	2	1, 1	R_5
331·7	1		S_2	021·8	2		R_4
331·0	1			019·7	10	0, 0	Q_5
329·9	Mn	1, 0	S_2*	017·9	8		Q_4
317·5	Mn	1, 0	R_5	014·1	4	2, 2	R_5
315·7	3		R_4 . R_5*	013·1	4		R_4
314·2	Mn		R_4* . R_3	010·9	4	1, 1	Q_5
313·0	3		R_3*	005·4	2	3, 3	R_5
311·7	3		R_2	002·6	5	2, 2	Q_5
310·3	2		R_2*	19999·2	2	4, 4	R_5
309·2	2	1, 0	R_1; 2, 1 R_5	995·8	2	3, 3	Q_5
308·1	2	2, 1	R_4	987·0	1	4, 4	Q_5
307·0	2	1, 0	R_1*; 2, 1 R_5*	743·1	1	2, 3	S_5*
306·1	2	2, 1	R_4*	741·3	1		S_5
303·4	3	1, 0	Q_5	733·3	1	1, 2	R_5*
292·3	2	2, 1	Q_5	731·5	1		R_5
049·4	5	0, 0	S_5	729·2	1		
048·3	3		S_4	728·1	1	0, 1	Q_5*
046·5	3		S_3	726·5	1		Q_5
045·2	1		S_2				

The heads of the molecule $Mn^{81}Br$ are marked with a star. In some cases manganese lines coincide with expected head positions and where this occurs the wave numbers of the lines are given and their presence indicated in the intensity column.

Table 2. Isotope Effect in the Π–Σ System of MnBr

v', v''	$\Delta\nu(Q)_{calc}$	$\Delta\nu(Q)_{obs}$	v', v''	$\Delta\nu(R)_{calc}$	$\Delta\nu(R)_{obs}$
0, 1	1·6	1·6	1, 0	1·7	1·5, 1·7, 1·8, 1·4
v', v''	$\Delta\nu(S)_{calc}$	$\Delta\nu(S)_{obs}$	2, 1	1·6	2·2, 2·0
1, 0	2·0	1·9, 1·9, 1·7, 1·8	1, 2	1·7	1·8
2, 3	2·0	1·8			

Table 3. Heads of MnBr in the Region λ 5068–5100 Å

(1) v', v''	(2) $\nu(R')_{vac}$	I	(3) $\nu(Q')_{vac}$	I	(4) $\nu(R)_{vac}$	I	(5) $\nu(Q)_{vac}$	I	(6)	I
0, 0	19724·2	3	19705·9	4	19684·9	1	19669·8	7	19720·6	4
1, 1	715·0	3	697·4	4	675·0	7	659·9	6	718·8	3
2, 2	708·6	7	689·6	5	664·9	6	650·2	6	716·8	3
3, 3	699·9	Mn	681·5	1	655·2	6	640·1	6	713·8	3
4, 4	691·7	5	672·9	2	644·4	6	629·7	5	710·7	5
5, 5	683·9	2	663·5	2	632·9	4	617·9	4		
6, 6	675·7	2	655·2	6	619·9	3	604·4	2		
7, 7	665·8	2								

The Π–Σ *System*

The heads of the $\Delta v = 0$ sequence of the system (figure 1 (*b*)) which begin at λ 4964 Å exhibit a close doubling which is discussed with the isotope effect arising from ^{35}Cl and ^{37}Cl. Each band, doubling neglected, appears to contain one R and one Q head. The bands of the $\Delta v = \pm 1$ sequences contain, in addition, a single S head suggesting that the system is a Π–Σ transition with a multiplicity of at least three and with the Π fine structure unresolved because of a close approximation to case *b*. The $\Delta v = +2$ sequence is observed in the region λ 4780–4825 Å but is too weak for measurement. The absence of well-defined S heads in the $\Delta v = 0$ sequence is noticeable. This is also observed in the complex infra-red MnCl bands (Hayes and Nevin 1955 b) where, however, weak S and T branches are seen running back to shorter waves from the R head of the (0, 0) band. The corresponding structure cannot be identified in the blue-green bands due to overlapping by the $\Delta v = +1$ sequence of the second system. It seems probable that the bands are the analogue of the $^5\Pi$–$^5\Sigma$ system of MnBr the difference in appearance being due to the stronger tendency to case *b* in MnCl.

The observed heads are classified in table 4. The number of unclassified heads is small. Faint structure the origin of which is obscure occurs between λ 5082 Å and λ 5098 Å and appears to contain some diffuse heads degraded to shorter waves. The Q heads of Mn^{35}Cl are represented with a mean error 1·4K by the equation

$$\nu = 20115{\cdot}4 + 378{\cdot}0\,(v' + \tfrac{1}{2}) + 0{\cdot}45\,(v' + \tfrac{1}{2})^2 - 385{\cdot}5\,(v'' + \tfrac{1}{2}) - 0{\cdot}50\,(v'' + \tfrac{1}{2})^2.$$

The signs of the coefficients of $(v' + \frac{1}{2})^2$ and $(v'' + \frac{1}{2})^2$ indicate an anomalous vibrational structure. The infra-red bands exhibit a similar anomaly.

The isotope effect arising from ^{35}Cl and ^{37}Cl exhibits some unusual features. The heads of the $\Delta v = 0$ sequence show a doubling of the order 1·7K, the close pairs of heads having an intensity ratio of about 3 to 1 with the weaker head on the long wave side. The calculated shift in the $\Delta v = 0$ sequence is about 0·3K and the weaker Mn^{37}Cl heads should lie on the short-wave side of the stronger Mn^{35}Cl heads. Examination of the $\Delta v = \pm 1$ sequences shows also a systematic discrepancy of the order 1·6K between the observed and calculated isotope shifts. All this would suggest that the origin of the Mn^{37}Cl bands is shifted by 1·6K to the low frequency side of the Mn^{37}Cl origin. A precisely similar effect of magnitude 0·5K has been observed in the infra-red MnCl bands. The effects may be due to an electronic isotope shift.

The differences between the observed and calculated isotope shifts are given in table 5. Allowance is made for the effect of the rotational shift on the position of the R and S heads.

The Bands in the Region λ 5011–5030 Å

The extensive group of heads beginning at λ 5011 Å (figure 2 (*b*)) contains five strong well-defined heads between λ 5013 Å and λ 5019 Å. From λ 5019 Å to longer waves, intense heads occur accompanied by a large number of weaker diffuse heads. The bands may be assigned to the $\Delta v = 0$ sequences of the first three components of a Π–Σ transition with a multiplicity at least five. The measured heads are classified in table 6. The two highest energy components contain Q, R, S and T heads, the heads of the weaker second component being marked with a dash. The third weakest component contains Q, R and S heads marked with two dashes. The multiplet separation appears to be of the order of 11K.

Table 4. Heads of MnCl in the Blue-Green. Π–Σ System

Vacuum Wave number	*I*	Classification	Vacuum Wave number	*I*	Classification
20518·0	0	2, 1 S	20101·1	8	4, 4 R
510·2	1	3, 2 S	098·1	12	2, 2 Q
508·2	1	1, 0 R	095·6	5	Q*
505·9?	1	4, 3 S	093·9	5	5, 5 R
504·6?	1		092·5	2	R*
501·9	2	5, 4 S	090·2	20	3, 3 Q
500·3	2	2, 1 R	089·0	12	Q*
597·7	0	4, 3 S*	085·9	15	6, 6 R
595·3	0	6, 5 S*	084·8	10	R*
593·6	1	5, 4 S	081·5	15	4, 4 Q
592·7	3	3,2 R; 1,0 Q; 2,1 R*	080·4	8	Q*
589·9	2	7, 6 S	077·2	10	7, 7 R
585·5	6	4,3 R; 2,1 Q; 3,2 R*	072·8	10	5, 5 Q
583·5	2	8, 7 S	067·2	10	8, 8 R
582·1	1	7, 6 S*	063·6	10	6, 6 Q
579·5	5	5, 4 R	058·7	4	9, 9 R
578·1	3	3, 2 Q	055·8?	2	
576·7	3	9,8 S; 4, 3 R*	053·7	2	7, 7 Q
574·4?	0	8, 7 S*	19750·3?	1	0, 1 R*
572·7	4	6, 5 R	745·7	1	R
570·8	4	4, 3 Q	742·0	Mn	5, 6 S; 1, 2 R*
569·5	1	10,9 S; 2,1 Q*	738·0	2	1, 2 R
568·6?	1	9, 8 S	734·9	0	2, 3 R*
566·2	4	7, 6 R	733·9?	2	6, 7 S
564·7	1	6, 5 R*	732·9?	1	
563·6	4	5, 4 Q	731·2	2	2, 3 R
561·5	0	10, 9 S*	729·6	1	0, 1 Q*
560·1	5	8, 7 R	728·3	1	7, 8 S
558·0	1	7, 6 R*	726·5	3	
557·1	3		725·2	2	0, 1 Q
552·2	2	6, 5 Q	723·2	1	3,4 R; 1,2 Q*
553·4	4	9, 8 R	721·0	2	8, 9 S
551·1	1	8, 7 R*	719·2	1	1, 2 Q
548·1	Mn	7,6 Q; 6,5 Q*	717·2	2	4, 5 R
544·4	3	10, 9 R	716·0	2	2, 3 Q*
542·8	1		712·9	2	5, 6 R*
541·0	2	7, 6 Q*	711·7	2	2, 3 Q
539·7	3	8, 7 Q	710·0	2	9, 10 S
534·1	2	11, 10 R	708·3	2	5, 6 R
531·5	2	9, 8 Q	705·4	4	10, 11 S; 6,7 R*
529·8	1		703·6	3	3, 4 Q
129·5	4	0, 0 R	699·7	Mn	6, 7 R
127·9	2	R*	697·7	1	4, 5 Q*
123·0	8	1, 1 R	695·3?	3	7, 8 R*
121·6	3	R*	692·5	2	4, 5 Q
115·8	10	2, 2 R	689·8	2	7, 8 R
113·9	4	R*	687·2	2	5, 6 Q*
112·0	4	0, 0 Q	684·4	1	8, 9 R*
110·0	2	Q*	682·6	2	5, 6 Q
108·7	14	3, 3 R	680·8	2	
106·5	5	R*	678·7	2	8, 9 R
105·4	4	1, 1 Q			
103·8	3	Q*			

Heads of the molecule $Mn^{37}Cl$ are marked with a star.
Doubtful heads are followed by a question mark.

The $\Delta v = -1$ sequence of the transition has been observed beginning at λ 5118 Å. The $\Delta v = +1$ sequence lies between the $\Delta v = +1$ and 0 sequences of the first system and its beginning and end are obscured by them. Heads are not recognized in these sequences which are faint. An approximate estimate of the vibrational constants gives $\omega' = 385\mathrm{K}$, $\omega'' = 410\mathrm{K}$.

Table 5. Isotope Effect in the Π–Σ System of MnCl

v', v''	$\Delta\nu(\mathrm{Q})_{\mathrm{obs}}$	obs − calc	v', v''	$\Delta\nu(\mathrm{Q})_{\mathrm{obs}}$	obs − calc
1, 0	8·8	2·5	2, 2	2·5	2·8
2, 1	8·6	2·4	3, 3	1·2	1·6
3, 2	9·3?	3·2	4, 4	1·1	1·7
4, 3	8·4	2·5	0, 1	−5·6	0·9
5, 4	7·1	1·3	1, 2	−4·0	2·6
6, 5	7·1	1·4	2, 3	−4·3	2·4
0, 0	2·0	2·1	3, 4	−4·7	2·2
1, 1	1·6	1·8	4, 5	−5·2	1·8
			5, 6	−5·0	2·1
v', v''	$\Delta\nu(\mathrm{R})_{\mathrm{obs}}$	obs − calc	v', v''	$\Delta\nu(\mathrm{R})_{\mathrm{obs}}$	obs − calc
1, 0	7·5	0·6	2, 2	1·9	1·6
2, 1	7·5	0·7	3, 3	2·2	2·0
3, 2	8·8	2·1	5, 5	1·4	1·5
4, 3	6·8	0·3	6, 6	1·1	1·3
5, 4	8·7	2·3	0, 1	−4·6	1·3
6, 5	8·2	1·9	1, 2	−4·0	2·0
7, 6	9·0	2·9	2, 3	−3·7	2·4
0, 0	1·6	1·1	5, 6	−4·6	1·9
1, 1	1·4	1·0	6, 7	−4·8	1·8
			7, 8	−5·5	1·2
			8, 9	−5·7	1·1
v', v''	$\Delta\nu(\mathrm{S})_{\mathrm{obs}}$	obs − calc	v', v''	$\Delta\nu(\mathrm{S})_{\mathrm{obs}}$	obs − calc
4, 3	8·2	0·9	7, 6	7·9	0·9
5, 4	8·3	1·1	8, 7	8·9	2·0
6, 5	7·7	0·6	9, 8	8·1	1·3
			10, 9	8·0	1·3

§ 5. THE SPECTRUM OF MnF

Under low dispersion the spectrum of MnF is similar in appearance to the spectra of MnCl and MnBr. Two strong groups of heads degraded to longer waves lie in the regions λ 4920–4989 Å and λ 4993–5100 Å. These are assigned to the $\Delta v = 0$ sequences of separate systems. The system of greater energy is interpreted as a Π–Σ transition.

The Π–Σ *System*

The bands of the $\Delta v = 0$ sequence of the system (figure 1 (*c*)) are double headed each band containing one R and one Q head. Heads are formed by R and Q branches also in the weak $\Delta v = \pm 1$ sequences. The $\Delta v = +1$ sequence begins at λ 4776 Å but the heads of the $\Delta v = -1$ sequence beginning at λ 5100 Å are not obvious due to slight overlapping by the $\Delta v = 0$ sequence of the second system. The heads could arise from a $^1\Pi$–$^1\Sigma$ transition but it is clear from the appearance of the system that the bands are complex. As with MnCl, it is likely that the

Table 6. Heads of MnCl in the Region λ 5011–5030 Å

Vacuum Wave number	*I*	Classification		Vacuum Wave number	*I*	Classification	
19943·4	10	0, 0	R	19871·4?	1		
928·6	3		Q	875·9	Mn	3, 3	T
924·4	8		R′	868·1	2		S
916·1	3		Q′ . R″	863·2	0		T′
906·0	2		Q″	860·9	7		R
933·4	7	1, 1	S	855·0	2		Q
919·5	7		R	853·7	1		S′
910·5	3		S′	845·1	3		R′
908·1	4		Q	841·5	6		Q′
899·8	3		R′	837·0	1		S″
898·6	1		S″	832·2	1		R″
890·4	7		Q′	843·1?	4		
888·1	3		R″	835·2	1	4, 4	T
880·3?	1		Q″	828·8	1		S
902·4	2			825·7	4		R
886·6?	3			823·0	2		Q
906·0	2	2, 2	S	812·1	2		Q′
896·4	0		T′	798·6?	0		
894·3	7		R	794·9	1	5, 5	T
884·4	3		Q	790·1	1		S
882·3	2		S′	780·1?	1		Q′
872·7	Mn		R′				
868·1	2		S″				
865·5	4		Q′				
859·4	4		R″				
853·7	1		Q″				

system is the analogue of the $^5\Pi$–$^5\Sigma$ bands of MnBr, the absence of S heads in MnF and the lack of resolution of the Π fine structure being due to a very close approximation to case *b*.

The classification of the observed heads is given in table 7. Unclassified heads might well be regions of high line density. The Q heads are represented with a mean error 1·8K by the equation

$$\nu = 20298{\cdot}2 + 637{\cdot}1\,(v' + \tfrac{1}{2}) - 1{\cdot}9\,(v' + \tfrac{1}{2})^2 - 649{\cdot}1\,(v'' + \tfrac{1}{2}) + 1{\cdot}5\,(v'' + \tfrac{1}{2})^2.$$

The Bands in the Region λ 4993–5100 Å

The strong group of heads beginning at λ 4993 Å (figure 2 (*c*)) appears to consist of two extensive sequences of single headed bands. What appear to be weak irregularly spaced heads are also observed especially in the region λ 5004 Å to λ 5034 Å but these are possibly fortuitous line accumulations. The structure is obviously complex and might arise from a transition of the type $0^{\pm}$–Σ^+ where the multiplicity of the Σ state is most likely five or seven. The properties of such transitions are discussed by Hayes and Nevin (1955 c). If this interpretation is correct the observed heads can be classified as R and Q heads. The absence of satellite heads is not surprising since large head–origin separations are not unlikely. The R heads are assigned to 0^+–Σ^+ and the Q heads to 0^-–Σ^+. The wave numbers of the observed heads, grouped in sequences, are given in table 8.

Table 7. Heads of MnF in the Blue-Green. Π–Σ System

Vacuum Wave number	I	Classification	Vacuum Wave number	I	Classification
20928·8	0	1,0 Q	20260·6	6	4, 4 R
910·7	0	2, 1 Q	237·2	2	Q
899·7	Mn	4, 3 R	247·3?	1	
891·7	0	3, 2 Q	246·0	3	5, 5 R
881·2	2	5, 4 R	241·6	6	
862·7	2	6, 5 R	233·8	3	
843·3	4	7, 6 R	231·6	1	6, 6 R
817·0	4		211·9	5	
789·8	3		19660·7	5	
308·9	1	0, 0 R	656·6	8	1, 2 R
293·5	3	Q	637·3	4	Q
299·2	2	1, 1 R	648·5	0	0, 1 Q
281·4	3	Q	651·9?	1	
285·9	Mn	2, 2 R	654·8	3	2,3 R
266·5?	1	Q	627·3	3	Q
275·9?	1		635·2?	1	3, 4 R
273·8	5	3, 3 R	614·8	1	Q
252·3	10	Q	622·7	1	4, 5 R
			618·7	4	
			609·6	1	5, 6 R

Table 8. Heads of MnF in the Region λ 4993–5100 Å

$\nu(\mathrm{R})_{\mathrm{vac}}$	I	$\nu(\mathrm{Q})_{\mathrm{vac}}$	I
20023·3	4	19971·6	6
19951·1	2	898·4	4
869·3	10	823·7	9
781·2	2	746·4	4
693·0	4	662·6	4

§ 6. DISCUSSION

In view of the progress made in the interpretation of the spectra of the manganese halides in recent years, a summary of the results so far obtained would appear to be of value.

Early work on the spectrum of MnF by Rochester and Olsson (1939) revealed the existence of an extensive band system of simple structure in the ultra-violet which they assigned to a $^1\Sigma$–Σ^1 transition. Later Bacher (1948) interpreted the system as $^7\Sigma$–$^7\Sigma$.

All the halides have strong complex systems of similar structure in the near ultra-violet. High dispersion measurements are given by Müller (1943). An analysis of these bands made by Bacher and extended by Rao (1949) showed the transition involved to be $^7\Pi$–$^7\Sigma$. There are a number of features of Bacher's analysis which appear to be unsatisfactory. Recently a new study of the MnCl and MnBr bands made by Hayes and Nevin (1955 a) has confirmed the assignment to a $^7\Pi$–$^7\Sigma$ transition but differs considerably in detail from Bacher's analysis.

New bands of MnF and MnBr in the red are interpreted by Hayes and Nevin (1955 c) as a transition of the type $0^{\pm}$–$^5\Sigma^+$. All the halides have extensive systems in the infra-red. The spectra of MnF and MnCl are described by Hayes and Nevin

(1955 b) and the spectrum of MnBr by Hayes (1955). The MnCl system appears to arise from a $\Pi-\Sigma$ transition with partial case *c* coupling in one or both of the states involved. The MnF bands comprise a single sequence which is possibly the analogue of the chloride system. The spectrum of MnBr contains two systems, one of which is assigned to a $\Sigma-\Sigma$ transition. The second MnBr system involving a $\Pi-\Sigma$ transition appears to be the analogue of the MnCl bands.

Table 9. List of Constants in the Spectra of the Manganese Halides

Transition	ν_e	ω_e'	ω_e''	$x_e'\omega_e'$	$x_e''\omega_e''$	Reference
			MnF			
$^7\Sigma-{}^7\Sigma$	41231·5	637·2	618·8	4·46	3·01	(11)
$^7\Pi_1-{}^7\Sigma$	∼28470	∼665	∼610	∼6·0	∼3·0	(1)
$\Pi-\Sigma$	20298·2	637·1	649·1	1·9	1·5	†
$0^{\pm}-\Sigma$	∼20000	—	—	—	—	†
$0^{\pm}-{}^5\Sigma$	14527·7	595·4	645·4	3·15	3·20	(5)
$\Pi-\Sigma$	∼12180	—	—	—	—	(4)
			MnCl			
$^7\Sigma-{}^7\Sigma$	∼40800	∼320	∼384	—	—	(1)
$^7\Pi_1-{}^7\Sigma$	27004·6	407·2	380·6	0·3	0·0	(3)
$\Pi-\Sigma$	20115·4	378·0	385·5	−0·45	−0·50	†
$\Pi-\Sigma$	∼19900	∼385	∼410	—	—	†
$\Pi-\Sigma$	11420·3	385·4	397·9	−0·56	−0·47	(4)
			MnBr			
$^7\Pi_1-{}^7\Sigma$	26303·7	302·3	286·7	0·6	0·8	(3)
$^5\Pi-{}^5\Sigma$	20024·6	286·6	295·9	1·4	1·6	†
$0^{\pm}-1$	∼19680	—	—	—	—	†
	∼16375	—	∼277	—	—	(5)
$0^{\pm}-{}^5\Sigma$	∼15910	∼275	∼272	—	—	(5)
$\Pi-\Sigma$	10682·1	290·4	291·3	0·13	0·01	(2)
$\Sigma-\Sigma$	10667·5	295·6	298·8	0·62	0·61	(2)
			MnI			
$^7\Pi-{}^7\Sigma$	∼24800	—	∼240	—	—	(1)

† Present paper.

A list of origins and vibrational constants of the various systems is given in the table. The fluoride bands described by Rochester and Olsson and the $^7\Pi-{}^7\Sigma$ bands in the near ultra-violet are both observed in absorption and would appear to have the $^7\Sigma$ ground state of the molecule in common. Analogous systems involving the ground state occur in MnCl. The presence of partial case *c* coupling in the red and infra-red bands suggests that highly excited states are involved. With the modes of excitation used so far no evidence is found for transitions between these states and the lower states of the molecule.

ACKNOWLEDGMENT

The author wishes to thank Professor T. E. Nevin for his encouragement and his interest in the work.

REFERENCES

BACHER, J., 1948 *Helv. Phys. Acta*, **21,** 379. (1)

HAYES, W., 1955, *Proc. Phys. Soc.* A, **68,** 670. (2)

HAYES, W., and NEVIN, T. E., 1955 a, *Proc. Roy. Irish Acad.*, **57,** 15; (3)
1955 b, *Nuovo Cim.*, in the press; (4)
1955 c, *Proc. Phys. Soc.* A, **68,** 665. (5)

MESNAGE, P., 1939, *Ann. Phys., Paris*, **12,** 5. (6)

MÜLLER, W., 1943, *Helv. Phys. Acta*, **16,** 1. (7)

RAO, P. T., 1949, *Indian J. Phys.*, **23,** 517; (8)
1952, *Proc. Nat. Inst. Sci. India*, **18,** 481; (9)
1953, *Ibid.*, **19,** 149. (10)

ROCHESTER, G. D., and OLSSON, E., 1939, *Z. Phys.*, **114,** 495. (11)

On the Levels of the p^2-Configuration in the Arc Spectra of Zn, Cd and Hg

By W. R. S. GARTON and A. RAJARATNAM
Department of Physics, Imperial College, London

MS. received 12*th July* 1955 *and in final form 3rd August* 1955

Abstract. The $p^2\ {}^3P_2$ level in the arc spectra of Zn, Cd and Hg has long been considered missing; the accepted explanation has been that transitions involving the level are excessively weakened by auto-ionization. By observation of the arc spectra of these elements in the range 1700–2350 Å, the level in question has been located in Zn and Cd and possibly in Hg. With increasing atomic number auto-ionization increases very greatly, so that one of two diffuse lines in Cd I has previously been considered a band of Cd_2. Intensity measurements on this line indicate a natural-broadening profile, and yield a value for the auto-ionization probability.

Previous placing of the $p^2\ {}^3P_0$ level of Hg I is considered erroneous, and a new position suggested.

---

§ 1. Introduction

One of the many apparently minor peculiarities of the simpler line spectra has concerned the missing $p^2\ {}^3P_2$ level in Zn I, Cd I, and Hg I. The $p^2\ {}^3P$ term lies above the normal series limit, and the $J=0$, 1 levels were recognized years ago, the $J=0$ level in Hg erroneously (see below), from combinations with sp ${}^3P^0$ which give rise in each case to a group of four fairly strong lines in the range 1700–2300 Å. The line pair sp ${}^3P^0_{1,2}$–$p^2\ {}^3P_2$, needed to complete the multiplet, has always been considered missing, and the explanation of this detail, which has come to be accepted, followed recognition of the effects of auto-ionization by Shenstone (1931) and Majorana (1931). The latter author was, in fact, concerned with the problem mentioned, and argued that, though no ${}^3P$-continuum of even parity was available for auto-ionization of $p^2\ {}^3P_2$, the coupling could be taken sufficiently removed from *LS* for ${}^3P_2$ and ${}^1D_2$ to share characteristics to the extent necessary for the former to auto-ionize readily into the continuum sE(d) ${}^1D_2$ attached to the sd ${}^1D_2$ series terms; the auto-ionization probability was supposed large enough to broaden and weaken the sp ${}^3P^0_{1,2}$–$p^2\ {}^3P_2$ combinations to the point of unobservability. As pointed out by Condon and Shortley (1935), this argument is not entirely convincing, in that the $p^2\ {}^3P_0$ level would be expected to auto-ionize freely into the sE(s) ${}^1S_0$ continuum, yet the line sp ${}^3P^0_1$–$p^2\ {}^3P_0$ appears sharp.

The missing lines have now been located definitely in Zn I and Cd I, and less definitely in Hg I; in proceeding from Zn to Hg the auto-ionization broadening increases greatly, so that in Hg, so far, only a single faint hazy patch has been obtained, which however, lies at the position to be expected. The three spectra are discussed in order below.

§ 2. Experimental

The Zn and Cd multiplets fall in the region 2050–2350 Å; spectra were photographed in the first and second orders of an aluminized 3-metre concave grating, with an arc in air at atmospheric pressure, or in helium or argon at reduced pressure, serving as light source.

In the case of Cd, photographic photometry was employed for intensity measurements. For this purpose, a Hilger medium-quartz spectrograph was used in conjunction with a stepped log-sector, to impress a calibration exposure on a plate which was afterwards transferred to the grating spectrograph for recording of the spectrum to be photometered; the calibration exposure could not be made with the latter instrument owing, of course, to astigmatism. The plates were subsequently examined with the Hilger recording microphotometer at Mill Hill Observatory.

In the case of Hg, the region concerned lies at 1700–2000 Å; accordingly, a one-metre normal-incidence vacuum spectrograph was used, and the light source consisted of a specialized form of constricted mercury arc carrying a window of lithium fluoride transparent to 1100 Å. All exposures were made on Ilford Q1 or Q2 plates.

§ 3. RESULTS AND DISCUSSION

(*a*) Zn I. The relevant portion of the spectrum of a Zn arc in air is reproduced in figure 1 (Plate) at (*a*). The singlet resonance line 2139 Å shows its usual heavy self-reversal. The four sharp lines 4s4p $^3P^0_{012}$–4p$^{2\,3}P_{01}$ marked were identified by Sawyer (1926); one of them is partially obscured by the longer wavelength member of the diffuse pair at 2070 and 2087 Å, but is clearly distinguishable on the original plate. The latter pair was also observed by Sawyer, who classified the lines as 4s4p $^3P^0_{12}$–4p$^{2\,1}D_2$ on account of their diffuseness; at that time, the auto-ionization process was unrecognized. Sawyer's classification is reproduced by Moore (1952); however, Sawyer recognized that the two diffuse lines fall in the places expected for the missing p$^{2\,3}P_2$ combinations, and a tentative classification of this sort was actually put forward by Selwyn (1929). Moreover, consideration of two- and three-electron spectra in general makes it apparent that the p$^{2\,1}D_2$ term is more likely to be found much deeper, mixed with the 4s*n*d $^1D_2$ series. In such case we expect to find the series terms considerably perturbed (Shenstone and Russell 1932), and in fact, a well-known anomaly occurring in most two-electron spectra, viz. that the ^1D terms lie deeper than the ^3D, has been explained by Bacher (1933) as a perturbation by p$^{2\,1}D$. Bacher assumed the perturbing term to lie above the series limit, but it is more probable that in these spectra the p$^{2\,1}D$ term has become fused with the lower terms of the series spectrum. As regards checks from iso-electronic spectra, positions for p$^{2\,1}D$ have been given by Lang (1929) and Rao (1931) for Ge III and As IV respectively, and if the assignments are correct they certainly point to a very deep position in Zn I.

On the whole, it seems established that the diffuse pair named completes the PP′ multiplet in Zn I, and the curious behaviour of the p$^{2\,1}D$ term in this and analogous spectra presents an interesting problem in theoretical interpretation.

(*b*) Cd I. The four sharp lines 5s5p $^3P^0_{012}$–5p$^{2\,3}P_{01}$ were found by Ruark (1925); he reported that a careful search did not reveal the missing line-pair. The four lines were later obtained in absorption in electrically excited Cd vapour by Foote *et al.* (1925), who suggested that absence of the p$^{2\,3}P_2$ combinations might be due to coincidence of the $J=1$ and 2 levels. Actually the expectation is that the p^2 ($^3P_2$–$^3P_1$) interval should approximate to sp ($^3P_2$–$^3P_1$), which leads us to seek a pair of diffuse lines near 2208 and 2267 Å. It is worth noting that the character of the p$^{2\,3}P$ levels was unmistakably ascertained by observation of the Zeeman pattern of the line 2306 Å 5s5p $^3P^0_1$–5p$^{2\,3}P_0$ (Paschen 1911).

Figure 1 (*b*) shows a portion of the spectrum of a Cd arc in air, obtained with the medium-quartz spectrograph. Ruark's four lines, which again fall close to the heavily reversed singlet resonance line, are marked. A notable feature is the very wide diffuse patch centred near 2212 Å, observed by one of us (Garton 1951) in a Cd arc, and, at the time, assumed identical with an absorption band of Cd_2 which occurs, as far as can be judged, at the same place. A similar feature was earlier found by Robertson (1932) in emission from a damped electrodeless ring discharge in Cd vapour, and likewise was taken to be the Cd_2 band. Cram (1934), in the most recent studies of the molecular bands of Cd_2, found that the 2212 Å feature was not produced in fluorescence or in Tesla excitation, and disposed of 'Robertson's band' as "probably due to an impurity".† The supposed observation of the 2212 Å band of Cd_2 in emission from an arc seemed to affect Cram's discussion of the relative dispositions of the potential-energy curves of the Cd_2 electronic states involved. The question now arises whether the feature observed by Robertson and by Garton is actually the line $sp\,{}^3P_1^0$–$p^2\,{}^3P_2$, which accidentally almost coincides with the Cd_2 absorption band. In this event, a companion line $sp\,{}^3P_2^0$–$p^2\,{}^3P_2$ should exist in the 2270 Å region. In the Cd arc in air, this region is obscured by the strong wing of the 2288 Å line; however, careful examination of the plates suggested the presence of a local darkening around 2270 Å. Now the extended wings of resonance lines in such cases are commonly ascribed to quasi-molecule formation (Herzberg 1950); reduction of vapour-density thus reduces the extent of the wings. At the same time, if lines having strongly auto-ionizing upper states in fact lie at 2212 and 2270 Å, their intensities are presumably assisted by higher ion densities, which promote inverse auto-ionization. Operation of an arc at reduced pressure can, therefore, be expected to diminish the wings of 2288 Å and lower the intensity of the suspected intrinsically broad lines. In the hope that the first of these effects would predominate, arcs were operated in helium and in argon at pressures from a few cm Hg upward. The hope was realized and, as can be seen from figure 1 (*c*), the line 2288 Å is now unreversed, its wings are no longer obtrusive, and the diffuse 2270 Å companion of 2212 Å is plainly distinguishable. There now seems little doubt that these two very wide features form the missing part of the PP′ multiplet.

Intensity Profiles and Auto-ionization Probability

If the suppositions of the preceding paragraph are correct, then the 2212 and 2270 Å features should possess profiles of the natural-broadening type, where the intensity at frequency ν is given by

$$I(\nu)=\frac{\text{const.}}{(\nu-\nu_0)^2+(\tfrac{1}{2}\Delta\nu)^2} \qquad \ldots\ldots(1)$$

with $\Delta\nu$ = half-breadth of the line centred at frequency ν_0
= (the auto-ionization probability)/2π.

A measurement of the intensity distribution will thus check whether the broad features are of the correct shape, and yield the auto-ionization probability of the $p^2\,{}^3P_2$ level.

Accordingly, intensity measurements were made over the region 2150–2350 Å, by the process of photographic photometry outlined in § 2, and the results are displayed in figures 2 and 3. In figure 2 the full line shows the course of the total relative intensity after allowance has been made for general background, consisting of continuum and stray light. This reduction isolates the 2212 Å feature fairly well, and in figure 3 the full line shows the experimental profile, and the broken curve represents equation (1), based on the measured half-breadth. The agreement is good enough to support the view that the 2212 Å feature is indeed a naturally broadened line. The most pronounced deviation lies towards shorter wavelengths, and may be at least partly due to the effects mentioned at the end of the next paragraph. The measured half-breadth is $\Delta\nu = 176{\cdot}1\ \mathrm{cm}^{-1} = 5{\cdot}28 \times 10^{12}\ \mathrm{sec}^{-1}$ which gives an auto-ionization probability of $3{\cdot}32 \times 10^{13}\ \mathrm{sec}^{-1}$.

---

† For an extensive general account of the details and interpretation of the supposed van der Waals type bands of Cd_2 etc. see Finkelnburg (1938).

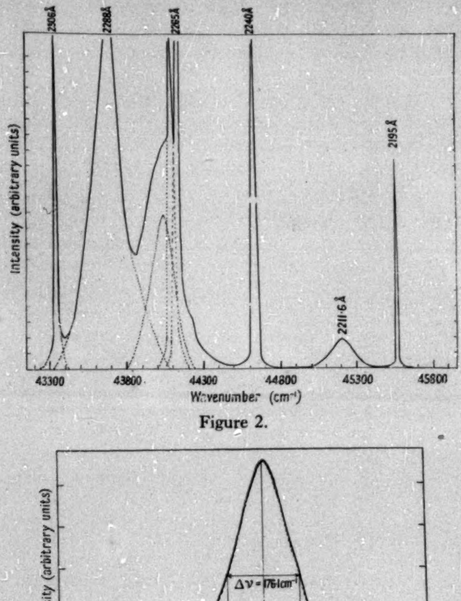

Figure 2.

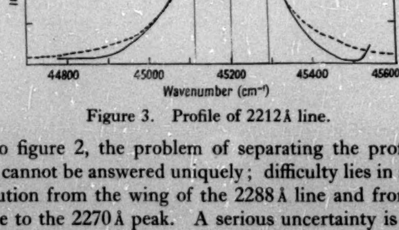

Figure 3. Profile of 2212 Å line.

Returning to figure 2, the problem of separating the profile of the 2270 Å companion line cannot be answered uniquely; difficulty lies in allowing properly for the contribution from the wing of the 2288 Å line and from the two strong sharp lines close to the 2270 Å peak. A serious uncertainty is presented by the fact that the 2288 Å reversal is undoubtedly asymmetrical; if this source of error is neglected, to first approximation, then the complete curve breaks down fairly naturally as indicated by the dotted lines in figure 2, when the half-breadth of the 2270 Å contribution is made as nearly as seems possible equal to that found for the 2212 Å line. However, this breakdown can be regarded as little more than illustrative. It may be noted that the total-intensity ratio of the 2270 to the 2212 Å line should lie between 3 : 1 for *LS* and 1 : 2 for *jj* coupling. From the curves of figure 2 the ratio appears more like 5 : 1; however, considerable uncertainty exists regarding spectrograph transmission, plate sensitivity and absorption by the air over the long light-path used, all of which vary rapidly with wavelength in this spectral region.

(*c*) HgI. The usual four sharp lines of the PP′ multiplet were identified in HgI by Sawyer (1926), as follows :

λ_{vac} (Å)	ν_{vac} (cm^{-1})	Classification
2002·7	49933	$6\,^3P^0_2$–$6p^2\,^3P_1$
1900·1	52629	$^3P^0_1$–$^3P_0$
1832·6	54567	$^3P^0_1$–$^3P_1$
1774·9	56341	$^3P^0_0$–$^3P_1$

$$\text{giving}\quad \begin{matrix} 6p^2\,^3P_0 = 92039 \\ ^3P_1 = 93977 \end{matrix}\quad \text{cm}^{-1}\ \text{above}\ 6s^2\,^1S_0.$$

There is little room to doubt three of these assignments; the line 1900·1 Å, however, which provides, of course, the sole basis for fixing $p^2\,^3P_0$, has a rather unnatural position in the multiplet.

Spectra have been photographed on the vacuum spectrograph, with 5–9 amp arcs in mercury vapour, arranged so that the arc column, constricted within a tube of a few millimetres diameter, was presented end-on to the slit. Three of the above four lines were found strongly developed, but no trace of a line was found near 1900·1 Å. It is noteworthy that Selwyn (1929) mentions no line at this wavelength. Selwyn's line at 1972·94 Å, not mentioned by Sawyer, is present on our plates in about the same intensity as 1832·6 Å, and has a much more natural position for the $^3P^0_1$–$^3P_0$ combination. Possibly some confusion may have arisen in the past from the existence of an HgII line at 1973·89 Å. We have distinguished the two lines near 1973 Å by the following observation. On first striking the Hg arc in helium as carrier gas, the spectrum shows strong HgII lines including 1973·89 Å; after the arc has warmed up the spark spectrum weakens and the latter line vanishes but is replaced by 1972·94 Å. As regards Sawyer's 1900 Å line, it is noticeable that a *raie ultime* of sulphur occurs at 1900·27 Å. From these considerations it is suggested that the second line of Sawyer's list should read :

$$1972{\cdot}94\ \text{Å}\qquad 50686\ \text{cm}^{-1}\qquad 6\,^3P^0_1\text{–}6p^2\,^3P_0.$$

$$\text{giving}\qquad 6p^2\,^3P_0 = 90096\ \text{cm}^{-1}\ \text{above}\ 6s^2\,^1S_0.$$

If we now assume that the overall splitting of $p^2\,^3P$ is of the same order as that of sp ^3P, we expect $6p^2\,^3P_2$ to lie about 96500 cm^{-1}, and to produce two very diffuse lines centred about 1750 Å and 1905 Å. The pictures obtained with the constricted mercury arc do suggest presence of a diffuse local darkening in the 1760 Å region, but the 1900 Å region is more affected by background and the wing of the 1849 Å reversal so that decision is not possible regarding the longer wavelength component. For these reasons further work is being done on Hg. The radiative transition probabilities of the $p^2\,^3P_2$ combinations are obviously quite high in Zn and Cd, and therefore presumably in Hg also, so that there seems a reasonable hope that the diffuse Hg lines sought may be obtainable in absorption by electrically excited vapour. Experiments in this direction are in hand.

ACKNOWLEDGMENTS

The thanks of the authors are due to Professor C. W. Allen for granting use of the recording microphotometer at the University of London Observatory, and to Mr. E. W. Foster, of the Observatory, for assistance in obtaining the traces.

REFERENCES

BACHER, R. F., 1933, *Phys. Rev.*, **43,** 264.

CONDON, E. U., and SHORTLEY, G. H., 1935, *Theory of Atomic Spectra* (Cambridge: University Press), Ch. 15.

CRAM, S. W., 1934, *Phys. Rev.*, **46,** 205.

FINKELNBURG, W., 1938, *Kontinuierliche Spektren* (Berlin: Springer).

FOOTE, P. D., TAKAMINE, T., and CHENAULT, R. L., 1925, *Phys. Rev.*, **26,** 165.

GARTON, W. R. S., 1951, *Proc. Phys. Soc.* A, **64,** 430.

HERZBERG, G. H., 1950, *The Spectra of Diatomic Molecules* (New York: van Nostrand), Ch. 7.

LANG, R. J., 1929, *Phys. Rev.*, **34,** 697.

MAJORANA, E., 1931, *Nuovo Cim.*, **8,** 107.

MOORE, C. E., 1952, *Atomic Energy Levels*, Vol. 2 (U.S. Nat. Bur. Stand. Circ. No. 467).

PASCHEN, F., 1911, *Ann. Phys., Lpz.*, **35,** 867.

RAO, K. R., 1931, *Nature, Lond.*, **123,** 244.

ROBERTSON, J. K., 1932, *Phil. Mag.*, **14,** 795.

RUARK, A. E., 1925, *J. Opt. Soc. Amer.*, **11,** 199.

SAWYER, R. A., 1926, *J. Opt. Soc. Amer.*, **13,** 431.

SELWYN, E. W. H., 1929, *Proc. Phys. Soc.*, **41,** 392.

SHENSTONE, A. G., 1931, *Phys. Rev.*, **38,** 873.

SHENSTONE, A. G., and RUSSELL, H. N., 1932, *Phys. Rev.*, **39,** 415.

The Scattering of Low-Frequency Lattice Waves by Static Imperfections

By P. G. KLEMENS

Division of Physics, Commonwealth Scientific and Industrial Research Organization, Sydney

Communicated by G. H. Briggs; MS. received 7th December 1954 *and in amended form* 12*th July* 1955

Abstract. The scattering of lattice waves by static imperfections is treated by second-order perturbation theory. The transition matrix is composed of contributions due to the mass difference of lattice points, changes in the elastic constants of linkages between lattice points, and elastic strain. Point imperfections are shown to scatter as the fourth power of frequency, dislocations as the first power, and grain boundaries independently of frequency. The magnitude of the scattering cross section is estimated for a variety of lattice defects in alkali halides, for screw and edge dislocations and for grain boundaries. These results are discussed in relation to thermal conduction by the lattice at low temperatures.

§ 1. INTRODUCTION

THE thermal conductivity of non-metals as well as the lattice component of the thermal conductivity of metals is sensitive at low temperatures to the type and concentration of lattice imperfections (Berman 1953, Olsen and Rosenberg 1953, Kemp, Klemens, Sreedhar and White 1954). The temperature dependence of the thermal resistance arising from these imperfections is governed by the frequency dependence of their scattering cross section for lattice waves (Klemens 1951), so that a study of the thermal conductivity gives information about the nature of the principal imperfections. To interpret such measurements it is necessary to know the frequency dependence of the cross sections of various model imperfections; if estimates of concentration are desired the absolute values of these cross sections must also be known. It is the purpose of this paper to discuss the quantum-mechanical theory of the elastic scattering of lattice waves by static imperfections, and to apply it to substitutional impurities, vacancies, dislocations and grain boundaries. To facilitate the calculations, the lattice is taken as simple cubic or, where the discreteness of the lattice is unimportant, the solid is treated as an isotropic elastic medium. Trigonometric ratios will be consistently replaced by root mean square values. Only waves of lowest frequency will be considered, so that dispersion can be disregarded.

The scattering probability may be calculated from the terms in the expression for the perturbation energy which are quadratic in the displacement of the lattice waves. An imperfection contributes in three ways to the perturbation energy by producing an alteration in (*a*) the kinetic energy due to a mass difference, (*b*) the potential energy due to a change in the elastic constant of some linkages, and (*c*) the potential energy due to an elastic strain field which alters the elastic constants of the linkages as a result of deviations from Hooke's law. It is the last-named effect which has been discussed by Peierls (1929) and Klemens (1951) in relation to the intrinsic thermal resistance of non-metallic solids.

§ 2. INTERACTIONS DUE TO STATIC IMPERFECTIONS

The energy of the lattice vibrations of a perfect crystal can be expressed (Peierls 1929) as

$$E=\tfrac{1}{2}M\sum_{\mathbf{k}}\omega_{\mathbf{k}}^2(a_{\mathbf{k}}a_{-\mathbf{k}}+a_{-\mathbf{k}}a_{\mathbf{k}}) \qquad \ldots\ldots(1)$$

where M is the mass of each atom† and the sum is taken over all normal modes. The displacement of an atom at the lattice-site $\mathbf{x}$ is given by

$$\mathbf{u}(\mathbf{x})=\frac{1}{G^{1/2}}\sum_{\mathbf{k}}b_{\mathbf{k}}\boldsymbol{\epsilon}_{\mathbf{k}}\exp\{i(\mathbf{k}\,.\,\mathbf{x}+\omega t)\} \qquad \ldots\ldots(2)$$

G being the number of atoms in the crystal, $\boldsymbol{\epsilon}$ the polarization vector, $\mathbf{k}$ the wave vector, ω the frequency and b the amplitude. The amplitudes in (1) and (2) are related by

$$a_{\mathbf{k}}=b_{\mathbf{k}}\,e^{i\omega t}. \qquad \ldots\ldots(3)$$

Since the displacements must be real, $a_{-\mathbf{k}}$ and $b_{-\mathbf{k}}$ are the complex conjugates (or adjoints) of $a_{\mathbf{k}}$ and $b_{\mathbf{k}}$ respectively, and $\omega_{\mathbf{k}}=-\omega_{-\mathbf{k}}$. The normal modes obey harmonic oscillator equations, so that the a's are represented quantum-mechanically by matrices whose non-vanishing elements are

$$(a_{\mathbf{k}})_{N,\,N-1}=\left(\frac{\hbar}{M\omega}N\right)^{1/2} \qquad \ldots\ldots(4a)$$

$$(a_{\mathbf{k}}^*)_{N,\,N+1}=(a_{-\mathbf{k}})_{N',\,N'-1}=\left(\frac{\hbar}{M\omega}(N+1)\right)^{1/2} \qquad \ldots\ldots(4b)$$

$$N'=-(N+1) \qquad \ldots\ldots(4c)$$

Thus

$$E=\sum_{\mathbf{k}}\hbar\omega\,(N+\tfrac{1}{2}) \qquad \ldots\ldots(5)$$

so that the excitation of a normal mode is equivalent to N phonons, each of energy $\hbar\omega$. The state of the crystal is specified by enumerating the number of phonons of each mode.

The above theory is applicable only to a crystal which is perfectly periodic and whose interatomic linkages are perfectly harmonic. In real crystals this is not so and energy can be interchanged between the lattice waves, which are no longer true normal modes. Thus the state of the crystal can alter. If E_{ij}' is the perturbation energy matrix, i and j being two states of the crystal, then the rate of change of W_i, the occupation probability of the ith state, is given by

$$t\frac{dW_i}{dt}=\sum_j(W_j-W_i)2E_{ij}'^2\,\frac{1-\cos(E_i-E_j)t/\hbar}{(E_i-E_j)^2} \qquad \ldots\ldots(6)$$

where E_i is the energy of the state i.

Elastic scattering of lattice waves is described by those terms of the perturbation energy matrix which are of the form

$$E'=\sum_{\mathbf{k},\,\mathbf{k}'}c_{\mathbf{k},\,\mathbf{k}'}\,a_{-\mathbf{k}'}\,a_{\mathbf{k}},\quad c_{\mathbf{k},\,\mathbf{k}'}=c^*_{\mathbf{k}',\,\mathbf{k}} \qquad \ldots\ldots(7)$$

---

† In polyatomic crystals M is the mass of each unit cell. This assumption that the lattice is monatomic does not lead to errors at low frequency.

each term representing the annihilation of a phonon **k** and the creation of a phonon **k**′, that is scattering of a phonon from a state **k** to **k**′. The resonance factor in (6) ensures conservation of energy, so that real transitions occur only if $\omega=\omega'$.

One can rewrite (6) in terms of the average values of N, that is in terms of $N=\Sigma_i W_i (N)_i$, namely

$$t\frac{dN}{dt}=\sum_{\mathbf{k}'} 2c_{\mathbf{k},\mathbf{k}'}^2 \frac{\hbar^2}{M^2\omega\omega'}\,\frac{1-\cos(\omega-\omega')t}{\hbar^2(\omega-\omega')^2}\,[(N+1)N'-N(N'+1)]. \quad \ldots\ldots(8)$$

If $N=N^0+n$, where N^0 is the equilibrium value of N, and n the deviation from equilibrium,

$$(N+1)N'-N(N'+1)=N'-N=n'-n \quad \ldots\ldots(9)$$

for real transitions, for which $N^0=N^{0\prime}$. Replacing the summation over **k**′ by an integration, one finds a relaxation time

$$\frac{1}{\tau}=-\frac{1}{n}\frac{dN}{dt}$$

$$=a^3G\int dS'\, 2c_{\mathbf{k},\mathbf{k}'}^2 \frac{1}{M^2\omega^2}\,\frac{\pi}{(2\pi)^3}\,\frac{dk'}{d\omega'}\left[1-\frac{n'}{n}\right] \quad \ldots\ldots(10)$$

where the integration is over the three surfaces $\omega'=\omega$ in **k**′-space, corresponding to the three modes of polarization of **k**′. The lattice parameter is a, and the volume of the crystal Ga^3.

If the material is isotropic, and if μ is the direction cosine of **k** relative to the temperature gradient,

$$n'/n=\mu'/\mu. \quad \ldots\ldots(11)$$

If the imperfection is spherically symmetrical, or if it is orientated at random, then the average value of μ'/μ is $\bar{\mu}$, the average of the cosine of the scattering angle.

§ 3. SCATTERING BY A SUBSTITUTIONAL ATOM OF DIFFERENT MASS

The perturbation energy arising from a substitutional impurity atom of mass $M+\Delta M$, otherwise identical with the normal atoms, and situated at **x**, is

$$E'=\tfrac{1}{2}\Delta M\left(\frac{du}{dt}\right)^2$$

$$=\frac{\Delta M}{2G}\sum_{\mathbf{k},\mathbf{k}'}(-1)\,b_{\mathbf{k}}b_{\mathbf{k}'}\,\omega\omega'\,(\boldsymbol{\epsilon}\cdot\boldsymbol{\epsilon}')\exp\{i(\mathbf{k}+\mathbf{k}')\cdot\mathbf{x}+i(\omega+\omega')t\}. \quad \ldots\ldots(12)$$

In this double sum there are terms $\mathbf{k}=-\mathbf{k}'$, whose sum is

$$\frac{\Delta M}{2G}\sum_{\mathbf{k}}\omega^2(b_{-\mathbf{k}}b_{\mathbf{k}}+b_{\mathbf{k}}b_{-\mathbf{k}})=\frac{\Delta M}{2G}\sum_{\mathbf{k}}\omega^2(a_{-\mathbf{k}}a_{\mathbf{k}}+a_{\mathbf{k}}a_{-\mathbf{k}}). \quad \ldots\ldots(13)$$

In the matrix representation these terms are diagonal, and denote the change in the expectation value of the vibrational energy of the crystal. From (1) and (13) this is simply

$$\Delta E=\frac{\Delta M}{GM}E. \quad \ldots\ldots(14)$$

In addition there are non-diagonal terms, which can be written as

$$-\frac{\Delta M}{2G}\sum_{\mathbf{k},\mathbf{k}'}a_{\mathbf{k}}a_{-\mathbf{k}'}\,\omega\omega'\,(\boldsymbol{\epsilon}\cdot\boldsymbol{\epsilon}')\exp\{i\mathbf{x}\cdot(\mathbf{k}-\mathbf{k}')\} \quad \ldots\ldots(15)$$

which is in the form of (7).

In the case of an isolated impurity, one can disregard the factor $\exp\{i\mathbf{x} \,.\, (\mathbf{k}-\mathbf{k}')\}$, because it does not affect the value of $c_{\mathbf{k},\mathbf{k}'}{}^2$. In the case of a group of impurities of definite arrangement, one must sum over the appropriate values of $\mathbf{x}$, leading to a restriction on the admissible values of $\mathbf{k}'$. Thus in the case of an infinite row of impurity atoms in the direction of the z-axis, $c_{\mathbf{k},\mathbf{k}'}$ vanishes unless $k_z = k_z'$.

For an isolated impurity atom, then

$$c_{\mathbf{k},\mathbf{k}'}{}^2 = \left(\frac{\Delta M}{2G}\right)^2 \omega^2 \omega'^2 (\boldsymbol{\epsilon} \,.\, \boldsymbol{\epsilon}')^2. \qquad \ldots\ldots(16)$$

In the average $(\boldsymbol{\epsilon} \,.\, \boldsymbol{\epsilon}')^2 = \frac{1}{3}$, $\mu/\mu' = 0$, and from (10)

$$\frac{1}{\tau} = \frac{a^3}{G}\left(\frac{\Delta M}{M}\right)^2 \frac{\omega^4}{4\pi v^3} \qquad \ldots\ldots(17)$$

where $v = \omega/k$ is the velocity of the waves. This is similar to an expression given without derivation by Pomeranchuk (1942), but exceeds his value by a numerical factor of order 10.

§ 4. SCATTERING BY AN ATOM OF DIFFERENT BINDING FORCE

If a foreign atom is bound to its neighbours by binding forces of different elastic properties from those of normal linkages, the resulting disturbance scatters phonons.

The contribution of the normal linkages to the unperturbed Hamiltonian is

$$E_p = \tfrac{1}{2} M \sum_{\mathbf{x}} \sum_{\mathbf{l}} \left\{ \left(\frac{v_{\mathrm{I}}}{a}\right)^2 [\mathbf{l} \,.\, (\mathbf{u}_{\mathbf{x}} - \mathbf{u}_{\mathbf{x}-\mathbf{l}})]^2 + \left(\frac{v_{\mathrm{II}}}{a}\right)^2 [\mathbf{l} \times (\mathbf{u}_{\mathbf{x}} - \mathbf{u}_{\mathbf{x}-\mathbf{l}})]^2 \right\} \qquad \ldots\ldots(18)$$

where v_{I} and v_{II} are the velocities of longitudinal and transverse waves respectively of long wavelength in the principal directions, $\mathbf{l}$ is a unit vector† in the direction of a linkage, and the sum is over all linkages, that is half the sum over all lattice points $\mathbf{x}$ and over all linkages $\mathbf{l}$ emanating from each lattice site. The first term in (18) is due to relative displacements parallel to the linkage, the second term due to relative displacements in the normal plane.

The interatomic forces between a foreign atom and its neighbours will differ from the normal forces; let the corresponding changes in the elastic constants be described by changes δv_{I} and δv_{II} in the v's. The perturbation Hamiltonian is then

$$E' = \tfrac{1}{2} M \sum_{\mathbf{l}} \left\{ \frac{2 v_{\mathrm{I}} \delta v_{\mathrm{I}}}{a^2} [\mathbf{l} \,.\, (\mathbf{u}_{\mathbf{x}} - \mathbf{u}_{\mathbf{x}-\mathbf{l}})]^2 + \frac{2 v_{\mathrm{II}} \delta v_{\mathrm{II}}}{a^2} [\mathbf{l} \times (\mathbf{u}_{\mathbf{x}} - \mathbf{u}_{\mathbf{x}-\mathbf{l}})]^2 \right\}. \qquad \ldots\ldots(19)$$

The sum is now over all linkages between the imperfection and its neighbours (six values of $\mathbf{l}$ for a simple cubic lattice).

It is now possible to express E' in the form (7). From (2) and (3)

$$\mathbf{l} \,.\, (\mathbf{u}_{\mathbf{x}} - \mathbf{u}_{\mathbf{x}-\mathbf{l}}) = \frac{1}{G^{1/2}} \sum_{\mathbf{k}} a_{\mathbf{k}} (\boldsymbol{\epsilon} \,.\, \mathbf{l}) \exp(i\mathbf{k} \,.\, \mathbf{x}) [1 - \exp(i\mathbf{k} \,.\, \mathbf{l}a)] \qquad \ldots\ldots(20)$$

$$\mathbf{l} \times (\mathbf{u}_{\mathbf{x}} - \mathbf{u}_{\mathbf{x}-\mathbf{l}}) = \frac{1}{G^{1/2}} \sum_{\mathbf{k}} a_{\mathbf{k}} [\mathbf{l} \times \boldsymbol{\epsilon}] \exp(i\mathbf{k} \,.\, \mathbf{x}) [1 - \exp(i\mathbf{k} \,.\, \mathbf{l}a)]. \qquad \ldots\ldots(21)$$

---

† But in the suffixes $\mathbf{l}$ denotes the displacement from an atom to its neighbour along the linkage.

The factor $\exp(i\mathbf{k} \,.\, \mathbf{x})$ will be omitted, as in § 3, since it merely introduces a phase-factor into the matrix element. In the case of long waves,

$$\exp(i\mathbf{k} \,.\, \mathbf{l}a) - 1 \simeq i(\mathbf{k} \,.\, \mathbf{l})a,$$

so that, after substituting (20) and (21) into (19), one has to evaluate expressions of the type

$$\sum_{T} (\mathbf{k} \,.\, \mathbf{l})(\boldsymbol{\epsilon} \,.\, \mathbf{l})(\mathbf{k}' \,.\, \mathbf{l})(\boldsymbol{\epsilon}' \,.\, \mathbf{l})\,[1 + \exp\{i(\mathbf{k} - \mathbf{k}') \,.\, \mathbf{l}a\}] \quad \ldots\ldots(22\,a)$$

$$\sum_{T} (\mathbf{k} \,.\, \mathbf{l})(\mathbf{k}' \,.\, \mathbf{l})\,[(\mathbf{l} \times \boldsymbol{\epsilon}) \,.\, (\mathbf{l} \times \boldsymbol{\epsilon}')]\,[1 + \exp\{i(\mathbf{k} - \mathbf{k}') \,.\, \mathbf{l}a\}]. \quad \ldots(22\,b)$$

The resulting expressions are in general quite complicated, but for the purpose of deriving the frequency dependence and the approximate magnitude of the relaxation time, the following simplifications seem permissible and will be made.

Expression (22 *a*) contains a product of four trigonometric ratios, depending on the relative orientations of **l**, **k**, **k**′ and the polarizations. In principle one should evaluate (22 *a*), square and then sum over all modes **k**′. Since in practice one requires, not the relaxation time of a wave **k**, but an average relaxation time over all modes of wave number **k**, one should then average over all directions of **k**, and all polarizations. This suggests the following approximation: the square of the matrix element is to be averaged for all interacting waves **k** and **k**′ of wave number *k*; treating the directions of **k**, **k**′, $\boldsymbol{\epsilon}$ and $\boldsymbol{\epsilon}'$ as uncorrelated, every trigonometric ratio will be replaced by its root mean square value $(1/3)^{1/2}$. As a further simplification the distinction between different polarizations will be disregarded†. For long waves one can approximate

$$1 + \exp\{i(\mathbf{k} - \mathbf{k}') \,.\, \mathbf{l}a\} \simeq 2 \quad \ldots\ldots(23)$$

so that (22 *a*) becomes simply

$$3\left(\tfrac{1}{3}\right)^{4/2} 2kk' = \tfrac{2}{3}kk' \quad \ldots\ldots(24\,a)$$

while (22 *b*), containing in addition the cosine of the angle between $(\mathbf{l} \times \boldsymbol{\epsilon})$ and $(\mathbf{l} \times \boldsymbol{\epsilon}')$, whose root mean square value is $(1/2)^{1/2}$, becomes similarly

$$3\left(\tfrac{1}{3}\right)^{4/2}\left(\tfrac{1}{2}\right)^{1/2} 2kk' = \frac{\sqrt{2}}{3}kk'. \quad \ldots\ldots(24\,b)$$

One thus obtains from (19)

$$c_{\mathbf{k},\mathbf{k}'} = -\frac{M}{3G}\exp\{i(\mathbf{k} - \mathbf{k}') \,.\, \mathbf{x}\}\, kk'\,(2v_{\mathrm{I}}\,\delta v_{\mathrm{I}} + \sqrt{2}v_{\mathrm{II}}\,\delta v_{\mathrm{II}}). \quad \ldots\ldots(25)$$

Substituting into (10) one obtains, on approximating $v = v_{\mathrm{I}} = v_{\mathrm{II}}$,

$$\frac{1}{\tau} = \frac{2}{\pi}\frac{a^3}{G}\left(\frac{\delta v}{v}\right)^2 \frac{1}{v^3}\omega^4 \quad \ldots\ldots(26)$$

for the inverse relaxation time. When squaring (25), the product of the two terms in the bracket is omitted, since phase relationships between them were lost by the present approximation.

§ 5. SCATTERING BY AN ELASTIC STRAIN FIELD

In a perfectly harmonic lattice an elastic strain field has no influence on the lattice vibrations. In real crystals the strain energy depends not only on the quadratic strain terms, but also on terms of higher order, so there is interaction due to a strain field. The cubic terms only will be considered here. These terms give rise to thermal expansion, and also to the three-phonon interactions, which are responsible for the intrinsic thermal resistance (Peierls 1929, Klemens 1951).

---

† This does not introduce a serious error in the thermal conductivity, because three-phonon processes will tend to equalize the effective relaxation times of modes of the same frequency but of different polarizations (Klemens 1951).

It is assumed that the contribution to the Hamiltonian arising from the cubic anharmonicities is of the form

$$E' = -\tfrac{1}{2}M \sum_{\mathbf{x}} \sum_{\mathbf{l}} \left\{ \frac{2\gamma_{\mathrm{I}}}{3a} \left(\frac{v_{\mathrm{I}}}{a} \right)^2 [\mathbf{l} \cdot (\mathbf{u}_{\mathbf{x}} - \mathbf{u}_{\mathbf{x}-\mathbf{l}})]^3 + \frac{2\gamma_{\mathrm{II}}}{a} \left(\frac{v_{\mathrm{II}}}{a} \right)^2 [\mathbf{l} \times (\mathbf{u}_{\mathbf{x}} - \mathbf{u}_{\mathbf{x}-\mathbf{l}})]^2 [\mathbf{l} \cdot (\mathbf{u}_{\mathbf{x}} - \mathbf{u}_{\mathbf{x}-\mathbf{l}})] \right\} \quad \ldots\ldots(27)$$

where the summation is as in (18) and γ_{I}, γ_{II} are two constants specifying the anharmonicities.

Equation (27) disregards interaction between different linkages and does not contain odd power terms in $[\mathbf{l} \times (\mathbf{u}_{\mathbf{x}} - \mathbf{u}_{\mathbf{x}-\mathbf{l}})]$. The latter is justified from symmetry considerations in cubic crystals. Expression (27) is related to the Grüneisen model of thermal expansion: it is easily seen that if $\gamma = \gamma_{\mathrm{I}} = \gamma_{\mathrm{II}}$, all lattice frequencies are changed by a factor $1 - \gamma\Delta$ in the case of a uniform dilatation Δ (positive if the volume is increased). In this case the coefficient of thermal volumetric expansion is

$$d\Delta/dT = \gamma S/\kappa \quad \ldots\ldots(28)$$

where S is the specific heat per unit volume and κ the compressibility. Bijl and Pullan (1954) generalized (28) for the case when γ_{I} and γ_{II} are not equal. Existing measurements of thermal expansion are usually not sufficiently accurate to warrant this refinement, so that it will be assumed here that

$$\gamma_{\mathrm{I}} = \gamma_{\mathrm{II}} = \gamma = \frac{\kappa}{S} \frac{d\Delta}{dT}. \quad \ldots\ldots(29)$$

Let the strain field be specified by displacement vectors $\mathbf{v}(\mathbf{x})$. For simplicity consider a simple cubic crystal and choose the coordinates to coincide with the crystal axes. Then

$$\frac{1}{a} \mathbf{l}_i \cdot (\mathbf{u}_{\mathbf{x}} - \mathbf{u}_{\mathbf{x}-\mathbf{l}}) = \frac{dv_i}{dx_i} \quad \ldots\ldots(30)$$

$$\frac{1}{a} \mathbf{l}_i \times (\mathbf{u}_{\mathbf{x}} - \mathbf{u}_{\mathbf{x}-\mathbf{l}}) = e_{ijk} \frac{dv_j}{dx_i} \mathbf{l}_k \quad \ldots\ldots(31)$$

where $\mathbf{l}_i$ is a unit vector in the direction of one of the crystal axes and where e_{ijk} is the permutor. One thus obtains for (27)

$$E' = \frac{M\gamma}{Ga^3} \sum_{\mathbf{k}, \mathbf{k}', \mathbf{l},} \int d\mathbf{x} \left\{ v_{\mathrm{I}}^2 \frac{dv_i}{dx_i} (\boldsymbol{\epsilon} \cdot \mathbf{l})(\boldsymbol{\epsilon}' \cdot \mathbf{l})(\mathbf{k} \cdot \mathbf{l})(\mathbf{k}' \cdot \mathbf{l}) + v_{\mathrm{II}}^2 \frac{dv_i}{dx_i} ([\mathbf{l} \times \boldsymbol{\epsilon}] \cdot [\mathbf{l} \times \boldsymbol{\epsilon}'])(\mathbf{k} \cdot \mathbf{l})(\mathbf{k}' \cdot \mathbf{l}) + 2v_{\mathrm{II}}^2 e_{ijk} \frac{dv_j}{dx_i} (\mathbf{l}_k \cdot [\mathbf{l} \times \boldsymbol{\epsilon}])(\mathbf{l} \cdot \boldsymbol{\epsilon}')(\mathbf{k} \cdot \mathbf{l})(\mathbf{k}' \cdot \mathbf{l}) \right\} \exp\{i(\mathbf{k} - \mathbf{k}') \cdot \mathbf{x}\} \quad \ldots(32)$$

If all trigonometric ratios are again replaced by their root mean square values, (32) can be simplified. Let

$$\Delta(\mathbf{x}) = \sum_i \frac{dv_i}{dx_i} \quad \ldots\ldots(33)$$

be the dilatation, and

$$\Pi_k = \mathbf{l}_k e_{ijk} \frac{dv_j}{dx_i} \qquad \ldots\ldots(34)$$

be a component of rotation, and define their inversions

$$D(\mathbf{q}) = \int \Delta(\mathbf{x}) \exp(i\mathbf{q} \cdot \mathbf{x})\, d\mathbf{x} \qquad \ldots\ldots(33\,a)$$

$$P_i(\mathbf{q}) = \int \Pi_i(\mathbf{x}) \exp(i\mathbf{q} \cdot \mathbf{x})\, d\mathbf{x} \qquad \ldots\ldots(34\,a)$$

then the approximate expression for (32) becomes

$$E' = \frac{M\gamma}{Ga^3} \sum_{\mathbf{k},\mathbf{k}'} \left\{ D(\mathbf{k}-\mathbf{k}') \left(\frac{v_{\mathrm{I}}^2}{9} + \frac{v_{\mathrm{II}}^2}{9\sqrt{2}} \right) + 2 \sum_i P_i(\mathbf{k}-\mathbf{k}') \frac{v_{\mathrm{II}}^2}{3\sqrt{6}} \right\} kk' a_{\mathbf{k}} a_{-\mathbf{k}'}. \qquad \ldots\ldots(35)$$

In the approximations made to derive (35), the relative signs of D and the P_i's were disregarded, because the terms in (35) are root mean square values. Hence to obtain $c_{\mathbf{k},\mathbf{k}'}{}^2$ each term in (35) must be squared separately, rather than the sum being squared, as should be done if (35) were an exact expression.

§ 6. SCATTERING BY THE ELASTIC FIELD AROUND A POINT IMPERFECTION

The displacement field $\mathbf{v}(\mathbf{x})$ is governed by the equation

$$\nabla^2 \mathbf{v} = 0. \qquad \ldots\ldots(36)$$

The field about a point imperfection is spherically symmetrical, all displacements being in the radial direction. The solution of (36) is thus

$$v_r = ar + br^{-2}. \qquad \ldots\ldots(37)$$

The first term corresponds to a uniform dilatation, whose Fourier inversion (33 a) vanishes except for $q=0$, so that it does not contribute to the scattering and can be disregarded. The dilatation is given by

$$\Delta = \frac{dv}{dr} + \frac{2v}{r} \qquad \ldots\ldots(38)$$

which vanishes for $v = br^{-2}$. Similarly each component of the rotation vanishes. Hence the elastic field about a point imperfection would not scatter lattice waves if treated according to the continuum theory and if the physically unreal singularity at the origin were excluded.

However, the continuum theory is not applicable in the immediate vicinity of the imperfection, so that changes in the elastic constants of individual linkages must be obtained from (27), and the perturbation matrix obtained from (25).

The linkages in the immediate vicinity of a point imperfection A (see figure 1)

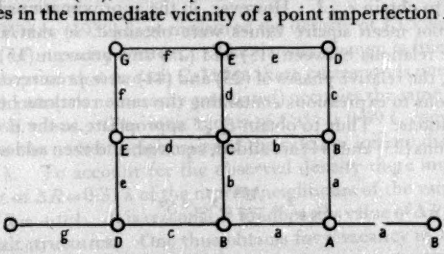

Figure 1. The linkages about an imperfection at A.

can be classified as follows : There are six nearest linkages a from A to sites B. There are six links of type c and 24 of type b. It follows from the elastic theory that the scattering contribution from any three mutually perpendicular linkages emanating from one point add up approximately to zero. Thus a link c cancels two links b, but 12 links of type b are not cancelled ; also links a are strained in the opposite sense of links c and thus in the same sense as links b. Similarly a g-link cancels two e-links, a d-link two f-links, etc., but there are residual links which cannot be thus grouped, namely links adjoining and perpendicular to the three planes formed by the six nearest links. The number of these residual links increases as the first power of the distance, but the strain decreases as the cube of the distance. Thus the contribution to the scattering matrix from the strains in such ungrouped linkages is equal to the contribution from the six nearest linkages, multiplied by

$$1+2(1+\tfrac{1}{4}+\tfrac{1}{9}+\ldots)\simeq 4{\cdot}2. \qquad \ldots\ldots(39)$$

For short waves there will be some destructive interference from different links, but for long waves all contributions to the scattering matrix are additive. It is easily seen that all strains on the residual linkages are in the same sense.

If the nearest neighbours B, distant R from A, are displaced radially by ΔR, then this corresponds to a change in v^2 which, according to (27), is

$$\frac{\delta(v^2)}{v^2}=-2\gamma\frac{\Delta R}{R} \qquad \ldots\ldots(40)$$

where ΔR is positive, if outward.

Substituting this into (25) and multiplying by the factor (39)

$$c_{\mathbf{k},\mathbf{k}'}=\frac{M}{G}\exp\{i(\mathbf{k}-\mathbf{k}')\,.\,\mathbf{x}\}\,.\,\omega\omega'\gamma\frac{\Delta R}{R}Q\left(\frac{2}{3}\right)^{1/2} \qquad \ldots\ldots(41)$$

where $Q\simeq 4{\cdot}2$ if the nearest linkages have the same anharmonicity as all other links, but $Q\simeq 3{\cdot}2$ if the anharmonicity of the nearest linkages is excluded.

§ 7. SCATTERING BY POINT IMPERFECTIONS

One must now consider the combined effect of the mass difference, the difference in the elastic constants of the nearest linkages, and of the strain field. Each effect is described separately by a matrix, namely (15), (25) and (41). If these were exact expressions, the correct precedure would be to add these together, then square the sum to obtain $c_{\mathbf{k},\mathbf{k}'}{}^2$. However, in the approximations leading to (25) and (41) only root mean square values were obtained, so that all information regarding phase relations between (15) and (25) and between (15) and (41) was lost. However, the relative phases of (25) and (41) were preserved, because they are approximations to expressions containing the same relations between **k**, **k′**, **l** and the polarizations. Thus to obtain $c_{\mathbf{k},\mathbf{k}'}{}^2$ appropriate to the present approximation, expressions (25) and (41) are added, squared, and then added to the square of (15). Thus

$$c_{\mathbf{k},\mathbf{k}'}{}^2=\frac{M^2}{G^2}\omega^2\omega'^2S^2 \qquad \ldots\ldots(42)$$

where

$$S^2=S_1{}^2+(S_2+S_3)^2 \qquad \ldots\ldots(43)$$

and where S_1, S_2 and S_3 are, from (15), (25) and (41),

$$S_1=\frac{\Delta M}{M}\frac{1}{2\sqrt{3}},\ S_2=\frac{\delta(v^2)}{v^2}\frac{1}{\sqrt{6}},\ S_3=-Q\gamma\frac{\Delta R}{R}\sqrt{\frac{2}{3}}. \qquad \text{......(44)}$$

The relaxation time is given by (10), and it follows that

$$\frac{1}{\tau}=\frac{3a^3}{G}S^2\frac{\omega^4}{\pi v^3}. \qquad \text{......(45)}$$

In (44), $\delta(v^2)$ is positive if the elastic constant of the nearest linkages is higher than that of the normal linkages, γ is positive for materials which expand on heating, and ΔR is positive if the nearest neighbours are displaced outwards.

Consider the effect of a *substitutional foreign atom*. The only well-known quantity is ΔM. To estimate ΔR it will be assumed that the interionic distances are the sum of the ionic radii, so that ΔR is the difference between the radii of the foreign and the normal ions. The constant γ is obtained from thermal expansion data (Grüneisen 1926). It is assumed that the nearest linkages have the same anharmonicity as the normal links, so that $Q=4{\cdot}2$. The change in the elastic constants of the nearest linkages can, in some cases, be deduced from elastic data: thus in the case of a K impurity in NaCl the foreign linkages are K–Cl, so that

$$\frac{\delta(v^2)}{v^2}=\frac{\kappa_2-\kappa_1}{\kappa_1} \qquad \text{......(46)}$$

where κ_2 is the compressibility of KCl, κ_1 that of NaCl. However, this method of estimation is not applicable in the case of divalent impurities in alkali halides, because the corresponding ionic compounds have a different crystal structure. In such cases all that is known is that $\delta(v^2)/v^2$ is positive.

For the above case of a K^+ ion in NaCl, $\Delta M/M=+0{\cdot}70$, $\Delta R/R=+0{\cdot}14$, $\delta(v^2)/v^2$ is estimated to be $+1/4$, and $\gamma=1{\cdot}6_5$. The K–Cl bonds are assumed to have the same anharmonicity as the Na–Cl bonds, since both substances have nearly the same value of γ, so that $Q=4{\cdot}2$. Thus $S_1=0{\cdot}20$, $S_2=0{\cdot}11$, $S_3=-0{\cdot}79$, and $S^2=0{\cdot}50$.

In the table the results of similar calculations are given for a number of substitutional impurities in alkali halides. For divalent impurities S_2 is only known to be positive, and the total scattering probability is correspondingly uncertain.

Consider now the case of a *vacancy*. In this case the absence of an atom implies $\Delta M/M=-1$, $\delta(v^2)/v^2=-1$, $Q=3{\cdot}2$. The displacement ΔR is, however, not so certain.

Pick and Weber (1950) have measured the density of KCl with $CaCl_2$ addition as a function of impurity content. The density change is linear and consistent with the assumption that to each Ca^{2+} ion there corresponds one K^+ vacancy, and that each such pair (not necessarily associated) occupies the same volume (to within 10%) as two K^+ ions. The ionic radius of Ca^{2+} is 0·99 Å, compared with 1·33 Å for K^+; thus the nearest neighbours of the calcium ion are displaced inward by $\Delta R=-0{\cdot}34$ Å. To account for the observed density there must be an outward displacement of $\Delta R=0{\cdot}31$ Å of the nearest neighbours of the vacancy, so that for a vacancy $\Delta R/R=+0{\cdot}1$. It is reasonable to adopt this value of $\Delta R/R$ for all vacancies in the rock salt structures. One thus obtains for a vacancy in KCl: $S_1=-0{\cdot}29$, $S_2=-0{\cdot}43$, $S_3=-0{\cdot}42$, and $S^2=0{\cdot}8$.

Scattering by Point Imperfections

	γ	Ω	$\Delta R/R$	$\Delta M/M$	$\delta(v^2)/v^2$	S_1	S_2	S_3	S^2
Impurities									
K^+ in NaCl	$1{\cdot}6_8$	4·2	+0·14	+0·70	$+0{\cdot}2_5$	+0·20	+0·11	−0·79	0·50
Na^+ in KCl	1·6	4·2	−0·12	−0·41	$-0{\cdot}2_0$	−0·12	−0·09	+0·67	0·35
Mg^{2+} in KCl	1·6	4·2	−0·22	−0·37	>0	−0·11	>0	+1·2	>1·5
Ca^{2+} in KCl	1·6	4·2	−0·11	+0·03	>0	+0·01	>0	+0·61	>0·4
Sr^{2+} in KCl	1·6	4·2	−0·06	+1·24	>0	+0·36	>0	+0·33	>0·24
Ba^{2+} in KCl	1·6	4·2	+0·01	+2·51	>0	+0·72	>0	−0·06	~0·5
Na^+ in LiF	2·4	4·2	+0·18	+2·31	+0·35	+0·67	+0·15	−1·50	2·7
Mg^{2+} in LiF	2·4	4·2	$+0{\cdot}02_6$	+2·50	>0	+0·72	>0	−0·22	~0·6
Ca^{2+} in LiF	2·4	4·2	+0·20	+4·8	>0	+1·38	>0	−1·65	<4·6
Br^- in KCl	1·6	4·2	$+0{\cdot}04_4$	$+1{\cdot}2_5$	$+0{\cdot}1_4$	+0·36	+0·06	−0·25	0·12
Vacancies									
K^+ in KCl	1·6	3·2	+0·1	−1	−1	−0·29	−0·43	−0·42	1·8
Cl^- in KCl	1·6	3·2	+0·1	−1	−1	−0·29	−0·43	−0·42	1·8
Li^+ in LiF	2·4	3·2	+0·1	−1	−1	−0·29	−0·43	−0·62	1·2
Na^+ in NaCl	$1{\cdot}6_8$	3·2	+0·1	−1	−1	−0·29	−0·43	−0·42	0·8

§ 8. Scattering by Single Dislocations

Consider a dislocation with its axis in the z direction, and a Burgers vector of magnitude b. If the dislocation is screw, the displacement in the z direction is

$$w=\frac{b\theta}{2\pi} \qquad \ldots\ldots(47)$$

so that

$$\Delta=0,\ \Pi_z=\frac{b}{2\pi r}\cos\theta,\ \Pi_y=\frac{b}{2\pi r}\sin\theta \qquad \ldots\ldots(48)$$

where $x=r\cos\theta$, etc. In the case of an edge dislocation with slip-plane $y=0$, it can be shown (Cottrell 1953) that

$$\Delta=-\frac{b}{2\pi}\,\frac{1-2\nu}{1-\nu}\,\frac{\sin\theta}{r}$$

$$\Pi_z=\frac{b}{2\pi}\,\frac{\cos\theta}{r} \qquad \ldots\ldots(49)$$

where ν is the Poisson ratio.

These expressions do not apply in the immediate vicinity of the dislocation line, where changes in the individual linkages must be considered, as in § 6. In this case, however, owing to the non-vanishing of Π, and of Δ for edge dislocations, and owing to their slow decrease with increasing r, most of the scattering arises from distant regions ($r\sim 1/k$), so that no serious error is incurred by applying the continuous theory also in the vicinity of the dislocation line.

To calculate P and D, the Fourier inversions of $\cos\theta/r$ and $\sin\theta/r$ are required. Thus

$$\iint\frac{\cos\theta}{r}\exp(i\mathbf{q}\,.\,\mathbf{r})\,d\mathbf{r}=\int_0^{2\pi}\int_0^{\infty}\cos\theta\exp\{iqr\cos(\theta-\phi)\}\,dr\,d\theta \qquad \ldots\ldots(50)$$

where $\mathbf{r}=(r\cos\theta,\ r\sin\theta)$, $\mathbf{q}=(q\cos\phi,\ q\sin\phi)$. Integrating first with respect to r, and then with respect to $\alpha=\theta-\phi$, (50) becomes

$$\frac{2\pi\cos\phi}{iq}-\lim_{R\to\infty}\int_0^{2\pi}\exp(iqR\cos\alpha)(1-\tan\alpha)\frac{\cos\phi}{iq}\,d\alpha. \qquad \ldots\ldots(51)$$

Consider the second term in (51). Since $\cos\alpha$ is an even function, and $\tan\alpha$ odd, the term in $\tan\alpha$ vanishes on integration. The other term can be written

$$\frac{\cos\phi}{iq}\,4\lim_{X\to\infty}\int_0^X\cos z\,\frac{dz}{(X^2-z^2)^{1/2}}. \qquad \ldots\ldots(52)$$

Owing to the oscillatory nature of the integrand, and because the denominator behaves as $1/X$ for small z, the only important region of integration is near $z=X$. Writing $\zeta=X-z$

$$\int_0^X\cos z\,\frac{dz}{(X^2-z^2)^{1/2}}=\int_0^X\cos(X-\zeta)\frac{d\zeta}{[\zeta(2X-\zeta)]^{1/2}}\simeq\cos X\int_0^X\frac{d\zeta}{(2X\zeta)^{1/2}}. \qquad \ldots\ldots(53)$$

This integral converges at $\zeta=0$, behaving as $\cos X(2)^{-3/2}(\zeta/X)^{1/2}$. Thus the second term in (51) vanishes, and

$$\iint\frac{\cos\theta}{r}\exp(i\mathbf{q}\,.\,\mathbf{r})\,d\mathbf{r}=\frac{2\pi\cos\phi}{iq} \qquad \ldots\ldots(54\,a)$$

and similarly

$$\iint\frac{\sin\theta}{r}\exp(i\mathbf{q}\,.\,\mathbf{r})\,d\mathbf{r}=\frac{2\pi\sin\phi}{iq}. \qquad \ldots\ldots(54\,b)$$

Consider now the case of a screw dislocation. Substituting (48) into (35), and using (54)

$$c_{\mathbf{k},\mathbf{k}'} = \frac{M\gamma}{Ga^3} kk' \frac{2v_{\mathrm{II}}^2}{3\sqrt{6}} b\,(\sin^2\phi + \cos^2\phi)^{1/2} \frac{1}{q} \int \exp(iq_z z)\, dz \qquad \ldots\ldots(55)$$

where $\mathbf{q} = \mathbf{k} - \mathbf{k}'$. Now

$$\int \exp(iqz)\, dz = a \sum_z \delta_q = aG_3 \delta_q \qquad \ldots\ldots(56)$$

where G_3 is the number of atoms along a line in the z direction in the crystal and $\delta_q = 0$ unless $q = 0$, when $\delta_q = 1$. Thus

$$c_{\mathbf{k},\mathbf{k}'}^2 = \frac{M^2\gamma^2}{G_0^2 a^4} \left(\frac{kk'}{|\mathbf{k} - \mathbf{k}'|} \right)^2 b^2 v_{\mathrm{II}}^2 \frac{2}{27} \qquad \ldots\ldots(57)$$

if $k_3 = k_3'$; otherwise it vanishes. Here $G_0 = G/G_3$. We must substitute (57) into (10); here

$$dS' = \frac{2\pi}{aG_3} dl' \qquad \ldots\ldots(58)$$

where dl' is an element of the intersection of the surface $\omega = \omega'$ and the plane $k_3' = k_3$.

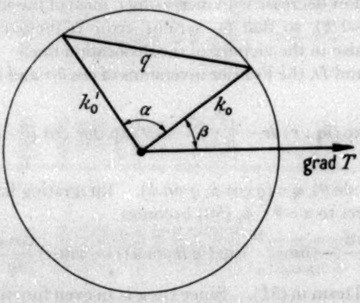

Figure 2. Projection of **k** and **k**′ in a plane perpendicular to the dislocation axis.

In figure 2 the plane $k_3' = k_3$ is shown; thus $dl' = k_0\, d\alpha$, where k_0 is the projection of **k**; $\mu = \cos\beta$, $\mu' = \cos(\alpha + \beta)$, and

$$1 - \mu'/\mu = 1 - \cos\alpha + \sin\alpha \tan\beta. \qquad \ldots\ldots(59a)$$

Also

$$\frac{k_0 k_0'}{|\mathbf{k} - \mathbf{k}'|} = k_0 (2 \sin \tfrac{1}{2}\alpha)^{-1} \qquad \ldots\ldots(59b)$$

and

$$\int dl' \frac{k_0^2 k_0'^2}{|\mathbf{k} - \mathbf{k}'|^2} \left(1 - \frac{\mu'}{\mu} \right) = \pi k_0^3. \qquad \ldots\ldots(60)$$

In figure 2 grad T has been taken to be perpendicular to the dislocation line. In the average $k_0 = (2/3)^{1/2} k$, so that for a dislocation perpendicular to the temperature gradient

$$\frac{1}{\tau} = \frac{1}{G_0} \frac{b^2}{a^2} \gamma^2 \omega \frac{2^{3/2}}{3^{7/2}}. \qquad \ldots\ldots(61)$$

If the dislocation line is in the direction of the temperature gradient, $1/\tau$ vanishes. More generally

$$1-\frac{\mu'}{\mu}=1-\frac{l_1l_1'+l_2l_2'+l_3l_3'}{l_1l_1''+l_2l_2''+l_3l_3''} \qquad \ldots\ldots(62)$$

where l_1, l_2, l_3 are the direction cosines of grad T, l_1' etc. of $\mathbf{k}'$ and l_1'' etc. of $\mathbf{k}$. Now $l_3'=l_3''$, so that $l_3l_3'=l_3l_3''=\cos\gamma$. Thus (62) is

$$1-\frac{\cos(\beta+\alpha)+\cos\gamma}{\cos\beta+\cos\gamma}=\frac{\cos\beta-\cos(\beta+\alpha)}{\cos\beta+\cos\gamma}. \qquad \ldots\ldots(63)$$

In (60) the average of $\{\cos\beta-\cos(\beta+\alpha)\}/\cos\beta$ was obtained; this is now reduced by a factor $\cos\beta/(\cos\beta+\cos\gamma)$. Consider now dislocation lines orientated at random: the average value of $\cos\beta$ is $1/\sqrt{2}$, and of $\cos\gamma$ it is $1/\sqrt{3}$, thus the average value of $\cos\beta/(\cos\beta+\cos\gamma)$ is 0·55, and (61) must be multiplied by this factor to obtain the scattering probability due to randomly orientated screw dislocations.

A similar calculation can be made for edge dislocations. In this case one obtains for a dislocation perpendicular to the temperature gradient

$$\frac{1}{\tau}=\frac{1}{G_0}\frac{b^2}{a^2}\gamma^2\omega\,\frac{2^{3/2}}{3^{7/2}}\left\{\frac{1}{2}+\left(\frac{1-2\nu}{1-\nu}\right)^2\frac{1}{24}\left[1+\sqrt{2}(v_{\mathrm{I}}/v_{\mathrm{II}})^2\right]^2\right\} \qquad \ldots\ldots(64)$$

which must again be multipled by a factor 0·55 in the case of dislocation lines orientated at random.

It is of interest to consider the order of magnitude of the scattering arising from the change in the crystal structure at the core of the dislocation, which has been neglected in the present treatment. To do so consider a line of atoms of mass difference $\Delta M=M$. By arguments similar to those of § 3, and noting that the component of $\mathbf{k}$ parallel to the dislocation line cannot change, it can be shown that

$$\frac{1}{\tau}=\frac{3}{4G_0}\omega k^2a^2\left(\frac{\Delta M}{M}\right)^2 \qquad \ldots\ldots(65)$$

so that the scattering from the dislocation core varies as the cube of the frequency, and becomes comparable with the scattering by the strain field only near the Debye frequency.

Both the frequency dependence and the order of magnitude of (61), (64) and (65) were deduced by Nabarro (1951) from general arguments. The present considerations apply only to sessile dislocations; in the case of mobile dislocations there is additional scattering due to re-radiation.

§ 9. SCATTERING BY GRAIN BOUNDARIES

Grain boundaries can be considered as an array of dislocations lying in the plane of the boundary. The strain field of the grain boundary can be obtained by summing the strain fields due to the individual dislocations. As would be expected, the displacement at large distances is thus found to be a constant rotation relative to a similar region on the other side of the grain boundary. The only case which will be considered here explicitly is the symmetrical boundary consisting of regularly spaced edge dislocations, all in the same sense, whose slip plane is perpendicular to the boundary. More complex boundaries can be treated similarly.

Consider a wall of edge dislocations, lying in the plane $y=0$, parallel to the z axis, the slip plane of each dislocation being $x=nH$, where n is an integer and H the spacing of the dislocations. The strain field of a single dislocation is given by (49)

$$\Delta^{(n)}=-\frac{b}{2\pi}\frac{1-2\nu}{1-\nu}\frac{x-nH}{(x-nH)^2+y^2},\quad \Pi_z^{(n)}=\frac{b}{2\pi}\frac{y}{(x-nH)^2+y^2}\qquad\ldots\ldots(66)$$

and the strain field due to this assembly is

$$\Delta=\sum_{n=-\infty}^{+\infty}\Delta^{(n)},\quad \Pi_z=\sum_{n=-\infty}^{+\infty}\Pi_z^{(n)}.\qquad\ldots\ldots(67)$$

Approximating this summation by an integration, one obtains

$$\Delta=0,\ \Pi_z=\frac{b}{2\pi}\frac{1}{H}\int_{-\infty}^{+\infty}\frac{y}{x^2+y^2}\,dx=\frac{y}{|y|}\frac{b}{2H}.\qquad\ldots\ldots(68)$$

These values are smoothed with respect to their dependence on x; superimposed there is a ripple, periodic with period H in x, whose amplitude decreases rapidly with y. Substituting (68) into (34a)

$$P_z(q)=a^2G_1G_3\delta_{q_1}\delta_{q_3}\frac{2i}{q}\lim_{R\to\infty}(\sin qR)\qquad\ldots\ldots(69)$$

where $G=G_1G_2G_3$, and $\delta_q=1$ if $q=0$, and vanishes otherwise. Squaring and replacing $\lim_{R\to\infty}(\sin^2 qR)$ by $\frac{1}{2}$ one obtains

$$c_{\mathbf{k},\mathbf{k}'}{}^2=\frac{M^2\gamma^2}{\alpha G_2{}^2}\frac{v^4}{54}k^2k'^2\left(\frac{b}{H}\right)^2\delta_{q_1}\delta_{q_3}\frac{1}{q^2}.\qquad\ldots\ldots(70)$$

The only possible value of $\mathbf{k}'$ is

$$\mathbf{k}'=(k_1,k_2,-k_3)\qquad\ldots\ldots(71)$$

so that

$$\int dS'=3\left(\frac{2\pi}{a}\right)^2\frac{1}{G_1G_3}\qquad\ldots\ldots(72)$$

and from (10)

$$\frac{1}{\tau}=\frac{v}{aG_2}\gamma^2\frac{1}{36}\left(\frac{b}{H}\right)^2\qquad\ldots\ldots(73)$$

since

$$(1/q)^2=(1/2k_3)^2\qquad\ldots\ldots(74)$$

and in the average

$$(1-\mu'/\mu)=1-\bar{\mu}=2(k_3/k)^2.\qquad\ldots\ldots(75)$$

In (73) the grain boundaries are assumed to be orientated at random, and the average distance between the intersections of grain boundaries on a random line is aG_2.

The scattering probability increases with decreasing H, that is with increasing angle of misfit. The dislocation picture breaks down for angles greater than about 15°, but presumably (73) still holds if b/H is replaced by the angle of misfit.

In (68) a possible periodic dependence of Π on x for small values of y has been disregarded. This would lead to scattering processes which not only change k_2, but also change k_1 by a multiple of $2\pi/H$, that is processes of diffraction by the array of dislocations. At low frequencies the probability of such processes varies as ω^2, and will thus be quite low.

The treatment also neglects the disorder in the immediate vicinity of each dislocation line, and by arguments similar to that in §8 it can be shown that the scattering from that cause varies as ω^2 and is of the order of

$$\frac{1}{\tau}\sim\omega^2\frac{a}{vG_2}\gamma^2\left(\frac{b}{H}\right)^2\qquad\ldots\ldots(76)$$

thus becoming equal to (73) only for frequencies of the order of the Debye frequency.

§ 10. Discussion

At the lowest frequencies all point imperfections scatter as the fourth power of frequency, so that the thermal resistance due to this cause is proportional to the absolute temperature T, and is given by

$$W = T\frac{3(2\pi)^2a^3}{hv^2}\frac{S^2}{G}\left\{\int_0^1 \frac{x^4e^x\,dx}{(e^x-1)^2} + \int_1^\infty \frac{e^x\,dx}{(e^x-1)^2}\right\}^{-1} \quad \ldots\ldots(77)$$

obtained by substituting (45) into the expressions for thermal conductivity given by Klemens (1951). De Haas and Biermasz (1937, 1938) have measured the thermal conductivity of a number of KCl crystals from the same source, and found that at liquid hydrogen temperatures

$$W/T = 3{\cdot}8\times10^{-2}\ \text{cm watt}^{-1} \quad \ldots\ldots(78)$$

with minor variations between specimens. This corresponds to a value of

$$\sum\frac{S^2}{G} = 1{\cdot}2\times10^{-4} \quad \ldots\ldots(79)$$

the sum being over all types of point imperfections. The principal impurities are stated to be Na^+ and Mg^{2+}, both in concentrations of somewhat less than 10^{-4}. For Na^+, $S^2=0{\cdot}3_5$, for Mg^{2+}, $S^2>1{\cdot}5$, and for the vacancy which occurs with every divalent impurity, $S^2=0{\cdot}8$. If both impurities were present to a concentration of 10^{-4}, the value of (79) would exceed $2{\cdot}6\times10^{-4}$, so that the observed value of (79) is consistent with the stated impurity content. Measurements of the thermal conductivity at liquid hydrogen temperatures of alkali halides of controlled impurity content would be extremely valuable in testing the present theory.

It is interesting to note that there is no systematic difference between the scattering power of vacancies and substitutional impurities. The author's earlier incorrect conclusion (Klemens 1951) that the scattering cross section of vacancies exceeds that of impurities by a factor of the order of 100 was based on the measurement of Eucken and Kuhn (1928) of KCl with 10% Br impurities. It is seen from the table that this impurity is a particularly weak scatterer, furthermore its scattering cross section was probably under-estimated because of the high (liquid oxygen) temperature and the high impurity concentration of these measurements.

The thermal resistance due to dislocations is given by

$$WT^2 = \frac{Avh^2}{2\boldsymbol{k}^3}\left\{\int_0^1 \frac{x^4e^x\,dx}{(e^x-1)^2} + \int_1^\infty \frac{x^3e^x\,dx}{(e^x-1)^2}\right\}^{-1} \quad \ldots\ldots(80)$$

where $\boldsymbol{k}$ is Boltzmann's constant, and the relaxation time for scattering due to dislocations is $1/\tau = A\omega$. From (61) one obtains for silver

$$WT^2 = 7{\cdot}3\times10^5/G_0\ \text{deg}^3\ \text{cm watt}^{-1}. \quad \ldots\ldots(81)$$

The thermal lattice resistance at low temperatures due to cold work was found to be inversely proportional to T^2 (Estermann and Zimmerman 1952) for Cu–10%Ni. The same temperature dependence was found in the case of Ag–2%Pd, Ag–2%Cd and Ag–20%Cd by Kemp, Klemens, Sreedhar and White (1954, and further data to be published). This agrees with the frequency dependence of dislocation scattering derived here but the density of dislocations required to account for the magnitude of the resistance of the silver alloys is, according to (81), of the order of 6×10^{12}, 8×10^{12} and 20×10^{12} per cm^2 respectively. The saturation density for pure silver has been estimated by various other means to be in the vicinity of 10^{11} to 10^{12} per cm^2 (Cottrell 1953). The densities derived here are an order of magnitude higher. This may be due to the uncertainty in the other methods of estimating dislocation densities. However, following a suggestion by Mott (1952) one may suppose the dislocations to be piled up in groups of 50 to 100, all of the same sign. Since the scattering probability of such a group is proportional to the square of the total Burgers vector, a total of 10^{11} dislocations, an appreciable fraction of which are thus grouped, can account for the observed resistances.

ACKNOWLEDGMENTS

The author wishes to thank Mr. A. F. A. Harper and Dr. W. Boas for helpful discussions.

REFERENCES

BERMAN, R., 1953, *Advances in Physics* (*Phil. Mag.* Suppl.), **2,** 103.
BIJL, D., and PULLAN, H., 1954, *Phil. Mag.*, **45,** 290.
COTTRELL, A. H., 1953, *Dislocations and Plastic Flow in Crystals* (Oxford: University Press).
ESTERMANN, I., and ZIMMERMAN, J. E., 1952, *J. Appl. Phys.*, **23,** 578.
EUCKEN, E., and KUHN, G., 1928, *Z. Phys. Chem.*, **134,** 193.
GRÜNEISEN, E., 1926, *Handb. d. Physik*, **10,** 1.
DE HAAS, W. J., and BIERMASZ, TH., 1937, *Physica*, **4,** 752; 1938, *Ibid.*, **5,** 47.
KEMP, W. R. G., KLEMENS, P. G., SREEDHAR, A. K., and WHITE, G. K., 1954, *Proc. Phys. Soc.* A, **67,** 728.
KLEMENS, P. G., 1951, *Proc. Roy. Soc.* A, **208,** 108.
MOTT, N. F., 1952, *Phil. Mag.*, **43,** 1151.
NABARRO, F. R. N., 1951, *Proc. Roy. Soc.* A, **109,** 278.
OLSEN, J. L., and ROSENBERG, H. M., 1953, *Advances in Physics* (*Phil. Mag.* Suppl.), **2,** 28.
PEIERLS, R. E., 1929, *Ann. Phys., Lpz.*, **3,** 1055.
PICK, H., and WEBER, H., 1950, *Z. Phys.*, **128,** 409.
POMERANCHUK, I., 1942, *J. Phys. U.S.S.R.*, **6,** 237.

The Free-Electron Network Model for Metals: II

By C. A. COULSON
Mathematical Institute, Oxford

MS. received 16th June 1955

Abstract. The free-electron network model for metals originally introduced by the writer is extended in two ways. First an allowance is made for the strong electron attraction towards the nuclei by inserting δ-function potential wells at the positions of these nuclei. Secondly, the potential between the nuclei is not regarded as constant but may be of arbitrary shape. Provided that this potential does not fluctuate too fast along the 'bonds', its influence on band shape is shown to be small, in agreement with the situation found without δ-functions by Raychaudhuri. Atoms of different kinds may be introduced into the lattice, and the particular cases of the diatomic cubic lattice AB and the planar hexagonal lattice of graphitic type (example, boron nitride) are studied in detail. A possible application to the problem of antiferromagnetism is pointed out, involving a splitting of one otherwise continuous energy band into two separated parts as a result of partial localization of electrons of similar spin on alternate atoms.

§ 1. Introduction

In a previous paper (Coulson 1954, subsequently referred to as I) the writer showed how to extend the so-called free-electron theory for conjugated molecules to make it apply to metals. Essentially all that was required was to suppose that the conduction electrons moved in a zero potential field, confined to the straight lines (i.e. bonds) which joined adjacent nuclei. It appeared that the resulting band distribution of the allowed energies was exceedingly similar to that found in the conventional tight-binding approximation.

There are several ways in which this model could be made more realistic, while still keeping to the network principle. Thus (*a*) we might suppose that the potential was not constant between the nuclei, but varied slowly. Raychaudhuri (1955) has recently shown that unless the variation of potential is rapid, the resulting band distribution is hardly affected. A second improvement (*b*) is to recognize that when a conduction electron is close to a nucleus it experiences a strong attraction. This may be simulated by adding a suitable delta function (δ-function) to the potential at each nucleus, while maintaining a constant potential between the nuclei. A third improvement (*c*), which is indeed essential if the method is to apply to diatomic and other intermetallic compounds, is to use different delta-function wells at the different nuclei. Finally (*d*) we may superpose on these delta-function potentials at the nuclei a varying potential between the nuclei, thus extending Raychaudhuri's work in which there were no δ-functions. Improvement (*a*) has already been made. In this note we show how to make the other three extensions (*b*)–(*d*). The essential point which is new concerns the type of boundary or continuity conditions to be satisfied at a nucleus where two or more bonds terminate in a δ-function potential well. For that reason we have discussed it carefully in §2. The later sections then follow fairly simply, and require relatively little detailed analysis.

§ 2. THE CONNECTION FORMULAE

Consider (figure 1) three lines Ox, Oy, Oz of the network which meet at O. Let us suppose that in the range $0 \leqslant x, y, z < \epsilon$ the potential is $-V_0$, where V_0 is large and positive, and that along the rest of the three lines the potential V is either constant, as in the older theories of I, or slowly varying. We first discuss the connection formulae for the wave functions in these three segments, and then let $\epsilon \to 0$ in such a way that the product $8\pi^2 m V_0 \epsilon / h^2$ tends to a finite value α. The quantity α measures the depth of the delta-function well at O.

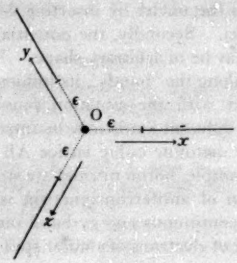

Figure 1.

Along the Ox segment, where x is measured from zero at O, the wave equation is

$$\frac{d^2\psi}{dx^2} + q^2\psi = 0$$

with $q^2 = 8\pi^2 m(E - V)/h^2$ when $x > \epsilon$, and $q^2 = 8\pi^2 m(E + V_0)/h^2 = (q')^2$, say, when $x < \epsilon$. In the range $x > \epsilon$ there are two independent solutions, which we will call $X_1(x)$ and $X_2(x)$. Analogously to Raychaudhuri (1955) these are conveniently normalized so that

$$X_1(0) = 1, \quad X_1'(0) = 0$$
$$X_2(0) = 0, \quad X_2'(0) = q_0 \qquad \ldots\ldots(1)$$

where q_0 is the value taken by q at the point O when ϵ shrinks to zero. In the particular case when $V = 0$ along the bonds,

$$X_1(x) = \cos qx, \qquad X_2(x) = \sin qx. \qquad \ldots\ldots(2)$$

We may write the wave function along Ox in the form

$$x > \epsilon, \quad \psi = A_1 X_1(x) + A_2 X_2(x)$$
$$x < \epsilon, \quad \psi = a_1 \cos q'x + a_2 \sin q'x \qquad \ldots\ldots(3)$$

where A_1, A_2, a_1, a_2 are certain constants. Similarly, along Oy :

$$y > \epsilon, \quad \psi = B_1 Y_1(y) + B_2 Y_2(y)$$
$$y < \epsilon, \quad \psi = b_1 \cos q'y + b_2 \sin q'y. \qquad \ldots\ldots(4)$$

There is a similar set of equations for each segment of the network that ends at O.

The continuity conditions are

(i) ψ continuous at $x=\epsilon, y=\epsilon, z=\epsilon$
(ii) ψ continuous at $x=0, y=0, z=0$
(iii) grad ψ continuous at $x=\epsilon, y=\epsilon, z=\epsilon$
(iv) Σ grad $\psi=0$ at $x=0, y=0, z=0$

where, in (iv), the gradient is measured outwards from O along each segment. This condition is the conservation of current condition of Griffith (1953), Ruedenberg and Scherr (1953) and Kuhn (1954 a).

Condition (ii) is satisfied if

$$a_1=b_1=c_1 \qquad \ldots\ldots(5)$$

Condition (iv) is satisfied if

$$a_2+b_2+c_2=0. \qquad \ldots\ldots(6)$$

Conditions (i) and (iii) require that

$$\begin{gathered} a_1 \cos q'\epsilon + a_2 \sin q'\epsilon = A_1X_1(\epsilon) + A_2X_2(\epsilon) \\ q'(-a_1 \sin q'\epsilon + a_2 \cos q'\epsilon) = A_1X_1'(\epsilon) + A_2X_2'(\epsilon) \end{gathered} \qquad \ldots\ldots(7)$$

with similar equations for the y and z directions. If we now let $\epsilon \to 0$ then the first equation in (7) requires that $a_1 \to A_1$, provided only that $q'\epsilon\, a_2 \to 0$. Similarly the second equation in (7) gives

$$q'a_2 - (q')^2\epsilon a_1 \to A_2 q_0.$$

Putting $(q')^2\,\epsilon=\alpha$, where in the limit, $\epsilon \to 0$ and $q' \to \infty$ in such a way that the product $(q')^2\epsilon$ remains finite, we have

$$q'a_2 \to A_2q_0 + \alpha A_1.$$

Substituting for a_1 and a_2, etc., in equations (5) and (6) we have

$$\begin{gathered} A_1=B_1=C_1 \\ q_0(A_2+B_2+C_2)+\alpha(A_1+B_1+C_1)=0. \end{gathered}$$

These may be written in a form which only involves the solutions of the wave equation in the segments outside the δ-function:

$$\begin{gathered} \psi \text{ is continuous at O} \\ \Sigma \operatorname{grad} \psi + n\alpha\psi = 0 \end{gathered} \qquad \ldots\ldots(8)$$

where n is the number of segments (here 3) which terminate at O. Thus the only effect of the δ-function in the potential is to replace the conservation condition Σ grad $\psi=0$ by the more general condition (8). Furthermore it is seen that the supplementary condition $q'\epsilon a_2 \to 0$ which was necessary for this analysis to apply, is indeed satisfied.

Equation (8) is not entirely new. A branching connection equation of this type has been suggested by Kuhn (1954 b) though his analysis gave no ground for identifying the parameter α with the strength of a δ-function potential well. It has also been used by Frost (1955) in a note published since this present work was completed, where, by analogy with a pseudo-atom in which an electron moves along a line under such a potential energy function, it is found that the correct 1s wave function is obtained. But we believe that the account given in this paper is more direct and general. The introduction of δ-functions at non-branching points in linear metals and molecules has been familiar for many years.

§ 3. Simple Cubic and Graphite Lattices

We are now ready to apply our analysis to particular problems. First let us consider the simple cubic lattice, of side l, as in I except that there is a δ-function of strength α at each lattice point. Entirely similar analysis to that of I § 2 shows that when the wave vector is $k_x\, k_y\, k_z$, the energy E is given by

$$\cos k_x l + \cos k_y l + \cos k_z l = 3 \cos ql - \frac{3\alpha}{q} \sin ql$$
$$q^2 = 8\pi^2 mE/h^2. \qquad \ldots\ldots(9)$$

Provided that ql is not large, the right-hand side of (9) takes the form

$$3(1-\alpha l) - \frac{4\pi^2 mEl^2}{h^2}(3-\alpha l) + O(q^4 l^4).$$

Thus the presence of the δ-function is mainly to shift the origin of energy and to alter the scale of energy in the ratio $1:(1-\frac{1}{3}\alpha l)$. Other features of the band density curve are unchanged.

A somewhat amusing situation occurs, though of no significance for the theory of metals, when k_x, k_y, k_z are all small. For then, since $\alpha > 0$, it follows that q^2 is negative, and the functions $\cos ql$ and $\sin ql$ need to be replaced by their hyperbolic analogues. The wave function is everywhere of exponential, and not sinusoidal, type. For a linear one-dimensional chain of atoms, the wave function for $k = 0$ is shown in figure 2.

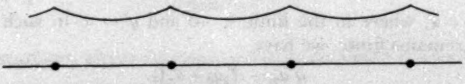

Figure 2. Wave function for $k=0$ in a linear chain. This function is everywhere of exponential, and not oscillatory, type.

Other cubic lattices can be dealt with similarly. The formulae given in I § 3 apply at once, with additional terms in α similar to (9).

The hexagonal plane layer lattice of graphite of side l was discussed in I § 4, where it was shown that in terms of a momentum vector (k_1, k_2) the energy is given by

$$\begin{aligned} q^2 &= 8\pi^2 mE/h^2, \\ \cos ql &= \pm \tfrac{1}{3} g(k_1, k_2), \\ g^2(k_1, k_2) &= 3 + 2\cos k_1 a + 2\cos k_2 a + 2\cos(k_1 - k_2)a, \qquad \ldots\ldots(10) \\ a^2 &= 3l^2. \end{aligned}$$

When there is a δ-function of strength α at each nucleus, the only change is that instead of the second of the above equations we have

$$\cos ql - \frac{\alpha}{q} \sin ql = \pm \tfrac{1}{3} g(k_1, k_2). \qquad \ldots\ldots(11)$$

The effect of this alteration on the energy associated with given k_1, k_2 is similar to that for the cubic lattice discussed earlier in this section.

§ 4. Diatomic Lattices

We can now pass to diatomic lattices, which is extension (c) of the introduction. Here, in the case of a cubic lattice, we suppose that there are different δ-functions, of strength α_1 and α_2, at adjacent lattice points. The analysis of I § 3 becomes rather more complicated, since there are now six 'bonds' in the unit cell instead of three. The number of continuity conditions is twelve instead of six. But it is found that the consistency equation reduces quite simply to

$$9\left\{\cos ql-\frac{\alpha_1}{q}\sin ql\right\}\left\{\cos ql-\frac{\alpha_2}{q}\sin ql\right\}=\{\cos k_x l+\cos k_y l+\cos k_z l\}^2. \qquad \ldots\ldots(12)$$

If we put $\alpha_2=\alpha_1$, this equation reduces to (9), as it ought to do. For most values of k_x, k_y, k_z the energy given by (12) is related to the energy without the δ-functions just as in § 3. But for values of k near the edges and centre of the band there are differences, which we shall discuss in a moment.

The case of the graphite lattice with unequal δ-functions is the case of lattices such as boron nitride (BN) (Taylor and Coulson 1952). It is not difficult, though a little tedious, to show that instead of (11) we have

$$\left\{\cos ql-\frac{\alpha_1}{q}\sin ql\right\}\left\{\cos ql-\frac{\alpha_2}{q}\sin ql\right\}=\frac{1}{9}g^2(k_1,k_2). \qquad \ldots\ldots(13)$$

The general forms of (12) and (13) are so similar that we may conveniently discuss them together. We shall show that if $\alpha_1\neq\alpha_2$ the complete band of energies is split into two separate parts. In the particular case of (13) as applied to the BN lattice, this means, as Taylor and Coulson showed, that the crystal is an insulator, with a completed band and an energy gap before the next available band begins. In the case of (12) there is an immediate application to antiferromagnetism. For if, as is usually supposed, in antiferromagnetic substances electrons of one spin tend to congregate on one set of atoms, and electrons of the other spin on the alternate set, then the Hartree–Fock equation for the first type of electron will involve an effective potential energy function (Coulomb + exchange) which is different from that for the second type of electron. In a rough sort of way we could express this by saying that electrons of one spin were attracted more to certain of the nuclei, and electrons of the other spin to the other nuclei. For a given electron, therefore, the potential wells α_1 and α_2 will differ: and this, as Slater (1954) has suggested, may easily lead to a significant splitting of the otherwise continuous energy band. It is not difficult to show this splitting in a one-dimensional model: it is much more difficult to show it in a more realistic three-dimensional one though Slater and Krutter have done this for the d-band in a body-centred cubic lattice, using a tight-binding approximation. For these reasons a short discussion of (12) and (13), which does show this splitting quite unequivocally, is worth giving. We shall do this in terms of (13), which may be written in the form

$$\{\cos k_x l+\cos k_y l+\cos k_z l\}^2/9=f(ql,\alpha_1)f(ql,\alpha_2) \qquad \ldots\ldots(14)$$

where

$$f(ql,\alpha)=\cos ql-\alpha l\left(\frac{\sin ql}{ql}\right). \qquad \ldots\ldots(15)$$

Now whatever the values of k_x, k_y, k_z, the left-hand side of (14) is positive. Thus only those values of ql are permitted which make the right-hand side positive. Since, from (10), q^2 gives the energy value, any limitation on q will involve limitation on E. The condition that the right-hand side of (14) shall be positive requires that $f(ql,\ \alpha_1)$ and $f(ql,\ \alpha_2)$ shall have the same sign. Figure 3 shows the graph of $f(ql,\ \alpha)$ when $\alpha=0$ and when $\alpha=\alpha_1$, and $\alpha=\alpha_2$. All three curves have common points at $ql=n\pi\,(n=1, 2, \ldots)$. It is immediately clear from this figure that there are certain forbidden ranges of the quantity ql, since in these ranges the curves for $\alpha = \alpha_1$ and $\alpha = \alpha_2$ lie on opposite sides of the axis of ql. These forbidden ranges of ql, corresponding directly to forbidden ranges of E, are shown by thick lines in the figure. It is evident that whatever the actual values of α_1 and α_2, provided only that they are different, the energy band is split up into two or more parts. To the extent that the model is a fair transcription of the antiferromagnetic situation, this confirms Slater's view regarding the total band structure. In the graphitic lattice, of course, this is merely another way of confirming what Taylor and Coulson had already shown for the BN lattice by using the tight-binding approximation—that this lattice should have insulating and not conducting character. It is a perfectly straightforward matter to calculate the energy gap between the bands, using (12) or (13).

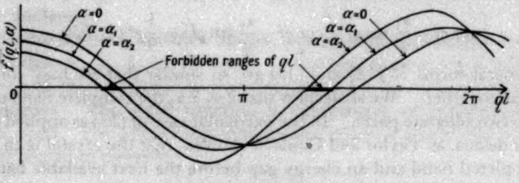

Figure 3. Diagram to show the forbidden ranges of ql (and so of energy). Those ranges are marked by thick lines.

It should perhaps be mentioned that if α_1 and α_2 are positive, the energy levels corresponding to small k_x, k_y, k_z are of the type described in figure 2. But no complication arises from this cause.

§ 5. NON-UNIFORM POTENTIAL

The previous analysis is easily extended to cover non-uniform potentials in a way analogous to that recently used by Raychaudhuri (1955). The simple cubic lattice will serve as an example. We suppose that at each lattice point there is a δ-function of strength α, and that between the lattice points the potential, although periodic, is not necessarily constant. In the i, j, k cell (figure 4) there are now six functions, which we may define as in (1). Thus X_1 and X_2 are the two basic independent solutions along the x-segment, and similarly for the Y_1, Y_2, Z_1, Z_2 functions.

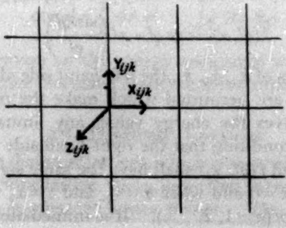

Figure 4.

The wave function in this cell, along the three positive directions has the form

$$\begin{aligned} \psi(x) &= X_1(x) + a\,X_2(x) && \text{along } x \text{ direction} \\ \psi(y) &= Y_1(y) + b\,Y_2(y) && \text{along } y \text{ direction} \\ \psi(z) &= Z_1(z) + c\,Z_2(z) && \text{along } z \text{ direction.} \end{aligned}$$

In view of condition (i) these definitions ensure continuity of ψ at $x=y=z=0$. The continuity with adjacent cells requires that

$$\exp(-ik_x l)\{X_1(l) + a\,X_2(l)\} = 1$$

and two similar relations in Y and Z. Finally the flux condition is

$$\begin{aligned} q_0(a+b+c) - \exp(-ik_x l)\{X_1'(l) + a\,X_2'(l)\} - \exp(-ik_y l)\{Y_1'(l) + b\,Y_2'(l)\} \\ - \exp(-ik_z l)\{Z_1'(l) + c\,Z_2'(l)\} + 6\alpha = 0 \end{aligned}$$

where, as before, q_0^2 is the value of $8\pi^2 m(E-V)/h^2$ at a lattice point. Eliminating a, b, c we obtain the fundamental relation (16), in which, following Raychaudhuri, we have used the Wronskian relation

$$X_1(x)X_2'(x) - X_1'(x)X_2(x) = \text{constant} = q_0, \text{ etc.}$$

$$2q_0 \sum \frac{\cos k_x l}{X_2(l)} = \sum \frac{X_2'(l) + q_0 X_1(l)}{X_2(l)} - 6\alpha. \qquad \ldots\ldots(16)$$

It is natural to suppose that the potential varies similarly along each direction, so that $X_2(l) = Y_2(l) = Z_2(l)$. Then (16) becomes

$$2q_0 \sum \cos k_x l = 3\{X_2'(l) + q_0 X_1(l)\} - 6\alpha\,X_2(l). \qquad \ldots\ldots(17)$$

This is essentially equation (9) of Raychaudhuri's paper, apart from the δ-function term $6\alpha X_2(l)$. In the case of constant potential, $X_1(x) = \cos q_0(x)$, $X_2(x) = \sin q_0 x$, and our equation (17) reduces to Raychaudhuri's (9), as of course it ought to do.

Similarly in the diatomic graphitic layer the fundamental equation (13) is replaced by

$$\left\{X_1(l) - \frac{\alpha_1}{q_0} X_2(l)\right\}\{X_2'(l) - \alpha_2 X_2(l)\} = \tfrac{1}{9} q_0 g^2(k_1, k_2) \qquad \ldots\ldots(18)$$

where α_1 is the δ-function at the end $x=0$, and α_2 at the end $x=l$ of the links in the fundamental unit cell. This also reduces to (13) when the potential is actually constant.

There is no need to discuss (17) and (18) in detail, for the arguments used by Raychaudhuri show that provided $q_0 l$ is not too large, the dominant effect of a non-uniform potential is a simple shift of energy, superimposed upon the effect of the δ-function which we have already shown to be a further shift of energy and a small change of scale. In this way we see that the range of applicability of the free-electron treatment is probably much wider than might at first have been expected. The argument used in I, that formulae such as those which we have developed may be employed as interpolation formulae between energy values calculated by more accurate methods for particular values of the wave vector **k**, receives additional support from the present work.

REFERENCES

COULSON, C. A., 1954, *Proc. Phys. Soc.* A, **67**, 608.

FROST, A. A., 1955, *J. Chem. Phys.*, **23**, 985.

GRIFFITH, J. S., 1953, *Trans. Faraday Soc.*, **49**, 345.

KUHN, H., 1954 a, *Z. Naturf*, **9a**, 989 ; 1954 b, *J. Chem. Phys.*, **22**, 2098.

RAYCHAUDHURI, A., 1955, *Proc. Phys. Soc.* A, **68**, 439.

RUEDENBERG, K., and SCHERR, C. W., 1953, *J. Chem. Phys.*, **21**, 1565.

SLATER, J. C., 1954, *Quarterly Progress Report of Solid State and Molecular Theory Group*, Massachusetts Institute of Technology, 15th April 1954, p. 5.

TAYLOR, R., and COULSON, C. A., 1952, *Proc. Phys. Soc.* A, **65**, 834.

The Liquid ‘Cell’ Model Applied to ^{3}He

By H. N. V. TEMPERLEY†

U.S. National Bureau of Standards, Washington

MS. received 1st *April* 1955 *and in amended form* 3rd *August* 1955

Abstract. It is shown that a sum of suitably chosen Debye and Schottky functions leads to a Gibbs free energy that satisfactorily represents the entropy, specific heat, and vapour pressure of liquid ^{3}He. It is further shown that such a free energy is a plausible consequence of the ‘cell’ model of the liquid. The model can be developed consistently with symmetry requirements by using the ‘pair-wise’ approximation of the Heitler–London–Heisenberg theory of ferromagnetism, in a way that enables the magnetic susceptibility to be described quantitatively. The model predicts that the lowest state of liquid ^{3}He is an antiferromagnetic one of zero entropy, and that a transition should occur at 0·1° to 0·2°K. A comparison is made with the ‘imperfect Fermi gas’ model considered earlier, which, although it can be further improved in various ways, seems to be inferior to the present one.

§ 1. Introduction

In a recent paper (Temperley 1954) it was shown that the ‘perfect Fermi gas’ model of liquid ^{3}He could be improved considerably by the introduction of van der Waals corrections. As with a classical liquid, it was found that reasonable choices of the van der Waals coefficients gave numerical agreement with some of the observed properties of the liquid, while others were predicted in order of magnitude. At the same time, it became clear that the actual energy levels of the liquid must depart considerably from those of the Fermi gas. These results were encouraging enough to prompt the consideration of more detailed liquid models. It has been found that an appropriate form of the ‘cell’ model of the liquid leads to a partition function that describes the specific heat, the magnetic susceptibility, the entropy and the vapour pressure with satisfactory accuracy. The corresponding vapour pressure equation, although differing in form, gives predictions differing only slightly from those of the equation proposed empirically by Chen and London (1953), and every single term of the proposed new equation can be given a definite physical significance. Since it involves several quantities that cannot be calculated *a priori* with any accuracy, it may be helpful to outline the reasoning by which it was reached.

§ 2. Choice of the Form of Model

The Fermi gas model fails badly in trying to describe the specific heat data which have recently been reported (Osborne *et al.* 1954, Sydoriak and Roberts 1954, de Vries and Daunt 1954). The data on magnetic susceptibility obtained by W. M. Fairbank *et al.* 1953, 1954) are also in ‘order of magnitude’ agreement only, the susceptibility following Curie's law down to much lower temperatures than the Fermi gas model predicts. Since the susceptibility and specific heat of such a model depend mainly on the distribution of levels near the critical Fermi energy, it is perhaps not surprising that the gas-like model fails in these respects. For example, we might try a 'Brillouin zone' type of treatment with a half-filled zone, which leads to some improvement. A further improvement results (de Vries and Daunt 1953) if we introduce a Debye-like contribution to the specific heat. This can be done quite consistently, because we can argue that sound waves of low frequency represent compressions and rarefactions involving the simultaneous motion of large numbers of atoms which we cannot expect models of 'one-atom' type to describe properly. However, even with this improvement, no simple model of this type could be found that could properly represent both the specific heat and susceptibility as functions of temperature.

---

† Present address: Riversdale, Grantchester, Cambridge.

Consideration of a 'cell' type of model was prompted by the empirical fact that the observed specific heats could all be satisfactorily extrapolated to $T=0$ along a simple Schottky curve, and further examination showed that the following formula represented all the data with an accuracy comparable with the disagreements between the different observers:

$$\frac{C}{N\boldsymbol{k}}=\frac{x^2\,e^x}{(1+e^x)^2}+0{\cdot}12T^3,\quad x=\frac{\Theta}{T} \qquad \ldots\ldots(1)$$

If Θ is chosen equal to 1·8°, we get a curve with an almost linear portion *not* pointing at the origin, as found by Osborne *et al.* (1954) and Sydoriak and Roberts (1954). A slightly lower value of Θ, 1·5°–1·6°, gives a curve that is almost flat between 1° and 0·5°, like the results reported by de Vries and Daunt (1954). (It is relevant to point out here that one sample used by the latter workers was not quite pure (96%) and that a slight decrease in energy-level spacing is a plausible result of dilution.) Equation (1) is compared with experiment in figure 1.

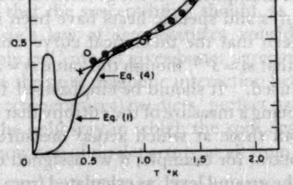

Figure 1. Calculated and observed specific heats.

The justification for introducing a Debye-like term in combination with the 'cell' model is the same as that for the 'zone' model. Since there is, as yet, no information about the compressibility, the coefficient of T^3 was chosen in order to get agreement with the upper portion of de Vries and Daunt's (1954) specific heat curve. An independent check on this choice has been found by Mikura (1955). It is readily verified numerically that an energy-level spacing of the order of $\boldsymbol{k} \times 1°–2°$ is a reasonable consequence of the cell model. We should expect the spacing to be of the order of $3\boldsymbol{h}^2/8md^2$ where d is the dimension of the cell, and this would call for an effective value of d of nearly twice the equivalent lattice distance. This is in line with the fact, pointed out by many writers, that the potential barriers between cells in liquid helium must be low because of the relatively large spacing of atoms.

§ 3. CHOICE OF THE NUMBER OF DISCRETE ENERGY LEVELS

In view of this, we assume also that only a few energy levels per cell need be mentioned explicitly in the partition function, the remainder being supposed to be 'smeared out' into the Debye-like spectrum already introduced, but it is less clear how we are to decide the numbers of such discrete levels. (It is seldom, if ever, possible to reconstruct a level scheme from specific heat data taken alone.) Expression (1) does not, of course, imply that, in each cell, we have a ground level and an excited level that are both simple; any model in which these two levels had the same multiplicity would lead to precisely the same specific heat curve.

Schottky functions of several other types were tried, corresponding to the excited level being of higher or lower multiplicity than the ground level, before expression (1) was finally adopted. It can be said that these other models failed to give as good a description of the observed specific heat because the Schottky peak, the height of which is independent of Θ, comes out to be too high or too low to represent the data properly, so we seem forced to conclude that the effective multiplicities are nearly equal. Something like a relative multiplicity of 1 to 3 or more seems to be definitely inconsistent with the data, though something like 2 to 3 or 4 cannot be excluded.

In addition to the specific heat data, Weinstock *et al.* (1953) and Sydoriak and Roberts (1954) have used the vapour pressure data to compute upper and lower limits to the entropy at various temperatures, and these figures can be used, in combination with the entropy that follows from expression (1), to fix the 'apparent multiplicity' of the ground level. The entropy that follows from expression (1) is, per atom,

$$S = \boldsymbol{k}\,[0{\cdot}04T^3 + \ln(1+e^{-x}) + x/(1+e^{x}) + \ln m] \qquad \ldots\ldots(2)$$

where m is the 'apparent multiplicity' of the ground level at the lowest temperature at which vapour pressures and specific heats have been measured (about 0·4°K). In figure 2 it will be seen that the theoretical curve would pass through all the 'gates' if we supposed that $m = 3^{1/2}$, though the value $m = 2$, leading to $S \to \boldsymbol{k} \ln 2$ as $T \to 0$ has actually been used. It should be emphasized that these figures have a real physical meaning, being a measure of the entropy that has still to be got rid of at lower temperatures than those at which actual measurements were made. (A value of $m = 2$ would follow, for example, if we assigned exactly one atom to each cell and supposed that the ground level, as calculated from Schrödinger's equation, was single, and then took account of the doubling of levels due to spin.)

§ 4. A SIMPLE MODEL CONSISTENT WITH THE SPECIFIC HEAT AND ENTROPY

The quantitative success of equations (1) and (2) prompts consideration of a very simple model. We suppose that a typical atom is moving in a cell whose

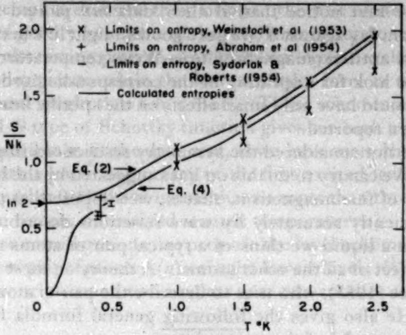

Figure 2.

barriers represent the interactions with other atoms, but that the pattern of discrete levels is smeared by fluctuations in the size of the cell, together with the fact that the barriers are fairly low, to the extent that only a few of the lowest levels can be specified explicitly as referring to one particle, the remainder merging into the continuum of many-particle levels, which certainly exists in all liquids and solids, and which we have represented by means of a Debye-like spectrum. The very simplest assumption of this kind that we can make is that it is only appropriate to specify explicitly the ground level and the first excited level for each cell, and we then note that these levels are both double because of spin. These assumptions lead directly to equations (1) and (2) with $m=2$. We are neglecting completely the symmetry requirements imposed by Fermi statistics, and this would be justifiable if each atom could be considered as 'completely localized' in one cell, in the same sense that an atom in a solid seldom leaves the neighbourhood of a lattice point. For a discussion of this see, for example, Rushbrooke (1949).

It is instructive to compare the predictions of this model with those of the slightly imperfect Fermi gas, for which symmetry requirements are the *dominating* factor. As shown by de Vries and Daunt (1953), a Fermi gas model cannot represent the specific heat very well, even with the addition of a Debye term. Although it can roughly represent the entropy and vapour pressure (Temperley 1954) the Fermi model predicts that the susceptibility should, as we have already pointed out, depart from Curie's law at temperatures considerably higher than are observed. The 'simple cell' model gives better agreement with the specific heat and entropy, but (since the pure magnetic interaction between spins is completely negligible at attainable temperatures) predicts 'perfect paramagnetism', an applied magnetic field being the only way in which the spin degeneracy can be lifted, so that the prediction is now one of no departure at all from Curie's law.

§ 5. CONSIDERATION OF THE MAGNETIC DATA, AND OF SYMMETRY AND EXCHANGE EFFECTS

We have already derived from experiment conclusions (§ 3) that limit fairly severely the possible numbers of energy levels in models of this type. A study of the magnetic susceptibility data of W. M. Fairbank *et al.* (1954) now gives us further clues. We first notice that, if their data are plotted in the 'routine' Curie–Weiss fashion, $1/\chi$ against T, we get a good straight line between 1° and 0·4°, extrapolating to an antiferromagnetic Curie–Weiss temperature of about 0·15°. This prompts us to look for a splitting of the corresponding order of magnitude, which, of course, would have only small effects on the specific heat at temperatures that have so far been reported.

So far, we have not considered the symmetry restrictions imposed by Fermi–Dirac statistics. We can try to do this on lines suggested by the Heitler–London–Heisenberg theory of ferromagnetism, that is, we suppose that the assembly can be described sufficiently accurately by wave functions describing neighbouring *pairs* of atoms. In a liquid we think of a typical pair of atoms moving in a field representing the effect of all the other atoms. A theory on these lines has, in fact, been set up by Price (1955), who tries to describe the pair of atoms by a 'rotator' wave function. He also gives the following general formula for the magnetic susceptibility of any model of this general type

$$\frac{\boldsymbol{k}T\chi}{N\mu^2}=\frac{4}{3}\frac{Z_0}{Z_0+Z_p}\,. \qquad \ldots\ldots(3)$$

Here Z_0 and Z_p correspond respectively to the partition functions associated with ortho- and para-type wave functions. By inserting into (3) the known partial partition functions for a rigid rotator Price (1955) obtained only qualitative agreement with the observed susceptibility. If we use instead a simple model consisting of a singlet para-level and a triplet ortho-level $0{\cdot}4^\circ\times\boldsymbol{k}$ higher, i.e. if we assume the lowest ortho-level to be *without* spatial degeneracy, we can get almost perfect agreement with experiment (table 1). At very low temperatures, only these two levels are effectively occupied and Z_0 and Z_p each reduce to one term, and we shall have approximately $Z_0/Z_p\simeq\exp(-0{\cdot}4/T)$. Rice (1955) retained the three-fold spatial degeneracy of the first ortho-level and neglected the higher levels. This would give $Z_0/Z_p\simeq 3\exp(-T_0/T)$ where T_0 is an adjustable constant. The agreement is then about as good.

Table 1. Observed Susceptibility Compared with Susceptibility predicted by Present Model

Temp. (°K)	0·2	0·3	0·5	0·6	0·8	1·0	1·2	1·5
Calculated	0·385	0·661	0·766	0·808	0·861	0·891	0·910	0·929
Observed	0·50	0·63	0·82	0·85	0·90	0·93	0·94	0·95

§ 6. The Proposed Form of Partition Function

We are guided in our choice of a scheme of discrete energy levels referring to a pair of atoms by the results of some of the possible approximate treatments of a system of two particles moving in a cell, and by the consideration that the model must lead to a specific heat and entropy not differing very much from expressions (1) and (2). The following level scheme for a *pair* would lead *exactly* to expressions (1) and (2), corresponding to a single atom in a cell, with a ground level and a first excited level both doubly degenerate: (*a*) a four-fold degenerate ground level; (*b*) an eight-fold degenerate first excited level of total energy $\boldsymbol{k}\Theta$; (*c*) a four-fold degenerate second excited level of total energy $2\boldsymbol{k}\Theta$. Group (*c*) can be neglected altogether without spoiling the agreement of the free energy and entropy, though there is a noticeable effect on the calculated specific heat.

We might attempt to describe the motion of the pair of atoms relative to their common centre of gravity by means of the oscillator or rotator models. Either of these leads to an alternating pattern of singlet and triplet levels, the lowest singlet level being non-degenerate while the lowest triplet level is also spatially triply degenerate, the total weight thus being nine. These schemes are excluded as they stand because a 1–9 type of Schottky function gives too high a peak in the specific heat to make it possible to fit the data, and, as we have seen, the magnetic data are also consistent with a lower degeneracy of the first excited level. (The measured entropy of the liquid at 0·4°–0·5°K means that no more than three or four levels per pair of atoms can remain unresolved at such temperatures.)

Based on these considerations, we propose the level scheme shown in figure 3, describing a typical pair of atoms: (*a*) a singlet lowest level; (*b*) a triplet at $\boldsymbol{k} \times 0{\cdot}4°$ above (*a*); (*c*) two triplets and two singlets near one another at $\boldsymbol{k} \times 2{\cdot}3°$ above (*b*).

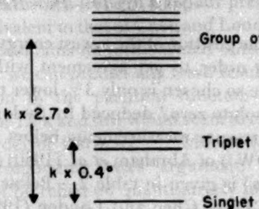

Figure 3. Proposed scheme of levels for typical pair of atoms.

It would only be possible to distinguish experimentally between, say, six, eight or ten levels in group (*c*) if one had extremely accurate data on the specific heat. To this scheme of discrete levels we add a Debye-like continuous spectrum as before. Above 0·5°, this scheme of levels has numerical consequences not differing greatly from those of equations (1) and (2), (see figures 1 and 2), while equation (3) gives a satisfactory description of the susceptibility.

Such a scheme differs in two ways from the consequences of an 'ordinary' type of cell model e.g. particle in box, oscillator, rotator etc. (i) the nearness of the lowest excited level to the ground level; (ii) this lowest excited level is, apparently, not spatially degenerate. Of these, (i) is not serious, and is a fairly plausible consequence of the interactions between the two atoms in a typical pair. Moreover, the existence of ferromagnetism shows that, in certain circumstances, a triplet level can actually be depressed *below* the lowest singlet level when interactions are taken into account. The possibility of such an occurrence was considered for ^3He by Goldstein (1949), who concluded that some depression of the triplet levels probably does occur but that it would still leave the assembly antiferromagnetic. Item (ii) is also a possible consequence of taking interactions into account. This might well lift the spatial degeneracy, and Rice (1955) has given a physical argument for this.

The log (partition function) that follows from the level scheme shown in figure 3 is, per atom,

$$\tfrac{1}{2}\ln(1+3\exp(-0{\cdot}4/T)+8\exp(-2{\cdot}7/T))+0{\cdot}0108T^3. \qquad \ldots\ldots(4)$$

We have increased the Debye term slightly to allow for the fact, already mentioned, that expression (4) would not be quite equivalent to expression (1) even if the singlet and triplet were brought into coincidence. From this we can derive the vapour pressure curve by equating the corresponding partial potential to Chen and London's (1953) expression for the partial potential of a slightly non-ideal vapour phase of ^{3}He

$$g_{\text{vap}} = \boldsymbol{Nk} + \ln\left(\frac{P_{\text{mm}}}{T^{5/2}}\right) - 5{\cdot}325 + BP - \frac{(BP)^2}{2\boldsymbol{Nk}T} \qquad \ldots\ldots(5)$$

where B is the second virial coefficient. Combining these two expressions, we arrive at the following equation for vapour pressure, which should be valid until the third and higher virial coefficients of the vapour become significant (probably at about 2·5°K).

$$\log_{10}\left(\frac{P_{\text{mm}}}{T^{5/2}}\right) = 2{\cdot}3126 - \frac{A}{T} - \tfrac{1}{2}\log_{10}(1 + 3\exp(-0{\cdot}4/T) + 8\exp(-2{\cdot}7/T))$$
$$- 0{\cdot}004705\,T^3 + Pv - BP - \frac{(BP)^2}{2\boldsymbol{R}T} \qquad \ldots\ldots(6)$$

where the constant A fixes the position of the lowest energy level shown in figure 3. We chose A arbitrarily in order to get agreement with the observed vapour pressure at 2°K. The value so chosen is only 3% lower than the value following from the 'latent heat at absolute zero,' deduced by Sydoriak and Roberts (1953, 1954) from their vapour pressure measurements below 1°K. A comparison of equation (6) with that ('AOW') of Abraham *et al.* (1950) (known to represent the data satisfactorily above 1°K) is given in table 2. Below 1°K comparison is also made with the equation 'CL' of Chen and London (1953). This is known to agree with AOW between 1° and 2·5°K, but there is evidence, which we shall summarize in a moment, that the Chen–London equation is better in the range below 1°K.

Table 2. Values of $\log_{10}(P_{\text{mm}}/T^{5/2})$

Temp. (°K)	0·3	0·6	1·0	1·2	1·5	2·0	2·5
Eqn. (6)	$\bar{2}{\cdot}4553$	+0·2367	0·9272	1·0971	1·2620	1·4280	1·5176
AOW	$\bar{2}{\cdot}6494$	+0·2828	0·9363	1·0999	1·2636	1·4284	1·5280
CL	$\bar{2}{\cdot}3849$	+0·2317	0·9379				

(P_{mm} = vapour pressure in millimetres of mercury.)

Since equation (4) gives a satisfactory description of the entropy of the liquid at least down to 0·5°, it is to be expected that the proper choice of the constant A would give an extremely good representation of the vapour pressure. Comparison with the AOW equation (representing the smoothed experimental data above 1°K) shows that this is indeed the case down to that temperature. Preliminary measurements by Sydoriak and Roberts (1953) between 1° and 0·4°K show that the new equation is satisfactory here also. They state that, over this range, their measurements agree with the CL equation 'to within 2%'.

In computing the correcting terms in equation (6), the data of Grilly, Hammel and Sydoriak (1949) and of de Boer *et al.* (1950) were used for the terms involving v and B.

§ 7. DISCUSSION

It may be helpful to make a few remarks about the effect of small alterations in the model. Minor changes in the spacing of the levels, e.g. supposing the group of eight to be 'spaced out' somewhat, would have very little effect. If the group of eight were set at $\boldsymbol{k} \times 2{\cdot}5°$K (instead of $2{\cdot}7°$K) the minimum in the specific heat would become slightly shallower, and the agreement with the specific heat at about $0{\cdot}5°$K would be slightly improved, at the expense of a slight impairment of the existing agreement between calculated and observed entropies in this region. We may sum up by saying that the degeneracies of the two lowest groups of levels are practically fixed at 1 and 3 by combining the evidence from the entropy with the magnetic data and symmetry considerations, and the multiplicity of the highest group is then fixed at about 8 by the specific heat between about $0{\cdot}8°$ and $1{\cdot}5°$, while the magnitude of the Debye term is fixed by the specific heat at the higher temperatures (up to $2{\cdot}3°$, the highest point measured). Within this rough framework, partial 'smearing out' of these discrete levels or minor changes in the spacing have no observable influence.

We have found a partition function that describes many of the equilibrium properties of the liquid, and which leads to a vapour pressure equation that is, for all practical purposes, equivalent to that of Chen and London (1953), but is superior to that equation in that it contains no terms which cannot be justified physically. It remains to ask whether we can predict any fresh results. We have introduced a Debye-like contribution to the partition function which implies a Debye temperature of the order of 12°K and this would seem to call for a velocity of propagation of sound of the order of 100 m sec^{-1}. Mikura (1955) has arrived at very similar figures by a 'corresponding states' argument. The proposed partition function can probably not be relied on quantitatively much below $0{\cdot}4°$K, because of the likelihood that the transition to the final state, in which the spins are aligned antiparallel, takes place via a Curie-type transition, instead of along a second Schottky curve with a peak at about $0{\cdot}1°$K, as equation (4) predicts. (The derivation of equation (4) neglected correlations between spins except between neighbouring pairs, an assumption that must certainly fail at low enough temperatures.) Whatever the form of the specific heat anomaly, we can safely predict a minimum in the specific heat at about $0{\cdot}3°$K. (Present theories of cooperative phenomena are almost useless for predicting the *form* of specific heat anomalies.)

§ 8. POSSIBLE APPLICATIONS TO OTHER LIQUIDS

These seem to be extremely limited. Any ordinary liquid would have solidified long before a possible Schottky contribution to the specific heat could be detected. In ^{4}He it has been repeatedly suggested that discrete levels, or a complete energy spectrum, exist apart from the Debye-like spectrum and it has been argued, with some justification, that some assumption on these lines is needed in order to account for superfluidity (see, for example, Zilsel 1953). Beyond pointing to the probable existence of discrete levels in ^{4}He as well as in ^{3}He the present investigation seems to make no predictions about ^{4}He that can be experimentally checked.

§ 9. CONCLUSIONS

It is possible to set up a simple model of ^{3}He, based on the liquid cell model, which gives good agreement with what is at present known about the specific heat, entropy, vapour pressure and magnetic susceptibility of the liquid. The very simple cell model (two discrete levels only) can be improved, on lines suggested by the magnetic properties, in such a way as to be consistent with symmetry considerations. The new model involves 'pair' and 'many-atom' energy-levels, and is therefore likely to be superior to the Fermi-gas model based on 'single-atom' levels. It is probable that a Curie type transition to an antiferromagnetic state occurs at about 0·1°–0·2°. Such a transition would follow as a consequence of improving the existing 'pair-wise' approximation on lines already familiar in the Heisenberg theory of ferromagnetism. A rapid rise in the specific heat seems certain as the transition approaches, whether this is actually of cooperative form or not. Measurement of the compressibility of the liquid would be of great interest, as would be an attempt to find a shift in the 'apparent Curie–Weiss temperature' of the liquid with increase of pressure, or to measure the effect of pressure on the specific heat.

Since I wrote this paper, Sydoriak and Roberts (1955) and Weinstock *et al.* (1955) have published new results on the specific heat and entropy. Above 0·5°K these agree with the model (if the T^3 law is replaced by the corresponding Debye function). Below 0·4°K they begin to depart from the theoretical curves in a way that is consistent with a co-operative transition at about 0·2°K. de Boer and Cohen (1955) have given results of a treatment based on the 'cell cluster' approach with results qualitatively similar to those of this paper.

ACKNOWLEDGMENTS

I wish to thank Drs. D. W. Osborne, P. J. Price and O. K. Rice for helpful discussions and correspondence. I also wish to thank the National Bureau of Standards for permission to publish this work, which was done during my stay at the Bureau in 1954–5. A preliminary account of this work has already been published (Temperley 1955).

REFERENCES

ABRAHAM, B. M., OSBORNE, D. W., and WEINSTOCK, B., 1950, *Phys. Rev.*, **80**, 366.

DE BOER, J., and COHEN, E. G. D., 1955, *Physica*, **21**, 79.

DE BOER, J., KRANENDONK, I., and COMPAAN, K., 1950, *Physica*, **16**, 545.

CHEN, T. C., and LONDON, F., 1953, *Phys. Rev.*, **89**, 1038.

FAIRBANK, W. M., ARD, W. B., DEHMELT, H. G., GORDY, W., and WILLIAMS, S. R., 1953, *Phys. Rev.*, **92**, 208.

FAIRBANK, W. M., ARD, W. B., and WALTERS, G. K., 1954, *Phys. Rev.*, **95**, 567.

GOLDSTEIN, L., 1949, *Massachusetts Institute of Technology Conference on Low Temperatures* (Cambridge, Mass. : M.I.T.)

GRILLY, E. R., HAMMEL, E. F., and SYDORIAK, S. G., 1949, *Phys. Rev.*, **75**, 1103.

MIKURA, Z., 1955, *Prog. Theor. Phys.*, **13**, 120.

OSBORNE, D. W., ABRAHAM, B. M., and WEINSTOCK, B., 1954, *Phys. Rev.*, **94**, 202.

PRICE, P. J., 1955, *Phys. Rev.*, **97**, 259.

RICE, O. K., 1955, *Phys. Rev.*, **97**, 263.

RUSHBROOKE, G. S., 1949, *Statistical Mechanics* (Oxford : University Press).

SYDORIAK, S. G., and ROBERTS, T. R., 1953, *Rice Institute Conference Report*; 1954, *Phys. Rev.*, **93**, 1418 ; 1955, *Ibid.*, **98**, 1672.

TEMPERLEY, H. N. V., 1954, *Proc. Phys. Soc.* A, **67**, 495; 1955, *Phys. Rev.*, **97**, 835.

DE VRIES, G., and DAUNT, J. G., 1953, *Phys. Rev.*, **92**, 1572; 1954, *Ibid.*, **93**, 631.

WEINSTOCK, B., ABRAHAM, B. M., and OSBORNE, D. W., 1953, *Phys. Rev.*, **89**, 787 ; 1955, *Ibid.*, **98**, 55.

ZILSEL, P. R., 1953, *Phys. Rev.*, **92**, 1106.

Equations of State of Elements from the Thomas–Fermi Theory II: Case of Incomplete Degeneracy

By N. H. MARCH
Department of Physics, University of Sheffield

MS. received 10*th May* 1955 *and in amended form* 18*th July* 1955

Abstract. The work described in part I of the series has been used to discuss the modified equations of state of elements given by the Thomas–Fermi method generalized to deal with non-zero temperatures. The equation of Marshak and Bethe can be solved in the limit of very high pressures by a Taylor expansion around the boundary point. The limiting forms of the thermodynamic functions given by Gilvarry are then regained and the present method enables these to be generalized. The equation is also solved numerically for three cases and a comparison of the results is made with the formulae given by Gilvarry. Some modifications of these are suggested and reliable results for the equations of state according to the Thomas–Fermi method are thus made available.

---

§ 1. INTRODUCTION

IN a previous paper (March 1955, to be referred to as I) a detailed investigation of the equations of state of elements as given by the Thomas–Fermi (TF) theory was carried out. Particular attention was given to the limiting forms of the equations of state for very high pressures and these forms were given explicitly for both the original TF theory, in which exchange is neglected, and for the Thomas–Fermi–Dirac theory, in which account is taken of exchange.

The theory as applied in I was restricted however to the completely degenerate case, whereas it is often necessary in astrophysics to deal with the case of elevated temperatures. Several investigators have considered the generalization of the theory to take account of this. Marshak and Bethe (1940, to be referred to as MB) gave a formulation appropriate for low temperatures, whilst the general case of arbitrarily high temperatures was considered by Sakai (1942) and Feynman, Metropolis and Teller (1949, to be referred to as FMT). These treatments all neglected exchange. The introduction of exchange was considered first by Yokota (1949) and later by Umeda and Tomishima (1953) (see also March 1953). Yokota's treatment was not satisfactory because, as he remarked, the simple Fermi–Dirac statistics are no longer applicable. Umeda and Tomishima and the present writer used an approximate variational distribution function to improve the treatment. However, the fundamental equations of the theory are then of a very complicated nature and in view of this we shall not attempt to deal with this case here.

In § 2 we summarize the results of I which we require here, in § 3 we consider the solution of the MB equation both analytically and numerically, and in § 4 we consider the connection between our results and those obtained previously by Gilvarry (1954).

§ 2. SUMMARY OF RESULTS FOR ZERO TEMPERATURE

In I, we showed how the boundary values $\phi(x_0)$ of the solutions of the dimensionless TF equation

$$\frac{d^2\phi}{dx^2}=\frac{\phi^{3/2}}{x^{1/2}} \qquad \ldots\ldots(1)$$

appropriate to describe solids could be found for the limiting case of extremely high pressures. The result was

$$\phi(x_0)=\frac{3^{2/3}}{x_0}\left[1-\frac{3^{1/3}}{10}x_0\right] \qquad \ldots\ldots(2)$$

to the approximation considered in I. This boundary value enabled the equations of state of elements at very high pressures to be written as

$$pv=\frac{h^2}{5m}\left(\frac{3}{8\pi}\right)^{2/3}\frac{Z^{5/3}}{v^{2/3}}\left[1-\frac{2\pi me^2}{h^2}(4Zv)^{1/3}\right]. \qquad \ldots\ldots(3)$$

This suggested some modifications to be made in the formulae given by Gilvarry, who fitted the available numerical data with analytical expressions having the correct limiting values, and the final results over the entire range of pressures were represented by

$$p^{2/5}\left[\sum_{n=2}^{6}A_n\left(\frac{3v}{4\pi b^3}\right)^{\frac{(n+2)}{6}}\right]=\left(\frac{Z^2e^2}{10\pi b^4}\right)^{2/5} \qquad \ldots\ldots(4)$$

where

$$b=\left(\frac{3}{32\pi^2}\right)^{2/3}\frac{h^2}{2me^2Z^{1/3}}.$$

The coefficients A_n are as follows : $A_2=4{\cdot}8075\times10^{-1}$, $A_3=0$, $A_4=6{\cdot}934\times10^{-2}$, $A_5=9{\cdot}700\times10^{-3}$, $A_6=3{\cdot}3704\times10^{-3}$. We can thus regard the results of the TF method for the equations of state of elements as completely known in the totally degenerate case. However the same is not true in the incompletely degenerate formulation although again in this case Gilvarry has given analytical formulae which at any rate fit the sparse numerical data and have the correct limiting forms. We propose in this paper to consider this case in detail.

§ 3. SOLUTIONS OF THE MARSHAK–BETHE EQUATION

To avoid undue length in the present discussion we refer the reader to the paper by Gilvarry for a concise summary of the equations corresponding to the generalized TF theory.

We are interested now in the first-order temperature perturbation in the terminology of Gilvarry. Then the basic TF function Φ we require is a generalization of the ordinary TF function ϕ of equation (1) and can be expressed in terms of ϕ by

$$\Phi=\phi+\chi\zeta(kT)^2 \qquad \ldots\ldots(5)$$

where k is Boltzmann's constant, T is the temperature, $\zeta=\pi^2b^2/8Z^2e^4$, and χ is a solution of the equation

$$\frac{\partial^2\chi}{\partial x^2}=\frac{3}{2}\left(\frac{\phi}{x}\right)^{1/2}\chi+\frac{x^{3/2}}{\phi^{1/2}}. \qquad \ldots\ldots(6)$$

We shall deal with this equation by the procedure referred to by Gilvarry as the method of MB. We shall not be concerned at all with the alternative method which he refers to as the method of FMT.

In the method of MB, the perturbation leaves the volume unchanged and if we put into equation (6) a solution ϕ corresponding to a dimensionless atomic sphere radius x_0, then we have to solve equation (6) subject to the boundary conditions

$$\left.\begin{aligned} \chi(0)&=0 \\ \frac{\chi(x_0)}{x_0}&=\left(\frac{\partial\chi}{\partial x}\right)_{x_0}. \end{aligned}\right\} \qquad \ldots\ldots(7)$$

We shall shortly consider the solutions of equation (6) subject to the conditions (7) by both analytical and numerical methods.

First however, as Gilvarry has discussed, it is important to note that all the thermodynamic functions of the generalized TF theory can be expressed in terms of two parameters σ and ω, to be obtained by solving equation (6) for χ, and the results for the completely degenerate case. We define these parameters, following Gilvarry, as

$$\sigma=\frac{\chi(x_0)}{\phi(x_0)}\,; \quad \omega=\frac{\chi_1'}{x_0^{1/2}\{\phi(x_0)\}^{5/2}} \qquad \ldots\ldots(8)$$

where χ_1' is the slope of χ at the origin. Two other parameters depending only on the results for $T=0$ are particularly important and are defined by

$$\tau=\left[\frac{x_0}{\phi(x_0)}\right]^2; \quad \epsilon_0=\frac{5}{6}\left[1-\frac{x_0}{\phi(x_0)}\frac{d\phi(x_0)}{dx_0}\right]. \qquad \ldots\ldots(9)$$

τ and ϵ_0 can be regarded as known from I; our purpose now is to calculate σ and ω. (Actually, see § 4, the equations of state depend only on σ and not at all on ω, and in this paper we shall consequently focus attention mainly on σ.)

Let us first of all attempt to develop an analytical solution of equation (6) in the limiting case of x_0 small. As in I, we try to solve by expanding the solution of equation (6) in a Taylor series around the boundary point x_0 and thus we write

$$\chi(x)-\chi(x_0)=\sum_{n=1}^{\infty}\frac{(-1)^n}{n\,!}h^n\chi^n(x_0)=\sum_{n=1}^{\infty}s_n h^n \qquad \ldots\ldots(10)$$

where $h=x_0-x$, $\chi^n(x)$ is the nth derivative of $\chi(x)$ and $s_n=(-1)^n\,\chi^n(x_0)/n\,!$ It is convenient to express the results in terms of two further parameters a and c. The first of these was introduced in I and was defined by

$$\frac{\phi(x_0)}{x_0}=\left(\frac{\partial\phi}{\partial x}\right)_{x_0}=a^2 \qquad \ldots\ldots(11)$$

and we choose to define the second by

$$\frac{\chi(x_0)}{x_0}=\left(\frac{\partial\chi}{\partial x}\right)_{x_0}=-c^2. \qquad \ldots\ldots(12)$$

We now differentiate equation (6) and find the coefficients s_n in terms of x_0, a and c. These for $n=1$ to 5 are as follows:

$$s_1=c^2$$

$$s_2=\tfrac{1}{2}\left[\frac{1}{a}-\frac{3}{2}ac^2\right]x_0 \qquad s_4=\frac{1}{24}\left[1-3\,a^2c^2\right]x_0$$

$$s_3=-\frac{1}{6}\left[\frac{1}{a}-\frac{3}{2}ac^2\right] \qquad s_5=-\frac{1}{120}\left[1-3\,a^2c^2\right]$$

The solution thus obtained satisfies the boundary conditions at x_0; we must find c (assuming a is known from I) by imposing the condition $\chi(0)=0$. We begin by neglecting coefficients s_n in equation (10) higher than s_3. Then we find

$$0=\frac{1}{3}\left[\frac{1}{a}-\frac{3}{2}ac^2\right]x_0^3 \qquad \ldots\ldots(13)$$

or

$$a^2c^2=2/3. \qquad \ldots\ldots(14)$$

Putting in the limiting form of a^2 from I, namely

$$a^2=3^{2/3}/x_0^2 \qquad \ldots\ldots(15)$$

we obtain

$$c^2=2x_0^2/3^{5/3} \qquad \ldots\ldots(16)$$

or

$$\chi(x_0)=-2x_0^3/3^{5/3} \qquad \ldots\ldots(17)$$

which is simply Gilvarry's result obtained by another method. However the present treatment now enables us to examine the next term in the expansion for small x_0. Retaining all coefficients up to and including s_5 in equation (10) we find

$$0=\frac{1}{3}\left[\frac{1}{a}-\frac{3}{2}ac^2\right]x_0^3+\frac{1}{30}\left[1-3a^2c^2\right]x_0^5. \qquad \ldots\ldots(18)$$

By substituting in the correction term for a^2 and c^2 from equations (15) and (16) and for a in the leading term from equations (11) and (2), it is easy to show that the coefficient of the term in x_0^4 in $\chi(x_0)$ is identically zero. Thus our argument demonstrates that equation (17) is in fact accurate to better than $O(x_0^4)$.

In a similar manner we can obtain χ_1' the slope of χ at the origin to the same order of accuracy from the Taylor expansion and the result is

$$\chi_1'=-2x_0^2/3^{5/3}. \qquad \ldots\ldots(19)$$

Again, the coefficient of the term in x_0^3 is identically zero, and equation (19) is simply Gilvarry's result. However, we have now established that equations (17) and (19) are more accurate than was evident from the derivation used by Gilvarry (equivalent in fact to the approximation implied by our equation (13)) and we can hence proceed to calculate the parameters σ and ω more accurately than was possible in Gilvarry's treatment. We then find

$$\sigma=-\frac{2x_0^4}{3^{7/3}}\left[1+\frac{3^{1/3}}{10}x_0\right], \quad \omega=-\frac{2x_0^4}{3^{10/3}}\left[1+\frac{3^{1/3}}{4}x_0\right] \qquad \ldots\ldots(20)$$

and for completeness we can write the parameters τ and ϵ_0, using equation (2), as

$$\tau=\frac{x_0^4}{3^{4/3}}\left[1+\frac{3^{1/3}}{5}x_0\right], \quad \epsilon_0=\frac{5}{3}\left[1+\frac{3^{1/3}}{20}x_0\right]. \qquad \ldots\ldots(21)$$

In all four cases the first terms agree of course with the results of Gilvarry, the second terms have not been given hitherto however. Further proof of the correctness of the results embodied in equations (20)–(21) is given by the fact that the parameters as expressed in these equations satisfy the relation

$$x_0\frac{d}{dx_0}(\sigma+3\omega)=(3\epsilon_0-2)\sigma+\left(\frac{6}{5}\epsilon_0-4\right)\tau+9(\epsilon_0-1)\omega \qquad \ldots\ldots(22)$$

which Gilvarry has shown must be obeyed by any exact solution. From these results the various thermodynamic functions can be easily obtained from the formulae given by Gilvarry, and these will not be reproduced here.

Of course, the results for $\chi(x_0)$ and χ_1' given in equations (17) and (19) are only computationally useful for small x_0 and in general one must solve equation (6) numerically. Since only three solutions have been obtained previously, and these for x_0 greater than 9·5, we have examined three further cases for smaller values of x_0. We have devised a direct method of solution of equation (6) subject to the boundary conditions (7) which is based on the Taylor expansion we have developed. Starting with a known solution $\phi(x)$, we must choose c for the particular value of x_0 to which $\phi(x)$ corresponds in order to obtain starting values from the Taylor series. Continuing the integration inwards, it will in general turn out that the solution will not pass through the origin, and hence a change must be made in c and another integration started. This means that a certain amount of trial and error is involved but the method is quite practicable because the form of the solutions near the origin, for a given x_0, depends rather critically on c. In this way we have obtained values of c, and hence of $\chi(x_0)$, for $x_0 = 0{\cdot}4976$, 2·800 and 5·401. The last two values were chosen because solutions of the TF equation (1) have been tabulated by the writer for these values of x_0 (March 1952). The first value was taken because it seemed desirable to have at least one solution for a smaller x_0 than 2·8. Our method, unfortunately, is not very suitable, without a good deal more effort, for the calculation of χ_1'. However from the present point of view

Table 1. Boundary Values of χ

x_0	$-\chi(x_0)$ by numerical integration	$-\chi(x_0)$ from Gilvarry's formula
0·4976	0·0402 ± 0·0002	0·0420
2·800	9·27 ± 0·03	9·94
5·401	92·6 ± 0·3	96·3

this is not a serious defect as we are primarily interested in equations of state and, as we have already mentioned, the parameter ω which involves χ_1' is not required for this purpose. The values of $\chi(x_0)$ obtained from these numerical integrations are collected in table 1. We are now in a position to discuss the connection between our results and those obtained previously by Gilvarry, and the final results of our work for the equations of state of elements.

§ 4. COMPARISON WITH GILVARRY'S RESULTS AND IMPROVED EQUATIONS OF STATE

In his work, Gilvarry expressed the quantities $\chi(x_0)$ and χ_1' by expressions having the correct behaviour in the two limits $x_0 \to 0$ and $x_0 \to \infty$. For $\chi(x_0)$ he used the formula

$$\chi(x_0) = \sum C_n x_0^{\,n} \qquad \ldots\ldots(23)$$

where $n = 3$, 4 and 5 and the coefficients C_3 and C_5 are determined by the two limiting forms. The remaining coefficient C_4 was chosen in order to fit the available numerical data (three solutions obtained by FMT). Similarly for χ_1' he wrote

$$\chi_1' = \left[\sum D_n x_0^{\,-n}\right]^{-1} \qquad \ldots\ldots(24)$$

where $n = 1 - \lambda_2$, 1 and 2, with $\lambda_2 = 0{\cdot}77200$. Again the coefficients $D_{1-\lambda_2}$ and D_2 are determined by the asymptotic forms, whilst D_1 was adjusted to fit the data.

The numerical values of the coefficients C_n and D_n as given by Gilvarry are recorded in table 2.

Table 2. Numerical Values of Coefficients in equations (23) and (24)

n	C_n	n	D_n
3	$-3{\cdot}205\times10^{-1}$	$1-\lambda_2$	$-5{\cdot}805\times10^{-3}$
4	$-4{\cdot}021\times10^{-2}$	1	$-3{\cdot}755\times10^{-1}$
5	$-2{\cdot}519\times10^{-3}$	2	$-3{\cdot}120$

It should be noted first of all that equations (23) and (24) fit data in the region $9{\cdot}5<x_0<16$ and that the reliability of the formulae for small x_0 must be open to doubt. In fact, whereas the coefficient of x_0^4 in equation (23) is not zero, we have shown that for small x_0 the exact coefficient is identically zero. We should expect therefore that Gilvarry's formula will lead to values of $|\chi(x_0)|$ which are too large when x_0 is small and the results shown in table 1 confirm this. It will be seen that around $x_0=2{\cdot}8$ there is an error of rather more than 7%. Gilvarry pointed out previously that by adjusting the exponent of the middle term in equation (23) a closer fit could be obtained, and adopting this suggestion we have found that an exponent of 4·2 and a coefficient of $-0{\cdot}0241$ will reproduce the existing data to within about 2%. The agreement for larger values of x_0 is rather less good than Gilvarry obtained. Even with the present exponent the numerical results indicate that the asymptotic form (17) is not being approached quite rapidly enough. We have no accurate data to enable us to improve formula (24) for χ_1' but it seems very likely that similar modifications will be required in this case also.

To obtain equations of state we now observe that we can write the pressure P in the incompletely degenerate formulation we have considered in this paper in terms of the pressure p in the completely degenerate case. We can regard p as known from equation (4). The result is (Gilvarry 1954, eqn (52))

$$P=p\left[1+\frac{5}{2}(\sigma+2\tau)\,\zeta\,(kT)^2\right]. \qquad \ldots\ldots(25)$$

The parameters σ and τ can be regarded as known from the work reported in I and the present paper, and thus reliable equations of state according to the TF method are made available over a wide range of pressures. For small x_0 we can write equation (25) in the form

$$P=p\left[1+\frac{10x_0^4}{3^{7/3}}\left(1+\frac{3^{1/3}}{4}x_0\right)\zeta(kT)^2\right] \qquad \ldots\ldots(26)$$

and x_0 is of course related to the volume v by $v=4\pi(bx_0)^3/3$.

Finally it should be pointed out that the results presented here using the first-order temperature perturbation treatment of MB can be used whenever the temperature is low in comparison with the maximum kinetic energy of electrons near the boundary of the atomic sphere. More precisely, the range of validity of the present treatment can be expressed by the inequality

$$kT\ll\frac{Ze^2}{b}\left[\frac{\phi(x_0)}{x_0}\right]. \qquad \ldots\ldots(27)$$

As Gilvarry has emphasized, since $\phi(x_0)/x_0\sim x_0^{-2}$ as $x_0\to 0$, it follows that in this case high temperatures fall within the range of the treatment given here. On the other hand, as $x_0\to\infty$, $\phi(x_0)/x_0\sim x_0^{-4}$ and thus in this limit the inequality (27) demands temperatures approaching zero.

§ 5. Conclusions

We have shown in this paper how the results of the TF theory derived in I can be utilized to discuss the equations of state of elements when it is not permissible to assume that we are dealing with zero temperature. The equation of MB has been solved for very high pressures by a Taylor expansion and the boundary value of the perturbation function χ can thus be found. In this way two parameters σ and ω, from which, when combined with the results of I, all thermodynamic functions can be calculated, are found in the very high pressure limit to a higher approximation than given previously. For smaller pressures equation (6) has been solved numerically for three cases in order to supplement existing data. A new expression has then been obtained which gives the value of $\chi(x_0)$ to 2% over a wide range of x_0. In this way, for the case of incomplete degeneracy, reliable results for the equations of state of elements according to the TF method are made available over a wide range of pressures.

References

Feynman, R. P., Metropolis, N., and Teller, E., 1949, *Phys. Rev.*, **75**, 1561.
Gilvarry, J. J., 1954, *Phys. Rev.*, **96**, 934.
March, N. H., 1952, *Proc. Camb. Phil. Soc.*, **48**, 665 ; 1953, *Phil. Mag.*, **44**, 346 ; 1955, *Proc. Phys. Soc.* A, **68**, 726.
Marshak, R. E., and Bethe, H. A., 1940, *Astrophys. J.*, **91**, 239.
Sakai, T., 1942, *Proc. Phys.-Math. Soc. Japan*, **24**, 259.
Umeda, K., and Tomishima, Y., 1953, *J. Phys. Soc. Japan*, **8**, 360.
Yokota, I., 1949, *J. Phys. Soc. Japan*, **4**, 82.

Note added in proof. Very recently Gilvarry and Peebles (*Phys. Rev.*, 1955, **99**, 550), have published some additional solutions of equation (6) and have suggested modifications of the formulae previously proposed by Gilvarry (1954). The revised formula which they give for $\chi(x_0)$ is in excellent agreement with that proposed in the present paper.

Calculation of Isotope Shifts in the Spectrum of Helium

By A. P. STONE
Clarendon Laboratory, University of Oxford

Communicated by H. G. Kuhn; *MS. received* 19*th July* 1955

Abstract. The isotope shift due to nuclear motion is calculated for the 2^1S, 2^3S terms of helium, using wave functions which take account of configuration interaction. Agreement is obtained with the experimental term shifts within the limits of experimental error. It is concluded that isotope shifts in helium are due mainly to nuclear motion.

---

§ 1. Introduction

For light elements, the main term in the atomic Hamiltonian which varies with different isotopes is the nuclear kinetic energy. In the centre-of-mass system of a 2-electron atom this takes the form

$$\frac{(\mathbf{p}_1+\mathbf{p}_2)^2}{2M} = \frac{\mathbf{p}_1{}^2+\mathbf{p}_2{}^2}{2M} + \frac{\mathbf{p}_1\cdot\mathbf{p}_2}{M}$$

where M is the nuclear mass and $\mathbf{p}_1$, $\mathbf{p}_2$ are the electronic momenta. The term $(\mathbf{p}_1{}^2+\mathbf{p}_2{}^2)/2M$ gives rise to the reduced mass of the electron, and if spin–orbit interaction is neglected the energy is $M/(M+m)$ times that for an infinitely heavy nucleus, m being the electron mass (Hughes and Eckart 1930). This is known as the 'normal mass effect'. The term $\mathbf{p}_1 . \mathbf{p}_2/M$ gives rise to the 'specific mass effect' and is treated as a perturbation.

Hughes and Eckart (1930) obtained a formula for the specific mass effect in 2-electron atoms, using hydrogen-like wave functions with different nuclear charges for each electron. This type of wave function leads to specific shifts which are zero for the S, D, ... states and non-zero for the P, F, ... states. Results of experiments on various line series in helium (Fred *et al.* 1951, Bradley and Kuhn 1951) show that Hughes and Eckart's treatment is inadequate in this case: Bradley and Kuhn found term shifts which were up to 20% greater than the predicted shifts, and the S, D terms showed definite residual shifts over and above the normal effect.

The suitability of a wave function for calculating the specific effect may be judged by two criteria, the calculated energy and the inclusion of possible configuration interaction, to which the expectation value of $\mathbf{p}_1 . \mathbf{p}_2$ is very sensitive.

In the ground state of helium the specific effect is due entirely to configuration interaction, which occurs to a considerable extent (Green *et al.* 1952, 1953). The specific effect calculated with Hylleraas' 6-term wave function contributes $-5{\cdot}2\ \mathrm{cm}^{-1}$ to the ionization potential of helium (Bethe 1933). A calculation made by the author (unpublished) with the 10-term wave function of Chandrasekhar, Elbert and Herzberg (1953) gave the effect as $-4{\cdot}6\ \mathrm{cm}^{-1}$.

The present paper describes a calculation of the specific effect for the 2^1S, 2^3S terms of helium, using the wave functions of Hylleraas and Undheim (1930) and Huang (1948). These have essentially the same form and satisfy the two criteria of suitability. A brief report of the results has appeared elsewhere (Stone 1955).

§ 2. The Wave Functions

In terms of the coordinates

$$s=r_1+r_2, \qquad t=r_2-r_1, \qquad u=r_{12}$$

the Hylleraas–Undheim wave functions are given by

$$\psi=\sum_{i=1} c_i\psi_i \qquad \ldots\ldots(1)$$

where the component functions ψ_i are

$$\left.\begin{array}{ll} 2^1\mathrm{S}: & \psi_1=\exp(-\tfrac{1}{2}s)\cosh\tfrac{1}{2}ct, \quad \psi_3=t\exp(-\tfrac{1}{2}s)\sinh\tfrac{1}{2}ct \\ 2^3\mathrm{S}: & \psi_1=\exp(-\tfrac{1}{2}s)\sinh\tfrac{1}{2}ct, \quad \psi_3=t\exp(-\tfrac{1}{2}s)\cosh\tfrac{1}{2}ct \end{array}\right\} \quad \ldots.(2a)$$

$$\psi_2=s\psi_1, \qquad \psi_4=u\psi_1, \qquad \psi_5=u\psi_2, \qquad \psi_6=u\psi_3. \qquad \ldots\ldots(2b)$$

The unit of length is $a_0/4k$, a_0 being the Bohr radius. The constants c, k and the coefficients c_i are parameters determined by the variation principle and are given in table 1. The parameters for the triplet state quoted in column 4 of table 1 were communicated privately to the author by Professor Hylleraas. They were obtained in re-calculating the triplet energy, which differs from that previously given by Hylleraas and Undheim owing to a numerical error. The parameters of the singlet wave function given in column 2 of table 1 were calculated by the author from the data of Hylleraas and Undheim.

Table 1. Parameters of the 2S Wave Functions (non-normalized)

	Singlet		Triplet	
	Hylleraas–Undheim	Huang	Hylleraas–Undheim	Huang
k	0·67	0·6755	0·675	0·676
c	0·55	0·54996	0·55	(see § 4)
c_1	1	1	1	1
c_2	−0·13746	−0·13575	−0·29048	−0·2865
c_3	−0·13039	−0·13599	−0·28390	−0·2842
c_4	0·0449	0·05316	−0·08218	−0·07978
c_5	−0·005389	−0·006629	−0·00663	−0·007053
c_6	0·0001446	0·0009538	0·01130	0·011718
Energy (*Ry*)	−4·28980	−4·28975	−4·350406	−4·35040

The Huang wave functions have the same form as (1) with component functions given by

$$\psi_1'=\tfrac{1}{2}\left[\exp(-ar_1-br_2)\pm\exp(-br_1-ar_2)\right],$$
$$\psi_3'=\tfrac{1}{2}(r_2-r_1)\left[\exp(-ar_1-br_2)\mp\exp(-br_1-ar_2)\right]$$

together with relations as in equations (2*b*). The upper and lower signs refer to the singlet and triplet states, respectively. Huang's values of the parameters for the singlet make $a+b=1$ and the wave functions for this state can be put into exactly the same form as in equations (2) with $c=2a-1$. This is not quite the case for the triplet for which $a+b=1{\cdot}000185$; however, the assumption of exact equality is made in the present calculation (see § 4). The values of the parameters given in columns 3, 5 of table 1 were obtained from Huang's paper.

§ 3. THE FORMULA FOR THE SPECIFIC SHIFT

By first-order perturbation theory one finds the specific term shift for an isotope of nuclear mass M to be

$$\Delta T = -32k^2 \frac{m}{M} Ry K_{ij}c_i c_j / I_{ij}c_i c_j$$

where

$$I_{ij} = \frac{1}{\pi^2}\iint \psi_i\psi_j \, d\mathbf{r}_1 \, d\mathbf{r}_2$$

and

$$K_{ij} = F_{ij} + \tfrac{1}{2}(G_{ij} + G_{ji}) - J_{ij}$$

where

$$F_{ij} = \frac{1}{\pi^2}\iint \cos\theta \frac{\partial\psi_i}{\partial r_1} \cdot \frac{\partial\psi_j}{\partial r_2} \, d\mathbf{r}_1 \, d\mathbf{r}_2$$

$$G_{ij} = \frac{2}{\pi^2}\iint \frac{r_2\cos\theta - r_1}{r_{12}} \frac{\partial\psi_i}{\partial r_1} \frac{\partial\psi_j}{\partial r_{12}} \, d\mathbf{r}_1 \, d\mathbf{r}_2$$

$$J_{ij} = \frac{1}{\pi^2}\iint \frac{\partial\psi_i}{\partial r_{12}} \frac{\partial\psi_j}{\partial r_{12}} \, d\mathbf{r}_1 \, d\mathbf{r}_2.$$

Ry is the Rydberg energy for infinite nuclear mass. The summation convention is employed with $i, j = 1, 2, \ldots, 6$, and the integrals are divided by π^2 for convenience. In deriving the expression for K_{ij} use is made of the easily proved formula for two functions v, w of r_1, r_2, r_{12}:

$$\nabla_1 v \,.\, \nabla_2 w = \cos\theta \frac{\partial v}{\partial r_1}\frac{\partial w}{\partial r_2} + \frac{r_1\cos\theta - r_2}{r_{12}}\frac{\partial v}{\partial r_{12}}\frac{\partial w}{\partial r_2} + \frac{r_2\cos\theta - r_1}{r_{12}}\frac{\partial v}{\partial r_1}\frac{\partial w}{\partial r_{12}} - \frac{\partial v}{\partial r_{12}}\frac{\partial w}{\partial r_{12}},$$

in which θ is the angle between the vectors $\mathbf{r}_1$, $\mathbf{r}_2$. After lengthy calculations the expressions for I_{ij}, K_{ij} given in the appendix are obtained, and hence the numerical results given in columns 4, 5 of table 2.

A check on many of the integrals occurring in the calculation may be made by differentiating them with respect to the parameter c.

Thus $$\frac{\partial}{\partial c} I_{11} = I_{13}, \ \frac{\partial}{\partial c} I_{12} = I_{23}, \ \frac{\partial}{\partial c} I_{13} = \tfrac{1}{2}(I_{33} + \tilde{I}_{33}) \qquad \ldots\ldots(3)$$

where $\tilde{I}_{ij}$ refers to the singlet state if I_{ij} refers to the triplet state, and vice versa. Six more relations are obtained on multiplying (3) bu u, u^2. Also

$$\frac{\partial}{\partial c} K_{14} = \tfrac{1}{2}(K_{34} + K_{16}), \ \frac{\partial}{\partial c} K_{44} = K_{46}.$$

§ 4. DISCUSSION

The expressions for the integrals given in the appendix depend, as stated in § 2, on assuming the equality $2a - 1 = 1 - 2b = c$ for the Huang wave functions. The values of $2a - 1$, $1 - 2b$ for his triplet wave function are 0·55030 and 0·54993 respectively; the calculated specific shift of 0·076 cm^{-1} is found in the approximation of taking $c = 0·55$, i.e. the same values of the integrals are used as for the Hylleraas–Undheim triplet wave function. The other parameters of these wave functions are very similar and the calculated specific shifts 'A' in table 2 agree to two significant figures, which is the estimated accuracy of the value obtained with the Huang wave function. For the singlet state, the Huang wave function gives the higher shift, which is also the one further from the experimental value.

Table 2. Term Shifts (cm^{-1})

Shift	Term	Wave function			Expt.
		Hughes–Eckart	Huang	Hylleraas–Undheim	
A	2^1S	0	0·159	0·149	0·13 ± 0·02
A	2^3S	0	0·076	0·0758	0·10 ± 0·02
B	2^1S	1·436	1·595	1·585	1·57 ± 0·02
B	2^3S	1·723	1·799	1·799	1·82 ± 0·02

A : total term shift minus normal term shift; B : total term shift.

The shifts found in this paper disagree with those calculated by Hamermesh and Eisner using the Huang wave functions and quoted by Fred *et al.* (1951).

The experimental shifts 'B' given in column 6 of table 2 were obtained by Bradley and Kuhn (1951) by extrapolating their measured shifts of the lines $2^{1,3}$S–$n^{1,3}$P to the series limits. Fred *et al.* observed only three lines of the triplet series, but found a residual shift 'A' of about 0·135 cm^{-1} for the 2^1S state, which agrees well with the value 0·13 cm^{-1} given by Bradley and Kuhn.

The total calculated term shifts 'B' given in columns 4, 5 of table 2 are all within the estimated limits of experimental error with the exception of the shift found with the Huang singlet wave function, which is just outside the limit of error. It is concluded that nuclear motion makes by far the most important contribution to isotope shift in helium.

ACKNOWLEDGMENTS

The author wishes to express his thanks to Dr. H. Kuhn, Dr. J. A. Spiers and Professor H. M. Foley for their interest in this work, and is indebted to the Department of Scientific and Industrial Research for a maintenance grant.

APPENDIX

The integrals I_{ij}, K_{ij} are given in terms of the quantities

$$A_n=(1-c)^{-n}+(1+c)^{-n},\quad B_n=(1-c)^{-n}-(1+c)^{-n},\quad C_n=(1-c^2)^{-n}$$

the upper and lower signs referring to the singlet and triplet states, respectively:

$$I_{11}=32(C_3\pm 1),\qquad I_{22}=192[(7+c^2)C_5\pm 7],$$

$$I_{12}=192(C_4\pm 1),\qquad I_{23}=1536cC_5,$$

$$I_{13}=192cC_4,\qquad I_{33}=192[(1+7c^2)C_5\mp 1],$$

$$I_{14}=12A_4+18A_3+20(A_2+A_1)\pm 140,$$

$$I_{24}=I_{15}=48A_5+90A_4+112A_3+120(A_2+A_1)\pm 980,$$

$$I_{34}=I_{16}=48B_5+54B_4+40B_3+20B_2,$$

$$I_{35}=I_{26}=24(10B_6+15B_5+14B_4+10B_3+5B_2),$$

$$I_{25}=8(30A_6+63A_5+87A_4+100A_3+105A_2+105A_1\pm 980),$$

$$I_{36}=8(30A_6+27A_5+15A_4+5A_3\mp 154),$$

$$I_{44}=768[(1+c^2)C_5\pm 1],\qquad I_{55}=9216[(6+13c^2+c^4)C_7\pm 6],$$

$$I_{45}=3072[(2+3c^2)C_6\pm 2],\qquad I_{56}=92160c(1+c^2)C_7,$$

$$I_{46}=3072c(3+2c^2)C_6,\qquad I_{66}=9216[(1+13c^2+6c^4)C_7\mp 1].$$

$$\begin{aligned}
K_{14} &= A_2 + \tfrac{3}{2}A_1 \pm 5(1-c^2) & K_{16} &= 3B_3 + \tfrac{5}{2}B_2 \\
K_{24} &= A_3 + \tfrac{5}{2}A_2 + 4A_1 \pm 5(3-7c^2) & K_{26} &= 6B_4 + 10B_3 + 8B_2 \\
K_{34} &= B_3 + \tfrac{1}{2}B_2 \mp 20c & K_{44} &= 16[C_3 \pm (1-3c^2)] \\
K_{15} &= 3A_3 + \tfrac{13}{2}A_2 + 8A_1 \pm 35(1-c^2) & K_{45} &= 96\,[C_4 \pm (1-4c^2)] \\
K_{25} &= 6A_4 + 14A_3 + 22A_2 + 28A_1 \pm 140\,(1-2c^2) & K_{46} &= 96c\,(C_4 \mp 1) \\
K_{35} &= 6B_4 + 8B_3 + 4B_2 \mp 140c & K_{55} &= 192\,[(3+c^2)\,C_5 \pm 3(1-6c^2)] \\
K_{36} &= 6A_4 + 2(A_3+A_2) + 4A_1 + 2c(B_3+B_2) & K_{56} &= 768c\,(C_5 \mp 1) \\
&\qquad \mp 28(1-c^2) & K_{66} &= 192[(1+3c^2)C_5 \mp (1-2c^2)].
\end{aligned}$$

REFERENCES

BETHE, H., 1933, *Handbuch der Physik*, Vol. 24/1 (Berlin : Julius Springer), p. 374.

BRADLEY, L. C., and KUHN, H., 1951, *Proc. Roy. Soc.* A, **209**, 325.

CHANDRASEKHAR, S., ELBERT, D., and HERZBERG, G., 1953, *Phys. Rev.*, **91**, 1172.

FRED, M., TOMKINS, F. S., BRODY, J. K., and HAMERMESH, M., 1951, *Phys. Rev.*, **82**, 406.

GREEN, L. C., MULDER, M. M., and MILNER, P. C., 1953, *Phys. Rev.*, **91**, 35.

GREEN, L. C., MULDER, M. M., UFFORD, C. W., SLAYMAKER, E., KRAWITZ, E., and MERTZ, R. T., 1952, *Phys. Rev.*, **85**, 65.

HUANG, S.-S., 1948, *Astrophys. J.*, **108**, 354.

HUGHES, D. S., and ECKART, C., 1930, *Phys. Rev.*, **36**, 694.

HYLLERAAS, E. A., and UNDHEIM, B., 1930, *Z. Phys.*, **65**, 759.

STONE, A. P., 1955, *Nature, Lond.*, **176**, 130.

The Ionization by Electrons of the Excited 2s and 2p States of Atomic Hydrogen

By P. SWAN
Physics Department, Melbourne University, Melbourne, Australia

Communicated by H. S. W. Massey; MS. received 10*th June* 1955

Abstract. The cross sections for ionization by electrons of H2s and H2p have been evaluated in the energy range 5–100 ev. First order perturbation theory is employed, the ejected electron being described by a Coulomb wave function, and the bombarding electron by plane waves both before and after collision. The H2s cross sections are larger than the H2p values, but both are much greater than the cross section for ionization of the ground state H1s. The classical cross section formula agrees roughly with the H2p ($m = \pm 1$) results, but is considerably smaller than the H2p ($m = 0$) and H2s cross sections.

When hydrogen gas is subjected to a heavy electric discharge, the concentration of excited atoms can become comparable with that of normal hydrogen atoms. In order to find the electron mobility, it is necessary to know the cross sections for elastic and inelastic scattering of electrons by the lowest excited states of atomic hydrogen, namely H2s and H2p.

The elastic cross sections have been evaluated by Swan (1954), so that it is the object of this paper to find the corresponding ionization cross sections.

The ionization of the K shell of atoms by electron impact has been studied theoretically by Bethe (1930), Massey and Mohr (1933), Graf Soden (1934), Massey and Burhop (1935), and Wetzel (1933, 1936). Burhop (1940) and Mandl (1952) have independently extended the theory to the L shell of atoms. However, there are a number of printing errors in the papers of Massey and Mohr and Burhop respectively, and some of Mandl's formulae are in a form inconvenient for computation. For this reason the formulae are restated below.

In the first order perturbation theory, the bombarding electron is described before and after collision by plane waves, the error involved in not using Coulomb waves being small provided the energy is large. In this case the motion of the electron is but little modified by the field of the nucleus.

However the atomic electron has in general only a small energy after ionization so that the correct Coulomb wave function must be used.

Electron exchange is neglected, and also the interaction between the two electrons, apart from the latter causing the transition from bound to free states. Both these approximations again require a high energy to be justified.

Writing $\mathbf{k}$ = incident electron momentum, $\mathbf{k}'$ = scattered momentum, $\boldsymbol{\varkappa}$ = ejected electron momentum, $\mathbf{K} = \mathbf{k} - \mathbf{k}'$ = change of momentum of the incident electron, $a_0 = \hbar^2/me^2$, the differential cross section for ionization of the K shell of a hydrogen-like atom is given by Mott and Massey (1949),

$$I(K,\kappa)\,dK\,d\kappa$$

$$= \frac{2^{11}\pi\mu_K^6\kappa}{a_0^2 k^2 K}\{1-\exp(-2\pi\mu_K/\kappa)\}^{-1}\exp\left\{-\frac{2\mu_K}{\kappa}\arctan\frac{2\mu_K\kappa}{(K^2-\kappa^2+\mu_K^2)}\right\}$$

$$\times\{K^2+\tfrac{1}{3}(\mu_K^2+\kappa^2)\}\{\mu_K^4+2\mu_K^2(K^2+\kappa^2)+(K^2-\kappa^2)^2\}^{-3}\,dK d\kappa \quad \ldots\ldots(1)$$

where $\mu_K = z/a_0$.

The differential cross sections for the 2s and 2p $(m=0)$ states are quoted from Burhop (1940). Taking $\mu_L = z/2a_0$,

$$I(K,\kappa)\,dK\,d\kappa = \frac{2^{14}\pi\mu_L^6}{15\,a_0^2}\frac{\kappa k'}{K^2 k}\exp\left\{-\frac{4\mu_L}{\kappa}\arctan\frac{2\mu_L\kappa}{(K^2-\kappa^2+\mu_L^2)}\right\}$$

$$\times\{\mu_L^4+2(K^2+\kappa^2)\mu_L^2+(K^2-\kappa^2)^2\}^{-5}\,A\,dK\,d\kappa \quad \ldots\ldots(2)$$

where for H2s,

$$A = 20\mu_L^{10}+\mu_L^8(85\kappa^2+47K^2)+\mu_L^6(140\kappa^4+100K^4)$$

$$+\mu_L^4(110\kappa^6-82\kappa^4K^2-310\kappa^2K^4+410K^6)+40\mu_L^2(\kappa^2-K^2)^2(\kappa^4+\kappa^2K^2-4K^4)$$

$$+5(\kappa^2-K^2)^4(\kappa^2+3K^2) \quad \ldots\ldots(3)$$

and for H2p $(m=0)$,

$$A = 23\mu_L^{10}+\mu_L^8(76\kappa^2+204K^2)+\mu_L^6(90\kappa^4+444\kappa^2K^2+218K^4)$$

$$+4\mu_L^4(\kappa^2-K^2)(11\kappa^4+80\kappa^2K^2+85K^4)$$

$$+\mu_L^2(\kappa^2-K^2)^2(7\kappa^4+50\kappa^2K^2+135K^4). \quad \ldots\ldots(4)$$

The formula for H2p $(m=\pm 1)$ uses (2), with A as given by Mandl (1952):

H2p $(m=\pm 1)$,

$$A = 4\mu_L^2(\mu_L^2+\kappa^2+5K^2)\{\mu_L^4+2(K^2+\kappa^2)\mu_L^2+(K^2-\kappa^2)^2\}(4\mu_L^2+\kappa^2). \quad \ldots(5)$$

By the conservation of energy principle, we have

$$k^2+2\epsilon_H = \kappa^2+k'^2,$$

where $\epsilon_H = -1/8$ is the energy of the L shell of hydrogen. Thus

$$\kappa = (k^2-0\cdot25-k'^2)^{1/2}, \quad \kappa_{\max} = (k^2-0\cdot25)^{1/2}. \quad \ldots\ldots(6)$$

The total cross section σ for ionization then becomes

$$\sigma = \int_{k-k'}^{k+k'} dK \int_0^{\kappa_{\max}} d\kappa\, I(K,\kappa). \quad \ldots\ldots(7)$$

Equation (7) gives the cross section per atomic electron so that the total cross section for ejection from the L shell is found by multiplying (7) by the factor 2.

J. J. Thomson (1912) has given a classical formula for ionization cross sections:

$$\sigma = \frac{\pi e^4}{E}\left(\frac{1}{E_{\mathrm{i}}}-\frac{1}{E}\right) \quad \ldots\ldots(8)$$

where E_{i} and E are the ionization and bombarding energies respectively. In atomic units, the L-shell result becomes

$$\sigma = \frac{\pi}{E}\left(8-\frac{1}{E}\right). \quad \ldots\ldots(9)$$

One would expect the classical result to hold for large quantum numbers l, that is highly excited atoms, but not for S states, which have no classical analogue.

Numerical Calculations

In the calculations the double integral expression (7) for the cross section was evaluated for a number of bombarding electron energies between 5 and 100 ev. Atomic units $m=e=\hbar=a_0=1$ were used. $I(K,\kappa)$ was plotted as a square table function of K and κ, an interval of 0·1 in atomic units a_0 being used for $0{\cdot}1 \leqslant K \leqslant 1{\cdot}0$, $0{\cdot}1 \leqslant \kappa \leqslant 1{\cdot}0$, and an interval of 0·2 for $1{\cdot}0 \leqslant K \leqslant 5{\cdot}6$, $1{\cdot}0 \leqslant \kappa \leqslant 2{\cdot}8$. Values of $I(K,\kappa)$ for $K \leqslant 0{\cdot}1$ were estimated individually.

The functions A in equations (3), (4) and (5) for H2s, H2p$(m=0)$ and H2p $(m=\pm 1)$ respectively were evaluated in the same intervals, and σ was found by double numerical integration of $I(K,\kappa)$ according to equation (7).

The cross section for H2p was found by suitably weighing the σ's obtained for the magnetic sub-states $m=\pm 1, 0$.

$$\sigma(2\text{p}) = \tfrac{2}{3}\sigma(2\text{p}, m=\pm 1) + \tfrac{1}{3}\sigma(2\text{p}, m=0). \qquad \ldots\ldots(10)$$

Results are shown in the table in units of $10^{-16}\,\text{cm}^2$, together with the classical cross section (8).

Ionization Cross Sections (in units of $10^{-16}\,\text{cm}^2$) for Atomic Hydrogen

k	E (ev)	H2s	H2p $(m=\pm 1)$	H2p $(m=0)$	H2p	Classical, $n=2$
0·6	4·87	21·27	9·77	16·77	12·10	11·88
0·8	8·66	31·80	16·81	37·92	28·85	13·32
1·0	13·53	26·80	15·71	35·52	22·31	10·49
1·2	19·48	21·60	12·33	30·08	18·25	8·03
1·8	43·83	12·46	6·29	16·29	9·62	3·99
2·3	71·57	8·76	4·18	10·92	6·43	2·52
2·7	98·63	6·73	3·34	8·27	4·99	1·85

The cross sections are shown graphically in the figure as a function of momentum k together with values for the ground state H1s interpolated from a table of

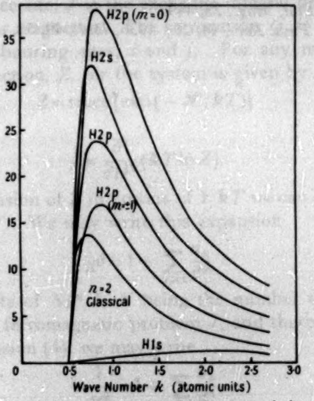

Cross sections in units of $10^{-16}\,\text{cm}^2$ for the ionization of the K and L shells of hydrogen by electron impact.

Massey and Mohr (1933). Below about 20 ev the condition for the perturbation treatment is not fulfilled so that the table cannot be relied on in this region.

The classical cross section agrees roughly with the H2p ($m = \pm 1$) curve but is smaller by a factor of 4 or more than the H2p ($m = 0$) curve. The former agreement is probably incidental as the quantum numbers involved are small. The H2s cross sections are also considerably larger than the classical values, and all the L shell results are greater by large factors than the ground state ionization cross sections. In this latter property the ionization results follow the same trend as the elastic scattering by H2s and H2p (Swan 1954). This was interpreted for elastic scattering as due to the potential acting between atom and bombarding electron having a much longer tail for excited atoms than for the ground state. Thus interactions involving high angular momenta become very important for excited atoms bombarded with electrons, resulting in considerably larger total cross sections.

The same reasons would explain the large ionization cross sections for excited hydrogen as compared to normal hydrogen.

ACKNOWLEDGMENTS

I would like to thank Professor H. S. W. Massey for the interest shown in this work and Professor C. B. O. Mohr for many useful discussions.

REFERENCES

BETHE, H. A., 1930, *Ann. Phys., Lpz.*, **5,** 325.

BURHOP, E. H. S., 1940, *Proc. Camb. Phil. Soc.*, **36,** 43.

MANDL, F., 1952, *A.E.R.E. Report*, T/R 1006 (London : H. M. Stationery Office).

MASSEY, H. S. W., and BURHOP, E. H. S., 1935, *Phys. Rev.*, **48,** 468.

MASSEY, H. S. W., and MOHR, C. B. O., 1933, *Proc. Roy. Soc.* A, **140,** 613.

MOTT, N. F., and MASSEY, H. S. W., 1949, *Theory of Atomic Collisions*, 2nd Ed. (Oxford : University Press), p. 235.

SODEN, D., 1934, *Ann. Phys., Lpz.*, **19,** 409.

SWAN, P., 1954, *Proc. Phys. Soc.* A, **67,** 1086.

THOMSON, J. J., 1912, *Phil. Mag.*, **23,** 449.

WETZEL, W. W., 1933, *Phys. Rev.*, **44,** 25; 1936, *Ibid.*, **49,** 53.

On the High-Temperature Susceptibility for the Heisenberg Model of a Ferromagnet

By G. S. RUSHBROOKE and P. J. WOOD
Physics Department, King's College, Newcastle-upon-Tyne,
University of Durham

Communicated by E. C. Stoner; MS. received 11*th July* 1955 *and in amended form* 17*th August* 1955

Abstract. The paper deals with the high-temperature expansions, in powers of T^{-1}, of the susceptibility, χ, and the inverse susceptibility, χ^{-1}, for the Heisenberg model of a ferromagnet. Expressions, valid for any lattice, are given for the coefficients in these expansions, up to and including the coefficient of T^{-5}. The results are discussed numerically, for particular lattices, in their bearing on the Curie temperature.

---

§ 1. Introduction

Series expansions in inverse powers of the temperature, of the susceptibility χ for the Heisenberg model of a ferromagnet have been given by Opechowski (1937, 1938) and Zehler (1950): see also Van Vleck (1951). The Heisenberg model associates one electron with each site of a regular crystal lattice, and takes the effective Hamiltonian, $\mathscr{H}$, of the system, in the presence of an external magnetic field $\mathbf{H}$, to be given by

$$\mathscr{H} = -\tfrac{1}{2}J \sum_{\langle i,j \rangle} \boldsymbol{\sigma}^{(i)}.\boldsymbol{\sigma}^{(j)} - \beta \sum_i \boldsymbol{\sigma}^{(i)}.\mathbf{H} \qquad \ldots\ldots(1)$$

where $\boldsymbol{\sigma}^{(i)}$ is the vector whose components are the Pauli spin-matrices for an electron on the ith lattice-site, J is the exchange-integral between neighbouring electrons and β the Bohr magneton. The summation $\langle i, j \rangle$ denotes summation over all pairs of neighbouring sites, i and j. For any matrix representation of $\mathscr{H}$, the partition-function, Z, for the system is given by

$$Z = \mathrm{trace}\,[\exp(-\mathscr{H}/\boldsymbol{k}T)] \qquad \ldots\ldots(2)$$

and then

$$\chi = \frac{\partial^2}{\partial H^2}(\boldsymbol{k}T \ln Z). \qquad \ldots\ldots(3)$$

Thus from an expansion of Z in powers of $1/\boldsymbol{k}T$ we can deduce an expansion of χ in powers of $1/\boldsymbol{k}T$. We may write this expansion

$$\chi\theta = 1 + \sum_{n\geqslant 1} \frac{a_n}{\theta^n} \qquad \ldots\ldots(4)$$

where now χ is in units of $N\beta^2/J$, N being the number of lattice-sites, and θ denotes $\boldsymbol{k}T/J$. In the ferromagnetic problem J, and therefore θ, is positive.

Inverting the expansion (4), we may write

$$\frac{1}{\chi\theta} = 1 + \sum_{n\geqslant 1} \frac{b_n}{\theta^n} \qquad \ldots\ldots(5)$$

where b_n is a combination of the coefficients $a_n, a_{n-1}, \ldots a_1$.

The expansions (4) and (5) are assumed to be valid above the Curie temperature of the model under consideration; and Opechowski and Zehler have determined this Curie temperature by curtailing the right-hand side of (5) after the few coefficients b_n which have been evaluated numerically, and then solving the resulting polynomial of low degree to find the value of θ for which $1/\chi$ vanishes. We shall criticize this procedure later.†

In general, of course, the coefficients a_n and b_n are functions of H, and should be written $a_n(H)$ and $b_n(H)$. Similarly $\chi=\chi(H)$. But we are principally interested physically in $\chi(0)$, the limit of χ for small H, and thus in $a_n(0)$ and $b_n(0)$. In this paper we shall confine ourselves to the discussion of $a_n(0)$ and $b_n(0)$ and, for brevity, shall use the simple notation a_n and b_n for these quantities.

The calculations of Opechowski produced numerical values for a_1, a_2 and a_3 for the face-centred cubic, simple cubic and diamond lattices, and a value for a_4 for the face-centred cubic lattice. This last result was later found by Zehler to be incorrect; and Zehler gives the true values of a_4 for both the face-centred and simple cubic lattices.

Using what is perhaps a rather different computational approach (Zehler does not give details), we have calculated a_1, a_2, a_3, a_4 and a_5 for an arbitrary lattice, the values for any particular lattice being obtained by substituting the appropriate lattice parameters in the general expressions. For the first four coefficients our results agree with those of Zehler, which is sufficient guarantee of their correctness. In the case of a_5 we have no previous results against which to check our formula.‡ But the general trend of coefficients, discussed below, does not suggest that there is anything markedly wrong with the answer.

After outlining the method used to tackle the problem we shall simply present the results without going into full computational details. We shall then discuss what conclusions may be drawn from these coefficients a_n or b_n, for various lattices.

§ 2. ALGEBRAIC METHOD

Taking σ_3 to correspond to the direction of $\mathbf{H}$, and writing

$$\sum_{\langle i,j\rangle} \boldsymbol{\sigma}^{(i)}\cdot\boldsymbol{\sigma}^{(j)}=P, \quad \sum_i \sigma_3^{(i)}=Q$$

equation (2) gives

$$Z=2^N\left[1+\sum_{r\geqslant 1}\frac{\mu_r}{r\,!}\left(\frac{1}{2\theta}\right)^r\right] \qquad \ldots\ldots(6)$$

where

$$\mu_r=\langle(P+\alpha Q)^r\rangle. \qquad \ldots\ldots(7)$$

---

† At the request of a referee, we add a brief comment on a paper by Tredgold (1953). Tredgold criticizes the Opechowski–Zehler procedure for finding the Curie temperature, on the ground that if equation (4) is curtailed after a few terms then its reciprocal will never vanish since the sum of a few terms from the right-hand side of (4) can never become infinite, except for $\theta=0$. He then proceeds, for the face-centred cubic lattice, to find a power series expansion for χ^{-1} by an alternative method, but fails to point out that the terms he obtains are precisely the first three terms (stopping at $n=3$) of equation (5), as calculated by Opechowski, so that his estimates of the Curie temperature are precisely those already given (see table 3). (Note, Tredgold's symbol γ stands for z/θ, i.e. $12/\theta$, in our notation.) While not disputing the interest of Tredgold's alternative computational approach, we do not believe his initial criticism to be well founded. For, as we argue in § 4 below, it is the radius of convergence of (4) which determines the Curie temperature, and the Opechowski–Zehler procedure is one way, though perhaps not the best, of estimating this radius of convergence.

‡ Both authors performed the calculations independently; but this is not a complete check since comparisons of our respective results were necessarily made from time to time and disagreements rectified.

Here $\varkappa$ stands for $2\beta H/J$, and $\langle A \rangle$ denotes $(\text{trace}\, A)/2^N$, where A is the matrix representation of a spin-operator in the 2^N-dimensional space which is the N-fold direct product of the 2-dimensional spin spaces of each electron.

Since P and Q commute, we are thus faced with having to calculate expressions of the form $\langle P^s Q^t \rangle$, and for $\chi(0)$ we require only $t=2$. Now

$$(A \times B).(C \times D) = AC \times BD \quad \text{and} \quad \text{tr}\,(A \times B) = \text{tr}\, A\,.\,\text{tr}\, B,$$

while $\boldsymbol{\sigma}^{(i)}.\boldsymbol{\sigma}^{(j)}$ is represented by

$$I_2 \times I_2 \times \ldots \times \sigma_\alpha \times \ldots \times \sigma_\alpha \times \ldots \times I_2$$

where I_2 is the two-dimensional unit matrix and the σ-matrices occur in the ith and jth places (summation over a repeated suffix being implied). Consequently, since $\sigma_\alpha \sigma_\beta = i\epsilon_{\alpha\beta\gamma}\sigma_\gamma + \delta_{\alpha\beta} I_2$ and $\text{tr}\,\sigma_\alpha = 0$, the factors 2, arising from $\text{tr}\, I_2$, cancel with the 2^N in the denominator of $\langle A \rangle$ so that we may ignore these factors and calculate $\langle A \rangle$ algebraically, using

$$\sigma_\alpha \sigma_\beta = i\epsilon_{\alpha\beta\gamma}\sigma_\gamma + \delta_{\alpha\beta}. \qquad \ldots\ldots(8)$$

Further, each contribution to $\langle P^s Q^t \rangle$ may be represented by a diagram, such as

=

in which each point of the diagram corresponds to a lattice-site, each line to a $\boldsymbol{\sigma}^{(i)}.\boldsymbol{\sigma}^{(j)}$ term and each cross to a $\sigma_3{}^{(i)}$ term. Diagrams pertaining to $\langle P^s Q^t \rangle$ comprise s lines and t crosses: and the only non-vanishing contributions to $\langle P^s Q^t \rangle$ arise from diagrams in which there are no isolated single crosses and no points which are solely the terminus of a single line.

Strictly, such a diagram corresponds to a group of terms in the expansion of $P^s Q^t$. For, firstly, the particular lattice-sites involved are immaterial in the calculation of the corresponding trace and, secondly, the simple triangle

for example (in which the numbers 1, 2, 3 denote the particular lattice-sites involved) arises from the six possibilities

$$(\boldsymbol{\sigma}^{(1)}.\boldsymbol{\sigma}^{(2)})(\boldsymbol{\sigma}^{(2)}.\boldsymbol{\sigma}^{(3)})(\boldsymbol{\sigma}^{(3)}.\boldsymbol{\sigma}^{(1)}), \qquad (\boldsymbol{\sigma}^{(1)}.\boldsymbol{\sigma}^{(2)})(\boldsymbol{\sigma}^{(3)}.\boldsymbol{\sigma}^{(1)})(\boldsymbol{\sigma}^{(2)}.\boldsymbol{\sigma}^{(3)})\ldots,$$
$$(\boldsymbol{\sigma}^{(3)}.\boldsymbol{\sigma}^{(1)})(\boldsymbol{\sigma}^{(1)}.\boldsymbol{\sigma}^{(2)})(\boldsymbol{\sigma}^{(2)}.\boldsymbol{\sigma}^{(3)}), \qquad (\boldsymbol{\sigma}^{(3)}.\boldsymbol{\sigma}^{(1)})(\boldsymbol{\sigma}^{(2)}.\boldsymbol{\sigma}^{(3)})(\boldsymbol{\sigma}^{(1)}.\boldsymbol{\sigma}^{(2)}).$$

We have thus (*a*) to multiply the calculated traces by the number of times the corresponding diagrams can 'occur on the lattice' and (*b*) to sum over all possible sequences of the factors pertaining to any particular diagram.

Although care is needed in the calculations involved in (*a*), the real complexity of the problem comes from (*b*), i.e. from the non-commutativity of the σ-functions. Each of the hundred or so different diagrams involved in calculating a_5, for example, since it involves 5 lines, may give rise to as many as 120 different permutations of the $\boldsymbol{\sigma}^{(i)}.\boldsymbol{\sigma}^{(j)}$ factors; a direct approach is clearly impracticable. But, without undue labour, the calculations can be performed as follows:

If, for brevity, we denote $\boldsymbol{\sigma}^{(1)}.\boldsymbol{\sigma}^{(2)}$ by (12), then there are a number of simple, first principle, relationships such as

$$(12)^2 = 3 - 2(12)$$
$$(23)[(12)+(13)] = (12)+(13)$$
$$(12)(23)+(23)(12) = 2(13)$$

which follow from equation (8), and which enable us to reduce the quantities we require to simpler terms, whose traces are elementary. For example, if $\sum_{(P)}$ denotes the sum over all permutations of the corresponding factors,

$$\sum_{(P)}$$ $$=18-4[(12)+(23)+(31)]$$

$$\sum_{(P)}$$ 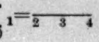 $$=20(24)-8(14)-8(13)(24)+8(14)(23)$$

$$\sum_{(P)}$$ 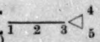 $$=200(13)-80(13)(45)-24(13)(24)-24(13)(25)+24(23)(14)+24(23)(15).$$

Although there does not seem to be any guarantee that such a reduction is always possible, to a result in which there is no repeated numeral in any term on the right-hand side, we have in fact succeeded in reducing all diagrams in this way (with just one exception, namely

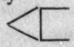

which defeated us, but for which the corresponding trace could be calculated without difficulty from the stage reached). There seems no point in giving a complete list of these results, but we would observe that from them we can obtain at once the corresponding traces pertaining not only to these diagrams without crosses (σ_3 terms) but also to these diagrams with any number of crosses added. Though we have in fact confined attention to $t=2$, it would not entail much additional labour to find how the coefficients $a_1, a_2, \ldots, a_5$ depend on H.

Before summarizing our results for the coefficients a_n and b_n, we would add only that whereas the coefficients (moments) μ_r in (6) can involve higher powers of N than the first (since the diagrams discussed above may involve more than one separate piece), the corresponding coefficients λ_r (cumulants) in the formula for the free energy F,

$$F=-N\boldsymbol{k}T\ln 2-\boldsymbol{k}T\sum_{r\geq 1}\frac{\lambda_r}{r!}\left(\frac{1}{2\theta}\right)^r \qquad \ldots\ldots(9)$$

are directly proportional to N. In fact λ_r is the term proportional to N in the expression for μ_r, and the well-known connections between moments and cumulants (e.g. Kendall, p. 64) need be used only as a check on the accuracy of the calculations. We have, of course, employed this check and verified that terms in N^2, N^3, do in fact cancel out.

§ 3. COEFFICIENTS IN χ AND $1/\chi$

In summarizing our results for the coefficients a_n and b_n occurring in the expansions, in powers of $1/\theta$, of χ (equation (4)) and $1/\chi$ (equation (5)), we introduce the following parameters characteristic of the particular lattice concerned: z = coordination-number, i.e. number of sites j which are neighbours of a given site i, and p_n = number of different routes on the lattice, $i, k_1, k_2, \ldots k_n, j$ where i and j are given neighbouring sites; each link in the route is from a site to a neighbouring site, and the n points $k_1, k_2, \ldots k_n$ are all different. Thus p_1 = number of triangles on a given base ij, p_2 = number of 'squares' on a given base ij, p_3 = number of 'pentagons' on a given base ij, though the 'squares' and 'pentagons' are not necessarily plane figures.

These parameters are easily determined for any given lattice, and we have worked throughout in terms of them. Their values for particular lattices are given in table 1.

Table 1

Lattice	z	p_1	p_2	p_3
Linear	2	0	0	0
Honeycomb	3	0	0	0
Plane square	4	0	2	0
Plane triangular	6	2	4	10
Diamond	4	0	0	0
Simple cubic	6	0	4	0
Body-centred	8	0	12	0
Face-centred	12	4	22	140

In terms of these parameters, we find

$$a_1 = \tfrac{1}{2}z$$
$$a_2 = \tfrac{1}{4}z(z-2)$$
$$a_3 = (z/24)(3z^2 - 12z + 8 - 5p_1)$$
$$a_4 = (z/48)(3z^3 - 18z^2 + 33z - 13 + 15p_1 - 10zp_1 - 5p_2)$$
$$a_5 = (z/480)(15z^4 - 120z^3 + 350z^2 - 380z + 122 - 245p_1 + 310zp_1 - 75z^2p_1 + 45p_1^2 + 90p_2 - 50zp_2 - 25p_3)$$

whence

$$b_1 = -\tfrac{1}{2}z$$
$$b_2 = \tfrac{1}{2}z$$
$$b_3 = (z/24)(5p_1 - 8)$$
$$b_4 = (z/48)(5p_2 - 15p_1 + 13 - 5z)$$
$$b_5 = (z/480)(25p_3 - 90p_2 - 45p_1^2 - 60zp_1 + 245p_1 - 122 + 90z).$$

The most striking feature of these results is the simplicity of the expressions for the coefficients b_n as compared with those for a_n.

As we have stated in the introduction, the numerical values of a_1, a_2, a_3 and a_4 agree with those given by Zehler for the simple cubic and face-centred cubic lattices, which is a sufficient check on our general expressions. We regret that there are no previous calculations of a_5 with which to compare our formula. But some confirmation is provided by the simplicity of the expression for b_5.

In table 2 we present the numerical values of these coefficients for the lattices specified in table 1.

Table 2

Lattice	a_1	a_2	a_3	a_4	a_5	b_1	b_2	b_3	b_4	b_5
Linear	1	0	$-\frac{1}{3}$	$\frac{5}{24}$	$\frac{7}{40}$	-1	1	$-\frac{2}{3}$	$\frac{1}{8}$	$\frac{29}{120}$
Honeycomb	$\frac{3}{2}$	$\frac{3}{4}$	$-\frac{1}{8}$	$\frac{5}{16}$	$\frac{107}{160}$	$-\frac{3}{2}$	$\frac{3}{2}$	-1	$-\frac{1}{8}$	$\frac{37}{40}$
Plane square	2	2	$\frac{4}{3}$	$\frac{13}{12}$	$\frac{71}{60}$	-2	2	$-\frac{4}{3}$	$\frac{1}{4}$	$\frac{29}{60}$
Plane triangular	3	6	$\frac{17}{2}$	$\frac{75}{8}$	$\frac{441}{40}$	-3	3	$\frac{1}{2}$	$-\frac{27}{8}$	$-\frac{51}{40}$
Diamond	2	2	$\frac{4}{3}$	$\frac{23}{12}$	$\frac{181}{60}$	-2	2	$-\frac{4}{3}$	$-\frac{7}{12}$	$\frac{119}{60}$
Simple cubic	3	6	11	$\frac{165}{8}$	$\frac{1561}{40}$	-3	3	-2	$\frac{3}{8}$	$\frac{29}{40}$
Body-centred	4	12	$\frac{104}{3}$	$\frac{575}{6}$	$\frac{2627}{10}$	-4	4	$-\frac{8}{3}$	$\frac{11}{2}$	$-\frac{241}{30}$
Face-centred	6	30	138	$\frac{2445}{4}$	$\frac{53171}{20}$	-6	6	6	$\frac{3}{4}$	$-\frac{71}{20}$

Before discussing any conclusions that may be drawn from these coefficients we shall simply present the expressions for the coefficients in an expansion of the internal energy E in powers of $1/\theta$, when $H=0$. To obtain these we proceed as above, but with $t=0$ instead of $t=2$. Writing

$$E=E_0-NJ\sum_{s=1}^{\infty}\frac{1}{2^{s+1}s!}\left(\frac{1}{N}\lambda_{s+1}{}^{(0)}\right)\frac{1}{\theta^s} \qquad \ldots\ldots(10)$$

we have

$$(1/N)\,\lambda_1{}^{(0)}=0$$
$$(1/N)\,\lambda_2{}^{(0)}=\tfrac{3}{2}z$$
$$(1/N)\,\lambda_3{}^{(0)}=3z(p_1-1)$$
$$(1/N)\,\lambda_4{}^{(0)}=3z(3-4z-4p_1+3p_2)$$
$$(1/N)\,\lambda_5{}^{(0)}=12z(10z-5-5p_2-10p_1z+5p_1+3p_3)$$

again in agreement with any particular results given by Zehler or Opechowski.

§ 4. THE CURIE TEMPERATURE

As we have said, the method hitherto used for determining the Curie temperature of this model of a ferromagnet on the basis of such high-temperature expansions, is to curtail equation (5) after m terms ($m=1, 2, 3\ldots$) and solve the resulting polynomial equation of degree m in θ to find that value of θ for which $1/\chi=0$. Attention has been restricted to positive real roots of these polynomials. Proceeding in this way we obtain the following table of values of θ for which $1/\chi=0$, a blank space indicating that the corresponding polynomial does not have a positive real root.

Table 3

Lattice	$m=1$	2	3	4	5	From $a_n{}^{1/n}$
Linear	1·000		0·7959	0·6042		0·89
Honeycomb	1·500		1·000	1·072		1·82
Plane square	2·000		1·253	1·095		1·56
Plane triangular	3·000			1·752	1·873	1·39
Diamond	2·000		1·253	1·447		1·72
Simple cubic	3·000		2·000	1·930	1·834	1·92
Body-centred	4·000	2·000	2·951	2·392	2·787	2·70
Face-centred	6·000	4·732	4·262	4·243	4·264	4·21

It is evident at once that there is considerable irregularity in these results (even if we disregard the column for $m=5$). The sequence for the body-centred cubic lattice is probably the most instructive, where we have alternate 'high' and 'low' values: but in no case can we draw particularly clear conclusions from these roots. But this, we suggest, is not surprising. For we ought really to be looking for the radius of convergence of the series (4). With only two trivial exceptions, this series is an inverse-power series with positive coefficients so that we should expect the first singularity of the function, represented by this series for small θ, to lie on the positive real θ-axis and correspond to the Curie point. It is true that we should expect the procedure adopted above, based on equation (5), eventually to lead to the same result, though we ought probably to consider the limit, for large m, of the modulus of the smallest root, real or complex of the corresponding polynomial. The numerical labour involved would be considerable, and, in any case, we see no ground for expecting good convergence. We prefer, therefore, to attempt a direct estimate of the radius of convergence of the series (4).

Either $\lim_{n\to\infty}(a_n/a_{n-1})$ or $\lim_{n\to\infty} a_n^{1/n}$ may be expected to yield the critical value of θ. For the few (five) coefficients that we have, trial shows that the numerical values of $a_n^{1/n}$† form a more regular sequence, in every case, than do those of a_n/a_{n-1} which is understandable since 'irregularities' in the early coefficients will be magnified, and persist longer, in the latter sequence of ratios. We have therefore plotted $a_n^{1/n}$ against $1/n$, with the intention of extrapolating to $1/n=0$. The results, for all the lattices, are shown in figure 1. The sequences, particularly for the three-dimensional cubic lattices, are fairly smooth. For estimating the critical value of θ, however, we have decided to use quadratic extrapolation on the last three points ($n=3$, 4, 5). This amounts to putting a parabola through these points and finding where it cuts the $1/n=0$ axis. The corresponding estimates of θ are enclosed in brackets on the left of each curve (and are repeated in the last column of table 3). Only in the case of the linear lattice have we departed from this procedure: for here the values of $a_n^{1/n}$ are alternately 'high' and 'low', and the value 0·89 given is the result of extrapolating on the points for $n=1$, 3 and 5. Extrapolation from the points for $n=3$, 4 and 5 gives 1·13 which, on inspection if for no other reason, is certainly too high.

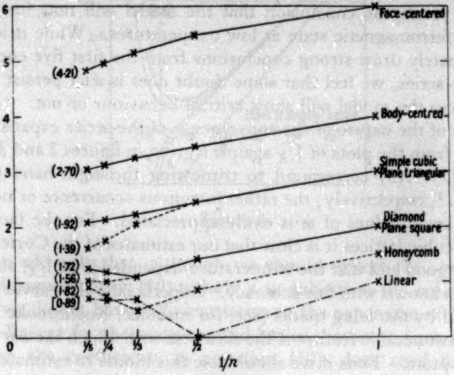

Figure 1.

§ 5. Discussion of the Results

For the three-dimensional cubic lattices our critical temperatures estimated from the coefficients a_n agree fairly well with those previously obtained by other methods. Thus Weiss (1948), using the Bethe–Peierls method, estimated values of 2·90 and 1·85 for the body-centred and simple cubic lattices, respectively: to be compared with our values of 2·70 and 1·92. For the face-centred cubic lattice our value of 4·21 is close to the value estimated by Zehler from the evidence of the roots of the polynomial approximations to $1/\chi$. For the body-centred lattice too the evidence of the roots is not inconsistent with that of the extrapolant of $a_n^{1/n}$. And we feel that the same may be said of the diamond lattice, though perhaps the extrapolant of $a_n^{1/n}$ is here a little too high.

---

† In the two cases where a_n is negative we have used $|a_n|$.

For the two-dimensional and linear lattices we have less good agreement between the evidence provided by the roots of the polynomial approximations to $1/\chi$ and that given by the values of $a_n^{1/n}$. For the honeycomb lattice, in particular, the extrapolant of $a_n^{1/n}$ almost certainly gives too high a value for the Curie temperature since in every other instance the linear approximation ($m=1$) leads to an estimate higher than the true value. Neither line of approach, however, would lead us to conclude that there should not in fact be a critical temperature for these lattices despite the fact that the spin-wave approximation (Bloch 1930) yields the conclusion that the model will not, for these lattices, give rise to a ferromagnetic state at low temperatures. While it is true that we cannot legitimately draw strong conclusions from the first five coefficients of an infinite power-series, we feel that some doubt does in fact persist as to whether for these lattices the model will show critical behaviour or not.

Some idea of the nature of the convergence of the series expansion (5) for $1/\chi$ can be gained from the plots of $1/\chi$ against θ given in figures 2 and 3. The curves labelled (1), (2)...(5) correspond to truncating the right-hand side of (5) at $n=m=1, 2\ldots 5$, respectively; the rather fortuitous occurrence or non-occurrence of $1/\chi=\theta$ for small values of m is easily appreciated. For the face-centred and body-centred cubic lattices it is clear that our estimates of the Curie temperatures are reasonably good and that the temperature-dependence of $1/\chi$, above the Curie temperature, is known with fair accuracy. Superficially the curves are not unlike those predicted by the Ising model (see, for instance, Rushbrooke 1952, Fig. 5): perhaps the most notable feature is the slowness with which the curve approaches its linear asymptote. Thus if we should use this model to estimate the exchange integral J by drawing a tangent along the approximately linear, high-temperature, part of an experimental plot of $1/\chi$ against T, assuming the tangent to cut the temperature axis at $\boldsymbol{k}T/J=z/2$, we should probably obtain an estimate of J some 10–20% too small.

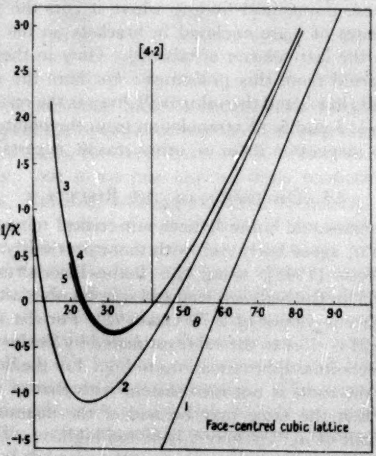

Figure 2.

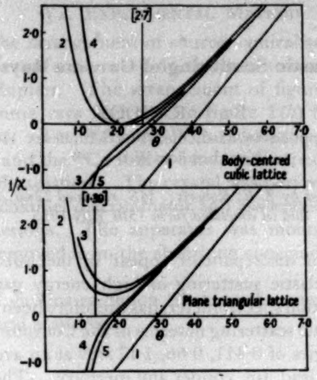

Figure 3.

Finally, we add only that, although we should expect the specific heat (for $H=0$) derived from equation (10) to have a singularity at the same critical Curie temperature, we do not have sufficient terms in the expansion of E to verify this supposition. Except for the body-centred lattice, however, such evidence as we do have, from the coefficients in equation (10), does tend to support this conclusion.

References

Bloch, F., 1930, *Z. Phys.*, **61**, 206.
Kendall, M. G., 1945, *Advanced Theory Statistics*, Vol. I, 2nd edn (London: Charles Griffin).
Opechowski, W., 1937, *Physica*, **4**, 181; 1938, *Ibid.*, **6**, 1112.
Rushbrooke, G. S., 1952, *Comptes Rendus de la 2e Réunion de Chimie Physique*, p. 177.
Tredgold, R. H., 1953, *Proc. Phys. Soc.* A, **66**, 421.
Van Vleck, J. H., 1951, *Ferromagnétisme et Antiferromagnétisme*, Grenoble Conference (Paris: C.N.R.S.), p. 239.
Weiss, P. R., 1948, *Phys. Rev.*, **74**, 1493.
Zehler, V., 1950, *Z. Naturf.*, **5A**, 344.

Elastic Scattering of Gamma Rays

By J. R. COOK
Department of Physics Applied to Medicine, The Middlesex Hospital Medical School, London W.1

Communicated by J. E. Roberts; MS. received 22nd April 1955
and in amended form 15*th July* 1955

Abstract. A number of discrepancies appear in the published values for the cross sections for the elastic scattering of high energy gamma rays. A direct method, using a scintillation spectrometer, has therefore been developed to measure the cross section for elastic scattering in terms of the Compton cross section. This has been done for energies of 0·411, 0·66, 1·17 MeV at an average scattering angle of approximately 80° in lead, tin, copper and mercury. The cross sections are in agreement with classical prediction in these elements for 0·411 and 0·66 MeV photons. The existence of Delbruck scattering is suggested in the case of 1·17 MeV scattering from lead.

---

§ 1. INTRODUCTION

THE cross sections for the elastic scattering of gamma rays have been determined experimentally by a number of workers (Moon 1950, Storruste 1950, Wilson 1951, 1953, Davey 1953, Stickler 1953).

In the case of ^{198}Au 0·411 MeV radiation and a lead scatterer, Storruste found good agreement with the theories of Rayleigh plus Thomson scattering as regards the absolute cross section and the angular dependence from 3° to 150°. Davey investigated the coherent scattering at 1·33 and 2·76 MeV from lead between 40° and 120° and found reasonable agreement with theory for 1·33 MeV. In the case of 2·76 MeV however the measured cross sections were found to be higher than the Rayleigh–Thomson predictions using the Fermi–Thomas model, and also higher than values calculated by Bethe (see Wilson 1953) using relativistic wave functions. This discrepancy was attributed either to secondary effects or to the occurrence of Delbruck scattering.

Wilson (1953) measured the angular dependence and cross section for 1·33 MeV gamma rays in several absorbers and found a value considerably less than the predictions of Bethe, which suggested that Delbruck scattering was occurring and was of an opposite phase to the Rayleigh plus Thomson scattering. Measurements by Stickler at 135° (where the potential scattering is negligible) with 1·33 MeV gamma rays in lead, have confirmed Bethe's calculation, though the experimental accuracy was low. He further suggested an additional process as contributing to the observed elastic scattering, depending on the fifth power of the atomic number. In view of the importance of deciding between these experiments, which disagree by considerable factors, a direct method has been used to measure the cross section for elastic scattering in terms of the Compton cross section. This was done for energies of 0·411, 0·66, 1·17 MeV at an average scattering angle approximately 80° in lead, tin, copper and mercury.

§ 2. Experimental Method

Figure 1 shows the arrangement of source, conical scatterer and scintillation crystal. The latter was of sodium iodide, thallium activated, and was mounted on an E.M.I. photomultiplier. The arrangement of figure 1 (*a*) was used for the 0·411 Mev ^{198}Au gamma rays and that in figure 1 (*b*) for the 0·661 ^{137}Cs and 1·17 ^{60}Co gamma rays. The ^{198}Au and ^{137}Cs radioactive sources were of strength approximately 1 mc, and the ^{60}Co source 3 mc, and were enclosed in glass or silver sheaths to filter any β-radiation. The crystal was part of a conventional spectrometer. The single channel discriminator and associated equipment were stable to 1% over long periods. The apparatus was mounted so that the conical scatterers could be removed from the absorbing cone and replaced in the position shown in figure 1.

The spectrum of gamma radiation reaching the crystal was determined with and without the conical scatterer.

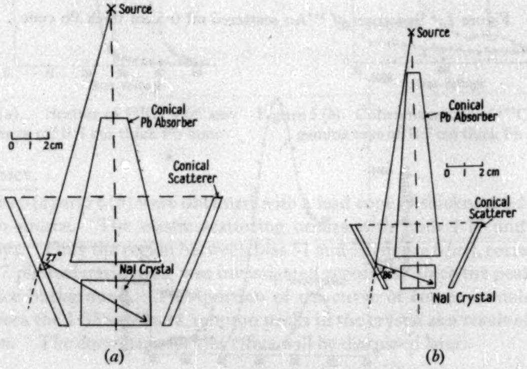

Figure 1. Experimental arrangement.

§ 3. Experimental Results

(i) 0·411 Mev.

Figures 2, 3 and 4 show the spectra obtained with various scatterers. The spectra with the scatterer present show three peaks which correspond to scatter from the walls of the room, Compton scatter from the cone, and a partly resolved peak which corresponds to the full energy of the incident rays and is therefore the elastic scatter. The background from the walls is reduced when the scatterer is present and does not contribute appreciably to the high-energy side of the gaussian curves which have been fitted to the scattered Compton peaks. The background count in the region of the elastic peak was unaltered when the scatterer was placed in position. This background is mainly due to cosmic rays.

(ii) 0·66 Mev.

Figures 5 (*a*) and 5 (*b*) show the similar behaviour with the arrangement of figure 1 (*b*) and a ^{137}Cs source.

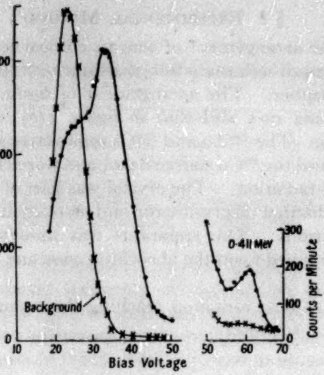

Figure 2. Spectrum of ^{198}Au scattered off 0·5 cm thick Pb cone.

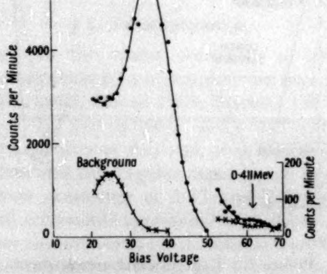

Figure 3. Spectrum of ^{198}Au gamma rays scattered off 1·5 cm thick Cu cone.

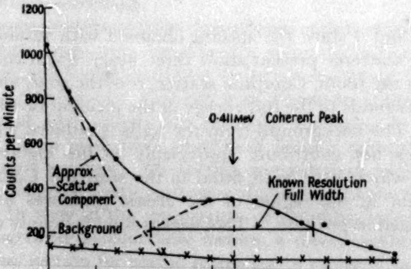

Figure 4. Coherent scatter of ^{198}Au 0·41 MEV gamma rays off 1 cm thick Hg cone.

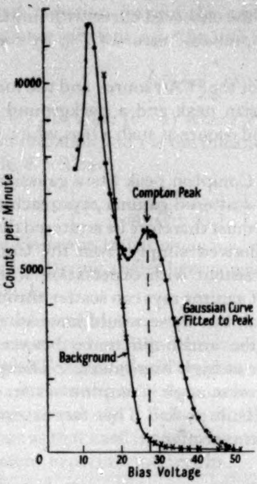

Figure 5 (*a*). Scatter of ^{137}Cs 0·66 Mev gamma rays off 0·5 cm thick Pb cone.

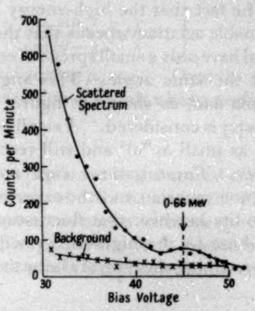

Figure 5 (*b*). Coherent scatter of ^{137}Cs 0·66 Mev gamma rays off 0·5 cm thick Pb cone.

(iii) 1·17 Mev.

Figures 6 (*a*) and 6 (*b*) were obtained with a lead cone of thickness 0·5 cm and a 3 mc ^{60}Co source. The elastic scattering occurs with both 1·17 and 1·33 Mev gamma rays. Only the region between bias 51 and 56 (figure 6 (*a*)), corresponding to the 1·17 photoelectric peak, was investigated accurately since the peak rate was about twice background. This portion of the curve of course contains contributions from the 1·33 Mev and Compton peaks in the crystal as a result of gaussian fluctuation. The correction for this effect will be discussed later.

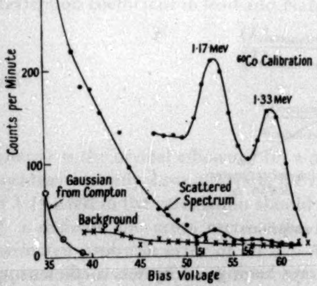

Figure 6 (*a*). Coherent scatter of ^{60}Co off 0·5 cm thick Pb cone.

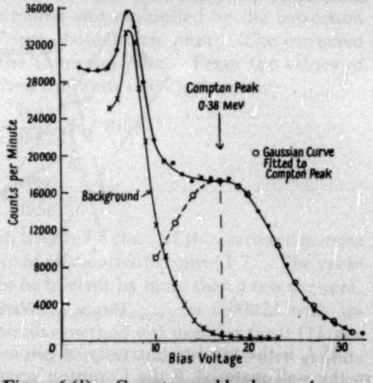

Figure 6 (*b*). Compton and background scatter of ^{60}Co off 0·5 cm thick Pb cone.

The area between the background rate and the observed curve with limits from 51 and 56 bias units was determined with a probable error of 7% by repeated measurements.

Figure 4 shows the region near 0·411 MeV for the ^{198}Au source and the mercury scatterer. This can be resolved into a gaussian peak and a background count (shown dotted). This gaussian has a width and occurs at such a bias which shows that it is the coherently scattered gamma ray.

The fact that the high-energy side of the Compton peak fits a gaussian with reasonable accuracy means that the Compton scattered gamma rays reaching the crystal have only a small spread of energies, and must therefore be scattered through about the same angle. This angle can be derived simply from the Compton formula and, as shown in figure 1 (*a*), is consistent with expectation when the geometry is considered. A small percentage of gamma rays can scatter through an angle as small as 50° and still reach the crystal, but these would have an energy 320 kev. These gamma rays account for the small difference between the Compton gaussian and the experimental curve at high bias values. There is no possibility however that fluctuations in the lowest angle Compton scatter could contribute to the high-energy side of the elastic peak. This fact is essential in determining the ratio of elastic to Compton cross sections.

§ 4. ANALYSIS OF RESULTS

In the case of 0·411 MeV scattered peaks the area on the high-energy side of the gaussian peaks was determined both for the coherent and Compton rays. This ratio was corrected for absorption in the walls of the scatterer, crystal efficiency, and ratio of photoelectric peak area to total area under the pulse spectrum. The corrections were determined as follows:

(i) *Wall absorption.*

Considering a parallel beam of monochromatic gamma rays incident on a slab of scatterer at angle α and undergoing absorption plus scattering, the ratio of the intensities of coherent and Compton scattered radiation leaving the slab can be obtained simply (figure 7).

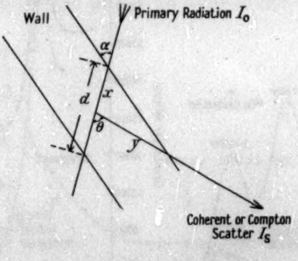

Figure 7. Wall absorption.

If I_0 is the incident intensity of gamma rays having absorption coefficient μ_1 in the wall material, θ the Compton scattered angle and I_s the intensity of the scattered radiation leaving the scatterer in the plane of the paper and having absorption coefficient μ_2 in the wall material, then

$$I_s \propto I_0 \int_0^d \exp(-\mu_1 x)\exp(-\mu_2 y)\,dx$$

since $y = x \sin\alpha/\sin(\theta-\alpha)$ where x is the thickness of absorber traversed by the incident radiation and y is the thickness of absorber traversed by radiation scattered at angle θ. Then

$$I_s \propto \left[\mu_1 + \frac{\mu_2 \sin\alpha}{\sin(\theta-\alpha)}\right]^{-1}\left[\exp\left(-\left\{\mu_1 + \frac{\mu_2 \sin\alpha}{\sin(\theta-\alpha)}\right\}d\right)-1\right].$$

For the Compton radiation $\mu_2 > \mu_1$, for the elastic scatter $\mu_2 = \mu_1$. Over the small range of scattering angles here considered, the variation of θ with x has a negligible effect on I_s.

(ii) *Peak to total ratios.*

The spectrum of monochromatic gamma rays produced in the crystal consists of the photoelectric plus Compton areas. The ratio of the area under the photoelectric peak to the total area under the pulse spectrum varies with energy of the primary gamma ray. Bell *et al.* (1952) have given this ratio for a crystal of the same size as that used in the present work. Their values have been used to correct the present experimental results.

(iii) *Crystal efficiency.*

In view of the large size of crystal used in these experiments the ratio of the detection efficiencies for Compton and scattered radiation does not vary appreciably with the angle of entry of the gamma ray into the crystal. The crystal diameter d is 3·8 cm and if μ_s is the absorption coefficient of the scattered radiation in NaI, the number of gamma rays stopped in the crystal is proportional to $1-\exp(-\mu_s d)$, assuming all the rays traverse a diameter.

As an example we may consider the application of these corrections in detail to the 1·17 MeV ^{60}Co radiation. A preliminary run of the incident ^{60}Co radiation showed that the 1·17 MeV photoelectric peak constituted 58% of the area under the spectrum between bias 51 and 56 volts, the remainder of this area being due to scatter and the 1·33 MeV peak. From the scatter spectrum of figure 1 (*a*), the area between bias 51 and 56 volts was determined and multiplied by the correction factor 0·58 to correspond with the 1·17 MeV photoelectric peak. The corrected area was then divided by the area of the Compton peak. From the values of absorption coefficient in lead and NaI given by White (1952), the ratio

$$\frac{(I_s)_{\text{Compton}}}{(I_s)_{\text{coherent}}} = \frac{0{\cdot}31}{0{\cdot}525} \text{ for } \theta = 84^\circ$$

and

$$\frac{\epsilon_{\text{Compton}}}{\epsilon_{\text{coherent}}} = \frac{0{\cdot}86}{0{\cdot}58} = 1{\cdot}48$$

where ϵ is the crystal efficiency for a path length 3·8 cm. If the scattered gamma rays traverse only 2 cm of crystal the ratio of efficiencies becomes 1·7. The value of 1·48 used in the calculation should not be in error by more than a few per cent. If σ denotes the cross section this gives $\sigma_{\text{coherent}}/\sigma_{\text{Compton}}$ as 0·00023 with an estimated probable error of 10%. A similar method was used for the 0·411 MeV gamma ray scattered from mercury, tin and copper, and the 0·66 MeV gamma ray from lead.

Theoretical values of the Rayleigh cross section were calculated using Franz's (1935) formula and Thomson's equation (Moon 1950) and are shown in the table with the experimental results.

The calculations of Bethe and Wilson at 1·33 Mev for coherent and Delbruck scattering have been taken as approximately correct at 1·17 Mev.

(1)	(2)	(3)	(4)	(5) (*a*)	 (*b*)	 (*c*)
0·411	77	Pb	0·010	0·013		
		Hg	0·017	0·013		
		Sn	0·0043	0·0045		
		Cu	0·0015	0·0017		
0·66	84	Pb	0·0043	0·003		
1·17	84	Pb	0·00023 ± 0·00002	0·0007	0·00037	0·00023

(1) Energy (Mev); (2) angle of scatter $\theta(^\circ)$; (3) scatterer; (4) experimental $\sigma_{\text{coh}}/\sigma_{\text{Compt}}$; (5) theoretical $\sigma_{\text{coh}}/\sigma_{\text{Compt}}$: (*a*) Rayleigh & Thomson, (*b*) Bethe, (*c*) Bethe & Delbruck.

§ 5. Discussion of Results

It can be seen from the table that the experimental and theoretical values for 0·411 Mev radiation scattered from Pb, Sn, Cu, Hg and 0·66 Mev scattered from Pb are in good agreement with expectation.

The value of the ratio for 1·17 Mev is in excellent agreement with the recent data of Wilson (1953) for 1·33 Mev, confirming the existence of Delbruck scattering which is in opposite phase to the coherent Rayleigh scattering, and supporting the calculation of Bethe. The early experiments of Wilson (1951) and of Storruste (1950) and Davey (1953) may therefore have been in error by a considerable factor. The experiment of Stickler (1953) is also subject to considerable uncertainty.

§ 6. Conclusion

The cross sections for coherent scattering are in agreement with classical prediction over a range of atomic numbers for 0·411 and 0·66 Mev gamma rays. The existence of Delbruck scattering is suggested in the case of 1·17 Mev scattering from lead.

Acknowledgment

The author is grateful to Professor J. E. Roberts for encouragement in this work.

References

Bell, P. R., Heath, R. L., Davies, R. C., 1953, *Oak Ridge National Laboratory Report* No. 1415.
Davey, W. G., 1953, *Proc. Phys. Soc.* A, **66,** 1059.
Franz, W., 1935, *Z. Phys.*, **98,** 314.
Moon, P. B., 1950, *Proc. Phys. Soc.* A, **63,** 1189.
Stickler, T. D., 1953, *Phys. Rev.*, **92,** 923.
Storruste, A., 1950, *Proc. Phys. Soc.* A, **63,** 1197.
White, G., 1952, *Nat. Bur. Std. Report* 1003.
Wilson, R. R., 1951, *Phys. Rev.*, **82,** 295 ; 1953, *Ibid.*, **90,** 720.

A Search for Low Intensity Gamma Rays in the ThC.C′ and ThC″.D Transitions

By D. G. E. MARTIN and G. PARRY
George Holt Physics Laboratory, University of Liverpool

Communicated by H. W. B. Skinner; *MS. received* 11*th July* 1955
and in amended form 5*th September* 1955

Abstract. A 180° spectrometer has been used to study the Compton electrons ejected from polythene radiators by the gamma rays from a radio-thorium source, in an attempt to detect gamma rays of low intensity between the energies of 1 Mev and 3·5 Mev. The only gamma rays detected in this region were a gamma ray at 1·62 Mev and the well-known 2·62 Mev ray, the intensity of the 1·62 Mev ray being about 3·5% of the 2·62 Mev ray. Upper limits are estimated for the intensities of gamma rays which have been previously reported by some workers. A possible decay scheme for ThC is discussed.

§ 1. INTRODUCTION

In the region between 0·86 Mev and 3·5 Mev, in addition to the strong 2·62 Mev γ-ray, some workers have reported low intensity γ-rays from thorium active deposit, which have not been found by others.

The existence of some of these γ-rays might be expected from consideration of the α-ray and β-ray spectra. Thus the α-disintegration energies, recalculated by Briggs (1954), suggest excited levels of ThC′ at 0·73, 1·67 and 1·80 Mev. The existence of a 0·726 Mev γ-ray is well established. The energy balance in the two branches of the ThC decay indicates that the β-ray end point of ThC″.D is on a level 3·2 Mev above the ground state of ThD, and this is the sum of the well-known 2·62 and 0·58 Mev γ-transitions. Thus there is a possibility of additional γ-rays with energies 0·94, 1·07, 1·67, 1·80 and 3·2 Mev.

Conversion electrons from γ-rays of 1·62 and 1·80 Mev were reported by Ellis (1934). Subsequently, Alichanow and Dzelepov (1938) reported γ-rays with energies 1·35, 1·50, 1·60, 1·80, 2·20 and 3·20 Mev, from measurements of internal positron production. Curran, Dee and Strothers (1940), using the Compton recoil electron spectrum reported a 15% intensity for a 1·68 Mev γ-ray, and the presence of a 1·1 Mev γ-ray. Latyshev and Kulchitsky (1941), using collimated γ-rays, confirmed the presence of recoil electrons corresponding to all the γ-rays found by Alichanow and Dzelepov except the 3·2 Mev γ-ray. Itoh and Watase (1941) found recoil groups corresponding to 0·96, 1·77 and 3·24 Mev. Mandeville (1942), using a similar technique to Curran *et al.*, claimed γ-rays at 1·58, 1·77 and 3·2 Mev. Johannson (1947) re-examined the Compton spectrum with a lens spectrometer and claimed γ-rays at 1·03, 1·34, 1·61 and 1·81 Mev with intensities of 11%, 9%, 14% and 14% respectively of the 2·62 Mev γ-ray. More recently, however, Fultz and Harding (1948) have measured the total γ-ray energy per disintegration of ThC.C′ and found their result of 0·14 Mev per α-disintegration to accord more closely with the simpler findings of Ellis, omitting the 1·6 Mev γ-ray and assuming the remaining rays at 1·8 and 0·73 MeV were both electric quadrupole. Bell and Elliott (1948) after a careful search for photo-electrons have stated that the intensity of the 3·2 MeV γ-transition must be less than 1 in 500 of that of the 2·62 MeV γ-ray.

§ 2. Apparatus

A 180° magnetic focusing spectrometer with equilibrium radius 9 cm, described by Martin, Richardson and Hsü (1948), has been used to study the Compton electrons ejected from a light target by the γ-rays from a radiothorium source. This source of about 20 mc was prepared and sealed in a glass capsule of length 1·5 cm, diameter 3 mm and wall thickness 0·8 mm, by the Radiochemical Centre, Amersham. To measure the magnetic field, a coil was rotated at a constant 1500 rev/min by a synchronous motor which was driven by a hard valve inverter circuit controlled by a 50 c/s tuning fork. The d.c. component of the voltage generated, after passing through a commutator and 10 c/s low-pass filter, was measured with a vernier potentiometer. The momentum calibration was obtained from well-known lines of thorium active deposit.

An absorber of non-magnetic G.E.C. heavy alloy (density 16·5 g cm^{-3}) was placed between the source and detector and the residual background due to γ-rays was practically eliminated by measuring coincidences between two small counters, each 2 cm long and 1 cm in diameter, separated by 2·5 cm in a reservoir containing an alcohol–argon mixture. Some of the electrons detected in the first counter missed the second counter as a result of scattering in the mica window or gas of the reservoir. The fraction of the beam lost increased with decreasing electron energy. A correction factor was obtained by measuring the ratio of the coincidence counting rate to the single rate in the first counter, which was sufficiently close to the mica window to collect most of the scattered electrons.

§ 3. Measurements

The glass capsule was surrounded by a copper tube, to absorb the primary electrons, and placed in contact with a polythene radiator. The experimental results corrected for the counter absorption and transmission of the spectrometer are shown in figure 1. If the intensity of the 2·62 MeV γ-ray is taken as 100%, then that of a γ-ray of 3·2 MeV is less than 0·1%. Due to the continuous distribution of the electrons it is difficult to detect electrons from low intensity γ-rays but there does seem to be a definite increase in the region corresponding to a γ-ray of about 1·7 MeV. The well known 0·86, 0·73 and 0·58 γ-rays are seen.

An electron ejected at an angle θ with the direction of the incident quantum has an energy E_c given by

$$E_c = E_\gamma 2a \cos^2\theta (1 + 2a + a^2 \sin^2\theta)^{-1}$$

where E is the energy of the primary quantum and $a = E_\gamma / m_0 c^2$, m_0 being the rest mass of the electron. Thus Compton 'lines' replace the broad Compton distributions of figure 1, when θ is restricted to small values by moving the source back from the target. This arrangement of the spectrometer (in which θ cannot exceed 6°) was similar to that used by Latyshev and Kulchitsky (1941). An investigation of the effect of different dispositions of the screening blocks near the source has been described by Martin and Parry (1952). With the final arrangement shown in figure 2 the background counting rate did not exceed 0·5 counts per minute at any part of the spectrum.

The polythene target, $0{\cdot}75 \times 0{\cdot}36\,\text{cm}^2$ and $28\,\text{mg cm}^{-2}$, was attached by fine silk threads to an aluminium frame, which could be rotated to put the target in the 'shadow' at the base of the spectrometer. In either position the aluminium frame was in 'shadow'. In this way background measurements could be alternated with spectrum measurements.

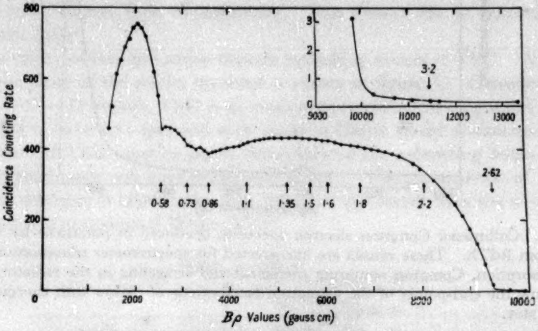

Figure 1. Compton electron distribution produced in a polythene radiator by the γ-rays from a RdTh source. Arrows show the end-points of the Compton distribution of γ-rays with energies marked in MeV.

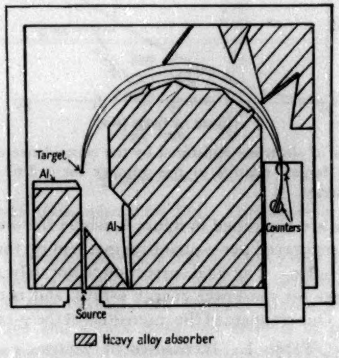

Figure 2. Arrangement of spectrometer for collimated γ-ray experiment.

Figure 3 shows the results with background subtracted and corrected for source decay. To obtain intensities, the curve must be corrected for the variation in transmission of the spectrometer, absorption between the coincidence counters, the Compton scattering coefficient and straggling of the electrons within the radiator. The Compton scattering coefficient was calculated from the Klein–Nishina formula. The rather uncertain straggling correction was estimated from the work of Warshaw and Chen (1950) and Kalil and Birkhoff (1953).

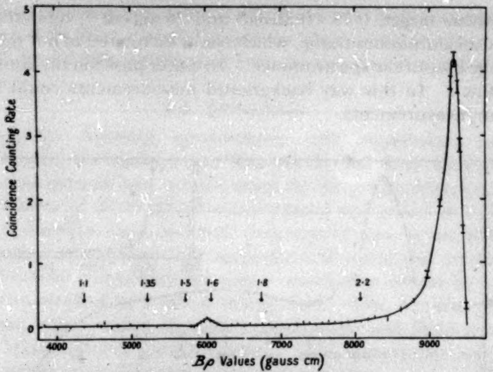

Figure 3. Collimated Compton electron spectrum produced in polythene by the γ-rays from RdTh. These results are uncorrected for spectrometer transmission, counter absorption, Compton scattering coefficient and straggling in the radiator. Arrows show the end-points of the Compton distributions of γ-rays with energies marked in Mev.

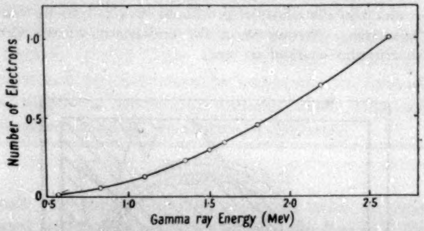

Figure 4. The number of electrons registered by the coincidence counter per γ-quantum incident on the target, relative to the number for a 2·62 Mev quantum, plotted against γ-ray energy.

These corrections are combined in figure 4, where the ordinates represent the number of electrons registered per γ-quantum incident on the radiator, relative to that for the 2·62 Mev γ-ray. The total correction factor to be applied to the results becomes rapidly larger for the lower energy γ-rays, and is certainly not reliable below about 1 Mev. Our estimate of the intensities of the γ-rays is given in table 1.

Table 1. Intensities of γ-rays

γ-ray energy (Mev)	2·62	1·62	0·58
Intensity	100, assumed	3·5	(50)

The value for the 0·58 γ-ray is uncertain because of the uncertainty in the correction factor, which is large at this energy.

Assuming that an area on the graph of 0·5% of that due to the 2·62 Mev γ-ray could be detected, an upper limit to the intensity of any undetected γ-rays may be estimated. Table 2 shows these limits for the γ-rays reported by Latyshev and Kulchitsky. The value for the 3·2 Mev γ-ray is obtained from the uncollimated Compton spectrum.

Table 2. Upper Limits of Intensity for Undetected γ-rays

Energy (Mev)	3·2	2·2	1·8	1·5	1·35	1·1
Intensity (% of 2·62 Mev γ-ray)	0·1	0·5	1·0	1·5	2·0	4·0

§ 4. DISCUSSION

In the interval between 1·0 Mev and 3·5 Mev we have found only γ-rays of 1·62 Mev and 2·62 Mev from radiothorium. The former has an intensity about 3·5% of the latter.

In the decay of thorium active deposit branching occurs at ThC. A possible scheme for some of the nuclei involved is shown in figure 5. Considering first the ThC → C′ → D branch, ThD is an even–even nucleus and its ground state can be assumed to have zero spin and even parity. Hence all the α-transitions to the ground state of ThD must be parity favoured and the α-emitting levels of ThC′ with even (odd) spin will have even (odd) parity. The ground state of ThC′, an even–even nucleus, is taken to be zero, even, in agreement with the α–γ angular correlation determination of Weale (1955).

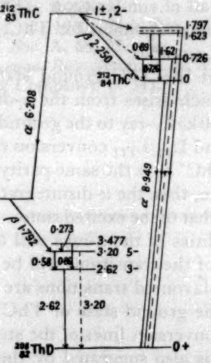

Figure 5. Possible decay scheme for ThC. Disintegration energies in Mev.

The internal conversion coefficient of the 0·73 Mev γ-ray as measured by Martin and Richardson (1950) is in agreement with the theoretical value for an E2 transition. Thus the first excited state of ThC′ should be 2^+. The ratio of intensity of the α-rays and γ-rays from this level is in good agreement with calculation, using the formulae of Blatt and Weisskopf (1952).

If the 1·62 Mev γ-ray is attributed to ThC′, rather than to ThD, the absence of an α-disintegration of 10·572 Mev may be the result of an unfavourable parity change, or a γ-transition of much shorter life than the α-transition. A rough calculation, using Ellis' (1934) estimate of the intensity of the conversion electrons of the 1·62 Mev γ-ray and the present intensity of 2% per disintegration for the photons, gives an internal conversion coefficient of about 6×10^{-3}. This suggests an M1, E2 or E3 transition. Thus a level at 1·62 Mev may be 1^+, 2^+ or 3^-. However, either the parity condition for the absence of an α-transition or the restriction of multipole order of the γ-ray would exclude 3^- and 2^+. Thus the level must be

1^+. There should be an M1 transition to the 0·73 level. This would have about 0·89 MeV energy and should be about one-sixth the intensity of the 1·62 MeV γ-ray. There is a conversion line (Pa) of 0·796 MeV (Surugue 1937), which, if attributed to the ThC.C′ disintegration, would indicate the existence of a 0·889 MeV transition, too weak to be detected in the Compton spectrum.

Since the calculated α-lifetime of the 1·797 MeV level is about 4×10^{-10} sec, the radiative transition must be either E3 or higher order or $0 \rightarrow 0$ to escape detection. Thus the spin and parity of the level may be 0^+, 3^-, 4^+, etc. An assignment of 3^- would give rise to a strong 1·06 MeV γ-transition which should have been detected.

Taking the strength of the 1·6 and 0·89 MeV γ-rays as 0·2 and 0·004 per disintegration respectively and obtaining the strength of the 0·73 γ-ray from the K-shell internal conversion line, assuming an E2 transition, the γ-ray energy of ThC′ is about $0{\cdot}105 \pm 0{\cdot}02$ MeV per α-disintegration. This is to be compared with the direct measurement of $0{\cdot}14 \pm 0{\cdot}014$ MeV per α-disintegration obtained in coincidence measurements by Fultz and Harding (1948).

Calculation of log *ft* values for the partial spectra of ThC.C′ indicates that the β-transitions are probably all of similar type. Therefore, if they are of allowed type, 1^+ is the only possible assignment for ThC ground state; if of forbidden type, then 0^+, 1^-, 2^- are all possible.

Further evidence about the ThC ground state may be obtained from the ThC→C″→D branch, which arises from the α-disintegration of ThC. Weale (1955) has shown that the 40 kev γ-ray to the ground state of ThC″ is M1. This is confirmed by the L_I/L_{II} and L_{II}/L_{III} conversion ratios. Therefore, the ground and first excited states of ThC″ have the same parity and a spin difference of 0 or 1. If the spin difference is zero, then the α-disintegration to the ground state should have twice the intensity of that to the excited state. If there is a difference of spins then the emission probabilities of the α-rays will differ due to the different spin changes involved and one of the transitions will be parity favoured and the other unfavoured. As parity unfavoured transitions are absolutely forbidden if one of the states has zero spin, the ground state of ThC cannot have zero spin. The intensity ratios of the L-conversion lines of the strong 238 kev transition of ThC require that it be M1, as is also suggested by the K-shell internal conversion coefficient. The most plausible interpretation of the β-transitions is then that the ground state of ThC is 1^- and the 238 kev level is 0^-. The ground to ground β-transitions of ThB.C and ThC.C′ are then first forbidden with spin change 1, in agreement with their log *ft* values of 6·81 and 7·22, and the β-transition to the 238 kev level of ThC is a $0 \rightarrow 0$ transition with change of parity and log *ft* of 5·17, in agreement with the assignment of Wu (1955).

Angular correlation measurements of the 0·58 and 2·62 MeV γ-rays by Elliott *et al.* (1954) have determined the spins and parities of the 2·62 and 3·20 MeV levels of ThD as 3^-, 5^-, respectively. The 2·62 MeV transition is then E3 and the 0·58 MeV transition is E2, in good agreement with the internal conversion coefficients measured by Martin and Richardson (1950). The probability of an E5 transition of 3·2 MeV is very small (approximately 10^{-7}) compared with that of a 0·58 MeV E2 transition. This explains our failure to find Compton electrons from a 3·2 MeV γ-ray and that of other workers to detect photoelectrons or internal conversion electrons (Bell and Elliott 1948, Bradt, Halter, Heine and Scherrer 1946, Martin and Richardson 1948).

References

Alichanow, A. I., and Dzelepov, V. P., 1938, *C. R. Acad. Sci. U.R.S.S.*, **20,** 113.

Bell, R. E., and Elliott, L. G., 1948, *Canad. J. Res.* A, **26,** 379.

Blatt, J. M., and Weisskopf, V. F., 1952, *Theoretical Nuclear Physics* (New York : John Wiley).

Bradt, H., Halter, J., Heine, H. G., and Scherrer, P., 1946, *Helv. Phys. Acta*, **19,** 431.

Briggs, G. H., 1954, *Rev. Mod. Phys.*, **26,** 1.

Curran, S. C., Dee, P. I., and Strothers, J. E., 1940, *Proc. Roy. Soc.* A, **174,** 546.

Elliott, L. G., Graham, R. L., Walker, J., and Wolfson, J. L., 1954, *Phys. Rev.*, **93,** 356.

Ellis, C. D., 1934, *Proc. Roy. Soc.* A, **143,** 350.

Fultz, S. C., and Harding, G. N., 1948, *Canad. J. Res.* A, **26,** 313.

Itoh, J., and Watase, Y., 1941, *Proc. Phys.-Math. Soc. Japan*, **23,** 142.

Johannson, A., 1947, *Arkiv. Mat. Astr. Fys.* A, **34,** No. 9.

Kalil, F., and Birkhoff, R. D., 1953, *Phys. Rev.*, **91,** 505.

Latyshev, G. D., and Kulchitsky, L. A., 1941, *J. Phys. U.S.S.R.*, **4,** 515.

Mandeville, C. E., 1942, *Phys. Rev.*, **62,** 309.

Martin, D. G. E., and Parry, G., 1952, *Physica*, **18,** 1157.

Martin, D. G. E., and Richardson, H. O. W., 1948, *Proc. Roy. Soc.* A, **195,** 287 ; 1950, *Proc. Phys. Soc.* A, **63,** 223.

Martin, D. G. E., Richardson, H. O. W., and Hsü, Y. K., 1948, *Proc. Phys. Soc.*, **60,** 466.

Surugue, J., 1937, *Ann. Phys., Paris*, **8,** 484.

Warshaw, S. D., and Chen, J. J. L., 1950, *Phys. Rev.*, **80,** 97.

Weale, J. W., 1955, *Proc. Phys. Soc.* A, **68,** 35.

Wu, C. S., 1955, *Beta and Gamma Ray Spectroscopy*, Ed. K. Siegbahn (Amsterdam : North Holland Publishing Company), p. 343.

Theory of a Dielectric Loss in Long Chain Polar Compounds

By P. G. HARPER and J. J. O'DWYER
Division of Electrotechnology, National Standards Laboratory, Commonwealth Scientific and Industrial Research Organization, Australia

MS. received 26th May 1955

Abstract. A new model is proposed which gives a dielectric absorption for long chain polar compounds. Under the influence of an alternating applied field the equilibrium distribution of the dipoles is disturbed and it is supposed that a steady state is attained by each dipole interacting with its own molecular chain, the chains themselves always maintaining their equilibrium distribution. The frequency dependent dielectric constant is found to be of the form $\epsilon(\omega) = \text{const.}\,(1 + i\omega\tau)^{-2}$ where τ is a collision time. The present theory does not preclude the co-existence of any of the other well-known types of dielectric absorption.

---

§ 1. Introduction

The theory of what has now become known as the low-frequency loss in long chain polar compounds has been treated extensively by Fröhlich (1949) who considers the basic process to be a rotational transition of the paraffin chain with its associated dipole from one position of equilibrium in the lattice to another. Various experimental workers have found results which support this theory and it must be considered as well established that this low-frequency loss is due to movement of the chain and the dipole as a whole. However, more recent experimental work (cf. Dryden and Welsh 1951, Hoffman 1952) has established the existence of another loss peak in many such compounds at a considerably higher frequency. The main characteristics of this absorption are that it is of approximate Debye shape, and that the frequency of maximum absorption shifts only slightly with variations in temperature and chain length compared with the shifts which such variations cause in the low-frequency absorption. It is the purpose of this paper to propose a mechanism which shows how dielectric loss can arise in a specified model the essential features of which may apply to the experimental situation.

§ 2. The Model

The present model considers the chain and the dipole as being free to rotate relatively to their surroundings and to each other. The dipole is supposed to interact with the molecular chain to which it is attached, but not with any of the neighbouring chains; it is supposed to interact with neighbouring dipoles only in so far as we replace the external field by the local field. In addition the chains are supposed to interact with each other and to preserve their equilibrium distribution of angular velocities even when the equilibrium distribution of the dipole angular velocities has been altered by an applied field. It is in this respect that the present model differs from the potential hole one, namely that the dipole distribution is not supposed to remain Maxwellian under the influence of a field, and it is indeed the main purpose of the paper to calculate this distribution.

§ 3. THE BOLTZMANN EQUATION

Let $f(\theta, d\theta/dt, t)$ be the average number of dipoles per unit volume oriented at an angle θ with the field and having an angular velocity $d\theta/dt$ at time t. Then

$$\frac{df}{dt}=\frac{\partial f}{\partial \theta}\frac{d\theta}{dt}+\frac{\partial f}{\partial(d\theta/dt)}\frac{d^2\theta}{dt^2}+\left(\frac{\partial f}{\partial t}\right)_{\text{int}} \qquad \ldots\ldots(1)$$

where the first two terms refer to the change produced by the field, and the last term to the interaction of the dipole with its own chain. Since we shall assume no dielectric saturation we need only consider quantities occurring to the first order in the field strength and with this in mind we put

$$f=f_0+gF\exp(i\omega t) \qquad \ldots\ldots(2)$$

where $F\exp(i\omega t)$ is the local field acting on the dipole and

$$f_0=N(\beta I_1/2\pi)^{1/2}\exp(-\beta I_1\Omega^2/2) \qquad \ldots\ldots(3)$$

is the equilibrium distribution of the dipoles in the absence of a field where $\beta=1/\boldsymbol{k}T$, N is the number of dipoles per unit volume, Ω is the angular velocity at a stationary value of $d\theta/dt$ and I_1 is the moment of inertia of the dipoles. Since for a dipole of moment μ in the local field $F\exp(i\omega t)$ we have

$$I_1\frac{d^2\theta}{dt^2}=-\mu F\sin\theta\exp(i\omega t)$$

and since restoring forces due to the chain will vanish on the average, equation (1) becomes to the required order in F

$$i\omega g=\Omega\frac{\partial g}{\partial\theta}-\frac{\mu}{I_1}\sin\theta\frac{\partial f_0}{\partial\Omega}+\left(\frac{\partial g}{\partial t}\right)_{\text{int}} \qquad \ldots\ldots(4)$$

and we have also noted that in the presence of a field $d\theta/dt=\Omega+O(\mu F/I_1\Omega^2)$.

§ 4. SPECIAL SOLUTIONS

4.1. *Solution assuming a Collision Time*

The most obvious thing to do is to describe the interaction term arbitrarily by

$$(\partial g/\partial t)_{\text{int}}=-g/\tau \qquad \ldots\ldots(5)$$

and we will work this case through before proceeding to a more detailed discussion of this term. Under these circumstances the equation (4) becomes quite simple and the solution is given by

$$g=X(\Omega)\cos\theta+Y(\Omega)\sin\theta$$

$$X(\Omega)=-\frac{\Omega}{\Omega^2+(i\omega+1/\tau)^2}\frac{\mu}{I_1}\frac{\partial f_0}{\partial\Omega}. \qquad \ldots\ldots(6)$$

We note that $Y(\Omega)$ is not required to calculate the polarization per unit volume which is given by

$$P=\mu\int f\left(\theta,\frac{d\theta}{dt}\right)\cos\theta\, d\left(\frac{d\theta}{dt}\right)d\theta$$

$$=-\frac{\mu^2F}{3I_1}\exp(i\omega t)\int_{-\infty}^{\infty}\frac{\Omega\,\partial f_0/\partial\Omega}{\Omega^2+(i\omega+1/\tau)^2}d\Omega \qquad \ldots\ldots(7)$$

where the average of $\cos^2\theta$ over all directions has been put as 1/3. Assuming τ to be independent of Ω the integral in (7) may be expanded in powers of $\boldsymbol{k}T\tau^2/I_1$ to give

$$P = +N\frac{2\mu^2 F}{3I_1}\exp(i\omega t)\left[\frac{1}{(i\omega+1/\tau)^2} - 3\frac{\boldsymbol{k}T}{I_1}\frac{1}{(i\omega+1/\tau)^4} + \mathrm{O}\left(\frac{\boldsymbol{k}^2T^2\tau^4}{I_1^2}\right)\right]. \qquad \ldots\ldots(8)$$

The properties of this solution and the assumptions made in the expansion will be discussed later.

4.2. *Solution with detailed Interaction Mechanism*

We now consider a detailed calculation of $(\partial f/\partial t)_{\mathrm{int}}$ in which f changes on account of collisions of the dipole with its own rotating chain. We shall suppose that the dipole has two, oppositely directed, equilibrium positions relative to its chain with a potential barrier V hindering transitions between them. Then, considering the relative motion of dipole and chain, if there is insufficient energy for the dipole to cross this barrier, a collision means simply a reversal of relative angular velocity. This may be conveniently described by

$$\begin{pmatrix}\Omega' \\ a\Omega+b\Omega'\end{pmatrix} \longleftrightarrow \begin{pmatrix}\Omega \\ a\Omega'+b\Omega\end{pmatrix}$$

where

$$a = \tfrac{1}{2}(1+I_1/I_2), \quad b = \tfrac{1}{2}(1-I_1/I_2). \qquad \ldots\ldots(9)$$

I_1 and I_2 are the moments of inertia of the dipole and chain, and Ω' and Ω the angular velocities of the dipole before and after collision respectively. This transition conserves energy and momentum and reverses relative angular velocity. If, on the other hand, the dipole possesses sufficient energy to overcome the potential barrier (i.e. if $I_1I_2\Omega_r^2/2(I_1+I_2) > V$ where Ω_r is the relative angular velocity) then a transition occurs from one potential minimum to the other across the barrier V. If the potential wells are of equal depth this leaves the velocities unaltered but changes the relative orientation of chain and dipole. Suppose now that $N(\theta, \Omega)$ describes the average number of chains with orientation and velocity θ and Ω respectively; then

$$\left(\frac{\partial f}{\partial t}\right)_{\mathrm{int}} = \int_{\Omega-\nu/a}^{\Omega+\nu/a}\{f(\theta,\Omega')N(\theta, a\Omega+b\Omega') - f(\theta,\Omega)N(\theta, a\Omega'+b\Omega)\}\nu_1 a\, d\Omega'$$
$$+\left[\int_{\Omega+\nu}^{\infty} + \int_{-\infty}^{\Omega-\nu}\right]\{f(\theta+\pi,\Omega)N(\theta,\Omega') - f(\theta,\Omega)N(\theta,\Omega')\}\nu_2\, d\Omega' \quad .(10)$$

where ν is defined by

$$I_1I_2\nu^2/2(I_1+I_2) = V \qquad \ldots\ldots(11)$$

and ν_1 and ν_2 are the frequencies of the low and high energy transitions respectively. It is clear that these transition frequencies are functions only of the relative velocity $|\Omega-\Omega'|$. For example ν_1 might be taken as constant and equal say to ν/π, while ν_2 may be approximated by $|\Omega-\Omega'|/2\pi$ which is its limiting value for high energies. (A rather less realistic model would be to assume an infinite potential barrier so that only 'hard' collisions occur and ν_1 is then accurately $|\Omega-\Omega'|/2\pi$. Only the first contribution would then remain.)

In application to the materials considered it will generally be the case that $I_2 \gg I_1$ on account of the disparity in masses. It should therefore be sufficient to assume that

$$a \simeq b \simeq \tfrac{1}{2} \qquad \ldots\ldots(12)$$

which amounts to neglecting the recoil of the heavy chain.

Substituting (2) in (10) and taking account of (12) we find

$$\left.\begin{aligned} \left(\frac{\partial g}{\partial t}\right)_{\text{int}} &= \int_{\Omega-2\nu}^{\Omega+2\nu} \{g(\theta,\Omega') - g(\theta,\Omega)\} \times N\{\theta, \tfrac{1}{2}(\Omega'-\Omega)\} \frac{\nu}{2\pi}\, d\Omega' \\ &\qquad + \{g(\theta+\pi,\Omega) - g(\theta,\Omega)\} R(\Omega) \\ \text{where} \qquad & \\ R(\Omega) &= \left[\int_{\Omega+\nu}^{\infty} + \int_{-\infty}^{\Omega-\nu}\right] N(\theta,\Omega') \frac{|\Omega-\Omega'|}{2\pi}\, d\Omega'. \end{aligned}\right\} \qquad \ldots\ldots(13)$$

Expanding

$$g(\theta,\Omega') - g(\theta,\Omega) = (\Omega'-\Omega) g'(\theta,\Omega) + \tfrac{1}{2}(\Omega'-\Omega)^2 g''(\theta,\Omega) + \ldots.$$

we find by taking the first two terms of the expansion

$$\left(\frac{\partial g}{\partial t}\right)_{\text{int}} = A \frac{d^2 g}{d\Omega^2} + R(\Omega)\{g(\theta+\pi,\Omega) - g(\theta,\Omega)\}$$

where we have put

$$\begin{aligned} A &= \frac{\nu}{2\pi}\left(\frac{\beta I_2}{8\pi}\right)^{1/2} \int_{-2\nu}^{2\nu} x^2 \exp(-\beta I_2 x^2/8)\, dx \qquad \ldots\ldots(14) \\ &\simeq 2\nu/\pi\beta I_2. \end{aligned}$$

The series expansion and the approximation for the integral converge provided $I_2\nu^2 > 8\boldsymbol{k}T$. The general equation (4) now becomes

$$i\omega g = \Omega \frac{\partial g}{\partial \theta} + \frac{\mu}{I_1} \sin\theta \frac{\partial f_0}{\partial \Omega} + A \frac{d^2 g}{d\Omega^2} + R(\Omega)\{g(\theta+\pi,\Omega) - g(\theta,\Omega)\}.$$

A solution is again

$$g(\theta,\Omega) = X(\Omega)\cos\theta + Y(\Omega)\sin\theta$$

where X and Y satisfy

$$\left.\begin{aligned} \left[i\omega + 2R(\Omega) - A\frac{d^2}{d\Omega^2}\right] X &= \Omega Y \\ \left[i\omega + 2R(\Omega) - A\frac{d^2}{d\Omega^2}\right] Y &= -\Omega X + \frac{\mu}{I_1}\frac{\partial f_0}{\partial \Omega}. \end{aligned}\right\} \qquad \ldots\ldots(15)$$

It is easily seen that $R(\Omega)$ is approximated by

$$\left.\begin{aligned} & R(\Omega) \simeq 0 \quad \text{or} \quad |\Omega| \\ \text{according as} \qquad & \Omega < \nu \quad \text{or} \quad \Omega > \nu \end{aligned}\right\} \qquad \ldots\ldots(16)$$

provided in both cases that $I_2\Omega^2 > 2\boldsymbol{k}T$. It can be shown that the approximation (16) remains reasonably good under the less stringent condition $I_2\nu^2 > 2\boldsymbol{k}T$. This could have been seen physically since for slowly rotating dipoles the probability that the relative angular velocity be sufficiently high to cross the barrier is very small (on account of the thermal equilibrium of the chains), whereas a rapidly rotating dipole can always interact with a slowly moving chain with a frequency equal to its own angular velocity.

We have then for the polarization

$$P = \mu F \overline{\cos^2\theta} \exp(i\omega t) \int_{-\infty}^{\infty} X(\Omega)\, d\Omega$$

$$= \frac{2}{3} \mu F \exp(i\omega t) \left\{ \int_0^{\nu} X_1(\Omega)\, d\Omega + \int_{\nu}^{\infty} X_2(\Omega)\, d\Omega \right\} \qquad \text{......(17)}$$

where X_1 and X_2 satisfy equations (15) with R equal to 0 and $|\Omega|$ respectively. In the approximation considered almost all the contribution to P will come from the first integral so we take as trial solutions of (15) for the case $R(\Omega) = 0$

$$\left.\begin{aligned} X_1(\Omega) &= \frac{\Omega}{\Omega^2 + b^2} \frac{\mu}{I_1} \frac{\partial f_0}{\partial \Omega} \\ Y_1(\Omega) &= \frac{b}{\Omega^2 + b^2} \frac{\mu}{I_1} \frac{\partial f_0}{\partial \Omega} \end{aligned}\right\} \qquad \text{......(18)}$$

which are suggested by (6). It is easily seen that $Y_1(\Omega)$ has a stationary point (a maximum) at some point $\Omega = \Omega_0$ and that in the vicinity of this point

$$\frac{Y_1''}{Y_1} = \frac{X_1''}{X_1} = \sigma \qquad \text{......(19)}$$

where σ is a constant. Substituting the trial solutions (18) in the equations (15) we find

$$b = i\omega - A\sigma \qquad \text{......(20)}$$

and $Y_1(\Omega)$ can now be made a good solution by determining σ in a self-consistent manner. It can be shown that the stationary point of $X_1(\Omega)$ is sufficiently close to $\Omega = \Omega_0$ to ensure that $X_1(\Omega)$ is also accurately represented in this region. Since the greatest contribution to $\int X_1\, d\Omega$ comes from this same region we may be confident of the approximation. The equation $dY_1(\Omega)/d\Omega = 0$ then becomes

$$(b^2 + \Omega^2)(1 - 2\alpha\Omega^2) - 2\Omega^2 = 0$$

where we have put $\alpha = I_1/2\boldsymbol{k}T$. The solution is

$$\Omega_0{}^2 = \left\{ \frac{b^2}{2\alpha} + \left(\frac{b^2}{2} + \frac{1}{4\alpha} \right)^2 \right\}^{1/2} - \left\{ \frac{b^2}{2} + \frac{1}{4\alpha} \right\}. \qquad \text{......(21)}$$

The appropriate approximation is for $b^2\alpha > 1$ and we find accordingly

$$\Omega_0{}^2 = \frac{1}{2\alpha} \left\{ 1 - \frac{1}{\alpha b^2} + \ldots . \right\} \qquad \text{......(22)}$$

Evaluating $Y_1''(\Omega)$ at $\Omega = \Omega_0$ we find

$$\sigma = \left(\frac{Y_1''}{Y} \right)_{\Omega = \Omega_0} = -4\alpha - \frac{4}{b^2 + \Omega_0{}^2} + \frac{4\Omega_0{}^2}{(b^2 + \Omega_0{}^2)^2} \simeq -4\alpha \left\{ 1 + \frac{1}{\alpha b^2} + \ldots . \right\} \qquad \text{......(23)}$$

with the help of (22).

We have now in effect determined b and find to first approximation

$$b = i\omega + \frac{4}{\pi} \frac{I_1}{I_2} \nu. \qquad \text{......(24)}$$

The polarization is thus given by equation (8) with the collision time $\boldsymbol{\tau}$ given explicitly by

$$\frac{1}{\tau} = \frac{4}{\pi} \frac{I_1}{I_2} \nu. \qquad \text{......(25)}$$

Higher approximations have been considered and are very complicated. They have been found to give small correction terms varying linearly with T both for the polarization and absorption and also for the frequency of maximum absorption.

§ 5. DISCUSSION

5.1. *Relation of the Solution to Experimental Results*

The first approximation for the dielectric constant is from (8) and (25)

$$\epsilon(\omega)=\epsilon_1(\omega)+i\epsilon_2(\omega)=\frac{\pi^2}{24}\frac{\mu^2N\gamma}{\nu^2}\frac{I_2^{\,2}}{I_1^{\,3}}\left\{1+i\frac{\omega}{\nu}\frac{\pi}{4}\frac{I_2}{I_1}\right\}^{-2} \qquad \ldots\ldots(26)$$

where γ is the ratio of the local field to the applied field.

The shape of the absorption curve derived from a complex dielectric constant $(1+i\omega\tau)^{-2}$ is of some interest and is shown in the figure with a Debye type curve derived from $(1+i\omega\tau)^{-1}$ for comparison. The absorption peak for the present case is asymmetrical and the frequency of maximum absorption $\omega_{\max}$ is given by

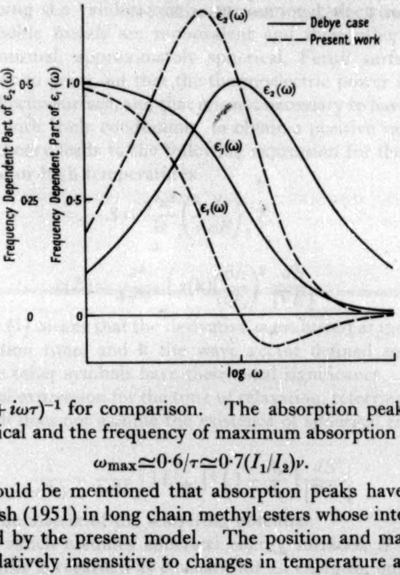

$$\omega_{\max}\simeq 0{\cdot}6/\tau\simeq 0{\cdot}7(I_1/I_2)\nu. \qquad \ldots\ldots(27)$$

Finally it should be mentioned that absorption peaks have been found by Dryden and Welsh (1951) in long chain methyl esters whose interpretation could possibly be fitted by the present model. The position and magnitude of these absorptions is relatively insensitive to changes in temperature and chain length. The small change of frequency of maximum absorption with chain length is in the right direction to be accounted for by (27). The temperature effects which are described by the second terms of (8), (22) and (23) are rather complicated. It can be shown, however, that the second term in (8) gives the next largest contribution, and that it results in increased maximum absorption and increased asymmetry in the absorption curve with increasing temperature.

5.2. *Validity of Approximations*

The solution expressed by (26) is essentially a low temperature solution which is valid only for sufficiently large values of ω. The most stringent requirement of the temperature is that stated by $b^2\alpha>1$ which becomes $(I_1/I_2)^2I_1\nu^2/\boldsymbol{k}T>1$ and we find putting $I_1/I_2 \sim 1/10$ and $I_1 \sim 10^{-37}$ g cm^2 that we must have $\nu \gtrsim 10^{13}$ sec^{-1} at room temperature. This is fairly high for a molecular vibration frequency, but even if the theory were applied in a case in which the approximations used in the derivation were no longer valid it is probable that the general form of the solution would be preserved though numerical factors may change.

The failure of the solution (26) for $\epsilon(\omega)$ at $\omega = 0$ is due to the treatment of the collision time as a constant. In order to obtain the correct static dielectric constant one must return to the general Boltzmann equation and omit the term $(\partial g/\partial t)_{\text{int}}$ rather than retain it as $-g/\tau$ since in an equilibrium state there will be no such change in the distribution function.

REFERENCES

DRYDEN, J. S., and WELSH, H. K., 1951, *Aust. J. Sci. Res.*, **4**, 616.

FRÖHLICH, H., 1949, *Theory of Dielectrics* (Oxford : University Press).

HOFFMAN, J., 1952, *J. Chem. Phys.*, **20**, 541.

RESEARCH NOTES

The Thermoelectric Power of Monovalent Metals

By H. JONES
Department of Mathematics, Imperial College, London

MS. received 25*th August* 1955

The thermoelectric powers of the noble metals copper, silver and gold are positive and rather small in magnitude. Observed values at 0°c are: Cu 1·73, Ag 1·3, Au 1·7 microvolts per degree. These results have led to doubts concerning the validity of the conventional electron theory of this effect, since the noble metals are monovalent and their other properties are compatible with normal, approximately spherical, Fermi surfaces. It is the purpose of this note to point out that the thermoelectric power is very sensitive to the form of the Fermi surface, and that it is not necessary to have the conditions usually associated with 'hole conduction' to obtain a positive value.

Conventional theory leads to the following expression for the thermoelectric power S at normal or high temperatures

$$S=\frac{\pi^2\kappa^2}{3e}\left(\frac{1}{\sigma}\frac{d\sigma}{dE}\right)_{\zeta}T, \qquad \ldots\ldots(1)$$

where

$$\sigma(E)=\frac{e^2}{4\pi^3\hbar^2}\int\tau(\mathbf{k})\left(\frac{\partial E}{\partial k_z}\right)^2\frac{dS}{|\nabla E|}. \qquad \ldots\ldots(2)$$

The subscript ζ in (1) means that the derivative is evaluated at the Fermi surface, $\tau(\mathbf{k})$ is the relaxation time, and $\mathbf{k}$ the wave vector defined so that $\hbar\mathbf{k}$ is the momentum. The other symbols have their usual significance.

A rather general expression for the time of relaxation, referring to unit volume of the metal, which does not assume the existence of spherical energy surfaces is as follows:

$$\frac{1}{\tau(\mathbf{k})}=\frac{1}{4\pi^2\hbar}\int|U_{\mathbf{kk}'}|^2\left(1-\frac{k_z'}{k_z}\right)\frac{dS'}{|\nabla E'|} \qquad \ldots\ldots(3)$$

in which $U_{\mathbf{kk}'}$ is the matrix of the scattering potential.

In the model which assumes spherical energy surfaces, S depends on the effective mass, if this is regarded as constant for all energies, only through ζ the Fermi energy.† In an actual monovalent metal, even when the Fermi surface is nearly spherical, $|\nabla E|$ is by no means constant over this surface; it is much smaller in the immediate neighbourhood of the Brillouin zone boundaries than elsewhere. It is this effect which gives rise to the peak in the density of states, $N(E)$, as shown, for example, in figure 1(*b*), for we have

$$N(E)=\frac{1}{4\pi^3}\int\frac{dS}{|\nabla E|}. \qquad \ldots\ldots(4)$$

---

† The reason a negative sign appears in conditions of pure hole conduction is that σ becomes the same function of E_0-E as it is of E in the negative electron case, where E_0 denotes the energy at the head of the band.

In order to evaluate the integral of equation (3) it is necessary to consider the properties of the matrix element $U_{\mathbf{kk}'}$. For given **k** this is not constant over the Fermi surface. It decreases steadily with increasing angle θ between the vectors **k** and **k**′. We adopt a common approximation and assume that $U_{\mathbf{kk}'}$ is constant for all angles less than θ_0, and zero for greater angles, where

$$2k\sin(\theta_0/2)=q_0 \qquad \ldots\ldots(5)$$

and q_0 is the radius of the Debye sphere in the space of the wave vector of the lattice vibrations, and k the mean radius of the Fermi surface. Thus, if we write

$$\frac{1}{\tau(\mathbf{k})}=\frac{1}{4\pi^2\hbar}\left\langle\frac{1}{|\nabla E|}\right\rangle_{\mathrm{av}}\int|U_{\mathbf{kk}'}|^2\left(1-\frac{k_z'}{k_z}\right)dS' \qquad \ldots\ldots(6)$$

the weighted average of $|\nabla E|^{-1}$ in (6) is taken over a certain area of the Fermi surface about the point fixed by **k**. This area will, in general, for any **k**, contain one of the regions in which $|\nabla E|$ becomes small. Thus a reasonable approximation to (3) is

$$\frac{1}{\tau}\propto N(E)\int_0^{2\sin^{-1}(q_0/2k)}(1-\cos\theta)2\pi\sin\theta\,d\theta, \qquad \ldots\ldots(7)$$

or

$$\tau\propto k^4/N(E), \qquad \ldots\ldots(8)$$

and, since we may assume for a slightly distorted sphere $E\propto k^2$, we have

$$\tau\propto E^2/N(E). \qquad \ldots\ldots(9)$$

In the integral of equation (2) the regions of small $|\nabla E|$ do not have the same importance as in (3) since $|\partial E/\partial k_z|\leqslant|\nabla E|$. In fact the regions of the Fermi surface responsible for carrying the current are those between the areas close to the Brillouin zone planes, i.e. between A and B, B and C, etc., as shown in figure 1(*a*). There is here an analogy with the two-zone theory as applied, for example, to the transition metals by Mott (1936). Part of the Fermi surface, those regions near A, B, C, etc., determines the rate of change of τ with E, and the remainder carries the bulk of the current. The first part would correspond to the 'd-band'; the second to the 's-band'.

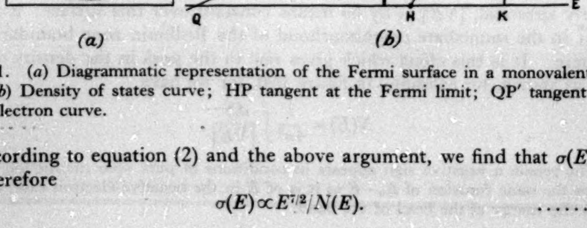

Figure 1. (*a*) Diagrammatic representation of the Fermi surface in a monovalent metal. (*b*) Density of states curve; HP tangent at the Fermi limit; QP′ tangent to free electron curve.

According to equation (2) and the above argument, we find that $\sigma(E)\propto\tau k^3$, and therefore

$$\sigma(E)\propto E^{7/2}/N(E). \qquad \ldots\ldots(10)$$

Hence, according to (1)

$$S=\frac{\pi^2\kappa^2}{3e\zeta}\left[\frac{7}{2}-\left(\frac{E}{N(E)}\frac{dN(E)}{dE}\right)_\zeta\right]T. \qquad \ldots\ldots(11)$$

The second term in brackets is equal to $\frac{1}{2}$ for free electrons, but for monovalent metals in which the Fermi surface lies close to the zone boundaries it may be very much greater. Figure 1(*b*) shows that it is equal to QK/2HK, where QK and HK are the subtangents to the parabola and the true $N(E)$ curve respectively. The difference between KP and KP′ is neglected. It is clear that if the Fermi surface lies sufficiently close to the Brillouin zone planes this factor may exceed 7/2, and therefore lead to a positive value of S (e is negative).

This theory suggests a reason why the alkali metals, except lithium, have negative values of S while the noble metals have positive values. The noble metals have face-centred cubic structures, and the Fermi surface lies close to the octahedral planes of the Brillouin zone; appreciably closer than the Fermi surface lies to the {110} planes of the Brillouin zone of the alkali metals. Thus in the alkali metals the Fermi level lies further from the peak of the $N(E)$ curve, and therefore leads to a much smaller value of the ratio QK/HK. The anomalous sign for lithium is undoubtedly connected with the fact that in this metal the electronic energies deviate markedly from free electron values as shown by Schiff's calculations (1954).

REFERENCES

MOTT, N. F., 1936, *Proc. Roy. Soc.* A, **153**, 699. (See also MOTT, N. F., and JONES, H., 1936, *Theory of Properties of Metals and Alloys* (Oxford : University Press).)

SCHIFF, B., 1954, *Proc. Phys. Soc.* A, **67**, 2.

Many-Body Scattering Problem in Momentum Space

BY S. N. BISWAS

Department of Theoretical Physics, Indian Association for the Cultivation of Science, Jadavpur, Calcutta

MS. received 21*st April* 1955 *and in final form* 1*st July* 1955

THE following second-order linear integro-differential equation,

$$\left[\frac{d^2}{dr^2}+k^2-\frac{l(l+1)}{r^2}-U(r)\right]f_l(r)=\lambda\int_0^\infty K_l(r,r')f(r')\,dr' \qquad \ldots\ldots(1)$$

occurs in many-body scattering problems. A reduction of this (1) to a Fredholm equation of the second type has been proposed for an iterative solution by Swan (1954).

In this note we reduce the problem in the momentum space (see Kohn 1951) by the aid of Hankel transform. This will reduce the equation (1) to a homogeneous integral equation of the Fredholm type in the momentum space. For the asymptotic nature of the function $f_l(r)$ as is required to obtain the asymptotic phase we have made use of Riemann–Lebesgue theorem of integral calculus to note that the singular nature of the f_l function in the p-space will characterize the corresponding asymptotic behaviour of the coordinate-space function.

We write

$$f_l(r)=\sqrt{\frac{\pi}{2}}\int_0^\infty \sqrt{(pr)}\,J_{l+\frac{1}{2}}(pr)\phi_l(p)\,dp \qquad \ldots\ldots(2)$$

and define

$$U(p,p')=\frac{2}{\pi}\int_0^\infty \sqrt{(pr)}\,J_{l+\frac{1}{2}}(pr)U(r)J_{l+\frac{1}{2}}(p'r)\sqrt{(p'r)}\,dr \qquad \ldots\ldots(3)$$

and

$$G_l(p,p')=\frac{2\lambda}{\pi}\int_0^\infty\int_0^\infty \sqrt{(pr)}\,J_{l+\frac{1}{2}}(pr)\sqrt{(p'r')}\,J_{l+\frac{1}{2}}(p'r')K_l(r,r')\,dr\,dr'. \qquad \ldots\ldots(4)$$

Introducing the value of $f_l(r)$ from (2) in (1) and multiplying the resulting equation by $\sqrt{(p'r)}J_{l+\frac{1}{2}}(p'r)$ on the left and then integrating over r from 0 to ∞ we get from (3) and (4) the following homogeneous integral equation in the momentum space.

$$(p^2-k^2)\phi(p)+\int_0^\infty \{U(p,p')+G_l(p,p')\}\phi(p')\,dp'=0 \qquad \ldots\ldots(5)$$

where both $U(p,p')$ and $G_l(p,p')$ are symmetric functions as is clear from (3) and (4).

In deducing (5) we have utilized the fact that

$$\int_0^\infty \sqrt{(pp')}\,J_{l+\frac{1}{2}}(pr)J_{l+\frac{1}{2}}(p'r)r\,dr=\frac{\pi}{2}\delta(p-p').$$

It is easily seen that the function which in coordinate space has the asymptotic behaviour

$$\underset{r\to\infty}{f_l(r)}=(kr)[j_l(kr)-\tan\eta\,.\,n_l(kr)]$$

($j_l(kr)$ and $n_l(kr)$ are spherical Bessel functions) satisfies the integral equation

$$\phi(p)=\delta(p-k)-(p^2-k^2)^{-1}\int_0^\infty [U(p,p')+G_l(p,p')]\phi(p')\,dp'. \qquad \ldots\ldots(5\,a)$$

Hence when η is the phase shift

$$\left(-\frac{2k}{\pi}\right)\tan\eta=\int_0^\infty [U(p,p')+G_l(p,p')]\phi(p')\,dp'. \qquad \ldots\ldots(6)$$

An iterative solution of $\tan\eta$ may be obtained from (6) by introducing (5 *a*) in (6).

An approximate integro-differential equation for the scattering of neutrons by deuterons (Buckingham and Massey 1942) is

$$\left(\frac{d^2}{dr^2}+k^2\right)f(r)=\lambda\int_0^\infty rr'\exp[-\alpha(r+r')]f(r')\,dr'.$$

This gives in the momentum-space the following for $\tan\eta$,

$$\left(-\frac{2k}{\pi}\right)\tan\eta=\lambda\int_0^\infty G_0(p,p')\phi(p')\,dp'$$

where

$$G_0(p,p')=\frac{2}{\pi}\left(\int_0^\infty \exp(-\alpha r)rJ_{\frac{1}{2}}(pr)\sqrt{(pr)}\,dr\right)\left(\int_0^\infty \exp(-\alpha r')r'\sqrt{(p'r')}\,J_{\frac{1}{2}}(p'r')\,dr'\right)$$

and

$$\phi(p)=\delta(p-k)-(p^2-k^2)^{-1}\int_0^\infty G_0(p,p')\phi(p')\,dp';$$

$\phi(p)$ is the Hankel transform of $f(r)$.

My thanks are due to Dr. D. Basu for his helpful comments.

References

Buckingham, R. A., and Massey, H. S. W., 1942, *Proc. Roy. Soc.* A, **179**, 123.
Kohn, W., 1951, *Phys. Rev.*, **84**, 495.
Swan, P., 1954, *Phys. Rev.*, **96**, 1144.

Angular Distribution of γ-Radiation from ^{9}Be(α, nγ)^{12}C

By N. W. TANNER
Cavendish Laboratory, Cambridge

MS. received 26th August 1955

§ 1. Introduction

At the present time seven resonances for γ-ray emission are known for the reaction $^9\mathrm{Be}(\alpha, \mathrm{n}\gamma)^{12}\mathrm{C}$ in the range of α-particle bombarding energies up to 5 Mev (Ajzenberg and Lauritsen 1955); several of these resonances have also been identified in the neutron yield. Presumably these resonances indicate excited states of the ^{13}C compound nucleus, and in principle the spins, and possibly the parities, of the states concerned can be deduced from a knowledge of the angular dependence of the radiations.

Jones (1953) and James (1952) made quite a thorough investigation of this reaction over the α-particle energy range 0·5 to 1·3 Mev. Their work included nearly all possible angular distributions and correlations and the results showed marked effects of interfering energy levels. An analysis by Jones of the ground state neutron angular distribution was made in terms of three overlapping levels, two corresponding to the known resonance at $E_\alpha = 0{\cdot}65$ Mev, width approximately 0·1 Mev, and at $E_\alpha = 1{\cdot}9$ Mev, width approximately 0·2 Mev, and a third remote level of large width; spins, parities were assigned as $\frac{1}{2}^+$, $\frac{1}{2}^-$ and $\frac{7}{2}^-$ respectively. Although the theoretical fit achieved was barely qualitative, there was a clear suggestion of greater simplicity at higher energies. In particular the $\frac{1}{2}^-$ character of the ^{13}C excited state corresponding to $E_\alpha = 1{\cdot}9$ Mev should make angular distribution somewhere in this energy region at least approximately isotropic.

§ 2. Experimental

The measurements were made using a 1 μA beam of He$^+$ ions to bombard a beryllium target about 1000 Å thick evaporated on to a 0·005 inch copper backing. This target thickness corresponds to 30 kev energy loss for 1·9 Mev α-particles. A sodium iodide scintillation counter was used for counting the 4·43 Mev γ-radiation and it was arranged to move around the target in a horizontal plane and to subtend a solid angle of 0·03 steradian at the target. A similar counter monitored the intensity of the α-particle beam. The energy calibration of the detectors was checked with a polonium–beryllium source.

An excitation curve for the 4·43 Mev γ-radiation was taken over the range $E_\alpha = 1{\cdot}2$ to 2·5 Mev. Agreement with the curve published by Talbot and

Heydenburg (1953) was very good, the resonance being placed at 1·905 ± 0·010 Mev and having a half-width at half-height on the low-energy side of 0·09 ± 0·01 Mev; the high-energy side of the curve appeared to be distorted by the tail of the 2·6 Mev resonance.

Angular distribution measurements of the γ-radiation were made at α-particle energies of 1·32, 1·52, 1·72, 1·82, 1·92 and 2·02 Mev. As the yield of the reaction is very large, counting was carried out at 30 angles for each energy, with a statistical accuracy to 2 or 3%. A further angular distribution measurement was taken with a small piece of ^{60}Co, waxed to the target, replacing the reaction as the source of radiation; this allowed accurate correction for eccentricity, absorption, scattering and the effect of the stray field of the magnetic analyser. Corrections for centre-of-mass motion and Doppler effect are sufficiently small to be neglected.

The final results were fitted by a least squares method with a curve of the form $A_2 + B_2 \cos^2\theta + C_2 \cos^4\theta$ (θ is the angle between the α-particle beam and the centre of the γ-counter), this being the highest order polynomial in $\cos^2\theta$ that can occur as the γ-radiation is known to be electric quadrupole. Curves of the form $A_1 + B_1 \cos^2\theta$ were also fitted in order to determine whether the coefficients C_2 were genuine. The table lists the results of the analysis together with the data of Jones and James taken at lower energies.

	Energy E_α (Mev)	γ–Angular Distribution
Jones and James	0·646	$1-(0{\cdot}07 \pm 0{\cdot}06)\cos^2\theta$
	0·703	$1-(0{\cdot}15 \pm 0{\cdot}06)\cos^2\theta$
	0·934	$1-(0{\cdot}60 \pm 0{\cdot}06)\cos^2\theta$
	1·140	$1-(0{\cdot}66 \pm 0{\cdot}06)\cos^2\theta+(0{\cdot}44 \pm 0{\cdot}06)\cos^4\theta$
	1·32	$1-(0{\cdot}02 \pm 0{\cdot}02)\cos^2\theta$
	1·52	$1-(0{\cdot}18 \pm 0{\cdot}04)\cos^2\theta+(0{\cdot}23 \pm 0{\cdot}04)\cos^4\theta$
	1·72	$1+(0{\cdot}02 \pm 0{\cdot}03)\cos^2\theta+(0{\cdot}12 \pm 0{\cdot}03)\cos^4\theta$
	1·82	$1-(0{\cdot}29 \pm 0{\cdot}03)\cos^2\theta+(0{\cdot}43 \pm 0{\cdot}02)\cos^4\theta$
	1·92	$1-(0{\cdot}00 \pm 0{\cdot}03)\cos^2\theta+(0{\cdot}16 \pm 0{\cdot}02)\cos^4\theta$
	2·02	$1+(0{\cdot}36 \pm 0{\cdot}02)\cos^2\theta$

By calibrating the efficiency of the γ-counter from the known strength of the polonium–beryllium source, absolute cross sections of the ^{9}Be(α, nγ)^{12}C reaction have been estimated to an accuracy of a factor of two. The figures for $E_\alpha = 1{\cdot}92$ Mev are $d\sigma(\alpha, n\gamma) = 0{\cdot}026$ barn sterad^{-1} at $\theta = 90°$, $\sigma(\alpha, n\gamma) = 0{\cdot}33$ barn.

An attempt by Dearnaley (1954, private communication) to obtain further information on the ^{9}Be(α, nγ)^{12}C reaction, by studying the elastic scattering of alpha particles from ^{9}Be, led to a negative result. No significant deviations from the Rutherford scattering were observed. An upper limit to the cross section was placed at $d\sigma(\alpha, \alpha) \leqslant 0{\cdot}0026$ barn sterad^{-1} at $\theta = 90°$, $E_\alpha = 1{\cdot}9$ Mev. Comparing $d\sigma(\alpha, \alpha)$ with $d\sigma(\alpha, n\gamma)$ and assuming the ground state neutron group to be one third as intense as the excited state group, gives $\Gamma_n/\Gamma_\alpha \geqslant 12$. Here Γ_n is width for neutron emission to both ground and first excited states of ^{12}C and Γ_α is width for α-particle emission.

§ 3. Discussion

It is clear that no obvious simplicity, certainly not isotropy, appears in the γ-angular distributions over the region of the resonance at $E_\alpha = 1{\cdot}9$ Mev. In fact the size and the variation of the coefficients are greater at this energy than at the energies studied by Jones and James.

No attempt has been made to find a theoretical fit in terms of interfering energy levels. The labour involved would be very great and the result almost certainly ambiguous and of doubtful significance. Moreover, the actual size of the cross section, 0·33 barn, and the failure of Dearnaley to observe resonant elastically scattered alpha particles, is not easy to explain except in terms of something like a continuum theory (Blatt and Weisskopf 1952) in which resonant states do not appear.

The conclusion reached is that in the region of 12 MEV excitation in ^{13}C, the states are not well defined and any attempt to assign such properties as spins and parities must be speculative.

I am indebted, for an Overseas Scholarship, to the Royal Commission for the Exhibition of 1851.

REFERENCES

AJZENBERG, F., and LAURITSEN, T., 1955, *Rev. Mod. Phys.*, **27**, 77.

BLATT, J. M., and WEISSKOPF, V. F., 1952, *Theoretical Nuclear Physics* (New York: John Wiley).

JAMES, D. B., 1952, *Ph.D. Thesis*, University of Cambridge.

JONES, G. A., 1953, *Ph.D. Thesis*, University of Cambridge.

TALBOT, F. L., and HEYDENBURG, N. P., 1953, *Phys. Rev.*, **90**, 186.

Inequalities for Molecular Integrals

BY A. WEINMANN

Department of Physics, University College, London

Communicated by H. S. W. Massey; *MS. received 2nd August* 1955

THE theory of molecular structure is beset with many difficulties, the chief of which is the evaluation of the integrals which occur in the quantum mechanical treatment of the problems. The wave functions used are mostly chosen so that these integrals can be evaluated, and even then it is not unusual for many terms to be neglected as 'small', or evaluated approximately (see, for example, Löwdin 1953).

It is thus desirable to have an upper bound which can be easily evaluated for these integrals.

All of the usual types of integral which occur, except the 'overlap' type, are contained in the following expressions

$$I=\int \Phi(\mathbf{r}_1)\frac{1}{r_{12}}\,d\tau_1 \qquad \ldots\ldots(1)$$

$$J=\int \Phi(\mathbf{r}_1)\frac{1}{r_{12}}\Psi(\mathbf{r}_2)\,d\tau_1\,d\tau_2 \qquad \ldots\ldots(2)$$

in which it is usual to have

$$\Phi(\mathbf{r})=\phi_1(\mathbf{r}).\phi_2(\mathbf{r}) \quad\text{and}\quad \Psi(\mathbf{r})=\psi_1(\mathbf{r}).\psi_2(\mathbf{r}) \qquad \ldots\ldots(3)$$

where the ϕ_1, ϕ_2, ψ_1, ψ_2 are functions 'centred' on various centres A, B, C, D, say (any of which may coincide). Now

$$|I| \leqslant \int |\Phi(\mathbf{r}_1)| \frac{1}{r_{12}} \, d\tau_1;$$

changing the origin of $\mathbf{r}_1$ coordinates by transformation

$$\mathbf{r}_1 = \mathbf{r}_2 + \mathbf{p} \qquad (\mathbf{r}_2 \text{ fixed})$$

and evaluating the integral in polar coordinates p, μ, ϕ we get

$$\begin{aligned} |I| &\leqslant \int_0^\infty \int_{-1}^{+1} \int_0^{2\pi} |\Phi(\mathbf{r}_2+\mathbf{p})| \frac{1}{p} p^2 dp\,d\mu\,d\phi \\ &= \int_0^1 \int_{-1}^{+1} \int_0^{2\pi} |\Phi(\mathbf{r}_2+\mathbf{p})| \frac{p^2}{p} dp\,d\mu\,d\phi + \int_1^\infty \int_{-1}^{+1} \int_0^{2\pi} |\Phi(\mathbf{r}_2+\mathbf{p})| \frac{p^2}{p} dp\,d\mu\,d\phi \\ &\leqslant \mathrm{Max}_S |\Phi| \int_0^1 \int_{-1}^{+1} \int_0^{2\pi} p\,dp\,d\mu\,d\phi + \int_1^\infty \int_{-1}^{+1} \int_0^{2\pi} |\Phi(\mathbf{r}_2+\mathbf{p})| p^2 \, dp\,d\mu\,d\phi \end{aligned}$$

and adding $\int_0^1 \int_{-1}^{+1} \int_0^{2\pi} |\Phi(\mathbf{r}_2+\mathbf{p})| p^2 \, dp\,d\mu\,d\phi$ to the right-hand side we get

$$|I| \leqslant \left[2\pi\, \mathrm{Max}_S |\Phi| + \int |\Phi(\mathbf{r})| \, d\tau\right] \leqslant \left[2\pi\, \mathrm{Max} |\Phi| + \int |\Phi(\mathbf{r})| \, d\tau\right] \quad \ldots(4)$$

in which $\mathrm{Max}_S |\Phi|$ is the maximum of $|\Phi(\mathbf{r})|$ for $|\mathbf{r} - \mathbf{r}_2| \leqslant 1$.

Also
$$|J| \leqslant \int |\Phi(\mathbf{r}_1)| \frac{1}{r_{12}} |\Psi(\mathbf{r}_2)| \, d\tau_1 \, d\tau_2.$$

Performing the $d\tau_1$ integration first and using the result (4)

$$|J| \leqslant \left[2\pi\, \mathrm{Max} |\Phi| + \int |\Phi(\mathbf{r})| \, d\tau\right] . \int |\Psi(\mathbf{r})| \, d\tau. \quad \ldots\ldots(5)$$

Equations (4) and (5) are the principal inequalities. They depend on the relative position of the four centres A, B, C, D. Further inequalities which are independent of the relative positions of A, B, C, D can be obtained from them by inserting the following inequalities (6) and (7) on the right-hand sides of (4) and (5).

$$\mathrm{Max} |\Phi| \leqslant \mathrm{Max} |\phi_1| . \mathrm{Max} |\phi_2| \quad \ldots\ldots(6)$$

and as
$$|\phi_1 \phi_2| \leqslant \tfrac{1}{2} [|\phi_1|^2 + |\phi_2|^2]$$
$$\left| \int \Phi(\mathbf{r}) \, d\tau \right| \leqslant \int |\Phi(\mathbf{r})| \, d\tau \leqslant \tfrac{1}{2} \left[\int |\phi_1|^2 \, d\tau + \int |\phi_2|^2 \, d\tau \right] \quad \ldots\ldots(7)$$

and thus if each of ϕ_1, ϕ_2, ψ_1, ψ_2 are 'normalized', (4) and (5) give simply

$$|I| \text{ and } |J| \leqslant [2\pi\, \mathrm{Max} |\phi_1| . \mathrm{Max} |\phi_2| + 1]. \quad \ldots\ldots(8)$$

The calculation of $\mathrm{Max} |\Phi| = \mathrm{Max} |\phi_1 \phi_2|$ for equations (4) and (5) is fairly easily done by the use of spheroidal coordinates, and the calculation of an upper bound for

$$\int |\Phi(\mathbf{r})| \, d\tau = \int |\phi_1(\mathbf{r})| . |\phi_2(\mathbf{r})| \, d\tau$$

requires the evaluation of an overlap type integral only. These calculations can be considerably simplified by replacing the 'angular factors' in the functions $|\phi_1(\mathbf{r})|$ etc. by their maximum values.

To illustrate the use of equation (5) the case of a two-centre 'exchange' integral with four 1S hydrogenic wave functions is considered. Accurate values of this integral were taken from Hirschfelder and Linnett (1950) for comparison with the upper bounds. The internuclear separation $AB=\rho$.

$$J=\frac{1}{\pi^2}\int \exp(-r_{1A})\exp(-r_{1B})\frac{1}{r_{12}}\exp(-r_{2A})\exp(-r_{2B})\,d\tau_1\,d\tau_2$$

$$\operatorname{Max}|\Phi|=\operatorname{Max}\left|\frac{1}{\pi}\exp(-r_{1A})\exp(-r_{1B})\right|=\frac{1}{\pi}\exp(-\rho)$$

$$\int|\Psi|\,d\tau=\int\frac{1}{\pi}\exp(-r_{2A})\exp(-r_{2B})\,d\tau=(1+\rho+\rho^2/3)\exp(-\rho).$$

The results are given in the table.

ρ	Upper bound	Actual value†	ρ	Upper bound	Actual value†
0	$3\cdot00$	$0\cdot625$	5	$1\cdot06\times10^{-2}$	$0\cdot372\times10^{-2}$
1	$1\cdot37$	$0\cdot437$	6	$2\cdot45\times10^{-3}$	$0\cdot814\times10^{-3}$
2	$5\cdot00\times10^{-1}$	$1\cdot842\times10^{-1}$	8	$1\cdot11\times10^{-4}$	$0\cdot329\times10^{-4}$
3	$1\cdot57\times10^{-1}$	$0\cdot585\times10^{-1}$	10	$4\cdot25\times10^{-6}$	$1\cdot138\times10^{-6}$
4	$4\cdot26\times10^{-2}$	$1\cdot563\times10^{-2}$	12	$1\cdot47\times10^{-7}$	$0\cdot345\times10^{-7}$

† Hirschfelder and Linnett (1950).

REFERENCES

HIRSCHFELDER, J. O., and LINNETT, J. W., 1950, *J. Chem. Phys.*, **18**, 130.

LÖWDIN, P. O., 1953, *J Chem. Phys.*, **21**, 374, where further references may be found.

Doubly Charged Diatomic Molecular Ions

BY D. R. BATES AND T. R. CARSON

Department of Applied Mathematics, Queen's University, Belfast

MS. received 19*th September* 1955

§1

DOUBLY charged diatomic molecular ions, which in general may be denoted by XY^{2+}, have received very little attention. In particular consideration does not appear to have been given to the factors governing their stability or even to whether stable species are likely to be rare or common.

The states of ions such as XY^{2+} may be classified into two main types depending on the nature of the products that result if the distance r between the nuclei is increased adiabatically to infinity. In one type (which we shall designate by the letter A) the products are X and Y^{2+}; and in the other type (which we shall designate by the letter R) they are X^+ and Y^+.

§2

For type-A states the polarization of X by Y^{2+} ensures that the interaction potential is attractive over a considerable range. The simplest example is $HeH^{2+}(2p\sigma)$. This has He^{2+} and H(1s) as its adiabatic products. Exact calculations show that the state is indeed bound, that the equilibrium internuclear separation r_e is 2·06 Å and that the dissociation energy D_e is 0·85 ev (Bates and Carson 1956). The looseness of the binding is characteristic.

Most interest is of course attached to the ground state. Clearly it can only be of type A if

$$\Delta(\mathrm{X}-\mathrm{Y}^+)\equiv I(\mathrm{X})-I(\mathrm{Y}^+) \qquad \ldots\ldots(1)$$

is positive, the I's being the ionization potentials of the systems indicated. Inspection of tables of ionization potentials shows that this condition is usually not satisfied. The most important exceptions are to be found in the group in which X is an inert gas atom and Y an alkaline-earth atom. It may be noted, for instance, that $\Delta(\mathrm{Ne}-\mathrm{Mg}^+)$ is $+6{\cdot}5$ ev so that the ground state of NeMg^{2+} is of type A and is therefore bound. The ions should be formed readily in three-body collisions

$$\mathrm{Mg}^{2+}+2\mathrm{Ne}\rightarrow\mathrm{NeMg}^{2+}+\mathrm{Ne}. \qquad \ldots\ldots(2)$$

Like the other members of the group NeMg^{2+} does not possess any low-lying excited states.

§3

In spite of the Coulomb repulsion between X^+ and Y^+ a number of XY^{2+} ions with type-R ground states are effectively stable.

Suppose that $\Delta(\mathrm{X}-\mathrm{Y}^+)$ is negative but not unduly so. In the zero-order approximation the potential energy curve $V_{\mathrm{R}}(r)$ associated with the ground state and the potential energy curve $V_{\mathrm{A}}(r)$ associated with the first type-A state would cross at some internuclear separation r_c but if certain selection rules are obeyed the curves cannot in fact cross and instead behave as if they repel each other (cf. Coulson 1952, p. 65). In this event $V_{\mathrm{R}}(r)$ has the repulsive Coulomb form characteristic of type-R states only for r greater than r_c while for part of the region in which r is less than r_c it is in general attractive. Though $V_{\mathrm{R}}(r_c)$ exceeds $V_{\mathrm{R}}(\infty)$ the ion concerned may be regarded as stable, dissociation by leakage through the potential barrier with maximum at r_c being so exceedingly slow that it may be ignored completely.

A list of the ions which owe their stability to pseudo curve-crossing need not be given. One such ion, SiO^{2+}, may be considered as representative of the others. It may be seen that $\Delta(\mathrm{O}-\mathrm{Si}^+)$ is $-2{\cdot}7$ ev and that r_c is more than 5 Å. Beyond r_c the potential $V(r)$ is approximately equal to $(14{\cdot}4/r(\text{Å}))$ev; and within the polarization of O by Si^{2+} is sufficient by itself to lead to a minimum.

In contrast to ions with type-A ground states ions with type-R ground states cannot be formed in three-body collisions at thermal energies for the required close approach is prevented by the Coulomb repulsion. They might however be produced by high energy ionizing impacts. Spectroscopic detection may be possible as some have low-lying excited states: thus in the case of SiO^{2+} a number of such states arise from the crossings of the $[\mathrm{Si}^+(^2\mathrm{P})+\mathrm{O}^+(^4\mathrm{S}, {}^2\mathrm{D}, {}^2\mathrm{P})]$ potentials and the $[\mathrm{Si}^{2+}(^1\mathrm{S})+\mathrm{O}(^3\mathrm{P}, {}^1\mathrm{D}, {}^1\mathrm{S})]$ potentials.

If $\Delta(\mathrm{X}-\mathrm{Y}^+)$ is very negative, as it is for many pairs, r_c may be so small that the zero order approximation to $V_{\mathrm{A}}(r)$ has become repulsive, or there may even be no pseudo-crossing. This does not necessarily mean that $V_{\mathrm{R}}(r)$ has not a minimum. In a few instances one may result from ordinary valence binding.

To survey the possibilities it is convenient to write

$$V_{\mathrm{R}}(r)=1/r+U(r) \qquad \ldots\ldots(3)$$

where the first term is the part of the potential due to the Coulomb repulsion between X^+ and Y^+, the second term is the remainder, and all quantities are now in atomic units. Adopting the Morse representation let

$$\left.\begin{aligned} U(r) &= D_e'\{1-\exp[-\beta'(r-r_e')]\}^2 - D_e' \\ \beta' &= hc\omega_e'(\mu'/2D_e')^{1/2} \end{aligned}\right\} \qquad \ldots\ldots(4)$$

where the symbols have the customary significance (cf. Herzberg 1950, p. 101) and the primes on them indicate that they refer not to XY^{2+} but to the fictitious system obtained by omitting the $1/r$ term from the expression for the potential. Provided the binding is homopolar the neutral molecule isoelectronic with XY^{2+} may be taken as a crude approximation to this fictitious system.

For given r_e' and $\omega_e'\sqrt{\mu'}$ one can find $D_e'(\mathrm{C})$ the value of D_e' which is just sufficient to let $V(r)$ have a minimum. The results of some computations are presented in figure 1 from which it may be seen that a minimum may occur even if $D_e'(\mathrm{C})$ is quite moderate in magnitude.

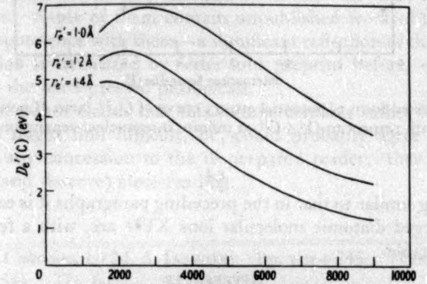

Figure 1. Dependence of $D_e'(\mathrm{C})$ on $\omega_e'\sqrt{\mu'}$ for $r_e' = 1{\cdot}0$ Å, $1{\cdot}2$ Å and $1{\cdot}4$ Å.

Besides being of interest in themselves the ions N_2^{2+} and O_2^{2+} serve as instructive illustrations of the general position. It is first noted that $\Delta(\mathrm{N{-}N^+})$ is $-15{\cdot}1$ ev and $\Delta(\mathrm{O{-}O^+})$ is $-21{\cdot}5$ ev both of which are large in magnitude. The neutral molecule isoelectronic with N_2^{2+} is C_2 so that for exploratory purposes r_e' may be taken to be $1{\cdot}3$ Å and ω_e' to be 1600 $\mathrm{cm^{-1}}$ from which it follows that $D_e'(\mathrm{C})$ is about $4{\cdot}2$ ev. Since D_e for C_2 is only $3{\cdot}6$ ev it would hence seem rather likely that N_2^{2+} is unstable. On the other hand O_2^{2+} is probably stable: thus by the same procedure $D_e'(\mathrm{C})$ for it is estimated to be $4{\cdot}1$ ev which is $5{\cdot}7$ ev smaller than D_e for N_2, the isoelectronic neutral molecule. In figure 2 the expected potential energy curve is sketched tentatively.

Hagstrum and Tate (1941) have reported that N_2^{2+} and O_2^{2+} are formed through

$$N_2 + e \rightarrow N_2^{2+} + 3e \qquad \ldots\ldots(5)$$

and

$$O_2 + e \rightarrow O_2^{2+} + 3e \qquad \ldots\ldots(6)$$

(cf. Massey and Burhop 1952, pp. 258, 266). The evidence should however be viewed with caution for the measured appearance potentials, $49{\cdot}5 \pm 0{\cdot}5$ ev and $50{\cdot}5 \pm 0{\cdot}5$ ev respectively, are anomalously high unless the ions are excited.

In the case of N_2^{2+} the discrepancy is slight but in the case of O_2^{2+} it is severe since if the ground state is bound the true appearance potential must be considerably *less* than

$$\{D(O_2) + 2I(O) + 1/r_e(O_2)\}\text{atomic units} = 44{\cdot}2\text{ ev.} \qquad \ldots\ldots(7)$$

Further work is required.

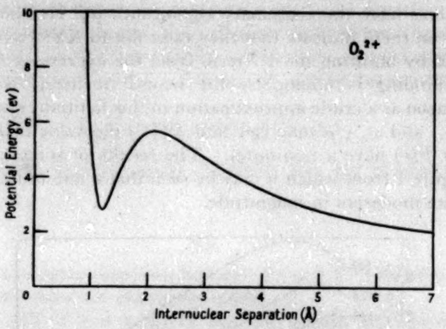

Figure 2. Suggested form of potential energy curve of O_2^{2+} (zero of potential is measured with respect to $O^+ + O^+$ at infinite internuclear separation).

§4

By reasoning similar to that in the preceding paragraphs it is easily established that trebly charged diatomic molecular ions XY^{3+} are, with a few unimportant exceptions, unstable.

REFERENCES

BATES, D. R., and CARSON, T. R., 1956, *Proc. Roy. Soc.* A, in the press.
COULSON, C. A., 1952, *Valence* (Oxford : Clarendon Press)
HAGSTRUM, H. D., and TATE, J. T., 1941, *Phys. Rev.*, **59**, 354.
HERZBERG, G., 1950, *Spectra of Diatomic Molecules*, 2nd Edn (London : Macmillan).
MASSEY, H. S. W., and BURHOP, E. H. S., 1952, *Electronic and Ionic Impact Phenomena* (Oxford : Clarendon Press).

REVIEWS OF BOOKS

Progress in Nuclear Physics. Volume 4, edited by O. R. Frisch. Pp. vii + 379. (London and New York: Permagon Press, 1955.) 70*s*.

As is said on the dust-jacket, " Sections of physics, such as nuclear physics, are in turn breaking up into specialities whose practitioners require aid from such progress reports as are contained in this volume ".

This year's specialities include the chemical and nuclear properties of the very heavy elements; focusing in high-energy accelerators and the acceleration of unusual ions in moderate energy ones; meson theory, scintillation spectrometer statistics, nuclear photodisintegration as studied by the emulsion technique, neutron spectroscopy and isotopic spin in relation to nuclear reactions. The authors are, as usual, wisely chosen from among those actively engaged in the work of which they write, and the articles include very full references to the original papers. Some of them contain unpublished work of the authors or of those in correspondence with them—a significant reflection of the extent to which new information is circulated by letter and preprint before, or instead of, its publication in the hard-pressed periodicals.

Though the editor claims that this volume contains rather less theory which experimenters might find difficult, he would probably agree that few of the authors make any concession to the ill-prepared reader; they write as experts and demand (and deserve) close reading.

P. B. MOON.

The Theory of Cohesion, by M. A. Jaswon. Pp. viii + 245. (London: Pergamon Press, 1954). 37*s*. 6*d*.

It seems to be a fairly common practice among chemists to reserve the word cohesion to specify the forces that stick molecules or aggregates together. Other forces, like those which operate between electrons and nuclei or atoms and atoms, are usually referred to as binding forces. Solid-state workers, on the other hand, do not always make this distinction and use the word cohesion with more latitude to include all attractive forces. It is in this latter sense that the author considers the theory of cohesion, so that chemical readers should not be disappointed when finding that, whereas most of the book is devoted to the treatment of binding in atoms and molecules, intermolecular forces are discussed in no more than two pages.

The first three chapters provide an account of quantum mechanics. This is a little sketchy. It is a pity also that one or two rather loose statements have slipped in here. For instance, on page 10 it seems to be implied that values of the probability distribution functions at an initial time determine those at any later time, and on page 20 it is stated, as a general condition for the wave function, that it should be finite everywhere.

In chapter IV a detailed discussion of the helium atom and exchange forces is given. Chapter V is a treatment of the hydrogen molecule, both from the Heitler and London and the molecular orbital approach. (Although of minor importance here, it is worth mentioning, as this is a mistake that appears in a number of textbooks, that the equilibrium interatomic distance for the hydrogen molecule given by the Weinbaum method is not 0·77 Å, as stated on page 115, but rather 0·75 Å.) Chapter VI deals with molecular orbitals. Bloch functions are introduced here for cyclic systems, and it would certainly have made this treatment more accessible for many readers if some justification for their use had been provided. The author then passes to the theory of metals, which is considered in the next two chapters on the basis of the tight-binding and the cellular approximations. The book ends with a chapter on covalent structures.

The whole approach to this book must be made by keeping in mind the author's frank statement in the introduction : " [This book] is not intended to be of direct use for solving problems or for correlating the theory with experimental data. Space has been devoted to points which have proved troublesome to the author but which may well appear as trivial matters to others." This attitude is certainly commendable, as a critical approach to many of the problems treated in this book has been needed for some time. It is, however, a very serious limitation, which robs the book of some unity and conciseness, and which reduces its attraction for those who do not share the viewpoint of the author.

The book is well produced but no doubt expensive for its size.

S. L. ALTMANN.

Méthodes de différentiation et d'intégration numériques (*applications*), par A. ZILLER. Pp. 150. (Paris : Publications Scientifiques et Techniques de l'Air, N. T. No. 50, 1955.) 1500 *fr*.

This book deals primarily with interpolation and the numerical evaluation of differential coefficients and integrals of tabulated functions. For example formulae are derived which approximate an integral as a linear combination of function values at points distributed over the range of integration. These are the usual formulae based on polynomial interpolation and there is little in this part that cannot be found in a standard textbook on numerical analysis.

The main value of the book however lies in the wealth of examples given to illustrate the preliminary analytical treatment which is very often necessary before a numerical formula can be applied, as for example, in the case of an integral where the integrand or a derivative has a singularity in the range of integration (for in this case polynomial approximation breaks down). Various transformations are suggested in such cases where the analytical form of the integrand is known.

A section on numerical integration of differential equations is included. The Taylor series method is described in relation to first- and second-order differential equations. For the latter class of equation two-point boundary conditions and eigenvalue problems are discussed.

R. A. BROOKER.

Siebenstellige Tafeln der elementaren transzendenten Funktionen, by F. LÖSCH. Pp. viii + 335. (Berlin – Göttingen – Heidelberg : Springer-Verlag, 1954.) DM. 49.80 (87*s*. 2*d*.)

The functions in tables I and II are : angle ϕ, $\sin x$, $\cos x$, $\tan x$, $\sinh x$, $\cosh x$, $\tanh x$, $\ln x$,e^x, e^{-x}, $\sin^{-1} x$, $\tan^{-1} x$, $\sinh^{-1} x$, $\cosh^{-1} x$, $\tanh^{-1} x$, $\coth^{-1} x$, where these functions are real. In both tables ϕ is given in degrees, minutes, seconds and 2 D of a second. Table I gives the remaining functions to 9 D for $x=0(0{\cdot}0001)0{\cdot}1$; table II gives them to 7 D for $x=0{\cdot}1(0{\cdot}0005)3{\cdot}15$, $x=3(0{\cdot}01)10$, $x=10(0{\cdot}1)20$ together with $\tan x$ for $x=1{\cdot}5680(0{\cdot}0001)1{\cdot}5730$, $\tanh^{-1}x$ for $x=0{\cdot}9980(0{\cdot}0001)1$ and $\coth^{-1}x$ for $x=1(0{\cdot}0001)1{\cdot}0020$. Table III gives several of the same functions as I and II, to 7 D for $x=0(1)100$. Table IV gives $\tfrac{1}{2}x\pi$ to 12 D for $x=0(1)100$. Table V gives $\sin\tfrac{1}{2}x\pi$, $\cos\tfrac{1}{2}x\pi$ to 7 D for $x=0(0{\cdot}001)0{\cdot}5$. Table VI gives $\exp(\pm\tfrac{1}{2}x\pi)$, $\sinh\tfrac{1}{2}x\pi$, $\cosh\tfrac{1}{2}x\pi$ to 7 D for $x=0(0{\cdot}01)2$; table VII gives the same functions of $x\pi/180$ to 7 D for $x=0(1)180$. Table VIII gives angle in degrees, minutes and seconds and also in degrees and decimals of a degree, as a function of angle in radians; table IX is the inverse of table VIII. Table X gives about 20 important constants and (as exact ratios) Bernouilli numbers as far as B_{40} (B_{20} in Glaisher's notation); factorials as far as 15 ! are also given.

English readers will naturally compare these tables with the second volume of Comrie's 1949 edition of *Chambers' Six-Figure Mathematical Tables*; these are six-figure or six-decimal, whichever is the less, whilst Lösch's gives not less than seven decimals. Again, Comrie's are tabulated only in the first quadrant, for the circular functions. On the other hand, Lösch's tables omit the reciprocal functions altogether and do not tabulate the circular functions against angle in degrees. Lösch's notes on interpolation are meagre in the extreme, not going beyond the ill-conceived recommendation of the Newton–Gregory forward formula. The contrast with Comrie's masterly introduction is as striking as the contrast in price. First differences are given where interpolation is supposed to be practicable and it is not perhaps surprising that the author gives up as soon as Δ''' becomes significant. No guidance is given to the reader as to how to enter such a table as e^x at $x\sim 5$, say, where, of course, special methods are available.

According to the preface, the *raison d'être* of the tables is that Hayashi's tables (Berlin : Springer 1926) are no longer available. It might have been added that they reached a level of unreliability rivalled only by the extensive "corrections" issued by Hayashi himself in 1932. We are told, however, that the present tables have been abbreviated from ten-decimal values, which had been checked by differencing. The quality of the paper is good and the type is clear, except that the italicized differences leave something to be desired in this respect.

J. C. E. JENNINGS.

Théories relativistes de la gravitation et de l'électromagnétisme, by A. LICHNEROWICZ. Pp. xii + 298. (Paris : Masson, 1955.) 2,800 *fr.*

This volume in the series of mathematical works for physicists is addressed to those with a good knowledge of tensor analysis, and some acquaintance with topology. Great care has been taken to achieve the utmost rigour in the mathematics, and to avoid undesirable reliance on physical intuition. The book is divided into two parts of roughly equal length. The first part is concerned with general relativity; here the author begins by considering exactly the nature of the space–time manifold, the systems of coordinates used, and the hypotheses about the existence of derivatives of various orders. The study of the energy-tensor and the field equations leads to Cauchy's problem. (That is, given the values of the field variables and their first derivatives on a hypersurface S, to find their values inside (or outside) S.)

The detailed consideration of Cauchy's problem, for the various theories, is an excellent feature of the book. In this, as in its elegance and exactness, it stands in the direct line of descent from the great French mathematical works. The interior and exterior forms of Cauchy's problem are connected by 'jump' conditions across S. The interpretation of the energy-tensor is then discussed in terms of hydrodynamics. Chapters are included on the relativistic hydrodynamics of a viscous fluid, and of a charged perfect fluid. Finally, new physical problems about the properties of the space–times in the large are considered; for example, static, everywhere regular, space–times are discussed.

The second part of the book deals with unified field theories. It opens with an excellent general introduction. The ideal of a unified field theory is traced to the combination of the electric and magnetic field strengths into a single six-vector, effected by the special theory of relativity. However, when the gravitational field receives an explanation by means of the extension to the general theory, the electromagnetic field is described in terms of concepts derived from general relativity, but by equations deduced by plausible extrapolation from the special theory. These modified Maxwell equations involve the metric, so that there is some interaction between the fields, and their laws of propagation are identical. The author concludes that such a theory, though an advance, is still only a provisional electromagnetic theory. The need is felt for a truly unified theory, in some sense. He distinguishes two senses; in the general sense a theory will be called unified if the gravitational and electromagnetic fields enter symmetrically, each coming from the same geometrical structure. In the strict sense, a theory is unified to the extent to which the exact equations represent one non-decomposable field, so that the separation into gravitational and electromagnetic field equations is possible only approximately under specially simple physical conditions.

The author divides the attempts to find a unified field theory into the two general classes of five-dimensional theories (including the so-called projective theories), and theories with an affine connection. As an example of the first class, he studies the Jordan–Thiry theory, with references to the earlier Kaluza–Klein theory. As the representative of the second class, the Einstein–Schrödinger theory is presented in a somewhat similar fashion to the presentation by Schrödinger in 'Space–Time Structure'.

The book can be earnestly recommended to specialists in general relativity who wish to consider seriously the problems raised. It is written throughout with the greatest care and precision, and printed very well; the alphabetical index, however, is wholly inadequate. C. W. KILMISTER.

Atomic and Nuclear Physics, by R. S. SHANKLAND. Pp. xv + 529. (New York: Macmillan, 1955.) 44*s*.

The need for a carefully prepared course on nuclear physics as part of undergraduate teaching in physics has been recognized by most Universities for many years. The lecturer about to prepare such a course at the present time is, however, faced with the difficulty that the underlying theory of the subject demands a working knowledge of quantum mechanics which is generally not reached in an undergraduate course. He therefore usually presents an account of the major experimental results eked out with a somewhat scanty theoretical background. This procedure has the advantage that the interest of the audience can be caught and sustained by the glamour of the subject while no great demands on analytical ability need be made. The large number of students whose future is likely to be concerned with the applications of nuclear energy fully justifies such an approach, and for these people Professor Shankland has written a book which could hardly be bettered.

The book presupposes a general knowledge of classical physics, including electrodynamics, and discusses in its early chapters the atomic and kinetic theory, the history of the electron, and atomic, molecular and x-ray spectra. Throughout these chapters the historical development of the subject is given adequate consideration, particularly in the matter of references, and often the excitement of a new discovery, such as x-rays, is well conveyed. Modern ideas are, however, introduced as soon as necessary to give the account coherence and completeness. There follows an interesting chapter on the solid state of matter which gives a brief but excellent review of the many physical phenomena for which the quantum theory of electrons provides an interpretation. The remainder of the book (rather less than half) is devoted to nuclear physics ; the chapters follow the logical order—isotopes, natural radioactivity, induced transformations, nuclear energy sources, high energy processes and cosmic rays. Altogether this is an enormous body of material, and it is a tribute to the author's ability as a teacher that it has been possible to produce such an admirable account of the whole subject, at a uniform level of excellence, within the confines of a single volume. The undergraduate will find it a stimulating textbook, not least for the genuine attempt which it makes to point out the features common between atomic and nuclear processes. Many advanced workers will find useful the up-to-date review of the subject as a whole which it provides ; topics as recent as the production of element 100 and the operation of the Berkeley Bevatron are mentioned.

In a book of such length and scope a reviewer is almost bound to find some points for criticism. It is for instance curious that in a chapter which describes fully the experiments on the wave nature of matter, the Schrödinger equation should not appear, but many students may regard this as an advantage. More might have been said on the theory of the hydrogen atom, particularly on the degeneracy due to the Coulomb field, and the physical reason for the energy separation between the terms of ortho- and parahelium is not well explained. The description of the operation of a Geiger counter is incomplete and the definition of nuclear temperature is not the most useful one. The treatment of beta-decay does not clearly show why beta-emitters have a range of lifetimes, and it is perhaps undesirable that internal conversion electrons should be treated in association with beta-spectra rather than with gamma-transitions. Nuclear isomerism has grown in importance and receives less attention than it deserves. The well-known cloud chamber picture of the disintegration of boron by protons does not show quite what the text implies, and the single-level cross section formula for a (p γ) resonance omits a factor.

Despite these small defects, the book contains many excellent expositions of involved branches of the subject, notably of nuclear resonance experiments and of nuclear energy sources. The references are well chosen and about right in number, although naturally they exhibit a preference for American journals. The book is well set out and produced and there are very few misprints ; it deserves to be widely read. W. E. BURCHAM.

CONTENTS OF SECTION B

PAGE

Mr. I. M. Mackintosh and Mr. J. W. Allen. The Lifetime of Added Carriers in InSb . . . 985

Dr. W. E. Spear. Electron Bombardment Effects in Thin Dielectric Layers . 991

Dr. W. R. Thomas and Dr. G. M. Leak. The Binding Energy of Nitrogen in a Dislocation . . . 1001

Mr. J. E. Bowman and Mr. G. B. F. Niblett. The Passage of a Plane Shock Wave Through a Wire Gauze . . . 1008

Dr. R. S. Tebble. The Barkhausen Effect . . . 1017

Dr. R. Street and Dr. E. O. Hall. Magnetic Domain Structure in Twinned Crystals of Silicon Iron . . . 1033

Dr. A. Fairweather. Dielectric Absorption in Dilute, Liquid, Polar Solutions: A New Approach . . . 1038

Dr. H. B. Huntington. Modification of the Peierls–Nabarro Model for Edge Dislocation Core . . . 1043

Prof. B. Dayal and Mr. R. S. Sharma. Inter-atomic Force Law and Equation of State of Solids . . . 1049

Dr. A. Franks. An Optically Focusing X-Ray Diffraction Camera . . . 1054

Mr. J. W. Gates. The Measurement of Comatic Aberrations by Interferometry 1065

Dr. F. D. Kahn. On the Basic Approximation in the Theory of the Phase Contrast Microscope . . . 1073

Dr. R. C. Faust. Refractive Index Determinations by the Central Illumination (Becke Line) Method . . . 1081

Dr. G. K. Batchelor, Mr. A. M. Binnie and Dr. O. M. Phillips. The Mean Velocity of Discrete Particles in Turbulent Flow in a Pipe . . . 1095

Dr. A. C. Jason and Dr. J. L. Wood. Some Electrical Effects of the Adsorption of Water Vapour by Anodized Aluminium . . . 1105

Prof. N. Ryde and Dr. B. Andersson. A Precision Curved Crystal Gamma-ray Spectrometer . . . 1117

Dr. P. B. Hirsch, Dr. A. Kelly and Dr. J. W. Menter. The Structure of Cold Worked Gold: I—A Study by Electron Diffraction . . . 1132

Research Notes:

- Mr. I. Brodie. D.C. and Pulsed Emission from L-Cathodes . . . 1146
- Mr. A. H. McIlraith. The Measurement of the Coherence of a Light Wave by means of a Lloyd Mirror . . . 1148
- Dr. K. W. Plessner and Mr. R. West. Replacement of Ti in $BaTiO_3$ Ceramic by Si and Ge . . . 1150
- Dr. J. Lees and Mr. S. Walton. Surface States on Germanium . . . 1152
- Mr. G. G. E. Low. Modulation of the Surface Conductance of Germanium by Pulsed Electric Fields . . . 1154
- Prof. R. M. Chaudhri. A Mercury Safety Valve for Electrolysis of Heavy Water . . . 1157

Corrigendum: Sampooran Singh . . . 1158

Reviews of Books . . . 1159

Contents of Section A . . . 1160

Subject Index, Section B, Vol. **68** . . . 1161

Index of Authors (with Titles), Section B, Vol. **68** . . . 1168

Index to Reviews of Books, Section B, Vol. **68** . . . 1175

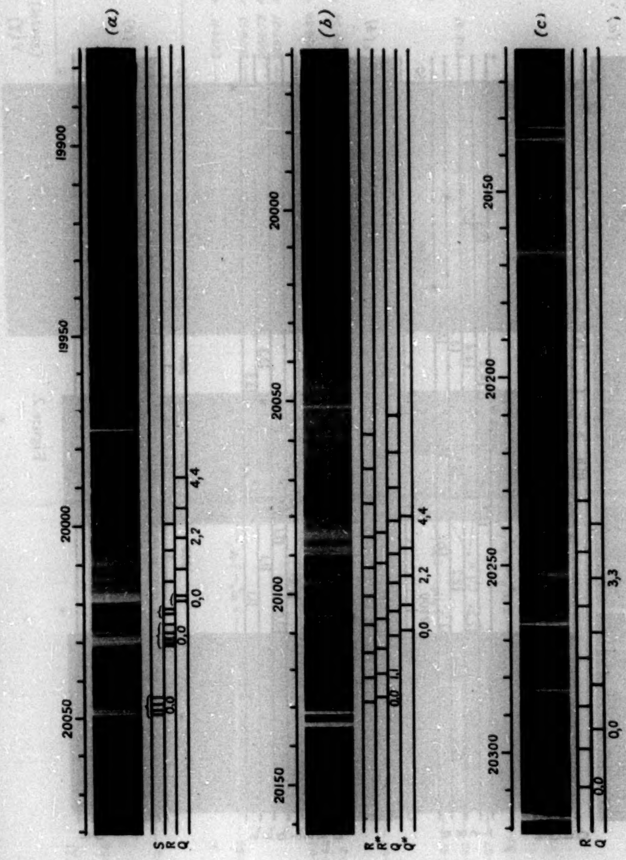

Figure 1.

PLATE I.

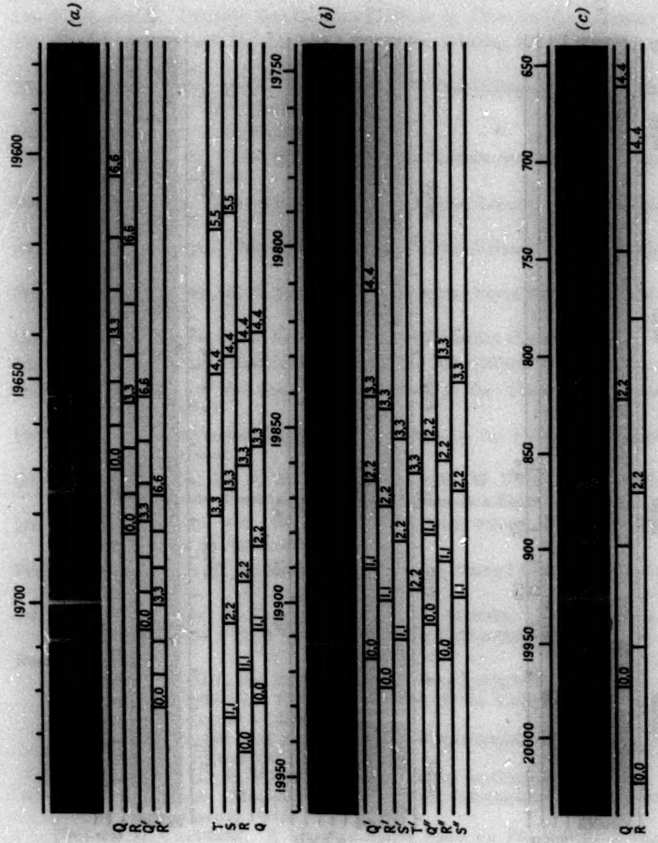
(a)
19600
19650
19700
Q
R
Q'
R'
T
S
R
Q
6,6
13,3
10,0
3,3
15,5
4,4
2,2
1,1
0,0
(b)
19750
19800
19850
19900
19950
Q'
R'
S'
T'
Q''
R''
S''
(c)
650
700
750
800
850
900
19950
20000
Q
R

Figure 2.

Plate II.

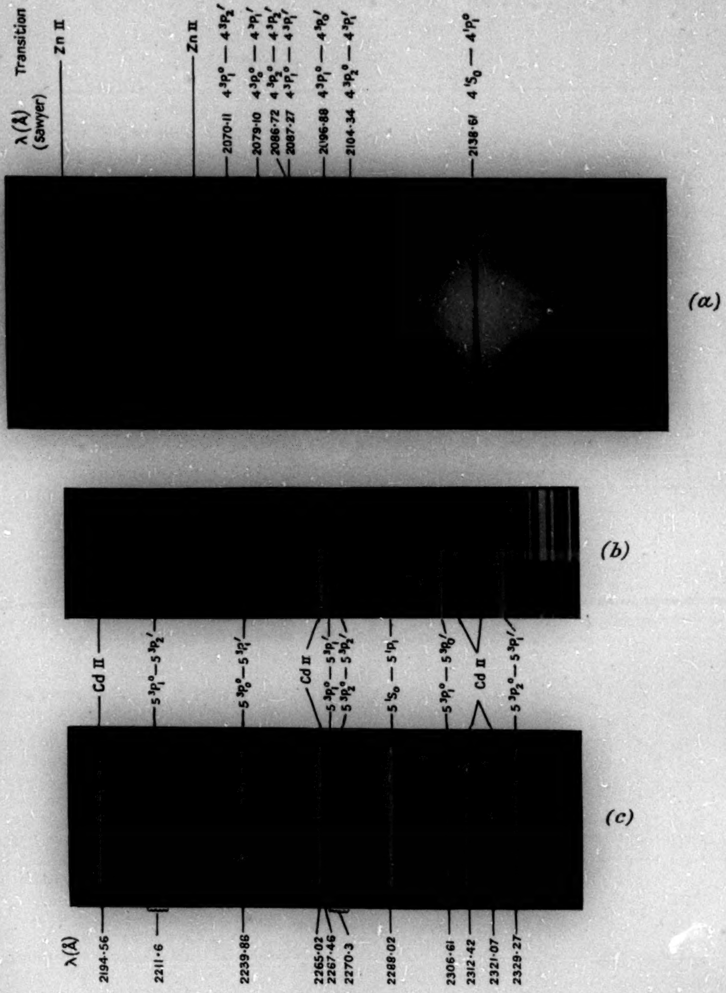

Figure 1.

(*a*) Spectrum of Zn arc in air showing PP′ multiplet; 3 metre grating spectograph.

(*b*) Spectrum of Cd arc in air showing PP′ multiplet; Fe arc comparison; medium quartz spectrograph.

(*c*) Spectrum of Cd arc in argon at 5 cm pressure; 3 metre grating spectrograph.

PROCEEDINGS OF THE PHYSICAL SOCIETY

SECTION A, 1955—VOLUME 68

SUBJECT INDEX

PAGE

Absorption, *see* Paramagnetic resonance
Absorption cross sections, *see* Cross sections
Absorption spectra, *see* under Spectra
Actinium X (^{223}Ra), radioactive decay, nuclear emulsion study 110
Alpha particles, radiative capture in ^{14}N 553
Aluminium 27, ground state, beta decay 1033
Aluminium $K\alpha_3\alpha_4$ lines in metal and oxide (R) 654
Aluminium monofluoride, triplet band systems 824
Angular correlation of annihilation radiation 304
Angular correlation parameters for oriented nuclei (L) 349
Angular correlations, α–γ, and internal conversion measurements in ThCC″ and ThC′D 35
Angular distribution of γ-radiation from ^{9}Be(α, nγ)^{12}C (R) 1187
Angular distribution of ^{7}Li(p, n)^{7}Be* neutrons for proton energies between 2·5 and 2·9 Mev (R) 1081
Angular distributions and angular correlations in reaction ^{23}Na(p, γ)^{24}Mg 369
Angular distributions from (d, n) reactions at 0·86 Mev deuteron energy 386
Angular momenta, quantized, proposed notation (L) 50
Anharmonicity and monomolecular reactions (R) 920
Annihilation radiation, angular correlation 304
Arc spectra, *see* Spectra, arc
Aromatic molecules, electronic spectra: II—Alternant hydrocarbon molecules, excited states 81
Aromatic molecules, electronic spectra: III—Effect of inductive substituents 329
Aromatic molecules, electronic spectra: IV—Excited states of odd alternant hydrocarbon radicals and ions 591
Aromatic molecules, electronic spectra: V—Interaction of two conjugated systems 601
Aromatic molecules, electronic spectra: VI—Mesomeric effect 969
Arsenic 70, produced by ^{14}N bombardment of Cu, decay (R) 760
Atomic heat of sodium (L) 762
Atomic systems, neutral, continuous atomic absorption cross sections for (R) 544
Atoms, mu-mesic, energy levels (L) 945

Band spectra, rotational analysis of $A^3\Pi_{0^+}$, $B^3\Pi_1-X^1\Sigma^+$ systems of InF 962
Band spectrum, 9·6μ band of ozone, line widths in 530
Band systems of CH, intensities (R) 547
Band systems, of MnF and MnBr in the red 665
Band systems, new, of PO and P$_2$, spectroscopic identification (R) 542
Band systems, triplet, of AlF 824
Band systems, *see also* Spectrum
Beryllium 8, spin, energy and lifetime 204
Beta decay of ground state of ^{27}Al 1033
Binding energy, *see* Energy, binding
Biot–Savart law and dislocations (L) 53
Bismuth, L levels, fluorescence yields 612, (L) 942
Bombardments, α-particle and deuteron, capture processes in (R) 535
Branching ratios of ^{86}Rb and ^{42}K (R) 346
Bremsstrahlung production, effect of finite nuclear size 165

Cadmium oxide, electrical conductivity at low temperatures 312
Caesium titanium alum, paramagnetism of (L) 57
Calibration, absolute, of neutron counters with Po–α–Be (L) 52
Capture processes in α-particle and deuteron bombardments (R) 535
Capture, radiative, *see also* Radiative capture

PAGE
Capture, radiative, of 669 kev protons in fluorine (R) 538
Carbon, production of ^{11}C by protons of energy 200–950 MEV 1001
Cell model, liquid, for ^{3}He 1136
Cellular method for close-packed hexagonal lattice, and applications to Ti 686
Charge transfer and ion–atom interchange collisions (R) 344
Charge transfer from negative ions of atomic H to protons in collisions 173
Charged particles, *see also* Particles, charged
Charged particles, spin 1/2, in constant magnetic field, effect of radiative corrections 316
Cloud chamber, *see* Wilson chamber
Cobalt 57, decay 701
Collisions of electrons with atoms, Layzer approximation for 377
Collisions, inelastic, heavy particle, involving crossing of potential energy curves: III—charge transfer from negative ions of atomic H to protons 173
Collisions, inelastic, between heavy particles: IV—Contribution of double transitions 90
Collisions, ion–atom interchange, and charge transfer (R) 344
Collisions of nucleons with deuterons 769
Combinatorial solution of triangular Ising lattice 145
Commutation relations between different fields 503
Conduction electrons, *see* Electrons
Conductivity, electrical, *see* Electrical conductivity
Configurations $(1s)^2$ $(2s)$ and $(1s)^2$ $(2s)^2$ in atoms and ions from He to C, search for simple analytic wave functions 297
Cosmic radiation and μ–e decay, positive temperature effect 893
Cosmic radiation, barometer effect on hard component 953
Cosmic radiation, positive temperature effect in 625
Cosmic-ray events in nuclear emulsions exposed below ground 829
Cosmic ray showers, second maxima in transition curve (L) 352
Cosmic ray transition curves, search for secondary maxima: I (L) 1086
Cosmic ray transition curves, search for secondary maxima: II (L) 1088
Counter, *see also* Proportional counter
Counter, proportional, pressure, energy loss distribution for minimum ionizing electrons (L) 549
Counters, neutron, absolute calibration with Po–α–Be (L) 52
Coupling, intermediate, studies: III—Lithium isotopes 189
Coupling, intermediate, studies: IV—Nuclei ^{13}C and ^{13}N 197
Covariant treatment of nucleon–nucleon interaction 577
Cross section, n–p, in range 60–550 kev (R) 1077
Cross section, slow neutron, of scandium 104
Cross sections, atomic absorption, continuous, for neutral atomic systems (R) 544
Cross sections, differential, absolute measurement, for nuclear scattering of low energy relativistic electrons (R) 928
Cross sections for 2s–2p transitions in H and 3s–3p transitions in Na produced by electron and proton impact 457
Cross sections, total, for nuclear scattering of high energy nucleons (L) 259
Crystal, nickel, temperature dependence of magnetostriction in 133
Crystals, single, of Fe and Si–Fe, [110] magnetostriction 65
Cyclotron, break-up of negative ions in 398

Decay of ^{70}As produced by ^{14}N bombardment of Cu (R) 760
Decay of ^{57}Co 701
Decay of ^{22}Na, electron capture in 681
Decay of RaD and 46·5 kev excited state of RaE 735
Decay, radioactive, of AcX (^{223}Ra), nuclear emulsion study 110
Diffusion, thermal, *see* Thermal diffusion
Deuterons, *see also* Scattering
Deuterons, collisions of nucleons with 769
Deuteron stripping by ^{23}Na, ^{27}Al, ^{31}P, neutron groups from 1008

PAGE
Dielectric loss in long chain polar compounds, theory 1175
Dielectric theory of electronic interaction in solids 976
Discharges in inert, gases, molecular ions in 11
Disintegration of phosphorus by 8 MEV deuterons, neutron groups from . . 754
Disintegration, radioactive, of ^{232}Th (R) 923
Dislocations and Biot-Savart law (L) 53

Einstein's unified field theory, new static spherically symmetric solution (L). . 260
Electrical conductivity of cadmium oxide at low temperatures . . 312
Electron capture in decay of ^{22}Na 681
Electron mass, effect on high energy electron scattering 741
Electron scattering, high energy, effect of electron mass 741
Electrons, conduction, in uniform magnetic field, general motion . . . 879
Electrons, conduction, in uniform magnetic field, single band motion . . 874
Electrons, detachment from negative hydrogen ions by impact with neutral atoms . 240
Electrons, high energy, scattering 559
Electrons, knock-on, transport of energy by (R). 1072
Electrons, 3pπ, effect of : energy levels of ethylene 72
Electrons, relativisitic, cross sections for nuclear scattering, absolute measurement (R) 928
Emission spectra, *see also under* Spectra . . . . . .
Emulsion, nuclear, study of radioactive decay of AcX (^{223}Ra) 110
Energy, binding, of ^{3}H and ^{4}He 265
Energy distribution of protons from reaction Cu(n, p)Ni (R) 925
Energy levels of ethylene; effect of 3pπ electrons 72
Energy levels, reduced widths, calculation from stripping curves . . . 512
Energies of normal and excited negative ions (R) 540
Energies, resonant, for radiative capture of protons by Na below 53 kev, absolute
  determination (R) 1079
Energy state, metastable, of negative helium ion 815
Energy, transport, by knock-on electrons (R) 1072
Entropy of superfluid helium (L) 939
Equations of state of elements from Thomas–Fermi theory 726
Equations of state of elements from Thomas–Fermi theory: II—Case of incomplete
  degeneracy 1145
Ethylene, energy levels : effect of 3pπ electrons 72
Europium 151 and 153, nuclear spins and ratio of magnetic moments (L) . . 55
Excitation functions for scattering of protons and deuterons by Be and Mg . . 97
Excitation, rotational, and inelastic scattering 656

Fermi gas, degenerate, effect of potential gradient on density 285
Ferrous ion, paramagnetic resonance absorption by (L) 258
Field, self-consistent, *see* Self-consistent field
Field theory, Einstein's unified, new static spherically symmetric solution (L) . 260
Fields, commutation relations between 503
Fluorescence yields of L levels of bismuth . . . . . . 612, (L) 942
Fluorine, radiative capture of 669 kev protons in (R) 538
Free-electron network model for metals : II 1129

Gamma radiation following surface scattering of nucleons 1037
Gamma radiation from ^{9}Be(α, nγ)^{12}C, angular distribution (R) 1187
Gamma radiation from reaction D(p, γ)^{3}He 781
Gamma rays, elastic scattering 1161
Gamma rays, low intensity, in ThC.C′ and ThC″.D transitions 1168
Gamma transition lifetimes, measurement by recoil methods 18
Gas, free electron, spin paramagnetism of (R) 644
Gases, inert, *see* Inert gases

PAGE

Hall effect in metals at high frequencies . . . 1026
Helium ion, negative, metastable energy state . . . 815
Helium, isotope shifts in spectrum, calculation . . . 1152
Helium II film, sub-critical flow in . . . 857
Helium 3, liquid cell model for . . . 1136
Helium 4 nuclei, scattering of 14·3 MeV neutrons by (R) . . . 43
Helium, superfluid, entropy (L) . . . 939
Holmium 165, nuclear magnetic moment (L) . . . 1090
Hot wire thermal diffusion columns, performance . . . 294
Hydrogen, atomic, ionization by electrons of excited 2s and 2p states . . . 1157
Hydrogen atoms, excited, interaction (R) . . . 444
Hydrogen atoms in fast encounters with other hydrogen atoms, contribution of double transitions . . . 90
Hydrogen ions, negative, detachment of electrons from, by impact with neutral atoms . . . 240
Hydrogen molecular ion, properties : V—Transitions connecting lowest even and odd π-states with higher σ-states . . . 565
Hydrogen molecular ion, properties : VI—Total electronic orbital angular momentum of $1s\sigma_g$, $2s\sigma_g$ and $3s\sigma_g$ states . . . 810
Hydrogen molecule, excited states, ionic configuration interaction in . . . 632
Hydrogen, solid, state of . . . 214
Hyperfine structure of praseodymium (L) . . . 936

Impact, electron, and proton, and 2s–2p transitions in H and 3s–3p transitions in Na 457
Inert gases, molecular ions in discharges . . . 11
Infra-red, *see also* Spectrum
Infra-red nitrogen spectra, electron excitation functions . . . 404
Integrals, molecular, inequalities for (R) . . . 1190
Interaction, electronic, in solids, dielectric theory . . . 976
Interaction of electrons in metals (R) . . . 441
Interaction, nucleon–nucleon, covariant treatment . . . 577
Interaction of two excited H atoms (R) . . . 444
Interaction, spin–orbit, determination, in scattering of nucleons by α-particles . 746
Internal conversion in ThCC″ and ThC′D and α–γ angular correlations . . . 35
Ion concentrations, mass spectrometric analysis, radio-frequency probe for . . . 1
Ionic configuration interaction in some excited states of hydrogen molecule . . . 632
Ionization by electrons of excited 2s and 2p states of atomic hydrogen . . . 1157
Ionization loss of relativistic μ-mesons in neon . . . 793
Ions, diatomic molecular, doubly charged (R) . . . 1192
Ions, molecular, in discharges in inert gases . . . 11
Ions, negative, break-up in cyclotron . . . 398
Ions, negative, normal and excited, energies (R) . . . 540
Iron, and silicon–iron, single crystals, [110] magnetostriction . . . 65
Isotope shifts in spectrum of helium, calculation . . . 1152

Kerr effect, theoretical studies : I—Deviations from linear polarization law 905, corr. 1091
Kerr effect, theoretical studies : II—Influence of pressure . . . 910, corr. 1091

Lanthanons, nuclear moments from paramagnetic resonance (L) . . . 937
Lattice, close-packed hexagonal, cellular method, and applications to Ti . . . 686
Lattice scattering in homopolar semiconductors . . . 675
Lattice, triangular Ising, combinatorial solution . . . 145
Lattice waves, low-frequency, scattering by static imperfections . . . 1113
Layzer approximation for treatment of collisions of electrons with atoms . . . 377
Line widths in $9{\cdot}6\mu$ band of ozone . . . 530
Lithium isotopes, intermediate coupling . . . 189
Low temperatures, electrical conductivity of cadmium oxide . . . 312

PAGE

Magnetic field, uniform, general motion of conduction electrons 879
Magnetic field, uniform, single band motion of conduction electrons 874
Magnetic ground state of UF$_3$ (L) 351
Magnetic moments, *see also under* Nuclear
Magnetic moments, ratio, and nuclear spins of Eu 151 and 153 (L) 55
Magnetic susceptibility of potassium manganicyanide 32
Magnetostriction constants for Ni, calculation 1066
Magnetostriction, [110] of single crystals of Fe and Si–Fe 65
Magnetostriction, temperature dependence, in nickel crystal 133
Mangenese halides, spectra in blue-green 1097
Mass spectrometric analysis of ion concentrations, radio-frequency probe for 1
Mesons, detection of mesic X-rays with proportional counter 801
Mesons, *see also* Mu-mesons
Metals, free-electron network model : II 1129
Metals, Hall effect in, at high frequencies 1026
Metals, interaction of electrons in (R) 441
Metals, monovalent, thermoelectric power (R) 1182
Metals, network approximation (R) 439
Metals, reflectivity, theory 121
Method of atoms in molecules 149
Molecular integrals, inequalities for (R) 1190
Molecular ion, hydrogen, properties : V—Transitions connecting lowest even and odd π-states with higher σ-states 565
Molecular ion, hydrogen, properties : VI—Total electronic orbital angular momentum of $1s\sigma_g$, $2s\sigma_g$ and $3s\sigma_g$ states 810
Molecular ions, diatomic, doubly charged (R) 1192
Molecular (monomolecular) reactions and anharmonicity (R) 920
Molecular orbitals, approximate : III—$2s\sigma_g$ and $3d\sigma_g$ states of H_2^+ 569
Molecules, aromatic, *see* Aromatic molecules
Molecules, structure, method of atoms in molecules 149
Moment, nuclear electric quadrupole, of ^{39}K (L) 450
Moments, quadrupole, of odd *A* nuclei (R) 1083
Momentum space, many-body scattering problem in (R) 1185
Momentum spectrum of μ-mesons at sea level : I—Range $5\times10^8-2\times10^{10}$ ev/c 409
Mu-mesic atoms, energy levels (L) 945
Mu-mesons, cosmic ray, stopped in carbon for detection of mesic X-rays by proportional counter 801
Mu-mesons, momentum spectrum at sea level : I—Range $5\times10^8-2\times10^{10}$ ev/c 409
Mu-mesons, relativistic, ionization loss in neon 793
Mu-mesons, scattering in lead and iron 1045
Mu-mesons, underground, star production 482

Negative ions, *see* Ions
Neon, K-series emission spectrum 717
Network approximation in metals (R) 439
Neutron cross section, *see* Cross section
Neutron–deuteron scattering in range 80–200 kev (R) 650
Neutron groups from deuteron stripping by ^{23}Na, ^{27}Al, ^{31}P 1008
Neutron groups from disintegration of phosphorus by 8 MeV deuterons 754
Neutron, *see also* Scattering
Neutronics, general perturbation theory 474
Neutrons, ^{7}Li(p, n)^{7}Be* yield for proton energies between 2·5 and 2·9 MeV (L) 452
Neutrons, 14·3 MeV, scattering by ^{4}He nuclei (R) 43
Neutrons, slow, mean free path in nuclear matter (R) 340
Nitrogen, active, new phenomenon 709
Nitrogen spectra, infra-red, electron excitation functions 404
Nuclear emulsion, variation of track length with angle of dip 852
Nuclear emulsions below ground, cosmic-ray events in 829

PAGE
Nuclear magnetic moments of holmium 165 (L) . . . 1090
Nuclear moments of lanthanons from paramagnetic resonance (L) . . . 937
Nuclear reactions, polarization in . . . 1041
Nuclear scattering, *see* Scattering
Nuclear size, finite, effect on bremsstrahlung production . . . 165
Nuclear spin and magnetic moment of terbium 159 (L) . . . 257
Nuclear spins and ratio of magnetic moments of Eu 151 and 153 (L) . . . 55
Nuclei, and Coulomb scattering of high energy electrons and positrons . . . 156
Nuclei, deformed, inelastic scattering of neutrons by . . . 994
Nuclei ^{13}C and ^{13}N, intermediate coupling . . . 197
Nuclei, complex, elastic scattering of polarized protons from . . . 361
Nuclei, odd A, quadrupole moments (R) . . . 1083
Nuclei, oriented, angular correlation parameters for (L) . . . 349
Nucleon–nucleon interaction, covariant treatment . . . 577
Nucleons, collisions with deuterons . . . 769
Nucleons, scattering, *see under* Scattering
Nucleons, surface scattering, γ radiation following . . . 1037
Nucleus, finite, effect on radiative correction (L) . . . 549

Oscillations, plasma-electron, spectroscopic study . . . 696
Ozone, $9{\cdot}6\ \mu$ band, line widths in . . . 530

Paramagnetic resonance, absorption by ferrous ion (L) . . . 258
Paramagnetic resonance, and nuclear moments of lanthanons (L) . . . 937
Paramagnetism of caesium titanium alum (L) . . . 57
Paramagnetism, spin, of free electron gas (R) . . . 644
Particles, charged, in solids, energy loss and plasma oscillations . . . 525
Particles, heavy, inelastic collisions involving crossing of potential energy curves :
  III—charge transfer from negative ions of atomic H to protons . . . 173
Particles, heavy, inelastic collisions between : IV—Contribution of double transitions 90
Penetrating showers at sea level, rates of . . . 585
Perturbation, *see* Variation
Perturbation theory, general, in neutronics . . . 474
Phase shifts, high order, in elastic scattering of slow protons in inert gases, approximation (R) . . . 932
Phase shifts in p–p scattering (R) . . . 930
Phosphors, Bi activated, absorption and emission spectra (R) . . . 647
Photodisintegration cross section of deuterium and radium equivalent of ^{24}Na sources 181
Plasma–electron oscillations, spectroscopic study . . . 696
Plasma oscillations and energy loss of charged particles in solids . . . 525
Polar compounds, long chain, theory of dielectric loss . . . 1175
Polarization in nuclear reactions . . . 1041
Positronium formation in gases and its pressure dependence (R) . . . 342
Potassium manganicyanide, magnetic susceptibility . . . 32
Potassium 39, nuclear electric quadrupole moment (L) . . . 450
Potential gradient, effect on density of degenerate Fermi gas . . . 285
Praseodymium, hyperfine structure (L) . . . 936
Proportional counter, pressurized, for detection of mesic x-rays . . . 801
Proton synchrotron beam size, determination with crystal scintillator (R) . . . 836
Proton synchrotron beam studies with induction electrode . . . 489
Protons of energy 200–950 Mev and production of ^{11}C from carbon . . . 1001
Protons *see also* Scattering

Quadrupole, electric, moment, of ^{39}K (L) . . . 450
Quantized angular momenta, proposed notation (L) . . . 50

RaD decay and $46{\cdot}5$ kev excited state of RaE . . . 735
Radiation, annihilation, angular correlation . . . 304
Radiation, cosmic, *see* Cosmic radiation
Radiation, *see also under* Capture, Gamma radiation
Radiative capture of α-particles in ^{14}N . . . 553

PAGE

Radiative capture of protons by Na, resonant energy determination (R) . . . 1079
Radiative correction, effect of finite nucleus on (L) . . . 549
Radiative corrections, effect on charged spin 1/2 particle in constant magnetic field . 316
Radioactive decay, *see* Decay
Radio-thorium source, low intensity γ-rays from . . . 1168
Radium equivalent of ^{24}Na sources and photodisintegration cross section of deuterium 181
Radium standards, comparison of British and U.S. (L) . . . 942
Reaction ^{11}B(d, n)^{12}C . . . 637
Reaction Cu(n, p)Ni, energy distribution of protons (R) . . . 925
Reaction D(p, γ)^{3}He, gamma radiation from . . . 781
Reaction ^{19}F(d, n)^{20}Ne, investigation using fast-neutron spectrometer . . . 1017
Reaction ^{23}Na(p, γ)^{24}Mg, angular distributions and angular correlations . . . 369
Reactions, (d, n), at 0·86 Mev deuteron energy, angular distributions . . . 386
Reactions, (d, p) and (d, n), theory : II—Coulomb corrections and numerical results 244
Reactions, nuclear, ^{7}Li(d, n) ^{8}Be and ^{11}B(d, n)^{12}C . . . 393
Reactions, *see also under* Cross sections, Nuclear, Stripping
Recoil methods for measurement of γ-transition lifetimes . . . 18
Reflectivity of metals, theory . . . 121
Relativistic cut-off (L) . . . 354
Resonance, paramagnetic, *see* Resonance

Scandium, slow neutron cross section . . . 104
Scattering, Coulomb, of high energy electrons and positrons by nuclei . . . 156
Scattering, elastic, of gamma rays . . . 1161
Scattering, elastic, of 80 kev neutrons (L) . . . 940
Scattering, elastic, of polarized protons from complex nuclei . . . 361
Scattering, elastic, of slow protons in inert gases, approximation for high order phase shifts (R) . . . 932
Scattering, electron, *see* Electron scattering
Scattering of high energy electrons . . . 559
Scattering, inelastic, of neutrons by deformed nuclei . . . 994
Scattering, inelastic, by rotational excitation (R) . . . 656
Scattering, lattice, in homopolar semiconductors . . . 675
Scattering of low-frequency lattice waves by static imperfections . . . 1113
Scattering, many-body, in momentum space (R) . . . 1185
Scattering, multiple, use of overlapping intervals in measurements (R) . . . 447
Scattering, neutron–deuteron, in range 80–200 kev (R) . . . 650
Scattering, nuclear, of electrons by uranium (L) . . . 348
Scattering, nuclear, of high energy nucleons, total cross sections (L) . . . 259
Scattering of μ-mesons in lead and iron . . . 1045
Scattering of 14·3 Mev neutrons by ^{4}He nuclei (R) . . . 43
Scattering of nucleons by α particles—determination of spin–orbit interaction . 746
Scattering, p–p, phase shifts in (R) . . . 930
Scattering of protons and deuterons by Be and Mg, excitation functions . . . 97
Scattering, surface, of nucleons, γ radiation following . . . 1037
Scattering, *see also* Cross sections
Scattering-in correction . . . 841
Scintillator, crystal, for determination of proton synchrotron beam size (R) . . . 836
Self-consistent field for Zr^{4+} . . . 987
Semiconductors, homopolar, lattice scattering in . . . 675
Showers, *see* Penetrating Showers
Showers, cosmic-ray, *see* Cosmic-ray showers
Sodium, atomic heat (L) . . . 762
Sodium 22, electron capture in decay . . . 681
Sodium 24 sources, radium equivalent, and photodisintegration cross section of deuterium . . . 181
Solid hydrogen, state of . . . 214
Solids, dielectric theory of electronic interaction . . . 976
Solids, energy loss of charged particles in, and plasma oscillations . . . 525

PAGE
Spaces, even and odd dimensional, wave propagation in 521
Spectra, *see also* Band Infra-red, Nitrogen
Spectra, absorption and emission, of Bi activated phosphors (R) 647
Spectra, Al $K\alpha_3\alpha_4$ lines in metal and oxide (R) 654
Spectra, arc, levels of p^2-configuration in Zn, Cd and Hg 1107
Spectra, electronic, of aromatic molecules : II—Alternant hydrocarbon molecules, excited states 81
Spectra, electronic, of aromatic molecules : III—Effect of inductive substituents 329
Spectra, electronic, of aromatic molecules : IV—Excited states of odd alternant hydrocarbon radicals and ions 591
Spectra, electronic, of aromatic molecules : V—Interaction of two conjugated systems 601
Spectra, electronic, of aromatic molecules : VI—Mesomeric effect 969
Spectra of manganese halides in blue-green 1097
Spectrometer, fast-neutron, for investigation of reaction $^{19}F(d, n)^{20}Ne$ 1017
Spectrometry, mass, *see under* Mass spectrometry
Spectroscopic identification of diatomic PS and new band systems of PO and P_2 (R) 542
Spectroscopic study of plasma-electron oscillations 696
Spectrum, atomic, of tin, isotope shifts and hyperfine structure 433
Spectrum, emission, K-series, on neon 717
Spectrum, MnBr, in photographic infra-red 670
Spectrum, yttrium, analysis 79
Spin paramagnetism of free electron gas (R) 644
Stripping curves, calculation of reduced widths from 512
Stripping reaction, *see under* Deuteron
Susceptibility, magnetic, *see* Magnetic susceptibility

Temperature dependence of magnetostriction in nickel crystal 133
Temperature effect, positive, in cosmic radiation 625
Temperature effect, positive, in cosmic radiation and μ–e decay 893
Terbium 159, nuclear spin and magnetic moment (L) 257
Thermal diffusion columns, hot wire, performance 294
Thermoelectric power of monovalent metals (R) 1182
Thomas–Fermi theory, equations of state of elements from 726
Thomas–Fermi theory, equations of state of elements from : II—Case of incomplete degeneracy 1145
Tin, atomic spectrum, isotope shifts and hyperfine structure 433

Uranium, nuclear scattering of electrons by (L) 348
Uranium trifluoride, magnetic ground state (L) 351

Variation–perturbation method : I 419
Variation–perturbation method : II 425

Wave function, analytic, for configurations $(1s)^2 (2s)$ and $(1s)^2 (2s)^2$ in atoms and ions from He to C 297
Wave propagation in even and odd dimensional spaces 521
Weizsäcker inhomogeneity correction term, validity 229
Wilson chamber, internal counter controlled, resolving time (add.) 58

X-ray satellites, identification 322
X-rays, mesic, detection with pressurized proportional counter 801

Yttrium spectrum, analysis 79

INDEX OF AUTHORS (WITH TITLES)

PAGE

Abraham, G., Cohen, L., and Roberts, A. S.: The binding energies of ^{3}H and ^{4}He . 265

Aghajanian, H., with Jaswon, M. A. : The interaction of two excited hydrogen atoms (R) . 444

Allan, D. L. : The energy distribution of protons from the reaction Cu(n,p)Ni at 14 Mev (R) . 925

Allan, H. R., with Sarma, N. : A search for capture processes in alpha-particle and deuteron bombardments (R) . 535

Allen, R. A., Burcham, W. E., Chackett, K. F., Munday, G. L., and Reasbeck, P. : Electron capture in the decay of sodium 22 . 681

Allen, T. K. : A spectroscopic study of plasma–electron oscillations . 696

Allen, W. D., and Ferguson, A. T. G. : Elastic scattering of 80 kev neutrons (L) . 940

Allen, W. D., and Ferguson, A. T. G. : The n–p cross section in the range 60–550 kev (R) . 1077

Allen, W. D., Ferguson, A. T. G. and Roberts, J. : Neutron-deuteron scattering in the range 80–200 kev . 650

Altmann, S. L. : The self-consistent field for Zr^{4+} . 987

Baker, J. M., and Bleaney, B. : The nuclear spin and magnetic moment of terbium 159 257

Baker, J. M., and Bleaney, B. : Hyperfine structure of praseodymium (L) . 936

Baker, J. M., and Bleaney, B. : The nuclear magnetic moment of holmium 165 (L) . 1090

Balazs, N. L. : Wave propagation in even and odd dimensional spaces . 521

Barrow, R. F., Glaser, D. V., and Zeeman, P. B. : Rotational analysis of bands of the $A^3\Pi_{0^+}$, $B^3\Pi_1$–$X^1\Sigma^+$ systems of indium monofluoride . 962

Barrow, R. F., with Dodsworth, P. G. : The triplet band systems of aluminium monofluoride . 824

Bastin, J. A., and Wright, R. W. : The electrical conductivity of cadmium oxide at low temperatures . 312

Batchelor, R. : The yield of ^{7}Li(p, n)^{7}Be* neutrons for proton energies between 2·5 and 2·9 Mev (L) . 452

Batchelor, R., and Morrison, G. C. : The angular distribution of ^{7}Li(p,n)^{7}Be* neutrons for proton energies between 2·5 and 2·9 Mev (R) . 1081

Batchelor, R., with West, D., and Bradley, E. F. : The detection of mesic x-rays with pressurized proportional counters using cosmic ray μ-mesons stopped in carbon . 801

Bates, D. R. : Charge transfer and ion–atom interchange collisions (R) . 344

Bates, D. R., and Carson, T. R. : Doubly charged diatomic molecular ions (R) . 1199

Bates, D. R., and Griffing, G. W. : Inelastic collisions between heavy particles : IV—Contribution of double transitions to certain cross sections including that associated with the ionization of hydrogen atoms in fast encounters with other hydrogen atoms . 90

Bates, D. R. and Lewis J. T. : Inelastic heavy particle collisions involving the crossing of potential energy curves : III—Charge transfer from negative ions of atomic hydrogen to protons . 173

Bates, D. R., and Moiseiwitsch, B. L. : Energies of normal and excited negative ions (R) 540

Bayman, B. F., and Ross, M. A. S. : A nuclear emulsion study of the radioactive decay of actinium X(^{223}Ra) . 110

Berg, R., and Wilets, L. : On the validity of the Weizsäcker inhomogeneity correction term . 229

Biel, S. J., and Burhop, E. H. S. : The effect of finite nuclear size on bremsstrahlung production . 165

Biswas, S. N. : Many-body scattering problem in momentum space (R) . 1193

Bleaney, B. : Nuclear moments of the lanthanons from paramagnetic resonance (L) 937

Bleaney, B., Bogle, G. S., Cooke, A. H., Duffus, H. J., O'Brien, M. C. M., and Stevens, K. W. H. : Paramagnetism of caesium titanium alum (L) . 57

PAGE

Bleaney, B., and Low, W. : Nuclear spins and ratio of magnetic moments of europium 151 and 153 (L) 55
Bleaney, B., with Baker, J. M. : The nuclear spin and magnetic moment of terbium 159 257
Bleaney, B., with Baker, J. M. : Hyperfine structure of praseodymium (L) . . 936
Bleaney, B., with Baker, J. M. : The nuclear magnetic moment of holmium 165 (L) . 1090
Bogle, G. S., with Bleaney, B., Cooke, A. H., Duffus, H. J., O'Brien, M. C. M., and Stevens, K. W. H. : Paramagnetism of caesium titanium alum (L) 57
de Borde, A. H. : The effect of radiative corrections on a charged spin 1/2 particle in a constant magnetic field 316
de Borde, A. H., and Massey, H. S. W. : The collisions of nucleons with deuterons . 769
Bovey, L. F. H., An extension of the analysis of the yttrium spectrum . . . 79
Bowcock, J. E. : Calculation of reduced widths from stripping curves 512
Boyd, R. L. F., and Morris, D. : A radio-frequency probe for the mass-spectrometric analysis of ion concentrations 1
Bradley, E. F. : Energy loss distribution for minimum ionizing electrons in a pressure proportional counter (L) 549
Bradley, E. F., with West, D., and Batchelor, R. : The detection of mesic x-rays with pressurized proportional counters using cosmic ray μ–mesons stopped in carbon 801
Brewer, D. F., Edwards, D. O., and Mendelssohn, K. : The entropy of superfluid helium (L) 939
Brink, D. M. : Inelastic scattering of neutrons by deformed nuclei . . . 994
Buckingham, A. D. : Theoretical studies of the Kerr effect : II—The influence of pressure . . . . 910, corr. 1091
Buckingham, A. D., and Pople, J. A. : Theoretical studies of the Kerr effect : I—Deviations from a linear polarization law . . . . . 905, corr. 1091
Bunbury, D. St. P., with Devons, S., and Manning, G. : Measurement of γ-transition lifetimes by recoil methods 18
Burcham, W. E., Symonds, J. L., and Young, J. D. : The production of ^{11}C from carbon by protons of energy between 200 and 950 Mev 1001
Burcham, W. E., with Allen, R. A., Chackett, K. F., Munday, G. L., and Reasbeck, P. : Electron capture in the decay of sodium 22 681
Burhop, E. H. S. and Biel, S. J. : The effect of finite nuclear size on bremsstrahlung production 165

Calvert, J. M., Jaffe, A. A., Litherland, A. E., and Maslin, E. E. : Neutron groups from deuteron stripping by ^{23}Na, ^{27}Al and ^{31}P 1008
Calvert, J. M., Jaffe, A. A., and Maslin, E. E. : An investigation of the reaction ^{19}F(d, n)^{20}Ne using a new fast-neutron spectrometer 1017
Campion, P. J., and Davies, W. T. : The resolving time of an internal counter controlled Wilson chamber (addendum) 58
Candlin, D. J. : On the identification of x-ray satellites 322
Carson, T. R., and Dalgarno, A. : Approximate molecular orbitals : III—The $2s\sigma_g$ and $3d\sigma_g$ states of H_2^+ 569
Carson, T. R., with Bates, D. R. : Doubly charged diatomic molecular ions (R) . 1199
Chackett, K. F., with Allen, R. A., Burcham, W. E., Munday, G. L., and Reasbeck, P. : Electron capture in the decay of sodium 22 681
Chalklin, F. C. (the late), with Moore, H. R. : The K-series emission spectrum of neon 717
Chandrasekhar, B. S., and Mendelssohn, K. : Sub-critical flow in the helium II film 857
Chapman, K. R., Matsukawa, E., Rose, P. H., and Stewardson, E. A. : The absolute measurement of differential cross sections for the nuclear scattering of low energy relativistic electrons (R) 928
Chartres, B. A., and Tidman, D. A. : The scattering-in correction . . . 841
Clegg, A. B., with Jones, G. A., and Wilkinson, D. H. : The radiative capture of protons of 669 kev in fluorine (R) 538
Cochran, A. J., with Ross, M. A. S., Hughes, J., and Feather, N. : Fluorescence yields of the L levels of Bi . . . . 612, (L) 942

PAGE

Coe, R. F., Riddiford, L., and van der Raay, H. B.: Some proton synchrotron beam studies with the induction electrode 489
Cohen, L.: A variation–perturbation method: I 419
Cohen, L.: A variation–perturbation method: II 425
Cohen, L., with Abraham, G., and Roberts, A. S.: The binding energies of ^{3}H and ^{4}He 265
Collie, C. H., with McMurray, W. R.: The radium equivalent of ^{24}Na sources and the photodisintegration cross section of deuterium 181
Cook, J. R.: Elastic scattering of gamma rays 1170
Cooke, A. H., and Duffus, H. J.: The magnetic susceptibility of potassium manganicyanide 32
Cooke, A. H., with Bleaney, B., Bogle, G. S., Duffus, H. J., O'Brien, M. C. M., and Stevens, K. W. H.: Paramagnetism of caesium titanium alum (L) . . 57
Corner, W. D., and Hunt, G. H.: The temperature dependence of magnetostriction in a nickel crystal 133
Coulson, C. A.: The free-electron network model for metals: II 1129
Curr, R. M.: The Coulomb scattering of high-energy electrons and positrons by nuclei 156

Dalgarno, A., with Carson, T. R.: Approximate molecular orbitals: III—The $2s\sigma_g$ and $3d\sigma_g$ states of H_2^+ 569
Dardis, J. G., with McCusker, C. B. A., and Wilson, B. G.: The rates of penetrating showers at sea level 585
Davies, W. T., with Campion, P. J.: The resolving time of an internal counter controlled Wilson chamber (addendum) 58
Devons, S., Manning, G., and Bunbury, D. St. P.: Measurement of γ-transition lifetimes by recoil methods 18
Dickson, J. M., Rose, B., and Salter, D. C.: Elastic scattering of polarized protons from complex nuclei 361
Dodsworth, P. G., and Barrow, R. F.: The triplet band systems of aluminium monofluoride 824
Donovan, B.: The Hall effect in metals at high frequencies 1026
Donovan, B., Lidiard, A. B., and March, N. H.: On the spin paramagnetism of a free electron gas: II 644
Dressler, K., and Miescher, E.: Spectroscopic identification of diatomic PS and new band systems of PO and P_2 (R) 542
Duffus, H. J., with Bleaney, B., Bogle, G. S., Cooke, A. H., O'Brien, M. C. M., and Stevens, K. W. H.: Paramagnetism of caesium titanium alum (L) . . 57
Duffus, H. J., with Cooke, A. H.: The magnetic susceptibility of potassium manganicyanide 32

Edwards, D. O., with Brewer, D. F., and Mendelssohn, K.: The entropy of superfluid helium (L) 939
El Bedewi, F. A., and El Wahab, M. A.: An investigation of the neutron groups from the disintegration of phosphorus by 8 Mev deuterons 754
Elton, L. R. B.: Effect of finite nucleus on the radiative correction (L) . . . 549
Elton, L. R. B.: Effect of electron mass on high energy electron scattering . . 741
El Wahab, M. A., with El Bedewi, F. A.: An investigation of the neutron groups from the disintegration of phosphorus by 8 Mev deuterons 754
Emery, E. W., and Veall, N.: The branching ratios of ^{86}Rb and ^{42}K (R) . . . 346
Erdman, K. L.: The angular correlation of annihilation radiation 304
Evans, J., with George, E. P.: Further observations of cosmic-ray events in nuclear emulsions exposed below ground 829
Eyeions, D. A., Owen, B. G., Price, B. T., and Wilson, J. G.: The ionization loss of relativisitic μ-mesons in neon 793

Feather, N., with Ross, M. A. S., Cochran, A. J., and Hughes, J.: Fluorescence yields of the L levels of Bi . . . . 612, (L) 942
Ferguson, A. T. G., with Allen, W. D.: Elastic scattering of 80 kev neutrons (L) . 940

PAGE

Ferguson, A. T. G., with Allen, W. D.: The n–p cross section in the range 60–550 kev (R) 1077
Ferguson, A. T. G., with Allen, W. D., and Roberts, J.: Neutron–deuteron scattering in the range 80–200 kev 650
Flack, F. C., with Grant, P. J., Rutherglen, J. G., and Hutchinson, G. W.: Angular distributions and angular correlations in the reaction ^{23}Na(p, γ)^{24}Mg 369
Fletcher, G. C.: Calculation of magnetostriction constants for nickel 1066
Flint, H. T., and Williamson, E. M.: A note on the relativistic cut-off (L) 354
Fowler, G. N.: On the scattering of high energy electrons 559
Fowler, G. N.: On star production by μ–mesons underground 482
Fremlin, J. H., and Spiers, V. M.: The break-up of negative ions in the cyclotron 398
Fröhlich, H., with Pelzer, H.: Plasma oscillations and energy loss of charged particles in solids 525

Gardner, J. W.: Transport of energy by knock-on electrons (R) 1072
Garton, W. R. S., and Rajaratnam, A.: On the levels of the p^2-configuration in the arc spectra of Zn, Cd and Hg 1107
Gatha, K. M., and Shah, G. Z.: The total cross sections for the nuclear scattering of high energy nucleons 259
George, E. P., and Evans, J.: Further observations of cosmic-ray events in nuclear emulsions exposed below ground 829
Glaser, D. V., with Barrow, R. F., and Zeeman, P. B.: Rotational analysis of bands of the $\mathrm{A}^3\Pi_{0^+}$, $\mathrm{B}^3\Pi_1-\mathrm{X}\Sigma^+$ systems of indium monofluoride 962
Grace, M. A., with Lemmer, H. R., and Segaert, O. J. A.: The decay of cobalt 57 701
Grant, I. P.: Theory of (d, p) and (d, n) reactions: II—Coulomb correction and numerical results 244
Grant, P. J., Rutherglen, J. G., Flack, F. C., and Hutchinson, G. W.: Angular distributions and angular correlations in the reaction ^{23}Na(p, γ)^{24}Mg 369
Grant, P. J., with Ward, A.: The reaction ^{11}B(d, n)^{12}C 637
Gray, T. P., and Satchler, G. R.: Angular correlation parameters for oriented nuclei (L) 349
Green, H. S.: Covariant treatment of the nucleon–nucleon interaction 577
Green, L. L., Scanlon, J. P., and Willmott, J. C.: Angular distributions from (d, n) reactions at 0·86 Mev deuteron energy 386
Greenlees, G. W.: Excitation functions for scattering of protons and deuterons by Be and Mg 97
Griffing, G. W., with Bates, D. R.: Inelastic collisions between heavy particles: IV—Contribution of double transitions to certain cross sections including that associated with the ionization of hydrogen atoms in fast encounters with other hydrogen atoms 90
Griffiths, G. M., and Warren, J. B.: The gamma radiation from the reaction D(p, γ)^{3}He 781

Hancock, D. A., and Verdaguer, F.: The absolute determination of resonant energies for radiative capture of protons by sodium in the energy range below 530 kev (R) 1080
Harding, G. N.: Absolute calibration of neutron counters with Po–α–Be (L) 52
Harding, J. B.: The second maxima in the transition curve of cosmic ray showers (L) 352
Harper, P. G.: Single band motion of conduction electrons in a uniform magnetic field 874
Harper, P. G.: The general motion of conduction electrons in a uniform magnetic field with application to the diamagnetism of metals 879
Harper, P. G., and O'Dwyer, J. J.: Theory of a dielectric loss in long chain polar compounds 1184
Hayakawa, S., and Yoshida, S.: Inelastic scattering by rotational excitation (R) 656
Hayes, W.: The spectrum of MnBr in the photographic infra-red 670
Hayes, W.: The spectra of the manganese halides in the blue–green 1097
Hayes, W., and Nevin T. E.: New band systems of MnF and MnBr in the red 665

PAGE

Haywood, C. A. : An approximation for the high order phase shifts in the elastic scattering of slow protons in the inert gases (R) 932
Hindmarsh, W. R., and Kuhn, H. : Isotope shifts and hyperfine structure in the atomic spectrum of tin 433
Hochberg, S., Massey, H. S. W., Robertson, H., and Underhill, L. H. : The scattering of nucleons by alpha particles—determination of the spin–orbit interaction 746
Holøien, E. : Note on a search for simple analytic wave functions for configurations $(1s)^2$ $(2s)$ and $(1s)^2$ $(2s)^2$ in atoms and ions from He to C 297
Holøien, E., and Midtdal, J. : On a metastable energy state of the negative helium ion 815
Hubbard, J. : On the interaction of electrons in metals (R) 441
Hubbard, J. : The dielectric theory of electronic interactions in solids 976
Hughes, J., with Ross, M. A. S., Cochran, A. J., and Feather, N. : Fluorescence yields of the L levels of Bi . . . . 612, (L) 942
Hunt, G. H., and Corner, W. D. : The temperature dependence of magnetostriction in a nickel crystal 133
Hurley, A. C. : On the method of atoms in molecules 149
Husain, A. : Electron scattering in photographic emulsions (R) 45
Hutchinson, G. W., with Grant, P. J., Rutherglen, J. G., and Flack, F. C. : Angular distributions and angular correlations in the reaction ^{23}Na(p, γ)^{24}Mg . . . 369

Ihsan, M. A. : An investigation of ^{7}Li(d, n)^{8}Be and ^{11}B(d, n)^{12}C nuclear reactions . 393

Jacobs, J. : The effect of $3p\pi$ electrons : energy levels of ethylene . . . 72
Jaffe, A. A., with Calvert, J. M., Litherland, A. E., and Maslin, E. E. : Neutron groups from deuteron stripping by ^{23}Na, ^{27}Al and ^{31}P 1008
Jaffe, A. A., with Calvert, J. M., and Maslin, E. E. : An investigation of the reaction ^{19}F(d, n)^{20}Ne using a new fast-neutron spectrometer 1017
Jaswon, M. A., and Aghajanian, H. : The interaction of two excited hydrogen atoms (R) 444
Jones, G. A., Clegg, A. B., and Wilkinson, D. H. : The radiative capture of protons of 669 kev in fluorine (R) 538
Jones, H. : The thermoelectric power of monovalent metals (R) 1191

Keller, A. : Phase shifts in p–p scattering (R) 930
Klemens, P. G. : The scattering of low-frequency lattice waves by static imperfections 1113
Kroener, E. : Dislocations and the Biot–Savart law (L) 53
Kuhn, H., with Hindmarsh, W. R. : Isotope shifts and hyperfine structure in the atomic spectrum of tin 433

Lane, A. M. : Studies in intermediate coupling : III—The lithium isotopes . 189
Lane, A. M. : Studies in intermediate coupling : IV—Further remarks on the nuclei ^{13}C and ^{13}N 197
Laubitz, M. J. : The beta decay of the ground state of ^{27}Al 1033
Ledley, B., and Riddiford, L. : Determination of proton synchrotron beam size with a crystal scintillator (R) 836
Lee, E. W. : The [110] magnetostriction of some single crystals of iron and silicon–iron 65
Lemmer, H. R., Segaert, O. J. A., and Grace, M. A. : The decay of cobalt 57 . 701
Lewis, G. M. : The decay of RaD and the 46·5 kev excited state of RaE . . 735
Lewis, J. T. : Ionic configuration interaction in some excited states of the hydrogen molecule 632
Lewis, J. T., with Bates, D. R. : Inelastic heavy particle collisions involving the crossing of potential energy curves : III—Charge transfer from negative ions of atomic hydrogen to protons 173

PAGE

Lewis, J. T., McDowell, M. R. C., and Moiseiwitsch, B. L. : Properties of the hydrogen molecular ion: V—Transitions connecting the lowest even and lowest odd π-states with higher σ-states 565

Lidiard, A. B., with Donovan, B., and March, N. H. : On the spin paramagnetism of a free electron gas : II 644

Litherland, A. E., with Jaffe, A. A., Calvert, J. M., and Maslin, E. E. : Neutron groups from deuteron stripping by ^{23}Na, ^{27}Al and ^{31}P 1008

Lloyd, J. L., and Wolfendale, A. W. : The scattering of μ-mesons in lead and iron 1045

Longuet-Higgins, H. C., and Murrell, J. N. : The electronic spectra of aromatic molecules : V—The interaction of two conjugated systems 601

Longuet-Higgins, H. C., and Pople, J. A. : The electronic spectra of aromatic molecules : IV—Excited states of odd alternant hydrocarbon radicals and ions 591

Longuet-Higgins, H. C., with Murrell, J. N. : The electronic spectra of aromatic molecules : III—The effect of inductive substituents 329

Low, W., with Bleaney, B. : Nuclear spins and ratio of magnetic moments of europium 151 and 153 (L) 55

McCarroll, R. W., and McDowell, M. R. C. : Properties of the hydrogen molecular ion : VI—The total electronic orbital angular momentum of the 1sσ_g, 2sσ_g and 3sσ_g states 810

McCormack, P. D., McCusker, C. B. A., and Wilson, B. G. : A search for secondary maxima in cosmic ray transition curves : II (L) 1088

McCusker, C. B. A., Dardis, J. G., and Wilson, B. G. : The rates of penetrating showers at sea level 585

McCusker, C. B. A., and Wilson, B. G. : A search for secondary maxima in cosmic ray transition curves : I (L) 1086

McCusker, C. B. A., with McCormack, P. D., and Wilson, B. G. : A search for secondary maxima in cosmic ray transition curves : II (L) 1088

McDowell, M. R. C., with Lewis, J. T., and Moisewitsch, B. L. : Properties of the hydrogen molecular ion: V—Transitions connecting the lowest even and lowest odd π-states with higher σ-states 565

McDowell, M. R. C., with McCarroll, R. W. : Properties of the hydrogen molecular ion : VI—The total electronic orbital angular momentum of the 1sσ_g, 2sσ_g and 3sσ_g states 810

McMurray, W. R., and Collie, C. H. : The radium equivalent of ^{24}Na sources and the photodisintegration cross section of dueterium 181

Manning, G., with Devons, S., and Bunbury, D. St. P. : Measurement of γ-transition lifetimes by recoil methods 18

March, N. H. : Equations of state of elements from the Thomas–Fermi theory . 726

March, N. H. : Equations of state of elements from the Thomas–Fermi theory : II—Case of incomplete degeneracy 1145

March, N. H., with Donovan, B., and Lidiard, A. B. : On the spin paramagnetism of a free electron gas : II 644

Marr, G. V. : The continuous atomic absorption cross sections for neutral atomic systems (R) 544

Martin, D. G. E., and Parry, G. : A search for low intensity gamma rays in the ThC.C′ and ThC″.D transitions 1177

Maslin, E. E., with Calvert, J. M., and Jaffe, A. A. : An investigation of the reaction ^{19}F(d, n)^{20}Ne using a new fast-neutron spectrometer 1017

Maslin, E. E., with Calvert, J. M., Jaffe, A. A., and Litherland, A. E. : Neutron groups from dueteron stripping by ^{23}Na, ^{27}Al and ^{31}P. 1008

Massey, H. S. W., with de Borde, A. H. : The collisions of nucleons with deuterons 769

Massey, H. S. W., with Hochberg, S., Robertson, H., and Underhill, L. H. : The scattering of nucleons by alpha particles—determination of the spin–orbit interaction 746

Matsukawa, E., with Chapman, K. R., Rose, P. H., and Stewardson, E. A. : The absolute measurement of differential cross sections for the nuclear scattering of low energy relativistic electrons (R) 928

PAGE
Mendelssohn, K., with Brewer, D. F., and Edwards, D. O. : The entropy of superfluid helium (L) 939
Mendelssohn, K., with Chandrasekhar, B. S. : Sub-critical flow in the helium II film 857
Midtdal, J., with Holøien, E. : On a metastable energy state of the negative helium ion 815
Miescher, E., with Dressler, K. : Spectroscopic identification of diatomic PS and new band systems of PO and P_2 (R) 542
Mohr, C. B. O. : The mean free path of slow neutrons in nuclear matter (R) . 340
Mohr, C. B. O. : Positronium formation in gases and its pressure dependence (R) . 342
Moiseiwitsch, B. L., with Bates, D. R. : Energies of normal and excited negative ions (R). 540
Moiseiwitsch, B. L., with Lewis, J. T., and McDowell, M. R. C. : Properties of the hydrogen molecular ion : V-Transitions connecting the lowest even and lowest odd π-states with higher σ-states 565
Moore, H. R., and Chalklin, F. C. (the late) : The K-series emission spectrum of neon 717
Morris, D. : Molecular ions in discharges in the inert gases 11
Morris, D., with Boyd, R. L. F. : A radio-frequency probe for the mass-spectrometric analysis of ion concentrations 1
Morrison, G. C., with Batchelor, R. : The angular distribution of ^{7}Li(p, n)^{7}Be neutrons for proton energies between 2·5 and 2·9 Mev (R) 1081
Munday, G. L., with Allen, R. A., Burcham, W. E., Chackett, K. F., and Reasbeck, P. : Electron capture in the decay of sodium 22 681
Murrell, J. N. : The electronic spectrum of aromatic molecules : VI—The mesomeric effect 969
Murrell, J. N., and Longuet-Higgins, H. C. : The electronic spectra of aromatic molecules : III—The effect of inductive substituents 329
Murrell, J. N., with Longuet-Higgins, H. C. : The electronic spectra of aromatic molecules : V—The interaction of two conjugated systems 601

Nevin, T. E., with Hayes, W. : New band systems of MnF and MnBr in the red . 665
Nordfors, B. : A note on the Al K$\alpha_3\alpha_4$ lines in metal and oxide 654

O'Brien, M. C. M. : The magnetic ground state of UF_3 (L) 351
O'Brien, M. C. M., with Bleaney, B., Bogle, G. S., Cooke, A. H., Duffus, H. J., and Stevens, K. W. H. : Paramagnetism of caesium titanium alum (L) . . . 57
O'Dwyer, J. J., with Harper, P. G. : Theory of a dielectric loss in long chain polar compounds 1184
Oneda, S., with Umezawa, H., and Podolanski, J. (the late) : Commutation relations between different fields 503
Öpik, U. : The Layzer approximation for the treatment of collisions of electrons with atoms 377
Owen, B. G., and Wilson, J. G. : Measurements of the momentum spectrum of μ-mesons at sea level : I—The momentum range 5×10^8 ev/c–2×10^{10} ev/c 409
Owen, B. G., with Eyeions, D. A., Price, B. T., and Wilson, J. G. : The ionization loss of relativisitic μ-mesons in neon 793

Palmer, R. B. J., and Simons, H. A. B. : The variation of track length with angle of dip in photographic nuclear research emulsion 852
Parkinson, D. H., and Quarrington, J. E. : The atomic heat of sodium (L) . . 762
Parry, G., with Martin, D. G. E. : A search for low intensity gamma rays in the ThC.C′ and ThC″.D transitions 1177
Pattenden, N. J. : The slow neutron cross section of scandium 104
Peat, S. W., and Ross, M. A. S. : Radioactive disintegration of ^{232}Th (R) . . 923
Pelzer, H., and Fröhlich, H. : Plasma oscillations and energy loss of charged particles in solids 525
Pendlebury, E. D. : General perturbation theory in neutronics 474
Perks, M. A. : The quadrupole moments of odd A nuclei (R) 1083
Perry, W. E. : Comparison of British and United States national radium standards (L) 942
Pillow, M. E. : Intensities in band systems of CH (R) 547

PAGE

Podolanski, J. (the late), with Umezawa, H., and Oneda, S.: Commutation relations between different fields 503

Pople, J. A.: The electronic spectra of aromatic molecules: II—A theoretical treatment of exctited states of alternant hydrocarbon molecules based on self-consistent molecular orbitals 81

Pople, J. A., with Buckingham, A. D.: Theoretical studies of the Kerr effect: I—deviations from a linear polarization law 905, corr. 1091

Pople, J. A., with Longuet-Higgins, H. C.: The electronic spectra of aromatic molecules: IV—Excited states of odd alternant hydrocarbon radicals and ions 591

Potts, R. B.: Combinatorial solution of the triangular Ising lattice 145

Price, B. T., with Eyeions, D. A., Owen, B. G., and Wilson, J. G.: The ionization loss of relativistic μ-mesons in neon 793

Price, P. C.: The radiative capture of alpha-particles in ^{14}N 553

Quarrington, J. E., with Parkinson, D. H.: The atomic heat of sodium (L) 762

van der Raay, H. B., Riddiford, L., and Coe, R. F.: Some proton synchrotron beam studies with the induction electrode 489

Radcliffe, J. M.: On lattice scattering in homopolar semiconductors 675

Rajaratnam, A., with Garton, W. R. S.: On the levels of the p^2- configuration in the arc spectra of Zn, Cd and Hg 1107

Raychaudhuri, A.: Note on the network approximation in metals (R) 439

Reasbeck, P., with Allen, R. A., Burcham, W. E., Chackett, K. F., and Munday, G. L.: Electron capture in the decay of sodium 22 681

Riddiford, L., van der Raay, H. B., and Coe, R. F.: Some proton synchrotron beam studies with the induction electrode 489

Riddiford, L., with Ledley, B.: Determination of proton synchrotron beam size with a crystal scintillator (R) 836

Ritter, G. J., and Series, G. W.: Nuclear electric quadrupole moment of potassium 39 (L) 450

Roberts, A. S., with Abraham, G., and Cohen, L.: The binding energies of ^{3}H and ^{4}He 265

Roberts, J., with Allen, W. D., and Ferguson, A. T. G.: Neutron-deuteron scattering in the range 80–200 kev 650

Robertson, H., with Hochberg, S., Massey, H. S. W., and Underhill, L. H.: The scattering of nucleons by alpha particles—determination of the spin–orbit interaction 746

Rose, B., with Dickson, J. M., and Salter, D. C.: Elastic scattering of polarized protons from complex nuclei 361

Rose, P. H., with Chapman, K. R., Matsukawa, E., and Stewardson, E. A.: The absolute measurement of differential cross sections for the nuclear scattering of low energy relativistic electrons (R) 928

Ross, M. A. S., Cochran, A. J., Hughes, J., and Feather, N.: Fluorescence yields of the L levels of Bi 612, (L) 942

Ross, M. A. S., with Bayman, B. F.: A nuclear emulsion study of the radioactive decay of actinium X(^{223}Ra) 110

Ross, M. A. S., with Peat, S. W.: Radioactive disintegration of ^{232}Th (R) 923

Runciman, W. A.: Absorption and emission spectra of bismuth-activated phosphors 647

Rushbrooke, G. S., and Wood, P. J.: On the high-temperature susceptibility for the Heisenberg model of a ferromagnet 1161

Rutherglen, J. G., with Grant, P. J., Flack, F. C., and Hutchinson, G. W.: Angular distributions and angular correlations in the reaction ^{23}Na(p, γ)^{24}Mg 369

Salter, D. C., with Dickson, J. M., and Rose, B.: Elastic scattering of polarized protons from complex nuclei 361

Sarma, N., and Allan, H. R.: A search for capture processes in alpha-particle and deuteron bombardments (R) 535

Satchler, G. R.: Gamma radiation following the surface scattering of nucleons 1037

PAGE
Satchler, G. R. : Polarization in nuclear reactions 1041
Satchler, G. R., with Gray, T. P. : Angular correlation parameters for oriented nuclei (L) 349
Scanlon, J. P., with Green, L. L., and Willmott, J. C. : Angular distributions from (d, n) reactions at 0·86 MEV deuteron energy 386
Schiff, B. : The cellular method for a close-packed hexagonal lattice, with applications to titanium 686
Schonland, D. S. : The use of overlapping intervals in multiple scattering measurements (R) 447
Seaton, M. J. : Cross sectoins for 2s–2p transitions in H and 3s–3p transitions in Na produced by electron and by proton impact 457
Segaert, O. J. A., with Lemmer, H. R., and Grace, M. A. : The decay of cobalt 57 . 701
Series, G. W., with Ritter, G. J. : Nuclear electric quadrupole moment of potassium 39 (L) 450
Shah, G. Z., with Gatha, K. M.: The total cross sections for the nuclear scattering of high energy nucleons 259
Shah, S. M. : Energy levels of mu-mesic atoms (L) 945
Shaw, D. F. : Scattering of 14·3 MEV neutrons by ^{4}He nuclei (R) 43
Sida, D. W. : The detachment of electrons from negative hydrogen ions by impact with neutral atoms 240
Simons, H. A. B., with Palmer, R. B. J. : The variation of track length with angle of dip in photographic nuclear research emulsion 852
Souch, A. E. : Decay of ^{70}As produced by ^{14}N bombardment of Cu (R) 760
Spiers, J. A. : A proposed notation for quantized angular momenta (L) 50
Spiers, V. M., with Fremlin, J. H. : The break-up of negative ions in the cyclotron . 398
Srivastava, R. C. : Performance of hot wire thermal diffusion columns 294
Stanley, C. R. : A new phenomenon associated with active nitrogen 709
Stevens, K. W. H., with Bleaney, B., Bogle, G. S., Cooke, A. B., Duffus, H. J., and O'Brien, M. C. M. : Paramagnetism of caesium titanium alum (L) 57
Stewardson, E. A., with Chapman, K. R., Matsukawa, E., and Rose, P. H. : The absolute measurement of differential cross sections for the nuclear scattering of low energy relativistic electrons (R) 928
Stewart, D. T. : Electron excitation functions of infra-red nitrogen spectra . . 404
Stone, A. P. : Calculation of isotope shifts in the spectrum of helium 1152
Swan, P. : The ionization by electrons of the excited 2s and 2p states of atomic hydrogen 1157
Swiatecki, W. J. : The effect of a potential gradient on the density of a degenerate Fermi gas 285
Symonds, J. L., with Burcham, W. E., and Young, J. D. : The production of ^{11}C from carbon by protons of energy between 200 and 950 MEV 1001

Tanner, N. W. : Angular distribution of γ-radiation from ^{9}Be(α, nγ)^{12}C (R) . . 1195
Temperley, H. N. V. : The liquid ' cell ' model applied to ^{3}He 1136
Tidman, B. A., with Chartres, D. A. : The scattering-in correction 841
Tinkham, M. : Paramagnetic resonance absorption by the ferrous ion 258
Tomita, Kazuhisa : On the state of solid hydrogen 214
Treacy, P. B. : The spin, energy and lifetime of ^{8}Be 204
Tredgold, R. H. : Anharmonicity and monomolecular reactions (R) 920
Trefall, H. : On the positive temperature effect in cosmic radiation . . . 625
Trefall, H. : On the positive temperature effect in the cosmic radiation and the μ–e decay 893
Trefall, H. : On the barometer effect on the hard component of the cosmic radiation 953

Umezawa, H., Podolanski, J., (the late) and Oneda, S. : Commutation relations between different fields 503
Underhill, L. H., with Hochberg, S., Massey, H. S. W., and Robertson, H. : The scattering of nucleons by alpha particles—determination of the spin–orbit interaction 746

PAGE

Vaidya, P .C. : A new static spherically symmetric solution of Einstein's unified field theory 260
Veall, N., with Emery, E. W. : The branching ratios of ^{86}Rb and ^{42}K (R) 346
Verdaguer, F., with Hancock, D. A. : The absolute determination of resonant energies for radiative capture of protons by sodium in the energy range below 530 kev (R) 1080

Walshaw, C. D. : Line widths in the 9·6μ band of ozone 530
Ward, A., and Grant, P. J. : The reaction ^{11}B(d, n)^{12}C 637
Warren, J. B., with Griffiths, G. M. : The gamma radiation from the reaction D(p, γ)^{3}He 781
Weale, J. W. : Alpha–gamma angular correlations and internal conversion measurements in ThCC″ and ThC′D 35
Weinmann, A. : Inequalities for molecular integrals (R) 1197
West, D., Batchelor, R., and Bradley, E. F. : The detection of mesic X-rays with pressurized proportional counters using cosmic ray μ-mesons stopped in carbon 801
Wilets, L., with Berg, R. : On the validity of the Weizsäcker inhomogeneity correction term 229
Wilkinson, D. H., Clegg, A. B., and Jones, G. A. : The radiative capture of protons of 669 kev in fluorine (R) 538
Williamson, E. M., with Flint, H. T. : A note on the relativistic cut-off (L) 354
Willmott, J. C., with Green, L. L., and Scanlon, J. P. : Angular distributions from (d, n) reactions at 0·86 Mev deuteron energy 386
Wilson, B. G., with McCormack, P. D., and McCusker, C. B. A. : A search for secondary maxima in cosmic ray transition curves : II (L) 1088
Wilson, B. G., with McCusker, C. B. A. : A search for secondary maxima in cosmic ray transition curves : I (L) 1086
Wilson, B. G., with McCusker, C. B. A., and Dardis, J. G. : The rates of penetrating showers at sea level 585
Wilson, J. G., with Eyeions, D. A., Owen, B. G., and Price, B. T. : The ionization loss of relativistic μ-mesons in neon 793
Wilson, J. G., with Owen, B. G. : Measurements of the momentum spectrum of μ-mesons at sea level : I—The momentum range 5×10^8 ev/c $-$ 2×10^{10} ev/c. 409
Wolfe, R. : The theory of the reflectivity of metals 121
Wolfendale, A. W., with Lloyd, J. L. : The scattering of μ-mesons in lead and iron 1045
Wood, P. J., with Rushbrooke, G. S. : On the high-temperature susceptibility for the Heisenberg model of a ferromagnet 1161
Wright, R. W., with Bastin, J. A. : The electrical conductivity of cadmium oxide at low temperatures 312

Yadav, H. N. : The nuclear scattering of electrons by uranium (L) 348
Yoshida, S., with Hayakawa, S. : Inelastic scattering by rotational excitation (R) 656
Young, J. D., with Burcham, W. E., and Symonds, J. L. : The production of ^{11}C from carbon by protons of energy between 200 and 950 Mev 1001

Zeeman, P. B., with Barrow, R. F., and Glaser, D. V. : Rotational analysis of bands of the $\mathrm{A}^3\Pi_{0^+}\mathrm{B}^3\Pi_1-\mathrm{X}^1\Sigma^+$ systems of indium monofluoride 962

INDEX TO REVIEWS OF BOOKS

PAGE
Asami, Y., and Higasi, K. (Eds.) : *Molecular Structure and Related Problems* 62
Bachman, C. H. : *Physics—A Descriptive Interpretation* 1095
Bacon, G. E. : *Neutron Diffraction* (*Monographs on the Physics and Chemistry of Materials*) 951
Beckerley, J. G., Kamen, M. D., and Schiff, L. I. (Eds.) : *Annual Review of Nuclear Science*, Vol. 4 660
Bell, E. T. : *Mathematics, Queen and Servant of Science* 61
Bellamy, E. H., and Moorhouse, R. G. : *Proceedings of the* 1954 *Glasgow Conference on Nuclear and Meson Physics* 949
Booth, A. D. : *Numerical Methods* 1093
Born, M., and Huang, K. : *Dynamical Theory of Crystal Lattices* 1092
Constant, F. W. : *Theoretical Physics—Mechanics of Particles, Rigid and Elastic Bodies, Fluids and Heat Flow* 129
Fretter, W. B. : *Introduction to Experimental Physics* 949
Frisch, O. R. : *Progress in Nuclear Physics*, Vol. 4 1203
Gentner, W., Maier-Leibnitz, H., and Bothe, W. : *An Atlas of Typical Expansion Chamber Photographs* 357
Goudet, G. : *Les fonctions de Bessel* (2nd Edition) 662
Guggenheim, E. A., and Prue, J. E. : *Physicochemical Calculations* 764
ter Haar, D. : *Statistical Mechanics* 356
Heitler, W. : *The Quantum Theory of Radiation* (3rd Edition) 128
Hirschfelder, J. O., Curtiss, C. F., and Bird, R. B. : *Molecular Theory of Gases and Liquids* 947
Hoel, P. G. : *Introduction to Mathematical Statistics* (2nd Edition) 765
Huntley, H. E. : *Nuclear Species* 358
Jaswon, M. A. : *The Theory of Cohesion* 1203
Johns, R. V., and Ware, W. F. : *Advanced Level Examples in Physics* 454
Klug, H. P., and Alexander, L. E. : *X-ray Diffraction Procedures* 263
Kronig, R. (Ed.) : *Textbook of Physics* 129
Lense, J. : *Reihenentwicklungen in der mathematischen Physik* 764
Lichnerowicz, A. : *Théories relativistes de la gravitation et de l'électromagnétisme* 1205
London, F., the late : *Superfluids*, Vol II—*Macroscopic Theory of Superfluid Helium* 662
Lösch, F. : *Siebenstellige Tafeln der elementaren transzendenten Funktionen* 1204
Mandl, F. : *Quantum Mechanics* 454
Pekar, S. I. : *Untersuchungen uber die Elektronentheorie der Kristalle* 947
Pohl, R. W. : *Einführung in die Physik, Band 3, Optik und Atomphysik* 130
Semat, H. : *Introduction to Atomic and Nuclear Physics* 766
Shankland, R. S. : *Atomic and Nuclear Physics* 1206
Struik, D. J. : *A Concise History of Mathematics* 359
Thirring, W. : *Einführung in die Quanten-Elektrodynamik* 948
U.S. Department of Commerce, N.B.S. Applied Mathematics Series 32 : *Table of Sine and Cosine Integrals for Arguments from* 10 *to* 100 358
U.S. Department of Commerce, N.B.S. Applied Mathematics Series 34 : *Table of the Gamma Function for Complex Arguments* 659
Wilson, A. H. : *The Theory of Metals* (2nd Edition) 62
Wilson, A. J. C. (Ed.) : *Structure Reports* Vols. 11 and 12 (1947–48, 1949) 59
Wilson, A. J. C. (Ed.) : *Structure Reports* Vol. 13 (1950) 60
Yourgrau, W., and Mandelstam, S. : *Variational Principles in Dynamics and Quantum Theory* 659
Ziller, A. : *Méthodes de différentiation et d'intégration numériques* (*applications*) 1204